EAC 2013, PRAGUE

European Aerosol Conference

1–6 September 2013

czech aerosol society

European Aerosol Conference 2013,

Prague, Czech Republic, September 1 to 6, 2013
Conference chair: Jiří Smolík, co-chair: Martin Braniš
Hosting Aerosol Association: Czech Aerosol Society (CAS)

Contents:

Welcome	p. 9
Technical information	pp. 13 - 16
Committees and Societies	pp. 17 - 18
Further Information	pp. 19 - 26
Conference Program Overview	pp. 29 – 31
Conference Program - orals	pp. 35 – 62
Conference Program – posters	pp. 73 - 113
Sponsors and exhibitors	pp. 115 – 131

Abstracts:

Monday, September 2, 2013

Plenary lecture: Aerosol particles in the marine environment by Merete Bilde	pp. 132 - 133
Session: Atmospheric Aerosols, *Remote sensing and optical properties of aerosols*	pp. 134 – 141
Session: Atmospheric Aerosols, *SOA and aerosol hygroscopicity*	pp. 142 - 149
Session: Aerosol Chemistry, *Chemistry of organic aerosols 1*	pp. 150 – 158
Session: Indoor and Working Place Aerosols, *Indoor environment*	pp. 159 - 166
Session: Instrumentation, *New techniques*	pp. 167 - 175
Special Session: PMx, *Source apportionment-AMS and carbon based*	pp. 176 - 184
Session: Instrumentation, *Combustion aerosol*	

and chemical measurements pp. 185 – 192
Session: Aerosol Modelling,
Models for aerosol emission and nucleation pp. 193 – 199
Session: Combustion Aerosols, *Characterization methods of combustion aerosols* pp. 200 – 208
Session: PMx, *Urban PMx* pp. 209 – 216
Session: Aerosol-based Nanotechnology
Applications of engineered nanoparticles pp. 217 – 224
Special Session: Aerosol Chemistry
Radical chemistry and aerosol formation pp. 225 – 232

Poster Session A: *Atmospheric Aerosols* pp. 233 - 451
Posters A001 to A229

Tuesday, September 3, 2013

Plenary lecture: Primary Biological Atmospheric Aerosols
By Ruprecht Jaenicke pp. 452 – 454

Session: Atmospheric Aerosols
Carbonaceous aerosols pp. 455 – 463
Session: Atmospheric Aerosols
New particle formation between ground and free troposphere pp. 464 – 472
Session: Aerosol Chemistry
Chemistry of organic aerosols 2 pp. 473 – 481
Session: Indoor and Working Place Aerosols
Workplace exposure pp. 482 - 490
Session: Instrumentation
Ambient aerosol instrumentation pp. 491 - 499
Special Session: *PMx, Source apportionment-intercomparisons and trends* pp. 500 – 508
Session: Atmospheric Aerosols
New particle formation pp. 509 – 516
Session: Aerosol Modelling
Modelling aerosols in different environments pp. 517 – 524
Session: Combustion Aerosols

Combustion and industrial aerosols pp. 525 – 532
Session: PMx, *Urban and regional PMx* pp. 533 – 540
Session: Aerosol-based Nanotechnology
Fabrication of nanostructured materials pp. 541 – 548

Poster session B,
Aerosol Chemistry, Posters B001 – B063 pp. 549 – 611
Aerosol Modelling, Posters B064 – B125 pp. 612 – 668
Aerosol-based Nanotechnology, B126 – B166 pp. 669 – 705
Combustion Aerosols, Posters B167 – B241 pp. 706 – 765
Reserve posters B223 – B237 pp. 766 – 780

Wednesday, September 4, 2013

Plenary lecture: The Dynamics of Indoor Aerosol:
What is important, where, when and why?
By Lidia Morawska pp. 781 - 782

Session: Atmospheric Aerosols,
Physico-chemical properties and transport pp. 783 – 791
Session: Atmospheric Aerosols, *Urban aerosols-*
from particle counts to chemical compostion pp. 792 – 799
Session: Aerosol Modelling,
Modelling atmospheric aerosols pp. 800 – 808
Session: Indoor and Working Place Aerosols,
Chemistry / Instrumentation pp. 809 – 817
Session: Aerosol-based Nanotechnology,
Nanoparticle synthesis in the gas phase pp. 817 – 827
Special Session: Particle-Lung Interactions
Bioaerosols and health pp. 828 – 835

Thursday, September 5, 2013

Plenary lecture: Nucleation of vapours-molecular content of critical clusters and activation of nanoparticles
By Paul E. Wagner and P.M. Winkler pp. 836 - 837

Session: Atmospheric Aerosols
Aerosol cloud interaction pp. 838 – 846
Session: Atmospheric Aerosols, *Turbulent exchange, transport and transformation* pp. 847 - 855
Session: Combustion Aerosols,
Engines related emissions pp. 856 – 864
Session: Electrical Effects, *Electrical effects* pp. 865 – 873
Session: Fundamentals,
Nucleation theory and experiments pp. 874 – 882
Session: Aerosol Chemistry
Heterogeneous chemistry of aerosol pp. 883 – 890
Session: PMx, *Source-specific emissions of carbonaceous aerosol from combustion processes* pp. 891 – 898
Session: Particle-Lung Interactions,
Exposure and dosimetry pp. 899 – 906
Special Session: Combustion Aerosols,
Composition and health effects pp. 907 – 914
Session: Atmospheric Aerosols
Biomass burning and bioaerosols pp. 915 – 921
Special Session: Aerosol Modelling, Atmospheric Aerosols
European Year of Air Quality 2013 pp. 922 – 928

Poster session C

Electrical effects, Posters C001 – C009 pp. 929 – 938
Fundamentals, Posters C010 – C043 pp. 939 – 970
Instrumentation, Posters C044 – C083 pp. 971 – 1010
Particle-Lung Interactions, C084 – C098 pp. 1011 – 1025
Indoor and Working Place Aerosols,
Posters C099 – C154 pp. 1026 – 1081
PMx, Posters C155 – C201 pp. 1082 – 1128
Reserve Posters, C202 – C216 pp. 1129 – 1144

Friday, September 6, 2013

Plenary lecture: Urban aerosol: tendencies and challenges
By Imre Salma pp. 1145 – 1146

Session: Atmospheric Aerosols, *Aerosol-cloud interaction and climate effects of aerosols* pp. 1147 – 1155
Session: Atmospheric Aerosols, *Mineral dust, marine aerosols and others* pp. 1156 – 1164
Session: Fundamentals, *Aerosol properties and dynamics* pp. 1165 – 1173
Session: Aerosol Chemistry, *Chemical characterisation techniques for aerosols* pp. 1174 – 1182
Session: Particle-Lung Interactions, *PM toxicity* pp. 1183 - 1190

Handbook
EAC 2013, PRAGUE

czech aerosol society

EAC 2013 PRAGUE
European Aerosol Conference
1-6 September 2013

CAMBUSTION Aerosol Science

Centrifugal Particle Mass Analyzer

Classifies aerosol particles by their mass: charge ratio.

Forms an aerosol mass standard, (when combined with a unipolar charger andaerosol electrometer):

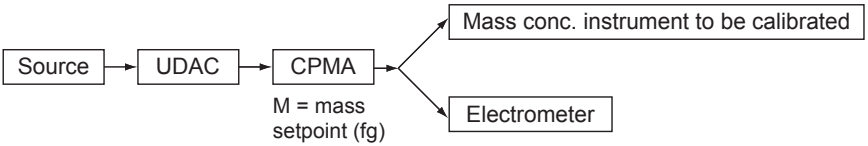

m_{total} = mass *setpoint* × indicated electrometer *concentration* + zero charge correction

(Symonds et al., Aerosol Science and Technology 47:8 i–iv)

Unipolar Diffusion Aerosol Charger

Places a high level of charge on aerosol particles.

Use in mass standard above.

Electrostatic Precipitator

Use in mass standard above, to quantify uncharged particles.

Includes high voltage supply

www.cambustion.com/aerosol
(+44) 1223 210250
sales@cambustion.com

AAAR - booth #204
EAC booth #14

Welcome to Prague

The 2013 European Aerosol Conference (EAC 2013) will be held in the historical city of Prague, Czech Republic, during the period of 1st-6th September 2013 under the auspices of the European Aerosol Assembly (EAA), a body that now represents 12 national or regional aerosol societies.
In the past, the European Aerosol Conference was organized in Prague under the umbrella of the Gesellschaft für Aerosolforschung in 1999 when the Czech Aerosol Society was established. During the EAC 2013 the Czech Aerosol Society will celebrate its 14th anniversary and the 11th year of membership in the European Aerosol Assembly. It is a pleasure and honour for the Czech Aerosol Society to organize such important meeting of scientists from all over the world.

Patronage

The conference will be held under the auspices of:

Prof. Jiří Drahoš
President of The Academy of Sciences of the Czech Republic

Prof. Václav Hampl
Rector, Charles University in Prague, Czech Republic

THE ACADEMY OF SCIENCES OF THE CZECH REPUBLIC

Table of Contents

Welcome to Prague 1

Patronage 1

Table of Contents 3

Maps 5

Conference Venue 5
Social Programme Venue 6

Committees 9

Organising Committee 9
Programme Committee 9
International Advisory Committee 9

The European Aerosol Assembly 10

The Czech Aerosol Society 10

General Information 11

Conference Venue 11
Conference Information 13

Social Programme 14

Welcome Reception 14
Concert 14
Conference Dinner 14

Meetings 15

Monday, September 2nd 15
Tuesday, September 3rd 15
Wednesday, September 4th 15
Thursday, September 5th 15
Friday, September 6th 15

EAA Working Group Meetings 16

Assembly 16

Presentation Information 17

Abstracts 17
Instructions for Oral Presentations 17
Poster Sessions Schedule 18

Programme Overview 21

Sunday, September 1st 21
Monday, September 2nd 21
Tuesday, September 3rd 22
Wednesday, September 4th 22
Thursday, September 5th 23
Friday, September 6th 23

Programme 27

Sunday, September 1st 27
Monday, September 2nd 29
Tuesday, September 3rd 37
Wednesday, September 4th 45
Thursday, September 5th 51
Friday, September 6th 59
Poster Session A 65
Poster Session B 79
Poster Session C 93

Sponsors and Exhibitors 107

Aerodyne Research, Inc. 107
Aerosol d.o.o. 107
AethLabs 108
Airmodus Ltd. 108
Cambustion Ltd. 109
Catalytic Instruments GmbH & Co. KG 109
Comde-Derenda GmbH 110
Copley Scientific Limited 110
Dekati Ltd. 111
DIGITEL Elektronik AG 111
Ecotech PTY Ltd. 112
Grimm Aerosol Technik GmbH & Co. KG 112
IONER® 113
Matter Aerosol 113
MCV, S.A. 114
Met One Instruments, Inc. 114
Metrohm Applikon B.V. 115
Naneos Particle Solutions GmbH 115
Palas® GmbH 116
Sunset Laboratory Inc. 116
Topas GmbH 117
TSI GmbH Germany 118
ECM ECO Monitoring 118
URG Corporation 119

Conference Secretariat 120

Exhibition Plan 121

Maps

Conference Venue

Clarion Congress Hotel Prague

Clarion Congress Hotel Prague representing a four-star comfort hotel with modern congress center is easily accessible by all means of transport - the Old Town can be reached within 10 minutes.

A.CLARION CONGRESS HOTEL PRAGUE

CLARION CONGRESS HOTEL PRAGUE

Social Programme Venue

Concert

Bethlehem Chapel / Betlémská kaple
Betlémské náměstí 255/4, 110 00 Prague 1

Take metro line B (yellow) from station "Vysočanská" to station "Můstek" (7 stops). The journey takes approximately 12 minutes.

A. CLARION CONGRESS HOTEL PRAGUE
B. BETHLEHEM CHAPEL

The Bethlehem Chapel is located about 500 meters from the "Můstek" metro station.

Conference Dinner

Municipal House / Obecní dům
Náměstí Republiky 1090/5, 110 00 Prague 1

Take metro line B (yellow) from station "Vysočanská" to station "Náměstí Republiky" (6 stops). The journey takes approximately 10 minutes.

A. CLARION CONGRESS HOTEL PRAGUE
B. BETHLEHEM CHAPEL

The Municipal House is located about 100 metres from the "Náměstí Republiky" metro station.

Committees

Organising Committee

- Martin Braniš (chair)
- Pavel Moravec
- Ludmila Mašková
- Pavel Mikuška
- Jakub Ondráček
- Naděžda Slezáčková Zíková
- Petr Vodička

Programme Committee

- Jiří Smolík (chair)
- Vladimír Havránek
- Zdeněk Kožíšek
- Jaroslav Schwarz
- Zbyněk Večeřa
- Vladimír Ždímal

International Advisory Committee

- Lucas Alados Arboledas
- Christoph Asbach
- Ari Asmi
- George Biskos
- Andrei Bologa
- David Broday
- Jeroen Buters
- Ian Colbeck
- Aladar Czitrovszky
- Yannis Drossinos
- Ian Ford
- Martin Gysel
- Regina Hitzenberger
- Yoshi Inuma
- Martina Krämer
- Mihalis Lazaridis
- Willy Maenhaut
- Francois-Xavier Ouf
- Manabu Shiraiwa
- Olli Sippula
- Wendelin Stark
- Birgit Wehner
- Sabine Wurtzer
- Caner Yurteri

The European Aerosol Assembly

The European Aerosol Assembly (EAA) is the organisation which has the responsibility to plan for the future hosting of European Aerosol Conferences, as well as to promote the development of the field of aerosol science through its working groups. It consists of 12 national or regional societies across Europe, though membership of these societies is not limited to European nationals, and operates under a formal constitution. The major activity of the EAA and its working groups takes place at the European Aerosol Conference, held in three out of every four years (the missing year being that in which the International Aerosol Conference, an event designed to foster links between research communities in all regions of the world, is held).

The Czech Aerosol Society

The Czech Aerosol Society (CAS) was formed in 1999 from the former Working Group on Aerosol Research of the Czech Society of Chemical Engineering at the ocassion of the Europen Aerosol Conference held in Prague in 1999. As given in its constitution the Society maintains a forum of researchers from various Czech Institutions and Universities in order to:

- **promote collaboration in all areas of aerosol research**
- **promote by means of meetings and publications the spread of information between the members and the public**
- **support education in aerosol related fields at all levels**
- **support international co-operation**

General Information

Conference Venue

The European Aerosol Conference 2013 is held at the Clarion Congress Hotel Prague represents a four-star comfort hotel with modern congress center and is easily accessible by all means of transport - the Old Town can be reached within 10 minutes.

Transport to the Conference Venue

By taxi

AAA Radiotaxi	+420 222 333 222, +420 729 331 133
CITY taxi	+ 420 257 257 257
Taxi PRAHA	+ 420 222 111 000

The maximum prices for taxi services in the district of the capital city of Prague:

Ride in the district of the capital city of Prague	**28,- CZK/km**
Boarding fee	**40,- CZK**
Waiting time	**6,- CZK/min**

A typical taxi fares:

From the Conference Venue to the city centre	**10-15 EUR**
From the Conference Venue to the Prague airport	**25-30 EUR**

By metro

Clarion Congress Hotel is located next door to Vysočanská metro station (yellow line B).

Basic ticket (ticket is valid for 90 minutes after validation)	**32,- CZK**
Short-term ticket (ticket is valid for 30 minutes after validation)	**24,- CZK**
1 day (24 hrs) ticket	**110,- CZK**
3 days (72 hrs) ticket	**310,- CZK**

Each fully registered participant will obtain FREE PASS FOR PRAGUE PUBLIC TRANSPORTATION valid for the period of September 1 – 6, 2013 together with registration materials at the registration desk.

Name Badges

Upon registration you will receive a name badge which should be worn at all conference sessions including social events.

Lunch, Coffee, Tea and Snacks

Coffee breaks will be served in the foyer of conference rooms (incl. in the registration fee). Lunches will be served in the hotel restaurant (tickets available at the registration desk). There are several other restaurants at the food court of the adjacent shopping mall Pheonix.

Internet

A Wi-Fi internet connection is available throughout the conference rooms.

Currency

The official currency of the Czech Republic is the Czech Crown = Česká koruna (CZK = Kč). Exchange of foreign currency is available at Prague international Airport and at most hotels, banks and exchange offices throughout the city. International credit cards are accepted for payments in hotels, restaurants and shops. Payment in cash in EUR is also available in some restaurants and shops, please ask for details on-site.

Drinking Water

Tap water is of good quality and can be consumed safely throughout the city. Bottled mineral and spring water is available in shops and restaurants.

Conference Information

Registration desk

Registration and information desk will be open at the conference floor of the Clarion Congress Hotel Prague as follows:

Sunday September 1	**10:00-21:00**
Monday September 2	**08:00-18:00**
Tuesday September 3	**08:30-18:00**
Wednesday September 4	**08:30-13:30**
Thursday September 5	**08:30-17:00**
Friday September 6	**08:30-14:00**

Contact details

Emergency number to the registration desk	**+420 606 918 277**
Email:	**eac2013@cbttravel.cz**

Exhibition

The exhibition is situated in the congress foyer of the Clarion Congress hotel, close to all meeting activities such as scientific sessions, poster exhibition, registration and coffee breaks and will be open to all participants throughout the duration of the conference.

Social Programme

Welcome Reception

Included in the registration fee.

Date:	**Sunday, September 1**
Venue:	**Foyer of the Clarion Congress hotel**
Time:	**19:00**

Concert

Included in the registration fee.

Date:	**Monday, September 2**
Venue:	**Bethlehem Chapel / Betlémská kaple**
Address:	**Betlémské náměstí 255/4, 110 00 Prague 1**
Time:	**19:00**

Bethlehem Chapel is located in the heart of Prague, the Old Town district. It was built as a holy place where sermons could be held in Czech. Jan Hus - university professor and Czech religious reformer - preached there between 1402 and 1413. As he was also the Rector of Charles University, it is believed that the Chapel was linked to this institution.

Conference Dinner

Date:	**Thursday, September 5, 2013**
Venue:	**Municipal House / Obecní dům**
Address:	**Náměstí Republiky 1090/5, 110 00 Prague 1**
Time:	**19:30**
Price:	**70€ per person (tickets available at the registration desk)**

The dinner will be served in a buffet style.

The Municipal House, a national cultural landmark, is among the most significant Art Nouveau buildings in Prague. It is located in the very centre of Prague, directly neighbouring the Powder Gate.

The most significant Czech painters and sculptors of the time participated in the decoration of the Municipal House. That list included: Jan Preisler, Mikoláš Aleš, Max Švabinský, František Ženíšek, Ladislav Šaloun, Josef Mařatka, Josef Václav Myslbek, Alfons Mucha.

Meetings

Monday, September 2nd

12:50-14:00	GAeF Board Meeting
18:00	Elsevier Board Meeting

Tuesday, September 3rd

12:50-14:00	IARA Meeting
18:00	GAeF General Assembly Meeting
18:00	Working Group Meetings

Wednesday, September 4th

12:50-14:00	EAA Board Meeting
afternoon	HEXACOMM
13:00-18:00	ACTRIS ACSM/AMS meeting

Thursday, September 5th

12:50-14:00	EAA Working Group Chairs Meeting

Friday, September 6th

13:00-18:00	ACTRIS ACSM/AMS meeting

EAA Working Group Meetings

The purpose of these meetings is to discuss general matters within the various topic areas to help plan future events, particularly the next EAC. All delegates are welcome.

Tuesday, September 3rd, 18:00, the following groups will meet at the Meridian Hall.

WG 1 **Aerosol-based Nanotechnology**
WG 2 **Aerosol Chemistry**
WG 3 **Aerosol Modelling**
WG 4 **Atmospheric Aerosols - Aerosol Processes and Properties**
WG 5 **Atmospheric Aerosols - Specific Aerosol Types**
WG 6 **Electrical Effects**
WG 7 **Fundamentals**
WG 8 **Combustion Aerosols**
WG 9 **Indoor and Working Place Aerosols**
WG 10 **Instrumentation**
WG 11 **Particle-Lung Interactions**
WG 12 **PMx**

Assembly

GAeF General Assembly will meet on Tuesday, September 3rd, 18:00, at the Aquarius & Taurus Hall.

Presentation Information

Abstracts

All abstracts will be published in electronic form and distributed to participants on USB memory key.

Instructions for Oral Presentations

Every speaker is entitled to speak for 20 minutes, including questions and answers. Due to the very tight schedule, we kindly ask that you respect these time limitations.

How to upload your oral presentation

All presentations should be brought to the Speaker´s Preview Room /QUADRANT/ any time during the official hours but at the least 2 hours before the section starts (or the day prior when your session is scheduled in the morning) or in the conference room one hour before your presentation.

A qualified technician will help you to upload your presentation to our system. Please use the USB key or CD / DVD-Rom. Speaker Preview Room opening times are the same as operating times of the registration desk.

Speaker's Preview Room opening times:

Sunday, September 1	**10:00-21:00**
Monday, September 2	**08:00-18:00**
Tuesday, September 3	**08:30-18:00**
Wednesday, September 4	**08:30-18:00**
Thursday, September 5	**08:30-17:00**
Friday, September 6	**08:30-14:00**

Instructions for oral reserve presentations

Oral reserve presentations are poster presentations that will also be offered a slot for oral presentation should a vacancy become available. Presenters should check with chairs at the start of the relevant oral session.

Poster Sessions Schedule

Posters will be located at the hall Zenit and Nadir. Participanst are kindly asked to display and also take down their poster according to this poster session schedule. For those who will not take down their poster on time please come to Quadrant room where they will be kept for you during the time of the conference. Presenting authors are kindly asked to be available to present their posters during the poster sessions time schedule.

Poster Session A:

Atmospheric Aerosols

Days:	**Sunday, September 1 - Monday, September 2**
Time to display:	**Sunday evening**
Time to uncover:	**Monday evening**
Presenatation time:	**Monday, 16:00-18:00**

Poster Session B:

Aerosol Chemistry, Aerosol Modelling, Aerosol-based Nanotechnology, Combustion Aerosols

Days:	**Tuesday, September 3 - Wednesday, September 4**
Time to display:	**Tuesday morning**
Time to uncover:	**Wednesday evening**
Presentation time:	**Tuesday, 16:00-18:00**

Poster Session C

Electrical Effects, Fundamentals, Indoor Working Place Aerosols, Instrumentation, Particle-Lung Interactions, PMx

Days:	**Thursday, September 5 - Friday, September 6**
Time to display:	**Thursday morning**
Time to uncover:	**Friday up to 12 o'clock**
Presentation time:	**Thursday, 16:00 - 18:00**

Late Posters

Late posters will be displayed according to their topics and will be located at the poster area (room Zenit and Nadir) as per poster sessions schedule.

WHAT'S NEW AT TSI SMPS™ 3938

Scanning Mobility
Particle Sizer™ Spectrometer

+ Very fast scans <10 second
+ High resolution 1% accuracy
+ Easy to use

TSI UNDERSTANDING, ACCELERATED

ECM ECO Monitoring

Understand more, visit:
www.tsi.com
www.ecomonitoring.com

or contact:
AnswersEU@tsi.com

Programme Overview

Sunday, September 1st

10:00-21:00	Registration
19:00	Welcome Reception, Exhibition Opening

Monday, September 2nd

8:00-18:00	Registration					
8:45-9:00	Opening Ceremony, A (Meridian)					
9:00-10:00	Plenary lecture: Merete Bilde - Aerosol particles in the marine environment, A (Meridian)					
10:00-10:30	Coffee break					
	A (Meridian)	B (Leo + Virgo)	C (Aquarius + Taurus)	D (Kepler)	E (Tycho)	F (Stella)
10:30-12:50	Atmospheric Aerosols	Atmospheric Aerosols	PMx (Special session)	Aerosol Chemistry	Indoor and Working Place Aerosols	Instrumentation
12:50-14:00	Lunch, GAeF Board Meeting					
14:00-16:00	Aerosol Modelling	Instrumentation	Combustion Aerosols	PMx	Aerosol Chemistry (Special Session)	Aerosol-based Nanotechnology
16:00-16:30	Coffee break					
16:00-18:00	Poster Session A - Authors' Presentations					
18:00	Elsevier Board Meeting					
19:00	Concert					

Tuesday, September 3rd

8:30-18:00	Registration					
9:00-10:00	Plenary lecture: Ruprecht Jaenicke - Primary Biological Atmospheric Aerosols, A (Meridian)					
10:00-10:30	Coffee break					
	A (Meridian)	B (Leo+Virgo)	C (Aquarius+Taurus)	D (Kepler)	E (Tycho)	F (Stella)
10:30-12:50	Atmospheric aerosols	Atmospheric aerosols	Aerosols chemistry	Indoor and Working Place Aerosols	Instrumentation	PMx (Special session)
12:50-14:00	Lunch, IARA Meeting					
14:00-16:00	Atmospheric aerosols	Aerosol modelling	Combustion Aerosols	PMx	Aerosol-based Nanotechnology	–
16:00-16:30	Coffee break					
16:00-18:00	Poster Session B - Authors' Presentations					
18:00	Working Group Meetings, GAeF General Assembly Meeting					

Wednesday, September 4th

8:30-13:30	Registration					
8:45-9:45	Plenary lecture: Lidia Morawska - The Dynamics of Indoor Aerosol: what is important, where, when and why?, A (Meridian)					
9:45-10:00	Smoluchowski Award, A (Meridian)					
10:00-10:30	Coffee break					
	A (Meridian)	B (Leo+Virgo)	C (Aquarius+Taurus)	D (Kepler)	E (Tycho)	F (Stella)
10:30-12:50	Atmospheric aerosols	Atmospheric aerosols	Aerosol modelling	Indoor and Working Place Aerosols	Aerosol-based Nanotechnology	Particle-Lung Interactions (Special session)
12:50-14:00	Lunch, EAA Board Meeting					
14:00	Free Afernoon					

Thursday, September 5th

8:30-17:00	Registration					
9:00-10:00	Plenary lecture: Paul E. Wagner - Nucleation of vapours - molecular content of critical clusters and activation of nanoparticles, A (Meridian)					
10:00-10:30	Coffee break					
	A (Meridian)	B (Leo+Virgo)	C (Aquarius+Taurus)	D (Kepler)	E (Tycho)	F (Stella)
10:30-12:50	Atmospheric aerosols	Atmospheric aerosols	Combustion Aerosols	Electrical Effects	Fundamentals	–
12:50-14:00	Lunch, EAA Working Group Chairs Meeting					
14:00-16:00	Atmospheric aerosols	Aerosol chemistry	PMx	Combustion Aerosols	Aerosols modeling, Atmospheric aerosols (Special session)	Particle-Lung Interactions
16:00-16:30	Coffee break					
16:00-18:00	Poster Session C - Authors' Presentations					
19:30	Conference Dinner					

Friday, September 6th

8:30-14:00	Registration					
9:00-10:00	Plenary lecture: Imre Salma - Urban aerosol: tendencies and challenges, A (Meridian)					
10:00-10:30	Coffee break					
	A (Meridian)	B (Leo+Virgo)	C (Aquarius+Taurus)	D (Kepler)	E (Tycho)	F (Stella)
10:30-12:50	Atmospheric aerosols	Atmospheric aerosols	Aerosols chemistry	Fundamentals	Particle-Lung Interactions	–
12:50-14:00	Lunch					

GRIMM Aerosol Technik
continuous research

EDM 465 UFPC

ENVIRONMENTAL
Ultra Fine Particle Counter

IAQ

Your all-in-one solution provider for the measurement of airborne particles

Sizes from 0.8 nm to > 30 µm
Indoor & Outdoor
Counts, size distributions
mass, surface area, PM 10 / 2.5 / 1
Inhalable, thoracic, alveolic
Filter & ventilation testing
Particle generators

Nano

Satisfied customers for over 30 years.
Just contact us
or meet us face-to-face at the EAC!

Phone: +49 (0)8654 . 578-0
contact@grimm-aerosol.com

Enviro

GRIMM

www.GRIMM-aerosol.com

Programme

Sunday, September 1st

10:00-21:00 Registration
Room: Conference foyer

19.00 Welcome Reception, Exhibition Opening
Room: Conference foyer

Monday, September 2nd

8:45-9:00 **Opening Ceremony**
Room: A (Meridian)

9:00-10:00 **Plenary lecture: Aerosol particles in the marine environment**
Plenary speaker: Merete Bilde
Plenary chairs: Regina Hitzenberger, Ilona Riipinen
Room: A (Meridian)

10:00-10:30 Coffee break
Room: Conference foyer

10:30-12:50 **Session: Atmospheric Aerosols**
Remote sensing and optical properties of aerosols
Chairs: Lucas Alados Arboledas, Arnaud Apituley
Room: A (Meridian)

10:30-10:50 **Relationship between oxidation level and optical properties of secondary organic aerosol**
A. T. Lambe, C. D. Cappa, P. Massoli, T. B. Onasch, S. D. Forestieri, A. T. Martin, M. J. Cummings, D. R. Croasdale, W. H. Brune, D. R. Worsnop, P. Davidovits

10:50-11:10 **Satellite and ground-based retrievals of aerosol optical properties in Arctic (2003-2011)**
P. Glantz, M. Tesche, K. Stebel, A. Herber, H. Struthers, J. Karlsson, A. Bourassa, L. Thomason, M. Maturilli

11:10-11:30 **iSPEX: First Results of Aerosols Measured by Smartphones in The Netherlands**
A. Apituley, iSPEX team

11:30-11:50 **Operational boundary layer height determination with in-situ and ground-based remote sensing instruments: validation and first climatology on the Swiss plateau**
C. Praz, M. Collaud Coen, A. Haefele, D. Ruffieux

11:50-12:10 **Assessment of parameterizations of optical properties and hygroscopic growth of aerosols**
A. R. Esteve, E. J. Highwood, W. T. Morgan, H. Coe, R. G. Grainger, P. Brown, C. L. Ryder, K. Szpek, J. A. Martínez-Lozano

12:10-12:30 **The optical properties of aerosols in Amazonia: from natural biogenic to biomass burning particles**
Paulo Artaxo, Xuguang Chi, Henrique M. J. Barbosa, Luciana V. Rizzo, Andrea Arana, Joel F. Brito, Elisa T. Sena, Joel Schaefer, Meinrat O. Andreae

12:30-12:50 **In-situ absorption measurement of HULIS and mineral dust components as well as winter time ambient aerosol using multi-wavelength photoacoustic instrument. A laboratory and a field study**
T. Ajtai, N. Utry, Á. Filep, Z. Bozóki, G. Szabó

Reserve paper **Black carbon aerosol concentrations and mixing state in Pallas, Finland**
T. Raatikainen, D. Brus, A.-P. Hyvärinen, J. Svensson, H. Lihavainen

10:30-12:50 Session: Atmospheric Aerosols

SOA and aerosol hygroscopicity

Chairs: U. Baltensperger, M.R. Alfarra
Room: B (Leo+Virgo)

10:30-10:50 **Vapour pressures of substituted polycarboxylic acids are much lower than previously reported**
A. J. Huisman, U. K. Krieger, A. Zuend, C. Marcolli, Th. Peter

10:50-11:10 **Investigation of the effects of chemical and physical factors on the phase state of SOA particles**
A. Pajunoja, M. R. Alfarra, A. Buchholz, W. T. Hesson, G. B. McFiggans, A. Virtanen

11:10-11:30 **Impact of semi-volatiles on hygroscopic growth and CCN activity of secondary organic aerosol**
A. Buchholz, M. R. Alfarra, W. T. Hesson, G. McFiggans

11:30-11:50 **A new inlet for simultaneous gas and particle phase measurements coupled to a chemical ionisation high-resolution time-of-flight mass spectrometer**
C. Mohr, F. Lopez-Hilfiker, B. H. Lee, D. S. Covert, D. R. Worsnop, J. A. Thornton

11:50-12:10 **Gas and Particle Phase Acids in a Ponderosa Pine Forest**
H. Stark, R. L. N. Yatavelli, S. L. Thompson, J. R. Kimmel, B. B. Palm, D. A. Day, P. Campuzano-Jost, M. J. Cubison, J. T. Jayne, D. R. Worsnop, J. A. Thornton, J. L. Jimenez

12:10-12:30 **Hygroscopic Properties and Mixing state of Ultrafine Aerosol Particles over two Urban Background Sites**
S. Bezantakos, E. Konstenidou, K. Florou, A. Bougiatioti, K. Eleftheriadis, N. Mihalopoulos, A. Nenes, S. Pandis, G. Biskos

12:30- 12:50 **Profiling of hygroscopic properties during the Po-Valley PEGASOS campaign 2012**
B. Rosati, E. Weingartner, P. Zieger, M. Gysel, G. Wehrle, U. Baltensperger

Reserve paper **Observations on atmospheric electricity and aerosol-cloud interactions**
Hanna E. Manninen, Hannes Tammet, Antti Mäkelä, Jussi Haapalainen, Sander Mirme, Tuomo Nieminen, Alessandro Franchin, Tuukka Petäjä, Markku Kulmala, Urmas Hõrrak

10:30-12:50 Session: Aerosol Chemistry

Chemistry of organic aerosols 1

Chairs: Ivan Kourtchev, Yoshi Iinuma
Room: D (Kepler)

10:30-10:50 **Revisiting the formation of secondary organic aerosol from the photooxidation of anthropogenic precursors**
M. R Alfarra, A. Buchholz, W. T. Hesson, R. Lidster, I. White , A. Pajunoja, J. F. Hamilton, P. Monks, A. Virtanen, G. B. McFiggans

10:50-11:10 **Gas-Phase Measurements of Oxidized Organic Compounds Generated by a Potential Aerosol Mass (PAM) Reactor using Acetate Chemical Ionization High-Resolution Time-of-Flight Mass Spectrometry**
P. Chhabra, A. Lambe, M. Canagaratna, H. Stark, P. Massoli, J. Kimmel, J. Jayne, D. Worsnop

11:10-11:30 **Time-resolved chemical composition of chamber generated SOA originated from monoterpene oxidation**
A. Mutzel, O. Böge, A. Kahnt, Y. Iinuma, H. Herrmann

11:30-11:50 **Dependence of α-pinene secondary organic aerosol formation on relative humidity and aerosol surface distribution**
L. Pfaffenberger, P. Barmet, R. Wolf, S. M. Platt, I. El-Haddad, J. G. Slowik, J. Dommen, A. S. H. Prévôt, U. Baltensperger

11:50-12:10 **Characterization of secondary organic aerosol from ozonolysis of β-pinene**
Ågot K. Watne, Eva U. Emanuelsson, Anna Lutz, Evert Ljungström, Mattias Hallquist

12:10-12:30 **Formation of anthropogenic secondary organic aerosol (SOA) and its influence on biogenic SOA properties**
E. U. Emanuelsson, M. Hallquist, D.-F. Zhao, B. Bohn, H. Fuchs, B. Kammer, A. Kiendler-Scharr, S. Nehr, F. Rubach, R. Tillmann, A. Wahner, H.-C. Wu, K. Kristensen, M. Glasius, Y. Rudich, Th. F. Mentel

12:30-12:50 **Effect of Nucleation Precursors on the Atmospheric Oxidation of Organic Compounds**
J. Elm, M. Bilde, K. V. Mikkelsen

Reserve paper **Secondary organic aerosol formation in the ozonolysis of biogenic volatile organic compounds performed in a laminar flow reactor**
T. Braure, V. Riffault, A. Tomas, M. Duncianu, Y. Bedjanian, P. Coddeville

10:30-12:50 Session: Indoor and Working Place Aerosols

Indoor environment
Chairs: Ian Colbeck, Martin Braniš
Room: E (Tycho)

10:30-10:50 **Number concentration and modal Structure of indoor/outdoor fine particles in four European Cities**
M. Lazaridis, K. Eleftheriadis, V. Ždímal, J. Schwarz, Z. Wagner, J. Ondracek, Y. Drossinos, T. Glytsos, S. Vratolis, K. Torseth, J. Smolík

10:50-11:10 **Spatial variation of air pollutants in a multilevel office building**
C. He, L. Morawska

11:10-11:30 **Effect of Anti-idling Campaign on the Outdoor and Indoor Aerosol Exposure at Schools**
S. A. Grinshpun, M. Yermakov, J. Y. Kim, T. Reponen, C. Shaffer, P. Ryan

11:30-11:50 **Exposure assessment to air pollutants in Elderly Care Centers**
Almeida-Silva, S. M. Almeida, H. T. Wolterbeek

11:50-12:10 **Exposure to ultrafine particles in indoor and outdoor school environments across Barcelona (Spain)**
M. Viana, I. Rivas, J. Sunyer, L. Bouso, M. Álvarez, C. Sioutas, X. Querol, A. Alastuey

12:10-12:30 **Sources, sinks, chemical composition and transport of aerosol particles in a university lecture hall**
I. Salma, K. Dosztály, T. Borsós, T. Weidinger, G. Kristóf, N. Péter, Zs. Kertész

12:30-12:50 **The effect of size, location, occupancy and microclimatic factors on air quality of university lecture rooms**
M. Branis, K. Stupkova

Reserve paper **Particulate Matter in Indoor Aor in two Schools in Vienna, Austria**
A. Kasper-Giebl, N. Jankowski, K. Kassin, E. Can Cetintas, H. Bauer, H. Grothe

10:30 -12:50 Session: Instrumentation

New techniques
Chairs: Martin Fierz, Christof Asbach
Room: F (Stella)

10:30-10:50 **A fast-scanning DMA train for the precision quantification of nanoparticle dynamics**
P. M. Winkler, J. Ortega, P. H. McMurry, J. N. Smith

10:50-11:10 **Fast scanning mobility particle sizing system and classifier**
J. Farnsworth, F. Quant, H-G. Horn, B. Osmondson, R. Caldow

11:10-11:30 **A Drift Tube Ion Mobility Spectrometer (DT-IMS) combined with a Condensation Particle Counter for Analysis of Sub 10 nm Aerosol Particles**
Derek R. Oberreit, Peter H. McMurry, Christopher J. Hogan Jr.

11:30-11:50 **A new version of the Particle Size Magnifier for detection of airborne molecular clusters and nano-particles as small as 1 nm**
K. Lehtipalo, A. Franchin, J. Mikkilä, J. Vanhanen, J. Kangasluoma, T. Petäjä, M. Kulmala

11:50-12:10 **First results of a new Gas Aerosol Nucleation Spectrometer: GANS**
P. Dohányosová, E. Montoya, E. Ramiro, S. López-Vidal

12:10-12:30 **The versatile Size Analyzing Nuclei Counter (vSANC)**
T. Pinterich , P. M. Winkler , P. E. Wagner , M. Kulmala , A. Vrtala

12:30-12:50 **Charging efficiency of the single-wire corona unipolar charger with radial sheath flow**
V. Wattanamekhinkul, C.L. Chein, C.J. Tsai

Reserve paper **Application of broadband optical cavity methods to studying the optical properties of aerosols at short wavelengths**
E. M. Wilson, J. C.Wenger, D. S. Venables

10:30-12:50 Special Session: PMx

Source apportionment-AMS and carbon based
Chairs: André S. H. Prévôt, Regina Hitzenberger
Room: C (Aquarius+Taurus)

10:30-10:50 **ME-2 analysis of long-term on-line mass spectrometric data of non-refractory submicron aerosol in the city of Zurich**
F. Canonaco, J. G. Slowik, U. Baltensperger, A. S. H. Prévôt

10:50-11:10 **A Year-long C-TOF-AMS Dataset in London: Investigating Chemical Composition, Seasonal Trends and Sources of Aerosols**
D. E. Young, J. D. Allan, D. C. Green, P. I. Williams, H. Coe,

11:10-11:30 **Primary and secondary organic aerosol origin by combined gas-particle phase source apportionment**
M. Crippa, F. Canonaco, J. G. Slowik, I. El Haddad, P. F. DeCarlo, C. Mohr, M. F. Heringa, R. Chirico, N. Marchand, B. Temime-Roussel, E. Abidi, L. Poulain, A. Wiedensohler, U. Baltensperger, A. S. H. Prévôt

11:30-11:50 **Long-term monitoring, chemical composition and source apportionment study of PM2.5 in Augsburg, Germany**
R. M. Qadir, G. Abbaszade, J. Schnelle-Kreis, R. Zimmermann

11:50-12:10 **Composition and Source Identification of Ambient Single Particles during the NANO-INDUS 2012 Campaign in Dunkirk, France**
J. Arndt, R. Healy, A. Setyan, K. Deboudt, V. Riffault, A. Blondel, A. Anderson, L. Y. Alleman, S. Mbengue, P. Flament, J. Wenger

12:10-12:30 **Radiocarbon-based source apportionment of elemental carbon and organic carbon at a regional background site on Hainan Island, South China**
Y. L. Zhang, J. Li, G. Zhang, A. S. H. Prévôt, S. Szidat,

12:30-12:50 **Wood-burning emissions within a continuous-flow photooxidation reactor: Soot-Particle Aerosol Mass Spectrometer characterization**
J. C. Corbin, A. Keller, H. Burtscher, B. Sierau, U. Lohmann, A. A. Mensah

Reserve paper **Micromarkers of source-specific combustion aerosols**
O. B. Popovicheva, E. D. Kireeva, N. M.Persiantseva

12:50-14:00 Lunch break

14:00-16:00 Session: Instrumentation

Combustion aerosol and chemical measurements

Chairs: Markus Pesch, Michal Vojtíšek-Lom
Room: B (Leo+Virgo)

14:00-14:20 **Measurement of chemisorption on metallic nanoparticles using aerosol photoemission spectroscopy**
S. Onel, M. Seipenbusch

14:20-14:40 **Validation of an online, real-time, soft photon ionisation (SPI) time of flight mass spectrometer for mainstream tobacco smoke analysis**
J. Hawke, M. Bente Von Frowein

14:40-15:00 **An accurate, real-time and low-cost method to measure biomass smoke**
Yungang Wang, Daniel L. Wilson, Philip K. Hopke, Ashok J. Gadgil

15:00-15:20 **Multi-wavelength characterization of carbonaceous aerosol**
P. Prati, V. Ariola, V. Bernardoni, M.C. Bove, G. Calzolai, M. Chiari, F. Lucarelli, D. Massabò, S. Nava, A. Piazzalunga, G. Valli, R. Vecchi

15:20-15:40 **Characterization of Black Carbon concentration, sources and age using an Aethalometer AE33**
L. Drinovec, G. Močnik, J. E. Petit, J. Sciare, O. Favez, P. Zotter, R. Wolf, A. S. H. Prévôt, A. D. A. Hansen

15:40-16:00 **Hyphenation of a Thermal/Optical Carbon Analyzer to photo-ionization mass spectrometry for determination of the organic content of aerosol particles**
T. Streibel, J. Grabowsky, J. C. Chow, J. G. Watson, R. Zimmermann

Reserve paper **Organic aerosol speciation with in-situ thermal desorption gas chromatography: a brief history of the TAG instrument**
N. M. Kreisberg, S. V. Hering, A. P. Teng, G. Isaacman, Y. Zhao, D. R. Worton, A. W. H. Chan, B. J. Williams, J. T. Jayne, A. T. Lambe, T. Hohaus, J. R. Kimmel, D. T. Sueper, W. Brooks, L. R. Williams, A. M. Trimborn, D. R. Worsnop, A. H. Goldstein

14:00-16:00 Session: Aerosol Modelling

Models for aerosol emission and nucleation

Chairs: Sabine Wurzler, Michael Boy
Room: A (Meridian)

14:00- 14:20 **Contribution of ion-assisted nucleation to new particle formation in a tropical boundary layer**
V. P. Kanawade, S. N. Tripathi, D. K. Siingh, A. S. Gautam A. K. Srivastava, A. K. Kamra

14:20-14:40 **The role of sulphuric acid in the formation of atmospheric particles based on a long-term explicit modelling approach**
M. Boy, L. Zhou, D. Mogensen, A. Sogachev, S. Smolander

14:40-15:00 **Hydration of Sulfuric Acid Clusters and the Impact of Bases**
H. Henschel, I. K. Ortega, O. Kupiainen, T. Olenius, T. Kurtén, H. Vehkamäki

15:00-15:20 **Simulations of SOA formation from alpha-pinene ozonolysis and photo-oxidation in chamber experiments**
G. Capes, D. Lowe, G. McFiggans

15:20-15:40 **Effects of electric vehicles on air quality in street canyons**
T. Schöllnhammer, F. Lommes, T. Schulz, H. Hebbinghaus, S. Wurzler

15:40-16:00 **Remapping of aerosol emissions in a modal models as a source of error**
T. Korhola, H. Kokkola, H. Korhonen, A.-I. Partanen, A. Laaksonen, S. Romakkaniemi

Reserve paper **Impact of biogenic emissions on PM2.5 concentration over Europe**
E. Tagaris, R. E. P. Sotiropoulou, N. Gounaris, S. Andronopoulos, D. Vlachogiannis

14:00-16:00 Session: Combustion Aerosols

Characterization methods of combustion aerosols
Chairs: F.X. Ouf, N. Ivleva
Room: C (Aquarius+Taurus)

14:00-14:20 **Automatized determination of the primary particles size of soot aggregates by TEM image analysis**
A. Bescond, J. Yon, C. Rozé, F. X. Ouf

14:20-14:40 **Electrical Conductivity Measurements in Combination with Raman Microspectroscopy and Temperature Programmed Oxidation for Analysis of Microstructure and Reactivity of Soot**
B. Grob, F. Knoller, N. P. Ivleva, R. Niessner

14:40-15:00 **Aerosol mass spectrometry of refractory black carbon containing particles**
T. B. Onasch, E. C. Fortner, P. Massoli, L. R. Williams, A. T. Lambe, A. M. Trimborn, J. T. Jayne, P. Davidovits, D. R. Worsnop

15:00-15:20 **REMPI-Laser-mass spectrometry: On-line and off-line analysis of the molecular signature of polycyclic aromatic hydrocarbons (PAH) in gas- and particle-phase of combustion aerosols**
R. Zimmermann, C. Radischat, O. Sippula, M. Kelbg, M. Sklorz, J. Passig, C. Busch, M. Oster, H. Harndorf, A. Walte, B. Stengel, T. Streibel

15:20-15:40 **Carbonaceous aerosols and variations in their light absorbing properties**
C. Linke, I. Ibrahim , R. Hitzenberger, M. Schnaiter

15:40-16:00 **Effective density of particles from different combustion conditions and engineered TiO2 nanoparticles**
J. Leskinen, M. Ihalainen, T. Torvela, J. Ruusunen, M. Miettinen, I. Nuutinen, J. Lyyränen, A. Auvinen, J. Joutsensaari, O. Sippula, J. Tissari, J. Jokiniemi

Reserve paper **Dilution affects particle properties originating from residential biomass combustion**
H. Lamberg, T. Kaivosoja, J. Leskinen, M. Kortelainen, A. Viren, H. Koponen, V. Tiihonen, M. Miettinen, J. Pyykönen, J. Jokiniemi, J. Tissari1

14:00-16:00 Session: PMx

Urban PMx
Chairs: Regina Hitzenberger, M. Van Poppel
Room: D (Kepler)

14:00-14:20 **Road surface dust load is dependent on road surface macro texture**
G. Blomqvist, M. Gustafsson, T. Lundberg

14:20-14:40 **Evaluating the use of dust suppressant to control local PM10 concentrations**
G. W. Fuller, B. Barratt, D. Carslaw, D. Green, A. H. Tremper

14:40-15:00 **CHEMKAR PM10: A year-long chemical characterization of PM10 in Flanders (Belgium) in 4 major cities and 3 types of locations**
J. Vercauteren , D. Roet, C. Matheeussen, E. Roekens, R. Vermeylen, W. Maenhaut, M. Claeys

15:00-15:20 **Non-exhaust PMx emissions from road traffic**
M. Maasikmets, , E. Teinemaa, T. Arumäe, V. Kimmel

15:20-15:40 **Atmospheric particulate mercury in the megacity Beijing – spatio-temporal variations, sources, and efficiency of mitigation measures**
N. J. Schleicher, J. Schäfer, G. Blanc, Y. Chen, F. Chai, S. Wang, S. Norra

15:40-16:00 **Air Quality Study within Steel Works Town in the UK**
R. Vecchi, S. Nava, G. Calzolai, F. Lucarelli, G. Valli, D. C. S. Beddows, A. M. Taiwo, R. M. Harrison

Reserve paper **Blue sky over the Ruhr – a review of the effectiveness of more than 50 years of air quality measures in Germany**
S. Wurzler, H. Hebbinghaus, P. Bruckmann, J. Friesel, U. Pfeffer

14:00-16:00 Session: Aerosol-based Nanotechnology

Applications of engineered nanoparticles
Chairs: J. Davis, G. Biskos
Room: F (Stella)

14:00-14:20 **Nanostructural engineering of Pt/C catalyst via spray drying for elec trocatalyst applications**
R. Balgis, G. M. Anilkumar, S. Sago, T. Ogi, K. Okuyama

14:20-14:40 **Gas sensors by flame aerosol deposition: Correlations between blood glucose and breath components from portable gas sensors and mass spectroscopy**
M. Righettoni, A. Schmid, A. Amann, S. E. Pratsinis

14:40-15:00 **Aerosol synthesis of porous Particles for structured layers as catalyst support for Fischer–Tropsch reaction**
L. Zeng, A. P. Weber

15:00-15:20 **Optical heating of nanorods in a laser tweezers**
P. B. Roder, B. E. Smith, P. J. Pauzauskie, E. J. Davis

15:20-15:40 **Correlation between Catalytic Activity and Production of Reactive Oxygen Species for Airborne Engineered Palladium Nanoparticles**
N. Neubauer, J. Palomaeki, H. Alenius, G. Kasper

15:40-16:00 **Substance release kinetics of spherical and non-spherical hybrid nanoparticles generated by aerosol-photopolymerization**
E. Akgün, M. Vranceanu, B. Sachweh, J. Hubbuch, M. Wörner

Reserve paper **Industrial by-products as precursors for gas-phase nanoparticle synthesis**
T. Karhunen, A. Lähde, T. Torvela, J. Jokiniemi

14:00-16:00 Special Session: Aerosol Chemistry

Radical chemistry and aerosol formation
Chairs: Thorsten Hoffman, Thomas Zeuch
Room: E (Tycho)

14:00-14:20 **Partially oxidized radicals – crucial intermediates during atmospheric aerosol formation**
J. Ahrens, P. T. M. Carlsson, C. Keunecke, M.-C. Maas, J. L. Wolf, T. Zeuch

14:20-14:40 **Formation of organosulfates from the sulfate radical induced oxidation of methacrolein and methyl vinyl ketone**
J. Schindelka, Y. Iinuma, D. Hoffmann, H. Herrmann

14:40-15:00 **The oxidation of alpha-pinene and limonene in a flow tube, investigated using the CI-APi-TOF**
M. P. Rissanen, M. Sipilä, M. Ehn, N. Sarnela, T. Jokinen, J. Kangasluoma, T. Petäjä, H. Junninen, D. Worsnop, M. Kulmala

15:00-15:20 **Ozonolysis of shikimic acid particles caught in the act**
S. Steimer, A. J. Huisman, U. K. Krieger, T. Peter, M. Lampimäki, G. Gržinić, E. Coz, B. Watts, J. Raabe, M. Ammann

15:20-15:40 **Aerosol particles in molecular beams: pickup of molecules, chemistry and photochemistry**
M. Fárník, V. Poterya, A. Pysanenko, J. Lengyel, J. Kočišek, J. Fedor

15:40-16:00 **Photoionization and infrared excitation of clusters with radical sites: Probing size and structure of neutral, sodium doped water clusters**
C. C. Pradzynski, U. Buck, R. M. Forck, F. Zurheide, T. Zeuch

Reserve paper **Pressure dependency of ozonolysis product formation of α-pinene focusing on low volatile compounds such as organic acids and dimeric compounds**
M. Beck, C. Keunecke, T. Zeuch, T. Hoffmann

16:00-16:30 Coffee break
Room: Conference foyer

16:00-18:00 Poster Session A - authors' presentations

19:00 Concert
Venue: Bethlemen Chapel

Tuesday, September 3rd

9:00-10:00 **Plenary lecture: Primary Biological Atmospheric Aerosols**

Plenary speaker: Ruprecht Jaenicke
Plenary chairs: Ian Colbeck, Andrei Bologa
Room: A (Meridian)

10:00-10:30 Coffee break
Room: Conference foyer

10:30-12:50 **Session: Atmospheric Aerosols**

Carbonaceous aerosols
Chairs: A. Petzold, U. Dusek
Room: A (Meridian)

10:30-10:50 **Recommendations for the interpretation of "black carbon" measurements**
A. Petzold, John A. Ogren

10:50-11:10 **Comparability of methods to measure black and elemental carbon in two European urban areas - site and seasonal similarities and differences**
R. Hitzenberger, J. Schwarz, I. Aschauer, R. Haindl, W. Ludwig, R Wagner, A. Wonaschuetz, G. Zecha, I. Ševčíková, P. Vodička , N. Zíková, V. Ždímal

11:10-11:30 **Seasonal variations of black carbon physical properties influenced by different sources in London urban environment**
Dantong Liu, James Allan, Michael Flynn, Dominique Young, Hugh Coe, Martin Gallagher

11:30-11:50 **Influence of vertical transport on the mixing state of black carbon at the high-alpine Jungfraujoch site**
M. Gysel, M. Laborde, N. Bukowiecki, E. Hammer, P. Zieger, U. Baltensperger, E. Weingartner

11:50-12:10 **Fossil and non-fossil sources of OC and EC in Switzerland for winter-smog episodes**
S. Szidat, P. Zotter, Y. L. Zhang,, V. G. Ciobanu, L. Wacker, Baltensperger, A. S. H. Prévôt

12:10-12:30 **Long-term variability of elemental and organic carbon in aerosols over Athens, Greece**
D. Paraskevopoulou, E. Liakakou, E. Gerasopoulos, N. Mihalopoulos

12:30-12:50 **Influence of the traffic on the black carbon particle mass concentration and particle number size distribution in La Paz, Bolivia**
A. Wiedensohler, K. Weinhold, M. Andrade, F. Velarde, I. Moreno, F. Avila

Reserve paper **Long-term observations of carbonaceous aerosols and related gaseous emissions near a crude-oil plant in South Italy**
M. Calvello, M. Lovallo F. Esposito, L. Mangiamele, G. Pavese

10:30-12:50 Session: Atmospheric Aerosols

New particle formation between ground and free troposphere

Chairs: Birgit Wehner, Michael Boy
Room: B (Leo+Virgo)

10:30-10:50 **Secondary particle formation in Arctic Russia**
E. Asmi, V. Kondratyev, D. Brus, H. Lihavainen, T. Laurila, M. Aurela, T. Uttal, V. Ivakhov, A. Makshtas

10:50-11:10 **New Aerosol Particle formation in Amazonia**
M. Matisans, P. Tunved, T. Hamburger, H. E. Manninen, J. Backman, L. Rizzo, P. Artaxo, I. Riipinen, E. Swietlicki, R. Krejci, M. Kulmala

11:10-11:30 **Formation and chemical properties of nano-sized particles in the lower free troposphere**
J. Tröstl, J. Duplissy, F. Bianchi, L. Rondo, H. Junninen, A. Adamov, A. P. Praplan, C. Fuchs, J. Dommen, E. Weingartner, U. Baltensperger

11:30-11:50 **Enhancement in CCN concentrations during new particle formation events**
Z. J. Wu, W. Birmili, L. Poulain, Z. B. Wang, A. Hamed, S. Henning, F. Stratmann, H. Herrmann

11:50-12:10 **NanoShip: Are there any new particle formation events over the North Sea?**
N. Kelbus, A. Massling, R. Lange, M. Fiebig, B. Henzing, M. Glasius, M. Bilde, Q. T. Nguyen, M. Moerman, G. de Leeuw, M. Dal Maso, Niku Kivekäs, A. Kristensson

12:10-12:30 **Onset of new particle formation in boundary layer**
H. E. Manninen, S. Mirme, M. Ehn, K. Leino, S. Schobesberger, H. Junninen, E. Järvinen, J. Kangasluoma, T. Nieminen, R. Tillmann, F. Angelini, G. P. Gobbi, A. Mirme, S. Decesari, A. Wahner, T. Petäjä, D. R. Worsnop, F. Rohrer, T. F. Mentel, M. Kulmala

12:30-12:50 **Events of increased particle number concentrations around trade wind cumuli near Barbados**
B. Wehner, F. Ditas, A. Wiedensohler, H. Siebert

Reserve paper **Characteristics of new particle formation events in Hungarian background air at K-puszta, 2008-2012**
Zs. Bécsi, Á. Molnár, K. Imre, P. P. Aalto

10:30-12:50 Session: Aerosol Chemistry

Chemistry of organic aerosols 2

Chairs: Magda Claeys, Josef Dommen
Room: C (Aquarius+Taurus)

10:30-10:50 **Novel smog chamber studies of wood burning emissions at low temperatures**
E. A. Bruns, I. El Haddad, S. M. Platt, B. Temime-Roussel, D. Kilic, J. G. Slowik, , A. Detournay, G. Močnik, N. Marchand, U. Baltensperger, A. S. H. Prévôt

10:50-11:10 **Atmospheric reactivity of biomass burning emitted compounds: methoxyphenols OH rate constants and Secondary Organic Aerosol formation**
A. Lauraguais, , C. Coeur-Tourneur, A. Cassez, J. C. Wenger, A. Seydi, K. Deboudt, , M. Fourmentin, M. Choël

11:10-11:30 **Particle-bound Methoxyphenols and their atmospheric nitration products as wood combustion tracers**
J. Orasche, J. Schnelle-Kreis, G. Abbaszade, M. Elsasser, R. Zimmermann

11:30-11:50 **Aqueous-phase photochemical oxidation and direct photolysis of vanillin as a model compound of methoxy-phenols from biomass burning**
Y. J. Li, H. Y. Cheung, D. D. Huang, W. H. Fan, L. E. Yu, C. K. Chan

11:50-12:10 **Secondary organic aerosol formation through aqueous phase photooxidation of aromatic compounds**
Z. Kitanovski, I. Grgić, A. Čusak, M. Claeys

12:10-12:30 **Photosensitized reactions at the air-sea interface: a potential source of aerosol**
R. Ciuraru, F. Bernard, S. Rossignol, L. Fine, C. George

12:30-12:50 **Black Carbon Containing Particles at a Rural Site Southeast of London during ClearfLo Winter IOP Detling Site**
L. R. Williams, S. Herndon, J. Jayne, A. Freedman, B. Brooks, J. Franklin, P. Massoli, E. Fortner, P. Chhabra, M. Zahniser, H. Stark, T. Onasch, M. R. Canagaratna, D. R. Worsnop, F. Lopez-Hilfiker, C. Mohr, J. Thornton, N. L. Ng, L. Xu, W. B. Knighton, M. Dubey, A. Aiken, K. Gorkowski, S. Liu, T. Martin, R. Coulter, S. Visser, M. Furger, P. Zotter, A. S. H. Prévôt

Reserve paper **Contribution of Inorganic aerosols and trace gases due to biomass burning during cooking hours at a rural site in India**
Sudha Singh, Gyan Prakash Gupta, Bablu Kumar, U. C. Kulshrestha

10:30-12:50 Session: Indoor and Working Place Aerosols

Workplace exposure

Chairs: Congrong He, Kaarle Hameri
Room: D (Kepler)

10:30-10:50 **Nanoparticle Release from Dental Composites during Restoration Grinding and Polishing**
C. Asbach, B. Hellack, B. Van Meerbeek, M. Peumans, P. Hoet, M. Wiemann, T. A. J. Kuhlbusch, K. L. Van Landuyt

10:50-11:10 **Micro and nanoparticles released from the thermal cutting of polystyrene foams and the associated isomerization of hexabromocyclododecane (HBCD) diastereomers**
Y.-Y. Kuo, H. Zhang, A. C. Gerecke, J. Wang

11:10-11:30 **Mixed dust exposure and health risk assessment in the ceramics industry**
B. Moroni, D. Cappelletti, F. Scardazza, S. Becagli, R. Traversi, R. Udisti

11:30-11:50 **A prototype of a new engineered nanoparticle monitoring device for workplaces: Device testing**
J. Ruusunen, J. Leskinen, T. Torvela, M. Ihalainen, T. Karhunen, I. K. Koponen, V. Niemelä, A. Lähde, J. Jokiniemi

11:50-12:10 **Occupational exposure to ultrafine particles – work place measurements**
A.-K. Viitanen, A. J. Koivisto, T. Kanerva, K. Hämeri

12:10-12:30 **The Use of Nuclepore Filter for Ambient and Workplace Nanoparticle Exposure Assessment**
Sheng-Chieh Chen, Jing Wang, Heinz Fissan, David Y.H. Pui

12:30-12:50 **Characterization and emission measurements of multi-walled carbon nanotube release during production**
L. Ludvigsson, C. Isaxon, P. T. Nilsson, M. Hedmer, H. Tinnerberg, M. E. Messing, J. Rissler, V. Skaug, A. Gudmundsson M. Bohgard, J. Pagels

Reserve paper **Particle characterization during abrasive treatment of composite material containing fibres by Cryo HRTEM**
K. I. Lieke, M. Levin, K. A. Jensen, I. K. Koponen

10:30-12:50 Session: Instrumentation

Ambient aerosol instrumentation

Chairs: Oliver Bischof, Wladyslaw Szymanski
Room: E (Tycho)

10:30-10:50 **Urban particulate matter monitoring on a mobile platform: a real time experiment on a long term scale**
B. Moroni, E. Scocchera, A. Piazzalunga, M. G. Ranalli , S. Castellini, D. Cappelletti

10:50-11:10 **A new aerosol conditioning system - Characterisation and first application**
M. Laborde, B. Rosati , P. Zieger, T. Petäjä, G. Kassell, D. Logan, E. Weingartner

11:10-11:30 **Particle number concentration monitor for atmospheric aerosols**
L. Hillemann, A. Zschoppe

11:30-11:50 **A new visual expansion-type Condensation Particle Counter**
B. Bühner, A. Wagner, A. Kürten, J. Curtius

11:50-12:10 **Development of a high volume air-into-liquid aerosol collector for PM2.5 and ultrafine particulate matter**
Dongbin Wang, Payam Pakbin, Arian Saffari, James J Schauer, Constantinos Sioutas

12:10-12:30 **Online Method for Size-Resolved Chemical Speciation of Nano-Particles**
A. Wagner, A. Kürten, C. Fuchs, J. Hoker, J. Curtius

12:30-12:50 **Development of an automated total carbon analyzer for atmospheric aerosols**
Y. Komazaki, Y. Kanaya

Reserve paper **Remotely operated PLUS-octocopter used as an aerosol measurement platform**
P. Madl, C. Oberauer, F. Steinhäusler

10:30-12:50 Special Session: PMx

Source apportionment-intercomparisons and trends

Chairs: Thomas Kuhlbusch, Willy Maenhaut
Room: F (Stella)

10:30-10:50 **European Intercomparison for Receptor Models Using a Synthetic Database**
C. A. Belis, F. Karagulian, F. Amato, M. Almeida, G. Argyropoulos, P. Artaxo, M. C. Bove , D. Cesari, D. Contini, E. Diapouli, K. Eleftheriadis, I. El Haddad, R. M. Harrison, S. Hellebust, E. Jang, H. Jorquera, D. Mooibroek, S.Nava, J. K. Nøjgaard, M. Pandolfi, M. G. Perrone, A. Pietrodangelo, G. Pirovano, P. Pokorná, P. Prati, C. Samara, D. Saraga, A. Sfetsos, G. Valli, R. Vecchi, M. Vestenius, E. Yubero, P. K. Hopke

10:50-11:10 **Ten-year study of fine aerosol at Sde Boker, Israel: time trends, seasonal variation, correlations, and source areas for anthropogenic elements**
W. Maenhaut, A. Karnieli, M. O. Andreae

11:10-11:30 **Impact of international shipping on European air quality**
M. Viana, A. Colette, J. van Aardenne, X. Querol, B. Degraeuwe, P. Hammingh, I. de Vlieger

11:30-11:50 **Hourly elemental composition and source identification of fine and coarse particulate matter in the high polluted industrial area of Taranto (Italy)**
F. Lucarelli, G. Calzolai, M. Chiari, S. Nava

11:50-12:10 **Source apportionment of size resolved particulate matter in European air pollution hot spot**
P. Pokorná, J. Hovorka, P. K. Hopke

12:10-12:30 **A mass closure and source apportionment study on PM1 in Milan (Italy)**
R. Vecchi, V. Bernardoni, M. Boretti, M. Elser, P. Fermo, A. Piazzalunga, R. Gonzalez Turrion, G. Valli

12:30-12:50 **Performance of the Chemical Mass Balance Model with Various Traffic Profiles**
Pallavi Pant, Jianxin Yin, Roy M. Harrison

Reserve paper **PMF source apportionment for fine and coarse PM in Athens, Greece: Evolution of source contributions over the last decade**
K. Eleftheriadis, E. Diapouli, A. Karanasiou, S. Vratolis, V. Vasilatou, M. Gini, D. Saraga, S. Pateraki, Th. Maggos

12:50-14:00 Lunch break

14:00-16:00 Atmospheric Aerosols

New particle formation
Chairs: Amar Hamed, Vladimír Ždímal
Room: A (Meridian)

14:00-14:20 **Role of organics in particle nucleation as viewed from a positive ion spectrometer**
F. Bianchi, J. Dommen, J. Tröstl, S. Schobesberger, H. Junninen, D. R. Worsnop, E. Weingartner, U. Baltensperger, the CLOUD collaboration

14:20-14:40 **Particle formation above natural and simulated salt lakes**
K. A. Kamilli, J. Ofner, T. Sattler, T. Krause, C. Zetzsch, A. Held

14:40-15:00 **Secondary aerosol formation from stress-induced biogenic emissions and possible climate feedbacks**
Th. F. Mentel, E. Kleist, S. Andres, M. Dal Maso, Th. Hohaus, A. Kiendler-Scharr, Y. Rudich, M. Springer, R. Tillmann, R. Uerlings, A. Wahner, J. Wildt

15:00-15:20 **Nanoparticle Growth Mechanisms During New Particle Formation**
M. V. Johnston, B. R. Bzdek, A. J. Horan, J. W. DePalma

15:20-15:40 **Comparative study of atmospheric particle formation using laboratory tools - COMPASS**
T.S. Sun, B. Bonn

15:40-16:00 **Estimating pre-existing aerosol effects on tropospheric aerosol production**
M. Dal Maso, L. Liao, H. Vehkamäki, H.Korhonen, K. E. J. Lehtinen

Reserve paper **Intercomparison of sulphuric acid measurements and neutral cluster composition in the lower free troposphere**
L. Rondo, M. Simon, H. Junninen, J. Duplisy, A. Praplan, A. Adamov, A. Kürten, M. Sipilä, F. Bianchi, J. Tröstl,E. Weingartner, U. Baltensperger, M. Kulmala, J. Curtius

14:00-16:00 Session: Aerosol Modelling

Modelling aerosols in different environments
Chairs: David Topping, Svetlana Tsyro
Room: B (Leo+Virgo)

14:00-14:20 **CFD prediction of the spatial distribution of particulate matter deposition indoors**
J. Grau-Bové , L. Mazzei , M. Strlič

14:20-14:40 **Correction of approximation errors with random forests applied to modelling of aerosol first indirect effect**
A. Lipponen, V. Kolehmainen, S. Romakkaniemi, H. Kokkola

14:40-15:00 **A simplified model to predict partitioning between the vapour and multiple condensed phases in mixed inorganic- organic aerosol particles**
D. Topping, G. McFiggans, M. Barley

15:00-15:20 **Wall losses of vapours distort yield calculations in SOA chamber experiments**
H. Kokkola, P. Yli-Pirilä, H. Korhonen, M. Vesterinen, H. Keskinen, S. Romakkaniemi, L. Hao, J. Joutsensaari, D. Worsnop, A. Virtanen, K. E. J. Lehtinen

15:20-15:40 **Development of the Secondary Organic Aerosol Processor (SOAP) model: multi-phase partitioning, non-ideality, phase separation and multi-layer representation of the semi-solid state of organic aerosols**
F. Couvidat, K. Sartelet

15:40-16:00 **Numerical studies of aerosol activation behaviour in warm clouds compared to in-situ measurements at the high-alpine site Jungfraujoch**
E. Hammer, C. R. Hoyle, B. P. Luo, M. Gysel, N. Bukowiecki, U. Lohmann, R. Vogt, C. Marcolli, T. Peter, U. Baltensperger, E. Weingartner

Reserve paper **Dependence of Aircraft Smoke Number on Black Carbon Size Distribution**
M. E. J. Stettler, J. J. Swanson, A. M. Boies

14:00-16:00 Session: Combustion Aerosols

Combustion and industrial aerosols
Chairs: A. Bologa, S. Grinshpun
Room: C (Aquarius+Taurus)

14:00-14:20 **Sulphuric Acid Aerosol Formation in Industrial Processes – Simulation and CPC measurement at a Pilot Plant**
L. Brachert, S. Sinanis, K. Schaber

14:20-14:40 **Inactivation of Aerosolized Spores in Combustion Environments Using Filled Nano-composite Materials: Study with Two Surrogates of Bacillus Anthracis**
S. A. Grinshpun, M. Yermakov, R. Indugula, X. He, T. Reponen, E. Dreizin, M. Schoenitz, S. Zhang, Y. Aly

14:40-15:00 **Size distribution and light scattering properties of standard test fire aerosols**
Zs. Jurányi, S. Lauber , A. Duric, M. Allemann, B. Schmid, M. Loepfe, H. Burtscher

15:00-15:20 **On-site estimation of secondary organic aerosol production potential from wood burning appliances**
A. Keller, J. C. Corbin, A. A. Mensah, B. Sierau, H. Burtscher

15:20-15:40 **Reference particles for toxicology studies of biomass combustion generated ash particles**
T. Torvela, O. Uski, A. Lähde, J. Grigonyte, T. Karhunen, T. Koponen, M.-R. Hirvonen, J. Jokiniemi

15:40-16:00 **Study of fine particle emissions from small scale wood chips combustion boiler**
A. Bologa, M. Ecker, H.-P. Rheinheimer, K. Woletz, H.-R. Paur

Reserve paper **Effects of severe congestion on PAH emissions from a heavy vehicle diesel engine**
M. Vojtisek-Lom, M. Pechout, M. Mazač, J. Topinka

14:00-16:00 Session: PMx

Urban and regional PMx

Chairs: Willy Maenhaut, Roberta Vecchi
Room: D (Kepler)

14:00-14:20 **EC/OC comparison exercise with same thermal protocols after temperature offsets correction**
P. Panteliadis, T. Hafkenscheid, B. Cary, W. Maenhaut

14:20-14:40 **The fossil fraction of carbon in PM2.5: Variations on seasonal and diurnal time scales**
U. Dusek, M. Monaco, A. Kappetijn, H. A. J. Meijer, S. Szidat, T. Röckmann

14:40-15:00 **Ultrafine particles at eight urban sites in Antwerp: instrument comparison and spatiotemporal variation in particle number concentration and size distribution**
J. Staelens, E. Frijns, P. Berghmans, G. P. A. Kos, C. Matheeussen, P. Panteliadis, B. Bergmans, E. P. Weijers, K. Wyche, E. Roekens

15:00-15:20 **Long term trend and weekly cycles of PM10 in the Po valley**
A. Bigi, G. Ghermandi

15:20-15:40 **Fugitive particle emissions from steel making: source characteristics and local air quality impact investigated with a mobile laboratory**
F. Drewnick, F. Freutel, S.-L. von der Weiden-Reinmüller, J. Fachinger, S. Borrmann

15:40-16:00 **Elemental composition and potential toxicity of airborne particles at some urban schools**
L. R. Crilley, G. A. Ayoko, E. Stelcer, D. D. Cohen, L. Morawaska

Reserve paper **Characterisation of the aerosol sources in Brindisi (Italy) harbour area within the CESAPO project: an overview of the experimental results**
D. Contini, D. Cesari, A. Donateo, A. Gambaro, A. Genga, G. Giovanelli, R. Giua, F.M. Grasso, E. Gregoris, P. Ielpo, S. Masieri, E. Merico, E. Morabito, A. Nocioni, T. Pastore, M. Siciliano

14:00-16:00 Session: Aerosol-based Nanotechnology

Fabrication of nanostructured materials with aerosol nanoparticles

Chairs: E. Kruis, J. Rosell-Llompart
Room: E (Tycho)

14:00-14:20 **Rapid synthesis of multi-layered & multi-functional polymer nanocomposite films**
C. O. Blattmann, G. A. Sotiriou, S. E. Pratsinis

14:20-14:40 **Electrostatic charging during electrospray deposition of polymer granular coatings**
E. Bodnár , N. Sochorakis , J. Grifoll , J. Rosell-Llompart

14:40-15:00 **Towards deposition of single layer graphene by an electrospray ion-assisted method**
L. B. Modesto-Lopez, O. V. Bilousov, J. M. Serres, J. Rosell-Llompart, J. J. Carvajal, F. Díaz

15:00-15:20 **Large-Area Patterning of Three-dimensional Nanoparticle Structure Arrays via Ion Assisted Aerosol Lithography (IAAL) and Multi-tip Spark Discharge**
K.-Y. Ha, H.-S. Choi, K.-N. Jung, K.-H. Han, J.-K. Lee, M. Choi

15:20-15:40 **Silver-decorated silica nanoparticles in a multilayered plasmonic structure**
J. Harra, M. Zdanowicz, M. Virkki, A. Rantamäki, M. Honkanen, G. Genty, M. Kauranen, J. M. Mäkelä

15:40-16:00 **Aerosol synthesis of semiconductor nanowires**
M. Heurlin, M. H. Magnusson, D. Lindgren, M. Ek, L. R. Wallenberg, L. Samuelson, K. Deppert

Reserve paper **Dry deposition of electrosprayed liquid suspensions**
S. Martin. B. Martinez-Vazquez, P. L. Garcia-Ybarra, J. L. Castillo

16:00-16:30 Coffee break
Room: Conference foyer

16:00-18:00 Poster Session B - authors' presentations

Wednesday, September 4th

8:45-9:45 **Plenary lecture: The Dynamics of Indoor Aerosol: what is important, where, when and why?**
Plenary speaker: Lidia Morawska
Plenary chairs: Mihalis Lazaridis, Erik Swietlicki
Room: A (Meridian)

9:45-10:00 **Smoluchowski Award**
Room: A (Meridian)

10:00-10:30 **Coffee break**
Room: Conference foyer

10:30-12:50 **Session: Atmospheric Aerosols**
Physico-chemical properties and transport
Chairs: J. Ström, E. Weingartner
Room: A (Meridian)

10:30-10:50 **Unmanned Aircraft Aerosol Sampling: Improvements in Capabilities and Sample Analyses**
C. F. Cahill, G. W. Walker, T. A. Cahill. C. R. Iceman, D. E. Barnes

10:50-11:10 **Aerosol mass spectrometry on a Zeppelin NT in the planetary boundary layer**
F. Rubach, A. Trimborn T. F. Mentel, A. Wahner, PEGASOS 0 Zeppelin Team

11:10-11:30 **Classification of aerosol size distributions observed at a tropical high altitude station**
T. Hamburger, M. Matisans, J. Ström, P. Tunved, G. Hoschild, J. Gross, S. Calderon, P. Hoffmann, T. Schmeissner, R. Krejci,

11:30-11:50 **Chemical composition (ions and selected metals) of size-segregated aerosol samples collected at Ny Alesund (Svalbard Island - Norway) during the 2010 and 2011 summer campaigns**
S. Becagli, M. Busetto, G. Calzolai, D. Cappelletti, D. Frosini, F. Lucarelli, A. Lupi, M. Mazzola, B. Moroni, S. Nava, M. Severi, R. Traversi, A. Viola, V. Vitale, R. Udisti

11:50-12:10 **Sub-micrometer non-refractory aerosol composition and their sources at Welgegund in the southern African grassland region**
P. Tiitta, V. Vakkari, M. Josipovic, P. Croteau, P. Beukes, P. Van Zyl, A. Venter, K. Jaars, J. Pienaar, S. Ng, M. Canagaratna, J. Jayne, V. Kerminen, M. Kulmala, A. Laaksonen, J. Jokiniemi, D. Worsnop, L. Laakso

12:10-12:30 **Chemical composition of the 300°C refractory fraction of the atmospheric aerosol at the Central European station Melpitz, Germany/Leibniz Institute for Tropospheric Research**
L. Poulain, W. Birmili, F. Canonaco, M. Crippa, Z. J. Wu, S. Nordmann, G. Spindler, A. S. H. Prévôt, A. Wiedensohler, H. Herrmann

12:30-12:50 **Seasonal and spatial variation of PM1 organic tracers in densely populated Mediterranean urban areas: Barcelona vs. Madrid**
B. L. van Drooge, M. Fontal, N. Bravo, P. Fernandez, M. A. Fernández, J. Muñoz-Arnanz, B. Jiménez, J. O. Grimalt

Reserve paper **Winter particulate matter (PM10) sources for an Austrian-Slovenian border region**
M. Kistler, E. C. Cetintas, H. Bauer, A. Kasper-Giebl

10:30-12:50 Session: Atmospheric Aerosols

Urban aerosols-from particle counts to chemical compostion
Chairs: Gary Fuller, Thomas Kuhlbusch
Room: B (Leo+Virgo)

10:30-10:50 **Nanoparticle emissions from road vehicles in Asian and European cities and allied health implications**
Prashant Kumar, Roy M. Harrison,

10:50-11:10 **Long-term Variations of Particle Sources in Beijing, China**
J. Gu, S. Breitner, A. Schneider, M. Hu, Z. J. Wu, Z. B. Wang, A. Wiedensohler, B. Wehner, U. Franck, J. Soentgen, A. Peters, J. Cyrys

11:10-11:30 **Road tunnels - particle properties, wet and dry conditions**
S. Janhall, M. Gustafsson, S. Abbasi, G. Blomqvist, A. Gudmundsson, C. Johansson, M. Norman, U. Olofsson, B. Sjovall

11:30-11:50 **Particle Number Size Distribution Statistics at Urban and Suburban Background and Remote Sites in Greece during Summer**
S. Vratolis, M. Gini, D. Siakavaras, S. Bezantakos, I. Stavroulas, N. Kalivitis, E. Kostenidou, E. Louvaris, G. Biskos, N. Mihalopoulos, S. Pandis, C. Pilinis, K. Eleftheriadis

11:50-12:10 **Highly time- and size-resolved measurements of trace elements in London during ClearfLo**
S. Visser, M. Furger, U. Flechsig, K. Appel, R. Dressler, P. Zotter, J. G. Slowik, A. S. H. Prevot, U. Baltensperger

12:10-12:30 **Exposure of schoolchildren to traffic-related air pollution: the HEAPS study**
Martine Van Poppel, Evi Dons, Luc Int Panis, S. De Prins, G. Koppen, Christina Matheeussen, Patrick Berghmans

12:30-12:50 **Aerosol particles from smoking, cooking, and various pyrotechnical devices: laboratory characterization and detection in a football stadium**
P. Faber, F. Drewnick, S. Borrmann

Reserve paper **Exposure of air pollutants inside vehicles while driving in road tunnels**
S. Silvergren, M. Norman, C. Johansson, B. Sjövall

10:30-12:50 Session: Aerosol Modelling

Modelling atmospheric aerosols
Chairs: Risto Makkonen, Ari Asmi
Room: C (Aquarius+Taurus)

10:30-10:50 **Linking climate change and air quality over Europe: Effects on aerosol concentrations**
A. G. Megaritis, C. Fountoukis, S. N. Pandis

10:50-11:10 **Particle Number Concentrations over Europe in 2030: The Role of Emissions and New Particle Formation**
L. Ahlm, J. Julin, C. Fountoukis, S. N. Pandis, I. Riipinen

11:10-11:30 **Predictions of aerosol extinction coefficients over Greece by means of a new modular software system**
P. E. Charalampidis Haralabidis, C. Pilinis , C. Fountoukis, A. Panagiotopoulou, S. N. Pandis

11:30-11:50 **Mitigation of Arctic warming by controlling European black carbon emissions (MACEB): modelling results**
J.-P. Pietikäinen, K. Kupiainen, Z. Klimont, A.-P. Hyvärinen, A. Laaksonen, H. Lihavainen

11:50-12:10 **Modeling biogenic secondary organic aerosol formation in the subarctic**
E. Hermansson, P. Roldin, A. Rusanen, D. Mogensen, S. Madronich, A. Hodzic, E. Swietlicki, M. Boy

12:10-12:30 **Taking the step from bulk to size-segregated aerosol description: Modelling of size distributions with the EMEP/MSC-W model**
M. Karl, S. Tsyro

12:30-12:50 **Contribution of primary emissions, secondary organic aerosol and nucleation on global aerosol number concentrations in NorESM**
R. Makkonen, Ø. Seland, A. Kirkevåg, T. Iversen, J. E. Kristjánsson

Reserve paper **Climate and biofuels in Brazil**
H. Vuollekoski, R. Makkonen, A. Asmi, R. Hillamo, T. Petäjä, M. Kulmala

10:30-12:50 Session: Indoor and Working Place Aerosols

Chemistry / Instrumentation
Chairs: Mihalis Lazaridis, Philip Hopke
Room: D (Kepler)

10:30-10:50 **The Effects of Mainstream and Sidestream Environmental Tobacco Smoke Composition for Enhanced Condensational Droplet Growth by Water Vapor**
X. Tang, Z. Zheng, H. S. Jung, A. Asa-Awuku

10:50-11:10 **A study on SVOC aerosol evaporation and its possible implications on workplace sampling**
G. C. Dragan, E. Karg, D. Breuer, M. Blaskowitz, H. Nordsieck, J. Schnelle-Kreis, R. Zimmermann

11:10-11:30 **Household products and indoor air quality: emission, reactivity and by-products in both gaseous and particulate phases**
A. Même, M. Nicolas, L. Chiappini, C. Rio, J. Nicolle, S. Rossignol, B. D'Anna

11:30-11:50 **Personal monitor for engineered nanoparticles using a MEMS cantilever balance**
S. Merzsch, H. S. Wasisto, I. Kirsch, A. Waag, E. Peiner, E. Uhde

11:50-12:10 **Test of indoor air cleaners**
B. Mølgaard, A. J. Koivisto, T. Hussein, K. Hämeri

12:10-12:30 **Use of portable particle counters for the assessment of residential exposure to indoor-generated particles**
A. Wierzbicka, G. Bekö, J. Toftum, G. Clausen

12:30-12:50 **Chemical composition of hookah smoke derived aerosol measured with an Aerosol Chemical Speciation Monitor**
P. L. Croteau, J. T. Jayne, D. R. Worsnop, T. Oh, C. DeForest Hauser

Reserve paper **An experimental approach to measure particle deposition in large circular ventilation ducts**
G. Da, E. Géhin, M. Ben-Othmane, M. Havet, C. Solliec, C. Motzkus

10:30-12:50 Session: Aerosol-based Nanotechnology

Nanoparticle synthesis in the gas phase

Chairs: A. Schmidt-Ott, S. Pratsinis
Room: E (Tycho)

10:30-10:50 **"Anti-agglomeration of spark discharge generated aerosols via unipolar air ions"**
Kyu-Tae Park, Massoud Massoudi Farid, Jungho Hwang

10:50-11:10 **A Controlled Spark Generator for Increased Nanoparticle Production**
T. V. Pfeiffer, P. Keijzer, A. Schmidt-Ott

11:10-11:30 **Experimental study on the transition from spark to arc discharge with respect to nanoparticle production**
E. Hontanon, J. M. Palomares, M. Stein, X. Guo, R. Engeln, H. Nirschl, F. E. Kruis

11:30-11:50 **Enclosed Flame Spray Pyrolysis: Control of Product Particle Characteristics by the Air Entrainment**
O. Waser, S. E. Pratsinis

11:50-12:10 **Flame spray synthesis of amorphous Indium-Zinc Oxide (IZO) nanoparticles and their electrical and optical properties - towards an application in field effect transistors**
D. Kilian, S. Polster, M.P.M. Jank, L. Frey, W. Peukert

12:10-12:30 **Parametric study of iron and iron-oxide nanoparticle synthesis via Aerosol Spray Pyrolysis**
G. Kastrinaki, S. Lorentzou, G. Karagiannakis, A. G. Konstandopoulos

12:30-12:50 **Aerosol synthesis of silicon germanium hybrid and alloy nanoparticles**
C. Mehringer, B. Butz, E. Spiecker, W. Peukert

Reserve paper **Synthesis of tailored organic-inorganic nanostructures by charge controlled coagulation**
S. Sigmund, E. Akgün, J. Meyer, M. Wörner, G. Kasper

10:30-12:50 Special Session: Particle-Lung Interactions

Bioaerosols and health

Chairs: Jeroen Buters, Otto Hanninen
Room: F (Stella)

10:30-10:50 **Daily values of bio-aerosols relevant in allergy: the biological exposome**
J. T. M. Buters, I. Weichenmeier, G. Pusch, E. Bartusel, D. Kupresanin, H. Behrendt, C. Schmidt-Weber

10:50-11:10 **Association of fungal tracers with biomass burning activity in northern Vietnam**
S. H. Chen, G. Engling

11:10-11:30 **Airborne influenza virus survival in the air environment**
O. Pyankov, O. Pyankova, E. V. Usachev, I. E. Agranovski

11:30-11:50 **Toxicological effects of the particulate emissions from diesel engines and wood combustion are affected by used technology**
P. I. Jalava, M. S. Happo, T. Brunner, I. Obernberger, T. Murtonen, P. Aakko-Saksa, J. Maki-Paakkanen, J. Jokiniemi, M.-R. Hirvonen

11:50-12:10 **Long-term effects of repeated exposure to fine and ultrafine particles on lung epithelial cells and fibroblasts**
L. Boublil, M. C. Borot, L. Martinon, J. Sciare, A. Baeza-Squiban

12:10-12:30 **Exposure and harm to combustion-derived particles: searching for biomarkers**
K. A. BeruBe, I. A. Guschina, A. J. Wlodarcyzk, Z. Prytherch, T. Jones, E. Karg, O. Sippula

12:30-12:50 **Studying the causes of health effects of combustion-derived aerosol in the framework of the HICE-Virtual Helmholtz Institute: First results on ship diesel and wood combustion aerosols**
R. Zimmermann, T. G. Dittmar, T. Kanashova, J. Buters, S. Öder, H. Paur, C. Schlager, S. Mülhopt, M. Dilger, C. Weiß, S. Diabate, H. Harndorf, B. Stengel, R. Rabe, K. Hiller, S. C. Sapccariu, K. A. BeruBe, A. J. Wlodarcyzk, O. Sippula, B. Michalke, T. Krebs, M. Kelbg, J. Tiggesbäumker, T. Streibel, E. Karg, S. Scholtes, J. Schnelle-Kreis, J. Lintelmann, M. Sklorz, M. Arteaga Salas, S. Klingbeil, J. Orasche, P. Richthammer, L. Müller, M. Elsasser, A. Rheda, B. Werner, J. Passig, T. Gröger, G. Abbaszade, C. Radischat

Reserve paper **Aerosol Deposition Measurement in the Model of Human Lungs**
F. Lizal, J. Jedelsky, J. Adam, M. Belka, M. Jicha

12:50-14:00 Lunch break

14:00 Free afternoon

Thursday, September 5th

9:00-10:00 **Plenary lecture: Nucleation of vapours-molecular content of critical clusters and activation of nanoparticles**

Plenary speaker: Paul E. Wagner

Plenary chairs: Ian Ford, Vladimír Ždímal

Room: A (Meridian)

10:00-10:30 Coffee break

Room: Conference foyer

10:30-10:50 **Session: Atmospheric Aerosols**

Aerosol cloud interaction

Chairs: Martin Gysel, Martina Krämer

Room: A (Meridian)

10:30-10:50 **Evaporation and condensation of semivolatile aerosol compounds in the DMT-CCN counter**
S. Romakkaniemi, A. Jaatinen, A. Laaksonen, A. Nenes, T. Raatikainen

10:50-11:10 **Long-term hygroscopic properties of ambient aerosol in a boreal environment, as measured by the size-resolved Cloud Condensation Nuclei counter (CCNc)**
M. Paramonov, M. Äijälä, P. P. Aalto, A. Asmi, N. Prisle, V.-M. Kerminen, M. Kulmala, T. Petäjä

11:10-11:30 **Mass spectrometric analysis of cloud droplet residuals in different orographic clouds**
J. Schneider, S. Mertes

11:30-11:50 **What controls cloud droplet number concentration of trade wind cumuli?**
F. Ditas, B. Wehner, H. Siebert, T. Schmeißner, M. Simmel, H. Wex, A. Wiedensohler

11:50-12:10 **Size-dependent aerosol activation properties measured in radiation and stratus lowering fog during the ParisFog 2012/13 field campaign**
E. Hammer, J. Hofer, M. Gysel, G. Roberts, N. Bukowiecki, J. C. Dupont, F. Burnet, M. Haeffelin, U. Baltensperger, E. Weingartner

12:10-12:30 **Assessment of cloud maximum supersaturation by size-resolved CCN measurements**
M. Krüger, D. Rose, Y. Cheng, H. Su, C. Pöhlker, J. Schneider, S. Schmidt, T. Klimach, S. Mertes, M. O. Andreae, U. Pöschl

12:30-12:50 **Comprehensive Investigations on the Ice Nucleation Efficiency of Natural Soil Dust Samples**
K. Höhler, I. Steinke, D. Cziczo, A. Danielczok, F. Frank, S. Garimella, O. Möhler, M. Raddatz, M. Schnaiter, O. Stetzer, E. Toprak

Reserve paper **Effect of local pollutant sources on aerosol-cloud interactions at Puijo measurement station**
H. Portin, A. Leskinen, A. Kortelainen, L. Hao, P. Miettinen, A. Jaatinen, S. Romakkaniemi, A. Laaksonen, K. E. J. Lehtinen, M. Komppula

10:30-10:50 Session: Atmospheric Aerosols

Turbulent exchange, transport and transformation

Chairs: Andreas Held, Birgit Wehner
Room: B (Leo+Virgo)

10:30-10:50 **Natural surfactants promote the uptake of soot-particles in aerosols**
T. Hede, C. Leck , L. Sun, Y. Tu, H. Ågren

10:50-11:10 **Annual cycle of Background Aerosol at Troll Station, Antarctica**
M. Fiebig, D. Hirdman, C. R. Lunder, J. A. Ogren, A. Stohl

11:10-11:30 **Monitoring ship emissions with continuous onshore SMPS measurements**
N. Kivekäs, R. Lange, A. Massling, Q. T. Nguyen M. Glasius, A. Kristensson

11:30-11:50 **Analysis of particle size distribution changes between three measurement sites in Northern Scandinavia**
R. Väänänen, E.-M. Kyrö, T. Nieminen, N. Kivekäs, H. Junninen, A. Virkkula, M. Dal Maso, H. Lihavainen, Y. Viisanen, B. Svenningsson, T. Holst, A. Arneth, P. P. Aalto, M. Kulmala, V.-M. Kerminen

11:50-12:10 **Airborne measurements of aerosol particle physical, optical and chemical properties in Finland**
E. Asmi, D. Brus, S. Carbone, R. Hillamo, J. Hatakka, T. Laurila, H. Lihavainen, E. Rouhe, S. Saarikoski, Y. Viisanen

12:10-12:30 **Annual measurement of size resolved particle fluxes in an urban environment**
M. J. Deventer, O. Klemm, F. Grießbaum

12:30-12:50 **New methods to quantify the contributions of rainout, washout and dry deposition to the total deposition flux of atmospheric aerosol on horizontal urban surfaces**
P. Laguionie, D. Maro, P. Roupsard, S. Percot, L. Solier, V. Ruban, M. Rozet, D. Hébert, O. Connan

Reserve paper **Air mass back trajectories and dry atmospheric aerosol mass size distributions in Prague**
J. Schwarz, L. Štefancová, W. Maenhaut, J. Smolík, V. Ždímal

10:30-10:50 Session: Combustion Aerosols

Engines related emissions

Chairs: J. Pagels, T. Rönkkö
Room: C (Aquarius+Taurus)

10:30-10:50 **Oxidation reactivity of (bio)diesel generated soot**
H. Bladt, N. P. Ivleva, R. Niessner

10:50-11:10 **Can scooter emissions dominate urban organic aerosol?**
I. El Haddad, S. M. Platt, A. A. Zardini, J. G. Slowik, M. Clairotte, C. Astorga, P. Barmet, R. Chirico, J. Dommen, U. Baltensperger, A. S. H. Prévôt

11:10-11:30 **Transformation of Black Carbon Aerosol in the Atmosphere – Observations from Smog Chamber Studies and Ambient Air**
J. H. Pagels, A. C. Eriksson, J. Rissler, E. Z. Nordin, C. Wittbom, P. T. Nilsson, A. Kristensson, P. Roldin, B. Svenningsson, E. Swietlicki

11:30-11:50 **Effect of atmospheric ageing on volatility and ROS of biodiesel exhaust nano-particles**
Alimohammad Pourkhesalian

11:50-12:10 **Real-world nanoparticle emissions of passenger cars and heavy duty diesel vehicles**
T. Rönkkö, L. Pirjola, P. Karjalainen, S. Saari, J. Keskinen

12:10-12:30 **Chemical composition of particulate and gas emissions from a 4-stroke marine diesel engine operated with heavy and distillate fuel oils**
O. Sippula, B. Stengel, M. Sklorz, T. Streibel, R. Rabe, H. Harndorf, J. Orasche, J. Lintelmann, B. Michalke, G. Abbaszade, C. Radischat, J. Schnelle-Kreis, R. Zimmermann

12:30-12:50 **Effects of secondary organic aerosols from gasoline exhaust on healthy and diseased respiratory epithelia**
M. Krapf, L. Künzi, N. Daher, J. Dommen, S. Schneider, N. Jeannet, S. Platt, J. G. Slowik, A. S. H. Prévôt, M. Kalberer, C. Sioutas, U. Baltensperger, M. Geiser

Reserve paper **Characterisation of solid and semi-volatile gas-turbine particulate matter using a catalytic stripper**
J. J. Swanson, T. J. Johnson, J. S. Olfert, M. P. Johnson, P. I. Williams, G. J. Smallwood, A. M. Boies

10:30-10:50 Session: Electrical Effects

Electrical effects
Chairs: Andrei Bologa, Caner Yurteri
Room: D (Kepler)

10:30-10:50 **Effects of induced gas flow on electrospray dynamics**
A. K. Arumugham, Jordi Grifoll, Joan Rosell-Llompart

10:50-11:10 **Reduction of fine particle emissions from small scale wood chips combustion boiler by use of compact electrostatic precipitator**
A. Bologa, M. Ecker, H.-P. Rheinheimer, K. Woletz, H.-R. Paur

11:10-11:30 **The formation of solid charged aerosol particles at the destruction of metal bodies and bodies of other materials**
A. B. Vatazhin, D. A. Golentsov, V. A. Likhter

11:30-11:50 **Generation of negative ion mobility standards using tetra-alkyl ammonium halide salts**
G. Steiner, J. Kangasluoma, M. Breitenlechner, E. Canaval, M. Sipilä, A. Hansel, M. Kulmala

11:50-12:10 **A New Effective Unipolar Charger for Calibration and Validation of Commercial Particle Number Measurement Systems**
B. Grob, R. Niessner

12:10-12:30 **The Unipolar Charging Rate and Bipolar Charge Distribution for Nonspherical Particles**
Ranganathan Gopalakrishnan, Christopher J. Hogan Jr.

12:30-12:50 **Bipolar diffusion charging of aerosol nanoparticles by means of AC-corona discharge and soft X-ray devices**
P. Kallinger, W. W. Szymanski

Reserve paper **Diurnal variation of small and large ion concentrations in an urban location**
E. R. Jayaratne, X. Ling, L. Morawska

10:30-10:50 Session: Fundamentals

Nucleation theory and experiments
Chairs: Paul M. Wikler, Yannis Drossinos
Room: E (Tycho)

10:30-10:50 **Nucleation in the Presence of Background Aerosol**
Charles Clement

10:50-11:10 **Numerical Investigation of the Effect of Hydrodynamic Mixing on Droplet Nucleation and Growth**
A. O. Alshaarawi, G. Scribano, K. Zhou, A. Attili, F. Bisetti

11:10-11:30 **Effect of Surface Energy Evolution on Particle Nucleation under GASP Conditions**
D. E. Rosner, M. Arias-Zugasti

11:30-11:50 **A heterogeneous nucleation theory with explicit account of vapor adsorption**
A. Laaksonen

11:50-12:10 **Heterogeneous Nucleation on Nanometer and Sub-Nanometer Sized Charged Atomic Clusters**
K. Barmpounis, A. Maisser, M. B. Attoui, G. Biskos, A. Schmidt-Ott

12:10-12:30 **Heterogeneous nucleation of sulfur vapor on tungsten oxide and NaCl nanoparticles: Determination of the radius and the contact angle of critical nucleus**
S. V. Valiulin, V. V. Karasev, S. V. Vosel, A. A. Onischuk, A. M. Baklanov

12:30-12:50 **A 19m deep well – a downward thermal diffusion cloud chamber?**
R. F. Holub, P. K. Hopke, J. Hovorka, P. Otahal, V. Ždímal

Reserve paper **Free energy barrier in the growth of sulfuric acid clusters**
T. Olenius, O. Kupiainen, I. K. Ortega, H. Vehkamäki

12:50-14:00 Lunch break

14:00-16:00 # Session: Aerosol Chemistry

Heterogeneous chemistry of aerosol
Chairs: Manabu Shiraiwa, Barbara D'Anna
Room: B (Leo+Virgo)

14:00-14:20 **Heterogeneous reaction of sulphur dioxide on Eyjafjallajökull's volcanic ash from the 2010 eruption**
Yoan Dupart, Laurence Burel, Pierre Delichere, Christian Geoage, Barbara D'Anna

14:20-14:40 **Estimating amorphous deliquescence time scales of SOA from biogenic and anthropogenic precursors: Implications for heterogeneous ice nucleation on glassy aerosols.**
T. Berkemeier, M. Shiraiwa, U. Pöschl, T. Koop

14:40-15:00 **Surfactants in cloud activation: do they matter?**
B. Mølgaard, J. Hong, M. Paramonov, T. Yli-Juuti, N. L. Prisle

15:00-15:20 **Gas-particle partitioning of atmospheric aerosols: Interplay of physical state, non-ideal mixing and morphology**
Manabu Shiraiwa, Andreas Zuend, Allan K. Bertram, John H. Seinfeld

15:20-15:40 **Role of organic and inorganic salts in atmospheric nanoparticle growth: a modelling study**
T. Yli-Juuti, K. Barsanti, L. Hildebrandt Ruiz, A.-J. Kieloaho, U. Makkonen, T. Petäjä, T. Ruuskanen, M. Kulmala, I. Riipinen

15:40-16:00 **Secondary organic aerosol production potential from diesel and gasoline vehicle exhaust under different ambient conditions**
S. M. Pieber, S. M. Platt, I. El Haddad, A. A. Zardini, R. Suarez-Bertoa, J. G. Slowik, R. Huang, S. Hellebust, B. Temime-roussel, N. Marchand, L. Drinovec, G. Mocnik, U. Baltensperger, C. Astorga, A. S. H. Prévôt

Reserve paper **Uptake of N2O5 to citric acid aerosol particles**
G. Gržinić, T. Bartels-Rausch, A. Türler, M. Ammann

14:00-16:00 Session: PMx

Source-specific emissions of carbonaceous aerosol from combustion processes

Chairs: Willy Maenhaut, Heinz Burtscher
Room: C (Aquarius+Taurus)

14:00-14:20 **Thermal/Optical Analysis of Major Elements (C, H, N, S, and O) for Particles from Different Emission Sources**
X. L. Wang, J. A. Robles, X. F. Yang, L.-W. A. Chen, J. C. Chow, J. G. Watson

14:20-14:40 **Assessing the Wintertime Contribution of Biomass Smoke to Organic Aerosol at 15 Sites in Switzerland by Analysing Filter Samples Using Aerosol Mass Spectrometry**
K. R. Dällenbach, I. El-Haddad, P. Zotter, J. Slowik, F. Canonaco, V. G. Ciobanu, A. Piazzalunga, P. Fermo, U. Baltensperger, S. Szidat, A. S. H. Prévôt

14:40-15:00 **Carbonaceous Aerosols Emitted from Light-Duty Vehicles Operating on Ethanol Fuel Blends**
M. D. Hays, R. Baldauf, B. J. George, J. Schmid, R. Snow, T. Long, W. Preston

15:00-15:20 **Emissions of a GDI vehicle operating with different composition engine oils**
L. Pirjola, T. Lähde, A. Malinen, J. Heikkilä, P. Karjalainen, T. Rönkkö, K. Kulmala, J. Keskinen

15:20-15:40 **Biodiesel with controlled physicochemical properties, a means to further reduce diesel engine particle emissions**
M. M. Rahman, A. M. Pourkhesalian, S. Stevanovic, M. J. Islam, H. Wang, B. Miljevic, P. Phamxuan, R. J. Brown, A. Masri, Z. D. Ristovski

15:40-16:00 **Preliminary measurement results on aerosol emission from materials combustion**
M. Targosz, C. Chivas-Joly, L. Saragoza, C. Motzkus, F. Gaie-Levrel

Reserve paper **Atmospheric tar balls: primary droplets from biomass burning?**
Á. Tóth, A. Hoffer, I. Nyírő-Kósa, M. Pósfai, A. Gelencsér

14:00-16:00 Session: Particle-Lung Interactions

Exposure and dosimetry

Chairs: Werner Hofmann, George Ferron
Room: F (Stella)

14:00-14:20 **Hygroscopic Particle Deposition Model for Rat Lungs**
G. A. Ferron, S. Upadhyay, R. Zimmermann, E. Karg

14:20-14:40 **Uptake of PM2.5 mass by respiratory tract region and particle size: Hypothetical estimates for the FINRISK Cohort, Helsinki, Finland**
O. Hänninen, R. Sorjamaa, P. Lipponen, L. Kangas, A. Karppinen, T. Yli-Tuomi

14:40-15:00 **Exposure to Particulate Matter and Pulmonary Function Status of Traffic wardens in Two Selected Local Government Areas in South-Western Nigeria**
Godson R.E.E Ana, Oluseye J. Olamijulo

15:00-15:20 **Dynamics of highly concentrated, fresh aerosols during inhalation**
L. Pichelstorfer, W. Hofmann

15:20-15:40 **Mechanistic exposure assessment of ultrafine PM**
D. A. Sarigiannis, Z. Samaras, E. Vouitsis, S. Karakitsios, V. Kalaitzis

15:40-16:00 **Using cloud motion for fast, efficient and realistic in vitro delivery of inhaled drugs to pulmonary cells**
A. G. Lenz, D. Cei, M. Schmidmeir, N. Pfister, G. Burgstaller, B. Lentner, O. Eickelberg, T. Stoeger, S. Meiners, O. Schmid

Reserve paper **Release of fine particles from birch pollen grains following impaction**
N. Visez, M. Choël, G. Loubert, G. Chassard, D. Petitprez

14:00-16:00 Special Session: Combustion Aerosols

Composition and health effects
Chairs: Ralf Zimmermann, Olli Sippula
Room: D (Kepler)

14:00-14:20 **Chemical Properties of Combustion Aerosols: An Overview**
M. D. Hays

14:20-14:40 **Chemical, physical and toxicological properties of biomass combustion aerosols**
M-R. Hirvonen, J. Jokiniemi

14:40-15:00 **Biological effects of ship diesel exposure on human bronchial epithelial cells – effects of gas phase vs. particle phase of different fuels at the air liquid interface**
S. Oeder, O. Sippula, B. Stengel, R. Rabe, H. Harndorf, H. Paur, C. Schlager, E. Karg, T. Streibel, C. Schmidt-Weber, R. Zimmermann, J. T. M. Buters

15:00-15:20 **Health relevant compounds in wood combustion and ship diesel aerosols: Evaluation of the toxicity due to polycyclic aromatic hydrocarbons**
J. Orasche, T. G. Dittmar, T. Kanashova, J. Buters, S. Öder, H. Paur, C. Schlager, S. Mülhopt, M. Dilger, C. Weiß, S. Diabate, H. Harndorf, B. Stengel, R. Rabe, K. Hiller, S. C. Sapccariu, K. A. BeruBe, A. J. Wlodarcyzk, O. Sippula, J. Jokiniemi, M.-R. Hirvonen, B. Michalke, T. Krebs, M. Kelbg, J. Tiggesbäumker, T. Streibel, E. Karg, G. Abbaszade, S. Scholtes, J. Schnelle-Kreis, J. Lintelmann, M. Sklorz, M. Arteaga Salas, S. Klingbeil, P. Richthammer, L. Müller, M. Elsasser, A. Rheda, B. Werner, J. Passig, T. Gröger, C. Radischat, R. Zimmermann

15:20-15:40 **Air-liquid interface exposure systems for the assessment of toxicity of combustion aerosols**
H.-R. Paur, S. Mülhopt, M. Dilger, C. Schlager, T. Krebs, R. Zimmermann, S. Diabaté, C. Weiss

15:40-16:00 **Oxidative potential of particulate matter in a major urban environment**
Frank J. Kelly, Ben Barratt, Cathryn Tonne, Ian Mudway

Reserve paper **A novel set-up for source characterization and human exposures of biomass combustion aerosols**
R. Nyström, E. Z. Nordin, J. H. Pagels, A. Blomberg, T. Sandström, C. Boman

14:00-16:00 Session: Atmospheric Aerosols

Biomass burning and bioaerosols
Chairs: J. Schneider, M.R. Alfarra
Room: A (Meridian)

14:00-14:20 **Particle characterisation during biomass burning events in Tasmania, Australia**
F. Reisen, C. P. Meyer, M. D. Keywood, S. Crumeyrolle

14:20-14:40 **Biomass burning layers measured during the Deep Convective Clouds and Chemistry experiment (DC3) with an airborne Single Particle Soot Photometer (SP2)**
K. Heimerl, B. Weinzierl, A. Minikin, D. Sauer, D. Fütterer, M. Lichtenstern, H. Schlager, J. P. Schwarz, M. Z. Markovic, A. E. Perring, D. W. Fahey, H. Huntrieser

14:40-15:00 **Airborne lidar observations of mineral dust and biomass burning aerosols**
F. Marenco, K. Turnbull, B. Johnson, J. Haywood, P. Rosenberg, L. Garcia-Carreras, J. B. McQuaid, V. Amiridis, E. Marinou, A. Tsekeri

15:00-15:20 **Primary particles and marker compounds from wood combustion in household stoves**
M. Maasikmets, , E. Teinemaa, K. Vainumäe, L. Parts, L. Lehes, T. Arumäe, V. Kimmel

15:20-15:40 **The comparison of long-term changes in the bioerosol components in Southwestern Siberia in the near-ground atmospheric layer and at the altitudes of 500 - 7000 m**
A. S. Safatov, G. A. Buryak, V. A. Vechkanov, I. S. Andreeva, S. T. Olkin, I. K. Reznikova, V. M. Generalov, M. Yu. Arshinov, B. D. Belan, D. V. Simonenkov, G. N. Tolmachev

15:40-16:00 **Filtration and inactivation of aerosolized bacteriophage MS2 with air ions and electric field**
J. Hyun, Y.-H. Joe, J. Hwang

Reserve paper **Measurements During The South American Biomass Burning Analysis (SAMBBA) Field Experiment**
J. D. Allan, W. T. Morgan, P. I. Williams, M. Flynn, E. Darbyshire, A. Hodgson, B. T. Johnson, J. M. Haywood, S. Freitas, K. Longo, P. Artaxo, H. Coe

14:00-16:00 Special Session: Aerosol Modelling, Atmospheric Aerosols

European Year of Air Quality 2013
Chairs: Alexander Schladitz, Markus Pesch, Sabine Wurzler
Room: E (Tycho)

14:00-14:20 **Experimental and modeling analyses of emission measurements for a heavy-duty diesel bus: the comparison between on-road and in-lab methods**
Y. J. Wang, Z. Tong, T. Rönkkö, J. Keskinen, L. Pirjola, K. M. Zhang

14:20-14:40 **Source apportionment of sub-micron particles in the urban background by Positive Matrix Factorization**
H. Yu, U. Quass, H. Kaminski, T. A. J. Kuhlbusch

14:40-15:00 **Air quality in a Mediterranean city-port: Particulate matter source apportionment using the WRF-CAMx modeling system**
A. Poupkou, N. Liora, A. Karagiannidis, T. Giannaros, D. Melas, A. Argiriou

15:00-15:20 **Size specific distribution of the atmospheric particulate persistent organic pollutants (POPs) on a seasonal scale**
Céline Degrendele, Krzysztof Okonski, Lisa Melymuk, Linda Landlová, Petr Kukučka, Jana Klánová

15:20-15:40 **Modelling multiphase night-time processes with WRF-Chem**
D. Lowe , S. Archer-Nicholls , W. Morgan , S. Utembe , G. McFiggans

15:40-16:00 **Air quality modeling of mega cities in Yangtze River Delta region**
L. L. Tang, B. Zhu, Y. J. Zhang, L. Tang

Reserve paper **Characterising the influence of anthropogenic emissions on regional background aerosols at the puy de Dome station in France**
E. J. Freney, E. Asmi, M. Hervo, C. Rose, A. Colomb, K. Sellegri

16:00-16:30 Coffee break
Room: Conference foyer

16:00-18:00 Poster Session C - authors' presentations

19:30 Conference Dinner
Venue: Municipal House

Friday, September 6th

9:00-10:00 **Plenary lecture: Urban aerosol: tendencies and challenges**

Plenary speaker: Imre Salma

Plenary chairs: Willy Maenhaut, Kostas Eleftheriadis

Room: A (Meridian)

10:00-10:30 Coffee break

Room: Conference foyer

10:30-12:50 **Session: Atmospheric Aerosols**

Aerosol-cloud interaction and climate effects of aerosols

Chairs: Helmut Horvath, Martin Gysel

Room: A (Meridian)

10:30-10:50 **Simplifying the water-affinity and CCN activation of complex organic aerosols: A model study**
I. Riipinen, N. Rastak, S. N. Pandis

10:50-11:10 **Marine Cloud Brightening - do implementation assumptions change its effectiveness?**
A. K. L. Jenkins, P. M. Forster

11:10-11:30 **The importance of organic compounds for the first aerosol indirect effect: sensitivity to cloud formation parameterizations and meteorological fields**
R. E. P. Sotiropoulou, E. Tagaris

11:30-11:50 **Local geological topsoil dust in the area of Rome: linking mineral composition, aerodynamic size and optical properties**
A. Pietrodangelo, R. Salzano, C. Bassani, S. Pareti, C. Perrino

11:50-12:10 **Modeling aerosol water uptake in the Arctic and its direct effect on climate**
N. Rastak, A. Ekman, S. Silvergren, P. Zieger, U. Wideqvist, J. Ström, B. Svenningsson, P. Tunved, I. Riipinen

12:10-12:30 **Pre-Industrial Atmospheric Black Carbon Concentrations in North America**
Liaquat Husain, Tanveer Ahmed

12:30-12:50 **Global model simulations of the impact of transport sectors emissions on atmospheric aerosol and climate**
M. Righi, J. Hendricks, R. Sausen

Reserve paper **Variations of levels of atmospheric electrical and meteorological parameters and natural radioactivity in response to heavy smog due to forest fires**
M. S. Cherepnev, A. V. Vukolov, I. I. Ippolitov, M. V. Kabanov, P. M. Nagorsky, Yu. A. Phalagov, S. V. Smirnov, V. S. Yakovleva

10:30-12:50 Session: Atmospheric Aerosols

Mineral dust, marine aerosols and others

Chairs: Alfred Wiedensohler, Francisco Jose Olmo
Room: B (Leo+Virgo)

10:30-10:50 **Below-cloud scavenging by snow and mixed precipitation events calculated from high temporal resolution in situ measurements**
G. Depuydt, O. Masson, J. L. Brenguier, C. Piot, J. L. Jaffrezo

10:50-11:10 **Diurnal and seasonal variations of (nano)aerosols in the Škocjan Caves, Slovenia, a natural treasure of planet Earth**
I. Grgić, I. Iskra, B. Podkrajšek, V. Debevec Gerjevič

11:10-11:30 **Aerosol Processes in PAH Infiltration and Population Exposure in Rome**
P. Lipponen, O. Hänninen, R. Sorjamaa, M. Gherardi, M. P. Gatto, A. Gordiani, A. Cecinato, P. Romagnoli, C. Gariazzo

11:30-11:50 **Two years of measured vertical profiles in the Arctic (Svalbard Islands): results from 2011-2012 spring-summer campaigns**
L. Ferrero, D. Cappelletti, B. Moroni, V. Vitale, R. Udisti, G. Sangiorgi, M. G. Perrone, M. Busetto, C. Lanconelli, M. Mazzola, A. Lupi, S. Becagli, R. Traversi, D. Frosini, M. Maturilli, R. Neuber, C. Ritter, J. Graeser, M. Fierz, G. Mocnik, E. Bolzacchini

11:50-12:10 **EMEP intensive measurements on mineral dust in PM10, summer 2012 and winter 2013**
W. Aas, X. Querol, F. Lucarelli, A. Alastuey, N. Pérez, H. Areskoug, V. Balan, J. N. Cape, M. Catrambone, D. Ceburnis, S. Conil, L. Gevorgyan, J. L. Jaffrezo, C. Hueglin, N. Mihalopoulos, M. Mitosinkova, T. Moreno, J.-P. Putaud, V. Riffault, K. Sellegri, G. Spindler

12:10-12:30 **The effect of hexanoic acid on the hygroscopic properties of sodium halide aerosols**
Lorena Miñambres, Estíbaliz Méndez, María N. Sánchez, Fernando Castaño, Francisco J. Basterretxea

12:30-12:50 **Marine Aerosol Hygroscopicity and Volatility, Measured on the Chatham Rise (New Zealand)**
L. Cravigan, M. Mallet, Z. D. Ristovski, P. Vaattovaara, N. Talbot, G. Olivares, M. Harvey, C. Law

Reserve paper **Assessment of emission sources in an industrial area using instrumental and biomonitoring techniques**
J. Lage, S. M. Almeida, M. A. Reis, P. C. Chaves, M. C. Freitas, T. Ribeiro, S. Garcia, J. P. Faria, B. G. Fernández, H. Th. Wolterbeek

10:30-12:50 Session: Fundamentals

Aerosol properties and dynamics

Chairs: Christopher J. Hogan Jr., Charles Clement
Room: D (Kepler)

10:30-10:50 **Evolution of the charge state z and the cross section W of mobility-selected protein ions held for tens of ms at temperatures from 25 to 100° C**
J. Fernandez de la Mora, M. Attoui

10:50-11:10 **Evaluation of the role played by multiple scattering on the radiative properties of soot fractal aggregates**
J. Yon, F. Liu, A. Bescond, C. Caumont-Prim, C. Rozé, F.-X. Ouf, A. Coppalle

11:10-11:30 **The role of the scaling-law prefactor in the morphology of fractal aggregates**
A. D. Melas, A. G. Konstandopoulos, L. Isella, Y. Drossinos

11:30-11:50 **The Collision Frequency of Fractal-like Aerosols in the Free Molecular Regime**
M. L. Eggersdorfer, S. E. Pratsinis

11:50-12:10 **Collision Cross Section Calculation and Differential Mobility Analysis-Mass Spectrometry (DMA-MS) of Po-210 and Electrospray Generated Ions**
Carlos Larriba-Andaluz, Hui Ouyang, Mark J. Meredith, Derek R. Oberreit, Christopher J. Hogan Jr.

12:10-12:30 **A new approach to the theory of Brownian coagulation**
M. S. Veshchunov, I. B. Azarov

12:30-12:50 **Oblique Impact Fragmentation of Nanoparticle Agglomerates**
M. Gensch, A. P. Weber

Reserve paper **Evaporation and growth dynamics of layered droplets: Theory and experiments**
H. H. Tu, A. K. Ray

10:30-12:50 Session: Aerosol Chemistry

Chemical characterisation techniques for aerosols
Chairs: Markus Kalberer, Rami Alfarra
Room: C (Aquarius+Taurus)

10:30-10:50 **Novel Viscosity Measurement Technique for Atmospheric Aerosols using Fluorescence Lifetime Imaging Microscopy (FLIM)**
C. Fitzgerald, N. Hosny, M. Kalberer, M. Kuimova, F. Pope

10:50-11:10 **Extractive electrospray ionisation: A novel mass spectrometry technique for the online characterisation of organic aerosol composition and reactivity**
P.J. Gallimore, M. Kalberer

11:10-11:30 **A Unique On-line Method to Infer Water-Insoluble Particulate Mass-Fractions**
Daniel Short, Michael Giordano, Yifang Zhu, Phillip Fine, Andrea Polidori, Akua Asa-Awuku

11:30-11:50 **Surface site density versus nucleation rate approaches of formulating ice formation in clouds – a comprehensive analysis based on AIDA cloud simulation experiments**
O. Möhler, N. Hiranuma, K. Höhler, C. Hoose, M. Hummel, M. Niemand, C. Oehm, T. Schmitt, I. Steinke, R. Wagner

11:50-12:10 **X-ray study of freshly emitted carbonaceous nano-aerosols by synchrotron radiation**
F.-X. Ouf, F.-A. Barreda, A. Coppalle, D. Ferry, X.-J. Liu, B. Marcillaud, C. Miron, J.-B. A. Mitchell, T. Mostefaoui, C. Nicolas, M. Patanen, P. Parent, E. Robert, O. Sublemontier, J. Yon

12:10-12:30 **Micro-Raman monitoring of photoevolution and hygroscopicity of single particles by using an environmental acoustic levitation cell**
Y. A. Tobon, M. Moreau, S. Sobanska, J. Barbillat

12:30-12:50 **Measurements of Oxidized Organic Compounds using Nitrate Chemical Ionization Time-of-Flight Mass Spectrometry coupled to an Atmospheric Pressure interface (NO3-CI-APi-ToF)**
P. Massoli, A. Lambe, T. Hohaus, M. Canagaratna, P. Chaabra, H. Stark, J. Kimmel, J. Jayne, D. Worsnop

Reserve paper **Quantitative single particle mass spectrometry with the Aerodyne aerosol mass spectrometer: development of a new classification algorithm and application to field data**
F. Freutel, F. Drewnick, J. Schneider, T. Klimach, S. Borrmann

10:30-12:50 Session: Particle-Lung Interactions

PM toxicity

Chairs: Otmar Schmid, Jenny Rissler
Room: E (Tycho)

10:30-10:50 **Translocation of fluorescently labelled SiO2 nanoparticles across human bronchial epithelial monolayers**
I. George, S. Vranic, S. Boland, A. Baeza-Squiban

10:50-11:10 **Air-liquid interface exposure system for in vitro toxicological studies of wood combustion aerosols**
S. Mülhopt, M. Dilger, C. Schlager, R. Zimmermann, S. Diabaté, C. Weiss, H.-R. Paur

11:10-11:30 **Effect of flue gas scrubber on the toxicological effects of particulate samples from a recovery boiler**
S. Kasurinen, O. Uski, P. Jalava, M. Happo, I. Nuutinen, M. Kortelainen, H. Koponen, J. Tirkkonen, K. Kuuspalo, A. Leskinen, K. Lehtinen, J. Jokiniemi, M.-R. Hirvonen

11:30-11:50 **Nanotoxicological studies in the Air-Liquid Interface using engineered metal NPs – Protein corona, gene analysis and dose response**
C. R. Svensson, S. Ameer, J. H. Pagels, T. Cedervall, M. Kåredal, L. Ludvigsson, K. Broberg, B. O. Meuller, M. E. Messing, J. Rissler

11:50-12:10 **Aerosol characterisation of e-cigarettes**
R. Cabot, A. Koc, C. U. Yurteri, J. J. McAughey

12:10-12:30 **Ecotoxicity of various types of urban particulate matter**
B. Jancsek-Turóczi, A. Hoffer, Á. Tóth, N. Kováts, A. Ács, A. Gelencsér

12:30-12:50 **The respiratory toxicity of coal fly ash**
T. P. Jones, P. Brown, K. A. BeruBe

Reserve paper **Trace elements bioaccessibility in fine and ultrafine particles from the industrial area of Dunkirk (France) during the NANO-INDUS project**
S. Mbengue, L. Alleman, P. Flament

12:50-14:00 Lunch break

tecora
A DIVISION OF OMNISENSE TECHNOLOGIES

Complete Solutions for Ambient Sampling

TÜV

Skypost PM HV

Sequential outdoor sampler for:
- PM10, PM2.5, PM1
- Total Particulate Matter
- Heavy metals

Delta MK2

Battery and electricity supply sampler, with built-in battery pack and integrated dry gas meter

Bravo Plus

Portable constant flowrate sampler, suitable for dust and gas sampling, both in stack and in ambient

Echo PM

PM10/PM2.5 low volume sampler, available for single filter or 2 lines sequential sampling

Echo Hi Vol

High Volume sampler for:
- IPA
- Heavy Metals
- Particulate matter

Headquarters: 211-215 rue la Fontaine - Fontenay sous Bois Cedex 94134 FRANCE
Italian Office: Via A. Volta 22 - 20094 Corsico ITALY
commercial@tecora.com www.tecora.com

Poster Session A

Monday, September 2nd
Room: Zenit + Nadir

16:00-18:00 **Authors' Presentations**
Room: Zenit + Nadir

Atmospheric Aerosols

A001 **Effective density measurements of different fresh soot types**
M. Abegglen, B. Sierau, A. A. Mensah, J. Wang, L. Durdina, M. Gysel, U. Lohmann

A002 **Atmospheric aerosol size distribution during winter period in Ostrava-Radvanice**
A. Baranova, J. Hovorka

A003 **Aerosol source analysis approach for a rural background site – identifying the chemical fingerprints of anthropogenic and biogenic aerosols**
M. Äijälä, H. Junninen, M. Ehn, T. Petäjä, M. Kajos, R. Väänänen, F. Canonaco, J. Slowik, A. Prévôt, P. Aalto, M. Kulmala, D. Worsnop

A004 **Monitoring of transatlantic particles over São Paulo (Brazil) by sun-photometry, ground-based lidar and CALIOP**
J. L. Guerrero-Rascado, F. J. S. Lopes, E. Landulfo, L. Alados-Arboledas

A005 **Measurements of aerosol light-scattering enhancement factors at the urban environment of Granada (Spain)**
G. Titos, H. Lyamani, A. Cazorla, Z.J. Wu, M. Sorribas, I. Foyo-Moreno, J. Cheng, H.J. Liu, A. Wiedensohler, L. Alados-Arboledas

A006 **Relating the wavelength dependency of the absorption coefficient and the aerosol type**
A. Cazorla, G. Titos, H. Lyamani, L. Alados-Arboledas

A007 **Evaluation of AERONET precipitable water vapour versus microwave radiometry, GPS and balloon-borne radiosondes at ARM sites**
Daniel Pérez-Ramírez, Alexander Smirnov, Hassan Lyamani, David Whiteman, Brent Holben, Lucas Alados-Arboledas

A008 **Aerosol Impact on cloud properties in Pakistan**
K. Alam, R. Khan

A009 **Remote Sensing of Aerosol optical property Over the Arabian Gulf**
F. M. Al-Kandari, H. K. Al-Jassar, K. S. Rao

A010 **Organic Fraction of Laboratory Generated Primary Marine Aerosol**
A. C. Butcher, S. M. King, T. Rosenoern, M. Bilde

A011 **Contribution of Fugitive Emissions in an Industrial Area of Portugal**
S. M. Almeida, A. V. Silva, S. M. Garcia, A. I. Miranda

A012 **Saharan dust contribution to PM10 levels and composition in Cape Verde**
S. M. Almeida, M. Almeida-Silva, C. A. Pio, T. Nunes, J. Cardoso, M. Cerqueira, M. A. Reis, P. C. Chaves, A. Taborda

A013 **Homologous series of organic compounds in aerosols impacted by sugar cane burning in São Paulo State, Brazil**
R. C. Urban, C. A. Alves, A. A. Cardoso, A. G. Allen, M. L. A. M. Campos

A014 **Emissions of carbonaceous aerosols and volatile organic com pounds by light-duty vehicles on a chassis dynamometer**
C. A. Alves, A. I. Calvo, D. Lopes, D. Custódio, S. Rocha, T. Nunes, M. Evtyugina, A. Charron, M. Goriaux, P. Tassel, P. Perret

A015 **Hydrocarbons in smoke samples from wildfire events in central Portugal in summer 2010**
A. M. Vicente, C. A. Alves, S. D. G. Acioli, A. P. Fernandes, T. Nunes, A. C. Monteiro, C. A. Pio

A016 **Evaluation of CMA as dust suppressant in Barcelona: Preliminary results from the AIRUSE LIFE+ Project**
F. Amato, A. Karanasiou, A. Alastuey, T. Moreno, F. Lucarelli, S. Nava, G. Calzolai, M. Chiari, M. Keuken, X. Querol

A017 **Temporal variation of urban atmospheric aerosol during smog episodes in Debrecen, Hungary**
A. Angyal, Zs. Kertész, Z. Ferenczi, E. Furu, Z. Szoboszlai, Zs. Török, Z. Szikszai

A018 **Aerosol profile retrieval algorithm development and validation for Sentinel-4**
A. Apituley , O. Vieitez, B. Sanders, P. Stammes, B. Veheilmann, Y. Meijer, R. Koopman

A019 **Modelling and impact of aerosols on climate variabilityover central Africa**
A. J. M.Komkoua, C. Tchawoua

A020 **Subgrid variability of CCN sized aerosol**
A. Asmi, R. Väänänen, R. Kredji, A. Minikin

A021 **Multi-criteria ranking and source apportionment of airborne particles**
G. A. Ayoko, A. J. Friend

A022 **A study of aerosol production at the cloud edge with direct numerical simulations**
N. Babkovskaia, M. Boy, S. Smolander, S. Romakkaniemi, M. Kulmala

A023 **The effect of cloudiness on new particle formation: investigation of radiation levels**
E. Baranizadeh, A. Arola, A. Hamed, T. Nieminen, A. Virtanen, M. Kulmala, A. Laaksonen

A024 **Influence of Mineral Dust Transport from North Africa in the Concentration and Size Distribution of Aerosol in León (Spain)**
E. Alonso-Blanco, A. I. Calvo, A. Castro, C. Alves, R. Fraile

A025 **UFIREG-Ultrafine particles and health**
S. Bastian, G. Löschau, J. Cyrys, J. Novak, M. Gobec, B. Mykhalchuk

A026 **Influence of stable weather on aerosol concentration and size distribution at K-puszta, Hungary**
A. Molnár, Zs. Bécsi

A027 **Wintertime distribution of PAH with aerosol particle size in two cities in the Czech Republic**
J. Bendl, J. Hovorka, J. Topinka

A028 **Hygroscopic Properties and Mixing State of Ultrafine Aerosol Particles over the Eastern Mediterranean Background Site of Finokalia**
S. Bezantakos, A. Bougiatioti, I. Stavroulas, K. Eleftheriadis, N. Mihalopoulos, A. Nenes, G. Biskos

A029 **Climatology of dust events at Mt. Cimone (2165 m a.s.l.), Italy**
L. Bourcier, G. Zaccaria, A. Marinoni, P. Cristofanelli, R. Duchi, D. Putero, T. C. Landi, F. Calzolari, P. Bonasoni

A030 **2011 Observations of Stratospheric Aerosol over Hampton, VA related to the Nabro volcanic Eruption in Africa**
N. Boyouk, P. M. McCormick, M. Hill, K. Leavor

A031 **Size-Resolved Source Apportionment of PM10 Organic Aerosol Measured with Aerosol Mass Spectrometry**
C. Bozzetti, I. El Haddad, R. Wolf, E. Bruns, A. Krepelova, K. Dällenbach, J. G. Slowik, U. Baltensperger, A. S. H. Prévôt

A032 **CANCELLED**

A033 **Lidar depolarization evolution during the CHARMEX intensive field campaign**
J. A. Bravo-Aranda , M. J. Granados-Muñoz, F. Navas-Guzmán, J. L. Guerrero-Rascado, F. J. Olmo, L. Alados-Arboledas

A034 **Ground-based observations of aerosol and cloud properties at sub-arctic Pallas GAW-station**
D. Brus, K. Neitola, E. Asmi, M. Aurela, U. Makkonen, J. Svensson, A.-P. Hyvärinen, A. Hirsikko, H. Hakola, R. Hillamo, H. Lihavainen

A035 **The concentrations of organic/elemental carbon and total protein in atmospheric aerosol of the near-ground atmospheric layer of Southwestern Siberia in the summer of 2012**
G. A. Buryak, A. S. Safatov, S. E. Olkin, I. K. Reznikova, V. I. Makarov, S. A. Popova, M. P. Shinkorenko, B. S. Smolyakov

A036 **Identification and characterization of black carbon aerosol sources in Lithuania**
S. Byčenkiene, V. Ulevicius, V. Dudoitis, J. Andriejauskiene

A037 **Influence of humidity on aerosol concentrationsin a subtropical region**
L. Caetano-Silva, A. G. Allen, M. Lima-Souza, A. A. Cardoso

A038 **CANCELLED**

A039 **Sugar markers in biomass burning particles from a Brazilian agro-industrial region**
R. C. Urban, A. A. Cardoso, A. G. Allen, M. E. C. Queiroz, C. A. Alves, M. L. A. M. Campos

A040 **Long-term time series of daily PM10 chemical composition in the area of Rome, Italy**
M. Catrambone, S. Dalla Torre, E. Rantica, T. Sargolini, C. Perrino, the Med-Particles Study Group

A041 **Organic characterization of particulate material from a Brazilian agro-industrial region impacted by biomass burning**
R. C. Urban, A. A. Cardoso, A. G. Allen, M. E. C. Queiroz, C. A. Alves, M. L. A. M. Campos

A042 **Thermal-optical analysis of elemental carbon (EC) in environmental samples – differences observed when using various protocols**
E. C. Cetintas, M. Kistler, C. Schmidl, H. Bauer, A. Kasper-Giebl

A043 **Coupling optical and chemical properties of primary and secondary carbonaceous aerosols**
F. Costabile, S. Gilardoni, F. Barnaba, M. Rinaldi, S. Ferrari, V. Poluzzi, G. P.Gobbi

A044 **Black carbon contribution to the particle matter in Madrid City during a local winter episode**
E. Coz, M. Becerril, Z. Chang, J. Pérez-Guldris, A. S. H. Prévôt, G. Ramos, B. Artiñano

A045 **Major ions particle size distribution from Baia de Todos os Santos, Northeastern Brazil**
G. O. da Rocha, J. S. S. Domingos, A. C. D. Regis, J. V. S. Santos, J. B. de Andrade

A046 **Extreme dust storms in Iceland**
P. Dagsson-Waldhauserova, H. Olafsson, O. Arnalds

A047 **Measurements of particulate matter hygroscopicity in Aerosol Exposure Chamber to prevent atmospheric corrosion in Data Center**
L. D'Angelo, G. Rovelli, L. Ferrero

A048 **Effect of the extensive use of fireplaces on carbonaceous particle concentration levels in Athens, Greece**
E. Diapouli, V. Vasilatou, S. Vratolis, M. Gini, D. Saraga, Th. Maggos, K. Eleftheriadis

A049 **Distribution of aerosol over coal strip mine**
V. Docekalova, J. Hovorka, F. Kobrzek, P. Marecek

A050 **Spatial-temporal variability of particle number concentrations between a busy street canyon and the urban background**
V. Dos Santos-Juusela, T. Petäjä, A. Kousa, K. Hämeri

A051 **Airborne Aldehydes as Altitude-Distributed Source of Particulate Matter in the Troposphere**
S. N. Dubtsov, T. A. Maksimova, G. G. Dultseva

A052 **The comparison of the light scattering coefficient measured in urban and coastal environments**
V. Dudoitis, V. Ulevicius, K. Plauškaite, G. Mordas

A053 **Variations of PM10 and its relationship with 7Be and 210Pb measurements at Malaga (Southeastern coast of Spain)**
C. Dueñas, M. C. Fernández, E. Gordo, E. Liger, S. Cañete, M. Pérez

A054 **Atmospheric fluxes of radionuclides on monthly time-scale in Malaga (Spain)**
C. Dueñas, M. C. Fernández, E. Gordo, S. Cañete, E. Liger, M. Pérez

A055 **The comparative analysis of variations of background radiation components and atmospheric electrical parameters**
M. S. Cherepnev, I. I. Ippolitov, M. V. Kabanov, P. M. Nagorsky, S. V. Smirnov, A. V. Vukolov, V. S. Yakovleva

A056 **13C measurements on organic aerosol – ambient samples versus source studies**
U. Dusek, C. Meusinger, B. Oyama, W. Ramon, P. A. de Wilde, R. Holzinger, T. Röckmann

A057 **Road Pavement Abrasion as the Source of Particulate Matter**
Dušan Jandačka, Daniela Ďurčanská

A058 **Time-resolved organic speciation at the Theodore Roosevelt National Park, North Dakota, USA**
A. Eiguren, G. Lewis, N. Kreisberg, D. R. Worton, A. H. Goldstein, S. V. Hering

A059 **Water activity measurement of pure and mixed organic/inorganic solutions**
M. M. Fard, and M. Bilde

A060 **Can lung-deposited surface area measurements serve as surrogate for black carbon?**
M. Fierz, D. Meier, C. Hüglin, H. Burtscher

A061 **Regional-scale modeling of organic aerosol composition in Europe: Insights from comparison with aerosol mass spectrometer factor analysis**
C. Fountoukis, A. G. Megaritis, K. Skyllakou, P. E. Charalampidis, C. Pilinis, S. N. Pandis

A062 **CANCELLED**

A063 **Year-round measurement of PM1 aerosol and its chemical composition in the Swiss high Alps using the Time-of-Flight Aerosol Chemical Speciation Monitor (ToF-ACSM)**
R. Fröhlich, M. J. Cubison, J. G. Slowik, A. S. H. Prévôt, U. Baltensperger, U. Rohner, M. Gonin, J. R. Kimmel, D. R. Worsnop, J. T. Jayne

A064 **Aerosol Activation and Scavenging during the Cloudy Test Campaign at the CERN CLOUD chamber**
C. Fuchs, J. Tröstl, J. Duplissy, E. Weingartner, U. Baltensperger, the CLOUD collaboration

A065 **The effect of the tramway track building on the aerosol pollution in Debrecen, Hungary**
E. Furu, I. Katona-Szabo, A. Angyal, Z. Szoboszlai, Zs. Török, Zs. Kertész

A066 **Contribution of fossil and modern carbon to PM2.5 and CO2 in the atmosphere of Debrecen, Hungary**
I. Major, E. Furu, I. Hajdas, Zs. Kertész, M. Mihály

A067 **The impact of extreme weather events on air quality in Budapest, Hungary**
V. Gácser, A. Molnár

A068 **Seasonal variation of urban aerosols in a sub-Saharan city: case study of Nairobi, Kenya**
S. M. Gaita, J. Boman, J. B. C. Pettersson, M. J. Gatari, S. Janhäll

A069 **Stable carbon isotopic values (δ13C) of biofuel in Lithuania**
A. Garbaras, A. Lipovec, A. Masalaite, V. Remeikis

A070 **Atmospheric aerosol episodes over Lithuania after the May 2011 volcano eruption at Grimsvötn, Iceland**
K. Kvietkus, J. Šakalys, J. Didžbalis, I. Garbariene, N. Špirkauskaite, V. Remeikis

A071 **Quantifying the relative contribution of different aerosol types over Eastern Mediterranean: A decadal high resolution satellite view**
A. K. Georgoulias, K. A. Kourtidis, G. Alexandri, P. Zanis, U. Pöschl

A072 **CLACE 2013: Cloud microphysics and physico-chemical characterization of ice residuals in mixed-phase clouds**
P. Kupiszewski, E. Weingartner, R. Färber, M. Gysel, E. Hammer, C. Fuchs, U. Baltensperger, P. Vochezer, M. Schnaiter, C. Linke, E. Toprak, S. Mertes, J. Schneider, T. Klimach, S. Schmidt

A073 **The UPUPA project: Ultrafine Particles in the Urban Piacenza Area, Italy**
M. Giugliano, G. Lonati, S. Ozgen, G. Ripamonti

A074 **DIAPASON: an user-oriented EC-LIFE+ Project to quantify the role of Saharan dust on European PM10 levels**
G. P. Gobbi, F. Barnaba, F. Costabile, L. Di Liberto, C. Tirelli, R. Sozzi, A. Bolignano, M. Morelli

A075 **Testing of aerosols in Barentsburg area (Spitsbergen)**
L. P. Golobokova, D. G. Chernov, U. S. Turchinovicn, V. V. Polkin

A076 **The Spanish network on environmental DMAs: the 2012 SMPS+UFP intercomparison campaign and study on particle losses in dryers**
F. J. Gómez-Moreno, E. Alonso, B. Artíñano, V. Juncal Bello, M. Piñeiro Iglesias, P. López Mahía, N. Pérez, J. Pey, A. Alastuey, B. A. de la Morena, M. I. García, S. Rodríguez, M. Sorribas, G. Titos, H. Lyamani, L. Alados-Arboledas

A077 **The potential role of ion-induced nucleation at a coniferous forest site in north eastern Bavaria**
S. G. Gonser, F. Klein, W. Birmili, J. Größ, A. Held

A078 **Analysis of aerosol hygroscopic properties by combination of lidar, microwave radiometer and radiosounding data**
M. J. Granados-Muñoz, F. Navas-Guzmán, J. A. Bravo-Aranda, J. L. Guerrero-Rascado, A. Valenzuela, J. Fernández-Gálvez, L. Alados-Arboledas

A079 **Hygroscopic growth parameterization of aerosol particles based on high humidity measurements in the Po-Valley, Italy**
J. Größ, I. Pap, W. Birmili, A. Hamed, A. Wiedensohler

A080 **Mixture of biomass-burning and urban aerosols analysis: a case study**
Marius Mihai Cazacu, Florin Unga, Adrian Timofte, Ioana Popovici, Alin Ionut Pascaru, Dan Dimitriu, Silviu Gurlui

A081 **Characterization of fine particles using Aerosol mass spectrometer during intensive campaign in three different sites in Kanto basin in summer of 2011**
H. Hagino, and T. Morikawa, S. Hasegawa, S. Yonemochi, K. Sekiguchi, K. Kumagai, N. Yamaguchi, A. Iijima, H. Shimadera, H. Hayami

A082 **Hygroscopicity of sub-6 nm sodium chloride particles**
J. Hakala, J. Kangasluoma, T. Petäjä

A083 **Semi-empirical parameterization for sub-20 nm particle growth**
S. A. K. Häkkinen, H. E. Manninen, T. Yli-Juuti, J. Merikanto, M. K. Kajos, T. Nieminen, S. D. D'Andrea, A. Asmi, J. R. Pierce, M. Kulmala, I. Riipinen

A084 **New particle formation at rural and mountain stations in north Italy: A comparative study during the joint PEGASOS and Supersito campaign**
A. Hamed, S. Decesari, S. Gilardoni, S. Niemelä, L. Tarozzi, C. Carbone, P. Vaattovaara, J. Joutsensaari, P. Cristofanelli, A. Marinoni, P. Bonasoni, G. Bonafe, D. Bacco, I. Ricciardelli, A. Virtanen, S. Ferrari, V. Poluzzi, M. C. Facchini, A. Laaksonen

A085 **Secondary New Particle Formation in Central Europe: Eight years of Aerosol Particle Size distribution data from Melpitz Site, Germany**
A. Hamed, Z. Wang, W. Birmili, G. Spindler, A. Wiedensohler

A086 **Measurement of atmospheric organic nitrate aerosols and its application in cloud events**
L. Q. Hao, S. Romakkaniemi, A. Kortelainen, A. Jaatinen, H. Portin, P. Miettinen, M. Komppula, A. Leskinen, J. N. Smith, D. Sueper, D. R. Worsnop, K. E. J. Lehtinen, A. Laaksonen, A. Virtanen

A087 **Ultrafine particle concentrations: importance of local sources and new particle formation in two central European cities**
A. Wonaschuetz, R. Wagner, I. Aschauer, R. Haindl, W. Ludwig, G. Zecha, J. Ondráček, P. Vodička, N. Ziková, V. Ždímal, J. Schwarz, R. Hitzenberger

A088 **Absorbing aerosol long-term trend at Mukteshwar, a pristine location in Central Himalayas foothills**
Rakesh K. Hooda, A.-P. Hyvärinen, V. P. Sharma, M. Komppula, E. Asmi, Y. Viisanen and H. Lihavainen

A089 **Vertical profiles of aerosol optical properties and wavelength dependent absorption at Maldives Climate Observatory Hanimaadhoo**
F. Höpner, F. Bender, P. S. Praveen, V. Ramanathan

A090 **Spatial variations and source apportionment of the marine organic aerosol over the Atlantic Ocean**
S. Huang, L. Poulain, Z. J. Wu, H. Herrmann, A. Wiedensohler

A091 **Chemical composition, concentration, size distribution and diurnal variation of atmospheric aerosol particles at the background and urban sites in Lithuania**
K. Kvietkus, J. Šakalys, J. Didžbalis, E. Meinore

A092 **Surface Aerosol Monitoring at Hada Al Sham, Western Saudi-Arabia**
A.-P. Hyvärinen, M. Alghamdi, T. Hussein, M. Khodeir, A. Shehata, H. Lihavainen, M. Kulmala, A. Laaksonen

A093 **Chemical composition, and mass closure of Siberia aerosols at ZOTTO, Russia, April 2010 to February 2011**
X. Chi, E. Mikhailov, A. Panov, M. O. Andreae

A094 **Estimation of emission rates of resuspended road dust using a mobile monitoring system**
Sehyun Han, Yongwon Jung

A095 **One-year monitoring of nitro-organic compounds in biomass burning PM10 filter samples**
A. Kahnt, S. Behrouzi, R. Vermeylen, M. Safi Shalamzari, J. Vercauteren, W. Maenhaut, M. Claeys

A096 **A case of CCN formation associated with atmospheric nucleation in eastern Mediterranean**
N. Kalivitis, V.-M. Kerminen, G. Kouvarakis, I. Stavroulas, A. Bougiatioti, A. Nenes, H. E. Manninen, T. Petäjä, M. Kulmala, N. Mihalopoulos

A097 **Nitration and oxidation of bioaerosols and allergenic proteins**
C. J. Kampf, K. Selzle, U. Pöschl

A098 **Effects of mineral dust and sea salt on global nitrate concentration field**
V. A. Karydis, A. P. Tsimpidi, J. Lelieveld

A099 **Particle size distribution of viable airborne microbes and particulate matter during pretreatment of wastewater**
E. Katsivela, E. Latos, L. Raisi, M. Lazaridis

A100 **Comprehensive studies of chemical composition of atmospheric aerosol above Lake Baikal surface area, Russia**
T. V. Khodzher

A101 **Airborne Measurements of Emissions from Oil and Gas Exploration and Production Activities in the Norwegian Sea**
J. Kim, A. Roiger, B. Weinzierl, M. Rose, A. Reiter, J. Thomas, L. Marelle, K. Law, H. Schlager

A102 **Development of Reference Film for Quality Control and Assurance for Beta Attentuation Particulate Matter Measurement**
H. H. Kim, J. Y. Lee, S. Lee

A103 **Soot on Snow (SoS) measurement campaigns 2011-2013**
N. Kivekäs, A. Virkkula, O. Järvinen, J. Svensson, A. Aarva, H. Lihavainen, D. Brus, A. Hyvärinen, O. Meinander, A. Heikkilä, R. Väänänen, J. Backman, G. De Leeuw

A104 **Characterization of particle formation in a spruce forest in north east Bavaria**
F. Klein, A. Held

A105 **Influence of different fuels and grillables on particle emissions during an outdoor barbeque**
S. H. Schmitt, C. Berberich, M. Glor, L. Güntner, T. C. Sluka, K. A. Kamili, S. G. Gonser, A. Held

A106 **Photophoretic effects for the black carbon aerosols at stratospheric altitudes**
L. B. Kochneva, S. A. Beresnev, V. I. Gryazin, M. V. Vasiljeva, K. G. Gribanov and V. I. Zakharov

A107 **Particle collection properties of high vegetation elements**
R. D. Kouznetsov, M. A. Sofiev

A108 **A scheme for particle deposition from turbulent flows above surfaces**
R. D. Kouznetsov, M. A. Sofiev

A109 **Intermodal fraction of aerosol from indoor and outdoor microenvironments**
J. Kozáková, M. Braniš

A110 **Acidic reaction products of mono- and sesquiterpenes in atmospheric fine particles in boreal forest in Hyytiälä, Finland**
M. Vestenius, H. Hellen, J. Levula, P. Kuronen, H. Hakola

A111 **Evidence for the presence of secondary phosphorus in continental fine aerosol**
K. Krassován, Z. Kertész, K. Imre, A. Gelencsér

A112 **Measurement of evaporation rates of atmospheric nanoparticles**
N. K. Kumar, S. N. Pandis

A113 **Organic compounds in PM2.5 aerosol in Ostrava (Czech Republic)**
P. Mikuška, K. Křůmal, Z. Večeřa

A114 **Laboratory characterization of a size-resolved CPC battery to infer the composition of freshly formed atmospheric nuclei**
C. Kuang, J. Kangasluoma, D. Wimmer, K. Lehtipalo, J. Wang, M. Kulmala, T. Petäjä

A115 **Detailed study of fine particulate matter during 2013 New Year's celebrations**
L. Kubelová, P. Vodička, J. Schwarz, V. Ždímal

A116 **DMA Train measurements of nanoparticle growth at a field site in Lewes, Delaware**
A. Kupc, P. M. Winkler, M. Lawler, P. H. McMurry, J. N. Smith

A117 **Source Identification and Apportionment of Finnish Arctic Aerosols**
James R. Laing, Philip K. Hopke, Eleanor F. Hopke, Liaquat Husain, Vincent A. Dutkiewicz, Jussi Paatero, Yrjö Viisanen

A118 **Forty-Seven Years of MSA Concentrations in the Finnish Arctic**
James R. Laing, Philip K. Hopke, Eleanor F. Hopke, Liaquat Husain, Vincent A. Dutkiewicz, Jussi Paatero, Yrjö Viisanen

A119 **Source apportionment of ten years' aerosol collected at Mt. Lulin in East Asia**
C.-T. Lee, S.-C. Wu, George N.-H. Lin, G.-C. Hong

A120 **On the potential of volcanic ash and powder sample investigation with FIB/SEM EBSD-EDS**
K. I. Lieke, H. Alimadadi

A121 **Analyses of long-term measurements (2005-2012) of 7Be concentrations in surface air aerosols**
E. Liger, C. Dueñas, M. C. Fernández, E. Gordo, S. Cañete, M. Pérez

A122 **Airborne measurements of ship emissions**
H. Lihavainen, E. Asmi, J.-P. Jalkanen, A. Hyvärinen, T. Laurila, J. Walden, R. Hillamo

A123 **Relationship between the tropospheric aerosol size distribution and cloud droplet effective radius in a rural region of São Paulo State**
M. Lima-Souza, A. G. Allen, L. Caetano-Silva, A. A. Cardoso

A124 **Characteristics of fine and coarse particles collected from open burning of jujube tree branches**
Chih-Chung Lin, Wen-Yinn Lin, Kuo-Lin Huang, Lien-Te Hsieh, Jen-Hsiung Tsai, Shui-Jen Chen

A125 **Investigating the Small-Scale Vertical and Horizontal Variability of the Atmospheric Boundary Layer Aerosol using Unmanned Aerial Vehicles**
B. Wehner, A. Lampert, A. Scholtz, J. Bange, A. Platis, M. Hermann

A126 **The association of children's lung function and air pollution in Kaohsiung, Taiwan**
C. L. Yeh, K. D. Mena, C. S. Ou, P. S. Chen

A127 **Seasonal physical and optical properties of atmospheric aerosol at Princess Elisabeth station, East Antarctica**
A. Mangold, H. De Backer, A. Delcloo, V. De Bock, C. Hermans, I. Gorodetskaya, W. Maenhaut

A128 **δ13C of size segregated aerosol particles collected in Preila and Baltic Sea**
A. Masalaite, A. Garbaras, V. Remeikis

A129 **Size distribution of airborne Uranium and Thorium-labelled aerosols near a UF4 processing plant**
O. Masson, G. Videau, X. Cagnat

A130 **Comparison of Aerosol Time of Flight Mass Spectrometer (ATOFMS) measurements with off-line techniques for determining metal concentration in atmospheric particles**
Eoin McGillicuddy, Robert Healy, Manuel Dall'Osto, Jean Sciare, Franco Lucarelli, Silvia Nava, Xavier Querol, Ian O'Connor, Deborah Gross, John Wenger, John Sodeau

A131 **Levels of polybrominated diphenyl ethers in the ambient air of automobile dismantling plants from southern Taiwan**
S. I. Shih, H. R. Chao, W. K. Wu, Y. Y. Guo, B. A. Jiang, C. Y. Chen, Y. M. Kuo, C. H. Tsai

A132 **Rotational Spectra and ab initio modeling of dicarboxylic acids: Succinic Acid**
Estíbaliz Méndez, Patricia Écija, Emilio J. Cocinero, Fernando Castaño, Francisco J. Basterretxea, Peter D. Godfrey, Don McNaughton, Michaela K. Jahn, K. P. Rajappan Nair, Jens-Uwe Grabow

A133 **The influence of the Sahara storm on the aerosol optical properties in Lithuania**
G. Mordas, V. Ulevicius, N. Prokopciuk

A134 **Measurements of the aerosol particle physical properties and particle chemical composition in Vilnius city**
G. Mordas, V. Ulevicius, I. Garbariene, K. Kvietkus

A135 **Exploring the effect of deep-convective cloud systems on particle mass and number: source or sink?**
B. N. Murphy, I. Riipinen, A. M. L. Ekman

A136 **Total sulphate vs. sulphuric acid monomer in nucleation studies**
K. Neitola, D. Brus, U. Makkonen, M. Sipilä, T. Jokinen, R. L. Mauldin III, K. Kyllönen, H. Lihavainen, M. Kulmala

A137 **Air mass history on 1-year long new aerosol particle formation dataset in Budapest**
Z. A. Németh, I. Salma

A138 **Comparison of particle concentrations obtained at urban and regional background environments**
J. F. Nicolás, J. Crespo, E. Yubero, R. Soler

A139 **Enhancement of the collision efficiency between basidiospores and cloud droplets by electrostatic charges carried on freshly emitted basidiospores**
M. Saar, M. Noppel, J. Salm

A140 **On the microphysical and optical aerosol properties during AMISOC-ARN campaign**
M. Sorribas, C. Córdoba-Jabonero, H. Lyamani, G. Titos, J. A. Adame, R. Fraile, B. A. de la Morena, F. J. Olmo, L. Alados-Arboledas, O. Puentedura, M. Gil

A141 **Bimodal particle concentration profile retrieved from ground-based Lidar and CIMEL measurements**
A. Quirantes, F. J. Olmo , A. Valenzuela, M. J. Granados-Muñoz, J. L. Guerrero-Rascado, J. A. Bravo-Aranda, F. Navas-Guzmán, L. Alados-Arboledas

A142 **On the contribution of ephemeral lakes to the aerosol load**
J. A. G. Orza, M. Cabello, E. Doménech, L. Pérez

A143 **Investigation of the truncation correction of the polar nephelometer Ecotech Aurora4000**
M. Paixão, T. Müller, S. Pfeifer, A. Wiedensohler

A144 **Estimation of viscosity of SOA particles based on coalescence times**
A. Pajunoja, J. Malila, L. Hao, K. E. J. Lehtinen, A. Virtanen

A145 **Studies of precipitable water vapor measurements with use of Microtops II Sun Photometer and Radiosonde RS92**
P. Pakszys, T. Zieliński, T. Petelski, P. Makuch, A. Strzałkowska, P. Markuszewski, J. Kowalczyk

A146 **Factor analysis of aerosol measurements in Tartu**
M. Palo, M. Eller

A147 **Continuous atmospheric boundary layer observations in Barcelona, Spain**
M. Pandolfi, G. Martucci, X. Querol, A. Alastuey, F. Wilsenack, S. Frey, C. D. O'Dowd, M. Dall'Osto

A148 **Hygroscopic properties of the anthropogenic aerosol in the Po-Valley, Italy**
I. Pap, J.Größ, A. Hamed, W. Birmili, A. Wiedensohler

A149 **Rainout, washout and dry deposition contributions to the total deposition flux of heavy metal aerosol onto surfaces of a small urban catchment (Pin Sec, Nantes)**
S. Percot, V. Ruban, P. Laguionie, D. Maro, P. Roupsard, D. Demare

A150 **Continuous Measurements with high Time Resolution of Semi-Volatile Components in the Atmospheric Aerosol**
H. Grimm, M. Pesch, M. Richter, A. Comouth

A151 **Mobile FINE DUST Aerosol Spectrometer**
M. Pesch, H. Grimm, M. Richter

A152 **Primary Biological DNA Database**
D. Pickersgill, J. Wehking, I. Müller-Germann, U. Pöschl, V. R. Després

A153 **Studying Atmospheric Aerosols by Acoustic Levitation: Linking Headspace Solid-Phase Microextraction (HS-SPME) with Gas Chromatography-Mass Spectrometry (GC-MS)**
S. Almabrok, G. Marston, C. Pfrang

A154 **The variation of the total aerosol particle number concentration in fog in southern and south-eastern regions of the Baltic Sea**
K. Plauškaite, N. Špirkauskaite, T. Zielinski, T. Petelski, V. Ulevicius

A155 **Autofluorescence of atmospheric bioaerosols – studies on biofluorophores and biological standard particles**
C. Pöhlker, J. A. Huffman, J.-D. Förster, U. Pöschl

A156 **CANCELLED**

A157 **Observations of cloud effects on aerosol light absorption and scattering**
A. Leskinen, H. Portin, A. Arola, S. Romakkaniemi, A.-P. Hyvärinen, A. Laaksonen, K. E. J. Lehtinen, M. Komppula

A158 **Meteorological impacts in the modification of PM10 concentration levels in the urban area of Volos, Greece**
G. T. Proias, K. P. Moustris, I. K. Larissi, P. T. Nastos, A. G. Paliatsos

A159 **Study of the Impact of the Natural Production, in the Mediterranean Sea, of Coastal Marine Aerosols on the Dynamics and Microphysical Behavior of a Convective Cloud**
R. Merrouchi, J. Piazzola, M. Chagdali, S. Mourdane

A160 **Black carbon aerosol concentrations and mixing state in Pallas, Finland**
T. Raatikainen, D. Brus, A.-P. Hyvärinen, J. Svensson, H. Lihavainen

A161 **Particle emissions from bushfires extending into the rural-urban interface**
F. Reisen, M. Bhujel, P. Selleck

A162 **Measurements of the variation in hygroscopic growth of organic aerosol with oxygen-to-carbon ratio (O/C)**
A. M. J. Rickards, R. E. H. Miles, J. F. Davies, F. H. Marshall, J. P. Reid

A163 **Overview of the French contribution to the EMEP 2012-2013 summer and winter campaigns**
V. Riffault, J. L. Jaffrezo, J. Sciare, K. Sellegri, S. Sauvage, V. Crenn, A. Waked, J. E. Petit, A. Colomb, S. Conil, J. L. Besombes, A. Setyan, E. Freney, T. Leonardis, N. Locoge, V. Gros, N. Bonnaire, R. Sarda-Estève, F. Dulac, M. Hervo, L. Chiappini, O. Favez, F. Gheusi, G. Athier, M. Mallet, T. Bourrianne, G. Roberts, N. Pascal, J. Descloitres

A164 **Dry deposition velocity measurements onto urban surfaces using atmospheric beryllium 7: development of a methodology and results**
P. Roupsard, D. Maro, A. Coppalle, V. Ruban, M. Rozet, M. Talbaut, S. Percot

A165 **Seasonality of biological aerosol particles associated with African dust storms**
Cristina Ruzene-Nespoli, Janine Fröhlich-Nowoisky, T. Nunes, J. Cardoso, C. Pio, Ulrich Pöschl

A166 **Fluorescence based real-time measurements of atmospheric PBAP in urban environment**
S. Saari, J.V. Niemi, T. Rönkkö, L. Pirjola, R. Hillamo, J. Keskinen

A167 **An observational study on air pollution conditions in two continuous haze periods in winter in Nanjing, China**
Y. J. Zhang, L. L. Tang, H. L. Zhang, L. Tang

A168 **Classification of Dust/Non-dust Particle from the Asian Dust Plumes and Retrieval of Microphysical Properties using Multiwavelength Raman Lidar System**
S. K. Shin, Detelf Müller, Y. M. Noh, D. H. Shin, K. H. Lee

A169 **Improvements to harmonize different soot measurement techniques in air quality monitoring networks**
A. Schladitz, G. Löschau, H. G. Kath

A170 **Single particle analysis of cloud residuals sampled at the research station Schneefernerhaus (2650 m) during ACRIDICON-Zugspitze 2012**
S. Schmidt, J. Schneider, T. Klimach, S. Mertes, L. Schenk, S. Borrmann

A171 **In-situ single particle composition analysis of ice residuals in mixed-phase clouds during INUIT-JFJ 2013**
S. Schmidt, J. Schneider, T. Klimach, S. Mertes, L. Schenk, U. Kästner, F. Stratmann, U. Bundke, B. Nillius, F. Frank, J. Curtius, S. Borrmann

A172 **New Homogeneous Ice Nucleation Results from Measurements at a Large Atmospheric Simulation Chamber**
T. Schmitt, O. Möhler, D. Duft, M. Haarig, K. Höhler, A. Kiselev, I. Steinke, T. Leisner

A173 **Processing of ambient aerosols during fog events**
A. Chakraborty, T. Gupta, S. N. Tripathi

A174 **Comparison of mass size distribution of PM and ions in Prague and Vienna in winter and summer**
J. Schwarz, N. Zíková , P. Vodička, I. Ševčíková, J. Kugler, A. Wonaschuetz, R. Wagner, I. Aschauer, W. Ludwig, R. Haindl, G. Zecha, R. Hitzenberger, V. Ždímal

A175 **Characteristics of Local and Regional Nucleation Events at an Urban Background Site during Summer Period in Thessaloniki, Greece**
D. Siakavaras, C. Samara, A. Kelessis, G. Biskos

A176 **Exposure of air pollutants inside vehicles while driving in road tunnels**
S. Silvergren, M. Norman, C. Johansson, B. Sjövall

A177 **Measurement capabilities of the Poland-AOD network**
A. Strzalkowska, P. Makuch, P. Pakszys, O. Zawadzka, P. Markuszewski, T. Zielinski, T. Petelski, K. M. Markowicz, I. Stachlewska, A. Ponczkowska, M. Wichorowski

A178 **Aerosol characteristics during dust storm in Middle East and South-Western Asia**
F. Subhan, K. Alam

A179 **CANCELLED**

A180 **Assessment of air pollution sources and implications for human health**
Afrim Syla

A181 **Structural analysis of fine particles using a Time-of-Flight Secondary Ion Mass Spectrometer**
A. Takami, N. Mayama, T. Sakamoto, K. Ohishi, S. Irei, A. Yoshino, S. Hatakeyama, K. Murano, Y. Sadanaga, H. Bandow, K. Misawa, M. Fujii

A182 **CANCELLED**

A183 **Estimating PM2.5 in the Stockholm region from spaceborne AOT measurements**
M. Tesche, P. Glantz

A184 **Reconciling aerosol light extinction from ground-based in-situ measurements and active satellite remote sensing**
M. Tesche, N. Rastak, P. Glantz, H.-C. Hansson, I. Riipinen, R. Charlson

A185 **Investigating the Formation of H2SO4 from ion-induced Oxidation of SO2**
N. T. Tsona, N. Bork, H. Vehkamäki

A186 **Chemical characterization of aerosol particles in Évora: comparison between summer and winter campaigns**
L. C. Tobias, N. Schiavon, K. Kandler, J. Mirão, F. Wagner

A187 **„Aerosol-fingerprint" of Europe in the atmosphere of Debrecen, Hungary**
Zsófia Török, Zsófia Kertész, Anikó Angyal, Enikő Furu, Zoltán Szoboszlai, Zita Szikszai, Ildikó Borbély-Kiss

A188 **Measurements of black carbon using the Transmissometer**
A. H. Tremper, D. C. Green, G. Fuller

A189 **Effect of organics and their hygroscopicity on cloud condensation nuclei (CCN) activity**
Deepika Bhattu, Sachchida Nand Tripathi

A190 **Estimation of source apportionment using the UNMIX model of ambient PM2.5 in Seoul area, Korea**
Yeong-Jin Jeong, Tae-Ho Lee and InJo Hwang

A191 **Ionic composition and metal content of PM10 samples collected along longitudinal and latitudinal transects in the Norwegian and Greenland Seas during the AREX 2011 cruise**
R. Udisti, S. Becagli, E. Bolzacchini, G. Calzolai, M. Chiari, L. Ferrero, D. Frosini, M. Marconi, M. G. Perrone, G. Sangiorgi, M. Severi, R. Traversi, W. Walczowski, R. Zanini, T. Zielinski

A192 **Project AEROLIT (Aerosol in Lithuania): Investigation of primary-secondary and regional-local contributions to particulate matter in the south-eastern Baltic region**
V. Ulevicius, A. S. H. Prévôt, K. Plauškaite, S. Byčenkiene, G. Mordas, V. Dudoitis, V. Remeikis, A. Garbaras, K. Kvietkus, I. Garbariene, J. Dommen, J. G. Slowik, C. Bozzetti, U. Baltensperger

A193 **Air masses types over the remote Alborán Island**
A. Valenzuela, F. J. Olmo, H. Lyamani, M. J. Granados Muñoz, J. L. Guerrero-Rascado, A. Quirantes, L. Alados-Arboledas

A194 **A LUR model for NO2 and BC to assess exposure of schoolchildren to traffic-related air pollution at their home address**
Martine Van Poppel, Evi Dons, Luc Int Panis

A195 **Košetice Observatory – The Czech Background Aerosol Supersite**
M. Váňa, J. Čech, A. Holubová, M. Pavelka, J. Ondráček, J. Schwarz, J. Smolík, N. Zíková, V. Ždímal

A196 **Source apportionment of carbonaceous PM2.5 with 14C analysis in Nagoya, Japan**
Fumikazu Ikemori, Koji Honjyo, Makiko Yamagami, Toshio Nakamura

A197 **Biomass burning in the Amazon Region: Characterization of airborne particle-phase Polycyclic Aromatic Hydrocarbons**
P. C. Vasconcellos, Nilmara de Oliveira Alves, Sofia Ellen da Silva Caumo, Paulo Artaxo, Sandra de Souza Hacon, Silvia Regina Batistuzzo de Medeiros

A198 **Optical and chemical characterization of biomass burning aerosols**
J. Vasilescu, L. Marmureanu, A. Nemuc, C. Talianu, L. Belegante

A199 **Chemical composition and hygroscopic properties of aerosol particles from Siberian boreal area**
S. Yu. Vasileva, G. N. Mironov, T. I. Rushkevich, S. S. Vlasenko, Xuguang Chi, A. V. Panov, M. O. Andreae, E. F. Mikhailov

A200 **Interpretation of Urban Particle-bound Polycyclic Aromatic Hydrocarbons Source Profiles of PMF with Known Site Specific Emission Characteristics**
E. H. Jang, M. S. Alam, R. M. Harrison

A201 **Water soluble ionic species of particulate matter in an urban road tunnel**
M. S. Vieira-Filho, R. Astolfo, J. J. Pedrotti, A. Fornaro

A202 **Determination of alkyl phenols in atmospheric aerosols by gas chromatography–ion trap mass spectrometry**
M. Visentin, M. C. Pietrogrande

A203 **Seasonal variations of organic carbon with different volatility at suburban site**
Petr Vodička and Jaroslav Schwarz

A204 **Ionic composition of PM10 and PM2.5 in the area of Thessaloniki, Northern Greece-Estimation of secondary inorganic aerosols and sea spray contribution**
D. Voutsa, C. Samara, E. Manoli, E. Gounari, D. Lazarou, P. Tzoumaka

A205 **One year analysis of sedimentation samples at Évora, Portugal**
F. Wagner, L. Tobias, K. Kandler, N. Schiavon, J. Mirão

A206 **Identification of parameters influencing the variability of particle number size distributions in Europe-a multi-site study**
C. von Bismarck-Osten, S. Weber

A207 **Vertical aerosol stratification above the Caribbean Sea near Barbados**
B. Wehner, F. Ditas, H. Wex, I. Serikov, A. Wiedensohler, H. Siebert

A208 **Methods and limits of unipolar charged aerosol inversion**
Z. N. Wei, L. Knobel, H.-J. Schmid

A209 **Alpha radioactive aerosols behavior in the ground atmosphere**
V. S. Yakovleva, M. S. Cherepnev, I. I. Ippolitov, P. M. Nagorsky, S. V. Smirnov, A. V. Vukolov

A210 **The role of condensable vapours in atmospheric new particle growth and shrinkage**
L.-H. Young, P.-S. Cheng, Y.-J. Liou, S.-H. Lee, V. P. Kanawade, T.-C. Hsiao

A211 **Evolution of n-Alkanes in PM samples collected in São Paulo, Brazil (2000-2010)**
P. C. Vasconcellos, Sofia Caumo, J. B. De Andrade

A212 **Comparison of particle number size distributions in three Central European capital cities**
N. Zíková, T. Borsós, D. Řimnáčová, J. Smolík, Z. Wagner, T. Weidinger, J. Burkart, G. Steiner, G. Reischl, R. Hitzenberger, J. Schwarz, I. Salma, V. Ždímal

A213 **CCN activation of insoluble silica aerosols mixed with soluble pollutants**
M. Dalirian, H. Keskinen, P. Miettinen, A. Virtanen, A. Laaksonen, I. Riipinen

A214 **CANCELLED**

Reserve Posters

A215 **Measurements During The South American Biomass Burning Analysis (SAMBBA) Field Experiment**
J. D. Allan, W. T. Morgan, P. I. Williams, M. Flynn, E. Darbyshire, A. Hodgson, B. T. Johnson, J. M. Haywood, S. Freitas, K. Longo, P. Artaxo, H. Coe

A216 **Characteristics of new particle formation events in Hungarian background air at K-puszta, 2008-2012**
Zs. Bécsi, Á. Molnár, K. Imre, P. P. Aalto

A217 **Long-term observations of carbonaceous aerosols and related gaseous emissions near a crude-oil plant in South Italy**
M. Calvello, M. Lovallo, F. Esposito, L. Mangiamele, G. Pavese

A218 **Wood-burning emissions within a continuous-flow photooxidation reactor: Soot-Particle Aerosol Mass Spectrometer characterization**
J. C. Corbin, A. Keller, H. Burtscher, B. Sierau, U. Lohmann, A. A. Mensah
CHANGED TO ORAL PRESENTATION

A219 **Characterising the influence of anthropogenic emissions on regional background aerosols at the puy de Dome station in France**
E. J. Freney, E. Asmi, M. Hervo, C. Rose, A. Colomb, K. Sellegri

A220 **Variations of levels of atmospheric electrical and meteorological parameters and natural radioactivity in response to heavy smog due to forest fires**
M. S. Cherepnev, A. V. Vukolov, I. I. Ippolitov, M. V. Kabanov, P. M. Nagorsky, Yu. A. Phalagov, S. V. Smirnov, V. S. Yakovleva

A221 **Road tunnels-particle properties, wet and dry conditions**
S. Janhäll, M. Gustafsson, S. Abbasi, G. Blomqvist, A. Gudmundsson, C. Johansson, M. Norman, U. Olofsson, B. Sjövall
CHANGED TO ORAL PRESENTATION

A222 **Winter particulate matter (PM10) sources for an Austrian-Slovenian border region**
M. Kistler, E. C. Cetintas, H. Bauer, A. Kasper-Giebl

A223 **Assessment of emission sources in an industrial area using instrumental and biomonitoring techniques**
J. Lage, S. M. Almeida, M. A. Reis, P. C. Chaves, M. C. Freitas, T. Ribeiro, S. Garcia, J. P. Faria, B. G. Fernández, H. Th. Wolterbeek

A224 **Relationship between oxidation level and optical properties of secondary organic aerosol**
A. T. Lambe, C. D. Cappa, P. Massoli, T. B. Onasch, S. D. Forestieri, A. T. Martin, M. J. Cummings, D. R. Croasdale, W. H. Brune, D. R. Worsnop, P. Davidovits
CHANGED TO ORAL PRESENTATION

A225 **Observations on atmospheric electricity and aerosol-cloud interactions**
Hanna E. Manninen, Hannes Tammet, Antti Mäkelä, Jussi Haapalainen, Sander Mirme, Tuomo Nieminen, Alessandro Franchin, Tuukka Petäjä, Markku Kulmala, Urmas Hõrrak

A226 **Effect of local pollutant sources on aerosol-cloud interactions at Puijo measurement station**
H. Portin, A. Leskinen, A. Kortelainen, L. Hao, P. Miettinen, A. Jaatinen, S. Romakkaniemi, A. Laaksonen, K. E. J. Lehtinen, M. Komppula

A227 **Intercomparison of sulphuric acid measurements and neutral cluster composition in the lower free troposphere**
L. Rondo, M. Simon, H. Junninen, J. Duplisy, A. Praplan, A. Adamov, A. Kürten, M. Sipilä, F. Bianchi, J. Tröstl, E. Weingartner, U. Baltensperger, M. Kulmala, J. Curtius

A228 **Air mass back trajectories and dry atmospheric aerosol mass size distributions in Prague**
J. Schwarz, L. Štefancová, W. Maenhaut, J. Smolík, W. Ždímal

A229 **Blue sky over the Ruhr – a review of the effectiveness of more than 50 years of air quality measures in Germany**
S. Wurzler, H. Hebbinghaus, P. Bruckmann, J. Friesel, U. Pfeffer

Poster Session B

Tuesday, September 3rd
Room: Zenit + Nadir

16:00-18:00 **Authors' Presentations**
Room: Zenit + Nadir

Aerosol Chemistry

B001 **Organic Aerosol Formation Photoenhanced by the Formation of Secondary Photo-sensitizers in ageing Aerosols**
Kifle Z. Aregahegn, Barbara Nozière, Christian George

B002 **H2SO4 formation from olefin ozonolysis in the presence of SO2: Influence of water vapour content and temperature**
T. Berndt, T. Jokinen, M. Sipilä, R. L. Mauldin III, H. Herrmann, F. Stratmann, H. Junninen, M. Kulmala

B003 **Development of a method to measure the δ13C for OC and EC in PM**
L. Bourcier, B. Geypens

B004 **Secondary organic aerosol formation in the ozonolysis of biogenic volatile organic compounds performed in a laminar flow reactor**
T. Braure, V. Riffault, A. Tomas, M. Duncianu, Y. Bedjanian, P. Coddeville

B005 **Geochemical anomalies in aerosol induced by mining and metallurgical activities in SW Spain**
J. de la Rosa, A. M. Sánchez de la Campa, Y. González-Castanedo, R. Fernández Camacho, J. C. Fernández Caliani, A. Alastuey, X. Querol

B006 **Synthesis and glass formation properties of compounds representative of low-volatility secondary organic aerosol particles**
H. P. Dette, M. Qi, D. C. Schröder, A. Godt, T. Koop

B007 **PM formation processes in the urban atmosphere: comparison between South and North Italy**
P. R. Dambruoso, G. de Gennaro, A. Di Gilio, P. Fermo, R. Gonzalez Turion, A. Piazzalunga

B008 **Formation mechanism and important implications of highly oxidized molecules (HOM) in the gas phase**
M. Ehn, E. Kleist, H. Junninen, M. Sipilä, T. Petäjä, I. Pullinen, M. Springer, S. Andres, M. Rissanen, J. Kontkanen, S. Schobesberger, F. Rubach, R. Tillman, B. H. Lee, F. Lopez-Hilfiker, V.-M. Kerminen, M. Kulmala, D. R. Worsnop, J. Thornton, J. Wildt, T. F. Mentel

B009 **Noise as an indicator of traffic and ultrafine particles in Huelva city**
I. M. Brito Cabeza, R. Fernández-Camacho, J. D. de la Rosa

B010 **Chemical characterization of PM2.5 belonging to a port city**
A. Genga

B011 **Temperature dependence of nopinone partitioning coefficient in organic aerosol**
B. Steitz, I. Gensch, T. Hohaus, H. Saathoff, A. Kiendler-Scharr

B012 **How did chemical composition of the Po Valley radiation fog change in the last twenty years?**
L. Giulianelli, M. C. Facchini, S. Gilardoni, S. Decesari, M. Rinaldi, C. Carbone, M. Paglione, S. Fuzzi

B013 **Speciation of metals in refinery emissions particles**
Y. González-Castanedo, D. A. Sánchez Rodas, C. Ferrer, J. de la Rosa

B014 **Thermal properties of secondary organic aerosols**
A. Lutz, E. U. Emanuelsson, Å. K. Watne, M. Hallquist

B015 **Diurnal variation of C2-C5 organosulfates detected during PEGASOS field campaign**
Yoshiteru Iinuma, Laurent Poulain, Dominik van Pinxteren, Hartmut Herrmann

B016 **Reactivity of chlorine radical on palmitic acid particles: kinetic measurements**
M. Mendez, R. Ciuraru, N. Visez, D. Petitprez

B017 **Characterization and interaction between bacterial community and chemical composition of Particulate Matter in two areas of Po Valley**
E. Innocente, G. Rampazzo, S. Squizzato, V. Bertolini, A. Franzetti, I. Gandolfi, G. Bestetti

B018 **Raman Microspectriscopic Identification and Characterization of Individual Airborne Volcanic Ash Particles**
N. P. Ivleva, S. Huckele, B. Weinzierl, C. Haisch, T. Baumann, R. Niessner

B019 **On the oxidation of gaseous iodine at elevated temperatures**
T. Kärkelä, J. Holm, A. Auvinen, C. Ekberg, J. K. Jokiniemi

B020 **Hygroscopicity of nucleated nanoparticles in the presence of sulfuric acid and organics**
J. Kim, H. Keskinen, P. Vaattovaara, P. Miettinene, J. Joutsensaari, A. Virtanen, CLOUD collaboration

B021 **Characterization of particulate matter in Kraków, Poland**
M. Kistler, L. Samek, K. Styszko, K. Szramowiat, L. Furman, M. Gerhardus, A. Kasper-Giebl

B022 **Molecular composition of PM2.5 aerosols from Cork Harbour, Ireland using ultrahigh resolution mass spectrometry**
I. Kourtchev, I. P. O'Connor, S. Fuller, K. Kristenen, W. Maenhaut, J. C. Wenger, J. R. Sodeau, M. Glasius, M.Kalberer

B023 **New experimental tools for characterization of nucleation and reactivity in small aerosols**
J. Lengyel, M. Fárník, P. Slavíček, T. Zeuch

B024 **NOx Effects on Secondary Organic Aerosol Formation of Biogenic and Anthropogenic Organic Gases**
J. H. Park, K. M. Jung, W. G. Woo, W. K. Jo, H. J. Lim

B025 **Temporal trends in the atmospheric concentration of selected metals in the PM10 aerosol collected in March-September 2010 at Ny-Ålesund (Svalbard Islands)**
M. Malandrino, A. Giacomino, O. Abollino, S. Becagli, D. Frosini, M. Severi, R. Traversi, R. Udisti

B026 **Within-city variability as a tool for source apportionment of trace elements. Application to the Barcelona metropolitan area**
M. C. Minguillón, M. Cirach, G. Hoek, B. Brunekreef, M. Nieuwenhuijsen, X. Querol

B027 **Real time chemical characterization of fine particulate matter in a Spanish regional background site**
M. C. Minguillón, A. Ripoll, N. Pérez, X. Querol, A. Alastuey

B028 **Vertical profiles and seasonal variation of aerosol particles in the PBL upon Ny Ålesund (Svalbard Islands): electron microscopy vs geochemical records**
B. Moroni, S. Becagli, E. Bolzacchini, M. Busetto , L. Ferrero, D. Frosini, C. Lanconelli, A. Lupi, M. Mazzola, R. Traversi, R. Udisti, V. Vitale, D. Cappelletti

B029 **Secondary organic aerosols (SOA) chemical characterization employing simulated NMR spectra of model compositions**
M. Paglione, F. Moretti, E. Tagliavini, E. Finessi, M. C. Facchini, S. Decesari

B030 **On the enigma of new particle formation in the atmosphere**
T.-E. Parts, A. Luts, K. Komsaare, M. Noppel, U. Hõrrak

B031 **Experimental studies of the formation of cluster ions formed by corona discharge in an atmosphere containing SO_2, NH_3 and H_2O**
Preben Hvelplund, Jens Olaf Pepke Pedersen, Kristian Støchkel, Martin B. Enghoff, Theo Kurtén

B032 **PAHs and ALKs in the Arctic (Svalbard Island) aerosol: results from the AREX2011 oceanographic campaign**
E. Bolzacchini, L. Ferrero, F. Marazzi, A. Molinelli, M. G. Perrone, G. Sangiorgi, S. Becagli, R. Traversi, R. Udisti, W. Walczowski, T. Zielinski

B033 **Chemical characterization of polar organic markers in PM 2.5 during an intensive campaign of Supersito Project in Po Valley (Italy)**
M. C. Pietrogrande, M. Visentin, D. Bacco, S. Ferrari, V. Poluzzi

B034 **Photodissociation dynamics of CF2Cl2 molecule in aerosol particles**
V. Poterya, A. Pysanenko, J. Lengyel, P. Svrčková, J. Kočišek, M. Fárník

B035 **Kinetic Measurements in Acoustically Levitated Terpene Droplets**
K. Rastogi, C. Yuan, R. Willoughby, S. Almabrok, C. Pfrang

B036 **Gas phase sampling and determination of carbonyl compounds in ship diesel emissions: Differences between light fuel oil and heavy fuel oil operation**
Ahmed A. Reda, G. Abbaszade, J. Lintelmann, H. Harndorf, R. Rabe, O. Sippula, T. Streibel, J. Schnelle-Kreis, R. Zimmermann

B037 **CANCELLED**

B038 **Regional scale oxidation of organic aerosol observed through HR-ToF-AMS measurements at Mt. Cimone (2165 m asl), Italy**
M. Rinaldi, S. Gilardoni, S. Decesari, S. Fuzzi, S. Ferrari, V. Poluzzi, M. C. Facchini

B039 **Investigation of the oxidation mechanism of limonene photosensitized by imidazole-2-carboxaldehyde and leading to aerosol growth**
S. Rossignol, L. Tinel, K. Aregahegn, L. Fine, B. Nozière, C. George

B040 **Impact on Air Quality operations cleaning and inspection of Natural Gas pipelines in Central Mexico**
L. M. Rodríguez, A. M. Sánchez de la Campa, Jesús D. Rosa

B041 **Characterization of fine particles in the near-field of a metallurgy plant: Overview of the NANO-INDUS project**
A. Setyan, P. Flament, N. Locoge, K. Deboudt, V. Riffault, L. Y. Alleman, C. Schoemaecker, J. Arndt, P. Augustin, F. Blond, F. Cazier, H. Delbarre, D. Dewaele, P. Dewalle, M. Fourmentin, P. Genevray, R. Healy, P. Le Louer, T. Leonardis, H. Marris, S. Mbengue, J. Wenger

B042 **Organic aerosol: distribution between fog water and interstitial air - a report for two mountainous sites in Germany**
S. Schüttauf, J. Matschullat, F. Zimmermann, D. van Pinxteren, H. Herrmann

B043 **Modelling the multiphase chemical processing of aerosol constituents in orographic hill cap clouds during HCCT-2010**
A. Tilgner, P. Bräuer, R. Wolke, H. Herrmann

B044 **Mass distribution of elements among four fractions of suspended dust in Zabrze, Poland**
W. Rogula-Kozłowska, K. Klejnowski, P. Rogula-Kopiec, B. Błaszczak, M. Mathews, S. Szopa

B045 **Thermal properties of SOA from Ozone and OH induced oxidation of terpenes**
J. Westerlund, Å. K. Watne, Å. M. Hallquist, M. Hallquist

B046 **Microstructural changes on the carbon functional groups of individual aerosol particles from cooking activities during photochemical oxidation**
E. Coz, I. El Haddad, S. Platt, J. G. Slowik, A. S. H. Prévôt, S. Steimer, G. Grzinic, M. Lampimäki, B. Artiñano, M. Ammann

B047 **Automatic hourly measurements of hydrocarbons (C2-C11) in Metropolitan Area of Sao Paulo: Spring campaign**
P. A. Dominutti, T. Nogueira, A. Fornaro, M. F. Andrade

B048 **Chemical composition of PM10 and PM1 at a remote mountain site in NE of Spain**
A. Ripoll, M. C. Minguillon, J. Pey, X. Querol, A. Alastuey

B049 **Profiles and seasonal-distribution of PAH and n-alkanes in the urban atmosphere of Elche, Spain**
J. Gil-Moltó, N. Galindo, M. Varea, C. Chofre

B050 **Organic and elemental carbon in the surroundings of a cement complex in southeastern Spain**
E. Yubero, N. Galindo, S. Nava, M. Chiari, J. Nicolás, G. Calzolai, F. Lucarelli, J. Crespo

B051 **ATD-GC-MS method for characterization and quantification of organic compounds associated to gunshot particles**
R. Magnusson, L. Hägglund, S. Hedenstierna, H. Wingfors

B052 **Differences between inorganic ion concentrations in an urban and a remote background station**
E. Yubero, J. F. Nicolás, N. Galindo, R. Soler, J. Crespo

B053 **Knudsen Cell measurements applied for the study of gaseous precursors and chemical process**
F. G. Di Lemma, J. Y. Colle, R. J. M. Konings

B054 **An ICP-MS analysis on aerosol from simulated nuclear fuel, to study the elemental**
F. G. Di Lemma, J. Y. Colle, G. Rasmussen, S. Van Winckel, R. J. M. Konings

B055 **Saturation vapour pressures of subcooled liquid oxodicarboxylic acids**
I. Crljenica, T. Yli-Juuti, A. A. Zardini, J. Julin, M. Bilde, I. Riipinen

B056 **Flow tube analysis of the chemical composition of freshly nucleated secondary organic aerosol particles**
S. G. Gonser , C. Berberich, A. Held

B057 **Secondary organic aerosol formation from gasoline and diesel vehicle emissions: first results from a new flow reactor**
R. J. Huang, J. G. Slowik, I. El Haddad, S. M. Platt, S. M. Pieber, A. A. Zardini, R. Suarez-Bertoa, S. Hellebust, B. Temime-Roussel, N. Marchand, L. Drinovec, G. Mocnik, C. Astorga, U. Baltensperger, A. S. H. Prévôt

B058 **Synthesis of Ag triangular nanoplates protected by glutathione and their interaction of hemoglobin**
N. Kinoshita, T. Ito, N. Nishida, H. Tanaka

B059 **First Steps in Atmospheric Particle Formation**
J. Fedor, J. Lengyel, J. Kocisek, V. Poterya, A. Pysanenko, P. Svrčková, M. Fárník

B060 **Interaction of gas-born Ag nanoparticles with DNAs of salmon testes**
M. Shibata, N. Nishida, H. Tanaka

B061 **Regional modelling of the tropospheric multiphase system using COSMO-MUSCAT: Sensitivity on detail of cloud microphysics and chemical mechanism**
R. Schroedner, A. Tilgner, R. Wolke

B062 **Extinction characteristics of SOA formed following the photolysis of 2-nitrophenol: A broadband study in the near-ultraviolet**
E. M. Wilson, J. C. Wenger, D. S. Venables

B063 **Changes of aerosol properties during the ozonolysis of unsaturated carboxylic acids in the absence and presence of oxygen**
C. Keunecke, M. Beck, T. Hoffmann, T. Zeuch

Aerosol Modelling

B064 **Long-Term Variability of Terrestrial, Terpenoid BVOC Emissions in the Last Millennium**
Juan C Acosta, Hamish Struthers, Eduardo Zorita, Annica ML Ekman, Alex Guenther, Ilona Riipinen

B065 **Applications of Multiple Regression Analysis to estimate Aerosol Optical Depth over the Arabian Gulf**
F. M. Al-Kandari, H. K. Al-Jassar, K. S. Rao

B066 **Simulation of ice nucleation in a parcel model**
C. Anquetil-Deck, C. Hoose, P. Conolly

B067 **Modelling Amazonian Biomass Burning Aerosol using WRF-Chem**
S. Archer-Nicholls, D. Lowe, W. Morgan, G. McFiggans

B068 **Modeling the chemical and radiative effects of aerosol during the wildfires of 2007 in Greece**
E. Athanasopoulou, D. Rieger, C. Walter, H. Vogel, B. Vogel, E. Gerasopoulos

B069 **Model simulations on the effects of deposition freezing in convective clouds**
K. Diehl, S. K. Mitra

B070 **On blow-up in some mathematical models related to phase transitions and turbulence**
E. I. Galakhov, O. A. Salieva

B071 **Modeling of optical properties sea-salt aerosol in the surface layer of the marine and coastal atmosphere**
G. A. Kaloshin

B072 **Coupled chemical mechanism and sectional aerosol developments within WRF-Chem**
D. Lowe, S. Archer-Nicholls, S. Utembe, D. Topping, M. Barley, R. Zaveri, G. McFiggans

B073 **WRF CHEM in the marine environment**
E. Miklos, D. Martin, C. D. O'Dowd

B074 **3D modeling of open-pored foams regarding particle deposition from aerosols**
K. Schmidt, A. Hellmann, S. Ripperger

B075 **Modelling the impact of mineral dust on air quality in Beijing during a dust event**
S. Schrader, B. Vogel, H. Vogel, K. Schaefer, R. R. Shen, R. Forkel, P. Suppan, G. Tang, Y. Wang, S. Norra

B076 **The model of propagation of acoustic signal on water surface with precipitated aerosol particles**
L. A. Uvarova, V. V. Zabolotin, I. V. Krivenko, T. V. Kazarova

B077 **Airport emissions characterized by multivariate nonlinear time series models**
G. Valotto, C. Varin, C. Gaetan, E. Pecorari, G. Rampazzo, D. Bassano, S. Sollecito, E. Rampado

B078 **Photophoresis of fractal-like aerosol particles: physical model and methodical approaches**
M. V. Vasiljeva, S. A. Beresnev, L. B. Kochneva, V. I. Gryazin

B079 **Modelling the chemically speciated PM2.5 over the French Northern region using the WRF-Chem system coupled to EMEP and regional emission inventories**
M. Mendez, V. Fèvre-Nollet, P. Lebègue, D. Petitprez, N. Visez, R. Borge

B080 **Black carbon and particle number emission factors of different vehicle types measured in real driving conditions**
I. Ježek, D. Westherdal, G. Močnik

B081 **Modelled and measured aerosol hygroscopicity for aerosol corrosion prevention and energy saving in green data center designing**
L. Ferrero, G. Sangiorgi, M. G. Perrone, M. Moscatelli, L. D'Angelo, G. Rovelli, A. Ariatta, R. Truccolo, E. Bolzacchini

B082 **CANCELLED**

B083 **The role of organic condensation on ultrafine particle growth during nucleation events**
D. Patoulias, I. Riipinen, S. N. Pandis

B084 **Computational modeling of aerosol formation and evolution using OpenFOAM®**
E. M. A. Frederix, A. K. Kuczaj, M. Nordlund, C. Winkelmann, B. J. Geurts

B085 **CANCELLED**

B086 **CANCELLED**

B087 **CANCELLED**

B088 **Modeling of long-term particle formation and growth in the planetary boundary layer**
L. Zhou, M. Boy, T. Nieminen, D. Mogensen, S. Smolander, M. Kulmala

B089 **Long range transport and chemical transformation of aerosols over the Aegean Sea during a recent Etesian period**
E. Athanasopoulou, A. Protonotariou, E. Bossioli, J. Allan, A. Dandou, G. Papangelis, H. Coe, A. Bacak, J. Kalogiros, N. Mihalopoulos, G. Biskos, M. Tombrou

B090 **On the influence of WRF schemes in reconstructing the Planetary Boundary Layer height in the Po Valley**
A. Balzarini, M. Moscatelli, F. Angelini, L. Ferrero, G. Pirovano, G. M. Riva, E. Bolzacchini

B091 **Multicomponent aerosol modelling with detailed chemical species**
A. Rusanen, M. Boy, S. Smolander, D. Mogensen, P. Roldin, E. Hermansson

B092 **Phenomenological modelling of particle resuspension on bubbling PMMA**
S. Delcour, F.-X. Ouf, N. Azema, A. Coppalle, J. Yon, L. Ferry, F. Gensdarmes, J.-M. Lopez-Cuesta

B093 **Ageing of Sodium Combustion Aerosols: a Theoretical and Experimental Study**
E. Mathé, M. P. Kissane, D. Petitprez

B094 **A modeling study of regional sources contributin to atmospheric PM2.5 of Taiwan**
Tu-Fu Chen, Wen-Yinn Lin, Ken-Hui Chang

B095 **The Contribution of Local and Regional Sources to Particulate Matter in European Megacities**
K. Skyllakou, A. G. Megaritis, C. Fountoukis, B. N. Murphy, P. E. Haralabidis, S. N. Pandis

B096 **Transport of aerosol particles from the Fukushima accident**
G. Lujaniene, S. Bycenkiene, P. P. Povinec

B097 **Cs, Am and Pu isotopes in the atmosphere: source terms and tracer studies**
G. Lujaniene, D. Valiulis, S. Byčenkiene, J. Šakalys, P. P. Povinec

B098 **Comparison of the results of two air quality models in the simulation of a turbo gas cogeneration plant PM emissions**
P. Ugolini, A.Trentini, G.Bonafé, V.Poluzzi

B099 **On an influence of a temperature jump on a molecular heat flow which is taken away from a surface of strongly heated solid spherical aerosol particle**
E. R. Shchukin, L. A. Uvarova, N. V. Malay, Z. L. Shulimanova

B100 **A novel method to determine the growth rate of a growing particle mode**
T. Anttila, J. Leppä, H. Lihavainen

B101 **Determination of geometrical length of airborne carbon nanotubes by filtration method**
Y. K. Bahk, J. Wang

B102 **Modelling of aerosol optical properties with CHIMERE and OPAC and validation with Brewer and Cimel measurements at Brussels, Belgium**
V. De Bock, A. Delcloo, A. Mangold, H. De Backer

B103 **Modelling of air quality: number of particles**
S. Deschamps, K. N. Sartelet, F. Freutel

B104 **Influence of the geometry of the aerosol conducting system on the deposition of particles from inhalable aerosols on cellular surfaces in vitro**
C. Brodbeck, D. Ritter, J. Knebel

B105 **Comparison of the atmospheric Chemistry Transport Model COSMO-MUSCAT with experimentally determined aerosol parameters**
C. Engler, R. Wolke, W. Birmili, A. Wiedensohler

B106 **Year-round modelling study on particle formation a South African savannah**
R. Gierens, L. Laakso, V. Vakkari, L. Zhou, D. Mogensen, J. P. Beukes, P. G. Van Zyl, M. Boy

B107 **Binary aerosol droplet formation**
X. Z. Zhen, H.-J. Schmid

B108 **Modelling the fine and coarse fraction of heavy metals in high resolution Spanish domains**
M. A. González, M. G. Vivanco

B109 **Measurement and 3D Simulation of NaCl aerosol deposition on electrically charged microfibers**
A. Hellmann, K. Schmidt, M. Pitz, S. Ripperger

B110 **Black carbon and organic carbon in Finland: Measurements vs. model**
A. Hienola, J.-P. Pietikäinen, D. O'Donnell, K. Saarnio, A. Laaksonen

B111 **Modelling aerosol agglomeration using molecular dynamics methodology**
G. Inci, A. Kronenburg

B112 **Identification of atmospheric PM2.5 sources using Non-negative Matrix Factorization modeling in urban-industrial mixed environments**
A. Kfoury, F. Ledoux, A. Limem, G. Delmaire, G. Roussel, D. Courcot

B113 **Mathematical study of penetration efficiency of aerosol particles for human breathing with protective facemask**
I. T. Mukhametzanov, S. K. Zaripov, A. K. Gilfanov

B114 **Diagrams for drift acceleration of inclusion in acoustic field**
D. A. Gubaidullin, P. P. Osipov

B115 **Comparison of two airports emissions and pollutants dispersion in urban areas**
E. Pecorari, G. Valotto, S. Squizzato, G. Rampazzo, D. Bassano, S. Sollecito, E. Rampado

B116 **CANCELLED**

B117 **A methodology to assess occupational exposure to MNMs by modeling**
M. Pilou, T. Oroz, C. Vaquero Moralejo, P. Neofytou, C. Housiadas

B118 **The charging of amine containing clusters using protonated acetone**
K. Ruusuvuori, P. Hietala, O. Kupiainen, T. Kurtén, H. Vehkamäki

B119 **Influence of the inlet particle diameter distribution on the experimental determination of cyclone collection efficiency**
B. Sagot, J. Giardi

B120 **CANCELLED**

B121 **Novel informatics software for automated individual aerosol component property predictions and complex ensemble predictions – an online community facility**
D. Topping, M. Bane, M. Barley, D. Lowe, R. Pinning, G. McFiggans

B122 **Modeling global secondary organic aerosol formation and growth: Integrating the volatility basis set into the EMAC chemistry climate model**
A. P. Tsimpidi, V. A. Karydis, S. N. Pandis, J. Lelieveld

B123 **Source apportionment of PM2.5 concentrations: comparison of source-oriented and receptor-oriented techniques**
G. Pirovano, C. Colombi, G. Lonati, A. Balzarini and G. M. Riva

B124 **Periodic changes in the parameters of finite coagulating systems with sources and sinks at steady state regime approach**
V. A. Zagaynov, A. Maslov, A. A. Lushnikov, I. E. Agranovski, A. B. Leontyev, Yu. G. Biryukov

B125 **Efficiency of inertial capture of aerosol particles by porous fiber in cylinder array**
S. K. Zaripov, O. V. Grigorieva, S. A. Soloviev

Aerosol-based Nanotechnology

B126 **Direct Transfer of Aerosol Particles into Liquid Suspensions**
C. Anderlohr, K. Schaber

B127 **Dependency of particle size on filtration mechanisms of nanofiber web**
H.-J. Choi, S. B. Kim, S. H. Kim, M.-H. Lee

B128 **Aerosol Synthesized Porous Catalytic Particles for Emission Control Applications**
G. Kastrinaki, M. Kostoglou, A. G. Konstandopoulos

B129 **Aerosol nanoparticles captured into colloids by using an electrospray cloud as a filter**
M. Valenti, G. Biskos, A. Kourmouli, A. Schmidt-Ott

B130 **CANCELLED**

B131 **The measurement of nanoparticle deposition efficiency in the lungs of Wistar rats**
S. G. Matveeva, A. M. Baklanov, T. G. Tolstikova, S. W. Ankow

B132 **Experimental study of homogeneous nucleation from the antimony supersaturated vapor**
O. V. Borovkova, A. M. Baklanov, S. V. Vosel, F. B. Baimasheva

B133 **CANCELLED**

B134 **Real-time Characterization of Fractal-like Aerosols**
M. L. Eggersdorfer, A. J. Gröhn, C. M. Sorensen, P. H. McMurry, S. E. Pratsinis

B135 **Potential exposure to nanoplates during blending of halloysite nanoclay powder**
E. Jankowska, J. Łukaszewska, W. Zatorski

B136 **Dustiness testing of engineered nanomaterials based on ZrO2 by vortex shaker method**
E. Jankowska, P. Sobiech, J. Łukaszewska, O. Witschger, S. Bau, B. Bianchi

B137 **An effort towards understanding the sources of impurities in generating nanoparticles via liquid-phase methods**
E. M. Faghihi, L. Morawska, C. He

B138 **New measurement system for PM and ultrafine particles**
J. Spielvogel, M. Weiß

B139 **Nanoparticles generation modes of the multi-spark discharge generator**
A. A. Efimov, V. V. Ivanov, I. V. Beketov, I. A. Volkov

B140 **Size Controlled Synthesis of Spherical Nanoparticles by Spark Discharge**
J. Feng, A. Maisser, T. Pfeiffer, G. Biskos, A. Schmidt-Ott

B141 **CANCELLED**

B142 **Fluid-Particle Dynamics of Nanoparticle Synthesis in Flame Spray Reactors**
A. J. Gröhn, S. E. Pratsinis, K. Wegner

B143 **Generation of Mn oxides nanoparticles**
P. Mikuška, Z. Večeřa, B. Dočekal, P. Moravec

B144 **Synthesis of N-modified TiO2 nano powder by plasma spray for visible light photocatalysis**
C. H. Tsai, Y. M. Kuo, Y. I. Tsai, L. C. Wang, Y. F. Wang

B145 **Experimental study of homogeneous nucleation from the sulfur supersaturated vapor: Evaluation of the surface tension of critical nucleus**
S. V. Valiulin, S. V. Vosel, A. A. Onischuk, V. V. Karasev

B146 **Cu-Ni spark discharge nanoparticles from alloy feedstock of varied composition**
M. Wagner, M. Seipenbusch

B147 **Simulation of the flow field in a nanoparticle synthesis spray flame reactor including a particle coating process**
C. Weise, I. Wlokas, A. Kempf

B148 **Emission spectroscopic investigation of the spark discharge used for Cu nano particle production**
A. Kohut, A. Metzinger, G. Galbács, L. Ludvigsson, B. O. Meuller, M. E. Messing, Zs. Márton, K. Deppert, Zs. Geretovszky

B149 **Characterization of Carbon Nano-Particles from the Clad of Nuclear Fuel in HTGR with Inherent Safety (I) - Qualitative Analysis**
H. Nishida, G. Iwanaka, H. Takano, M. Itoh

B150 **Synthesis and characterization of calcium oxide based particles for CO2 adsorption applications**
K. G. Sakellariou, G. Kastrinaki, G. Karagiannakis, A. G. Konstandopoulos

B151 **Detection of Airborne Carbon Nanotubes via Embedded Nickel Catalysts in Quasi-Real Time**
N. Neubauer, G. Kasper

B152 **Acute respiratory response on workers exposure to nanoparticles in different occupational settings**
I. Szadkowska-Stańczyk, S. Bujak-Pietrek, U. Mikołajczyk

B153 **Testing particulate matter toxicity via in vitro methods: what should be tested?**
A. J. Wlodarczyk, K. A. BéruBé

B154 **The impact of zinc oxide nanoparticles on metabolic activity in the cells of respiratory and reproductive system**
L. Zapór

B155 **A new device for continuous unattended measurements of UFP**
M. Pesch, H. Grimm, R. Albrecht, A. Edfelder

B156 **Portable device for simultaneous measurements of Nano particles and it agglomerations at workplaces**
H. Grimm, M. Pesch, M. Richter, A. Comouth

B157 **Combustion of CNT-containing composite materials in a laboratory scale incinerator**
A. M. Todea, B. Stahlmecke, C. Asbach, T. A. J. Kuhlbusch

B158 **Characterization of Polyamide Nanofiber Media for Aerosol Filtration Applications**
J. Matulevicius, L. Kliucininkas, D. Martuzevicius

B159 **Sublimation growth of 3C-SiC in induction heating of preceramic Si-C nanoparticles**
M. Miettinen, J. Hokkinen , T. Karhunen, T. Torvela, U. Tapper, J. Jokiniemi, A. Lähde

B160 **Generation of Pb/PbOx nanoparticles for inhalation experiments**
P. Moravec, J. Smolík, J. Ondráček, P. Vodička, R. Fajgar

B161 **Batch-to-batch reproducibility - a challenge for safety assessment and regulation**
H.-R. Paur, C. Adelhelm, S. Diabaté, J. Forsgren, E. Mahon, S. Mülhopt, J. P. Bagaria, V. Puntes, R. Schneider, C. Weiss, T. Wilkins, Y. Jiang

B162 **Contrasting manufactured nano objects emitted during maintenance of common particle generators with originally synthesized particles**
P. T. Nilsson, L. Ludvigsson, J. Rissler, M. E. Messing, C. Isaxon, A. C. Eriksson, M. Hedmer, H. Tinnerberg, K. Deppert, A. Gudmundsson, J. Pagels

B163 **Fragmentation of nanoparticle agglomerates by collisions in supersonic flows**
Y. Okada, N. Oshio, K. Oda, M. Yabuhana

B164 **High-throughput multi-jet electrospinning for two fluids using a coaxial grooved nozzle**
I. Park, W. Kim, S. S. Kim

B165 **Impact of size and concentration on the particle charging properties of an annular DBD**
M. Pesch, H. Grimm, T. Külz, M. Richter, R. Albrecht

B166 **Positioning of nano-sized noble metal aerosols in an organic light-emitting diode for enhanced quantum efficiency**
H.-K Sung, J.-C. Lee, J.-K. Lee, C. Kim, M. Choi

Combustion Aerosols

B167 **Penetration of Combustion Aerosol Particles through an N95 FFR Respirator Filter**
S. A. Grinshpun, X. He, J. Y. Kim, T. Reponen

B168 **Selective catalytic reduction nitrogen oxides with methane over nanosized CuO supported on Al2O3. Part 1. Materials structural characterization**
Chang-Mao Hung, Mu-Hsing Kuo, Shui-Jen Chen, Wei-Bang Lin, Wen-Liang Lai

B169 **Selective catalytic reduction nitrogen oxides with methane over nanosized CuO supported on Al2O3. Part 2. Catalytic activity and mechanism study**
Chang-Mao Hung, Mu-Hsing Kuo, Shui-Jen Chen, Wei-Bang Lin, Wen-Liang Lai

B170 **Selective catalytic reduction nitrogen oxides with methane over nanosized CuO supported on Al2O3. Part 3. Reaction kinetic behavior study**
Chang-Mao Hung, Mu-Hsing Kuo, Shui-Jen Chen, Wei-Bang Lin, Wen-Liang Lai

B171 **Characterization of aerosols emitted during the incineration of nanocomposites**
G. Ounoughene , O. Le Bihan, C. Chivas-Joly, C. Longuet, A. Joubert, C. Motzkus, D. Venditti , S. Durécu, B. Debray, J-M. Lopez-Cuesta, L. Le Coq

B172 **Particle Emission from the Aircraft Engine Testing Cycles**
J. J. Rodríguez-Maroto, V. Archilla, D. Sanz-Rivera, E. Rojas-García, M. Pujadas, J. L. Mosquera, D. Mercader, A. Gonzalez (ISDEFE), A. Jimenez, J. Mena, A. Entero (ISDEFE), J. M. Fernández-Mainez, J. C. Bezares

B173 **Gas-droplet flows in fire safety engineering**
K. Volkov, V. Emelyanov

B174 **The nanofraction of fly ashes in Swiss waste incineration plants (WIP) and the respective modelled contributions of engineered nanomaterials (ENM)**
J. Buha, N. Müller, B. Nowack, A. Ulrich, J. Wang

B175 **Tandem-DMA measurements of gases and particles in large-scale biomass combustion and gasification**
D. Gall, M. Pushp, C. Forsman, K. O. Davidsson, M. Hallquist, J. B. C. Pettersson

B176 **Condensing Heat Exchanger for Fine Particle Precipitation and Efficient Heat Recovery in Small Scale Wood Combustion**
J. Grigonyte, O. Sippula, I. Nuutinen, T. Koponen, H. Lamberg, T. Kaivosoja, J. Jokiniemi

B177 **Effect on pore size distribution on filtration performance of ceramic filter media**
J.-U. Kim, H.-J. Choi, S.-H. Kim, M.-W Lee

B178 **Characterizing physical properties of aerosol particles in a bubbling fluidized bed boiler**
H. Kuuluvainen, P. Karjalainen, J. Maunula, J. Kauppinen, M. Räsänen, R. Taipale, P. Vainikka, J. Roppo, J. Keskinen, T. Rönkkö

B179 **Diagnostics of burning tungsten particles by two-color imaging pyrometry**
S. G. Orlovskaya, F. F. Karimova, M. S. Shkoropado

B180 **Fate of hazardous elements from biomass burned in stoves and boilers**
Torben Seidel, Hans Ruppert

B181 **Biomass Combustion in Stoves - Influence on Emissions and Toxic Potential of Particles**
C. Schön, H. Hartmann, J. Gerth

B182 **Ultrafine particulate matter emissions from a gasoline direct injection engine**
B. R'Mili, A. Boréave, W. Y. Hernandez, M. N. Tsampas, N. Charbonnel, L. Retailleau-Mevel, B. D'Anna, ¨ P. Vernoux, M. Leblanc, S. Zinola, S. Raux

B183 **Fractional cabin air recirculation: A simple and robust way to reduce PM exposure for passengers**
H. Jung, M. Grady

B184 **Particle emissions of a heavy duty diesel engine fuelled with fossil diesel and hydrotreated vegetable oil**
P. Karjalainen, J. Heikkilä, T. Rönkkö, M. Happonen, F. Mylläri, L. Pirjola, T. Lähde, D. Rothe, J. Keskinen

B185 **Particle number and size distribution of Euro 5 and Euro 6 passenger cars at 22°C and -7°C**
F. Riccobono, U. Manfredi, G. Martini

B186 **Investigations on the removal of volatile components from diesel exhaust**
B. Kiwull, J. C. Wolf, R. Niessner

B187 **Effects of severe congestion on PAH emissions from a heavy vehicle diesel engine**
M. Vojtisek-Lom, M. Pechout, M. Mazač, J.Topinka

B188 **Emissions of gases and PM2.5 during combustion of wood logs in a stove or a fireplace**
V. Martins, A.I. Calvo, C. Alves, T. Nunes, R. Hillamo, K. Teinilä, M. Duarte, L. Mendes, L. A. C. Tarelho

B189 **Combustion of forest residues in a bubbling fluidised bed: characterisation of particulate matter emissions**
A. I. Calvo, L. A. C. Tarelho, E. R. Teixeira, R. Modolo, C. Alves, T. Nunes, M. Duarte, E. Coz, D. Custódio, A. Castro, B. Artiñano, R. Fraile

B190 **Prospecting analysis of soot for post-fire investigation**
A. Bellivier, M. Meneceur, H. Bazin

B191 **Nanoparticles Emissions from Pottery Manufacturing**
A. Voliotis, S. Bezantakos, M. Giamarelou, G. Biskos

B192 **Wildfires in North Spain: Smoke aerosol and its radiative effects**
A. Castro, E. Alonso-Blanco, A. I. Calvo, V. Pont, M. Mallet, C. Alves, R. Fraile

B193 **Influence of biodiesel-to-diesel addition on major ions and trace elements in fine particulate matter exhausted by a diesel engine**
G. O. da Rocha, J. V. S. Santos, A. C. D. Regis, L. Tormen, A. L. N. Guarieiro, J. D. S. da Silva, A. J. Curtis, J. B. de Andrade

B194 **Effective density of particulate matter emitted from aircraft gas turbine engine sources**
L. Durdina, B. Brem, M. Abegglen, B. Sierau, J. Wang

B195 **Particulate matter generated by heating/cooking plants in traditional homes of Mt. Everest region in central southern Himalaya (Nepal)**
P. Fermo, A. Piazzalunga, R. Gonzalez, D. Comunian, G. Tartari, F. Salerno, G. Viviano, P. Ielpo

B196 **New CO2 Mitigation Process with Diesel Dynamo Power Plant Associated by Optimized Aerosol Driven Technique**
K. Fukamizu, H. Takano, M. Itoh

B197 **Investigating the aethalometer model to estimate black carbon and airborne particles from wood burning**
G. W. Fuller

B198 **CANCELLED**

B199 **Reduction of PAHs emitted from a generator fuelled by waste-edible-oil-biodiesel with acetone and isopropyl alcohol addition**
Jen-Hsiung Tsai, Shui-Jen Chen, Wen-Yinn Lin, Kuo-Lin Huang, Chih-Chung Lin, Yung-Shun Chen

B200 **Cytotoxicity of exhaust emissions from a generator fuelled by waste-edible-oil-biodiesel with acetone and isopropyl alcohol addition**
Jen-Hsiung Tsai, Shui-Jen Chen, Kuo-Lin Huang, Wen-Yinn Lin, Yi-Chu Huang, Te-San Chen

B201 **Characteristics of SO2 removal by using CaCO3 sorbent particle in an oxy-PC combustion system**
Seongha Jeong, Kang Soo Lee, Sang In Keel, Jin Han Yun, Sang Soo Kim

B202 **Dry absorption of SO2 with hydrated lime in spout-bed circulating dry scrubber system**
Young-Ok Park, Seong-Min Cheon, Yong-Ha Kim

B203 **Real-time chemical composition analysis of particle emissions from woodchip combustion**
A. Kortelainen, J. Joutsensaari, P. Tiitta, A. Jaatinen, P. Miettinen, L. Hao, J. Leskinen, A. Virén, T. Torvela, J. Tissari, J. Jokiniemi, D. R. Worsnop, A. Laaksonen, A. Virtanen

B204 **Ash behaviour and emission formation in co-combustion of wood and two agricultural fuels**
M. Kortelainen, J. Tissari, T. Torvela, T. Karhunen, H. Lamberg, I. Nuutinen, O. Sippula, J. Jokiniemi

B205 **Characteristics of the particulate matter from road tunnel environment**
R. Licbinsky, J. Huzlik, J. Faimon, K. Kreislova

B206 **On the relation between aerodynamic and mobility diameter distributions for aggregates consisting of few monomers**
A. Melas, M. Kostoglou, P. Baltzopoulou, Y. Drossinos, A. G. Konstandopoulos

B207 **Immunomodulatory effects of short-term exposure to fine particulate matter from smog episode in Ostrava region: in vitro study**
T. Brzicová, I. Lochman, P. Danihelka, A. Lochmanová, K. Lach, V. Mička

B208 **PAH, PCDD/F and HCB emissions from residential wood combustion**
K. Mõts, M. Maasikmets, E. Teinemaa, K. Vainumäe, L. Lehes, T. Arumäe, V. Kimmel

B209 **Toxicological Responses to Ozone Aging of Aerosols from Small-scale Biomass Combustion**
E. Z. Nordin, O. Uski, R. Nyström, P. Jalava, J. Genberg, A. C. Eriksson, C. Bergvall, R. Westerholm, C. Boman, J. Jokiniemi, J. Pagels, M.-R. Hirvonen

B210 **Fourier-transform-ion-cyclotron-resonance mass spectrometry with laser-desorption-ionization of primary ship diesel exhaust particles**
C. Rüger, T. Schwemer, M. Sklorz, R. Zimmermann

B211 **Removal Characteristics of Iron Particles by Ceramic Candle Filters and the Effect of the flue Gas Inlet Configuration in Particulate Collectors**
Y. O. Park, N. Hasolli

B212 **Chemical profile of wood burning PM2.5 and PM1 in the two largest cities of Greece, Athens and Thessaloniki**
St. Pateraki, Th. Maggos, D. A. Sarigiannis, M. Kermenidou, S. K. Karakitsios, V. D. Assimakopoulos, A. Zagkos, D. N. Asimakopoulos

B213 **Emissions of volatile organic compounds from ritual burning practices**
Shamsh Perver, Rajan Chakrabarty, Barbara Zielinska, Shippi Dewangan

B214 **Particle and gas phase distribution of toxic metals during biomass combustion**
D. Pudasainee, H.-R. Paur, A. Bologa, H. Seifert

B215 **Laboratory particle-phase emissions from sugarcane burning: chemical and mutagenicity**
E. R. Dias, K. F. Souza, D. A. Morales, F. Kummrow, G. A. Umbuzeiro, L. R. F. Carvalho

B216 **Characterisation of different soot types regarding morphology and black carbon content**
H. Saathoff, A. Comouth, B. Altstädter, C. Linke, A. Kiselev, K.-H. Naumann

B217 **Characterization of indoor and outdoor aerosol during extreme pollution events from winter heating in single-family home districts**
I. Stasiulaitiene, E. Krugly, L. Kliučininkas, T. Prasauskas, M. Tichonovas, A. Garbaras, D. Martuzevičius

B218 **Verifying modified EAD (MEAD) used in measuring metal fume nanoparticle and charactering its exposure concentration during gas metal arc and flux cored arc welding processes**
P. J. Tsai, Y. F. Wang

B219 **Particle size distributions of PAHs in workplace atmospheres and their exposure concentrations to workers in a steal and iron manufacturing factory**
Y. F. Wang, P. J. Tsai

B220 **Comprehensive analysis of anthropogenic aerosol using automated classification for GCxGC-TOF analysis**
B. A. Weggler, J. Orasche, T. Groeger, R. Zimmermann

B221 **Physical and chemical characterisation of PM emissions from in-operation ship engines**
J. Moldanová, E. Fridell, H. Winnes, J. Boman, V. Tishkova, B. Demirdjian, S. Joulie, H. Bladt, N. Ivaleva

B222 **Exposure to airborne (1-3)-B-D-glucans during metalworking processes**
M. Cyprowski, A. Lawniczek-Walczyk, R. L. Górny

B238 **Nanoparticle release from nanostructured powders during low- and high-energetic dry dispersing processes**
D. Göhler, M. Stintz

B239 **Characterization of Carbon Nano-Particles from the Cladof Nuclear Fuel in HTGR with Inherent Safety(II) –Quantitative Analysis**
G. Iwanaka, H. Nishida, H. Takano, M. Itoh

B240 **Risk assessment of airborne engineered nanomaterials**
A. J. Koivisto, A.-K. Viitanen, T. Hussein, T. Kanerva, T. Tuomi, H. Stockmann-Juvala, K. Hämeri

B241 **Stability of nanoparticle agglomerates in flames - First results of investigations on the release during waste incineration**
I.-M. Liesen, W. Baumann, M. Hauser, H. Mätzing, H.-R. Paur, H. Seifert

Reserve Posters

B223 **Uptake of N2O5 to citric acid aerosol particles**
G. Gržinić, T. Bartels-Rausch, A. Türler, M. Ammann

B224 **Pressure dependency of ozonolysis product formation of α-pinene focusing on low volatile compounds such as organic acids and dimeric compounds**
M. Beck, C. Keunecke, T. Zeuch, T. Hoffmann

B225 **Dry deposition of electrosprayed liquid suspensions**
S. Martin. B. Martinez-Vazquez, P. L. Garcia-Ybarra, J. L. Castillo

B226 **Effect of Nucleation Precursors on the Atmospheric Oxidation of Organic Compounds**
J. Elm, M. Bilde, K. V. Mikkelsen
CHANGED TO ORAL PRESENTATION

B227 **Quantitative single particle mass spectrometry with the Aerodyne aerosol mass spectrometer: development of a new classification algorithm and application to field data**
F. Freutel, F. Drewnick, J. Schneider, T. Klimach, S. Borrmann

B228 **Smoke particle morphology for different fire types determined by equivalent ratio tube furnace method**
Jaehark Goo

B229 **Industrial by-products as precursors for gas-phase nanoparticle synthesis**
T. Karhunen, A. Lähde, T. Torvela, J. Jokiniemi

B230 **Dilution affects particle properties originating from residential biomass combustion**
H. Lamberg, T. Kaivosoja, J. Leskinen, M. Kortelainen, A. Viren, H. Koponen, V. Tiihonen, M. Miettinen, J. Pyykönen, J. Jokiniemi, J. Tissari

B231 **A novel set-up for source characterization and human exposures of biomass combustion aerosols**
R. Nyström, E. Z. Nordin, J. H. Pagels, A. Blomberg, T. Sandström, C. Boman

B232 **Synthesis of tailored organic-inorganic nanostructures by charge controlled coagulation**
S. Sigmund, E. Akgün, J. Meyer, M. Wörner, G. Kasper

B233 **Contribution of Inorganic aerosols and trace gases due to biomass burning during cooking hours at a rural site in India**
Sudha Singh, Gyan Prakash Gupta, Bablu Kumar, U. C. Kulshrestha

B234 **Dependence of Aircraft Smoke Number on Black Carbon Size Distribution**
M. E. J. Stettler, J. J. Swanson, A. M. Boies

B235 **Characterisation of solid and semi-volatile gas-turbine particulate matter using a catalytic stripper**
J. J. Swanson, T. J. Johnson, J. S. Olfert, M. P. Johnson, P. I. Williams, G. J. Smallwood, A. M. Boies

B236 **Impact of biogenic emissions on PM2.5 concentration over Europe**
E. Tagaris, R. E. P. Sotiropoulou, N. Gounaris, S. Andronopoulos, D. Vlachogiannis

B237 **Climate and biofuels in Brazil**
H. Vuollekoski, R. Makkonen, A. Asmi, R. Hillamo, T. Petäjä, M. Kulmala

Poster Session C

Thursday, September 5th
Room: Zenit + Nadir

16:00-18:00 **Authors' Presentations**
Room: Zenit + Nadir

Electrical Effects

C001 **Incineration of the diesel particulate matter using the dielectric barrier discharge on the electrostatic precipitator**
Y. Ehara, M. Kobayashi, H. Muramatsu, A. Zukeran, H. Kawakami, T. Inui

C002 **Manipulation of aerosol particles with nonlinear polarizability**
K. V. Generalov, D. V. Korneev, V. M. Generalov, M. V. Kruchinina, B. N. Zaycev

C003 **An ESP nanoparticle generator**
C. W. Lin, W. Y. Lin, T. C. Hisao, Y. M. Kuo, C. C. Chen

C004 **Experimental study of a louvered electrostatic precipitator**
Hso-Chi Chaung, Tsai-Yun Wu

C005 **Open Channel Electrospray System**
J. S. Kang, J. H. Jung, G.-N. Bae

C006 **Effect of aperture rate on improving collection efficiency in hole-type electrostatic precipitator**
H. Kawakami, A. Osako, Y. Watanabe, Y. Ehara, Y. Nitta, A. Zukeran, T. Inui

C007 **The Effect of Surface Charge on Characteristics of Fibrous Membrane**
Y. R. Jhong, H. Y. Lin, S. K. Chan, T. M. Tu, Y. C. Cheng, Y. Y. Chang, C. W. Chen, W. Y. Lin

C008 **Characterization of an ion jet unipolar electrical aerosol diffusion charger**
Wen-Yinn Lin, Ken-Hui Chang, Chih-Chieh Chen, Shao-Hao Lu, Yuan-Yi Chang, Jin-Yuan Syu

C009 **SO2 Reduction by water condensation for marine diesel**
A. Zukeran, K. Ninomiya, Y. Ehara, K. Yasumoto, H. Kawakami, T. Inui

Fundamentals

C010 **Modifications to the bipolar charging theory for spherical particles**
J. L. de La Verpillière, J. J. Swanson, A. M. Boies

C011 **Restructuring of Aggregates and their Primary Particle Size Distribution during Sintering**
M. L. Eggersdorfer, S. E. Pratsinis

C012 **Acoustic waves in vapour-gas mixtures with polydispersed particles and droplets**
Yu. V. Fedorov, D. A. Gubaidullin, D. D. Gubaidullina

C013 **Multiscale design of aerosol synthesis of materials: Effect of structure on TiO2 & SiO2 particle growth by coagulation and sintering**
E. Goudeli, M. L. Eggersdorfer, S. E. Pratsinis

C014 **Dynamics of aerosols and particles at nonlinear oscillations in tubes**
D. A. Gubaidullin, R. G. Zaripov, L. A. Tkachenko

C015 **De-agglomeration and bounce of the iron oxide agglomerates due to the impaction**
M. Ihalainen, T. Lind, T. Torvela, J. Ruusunen, A. Lähde, P. Tiitta, J. Jokiniemi

C016 **Propagation of acoustic disturbances in N-fractional gas-liquid systems**
D. A. Gubaidullin, A. A. Nikiforov, E. A. Teregulova, R. N. Gafiyatov

C017 **Experimental investigation dynamics of aerosols at oscillations in tubes in a no shock-wave mode**
D. A. Gubaidullin, R. G. Zaripov, L. A. Tkachenko

C018 **Calculation of deposition on fibrous filters due to impaction – critical trajectories**
S. J. Dunnett, C. F. Clement

C019 **Study of filtration performances of fibrous media: comparison between flat and industrial-geometry prototypes filters**
L. F. Gonzalez, A. Joubert, Y. Andrès, C. Delahaye, N. Berthelot, X. Chaucherie, L. Le Coq

C020 **Degradation of glass fiber filter media exposed to acidic and alkaline contaminants**
Myong-Hwa Lee, Jeong-Uk Kim, Eunsol Kim

C021 **Filtration characteristics of air filter loaded with differently charged particles**
H. S. Park

C022 **Influence of particle and filter charge on collection efficiency of air filters in an externally applied electric field**
H. S. Park

C023 **The analytical description of the dynamics of the impurity redistribution in the composite particles by coagulation**
D. V. Tsaplin, V. N. Piskunov

C024 **Detection of the negative thermophoresis phenomenon in microgravity experiments**
A. A. Vedernikov, S. A. Beresnev, A. V. Markovich

C025 **Contribution to the study of particle resuspension kinetics during thermal degradation of polymers**
S. Delcour, F.-X. Ouf, N. Azema, A. Coppalle, J. Yon, L. Ferry, F. Gensdarmes, J.-M. Lopez-Cuesta

C026 **Determining the mass accommodation coefficient of dicarboxylic acids using molecular dynamics simulations**
Jan Julin, Ilona Riipinen

C027 **Size dependence of incorporation of gas molecules into aerosol nanoparticles**
V. V. Levdansky, J. Smolík, V. Ždímal, P. Moravec

C028 **Influence of size effect on chemical reactions on surface of aerosol nanoparticles**
V. V. Levdansky, J. Smolík, V. Ždímal, P. Moravec

C029 **Evolution of Size and Temperature of Droplets in the Process of Bulk Condensation**
N. M. Kortsenshteyn, A. K. Yastrebov

C030 **Nucleation near critical supersaturation**
Z. Kožíšek, P. Demo

C031 **Heterogeneous nucleation on partially wettable charged conducting seed particle**
M. Noppel, H. Vehkamäki, P. M. Winkler, M. Kulmala, P. E. Wagner

C032 **The Role of Highly Oxidized Organics in New Particle Formation**
I. K. Ortega, H. Vehkamäki

C033 **Linking Neutral and Charged Sulfuric Acid - Ammonia and Sulfuric Acid - Dimethylamine Clusters**
I. K. Ortega, O. Kupiainen, T. Olenius, V. Loukonen, T. Kurten, H. Vehkamäki

C034 **Determination of Nanoparticles Surface Tension from Experimental Data on Homogeneous Nucleation of Ibuprofen Vapors**
A. V. Samodurov, A. M. Baklanov, S. V. Vosel

C035 **Development of an Experimental Flow Configuration for the Study of the Effects of Mixing on the Nucleation and Growth of Liquid Droplets**
G. Scribano, A. O. Alshaarawi, K. Zhou, A. Attili, F. Bisetti

C036 **Systematic correlation between aerodynamic shape factor and optical properties**
S. Pfeifer, T. Mueller, A. Wiedensohler

C037 **CANCELLED**

C038 **Experiments on neutral cluster generation and detection below 2 nm size**
J. Kangasluoma, H. Junninen, M. Sipilä, M. Kulmala, T. Petäjä

C039 **A method to determine the size distribution of recombination products from atmospheric measurements**
J. Kontkanen, T. Nieminen, H. E. Manninen, K. Lehtipalo, V-M. Kerminen, K. E. J. Lehtinen, M. Kulmala

C040 **Generation of sub-Nanometer Atomic Clusters in the Aerosol Phase using Spark Discharge Generation (SDG)**
A. Maisser, K. Barmpounis, M. B. Attoui, G. Biskos, A. Schmidt-Ott

C041 **Calculation of dynamic properties of fractal aggregates in the transition regime**
A. D. Melas, A. G. Konstandopoulos, L. Isella, Y. Drossinos

C042 **Analysis of the Current Models of Aerosol Dry Deposition**
V. N. Piskunov

C043 **CANCELLED**

Instrumentation

C044 **Comparisons of Rman- and WALI- derived aerosol optical properties during HyMeX**
M-L. Boytard, P. Royer, P. Chazette, J. Totems, X. Shang, F. Marnas

C045 **Determining effective density of nanostructured particles by tandem electrical mobility and mass measurement (tandem DMA/APM): application to thermal spraying fumes**
S. Bau, A. Charvet, D. Bémer, D. Thomas

C046 **Direct analysis of secondary organic aerosol using atmospheric-pressure glow discharge mass spectrometry**
M. Brüggemann, T. Hoffmann

C047 **Aerosol detection and ranging: fast laser imaging optical emission spectroscopy (DARLIOES)**
S. Mitachi, M. M. Cazacu, A. Timofte, D. Dimitriu, S. Gurlui

C048 **Measurement of solid particle concentration is aided by catalytic stripper technology**
J. J. Swanson, H.-J. Schulz

C049 **A new Instrument to Observe Contact Freezing of Single Supercooled Levitated Water Droplets**
H.-J. Tong, F. D. Pope, M. Kalberer

C050 **On-board study of nano- and micrometer-particle characteristics of a running electric train**
S. Abbasi, U. Olofsson, T. Tritscher, T. Krinke

C051 **A new device for the investigation of nucleation, dynamic growth and surface properties of single ice crystals**
J. Voigtländer, C. Chou, H. Bieligk, T. Clauss, P. Herenz , D. Niedermeier, J. Z. Ulanowski, F. Stratmann

C052 **A real-time analyzing and weighing system**
D. Weidauer, C. Bey, F. Freyer, N. Derenda

C053 **Review of the field experiments on the transfer of pollution in urban areas in 1979 and 2003**
Yu. S. Balashov, V. N. Piskunov

C054 **Comparing particle number size distributions and number concentrations for airborne nanoparticles measured by SMPS, FMPS and UWCPC**
S. Bau, V. Hase, P. Danihelka, O. Witschger

C055 **UFP measurement: comparison of commercial equipments using different measuring principles**
B. Bergmans, F. Lenartz, J. Mertens, N. Faniel, T. Krinke

C056 **Comparison among un-denuder filter based, denuder filter pack and continuous techniques for inorganic artefact assessment**
P. R. Dambruoso, G. de Gennaro, A. Di Gilio, P. Fermo, R. Filardi, A. Piazzalunga, R. Gonzalez Turion, R. Vecchi

C057 **Comparison of On-line and Off-line methods for the quantification of particle bound Reactive Oxygen Species**
S. J. Fuller, F. P. H. Wragg, M. Kalberer

C058 **Inter-comparison of size distribution measurements in cloud expansion studies**
E. Järvinen, M. Schnaiter, P. Vochezer, K. Höhler, N. Hiranuma, O. Möhler

C059 **Validating SMPS-measured size distribution of double-mode spherical Silica nanoparticles by Transmission Electron Microscope (TEM)**
E. M. Faghihi, L. Morawska, G. Johnson, T. Bostrom

C060 **Application and recalibration of a GRIMM spectrometer in the monitoring of Sahara dust**
C. Pio, J. Cardoso, T. Nunes, C. Alves, M. Cerqueira, S. M. Almeida, M. Almeida-Silva, M. C. Freitas

C061 **Description of the aerosol size distribution of the atmosphere during a Saharan dust intrusion over South Spain with airborne and ground based instrumentation: AMISOC**
N. Seoane Vieira, J. Andrey-Andrés, M. Sorribas, A. Corrales Sierra, R. González-Armengod, M. Gil, B. de la Morena, B. Marqués

C062 **Model 3088 Advanced Aerosol Neutralizer: Comparisons with Previous Generation**
J. H. Scheckman, S. Elzey, J. E. Farnsworth, B. Osmondson

C063 **Black carbon measurements in snow with the single particle soot photometer**
J. Svensson, D. Brus, A.-P. Hyvärinen, H. Lihavainen

C064 **RADES (RAdiological Dispersion Events Set-up) set-up and result from the characterization of the aerosol from simulated RDE´s (Radiological Dispersion Events)**
F. G. Di Lemma, J. Y. Colle, H. Thiele, M. Ernsteberg, R. J. M. Konings

C065 **A laboratory evaluation of four commercial particle sizers under several aerosol types**
G. C. Dragan, J. Schnelle-Kreis, E. Karg, R. Zimmermann

C066 **On-line Diagnostics for Particle Size in Nanoparticle Manufacturing**
A. J. Gröhn, M. L. Eggersdorfer, S. E. Pratsinis, K. Wegner

C067 **XPS analysis of size-segregated aerosol collected in an urban background site in Lecce (Italy)**
M. R. Guascito, P. Ielpo, D. Cesari, A. Genga, C. Malitesta, D. Chirizzi, D. Contini

C068 **Characterization of filter materials for aerosol research – size resolved penetration**
J. Ondráček, N. Zíková, V. Ždímal

C069 **Data Merging of Size Distributions from Electrical Mobility and Optical Measurements**
T. Tritscher, A. F. Zerrath, S. Elzey, H. S. Han

C070 **Tandem of Differential Mobility Analyzer and Centrifugal Particle Mass Analyzer: application to hygroscopic growth of aerosol particles**
S. S. Vlasenko, E. F. Mikhailov

C071 **Steady-state mass-mobility measurements of cigarette smoke using a CPMA**
T. J. Johnson, R. Cabot, C. Treacy, C. Dickens, J. McAughey, C. U. Yurteri, J. P. R. Symonds, J. S. Olfert

C072 **Assessment of Voltage Shift in Tandem DMAs by Brownian Particle Trajectory Simulation**
M. Alonso, F. J. Alguacil, J. P. Santos, V. Gómez

C073 **Instrumental optimization of the compact laser mass spectrometer LAMPAS 3 for on-line single particle analysis under various field conditions**
K.-P. Hinz, A. Fendt, B. Spengler

C074 **Multi-Element Scanning Thermal Analysis (MESTA) of Aerosols and Nano-Carbon Particles**
Y. P. Hsieh, G. Bugna, K. Robertson

C075 **Study on particle capture characteristics and numerical analysis for impaction sizer**
C-H Huang, C-J Wu, Y-Y Chang

C076 **Consistency of Long-term Black Carbon Trends from Thermal and Optical Measurements in the U.S. IMPROVE Network**
L.-W. A. Chen, J. C. Chow, J. G. Watson, B. A. Schichtel

C077 **Black Carbon in Dust and Geological Material: Reconciling Thermal/Optical and Spectral Quantification Methods**
L.-W. A. Chen, Y. M. Han, J. A. Robles, J. C. Chow, J. J. Cao, J. G. Watson

C078 **Airspace Dimension Test (ADT) – A novel technique for diagnosis of chronic obstructive pulmonary disease with nanoparticles**
J. Jakobsson, J. Kumlin, J. Hedlund, P. Wollmer, J. Löndahl

C079 **Remotely operated PLUS-octocopter used as an aerosol measurement platform**
P. Madl, C. Oberauer, F. Steinhäusler

C080 **A CAPS-Based Single Scattering Albedo Monitor**
T. B. Onasch, P. Massoli, P. L. Kebabian, A. Freedman

C081 **Performance Enhancements to TSI Water-based Condensation Particle Counters**
J. H. Scheckman, S. Morell and F. Quant

C082 **Evaluation and development of Scanning Flow CCN Analysis**
C. Wittbom, B. Svenningsson, S. Sjogren, E. Swietlicki

C083 **Generation and growth of aerosol particles on nucleus of radioactive decays**
V. A. Zagaynov, N. A. Klyachin, N. P. Kalashnikov, A. A. Lushnikov, I. E. Agranovski, Yu. G. Biryukov

Particle-Lung Interactions

C084 **Biological response in lung cells by brake dust from a novel set-up to generate one source wear particles**
S. Abbasi, B. Ekstrand-Hammarström, U. Bergström, A. Bucht, U. Olofsson, U. Sellgren, A. Jansson

C085 **A multiculture cell exposure chamber for the assessment of airborne and engineered nanoparticles effects on health**
A. Asimakopoulou, E. Daskalos, N. Lewinski, E. Papaioannou, A. G. Konstandopoulos

C086 **Effect of flow rate on fiber deposition in the model of human lungs**
M. Bělka, F. Lízal, M. Jicha, J. Jedelsky

C087 **A portable device to measure puffing behaviour and tobacco smoke exposure**
C. Graham, S. Slayford

C088 **In vivo measurements of nanometer-sized particle deposition in the nasal cavities of Taiwanese adults**
D. J. Hsu and C. W. Lee

C089 **Role of size and composition of traffic and wood burning aerosols in the molecular responses induced in airway epithelial and pulmonary artery endothelial cells**
L. Boublil, M. Lisbonne-Autissier, M. Thierry-Mieg, M. Leroux, J. P. Savineau, L. Martinon, J. Sciare, K. Andreau, A. Baeza-Squiban, I. Baudrimont

C090 **In vitro efficiency measurements of the deposition of pMDI generated aerosols in a realistic central airway geometry**
A. Kerekes, A. Nagy, M. Veres, D. Oszetzky, A. Czitrovszky

C091 **Aerosol Deposition Measurement in the Model of Human Lungs**
F. Lízal, J. Jedelský, J. Adam, M. Bělka, M. Jícha

C092 **Airspace dimension test (ADT) with nanoparticles for identification of patients with respiratory disease**
J. Löndah, J. Jakobsson, T. Andersson, P. Wollmer

C093 **CANCELLED**

C094 **Experimental investigation of the transport and deposition of ambient aerosols in the human airways**
A. Nagy, A. Kerekes, A. Czitrovszky

C095 **Coincidental study of inhalation and intratracheal instillation for hazard assessment of nanoparticles**
T. Oyabu, Y. Morimoto, M. Horie, Y. Yoshiura, M. Shimada, M. Kubo, B. W. Lee, T. Okada, T. Myojo

C096 **HEAPS study design: Health Effects of Air Pollution in Antwerp Schools**
E. Dons, M. Van Poppel, S. De Prins, L. I. Panis, G. Koppen

C097 **Differential uptake kinetics of nitrogen dioxide on various pollen grains**
N. Visez, G. Chassard, S. Gosselin, M. Choël, D. Petitprez

C098 **Characterisation of an analysis system used to quantify health-relevant reactive oxygen species (ROS) in atmospheric aerosol particles**
F. P. H. Wragg, S. J. Fuller, M. Kalberer

Indoor and Working Place Aerosols

C099 **Analysing biological activity of dust from moisture damaged buildings: Relation of microbial components with toxicity**
K. Huttunen, J. Tirkkonen, E. Krop, M. Täubel, J. Pekkanen, A. Hyvärinen, D. Heederik, J.-P. Zock, M.-R. Hirvonen

C100 **Environmental monitoring to inform built environments vulnerability to airborne disease transmission**
Z. A. Nasir, L. Campos, M. Canales, L. Ciric, I. Colbeck

C101 **Air concentration of ultra-fine particles released from the Diesel engines**
S. Bujak-Pietrek, U. Mikołajczyk, I. Szadkowska-Stańczyk

C102 **Workers exposure to carbon black dust containing nano-sized particles**
U. Mikołajczyk, S. Bujak-Pietrek, I. Szadkowska Stańczyk

C103 **Tests of the personal respiratory protective equipment using radioactive aerosols**
P. Otahal, J. Vosahlik, I. Burian

C104 **Verification of airflow patterns and leakage of contaminants from fume cupboard**
T. Jankowski

C105 **Effect of air exchange rate on the removal of aerosol in a test chamber**
T. Prasauskas, L. Gagyte, A. Jurelionis, D. Ciuzas, E. Krugly, L. Seduikyte, D. Martuzevicius

C106 **Coarse and fine particulate emissions from drilling activity**
F. Azarmi, P. Kumar, M. Mulheron

C107 **Particle concentrations and radon equilibrium ratios in an occupied auditorium**
I. Bilska, M. R. Dudzinska, K. Kozak, J. Mazur, B. Polednik

C108 **Assessment of fungal aerosol in different type of residential buildings located in the city free of flood**
K. Bródka, M. Sowiak, M. Wojtania, A. Kozajda, I. Szadkowska-Stańczyk

C109 **Indoor air in child homes related to selected home characteristic**
M. Sowiak, K. Bródka, A. Kozajda, M. Wojtania, I. Szadkowska-Stańczyk

C110 **Indoor particles collected passively in urban and rural primary schools of Portugal**
N. Canha, S. M. Almeida, M. C. Freitas, H. T. Wolterbeek

C111 **Filtration of an ultrafine aerosol produced by thermal spraying using a granular bed**
D. Bémer

C112 **Physical parameters of powders and release of aerosol**
P. Görner, R. Wrobel, M. Knider, A. Boivin, F. Clerc

C113 **PM10 and PM2.5 air pollution in Chinese village homes in the Xuanwei region**
Fengxia Li, Jürgen Schnelle-Kreis, Gülcin Abbaszade, Bernhard Michalke, Ralf Zimmermann, Jing Wang, Shao Longyi

C114 **Indoor particle load caused by burning of different types of candles and incense**
C. Heuck, S. A. Hofmann, A. Hubach, J. Mehlhorn, S. Titel, K. Wissmüller, K. A. Kamilli, S. G. Gonser, A. Held

C115 **Influence of food surface area on PM2.5 and particle number concentration during frying**
M. Amouei Torkmahalleh, Y. Zhao, P. K. Hopke, A. Rossner, A. R. Ferro

C116 **Air Quality in London Paddington Train Station**
U. Chong, J. J. Swanson, A. M. Boies

C117 **Source characterisation and estimation of daily residential exposure to ultrafine particles**
C. Isaxon, A. Wierzbicka, E. Z. Nordin, A. Dahl, G. Wieslander, M. Bohgard

C118 **VOC and particle emissions from a household cleaning product**
A. W. Nørgaard, J. D. Kudal, I. K. Koponen, P. Wolkoff

C119 **Radon progeny particle concentration changes in an air-conditioned auditorium**
B. Polednik, M. R. Dudzinska, K. Kozak, J. Mazur, D. Grzadziel

C120 **Exposure to indoor air pollutants during physical activity in gymnasiums**
C. A. Ramos, S. M. Almeida, H. T. Wolterbeek

C121 **Investigation of particulate matter from wave soldering processes at a printed circuit board manufacturing company**
Z. Szoboszlai, Zs. Kertész, Z. Szikszai, A. Angyal, E. Furu, Zs. Török, L. Daróczi, Á. Z. Kiss

C122 **Comparative study of indoor aerosols collected at educational institutions: kindergarten, elementary school, and secondary grammar school**
Z. Szoboszlai, E. Furu, A. Angyal, Zs. Török, Zs. Kertész

C123 **Seasonal behavior of indoor and outdoor PAHs in different microenvironments of Rome, Italy**
M. P. Gatto, A. Gordiani, P. Romagnoli, C. Balducci, M. Perilli, A. Cecinato, M. Gherardi

C124 **Indoor/outdoor ratio and percent distribution behaviours of PAHs in Rome, Italy**
P. Romagnoli, C. Balducci, M. Perilli, A. Cecinato, M. Gherardi, M. P. Gatto

C125 **Seasonal and weekly modulations of Psychotropic Substances (PSs) in Rome, Italy**
P. Romagnoli, F. Sacco, C. Balducci, M. Perilli, A. Cecinato

C126 **Spatial and seasonal variation of nitrogen dioxide and ozone in modern office buildings**
T. Szigeti, V. G. Mihucz, P. M. Bluyssen, P. Carrer, A. Cattaneo, D. Cavallo, H. J. M. Cornelissen, S. Dimitroulopoulou, S. Fossati, C. Mandin, E. Oliveira de Fernandes, K. K. Kalimeri, Y. de Kluizenaar, R. Pereira, Y. Sakellaris, D. E. Saraga, J. G. Bartzis

C127 **Indoor air quality in Lahore, Pakistan**
I. Colbeck, Z. A. Nasir, Z. Ali, S. Safdar

C128 **Indoor air quality in university**
S. W. Chen, K. D. Mena, P. S. Chen

C129 **Concentrations of Indoor Submicrometer and Supermicrometer Particulate Matter in a Primary School in Prague**
J. Stolcpartova, M. Branis, J. Hromadka

C130 **PM2.5 in modern office buildings: elemental characterization and oxidative potential**
T. Szigeti, C. Dunster, F. J. Kelly, Zs. Kertész, A. Cattaneo, Gy. Záray, V. G. Mihucz

C131 **Characterization of the bacterial and fungal bioaerosols in three elementary schools in Kaohsiung**
M. C. Wang , K. D. Mena, P. S. Chen

C132 **Exposure Assessment of Ozone in Elementary Schools in Kaohsiung, Taiwan**
Y. C. Lin, K. D. Mena, P. S. Chen

C133 **Real-time Monitoring Of PM2.5 In Primary School**
Y. C. Lin, K. D. Mena, P. S. Chen

C134 **Ultrafine particles counts in elementary school in Taiwan**
M. C. Wang, K. D. Mena, P. S. Chen

C135 **The distribution of PM10, PM2.5, and PM1 concentrations in primary schools in Kaohsiung, Taiwan**
S. W. Chen, K. D. Mena, P. S. Chen

C136 **Clean air delivery rate (CADR) analysis based on energy consumption for different air flow rates of air cleaners**
B. Han, J. S. Kang, H. J. Kim, Y. J. Kim

C137 **Characterization of particular matters in subway HAVC system**
S. Huang, Y. M. Jo

C138 **The effect of controlled indoor activities on the particulate matter mass and number**
S. E. Chatoutsidou, N. Serfozo, I. Kopanakis, T. Glytsos, M. Lazaridis

C139 **Survivability of yeast in an electrodynamic balance**
Y. M. Kuo, S. H. Huang, W. Y. Lin, S. C. Teng, C. C. Chen

C140 **Evaluation on removal performance of air cleaning devices against airborne allergen particles using an optical particle counter and ELISA method**
H. J. Kim, B. Han, Y. J. Kim

C141 **Aerosol Particles in the Indoor Environment of the Týn Church in Prague**
L. Mašková, J. Smolík

C142 **Air Quality in Different Types of Archives**
L. Mašková, J. Smolík

C143 **Alveolar dose of ultrafine particles for children in urban environments**
M. Mazaheri, S. Clifford, M. A. Megat Mokhtar, F. Fuoco, G. Buonanno, L. Morawska

C144 **Subway platform air quality: assessing the influences of tunnel ventilation, train "piston effect" and station design**
T. Moreno, N. Pérez, C. Reche, E. de Miguel, M. Capdevila, S. Centelles, J. Jaume, A. Alastuey, X. Querol

C145 **The effect of biomass burning on PM exposure during wintertime**
D. A. Sarigiannis, S. Karakitsios, M. Kermenidou

C146 **Particle release from open ethanol fireplaces into the indoor environment**
T. Schripp, E. Uhde, S. Wientzek, M. Wensing, T. Salthammer

C147 **Nanoparticle Enhanced PCR Detection of Bacterial Aerosols**
Siyu Xu, Maosheng Yao

C148 **Direct Viral Aerosol Inactivation by Microwave Irradiation and its Mechanisms**
Yan Wu, Maosheng Yao

C149 **Improving the Efficiencies of Andersen Impactors Using Mineral-Oil-Spread Agar Plate**
Maosheng Yao, Zhenqiang Xu, Kai Wei, Yan Wu, Fangxia Shen, Qi Chen, Mingzhen Li

C150 **Cancer risk assessment for the inhalation exposure to particulate matters and polycyclic aromatic hydrocarbons from household cooking in northern Taiwan**
K.-P. Yu, K. R. Yang, S. C. Lung, C.-H. Liu

C151 **Enhancement effect of O3 on the antifungal efficacy of nano-metals supported TiO2 on resistant mold spores**
K.-P. Yu, Y.-T. Huang, S.-C. Yang

C152 **Organic composition of indoor/outdoor particles in an elementary school**
C. A. Alves, R. C. Urban, P. N. Pegas, T. Nunes

C153 **Indoor air quality in school buildings in the city of Sosnowiec, Poland**
P. Z. Brewczyński, E. Krakowiak, J. Kurek, A. Wlazło, M. Zaciera

C154 **Assessing the contribution of indoor particulate matter sources in residential homes in a northern province of Italy**
P. Fermo, A. Piazzalunga, J. Tarlassi, A. Cattaneo, P. Urso, M. G. Perrone

C155 **Assessment of population exposure to PM2.5 and PM10 in the Athens metropolitan area**
V. Aleksandropoulou, M. Lazaridis

C156 **Measurement of Non-Volatile Particulate Matter Mass Emission Indices of Aircraft Gas Turbine Sources**
B. T. Brem, L. Durdina, J. Wang

C157 **CANCELLED**

C158 **Dynamic Changes of the Aerosol Composition and Concentration During Different Burning Phases of Wood Combustion**
M. Elsasser, C. Busch, J. Orasche, C. Schön, H. Hartmann, J. Schnelle-Kreis, R. Zimmermann

C159 **PM10 chemical composition in at street canyon and urban locations in London, UK**
D. C. Green, A. H. Tremper

C160 **Particles in road and railroad tunnel air - properties, sources and abatement possibilities**
M. Gustafsson, S. Abbasi, G. Blomqvist, A. Gudmundsson, S. Janhäll, C. Johansson, M. Norman, U. Olofsson, B. Sjövall, H. Wilhelmsson

C161 **Study on design optimization of HI-FILTER SYSTEM by using CFD**
Youn Suk Kang, Hye Mi Lim, Cheol-Gyu Lee, Du-Hun Jang

C162 **PM trends, chemical composition and source apportionment of particulate matter in Mediterranean countries: Results from the Med-Particles project**
A. Karanasiou, X. Querol, A. Alastuey, C. Perrino, J. de la Rosa, G. Berti, B. Artiñano, J. Sunyer, F. Forastiere, M. Stafoggia, the Med-Particles Study Group

C163 **Overview of the AIRUSE project: Testing and Development of air quality mitigation measures in Southern Europe**
A. Karanasiou, F. Amato, T. Moreno, A. Alastuey, M. Viana, F. Lucarelli, S. Nava, G. Calzolai, C. Pio, C. Alves, T. Nunes, K. Eleftheriadis, E. Diapouli, V. Vasilatou, E. Monfort, I. Celades Lopez, R. M. Harrison, D. Beddows, X. Querol

C164 **Particle size distributions of combustion aerosol of various local fuel mixtures**
E. Krugly, E. Puida, K. Buinevičius, L. Kliučininkas, I. Stasiulaitiene, A. Minikauskas, D. Martuzevičius

C165 **Analysis of intrapersonal variance of hourly PM exposures**
P. Lipponen, O. Hänninen, J. Kolomazníková, M. Braniš

C166 **Real-time relationship between digital visibility and PM2.5 at the middle of Taiwan**
C.-H. Luo, S. Yang

C167 **On the fine and the coarse fractions of atmospheric aerosol**
M. Manigrasso, A. Febo, P. Avino

C168 **Nanoparticle contribution to elemental concentration in atmospheric particulate matter**
S. Canepari, M. L. Astolfi, M. Marcoccia, D. Frasca, C. Perrino

C169 **Primary aerosols from ship diesel engine exhaust within the framework of HICE measurement campaign**
L. Mueller, G. Jakobi, M. Elsasser, B. Stengel, R. Rabe, O. Sippula, E. Karg, M. Sklorz, T. Streibel, J. G. Slowik, A. S. H Prevot, J. Schnelle-Kreis, R. Zimmermann

C170 **Study of the aerosol elemental composition with high time resolution: preliminary results from the AIRUSE LIFE+ Project**
S. Nava, G. Calzolai, M. Chiari, F. Lucarelli, F. Amato, A. Karanasiou, X. Querol, C. Alves, M. Duarte, T. Nunes, C. Pio, K. Eleftheriadis, D. Beddows, R. M. Harrison

C171 **Characterisation of winter aerosols in the Helsinki region by TEM/EDX individual particle analysis**
J. V. Niemi, S. Saarikoski, K. Saarnio, A. Frey, A. Kousa, H. Kuuluvainen, L. Pirjola, T. Rönkkö, R. Hillamo

C172 **Development of a non-destructive method based on infrared analysis for quantification of ionic components in atmospheric particulate matter**
A. Piazzalunga, D. Ballabio, V. Bernardoni, P. Fermo, U. Molteni, P. Prati, R. Vecchi, G. Valli

C173 **Micromarkers of source-specific combustion aerosols**
O. B. Popovicheva, E. D. Kireeva, N. M. Persiantseva

C174 **Meteorological and chemical factors triggering an exceptional PM pollution episode in wintertime in the Po Valley, Italy**
V. Poluzzi, D. Bacco, G. Bonafé, C. Maccone, S. Ferrari, R. Vecchi, S. Decesari, I. Ricciardelli

C175 **Comparison of particle number concentration and PM2.5 chemical species in urban and rural sites in Po Valley (I) during measurement program in the Supersito project**
I. Ricciardelli, D. Bacco, F. Scotto, A. Trentini, A. Vagheggini, V. Poluzzi

C176 **Organic aerosols from residential wood burning emissions analysed by Ultra-high resolution mass spectrometry**
A. G. Rincón, C. Alves, M. Dietzel, M. Kalberer

C177 **A highway study of PM and black carbon (BC) in Flanders (Belgium)**
D. Roet, J. Vercauteren, C. Matheeussen, E. Roekens

C178 **Urban organic aerosols ultrafine particles compositions: a high-resolution mass spectrometry characterization**
G. Salque-Moreton, R. Jacob, D. Voisin, F. Donnaz, J.-L. Jaffrezo, J.-L. Besombes, R. Thissen

C179 **Organic and elemental carbon associated to PM10 and PM2.5 in the urban atmosphere - Estimation of secondary organic carbon**
C. Samara, D. Voutsa, A. Kouras, K. Eleftheriadis, Th. Maggos, D. Saraga, M. Petrakakis

C180 **Study of Trace Metals and Free Radical Generation in Particulate Matter in Pune**
P. G. Satsangi, Suman Yadav, Amruta P. Kodre, Ritwika Roy

C181 **The influence of children jumping on the bed on PM10/PM2.5/PM1 concentration profile**
C. L. Yeh, K. D. Mena, P. S. Chen

C182 **Summer and winter time aerosol levels at an urban Mediterranean environment: Impacts of biomass burning**
M. Psichoudaki, E. Kostenidou, A. Bougiatioti, S. Bezantakos, G. Biskos, A. Nenes, S. N. Pandis

C183 **An integrated source apportionment study: Positive Matrix Factorization vs. the Chemical Transport Model CAMx**
M. C. Bove, P. Brotto, F. Cassola, E. Cuccia, D. Massabò, A. Mazzino, P. Prati

C184 **Characterization of PM10 sources in the central Mediterranean Basin**
G. Calzolai, S. Nava, M. Chiari, F. Lucarelli, S. Becagli, R. Traversi, M. Marconi, F. Rugi, R. Udisti, A. di Sarra, G. Pace, D. Meloni, C. Bommarito, D. M. Sferlazzo

C185 **Size-segregated source apportionment of aerosol using water soluble components**
D. Cesari, D. Contini, A. Genga, M. Siciliano, P. Ielpo, M. R. Guascito, M. Conte

C186 **The Impact of Select Pollutant Sources on Air Quality for Ostrava and the Moravian-Silesian Metropolitan Region by the Positive Matrix Factorization model**
L. Černikovský, J. Novák, H. Plachá, B. Krejčí, I. Nikolova, E. Chalupníčková, T. Conner, G. Norris, K. Kovalcik, D. Olson, J. Turlington, C. Croghan, R. Willis, R. Williams

C187 **Source apportionment of PM2.5 at Abu Dhabi sites**
C. Hak, S. López-Aparicio

C188 **Comparison of PMx collected at sites with different level of air pollution using iron oxides as magnetic tracers**
E. Petrovský, B. Kotlík, A. Kapička, M. Mikešová, R. Zbořil, H. Grison

C189 **Seasonal variability of the PMx chemical composition and ammonia concentration in loose-housing cowshed**
M. Maasikmets, A. Kaasik, A. Ruus, E. Teinemaa

C190 **Contribution from wood burning to the PM10 aerosol at four urban background sites in Flanders, Belgium**
W. Maenhaut, R. Vermeylen, M. Claeys, J. Vercauteren, C. Matheeussen, E. Roekens

C191 **Characterization of submicron organic aerosol in Prague by ME 2 factor analysis of summer AMS data**
O. Makeš, P. Vodička, J. Schwarz, F. Canonaco, A. S. H. Prévôt, V. Ždímal

C192 **Source apportionment in suburban environment during summer**
L. Marmureanu, J. Vasilescu, D. Nicolae, F. Canonaco, J. G. Slowik, A. S. H. Prévôt

C193 **The contribution of winter sanding to PM10 concentrations at traffic stations in the Czech Republic in 2011**
L. Matoušková

C194 **Size distributed metallic elements in submicron and ultrafine atmospheric particles from urban and industrial areas: a source assessment**
S. Mbengue, L. Alleman, P. Flament

C195 **Estimation of Non-Exhaust Emissions in PM10 Road Dust in Birmingham, UK**
Pallavi Pant, R. M. Harrison

C196 **Elemental composition and source identification of PM0.09-0.26 in European air pollution hot-spot**
P. Pokorná, J. Hovorka, P. K. Hopke

C197 **PM2.5 chemical composition and source apportionment in the Po Valley: the Med Particles and Supersito projects preliminary results**
F. Scotto, S. Ferrari, I. Ricciardelli, R. Vecchi, G. Valli, A. Piazzalunga, V. Poluzzi

C198 **Traffic-generated changes in the chemical composition of 13 fractions of PM in an urban area of Upper Silesia, Poland**
W. Rogula-Kozłowska

C199 **PM1 chemical and mineralogical characterization near a crude oil pre-treatment plant (Agri Valley) during an emergency procedure**
S. Trippetta, R. Caggiano, S. Margiotta, S. Sabia, A. Speranza, V. Summa

C200 **Sources and trends of atmospheric pollutants at Pallas, Finland, during 1996-2009**
M. Vestenius, P. Anttila, S. Leppänen, K. Hansson, E. Brorström-Lunden, H. Hakola

C201 **High-time resolved characterization of PM1.0 in a peri-urban site near Rome, Italy**
R. Salzano, M. Giusto, M. Montagnoli, M. Catrambone, E. Rantica, T. Sargolini, C. Perrino

Reserve Posters

C202 **Urban particulate matter monitoring on a mobile platform: a real time experiment on a long term scale**
B. Moroni, E. Scocchera, A. Piazzalunga, M. G. Ranalli, S. Castellini, D. Cappelletti
CHANGED TO ORAL PRESENTATION

C203 **Characterisation of the aerosol sources in Brindisi (Italy) harbour area within the CESAPO project: an overview of the experimental results**
D. Contini, D. Cesari, A. Donateo, A. Gambaro, A. Genga, G. Giovanelli, R. Giua, F. M. Grasso, E. Gregoris, P. Ielpo, S. Masieri, E. Merico, E. Morabito, A. Nocioni, T. Pastore, M. Siciliano

C204 **An experimental approach to measure particle deposition in large circular ventilation ducts**
G. Da, E. Géhin, M. Ben-Othmane, M. Havet, C. Solliec, C. Motzkus

C205 **PMF source apportionment for fine and coarse PM in Athens, Greece: Evolution of source contributions over the last decade**
K. Eleftheriadis, E. Diapouli, A. Karanasiou, S. Vratolis, V. Vasilatou, M. Gini, D. Saraga, S. Pateraki, Th. Maggos

C206 **Toxicological effects of the particulate emissions from diesel engines and wood combustion are affected by used technology**
P. I. Jalava, M. S. Happo, T. Brunner, I. Obernberger, T. Murtonen, P. Aakko-Saksa, J. Mäki-Paakkanen, J. Jokiniemi, M-R. Hirvonen
CHANGED TO ORAL PRESENTATION

C207 **Diurnal variation of small and large ion concentrations in an urban location**
E. R. Jayaratne, X. Ling, L. Morawska

C208 **Particulate Matter in Indoor Aor in two Schools in Vienna, Austria**
A. Kasper-Giebl, N. Jankowski, K. Kassin, E. Can Cetintas, H. Bauer, H. Grothe

C209 **Organic aerosol speciation with in-situ thermal desorption gas chromatography: a brief history of the TAG instrument**
N. M. Kreisberg, S. V. Hering, A. P. Teng, G. Isaacman, Y. Zhao, D. R. Worton, A. W. H. Chan, B. J. Williams, J. T. Jayne, A. T. Lambe, T. Hohaus, J. R. Kimmel, D. T. Sueper, W. Brooks, L. R. Williams, A. M. Trimborn, D. R. Worsnop, A. H. Goldstein

C210 **Particle characterization during abrasive treatment of composite material containing fibres by Cryo HRTEM**
K. I. Lieke, M. Levin, K. A. Jensen, I. K. Koponen

C211 **Trace elements bioaccessibility in fine and ultrafine particles from the industrial area of Dunkirk (France) during the NANO-INDUS project**
S. Mbengue, L. Alleman, P. Flament

C212 **Free energy barrier in the growth of sulfuric acid clusters**
T. Olenius, O. Kupiainen, I. K. Ortega, H. Vehkamäki

C213 **Evaporation and growth dynamics of layered droplets: Theory and experiments**
H. H. Tu, A. K. Ray

C214 **Atmospheric tar balls: primary droplets from biomass burning?**
Á. Tóth, A. Hoffer, I. Nyírő-Kósa, M. Pósfai, A. Gelencsér

C215 **Application of broadband optical cavity methods to studying the optical properties of aerosols at short wavelengths**
E. M. Wilson, J. C. Wenger, D. S. Venables

C216 **Release of fine particles from birch pollen grains following impaction**
N. Visez, M. Choël, G. Loubert, G. Chassard, D. Petitprez

Sponsors and Exhibitors

Aerodyne Research, Inc.

Address: **45 Manning Road, Billerica**
MA 01821-3976

Phone: **(978) 663-9500**
Email: **info@aerodyne.com**
Website: **www.aerodyne.com**

Aerodyne Research, Inc. (ARI) has provided research and development (R&D) services to commercial and government clients working to solve national and international problems since 1970. Our R&D staff is organized into six technology centers which address such critical issues as global and regional environmental quality and development of clean and efficient energy and propulsion technologies.

In conjunction with ARI's research activities, we also manufacture and sell high sensitivity, fast time response instrumentation for environmental air quality monitoring and atmospheric research. These instruments include Aerosol Mass Spectrometers, Quantum Cascade Laser Trace Gas Detectors, Aerosol Chemical Speciation Monitors (ACSM), Particle Optical Extinction (CAPS PMex) monitors, and ultrasensitive nitrogen dioxide (CAPS NO2) monitors.

ARI also designs, builds and utilizes remote sensing, surveillance, image processing, tracking and recognition systems for commercial and environmental applications and national defense.

Aerosol d.o.o.

Address: **Kamniska 41**
SI-1000 Ljubljana
Slovenia

Phone: **+386 59 191 220**
Fax: **+386 59 191 221**
Website: **www.aerosol.si**

Magee Scientific Aethalometers, instruments for measurement of Black Carbon, are manufactured at "Aerosol d.o.o." in Ljubljana, Slovenia. The Aethalometers provide an on-line measurement of aerosol absorption on up to 7 wavelengths: 370, 470, 520, 590, 660, 880, 950 nm. Black Carbon is the second most important climate forcer and highly correlated with detrimental health effects of air pollution. Measurements by the Aethalometer of aerosol absorption at different wavelengths of light provide information specific to sources and enable discrimination between biomass and fossil fuel combustion aerosols by ambient measurements, and detection of mineral dust events.

The 'Next Generation' Aethalometer®, Model AE33, incorporates scientific and technical advances designed to offer improved measurement performance, user features, communications and interface, and the ability to perform routine performance tests to verify correct operation. Most importantly, the new instrument incorporates the patented DualSpot™ measurement method. This provides two significant advantages: elimination of the changes in response due to 'aerosol loading' effects; and a real-time calculation of the 'loading compensation' parameter which offers insights into aerosol optical properties.

AethLabs

Address: **2180 Folsom St, 3rd Floor**
San Francisco, CA 94110
United States of America

Phone: **+1 (415) 529-2355**
Website: **www.aethlabs.com**

AethLabs is the manufacturer of the microAeth® Model AE51 for measuring Aerosol Black Carbon. The microAeth® is battery powered, easy to use, and small enough to fit in your pocket. With Aethalometer® measurement technology inside, the microAeth® is built on proven technology that has been used world-wide for 30 years.

Airmodus Ltd.

Address: **Gustaf Hällströmin katu 2a**
FIN-00560 Helsinki
Finland

Phone: **+358 44 544 5694**
Email: **info@airmodus.com**
Website: **www.airmodus.com**

Airmodus manufactures instruments for the counting of individual aerosol particles and the detection of clusters and gas molecules.

Airmodus offers Particle Size Magnifier systems that allow you to detect particles as small as 1 nm in diameter; easy to use Condensation Particle Counters with a cut-off size fit for your measurement needs; and special mass spectrometer inlets for the detection of challenging gaseous compounds (e.g. sulfuric acid, ammonia, amines).

Cambustion Ltd.

Address: **J6 The Paddocks**
347 Cherry Hinton Road
CB1 8DH Cambridge
United Kingdom

Phone: **+44 1223 210250**
Fax: **+44 1223 210190**
Email: **cambustion@cambustion.com**
Web: **www.cambustion.com**

New in 2013, Cambustion's UDAC is a standalone unipolar diffusion charger, capable of placing a high level of charge on aerosols, and forming a building block of many laboratory experiments.

A novel application (the subject of an AS&T letter) combines a UDAC, a Cambustion Centrifugal Particle Mass Analyzer (CPMA) and an aerosol electrometer, to provide an aerosol mass standard.

The CPMA continues to find new applications as an aerosol laboratory tool, with a growing group of researchers publishing around the world since 2012.

Cambustion's aerosol product range continues to develop, with the addition of an aerosol flow meter accessory for the UDAC/CPMA and a standalone electrostatic precipitator.

Our established DMS series instruments offer the fastest real-time electrical mobility size/number spectra available (from 200 ms T10-90% at 10Hz); particle size measurement range from 5nm – 2.5μm, with unrivalled sensitivity. Applications include ambient monitoring, combustion aerosol, workplace exposure and engineered nanoparticle research.

With fully integrated sampling and dilution options, DMS series instruments can be used for both ambient applications and straightforward direct sampling of high concentration aerosol sources through software selection of appropriate dilution.

Meet us at the Cambustion exhibit – booth No. 14

Catalytic Instruments GmbH & Co. KG

Address: **Lug ins Land 53**
D-83024 Rosenheim
Germany

Phone: **+49 8031 901 777-6**
Mobile: **+49 171 621 6947**
Fax: **+49 8031 901 777-5**
Email: **hans-joachim.schulz@catalytic-instruments.com**

Catalytic Instruments is a German company specializing in the production of innovative aerosol instruments based on "catalytic stripper" technology. A catalytic stripper is a heated catalytic element used to remove the particle and gas phase semi-volatile fraction of an aerosol. Applications include measurement of diesel, locomotive, and gas turbine exhaust.

Current products include the CS08 and CS015 - catalytic strippers designed for aerosol flowrates of 8 and 1.5 L/min, respectively. A CVF100 or Catalytic Vapor Filter is also offered for the removal of CPC exhaust vapor. For unique applications, Catalytic Instruments will work with the customer to provide individual solutions.

Comde-Derenda GmbH

Address: **Kieler Strasse 9**
14532 Stahnsdorf
Germany

Phone: **+49 3329 690 27 10**
Fax: **+49 3329 690 27 19**
Email: **info@derenda.de**
Website: **www.comde-derenda.de/index.php/en**

Comde-Derenda GmbH was originally founded under the name of Norbert Derenda Engineering Office in Berlin in the year of 1972. Today the company is located in Stahnsdorf near Berlin where new facilities were erected in the year of 2007. The firm's products are being used to an ever increasing extent within the European Union to monitor outdoor air quality.

In the years 1999 and 2000 the company was certified as per the DIN EN ISO 9001 quality assurance standards. In 2002 the quality management system was audited to the requirements set forth in DIN EN ISO 9001:2000. Norbert Derenda, the owner of the company, has, since the year 2000, also been a member of the Sponsors' Circle for the Commission on Air Quality Maintenance (KRdL) in the VDI and DIN organizations.

In October of 2007 Norbert Derenda was appointed to membership in "KRdL Working Group 4/2/09 on Measurement of Particles in Outdoor Air".

The product range now includes complete sampling systems and measurement instruments for direct and continuous analysis of gas and particle concentrations in the atmosphere.

In detail the available products are the following:

Equipment and systems for sampling and measuring fine dust from the ambient air. Low volume sampler (reference devices in compliance with CEN standards). Automatic dust sampling systems for low-, medium- and high-volume sampler units. Air pollution monitors (on-line) for direct and continuous determination of the concentration of suspended dust particles. Automatic weighing systems for gravimetric evaluation of dust-loaded filters or other sample carriers. Air monitoring stations for up to 8 immission values (fine dust and gases) for environmental monitoring purposes. Gas collection units for exposing gas absorption tubes.

Comde-Derenda GmbH employs highly competent and dedicated personnel who can also be set to work on special solutions and custom equipment at any time.

Copley Scientific Limited

Address: **Colwick Quays Business Park**
Private Road No. 2
Colwick, Nottingham
NG4 2JY, United Kingdom

Phone: **+44 (0)115 961 6229**
Fax: **+44 (0)115 961 7637**
Email: **sales@copleyscientific.co.uk**
Website: **www.copleyscientific.com**

Copley Scientific is considered the world's leading manufacturer of test equipment for Metered-Dose Inhalers (MDIs), Dry Powder Inhalers (DPIs), Nebulizers and Nasal Sprays. In cooperation with aerosol characterisation equipment experts, MSP Corporation (MN, USA), Copley Scientific also offers a comprehensive range of aerosol sampling and particle sizing equipment for use in industrial and academic applications. This includes the world-renowned MOUDI and Nano-MOUDI range of cascade impactors, the Wide Range Particle Spectrometer Model 1000XP, the Real-Time Fibre Monitor Model 7400AD and Water-based Condensation Particle Counters (WCPCs). Copley Scientific has offices and product experts based in Nottingham, UK and Basel, Switzerland, serving the European market.

Dekati Ltd.

Address: **Tykkitie 1**
36240 Kangasala
Finland

Phone: **+358 3357 8100**
Email: **sales@dekati.fi**
Website: **www.dekati.com**

Dekati Ltd. develops, manufactures and markets instrumentation needed in fine particle measurement and sampling. In 1995, Dekati introduced the world's first real-time fine particle concentration and size distribution measurement instrument, ELPI™. Since then, our product line has been continually expanding and it now includes several instruments for both particle detection and aerosol sample conditioning and dilution. The latest addition in the Dekati® Product Line is the Dekati® Bipolar Charge Analyzer (BOLAR™) for particle bipolar charge size distribution measurements.

Dekati develops new products in close co-operation with the world's leading universities and companies. Our mission is to provide our customers with innovative fine particle measurement solutions that guarantee accurate results even in demanding environments.

Dekati instruments are used for example in the following application areas:

- Combustion Processes (Diesel, Gasoline, Oil, Coal, Bio-fuels etc.)
- Environmental Ambient Aerosol Research and Monitoring
- Occupational Health and Safety Measurements
- Pharmaceutical Drug Screening and Inhalator R&D
- Nanotechnology and Material Processing

Visit www.dekati.com for more details on our company and our products, or contact us at sales@dekati.fi for further information.

DIGITEL Elektronik AG

Address: **Alte Gasse 18**
CH-8604 Hegnau
Switzerland

Phone: **+41 44 908 20 30**
Fax: **+41 44 908 20 31**
Email: **info@digitel-ag.com,**
Website: **www.digitel-ag.com**

Since 1970 Digitel Elektronik AG designs and manufactures successfully measurement instrumentation for environmental monitoring. Digitel Elektronik AG is located in Switzerland and sells worldwide over a network of local resellers. Their experience and the state-of- the- art production processes stand for approved first-class quality products.

Digitel provides a full range of High and Low Volume sampler products for immission measurement such as PM10 according to the directives EN12341 and PM2,5 according to the directives EN 14907 as well as for other measuring purposes with different flow rates and cut-off point characteristics.

In addition to their standard products Digitel offer customer-specific solutions with specialised know-how and profound experience of over 40 years as environmental professionals. Digitel sets high quality standards and is well know to be the leading company when it comes to precision and reliability. All instruments made by Digitel hav a long lifetime, low power consumption and a low noise level.

Digitel Enviro-Sense – We Care

Ecotech PTY Ltd.

Address: **1492 Ferntree Gully Road**
Knoxfield, VIC, 3180
Australia

Phone: **+613 9730 7800**
Email: **info@ecotech.com**
Website: **www.ecotech-research.com**

Ecotech's tailored and innovative monitoring solutions assist our customers in quantifying environmental impacts all around the world. From our range of gas analysers through to our particulate instrumentation and also our sophisticated data software, Ecotech provides solutions that ensure air quality and climate data are accessible to everyone.

Our series of integrating nephelometers ranges from single to multiple wavelength versions and incorporates both polar and particle correlating options. Ecotech's Aurora range of integrating nephelometers are gaining a world-wide reputation for quality and reliability.

The newest addition to our aerosol family is the Aerosol Conditioning System (ACS1000). By exposing the aerosol to different relative humidity, the system enables their hygroscopic properties to be measured and analysed by a wide range of instrumentation. The dual channel provides real-time comparison between humid and dry samples.

Visit our booth at the EAC to view both our polar nephelometers and ACS1000. We will also be conducting an open workshop on Saturday 7th September at the Clarion Congress Hotel to discuss these instruments and much more. Register your interest at our booth today.

Grimm Aerosol Technik GmbH & Co. KG

Address: **Dorfstrasse 9**
83404 Ainring
D – Germany

Phone: **+49 (0)8654 / 578-0**
Fax: **+49 (0)8654 / 578-35**
Website: **www.grimm-aerosol.com**

The company GRIMM Aerosol Technik has been established 30 years ago by Hans Grimm in Bavaria/Germany. Meanwhile, GRIMM Aerosol Technik is one of the worldwide leading companies in the field of particle sizing and counting down to a few nanometers due to its innovative developments and manufacturing.

The company offers a product range of portable and stationary solutions for the continuous measurement of fine and ultrafine aerosols, for applications such as Environmental Dust Monitors, Aerosol Spectrometers, Particle Counters and Sizers, Filter and Motor Testers, as well as appropriate Aerosol Generators. Our products and technologies are of newest technology, such as wireless data transfer and logging, remote control, automatic operation. Specialists in-house will advise about the correct instruments for particular applications, e.g. for ambient air, emission, occupational health, filter efficiency and exhaust gas measurements, for quality control and for pharmaceutical, atmospheric or epidemiological studies.

Worldwide direct customer support and service is offered through our subsidiaries in the US, Canada, UK, Middle East and Asia, Australia, etc. and supplemented by our strong network of international representatives.

GRIMM Aerosol Technik:

- Environmental Dust Monitors
- Portable Dust Monitors and Aerosol Spectrometers
- Nanoparticle measuring systems (portable, mobile, stationary)

IONER®

a trademark of RAMEM S.A.

Address: **C/ Sambara, 33**
28027 - Madrid
Spain

Phone: **+34 91 404 45 75**
Fax: **+34 91 403 45 96**
E-mail: **sales@ioner.eu**
Websites: **www.ioner.eu, www.ramem.com**

RAMEM-IONER® is a Spanish company devoted to the development of innovative aerosol instruments. RAMEM-IONER has a main goal: taking the DMA technology and applications to the smaller particles possible. RAMEM-IONER develops DMAs based on patented parallel plate technology and with different chargers and ion sources. Very high resolutions are reached with high sheath flows. Complete DMAs with sheath flow and aerosol flow control, chargers and electrometers are commercialised. Also, separate modules like ElectroSpray sources, Corona discharge sources, High Voltage sources or modules for flow control are sold.

RAMEM, the main branch of the company, designs and manufactures special needs of prototypes in scientific instrumentation or scientific installation. Short series or even single prototypes can be considered.

The latest RAMEM-IONER project is GANS: A DMA for early stage of nucleation studies. In this project, RAMEM-IONER ion sources for organic compounds and for inorganic compounds are coupled to a high resolution DMA (or HRIMS) for ions. The detection stage is done coupling a Particle Size Magnifier (PSM) with a Condensation Particle Counter (CPC) developed by Airmodus. Further information about GANS project and RAMEM-IONER can be found in: http://www.gans-project.eu/

Matter Aerosol

matter aerosol
a testo company

Address: **Bremgarterstrasse 62**
CH-5610 Wohlen
Switzerland

Phone: **+41 (0)56 618 66 30**
Fax: **+41 (0)56 618 66 39**
Website: **www.matter-aerosol.ch**

Matter Aerosol continues its successful specialization in the measurement and characterization of nanoparticles from combustion processes and nanoparticles in ambient air.

Matter Aerosol combines over 50 years experience in instrument design and development with latest research results about nanoparticles, for application in laboratories to real-world problems.

Matter Aerosol's NanoMet3 is a new Portable Emissions Measurement System – PEMS for nanoparticle counting and classification. Come and see yourself!

MCV, S.A.

Address: **Highway A-2, km 575**
ES08293 Collbató (Barcelona)
Spain

Phone: **+34 93 777 05 00**
Fax: **+34 93 777 05 50**
Email: **cial@mcvsa.com,**
Website: **www.mcvsa.com**

MCV is a company established for more than 30 years in order to design and develop instrumentation, equipment and systems related to the environment, especially in the areas of air quality control and meteorology. The main field of activity of the company includes the design of equipments, management, control and monitoring systems, data acquisition systems, software and civil works.

MCV due to its experience and leadership in the environmental engineering field offers their clients the development of customize solutions to their needs.

The facilities of the company allow us to face any kind of project as the construction of mobile units, monitoring stations for automatic networks, radars and meteorological towers, production of equipments for the sampling of gases and particles or data acquisition systems.

MCV has the certifications for quality and environmental management systems ISO9001, ISO 14001 and EMAS.

MCV develops, manufactures and distributes equipment to measure and control the air quality as: HVS (PM10, PM2.5, PM1, HAP, TSP heads), VOC's samplers, Calibration systems with aire zero generator and automatic analysers for SO2, NOx, O3, CO, H2S, BTX…

MCV carries out tasks of maintenance, repairmen, verification and calibration of the measurement instruments either on site or in the company features. Our team possesses the means and technical resources to give and effective response to the customer requirements and incorporates the last updates and innovations. MCV supports their customers with its features and technical assistance in order to give an integral service.

This company will not be present at the Conference.

Met One Instruments, Inc.

Address: **Met One Instruments Inc**
1600 Washington Blvd
Grants Pass, Oregon, 97526
United States of America

Phone: **+1 (541) 471-7111**
Fax: **+1 (541) 471-7116**
Email: **sales@metone.com**
Website: **www.metone.com**

Met One Instruments, Inc. located in Oregon, USA designs and manufactures meteorological instruments, handheld/portable particle counters, aerosol monitors, and regulatory particulate matter (PM) samplers/monitors. Our BAM-1020 Monitor is the first continuous PM measurement method to receive both PM2.5 and PMcoarse U.S. EPA Federal Equivalence Method designation. It also passed the newest European Equivalency testing for PM10 and PM2.5 and is certified to EN 15267 the highest EU quality standard for ambient monitors.

We are committed to meet the needs of our worldwide customers for ambient and indoor monitoring requirements and offer specialized solutions for various applications including data logging and software instruments. We are in business since more than 20 years and bring our experience to work for you.

See the new additions to our aerosol instrumentation product line at www.metone.com.

Metrohm Applikon B.V.

Address: **P. O. Box 149,**
3100 AC Schiedam
The Netherlands

Phone: **+31 (0)10 29 83 555**
Fax: **+31 (0)10 437 96 48**
Email: **ELe@metrohm-applikon.com**
Website: **www.metrohm-applikon.com**

Metrohm Applikon, headquartered in Schiedam, the Netherlands has more than 35 years experience in delivering solutions for laboratory, at-line and on-line wet chemical analysis. Part of the worldwide Metrohm AG group, Metrohm Applikon has access to Metrohm's know-how and expertise in ion analysis.

MARGA (Monitor for AeRosols and Gases in ambient Air) is an on-line ion chromatograph that measures the concentration of soluble inorganic species in aerosols and their related gas phase components in ambient air. Hourly simultaneous results for gases and aerosols can be accessed from a remote workstation, with result quality being maintained by an internal standard and detailed system diagnostics.

Jointly developed with ECN, The Netherlands, MARGA is distributed world-wide through Metrohm Applikon's distributor network; most members of which belong to the Metrohm group of companies.

Naneos Particle Solutions GmbH

Address: **Dorfstrasse 69**
CH-5210 Windisch

Phone: **+41 56 560 20 70**
Website: **www.naneos.ch**

Naneos builds nanoparticle detectors that are easy to use, small and reliable. They can be used in workplace safety, for ambient monitoring and health studies.

Palas® GmbH

Address: **Greschbachstr. 3b**
76229 Karlsruhe
Germany

Phone: **+49 (0)721 96213-0**
Fax: **+49 (0)721 96213-33**
Email: **mail@palas.de**
Website: **www.palas.de**

With more than 60 submitted patents, the Palas® GmbH has effectively set standards in the aerosol technology since 1983. Today, Palas® offers a complete product range for the continuous aerosol generation and measurement from 5 nm to 100 μm.

Our innovations result in superior quality and durability of the products that lead to unique technical and economic advantages for our customers.

Our core competencies are:

- Particle generation
- Particle measurement systems (for high pressures up to 10 bar, temperatures from -120°C up to 470°C, processes, environment and workplace, inhalation)
- Nanoparticle measurement systems (U-SMPS, UF-CPC etc.)
- Filter test and filter media test systems
- Continuous fine dust monitoring systems
- Dilution systems
- Cleanroom particle technology
- Calibration systems

Well-known industrial enterprises and research institutions worldwide have decided in favour of Palas® products and have thus established Palas® as a worldwide market leader.

Sunset Laboratory Inc.

Address: **10180 SW Nimbus Avenue**
Suite J/5
Tigard, OR 97223-4341

Phone: **503-624-100**
Fax: **503-620-3505**
Website: **www.sunlab.com**

Sunset Laboratory Inc. has specialized in the analysis of air pollution for carbon aerosols since 1984. As well as performing the OCEC analysis, Sunset Laboratory also provides instrumentation for carbon aerosol analysis. Our equipment is suitable for the laboratory or in the field, and ready for use with the NIOSH method 5040, IMPROVE-A, and EUSAAR 2 protocols.

Clients include researchers working for government regulatory agencies, private companies, commercial laboratories, and universities.

Topas GmbH

Address: **Oskar-Röder-Str. 12**
01237 Dresden
Germany

Phone: **+49 (351) 21 66 43-0**
Fax: **+49 (351) 21 66 43 55**
Email: **office@topas-gmbh.de**
Website: **www.topas-gmbh.de**

Topas GmbH Dresden is a specialist company in the field of aerosol and particle technology.

Our standard product range comprises:

- aerosol generators (mono- and polydisperse, solid and liquid particles)
- particle size measuring instruments for aerosols and liquids
- aerosol dilution systems
- electrostatic aerosol neutralizers
- process aerosol monitors
- filter testing technology and instruments
- clean room measuring equipment
- pore size measuring instruments

Topas also provides solutions for special applications like the dispersion of complex powders, test systems for particle filters and for adsorptive filters, filter media testing, blow-by measuring etc. Our corporate philosophy allows us to meet a variety of customer needs. Many years of experience, our know-how as well as close cooperation with universities, research centres and industrial partners is the ideal basis for the development of new and innovative solutions. Our reliable measuring and testing equipment has proven successful worldwide.

TSI GmbH Germany

Address: **Neuköllner Strasse 4**
52068 Aachen
Germany

Phone: **+49 241-52303-0**
Fax: **+49 241-52303-49**
Email: **answersEU@tsi.com**
Website: **www.tsi.com**

As an international leader in measurement technology for over 50 years, TSI Incorporated (www.tsi.com) designs and manufactures precision instruments used for aerosol research, contamination control, indoor air quality and serves the needs of industry, governments, research institutions and academia.TSI researchers and engineers have developed instruments that are recognized worldwide. During EAC 2013 in Prague TSI's team will show new products like the Model 3938 which is the 3rd generation of the SMPS; trusted by researchers for over 30 years. The new generation has an improved accuracy, does not require an external computer, and offers new features like fast size measurements with scan times below 10s.

Stop by our booth and learn more about the new.

Multi-Instrument-Software (MIM), Highlights of Sizing Nanoparticles with NanoScan SMPS and OPS Combination System Model 3914 and our 30 % CPC Trade-In offer for selected CPCs.

We look forward to seeing you at our booth.

ECM ECO Monitoring

ECM ECO Monitoring

Address: **Nevädzová 5**
821 01 Bratislava
Slovak Republic

Phone: **00421 2 4342 9417**
Fax: **00421 2 4342 7465**
Email: **ecm@ecm.sk**

ECM is a TSI company operating in area of Central/Eastern Europe and CIS countries. Besides of TSI particle monitoring products also OC/EC, carbon black and complex analytic solutions for monitoring of gases, liquids and particles are provided.

For detailed information in different languages refer to www.ecomonitoring.com

URG Corporation

Adress: **116 South Merritt Mill Rd.**
Chapel Hill,
North Carolina
27516 USA

Phone: **919-942-2753**
Email: **info@urgcorp.com**
Website: **www.urgcorp.com**

URG Corporation manufactures the Ambient Ion Monitor (AIM) System for the continuous direct measurement of particulate Cl-, NO3-, SO42-, NH4+, NA+, K+, CA2+, MG2+ in PM2.5 plus gas measurements of HCl, HNO3, HNO2, SO2, NH3. The AIM System analyzes particles, gases and organics. The AIM System incorporates Thermo Scientific Dionex Reagent-Free Ion Chromatographs. The AIM System has detection limits of 0.05μg/m3 for each of the required analytes. The multi-pollutant data is instantly available on an hourly basis and with the option of every 15-30 minutes.

URG provides a wide variety of instruments for indoor and outdoor air sampling. Our Annular Denuder System (ADS) collect both acidic and basic gases and is designed to meet USEPA's Compendium Method IO-4.2. URG's complete collection of aluminum cyclone inlets are Teflon© coated, a patented process that minimizes the losses of reactive gases such as HNO3 and NH3 to the internal surfaces of the cyclone. URG provides stainless steel cyclones and filter holders for diesel emissions.

URG air sampling instrumentation is used in Europe, Asia, North America, Australia, Antarctica, Africa and South America.

Conference Secretariat:

Congress Business Travel Ltd.

Lidická 43/66, 150 00 Praha 5 – Anděl, Czech Republic

Phone: +420 224 942 575
+420 224 942 579

Fax: +420 224 942 550

E-mail: eac2013@cbttravel.cz

Exhibition Plan

Clarion Congress Hotel - Congress floor

EXHIBITOR	BOOTH
TSI GMBH	1
DIGITEL ELEKTRONIK AG	2
GRIMM AEROSOL TECHNIK GMBH	3
COPLEY SCIENTIFIC LIMITED	4
AETH LABS	5
DEKATI LTD	6
METROHM	7
COMDE-DERENDA GMBH	8
PALAS GMBH	9
NANEOS PARTICLE SOLUTIONS	10
URG CORPORATION	11
ECOTECH PTY LTD	12
SUNSET LABORATORY INC	13
CAMBUSTION	14
CATALYTIC INSTRUMENTS	15
MATTER AEROSOL	16
TOPAS GMBH	17
RAMEM-IONER	18
AIRMODUS	19
AERODYNE RESEARCH	20
AEROSOL	21
MET ONE INSTRUMENTS	22

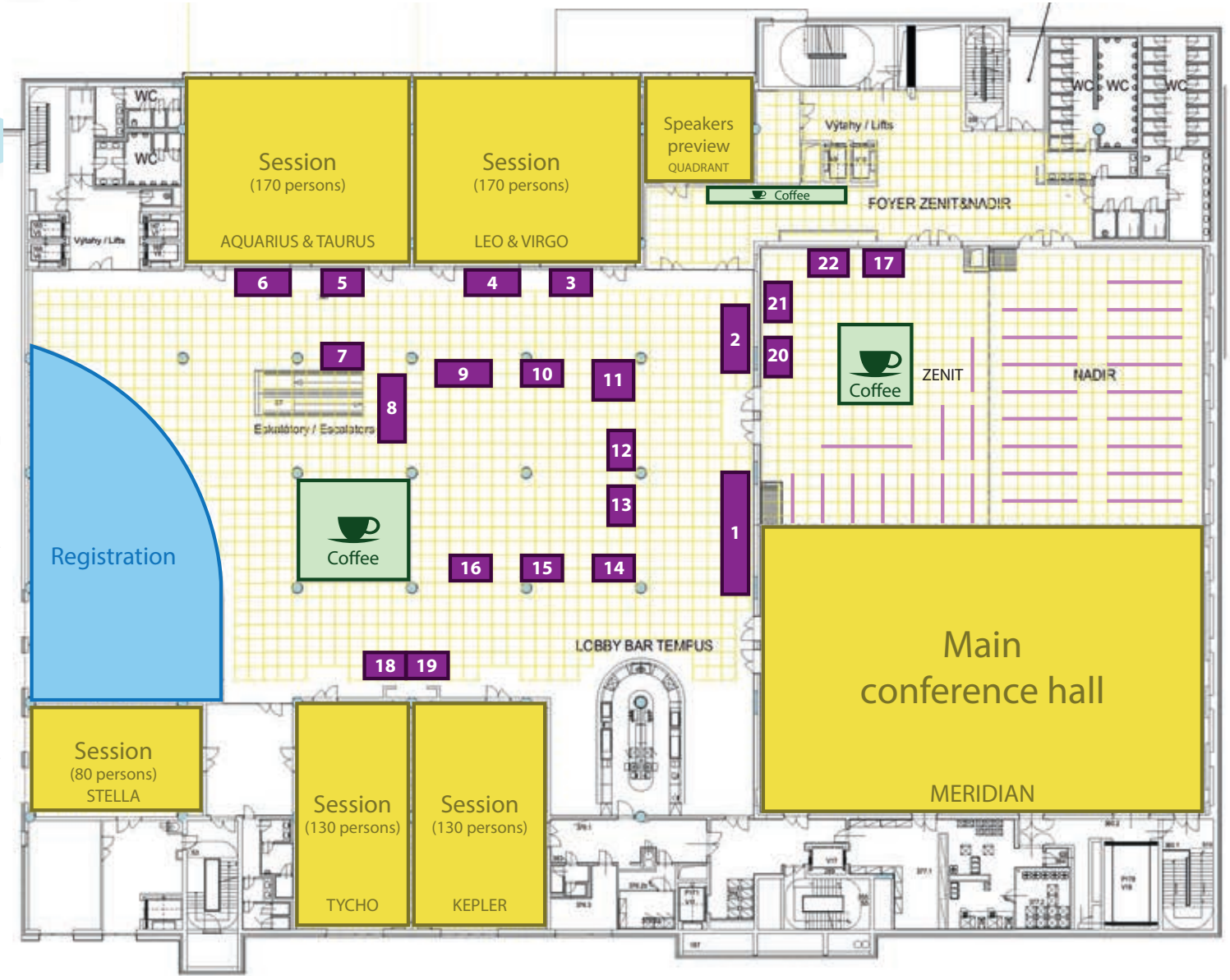

Sponsors and Exhibitors

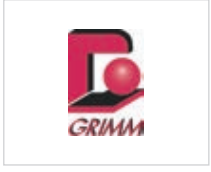

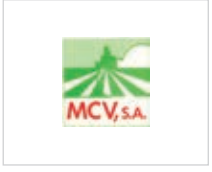

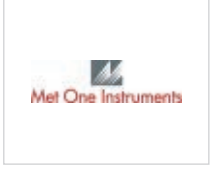

E.A.C. Essentials

VISIT

The Ecotech booth to see our:

- **ACS 1000 Aerosol Conditioning System**
- **Aurora 4000 Polar Integrating Nephelometer**

LISTEN

Tuesday morning September 3, 2013
Session 5 - Instrumentation
A new aerosol conditioning system - Characterisation and first application
M. Laborde, B. Rosati, P. Zieger, T. Petäjä, G. Kassell, D. Logan, E. Weingartner

ATTEND

Ecotech's Nephelometer Workshop
Saturday 7th September,
Clarion Congress Hotel
Visit our booth to register

ecotech
environmental monitoring solutions

www.ecotech-research.com
info@ecotech.com

Monday, September 2, 2013

Plenary lecture: Aerosol particles in the marine environment

by Merete Bilde

Aerosol particles in the marine environment

M. Bilde

Department of Chemistry, Aarhus University, Langelandsgade 140, DK-8000 Århus, Denmark

Keywords: Sea spray aerosol, CCN, soot.
Presenting author email: bilde@chem.au.dk

Aerosol particles in the marine environment stem from several sources including primary production of sea-spray particles via wind-driven air-entrainment and subsequent bubble bursting, transport from land sources, new particle formation and emissions from ships.

Large uncertainties are associated with the source strength, properties and climate impact of particle from these different sources.

This talk provides a general introduction to aerosol particles in the marine environment with focus on particle properties. The results presented address properties of particles generated from bubble bursting processes in a laboratory environment. In addition, properties of particles sampled from a low-speed ship engine will be presented. Outcomes will be discussed in the context of atmospheric science.

Methods

In *Sea-spray experiments* particles were generated by air-entrainment and bubble bursting processes in laboratory tanks. Bubbles were generated either by aeration through a diffuser or by water jet impingement on the water surface of the tank. Particle properties were determined using a suite of aerosol instruments including SMPS systems and CCN-counter.
In *ship-engine experiments* particles were collected during a 3-week measurement campaign at a MAN B&W low-speed ship engine on test bed in Copenhagen and analyzed using Transmission Electron Microscopy.

Results

Sea-spray aerosols constitute a major fraction of marine aerosols. They can be formed when air bubbles entrained in ocean water as a result of breaking waves rise and burst at the surface (e.g. de Leeuw et al. 2011). Sea-spray aerosol has been shown to contain not only sea salt but also organic molecules and field studies (O'Dowd et al. 2004) have suggested that smaller sub-micron particles are enriched in organic material compared to the ocean water.

In this work a series of laboratory experiments were performed to investigate the mechanism of sea-spray aerosol formation, organic enrichment and physico-chemical properties of sea-spray aerosols. For example, the effect of bubble residence time in the bulk seawater solution on particle size and CCN activity was investigated for artificial seawater containing different organic molecules. CCN activity of particles produced from water jet impingement was compared with CCN activities of particles produced from aeration through a diffuser and suggests a considerable amount of organic enrichment in the particles produced via jet-impingement when the salt water contained an organic surfactant (sodium laurate) (King et al. 2012).

Another type of complex aerosol particles in the marine environment are particles emitted from marine diesel engines. Results will be presented from a study comparing particle properties before and after an exhaust gas recirculation scrubber for a low-speed ship engine on test bed.

Acknowledgements

This work was supported by The Carlsberg Foundation, the Danish Agency for Science Technology and Innovation and the Nordic Center of Excellence on Cryosphere-atmosphere interactions in a changing Arctic climate (CRAICC).

References

King, M, Butcher AC, Rosenoern T, Coz, E, Lieke KI, de Leeuw G, Nilsson D and Bilde M. "Investigating Primary Marine Aerosol Properties: CCN Activity of Sea Salt and Mixed Inorganic-Organic Particles" (2012) *Environ. Sci. Technol*. 46, 10405-10412.

de Leeuw G, Andreas E L, Anguelova MD, Fairall CWR, O'Dowd C, Schulz M and Schwartz SE "Production flux of seaspray aerosol." (2011) *Reviews of Geophysics* 49.

Lieke KI, Thomas Rosenørn, Pedersen J., Larsson D., Kling J., Fuglsang K. and Bilde M. "Micro- and Nanostructural Characteristics of Particles
Before and After an Exhaust Gas Recirculation System Scrubber" (2013) *Aerosol Sci. Technol.* 47, 1038–1046.

O'Dowd, C. D., M. C. Facchini, F. Cavalli, D. Ceburnis, M. Mircea, S. Decesari, S. Fuzzi, Y. J. Yoon and J. P. Putaud "Biogenically driven organic contribution to marine aerosol." (2004) *Nature* 431, 676-680.

Monday, September 1, 2013

Session: Atmospheric Aerosols,
Remote sensing and optical properties of aerosols

Relationship between oxidation level and optical properties of secondary organic aerosol

A. T. Lambe[1,2], C. D. Cappa[3], P. Massoli[2], T. B. Onasch[1,2], S. D. Forestieri[3], A. T. Martin[1], M. J. Cummings[1], D. R. Croasdale[1], W. H. Brune[4], D. R. Worsnop[2], P. Davidovits[1]

[1]Chemistry Department, Boston College, Chestnut Hill, Massachusetts, 02467, U.S.
[2]Aerodyne Research, Inc., Billerica, Massachusetts, 01801, U.S.
[3]Department of Civil and Environmental Engineering, University of California - Davis, Davis, California, 95616, U.S.
[4]Department of Meteorology and Atmospheric Sciences, The Pennsylvania State University, University Park, Pennsylvania, 16802, U.S.

Keywords: SOA, oxidative aging, optical properties, aerosol mass spectrometry.

Presenting author email: lambe@aerodyne.com

Brown carbon (BrC), which may include secondary organic aerosol (SOA), can be a significant climate-forcing agent via its optical absorption properties. However, the overall contribution of SOA to BrC remains poorly understood. Here, correlations between oxidation level and optical properties of SOA are examined. SOA was generated in a flow reactor in the absence of NO_x by OH oxidation of gas-phase precursors used as surrogates for anthropogenic (naphthalene, tricyclo[5.2.1.$0^{2,6}$]decane [JP-10]), biomass burning (guaiacol), and biogenic (α-pinene) emissions. SOA chemical composition was characterized with a time-of-flight aerosol mass spectrometer. The mass spectra yielded oxygen-to-carbon (O/C) ratios, used as a measurable surrogate for SOA oxidation level, that ranged from 0.29 to 1.29.

SOA mass-specific absorption cross sections (MAC) and refractive indices were calculated from real-time cavity ring-down photoacoustic spectrometry (CRD-PAS) measurements at 405 and 532 nm and from UV-Vis spectrometry measurements of methanol extracts of filter-collected particles (300 to 600 nm). At 405 nm, SOA MAC values and imaginary refractive indices ranged from $<$0.001 to 0.088 $m^2\ g^{-1}$ and 1.9×10^{-4} to 3.6×10^{-3}, respectively, increasing with SOA oxidation level. SOA light absorption decreased with increasing wavelength, leading to negligible absorption at 532 nm. Real refractive indices (n) of SOA at 405 nm ranged from 1.45 to 1.66 and for a given precursor changed at a rate of $\Delta(n)/\Delta(O/C)$ = -0.055 to -0.11. Comparison with literature studies suggests that under typical polluted conditions the effect of NO_x on SOA absorption is small. SOA may contribute significantly to atmospheric BrC, with the magnitude dependent on both precursor and oxidation level.

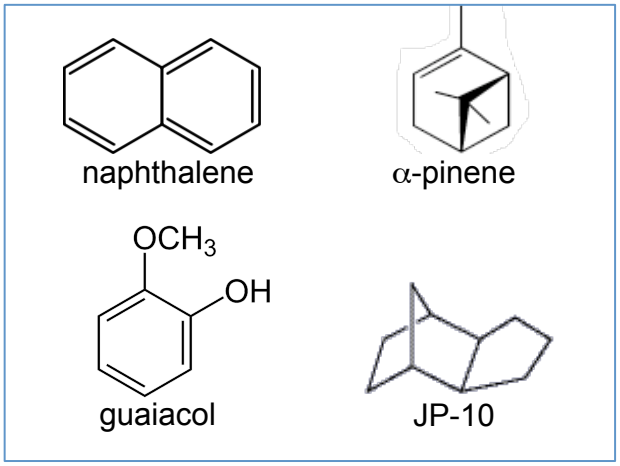

Figure 1: Molecular structures of SOA precursors used in this work.

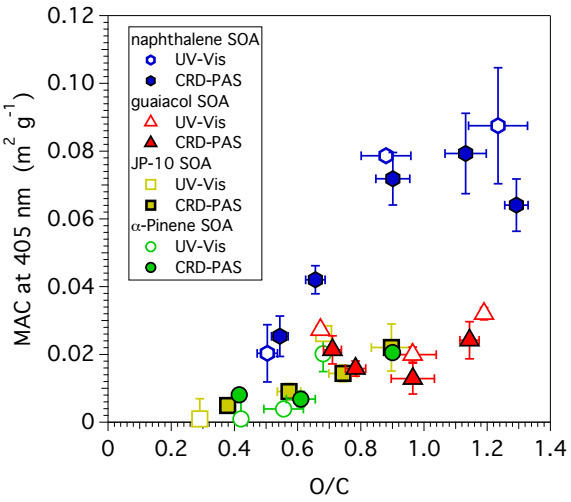

Figure 2: Mass-specific absorption cross sections (MAC) of SOA obtained at λ = 405 nm as a function of O/C ratio. MAC values are calculated from CRD-PAS and UV-Vis spectrometer measurements.

This research was supported by the Office of Science (BER), Department of Energy (Atmospheric Science Program) grants No. DE-SC0006980 and DE-FG02-05ER63995, and the Atmospheric Chemistry Program of the National Science Foundation grants No. ATM-0854916 and AGS-0904292 to Boston College and Aerodyne Research, Inc., ATM-0837913 to UC Davis, and and AGS-0855135 to Pennsylvania State University.

Cappa, C. D., Che, D. L., Kessler, S. H., Kroll, J. H., and Wilson, K. R. (2011) *J. Geophys. Res.*, **116**, D15204.

Lack, D. A., Lovejoy, E. R., Baynard, T., Pettersson, A., and Ravishankara, A. R. (2006) *Aerosol Sc. & Tech.*, **40**, 697–708.

Lambe, A. T., Ahern, A. T., Williams, L. R., Slowik, J. G., Wong, J. P. S., Abbatt, J. P. D., Brune, W. H., Ng, N. L., Wright, J. P., Croasdale, D. R., Worsnop, D. R., Davidovits, P., and Onasch, T. B. (2011) *Atmos. Meas. Tech.*, **4**, 445–461.

Updyke, K. M., Nguyen, T. B., and Nizkorodov, S. A. (2012) *Atmos. Environ.*, *63*, 22–31.

Zhong, M. and Jang, M. (2011) *Atmos. Environ.*, **45**, 4263–4271.

Satellite and ground-based retrievals of aerosol optical properties in Arctic (2003-2011)

P. Glantz[1], M. Tesche[1], K. Stebel[2], A. Herber[3], H. Struthers[4], J. Karlsson[5], A. Bourassa[6], L. Thomason[7], M. Maturilli[8]

[1]Department of Applied Environmental Science, Stockholm University, Stockholm, Sweden
[2]Norwegian Institute for Air Research, Kjeller, Oslo, Norway
[3]Alfred Wegener Institute for Polar and Marine Research, Bremerhaven, Germany
[4]National Supercomputer Centre, Linköping University, Linköping, Sweden
[5]Department of Meteorology, Stockholm University, Stockholm, Sweden
[6]Institute of Space and Atmospheric Studies, University of Saskatchewan, Canada
[7]NASA Langley Research Center, Hampton, Virginia, USA
[8]Alfred Wegener Institute Helmholtz Centre for Polar and Marine Research, Potsdam, Germany

Keywords: AOT, remote sensing, arctic marine atmosphere
Presenting author email: paul.glantz@itm.su.se

Aerosol particles influence the Earth's radiation balance directly by scattering or absorbing incoming solar radiation. Improving our knowledge of Arctic aerosols and their radiative impacts is important, particularly at present day when albedo is decreasing due to reductions in sea ice and snow cover. Realistic simulations of aerosol radiative forcing at the top of the atmosphere and at the surface require knowledge of the aerosol optical thickness (AOT).

In this study 9 years (2003-2011) of MODIS-Aqua aerosol observations have been combined with ground-based long-term sun-photometer and dry nephelometer measurements as well as with climate model simulations to examine the accuracy in estimations of aerosol optical properties in the Svalbard region (82°N-75°N, 10°W-40°E). MODIS 555-nm AOT was compared to ground-based sun-photometer measurements. For the 642 matches that was obtained it was found that MODIS AOT on the whole varies within the expected uncertainty for one standard deviation of the retrieval over ocean ($\Delta AOT = \pm 0.03 \pm 0.05 \cdot AOT$).

Figure 1 shows the annual variation of MODIS median 555-nm AOT, for the period under investigation,

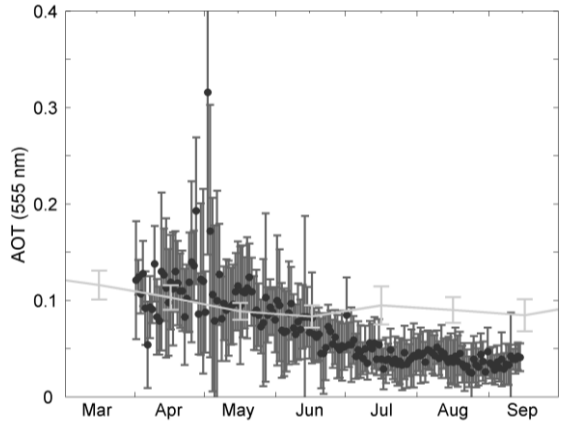

Figure 1. MODIS median AOT at 555 nm (black circle) and one standard deviation (dark gray line) averaged over all pixels that correspond to a day of the year in the 9-years period of observations (2003 – 2011). The light grey solid line denotes CAM3-Oslo model simulation of clear-sky AOT, using boundary conditions representative of the year 2000 and IPCC AR5 aerosol emissions.

compared to clear-sky AOT as simulated with the CAM3-Oslo global climate model. The latter values were obtained at 555 nm wavelength and averaged over the area investigated. Figure 1 shows that reasonable agreement occurs for the spring season while the simulated AOT is approximately a factor of 2 higher than the MODIS observations for the summer season.

Table 1 compares mean tropospheric AOT at 555 nm obtained in the framework of this study with AOT at 533 nm as obtained at Svalbard in the 1990's (Herber et al., 2002). The tropospheric AOT for the time period 2003-2011 was screened for the contribution of volcanic events by subtracting stratospheric AOT from Odin/OSIRIS measurements. In the present study we found June to mark the transition between spring- and summer-time aerosol conditions. Fig. 7 in Herber *et al.* (2002) on the other hand suggests that the transition occurred over a rather short period in late May in the 90's. The difference in AOT between June and July/August for the present period is statistical significant at the 99.9% confidence level (unpaired t-test) for all three platforms. This change in aerosol conditions suggests that Arctic was isolated during a longer period in the 90's compared to the last decade, in in line with weakened zonal winds and increased wave amplitude during 2000-2010, thus, moving the Rossby waves poleward (Francis and Vavrus, 2012).

Table 1. Tropospheric mean AOT at 555 nm (this study) and 532 nm (Herber et al. 2001, 1991 – 1999) resolved according to different times of the year.

Season	AOT (555 nm)			AOT (532 nm)
	2003 - 2011			1991 - 1999
	$MODIS_{C005}$	AERONET	Polar-AOT	Polar-AOT
Apr -May	0.113 ±0.069	0.092 ±0.050	0.070 ±0.036	0.089 ±0.033
Jun	0.071 ±0.045	0.066 ±0.037	0.063 ±0.035	
Jul - Aug	0.040 ±0.026	0.040 ±0.025	0.035 ±0.023	
Jun - Aug				0.046 ±0.024
Sep	0.032 ±0.021	0.036 ±0.020	0.025 ±0.058	0.031 ±0.014

This work was supported by FORMAS under grant 216-2010-910.

Francis, J. A. and Vavrus, S. J. (2012) *Gephys. Res. Let.*, **39**, L06801, doi:10.1029/2012GL051000, 2012.
Herber, A. *et al.* (2002) *J. Geophys. Res.*, **107 (D10)**, doi:10.1029/2001JD000536.

Operational boundary layer height determination with in-situ and ground-based remote sensing instruments: validation and first climatology on the Swiss plateau.

C. Praz, **M. Collaud Coen,** A. Haefele, and D. Ruffieux

MeteoSwiss, 1530 Payerne, Switzerland
Keywords: PBL, Lidar, Windprofiler, Radiometer, parcel and bulk Richardson, NWP model.
Presenting author email: martine.collaudcoen@meteoswiss.ch

The planetary boundary layer (PBL) is the lowest part of the troposphere that is directly influenced by the Earth's surface and concentrates the major part of aerosols as well as others pollutants. Continuous determination of PBL height is of prime importance for air quality analysis, for predicting aerosols, pollens and pollutants dispersion, and for local meteorological climate comprehension.

The top of the PBL is characterized by a strong decrease of the aerosol concentration and humidity content as well as by strong turbulences. It can be consequently estimated by measuring various physical parameters such as the aerosol scattering ratio (ASR) measured by the Raman-lidar, the RH gradient measured by the radiosonde (RS) or the Raman-lidar, or the turbulence signature in the signal to noise ratio (SNR) of the windprofiler. The radiosonde and the microwave radiometer provide temperature profiles to which both Parcel Method (PM) and bulk Richardson (bR) can be applied to detect the PBL height by the elevation of air masses adiabatically raised by convection. The numerical weather prediction (NWP) model COSMO-2 also used the bulk Richardson method to determine the PBL height.

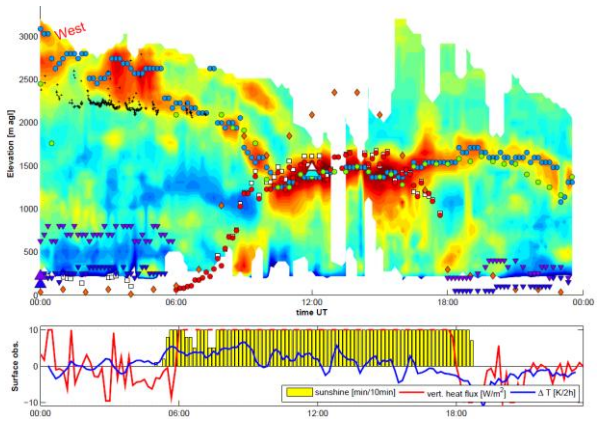

Figure 1: PBL height detected by the PM (red circles + triangle) and the bR (white squares +triangle) applied on the radiometer and radioSonde T profiles, on the SNR (blue circles) on the ASR (green circles) and nocturnal SBL height detection (blue and violet triangles), as well as COSMO-2 output (orange diamond), 31 July, 2012 at Payerne. The sunshine duration, the vertical heat flux and the temperature gradient are plotted on the second panel.

All the PBL height detection methods are operationally applied to all instruments in Payerne (491 m asl) and Schaffhouse (437 m asl) situated on the Swiss plateau. The 2012 data were used to validate the detection methods taking the PM applied on the radiosonde or the radiometer T profiles as a reference method and to calculate a climatology of both the CBL and the SBL at both measuring sites. Figure 1 presents an example of clear sky convective day, where 1) the convective boundary layer (CBL) height's increase and decrease can be detected by the PM applied to the radiometer data, 2) all detection methods show a very good agreement for the CBL height during the afternoon, 3) the residual layer is detected by both the windprofiler and lidar, 4) the nocturnal stable layer (NSL) is evaluated by the radiometer and radiosonde T profiles, and 5) the COSMO model shows a clear overestimation of the CBL height for this day.

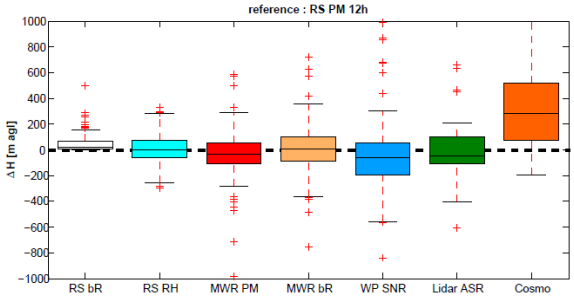

Figure 2: Boxplots of ΔH between PBL height computed at 12:00 UT with various methods and the reference RS PM. The central mark is the median, the edges of the box are the 25th and 75th percentiles q1 and q3, the whiskers extent covering 99% of data assuming a normal distribution, and the red crosses are the outliers.

The validation (Fig. 2) done on 107 convective days during January-October 2012 shows that all the detection methods based on remote sensing and radiosonde measurements are in very good accordance (mean at ± 50m, 25th and 75th percentiles at ± 200 m). The COSMO CBL height being on the contrary regularly overestimated for part of the summer days.

One year climatology shows that both in Payerne and Schaffhouse, the PBL height obeys a remarkable annual cycle, varying between about 400 m agl in winter up to nearly 1400 m agl in July. The PBL maximal height appears to be reached from May to August.

Assessment of parameterizations of optical properties and hygroscopic growth of aerosols

A.R. Esteve[1,2], E.J. Highwood[2], W.T. Morgan[3], H. Coe[3], R.G. Grainger[4], P. Brown[5], C.L. Ryder[2], K. Szpek[5] and J.A. Martínez-Lozano[1]

[1]Department of Earth Physics and Thermodynamics, University of Valencia, Burjassot, 46100, Spain
[2]Department of Meteorology, University of Reading, Reading, RG6 6BB, UK
[3]Centre for Atmospheric Science, University of Manchester, Manchester, M13 9PL, UK
[4]Atmospheric, Oceanic and Planetary Physics, University of Oxford, Oxford, OX1 3PU, UK
[5]Observation Based Research, Met Office, Exeter, EX1 3PB, UK
Keywords: anthropogenic aerosols, optical properties, aircraft measurements, aerosol modelling.
Presenting author email: Anna.Esteve@uv.es

Atmospheric aerosols affect the Earth's climate both directly, through the scattering and absorption of radiation, and indirectly, via changes to cloud microphysics and properties. In order to estimate the "direct effect", climate models generally require aerosol optical properties such as the extinction coefficient, the single scattering albedo and the asymmetry parameter. And for these, they need to quantify first the spectral refractive index, the size distribution, the influence of relative humidity and the mixing state of atmospheric aerosols. This complexity of the atmospheric aerosols requires synergistic use of models and measurements in order to provide the information needed in climate models.

The Facility for Airborne Atmospheric Measurements (FAAM) BAe-146 aircraft has recently provided a new body of measurements of the chemical composition, microphysical, optical and hygroscopic properties of the atmospheric aerosols (Johnson *et al.*, 2000; Osborne *et al.*, 2007), which allow us to explore the agreement between models and measurements of the aerosol optical properties.

In this work we have used a flexible framework for assessing parameterizations of optical properties and hygroscopic growth of aerosols. We have used this framework to calculate aerosol optical properties at a given relative humidity based on composition, and then we have compared with measured values of the same. For this, we have used data collected by the FAAM BAe-146 aircraft over Western Europe during the EUCAARI-ADIENT project (Kulmala *et al.*, 2009) and over the South East Pacific region during the VOCALS-UK project (Wood *et al.*, 2011).

The methodology used in this work consists in using the measurements of the aerosol composition made by a Time-of-Flight Aerosol Mass Spectrometer (ToF-AMS) and a Single Particle Soot Photometer (SP2) and the measurements of the size distribution made by a Passive Cavity Aerosol Spectrometer probe (PCASP-100x) together with volume weighted mixing rules, best estimates of refractive indices and assumptions about the growth factors of the aerosol components to determine the ambient size distribution and the refractive indices of an internally mixed aerosol at a given relative humidity. The scattering and absorption by the internally mixed aerosol can be then calculated using a Mie scattering code (Wiscombe, 1979). Finally, the resulting scattering and absorption are compared against coincident scattering and absorption measurements from a TSI 3563 integrating nephelometer and a Particle Soot Absorption Photometer (PSAP) (Figure 1).

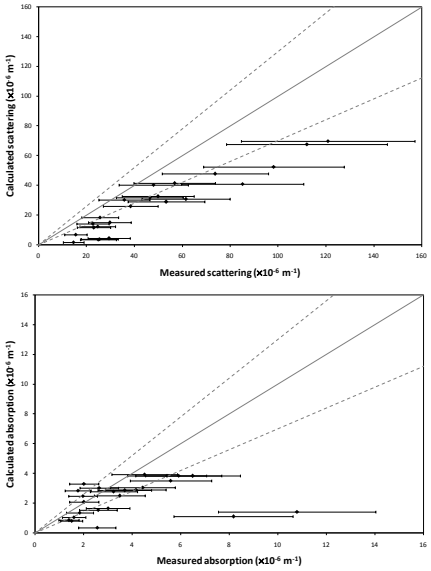

Figure 1. Comparison of modelled and measured scattering and absorption during the EUCAARI-ADIENT project.

This work was supported by NERC ADIENT project NE/E011101/1 and EUCAARI project 036833-2. VOCALS-UK was funded by NERC (ref.: NE/F019874/1). The collaboration of A.R. Esteve was possible thanks to the VALi+d postdoctoral fellowship APOSTD/2012/078 and the project PROMETEO/2010/064 of the Valencian Autonomous Government.

Johnson, D.W. *et al.* (2000) *Tellus*, **52B**, 290–320.
Kulmala, M. *et al.* (2009) *Atmos. Chem. Phys.*, **9**, 2825-2841.
Osborne, S.R. *et al.* (2007) *Q. J. Roy. Meteorol. Soc.*, **133**, 17–32.
Wiscombe, W.J. (1979) *NCAR/TN-140+STR NCAR Tech. Note*, National Center for Atmospheric Research, Boulder, Colorado, USA.
Wood, R. *et al.* (2011) *Atmos. Chem. Phys.*, **11**, 627-654.

The optical properties of aerosols in Amazonia: from natural biogenic to biomass burning particles

Paulo Artaxo[1], Xuguang Chi[4], Henrique M. J. Barbosa[1], Luciana V. Rizzo[2], Andrea Arana[1], Joel F. Brito[1], Elisa T. Sena[1], Joel Schaefer[3], Meinrat O. Andreae[4].
[1] Institute of Physics, University of São Paulo,
Rua do Matão, Travessa R, 187. CEP 05508-090, São Paulo, S.P., Brazil.
[2] Departamento de Ciências Exatas e da Terra, UNIFESP - Campus Diadema,
Rua Prof. Artur Riedel, 275 , CEP 09972-270, Diadema - São Paulo, Brazil.
[3] NASA Goddard Space Flight Center, Code 618, Bldg. 33, Rm. F541. Greenbelt, MD 20771-0001, USA
[4] Biogeochemistry Department, Max Planck Institute for Chemistry, P.O. Box 3060, 55020 Mainz, Germany.

Keywords: Aerosol particles, Amazonia, biosphere-atmosphere interactions, Biomass Burning,
Presenting author email: Artaxo@if.usp.br

Amazonia is one of the most pristine continental areas in the wet season, with very low aerosol particles concentration. Over the last 20 years, the Large Scale Biosphere Atmosphere Experiment in Amazonia (LBA) has implemented research projects aiming to study aerosol optical properties (Davidson et al., 2012). Three aerosol components are the most visible: 1) The natural biogenic emissions of aerosols; 2) Secondary organic aerosols from biogenic VOCs emissions; and 3) the biomass burning component. Long term monitoring of aerosols and trace gases were performed in two sites: a background site in Central Amazonia, 55 Km North of Manaus (called ZF2 ecological reservation) and a monitoring station in Porto Velho, Rondonia state, a site heavily impacted by biomass burning smoke. Recently, two new sites are providing new information on aerosol optical properties: the so called ATTO (Amazon Tall Tower Observatory) that is a very clean site North of Manaus and the EMBRAPA site, 50 Km NE of Manaus, with the long term operation of a Raman Lidar and other instruments. At these sites, detailed aerosol characterization is being performed, with the measurements of aerosol size distribution from 10 to 600 nm, spectral light absorption measured with Aethalometer and MAAPs, light scattering with the use of TSI and Ecotech 3 lambda nephelometers. In parallel, aerosol composition is being measured for inorganic components (measured using XRF) and organic and elemental carbon determined with a Sunset OC/EC instrument. We are also operating a network of 6 CIMEL sunphotometers from AERONET and the use of MODIS AOD allows to obtain the large scale aerosol distribution. Combination of MODIS and CERES allowed the calculation of top of the atmosphere large scale aerosol radiative forcing.

Aerosol optical depths (AOD) of more than 4 at 550nm was observed frequently over biomass burning areas, while in the wet season, central Amazonia shows very low AOD of about 0.05 to 0.1 at 550 nm. At the ZF2 site, dry particle median scattering coefficients at the wavelength of 550 nm increased from 6.3 Mm−1 to 22 Mm−1, whereas absorption at 637 nm increased from 0.5 Mm−1 to 2.8 Mm−1 from wet to dry season. Angstrom exponents for scattering were lower during the wet season (1.6) in comparison to the dry season (1.9), which is consistent with the shift from fine mode biomass burning aerosols, to biogenic aerosols, predominant in the coarse mode. Single scattering albedo (SSA), calculated at 637 nm, did not show a significant seasonal variation, averaging 0.86±0.08 for dry particles. AERONET SSA at 550 nm for the region shows an average of 0.91±0.04. A detailed analysis of aerosol optical properties was provided in Rizzo et al., 2012.

Combined analysis of MODIS and CERES for a 10 years study shows that the mean direct radiative forcing of aerosols at the top of the atmosphere (TOA) during the biomass burning season was $-5.6\pm1.7 Wm^{-2}$. It was observed that for high AOD (larger than 1 at 550 nm) the maximum daily direct aerosol radiative forcing at the TOA may be as high as $-20 Wm^{-2}$ locally. Details of this analysis can be found in Sena et al., 2012.

At the ATTO site, very low aerosol light scattering and absorption was observed, with a wet season light scattering typical values of 6 Mm-1 at 550 nm, while BC typical values are in the range of 70-100 ng/m³. The average SSA at ATTO is about 0.89, a value slightly higher than observed at the ZF2 site (0.86).

Elemental composition of aerosols shows that sharp increases in Al, Si, Ti and Fe are associated with Sahara dust input into Central Amazonia that is also easily observed with our Raman Lidar.

This work presents a general description of the aerosol optical properties in Amazonia, both during the Amazonian wet and dry seasons.

We would like to thank the INPA LBA central office in Manaus for logistical support for the ZF2 and ATTO sites. This research was funded by the FAPESP Thematic project AEROCLIMA, 2008/58100-2, and CNPq/INCT projects.

Rizzo, L.V., et al, Atmos. Chem. Phys. Discuss., 12, 23333–23401, 2012.
Sena, E. T. et al., Atmospheric Chemistry and Physics, 13, 1261–1275, 2013.
Davidson, E. A. et al., The Amazon Basin in Transition. Nature, 481, 321-328, 2012.

In-situ absorption measurement of HULIS and mineral dust components as well as winter time ambient aerosol using multi-wavelength photoacoustic instrument. A laboratory and a field study

T.Ajtai[1], N. Utry[1], Á. Filep[1], Z. Bozóki[1], G. Szabó[1]

Department of Optics and Quantum Electronics, University of Szeged, Hungary
Keywords: Aerosol absorption, minerals, HULIS, photoacoustic
Presenting author email: ajtai@physx.u-szeged.hu

Aerosol can interact with solar radiation via absorption and scattering. While backward scattering directly cooling the atmosphere, forward scattering redistribute the electromagnetic energy without affecting the annual global average of atmospheric temperature. The absorption processes directly heat the atmosphere. The net effect is cooling, but the accuracy of its amplitude is really questionable, in part since, the lack of the reliable instrumentation for in-situ absorption measurement (Lack et al., 2006). The only method which could directly measure light absorption by aerosol is photoacoutic, but it is not widespread in its application yet (Meinrat. O. Andreae, 2005). Very recently, multi-wavelength photoacoustic instruments become available for in-situ spectral characterisation of aerosol and open up a new perspective for reliable and selective in-situ carbon content identification (Lewis et al, 2008 , Ajtai et al, 2010).

In this study we present mass specific light absorption coefficient of re-dispersed dust components such as illit, caolinite, quartz, calcite, rutile, hematite as well as HULIS aerosols in the whole climate relevant and the photochemically active UV region. The measurements were made by our state-of-the-art multi-wavelength photoacoustic instrument (4λ-PAS, Ajtai et al, 2010). Based on the photoacoustic absorption measurement we calculated the two wavelengths Absorption Angström Exponent (AAE) of the investigated aerosols refer to UV, VIS, and Near-IR spectral region. We experimentally demonstrated that the absorption feature of mass specific aerosol absorption (MAC) could be used as chemically selective parameter. We also demonstrated that the selectivity of the composition identification through in-situ measured absorption feature might be increased by taking into account the wavelength dependency of AAE. Moreover, we demonstrate that forcing calculation based on the wavelength dependent AAE is more accurate than forcing calculation used the commonly applied single wavelength AAE approach.

We also present here results of in-situ spectral responses of ambient aerosol under wintry conditions in urban environment. The hourly concentration of gaseous pollutants (CO and NOx), trace elements (i.e. K, Ca, Fe, and Si) as well as the size distribution of ambient aerosol were also analyzed during the whole measurement campaign. The levoglucosan measurement was made to confirm that the daily fluctuation of ambient AAE governed by the changes in the relative strength between the traffic and residential heating emission. Finally, we demonstrate correlations between the measured two wavelengths AAEs and the concurrently measured other aerosol variables such as size distribution, gas and trace elements concentrations. All the correlations are quantified using both single wavelength and wavelength dependent AAE.

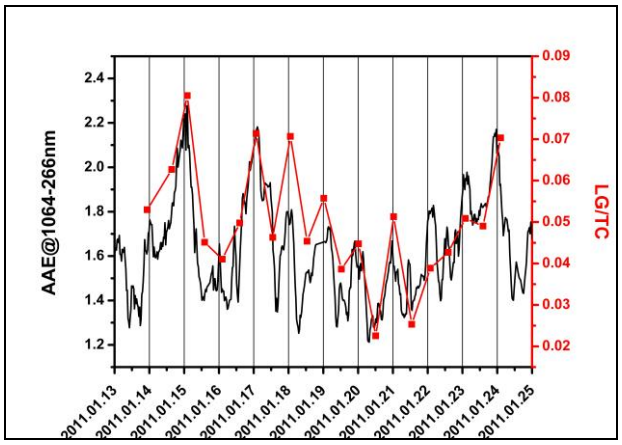

Figure 1. The time series of AAE and the relative strengths of levoglucosan/TC concentration

These researches were funded by Hungarian Scientific Research Foundation (OTKA, Grant no. K101905). The European Union and the European Social Fund have provided financial support to the projects under the grant no. TÁMOP 4.2.2.A-11/1/KONV-2012-0047 and TÁMOP 4.2.2.A-11/1/KONV-2012-0060.

Lack, D. A., Lovejoy, E. R., Baynard, T. & Pettersson, A. (2006). Aerosol absorption measurement using photoacoustic spectroscopy: sensitivity, calibration and uncertainty developments. *Aerosol Sci.Technol.*, 40, 697–708.

Meinrat O. Andreae, (2005) The dark side of the aerosols, Nature **409**, 671-672

Ajtai, T., Filep, Á., Schnaiter, M., Linke, C., Vragel, M., Bozóki, Z., Szabó, G. and Leisner, T., 2010. A novel multi-wavelength photoacoustic spectrometer for the measurement of the UV-vis_NIR spectral absorption coefficient of atmospheric aerosols. Journal of Aerosol Science, 41, 1020-1029.

Lewis, K., Arnott, W. P., Moosmüller, H., Wold, C. E. (2008). Strong Spectral Variation of Biomass Smoke Light Absorption and Single Scattering Albedo Observed with a Novel Dual-Wavelength Photoacoustic Instrument, *J. Geophys. Res.*, 113.

Black carbon aerosol concentrations and mixing state in Pallas, Finland

T. Raatikainen[1], D. Brus[1], A.-P. Hyvärinen[1], J. Svensson[1] and H. Lihavainen[1]

[1]Finnish Meteorological Institute, Helsinki, Finland
Keywords: SP2, black carbon, soot particles, aerosol coating.
Presenting author email: tomi.raatikainen@fmi.fi

Black carbon (BC) aerosols have various climate effects. In addition to directly absorbing solar radiation, they have an effect on aerosol-cloud interactions and snow and ice albedo. Single Particle Soot Photometer (SP2) detects BC by using laser-induced incandescence and non-absorbing particles are identified from the scattered light (Stephens et al, 2003). Absorbing particles, with or without coating, are quickly heated to the incandescence temperature and the resulting peak signal, which is seen before evaporation, is proportional to the BC mass. Sizes of the purely scattering particles can be calculated from the peak intensity of the scattered light, which is seen when the particle is at the centre of the laser beam. However, particles containing both BC and scattering material heat up rapidly so that the scattering material evaporates before the centre of the laser beam. In this case, the initial scattering particle size can be extrapolated.

Two commonly used methods to extrapolate scattering sizes for evaporating particles are Leading Edge Optimization (LEO; Gao et al, 2008) and Normalized Derivative Method (NDM; Moteki and Kondo, 2008). The NDM is computationally demanding, and both methods can fail when, for example, the sample flow rate fluctuates. Significant flow rate fluctuations were observed in the SP2 measurements conducted at Pallas station in northern Finland during winter 2011-2012. To improve the coating thickness calculations, we have improved the NDM method so that the computationally heavy a priori estimate of the scattering signal is replaced by a linear fit to the normalized derivative and a fast posteriori likelihood test.

Figure 1 shows number concentrations of the different particle types. Concentrations are low in this pristine environment, but about 10 % of the observed (150-500 nm) particles contain BC. In addition, practically all BC particles are coated.

Figure 2 shows coating thickness distributions based on the original scattering sizes and those calculated with LEO, NDM and the new method. Due to the fluctuating flow rate, the NDM often fails to find a solution. The LEO method can find a solution, but it could overestimate coating thickness. The new method finds a reasonable solution for most particles (4715 of 5973) and the results show that most particles are thinly coated (68 % have less than 50 nm coating). This finding is in good agreement with the observation that 73 % of these particles experienced rapid coating evaporation determined from the lag time between scattering and incandescence peak signals. Further calibration experiments with mixed particles will be used to show that the new method finds the correct scattering size.

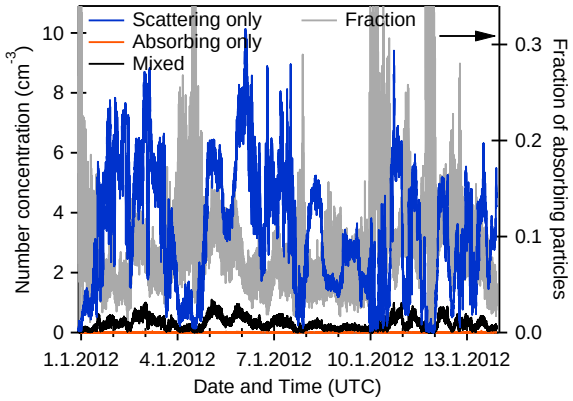

Figure 1. Total concentrations of scattering, absorbing and mixed particles from the 150-500 nm size range, and the fraction of absorbing particles.

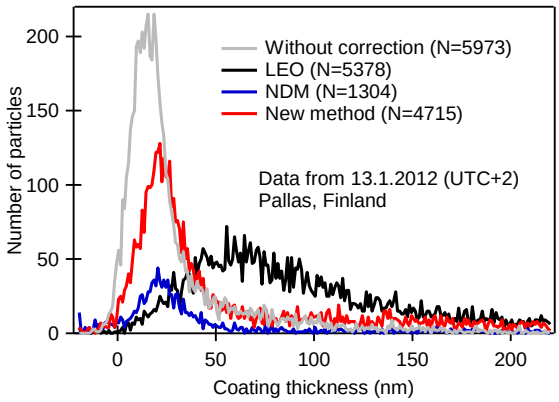

Figure 2. Coating thickness distributions for mixed particles which BC core diameter is 150-170 nm.

The work is supported by the EU LIFE+ project MACEB (project no. LIFE09 ENV/FI/000572), the Academy of Finland through the FCoE in Physics, Chemistry, Biology and Meteorology of Atmospheric Composition and Climate Change (program no. 1118615), black and brown carbon influence on climate and climate change in India – from local to regional scale (project no. 264242), Arctic Absorbing Aerosols and Albedo of Snow (project no. 3162) and the Nordic research and innovation initiative CRAICC.

Gao, R.S., et al. (2007) *Aerosol Sci. Technol.* **41**, 125-135.

Moteki, N. and Kondo, Y. (2008) *J. Aerosol. Sci.* **39**, 348-364.

Stephens, M., Turner, N. and Sandberg, J. (2003) *Appl. Opt.* **42**, 3726-3736.

Monday, September 1, 2013

Session: Atmospheric Aerosols,
SOA and aerosol hygroscopicity

Vapour pressures of substituted polycarboxylic acids are much lower than previously reported

A. J. Huisman[1], **U. K. Krieger[2]**, A. Zuend[2], C, Marcolli[2] and Th. Peter[2]

[1]Chemistry Department, Union College, Schenectady, N.Y. 12308, USA
[2]Institute for Atmospheric and Climate Science, ETH Zurich, 8092 Zurich, Switzerland
Keywords: vapour pressure, polycarboxylic acids, electrodynamic balance, Mie resonance spectroscopy
Presenting author email: ulrich.krieger@env.ethz.ch

The formation and fate of secondary organic aerosol (SOA) is governed by the partitioning of compounds between the aerosol and gas phase. This gas-particle partitioning of SOA is generally represented by an equilibrium partitioning model. A key physical parameter which governs gas-particle partitioning is the pure component vapour pressure (p^0) over the liquid state, which is difficult to accurately measure at atmospheric temperatures for low- and semi-volatile organic compounds such as polycarboxylic acids. Subcooled liquid state vapour pressures of substituted polycarboxylic acids inferred from measurements made in the solid state differ by many orders of magnitude from the predictions of current vapour pressure estimation methods, leading to large uncertainties in predictions of SOA partitioning. In this study, vapour pressures are inferred from the evaporation rate of single liquid particles levitated in an electrodynamic balance.

We present measurements of the liquid pure component vapour pressure for 2-Methylmalonic (isosuccinic) acid, 2-Hydroxymalonic (tartronic) acid, 2-Methylglutaric acid, 3-Hydroxy-3-Carboxyglutaric (citric) acid and 2,3-Dihydroxysuccinic (tartaric) acid which were measured in the subcooled liquid state (Huisman et al, 2013). Here we report also on measurements for 2-Oxoglutaric acid and compare those with literature data.

While the measurements of isosuccinic and 2-Methylglutaric acids agree with previous measurements, the data for tartaric and citric acid are 6 orders of magnitude lower than those previously reported, see Fig. 1. Also, our data of tartronic acid and 2-Oxoglutaric acid are significantly lower (2-3 orders of magnitude) lower than those inferred from measurements in the solid state by Booth et al. (2010). Please note that the agreement between our data and those of the vapour pressure estimation method by Compernolle et al. (2011) is significantly better when neglecting the empirical correction terms introduced to model the inexplicably high vapour pressures of some of substituted dicarboxylic acids reported by Booth et al. (2010). This holds particularly true for tartaric and citric acid.

We conclude first, that vapour pressure measurements should be performed in the liquid state whenever possible, second, that the empirical correction term introduced within the estimation model by Compernolle et al. (2011) should not be used and third, that more measurements using different techniques are needed to elucidate the reason for the many order of magnitude differences between our measurements and those of Booth et al. (2010).

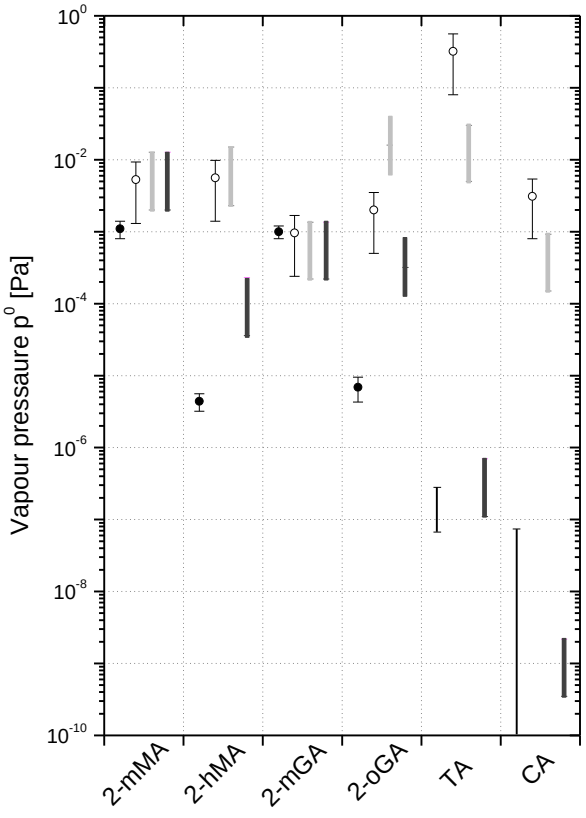

Fig. 1. Vapour pressures (T=298 K) of the liquid for 2-Methylmalonic acid (2-mMA), 2-Hydroxymalonic acid (2-hGA), 2-methlyglutaric acid (2-mGA), 2-oxoglutaric acid (2-oGA), tartaric acid (TA), and citric acid (CA), from this work (solid symbols and bars, when only a data range is reported), Booth et al. (open symbols), model prediction (Compernolle et al.) with correction (light gray) and without empirical correction term (dark gray).

Booth, A.M., Barley, M.H., Topping, D.O., McFiggans, G., Garforth, A., and Percival, C. J. (2010) *ACP* **10**, 4879-4892.

Compernolle, S., Ceulemans, K., and Müller, J.-F. (2011) *ACP* **11**, 9431-9450.

Huisman, A. J., Krieger, U. K., Zuend, A., Marcolli, C. and Peter, T. (2013) *ACPD* **13**, 1133-1177.

Investigation of the effects of chemical and physical factors on the phase state of SOA particles

A. Pajunoja[1], M. R. Alfarra[2,3], A. Buchholz[2], W.T. Hesson[2], G.B. McFiggans[2], A. Virtanen[1]

[1]Department of Applied Physics, University of Eastern Finland, Kuopio, FI-70210, Finland
[2]Centre for Atmospheric Science, The University of Manchester, Manchester, M13 9PL, UK
[3]National Centre for Atmospheric Science, The University of Manchester, Manchester, M13 9PL, UK
Keywords: SOA, phase state, viscosity, VOC.
Presenting author email: aki.pajunoja@uef.fi

Secondary organic aerosol (SOA) formed from partitioning of oxidation products of volatile organic compounds (VOC) accounts for a significant portion of atmospheric particulate matter. Behaviour of SOA particles in the atmosphere is affected by the phase of particles; not heeding these effects can result in errors when the atmospheric implications of SOA particles are predicted. Phase change of the particles can be induced e.g. by temperature change, absorption of water, or other solvent, or by chemical aging.

The phase state of SOA particles cannot be measured directly. Present studies show that particle bounce correlates with the phase state of particles (Virtanen et *al.* (2010), Saukko et *al.* (2012a), Saukko et *al.* (2012b)). A similar but modified method was employed in this study. The schematic of the new measurement system is shown in Figure 1. The system consists of a size classification DMA (selected sizes 70-150 nm), humidity control unit, a single MOUDI-type impactor stage (cut-off size 67 nm) and two CPCs. Upstream and downstream pressures of the impactor stage were stabilized to 0.85 bar and 0.7 bar.

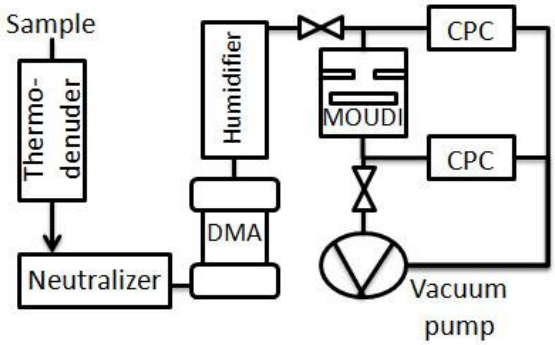

Figure 1: Schematic representation of the measurement system.

The chamber experiments were performed in the Manchester Photochemical Aerosol Chamber (Alfarra et al., 2012). In these experiments both biogenic and anthropogenic precursors were used (α-pinene, 1,3,5-trimethylbenzene, β-caryophyllene, limonene and n-heptadecane). The measurement schedule for different VOC mixtures is shown in Table 1. Mixtures of one to three precursors were investigated with and without the presence of ammonium sulphate seeds.

The oxidation conditions in the chamber were altered, namely the NO_x-level (20-115 ppb) and the UV exposure (filter on/off) while the O_3 level and relative humidity (RH) in the chamber were constantly 40 ppb and 60%, respectively. The exposure to light (visible and UV) varied between 0 and 5 hours.

The particle bounce was investigated for RH between 5 and 80% in the impactor. These RH scans were conducted for several thermodenuder temperatures (25 - 75°C).

Table 1. Chamber experiment schedule for four VOCs and specific NO_x and O_3-levels (ppb). X means the existence of ammonium sulphate seeds or usage of UV filter.

1	2	3	NO_x	O_3	seed	filter
α-pin.	TMB		20	40		X
α-pin.	TMB		20	40		
α-pin.	TMB		115	40		X
α-pin.	TMB		20	40	X	X
α-pin.	β-car.		20	40		X
α-pin.	β-car.		20	40	X	X
limon.			20	40		X
α-pin.	β-car.		20	40		
α-pin.	TMB	β-car.	20	40		
α-pin.	TMB	β-car.	20	40	X	X
α-pin.	TMB	β-car.	20	40		X
α-pin.	limon.		20	40		X
β-car.	limon.		20	40		X
α-pin.	β-car.	limon.	20	40		X
n-hept			50	80		

In this paper, results of the particle bounce measurements will be compared to findings from measurements of particle composition and sub- and super-saturated water uptake determined by high resolution AMS, HTDMA and CCNc, respectively. Clear effects of chemical composition and aging, hygroscopicity and relative humidity on the phase state of the SOA particles were observed. In addition differences between the bounce fractions in the SOA-coated seed experiments with different temperatures and aging times were found.

Research has been supported by Academy of Finland (decision no: 259005 & 264989) and by the strategic funding of University of Eastern Finland.

Alfarra et al. (2012), *Atmos. Chem. Phys.*, 12, 6417-6436.
Saukko E, et *al.* (2012a) *Atmos. Meas. Tech.* 5:259-265
Saukko E, et *al.* (2012b) *Atmos. Chem. Phys.* 12:7517-7529
Virtanen A, et *al.* (2010) *Nature* 467:824-827

Impact of semi-volatiles on hygroscopic growth and CCN activity of secondary organic aerosol

A. Buchholz[1], M. R. Alfarra[1,2], W.T. Hesson[1] and G. McFiggans[1]

[1]Centre for Atmospheric Sciences, The University of Manchester, Manchester, M13 9PL, UK
[2]National Centre for Atmospheric Science (NCAS), The University of Manchester, Manchester, M13 9PL, UK
Keywords: hygroscopic growth, CCN, SOA, semi-volatiles.
Presenting author email: angela.buchholz@manchester.ac.uk

Secondary organic aerosols (SOA) are an important constituent of the global aerosol load. They are formed via gas to particle conversion of low- and semi-volatile oxidation products of volatile organic compounds (VOCs) from both biogenic and anthropogenic sources. In smog chamber studies semi-volatile compounds may play an important role. These compounds could be over-represented at the beginning of experiments because of relatively high precursor concentrations and the limited volume of chambers. As an additional complication, these compounds might leave the particle phase when subjected to higher temperatures e.g. in measurement instruments. In this paper we focus on the influence of semi-volatiles on the microphysical properties (i.e. the hygroscopic growth and cloud condensation nuclei (CCN) activity) of SOA. Knowledge of the microphysical properties is important to understand the impact of atmospheric aerosols on climate.

Experiments were conducted in the Manchester Aerosol Chamber (Alfarra et al., 2012) using biogenic (α-pinene, β-caryophyllene, limonene) and anthropogenic precursor VOCs (1,3,5-trimethylbenzene (TMB), n-heptadecane) both individually and in binary or ternary mixtures. In some experiment ammonium sulphate was used as seed aerosol. In order to produce SOA with a range of different composition and properties the oxidation conditions were varied (namely the NO_x to VOC ratio, the starting O_3 concentration, and the spectrum of the UV lamp). All experiments were conducted at approx. 25°C and under humid conditions (RH ~60%).

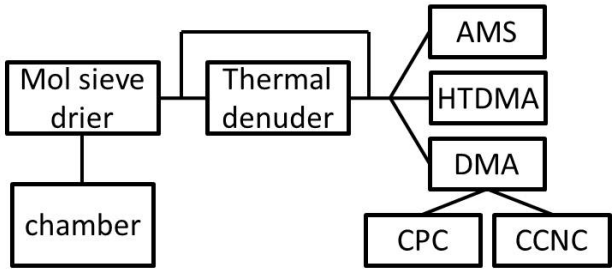

Figure 1. Schematic representation of instrument set up

The aerosol was treated in a thermal denuder (TD) at temperatures between 25 °C (room temperature) and 100 °C to investigate the influence of semi-volatile compounds on the properties of the particles (see Fig. 1). This alternated with sampling directly from the chamber to fully characterise the SOA. The chemical composition was investigated with an Aerodyne Time-of-Flight Aerosol Mass Spectrometer (HR-ToF-AMS). The hygroscopic growth at 90% RH was measured with a hygroscopicity tandem differential mobility analyser (HTDMA). A differential mobility analyser (DMA) was coupled with a CPC to measure the size spectra and with a Droplet Measurement Technology cloud condensation nuclei counter (CCNC).

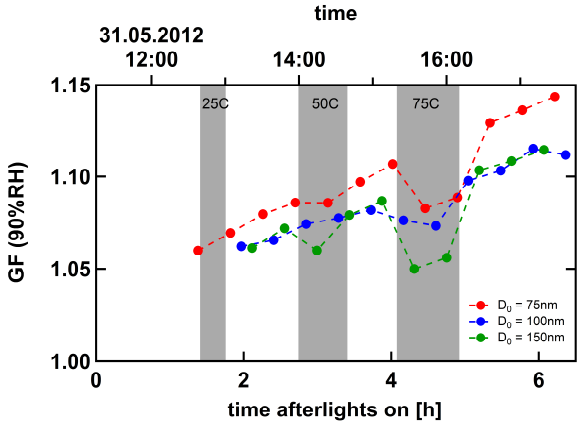

Figure 2. Time series of GF(90%) for an α-pinene experiment.

Figure 2 shows an example for one of the α-pinene experiments. In this case hygroscopic growth was reduced for particles which passed through the TD. A similar effect could be seen for the CCN activity of these particles. We will investigate how the HTDMA and CCNC reconciliation varies with TD temperature and if this can be related to changes in the AMS mass spectra.

This work was supported by the UK Natural Environment Research Council (NERC) through the ACIDPRUF programmes.

Alfarra et al. (2012), *Atmos. Chem. Phys.*, 12, 6417-6436.

Gas and Particle Phase Acids in a Ponderosa Pine Forest

H. Stark[1,2,3], R.L.N. Yatavelli[2,3], S.L. Thompson[2,3], J.R. Kimmel[1,4], B.B. Palm[2,3], D.A. Day[2,3], P. Campuzano-Jost[2,3], M.J. Cubison[4], J.T. Jayne[1], D.R. Worsnop[1,5], J.A. Thornton[6], J.L. Jimenez[2,3]

1. Aerodyne Research Inc., 45 Manning Road, Billerica, MA , USA
2. Cooperative Institute for Research in Environmental Sciences, University of Colorado, Boulder, CO, USA
3. Department of Chemistry and Biochemistry, University of Colorado, Boulder, CO, USA
4. Tofwerk AG, Thun, Switzerland
5. University of Helsinki, Finland
6. Department of Atmospheric Sciences, University of Washington, Seattle, WA, USA

Keywords: Secondary organic aerosol, chemical ionization mass spectrometry, biogenic emissions, data analysis.

Presenting author email: harald.stark@aerodyne.com

We use data from a high-resolution time-of-flight chemical ionization mass spectrometer (HRToF-CIMS, Yatavelli et al 2012) to derive chemical formulas for aerosol particles and gas-phase acids measured continuously for a 10-day period during August 2011 in a Ponderosa Pine forest in South-Western Colorado, USA. This study was part of the "Bio-hydro-atmosphere interactions of Energy, Aerosols, Carbon, H2O, Organics & Nitrogen - Rocky Mountain Biogenic Aerosol Study" (BEACHON-RoMBAS) project focused on the study of secondary organic aerosol (SOA) precursors, and their transformations and impacts in the atmosphere.

The newly developed MOVI technique (Yatavelli *et al*, 2010) was used to simultaneously study gas phase and aerosol particles. The use of acetate as reagent ion (Veres et al, 2008) in combination with the HRToF-CIMS allowed us to selectively and simultaneously measure the entire population of inorganic and organic acids at the same time. Data were acquired at 2Hz, MOVI cycles were repeated every 90 min. Data analysis was performed using the analysis package "Tofware", embedded within the commercial data analysis program "Igor Pro" (Wavemetrics, Inc.).

We will describe the specific methods developed to assign chemical formulas to all ion peaks measured in each mass spectrum, resulting in more than 1800 different unique formulas. The formulas, together with their ion peak areas, were used to perform elemental analysis and derive chemical properties such as elemental ratios (e.g. O:C, H:C, N:C) and average carbon oxidation state (OS_c), both for the bulk composition as well as a function of carbon number.

Figure 1 shows a diagram of approximate oxidation state as a function of carbon number for the aerosol during a 24-hr period of the campaign ("Kroll diagram", Kroll et al, 2011).

These data help to understand the volatile organic compound (VOC) emissions from a Ponderosa Pine forest, their gas-phase chemical transformations as well as the formation of secondary organic aerosol (SOA).

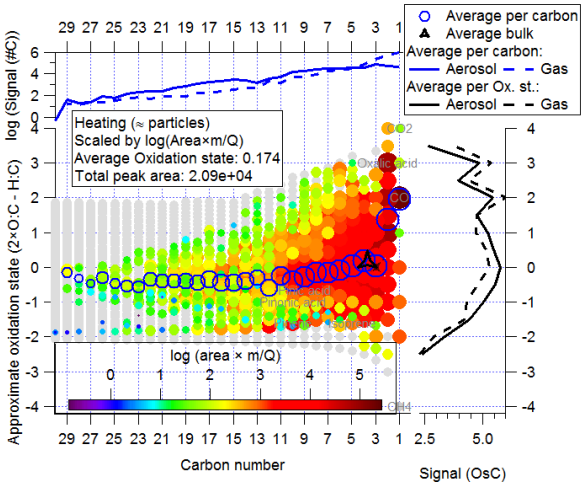

Figure 1: "Kroll diagram" for 24-hour average of "heating" (≈ aerosol) on August 20th, 2011. Colored circles: individual data; blue circles: average data per carbon number, sized by log(ion peak area×m/Q), black triangle: bulk average OS_c, blue line: avg. log(ion peak area×m/Q) vs. carbon number: solid: aerosol, dashed: gas phase, black line: avg. log(ion peak area×m/Q) vs. oxidation state: solid: aerosol, dashed: gas phase; grey circles: expected possible data range

The data show wide ranges of carbon numbers and oxidations states, suggesting a variety of VOC emissions and chemical processing. In general, gas-phase signals show higher signal at lower carbon numbers and higher bulk oxidation states than aerosol signals.

We also compare our results for acids to total organic aerosol mass (OA), measured by the AMS, and find that a significant fraction of OA consists of acids.

Yatavelli, R. L. N. et al. (2012), Aerosol Science and Technology, 2012.

Yatavelli, R. L. N. and J. A. Thornton (2010), Aerosol Science and Technology ***44****(1): 61-74.*

Veres, P., J. M. Roberts, et al. (2008), International Journal of Mass Spectrometry ***274****(1-3): 48-55.*

Kroll, J. H., N. M. Donahue, et al. (2011), Nature Chemistry ***3****(2): 133-139.*

Hygroscopic Properties and Mixing state of Ultrafine Aerosol Particles over two Urban Background Sites

S. Bezantakos[1,2], E. Konstenidou[3], K. Florou[3], A. Bougiatioti[5], K. Eleftheriadis[2], N. Mihalopoulos[4], A. Nenes[5,3], S. Pandis[3,6], G. Biskos[1]

[1]Dept. of Environment, University of the Aegean, Mytilene, 81100, Greece
[2]Inst. of Nuclear Tech. & Rad. Protection, NCSR Demokritos, 15310 Ag. Paraskevi, Attiki, Greece
[3]Institute of Chemical Engineering, ICE-HT, Patras, 26504, Greece
[4]Environmental Chemical Processes Laboratory, Dept. of Chemistry, University of Crete, Heraklion, 71003, Greece
[5]Schools of Earth & Atmospheric Sciences & Chemical & Biomolecular Engineering, GeorgiaTech, Atlanta, GA, USA
[6]Depts. of Chemical Engineering & Engineering & Public Policy, Carnegie Mellon University, Pittsburgh, PA, U.S.A

Keywords: Aerosol Measurement, Particle size, Particle growth, H-TDMA, Mediterranean
Presenting author email: bezantakos@env.aegean.gr

Ultrafine aerosol particles in the atmosphere affect the global climate by absorbing and scattering radiation and by acting as Cloud Condensation Nuclei (CCN). Due to the high variability of their physical and chemical properties, however, quantifying the contribution of airborne particles on climate is a challenging task. Particle properties may change depending on the activity of their sources and the meteorological conditions. In addition their mixing state can vary with time and location. Having information about the variation of the properties and the mixing state is therefore very important for understanding the contribution of atmospheric particles on climate.

In this work we report in situ measurements of the hygroscopicity and the mixing state of the particles observed in the atmosphere over two urban background sites in Greece: one in Patras and one in Athens. Measurements were conducted from 8 to 27 June in Patras and from 4 to 25 July 2012 at the NCSR Demokritos Global Atmosphere Watch (GAW) in Athens using a Hygroscopic Tandem Differential Mobility Analyzer (HTDMA; Rader & McMurry, 1986). In brief, dried aerosol particles having mobility diameter of 40, 60, 80, 100, and 120 nm were selected by the first DMA of the system. The monodisperse particles downstream of DMA-1 were conditioned at a relative humidity (RH) of 87±2% and measured by the second DMA and the CPC. A curve-fitting algorithm was used to fit up to three lognormal distributions depending on the spread of the selected monodisperse size distributions, revealing the aerosol's mixing state.

Figure 1 shows the HTDMA measurements of particles having dry diameter of 120 nm in Patras and in Athens. Particles observed over the Athens GAW station were more hygroscopic and more frequently externally mixed. The measured hygroscopic growth factors ranged from 1.01 to 1.63 with an average value of 1.26 and from 1.01 to 2.0 with an average value of 1.37, over the urban background sites of Patras and Athens respectively.

Table 1 provides a summary of all the HTDMA measurements recorded during the campaign.

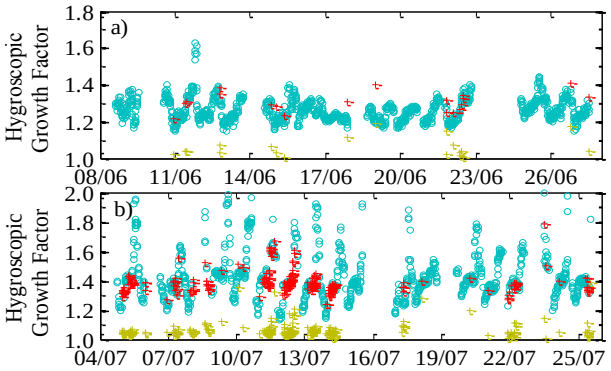

Figure 1. Particle hygroscopic growth factors in (a) Patras and (b) Athens. The growth factors correspond to particles having dry mobility diameter of 120 nm when exposed to 87±2% RH. Circles indicate internally mixed particles and crosses externally mixed particles (bimodal).

Table 1: Summary of the HTDMA measurements. Key: d_{dry} is the mobility diameter selected by DMA-1; P_u and P_b are the relative frequencies of occurrence for unimodal and bimodal distributions, respectively; g_1, g_{21}, and g_{22} are the average growth factors ± one standard deviation for the measurements showing unimodal and two bimodal distributions, respectively.

	D_0	Gf 1	P_u (%)	Gf 21	Gf 22	P_b (%)
Patras Background Urban Station	40	1.21 ±0.07	74.2	1.11 ±0.04	1.34 ±0.06	25.4
	80	1.25 ±0.06	87.3	1.06 ±0.03	1.30 ±0.05	12.7
	120	1.26 ±0.06	96.8	1.06 ±0.05	1.31 ±0.05	3.2
Athens Background Urban Station	40	1.27 ±0.17	42.9	1.08 ±0.05	1.37 ±0.10	54.8
	80	1.41 ±0.17	65.1	1.06 ±0.03	1.37 ±0.08	34.6
	120	1.43 ±0.17	72.4	1.06 ±0.05	1.39 ±0.09	27.6

Acknowledgement:
This research has been co-financed by the European Union (European Social Fund – ESF) and Greek national funds through the Operational Program "Education and Lifelong Learning" of the National Strategic Reference Framework (NSRF) - Research Funding Program: **THALES**. Investing in knowledge society through the European Social Fund.

References

Rader, D. and McMurry,P. (1986), *Journal of Aerosol Science*, 17,771-787.

Profiling of hygroscopic properties during the Po-Valley PEGASOS campaign 2012

B. Rosati[1], E. Weingartner[1] , P. Zieger[1], M. Gysel[1], G. Wehrle[1], U. Baltensperger[1] and the PEGASOS collaboration

[1]Laboratory of Atmospheric Chemistry, Paul Scherrer Institute, CH-5232 Villigen PSI, Switzerland
Keywords: hygroscopicity, growth factor, OPS, refractive index, mixing state.
Presenting author email: bernadette.rosati@psi.ch

Aerosol particles influence the Earth's radiation budget by interacting with the incident sunlight. If they directly scatter or absorb the incoming solar radiation it is referred to as *aerosol direct effect*. The magnitude of this effect depends on several factors, including the chemical composition and size of the particles as well as their ability to take up water. If the particles are hygroscopic, this will itself lead to an increased size and change in index of refraction which will significantly vary their optical properties (Zieger et al., 2011). In addition, aerosols can exist in different mixing states that are usually described as internal and external mixtures. While an internal mixture implies that all particles of the same size have an identical chemical composition, an external mixture is composed by different substances that are chemically and physically independent. By analyzing the water uptake, the mixing state can be inferred. An internally mixed aerosol will grow uniformly with increasing relative humidity (RH), whereas the different species present in the external mixture will lead to a polymodal or broad size distribution. Since the chemical composition and ambient RH are known to change with altitude (Morgan et al., 2010), vertical profiles are important to quantify the actual optical properties and mixing states which particles have at different heights. This information is finally needed to e.g. determine the direct aerosol radiative forcing or to validate remote sensing with in-situ data.

Within the **P**an-**E**uropean **G**as-**A**ero**so**ls-climate interaction **S**tudy (PEGASOS) a Zeppelin is used to explore the planetary boundary layer. Two main measurement campaigns took place in the Netherlands and in the Po-Valley in Italy in 2012. As a new way to explore hygroscopic and optical properties on the platform, the white-light humidified optical particle spectrometer (WHOPS) was developed. Due to its ability to record data each second, it is highly suited for airborne measurements. The working principle can be explained as follows: First, the particles are dried and led through a differential mobility analyzer to select particles with a specific mobility diameter (d_{mob}). This monodisperse aerosol is then exposed to a defined high RH (typically 94%) and the new size is detected with a white-light optical particle spectrometer (WELAS). In this way, the hygroscopic growth factor can be determined. In addition, the humidification system is periodically bypassed. This allows retrieving information on the particle's effective refractive index by comparing the particle's dry mobility diameter with the optical response from the WELAS.

In this work we will present the hygroscopic growth and mixing state of aerosols, measured during the PEGASOS campaign in the Po-Valley in Italy in June 2012. Figure 1 shows an example for such a profile flown above San Pietro Capofiume (SPC), where the response of the WHOPS to dry, monodisperse particles (d_{mob}= 300 nm) is shown. The lower graph depicts the size distribution of the humidified particles and clearly shows a bimodal distribution with a more and a less hygroscopic mode. This is a clear indication of an externally mixed aerosol. Comparing the results for the two selected heights (i.e. 100 m and 700 m above ground), a similar behavior can be seen. Different results (i.e. non hygroscopic particles) were found for the larger sizes (d_{mob}= 500 nm) on days with Saharan dust intrusions.

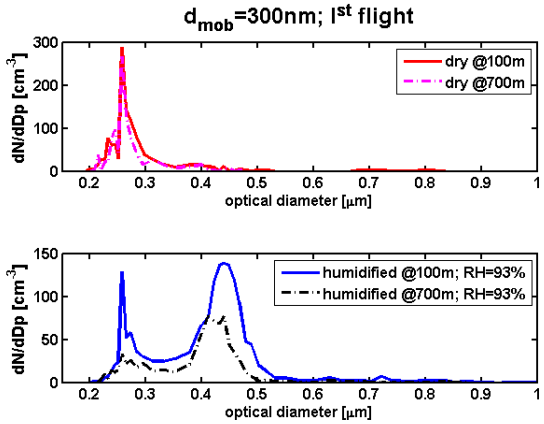

Figure 1: Data from a flight at SPC on the 20th of June 2012; for both plots a dry d_{mob} of 300 nm was selected; solid and dashed lines: flights at 100m and 700m above ground, respectively; the upper and lower graph show the dry and wet size distributions, respectively.

This work is supported by the EU-funded project PEGASOS.

W.T. Morgan *et al.*, Enhancement of the aerosol direct radiative effect by semi-volatile aerosol components: Airborne measurements in North-Western Europe, *Atmospheric Chemistry and Physics* **10**(2010), pp. 8151-8171.

P. Zieger *et al.*, Comparison of ambient aerosol extinction coefficients obtained from in-situ, MAX-DOAS and LIDAR measurements at Cabauw, *Atmospheric Chemistry and Physics* **11**(2011), pp. 2603-2624.

Observations on atmospheric electricity and aerosol-cloud interactions

Hanna E. Manninen[1,2], Hannes Tammet[1], Antti Mäkelä[3], Jussi Haapalainen[3], Sander Mirme[1], Tuomo Nieminen[2,4], Alessandro Franchin[2], Tuukka Petäjä[2], Markku Kulmala[2], and Urmas Hõrrak[1]

[1]Institute of Physics, University of Tartu, Ülikooli 18, 50090 Tartu, Estonia
[2]Department of Physics, P.O. Box 64, 00014 University of Helsinki, Finland
[3]Finnish Meteorological Institute, P.O. Box 503, 00101 Helsinki, Finland
[4]Helsinki Institute of Physics, P.O. Box 64, 00014 University of Helsinki, Finland
Keywords: atmospheric electricity, small ions, earth's electric field, lightning, aerosol-cloud interactions.
Presenting author email: hanna.manninen@helsinki.fi

Atmospheric ions play an important role in the fair weather electricity. Atmosphere's fair weather condition concerns the electric field and the electric current in the air as well as the air conductivity. On the other hand, atmospheric ions are important for Earth's climate, due to their potential role in secondary aerosol formation. This can lead to increased number of cloud condensation nuclei (CCN), which in turn can change the cloud properties. Our aim is to quantify the connections between these two important roles of air ions based on field observations and existing data archives.

When studying atmospheric electricity, the air ions are essential. Small ions, or charged molecular clusters, carry electric currents in the atmosphere. These small ions are continuously present, and their lifetime in lower atmosphere is about one minute. It's essential to find out a connection between the production rate of cluster ions, ion-ion recombination, and ion-aerosol attachment, and their ambient concentrations, in order to understand electrical properties of air istelf.

Currently, there's an intensive discussion about the connection between the atmospheric electricity and climate change. Recently, changes in atmosphere's electric properties caught new interest, as a possible connection between ionizing galactic cosmic rays, cloud cover and climatic effects was suggested (Carslaw, Harrison and Kirkby, 2002; Kirkby et al. 2011). The most significant factor of uncertainty in climate research is caused by atmospheric aerosols, especially due to small particle effects. Secondary formation of new particles through a process of gas-to-particle conversion, beginning with a few gas molecules colliding to form a cluster of 1-2 nm in diameter, is believed to be the dominant source of aerosol particles in the atmosphere. Some studies suggest that the contribution of air ions is important or even dominant to secondary aerosol formation, whereas other studies show that their role is negligible.

We studied the interactions between atmospheric electricity (air conductivity, electric field, and ambient concentartion of small ions), aerosol particles, and cloud properties. In other words, the correlations and trends in atmospheric ionization, electricity, aerosols, and CCN properties were studied. Most of the work here is based on analysis of already existing data archives, and some new measurements are established as a part of already existing measurement networks. The electrical properties of the atmosphere have been measured over a century now, whereas the longest continuous time series of aerosol particle data available is little over decade old. Tammet (2009) has collected a dataset, which comprises the measurements of atmospheric electric field, positive and negative conductivities, air ion concentrations, and accompanying meteorological measurements at 13 stations, including 7 stations of the former World Data Centre network on Atmospheric Electricity at the Main Geophysical Observatory, St. Petersburg, Russia.

The ongoing field observations of atmospheric aerosols are mainly performed at Hyytiälä SMEAR site, Southern Finland (Station for Measuring Ecosystem-Atmosphere Relations). Hyytiälä provides extensive dataset of measured aerosol particle (physical, chemical, and optical) properties, external and radon radiation, CCN properties, trace gases, meteorological parameters, different flux measurements (micrometeorology), and forest ecology observations. The atmosphere's electricity is measured with the air ion spectrometers (Manninen et al. 2010) to determine air conductivity and with the electric field mills, which measures the strength of atmospheric electric field. The plan is to extend the measurements of atmospheric electricity to the Finnish Meteorological Institute (FMI) site at Pallas, Northern Finland, and to SMEAR site at Järvselja, Estonia. Hyytiälä and Pallas stations are part of ACTRIS (Aerosols, Clouds, and Trace gases Research InfraStructure Network) and GAW (Global Atmosphere Watch) networks.

The lightning activity and ion concentration was also investigated. The lightning flash counter data for Hyytiälä, Pallas, and Järvseljä is collected by FMI. The systematic ground lightning observations are performed with eight ground-based sensors in Finland. The Norwegian, Swedish, and Estonian sensors have been integrated, completing the coverage up to the whole Nordic countries.

The support by the Finnish Cultural Foundation and the Academy of Finland Centre of Excellence program (project no. 1118615) are gratefully acknowledged.

Carslaw K. S., Harrison R. G., and Kirkby J. (2002) *Science* **298**, 1732-1736.
Kirkby J. et al. (2011) *Nature* **476**, 429-433.
Manninen et al. (2010) *Atmos. Chem. and Phys.* **10**, 7907-7927.
Tammet H. (2009) *Atmospheric Research* **91**, 194-200.

Monday, September 1, 2013

Session: Aerosol Chemistry,
Chemistry of organic aerosols 1

Revisiting the formation of secondary organic aerosol from the photooxidation of anthropogenic precursors

M.R Alfarra[1,2], A. Buchholz[2], W.T. Hesson[2], R. Lidster[3], I. White[4] , A. Pajunoja[5], J.F. Hamilton[3], P. Monks[4], A. Virtanen[5] and G.B. McFiggans[2]

[1]National Centre for Atmospheric Science (NCAS), The University of Manchester, Manchester, M13 9PL, UK
[2]Centre for Atmospheric Sciences, The University of Manchester, Manchester, M13 9PL, UK
[3]Deparment of Chemistry, University of York, Heslington, York, YO10 5DD, UK
[4]Department of Chemistry, University of Leicester, Leicester, LE1 7RH, UK
[5]Department of Applied Physics, University of Eastern Finland, Kuopio, FI-70210, Finland

Keywords: SOA, Smog Chamber, anthropogenic VOCs, Aerosol mass spectrometry
Presenting author email: rami.alfarra@manchester.ac.uk

Atmospheric aerosols are known to affect climate and human health. The organic component of aerosol particles comprises about one half of the fine-particle mass on average. Recent work has shown that most of the organic-aerosol mass is oxygenated organic aerosol (OOA) (Zhang et al., 2007), which is expected to be formed mostly as secondary organic aerosol (SOA) from the oxidation of biogenic and anthropogenic volatile and semi-volatile organic compounds (VOCs and SVOCs). Air-quality models currently under-predict the concentrations of organic aerosol in the atmosphere, especially in the summer and in urban areas (Volkamer et al., 2006), suggesting that anthropogenic SOA formation is still not well understood.

A wide range of SOA mass yield values have been reported in the literature for a number of the most commonly studied anthropogenic VOCs (e.g. toluene and 1,3,5-trimethylbenzene). In this paper, we present results suggesting that the ability of key anthropogenic precursors to form SOA may have been over-estimated in the literature. The paper will discuss a series of smog chamber experiments conducted using single anthropogenic and biogenic precursors, as well as mixtures of anthropogenic and biogenic VOCs at different experimental conditions. Investigated compounds included touluene, 1,3,5-trimethylbenzene (TMB), n-heptadecane, α-pinene, β-caryophyllene and limonene. Among the studied parameters, the influence of different characteristics of chamber light spectrum on SOA formation will be discussed and related to previous anthropogenic SOA studies.

The experiments reported in this paper were conducted at the Manchester aerosol chamber (Alfarra et al., 2012), which is an 18 m^3 photochemical batch reactor designed to study atmospheric processes of multicomponent aerosols under controlled and realistic conditions. An array of state-of-the-art instruments measuring aerosol composition and properties as well as VOC precursors and their oxidation products were employed. The chemical composition of the formed SOA was measured on-line using an Aerodyne Time-of-Flight Aerosol Mass Spectrometer (HR-ToF-AMS). A hygroscopicity tandem differential mobility analyser (HTDMA) and a cloud condensation nuclei (CCN) counter were used to probe the hygroscopic properties and CCN activity of the aerosols in the sub- and super-saturated regimes, respectively. A proton transfer reaction mass spectrometer was used to study the evolution of the gas-phase oxidation products. The phase-state of the formed particles was inferred using a particle bounce method (Virtanen et *al.* (2010), Saukko et *al.* (2012)). A thermodenuder was used to study the volatility of secondary organic aerosol at 50 and 75 ^oC.

Particles from a range of experiments were collected on filters for off-line chemical speciation by liquid-chromatography coupled to mass spectrometry (LC/MS-MS). Results from this detailed analysis will be used to investigate the contribution of specific precursors to the formed SOA, and will also be linked to the particle phase state and precursor type.

This work was supported by the UK Natural Environment Research Council (NERC) through the ACIDPRUF programmes. The particle phase-state studies were performed as part of a EUROCHAMP-2 transnational activity.

Alfarra et al. (2012), *Atmos. Chem. Phys.* 12, 6417-6436
Saukko et al. (2012) *Atmos. Chem. Phys.* 12:7517-7529
Virtanen et al. (2010) *Nature* 467:824-827
Volkamer et al. (2006) *Geoph. Res. Lett.*, 33, 2006.
Zhang et al. (2007) *Geoph. Res. Lett.*, 34, L13801

Gas-Phase Measurements of Oxidized Organic Compounds Generated by a Potential Aerosol Mass (PAM) Reactor using Acetate Chemical Ionization High-Resolution Time-of-Flight Mass Spectrometry

P. Chhabra[1], A. Lambe[1,2], M. Canagaratna[1], H. Stark[1,3], P. Massoli[1], J. Kimmel[1,4], J. Jayne[1], and D. Worsnop[1]

[1]Aerodyne Research Inc., 45 Manning Road, Billerica, MA 01821, USA
[2]Department of Chemistry, Boston College, Chestnut Hill, MA 02467, USA
[3]Cooperative Institute for Research in Environmental Sciences, University of Colorado, Boulder, CO 80303, USA
[4]Tofwerk, AG, Uttigenstrasse 22 CH-3600 Thun, Switzerland

Keywords: organic molecules, mass spectrometry, secondary organic aerosol, CIMS
Presenting author email: puneet@aerodyne.com

We present gas-phase measurements of laboratory generated oxidized organic compounds using acetate chemical ionization mass spectrometry (Acetate-CIMS). This relatively new detection scheme uses acetate ions ($CH_3C(O)O^-$) to initiate proton transfer reactions with trace organic and inorganic acids with gas-phase acidities higher than that of acetic acid (Veres *et al*, 2008; Bertram *et al*, 2011). This technique has been used in conjunction with recently developed aerosol inlets to study secondary organic aerosol in both the field and laboratory (Yatavelli *et al*, 2009, 2012).

Here, we present acetate-CIMS spectra of oxidized organic vapors generated from the ozonolysis of α-pinene and photooxidation of α-pinene, isoprene, and naphthalene in a Potential Aerosol Mass (PAM) flow reactor over multiple days of equivalent atmospheric OH oxidation (Lambe *et al*, 2011). By taking advantage of the high-resolution capabilities of the Tofwerk HToF on the CIMS, we are able to explore the elemental composition of the oxidized organic vapors as a function of OH exposure and precursor. Such vapors are of interest because low volatility organics have been implicated in aerosol nucleation processes (Riipinen *et al*, 2012).

Within the range of our measurements, we investigate commonly used metrics for oxidation level such as the average oxygen to carbon (O/C) ratio, carbon oxidation state (OS_c), and carbon number (C_n) of the oxidized vapors relative to C_n of the precursor. Figure 1 shows O_{sc} as a function of C_n of oxidized vapors produced from the ozonolysis of α-pinene, referred to here as a Kroll diagram (Kroll *et al*, 2011). Average O/C ratios and OS_c values typically range from 0.7 to 1.1 and -0.1 to 0.9, respectively, across the entire simulated OH exposure.

To gain insight into the relative acidity of these oxidized organic vapors, we compare acetate-CIMS spectra with NO_3-CIMS spectra obtained for the same systems in the laboratory and for ambient measurements obtained during the Southern Oxidant and Aerosol Study (SOAS) at the forest supersite in Centreville, AL. The NO_3-CIMS method is specific to species with gas-phase acidities higher than that of nitric acid, thus producing spectra that represent a subset of the acetate-CIMS spectra.

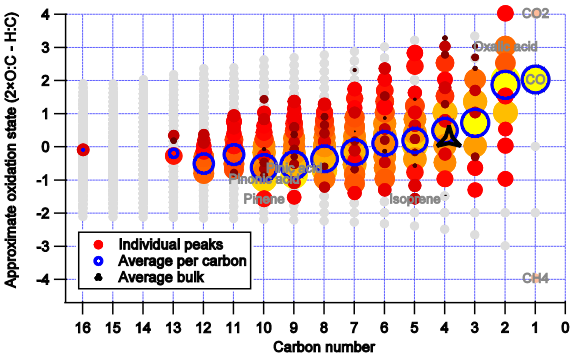

Figure 1: Kroll diagram of oxidized organic vapors produced from the ozonolysis of α-pinene.

Bertram, T. H. *et al*, (2011), *Atmos. Meas. Tech.* 4, 1471-1479.

Kroll, J. H. *et al*, (2011), *Nature Chem.*, 3, 133-139.

Lambe, A. T. *et al* (2011), *Atmos. Meas. Tech.*, 4, 445-461.

Riipinen, I. *et al* (2012), *Nature Geosci.*, 5, 453-458.

Veres, P. *et al* (2008), *Int J Mass Spectrom*, 274, 48-55.

Yatavelli, R. L. N., and Thornton, J. A. (2009), *Aerosol Sci Tech*, 44, 61-74.

Yatavelli, R. L. N. *et al* (2012), *Aerosol Sci Tech*, 46, 1313-1327.

Time-resolved chemical composition of chamber generated SOA originated from monoterpene oxidation

A. Mutzel[1], O. Böge[1], A. Kahnt[2], Y. Iinuma[1] and H. Herrmann[1]

[1]Leibniz-Institut for Tropospheric Research, Permoserstr. 15, Leipzig 04318, Germany
[2] University of Antwerp, Universiteitsplein 1, 2610 Wilrijk, Belgium
Keywords: VOCs, SOA, Aerosol characterization
Presenting author email: mutzel@tropos.de

The oxidation of biogenic volatile organic compounds (BVOCs) yields a wide range of oxidation products with multifold functional groups. Depending on the chemical and physical properties of the formed products they are able to undergo gas to particle conversion contributing significantly to the formation of secondary organic aerosol (SOA). Although several studies exist about the formation of SOA originating from the monoterpene oxidation (see review by Hallquist *et al.*, 2009) there is a gap in the knowledge about the involved species. To overcome this issue, the condensation growth and impacting system (C-GIS, Sierau *et al.*, 2003) was connected to the aerosol chamber LEAK (Leipziger Aerosol Kammer) that enables a time-resolved sampling and analysis of chamber generated SOA.

Several experiments were conducted examining the oxidation of monoterpenes (α- and β-pinene) and their first generation oxidation products (pinonaldehyde and nopinone). The oxidation was carried out using OH radicals originated from the photolysis of hydrogenperoxide (H_2O_2) as well as from the ozonolysis of tetramethylethylene (TME). All experiments were conducted in the presence of acidic seed particles (78 mM NH_4HSO_4). The generated SOA was sampled during the course of the experiment for 10 minutes using C-GIS. The suitability of C-GIS was evaluated conducting a comparison between filter measurements and C-GIS using three SOA compounds (Table 1) terpenylic acid, pinic acid, and 3-methyl-1,2,3-tricarboxylic acid (MBTCA).

Table 1. Mean value of the deviation between filter and C-GIS measurements

Compound	Deviation [%] (n=3)
Terpenylic acid	39 ± 2
Pinic acid	21 ± 4
MBTCA	48 ± 3

Despite the underestimation the data obtained by C-GIS show only small deviations from the mean value (below 5%) indicating the suitability of C-GIS for the time-resolved SOA analysis.

From the analysis of the C-GIS samples a time profile of the three SOA compounds can be obtained. It was found that terpenylic acid and pinic acid are early generation oxidation products whereas MBTCA is formed secondary.

These observations are in consistence to the literature (Claeys *et al.*, 2009, Christoffersen *et al.*, 1998). In addition, a correlation was found between the time-profile of the terpenylic acid concentration and the particle growth ΔM (Figure 1) indicating a central role of terpenylic acid for the SOA formation (Claeys *et al.*, 2009). Nevertheless, such a correlation was not found for all of the conducted experiments. Those missing correlations might be explained by additional compounds causing particle growth which are not indentified and quantified jet.

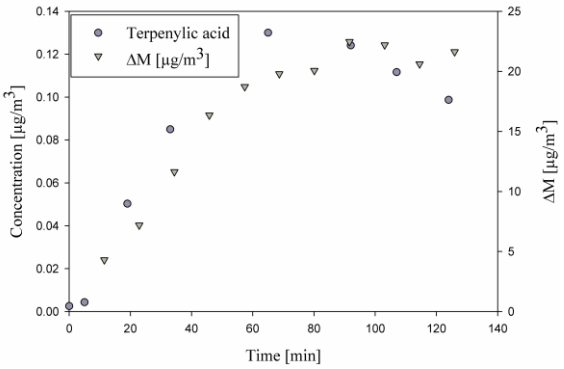

Figure 1: Relationship between the concentration profile of terpenylic acid and the particle growth during the oxidation of nopinone with OH radicals.

The decay of terpenylic acid concentration after 90 minutes of the experiments might be a result of the formation of higher molecular weight compounds (HMWCs). From the analysis it was found that a compound with *m/z* 357 is also formed which corresponds to $C_{17}H_{25}O_8$. Therefore it can be assumed that besides the central role of terpenylic acid for the particle growth it might be also an important precursor compound for the formation of HMWCs.

Christoffersen, T.S. *et al*., (1998), Atmos. Environ. 32, 1657-1661.
Claeys, M. *et al*., (2009), Environ. Sci. Technol. 43, 6976-6982.
Hallquist, M. *et al*., (2009). Atmos. Chem. Phys. 9, 5155-5236.
Sierau, B. *et al*., (2003) J. Aerosol. Sci. 34, 225-242.

Dependence of α-pinene secondary organic aerosol formation on relative humidity and aerosol surface distribution

L. Pfaffenberger, P. Barmet, R. Wolf, S. M. Platt, I. El-Haddad, J. G. Slowik, J. Dommen, A. S. H. Prévôt and U. Baltensperger

Laboratory of Atmospheric Chemistry, Paul Scherrer Institute PSI, Villigen, 5232, Switzerland

Keywords: AMS, Photochemical processes, SOA (Secondary Organic Aerosols), Water soluble organic compounds

Organic aerosol (OA) represents a major fraction (20-90%) of the submicron aerosol (Jimenez et al., 2009). Potential sources and processes leading to the formation of secondary organic aerosol (SOA) are still rather poorly understood, although SOA contributes significantly to the global OA burden. To determine parameters relevant to SOA yields, in particular volatility and degree of oxygenation, the formation and aging of particles has to be investigated more thoroughly.

Several laboratory studies suggest that aqueous phase SOA formation can be almost as important as gas phase oxidation of volatile organic compounds and their subsequent partitioning to the aerosol phase (Ervens et al., 2011).

In this study, the aerosol chemical composition as a function of the vacuum aerodynamic diameter (d_{va}) was investigated using an Aerodyne aerosol mass spectrometer (AMS) equipped with a $PM_{2.5}$ lens. In the PSI smog chamber, the aerosol precursor α-pinene was irradiated in the presence of low (~30%) or high (~80%) relative humidities (RH) and various NO_x concentrations. NH_4HSO_4 was used as a hygroscopic seed, providing a large water volume at high humidity. A wide diameter range, ~50 to 2500 nm, was covered by the particle phase instruments. The aging time in the chamber was related to the atmospheric oxidation time using OH exposures derived from the decay of an OH tracer injected into the chamber (Barmet et al., 2012).

For a similar NO_X concentration, higher SOA yields were observed at higher RH compared to lower RH. Fig. 1 shows mass distributions of organics, sulfate, ammonium, and nitrate, as well as organic mass fractions f_{44} (m/z 44 / total organics, a surrogate for the degree of oxygenation) and f_{43} (m/z 43 / total organics, a surrogate for less oxygenated compounds like aldehydes, ketones and alcohols) as a function of particle diameter. The data is averaged over the experiment period when aerosol aging dominates. The wet aerosol surface distribution shown in Fig. 1 was calculated using a volume-mixed growth factor and the measured RH (72 ± 1 %). This particular experiment was conducted with 16 ppb α-pinene and 20 ppb NO_x.

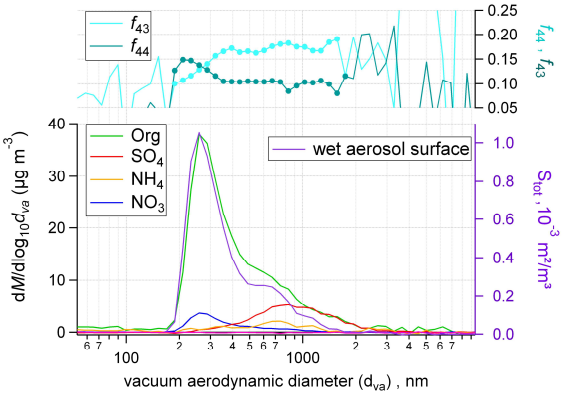

Figure 1. Averaged mass distribution of chemical species, calculated wet surface distribution and organic mass fractions f_{44} and f_{43} as a function of particle diameter. Dots (f_{44}, f_{43}) represent data when $d(org)/dlog_{10}d_{va}$ is above a threshold of $2 \mu g \cdot m^{-3}$.

The organic mass distribution follows the wet surface distribution of the aerosol, suggesting a fast, surface dependent, SOA formation process. Secondly, the chemical composition is dependent on particle size, indicated by the increase of f_{44} with diameter. This could be due to the larger available water volume, favouring aqueous phase processes that lead to more highly oxygenated products like acids.

The effect of particle size will also be assessed by analysis of single particle mass spectra acquired using a light scattering module integrated with the AMS. The combined effects of varied relative humidity and NO_x concentration on SOA yields and composition will be investigated and discussed in this study.

This work was supported by EUROCHAMP-2, a project within the EC 7th Framework Programme, as well as the Swiss National Science Foundation.

Jimenez, J. L. et al. (2009) *Science*, **326**(5959), 1525-1529.

Ervens, B. et al. (2011) *Atmos. Chem. Phys.*, **11**, 11069–11102.

Barmet, P. et al. (2012) *Atmos. Meas. Tech.*, **5**, 647–656.

Characterization of secondary organic aerosol from ozonolysis of β-pinene

Ågot K. Watne, Eva U. Emanuelsson, Anna Lutz, Evert Ljungström and Mattias Hallquist

Department of Chemistry and Molecular Biology, University of Gothenburg, Gothenburg, Sweden
Keywords: Aerosol Chemistry, Flow Reactor, Volatility, Terpenes
Presenting author email: agot.watne@chem.gu.se

A large fraction of the atmospheric aerosol contains organics. Particulate organics can be formed in the atmosphere through oxidation of gaseous precursors to secondary organic aerosol (SOA). The processes of formation of SOA are currently not well understood. In order to predict and represent SOA influence on for instance cloud formation and climate, an accurate description of formation and properties of SOA is needed (Hallquist *et al*., 2009).

The effects of humidity, temperature and radical chemistry on the SOA formed from the ozonolysis of β-pinene were studied in Gothenburg Flow Reactor for Oxidation Studies at low Temperatures (G-FROST). G-FROST is a laminar flow reactor where SOA can be formed under well-controlled conditions (Figure 1). Through the flow reactor there is a continuous laminar flow. This creates a stable aerosol output and imposed changes to the chemistry can be monitored and analyzed.

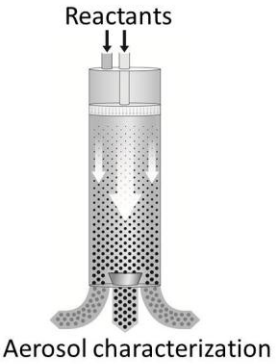

Figure 1: Schematic of G-FROST.

The relative humidity (RH) was varied in experiments conducted at 288 K and at 298 K for three different β-pinene concentrations: low, intermediate and high. In addition, the effect of using 2-butanol or cyclohexane as OH-scavenger was studied. In all experiments, the RH was changed in four steps aiming at 12, 15, 30 and 50 %. Figure 2 shows an example of an experiment.

In addition to the number and mass of SOA produced, thermal properties of the aerosol were characterized using a Volatility Tandem Differential Mobility Analyser (VTDMA). The VTDMA provides several aspects of thermal properties. An example is volume fraction remaining at 383K, VFR(383K), which is a general measure of volatility.

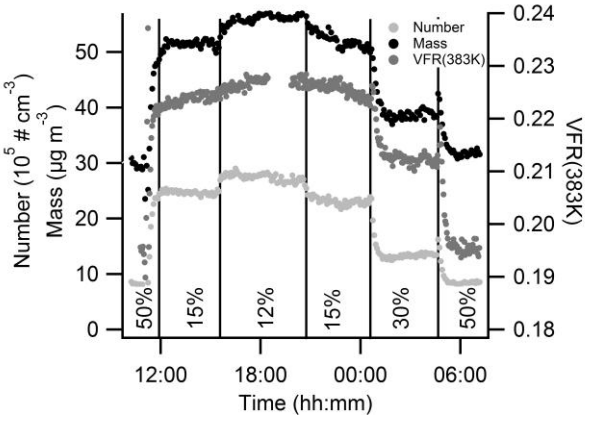

Figure 2: Change in particle number, mass concentration and VFR(383K) in with stepwise change in RH.

As can be seen in Figure 2, the SOA formed from ozonolysis of β-pinene shows a negative RH dependence. This was valid for all experiments and is the opposite RH dependence of what has been observed from the ozonolysis of α-pinene (e.g. Jonsson *et al*, 2008).

Regarding the thermal properties, several aspects were revealed. It was demonstrated that thermal properties of the SOA did change for the different conditions (e.g. temperature, RH and use of scavenger). For instance, as shown in Figure 2, the SOA got more volatile with increasing RH. This was observed as an decrease in VFR(383K) at higher RH and was valid in all experiments. These features can be linked to the changes in chemical mechanism affecting SOA number and mass (Emanuelsson *et al*,. 2013).

The results from this study suggest inclusion of new chemistry in atmospheric chemical models in order to cover relevant atmospheric changes in humidity, temperature and oxidant levels that affect SOA formation and properties.

The research presented is a contribution to the Swedish strategic research area ModElling the Regional and Global Earth system, MERGE. This work was supported by Formas (214-2010-1756) and the Swedish Research Council (80475101).

Emanuelsson et al, (2013), *manuscript submitted to Journal of Physical Chemistry*
Hallquist et al, (2009) *Atmospheric Chemistry and Physics*, 9, 5155-523
Jonsson et al, (2008) *Environmental Science and Technology*, 42, 5938-5944

Formation of anthropogenic secondary organic aerosol (SOA) and its influence on biogenic SOA properties

E. U. Emanuelsson[1], M. Hallquist[1], D.-F. Zhao[2], B. Bohn[2], H. Fuchs[2], B. Kammer[2], A. Kiendler-Scharr[2], S. Nehr[2], F. Rubach[2], R. Tillmann[2], A. Wahner[2], H.-C. Wu[2], K. Kristensen[3], M. Glasius[3], Y. Rudich[4], Th. F. Mentel[2]
[1]Department of Chemistry and Molecular Biology, University of Gothenburg, Göteborg, SE-41296, Sweden
[2]Institut für Energie und Klimaforschung: Troposphäre (IEK-8), Forschungszentrum Jülich, Jülich, D-52428, Germany
[3]Department of Chemistry, Aarhus University, Aarhus, DK-8000, Denmark
[4]Department of Environmental Sciences and Energy Research,Weizmann Institute of Science, Rehovot, 76100, Israel
Keywords: secondary organic aerosol, anthropogenic enhancement, volatility, OH dose
Presenting author email: d.zhao@fz-juelich.de

Recent field data and model analysis show that SOA is enhanced under anthropogenic influences although the SOA material itself is mainly biogenic (de Gouw et al. 2005; Spracklen et al. 2011). Such anthropogenic enhancement may affect the global SOA loading significantly. However, its mechanism is still not clear. Direct chemical interaction of BSOA and ASOA components may contribute to anthropogenic enhancement.

In order to investigate the interaction of anthropogenic SOA(ASOA) with biogenic SOA(BSOA) we studied mixtures aromatics and monoterpenes as representatives of anthropogenic VOC and biogenic VOC in the large chamber SAPHIR in Juelich, Germany (Emanuelsson et al. 2012). SAPHIR chamber allows for studies under natural OH concentrations. Particle chemistry and properties including volatility were characterized by a High resolution Time-of-Flight aerosol mass spectrometer (TAMS), off-line filter analysis by HPLC-ESI-qTOF-MS(Kristensen and Glasius 2011), and Volatile Tandem Differential Mobility Analyzer (VTDMA, (Jonsson et al. 2007)). Gas phase OH concentration was measured by a Laser Induced Fluorescence (LIF) to quantify the OH dose to which the reaction mixtures were exposed.

We found two major drivers for the time evolution of SOA volatility: OH dose and ASOA fraction. Volatility decreases with OH dose for both BSOA and ASOA (Figure 1). ASOA has lower volatility and higher O/C since its precursor needs higher OH dose before it generate significant amount of materials to condense on the particle due to their low reactivity.
Generally, volatility of particle also decreases as ASOA fraction increase (Figure 1). However, ASOA components decrease the volatility of mixed ABSOA more efficient than expected by a simple linear combination of properties of pure ASOA and BSOA systems. Already a very small fraction of ASOA can decrease the volatility of ABSOA significantly likely initiating oligomerization(Kalberer et al. 2004), as shown in Figure 1 for case 10/6.

In contrast, mass yield, f44, O/C can be described by the linear combination of the corresponding properties of pure ABSOA and BSOA systems (Emanuelsson et al. 2012). Decreased volatility increases thermal persistence, suppresses one loss channel, evaporation by heating and dilution and therefore increases the lifetime of ABSOA compared to BSOA under same conditions. Since aromatic VOCs are mainly anthropogenic (and correlate with CO), this phenomenon may contribute to the anthropogenic enhancement. This phenomenon was further investigated in a second study in order to detect oligomerization and relate it to change of optical properties.

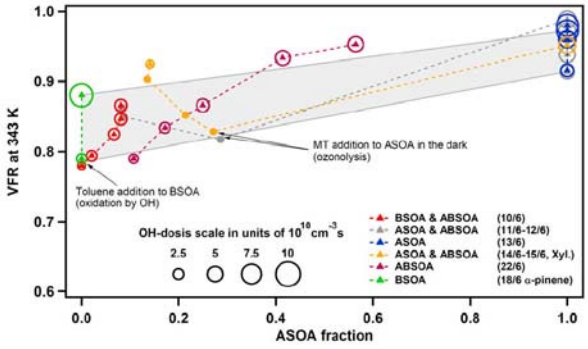

Figure 1 VFR (343K) for ABSOA experiments and BSOA experiment (18/6) as a function of the model derived ASOA fraction (triangles) with OH dose indicate by the size of the circles. The lower boundary of the shaded area is given by VFR (343K) for freshly formed aerosol at OH doses of ≈ 1-2x10^{10} cm^{-3} s for pure BSOA and of 3.6x10^{10} cm^{-3} s for pure ASOA. The upper boundary line connects pure BSOA (18/6) and pure ASOA (13/6) at about the same OH dose ≈ 9x10^{10} cm^{-3} s.

This study was supported by EUROCHAMP-2 (Integration of European Simulation Chambers for Investigating Atmospheric Processes)-EC 7th framework, Swedish Formas (214-2010-1756), the Swedish Research Council (80475101) and the Tellus research platform at University of Gothenburg.

de Gouw, J. A., Middlebrook, A. M., et al. (2005). *J. Geophys. Res.-Atmos.* **110**(D16).
Emanuelsson, E. U., Hallquist, M., et al. (2012). *Atmos. Chem. Phys. Discuss.* **12**(8): 20311-20350.
Jonsson, A. M., Hallquist, M., et al. (2007). *J. Aerosol Science* **38**(8): 843-852.
Kalberer, M., Paulsen, D., et al. (2004). *Science* **303**(5664): 1659-1662.
Kristensen, K. and Glasius, M. (2011). *Atmos. Environ.* **45**(27): 4546-4556.
Spracklen, D. V., Jimenez, J. L., et al. (2011). *Atmos. Chem. Phys.* **11**(23): 12109-12136.

Effect of Nucleation Precursors on the Atmospheric Oxidation of Organic Compounds

J. Elm[1], M. Bilde[2], K. V. Mikkelsen[1]

[1]Department of Chemistry, University of Copenhagen, Copenhagen, Universitetsparken 5, 2100, Denmark
[2]Department of Chemistry, Aarhus University, Aarhus, Langelandsgade 140, 8000, Denmark
Keywords: Nucleation, QM, Kinetics, SOA.
Presenting author email: elm@chem.ku.dk

The goal of this work is to determine the effect of common aerosol precursors H_2O, NH_3 and H_2SO_4 on the OH initiated oxidation mechanism of volatile organic molecules in the atmosphere. We use methanol as a model compound due to its relatively high atmospheric abundance and long residence time. We have investigated the interaction between methanol and each of the molecules H_2O, NH_3 and H_2SO_4 to assess cluster stabilities. This has been done by calculating statistical Gibb's free energies of formation. Subsequently the effect of the aerosol precursors on the reaction rate and mechanism of hydrogen abstraction reactions by the OH radical have been calculated.

Theory

To evaluate the rate constant of the i'th hydrogen abstraction conventional transition state theory is applied:

$$k_i = \sigma_i \kappa_i(T) \frac{k_B T}{h} \frac{Q_{TS,i}}{Q_R Q_{OH}} \exp\left[-\frac{\Delta E_i^{\ddagger}}{k_B T}\right]$$

The tunnelling correction κ_i is evaluated using an asymmetrical Eckart barrier. σ_i is the symmetry factor which denotes the reaction path degeneracy. From the individual rate constants the total rate constant (k_{total}) and branching ratio (Γ_i) can be calculated.

Methodology

To systematically scan the configurational space each nucleation step was performed by adding 1000 randomly oriented nucleate molecules (H_2O, NH_3 and H_2SO_4) randomly distributed around the target methanol molecule/complex. The 1000 generated structures were geometry optimized using the semi-empirical PM6 method to yield initial guesses. The identified conformations were then optimized with M06-2X/6-311++(3df,3pd) to yield the final structures. All local minima within 3 kcal/mol of the identified "global" minima were then thermally averaged to calculate the statistical Gibb's free energy of formation. For calculating the rate constants and branching ratios BH&HLYP/aug-cc-pVTZ geometries and frequencies were used. The single point energy was corrected with a high level explicitly correlated Coupled Cluster Singles Doubles with perturbative triples CCSD(T)-F12a calculation using the VDZ-F12 basis set.

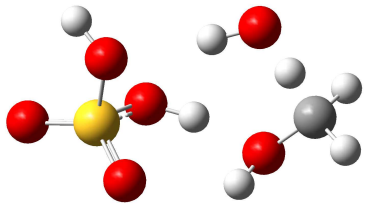

Figure 1: Transition state structure of C-H hydrogen abstraction by the OH radical from methanol in the $(CH_3OH)(H_2SO_4)$ complex.

Conclusions

The interaction between methanol and H_2O/NH_3 is found to be thermodynamically unfavourable suggesting that neither water nor ammonia catalyse the gas phase reaction of methanol with the OH radical.. We find that methanol is able to form stable complexes with H_2SO_4 which is more favourable than the corresponding hydrate. The incorporation of methanol into a pre-nucleation cluster does not hinder the subsequent addition of nucleation precursors. Due to stabilization of the transition state complex trough hydrogen bonding the complex formation is found to be able to both catalyse and change the reaction mechanism of the hydrogen abstraction reactions of methanol by the OH radical depending on collision mechanism. This intriguing result indicates that complex formation with sulfuric acid is able to alter the reaction mechanism of a simple organic compound by acting as a stabilizing scaffold and it thereby indicates an alternative new pathway for oxidation products of various organic compounds.

The authors thank the Danish Center for Scientific Computing for providing computer resources, and the Villum Kann Rasmussen Foundation for financial support

Secondary organic aerosol formation in the ozonolysis of biogenic volatile organic compounds performed in a laminar flow reactor

T. Braure[1,2], V. Riffault[1,2], A. Tomas[1,2], M. Duncianu[1,2], Y. Bedjanian[3] and P. Coddeville[1,2]

[1] Université Lille Nord de France, F-59000, Lille, France
[2] Mines Douai, CE, F-59508 Douai, France
[3]Institut de Combustion Aérothermique Réactivité et Environnement, F-45071, Orléans, France
Keywords: limonene, α-pinene, nucleation, aerosol yield.
Presenting author email: tristan.braure@mines-douai.fr

The oxidation of Biogenic Volatile Organic Compounds (BVOC) emitted by vegetation, such as monoterpenes ($C_{10}H_{16}$) or sesquiterpenes ($C_{15}H_{24}$) is an important source of Secondary Organic Aerosol (SOA). Because of their large global emissions and high reactivity with the major atmospheric oxidants (Atkinson and Arey, 2003) – and particularly with ozone (O_3) – they are believed to be the dominant contributors to global SOA formation (Kanakidou *et al*, 2005).

α-Pinene and limonene are two of the three most important BVOC emitted in the atmosphere (Griffin *et al*, 1999), with conifers as major sources (Geron *et al*, 2000, Pokorska *et al*, 2012). These two BVOC (especially limonene) are also emitted in indoor air by air fresheners and cleaning products such as kitchen cleaners and dishwashing detergents (Huang *et al*, 2011). It has been highlighted in previous studies that their reactions with ozone could produce SOA (Chen *et al*, 2011, Waring *et al*, 2011, Bernard *et al*, 2012) either in atmospheric or indoor environments, and could then lead to significant climate (Myhre *et al*, 2001) and health (Gaschen *et al*, 2010) effects.

In the present work, the ozonolysis reactions of limonene and α-pinene have been investigated at room temperature and atmospheric pressure using a laminar flow reactor newly developed in our laboratory (Figure 1, Duncianu *et al*, 2012), which allows the monitoring of the first steps of ozonolysis reactions (typically ~30 seconds to 5 minutes) providing complementary data to more widely performed smog chamber experiments.

The rate coefficients have been measured under pseudo first-order conditions in excess of the BVOC. The decay of ozone has been monitored with an O_3 analyser while BVOC concentrations have been determined using online sampling onto adsorbent cartridges followed by thermodesorption and subsequent analysis in a GC/FID-MS system. Specific experiments have been performed to identify and quantify both gas-phase and particulate products using a TD/GC/FID-MS system, a SMPS and a HR-ToF-AMS, respectively.

Results will be further discussed and compared to literature data.

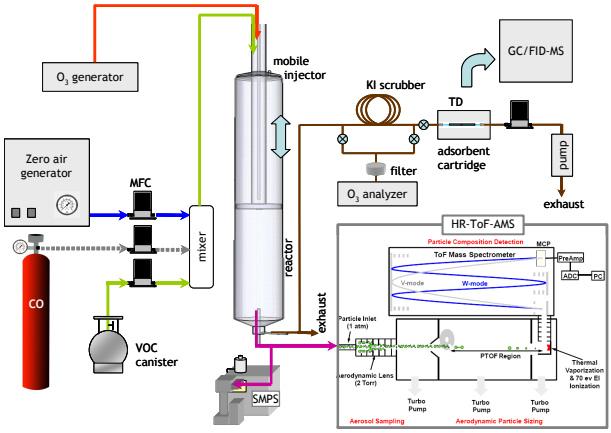

Figure 1. Schematic of the experimental setup and instrumentation (MFC: mass flow controller) (adapted from Duncianu *et al*, 2012).

Our laboratory participates in the Research Institute of Industrial Environment (IRENI) which is financed by the Communauté Urbaine de Dunkerque, the Nord-Pas de Calais Regional Council, the French Ministry of Education and Research, and European funds (FEDER). The CaPPA project (Chemical and Physical Properties of the Atmosphere) is funded by the French National Research Agency (ANR) through the PIA (Programme d'Investissements d'Avenir) under contract ANR-10-LABX-005. M. Duncianu and T. Braure are grateful for PhD scholarships from the Nord-Pas de Calais Regional Council and Armines.

Atkinson, R. and Arey, J. (2003) *Atm. Env.* **37**, S197-S219.
Bernard, F. *et al.* (2012) *J. Aer. Sci.* **43**, 14-30.
Chen, X. *et al.* (2011) *Env. Sci. Tech.* **45**, 276-282.
Duncianu, M. *et al.* (2012) *J. Phys. Chem. A* **116**, 6169-6179.
Gaschen, A. *et al.* (2010) *Env. Sci. Tech.* **44**, 1424-1430.
Geron, C. *et al.* (2000) *Atm. Env.* **34**, 1761-1781.
Griffin, R.J. *et al.* (1999) *Geophys. Res. Lett.* **26**, 2721-2724.
Huang, Y. *et al.* (2011) *Atm. Env.* **45**, 6191-6196.
Kanakidou, M. *et al.* (2005) *Atm. Chem. Phys.* **5**, 1053-1123.
Myhre, G. *et al.* (2001) *Atm. Env.* **35**, 2361-2373.
Pokorska, O. *et al.* (2012) *Atm. Env.* **59**, 501-508.
Waring, M.S. *et al.* (2011) *Atm. Env.* **45**, 4235-4242.

Monday, September 1, 2013

Session: Indoor and Working Place Aerosols, *Indoor environment*

Number concentration and modal Structure of indoor/outdoor fine particles in four European Cities

M. Lazaridis[1], K. Eleftheriadis[2], V. Ždímal[3], J. Schwarz[3], Z. Wagner[3], J. Ondracek[3], Y. Drossinos[4], T. Glytsos[1], S. Vratolis[2], K. Torseth[4] and J. Smolík[3]

[1]Department of Environmental Engineering, Technical University of Crete, Chania 73100, Greece,
[2]Institute of Nuclear Technology & Radiation Protection, N.C.S.R. "Demokritos", 15310 Ag. Paraskevi, Attiki, Greece,
[3] Institute of Chemical Process Fundamentals, Laboratory of Aerosol Chemistry and Physics, Rozvojová 135, CZ-16502 Praha 6, Prague, Czech Republic,
[4]European Commission, Joint Research Centre, I-21027 Ispra (Va), Italy.
[5] Norwegian Institute for Air Research (NILU), Instituttvien 18, N-2020 Kjeller, Norway
Keywords: Indoor number concentration, indoor sources, modal structure.
Presenting author email: thodoros.glytsos@enveng.tuc.gr

Indoor/outdoor measurements campaigns were performed in naturally ventilated houses and offices in four European cities to investigate the relationship between indoor and outdoor particle number concentrations and aerosol modal structures. The measurements sites were located in Oslo (Norway), Prague (Czech Republic), Milan (Italy) and Athens (Greece). A number of ordinary indoor activities (cooking, smoking, candle burning, etc.) were performed during the measurements to quantify the contribution of particles emitted from indoor sources and the contribution of outdoor particles to the change of the indoor aerosol size spectra.

The size and time resolved particle concentrations in the size range 10 nm – 600 nm were measured by scanning mobility particle sizers (SMPS). The results were analysed, and the modal structure of the measured particle number size distribution data, along with the number concentration in each of the modes comprising the aerosol size distribution, were computed.

The analysis of the measurements showed that in absence of indoor sources, indoor number concentration followed the variations of the outdoor concentration. Figure 1 presents the correlation between diurnal median values of indoor and outdoor number concentrations for the measurements conducted in Prague. Indoor concentration was highly correlated to the outdoor concentration when the apartment was unoccupied, but poor correlation was observed during periods with indoor activities (e.e., cooking).

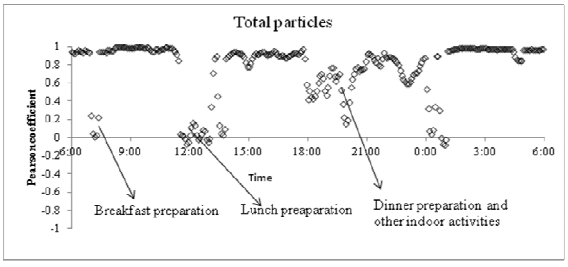

Figure 1. Correlation of indoor and outdoor diurnal median number concentrations for the measurements conducted in Prague (Czech Republic).

Emissions from indoor sources resulted in elevated indoor number concentrations and I/O ratios. Furthermore, the aerosol spectra presented different characteristics during periods with indoor activities as depicted in Table 1. The outdoor size distribution was similar to the indoor size distribution suggesting that in naturally ventilated buildings the indoor size spectra is formed according to the penetration efficiency of the outdoor particles to the indoor environment and to the emission characteristics of indoor sources.

Table 1a,b: Median values of GMDs, for the first and second mode, sorted according to time period without indoor activities(a) and with indoor activities (b) in the measurements sites of Oslo, Prague and Milan.

Median values for time periods without indoor activities

		GMD [nm]	
		1	2
Unimodal	Prague	120	
	Oslo	57	
	Milan	74	
Bimodal	Prague	34	132
	Oslo	23	91
	Milan	41	128

(a)

Median values for periods with indoor activities

		GMD [nm]	
		1	2
Unimodal	Prague	85	
	Oslo	85	
	Milan	129	
Bimodal	Prague	45	182
	Oslo	20	101
	Milan	48	150

(b)

The data analysis has received funding from the European Union Seventh Framework Programme HEXACOMM *FP7/2007-2013* under *grant agreement* n° *315760*. The data were obtained during the European Union Fifth Framework Programme Urban-Aerosol *FP5/EEDS*

Spatial variation of air pollutants in a multilevel office building

C. He and L. Morawska

International Laboratory for Air Quality and Health, Institute of Health and Biomedical Innovation, Queensland University of Technology (QUT), Brisbane, 4001, Australia

Keywords: indoor, aerosol, particle number, $PM_{2.5}$, CO
Presenting author email: c.he@qut.edu.au

Within-building spatial variability of indoor air quality may influence substantially the reliability of human exposure assessments based on single point samples, but have hitherto been little studied. To investigate and understand the within-building spatial variation of air pollutants, field measurements were conducted in a 7 level office building in Brisbane, Australia. The building consists of 3 sections (A side, Meddler and B side).

A portable unit consisting of a P-Trak, DustTrak and Q-Trak, was assembled on a small trolley and moved to the various locations around the building. The average particle number (PN) concentration (in the range 0.020-1.0μm), particle mass concentration ($PM_{2.5}$) and CO and CO_2 levels, as well as temperature and relative humidity, were simultaneously measured by P-Trak, DustTrak and Q-Trak Plus, at diffident locations inside and outside of the building during working hours in two typical weather conditions in Brisbane. At each sampling location, the sampling period was 5 minutes (with a logging interval of 10 seconds), and average measurements were obtained by sampling at different sub-locations within the office area including the working area, corridor, conference room and rest areas. The measurements were repeated twice at each location.

The average PN and $PM_{2.5}$ concentrations at various locations are presented in Figure 1. From Figure 1, some results can be drawn. Average particle concentration levels varied from location to location within the building, especially for PN. Indoor PN and $PM_{2.5}$ concentration levels in the underground car park, lifts and entrances were considerably higher (about 3 times for PN and 40% for $PM_{2.5}$) than those measured in the offices. Average PN concentration levels also varied from office to office within the building, in the range from 1.17×10^3 particle cm^{-3} to 6.68×10^3 particle cm^{-3}. Average indoor PN concentrations at level 7 were higher than those at other levels. This is due to there being an entrance at level 7 to the roof area of the building. It was found that the particle concentration in a printer room (24.0×10^3 particle cm^{-3} for PN and 7 μg m^{-3} for $PM_{2.5}$) was significantly higher than the average office concentration (3.7×10^3 particle cm^{-3} for PN and 5 μg m^{-3} for $PM_{2.5}$), which indicated that printers are a major indoor source of particles in this building.

A summary of the average indoor and outdoor PN, $PM_{2.5}$ and CO_2 concentration levels is given in Tables 1. From Table 1, it can be seen that both outdoor average PN and $PM_{2.5}$ concentration levels were higher (about 3 times for PN and 2 time for $PM_{2.5}$) than indoor average particle concentration levels. However, outdoor CO_2 levels were lower than indoor levels. It also can be noted that the highest $PM_{2.5}$ concentration for both indoor and outdoor was collected from the underground car park. There were also clear particle concentration differences between A side and B side for both outdoors and entrances.

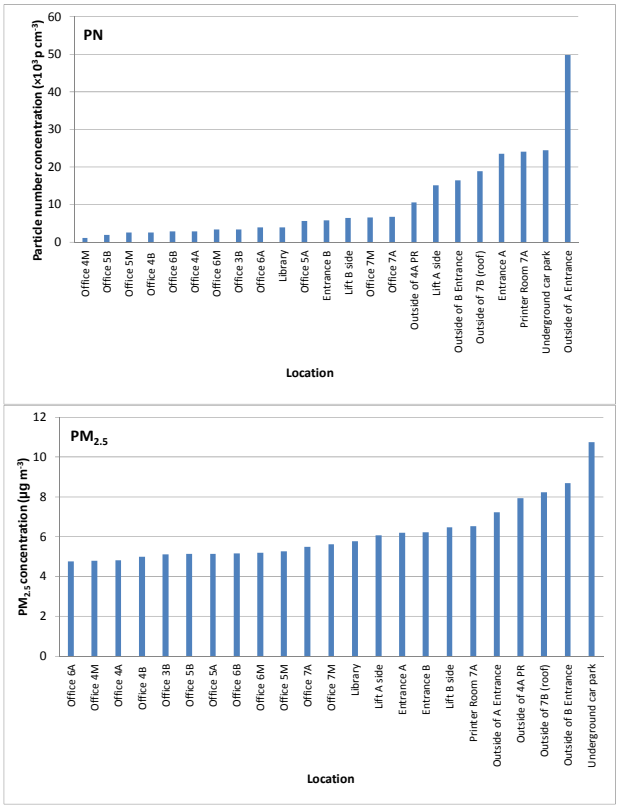

Figure 1. The average PN and $PM_{2.5}$ concentrations at various locations

Table 1. Summary of indoor and outdoor average concentration of the pollutants

	PN ($\times 10^3$ p cm^{-3})		$PM_{2.5}$ (μg m^{-3})		CO_2 (ppm)	
	In	Out	In	Out	In	Out
Average	7.74	24.0	6	8	767	496
S.D	7.84	17.6	1	1	206	115
Min	1.17	10.6	5	7	459	435
Max	24.4	49.9	11	9	1192	668
Median	3.98	17.7	5	8	795	439

CO concentration levels also varied from location to location within the building. However, CO concentration levels were clearly lower than the NEPM ambient air quality standards (8 hours: 9.0 ppm).

Effect of Anti-idling Campaign on the Outdoor and Indoor Aerosol Exposure at Schools

S.A. Grinshpun[1], M. Yermakov[1], J.Y. Kim[1], T. Reponen[1], C. Schaffer, P. Ryan[2]

[1]Center for Health-Related Aerosol Studies, University of Cincinnati, Cincinnati, Ohio, USA
[2]Cincinnati Children's Hospital Medical Center, Cincinnati, Ohio, USA

Keywords: traffic aerosol, PM2.5, exposure, indoor/outdoor, school
Presenting author email: sergey.grinshpun@uc.edu

Exposure to traffic aerosols, including diesel exhaust particles, may be elevated at schools, partially because of the emission from cars and buses transporting students daily. Idling of vehicles in the school proximity may increase the outdoor aerosol concentration of fine particulate matter (PM2.5) as well as the concentrations of its constituents, including traffic-related elements. We hypothesize that an anti-idling campaign implemented at schools reduces the children exposure outdoors and indoors.

The objective of this study was to evaluate the impact of an anti-idling campaign on outdoor and indoor air quality at four urban schools in Cincinnati (Ohio, USA) with varying exposure to the school bus emission. Table 1 presents some of the characteristics of the selected schools. At each school, Harvard-type PM2.5 impactors (Air Diagnostics and Engineering, Inc. Harrison, ME, USA) operated in parallel – two indoors and two outdoors; in each pair, one was equipped with Teflon filter and one with quartz filter. The PM2.5 mass concentration was determined using gravimetric technique; the mass concentration of ten elements (Si, S, Ti, V, Mn, Fe, Cu, Zn, Br, Pb) was obtained using X-ray fluorescence analysis on Teflon filters. The quartz filter samples were analyzed for elemental and organic carbon (EC and OC) with thermal-optical transmittance.

Table 1. Characteristics of school A - D.

School	Average number of school buses operating	Average number of cars dropping-off students	Distance from highway (m)
A	5	18	303
B	39	77	526
C	11	27	243
D*	9	24	2,083

* A metro-bus stop is in the proximity

The outdoor concentrations of PM2.5 decreased at school B and D following the anti-idling campaign; no significant changes in PM2.5 were identified at school A and C. Some elemental constituents of PM2.5 decreased at all schools after the campaign was implemented; however, this decrease was mostly insignificant, except for school B, which had the greatest number of school buses and cars. For this school, we identified a statistically significant reduction of organic carbon as well as Si, Fe, and Zn. Furthermore, the levels of all traffic-related elements in the outdoor environment of school B measured before the anti-idling campaign exceeded the corresponding area levels (measured as a surrogate for the school B's community). The latter finding suggests that traffic emission was the dominant air pollution source at school B. In contrast to school B, the anti-idling campaign did not have a definitive effect on the outdoor elemental concentrations determined at other three schools. Most of the results seem to have been influenced by the time variability of the background aerosol, which represents a limitation of the present study.

A significant ($p<0.05$) positive association was found for the changes in outdoor and indoor elemental concentrations observed at school B (the one with the most intense local traffic). No statistically significant association was identified for any of the three other schools. The data for school B are presented in Fig. 1. Elements such as Br and Cu that fell outside the plot are marked with arrows (the outdoor concentrations of these elements did not change significantly following the anti-idling campaign). For most elements measured at school B, the decrease in outdoor concentrations followed by a corresponding decrease in indoor concentrations.

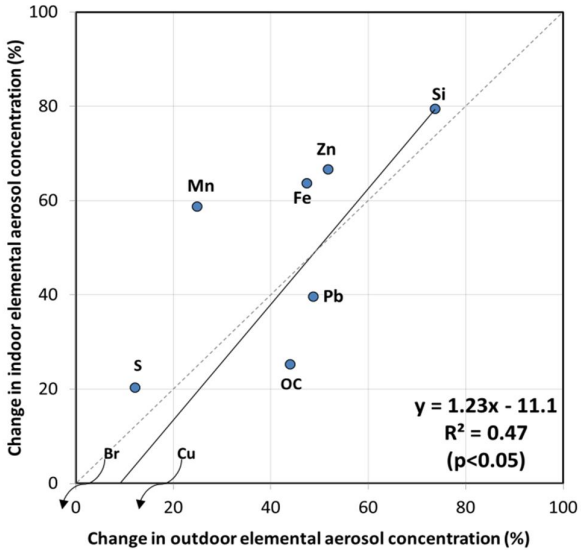

Fig. 1. Association between the changes in outdoor and indoor elemental concentrations at school B following the anti-idling campaigns. Elements detected at levels below uncertainty in at least 50% of samples were excluded.

This research was funded by the National Institute of Environmental Health Sciences, through Grant NIEHS R21ES017957. The authors appreciate this support.

Exposure assessment to air pollutants in Elderly Care Centers

M. Almeida-Silva[1], S. M. Almeida[1*], H. T. Wolterbeek[2]

[1] IST/ITN, Instituto Superior Técnico, Universidade Técnica de Lisboa, Estrada Nacional 10, 2686-953 Sacavém, Portugal;

[2] Faculty of Applied Sciences, Department of Radiation, Radionuclides and Reactors, Section RIH (Radiation and Isotopes in Health), Technical University of Delft, Delft, The Netherland.

* Correspondent author: smarta@ctn.ist.utl.pt

Keywords: Elderly, Indoor, Exposure

Presenting author email: marina@ctn.ist.utl.pt

According to the United Nations the proportion of total population aged 60 years or over for the Europe is 22% for the year 2012 and prospects 34% for 2050[1]. In general, people spend about 19-20 hours indoors. These values could increase considering the older people who are institutionalized in Elder Care Centers (ECC)[2]. By these reasons and by the fact that old people are considered a susceptible group becomes increasingly important to mitigate their exposure to air pollutants. The main goal of this work was to characterize the indoor air quality in ECC in order to understand the elderly exposure to air pollutants. The current study was developed in Loures and Lisbon (Fig. 1).

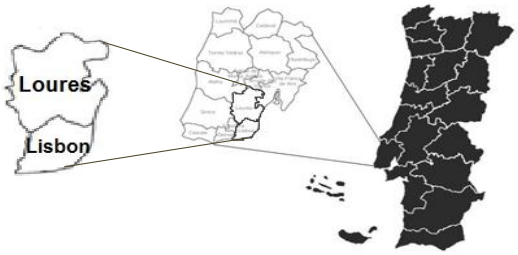

Figure 1 - Localization of the sampling sites

A time-budget survey was carried out with more than 300 elderly in order to define the time spent by the old people. This data will be used to achieve the exposure to air pollutants, according to the follow equation:

$$Exposure = \sum_{i=n}^{n} C_{z,n} \cdot t_n$$

Where *n* corresponds to the different micro-environments, *C* is the concentration of the pollutant *z* and *t* is the time spends in each micro-environment.

A set of pollutants has been selected to characterize the indoor air quality inside two micro-environments – Room (R) and Living-Room (LR) – in 4 ECC, such as air temperature, relative humidity, carbon dioxide (CO_2), carbon monoxide, particulate matter with 5 different sizes, namely $PM_{0.5}$, PM_1, $PM_{2.5}$, PM_5, PM_{10}, total volatile organic compounds. Measurements in each outdoor environment were performed simultaneously.

PM_{10} were also collected in Teflon filters and were gravimetrically assessed in a clean room (class 10,000), as well their chemical content by Instrumental Neutron Activation Analysis, in Portuguese Research Reactor.

Results showed that CO_2 and PM_{10} exceeded the Portuguese legal value (1800 and 0.15 $mg.m^{-3}$, respectively) in some periods of the day.

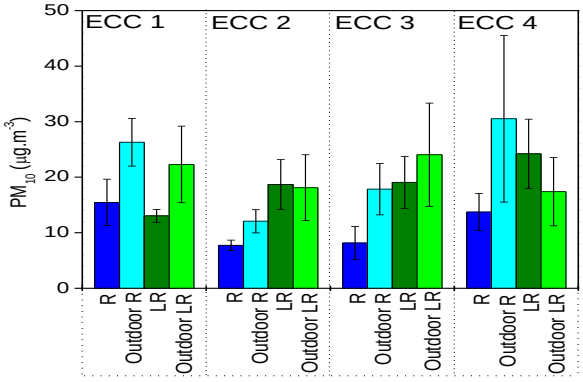

Figure 2 - Mass concentration in PM_{10} sampled for each ECC.

Fig. 2 shows the gravimetric PM_{10} concentration measured in each ECC. The outdoor levels associated with the R's were always higher, comparing with the PM_{10} concentrations determined inside the R's. In the other hand, two different ECC's presented higher values in the LR's than in the corresponding outdoors. This last evidence shows the importance of indoor sources inside of the LR's, e.g. elderly, collaborators, plants, etc.

In/Out ratio are showed in Fig. 3. Ratios for R and LR in EEC2 presented the best correlation (0.78 and 0.90, respectively) and confirm an outdoor origin of the PM_{10}.

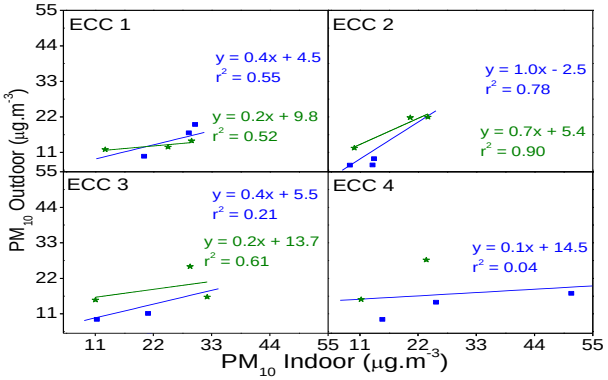

Figure 3 - Ratio In/Out per ECC for R (--) and LR (--).

We gratefully acknowledge the assistance of the Câmara Municipal de Loures, ESTeSL, Dr.º Amádis Santos of EFACEC and Dr.ª Célia Alves and Dr.ª Teresa Nunes of Aveiro University, for their collaboration. We also gratefully acknowledge FCT for funding M. Almeida-Silva by PhD fellowship (SFRH/BD/69700/2010).

[1] United Nations. Population Ageing and Development 2012. New York : United Nations, 2012. 978-92-1-151494-0.

[2] Bradshaw, S. A., Playford, E. D. and Riazi, A. Living well in care homes: a systematic review of qualitative studies. Age and Ageing. 2012, Vol. 41, pp. 429-440.

Sources, sinks, chemical composition and transport of aerosol particles in a university lecture hall

I. Salma[1], K. Dosztály[1], T. Borsós[1], T. Weidinger[2], G. Kristóf[3], N. Péter[3], Zs. Kertész[4]

[1]Institute of Chemistry, Eötvös University, H-1518 Budapest, P.O. Box 32, Hungary
[2]Department of Meteorology, Eötvös University, H-1518 Budapest, P.O. Box 32, Hungary
[3]Department of Fluid Mechanics, Budapest University of Technology and Economics, H-1111 Budapest, Bertalan L. u. 4–6., Hungary
[4]Laboratory of Ion Beam Applications, Institute of Nuclear Research, H-4001 Debrecen, P.O. Box 51, Hungary
Keywords: emission rate, residence time, enrichment factor, dust particles, ultrafine particles
Presenting author email: salma@chem.elte.hu

An intensive aerosol research program was conducted in a university lecture hall at the Eötvös University, Faculty of Science, Budapest, Hungary to determine time-resolved aerosol mass and number concentrations, CO_2 concentration, size-resolved chemical composition of aerosol particles, and to evaluate them together with micro-meteorological variables. A computational fluid dynamics (CFD) model was developed to estimate the spatial distribution of the experimental and derived data within the hall and the transport of aerosol particles.

PM_{10} mass, particle number (N) and CO_2 concentrations, particle number size distributions and meteorological parameters were determined with high time resolution, and daily aerosol samples were collected in the $PM_{10-2.0}$ and $PM_{2.0}$ size fractions for chemical analysis in the middle of the lecture hall for one week. Median concentrations for the PM_{10} mass and N of 15.3 $\mu g\ m^{-3}$ and $3.7\times10^3\ cm^{-3}$, respectively were derived. The data are substantially smaller than the related outdoor levels or typical values for residences. There were considerable concentration differences for workdays, weekends and various lectures. Main sources of PM_{10} mass include the usage of chalk sticks for writing, wiping the blackboard, ordinary movements and actions of students and cleaning. High PM_{10} mass concentration levels up to 100 $\mu g\ m^{-3}$ were realised for short time intervals after wiping the blackboard. The mass concentrations decreased rapidly after the emission source ceased to be active. Two classes of coarse particles were identified. General indoor dust particles exhibited a residence time of approximately 35 min, while the residence time for the chalk dust particles was approximately 15 min as lower estimates. Emission source rate for wiping the blackboard was estimated to be between 8 and 14 $mg\ min^{-1}$. This represents a substantial emission rate but the source is active only up to 1 min. Most aerosol constituents have smaller indoor concentrations than their outdoor counterparts. At the same time, Ca and S showed larger indoor enrichment factors than the other constituents. This is explained by the chalk (made mainly of gypsum) usage for writing and drawing, and suspension of the chalk dust particles. The crustal enrichment factors and $PM_{2.0}/PM_{10-2.0}$ concentration ratios revealed that mechanical disintegration is the major source for many aerosol constituents. Contribution of ambient aerosol via the heating, ventilation and air conditioning (HVAC) facility was considerable for time intervals when the indoor sources of PM_{10} mass were not intensive. The HVAC facility introduces, however, the major amount of aerosol particles from the outdoors as far as their number concentration is regarded. Mean contribution of ultrafine particles to the total particle number was (69±7)%, which is smaller than for the related outdoor urban environment. This can indicate aged ultrafine aerosol. The major amounts of CO_2 arrive from the corridors through open doors by infiltration.

Spatial distribution of the PM_{10} mass concentration within the hall was derived by CFD modelling, and spatial inhomogeneities were obtained as indicated in Figure 1. A plume of particles is created along the central longitudinal band of the hall. Sitting at the outermost seats seems favourable, and the lecturers who use chalk sticks intensively are exposed to higher concentration levels than the students.

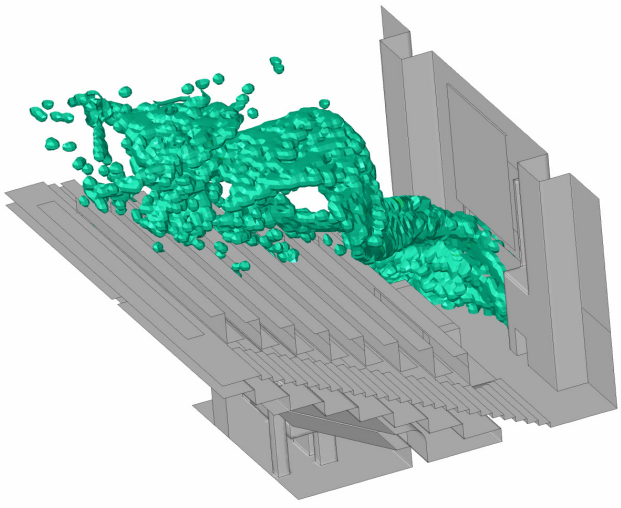

Figure 1. Modelled three-dimensional spatial distribution of PM_{10} aerosol particle after wiping the blackboard.

This work was supported by the Hungarian Scientific Research Fund under grant K84091.

Salma, I., Dosztály, K., Borsós, T., Süveges, B., Weidinger, T., Kristóf, G., Péter, N., Kertész, Zs. (2013) *Atmos. Environ.* **64**, 219–228.

The effect of size, location, occupancy and microclimatic factors on air quality of university lecture rooms

M. Braniš[1] and K. Stupková[1]

[1] Charles University in Prague, Faculty of Science, Institute for Environmental Studies, Albertov 6, 128 43 Prague 2, Czech Republic

Keywords: indoor air quality, school, particulate matter, microclimate

Presenting author email: brains@natur.cuni.cz

As has been repeatedly documented in scientific literature, one of the most polluted indoor microenvironment can be found at schools. School buildings and classrooms suffer from poor air quality from two reasons: (1) Schools in cities are frequently situated in quarters or near streets with dense traffic and the infiltration of freeway particles into the school buildings represents an important source of pollutants (Janssen et al. 2001; Green et al. 2004) and (2) High levels of particulate matter in schools are frequently attributed to human activity and insufficient frequency of cleaning which is not capable in removing deposited particles (Branis et al., 2005; Fromme et al., 2007). Since these particles are only partly removed, they can be resuspended again and again. To ascertain the effect of infiltration and resuspension under various conditions (such as position of the classroom with respect to outdoor sources, its size and occupancy) we performed a year long project in three university lecture rooms situated in the centre of Prague.

Twenty-four hour mass concentrations of size-segregated aerosol were measured simultaneously in three university lecture rooms and outdoors in the central part of Prague (Czech Republic) by a five-stage A - F (<0.25µm, 0.25-0.5µm, 0.5-1.0µm, 1.0-2.5µm and 2.5-10µm) Personal Cascade Impactor Sampler (PCIS). Identical sets of instruments were deployed at the outdoor and indoor sites. Other variables such as CO_2, ventilation, temperature, relative humidity, occupancy were monitored as well. The measurements were performed during all seasons of the year during 11 three to four-day long campaigns involving working days as well as weekends and holidays.

The results documented that finer indoor size fractions (below 500nm) were significantly affected by outdoor concentrations while coarse particulate matter levels ($PM_{2.5-10}$) were predominantly dependent on the number of students in the lecture rooms. Nevertheless, some effect of human presence on the PM below 500nm was recorded as well, indicating a possible effect of the so called personal cloud (Table 1; Figure 1). The level of particulate matter concentrations corresponded to the proximity to the adjacent street (the closer the lecture room the higher the average PM concentration) and to the size of the size of the lecture room (the smallest was the space the highest PM concentrations were recorded).

In addition, concentrations of carbon dioxide frequently reached values over 1500ppm and higher. One of the common problems in all the three lecture rooms was very low relative humidity (around 30-35%). The results of the study not only confirmed previous results but also showed that measurements in one classroom per school may be insufficient because differences in position, size and occupancy may affect the concentrations of aerosol from which the estimates of exposure are made for the whole population of students in a particular school.

Table 1. The effect of occupancy on size resolved aerosol. OC - occupied; UOC - unoccupied periods; A, B, C, D, F - impactor stages; CPM ($PM_{10-1.0}$). B11, B12, B14 - lecture rooms.

	B11		B12		B14	
	OC	UOC	OC	UOC	OC	UOC
A	2.18	0.78	2.56	0.49	2.88	0.50
B	1.50	0.66	1.32	0.56	1.45	0.78
C	1.14	1.01	1.01	0.61	1.07	0.88
D	4.64	4.03	5.13	3.50	4.24	4.49
F	10.15	10.02	10.06	6.22	9.96	7.79
PM_{10}	18.30	15.78	20.08	11.38	20.03	11.77
CPM	3.68	1.44	3.88	1.05	4.33	1.29

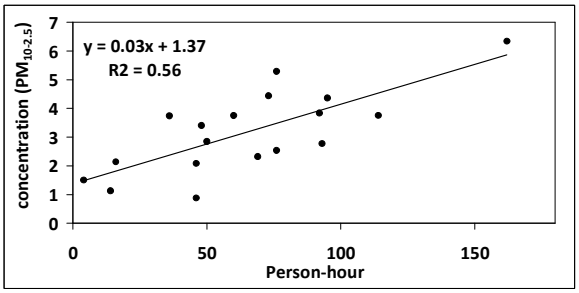

Figure 1. The relationship between coarse PM ($PM_{10-2.5}$) and occupancy (in person-hours) in one lecture room.

This work was supported by Ministry of Education, Youth and Sports of the Czech Republic under program NPV II, project No. 2B08077.

Branis, M., Rezacova, P., Domasova, M. (2005) *Environ. Res.* **99(2)**:143–149.

Green, R.S., Smorodinsky, S., Kim, J.J,, McLaughlin, R., Ostro, B. (2004) *Environ. Health. Perspect.* **112**:61–66.

Janssen, N.A.H., van Vliet, P.H.N., Aarts, F., Harssema, H., Brunekreef, B. (2001) *Atmos. Environ.* **35**:3875–3884.

Fromme, H., Twardella, D., Dietrich, S., Heitmann, D., Schierl, R., Liebl, B., Ruden, H. (2007) *Atmos. Environ.* **41**:854–866.

Particulate Matter in Indoor Air in two Schools in Vienna, Austria

A. Kasper-Giebl[1], N. Jankowski[1,2], K. Kassin[1,3], E. Can Cetintas[1], H. Bauer [1,†] and H. Grothe[4]

[1]Institute of Chemical Technologies and Analytics, Vienna University of Technology, Vienna, A-1060, Austria
[2]now at: Amag, Austria Metal AG, Braunau am Inn - Ranshofen, A-5282, Austria
[3]now at: Umweltbundesamt, Vienna, A-1090, Austria
[4]Institute of Materials Chemistry, Vienna University of Technology, Vienna, A-1060, Austria

Keywords: indoor air, source apportionment, chemical composition, carbonaceous aerosols
Presenting author email: akasper@mail.tuwien.ac.at

Sampling of particulate matter was performed in two schools in Vienna in 2011. The first campaign started in January and lasted until April, the second from October till December, respectively. Particulate matter (PM10) was collected in parallel with a high-volume sampler (Digitel DHA80) using quartz fibre filters, a low-volume sampler (Leckel, SEQ47/50) using cellulose acetate filters and a beta particulate monitor (ESM, Eberline). In addition to the characterization of indoor air the sampling equipment was also installed outside the buildings for at least one week during both campaigns. This allowed to determine the ambient PM10concentrations in the vicinity of the two schools and to compare them with the air quality network in Vienna. This comparison showed very good agreement and allowed to take data from the air quality network as ambient concentration data for the time of the indoor sampling. Filter samples were analysed for aerosol mass, water soluble ions, carbon parameters (total carbon, elemental carbon, organic carbon, carbonates) selected anhydrosugars and other saccharides, cellulose, humic like substances and metals using protocols described in Bauer et al. (2007).

Both sampling sites were located in the western part of Vienna. The vicinity of HBLVA Rosensteingasse (RG) can be characterized as a densely populated residential area with some influence of local traffic. The other site, BG Fichtnergasse (FG), is also a residential area with a large number of single family houses and private gardens around. Average concentrations of particulate matter in the ambient were ranging from 20 µg/m³ (April at FG) to 81 µg/m³ (November at RG). Sampling times comprised most of the exceedances of the 24h-limit value of PM10 observed in Vienna during 2011.

As expected indoor particulate matter concentrations showed distinct daily and weekly cycles reflecting the activity of students and teachers moving around the building and vaccations or weekends. Superimposed to these short time fluctuations the concentrations are driven by the ambient air concentrations monitored within the air quality network in Vienna.

Chemical analyses accounted for approx. 90 % of aerosol mass using a macro-tracer model (Bauer et al. 2007) which allows to quantify the contributions of inorganic secondary aerosols, mineral dust, wood smoke, other organic material and traffic to aerosol mass. For indoor samples organic material gave the highest contribution to aerosol mass, with cellulose being the most dominant single compound measured. Furthermore pronounced differences of saccaride concentration patterns were observed by comparing indoor and ambient air samples. Thus sugar alcohols being tracers for fungal spores (Bauer et al. 2008) were only determined outside, while e.g. glucose, fructose and succrose were only determined in indoor air samples. In FG mineral dust and in RG inorganic ions were the second important contributors to aerosol mass, respectively. Traffic showed a similar and rather small contribution at both sampling sites.

For ambient air samples inorganic secondary aerosol is the most important contributor to aerosol mass, followed by mineral dust, wood smoke and other organic material.

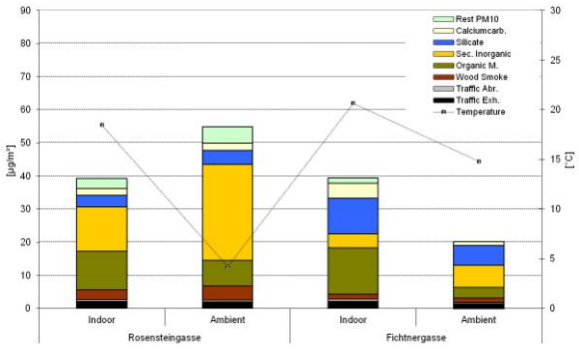

Figure 1. Source apportionment in the first campaign.

This work was supported by the Austrian Federal Ministry for Science and Research, within the Sparkling Science programme (SPA03-33). We thank the Environment Agency Austria and the municipal authority (MA22) for providing part of the sampling equipment. Support in the lab by H. Zbiral, C. Ramirez Santa Cruz, J. Firmkranz, L. Sampaio Cordeiro Wagner, J. Kirchbacher, B. Meixner, L. Striok and N. Wolf is gratefully acknowledged.

Bauer H. et al. (13 authors) (2007) AQUELLA Steiermark, Report LU08/07 (available at: http:// umwelt.steiermark.at/)
Bauer H. et al. (2008) *Atmos. Environ.* **42**, 588-593

Monday, September 1, 2013

Session: Instrumentation, *New techniques*

A fast-scanning DMA train for the precision quantification of nanoparticle dynamics

P.M. Winkler[1,2], J. Ortega[1], P.H. McMurry[3], J.N. Smith[1,4]

[1]Atmospheric Chemistry Division, National Center for Atmospheric Research, Boulder, CO, USA
[2]Fakultät für Physik, Universität Wien, 1090 Vienna, Austria
[3]Department of Mechanical Engineering, University of Minnesota, Minneapolis, MN, USA
[4]Department of Applied Physics, University of Eastern Finland, Kuopio, Finland
Keywords: Nanoparticle dynamics, size distribution, time resolution, DMA train.
Presenting author email: paul.winkler@univie.ac.at

Nanoparticle dynamics can be measured reliably by SMPS if the size distribution is changing slowly in the course of a single scan. Once the size distribution changes significantly during one scan, the resulting distortion may heavily impact the correct interpretation of the relevant distribution parameters. The need for instruments reliably analyzing nanoparticle growth at high time resolution has been pointed out recently (Winkler et al., 2012).

In this study we report on a new experimental device dedicated to the precision measurement of freshly formed growing nanoparticles. To this end, we combine a set of five differential mobility analyzers (DMAs) into a so-called DMA train in which each DMA is set to classify a single fixed particle size. The DMA train is specifically designed to resolve growth rates exceeding the time resolution provided by conventional SMPS.

The DMA train presented here utilizes five TSI 3085 nanoDMAs together with four TSI 3025 ultrafine condensation particle counters (UCPC) and one diethylene-glycol (DEG) based CPC (Iida et al., 2009). Thereby, size information can be retrieved from large clusters around 2 nm mobility diameter and upwards. DMAs were usually operated with sheath and excess flow rates of 15 L min^{-1} and a 1.5 L min^{-1} aerosol flow. The DMA in combination with the DEG-CPC, however, was operated at 20 and 2 L min^{-1}, respectively. In order to minimize particle losses in the lines to the DMAs transport flows of 8.7 and 2.3 L min^{-1} were used for particle sizes below and above 5 nm, respectively.

The performance of the DMA train was tested under laboratory conditions using the NCAR biogenic aerosol chamber. The 10 m^3 chamber is continuously flushed with HEPA filtered dry zero air together with the precursor vapor until a steady-state monoterpene (α-pinene) concentration of ~4 ppb is reached. Particle formation is subsequently initiated by increasing ozone to about 40 ppb. Gas-phase products were monitored using a proton transfer reaction time-of-flight mass spectrometer (PTR-TOF-MS). Particle evolution was monitored with the DMA train.

Figure 1 illustrates the time evolution of different particle sizes as measured by the DMA train. The particle sizes shown were obtained from two consecutive chamber runs under identical conditions. The reproducibility of size distribution data clearly indicates stable conditions in the chamber and supports the reliable operation of the DMA train. As can be seen, all particle sizes show a steep increase in concentration from basically zero to full appearance within 7-8 minutes. Obviously, a regular SMPS with a typical 5 minute scan time would not be able to resolve the particle dynamics correctly. Also it is important to note that the results shown here are statistically significant for raw counts as low as 0.1 cm^{-3}. This is a consequence of the averaging that can be performed due to the sampling at fixed sizes.

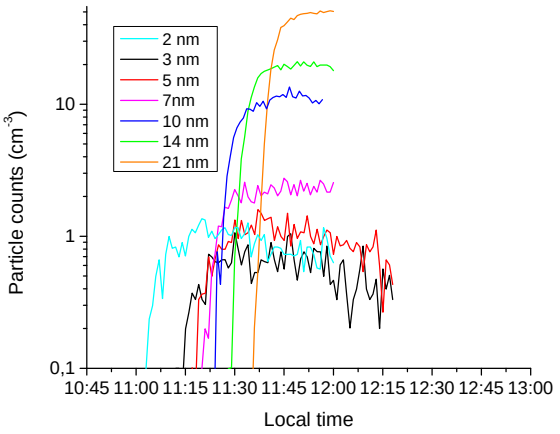

Figure 1. Raw data obtained from two consecutive formation events in the NCAR biogenic aerosol chamber under identical conditions. Chemical reaction was initiated at 10:45.

For the study of early nanoparticle growth we have designed a DMA train operating five DMAs equipped with CPCs in parallel at fixed sizes. Features of the DMA train include size distribution scan times of one second for a size range between 2 and 20 nm. Statistically significant data could be obtained for classified particle concentrations as low as 0.1 cm^{-3}. The performance test in a chamber study of α-pinene ozonolysis under close-to-ambient conditions demonstrates the superiority of this set-up over regular SMPS for the purpose of growth analysis.

This work was supported by the Austrian Science Fund (FWF): J3198-N21. The National Center for Atmospheric Research is supported by NSF.

Winkler, P. M., et al., *Geophys. Res. Lett.* **39**, L20815 (2012).
Iida, K., et al., *Aerosol Sci. Technol.* **43**, 81 (2009).

Fast scanning mobility particle sizing system and classifier

J. Farnsworth, F. Quant, H-G. Horn, B. Osmondson, and R. Caldow

TSI Incorporated, Shoreview, MN, 55126, USA
Keywords: SMPS, DMA, 15900, CPC
Presenting author email: jim.farnsworth@tsi.com

Since the scanning concept was introduced by Wang and Flagan in 1990, differential mobility classification has become the measurement principle of choice for making aerosol size distribution measurements in the 1 nm to 1 µm size range. Devices such as the TSI Model 3080 Classifier, typically used as part of a Scanning Mobility Particle Sizer (SMPS) system, operate by this principle. While the technique has a reputation for reliability because it is based on basic physical principles, its primary drawback is response time: it typically takes 60 seconds or more to complete a scan.

In order to meet the need for faster measurements while leveraging the reliability of differential mobility classification, a new classifier (TSI Model 3082) is presented to enable scanning at rates down to 5-seconds (see Figure 1).

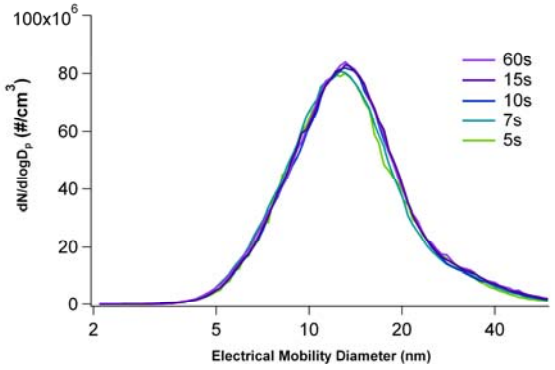

Figure 1. Polydisperse silver aerosol size distribution obtained at various scan times between 5s and 60s.

The 3082 retains the functions of the 3080 with the following additions:

1. Dual polarity DMA high voltage control with <50 ms response time for faster scanning
2. 50 Hz data sampling for higher time resolution
3. 30 L/min sheath flow capability for higher size resolution and wider size range
4. Integrated and removable x-ray bi-polar charge neutralizer (Scheckman *et al*)
5. Integrated and removable inlet impactors for aerosol flow measurement and particle pre-separation
6. Tool-free installation of DMAs and impactor set

Precise control of high voltage and sheath flow coupled with well-characterized CPC response time allows for ±1% size accuracy at 100 nm. Calibration of the device complies with ISO 15900 Standard, which was put in place to provide methodology for adequate quality control of differential mobility devices.

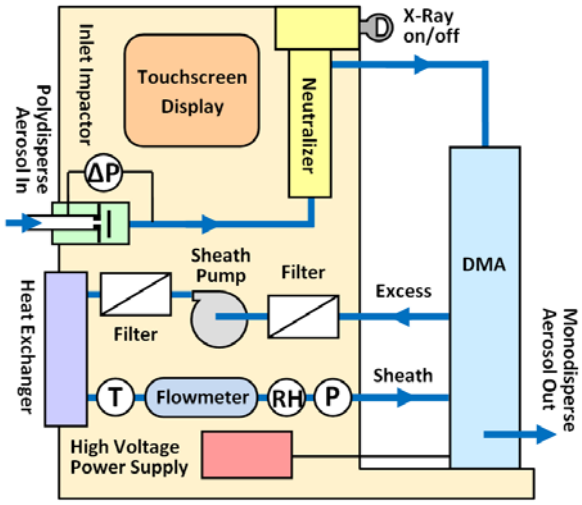

Figure 2. Flow schematic for the TSI Model 3082 Classifier.

Equivalence data comparing SMPS scans using the TSI Model 3082 Classifier versus the TSI Model 3080 Classifier are presented. These data demonstrate the agreement of both classifiers at traditional scanning rates as well as the advantages of the new model at reduced scan times.

Wang, S.C. and Flagan, R.C. (1990) *J. Aerosol Sci.* 13:230-240.

Scheckman J.H., Elzey S., Farnsworth J.E., Horn H.-G., and Osmondson B. (2013) *Proc. of Euro. Aerosol Conf.* In Preparation.

ISO 15900:2009(E) Determination of particle size distribution – Differential electrical mobility analysis for aerosol particles.

A Drift Tube Ion Mobility Spectrometer (DT-IMS) combined with a Condensation Particle Counter for Analysis of Sub 10 nm Aerosol Particles

Derek R. Oberreit[1], Peter H. McMurry[1], & Christopher J. Hogan Jr.[1]

[1]Department of Mechanical Engineering, University of Minnesota, Minneapolis, Minnesota, 55455, USA
Keywords: Electrical Mobility Analysis, Size Distribution Measurement, Nanoparticles, Drift Tube
Presenting author email: hogan@me.umn.edu

Drift tube-ion mobility spectrometer (DT-IMS) devices allow for determination of the electrical mobilities of charged particles through measurement of the time necessary for a particle to travel a fixed distance through a tube in the presence of an electrostatic gradient. These instruments have traditionally been limited to measurements of ionized molecules and small (~1 nm) cluster ions. Previously developed devices are not able to sample charged aerosol particles from the ambient because of the high electric fields present at the beginning of the drift region. An additional limitation of existing DT-IMS devices is the low sensitivity of the Faraday Cup Electrometers at concentrations found in typical aerosols. Conversely, DT-IMS devices have the advantages of mobility invariant high resolving power (>R~20), low drift gas flow rates compared to differential mobility analyser (DMA) sheath gas flowrates and shorter measurement times as compared to most scanning differential mobility analyses. Therefore, modification of such devices, such that they can be coupled to sensitive condensation particle counters (CPCs) and used for aerosol particle electrical mobility measurement is of interest.

We have made such modifications, developing a DT-IMS applicable for 2-10 nm aerosol particle analysis, which is described in this presentation. The modifications to traditional DT-IMS devices required for application in ambient pressure aerosol measurement include a novel gateless sample introduction scheme, and the ability to couple to an aspirating CPC. The gateless sample introduction, with particle pathlines and electrical field strengths depicted in Figure 1, uses a combination of a controlled flow path and stepped voltage at the start of a measurement to effectively select a 'packet' of aerosol. Additional aerosol is not able to enter the sample region after the start of a measurement due to the presence of an electrostatic field. The coupling to a CPC requires a controlled flow that splits to provide the drift gas and the gas aspirated by the CPC at the drift tube outlet. A prototype device with these inlet and outlet modifications has been constructed and tested. Example results for charge reduction electrospray generated Cytrochrome C aerosol particles are shown in Figure 2. The prototype DT-IMS has a linear relationship between drift time and mobility, a resolving power greater than 10, and can measure 2-10 nm aerosol particle electrical mobility distributions in less than 5 seconds.

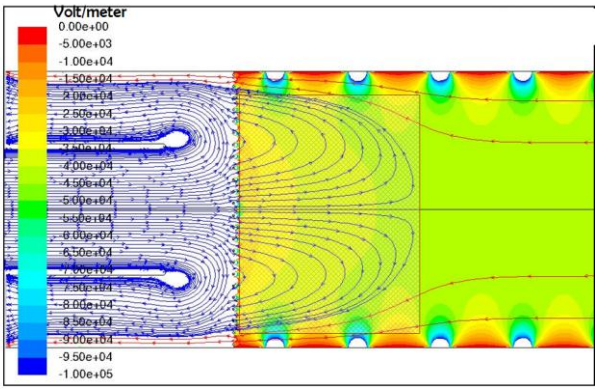

Figure 1. The pathlines (blue) of aerosol particles entering the inlet of the DT-IMS when the electric field is not applied. Color contours reveal the intensity of the electric fields when applied; these fields drive aerosol particles within the sample packet zone down drift tube (to the detector).

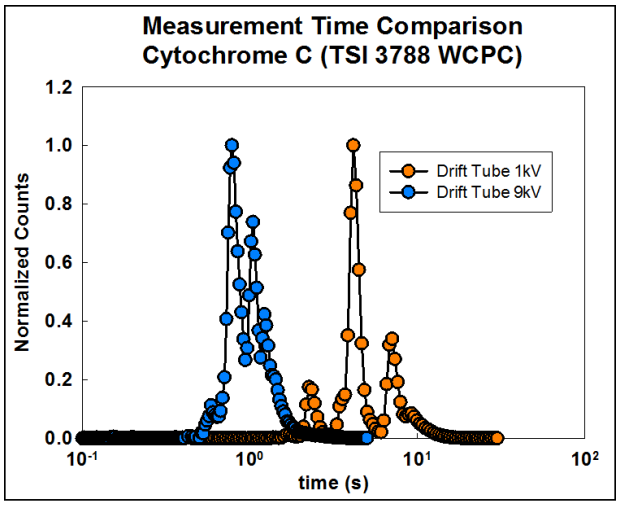

Figure 2. Normalized CPC signal intensity as a function of drift time (inversely proportional to electrical mobility) for electrosprayed Cytochrome C in the DT-IMS. The most prominent peaks in the displayed distributions correspond to the singly charged monomer ion at 3.15 nm mobility diameter, with the peak to the right corresponding to the Cytrochome C dimer (4.35 nm). Longer drift times enable greater peak separation.

This work was support by National Science Foundation grant CHE- 1011810.

A new version of the Particle Size Magnifier for detection of airborne molecular clusters and nano-particles as small as 1 nm

K. Lehtipalo[1,2], A. Franchin[1,2], J. Mikkilä[2], J. Vanhanen[2], J. Kangasluoma[1], T. Petäjä[1], and M. Kulmala[1]

[1]Department of Physics, University of Helsinki, 00560 Helsinki, FINLAND
[2]Airmodus Oy, 00560 Helsinki, FINLAND

Keywords: condensation particle counters, nucleation, nano-particles
Presenting author email: katrianne.lehtipalo@helsinki.fi

There is a growing demand on measuring airborne particles and clusters even down to the size of 1 nm. For instance, the new particle formation process is not yet completely understood on a molecular level, mainly due to the lack of suitable instrument to detect the recently formed particles. The new generation of condensation particle counters (*e.g.* Vanhanen *et al.,* 2011, Jiang *et al.,* 2011, Wimmer *et al.,* 2013) allow deriving parameters describing the new particle formation process, *e.g.* the formation and growth rates, directly from measurements also in the size range below 2 nm (Kirkby *et al.,* 2011; Kuang *et al.*, 2012; Kulmala *et al.,* 2013).

The Airmodus Particle Size Magnifier (PSM; Vanhanen *et al.,* 2011) can be used to resolve the size distribution of particles below about 3 nm. The cut-off size of the instruments was varied between 1-2.5 nm by altering the mixing ratio of saturator and aerosol flow and thus changing the supersaturation created. A schematics of the instrument is presented in Fig. 1.

The relation between the flow mixing ratio and activation diameter in the PSM has been determined in laboratory calibrations using size-selected ammonium sulphate ions. The PSM was found to activate ammonium sulphate clusters consisting of just a few molecules, and it was able to detect even single large molecules, for example tetra-alkyl ammonium halides. Clusters and particles of different composition activate at slightly different flow rate, indicating that there is a material dependency. This is further studied in Kangasluoma *et al.,* (2013).

The A09 PSM have been used to measure the size distribution of particles between 1 – 3 nm in field measurements *e.g.* at the Hyytiälä SMEAR II measurement station in southern Finland (Kulmala et al., 2013) and at the CLOUD experiments in CERN (Kirkby et al., 2011). The data was compared to neutral clusters measured with the CI-APi-TOF mass spectrometer (Jokinen *et al.,* 2012), and to ion clusters measured with the APi-TOF (Junninen *et al.,* 2011). By combining the PSM and the new mass spectrometric methods it is possible to cover the whole size range from molecules to aerosol particles.

A new version of the Particle Size Magnifier, A10, was developed during 2012-2013. It includes modifications especially in the air and liquid flow design. A special care has been taken in making the instrument stable in varying operating conditions. The A10 PSM has been tested in the laboratory, and it will be take part in atmospheric field measurement campaigns during spring 2013.

A special version of the A10 PSM will be used as a counter in the Gas Aerosol Nucleation Spectrometer built in the GANS project (http://www.gans-project.eu/, Dohányosová et al. 2013).

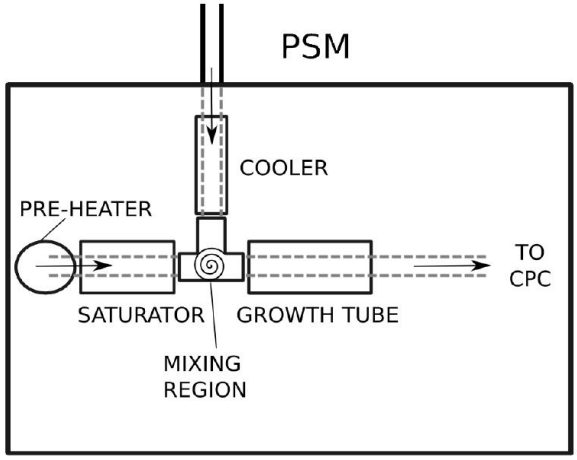

Figure 1. Schematics of the Particle Size Magnifier. Sample air is going from the inlet through a cooler before being mixed with saturated clean air in the mixing region. Particles grow to about 90 nm in the growth tube before they are directed to a counter CPC.

This research has been partly funded by the ERC-Advanced "ATMNUCLE" grant no. 227463), the Academy of Finland (Center of Excellence project no. 1118615), and the Eurostars Programme under contract no. E!6911

Dohányosová, P., *et al.,* (2013). This abstract book.
Jiang, J. *et al.* (2011) *Aerosol Sci. Technol.* **45**, 510–521.
Jokinen et al. (2012) *Atmos. Chem. Phys.,* **12**, 4117-4125
Junninen, H. *et al.* (2010) *Atmos. Meas. Tech.*, **3**, 1039-1053.
Kangasluoma et al., (2013). Aerosol Sci. Technol. in press
Kirkby, J. *et al.* (2011) *Nature* **476**, 429-433.
Kuang, C. *et al.* (2012). Atmos. Chem. Phys. **12**, 3573-3589.
Kulmala, M. *et al* (2013). *Science*, **22**, 911-912.
Vanhanen, J. *et al.* (2011) *Aerosol Sci.Tech.* **4**, 533-542.
Wimmer et al., (2013). *Atmos. Meas. Tech. Discuss* **6**, 2151-2181.

First results of a new Gas Aerosol Nucleation Spectrometer: GANS

P. Dohányosová, E. Montoya, E. Ramiro, S. López-Vidal

RAMEM SA., Madrid, 28027, Spain
Keywords: instrumentation, DMA, nucleation.
Presenting author email: slopez@ioner.net

Nucleation is currently a hot issue in the aerosol science field and much attention has been dedicated to the problem (e.g. special issue in the Journal of Aerosol Science and Technology in April, 2011). One of the most important difficulties for the study of aerosol nucleation is the lack of available instrumentation with good performance and enough sensitivity for size-classifying the sub-2nm nanoparticles.

GANS (http://www.gans-project.eu/) is a project whose aim is to develop a commercial mobility-based particle sizer based on a planar DMA. The new instrument covers the particle sizes where the nucleation phenomena take place and where particles and ions coexist (< 5 nm). Several important innovations can be found in GANS instrument. The first one is a multipurpose ion source suitable for inorganic and organic ions (Ultra-Violet (UV) light ion source and Atmospheric Pressure Chemical Ionization (APCI) source designed by Ramem/Ioner). As the ion source can be switched off, free ions can also be detected. The second innovation of GANS project is the development of an instrument achieving much higher resolution than the resolution obtained in conventional Ion Mobility Spectrometers (IMS). The expected resolution of new GANS instrument is 80, even though the actual state of the instrument allows a resolution around 60. GANS is available with two detectors. The first detector is an electrometer with a sensibility of femtoAmpers. The second detector, and one of the main innovations in GANS project, is the inclusion of a Particle Size Magnifier (PSM) developed by Airmodus. The PSM is a special type of Condensation Particle Counter (CPC) for ions smaller than 2nm (Lehtipalo *et al*., 2013).

In this work we present first results of GANS instrument performance. To test the instrument, an aerosol of tetraheptylammonium (THA) ions was formed from a solution of THABr with IONER® ES-3020 electrospray source. In order to optimize the Resolving Power (RP) various experimental conditions were tested. As can be observed in Figure 1, the instrument can achieve RP higher than 60.

Regarding the ion source, the inorganics will be ionized using an APCI source. The new Ramem/Ioner´s ACPI ion source was tested with ammonium sulphate under various experimental settings. The results are compared with a radioactive ion source in Figure 2. As can be seen, the APCI source can charge ammonium sulphate aerosol as efficiently as radioactive source under optimal setting.

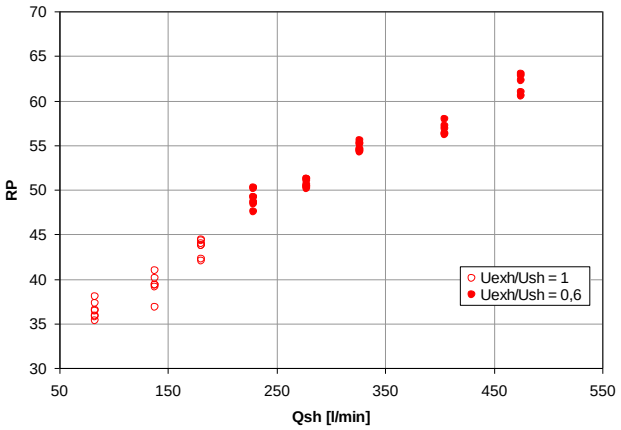

Figure 1: RP of GANS instrument for the monomer ion THA^+.

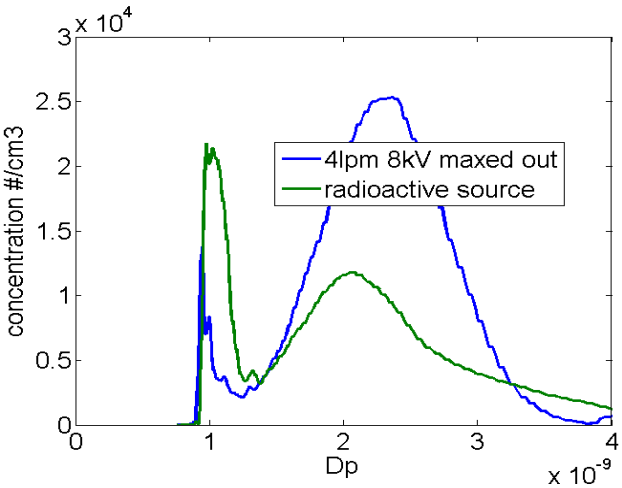

Figure 2: Comparison between Ramem/Ioner´s APCI and radioactive source for ammonium sulphate clusters.

This work was supported by the Eurostars Programme under contract no. E!6911.

Special Issue (2011) *Aerosol Sc.i and Tech.*, **45** (4).
Lehtipalo,K., *et al.*, (2013) This abstract book.

The versatile Size Analyzing Nuclei Counter (vSANC)

T. Pinterich[1], P. M. Winkler[1], P. E. Wagner[1], M. Kulmala[2], A. Vrtala[1]

[1]Faculty of Physics, University of Vienna, Vienna, A-1090, Austria
[2]Department of Physics, University of Helsinki, Helsinki, P.O. Box 64, 00014, Finland
Keywords: Nanoparticles, nucleation studies, CPC
Presenting author email: tamara.pinterich@univie.ac.at

We present a newly developed expansion chamber condensation particle counter - the versatile Size Analyzing Nuclei Counter - suitable for studies on nanoparticles from diameters of 1-2nm upwards. The vSANC is applicable for both, laboratory as well as long-term field measurements at temperatures ranging from $-20°C$ to $+40°C$ and inlet gas pressures ranging from 0.2bar to 1.2bar.

The operation is based on heterogeneous nucleation of supersaturated vapor on aerosol particles and subsequent droplet growth, whereby well-defined uniform supersaturation inside the measuring chamber is achieved by adiabatic expansion. Thereby small particles grow to visible sizes where they can be detected by applying the multiple Constant Angle Mie Scattering method. The measuring principle was adopted from the Size Analyzing Nulcei Counter and can be found elsewhere (see Wagner *et al*, 2003). Here the droplets, growing in the expansion chamber are illuminated by a solid state laser beam ($\lambda = 488nm$). The resulting scattered light fluxes are then monitored simultaneously at 10 different scattering angles.

In order to enable an automatic establishment of a correspondence between experimental and theoretical (Mie-theory) light scattering extrema, a tailormade software was developed dividing scattering intensities for two specifically selected angles by each other. The resulting structure has strongly pronounced extrema, which make an automated data evaluation possible (Hollaender *et al*, 2002). By additionally measuring the transmitted light flux, absolute determination of particle number concentrations ranging from 50/cc to 10^7/cc is enabled without the need of external calibration. Moreover well-defined uniform conditions in the expansion chamber allow for an automated determination of droplet growth rates for precision verification of vapor supersaturation ranging from 5% up to the limit of homogeneous nucleation.

The design of the experimental setup, including expansion chamber, subpressure vessel, valves, tubing, pumps and critical orifices, enables constant and continuous aerosol flow during measurements. In addition the sampling flow through the chamber can be controlled either by means of critical orifices (active sampling mode) or externally (passive sampling mode). Particularly the latter is of advantage when performing measurements in combination with a uDMA. The redundant system layout allows the exchange of filters and dryers during experiment. Thus continuous long-term measurements are possible.

Furthermore the system pressure can be chosen independent from the ambient air pressure. The only limitation is given by the measuring range of pressure sensitive components, such as pressure gauges. Hence the input gas pressure can range from 0.2bar to 1.2bar.

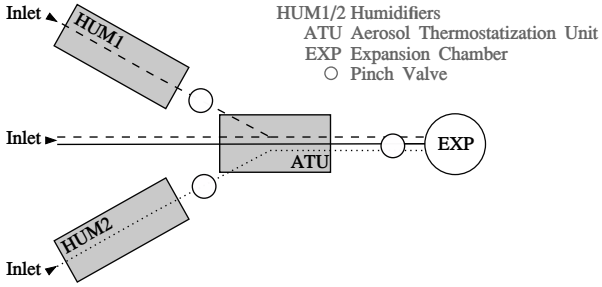

Figure 1: Schematic diagram of the aerosol inlet system. Either the aerosol is already humidified and is passed directly into the expansion chamber (solid line) or it first passes through one of the two humidifiers (dotted line) or it gets mixed with humidified air in the aerosol thermostatisation unit (dashed line).

To minimize particle losses along the sampling line the inlet system was designed as short and straight as possible using only stainless steel tubing and pinch valves with complete and true full bore, when open. The inlet system includes three alternative aerosol inlets, two humidifiers, and the aerosol thermostatization unit. Its design provides flexibility with respect to aerosol presampling conditions (see figure 1). In addition it is possible to alter two different condensing liquids, e.g. polar and non-polar, or use binary vapors.

In conclusion, the vSANC provides a powerful tool to investigate nanoparticles from diameters of 1-2nm upwards. It enables the determination of droplet growth rates and absolute number concentrations ranging from 50/cc to 10^7/cc. The vSANC was optimized to achieve high flexibility with respect to temperature, inlet gas pressure, and condensing liquid. Its mobility and the redundant system layout even enable long-term field measurements. We present first measurement results providing determinations of heterogeneous nucleation probabilities and allowing evaluations of sizes of molecular clusters.

This work was supported by the Austrian Science Fund (Project No. AL0059321).

Hollaender, W. *et al.* (2002) *J. Atmos. Oceanic Technol.* **19**, 1811.
Wagner, P. E. *et al.* (2003) *Phys. Rev. E.* **67**, 021605.

Charging efficiency of the single-wire corona unipolar charger with radial sheath flow

V. Wattanamekhinkul[1], C.L. Chein[1] and C.J. Tsai[1]

[1]Institute of Environmental Engineering, National Chiao Tung University, Hsinchu, 30010, Taiwan
Keywords: unipolar aerosol charger, charging efficiency, nanoparticles, aerosol instrumentation.
Presenting author email: w_virat@yahoo.com

A single-wire corona unipolar charger has been developed and investigated to enhance the extrinsic charging efficiency of nanoparticles by using radial sheath air to minimize charged particle loss. Experimental charging efficiencies were obtained at a fixed aerosol flow rate of 0.5 and 1.0 L/min using monodisperse silver nanoparticles of 2.5 to 20 nm in diameter. The applied sheath air flow rates range from 0.5 to 2.0 L/min, while the applied corona voltage range from ±1.80 to ±2.70 kV respectively.

Figure 1 shows the schematic diagram of the present unipolar charger which is a modification of the nanoparticle charger with multiple discharging wires developed by Tsai et al. (2010) and the nanoparticle charger with sheath air developed by Chien et al. (2011). The outer stainless steel cylindrical casing of 30 mm in diameter is grounded. A 6 mm long grounded porous metal tube (inner diameter ID = 6.35 mm) with a Teflon tube inserted at the end from which radial sheath air is introduced, and a discharge gold wire of 50 μm in ID and 6 mm in effective length is used as the discharge electrode, on which a high DC voltage is applied from the top of the charger. The space between the gold wire and the stainless steel casing is the charging zone where aerosol charging takes place.

The aerosol flow is introduced into the charger from the top aerosol inlet through an annular slit of 0.05-mm gap formed by the stainless steel shroud and the outer casing, and filtered high-speed sheath airflow with the velocity of 0.07–0.28 m/s is introduced through the inner wall of the porous tube to avoid charged particle loss. The charged particles are accelerated to exit the charger quickly through the bottom aerosol outlet after the charging zone.

Four parameters are used for the performance evaluation of unipolar electrical aerosol chargers (Marquard et al. 2006), including intrinsic charging efficiency (η_{int}), extrinsic charging efficiency (η_{ext}), electrostatic loss (L_{el}), and diffusion loss (L^0_d).

The obtained experimental data will be used to validate with numerical results of Chien and Tsai (2012) which shows that the extrinsic charging efficiency ranges from 17.2% - 70.5% for particles ranging from 2.5 to 10 nm in diameter.

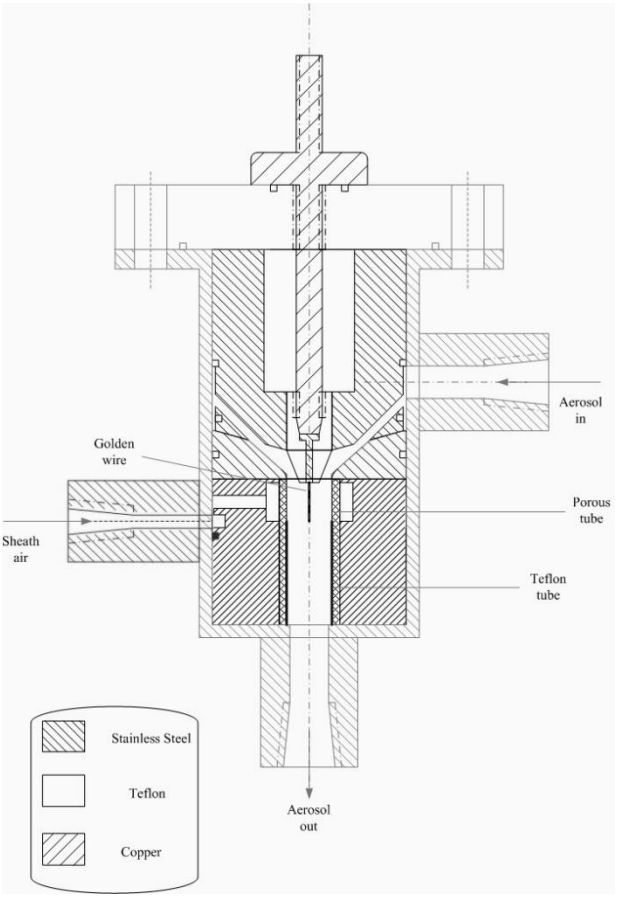

Figure 1. Schematic diagram of the present unipolar charger

Chien, C.L., Tsai, C.J., Chen, H.L., Lin, G.Y., and Wu, J.S. (2011) *Modeling and Validation of Nanoparticle Charging Efficiency of a Single-Wire Corona Unipolar Charger*. Aerosol Sci. Technol. **45**, 1468-1479.

Chien, C.L., Tsai, C.J. (2013) *Improvement of the nanoparticle charging efficiency of a single-wire corona unipolar charger by using radial sheath air flow: numerical study*, Aerosol Sci. Technol. **7**, 417–426.

Marquard, A., Meyer, J., and Kasper, G. (2006) *Characterization of Unipolar Electrical Aerosol Chargers—Part I: A Review of Charger Performance Criteria*, J. Aerosol Sci. **37**, 1052–1068.

Tsai, C.J., Lin, G.Y., Chen, H.L., Hunag, C.H., and Alonso, M. (2010) *Enhancement of Extrinsic Charging Efficiency of a Nanoparticle Charger with Multiple Discharging Wires*, Aerosol Sci. Technol. **44**, 807–816.

Application of broadband optical cavity methods to studying the optical properties of aerosols at short wavelengths

E. M. Wilson[1,2], J.C.Wenger[1,2], D. S. Venables[1,2]

[1] Department of Chemistry, University College Cork, Cork, Ireland
[2] Environmental Research Institute, University College Cork, Cork, Ireland

Keywords: optical properties, near-ultraviolet, optical cavity, IBBCEAS, nitroaromatic, nitrophenol, SOA, simulation chamber
Presenting author email: eoin.wilson@umail.ucc.ie

There is currently much interest in light absorption by atmospheric aerosols. Recent research has shown that some types of atmospheric particles start to absorb strongly at blue and ultraviolet wavelengths, but there are few techniques to probe the aerosol optical properties at these wavelengths. Varma et al. (2009) first showed that *incoherent broadband cavity-enhanced absorption spectroscopy* (IBBCEAS) is a promising approach to measure aerosol extinction with high sensitivity. Several groups are now using IBBCEAS for studying aerosol optical properties across a continuous spectral region and at short wavelengths (Washenfelder et al., 2012; Zhao et al., 2013). Our aim in this presentation is to describe our recent work to extend IBBCEAS aerosol measurements to very short wavelengths (Chen et al., 2011; Wilson et al., 2012).

A schematic of the experimental system is shown in Fig. 1. The IBBCEAS system was coupled directly across a 4 m^3 atmospheric simulation chamber in the Centre for Research into Atmospheric Chemistry at University College Cork. The system is unusual in that it is a single channel optical cavity spectrometer with continuous spectral coverage from 320 to 405 nm. The 4 m long optical cavity partially compensated for the reduced mirror reflectivity across this broad range. A xenon short arc lamp was used as a light source across the spectral region.

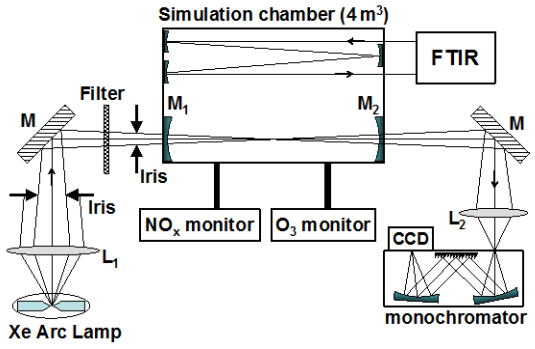

Figure 1. Layout of the atmospheric simulation chamber, IBBCEAS spectrometer, and ancillary equipment.

The stability and sensitivity of the system's extinction measurements were evaluated in a series of SOA experiments. The SOA was formed by photolysing strongly absorbing nitroaromatic compounds, which have been implicated in reducing levels of actinic radiation in large urban centres. The analysis of the total extinction spectrum is discussed, particularly how the contributions of gas phase absorption and particle extinction can be separated. We consider key elements of the experimental system and compare our approach to those of other groups. Finally, the future prospects for using IBBCEAS in field and chamber studies are assessed.

We gratefully acknowledge financial support from Science Foundation Ireland through grant 11/RFP/GEO3200.

Chen, J., Wenger, J.C., and Venables, D.S. (2011) *J. Phys. Chem. A*, **115**, 12235–12242.
Varma, R.M., Venables, D.S., Ruth, A.A., Heitmann, U., Schlosser, E., Dixneuf, S. (2009) *Appl. Opt.* **48**, B159.
Washenfelder, R.A., Flores, J.M., Brock, C.A., Brown, S.S., and Rudich, Y. (2012) *Atmos. Meas. Tech. Discuss.*, **6**, 113-157.
Wilson, E.M., Chen, J., Varma, R.M., Wenger, J.C. and Venables, D.S. (2012); *Proc. Int. Rad. Symp.*, AIP (in press).
Zhao, W., Dong. M., Chen, W., Gu, X., Hu, C., Gao, X., Huang, W., and Zhang, W. (2013) *Anal. Chem.*, **85**, 2260.

Monday, September 1, 2013

Special Session: PMx
Source apportionment-AMS and carbon based

ME-2 analysis of long-term on-line mass spectrometric data of non-refractory submicron aerosol in the city of Zurich

F. Canonaco[a], J. G. Slowik[a], U. Baltensperger[a], A.S.H. Prévôt[a]

[a]Laboratory of Atmospheric Chemistry, Paul Scherrer Institut, 5232 Villigen PSI, Switzerland
Keywords: AMS, PMF, ME2, ACSM
Presenting author email: francesco.canonaco@psi.ch

The role of aerosols in the atmosphere is of importance, because they affect climate (Forster *et al.,* 2007), human health (Peng *et al.,* 2005), ecosystems, e.g., acidification (Matson *et al.,* 2002), and visibility (Watson, 2002). Thus, the identification and quantification of formation mechanisms and sources is of high priority. However, this task is complicated due to the complexity of particle composition.

Long-term monitoring of aerosol composition provides a powerful tool for the analysis of the aforementioned effects. Long-term measurements allow capturing the seasonal variability of different aerosol constituents, which is not possible with shorter-term campaigns. Furthermore, long-range, mesoscale, and local air quality models can be improved through comparison with long-term datasets. Finally, the existence of long-term sampling records at a given site provides a framework for the interpretation of datasets from short-term intensive measurement campaigns.

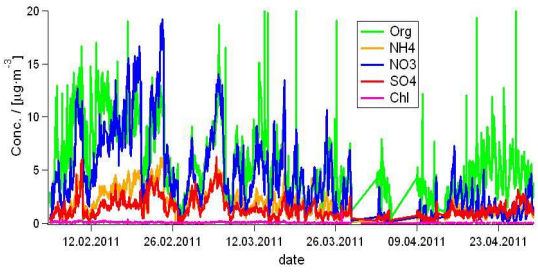

Fig. 1. Preliminary time series of the ACSM including SO_4, NO_3, NH_4, Cl and organics. For the sake of simplicity the figure contains only the winter data.

We present measurements of submicron aerosol composition from an aerosol chemical speciation monitor (ACSM, Aerodyne Research, Inc.) deployed in downtown Zurich. The ACSM yields quantitative mass spectra of the non-refractory aerosol component with an averaging period of 15 to 30 minutes. These are one of the first full-year measurements in Europe using this technique. As shown in Fig. 1, the ACSM is capable of resolving inorganic species such as NH_4, SO_4, NO_3, Cl, and the organics. The data can be further deconvolved in order to identify and apportion the sources, in particular for the complex organic fraction.

There are several possible techniques for the deconvolution of a data set. Positive matrix factorization (PMF) has been extensively exploited for this type of data. However, the multilinear engine 2 (ME2) offers advantages compared to PMF, due to the fact that the user has the possibility to introduce a priori information in form of e.g. known factor profiles into the model (Paatero, 1999).

The aim of this work is to make use of the multiple approaches available in ME2 on a large dataset, in particular on the obtained data from downtown Zurich during the full year 2011. For this purpose we implemented a user-friendly interface in the software IGOR Pro (Wavemetrics, Inc.) which shall be shared in the next future with other research groups.

We will discuss identification and source apportionment of ACSM organic data at an urban site over the full year of 2011 with the ME-2 algorithm. Different techniques, like the a-value (Lanz et al., 2008) or the pulling approach (Paatero, P. and Hopke, P.K., 2009), as highlighted in Fig.2 have been tested. Moreover, studying and comparing the outcomes of these just mentioned techniques provides useful information for estimating of the model uncertainty.

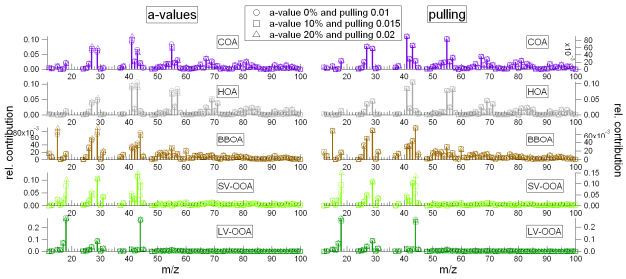

Fig. 2. Preliminary factor profiles of the source apportionment of the ACSM organic winter data. For the sake of simplicity the figure comprises only the winter data.

This work was supported by the Swiss Federal Office for the Environment (FOEN) and the Swiss National Science Foundation through the Ambizione program.

Forster, P. et al. (2007) Cambridge University Press.
Lanz, V.A. et al. (2008) *Environ. Sci. Technol.* **42**, 214 220.
Matson, P. et al. (2002) *Ambio* **31**, 113-119.
Peng, R. et al. (2005) *Am. J. Epidem.* **161**, 585-594.
Paatero, P. (1999) *J. Comp. Graph. Stat*. **8**, 854-888.
Paatero, P. and Hopke, P.K. (2009) *J. Chemometrics.,***23**, 91-100.
Watson, J.G. (2002) *J. Waste Air Manage.* **52**, 628-713.

A Year-long C-TOF-AMS Dataset in London: Investigating Chemical Composition, Seasonal Trends and Sources of Aerosols

D.E Young[1], J.D. Allan[1,2], D.C. Green[3], P.I. Williams[1,2] and H. Coe[1,2]

[1]School of Earth, Atmospheric and Environmental Sciences, University of Manchester, Oxford Road, Manchester, M13 9PL, UK
[2]National Centre for Atmospheric Science, University of Manchester, Oxford Road, Manchester, M13 9PL, UK
[3]King's College London, Environmental Research Group, Franklin-Wilkins Building, 150 Stamford Street, London, SE1 9NH, UK
Keywords: aerosols, London, AMS, PMF.
Presenting author email: dominique.young@postgrad.manchester.ac.uk

An Aerodyne compact Time-of-Flight Aerosol Mass Spectrometer (cToF AMS) was deployed in London as part of the Clean Air for London (ClearfLo) project. A full calendar year of data were collected, covering the two major intensive observation periods (IOPs) in the winter and summer of 2012 during which aerosols, radicals, gases and meteorological parameters were measured by a suite of state-of-the-art instrumentation. Measurements were also conducted before, during, and after the 2012 summer Olympic Games which were held in the city.

The cToF AMS was located in a permanent London Air Quality Network (LAQN) monitoring station representative of an urban background environment from 11 January 2012 until 23 January 2013 (Fig. 1). The IOP measurements also took place at this site in North Kensington. Both clean westerly conditions and more polluted conditions including transported European plumes were experienced at the site. Contrasting meteorological conditions, such as inversions and heat waves, also influenced the site throughout the year.

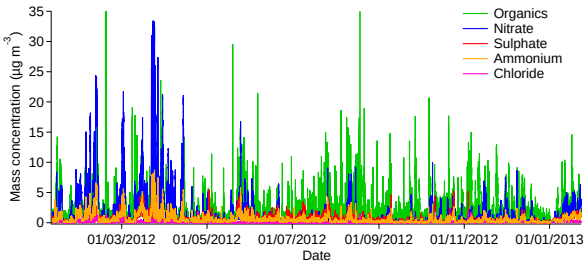

Figure 1. Time series of organic and inorganic mass concentrations measured by the cToF AMS.

Distinct diurnal profiles (Fig. 2) for the entire year of data are observed for the organic aerosols with peaks in concentration either side of midday and a large evening peak. The diurnal profile of nitrate exhibits a morning peak and afternoon trough. Seasonal trends are also evident with a change in the dominant species from nitrate to organic between winter and summer.

Preliminary positive matrix factorization (PMF) analysis identified at least five factors (Fig. 3) as potential sources for the organic aerosols in this urban environment. Primary organic aerosols include hydrocarbon-like (HOA), solid fuel (SFOA), and cooking (COA). Both type 1 and type 2 oxygenated secondary organic aerosols are identified.

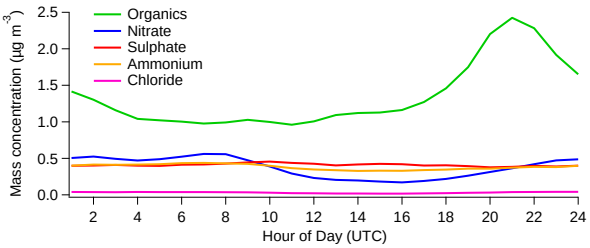

Figure 2. Median diurnal profiles of organic, nitrate, sulphate, ammonium, and chloride species.

There is a near equal contribution of primary and secondary aerosols to the total organic mass of the whole year, where primary aerosol dominate in the winter and secondary aerosols dominate in the summer.

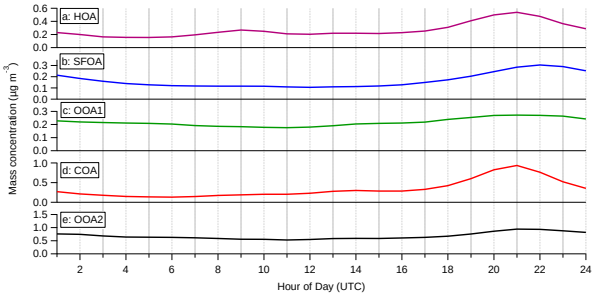

Figure 3. Median diurnal profiles of 5-factor solution from preliminary PMF analysis of organic data.

Long-term cToF AMS data, including solutions from PMF analysis will be presented, highlighting diurnal and seasonal characteristics of London urban background pollution. These data will be used to identify sources of organic aerosols and how these change with time. Furthermore the factors from PMF analysis can be used to target factors in future Aerosol Chemical Speciation Monitor (ACSM) studies at the same site.

This work was supported by the UK Natural Environment Research Council under grant NE/H003150/1.

Primary and secondary organic aerosol origin by combined gas-particle phase source apportionment

M. Crippa[1], F. Canonaco[1], J. G. Slowik, I. El Haddad, P. F. DeCarlo[1*], C. Mohr[1**], M. F. Heringa[1***], R. Chirico[1****], N. Marchand[2], B. Temime-Roussel[2], E. Abidi[2], L. Poulain[3], A. Wiedensohler[3], U. Baltensperger[1], A. S. H. Prévôt[1]

[1] Laboratory of Atmospheric Chemistry, Paul Scherrer Institute, PSI Villigen, 5232, Switzerland
[2]Aix-Marseille Université, CNRS, LCE FRE 3416, 13331, Marseille, France
[3]Leibniz Institut for Tropospheric Research, Permoserstr 15, 04318, Leipzig, Germany
[*]now at: Department of Civil, Architectural, and Environmental Engineering and Department of Chemistry, Drexel University, Philadelphia, PA, USA, 19104
[**]now at: Department of Atmospheric Sciences, University of Washington, Seattle WA 98195, USA
[***]now at: WIL Research, 5203 DL 's-Hertogenbosch, The Netherlands
[****]now at: Italian National Agency for New Technologies, Energy and Sustainable Economic Development (ENEA), UTAPRAD-DIM, Via E. Fermi 45, 00044 Frascati, Italy

Keywords: source apportionment, ME-2, organic aerosols, VOCs.
Presenting author email: monica.crippa@psi.ch

Secondary organic aerosol (SOA), typically the dominant fraction of particulate organic mass (OA), remains poorly constrained. Its formation involves several unknown precursors, formation and evolution pathways and multiple natural and anthropogenic sources. In our work a combined gas/particle-phase source apportionment is applied to wintertime and summertime data collected in the megacity of Paris within the MEGAPOLI project to investigate SOA origin during both seasons (Crippa et al., submitted). Source apportionment was conducted by positive matrix factorization (PMF) analysis of combined mass spectra from an Aerodyne aerosol mass spectrometer (AMS) and a proton transfer reaction mass spectrometer (PTR-MS). PMF was implemented within a new source apportionment toolkit based on the multi-linear engine (ME-2) algorithm (Canonaco et al., in prep.).

The combined method improved apportionment of primary OA (POA) sources by the inclusion of gas-phase tracers. These tracers further allowed distinguishing between biogenic-influenced and continental/anthropogenic sources of SOA. We found that continental SOA was dominant during both seasons (24-50% of total OA), while contributions from photochemistry-driven SOA (9% of total OA) and marine emissions (13% of total OA) were also observed during summertime. A semi-volatile nighttime component was also identified (up to 18% of total OA during wintertime). The presence of benzene and PAN in the wintertime oxygenated continental factor suggested that this secondary fraction could be influenced by biomass smoke in aged air masses, consistent with ^{14}C data.

Apportionment of the volatile organic compounds (VOCs, see Fig.1) indicated that traffic was mostly the dominant source of the aromatic fraction. However, aged air masses (during winter) and nighttime air (during summer) were also significant sources. Cooking contributed an unexpectedly high fraction of the total aromatics, possibly due to the overlap of traffic and cooking emissions influenced by meteorology. The source apportionment of oxygenated VOCs revealed that secondary species dominated in both seasons, but especially summer. During wintertime acetic acid was also produced by wood burning emissions. Finally, biogenic emissions were produced by biomass burning during wintertime while “fresh” secondary species dominated in summer.

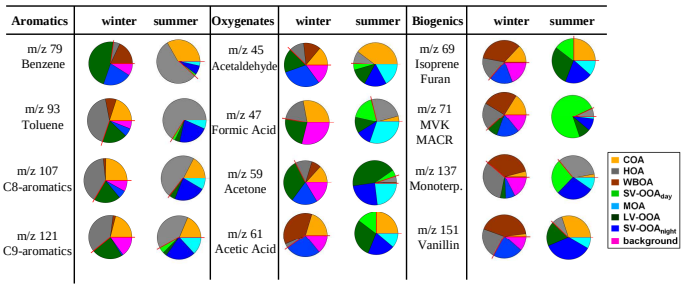

Figure 1. Source apportionment of aromatic, oxygenated and biogenic VOCs.

This research in the context of the MEGAPOLI project is financially supported by the European Community’s Framework Program FP/2007-2011 under grant agreement n°212520, as well as the Swiss Federal Office for the Environment and Swiss National Science Foundation.

Canonaco, F., et al.., in preparation.
Crippa, M., et al., submitted ACP-2013-94.
Crippa, M., et al., ACP, 13, 961-981, 2013.
Freutel, F., et al., ACP, 13, 933-959, 2013.
Crippa et al., JGR, 118, 1-19, 2013.

Long-term monitoring, chemical composition and source apportionment study of $PM_{2.5}$ in Augsburg, Germany

R.M. Qadir[1,2], G. Abbaszade[1], J. Schnelle-Kreis[1] and R. Zimmermann[1,2]

[1]Institute of Chemistry, University of Rostock, Dr.-Lorenz-Weg 1, D-18051 Rostock, Germany
[2]Joint Mass Spectrometry Centre -"Comprehensive Molecular Analytics", Helmholtz Zentrum München, Ingolstädter Landstraße 1, D-85764 Neuherberg, Germany

Keywords: $PM_{2.5}$, Particulate organic compounds (POC), PMF.
Presenting author email: raeed.qadir@helmholtz-muenchen.de

Knowledge of the temporal and spatial variation of particulate organic matter (POM) and its chemical composition are clearly needed to understand its climate and adverse human health effects. To protect both human health and the environment, it is important to combat pollutant emissions at the source and identify and implement the most effective reduction measures at local, national and international levels. Comprehensive studies are therefore necessary to evaluate the characteristics of PM at the different sources. Organic compounds of biogenic and anthropogenic origin often represent a large fraction, up to 40%, of total PM mass. The concentrations of organic compounds ranging from below $pg.m^{-3}$ to $mg.m^{-3}$[1].

A monitoring site for detailed physical and chemical characterization of ambient fine and ultrafine particles was established in Augsburg in October 2004. The station is located on the premises of the University of Applied Sciences (Fachhochschule) Augsburg (Fig.1). Daily samples of $PM_{2.5}$ were collected at the monitoring site of Fachhochschule in Augsburg city. Allowing for a thorough monitoring of particle associated organic substances and the different sources of PM pollution. The long-term monitoring data, every fifth day samples (from 2007 to 2012) are analyzed for their particulate organic compounds (POC) and carbon fraction (EC/OC) and will be considered in our investigation.

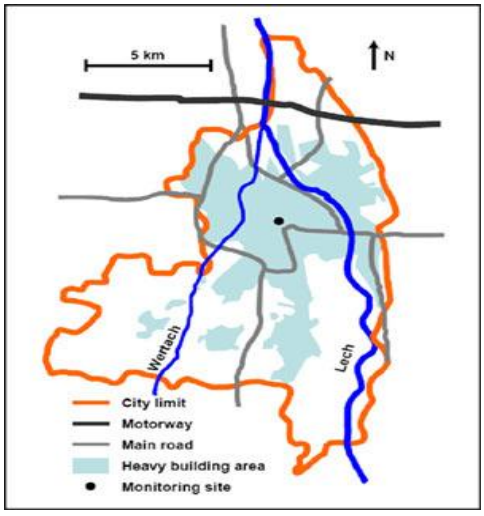

Figure1. Monitoring site in Augsburg

In-situ derivatization thermal desorption gas chromatography time of flight mass spectrometry (IDTD-GC-ToF-MS) [2] is used for the chemical characterization of POC. Elemental and organic carbon fraction (EC/OC) are analyzed by thermal-optical analysis IMPROVE-A protocol.

Results of source apportionment analysis of PM_{10} in Augsburg have been published recently. In our present study, the main sources of POC were identified using positive matrix factorization (PMF) [3]. More than 80 organic species under investigation will be used for PMF analysis, including PAH, oxidized PAH, n-alkanes, iso & anteiso alkanes, hopanes, resin acids, fatty acids, anhydrous sugars and phenolic compounds.

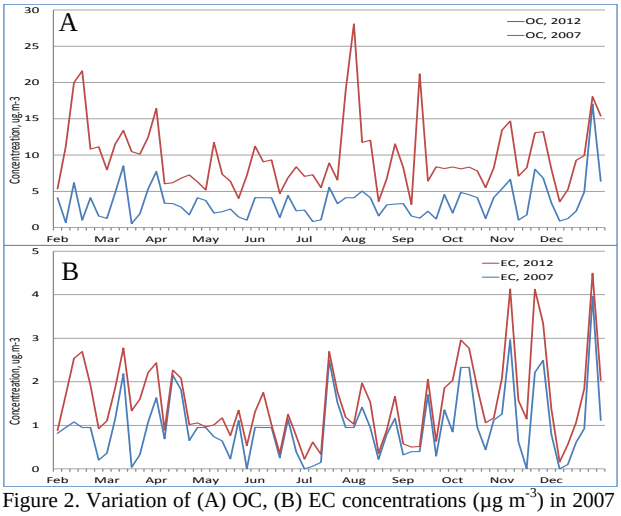

Figure 2. Variation of (A) OC, (B) EC concentrations (µg m^{-3}) in 2007 and 2012

The health effects of organic compounds in aerosols are currently investigated in the framework of the Helmholtz Virtual Institute of Complex Molecular Systems in Environmental Health, HICE (www.hice-vi.eu).

1. Orasche, J., Schnelle-Kreis, J., Abbaszade, G. And Zimmermann, R. (2011). *Atmos. Chem. Phys.* **11**, 8977–8993.
2. Tsapakis, M., Lagoudaki, E., Stephanou, E.G., Kavouras, I.G., Koutrakis, P., Oyola, P., von Baer, D. (2002). *Atmospheric Environment* **36**, 3851-3863.
3. Paatero, P. and Tapper, U., (1994). *Environmetrics* **5**, 111–126.

Composition and Source Identification of Ambient Single Particles during the NANO-INDUS 2012 Campaign in Dunkirk, France

J. Arndt[1], R. Healy[1], A. Setyan[2,3], K. Deboudt[2,3], V. Riffault[2,4], A. Blondel[2,3], A. Anderson[2,3], L. Y. Alleman[2,4], S. Mbengue[2,4], P. Flament[2,3] and J. Wenger[1]

[1]Department of Chemistry and Environmental Research Institute, University College Cork, Cork, Ireland
[2]Université Lille Nord de France, 59000 Lille, France.
[3]Laboratoire de Physico-Chimie de l'Atmosphère, EA 4493-Université du Littoral Côte d'Opale, 59140 Dunkerque, France.
[4]Mines Douai, CE, 59508 Douai, France.

Keywords: Single particle analysis, industrial aerosols, heavy metals, aerosol chemistry
Presenting author email: 104531485@umail.ucc.ie

Situated on the north coast of France, Dunkirk's air quality is subject not only to the high volume of shipping traffic passing through the Dover Strait, but also to the emissions from a considerable industrial sector. The city is host to the largest steel manufacturing plant in France, an oil refinery and an industrial facility with the largest manganese ferroalloy furnace (Fe-Mn furnace) in the world.

The aim of the NANO-INDUS campaign was to characterise the transient emissions from this facility. To this end a suite of online instruments and offline techniques were located approximately 1 km to the southwest of the alloy manufacturing plant, from 15th May – 10th June 2012. An aerosol time-of-flight mass spectrometer (ATOFMS, TSI model 3800), was used to determine the chemical composition and size of individual ambient particles in the vicinity of the Fe-Mn furnace in real time.

Over 700,000 single particle mass spectra were generated and then classified using the *K*-means algorithm. Based on their mixing state, size distributions and temporality, 18 major particle types were identified including: shipping, sea salt, several elemental and organic carbon types, along with some sulfur, calcium, and various Fe-containing types emitted from nearby industrial sources.

Particles containing internally mixed potassium and chloride, typically associated with biomass burning (specifically from domestic wood combustion) were found instead to be industrial in origin. This was supported by the absence of biomass burning organic aerosol (BBOA) in the co-located Aerodyne high-resolution time-of-flight aerosol mass spectrometer (HR-ToF-AMS) dataset. The latter instrument was used to identify a number of sources of organic aerosol (OA) and comparison of these OA factors with the ATOFMS data has provided valuable information on the mixing state of organic aerosol in Dunkirk.

A calcium-containing particle type, usually associated with vehicular traffic emissions in urban field studies, was also found to be industrial in origin. Mass spectra for these particles were dominated by calcium (*m/z* 40, $[Ca]^+$) and carbonate (*m/z* -60, $[CO_3]^-$) and displayed a strong northeasterly wind dependence, the direction of the Fe-Mn furnace. Calcium carbonate is used as an additive in the sintering process and it is thus likely that these particles are emitted from one of the main stacks of the plant.

Fe and Mn particle types, originating from the Fe-Mn furnace were also identified. These included two Fe-containing types, one internally mixed with Na and K, the other internally mixed with Mn (Figure 1). Further Mn-containing particle types were identified and found to contain Pb and K, but not Fe. Zn-containing particles were also observed, with and without Pb. Thus, single particle mixing state was observed to be highly heterogeneous in the vicinity of the industrial facility.

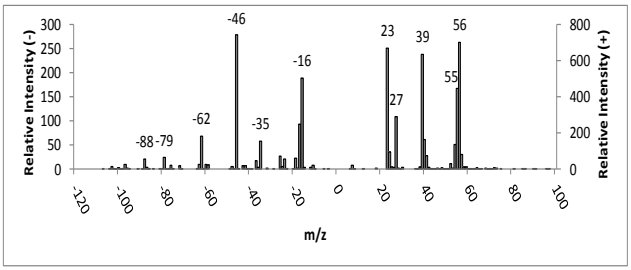

Figure 1. Average mass spectrum of Fe-Mn particles observed in the vicinity of an industrial plant in Dunkirk.

Further information on these metal-containing particles has been obtained by quantitative analysis of filter extracts using ICP-AES and ICP-MS, as well as measurements of single particles using SEM/EDX. The use of these techniques in combination with the mixing state information and high temporal resolution of the ATOFMS provides valuable insights into the sources, composition, variability and chemical processing of single particles from industrial emissions.

The NANO-INDUS project was supported by the French Environment and Energy Management Agency (ADEME) under grant N° 11-81-C0089 and by the Institut de Recherche en ENvironnement Industriel (IRENI). Jovanna Arndt was supported by the Irish Research Council.

Radiocarbon-based source apportionment of elemental carbon and organic carbon at a regional background site on Hainan Island, South China

Y.L. Zhang[1,2,3], J. Li[4], G. Zhang[4], A.S.H. Prévôt[2] and S. Szidat[1,3]

[1]Department of Chemistry and Biochemistry, University of Bern, Berne, 3012, Switzerland
[2]Paul Scherrer Institute (PSI), Villigen, 5232, Switzerland
[3]Oeschger Centre for Climate Change Research, University of Bern, Berne, 3012, Switzerland
[4]State Key Laboratory of Organic Geochemistry, Guangzhou Institute of Geochemistry, Chinese Academy of Sciences, Guangzhou, 510640, China
Keywords: Source apportionment, radiocarbon (^{14}C), carbonaceous particles, elemental carbon, organic carbon
Presenting author email: yanlin.zhang@dcb.unibe.ch

Carbonaceous particles (total carbon, TC) are major fraction of fine particles and are of worldwide concern due to their important impacts on climate and human health. TC is often operationally classified into two sub-fractions: elemental carbon (EC) and organic carbon (OC) (Pöschl, 2005). Radiocarbon (^{14}C) analysis of EC and OC separately allow a quantitative and unambiguous measurement of their contemporary and fossil contributions, thereby potentially reducing a major uncertainty in the present understanding of organic aerosols emissions (Szidat *et al*. 2006).

Both fossil-fuel emissions and biomass/biofuel burning in Southeast Asia may have an important impact on regional EC and OC emissions. Here, we present a ^{14}C-based source apportionment study at a regional background site of Jianfeng (JF) on Hainan Island, South China. This is an ideal site to study air pollutions outflows from mainland China, as well as the impact of Southeast Asian biomass burning emission.

PM2.5 samples were collected about once per week from May 2005 to August 2006 using a high volume sampler (~1 m^3/min) for 24 h. All samples were measured for the EC and OC concentrations by the thermal-optical transmittance method. The EC and OC isolation for subsequent ^{14}C measurements were prepared with an optimized thermo-optical protocol (Swiss_4S) on the selective samples (Zhang *et al*. 2012).

As shown in Figure 1, both EC and OC are characterized by the lowest abundances during the wet summer season (i.e. from the Mid-May to September) and the highest levels in winter (i.e. from mid-November to February). This is most likely due to the high wash-out effect and the prevailing clean maritime air mass origins in summer on the one hand and the anthropogenic air pollutions (biomass and fossil fuel combustions) transportation from continental China with the northeast winds on the other hand.

As an example illustrated in Figure 2, the combination of the analysis of the air mass back trajectories and fire counts on the day of the highest carbonaceous particles levels during the entire study period indicate a significant contribution from open biomass burning to the carbonaceous particles. This idea is further confirmed by ^{14}C measurements, which show the non-fossil sources account for 69% and 88% to the total EC and OC, respectively. Biofuel combustion may be another important non-fossil contributor to EC and OC in Southeast China during the heating season. ^{14}C measurements of the carbon faction of interest on other samples with different air mass origins and seasons will be present as well.

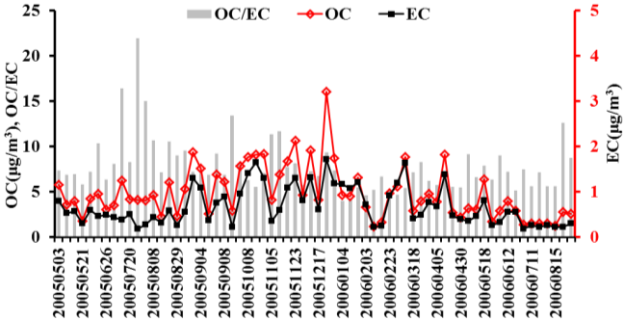

Figure 1. Temporal variations of OC, EC concentrations (μg/m^3) and the OC-EC ratios

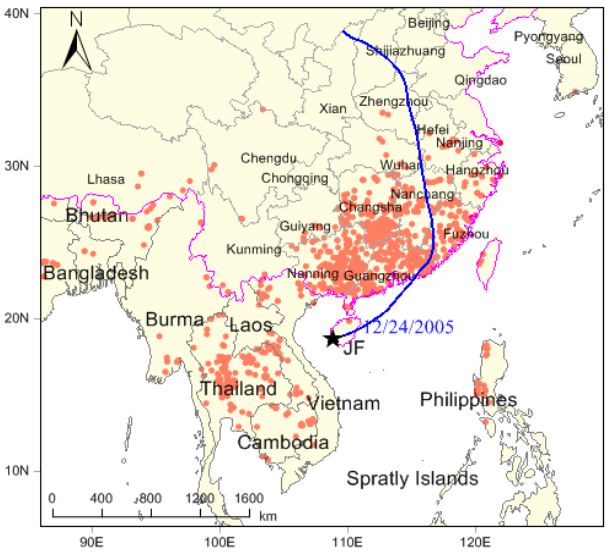

Figure 2. 5-day air mass back trajectories reaching JF and MODIS fire counts on 24 Dec 2005.

Pöschl, U. (2005). *Angew. Chem. Int. Ed.*, **44**, 7520-40.
Szidat, S. *et al*. (2006). *J. Geophys. Res*. **111**, D07206.
Zhang, Y. L. *et al*. (2012). *Atmos. Chem. Phys*. **12**(22), 10841-56.

Wood-burning emissions within a continuous-flow photooxidation reactor: Soot-Particle Aerosol Mass Spectrometer characterization

J. C. Corbin[1], A. Keller[2], H. Butscher[2], B. Sierau[1], U. Lohmann[1], and A. A. Mensah[1]

[1]Institute for Atmosphere and Climate Science, ETH Zürich, Universitätstrasse 16, 8092 Zürich, Switzerland.
[2]Institute of Aerosol and Sensor Technology, FHNW, Klosterzelgstrasse 2, 5210 Windisch, Switzerland.

Keywords: wood-burning, photooxidation, AMS, SP-AMS
Presenting author email: joel.corbin@env.ethz.ch

Wood-burning stoves, used worldwide for heating and cooking, can be an important atmospheric source of primary and secondary aerosols. Current legislation restricts only the primary aerosol emissions of such stoves, which include primary organic aerosol particles (POA), ash, and soot. Such legislation neglects the potential formation of secondary organic aerosol (SOA), which may nucleate or condense after the atmospheric oxidation of volatile organic compounds. For example, smog chamber photooxidation experiments have observed wood-burning SOA concentrations up to four times higher than the corresponding POA emissions (Grieshop et al., 2009; Heringa et al., 2011).

To characterize the SOA-formation potential of wood-burning stoves and similar emissions, Keller and Burtscher (2012) have developed a continuous-flow photooxidation reactor for monitoring potential SOA in real-time. The short residence time (seconds) of this chamber allows the time-resolved measurement of potential SOA. However, the small chamber also necessitates higher-than-ambient irradiation conditions.

Here, we present results from high-resolution Aerosol Mass Spectrometer (AMS) and Soot-Particle AMS (SP-AMS) analysis of wood-stove emissions under three different conditions: filtered and photooxidized ("SOA"), unfiltered and photooxidized ("OxPOA"), and unfiltered emissions ("POA").

Figure 1 shows the increase in aerosol oxidation after photooxidation, as measured by the AMS. The figure shows the difference of the normalized SOA and POA organic mass spectra, averaged over multiple burns. High-resolution analysis has been used to identify organic species as C_xH_y (*green*), $C_xH_yO_{z=1}$ (*purple*), or $C_xH_yO_{z>1}$ (*pink*). However, data are presented on a unit-mass scale for clarity. As shown, the relative intensity of CO_x ions was higher for SOA, whereas C_xH_y was higher for POA. The pie charts (inset) summarize all three cases, showing $C_xH_yO_z$ increasing and C_xH_y decreasing, from left to right. For POA, the contribution of hydrocarbons C_xH_y was more than double that of SOA. Also, SOA contained more $C_xH_yO_{z>1}$ relative to OxPOA. Elemental analysis indicated that the shift of H:C and O:C ratios due to oxidation was comparable to, but significantly greater than, observations in Mexico City (Heald et al., 2010).

In these experiments, refractory species (those involatile below 600 °C) were also characterized with an SP-AMS laser equipped on the same AMS. High-resolution SP-AMS analysis yielded similar results to the AMS, with the major spectral change due only to pure-carbon ions (C_x). Detailed AMS and SP-AMS results will be presented and compared.

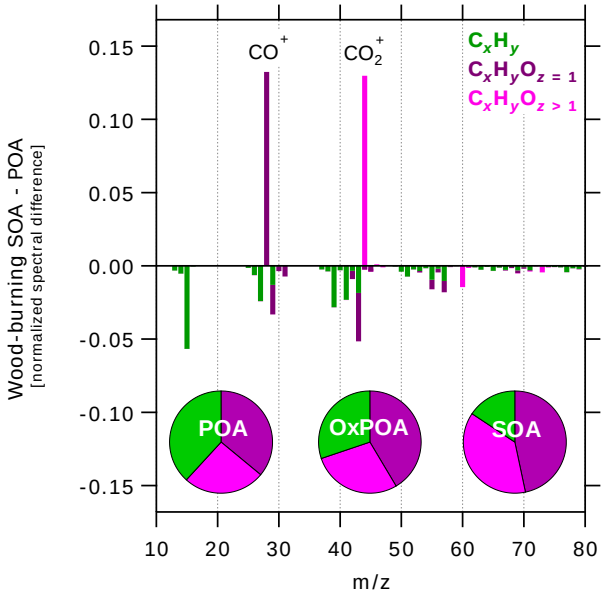

Figure 1. AMS difference mass spectrum for wood-stove SOA minus POA. Inset: pie charts of the organic composition for the three cases.

This work was supported by the Swiss National Fund, Swiss Federal Office for Energy, Swiss Federal Office for the Environment, and the IMBALANCE project of the ETH Zürich.

Grieshop, A.P., J.M. Logue, N.M. Donahue and A.L. Robinson (2009). Atmos. Chem. Phys., 9, 1263-1277. *doi:10.5194/acp-9-1263-2009*

Heringa, M.F., P.F. DeCarlo, R. Chirico, T. Tritscher, J. Dommen, E. Weingartner, R. Richter, G. Wehrle, A.S.H. Prévôt, U. Baltensperger (2011). Atmos. Chem. Phys., 11, 5945-5957. *doi:10.5194/acp-11-5945-2011*

Heald, C.L., J.H. Kroll, J.L. Jimenez, K.S. Docherty, P.F. DeCarlo, A.C. Aiken, Q. Chen, S.T. Martin, D.K. Farmer, P. Artaxo (2010). Geophys. Res. Lett., 37, L08803, *doi:10.1029/2010GL042737*

Keller and Burtscher (2012). J. Aerosol. Sci., 49, 9-20. *doi:10.1016/j.jaerosci.2012.02.007*

Micromarkers of source-specific combustion aerosols

O.B. Popovicheva[1], E.D. Kireeva[1], N.M.Persiantseva[1]

[1]Institute of Nuclear Physics, Moscow State University, Moscow, 119991, Russia
Keywords. combustion aerosols, characterization, source of emission
Presenting author email: polga@mics.msu.su

Aerosols generated by incomplete combustion of fossil fuels (FF) and biomass burning (BB) are major air pollutants. Open BB relating to wildfires contributes to almost a half of the combustion aerosol global inventory. Aerosol emissions of transport systems are currently acknowledged to be a largest source of uncertainties in understanding the impacts on the regional air quality. Ship emission is among the world's highest polluting sources per quality of fuel consumed. Combustion aerosols may serve tracers allowing a link to distinct combustion sources in apportionment studies if their key physico-chemical characteristics representative the emission sources are defined. The estimations of the source contribution to ambient particulates assume specific markers different from other combustion sources.

A complexity of multicomponent and source-specific PM emissions requires the characterization of individual particles. The classification of combustion aerosols may be done by representative particle types according to their chemical specification. This approach allows quantifying the various diesel and biomass burning sources and identifying the specific characteristic features that can serve as micromarkers emission source.

Presently, the hierarchical cluster analysis (HCA) is a data analysis technique which is used for the interpretation of electron microprobe analysis data and the determination of particle types in ambient air with a large number of pollution sources. Here, we present the development of HCA for characterization the FF and BB emissions by classification of individual particle data on characteristic groups with similar morphological and chemical composition according to the source and type of fuel used. Scanning electron microscopy (SEM) coupled with energy-dispersive X-ray spectroscopy (EDX) is used for characterization of morphology and composition of a large number of individual particles. FTIR spectroscopy and ion content measurements provide the bulk composition data for clustering expert analysis that assures that the mean composition of a cluster is close to physico-chemical identifiable type of particles. Impact of Fe content in laboratory-produced soot aerosol on its composition and structure was analysed in Bladt *et al.* (2012) to demonstrate the elaborated approach for separation individual particles into characteristic groups representing the particle types in dependence of iron content in soot.

This review presents micromarkers of source-specific combustion aerosols emitted by transport systems (road and marine diesel engines) and in open fire experiments. Microscopic and chemical characterization of Opel Astra diesel engine exhaust operated at 35 km/h speed and used diesel B0 fuel with various lube oil (low and high SAPS) and biodiesel fuel B20 with high SAPS are performed. The most abundant group (around 50%) in each exhaust is polluted soot. In diesel B0 exhaust particles, low SAPS groups of silicates, iron and aluminum oxides are found. Using high SAPS with larger ash content leads to abundance of groups of Al oxide and Al fused with Fe. The most prominent impact of high SAPS using relates with presence of well-separated groups of Nb oxides and W particles. Biodiesel exhaust particles, high SAPS contain groups of Fe and Zn oxides, and W particles. The source specific micromarker of biodiesel particles is a separate group enriched by Cl, K, and Na, the elements which are commonly recognized as biomarkers of biofuel combustion.

Exhausts from the main and auxiliary engines operated onboard of a RoRo/casetter carrier ship during TRANSFORM campaign, burning heavy and distillated fuels, respectively, are analyzed (Popovicheva *et al*., 2012). SEM/EDX observations of emitted aerosols indicate carbonaceous particles internally and externally mixed with inorganic species in the combination of spherical and irregular shapes. The composition of individual particles is varying in a wide concentration range of major elements (C, O) and impurities (S, Fe, Si, Ca, Zn, V, Ni, K, Mn) representative the origin of fuels. In distillated fuel (DF)-derived aerosols we identify groups of soot, Ca- and Fe/Si-rich particles. Calcium sulfate/oxide/carbonates and iron oxides are found to compose the group of Ca- and Fe-rich particles, respectively, while silicon oxide and silicate determine the group of Si-rich particles in heavy fuel (HF)-derived emission. Transition metals (V, Ni) containing particles specify the separate group which may serve as a specific micromarker of heavy fuel combustion.

Characterization of freshly-generated smoke particles produced in small-scale spruce open fire experiments shows the groups of soot, Ca- and Fe-rich particles while K- and Mn- rich groups identify the specific micromarkers of BB.

Thus, state-of-the-art characterization of complex multicomponent aerosols improves the quantification of contribution of various fossil fuel and biomass burning emissions to ambient particulates and the identification of a source type in the apportionment studies.

This work was supported by RFBR projects 12-05-00395_a and 12-05-92002.

Bladt, H., Schmid, J., Kireeva, E., Popovicheva, O.B. et al. (2012). *Aerosol Science and Technology*, 46, 1337-1348.

Popovicheva O., Kireeva E. et al. (2012). *J. Environ. Monit.*, **14**, 3101 – 3110.

Monday, September 1, 2013

Session: Instrumentation
Combustion aerosol and chemical measurements

Measurement of chemisorption on metallic nanoparticles using aerosol photoemission spectroscopy

S. Onel and M. Seipenbusch
Institute for Mechanical Process Engineering and Mechanics, Karlsruhe Institute of Technology, Karlsruhe, 76131, Germany
Keywords: nanoparticles, surface chemistry, photoemission spectroscopy.
Presenting author email: santiago.onel@kit.edu

Chemisorption on metallic nanoparticles is not only a fundamental step in heterogeneous catalysis, but also builds the basis for self-assembled monolayers. We address this topic by working with gas-carried metallic nanoparticles using aerosol photoemission spectroscopy as a highly sensitive analysis tool.

Aerosol photoemission spectroscopy (APES) is a surface sensitive method, which was successfully used in the past showing a correlation between catalytic and photoelectric activity of gas-carried nickel and platinum nanoparticles (Weber et al, 2001). Changes on the particle surface modify the electronic structure, therefore leading to a variation of the photoemission parameters: work function and emission constant. As a result of this, this method shows potential for the study of adsorption on particle surfaces.

In this work we show that APES can be used for the quantitative determination of adsorbates on metallic nanoparticles. This opens up the possibility of measuring size dependent adsorption effects without metal-support interactions or mass transfer limitations due to a support. This online method can be used as well in order to monitor surface functionalization of particles in the gas phase without collecting them or having to perform any other sample preparation step.

Photoemission studies were conducted in an energy range between 5,5 and 6,5 eV, using a deuterium lamp and a monochromator for wavelength selection. The photon energy is just above the work function of metals, but considerably below the ionization energies of the gases used. Work function and emission constant were obtained using the Fowler-Nordheim equation, which describes the photoelectric yield as a function of photon energy near the photothreshold.

Au and Pt nanoparticles were produced in nitrogen 5.0 using a spark discharge generator. The generated particles were mainly aggregates with mean diameters as measured with a scanning mobility particle sizer of 16,6 nm and 18,7 nm, respectively. The primary particle size was determined using TEM being 3,4 nm and 3,8 nm, respectively. The particle number concentration used in both cases was in the order of 10^6 cm^{-3}. The aerosol flow was mixed with the reactant flows: carbon monoxide and 1-hexanethiol. Carbon monoxide 4.7 was dosed using a mass flow controller up to a concentration of 1300 ppm. 1-hexanethiol is liquid at room temperature; consequently, the dosage took place by passing a nitrogen flow through a bubbler filled with 95% 1-hexanethiol. By regulating the nitrogen flow rate and assuming the nitrogen flow is saturated, a maximum concentration of 300 ppm was used.

A positive shift of the work function was observed due to the interaction of CO with Pt. The work function shift increased with increasing CO concentration. The work function shift reached a maximum of 0,23 eV. The data points could be approximated by a Langmuir adsorption isotherm (Figure 1). This can be explained through a growing coverage of the surface with CO and shows consistency with previous results using traditional ultraviolet photoemission spectroscopy for a Pt sheet (Collins et al, 1976). No change in the work function of gold was observed when CO was added, even with higher CO concentrations.

Exposing gold nanoparticles to 1-hexanethiol led to a much larger negative shift of the work function. The effective work function decreased with higher concentration of hexanethiol and reached a saturation value 1,5 eV lower than the work function of the clean surface (5,1 eV). The dependence of the work function on concentration (coverage) was non linear. This behaviour, as well as the maximum value, is in good agreement with theoretical studies (Fragouli et al, 2007)

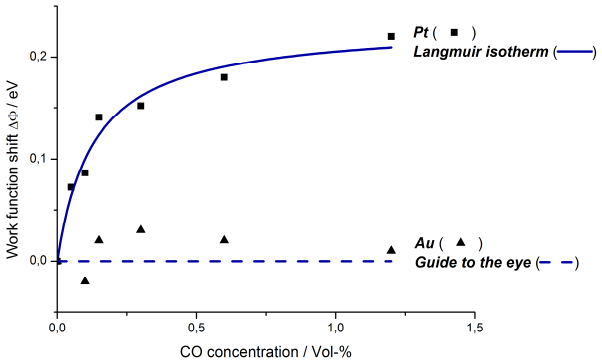

Figure 1. Work function shift as a function of CO concentration

This work was supported by the Deutsche Forschungsgemeinschaft (DFG).

Collins, D., Lee, J., & Spicer, W. (1976). *Surface Science*, *55*, 389–402

Fragouli, D., Kitsopoulos, T. N., Chiodo, L., Della Sala, F., Cingolani, R., Ray, S. G., & Naaman, R. (2007). *Langmuir*, *23*(11), 6156–62

Weber, A. P., Seipenbusch, M. & Kasper, G. (2001). *Journal of Physical Chemistry A*, 105(39), 8958-8963

Validation of an online, real-time, soft photon ionisation (SPI) time of flight mass spectrometer for mainstream tobacco smoke analysis

J. Hawke[1] and M. Bente Von Frowein[2]

[1]British American Tobacco, Group R&D, Southampton, SO15 8TL, UK
[2]Photonion GmbH, Hagenower Str. 73, 19061 Schwein, Germany
Keywords: time of flight, mass spectrometry, soft photon ionisation, tobacco smoke
Presenting author email: jenni_hawke@BAT.com

Mainstream tobacco smoke is a complex and dynamic aerosol, consisting of both particulate and vapour phases. Most analytical approaches for the determination of mainstream tobacco smoke toxicant yields employ off-line per-cigarette analytical techniques that limit understanding of the processes leading to smoke formation. Therefore analytical techniques which allow for online, real time, per-puff quantifiable yield measurements offer many advantages over traditional techniques. The LM2X-TOFMS (Borgwaldt GmbH, Munich, Germany), a coupling of a linear smoking engine and time of flight mass spectrometer is an example of a real-time per-puff analysis system for the vapour phase of mainstream cigarette smoke.

The system uses an E-Lux 126 vacuum ultraviolet (VUV, 126nm) lamp as its light source for soft photon ionisation (SPI), an ionisation technique which causes almost no fragmentation of the chemical species present in the sample (photons of 9.8eV). SPI allows substances to be measured directly in complex mixtures, such as mainstream tobacco smoke whilst not ionising background gases such as O_2, N_2 and CO_2. Currently, seven constituents of mainstream smoke can be quantified (Table 1) on the system (Adam, 2006). Three of which are present on the WHO eighteen priority toxicant list (WHO, 2008).

Table 1: Quantifiable vapour phase analytes on the LM2X-TOFMS.

Class	Analyte
Alkenes	1,3-Butadiene (m/z 54)*
	Isoprene (m/z 68)
Aromatics	Benzene (m/z 78)*
	Toluene (m/z 92)
Carbonyls	Acetaldehyde (m/z 44)*
	Acetone (m/z 58)
	2-Butanone (m/z 72)

*identified as toxicants of concern by a WHO study group

Validation of the system was split into two studies based on recommendations of the International Committee on Harmonisation (ICH). Initially, robustness testing was performed to determine whether the LM2X-TOFMS was able to remain unaffected by small but deliberate changes in operational factors such as capillary length, ferrule, time of day and the day on which measurements are performed. Secondly, measurements were performed to evaluate the linear response of the system based on an individual concentration range for each analyte.

3R4F Kentucky reference cigarettes, (9.4mg ISO pack tar) were used during the first part of the study; all samples were conditioned under ISO parameters: T: 22 ± 1°C RH: 60 ± 3%, and smoked using ISO puffing parameters (35ml puff over 2s every 60s). For the linearity measurements, six certified gas mixtures of varying concentrations as well as a 'blank' were analysed in 2L gas bags over three days. Gas bag analysis was performed using sampling parameters of ten 35ml, 2s "puffs" with a frequency of 20s. Separate gas bags were used for each gas mixture to avoid contamination.

The robustness results were analysed by One-way ANOVA, it showed that no vapour phase constituent had a statistically significant difference for any of the identified changes ($p = \geq 0.05$). I-MR control charts confirm that although there is day to day variation, some of which could be attributed to cigarette variation, the overall process shows good stability and control.

To establish analyte linearity, the measured puff yield (µg/puff) for each analyte was plotted against the relevant bottle concentration range. Figure 1 shows a comparison plot of measured benzene yields vs. calculated benzene yields (assuming ideal gas law).

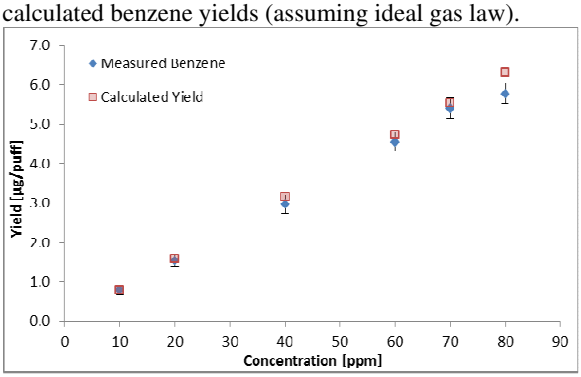

Figure 1. calculated vs. measured values for benzene.

These data will be used to determine reproducibility, repeatability and limits of detection (LOD) and quantification (LOQ).

WHO Study Group on Tobacco Product Regulation (2008). The scientific basis of tobacco product regulation: Second report of a WHO Study Group (WHO Technical Report Series No 951) (pp 45-277) Geneva Switzerland: World Health Organization. Retrieved from http://www.who.int/tobacco/global_interaction/tobreg/en

Adam, T., Mitschke, S., Streibel, T., Baker, R. R., Zimmermann, R. (2006). Quantitative puff-by-puff-resolved characterization of selected toxic compounds in cigarette mainstream smoke. Chemical Research in Toxicology. 19 (4): 511-520

An accurate, real-time and low-cost method to measure biomass smoke

Yungang Wang[1], Daniel L. Wilson[2], Philip K. Hopke[3], Ashok J. Gadgil[1]

[1]Lawrence Berkeley National Laboratory, Berkeley, California
[2]University of California – Berkeley, Berkeley, California
[3]Clarkson University, Potsdam, New York
Keywords: biomass cookstove, aethalometer, emission, water boiling test
Presenting author email: phopke@clarkson.edu

Background

In the developing world, approximately 3 billion people cook their food by burning solid fuels with the majority using biomass in polluting and inefficient rudimentary stoves. This number is expected to increase in the coming decades. This use of biomass fuels represents a significant part of energy use in developing regions. The products of incomplete combustion from biomass cookstoves include methane, ozone-precursors, organic carbon and black carbon (BC), which are important greenhouse pollutants. Emissions from cookstove use also have been linked to adverse respiratory, cardiovascular, neonatal, and cancer outcomes. Exposure to cookstove emissions leads to an estimated 4 million deaths each year. Given the substantial threat to public health particularly for women and children, and the uncertainty about the climate effect resulting from cookstove use in developing countries, further study is needed to pinpoint the most beneficial strategies for reducing emissions from this source.

Problem

Mitigating emissions from biomass cookstoves depends first on identifying technologies that are proven effective in reducing emissions, and second on disseminating these technologies on a large scale. Currently, a wide range of improved stove technologies is available including Berkeley Darfur Stoves (BDS), electric stoves, advanced biomass stoves, rocket stoves, solar cooker, etc, but the potential climate and health benefits vary substantially by technology and fuel options. The ability to accurately characterize cookstove emissions in the laboratory and in the field is essential but currently very weak.

Solution

Automated on-line measurements can quantify emission reductions and exposure under actual operating conditions. Prior work has shown that organic components in biomass smoke particles absorb light at 370 nm more effectively than 880 nm in two-wavelength aethalometer (Magee Scientific, Berkeley, CA) measurements. This enhanced absorption (Delta-C = BC370nm – BC880nm) can serve as an indicator of biomass combustion emissions. A strong linear relationship between Delta-C and levoglucosan (a classic biomass combustion marker) was recently observed in Rochester, NY during the winter heating season (Wang et al., 2011). Compared to filter-based levoglucosan measurement, this aethalometer method is simpler, cheaper, more readily accessible, and has higher time resolution for indicating the contributions of biomass smoke to ambient or indoor pollution. In our study, this method will be tested using the BDS under laboratory controlled cooking conditions – water boiling tests (WBT, version 4, http://www.pciaonline.org/node/1048).

Implication

The discrepancies between laboratory and field testing have hindered previous cookstoves development efforts. Improved laboratory studies and testing protocols that can recreate field conditions are needed. This discrepancy suggests a need to undertake further validation of the Delta-C method for different biomass fuels (e.g. waste, charcoal, animal dung, twigs) over a range of burning conditions. Once validated broadly, the Delta-C method would make it easier and cheaper to accurately quantify the cookstove emission levels in the field.

Standardized tests using aethalometer Delta-C measurement performed for the variety of fuels, field conditions, and cooking practices could help determine which stoves are most successful in the field for improving fuel efficiency, emissions, and health, and shed light on the persistent discrepancy in measured emissions in the field versus in the laboratory.

References

Wang, Y., Hopke, P. K., Rattigan, O. V., Xia, X. (2011) *Environ. Sci. Technol.* **45** (17), 7387-7393.

Multi-wavelength characterization of carbonaceous aerosol

P. Prati[1], V. Ariola[1], V. Bernardoni[2], M.C. Bove[1], G. Calzolai[3], M. Chiari[3], F. Lucarelli[3], D. Massabò[1], S. Nava[3], A. Piazzalunga[4], G. Valli[2] and R. Vecchi[2]

[1] Department of Physics & INFN, University of Genoa, via Dodecaneso 33, 16146, Genova, Italy
[2]Department of Physics & INFN, Università degli Studi di Milano, Via Celoria 16, 20133, Milano, Italy
[3] Department of Physics & INFN, University of Florence, via Sansone 1, 50019 Sesto Fiorentino Firenze, Italy
[4]Department of Environmental and Territorial Sciences, Università degli Studi di Milano-Bicocca, Piazza della Scienza 1, 20122 Milan, Italy

Keywords: carbonaceous aerosol, light absorption, light scattering, source apportionment
Presenting author email: prati@ge.infn.it

Carbonaceous aerosol is a major component of the urban PM. It mainly consists of organic carbon (OC) and elemental carbon (EC) although a minor fraction of carbonate carbon could be also present. Elemental carbon is mainly found in the finer PM fractions (PM2.5 and PM1) and it is strongly light absorbing. When determined by optical methods, it is usually called black carbon (BC). The two quantities, EC and BC, even if both related to the refractory components of carbonaceous aerosols, do not exactly define the same PM component (Bond and Bergstrom, 2006; and references therein). Moreover, another fraction of light-absorbing carbon exists which is not black and it is generally called brown carbon (Andreae and Gelencsér, 2006).

We introduce a simple, fully automatic, multi-wavelength and non-destructive optical system, actually a Multi-Wavelength Absorbance Analyzer, MWAA, to measure off-line the light absorption in Particulate Matter (PM) collected on filters and hence to derive the black and brown carbon content in the PM (Figure 1)

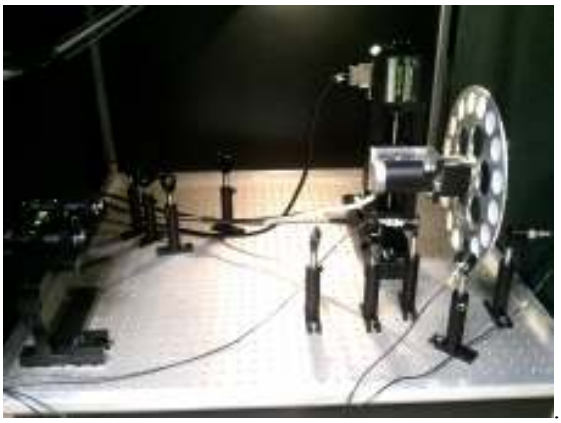

Figure 1: Set-up of the MWAA

This gives the opportunity to measure in the same sample the concentration of total PM by gravimetric analysis, black and brown carbon, metals by, for instance, X Ray Fluorescence, and finally ions by Ion Chromatography. Up to 16 samples can be analyzed in sequence and in an automatic and controlled way within a few hours. The filter absorbance measured by MWAA was successfully validated both against a MAAP, Multi Angle Absorption Photometer (Petzold and Schönlinner, 2004), and the polar photometer of the University of Milan.

The measurement of sample absorbance at three wavelengths gives the possibility to apportion different sources of carbonaceous PM, for instance fossil fuels and wood combustion. This has been done following the so called "aethalometer method" (Sandradewi et al., 2008;) but with some significant upgrades that will be discussed together the results of a field campaign presently on going in a mountain site in the Ligurian Appennines. The apportionemnt of the combustion source derived from the optical analysis, will be compared with the results of other techniques (i.e chemical characterization of biomass burning tracers and radiocarbon determination by Accelerator Mass Spectrometry).

Results of the application of the MWAA to the analysis of collecting stages of cascade impactors will be also also shown.

This work was supported by INFN, under the grant MANIA and by Amministrazione Provinciale di Genova

Andreae, M.O, and Gelencsér, A. (2006). *Black Carbon or Brown Carbon? The nature of light-absorbing carbonaceous aerosol.* Atmospheric Chemistry and Physics, 6, 3131-3148.

Bond, T., Bergstrom, R. W. (2006*). Light absorption by carbonaceous particles: an investigative review.* Aerosol Science and Technology, 40, 27-67.

Petzold, A., Schölinner, M. (2004). *Multi-angle absorption photometry—a new method for the measurement of aerosol light absorption and atmospheric black carbon.* Journal of Aerosol Science, 35, 421-441.

Sandradewi, J., Prevot, A.H., Zidat, S., Perron, N., Rami Alfarra, M., Lanz, V., Weingartner, E., Baltensperger, U. (2008). *Using Aerosol Light Absorption Measurements for the Quantitative Determination of Wood Burning and Traffic emission Contributions to Particulate Matter.* Environmental Science & Technology, 42, 3316-3323.

Characterization of Black Carbon concentration, sources and age using an Aethalometer AE33

Luka Drinovec[1], Griša Močnik[1], Jean-Eudes Petit[2,3], Jean Sciare[2], Olivier Favez[3], Peter Zotter[4], Robert Wolf[4], André S.H. Prévôt[4], and Anthony D.A. Hansen[1,5]

[1] Aerosol d.o.o., Kamniška 41, SI-1000 Ljubljana, Slovenia
[2] LSCE (CEA-CNRS-UVSQ), Orme des Merisiers, Gif-sur-Yvette, France;
[3] INERIS, Verneuil-en-Halatte, France
[4] Paul Scherrer Institut, CH-5232 Villigen PSI, Switzerland
[5] Magee Scientific, 1916A M.L. King Jr. Way, Berkeley, CA 94704, USA
Keywords: Aethalometer, source apportionment, ACSM, AMS, PSCF
Presenting author email: luka.drinovec@aerosol.si

Filter-based measurements of aerosol optical absorption are widely used to determine Black Carbon (*BC*) concentrations in real time. Measurements at multiple wavelengths permit the separation of contributions of *BC* from different combustion sources (Sandradewi 2008). However, filter-based methods can suffer from non-linearity due to a »loading« effect as a function of increasing deposit density on the filter (Gundel 1984, Weingartner 2003, Arnott 2005, Virkkula 2007). Static algorithms to compensate for the effect fail to capture the details and potential variability of these aerosol optical properties. This impacts the accuracy of source apportionment using the data.

The dual-spot Aethalometer (Magee Scientific model AE33) provides a real-time the model introduced determination of a loading effect, based on the model introduced by Virkkula (2007): $BC_{compensated} = BC\ (1-k*ATN)$. The compensation parameter k is determined in real time for each of the operational wavelengths, and is used in the same manner as has been developed for off-line post-processing. This provides a time resolved specific spectral fingerprint that may be interpreted in terms of aerosol composition.

Optical and chemical properties of aerosols were measured with high time resolution during summer and winter EMEP campaigns in Paris (France) and Payerne (Switzerland). An Aerosol Chemical Speciation Monitor (ACSM) and an Aerodyne High Resolution Time-of-Flight Aerosol Mass Spectrometer (AMS) were used to measure quantitative chemical composition for non-refractory aerosol particles. During summer we observed complex temporal variation of k, where k(880 nm) changed from approximately 0.006 for fresh aerosols to near zero for aged aerosols as shown using Potential Source Contribution Function (PSCF) method for back trajectory analysis.

We have combined the Aethalometer and ACSM/AMS measurements, and normalized the sum of inorganic secondary and organic aerosol mass to BC. Values of this ratio are expected to be high for air parcels containing aged aerosols. The ratio correlates well with the loading compensation parameter k measured by the Aethalometer at 880 nm (Figure 1). This indicates that the compensation parameter k can be used for discrimination between local (fresh) and regional (aged) air pollution aerosols.

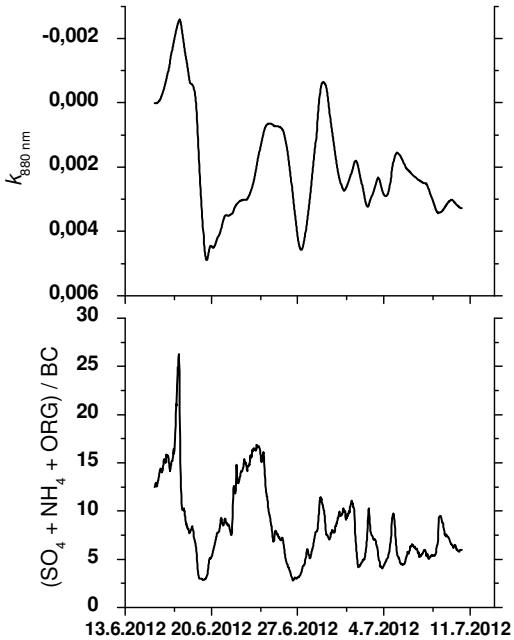

Figure 1. Time series of loading effect compensation parameter k(880 nm), compared to sum of inorganic secondary and organic aerosol mass normalized to BC, during the summer EMEP campaign at the Paris SIRTA-LSCE site.

Arnott, W. et al. (2005) Aerosol Sci. Technol. 39, 17- 29;
Gundel, L.A., et al. (1984) Sci. Total Environment 36, 197-202;
Sandradewi, J. et al. (2008) Environ. Sci. Technol. 42, 3316–3323;
Virkkula, A. et al., (2007) J. Air & Waste Manage. Assoc. 57, 1214-1222;
Weingartner, E., et al. (2003) J. Aerosol Sci. 34, 1445-1463;

Acknowledgements: The work described herein was co-financed by the EUROSTARS grant E!4825 and JR-KROP grant 3211-11-000519. The measurements in Payerne were conducted by the Swiss Federal Office for the Environment (FOEN). Measurements performed at SIRTA (LSCE) were funded by CNRS, CEA, the EU-FP7(2007-2013) 'ATRIS' project under grant agreement n°262254, the Primequal Predit 'PREQUALIF' project (ADEME contract n°1132C0020), and the DIM R2DS (AAP 2010) 'PARTICUL'AIR' project.

Hyphenation of a Thermal/Optical Carbon Analyzer to photo-ionization mass spectrometry for determination of the organic content of aerosol particles

T. Streibel[1,2,4], J. Grabowsky[1], J.C. Chow[3], J.G. Watson[3], R. Zimmermann[1,2,4]

[1]Joint Mass Spectrometry Centre / Chair of Analytical Chemistry, University of Rostock, 18051 Rostock, Germany
[2]Joint Mass Spectrometry Centre, Cooperation Group Comprehensive Molecular Analytics, Helmholtz Zentrum München, Ingolstädter Landstr. 1, 85764 Neuherberg, Germany
[3]Division of Atmospheric Sciences, DRI Research Institute, 2215 Raggio Parkway, Reno, Nevada 89512-1095
[4]HICE – Helmholtz Virtual Institute of Complex Molecular Systems in Environmental Health – Aerosols and Health, www.hice-vi.eu

Keywords: OC/EC analysis, mass spectrometry, photo ionization, hyphenated technique
Presenting author email: thorsten.streibel@uni-rostock.de

The identification of carbonaceous fractions of particulate matter on a molecular level still provides an analytical challenge. Knowledge of organic composition is of great importance with respect to health effects or aerosol particles. The determination of sum parameters such as total organic and elementary carbon (OC and EC) following thermal desorption at different temperatures already yields valuable information. However, the method provides no insight of the molecular composition of the distinct thermal fractions. Therefore, hyphenation between a commercial thermal/optical carbon analyzer and a time-of-flight mass spectrometer equipped with photo-ionization has been developed. With this new setup, desorbed organic compounds can be analyzed prior to their oxidation to carbon dioxide by sidelining a small part of the gas flow. For this, the quartz tube between sample holder and oxidizer had to be modified. The new coupling piece extends into an aluminum box, which is heated to 230 °C to prevent condensation. The modified quartz tube is coupled inside the box to a capillary running inside a heated curing tube, which guides the molecules to the ion source of the mass spectrometer. In total a flow of 5 ml/min is led to the mass spectrometer. Ionization is carried out with two soft methods, viz. resonance enhanced multi photon ionization (REMPI), which is selective for (poly)aromatic compounds as well as single photon ionization (SPI), which allows a more universal analysis of aliphatic and aromatic species. By doing this, the molecular pattern of each organic fraction is obtained. Figure 1 depicts a scheme of the instrumental setup and an exemplary two-dimensional graph of the mass spectrometric pattern of a complete OC/EC experiment of diesel exhaust particles.

With the new instrumentation ambient aerosols as well as source particles from combustion processes have been investigated. Furthermore, particles from smog chamber experiments with α- und β-pinene and toluene as precursors were analyzed.

With the new instrumentation ambient aerosols as well as source particles from combustion processes have been investigated. Furthermore, particles from smog chamber experiments with α- und β-pinene as precursors were analyzed. Ambient samples taken in winter showed a big influence from wood combustion, whereas samples taken in summer at the same location missed wood combustion markers, but were dominated by secondary organic aerosol (SOA). Comparison with smog chamber filter samples experiments revealed typical mass to charge signals (at m/z 58 and 82, respectively) that are not observable in any other sample. These could therefore be potential marker substances for SOA. Particles from cold start emissions of gasoline cars showed larger polycyclic aromatic hydrocarbons than those from diesel cars. With diesel cars, there was also a significant influence of the biodiesel content on the product pattern. In general, at higher desorption temperatures the spectra are shifted to smaller molecules, which are formed by thermal decomposition of larger oligomeric and polymeric species, suggesting the possibility to learn more about the nature of such larger structures.

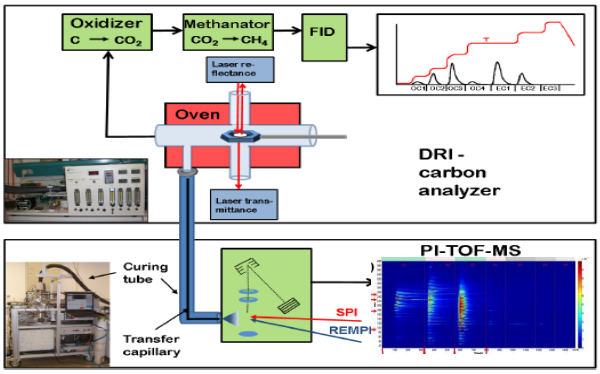

Figure 1: Experimental setup of the hyphenation between a thermal/optical carbon analyzer and photo-ionization mass spectrometry depicting a two-dimensional mass spectrometric pattern of a complete OC/EC analysis of diesel exhaust particles

This work was financially supported by the Deutsche Forschungsgemeinschaft (DFG). For the provision of filter samples the authors are gratefully indebted to A. Mamakos (JRC Ispra, Italy) and F. Lee (Hong Kong Polytechnic University)

Grabowsky, J., Streibel, T., Sklorz, M., Chow, J.C., Watson, J.G., Mamakos, A. and Zimmermann, R. (2011) *Anal. Bioanal. Chem.* **401**, 3153-3164.

Organic aerosol speciation with in-situ thermal desorption gas chromatography: a brief history of the TAG instrument

N.M. Kreisberg[1], S.V. Hering[1], A.P. Teng[1], G. Isaacman[2], Y. Zhao[2], D.R. Worton[2], A.W.H. Chan[2], B.J. Williams[3], J.T. Jayne[4], A.T. Lambe[4], T. Hohaus[4], J.R. Kimmel[4], D.T. Sueper[4], W. Brooks[4], L.R. Williams[4], A.M. Trimborn[4], D.R. Worsnop[4] and A.H. Goldstein[2]

[1]Aerosol Dynamics Inc., Berkeley, CA, 94806, USA
[2]Depart. of Environmental Science, Policy & Management, University of California, Berkeley, CA, 94720, USA
[3]Depart. of Energy, Environmental & Chemical Engineering, Washington University in St. Louis, MO, 63130, USA
[4]Aerodyne Research Inc., Billerica, MA, 01821, USA
Keywords: organic aerosol, thermal desorption, gas chromatography, mass spectrometry
Presenting author email: nathan@aerosol.us

Speciation at the molecular level is necessary to more fully understand the sources, sinks, transport and transformation of organic matter in the atmosphere. The thermal desorption aerosol gas chromatograph (TAG) is a mature instrument successfully deployed in five distinct field campaigns and offers a proven method for in-situ, hourly speciation of organic aerosols.

Multiple versions of this evolving instrument will be reviewed but all have in common the use of chemical separation using gas chromatography following thermal desorption. The first TAG to be deployed relied on inertial impaction to collect particulates and filter blanks to estimate vapour adsorption. Figure 1 illustrates the ability to acquire hourly time series of useful aerosol markers (primary norhopane and secondary phthalic acid) in the LA basin as part of the SOAR campaign (Williams et al., 2010). A subsequent deployment in the California Sierra Foothills (Worton et al., 2011) provided important information about the interaction of biogenic primary gases with anthropogenic pollutants that dominates secondary organic aerosol production.

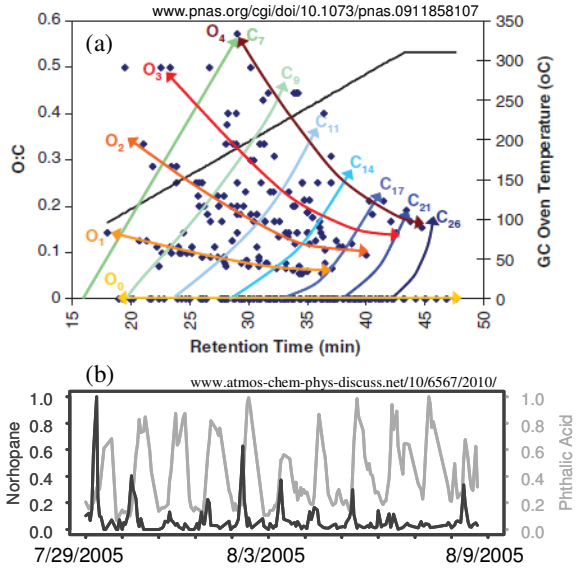

Figure 1. (a) O:C ratio, carbon and oxygen numbers vs. volatility as indicated by column retention time for ~300 compounds and (b) time series of representative source markers as measured in Riverside, CA in 2005.

To measure semi-volatile organics, which are important to secondary aerosol formation, a new version of the instrument has been developed to collect both particle and semi-volatile vapor phases (Zhao et al., 2013). Using a high efficiency carbon-based gas phase denuder and a new collection system with a reusable metal-fiber filter, alternate samples with and without the denuder provide direct partitioning measurements of organic compounds.

A parallel development has focussed on adapting the TAG instrument to function as a parallel collection system to be added to the Aerodyne Aerosol Mass Spectrometer (AMS; Canagaratna et al., 2007). This hybrid instrument (Williams et al., 2013) shares a detector to provide simultaneous size-dependent bulk and speciated organic aerosol information in one instrument. Comparing measurements from these separate instruments has proven the utility of being able to identify individual marker species corresponding to traditional AMS organic classes based on oxygen to carbon ratios such as HOA, OOA etc. (Williams et al., 2010; Worton et al., 2011).

Current efforts are directed towards expanding the range of compounds that can be analysed using in-situ derivatization of highly polar species. A dual cell version of the semi-volatile oriented instrument for initial deployment as part of a southeast US summer of 2013 field campaign seeks to ascertain the origin and fate of the large secondary organic aerosol levels present throughout the region. The paired filter cells provide simultaneous collection of denuded and undenuded aerosol streams for unique hourly measurements of derivatized SOA markers stemming from the oxidation of isoprene and other (bio-)anthropo-genic precursors.

Work supported under U.S. DOE SBIR/STTR grants DE-FG02-02ER83825, DE-FG02-05ER 86235, DE-FG02-08ER86335 and DE-FG02-08ER85160 and California Air Resources Board award number 03-324.

Canagaratna et al (2007) *Mass Spec Revs, 26*, 185-222.
Williams et al (2010) *Atmos Chem Phys, 10*, 11577-603.
Worton et al (2011) *Atmos Chem Phys, 11*, 17071-125.
Zhao (2013). *Aerosol Sci Technol, 47*(3), 258-266.
Williams et al (2013) submitted *Aerosol Sci and Technol*

Monday, September 1, 2013

Session: Aerosol Modelling
Models for aerosol emission and nucleation

Contribution of ion-assisted nucleation to new particle formation in a tropical boundary layer

V.P. Kanawade[1], S.N. Tripathi[1], D.K. Siingh[2], A.S. Gautam[2] A.K. Srivastava[3], A.K. Kamra[2]

[1]Department of Civil Engineering, Indian Institute of Technology, Kanpur, Uttar Pradesh, 208016, India
[2]Indian Institute of Tropical Meteorology, Pune, Maharashtra, 411008, India
[3]Indian Institute of Tropical Meteorology (Branch), New Delhi, 110060, India
Keywords: aerosol size distribution, nucleation, aerosol microphysics, tropical boundary layer
Presenting author email: snt@iitk.ac.in

Aerosols are ubiquitous in Earth's atmosphere and their interactions with clouds via activation of cloud condensation nuclei (CCN) constitute the largest uncertainty in climate forcing. Nucleation (as a result of gas-to-particle conversion) is a predominant source of new particles in the atmosphere and thus is an important process that controls aerosol and cloud abundance.

New particle formation (NPF) occurs nearly everywhere in the Earth's atmosphere [Kulmala et al., 2004]. A variety of species may contribute to nucleation and growth processes, such as sulfuric acid (H_2SO_4) [Kuang et al., 2008], ammonia (NH_3) [Ball et al., 1999], amines [Yu et al., 2011], organic acids [Metzger et al., 2010], and ion clusters [Yu, 2010]. Previous field study by Boy et al. [2008] reported ~15% contribution of ion-assisted nucleation to NPF in the boundary layer in Hyytiälä, Finland. On the contrary, modeling approach including the association of ion–ion recombination to neutral clusters showed 100% contribution of ion–mediated nucleation (IMN) to NPF in Hyytiälä [Yu and Turco, 2008]. A recent cloud chamber study revealed that ion-assisted nucleation contribution to the boundary layer NPF is negligible but is nevertheless taking place [Kirkby et al., 2011].

We conducted measurements of particle size distributions in an Indian tropical boundary layer during March 20–May 23, 2012. Eighteen regional NPF events were observed, all of these likely occurred under the influence of transported anthropogenic plumes. We used particle growth and nucleation (PARGAN) model to calculate total particle nucleation rate (J_1) from the measured particle size distributions along with aerosol microphysics box model [Kanawade and Tripathi, 2006] incorporated with binary homogeneous nucleation (BHN) [Vehkamaki et al., 2002], ion-induced nucleation (IIN) [Modgil et al., 2005] and IMN [Yu, 2010] schemes to simulate observed NPF events. The aerosol microphysical model simulations revealed that none of these nucleation mechanisms could explain NPF solely, suggesting that two or more processes occurring simultaneously. The other nucleation mechanisms, involving species such as NH_3 or organics, may be crucial in the boundary layer NPF but these were not possible to examine. For example, NH_3 concentrations in such heavily polluted environment vary from ~3 to 42 ppbv (Singh and Kulshrestha, 2012), which exceeds the limit currently treated in the ternary homogeneous nucleation (THN) parameterization.

Our simulations further indicated that ion-induced and –mediated nucleation could be an important contributor to NPF at this location whereas BHN failed to explain NPF at all. The median contributions of IIN and IMN were about 28% and 87%, respectively . These results demonstrate the importance of ion-assisted nucleation to the tropical boundary layer NPF.

This work was supported by Indian Ministry of Earth Sciences (MoES).

Ball, S. M., Hanson, D. R, Eisele, F. L. and McMurry, P. H. (1999) *J. Geophys. Res.* **104**.
Boy, M. et al. (2008) *Atmos. Res.* **90**, 151-158.
Kanawade, V. P., and Tripathi, S. N. (2006) *J. Geophys. Res.* **111**.
Kirbky, J., et al. (2011), *Nature*, **476** (7361), 429-433.
Kuang, C., McMurry, P. H., McCormick, A. V., and Eisele, F. L. (2008) *J. Geophys. Res.* **113**.
Kulmala, M., et al. (2004), *J. Aerosol Sci.* **35**, 143-176.
Metzger, A., et al. (2010) *Proc. Natl. Acad. Sci., USA* **107**, 6646.
Modgil, M. S., Kumar, S., Tripathi, S. N., and Lovejoy, E. R. (2005), *J. Geophys. Res.*, **110**.
Singh, S. and Kulshrestha, U. C. (2012) *Biogeosciences*, **9**, 5023-5029.
Sparcklen et al., (2008), *Geophys. Res. Lett.* **35** (6).
Vehkamaki, H., et al. (2002) *J. Geophys. Res.*,**107**.
Yu, F. (2010) *J. Geophys. Res.*, **115**, D03206.
Yu, H., McGraw, R., and Lee, S.-H. (2011) *Geophys. Res. Lett.*, **39**(2).
Yu, F. and Turco, R. P. (2008) *Atmos. Chem. Phys.*, **8**, 6085-6102.

The role of sulphuric acid in the formation of atmospheric particles based on a long-term explicit modelling approach

M. Boy[1], L. Zhou[1], D. Mogensen[1], A. Sogachev[2] and S. Smolander[1]

[1]Department of Physics, University of Helsinki, Helsinki, P.O. Box 48 FI-00014, Finland
[2]Wind energy department, Technical University of Denmark, P.O. Box 49, 4000, Roskilde, Denmark

Keywords: new particle formation, long-term, boundary layer, modelling
Presenting author email: michael.boy@helsinki.fi

The role of atmospheric aerosols is perhaps the largest unknown concerning our climate and greenhouse warming. New particle formation has been observed at almost all sites, where particle size distributions have been measured (Kulmala et al., 2004). Although many field campaigns, laboratory experiments and new modelling approaches have led to increased understanding, detailed mechanisms responsible for the formation of new particles in the troposphere have still not been completely elucidated. One of the most controversial topics is the role or importance of sulphuric acid in the formation process.

In this study we present results achieved by SOSA (Boy et al., 2011). This model was developed at the University of Helsinki. The meteorology is based on a 1-D version of the model SCADIS (Sogachev et al., 2002) and the Model for Emissions of Gases and Aerosols in Nature (MEGAN) is used to simulate the emission of organic vapours from the biosphere (Guenther et al., 2006). The gas phase chemistry is solved with the Kinetic Pre-Processor (KPP) in combination with the Master Chemical Mechanism from the University of Leeds. It is a parallelized model operating on a high-performance super-cluster at the CSC - IT Centre for Science in Finland, which gives the possibility to run detailed processes in chemistry, aerosol dynamic and meteorology over long periods with reasonable model runtime.

We will present different model results for 10 years of simulations (2003-2012) and comparison with measurements. Our aim is to demonstrate the role of sulphuric acid when considering the question: What are the crucial molecules for new particle formation in the atmosphere?

One possible way to get some hints to solve this question is the use of long-term comparisons between different parameters simulated with the new model SOSA and the frequency of particle formation events (Boy et al., 2002). In this context we calculated different combinations of parameters like e.g. RP-1:

$$RP-1 = \frac{[H_2SO_4]}{CS}$$

This equation gives the concentration of sulphuric acid divided by the condensation sink of the pre-existing aerosols. Figure 1 presents the number of event days in three different classes (Boy et al., 2002) and the amount of days per month where the daytime (9-15) mean value exceed the mean value by 0, 10, 25 %, respectively.

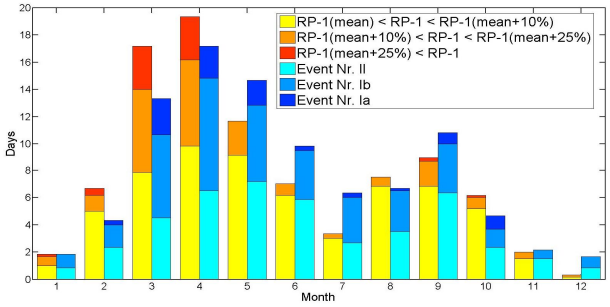

Figure 1: Monthly trend for RP-1 and observed frequency of nucleation event days

The figure shows a clear correlation in monthly distribution between sulphuric acid and nucleation event frequency. Including the monoterpenes, temperature and water vapour into the equation shifts the distribution more towards the summer months but also decrease the amount of days during the second observed event peak in autumn.

This work was supported by the Helsinki University Centre for Environment (HENVI).

Boy, M. and Kulmala, M. (2002) Nucleation events in the continental boundary layer: Influence of physical and meteorological parameters, *Atmos. Chem. Phys., 2, 1-16.*

Boy, M., Sogachev, A., Lauros, J., Zhou, L., Guenther, A. and Smolander, S. (2011) SOSA- a new model to simulate the concentrations of organic vapours and sulphuric acid inside the ABL- Part 1: Model description and initial evaluation, *Atmos. Chem. Phys., 11, 43-51.*

Guenther, A., Karl, T., Harley, P., Wiedinmyer, C., Palmer, P. I. and Geron, C. (2006) Estimates of global terrestrial isoprene emissions using MEGAN (Model of Emissions of Gases and Aerosols from Nature), *Atmos. Chem. Phys., 6, 3181-3210.*

Kulmala, M., Vehkamäki, H., Petajda, T., Dal Maso, M., Lauri, A., Kerminen, V., Birmili, W., and McMurry, P. (2004) Formation and growth rates of ultrafine atmospheric particles: a review of observations, *J. Aerosol Sci., 35, 143–176.*

Sogachev, A., Menzhulin, G., Heimann, M., and J. Lloyd (2002) A simple three-dimensional canopy – planetary boundary layer simulation model for scalar concentrations and fluxes. *Tellus 54B (5), 784-819.*

Hydration of Sulfuric Acid Clusters and the Impact of Bases

H. Henschel[1], I. K. Ortega[1], O. Kupiainen[1], T. Olenius[1], T. Kurtén[2] and H. Vehkamäki[1]

[1]Division of Atmospheric Sciences, Department of Physics, P.O. Box 64, 00014 University of Helsinki, Finland
[2]Laboratory of Physical Chemistry, Department of Chemistry, P.O. Box 64, 00014 University of Helsinki, Finland
Keywords: sulfuric acid, ammonia, water, quantum chemistry, nucleation.
Presenting author email: henning.henschel@helsinki.fi

The formation of new particles in the atmosphere is generally agreed to involve sulfuric acid and water. However, it is known that these alone can not explain the observed particle formation rates. Therefore, other substances must be invoved in the process. One substance known to enhance the formation rate is ammonia, though not either this can fully explain the observed rates.

An important goup of substances that could explain the elevated nucleation rates are amines. Especially dimethylamine has been found to be involved in particle formation events (Mäkelä, 2001).

We present here a study of the hydration of clusters formed by sulfuric acid, and sulfuric acid together with ammonia and dimethylamine, respectively.

Clusters containing up to four molecules of sulfuric acid with up to three molecules of ammonia or diemthylamine together with up to five water molecules were modelled using a RICC2/aug-cc-pVTZ//B3LYP /CBSB7 level of theory. Based on these results the realtive populations of the repsective hydrates were simulated for different relative humidities.

Clusters consisting only of sulfuric acid form in general stable hydrates with an increasing energy of hydration with increasing number of sulfuric acid molecules. Only in case of the cluster containing four molecules of sulfuric acid one hydrate was found to be considerably more stable than would be expected from the trend in energies. Consequently this hydrate is also predominantly populated over a wide range of relative humidities.

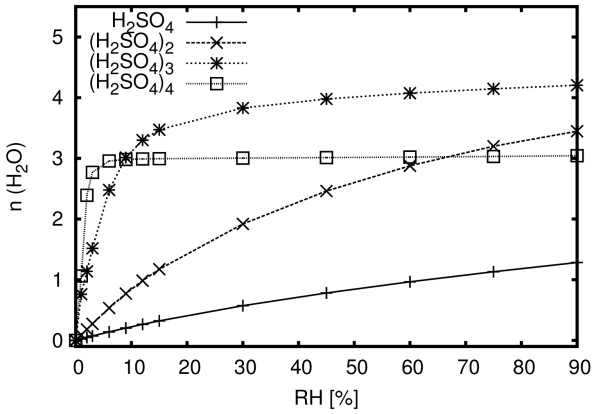

Figure 1. Hydration profiles for sulfuric acid clusters.

The resulting average hydration of clusters containing no base can be found in Fig. 1.
For systems containing both sulfuric acid and ammonia in general smaller hydration energies were found as compared to the base free system. Also, these systems do not exhibit broad distribution of hydration energies as the systems containing only acid, and show average hydration umbers between approximately 1.5 and 2.5 for relative humidity approaching 100 %.

Clusters containing both sulfuric acid and dimethylamine show an even lower affinity for water. For all clusters studied, the energy for at least one hydration step has been found to be positive. In case of the cluster consisting of two molecules of sulfuric acid and dimethylamine, all hydration energies were positive. Consequently, the average hydration of the dimethylamine-containing clusters is lower than for the other systems (cf. Fig. 2).

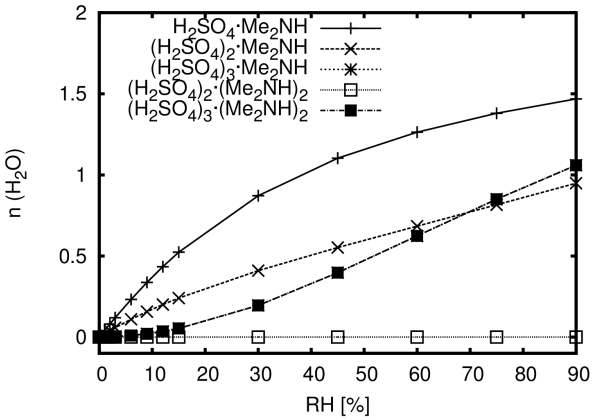

Figure 2. Hydration profiles for clusters containing sulfuric acid and dimethylamine.

At the same time, the profiles of the average hydrations of these clusters are not as uniform as for the other systems studied.

The observed differences in the hydration profiles will clearly have consequences on new-particle formation. Due to the differences in stability of certain hydrates, pathways towards particle formation can both become more and less likely, potentially altering the importance of different factors for the overall process significantly.

We thank the CSC–IT Center for Science in Espoo, Finland, for computing time, and ERC StG 257360 MOCAPAF, and the Academy of Finland (Center of Excellence program project #1118615, LASTU program project #135054) for funding.

Mäkelä, J. M., Yli-Koivisto, S., Hiltunen, V., Seidl, W., Swietlicki, E., Teinilä, K., Sillanpää, M., Koponen, I. K., Paatero, J., Rosman, K., and Hämeri, K. (2001) *Tellus B* **53**, 380–393.

Simulations of SOA formation from alpha-pinene ozonolysis and photo-oxidation in chamber experiments

G. Capes[1], D. Lowe[1], G. McFiggans[1]

[1]Centre For Atmospheric Science, University of Manchester, Manchester, M13 9PL, U.K.
Keywords: SOA, chamber, MCM, alpha-pinene.
Presenting author email: gerard.capes@manchester.ac.uk

Model description

We present here simulations of secondary organic aerosol formation from ozonolysis and photo-oxidation of alpha-pinene in a smog chamber. Simulations were performed using the MANIC model (Lowe et al., 2009), which uses gaseous VOC photochemistry from the MCM (Jenkin et al., 1997; Saunders et al., 2003) coupled to aerosol microphysics through mass transfer driven by Raoult's Law using predicted vapour pressures. The aerosol size distribution and size-resolved composition are represented by 16 size bins, which can use either moving-centre or moving-grid numerical schemes to follow particle growth.

Results

Two nucleation (i.e. unseeded) test cases will be presented:

1. ozonolysis of 100 ppb alpha-pinene by 135 ppb ozone, in the absence of NOx. This experiment was performed in the EUPHORE chamber, and is taken from Jenkin et al. (2004). Measurements of ozone, alpha-pinene and aerosol mass are compared with model output.

2. photo-oxidation of 55 ppb alpha-pinene, with initial concentrations 15 ppb NO2, 3 ppb NO and no ozone. This experiment was performed in the University of Manchester aerosol chamber, and measurements of NO, NO2, O3 and aerosol concentration are compared with the simulated quantities.

In both test cases, simulated aerosol mass concentrations reproduced measured aerosol mass concentrations to within a factor of 5, without the need to tune vapour pressures. Aerosol nucleation rate was tuned to the measured number concentration, and wall loss rates were also derived from the measured aerosol number distributions (Verheggen et al., 2006).

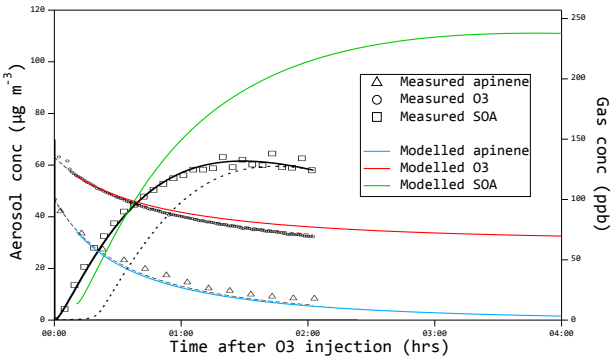

Figure 1: Preliminary results from the ozonolysis simulation. SOA mass is over-predicted by a factor of two.

This work was supported by EUROCHAMP–2.

Jenkin, M. E., Saunders, S. M., and Pilling, M. J., (1997) *Atmos. Environ.*, **31** 81–104.

Jenkin, M., E. (2004) *Atmos. Chem. Phys.*, **4**, 1741-1757.

Lowe, D., Topping, D., and McFiggans, G. (2009) , *Atmos. Chem. Phys.* **9**, 4559–4573.

Saunders, S. M., Jenkin, M. E., Derwent, R. G., and Pilling, M. J. (2003) *Atmos. Chem. Phys.*, **3**, 161–180.

Verheggen, B, and Mozurkewich, M. (2006) *Atmos. Chem. Phys.* **6**, 2927–2942.

Effects of electric vehicles on air quality in street canyons

T. Schöllnhammer[1], F. Lommes[2], T. Schulz[3], H. Hebbinghaus[3], and S. Wurzler[3]

[1]Department of Civil and Environmental Engineering, Ruhr University Bochum, Bochum, Germany
[2]Meteorological Institute, University of Hamburg, Hamburg, Germany
[3]North Rhine Westphalia State Agency for Nature, Environment, and Consumer Protection, Recklinghausen, Germany
Keywords: electric vehicles, air quality, street canyon.
Presenting author email: sabine.wurzler@lanuv.nrw.de

Road traffic is one of the main causes of poor air quality in European cities. Electric vehicles (EV) are often presented as solution for air quality problems in cities. In addition they are claimed to be a climate friendly means of transport owing to their non-existent exhaust emissions. The German government has formulated the ambitious goal to increase the amount of electric vehicles in Germany to 1 million in 2020 and 6 million in 2030. The aim of this paper is to investigate how much of this claim is true. While traffic is a major source of air pollutants in street canyons, it is often forgotten that electricity production nowadays is a significant source of air pollutants on the regional scale.

Focus of the present study is the air quality in street canyons, to be more precise the PM10 and NO_2 concentrations. We concentrate our investigation on road traffic, taking the fleet composition into account. We have investigated the following questions:

- Is the goal of the German government effective with regard to an improvement of the air quality?
- What share of electric vehicles would be needed to
a) significantly reduce the annual immission load (5 µg/m³ for NO_2 and 3 µg/m³ for PM10)?
b) comply with the EC limit values?
- Which vehicle type is most promising with regard to an efficient immission reduction? E.g., passenger cars? Busses? Heavy duty vehicles?
- What is the impact of the reduced traffic emissions on the regional background concentration of PM10 and NO_2?
- How much electricity is consumed by the vehicles? What is the resulting effect on power plant emissions?

We present results for two street canyons in Germany with moderate EC air quality limit value exceedances: Gladbecker Street in Essen, and Friedrich-Ebert-Street in Mönchengladbach. The air quality analyses were carried out using the canyon plume box model Immis^{Luft} for the contribution of local traffic, combined with field observations of air quality and model results of the chemical transport model EURAD (Memmesheimer et al., 2004). The change in power plant emissions was estimated based on the emission inventory of LANUV NRW. The energy consumption by the vehicles was estimated based on values from the recent literature, such as product information (Schöllnhammer, 2012).

As already mentioned the German government wants to increase the amount of electric vehicles in Germany. An example of the effects of this program on the air quality is shown in Table 1 for the annual average PM10 concentration. Reference year is 2009. We have assumed that the replacement of vehicles with combustion engines by electric vehicles would happen instantaneously. The proportion of electric vehicles in our street canyon was assumed to be the same as for the vehicle fleet in Germany. The findings are rather daunting for PM10, the results for NO_2 are somewhat better. The good news for these scenarios is that the effect of the increased electricity production on the regional air quality is leveled out by the emission reduction by the vehicle fleet on the regional scale.

Table 1: PM10 annual average concentration in µg/m³ in Friedrich-Ebert-Street for different scenarios: no electric vehicles (None), 1 or 6 million electric vehicles (EV) of the different vehicle types in Germany. HDV = heavy duty vehicles; LDV = light duty vehicles.

PM10 annual average concentration in µg/m³					
EV	None	Cars	HDV	Busses	LDV
1 mio.	29,6	29,6	29,5	29,4	29,6
6 mio.	29,6	29,4	29,5	29,4	29,6

One general finding of our study is that electric vehicles can reduce the NO_2 burden but are not the right measure to significantly influence the PM10 concentration in a street canyon. Only a minor share of the PM10 emissions is caused by vehicle exhaust. The lions share is produced by friction and abrasion processes. Those are present anyhow no matter of the engine type.

What amount of electric vehicles would be necessary to find a major impact on air quality will be addressed further in the presentation. The tradeoff between local emissions by the vehicles and the more regional emissions by the power plants will be critically discussed.

Major parts of this work were performed as diploma thesis at the Department of Civil and Environmental Engineering, Ruhr University Bochum, with the advisors Prof. R. Höffer and C. Wevers.

Memmesheimer, M., Friese, E., Ebel, A., Jakobs, H. J., Feldmann, H., Kessler, C., Piekorz, G. (2004), IJEP, **22**, 108 – 132.

Schöllnhammer, T. (2012): Wirkung der Elektromobilität auf die Luftqualität im innerstädtischen Gebiet. Diploma Thesis, Ruhr University Bochum, 95pp.

Remapping of aerosol emissions in a modal models as a source of error

T. Korhola[1], H. Kokkola[2], H. Korhonen[2], A.-I. Partanen[2], A. Laaksonen[1,3], S. Romakkaniemi[1]

[1] Department of Applied Physics, University of Eastern Finland, Finland
[2] Finnish Meteorological Institute Kuopio Unit, Kuopio, Finland
[3] Finnish Meteorological Institute, Climate change, Helsinki, Finland
Keywords: modelling, modal representation, emission inventories, activation
Presenting author email: tapani.korhola@uef.fi

Prescribed datasets for natural and anthropogenic aerosol emissions are widely used in global climate modelling. These inventories include i.a. recommendations for size distributions for emitted aerosol particles often given as parameters for log-normal modes. Most aerosol models use log-normal modes to describe the aerosol distributions. In these global models, the maximum mode diameter is often restricted due to technical reasons. These restrictions cause artificial minima in the model's aerosol size distribution at certain fixed sizes.

We have noticed that if the recommended mode diameters (Dentener *et al* 2006) in emission inventories are close to these artificial minimums, the model then remaps the emitted particles between two adjacent modes and never uses the actual emission distribution that is described in the inventories. In this work, we study how this affects the cloud droplet number concentration (CDNC) and aerosol-cloud interaction (ACI) parameter.

The simulations were done by using a box model, which allows the use of both free and restricted modes and a better control over physical, technical and statistical phenomena compared to a global model. The CDNC was calculated by using the Fountoukis and Nenes (2005) parametrization. The ACI was defined by

$$\mathrm{ACI} = \frac{d\log(\mathrm{CDNC})}{d\log \mathrm{N}}, \qquad (1)$$

where N is the total number concentration of the emitted (inventory based) aerosol. The ACI parameter fundamentally describes the sensitivity of droplet formation to aerosol distribution.

To study the effects of the mode size restrictions and the following remapping on the CDNC and ACI, we calculated both parameters with the unaltered emission size distribution recommended by the inventories and with the emissions that were forced under the global model restrictions. We did the same simulations with and without background aerosol.

The CDNC and ACI were evaluated as a function of N and vertical velocity of the cloud forming air parcel. Finally, we calculated the relative difference of these parameters between the unaltered and remapped emission.

The mode remapping effectively reallocates the mass and number concentration that exceeds the set upper diameter limit of a given mode (Binkowski and Roselle 2003). This reallocation decreases the mode average diameter and creates a new larger mode, or increases the number concentrations of pre-existing larger mode (Figure 1).

Our results show clearly that the mode remapping causes underestimation of both the CDNC (Figure 2) and ACI. The underestimation of the CDNC is most evident in the case with no background aerosol, where the relative difference is more more than 50 %. With the background aerosol, it is still more than 30 %. The underestimation due to remapping is because the critical diameter is smaller than the average diameter of the emission mode, but bigger than the smallest particles in the mode resulting from mode remapping. When the mode is remapped, significant number of the particles that would activate, are moved to a mode that is mostly below the critical diameter. For the same reason, as mentioned above, the ACI parameter shows stronger correlation between the unaltered emission and CDNC compared to the remapped emission. The underestimation of ACI by remapped emissions is up to 40 % with background and up to 20 % without background aerosol.

Depending on the emission inventories and aerosol models used, the widespread method of aerosol reallocation and mode remapping can cause a clear underestimation of cloud droplet number concentration and aerosol-cloud interaction parameter.

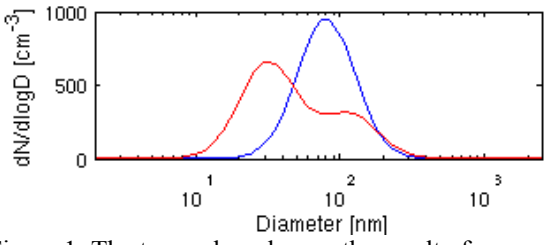

Figure 1: The two red modes are the result of remapped blue mode.

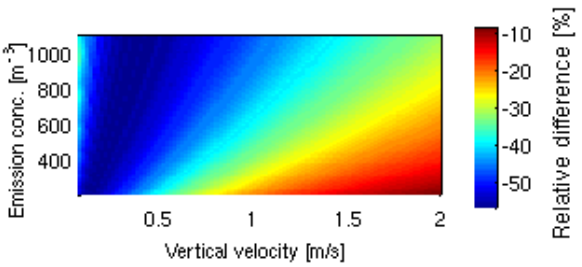

Figure 2: The relative difference between unaltered and remapped emission modes without background aerosol.

This study has been supported by the strategic funding of the university of Eastern Finland.

Dentener F. et al. (2006) *Atmos. Chem. Phys.*, **6**, 4321–4344.

Binkowski, F., Roselle S., (2003) *J. Geophys. Res.*, **108**, 4183, 18 PP.

Fountoukis, C., Nenes, A., (2005) *J. Geophys. Res.*, **110** D11212.

Impact of biogenic emissions on $PM_{2.5}$ concentration over Europe

E. Tagaris, R.E.P. Sotiropoulou, N. Gounaris, S. Andronopoulos and D. Vlachogiannis

Environmental Research Laboratory, NCSR Demokritos, Aghia Paraskevi Attikis, 15310 Athens, Greece
Keywords: biogenic emissions, particulate matter, Europe
Presenting author email: tagaris@ipta.demokritos.gr

Natural and biogenic emissions are contributing to atmospheric pollution in addition to anthropogenic emissions. Over 90% of the total Volatile Organic Compounds (VOCs) entering the atmosphere are biogenic (Greenberg et al., 1999), having an important role in regulating the atmospheric composition. The impact of both anthropogenic and biogenic emissions on air quality is very important, as only the anthropogenic part can be influenced by abatement measures. Curci et al. (2009) estimated that biogenic VOC emissions increased on average summer daily ozone maxima over Europe by 5% (2.5 ppbv) using the CHIMERE chemistry-transport model. Sartelet et al. (2012) using the Polyphemus air quality modeling platform estimated that ozone decreased by 10-11% on average over Europe (locally up to 35%) while secondary organic aerosols decreased by 72-88% when removing biogenic emissions. The objective of this study is to estimate the effect of biogenic emissions on $PM_{2.5}$ concentration and chemical composition over Europe.

Meteorological fields are derived using the Penn State/NCAR Mesoscale Model (MM5) (Grell et al., 1994).

Emissions are processed by the Sparse Matrix Operator Kernel Emissions (SMOKE v2.6) Modeling System (http://www.smoke-model.org). The TNO gridded anthropogenic emissions inventory for the year 2006 over Europe in a 0.1 × 0.1 degrees resolution (ftp://neptunus.tno.nl) is used. The Biogenic Emission Inventory System, version 3 (BEIS3) is used for processing biogenic source emissions (http://www.epa.gov/asmdnerl/biogen.html) using the USGS gridded land use data in 1 Km resolution (http://edc2.usgs.gov/glcc/glcc.php).

The Community Multiscale Air Quality (CMAQ v 4.7) Modeling System with the Carbon Bond mechanism (CB05) (http://www.camx.com/publ/pdfs/CB05_Final_Report_120805.pdf) is used for the regional air quality modeling (177 × 217 grid cells of 35 km × 35 km, with 14 vertical layers) (Byun et al., 2006).

$PM_{2.5}$ concentrations are simulated with and without biogenic emissions for July, 2006. The effect of the addition of biogenic emissions to anthropogenic ones is computed to reduce the average monthly mean $PM_{2.5}$ concentration over European land by 2% with both positive and negative responses regionally (Fig. 1). The addition of biogenic emissions increases the average monthly mean organic carbon concentration by 14% (Fig. 2) and decreases the monthly mean inorganic component concentrations (SO_4: -6%, NO_3: -4%, and NH_4: -6% on average) due to the reduction in oxidant levels (OH: -30% on average). However, regional changes in inorganic concentrations with both positive and negative responses are simulated.

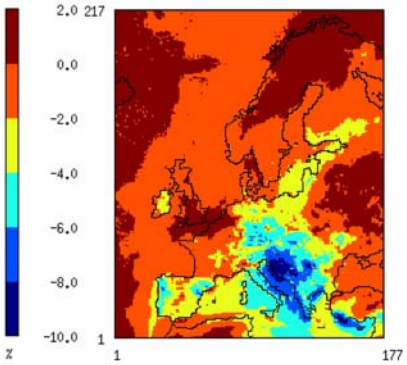

Fig. 1: Average change in $PM_{2.5}$ concentration (%) for July 2006 when biogenic emissions are added to anthropogenic emissions

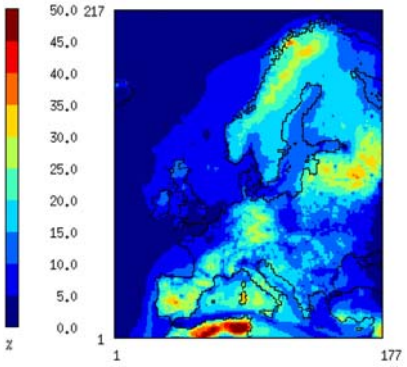

Fig. 2: Average change in OC concentration (%) for July 2006 when biogenic emissions are added to anthropogenic emissions

This work was supported by the National Strategic Reference Framework (NSRF) 2007-2013 grand No 09SYN-31-667.

Byun, D. W., and K. L. Schere (2006), *Appl. Mech. Rev.*, **59**, 51–77.

Curci, et al., (2009), *Atmos. Environ.*, **43**, 1444–1455.

Grell, G., et al. (1994), *Tech. Note NCAR/TN-398+STR*, Natl.Cent. for Atmos. Res., Boulder, Colo.

Greenberg, et al. (1999), *Atmos. Environ.*, **33**, 855– 867.

Sartelet et al. (2012), *Atmos. Environ.*, **53**, 131-141.

Monday, September 1, 2013

Session: Combustion Aerosols,
Characterization methods of combustion aerosols

Automatized determination of the primary particles size of soot aggregates by TEM image analysis

A. Bescond[1], J. Yon[1], C. Rozé[1] and F. X. Ouf[2]

[1]UMR 6614 CORIA, Avenue de l'université, 76801 Saint-Etienne du Rouvray, France
[2]Institut de Radioprotection et de Sureté Nucléaire (IRSN), 91192 Gif-sur-Yvette Cedex, France
Keywords: soot, morphology, TEM, EDM.
Email: alexandre.bescond@coria.fr

The needs for reference methods to analyse the physico-chemical properties of combustion aerosol have been of rising concern of the scientific community over the last three decades. The morphological characterization of soot aggregate is possible by analysing images obtained by Transmission Electron Microscopy (TEM). Indeed, it is shown that maximum projected length is related to the gyration radius size parameter. The 3D number of primary spheres in the aggregate can also be determined from the measurement of the particle projected area. Finally, these parameters are linked by a power law that permits to determine the soot fractal dimension (Brasil, et al., 1999; Köylü, et al., 1995). These measurements can be achieved automatically over a set of numerous TEM images in order to determine statistically the fractal dimension. However, the size of the primary particles is also needed and the classical method for determine it from TEM pictures is manual, time consuming and tedious.

Recently, an automatized method based on the Hough transform has been proposed in order to determine the primary particle size (Bradski and Kaehler, 2008). Here, we present another approach based on the Euclidian Distance Mapping (EDM) method which is robust, rapid and easy to implement. Indeed, EDM is often used to characterize the morphology of complexes objects as human cells (Ballerini and Franzen, 2001) or atomizing liquid flows (Grout, et al., 2007). In addition to its ability to determine the size of primary spherules, this method is promising to inform us of the fractal dimension of the particles.

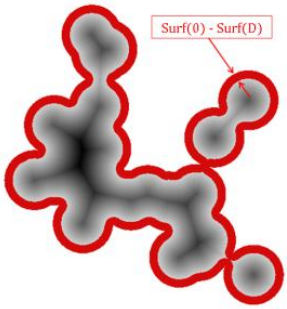

Figure 1. Illustration of the EDM method

The EDM analysis permits to determine, for each position in the image, the smallest distance to the border of the particle. This distance is represented in gray levels in figure 1. The more the Euclidian distance is, the more the gray level is dark. From this EDM map, we define a surface $S(D)$ corresponding to the part of the aggregate whose distance to the border is less than D, a scaling parameter. This surface is illustrated in red in figure 1. A dimensionless function ranging from 0 to 1 is finally defined:

$$S(D) = 1 - Surf(D)/Surf(0)$$

This function is established over a set of images of virtual aggregates generated by a DLCA (Diffusion Limited Cluster Aggregation) code (Meakin, 1999). The interest of this numerical investigation is to control the primary particle size (mode and standard deviation).

The Figure 2 presents the $S(D)$ functions determined for aggregates made of different sizes of primary particles. For each case, 200 aggregates whose number of primary spheres ranges from 10 to 60 are considered. In case of monodisperse primary particles, the representation of $S(D)$ as a function of D is shown to indicate that primary particle size can be determined easily from EDM analysis.

Based on different sets of DLCA aggregates, the way to determine simultaneously the primary spheres mean diameter and standard deviation is discussed.

After all, the EDM method is applied to TEM pictures coming from thermophoretic sampling of real soot aggregates of ethylene diffusion flame and CAST5201© generator.

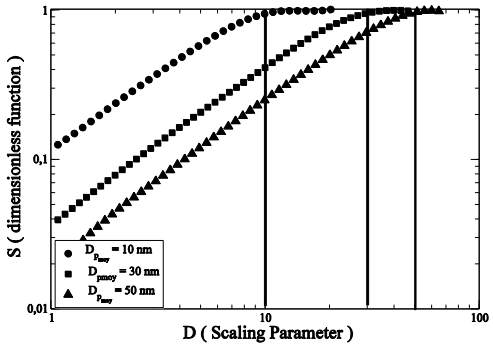

Figure 2. Representation of normalized surface function S

This work was supported by the French Civil Aviation Direction for MERMOSE Project.

Ballerini, L. and Franzen, L. (2001) *WSEAS Trans. on Circuit*, **11**, 7.

Bradski, G. and Kaehler, A. (2008) *Learning OpenCV: Computer vision with the OpenCV library*. O'Reilly Media, Incorporated.

Brasil, A., Farias, T. and Carvalho, M. (1999) *Journal of Aerosol Science*, **30**, 1379.

Grout, S., Dumouchel, C., Cousin, J. and Nuglisch, H. (2007) *Int. J. Multiphase Flow*, **33**, 1023-1044.

Köylü, Ü.Ö., FaethT L, G. and Carvalho, M. (1995) *Combustion and Flame*, **100**, 621-633.

Meakin, P. (1999) *J. Sol-Gel Sci. Technol.*, **15**, 97-117.

Electrical Conductivity Measurements in Combination with Raman Microspectroscopy and Temperature Programmed Oxidation for Analysis of Microstructure and Reactivity of Soot

B. Grob[1], F. Knoller[1], N. P. Ivleva[1], R. Niessner[1]

[1]Chair for Analytical Chemistry, Technical University of Munich, Munich, 81377, Germany
Keywords: electrical conductivity, Raman microscopy, temperature programmed oxidation, soot reactivity, real-time detection
Presenting author email: benedikt.grob@mytum.de

Soot particles emitted by diesel engines are a well known problem especially in urban areas due to their influence on the human health but they can have a significant influence on the climate as well. Therefore the emission regulations for light and heavy duty vehicles prescribe a strict limit of diesel soot particle emission. This can only be accomplished by diesel particle filters (DPF). To control the back pressure of this filters a continuous or periodically gasification of the deposited particles is necessary. The efficiency of this regeneration step is mainly affected by the oxidation behaviour of the soot, which is directly connected to its microstructure.

To optimize the engine in the way that they produce highly reactive soot, tools are required to analyse soot samples regarding their oxidation behaviour. Currently, the temperature controlled oxidation of soot samples is used as a common method for engine optimization. But as we could show in early publications Raman microspectroscopy as well as the electrical conductivity measurement are a promissing tool for soot microstructure characterization (Schmid 2011 & Grob 2012) Especially the conductometric measurement method is very attractive, because it is a simple, rapid and cheap tool compared to the other techniques. So far we could show in basic experiments the possibilities and the limitations of this method (Grob 2012).

Our approach is now to develop a device which makes it possible to investigate the influence of the microstructure and the oxidation behaviour of soot on the electrical conductivity combined with the monitoring of the processes by the Raman microspectroscopy (RM) and the temperature programmed oxidation in one setup. Therefore we developed a flowcell (Fig. 1) which can be heated up to 1273 K and can be placed under the Raman microscope, due to a good isolation and a effective cooling of the cell frame. Through a quartz glass window it is possible to observe the soot layer on the conductometric sensor (Fig. 2) inside the cell. On the outlet of the cell a FTIR can be plugged as a gas detector of the controlled oxidation. The soot particles are collected by a thermophoretic particle precipitator on the conductometric sensor surface, which consists of a oxidized silicon substrate with interdigitated AlSiCu electrodes on it.

The setup allows us to change the graphitization of a soot sample under controlled atmosphere. By cooling down the sample under protective gas atmosphere in the same device a contamination or further oxidation of the sample can be prohibited. In the second step the measurement of the electrical conductivty of the sample follows and can be correlated with the fingerprint spectra of the RM provided through the window of the cell.

So far the conductometric sensor principle is only used for on board particle detection to monitor the DPF in light duty vehicles. We hope that we are able to extend the use of the principle by this experminental setup for soot microstructure and reactivity analysis.

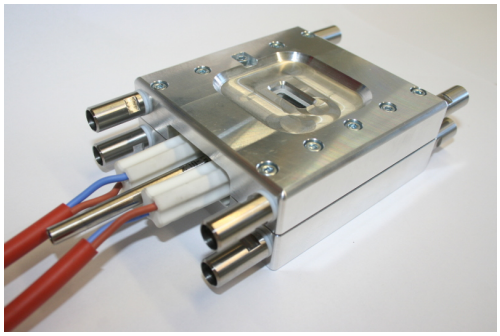

Figure 1: The heatable flow cell covered with a water cooled aluminum block.

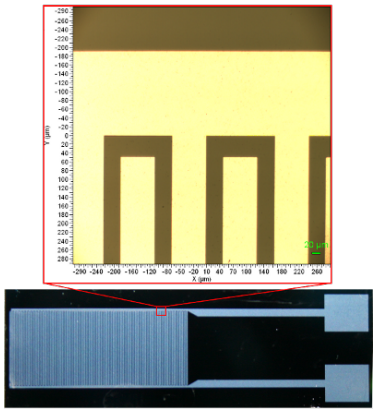

Figure 2: The interdigitated electrodes with a distance of 50 µm between the fingers.

Grob, B., Schmid, J., Ivleva, P. N., Niessner, R. (2012) *Anal. Chem.* **84**, 3586–3592.

Schmid, J., Grob, B., Niessner, R., Ivleva, N. P. (2011) *Anal. Chem.* **83**, 1173–1179.

Aerosol mass spectrometry of refractory black carbon containing particles

T.B. Onasch[1,2], E.C. Fortner[1], P. Massoli[1], L.R. Williams[1], A.T. Lambe[1,2], A.M. Trimborn[3], J. T. Jayne[1], P. Davidovits[2], and D.R. Worsnop[2]

[1]Center for Aerosol and Cloud Chemistry, Aerodyne Research, Inc., Billerica, MA, 01821, USA
[2]Department of Chemistry, Boston College, Chestnut Hill, MA, 02467, USA
[3]Aeromegt GmbH, Hilden, 40723, Germany
Keywords: aerosol mass spectrometry, refractory black carbon, combustion soot.
Presenting author email: onasch@aerodyne.com

The soot particle aerosol mass spectrometer (SP-AMS) instrument, recently developed by Aerodyne Research, Inc., combines the ability to measure the mass and chemical composition of size-resolved particulate matter, including refractory black carbon components (Onasch et al. 2012). This instrument was developed to address the issue that refractory black carbon-containing particles formed in incomplete combustion processes are strong light-absorbers with significant climate forcing impacts and potential health effects. The complex nature of these particles makes their characterization (microphysical, chemical and optical) challenging. The SP-AMS technique represents a new method for characterizing and quantifying the chemical and physical properties of particulate refractory black carbon. Using the SP-AMS, we have participated in a growing number of laboratory studies and field campaigns to characterize refractory black carbon-containing particles from a range of sources and over a range of atmospheric aging. We will present selected highlights from these studies.

The SP-AMS is equipped with an intracavity Nd:YAG CW laser vaporizer (1064 nm). Only light absorbing particles, such as refractory black carbon containing particles, will vaporize in the laser beam. Both the nonrefractory and refractory components are vaporized. Particulate vapors are ionized by electron ionization (70 eV) and detected with high resolution time-of-flight mass spectrometry. The SP-AMS can be operated with or without a resistively heated (600°C) tungsten vaporizer; with both vaporizers, the SP-AMS measures all refractory and non-refractory particles.

Laboratory results have focused on characterizing the chemical and physical properties of laboratory-based flame soot and manufactured refractory black carbon particles as a function of coating with organic compounds and sulfuric acid and thermal denuding (Eben S. Cross et al. 2010). These studies have provided the foundation for using the SP-AMS instrument to constrain measurements of the optical properties of ambient soot particles, specifically relating to the absorption enhancement due to atmospheric aging.

In addition, we are characterizing the carbon ion distributions generated by different refractory black carbon particle types. These mass spectral signatures may provide unique information on different types of refractory black carbon sources. Figure 1 shows five carbon ion mass spectra for laboratory and field measured rBC particle types and illustrates a trend towards larger carbon clusters.

The field measurements conducted include biomass burning (FLAME3), flare emissions (Fortner et al. 2012) internal combustion engine sources (Massoli et al. 2012; Cross et al. 2012; NYC, MIT Engine Lab, and Caldecott Tunnel), and urban environments (Cappa et al. 2012; CalNex 2010 and ClearfLo 2012). Mass spectral features and size distribution results for several field deployments will be presented with emphasis on source characterization and the characterization of the chemical and physical changes that rBC particles undergo as a function of atmospheric aging.

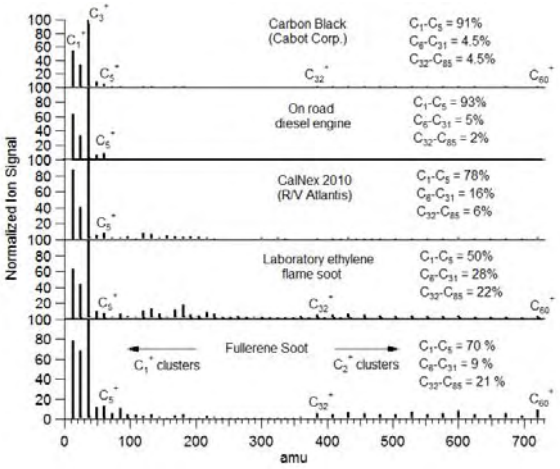

Figure 1. Refractory black carbon mass spectra for laboratory and field particulate sources.

This work was supported by the DOE SBIR, NOAA Global Climate Change, and EPA STAR programs.

Cappa, C. D., et al. (2012) *Science* 337 (6098) (August 30): 1078–1081.

Cross, E. S., et al. (2012) *Journal of Engineering for Gas Turbines and Power* 134 (7): 072801.

Cross, E. S., et al. (2010) *Aerosol Science and Technology* 44 (8) (June 30): 592–611.

Fortner, E. C., et al. (2012) *Industrial & Engineering Chemistry Research* 51 (39) (May 3): 12586–12592.

Massoli, P., et al. (2012) *Aerosol Science and Technology* 46 (11) (November): 1201–1218.

Onasch, T. B., et al. (2012) *Aerosol Science and Technology* 46 (7) (July): 804–817.

REMPI-Laser-mass spectrometry: On-line and off-line analysis of the molecular signature of polycyclic aromatic hydrocarbons (PAH) in gas- and particle-phase of combustion aerosols

R.Zimmermann[1,4], C.Radischat[1,4], O.Sippula[1,4], M.Kelbg[2,4], M.Sklorz[1], J.Passig[1,4], C. Busch[1], M. Oster[1], H.Harndorf[2,4], A. Walte[3], B Stengel[2,4], T.Streibel[1]

[1]Joint Mass Spectrometry Centre, Rostock University (Analytical Chemistry) & Helmholtz Zentrum München (HMGU/CMA), Germany; [2]University of Rostock (Inst. of Piston Machines & Int. Combust. Engines and Inst. of Physics), Germany; [3]Photonion GmbH, Schwein, Germany; [4]HICE – Helmholtz Virtual Institute of Complex Molecular Systems in Environmental Health-Aerosols and Health, www.hice-vi.eu

Presenting author email: ralf.zimmermann@helmholtz-muenchen.de *or* ralf.zimmermann@uni-rostock.de

Keywords: combustion aerosol, on-line mass spectrometry, aromatic compounds, ship diesel-/wood-combustion

Polycyclic aromatic hydrocarbons (PAH) and benzene derivatives represent important compound classes, present in combustion aerosols. On the one hand, PAH and their derivatives are known to be of high health relevance (chronic and acute lung and cardiovascular diseases). On the other hand, the signatures of the aromatic molecules in combustion aerosols characterize the combustion process and allows conclusion on the molecular formation mechanisms of soot and other pyrolysis and combustion by-products. Photoionisation mass spectrometry is an ideal approach for on-line-detection of the molecular signature of combustion aerosols. When the laser based resonance-enhanced multiphoton ionization method (REMPI) and a time-of-flight mass analyser (TOFMS) are used, unsurpassed sensitivities (ppb/ppt) and time resolutions (sub-second) are achieved for detection of aromatic molecular species. In Fig. 1A an on-line measured REMPI-TOFMS mass spectrum of wood combustion aerosol is depicted. The

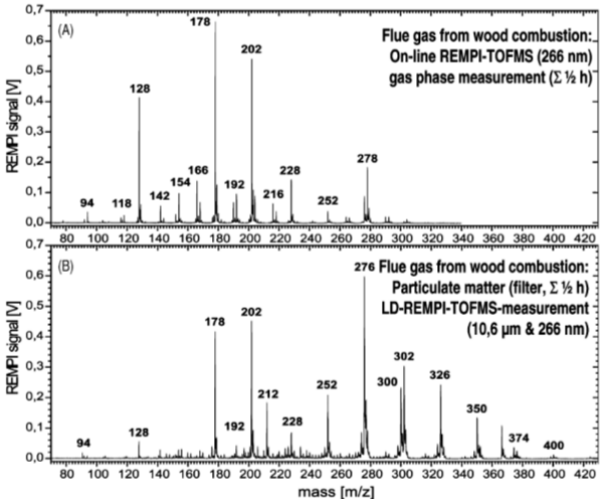

*Figure 1) REMPI mass spectra of **wood combustion aerosol** A) Signal of the aromatic compounds in the **gas phase** of a wood combustion experiments: more volatile aromatics are detected B) Laser desorption-REMPI mass spectrum of the aromatic compounds from the **particulate phase** (collected simultaneously to measurement of A): larger PAH are observed*

selectivity of the REMPI ionisation for aromatic compounds allows a straight-forward assignation of the observed mass peaks in the mass spectrum (e.g. for Fig. 1A: 94 m/z-phenol, 118 m/z-indane, 128 m/z-naphthalene, 166 m/z-fluorene, 178 m/z-phenanthrene, 202 m/z-pyrene, 228 m/z-chrysene, 252 m/z-5-ring PAH including Benz[a]pyrene, 278 m/z 6-ring-PAH). By

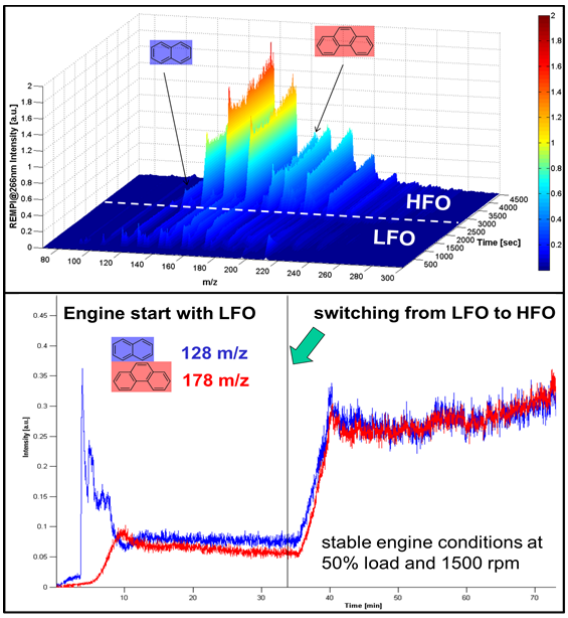

*Figure 2 On-line measurement of the gas-phase aromatics (PAH and alkylated-PAH) in combustion aerosol from a **ship diesel engine** operated with distillate fuel (light fuel oil, LFO) and residual fuel (heavy fuel oil, HFO) top) 3D-representation of the changes in aromatic REMPI mass spectral signature over time during a switch from "clean"LFO -fuel to"dirty" HFO-fuel. The lower part of the figure depicts the time-intensity curves for 2 selected PAH, naphthalene and phenanthrene.,*

using laser desorption (LD, e.g. direct from PM on filter) also the particle-bound aromatics can be rapidly analysed (Fig. 1B). It is obvious from Fig. 1 that the larger PAH are predominately particle bound.
During the HICE campaign at a ship diesel engine test bench, REMPI-TOFMS was used to follow the switch from LFO to HFO fuel in real time (Fig. 2). During the engine-start period, the large ship diesel engines are operated with LFO. The HFO fuel (melting point ~ 60 °C) is only introduced when the engine is at operational temperature. Fig. 2 shows clearly, that the emission of aromatic compounds, including the toxic polyaromatics, is increased significantly after the transition to HFO. The PM from ship diesel and wood combustion aerosol was furthermore investigated by a new coupling of an EC/OC-thermal analyser to a REMPI-TOFMS system, showing the aromatic signature of different thermal steps in the thermo-optical EC/OC measurement.

This work is supported by the Helmholtz association (HGF) via the Virtual Helmholtz Institute HICE (www.hice-vi.eu).HICE investigates the health effects of anthropogenic combustion aerosols

Carbonaceous aerosols and variations in their light absorbing properties

C. Linke[1], I. Ibrahim[1] , R. Hitzenberger[2] and M. Schnaiter[1]

[1]Institute for Meteorology and Climate Research, Karlsruhe Institute of Technology (KIT), Hermann-von-Helmholtz-Platz 1, 76344 Eggenstein-Leopoldshafen, Germany
[2]Faculty of Physics, Aerosol Physics and Environmental Physics, University of Vienna, Boltzmanngasse 5, 1090 Vienna, Austria

Keywords: absorption, black carbon, brown carbon, optical properties
Presenting author email: claudia.linke@kit.edu

In urban environments carbonaceous aerosols have serious impact on air quality and therfore on human health. Moreover due to their strong absorption properties in the visible spectral region they directly contribute to radiative forcing on regional and global scales.

In spite of various analytical and/or optical methods the accurate determination of atmospheric burdens by carbonaceous aerosol is still challenging (Cavalli et al., 2010, Lack et al., 2008).

In a combined laboratory and field study we characterised the spectral light absorption properties of soot with a single cavity multi wavelength photoacoustic spectrometer. During laboratory experiments we studied artificially generated combustion soot (mini-CAST) of increasing organic content. Therefore the burning conditions were stepwise changed towards more and more incomplete combustion (Schnaiter et al., 2006). From these experiments we can show that different burning conditions correlate to different wavelength dependencies of the measured absorption coefficients. Moreover, absorption cross sections were independently calculated from off-line filter measurements analysed by Sunset EC/OC.

Table 1. Absorption cross sections (ACS) of CAST soot for different burning conditions and for a wavelength of 532nm

CAST soot C/O ratio	ACS from PAS and EC (m2/g)	ACS from PAS and TC (m2/g)
0.29 (35%EC,65%OC)	14.5 ±1.6	5.4 ±0.4
0.4 (10%EC,90%OC)	18.6 ±4.2	1.6 ±0.1

For the first time we operated the multi-wavelength photoacoustic spectrometer during an urban field campaign (AIDA mobil urban) in autumn 2012 at Durlacher Tor in Karlsruhe, Germany. At that time, the measurement site was characterised by intense road works (construction of subway tube) and high traffic volume. In combination with concurrently determined refractory black carbon mass concentrations from a single particle soot photometer (SP-2), we derived absorption cross sections for the three photoacoustic wavelengths.

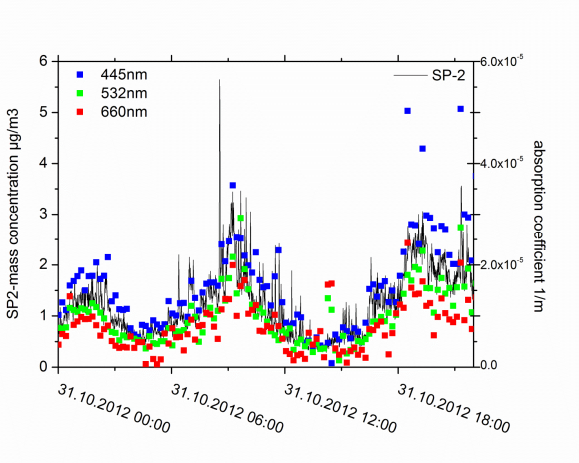

Figure 1. Diurnal variations of incandescence derived refractory BC mass concentration (SP-2) and photoacoustic absorption coefficients in the blue, green and red wavelength range during the field campaign at Durlacher Tor, Karlsruhe, Germany, in autumn 2012

This work was supported by a KIT start-up project within the Kompetenzbereich *Erde und Umwelt*.

Cavalli, F.et al. (2010) *Toward a standardised thermal-optical protocol for measuring atmospheric organic and elemental carbon: the EUSAAR protocol*, Atmos. Meas. Tech. 3, 79-89

Lack, D. et al. (2008) *Bias in filter-based aerosol light absorption measurements due to organic aerosol loading* Aerosol Sci. Technol. 42, 1033-1041

Schnaiter, M. et al. (2006) *Strong spectral dependence of light absorption by organic carbon particles formed by propane combustion,* Atmos. Chem. Phys. 6, 2981-2990

Effective density of particles from different combustion conditions and engineered TiO_2 nanoparticles

J. Leskinen[1], M. Ihalainen[1,4], T. Torvela[1], J. Ruusunen[1], M. Miettinen[1], I. Nuutinen[1], J. Lyyränen[3], A. Auvinen[3], J. Joutsensaari[2], O. Sippula[1], J. Tissari[1] and J. Jokiniemi[1,3]

[1]Department of Environmental Science, University of Eastern Finland, Kuopio, FI-70101, Finland
[2]Department of Applied Physics, University of Eastern Finland, Kuopio, FI-70101, Finland
[3]VTT Technical Research Centre of Finland, P.O. Box 1000, FI-02044 VTT, Espoo, Finland
[4]Department of Nuclear Energy and Safety, Paul Scherrer Institut (PSI), CH-5232 Villigen PSI Switzerland
Keywords: effective density, particle characterization, biomass burning, nanoparticle
Presenting author email: Jani.Leskinen@uef.fi

It is widely accepted that combustion derived particulate matter (PM) is related to adverse health effects in humans. However, it is still unclear, what is the mechanism behind these effects, and which properties of the PM (size, shape, chemical composition, surface properties) besides of mass concentration are relevant (Mills et al. 2009). Therefore, detailed analyses of the PM properties are needed.

Density is a fundamental property of particles, and by one definition, links the particle mass m_p and mobility diameter in relation of

$$\rho_{ef} = \frac{m_p}{\frac{\pi}{6} d_{el}^3}$$

Density is also the link between electrical mobility diameter d_{el} and aerodynamic diameter d_{ae}, which enables measurements with impactors and classifiers to be compared. However, errors in determination of particle size arise as particles deviate from ideal spheres with standard density. One of the key properties in particle sizing is the fractal dimension D_f,

$$\rho_{ef} = D' d_{el}^{D_f - 3},$$

where D' = constant and D_f = mass related fractal dimension (Park *et al.*, 2003). Combustion derived soot agglomerates, readily found in atmospheric samples, are a typical example of non-standard, fractal particles that are shown to have significant role in particle mediated health issues.

In this study, we compared experimental results as follows: the effective densities ρ_{ef} of particles in various size fractions (<1 µm) from i) different biomass grate combustion situations (Torvela et al. 2011), ii) biomass gasification combustion experiments (Nuutinen et al. 2010) and iii) synthesis of TiO_2 nanoparticle (Backman et al. 2009). An APM-SMPS method was applied to determine effective densities of particles.

In Fig. 1 the measured effective densities are shown as function of d_{el}. According to the equation above, the slope of these graphs is related to the fractal dimensions of those particles.

The effective density was found to be connected with the source of the particles and with combustion conditions. In biomass combustion a relatively small change in the combustion conditions (air staging and fuel feeding) caused significant differences to ρ_{ef}, even for particles of approximately same mobility diameter. This was due to differences in both chemical composition and morphological properties of the particles, observed by single particle analyses by TEM.

The fractal dimension was not constant for the smallest particles in Fig 1 (slope of the graph). However, larger particles seem to have a clear fractal structure (close to constant D_f).

As a conclusion, no single value can be used for effective density of biomass combustion particles. Rather, effective density should be determined for each particle type separately.

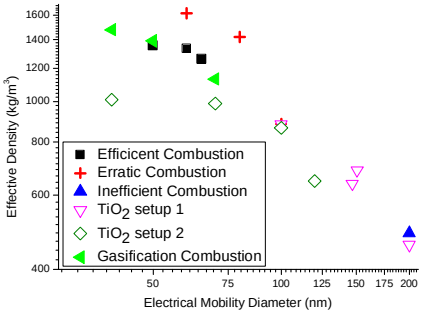

Figure 1. Effective density of particles from biomass combustion (Efficient: low CO-emission, Erratic: elevated CO and Inefficient: high CO), gasification combustion and TiO_2 particles in log-log graph.

The authors acknowledge Finnish Funding Agency for Technology and Innovation (grants 40392/09, 70004/09 and 40154/08) and partners in these projects, strategic funding of the University of Eastern Finland for project sustainable bioenergy, climate change and health, Finnish Cultural Foundation North Savo Regional fund and M.Sc.(Tech.) Tapio Kettunen.

Mills, N.L. et al. (2009). Nature Clinical Practice Cardiovascular Medicine 6:36-44.
Torvela T. et al. Abstract 554 in EAC 2011
Nuutinen, I. et al. Abstract 952 in IAC 2010
Backman, U. et al. (2009) Abstracts of the 4th Int. Conf. on Nanotech. – Occup. and Environ. Health, Helsinki (PK-Paino OY, Tampere), 42.
Park, K. et al., J. Environ. Sci. Technol 2003, 37, 577-583

Dilution affects particle properties originating from residential biomass combustion

H. Lamberg[1], T. Kaivosoja[1], J. Leskinen[1], M. Kortelainen[1], A. Viren[1], H. Koponen[1], V. Tiihonen[1], M. Miettinen[1], J. Pyykönen[2], J. Jokiniemi[1,2] and J. Tissari[1]

[1]Department of Environmental Science, University of Eastern Finland, Fine Particle and Aerosol Technology Laboratory, P.O. Box 1627, FI-70211 Kuopio, Finland
[2] VTT, Technical Research Centre of Finland, Fine Particles, P.O. Box 1000, FI-02044 VTT, Espoo, Finland
Keywords: dilution, biomass combustion, sampling.
Presenting author email: heikki.lamberg@uef.fi

Residential biomass combustion is known to be a significant source of particulate matter (PM) in regions where it is in common use. Sampling of fine particles from residential combustion appliances is of great significance because of a need to create standards for particulate emission measurements. Small-scale biomass combustion sources often emit fine particles that contain substantial amounts of organic compounds that condense at relatively low temperatures. Sampling procedures, such as temperature control and dilution ratio (DR), are known to affect sampled particles, especially as concerns their organic constituent (Lipsky et al. 2006). The aim of this study was to identify the effect of DR on fine particles, and to study the use of porous tube diluter in this type of measurements.

Batch combustion appliance with simple combustion technology, a sauna stove, was used in the experiments. Sampling of flue gases was done with a setup of porous tube and ejector diluters (Tissari et al. 2007). Three different DRs, 15, 40 and 115, were used. DRs were controlled with simultaneous CO_2 concentration measurements in the flue gas and in the diluted sample gas. Two similar dilution and sampling systems were operated during each measurement at different DRs. This ensured that the samples were comparable even if the combustion process varied slightly between each individual experiment, which is often present in batch-combustion process.

Overall, only a minor effect of DR on sampled PM mass was observed in the experiments. As expected, the smallest DR seemed to lead to the highest PM mass. While the total PM mass remained rather constant, a large variation as a function of DR was observed in measured particulate form PAH content, in the studied combustion conditions. The total particulate PAH at DR 15 was 1.8-fold to 2.9-fold compared to DRs 40 and 115, respectively (Fig. 1). The PAH/PM_1 ratio decreased from 9.4% to 5.8% and 2.5%, while DR increased from 15 to 40 and 115. The effect of DR was the largest for light PAH compounds. Heavy PAH species have most likely condensed prior to sampling. The fact that their measured concentrations scaled very well with DRs indicated that the porous tube diluter worked in a reliable way.

Computational fluid dynamics (CFD) modelling was used to obtain a better understanding of flows and losses inside the porous tube diluter. The studies identified the tip of the porous tube nozzle as the critical region for condensable organic vapour and fine particle losses. Right at the tip, the porous flow does not provide protection. Overall, only minor sampling losses are predicted for typical small-scale biomass combustion conditions. Model considerations of dynamics involved in gas-to-particle conversions indicate that the residence times in the diluter are sufficient for equilibrium, provided that no chemical reactions are involved. This is the case for PAH compounds that are the same in the gaseous and condensed forms. Indeed, vapour pressures seem to provide sufficient explanation of the observed trends in PAH contents.

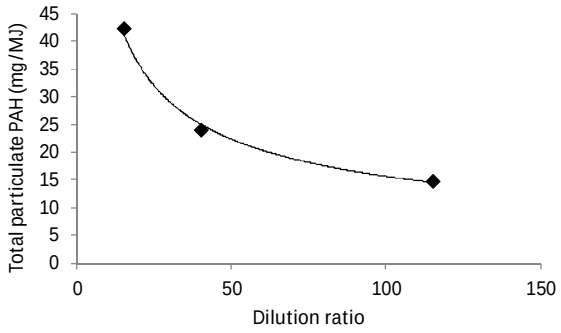

Figure 1. The effect of dilution ratio on total particulate PAH.

The porous tube diluter worked in a consistent and reliable way in the measurements. The experiments indicate that, even in cases where total PM emissions only show weak DR dependence, particulate properties may still be significantly affected by DR. This is especially true of health effect studies. The samples have large variation in their PAH contents, and consequently, possibly in their health effects as well.

This work is part of the ERA-NET joined project EN-PME-TEST. The work at UEF and VTT is funded by the Finnish Funding Agency for Technology and Innovation (TEKES). This work was further supported in part by the strategic funding of the University of Eastern Finland for project Sustainable Bioenergy, Climate change and Health (SUBI).

Lipsky, E.M. and Robinson, A.L. (2006). *Environ. Sci. Technol.* **40**, 155–162.
Tissari, J., Hytönen, K., Lyyränen, J., Jokiniemi, J. (2007). *Atmos. Environ.* **41**, 8330–8344.

Monday, September 1, 2013

Session: PMx, *Urban PMx*

Road surface dust load is dependent on road surface macro texture

G. Blomqvist, M. Gustafsson and T. Lundberg

VTI – Swedish National Road and Transport Research Institute, Linköping, SE-58195, Sweden
Keywords: road, dust, texture, abatement.
Presenting author email: goran.blomqvist@vti.se

Emission of road dust into the air is negatively dependent on the road surface macro texture (Blomqvist *et al*, 2011; China and James, 2012). That statement is, however, based on controlled experiments where equal amounts of dry dust were applied on clean road surfaces.

This abstract concludes that the actual dust load in city streets are positively related to the road surface macro texture and also strongly related to the season (Figure 1). The amount of vehicle induced emission of the road dust suspended into the air will, however, not only be dependent on the dust load amount on the road surface, but also to its emission availability, which to a very large degree depends on the road surface wetness. The large seasonal variation of the dust load is to large extent due to the studded tire wear of road surfaces, and winter sanding material spread on roads and sidewalks.

The road dust was sampled with the VTI Wet Dust Sampler (Jonsson *et al* 2012) on four test sites, representing different city streets, at eight different occasions from October 2011 to January 2013. The road surface macro texture (Table 1) was measured at each sampling site by the sand patch method (CEN-standard EN 13036-1). The macro texture was also measured along the entire road lengths of the sampled streets using the VTI Laser Road Surface Tester, RST.

Table 1. Road lengths and texture at sampling sites.

Testsites (Street name)	Road length (km)	Road surface macro texture (mean texture depth) (mm)	
		Wheel track	Between tracks
Hornsgatan	2.4	1.5	2.0
Folkungagatan	0.6	1.7	1.0
Sveavägen	1.6	1.3	1.1
Norrlandsgatan	0.3	1.2	0.9

The mode and standard deviation of the road surface macro texture histograms differ largely between and within the four studied city streets (Figure 2). This points out that the geographic variation of the road surface texture and, hence, the amount of road dust load can be very large.

Together with the fact that the road dust load also shows a large seasonal variation, this knowledge could be used from an abatement strategy point of view as it gives information regarding the questions of *when* and *where* abatement activities such as street cleaning should take place. That will, however, require knowledge of the road surface texture along the city road network.

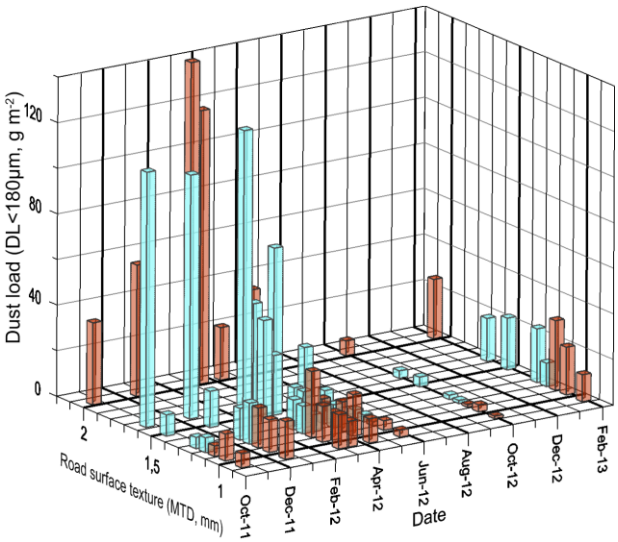

Figure 1. Road surface dust load as related to road surface macro texture and time of year. Red = between wheel tracks, Blue = in wheel tracks. Data partly from Gustafsson *et al* (2012).

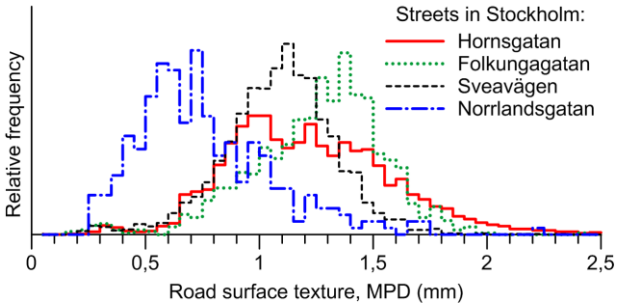

Figure 2. Histogram of road surface macro texture (mean profile depth) in the left wheel track in four city streets.

This work was supported by the City of Stockholm and BVFF; a research program financed by the Swedish Transport Administration, KTH Royal Institute of Technology, and Swedish National Road and Transport Research Institute. Grant No. BVFF 2012-055 and -056.

Blomqvist, G., Gustafsson, M., Bennet, C. and Halldin T. (2011) *Proc. 2011 European Aerosol Conference*.

China, S. and James, D.E. (2012) *Atm. Env.* **63**, 313–326.

Gustafsson, M., Blomqvist, G., Johansson, C. and Norman, M. (2010) Report, *VTI-rapport* **767**, Swedish National Road and Transport Research Institute. (In Swedish with English summary)

Jonsson, P., Blomqvist, G. and Gustafsson, M. (2008) *Transportation Research Circular*, **E-C126**, 102–111

Evaluating the use of dust suppressant to control local PM_{10} concentrations

G. W. Fuller, B. Barratt, D. Carslaw, D. Green, A.H. Tremper

MRC HPA Centre for Environment and Health, King's College London, London, SE1 9NH, UK
Presenting author email: gary.fuller@kcl.ac.uk

Introduction

Around Europe cities are struggling to meet EU Limit Values for PM_{10} requiring ever more creative measures to control concentrations in PM_{10} hotspots. Trials have found that street sweeping alone is not effective. The combination of street sweeping and washing has led to decreased PM_{10} in some locations with decreases of 7-10% at the kerbside in Barcelona (Amato et al 2009) but other studies have found no effects. Similarly dust suppressants have had impressive results in some studies such as those in Sweden where Norman and Johansson (2006) found a reduction of 35% in ambient air PM_{10} levels and 29– 43% decreases were found in Klagenfurt, Austria (Hafner, 2007) but other studies have reported no benefits at all (Amato et al 2010).

The application of calcium magnesium acetate (CMA) dust suppressant was tested over two years at nine locations in London ranging from a busy urban centre street canyon to suburban streets around industrial areas; each location having its own distinct geographical and emissions characteristics, allowing an assessment of the impact of CMA in differing situations and at varying application rates.

Methods

Changes in ambient PM_{10} as a result of CMA application were tested using different assessment methods each with their own controls:

a) NO_X tracer methods which sought changes in NO_X:PM_{10} emissions ratios from CMA applications reasoning that CMA would affect PM_{10} but not tailpipe NO_X.

b) Meteorological statistical modelling to remove as much of the interfering behaviour of meteorology, giving a much better chance of observing the effect of an intervention or emissions change.

c) PM_{10} mass closure from measured PM chemical components.

d) Detailed analysis of PM_{10} measurements looking at diurnal variations in PM10 from road sources on days with CMA and days with no CMA.

Results

Three roads showed no decrease in PM_{10} concentrations. This may be explained by low concentrations of PM_{10} from sources that may be susceptible to control by CMA; the mean contribution of mineral PM to total PM_{10} mass concentration was 5%, tyre wear 6% and brake wear 14%. These are typical of most roads in London.

Decreases in local PM_{10} were found in an underpass but only during high CMA dosing. CMA led to a decrease of ~ 12% in annual mean PM_{10} at one road near a construction site and the local increment in PM_{10} concentrations decreased by between 18 and 41% when CMA was used on industrial sites and surrounding residential roads.

Conclusions

Although CMA is not an effective method to decrease PM_{10} on typical London roads it may have a role to play in controlling local PM_{10} on roads around industrial and construction sites. Local PM_{10} at locations with greater than expected NOX:Primary PM_{10} emissions ratios (those above the regression line in Figure 1) would be most amenable to control by CMA.

Assessment methods developed for this programme can be useful to assess other air quality management interventions.

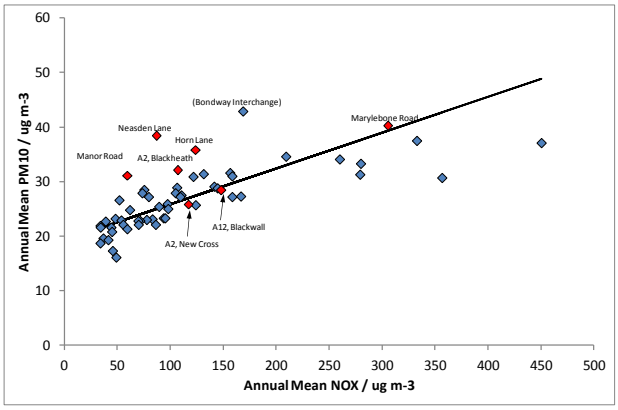

Figure 1 Annual mean PM_{10} vs NO_X; the regression line indicating a typical NO_X:Primary PM_{10} emissions ratio. Red diamonds = CMA study locations.

References

Amato F, Querol X, Alastuey A, Pandolfi M, Moreno T, Gracia J, et al. 2009 Atmos Env 43:4472–80.

Amato F, Querol X, Johansson C, Nagl C., Alastuey, A, 2010 Sci Total Environ 408: 3070–308.

Hafner, 2007 International Congress on the EU-LIFE-Environment Project KAPA GS Klagenfurt, Austria.

Norman M, Johansson C., 2006. Atmos Env 40:6154–6164.

This work was funded by the Mayor of London's Clean Air Fund.

CHEMKAR PM_{10}
A year-long chemical characterization of PM_{10} in Flanders (Belgium) in 4 major cities and 3 types of locations

J. Vercauteren[1], D. Roet[1], C. Matheeussen[1], E. Roekens[1], R. Vermeylen[2], W. Maenhaut[2] and M. Claeys[2]

[1] Flemish Environment Agency (VMM), Kronenburgstraat 45, 2000 Antwerpen, Belgium
[2]University of Antwerp (UA), Dept. of Pharmaceutical Sciences, Universiteitsplein 1, 2610 Antwerpen, Belgium

Keywords: PM_{10}, chemical characterization, elemental carbon, streetcanyon

Presenting author email: d.roet@vmm.be

From July 2011 until July 2012 the Flemish Environment Agency (VMM) carried out its fourth "*Chemkar PM_{10}*" campaign as part of the European Life+ ATMOSYS project. This was a large scale chemical characterization project of PM_{10} in Flanders (Belgium) in four major cities (Antwerp, Ghent, Bruges and Ostend; see also *Figure 1*). In each city measurements were done at 3 types of locations: a streetcanyon, an urban background and a regional road. The focus of the current project was to compare the results on both a city and location type level. Such comparison allows us to assess the contribution to PM_{10} that can be attributed to local contributions like a streetcanyon. Besides the total PM_{10} mass, ions, metals also elemental- and organic carbon (EC/OC) and levoglucosan (wood burning tracer) were analysed.

Experimental setup:

During one full year PM_{10} was sampled simultaneously on every 4th day at each location type in each city totaling **about 1000 samples** (including field blanks).

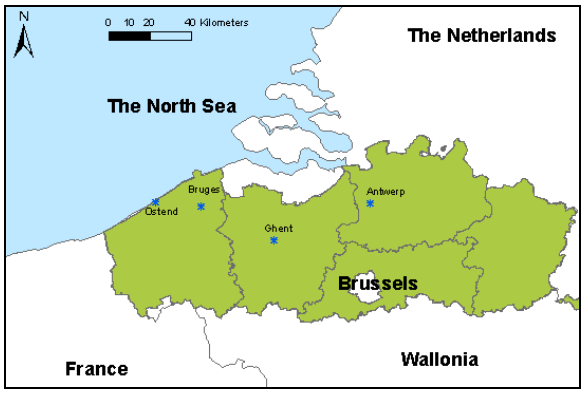

Figure 1: Location of the project cities

Sampling was done for 24h with one Leckel SEQ 47/50 low volume sampler at 2.3 m^3/h on 47mm Pallflex® Tissuquartz™ 2500 QAT-UP filters. After sampling the PM_{10} mass concentration was determined by dual weighing of the filters according to the European reference method EN14907. Next, the filters were punched for chemical analysis and stored at -18°C until analysis. One punch (1.5 cm^2) was used for the determination of **elemental and organic carbon** (thermal/optical transmittance) with the NIOSH protocol. Another punch (1.5 cm^2) was used for determination of **levoglucosan** by means of GC/MS after derivatisation with *N*,*O*-bis(trimethylsilyl)trifluoroacetamide (BSTFA) containing 1% trimethylchlorosilane (TMCS).

Results:

On average, concentrations in the **street canyons** were 7.5 µg/m^3 higher than at the urban background sites. This local contribution was mainly due to the resuspension of mineral dust (+ 3 µg/m^3), organic matter (+2 µg/m^3) and elemental carbon (+ 1 µg/m^3). *Figure 2* shows more detailed results for the streetcanyons in each city.

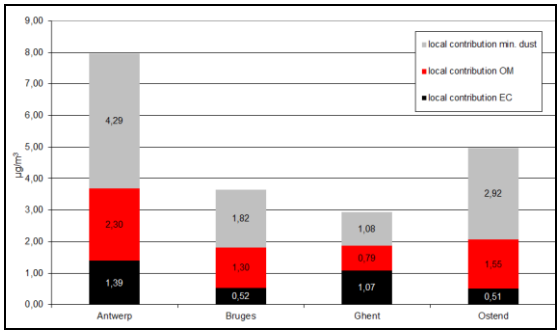

Figure 2: Local contributions to PM_{10} in streetcanyons in different cities.

More results and extended analysis will be presented at the conference.

Non-exhaust PMx emissions from road traffic

M. Maasikmets[1, 2], E. Teinemaa[1], T. Arumäe[1], V. Kimmel[2]

[1]Estonian Environmental Research Centre (EERC), Marja 4d, 10617 Tallinn, Estonia; [2]Estonian University of Life Science (EULC), Institute of Agricultural and Environmental Sciences, Kreutzwaldi 5, 51014 Tartu, Estonia
Keywords: non-exhaust emissions, studded tyres, PMx
Presenting author email: marek.maasikmets@klab.ee

Non-exhaust vehicle emissions are formed from wear particles of vehicle components such as brakes, clutches, chassis and tires. Although the non-exhaust particles are relatively minor contributors to the overall ambient air particulate load, reliable exposure estimates are few. (Panko et al. 2013). Suspended road dust will remain a problem because of an increasing number of vehicles in urban and rural areas. Only few real-world measurements of road dust resuspension have been performed to date. There is still a knowledge gap regarding the dominant mechanisms leading to road dust emissions, although resuspension of surface particle loading obviously plays an important role. (Pirjola et al. 2010). In practice, quantification of road dust emissions is complicated because of the many different factors that might need to be controlled —vehicle type and speed, tire type, pavement type and conditions, the use of road salt and sand (Hussein et al. 2008).

In current study the mobile measurement system was used to quantify the relative importance of road PMx emission and suspension of accumulated dust versus direct pavement wear, tire type (studded, non-studded and summer), pavement type, and vehicle speed. The mobile sampling cart was built, which enables simultaneously measure PMx concentrations directly behind the both rear tyres and the background air from the front of the vehicle. Simultaneously road and tire temperature were measured with infrared thermometer system. The tire pressure and ambient conditions were measured before and after each driving test. Measurements were performed during March-September on selected roads with different pavements and traffic conditions in Estonia. Particle number concentration and size distribution from 30 nm to 10 µm with 1-sec time resolution were measured by ELPI (Electrical low pressure impactor, Dekati Ltd.), behind the tires with the sampling rate of 2 x 29.25 l/min. The minimum detection level at 1 stage for the mass concentration is 0.01 µg/m^3 and for the number concentration 142 1/cm^3. The upper concentration limit at 13 stage for the mass concentration is 8269 mg/m^3 and for the number concentration 2.7E+04 1/cm^3. Simultaneous particle measurements were carried out using TSI optical particle counter OPC Model 3330 and DustTrak DRX. PM samples on impactor plates were also analysed by SEM (scanning electron microscopy, Zeiss EVO MA15 with Inca EDS) technique for chemical composition and morphology.

Results

The initial data show clear relationship between the vehicle speed and total PM emitted. Humidity of the road surface had strong implication on the PMx emission. Pavement composition has significant impact to the road wear and therefore PMx emission.

Studded tyres are generating more coarse PM emission compared to the non-studded winter and summer tyres.

There was a clear indication that the smallest particles with diameter less than 200 nm originate from the tires and not from the pavement. During the ride the tyre temperature is increasing, which leads to emissions of loosely bound reinforcing filler material and evaporation of semi-volatile softening oils. Particles larger than 300 nm consist mostly carbon reinforcement filler from the stone material in the pavement.

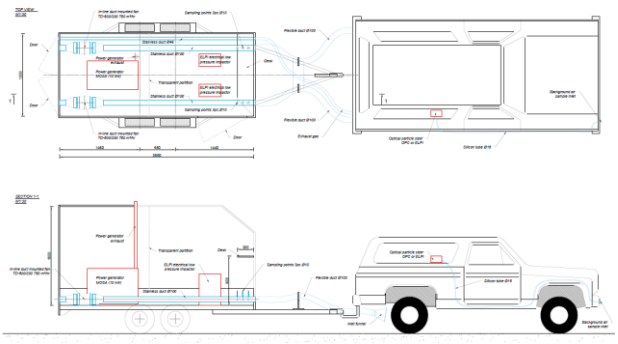

Figure 1. Scheme of the sampling device

This work was supported by the Estonian MoE and by the Ministry of Education and Research.

Hussein, T., Johansson, C., Karlsson, H., Hansson, H.C. 2008. Factors affecting non-tailpipe aerosol particle emissions from paved roads: On-road measurements in Stockholm, Sweden. Atmospheric Environment. 688–702.

Panko, J.M., Chu, J., Kreider, M.L., Unice, K.M., Measurement of airborne concentrations of tire and road wear particles in urban and rural areas of France, Japan, and the United States, Atmospheric Environment (2013), doi: 10.1016/j.atmosenv.2013.01.040.

Pirjola, L., Johansson, C., Kupiainen, K., Stojiljkovic, A., Karlsson, H., Hussein, T. 2010. Road Dust Emissions from Paved Roads Measured Using Different Mobile Systems. Journal of the Air & Waste Management Association. 1422-1433.

Atmospheric particulate mercury in the megacity Beijing – spatio-temporal variations, sources, and efficiency of mitigation measures

N.J. Schleicher[1,2], J. Schäfer[3], G. Blanc[3], Y. Chen[4], F. Chai[4], S. Wang[4] and S. Norra[1]

[1]Institute of Mineralogy and Geochemistry, Karlsruhe Institute of Technology, Karlsruhe, 76131, Germany
[2]Institute of Geography and Geoecology, Karlsruhe Institute of Technology, Karlsruhe, 76131, Germany
[3]Traceurs Géochimiques et Minéralogiques (TGM), UMR CNRS 5805 EPOC, Université Bordeaux I, F.33405 Talence Cedex, France
[4]Institute of Urban & Regional Atmospheric Environmental Research, China Research Academy of Environmental Sciences, Beijing, 100012, China

Keywords: Mercury, Urban Aerosols, Source Apportionment, Mitigation Measures
Presenting author email: nina.schleicher@kit.edu

Air quality remains one of the major challenges for the megacity Beijing. Mercury is known as a global pollutant, which is highly mobile in the environment and toxic to humans as well as to wildlife at extremely low levels (Carpy, 1997). However, unlike other heavy metals, only few studies investigated total particulate Hg (HgT_P) concentrations in atmospheric particles in Asian megacities. Sources for HgT_P are abundant in a city like Beijing. Coal combustion for industrial and residential use as well as coal-fired power plants constitutes a major source. Other potential sources are non-ferrous metal smelting, cement production, Hg mining, biofuel and biomass combustion, or waste incineration (Fu *et al.* 2012).

Within this study, weekly $PM_{2.5}$ (particles ≤ 2.5 µm, separately for day- and night-time) and total suspended particles (TSP) were investigated continuously for the whole year 2006 at one central sampling site in Beijing. Additionally, three months (Jan, Feb, Mar) within this period were selected for comparing HgT_P concentrations at four different sampling sites within the city. This approach aimed at (i) assessing the major HgT_P sources in Beijing and (ii) investigating the spatio-temporal variations in detail.

Furthermore, the period of the Olympic Summer Games in August 2008 with its strictly enforced mitigation measures (including traffic reductions and industry closures) provided the unique opportunity to investigate the efficiency of these comprehensive actions taken to reduce air pollution. The data set presented here includes TSP samples of each August from 2006 to 2010 in order to gain knowledge about HgT_P concentrations before, during, and after the Olympic Games period.

All samples were collected actively on quartz fibre filters (Mini-VS, 200 L/h, for $PM_{2.5}$ and TSP sampler, 1 m^3/h for TSP, Leckel, Germany). Mass concentrations were determined gravimetrically. Total particulate Hg was analyzed from circular filter punches by cold vapor atomic absorption spectrometry after calcination in an O_2 stream and amalgamation on an Au trap using a Direct Mercury Analyzer (DMA-80, Milestone, Italy).

Results show strong seasonal differences in HgT_P concentrations (Fig. 1). Lowest HgT_P concentrations occurred during summer months, while winter concentrations were up to 15-times higher. Both, meteorological conditions and seasonal sources were responsible for these high variations over the annual course. Usually, day-time HgT_P concentrations were higher compared to those during night. However, during the summer months (Jun, Jul, Aug, and also Sep), night-time concentrations were higher (Fig. 1).

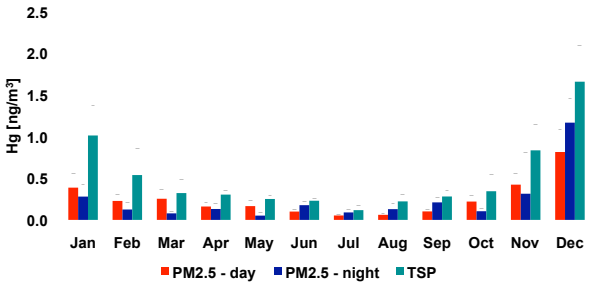

Figure 1. Average monthly HgT_P concentrations in ng/m^3 for $PM_{2.5}$ and TSP samples in 2006.

In Aug-08, the mitigation measures reduced not only overall mass and metal concentrations in Beijing (Schleicher *et al.* 2012) but also HgT_P (Fig. 2). On average, HgT_P in Aug-08 was reduced by about 60% compared to the previous two years. However, after the Olympic Games, HgT_P increased again to pre-Olympic levels. Generally, HgT_P concentrations in Beijing are comparably high and sustainable urban planning needs to include comprehensive reduction measures for Hg.

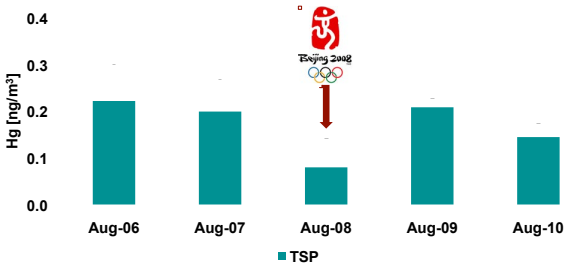

Figure 2. Average HgT_P concentrations in ng/m^3 for each August from 2006 to 2010.

Part of this work was supported by the German Research Foundation (DFG) under grant STU 169/32-1,2.

Carpi, A. (1997) *Water Air Soil Pollut.* **98**: 241-254.
Fu, X., Feng, X. Sommar, J., and Wang S. (2012) *Sci. Tot. Environ.* **421-422**: 73-81.
Schleicher, N., Norra, S., Chen, Y., Chai, F., and Wang, S. (2012) *Sci. Tot. Environ.* **427-428**: 146-158.

Air Quality Study within Steel Works Town in the UK

R. Vecchi[1], S. Nava[2], G. Calzolai[2], F. Lucarelli[3], G. Valli[1], D.C.S. Beddows[4], A.M Taiwo[4] and R.M. Harrison[4]

[1]Department of Physics, Università degli Studi di Milano & INFN, Milan, 20133, Italy
[2]INFN (Istituto Nazionale di Fisica Nucleare), Florence, 50019, Italy
[3] Department of Physics and Astronomy, Università degli Studi di Firenze & INFN, Florence, 50019, Italy
[4]National Centre for Atmospheric Science, University of Birmingham, Edgbaston, Birmingham, B15 2TT,UK

Keywords: Steel Works, MOUDI, Streaker, Particle Number
Presenting author email: roberta.vecchi@unimi.it

In April/May 2012, aerosol filter measurements were carried out in and around the coastal town of Port Talbot in South Wales which has an approximate population of 35,000 and is located on the M4 corridor (51 34' N and 3°46' W). The town sites one of the UK steel manufacturing plants owned by Tata and is the main source affecting air quality in the area (AQEG, 2010). The site covers approximately 28 km^2, comprises of ~50km of roads, 100 km of railway, and 25,000 vehicle movements per day. The production capacity is around 5m tonnes per year with the main processes in the steelworks being iron-making (sintering, blast furnace and raw materials), steel-making (basic oxygen steel-making (BOS) and coking) and rolling mills (hot and cold mills) (Moreno et al., 2004; Dall'Osto et al., 2008).

Instruments were deployed at four sites around the perimeter of the steel works (one at a coastal site (Little Warren LW) and the remain in 3 inland sites placed along the length of the works (Fire Station FS, Prince Street PS and Dyffryn School DS) in the study area for a four-week campaign (16th April to 16th May, 2012) (see Figure 1). With a view to measuring elements and water soluble ions within the fine and coarse fraction, our main site was located at FS where we deployed: a micro-orifice uniform deposit impactor (MOUDI) (3 day samples); a Partisol Dichotomous sampler (daily sample); a Streaker sampler (hourly samples); an Aerosol time-of-flight Mass Spectrometry (ATOFMS); a GRIMM particle size spectrometer and an Aethalometer.

Figure 1. Overview of the sampling sites used in Port Talbot.

Gaseous and meteorological data measured during the period of sampling were also collected from the Automatic Urban and Rural Network (AURN) located next to the FS site. This main site was in itself complemented by 3 other sampling sites where we deployed another 3 Partisol samples (24 hr sampling rate). At our coastal site, we ran a second Streaker sampler, which when paired with the FS Streaker, collected data to measures the increment in PM caused by the steel works.

An example the results with huge peaks of Fe and Mn detected in one of the sites nearby the steel works is reported in Figure 2.

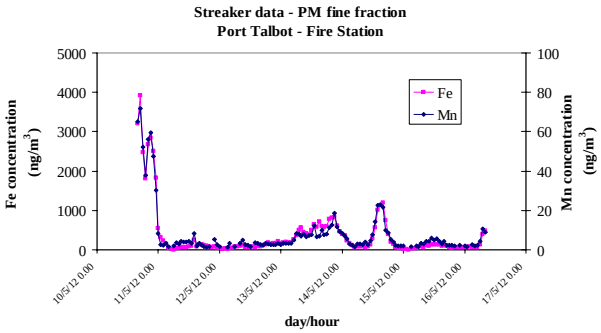

Figure 2. Fe and Mn hourly concentration (in ng/m^3) detetcted in Port Talbot (FS site).

Given this large data set of elements, ions and chemical species, our aim was to assess the impact of the steel works on the local area and in particular understand the nature of PM episodes detected by ongoing continuous PM measurements within the area which were suspected to be generated by fugitive dusts.

References.

Dall'Osto, M., Booth, A, M.J., Smith, W., Fisher, R., Harrison, R.M., 2008. Study of the size distributions and the chemical characterization of airborne particles in the vicinity of a large integrated steelworks. Aerosol Science and Technology 42, 981–991.

Moreno, T., Jones, T.P., Richards, R.J., (2004), Characterisation of aerosol particulate matter from urban and industrial environments: examples from Cardiff and Port Talbot, South Wales, UK, Science of The Total Environment Volumes 334–335, 1 December 2004, Pages 337–346.

The National Centre for Atmospheric Science, University of Birmingham, is gratefully acknowledged for funding the fieldwork.

Blue sky over the Ruhr – a review of the effectiveness of more than 50 years of air quality measures in Germany

S. Wurzler, H. Hebbinghaus, P. Bruckmann, J. Friesel, U. Pfeffer

North Rhine Westphalian State Agency for Nature, Environment and Consumer Protection, Recklinghausen, Germany
Keywords: air quality
Presenting author email: sabine.wurzler@lanuv.nrw.de

In January and February 2013, the poor air quality in many major cities in parts of Asia, such as Peking and Delhi, made headlines worldwide. The high concentrations of air pollutants and the accompanying pictures and effects look very familiar to those, who lived in the area Rhine Ruhr during the fifties and sixties. Notable was, e. g., the smog episode in December 1962, leading to an increase of mortality by 30 %. This drastically increased number of deaths owing to poor air quality made very apparent that something had to be done.

Already the year 1961 marked a turning point in German air quality planning, because of a notable speech of the subsequent chancellor, Willy Brandt, who demanded a change in politics concerning air quality with the catch phrase of blue sky over the Ruhr area. This was the first time that someone so prominently focussed on the combination of air quality, health effects and social justice, turning smoking stacks into something more than just a sign for economic success.

While this single talk did not mean an immediate change in politics and public awareness, it was a popular vision from which future activities could build. These activities included monitoring air quality as well as measures for emission reduction. The awareness of air quality as a challenging problem has grown in the public since then. Now, the blue sky is again visible over the Ruhr area, at least on sunny days. The European Commission has declared the year 2013 as the year of air quality. When comparing today's air quality in Europe to the situation in the past and to the present situation in Asia, this might seem a bit exaggerated at the first glance. But is this true? Are all problems already solved? Therefore, we review the past, present and possible future activities in Germany and Europe and their results for air quality. It can be seen, that the work on clean air includes some success stories. As an example, figure 1 shows the SO_2 concentration in the area Rhine Ruhr from 1964 till 2011. The TSP and PM10 trend from 1968 to 2011 can be seen in figure 2. These figures well illustrate the success stories of air quality measures – as well as some less favourable measures. It can be seen that the general trend shows a clear decrease in SO_2, PM10, and TSP concentrations. Measures like dust separation in industrial facilities, substituting solid fuels in space heating as well as the structural change in the Ruhr area all led to a reduction of SO_2, PM10, and TSP, while the policy of high stacks only led to a change in distribution, causing acidification and eutrophication in ecosystems. Particularly the desulphurisation of power plants since 1977 enhanced the decrease and it can be stated that today the concentrations of SO_2 in Germany are no longer problematic with respect to human health.

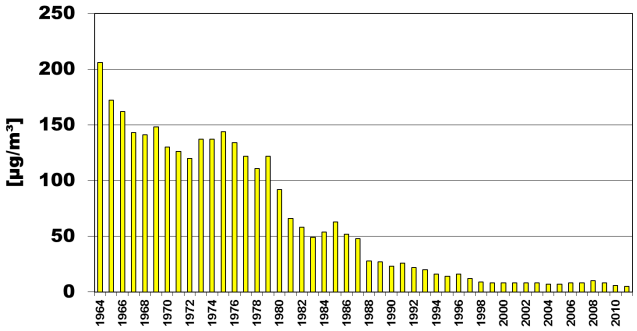

Fig. 1: Trend of annual average SO_2 concentrations in µg/m³ in the area Rhine Ruhr from 1964 to 2011. The highest concentrations correspond to values above 200 µg/m³, the lowest are below 10 µg/m³

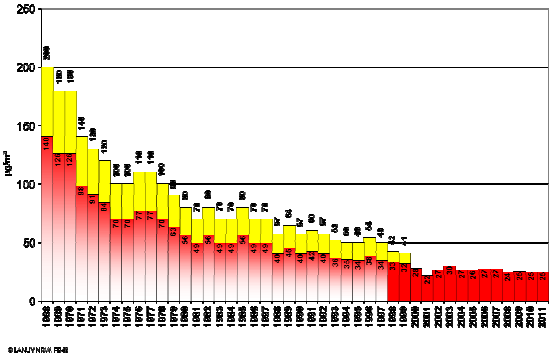

Fig. 2: Trend of annual average total suspended particle (TSP, yellow bars) and PM10 (red bars) concentrations in µg/m³ in the area Rhine Ruhr from 1968 to 2011. The highest concentrations correspond to values above 200 µg/m³, the lowest are below 50 µg/m³

But despite all advances, there are still problems to face. E. g., the high amount of road traffic is a main source for high NO_2 concentrations in cities. The number of PM10 exceedance days is still occasionally too high. Another challenge is the preservation of nature protection areas that can be adversely affected by high depositions of nitrogen, acid, or heavy metals.

Our presentation will give an overview of the last 50 years' challenges, success stories and memorable events as well as a reflection on current and future challenges in the area of air quality planning.

Monday, September 1, 2013

Session: Aerosol-based Nanotechnology
Applications of engineered nanoparticles

Nanostructural engineering of Pt/C catalyst via spray-drying for electrocatalyst applications

R. Balgis[1], G.M. Anilkumar[2], S. Sago[2], T. Ogi[1] and K. Okuyama[1]

[1]Department of Chemical Engineering, Hiroshima University, Higashi-Hiroshima, Hiroshima, 739-8527, Japan
[2]Research and Development Centre, Noritake, Co., Ltd., Miyoshi, Aichi, 470-0293, Japan
Keywords: spray-drying, electrocatalyst, mass activity.
Presenting author email: ratna-balgis@hiroshima-u.ac.jp

The great advantages of proton exchange membrane fuel cell (PEMFC) drive us to develop industrially friendly processing techniques and technologies for the production of its components such as a fuel cell catalyst. Platinum nanoparticles supported on carbon (Pt/C) are the most widely used catalyst material. Many researchers have demonstrated intense effort in the development of Pt/C catalysts. They were concerned with not only reducing Pt consumption, but also with keeping the catalytic performance at a reasonable level by means of structural engineering of the catalyst support materials to provide a high surface area. However, the common methods have been relatively time consuming (Balgis *et* al, 2012 and Balgis *et* al, 2013). In this work, we report development of a facile in-situ synthesis route to control the morphology and atomic content of Pt/C catalyst using spray-drying technique. The prepared catalyst showed high performance catalytic activity with excellent durability. The present method, described herein, is simple and cost-effective with a short processing time, which presents high opportunity for large-scale commercialization.

A precursor containing polystyrene latex (PSL, 300 nm), carbon black (40 nm), H_2PtCl_6 solution, and Polyvinyl alcohol (PVA, Mw = 500, at a mass ratio of 16:1) was spray-dried at 180°C with an air flow of 11.1 l/min as shown in Figure 1. Ammonia solution, $(NH_3)_{aq}$, was added into the precursor to intrude Nitrogen atom to the catalyst support (carbon). As-sprayed composite particles were calcined at 700°C for 30 min, under a nitrogen atmosphere in order to decompose PSL particles, to allow for a reduction process and for the crystal growth of platinum, accomplish N-doping process, and to obtain spherical microflower architecture. Electrocatalytic activity was performed using cyclic voltammetry (CV) and rotating disc electrode (RDE) measurement.

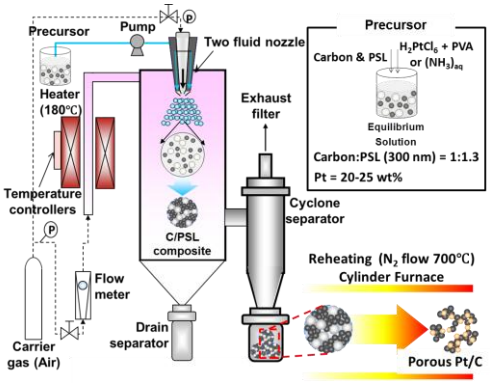

Figure 1. Schematic diagram of the experimental setup.

The prepared Pt/C catalysts have a unique porous structure that appears as a flower bunch in micrometer scale, namely spherical microflower catalyst (Pt/C_{SMF}) and Pt/C_N for sample with N-doping, as shown in Figure 2(a) and (b), respectively. Pt nanoparticles were very well dispersed on both catalysts, without any sintering, even after exposed at high temperature. The average particle size of Pt was 3.34 and 4.01 nm for Pt/C_{SMF} and Pt/C_N, respectively. The XRD pattern of both catalysts (data not shown) was indicating face-centered cubic crystal structure, which means complete reduction of H_2PtCl_6 was achieved.

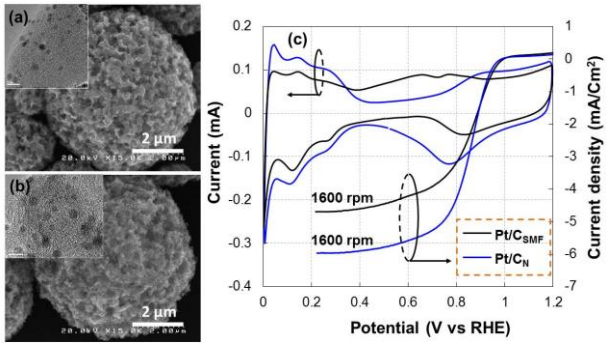

Figure 2. SEM and TEM image of: (a) Pt/C_{SMF} and (b) Pt/C_N; and (c) polarization curve of CV and ORR at 1600 rpm of Pt/C_{SMF} and Pt/C_N

The electrochemical characteristics of the prepared catalysts are presented by CV and ORR polarization curve shown in Figure 2(c). The electrochemical surface area (ECSA), mass activity (MA), and specific activity (SA) values of the catalysts summarized in Table 1. This work demonstrates an ample opportunity for the large-scale commercialization of a high-performance Pt/C catalyst with an exotic architecture.

Table 1. Catalyst characterization results.

Sample	Pt loading (wt%)	ECSA (m^2/g_{Pt})	MA (mA/mg_{Pt})	SA ($\mu A/cm^2_{Pt}$)
Pt/C_{SMF}	20.1	63.70	132.26	207.62
Pt/C_N	25.1	68.00	564.00	834.00

Balgis, R., Anilkumar, G.M., Sago, S., Ogi, T., Okuyama, K. (2012) *Fuel Cells* **12**, 665-669.
Balgis, R., Anilkumar, G.M., Sago, S., Ogi, T., Okuyama, K. (2013) *J. Power sources* **229**, 58-64.

Gas sensors by flame aerosol deposition: Correlations between blood glucose and breath components from portable gas sensors and mass spectroscopy

M. Righettoni[1], A. Schmid[2,3], A. Amann[2,3] and S. E. Pratsinis[1]
[1]Particle Technology Laboratory, Department of Mechanical and Process Engineering
ETH Zurich, CH-8092 Zurich, Switzerland
[2]Univ.-Clinic for Anesthesia, Innsbruck Medical University, A-6020 Innsbruck, Austria
[3]Breath Research Institute of the Austrian Academy of Sciences, A-6850 Dornbirn, Austria
Keywords: breath, gas sensor, acetone, blood glucose.
Presenting author email: righettoni@ptl.mavt.ethz.ch

Breath analysis has become increasingly significant for its potential in clinical diagnoses (Manolis, 1983). It is also one of the least invasive procedures for monitoring diseases and particularly attractive for patients who have to control body parameters such as glycemia for diabetics. Among all volatile organic compounds and gases in the human breath, acetone is one of the most abundant. Its breath concentration increases in patients with uncontrolled diabetes (Cao and Duan, 2006) and during normal overnight sleep of healthy persons (King et al., 2012).

Several methods (e.g. GC-MS, PTR-MS) can be used for measurements of breath composition (Risby and Solga, 2006). They provide detailed characterization of breath composition but are usually bulky. So there is considerable interest in the development of hand-held devices for reliable monitoring of specific breath markers. For this, chemo-resistive gas sensors based on semiconductor nanoparticles are attractive for breath analysis (Righettoni et al., 2010) offering low fabrication costs, high sensitivity and high miniaturization potential (Tricoli et al., 2010). Portable gas sensors made of Si:WO_3 nanoparticles were already applied to continuous monitoring of the breath acetone from healthy subjects during rest or physical activity and these measurements were in agreement (>98%) to simultaneous PTR-MS analysis (Righettoni et al., 2012).

Here, a portable acetone sensor consisting of flame made Si-doped WO_3 nanostructured films (Righettoni et al., 2010) was used to analyze the end tidal fraction of the breath collected in Tedlar bags from eight volunteers after overnight fasting and after lunch. These samples were analyzed simultaneously by proton transfer reaction, time-of-flight, mass spectrometry (PTR-TOF-MS). Furthermore, blood glucose levels were measured for each person after breath sampling to investigate possible correlations with specific breath markers and sensor response. Figure 1 shows the PTR-TOF-MS signals of acetone (red broken line) and ethanol (blue dotted line) compared to the Si:WO_3 sensor signal (black line) of the exhaled breath of three different subjects or persons after overnight fasting. Subjects S1 and S3 showed similar acetone signals in agreement with their corresponding sensor responses. Subject 2, in contrast, showed a higher acetone signal by PTR-TOF-MS that is captured nicely by the sensor response. Additionally, the strong difference in breath ethanol content between S1 and S3 hardly affected the sensor response, confirming the high selectivity against ethanol of these sensors. These results showed a reliable sensor response to different breath acetone concentrations from different subjects independent of ethanol and other breath gas concentrations. Similar agreement was obtained for most of the subjects in the afternoon. Statistical analysis showed indeed strong correlations in the morning (after overnight fasting) between blood glucose and breath acetone (0.98), sensor response (0.96) that became, however, weaker after lunch. These results are promising for future breath-based glucose testing for further development of portable devices based on chemo-resistive gas sensors in clinical applications.

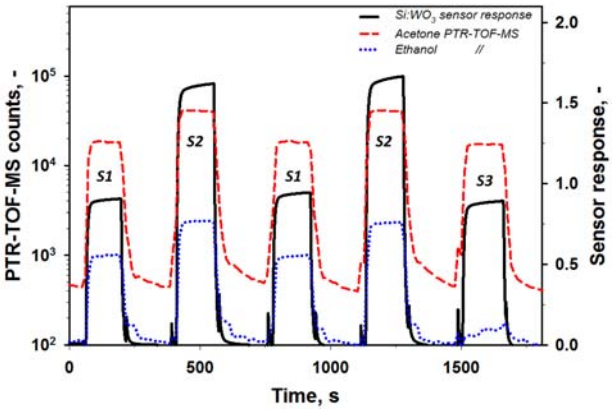

Figure 1. Exhaled breath concentrations of acetone (red broken line) and ethanol (blue dotted line) measured by PTR-TOF-MS for three different persons along with the portable sensor response (black line).

This research was supported by the Swiss National Science Foundation, grant 200021_130582/1 and the European Research Council under the European Union's Seventh Framework Program (FP7/2007-2013, ERC grant agreement n° 247283).

Manolis A (1983) *Clin. Chem.* **29** 5-15.
Cao W Q and Duan Y X (2006) *Clin. Chem.* **52** 800-811.
King J, Kupferthaler A, Frauscher B, Hackner H, Unterkofler K, Teschl G, Hinterhuber H, Amann A and Hogl B (2012) *Physiol. Meas.* **33** 413-428.
Risby T H & Solga S F (2006) *Appl Phys B* **85** 421-426.
Tricoli A, Righettoni M and Teleki A (2010) *Angew. Chem. Int. Ed.* **49** 7632-7659.
Righettoni M, Tricoli A and Pratsinis S E (2010), *Anal. Chem.* **82** 3581-3587.
Righettoni M, Tricoli A, Gass S, Schmid A, Amann A, Pratsinis S E (2012) *Anal. Chim. Acta.* **738** 69-75.

Aerosol synthesis of porous Particles for structured layers as catalyst support for Fischer–Tropsch reaction

Lintao Zeng and Alfred P. Weber

Institute of Particle Technology, TU Clausthal, Leibnizstrasse 19, 38678, Clausthal-Zellerfeld, Germany
Keywords: spray drying, porous silica particles, catalyst support, Fischer–Tropsch synthesis
Presenting author email: zeng@mvt.tu-clausthal.de

Using materials with well-defined porous structures as catalyst support provide new possibilities for tuning the catalytic properties (particularly the selectivity) for the Fischer-Tropsch (FTS) synthesis [Zhang 2010]. Saib et al found that the pore size of the support has a strong effect on the activity and selectivity of the catalyst [Saib 2002].Therefore, for FTS, it is desirable to develop a new method to prepare a catalyst support with controllable pore size distribution.

In this paper, we present a novel aerosol approach towards the preparation of well-defined trimodal porous layered structure as catalyst support for Fischer–Tropsch synthesis, which consists of two layers of porous SiO_2-building blocks and one layer of spherical glass particles (Fig. 1).

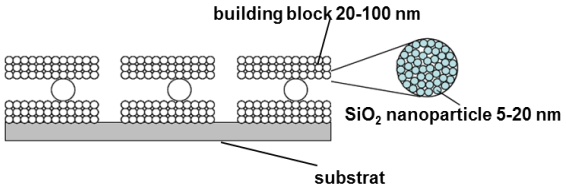

Fig. 1 Schematic representation of porous structured layers of building blocks

Firstly, porous silica particles were synthesized by spray drying process. The synthesis setup consists of an aerosol generator, a tube furnace and a filtration station. Templates (Polyvinylpyrrolidone, PVP) containing silica aerosols were generated by an atomizer operated with compressed air. The droplets were tempered in a tube furnace at 400-500°C. The dry particles were collected on a filter in a filtration station which was heated to 100°C during the synthesis.

The collected particles were heat treated at 500°C for 6 h to remove PVP. After calcination the products were characterized by SEM, TEM and nitrogen sorption.

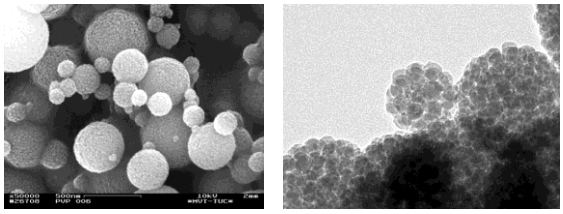

Fig. 2 SEM (left) and TEM (right) micrographs of porous particles

Through surface filtration or impaction of the aerosol, two layers of building blocks were deposited and reinforced by pressure and thermal treatment. The two single layers were then bound by partially melted glass particles.

In this contribution the aerosol synthesis of the different building blocks will be outlined together with the results of the porosity characterization. It will be shown that pore size and the porosity can be tailored by controlling the amount of polymer template and the type of colloids. In addition, the thermal stability of the porous particles will be presented.

This work was supported by the Deutsche Forschungs Gemeinschaft (DFG) under grant DFG-We 2331/13-1.

[1] Q. Zhang, J. Kang and Y. Wang, (2010), ChemCatChem 2, 1030-1058

[2] A.M. Saib,M. Claeys and E. Van Steen, (2002), Cataly. Today 71, 395-402

Optical heating of nanorods in a laser tweezers

P.B. Roder[1], B.E. Smith[1], P.J. Pauzauskie[1] and E.J. Davis[2]

[1]Department of Materials Science and Engineering, University of Washington, Seattle, WA 98195-2120, USA
[2]Department of Chemical Engineering, University of Washington, Seattle, WA, 98195-1750, USA
Keywords: Electromagnetic heating, optical tweezers, nanorods
Presenting author email: davis@cheme.washington.edu

The capture of nanoparticles with the optical tweezers makes it possible to perform a variety of measurements of physical and chemical properties, but the high irradiances usually encountered can lead to excessive heating of the particles. In a previous paper we (Roder et al., 2012) analyzed the heating of nanowires illuminated at right angles to the wire axis using Mie theory to determine the heat source function. Here we extend the analysis to finite length nanorods illuminated end-on in a laser trap. The theoretical predictions of the rod temperature are compared with optical tweezer studies which involve measurement of the Brownian motion of trapped particles using the methods of Peterman et al. (2001) and Marago et al. (2008) to determine the particle temperature.

The temperature distribution in a circular nanorod satisfies the energy equation given by

$$\frac{\partial T}{\partial t} = \alpha \nabla^2_{r,\theta,z} T + S(r,\theta,z) , \qquad (1)$$

in which α is the thermal diffusivity of the rod, and $S(r,\theta,z)$ is the volumetric rate of heat generation, which must be determined from the internal electric field, that is,

$$S(r,\theta,z) = \frac{1}{2\rho C}\sigma(\mathbf{E}\cdot\mathbf{E}^*) , \qquad (2)$$

where ρ is the particle density, C is its specific heat per unit mass, σ is its electrical conductivity, which is a function of the complex refractive index of the particle. The electric vector **E** and its complex conjugate **E*** depend on the optical characteristics of the irradiation. It is assumed that the heat source is not a function of time, and for the special case of infinitely long cylinders it is not a function of the axial position, z.

Equation (1) has been solved for boundary conditions and initial conditions appropriate for a rod (or wire) trapped in a stagnant fluid for three cases of possible applications: (i) illumination at right angles to the cylinder axis, the case examined by Roder et al. (2012), (ii) illumination of the lower end of a highly absorbing rod by a plane wave, and (iii) the more general case of a rod illuminated by a plane wave propagating in the z-direction.

Examples of the dimensionless source function and temperature distribution for case (i) are shown in Figures 1a and 1b, respectively, for a strongly absorbing carbonaceous rod. In this case Mie theory was used to compute the internal electric field, and the dimensionless source function is seen to have a complex structure of peaks and valleys. The dimensionless temperature distribution, $(T-T_\infty)/T_\infty$, is seen to be highly non-uniform.

Computations for nanoparticles show that even though the heat source function can be very non-uniform, the temperature can be uniform due to internal conduction, eliminating the possibility of photophoresis. For a carbonaceous rod with the temperature distribution shown in Figure 1b photophoresis can be expected.

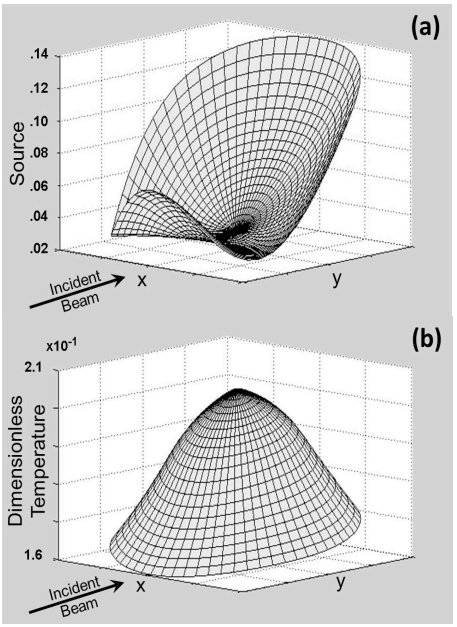

Figure 1. The dimensionless source function (a) and dimensionless temperature distribution (b) for a carbon rod with a radius of 100 nm in air irradiated at 1,000 W/cm^2 at a wavelength of 488 nm .

For case (ii), which applies to strong absorbers such a carbonaceous particles, we have applied the Fresnel equations to obtain an approximation for the internal field, and used that in the general solution of the energy equation to determine the temperature distribution. Very high temperatures are predicted for the high irradiances usually used for laser traps. For case (iii), which is a much more difficult problem, we have used numerical methods to determine the internal electric field, and then inserted the results in the general solution of Eq. (1).

Roder, P.B., Pauzauskie, P.J. and Davis, E.J.(2012) *Langmuir* **28**, 16177-16185.

Peterman, E.J., Frederick, G. and Schmidt, C.F. (2003) *Biophys. J.* **84**, 1308-1316.

Marago, O.M., Jones, P.H., Bonaccorso, F., Sardaci, V., Gucciardi, P.G. Rozhin, A.G. and Ferrari, A.C. (2008) *Nano Letters* **8**, 3211-3216.

Correlation between Catalytic Activity and Production of Reactive Oxygen Species for Airborne Engineered Palladium Nanoparticles

N. Neubauer[1], J. Palomaeki[2], H. Alenius[2] and G. Kasper[1]

[1]Karlsruhe Institute of Technology (KIT), Institute for Mechanical Process Engineering and Mechanics, Karlsruhe, 76131, Germany
[2]Finnish Institute of Occupational Health (FIOH), Unit of System Toxicology, Helsinki, 00250, Finland

Keywords: catalytic activity, reactive oxygen species, palladium nanoparticles
Presenting author email: nicole.neubauer@kit.edu

Catalyts are widely used in industry, and the catalytic functionality of nanoparticles is a major scientific topic for engineered nanomaterials. However, their influence on human health and biological systems is currently not understood because studies linking the catalytic activity with biological effects are largely unavailable. Therefore, we were investigating correlations between catalytic and biological activity for airborne palladium aerosols as a basis for better understanding of biological effect pathways.

Methods
The catalytic activity of palladium nanoparticles was investigated by the Catalytic Activity Aerosol Monitor (CAAM) which allows the detection of catalytically active nanoparticles (e.g. palladium) with a high sensitivity (Neubauer et al., 2013). As the ability to produce reactive oxygen species (ROS) is believed to be one of the key factors of nanotoxicology (Nel et al., 2006), the generation of ROS was measured by using the DCF method (Le Bel et al., 1992) both in a cell-free environment and with THP-1 cells (human monocytic leukaemia cells).

Experimental
Palladium aerosols produced by spark discharge were thermally conditioned in a tube furnace to generate differently sized palladium primary particles. These aerosols were characterized by an electrical mobility spectrometer for number concentrations and agglomerate size distributions. The mass concentration of the aerosols was determined from filter samples by inductively coupled plasma optical emission spectroscopy (ICP-OES). The geometric diameters of the primary particles were investigated by electron microscopy (TEM).

Detection of the catalytic activity by the CAAM is based on sampling defined volumes of the palladium aerosols onto filters, and then immediately initiating a substance specific chemical reaction on the filter – in this case the hydrogenation of ethene. For this purpose pre-mixed gaseous reaction educts are added to the deposit. The composition of the gaseous reaction products was measured by an IR sensor. Their concentration provides a measure for the catalytic activity of the palladium particles.

For the ROS measurements, the aerosols were transferred into suspension using a phosphate buffered saline. The production of ROS was then determined from these suspensions of differently sized palladium particles via the DCF method. A fluorescence spectrophotometer was used to detect DCF which was formed via the oxidation of non-fluorescent DCFH by ROS. TEM pictures of the suspended palladium were also taken to investigate potential changes in particle size or morphology.

Results
TEM analysis of the palladium aerosols directly after the production gave median primary particle sizes between 3 and 30 nm, depending on preparation. It was also determined that the primary particles did not change their size while the catalytic activity measurements took place, or during their transfer into the liquid.

The measurements with the CAAM showed a pronounced dependence of the activity on the primary palladium particle size, with a sharp maximum at 6 nm. The ROS production also showed a strong size dependence with a maximum in the same size range as the catalytic activity.

Conclusion
The catalytic activity of palladium nanoparticles as determined by a gas-phase reaction correlates strongly with their ability to produce ROS in suspension. This coincidence points to a link between the biological and catalytic activities of palladium nanoparticles. It also demonstrates the usefulness of the CAAM for quasi-real time detection of airborne catalysts.

References
Le Bel CP, Ischiropoulos H and Bondy SC. (1992) *Chemical Research Toxicology 5*, 227-231

Nel A, Xia T, Maedler L and Li N. (2006) *Science 311, 622-627*

Neubauer N, Seipenbusch M and Kasper G. (2013) *Annals of Occupational Hygiene (accepted)*

The research leading to these results has received funding from the European Commission's Seventh Framework Programme (FP7/2007-2013) under grant agreement n° 211464-2 (Nanodevice).

Substance release kinetics of spherical and non-spherical hybrid nanoparticles generated by aerosol-photopolymerization

E. Akgün[1], M. Vranceanu[2], B. Sachweh[2], J. Hubbuch[1], M. Wörner[1]

[1]Process Engineering in Life Sciences, Karlsruhe Institute of Technology, Karlsruhe, 76131, Germany
[2]BASF SE, Ludwigshafen, 67056, Germany
Keywords: controlled release, hybrid nanoparticles, photopolymerization, nanocaps
Presenting author email: ertan.akguen@kit.edu

Release of the absorbed or encapsulated material from polymeric environments in a controlled manner has extensive and emerging applications as, for example, self-healing coatings (Suryanarayana *et al*, 2010) and controlled release platforms in the pharmaceutical and medical fields (Pinto Reis *et al*, 2006). The main advantages of such nano – and microscale particles are storing and protecting the inner material from the environment and performing controlled and sustained release (Suryanarayana *et al*, 2010).

Romero-Cano and Vincent (2002) compared the controlled release kinetics from poly(lactic acid) nanoparticles with different morphologies. All of the morphologies were spherical, but the active ingredient to be released was at different locations within the spheres. In this contribution, we compare the release kinetics of spherical and non-spherical (nanocaps) nanoparticles.

In our previous contributions, aerosol-photopolymerization has already been shown to be suitable for the generation of differently structured polymeric and hybrid nanoparticles. Figure 1 illustrates such polymer particles not hybridized yet. This contribution deals with loading of the produced spherical nanoparticles and nanocaps with specific substances such as caffeine and comparing their release kinetics from nanopolymers with different structures. A power of this method is the possibility of loading the nanoparticles *in situ*. Apart from this, photoinitiation serves for fast initiation rates, contributing to increased overall polymerization rates. Fast kinetics is favoured due to the sub-minute average aerosol residence time in the process. Photoinitiation permits an operation at ambient temperature, minimizing monomer droplet evaporation before polymerization. The aerosol-based process results in a continuous hybrid particle generation process. In addition, the incorporation of surfactants, required for many liquid phase processes, may be avoided, leading to highly pure particulate products.

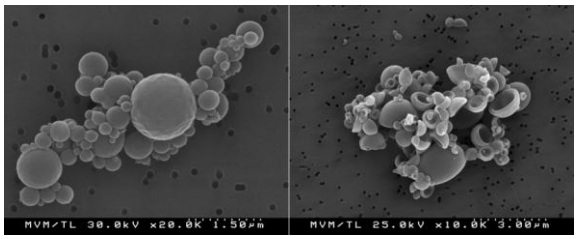

Figure 1. Spherical and non-spherical polymer nanoparticles generated by aerosol-photopolymerization.

The structure of the produced hybrid nanoparticles loaded with a specific substance was characterized by scanning electron microscopy. Transmission electron microscopy was also performed for further investigations on the hybrid character of particles before and after substance release.

The released amounts of caffeine from spherical nanopolymers and nanocaps were measured by HPLC. Figure 2 illustrates an exemplary comparison of the two particle types for low caffeine loadings of polymer particles.

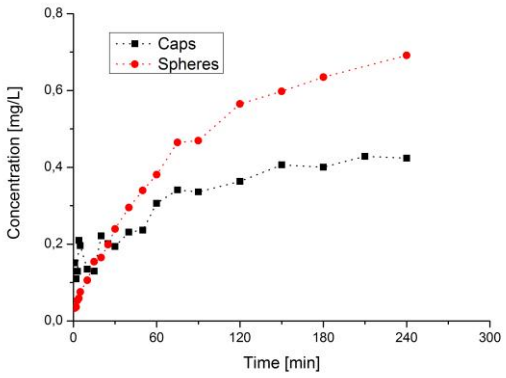

Figure 2. Caffeine release profiles from nanocaps and nanospheres produced by aerosol-photopolymerization.

Release profiles of higher concentrated hybrid particles and other material combinations will be illustrated as well.

This project is part of the JointLab IP3, a joint initiative of KIT and BASF. Financial support by the ministry of science, research and the arts of Baden-Württemberg (Az. 33-729.61-3) is gratefully acknowledged.

Suryanarayana, C., Chowdoji Rao, K., and Kumar, D. (2008) *Progress in Organic Coatings* **63**, 72-78

Pinto Reis, C., Neufeld, R., J., Ribeiro, A., J., and Veiga, F. (2006) *Nanomedicine* **2**, 8-21

Romero-Cano, M. S. and Vincent, B. (2002) *Journal of Controlled Release* **82**, 127-135

Industrial by-products as precursors for gas-phase nanoparticle synthesis

T. Karhunen[1], A. Lähde[1], T. Torvela[1], J. Jokiniemi[1,2]

[1]Fine Particle and Aerosol Technology Laboratory, University of Eastern Finland, Kuopio, 70211, Finland
[2]Fine Particles Team, Technical Research Center of Finland, Espoo, 02044 VTT, Finland
Keywords: $LiFePO_4$, CVS, phase composition.
Presenting author email: tommi.karhunen@uef.fi

The structure of global energy supply is changing rapidly towards sustainable energy solutions. However, all forms of sustainable and intermittent energy production (e.g. wind power, photovoltaics) and sustainable transportation (e.g. hybrid and full electric vehicles) require excellent energy storage systems in order to increase their effectiveness (Hall and Bain, 2008).

Li-ion secondary cells are one of the most advanced battery energy storage systems currently available due to their high energy density (Du Pasquier *et al*, 2003). One of the main obstacles in their wide scale adoption, however, is the high cost of such batteries.

This obstacle can be overcome, firstly, by increasing the operational life time of the batteries. $LiFePO_4$ is a very promising electrode material for achieving this. In proper combination with an conductive additive it can be used to make Li-ion batteries that can undergo at least 1000 charge/discharge cycles without significant degradation in performance (Song *et al*, 2011). Furthermore, $LiFePO_4$ and its precursors are environmentally friendly.

Secondly, the cost of the precursor materials can be reduced by utilising alternative sources, such as industrial by-products. At least iron and phosphorus are available in the industrial waste streams. Utilising these streams will also reduce the environmental impact of the production.

Lastly, the synthesis process itself can be optimised. Gas-phase processes are highly material and energy efficient routes for synthesis of nanoparticles with controlled composition and particle size. With the proper selection of the process environment the waste streams can also be easily utilised in these processes.

In this paper we present a gas-phase method for the synthesis of LiFePO4 nanoparticles utilising industrial waste stream of FeSO4·7H2O. The precursors were dissolved in water and atomized using an ultrasonic nebuliser. The produced droplets were then carried to the heated zone of the reactor. Experiments were carried out at temperatures between 200 and 1000 °C in atmospheres with varying reduction potentials. The aerosol exiting the heated zone was rapidly cooled with a large volume of dilution gas (air or N2) at ambient temperature.

With increasing temperature the particles became more solid with increasing fraction of $LiFePO_4$ (Figure 1). Increasing the reducing potential of the synthesis atmosphere increases the ratio of the Pnma-to-Cmcm polymorphs of $LiFePO_4$ (Figure 2). The effects of temperature, precursor composition and process atmosphere on the product composition will be presented.

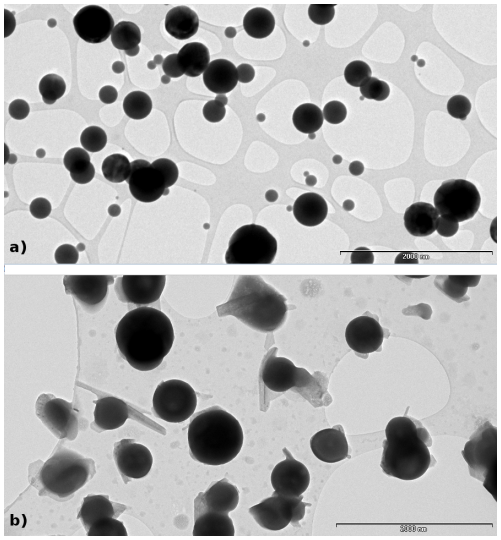

Figure 1: TEM images of $LiFePO_4$ samples synthesised at (a) 800 °C and (b) 600 °C.

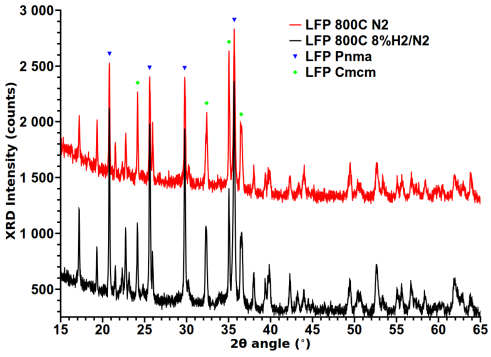

Figure 2: XRD diffractiograms of $LiFePO_4$ samples synthesised in N2 (red) and 8%H2/N2 (black).

This work was supported by Foundation for Research of Natural Resources in Finland (grant 1749/12), the Fortum Foundation (grant 12-072), and the strategic funding of the University of Eastern Finland (NAMBER spearhead project).

Hall, P. J. and Bain E. J. (2008) *Energy Policy* **36**, 4352–4355.

du Pasquier, A., Plitz, I., Menocal, S. and Amatucci, G. (2003) *J. Power Sources* **115** (1), 171–178.

Song, M.-K., Park, S., Alamgir, F. M., Cho, J., Liu, M. (2011) *Mat. Sci. Eng. R* **72**, 203–252.

Monday, September 1, 2013

Special Session: Aerosol Chemistry
Radical chemistry and aerosol formation

Partially oxidized radicals – crucial intermediates during atmospheric aerosol formation

J. Ahrens, P. T. M. Carlsson, C. Keunecke, M.-C. Maas, J. L. Wolf and T. Zeuch

Institut für Physikalische Chemie, Universität Göttingen, Göttingen, 37077, Germany

Keywords: radical chemistry, aerosol formation, sulfur dioxide, Criegee intermediates.
Presenting author email: tzeuch1@gwdg.de

The dynamics of reactive mixtures under conditions being typical for important environmental issues and technical applications are driven by chemical kinetics being related to the elementary reaction steps of a zoo of stable and transient species. This complexity limits our current understanding of important phenomena like the atmospheric formation of secondary organic aerosol.

Reactions of partially oxidized, transient species like alkoxy and peroxy radicals or Criegee intermediates (CIs) represent key mechanistic branch points in hydrocarbon degradation schemes. However, for some crucial reaction steps like the atmospheric oxidation of SO_2 by CIs the rate coefficient was not accessible until recently (see Welz et al., 2012). Such knowledge gaps are critical since incorrect data for sensitive elementary steps can drastically mislead predictions of atmospheric models with regard to aerosol formation.

In recent years we applied and combined different experimental and modeling techniques for dealing with the complexity being inherent to atmospheric and combustion chemistry. This overall examination approach helped us to derive e.g. a compact and consistent kinetic model with fully validated peroxy radical chemistry (Zeuch et al., 2008). For the study of atmospherically relevant reactions we apply a specially designed reactor experiment featuring fast initial reactant mixing and aerosol characterization at the end of main reactive processes (Carlsson et al., 2012). The final product analysis at the end of β-pinene ozonolysis in the presence and absence of SO_2 revealed the high influence of SO_2 on mechanistic branching in the chemistry of CIs (Figure 1) and aerosol formation (Figure 2).

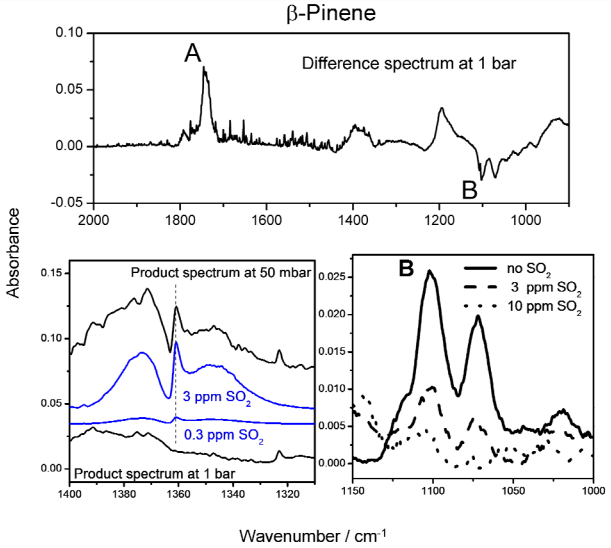

Figure 1. IR spectra of final products from β-pinene ozonolysis at 1 bar and 50 mbar. The difference spectrum in the upper panel shows the suppression of secondary ozonide formation (feature B) and highly increased nopinone formation (A). The lower panels show the consumption of SO_2 at high pressure and the suppression of secondary ozonide formation by SO_2.

The combined use of time resolved infrared spectroscopy and kinetic modeling gives reliable constraints for the rate coefficient of SO_2 + CI from biogenic terpenes under ambient conditions. In (cis and trans) 2-butene ozonolysis experiments the measured particle numbers in the presence of SO_2 show a slope of ~2 in a double logarithmic plot against predicted sulfuric acid concentrations in support of atmospheric and smog chamber observations (Carlsson et al., 2012), which represent much different reactive environments.

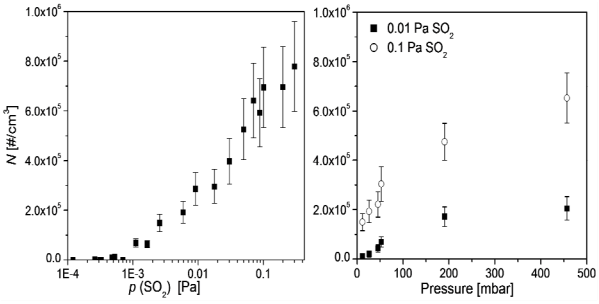

Figure 2. Aerosol formation during 2-butene ozonolysis as a function of SO_2 concentration and pressure.

This work was supported by the Deutsche Forschungsgemeinschaft, GRK 782.

Welz, O., Savee, J. D., Osborn, D. L. et al. (2012) *Science* **335**, 204-207.

Zeuch, T., Moréac, G., Ahmed, S. S., Mauß, F. (2008) *Combust. Flame* **155**, 651-674.

Carlsson, P. T. M., Dege, J. E., Keunecke, C., Krüger, B. C., Wolf, J. L., and Zeuch, T. (2012) *Phys. Chem. Chem. Phys.* **14**, 11695-11705.

Carlsson, P. T. M., Keunecke, C., Krüger, B. C., Maaß, M.-C., and Zeuch, T. (2012) *Phys. Chem. Chem. Phys.* **14**, 15637-15640.

Formation of organosulfates from the sulfate radical induced oxidation of methacrolein and methyl vinyl ketone

J. Schindelka[1], Y. Iinuma[1], D. Hoffmann and H. Herrmann[1]

[1] Leibniz Institute for Tropospheric Research (TROPOS), Leipzig, D-04318, Germany

Keywords: Isoprene, Sulfate radical, SOA
Presenting author email: schindelka@tropos.de

Recent studies show that organosulfates are an important fraction of ambient secondary organic aerosol (SOA). The contribution to the organic mass was estimated to be up to 30% in ambient aerosols and up to 20% for isoprene-derived organosulfates (Froyd et al., 2010, Surratt et al., 2008). The isoprene-derived organosulfate with *m/z* 215 ($C_5H_{11}O_7S^-$) is often reported to be the most abundant single organosulfate compound. Its formation is explained by the acid catalyzed sulfation of isoprene epoxydiol (IEPOX) that is suggested to form from the OH oxidation of isoprene under NO_x-free conditions(Paulot et al., 2009, Iinuma et al., 2007).

C_2 to C_4 organosulfates are found in ambient and laboratory generated SOA that can be related to isoprene oxidation products (Froyd et al., 2010, Surratt et al., 2007, Gómez-González et al., 2008). These compounds have been suggested to form from the sulfate radical induced oxidation of semi-volatile isoprene oxidation products in the particle phase (Galloway et al., 2009, Perri et al., 2010, Nozière et al., 2010). Here, the formation of organosulfates originating directly from methacrolein (MACR) or methyl vinyl ketone (MVK) with *m/z* of 199 and 183, are of interest because their existence was shown in studies of ambient aerosols (Froyd et al., 2010, Gómez-González et al., 2008). A sulfate radical reaction with unsaturated compounds is as fast as other organosulfate formation mechanisms and is even competitive to the reaction with hydroxyl radicals (Nozière et al., 2010, Buxton et al., 2000). Supporting the theory of the contribution of a radical mechanism in the formation, a very recent study reports a dependency of the fraction of organosulfates in particle mass on the season and photochemical activity (Tolocka and Turpin, 2012). This might indicate the involvement of solution phase radical chemistry.

In the present study, experiments on the sulfate radical induced oxidation of methacrolein and methyl vinyl ketone were performed in bulk aqueous phase as well as in an aerosol chamber, to investigate their relevance in aqueous phase SOA formation. Samples from aqueous phase experiments and extracts from filters collected after chamber experiments were analysed with UPLC/(-)ESI-IMS-QTOFMS.

All the samples showed the abundance of highly oxidized organosulfates with *m/z* values corresponding to the species found in ambient particle samples (see Table 1). Chamber experiments showed a distinct increase in particle mass for experiments with sulfate radical precursor ($K_2S_2O_8$) in the seed particles (see Figure 1).

Table 1. Selected organosulfate species of MACR and MVK with elemental composition.

Reactant	m/z [M-H]	Formula
MVK/ MACR	153	$C_3H_5O_5S$
	183	$C_4H_7O_6S$
	199	$C_4H_7O_7S$

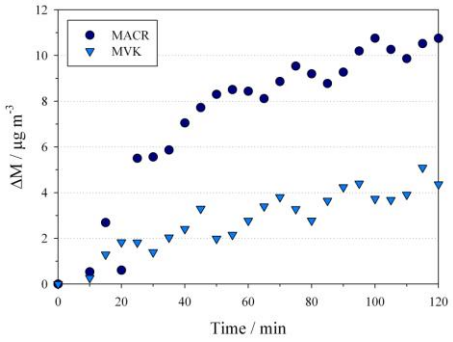

Figure 1. Time series of particle mass increase (ΔM) for MACR and MVK with $K_2S_2O_8/H_2SO_4$ as seed particles.

This study shows that sulfate radical reactions in the aqueous phase can partly explain the formation of these organosulfates from methacrolein and methyl vinyl ketone.

Froyd, K. D., et al. (2010) *Proc. Natl. Acad. Sci. U. S. A.* **107**, 21360-21365

Surratt, J. D., et al. (2008) *J. Phys. Chem. A* **112**, 8345-8378

Paulot, F., et al. (2009) *Science* **325**, 730-733

Iinuma, Y., et al. (2007) *Environ. Sci. Technol.* **41**, 6678-6683

Surratt, J. D., et al. (2007) *Environ. Sci. Technol.* **41**, 517-527

Gómez-González, Y., et al. (2008) *J. Mass Spectrom.* **43**, 371-382

Galloway, M. M., et al. (2009) *Atmos. Chem. Phys.* **9**, 3331-3345

Perri, M. J., et al. (2010) *Atmos. Environ.* **44**, 2658-2664

Nozière, B., et al. (2010) *Geophys. Res. Lett.* **37**

Buxton, G. V., et al. (2000) *J. Atmos. Chem.* **36**, 111-134

Tolocka, M. P. and Turpin, B. (2012) *Environ. Sci. Technol.* **46**, 7978-7983

Ozonolysis of shikimic acid particles caught in the act

S. Steimer[1,2], A.J. Huisman[3], U.K. Krieger[2], T. Peter[2], M. Lampimäki[1], G. Gržinić[1], E. Coz[4], B. Watts[5], J. Raabe[5] and M. Ammann[1]

[1]Laboratory of Radiochemistry and Environmental Chemistry, Paul Scherrer Institute, Villigen, 5232, Switzerland
[2]Institute of Atmospheric and Climate Sciences, ETH Zürich, Zürich, 8092, Switzerland
[3]Union College, Schenectady, NY 12308, USA
[4] Department of Environment, CIEMAT, Madrid, 28040, Spain
[5]Swiss Light Source, Paul Scherrer Institute, Villigen, 5232, Switzerland
Keywords: aerosol aging, ozonolysis, semi-solid, glassy aerosol.
Presenting author email:markus.ammann@psi.ch

It has been shown that organic compounds may become solid or semi-solid under atmospheric conditions (Virtanen et al., 2010). It is therefore important to understand how the physical state of aerosol components might affect chemical ageing and thus their environmental impact (Shiraiwa et al., 2011). Shikimic acid is a plant metabolite, which has been found to be present in biomass burning aerosol (Medeiros et al., 2008), and which has convenient physical properties at low relative humidity for the purpose of the present experiment. Here, we studied the chemical aging of individual submicron shikimic acid particles on a substrate as a function of size and humidity in situ using scanning transmission X-ray microscopy (STXM) and near edge X-ray absorption fine structure spectroscopy (NEXAFS).

Shikimic acid particles were generated by ultrasonic nebulisation of solution, dried with a diffusion drier, size-selected by a differential mobility analyzer (DMA) and then impacted on a silicon nitride membrane. A temperature controlled environmental micro reactor (Huthwelker et al., 2010; Zelenay et al., 2011) was used to adjust relative humidity during the experiment (13%-83% RH) and facilitate in situ exposure to ozone. All STXM and NEXAFS experiments were conducted at the Pollux beamline at the Swiss Light Source.

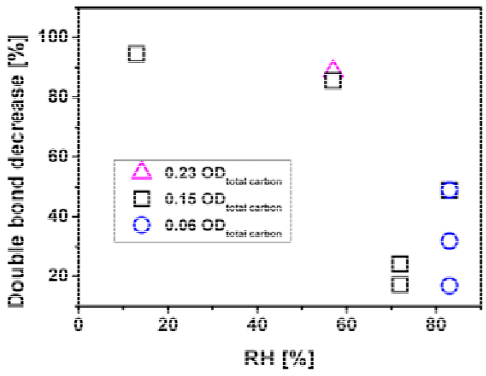

Figure 1. Humidity dependence of oxidation after 211 min exposure to 2.5 ppm ozone. Different symbols mark particles of different total carbon optical density, which is a measure of particle thickness.

Upon oxidation, the carbon K-edge spectra for shikimic acid particles show a clear decrease of the optical density (OD) at 284.5 eV, where resonant absorption occurs due the carbon-carbon double bond of shikimic acid. Figure 1 demonstrates the increasing degree of oxidation with increasing humidity. It is likely due to water acting as a plasticizer for shikimic acid, which leads to a decrease in viscosity and thus increase in diffusivity of reactants. Detailed analysis shows that no gradient is observed within the particles. Combined with the size dependence of the oxidation shown in figure 2, this points to either a shallow gradient or a surface limited process.

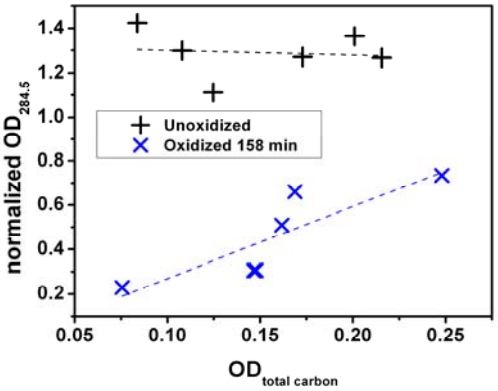

Figure 2. Double bond peak height at 72% before (black +) and after (blue ×) oxidation with 2.5 ppm ozone as a function of particle size, expressed as optical density of total carbon (310-320 eV).

This work is supported by the EU FP7 project PEGASOS and the Swiss National Science Foundation (grant no. 130175).

Huthwelker, T., Zelenay, V., Birrer, M., Krepelova, A., Raabe, J., Tzvetkov, G., Vernooij, M.G.C., & Ammann, M. (2010). *Rev. Sci. Instrum.*, **81**, 113706-113709.

Medeiros, P.M., & Simoneit, B.R.T. (2008). *Environ. Sci. Technol.*, **42**, 8310-8316.

Shiraiwa, M., Ammann, M., Koop, T., & Pöschl, U. (2011). *Proc. Natl. Acad. Sci.*, **108**, 11003-11008.

Virtanen, A., Joutsensaari, J., Koop, T., Kannosto, J., Yli-Pirila, P., Leskinen, J., Makela, J.M., Holopainen, J.K., Poschl, U., Kulmala, M., Worsnop, D.R., & Laaksonen, A. (2010). *Nature*, **467**, 824-827.

Zelenay, V., Ammann, M., Krepelová, A., Birrer, M., Tzvetkov, G., Vernooij, M.G.C., Raabe, J., & Huthwelker, T. (2011). *J. Aerosol Sci.*, **42**, 38-51.

Aerosol particles in molecular beams: pickup of molecules, chemistry and photochemistry

M. Fárník[1], V. Poterya[1], A. Pysanenko[1], J. Lengyel[1], J. Kočišek[1] and J. Fedor[2]

[1]J. Heyrovský Intsitute of Physical Chemistry, ASCR, Dolejškova3, Prague 8, 18223, Czech Republic
[2]Department of Chemistry, University of Fribourg, Chemin du Museé, Fribourg, CH-1700, Switzerland
Keywords: nucleation, photodissociation, ice nanoparticles.
Presenting author email: michal.farnik@jh-inst.cas.cz

A unique versatile molecular beam CLUB (CLUstr Beam) apparatus has recently been exploited for various studies of atmospherically relevant aerosol particles in vacuum. These studies will be briefly reviewed demonstrating the significant potential which the implementation of the molecular beam techniques has for the aerosol studies.

In molecular beams clusters are prepared by expansion of suitable gases into the vacuum through supersonic nozzles. Depending on the expansion conditions the clusters of various sizes can be generated ranging from a few molecules to small aerosol particles with sizes in the nanometer range composed of hundreds molecules. Our CLUB apparatus enables various experiments with these particles: (1) doping them with different molecules; (2) investigating photodissociation and photochemistry in/on the clusters by the fragment velocity imaging method; (3) studying the composition, dynamics and reactions by a unique reflectron time-of-flight mass spectrometer.

Several experiments will illustrate the variety of information about the small aerosol particles gained with the CLUB apparatus. First, we will exemplify the pickup cross sections of small ice nanoparticles for uptake of various atmospheric molecules (Lengyel, Kočišek *et al*, 2012). The cross sections were measured by precise velocity measurements of particles after their passage through a pickup cell filled with the particular gas. The cluster velocity change in dependence on the pickup pressure allows the pickup cross section determination. The experimental results are in good agreement with molecular dynamics simulations. They show that the actual cross section for the pickup is significantly larger than the geometrical cross section. This effect should be considered in the atmospheric models and nucleation theories.

Photochemistry of ice nanoparticles doped by hydrogen halide molecules HX (X= Cl, Br, I) is highly relevant to the stratospheric ozone depletion process. We have studied $HX{\cdot}(H_2O)_n$, n= 10^2-10^3, clusters under the influence of UV laser radiation at 193 nm and 243 nm. A series of experiments and theoretical calculations (Poterya, 2007) (Poterya, 2011) (Ončák, 2011) revealed that the HX molecule is acidically dissociated on the ice particle and a neutral hydronium radical H_3O is generated upon the UV excitation. This radical also represents a cluster model for solvated electron.

Most recently we have also investigated the photodissociation of CF_2Cl_2 molecule in clusters revealing the detailed dynamics of the molecular dissociation, and Cl-fragment caging and escape from the clusters.

Finally, we have studied mixed nitric acid/water ice nanoparticles in two different mass spectrometric experiments (Lengyel, Pysanenko *et al*, 2012). The comparison between the electron ionization and photoionization after Na-pickup showed that HNO_3 molecules act as very effective condensation nuclei, and no pure water clusters were generated even from vapors with 100 fold excess of water molecules. Besides, we have demonstrated that the Na doping can be used for detection of species reacting with Na or solvated electron in the aerosols.

In general, all these results are relevant for the ozone depletion process in the stratosphere.

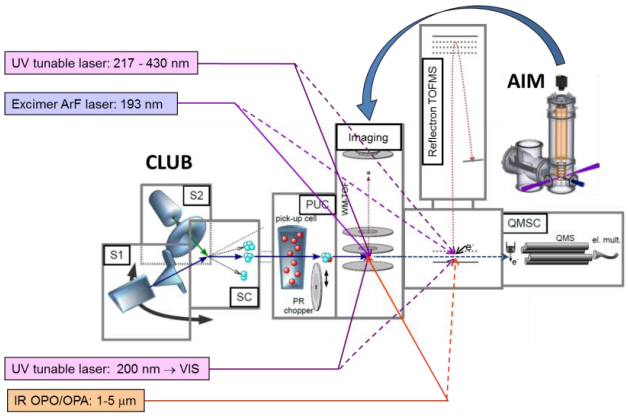

Figure 1. Schematic picture of molecular beam CLUB (CLUstr Beam) apparatus for small aerosol studies.

This work was supported by the Grant Agency of the Czech Republic under grants P208/11/0161 and 203/09/0422.

Lengyel, J., Kočišek, J., Poterya, V., Pysanenko, A., Svrčková, P., Fárník, M., Zaouris, D. K. and Fedor, J. (2012) *J. Chem. Phys.* **137**, 034304.

V. Poterya, M. Fárník, P. Slavíček, U. Buck, V. V. Kresin, J. (2007) *J. Chem. Phys.* **127**, 071101.

V. Poterya, J. Fedor, A. Pysanenko, O. Tkáč, J. Lengyel, M. Ončák, P. Slavíček, and M. Fárník, (2011) *Phys. Chem. Chem. Phys.* **13**, 2250-2258.

M. Ončák, P. Slavíček, M. Fárník, U. Buck, (2011) *J. Phys. Chem. A* **115**, 6155-6168.

Lengyel, J., Pysanenko, A., Kočišek, J., Poterya, V., Pradzynski, C. C., Zeuch, T., Slavíček, P. and Fárník, M. (2012) *J. Phys. Chem. Lett.* **3**, 3096-3101.

Photoionization and infrared excitation of clusters with radical sites: Probing size and structure of neutral, sodium doped water clusters

[1]C. C. Pradzynski, [2]U. Buck, [1]R. M. Forck, [1]F. Zurheide, and [1]T. Zeuch

[1]Institut für Physikalische Chemie, Georg-August-Universität Göttingen, Göttingen, 37077, Germany
[2]Max-Planck-Institut für Dynamik und Selbstorganisation, Göttingen 37077, Germany

Keywords: sodium doping, neutral clusters, water crystallization, photoionization, infrared spectroscopy
Presenting author email: cpradzy@gwdg.de

An interesting application of the sodium doping technique is the size selection of neutral clusters or aerosol particles (Bobbert et al. 2002, Yoder et al. 2011). The most general method to prepare size selected clusters is a crossed beam scattering experiment, where the mass dependency of cluster deflection by the second beam is exploited. However, this approach is experimentally demanding and restricted to cluster sizes up to around 12 molecules (Pradzynski et al., 2012). Tagging neutral clusters with a sodium atom has emerged in the last decade as a general and experimentally much less complicated method for neutral particle sizing in laboratory experiments.

A key idea of this technique is the formation of a solvated electron when the alkali metal (usually sodium, but lithium and caesium atoms work very similar) interacts with the cluster after pick-up. The site where the metal atom is attached features a single or multi radical type chemical environment, which is crucial for the photoionzation of the cluster. This effect is quite general and works with many hydrogen bonded complexes (secondary organic aerosol are highly hydrogen bonded aggregates) and even rare gas clusters. This first stage of the method has the character of chemical pre-ionization. The sodium atom is ionized at the particle surface which decreases the binding energy of the Na 3s electron such that photoionization with tuneable, commercially available lasers becomes possible. When photoionized at the threshold only the most sodium centered clusters become visible. In this case the zwitterionic type potential of the neutral and the cationic potential of the photoionized clusters are quite similar near the energy minimum. This property explains the formation of cold cations without fragmentation because in the cation only low energy modes are populated. The method has a hybrid character. It combines the softness of chemical ionization with the universal applicability of single photon ionization, which is also a rather soft method, even for clusters. The chemical pre-ionization component can be modulated by IR excitation, which provides an additional dimension – the generation of size resolved infrared spectra of the clusters (see Figures 1 and 2).

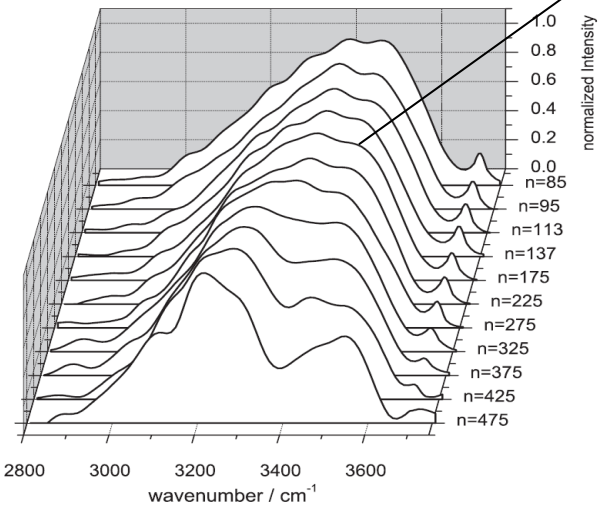

Figure 1. Evolution of crystalline core of water clusters with increasing cluster size (Pradzynski et al., 2012).

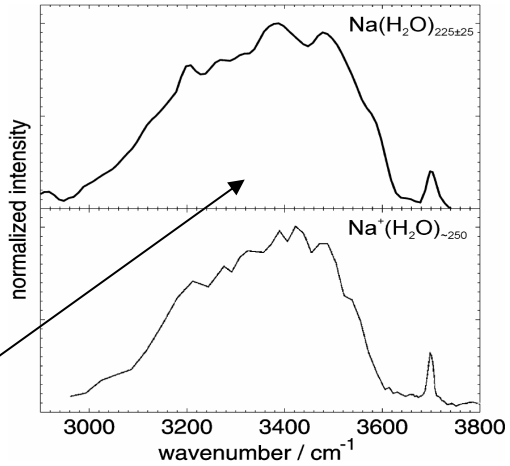

Figure 2. Comparison of infrared spectrum of $Na(H_2O)_{225\pm25}$ with $Na^+(H_20)_{\sim250}$ clusters (O´Brien and Williams, 2012).

In recent years we applied and refined the sodium doping technique and tested some new applications. In a recent work we could experimentally observe for the first time in the cluster size range between 250 to 500 molecules the transition between amorphous and crystalline ice on the basis of precisely size selectively determined infrared spectra in the OH stretching region, see Pradzynski et al., 2012.

Bobbert, C. et al. (2002) *Eur. J. Phys*. D **19**, 183-192.
Yoder, B. L., et al. (2011) *Phys. Chem. Lett.* **2**, 2623-2628.
Pradzynski, C. C. et al. (2012) *Science* **337**, 1529-1532.
O´Brien, J. T. and Williams, E. R. (2012) *J. Am. Chem. Soc*., 134, 10228-10236.

The oxidation of alpha-pinene and limonene in a flow tube, investigated using the CI-APi-TOF

M.P. Rissanen[1], M. Sipilä[1], M. Ehn[1], N. Sarnela[1], T. Jokinen[1], J. Kangasluoma[1], T. Petäjä[1], H. Junninen[1], D. Worsnop[1,2] and M. Kulmala[1]

[1]Division of Atmospheric Sciences, Department of Physics, University of Helsinki, P. O. Box 64, Fin-00014, Finland
[2]Aerodyne Research, Inc., 45 Manning Road, Billerica, MA 01821, USA
Presenting author email: matti.p.rissanen@helsinki.fi

The oxidation of alpha-pinene and limonene were studied in a Pyrex flow tube reactor using nitrogen (N_2) or synthetic air (N_2 and O_2) as the bath gas. The products of the reactions investigated were detected using a novel CI-APi-Tof (Chemical Ionization Atmospheric Pressure interface Time-of-flight mass spectrometer) technique with a nitrate ion (NO_3^-) based detection scheme (Jokinen *et al.* 2012). The detection scheme and the measurement routines have been described previously (Ehn *et al.* 2010, Jokinen *et al.* 2012, Junninen *et al.* 2010).

The setup used has three major advantages in studying oxidation reactions with atmospheric relevance: (i) the design of the atmospheric pressure interface (APi) allows the studies to be performed at ambient pressure, regardless of the mass spectrometric detection method – which significantly decreases uncertainties associated with extrapolating research results into atmospherically relevant conditions. (ii) The chemical ionization method is a fairly sensitive ionization method, and hence, enables the detection of molecular clusters that can provide insight into atmospheric new particle formation. (iii) Time-of-flight technique measures the whole mass spectrum at a time, up to a finite maximum mass, which helps in the product identification tremendously

In the experiments, alpha-pinene and limonene were exposed to differing levels of oxidants (O_3 and OH) in a flow tube coupled to the mass spectrometer. By varying the levels of oxidizers, the amount of organic precursor, their residence time in the reactor, as well as the water content, the important steps of the oxidation processes can be tracked.

The aim of the present experiments was to study the formation of highly oxidized molecules - HOMs – (Ehn *et al.* 2012) from two biogenic terpenes [terpene = organic hydrocarbon molecule with a chemical formula $(C_5H_8)_n$] limonene and alpha-pinene. The HOMs have recently started to attract considerable attention due to their possible relevance in the atmospheric new particle formation. Hence, the two reaction systems were investigated with the CI-APi-Tof, in order to gain insight into these processes.

Ehn, M., Junninen, H., Petäjä, T., Kurtén, T., Kerminen, V.-M., Schobesberger, S., Manninen, H. E., Ortega, I. K., Vehkamäki, H., Kulmala, M. and Worsnop, D. R. (2010) *Atmos. Chem. Phys.* **10**, 8513–8530.

Ehn, M., Kleist, E., Junninen, H., Petäjä, T., Lönn, G. Schobesberger, S., Dal Maso, M., Trimborn, A.,
Kulmala, M., Worsnop, D. R., Wahner, A., Wildt, J. and Mentel, Th. F. (2012) *Atmos. Chem. Phys.* **12**, 5113-5127.

Jokinen, T., Sipilä, M., Junninen, H., Ehn, M., Lönn, G., Hakala, J., Petäjä, T., Mauldin III, R. L., Kulmala, M. and Worsnop, D. R. (2012) *Atmos. Chem. Phys.* **12**, 4117-4125.

Junninen, H., Ehn, M., Petäjä, T., Luosujärvi, L., Kotiaho, T., Kostiainen, R., Rohner, U., Gonin, M., Fuhrer, K., Kulmala, M. and Worsnop, D. R. (2010) *Atmos. Meas. Tech.* **3**, 1039–1053.

Pressure dependency of ozonolysis product formation of α-pinene focusing on low volatile compounds such as organic acids and dimeric compounds

M. Beck[1], C. Keunecke[2], T. Zeuch[2] and T. Hoffmann[1]

[1]Institut für Anorganische und Analytische Chemie, Johannes Gutenberg-Universität Mainz, Mainz, 55128, Germany
[2]Institut für Physikalische Chemie, Georg-August-Universität Göttingen, Göttingen, 37077, Germany

Keywords: SOA, ozone, monoterpene oxidation, organic acids.
Presenting author email: hoffmant@uni-mainz.de

Secondary organic aerosols (SOA) are important for air quality and the global climate. Therefore, a better understanding of formation mechanism, growth, sources and also quantity of SOA is necessary. Today many details concerning these aspects are unknown.

SOA is formed by volatile organic compounds (VOCs) oxidized by ozone, OH- and NO_3-radicals in the atmosphere. The products of these oxidations have different kinds of functional groups (e.g. acid- and aldehyde-groups). Thus the volatility of the compounds decreases and nucleation or condensation on existing particles occurs. As monoterpenes are an important part of VOCs, the atmospheric oxidation is of high interest in aerosol research. α-Pinene is a very common monoterpene and therefore an often used model substance for mechanistic studies (Müller *et al.* 2009).

Besides oxidation products with monomeric structure, such as pinic acid for example, dimers were found in SOA. The formation of these is discussed intensively. Various reactions in the gas- and/or particle phase are possible. The dimers of α-pinene are of high interest due to the quantity of this terpene in the atmosphere. A lot of research hereby is focused on the compounds with the molecular mass 358 and 368. For the former very different formation pathways and chemical structures are suggested in the literature. These two dimers are of special interest because they were also observed in environmental samples. Therefore the possibility of using them as marker substances for various atmospheric conditions is discussed. A much higher number of dimeric compounds can be detected in atmospheric simulation chambers. This is due to the higher concentration of monoterpene and ozone used especially in mechanistic studies (Kundu *et al.* 2012).

Ozonolysis of α-pinene in the reaction chamber at the University of Göttingen, which can be operated at reduced pressures, is used to get more information about the formation process. This spheric reaction cell has a volume of 64 L with ozone and alkene premixing chambers, which allow well-controlled reactant mixing within two seconds. A FTIR- spectrometer for gas phase species analysis and a SMPS system for measuring particle size distributions and mass are attached to the chamber (Wolf *et al.* 2011). The aerosol particles were sampled on filters after the reaction in the chamber was finished (typically after five minutes) and the chamber was filled to ambient pressure. A methanol-water-solution was used for extraction of the filters. RP-HPLC-ESI-IT/MS^n was used for analysis.

Experiments were performed at three different reaction pressures (10, 20 and 460 mbar) with almost identically concentrations of ozone (5 ppm at 1 bar) and excess α-pinene. In general lower pressure yields lower particle number concentrations and smaller aerosol masses.

Therefore, the samples of the high pressure experiments at 460 mbar were used to identify the ozonolysis products. The often reported monomeric products such as terpenylic acid, pinic acid and hydroxypinonic acid were detected. About twenty dimeric compounds with a mass-to-charge ratio (m/z) between 300 and 400 were observed including the above mentioned dimers 358 and 368. For most of these dimers no confirmed or even suggested chemical structures are available in the literature. The MS/MS-experiments showed for the majority of the dimers a fragment with m/z 185 like pinic acid. Therefore, it is assumed that most of these compounds contain a pinic acid analogue or a closely related chemical structure.

The analysis of the filter samples confirmed a decreasing yield with decreasing reaction pressure for most of the compounds. Due to the lack of authentic standards for almost all substances only a semi-quantitative analysis was performed by comparison of the peak area. A roughly classification in six groups was performed (as shown in table 1).

The strong influence of pressure on the relative yields of SOA components seems to be related to the presence and absence of stabilized Criegee intermediates and different degrees of chemical activation of other intermediate species at high and low pressures. After further analysis the results are expected to provide constraints for suggested dimer formation mechanisms.

Table 1. Classification of pressure dependency. 100% represents the product yield at 460 mbar.

Group	1	2a	2	2b	3	4
10 mbar	< 1%	< 1%	1-3%	3-10%	3-25%	>50%
20 mbar	< 5%	5-20%	5-20%	5-20%	20-50%	>50%

L. Müller, M.C. Reinnig, H. Hayen, T. Hoffmann, *Rapid Commun. Mass Spectrom.*, **23** (2009) 971
S. Kundu, R. Fisseha, A.L. Putman, T. A. Rahn, and L. R. Mazzoleni, Atmos. Chem. Phys., **12** (2012) 5523
J. L. Wolf, S. Richters, J. Pecher, and T. Zeuch, *Phys. Chem. Chem. Phys.*, **13** (2011) 10952.

Monday, September 1, 2013

Poster Session A: *Atmospheric Aerosols*
Posters A001 - 229

Effective density measurements of different fresh soot types

M. Abegglen[1], B. Sierau[1], A. A. Mensah[1], J. Wang[2,3], L. Durdina[2,3], M. Gysel[4], U. Lohmann[1].

[1]ETHZ, Institute for Atmospheric and Climate Science, Zurich, 8092, Switzerland.
[2]Swiss Federal Laboratories for Materials Science and Technology (EMPA), Dubendorf, 8600, Switzerland.
[3]ETHZ, Institute of Environmental Engineering, Zurich, 8093, Switzerland.
[4]Paul Scherrer Institute, Laboratory of Atmospheric Chemistry, Villigen, 5232, Switzerland.
Keywords: soot, effective density, aircraft engine exhaust.
amanuel@ethz.ch

Introduction

In the atmosphere, black carbon is known to reduce visibility and affect the global radiation budget. A recent study has estimated the direct radiative forcing due to present-day black carbon emissions to be in the range from +0.17 W/m² to +1.48 W/m², with a certainty of 90 % (Bond et al., 2013). In order to better understand the role of black carbon in the atmosphere, a detailed characterization of freshly emitted particles and their subsequent ageing processes, involving coating due to condensation of secondary material, and possible restructuring of soot agglomerates, is needed. The knowledge of the particles' density is crucial because it is directly influenced by restructuring of soot particles.

Herein, we present size, density and mass distributions of freshly produced soot particles from several sources. The particles are characterized using a Differential Mobility Sizer (DMA) system and a Centrifugal Particle Mass Analyzer (CPMA), in series.

Another reason for conducting these measurements are mass-based thresholds used in air quality monitoring. Since the CPMA classifies particles according to their mass-to-charge ratio (Olfert & Collings, 2005) the mass distribution measurements can be a powerful application to determine the mass-based net output from any source. The results could then be compared with values obtained from currently used instruments.

Experimental

The actual experiments were performed in our laboratory at ETHZ. Four types of soot particles were generated. In more detail, two types using a Combustion Aerosol Standard (CAST) burner (fuel-rich (1) and fuel-lean (2)), one type (3) from a PALAS GFG aerosol generator and a (4) carbon black (Cabot Regal Black). Soot type 1, 2 and 3 are especially marked as surrogates for diesel soot by the manufacturers. In addition, soot particles from aircraft engine exhaust were investigated at the airport in Zurich during the Aviation Particle Regulatory Instrumentation Demonstration Experiments (A-PRIDE) campaign in November 2012. Here, sampling was performed directly behind the engine.

The freshly generated soot particles are first charge equilibrated to account for multiple charging and selected according to their mobility size (d_m) by a DMA. The monodisperse flow then enters the CPMA that records the mass distribution by scanning over the relevant mass range. A condensation particle counter counts the corresponding particle number concentration.

Results

Fig. 1 exemplarily depicts the effective density (ρ_{eff}) of soot from aircraft engine exhaust for different selected d_m measured during A-PRIDE. This can be mathematically derived by using the fractal relationship between the mass and the mobility size and the definition of the effective density. As can be seen, the effective density decreases with increasing mobility diameter. This effect will be discussed in detail for all datasets.

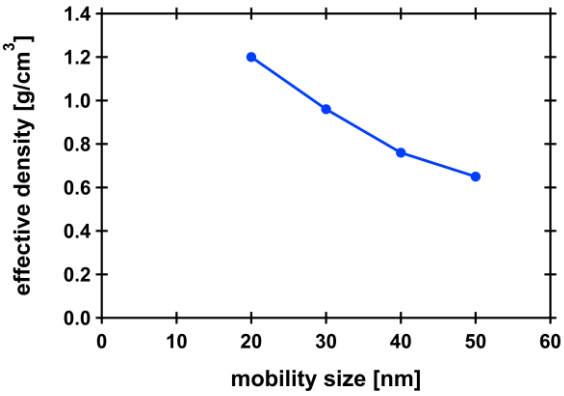

Fig. 1 Effective density of aircraft engine exhaust particles

Furthermore, we will compare our data to those from Gysel et al., 2012, who used an Aerosol Particle Mass analyser (APM) based on a very similar working principle as the CPMA.

Bond, T. C., *et al.* (2013). Bounding the role of black carbon in the climate system: A scientific assessment. *Journal of Geophysical Research: Atmospheres*, n/a–n/a. doi:10.1002/jgrd.50171

Gysel, M., *et al.* (2012). Technical Note: The single particle soot photometer fails to reliably detect PALAS soot nanoparticles. *Atmospheric Measurement Techniques*, *5*(12), 3099–3107. doi:10.5194/amt-5-3099-2012

Olfert, J. S., & Collings, N. (2005). New method for particle mass classification—the Couette centrifugal particle mass analyzer. *Journal of Aerosol Science*, *36*(11), 1338–1352. doi:10.1016/j.jaerosci.2005.03.006

Atmospheric aerosol size distribution during winter period in Ostrava-Radvanice

A. Baranova, J. Hovorka

Institute for Environmental Studies, Faculty of Science, Charles University in Prague, Prague 2, 12801, Czech Republic

Keywords: urban atmosphere, smog, SMPS, APS

Presenting author email: alexandra.baranova@natur.cuni.cz

Airborne particulate matter is one of the most important components of urban air pollution that affects health condition of human population. Fine aerosol particles have the highest impact on human health s, since they can bind carcinogenic substances and cause severe respiratory problems (Kim *et al.* 2007). Submicron particles are also substantial atmospheric component of urban smog. However, coarse aerosol particles contribute to air pollution level as well. With this reason, atmospheric aerosol investigation and aerosol size distribution particularly is considered to be very important. The location in the center of the Moravian-Silesian region - the city of Ostrava – was selected for measuring campaign. According to numerous studies, Ostrava is a city with the worst air quality not only in the Czech Republic, but in Europe as well (Rossnerova *et al*. 2011).

The measurement was performed using isothermal mobile container of the Laboratory for air quality measurements of the Institute for Environmental Studies, Faculty of Science, Charles University in Prague. It was located in Ostrava-Radvanice and Bartovice (49°48'40.4"N, 18°20'15.8"E) during the winter period 25.1-22.02.2012. 5 minute integrates of number size distribution of particles with aerodynamic diameter 14-10000 nm were determined, by combination of Scanning Mobility Particle Sizer (SMPS 3936L25) and Aerodynamic Particle Sizer (APS 3321). Also 5 min concentrations of gaseous components NO_x, O_3, CO, SO_2, CH_4 and NMHC and meteorological parameters: wind speed, wind direction, temperature, relative humidity and global radiation were determined.

Two periods can be distinguished within the campaign: smog and after smog. Smog period (25.01.-15.02.) is characterized by low air temperature (median T = -14.8 °C), low wind speed (median WS = 0,7 ms^{-1}) and inverse layering of atmospheric boundary layer. As results, high median concentrations of $PM_{2.5}$ = 104 μgm^{-3} were observed. Smog period continued until a warm front moved over the locality. Air temperature and wind speed increased (median T = -1.7 °C, median WS = 1.1ms^{-1}) substantially. Also heavy snow storms occurred at the beginning of the period. As result, median concentration of $PM_{2.5}$ dropped to 38 μgm^{-3}.

Particle number concentrations are dominated by particles of less than 0.6µm of aerodynamic diameter both in smog and after smog periods (Fig.1). Nevertheless, number size distribution averaged over smog period was found near monomodal with mode at 150 nm, while there was clear bimodality, the first mode at 25nm and the second at 55 nm, for the distribution in after smog period (Fig.1). Both disappearance of the first mode and the increase in particle diameter of the second mode are consequences of ultrafine particle coagulation on particles of accumulation mode produced during the smog period.

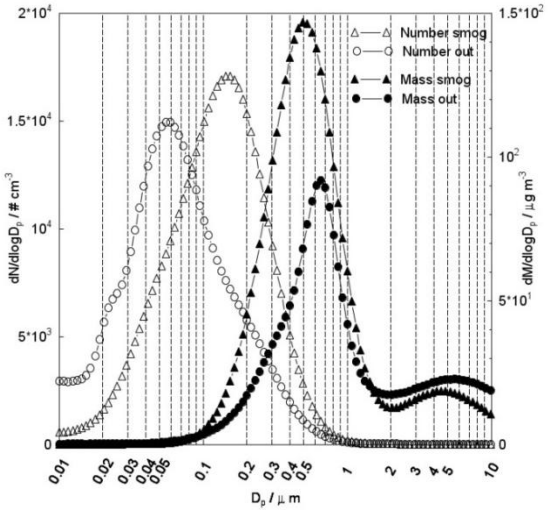

Figure.1 Aerosol particle number and mass size distributions during smog (25.1-15.2) and after smog (15.2.-22.2) periods in Ostrava-Radvanice, in winter 2012

Similarly to particle number submicron particles aerosol particles dominated the aerosol mass. But contrary to number size distributions, mass size distributions were bimodal for both the periods. The first mode was at 0.5µm for smog period and 0.65 µm for after smog period respectively while the second mode at about 5 µm was common to both the periods. The increased mass due to coarse aerosol after smog period is caused by meteorological changes when particles of greater size could be raised upwards because of increased wind speed.

The work was supported by the Grant Agency of the Czech Republic, project CENATOX, under grant P503/12/G147.

Kim, H.-S., Huh, J.-B., Hopke, P.K., Holsen, T.M., Yi, S.-M. (2007), *Atmospheric Environment*, **41(32)**, 6762-6770

Rossnerova, A., Spatova, M., Rossner P.Jr., Novakova, Z., Sram, R.J. (2011), *Mutation Research* **708**, 44-49

Monitoring of transatlantic particles over São Paulo (Brazil) by sun-photometry, ground-based lidar and CALIOP

J.L. Guerrero-Rascado[1,2], F. J. S. Lopes[3,4], E. Landulfo[4] and L. Alados-Arboledas[1,2]

[1]Andalusian Center for Environmental Research (CEAMA), University of Granada, Autonomous Government of Andalusia, Av. del Mediterráneo, s/n, 18006, Granada, Spain
[2]Dpt. of Applied Physics, University of Granada, Fuentenueva s/n, 18071, Granada, Spain
[3]Universidade de São Paulo, Instituto de Astronomia, Geofísica e Ciências Atmosféricas, Rua do Matão, 1226, Cidade Universitária, CEP 05508-090, São Paulo, SP, Brazil
[4]Instituto de Pesquisas Energéticas e Nucleares, Centro de Lasers e Aplicaçoes Avenida Lineu Prestes, 2242 Cidade Universitária, CEP 05508-000, São Paulo, SP, Brazil
Keywords: aerosol particles, Brazil, CALIPSO, lidar, sun-photometry, transatlantic transport
Presenting author email: alados@ugr.es

Two aerosol types have been traditionally reported over the Brazilian area. On the one hand, it is well recognized that the biomass burning activity has an important impact on the air quality in Brazil. According to CPTEC/INPE (www.cptec.inpe.br/queimadas), between $11.5 \cdot 10^4$ and $20.5 \cdot 10^4$ actives fires per year were detected in 2006-2012 period. In particular, biomass burning activities related to sugarcane crops is especially relevant in the Northeastern and Southeastern areas. Several works reported studies related to biomass burning covering different aspects such as gases, particulate matter and their transport. On the other hand, the largely local emission sources determine the chemical composition of the atmospheric aerosol in all metropolitan regions, with the most populated and industrialized areas in the Southeastern Brazil. This results in a small influence of long-range transported particles from elsewhere in term of aerosol load in Brazil and traditionally other different long-range transported aerosol types have been ignored over the Southeastern metropolitan areas as the State of São Paulo. However, it is possible to detect their presence on intensive optical properties such as the lidar ratio.

In order to achieve a better understanding of the spatial and temporal variability of the complex aerosol distributions on both regional and global scales, the transcontinental transport of different aerosol types is of the special importance and must be understood. Regarding Saharan dust, many field campaigns and studies have been conducted during the last years. However, most of them were performed close to source regions or considering short-range transport, and therefore the evolution of dust properties during transport is still misunderstood. The Atlantic Ocean is the major pathway of dust transport from North Africa, the latter being the Earth's largest source of mineral dust. Several studies have already been conducted to understand the physic-chemical properties of Saharan mineral dust. However, most of them were performed close to source regions or considering short-range transport, therefore the evolution of dust properties during transport is still misunderstood and many examples illustrate the need of a thoroughly understanding on the transcontinental transport of aerosols. Although the location of the Inter Tropical Convergence Zone (ITCZ) can be an indicator of the dust meteorology as a rough approximation, both meteorology and source features are the overriding factors determining the transport of dust in the atmosphere. Synoptic scale system provides a mechanism in the western Atlantic to inject dust across an active ITCZ. Up to now, the vertical distribution of Saharan mineral dust over South America is almost limited to a case study and a medium-term analysis of systematic (1 year) multiwavelength polarization Raman lidar observations of optical and microphysical particle properties, both over the Amazon Basin.

The analyses presented in this study are an evidence of the arrival of the transcontinental advection of Saharan dust and its subsequent detection in São Paulo, at latitudes very far from the Equator. For that goal, the synergetic combination of several approaches, including active (lidar) and passive (sun-photometer) remote sensing from ground and satellite platform (CALIPSO), were used.

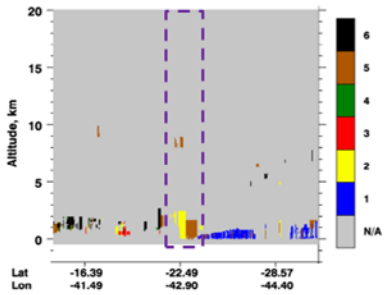

Figure 1. Aerosol subtype from CALIPSO on 26/12/2007 (night) around São Paulo (shaded box) detecting dust (yellow) and polluted dust (brown).

This work was supported by the Santander Bank through the fellowship program "Becas Iberoamérica. Jóvenes Profesores e Investigadores. Santander Universidades. Convocatoria España, 2012", the Andalusia Regional Government through projects P08- RNM-3568 and P10-RNM-6299, by the Spanish Ministry of Science and Technology through projects CGL2011-16124-E, CGL2010-18782, CSD2007-00067 and CGL2011-13580-E/CLI, and by the EU through the ACTRIS project (EU INFRA-2010-1.1.16-262254).

Measurements of aerosol light-scattering enhancement factors at the urban environment of Granada (Spain).

G. Titos[1,2], H. Lyamani[1,2], A. Cazorla[1,2], Z.J. Wu[3], M. Sorribas[1,2], I. Foyo-Moreno[1,2], J. Cheng[4], H.J. Liu[4], A. Wiedensohler[3] and L. Alados-Arboledas[1,2]

[1]Centro Andaluz de Medio Ambiente, Universidad de Granada, Junta de Andalucía, Granada, 18006, Spain
[2]Department of Applied Physic, University of Granada, Granada, 18071, Spain
[3] Leibniz Institute for Tropospheric Research, 04318 Leipzig, Germany
[4] Department of Atmospheric and Oceanic Sciences, School of Physics, Peking University, Beijing, China
Keywords: hygroscopicity, scattering enhancement factor, absorption coefficient
Presenting author email: alados@ugr.es

Microphysical and optical properties of aerosol particles present a strong dependence on relative humidity (RH). A better understanding of this RH effect is, therefore, very important for climate forcing calculations. Here, we present results from a campaign performed in an urban environment in southern Spain (Granada, 37.18ºN, 3.58ºW, 680 m a.s.l) during winter season. The aerosol light-scattering coefficient ($\sigma_{sp}(\lambda)$) was measured with two integrating nephelometers (TSI 3563) at dry (Dry-neph) and at a predefined RH (Wet-neph). The light scattering enhancement factor (f(RH) = σ_{sp}(RH)/ σ_{sp}(dry)) was used to quantify the dependence of σ_{sp} on RH. We defined two operation procedures: 1) Keep the RH of the Wet-neph at a constant value (85%) and 2) Scan the RH between 30-90%. Additionally, the aerosol light-absorption coefficient was measured with a MAAP (Multi-Angle Absorption Photometer) and an aethalometer AE-31. Filter samples were also collected in PM_1 and PM_{10} fractions for chemical analysis.

During the campaign, dry light-scattering and absorption coefficients showed a mean value (± standard deviation) of 40±40 Mm^{-1} at 550 nm and 17±18 Mm^{-1} at 637 nm, respectively. Both coefficients showed a high variability due to the diurnal changes in the local emissions (mainly caused by traffic) and in the meteorological conditions during the campaign. The dry scattering Angstrom exponent calculated between 450 and 700 nm was 1.7±0.4 and the single scattering albedo at 637 nm was 0.7±0.1, denoting a predominance of fine particles and a significant fraction of absorbing particles. These values are typical of our urban station during winter season (Lymani et al., 2010; Titos et al., 2012). f(RH=85%) at 550 nm presented a mean value of 1.5±0.2, reaching values up to 3.4. The mean value is in accordance with the value of 1.4 reported by Yan et al. (2009) at an urban station in Beijing. The average diurnal evolution of f(RH=85%) and the single scattering albedo is shown in Figure 1. f(RH=85%) presented two minima during morning and afternoon traffic rush hours, probably due to the relative increase of non-hygroscopic fraction (like black carbon) due to traffic emissions. This fact can be observed in the diurnal evolution of ω_0(637 nm) that also presented two minima denoting an increase in the relative contribution of absorbing particles during the traffic rush hours. The afternoon minimum in the f(RH=85%) is lower than the morning minimum in contrast with the single scattering albedo which presented the minimum value during the morning. This fact evidences that not only the increase in the contribution of BC to the total aerosol load is responsible of the decrease of f(RH=85%). In this sense, it could be related to aging processes that lead to lower f(RH) during the afternoon than during the morning. In the early morning (around 3-4 GMT) the f(RH=85%) reached it maximum value, probably due to the decrease in BC concentrations as a result of the reduction in local anthropogenic emissions and an increase in the water soluble fraction. This increase in the water soluble fraction can be related with higher levels of ammonium nitrate during the cooler time of the day (Park et al. 2005).

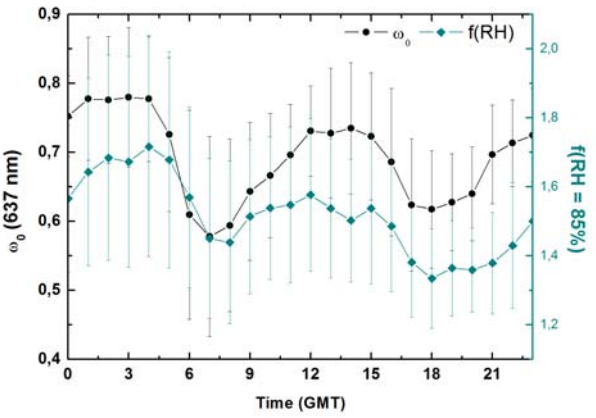

Figure 1. Average diurnal evolution of f(RH=85%) and single scattering albedo at 637 nm. The error bars represent the standard deviations.

Acknowledgments: This work was supported by the Andalusia Regional Government through projects P08-RNM-3568 and P10-RNM-6299, by the Spanish Ministry of Science and Technology through projects CGL2010-18782, CSD2007-00067, CGL2011-13580-E/CLI, CGL2011-16124-E and CGL2011-15008-E; and by EU through ACTRIS project (EU INFRA-2010-1.1.16-262254). G. Titos was funded by the Spanish Ministry of Science.

Park et al. (2005) *Atmos. Environ*. 39 2011-2020.
Yan et al. (2009) *Particuology 7 52-60.*
Lyamani et al. (2010*) Atmos. Chem. Phys.,* 10, 239–254.
Titos et al. (2012) J. Geophys. Res. 117, D04206, doi:10.1029/2011JD016671.

Relating the wavelength dependency of the absorption coefficient and the aerosol type

A. Cazorla[1,2], G. Titos[1,2], H. Lyamani[1,2] and L. Alados-Arboledas[1,2]

[1]Centro andaluz de Medio Ambiente, University of Granada, Junta de Andalucía, Granada, 18006, Spain
[2]Departmento de Física Aplicada, University of Granada, Granada, 18071, Spain
Keywords: absorption coefficient, absorption Ångström exponent, aerosol type.
Presenting author email: alados@ugr.es

Absorption of solar radiation due to aerosol particles is mainly caused by carbonaceous particles and mineral dust. The Absorption Ångström Exponent (AAE) describes the wavelength dependency of the absorption coefficient and it can give information about the type of aerosol or source (Cazorla et al., 2013). In this sense, black carbon (BC) absorption follows a λ^{-1} spectral dependency, yielding an AAE equal to 1 (Bergstrom et al., 2002), while brown carbon and mineral dust have a higher contribution to absorption in the ultraviolet and blue spectral regions yielding an AAE greater than 1 (Kirchstetter et al., 2004).

In this study, we analyzed data from an aethalometer AE31, that measures the aerosol light-absorption coefficient at 7 wavelengths (370, 470, 520, 590, 660, 880, 950 nm), installed in Granada; an urban city in the southeast of Spain (37.18ºN, 3.58ºW, 680 m a.s.l). The period of study comprises from September 2012 to January 2013.

We calculated the AAE using all the aethalometer wavelengths (AAE), using the three shorter wavelengths (AAE_UV), and using the three longer wavelengths (AAE_IR). Daily AAE values reveal that there are two distinct periods, one comprised from the beginning of the study period to November 15, and another from November 16 to the end of the study period (Fig.1).

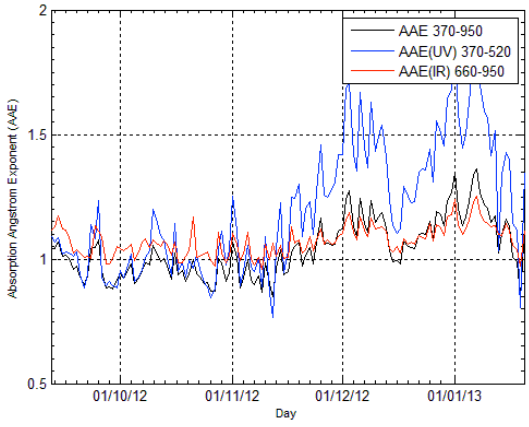

Figure 1. Aethalometer daily AAE

The first period has an AAE, AAE_UV and AAE_IR mean value of 1.0±0.3, 1.0±0.5 and 1.0±0.5 respectively; indicating the predominance of BC particles emitted by traffic source. On the other hand the second period presents an AAE, AAE_UV and AAE_IR mean value of 1.1±0.3, 1.4±0.5 and 1.1±0.3. A value of AAE greater than 1 indicates a change in the dominant absorbing type of aerosol. This change is related to seasonal changes in the emission sources; in winter domestic heating (based on fuel-oil and biomass combustion) is an additional local anthropogenic source. As we can see, this change is more pronounced for AAE calculated using the shorter wavelengths (AAE_UV), pointing out an increased contribution of brown carbon to aerosol population.

The results show the importance of measuring absorption coefficient in a wide range of wavelengths (from UV to near IR) for identifying aerosol types.

This work was supported by the Andalusia Regional Government through projects P08-RNM-3568 and P10-RNM-6299, by the Spanish Ministry of Science and Technology through projects CGL2010-18782, CSD2007-00067, CGL2011-13580-E/CLI, CGL2011-15008-E and CGL2011-16124-E; and by EU through ACTRIS project (EU INFRA-2010-1.1.16-262254).

Bergstrom, R.W., Russell, P.B. and Hignett, P. (2002) *J. Atmos. Sci.*, **59**, 567–577.

Cazorla, A., Bahadur, R., Suski, K. J., Cahill, J. F., Chand, D., Schmid, B., Ramanathan, V., and Prather, K. (2013) *Atmos. Chem. Phys. Discuss.*, **13**, 3451-3483.

Kirchstetter, T.W., Novakov, T., and Hobbs, P.V. (2004). *J. Goephys. Res.*, **109**(D21208), 1–12

Evaluation of AERONET precipitable water vapour versus microwave radiometry, GPS and balloon-borne radiosondes at ARM sites.

D. Pérez-Ramírez[1,2,3], A. Smirnov[4,5], H. Lyamani[2,3], D. Whiteman[1], B. Holben[4] and L. Alados-Arboledas[2,3]

[1] Mesoscale Atmospheric Processes Laboratory, NASA Goddard Space Flight Center, 20771, Greenbelt, Maryland, United States
[2] Andalusian Centre for Environmental Research, University of Granada, Granada, Andalucía, 18006, Spain
[3] Department of Applied Physics, University of Granada, Granada, Andalucía, 18071, Spain
[4] Biospheric Sciences Branch, NASA Goddard Space Flight Center, 20771, Greenbelt, Maryland, United States
[5] Sigma Space Corporation, 20771, Lanham, Maryland, United States

Presenting author email: alados@ugr.es

Measurements of the precipitable water vapour (*W*), defined as the total amount of water vapour in the atmospheric column, are being very important to characterize water vapour role in radiative forcing, hydrological cycle and climate. From several decades ago sun-photometry measurements at the water vapour absorption bands around 940 nm are being used to retrieve W. But it faced with problems related to an appropriate methodology and calibration. AERONET network addresses those problems and standardizes calibration and measurement protocols, as well as data quality [Smirnov et al., 2004]. But to date, evaluation of AERONET retrievals of W are sparse.

Balloon-borne radiosondes have been used as standard to retrieve W from decades ago, but faces with problems as the drift of the sonde, the 'dry' bias or the batch dependence [Milosevich et al., 2006]. Moreover, zenith wet delays measured by GPS allow the retrievals of W under almost all weather conditions. Similarly, W retrievals (and also atmospheric profiles of water vapour) can be obtained from sky brightness temperature measurements around 22.235 GHz water vapour absorption band by microwave radiometers. The uncertainties of these techniques to retrieve W stated in the bibliography are of ~5% for MWR and GPS and ~10-15% for balloon-borne.

The scope of this work is to evaluate AERONET retrievals of W versus those by MWRs, GPS and balloon borne. To this end, we use the large database of MWRs and balloon-borne measurements made at the three major sites of the U.S. Department of Energy Atmospheric Radiation Measurement (ARM), located at Southern Great Plains (36.61ºN, 97.49 ºW, 318 m a.s.l.), Nauru Islands (0.52 ºS, 166.92 ºE, 7 m a.s.l.) and Barrow (71.31 ºN, 156.67 ºW, 0 m a.s.l.). GPS retrievals of W at these sites are provided by SUOMINET network managed by the University Corporation for Atmospheric Research (UCAR).

For 10 years of correlative measurements between the different instrumentation at the Southern Great Plain, Figure 1 present number density plots of W obtained by MWRs, GPS and balloon-borne as function of those obtained by AERONET. The linear fits forced through zero revealed slopes of 1.10 ± 0.01, 1.05 ± 0.01 and 1.04 ± 0.01 for the evaluations versus MWR, GPS and balloon-borne. These values indicate underestimation of W retrieved by AERONET. The extended study, including also the other ARM sites, indicates underestimations by AERONET of ~7.8% versus MWR, ~3.8% versus GPS and ~4.8% versus balloon-borne radiosondes. But assuming an the uncertainty of AERONET retrievals of W is ~10%, the stated differences within the different instrumentation are within the error margins. Therefore, we conclude that within a 10% uncertainty there is no golden instrument to retrieve precipitable water vapour. The largest differences found between AERONET sun-photometers and MWRs can be explained by the differences in the spectral databases and radiative transfer models between sun-photometry and microwave radiometry. Actually, the strength of the water vapor absorption currently remains a subject of discussion in the scientific community [e.g. Alexandrov et al., 2009]. A better agreement between these two techniques should imply combined efforts to use the same spectral database with similar constraints.

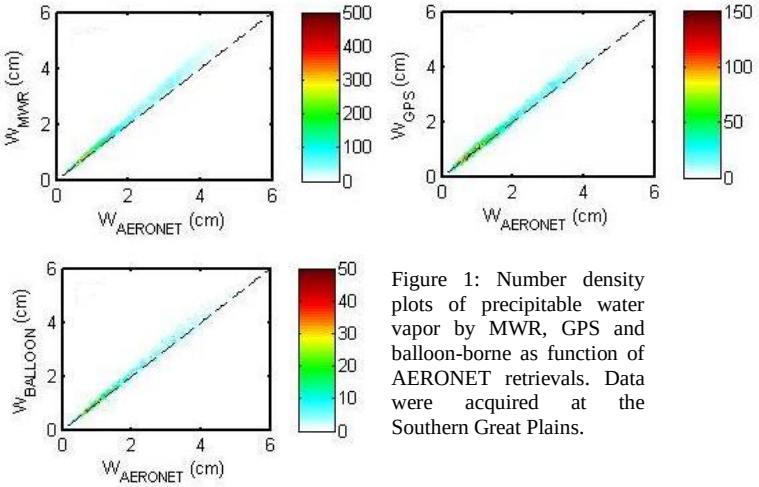

Figure 1: Number density plots of precipitable water vapor by MWR, GPS and balloon-borne as function of AERONET retrievals. Data were acquired at the Southern Great Plains.

Alexandrov, M.D., et al. (2010) *J. Geophys. Res.*, 114, doi:10.1029/2008.jd010543.

Miloshevich, L.M., et al., (2006) *J. Geophys. Res.*, 111, D09S10, doi:10.1029/2005JD006083.

Smirnov, A., et al., (2004) *Proceedings of AERONET workshop*, El Arenosillo, Spain.

Aerosol Impact on cloud properties in Pakistan

K. Alam[1,2], R. Khan[1]

[1]Institute of Physics & Electronics, University of Peshawar, Peshawar,25120, Pakistan
[2]Higher education commission (HEC), Pakistan

Keywords: Aerosol, Cloud, Cloud fraction, Liquid water path, Pakistan.
Presenting author email: khanalamso@gmail.com

This study investigates aerosol impact on various properties of clouds over different cities of Pakistan using Moderate Resolution Imaging Spectroradiometer (MODIS) data during the period (2001-2011). The relationship between AOD and other cloud parameters, namely water vapor (WV), cloud fraction (CF), cloud optical thickness (COT), cloud liquid water path (CLWP), cloud top temperature (CTT), and cloud top pressure (CTP) were analyzed. On smaller temporal scales, latitudinal variations of both WV and AOD produce high correlations (> 0.8) in some regions and moderate (> 0.6) in the other regions. An increasing trend in CF with AOD was found over urban region in the period of observations. The CF values were higher for Lahore than the other selected regions during the whole period.

The correlation between AOD and CWPL was found to be positive during autumn and winter seasons, while negative correlation was observed during the other seasons for all the selected regions. COT showed negative correlation with AOD at all locations except Karachi during spring and summer seasons. AOD showed a positive correlation with CTP and CTT for spring season and a negative correlation was observed for summer for the all investigated regions. Furthermore, in warm clouds AOD and CTP were negatively correlated for all regions except Peshawar, whereas AOD and CTT were positively correlated for all regions except Karachi. In cold clouds the relationships between AOD and CTP, and AOD and CTT were negative except Karachi. Thus meteorological parameters, geographical conditions, as well as warm and cold clouds are the causative factors for AOD and CTP, and AOD and CTT variations.

References

Ackerman, A. S., Toon, O. B., Stevens, D. E., Heymsfield, A. J., Ramanathan, V., 2000. Reduction of tropical cloudiness by soot, Science 288 (5468), 1042–1047.

Alam, K., Iqbal, M.J., Blaschke,T., Qureshi, s., Khan, G., 2010. Monitoring spatio- temporal variations in aerosols and aerosol cloud interaction over Pakistan using MODIS data. Advance in space research 46, 1162-1176.

Remote Sensing of Aerosol optical property Over the Arabian Gulf

F.M. Al-Kandari, H.K. Al-Jassar and K.S. Rao

Department of Physics, University of Kuwait, Khaldiya, Kuwait, 13060, Kuwait
Keywords: Aerosol Optical depth, sun photometer, Aeronet, Absorption factor
Presenting author email: fatma.alkandri@gmail.com

The aim of the study is to detect the pollution periods associated with dust emissions according to aerosols spectral behaviour and the change of wind regimes over the Arabian Gulf. Three Aerosol Robotic Network (AERONET) sites are involved in the study - Kuwait University, Kuwait (29.32°N, 47.97°E), Solar Village, Riyadh (24.91°N, 46.41°E) and Dhadnah Al Fujairah, UAE (25.51°N, 56.327°E).

In Gulf sites fine mode particles lie in a geometric mean radius range of $0.05 < r < 0.33 - 0.44$ μm, while coarse mode lie particles in the range $0.33 - 0.44 < 1 < 15$ μm (figure 1).

Clarke et. Al., (2004) separated soot from dust by taking into assumption that sub micrometer particles have radii within range ≤ 0.75 μ. Sub micrometer particles are divided into two categories. In Kuwait site we found particles with radii between 0.75 and 0.35 μm have positive significant correlation ~ 0.4 between total volume concentration and absorption factor σ_{abs} in Kuwait. Such trend is related to existence of urban dust. The results of the other sites are demonstrated in Table (1).

Single Scattering Albedo (SSA) is retrieved for wavelengths corresponding to sky radiance measurements. SSA daily averages are computed from hourly data of level 1.5 with solar zenith angle $\leq 55^{o}$. In Kuwait SSA increases with wavelength in spring and summer with associated high absorption at 470 nm wavelength. This situation occur when dust work as a carrier for soot. Soot signature is found in winter season. In Solar village SSA has almost neutral trend in all seasons. Finally in Dhadnah SSA reveal dust dominance with soot emissions in spring and dry summer interval and neutral in humid summer & autumn.

Table 1: Summarize the results of the urban dust correlation with absorption factor as well as the soot percentage in AERONET data.

Aeronet Site	Radii (μm) Division	$r_{VOL-\sigma abs}$	Aerosol Load Percentage
Kuwait	$0.35 \leq r < 0.75$	0.40**	Urban dust
	$r < 0.35$	0.05**	5.5% (soot)
Solar Village	$0.35 \leq r < 0.75$	0.525**	Urban dust
	$r < 0.35$	0.41*	2.9% (dust carrying soot)
Dhadnah	$0.35 \leq r \leq 0.75$	0.632*	Urban dust
	$r < 0.35$	0.005	4.87%

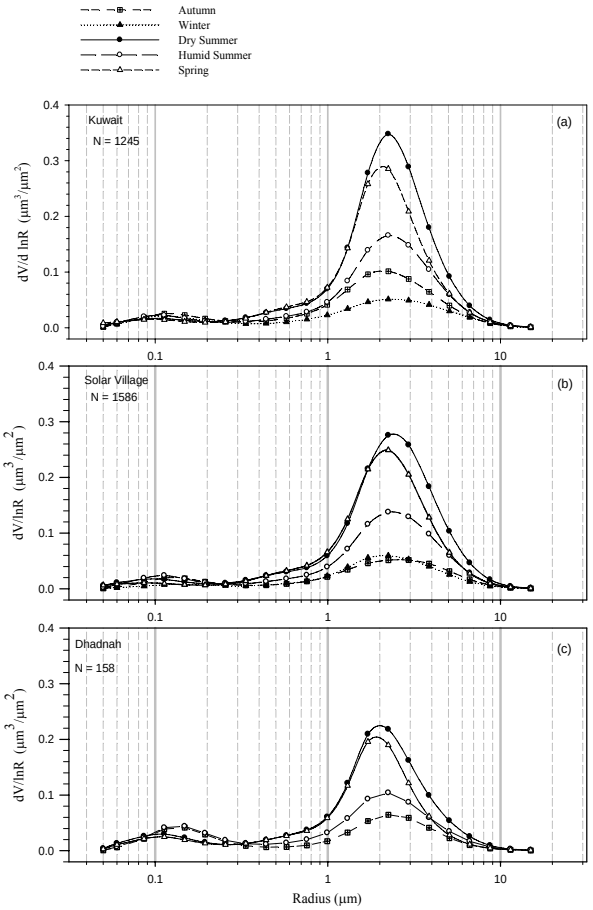

Figure 1: Seasonal aerosol volume size distribution versus geometric mean radius in Kuwait, Solar village and Dhadnah. The number for averaged retrieval is shown for each season.

This work was supported by The Research Administration Department of Kuwait University, under Project Code: SP02/09. We are grateful to the principal investigators of the Gulf AERONET sites, Naif Al-Abbadi (Solar Village) and Brent Holben (Dhadnah), all the sites staff and the responsible Institutions in Saudi Arabia and United Arab of Emirates for their efforts in maintaining AERONET Data.

Clarke, A.D., Shinozuka, Y., Kapustin, V.N., Howell, B., Huebert, S., Doherty, S., Anderson, T., Covert, D., Anderson, J., Hua, X., Moore II, K.G., McNaughton, C., Carmichael, G., and Weber, R. (2004). *Size distributions and mixtures of dust and black aerosol in Asian outflow: Physiochemistry and optical properties, J. Geophys. Res.*, 109, *D* 15*SO*9, *doi:* 10.1029 / 2003JD004378.

Organic Fraction of Laboratory Generated Primary Marine Aerosol

A. C. Butcher[1], S. M. King[2], T. Rosenoern[3], and M. Bilde[4]

[1]Copenhagen Center for Atmospheric Research (CCAR), Department of Chemistry, University of Copenhagen, Copenhagen, DK-2100, Denmark
[2]Formerly at CCAR, now at Haldor Topsoe, Denmark
[3]Formerly at CCAR, now at Force Technoology, Denmark
[4]Institut for Kemi, Aarhus Universitet, Aarhus, DK-8000, Danmark
Keywords: marine aerosols, organics, thermodenuder, VTDMA
Presenting author email: andrew@chem.ku.dk

Marine aerosols are an important source of aerosols in the Earth's climate system. Despite their importance, much remains unknown about the characteristics of these aerosols. The largest uncertainty remains in the submicron aerosol size range, where flux estimates span several orders of magnitude (de Leeuw *et al.* 2011). In addition to this, the organic fraction of these particles remains a large open question.

Building on previous work with a simulated sea spray aerosol tank at the University of Copenhagen (King *et al.* 2012), the organic fraction of laboratory produced aerosol is probed with the use of a thermo-denuder forming a Volatility-Tandem Differential Mobility Analyzer (VTDMA) operating at high temperatures (∼400°C). By selecting specific proxy sea water solutions with known organics and salts, the organic volume fraction volatilized from aerosols at specific mobility sizes can be determined, yielding the organic fraction of aerosols.

Several organic-salt systems were investigated, with results presented here from L-Serine, an amino acid found in the sea micro layer, with respect to varying concentrations of sodium chloride (NaCl) and an artificial sea salt, Tropic Marin Sea Salt (TMSS). A 1 g sample of organic in 10 L of Milli-Q (18MΩ) is bubbled using a vertical plunging jet producing bubble burst-aerosols characteristic of primary marine aerosols. Salt concentration is increased in the tank while the first DMA is set to several diameters with sufficient concentration for VTDMA study. Resulting modal diameters of the size distribution before and after the thermo-denuder are then used to calculate the volume fraction remaining (VFR). This results in the VFR plot shown in Figure 1.

Figure 1 shows that the volume fraction remaining, following passage of aerosols through the thrermodenude, decreases for all sample aerosols. For the TMSS:Serine system, the volume fraction remaining increases with increase in salt:organic ratio. A similar trend is seen for the NaCl:Serine system, however less pronounced.

A trend of volume fraction remaining with particle diameter is seen for TMSS:Serine ratios of 10:1 and 100:1, repectively, with a slight decrease in VFR near 100 nm. The low VFR for 20 nm particles implies a high organic fraction in the original particles and when considered relative to VFR of 60 nm particles, gives evidence for a size dependent organic fraction.

These results indicate a promising avenue with which to investigate the organic fraction of laboratory produced aerosols, which allows for the careful control of the precise organic and salt concentrations of a sea water proxy. Estimates of specific organics within the surface layer of the ocean can then be tied to aerosol production and organic mass flux over the ocean. Further work is to include more sample matrices and characterization of experimental error.

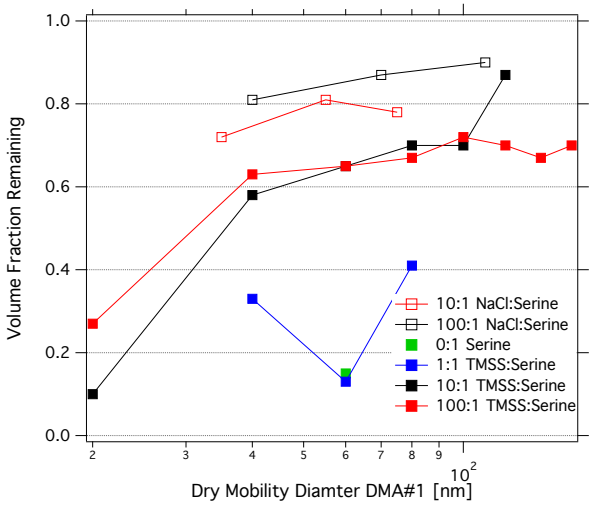

Figure 1: Volume Fraction Remaining for aerosols produced by plunging jet aerosol production in Salt:Organic sea water proxies

This work is supported by The Carlsberg Foundation and Cryosphere-atmosphere interactions in a changing Arctic climate (CRAICC).

G. de Leeuw, E. L. Andreas, M. D. Anguelova, C. W. Fairall, E. R. Lewis, C. O'Dowd, M. Schulz, and S. E. Schwartz (2011) *Production flux of sea spray aerosol*, Rev. Geophys., 49(2).

S. M. King, A. C. Butcher, T. Rosenoern, E. Coz, K. I. Lieke, G. de Leeuw, E. D. Nilsson, and M. Bilde. (2012) *Investigating primary marine aerosol properties: CCN activity of sea salt and mixed inorganic-organic particles.*, Environmental Science & Technology, DOI:10.1021/es300574u.

Saharan dust contribution to PM_{10} levels and composition in Cape Verde

S. M. Almeida[1], M. Almeida-Silva[1]*, C.A. Pio[2], T. Nunes[2], J. Cardoso[2, 3], M. Cerqueira[2], M.A. Reis[1], P.C. Chaves[1], A. Taborda[1]

[1] IST/ITN, Instituto Superior Técnico, Universidade Técnica de Lisboa, Estrada Nacional 10, 2686-953 Sacavém, Portugal
[2]CESAM, Aveiro University, 3810-193 Aveiro, Portugal
[3]Cape Verde University, Campus do Palmarejo, Praia, Cape Verde

Keywords: PM_{10}, Source Apportionment, Cape Verde, Sahara Desert.
Presenting author email: smarta@ctn.ist.utl.pt

Sahara Desert is the most important source of mineral dust, contributing more than 1900 million tons per year (Goudie, 2009; Goudie and Middleton, 2006; Prospero, 1996; D'Almeida, 1986) and responsible for almost half of all the aeolian material provided to the world's oceans. Due to its geographical position, Cape Verde is highly affected by the transport of dust from the Sahara desert. Therefore, it is essential to elucidate the role of Saharan dust may play in the degradation of Cape Verde air quality, human health, wellbeing, visibility, tourism and economy.

The objective of this study was (1) to perform a chemical characterization of the airborne particles sampled in Cape Verde, (2) to identify the main sources and origins of the particles and (3) to assess the influence of Sahara desert on local suspended particles.

PM10 was sampled during 2011 and chemical characterization of particles was performed by Neutron Activation Analysis and Particle Induced X-ray Emission for elemental measurements, by Ion Chromatography for the determination of water soluble ions and by a Thermal-optical system for the measurement of carbonaceous aerosol. Source apportionment was performed by integrating Principal Component Analysis with Multilinear Regression Analysis, Positive Matrix Factorization and Cluster Analysis of Backward Trajectory.

Results showed that Cape Verde aerosol is affected principally by natural sources: dust coming from Sahara desert contributes on average to 48% of the total PM_{10} mass and sea salt spray contributes on average to 20%. During air mass trajectories from Sahara, dust contribution increases to more than 60% and PM_{10} reach concentrations 10 times higher than the EC limit values and WHO guidelines.

This work was supported by the Portuguese Fundação para a Ciência e Tecnologia – FCT, under the project CVDust: Atmospheric Aerosol in Cape Verde Region: Seasonal Evaluation of Composition, Sources and Transport, PTDC/AAC-CLI/100331/2008. J. Cardoso and M. Almeida-Silva acknowledge the FCT PhD grants SFRH/BD/6105/2009 and SFRH/BD/69700/2010, respectively.

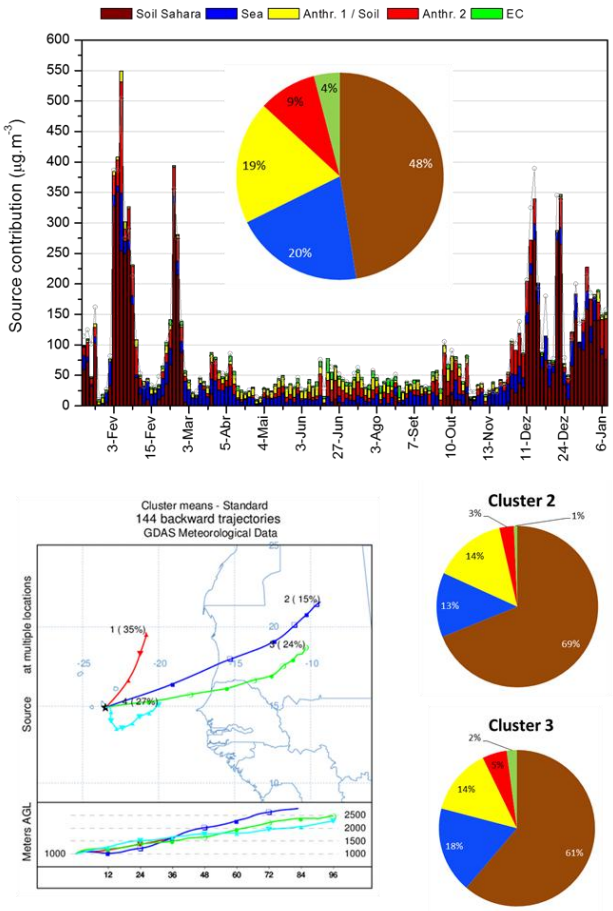

Figure 1. Source contribution for PM_{10} concentrations measured in Cape Verde during 2011. Cluster analysis applied to the backward trajectories and relative source contribution for trajectories coming from Sahara desert.

Goudie, A. (2009). Dust storms: recent developments. Journal of Environmental Management, 90, 89-94.

Goudie, A., & Middleton, N. (2006). Desert dust in the global system. Germany: Springler.

Prospero, J. (1996). Saharan dust transport over the north atlantic ocean and mediterranean: an overview. Kluwer Academic Publishers, The Netherlands. 133-151.

D'Almeida, G. (1986). A model for Saharan dust transport. Journal of Climate and Applied Meteorology, 25, 903-916.

Homologous series of organic compounds in aerosols impacted by sugar cane burning in São Paulo State, Brazil

R. C. Urban[1], C. A. Alves[2], A. A. Cardoso[3], A. G. Allen[3] and M. L. A. M. Campos[1]

[1]Department of Chemistry, University of São Paulo, Ribeirão Preto, SP, 14040-901, Brazil
[2]Centre for Environment and Marine Studies, Department of Environment, University of Aveiro, 3810-193 Aveiro, Portugal
[3]Institute of Chemistry, São Paulo State University, Araraquara, SP, 14800-900, Brazil
Keywords: TSP, sugar cane burning, organic speciation, homologous compounds.
Presenting author email: celia.alves@ua.pt

Sugar cane burning is carried out before manual harvesting to make the process easier and less labour-intensive. It takes place during the dry season, lasting from May to November. São Paulo State is the largest sugar cane producer in Brazil, accounting for 51% of the total production. The planted area in the State was 4.6 million hectares in 2010/2011 (IBGE, 2011). Around 40-50% of this area was burned before manual harvesting.

To evaluate the impact of sugar cane burning emissions on the atmospheric aerosol composition, samples of total suspended particles (TSP) were collected in two agricultural regions of São Paulo State (Araraquara and Ourinhos) using a high-volume sampler at a flow rate of 1140 L min^{-1}. Punches of the filters were solvent-extracted and fractionated into different classes of organic compounds by vacuum flash chromatography. The detailed organic speciation was performed by gas chromatography-mass spectrometry. Polar oxygenated compounds bearing carboxylic or hydroxyl groups were derivatised prior to injection into the chromatograph.

A series of *n*-alkanes were identified in the aerosol samples, ranging from C_{11} to C_{36}. The highest concentrations were observed for the C_{24}-C_{30} homologues. All the samples presented carbon preference indices (the ratio between odd and even carbon number homologues) around 1, which have been described as typical of petrogenic inputs (Alves, 2008). Vascular plants synthesise epicuticular waxes containing odd C number *n*-alkanes, usually in the C_{25} to C_{33} range with C_{29} or C_{31} as dominant homologues. The lack of odd C number predominance in this study could be due to the lesser amount of waxy hydrocarbons in the stems and leaves of the herbaceous biomass crops. The *n*-alkanes derived from plant waxes were calculated by subtraction of the average of the next higher and lower even carbon numbered homologues, taking as zero the negative values. Except for one sample (13/08/2010), in which 33% of the *n*-alkane content was attributable to plant waxes, the waxy fraction of aliphatics in the remaining samples ranged from 4.5 to 7%. The highest concentrations of *n*-alkanes were observed in samples more impacted by emissions from sugar cane burning at nighttime (Figure 1). These concentrations are much higher than those obtained in 24-h samples of PM_{10} in Piracicaba, a city in São Paulo State impacted by the same agricultural activities (Vasconcellos *et al*., 2010).

A discontinuous series of *n*-alkanols (C_{10}-C_{30}) was detected, peaking at C_{18}, C_{28} and C_{30}. Total concentrations ranged from 9.37 to 161 ng m^{-3}. The lowest level of *n*-alkanoic acids (9.66 ng m^{-3}) was obtained during the non-harvest period, while values up to 374 ng m^{-3} were reached in samples strongly impacted by smoke. In the aerosol samples of the harvest season, the homologous series encompassed acids from C_8 to C_{24} with a strong even carbon number predominance, currently associated with vegetative detritus. A series of *n*-di-acids, ranging from propanedioic to hexadecanedioic, were also present in TSP. Malic acid varied from undetectable levels for the non-harvest period to nearly 3300 ng m^{-3} during the dry season.

Taking into account the high concentrations observed for many of the homologous compounds, the exposure to these aerosols by inhalation or skin contact may be of concern due to the hazardous properties of some constituents (e.g. *n*-alkanes > C_{16}).

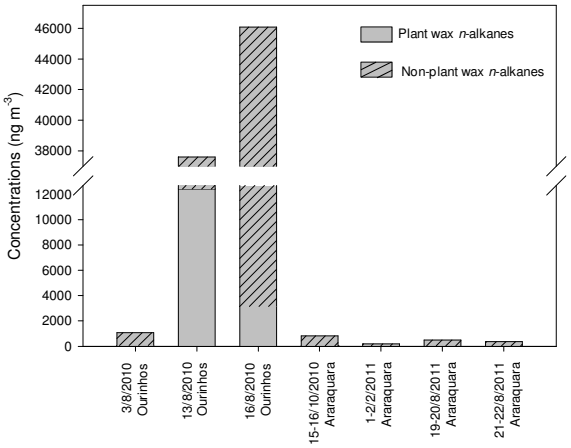

Figure 1. Concentrations of *n*-alkanes in samples from Ourinhos (nighttime samples) and Araraquara (24-h samples).

This work was supported by FAPESP (Processes 08/58073-5, 10/50236-2, and 2009/07415-6) and CNPq (Process 311668/2011-9).

Alves C. (2008) *An. Acad. Bras. Cienc*. **80**, 21-82.
IBGE (2011) Levantamento Sistemático da Produção Agrícola. Instituto Brasileiro de Geografia e Estatística (IBGE), Rio de Janeiro, December 2011.
Vasconcellos *et al.* (2010) *Sci. Tot. Environ*. **408**, 5836-5844.

Emissions of carbonaceous aerosols and volatile organic compounds by light-duty vehicles on a chassis dynamometer

C.A. Alves[1], A.I. Calvo[1], D. Lopes[1], D. Custódio[1], S. Rocha[1], T. Nunes[1], M. Evtyugina[1], A. Charron[2], M. Goriaux[2], P. Tassel[2] and P. Perret[2]

[1]Centre for Environment and Marine Studies, Department of Environment, University of Aveiro, 3810-193 Aveiro, Portugal
[2] French Institute of Science and Technology for Transport, Spatial Planning, Development and Networks (IFSTTAR) 25, Avenue François Mitterrand, Case 24, Cité des Mobilités, F-69675 Bron Cedex, France
Keywords: vehicle exhaust, dynamometer, OC, EC, VOC.
Presenting author email: celia.alves@ua.pt

While advances in engine technology have led to considerable improvements in emissions in recent years, particulate matter (PM) from motor vehicles, especially from diesel, continues to be a major source of urban aerosol pollution. PM has been identified as one of the priority mobile source air toxics. Motor exhaust also contains volatile organic compounds (VOCs) that have direct health implications and act as precursors to photochemical ozone formation.

In this study, a total of 8 light-duty diesel and gasoline vehicles representative of the Southern European fleet were tested on a chassis dynamometer. Sampling of vehicle exhausts was performed using two real-world driving cycles: the ARTEMIS Road (ArtRoad with cold and hot starts) and the ARTEMIS Urban (ArtUrb) (André *et al*., 2006). The organic and elemental carbon (OC and EC) content in the PM filters was determined by a thermal-optical transmission technique. VOCs sampled in sorbent tubes were analysed by a thermal desorption/cryogenic concentration method on a gas chromatograph equipped with a thermal desorption injector and a flame ionisation detector.

The particulate carbon emission factors were significantly lower under the ArtRoad compared to ArtUrb driving cycle with cold start. In general, hot start-up driving conditions produced the lowest emission factors (Fig. 1). A tendency to the decline of carbonaceous emissions from Euro 3 to Euro 5 diesel vehicles is observed, whereas this trend is not registered for petrol-powered cars. The fraction of TC composed of EC is much lower in particles emitted by petrol vehicles (< 10%) than by diesel engines (50-95%). However, the EC content in emissions from more modern vehicles equipped with DPF (diesel particulate filter) is almost negligible.

The measurement of unregulated pollutants comprised about 20 different VOCs in the C_5–C_{11} range. Among these, benzene, toluene and xylenes (BTX) were generally the dominant species. A significant decrease in emissions from Euro 4 to Euro 5 petrol-powered vehicles was observed (Table 1). The trend in VOC emissions is unclear when diesel engines are considered. During DPF regeneration cycles, emissions are several times larger than those during normal engine operation.

Taking into account the small number of vehicles per category, these results should be faced as indicative and complementary tests are strongly encouraged.

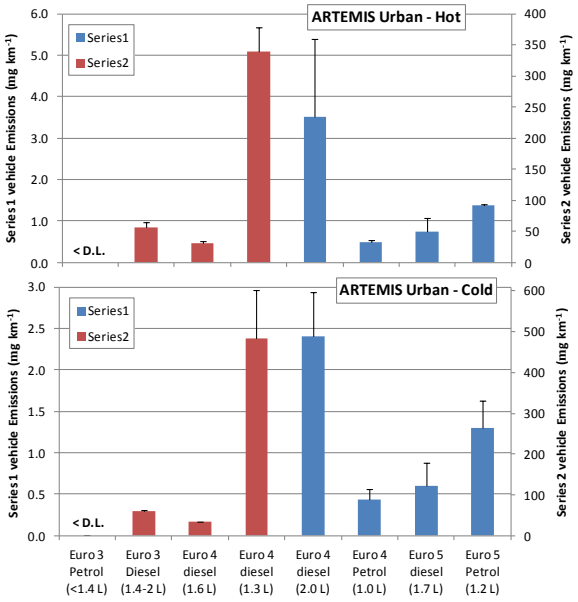

Figure 1. Total carbon (TC=OC+EC) emission factors (< D.L. means lower than detection limit)

Table 1. BTX emission factors (μg km^{-1}) for petrol-powered vehicles.

Compound	Vehicle	Art. Road	ArtUrb cold	ArtUrb hot
Benzene	Euro 4, 1.0 L	139	70.8	51.0
	Euro 5, 1.2 L	5.20	36.6	12.9
Toluene	Euro 4, 1.0 L	191	250	6.4
	Euro 5, 1.2 L	39.2	81.9	16.6
m,p-Xylene	Euro 4, 1.0 L	195	465	75.9
	Euro 5, 1.2 L	44.0	107	2.33
o-Xylene	Euro 4, 1.0 L	66.4	174	25.4
	Euro 5, 1.2 L	14.8	37.8	7.76

This work was funded by the Portuguese Science Foundation (FCT) through the project "Source apportionment of URBan Emissions of primary particulate matter", PTDC/AAC-AMB/117956/2010 (URBE). Ana Calvo acknowledges the postdoctoral grant SFRH/BPD/64810/2009 from FCT.

André, M., Joumard, R., Vidon, R., Tassel, P. and Perret, P. (2006) *Atmos. Environ*. **40**, 5944-5953.

Hydrocarbons in smoke samples from wildfire events in central Portugal in summer 2010

A.M. Vicente, C.A. Alves, S.D.G. Acioli, A.P. Fernandes, T. Nunes, A.C. Monteiro and C.A. Pio

Centre for Environmental and Marine Studies, Department of Environment, University of Aveiro, 3810-193 Aveiro, Portugal
Keywords: wildfires, $PM_{2.5}$, $PM_{2.5-10}$, hydrocarbons
Presenting author email: celia.alves@ua.pt

In summer 2010, smoke samples were collected from six wildfires occurring over central Portugal.

In order to collect sequentially, on pre-fired quartz fibre filters, coarse ($PM_{2.5-10}$) and fine ($PM_{2.5}$) smoke particles from the plumes, a tripod high volume sampler operating at a flow of 1.13 m^3 min^{-1} was used. Sampling was performed at 1.5 m above ground, downwind from the burning areas, at distances of 10-100 m from the fire fronts. The organic and elemental carbon content (OC and EC) of particulate matter was analysed by a thermal-optical transmission technique. The detailed speciation of organic compounds in smoke samples was carried out by gas chromatography-mass spectrometry (Alves *et al*., 2011).

The chromatographically resolved organics, object of this study, are *n*-alkanes, *n*-alkenes, polycyclic aromatic hydrocarbons (PAHs), carbonyl compounds and acid methyl esters.

The smoke particle concentrations were in the ranges 0.69-12 mg m^{-3} for $PM_{2.5}$ and 0.085-0.66 mg m^{-3} for $PM_{2.5-10}$. Fine particles represented 92±4.1% of the PM_{10} mass. On average, 47±13% of the $PM_{2.5}$ emissions consisted of organic carbon, whilst the OC mass fraction obtained for coarse particles was 27±13%.

Aliphatic compounds comprised the *n*-alkane homologous series from C_{10} to C_{34} without a clear odd-to-even carbon number predominance. The homologues with the highest concentrations (C_{max}) were C_{22}, for fine particles, and C_{29}, for coarse particles. The *n*-alkene homologous series ranged from C_{14} to C_{30}, with C_{max} at C_{20}, for both size fractions, showing an even-to-odd carbon number predominance. *n*-Alkenes derive mostly from the thermal dehydration of *n*-alkanols and, in smaller amounts, from the oxidation of *n*-alkanes during incomplete combustion (Oros and Simoneit, 2001). The *n*-alkane and *n*-alkene contents in the wildfire smoke particles were in the ranges 0.0022-1.2 mg g^{-1} OC and 0.0035-0.37 mg g^{-1} OC, respectively.

PAHs are formed as a result of incomplete combustion or thermal decomposition (pyrolysis) of the organic material. The OC-normalised concentrations of the dominant PAHs identified in coarse and fine smoke particles are presented in Figure 1. Retene was the dominant polyaromatic hydrocarbon found in both particle sizes. It is the fully aromatised thermal alteration product of the resin acids present in conifer woods (Ramdahl, 1983). Besides retene, fluoranthene and chrysene were the most abundant PAHs found in both size fractions. Benzo[a]anthacene, benzo[a]pyrene and benzo[e]pyrene, components with high mutagenic and genotoxic potential (Medeiros and Simoneit, 2008), were also identified in smoke samples. PAHs in biomass burning emissions are common to those emitted by other combustion sources. Diagnostic ratios are used as a tool for assessing the possible contribution of different sources (Alves, 2008). The ratios obtained in this study are listed in Table 1.

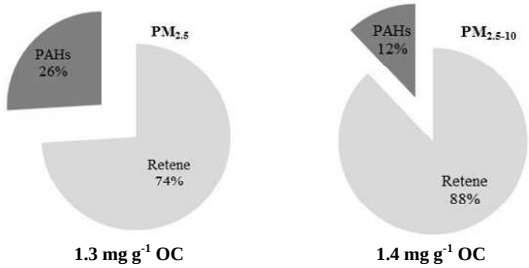

Figure 1.OC-normalised concentrations of PAHs detected in fine and coarse particles.

The dominant carbonyl compound in the wildfire aerosols was 6,10,14-trimethyl-2-pentadecanone. Alkanoates and vanillin were also found to be abundant in the majority of samples.

Table 1. PAH diagnostic ratios obtained in this study.

	$PM_{2.5}$	$PM_{2.5-10}$
Flu/(Flu+Pyr)	0.46-0.60	0.50-0.73
IcdP/(BghiP+IcdP)	0.74-0.84	0.75-0.82
BFs/BghiP	2.4-5.7	3.8-4.9
BeP/(BeP+BaP)	0.33-0.57	0.37-0.51
BghiP/BaP	0.29-0.66	0.41-0.63
Phe/(Phe+Ant)	0.47-0.80	0.53-1.0

Flu – Fluoranthene; Pyr – Pyrene; IcdP – Indeno[1,2,3-cd]pyrene; BghiP – Benzo[ghi]perylene; BFs – Benzofluoranthenes ; BeP – Benzo[e]pyrene; BaP – Benzo[a]pyrene; Phe – Phenanthrene; Ant – Anthracene

This work was supported by the Portuguese Science Foundation (FCT), through the project PTDC/AMB/65706/2006 (BIOEMI). Ana Vicente acknowledges the PhD grant SFRH/BD/48535/2008.

Alves, C. (2008) *An. Acad. Bras. Ciênc.* **80**, 21-82.
Alves *et al*. (2011) *Sci. Total Environ.* **409**, 1466-1475.
Medeiros, P., Simoneit, B. (2008) *Environ. Sci. Technol*. **42**, 8310-8316.
Oros, D.R., Simoneit, B.R.T., (2001) *Appl. Geochem.* **16**, 1545-1565.
Ramdahl, T. (1983) *Nature* **306**, 580-582.

Evaluation of CMA as dust suppressant in Barcelona: Preliminary results from the AIRUSE LIFE+ Project

F. Amato[1], A. Karanasiou[1], A. Alastuey[1], T. Moreno[1], F. Lucarelli[2], S. Nava[2], G. Calzolai[2], M. Chiari[2], M. Keuken[3] and X. Querol[1]

[1]Institute of Environmental Assessment and Water Research, Spanish Research Council (IDÆA-CSIC), c/Jordi Girona 18-26, 08034 Barcelona, Spain
[2]National Institute of Nuclear Physics (INFN) and Physics Department, University of Florence, via Sansone 1, 50019 Sesto Fiorentino, Italy
[3]TNO, Applied Research Organization, The Netherlands

Keywords: road dust, mitigation, resuspension, PM10.
Presenting author email: fulvio.amato@idaea.csic.es

Calcium-Magnesium Acetate (CMA) has been proposed as dust binder and its application on paved roads was recently tested in Sweden, Austria, Germany and UK in order to mitigate road dust emissions (Norman and Johansson, 2006; www.life-cma.at; www.tfl.gov.uk/corporate/projectsandschemes/17246.aspx). These previous studies showed that in most cases a reduction of kerbside PM10 concentrations was reached, even if short lived (few hours). The effectiveness of CMA in binding deposited particles seems to be closely related to the degree of road moisture (Gustafsson et al., 2010). This is a crucial aspect, mostly when evaluating the potential effectiveness in South European environments, where the higher solar radiation might further reduce the life-time of the air quality benefit.

In the framework of the LIFE+ AIRUSE project (www.airuse.eu), a measurement campaign will be carried out in April-May 2013 in the city of Barcelona (NE Spain), a typical Mediterranean city, spreading a 25% CMA aqueous solution (ICE & DUST-AWAY, Nordisk Aluminat) on a 1400 m stretch of a centric street (*Industria Av.*) counting typically 18000 vehicles/day. During the two months measurements the CMA solution will be spread 10 times during different mornings.

Given that the air quality benefit is expected to be short lived, CMA will be applied at 6 am local time, in order to exploit its effectiveness during the most-polluted hours due to traffic emissions (7-10 am).

Air pollutants will be monitored continuously at five monitoring sites:

- Two kerbside mobile laboratory vans installed at the kerbside of the road stretch treated with CMA;
- One control kerbside mobile laboratory van installed at the same road but on an untreated stretch, located 1 km away from the CMA stretch;
- One control kerbside mobile laboratory van installed at a parallel road (*Valencia Av.*) also untreated at a perpendicular distance of 650 m from *Industria Av.;*
- One control urban background monitoring station, located 5.5 km away from *Industria Av.*

Each monitoring site will be equipped with the following instrumentation:

- Optical counters (TSI Dust Track, TEOM and GRIMM);
- High volume samplers for PM10 (DIGITEL and MCV). PM10 samples will be chemical characterized for elemental composition (ICP-AES and ICP-MS), ECOC (thermo-optical analysis) and ions (HPLC and specific electrode for ammonium), following the procedure of Querol et al., (2001);
- Streaker low-volume samplers for hourly elemental composition of $PM_{2.5}$ and $PM_{2.5-10}$ by means of PIXE at two sites (Chiari et al., 2005);
- BC monitors (Mini-Aethalometers and Multi Angle Absorption Photometers);
- NOx, O_3 and SO_2 monitors;
- Meteo towers.

After the CMA treatment, conductivity tests will be carried out by means of the SOBO sensor (Boschung) to monitor the residual amount of CMA on the road surface. For traffic safety, friction tests will be also carried out following the UNE-EN 13036 protocol.

Results on air quality benefits will be shown.

This work is being funded by the AIRUSE LIFE+ ENV/ES/584 project. Authors would like to acknowledge the City hall of Barcelona (E. Aulí and R. Alsina, *Serveis d'Intervenció i Innovació Mediambiental)* the instrumental support provided by Springer KommunalTechnik and Provincial Capital Klagenfurt on Lake Wörth, Department for Environmental Protection, Austria

Chiari, M., Lucarelli, F., Mazzei, F., Nava S., Paperetti, L., Prati, P., Valli, G., Vecchi, R. (2005). *X-Ray Spectrom.* **34**(4), 323–9.

Gustafsson M. (2010). *CMA+ Congress. 30th September 2010, Lienz, Austria*

Norman, M., Johansson, C. (2006). *Atmos. Environ.* **40**, 6154–64.

Querol, X.., Alastuey, A., Rodríguez, S., Plana, F., Mantilla, E., Ruiz, C.R. (2001). *Atmos. Environ.* **35**, 845–58

Temporal variation of urban atmospheric aerosol during smog episodes in Debrecen, Hungary

A.Angyal[1], Zs. Kertész[1], Z. Ferenczi[2], E. Furu[13], Z. Szoboszlai[1], Zs. Török[13] and Z. Szikszai[1]

[1]Laboratory of Ion Beam Applications, Institute for Nuclear Research, Hungarian Academy (MTA ATOMKI), H-4026, Debrecen, , P. O. Box 51, Hungary
[2] Hungarian Meteorological Service, H-1675 Budapest, P. O. Box 39, Hungary
[3]University of Debrecen, H-4032 Debrecen, Egyetem tér 1, Hungary
Keywords: smog, source, PBL, PMF.
email: angyal.aniko@atomki.mta.hu

One of the leading environmental problems is the atmospheric particle matter (APM) in densely populated urban. High pollution levels regularly occur in most cities all around the world. Debrecen, the second largest city in Hungary and the regional centre of the Northern Great Plain region is no exception. There are several days every year when the particle matter concentration level exceeds the alarm threshold value (100 μg/m^3 for PM_{10} in 24- hours average). It is called "smog" by the authorities when the increased pollution level remains over the limit value for days.

The aim of this work was to study the variation of elemental components and sources of PM_{10}, $PM_{2.5}$ and $PM_{2.5-10}$ as well as their dependence on meteorological conditions during two smog episodes occurred in November 2011.

Aerosol samples were collected with two-stage PIXE International sequential streaker to study the hourly evolution of atmospheric aerosol concentration. Furthermore, 9-stage cascade impactors were also applied to get information about the size distribution of the elemental components.

Particle Induced X-ray Emission (PIXE) at IBA Laboratory (MTA Atomki) was employed to determine the elemental composition ($Z \geq 13$). Concentrations of black carbon were evaluated by smoke stain reflectometer. Weather prediction model (WRF) was applied to determine the planetary boundary layer (PBL) height values. Source apportionment was carried out on obtained data using the positive matrix factorisation (PMF) method.

The result of the elemental mass size distributions indicates that the elements can be classified into three groups. The first group comprising of minerals is with a dominant peak at the 8-16 μm range. The second group composed of K, Cl, S and Zn. One prevalent peak can be found in the droplet mode (0.5-1 μm) and another lower peak at 4-8 μm. High temperature processes such as combustion processes, particularly woody biomass burning release these elements. The third group contains Br and Pb. The low concentration of these elements seems to be considerable in droplet mode (0.5-1 μm) too, implying that these particles (comprising Br, Pb) used to have a major common source in gasoline.

The time pattern of the aerosol elemental components and PM sources exhibited strong dependence on the planetary boundary layer thickness. The concentration of some elements (K, Cl, BC) showed inverse tendency compared to PBL in the fine fraction in the first week (2-8 November 2011). This result is represented in Figure 1.

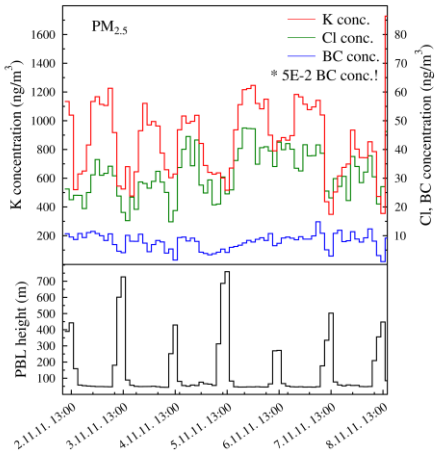

Figure 1. Temporal variation of the concentrations of the elements (K, Cl, BC) and the planetary boundary layer from the 2nd till 8th of November

Traffic derived elements (Fe, Cu, Zn, Pb) and elements from combustion processes (K, Cl, BC) showed also negative correlations with the PBL in the second week (15-21 November 2011).

PMF modelling determined four factors in both size fractions. The sources were identified as soil, biomass burning, traffic and oil combustion in case of fine fraction. Soil with soil improvement agent, two biomass burning, and road dust were recognised in $PM_{2.5-10}$. Due to above mentioned reasons, biomass burning as domestic heating was the main contributor to formation of smog and the meteorological condition was responsible for the accumulation of combustion aerosols during nights when the planetary boundary layer was the lowest.

Acknowledgement

This work was carried out in the frame of the János Bolyai Research Scolarship ogf the Hungarian Academy of Sciences and TÁMOP-4.2.2/B-10/1-2010-0024 project.

Aerosol profile retrieval algorithm development and validation for Sentinel-4

Arnoud Apituley[1], Ofelia Vieitez[1], Bram Sanders[1], Piet Stammes[1], Ben Veihelmann[2], Yasjka Meijer[2], Rob Koopman[2]

[1]Royal Netherlands Meteorological Institute (KNMI), De Bilt, The Netherlands
[2]ESA-ESTEC, Noordwijk, The Netherlands
Keywords: aerosol layer height, oxygen A-band, validation, Sentinel-4, GOSAT, lidar
Presenting author email: apituley@knmi.nl

In the ESA AEROPRO project we develop and validate an oxygen A-band aerosol profile retrieval concept for ESA's Sentinel-4 mission.

Sentinel-4

Sentinel-4 is an ESA mission (Ingmann, 2012) that is part of of the Global Monitoring for Environment and Security (GMES) space component. The primary mission objective is the observation of the diurnal cycle of the tropospheric composition in support of the operational air quality applications of the GMES Atmosphere Services. The Sentinel-4 instrument is an Ultra-violet Visible Near infrared spectrometer (S4/UVN) which is embarked on the geostationary Meteosat Third Generation-Sounder (MTG-S) platforms. Key features of the S4/UVN instrument are the spectral range from 305 nm to 500 nm with a spectral resolution of 0.5 nm, and from 750 nm to 775 nm with a spectral resolution of 0.12 nm. The instrument shall observe Europe with a revisit time of one hour. The spatial sampling distance varies across the geographic coverage area and takes a value of 8 km at a reference location at 45° N. The expected launch date of the first MTG-S platform is 2019, and the expected lifetime is 15 years (two S4/UVN instruments in sequence on two MTG-S platforms).

Aerosol Layer Height Retrieval

In the AEROPRO project measured oxygen A-band spectra (758–778 nm) from the Japanese GOSAT Fourier Transform Spectrometer (Kuze, 2009) are being used as proxy for the Sentinel-4 data. The spectral resolution of GOSAT is downgraded to 0.12 nm, which is the Sentinel-4 resolution. This also helps to improve the Signal-to-Noise ratio of GOSAT data. The AEROPRO O_2 A-band algorithm, with heritage from the Sentinel-5P/Tropomi (Veefkind, 2012) algorithm (Sanders, 2012), is based on optimal estimation and a forward model with full multiple scattering, using a simple aerosol microphysics model. The basic set of fit parameters comprises aerosol optical thickness, aerosol layer pressure and surface albedo. For vegetated land, we also fit fluorescence emission. Sensitivity studies show that aerosol cases for which the algorithm will be specifically suited include elevated, optically thick aerosols, such as volcanic ash plumes, desert dust and biomass burning aerosols. The retrieval is independent of the aerosol microphysics assumption.

Validation Approach

Since the altitude of aerosols is difficult to determine from space using passive sensors, validation of the AEROPRO algorithm is essential. During the ESA CarbonExp aircraft campaign, which took place over Greece and Turkey in August-September 2011, a GOSAT special pointed observation request was executed. This campaign offered a unique opportunity to validate the O_2 A-band aerosol profile retrievals from GOSAT, since the aircraft's actively sensed lidar data give the vertical structure of the atmosphere in an unambiguous way. Additional ground-based lidar data from the European Aerosol Research Lidar Network (Earlinet) and the Micropulse Lidar network (MPLnet) are used to validate the aerosol height retrievals from GOSAT for selected cases of strong aerosol events in between July 2010 and June 2012.

First results from the AEROPRO study will be shown.

Acknowledgement
This work was supported by the ESA project AO/1-7017/11/NL/MP.

References

P. Ingmann, et al., Requirements for the GMES atmosphere service and ESA's implementation concept: Sentinels-4/-5 and -5p. *Rem. Sens. Env.*, 120(0):58–69, 2012.

A. Kuze, at al., Thermal and near infrared sensor for carbon observation Fourier-transform spectrometer on the greenhouse gases observing satellite for greenhouse gases monitoring. *Appl. Opt.*, 48(35):6716–6733, 2009.

J. Veefkind, et al., Tropomi on the esa Sentinel-5 precursor: A GMES mission for global observations of the atmospheric composition for climate, air quality and ozone layer applications. *Rem. Sens. Env.*, 120(0):70–83, 2012.

A. F. J. Sanders, et al., Retrieval of aerosol height from the oxygen A-band with Tropomi. In F. Marzano, V. Rizi, P. DiGirolamo, and N. Cimini, editors, Proceedings of the 9th International Symposium on Tropospheric Profiling, ISBN/EAN: 978-90-815839-4-7, 2012.

Abstract preparation for EAC2013

A.J.M.Komkoua.[1] and C. Tchawoua[1]

[1]Department of Physics , University of Yaounde I, Yaounde, 812, Cameroon

Keywords: Aerosols, RegCM4, Central Africa.
Presenting author email: kombiend@yahoo.fr

The direct and inderect effects of aerosols lead the reductions in the amount of solar radiation reaching Earth's surface, thus causing a nagative radiative forcing . Atmospheric aerosols are still considered one of the main sources of uncertainty in the climate change (IPCC 2007). To study the climate feedback of aerosols, it is necessary to couple climate and aerosol models. However, the relatively short lifetime of aerosols, in the order of a few days and their inhomogeneity indicates the importance of regional scales when studying aerosol effects.

Our work investigated the effect of aerosols on the surface temperatures over Centra Africa based on simulation performed by the regional climate model RegCM4.

Subgrid variability of CCN sized aerosol

A. Asmi[1], R. Väänänen[1] and R. Kredji[1,2], A. Minikin[3], and airborne aerosol data providers

[1]Department of Physics, University of Helsinki, FI-00014, Finland
[2] Department of Applied Environmental Science (ITM), Stockholm University, S-10691, Sweden
[3] Institute of Atmospheric Physics, German Aerospace Center (DLR), 82234 Oberpfaffenhofen-Wessling, Germany
Keywords: CCN, Subgrid variability, Aircraft measurements, Spatio-temporal variability
Presenting author email: ari.asmi@helsinki.fi

General Circulation Models (GCMs) are the key method to figure out the impacts of atmospheric aerosol to climate system. Unfortunately, the computational limitations require such models to use relatively large grid sizes, typically of kilometres. Many clouds are much smaller than this, and such parameterizations are already used to approach the subgrid scale cloud formation for e.g. convective clouds (see e.g. Lohmann et al, 2007). However, the subgrid scale variation of cloud condensation nuclei (CCN) sized aerosol is far less studied.

We approach this issue by analysing the spatial variability of CCN sized aerosol from several aircraft campaigns around the world, mainly from EUCAARI LONGREX, ATAR, INCA, INDOEX, CLAIRE and several national aircraft campaigns in Finland. The aim is to find out the typical distribution shapes and usable mean parameters to describe such distributions. These values could then be used to parameterize such variability in GCMs, or at least diagnose potential variability in the results from this variation.

Analysing the aerosol measurements in the aircraft data shows a clear lognormal distribution of values, although with variable and location dependent modal parameters. The shape of the distribution is maintained in smaller scales (representing finer resolution models), but naturally with smaller geometric standard deviations as the variability is reduced. Figure 1 shows an example of gained coefficients of variation calculated from EUCAARI Falcon OPC datasets during 2008 LONGREX experiments (Hamburger et al., 2012).

The modelled grid box concentration is often assumed to be arithmetic mean value of the concentrations within the grid-box. Using such mean value (if correctly modelled, of course) could then significantly vary from the true number concentration of CCN sized particles on the most cases where the cloud activation would happen in the grid box. Thus, there might be a bias in aerosol-cloud interactions in GCMs and Chemical Transport Models (CTMs) related to the representation of aerosol number concentration spatial variability.

We will also evaluate the possibility to include Eulerian (fixed station) measurements to approximate spatial variability. This approach, if found feasible, will increase the temporal coverage significantly from individual aircraft campaigns to decades.

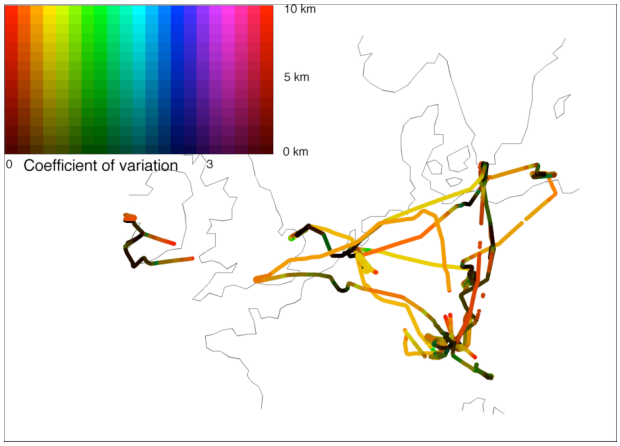

Figure 1. Example of spatial scale dependent differences around Europe, based on EUCAARI DLR Falcon measurements. Plotted is the coefficient of variation (CV=STD(x)/MEAN(x)) of the OPC aerosol concentrations (approx.. 250 nm to 1.1 µm), corrected to STP conditions, from 100 km spatial and 1 km vertical distance from each measurement point. The hue gives CV values, and the colour brightness is related to altitude. Only cloud-free data is shown.

This work was supported by the ATM Finnish National Centre of Excellence program. The measurements presented are from EUCAARI LONGREX campaigns, part of FP6 project EUCAARI.

Hamburger, T., McMeeking, G., Minikin, A., Petzold, A., Coe, H., and Krejci, R. (2012) *Atmos. Chem. Phys*., **12**, 11533-11554

Lohmann, U., Stier, P., Hoose, C., Ferrachat, S., Kloster, S., Roeckner, E., and Zhang, J. (2007) *Atmos. Chem. Phys*., **7**, 3425-3446

Multi-criteria ranking and source apportionment of airborne particles

Godwin A. Ayoko[1*] and Adrian J. Friend[1]

[1]*International Laboratory for Air Quality and Health, School of Chemistry, Physics and Mechanical Engineering, Science and Engineering Faculty, Queensland University of Technology, Brisbane QLD 4001, Australia*

Keywords : airborne particles, multicriteria ranking, source apportionment.

Presenting author email: g.ayoko@qu.edu.au

Source apportionment studies have become very widespread since the availability of EPA PMF. Some of the drivers for such studies include the desire for (a) source identification and (b) quantification of the contribution of each of the identified sources to the pollution level at a receptor site. In addition to the information on source profile and source contribution obtained from receptor modeling such PMF analyses, the results can be coupled with meteorological data, in order to estimate the location of each of the sources resolved by the receptor model.

Based on the above outcomes, it may be necessary to devise source control strategies and where there are multiple sites, the next logical step is to work out which of the affected sites should be addressed first. Fortunately, formal procedures for multi-criteria decision-making are available (e.g. Massart *et al* 1997). One of these multi-criteria decision making methods, the Preference Ranking Organization METHods for Enrichment Evaluation (PROMETHEE) and Graphical Analysis for Interactive Assistance (GAIA) PROMETHEE was originally developed to aid the selection of the best location for factories (Brans & Mareschall, 1989) but it is finding increasing application in air quality research. PROMETHEE is an outranking method that ranks alternatives on the basis of a set of criteria. GAIA (Graphical Analysis for Interactive Assistance), on the other hand, is a visual display tool.

This paper reports the application of multicriteria decision making techniques, PROMETHEE and GAIA, and receptor models (such as Principal Component Analysis/ Absolute Principal Component Scores (PCA/APCS) and Positive Matrix Factorization (PMF) to data air quality data collected at various locations. The data consisted of the concentrations of elemental species, gaseous species or particle number concentration and meteorological data.

Each factor obtained by PCA/APCS and PMF had distinctive compositions that suggested that motor vehicle emissions, controlled burning of forests, secondary sulfate, sea salt, and road dust/soil were the most important sources of fine particulate matter in the sites. The most plausible locations of the sources were identified by combining the results obtained from the receptor models with meteorological data.

Then the air quality data were further analysed with PROMETHEE to facilitate multi-criteria ranking and the choice of the least and the most polluted sites based on several air quality indicators. This procedure compared all objects (e.g. sites or years that sampling was conducted) based on the values of the variables (e.g. chemical species, particle number concentrations), and ranks the objects (e.g. sites) from the least to the most polluted (Ayoko et al., 2004; Friend and Ayoko, 2009).

The overall results provided insights which can aid the prioritization mitigation measures not only for outdoor (Friend and Ayoko, 2009, Friend et al, 2011a, Friend et al, 2011b) but also indoor (Ayoko et al, 2004) microenvironments. In addition, the studies demonstrated the potential benefits of combining results from multi-criteria decision making analyses with those from receptor models to enhance the development of air pollution control measures.

Ayoko G.A., Morawska L., Kokot S., Gilbert D. (2004) *Environ Sci Technol*. 38,2609-16.

Brans J.P. and Mareschall B. 1989, *PROMETHEE-GAIA visual interaction modeling for mulitcriteria location problems*, Internal Report, University of Brussels, STOOTW/244.

Friend, A.J., Ayoko, G.A., Guo, H., (2011a) *Sci. Total Environ.*, 409, 719-737.

Friend, A.J. Ayoko, G.A. (2009) *Environ. Chem*., 6, 398-406.

Friend, A.J., Ayoko, G.A., Elbagir, S.G., (2011b), *Environ. Chem*., 8, 163-173.

Massart D. L., Vandegisnte B.G.M., Buydens L.M.C., de Jong S., Lewi P.J., Smeyers-verbeke J (1997), in Handbook of Chemometrics and Qualimetrics: Part A : Data handling in science and technology, Vandegisnte B.G.M and Rutan S.C. (eds), Elsevier, Amsterdam, 20A : 771-804.

A study of aerosol production at the cloud edge with direct numerical simulations

N. Babkovskaia[1], M. Boy[1], S. Smolander[1], S. Romakkaniemi[2], M. Kulmala[1]

[1]Department of Physics, University of Helsinki, PO Box 48, Erik Palmenin aukio, 1, 00014, Finland
[2]Department of Applied Physics, University of Eastern Finland, P.O. Box 1627, 70211 Kuopio, Finland
Keywords: DNS, aerosol particles, clouds.
Presenting author email: NBabkovskaia@gmail.com

Introduction

Aerosol clouds are dynamic systems with spatially and temporally varying properties. More cloud droplets may form due to in-cloud activation or due to entrainment of air from cloud edges that might lead to formation of fresh cloud droplets. On the other hand, cloud droplets may be evaporated because of mixing at cloud boundaries or in-cloud dynamics causing part of droplets to evaporate. The latter of these can be important in stratus type clouds with long in-cloud residence time of air parcel. The mixing at cloud boundaries takes place in all clouds, and the type of mixing is dependent on the conditions and mixing time scales.

Methods

To study the structure of the cloud edge area we use the direct numerical simulation (DNS) high-order public domain finite-difference PENCIL Code for compressible hydrodynamic flows. The PENCIL Code is a powerful tool for studying the aerosol dynamics in a turbulent medium with complicated chemical composition (PENCIL Code, 2001; Babkovskaia et al., 2011). The scientific goals for the construction of the new model are to investigate the spatial distribution of aerosol particles, turbulent mixing of clouds with the environment and the influence of turbulence on aerosol dynamics (and vice versa).

Results

We study the activation process at the cloud edge. We consider the flux of aerosol particles, which goes through the boundary between the dry and wet air. For a test purpose we start from a zero-dimentional problem. Following by Andrejczuk et al. (2004), we take into account the condensation and evaporation of the aerosol particles covered by liquid water. Next, we consider a one dimensional problem to study a motion and evolution of the front between the dry and wet air. This approach allows us to analyze the effect of the fluid mechanics on the aerosol dynamics (and vice versa) in a laminar regime. Finally, we make two- and three-dimentional simulation with a more complicated velocity field at the cloud edge. We assume that the dry air flux is coming into the computational domain in its middle part and coming out near its boundaries. Wet air is moving in horizontal direction with velocity $U_x = 50 - 100$ cm/s. The third velocity component initially equals to zero, $U_z = 0$ cm/s. We study the effect of air mixing, comparing the results of simulation with zero, $U_{in} = 0$ cm/s, and non-zero, $U_{in} = 20$ cm/s, inlet velocity. We find that for $U_{in} = 0$ cm/s (no mixing) the most efficient growing of particles due to condensation occurs inside the front. In a case of $U_{in} = 20$ cm/s the intensive mixing of air results to evaporation and increasing of the supersaturation in the front area. Additionally, comparing the results of simulation for such two cases (with $U_{in} = 0$ cm/s and $U_{in} = 20$ cm/s) we conclude that the air mixing leads to increase of the number of activated particles (with the size larger than 5 μm). It happens because of extending of the front area where the most efficient growing of particles occurs. Also, we compare the results of 2D and 3D simulations and of the 3D simulations with different grid sizes and analyze how such approaches are valid for the correct description of aerosol production at the cloud edge.

We thank the Helsinki University Centre for Environment (HENVI), the Academy of Finland (251427, 139656) and computational resources from CSC – IT Center for Science Ltd are all gratefully acknowledged. This work was supported by the Magnus Ehrnrooth Foundation.

Andrejczuk, M., Grabowski, W., Malinowski, S., Smolarkiewicz, P. (2004). *J. of Atmospheric Sciences*, **61**, 1726-1739.

Babkovskaia, N., Haugen, N., Brandenburg, (2011). *J. of Computational Physics*, **230**, 1-12.

The PENCIL Code, http://pencilcode.googlecode.com, (2001).

The effect of cloudiness on new particle formation: investigation of radiation levels

E. Baranizadeh[1], A. Arola[2], A. Hamed[1], T. Nieminen[3], A. Virtanen[1], M. Kulmala[3] and A. Laaksonen[1,4]

[1]Department of Applied Physics, University of Eastern Finland, Kuopio, Finland
[2]Finnish Meteorological Institute, Kuopio Unit, Kuopio, Finland
[3]Department of Physics, University of Helsinki, Helsinki, Finland
[4]Finnish Meteorological Institute, Climate Change Unit, Helsinki, Finland

Keywords: Nucleation, New particle formation, Solar radiation.
Presenting author email: elham.baranizadeh@uef.fi

The importance of solar radiation as a driver of new particle formation has been firmly confirmed in the literature. Boy and Kulmala (2002) showed that appearance of clouds during new particle formation (NPF) events in May 1999 did sometimes stop the nucleation. However, seasonal cloud effects on NPF events have not been systematically investigated. In this research, we look into this question by analysis of the ratio Half-hourly measured global-radiation (I) divided by calculated half-hourly clear-sky global radiation (I_{max}) during NPF events recorded at Hyytiälä station in 2008-2011. The time during which the ratio I/I_{max} was analyzed (hereafter the time range) for each NPF event corresponded to the period of appearance of newly formed 3nm particles. The time range was defined visually from the so called banana. The global radiation (I) data are actual measurement data downloaded from SMEAR II station and I_{max} data are modelled data downloaded from AERONET website (http://aeronet.gsfc.nasa.gov/).

We classified the event days as "quantifiable" and a "Non-quantifiable" according the criterion introduced by Dal Maso *et al* (2005) which is whether the event is homogeneous enough to quantify the basic characteristics such as formation rate and growth rate or not. The half-hourly ratio of I/I_{max} on event days versus hour of day has been plotted for four seasons winter (Dec-Jan-Feb), spring (Mar-Apr-May), summer (Jun-Jul-Aug), see Fig. 1, and autumn (Sep-Oct-Nov). The results show that in the winter, the NPF events only start when I/I_{max} have high values (> 0.65). Also, in the three other seasons the radiation level is mostly high at the start time of the NPF events.

Table 1. Frequency (%) of ratio (I/I_{max}) values in the given ranges, at start time of event days

Season	[0-0.5] Quant	[0.5-1] Quant	[0-0.5] Non-Quant	[0.5-1] Non-Quant
Winter	0	100	0	100
Spring	11.11	88.9	5.26	94.8
Summer	0	100	8	92
Autumn	20	80	25	75

Table 1 shows that in the summer, all quantifiable events and 94.8% of non-quantifiable events happen when I/I_{max} > 0.5. The frequency of quantifiable events in the range [0-0.5] is 11.11% and 20 % in spring and autumn, respectively. This means there is a possibility that NPF events occur also at cloudy conditions in spring and autumn (note, however, that the amount of data is limited so that we cannot exclude the possibility of NPF in cloudy conditions also in winter and summer).

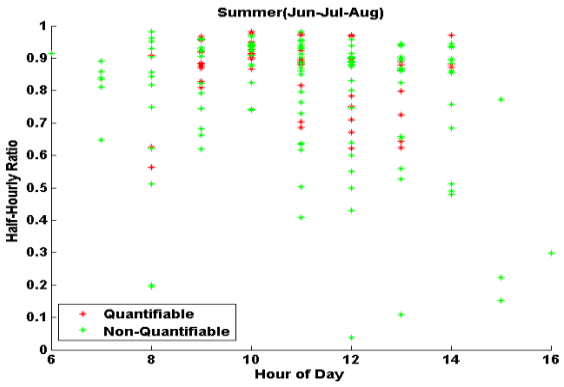

Figure 1. Half-hourly ratio (I/I_{max}) during the time range during 2008-2011at Hyytiälä .

In future work we will extend the study to longer periods and other stations beside Hyytiälä. We will also investigate the relations between I/I_{max} and particle formation and growth rates.

Boy, M. and Kulmala, M.: *Nucleation events in the continental boundary layer: Influence of physical and meteorological parameters* (2002), Atmos. Chem. Phys., 2, 1-16.

Dal Maso, M. , Kulmala, M. , Riipinen, I. , Wagner, R. , Hussein, T. , Aalto, P. P. & Lehtinen, K. E. J. 2005: *Formation and growth of fresh atmospheric aerosols: eight years of aerosol size distribution data from SMEAR II, Hyytiälä, Finland*, Boreal Environment Research. 10, 5, p. 323-336. 14 p.

This work was funded by Cryosphere-Atmosphere Interactions in a Changing Arctic Climate project (CRAICC).

Influence of Mineral Dust Transport from North Africa in the Concentration and Size Distribution of Aerosol in León (Spain)

E. Alonso-Blanco[1], A.I. Calvo[2], A. Castro[3], C. Alves[2] and R. Fraile[3]

[1]Centre for Energy, Technological and Environmental Research (CIEMAT), Madrid, Spain
[2]Centre for Environmental and Marine Studies (CESAM), University of Aveiro, Portugal, 3810-193
[3]Department of Physics, IMARENAB, University of Léon, Spain

Keywords: Aerosol Size Distribution, Mineral Dust, PCASP-X
Presenting author email: acasi@unileon.es

During the summer months, the Iberian Peninsula is exposed to intrusions of mineral dust from North Africa. These intrusions lead to an alteration in the atmospheric particulate content, contributing to coarse sized particles mainly composed of minerals. Mineral dust makes the highest contribution to atmospheric particulate material at global level (IPCC, 2001), which means that characterising its properties is essential to understand its repercussions on the climate.

This study presents a series of particle measurements made in the city of Léon, in north western Spain, on the 28th and 29th of June 2012, during the final stage of an event involving the arrival of Saharan dust into the Iberian Peninsula.

In order to characterise the atmospheric particle content, a laser spectrometer (Passive Cavity Aerosol Spectrometer Probe, PMS Model PCASP-X) was set up in the north east of the city. This device makes it possible to measure discrete particle sizes ranging between 0.1 and 10 μm in 31 channels. During the study period, measurements were taken at 15-minute intervals each hour. As environmental particles present a different refractive index to that used for PCASP-X calibration (latex particles: 1.59 -0 i), raw size bins were corrected using a program based on Mie Theory. Different refractive indices were used: i) $1.59 - 9\times10^{-3}$ i for measurements affected by mineral dust intrusions (Kandler *et al*., 2007) and ii) $1.574 - 9.13\times10^{-2}$ i for urban aerosol measurements not affected by dust intrusions and considering the relative humidity (Kim and Boatman, 1990).

The meteorological data used in this study were obtained from a weather station located next to the probe, which allowed us to gather one-minute measurements of the pressure, temperature, humidity, precipitation and wind speed and direction.

The PM_{10} measurements recorded at the three air quality stations in the city of Léon were also taken into account.

This study examined the incidence of the mineral dust on the number of particles and their size distributions in the city of León, and the influence of meteorological variables in recovering the atmospheric particle content. An analysis was also made of the implications of this intrusion of Saharan dust on the legal air quality controls in relation to PM_{10} concentrations.

On the 24th of June 2013, the first mass of Saharan dust of the summer entered the Iberian Peninsula from the south west, remaining until the 29th of June 2012. From the 27th of June onwards, this intrusion began to affect the atmospheric particle content of the city of Léon. The highest particle concentrations were recorded on the 28th, with an average daily value of 535 ± 220 particles cm^{-3}. From the aerosol size distributions, it was observed that these particles corresponded to sizes in excess of 0.3 μm. This increase corresponds to the largest fraction of fine mode and coarse mode.

The recovery of the local particulate content was conditioned by the wind speed and direction recorded on the 28th. Between 1759 UTC and 1800 UTC, predominant winds from the WSW and W were recorded, with an average speed of 3.9 ± 0.1 m s^{-1}. These winds blew the mineral dust towards the city, as a result of which the average number of particles for this time interval was very high: 790 ± 210 particles cm^{-3}. However, between 1800 UTC and 2300 UTC, the average wind speed was 2.6 ± 1.1 m s^{-1} from the WSW, allowing clean air to enter and facilitating the recovery of the local particulate content. During this time interval, an average number of particles of 420 ± 80 particles cm^{-3} was recorded.

On the 29th of June, the local particulate content was fully recovered. During this day, the average number of particles recorded was 320 ± 80 particles cm^{-3}.

The arrival of this intrusion of Saharan dust in the city affected the legal controls of air quality. On the 28th of June it exceeded the daily PM_{10} limit (defined in Royal Decree 102/2011 as 50 μg m^{-3}) in the three air quality stations of León City Council, with values of 122, 155 and 139 μg m^{-3}. On the 29th of June this value did not exceed 20 μg m^{-3} in any of the air quality stations, which confirms the recovery that was observed in the numeric concentration of particles.

This work was supported by the Spanish Ministry of Science and Innovation (Grant TEC2010-19241-C02-01). Elisabeth Alonso and Ana I. Calvo acknowledge the pre-doctoral (CGL2010-1777 from the Spanish Ministry Science and Innovation) and posdoc (SFRH/BPD/64810/ 2009 from FCT) grants, respectively.

IPCC (2001). *Climate Change 2001: The Scientific Basis*. Cambridge University Press.

Kandler, K., Benker, N., Bundke, U., Cuevas, E., Ebert, M., Knippertz, P., Rodríguez, S., Schüz, L. and Weinbruch, S. (2007). *Atmos. Environ.* **41**, 8058-8074.

Kim, Y.J. and Boatman, J.F. (1990). *Aerosol Sci. Technol*. **12**, 665-672.

UFIREG – Ultrafine particles and health

S. Bastian[1], G. Löschau[1], J. Cyrys [2], J. Novak[3], M. Gobec[4] and, B. Mykhalchuk[5]

[1]Saxon State Office for Environment, Agriculture and Geology, Dresden, Saxony, 01309, Germany
[2]Helmholtz Zentrum München, German Research Center for Environmental Health, Neuherberg, 86754, Germany
[3]Czech Hydrometeorological Institute, Prague, 14306, Czech Republic
[4]Institute for Public Health Celje, Celje, 3000, Slovenia
[5]Medved's Institute of Ecohygiene and Toxicology, Chernivtsi, 58022, Ukraine
Keywords: ambient particle number concentrations, air quality, health effects
Presenting author email: susanne.bastian@smul.sachsen.de

Information on health impacts of ultrafine particles (UFP) is still limited. Only few studies have been conducted so far. Therefore, the aim of the UFIREG-project which started in July 2011 is to investigate short-term effects of different size classes of (ultra)fine particles on mortality and morbidity, especially on cardiovascular and respiratory diseases. Further objectives of UFIREG are the preparation of a cost-efficient UFP measurement strategy applicable in European cities, analyzing temporal and spatial variation of UFP among the cities and raising the overall awareness of the population as well as environmental and public health authorities.

UFP measurements within UFIREG are performed using Differential or Scanning Mobility Particle Sizer (DMPS/SMPS) in five cities: Dresden, Augsburg, Prague, Ljubljana, and Chernivtsi. In addition, two Ultrafine Particle Monitors, recently developed within the former EU project UFIPOLNET, are operated in Prague and Augsburg. Most of the measurement stations are integrated in local air quality monitoring networks and are located at urban background sites. At these sites, other air pollution parameters such as PM_{10}, $PM_{2.5}$, NO_x, SO_2, O_3, and partially black carbon as well as meteorological parameters are determined. On the basis of the measured air quality data, epidemiological studies will be carried out in all participating cities.

An extensive quality assurance program is an essential part of UFIREG aiming at a high and comparable data quality. It comprises staff training, an initial intercomparison of all SMPS used in UFIREG, frequent on-site comparisons against reference instruments and automatic control units at two sites. During the initial intercomparison and the on-site comparisons which have been carried out so far, none of the SMPS deviated more than 20 % against the reference instrument in the size range from 20 to 200 nm.

Preliminary results of the year 2012 indicate no large differences between annual averages of particle number concentrations (PNC) in a size range from 20 to 200 nm at all stations (except Chernivtsi). The annual means ranged between 6.000 and 6.500 particles per cm³. However, more pronounced differences were observed for monthly averages. First measurements in Chernivtsi where the SMPS could be installed only in January 2013 showed a greater fraction of particles larger than 100 nm in comparison to the other cities.

As shown in Table 1 for Dresden and Ljubljana the coefficients of determination between PNC and other air pollutants varied between different sites. For Dresden the highest R^2 was observed for PNC (20-200 nm) and NO_2 during the colder months (Nov to Apr, Fig.1).

Table 1. Coefficients for determination (R^2) for linear regression (y=ax+b) for Dresden and Ljubljana, April to December 2012, preliminary data

	PM_{10}	NO	NO_2
PNC Dresden	0.11	0.09	0.15
PNC Ljubljana	0.39	0.49	0.56

Further analyses of the air pollution data within UFIREG will include meteorological cluster analysis based on backtrajectories and source apportionment by applying Positive Matrix Factorization.

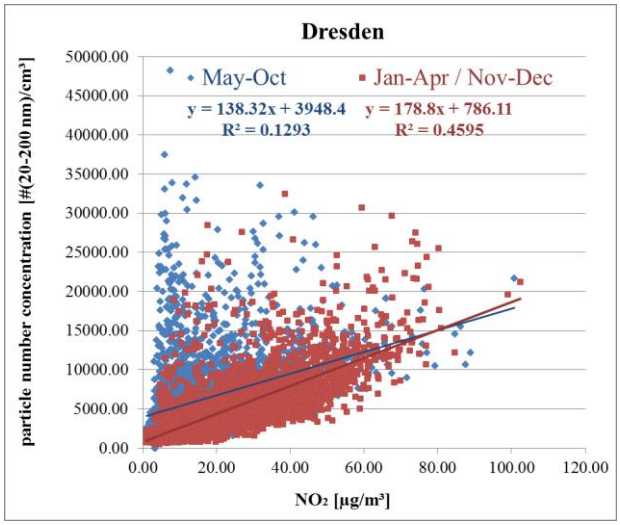

Figure 1. Correlation of PNC and NO_2 for Dresden, blue: May to October 2012, red: January to April and November to December 2012

This project is funded by the European Regional Development Fund Financing Programme Central Europe and led by the Technische Universität Dresden. Many thanks to Vladimir Zdimal from the Institute for Chemical Process Fundamentals, AS CR, for providing the SMPS data from Prague and to the research group "Tropospheric Aerosol" from TROPOS for scientific and technical support of the project.

Influence of stable weather on aerosol concentration and size distribution at K-puszta, Hungary

A. Molnár[1] and Zs. Bécsi[2]

[1]MTA-PE Air Chemistry Research Group, Veszprém, P.O. Box 158, H-8201, Hungary
[2]Department of Earth and Environmental Sciences, University of Pannonia, Veszprém, P.O. Box 158, H-8201, Hungary
Keywords: aerosol, ageing, dry deposition.
Presenting author email: becsi.zsuzsanna@gmail.com

Living in the Anthropocene, among the Earth-system processes climate change is already beyond our planetary boundaries (Rockström *et al* (2009). Changing climate leads to changes in the frequency, intensity, temporal and spatial extent of extreme weather and climate events (IPCC, 2012). Some of these extreme events – e.g. heat waves, droughts – are frequently connected to high atmospheric stability that inhibits the vertical and horizontal mixing of the air in the lower troposphere.

It is well known that physical characteristics of the atmosphere (meteorological parameters) can significantly affect the air quality. In summer the high pressure weather systems may lead to deterioration of air quality resulting in very high concentrations of atmospheric trace constituents. On the other hand, air pollution episodes can also be formed in winter due to persistent stable weather. These episodes can cause serious air pollution mainly in urban environments; however, persistent anticyclones with large spatial extent can result in high level of air pollutants even in regional background air.

Beside ground level ozone, aerosol particles play an important role in air pollution episodes with special regard to their adverse health effects (IPCC, 2012). The number and mass concentration, as well as the size distribution of the particles are the most important parameters which affect significantly the human respiratory system; and their ecological influence due to aerosol deposition is also important.

In this work the change in aerosol size distribution and dry deposition velocity is studied as a function of weather conditions in background air. We focus mainly on the changes of aerosol size distribution under stable atmospheric conditions both in summer and winter.

The aerosol size distribution has been monitored at K-puszta, Hungary between 2010 and 2012. The weather in 2010 was rather changeable with extremely high amount of precipitation, while 2011 and 2012 were excessively dry and warm resulting severe drought and heat-waves. For the selection of periods with stable weather conditions, meteorological data (temperature, precipitation, air pressure) (Hungarian Meteorological Service) and the synoptic weather maps (www.met.hu) are evaluated.

Aerosol data are obtained by means of DMPS and ELPI samplers. The size distribution of the particles between 3-800nm as well as in the size range of 30nm and 10.8μm is monitored by the DMPS and ELPI, respectively.

The aerosol size distribution is controlled by a number of different processes as new particle formation, condensation and coagulation, cloud and photochemical ageing processes, hygroscopicity, etc. In this work the results of these complex processes are discussed in detail.

The research leading to these results has received funding from the European Union Seventh Framework Programme (FP7/2007-2013) under grant agreement n° [262254], [ACTRIS]; and TÁMOP-4.2.2.A-11/1/KONV-2012-0064 (The project is realized with the support of the European Union, with the co-funding of the European Social Fund). The authors also gratefully acknowledge the Hungarian Meteorological Service for providing meteorological data.

IPCC, 2012: Managing the Risks of Extreme Events and Disasters to Advance Climate Change Adaptation. A Special Report of Working Groups I and II of the Intergovernmental Panel on Climate Change [Field, C.B., V. Barros, T.F. Stocker, D. Qin, D.J. Dokken, K.L. Ebi, M.D. Mastrandrea, K.J. Mach, G.-K. Plattner, S.K. Allen, M. Tignor, and P.M. Midgley (eds.)]. Cambridge University Press, Cambridge, UK, and New York, NY, USA, 582 pp.

Rockström, J., et al., 2009. A safe operating space for humanity, Nature 461, 472-475.

www.met.hu

Wintertime distribution of PAH with aerosol particle size in two cities in the Czech Republic

J. Bendl[1], J. Hovorka[1], J. Topinka[2]

[1] Institute for Environmental Studies, Faculty of Science, Charles University in Prague, Albertov 6, Prague 2, 128 34, Czech Republic

[2]Department of Genetic Ecotoxicology, Institute of Experimental Medicine, Acad. Sci., Vídeňská 1083, Prague 4, 142 20, Czech Republic

Keywords: PAHs, Hi-Vol, artifact, distribution

Presenting author email: honzabendl@seznam.cz

Distribution of Polycyclic Aromatic Hydrocarbons - PAH with aerosol particles is part of the comprehensive characterization of winter urban aerosol conducted in two cities in the Czech Republic – Ostrava and Mladá Boleslav. Both cities are industrial, but air pollution in each has a different source. Measurements were conducted during smog and non-smog periods in both cities.

In Ostrava, steel industry is supposed to be a major source of nanoparticles with high amount of carcinogenic c-PAH. Concentrations of B(a)P were measured in winter 2012 and reached up to 300 ng/m^3. Such concentration represents one of the worst situations in Central Europe.

Large industry (Škoda auto a.s.) is also located in the city of Mladá Boleslav. However, this automotive industry is not expected to be a significant air polluter. We assume that transportation and local heating in suburb areas are the main sources of air pollution in Mladá Boleslav. Measurements were conducted in winter 2013 and our results will be concluded soon.

In both cities, daily characterizations of aerosol were carried out for at least 14 day-long periods, including measuring with high-volume cascade impactor BGI 900 used for analyzing amount and distribution of c-PAH. Subsequently, our samples are used for a toxicology study of c-PAHs within the CENATOX project. Other measured parameters were NOx, O_3, CO, SO_2, CH_4, NMHC, PM_{10}, $PM_{2,5}$, and particle number concentrations of 14-20 000 nm with integrating time of 5 minutes. With integrating time of 1 hour, $PM_{2,5}$ OC/EC and 27 chemical elements were recorded.

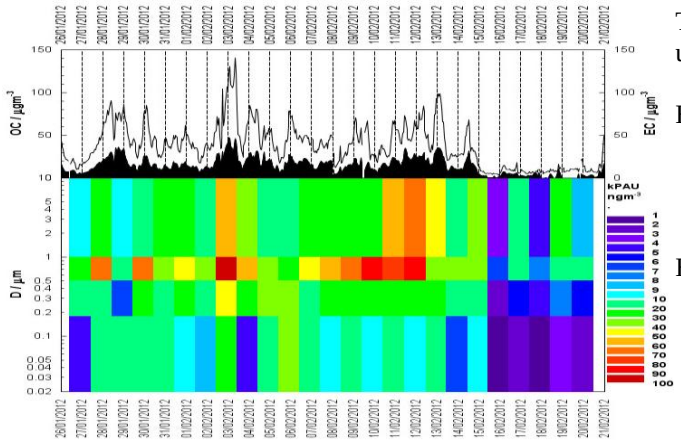

Figure 1. Temporal variation of c-PAH size-distribution and OC/EC concentration in Ostrava (26.1.-26.2. 2012)

For spatial variability assessment and verification of correctness, a network of DustTrak's ($PM_{2,5}$) was deployed in strategic places of both cities.

Remarkable positive sampling artifact - PSA for the high-volume cascade impactor BGI 900 was evaluated in Ostrava (2012). Significant amounts of gaseous phase of phenanthrene, anthracene, fluoranthene, pyrene and benzo(a)anthracene were captured in the experimental PUF (polyurethane foam) after 24 hour air exposure. The extent of the captured gaseous PAHs positively correlated with their individual vapor pressures (ranging from 10^{-4} to 10^{-1} Pa). Other measured PAHs (coronene, benzo(ghi)perylene, chrysene, benzo(b)fluoranthene, benzo(k)fluoranthene, benzo(a)pyrene, dibenzo(a,h)anthracene and indeno(1,2,3-cd)pyrene) with vapor pressures from 10^{-5} to 10^{-10} Pa did not exhibit the PSA. Based on this finding, a correction for the capture of gaseous phase in the particle size fractions of PAHs captured in BGI 900 was calculated. The deduction for the captured gaseous volatile PAHs ranged from units to tens of percent of measured particle size fractions of PAHs.

In Mladá Boleslav (2013), the same experiment was conducted in larger extent, and we are looking forward to the laboratory results. Afterwards, a general model will be designed for calculating the ratio between solid and gaseous fractions of PAHs captured on the PUF substrates in Hi-Vol BGI 900. This ratio is temperature dependent and will be applicable to future measurements of PAHs by HiVol BGI 900 using the PUF substrates.

This work was supported by the project CENATOX under grant GAČR P503/12/G147.

Hovorka, J., Topinka, J., Bendl, J., Baranová, A., Pokorná P. and Braniš, M. (2012) *European Air Pollution Hot Spot in Winter 2012: Distribution of PAH with Aerosol Particle Size*, 31st AAAR Annual Conference 2012

Hovorka, J., Topinka, J., Bendl, J., Baranová, A., Pokorná P. and Braniš, M. (2012) *Podrobná charakterizace atmosférického aerosolu v lokalitě Ostrava-Radvanice v zimě 2012: Velikostní distribuce k-PAU.* Ochrana ovzduší. 2012, 24 (44), 5, s. 40 – 43. ISSN 1211-0337

Hygroscopic Properties and Mixing State of Ultrafine Aerosol Particles over the Eastern Mediterranean Background Site of Finokalia

S. Bezantakos[1,2], A. Bougiatioti[5], I. Stavroulas[4]
K. Eleftheriadis[2], N. Mihalopoulos[4], A. Nenes[5,3], G. Biskos[1]

[1]Dept. of Environment, University of the Aegean, Mytilene, 81100, Greece
[2]Inst. of Nuclear Tech. & Rad. Protection, NCSR Demokritos, 15310 Ag. Paraskevi, Attiki, Greece
[3]Institute of Chemical Engineering, ICE-HT, Patras, 26504, Greece
[4]Environmental Chemical Processes Laboratory, Dept. of Chemistry, University of Crete, Heraklion, 71003, Greece
[5]Schools of Earth & Atmospheric Sciences & Chemical & Biomolecular Engineering, GeorgiaTech, Atlanta, GA, USA
[6]Depts. of Chemical Engineering & Engineering & Public Policy, Carnegie Mellon University, Pittsburgh, PA, U.S.A

Keywords: Aerosol Measurement, Particle size, Particle growth, H-TDMA, Mediterranean
Presenting author email: bezantakos@env.aegean.gr

Quantifying the contribution of aerosol particles on local and regional climate is complex due to the diversity of their sources and the various physicochemical processes they participate during their lifetime (Hallquist et al., 2009). The Eastern Mediterranean for example is affected by anthropogenic and natural aerosol emissions (Mihalopoulos et al., 1997), which in many cases blend resulting in increased particle concentrations (Salisbury et al., 2003). In addition due to their interactions with the intense incident solar radiation of the area, the properties of airborne particles can change drastically with time. Having information about the variation of the physicochemical properties of the aerosol in this region is therefore very important for better understanding the contribution of atmospheric particles on climate.

In this work we report on measurements of the hygroscopicity of the particles observed in the atmosphere over a background site in eastern Mediterranean, and use them to determine their mixing state. The site of Finokalia is located on the north coast of Crete (35° 20'N, 25° 40'E) at 250 m a.s.l. Measurements were conducted from 21 August to 28 November 2012, using a Hygroscopic Tandem Differential Mobility Analyzer (HTDMA; Rader & McMurry, 1986). In brief, sampled air was first dried in a nafion tube humidity exchanger to ca. 40% relative humidity (RH). The voltage on the first DMA was adjusted to select and particles having mobility diameter of 40, 60, 80, 100, and 120 nm. The monodisperse particles downstream of DMA-1 were conditioned at a 86±2% RH and measured by the second DMA and the CPC. A curve-fitting algorithm was used to fit up to three lognormal to the measurements depending on their spread. The number of the fitted distributions to each sample was used to determine the mixing state of the particles.

Figure 1 gives an overview of the measurements throughout the whole period of the campaign. Figure 1a shows the daily average hygroscopic growth factor of particles having mobility diameter of 40 nm when selected by DMA-1, whereas Fig. 1b shows the occurrence of samples with more than one distinct modes that indicate externally mixed particles. Until the end of September almost all the samples exhibited internally mixed particles. From October until the end of the measuring period, however, externally mixed particles were more often observed, reaching up to 40% of the total samples on some days. The daily average hygroscopic growth factors of internally mixed particles were ranging from 1.11 to 1.27 with a median value of 1.23. Externally mixed particles average daily hygroscopic growth factors ranged from 1.01 to 1.27 with a median value of 1.08 and from 1.18 to 1.65 with a median value of 1.28 for the first and the second hygroscopic mode.

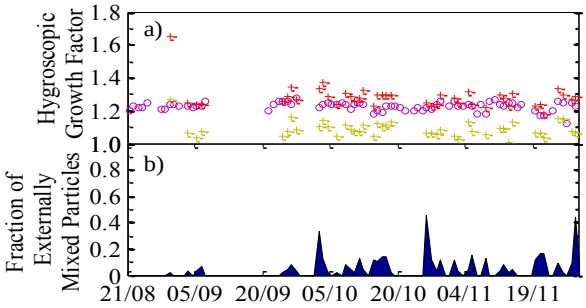

Fig. 1. Daily average hygroscopic growth factors of particles measured at Finokalia (a) and fraction of samples in which externally mixed particles were revealed (b). The hygroscopic growth factors correspond to particles having selected mobility diameter of 40 nm at 40% RH and then exposed to 86±2% RH. Circles indicate internally mixed particles and crosses externally mixed particles (bimodal).

Acknowledgement:
This research has been co-financed by the European Union (European Social Fund – ESF) and Greek national funds through the Operational Program "Education and Lifelong Learning" of the National Strategic Reference Framework (NSRF) - Research Funding Program: **THALES**. Investing in knowledge society through the European Social Fund.

References

Hallquist, M., Wenger, J.C., Baltensperger, U., Rudich, Y., (2009), Atmospheric Chemistry and Physics, 9, 5155-5236.
Mihalopoulos, N., Stephanou, E., Kanakidou, M., Pilitsidis, S., (1997), Tellus B, 49B, 314326.
Rader, D. and McMurry,P. (1986), *Journal of Aerosol Science*, 17,771-787.
Salisbury, G., Williams, J., Holzinger, R., Gros, V., (2003), Atmospheric Chemistry and Physics,3, 925-940

Climatology of dust events at Mt. Cimone (2165 m a.s.l.), Italy

L. Bourcier[1], G. Zaccaria[1], A. Marinoni[1], P. Cristofanelli[1], R. Duchi[1], D. Putero[1], T.C. Landi[1], F. Calzolari[1] and P. Bonasoni[1]

[1]CNR - Institute for Atmospheric Sciences and Climate, Via Gobetti 101, 40129 Bologna, Italy

Keywords: dust, climatology, microphysical, optical.
Presenting author email: l.bourcier@isac.cnr.it

Mediterranean basin is a key area in the climate studies, because of its high vulnerability and temperature rise predictions higher than the global average. Dust aerosol plays an important role in climate system, by affecting the radiation budget of the atmosphere. The optical and microphysical properties of aerosol particles are monitored since 2002 at global GAW station of Mt. Cimone (MTC; 44° 11' N, 10° 42' E). Its location in the Mediterranean region, its physical characteristics (highest peak of the Italian northern Apennines, 2165m a.s.l.), makes it particularly suitable to study the transport of air masses from the north African desert area to Europe.

The monitoring of the aerosol particle number with an optical particle counter (OPC-GRIMM 1108) has shown a mean concentration of 22.9 ± 28.6 # cm^{-3} for fine particles (Dp<1µm) and of 0.19 ± 0.41 # cm^{-3} for coarse particle (1µm<Dp<20µm). Particles number observed with the SMPS (1540 ± 1460 # cm^{-3}) was much higher due to the different size range of two instruments and in the same order that was has been observed at the remote station of puy de Dome (Venzac et al 2008). In addition, the mean scattering coefficient is 21 ± 24 Mm^{-1} and the mean absorption coefficient is 1.5 ± 5.0 Mm^{-1}.

Moreover, the analysis of back-trajectories allows us to make a statistical climatology of the optical and microphysical properties of the aerosol according to the origin of the air masses. We used the Lagrangian model FLEXTRA (Stohl et al 1995) to calculate three-dimensional 6-d back-trajectories (3d-BTJ) arriving at MTC every 6 h (00, 06, 12, 18 UTC).

In order to identify dust transport events (DTE) at MTC, we analysed the variability of number of coarse particles, considered a tracer for mineral dust. The analysis of 3D-BTJ and of transport model (NAAPS) was considered to identify the days characterized by transport of desert dust from North Africa.

We identified 380 DTE, corresponding to 15% of the days at MTC; in these days the coarse particle number is 685% higher than with respect to rest of the time (Fig 1). It can be noted that 65% of DTE occurs in spring and summer.

Regarding the aerosol particle number concentration, the coarse mode showed a spring-summer maximum and a winter minimum. In addition to this, the size distribution of dust particles evolves within the year, with a mean mode diameter higher in winter.

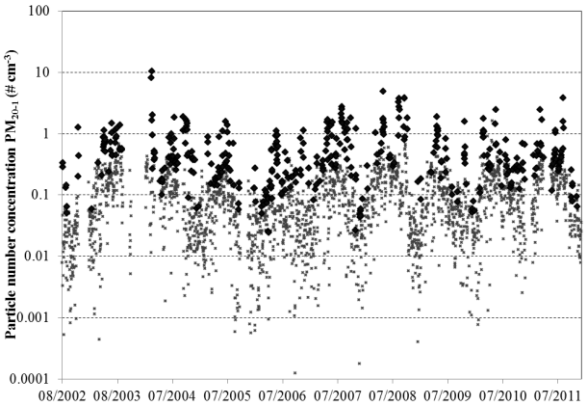

Figure 1. Time series of the coarse aerosol particle number concentrations (# cm^{-3}) at MTC for PM_{20-1}. The black diamond represents the DTE.

The absorption and scattering coefficients in DTE days have been calculated on a seasonal basis, with the aim to study the impact of dust transport on aerosol properties at MTC (Fig.2). It clearly shows an increase of the absorption coefficient in presence of dust, while the scattering coefficient is less affected.

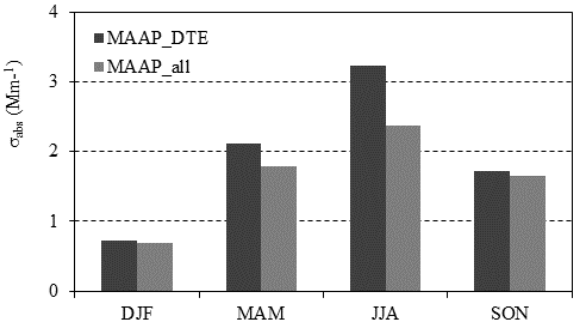

Figure 2. Seasonal average of the absorption coefficient (Mm^{-1}) during the dust events and in the rest of the year 2009 at MTC.

This work was supported by EU-ACTRIS; MIUR-NEXTDATA and EvK2CNR-SHARE projects.

Stohl, A. (1998) *Atmos. Environ.* **32**, 947-966.
Venzac, H., Sellegri, K., Villani, P., Picard, D. and Laj, P. (2009) *Atmos. Chem. Phys.* **9**, 1465-1478.

2011 Observations of Stratospheric Aerosol over Hampton, VA related to the Nabro volcanic Eruption in Africa

Boyouk, Neda[1], M. T. Hill[1], Kevin Leavor[1], M. Patrick McCormick[1]
[1]*Department of Atmospheric and Planetary Sciences, Hampton University, 23 Tyler St., Hampton, VA 23668, USA,*

Keywords: Nabro, Stratospheric aerosol
Presenting author email: neda.boyouk@gmail.com

Lidar observations from Hampton University, Hampton, VA (37.02°N, 76.33°W) show several stratospheric aerosol layers between 15.3 and 18.8 km altitude beginning 14 July 2011 and continuing throughout August, September and October. These layers are showed to be due to the June 2011 Nabro volcanic eruption, Africa (13.37° N and 41.70° E). A trajectory analysis was conducted using HYSPLIT to investigate the air mass history of the stratospheric layer and determine its source. Backtrajectories from observations made on 20 July clearly show the transport of stratospheric aerosol layers between 16 km and 18 km from Africa to Hampton. A nighttime CALIPSO overpass on 21 July, 327 km from Hampton, confirms a stratospheric layer at approximately the same height.. The backscatter and extinction coefficients of these stratospheric aerosols are reported using the Klett method and an estimated lidar ratio.

Three 20-day back trajectories were computed starting from 17.80, 17.83, and 17.86 km above mean sea level directly over Hampton University's observatory (37.02°N, 76.33°W) on 20 July 2011 at 1500 UTC. The distance between the HYSPLIT backtrajectories and same-day coincident CALIPSO overpasses is calculated. The closest CALIPSO overpasses to the backtrajectories are used to confirm the presence of stratospheric aerosols related to the Nabro eruption.

In figure 1 we present the range-corrected elastic backscatter signal on 20 July 2011, the day of the strongest observed range-corrected signal of stratospheric aerosol over Hampton. The lidar measurement starts at 10:30 and continues until 15:30 local time. An increase in the 1064 nm range-corrected backscatter signal was observed in the stratosphere between 17.3 and 18.3 km (Figure 1) with a peak signal observed at 17.8 km. For contrast, a cloud layer has also been observed between 12.7 km and 13.6 km from approximately 12:45 local time onward.

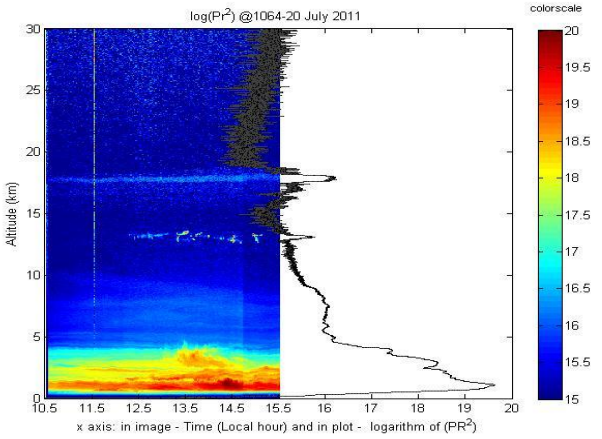

Figure 1 The range-corrected elastic backscatter signal measured on 20 July 2011 between 10:30 and 15:30 local time. The black line is the average of range-corrected signals between 14:00 and 15:00. The color scale is the Logarithm of PR2 in the image.

Multiple observations over different days show stratospheric aerosols in July, August, September and October, all of which appear to be related to aerosol produced by the Nabro eruption aerosol layer, corroborating the long life of these aerosols, the CALIOP lidar measurement aboard CALIPSO, and the HYSPLIT model of aerosol transport in the lower stratosphere.

This project is supported by the PIRT project funded by US Army Research, Development, and Engineering Command (AQC) Center (DOD) under HU PIRT Award # 551150-211150) and by NASA under Grant #NNX10AM23G.

Sawamura, et al, R. M. Hoff 2012 Stratospheric AOD after the 2011eruption of Nabro volcano measured by lidars over the Northern Hemisphere, *Eniron. Res. Lett, 7* (034013).

Bourassa A E, et al 2012 Large Volcanic Aerosol Load in the Stratosphere Linked to Asian Monsoon Transport *Science **337*** 78-81.

Size-Resolved Source Apportionment of PM_{10} Organic Aerosol Measured with Aerosol Mass Spectrometry

C. Bozzetti[1], I.El Haddad[1], R. Wolf[1], E. Bruns[1], A. Krepelova[1], K. Dällenbach[1], J.G. Slowik[1], U. Baltensperger[1] and A.S.H. Prevot[1]

[1]Laboratory of Atmospheric Chemistry, Paul Scherrer Institut, Villigen, Aargau, 5232, Switzerland
Keywords: offline analysis, AMS, PM_{10}, source apportionment, primary biological particles
Presenting author email: carlo.bozzetti@psi.ch

Atmospheric particles affect human health, climate and visibility. The extent and impact of these effects depend on both particle size and chemistry, which concurrently evolve in the atmosphere via direct emission or formation of new particles and subsequent condensation of semi-volatile species. Thus aerosol size and chemical composition are directly linked, and ideally should be measured simultaneously.

The Aerodyne aerosol mass spectrometer (AMS, DeCarlo et al., 2006) offers real-time, quantitative measurements of the size-resolved chemical composition of non-refractory submicron aerosol (organic aerosol (OA), Cl^-, NO_3^-, NH_4^+, SO_4^{2-}). The application of positive matrix factorization (PMF) techniques to AMS data have demonstrated that the mass spectra of bulk OA contain enough information to differentiate several factors, which can be related to different aerosol emission sources and/or formation processes. These factors typically include those related to primary emissions, such as hydrocarbon-like organic aerosol (HOA) from traffic, biomass smoke (BBOA), and cooking emission (COA). Secondary OA formed via the oxidation of volatile organic compounds can also be identified by this technique, termed oxygenated organic aerosol (OOA).

Most recently, the application of three dimensional PMF to online AMS data has been proposed to factorize the chemical composition data from particles in different size ranges (Ulbrich et al., 2012). However, such analysis is limited by the low signal-to-noise ratio of size-resolved AMS spectra (compared to those of bulk OA) and the negligible transmission efficiency of the conventional AMS for supermicron particles, although a newly developed aerodynamic lens system extends measurements into the $PM_{2.5}$ range (Williams et al., in prep). Although supermicron particles constitute a considerable fraction of the total suspendend particles, the chemical composition of their organic fraction remains largely unknown. It is thought that these particles include primary biological material (e.g. pollen, bacteria and spores) that can act as allergens and ice nuclei, affecting both public health and climate (Schneider et al., 2011).

In order to measure size-fractionated mass spectra, we explored the application of laboratory AMS measurements to aerosol filter samples. Such methodology based on offline sampling offers the separation of particles in discrete size ranges and allows measurement of particles through the PM_{10} size range. The approach involves water extraction of the particulate matter from quartz filters by sonication and subsequent nebulisation of the aerosol extract into the AMS. The OA extraction efficiency has been evaluated by comparison with AMS online measurements performed during the same period and is estimated at 80%. Method detection limits are estimated for organic aerosol, NO_3^-, SO_4^{2-}, and NH_4^+ as 410 mgL^{-1}, 210 mgL^{-1}, 260mgL^{-1}, and 200 $mg\ L^{-1}$, respectively. Here, we present the application of the offline AMS approach to PM_1, $PM_{2.5}$ and PM_{10} filter samples collected at a rural site in Switzerland during summer and winter. Differences in aerosol fingerprints across particle sizes are examined and indicate a significantly different composition of coarse particles with higher contributions from fragments that are likely related to carbohydrates (e.g. m/z 29 and 60). Size-resolved PMF applied to these measurements will be discussed and compared with online AMS measurements to identify the contribution of primary biological particles.

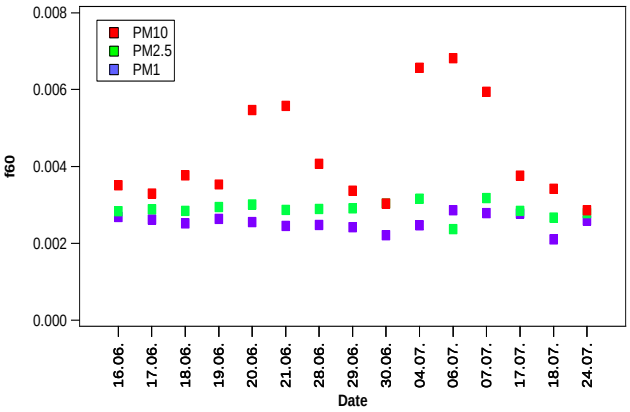

Figure 1. Time series of the f_{60} marker in 3 size fractions on 15 selected days with highest pollution during the EMEP campaign in Payerne 2012.

This work was supported by the Federal Office for the Environment in Switzerland and the Swiss National Science foundation..

DeCarlo, P.F. et al. (2006) *Anal. Chem.* **78**, 8281-8289.
Ulbrich et al. (2012) *Atmos. Meas. Tech.* **5**, 195-224.
Williams et al (2012) *Aerosol Sci. Tech.* In prep.
Schneider, J., et al. (2011) *Atmos. Chem. and Phys.* **11**, 11415-11429.

Lidar depolarization evolution during the CHARMEX intensive field campaign

J.A. Bravo-Aranda [1,2], M.J. Granados-Muñoz [1,2], F. Navas-Guzmán [1,2], J.L. Guerrero-Rascado [1,2], F. J. olmo [1,2] and L. Alados-Arboledas [1,2]

[1]Centro Andaluz de Medio Ambiente, Universidad de Granada - Junta de Andalucía, Av. del Mediterráneo s/n, 18006-Granada, Spain

[2]Dep. Física Aplicada, Universidad de Granada, Av. Fuentenueva s/n, 18071-Granada, Spain

Keywords: aerosol, depolarization, lidar

Presenting author email: jabravo@ugr.es

Atmospheric aerosol directly and indirectly affects the Earth-Atmosphere energy budget. Regarding the direct effect, the uncertainties related to the radiative forcing of the atmospheric aerosol are still too large as the IPCC showed up in 2007. A better knowledge about the radiative and physical properties of the atmospheric aerosol (e.g. refractive index, volume size distribution and shape) is necessary to reduce these uncertainties. Particularly, microphysical inversion codes developed in recent years model aerosol particles as spheroids. In this sense, particle linear depolarization ratio (δ^p), directly related to its shape, is becoming a key property for the microphysical characterization.

The main objective of CHARMEX (Chemistry-Aerosol Mediterranean Experiment) is developing and coordinating regional research actions for a scientific assessment of the present and future state the atmospheric environment in the Mediterranean Basin, and of its impacts on the regional climate, air quality, and marine biogeochemistry. Concretely, CHARMEX intensive campaign provides a real data base with vertical resolution for checking 3-D modelling of African dust aerosol radiative impact. During this campaign, lidar measurements were performed continuously during 72 hours.

In this work, the temporal evolution of δ^p is analysed in order to investigate the variability of this property. δ^p is calibrated by means of ±45º-calibration method (Bravo-Aranda *et al.*, 2012) and only values where the backscattering ratio (aerosol-to-molecular backscatter coefficient ratio) is higher than 1.2 are used as the equation is instable for lower backscattering ratios. This property is analysed in synergy with the backscatter-related Angström exponent ($å_\beta$) derived from lidar. Also, air masses analysis is performed using the backward trajectories from HYSPLIT model (www.arl.noaa.gov/HYSPLIT.php).

Figure 1 shows δ^p at 532 nm obtained during CHARMEX campaign. The upper layer (3.52-5.49 km asl), detected at 12:30-13:00 on 9th July, presented δ^p and $å_\beta$ values with mean and standard deviation of 0.36±0.01 and -0.06±0.05, respectively. These values are typically representative of pure Saharan dust. In fact, backward trajectories show that air masses that reached Granada between 3 and 5 km asl came from the centre of the Sahara Desert between 2 and 4 km asl. However, during following days, δ^p in the upper layers decreases up to values around 0.25 whereas $å_\beta$ increases up to values around 0.5. This change can be related to mixing process of dust particles with marine or biomass burning aerosol. In this sense, backward trajectories show that air masses came from Atlantic Ocean or regions near to Central Africa where FIRMS locates several forest fires (http://firms.modaps.eosdis.nasa.gov/firemap).

In the lowermost troposphere, δ^p remains almost constant (during the whole period) around 0.12 with $å_\beta$ values around 2. Low values of $å_\beta$ indicate the predominance of the fine mode while lower δ^p indicate more spherical particles. Therefore, the mixing between the anthropogenic and Saharan aerosol was detected in these layers.

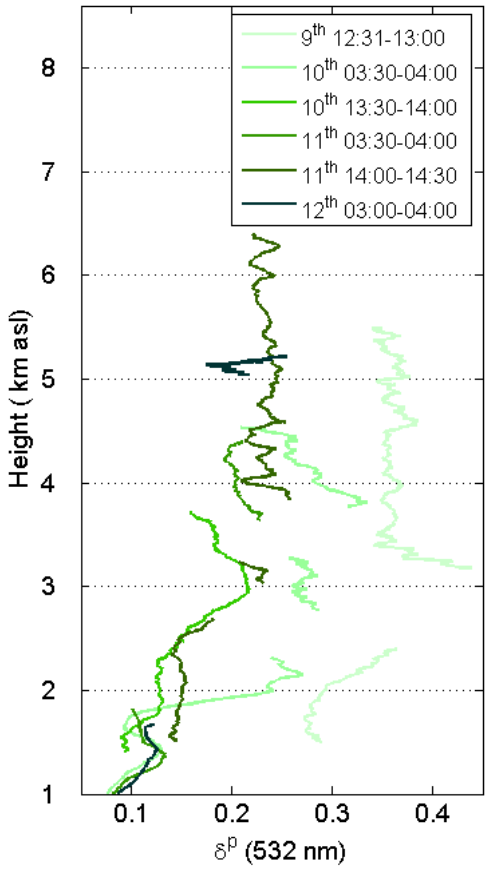

Figure 1: δ^pat 532 nm each ~15 hours during CHARMEX from 9th to 12th July 2012.

Acknowledgments: This work was supported by the Andalusia Regional Government through projects P08-RNM-3568 and P10-RNM-6299, by the Spanish Ministry of Science and Technology through projects CGL2011-16124-E, CGL2010-18782, CSD2007-00067 and CGL2011- 13580-E/CLI; and by the EU through the ACTRIS project (EU INFRA-2010-1.1.16-262254)

Bravo-Aranda, J.A., Navas-Guzmán, F., Guerrero-Rascado, J.L., Pérez-Ramírez, D., Granados-Muñoz, M.J. and Alados-Arboledas, L. (2012). Inter. J. Rem. Sen. 10.1080/01431161.2012.716546

Ground-based observations of aerosol and cloud properties at sub-arctic Pallas GAW-station

D. Brus[1], K. Neitola[1], E. Asmi[1], M. Aurela[1], U. Makkonen[1], J. Svensson[1], A.-P. Hyvärinen[1], A. Hirsikko[1,2], H. Hakola[1], R. Hillamo[1], and H. Lihavainen[1]

[1] Finnish Meteorological Institute, Erik Palménin aukio 1, P.O. Box 503, 00101 Helsinki, Finland
[2] Forschungszentrum Jülich GmbH, Institut für Energie und Klimaforschung: Troposphäre, Jülich, Germany
Keywords: cloud properties, CCN, kappa.
Presenting author email: david.brus@fmi.fi

Clouds constitute perhaps the largest source of uncertainty in predicting the behaviour of the Earth's climate system. Vulnerable Arctic region is slowly heading towards a new climatic state with substantially decreased permanent ice cover. However, due to poorly understood feedback mechanisms, the rate of Arctic climate response to changes is very hard to predict with current global models. Arctic clouds are supposed to play a central role in these feedback processes (Vavrus, 2004).

The 4th cloud campaign was carried out six weeks, between September 17th and October 30th 2012, at Finnish Meteorological Institute's Pallas Global Atmosphere Watch (GAW) station in northern Finland (Hatakka et al., 2003). The measuring site - Sammaltunturi station (67°58′N, 24°07′E) - resides on a top of the second southernmost fjeld at an elevation of 565 m a.s.l. Sammaltunturi station is, due to topography of the surrounding terrain, a great place for ground-based observations of orographic clouds (Lihavainen et al., 2008; Anttila et al., 2012).

In autumn, probability the station to be inside cloud is high, during the campaign it was 50 % of time. The maximum and minimum temperatures were between 8 and -13 °C. The temperature was below 0 °C during half of time. The winds were mostly western and north-eastern with average wind speed of 6.5 m/s (1 m/s to 15.4 m/s). Time series of selected aerosol particle and CCN properties measured during the campaign are presented in Fig. 1.

The measurements at Pallas (GAW) station included instrumentation for: aerosol number size distribution with differential mobility particle sizers (DMPS), total number particle counters (CPC, TSI 3010), particle absorption with Aethalometer (model AE 31, Magee Scientific), Multi-Angle Absorption Photometer (MAAP, Thermo Scientific) and the Single Particle Soot Photometer (SP2, DMT), and particle scattering with the integrating Nephelometer (model 3563, TSI). The ambient RH was measured with Vaisala HUMICAP sensor, and visibility and temperature were measured with Vaisala FD12P weather sensor.

In addition to above mentioned equipment, the aerosol CCN and hygroscopic properties were measured with the HTDMA (Hygroscopicity Tandem Differential Mobilitity Analyzer) and the Cloud Condensation Nuclei Counter (CCNC, DMT model CCN-100). In situ cloud properties were measured with a Forward Scattering Spectrometer Probe (FSSP, 3-47µm, model SPP-100, DMT) and the Cloud, Aerosol and Precipitation Spectrometer (CAPS, DMT), which includes three instruments: the Cloud Imaging Probe (CIP, 12.5 µm-1.55 mm), the Cloud and Aerosol Spectrometer (CAS-DPOL, 0.51-50 µm) with depolarization feature, and the Hotwire Liquid Water Content Sensor (Hotwire LWC, 0 - 3 g/m^3).

Mass and chemical composition of non-refractory submicron particulate matter was characterized with Aerosol Chemical Speciation Monitor (ACSM, Aerodyne) and the chemical composition of gas and aerosol phase was measured with an online ion chromatograph for Measuring AeRosols and GAses (MARGA 2S ADI 2080, Metrohm Applikon Analytical BV).

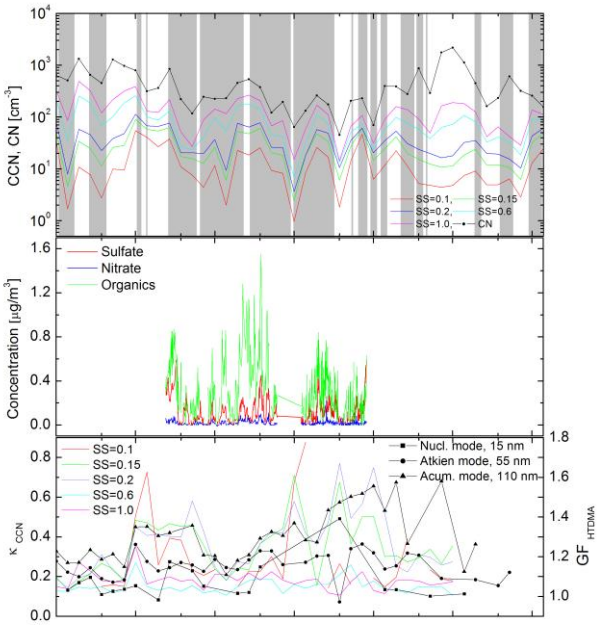

Figure 1. Example of measured properties: from the top total particle count CN together with CCN (gray areas represent cloud events), observed mass concentrations of sulfate, nitrate and organic aerosol, and derived kappa values from size-resolved CCN measurements together with growth factor from HTDMA measurements.

Authors would like to acknowledge financial support provided by Academy of Finland Centre of Excellence program (project no. 1118615)

Vavrus, S. (2004) *J. Climate*, **17**, 603-615.
Hatakka, J. et al. (2003) *Boreal Environ. Res.*, **8**, 365–384.
Lihavainen, H, et al. (2008) *Atmos. Chem. Phys.*, **8**, 6925-6938, doi:10.5194/acp-8-6925-2008.
Anttila, T., et al. (2012) *Atmos. Chem. Phys.*, **12**, 11435-11450, doi:10.5194/acp-12-11435-2012.

The concentrations of organic/elemental carbon and total protein in atmospheric aerosol of the near-ground atmospheric layer of Southwestern Siberia in the summer of 2012

G.A. Buryak[1], A.S. Safatov[1], S.E. Olkin[1], I.K. Reznikova[1], V.I. Makarov[2], S.A. Popova[2], M.P. Shinkorenko[3] and B.S. Smolyakov[3]

[1]FSRI State Research Center of Virology and Biotechnology "Vector", Novosibirsk Region, 630559, Koltsovo, Russian Federation
[2]Institute of Chemical Kinetics and Combustoin, SB RAS, 630090, Novosibirsk, Russian Federation
[3]Institute of Inorganic Chemistry, SB RAS, 630090, Novosibirsk, Russian Federation
Keywords: atmospheric aerosol, organic/elemental carbon, bioaerosol, monitoring.
Presenting author email: buryak@vector.nsc.ru

An extreme situation related to air pollution was recorded in Southwestern Siberia due to extensive forest fires in the summer of 2012. The paper presents the results of the study of atmospheric aerosol samples collected in 2 points separated by a distance of 80 km from each other. Previously it was shown (Buryak *et al.*, 2011) that the results of measurements in these points were highly correlated; therefore, they can be considered similarly. In the first point, samples were collected from June 20 to July 19, and in the second point series of observations were performed from June 21 to 30, from July 30 to August 10 and from August 30 to September 6.

Aerosol sampling was performed by pumping the air at a flow rate of 13 m^3/h for a day through fiber filters of AFA-HA-20 type and glass fiber filters.

Macc The mass of deposited aerosol was determined by the gravimetric method.

The concentrations of organic (OC) and elemental carbon (EC) were determined by the thermal method (reaction gas chromatography) described in (Popova *et al.*, 2007). The reaction chromatography method allows us to determine OC and EC concentrations by high-temperature separation in inert atmosphere. Each component is oxidized to CO_2, converted into CH_4 and recorded by a plasma-ionization detector. Thus, when the sample is heated (up to 700ºC) in inert atmosphere, organic substances evaporate and are determined as organic carbon, and elemental carbon is determined at burning in an oxidizing atmosphere.

The total protein masses in the samples were determined using a fluorescent dye (You *et al.*, 1997).

The measurement results are presented in Figures 1 and 2. During the period of the maximal smoke in the air in June and July, the total aerosol mass was always (and on some days exceeded) 100 μg/m^3. In August – September this concentration decreased to approximately 30 μg/m^3. OC and EC concentrations also changed during the period of the maximal smoke practically in proportion to the total mass of aerosol, and OC concentration was higher than that of EC during all days of observation. The concentration of the total protein in atmospheric aerosol remained at a normal level for this year all the time: 0.5 – 1.0 μg/m^3. Thus, forest fires in the region did not produce any significant influence on the total protein concentration in atmospheric aerosol.

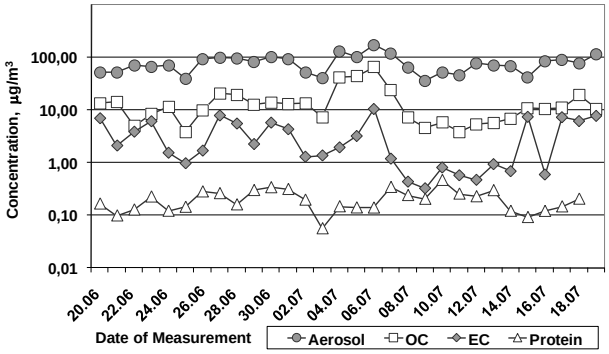

Figure 1. The results of measuring the concentrations of aerosol, organic/elemental carbon and total protein in 1 sampling point.

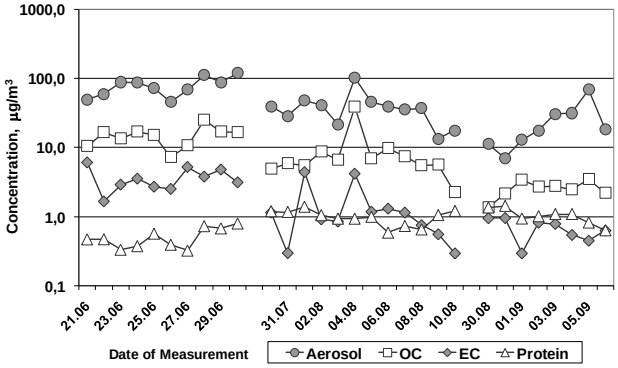

Figure 2. The same for sampling point 2.

The work was partially supported by the SB RAS Integrated Project under grant 35-2012.

Popova, S.A., et al. (2007) *Chem. Sustain. Develop*. **15**, 97-103.

Buryak G.A., et al. *Abstracts of the XVIII Meeting of the Working Group "Siberian Aerosols".* Tomsk, 2011. P. 63 (in Russian)

You, W.W., et al. (1997) *Annal. Biochem.*, **244**, 277-282.

Identification and characterization of black carbon aerosol sources in Lithuania

S. Byčenkienė, V. Ulevicius, V. Dudoitis, J. Andriejauskienė

Center for Physical Sciences and Technology, Vilnius, LT-02300, Lithuania
Keywords: black carbon aerosol, organic carbon, Ångström exponent of the absorption coefficient.
Presenting author email: bycenkiene@ar.fi.lt

Black carbon (BC) is the most ubiquitous aerosol component which absorbs visible light and affects climate through both direct and indirect mechanisms. The term BC refers to light absorbing carbon aerosols produced by incomplete combustion processes. Due to the molecular structure, which is characterized by valence electrons in π-orbitals, BC able to absorb visible light (380–880 nm). BC is a major component of "soot", a complex light-absorbing mixture that also contains organic carbon. Due to high sorption capacity and optical properties, BC originated from biomass burning (BB) is of great importance to the atmosphere processes. A carbonaceous aerosol component has been observed in fresh volcanic clouds from several volcanoes. The ash plume of the Grimsvötn eruption on 21 May 2011 offered an exceptional opportunity to characterize the volcanic aerosols.

The aim of this experimental study was to investigate BC aerosol source and particles size distributions and their dynamics in the marine environment.

Data set and methodology

The data from the monitoring site located at the EMEP Preila environmental pollution research station (55°55'N, 21°00'E, 5 m asl) in the coastal/marine environment were presented. This station is located on the Curonian Spit, which separates the Curonian Lagoon and the Baltic Sea, and thus can be characterized as a regionally representative background area.

A Magee Scientific Company AethalometerTM, Model AE31 Spectrum, manufactured by Aerosol d.o.o., Slovenia, was deployed at the site and provided real-time, continuous measurements of the BC mass concentration. The optical transmission of carbonaceous aerosol particles was measured sequentially at seven wavelengths λ (370, 450, 520, 590, 660, 880 and 950 nm). The concentration of BC corresponds to the 880 nm wavelength.

The aerosol size distribution was measured by using the Scanning Mobility Particle Sizer (SMPS) built by the Leibniz Institute for Tropospheric Research, Germany. The SMPS is composed of a differential mobility analyzer and CPC UF-02proto. This system had the following general specifications: size range 8 - 900 nm; scan time 5 min; resolution 71 size channels.

We analyzed the aerosol characteristics with respect to categorized air mass backward trajectories for the initial estimation of the BB potential source locations and quantitative contribution. Backward trajectories were produced using the Flextra model (NILU) and meteorological data provided from ECMWF (European Centre for Medium Range Weather Forcast).

Results

Discernible influence of the BB can be seen in Figure 1, where the exponents of the absorption coefficients $\alpha_{370-520}$ are depicted. This is a strong indication that the aerosol particles over the site containing the different amount of UV-absorbing material depend on the source. The Ångström exponent of the absorption coefficient for organic species depends on the wavelength. The dependence of α on the wavelength can be seen in Fig. 1.

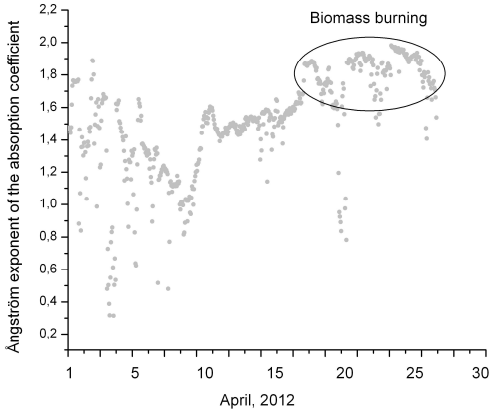

Figure 1. The spectral variation of instantaneous measurements of the Ångström exponent of the absorption coefficient for April 2012

The surface measurements and analysis of the Ångström exponent of the absorption coefficient done separately for shorter and longer wavelengths (i.e., α=370–520 nm and α=660–950 nm) showed that high levels of aerosol BC were related to the transport of air masses rich in BB products caused by active grass burning. During the events the highest mean values of the Ångström exponent of the absorption coefficient $\alpha_{370-520}$ and $\alpha_{590-950}$ nm were observed (2.4±0.1 and 1.5±0.1, respectively).

The observational data and analysis demonstrated that new secondary particle formation event could occur within the lower troposphere at a large distance from the eruptive activity.

This work was supported by the Lithuanian-Swiss cooperation programme "Research and development" project AEROLIT (Nr. CH-3-ŠMM-01/08).

Influence of humidity on aerosol concentrations in a subtropical region

L. Caetano-Silva, A. G. Allen, M. Lima-Souza and A. A. Cardoso

Department of Analytical Chemistry, Universidade Estadual Paulista, Araraquara, São Paulo, 14800-900, Brazil
Keywords: aerosol, hygroscopic growth, humidity, subtropical region
Presenting author email: leticiacaetanno@gmail.com

The climatic characteristics of subtropical southeast Brazil include large-amplitude fluctuations of relative humidity (RH), both diurnally and between seasons. This work investigated the influence of these shifts on ambient aerosol concentrations. Particle numbers were measured in six size fractions using an optical particle counter (Aerotrak, TSI), and the bulk aerosol chemical composition (soluble ions: sodium, ammonium, potassium, calcium, magnesium, formate, acetate, nitrate, sulfate, phosphate, and oxalate) was determined for 85 samples by ion chromatography (Dionex DX120). Meteorological parameters included relative humidity (RH), wind speed, and temperature. The measurements were made in August 2010. The data were treated by agglomerative hierarchical clustering (AHC), and comparison between wet (RH above 70%) and dry periods (RH below 50%) (Zentzsch *et al.*, 2013) enabled elucidation of the influence of relative humidity on aerosol growth and chemical composition.

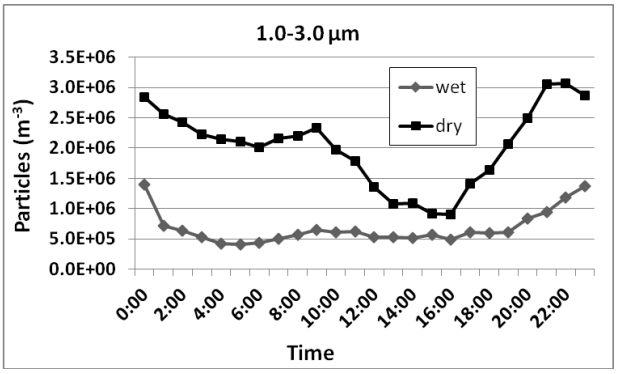

Figure 1. Diurnal number concentrations of aerosols in the size range 1.0-3.0 µm, during dry and wet periods.

Particle number concentrations (in the measured size range) were higher at night (higher RH) than during the daytime (lower RH), and diurnal fluctuations were lower under more humid conditions (Fig. 1). The 1.0-3.0 µm size fraction was most affected by RH, although aerosols of all sizes showed clear humidity-related trends, with number concentrations either increasing or decreasing (Fig. 2). The 1.0-3.0 µm size range appeared to represent a neo-equilibrium in terms of the uptake and loss of water vapor by the particles.

The shifts in RH (the minimum and maximum values were 12% and 95%, respectively) were sufficient to cover the range of deliquescence and efflorescence points (Freney *et al.*, 2009) of many of the salts present in the composition of the aerosols analyzed, including compounds of ammonium and potassium. NH_4^+ and K^+ accounted for 31.5% and 16.7% of the mass of measured cations, respectively, and the hygroscopic behavior of the corresponding compounds could explain the diurnal fluctuations in the number concentrations of aerosols in the 0.5-5.0 µm size range. Overall, there was an excess of cations, relative to anions (Table 1), which could be explained by the presence of calcium carbonate (carbonate was not determined), since this material is widely used in the region for soil pH correction, and was therefore probably the main source of aerosol basicity.

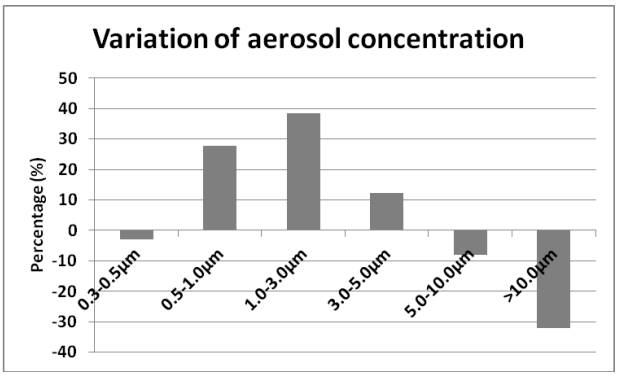

Figure 2. Percentage difference in aerosol concentrations, comparing wet periods (RH >70%) with dry periods (RH <50%).

Table 1. Ion balances for wet and dry periods.

Period	Anions neq/m^3	Cations neq/m^3	Cation/ Anion
Wet	52.7	199.7	3.8
Dry	47.6	226.5	4.8

The results revealed a substantial influence of diurnal changes in relative humidity on the hygroscopic growth of ambient aerosols derived predominantly from biomass burning and soil dust resuspension. Cyclical growth and evaporation of the particles favored both the production of secondary chemical species via aqueous phase reactions and the formation of internal mixtures of chemical components.

Acknowledgments: FAPESP (Process 2008/58073-5) and CNPq (Process 311668/2011-9).

Freney, E. J., Martin, S. T. and Buseck, P. R. (2009) *Aerosol Sci. Technol.* **43**, 799-807.

Zentzsch, P. V., Ciobota, V., Rosch, P. and Popp, J. (2013) *Angew. Chem. Int. Ed.* **52**, 1410-1413.

Influence of humidity on aerosol concentrations in a subtropical region

L. Caetano-Silva, A. G. Allen, M. Lima-Souza and A. A. Cardoso

Department of Analytical Chemistry, Universidade Estadual Paulista, Araraquara, São Paulo, 14800-900, Brazil
Keywords: aerosol, hygroscopic growth, humidity, subtropical region
Presenting author email: leticiacaetanno@gmail.com

The climatic characteristics of subtropical southeast Brazil include large-amplitude fluctuations of relative humidity (RH), both diurnally and between seasons. This work investigated the influence of these shifts on ambient aerosol concentrations. Particle numbers were measured in six size fractions using an optical particle counter (Aerotrak, TSI), and the bulk aerosol chemical composition (soluble ions: sodium, ammonium, potassium, calcium, magnesium, formate, acetate, nitrate, sulfate, phosphate, and oxalate) was determined for 85 samples by ion chromatography (Dionex DX120). Meteorological parameters included relative humidity (RH), wind speed, and temperature. The measurements were made in August 2010. The data were treated by agglomerative hierarchical clustering (AHC), and comparison between wet (RH above 70%) and dry periods (RH below 50%) (Zentzsch *et al.*, 2013) enabled elucidation of the influence of relative humidity on aerosol growth and chemical composition.

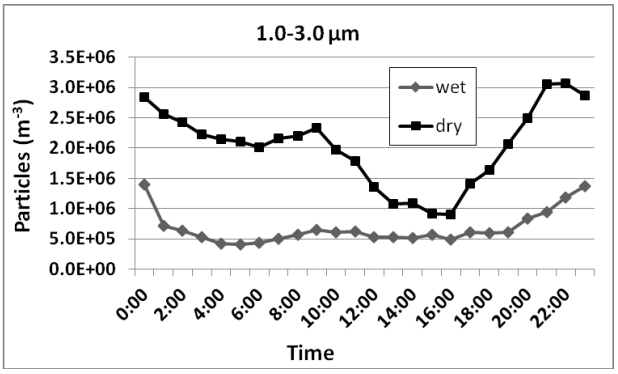

Figure 1. Diurnal number concentrations of aerosols in the size range 1.0-3.0 µm, during dry and wet periods.

Particle number concentrations (in the measured size range) were higher at night (higher RH) than during the daytime (lower RH), and diurnal fluctuations were lower under more humid conditions (Fig. 1). The 1.0-3.0 µm size fraction was most affected by RH, although aerosols of all sizes showed clear humidity-related trends, with number concentrations either increasing or decreasing (Fig. 2). The 1.0-3.0 µm size range appeared to represent a neo-equilibrium in terms of the uptake and loss of water vapor by the particles.

The shifts in RH (the minimum and maximum values were 12% and 95%, respectively) were sufficient to cover the range of deliquescence and efflorescence points (Freney *et al.*, 2009) of many of the salts present in the composition of the aerosols analyzed, including compounds of ammonium and potassium. NH_4^+ and K^+ accounted for 31.5% and 16.7% of the mass of measured cations, respectively, and the hygroscopic behavior of the corresponding compounds could explain the diurnal fluctuations in the number concentrations of aerosols in the 0.5-5.0 µm size range. Overall, there was an excess of cations, relative to anions (Table 1), which could be explained by the presence of calcium carbonate (carbonate was not determined), since this material is widely used in the region for soil pH correction, and was therefore probably the main source of aerosol basicity.

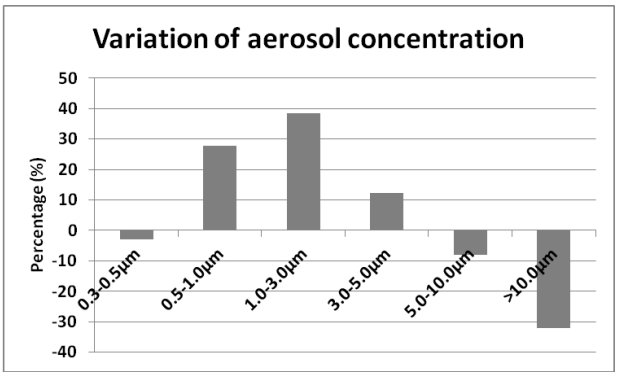

Figure 2. Percentage difference in aerosol concentrations, comparing wet periods (RH >70%) with dry periods (RH <50%).

Table 1. Ion balances for wet and dry periods.

Period	Anions neq/m^3	Cations neq/m^3	Cation/ Anion
Wet	52.7	199.7	3.8
Dry	47.6	226.5	4.8

The results revealed a substantial influence of diurnal changes in relative humidity on the hygroscopic growth of ambient aerosols derived predominantly from biomass burning and soil dust resuspension. Cyclical growth and evaporation of the particles favored both the production of secondary chemical species via aqueous phase reactions and the formation of internal mixtures of chemical components.

Acknowledgments: FAPESP (Process 2008/58073-5) and CNPq (Process 311668/2011-9).

Freney, E. J., Martin, S. T. and Buseck, P. R. (2009) *Aerosol Sci. Technol.* **43**, 799-807.

Zentzsch, P. V., Ciobota, V., Rosch, P. and Popp, J. (2013) *Angew. Chem. Int. Ed.* **52**, 1410-1413.

Sugar markers in biomass burning particles from a Brazilian agro-industrial region

R. C. Urban[1], A. A. Cardoso[2], A. G. Allen[2], M. E. C. Queiroz[1], C. A. Alves[3] and M. L. A. M. Campos[1]

[1]Department of Chemistry, University of São Paulo, Ribeirão Preto, SP, 14040-901, Brazil
[2]Institute of Chemistry, São Paulo State University, Araraquara, SP, 14800-900, Brazil
[3]Centre for Environment and Marine Studies, University of Aveiro, 3810-193 Aveiro, Portugal
Keywords: levoglucosan, sugar cane, agricultural impact
Presenting author email: lcampos@ffclrp.usp.br

The State of São Paulo (SP) alone accounts for over 50% of the total area (96,166 km^2) used for sugar cane plantations in Brazil. Burning of the sugar cane foliage before harvesting still occurs in about 40% of the cultivated land in SP, and there is not an official program to phase out burning in other States. Consequently, large amounts of gases and aerosol are released into the atmosphere during the harvest period (April – November) each year. In addition to human health effects, these emissions potentially affect cloud formation, precipitation, and radiative fluxes.

In this study, sugar markers in total aerosol samples from highly impacted agro-industrial regions (Araraquara and Ourinhos - SP) were used to improve understanding of the contribution of smoke particles from sugar cane burning to the chemical composition of the lower troposphere. We also intend to discuss other markers (K^+, Ca^{2+}, Soluble Organic Carbon, PAHs) and solubility properties of the aerosol.

Aerosol samples (n = 112) were collected using a high-volume sampler fitted with glass fiber filters. Sugars were extracted with dichloromethane /methanol, and sugar speciation was conducted for seven samples (Alves *et al*., 2011).

Levoglucosan (L) was the anhydrosugar that most contributed to the aerosol mass. Concentrations were in the ranges (i) 25 - 1406 ng m^{-3} at night, (ii) 50 - 397 ng m^{-3} during the daytime, and (iii) 12 - 382 ng m^{-3} for 24-h averages. The latter range was similar to those obtained for other locations where there is intense sugar cane production (Urban *et al*., 2012; Souza, 2011). Concentrations of mannosan (M) (2.40 - 274 ng m^{-3}) and galactosan (G) (1.81 - 274 ng m^{-3}) were about 10 times lower than levoglucosan at all times. Since burning operations were normally conducted in the evening and during the sugar cane harvest period, there were distinct diurnal and seasonal trends that were similar for the three anhydrosugars (Figure 1).

Although the majority of fires occurred during the dry season, it was still possible to detect and quantify several biomass burning markers during the wet season (November–February; non-harvest period). This could be due to the use of fire for land clearance (rural and urban fires) and to the combustion of sugar cane bagasse (the crushed solid cane residue), which returns to the production process as an energy source or is used to generate electricity.

In addition to anhydrosugars, 17 other sugars were quantified. Four of these (erythrose, maltose, arabinose, and ribose) showed behavior similar to that of levoglucosan. Overall L/M and L/G ratios were 8.64 ± 5.70 (n = 109) and 12.1 ± 7.93 (n = 109), respectively. These values are similar to those obtained for controlled sugar cane burning (Hall *et al.*, 2012) and for other regions within the State of São Paulo (Vasconcellos *et al.*, 2010). The L/M ratios for the aerosols collected during the harvest period (9.54 ± 4.39) and the non-harvest wet season (7.60 ± 3.67) were not significantly different. An L/M ratio of 10.8 was obtained for aerosols collected near a fire on pasture with scrub, which is similar to that for sugar cane leaves. Aerosol from the Amazon region did not seem to affect the study region, given the much higher L/M ratios reported for Amazonia (ca. 20; Kundu *et al.*, 2010). Combustion of different types of wood from Europe and the USA resulted in L/M values that were mostly between 1 and 6 (Gonçalves *et al.*, 2011; Medeiros and Simoneit, 2008).

In conclusion, smoke particles were generated on a regional scale and were derived from agricultural practices. Burning of sugar cane leaves will be totally eliminated by the year 2017, which will result in a major shift in the trace component chemistry of the lower troposphere in rural areas of São Paulo State.

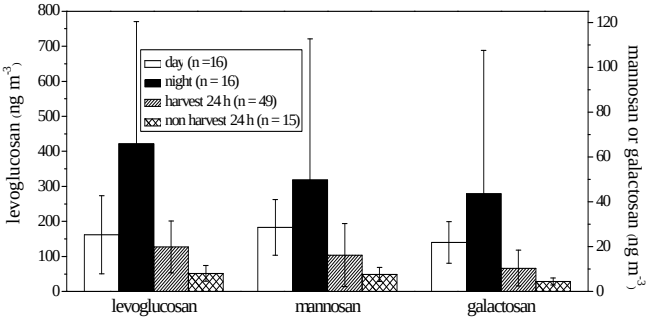

Figure 1: Average concentrations of monosaccharides during different periods.

This work was supported by FAPESP (08/58073-5 and 10/50236-2) and CNPq (311668/2011-9).

Alves, C. *et al*. (2011) *Sci. Tot. Environ*. **409**, 1466-75.
Gonçalves, C. *et al.* (2011) *Atmos. Environ.* **45**, 4533-45.
Hall, D. *et al.* (2012) *Atmos. Environ.* **55**, 164-172.
Kundu, S. *et al.* (2010) *Aerosol Sci.* **41**, 118-133.
Medeiros, P. M. and Simoneit, B. R. T. (2008) *Environ. Sci. Technol.* **42**, 8310-8316.
Souza, D. Z. (2011) *PhD Thesis. Universidade de São Paulo.*
Vasconcellos P. C. *et al.* (2010) *Environ. Sci. Technol.* **408**, 5836-5844.
Urban, R. C. *et al.* (2012) *Atmos. Environ.* **61**, 562-569.

Long-term time series of daily PM_{10} chemical composition in the area of Rome, Italy

M. Catrambone[1], S. Dalla Torre[1], E. Rantica[1], T. Sargolini[1], C. Perrino[1], the Med-Particles Study Group

[1]CNR Institute of Atmospheric Pollution Research, Monterotondo St. (Rome), 00015, Italy
Keywords: macro-sources, mass closure, composition
Presenting author email: catrambone@iia.cnr.it

MED-PARTICLES (Particles size and composition in Mediterranean countries: geographical variability and short-term health effects, http://www.epidemiologia.lazio.it/medparticles/index.php/en/) is a LIFE+ project aimed to investigate the health effects of short-term exposure to ambient air pollution in the Mediterranean Basin and to obtain a better understanding of particulate air pollution characteristics in some cities of the Mediterranean area. In the framework of this project, particular attention is drawn to the study of the interconnections between respiratory / cardio-vascular health and chemical composition of atmospheric particulate matter. To obtain this goal of the project, long-term data series of PM components are required.

Two sites in Central Italy provided data to the MED-PARTICLES project: the urban background site of Villa Ada, located inside a green area in the centre of Rome and at the peri-urban site of Montelibretti, sited at the distance of 22 km, NW of the city. At these two sites, both run by the CNR Institute of Atmospheric Pollution Research, daily PM_{10} composition was continuously investigated for three years at Villa Ada (2005 – 2007) and for six years at Montelibretti (2005 – 2010).

Each day PM_{10} was sampled on two side-by-side membrane filters: the first one (quartz) was devoted to the determination of elemental and organic carbon by thermo-optical analysis, the second one (Teflon) was aimed at measuring the mass concentration by the beta attenuation method and at determining element concentration by energy dispersion X-ray fluorescence and ion concentration by ion chromatography. A total of 24 daily chemical determinations were carried out during the six investigated years.

By using a few simple algorithms, the obtained chemical composition data were re-arranged in order to obtain the mass closure (agreement between the determination of the PM mass and the sum of the chemical components) and to estimate the strength of the main PM macro-sources: soil, sea, secondary reactions of inorganic species, combustion processes, biosphere (primary and secondary organics), as described in Perrino *et al.* (2009) and Perrino *et al*. (2010).

Seasonal and annual variations of PM composition were evaluated, both as single chemical components and as macro-sources. Figure 1 reports an example of the variations in the strength of the five macro-sources during the years 2005 and 2006 at the Montelibretti site.

Seasonal variations were observed particularly for soil components (increase during the summer due to higher soil dryness) and for organics (higher values during the winter, up to reach about 50% of the total PM_{10} mass).

The differences in the PM_{10} mass concentration and chemical composition at the urban background and the peri-urban sites were also evaluated. Very similar results between the two sites were obtained for crustal components (mainly for Al, Si and Ti), for secondary species (ammonium, sulphate and, at a less extent, nitrate), which are almost homogeneous on a regional space scale, and for the main sea-spray components (sodium and chloride). Higher values were found at the urban background site for the species that are mainly generated by exhaust and non-exhaust traffic emission (elemental carbon, iron, copper, manganese, lead, zinc, Canepari *et al*., 2008), while variable difference were found for organic components, which are emitted by a variety of different sources.

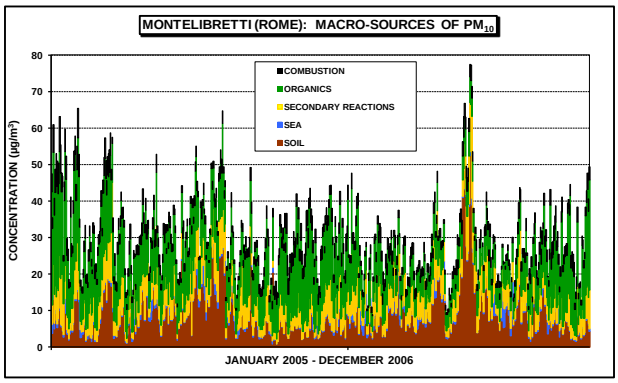

Figure 1. Macro-sources of PM_{10} in the peri-urban site of Montelibrettti during 2005 and 2006.

This work was supported by the European Community (LIFE + Environment Policy and Governance, LIFE10 ENV/IT/327)

Canepari, S., Perrino, C., Olivieri, F., Astolfi, M.L. (2008) *Atmos. Environ*. **42**, 8161–8175.

Perrino, C., Canepari, S., Catrambone, M., Dalla Torre, S., Rantica, E., Sargolini, T. (2009) *Atmos. Environ*. **43**, 4766–4779.

Perrino, C., Canepari, S., Pappalardo, S., Marconi, E. (2010) *Chemosphere* **80**, 1291-1300.

Organic characterization of particulate material from a Brazilian agro-industrial region impacted by biomass burning

R. C. Urban[1], A. A. Cardoso[2], A. G. Allen[2], M. E. C. Queiroz[1], C. A. Alves[3] and M. L. A. M. Campos[1]

[1]Department of Chemistry, University of São Paulo, Ribeirão Preto, SP, 14040-901, Brazil
[2]Institute of Chemistry, São Paulo State University, Araraquara, SP, 14800-900, Brazil
[3]Centre for Environment and Marine Studies, University of Aveiro, 3810-193 Aveiro, Portugal
Keywords: biomarkers, biomass burning, PAH, organic acids, phenols, sterols.
Presenting author email: rocerasiurban@pg.ffclrp.usp.br

Biomass burning is widely used in Brazil for deforestation and in agricultural practices. Rural areas within São Paulo State emit large quantities of particulate matter to the atmosphere due to extensive biomass burning during sugar cane plantation management. This practice is used to remove the outer leaves of the cane and facilitate manual harvesting.

The objective here was to perform a chemical characterization (including marker compounds) of the atmospheric particulate matter in an agro-industrial region of Brazil impacted by biomass burning (Araraquara and Ourinhos - SP). Ultimately, better knowledge of the chemical composition of these aerosols should improve our understanding of the role played by biomass burning particles in terms of both the regional climate and human health.

Seven samples of ambient total particulate matter (TPM) were collected on glass fiber filters using a high-volume sampler. Samples were extracted using dichloromethane and methanol, fractionated into five different classes by vacuum flash chromatography, and analyzed by GC-MS (Alves *et al.*, 2011).

Hydroxy-acids, oxy-acids, and aromatic acids were found at relatively high concentrations, as expected for biomass burning particles (Graham *et al.*, 2002). The most abundant acid in the aerosol was glycolic acid (4.3 - 300 ng m^{-3}), which has been described as a product of the hydrolysis of hemicelluloses (Girisuta, 2007).

Among the phenolic compounds, coumaryl-type was the most abundant (60 - 94%), followed by syringyl (5.3 - 37%) and vanillyl (0.87 - 16%). Coumaryl compounds are formed preferentially during the burning of *Gramineae* species (Alves, 2008). The most abundant sterol was *β*-sitosterol (50 - 60%), also characteristic of *Gramineae* burning (Oros *et al.*, 2006), followed by cholesterol (4.0 - 33%) and stigmasterol (7.5 - 46%).

The concentrations of polycyclic aromatic hydrocarbons (PAH) ranged from 1.93 to 38.7 ng m^{-3} (average: 19.1 ± 16.1 ng m^{-3}). These values are similar to those reported for other regions where burning is used in sugar cane fields (Vasconcellos *et al.*, 2003).

Retene, a biomass-burning marker, was the most abundant PAH found in the samples (14 – 84%; Figure 1). Benzo[a]pyrene (BaP) concentrations ranged from 0.03 to 2.2 ng m^{-3}. This compound has carcinogenic and mutagenic characteristics, and the World Health Organization recommends a maximum limit concentration of 1 ng m^{-3}. Four out of six samples collected during the harvest period had BaP concentrations (0.94, 0.98, 1.1, and 2.2 ng m^{-3}) either close to or higher than the limit value. Similar observations were made in earlier work by Godoi *et al.* (2004).

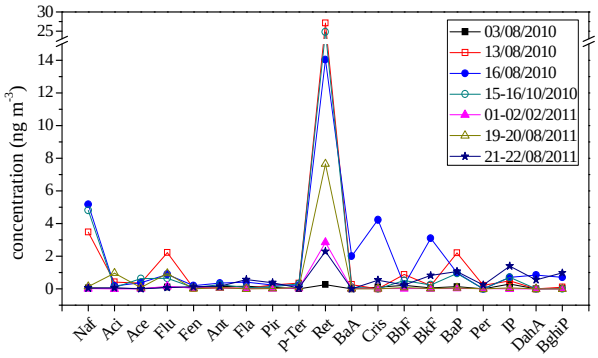

Figure 1. Concentrations of PAHs.

The most polar compounds extracted were alcohols (fraction 4) and sugars and acids (fraction 5). These two fractions corresponded to between 4.0 and 72% of the total measured mass of organic carbon. The lowest percentages of polar compounds (4.0 and 6.8%) were found in the two samples with the strongest influences of biomass burning (collected on 13/08/2010 and 16/08/2010). The percentages of *n*-alkanes in these samples were 95.7 and 92.7%, and the total concentrations of organic compounds were 115 and 123 µg m^{-3} respectively, compared to a range of 0.8 - 2.9 µg m^{-3} for the remaining samples. The highest percentage (72%) of polar compounds was found in a sample collected during the non-harvest period.

In conclusion, although biomass burning made an important contribution to the aerosol loading, the particles concerned were mostly non-polar and therefore might be unable to act effectively as cloud condensation nuclei. The proximity of plantations to urban areas could present a health hazard to the local population due to the emissions of carcinogenic compounds.

This work was supported by FAPESP (processes 08/58073-5 and 10/50236-2), and CNPq (process number 311668/2011-9).

Alves, C. (2008) *An. Acad. Bras. Cienc*. **80**, 21-82.
Alves, C. *et al.* (2011) *Sci. Tot.Environ*. **409**, 1466-1475.
Girisuta, B. (2007) *Levulinic Acid from Lignocellulosic Biomass.* PhD thesis, University of Groningen.
Godoi, A. *et al.* (2004) *J. Chromatogr. A* **1027**, 49-53.
Graham, B. et al. (2002) *J. Geophys. Res.* **107**, 14-1-15
Oros, D.R. *et al.* (2006) *Appl. Geochem.* **21**, 919-940.
Vasconcellos P.C. *et al.* (2003) *Atmos. Environ.* **37**, 3009-3018.

Thermal-optical analysis of elemental carbon (EC) in environmental samples – differences observed when using various protocols

E.C. Cetintas[1], M. Kistler[1], C. Schmidl[2], H. Bauer[1,†] and A. Kasper-Giebl[1]

[1]Institute of Chemical Technologies and Analytics, Vienna University of Technology, Vienna, A1060, Austria
[2]Bioenergy2020+, Wieselburg - Land, A3250, Austria
Keywords: EC, PM10, EUSAAR2, *quartz.par*.
Presenting author email: eylemcan@gmail.com

Several methods are used nowadays for assessing of elemental- and organic carbon (EC, OC) in the atmospheric samples. Their classification and selection depends on the principle of the measurement (e.g., thermal, optical) and furthermore also on the type (e.g., solid, liquid, gaseous), quality and quantity of the sample. Due to basic differences a comparison between methods need not result in perfect agreement, especially when analyzing environmental samples. More demanding is the task, that it was already noticed that even the same method reveals often not uniform resuts, depending on applied settings (e.g., Baumgardner *et al.*, 2012)

Thermal-optical carbon analysis is a standard method applied and recommended for analysis of EC and OC in atmospheric aerosols collected on filter media. For this purpose several protocols (IMPROVE, NIOSH 5040, EUSAAR2, NIOSH-like protocols - e.g., *quartz.par*) are available (Chow et al., 1993, Birch and Cary, 1996, Cavalli et al., 2009). Applying of different temperature steps with varying length and a diverse optical correction mode (transmission or reflection mode) might significantly affect the result.

With relation to the samples presented below following analytical questions are to be answered:

- How do pure wood burning emission PM10 behave during EC-OC analysis with different protocols?
- How do ambient particulate matter with a significant wood combustion PM10 behave during EC-OC analysis with different protocols?
- Which factors influence the observed differences (if any)?
- How could the choice of the protocol for analysis be simplified?

Wood burning emission samples (PM10) have been taken during stove tests conducted at TU Vienna (AQUELLIS FB Project, Schmidl *et al.*, 2008). Particles were sampled from a dilution exhaus on quartz fibre filters (Pall, 47mm), using Low-Vol PM10 separators (~1m³/h). The samples were highly loaded (3-5 mg/filter) with dark brown or black particles. Another set of emission samples was collected at Bioenergy 2020+. Again particles were sampled on quartz fibre filters (Pall, 47 mm) and were chosen to reflect different conditions of wood burning. Filters showed lower mass loadings during this smpling campaign.

Ambient air particulate matter (PM10) samples were collected on quartz fibre filters (Pallflex, 150 mm) with Hi-Vol samplers (~30m³/h) during winter (February 2011) and summer (July 2011) campaigns conducted in Austria and Slovenia (PMinter Project, Kistler *et al.*, 2013).

The winter samples were highly concentrated with dark brown/black loadings exceeding 35 mg/filter. Summer sample loadings were only about 10 mg/filter with no visible soot (grey dust).

Measurements of EC and OC in both ambient air and emission samples were conducted with an Sunset Laboratory Lab OCEC Analyser using EUSAAR2 and *quartz.par* temperature protocols. Measurements with *quartz.par* method were additionally evalueted in reflectance mode.

Aditional analyses of the filters (inorganic ions, saccharides, HULIS (humic like substances), selected elements) were performed and are available to gain a general chemical characteristic of the samples.

Among ambient air samples the problem of overloading did not occur. Nevertheless the agreement between results for measurement with both protocols was not constant. In several cases (concerning whole measurement series) EC differ more than 3 times, showing an evident coherrence with factors describing the collected aerosol (age and chemical composition).

Authors acknowledge a cooperation between TU Vienna, Bioenergy 2020+ and PMinter project consortium. We thank to the group members involved in the study.

Baumgardner, D., et al. (2012*). Atmos. Meas. Tech. Discuss.*, **5**, 2315–2362.

Birch, M.E., & Cary, R.A. (1996). *Aerosol Sci. & Technol.* **25**, 221-241.

Cavalli, F., Viana, M., Yttri, K.E., Genberg, J., Putaud, J.-P. (2010). *Aerosol Meas. Techn.* **3**, 79-89.

Chow, J.C., Watson, J.G., Pritchett, L.C., Pierson, W.R., Fraizer, C.A., Purcell, R.G. (1993). *Atmos. Environ.* **27A**, 1185-1201

Kistler, M., Cetintas, E.C., Bauer, H., Kasper-Giebl, A., (2013). *Submitted for European Aerosol Conference*, Prague, 2013.

Schmidl, C., Peng., G, Bauer., H., Puxbaum, H., (2008). *Project Report*. Vienna University of Technology, Vienna.

Coupling optical and chemical properties of primary and secondary carbonaceous aerosols

F. Costabile[1], S. Gilardoni[2], F. Barnaba[1], M. Rinaldi[2], S. Ferrari[3], V. Poluzzi[3], G. P.Gobbi[1]

[1]ISAC-CNR, via Fosso del Cavaliere, Rome, Italy
[2]ISAC-CNR, via Gobetti 101, Bologna, Italy
[3]ARPA Emilia Romagna, via Rocchi 19 ,Bologna, Italy
Keywords: Black carbon, organic aerosol, optical properties.
Presenting author email: f.costabile@isac.cnr.it

Carbonaceous aerosol particles are one of the most abundant aerosol components in the urban atmosphere. They are composed by black carbon (BC) and organic carbon (OC) plus additional quantities of trace elements; their particle size ranges over several orders of magnitude from the ultrafine (particle diameter, $D_p < 100$nm) to the fine region ($< 100\text{nm} < D_p < 1\mu$m). Relating their optical properties to chemical properties is necessary to assess their contribution on air pollution and on the radiative balance in the atmosphere .

On one hand, BC-rich aerosols show high absorption: their BC content cause those aerosols to strongly absorb light with a flat spectral variability. On the other hand, optical properties of BC-rich aerosols do vary with varying D_p: their D_p vary from the ultrafine (soot mode, 60-100 nm in D_p, i.e., motor vehicle emissions) to the small accumulation mode (100-300 nm, typical of lower temperature combustion processes such as biomass smoke). Clearly defining BC-rich aerosol properties requires to separate them with regard to homogeneous properties (i.e.,D_p, chemical composition, and spectral optical properties). Similar definitions are still missing.

Aerosols with large OC content also exhibit a variety of optical properties varying with varying the type of organic molecular species. Some organic molecular species cause the aerosol to mainly produce light scattering effects. Other aerosol organic molecular species show, on the contrary, absorption effects with a strong spectral variability. The absorption spectral variability depends on the OC content referred to as brown carbon (BrC) (Kirchstetter et al., 2004). A clear understanding of optical properties in BrC-rich organic aerosols is still far to be reached.

In this work we analyze optical, chemical and microphysical properties of carbonaceous aerosol particle in the urban area of Bologna during an intensive campaign of the "Supersito" project. The objective is to relate aerosol spectral optical properties to relevant chemical properties for selected types of organic aerosols varying with varying BC and BrC contents, and particle diameters.

Aerosol chemical composition, species size distribution, and organic aerosol chemical properties are measured by an High Resolution Time of Flight Aerosol Mass Spectrometer (HR-TOF-AMS). Aerosol spectral optical properties are measured by a 3-wavelenght PSAP and a 3-wavelenght integrating nephelometer operating in the visible region. Particle number size distributions are measured by SMPS+APS (TSI).

The bulk aerosol is separated in primary and secondary carbonaceous aerosol populations through the analysis of the aerosol spectral optical properties: Scattering Angstrom Exponent (SAE), Absorption Angstrom Exponent (AAE), Single Scattering Albedo (SSA) and its variability dSSA. Aerosol absorption is separated in the absorption due to BC, and the one due to BrC. The identified aerosol types are analysed in terms of chemically-resolved size distributions (fig.1).

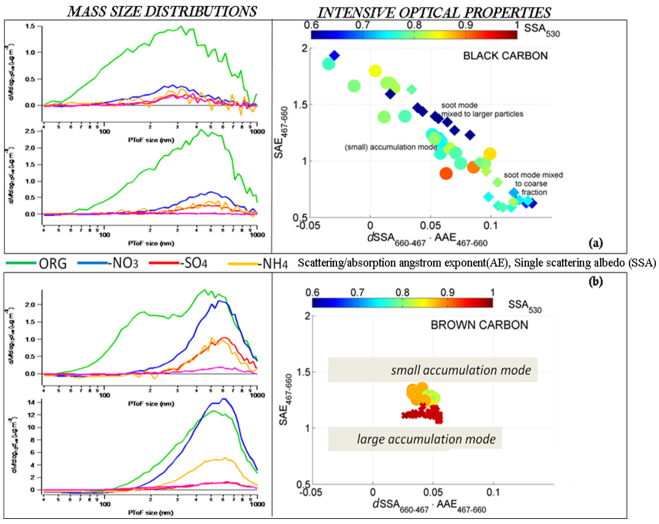

Figure 1: Optical properties and mass size distribution of major chemical constituents of: (a) mixed aerosols dominated by black carbon (soot-BC and not-soot-BC); (b) organic aerosols rich in Brown Carbon (small and large accumulation mode).

The results, still in progress, will be analyzed to obtain optical properties of carbonaceous aerosols concerning both freshly emitted particles (motor vehicles and biomass smoke), and aged secondary organic aerosols. Major conclusions will constrain spectral absorption properties of the selected aerosol types to estimate in particular refractive indices, Angstrom exponents, and mass absorption efficiencies. Conclusions will also target chemical properties of the organic molecular species contributing to the spectral absorption.

This work was supported by the Emilia-Romagna Region project SUPERSITO (DGR 428/10).

Black carbon contribution to the particle matter in Madrid City during a local winter episode

E. Coz[1], M. Becerril[1], Z. Chang[2], J. Pérez-Guldris[2], A.S.H. Prévôt[3], G. Ramos[2], B. Artiñano[1]

[1]Department of the Environment, CIEMAT, Madrid, ES-28040, Spain
[2]Department of Analytical Chemistry and Chemical Engineering, University of Alcalá de Henares, Alcalá de Henares, ES-28801, Spain
[3]Laboratory of Atmospheric Chemistry, PSI, Villigen-PSI, CH-5232, Switzerland
Keywords: black carbon, thermal inversion
Presenting author email: esther.coz@ciemat.es

Black carbon (BC), a product of inefficient combustion from fossil fuel and/or biomass burning, is considered a major contributor to global warming (Ramanathan and Carmichael, 2008). In a highly populated urban metropolis, such as Madrid, with no industry nearby and where traffic and domestic activities are the dominant sources, BC can be regarded as one of the most important components within the chemical atmospheric pool. Thus, BC monitoring has become an urgent challenge to achieve for the city.

For the first time, PM_{10} BC concentrations have been recorded through aerosol light absorption using a 7 multi-wavelength Aethalometer (Magee Sci. mod. AE33, Aerosol d.o.o.) during a small thermal inversion period (Fig.1) -typical meteorological scenario from the winter season in Madrid-, at the CIEMAT urban background site (Plaza et al., 2011). The instrument took part in an ACTRIS intercomparison showing extremely good agreement with the other instruments (same and previous model, AE31) and the MAAP used as reference.

Results showed that the evolution of the BC concentrations during the sampling tests conducted at CIEMAT were in good agreement with the averaged $PM_{2.5}$ and PM_{10} concentration levels of all the stations from the city Authority air quality monitoring network (http://www.mambiente.munimadrid.es/svca/index.php?lang=en), confirming the site as representative of the atmospheric aerosol composition within the urban limits during this type of events. Hourly BC concentrations, which reached more than 20 $\mu g \cdot m^{-3}$ in part of the period, represented, on average, 40% of the network averaged $PM_{2.5}$ during the episode in comparison with 10% during the previous and subsequent days.

A first evaluation of the responses at the ultraviolet (UVPM, 370nm) and near-infrared (nIR-BC, 880nm) wavelengths (Sandradewi et al., 2008), suggests there was no important contribution from biomass burning origin to these high BC concentrations during the event. The mean UVPM/n-IR-BC ratio was 1.07±0.05. Relatively higher concentrations of the UVPM signal are expected from the derived organic compounds when the contribution of wood smoke aerosols becomes important. Nevertheless, further analysis ^{14}C analyses and further data analyses need to be done to quantitatively estimate each contribution.

This finding is of special importance since biomass burning seems to be a significant source in most of the European highly populated cities, giving Madrid a unique position regarding atmospheric aerosol /BC sources at least in this time of the year.

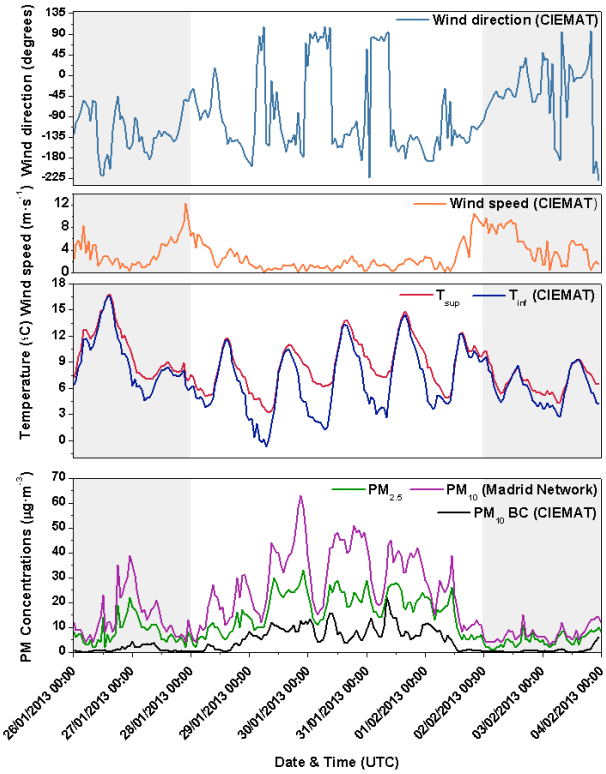

Fig 1. Meteorological parameters and BC concentrations during the thermal inversion in the station at Ciemat. T_{sup} and T_{inf} are temperature at high and low levels of the CIEMAT tower. Averaged PM_{10} and $PM_{2.5}$ concentration levels from the stations in the local Authority network.

The authors especially acknowledge Dr. Müller and the participant team in the ACTRIS WP3 Absorption Photometer and Nephelometer Workshop in February 2013. This work has been funded by the AEROCLIMA project (CIVP16A1811, Fundación Ramón Areces) and the MICROSOL project (CGL2011-27020).

Plaza et al. (2011). *Atmos. Environ.* **35 (11)**, 2496–2506.
Ramanathan, V. and Carmichael, G. (2008). *Nature Geosci.* **1**, 221–227.
Sandradewi et al. (2008), *Atmos. Environ.* **42**, 101-112.

Major ions particle size distribution from Baia de Todos os Santos, Northeastern Brazil

G.O. da Rocha[1,2,3,*], J.S.S. Domingos [1,3], A.C.D. Regis[1,3], J.V.S. Santos[1,3,4], J.B. de Andrade[1,2,3]

[1]Institute of Chemistry, Universidade Federal da Bahia, 40170-290, Salvador-BA, Brazil
[2] Centro Interdisciplinar de Energia e Ambiente – CIEnAm, Universidade Federal da Bahia, 40110-040, Salvador-BA, Brazil
[3] INCT for Energy & Environment, 40170-290, Salvador-BA, Brazil
[4] Instituto Federal de Educação, Ciência e Tecnologia Baiano, 45995-000, Teixeira de Freitas-BA, Brazil
Keywords: particle size distribution, major ions, atmospheric aerosol, Baia de Todos os Santos
Presenting author email: giseleor@ufba.br

Organic and inorganic ions are major particulate matter (PM) constitutents, being commonly used as source tracers. They may also be good representatives of secondary atmospheric pollutants mainly associated with crustal cations (Na^+, K^+, NH_4^+, Mg^{2+} and Ca^{2+}). Furthermore, major ions are ubiquitous in atmosphere. In terms of particle's size, it is accepted the following classification particles in nuclei mode (3 nm < dp < 30 nm), nanoparticles (dp < 50 nm), accumulation mode (0.1 µm < dp < 2.5 µm) and coarse mode (2.5 µm < dp < ~100 µm). Yet PM at dp < 1 µm are also called ultrafine particles. In this study, we studied major ions size distribution from three sites in Baia de Todos os Santos (BTS).

BTS is the second largest coastal bay in Brazil (Fig. 1). Its surroundings comprises an urban area with more than 3 million inhabitants with intense vehicular and port activities and an extensive industrial area. The bay is close to a Nave Base and the largest petrochemical complex in the southern hemisphere. Although all those activities in BTS are potential sources of compounds to be realeased to atmosphere, studies about PM size distribution and the content of major ions and other species on that are scarce.

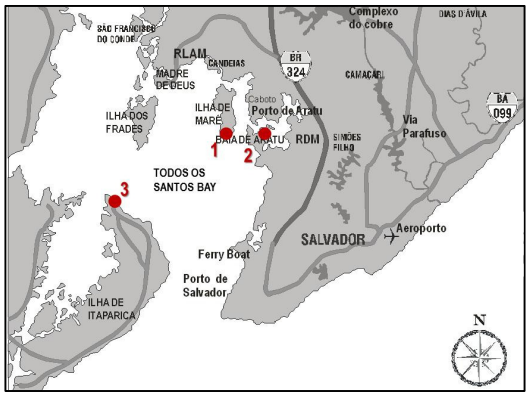

Fig. 1. Map of TSB and the three sampling sites: #1 is Botelho, #2 is Base Naval de Aratu (BNA) and #3 is Itaparica.

Samples were collected by using a NanoMOUDI sampler set with PTFE filters, at 30 L min^{-1}, during 7 days (n=2) in each site. Sampling was done during August 2010 in Botelho, September 2010 in Base Naval de Aratu (BNA), and October 2010 in Itaparica (Fig. 1). During sampling there were contributions of oceanic (90%) and continental (10%) air masses with prevailing NNE direction. Major ions analysis (F^-, Cl^-, NO_3^-, SO_4^{2-}, PO_4^{3-}, lactate, formate, acetate, succinate, oxalate, Na^+, K^+, NH_4^+, Mg^{2+}, and Ca^{2+}) was done by an ion chromatograph with conductivity detection (Domingos *et al,* 2012). Size distributions of selected ions are shown in Fig. 2.

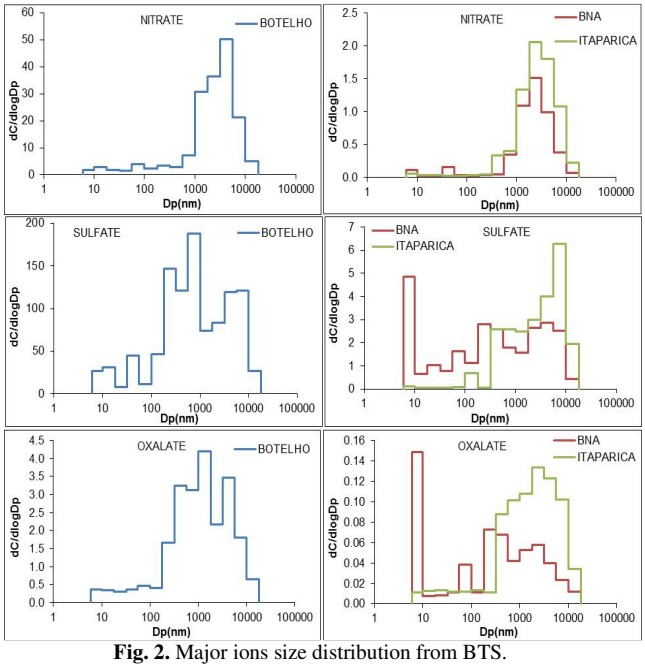

Fig. 2. Major ions size distribution from BTS.

It was observed that the ions Cl^-, NO_3^-, Na^+, K^+ and Ca^{2+} showed monomodal distribution (in the coarse fraction), SO_4^{2-}, PO_4^{3-} and oxalate had bimodal distribution (coarse fraction and in the range of accumulation), and succinate, formate, NH_4^+, Mg^{2+} and lactate showed trimodal distribution (coarse particles, nanoparticles, and accumulation mode). The species present in the coarse fraction showed biogenic sources (sea spray and resuspension of particles), while the source contributions for accumulation mode and nanoparticles were anthropogenic (fuel burning and industrial).

This work was supported by PETROBRÁS, FAPESB, CAPES, CNPq, INCT for Energy & Environment.

Domingos, J.S.S., Regis, A.C.D., Santos, J.V.S., de Andrade, J.B., da Rocha, G.O. (2012) *J. Chrom. A* **1266**, 17-23.

Extreme dust storms in Iceland

P. Dagsson-Waldhauserova[1,2], H. Olafsson[1,3,4] and O. Arnalds[2]

[1]Department of Physics, University of Iceland, Reykjavik, 101, Iceland
[2]Faculty of Environment, Agricultural University of Iceland, Hvanneyri, 311, Iceland
[3]Geophysical Institute, Bergen School of Meteorology, University of Bergen, Bergen, 5020, Norway
[4]Icelandic Meteorological Office, Reykjavik, 150, Iceland
Keywords: glaciogenic dust, HYSPLIT, volcanic ash, dust plume.
Presenting author email: e-mail: pavla@lbhi.is

Iceland, an island in the North Atlantic Ocean, is an active source of dust from glaciogenic and volcanic sediments. Frequent strong winds drive the soil into suspension and transport the dust several hundreds of km over the N-Atlantic Ocean and the Arctic Ocean.

We observed 1033 dust days from the meteorological observations in NE Iceland in 1949-2011. A total of 192 dust events were severe in the sense that the visibility was less than 5 km. An annual mean of 55 days of atmospheric dust observation was reported for the first decade of the 2000s in Iceland (our data and Georgsdottir, 2012). We chose two of the most severe dust storms for each region - N and S Iceland - with different dust sources and deposition areas. The South-Iceland Dust Storm (SDS) occurred on slope of the Eyjafjallajokull volcano five months after the eruption on September 14th 2010. The major source of resuspended material was volcanic ash and the deposition area was over the North Atlantic Ocean and further over Europe. We measured an aeolian particle transport with BSNE wind erosion samplers (Fryrear, 1986), total particle number with saltation sensor (SENSIT) and employed an automatic weather station *in situ* during this event. The North-Iceland Dust Storm (NDS) took place in outwash plains north of Vatnajokull glacier on September 17th 2008. The major source was glaciogenic dust and the deposition area was over the Arctic Ocean and Greenland. We calculated PM_{10} mass concentration from *in situ* meteorological and visibility observations. The aim of this study was to quantify aerosol particle transport of volcanic aerosol during extreme dust storms when the conventional aerosol measurements *in situ* fail. An attempt is made to detect the deposition area of dust storms by calculating forward trajectory and determining the Absorption Aerosol Index.

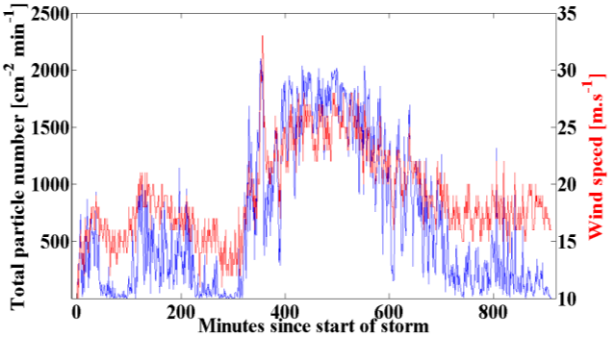

Figure 1. Total particle number measured with saltation sensor and mean wind speed during the SDS.

The SDS lasted for 23 hours and we measured max wind speed of 38.7 ms^{-1}, max total particle number of 2,100 $cm^{-2}min^{-1}$ and max saltation of 6,825 counts min^{-1} (Fig. 1). Total aeolian particle transport was calculated as 11,000 kg m^{-1} (Arnalds et al., 2013). The desposition area extended from the North Atlantic Ocean to Ireland, Great Britain and several trajectories arrived as far as to the Czech Republic. The NDS was observed for seven days with reduced visibility to 1500 m and calculated mean PM_{10} concentration of 231 µg m^{-3}. Depostion area was over the Greenland sea and air parcels travelled over northwestern Greenland (Fig. 2).

Icelandic dust storms are frequent and among the most severe dust storms observed on Earth (Arnalds et al., 2013). Fine glaciogenic particles can be rapidly activated and resuspended after recurrent flooding and travel over 1800 km within 24 hours. Deposition area is in the Arctic environment. Freshly deposited volcanic material under severe meteorological conditions such as in Iceland prolongs impacts of volcanic eruptions.

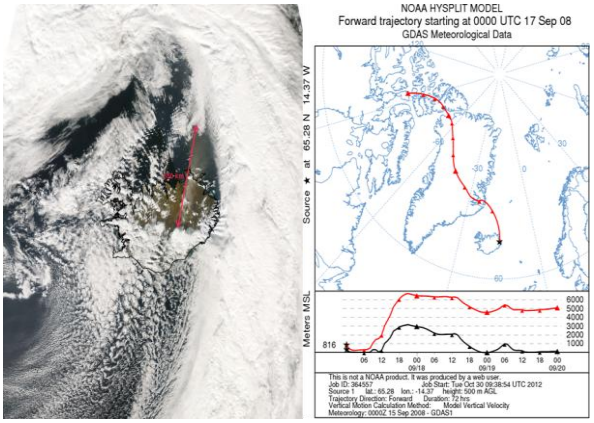

Figure 2. MODIS Aqua picture (left) and NOAA HYSPLIT 72-hr forward trajectory for air parcels released in Egilsstadir (right) during the NDS.

Arnalds, O., Thorarinsdottir, E.F., Thorsson, J., Dagsson-Waldhauserova, P., Agustsdottir, A.M. (2013) *Nature Scientific Reports* **3**, 1257.

Fryrear, D.W. (1986) *Journal of Soil and Water Conservation* **41**,117-120.

Georgsdóttir G.I. (2012) *M.Sc. thesis*, Faculty of Earth Sciences, University of Iceland Press.

Measurements of particulate matter hygroscopicity in Aerosol Exposure Chamber to prevent atmospheric corrosion in Data Center

L. D'Angelo[1], G. Rovelli[1], L. Ferrero[1], G. Sangiorgi[1], M. G. Perrone[1], M. Moscatelli[1] and E. Bolzacchini[1]
[1] Environmental Science and Technologies, University of Milano-Bicocca, Piazza della Scienza 1, 20126, Milano, Italy
Keywords: hygroscopicity, deliquescence, crystallization, chamber.
Presenting author email: l.dangelo6@campus.unimib.it

Data Center energy consumption amounts to ~27% of energy demand in Western Europe. About 35-50% of this energy is used by air-cooling system to remove the heat generated by electronic circuit activities (Shehabi, 2009). A recent solution to save energy consists in using an outside airflow to cool informatic technology (IT) equipment. This system, called Direct Free-Cooling, involves the risk to introduce particulate matter (PM) which can operate electrochemical corrosion once it deposits on ITs and reaches deliquescence conditions. Furthermore PM can arrange electrical conductive bridges which can cause the failure of ITs (Shehabi et al., 2008). ASHRAE (American Society of Heating, Refrigerating and Air-Conditioning Engineers) Technical Committee 9.9 guidelines recommend air thermodynamic conditions only to prevent corrosion process. It suggests to estimate deliquescence relative humidity (DRH), but it avoids to consider both the aerosol chemical composition – which drives the aerosol DRH – and the crystallization relative humidity (CRH).
Systematic studies of DRH and CRH changes related to the aerosol chemical composition, which in turn varies in space and time, are missing.
For these reasons, DRH and CRH were experimentally investigated in this study by electrical conductive measurements. In this respect, PM2.5 atmospheric samples collected at two sites, Milan (45°31'19"N, 9°12'46"E) and Oasi Le Bine (45°8'17.24"N, 10°26'10.99"E), were used to characterize respectively the urban and rural PM hygroscopic behaviour in the Po Valley (North Italy). Conductivity was measured in an Aerosol Exposure Chamber (AEC) – specifically designed for this study by Atmospheric Chemistry Research Group in Milano–Bicocca University – as a function of the relative humidity (RH) which was controlled by 1% step. Conductivity measurements were carried out using the Hewlett-Packard 3421A Data Acquisition Module while RH was monitored by LSI-Lastem termoigrometer sensor.
The inorganic ionic chemical composition of the 15 samples was also determinated by ionic cromatography (for cations: Dionex ICS-90 and for anions: Dionex ICS-2000) system. Data from chemical analysis were used to model hygroscopicity of collected particles by using the water moles output of the thermodynamic Extended-Aerosol Inorganics Model (E-AIM II, Clegg et al., 1998) Experimental data from AEC and model result were then compared (Figure 1).
Conductivity analysis on PM2.5 show hysteresis behaviour (Figure 2).
Data from AEC analysis of the 15 $PM_{2.5}$ show an average DRH of 61.38±1.68% and CRH of 47.12±1.58%. E-AIM modelled results estimate an average DRH of 63.00±2.16%.
These results are very useful to improve knowledge about the thermodynamic conditions which can cause corrosion processes triggered by atmospheric aerosols.

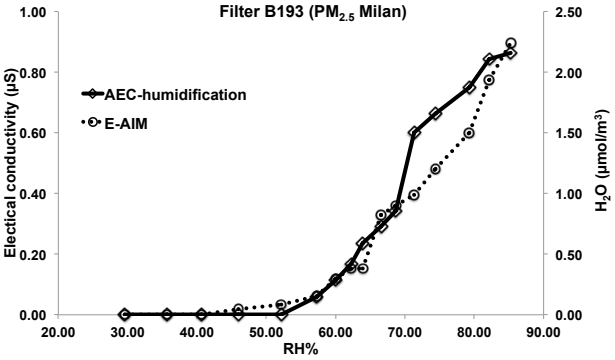

Figure 1. Aerosol conductivity curve (electrical conductivity; µS) during AEC air humidification and hygroscopic growth (H_2O; µmol/m^3) modelled by E-AIM II.

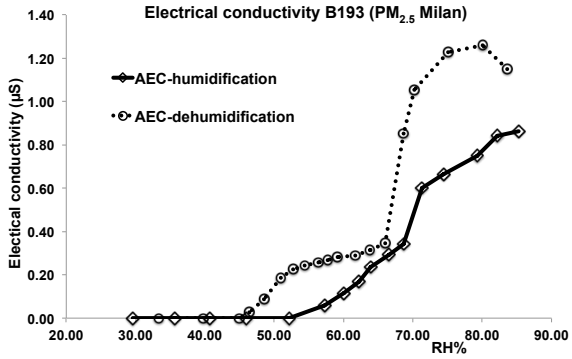

Figure 2. Aerosol conductivity curve during indoor AEC air humidification and dehumidification.

ASHRAE whitepaper (2011), *Gaseous and particle contamination guidelines for data center*.
Clegg, S. L., Brimblecombe, P. and Wexler, A. S. (1998) *Thermodynamic Model of the System H^+- NH_4^+ - SO_4^{2-} - NO_3^- - H_2O at Tropospheric Temperatures*, Journal of Physical Chemistry, **102**, 2137-2154.
Shehabi, A. (2009) *Energy Demands and Efficiency Strategies in Data Center Buildings*, PhD Dissertation [Online], Civil and Environmental Engineering University of California, Berkeley. September **2009**.
Shehabi, A., Horvath A., Tschudi, W., Gadgil, A.J., Nazaroff, W. W. (2008), *Particle concentrations in data centers*, Atmospheric Environment, **42**, 5978-5990.

Effect of the extensive use of fireplaces on carbonaceous particle concentration levels in Athens, Greece

E. Diapouli, V. Vasilatou, S. Vratolis, M. Gini, D. Saraga, Th. Maggos, K. Eleftheriadis

Institute of Nuclear & Radiological Sciences & Technology, Energy & Safety,
National Centre of Scientific Research "Demokritos", 15310 Ag. Paraskevi, Attiki, Greece
Keywords: carbonaceous aerosol, biomass burning, urban background site, $PM_{2.5}/PM_{10}$.
Presenting author email: ldiapouli@ipta.demokritos.gr

The main factors contributing to reported exceedances of the particulate matter (PM) air quality limit values, in Athens are the high urbanization of the city, mostly reflected by intense traffic, along with meteorological conditions that favour the accumulation of the emitted pollutants. During the last two years, the financial crisis has greatly affected every aspect of the country's economic and other activity, including significant changes in the emission strength of certain sources. Instead of diesel fuel oil, which was traditionally used for residential heating, massive use of fireplaces or wood stoves became a regularphenomenon across the city. The objective of the present work was to investigate the long term effect of this intense biomass burning activity on the concentrations of PM and in particular its carbonaceous constituents.

The results presented correspond to winter measurements (November – January) collected during 2010 – 2013 at Demokritos urban background station (GAW-DEM, 2007). 24-hr $PM_{2.5}$ concentrations were measured gravimetrically, while elemental (EC) and organic (OC) carbon concentrations were monitored on a 3-hr basis by Semi-Continuous OCEC Field Instrument (Sunset Laboratory Inc.).

During January 10 – February 10, 2013 an intensive campaign was conducted, targeted specifically on the effects of biomass burning. $PM_{2.5}$ and $PM_{2.5\text{-}10}$ concentrations were measured gravimetrically by means of a low volume custom-made two stage impactor. Two samples were collected daily starting at 8:00 am and 6:00 pm, in order to characterize separately the day-time and night-time periods. In addition, 6-hr PM_{10} samples were collected on quartz filters, to be analyzed for OC and EC (Lab OC-EC Aerosol Analyzer, Sunset Laboratory, Inc.).

Initial results clearly demonstrated an increase in $PM_{2.5}$ and organic carbon concentrations during the present and last winter, in comparison to 2010-11 (Figure 1). The largest difference corresponded to the contribution of OC to $PM_{2.5}$ mass, which has more than doubled during the last two winter seasons (mean OC-to-$PM_{2.5}$ concentration ratios for the three consecutive periods: 0.21, 0.55 and 0.47). This effect was more pronounced in 2011-12 when temperatures were generally lower than the following year. January 2013 was rather mild (mean value around 10°C), with frequent south winds and a number of Sahara dust transport events. On the other hand, the drop of temperature was followed by a sharp increase in OC levels, especially during the night, clearly indicating the use of fireplaces (Figure 2).

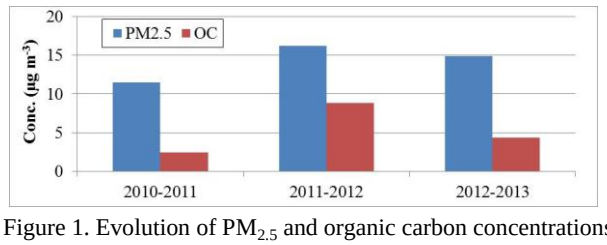

Figure 1. Evolution of $PM_{2.5}$ and organic carbon concentrations during wintertime of 2010 - 2013.

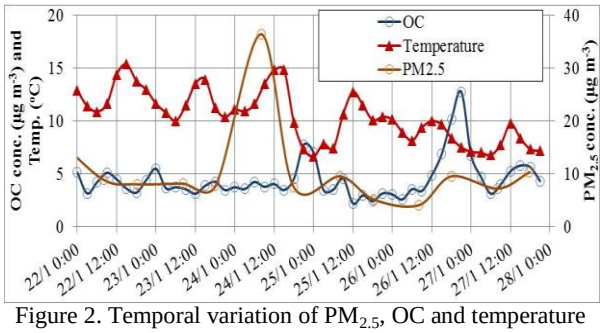

Figure 2. Temporal variation of $PM_{2.5}$, OC and temperature during 22 – 27/1/2013.

Elemental carbon concentrations were similar during 2010/11 and 2012/13(0.72 μg m^{-3} and 0.68 μg m^{-3} on average, respectively) and much higher during 2011/12 (2.53 μg m^{-3}). These results reflect changes in anthropogenic activities caused by the financial crisis of the two last years. In the previous years the main source of EC in the area was vehicular traffic. During winter of 2011/12 biomass burning emissions were added to traffic causing a great increase in concentration levels. During winter 2012/13 lower traffic densities were observed, while the change in source contributions is highlighted by the EC/OC concentrations ratio which has decreased from a value of 0.30 to 0.15, indicative of biomass burning aerosol (Schmidl et al., 2008).

Acknowledgement: This research has been partly co-financed by the European Union (European Social Fund – ESF) and Greek national funds through the Operational Program "Education and Lifelong Learning" of the National Strategic Reference Framework (NSRF) - Research Funding Program: **THALES**, Investing in knowledge society through the European Social Fund.

GAW-DEM (2007) http://gaw.empa.ch/gawsis/reports. asp?StationID=2076202728.
Schmidl, S. et al. (2008) *Atmos. Environ.*, **42**, 9070.

Distribution of aerosol over coal strip mine

V. Docekalova[1], J. Hovorka[1], F. Kobrzek[2], P. Marecek[2]
[1]Institute for Environmental Studies, Faculty of Science, Charles University in Prague, Benatska 2, 128 01 Prague 2, Czech Republic
[2] AirshipClub.com, Nad Salkovnou 9, 147 00 Praha 4, Czech Republic

Keywords: coal strip mine, PM_{10}, flight measurement.
Presenting author email: venikae@gmail.com.

Coal strip mine is supposed to be significant source of coarse atmospheric aerosol to surroundings of the mine. Contribution of the mine aerosol to the air pollution in the surroundings are usually modelled (Chakraborty et al., 2002; Guidebook, 2009) and rarely directly measured (Hovorka et al., 2011), since vertical transport of the mine aerosol directly from the source is difficult to measure.

Therefore, objective of this study was to measure vertical and horizontal distribution of PM_{10}, PM_1 and coarse aerosol in atmospheric boundary layer above the area of coal strip mine through unique experimental flight measurements.

Electrically powered airship was used with specially designed gondola carrying aerosol monitors DustTrak DRX Aerosol Monitor 8533, TSI, P-Trak Ultrafine Particle Counter 8525, TSI. Temperature and relative humidity data were also recorded. Detailed information is summarised in table 1.

Table 1. Parameters measured during flights.

Parameter	Instrument	Logging interval
PM_{10}, $PM_{2,5}$, PM_1	DRX	1 s
20 nm – 1000 nm particles number concentration	P-Trak	1 s
Temperature, RH	Commeter	10 s

Repeated flights were carried out in several heights according to mine edge level (- 50 m, 0 m, 50 m, 100 m, 150 m). Airship position data were recorded also every second. Airship velocity was in the range from 2 to 7 ms^{-1}.

Figure 1 shows how mass concentration of coarse mode of aerosol depends on distance from the mine surface: the closer distance, the higher concentration.

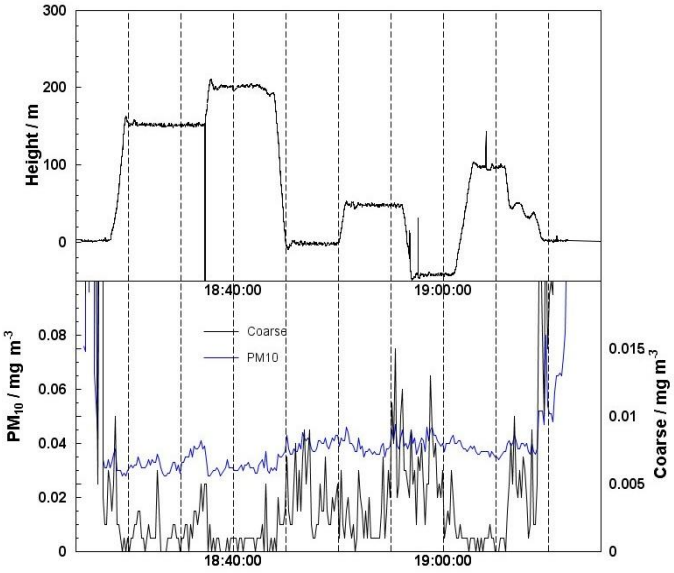

Figure 1. Vertical distribution of PM_{10} and coarse mode-particles over coal strip mine.

Flight measurements were also compared to ground-based measurements of PM_{10} and PM_1 and meteorological data.

Chakraborty M. K., Ahmad M., Singh R. S., Pal D., Bandopadhyay C. and Chaulya S. K. (2002) *Environmental Modelling & Software* **17**, 467-480.

Guidebook (2009) *EEA (European Environmental Agency) Emission Inventory Guidebook.* http://www.eea.europa.eu/

Hovorka J., Gregr M. and Civis M. (2011) *Acta Environmentalica Universitatis Comenianae* **19,** 113-116.

Spatial - temporal variability of particle number concentrations between a busy street canyon and the urban background

V. Dos Santos-Juusela[1], T. Petäjä[1], A. Kousa[2], and K. Hämeri[1,3]

[1] Department of Physics, University of Helsinki, P.O. Box 64, FI-00014 Helsinki, Finland
[2] Helsinki Region Environmental Services Authority HSY, P.O. Box 100, FI-00066 HSY, Helsinki, Finland
[3] Finnish Institute of Occupational Health, Topeliuksenkatu 41 A, FI-00250 Helsinki, Finland
Keywords: Ultrafine particles, Helsinki, street canyon, spatial variations.
Presenting author email: vanessa.dossantos-juusela@helsinki.fi

Road traffic is a major source of airborne ultrafine particles (UFP, diameter < 100 nm) in urban areas. As these particles concentrate close to the sources, their number can vary considerably from site to site (Seinfeld and Pandis, 2006). Since exposure to UFP is suspected to cause serious adverse health effects (Franck et al., 2011, Oberdörster et al., 2004), understanding the spatial-temporal variations of UFP in urban areas is of great importance, especially for epidemiological studies. We evaluated the spatial-temporal variations of UFP by measuring particle total number concentrations (PNC) continuously in a busy street canyon and an urban background site of Helsinki, from 20.01 to 10.06.2010, using condensation particle counters. In addition, we evaluated the influence of roof-top wind speed, wind direction and temperature on PNC inside the street canyon, as well as the correlation between PNC and PM_{10}, $PM_{2.5}$ and black carbon (BC).

We found that the median PNC in the street canyon (16 500 cm^{-3}) was 3 times higher than in the urban background (5 300 cm^{-3}) for 1-min time series, and were moderately correlated (R^2 = 0.50, for 1-hour medians time series). The peak median number concentration in the street canyon during the morning rush hours was 40 200 cm^{-3} while in the urban background it was nearly 5 times lower, 8 400 cm^{-3}. The analysis of meteorological conditions showed that PNC in the street canyon were inversely proportional to wind speed and temperature, and highly dependent on wind direction. The highest concentrations were during northeastern winds and the lowest during southwestern winds. As both directions are perpendicular to the street axes, we speculate that the higher PNC during northeastern winds may result from wind vortex formation inside the canyon, as suggested by previous studies. The PNC in the street canyon were best correlated with black carbon (R^2 = 0.78) than with $PM_{2.5}$ (R^2 = 0.34) or PM_{10} (R^2 = 0.05) for 1-hour medians of weekdays. The result was expected since $PM_{2.5}$ and PM_{10} are also affected by sources other than traffic, such as long range transport and street dust.

The results confirm that the combination of high traffic intensity and slow dispersion rates in the street canyon yield in PNC considerably higher than the urban background levels. This indicates that people spending time in the street canyon are exposed to considerably higher UFP concentrations than people spending time in the urban background. Thus, air pollution hotspots should be considered in epidemiological evaluations.

The aerosol data was partly produced in the MMEA Programme (Measurement, Monitoring and Environmental Assessment). MMEA is supported by TEKES (the Finnish Funding Agency for Technology and Innovation) and coordinated by the Finnish energy and environment cluster – CLEEN Ltd. We would like to thank the Helsinki City Planning Department for providing the traffic data and Pasi Aalto for providing the technical support.

Franck, U., Herbarth, O., Röder, S., Schlink, U., Borte, M., Diez, U., Krämer, U. & Lehmann, I. 2011. Respiratory effects of indoor particles in young children are size dependent. *Science of the Total Environment,* 409**,** 1621-1631.

Oberdörster, G., Sharp, Z., Atudorei, V., Elder, A., Gelein, R., Kreyling, W. & Cox, C. 2004. Translocation of inhaled ultrafine particles to the brain. *Inhal Toxicol,* 16**,** 437-45.

Seinfeld, J. H. & Pandis, S. N. 2006. *Atmospheric chemistry and physics : from air pollution to climate change,* Hoboken, Wiley

Airborne Aldehydes as Altitude-Distributed Source of Particulate Matter in the Troposphere

S.N. Dubtsov, T.A. Maksimova, G.G. Dultseva

Institute of Chemical Kinetics and Combustion, Siberian Branch of the Russian Academy of Sciences, Novosibirsk, 630090, Russia

Keywords: atmospheric aerosol, aldehydes.

Presenting author email: dubtsov@kinetics.nsc.ru

Aldehydes emitted into the atmosphere from natural and anthropogenic sources, as well as aldehydes formed as secondary pollutants in the atmospheric photooxidation of various hydrocarbons, are precursors of particulate matter. Our previous studies proved that even the simplest aliphatic and aromatic aldehydes form aerosol particles of nanometer size under photolysis (Dultseva et al., 2008). Surface sources of aldehydes have been assessed by researchers but the vertical (altitudinal) distribution of aldehydes in the troposphere remains unknown though the local concentration of aerosol-forming species is a very important characteristic to evaluate the rates and mechanisms of atmospheric photonucleation. In the present study we describe our approach to process the data on aldehyde concentrations at different altitudes to reveal the contributions from ground-based sources and chemical transformations of hydrocarbons in the troposphere.

Airborne measurements of aldehyde concentrations were carried out over the southern part of West Siberia in summer and autumn 2012, and in winter-spring 2013. Air samples were collected with an aircraft-mounted sampling device at the altitudes of 500 to 7000 m. Aldehyde concentrations were measured by means of HPLC using the procedure based on the reaction with 2,4-dinitrophenylhydrazine. Measurements revealed episodes with unexpectedly high [H_2CO] at some altitudes up to 7000 m, with nonmonotonic dependence on altitude, while aromatic aldehydes were not detected at altitudes above 2000 m. Keeping in mind the fact that benzaldehyde can be considered as a marker of anthropogenic air pollution, and our previous results on urban air pollution indicating that benzaldehyde in cities with high traffic usually accounts for *ca.* 10 % of formalehyde concentration, we used the relations between measured [H_2CO] and [C_6H_5CHO] as the basis to distinguish between anthropogenic and natural formaldehyde sources.

Formaldehyde at the altitude of 7000 m was thus related to natural sources. To reveal whether natural sources may account for high (> 0.3 mg/m^3) formaldehyde concentrations, we carried out modelling of the chemical mechanism of hydrocarbon photooxidation at the level of elementary stages, leading to gas-to-particle conversion under tropospheric conditions. We chose isoprene as a model compound emitted by vegetation and compiled the scheme of its transformations in the atmosphere according to Carter (2007), with focus on aldehydes formed at some stages as intermediate products. Rate constants for elementary stages were taken from the NIST Database when available, and the values for unknown rate constants were chosen on the basis of known ones for similar stages with other hydrocarbon species. This approach, together with the simulation of nucleation according to Smolukhowski's algorithm, allowed us to assess the biogenic contribution into formaldehyde concentration in middle troposphere. The general scheme of transformations can be represented as

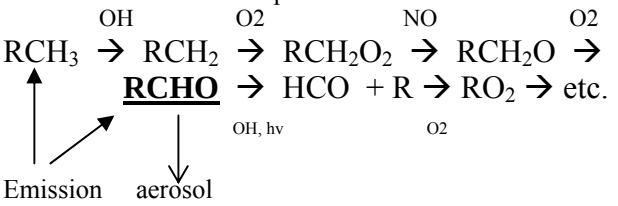

This general scheme involves specific stages for the cases of R = alkenyl (hydrocarbon radical with double bonds) and R = alkyl. Hydrocarbons present in industrial emissions and those emitted by the vegetation can be clearly distinguished from each other in the samples collected in winter when only the contribution from coniferous trees is to be taken into account, while foliaceous trees, bushes and herbs do not emit organic compounds into the atmosphere. Aldehydes also exhibit a clear distinction of natural origin from the industrial sources. This evaluation allowed us to state that the origin of substituted aromatic aldehydes in the atmosphere is commonly biogenic, while benzaldehyde is an industry-related pollutant. Aliphatic aldehydes, including formaldehyde, originate both from vegetation and from industry; these contributions can be quantified through a comparison between summer and winter samples. Our results suggest that in summer about 80 % of airborne formaldehyde in the troposphere at an altitude of 5000 m and above has the biogenic origin, and among this amount, more than a half is formed as the secondary pollutant in alkene and alkane photooxidation, while the fraction of industry-related contribution reaches more than 90 % in winter but accounts for notmore than 20 % in summer. This feature may be significant for any region with climatic conditions close to those existing in the southern part of West Siberia.

Acknowledgements**.** The work was supported by the Russian Foundation for Basic Research (Project No. **11-**05-00921) and Integration Project of SB RAS.

Dultseva, G.G., Dubtsov, S.N. and Dultsev, F.N. (2008) *J. Phys. Chem. A,* **112** (23), 5264–5268.

Carter, W.P.L. (2007) *Atm. Environ.,***41**, S80-S117.

The comparison of the light scattering coefficient measured in urban and coastal environments

V. Dudoitis, V. Ulevicius, K. Plauškaitė and G. Mordas

Center for Physical Sciences and Technology, Savanoriu av. 231, LT-02300, Vilnius, Lithuania
Keywords: light scattering, angstrom exponent, nephelometer
Presenting author email: vadimas.dudoitis@ftmc.lt

Atmospheric aerosols affect the Earth's climate directly through absorbing and scattering the solar radiation. The light scattering coefficient is depended on the aerosol particle chemical composition and is different in various environments. In this work, we determined and compared light scattering coefficients for urban and coastal environments. The most common component of coastal aerosol is sea-salt, which has a significant influence on the light scattering properties Chamaillard *et al* (2006). One of such property is a wavelength dependence of the optical thickness described by the Ångström wavelength exponent α. According to Smirnov *et al* (2002) average α values estimated for marine environments were in range from 0.3 to 0.7.

Table 1. Monthly observations of aerosol light scattering coefficients.

	AVG, Mm^{-1}	MAX, Mm^{-1}	MIN, Mm^{-1}	25‰, Mm^{-1}	50‰ Mm^{-1}	75‰, Mm^{-1}
Vilnius city						
σ_{sp}^{450}	30.5	369.1	8.9	16.8	23.9	37.8
σ_{sp}^{550}	20.2	276.2	5.6	10.9	15.7	24.9
σ_{sp}^{700}	12.8	194.6	3.5	6.7	9.7	15.8
Environment Pollution Research station in Preila						
σ_{sp}^{450}	109.6	279.4	13.2	61.6	96.2	158.1
σ_{sp}^{550}	84.5	223.5	9.3	49.1	71.9	119.4
σ_{sp}^{700}	61.7	167.5	7.7	36.2	52.5	85.0

An integrating nephelometer TSI 3563 was used to measure the light scattering coefficient during the whole measurement campaign. Measurements were performed in Preila (55°22'39.24", 21°1'54.34"; coastal area; 2012 December) and Vilnius (54°38'36.31", 25°10'58.81"; urban-background area; 2012 July).

The statistical analysis (Table 1) revealed that almost all total scattering coefficient values were higher in Preila than in Vilnius. Though exceptionally high (MAX) values in Vilnius were reported during the Saharan dust event Mordas *et al* (2013). However, such event is not common for this area and doesn't correctly represent the monthly variations. Thus, the comparison of 99th percentile shows that the aerosol scattering coefficient in Preila is 2.4 times higher than in Vilnius.

Klaipėda meteorological station data and HYSPLIT4 air mass backward trajectories, were compared with α values in Preila and in Vilnius. Preila wind directions can be combined in two categories: from the sea (SW, W, NW, N) and from the land (NE, E, SE, S). Lowest α values were reported from the sea directions, except from the North. In this case, average Ångström values were in range: α_1 = 0.46 – 0.79; α_2 = 0.24 – 0.25; α_3 = 0.42 - 0.58. On the contrary, the wind direction from the land resulted in higher Ångström values, which can be classified as continental aerosol. Average α values for land directions were in range: $\alpha_1=\alpha_2=\alpha_3$=1.32 – 1.48.

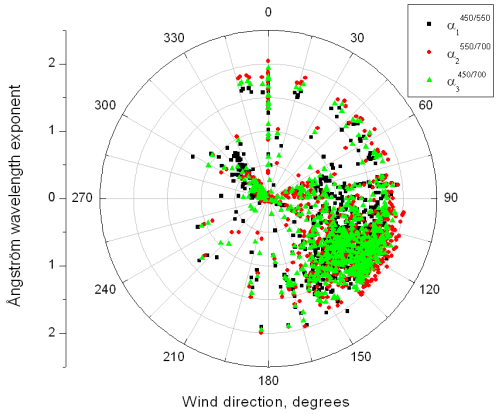

Fig. 1. The dependence of Ångström wavelength exponent α on the wind direction in Preila.

This work was supported by the Lithuanian-Swiss cooperation programme "Research and development" project AEROLIT (Nr. CH-3-ŠMM-01/08).

Chamaillard, K., Kleefeld, C., Jennings, S.G., Ceburnis, D. and O'Dowd, C.D. (2006), J. Quant. Spectrosc. Radiat. Transfer **101**, 498–511.

Smirnov, A., Holben, N. B., Kaufman, Y. J., Dubovik, O., Eck, T. F., Slutsker, I., Pietras, C. and Halthore, R. N. (2002), *J. Atmos. Sci.* **59 (3)**, 501–523.

Mordas, G., Prokopciuk, N. and Ulevicius, V. (2013 in press), *Boreal Env. Res.*

Variations of PM_{10} and its relationship with ^{7}Be and ^{210}Pb measurements at Malaga (Southeastern coast of Spain)

C. Dueñas[1], M.C. Fernández*[1], E. Gordo[1],E.Liger[2] S. Cañete[1] and M. Pérez[3]

[1]Department of Applied Physics I, Faculty of Science, [2]Department of Applied Physics II, Faculty of Computer Engineering, [3]Department of Radiology and Health Physics, Ophthalmology and OTL, Faculty of Medicine. University of Málaga, 29071 Málaga, Spain.

Keywords: ^{7}Be, ^{210}Pb, atmospheric aerosols, gamma spectrometry, particulate matter (PM_{10}).

*Presenting author email: mafeji@uma.es

Levels of particulate matter fraction PM_{10} were monitored between 2009 and 2011 in Málaga (Spain). PM_{10} concentrations were measured at "Carranque" station by the beta attenuation method. This station is one of the Atmospheric Pollution Monitoring network managed by the Environmental Health Service of the Andalusian Government.

Weekly ^{7}Be and ^{210}Pb concentrations in air were continuously monitored (4º 28' 4" W; 36º 43' 40"N) with a high-volume air sampler (ASS-500C). This sampler uses polypropylene square filters (44 x 44 cm^2) with a collection efficiency 93-99%, at a flow rate of 90,000 L min^{-1}. Measurements by gamma-spectrometry were performed to determine the activities of the samples using an intrinsic REGe detector.

Long-term measurements of cosmogenic radionuclides such as ^{7}Be provide an important data in studying global atmospheric processes and comparing environmental impact of radioactivity from man-made sources to natural ones. On the other hand, ^{210}Pb is produced by radioactive decay from its progenitor, ^{222}Rn, which emanates primarily from land surface. Therefore, ^{210}Pb in the air is an effective tracer of the continental surface air mass. The variation of the data with time was studied by time series analyses and seasonal patterns were identified. The study of air back-trajectories were computed by means of the Hybrid Single-Particle Lagrangian Integrated Trajectories (HYSPLIT) trajectory model (Draxler, 1994) using meteorological data supplied by the US National Climatic Data Centre.

Table 1 provides arithmetic mean (AM) and related statistical information such as geometric mean (GM), standard deviation (SD), variation coefficient (CV), maximum (MAX) and minimum (MIN) values.

Table 1. Statistical parameters of the different measurements.

	AM	GM	SD	CV(%)	MAX	MIN
^{7}Be (mBq/m^3)	5.1	4.8	1.7	34.7	10.2	2.1
^{210}Pb (mBq/m^3)	0.55		0.31		2.04	0.1
PM_{10} ($\mu g/m^3$)	40.3	37.8	14.3	35.5	86.3	17.4

The concentration data of ^{7}Be, ^{210}Pb and PM_{10} with meteorological variables were correlated to understand the weekly variation of these radionuclides in air. This study has shown that ^{7}Be and PM_{10} are associated with different sources in Málaga and they may reach high concentrations simultaneously. The reason for this is the concurrent occurrence of subsidence processes over North Africa (resulting in the downward transport of ^{7}Be from the mid-troposphere) and the suspension of mineral dust over desert region with a subsequent transport to Málaga. Additionally, in order to simplify the analysis, the events have been grouped into: (a) High PM_{10} and ^{210}Pb concentrations with low ^{7}Be concentrations; (b) High PM_{10} and ^{210}Pb concentrations with high ^{7}Be concentrations; (c) Low PM_{10} and ^{210}Pb concentrations with low ^{7}Be concentrations.

Several events of high ^{7}Be concentrations are mainly caused by downward transport of ^{7}Be from the mid-troposphere at mid-latitudes. The meteorological situation was characterised by an Atlantic anticyclone system with a low-pressure area over central European North Atlantic. High ^{7}Be concentrations were also found associated with low aerosol mass concentrations. These values were attributed to downward transport from mid-to-upper troposphere over the North Atlantic. The meteorological situation was characterised by a south Europe anticyclone located in the South Atlantic Ocean that favoured the development of a blocking system with a low-pressure area over north Europe. Under these conditions, a slanting stratospheric air mass can penetrate into the troposphere (Hernández et al., 2008). The distribution of ^{210}Pb in the atmosphere show both spatial and temporal variations depending on the geographical location, atmospheric circulation and scavenging processes. High concentrations for ^{210}Pb are obtained with air masses from the Sahara area.

The authors gratefully acknowledge the NOAA Air Resources Laboratory (ARL) for the provision of the HYSPLIT transport and dispersion model and/ or READY website (http://www.arl.noaa.gov/ready.html) used in this study.

Hernández F., Rodríguez S., Karlsson L., Alonso-Pérez S., López-Perez M., Hernández-Armas J. and Cuevas E., (2008). *Atmos. Environ.* **42**, 4247-4256.

Draxler, R.R., 1994. *Hybrid single-Particle Lagrangian Integrated Trajectories, Version 3.2. NOAA-ARL.*

ATMOSPHERIC FLUXES OF RADIONUCLIDES ON MONTHLY TIME -SCALE IN MALAGA (SPAIN)

C. Dueñas[1], M.C. Fernández[1], E. Gordo[1], S. Cañete[1], E. Liger[2] and M. Pérez[3]
1 Department of Applied Physics I, Faculty of Sciences, [2]Department of Applied Physics II, Faculty of Computer Engineering, [3]Department of Radiology and Health Physics, Ophthalmology and OTL, Faculty of Medicine. University of Málaga 29071 Málaga (SPAIN)
Keywords: atmospheric aerosol, deposition, ^{7}Be, ^{210}Pb, precipitation
E-mail: mcduenas@uma.es

ABSTRACT.- Bulk atmospheric deposition of gamma radionuclides (^{7}Be, ^{210}Pb and ^{40}K) has been measured at Málaga (4º 28′ 80″ W; 36º 43′ 40″ N) at a coastal Mediterranean station in the south of Spain, from January 2005 through December 2012 for monthly periods

INTRODUCTION Berylium-7 is one of the radionuclide produced by spallation reactions of cosmic rays with light atmospheric nuclei.^{7}Be rapidly associates primarily with submicron-sized aerosol particles. Lead-210 which is one of the natural radionuclide of the ^{238}U decay series is widely used as a tracer. ^{210}Pb depositional pattern gave us information on continental aerosols in lower troposphere. These two radionuclides with their different sources and therefore are useful to understand the mechanisms of aerosol removal from the atmosphere. These radionuclides have been measured routinely in many places of the word in order to study the description of environmental processes such as aerosol transit and residence times in the troposphere and aerosol deposition velocities. ^{40}K is found in most types of soil and can easily be transported by re-suspended material. Potassium is an important constituent of fertile soil and is an essential nutrient for plant growth and in the human diet. This nuclide has been previously associated with the arrival of coarse re-suspended material (PM10, particulate matter with diameter below 10 µm) from the African continent (Hernández et al., 2005).

MATERIAL AND METHODS.- The sampling site is one of the environmental radioactivity monitoring network stations operate by the Spanish Nuclear Security Council (CSN). The sampling point was located above the ground, on the roof of the Faculty of Sciences, University of Málaga.

Monthly precipitation and dry fallout samples were routinely collected using a steel tray 1m^2 in area as a collecting system and polyethylene vessels of 50 l capacity for rainwater samples reservoirs. Measurements by gamma spectrometry were performed to determine the ^{7}Be, ^{210}Pb and ^{40}K activities of the samples using an intrinsic REGe detector. The peak analysis of ^{7}Be (I= 10.52 %, 477.7 keV), ^{210}Pb (I = 4%, 45 keV) and ^{40}K (I = 11%, 1460.8 keV) was done using GENIE 2000 peak analysis software. The counting time was 172800s.

RESULTS.- Table 1 summarises the main statistical variables calculated for the measured gamma emitting radionuclides (^{7}Be, ^{210}Pb and ^{40}K) in Bq/l over the whole sampling period.

	^{7}Be	^{210}Pb	^{40}K
Average	2,66	0.41	0.23
Geometric mean	2.19	0.34	0.18
Standard deviation	1.70	0.24	0.15
Coeff. of variation	63.9 %	58.7%	68.0%
Minimum	0.6	0.05	0.02
Maximum	8.3	1.32	0.84

The results from fluxes of ^{7}Be, ^{210}Pb and ^{40}K were correlated with five parameters: rainfall amount, rainfall duration, number of dry days and number of wet days. The next table provides the correlation coefficients between the fluxes and the mentioned parameters.

	Flux ^{7}Be	Flux ^{210}Pb	Flux ^{40}K
Precipitation (mm)	0.84	0.89	0.66
Duration of precipitation (min)	0.7,	0.82	0.59
Number of dry days	-0.45	-0.63	0.55
Number of wet days	0.51	0.68	0.61

The depositions of ^{7}Be and ^{210}Pb were well correlated with the amount of precipitation . Such relations have been commonly observed and explained by the fact that rainfall constitutes the major depositional pathway of these radionuclides. As previously observed, correlation of rainfall with ^{210}Pb seems better than with ^{7}Be (Caillet el al., 2001) likely due to a relatively greater contribution of ^{210}Pb from dry deposition.

BIBLIOGRAPHY

Caillet, S., P. Arpagaus, F. Monna and J. Dominik (2001).J. Environ. Radioactivity 53, 241-256 Hernandez, F. Hernández Armas CatalánA., Fernández Aldecoa, J.C. and Karlson, L.2005. Atmospheric Environment, 39, 4057-4066.

The comparative analysis of variations of background radiation components and atmospheric electrical parameters

M.S. Cherepnev[1], I.I. Ippolitov[2], M.V. Kabanov[2], P.M. Nagorsky[2], S.V. Smirnov[2], A.V. Vukolov[1], V.S. Yakovleva[1]

[1]Department of Applied Physics, Tomsk Polytechnic University, Tomsk, 634050, Russian Federation
[2]Department of Climatic System, Institute of Monitoring of Climatic and Ecological System (IMCES) SB RAS, Tomsk, 634050, Russian Federation
Keywords: background radiation, light ions, atmosphere, variation
Presenting author email: maxcherepnev@gmail.com

Interest to investigation of natural background radiation levels is caused by the need to assess the role of ionizing radiation variations in the dynamics of aerosol atmosphere. The main purpose of the work was a comparative evaluation of the spectral-temporal variations of the ionizing radiation measured at series of heights and depths, and identification of their mutual relations with meteorological and electrical parameters of the surface layer. The monitoring method and equipment are detail described in [1].

3-years experiment in Tomsk revealed that variations of β-background radiation of atmosphere are relatively poorly associated with pressure variations of synoptic-scale and is closely related to daily variations of temperature and moisture. Annual behavior of β-background changes from year to year as opposed to γ-background for which the maximum is observed in November and a minimum in February and March. Synchrony in the dynamics of β- and γ-radiation fields was registered in summer-autumn period.

In soil, the duration of increase of background radiation component levels was from 6 up to 12 hours, the duration of recovery was about some days. Variations of α-, β-and γ-radiation in atmosphere and soil with a one-day period were in opposition. Relationship of variations of atmospheric meteorological parameters and subsurface radiation components has fundamentally different nature in winter and summer conditions. Namely, in winter pressure increase is accompanied by an increase in the subsurface radiation components but in summer there is no such relationship between them. Typical example of the dynamics of atmospheric (height) and subsurface (depth) components of β-background in early winter is represented in Fig. 1. Here are the variations of: β-background levels at a height of 10 m (h=10 m) and at a depth of 50 cm (h=-0.5 m); positive and negative conductivities (light ions) $\lambda_{\pm}$ (data1 – λ_-; data2 – λ_+), pressure ***P*** and temperature ***T***.

If for $\lambda_{\pm}$ the correlation with variations of pressure is negative, then the β-background in the soil it is positive. A situation with variations in the temperature is reversed: the correlation between above mentioned parameters and the temperature changes its sign compared to the pressure. β-background radiation in the air rise sharply with amplitude of up to several hundred percent and duration from a few hours to half a day with changing pressure (temperature). Temporal variations of β-radiation in soil are not some hours but some days.

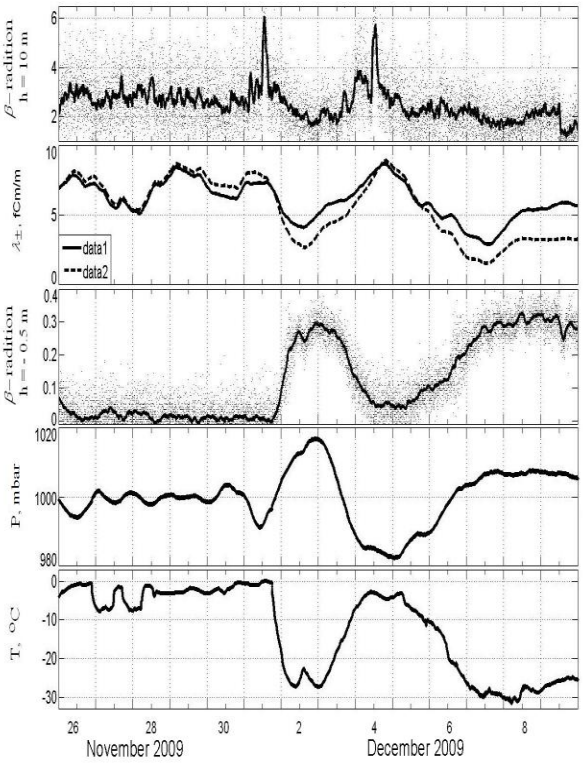

Figure 1. Variations β-background radiation and meteorological parameters in winter season

3-years monitoring revealed some important futures in variations of background ionizing radiation at series of heights and depths during such events as heavy rainfall.

It was also observed that on synoptic and annual scales the variations of atmosphere γ-background and the neutron component of cosmic rays are closely related with atmospheric pressure changes. As a result, cyclonic activity leads to concerted fluctuations in the γ-background levels of terrestrial origin and cosmic rays, and the restructuring of the atmospheric circulation in large areas, which is related with global climate changes, leads to concerted changes in the γ-background level.

Yakovleva,V., Ippolitov, I., Kabanov, M., Nagorsky, P., Firstov, P., Karataev, V., Vukolov, A., Smirnov, S., Parovik, R. (2009)
A coordinated multifactor experiment to analyze of transport processes of soil radon in surface atmosphere, ANRI Journal, **4,** 55-60.

13C measurements on organic aerosol – ambient samples versus source studies

U. Dusek[1], C. Meusinger[2], B. Oyama[1,3], W. Ramon[1], P.A. de Wilde[1], R. Holzinger[1], T. Röckmann[1]

1 Institute for Marine and Atmospheric research Utrecht (IMAU), Utrecht University, The Netherlands
2 Copenhagen Center of Atmospheric Research (CCAR), University of Copenhagen, Denmark
3 Department of Atmospheric Sciences, Institute of Astronomy, University of São Paulo

Keywords: organic aerosol, carbon isotopes, volatility, SOA.
Presenting author email: u.dusek@uu.nl

The stable carbon isotopes ^{12}C and ^{13}C can be used to get information about sources and processing of organic aerosol (OA). We developed and tested a method to measure $\delta^{13}C$ values of OA collected on filter samples in different volatility classes. These filter samples are introduced into an oven, where organic compounds are thermally desorbed in He at different temperatures. The compounds released at each temperature step are oxidized to CO_2 using a platinum catalyst at 550 °C. The CO_2 is then passed on to an isotope ratio mass spectrometer (IRMS) to measure $\delta^{13}C$ ratios. With a similar setup the chemical composition at each temperature step can be determined using a Proton Transfer Reaction Time-of-Flight Mass Spectrometer (PTR-ToF-MS).

System evaluation with controlled test compounds showed that organic compounds usually start evaporating from the filter when their melting point is reached. Isotopic fractionation occurs only if one temperature step is within a few degrees of the melting point of the substance, so that the substance only partially evaporates. However, this effect should be limited in an ambient sample containing thousands of individual chemical compounds. $\delta^{13}C$ values of aerosol filter samples do not depend on the sample amount used, i.e. the system shows good linearity. The reproducibility depends somewhat on the sample amount and is usually $< \pm$ 0.3 ‰ for oven temperatures up to 200 °C and $< \pm$ 0.5 ‰ for oven temperatures greater than 200 °C.

We analysed aerosol samples collected in a tunnel in Brazil (vehicular emissions), laboratory generated secondary organic aerosol (SOA) from alpha-pinene ozonolysis, and ambient filter samples from a regional site in the Netherlands and an urban site in Belgium. First results indicate that the SOA produced in our experiments is slightly enriched in $\delta^{13}C$ compared to the precursor alpha-pinene. It is also more volatile than organic aerosol from ambient or tunnel filters. The $\delta^{13}C$ ratios of SOA and vehicular emissions do not change strongly with oven temperature, i.e. the more refractory organic compounds have similar isotopic composition as the more volatile compounds.

This is in contrast to many ambient organic aerosol samples, where the more volatile compounds evaporating below 200°C are often depleted with respect to the refractory compounds (see Figure 1).

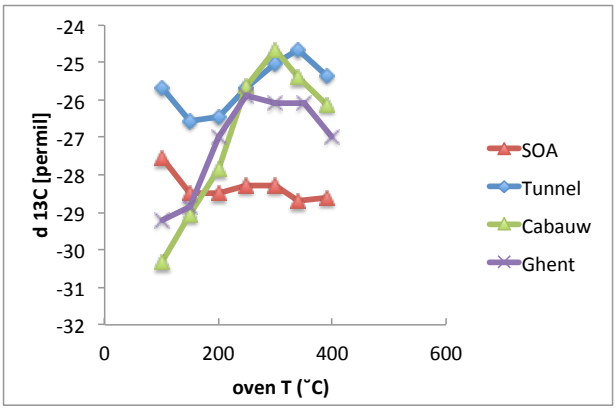

Figure 1. $\delta^{13}C$ of organic compounds released at a given oven temperature for aerosol filter samples taken in a tunnel in Brazil, SOA produced from alpha-pinene ozonolysis compared with typical ambient samples taken in the polluted regional background location of Cabauw, and the urban area of Ghent

Measurements at the Cabauw site show interesting differences between $\delta^{13}C$ measured in polluted air masses and relatively clean air with marine air mass origin. In polluted, continental air masses $\delta^{13}C$ is only weakly dependent on oven temperature, similar to the tunnel samples. In air masses with marine origin, organic compounds evaporating at low temperatures are strongly depleted in ^{13}C, see figure 1.

Possible reasons for the difference between source profiles and ambient samples (mixture of sources vs. the role of heterogeneous oxidation in the ambient filter samples vs. sampling artefacts) will be discussed and related to the chemical composition of the aerosol.

Road Pavement Abrasion as the Source of Particulate Matter

Dušan JANDAČKA, Daniela ĎURČANSKÁ

University of Žilina, Faculty of Civil Engineering, Department of Highway Engineering, Žilina, Slovakia
Key words: aerosol, particulate matter (PM), air pollution, asphalt mixture
Email: dusan.jandacka@fstav.uniza.sk

Sources of pollution with reference to particulate matter which originate from the automotive traffic can equally come from combustion processes or non-combustion processes. Non-combustion related emissions of particulate matter as of the automotive traffic may come from the tear and wear of tires, wear of the braking pads and callipers, lining of brakes [1], **abrasion of road pavement,** wear of mechanical clutches, car bodies and re-suspension of collected dust by virtue of the automotive traffic and their presence on the road, frequenting the road. It can prove rather complex and intricate to identify the road pavement abrasion directly in field as the source of particulate matter and separate it from other sources as well as quantify its share on the origination and presence of particulates. One of the possible ways is to approach the chemical analyses of particulate matter as well as multi-layer statistical analyses. But even then it is indispensable to be aware of which chemical substances are to be considered as prime suspects for a given source – to be contained and released by the road pavement, surface. The main goal of that experiment was to determine the presence, production or presence of aerosol in various samples of tarmac compounds (various in composition – hard-core aggregate and type of asphalt, tar used). Samples marked as A3 – tarmac concrete (AC), S3 – stone mastic asphalt (SMA), P3 – Single layer drainage asphalt (PA).

During the process of wearing the carriageways the ambient air was sampled inside the sampling device by means of the following apparatus - Aerodynamical Particle Sizer Spectrometer /APS/- Model 3321 and low volume flow sampler of Leckel LVS3.

Following the experimental measurements while focusing on the determination of the aerosol production originating in various road pavements and asphalt substances there were several differences uncovered among the tried samples. First of all the highest amount of the aerosol being released happened during the experimental phase, whereas it was determined to be with the sample of S3 – stone mastic asphalt (SMA). When comparing the overall mean concentrations, this was almost a twofold value. A numerous distribution of aerosol in all the three samples had a similar course. In relation to the weight distribution, a similar trend was carried over by samples of A3 and S3, the sample of P3 showed a more even weight distribution of aerosol without a significant peak values. At the same time, weight wise the most numerous aerodynamic diameter was greater than with A3 and S3 samples. In all the three cases of tested samples, the weight concentration when compared to the volumetric concentration of particulate matter, particulates were shifted towards the greater aerodynamic diameters. Each of the tested samples is a specific one, when relating to their composition – asphalt type, amount of asphalt, kind of aggregate, various lines of granularity and fraction in the composites. With regard to the materials used, there are various samples created observing similar surface structures, which can in the long run influence the abrasion of these road pavements.

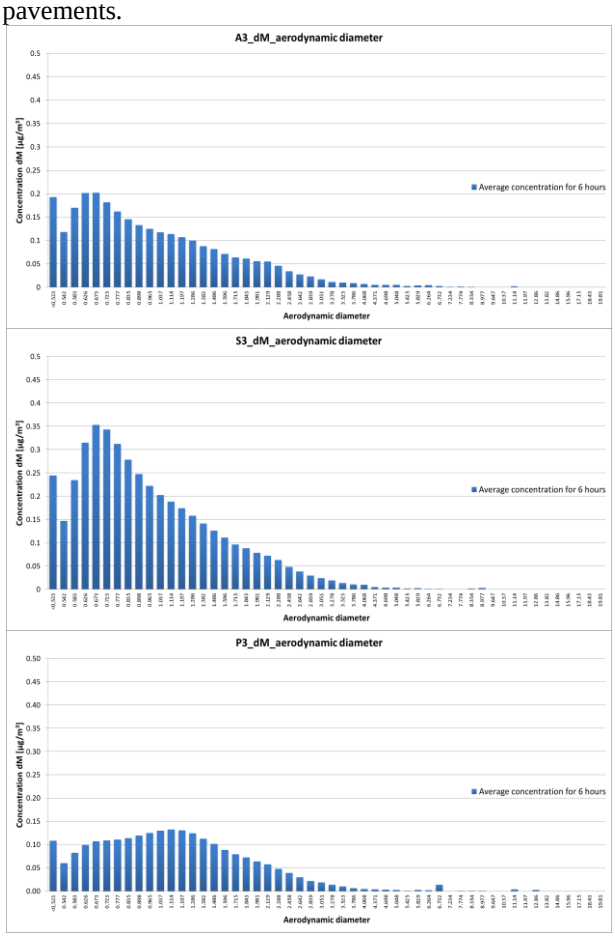

Figure 1 Mass concentration of aerosol from different asphalt mixture

References

[1] P. Moravec, J. Smolík, J. Schwarz, I. Ševčíková, J. Kukutschova, V. Tomášek: Sampling and characterization of airborne particles from car brakes testing, Conference Proceedings of the Czech Aerosol Society Conference, Čelkovice 2009, Issued by ČAS 2009, ISBN 978-80-86186-20-7.

This contribution is the result of the project implementation: "Promotion & Enhancement of Transportation Research Centre " (ITMS: 26220220160) supported by the Research & Development Operational Programme funded by the ERDF.

Time-resolved organic speciation at the Theodore Roosevelt National Park, North Dakota, USA

A.Eiguren[1], G. Lewis[1], N. Kreisberg[1], D.R. Worton[2], A.H. Goldstein[2], S.V. Hering[1]

[1]Aerosol Dynamics Inc., Berkeley, CA, USA
[2]Department of Environmental Science, Policy and Management, University of California, Berkeley, CA, USA

Keywords: time-resolved PM collection, organic speciation, oil fracturing, methane combustion.
Presenting author email: arantza@aerosol.us

National Parks and Wilderness Areas in United State possess many stunning vistas and scenery. Unfortunately, these scenes are diminished as result of increased air pollution. To maintain visual air quality, congress included legislation in the 1977 Clean Air Act to prevent future and remedy existing visibility problems. In 1985, the IMPROVE program (Interagency Monitoring of Protected Visual Environments) was initiated. This program implemented an extensive long term monitoring program to establish the current visibility conditions, track changes in visibility and determine causal mechanism for the visibility impairment in the National Parks and Wilderness Areas. (http://vista.cira.colostate.edu/improve/)

Since 2000 the total number of sites in the IMPROVE network is 110. These sites are under the supervision of the IMPROVE committee and represent 155 of the 156 areas of concern (figure 1).

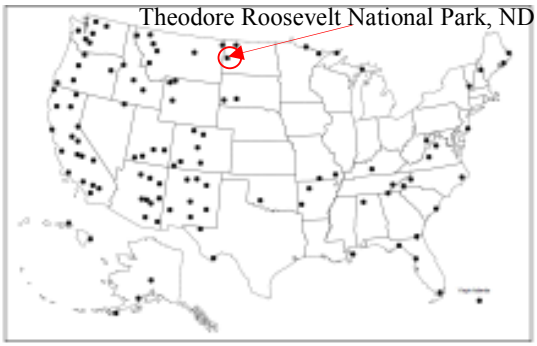

Figure 1. IMPROVE Monitoring Network (IMPROVE aerosol QMP, 2002) and location of this study's site.

The current study was focused on the Theodore Roosevelt National Park (North Dakota). This park is surrounded by oil and gas production wells (figure 2).

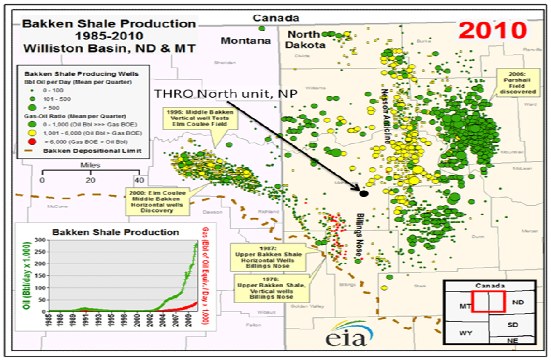

Figure 2. Distribution of Bakken Shale Producing Wells as 2010, and Monitoring Station location

Emissions from well development and production phases, including hydraulic fracturing "fracking" processes and open flame combustion of the extracted methane gas (figure 3), are not well characterized and their impact on visibility is unknown.

Figure 3. Oil wells and open flame near Watford City, ND

Three spot samplers have been deployed at the park's north site monitoring station, for the collection of time-resolved dry, concentrated $PM_{2.5}$ samples. Collection will be conducted from mid February to beginning of April. Samples for inorganic anion analysis (IC-ECD) are collected for 6 hr, and samples for polycyclic aromatic hydrocarbon characterization (HPLC-FL) and organic speciation by Thermo-desorption HR-GCxGC-MS are collected for 24hr.

Results obtained in this pilot study will help better understanding and characterizing emissions from oil production wells and fracking processes and their impact on the visibility and air quality of the park as well as surrounding communities.

Acknowledgements:
This work was supported by the IMPROVE network and National Parks, and by the NIH Grant 1 RC3 ES019081-01

References:
QUALITY MANAGEMENT PLAN for the Aerosol Monitoring Network Component of the IMPROVE Visibility Monitoring Program, 2002
(http://vista.cira.colostate.edu/improve/Publications/QA_QC/IMPROVEAerosolQMP_May2002.PDF)

Water activity measurement of pure and mixed organic/inorganic solutions

Mehrnoush M. Fard[1], and Merete Bilde[2]

[1] Department of Chemistry, University of Copenhagen, DK-2100 Copenhagen, Denmark
[2] Department of Chemistry, Aarhus University, Langelandsgade 140, DK-8000 Århus, Denmark
Keywords: Water Activity, Hygroscopicity, CCN Activity.
Presenting Author e-mail: fhb487@alumni.ku.dk

Atmospheric aerosols play an important role on Earth's climate, atmospheric chemistry, visibility and human health. Aerosols are complex mixtures of organic and inorganic matters and several studies show that organic and inorganic constituents of the atmospheric aerosol are internally mixed.

The water activity of solutions comprising atmospheric particles is a key parameter to calculate the super-saturation required for particles to activate as cloud condensation nuclei (CCN). It is also needed to determine water uptake properties below 100% relative humidity which impacts visibility, direct radiative forcing, and hydrological cycle in the atmosphere.

Early experimental studies on the water activity of different constituents of the atmospheric aerosol acting as cloud condensation nuclei (CCN) mainly focused on common atmospheric inorganic salts such as ammonium sulfate and sodium chloride. However, organics have been shown to be a significant fraction of the aerosol mass (Kanakidou et al. 2005) in different environments, and the presence of organic species in atmospheric aerosol can affect both the aerosol hygroscopicity and the ability of mixed particles to serve as CCN (Raymond and Pandis, 2002, Kanakidou et al. 2005, Kristensen et al. 2012).

The focus of this study is to measure the water activity of several atmospherically relevant pure and mixed Organic/Inorganic systems in wide concentration range and provide data required to determine hygroscopic growth factor (Gf) and cloud-nucleating behavior of aerosol particles.

Methods

Water activities, a_w, are measured using an AquaLab water activity meter (Model 4TE, Decagon Devices, U.S.A.) covering the temperature range from 289-313K.

Results

Figure 1 shows measured water activity as a function of total concentration of solute for aqueous solutions of pure NaCl, solutions containing NaCl and the amino acid Glycine and pure Glycine.

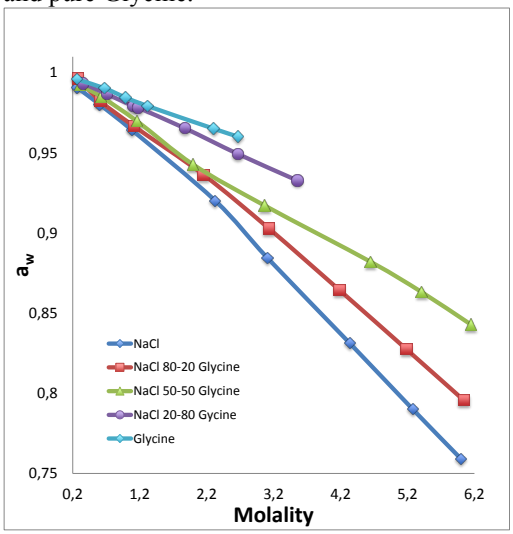

Figure 1: Water activity of pure and mixed NaCl/Glycine solutions (mass ratios are provided in the legends) measured at different concentrations at 298 K.

Measured water activities will be compared with thermodynamic modeling results. Hygroscopic growth factors calculated from the measured water activities will be presented and discussed.

We acknowledge the Carlsberg Foundation and the Nordic Center of Excellence on Cryosphere-atmosphere interactions in a changing Arctic climate (CRAICC).

Reference

Kanakidou, M., Seinfeld, J. H., Pandis, S. N., Barnes, I., Dentener, F. J., Facchini, M. C., Van Dingenen, R., Ervens, B., Nenes, A., Nielsen, C. J., Swietlicki, E., Putaud, J. P., Balkanski, Y., Fuzzi, S., Horth, J., Moortgat, G. K., Winterhalter, R., Myhre, C. E. L., Tsigaridis, K., Vignati, E., Stephanou, E. G., and Wilson, J. (2005) *Chem. Phys*. **5**, 1053-1123.

Kristensen, T. B., et al. (2012), *J. Geophys. Res*. **117**, D22203.

Raymond, T. M. and Pandis, S. N. (2002) *J. Geophys. Res. Atmos*. **107** (D24).

Can lung-deposited surface area measurements serve as surrogate for black carbon?

M.Fierz[1,2], D.Meier[2], C.Hüglin[3] and H. Burtscher[1]

[1] University of Applied Sciences Northwestern Switzerland, 5210 Windisch, Switzerland
[2] naneos particle solutions llc, 5210 Windisch, Switzerland
[3] Swiss Federal Laboratories for Materials Science and Technology (EMPA), 8600 Dübendorf, Switzerland
Keywords: lung-deposited surface area, elemental carbon, measurement networks
Presenting author email: martin.fierz@naneos.ch

Mass-based limit values for particulate matter, based on size cut-offs at a few micron such as PM2.5 and PM10, are used all over the world for legal purposes, but the awareness is growing that these measurements may not adequately reflect the negative health impact of ultrafine particles. In particular, the world health organization (WHO) declared diesel soot particles to be carcinogenic in 2012, and these soot particles with typical diameters of around 70nm only contribute very little to PM2.5 and PM10 mass. Therefore, the search is on for alternative particle metrics that might be more health relevant with respect to ultrafine particles, and which could complement today's PMx standards. Due to the toxic properties of soot, the most obvious candidate is elemental carbon or black carbon (EC or BC), the latter can be continuously measured e.g. with an Aethalometer.

Another recent trend in urban air pollution monitoring is the move to multiple small and possibly mobile monitoring stations to complement today's fixed monitoring sites. These two trends are actually connected: The characteristic length scale over which PM mass based metrics vary is much larger than the length scale over which ultrafine particles vary, and therefore, if ultrafine particles are to be measured properly in an urban environment, a single fixed central measurement station – which was fine for PM10 - is no longer sufficient.

Since common instruments for BC measurements are bulky and expensive, they cannot be used in such sensor networks, and here we explore the use of another alternative metric, the lung-deposited surface area (LDSA), as a surrogate for BC in urban environments. LDSA is also interesting in its own, since the interaction of inhaled particles with the human body takes place on the particle surface; and a number of toxicology studies have found a better link between health effects and particle surface area than either particle mass or number (e.g. Waters, 2009). The lung-deposited surface area can be measured approximately with diffusion charging sensors (Wilson, 2007), which can be miniaturized easily. Such miniature diffusion charging sensors are interesting, because they can be incorporated in large numbers in sensor networks due to their low power consumption, comparatively low price, and long maintenance intervals. Moreover, they provide a much higher time resolution than common instruments for BC (on the order of seconds), which is necessary for mobile sensing platforms.

Our hypothesis is that LDSA and BC correlate well in urban environments, since both are dominated by combustion related aerosol. We verified the hypothesis by computing LDSA from SMPS data of the Swiss air pollution monitoring network (NABEL) and comparing it to BC. Figure 1 shows the two pollutants for the urban background site Zürich-Kaserne.

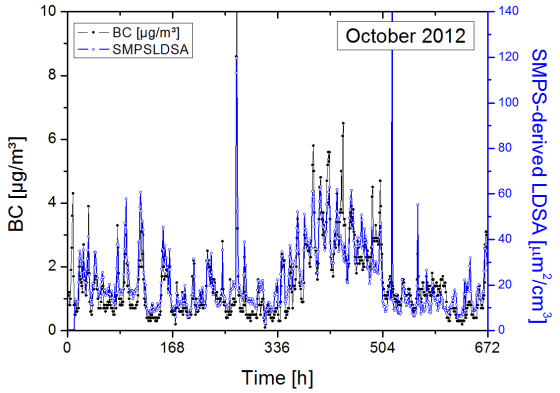

Figure 1. Time series of BC and SMPS-derived LDSA at the urban background site Zürich-Kaserne during 4 weeks in October 2012.

We have now deployed four miniature LDSA sensors (naneos partector) at four selected NABEL sites with BC monitoring (Basel, Bern, Lugano and Zürich). These four sites represent different environments: Lugano and Zürich are urban background sites; Bern is an urban street canyon site while Basel is a suburban site.

The LDSA sensors will run for the first half of 2013, providing us with a lot of useful information. We will learn more about the reliability and the applicability of these sensors for deployment in unattended sensor networks; and at the same time we will be able to answer the question whether or not BC can be approximated by LDSA as surrogate measurement in urban environments.

Wilson W.E. et al. (2007) *J. Air & Waste Manage. Assoc.* **57**:211-220.
Waters K.M. et al. (2009) *Tox Sci* **107**:553-569

Regional-scale modeling of organic aerosol composition in Europe: Insights from comparison with aerosol mass spectrometer factor analysis

C. Fountoukis[1], A.G. Megaritis[1,2], K. Skyllakou[1,2], P.E. Charalampidis[3], C. Pilinis[3], and S.N. Pandis[1,2,4]

[1]Institute of Chemical Engineering Sciences (ICEHT), Foundation for Research & Technology-Hellas (FORTH), Patras, Greece
[2] Department of Chemical Engineering, University of Patras, Patras, Greece
[3]Department of Environment, University of the Aegean, Mytilene, Greece
[4]Department of Chemical Engineering, Carnegie Mellon University, Pittsburgh, PA 15213, USA
Keywords: PMCAMx, Regional air quality, Positive Matrix Factorization, AMS data
Presenting author email: cfountoukis@iceht.forth.gr

Recently, the volatility basis set framework (VBS) has been implemented in several Chemical Transport Models (CTMs) improving predictions of organic aerosol (OA) concentrations (Fountoukis et al., 2011). However, uncertainties still exist in these models regarding the volatility distribution of the primary OA emissions, the chemical aging of the OA or errors in either the anthropogenic or biogenic emissions.

The increasing availability of Aerosol Mass Spectrometer (AMS) field measurements analyzed by Positive Matrix Factorization (PMF) provides an opportunity to further evaluate and constraint CTMs based on their ability to predict concentrations of the different OA components. In this work we apply PMCAMx-2008 over Europe (Fountoukis et al., 2011) during 3 periods representative of different seasons, and use an extensive set of AMS measurements (15 datasets in total) to evaluate the model and (using PMF results) gain more insight into the sources and physical and chemical transformations of OA, as well as identify strengths and limitations of our current OA modeling framework.

In this study we simulate 3 periods (1–29 May 2008, 25 February – 24 March 2009, and 15 September – 17 October 2008) during which 3 intensive measurement campaigns took place as part of large-scale projects of the EU. During all three campaigns, AMS measurements of aerosol mass composition were performed at several sites in Europe while further analysis of the OA composition was performed using PMF. The modeling domain covers a 5400×5832 km^2 region in Europe with 36×36 km grid resolution and 14 vertical layers extending up to approximately 6 km in height with a surface layer depth of 55 m.

Fig. 1 shows a comparison of predicted vs. observed PM_1 oxygenated OA (OOA) from all three measurement datasets. The overall agreement between AMS measurements and model predictions is encouraging. The OA formation during the late spring and autumn period is mostly dominated by enhanced photochemical activity while during the winter period by direct primary emissions. Predictions of fresh primary OA (POA) are the highest during the winter period ranging from 0.5 to 1.5 μg m^{-3} on average, with peak values up to 10 μg m^{-3} at urban centers. On average, the model predicts that oxygenated OA contributes 93% to total OA during May, 87% during winter and 96% during autumn with the rest comprising fresh POA.

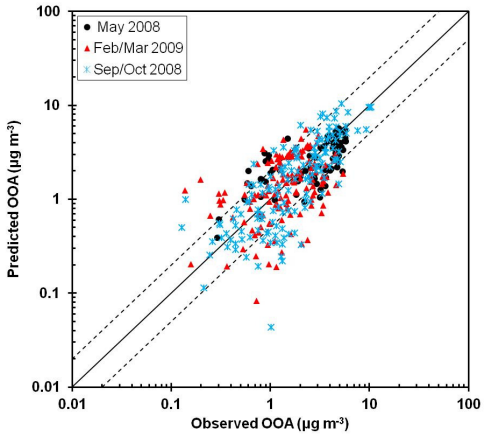

Figure 1. Comparison of predicted vs. observed PM_1 oxygenated organic aerosol from 3 measurement periods. Each point corresponds to a daily average value. Also shown the 1:1, 2:1 and 1:2 lines. Observed data represent AMS measurements. The slope of the line for OA is 0.893 (R^2 = 0.49).

Oxidized POA and OOA from intermediate volatility organic compounds (IVOCs) is predicted to be a major OA component with a contribution of ~50% to total OOA in all three periods. Biogenic SOA (BSOA) comprises around one third of OOA during May and around 40% during the other two periods. In each one of the simulation periods, the spatial pattern of concentrations for OPOA, ASOA and BSOA is quite similar, while the fresh POA pattern is different indicating differences in sources and production mechanisms. Inferences regarding the nature of LV-OOA and SV-OOA measured components and their representation in the model will be discussed.

This work was funded by the European Community's 7th Framework Programme EU project PEGASOS (contract 265307).

Fountoukis, C., et al. (2011) Evaluation of a three-dimensional chemical transport model (PMCAMx) in the European domain during the EUCAARI May 2008 campaign, *Atmos. Chem. Phys.*, 11, 10331–10347.

Year-round measurement of PM_1 aerosol and its chemical composition in the Swiss high Alps using the Time-of-Flight Aerosol Chemical Speciation Monitor (ToF-ACSM)

R. Fröhlich[1], M. J. Cubison[2], J. G. Slowik[1], A. S. H. Prévôt[1], U. Baltensperger[1], U. Rohner[2], M. Gonin[2], J. R. Kimmel[2, 3], D. R. Worsnop[3], J. T. Jayne[3]

[1]Laboratory of Atmospheric Chemistry, Paul Scherrer Institute, CH-5232 Villigen PSI, Switzerland
[2]TOFWERK AG, CH-3600 Thun, Switzerland
[3]Aerodyne Research, Inc., Billerica, MA-01821, United States
Keywords: AMS, Aerosol mass spectrometry, ACSM, Monitoring, Free troposphere.
Presenting author email: roman.froehlich@psi.ch

The newly-developed Time-of-Flight Aerosol Chemical Speciation Monitor (ToF-ACSM) is conceptually related to the Q (quadrupole)-ACSM (Ng, 2011), which itself is based on Aerosol Mass Spectrometer (AMS, Jayne, 2000) technology. The ACSM systems are designed for long-term, low-maintenance operation. These features, combined with their lower cost relative to the AMS, makes them suitable for long-term deployment (> years) and integration into monitoring networks. The ToF-ACSM provides online measurements with high sensitivity (e.g. detection limit for sulfate: 3.1 ng/m^3 at 30 min time resolution) of the major non-refractory species of the submicron aerosol (organics, NO_3, SO_4, NH_4 and chloride).

Initial deployment of the ToF-ACSM was performed at the Sphinx research station on the Jungfraujoch (JFJ, 3570 m a.s.l.) in the Bernese Alps. For many years measurements at the JFJ have provided excellent insights into the properties of high alpine aerosols. Most of the winter the station lies within the free troposphere while in summer aerosol generated at lower altitudes can reach the Jungfraujoch due to vertical exchange processes (Henne, 2004). However, despite the vast number of experiments performed there, we here present the first dataset of an online year-round measurement (resolution: 15 - 30 min) of the aerosol chemical composition at the Jungfraujoch.

This one-year exercise proved the measurements and tested the operational stability of the new instrument. The deployment included an intercomparison between the ToF- and Q-ACSM for a period of five months. The instrument time series were strongly correlated (e.g. organics July 27 - August 05: slope = 0.98; R^2 = 0.95) and the ToF-ACSM improved on Q-ACSM detection limits by a factor of 4 to 62, depending on the species measured. Furthermore, we plan to report the correlation to a CToF-AMS instrument from measurements during the CLACE2013 campaign in the first months of 2013.

The aerosol data shows a distinct seasonal cycle with higher concentrations in summer ($C_{av(26Jun-07Sept)}$ = 3.3 μg/m^3, $C_{max(26Jun-07Sept)}$ = 27.8 μg/m^3)† and low concentrations during wintertime ($C_{av(01Nov-07Jan)}$ = 0.5 μg/m^3)†. In summer the aerosol consists mainly of organics (58 %) with some sulfate (25.2 %), ammonium (9.4 %) and nitrate (6.8 %) and exhibits a regular diurnal cycle corresponding to PBL movement; that is, the aerosol concentration increases during the day with a maximum around 16:00 and decreases again after sunset. The concentrations of all measured species follow this cycle more or less the same way. In winter this diurnal pattern disappears and the concentration stays relatively constant on a low level with the exception of a few rare pollution events (see Fig. 1). This suggests that the JFJ research station is situated in the free tropsphere during the cold season. Sulfate becomes the major fraction in winter with a share of 54.6 %. 30.1 % of the aerosol are organics and the fractions of ammonium and nitrate are similar to summer (8.7 % and 6.0 %)

Preliminary analyses with statistical techniques (Multilinear Engine version 2, Paatero, 1999) show that the organic fraction in summer mainly exists of highly oxidized species, i.e. "aged" aerosol (mostly LV-OOA, some SV-OOA). As expected, the influence of fresh aerosol from local sources like HOA or BBOA is low at the Jungfraujoch (< 15 % of total).

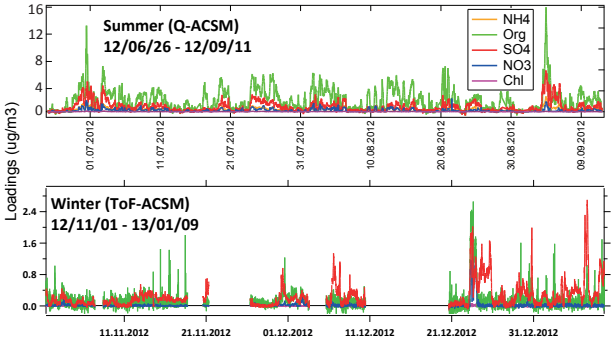

Figure 1: Sample time series recorded at the Jungfraujoch. Top: 2.5 months in summer measured with the Q-ACSM. Bottom: 2 months in winter measured with the ToF-ACSM. Note the different scaling of the y-axis.

This work was supported by the Swiss Commission for Technology and Innovation, the European FP-7 project ACTRIS, the Federal Office for the Environment as well as the Swiss National Science Foundation.

We acknowledge Joan & Martin Fischer and Maria & Urs Otz who always make sure things are going smoothly on the Jungfraujoch.

Ng, N. L. *et al.* (2011) *Aerosol Sci. Tech.*, **45**, 770-784.
Jayne, J. T. *et al.* (2000) *Aerosol Sci. Tech.*, **33**, 49-70.
Henne, S. *et al.* (2004) *Atmos. Chem. Phys.*, **4**, 497-509.
Paatero, P. (1999) *J. Comput. Graph. Stat.*, **8**, 854-888.

†all values calculated assuming collection efficiency CE = 0.5

Aerosol Activation and Scavenging during the Cloudy Test Campaign at the CERN CLOUD chamber

C. Fuchs[1], J. Tröstl[1], J. Duplissy[2], E. Weingartner[1], U. Baltensperger[1] and the CLOUD collaboration

[1]Laboratory of Atmospheric Chemistry, Paul Scherrer Institut, CH-5232 Villigen PSI, Switzerland
[2] Department of Physics, University of Helsinki, FI-00014 Helsinki, Finland
Keywords: cloud formation, aerosol growth, GCR, CLOUD.
Presenting author email: claudia.fuchs@psi.ch

Besides aerosol nucleation, which has been observed almost everywhere in the atmosphere (Kulmala et al., 2004), the growth of these newly formed aerosol particles and the formation of cloud droplets and ice crystals play a major role in atmospheric research. In previous studies at the CERN CLOUD chamber mainly nucleation events have been studied (Kirkby et al., 2011). However, the CLOUD 6 campaign mainly focused on the formation of cloud hydrometeors. The CLOUD chamber with a very low contaminant background, stable temperature conditions and a fast adiabatic expansion system allowed obtaining new scientific findings by determining which particles or particle fractions act as **c**loud **c**ondensation **n**uclei (CCN) and **i**ce **n**uclei (IN). Due to adiabatic expansion the relative humidity increases until the chamber is supersaturated and cloud droplets and ice crystals are formed. Cloud formation was investigated applying different pressure drops, expansion times and temperatures. In addition CERN's **P**roton **S**ynchrotron (PS) was used to simulate ion conditions of the atmosphere from ground level to the upper troposphere (Kirkby et al., 2011).

The purpose of this study was to investigate the activated fraction and the scavenging of aerosols during cloud events with a new CLOUD chamber setup. One SMPS and one TSI CPC 3010 were installed at the CERN CLOUD chamber to measure the aerosol particle size distribution and aerosol concentration. In addition, two cyclones were attached in order to remove all particles and hydrometeors larger than 1 µm from the sampling flow. Hence, the number concentration and the dry size distribution of interstitial aerosols (i.e. the non-activated particles) could be measured during the presence of clouds. During all other times the total dry size distribution was measured. By comparing the pre (total), inter (interstitial) and post (total) particle size distribution, aerosol activation and scavenging were investigated. In addition, charged and neutral conditions were tested.

Figure 1 shows an example of aerosol activation during a cloud event at T=-34°C. The concentration is plotted against the particle diameter where the green line denotes the concentration (dN/dlogD) before the cloud was formed and the red line the concentration while the cloud was present.

First tests of the new expansion system were successful, showing aerosol activation and scavenging. The cyclones removed droplets and ice crystals successfully to measure the interstitial aerosol concentration during cloud events.

For the upcoming campaign (CLOUD 8) further improvements of the system are planned to ensure that a longer cloud presence is possible. In addition, the possible influence of **g**alactic **c**osmic **r**ays (GCR) will be investigated.

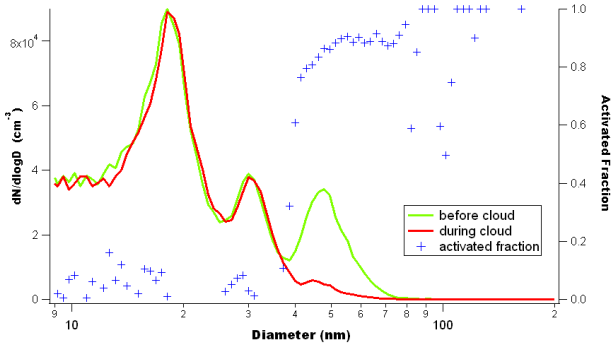

Figure 1. Number site distributions before and during the presence of a cloud. Particles larger than ~ 40 nm were activated to cloud droplets.

Acknowledgements: We would like to thank CERN for supporting CLOUD with important technical and financial resources, and for providing a particle beam from the CERN Proton Synchrotron. This research has received funding from the EC Seventh Framework Programme (Marie Curie Initial Training Network "CLOUD-ITN" no. 215072, MC-ITN "CLOUD-TRAIN" no. 316662, and ERC-Advanced "ATMNUCLE" grant no. 227463), the German Federal Ministry of Education and Research (project nos. 01LK0902A and 01LK1222A), the Swiss National Science Foundation (project nos. 200020_135307 and 206620_130527), the Academy of Finland (Center of Excellence project no. 1118615), the Academy of Finland (135054, 133872, 251427, 139656, 139995, 137749, 141217, 141451), the Finnish Funding Agency for Technology and Innovation, the Nessling Foundation, the Austrian Science Fund (FWF; project no. P19546 and L593), the Portuguese Foundation for Science and Technology (project no. CERN/FP/116387/2010), the Swedish Research Council, Vetenskapsrådet (grant 2011-5120), the Presidium of the Russian Academy of Sciences and Russian Foundation for Basic Research (grants 08-02-91006-CERN and 12-02-91522-CERN), and the U.S. National Science Foundation (grants AGS1136479 and CHE1012293).

Kulmala, M. et al. (2004) *J. Aerosol Sci.* **35**, 143-176.

Kirkby, J. et al. (2011) *Nature.* **476**, 429-433.

The effect of the tramway track building on the aerosol pollution in Debrecen, Hungary

E. Furu[1,2], I. Katona-Szabo[2], A. Angyal[1], Z. Szoboszlai[1,] Zs. Török[1,2], and Zs. Kertész[1]

[1]Institute of Nuclear Research of the Hungarian Academy of Sciences, Laboratory of Ion Beam Applications, H-4001 Debrecen, P.O. Box 51, Hungary
[2]University of Debrecen, H-4032 Debrecen, Egyetem tér 1, Hungary
Keywords: urban aerosol pollution, tramway construction, PM concentration, PM elemental composition
Presenting author e-mail: furu.eniko@atomki.mta.hu

In this study atmospheric aerosol concentration and composition were investigated along the tramway track construction in Debrecen, Hungary. Aerosol samples were collected with personal samplers between 21. and 30. 09. 2011 - four hours a day, during working hours. The sample collection was made by walking on the pavement next to the building. The weather was dry and warm on the sampling days.

Nuclepore two-stage samplers equipped with Nuclepore polycarbonate filters of 8 μm and 0.4 μm pore diameter were used. Mass concentrations and elemental composition were determined separate for coarse (particles with aerodynamic diameter larger than 2.5 μm) and fine size fractions (particles with aerodynamic diameter smaller than 2.5 μm). The elemental composition ($Z \geq 13$) was determined by particle induced X-ray emission (PIXE) analytical method. The concentration of particulate matter (PM) was measured by gravimetry using a microbalance.

The measured PM10 and PM2.5 concentrations are shown in Table 1. PM10 concentrations were compared with the data of the Hungarian Air Quality Network (http://www.kvvm.hu/olm/index.php?lang=en). In every case the PM10 concentration were 8-20 times higher along the building than the data of the Hungarian Air Quality Network. In the second week the weather was rather windy which explains the increased PM10 level along the tramline building.

Table 1. PM2.5 and PM10 concentration data along the tramline track construction and at the AQ monitoring stations of the Hungarian Air Quality Network

Date	tramline building PM2.5 (μg/m^3)	tramline building PM10 (μg/m^3)	Hungarian Air Quality PM10(μg/m^3) average data
21.09.11	24	292	26
22.09.11	36	291	49
23.09.11	36	232	37
26.09.11	39	322	38
27.09.11	51	647	48
28.09.11	43	408	42
29.09.11	33	617	22
30.09.11	40	559	30

The elemental concentration of the samples which were collected along the building were compared with the elemental concentration of samples from our urban background station (garden of Atomki), which is situated ~ 500 m from the new tramline track building. For comparison we show data from September 2010 (no building), and from September 21-30. 2011 (Table 2). For both size fractions significant increase were observed from 2010 to 2011. In the case of PM2.5 the concentration of all measured elements increased by a factor between 8 and 15 in the garden of Atomki. The elemental concentrations measured along the tramline construction were 1.5-5 times higher than at the Atomki. In the case of the coarse fraction the increase from 2010 to 2011 were only around a factor of 2 at the garden of Atomki. However, along the tramline constructions we measured 10-100 times higher elemental concentration values than 500 m away.

Table 2. Average elemental concentrations in the coarse fraction at an urban background station in 2010 and 2011 (A) and along the tramway track construction (B)

	Coarse fraction		
	A(2010) ng/m^3	A(2011) ng/m^3	B(2011) ng/m^3
Al	395	415	5360
Si	650	1250	35400
P	30	15	190
S	120	155	780
Cl	25	20	645
K	115	205	3795
Ca	275	480	17700
Ti	16	34	700
V	0.5	1.6	25
Cr	0.6	60	90
Mn	4.7	13.4	210
Fe	285	535	8200
Co	<0.8	4.5	30
Ni	1.0	18	14
Cu	3.4	4.3	48
Zn	7.9	6.6	125
Br	1.0	0.6	8.6
Sr	<1.9	5.1	90
Ba	6.2	13.7	310
Pb	1.9	4.1	125

Acknowledgement
This work was supported by the TÁMOP-4.2.2/B-10/1-2010-0024 project and co-financed by the European Union and the European Social Fund. This work was carried out in the frame of the János Bolyai Research Scholarship of the Hungarian Academy of Sciences.

Contribution of fossil and modern carbon to PM2.5 and CO_2 in the atmosphere of Debrecen, Hungary

I. Major[1,2], E. Furu[1,2], I. Hajdas[3], Zs. Kertész[1], M. Mihály[1],

[1]Institute for Nuclear Research, Hungarian Academy of Sciences, H-4001 Debrecen, P.O. Box 51, Hungary
[2]University of Debrecen, H-4032 Debrecen, Egyetem tér 1, Hungary
[3]Swiss Federal Institute of Technology (ETHZ), Rämistrasse 101, 8006 Zürich, Switzerland
Keywords: urban aerosols, PM2.5, fossil - non fossil carbonaceous component, radiocarbon dating by AMS
Presenting author email: furu.eniko@atomki.mta.hu

Atmospheric fossil CO_2 observations have been running in Debrecen, Hungary since the autumn of 2008 (Molnár et al., 2010). From the winter of 2010 synchronized aerosol sampling and C-14 analyses started to compare the aerosol fossil carbon content to the fossil carbon-dioxide results in the same time period and the same location.

Integrated bulk aerosol PM2.5 samples were collected on prebaked quartz filers with 10 L/min flow rate over the months at an urban background site in Debrecen, Hungary. One or two weeks long integrated samples were collected on a filter and those periods were synchronized with the parallel monthly atmospheric CO_2 observations. The collected total aerosol mass was determined by gravimetry, and its carbon content was measured through the amount of CO_2 produced after its combustion in the AMS C-14 sample preparation line.

Atmospheric fossil CO_2 measurements were done using the ATOMKI gas proportional counting based C-14 dating facility. C-14 measurement of the aerosol samples was carried out at the new EnvironMICADAS AMS facility of ATOMKI. The applied sample pretreatment steps were tested by multiple pretreatment of different sections of several real samples. Test results showed very good reproducibility for the applied aerosol sample preparation method and AMS C-14 analyses.

During the year from November 2010 to November 2011 in Hungary there were very high PM concentrations in the city air several times, particularly during the heating season.

The atmospheric CO_2 and $PM_{2.5}$ concentrations showed high similarity for Debrecen. During the winter heating period significantly higher total $PM_{2.5}$ concentrations could be observed which was also reflected in the quantity of the total carbon. The fossil CO_2 excess was very similar to the fossil carbon content of the $PM_{2.5}$. In the case of CO_2 the role of fossil excess from natural gas, oil and carbon combustion was the dominant for the heating period. For PM2.5 the contribution of modern carbon from biomass burning seems to be the determinant, since not the fossil but the biogenic carbon caused the elevated PM concentrations in the city of Debrecen. In absolute terms, the fossil part of the $PM_{2.5}$ increased, as well, in the heating period, however, even this value was exceeded by the increment of the modern carbon showing that the dominant process of aerosol emission is biomass burning due to municipal wood combustion.

These results clearly show the very different fossil/biogenic contribution in the atmospheric aerosol compared to the carbon-dioxide fraction.

Our results are in good agreement with other published city fossil aerosol results (e.g.. from Zürich) (Szidat et al., 2004). To help the source apportionment of the collected urban aerosol samples also $\delta^{13}C$ stable isotope ratio of the combusted carbon fraction was measured using a Finningan Delta XP plus stable isotope mass spectrometer.

Acknowledgement

This work was supported by the TÁMOP-4.2.2/B-10/1-2010-0024 project and co-financed by the European Union and the European Social Fund, by the János Bolyai Research Scholarship of the Hungarian Academy of Sciences and by the Hungarian NSF (OTKA-81515 and OTKA-77550). This reasearch was perfomed in part of the New Hungary Development Plan under Project No. GOP-1.3.1-09/A-2009-0032.

References

M. Molnár, L. Haszpra, É. Svingor, I. Major, I. Svetlik. *Atmospheric fossil fuel CO_2 measurement using a field unit in a CentralEuropean city during the winter of 2008/09.* Radiocarbon 52 (2010) 2-3: 835-845

S Szidat, T.M Jenk, H.W Gäggeler, H.-A Synal, R Fisseha, U Baltensperger, M Kalberer, V Samburova, S Reimann, A Kasper-Giebl, I Hajdas. *Radiocarbon (^{14}C)-deduced biogenic and anthropogenic contributions to organic carbon (OC) of urban aerosols from Zürich, Switzerland.* Atmospheric Environment, Volume 38, Issue 24, August 2004, Pages 4035-4044

The impact of extreme weather events on air quality in Budapest, Hungary

V. Gácser[1], A. Molnár[2]

[1]Department of Earth and Environmental Sciences, University of Pannonia, Veszprém, P.O. Box 158, H-8201, Hungary
[2]MTA-PE Air Chemistry Research Group, University of Pannonia, Veszprém, P.O. Box 158, H-8201, Hungary
Keywords: heat-wave, air pollutants, visibility
Presenting author email: gacserv@mk.uni-pannon.hu

Weather and climate extreme events frequently lead to negative effect on air quality, mainly in urban areas. It is well known, that atmospheric stability highly influences the concentrations of different air pollutants due to hindering both the vertical and the horizontal movements in the air. High pressure weather systems which bring typical stable situations occur frequently in the Carpathian Basin both in summer and wintertime.

In winter, when a high pressure builds over Hungary, it usually develops low-level inversion and fog that can become persistent. Consequently this results in extremely low visibility as well as elevated concentrations of the air pollutants, like PM10, SO_2, soot, etc., which frequently exceeds the health limit. High pressure system can also cause stable air stratification in summertime. Due to high irradiation and temperature intensive photochemical reactions take place in the lower troposphere. Among others the higher concentration of tropospheric O_3, NO_X, and decreasing visibility allude to development of photochemical smog. These air pollution episodes take place usually in dry, hot periods which frequently related to heat-waves. Climate simulations indicate a drying climate in Hungary with more extreme temperature events (IPCC 2012; HREX 2012). On the basis of long term data analysis more hot days, longer heat-waves and longer dry periods can already be registered in Hungary (Bartholy *et al*, 2007, 2010)

The aim of this work is to study how weather situations leading to extreme air pollution episodes. Two special years, 2010 and 2011 were chosen for this analysis. In 2010 excessively high amount of precipitation (170% of the yearly average amount) has occurred, while 2011 was extreme dry (yearly precipitation 70% of average amount) and warm with a few heat-waves. In this work the air quality (SO_2, NO_2, NO_x, O_3, PM10) (www.kvvm.hu/olm), as well as meteorological data (temperature, precipitation, air pressure, visibility) are evaluated (Integrated Surface Hourly Observations, NOAA National Data Center) at Marczell György Main Observatory, Budapest. In addition, the analyzed synoptic weather maps from these periods (www.met.hu) are also studied.

Our preliminary result show, that especially the concentration of the PM10 and tropospheric ozone follows the changing of the weather situation. PM10 episodes were monitored in both years that were connected to high pressure systems in fall and wintertime. During these events PM10 concentration frequently exceeded the heath limit (24-hours, 50 μgm^{-3}). On the other hand in summer the severe air pollution episodes can be characterized by ozone concentration. In 2010 – the whole summer was rather changeable and wet – the daily ozone concentration ranged between 40 and 70 $\mu g/m^3$; and during only two shorter stable periods the ozone concentration exceeded 70 $\mu g/m^3$. The summer in 2011 was much dryer with much more sunshine, and even the means daily ozone concentration was higher than in 2010; it ranged between 55 and 85 $\mu g/m^3$.

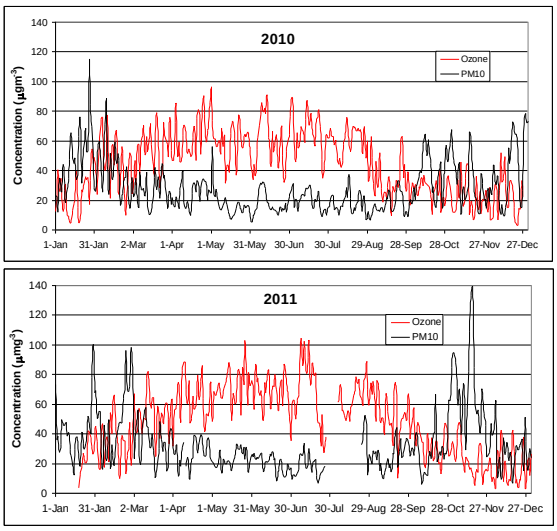

Figure 1: Daily PM10 and ozone concentration in Budapest, Hungary.

This work was supported by TÁMOP-4.2.2.A-11/1/KONV-2012-0064 Project.

IPCC, 2012: Managing the Risks of Extreme Events and Disasters to Advance Climate Change Adaptation. A Special Report of Working Groups I and II of the Intergovernmental Panel on Climate Change [Field, et al (eds.)]. Cambridge University Press.

HREX: Hungarian Report on Extreme Events; 2012

Bartholy, J, Pongrácz, R. (2010) *Physics and Chemistry of the Earth* **35**, 43-51

Bartholy, J, Pongrácz, R. (2007) *Global Planetary Change* **57**, pp. 83-95

Seasonal variation of urban aerosols in a sub-Saharan city: case study of Nairobi, Kenya

S.M. Gaita[1], J. Boman[1], J.B.C. Pettersson[1], M.J. Gatari[2] and S. Janhäll[3]

[1]Department of Chemistry and Molecular Biology, University of Gothenburg, SE-412 96, Göteborg, Sweden
[2]Institute of Nuclear Science and Technology, University of Nairobi, P. O. Box 30197-00100, Nairobi, Kenya
[3]Swedish National Road and Transport Research Institute – VTI, P.O. Box 8072, SE-402 78, Göteborg, Sweden

Keywords: $PM_{2.5}$, seasonal variation
Presenting author´s email: samuel.gaita@chem.gu.se

Seasonal variation of urban aerosols is poorly understood in sub-Saharan Africa due to lack of long-term measurement data. Available scientific information is usually based on short term measurement campaigns (e.g. Gatari and Boman, 2003; Kinney *et al.*, 2010). This predicament is further compounded by the fact that sub-Saharan cities are characterised by lack of long-term air pollution monitoring strategies and concrete policies on air quality and climate change, (UN, 2013).

In the view of the above, measurements of airborne fine particles (equivalent aerodynamic diameter < 2.5 µm, $PM_{2.5}$) were carried out from April, 2008 to May, 2010. The main objective was to get a better understanding of physical and chemical properties of Nairobi aerosol based on long-term measurement data. Observations would then be linked to perceived aerosol sources (local and regional) especially anthropogenic activities within the metropolitan area and their effects on urban air quality and local micro-climate.

Sampling was carried out at two sites within Nairobi metropolitan area. One site was at University of Nairobi main campus (UoN) and the other at the United Nation Environmental Programme (UNEP) headquarters, 5 km to the north of UoN site.

$PM_{2.5}$ samples were collected on pre-weighed polycarbonate filters using cyclone samplers for 24 h, per sample, at a flow rate of 3 L/min, except on weekend when samples were collected for 48 h. At the UoN site, a cyclone sampler was placed 17 m above the ground (agd), on the rooftop of Engineering building. This site being close to the central business district was a good representation of an urban background setting. At the UNEP site, a cyclone sampler placed on the rooftop of Urban Environment Unit offices, 10 m agd.

Particulate mass were determined using a Mettler Toledo TM5 microbalance, BC concentration using a black smoke detector (FH62 1-N) whereas elemental concentrations were analysed using an Energy Dispersive X-ray Fluorescence (EDXRF) spectrometer.

Results presented here are from the UoN site. Observed trend in $PM_{2.5}$ mass concentration (Figure 1), followed the normal rainfall pattern experienced in Kenya. Two troughs were observed and they coincided with two rainy seasons (long rains; March to May, Julian days 75 to 135: short rains; October to early December, Julian days 268 to 329). Importantly, higher concentrations were observed in 2009 due to draught that was being experienced in the country. WHO 24 h guideline limit of 25 µg/m^3 for $PM_{2.5}$ was frequently exceeded in 2009. This highlights the influence of natural phenomenon to air pollution monitoring. Results from elemental concentrations analysis and Positive Matrix Factorisation will be presented on the poster.

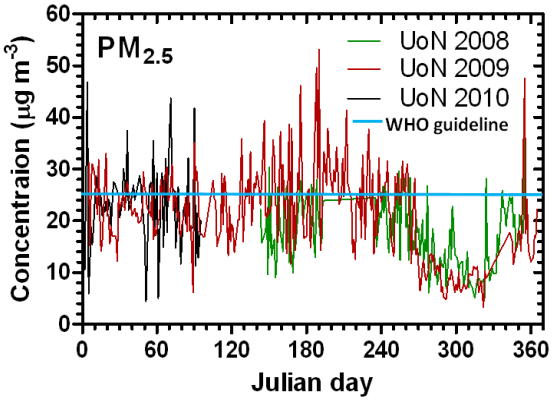

Figure 1: Seasonal variation of $PM_{2.5}$ sampled in Nairobi, Kenya.

In conclusion, it is worth noting that seasonal variation is evident in Nairobi city despite the unpredictability of the weather as experienced in 2009 when rainfall pattern became erratic. This observed variation can be exploited for modelling purposes as a way of planning for mitigation strategies to counteract the effects of aerosols on human health and local climate.

This work was funded by the Swedish International Development Cooperation Agency (SIDA) and the International Programme in the Physical Sciences (IPPS), Uppsala University, Sweden. We recognise the participation of Mr. Kagai at the UNEP site and support by the UNEP Environment Unit.

Gatari M. J. and Boman J. (2003). Black carbon and total carbon measurements at urban and rural sites in Kenya, East Africa. *Atmospheric Environ., 37: 1149 – 1154*

Kinney, P. L., Gatari, M. G., Volavka-Close, N., Ngo, N., Ndiba, P. K., Law, A., Gachanja, A., Gaita, S.M., Chillrud, S.N. and Sclar E. (2011). Traffic impacts on PM2.5 air quality in Nairobi, Kenya. *Environmental Science & Policy 14(4): 369-378.*

United Nations Environment Program (UNEP). Urban AirPollution,http://www.unep.org/urban_environment/issues/urban_air.asp (accessed on 23.02.2013)

Stable carbon isotopic values ($\delta^{13}C$) of biofuel in Lithuania

A. Garbaras[1], A. Lipovec[1,2], A. Masalaite[1] and V. Remeikis[1]

[1]Center for Physical Sciences and Technology, Vilnius, LT-02300, Lithuania
[2]Faculty of Physics, Vilnius University, Vilnius, LT- 10222, Lithuania
Keywords: $\delta^{13}C$, aerosol particles, biofuel.
Presenting author email: garbaras@ar.fi.lt

Introduction

Research on the origin of aerosol particles is important for understanding the climate change, environmental pollution and environmental self-cleaning processes. Atmospheric aerosol absorbs and reflects radiation from the Sun and heat radiation from the Earth, thus changing thermal balance of the planet. Aerosol absorbs gases, chemical elements and compounds, influences water condensation processes, stimulates photocathalytical reactions and has influence on the global chemical processes in the atmosphere [Ceburnis et al., 2005].

Stable carbon isotope method is one of the methods which are more and more implemented in the source apportionment studies [Ceburnis et al., 2011]. Due to the ability to preserve source isotopic ratio this method can be used as source fingerprint and allows distinguish an aerosol sources if they differ in the isotopic ratios. Because of that, the need to have the database of the possible aerosol sources arises. The $\delta^{13}C$ values of main aerosol source pools are known, but there is a lack of data on more precise spatial distribution of isotopic ratios, as these ratios are varying depending on the geographical region.

As biofuel is becoming more popular comparing to the fossil fuel, the demand to know the isotopic ratios of different types of biofuel arises, and usage of these isotopic ratios to assess the part of aerosol particles which is coming from the biofuel. Carbon isotopic ratio of the emitted aerosol particle depends not only on the burning conditions but also on the plants used. Therefore, the knowledge of the plants carbon isotopic ratio is highly needed

The aim of this work is to measure the carbon isotopic ratio of the main plants, which can be used as biofuel in the regional scale. In the future this database will be used in source apportionment studies.

Methods

In this work $\delta^{13}C$ values of the 24 different plants are presented. Wood, leafs, bark, grain, seeds were measured, 77 positions in total. The samples were collected in the Ignalina region (East Lithuania) during August 2012.

Samples were dried and measured with the elemental analyzer connected to the stable isotope ratio mass spectrometer (*Thermo Flash EA 1112 – Delta V Advantage*).

Results

One C_4 plant was found (maize, $\delta^{13}C$ = -13 ‰). The stable carbon isotopic ratios for the rest of the plants (C_3 type) varied from the -25 ‰ to the -33 ‰. In the Fig. 1 are presented some measurements of the wood $^{13}C/^{12}C$ ratios In order to assess the net aerosol input from the biofuel, the data on the composition of burned biofuel is needed because the biofuel isotopic ratio interfere with the fossil fuel isotopic ratio [Masalaite et al., 2012].

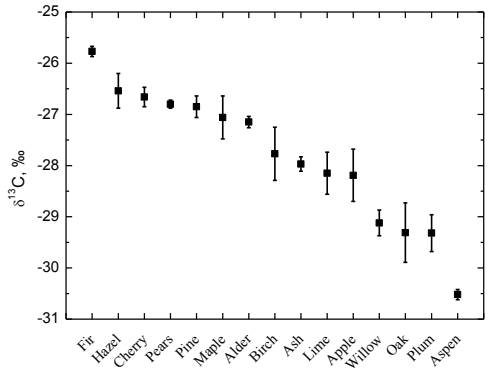

Figure 1. The carbon isotopic ratio of trees which grow in Lithuania and can be used as biofuel. (Wood part isotopic ratio is presented).

Integrated isotopic data from different sources (transportation, domestic heating, fires etc) can be used to perform source apportionment studies of the atmospheric aerosol particles.

This work was supported by the Research Council of Lithuania under grant “Pollution control in biomass combustion: from pollutant formation to human exposure (BioMassPoll) No. ATE05/2012.

Ceburnis, D., Ovadnevaite, J., Kvietkus, K., Remeikis, V., and Ulevicius, V. (2005). *Lith. J. Phys.*, **45**(5), 323-332.

Ceburnis D, Garbaras A., Szidat S., Rinaldi M., Fahrni S., Perron N., Wacker L., Leinert S., Remeikis Facchini V. M. C., Prevot A. S. H., Jennings S. G., and O'Dowd C. D. (2011) *Atm. Chem. Phys*, **11**, 8593-8606.

Mašalaitė A., Garbaras A., and Remeikis V. (2012) *Lith. J. Phys.* **52**, 261–268.

Atmospheric aerosol episodes over Lithuania after the May 2011 volcano eruption at Grimsvötn, Iceland

K. Kvietkus, J. Šakalys, J. Didžbalis, I. Garbarienė, N. Špirkauskaitė, V. Remeikis

State Research Institute Center of Physical Science and Technology, Savanorių Ave. 231, LT-02300 Vilnius, Lithuania
Keywords: PM_1, volcanic sulfate, Grimsvötn.
Presenting author email: ingar@ar.fi.lt

Volcanic eruptions emit large amounts of gaseous and particulate material into the atmosphere. In particular, SO_2 is abundant in volcanic gases (Hobs et al. 1991). SO_2 emitted from volcano could act as a precursor of the formation of sulfuric acid particles. Information of the composition and size distribution of volcanic aerosol particles in the troposphere is important to evaluate their effects on atmospheric radiation and cloud formation.

We present measurements of PM_1 components concentration and size distribution in the vicinity of Vilnius at the Institute of Physics (54°38'N; 24°11'E) on 24-29 May 2011 after the eruption of the volcano at Grimsvötn in Iceland. An Aerodyne Quadrupole Aerosol Mass Spectrometer (Q-AMS) has been used to provide on-line measurement of size dependent chemical composition of non-refractory components (ammonium, nitrate, nss-sulfate, organics) in submicron aerosol particles (PM_1). In order to determine air mass transport routes to Vilnius, forward and backward trajectories were calculated every 1-3 h with a total of 120 h duration for the sites (Grimsvötn and Vilnius) using the National Oceanic and Atmospheric Administration (NOAA) Hybrid Single-Particle Lagrangian Integrated Trajectory (HYSPLIT) model (Draxler and Rolph, 2003).

To distinguish volcanic and non-volcanic origin of PM_1 components four concentration episodes at Vilnius during 24-29 May 2011 have been selected for analysis. Episode 1 (0700-1400 UTC 25 May) and 2 (0400-1100 UTC 26 May) were selected according to trajectories of air masses which travelled from Iceland over North Atlantic Ocean before the arrival to Vilnius. Episode 3 (1200-2300 UTC 26 May) was selected as transitional one when the air masses originated from Iceland travelled over North Atlantic Ocean, and over Scandinavia and partly passed over polluted industrial regions (Great Britain, Germany). During Episode 4 (from 0600 UTC 27 May to 0000 UTC 28 May) air masses were mainly passing over Central Europe.

This study shows that the sulfate emissions from the volcano at Grimsvötn in Iceland reached distances farther than 3000 km, and they can have an influence on the local concentration and size distribution spectra of PM_1 chemical components. Over the period of the volcanic eruption (Episode 1) the sulfate concentrations increased by a factor of 3 and reached 90% of PM_1, while the nitrate and organic levels remained low and unchanged (Fig.1). Air mass trajectory analysis indicates that the volcanic aerosol from Iceland was carried to Vilnius by air masses at the height of 3000–4500 m. The ammonium to sulfate molar ratio (ASR) during Episodes 1 and 2 is 0.81, suggesting that sulfate particles were partially neutralized by ammonium and determined by volcanic eruptions. However, during Episodes 3 and 4 the ASR was higher (1.0) and determined by both volcanic and non-volcanic origin components.

Combining air mass transport analysis as well as investigations of aerosol chemical composition and size distribution parameters, allowed us to explain possible sources of atmospheric submicron aerosol particles.

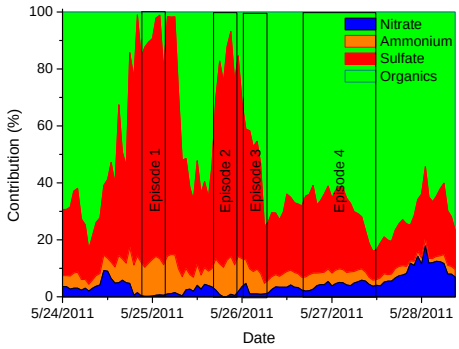

Figure 1. Relative contribution of chemical components of PM_1 measured at Vilnius from 24-29 May 2011.

This work was supported by the Research Council of Lithuania under project No. MIP-105/2010.

Hobbs, P.V., Radke, L.F., Lyons, J.H., Ferek, R.J. and Coffman, D.J. (1991) *J. Geophys. Res.* **96**, 18735–18752.

Draxler, R.R. and Rolph, G.D. (2003) *HYSPLIT Model* access via NOAA ARL READY Website (http://ready.arl.noaa.gov/HYSPLIT.php). NOAA Air Resources Laboratory, Silver Spring, MD

Note: This paper have been printed in *Atmos. Res.* (2013) **122**, 93-101.

Quantifying the relative contribution of different aerosol types over Eastern Mediterranean: A decadal high resolution satellite view

A.K. Georgoulias[1,2], K.A. Kourtidis[3], G. Alexandri[4], P. Zanis[1] and U. Pöschl[2]

[1]Department of Meteorology and Climatology, School of Geology, Aristotle University of Thessaloniki, Thessaloniki, Macedonia, 54124, Greece
[2]Multiphase Chemistry Department, Max Planck Institute for Chemistry, Mainz, 55128, Germany
[3]Department of Environmental Engineering, Democritus University of Thrace, Xanthi, Thrace, 79100, Greece
[4]Laboratory of Atm. Physics, Physics Department, Aristotle University of Thessaloniki, Thessaloniki, 54124, Greece
Keywords: MODIS, aerosols, anthropogenic, Eastern-Mediterranean.
Presenting author email: ageor@auth.gr

Satellite observations from MODIS have been extensively used in combination with observations from other satellite sensors or model simulations to quantify the optical properties of different aerosol types at a global as well as regional scale. Based on the pioneer results of Kaufman *et al* (2005) and a number of other studies that used a similar approach, Bellouin *et al* (2008) presented an algorithm that combines aerosol optical depth (AOD) and fine-mode ratio (FMR) at 550 nm from MODIS, Aerosol Index from TOMS and surface wind speed over oceans from SSM/I. This algorithm is capable of distinguishing the anthropogenic (fossil fuel and biomass burning) AOD from the corresponding sea salt and dust AOD on a daily basis. However, this is possible over oceans only, since, the FMR retrieval is not considered reliable over land. Over land they used regional anthropogenic fractions as derived from five global models that participated in the AEROCOM project (Bellouin *et al*, 2005). A similar approach was also used in a recent paper by Bellouin *et al* (2012) with data from MACC aerosol reanalysis. The fraction of different aerosol types to the total AOD is crucial for the calculation of the radiative forcing of each type separately (Quaas *et al*, 2008; Jones *et al*, 2009).

A common characteristic is that all the studies referenced above are focused on global observations using daily 1^ox1^o gridded level-3 MODIS data. Since the methodologies are now well established, we have to go a step further and investigate the relative contribution of different types of aerosols at a regional scale taking into account the special characteristics of each region. Here, we focus on Eastern Mediterranean [30^oN-$45N^o$, 17.5^oE-37.5^oE], a region subject to aerosol contributions from a variety of sources. Human activities, like industry and transport (anthropogenic aerosols), occasional Saharan dust intrusions (dust particles), sea spray (marine aerosols) and agricultural fires in Southeastern and Eastern Europe as well as occasional fire events in the region (biomass burning aerosols) contribute to the total aerosol burden. Hatzianastassiou et al (2009) used 1^ox1^o MODIS and TOMS monthly data to investigate the existence of anthropogenic and natural aerosols over Eastern Mediterranean but at a qualitative way rather than a quantitative one. In this work, the relative contribution of different aerosol types over the region is presented at a high resolution of 0.1^ox0.1^o on a daily basis along with the corresponding uncertainties. MODIS TERRA and AQUA level-2 datasets (10 km resolution at nadir) that span from 3/2000 and 7/2002 respectively are used for the compilation of two 0.1x0.1 degree gridded datasets that consist of 30000 grid cells each (see Georgoulias and Kourtidis, 2012 for more details). The use of these datasets in conjunction with Aerosol Index data from Earth Probe TOMS and OMI satellite sensors and wind field data from ERA-interim reanalysis within an algorithm similar to Bellouin *et al* (2008) allows for the calculation of the aerosol type fraction per grid and day. The seasonal and interannual variability of the relative contribution of each aerosol type is discussed while a Fourier-based method is used for the calculation of the trend (and its statistical significance) of AOD_{550} for each aerosol type.

This work was funded by QUADIEEMS project which is co-financed by the European Social Fund (ESF) and national resources under the operational programme Education and Lifelong Learning (EdLL) within the framework of the Action "Supporting Postdoctoral Researchers".

Bellouin, N., Boucher, O., Haywood, J. and Reddy, M.S. (2005) *Nature* **438**, 1138-1141.

Bellouin, N., Jones, A., Haywood, J. and Christopher, S.A. (2008) *J. Geophys. Res.* **113**, D10205, doi:10.1029/2007JD009385.

Bellouin, N., Quaas, J., Morcrette, J.-J. and Boucher, O. (2012) *Atmos. Chem. Phys. Discuss.* **12**, 20073-20111, doi:10.5194/acpd-12-20073-2012.

Georgoulias, A.K. and Kourtidis, K.A., (2012) Atmos. Res. **107**, 145-160, doi:10.1016/j.atmosres.2012.01.003.

Hatzianastassiou, N., Gkikas, A., Mihalopoulos, N., Torres, O. and Katsoulis, B.D. (2009) *J. Geophys. Res.* **114**, D24202, doi:10.1029/2009JD011982.

Jones, T.A., Christopher, S.A. and Quaas, J. (2009) *Atmos. Chem. Phys.* **9**, 4091-4114, doi:10.5194/acp-9-4091-2009.

Kaufman, Y.J., Boucher, O., Tanre, D., Chin, M., Remer, L.A. and Takemura, T. (2005) *Geophys. Res. Lett.* **32**, L17804, doi:10.1029/2005GL023125.

Quaas, J., Boucher, O., Bellouin, N. and Kinne, S. (2008) *J. Geophys. Res.* **113**, D05204, doi:10.1029/2007JD008962.

CLACE 2013: Cloud microphysics and physico-chemical characterization of ice residuals in mixed-phase clouds

P. Kupiszewski[1], E. Weingartner[1], R. Färber[1], M. Gysel[1], E. Hammer[1], C. Fuchs[1], U. Baltensperger[1], P. Vochezer[2], M. Schnaiter[2], C. Linke[2], E. Toprak[2], S. Mertes[3], J. Schneider[4], T. Klimach[4], S. Schmidt[4]

[1]Laboratory of Atmospheric Chemistry, Paul Scherrer Institute, CH-5232 Villigen PSI, Switzerland
[2]Institute for Meteorology and Climate Research, Karlsruhe Institute of Technology, D-76021 Karlsruhe, Germany
[3] Leibniz Institute for Tropospheric Research, Leipzig, Germany
[4]Max Planck-Institute for Chemistry, Mainz, Germany
Keywords: ice nucleation, mixed-phase clouds, CLACE 2013
Presenting author: piotr.kupiszewski@psi.ch

Much of the uncertainty in climate projections is due to an insufficient understanding of aerosol-cloud interactions. In particular, the formation of mixed-phase clouds via heterogeneous nucleation, their temporal and spatial evolution and the physico-chemical characteristics of ice nuclei (IN), the aerosol sub-population facilitating formation of ice crystals, is not well known. Meanwhile, cloud glaciation enhances precipitation formation, decreasing cloud cover and lifetime, and affects cloud radiative properties. Analysis of ice residuals (IR) in mixed-phase clouds is a difficult task: small, freshly formed ice crystals (where the IR contained within can be considered representative of the original IN) must be separated from super-cooled droplets with similar aerodynamic sizes, as well as the orders of magnitude more abundant interstitial particles.

A new Ice Selective Inlet (ISI) has been designed to extract small ice crystals from mixed-phase clouds, simultaneously counting, sizing and imaging the hydrometeors contained in the cloud with the use of Welas optical particle counters (OPC) and a Particle Phase Discriminator (PPD). The core of the ISI is an evaporation unit with ice-covered inner walls, removing droplets using the Wegener-Bergeron-Findeisen process, while transmitting a relatively high fraction of ice crystals (Fig. 1).

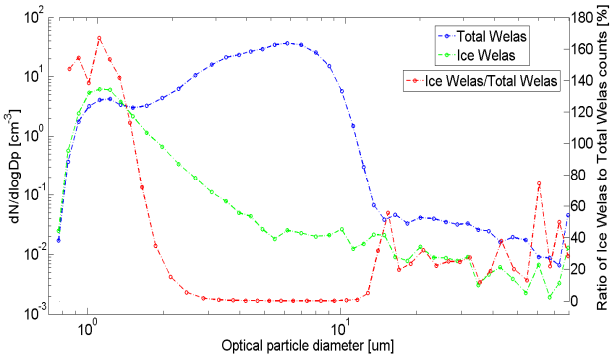

Figure 1. Particle and hydrometeor number size distributions measured by Welas OPCs upstream (blue) and downstream (green) of the droplet evaporation unit during a mixed-phase cloud event.

The ISI was deployed in winter 2013 at the high alpine Jungfraujoch site (3580 m.a.s.l) during the intensive CLACE 2013 field campaign. The measurements obtained shed light on both the microphysics of mixed-phase clouds and the physico-chemical characteristics of IR. Droplet and ice crystal size distributions measured with the optical spectrometers in the ISI are compared with those measured in situ by the Small Ice Detector (SID-3). A number of online instrumentation was deployed downstream of the inlet, including a scanning mobility particle sizer (SMPS) and a Grimm OPC for number size distribution measurements, as well as a single particle mass spectrometer (ALABAMA), single particle soot photometers (SP2) and a Waveband Integrated Bioaerosol Sensor (WIBS-4) for analysis of the chemical composition, with particular focus on the content of black carbon and biological particles in IR. Simultaneously, similar instruments were deployed downstream of a total inlet, which samples the bulk aerosol. A comparison of measurements from the total inlet and the ISI provides information on the characteristics of ice residuals relative to the total aerosol. First results show that the measured IR are generally larger than the bulk aerosol (Fig. 2).

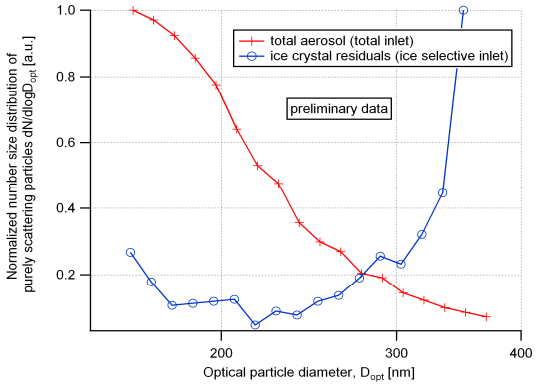

Figure 2. Normalized dry size distributions of the total aerosol (red) and ice residuals (blue)

This work is funded by the Swiss National Science Foundation and the German Research Foundation (SCHN 1140/2-1).

The UPUPA project: Ultrafine Particles in the Urban Piacenza Area, Italy

M. Giugliano, G. Lonati, S. Ozgen and G. Ripamonti

Civil and Environmental Engineering Department, Politecnico di Milano, P.za L. da Vinci 32 – 20133 Milano, Italy
Energy and Environment Laboratory Piacenza, Politecnico di Milano, Via Nino Bixio, 27C – 29121 Piacenza, Italy
Keywords: ultrafine particles, particle number concentration, size distribution, urban areas, Po valley.
Presenting author email: michele.giugliano@polimi.it

Emerging epidemiological and toxicological evidence indicates particle toxicity to be dependent on particle size. Ultrafine particles (UFP, d_p<0.1 µm) are believed to be more toxic than larger particles because of their higher number and surface area per given mass, and higher deposition probability in the deep lung region (Chio & Liao, 2008; Hoek et al., 2010). Nevertheless, regularly monitoring are scarce and the available knowledge on urban UFP appears still lacking compared with the complexity and variability of the phenomenon. For instance, scarce evidence exists on UFP levels in areas like the Po Valley, Northern Italy, a well-known European hot-spot for air pollution due to the particular local orography and to the high density of emission sources.

In 2011-2012 the UPUPA project took place in Piacenza (45.03 °N, 9.41 °E, 67 m a.s.l), a mid-sized city (about 100.000 inhabitants) located in the centre of the Po Valley, aiming to provide information on UFP levels in the urban area, on the diurnal and seasonal variation of particle number concentration (PNC) and particle number size distribution (PNSD). For the urban area of Piacenza about 60-120 events per year of PM10 daily limit exceedances have been reported in 2007-2011, with PM10 and PM2.5 annual averages in the 34-45 µg m^{-3} and 24-27 µg m^{-3} range, respectively.

Measurements of PNC and PNSD were performed at three different sites: a traffic exposed site (TR), about 20 meters from a highway flyover; an urban background (UB) site, in a park in a residential area at the outskirts of the city; a rural site (RU) located at about 20 km South-West of the urban area on the first hills of Apennine mountains. At each site measurements were performed either during cold period (October-March) and warm period (April-September). PNC in the 7 nm-10 µm ($PNC_{7\text{-}10000}$) and related PNSD in 12 size bins were measured by an ELPI™ (Electrical Low Pressure Impactor, - Dekati Ltd., Finland) that was displaced between sites.

Hierarchical cluster analysis applied to PNSD from ELPI data identified 4 size intervals with peculiar time patterns: $PNC_{7\text{-}29}$ (7<d_p<29 nm), $PNC_{29\text{-}95}$ (29<d_p< 95nm), $PNC_{95\text{-}264}$ (95<d_p<264nm), and $PNC_{264\text{-}10000}$ (264<d_p<10000nm). $PNC_{7\text{-}10000}$ levels were higher at TR site compared to UB site and RU site, with the latter site displaying the lowest average levels in any season and day of the week considered (Figure 1). Daily average $PNC_{7\text{-}10000}$ at TR site were in the 8.7-17.2·10^3 cm^{-3} range (lowest levels on warm Sundays, highest on cold workdays). Workdays' to Sundays' ratio for $PNC_{7\text{-}10000}$ varied from 1.6 during cold period to 1.3 during warm period, as reported for other urban areas (Jeong et al., 2006; Wang et al., 2011).

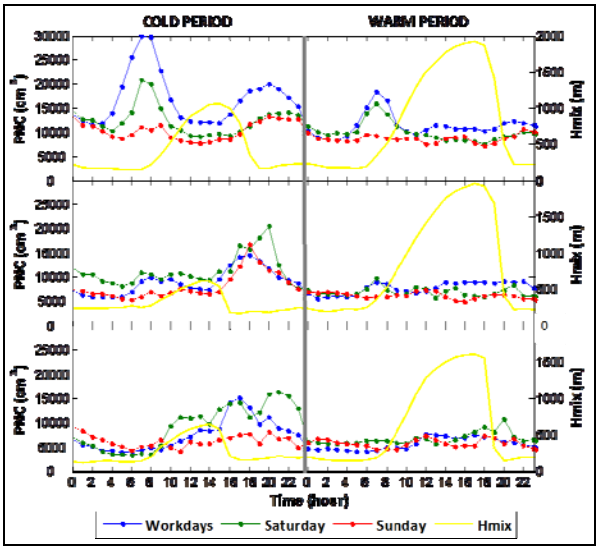

Figure 1. Average diurnal patterns of $PNC_{7\text{-}10000}$ on workdays, Saturdays and Sundays and of the atmospheric mixing height (Hmix)

UFP contribution to $PNC_{7\text{-}10000}$ was between 65-78% at TR site, 58-75% at UB and 56-78% at RU site, somewhat smaller than the European mean ratio (76%) reported by Putaud et al., 2010. At urban sites, all size fractions generally followed the same daily cycle of $PNC_{7\text{-}10000}$ but $PNC_{7\text{-}29}$ and $PNC_{29\text{-}95}$ levels increased on traffic rush hours (especially on cold season mornings). At TR site on warm workdays a third peak for $PNC_{7\text{-}29}$ was observed in the early afternoon (12.00-14:00); not correlated with traffic markers, this peak was likely of secondary origin, via photochemical nucleation of gaseous precursors.

Chio, C.-P., Liao, C.-M. (2008) *Atmos. Environ.* 42, 8575–8584.
Hoek, G. et al. (2010) *Environ. Sci. Technol.* 44, 476-482.
Jeong, C., Hopke, P., Chalupa, D., Utell, M. (2004) *Environ. Sci. Tech.* 38, 1933-1940.
Putaud et al. (2010) *Atmos. Environ.* 44, 1308–1320.
Wang, Y., Zhu, Y., Salinas, R., Ramirez, D., Karnae, S., John, K., (2008) *J. Air Waste Manage. Assoc.* 58, 1449-1457.

DIAPASON: an user-oriented EC-LIFE+ Project to quantify the role of Saharan dust on European PM10 levels

G.P. Gobbi[1], F. Barnaba[1], F. Costabile[1], L. Di Liberto[1], C. Tirelli[1], R. Sozzi[2], A. Bolignano[2] and M. Morelli[2]

[1]ISAC-CNR, Rome, Italy
[2]ARPA-Lazio, Rome, Italy
Keywords: Desert Dust, Air Quality, Particulate Matter, Lidar
Presenting author email: g.gobbi@isac.cnr.it

PM10 is a widely-employed to assess air quality. The current European Union Air Quality Directive 2008/50/EC allows no more than 35 exceedances per year of the daily-average threshold of 50 µg/m^3 while the PM10 yearly average should not exceed 40 µg/m^3. Considering the high levels of PM10 observed over a large part of Europe, these limits might result as rather stringent. The Directive 2008/50/EC also allows for subtraction of the natural contributions to the PM10 concentrations, after assessing the natural origin and relevant amount. In Mediterranean Europe the natural phenomenon which mostly affects PM10 concentrations is the transport of mineral dust from the nearby Sahara desert. In the central and western Mediterranean, such outflow of mineral dust reaches its maximum between Spring and Autumn, while minimizing in winter.

Under the Directive 2008/50/EC, the European Commission has recently released specific 'Guidelines' to quantify the contribution of natural sources to PM10 (EC, 2011). For Saharan dust, these Guidelines rely on back-trajectories, dust model forecasts and satellite observations coupled to ground PM10 concentration monitoring. The EC LIFE+2010 DIAPASON Project (*Desert dust Impact on Air quality through model-Predictions and Advanced Sensors ObservatioNs*, 2011-2015), intends to build on the capabilities of the current 'Guidelines' and explore possible improvements from the use of remote sensing devices. In this respect, at the core of DIAPASON is the prototyping of affordable Polarization Lidar-Ceilometers (PLCs) able to 'observe' the presence of dust plumes and thus 'certify' their loading in the lowermost atmosphere. Within DIAPASON PLC measurements will be used to define and validate an upgraded Saharan dust detection Methodology. The Project is implemented in the Pilot Region of Rome, in Central Italy, where three networked PLCs will monitor the altitude-resolved advections of Saharan dust for one year.

As the observational phase of DIAPASON has not started yet, an initial phase of the Project was devoted to the development of an effective, user-oriented tool to implement the current EC-Guidelines. To this purpose, DIAPASON has implemented a Graphic User Interface (GUI) (Fig.1) to allow an easy evaluation of the Saharan dust contribution to the PM10 records in a given area. This tool, adaptable to any European site/region/area and freely available upon request, is currently routinely used by the Italian Regional Agency in charge of Air Quality monitoring in the Lazio region (ARPA-Lazio).

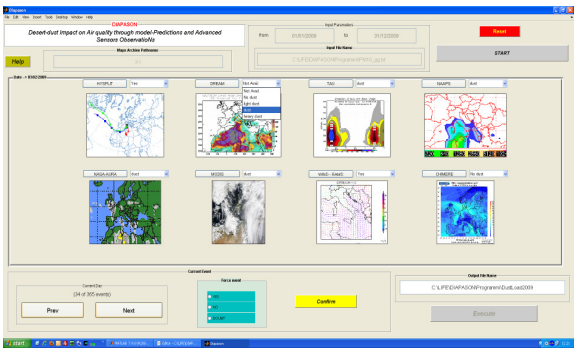

Figure 1. DIAPASON GUI to apply the EC Guidelines

Potential improvements of the current EC-Guidelines are also under evaluation. These include overcoming the selection of a Regional Background site (RB), as prescribed by the EC Guidelines. In fact, in Italy, PM10 monitoring sites "purely" representative of rural background conditions are difficult to find and the choice of the RB was found to be critical in the EC-Methodology outcome. DIAPASON is therefore investigating the use of the out-of-dust record in each single PM10 monitoring site as a 'background reference' for the evaluation of a Saharan dust load at the same site (self-calibration method, Gobbi et al. 2013). An example of the outcome of such a modified approach is given in Fig. 2. Major pro and cons of the new approaches under investigations will be discussed.

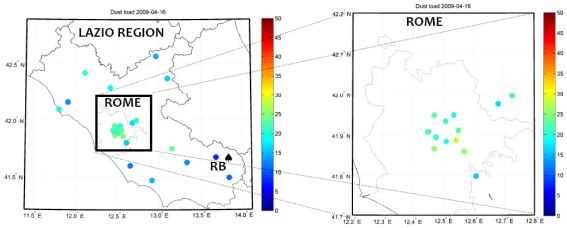

Figure 2. Example of dust load (µg/m^3) derived from a modified version of the EC Guidelines.

This work is supported by the EU LIFE+2010 DIAPASON project (ENV/IT/391). More details can be found at: http://www.diapason-life.eu.

EC (2011) *Establishing guidelines for demonstration and subtraction of exceedances attributable to natural sources under the Directive 2008/50/EC on ambient air quality and cleaner air for Europe,* SEC(2011), 208, 2011.

Gobbi et al. (2013), *Atm. Chem. Phys. Disc.*, 13, 4963-88

Testing of aerosols in Barentsburg area (Spitsbergen)

L.P. Golobokova[1], D.G. Chernov[2], U.S. Turchinovicn[2], V.V. Pol'kin[2]

[1]Limnological Institute SB RAS, Irkutsk, 664033, Russia
[2] V.E. Zuev Institute of Atmospheric Optics SB RAS, Tomsk, 634021, Russia
Keywords: aerosols, correlation, share factors, the sum of ions
L.P. Golobokova: lg@lin.irk.ru

In Spring to Summer periods of 2001-2012 (table 1) testing of aerosols air characteristics were conducted on the territory of the Spitsbergen archipelago (western Artic section) in the area of Zonal Hydrometeorological Observatory (ZHO), in Barentsburg (78.1°N 14.2°E, eastern part of the Grenfjord bay of the Greenland sea). Aerosols samples were taken on PTFE filters with 0.8 μm pore size. Chemical composition of aerosols water soluble fraction was done on ion chromatographer ICS-3000 (Dionex, USA).

During testing periods in the area of Barentsburg northern and western (Greenland island side) air mass transports were observed. During Summer seasons higher temperatures and lower wind speeds were observed. In summer it was often that foggy and thick weather was observed. Atmospheric pressure and relative air humidity varied within short ranges.

Mean concentration of ions within aerosols soluble fraction in April-May 2011 was twice higher as compared to their concentration in August. Maximum concentration of ions (5.6 $\mu g \cdot m^{-3}$) was recorded on May 16, and the minimum (0.48 $\mu g \cdot m^{-3}$) was recorded on August 02, 2011. In spring there was significant correlative interrelation of concentrations between the ion pairs NH_4^+–SO_4^{2-}, Na^+–Cl^-, Mg^{2+}–Cl^-, Ca^{2+}–NO_3^- with correlation ratios equal to 0.79, 0.97, 0.96 и 0.90 accordingly. In summer period this interrelation went down (0.68, 0.63, 0.61, 0.58) while higher positive correlation between the other pairs especially cations and nitrate- and chloride ions was indicated.

Mean cumulative ratio of ions in 2012 as compared to the previous testing was one and a half times higher during summer season. Exceeding of concentrations was due to ions of marine origin - Na^+ and Cl^- that together with ions NH_4^+ and SO_4^{2-} prevailed in aerosols composition. To this effect, during summer season higher correlative interrelation of concentrations between ion pairs Cl^- and Na^+, NH_4^+, Mg^{2+}, Ca^{2+} (r = 0,93-0,98) was observed. Comparison of aerosols compositions sampled in Barentsburg in 2011-2012 was indicative of its identity. Although similarity of qualitative composition there were differences in quantitative relation. During spring season number of soluble substances in aerosols composition during both testing years was more or less similar, however, in summer 2012 amount of ions rose three times as compared to 2011. Concentrations of Na^+ were 8.5 times higher, Mg^{2+}- - 3.7 times higher, K^+ and NO_3^- - 2.9 times higher, Cl^- and NH_4^+ - 1.8 times higher, and SO_4^{2-} - 1.6 times higher. During the same period increase of mass concentration of smock black within Barentsburg atmosphere was 1.5 times higher as compared to spring time. Similar increase of smoke black ratio was observed in 2011 when mean values in summer seasons were 3 times higher.

For identifying input of different sources into building chemical composition of aerosols FM_{cont} and FM_{ocean} share factors were used [1]. Relations of K^+, Mg^{2+}, Na^+, Ca^{2+}, Cl^-, SO_4^{2-} concentrations being the main ones both in sea water, and in aerosols. It was found out that prevailing factor of impact on building chemical composition of aerosols is continental. However, in summer season 2012 increase of sea factor input reaches up to 30 %.

This work was supported in part by the Program of Basic Researches No. 23 of the Presidium of the Russian Academy of Sciences «Basic problems of oceanology: physics, geology, biology, ecology».

This work was supported in part by the Program of Basic Researches No. 23 of the Presidium of the Russian Academy of Sciences «Basic problems of oceanology: physics, geology, biology, ecology».

1. Golobokova L.P., Fillipova U.G., Chipanina E.V., Pol'kin V.V., Terpugova S.A., Tikhomirov A.B. Chemical composition of near water aerosols in the area of Antarctica // Ice and snow. 2011; (4): 105-111.

Table 1. Mean chemical composition of aerosols in the area of Barentsburg, $\mu g \cdot m^{-3}$

Period	Na^+	NH_4^+	K^+	Mg^{2+}	Ca^{2+}	Cl^-	SO_4^{2-}	NO_3^-
2011								
19.04- 26.05	0,21±0,16	0,29±0,24	0,06±0,03	0,07±0,07	0,13±0,15	0,80±0,65	0,97±0,60	0,19±0,35
26.07 -31.08	0,08±0,04	0,13±0,14	0,07±0,05	0,02±0,01	0,14±0,21	0,30±0,24	0,57±0,53	0,07±0,04
2012								
26.04-06.06	0,33±0,22	0,22±0,28	0,14±0,11	0,02±0,02	0,15±0,18	0,45±0,44	1,18±1,21	0,17±0,53
21.07-25.08	0,70±0,83	0,24±0,26	0,20±0,13	0,06±0,11	0,25±0,25	1,63±1,65	0,90±0,98	0,15±0,55

The Spanish network on environmental DMAs: the 2012 SMPS+UFP intercomparison campaign and study on particle losses in dryers

F. J. Gómez-Moreno[1], E. Alonso[1], B. Artíñano[1], V. Juncal Bello[2], M. Piñeiro Iglesias[2], P. López Mahía[2], N. Pérez[3], J. Pey[3], A. Alastuey[3], B. A. de la Morena[4], M. I. García[5], S. Rodríguez[5], M. Sorribas[6,7], G. Titos[6,7], H. Lyamani[6,7] and L. Alados-Arboledas[6,7]

[1]Department of Environment, CIEMAT, Madrid, E-28040, Spain
[2]Institute of Environment, University of A Coruña (IUMA-UDC), A Coruña, E-15179, Spain
[3]Institute of Environmental Assessment and Water Research (IDAEA-CSIC), Barcelona, E-08034, Spain
[4]Atmospheric Sounding Station 'El Arenosillo', INTA, Mazagón-Huelva, E-21130, Spain
[5]Izaña Atmospheric Research Centre, (IARC/CIAI), AEMet, Santa Cruz de Tenerife, E-38001, Spain
[6]Andalusian Environmental Centre (CEAMA), University of Granada, E-18071 Granada, Spain
[7]Applied Physics Department, University of Granada, E-18071 Granada, Spain
Keywords: Atmospheric aerosols, Particle size distribution, Aerosol dryers, SMPS
Presenting author email: fj.gomez@ciemat.es

The Spanish network on environmental DMAs (Red Española de DMAs Ambientales, REDMAAS) is currently formed by six groups involved in the measurement of atmospheric particle size distributions by means of Differential Mobility Analyzers (DMAs). These groups are: IUMA-UDC, IDÆA-CSIC, INTA, IARC-AEMET, University of Granada and CIEMAT. The network has been working during the period 2010-2012 (Gómez-Moreno et al., 2011 & 2012). The REDMAAS has as main objective the cooperation between the groups to solve common problems and to optimize their facilities and protocols. The main activities developed in the network include: DMA calibration; CPC, SMPS and UFP intercomparison; measurement quality control program; losses in sampling lines; support for the radioactive facility license; webpage; and new DMA applications. In this work, the main results obtained during the 2012 SMPS+UFP intercomparison campaign, including the DMA calibrations and a study on particle losses in dryers are shown.

The field intercomparison exercise was performed during November 2012 in the INTA facilities (El Arenosillo, Huelva). There were 5 complete SMPS systems, an UFP and two additional CPCs. After calibrating all the flow rates, a CPC intercomparison was performed obtaining good results. The results for the DMA calibration was better than the previous campaigns, with a maximum deviation of 2% for 80 nm latex particles and only one SMPS above 5% for 190 nm latex particles. The SMPS intercomparison showed similar results to those obtained in the previous years (Gómez-Moreno et al., 2011 & 2012). The UFP showed good results when the adequate correction matrix was used.

One of the problems to study was the particle losses in the lines, especially in the dryers because of the few results published. The setup was as followed: the sampled air went through a dryer after which there was a flow splitter. Two SMPSs in parallel measured the particle size distribution, the first of them had the testing dryer and the second didn't have any. These two SMPSs were selected because they previously had shown to measure the same distributions. The pipes lengths from the splitter to the SMPS were the same for both of them, so the differences in the measurements were caused by the particle deposition in the dryer. Six dryers (5 Permapure Nafion dryers SS12" and 1 dryer SS24") were tested. An example of the results can be found in figure 1

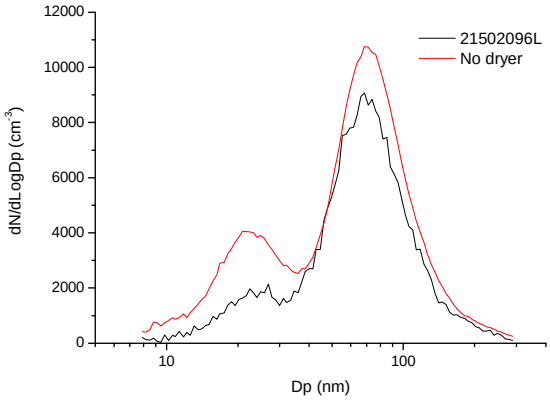

Figure 1. Comparison of a dry aerosol (flow rate: 1 lpm) measured with and without dryer (Nafion SS24"). The difference between the two measurements is the particle deposition in the dryer.

A comparison with theoretical deposition has been done. To calculate diffusional particle losses in the dryers, Wiedensohler et al (2012) recommended to consider the Permapure Nafion dryers SS12" and SS24" as pipes with equivalent lengths of 1.25 and 2.5 m respectively. These same equivalent lengths have been used to consider other different mechanisms for deposition.

This network is financed by the Ministry of Science and Innovation (CGL2011-15008-E & CGL2011-27020).

Gómez-Moreno et al. (2011) European Aerosol Conference, 4P291, Manchester.
Gómez-Moreno et al. (2012) European Aerosol Conference, B-WG01S2P30, Granada.
Wiedensohler et al. (2012) Atmos. Meas. Tech., 5, 657-685.

The potential role of ion-induced nucleation at a coniferous forest site in north eastern Bavaria

S. G. Gonser[1], F. Klein[1,2], W. Birmili[3], J. Größ[3] and A. Held[1]

[1] Junior Professorship in Atmospheric Chemistry, University of Bayreuth, 95440 Bayreuth, Germany
[2] Now at: Gasphase and Aerosol Chemistry Group, Paul Scherrer Institute, 5232 Villigen, Switzerland
[3]Leibniz-Institute for Tropospheric Research, 04318 Leipzig, Germany
Keywords: Ion-induced nucleation, Nucleation, Growth, Ions.
Presenting author email: stefan.gonser@uni-bayreuth.de

Mechanisms governing the nucleation process of secondary aerosol formation are widely discussed. In particular, there is no general consensus on the relevance of ion-induced nucleation. Over the last decade a set of new instruments has become available capable of measuring the number size distribution of neutral and charged clusters in size ranges relevant for nucleation. One of these instruments is the neutral cluster and air ion spectrometer (NAIS) which measures neutral clusters down to 2 nm diameter and ions down to diameters of 0.9 nm. Field based measurements in the lower troposphere using the NAIS indicate a minor impact of ions on nucleation (~10% or less, see e.g. Manninen *et al*, 2010), whereas modelling results as well as different approaches towards interpretation of the field data point at a major role of ion induced nucleation (Yu and Turco, 2011).

During an eight-week measurement campaign we applied a NAIS as well as a scanning mobility particle sizer (SMPS) to study new particle formation events at the "Waldstein" ecosystem research site in the Fichtelgebirge mountain range, NE Bavaria, Germany. The measurements were performed from mid of June to mid of August 2012. In the summer season, new particle formation is a frequently observed phenomenon at this site (e.g. Held *et al*, 2004).

The Fichtelgebirge mountains are well known for their elevated background radiation levels. The radiation originates from the bedrock, containing an increased concentration of uranium and thorium. Additionally, the fissured granitic bedrock promotes the molecular diffusion of gaseous radon. The radioactive background shows a diurnal variation with highest values during the night and decreasing radiation during day time. Thus, ion concentrations may be elevated at times and may play a role in particle nucleation.

During the campaign a total of 18 clear nucleation event days were observed with nucleation rates J_{2nm} between 1-38 cm^{-3} s^{-1} and growth rates in the range of 0.5-5 nm h^{-1}. In Fig. 1 the evolution of a new particle formation event is shown. The lower panel shows the ion fraction of the total particle number in the diameter range 2-3 nm. An increase in the ion fraction was observed shortly prior to the onset of the nucleation event, indicating the potential role of ions on nucleation.

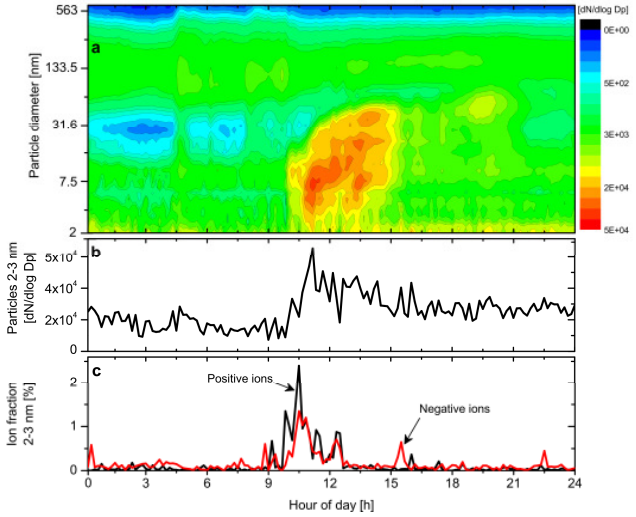

Figure 1. Time evolution of a new particle formation event on 4th July 2012. **a**) total particle number size distribution, **b**) total particle sum in the diameter range 2-3 nm, **c**) fraction of positive and negative ions of total particle number between 2-3 nm.

Daily mean small ion (< 2 nm mobility diameter) concentrations were found to be in the range from 90 cm^{-3} to more than 400 cm^{-3}. Further detailed analysis of the role of ion-induced new particle formation at this forest site will be presented.

This work is funded by the Deutsche Forschungs-gemeinschaft (DFG) under grant DFG HE 5214/3-1.

Held, A., Nowak, A., Birmili, W., Wiedensohler, A., Forkel, R., and Klemm, O. (2004) *J. Geophys. Res.* **109**, D23204.

Manninen, H. E., Nieminen, T., Asmi, E., Gagné *et al.* (2010) *Atmos. Chem. Phys.* **10**, 7907–7927.

Yu, F. and Turco, R. P. (2011) *Atmos. Chem. Phys.* **11**, 9451-9463.

Analysis of aerosol hygroscopic properties by combination of lidar, microwave radiometer and radiosounding data

M.J. Granados-Muñoz[1,2], F. Navas-Guzmán[1,2], J.A. Bravo-Aranda[1,2], J.L. Guerrero-Rascado[1,2], A. Valenzuela[1,2], J. Fernández-Gálvez[1,2] and L. Alados-Arboledas[1,2]

[1]Centro Andaluz de Medio Ambiente, Universidad de Granada, Junta de Andalucía, Av. del Mediterráneo s/n, 18006-Granada, Spain
[2]Departamento de Física Aplicada, Universidad de Granada, Av. Fuentenueva s/n, 18071-Granada, Spain

Keywords: hygroscopicity, lidar, radiosounding, microwave radiometer
Presenting author email: mjgranados@ugr.es

Aerosol particles are a key component in the atmosphere regarding its contribution to climate change. They can affect the Earth-Atmosphere energy budget by means of direct and indirect effects. An improved knowledge about the effects of the size increase of the aerosol particles due to water uptake (hygroscopic growth) is necessary for better understanding these effects. It directly affects the scattering of radiation and also the indirect effect. There are already many in-situ studies about the hygroscopicity effects on the aerosol properties. Under ambient conditions, analysis have usually been performed using humidified nephelometers or humidified tandem differential mobility analyzers. These instruments present mainly two limitations: firstly, they are unable to provide accurate results above 85% relative humidity (RH); secondly, they modify the ambient conditions by drying the air sample and then re-exposing it to varying RH. Remote sensing systems can overcome these difficulties, e.g, by sampling the atmosphere without modifying ambient conditions. Moreover, they can also detect RH close to saturation, which is of great importance since the region between 85 and 100% RH is where particles are more affected by hygroscopic growth. The combination of aerosol backscatter (or extinction) and relative humidity profiles retrieved from remote sensing systems are the needed information to perform hygroscopic studies. For this purpose, it is necessary to detect an aerosol layer with a RH increase large enough to observe the variations in the growth factor while the same type of aerosol is present in the corresponding portion of the layer. In that sense, the detected increase in the backscatter (or extinction) would be associated with the change in aerosol size due to the water uptake but not to changes in aerosol composition.

In this study, a combination of Raman lidar, radiosounding (RS) and microwave radiometer (MWR) data over the city of Granada (37.16ºN, 3.60ºW and 680 m asl) has been used to analyse aerosol hygroscopic growth with increasing RH in the vertical profile. In order to guarantee that the same type of aerosol was present along the profile, only situations with a good mixing in the boundary layer were analysed. As a first step, a backtrajectory analysis was performed using the HYSPLIT model. Only when the origin of the air masses was independent of the altitude in the range of interest, the same type of aerosol might be present along the profile (Veselovskii et al., 2009). To confirm good mixing within the boundary layer, potential temperature (θ) and water vapour mixing ratio (*r)* profiles were obtained. Constant profiles of θ and *r* are considered as indicators of well mixed conditions within the boundary layer. Usually RH profiles are obtained from RS, however, in this analysis also a combination of lidar *r* profiles with MWR temperature profiles was used to obtain RH. The accuracy of these RH profiles was checked against RH from RS, thus the analysis of aerosol hygroscopic properties can be extended to cases when radiosoundings are not available. The hygroscopic growth factor is defined as

$$f(RH) = \frac{X_\lambda(RH)}{X_\lambda(RH_{dry})}$$

where X_λ represents whether the backscatter or the extinction coefficient. To obtain *f*(RH) it is necessary to combine the backscatter or extinction coefficient profiles provided by the lidar with the RH profiles. The reference RH_{dry} is usually chosen as the lowest value of the RH in the profile.

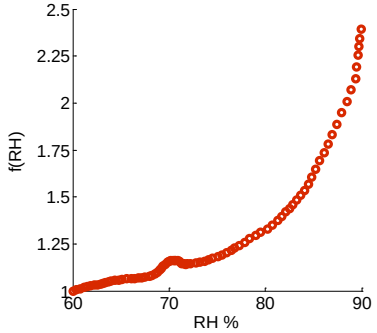

Figure 1. Hygroscopic growth factor for 22 July 2011 between 20:30 and 21:00 corresponding to a layer between 1200 and 2500 m asl. RH_{dry} = 60%.

Acknowledgments: This work was supported by the Andalusia Regional Government through projects P08-RNM-3568 and P10-RNM-6299, by the Spanish Ministry of Science and Technology through projects CGL2010-18782, CSD2007-00067, CGL2011- 13580-E/CLI and CGL2011-16124-E; and by the EU through the ACTRIS project (EU INFRA-2010-1.1.16-262254)

Veselovskii, I., D. N. Whiteman, A. Kolgotin, E. Andrews, M. Korenskii, (2009), *J. Atmos. Oceanic Technol.*, **26**, 1543–1557. doi: http://dx.doi.org/10.1175/2009JTECHA1254.1

Hygroscopic growth parameterization of aerosol particles based on high humidity measurements in the Po-Valley, Italy

J. Größ[1], I. Pap[1], W. Birmili[1], A. Hamed[1, 2] and A. Wiedensohler[1]

[1]Department of Physics, Leibniz Institute for Tropospheric Research, Leipzig, 04318, Germany
[2]Department of Applied Physics, University of Eastern Finland, Kuopio, P. O. Box 70211, Finland

Keywords: Hygroscopic growth, Hygroscopicity parameter
Presenting author email: johannes.groess@tropos.de

The hygroscopic behaviour of atmospheric aerosol particles was determined during the PEGASOS measurement campaign in 2012. The measurements were performed at the regional site in San Pietro Capofiume (SPC) in the PO-Valley, Italy, from June 9 to July 12, 2012. A High Humidity Tandem Differential Mobility Analyzer (HH-TDMA) was used for the hygroscopicity measurements. The HH-TDMA was developed to quantify the hygroscopic growth factor (HGF) and the mixing state of the aerosol particles for relative humidities (RH) ≥ 90 % under highly temperature-stabilized conditions (Hennig, T. et al., 2005). The HH-TDMA was applied to measure the hygroscopic properties at 90, 93 and 95 % RH for the particle size with 75, 100, 200 and 300 nm. Based on the measured HGFs and under use of the single-parameter κ-Köhler model, the hygroscopic growth behaviour was analysed. κ is the so called hygroscopicity parameter and enables the comparison between measurements at different RHs at a certain dry diameter (Liu et al., 2011). According to Petters, M. D. et al. (2007), κ can be estimated by the following equation:

$$\kappa = \left(HGF^3 - 1\right)\left[\frac{1}{S}\exp\left(\frac{4\sigma_{s/a}M_W}{RT\rho_W D_P HGF}\right) - 1\right] \quad (1)$$

where S is the saturation ratio, $\sigma_{s/a}$ the surface tension of the interface solution/air, M_W the molecular weight of water, R the universal gas constant, T the absolute temperature, ρ_W the density of water, and D_P the particle dry diameter. In order to obtain a parameterized κ, some analysis steps are required. First, for each D_P and S the measured HGF was averaged over the whole measurement period. In a second step the Köhler equation (1) was aligned to the point quantity (S, HGF) with κ as variable fitting parameter. The results are shown in Fig. 1. To get a parameterized κ in dependence on D_P a sigmoid curve (Fig. 2) approach was used:

$$\kappa\left(D_P\right) = A_2 + \frac{A_1 - A_2}{1 + \exp\left(\frac{D_P - D_0}{\Delta D}\right)} \quad (2)$$

with the fitting parameter A_1, A_2, D_0 and ΔD.

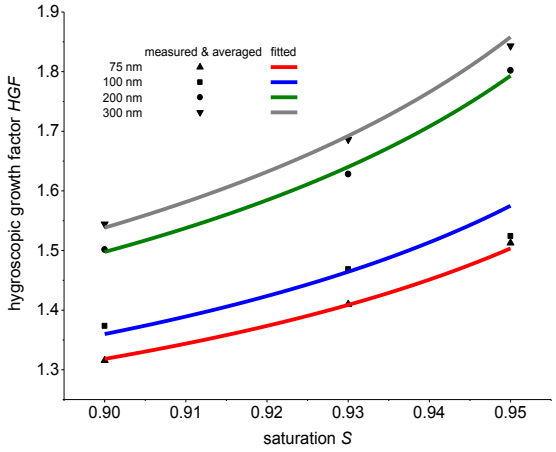

Fig. 1: The hygroscopic growth of different particles sizes (75, 100, 200 and 300 nm). The HGFs are the mean values of the measured HGF corrected to their target RHs (90, 93, 95 %). The red, blue, green and grey lines represent the fitted κ-Köhler curves.

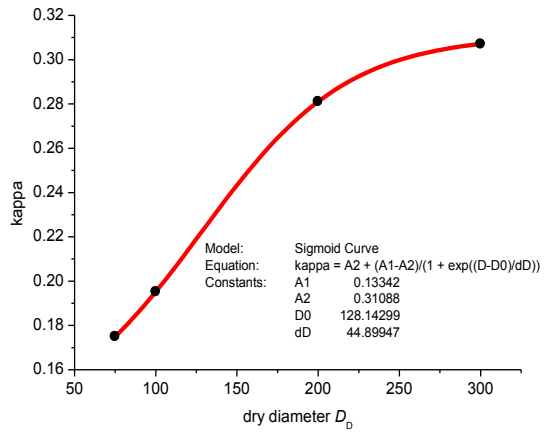

Fig. 2: The hygroscopicity parameter κ for four different particle sizes (75, 100, 200 and 300 nm). The black points are the fitted κs from the Köhler equation (1). The κ sigmoid curve (eq. 2) is displayed as red line.

References:

Hennig, T. et al., J. Aerosol Sci., 36, 1210–1223, 2005
Liu, P. et al., Atmos. Chem. Phys., 11, 3479–3494, 2011
Petters, M. D. et al., Atmos. Chem. Phys., 7, 1961–1971, 2007

MIXTURES OF BIOMASS-BURNING AND URBAN AEROSOLS ANALYSIS: A CASE STUDY.

Marius Mihai CAZACU[1], Florin UNGA[1], Adrian TIMOFTE[1, 2], Ioana POPOVICI[1], Alin Ionut PASCARU[1], Dan DIMITRIU[1], Silviu GURLUI[1]

1 "Alexandru Ioan Cuza" University of Iasi, Faculty of Physics, Atmosphere Optics, Spectroscopy and Lasers Laboratory, 11 Carol I Blvd., 700506 Iasi, Romania
[2] National Meteorological Administration, Regional Forecast Center Bacau, 1 Cuza Voda Str., 600274 Bacau, Romania
Keyword: aerosols, biomass, AERONET, lidar,
Presenting author email: sgurlui@uaic.ro

Iasi is a municipality from North-Eastern part of Romania and one of the largest cities in the country. Being a city in continuous development, several urban projects were started in the spring of 2012, with the purpose of improving the city's infrastructure and restoration of some cultural buildings and parks.

Urban and industrial aerosols type is a major component of the tropospheric aerosol load over IASI LOA-SL site monitoring station (47N, 27E). This study presents the results from optical properties analysis (from May 2012 to February 2013 period) on biomass-burning and urban aerosols mixtures by means of lidar and sun-photometer measurements.

In order to both identify and categorize the biomass burning types influences, Aerosol Robotic Network (AERONET) Version 2 data criteria (Level 1.5, solar zenith angle larger than 50° and retrieval error less than 5%) have been used to compute parameters such as: optical thickness, spectral dependence of Ångström exponent (α), spectral dependence of Single Scattering Albedo and the dominating size mode. Both biomass burning and urban-industrial aerosols are characterized by very small particles, so that fine mode is predominating in the particle size distribution.

The decreasing of Single Scattering Albedo's total average with the increasing of the wavelength (440, 675, 870, 1020 nm) from 0.95 (± 0.1) to 0.81 (± 0.1) agree on dominant aerosol type (Fig. 1).

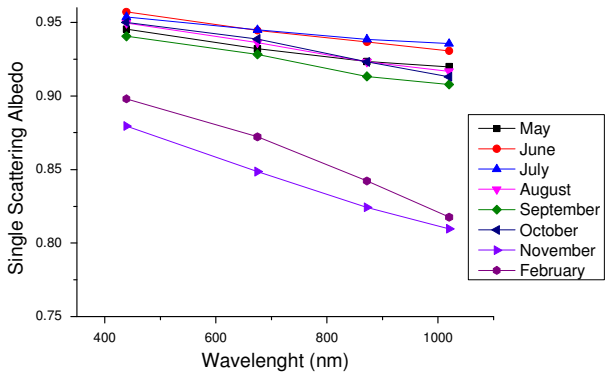

Fig. 1 Spectral single scattering albedo, monthly averages.

The lidar ratio has been calculated from both AERONET inversion and Fernald – Klett inversion (Nicolae et al., 2008). Single Scattering Albedo, Phase Function and Aerosol Optical Thickness were used to determine the lidar ratio and the extinction coefficient. An event on 5 July, 2012 shows that the AERONET lidar ratio calculated at 532 nm (S_{532aer}) is between 55~75 sr with an Ångström exponent between 1.3~1.7 for urban/industrial aerosol and 1.6~1.9 for biomass burning. The lidar measurements were performed by a mini-lidar system described in details in previous papers (Cazacu et al, 2012), developed in the framework of ROmanian LIdar NETwork (ROLINET) and RADO (Romanian Atmospheric Research 3D Observatory) research projects. The values of lidar-lidar ratio (S532) were in the range of 41 ~ 70 sr.

Furthermore, a good method to determine the dominating aerosol type is a/the correlation between the Absorption Ångström exponent (440 – 870 nm) and the Extinction Ångström exponent (440 – 870 nm). Aerosol absorption provides uncertainties in determining the dominance of aerosol types, while applying an aerosol particle size parameter (e.g., Extinction Ångström exponent at 440 – 870 nm) to separate larger particles, improves this method. (Giles et al., 2012; Russell et al., 2010).

Cazacu M. M., et al., (2012), *Grimsvotn Volcano: atmospheric volcanic ash cloud investigations, modelling-forecast, and experimental environmental approach upon the Romanian area*, Journal of Optoelectronics and Advanced Materials, 14, 5-6, 517-522;

Giles D. M., et al., (2012), *An analysis of AERONET aerosol absorption properties and classifications representative of aerosol source regions*, Journal of Geophysical Research, 117, d17203, doi:10.1029/2012JD018127.

Nicolae D., et al., (2008), *Air mass modification processes over the Balkans area detected by aerosol LIDAR techniques*, Journal of Optoelectronics and Advanced Materials – Rapid communications, 2, 405 – 412.

Russell P.B., et al., (2010), *Absorption Ångström Exponent in AERONET and related data as an indicator of aerosol composition*, Atmos. Chem. Phys., 10, 1155–1169;

Characterization of fine particles using Aerosol mass spectrometer during intensive campaign in three different sites in Kanto basin in summer of 2011

H. Hagino[1], and T. Morikawa[1], S. Hasegawa[2], S. Yonemochi[2], K. Sekiguchi[3]
K. Kumagai[4], N. Yamaguchi[4], A. Iijima[5], H. Shimadera[6], H. Hayami[6]

[1] Energy and Environmental Research Division, Japan Automobile Research Institute, Tsukuba, Ibaraki, Japan
[2] Center for Environmental Science in Saitama, Kazo, Saitama, Japan
[3] Graduate School of Science and Engineering, Saitama University, Saitama, Saitama, Japan
[4] Gunma Prefectural Institute of Public Health and Environmental Sciences, Maebashi , Gunma, Japan
[5] Takasaki City University of Economics, Takasaki , Gunma, Japan
[6] Central Research Institute of Electric Power Industry, Abiko, Chiba, Japan

Keywords: Aerosol mass spectrometry, Source Apportionment, PMF
Presenting author email: hhagino@jari.or.jp

The atmospheric aerosols, especially fine particles, are known to have adverse health effects on human populations. Understanding the composition of fine particles is necessary to identify their sources and to predict their effect on various atmospheric processes. Although organic aerosols are major components of the fine particles in urban atmospheres, the composition, formation mechanisms, and seasonal variation of concentrations of organic aerosols (OA) are not well understood. To study the organic aerosol source apportionment, the AMS data has been used to chemically characterise the sources and evolution of OA at many worldwide (Zhang *et al*., 2007).

The Aerodyne AMS were operated at Saitama University (C-ToF-AMS), Center for Environmental Science in Saitama (Q-AMS), Gunma Prefectural Institute of Public Health and Environmental Sciences in Maebashi (H-ToF-AMS), Japan, from 23 to 30 July 2011, except for occasional periods of maintenance and calibration (Figure 1). PMF (PMF2 ver4.2 ; Paatero (2000)) and PET (Ulbrich *et al*., 2009) were used to analyze datasets for each organic aerosol mass spectra from three differnt site.

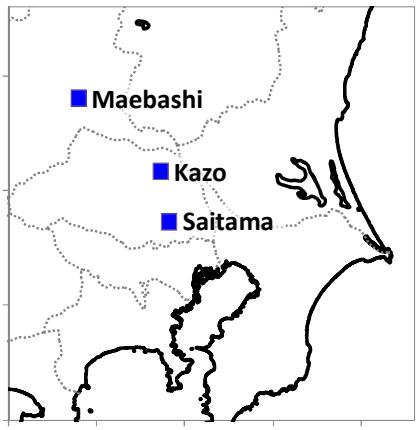

Figure 1. Sampling Sites

Organic aerosol (OA) was detected as major component in this sampling campaign. The organic aerosol mass spectra was divided into two types of OA components, oxygenated organic aerosol (OOA) and hydrocarbon-like organic aerosol (HOA), using positive matrix factorization (PMF) (Figure 2). The OOA was ubiquitous in various atmospheric environments, on average accounting for 44%, 49% and 55% of the total OA in Saitama (urban), Kazo (rural), and Maebashi (rural), respectively.

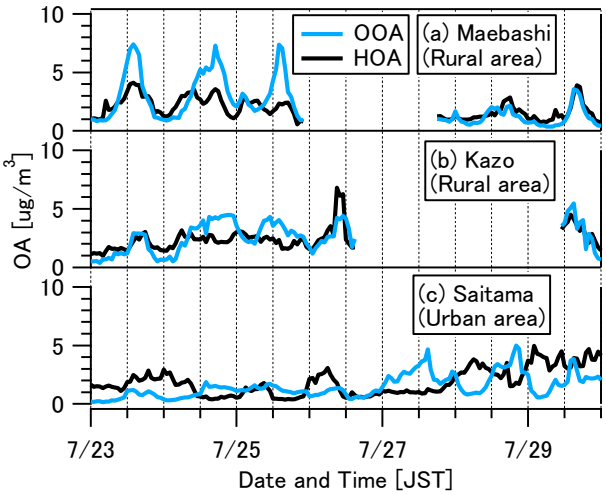

Figure 2. Variations of OOA (Oxygenated Organic Aerosol) and HOA (Hydrocarbon-like Organic Aerosol) concentration at Saitama, Kazo, and Maebashi, as 1 hour averages.

This research was supported by the Environment Research and Technology Development Fund (C-1001) of the Ministry of the Environment, Japan.

Paatero, P. User's Guide for Positive Matrix Factorization Programs PMF2 and PMF3; University of Helsinki: Finland, 2000.
Ulbrich *et al*., Atmos. Chem. Phys., **9**, 2891-2918, 2009.
Zhang, Q. *et al*. (2007) *Geophys. Res. Lett.* **34**, L13801.

Hygroscopicity of Sub-6 nm Sodium Chloride Particles

J. Hakala[1], J. Kangasluoma[1] and T. Petäjä[1]

[1]Division of Atmospheric Sciences, Department of Physics, University of Helsinki, Helsinki, 00560, Finland
Presenting author email: jani.hakala@helsinki.fi

Some studies suggest that the hygroscopic growth of water soluble salt particles may not follow the Köhler theory with particles below the diameter of 8 nm (Biskos et al., 2006a; Hakala et al., 2013). So far the hygroscopic growth of sodium chloride (NaCl) particles has not been studied below the mobility diameter of 6 nm (Biskos et al., 2006a, 2006b). In this study we present our investigations in hygroscopic growth of NaCl measured with a specially made nano Hygroscopicity Tandem Differential Mobility Analyzer (nHTDMA) from mobility diameter of 2.5 nm to 6 nm and in relative humidities from 10% to 95%.

Methods

The nHTDMA is consisted of a high resolution Herrmann Differential Mobility Analyzer (HDMA) for selecting the initial mobility diameter, a humidifier, and a TSI nano Differential Mobility Analyzer (nDMA, TSI DMA 3085) for measuring the mobility diameter after the humidifying. The nDMA was used in a closed loop arrangement. This way the humidifying is easy to achieve and keep stable with just one humidifier. The particles were produced in a tube furnace by vaporization-condensation method in ultrapure nitrogen carrier gas flow (Kangasluoma et al., 2013). To convert the agglomerates produced by this method (Krämer et al., 2000) into cubical crystals, the sample aerosol flow was humidified with an additional humidifier and cooled to 2°C. The aerosol experienced supersaturated conditions inside the cooling unit undergoing a phase transition into solute droplets. After drying in a silica gel diffusion dryer the NaCl particles were assumed to be cubical crystals.

Results

The Hygroscopic Growth Factors (HGF=diameter of humidified particle/diameter of dry particle) in different RH conditions were measured for NaCl particles with mobility diameters of 2.5 nm, 3 nm, 4 nm, 5 nm and 6 nm. The results showed clearly that the HGFs were lower for smaller particles due the Kelvin effect. Also the Deliquescence Relative Humidities (DRH) were determined for 4 nm, 5 nm and 6 nm NaCl particles. The DRH was higher the smaller the particle was. Particles below the mobility diameter of 4 nm had higher DRH than 95%. In Fig. 1. are the HGF distributions for 2.5 nm and 6 nm NaCl particles at different RHs. 2.5 nm particles have significantly lower HGF in same RH than 6 nm particles. The DRH is between 85% and 90% for 6 nm particles. This is marked by disappearance of the mode near HGF 1.1. The bimodal nature of the distribution for 2.5 nm particles is not as clear as for 6 nm particles at high RHs, but the widening of the distribution at RH of 95% shows that the DRH is not yet reached. The bimodal distribution near DRH is caused by different RH histories the particles have experienced before the size classification in nDMA.

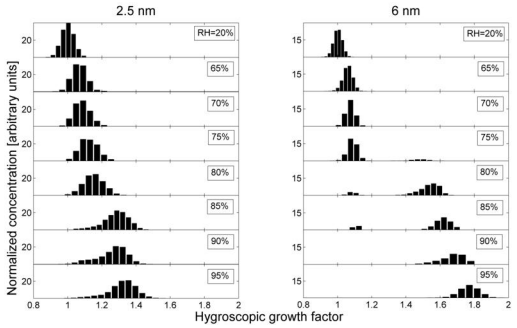

Figure 1. The hygroscopic growth factor distributions for 2.5 nm and 6 nm (mobility diameters) NaCl particles.

This research was supported by Academy of Finland (project 139656) and Finnish Center of Excellence.

Biskos, G., Russell, L. M., Buseck, P. R., and Martin S. T. (2006a) *Geophys. Res. Lett.* . **33**, L07801, doi:10.1029/2005GL025199.

Biskos, G., Malinowski, A., Russell, L. M., Buseck, P. R., and Martin S. T. (2006b) *Aerosol Sci. Technol.* **40**, 97-106.

Hakala, J., Manninen, H. E., Petäjä, T., and Sipilä, M. (2013) *Aerosol Sci. Technol.* **47**, 482-487.

Kangsluoma, J., Junninen, H., Lehtipalo, K., Mikkilä, J., Vanhanen, J., Attoui, M., Sipilä, M., Worsnop, D., Kulmala, M., and Petäjä. T (2013) *Aerosol Sci. Technol.*, DOI:10.1080/02786826.2013.773393.

Krämer, L., Pöschl, U., and Niessner. R. (2000) *J. Aerosol Sci.*, **31**, 673–685.

Semi-empirical parameterization for sub-20 nm particle growth

S.A.K. Häkkinen[1], H.E. Manninen[1, 2], T. Yli-Juuti[1], J. Merikanto[1], M.K. Kajos[1], T. Nieminen[1], S.D. D'Andrea[3, 4], A. Asmi[1], J.R. Pierce[4, 3], M. Kulmala[1] and I. Riipinen[5, 1]

[1]Department of Physics, University of Helsinki, 00014 Helsinki, Finland
[2]Institute of Physics, University of Tartu, 50090 Tartu, Estonia
[3]Department of Physics and Atmospheric Science, Dalhousie University, Halifax, Nova Scotia B3H 4R2, Canada
[4]Department of Atmospheric Science, Colorado State University, Fort Collins, CO 80523, USA
[5]Department of Applied Environmental Science and Bert Bolin Centre for Climate Research, Stockholm University, 10691 Stockholm, Sweden
Keywords: particle formation, growth
Presenting author email: silja.hakkinen@helsinki.fi

New particle formation occurs frequently in the atmosphere (Kulmala *et al*, 2004). According to global model estimations these newly formed particles contribute significantly to global CCN (cloud condensation nuclei) concentrations after growing large enough (Spracklen *et al*, 2008).

It has been observed that sub-20 nm particle growth is size-dependent (Manninen *et al*, 2010; Yli-Juuti *et al*, 2011) and has in some environments seasonal pattern comparable to that of atmospheric biogenic organics, e.g. monoterpenes (Yli-Juuti *et al*, 2011). These results among others suggest that atmospheric nanoparticles are growing mainly by condensation of low-volatile organic vapors and that different fractions of these condensable organics are condensing onto different sized particles due to Kelvin effect.

The challenge in current atmospheric models is to accurately yet efficiently represent atmospheric nanoparticle growth by biogenic and anthropogenic organics. In this work we introduce a simple semi-empirical parameterization for sub-20 nm particle growth that distributes secondary organics to the nanoparticles according to their size (1.5-3 nm, 3-7 nm, 7-20 nm) and this way captures particle growth rates observed in the atmosphere. The parameterization includes particle condensational growth by sulfuric acid, by secondary organics from monoterpene oxidation ($SORG_{MT}$) and by additional condensable non-monoterpene organics ("background") (Eq. 1).

$$I_{tot}(d_p)=I_{SA}(d_p)+k(d_p)I_{SORG,MT}(d_p)+k_{bg}(d_p)I_{SORG,bg}(d_p), \quad (1)$$

where I_{tot} is the total mass flux onto particles with a diameter of d_p, I_{SA} is the mass flux of sulfuric acid, $I_{SORG,MT}$ and $I_{SORG,bg}$ are the mass fluxes of the $SORG_{MT}$ and the background organics, respectively. $k(d_p)$ and $k_{bg}(d_p)$ are factors for distributing the $SORG_{MT}$ and the background organics to particles with diameter of d_p. I_{tot}, I_{SA} and $I_{SORG,MT}$ were obtained from ambient data. $I_{SORG,bg}$, k and k_{bg} values for the three particle sizes were obtained with a least-square method by fitting Eq. 1 to the ambient data. Ambient growth rate data was acquired from particle number size distribution measurements at six continental sites over Europe. The longest time series of 7 years (2003 to 2009) was obtained from a boreal forest site in Hyytiälä, Finland.

The parameterization was able to reproduce observed particle growth rates and their seasonal cycles with good accuracy (see Figure 1 for Hyytiälä as an example). The weighting factors (k) for distributing the $SORG_{MT}$ were 0 for 1.5-3 nm, 0.7 for 3-7 nm and 1 for 7-20 nm. The concentration of the background organics was comparable to the concentrations of the $SORG_{MT}$ and sulfuric acid, around $6 \cdot 10^7$ cm^{-3}. The weighing factors (k_{bg}) for distributing the background organics were 0.3 for 1.5-3 nm, 0.8 for 3-7 nm and 1 for 7-20 nm. Simulations with a global model, GEOS-Chem-TOMAS (Pierce *et al*, 2012), suggest that the "background" can be linked to biogenic organics that are oxidized in the presence of anthropogenic pollution (Spracklen *et al*, 2011).

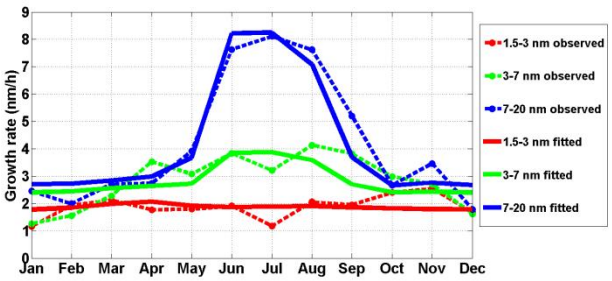

Figure 1. Comparison between particle growth rates (1.5-3, 3-7 and 7-20 nm sizes) obtained from ambient observations and from the parameterization in Hyytiälä.

This work was financially supported by the University of Helsinki three-year research grant (No. 490082), by Maj and Tor Nessling Foundation (No. 2010143), Academy of Finland (No. 139656), Finnish Center of Excellence grant (No. 141135), European Research Council grant ATMNUCLE (No. 227463) and ATMOGAIN (No. 278277), and Finnish Academy of Science and Letters (Vilho, Yrjö and Kalle Väisälä Foundation), which are gratefully acknowledged.

Kulmala *et al* (2004) *J. Aerosol Sci.*, 35, 143–176.
Manninen *et al* (2010) *Atmos. Chem. Phys.*, 10, 7907–7927.
Pierce *et al* (2012) *Atmos. Chem. Phys. Discuss.*, 12, 33127–33163.
Spracklen *et al* (2008) *Geophys. Res. Lett.*, 35, L06808.
Spracklen *et al* (2011) *Atmos. Chem. Phys.*, 11, 12109–12136.
Yli-Juuti *et al* (2011) *Atmos. Chem. Phys.*, 11, 12865–12886.

New particle formation at rural and mountain stations in north Italy: A comparative study during the joint PEGASOS and Supersito campaign

A. Hamed[1], S. Decesari[2], S. Gilardoni[2], S. Niemelä[3], L.Tarozzi[2], C. Carbone[2], P. Vaattovaara[1], J. Joutsensaari[1], P. Cristofanelli[2], A. Marinoni[2], P. Bonasoni[2], G. Bonafe[4], D. Bacco[4], I. Ricciardelli[4], A. Virtanen[1], S. Ferrari[4], V. Poluzzi[4], M.C. Facchini[2] and A. Laaksonen[1, 3]

[1]Department of Applied Physics, University of Eastern Finland, P. O. Box 70211, Kuopio, Finland
[2]Institute of Atmospheric Sciences and Climate, National Research Council of Italy, Bologna, Italy
[3]Finnish Meteorological Institute, P.O. Box 503, 00101 Helsinki, Finland
[4]Arpa Emilia-Romagna, Via Rocchi 19, 40138 Bologna, Italy
Keywords: New particle formation events, Condensational sink, Particle growth, Comparative study
Presenting author email: Amar.Hamed@uef.fi

New particle formation (NPF) events occur frequently in the atmosphere in both clean and polluted environments. It is not, however, yet possible to predict, a priori, rates at which particles are formed and grow, or even to know with certainty which chemical species are involved. To improve the understanding of atmospheric NPF, numerous field measurements, laboratory experiments and models studies are devoted to monitor the gas-phase nucleating vapors and chemical compositions of NPFs. Advanced field measurements are crucial to provide information about the spatial distribution of the rate coefficient in the nucleation parameterizations to assess the impacts of aerosols on climate, weather, air quality, and human health.

Recently, an intensive field campaign (a joint campaign between the Supersito project and the PEGASOS FP7-project) was conducted at San Pietro Capofiume (SPC) (44° 39' N, 11° 37' E; 11 m a.s.l; polluted rural site); and Mt.Cimone (MTC) (44°12' N, 10°42' E; 2165 m a.s.l.; mountain site) measurement stations in the Po Valley region from June 9th to July 10th 2012. Simultaneous measurements of NPF at different parts of the Po Valley give us a good opportunity to study the driving factors of NPF at different sectors of the PoValley region. Particle size distribution (PSD) measurements in diameter range from 3 to 600 nm were measured by a twin Differential Mobility Particle Sizer (DMPS) at the SPC site since March 2002 (Hamed et al., 2007). In November 2005, similar DMPS system but with diameter range from 10-500 nm was established at MTC site in the frame of EUSAAR and ACTRIS projects.

Here, we are presenting the NPF analysis for the first time at MTC station, in addition to SPC site, during the joint PEGASOS/Supersito campaign period. As a summary, 28 NPF event days were identified at SPC site while 9 NPF event days at MTC site. Figure 1 shows surface plots of PSD data as measured with a DMPS system from July 1st to July 7th at both SPC and MTC stations. It is clearly seen that NPF events at SPC are more frequent and more intense (in terms of clear formation and growth for several hours) than NPF events at Mt.Cimone site.

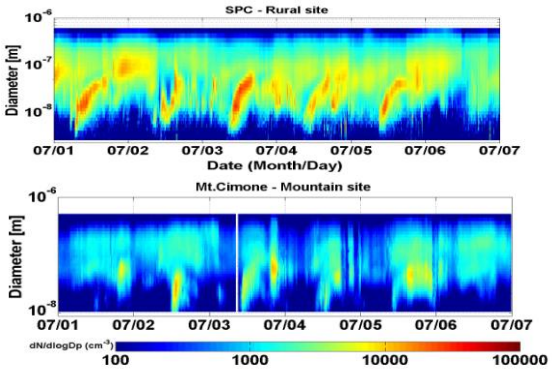

Figure1. Example of one week particle formation bursts observed at SPC (upper panel) and at Mt.Cimone (lower panel), in frame of PEGASOS/Supersito campaign.

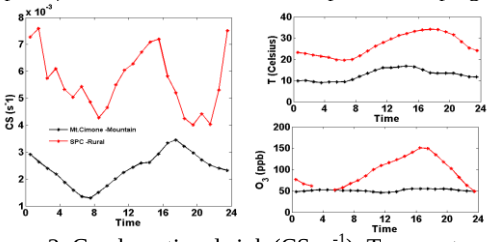

Figure 2. Condensational sink (CS; s^{-1}); Temperature (T; Celsius) and O_3 concentrations (ppb) at Mt.Cimone (black) and SPC (red) on the NPF day of July 3rd.

Our preliminarily results show that CS and T were both lower in MTC than SPC (Fig. 2), which could be possible driving factors of NPF occurrence at MTC site. These two combinations of conditions (low T and low CS), were also shown to favour NPF occurrences at the Finnish boreal station, Hyytiälä (Boy and Kulmala 2002). On the other hand, in SPC both T and O_3 were higher (Fig.2), therefore it is possible that volatile organic compounds (VOCs) and their oxidation products were at higher level in SPC. If VOC oxidation products participate in NPF events at SPC, then that favors NPF events more in SPC than in MTC. The above differences in NPF events hint that different processes are controlling the particle formation events at different parts of Po Valley. More details on characterization of NPF events at PoValley will be discussed in our presentation.

Boy and Kulmala (2002) *Atmos.Chem.Phys.*,***2***,1–16.
Hamed, et al. (2007) *Atmos. Chem. Phys.*,***7***,55-376.

Secondary New Particle Formation in Central Europe: Eight years of Aerosol Particle Size distribution data from Melpitz Site, Germany

A.Hamed[1,2], Z.Wang[1], W.Birmili[1], G.Spindler[1], A.Wiedensohler[1]

[1]Institute for Tropospheric Research (TROPOS), Leipzig, Germany
[2]Department of Applied Physics, University of Eastern Finland, P. O. Box 70211, Finland
Keywords: New particle formation, DMPS, Particle growth.
Presenting author email: Amar.Hamed@uef.fi

New particle formation (NPF) in the atmosphere is a global phenomenon that has been shown to take place in a wide variety of environments (Kulmala et al., 2004). However, the formation mechanisms and the participating substances have not been resolved yet. Long-term data continuous measurements are valuable as they are expected to reveal useful information that enable studies into the dynamics of the NPFs and present control data for climate modelers to predict with more accurately the future climatic conditions.

Here, we present eight years data set (2003-2011) of NPF conducted at the atmospheric research station Melpitz in Eastern Germany (51°32´ N; 12°54´ E; 87 m a.s.l.).The Melpitz station is part of the observation net works German Ultrafine Aerosol Network (GUAN; Birmili et al., 2009) and ACTRIS (Aerosols, clouds, and trace gases research Infrastructure network). Particle size distribution measurements were carried out using dual DMPS systems (Differential Mobility Particle Sizers) with particle size ranges of 3-800 nm.

The particle formation events were identified and classified into two categories i.e., NPF events and non-events. Figure 1a illustrates the total number of NPF events and non events over the period of eight years; while figure 1b shows the monthly frequency of NPF events and non-events for the same period. Earlier study shows that particle formation event days are observed at Melpitz measurement station on 60–100 days in a year (Birmili and Wiedensohler, 2000; Hamed et al., 2010).

Interestingly, for this long-data set, we have observed that number of intensive NPF events shows clear declination, more pronounced, after year 2006. In our earlier study, Hamed et al. (2010) showed that decreasing anthropogenic SO_2 emissions from years 1996/1997 to years 2003/2006 decreased the intensity of new particle formation and thus their frequency and formation rate in Melpitz rural site. Figure 1b shows that the event frequency (the event frequency has been calculated by dividing the total number of days with new particle formation by the total number when the DMPS was working efficiently -we excluded the days when the DMPS system malfunctioned-) was higher during spring and summer months with maximum values in April and May while the minimum was in winter and autumn months. Such high seasonal event frequency in spring has been observed quite often in clean and polluted areas as well. However, the high event frequency in summer contrasts with the observations performed in other rural German site, Hohenpeissenberg (Birmili et al., 2003), which shows a pronounced minimum in the summer (0.075 events per day at Hohenpeissenberg) but at the same time agreed with the observation at the SPC rural site in Italy (Hamed et al., 2007).

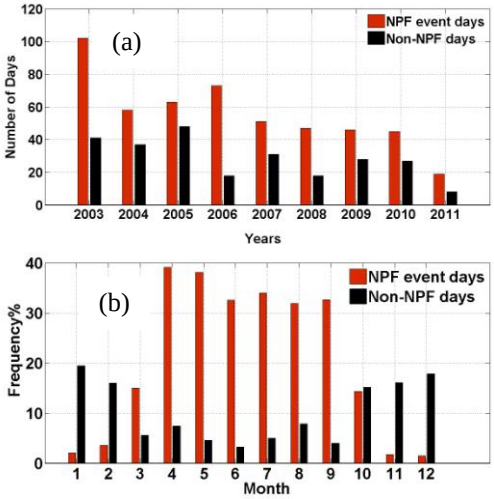

Figure 1: (a) the total numbers of New Particle formation days (NPF-event days; red bar) and non-event days (Non-NPF days; black bar) during each year; (b) monthly frequency of NPF events in Melpitz station, Germany during 2003-2011.

We will show a comprehensive statistical comparison of Melpitz data sets with respect to meteorological and trace gases of NPF events to elucidate the process govern particle formation at Melpitz station. Moreover, comparison of NPF events between Melpitz and other GUAN stations will be discussed in our future presentation.

Birmili, W. & A. Wiedensohler (2000) *Geophys. Res. Lett.* 27: 3325–3328.
Birmili et al., (2003) *Atmos. Chem. Phys., 3, 361–376.*
Birmili et al., (2009) *Gefahrst. Reinh. Luft, 69(4):* 137-145.
Hamed, A., et al., (2007) *Atmos. Chem. Phys.*,7, 355-376.
Hamed, A., et al.,(2010) *Atmos. Chem. Phys.,10 1071–1091, 2010*
Kulmala et al.,(2004) *J. Aerosol Sci*., 35,143–176.

Measurement of atmospheric organic nitrate aerosols and its application in cloud events

L.Q. Hao[1], S. Romakkaniemi[1], A. Kortelainen[1], A. Jaatinen[1], H. Portin[1,2], P. Miettinen[1], M. Komppula[2], A. Leskinen[2], J.N. Smith[1,4], D. Sueper[5], D.R. Worsnop[1,6], K.E.J. Lehtinen[1,2], A. Laaksonen[1,3] and A. Virtanen[1]

[1]Department of Applied Physics, University of Eastern Finland, Kuopio 70211, Finland
[2]Finnish Meteorological Institute, Kuopio Unit, Kuopio 70211, Finland
[3]Finnish Meteorological Institute, Climate Change, Helsinki 00101, Finland
[4]National Centre for Atmospheric Research, Boulder, CO 80305, USA
[5]Aerodyne Research, Inc., Billerica, MA 08121-3976, USA
[6]Department of Physics, University of Helsinki, Helsinki 00014, Finland
Keywords: Organic nitrate, Cloud events, HR-Tof-AMS
Presenting author email: hao.liqing@uef.fi

Boreal forests emit large amounts of biogenic volatile organic compounds (VOCs), primarily in the form of mono- and sesquiterpenes, which react with anthropogenic oxidant nitrate radical (NO_3) or undergo photochemical chemistry in the daytime to produce large, multifunctional organic nitrate with vapor pressures low enough to contribute new particle formation and growth. The organic nitrate aerosols, as a significant contribution to the global aerosol burden, can grow to cloud condensation nuclei (CCN) size and be activated into cloud droplets. However, the knowledge of organic nitrate aerosol-cloud interaction is poorly understood.

Observation of cloud events was carried out in a cloud observation station in Kuopio, Finland in 2010 (Hao et al., 2003, Leskinen et al., 2009). Samples from the cloud are introduced into the instruments through twin sampling lines. The first one is the total inlet line to collect the mixed information of cloud residual (RES) and interstitial particles (INT). The other is PM1.0 line to measure the cloud interstitial particles. The difference of both allows the estimation of composition of cloud residual. An Aerodyne high resolution aerosol time-of-flight mass spectrometer (TOF-AMS) was used to measure the chemical composition of cloud particles. We also applied positive matrix factorization (PMF) analysis to track the aerosol origin (Ulbrich et al., 2009). NO^+ and NO_2^+ ions were also integrated into the organic matrix for PMF analysis to separate the organic and inorganic nitrate components.

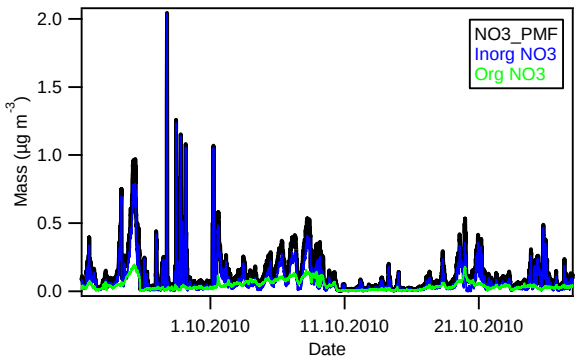

Figure 1. The time series of organic nitrate and inorganic nitrate mass concentrations from PMF fitting.

PMF analysis of the high resolution mass spectra of organics together with NO^+ and NO_2^+ ions allows for the separation of organic and inorganic species. Figure 1 shows the time series of organic nitrate and inorganic nitrate from PMF fitting results. Organic nitrates accounts for 34.7% of total nitrates and contributed to 1.9% of total aerosol masses, suggesting the significance as one of the global aerosol sources.

The investigation of chemical composition in cloud has showed in Table 1. The organic nitrates account for 51±7 % of total nitrate signals in the cloud interstitial particles, whereas its portion in the cloud residual particles was 26%. The difference between two can be explained by the cloud processing and particle size effects. However, the observations in this study highlight the potential important role of organic nitrates compounds playing in the cloud formation.

Table 1 Distribution of organic and inorganic nitrates compounds in cloud.

Mass conc. (µg m^{-3})	AMS measurements			PMF fitting		
	TOT	INT	RES	TOT	INT	RES
NO_3^-,org	-	-	-	0.11	0.050	0.060
NO_3^-,inorg	-	-	-	0.22	0.048	0.172
NO_3^- total	0.31	0.094	0.22	0.33	0.098	0.23
Fra. NO_3^-, org (%)	-	-	-	34	51	26
Fra. NO_3^-, inorg (%)	-	-	-	66	49	74

This work was supported by Magnus Ehrnrooth Foundation and Academy of Finland Centre of Excellence program.

Hao, L.Q., et al. (2013). *Environ. Sci. Technol.*, in press
Leskinen, A., et al. (2009) *Boreal Environ. Res.*, **14**, 576-590.
Ulbrich, I.M., et al., (2009) *Atmos. Chem. Phys.*, **9**, 2891-2918

Ultrafine particle concentrations: importance of local sources and new particle formation in two central European cities

A. Wonaschuetz[1], R. Wagner[1], I. Aschauer[1], R. Haindl[1], W. Ludwig[1], G. Zecha[1], J. Ondráček[2], P. Vodička[2], N. Zíková[2], V. Ždímal[2], J. Schwarz[2], R. Hitzenberger[1]
[1]Faculty of Physics, University of Vienna, Vienna, 1090, Austria
[2]Department of Aerosol and Laser Studies, Institute of Chemical Process Fundamentals, Prague, 16502, Czech Republic
Keywords: atmospheric aerosols, new particle formation, ultrafine particles
Presenting author email: anna.wonaschuetz@univie.ac.at

Ultrafine particle concentrations in urban areas are a major concern regarding air quality and public health. Local direct emissions of small, often carbonaceous, particles as well as new particle formation events are sources of fine and ultrafine particles, but meteorological conditions and the properties of the background aerosol moderate both the production and the fate of freshly produced particles. Concentrations of ultrafine particles from local sources are governed by human activity patterns and meteorology (Borsos *et al*, 2012, Kalafut-Pettibone *et al*, 2011, Salma *et al*, 2011), in particular boundary layer characteristics (Olofson *et al*, 2009). The timing and extent of new particle formation in urban areas is linked to precursor gas concentrations, solar radiation and condensational sink strength (Cheung *et al*, 2012, Stanier *et al*, 2004, Zhang *et al*, 2004), and often shows a strong seasonal dependence (Borsos *et al*, 2012, Salma *et al*, 2011, Stanier *et al*, 2004).

In this study, the importance of local primary sources and new particle formation as sources of fine and ultrafine particles is investigated for winter and summer in two central European cities. Particular attention is given to the impact of local meteorological characteristics: air mass origins play a large role in the characteristics of the background aerosol and the concentrations of trace gases associated with new particle formation and growth, and precipitation and thus the condensational sink.

The measurements were conducted in Prague (June 25 - July 9, 2012 and Jan. 14 - 30, 2013) and Vienna (July 16 - 30, 2012 and Feb. 4 - 16, 2013). Particle size distributions were measured continuously with an SMPS (Prague: TSI 3034 ,Vienna: DMA with CPC 3760A, TSI, Inc.). Black, brown, elemental and organic carbon concentrations were measured using a variety of methods (Hitzenberger *et al*, 2013). These measurements of carbonaceous aerosol concentration served as an indicator of human activity patterns and local anthropogenic emissions. Size-resolved chemical information was obtained from impactor data (ion chromatography). Meteorological data (temperature, relative humidity, precipitation, wind speed and direction) as well as solar radiation and concentrations of O_3, SO_2 and NH_3 were obtained from measurement networks. Air mass origin trajectories were calculated using the HYSPLIT model.

First results show that new particle formation events, which occurred mainly in summer, were often, but not always, linked to diurnal peaks in solar irradiation, and contributed substantially to fine particle concentrations. New particle formation events were absent in winter, due to both higher background aerosol concentrations and lower solar radiation in winter. Correspondingly, the contribution of fine and ultrafine particles to total number concentrations in winter was dominated by local anthropogenic sources.

This work was supported by the ÖAD, WTZ grant No. CZ 03/2012, the MEYS MOBILITY grant No. 7AMB12AT021, and the Czech Science Foundation grant No. P209/11/1342. We acknowledge the Austrian Central Institute for Meteorology and Geodynamics (ZAMG) for providing meteorological data, and the Viennese Environmental Department (MA 22) and for access to the data from the air quality monitoring network and the Czech Hydrometeorological Institute for both meteo and air quality data.

Borsos, T., Rimnacova, D., Zdimal, V., Smolik, J., Wagner, Z., Weidinger, T., Burkart, J., Steiner, G., Reischl, G., Hitzenberger, R., Schwarz, J., and Salma, I. (2012) *Sci. Total Environ.*, **38**, 0048-9697, doi: 10.1016/j.scitotenv.2012.06.052.

Cheung, H.C., Morawska, L., Ristovski, Z.D., and Wainwright, D. (2012) *Atmos. Chem. Phys.*, **24**, 1680-7316, doi: 10.5194/acp-12-4951-2012.

Kalafut-Pettibone, A.J., Wang, J., Eichinger, W.E., Clarke, A., Vay, S.A., Blake, D.R., and Stanier, C.O. (2011) *Atmos. Chem. Phys.*, **75**, 1680-7316, doi: 10.5194/acp-11-8861-2011.

Salma, I., Borsos, T., Weidinger, T., Aalto, P., Hussein, T., Dal Maso, M., and Kulmala, M. (2011) *Atmos. Chem. Phys.*, **56**, 1680-7316, 10.5194/acp-11-1339-2011.

Stanier, C.O., Khlystov, A.Y., Pandis, S.N. (2004) *Aerosol Sci. Technol.*, **28**, 0278-6826, doi: 10.1080/02786820390229570

Olofson, K.F.G., Andersson, P.U., Hallquist, M., Ljungstrom, E., Tang, L., Chen, D.L., and Pettersson, J.B.C. (2009) *Atmos. Environ.*, **20**, 1352-2310, doi: 10.1016/j.atmosenv.2008.09.080.

Zhang, Q; Stanier, CO; Canagaratna, MR; Jayne, JT; Worsnop, DR; Pandis, SN; Jimenez, JL (2004) *Environ. Sci. Technol.*, **52**, doi: 10.1021/es035417u

Hitzenberger, R., Schwarz, J., Aschauer, I., Haindl, R., Ludwig, W., Wagner, R., Wonaschuetz, A., Zecha, G., Vodicka, P., and Zikova, N. (2013), *European Aerosol Conference*

Absorbing aerosol long-term trend at Mukteshwar, a pristine location in Central Himalayas foothills

Rakesh K. Hooda[1, 2], A.-P. Hyvärinen[1], V.P. Sharma[2], M. Komppula[1,3], E. Asmi[1], Y. Viisanen [1] and H. Lihavainen[1]

[1] Finnish Meteorological Institute, P.O.Box 503, FIN-00101 Helsinki, Finland
[2] The Energy and Resources Institute, IHC, Lodhi Road, New Delhi -110003, India
[3]Finnish Meteorological Institute, Yliopistonranta 1F, P.O. Box 1627, FI-70211 Kuopio, Finland
Keywords: long-term trend, absorbing aerosols, Himalayas foothills
Presenting author email: rakesh.hooda@fmi.fi

Only recently have we become aware that anthropogenic absorbing aerosols, particularly BC (black carbon), can potentially play a major role in the global scale changes in hydrological cycle (Ramanathan et al., 2001; Liepert et al., 2004). Thus, the Finnish Meteorological Institute together with The Energy and Resources Institute have conducted continuous measurements of aerosol physical and optical properties in Mukteshwar, about 350 km northeast of New Delhi in India since 2006. The site is located at 2180 m above the sea level at the Himalayan Mountains. This is a background location in the foothills of Central Himalayas, and absorbing aerosol measurements with such a time span are unique from the area. Long-term trends in absorbing aerosol concentrations can be observed to emerge from the data set.

The black carbon concentrations were measured with a Magee AE 31 Aethalometer. The PM_{10} and $PM_{2.5}$ measurements were carried out using real-time beta attenuation particulate monitors (FH 62 I-R) manufactured by Thermo Scientific. In addition, other measurements included the particle number size distribution from 10nm to 800nm, aerosol scattering coefficient, and meteorological parameters including temperature, pressure, relative humidity and wind speed/direction (Hyvärinen et al., 2009). The black carbon concentrations were sampled from a $PM_{2.5}$ inlet.

The black carbon and $PM_{2.5}$ concentrations for the 7-year measurement period show high seasonal variability (Fig. 1). The maximum concentrations are observed in April, before the annual monsoon season. The average value of $PM_{2.5}$ fraction of PM_{10} was about 66%, indicating dominance of fine particles. The annual $PM_{2.5}$ concentrations during last 7-year measurements have not shown a clear increasing trend. In contrast, long-term trend of BC in $PM_{2.5}$ has shown a clear increase (Fig. 2). This reveals that anthropogenic activities which emit black carbon have increased during the time.

The highest concentrations of black carbon observed during the warm summer could be due to air lofted from the Indo-Gangetic plains below, when the boundary layer height is at its yearly maximum. It was noted that the $PM_{2.5}/PM_{10}$ ratios between 0.50 and 0.75 and the monthly mean ratio of BC to $PM_{2.5}$ mass lies between 3.0 and 7.5 % (Panwar et al., 2012). Furthermore, it is also observed that the winter months have a higher ratio of BC to $PM_{2.5}$ since the biomass burning is increased due to heating requirements. Therefore, it is not well evident which is the most vital factor for BC variations at this remote location: far emitting sources or changes in meteorological conditions.

In near future, our expanded study in the region would enhance knowledge of absorbing aerosols (brown and black carbon) horizontal variation, ageing processes and influence on climate. India has recently launched an ambitious program NCAP (National Carbonaceous Aerosol Program). The main focus of NCAP is on elemental carbon (EC) while our main aim is to chemically as well as optically characterize both brown and black carbon.

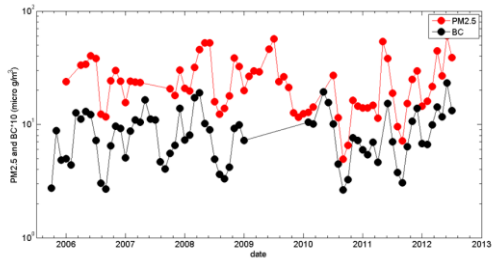

Figure 1. Trend in properties of aerosols

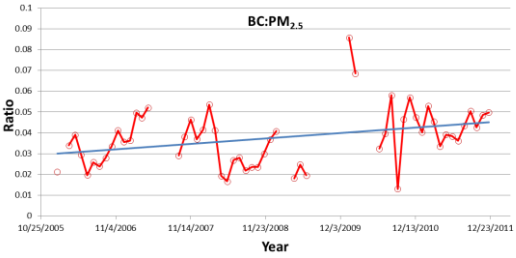

Figure 2. Mass fraction of BC (absorbing aerosol)

This work was supported by the Ministry of Foreign Affairs of Finland.

Ramanathan, V., et al. (2001), *Science*, **294**, 2119-2124.

Liepert, B., G., et al. (2004), *Geophys. Res. Lett.*, **31**, L06207, doi:10.1029/2003GL019060.

Hyvärinen, A.-P., et al. (2009), *J. Geophys. Res.*, **114**, D08207, doi:10.1029/2008JD011489.

Panwar, T., S., et al. (2012), *Environ. Monit. Assess.*, DOI 10.1007/s10661-012-2902-8.

Vertical profiles of aerosol optical properties and wavelength dependent absorption at Maldives Climate Observatory Hanimaadhoo

F. Höpner[1], F. Bender[1], P. S. Praveen[2], V. Ramanathan[2]

[1]Department of Meteorology, Stockholm University, Stockholm, 10691, Sweden
[2]Scripps Institution of Oceanography, University of California San Diego, La Jolla, California, 92093, USA
Keywords: absorbing aerosol, aerosol profiling, radiative forcing.
Presenting author email: friederike@misu.su.se

Aerosol radiative forcing is strongly dependent on the vertical distribution of aerosol. Especially, aerosol particle number and size distribution, particle optical properties and chemical composition are important features for calculating the radiative forcing (Kinne et al., 2006). Satellite based as well as surface based remote sensing instruments like Aeronet sun photometers can provide information about amongst other things columnar aerosol optical depth (AOD) and single scattering albedo (SSA). In addition, surface based as well as space borne lidar measurements can provide profiles of atmospheric backscatter and extinction. Meanwhile vertical in situ aerosol measurements are rare but also necessary to obtain actual particle concentrations and particle size information.

One focus of contemporary in situ aerosol measurements is the quantification of surface as well as vertically resolved carbonaceous aerosol (CA). CA consists mainly of black carbon (BC) and organic material (OM). BC, a product of incomplete combustion processes, is a main absorber of solar radiation and hence plays an important role in the climate system (Bond et al., 2012). Hence, it is important to incorporate BC properly in models. A good parameterization based on actual aerosol data leads to reducing uncertainty in model estimations of aerosol radiative forcing.

We will here present data from Cloud Aerosol Radiative Forcing Dynamics EXperiement (CARDEX) at Maldives Climate Observatory in Hanimaadhoo (Maldive Islands) in February and March 2012. This time of year is part of the dry monsoon season with arriving polluted air masses from the Asian continent. Thus air with high BC loading can be investigated. During CARDEX, aerosol profile measurements with lightweight unmanned aerial vehicles (UAVs) were performed. Amongst other instruments, a condensation particle counter (CPC), aethalometer and optical particle counter (OPC) were installed on board. Furthermore, surface instrumentation included a ground based lidar, nepholometer, aethalometer, CPC and an Aeronet sun photometer were in use.

Surface and vertical measurements from the CARDEX field campaign are used to calculate particle scattering, absorption as well as extinction profiles as functions of total particle concentration and relative humidity. A comparison between calculated profiles and measured absorption values from the on board aethalometer as well as from the lidar results will be presented. Reasons for potential discrepancies will be discussed. Figure 1 shows an example of calculated and measured vertical profiles of scattering, extinction and absorption on a day with an elevated aerosol layer present above the boundary layer.

Determined AOD and absorption AOD (AAOD) from vertically integrated extinction and absorption profiles respectively will also be compared to sun photometer based AOD results. Furthermore wavelength dependent AOD and AAOD will be analysed to separate the influence of dust, biomass and fossil fuel burning products (Chung et al, 2012).

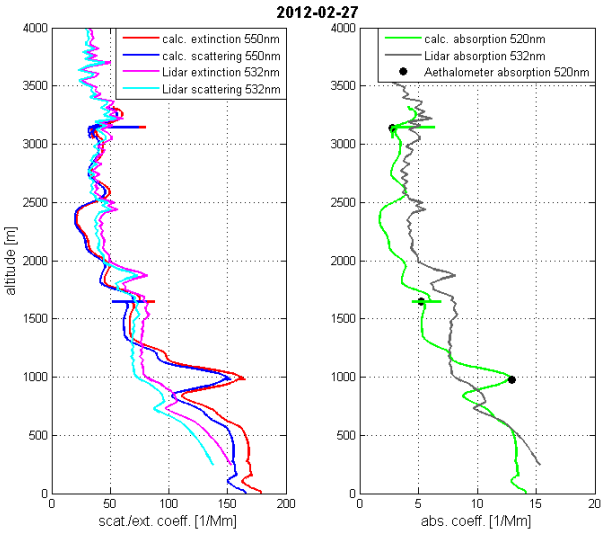

Figure 1: Calculated and measured vertical profiles of scattering, extinction and absorption. The calculated profiles (red, blue, green) and the measured absorption from an on board aethalometer (black) are results from a downward flight on Feb.27th 2012 between 10:00 and 11:00 local time. The lidar profiles (magenta, cyan, grey) are determined the same day at 10:00 local time.

Bond, T. C. et al. *Bounding the role of black carbon in the climate system: A scientific assessment*, J. Geophys. Res. Atm., doi:10.1002/jgrd.50171.

Kinne, S. et al. *An AeroCom initial assessment Ű optical properties in aerosol component modules of global models*, Atm. Chem. and Phys., 6, 1815-1834.

Chung, C. E., Ramanathan, V., and Decremer, D. (2012) *Observational constrained estimates of carbonaceous aerosol radiative forcing.*, PNAS.

Spatial variations and source apportionment of the marine organic aerosol over the Atlantic Ocean

S. Huang, L. Poulain, Z. J. Wu, H. Herrmann, A. Wiedensohler

Leibniz Institute for Tropospheric Research, Leipzig, 04318, Germany
Keywords: marine aerosol, organic compounds, methane sulfonic acid, source apportionment.
Presenting author email: huang@tropos.de

The marine aerosol plays an important role in global climate regulation and marine biogenic system. The organic compounds are found in both primary and secondary marine aerosol and related to the number size distribution, hygroscopic growth and optical properties of particles. However, the contribution and formation mechanisms of marine organic aerosol are still poorly understood (O'Dowd and De Leeuw, 2007). In this study, physicochemical properties of the marine boundary layer aerosol were measured by a comprehensive suite of on-line instrumentation on the research vessel Polarstern during 4 cruises over the Atlantic Ocean. The cruises details are shown in Table 1.

Table 1. The starting/terminal ports and duration of 4 cruises

Expedition	Port	Duration
Cruise I (ANT-XXVII/4)	Cape Town - Bremerhaven	20.04.2011 - 20.05.2011
Cruise II (ANT-XXVIII/1)	Bremerhaven - Cape Town	28.10.2011 - 01.12.2011
Cruise III (ANT-XXVIII/5)	Punta Arenas - Bremerhaven	10.04.2012 - 15.05.2012
Cruise IV (ANT-XXIX/1)	Bremerhaven - Cape Town	27.10.2012 - 27.11.2012

Table 2. Mass fraction of the main species for 3 cruises

Species	Cruise I	Cruise II	Cruise III
Organics	24%	29%	30%
Sulfate*	58%	56%	54%
Ammonium	13%	10%	11%
Nitrate	4%	3%	4%
Chloride*	1%	2%	1%

*non-sea salt sulphate and non-sea salt chloride

The chemical composition of non-refractory submicrometer particles was derived from High Resolution Time of Flight Aerosol Mass Spectrometer (HR-ToF-AMS) measurements from the first 3 Polarstern cruises. Table 2 provides the mass fraction of each main species measured by AMS. Sulfate is the dominant component, accounting for more than 50% of the total measured particle mass concentration. Organics are the second important species, taking 24-30% of total particle mass concentration. Ammonium contributes 10-13% to the total particle mass concentration. Nitrate and non-sea salt chloride showed very low concentrations during the cruises.

As an example, the spatial variations of organic component mass concentration for cruise I-III are given by Figure 1. High concentrations are observed when the ship is close to the continent, possibly influenced by both the air mass transport from the continents and the phytoplankton blooming depending on the season.

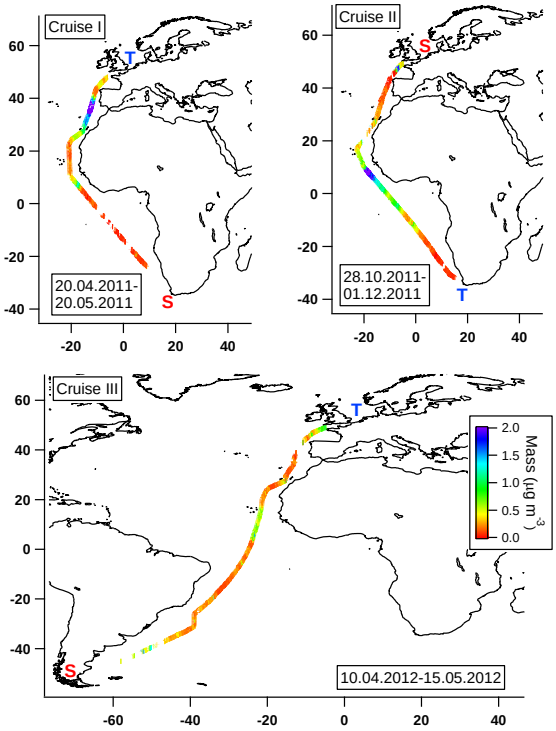

Figure 1. Organics mass concentration along the ship track for the first 3 cruises (S: starting port, T: terminal port)

Based on the high resolution mass spectra of HR-ToF-AMS, methane sulfonic acid (MSA) and sodium chloride (NaCl) are extracted from the original signals, providing clues of the secondary marine aerosol and the primary marine aerosol, respectively. They are being validated by filter sample results and being used to improve the source apportionment by Positive Matrix Factorization (PMF) method. The AMS-PMF analysis is on-going and more detailed results will be shown in the presentation.

C.D. O'Dowd and G. De Leeuw, Marine aerosol production: a review of the current knowledge, *Philos T R Soc A* **365**(2007), pp. 1753-1774.

Chemical composition, concentration, size distribution and diurnal variation of atmospheric submicron aerosol particles at the background and urban sites in Lithuania

K. Kvietkus, J. Šakalys, J. Didžbalis, E. Meinorė

State Research Institute Center for Physical Science and Technology, Savanoriu 231, LT-02300 Vilnius, Lithuania

Keywords: PM_1 chemical composition, concentration, size distribution, diurnal variation
Presenting author email: ernesta.pesliakaite@gmail.com

The aim of this study is to analyze PM_1 chemical composition, concentration, size distribution and diurnal variation of submicron aerosols particles at the background and urban sites in Lithuania. The quantitative size and chemical composition measurements of PM_1 are essentially important in determining aerosol particles effect on global climate as the major part of all aerosols volume is occupied by PM_1. PM_1 concentration and size-resolved chemical composition were measured with an *Aerodyne* Quadrupole Aerosol Mass Spectrometer (Q-AMS) during campaign in 2011. The detailed description of instrument performance is available in Jayne *et al.* (2000). The measurements of non-refractory particles were performed with a time resolution of 5 min in every sampling site, thus during campaign there were evaluated over 21 million values of measurements.

Rūgšteliškis sampling site is located in a forested area (55º27´48´´N, 26º03´60´´E) at national park of Aukštaitija with the highest point of 188,6 m a.s.l. and with mean average air temperature of 5,8 °C. Preila station is located nearby the Baltic Sea (55º22´24,4´´N, 21º4´4,5´´E) 5 m a.s.l. Rūgšteliškis and Preila sites are considered to be rural/background sites. Urban sampling site is located in the vicinity of Vilnius city, which is industrial centre with a population over 550 000 and residential area of about 400 km^2.

The average concentrations of non-refractory PM_1 chemical components (ammonium NH_4^+, nitrate NO_3^-, sulfate SO_4^{2-}, chloride Cl^- and organics) are presented in Table 1. The concentration of nitrates at polluted site in Vilnius was about twice as high as at Rūgšteliškis and Preila sites. According to O'Dowd *et al.* (2011) the source of nitrate at polluted areas is nitrate oxides from exhaust gases.

Clear diurnal variation of organics and nitrates components was indicated in Vilnius site, whereas in Preila site clear diurnal variation was observed only for chloride component. Clear diurnal variation was observed only at the presence of Northeast wind in Vilnius site.

PM_1 size distribution spectra at Preila site for ammonium and nitrates particles were shifted towards coarse particle size. Possible reason of the spectra shift is conditioned of hydrophilic aerosol particles in Preila station.

Table 1. Average concentration of PM_1 chemical components ($\mu g/m^{-3}$).

Period	NH_4^+	NO_3^-	SO_4^{2-}	Cl^-	Org
Vilnius city site					
03.23-03.28	0,078	0,190	0,253	0,0389	4,11
03.28-04.01	0,299	0,853	0,767	0,0783	6,82
04.02-04.07	0,372	1,20	0,996	0,0714	7,46
04.07-04.18	0,298	0,958	0,888	0,0703	5,86
04.18-04.22	0,113	0,471	0,292	0,0334	5,66
04.22-05.04	0,494	0,921	2,46	0,0675	13,0
05.04-05.13	0,166	0,437	0,775	0,0291	6,80
05.13-05.19	0,128	0,240	0,721	0,0193	2,44
Rūgšteliškis background site					
06.17-06.24	0,193	0,161	0,945	0,0221	4,01
06.24-07.01	0,092	0,055	0,508	0,0115	2,67
Preila background site					
07.03-07.16	0,161	0,070	1,017	0,0104	3,38
07.16-07.27	0,151	0,057	0,962	0,0103	2,20
07.31-08.08	0,115	0,069	0,802	0,0123	3,56
08.08-08.18	0,089	0,055	0,622	0,0112	1,02
08.18-08.24	0,154	0,066	0,865	0,0603	1,68

This work was supported by the Research Council of Lithuania under project No. MIP-105/2010.

Jayne, J.T., Leard, D.C., Zhang, X.F., Davidovits, P., Smith, K.A., Kolb, C.E., Worsnop, D.R. (2000) *Development of an aerosol mass spectrometer for size and composition analysis of submicron particles, Aerosol Sci. Technol*, 33, 49-70.

O'Dowd, C., Ceburnis, D., Ovadnevaite, J., Martucci, G., Bialek, J., Monahan, C., Berresheim, H., Vaishya, A., Grigas, T., Jennings, S.G., McVeigh, P., Varghese, S., Flanagan, R., Martin, D., Moran, E., Lambkin, K., Semmler, T., Perrino, C., McGrath, R. (2011) *The Eyjafjallajökull ash plume – Part I: Physical, chemical and optical characteristics, Atmos.Environ.*,doi:10.1016/j.atmosenv.2011.07.004.

Surface Aerosol Monitoring at Hada Al Sham, Western Saudi-Arabia

A.-P. Hyvärinen[1], M. Alghamdi[2], T. Hussein[3], M. Khodeir[2], A. Shehata[2], H. Lihavainen[1], M. Kulmala[3], A. Laaksonen[1]

[1]Finnish Meteorological Institute, Erik Palménin aukio 1, P.O. Box 503, FI-00101, Helsinki, Finland
[2]Department of Environmental Sciences, Faculty of Meteorology, Environment and Arid Land Agriculture, King Abdulaziz University, P. O. Box 80208, Jeddah 21589, Saudi Arabia
[3]Department of Physics, University of Helsinki, P.O. BOX 64, 00014 Helsinki, Finland
Keywords: aerosols, climate change, air quality, Saudi Arabia
Presenting author email: antti.hyvarinen@fmi.fi

The Arabian Peninsula has one of the largest aerosol particle burdens in the world because of the frequent presence of dust storms, smoke advection from South Asia, and its own pollution emissions from road traffic, the petroleum industry and local construction. In addition, the Arabian Peninsula exhibits extremely complicated meteorology with variable sea surface temperatures, enormous latent heat fluxes, abrupt topography, and strong mesoscale circulation, making both modeling and remote sensing of aerosols extremely difficult in this region.

The object of this study is to establish an aerosol measurement station in the Western Saudi Arabia to evaluate the quantities and properties of both natural and anthropogenic aerosols in the area, and their effect on climate change and air quality. The measurements were begun October 2012 with a projected length of three years.

The Hada Al Sham site (21.802° North, 39.729° East, 254 m a.s.l.) is situated about 60 km east of the coastal city of Jeddah. The surroundings represent a rural area. The following in situ measurements are conducted at the station: $PM_{2.5}$ and PM_{10} mass concentrations, total particle number concentration, particle number size distribution from 7 nm to 10 µm, aerosol black carbon concentration (absorption coefficient) and aerosol scattering coefficient. Cimel sunphotometer is used for measuring the columnar properties of the atmosphere. In addition, weather parameters are measured.

The early results from Hada Al Sham show a wide diversity of different aerosol sources. In December 2012, 85 % of the recorded days exhibited a new particle formation event (Fig 1.). This can be related to sulphate emissions from heavy oil combustion occurring in the Western Saudi Arabia, such as oil refining (Khodeir et al. 2012).

The scattering and absorption coefficients measured during December 2012 showed a clear diurnal variation (Fig 2.). While the scattering coefficient showed two daily maxima, occurring at 7 am and 5 pm, the absorption coefficient was elevated from 12 am to 7 am. This illustrates that the absorbing aerosols related to anthropogenic activities have different sources than scattering aerosols, which also have natural sources, such as mineral dust.

In the future, the seasonal variation of aerosols in Hada Al Sham, together with their spatial sources will be investigated.

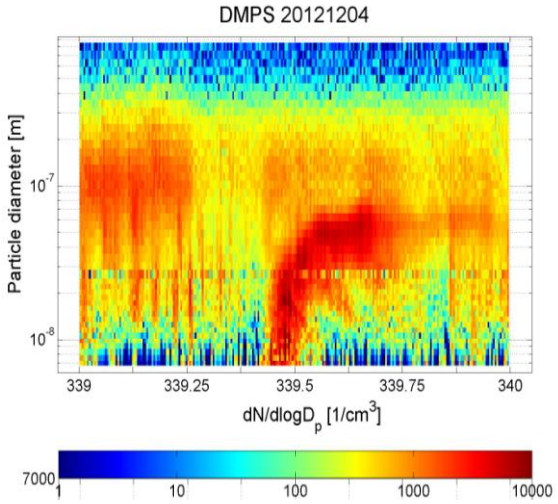

Figure 1. Example particle size distribution as a function of time on 4.12.2012.

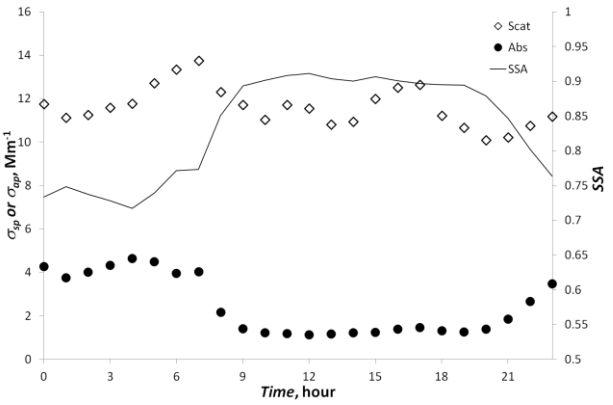

Figure 2. Diurnal variation of scattering coefficient (σ_{sp}), absorption coefficient (σ_{ap}), and single scattering albedo (*SSA*) at 525 nm on December 2012.

This study was funded by King Abdulaziz University (KAU), Jeddah, Saudi Arabia (under grant No. 1220/430). The authors acknowledge the technical support of KAU.

Khodeir, M., Shamy, M., Alghamdi, M., Zhong, M., Sun, H., Costa, M., Chen, L.-C., and Maciejczyk, P. (2012) *Atm. Pollut. Res.* **3**, 331-340.

Chemical composition, and mass closure of Siberia aerosols at ZOTTO, Russia, April 2010 to February 2011

X. Chi[1], E. Mikhailov[2] A. Panov[3] and M.O. Andreae[1]

[1] Biogeochemistry Department, Max Planck Institute for Chemistry, Mainz, D-55020, Germany
[2] Atmospheric Physics Department, Institute of Physics, St. Petersburg State University, St. Petersburg, 199026, Russia
[3] V.N. Sukachev Institute of Forest, Krasnoyarsk, 660036, Russia
Keywords: Siberia Aerosol, chemical composition, mass closure
Presenting author email: xuguang.chi@mpic.de

Atmospheric aerosols are currently a subject of high scientific and political interest mainly due to their role in climate and their effects on human health (Andreae and Crutzen 1997). Aerosols are a complex mixture of many different chemical species originating from a variety of natural and anthropogenic sources. Their chemical composition is determined by their sources and subsequent transformation while airborne, and is temporally and spatially highly variable. The major aerosol components (aerosol types) normally include organic matter (OM), elemental carbon (EC) or Black carbon (BC), sulfate, nitrate, ammonium, crustal matter, and sea salt. Data on aerosols chemical composition are necessary for source identification and apportionment, and also needed for the testing and validation of numerical aerosol models, which are becoming tools to extrapolate monitoring data. During the last decades, a growing number of scientific studies have been investigating the chemical composition of aerosols at various sites around world. However, the data for chemical aerosols composition in Siberia, a vast region in Central Eurasia, are still lacking. This is highly contradictory to the global relevance of the Siberian landmass as a source and sink for aerosol particles, and their role in the global radiation budget.

In order to characterize the Siberia aerosols, filter sampling were started at Zotto site (60.80°N and 89.35°E, 114 m a.s.l.), Russia in April 2010. Nuclepore polycarbonate and quartz fibre filter samples were taken in parallel with real time aerosols optical properties measurements and some tracer gas measurements. Up to March 2011, 66 samples were taken for each samplers. The quartz fibre filters were analysed for the particulate mass by weighing, and analysed for organic carbon (OC) and elemental carbon (EC) by sunset OC/EC analyser. The Nuclepore filters were analysed for major anions and cations by ion chromatography (Dionex, ics-1100), and for water soluble organic carbon (WSOC) with a Shimadzu TOC analyzer. With help from high time resolution CO and light absorption results and Hysplit back trajectories calculations, the filter samples were separate to episode samples and non-episode samples. The aerosols chemical compositions were clearly different between episode and non-episode samples, and between winter and other three seasons. The winter episodes associated with elevated concentrations for most of species, and were usually related to anthropogenic pollution, the air masses during such episodes had passed over the central Siberian region around Omsk and Novosibirsk – a heavily industrialized area. During spring and fall, a number of samples exhibited high K^+, and oxalate levels, indicating an impact from biomass burning. In addition a notable episode with extreme high Na^+, Cl^-, and Mg^{2+} were observed for the samples collected between 20 to 24 December 2010, which may result from long range transport of sea salt from North. More than 80% of OC are found to be Water soluble in summer non-episode period, which may due to the enhancement of secondary organic aerosols formation.

In the aerosol chemical mass closure calculations, six aerosol types were considered. Organic matter (OM) contributed by far the most to the PM mass; it accounted for about 40-70% of the average PM mass. Followed by Secondary Inorganic Aerosols species (SO4, NH4, and NO3), more than 30% of PM mass. OM contribution to PM mass was lower in winter than that in the other three seasons, while EC, Ammonium and Nitrite show higher contribution in winter. The mean PM mass attribution to the different aerosol types for April to November 2010 at Zotto during non-episodes periods were similar to those for the 2007 campaign at the forested site of Hyytiälä, Finland. EC and Nitrate were more important and Ammonium was clearly less important at Zotto, though.

Andreae, M O, and P J Crutzen (1997) *Atmospheric aerosols: Biogeochemical sources and role in atmospheric chemistry*, Science 276 (5315):1052-1056.

Maenhaut et al., (2011) *Chemical composition, impact from biomass burning, and mass closure for PM2.5 and PM10 aerosols at Hyytiälä, Finland, in summer 2007*, X-ray spectrometry, 40: 168-171.

Estimation of emission rates of resuspended road dust using a mobile monitoring system

Sehyun Han and Yongwon Jung

Department of Environmental Engineering, Inha University, 253 Yonghyun-Dong, 402-751, Incheon, Korea
Keywords: PM10, PM2.5, resuspended road dust, emission factor
Presenting author email: jungyw@inha.ac.kr

Resuspended road dust has been one of the main PM10 emission sources in Western United States and some of European countries including Norway during winter. According to the previous study based on CAPSS(Clean Air Policy Support System) developed by Korean Ministry of Environment, resuspended road dust is likely to contribute with significant amount to PM10 emission not only in road transport sector but also in entire PM10 emission inventory in Seoul metropolitan area including the city of Incheon. One of the main problems in estimating PM10 emission rate of resuspended road dust using the emission estimation equation in AP-42 of US EPA is that there are very large uncertainties in estimated values, which often result in overestimation of the PM10 emission rate of resuspended road dust. This study focuses on reducing uncertainties in estimating PM10 and PM2.5 emission rate of resuspended road dust.

To estimate PM10 emission rate of resuspended road dust, a mobile monitoring system was developed in this study, which is similar to the SCAMPER(System for the Continuous Aerosol Monitoring of Particle Emission Rates from Roads, Fitz and Bumiller, 2005) in principle. Originally, the mobile system was designed in 2005 using the principle of the TRAKER(Testing Re-Entrained Kinetic Emissions from Roads, Kuhns *et al*, 2001) and has been employed to measure silt loading on paved roads in Seoul metropolitan area(Han and Jung, 2012). Therefore, our system employs principles of both TRAKER and SCAMPER and thereby the silt loading data and emission rate of resuspended road dust can be estimated on a test road simultaneously. A schematic of a hybrid type mobile monitoring system is shown in Figure 1.

PM10 emission factors of resuspended road dust on a test road section can also be estimated using the emission estimation equation in AP-42 of US EPA, which uses silt loading and vehicle weight as parameters in the equation. Therefore, if one compares the emission factors (*i.e.* g/km) obtained using the emission estimation equation in AP-42 of US EPA with those obtained using SCAMPER principle, one can correct the predicted emission factors from the emission estimation equation in AP-42 of US EPA. By doing so, uncertainties in the emission estimation equation in AP-42 of US EPA can be reduced and possibility of modification of the equation, for example, by adding a vehicle speed dependency term to the equation as an additional parameter can also be verified. For this, we attempted to correlate the correction factors (or scaling factors hereafter) obtained at different test conditions with vehicle speed and silt loading as parameters.

It was found that the resulting correlation for the scaling factor is approximately proportional to the square of vehicle speed, whereas it has relatively weak dependency of silt loading. Detailed results will be presented in the conference.

Figure 1. A hybrid type mobile monitoring system

This work was supported by the Korea Ministry of Environment (MOE) as "The Eco-Innovation Program".

Fitz, D. and Bumiller, K. (2005) *Proc. 14th Int. Conf. on Emission Inventory*, EPA.

Kuhns, H., Etyemezian, V., Landwehr, D., MacDougall, C., Pitchford, M., and Green, M. (2001) *Atmospheric Environment* **35**, 2815-2825.

Han, S. and Jung, Y. (2012) *J. of the Air & Waste Management Association* **62**, 846-862

One-year monitoring of nitro-organic compounds in biomass burning PM_{10} filter samples

A. Kahnt[1], S. Behrouzi[1], R. Vermeylen[1], M. Safi Shalamzari[1], J. Vercauteren[2], W. Maenhaut[1,3] and M. Claeys[1]

[1]Department of Pharmaceutical Sciences, University of Antwerp, BE-2610 Antwerp, Belgium
[2]Flemish Environment Agency (VMM), BE-2000 Antwerp, Belgium
[3]Department of Analytical Chemistry, Ghent University, BE-9000 Gent, Belgium

Keywords: Biomass Burning, Nitro-aromatics, Nitrooxy organosulfates, Resin acid.
Presenting author email: Ariane.Kahnt@ua.ac.be

Biomass burning aerosol (BBA) contains a significant fraction of nitro-aromatic compounds and recent studies identified nitrocatechols ($C_6H_5NO_4$, MW 155) and methyl-nitrocatechols ($C_7H_7NO_4$, MW 169) as main constituents. These compounds were proposed as tracer compounds for processed (secondary) BBA (Iinuma *et al.*, 2010). Higher homologues of methyl-nitrocatechols ($C_8H_9NO_4$, MW 183) were described also recently as abundant compounds in ambient filter samples (Kitanovski *et al*., 2012a, b). Furthermore, nitrocatechols and their methyl homologues were shown to correspond to the abundant yellow-coloured compounds of humic-like substances that were isolated from BBA (Claeys *et al.*, 2012). Taking into account the abundance of nitro-aromatic compounds in atmospheric aerosol samples and their potential effects on health and climate, the aim of the present study was to examine their time series over a whole year and their relationships with other known tracers for BBA and biogenic secondary organic aerosol.

PM_{10} filter samples were collected from a rural station in Hamme, Belgium, which was recently shown to be largely impacted by biomass burning (Maenhaut *et al.*, 2012). The extracted filter samples were further investigated in terms of liquid chromatography combined with negative ion electrospray ionisation mass spectrometry and different compounds were quantified. The targeted compounds included four nitro-aromatic compounds (MWs 139, 155, 169, and 183), nitrooxy organosulfates (MW 295) originating from α-pinene and the resin acid dehydroabietic acid, DHAA (MW 300) (Figure 1).

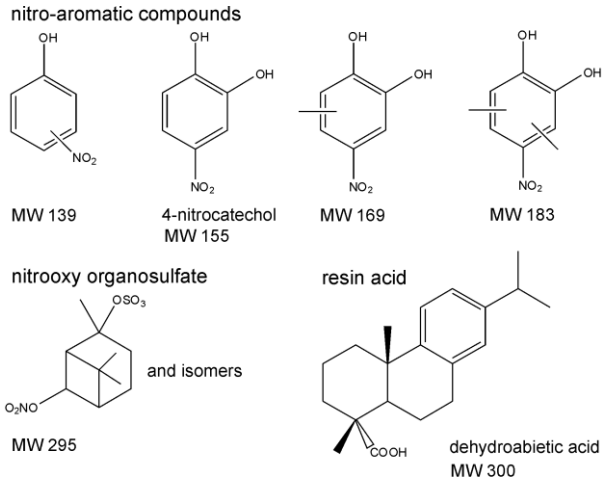

Figure 1. Targeted compounds in the present study.

A strong seasonal variation was observed for the nitro-compounds with highest concentrations during the winter months (Figure 2), followed by the autumn, spring and summer periods. In agreement with a previous study (Kitanovski *et al.*, 2012b), high correlations between the nitrocatechols and methyl-nitrocatechols were observed, with r-values up to 0.97. There were also substantial correlations (r-values up to 0.68) between these BBA tracers and the primary BBA tracer levoglucosan.

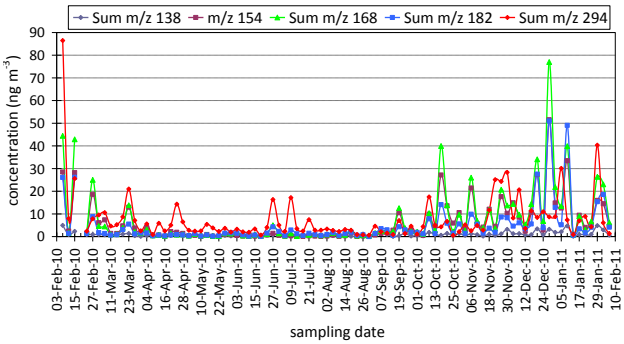

Figure 2. Time series for PM_{10} nitro-aromatic compounds in Hamme, Belgium.

Based on the DHAA measurements and the correlation analysis, the burning of softwood and foliage of coniferous trees is likely an important source for the formation of all of the targeted species.

This work was supported by the Belgian Federal Science Policy Office through the network project "Biogenic Influence on Oxidants and Secondary Organic Aersosol: theoretical, laboratory and modeling investigations (BIOSOA).

Claeys, M., *et al.* (2012), *Environ. Chem*. **9**, 273-284.
Iinuma, Y., *et al.* (2010), *Environ. Sci. Technol*. **44**, 8453-8459.
Kitanovski, Z., et al. (2012a), *Rapid Commun. Mass Spectrom.* **26**, 793-804.
Kitanovski, Z., *et al.* (2012b), *J. Chromatogr. A*, **1268**, 35-43.
Maenhaut, W., *et al.* (2012), *Sci. Total Environ*. **437**, 226-236.

A case of CCN formation associated with atmospheric nucleation in eastern Mediterranean

N. Kalivitis[1,2], V.-M. Kerminen[2], G. Kouvarakis[1], I. Stavroulas[1], A. Bougiatioti[3], A. Nenes[3], H.E. Manninen[2,4], T. Petäjä[2], M. Kulmala[2] and N. Mihalopoulos[1]

[1]Environmental Chemical Processes Laboratory, Department of Chemistry, University of Crete, 71003, Heraklion, Greece
[2]Department of Physics, University of Helsinki, P.O. Box 64, FI-00014, University of Helsinki, Finland
[3]School of Earth and Atmospheric Sciences, Georgia Institute of Technology, Atlanta, GA 30332,USA
[4]Institute of Physics, University of Tartu, Ülikooli 18, 50090, Tartu, Estonia

Keywords: nucleation, growth, Mediterranean, CCN
Presenting author email: nkalivitis@chemistry.uoc.gr

Quantifying the contribution of atmospheric nucleation processes as source of cloud condensation nuclei (CCN) is an important step towards the understanding of the interactions between aerosols and clouds, and subsequently the radiative forcing of the atmosphere (Kerminen et al., 2012).

During the FRONT (Formation and growth of atmospheric nanoparticles) project both nucleation and growth of atmospheric aerosols are studied, with special emphasis given to the precursor gases driving these processes. Continuous measurements of aerosol and ion size distributions and real time aerosol chemical composition are performed at Finokalia station, Greece.

In Fig. 1 an event of consecutive nucleation days observed at Finokalia is presented. Aerosol size distributions were measured with an SMPS in the size range 10-900nm and real time chemical composition of fine particles was monitored with an ACSM (Aerosol Chemical Speciation Monitor). The onset of new particle formation sequence took place when the origin of the air masses changed from west to north. Back trajectories analysis showed that air mass penetration from higher altitudes resulted to a drastic drop of condensation sink (CS). For the days presented the air mass origin remained the same. There were 4 events of atmospheric nucleation observed. The chemical composition of aerosols showed that the change of air masses origin, except of the drop of CS resulted additionally to a cations/anions (C/A) ratio well above 1. As has been shown in the past (Pikridas et al., 2012) under these conditions nucleation is favored, high C/A ratio is an indication of NH_3 excess in a sulfate rich environment as Finokalia.

Number concentration for particles with D_p<20nm (N_{nuc}) and D_p>100nm (N_{acc}) were calculated, N_{nuc} to demonstrate the nucleation and N_{acc} as representative for CCN number. In previous experiments during summer at Finokalia it was observed that N_{acc} is well correlated to CCN number for supersaturation of 0.2% (not shown). As can be seen in Fig. 1, the variation of N_{acc} follows closely that of sulfate indicating that sulfate is the major species that result to growth to CCN sizes. On the other hand, organic compounds present a weaker correlation to N_{acc}, playing important role though in the determination of CCN number. However, it is expected that the contribution of different species in the growth process changes on annual basis as a subject of the abundance of each species. Future work will provide supplementary information on VOCs and their potential role in the formation and growth processes.

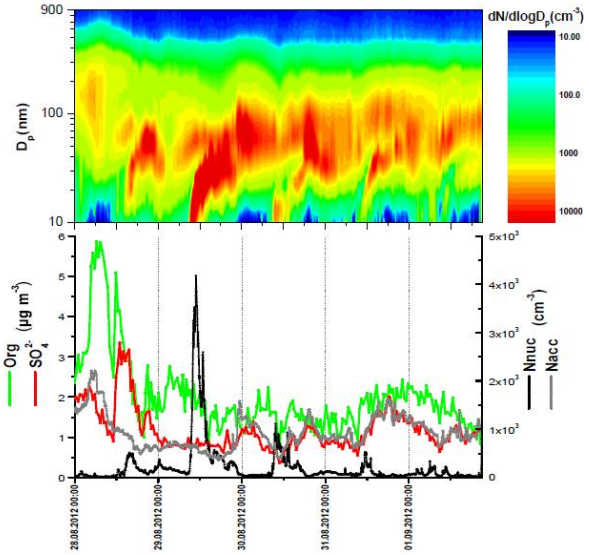

Figure 1. Nucleation events observed at the Finokalia station during the period 28/8-1/9/2012. Upper panel, number size distributions of atmospheric aerosols (D_p 10-900 nm). Lower panel, time series of aerosol chemical composition (major components) and number concentration of nucleation and accumulation mode particles.

The research project is implemented within the framework of the Action «Supporting Postdoctoral Researchers» of the Operational Program "Education and Lifelong Learning" (Action's Beneficiary: General Secretariat for Research and Technology), and is co-financed by the European Social Fund (ESF) and the Greek State. This research is supported by the Academy of Finland Center of Excellence program (project number 1118615).

Kerminen, V.-M, et al. (2012) *Atmos. Chem. Phys*., **12**, 12037-12059.
Pikridas, M., et al. (2012*) J. Geophys. Res*., **117**,D12205.

Nitration and oxidation of bioaerosols and allergenic proteins

C. J. Kampf[1], K. Selzle[1], and U. Pöschl[1]

[1]Multiphase Chemistry Department, Max Planck Institute for Chemistry, Mainz, 55128, Germany
Keywords: nitro-protein, reactive oxygen intermediates (ROI), bioaerosol
c.kampf@mpic.de

Primary biological aerosol particles, e.g. pollen, fungal spores, bacteria, etc., significantly contribute to the coarse mode particulate matter in urban, rural, and pristine environments (Elbert et al., 2007; Després et al., 2012). Up to ~5% of the total urban particulate matter are proteins. These proteins influence the physico-chemical properties of atmospheric particles and play a major role as airborne allergens (Franze et al., 2003)

Protein nitration was found to occur at the tyrosine residues, and to proceed at timescales and NO_2 and O_3 concentrations relevant to the ambient atmosphere (Franze et al., 2005). Moreover, recent studies suggest that nitration affects the allergenicity of proteins (Gruijthuijsen et al., 2006; Untersmayr et al., 2010).

For this study, the reaction products and pathways of protein nitration were investigated using 3 different nitration agents. Nitration of the investigated proteins was carried out in solution using 1) tetranitromethane (TNM), 2) peroxynitrite, and by passing gaseous nitrogen dioxide and ozone (NO_2+O_3) over protein spiked filters as illustrated in Fig 1. The nitration degrees of individual tyrosine residues (ND_Y) were determined by site-specific quantification using HPLC-MS/MS (Zhang et al., 2011) and compared to the total protein nitration degrees (ND) determined by photometric detection with HPLC-DAD (modified Yang et al., 2010).

The observed nitration patterns revealed that the site selectivity of the reaction depends on 1) the nitrating agent, 2) reaction conditions, and 3) molecular structure of the protein. Therefore, different nitration mechanisms in endogenous and exogenous processes lead to specific post-translational modifications of proteins under summer smog conditions in the atmosphere (NO_2 and O_3), or during inflammatory processes in the human body (peroxynitrite). Further, a correlation of ND and relative humidity (RH) was observed for protein nitration by gaseous NO_2 and O_3. Meteorological conditions therefore seem to play an important role in the ambient protein nitration. Atmospheric aerosol samples will be analyzed to investigate the extent of protein nitration and oxidation under ambient conditions.

The chemical mechanisms and molecular processes responsible for the adverse health effects of NO_2 and O_3 are still not well understood. We suggest that protein nitration by air pollutants plays a major role in the increase of allergies in the western countries besides nutrition effects and excessive hygiene practices.

This work was supported by the Max-Planck Society (MPG), the International Max-Planck Research School for Atmospheric Chemistry and Physics (IMPRS), and the Max-Planck Graduate School (MPGC). The authors gratefully acknowledge support by numerous collaboration partners in the Earth, environmental, and life sciences.

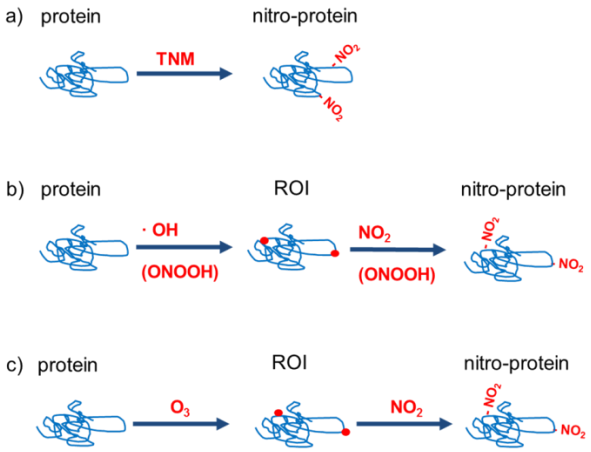

Figure 1: Protein nitration pathways. (modified from Shiraiwa et al., 2012)

Elbert, W., Taylor, P.E., Andreae, M.O., and Pöschl, U. (2007) *Atmos. Chem. Phys.*, 7, 4569-4588.

Després, V., Huffmann, J. A., et al. (2012) *Tellus B*, 64, 15598, DOI: 10.3402/tellusb.v64i0.15598

Franze, T., Weller, M. G., Niessner, R., and Pöschl, U. (2003) *J. Aerosol Sci.*, 34, S777-S778.

Franze, T., Weller, M. G., Niessner, R. and Pöschl, U. (2005) *Environ. Sci. Technol.*, 39, 1673-1678.

Gruijthuijsen, Y. K., Grieshuber, I., et al. (2006) *Int. Arch. Allergy Immunol.*, 141, 265-275.

Untersmayr, E., Diesner, S. C., et al. (2010) *PLoS ONE*, 5(12): e14210, doi:10.1371/journal.pone.0014210.

Zhang, Y., Yang, H., and Pöschl., U. (2011) *Anal. Bioanal. Chem.*, 399, 459-471.

Yang, H., Zhang, Y., and Pöschl., U. (2010) *Anal. Bioanal. Chem.*, 397, 879-886.

Shiraiwa, M., Selzle, K., and Pöschl, U. (2012) *Free Radical Research*, 46, 927-939.

Effects of mineral dust and sea salt on global nitrate concentration field

V.A. Karydis[1], A.P. Tsimpidi[1], and J. Lelieveld[1,2]

[1]Max Planck Institute for Chemistry, Mainz, 55128, Germany
[2]Energy, environment and water research center, Cyprus Institute, Nicosia, 1645, Cyprus

Keywords: Nitrate Aerosols, Aerosol Thermodynamics, Mineral Dust, Sea Salt.
Presenting author email: v.karydis@mpic.de

Inorganic particulate nitrate constituents contribute significantly to the total aerosol mass; i.e. over Europe particulate nitrate accounts for about 10–20% of the total dry aerosol mass (Putaud et al., 2004). While nitrate is predominantly present in the submicron mode, coarse mode aerosol nitrate can also be produced by adsorption of nitric acid onto sea salt particles and soil particles. Naturally emitted particles affect the phase partitioning of nitrate and ammonium, especially in areas where dust or sea salt comprises a significant portion of total particulate matter, and the simulation of these effects can considerably improve model predictions. However, most thermodynamic models used in global studies lack a realistic treatment of crustal species. Furthermore, assuming thermodynamic equilibrium between the gas and aerosol phases may not be appropriate for coarse mode aerosols in global models.

The project aims to improve the representation of nitrate aerosols in a global chemistry climate model, the ECHAM/MESSy Atmospheric Chemistry (EMAC) model (Jöckel et al., 2006), and address the shortcomings of previous models. EMAC calculates the aerosol microphysics and gas/aerosol partitioning by using the Global Modal-aerosol eXtension (GMXe) aerosol module (Pringle et al., 2010). Aerosol microphysics are treated using an extended version of the M7 modal aerosol scheme (Vignati et al., 2004), which describes the aerosol size distribution by 7 interacting lognormal modes (4 hydrophilic and 3 hydrophobic modes). An advanced dust emission module also accounts for the soil particle size distribution of different deserts worldwide (Astitha et al., 2012). Gas/aerosol partitioning is simulated using the EQSAM (Metzger and Lelieveld, 2007) and ISORROPIA-II (Fountoukis and Nenes, 2007) thermodynamic equilibrium models. The EQSAM model is a simplified, non-iterative, treatment of gas/aerosol partitioning that uses analytical expressions based on the species solubility. EQSAM can be run in a range of complexities; in this work we consider the interaction of K^+-Ca^{2+}-Mg^{2+}-NH_4^+-Na^+-SO_4^{2-}-NO_3^--Cl^--H_2O aerosol components. ISORROPIA-II uses the same suit of components and solves for the equilibrium state by considering the chemical potential of the species.

Simulation of the effects of mineral dust and sea salt on nitrate aerosol partitioning and size distribution requires an accurate description of the aerosol dynamics in the coarse mode, while it is desirable for the model to remain computationally efficient. In this project we use the hybrid method for aerosol dynamics developed by Capaldo et al. (2000) in which only the aerosol particles in the fine (nucleation, aitken, and accumulation) mode are simulated assuming equilibrium by applying EQSAM or ISORROPIA-II. For coarse particles the mass transfer differential equations are solved using the gas-phase concentrations calculated by the equilibrium step.

The proposed modeling framework combines the accuracy of the dynamic approach with the speed and simplicity of the equilibrium approach, which makes it ideal for the accurate prediction of the nitrate global concentration fields. The new model is tested in long-term simulations covering the years 2005-2008. Model predictions are compared with data from the European Monitoring and Evaluation Programme (EMEP), the Clean Air Status and Trends Network (CASTNet), the Acid Deposition Monitoring Network in East Asia (EANET)

References

Astitha, M., Lelieveld, J., Kader, M. A., Pozzer, A., and Meij, A. d. (2012) *Atmos. Chem. Phys. Discuss.*, 12, 13237-13298.

Fountoukis, C., and Nenes, A. (2007) *Atmos. Chem. Phys.*, 7, 4639-4659.

Jöckel, P., Tost, H., Pozzer, A., Bruehl, C., Buchholz, J., Ganzeveld, L., Hoor, P., Kerkweg, A., Lawrence, M. G., Sander, R., Steil, B., Stiller, G., Tanarhte, M., Taraborrelli, D., Van Aardenne, J., and Lelieveld, J. (2006) *Atmos. Chem. Phys.*, 6, 5067-5104.

Metzger, S., and Lelieveld, J. (2007) *Atmos. Chem. Phys.*, 7, 3163-3193.

Pringle, K. J., Tost, H., Message, S., Steil, B., Giannadaki, D., Nenes, A., Fountoukis, C., Stier, P., Vignati, E., and Leieved, J. (2010) *Geosc. Mod. Devel.*, 3, 391-412.

Putaud, J. P., Raes, F., Van Dingenen, R., Bruggemann, E., Facchini, M. C., Decesari, S., Fuzzi, S., Gehrig, R., Huglin, C., Laj, P., Lorbeer, G., Maenhaut, W., Mihalopoulos, N., Mulller, K., Querol, X., Rodriguez, S., Schneider, J., Spindler, G., ten Brink, H., Torseth, K., and Wiedensohler, A. (2004) *Atmos. Environ.*, 38, 2579-2595.

Vignati, E., Wilson, J., and Stier, P.: M7 (2004) *J. Geoph. Res.*, 109, 10.1029/2003jd004485.

Particle size distribution of viable airborne microbes and particulate matter during pretreatment of wastewater

E. Katsivela[1], E. Latos[2], L. Raisi[1], and M. Lazaridis[2]

[1]Department of Natural Resources and Environment, Technological Educational Institute of Crete, Romanou 3, 73133 Chania, Creece
[2]Department of Environmental Engineering, Technical University of Crete, Polytechneioupolis, 73100 Chania, Greece
Keywords: bioaerosols, bacteria, fungi, particle size distribution, indoor working place
Presenting author email: katsivela@chania.teicrete.gr

The aim of the present work was to determine the size distribution of the viable, cultivable, airborne bacteria and fungi, as well as of the inhalable particulate matter emitted from the coarse bubble aerated grit chambers (indoors) as well as from the primary settling tanks (outdoors, partially covered) of a Municipal Wastewater Treatment Plant. Measurements were conducted at a Mediterranean site (Chania) from March to July 2008.

Air samples were taken with an Andersen six stage viable particle impactor (Thermo Electron Corporation, USA). The heterotrophic bacteria were grown in Tryptone Soy Agar at 37°C for 48 h, whereas the mesophilic fungi were cultivated in Malt Extract Agar at 20°C for 72 h. The total coliforms were grown in Membrane Lauryl Sulphate Agar at 37°C for 48 h. Mass and number concentrations of particulate matter (PM) were determined using portable aerosol monitors (Dust-Trak and P-Trak instruments, TSI, Germany). Hydrogen sulfide measurements were performed using a Jerome 631-X sampler (Arizona Instruments, USA).

Table 1 summarizes the arithmetic mean concentrations of all measured parameters in the two stages of the wastewater treatment plant as well as of the control at a background site.

Table 1. Arithmetic mean values of parameters measured.

Parameter	Aerated Grit Chambers	Primary Settling Tank	Urban Background (control)
Sum Heterotrophic bacteria	3,145 cfu/m^3	36 cfu/m^3	89 cfu/m^3
Sum Mesophylic fungi	204 cfu/m^3	70 cfu/m^3	318 cfu/m^3
Sum Total coliforms	29 cfu/m^3	0 cfu/m^3	0 cfu/m^3-
PM_{10}	136 μg/m^3	38 μg/m^3	39 μg/m^3
$PM_{2.5}$	76 μg/m^3	28 μg/m^3	26 μg/m^3
PM_1	62 μg/m^3	23 μg/m^3	20 μg/m^3
PM_1	160,668 pt/cm^3	5,250 pt/cm^3	4,312 pt/cm^3
H_2S	8,121 ppb	195 ppb	4 ppb
T		23.6 °C	
RH		51 %	
υ		8.7 m/s	

A gradual decrease of bioaerosol concentrations was observed during the advanced wastewater treatment from the pretreatment to the primary treatment in agreement with a previous study (Karra and Katsivela, 2007). It is observed that the mean concentration of the airborne heterotrophic bacteria at the aerated grit chambers was 87 times higher than those at the primary settling tanks, and 35 times higher to the values measured at an urban background site. Similarly, the highest concentrations of the total coliforms as well as the mass and particle number concentrations of the inhalable particulate matter (PM_{10}, $PM_{2.5}$, PM_1) as well as the concentration of hydrogen sulfide were observed at the aerated grit chambers of the wastewater pretreatment. Only the mean concentration of mesophilic fungi at the aerated grit chambers had similar values to the background site.

Although, the size distribution profile of the mean concentrations of the airborne heterotrophic bacteria at the primary settling tanks and the urban background site was typical for this taxonomic group (Raisi *et al*, 2012), their profile at the aerated grit chambers was different and showed a maximum aerodynamic diameter concentration at the 3.3-4.7 μm size range (Figure 1).

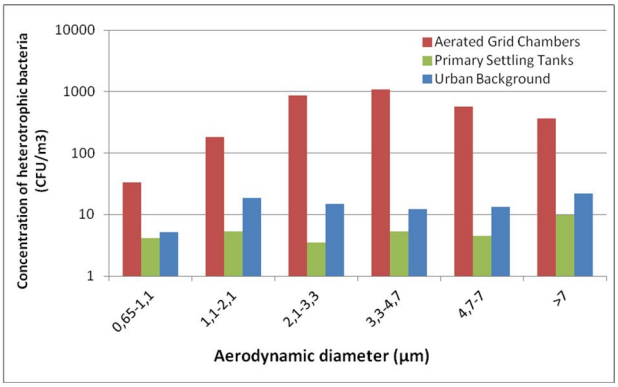

Figure 1. Mean concentration size distribution of viable, cultivable, airborne heterotrophic bacteria during the whole measurement period.

The current study concludes that the advanced wastewater treatment leads to the diminution of health risks associated emissions of potentially pathogenic microbes (heterochthonous heterotrophic bacteria and total coliforms), inhalable particles and hydrogen sulfide.

The research leading to these results has received funding from the European Union Seventh Framework Programme HEXACOMM *FP7/2007-2013* under *grant agreement* n° *315760*.

Karra, S. and Katsivela E. (2007) *Water Research* **41**, 1355-1365.
Raisi L., Aleksandropoulou, V., Lazaridis, M. and Katsivela E. (2012) *Aerobiologia* DOI 10.1007/s10453-012-9276-9.

Comprehensive studies of chemical composition of atmospheric aerosol above Lake Baikal surface area, Russia

T.V. Khodzher

Limnological Institute SB RAS, Irkutsk, 664033, Russia
Keywords: aerosols, Baikal, elements, n-alkanes, PAH
T.V. Khodzher: khodzher@lin.irk.ru

Long-term studies of the chemical composition of aerosols above the surface area of Lake Baikal (53º30' N, 108º0' E) were performed. This lake is one of the world's deepest lakes (1,637 m) which contain 20% of the world's surface fresh water.

Natural aerosol was sampled from the forebody of the research vessel at a height of 6 m above the water surface. Two types of sampling equipment were used – a standard high-volume pump and a six-phase high-volume slit cascade impactor TE-236 (Tisch Environmental Inc.) for particle sampling of the following size fractions – <10.2 μm and 10.2-4.2; 4,2-2.1; 2.1-1.3; 1.3-0.69; 0.69-0.39. "Whatman 41" served as a substrate for mineral particles. Persistent organic pollutants (POPs) were collected onto a fibrous glass filter.

Mean annual total concentration of ions amounted to 1.0-1.3 $\mu m/m^3$ in aerosol particles above the central areas of the lake water surface, which made up 25-30% of the total aerosol.

The majority of aerosols above Lake Baikal were represented by fractions of less than 1 μm, 60% of them being within the range less than 0.7 μm. Bicarbonates, sulphates, calcium and ammonium dominated in their composition. Differences in chemical composition of aerosol particles were mainly attributed to local sources of their origin which were located on the lake shore. Elevated concentrations of components were recorded in aerosol above the southern basin of Lake Baikal in the vicinity of settlements where total ions increased up to 2.0-4.0 $\mu m/m^3$. In the coastal area near the town of Baikalsk, the contribution of sodium and chloride ions was higher due to Baikalsk Pulp and Paper Plant located on the lake shore.

Distribution of microelements was also studied in aerosol particles of different sizes. Coarse-dispersion fraction (over 2 μm) was dominated by typical terrigenous elements (Ca, Mg K, Ti, Fe, Al, and Si). Such elements as Br, Zn and Pb prevailed in the fractions less than 0.7 μm. Some elements (V, Ni and Cu) had two peaks of maximal distribution in coarse (2.1-1.3 μm) and fine (0.69-039 μm) particles. To study remote and regional transfer of components to Lake Baikal (at tens and hundreds of kilometres), element composition of aerosol particles of 0.39-0.69 μm was analysed. Among 20 elements analysed by XRFA-SR, Mn, Ni, Cu, Zn, Ga, Sr, Br, and Pb were the most informative elements.

The concentration of the majority of microelements in aerosol particles above the Baikal surface area corresponded to the clarkes of the Earth's crust. The enrichment factor for such elements as Mn, Ni, Cu, Zn, Ga, Sr, Br, and Pb was by 1-2 orders higher compared to that of the soil. Therefore, there were some other sources for these elements besides terrigenous ones.

Electron microscopic analysis (X-ray spectral microanalysis) showed a high diversity of aerosol particles above the lake. Faceted particles were the most common in Northern Baikal. Particles >1 μm of oval or spherical shapes were registered above all three basins of the lake. The composition of rounded particles together with organic material (~ 80 %) consisted of inclusions of Al, Si, K, Ca, and Mg of terrigenous origin. Faceted particles and aggregations of particles like conglomerates contained C, O, Al, Ca, Si, and Mg. A more diverse range of elements (O, C, Si, K, Fe, Al, S, Ca, Na, and Mg) was recorded in particles of other shapes.

Twelve polycyclic aromatic hydrocarbons (PAH) and n-alkanes were analysed in Baikal aerosol. Maximal PAH concentration was detected in the size fraction less than 0.7 μm. The atmosphere above Southern Baikal contained benz(a)pyrene and chrysene – dominant components of forest fires, and benz(g,h,i)perylene and indeno(1,2,3-c,d)pyrene, indicators of atmospheric pollution by automobile transport. The ratio between PAH concentrations showed that the submicron fraction was represented by "aged" particles existing in the atmosphere for a long time and by aerosol of local origin in the coarse-dispersion fraction. The highest content of n-alkanes was registered in aerosol of Central Baikal where there are natural oil seepages. The dominance of odd homologues from n-C_{23} to n-C_{33} was observed in the fraction of higher homologues which is evident of their natural origin.

The results obtained allow us to conclude that the atmosphere above Lake Baikal remains relatively pure, and the components in it are mainly of natural origin. The southern part of the lake experiences some anthropogenic impact. However, the concentration of contaminants here is rather low.

Airborne Measurements of Emissions from Oil and Gas Exploration and Production Activities in the Norwegian Sea

J. Kim[1], A. Roiger[1] , B. Weinzierl[1], M. Rose[1], A. Reiter[1], J. Thomas[2], L. Marelle[2], K. Law[2], and H. Schlager[1]

[1] Institute of Atmospheric Physics, German Aerospace Centre (DLR), 82234 Oberpfaffenhofen, Germany
[2]UPMC Univ. Paris 06, Université Versailles St-Quentin, CNRS/INSU, UMR 8190, LATMOS-IPSL, Paris, France
Keywords: Arctic pollution, Emissions, Combustion aerosols, In-situ measurements.
Presenting author email: Jin.Kim@dlr.de

Over the past few decades, a rapid decline in Arctic sea ice has been observed. Unlocking of the Arctic Ocean is expected to promote hydrocarbon extraction in the Arctic, which in turn will increase emissions of climate-relevant pollutants such as black carbon (Ødemark *et al*, 2012). Despite the anticipated impact, there are still insufficient in-situ measurements of emissions from oil and gas activities.

In July 2012, an aircraft campaign based in northern Norway was conducted, as a part of the EU ACCESS (Arctic Climate Change Economy and Society) project, to investigate impacts of different pollution sources on the Arctic atmosphere. Among 13 flights performed, the flight on 19 July focused on measuring emissions from various oil/gas platforms, drilling rigs and tankers in the Norwegian Sea.

The DLR research aircraft Falcon was extensively equipped with aerosol instrumentations: Condensation Particle Counters to measure total, non-volatile and nucleation mode particle number concentrations, Optical Particle Counters, Ultra-High Sensitivity Aerosol Spectrometer, Passive Cavity Aerosol Spectrometer Probe and Forward Scattering Spectrometer Probe to measure particle size distributions across a wide range of particle sizes, Particle Soot Absorption Photometer to measure absorption coefficient and Single Particle Soot Photometer to measure black carbon concentrations. Aerosol measurements were complemented by measurements of trace gas (NO_x, SO_2, O_3 and CO) concentrations and meteorological parameters.

Particle size distributions measured within exhaust plumes from all facilities showed large enhancement in the number concentrations for particles < ~150 nm, which is characteristic of combustion emissions. However, different types of facilities emitted plumes with distinct chemical compositions as can be seen in Fig 1 as an example. Plumes from shuttle tanker and condensate storage tanker (*e.g.* Åsgard C in Fig 1) operating on fuel oil were characterised by high SO_2 concentration and high fraction of non-volatile particles (> 45%). Drilling rigs (*e.g.* Deepsea Bergen in Fig 1) were also high emitters of non-volatile particles.

On the other hand, oil/gas platforms (*e.g.* Heidrun in Fig 1), which combust large amounts of fuel gas, emitted low levels of SO_2 and mostly volatile particles with non-volatile particle fractions < 10%. Also, a significant increase in the nucleation mode particle concentration (up to 50% of total particle concentration) was observed which suggests new particle formation in the plumes, possibly due to high levels of co-emitted VOC. Especially high particle concentrations (> 20,000 cm^{-3} but < 2% non-volatile fraction) were measured for a platform which was flaring at the time of the measurement.

In addition to the freshly emitted plumes, relatively aged (1.5 – 2.5 hour old) pollution plumes were also sampled. Even in the aged plumes, total particle concentrations were more than 6 times higher than the background concentration. Therefore, emissions from oil and gas activities are expected to have a significant impact on the local air quality.

The results from this study will be used to improve current emission inventories and to validate regional and global chemical transport models. This will ultimately allow better prediction of future Arctic air pollution and associated warming.

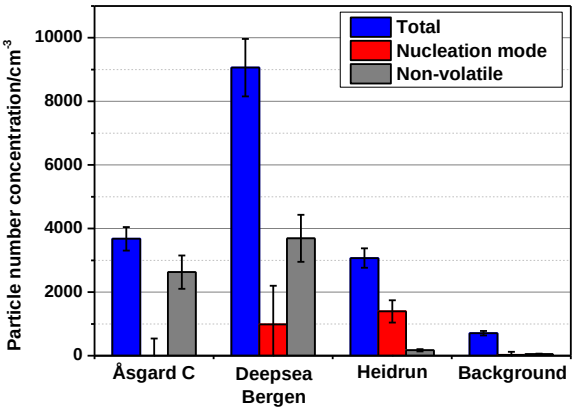

Figure 1. Maximum particle number concentrations measured in the pollution plumes from different oil/gas facilities (*n.b.* plume dilutions have not been taken into account yet). Average background concentrations measured in the marine boundary layer are also shown.

Research flights were funded by the EU project, ACCESS (Arctic Climate Change Economy and Society). The authors would like to thank the DLR flight department, Statoil, scientists and engineers from DLR and LATMOS for their valuable support during the campaign.

Ødemark, K., Dalsøren, S. B., Samset, B. H., Berntsen, T. K., Fuglestvedt, J. S. and Myhre, G. (2012) *Atmos. Chem. Phys.* **12**, 1979–1993.

Development of Reference Film for Quality Control and Assurance for Beta Attenuation Particulate Matter Measurement

H.H. Kim[1], J.Y. Lee[1] and S. Lee[2]

[1]Center for Analytical Measurement Service, Korea Research Institute of Standards and Science, Daejeon, 305-340, Republic of Korea
[2]Center for Gas Analysis, Korea Research Institute of Standards and Science, Daejeon, 305-340, Republic of Korea
Keywords: particulate matter, beta attenuation, air quality, reference film.
Presenting author email: hhkim@kriss.re.rk

Beta attenuation method is widely used to determine particulate matter mass concentration for air quality monitoring. Results from the beta attenuation method are used to determine whether air quality standards for particulate matter are attained.

Particulate matter mass concentration by the beta attenuation is determined by the equation

$$I = I_0 e^{-\mu x} \quad (1)$$

where I is the measured beta ray intensity with particulate matter, I_0 is the measured beta ray intensity without particulate mater, μ is the mass absorption coefficient (cm^2/mg), x is the areal density of the sampled particulate matter (mg/cm^2).

A reference beta attenuation instrument and film were developed to establish a harmonized method for the quality control and assurance of the beta attenuation method. Multiple particulate matter samples were prepared to measure I, I_0, x and then μ (0.291 ± 0.001 cm^2/mg) was determined by using the equation 1 and linear regression. The estimated mass absorption coefficient was applied to the reference beta attenuation instrument to determine the areal density of reference films. The masses of the reference films were determined by the reference beta attenuation instrument and gravimetric method. Results show that the estimated masses by two independent methods agree well, indicating that the developed reference films are valid. The results from this study illustrate that the reference film can be an effective tool for the quality control and assurance of the beta attenuation for particulate matter mass determination.

This work was supported by Project Measurement Standards and Technology Services from Korea Research Institute of Standards and Science.

Macias, E. S. and Husar, R.B. (1976) *Environ. Sci. Technol.* **10**, 904-907.

Soot on Snow (SoS) measurement campaigns 2011-2013

N. Kivekäs[1,2], A. Virkkula[1,3], O. Järvinen[3], J. Svensson[1], A. Aarva[4], H. Lihavainen[1], D. Brus[1], A. Hyvärinen[1], O. Meinander[1], A. Heikkilä[1], R. Väänänen[3], J. Backman[3], And G. De Leeuw[1,3]

[1]Climate change unit, Finnish Meteorological Institute, Helsinki, PO.Box 503, 00101 Finland.
[2]Department of Physics, Lund University, Box 117, SE-221 00, Lund, Sweden
[3]Department of Physics, Helsinki University, Helsinki, 00101, Finland.
[4]Weather and safety, Finnish Meteorological Institute, Helsinki, PO.Box 503, 00101 Finland.

Keywords: Soot particles, Absorption, Aerosol impacts, Climate effect.
Presenting author email: niku.kivekas@fmi.fi

Soot consists mainly of light absorbing carbon. When deposited on snow, it decreases the snow albedo, increases the absorption of radiation in snow and thereby enhances melting. This process has been studied for decades (e.g. Clarke and Noone, 1985) and it has been recognized to be one of the major sources of warming in the Arctic regions (Flanner et al., 2007). The link between soot, snow albedo, and climate change is still not known in enough detail for quantitative analysis (Hansen and Nazarenko, 2004). To provide more insight into these connections, the Finnish Meteorological Institute and Helsinki University have started a series of Soot on Snow (SoS) measurement campaigns during years 2011-2013. In these campaigns soot is deposited on snow in the beginning of the melting season and then the properties of the snow pack are measured throughout the whole melting season until the snow is gone (Kivekäs et al., 2012).

The first experiment, SoS-2011 was conducted on a farming field at Nurmijärvi, Southern Finland some 40 km outside Helsinki. The soot was produced by burning rubber and firewood in a portable stove. The smoke was led through a pipe, cooled by snow surrounding the pipe, and led into a garage tent that was built on top of the snow. The smoke drifted out from the other end of the garage tent that was left open. This method produced a clear gradient (in both concentration and particle size) of soot on the snow.

We measured albedo and melting of the snow at the area with most soot and at a reference area with no added soot. After the soot was deposited the albedo of the dirty snow was roughly 0.4 and that of the reference area roughly 0.8. After snowfall the albedos were equal, but 1-2 days the albedo of the dirty snow had decreased to about 0.1 lower than that of the clean snow. The dirty snow also melted earlier than the clean one and the melting rate was faster.

SoS-2012 was conducted on an agricultural field outside the meteorological observatory of Jokioinen in southern Finland, about 100 km from Helsinki. This time we used soot collected by chimney cleaners from residential fire places in eastern parts of Helsinki. The soot was deposited on the snow by blowing it through a cyclone removing particles larger than about 3 μm into a specially manufactured cylindrical tent. This method produced a more uniformly distributed soot layer on the surface of snow. Three spots with different amounts of soot and one reference spot were produced.

This time the results were not so clear. A snowfall with high winds covered the spots with 10 cm of new snow soon after the measurements were started. After that all spots had very similar albedos, and the melting time of the snow depended mostly on the amount of snow in each spot. In later snow sample analysis it was also found that the wind had possibly blown away the top layer of snow, containing the added soot.

SoS-2013 is planned to take place at the old airport of Sodankylä in Northern Finland north from the Arctic Circle. The conditions there represent better those on the Arctic. There is more snow, and the melting of the snow continues further to the spring, making solar radiation a more prominent forcer in melting the snow.

The soot will be deposited similarly to the method in 2012, but with some improvements to be able to produce more homogenous soot spots with better controlled concentrations of soot. This time we will also make some spots with volcanic dust. Our planned time window for depositing the soot is two weeks, allowing us to time the experiment better related to weather. The snow albedo will be measured continuously, and the snow depth daily. Also snow samples will be taken weekly throughout the melting season to understand better how the soot is penetrating through the snow. Results from this experiment are to be analysed before the EAC conference in September 2013.

This work was supported by the Tor and Maj Nessling Foundation and by the Academy of Finland through project A4 (Arctic Absorbing Aerosols and Albedo of Snow, project number 3162). The work is also a part of the Finnish Centre of Excellence in Physics, Chemistry, Biology and Meteorology of Atmospheric Composition and Climate Change (program number 1118615) as well as the Nordic research and innovation initiative CRAICC (Cryosphere-atmosphere interactions in a changing Arctic climate). We also thank Consti Talotekniikka for providing us the soot.

Clarke, A. D. and Noone, K. J. (1985), *Atmos. Environ.*, **19**, 2045–2053.

Flanner, M. G., C. S. Zender, J. T. Randerson, and P. J. Rasch (2007)., J. Geophys. Res., **112**, D11202, doi:10.1029/2006JD008003.

Hansen, J. and Nazarenko, L. (2004), *Proc. Nat. Acad. Sci.*,**101**, 423–428.

Kivekäs, N., et al (2012) *Proc. CRAICC annual meeting 2012*, Oslo, Norway.

Characterization of particle formation in a spruce forest in north east Bavaria

F. Klein[1,2], A. Held[1]

[1]Atmospheric Chemistry research group, University of Bayreuth, Bayreuth, 95445, Germany
[2]Laboratory of Atmospheric Chemistry, Paul Scherrer Institute, 5232 Villigen, Switzerland
Keywords: NAIS, nucleation, H2SO4, spruce
Presenting author email: felix.klein@psi.ch

Particle formation is happening all over the world (Kulmala et al., 2007) and influences human health and the global climate. However the processes leading to particle formation are not sufficiently understood until today. The formation and growth rate are essential parameters for the characterization of particle formation events (Kulmala et al., 2012). We tried to characterize particle formation and searched for connections between meteorological parameters and particle formation events.

We conducted particle and meteorological measurements during the summer 2012 in a spruce forest in north east Bavaria to increase the knowledge of particle formation events. For the particle measurements we used a scanning mobility particle spectrometer and a neutral cluster and air ion spectrometer which allows to measure particles down to a diameter of about 2 nm. The data of both instruments was used to generate a combined particle distribution for the calculation of nucleation and growth rates. We estimated the condensation and coagulation sink and parametrized sulphuric acid concentrations from measured sulphur dioxide concentrations and parametrized hydroxide radical concentrations.

We identified 18 event days which could be divided into three classes by their nucleation and growth behaviour. We also used 8 non event days without a rise in ultra fine particle concentration for comparison with the meteorological parameters. The overall growth rates were between 0 and 5.5 nmh^{-1}, the nucleation rates mostly under 10 $cm^{-3}s^{-1}$. We observed the highest relative humidity on non event days which is in good agreement with observations made by Boy and Kulmala (2002) who proposed that low water concentrations in the atmosphere favour nucleation events. Drops of the precursor sulphur dioxide concentration often during changes of wind direction or a decrease of radiation due to clouds often led to an interruption of the particle formation events. Correlations between air temperature and growth indicate an influence of oxidation products of volatile organic compounds (VOC) on particle growth. Particle formation occurred mainly on days with easterly winds. One reason for this finding could be wast forested areas in the east of the research area providing large amounts of precursor VOCs needed for the growth of the particles. Furthermore, rise of sulphur dioxide concentrations, a precursor for sulphuric acid, was often connected to easterly winds. The results of the correlation between sulphuric acid concentrations and nucleation rates are consistent with the homogenous binary nucleation of two sulphuric acid molecules. There was a clear connection between the rise of sulphuric acid concentrations and the rise of ultra fine particle concentration with a time delay of about 1.5 hours (c.f. Fig.1). In contrast we observed that the influence of sulphuric acid on the growth is under 7 % (c.f. Tab.1).

In summary our study emphasizes the influence of sulphuric acid on the nucleation and hints at the importance of VOC for the further growth of the newly formed clusters.

Table 1: Growth [nm/h] calculated from the geometric mean (observed growth), explained by the condensation of sulphuric acid (explained growth), in per cent on 5 event days

Day	Observed growth	Explained growth	[%]
24.07.	1.5	0.05	3
12.08.	4.6	0.06	1
13.08.	1.2	0.09	7
14.08.	1.8	0.11	6
15.08.	3.4	0.08	2

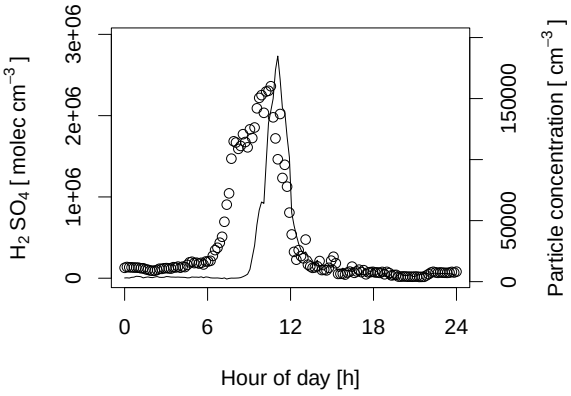

Figure 1: Mean sulphuric acid concentrations (dots) and ultra-fine particle concentrations (lines) on Class I event days

Many thanks to Andreas Held for the support with the study and the funding and special thanks to Wolfram Birmili (IfT Leipzig) for providing the NAIS.

M. Kulmala, et al. (2007) *Science* **318(5847)**, 89–92.
M. Kulmala, et al. (2012) *Nature Protocols* **7(9)**, 1651–1667.
M. Boy and M. Kulmala (2002) *Atmos. Chem. Phys.* **2**, 1–16.

Influence of different fuels and grillables on particle emissions during an outdoor barbeque

S.H. Schmitt[1], C. Berberich[1], M. Glor[1], L. Güntner[1], T. C. Sluka[1], K. A. Kamili[1], S. G. Gonser[1], A. Held[1]

[1]Junior Professorship in Atmospheric Chemistry, University of Bayreuth, 95448 Bayreuth, Germany

Keywords: Aerosol formation, Barbeque, Fuel, Grillables
Presenting author email: sebastian.schmitt@uni-bayreuth.de

Barbecueing is conducted in different styles as a recreational activity in many countries around the world even though early studies (Elmenhorst and Dontenwill 1967; Dyremark and Westholm 1994) had shown severe health risks due to particle formation from hazardous substances. Following studies mainly dealt with indoor cooking activities because of the more controllable experimental conditions. This study was conducted outside under realistic winter time conditions in order to test for influences of fuel and grillables on particle formation and their potential health risk.

The experiment was conducted in two separate runs. First, wood, charcoal (loose and briquettes), gas and pine cones have been used as fuel and a mixed beef-pork burger as grillable in order to test for the influence of different fuels. Second, gas was used as a low emission fuel and the grillables were vegetables (with and without oil), pork (lean and fatty), turkey, pork sausages and a mixed beef-pork burger in order to test the influence of different grillables. Temperature was tracked in order to take into account differences caused by different fuels.

Particles in the range of 10 – 750 nm were measured using a stationary Scanning Mobility Particle Sizer (SMPS) with an inlet installed one meter above the grill. Additionally, the grill master was equipped with a portable optical particle spectrometer (OPC; diameter range 0.3 µm to 10 µm, 6 channels) with an inlet of a 30 cm PTFE-tube placed at his breast. During the first run of the experiment particles were additionally collected on a quartz-filter placed next to the SMPS inlet. These filters and samples of the solid fuels and of the meat have been analyzed via temperature-programmed-pyrolysis mass-spectrometry (TPP-MS) to gain information about the composition of the pyrolysed material.

SMPS measurements show the highest particle emissions for pine cones in comparison to the other solid fuels (Fig. 1). Charcoal and briquettes have lower emissions than wood. As gas exhibits the lowest total aerosol emissions it was used as standard fuel for the comparison of various grillables. As indicated by mean PM1/PM10 ratios derived from OPC measurements, gas has the highest fraction of small particles which is supported by SMPS data.

The amount of fat in grillables does not only influence the total emitted aerosol concentration but also impacts the size distribution of the emitted particles. As a general result, our hypothesis that more fatty grillables tend to emit larger particles was confirmed. Nevertheless, most particles have diameters below 200 nm, which cannot be neglected for discussing health risks.

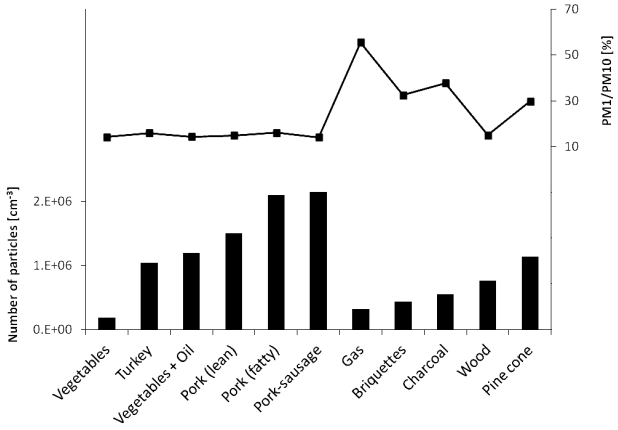

Figure 1. Numbers of emitted particles per cm³ during the main grill process (SMPS), and PM1/PM10 ratio (OPC)

TPP-MS results show that emitted organic aerosols are mainly oxidized, especially for larger molecules in both charcoal and briquettes. Within single measurements the most larger molecules were emitted at a pyrolysis – temperature of 550-600 °C for the solid fuels. The pyrolysed meat did not show this unique pattern. In consequence, aerosol samples are considered a mixture of meat- and fuel-derived particles.

Altogether the described experiments show that total number, size resolution and composition in chemistry differ significantly as a function of both grill fuel and grillables. Fat seems to be a major control for total particle number and dominant particle size.

Dyremark, A.; Westerholm, R; Övervik, E.; Gustavsson, J. (1994): *Polycyclic aromatic hydrocarbon (PAH) emissions from charcoal grilling*. Atmospheric Environment, 29, No.13, pp. 1553-1558.

Elmenhorst, H.; Dontenwill, W. (1967): *Nachweis cancerogener Kohlenwasserstoffe im Rauch beim Grillen über Holzkohlenfeuer.* Zeitschrift für Krebsforschung, 70, pp.157-160.

Photophoretic effects for the black carbon aerosols at stratospheric altitudes

L.B. Kochneva, S.A. Beresnev, V.I. Gryazin, M.V. Vasiljeva, K.G. Gribanov and V.I. Zakharov

Ural Federal University, Ekaterinburg, 620083, Russia
Keywords: fundamental aerosol physics, stratospheric aerosols, photophoresis, soot aerosol
Presenting author email: Louisa.Letfulova@usu.ru

This report continues and summarizes analysis and estimations of the photophoretic effects for soot aerosols in stratosphere. One of possible mechanisms of aerosol transport in the thermally and mechanically stable stratosphere can be radiometric photophoresis as the regular factor of aerosol vertical motion on the synoptic and global temporal scales. It can lead, for example, to the uncontrollable accumulation of soot particles at the certain altitudes in stratosphere from aircraft engines and biomass burning.

At the first stage of studies the estimations of transport opportunities of negative "solar" (motion of particles in the field of short-wave solar radiation against gravity) and positive "thermal" (motion in the field of thermal outgoing radiation) photophoresis of soot particles have been given at the assumptions of the highest possible intensities of atmospheric radiation fluxes. In this report we present updated and expanded calculations of the photophoretic motion characteristics according to the advanced radiation block of the model. Firstly, the results for “solar” photophoretic motion are calculated in the framework of advanced model for short-wave solar radiation (Beresnev *et al*, 2012a). Secondly, the characteristics for “thermal” photophoresis are specified taking into account the downward flux of the long-wave thermal radiation (Beresnev *et al*, 2011).

The results of theoretical analysis of photophoretic motion of soot particles in the short-wave solar radiation field for stationary atmosphere are presented. The integrated fluxes of solar radiation were calculated by the Monte Carlo method with approximation of a plane-parallel, horizontal-homogeneous molecular-aerosol atmosphere. The analysis confirms again an opportunity essential photophoretic effects for soot aerosol particles in stratosphere: the "sun" photophoresis can be considered as the effective mechanism of vertical transport of well-absorbing sub-micrometer particles up to heights of the middle stratosphere. The forces of "sun" photophoresis can compete to gravities up to heights 30-35 km for particles of sub-micrometer and micrometer sizes. On other hand, the estimations have shown again the small efficiency of radiometric photophoresis for weakly-absorbing, dense and high-conducting particles of atmospheric aerosol. The results for photophoretic motion of soot particles in the field of the Earth’ thermal radiation in a stationary atmosphere are also presented. In calculations the up- and down-fluxes of thermal radiation are taken into account. It is shown that positive "thermal" photophoresis potentially can be the effective mechanism of vertical transport for micron-sized soot particles at stratospheric altitudes.

Besides, in this report the theoretical and experimental estimations for so-called “accommodation” (gravito-photophoretic) forces which can compete partly with radiometric photophoretic forces are presented. We discuss, first, the independent development of the consecutive and rigorous gas-kinetic theory of the phenomenon for the free-molecular regime with detailed consideration of gas-surface interaction features and, second, an attempt of the measurement of predicted forces using an experimental technique with model macroparticles for quantitative comparison with the theoretical predictions (Beresnev *et al*, 2012b).

The theoretical estimations show that in the upper troposphere and in the middle stratosphere the “accommodation” (gravito-photophoretic) forces can be comparable with the radiometric photophoretic forces, but do not exceed the gravity force. These conclusions both qualitatively and quantitatively differ from the conclusions of the semi- empirical theory of gravito-photophoresis by Rohatschek (1984).

The measurements with the appropriate model macroparticles in vacuum chamber have confirmed the existence of “accommodation” forces affecting a particle with artificial asymmetry of surface characteristics together with the forces of radiometric photophoresis. The experimental values for the system “steel particle–helium” are in good agreement with theoretical predictions, and the ratio of the “accommodation” force to the photophoretic force does not exceed 3%.

Thus, the action of "accommodation" (gravito-photophoretic) forces, in our opinion, is not capable to provide effective vertical transport of aerosol particles against gravity at stratospheric altitudes.

This work was supported by the Ministry of Education and Science of the Russian Federation (research project implemented by leading scientist at Russian institution of higher education, agreement No.11.G34.31.0064).

Beresnev, S.A., Kochneva, L.B., Zhuravleva, T.B. and Firsov, K.M. (2012a) *Atmos. Oceanic Opt.* **25(4)**, 286-291.

Beresnev,S.A., Vasiljeva, M.S. and Suetin, D.V. (2012b) *Vacuum*. **86**, 1663-1668.

Beresnev, S.A., Kochneva, L.B., Zakharon, V.I. and Gribanov, K.G. (2011) *Atmos. Oceanic Opt.* **24(7)**, 597-600 (in Russian).

Rohatschek, H. (1984) *J. Atmos. Chem.* **1(4)**, 377–89.

Particle collection properties of high vegetation elements

R. D. Kouznetsov[1,2], M. A. Sofiev[1]

[1]Finnish Meteorological Institute, PL 503, 00101 Helsinki, Finland
[2]A. M. Obukhov Institute of Atmospheric Physics, Moscow, Russia
Keywords: aerosols, dry deposition, air pollution, mechanistic models, high vegetation
Presenting author email: rostislav.kouznetsov@fmi.fi

A new scheme for dry deposition of atmospheric aerosols onto surfaces is developed by the authors (2012, hereafter KS2012). For rough surfaces it utilizes a similarity between deposition processes for momentum and matter. The scheme considers deposition via three main processes: inertial impaction, interception and Brownian diffusion, controlled by three basic particle properties: inertial relaxation time τ_p, physical size d_p, and Brownian diffusivity D. It was found that there is a parameter a, called "collection scale" that, together with aerodynamic roughness, fully describes surface properties with respect to the deposition processes. The values of this parameter for few surface types including low vegetation were found from published wind-tunnel data. Current study attempts to evaluate the collection scales for high vegetation from three wind-tunnel experiments with vegetation elements.

In the experiments by Beckett et al. (2000), Freer-Smith et al. (2004) and Reinap et al. (2009), branches or small trees were exposed to a flow of particles NaCl particles of size $d_p \sim 1$ μm. The wind speeds U in these experiments were within 1-10 m/s, which is higher than normally observed in natural canopies, but provides some dynamic range to evaluate collection scales. The deposition rates were evaluated as mass fluxes per unit of projected leaf area whereas the concentrations were measured as number densities.

Simple calculations with KS2012 scheme show that main deposition mechanism in the experiments is interception, i.e. capture of particles due to their finite size. The deposition velocity to a rough surface surface due to interception v_{int} is proportional to square of particle size:

$$v_{int} = u_* \cdot 80\,(d_p/a)^2\,\mathrm{Re}_*^{1/2}, \qquad (1)$$

where $\mathrm{Re}_* = u_* a/\nu$ is a collector Reynolds number, ν is the kinematic viscosity of the air, $a = d_c u_*/U_{top}$ is the collection scale, that fully describes the deposition within the canopy layer for diffusion and interception, d_c is a collector size (leaf width or needle diameter) and U_{top} is the wind speed at the canopy top. In the context of KS2012, the scale a can be considered as a surface parameter without its actual connection with actual collector geometry.

To match the experimental data with KS2012 few assumptions have to be made. Firstly, the drag coefficient of canopy elements $C_d = 1$ is assumed, which means that they have poor aerodynamics and shadowing is neglected. Secondly, the ratio $U_{top}/u* = 3$ is assumed. Then a single-element collection efficiency for a canopy element:

$$\eta = \frac{9}{2} \cdot 80\,(d_p/d_c)^2\,\mathrm{Re}^{1/2}, \qquad (2)$$

where $\mathrm{Re}_* = u_* d_c/\nu$. The collector size d_c can be obtained from best fit for each of the plant species (Fig. 1).

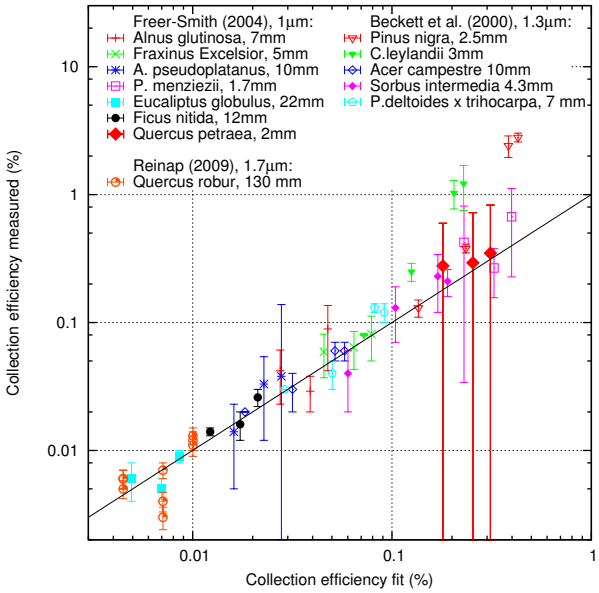

Figure 1: The fitted collection efficiencies for best-fit values of collector size d_c of each species

In general the relation $V_d \propto U^{3/2}$ (1:1 line in the plot) holds well for each species, except for the coniferous species (*Pinus nigra* and *Cupressus leylandii*) at high wind speeds when inertial impaction becomes significant. The collection scales obtained in different experiments appear incomparable for two oak species (*Q. robur* and *Q. petraea*), most probably due to significant effect of coarse tail in particle size distribution. The missing information on actual aerodynamic drag and uncertain coarse tails in particle-size distributions in the experiments prevented more accurate evaluation.

Acknowledgements: FP7-PBL-PMES, FP7-MEGAPOLI and Academy of Finland ASTREX projects.

Global Change Biol., *6*(8), 995–1003, doi:10.1046/j.1365-2486.2000.00376.x.

Freer-Smith, P., A. El-Khatib, and G. Taylor (2004) *Water, Air, & Soil Pollution*, *155*, 173–187, doi:10.1023/B:WATE.0000026521.99552.fd.

Kouznetsov, R., and M. Sofiev (2012) *J. Geophys. Res.*, *117*, D01,202, doi:10.1029/2011JD016366.

Reinap, A., B. Wiman, B. Svenningsson, and S. Gunnarsson (2009) *Trees – Structure and Function*, *23*, 1263–1274, doi:10.1007/s00468-009-0366-4.

A scheme for particle deposition from turbulent flows above surfaces

R. D. Kouznetsov[1,2], M. A. Sofiev[1]

[1]Finnish Meteorological Institute, PL 503, 00101 Helsinki, Finland
[2]A. M. Obukhov Institute of Atmospheric Physics, Moscow, Russia
Keywords: aerosols, dry deposition, air pollution, mechanistic models
Presenting author email: rostislav.kouznetsov@fmi.fi

A new scheme for dry deposition of atmospheric aerosols is developed by the authors (2012, hereafter KS2012 scheme). Unlike earlier schemes, it is based on physical considerations and contains minimum of empirical parameters. This makes the scheme applicable in atmospheric transport models at various scales. The scheme provides simple relationships that can be tested both in laboratory and in outdoor experiments.

The scheme expresses the deposition velocity V_d – steady-state deposition flux per unit concentration at given height – through the physical properties of a species, flow, and surface. Particles are given by three basic properties: inertial relaxation time τ_p, physical size d_p, and Brownian diffusivity D. These properties can be related to diameter of a spherical particle of a given density at particular air temperature and pressure, however arbitrary particles can be handled as long as their basic properties can be expressed. This approach allows in particular to account for non-spherical particles, particle size growth with humidity, *etc*. The flow is characterized by the turbulent velocity scale at the surface. In case of thermally homogeneous flow this scale is a friction velocity u_*.

The surface properties are given only with two parameters that have clear physical meaning and can be derived from basic surface properties. One of them – aerodynamic roughness length z_0 is used to distinguish between smooth and rough flow regimes. This distinction is based on the roughness Reynolds number $u_* z_0/\nu$, where ν is air viscosity. The expression for the deposition rate onto smooth surface results from the solution of the steady-flux equation with turbophoresis term and has no tuning parameters.

Rough surfaces are characterized by z_0 and newly-introduced "collection scale" which accounts for the effective size of collectors and ratio of the velocity at the roughness top to the friction velocity. The collection scale was found to characterize the deposition with three main processes: inertial impaction, interception and Brownian diffusion, corresponding to the basic particle properties. The expressions for deposition rates are found and verified against the data of wind tunnel measurements and numerical simulations.

The results of the scheme agree well to the available experimental data on particle deposition onto solid and water surfaces at least up to 20 m/s wind speeds. The scheme agrees well with the data of wind tunnel studies of deposition onto low-vegetated and gravel surfaces. The scheme also agrees with wind-tunnel experiments on the deposition to vegetation elements, but no quantitative conclusion can be made due to the experimental uncertainties. The data of outdoor experiments have too much scattering to judge on the performance of the parameterization.

The resulting scheme for chemical transport models is shown in Fig. 1. The deposition fluxes are evaluated at height z_1. Each model grid cell is assumed to have "smooth" and "rough" tiles with corresponding velocity scales. The resulting flux is a weighted sum of fluxes onto tiles. The fluxes for "smooth" tiles are evaluated directly from height z_1. For "rough" tiles the deposition pathway is split into above-canopy- and in-canopy layer. The latter is assumed to start at z_0. $V_d(z_0)$ is calculated as a sum of deposition velocities due to different mechanisms and then the above-canopy layer is accounted with standard Monin-Obukhov profiles for eddy diffusivity and exponential scheme that treats diffusion and regular velocity (settling) consistently, and unlike earlier resistance-based schemes, allows for the concentration evaluation at particular height z_{obz}.

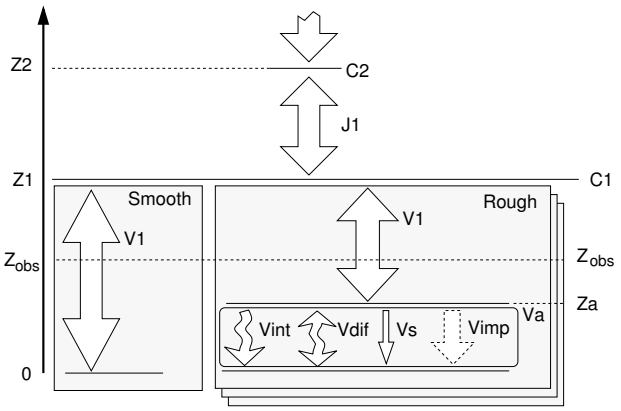

Figure 1: The outline of KS2012 dry deposition scheme

The scheme in a reduced form is implemented into SILAM chemical transport model (http://silam.fmi.fi). The full implementation requires a knowledge of collection scales for various land-use types. Few of them were found from available data of experiments with calibrated aerosols. Unfortunately, such experiments are very few in literature so more experiments for various surfaces are needed (see our poster).

Acknowledgements: FP7-PBL-PMES, FP7-MEGAPOLI and Academy of Finland ASTREX projects.

R. Kouznetsov and M. Sofiev *J. Geophys. Res.*, 117: D01202, 1–17, 2012. doi:10.1029/2011JD016366.

Intermodal fraction of aerosol from indoor and outdoor microenvironments

J. Kozáková[1] and M. Braniš[1]

[1] Institute for Environmental Studies, Faculty of Science, Charles University in Prague, Benátská 2, 128 01, Prague 2, Czech Republic
Keywords: cascade impactor, intermodal fraction, $PM_{2.5-1}$, indoor air quality
Presenting author email: jana.kozakova@gmail.com

Coarse and fine particles overlap in a particle size interval between 1 µm and 2.5 µm (aerodynamic diameter). Since this interval appears between the accumulation and coarse mode it is called intermodal fraction ($PM_{2.5-1}$). Sources of both coarse and fine aerosols contribute to intermodal fraction to a xcertain extent and the contributions of individual sources may vary under different meteorological and/or spatial conditions. According to several studies, intermodal fraction correlates more with coarse aerosol during higher wind velocities and windstorms in arid regions (*Kegler et al., 2010, Claiborn et al., 2011*). In contrast, other studies have shown ambiguous or different results (*Jalava et al., 2006, Geller et al., 2012*). Intermodal fraction has not been so far investigated sufficiently.

Concentrations of size-resolved PM were monitored indoors and outdoors by a low volume (9 litres per minute) Personal Cascade Impactor Sampler (PCIS) with 5 stages A to F (A: 2.5-10 µm; B: 1.0-2.5 µm; C: 0.5-1.0 µm; D: 0.25-0.5 µm; and F-backup <0.25 µm) during various seasons in three different urban and rural locations. Basic meteorological parameters (temperature, relative humidity, wind velocity) were monitored as well. Presence of persons in the buildings was recorded in a diary.

Generally, outdoor and indoor concentrations of $PM_{2.5-1}$ correlated strongly with coarse aerosol.

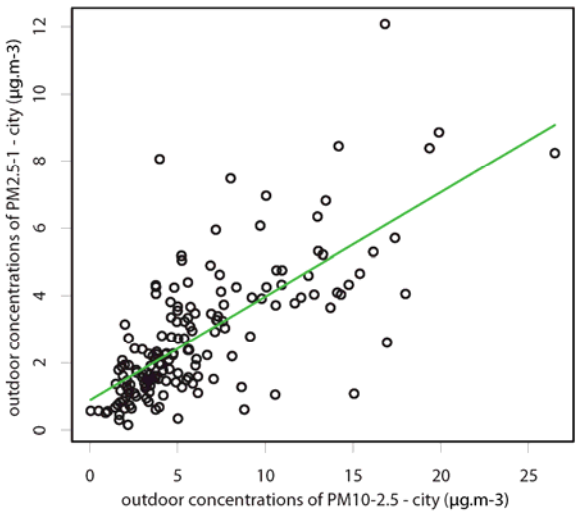

Figure 1. The association between outdoor concentrations of coarse aerosol and PM2.5-1 in Prague.

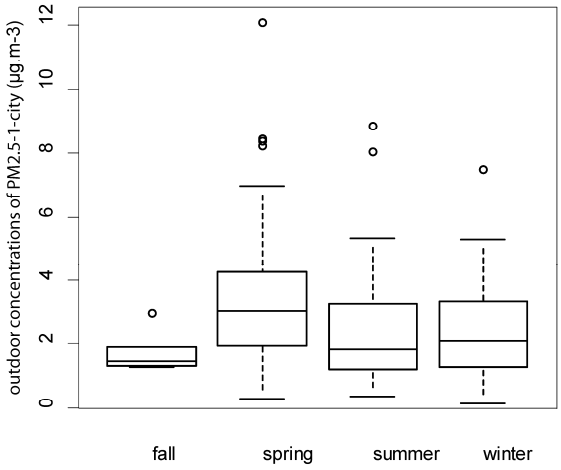

Figure 2. Comparison of outdoor concentrations in different seasons in Prague.

Correlation between the intermodal and fine fraction (PM_1) was also documented, however, it was much lower than the above mentioned coarse-intermodal association. In the indoor environment, the intermodal fraction was also associated with the number of persons present indoors.

This work was supported by the Czech Ministry of Education, Youth and Sports under the program NPV II, project No. 2B08077.

Claiborn, C.S. , Finn, D., Larson, T.V. and Koenig, J.Q. (2011) *Windblown dust contributes to high PM2.5 concentrations*, Journal of the Air & Waste Management Association, 50, 1440-1445

Geller, G.D., Fine, P.M. and Sioutas, C. (2012) *The Relationship between real-time and time-integrated coarse (2.5–10 µm), intermodal (1–2.5 µm), and fine (<2.5 µm) particulate matter in the Los Angeles basin*, Journal of the Air & Waste Management Association, 54, 1029–1039

Jalava, P.I., Salonen, R.O., Hälinen, A.I., Penttinen, P., Pennanen, A.S., Sillanpää, M., Sandell, E., Hillamo, R., Hirvonen, M.-R. (2006) *In vitro inflammatory and cytotoxic effects of size-segregated particulate samples collected during long-range transport of wildfire smoke to Helsinki,* Toxicology and Applied Pharmacology 215 (2006), 341–353

Kegler, S.R., Wilson, W. E. and Marcus, A.H. (2010) *PM 1, intermodal ($PM_{2.5-1}$) mass, and the soil component of PM 2.5 in Phoenix, AZ, 1995-1996*, Aerosol Science and Technology, 35 (2001), 914-920

ACIDIC REACTION PRODUCTS OF MONO- AND SESQUITERPENES IN ATMOSPHERIC FINE PARTICLES IN BOREAL FOREST IN HYYTIÄLÄ, FINLAND

M.Vestenius[1], H.Hellen[1], J.Levula[2], P.Kuronen[1] and H.Hakola[1]

[1]Finnish Meteorological Institute, P.O.Box 503, 00101 Helsinki, Finland
[2]Hyytiälä Forestry Field Station, University of Helsinki, Hyytiäläntie 124, 35500 Korkeakoski, Finland
Keywords: biogenic acids, boreal forest
Presenting author email: mika.vestenius@fmi.fi

A large amount of biogenic VOCs (monoterpenes and sesquiterpenes) is emitted to the atmosphere by vegetation, especially in the densely forested boreal regions (Hakola et al., 2006). In the atmosphere, these compounds are oxidized producing reaction products, which may take part in the formation and growth of new particles (Tunved et al., 2006). Even though organic compounds account for 20-90 % of the total fine particle mass concentration in a wide variety of atmospheric environments (Kanakidou et al., 2005), only little is known about their detailed composition.

For many sesquiterpenes atmospheric lifetimes are so short that their concentrations in the air cannot even be measured. Therefore knowledge about real atmospheric concentrations of the reaction products of terpenes is essential for different kind of aerosol studies. In this study, acidic reaction products of biogenic VOCs, which affect the formation and growth of fine particles, were analyzed from PM 2.5 aerosol samples taken at Hyytiälä, Finland.

Highest concentrations for all studied compounds were measured in summer, except pinonic acid in 2010. (Table 1). Concentrations peaking in summer are most clear for caryophyllic acid. It is known to be emitted from typical boreal trees only in July and August (Hakola et al. 2006). Limonic acid concentrations increased already in spring. Pinonic acid is showing relatively high concentrations also in winter. Pinonic acid is more volatile compared to other acids measured here so that cold winter temperatures may have more effect on it's gas-particle distribution. In summer 2010 concentrations of pinonic and pinic acids were clearly lower than in 2011.

Concentrations of pinonic and pinic acids had relatively good correlation during summer months. This was expected since they have same precursors i.e. they are both reaction products of a- and b-pinene. Average concentrations for pinonic acid were 40% higher than for pinic acid. Ambient monoterpenes pinic and caric acids show clearly the highest concentrations during summer months concomitant with their precursors (Hakola et al., 2012). β-caryophyllinic acid also has highest concentrations in summer, but it's precursor β-caryophyllene cannot be found in ambient air due to it's high reactivity. Limonic acid concentrations increase already in spring even though limonene concentrations are still low.

Table 1. Average concentrations of bio acids during different seasons (summer 2010 - summer 2011).

		Average concentrations (ng m^{-3})					
Bio acid	Precursor	Sum 10	Aut 10	Win 10/11	Spr 11	Sum 11	Aut 11
Pinonic acid	α-pinene	5.7	7.4	9.5	5.8	14.8	8.8
Pinic acid	α-pinene	2.6	4.4	1.5	0.8	10.1	2.0
Caric acid	3-carene	7.0	2.1	2.5	3.5	7.3	4.0
Limonic acid	limonene	1.0	0.9	0.5	1.8	1.7	1.2
β-caryophyllinic acid	β-caryophyllene	3.3	0.8	0.5	0.6	2.8	1.2

Bioacids and their precurosors show a similar trend, α-pinene and its reaction products (pinic acid+pinonic acid) having the highest concentrations and limonene and its reaction product limonic acid the lowest.

Hakola H., Tarvainen V., Bäck J., Rinne J., Ranta H., Bonn B., and Kulmala M., 2006. Seasonal variation of mono- and sesquiterpene emission rates of Scots pine. Biogeosciences, SRef-ID: 1726-4189/bg/2006-3-93, 93-101.

Hakola H., Hellén H., Rinne J., Henriksson M., and Kulmala M., 2012. In situ chromatographic measurements of volatile organic compounds in Boreal Forest. Atmospheric Chemistry and Physics Discussion **12**, 15565-15596.

Kanakidou M., Seinfeld J.H., Pandis S. N., Barnes I., Dentener F. J., Facchini M.C., Van Dingenen R., Ervens B., Nenes A., Nielsen C. J., Swietlicki E., Putaud J.P., Balkanski Y., Fuzzi S., Horth J., Mootgat G.K., Winterhalter R., Myhre C. E. L., Tsigaridis K.,Vignati E., Stephanou E. G., Wilson J, Organic aerosol and global climate modelling: a review. Atmos. Chem. Phys. 2005, **5**, 1053-1123.

Tunved P., Hansson H.-C., Kerminen V.-M., Ström J., Dal Maso M., Lihavainen H., Viisanen Y., Aalto P.P., Komppula M., and Kulmala M., 2006. High natural aerosol loading over boreal forests. Science **312**, 261-263.

Evidence for the presence of secondary phosphorus in continental fine aerosol

K. Krassován[1], Z. Kertész[2], K. Imre[3] and A. Gelencsér[1,3]

[1]Institute of Environmental Sciences, University of Pannonia, Veszprem, 8200, Hungary
[2]Institute of Nuclear Research, Section of Ion Beam Physics, University of Debrecen, Debrecen, 4032, Hungary
[3]Air Chemistry Research Group of the Hungarian Academy of Sciences, Veszprem, 8200, Hungary
Keywords: phosphorus, secondary aerosol, biogeochemical cycle.
Presenting author email: krassovan@gmail.com

The role of the atmosphere in the biogeochemical cycle of phosphorus is generally associated with the emission of soil dust, sea-salt particles, bioaerosols and industrial aerosols Mahowald *et al* (2008). Quite independently, a reduced gaseous phosphorus compound (phosphine, PH_3) was measured over various sources such as marshes and sewage plants Dévai *et al* (1988) and also in the global troposphere. Given that phosphine is a reactive gas that rapidly yields low-volatility phosphoric acid in the atmosphere Frank and Rippen (1987), secondary aerosol formation can be an important sink that has never been considered in the global phosphorus cycle.

In our study we present mass size-distribution measurements of phosphorus in aerosol samples collected at three locations in Hungary. The elemental compositions of the samples were determined by proton induced X-ray emission (PIXE). The evaluation of the X-ray spectra was performed with the PIXEKLM program code. The bimodal size distribution of phosphorus indicated two distinct formation mechanisms in the fine and coarse modes.

As expected, the mass concentration of phosphorus was dominated by the coarse particles (aerodynamic diameter >1 μm) Vicars *et al* (2010), the contribution of fine mode phosphorus was in the range of 10–27 % (median 19 %) of the total. The contribution of biomass burning to the fine mode phosphorus was inferred from measured K concentrations and P/K ratios reported for biomass smoke (Echalar, 1995).

It was found that biomass burning just partly accounted for fine mode phosphorus, the major part of which likely formed as secondary aerosol component from the photooxidation product of gaseous phosphine.

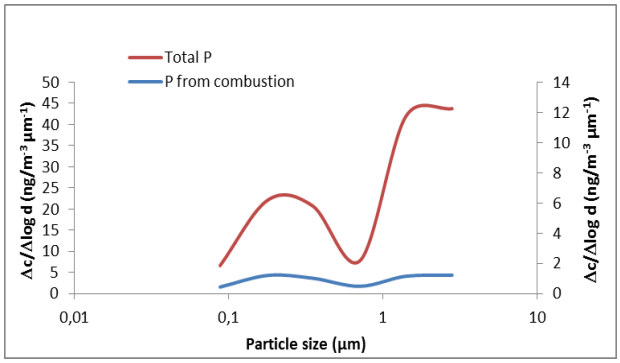

Figure 1. Measured size distribution of phosphorus in rural aerosol collected on 21st of July in 2003.

Secondary aerosol phosphorus can be even more important in providing this essential nutrient for remote ecosystems since it is associated with fine aerosol particles which have longer residence time and thus are more prone to long-range atmospheric transport than coarse primary particles.

This work was supported by the TÁMOP-4.2.2.A-11/1/KONV-2012-0064. The project is realized with the support of the European Union, with the co-funding of the European Social Fund.

Dévai, I., Delföldy, L., Wittner, I., Plosz, S. (1988). *Detection of phosphine: new aspects of the phosphorus cycle in the hydrosphere.* Nature 333, 343–345.

Echalar, F., Gaudichet, A. (1995) *Aerosol emissions by tropical forest and savanna biomass burning: characteristic trace elements and fluxes.* Geophysical Research Letters 22, 3039–3042.

Frank, R., Rippen, G. (1987). *Verhalten von Phosphin in der Atmosphiire*. Lebensmitteltechnik 7-8, 409-411.

Mahowald, N., et al. 2008. *Global distribution of atmospheric phosphorus sources, concentrations and deposition rates, and anthropogenic impacts.* Global Biogeochem. Cycles 22. GB4026.

Vicars, W. C., Sickman, J.O., Ziemann, P.J. (2010). *Atmospheric phosphorus deposition at a montane site: Size distribution, effects of wildfire, and ecological implications.* Atmospheric Environment 44, 2813–2821.

Measurement of evaporation rates of atmospheric nanoparticles

N.K. Kumar[1, 2] and S.N. Pandis[1]

[1]Department of Chemical Engineering, Carnegie Mellon University, Pittsburgh, PA 15213, USA
[2]Laboratory of Atmosphric Chemistry, Paul Scherrer Institute (PSI), CH-5232 Villigen PSI, Switzerland
Keywords: organic aerosol, volatility
Presenting author email: niveditk@andrew.cmu.edu

Atmosphereic organic aerosol (OA) is a complex mixture of thousands of individual organic compounds (Hildemann et al., 1991; Fraser et al., 1997, 1998; Goldstein et al., 2008). Large fractions of OA consist of organic compounds that are difficult to separate by gas chromatography (Schauer et al., 1996), and the majority of the OA consists of highly oxidized organic molecules. A critical determinant of whether an organic compound is found in OA (as opposed to the gas phase) is its saturation vapor pressure (often referred to as volatility). An accurate understanding of OA volatility is therefore important to properly predict the chemistry and phase partitioning of both natural and anthropogenic OA species, and to properly interpret OA measurements.

The current study was undertaken to extend the existing database of vapor pressures of semivolatile organic compounds in the atmosphere. The Tandem Differential Mobility Analyzer (TDMA) technique using a long temperature-controlled laminar reactor between the two DMAs was evaluated. The vapor pressure and surface free energy of glutaric acid have been previously measured by Bilde and Pandis (2001). This system was therefore studied to evaluate our experimental system. The saturation mixing ratio of glutaric acid was found to be 9.5 ppb at 303 K using a surface free energy of 0.1 Jm^{-2} and an accomodation coefficient equal to 1. This is in close agreement to the results obtained by Bilde and Pandis (2001) of a saturation mixing ratio of 11.5 ppb.

The other pure component organic aerosols studied were squalane and docosane.The vapor pressure of squalane was measured after flash-vaporizing it in a smog chamber. The saturation mixing ratio of squalane was found to be 0.03 ppb at 323 K. Docosane 100 nm particles evaporated in less than 2 seconds (before reaching the first sampling port of the TDMA) at 306 K. This behavior is consistent with a saturation mixing ratio of more than 6 ppb at 306 K. However, the results obtained at 298 K are inconsistent with this behavior as the measured saturation mixing ratio was 0.2 ppb. A possible explanation is that docosane particles existed as liquid at higher temperatures and solid at lower temperatures in our experiments. When the docosane particles are injected into the chamber by flash vaporization they exist in the liquid state and do not form solid particles until they reach temperatures below their melting point. Therefore they could be present as supercooled drops at 306 K and solid particles at 298 K.

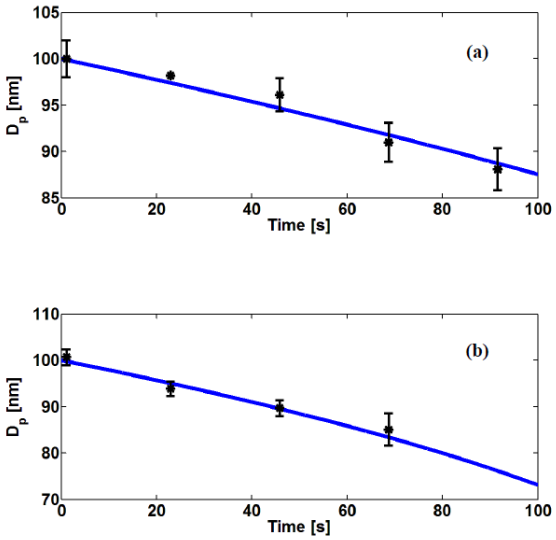

Figure 1. Measured (symbols) and predicted (line) diameters of squalane particles as a function of their evaporation time at (a) 313 K and (b) 323 K.

References

Bilde, M.; Pandis, S. N.; Evaporation rates and vapor pressures of individual aerosol species formed in the atmospheric oxidation of α- and β-pinene, *Environ. Sci. Technol., 35*, 3344-3349, 2001.

Fraser, M. P.; Cass, G. R.; Simoneit, B. R. T.; Rasmussen, R. A.; Air quality model evaluation data for organics. 4. C_2-C_{36} non-aromatic hydrocarbons, *Environ. Sci. Technol., 31*, 2356–2367, 1997.

Goldstein, A. H.; Worton, D. R.; Williams, B. J.; Hering, S. V.; Kreisberg, N. M.; Panic,O.; Gorecki, T., Thermal desorption comprehensive two-dimensional gas chromatography for in-situ measurements of organic aerosols, *Journal of Chromatography, 1186*, 340–347, 2008.

Hildemann, L. M.; Markowski, G. R.; Cass, G. R.; Chemical composition of emissions from urban sources of fine organic aerosol, *Environ. Sci. Technol, 25*, 744-759, 1991.

Organic compounds in PM2.5 aerosol in Ostrava (Czech Republic)

P. Mikuška, K. Křůmal and Z. Večeřa

Institute of Analytical Chemistry of the ASCR, v.v.i., Veveří 97, 602 00 Brno, Czech Republic
Keywords: organic tracer, urban aerosol.
Presenting author email: krumal@iach.cz

Atmospheric particulate matter (PM) is known to play an important role in many environmental problems. During last years much attention has been paid to the identification of emission sources of PM. To track the contributions of the main sources to composition of atmospheric aerosols, various source-specific organic and inorganic tracers are analysed in collected PM (Křůmal *et al.*, 2010; Křůmal *et al.*, 2013).

Atmospheric aerosols in the size fraction PM2.5 were sampled over 24-h periods using the high-volume sampler (DHA-80, Digitel, 30 m^3/h) on quartz filters during winter period of 2012 (26. 1. – 20. 2.) in industrial city Ostrava.

Collected aerosols were analysed for monosaccharide anhydrides (MAs), resin acids (RAs), methoxyphenols (MPs), monosaccharides (MSs), disaccharides (DSs), sugar alcohols (SAs), alkanes, hopanes/steranes (H/S) and polyaromatic hydrocarbons (PAHs). Analysis of MAs, RAs, MPs, MSs, DSs and SAs includes extraction of parts of filters with mixture dichloromethane/methanol (1:1 v/v) under ultrasonic agitation, derivatization of extracts with mixture of MSTFA/TMCS, dryness, redissolution in hexane and GC-MS analysis. Analysis of alkanes, H/S and PAHs includes extraction of parts of filters with mixture of dichlormethane/hexane (1:1 v/v), fractionation on column with silicagel, dryness to 1 mL and GC-MS analysis.

Analysed compounds include:

- MAs: levoglucosan, mannosan and galactosan.
- RAs: abietic and dehydroabietic acid.
- MPs: vanillic and syringic acid, vanillin and syringol
- MSs: xylose, fructose, galactose and glucose.
- DSs: sucrose and trehalose.
- SAs: arabitol, manitol, sorbitol and inositol.
- Alkanes: C8 – C40.
- H/S: 17*α*(H),21*β*(H)-hopane, 22*RS*-17α(H),21β (H)-homohopane, 17*α*(H),21*β*(H)-norhopane and *ααα* (20*R*)-cholestane.
- PAHs: fluorene, phenanthrene, anthracene, fluoranthene, pyrene, retene, benzo[*a*]anthracene, chrysene, benzo[*b*+*k*]fluoranthene, benzo[*e*]pyrene, benzo[*a*]pyrene, perylene, indeno[1,2,3-*c*,*d*]pyrene, dibenzo[*a*,*h*]anthracene benzo[*g*,*h*,*i*]perylene and picene.

Figure 1 compares the concentrations of PM2.5 aerosol and sum of analysed organic compounds in Ostrava. It is evident that course between the concentrations of PM2.5 and sum of organic compounds is similar. The atmosphere in industrial city Ostrava was very polluted by PM2.5 particles.

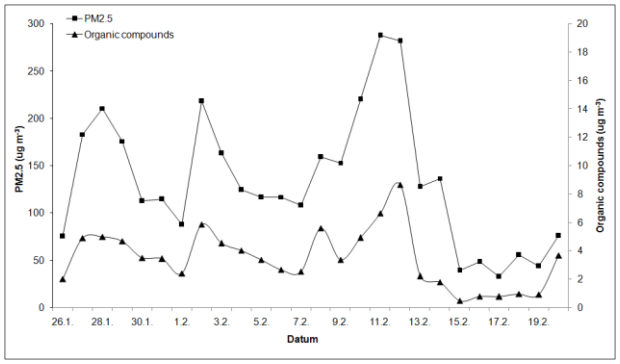

Figure 1. Mass concentrations of PM2.5 (μg.m^{-3}) and sum of analysed organic compounds (μg.m^{-3}) in Ostrava.

Detailed results including comparison of analysed organic compounds in winter in Ostrava will be presented.

This work was supported by Grant Agency of the Czech Republic under grant P503/12/G147 and by Institute of Analytical Chemistry of ASCR under an Institutional research plan No. RVO:68081715.

Křůmal, K., Mikuška, P., Vojtěšek, M., Večeřa, Z. (2010) Atmos. Environ. **44**, 5148-5155.
Křůmal, K., Mikuška, P., Večeřa, Z. (2013) Atmos. Environ. **67**, 27-37.

Laboratory characterization of a size-resolved CPC battery to infer the composition of freshly formed atmospheric nuclei

C. Kuang[1], J. Kangasluoma[2], D. Wimmer[2,3], K. Lehtipalo[2,4], J. Wang[1], M. Kulmala[2], T. Petäjä[2]

[1] Atmospheric Sciences Division, Brookhaven National Laboratory, Upton, New York, 11789, USA
[2] Department of Physics, P.O. Box 64, 00014, University of Helsinki, Helsinki, Finland
[3]Institute for Atmospheric and Environmental Sciences, Goethe University of Frankfurt, Frankfurt am Main, Germany
[4]Airmodus, Ltd., Finland, Gustaf Hällströmin katu 2 A, 00560 Helsinki, Finland

Keywords: CPC calibration, heterogeneous nucleation, particle activation.
Presenting author email: juha.kangasluoma@helsinki.fi

Atmospheric particle nucleation is an important environmental nano-scale process, with climate models indicating that nearly half of the global cloud condensation nuclei (CCN) may be formed from freshly nucleated particles. However, our understanding of atmospheric nucleation and its influence on climate is limited since few direct measurements have been made of either the nucleation rate or the chemical composition of the freshly formed clusters, both of which are necessary to constrain the mechanism and develop a nucleation model. In our study, we have developed an instrument to infer the size-resolved composition of freshly formed atmospheric particles, addressing a key knowledge gap in the composition of nucleated aerosol below 3 nm. This size-resolved condensation particle counter battery (SR-CPCb), is an extension of the CPCb concept [1] developed and used to infer the composition of nucleation mode particles between 2 and 9 nm [2]. In the SR-CPCb, the CPCb measurement principle has been extended down to 1 nm by combining a conventional nanoparticle mobility classifier with a CPCb composed of CPCs designed for the detection of sub 2 nm aerosol [3-7]. By sampling mobility-classified particles, the size resolved CPCb (SR-CPCb) eliminates the strong dependence of CPC response on particle size and charge below 2 nm [4-10]. Therefore, any measured differences in CPC response are then attributed solely to composition-specific interactions between the particle and the various working fluids.

The SR-CPCb is composed of a nanoparticle mobility spectrometer that has been optimized for the sampling and mobility classification of sub 3 nm particles [9]. The particle detector is composed of a CPCb containing the following CPCs with their accompanying working fluids: a Particle Size Magnifier [3] (diethylene glycol), a DEG-UCPC [5] (diethylene glycol), a TSI 3786 UCPC (water), a TSI 3025A UCPC [5] (butanol), and a pulse height UCPC [6] (butanol). The experimental schematic for determining the size, charge, and composition dependent particle detection efficiencies of the CPCb is described in [10]. The following methods were used to generate challenge aerosols for the characterization of the CPCb: (1) electrospray generation of molecular ion mobility standards, (2) evaporation of solid sodium chloride via tube furnace, (3) evaporation of ammonium sulfate via tube furnace, (4) tungsten oxide formation via a wire generator, and (5) candle aerosol generation. Presented results will include the particle composition dependent response of the SR-CPCb and size-dependent transmission efficiencies associated with the nanoparticle mobility spectrometer.

1 Kulmala M. et al. (2007) Journal of aerosol science, 38(3): p. 289-304.
2 Riipinen I. et al. (2009) Atmos. Chem. Phys., 2009. 9: p. 3317-3330.
3 Vanhanen, J. et al. (2011) Aerosol Sci.Tech. 4, 533-542.
4. Iida K. et al. (2009) Aerosol Science and Technology, 43(1): p. 81-96.
5. Kuang, C., et al. (2012) Aerosol Science and Technology 46, 309-315 DOI: 10.1080/02786826.2011.626815.
6. Sipilä M., et al (2009) Aerosol Science and Technology 43(2): p. 126-135.
7. Wimmer D. et al. (2013) Atmospheric Measurement Techniques Discussions.
8. Winkler P.M., et al. (2008) Science, 319(5868): p. 1374.
9. Jiang J. et al. (2011) Aerosol Science and Technology. 45(4): p. 510 - 521.
10. Kangasluoma J. et al. Aerosol Science and Technology, 2013: 47(5) p. 556-563

This work was supported by the US Department of Energy (DOE) Atmospheric System Research Program (Office of Science, OBER) under contract DE-AC02-98CH10886, US DOE Grant Number DE-FG-02-05ER63997, the Academy of Finland (project nos. 1251427, 1139656, 141451, 133872), the Finnish Center of Excellence (project no. 1118615), and the European Research Council (ATMNUCLE).

Detailed study of fine particulate matter during 2013 New Year's celebrations

L.Kubelová[1,2], P.Vodička[1], J.Schwarz[1] and V. Ždímal[1]

[1]Department of Aerosol and Laser Studies, Institute of Chemical Process Fundamentals, Academy of Sciences of the Czech Republic, Prague, Czech Republic
[2]Institute of Environmental Studies, Faculty of Science, Charles University, Prague, Czech Republic
Keywords: fine particulate matter, fireworks, aerosol mass spectrometry.
Presenting author email: kubelova@icpf.cas.cz

In this work we investigated rapid changes in chemical composition of fine particulate matter during the celebrations of New Year 2013. The measurements were carried out at the urban background site Prague-Suchdol. The compact time-of-flight aerosol mass spectrometer (c-ToF-AMS, Aerodyne), Drewnick *et al* (2005), was used to analyze highly time-resolved samples of non-refractory aerosol components. We focused on four episodes with significantly elevated total aerosol mass concentration. The scrutinized intervals are highlighted in Figure 1. We assume that the increased concentrations are due to: smoke plume from wood burning in Episode 1, fireworks in Episode 2, arrival of another air mass in Episode 3, and an uncategorized source of poly-aromatic hydrocarbons in Episode 4. The highest attention was given to the time interval between midnight and 3 a.m. on the New Year (marked in Figure 1 as Episode 2) as the aerosol composition was significantly affected by the occurring annual celebrations. In this period, the most significant increase in mass concentration was observed by sulfate, chlorides, and potassium (involved in the mass spectra for fragment 39). At the same time, nitrate and ammonium were unaffected. Those trends were compared to other measurements with c-ToF-AMS during annual celebrations, Drewnick *et al* (2006).

Available meteorological data from a nearby measuring site were taken into account for explanation of the observed trends.

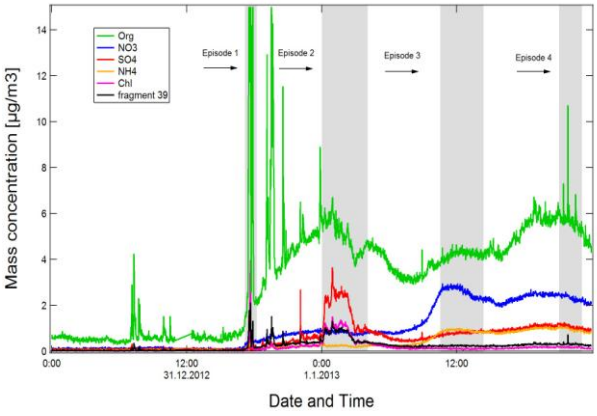

Figure 1. Time course of mass concentrations for various species determined by the c-ToF-AMS. Values over 15 µg are not shown.

Figure 2 shows mass size distributions for the whole period investigated and for the four selected episodes. Similar analyses were carried on for particular species. It is clearly seen that during the first event the particle size distribution was markedly shifted towards smaller sizes. It can be hypothesized that the source of these particles was in close vicinity to the measurement site.

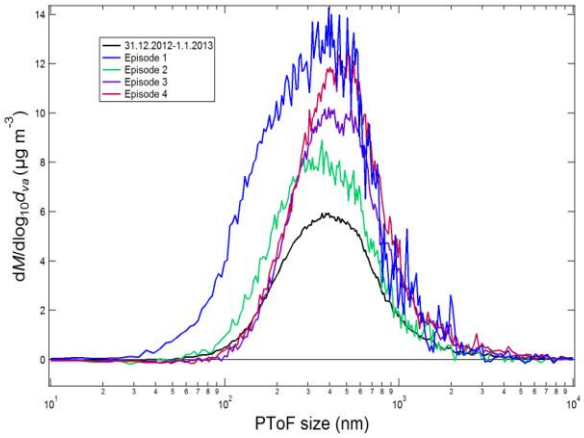

Figure 2. Average mass size distributions measured by c-ToF-AMS for the whole measurement period and for the selected episodes.

Generally, the analysis illustrates the possibilities and advantages of such highly time- and size-resolved measurement of the aerosol chemical composition. It is possible to characterize the individual events thoroughly when a shorter time period is taken into account. Nevertheless, it is necessary to pay attention to correct evaluation of such short events during data analysis.

Acknowledgement
The authors of this work gratefully appreciate financial support by the Czech Science Foundation under project No. CSF P209/11/1342.

Drewnick, F., Hings, S., DeCarlo, P.F., Jayne, J.T., Gonin, M.,Fuhrer, K., Weimer, S., Jimenez, J.L.,Demerjian, K.L., Borrman, S., Wornsnop, D.R. (2005) *Aerosol Sci. Technol.* **39,** 637-658.

Drewnick, F., Hings, S., Curtius, J., Eerdekens, G., Williams, J. (2006) *Atmos. Environ.* **40**, 4316-4327.

DMA Train measurements of nanoparticle growth at a field site in Lewes, Delaware

A. Kupc[1], P. M. Winkler[1,2], M. Lawler[2,3] , P. H. McMurry[4], and J. N. Smith[2,3]

[1]Faculty of Physics, University of Vienna, Vienna, AT-1090, Austria
[2]Atmospheric Chemistry Division, National Center for Atmospheric Research (NCAR), Boulder, CO, USA
[3]Department of Applied Physics, University of Eastern Finland, Kuopio, Finland
[4] Department of Mechanical Engineering, University of Minnesota, MN, USA

Keywords: growth rate, DMA Train, nanoparticle growth, new particle formation
Presenting author email: agnieszka.kupc@univie.ac.at

Knowledge of the mechanisms leading to atmospheric new particle formation and growth is of significant importance to the understanding of climate relevant aerosol radiative forcing. New particle formation (NPF) can be characterized by means of formation and growth rates (Kulmala, 2003). These parameters are usually determined using condensation particle counters (CPC) for measuring particle number concentration and scanning mobility particle sizers (SMPS) for measuring the size distribution.

At the moment, however, the main obstacles in aerosol research are related to detection limits and time-resolution of instrumentation for characterizing nanometer-sized particles (nanoparticles). Since nanoparticles may grow fast, high time-resolution instruments are required to precisely follow these processes.

A new measurement technique proposed by Winkler *et al.*, (2013), the DMA Train, provides precise and rapid measurements of the size distribution of growing nanoparticles. The DMA Train (Figure 1) consists of a set of differential mobility analysers (DMAs), each set to select particles of a specific mobility diameter. Size-selected particles from each DMA are subsequently counted by a dedicated CPC placed downstream. The DMA Train provides an alternative way of studying the dynamics of NPF by offering measurements of particle size distributions at high time-resolution (1 sec.).

In recent chamber experiments (Winkler *et al.*, 2013), the DMA Train was shown to provide definite growth rates even at low size-selected particle number concentrations. While the laboratory experiments describe measurements in well-defined and controlled conditions, it is important to confirm whether (1) the same behaviour can be observed in real atmospheric conditions and (2) the DMA Train measurement technique is suitable to be used in field studies. Thus, the DMA Train was deployed at a field site in Lewes, Delaware in August 2012 to perform size-resolved measurements of growth and formation rates for a particle size range between 3 and 10 nm.

The DMA Train at the Lewes Field Campaign measurement site utilized a parallel arrangement of four CPCs: a di-ethylene-glycol-based CPC (DEG-CPC; Iida *et al.*, 2009) and three butanol-based ultrafine CPCs (UCPCs, TSI 3025; Stolzenburg and McMurry, 1991) each coupled to a nano-DMA (TSI 3085) and a Po^{210} radioactive source (Figure 1). Further, each DMA was set at a fixed voltage and sample flow (1.5 L/min) for measuring ambient particle number concentration in a narrow range of mobility diameters. For this study the sampled mobility diameters were 3, 6, 8 and 10 nm.

Results from the Lewes field study, obtained using the DMA Train, will be presented and compared to data provided by the Particle Size Distribution (PSD) instrument.

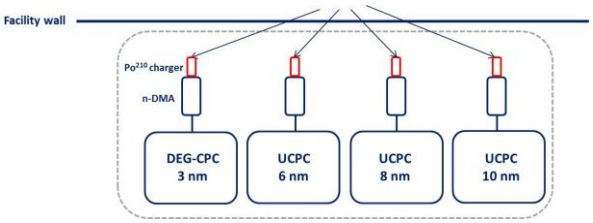

Figure 1. Schematic of experimental set-up includes DEG-CPC and three UCPC set to diameters of 3, 6, 8 and 10 nm respectively.

This work was supported by the Advanced Study Program (ASP), National Center for Atmospheric Research (NCAR), Boulder, CO, USA.

Kulmala, M. (2003), *Science*, **302**, 1000
Iida, K. *et al.* (2009), *Aerosol Sci. Technol.* **43**:1, 81-96
Stolzenburg, M.R and P.H. McMurry (1991), *Aerosol Sci. Technol.* **14**:48-65
Winkler, P.M *et al.* (2013), *A Fast-Scanning DMA Train for Precision Quantification of Early Nanoparticle Growth*, Abstract submitted to the ICNAA 2013

Source Identification and Apportionment of Finnish Arctic Aerosols

James R. Laing,[1] Philip K. Hopke,[1] Eleanor F. Hopke[1], Liaquat Husain,[2,3]
Vincent A. Dutkiewicz,[2,3] Jussi Paatero,[4] Yrjö Viisanen[4]

[1]Center for Air Resources Engineering and Science, Clarkson University, Potsdam, NY 13699, USA
[2]New York State Department of Health, Wadsworth Center, Empire State Plaza, Albany, NY 12201-0509, USA
[3]Department of Environmental Health Sciences, School of Public Health, SUNY, Albany, NY 12201-0509, USA
[4]Finnish Meteorological Institute, Helsinki, Finland
Keywords: Arctic, aerosol, time-series, PMF.
Presenting author email: laingjr@clarkson.edu

The Arctic aerosol has been studied since the early 1970s, but there are few available long-term datasets of the particulate chemical composition. There have been significant changes in the Arctic in the past half century. Long-term trends in aerosol chemical composition, specifically sulfate and black carbon, can provide a better understanding of the changes in these climatic forcing particles that have occurred. Changes in anthropogenic and natural sources can also be determined.

Week-long historical filter samples collected at Kevo, Finland from 1964 to 2010 have been analyzed for various chemical species. Major ions and methane sulfonate (MSA) have been analyzed by ion chromatography (IC), trace elements by inductively coupled plasma - mass spectrometry (ICP-MS), and BC by light transmission. Positive Matrix Factorization (PMF) and Potential Source Contribution Function (PSCF) analysis will be applied to the 47-year data set to determine possible source areas.

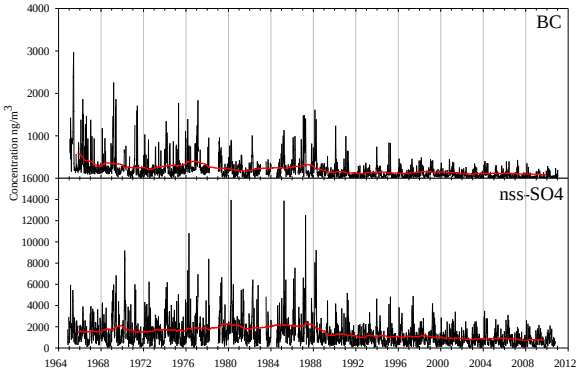

Figure 1. Black carbon and non-sea salt sulphate time series with 1-year moving average.

Time-series trend analysis will be performed to evaluate the evolution of sources over time. Black carbon and nss-SO_4 concentrations have decreased over the past five decades, most dramatically around 1990 coinciding with the fall of the Soviet Union (Figure 1). This decrease matches global inventories of anthropogenic emissions (Bond, 2007; Smith, 2011). Concentrations of lead have steadily decreased as a result of bans and regulations on the use of leaded gasoline.

Forest and agricultural fires have recently been shown to be a major source of Arctic BC during the spring/summer (Stohl, 2007; Warneke, 2010). It has been predicted that climate change has increased forest fires in central Canada and Russia (Stocks 1998). This prediction will be assessed and source areas of forest fires will be determined (Figure 2).

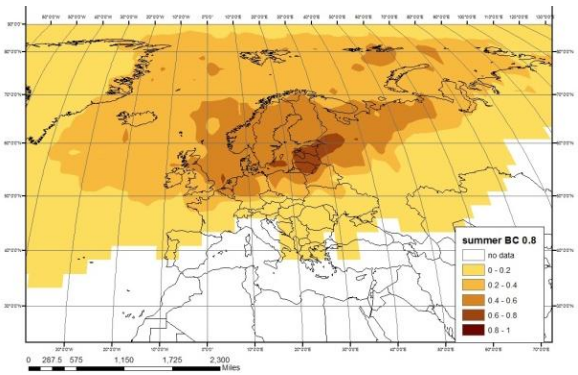

Figure 2. PSCF plot of BC during summer months.

This work was supported by the National Science Foundation under grant ATM 1007329.

Bond, T.C., Bhardwaj, E., Dong, R., Jogani, R., Jung, S., Roden, C., Streets, D.G., and Trautmann, N.M. (2007) Global Biogeochemical Cycles 21, GD2018.

Smith, S.J., Aardenne, J.v., Klimont, Z., Andres, R.J., Volke, A., and Arias, S.D. (2011) Atmos. Chem. Phys. 11, 1101–1116.

Stocks, B.J., Fosberg, M.A., Lynham, T.., Mearns, L., et al. (1998) Climate Change. 38, 1-13.

Stohl, A., Berg, T., Burkhart, J.F., Fjaeraa, A.M. et al. (2007) Atmospheric Chemistry & Physics 7, 511-534.

Forty-Seven Years of MSA Concentrations in the Finnish Arctic

James R. Laing[1], Philip K. Hopke[1], Eleanor F. Hopke[1], Liaquat Husain[2,3], Vincent A. Dutkiewicz[2,3], Jussi Paatero[4], Yrjö Viisanen[4]

[1]Center for Air Resources Engineering and Science, Clarkson University, Potsdam, NY 13699, USA
[2]New York State Department of Health, Wadsworth Center, Empire State Plaza, Albany, NY 12201-0509, USA
[3]Department of Environmental Health Sciences, School of Public Health, SUNY, Albany, NY 12201-0509, USA
[4]Finnish Meteorological Institute, Helsinki, Finland
Keywords: MSA, SST anomalies, PSCF.
Presenting author email: laingjr@clarkson.edu

In the northern hemisphere 7.5% of total sulfur emissions are from oceanic sources and for arctic regions (65° to 80°N) oceanic sulfur emissions constitute 42% of total emissions (Bates, 1992). MSA (Methane Sulfonate) is a unique sulfate that can be used as a marker for these biogenic oceanic sources. Marine planktonic algae excrete DMS (dimethylsulfide) which is transported to the air and oxidized to MSA (methane sulfonate) as well as nss-sulfate (Bates, 1992).

Week-long historical filter samples collected at Kevo, Finland from 1964-2010 have been analyzed for methane sulfonate (MSA) as well as various other species.

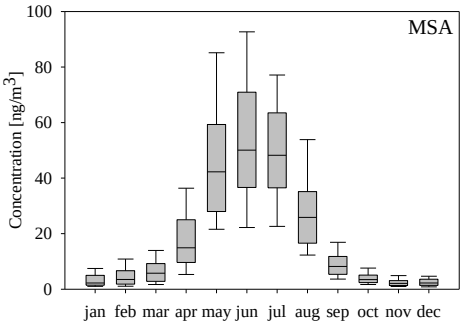

Figure 1. Seasonality of MSA concentrations.

MSA has a distinct summer maximum during the months of May, June and July associated with warmer waters and increased primary productivity in the surrounding oceans (Figure 1).

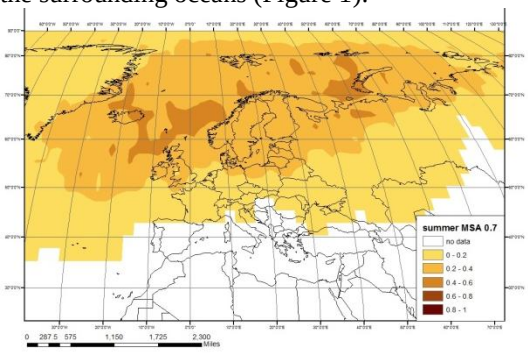

Figure 2. PSCF plot for MSA during summer months.

PSCF (potential source contribution function) results using HYSPLIT 5-day back-trajectories show for MSA in the summer show source areas primarily in the Norwegian and Barents Seas (Figure 2). Sea surface temperatures in the northern hemisphere have risen since the early 1970s, most dramatically in the North Atlantic (Thompson, 2010). Using the HadSST2 Dataset (Rayner, 2006), a significant correlation was found between average yearly MSA concentrations for the months of peak concentration (May, June, and July) and yearly SST anomalies in the region from 30W to 80E and 40N to 90N (Figure 3).

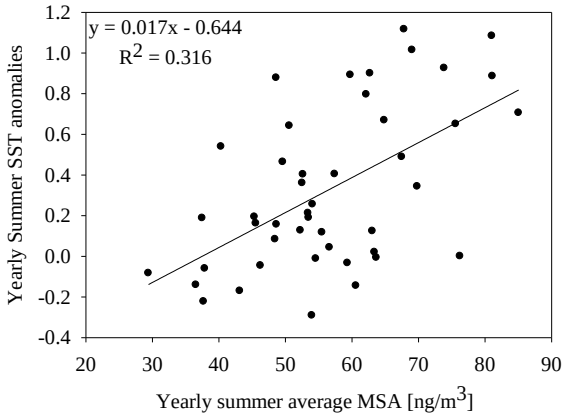

Figure 3. Yearly average summer (may, june, july) MSA concentrations and sea surface temperature anomalies.

This work was supported by the National Science Foundation under grant ATM 1007329.

Bates, T.S, Lambn, B.K., Guenther, A., Dignon, J., and Stoiber, R.E. (1992) Journal of Atmospheric Chemistry 14, 315-337.

Rayner, N.A., Brohamn, P., Parker, D.E., Folland, C.K., Kennedy, J.J., Vanicek, M., Ansell, T.J., andTett, S.F.B. (2006) Journal of Climate 19, 446-469.

Thompson, D.W.J., Wallace, J.M., Kennedy, J.J., and Jones, P.D. (2010) Nature 467, 444-447.

Source apportionment of ten years' aerosol collected at Mt. Lulin in East Asia

C.-T. Lee[1], S.-C. Wu[1], George N.-H. Lin[2] and G.-C. Hong[1]

[1]Graduate Institute of Environmental Engineering, National Central University, Jhong-Li, 32001, Taiwan
[2]Department of Atmospheric Science, National Central University, Jhong-Li, 32001, Taiwan
Keywords: biomass burning aerosol, aerosol chemical composition, long-range transport, source apportionment.
Presenting author email: ctlee@cc.ncu.edu.tw

Biomass burning (BB) in Indochina draws a great attention because its plume spreads in a regional scale to cause significant effects on solar radiation budget in East Asia (Street et al., 2003). Taiwan is located downstream of the prevailing westerly for receiving the air masses transported from BB source area in Indochina.

Atmospheric aerosol has been collected at Mt. Lulin (2,862 m a.s.l.) from 2003 to 2012. Comprehensive aerosol properties were resolved for $PM_{2.5}$ water-soluble ions, carbonaceous content (using the U.S. IMPROVE protocol), water-soluble/insoluble organic carbons (WSOC/WIOC), low-molecular-weight dicarboxylates (C2-C5), and monosaccharide anhydrides. In this study, K^+, NO_3^-, levoglucosan, OC3, and EC1-OP of $PM_{2.5}$ were found enhanced greatly in the transported BB plume than that of Non-BB (NBB). The aforementioned aerosol species are thus used as tracers to represent BB source contributions.

To apportion source contributions of aerosol to Mt. Lulin, a statistical method Positive Matrix Factorization (PMF) (USEPA, 2008) was adopted. Figure 1 shows that six major source types are identified for the air masses transported from BB source region during BB period. When arranged in terms of $PM_{2.5}$ contribution from high to low, these source types are secondary sulfate plus WSOM plus BB (28.7%), BB plus organic matter (OM) plus soil (25.4%), BB plus WSOM (17.6%), secondary aerosol plus dicarboxylates plus BB (12%), WSOM plus BB plus Diesel emissions (10.0%), and secondary aerosol plus sea salt (6.2%).

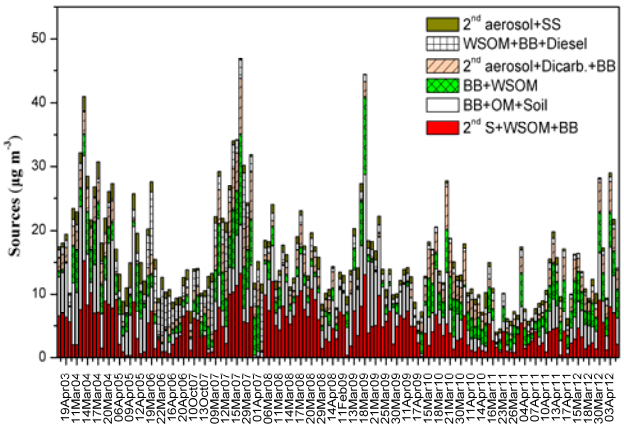

Figure 1. Time series of source contributions to the aerosol collected at Mt. Lulin for the air masses transported from BB source region during BB period.

It is noted that 93.8% of $PM_{2.5}$ mass concentration is contributed from BB source region during BB period. This confirms the consistency between PMF source apportionment and trajectory classification for the transported BB aerosol. It also implies that BB plume was mixed with other air masses during its transport before reaching the downstream Mt. Lulin site.

In contrast, WSOM, secondary sulfate, and OM contributed more than other sources to $PM_{2.5}$ during NBB period. The air masses were mostly originated from ocean (including Pacific Ocean and South China Sea) except for some mixing with marine and anthropogenic primary pollutants transported from the coastline of China mainland to the Mt. Lulin site.

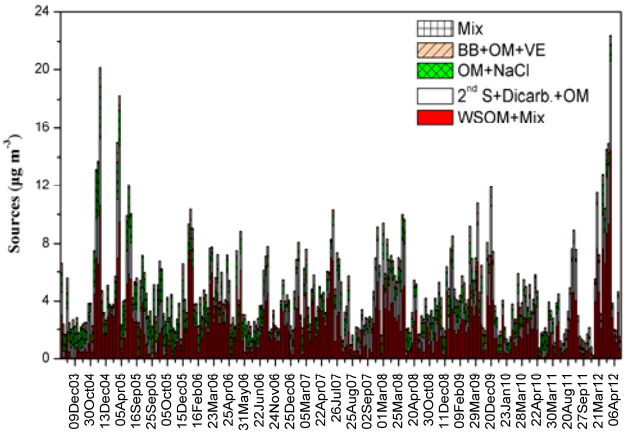

Figure 2. Time series of source contributions to the aerosol collected at Mt. Lulin for the air masses transported from non-BB source region.

In summary, ten years' aerosol data collected at Mt. Lulin shows that the air masses in the free atmosphere are enriched with organic aerosol. Meanwhile, aerosol source apportionment indicates that BB plume could mix with other minor sources during long-range transport and NBB air masses mainly contain secondary aerosol.

This work was supported by the National Science Council in Taiwan under grant NSC 98-2111-M-008 -023 -MY3.

USEPA (2008) EPA Positive Matrix Factorization (PMF) 3.0 Office of Research and Development, U.S. Environmental Protection Agency.

On the potential of volcanic ash and powder sample investigation with FIB/SEM EBSD-EDS

K.I. Lieke[1,2] and H. Alimadadi[1]

[1]Center for Electron Nanoscopy, Technical University of Denmark, 2800 Kgs. Lyngby, Denmark
[2] National Research Center for the Working Environment, 2100 Copenhagen, Denmark
Keywords: EBSD, FIB/SEM, volcanic ash.
Presenting author email: KirstenLieke@gmx.de

We present a method for sample preparation of single particles and powder samples for characterization with microscopic techniques, i.e. focused ion beam (FIB), electron backscatter diffraction (EBSD) and energy dispersive X-ray fluorescence (EDS).

In terms of analytical and preparation methods, particulate matter are non-ideal samples. Particles have rough surfaces and may consist of multiple mineral phases and glasses. These phases may have different hardness and densities. Furthermore, charging may occur depending on the conductivity of the material. All of these can potentially impede proper microscopic data acquisitions. In case of EBSD, due to the 60° - 80° tilting which is normally applied, the prepared surface should be as flat as possible, otherwise backscatter electrons are shadowed and do not reach the detector. EDS measurement may also suffer from irregular surfaces due to shadowing as well as deflection of the electron beam or outgoing X-rays. Because of different sputtering rate of different phases, ion milling may be far from optimal for multiphase materials and re-deposition of milled material can be an issue on irregular surfaces.

Determination of the chemical and mineralogical composition of volcanic ash is crucial for estimating their hardness, density and melting points, which are needed to calculate radiative properties (optical properties for detection and recognition, climate effects) their transport trajectories (plume development and atmospheric live time) and harm to aircrafts (sand blasting effect to aircraft windows and engine failure by plugging of engine parts).

To determine the mineral content in single particles or grains, bulk methods such X-ray powder diffraction fail, since large diffracting volume is needed. In contrast, EBSD combined with EDS provides crystallographic and chemical information on a sub-micrometer scale. By simultaneous utilization of the two techniques, phase boundaries and grain boundaries can be confidently determined. Hence, the surface area fraction of mineral grains can be estimated. In addition, by acquisition of maps from various cross-sections, i.e. improving the statistics, a volumetric estimations of mineral and glass content of the bulk can be obtained.

Transported volcanic ash particles are large (2-50 µm e.g. Schumann et al. 2011), they are non-conductive in large parts and the matrix is supposedly glassy (Lieke et al. 2013), they have rough surfaces and their mineral composition may vary. Hence, they are far from ideal for the mentioned microscopic characterization techniques.

To overcome the mentioned shortcomings, samples were prepared by embedding small amounts of powder in an epoxy blended with colloidal graphite and silver particles. The blend is designed for satisfactory conductivity, stability under electron beam and for mechanical milling. Careful evacuation is applied to make the embedding material porosity-free. The dried mixture was cut, grinded and polished under angles of 45 and 54 degrees, to enable mounting the sample in ion milling (52°) and EBSD (70°) positions. Ion milling can optionally be applied for further sample preparation or for extension of analysis in the third dimension. Silver paint was used to glow the samples to a holder. Coating (gold or copper) was applied before the last polishing step (0.05 µm), to remain conductivity over gaps, holes and cavities that may have formed during grinding.

The preparation method was successful for data acquisition in a Helios Nanolab 600 DualBeam instrument (FEI, Eindhoven, The Netherlands) equipped with EDAX (Mahwah, IL, USA) EDS and EBSD detectors.

Identified phases embedded in glassy matrix were Rutile and Plagioclase, whereas Olivine was identified as single grains.

In the present work, the microscopic characterization of particles is shown on the example of volcanic ash particles from the recent Eyjafjalla eruption on Iceland, collected upon deposition in the vicinity of the volcano. That opens future perspectives for the investigation of other challenging particulate samples.

The particle samples were kindly provided by Andreas Vogel, FH Düsseldorf, Germany. We gratefully acknowledge an inspiring working environment at DTU-CEN. Excellent technical assistance, expertise and fruitful discussion were provided by Adam Fuller, Zoltan Imre Balogh and Berit Wenzel.

Schumann, U., et al. (2011). Airborne observations of the Eyjafjalla volcano ash cloud over Europe during air space closure in April and May 2010. Atmospheric Chemistry and Physics 11: 2245-2279.

Lieke, K. L., Kristensen, T. B., Korsholm, U. S., Sørensen, J. H., Kandler, K., Weinbruch, S., Ceburnis, D., Ovadnevaite, J., O'Dowd, C. D. and Bilde, M. (2013). The 2011 Grímsvötn volcano eruption: characterization of long range transported single volcanic ash particles. Submitted to Atmospheric Environment.

Analyses of long-term measurements (2005-2012) of ^{7}Be concentrations in surface air aerosols.

E. Liger[2], C. Dueñas[1], M.C. Fernández[1], E. Gordo[1], S. Cañete[1] and M. Pérez[3]
1 Department of Applied Physics I, Faculty of Sciences, [2]Department of Applied Physics II, Faculty of Computer Engineering, [3]Department of Radiology and Health Physics, Ophthalmology and OTL, Faculty of Medicine. University of Málaga 29071 Málaga (SPAIN)
Keywords: ^{7}Be, cosmogenic radionuclide, atmospheric aerosols, meteorology.
Presenting author email: eliger@uma.es

Cosmogenic particles hitting the atmosphere lead to the production of ^{7}Be ($T_{1/2}$=53.3 days) in the lower stratosphere and upper troposphere. Once ^{7}Be is formed is rapidly associated with submicron aerosol particles and participates in the formation and growth of the accumulation mode (from 0.07 to 2 μm) aerosols, which is a major reservoir of pollutants in the atmosphere (Ioannidou *et al.*, 2011). This naturally occurring radionuclide is a most important isotope in studying atmospheric processes because of its convenient half-life and sufficiently detectable γ-radiation (Eγ = 0.477 MeV), which has served for studying precipitation scavenging, vertical and horizontal removal of air masses, aerosol transit and residence times in the troposphere. ^{7}Be surface air activity shows a strong dependence on altitude, latitude, local climate and seasonal variations.

The aim of the present study is to explain the behaviour of aerosols, associated with ^{7}Be, in the surface atmosphere using exploratory data analysis in order to obtain information on their possible mechanisms of transport and deposition. Long-term variations of the radionuclide concentrations are discussed in relation with precipitation, temperature, temperature interval, relative humidity, solar radiation, pressure, wind and Saharan dust events. Least significant difference test (LSD) and principal component analysis (PCA) with varimax rotation have been applied to study the datasets.

Airborne particulate samples were collected weekly during an 8 years period (January 2005 till December 2012) at Malaga, on the Southeastern coast of Spain, (36° 43′ 40″ N; 4° 28′ 8″ W; 54 m a.s.l). The sampling point is located approximately 5 km away from the coastline and the local sources of anthropogenic aerosols are limited to emissions from cars. Due to its geographical vicinity with the African continent, our study area is frequently affected by intrusions of Saharan air. The Sahara desert is one of the principal sources of natural dust in the northern hemisphere.

Aerosol particles were continuously collected in cellulose filter with 0.8-μm pore size. Gamma measurements were performed with a coaxial-type germanium detector. A total of 96 samples of aerosols were analyzed and ^{7}Be specific activity was determined. The meteorological parameters studied during the sampling period were provided by the Spanish National Institute of Meteorology (AEMET). Data for the number of days with high probability of episodes of Saharan intrusions have been obtained from the CALIMA project which is the result of Commendation of Management Agreement between the Ministry of Environment and Rural and Marine Affairs (MARM) and the State Agency National Research Council.

The mean specific activity of ^{7}Be in near-surface air measured over the 8-year studied period was 4.28 ±1.88 mBq m^{-3}, with a minimum of 0.34 mBq m^{-3} and a maximum of 14.9 mBq m^{-3}. Concentrations show seasonal variations with values above the annual mean occurring mainly in the spring and summer months of each year. LSD test was applied to find which months differed significantly in order to put the samples into homogeneous groups.

The activity concentrations of ^{7}Be have a significant positive relationship with Saharan dust events (r=0.519), temperature (r=0.44) and solar radiation (r=0.399). On the contrary, a negative correlation was observed with the amount of precipitation (r= -0.33) and relative humidity (r=-0.31). In the period January–June transport of Saharan dust toward Spain is mainly due to the cyclonic activities over the West or South of Portugal, while in the summer this transport is governed by the anti-cyclonic activities over the East or Southeast of Iberian Peninsula (Rodríguez *et al.*, 2001).

The results of the PCA analysis showed that the monthly behaviour of ^{7}Be aerosols in our sampling coastal site was represented by three groups which explain 71.55% of total variance. The first principal component explained 42.45% of the total variance of the dataset and it was positively correlated with ^{7}Be, Sahara dust events, temperature and radiation and negatively with relative humidity and precipitation.

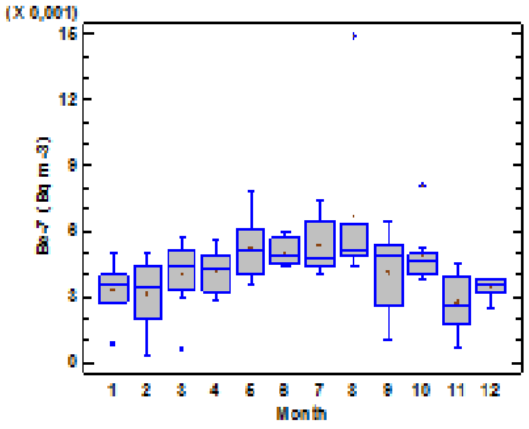

Figure 1. Boxplot of the ^{7}Be concentrations on a monthly basis.

Ioannidou A, Kotsopoulou E, Papastefanou C (2011). *J Radioanal Nucl Chem* **289**, 395–400.
Rodríguez, S., X. Querol, A. Alastuey, G. Kallos, and O. Kakaliagou (2001). *Atmos. Environ.*, **35**, 2433- 2447.

Airborne measurements of ship emissions

H. Lihavainen, E. Asmi, J.-P. Jalkanen, A. Hyvärinen, T. Laurila, J. Walden and R. Hillamo

Finnish Meteorological Institute, Helsinki, FI-00101, Finland
Keywords: ship emissions, health, climate, aerosol
Presenting author email: heikki.lihavainen@fmi.fi

Baltic Sea and North Sea, including the English Channel, were designated as SOx Emisson Control Areas (SECA) in May 2006 and November 2007 by the International Maritime Organization. In these sea regions the maximum sulphur content of marine fuels was restricted to 1.5% (weight/weight) and further reduced to 1.0% from July 2010 in SECA countries. These actions have significantly reduced the ship emitted SOx and sulphur containing fractions of particulate matter thus mitigating some of the detrimental effects to human health. Further, from Jan. 1st, 2010 a requirement for the use of 0.1% of sulphur (0.1%S) fuel in the European port areas became effective. From the beginning of 2015 sulphur is to be removed from marine fuels and only the use of 0.1%S marine gas oil is allowed in SECAs according to the new EU directive (2012/33/EC), whereas shipping globally have to switch to 0.5%S fuel by 2020. There should exist methods how to monitor the fuel sulfur content of the ships. One method is to measure gas phase SO_2 and CO_2 ratio from ship plume.

The analysis of costs and effects of the sulphur reductions have mostly included only the effects on human health, but they can also have impacts on the climate (Lauer *et al*., 2009). Emissions of sulphate aerosol are thought to have significant climate cooling impacts, either directly by scattering incoming solar radiation or indirectly by acting as cloud condensation nuclei and thus modifying cloud albedo. On the other hand, black carbon (BC) aerosol can warm the climate when it absorbs solar radiation in the atmosphere as well as by reducing the surface albedo in snow and ice covered regions, such as the. The emissions of these two aerosol types were recently connected to ship fuel sulphur content and the operational conditions of marine engines (Lack and Corbett, 2012). Current widely available ship emission inventories offer only limited support in assessing the climate impact of international shipping, because they lack the information how and where the ships are run during voyages and port stays. Significant uncertainties can exist in determining the time spent at sea, engine load profiles used, emission factors applied and emissions occurring during port operations.

Recently, Jalkanen *et al.* (2009) introduced the Ship Traffic Emission Assessment Model (STEAM) which uses Automatic Identification System (AIS) and is able to track individual vessels with unprecedented accuracy. However, in order to model the effects of fuel sulphur content, engine load profiles and ship operations accurately, a solid experimental groundwork is needed. Comprehensive studies, especially experimental, on ship emissions are rare (Murphy et al., 2009).

We had two major goals in this study; to test the method to monitor marine fuel sulphur content and to make detailed measurements on aerosol properties to gain better understanding on climate and health effect of ship emitted aerosols now and in the future. We studied ship emission with various flying platforms with different kind of instrumentation. Used platforms were one engine Cessna 172, two engine SHORT SC-7 Skyvan and AS350 helicopter. In Cessna and helicopter had the most simple instrumentation since the instrumentation are run by batteries, whereas Skyvan is prepared to carry heavier loads, like aerosol mass spectrometer. It has also electricity available on board.

With the basic instrumentation gas phase CO_2, CH_4, H_2O and SO_2 and particle number concentration (>4 nm), temperature and humidity was measured. In figure 1 is example from one flight in ship plume with Cessna. It shows that this method could be developed to a standard method to monitor the sulphur content of the ship fuel as well as for detailed studies of chemical, physical and optical properties of ship plumes.

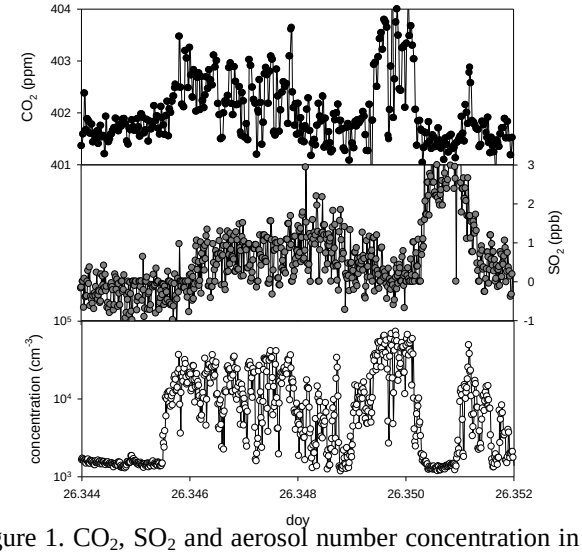

Figure 1. CO_2, SO_2 and aerosol number concentration in ship plume when approaching a vessel.

The work was supported by the European Regional Development Fund, Central Baltic INTERREG IV A Programme (project SNOOP). We would like to thank Airspark Oy, Aalto University Skyvan team and Helitour for flying platforms.

Jalkanen J.-P., A. Brink, J. Kalli, H. Pettersson, J. Kukkonen, and T. Stipa, (2009), *Atmos. Chem. Phys.*, **9**, 9209-9223

Lack D. and J. J. Corbett (2012), *Atmos. Chem. Phys.*, **12**, 3985-4000.

Lauer et al. (2009) *Environ. Sci. Technol.* **43**, 5592–5598.

Murphy, S. M. et al. (2009), *Environ. Sci. Technol*., **43**, 4626–4640.

Relationship between the tropospheric aerosol size distribution and cloud droplet effective radius in a rural region of São Paulo State

M. Lima-Souza[1], A. G. Allen[1], L. Caetano-Silva[1] and A. A. Cardoso[1]

[1]Department of Analytical Chemistry, Universidade Estadual Paulista, Araraquara, São Paulo, 14800-900, Brazil
Keywords: Aerosols, size distribution, clouds, SMPS, Aqua, Terra
Presenting author email: michelelsouza@gmail.com

The composition of the aerosol in the lower troposphere of the central region of the Brazilian State of São Paulo is governed mainly by the relative intensities of different anthropogenic sources: sugar cane burning, soil dust resuspension, industrial emissions, and road transport.[1,2] The resulting primary and secondary aerosols are present at concentrations that far exceed natural background levels.

Because of these emissions, the regional aerosol is substantially modified in terms of its chemical composition and its hygroscopic characteristics, and this is expected to affect the processes involved in cloud formation and, consequently, precipitation. The solubility of the particles suggests that they should be able to act efficiently as cloud condensation nuclei (CCN). It is therefore important to understand how different categories of aerosol might influence the processes of cloud formation and precipitation, due to the potential impacts on both agriculture and the water supply.

Size distributed number concentrations of ambient aerosols were measured at a rural site in the municipality of Araraquara, located in the interior of São Paulo State within one of Brazil's most important intensive sugar cane producing regions. Other significant economic activities here include citrus production and the industrial processing of the agricultural products.

The number concentrations of the aerosols were measured as a function of particle size using a TSI Model 3080 electrostatic classifier fitted with a Model 3081 differential mobility analyzer, connected to a condensation particle counter (CPC, TSI Model 3775) and operated in the scanning mobility particle sizer (SMPS) configuration. The size interval of the particles measured was 14.6-661.2 nm, and data were collected continuously, every 10 minutes, between August 2011 and November 2012.

In parallel with the ground-level measurements, the cloud droplet effective radius (r_e) corresponding to clouds present above the sampling site was retrieved from the database of the MODIS (Moderate Resolution Imaging Spectroradiometer) instruments carried on board NASA's Terra and Aqua satellites. The area considered for the satellite data was a rectangle (approximately 47 km x 47 km) described by the geographical coordinates: -21.564S, -48.452W (upper left corner); -22.063S, -47.953W (lower right corner). The satellite overpasses occurred during the periods (UTC): 12:30-14:30 (Terra); 16:00-17:30 (Aqua).

The SMPS data used considered an average of five individual measurements, centered on the time of the satellite overpass. The data were grouped according to both the total number concentration and the type of aerosol size distribution observed, considering the presence of an Aitken mode or an accumulation mode (as well as a number of mixed cases). The existence of an Aitken mode, without any obvious accumulation mode, was considered to reflect the presence of fresh particles, including those derived from recent nucleation, while a single accumulation mode was indicative of the presence of particles that had experienced aging within the atmosphere (Fig. 1).

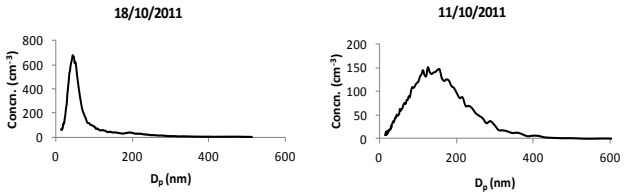

Fig.1. Examples of events characterized by Aitken (left) and accumulation (right) modes in the size distribution.

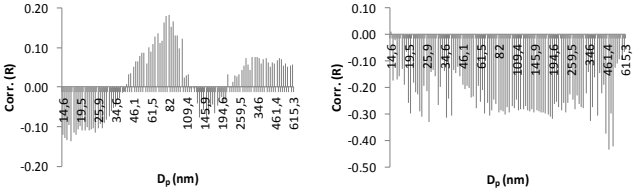

Fig. 2. Correlations obtained between r_e (Aqua data) and the size distributed aerosol number concentration during Aitken mode (left) and accumulation mode (right) events.

During Aitken events, the value of the coefficient (R) for the correlation between r_e and aerosol number concentrations showed a variable relationship as a function of particle size, while during accumulation mode periods, negative values of R were obtained for all size fractions (Fig. 2). The findings suggest that the relationship between tropospheric aerosol loadings and cloud properties in the study region may be more complex than previously thought, since cloud droplet size can show either a positive or a negative relationship with the aerosol number population in the lower troposphere.

Acknowledgments: FAPESP (Process 2008/58073-5), CNPq (Process 311668/2011-9) and CNPq (Process 162766/2011-4).

[1]Allen, A.G. *et al*. (2004) *Atmos. Environ*. **38**, 5025-5038.
[2]Da Rocha, G.O. *et al*. (2005) *Environ. Sci. Technol*. **39**, 5293-5301.

Characteristics of fine and coarse particles collected from open burning of jujube tree branches

Chih-Chung Lin[1], Wen-Yinn Lin[2], Kuo-Lin Huang[1], Lien-Te Hsieh[1], Jen-Hsiung Tsai[1] and Shui-Jen Chen[1,*]

[1] Department of Environmental Science and Engineering, National Pingtung University of Science and Technology, Pingtung County, Nei Pu, 91201, Taiwan
[2]Institute of Environmental Engineering and Management, National Taipei University of Technology, Taipei City, 10608, Taiwan
Keywords: open burning, water-soluble ions, agricultural waste, size distribution.
Presenting author email: lincc@mail.npust.edu.tw

This study investigates the chemical characteristics of particles that were collected from the open burning of jujube tree branches (agricultural waste), and evaluates the impact of such burning on regional air quality. The atmospheric particulate samples were collected in a jujube farm at Pingtung City in southern Taiwan. The area of jujube farm was 800 m^2 and the weight of jujube tree branch waste was 4.5 T. The sampling time was divided into three periods: before (background), during, and after open burning. During the open burning period, the A, B, C, and D samples were taken from four locations with distances of 1, 7, 11, and 16 m, respectively, away from the open burning site. The particle size distribution was collected using a micro-orifice uniform deposition impactor (MOUDI) and the particulate water-soluble ions in fine (D_p < 2.5 μm) and coarse (2.5 < D_p < 10 μm) particles (or particulate matter (PM)) were collected using a Dichot sampler. The masses and water soluble ions of particles collected on filters were analyzed using a digital balance and an ion chromatographer (IC, DIONEX ICS-3000), respectively.

The results indicate that the $PM_{2.5}$ concentrations at sampling sites A, B, C, and D during open burning were 103, 17.2, 13.5, and 5.59 times the background value, respectively, or on average, 34.9 times the background value. The average $PM_{2.5}/PM_{10}$ ratio at sample sites A during open burning (0.91) was higher than those before (0.62) and after burning (0.52). Also, the concentrations of $PM_{2.5}$ and $PM_{2.5\text{-}10}$ sharply dropped as the distance between the sampling point and the burning source increased. Ryu *et al.* (2007) also found that the average concentrations of fine or coarse particles in the early summer in the rural areas of Korea were higher during biomass burning than during a haze or normal period. In this study, the average $PM_{2.5}/PM_{10}$ ratio during open burning was 0.90, which exceeded that (0.79) obtained in Korea during a season of extensive open burning (Ryu *et al.*, 2007). In this study, before open burning, the particles had a bi-modal size distribution with one main peak in the coarse size range (3.2–5.6 μm) and the other peak in the fine size range (1–1.8 μm); during open burning, the particle size distribution was uni-modal, with a peak in the fine size range (Figure 1).

As shown in Figure 2, before and after jujube fruit branches were burned in the open space, NO_3^- had the highest concentration of all of the water-soluble ions in the particles, followed by SO_4^{2-}, and then NH_4^+. This result is similar to that obtained for particulate matter in the atmosphere. However, the concentrations of particle-bound Cl^- and K^+ rose sharply during open burning. Before burning, the concentration of Cl^- in $PM_{2.5}$ was 1.69 μg m^{-3}. The Cl^- concentrations in $PM_{2.5}$ that was collected at samples sites A, B, C, and D during open burning were 136, 61.8, 57.3, and 18.0 μg m^{-3}, respectively. The highest of these values was 84.5 times the background value. The K^+ concentration of samples that were collected at sites A, B, C, and D were 5–197 times higher than the background value, 0.87 μg m^{-3}. Khalil and Rasmussen (2003) indicated that K and Cl can be used as a tracer of wood smoke.

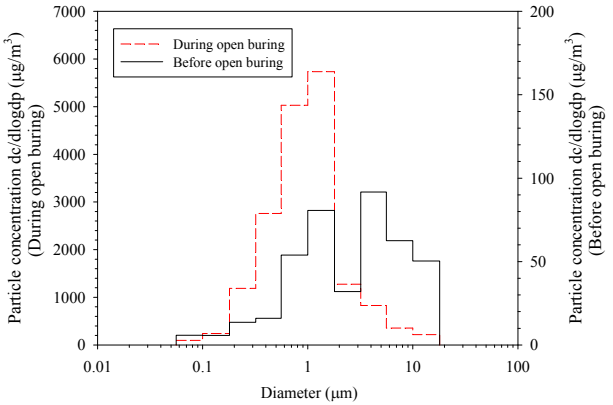

Figure 1. Size distributions of the particles collected before and during open burning.

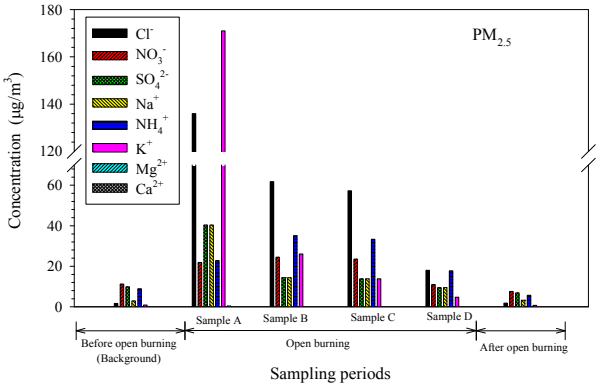

Figure 2. Concentrations of water-soluble ion in fine particles. (Sites A, B, C, and D were 1, 7, 11, and 16 m, respectively, from the open burning site.)

Ryu, S.Y., Kwon, B.G., Kim, Y.J., Kim , H.H., Chun, K.J. (2007) Atmos. Res. **84**, 362–373.

Khalila, M.A.K., Rasmussen, R.A. (2003) *Atmos. Environ.* **37**, 1211–1222.

Investigating the Small-Scale Vertical and Horizontal Variability of the Atmospheric Boundary Layer Aerosol using Unmanned Aerial Vehicles

B. Wehner[1], A. Lampert[2], A. Scholtz[2], J. Bange[3], A. Platis[3], and M. Hermann[1]

[1]Leibniz Institute for Tropospheric Research (TROPOS), 04318 Leipzig, Germany
[2]Institute of Aerospace Systems, TU Braunschweig, 38108 Braunschweig, Germany
[3]Universität Tübingen, Center for Applied Geophysics, 72076 Tübingen, Germany
Keywords: new particle formation, UAV, boundary layer aerosol.
Presenting author email: birgit@tropos.de

Introduction

Beside numerous ground based measurements only few aerosol data from higher altitudes taken by airborne instrumentation are available. These data showed a number of interesting phenomena, such as new particle formation often induced by turbulence. However, such data are rare and more continuous aerosol and turbulence measurements in higher altitudes are needed to close this gap.

One approach to realize airborne measurements with low logistical effort compared to aircraft measurements is the application of unmanned aerial vehicles (UAV) for atmospheric studies. The new UAV Carolo P360 “ALADINA” (see Figure 1) equipped with aerosol instrumentation provides a unique and flexible tool for characterizing the vertical and horizontal variability of the boundary layer aerosol. The Carolo P360 with a wingspan of 3.6 m is designed to carry up to 2.5 kg of payload in the front compartment. With electrical propulsion, it has an endurance of about 40 minutes. The cruising speed is 25 m/s.

Figure 1. Picture of the UAV ALADINA.

Instrumentation

For aerosol measurements, ALADINA will be equipped with a set of light-weight instruments. To reach the weight limit of 2.5 kg for the payload, commercially available instruments were chosen and modified in terms of space and weight. Two Condensation Particle Counters, CPCs, (TSI, model 3007, TSI Inc., St. Paul, USA) with different lower cut-offs will be used to measure the total particle number concentration between ~6 nm and 1 μm (N_6) and ~12 nm and 1 μm (N_{12}), respectively. The difference between N_6 and N_{12} will be used as indicator for new particle formation. To reduce weight, housing, internal batteries, and display of the CPCs were removed.

Larger aerosol particles will be measured using an Optical Particle Counter, OPC (Met One, model GT-526, Met One Instruments Inc., Washington, USA). This OPC counts particles in 6 size channels from 0.3 to 5.0 μm. Again, housing, battery, and display were removed.

The aerosol instruments will be characterized and improved in the laboratory with respect to the lower detection diameter and the response time of the CPCs.

Moreover, an additional meteorological payload for measuring the turbulent 3D wind vector, temperature and humidity is constructed by Tübingen University. These sensors and an aerosol inlet will be mounted in front of the UAV.

Electrical power for all three instruments will be provided by a common battery. A measurement and data acquisition system is developed at Tübingen University with the possibility of real-time data transfer by a telemetry downlink. This new UAV system will be flight tested for proper instrument operation while airborne.

Experiment

A first field experiment is planned in September 2013 in Melpitz, the research site of TROPOS. Here, the UAV aerosol and meteorological measurements will be completed by ground-based and helicopter-borne measurements. In addition, Lidar measurements will provide continuous measurements of the vertical structure. The UAV has the potential to close the gap of atmospheric aerosol measurements between long-term ground-based observations and expensive helicopter-borne measurements. Complementary to these measurements, UAV observations allow for investigating the small-scale and short-term aerosol variability in vertical and horizontal direction at low cost and with minimal logistical requirements. Two additional UAV of type MASC of Tübingen University equipped with turbulence instrumentation add the opportunity to study the interaction of the aerosol concentration with turbulent transport and exchange processes of the surface and the atmosphere. The combination of different flight patterns of the three UAV allows new insights in atmospheric boundary layer processes.

This work is supported by the Deutsche Forschungsgemeinschaft (LA 2907/5-1, WI 1449/22-1, BA 1988/14-1).

The association of children's lung function and air pollution in Kaohsiung, Taiwan

Yeh, CL[1], Mena, KD.[2], Ou, CS[3], and Chen, PS[1*]

[1]Department of Public Health, Kaohsiung Medical University, Kaohsiung, 80708,Taiwan
[2]Department of Public Health, University of Texas Health Science Center, Houston, El Paso, 79902,USA
[3]Graduate Institute of Occupational Safety and Health, Kaohsiung Medical University, Kaohsiung, 80708,Taiwan
Keywords: lung function, air pollution, children.
Presenting author email:protamine1199@yahoo.com.tw

Introduction

Recently, the association between the air pollution and human health has been widely mentioned. Children are more sensitive to air pollution then adult due to their higher metabolism rate and smaller body size. In most of the previous studies, data from air monitoring station were used to evaluate children exposure whereas questionnaire was used to evaluate their health effect. In the present study, we measured children`s lung function and air pollutants including CO, CO_2, NO_2, O_3, PM_1, $PM_{2.5}$, PM_{10}, ultrafine particles, fungal and bacterial bioaerosols in classrooms to evaluate the association between air pollutants and children's lung function.

Materials and Methods

Three elementary schools, reference, industry and traffic school, were selected in Kaohsiung, Taiwan. Twenty classrooms were randomly selected in each elementary school with a total sample size of sixty classrooms. Temperature, relative humidity, CO, CO_2, NO_2 (Airboxx, KD UK), O_3 (Ozone Monitor, Model 202, 2B Technologies, Inc),PM_1,$PM_{2.5}$, PM_{10} (DUSTTRAK™ DRX Aerosol Monitor; Model 8533, TSI USA), ultrafine particles (P-TRAK® Ultrafine Particle Counter ; Model 8525, TSI USA) were monitored in real-time from 8 am to 4 pm between April 2009 and November 2009. We also sampled fungal and bacterial bioaerosols indoor and outdoor of classroom at 8 am and 4 pm (MAS-100, MERCK USA). Tryptic soy agar (TSA) and Malt extract agar (MEA) was used for cultivated of bacteria and fungus, respectively. Lung function was measured for 1026 schoolchildren (HI-801, JAPAN). To investigate the explainability of air pollution for children's lung function, we analyze the air pollution concentration and the abnormal rate of lung function in the same classroom by using multiple regression.

Results and Discussion

The abnormal rate of lung function's parameter was analyzed as the product variables, and the concentrations of air pollutants were analyzed as the explain variables. If combining the data of three schools, ultrafine particles (R^2=10%) and $PM_{2.5}$ (R^2=13.3%) could significantly affect vital capacity (VC)'s abnormal rate. The abnormal rate of VC is defined as (measured VC/predicted VC)*100% below 70%. Ultrafine particles and $PM_{2.5}$ could explain 10%, and 13% of VC's abnormal rate, respectively. For traffic school, ultrafine particles (R^2=13.2%), $PM_{2.5}$ (R^2=19.9%), and O_3 (R^2=19.9%) could significantly explain each R^2= 20% of VC's abnormal rate, respectively. In industry school, the significant factors for VC's abnormal rate were ultrafine particles (R^2=13.1%), indoor fungi (R^2=7.1%), bacteria (R^2=7.5%), and CO (R^2=39.4%). In referece school, ultrafine particles (R^2=12.1%) could significantly affect VC's abnormal rate. Regarding forced expiratory volume (FVC), the significant affecting factors for FVC's abnormal rate were ultrafine particles (R^2=10.92%) and $PM_{2.5}$ (R^2=6.25%). Ultrafine particles, the only significant factor for both industry and traffic school, could explain 12% and 27% of FVC's abnormal rate in traffic and industry school, respectively. In background school, ultrafine (R^2=8.4%), indoor fungi (R^2=6.87%), and CO (R^2=39.4%) were the significant factors.

Table1. The explainability of significant air pollutants for the abnormal rate of children's Vital capacity (VC) by Stepwise model

Traffic	pollutant	Ultrafine	$PM_{2.5}$	O_3	
	partial R^2	13.2%	19.9%	7.0%	
Industry	pollutant	CO	Ultrafine	Bacteria	Fungi
	partial R^2	39.4%	13.1%	7.5%	7.1%
Reference	pollutant	Ultrafine			
	partial R^2	12.1%			
Three schools	pollutant	Ultrafine	$PM_{2.5}$		
	partial R^2	10.0%	13.3%		

Table2. The explainability of significant air pollutants for the abnormal rate of children's forced expiratory volume (FVC) by Stepwise model

Traffic	pollutant	Ultrafine	
	partial R^2	12.1%	
Industry	pollutant	Ultrafine	
	partial R^2	27.4%	
Reference	pollutant	Ultrafine	Indoor fungi
	partial R^2	8%	6.9%
Three schools	pollutant	$PM_{2.5}$	Ultrafine
	partial R^2	6.3%	10.9%

Seasonal physical and optical properties of atmospheric aerosol at Princess Elisabeth station, East Antarctica

A. Mangold[1], H. De Backer[1], A. Delcloo[1], V. De Bock[1], C. Hermans[2], I. Gorodetskaya[3] and W. Maenhaut[4]

[1]Royal Meteorological Institute of Belgium, Brussels, Belgium; [2]Belgium Institute for Space Aeronomy, Brussels, Belgium; [3]Catholic University of Leuven, Leuven, Belgium; [4]Ghent University, Ghent, Belgium
Keywords: Antarctica, atmospheric aerosol, optical properties, physical properties
Presenting author email: alexander.mangold@meteo.be

Aerosol optical and physical properties have been measured during recent austral summers and winters at the Belgian Antarctic research station Princess Elisabeth, inaugurated in February 2009. Princess Elisabeth station is situated around 180 km inland from the coast, north of the Sør Rondane Mountains in Dronning Maud Land, East Antarctica, on the Utsteinen ridge (71°57'S, 23°20'E, 1390 m asl; Pattyn *et al.*, 2010). The station is manned during austral summer. In winter, the station operates in automatic mode with remote control.

Measured aerosol properties comprise aerosol size distribution (laser aerosol spectrometer, LAS, TSI3340), total aerosol number (condensation particle counter, CPC, TSI3776), total aerosol mass concentration (TEOM-FDMS), mass concentration of light-absorbing aerosol and absorption coefficient (Magee 7-wavelength aethalometer) and total scattering coefficients (Ecotech 3-wavelength nephelometer).

All instruments were in simultaneous operation during summers 2011/12 and 2012/13 and are currently installed for continuous operation, including this austral winter. The aethalometer and TEOM-FDMS have been measuring since December 2010 and also during two winter months in 2011 and six in 2012. The LAS could measure during two winter months in 2012.

Besides these instruments for boundary layer aerosol characterisation, a 8-wavelength sunphotometer, (AErosol RObotic NETwork; aeronet.gsfc.nasa.gov; CIMEL CE318), provides aerosol information like aerosol optical depth (AOD) for the total atmospheric column during austral summer since February 2009.

Since February 2009, there are continuous data of an automatic weather station (Gorodetskaya *et al*., 2013) in order to interpret the meteorological conditions.

The aethalometer is operated at a nominal flow of 5.5 litre/min and an integration time of 60 min. The mean mass concentration of light-absorbing particles in winter 2011 was 6.0±4.7 ng/m^{-3} at 660/880 nm, and 10.5±5.6 ng/m^{-3} at 370/470 nm. The respective values for summer 2011/12 were 7.6±6.1 ng/m^{-3} and 11.6±6.8 ng/m^{-3}. The mean absorption coefficients, calculated using the instrument's cross sections, were 0.10±0.08 Mm^{-1} at 880 nm (soot particles absorb strongest at this wavelength) and 0.43±0.22 Mm^{-1} at 370 nm in winter 2011. The values for summer 2011/12 were 0.13±0.12 Mm^{-1}, and 0.49±0.28 Mm^{-1}, respectively. The mean absorption Angström exponent (370/470 to 660/880/950 nm) was 2.0±1.2 in winter 2011 and 1.8±1.2 in summer 2011/12. The differences between the wavelengths indicate that several absorbing aerosol types were present, as, e.g., pure soot has an absorption Angstrom exponent around 1. The single scattering albedo (SSA) could be derived from simultaneous aethalometer and nephelometer measurements in February 2012 (Table 1). The aethalometer data has been interpolated between wavelengths. SSA values showed high uncertainty, mainly due to low aerosol concentrations and the uncertainties of the absorption coefficient determination. SSA values around 0.9 would have been expected.

Table 1: Optical parameters February 2012:

λ	total scatter Mm^{-1}	absorption Mm^{-1}	single scatt. albedo (= sca/(sca+abs))
425nm	1.07±0.53	0.48±0.23	0.69±0.34
525nm	1.06±0.50	0.35±0.19	0.75±0.35
635nm	0.94±0.61	0.20±0.13	0.82±0.38

The CPC measures particles in the diameter range 3 to 3000 nm. Figure 1a shows data of February 2012. Simultaneous size distribution measurements revealed diurnal cycles in the size range 3–90 nm for 12 and 13 February 2012, indicative of locally formed aerosol.

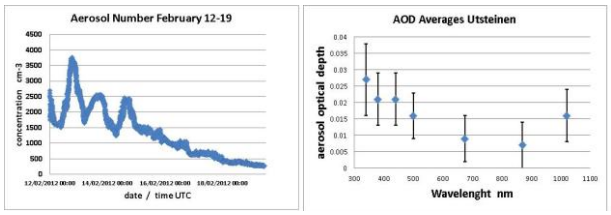

Figure. 1: a) CPC number concentration February 2012; b) total AOD averages February 2009 to February 2013

Figure 1b shows the average AOD values from the sunphotometer for all summer seasons. The average Angström exponent (440–880 nm) was 2.0±0.6, indicating a dominance of sub-micron particles.

We will present further seasonal aerosol properties from austral winters 2011/2012/2013 and respective summers.

This work was supported by the Belgian Federal Science Policy under grants EA/34/1A and EA/34/1B. Many thanks go to the Antarctic expedition teams, in particular Erik Verhagen, the station's science liaison officer.

Gorodetskaya, I. V., Van Lipzig, N. P. M., Van den Broeke, M. R., Mangold, A., Boot, W. and C. H. Reijmer (2013), *J. Geophys. Res Atmos.*, **118**, doi:10.1002/jgrd.50177.

Pattyn, F., Matsuoka, K. and Berte, J. (2010), *Antarctic Science*, **22(1),** 79-85.

$\delta^{13}C$ of size segregated aerosol particles collected in Preila and Baltic Sea

A. Masalaite, A. Garbaras and V. Remeikis
Center for Physical Sciences and Technology, Vilnius, LT-02300, Lithuania
Keywords: size segregated aerosol particles, carbon isotopic ratio
Presenting author email: agne.masalaite@ftmc.lt

Marine aerosol contributes significantly to the global aerosol load and consequently has an important impact on both the Earth's albedo and climate (O'Dowd, 2004).

The aim of this work was to identify size segregated aerosol particles origin using the carbon stable isotopes method.

Experimental

The aerosol samples were collected at the Air pollution research station in Preila (55°55′N, 21°00′E, 5 m above sea level) which is located in western Lithuania on the coast of the Baltic Sea, on the Curonian Spit from 26 November 2012 to 12 January 2013 and in Baltic Sea during the cruise with the R/W "Oceania" on 09 – 17 November 2012. The nearest source of anthropogenic pollution, the Klaipeda city, is at the 50 km distance. Thus, carbonaceous atmospheric aerosols were transported to the Preila site by continental and marine air masses. A Micro-Orifice Uniform Deposition Impactor "MOUDI 110" was used to collect samples in size intervals ranging from 18 μm to 0.056 μm. Aluminium foils of 47mm diameter (pre-fired for 5 h at 600^0C) were used. A total of 7 collections in Preila and 2 collections in Baltic Sea were done. In addition, the low volume PM_1 sampler was used. As the main aim of the study was to identify the origin of incoming carbonaceous aerosols, the HYSPLIT air mass backward trajectory model was used for the analysis of results (Draxler, 2003).

Total carbon isotopic ratios ($\delta^{13}C$) were measured at each stage of MOUDI and at quartz fibre filters of PM_1 using the elemental analyzer (FlashEA 1112) connected to the stable isotope ratio mass spectrometer (ThermoFinnigan Delta Plus Advantage). Simultaneously the carbon amount at each stage was measured using the elemental analyzer with a thermal conductivity detector (Garbaras, 2008). The 1/4th part of the foil/ quartz fibre filter was placed into the tin capsule and combusted in the oxidation furnace at the temperature of 1020º C and with the oxygen excess. Carbon of the sample oxidized into CO_2 gas, which passed to the mass spectrometer ionization cell through the gas distribution device ConFlow III.

Results

During the experiment the aerosol carbon isotopic ratio variation between accumulation and coarse modes in Preila ranged from -24.3 ‰ to -29.3 ‰ and in Baltic Sea from -24.7 ‰ to -28.2 ‰. It implies that in both cases the carbonaceous particles in the same size range were from almost the same sources. The $\delta^{13}C$ values for the aerosol particles PM_1 transported from longer distances depended on the air mass transport directions. Air mass transports during the Preila experiment were few characters. At first it was mainly from West and Southwest - more from the continent (United Kingdom, Germany, Denmark, Belgium, Netherland, Poland, and Russia) in such transport scenario the main source of carbonaceous aerosols in accumulation mode could be transport emissions and coal burning, moreover average of carbon isotopic ratio for accumulation mode was -28.1‰. However after ten days when it was from West and one episode was purely from Russia, Sweden and Norway the average $\delta^{13}C$ = -26.2‰.. The last episode was from South with the average $\delta^{13}C$ = -26.5‰. All these air mass transports changes have a good agreement with aerosol carbon isotopic ratio taking into account influence of coal burning, transport emissions and marine aerosol.

Results from Baltic Sea (Fig.1) demonstrate a good agreement of MOUDI and PM_1.

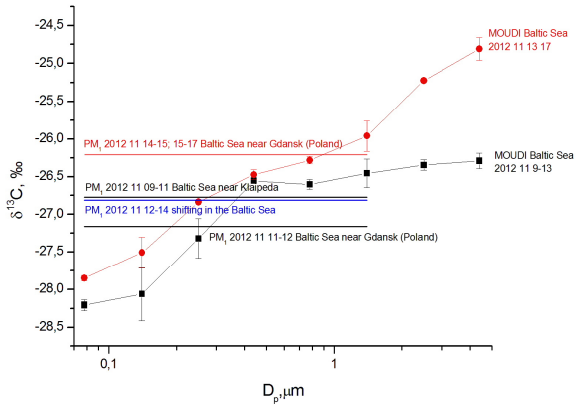

Figure 1. Experimental data from Baltic Sea.

Postdoctoral fellowship is funded by the European Union Structural Funds Project Postdoctoral Fellowship Implementation in Lithuania.

Draxler, R.R. and Rolph, G.D. (2003) HYSPLIT (Hybrid Single-Particle Lagrangian Integrated Trajectory) Model access via NOAA ARL READY Website (http://arl.noaa.gov/ready/hysplit4.html) (NOAA Air Resources Laboratory, Silver Spring, MD.

Garbaras, A., Andriejauskiene, J., Bariseviciute, R. and Remeikis V. (2008) *Lithuanian J. Phys.* **48**, 259–264.

O'Dowd, C.D., Facchini, M.C., Cavalli, F., Ceburnis, D., Mircea, M., Decesari, S., Fuzzi, S., Yoon, Y.J., and Putaud, J-P. (2004) *Nature* **431**, 676-680.

Size distribution of airborne Uranium and Thorium-labelled aerosols near a UF4 processing plant

O. Masson[1], G Videau[2], X. Cagnat[3]
[1] Nuclear Safety and Radioprotection Institute, IRSN, bât 153, 13115 St Paul lez Durance, France
[2] AREVA NC – COMURHEX, Usine de Malvesi - BP 222 - 11102 Narbonne Cedex, France
[3] Nuclear Safety and Radioprotection Institute, IRSN, bât. 501, Bois des Rames, 91400 Orsay, France

Keywords: Size distribution, uranium, thorium.
Presenting author email: olivier.masson@irsn.fr

Uranium and thorium-labelled aerosols are emitted by the stack of a UF_4 processing plant. Labelled-aerosols may also come from resuspension of soils particles from the surrounding environment and from areas devoted to the storage of waste. At 1.1 km from the plant stack, a size distribution study of aerosol carriers of the radionuclides of interest was conducted. This was performed during two distinct periods: one when the facility shut down for servicing (no atmospheric release) and the other when the facility was in operation. These trials were conducted using simultaneously six High Volume Impactors (HVI, Tisch TE-235) having 5+1 stages. Each sampling lasted two weeks at a flow rate of ~70 m^3/h per impactor and thus an overall flow rate of around 430 m^3/h. Thanks to the elevated air volume sampled (~ 92000 m^3) and very sensitive measurements, activity levels of thorium-234 (^{234}Th) of the ^{238}U decay series were quantified for each stage at some µBq/m^3 corresponding to a cumulative airborne activity of about 15 µBq/m^3 during the shutdown period. (Fig. 1).

Airborne activity levels are on average 5 times higher during operation of the facility except for the finest fraction that remains poorly affected by the releases. During the shutdown period, activity higher levels onto coarse particles can be explained by resuspension of former deposit onto soils. The corresponding Activity Median Aerodynamic Diameter (AMAD) and respective Geometric Standard Deviation (GSD) are listed in Table 1. The presented values are within the range of those compiled by Dorrian and Bailey (1997) but significantly lower than the default AMAD value (5µm) used for occupational exposures (ICPR 66) or those found in the fluoridation and precipitation workplaces of this facility (5.1 and 6.4 µm, respectively; Ansoborlo et al., (2001). The larger AMAD during operation is due to the release of coarse particles from the stack. Some of them remain suspended at 1.1 km. Regardless of the dust concentration, particles having the higher ^{234}Th load are within the [0.95-1.5µm[size range (Fig. 2).

	AMAD (µBq/m^3)	GSD (µBq/m^3)
Shutdown	0.84	17.0
Operation	1.6	4.7

Table 1. AMAD and GSD for ^{234}Th between shutdown and operation conditions

Compared to the typical weighted activity found in the uranium concentrate (yellow-cake), the weighted activity of the aerosols are ~ 4500 times lower.

Such information is useful to strikes and validate environmental dispersion/deposition model at short distance scale. Further investigations on the finest fraction are required to precise the contribution of the particle that enter deeply into the lungs.

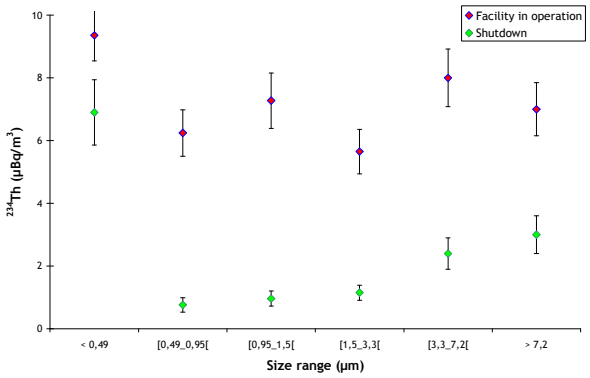

Figure 1. Size distribution of ^{234}Th aerosol carriers

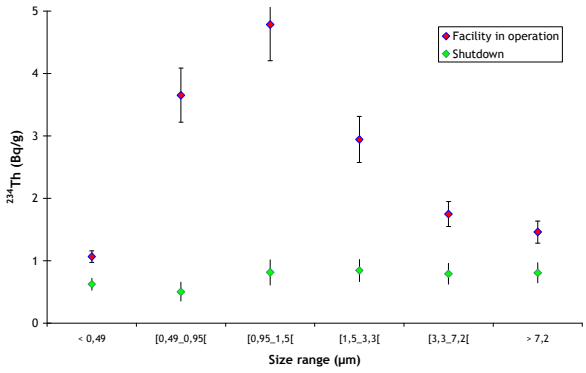

Figure 2. Size distribution of the weighted ^{234}Th

This work was supported by AREVA NC and IRSN.

Dorrian, M.D. and Bailey, M.R. (1997). Radiation Protection Dosimetry.Vol. 60, 2, 1995, 119-133.

International Commission on Radiological Protection. *Human respiratory tract model for radiological protection*. Oxford: Elsevier Science Ltd.; Ann. ICRP 24(1–4): Publication 66;1994a.

Ansoborlo et al., (2001) Health Physics, Vol. 82, 3, 2002, 279-289.

Comparison of Aerosol Time of Flight Mass Spectrometer (ATOFMS) measurements with off-line techniques for determining metal concentration in atmospheric particles

Eoin McGillicuddy [1], Robert Healy [1], Manuel Dall'Osto [2], Jean Sciare [3], Franco Lucarelli [4], Silvia Nava [5], Xavier Querol [2], Ian O'Connor [1], Deborah Gross [5], John Wenger [1], John Sodeau [1].

[1] Department of Chemistry and Environmental Research Institute, University College Cork, Ireland
[2]Institute for Environmental Assessment and Water Research (IDAEA-CSIC), Barcelona, Spain
[3] LSCE, Laboratoire des Sciences du Climat et de l'Environnement, CEA-CNRS-UVSQ, Gif-sur-Yvette, France
[4] Dipartimento di Fisica e Scienze dello Spazio, Universita degli Studi di Firenze, Via Sansone 1, 50019 Sesto Fiorentino, Italy
[5] INFN, Istituto Nazionale di Fisica Nucleare, Sezione di Firenze, Via Sansone 1, 50019 Sesto Fiorentino,Italy
[6] Department of Chemistry, Carleton College, 1 N. College Street, Northfield, MN 55057, USA

Keywords: ATOFMS, Aerosol Mass Spectrometry, Off-line, Metals.
Presenting author email: e.j.mcgillicuddy@mars.ucc.ie

Metals present in atmospheric particulate matter are associated with both natural and anthropogenic processes. Natural sources of metals in the atmosphere include volcanic activity and wind-blown dust, while anthropogenic sources include industrial processes, traffic emissions, incineration and fossil fuel combustion (Allen, Nemitz et al. 2001). The presence of certain metals in the atmosphere is of interest due to associated health effects.

The concentration of metals in atmospheric aerosols is traditionally measured using off-line techniques with particles being collected onto a substrate which is later analysed using techniques such as ICP-MS (Inductively Coupled Plasma - Mass Spectrometry), XRF (X-Ray Fluorescence) and IC (Ion Chromatography). These methods can quantitatively determine the metal component of particulate matter, but typically suffer from poor time resolution. This can lead to short-lived events being missed. More recent techniques such as PIXE (Particle induced X-ray Emission) allow samples to be analysed with an hourly temporal resolution (Chiari, Lucarelli et al. 2005). However, none of these off-line techniques can provide information on the mixing state of metals in the particles, which is useful for identification of their sources.

The interest in measuring the mixing state of individual aerosol particles has led to the development of single particle mass spectrometers. One such single particle instrument is the Aerosol Time of Flight Mass Spectrometer (ATOFMS), which provides size resolved single particle dual ion mass spectra of particles in the size range 100 nm to 3000 nm. This allows the characterisation of the primary composition of single particles (e.g. elemental/organic carbon and transition metals) along with the determination of secondary species present in the particle (such as nitrate and sulfate ions).

The ability of the ATOFMS to determine the presence of metals in ambient particles was utilised during several sampling campaigns to determine if ATOFMS can be used to measure metal concentrations in real-time. The comparisons were made during campaigns held in Cork (Ireland), Paris (France) and Barcelona (Spain). The ATOFMS ion signals for the metals of interest were compared with measurements made using IC, PILS-IC and PIXE.

Several comparisons between the ATOFMS ion signal and the quantitative techniques provided poor correlations, with the ATOFMS ion signal intensity not being proportional to the ambient concentration. The reason for the poor correlations with the quantitative techniques may be due to the matrix effects associated with the mixing state of the particle being sampled. The mixing state can affect the ionisation of the metal in sampling with the ATOFMS. The strongest correlations were found for comparisons between the ATOFMS and PIXE measurements for several metals including Al, Fe, Zn, Mn and Pb. Fig. 1 shows the correlation between ATOFMS and PIXE measurements for aluminium. The improved correlations for these metals is likely due to them having a specific source, with several of the metals such as Pb, Zn and Mn also occurring in short sharp peaks in concentration these factors may result in the ATOFMS ion signal responding to changes in concentration in a more proportional fashion.

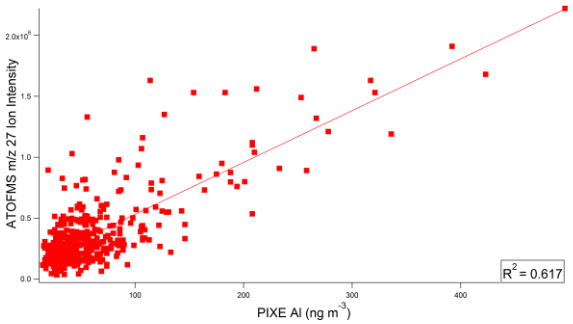

Fig. 1. Correlations between ATOFMS ion intensity (m/z 27) and PIXE mass concentrations for aluminium.

Allen, A. G., E. Nemitz, et al. (2001). "Size distributions of trace metals in atmospheric aerosols in the United Kingdom." Atmospheric Environment **35**(27): 4581-4591.

Chiari, M., F. Lucarelli, et al. (2005). "Characterization of airborne particulate matter in an industrial district near Florence by PIXE and PESA." X-Ray Spectrometry **34**(4): 323-329.

Levels of polybrominated diphenyl ethers in the ambient air of automobile dismantling plants from southern Taiwan

S.I. Shih[1], H.R. Chao[2], W.K. Wu[2], Y.Y. Guo[2], B.A. Jiang[2], C.Y. Chen[2], Y.M. Kuo[3] and C.H. Tsai[4]

[1]Department of Environmental Engineering, Kun Shan University, Yung Kang District, Tainan, 71003, Taiwan
[2]Department of Environmental Science and Engineering, National Pingtung University of Science and Technology, Neipu Township, Pingtung County, 91201, Taiwan
[3]Department of Safety Health and Environmental Engineering, Chung Hwa University of Medical Technology, Rende District, Tainan, 71703, Taiwan
[4]Department of Chemical and Materials Engineering, National Kaohsiung University of Applied Technology, SanMing District, Kaohsiung City, 80778, Taiwan
Keywords: PBDEs, dismantling, indoor, outdoor.
Presenting author email: ssi10@mail.ksu.edu.tw

As a class of brominated fire retardants (BFRs), polybrominated diphenyl ethers (PBDEs) are only used to decrease the flammability of consumer products including electronics (e.g. air conditioner, TV sets, and cellular phones), automobiles, furniture, and electrical wirings and textile application (Alaee *et al.*, 2003). PBDE contamination has been raising the global concern due to their lipophilicity, persistence, and bioaccumulation. PBDEs are ubiquitously existed in indoor environment due to their persistence and the widespread use in consumer products. Therefore, PBDEs have been recognized as the significant persistent pollutants of the indoor environment in recent years.

Since PBDEs are highly lipophilic and can accumulate in human fatty tissues, they have been investigated in most human tissues including breast milk (Chao *et al.*, 2007), cord blood (Lin *et al.*, 2011), venous blood (Lim *et al.*, 2008), placenta (Gómara *et al.*, 2007), and adipose tissue (Petreas *et al.*, 2010). PBDE levels in blood from workers of e-waste dismantling plants were significantly higher than those from computer clerks and hospital cleaners (Sjödin *et al.*, 1999). The recent report indicated that emission levels of predominant PBDE congeners (i.e. BDE-209) from indoor air to outdoors were roughly accounted for 90% of total PBDE emissions to outdoor air in Sweden, indicating that contaminated indoor air is an important source of PBDE contamination to outdoor air (Björklund *et al.*, 2012). Recently, PBDEs in car dust was found (Kalachova *et al.*, 2012). Little is known about PBDEs in indoor and outdoor air from automobile dismantling plant.

In this study, three automobile dismantling plants were selected in southern Taiwan to be investigated in 2012/10 and 2013/1. Indoor air in dismantling plants and ambient air nearby the corresponding plants was simultaneously sampled by high-volume PS-1 air samplers for 48 h. Air samples in on-duty and off-duty time were separately collected. $^{13}C_{12}$-labeled PBDEs were added into the samples before the extraction. The extract was cleaned up as follows. After the extraction, gas and particle phase was combined together. The first cleanup involved treatment with concentrated sulfuric acid. The next cleanup procedure involved a multi-layered silica column. The final cleanup procedure involved an acid alumina column. The eluate was collected, concentrated to near dryness by using N_2, and then transferred to a vial. A total of 50 μl of ^{13}C-labeled BDE-139 was added to a vial containing the eluate as an internal standard after the clean-up prior to injection. The final extract was reduced in volume to 0.2 mL under a stream of nitrogen. Fourteen PBDEs (BDE-28, 47, 49, 99, 100, 153, 154, 183, 196, 197, 203, 207, 208, and 209) were analyzed by high resolution gas chromatograph with high resolution mass spectrometry.

Levels of Σ_{14}PBDEs were 1200-8750 pg/m^3 in indoor air from automobile dismantling plants and 254-2740 pg/m^3 in the ambient air from corresponding plants, respectively. BDE-209 was the predominant congener consisting for 63-86% of the total in indoor and outdoor air. Although PBDEs in indoor air was higher than that in outdoor from dismantlers, no statistically significant differences were found for individual PBDE levels in paired of indoor and outdoor air samples, indicating that air PBDE levels in indoor and outdoor were not different.

This work was supported by the National Science Council, Taiwan under grant NSC 101-2221-E-168-026.

Alaee, M., Arias, P., Sjödin, A., Bergman, A. (2003) *Environ. Int.* **29**, 683-689.

Björklund, J.A., Thuresson, K., Palm Cousins, A., Sellström, U., Emenius, G., de Wit, C.A. (2012) *Environ Sci Technol*. **46**, 5876-5884.

Chao, H.R., Wang, S.L., L ee, W.J., Wang, Y.F., Papke, O. (2007) *Environ. Int.* **33**, 239-245.

Gómara, B., Herrero, L., Ramos, J.J., Mateo, J.R., Fernández, M.A., García, J.F., González, M.J. (2007) *Environ. Sci. Technol*. **41**, 6961-6968.

Kalachova, K., Hradkova, P., Lankova, D., Hajslova, J., Pulkrabova, J. (2012) *Sci. Total Environ*. **441**, 182-193.

Lim, J.S., Lee, D.H., Jacobs, D.R. Jr. (2008) *Diabetes Care* **31**, 1802-1807.

Lin, S.M., Chen, F.A., Huang, Y.F., Hsing, L.L., Chen, L.L., Wu, L.S., Liu, T.S., Chang-Chien, G.P., Chen, K.C., Chao, H.R. (2011) *Int. J. Hyg. Environ. Health* **214**, 115-120.

Petreas M., Nelson D., Brown F.R., Goldberg D., Hurley S., Reynolds P. (2010) *Environ. Int.* **37**, 190-197.

Sjödin, A., Hagmar, L., Klasson-Wehler, E., Kronholm-Diab, K., Jakobsson, E., Bergman, A. (1999) *Environ. Health Perspect*. **107**, 643-648.

Rotational Spectra and *ab initio* modeling of dicarboxylic acids: Succinic Acid

Estíbaliz Méndez[1], Patricia Écija[1], Emilio J. Cocinero[1], Fernando Castaño[1], Francisco J. Basterretxea[1], Peter D. Godfrey[2], Don McNaughton[2], Michaela K. Jahn[3], K. P. Rajappan Nair[3], Jens-Uwe Grabow[3].

[1]*Department of Physical Chemistry, University of The Basque Country UPV/EHU, Leioa, Biscay, 48940, Spain*
[2]*School of Chemistry, Box 23 Victoria 3800 Monash University, Australia*
[3]*Institut für Physikalische Chemie & Elektrochemie, Gottfried-Wilhelm-Leibniz-Universität, 30167 Hannover, Germany*

Keywords: New particle formation, Microwave spectroscopy, Succinic Acid, Sulfuric Acid
Presenting author email: estibaliz.mendez@ehu.es

Atmospheric aerosols affect terrestrial visibility by absorbing and reflecting incoming solar radiation, and they also influence climate and alter human health. Aerosols can be directly emitted from natural and anthropogenic sources or formed directly in the atmosphere through nucleation from gas phase species. New particle formation events have been observed frequently and worldwide but it is not fully understood how particles form at molecular level, creating one of the largest sources of uncertainty in atmospheric models and climate predictions (Zhang, 2010).

Several mechanisms have been proposed to explain nucleation events in the continental troposphere, including binary H_2SO_4/H_2O and ternary $H_2SO_4/H_2O/NH_3$ nucleation, ion-mediated nucleation, and nucleation enhanced by organic compounds (Metzger et al., 2010). In particular, dicarboxylic acids present in the troposphere have been proposed as favorable candidates to enhance the formation of the critical nucleus, as one of their carboxylic groups would be strongly hydrogen-bonded to H_2SO_4, whereas the free –COOH group would allow the growth of the complex until an aerosol particle is formed (Xu and Zhang, 2010; Gao-Lei Hou et al., 2013).

As a first step in exploring the configuration of the critical nucleus, we have conducted a rotational spectroscopic study of succinic acid (SA), which is a relatively simple dicarboxylic acid that has been detected in the troposphere. Rotational spectroscopy provides the most accurate vision of the molecular structure through precise moments of inertia.

In this work, we have applied the technique of Fourier Transform Microwave Spectroscopy (FTMW) in a supersonic jet, which is a high sensitivity and resolution technique. Expansion of a gaseous sample in a supersonic jet allows rapid cooling of the sample to only a few Kelvin so most molecules relax to the lowest ro-vibrational energy levels. SA was vaporized by UV ultrafast laser ablation avoiding any decomposition of the sample via heating conventional methods (Cocinero et al., 2012). The vaporized sample was seeded into an expanding stream of Ne forming a supersonic jet, where the molecules were probed by time-domain rotational spectroscopy. The experimental study was supplemented by *ab initio* (MP2) and DFT (M062X and B3LYP) calculations describing the conformational landscape and rotational parameters.

The rotational spectrum detected the presence of a single most stable conformation, for which accurate rotational and centrifugal distortion parameters have been determined. The rotational parameters were found in good agreement with the predictions for the predicted global minimum. The study was extended to all monosubstituted isotopic species (^{13}C, ^{18}O, D(O)), which were positively identified, leading to an accurate determination of the effective and substitution structures of the molecule, and hence, we were able to accurately determine all bond lengths, valence and dihedrals angles.

The next step of this study will be to detect intermolecular complexes formed by succinic acid and sulfuric acid. The ultimate goal is to provide experimental microscopic evidence of the geometric arrangement and energetic stability of a feasible critical nucleus to account for new particle formation in the atmosphere.

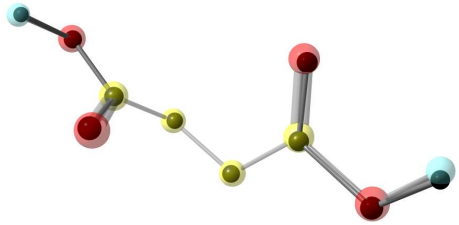

Figure 1: A comparison of the substitution and *ab initio* structures of SA. The full molecular structure is the theoretical structure. The smaller dark spheres are the experimental atom positions.

This work was supported by Ministerio de Ciencia e Innovación (Madrid, CGL2011-22441, CTQ2011-22923 and Consolider CSD-2007-00013), to Gobierno Vasco/Eusko Jaurlaritza (Vitoria-Gasteiz), (IT520-10), and UPV/EHU (UFI11/23 and general support). It was also supported by the Deutsche Forschungsgemeinschaft (DFG), the Land Niedersachsen, and the NCI Australia National Facility through the National Computational Merit Allocation Scheme for computational resources (DMcN, PDG).

Renyi Zhang (2010), *Science*, **328**, 1366-1367.
Axel Metzger et al. (2009), *Proceedings of the National Academy of Sciences*, **107,** 6646 - 6651.
Wen Xu and Renyi Zhang (2012), *The Journal of Physical Chemistry A*, **116**, 4539 – 4550.
Gao-Lei Hou et al. (2013), *The Journal of Physical Chemistry Letters*, **4**, 779 - 785.
Emilio J. Cocinero et al. (2012), *Angewandte Chemie International Edition,* **51,** 3119 – 3124.

The influence of the Sahara storm on the aerosol optical properties in Lithuania

G. Mordas, V. Ulevicius and N. Prokopciuk

Center for physical sciences and technology, Savanorių 231, LT-02300 Vilnius, Lithuania.
Keywords: Light scattering coefficient, number concentration, long range transport.
Presenting author email: genrik@ftmc.lt

Introduction

Atmospheric aerosol particles have direct and indirect effects on a human health, people life conditions and the global climate. The effects are dependent on aerosol particle physicochemical properties, which are formatted by natural and anthropogenic aerosol sources located in this region. In this study, we assembly ground based measurements, satellite measurements, a modelling of dust distribution and calculations of the backward trajectories with aim to show the effect of the far located (several thousand km) Sahara storm on the aerosol optical properties in Lithuania.

Methods

The ground-based measurements were performed in the in Vilnius city (54°38'36", 25°10'58") during July 2012. They give insights into the physical and optical properties of the urban aerosols measuring the aerosol scattering coefficient with the particle size distribution. The aerosol scattering coefficient was measured with the integrating nephelometer TSI 3563 at three wavelength λ=450, 550 and 700 nm. Measurements of the particle number concentration (D_{pa}>0.5µm) and the particle size distribution in the range from 0.5 to 10.0 µm was performed by aerodynamic particle sizer TSI 3321. The ground based measurements was reached by analyse of the air mass backward trajectories HYSPLIT4. That allows selecting the air masses by sectors, which have characterised properties of the aerosol particles. Helpful, it was an investigation of the regional dust distribution by Met Office Unified Model. The Met Office provides quantitative SEVIRI satellite retrievals of the aerosol optical depths (AOD) at 550 nm.

Results

The analyse of the air mass backward trajectories allowed dividing measurement period on several episodes. From 1 to 8 of July, the South-West sector (Mediterranean see, North Africa was dominated. The West sector (Atlantic Ocean, Great Britain, Norway) was observed at 9-24 of July. From 25 to 31, there were continental air mass from Ukraine and Russia. The significant differences were measured in the aerosol particle scattering coefficient and the particle number concentration (D_{pa}>0.5µm). The cleanest air mass came from West sector. The South-West sector was characterised the highest values of the particle number concentration (D_{pa}>0.5µm) and the aerosol scattering coefficient. So, the scattering coefficient was varied from 3.5 to 369 Mm^{-1} during measured period. The clean air mass from Atlantic Ocean had averaged scanning coefficient of 10 Mm^{-1} comparing with 70 Mm^{-1} from Mediterranean see. The highest pick was 369 Mm^{-1} at 3 of July. The averaged Angstram exponent for 450/700nm wavelength pair was 2.0. That is typical for aerosols affected by urban (Vrekoussis *et al.*, 2005). However, the Angstram coefficient decreased rapidly at 3 of July, it was 1.4, when the value of the aerosol scattering coefficient and the particle number concentration (D_{pa}>0.5µm) had the highest values (Fig.1) The calculation of the backward trajectories showed that the air masses came from the Nord Africa. In the Sahara desert, it was a storm during several days. The regional dust distribution based on the AOD measurements and dust transport were modeled. The results showed the invasion of the dust polluted air mass from Sahara on the Baltic region (Fig.2). Additionally, the chemical composition of a precipitation indicates increase in calcium which air masses brought from the region of North Africa.

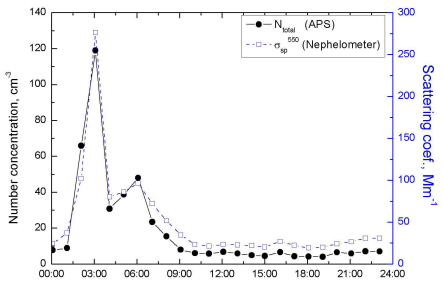

Fig.1. Aerosol scattering coefficient and particle number concentration (D_{pa}>0.5µm) during 3 of July.

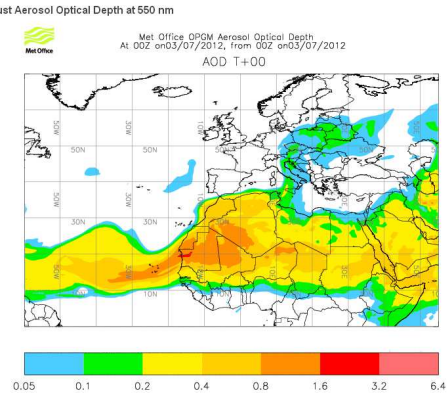

Fig.2. The AOD regional distribution.

This work was supported by the Lithuanian-Swiss cooperation programme "Research and Developing" project AEROLIT (Nr. CH-3-ŠMM-01/08).

Vrekoussis M., Liakakou E., Kocak M., Kubilay N., Oikonomou K., Sciare J., Mihalopoulos N. (2005). *Atm. Env.* **39**, 7083–7094

Measurements of the aerosol particle physical properties and particle chemical composition in Vilnius city

G. Mordas, V. Ulevicius, I. Garbariene and K. Kvietkus

Center for physical sciences and technology, Savanorių 231, LT-02300 Vilnius, Lithuania.
Keywords: Chemical composition, size distribution, light scattering coefficient.
Presenting author email: genrik@ftmc.lt

The investigation of the atmospheric aerosols physical properties and the particle chemical composition allow understanding the aerosol particle dynamical processes in the atmosphere, finding danger pollution sources and solving important problems for human health, live conditions and climate. In this work, we concentrated on a study of the atmospheric aerosols in the urban environment of Vilnius city. The study gives insights into the aerosol chemical composition, particle optical and physical properties measuring the chemical composition of the non-refractory fraction of submicron aerosol particles, the light scattering coefficient and the particle size distribution. The measurements were reached by modelling of the backward trajectories of the coming air mass and calculations of the aerosol optical depths.

The aerosol chemical composition was measured by Quadrupole Aerosol Mass Spectrometer (Q-AMS). The light scattering coefficient was examined for the wavelength of 450, 550 and 700 nm using the integrating nephelometer TSI3563. The aerosol particle size distribution was measured with scanning mobility particle sizer TSI3936 and with the aerodynamical particle sizer TSI3321. Thus, the range of the measured particle size distribution was from 3 nm to 10 µm. The bottom range was determined by detection efficiency of the used condensation particle counter TSI3076 and particle diffusion losses in the sampling line. The upper limit is affected by geometry of the used sampling system and ambient conditions. The ambient conditions were measured at 10 m height meteorological station. In the macro scale, the coming air masses were characterised by HYSPLIT 4. A model of Navy Aerosol Analysis and Prediction System gives information about aerosol optical depths measured by MODIS satellite and regional dust and sulfate distributions.

The particle chemical composition (organic matter, sulfate, nitrate and ammonium) of the non-refractory fraction of submicron aerosol particles (D_{va}<1µm) were investigated during spring. The typical measured particle chemical composition is presented in Fig. 1. It shows that the organic matter comprised the largest fraction (74%) of the non-refractory fraction of submicron aerosol particles, while sulfate, nitrate and ammonium made up 14%, 8% and 4%. The average concentrations of organic matter, sulfate, nitrate and ammonium were 7.40, 1.36, 0.76, 0.39 µg m^{-3}, respectively. The average mode diameter of the organic matter and nitrate was 300 nm. However, the sulfate had a characterized mode diameter of 400 nm. The typical particle size distribution is presented in the Fig. 2. It illustrates the increasing of the total particle number concentration affected by production of the primary and secondary aerosol particles of nucleation and Aitken modes. The primary organic particles detected in the urban environment are manly directly emitted from local combustion sources: light and heavy vehicles, house heating and industry. The emitted particles are modified immediately by various atmospheric oxidants. As result, the physicochemical properties (size, scattering coefficient and particle chemical composition) changed a lot comparing to their precursor primary particles (Donahue et al., 2009). The secondary organic particles are formed from the reactions of the volatile organic compounds affected by meteorological conditions. Thus, the assembly of different processes: primary aerosol particle emissions, secondary particle formations with continuous particle growth, the effect of the far located pollution sources on the regional environment, were investigated in our study.

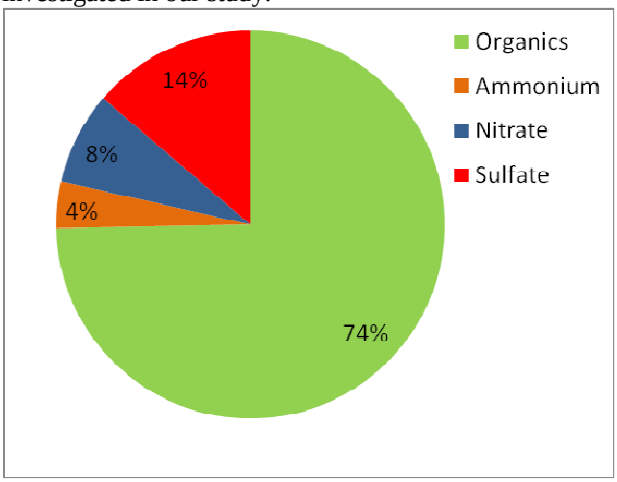

Fig. 1. The typical particle chemical composition in Vilnius city during spring.

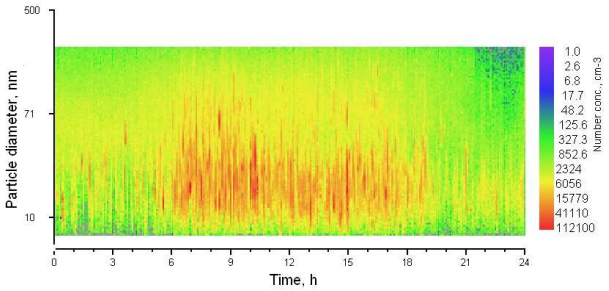

Fig. 2. The typical particle size distribution in Vilnius.

This work was supported by Lithuanian-Swiss cooperation programme “Research and developing” project AEROLIT (Nr. CH-3- ŠMM-01/08).

Donahuea N.M., Robinsona A.L., Pandis S.N. (2009) *Atm.Env.***43(1)**, 94-106.

Exploring the effect of deep-convective cloud systems on particle mass and number: source or sink?

B.N. Murphy[1, 2], I. Riipinen[2], and A. M. L. Ekman[1]

[1]Department of Meteorology, Stockholm University, Stockholm, 10691, Sweden
[2]Department of Applied Environmental Engineering, Stockholm University, Stockholm, 11148, Sweden
Keywords: cloud-aerosol interactions, nucleation, organic aerosol, aqueous-phase chemistry
Presenting author email: Benjamin.murphy@itm.su.se

Incomplete knowledge of aerosol-cloud interactions contributes significant uncertainty to the understanding of the Earth's climate sensitivity, and thus to the large-scale theoretical models used to predict future climate properties. The total number, size, and composition of an aerosol population entrained into a cloud system can affect cloud physical features (e.g. updraft velocity or precipitation rate) while cloud properties can affect features of the aerosol population (e.g. through wet scavenging efficiency or aqueous-phase chemical processing) (Yin *et al.*, 2005; Ekman *et al.*, 2006). This tightly-coupled system exhibits complicated feedbacks that are hard to discern in a theoretical model without faithfully representing the detailed transport, microphysical and chemical processes taking place. We present a new three-dimensional cloud-resolving model, CRM-ORG, which accounts for the processing of inorganic and organic aerosol components in a fully-coupled, dynamic simulation. We apply this model to a case study of a deep convective cloud under clean conditions above the tropical Amazon, and use it to elucidate the net influence of the cloud system on aerosol mass, number, and composition throughout the atmospheric column.

Following the Volatility Basis Set approach of Donahue *et al.* (2006), the CRM-ORG model incorporates a suite of lumped species to describe the oxidation products of isoprene and monoterpene compounds across a spectrum of volatility. The mass transfer of these species to/from particles and cloud drops is treated dynamically along with explicit representation of aqueous-phase chemical reactions relevant to the production of low-volatility organic compounds that partition significantly to the particulate phase after cloud drop evaporation. The model also accounts for particle nucleation and growth due to condensation of inorganic as well as organic vapors, and this work probes the sensitivity of the model's results to both the formulation of the nucleation mechanism and the volatility of condensable organic vapors.

The detailed considerations of organic aerosol formation and growth are implemented into the three-dimensional cloud-resolving model described by Wang *et al.* (1993) and Ekman *et al.* (2006). This elastic, non-hydrostatic model solves prognostic equations for momentum, air mass density, ice-liquid potential temperature, water vapor and four hydrometeor types. The model then considers chemical species in the gas, particulate and aqueous phases in addition to species adsorbed onto solid water particles. The sulfate and organic aerosol species are represented with three internally-mixed modes (one each in the nucleation, Aitken and accumulation size ranges). Important aerosol microphysical processes, such as coagulation and condensation, are considered in the model.

We compare the predicted aerosol and cloud properties from CRM-ORG to airborne measurements made during actual deep convective events in the Amazon. These observational constraints will gives us confidence in the ability of the model to faithfully represent the complex effects of clouds on aerosol mass and number in the tropical environment. In order to gain a more general understanding of these interactions, we report the net effect of cloud processing on aerosol mass and number at various altitudes throughout the column. Of particular focus is the generation of new particles in the relatively clean background environment of the upper troposphere where substantial amounts of trace gases and particles are injected within the cloud outflow.

Several other models have explored the effects and feedbacks between organic aerosols and clouds in adiabatic parcel or two-dimensional models (Ervens *et al.*, 2005; Yin *et al.*, 2005). These studies opted to consider more detailed representations of chemistry or spectrally-resolved microphysics while sacrificing an atmospherically relevant description of transport. The configuration of CRM-ORG, on the other hand, achieves a realistic description of the spatial complexity of a deep convective system, while maintaining enough chemical and microphysical detail to explore aerosol-cloud interactions in depth. We compare our model's results and sensitivities to those of past studies to highlight the influence of model configuration.

This work is supported by the Marie Curie Fellowship awarded under the European Commission's People program (FP7).

Ervens, B., Feingold, G. and Kreidenweis, S. (2005) *Jour. Geophys. Res.* **110**, D18211.

Yin, Y., Carslaw, K. and Feingold, G. (2005) *Q. J. R. Meteorol. Soc.* **131**, 221-245.

Ekman, A.M.L., Wang, C., Ström, J. and Krejci, R. (2006) *J. Atmos. Sci.* **63**, 682-696.

Wang, C. and Chang, J. (1993) *Journ. Geophys. Res.* **98**, D8, 827-844.

Donahue, N.M., Robinson, A.L., Stanier, C.O. and Pandis, S.N. (2006) *Environ. Sci. Technol.* **40**, 2635-2643.

Total sulphate vs. sulphuric acid monomer in nucleation studies

K. Neitola[1], D. Brus[1, 2], U. Makkonen[1], M. Sipilä[3], T. Jokinen[3], R. L. Mauldin III[3, 4], K. Kyllönen[1], H. Lihavainen[1] and M. Kulmala[3]

[1]Finnish Meteorological Institute, Erik Palménin aukio 1, P.O. Box 503, 00100 Helsinki, Finland
[2]Laboratory of Aerosol Chemistry and Physics, Institute of Chemical Process Fundamentals Academy of Sciences of the Czech Republic, Rozvojová 135, 165 02 Prague 6,Czech Republic
[3]Department of Physical Sciences, University of Helsinki, P.O. Box 64, 00014 Helsinki, Finland
[4]Institute for Arctic and Alpine Research, University of Colorado, Boulder, CO 80309, USA
Keywords: nucleation, sulphuric acid.
Presenting author email: kimmo.neitola@fmi.fi

Exact determination of sulphuric acid concentration is crucial for predicting the nucleation rates and subsequent growth. In our study, we have noticed a discrepancy of about one to two orders of magnitude between sulphuric acid monomer and total sulphate concentrations measured from the same source of sulphuric acid vapour, with similar particle formation rates.

A thermally controlled saturator half filled with neat sulphuric acid (~97%) was used to produce the sulphuric acid vapour. The production method was first tested and then used in combination with a flow tube in a H_2O – H_2SO_4 nucleation experiment. Particle formation rates and size distributions were measured with several CPCs (TSI models 3776, 3025A and PSM) and with a DMPS system, respectively.

Sulphuric acid concentrations were detected with two independent methods. First, with two different mass spectrometers, CIMS (e.g. Eisele and Tanner, 1993) and CI-APi-TOF (Junninen et al., 2010). Second, with online ion chromatograph MARGA 2S ADI 2080 (ten Brink et al., 2007). MARGA was used also to detect background concentration of ammonia. Mass spectrometers were used to detect sulphuric acid monomer concentration, whereas MARGA measures the total sulphate concentration.

Results were compared to the previous measurements done in our laboratory (Brus et al., 2010), where a furnace was used as a source of sulphuric acid vapour and Bubblers were used to measure total sulphate concentration. Bubbler method is analogous to the MARGA with the difference that it is offline method. Results were also compared to the predicted values calculated using vapour pressure of sulphuric acid (Kulmala and Laaksonen 1990).

Figure 1 shows comparison of observed nucleation rates as a function of total sulphate or sulphuric acid monomer concentration between two different production methods and between two independent sulphuric acid detection methods. All results were obtained in similar conditions (RH 30%, T = 298K). Here one can observe that with similar nucleation rates and experimental conditions total sulphate and sulphuric acid monomer concentrations has a discrepancy of one to two orders of magnitude.

The discrepancy between the total sulphate and sulphuric acid monomer concentration cannot be explained by formation of larger clusters (dimer, trimer, etc.) as the concentration of dimer was always 1% or less of monomer concentration, with decreasing trend when moving to larger clusters. Losses of sulphuric acid to particles and to the walls were determined and it is shown that losses cannot explain the discrepancy either.

We suggest that the sulphuric acid is hidden into pool of clusters that are not detected by the particle counters nor identified from the mass spectra of CI-APi-TOF.

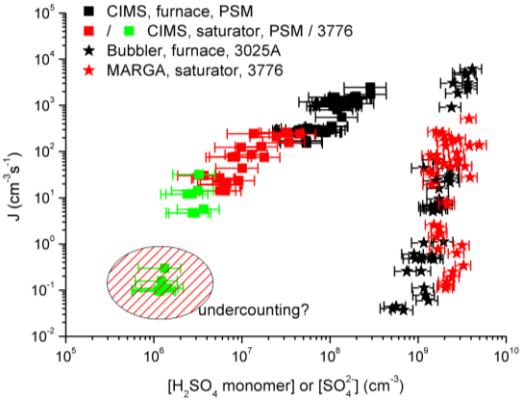

Figure 1. Comparison between our previous results and the results from this study from H_2O - H_2SO_4 nucleation experiment (Neitola et al., 2013).

This work was financially supported by the Finnish Academy Centre of Excellence program (project no. 1118615) and by the Maj and Tor Nessling Foundation.

Brus, D., Hyvärinen, A.-P., Viisanen, Y., Kulmala, M. and Lihavainen H. (2010) *Atmos. Chem. Phys.*, 10, 2631–2641.

Eisele, F. and Tanner, D. (1993) *J. Geophys. Res.*, 98, D5, 9001-9010.

Junninen, H., Ehn, M., Petäjä, T., Luosujärvi, L., Kotiaho, T., R. Kostiainen, R., Rohner, U., Gonin, M., Fuhrer, K., Kulmala, M. and Worsnop, D. (2010) *Atmos. Meas. Tech.*, 3, 1039–1053.

Kulmala M. and Laaksonen, A. (1990) *J. Chem. Phys.*, 93 (1), 1.

Neitola, K., Brus, D., Makkonen, U., Sipilä, M., Jokinen, T., Mauldin III, R. L., Kyllönen, K., Lihavainen, H. and Kulmala, M. (2013) *Atmos. Chem. Phys. Discuss.*, 13, 2313–2350.

ten Brink, H., Otjes, R., Jongejan, P. and Slanina S. (2006) *Atmos. Env.*, 41, 13, 2768-2779.

Air mass history on 1-year long new aerosol particle formation dataset in Budapest

Z.A. Németh and I. Salma

Institute of Chemistry, Eötvös University, H-1518 Budapest, P.O. Box 32, Hungary
Keywords: atmospheric nucleation, DMPS, backward trajectory.
Presenting author email: nemeth@caesar.elte.hu

As part of an urban aerosol research project, number size distributions of particles were measured at Lágymányos Campus of the Eötvös University, located in central Budapest, Hungary continuously between November 2008 and November 2009. The measurements were performed by a flow-switching type differential mobility particle sizer (DMPS) in the electric mobility diameter range of 6–1000 nm in 30 channels with a time resolution of ca. 10 min. Meteorological data were obtained from the Urban Climatological Station of the Hungarian Meteorological Service operated within the university campus.

The measurement days were classified on the basis of Dal Maso et al. (2005). For the 1-year period, there were 31 days that belonged to the nucleation event, class 1A (Salma et al., 2011). The start (t1) and end (t2) times of the beginning of the nucleation, and the end times of the condensational particle growth were determined from the contour plots by examining the changes in the channel contents and meteorological data (Kristensson et al., 2008). The times t1 and t2 were shifted by an interval that was needed for the particles to grow from 2 to 6 nm utilizing the actual growth rate between 2.0 and 13.3 nm/h.

Wind roses were constructed by taking the wind speed and wind direction data into consideration from t1−1 h to t1+6 h for the nucleation events, and for 0–24 h for the non-nucleation days. Wind speed varied from 0.15 to 13.2 m/s with a median of 2.7 m/s for the nucleation events. The prevailing wind direction was SE as shown in Figure 1.

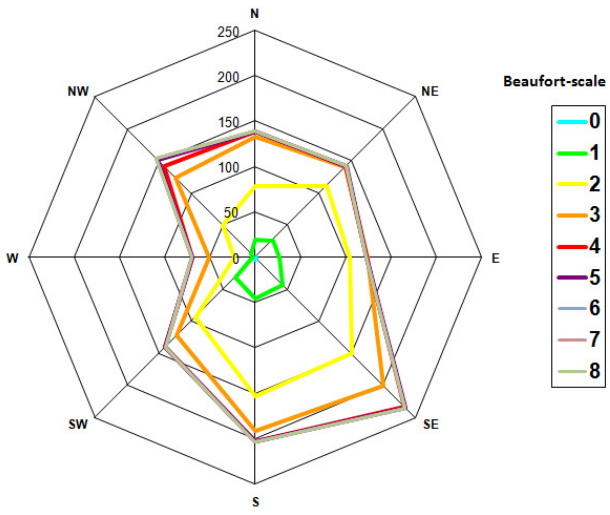

Figure 1. Wind rose for class 1A nucleation events.

For the non-nucleation days, the wind speed changed from 0.10 to 15.8 m/s with a median of 2.4 m/s, and the prevailing wind direction was NE. For the nucleation events, the range of the wind speed was smaller while the mean wind speed was somewhat larger than the non-nucleation days.

Air mass history was also investigated for class 1A nucleation events. Backward trajectories were calculated by the HYSPLIT code of the National Oceanic and Atmospheric Administration Air Resources Laboratory using meteorological data from the GDAS database (Draxler and Rolph, 2013). The trajectories arriving at the receptor site (47.474° N, 19.062° E) in a height of 200, 500, 2300 m above ground level were derived. The most distant (starting) point of the trajectories corresponded to the times when the particle growth was finished or by which the nucleation mode could be separated from the Aitken mode. The trajectories were calculated for every individual event with a resolution of 1 h to the ending time. The coordinates from the trajectories were plotted on a single geographical map. The plot revealed that the estimated horizontal dimension of the nucleating air mass extends far beyond the city, and that there are several distinct directions within the Carpathian basin where the nucleating air mass originates from. These directions were similar to the prevailing wind direction of the wind rose generated for the nucleation events.

Financial support of the Hungarian Scientific Research Fund (contract K84091) is appreciated.

Dal Maso, M., Kulmala, M., Riipinen, I., Wagner, R., Hussein, T., Aalto, P. P. and Lehtinen, K.E.J. (2005) *Boreal Environ. Res.* **10**, 323–336.

Draxler, R.R. and Rolph, G.D. (2013) HYSPLIT Model access via NOAA ARL READY Website (http://ready.arl.noaa.gov/HYSPLIT.php). NOAA Air Resources Laboratory, Silver Spring, MD.

Kristensson, A., Dal Maso, M., Swietlicki, E., Hussein, T., Zhou, J., Kerminen, V.-M. and Kulmala, M. (2008) *Tellus* **60B**, 330–344.

Salma, I., Borsós, T., Weidinger, T., Aalto, P., Hussein, T., Dal Maso, M. and Kulmala, M. (2011) *Atmos. Chem. Phys.* **11**, 1339–1353.

Comparison of particle concentrations obtained at urban and regional background environments

J.F. Nicolás[1], J. Crespo[1], E. Yubero[1], R. Soler[1]

[1]Atmospheric Pollution Laboratory, Miguel Hernández University, Avda. Universidad, 03202, Elche, Spain
Keywords: Particle concentration, Mountain station, Mineral dust, Urban aerosol.
Presenting author email: j.nicolas@umh.es

The study focuses on characterizing the particle number concentration registered at a regional background station (RS) and comparing it with the one obtained at an urban background site (US).

The stations are inside the province of Alicante in southeastern Spain. This region belongs to the Western Mediterranean Basin. RS (38°39´N; 0°16´W; 1558 m a.s.l) is located on top of a mountain range, in a military area (EVA nº 5) of the Ministry of Defence, 25 km from the Mediterranean coast. The station is located specifically at the named "Aitana peak". US (38°16´N; 0°41´W; 95 m a.s.l), is located in the city of Elche, 12 km from the coast. Specifically, the measurement site is placed on the roof of a building at the Miguel Hernández University, approximately 15 m a.g.l. The study period comprised from October 2011 to September 2012. The instruments used to measure particle concentrations were two optical counters. The instruments permit the determination of a fraction of fine mode (from 0.25 to 1 μm) and the coarse mode particles (size >1 μm).

Table 1 shows monthly and global average values of the coarse and fine particles at RS and US. Regarding the fine particle concentration at US (N_{FUS}), the winter and summer months were when the highest levels were registered. N_{FUS} obtained an absolute peak during August. The coarse particle concentration at US (N_{CUS}) showed a clear discontinuity between the colder months (November-March), with values below 0.15 cm^{-3}, and the warmer ones, in which the concentration became three times higher with a maximum in June (0.57 cm^{-3}).

Table 1. Monthly average values (cm^{-3}) of fine and coarse particles at RS and US.

Month	N_{FUS}	N_{FRS}	N_{CUS}	N_{CRS}
Oct-11	136.92	61.47	0.34	0.23
Nov-11	99.49	n.d	0.15	n.d
Dec-11	92.11	18.72	0.11	0.14
Jan-12	125.89	24.90	0.14	0.06
Feb-12	101.92	59.80	0.13	0.12
Mar-12	133.94	83.68	0.15	0.24
Apr-12	73.36	31.93	0.37	0.16
May-12	86.79	45.83	0.43	0.30
Jun-12	104.81	57.51	0.57	0.72
Jul-12	115.05	96.41	0.31	0.63
Ago-12	139.71	69.41	0.44	0.86
Sep-12	137.38	75.43	0.30	0.30
Annual	112.28	54.95	0.29	0.33

At RS, the fine particles showed a similar monthly tendency as the one seen at US. Fine particle concentration at RS (N_{FRS}) obtained maximum levels during the warmer period (from July to September). Although slightly lower than in summer, N_{FRS} showed high values during February and March as well. N_{FRS} made up between 20 and 85% of N_{FUS}. This percentage varies according to the season, with minimum values in January and February and maximum values in spring and summer. The annual average was: $N_{FRS}=0.5 \cdot N_{FUS}$. The coarse particle concentration at RS (N_{CRS}) was quite higher during summer than the rest of year. Standing out in a significant way as $N_{CRS}>N_{CUS}$ during summer-time. It is likely to due to between June and August the 55% of days were affected by Saharan dust outbreaks and these air mass entrances affected more at RS than at US. For this reason, N_{CRS} annual average value was slightly higher than N_{CUS} one.

In Fig. 1 we can compare the particle size distributions obtained at RS and US. The distributions are calculated for the colder (December-January and February) and warmer (June-July and August) months.

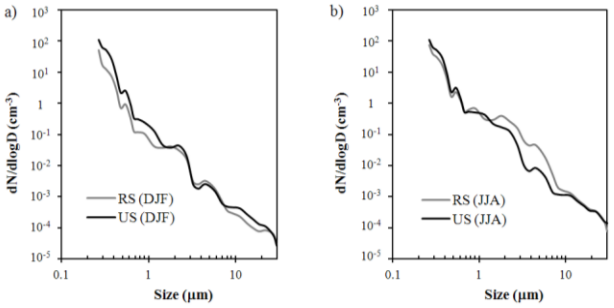

Figure 1. Average number size distributions obtained at RS and US during: a) cold months; b) warm months.

In general, the size distributions at both stations during the cold period (Fig. 1a) were quite similar, although the particle number concentration up to 2 μm registered at US was higher. In the warm months (Fig. 1b), we observe two differences with respect the distributions obtained in winter. First, the particle concentration difference in the accumulation mode particles between RS and US decreased, although the concentration at US remained slightly higher. On the other hand, the particle concentration in coarse mode up to 10 μm was higher at RS, establishing the major difference in the range 3-5 μm as a result of the significant impact of Saharan dust outbreaks at RS.

This work was supported by the Spanish Ministry of Science and Innovation under the CGL2009-08036 (PASSE) project and by the Spanish Ministry of Economy and Competitivity under the CGL2012-39623-C02-02 (PRISMA-AITANA) project. We would like to thank the military area (EVA nº 5) for its assistance in this work.

Enhancement of the collision efficiency between basidiospores and cloud droplets by electrostatic charges carried on freshly emitted basidiospores

M. Saar[1], M. Noppel[2] and J. Salm[2]

[1]Department of Botany, Institute of Agricultural and Environmental Sciences, Estonian University of Life Sciences, Tartu, 51014, Estonia
[2]Institute of Physics, University of Tartu, Tartu, 50090, Estonia
Keywords: bioaerosols, coagulation, ballistospore, washout.
Presenting author email: madis.noppel@ut.ee

In the coarse biogenic particles of the atmospheric aerosol, basidiospores are among the main fungal components (Fröhlich-Nowoiskya *et al.*, 2009). In bulk (about 20 000 species) of basidiomyceteous fungi, sexual spores expel themselves from their perches. Becoming airborne, these ballistic basidiospores (diameter 2−16 μm) carry an electrostatic charge (from tens to one thousand elementary charges) (Saar and Salm, 2013). Washout is one of mechanisms of sedimentation of fungal spores, but the role of basidiospore primary electric charges in this process is not yet studied. The effect of electric charges on collisions between water droplets or between water droplets and aerosol particles has been studied for a long time, up to the present time (Fletcher, 2012). In (Tripathi and Harrison, 2002), the considered ranges of the size and density of aerosol particles include those of basidiospores (Table 1). Based on this result, we evaluated the effect of charges for basidiospores of *Phellinus tremulae* and *P. nigricans*, members of the *P. igniarius* group, one of the most important wood-rotting fungi of many of deciduous trees.

These basidiospores are subglobose, smooth, with density of 1 g cm^{-3} or a bit more (1.2 g cm^{-3}), and represent the smallest and the biggest spores in the group. In *P. tremulae*, the mean equivalent diameter is 4.4 μm (99.7% of the variation of mean spore sizes is within the range of 3.9−4.7 μm) and the mean primary electric charge is 117 e (95% confidence intervals of mean spore charges is within the range of 46−222 e), and in *P. nigricans*, 6.1 μm (5.6−6.5 μm) and 204 e (107−496 e) (Saar, 2013). In the case of the droplet diameter D = 84 μm, the particle charge q enhances the collision efficiency if it has magnitude $|q|\geq 50$ e in particles of 4 μm or $|q|\geq 100$ e in particles of 6 μm. This shows, that in both *P. nigricans* and *P. tremulae* the primary charge enhances collision efficiency between basidiospores and cloud, fog or drizzle droplets of diameter about 80 μm.

Results of Tripathi and Harrison (2002) for the droplets D = 104 μm and the particles with density 2 g cm^{-3} show that the enhancement of collision between *P. nigricans* and *P. tremulae* spores and droplets may cease in the vicinity of D = 100 μm. Here as well as in the case of medium size cloud droplets the numerical calculation of particle's trajectories is needed to investigate collision efficiency.

Table 1. Collision efficiency for a droplet of diameter 84 μm and charged particles of 1 g cm^{-3} and 4−8 μm, expressed with respect to the collision efficiency in the case of neutral particles (0.00063 for d=4 μm, 0.0013 for d=5 μm, 0.0028 for d=6 μm, and 0.04 for d=8 μm).

Particle charge (e)	Particle diameter (μm)			
	4	5	6	8
10	1	1	1	1
20	1	1	1	1
50	1.4	1.2	1	1
100	2.4	1.5	1.1	1
500	28.6	11.5	5.0	1.1

The primary electrostatic charges of basidiospores could enhance the collision efficiency between spores and water droplets with D<100 μm not only near the ground, but also in the higher layers of the atmosphere. Due to the relaxation time of 23 minutes, highly charged spores can spread over a considerably area depending on the wind velocity (Saar and Salm, 2013).

This work was supported by the Doctoral School of Earth Sciences and Ecology created under the auspice of European Social Fund and, in part, by the Estonian Science Foundation through grant 8342.

Fletcher, N. (2012) Effect of electric charge on collisions between cloud droplets. *Journal of Applied Meteorology and Climatology*. Doi: 10.1175/JAMC-D-12-093.1. In press.

Fröhlich-Nowoiskya, J., Pickersgilla, D.A., Despresac, V.R., and Pöschl, U. (2009) *PNAS* **106**(31), 12814-12819.

Saar, M. (2013) Investigation of the electrostatic charge of basidiospores of the *Phellinus igniarius* group. *Central European Journal of Biology*. In press.

Saar, M. and Salm, J. (2013) Emission rate of charged spores in basidiomyceteous fungi and the relaxation time of their electric charges. *Aerobiologia*. Submitted

Tripathi, S.N. and Harrison, R.G. (2002) *Atmospheric Research* **62**, 57-70.

On the microphysical and optical aerosol properties during AMISOC-ARN campaign

M. Sorribas[1,2], C. Córdoba-Jabonero[3], H. Lyamani[1,2], G. Titos[1,2], J.A. Adame[3], R. Fraile[4], B.A. de la Morena[3], F.J. Olmo[1,2], L. Alados-Arboledas[1,2], O. Puentedura[3], and M. Gil[3]

[1]Centro Andaluz de Medio Ambiente, Universidad de Granada, Junta de Andalucía, Granada, 18006, Spain
[2]Department of Applied Physic, University of Granada, Granada, 18071, Spain
[3]Instrumentation and Research Branch, INTA, Huelva, Mazagón, 21130, Spain
[4]Department of Applied Physics, University of León, León, 24071, Spain
Keywords: particle size distribution, scattering coefficient, absorption coefficient, AOD
Presenting author email: fjolmo@ugr.es

Gas-aerosol interaction can significantly alter the concentration of gases in the atmosphere thus playing a role in the global heat balance and climate change. In particular, the atmospheric minor gases behaviour under high aerosol loading conditions such as desert dust episodes or nucleation processes are tasks demanding growing attention in last years due to their potential impact even at large scale. The AMISOC Project (Atmospheric Minor Species relevant to the Ozone Chemistry at both sides of the Sub-tropical jet) aims to improve the knowledge of the minor constituents of the atmosphere playing a role in the ozone chemistry. The core of the project is: two coordinated field campaigns, the development and improvement of instrumentation, modeling and applications system.

AMISOC started with an experimental campaign carried out at 'El Arenosillo' – Atmospheric Sounding Station from 20 May to 15 June 2012. This observatory is located southwestern Spain (37.1ºN, 6.7ºW) on the Atlantic Ocean coast. The location allows the first detection of Saharan dust plumes transported northward to Europe (Córdoba-Jabonero et al., 2011), and can be also affected by events with high levels of surface ozone (Adame et al., 2010) and ultrafine particles (Sorribas et al., 2011), due to natural or anthropogenic emissions under high levels of solar radiation.

This work shows the preliminary analysis of the microphysical and optical aerosol properties during the AMISOC-ARN campaign, as a first step to extend our understanding about the gas-aerosol interaction.

Mean value ± standard deviation for total particle concentration within (14-604) nm was 7750±6500 cm^{-3}, showing the highest levels at noon during the new particle formation events. Depending on wind direction, formation and growth properties of the new particles, seven new particle formation episodes were selected with the aim to analyze them with regard to iodine monoxide (IO), glyoxal (C_2) and sulfate (SO_2) concentrations.

Two desert dust episodes with impact on the columnar-integrated aerosol properties were detected during the AMISOC campaign: (1) 30 May - 3 June 2012 and (2) 6 - 7 June 2012. Mean AOD and Angström parameter (α) during the first episode were 0.30 and 0.61, respectively, and those same aerosol properties during the second one were 0.21 and 0.39. So, the particle contribution of fine size range was higher during the event from 30 May to 3 June (higher α) and the extinction process was strongest (higher AOD) than the other episode. Moreover, the impact on surface level of the first desert dust episode was also observed within the sub-micron and super-micron aerosol size ranges. Figure 1 shows the evolution of the particle volume size distribution during the episode, showing the strong impact on particle diameter about 10 μm was during the first hours of the episode.

The influence of the episode on the global heat balance was also observed with an increase of the scattering light with respect to non-dusty days from 32 Mm^{-1} to 69 Mm^{-1} and absorption light from 2.5 Mm^{-1} to 4.2 Mm^{-1}. It produces an increase of the radiative forcing from -4 W m^{-2} to -12 W m^{-2}.

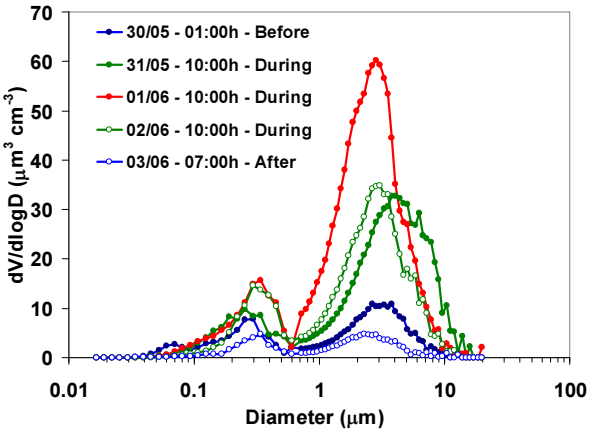

Figure 1. Evolution of the volume size distribution during a desert dust event from 30 May to 3 June 2012

Acknowledgments: M. Sorribas thanks MINECO for the award of a Juan de la Cierva post-doctoral grant. This work was supported by MINECO through project CGL2011-24891, by the Andalusian Regional Government through projects (P10-RNM-6299 and P08-RNM -03568), and by EU through ACTRIS project (EU INFRA-2010-1.1.16-262254). The authors thank the NOAA for the HYSPLIT back-trajectories and for providing technical support with the nephelometer.

Adame et al. (2010) *Environ. Sci. Pollut. Res.*, **17**, 355-368.
Córdoba-Jabonero et al. (2011) *Atmos. Chem. Phys.*, **11**, 3067-3091.
Sorribas et al. (2011) *Atmos. Chem. Phys.*, **11**, 11185-11206.

Bimodal particle concentration profile retrieved from ground-based Lidar and CIMEL measurements

A. Quirantes[1], F.J. Olmo[1,2] , A. Valenzuela[1,2], M.J. Granados-Muñoz[1,2], J.L. Guerrero-Rascado[1,2], J.A. Bravo-Aranda[1,2], F. Navas-Guzmán[1,2], and L. Alados-Arboledas[1,2]

[1]Department of Applied Physics, University of Granada, Granada, 18071 Spain
[2]CEAMA – Centro Andaluz de Medio Ambiente, Av. Mediterráneo s/n, 18006 Granada, Spain
Keywords: Lidar, T-matrix, light-scattering , layer
Presenting author email: fjolmo@ugr.es

Photometric measurements of solar extinction and sky radiance are currently used in inversion methods to retrieve microphysical values such as size and refraction index. However, this method cannot yield proper information regarding some microphysical (particle shape) and optical (backscatter, depolarization, lidar ratio) properties; and concentration values can be retrieved at a column-integrated basis only, lacking access to layer-by-layer information.

In the case of bimodal particle populations, accurate data is difficult to obtain concerning shape or composition for both modes. Such is, for example, the case in large-scale dust episodes, where North African dust is carried across the Mediterranean basin to Europe, and across the Atlantic Ocean to the Caribbean and the United States.

In these cases, dust episodes form mixtures with other particles produced in combustion processes, either natural or anthropogenic. The resulting population can be described as a mixture of two particle modes: a submicron-sized (fine) mode of combustion-produced particles, and a micron-sized (coarse) mode of dust particles. The assessment of the concentration of both particle modes is necessary to determine the physical and optical properties of the aerosol, with consequences in both local and global environments.

In the present work, a combination of column-integrated (CIMEL) and layer-by-layer (Lidar) measurements are used to retrieve detailed information regarding the distribution of both fine and coarse particle modes in each particular layer The particle size distribution (PSD) as retrieved from CIMEL inversion data is fitted to a bimodal log-normal size distribution. A solution is then chosen as a set of input parameters describing the composition (refraction index) and shape of both modes (fine and coarse), as well as the fine/coarse ratio. Particles in each mode are modelled as a 50% volume mixture of prolate and oblate spheroids with the same axial ratio.

A pre-calculated database of kernel functions (“BETA”), based on the T-matrix theory, is used to fit simulated data to experimental layer-specific parameters like particles extinction, backscatter and depolarization at several wavelengths, in order to retrieve the fine/coarse mode ratio and the full (fine+coarse) particle concentration. Once the full, layer-by-layer particle concentration has been obtained, simulated data can be compared to other CIMEL experimental measurements (asymmetry parameter at several other wavelengths).

Our approach does not resort to least-squares methods to obtain the best solution (“best” meaning “minimizing the difference between experimental and simulated data”). Instead, our approach is statistical: all solutions are considered acceptable as long as they agree to experimental data to within experimental uncertainty. By iterating the procedure for all possible kinds of particle shape and composition values, a set of acceptable solutions is obtained that can yield statistical information about fine and coarse mode distributions within each layer. The experimental uncertainty level can also be modified in order to get an assessment of the model's sensitivity

ACKNOWLEDGMENTS: This work was supported by the Andalusia Regional Government through projects P08-RNM-3568 and P10-RNM-6299, by the Spanish Ministry of Science and Technology through projects CGL2010-18782, CSD2007-00067 and CGL2011-13580-E/CLI; and by EU through ACTRIS project (EU INFRA-2010-1.1.16-262254). The authors thankfully acknowledge the computer resources, technical expertise and assistance provided by the Barcelona Supercomputing Center. T-matrix database computation was partly supported by RES (Spanish Supercomputation Network) computing resources (projects AECT-2009-1-0012, AECT-2011-3-0016).

On the contribution of ephemeral lakes to the aerosol load

J.A.G. Orza, M. Cabello, E. Doménech, L. Pérez

SCOLAb and Aeolian Research Group, University Miguel Hernández, Elche 03202, Spain
Keywords: mineral dust, resuspension, meteorology.
Presenting author email: ja.garcia@umh.es

The role of dry lakebeds as sources for aeolian export of soil particulates is studied in relation to their inundation extent and meteorological conditions. We focus on two areas: (1) El Hondo Nature Park in southeastern Spain, 2,400 ha, composed by two large reservoirs and several natural lagoons and pools surrounded by a salt marsh, and (2) the region of the Chotts in southern Tunisia, including el-Djerid and el-Gharsa vast saline lakes of 495,000 and 42,000 ha, respectively. The period 2005-2012 is considered.

Despite their differences in spatial extension and some geomorphologic features, both settings are topographic lows with flat terrain and scarce or absent vegetation, which experience ephemeral variations in inundation extent. The desiccated surface is susceptible to deflation by wind, resulting in soil emissions from the sediments lying on the surface and from evaporite minerals.

Several field campaigns were conducted in El Hondo during the period 2009-2012, aimed to analyze wind erosion and suspended particulate levels downwind in connection with the atmospheric and soil conditions. Measurements included size distribution of suspended particles, PM10 concentration and chemical composition; saltation profiles, composition and granulometry; and meteorological and soil parameters.

Previous studies in the Chotts have used very coarse inundation data and the TOMS AI to measure the dust loading (Mahowald et al., 2003). An indication of an increase in dust loading when lake beds are dry was obtained, but no clear conclusions could be drawn due to the additional contribution of the Saharan dust in the area. We make use of more detailed inundation data and the `present weather´ observations of local dust recorded in SYNOP reports at Tozeur, as well as meteorological and visibility data in the area (METARs and SYNOPs).

Variations in water sheet and salt crusted surface, as retrieved from the 7-2-1 spectral bands of MODIS, are driven primarily by the precipitation regime. In El Hondo, conditions may change dramatically due to additional anthropic intervention, as inflow and outflow are ultimately managed by humans.

The majority of the dust storms registered at El Hondo were associated to the passage of Atlantic frontal systems with no rainfall. W/NW/SW winds > 9 m/s (at 2 m above the ground) and average friction velocity of 0.46 m/s triggered these erosion events. Soil emissions from El Hondo had an impact on coastal touristic villages and some of the dust plumes could be observed in MODIS images.

Dust locally entrained in Tozeur was associated (80% of the cases) to horizontal visibility < 5 km, relative humidity < 75% and windspeed ≥ 8 m/s (at 10 m above the ground), mostly of E component (55%) and then W (28%). Events were primarily of synoptic origin and were registered from March to May.

Dust storms occurred in both settings when, in addition to high wind conditions, large dried areas were available. The inundation extent in the Chotts was large in March-May 2009 leading to a decrease in the frequency of erosion events in that period with respect to other years.

We acknowledge support from the Spanish Government (EroHondo, CGL2008-05160).

Mahowald, N. M., Bryant, R. G., del Corral, J., and Steinberger, L. (2003) *Geophys. Rev. Lett.* **30**(2), 1074.

Investigation of the truncation correction of the polar nephelometer Ecotech Aurora4000

M. Paixão[1], T. Müller[1], S. Pfeifer[1] and A. Wiedensohler[1]

[1]Department of Physics, Leibniz Institute for Tropospheric Research, Leipzig, Germany
Keywords: aerosol optics, nephelometer, scattering coefficient, phase function.
Presenting author email: paixao@tropos.de

In this work we present an investigation of the truncation of near-forward scattering of the polar nephelometer Aurora4000, Ecotech Pty Ltd.

Aerosol particles are known to contribute to climate change (Forster, 2007). The asymmetry parameter or phase function of aerosol particles plays a key role in a proper evaluation of its radiative forcing effect. The polar nephelometer measures the scattering coefficient of the aerosol for up to 18 angular sectors between 0 and 90 degrees. In this way, it's possible to evaluate a quasi-phase function of the aerosol.

Methods for reducing the uncertainties of angular non idealities of the nephelometer intensity function are widely discussed in literature (Anderson and Ogren, 1998; Massoli et al., 2009; Bond et al., 2009; Müller et al., 2011) and correction factors are based on Mie calculation or on parameterization of the Angström exponent. The truncation angle, generally accepted as 10 degrees for Aurora4000, is based on technical drawings and was never measured experimentally.

In order to investigate the truncation error, measurements of aerosol extinction and scattering coefficients were made. Polystyrene latex spheres (PSL) with diameter of 491 ± 4 nm were used, with concentration varying from 20 – 73 #/cm^3. As these particles are non-absorbing, the extinction is equal to the scattering coefficient. For extinction measurements we used a Cavity Attenuated Phase Shift Spectroscopy (CAPS), Aerodyne Ltd., at the wavelength 530 nm.

Preliminary results

Three methods for truncation correction were tested: a) Polar correction (Müller et al., 2012), using the information of the scattering coefficient sectors 10 and 20 degrees; b) Angström exponent measured by the nephelometer itself (Müller et al., 2011); c) calculations using Mie theory and the size distribution of the latex spheres. The Figure 1 shows the comparison of those methods and the error bars correspond to the standard deviation of 5 minutes average of extinction coefficient. The corrections are in good agreement in the region of 20 – 50 Mm^{-1}, probably because the concentration reached a more constant level.

Also the angular scattering was investigated and the measurements are in good agreement with the expected from Mie theory, as seen in Figure 2.

More experiments will be done furthermore with different particle sizes and ambient aerosol. The purpose is to test the instrument limits and improve accuracy.

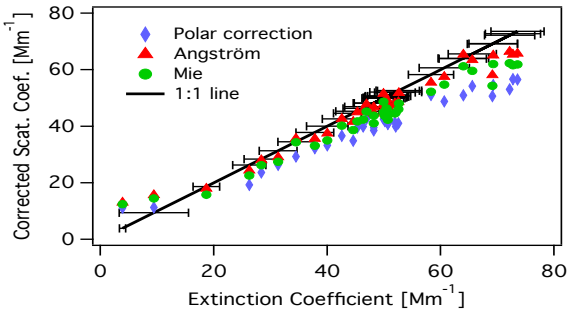

Figure 1. Correlation plot of the scattering coefficient measured by the polar nephelometer corrected using: a) polar correction; b) Angström exponent (Müller et al., 2011); c) Mie calculations using the nominal size distribution of latex spheres; and the extinction coefficient measured by CAPS. The error bars are the standard deviation of the extinction measurements.

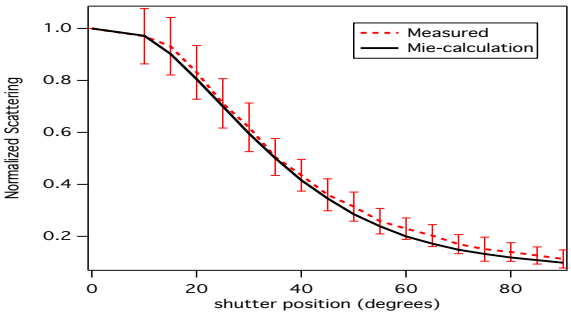

Figure 2. Scattering coefficient of angular sectors normalized by the total scattering measured by the polar nephelometer and calculated using Mie theory. The error bars are standard deviation of the average.

Anderson, T. L. and J. A. Ogren (1998) Aerosol Science and Technology 29(1): 57-69.

Bond, T. C., D. S. Covert and T. Muller (2009) Aerosol Science and Technology 43(9): 866-871.

Forster, P., Ramaswamy, V., Artaxo, P., Berntsen, T., Betts, T., and Fahey, D. (2007) *IPCC*, Cambridge University Press.

Massoli, P., Murphy,D., Lack, D., Baynard, T., Brock, C., and Lovejoy, E. (2009) Aerosol Science and Technology 43(11), 1064-1074.

Müller, T., M. Laborde, G. Kassell and A. Wiedensohler (2011) Atmospheric Measurement Techniques **4**: 1291-1303.

Müller, T., Paixao, M., Wiedensohler, A. (2012) *European Aerosol Conference*, Granada, Spain.

Estimation of viscosity of SOA particles based on coalescence times

A. Pajunoja[1], J. Malila[1], L. Hao[1], K. E. J. Lehtinen[1,2], and A. Virtanen[1]

[1]Department of Applied Physics, University of Eastern Finland, P. O. Box 1627 FI-70210 Kuopio, Finland
[2]Finnish Meteorological Institute, Kuopio Unit, P. O. Box 1627, FI-70210 Kuopio, Finland
Keywords: SOA, coalescence, viscosity, VOC
Presenting author email: aki.pajunoja@uef.fi

Secondary organic aerosol (SOA) formed from partitioning of oxidation products of volatile organic compounds (VOC) accounts for a significant portion of atmospheric particulate matter. The phase of SOA particles affects their behaviour in the atmosphere and ultimately also the climate in ways that fall under topical scientific interests (Riipinen *et al.*, 2012).

Virtanen *et al.* (2010) concluded that biogenic SOA particles can be amorphous solids. In a recent study, Abramson *et al.* (2013) estimated that the viscosity of α-pinene SOA particles is approximately 10^8 Pa·s, implying highly viscous (*i.e.* semi-solid) liquid particles. In this study we analyze the coalescence of agglomerates to estimate the viscosity of SOA particles. In the coalescence process, the (surface) free energy of agglomerated particles is minimized by reconstruction of the particles into spheres. For viscous amorphous particles, the characteristic time for coalescence is (Frenkel, 1945)

$$\tau = \mu d_p / \sigma, \quad (1)$$

where μ is the viscosity of particles, d_p particle diameter, and σ surface tension. A similar analysis recently used for levitated polystyrene microspheres was by Trevitt *et al.* (2009).

We performed chamber experiments using living Scots Pine (*Pinus sylvestris* L.) trees as a biological source of VOCs (Hao *et al.*, 2009). Other precursors (α-pinene, SO_2) were also investigated and the levels of ozone and trimethylethylene (TME), to produce OH, were controlled. The filter samples for scanning electron microscope (SEM) analysis were collected from the chamber (flow 0.2 l/min, sampling times 5–10 min).

The results of scanning mobility particle sizer (SMPS), aerosol mass spectrometer (AMS) and SEM were compared to characterize the particle size, O:C-ratio, SO_4/ORG-ratio, NH_4/SO_4 ratio and particle shape. O:C-ratio was calculated to be around 0.3 for every samples. Scanning electron microscope images of the SOA particles are shown in Figure 1. In Fig. 1a individual agglomerates with primary particle size around 40–80 nm and in Fig. 1b spherical SOA particles with particle size around 30–90 nm are shown. The storage time of these samples was two (2) months before image analysis was performed and agglomerates were still observed. Thus the structural deformation from agglomerates to spheres is remarkably slow and the characteristic coalescence time, τ, is longer than two months.

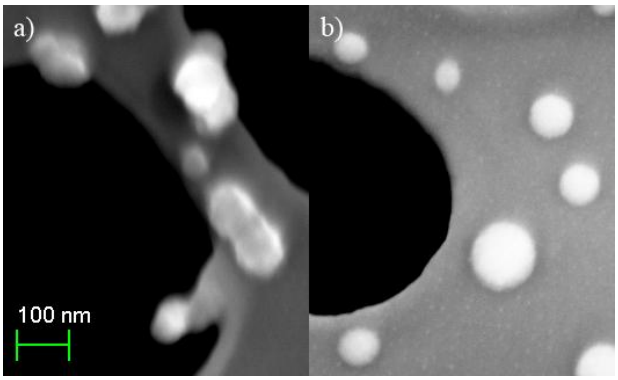

Figure 1: SEM images of the agglomerated SOA particles formed from pine + SO_2 + TME **(a)** and spherical SOA particles formed from oxidation of α-pinene **(b)**.

By using the equation (1), the viscosity of SOA particles can be estimated. As we do not know the detailed molecular composition of SOA, we used the estimated O:C-ratio to pinpoint a suitable model compound, *cis*-pinonic acid, with σ = 35 mJ/m^2. (www.chemspider.com/Chemical-Strucure.209536.html) This yields $\mu \geq 10^{12}$ Pa·s for SOA particles from pine + SO_2 + TME, and $\mu << 10^{12}$ Pa·s for SOA from pure α-pinene oxidation products. These results are consistent with earlier research (Virtanen *et al.*, 2010: Saukko et al., 2012; Abramson *et al.*, 2013), and bear out the hypothesis of highly viscous or even glassy SOA particles in the ambient atmosphere.

This research has been supported by the Academy of Finland (decision no 1118615, 259005 & 264989) and by the strategic funding of the University of Eastern Finland.

Abramson, E. *et al.* (2013) *Phys. Chem. Chem. Phys.* **15**, 2983–2991.
Frenkel, J. (1945) *J. Phys.* (Moscow) **9**, 385–391.
Hao, L. *et al.* (2009) *Atmos. Chem. Phys.* **9**, 8121–8137.
Riipinen, I. *et al.* (2012) *Nat. Geosci.* **5**, 453–458.
Saukko, E. *et al.* (2012) *Atmos. Chem. Phys.* **12**, 7157-7529.
Trevitt, A. J. *et al.* (2009) *J. Aerosol Sci.* **40**, 431–438.
Virtanen, A. *et al.* (2010) *Nature* **467**, 824–827.

Studies of precipitable water vapor measurements with use of Microtops II Sun Photometer and Radiosonde RS92

P.Pakszys[1], T. Zieliński[1], T.Petelski[1], P.Makuch[1], A.Strzałkowska[1], P.Markuszewski[1], J.Kowalczyk[1]

[1]Institute of Oceanology PAS, ul. Powst. W-wy 55, 81-712 Sopot, Poland
Keywords: water vapor, Microtops, radiosonde, AOD.
Presenting author email: pakszys@iopan.gda.pl

Information about vertically integrated content of water vapor in the atmosphere and type, composition and concentration of aerosols is relevant in many types of atmospheric studies. Such information is required to understand mechanisms of global climate and its further modeling (Smirnov et al., 2000).

This work is devoted to analyses of Columnar Water Vapor values obtained from two instruments.

The measurements were carried out using Microtops II Sunphotometer during the cruise onboard s/y Oceania between 29 March and 20 April 2011 in the southern Baltic Sea, near the Polish town of Leba. Measurements were collected for the NASA program Maritime Aerosol Network. Data at the Leba station were collected with a Radiosonde DiGICORA RS92.

The first instrument, sunphotometer, allows us to collect data on days that are cloud-free. The Microtops II is capable of measuring the total ozone column, total precipitable water vapor and aerosol optical depth at 1020 nm (Morys et al. 2001; Ichoku et al., 2002). Each of these parameters is automatically derived.

The water vapor measurement is based on pair of radiometric measurements in the IR band. Simultaneous observations are performed through two filters with different transmission bandwidths centered around the same wavelength located in the water vapor band (Plana-Fattori, 1997). The 936 nm wavelength is strongly affected by water vapor absorption, the 1020 nm filter only by aerosol scattering.

Data collected by Microtops have been processed with the pre- and post-field calibration and automatic cloud clearing. Precipitable water vapor in the column was derived from the 936nm channel. Detailed data description is available on the AERONET webpage.

Radiosonde observations also play an important role in conducting research to help develop satellite techniques for retrieving temperature and humidity profiles (Garand et al. 1992; Connell et al.,1995).

The total precipitable water is the water that occurs in a vertical column of a unit cross-sectional area between any two specified levels, commonly expressed as from the earth's surface to the "top" of the atmosphere. The Integrated Precipitable Water Vapor (IPWV) is the height of liquid water that would result from the condensation of all water vapor in a column.

During the study 241 Microtops measurements were made, each of them in a series of five "shots". Then only the lowest value was used. Then the data were matched with the radiosonde data, based on date and time. As a result 12 measurements were left to compare.

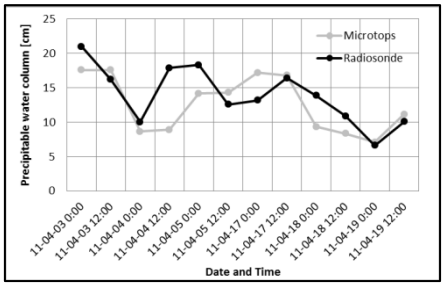

Figure 1. Comparison of data from Microtops II and a Radiosonde

The correlation is strong for both instruments (0.67). The correlation between aerosol optical depth and water vapor content in the total atmospheric column is strong (0.42). Also diurnal variations of the aerosol optical depth and precipitable water were insignificant ($\overline{AOD}$=0.09±0.03; $\overline{PWV}$=11.42±3.50).

These analyses are presented in order to quantify the accuracy of different techniques and algorithms to estimate WV present in the Earth's atmosphere. Nevertheless, the data comparison shows discrepancy at a lower level between the instruments.

Connell H. Bernadette, Miller R. David (1995) *An Interpretation of Radiosonde Errors in the Atmosphere Boundary Layer*. Journal of Applied Meteorology, vol 34, 1070-1081.

Garand L., C. Grassotti, J.Halle, G. Klein (1992) *On differences in radiosonde humidity – Reporting Practices and their implications for numerical weather prediction and remote sensing*. Bull. Amer. Soc., 73, 1417-1423.

Ichoku C. et al. (2002) *Analysis of the performance characteristics of the five-channel Microtops II Sun photometer for measuring aerosol optical thickness and precipitable water vapor*. Journal of Geophysical Research vol. 107.

Morys, M., F. M. Mims III, S. Hagerup, S. E. Anderson, A. Baker, J. Kia, and T. Walkup (2001). Design, calibration, and performance of Microtops II handheld ozone monitor and Sun photometer, J.Geophys. Res., 106, 14,573–14,582.

Plana-Fattori A. et al. (1997) *Estimating the Atmospheric Water Vapor content from Sun Photometer Measurements*. Journal of Applied Meteorology, vol. 37, 790-804.

Smirnov A. et al. (2000) *Atmospheric Aerosol Optical Properties in Maritime Environments*. Special issue of Journal of the Atmospheric Sciences 2000.

Factor analysis of aerosol measurements in Tartu

M. Palo and M. Eller

Institute of Physics, University of Tartu, Ülikooli 18, 50090, Tartu, Estonia
Keywords: urban aerosol, factor analysis
Presenting author email: marispalo@hotmail.com

The aim of this work was to study the spectrum characteristics of urban aerosol measured in Tartu, Estonia and to test, whether it is possible to use factor analysis to describe the formation processes and possible sources of the measured aerosol.

The concentrations of particles were measured with electrical aerosol spectrometer (EAS), developed by Airel Ltd. EAS (Tammet *et al*., 2002) can measure size distribution of particles in 3.16 nm to 10 µm diameter range and has the size resolution of 8 channels per size decade and time resolution up to 1 second.

Factor analysis was used to investigate spectrum characteristics during nucleation events and non-event periods. Periods were determined visually by examination of aerosol size spectrum.

In the analysis, the number of factors was determined by the Kaiser criterion. Factors characterize correlative tendencies in aerosol size spectrum and can be associated with the formation processes and sources of the aerosol. Results of factor analysis were explained according to knowledge of human activities in the area, weather conditions and particle formation-, growth- and loss processes.

Aerosol spectrum from the periods without nucleation events had a lot of variability. In spring, the spectrum showed unsteady conditions, while in autumn and winter periods the spectrum demonstrated a daily pattern. The pattern is caused by local heating, traffic and stable weather conditions. On figure 1 factor 1 shows the accumulation of particles from local heating and traffic due to little dispersion.

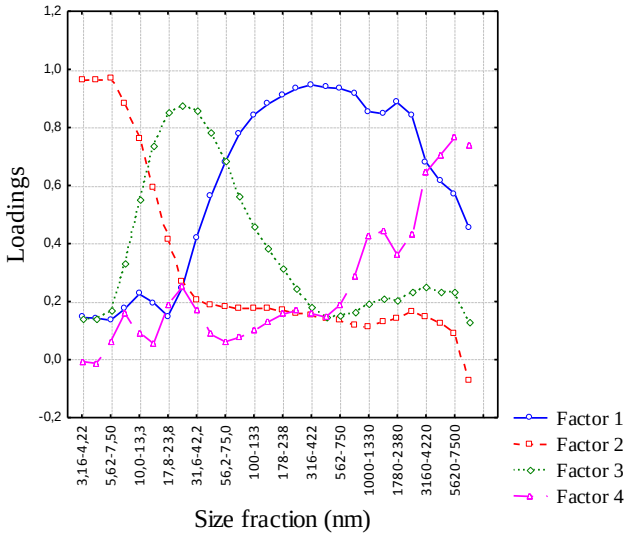

Figure 1. Results of factor analysis on a non-event period (12.12.2011-16.01.2012)

The factor analysis of nucleation periods revealed five factors. Nucleation mode was divided into three components; accumulation mode and coarse mode were also detected. The three factors in the nucleation mode were only present during nucleation events. These three modes can be linked with particle formation and growth from exhaust gases of traffic. Factor 2 on figure 2 shows accumulation of particles after growth processes and factor 1 is most likely connected to primary sources.

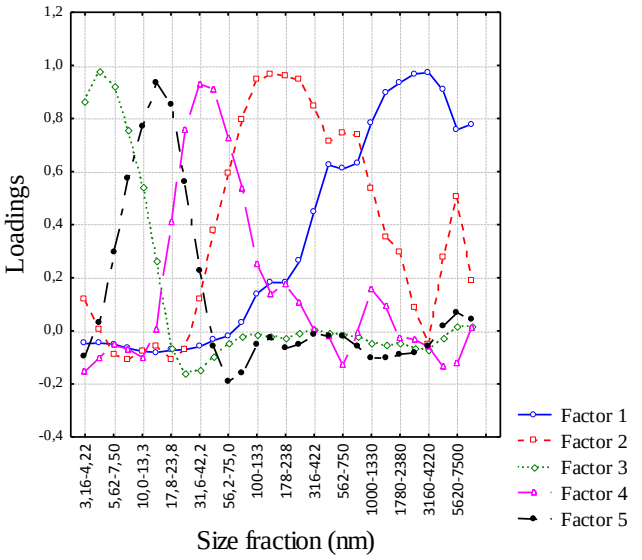

Figure 2. Results of factor analysis on nucleation event periods.

Factor analysis has previously been used to describe rural aerosol in North Estonia (Pugatšova, 2004) and urban air in other countries. However, it has rarely been used on multi-channel data. EAS measurements could also be performed with very high temporal resolution, to study aerosol distribution and development processes even in more detail in the future.

Tammet, H., Mirme, A., Tamm, E. (2002) *Electrical Aerosol spectrometer of Tartu University*, Atmospheric Research, 62, 315-324.

Pugatšova, A. (2004) *On the characteristics of the size spectrum and particle total concentration of the atmospheric aerosol depending on air mass origin*. Master's thesis, University of Tartu, Estonia. In Estonian, summary in English.

Hygroscopic properties of the anthropogenic aerosol in the Po-Valley, Italy

I. Pap[1], J.Größ[1], A. Hamed[1, 2], W. Birmili[1] and A. Wiedensohler[1]

[1]Department of Physics, Leibniz Institute for Tropospheric Research, Leipzig, 04318, Germany
[2]Department of Applied Physics, University of Eastern Finland, Kuopio, P. O. Box 70211, Finland

Keywords: hygroscopic growth, hydrophobic, hydrophilic, hygroscopicity parameter

Presenting author email: pap@tropos.de

The High Humidity Tandem Differential Mobility Analyzer (HH-TDMA) is designed to measure the hygroscopic growth factors (HGF) at sub-saturated conditions (up to 99 % RH) under highly temperature stabilized conditions. The HH-TDMA was employed to measure the water uptake of aerosol particles in the Po Valley region, which give us a good opportunity to measure the hygroscopic behaviour of these particles during the summer time. The campaign was performed in frame of the EU-PEGASOS project. The measurements were taken in the period at the station San Pietro Capofiume (SPC) in the time period from June 9 to July 10, 2012. HGF probability functions were calculated for four particle sizes (75, 100, 200 and 300 nm). These particles were measured at different RH: 90, 93 and 95.5 %. The HGF probability functions contain a hydrophobic and a hydrophilic mode, leading to a bimodal character in 62 % of the cases, during the whole measured period.

In order to describe the hygroscopic properties of particles, the hygroscopicity parameter κ was calculated using the Köhler theory. This was achieved by using the equation given by Petters and Kreidenweis, 2007. The hygroscopicity parameter κ was applied to all measured HGF probability functions.

The value of parameter κ classifies a certain aerosol fraction as hydrophobic or hydrophilic, similarly to the classification according to HGF. In general, a value close to 0 indicates that the aerosol fraction is hydrophobic. The aerosol fraction for 100 nm particles at 90 % is hydrophilic for a κ value higher than 0.2 (Liu, 2011).

The averaged HGF probability functions and the averaged κ probability functions over the measured period are shown in Figure 1. The distribution is shown for three different RHs for 200 nm particles. The distribution of κ is similar to the HGF distribution. Both, a hydrophilic and smaller, hydrophobic mode can be seen here. The difference between the HGF and the κ distribution is that, in the GF distribution, the hydrophilic peak is shifted with the change of RH, while this shift is negligible in the κ distribution. Due to these results, it can be concluded that κ is relatively constant with relative humidity, meaning no further material gets in solution with increasing RH.

The time series, shown in Figure 2, indicate that the number fraction of hydrophobic and hydrophilic particles varies greatly during the day and the external mixture of 100 nm particles changes drastically. More analysis on hygroscopicity at the SPC station related to the black carbon mass concentration will be presented in our studies.

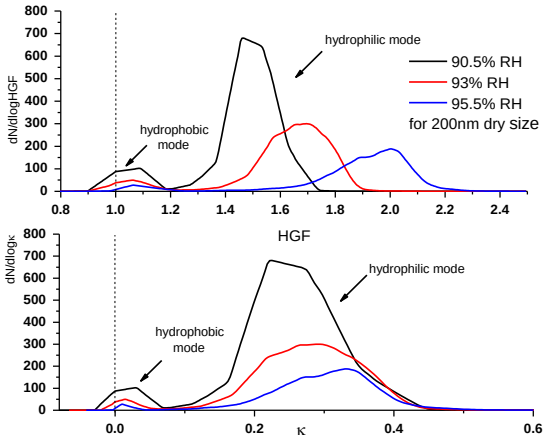

Figure 1: The averaged κ and HGF distribution for 200 nm at different RH. The black, red and blue line represents the particle number concentration density at 90.5, 93 and 95.5 % RH. The dashed line represents the original dry particle state.

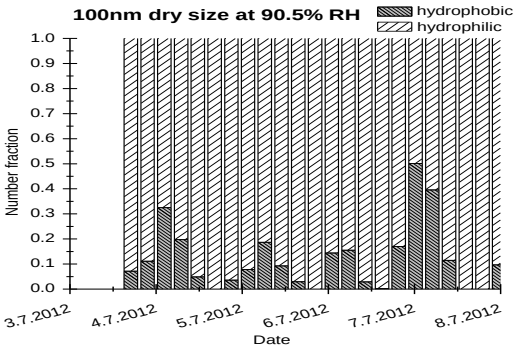

Figure 2: The number fractions of hydrophobic and hydrophilic particles of 100 nm particles at 90.5 % RH. Gray and brighter boxes represent the hydrophobic and hydrophilic number fraction

References

Liu et al. (2011), Atmos. Chem. Phys. ,11, 3479-3494
Petters and Kreidenweiss (2007), Atmos. Chem. Phys., 7, 1961-1971

Rainout, washout and dry deposition contributions to the total deposition flux of heavy metal aerosol onto surfaces of a small urban catchment (Pin Sec, Nantes)

S. Percot[1], V. Ruban[2], P. Laguionie[1], D. Maro[1], P. Roupsard[1], D. Demare[2]
[1] Institut de Radioprotection et de Sûreté Nucléaire (IRSN), PRP-ENV/SERIS/LRC, Cherbourg-Octeville, 50130, France
[2] Institut Français des Sciences et Technologies des Transports, de l'Aménagement et des Réseaux (IFSTTAR), GER7, Bouguenais, 44344, France.
Keywords: rainout, washout, dry deposition, heavy metals.

Pollutants associated to atmospheric particles in urban areas throughout the world have been characterized in many studies. Pollutant sources are either natural (e.g. volcanoes, forest fires) or anthropogenic (traffic, industries, central heating). The nature of surfaces as well as weather conditions and atmospheric turbulence influence the aerosol deposition. Previous studies in Nantes (France) on the Pin Sec catchment allowed the estimation of wet and dry atmospheric deposition fluxes. Thanks to these results further studies can now estimate the origin of atmospheric heavy metals by distinguishing rainout (long range transport) and washout (local scavenging) processes (Bertrand *et al.*,2008). The objective of this communication is to present the rainout, washout and dry deposition contributions to the total deposition flux of heavy metal aerosol (Zn, Cu, Ni, Pb and V) on the Pin Sec catchment.

The experiment was conducted between the 1st of September 2010 and the 31st of August 2011. The dry deposition of heavy metals was estimated by Percot *et al.* (2012) using the dry deposition velocity of the tracer Beryllium 7 measured on urban surfaces by Roupsard *et al.* (2012). Regarding monthly wet deposition, the flux is calculated as the ratio of the mass of pollutants collected in a covered pluviometer. The rainout/washout ratio was determined by the Laguionie *et al.* (2013) method. This method uses monthly integrated data: heavy metal elements concentrations in rainwater and in aerosol particle sampled by Partisol ™, scavenging coefficient Λ (s^{-1}) determined by Laguionie *et al.* (2011) method, reload rate of the local atmosphere in heavy metal elements, and meteorological parameters.

In average, over the 10-month survey period, heavy metals (except for vanadium and lead) are mainly deposited by rainout process, showing evidence of long range sources (Figure 1). The rest of the atmospheric deposition is composed of dry deposition and washout which is the lowest part of deposition (4 % for zinc and nickel to 14 % for lead). These results are in good agreement with results of source emission showing that there is no evidence of emission of pollutants from local activity (traffic, industry,…) (Percot, 2012). Lead behaves differently: dry deposition and washout contributions (respectively 60 % and 26%) suggest the existence of a local source.

The consequences of these results and perspectives will be further discussed at the conference. Further experiments will be lead to better understand the impact of particle size and hygroscopicity on the scavenging coefficient.

This work was supported by the French National Research Agency (INOGEV research program), the French Institute of Science and Technology for Transport Development and Network and the French Institute of Radioprotection and Nuclear Safety.

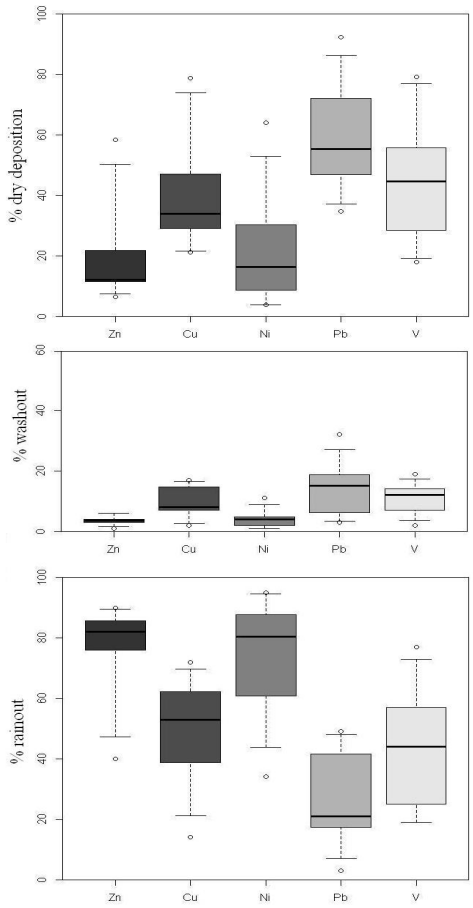

Figure 1. Contribution of heavy metal dry deposition, washout, and rainout to total deposition flux versus time on Pin Sec watershed, Nantes, France.

Bertrand, G. *et al.* (2008) J Atmos Chem, 60 :253-271
Percot, S. *et al.* (2012) Proc. European Aerosol Conference, 2-7 Sept, Granada, Spain.
Roupsard, P. *et al.* (2012) Proc. European Aerosol Conference, 2-7 Sept, Granada, Spain.
Laguionie, P. *et al.* (2013) Proc. European Aerosol Conference, 1-6 Sept., Prague, Czech Republic.
Laguionie, P. *et al.* (2011) Proc. European Aerosol Conference, 4-9 Sept., Manchester, UK.
Percot, S. (2012) Phd thesis, Nantes, France.

Continuous Measurements with high Time Resolution of Semi-Volatile Components in the Atmospheric Aerosol

H. Grimm[1], M. Pesch[2], M. Richter[3], A. Comouth[4]

Grimm Aerosol Technik GmbH & Co. KG, 83404 Ainring, Germany
Keywords: aerosol instruments, atmospheric aerosol, PM10, semi volatile components (SVC)
Presenting author email: mp@grimm-aerosol.com

EU limit and guideline values for the protection of human health (DIRECTIVE 2008/50/EG) demand a continuous monitoring of the atmospharic aerosol, more precisely its fine dust fraction PM10 and PM2.5. The tresholds are being exceeded in many areas in Europe, primarily in congested urban areas, where many people are affected. Fine dust is rated harmful to health which therefore strongly needs action to be taken, in order to minimize this exposure.

The EU regulates, when exceeding the set limit and guideline values, to develop clean air plans, in which efficient reduction strategies have to be enlisted. These plans are based upon cause analysis, which assigns certain dust exposure to certain sources.
For monitoring the thresholds, many measuring technologies proved well, whereas in the past years especially the optical measuring technology gained in importance. The optical detection of the aerosol enables a non-contact, continuous, and temporally high resolved measurement of the aerosols in real-time, where next to the PM fractions also particle size as well as particle counts can be determined.

A significant part (up to 60% of the particle mass) of the atmospheric aerosol is determined by semi-volatile components (SVC), which varies depending on location and season. This meaningful fraction of the SVC impedes the exact determination of the aerosol mass: The volatile components get lost, when heating the aerosol while sampling, e.g. when using a heated sampling probe for drying the sample, or when dust clogged filters remain several days without cooling inside the sampler.

Thus it is important to determine the volatile fraction of the aerosol for two reasons: On the one hand this fraction is very helpful for the source identification of the dust, because different sources create different SVC fractions, and on the other hand it is very important to measure the SVC for comparing the results of different fine dust measuring devices, which reveal the difference in their losses of SVC while measuring.
Thus the gas-particle-conversion from nitrogen oxides to nitrates and ammonium compounds, or the condensation from gaseous emitted carbon hydrides leads to organic aerosols.

The company Grimm Aerosol Technik GmbH & Co. KG developed a compact, mobile, and highly efficient measuring instrument, which enables the continuous determination of the volatile fraction within the atmospheric aerosol. This device is in possession of two sampling probes with complementary characteristics:
One probe dries the particles by a nafion membrane in such a way, that no volatile aerosols get lost, while in the other probe the aerosol can be heated to a temperature of up to 300 °C. The aerosol is alternating being sucked through the sampling probes and subsequently analyzed inside the same optical chamber. This means, that in one interval all aerosol are analyzed and in the other one only the thermically stabilized aerosols. Forming this difference of both intervals, a determination of the volatile fraction is possible. There the volatile components are classified simultaneously into 31 size channels from 250 nm up to 32 µm, as well as a simultaneous detection of the PM10, PM2.5, and PM1 fractions (figure 1).

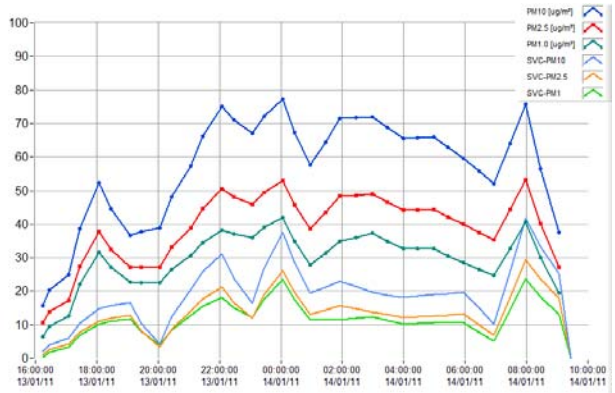

Figure 1: Temporal course of the PM fractions and its volatilecomponents at 100°C

The temporal resolution is 6 seconds. By limiting the size channels, measurements can be executed at 1 Hz, which enables the application of the Eddy-Correlation calculation for determination of aerosol flows.

Measurements at different locations prove the high temporal and spatial variability of the volatile aerosol components, and moreover provide valuable indication for the causes of fine dust exposure as well as a better understanding of the aerosol formation within the lower atmosphere.

Reference

REGULATION 2008/50/EG OF THE EUROPEAN PARLIAMENT AND THE COUNCIL for air quality and clean air for Europe

Mobile FINE DUST Aerosol Spectrometer

M. Pesch[1], H. Grimm[2] and M. Richter[2]

[1] Grimm Aerosol Technik Gmb, 83404 Ainring, Germany
[2]G.I.P. Messgeräte GmbH, Mühlbecker Weg 18, 06774 Pouch, Germany
Keywords: Spectromter, dust cloud, in-flight, high altitutes
Presenting author email: hg@grimm-aerosol.com

The impact of the new guidelines for aviation introduced in Europe during some volcanic eruptions and the consequences were studied by the EU. On requests by several users in Europe we build a compact, light weight flying device for aircrafts to monitor the movement of the ash cloud as event by using various instrumentations as remote sensing techniques.

Our contribution to this concept was to build a fast monitoring sensor measuring the Aerosol
.

:

size distribution in the NANO and MICRO size range at any altitude and air speed, so that ash plume model forecasts could be evaluated against actual remote sensing data based on satellites and ground-based instruments.

The paper will describe the technology, evaluation tests and the experiences made at different installations allowing volcanologists, chemists and geological expert to monitor all of over Europe for disciplines.

Primary Biological DNA Database

D. Pickersgill[1,2], J. Wehking [2], I. Müller-Germann[1,2], U.Pöschl[1], V.R.Després[2]

[1]Multiphase-Chemistry, Max Planck Institute for Chemistry, P.O. Box 3060, D-55020 Mainz, Germany
[2]General Botany, Johannes Gutenberg University, Saarstraße 1, D-55099 Mainz, Germany

Keywords: Biological Aerosol, database, pollen

This work focuses on the design and implementation of a Database (DB) for DNA fragments isolated from primary biological aerosol particle (PBAP) samples (Després et al. 2012 and references therein), along with all relevant information such as taxonomic, sampling, locational and meteorological information. A data structure was designed, according to the relational model (Codd 1970), that maximises flexibility, eliminates data redundancy and logically links all relevant data needed for analyses. The data structure was implemented using the open-source relational DB management system (RDBMS) MySQL.

For testing and subsequent analysis, data from 1179 plant sequences were imported, that were sampled in Mainz from March 2006 to April 2007. The sequences were attributed to 158 plant OTUs (Blaxter et al., 2005) which were used for taxonomic identification. Taxonomic tree information for the OTUs was stored according to the Nested-Set-Model (Celko, 2004).

Using SQL-queries, the plant data-set was analysed. Generalised queries were written that calculate Chao1, Shannon index, Shannon evenness, Simpson index, Simpson Diversity and the normalised species richness for the meteorological seasons including the normalised standard error. Using the generalised queries, values were extracted for various subsets of the data-set. Three methods were developed to normalise OTUs found on a sample, which were used for statistical analysis (Pickersgill 2013).

In addition data from a literature search concerning the discovered plant species was imported e.g. the pollen size, pollen count, or flowering period. This allows in-depth analysis e.g. the comparison of pollen size and species detection on coarse vs fine particle filter samples with a cut-off at 3 µm. Even though the literature shows that the pollen size starts at ~20 µm for the smallest pollen (Fig. 1), 42% of the total OTUs from Mainz were sampled on the fine particle filters. We assume that this plant-DNA originates either from other fragmented plant tissues or from pollen that have burst. This is interesting, as by this bursting process respirable allergens become free and cause pollinosis in humans.

There is a need for using DB management systems to research and analyze the growing data set under the background of pollinosis and other interactions of bioaerosols with the biosphere and the atmosphere.

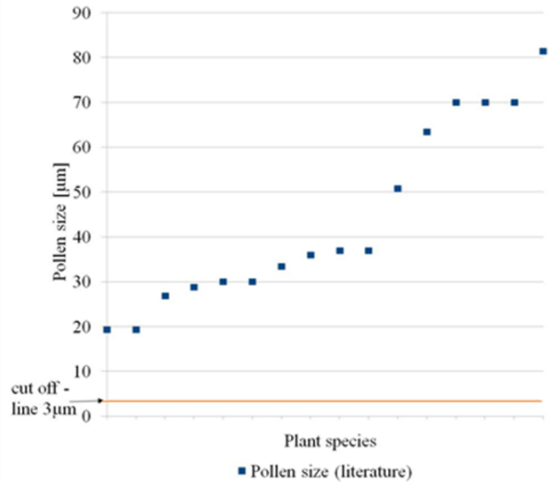

Figure 1. Pollen size (blue) of analyzed plant species of a fine particle filter with a cut-off of 3 µm (orange) in Mainz, Germany.

Achnowledgements

Max Planck Society are gratefully acknowledged for funding, J. Fröhlich-Nowoisky for sampling and DNA extraction, H. Schröder, M. Krupp and M. Geilke for informatics support.

References

Blaxter, M., Mann, J., Chapman, T., Thomas, F., Whitton, C., Floyd, R., & Abebe, E. (2005). *Series B, Biological sciences*, 360(1462), 1935–43

Celko, J. (2004). *Trees and Hierarchies in SQL for Smarties. Elsevier Inc*.

Després, Viviane R., Alex Huffman, J., Burrows, S. M., Hoose, C., Safatov, A. S., Buryak, G., Fröhlich-Nowoisky, J., et al. (2012). *Tellus B*, 64.

Pickersgill, Daniel. Design and Implementation of a Primary Bioaerosol DNA Database. Diploma thesis at the University Mainz, 2013.

Solomon, P. A., Moyers, J. L., & Fletcher, R. A. (1983). *Aerosol Science and Technology*, 2(4), 455–464.

Studying Atmospheric Aerosols by Acoustic Levitation: Linking Headspace Solid-Phase Microextraction (HS-SPME) with Gas Chromatography-Mass Spectrometry (GC-MS).

S. Almabrok, G. Marston and C. Pfrang

Department of Chemistry, University of Reading, P.O. Box 224, RG6 6AD Reading, Berkshire, UK
Keywords: Solid-Phase Micro-extraction, Acoustic Levitation, α-Pinene, Ozone.
Presenting author email: samihus2009@googlemail.com

Abstract

Climate change is one of the most important global environmental problems affecting natural ecosystems, food production, availability of fresh water as well as human health.(1) In acoustic levitation, a sound wave is generated between a piezoelectric transducer and a flat or concave reflector; therefore, by altering the distance between transducer and reflector a standing wave can be created and small samples of solids or liquids can be levitated.(2) This study has been conducted to improve our understanding of the reactions of O_3 and NO_3 with a range of terpenes found in the Earth's atmosphere and of the formation and properties of associated organic aerosols. Combination of acoustic levitation with gas chromatography-mass spectrometry (GC-MS) has been achieved for the first time using headspace solid-phase micro-extraction (HS-SPME); this combination leads to identification of several products, during reaction of oxygen, ozone and nitrate radicals with acoustically levitated droplets of α-pinene and d-limonene. The experimental set-up is illustrated in Fig.1.

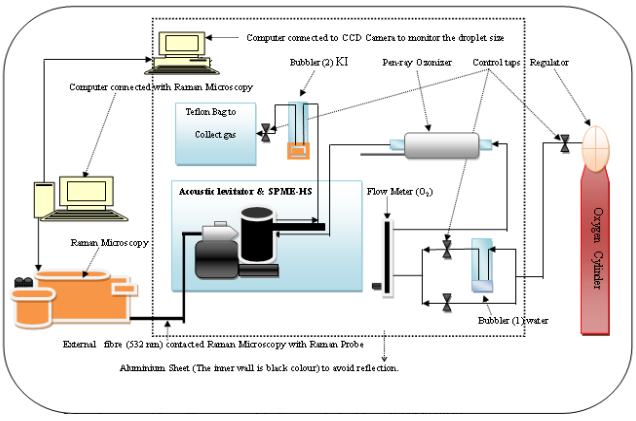

Fig.1: Experimental set-up for the acoustic levitator with HS-SPME-GC-MS analysis. The following conditions were employed: 174 mlmin^{-1} flow of N_2, 5 min extraction time, and using a 100-µm polydimethylsiloxane (PDMS) coated fibre.

Oxidation by oxygen and ozone of acoustically levitated droplets of α-pinene and d-limonene has been studied in an environmental chamber that allowed control of the gas-phase surroundings and relative humidity.
Several products for the reaction α- pinene with O_2 and O_3 could be identified mostly by comparison with reference samples in the same conditions including acetone, α-pinene epoxide, β-pinene, pinocarveol, verbenol, myrtenol, verbenone, pinenol, norpinone, norpinonaldehyde, and pinonoaldehyde. For the reaction of d-limonene with O_2 and O_3 the identified products are d-limonene oxide, carvone, carveol, limononaldehyde, carveol, keto-limononaldehyde, and limononic acid (see examples in Fig. 2 and Fig. 3).

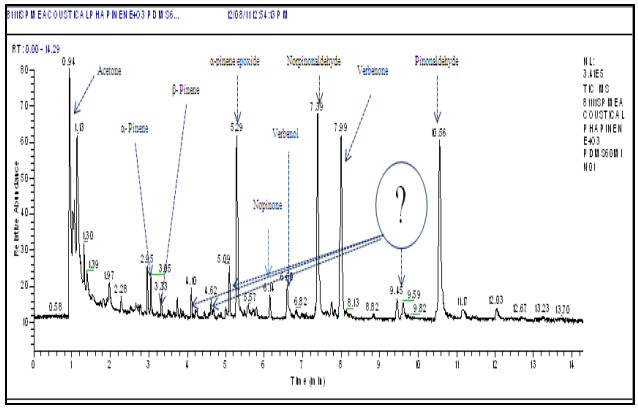

Figure 2: Products identified by HS-SPME-GC-MS for an acoustically levitated droplet of α-pinene after oxidative ageing (only GC trace shown for visual clarity).

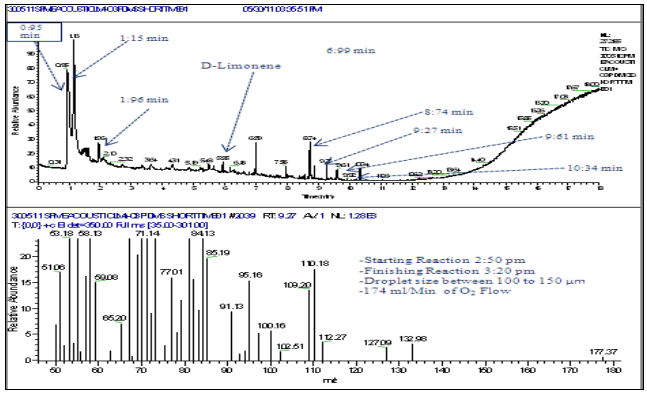

Fig. 3: Products identified by HS-SPME-GC-MS for a levitated droplet of d-limonene after oxidative ageing.

References.

1- Ravindranath, N.H., and J. A. Sathaye, *Climate Change and Developing Countries*, 2003, Kluwer Academic Publishers.
2- Priego-Capote, F., and L. Decastro, *Trends in Analytical Chemistry*, 25, 9 (2006).

The variation of the total aerosol particle number concentration in fog in southern and south-eastern regions of the Baltic Sea

K. Plauškaitė[1], N. Špirkauskaitė[1], T. Zielinski[2], T. Petelski[2] and V. Ulevicius[1]

[1]Department of Environmental Research, SSRI Center for Physical Sciences and Technology, Savanoriu 231, 02300 Vilnius, Lithuania
[2]Physical Oceanography Department, Institute of Oceanology PAS, Powstańców Warszawy 55, PL-81-712 Sopot, Poland
Keywords: aerosol particle number concentration, marine boundary layer, coastal site, fog.
Presenting author email: kristina@ar.fi.lt

The objective of this study was to determine the effect of air masses and meteorological conditions on the variation of total aerosol particle number concentration in marine boundary layer and simultaneously at the coastal site (Preila Environmental pollution research station, Lithuania) during the fog in the spring and autumn.

Measurements were performed during three cruises of r/v "Oceania" (Institute of Oceanology of PAS) in 2008 – 2010 mostly in southern and south-eastern parts of Baltic Sea. The total aerosol particle number concentration over open sea and at the Preila station was measured by using CPC (cut-off size 4.5 nm). Additionally, at the Preila station was measured aerosol size distribution by SMPS for the range 9 – 840 nm. To analyze transport pathways of air masses arriving at investigation sites (open sea and Preila station) the 72 hours air mass backward trajectories at 50, 500, 1000, 2000 and 2500 m heights above the sea or ground levels were calculated using the HYSPLIT-4 model, developed by NOAA/ARL (http://www.arl.noaa.gov/ready.htm, 2008). Meteorological parameters (air temperature, wind speed and direction, relative humidity) were measured at the Preila station and by the on-board system.

The analysis of data showed, that the variation of the total aerosol particle number concentration both in marine boundary layer and coastal zone (Fig. 1B) was smallest during evaporation fog, which was created by cold Polar air passing over warmer sea water. This type of fog is the most localized form (Heo *et al*, 2010) and was observed in Gulf of Gdansk during cruise on 26 September 2009. On the same time at the coastal site aerosol particle number concentration was typical of clean polar air mass. During the cruise on 22 – 23 September 2008, when fog was observed in more polluted polar continental air arriving from north-eastern directions and entering coastal site and the marine boundary layer, the aerosol particle number concentration over the open sea was similar to the case of 2009 but with higher variation of the concentration. However, at the same time at the aerosol particle number concentration at the Preila station was similar to the open sea concentration but with smaller variations in time (Fig. 1A).

The long continuous advection fog (~15 hour), which occurred when warm air mass from south-eastern direction passed over a cool water surface (Baltic Sea), was observed during cruise on the 7 – 8 April 2010 (Fig. 1C). The fog was observed simultaneously over open sea and coastal site causing the similar variations of aerosol particle number concentrations (the values of correlation coefficient were 0.79 and 0.82). Especially interesting phenomena is that during fogs, which were formed in calm anticyclone weather conditions, the total aerosol particle number concentrations over open sea during all cruises were about 4000 cm^{-3} level and may be conditioned by the specific environment of the Baltic Sea (e.g., 7‰ water salinity, typical amount of various phytoplankton (Chl-a (algal biomass) concentration varied from 3 to 30 mg m^{-3})) as a source of particles condensation nuclei in marine boundary layer.

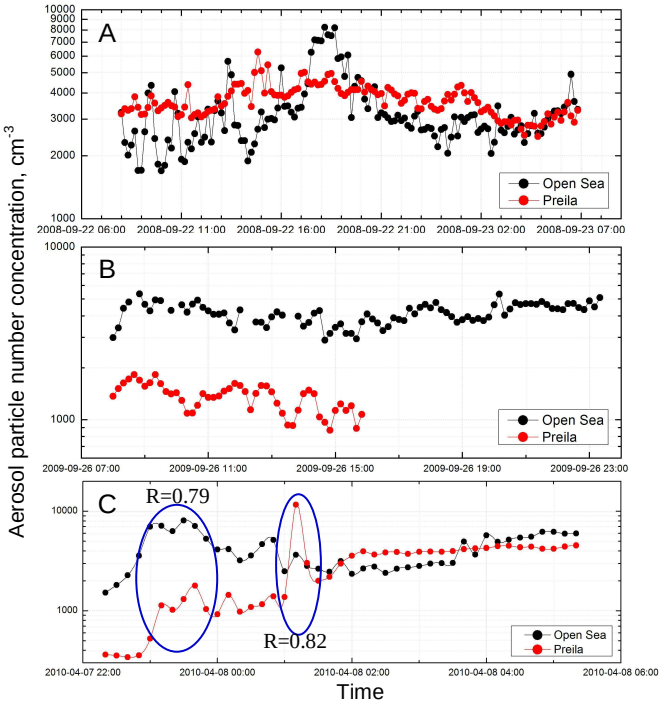

Figure 1. Variations of total aerosol number concentration during fog in marine boundary layer and at the coastal site in 2008 – 2010.

Heo, K.-Y., Ha, K.-J., Mahrt, L. and Shim, J.-S. (2010) *Atmospheric research* **98**, 426-437.

Autofluorescence of atmospheric bioaerosols – studies on biofluorophores and biological standard particles

C. Pöhlker[1], J. A. Huffman[1,2], J.-D. Förster[1], U. Pöschl[1]

[1]Biogeochemistry Department, Max Planck Institute for Chemistry, Mainz 55020, Germany
[2]Department of Chemistry and Biochemistry, University of Denver, Denver, Colorado 80208, USA
Keywords: Bioaerosols, Fluorescence, Pollen.
Presenting author email: c.pohlker@mpic.de

Primary biological aerosol particles (PBAP) such as pollen, fungal spores, bacteria, biogenic polymers and debris from larger organisms are known to influence atmospheric chemistry and physics, the biosphere and public health. PBAP account for up to ~30% of fine and up to ~70% of coarse particulate matter in urban, rural and pristine environment and are released with estimated emission rates of up to ~1000 Tg/a (Elbert et al. 2007).

Continuous measurements of the abundance, variability and diversity of PBAP have been difficult until recently, however. The application of online instruments able to detect autofluorescence from biological particles in real-time has been a promising development for the measurement of PBAP concentrations and fluxes in different environments (Huffman et al. 2010; Pöschl et al. 2010). The detected fluorescent biological aerosol particles (FBAP) can be regarded as a subset of PBAP, although the exact relationship between PBAP and FBAP is still being investigated.

Autofluorescence of FBAP is usually a superposition of fluorescence from a mixture of individual fluorescent molecules (fluorophores). Numerous biogenic fluorophores such as amino acids (e.g., tryptophan, tyrosine), coenzymes (e.g., NAD(P)H, riboflavin) and biopolymers (e.g., cellulose) emit fluorescent light due to heterocyclic aromatic rings or conjugated double bonds within their molecular structures. The tryptophan emission peak is a common feature of most bioparticles because the amino acid is a constituent of many proteins and peptides. The influence of the coenzymes NAD(P)H and riboflavin on the autofluorescence of bacteria can be regarded as an indicator for bacterial metabolism and has been utilized to discriminate between viable and non-viable organisms (Lakowicz 1999). However, very little information is available about other essential biofluorophores in fungal spores and pollen.

In order to better understand the autofluorescence behavior of FBAP, we have used fluorescence spectroscopy and fluorescence microscopy to analyze standard bioparticles, atmospherically relevant chemical substances and ambient aerosol samples (Pöhlker et al. 2012). In particular, we focused on pollen as an adequate bioaerosol type for this kind of explorative studies (Pöhlker et al. in prep.). Our aim is (i) to give a clear and general picture on the autofluorescence properties of native pollen and (ii) to illustrates, by means of *one* standard particle type, how offline fluorescence techniques can support the application of LIF in ambient air. Moreover, pollen represents atmospheric particles of high relevance, particularly due to its high allergenic potential with severe social and economic impacts. We suggest that our results can support the development and application of autofluorescence-based detectors for a specific monitoring of allergenic pollen in the atmosphere.

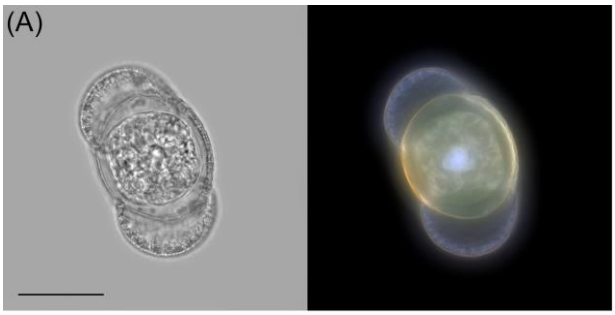

Figure 1. Microscopy images of *Pinus sylvestris* pollen in bright field (left) and fluorescence (right) mode. Micrographs illustrate the diverse autofluorescence properties with contributions from cell wall, cytosol, and organelles. Scale bar = 30 µm.

This work has been supported by the Max Planck Society, the Max Planck Graduate Center and the LEC Geocycles Mainz. The authors gratefully acknowledge support by M. O. Andreae.

Elbert, W., Taylor, P. E., Andreae, M. O., & Pöschl, U. (2007). *Atmos. Chem. Phys.*, 7, 4569-4588.

Huffman, J. A., Treutlein, B., & Pöschl, U. (2010). *Atmos. Chem. Phys.*, 10, 3215-3233.

Lakowicz, J., Principles of fluorescence spectroscopy, Plenum publishers, New York, 1999.

Pöhlker, C., Huffman, J. A., & Pöschl, U., (2012). *Atmos. Meas. Tech.*, 5, 37-71.

Pöschl, U., et al. (2010). *Science*, 329, 1513-1516.

Observations of cloud effects on aerosol light absorption and scattering

A. Leskinen[1], H. Portin[1,2], A. Arola[1], S. Romakkaniemi[2], A.-P. Hyvärinen[3], A. Laaksonen[3], K.E.J. Lehtinen[1,2] and M. Komppula[1]

[1]Finnish Meteorological Institute, Kuopio Unit, P.O.Box 1627, FI-70211, Kuopio, Finland
[2]University of Eastern Finland, Department of Applied Physics, P.O.Box 1627, FI-70211, Kuopio, Finland
[3]Finnish Meteorological Institute, Research and Development, P.O.Box 503, FI-00101 Helsinki, Finland
Keywords: aerosol cloud interaction, atmospheric aerosols, optical properties, scavenging.
Presenting author email: Harri.Portin@fmi.fi

The direct effect of aerosols to radiative forcing arises from light extinction by aerosol particles, i.e. light scattering from and absorption to the aerosols, and it still has a great uncertainty. Evaluation of its magnitude is complicated, because the optical properties depend on the wavelength of the incident light and the angular distribution of the scattered light, which, in turn, depends, e.g., on the size, concentration, and chemical composition of the aerosol particles.

The Puijo measurement station on the top of an observation tower (306 m a.s.l. and 224 m above the surrounding lake level) near the town of Kuopio in Finland has provided continuous data on aerosol-cloud interactions since 2006. Since then the station has been covered by clouds 15 % of the time and is occasionally influenced by e.g. sulphurous compounds and black carbon emitted from local sources. The former are good scatterers of light and the latter absorbs light efficiently.

With a special inlet setup (total and interstitial inlets) and a switching valve system we are able to separate the activated particles from the interstitial (non-activated) particles. This enables us to define the activation properties for aerosol size distribution between 3–800 nm, measured with two differential mobility particle sizers, light scattering at the wavelengths of 450, 550, and 700 nm, measured with a nephelometer (TSI Model 3563) and light absorption at the wavelength of 670 nm, measured with a Multi-Angle Absorption Photometer (Thermo Model 5012).

The level of cloud scavenging depends not only on the aerosol size but also its chemical composition and atmospheric age. We have found that during a cloud event the scattering and absorption values for non-activated particles compared to those for the activated particles are sometimes smaller and sometimes not (Leskinen *et al.* 2012). The decrease is, on an average, -22 % for absorption and -76 % for scattering.

The stronger decrease in scattering may be due to the fact that the absorptive material, e.g. fresh soot, is generally hydrophobic and therefore inhibits activation.. This results in a decrease in the single scattering albedo (SSA), which is the ratio of scattering to extinction (scattering + absorption). The SSA determines whether an aerosol layer causes net heating or cooling. For example, during two cloud events the SSA dropped from its initial value of 0.80–0.85 to as low as 0.4–0.5, on an average (Figure 1). A similar, but not as intensive, decrease in the SSA was observed by Berkowitz *et al.* (2011) in a foggy situation.

The scavenging is less efficient when the wind blows from the direction of local pollutant sources (the first cloud event in Figure 1) than when it blows from a cleaner sector with no local sources (the second cloud event in Figure 1). A similar observation was done by Sellegri *et al.* (2003) who concluded that the scavenging efficiency in clouds is enhanced by aging of organic species and subsequent mixing.

After the second cloud event the incoming air was clean and the scattering and absorption coefficients decreased to the same levels as during the second cloud. The low SSA values can be explained by the uncertainties in the low scattering and absorption coefficients and by the sensitivity of the SSA to the scattering coefficient value, especially in dry conditions.

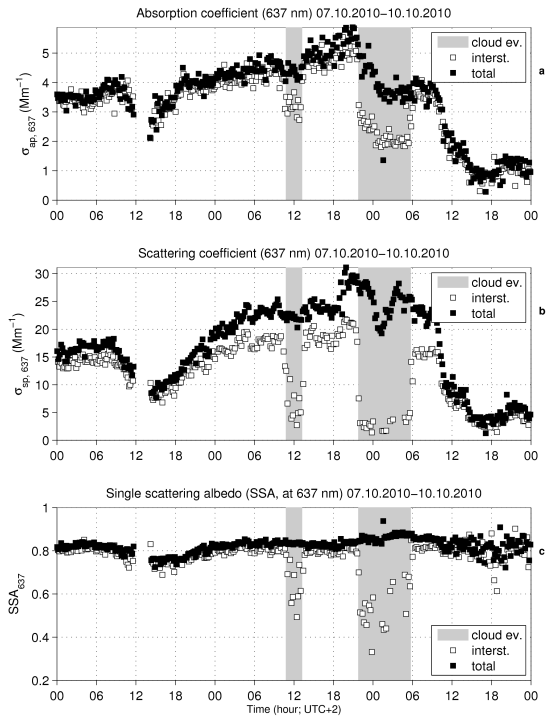

Figure 1. The evolution of (a) aerosol light absorption, (b) light scattering, and (c) single scattering albedo (SSA) around cloud events at Puijo in October 2010.

Berkowitz, C.M., Berg, L.K., Yu, X.-Y., Alexander, M.L., Laskin, A., Zaveri, R.A., Jobson, B.T., Andrews, E. and Ogren, J.A. (2011) *Atmos. Environ.* **45**, 2559-2568.

Leskinen, A., Arola, A., Komppula, M., Portin, H., Tiitta, P., Miettinen, P., Romakkaniemi, S., Laaksonen A. and Lehtinen, K.E.J. (2012) *Atmos. Chem. Phys.* **12**, 5647-5659.

Sellegri, K., Laj, P., Dupuy, R., Legrand, M., Preunkert, S. and Putaud, J.-P. (2003) *J. Geophys. Res.* **108**, D11, 4334.

Meteorological impacts in the modification of PM_{10} concentration levels in the urban area of Volos, Greece

G.T. Proias[1], K.P. Moustris[2], I.K. Larissi[3], P.T. Nastos[4] and A. G. Paliatsos[5]

[1]Department of Planning and Regional Development, University of Thessaly, Volos, 38334, Greece
[2]Department of Mechanical Engineering, Technological and Education Institute of Piraeus, Athens, Aegaleo, 12244, Greece
[3]Laboratory of Environmental Technology, Electronic Computer Systems Engineering Department, Technological and Education Institute of Piraeus, Athens, Aegaleo, 12244, Greece
[4b]Laboratory of Climatology and Atmospheric Environment, Department of Geology and Geoenvironment, University of Athens, Panepistimiopolis, Athens, Zografou, 15784, Greece
[5]General Department of Mathematics, Technological Education Institute of Piraeus, Athens, Aegaleo, 12244, Greece

Keywords: PM_{10}; Saharan dust events; Volos; Greece.
Presenting author email: giproias@prd.uth.gr

Volos, a coastal medium-sized city in the region of Thessaly extended along the northern part of the Pagassitikos Gulf at the eastern seaboard of Central Greece, is among the cities which suffer from the air pollution in Greece. The case of Volos is an interesting example, where in the last decades the urbanization and the increased industrialization have resulted in the degradation of the air quality within the area, triggering health impacts. Meteorological factors play an important role in the air pollution development, while the complex topography of Volos exacerbates air pollution episodes.

In this study, the relationships between PM_{10} (particulate matter with diameter less than 10 μm) and meteorological parameters such as wind speed, relative humidity and air temperature have been analyzed from 2005 to 2009 on the basis of 24-hour continuous measurements. According to the results obtained from the multiple linear regression analysis, there is a strong relation between meteorological parameters and the particulate matter (Table 1) concentrations in Volos city. More specifically, the PM_{10} concentrations remain above the European Union (EU) limit values (Figure 1) for the whole part of the examined period (2005-2009) and this can be attributed to anthropogenic (industry and car traffic) and natural sources (Saharan episodes) of particulate pollution. The percentage of the total variance of PM_{10} concentrations explained by a single meteorological parameter for the cold period gets up to 10.6% (r^2) whereas, for the 5-year period, up to 6.8%. On the contrary, for the warm period it appears that the percentage of the total variance of PM_{10} concentrations explained by a single meteorological parameter gets up to only 2.5%.

Table 1. Pearson's correlation coefficients between the mean daily PM_{10} concentrations (μg/m^3) and the three meteorological parameters. Statistically significant values (at the 99% confidence level) are presented in bold.

Period	WS (m/s)	T (°C)	RH (%)
2005-2007	**-0.260**	**-0.184**	**-0.213**
Cold	**-0.326**	-0.092	**0.243**
Warm	**-0.159**	0.107	-0.078

Moreover, the calculation of the 72-hour air mass back trajectories during (eight) Saharan dust events, took place within the examined period, was carried out by applying the HYSPLIT 4 model of Air Resources Laboratory of NOAA for three different levels: 500, 1500 and 4000 m (a.m.s.l.). It is worthy to remark the high PM_{10} values observed, indicating the contribution of such natural events in exacerbating the air quality in the area of Volos.

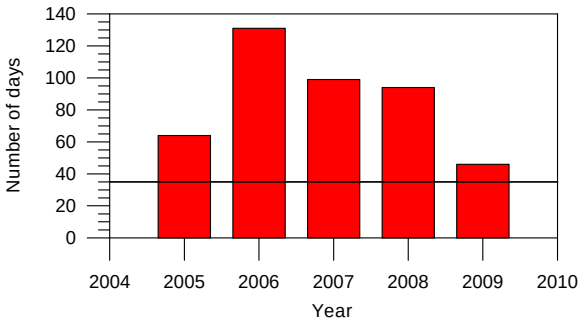

Figure 1. Temporal evolution of annual exceedances of mean daily PM_{10} concentrations at the city of Volos (2005-2009; the horizontal line indicates EU limit).

Larissi, I.K., Koukouletsos, K.V., Moustris, K.P., Antoniou, A. and Paliatsos, A.G. (2010) *Fresen. Environ. Bull.*, **19**, 226-231.

Larissi, I.K., Antoniou, A., Nastos, P.T. and Paliatsos, A.G. (2010) *Fresen. Environ. Bull.*, **19**, 1989-1996.

Nastos, P.T., Paliatsos, A.G., Anthracopoulos, M.B., Roma, E.S., Priftis, K.N. (2010) *Environ. Health*, **9:**45, doi:10.1186/1476-069X-9-45.

Paliatsos, A.G. and Amanatidis, G.T. (1994) *Sci. Total Environ.*, **144**, 137-144.

Proias, G.T., Nastos, P.T., Larissi, I.K. and Paliatsos, A.G. (2009) *AIP Conf. Proc., vol. 1203, 7th Int. Conf. of the Balkan Physical Union,* American Institute of Physics.

Samoli, E., Nastos, P.T., Paliatsos, A.G., Katsouyanni, K., Priftis, K.N. (2011) *Environ. Res.*, doi:10.1016/j.envres.2011.01.014.

Study of the Impact of the Natural Production, in the Mediterranean Sea, of Coastal Marine Aerosols on the Dynamics and Microphysical Behavior of a Convective Cloud

R. Merrouchi[1], J. Piazzola[2], M. Chagdali[3] and S. Mourdane[3]

[1]National Meteorological Service of Morocco, BP 8106 Oisis. Casablanca, 20000, Morocco
[2]Faculty of sciences Ben M'sick, Casablanca, 20000, Morocco
[3] Laboratory of Electromagnetic sounding of Terrestrial Environment-(LSEET), University of Toulon-Var, France
Keywords: Clouds Coastal Marine Aerosols
Presenting author email: rabia.merrouchi@gmail.com

The coastal marine area represents a specific zone for cloud formation. Aerosols caught in updrafts in these areas may have a mixed origin: sea spray aerosols punctually generated at the sea surface are added to a continental contribution issued from natural and/or anthropogenic sources.

The aerosol mixture in coastal zones is strongly related to the changes in the wind direction that could be in turn accompanied by variations in meteorological parameters.

To study the impact of marine aerosols, especially those generated in coastal areas, on the dynamics and microphysical behavior of the clouds, two numerical models were coupled. The first, calculates the coastal marine aerosol spectrum that could be generated under a given weather condition at the sea surface. The predicted spectrum is then introduced, as initial aerosol spectra, to a cloud model with a detailed microphysics.

Design of Numerical Experiments

The cloud model ExMix (External Mixture) has been developed to study mixed-phase clouds by integrating a detailed microphysics of the whole process of formation, growth and precipitation (Monier et al, 2006). EXMIX is dedicated to the different mechanisms behind the cloud formation and decay. The microphysics processes governing the growth of the water droplets inside the cloud depend on both the initial size spectrum and the chemical composition of aerosols caught in the updrafts feeding the cloud.

To include coastal effects in the aerosol model for the prediction of aerosol concentrations, Piazzola et al, (2003) proposed the coastal Mediterranean aerosol model (MEDEX) based on an extensive series of measurements on the island of Porquerolles (off the French Mediterranean coast, located at about 5 km from the coastline). The main inputs of the coastal Mediterranean aerosol model are both the wind speed and the fetch. The Mediterranean coastal aerosol model is a modification of the Navy Aerosol Model (NAM) developed by Gathman (1983) and it is formulated analogously to the model Medex on the basis of an aerosol data set acquired on the island Inisheer.

The simulations performed have focused on a convective cloud (mixed phase) using three distinct initial aerosols spectra of different origins: the first concern an unpolluted continental aerosol spectrum observed in Puy de Dome-France. The second one is for marine aerosol spectra developed by Jaenicke (1988) and the last one is produced by the MEDEX model.

Results:

The transition from a continental aerosol spectrum to a marine aerosol spectrum is synonymous to the introduction of aerosol particles of large size. The impact of such change in the initial spectrum of aerosol is much felt in terms of dynamic and microphysical responses of the cloud. The results obtained show that in presence of marine aerosols, some microphysical properties of the cloud evolution as well as the conditions for triggering rainfall are affected, and hence, the collected quantities on the ground. In particular, results indicate that precipitations are formed earlier, at lower altitudes and induce a larger rain accumulation at the surface. Moreover, simulations also showed pronounced changes when taking into account the natural production of coastal marine aerosols with more pronounced changes inducing greater amounts of water contents within the cloud, and hence, more important rain accumulation on the ground (Figure 1).

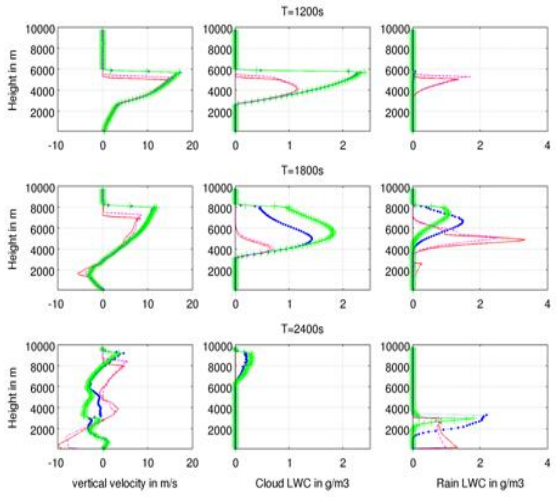

Figure 1. Comparison of vertical profiles obtained using the different aerosol spectrum.

Monier, M., Wobrock, W., Gayet, JF., Flossmann, AI.,(2006) *Development of a detailed microphysics cirrus model tracking aerosol particles histories for interpretation of the recent INCA campaign*, Journal of Atmospheric Science

Piazzola, J., Bouchara, F., Van Eijk, AMJ., De Leeuw, G., (2003), *Development of the Mediterranean extinction code MEDEX*, Optical Engineering, Vol.42, pp.912-924

Jaenicke, R., (1988), *Aerosol physics and chemistry*, V 4b, G. Fischer, Editor, Springer, pp.391-457

Black carbon aerosol concentrations and mixing state in Pallas, Finland

T. Raatikainen[1], D. Brus[1], A.-P. Hyvärinen[1], J. Svensson[1] and H. Lihavainen[1]

[1]Finnish Meteorological Institute, Helsinki, Finland
Keywords: SP2, black carbon, soot particles, aerosol coating.
Presenting author email: tomi.raatikainen@fmi.fi

Black carbon (BC) aerosols have various climate effects. In addition to directly absorbing solar radiation, they have an effect on aerosol-cloud interactions and snow and ice albedo. Single Particle Soot Photometer (SP2) detects BC by using laser-induced incandescence and non-absorbing particles are identified from the scattered light (Stephens et al, 2003). Absorbing particles, with or without coating, are quickly heated to the incandescence temperature and the resulting peak signal, which is seen before evaporation, is proportional to the BC mass. Sizes of the purely scattering particles can be calculated from the peak intensity of the scattered light, which is seen when the particle is at the centre of the laser beam. However, particles containing both BC and scattering material heat up rapidly so that the scattering material evaporates before the centre of the laser beam. In this case, the initial scattering particle size can be extrapolated.

Two commonly used methods to extrapolate scattering sizes for evaporating particles are Leading Edge Optimization (LEO; Gao et al, 2008) and Normalized Derivative Method (NDM; Moteki and Kondo, 2008). The NDM is computationally demanding, and both methods can fail when, for example, the sample flow rate fluctuates. Significant flow rate fluctuations were observed in the SP2 measurements conducted at Pallas station in northern Finland during winter 2011-2012. To improve the coating thickness calculations, we have improved the NDM method so that the computationally heavy a priori estimate of the scattering signal is replaced by a linear fit to the normalized derivative and a fast posteriori likelihood test.

Figure 1 shows number concentrations of the different particle types. Concentrations are low in this pristine environment, but about 10 % of the observed (150-500 nm) particles contain BC. In addition, practically all BC particles are coated.

Figure 2 shows coating thickness distributions based on the original scattering sizes and those calculated with LEO, NDM and the new method. Due to the fluctuating flow rate, the NDM often fails to find a solution. The LEO method can find a solution, but it could overestimate coating thickness. The new method finds a reasonable solution for most particles (4715 of 5973) and the results show that most particles are thinly coated (68 % have less than 50 nm coating). This finding is in good agreement with the observation that 73 % of these particles experienced rapid coating evaporation determined from the lag time between scattering and incandescence peak signals. Further calibration experiments with mixed particles will be used to show that the new method finds the correct scattering size.

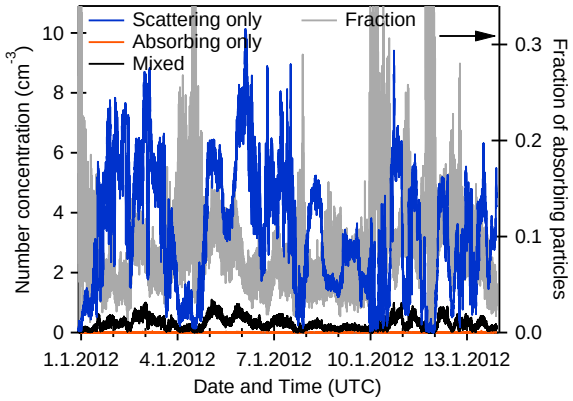

Figure 1. Total concentrations of scattering, absorbing and mixed particles from the 150-500 nm size range, and the fraction of absorbing particles.

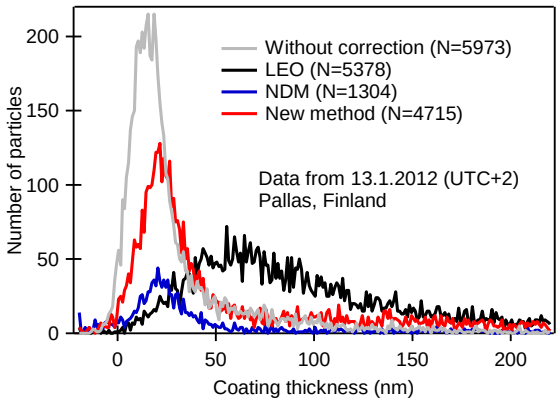

Figure 2. Coating thickness distributions for mixed particles which BC core diameter is 150-170 nm.

The work is supported by the EU LIFE+ project MACEB (project no. LIFE09 ENV/FI/000572), the Academy of Finland through the FCoE in Physics, Chemistry, Biology and Meteorology of Atmospheric Composition and Climate Change (program no. 1118615), black and brown carbon influence on climate and climate change in India – from local to regional scale (project no. 264242), Arctic Absorbing Aerosols and Albedo of Snow (project no. 3162) and the Nordic research and innovation initiative CRAICC.

Gao, R.S., et al. (2007) *Aerosol Sci. Technol.* **41**, 125-135.

Moteki, N. and Kondo, Y. (2008) *J. Aerosol. Sci.* **39**, 348-364.

Stephens, M., Turner, N. and Sandberg, J. (2003) *Appl. Opt.* **42**, 3726-3736.

Particle emissions from bushfires extending into the rural-urban interface

F. Reisen[1], M. Bhujel[1] and P. Selleck[1]

[1]Centre for Australian Weather and Climate Research, CSIRO Marine and Atmospheric Research, Aspendale, Victoria 3195, Australia

Keywords: combustion, building materials, carbon, PAHs.

Presenting author email: Fabienne.Reisen@csiro.au

Bushfires extending into the rural urban interface (RUI) have become more common, particularly in Southern Australia, California and southern Europe and have resulted in losses of life and properties. Climate change is predicted to increase both fire severity and fire season duration while a forecasted population growth in the RUI will expose more residents and homes to an increased bushfire risk.

Bushfires can release substantial quantities of particulate matter into the air environments of communities, both nearby and distant. When bushfires extend into the RUI, vegetation fuels but also structural fuels will burn and release additional chemicals into the air which may cause an increased health risk. Currently information on the composition of emissions and smoke plumes from fires at the RUI is scarce.

In order to assess the particle emissions from fires in the RUI, small-scale fire tests using a cone calorimeter were conducted on 11 selected building and furnishing materials. Samples were collected for analysis of gravimetric mass, organic (OC) and elemental (EC) carbon and polycyclic aromatic hydrocarbons (PAHs) along with continuous measurements of CO, CO_2 and fine particles ($PM_{2.5}$).

The time series analysis of $PM_{2.5}$ showed highest emissions during combustion of polyester insulation and a wool/nylon carpet. Maximum $PM_{2.5}$ concentrations were approximately 5-8 times higher than those measured during combustion of pine. Among wood-based products, combustion of medium-density fibreboard (MDF) resulted in highest peak $PM_{2.5}$ concentrations.

Emission yields expressed as mass of compound generated per mass of material combusted were calculated for CO, CO_2, $PM_{2.5,}$ EC, OC and PAHs. Highest emission yields of $PM_{2.5}$ were measured for polyester and polystyrene, both materials emitting about 20 times more particles compared to wood. Wood-based products had the lowest $PM_{2.5}$ yields.

Wood-based materials had the lowest carbon emission yields while polyester, carpet and polystyrene had the highest carbon emission yields (approximately 10 times higher). In general there was a larger fraction of EC compared to OC, with the exception of plasterboard and polystyrene where we observed a significant OC fraction (70-98%). The presence of glues and resins in manufactured wood products also increased the organic fraction of particles.

Highest PAH yields were observed for polyester, followed by polystyrene and carpet. The wood-based products had the lowest PAH yields (Figure 1). Naphthalene made up the majority of the total PAH yields (37-90%). Other PAHs with significant contributions included phenanthrene, fluoranthene and pyrene. Benzo(a)pyrene, a known human carcinogen contributed between 0.6 and 4.2% to the total PAH yields, with the highest contribution from the combustion of polyester.

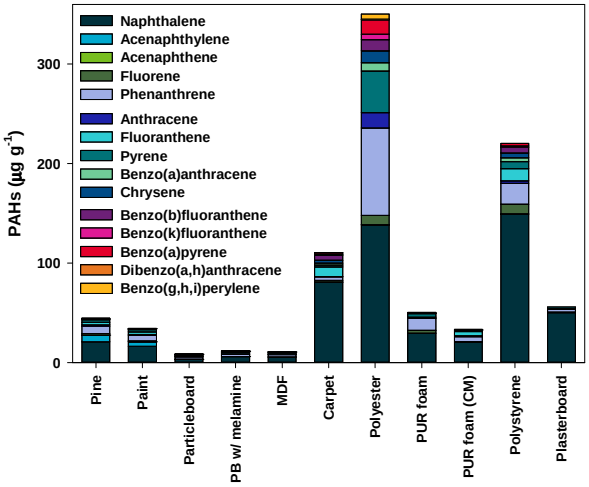

Figure 1. Distribution of individual PAHs emitted during combustion of selected materials

The study revealed that among the 11 materials that were tested, the most pollution resulted from the combustion of a wool/nylon carpet and polyester insulation. These materials ranked high in emissions of CO, particles, EC, OC and PAHs. However, as wood-based products make up the majority of mass in structures, the emissions from those materials may contribute more significantly to total emissions and hence to exposures. The emissions characterized in the small-scale fire tests will serve as input into a high time-resolution dispersion model that will enable to determine short-term modelled ground concentrations and provide an estimate of potentially hazardous exposures.

This work was funded by the Bushfire Cooperative Research Centre.

Measurements of the variation in hygroscopic growth of organic aerosol with oxygen-to-carbon ratio (O/C)

A.M.J. Rickards, R.E.H. Miles, J.F. Davies, F.H. Marshall, and J.P. Reid

Bristol Aerosol Research Centre, School of Chemistry, University of Bristol, Bristol, BS8 1TS, United Kingdom
Keywords: hygroscopicity, kappa, O/C, single particle analysis.
Presenting author email: Andrew.Rickards@bristol.ac.uk

Aerosols play a vital role in influencing radiative forcing through both the direct and indirect effect. The radiative forcing due to the indirect effect, where the aerosol droplets act as cloud condensation nuclei, has been shown by the IPCC to have an uncertainty similar in magnitude to the effect from carbon dioxide and to be of opposite sign (Forster et al., 2007). To reduce this uncertainty it is important to characterise how aerosol droplets of different compositions grow in size when exposed to increasing relative humidity (RH). This is referred to as aerosol hygroscopicity, and quantifies the equilibrium size of particles and also the extent of their light extinction.

Hygroscopic growth can be represented by a radial growth factor (GF). This is the ratio of the wet to dry particle sizes, and varies as a function of RH. To create a universal measure of hygroscopicity, Petters and Kreidenweis (Petters & Kreidenweis, 2007) have parameterised the GF in terms of a hygroscopicity parameter kappa, κ, and RH. It has been suggested in various studies that κ correlates with the magnitude of the m/z 44 ion fragment expressed as a fraction of the total organic ion signal, taken from aerosol mass spectrometry measurements. This ion fragment is usually attributed to the presence of a CO_2^+ ion, and has in turn been suggested to correlate with the oxygen to carbon ratio (O/C), indicative of the photochemical age of secondary organic aerosol (SOA) (Duplissy et al., 2011).

In this study, hygroscopicity measurements on single aerosol droplets of known composition were made using both aerosol optical tweezers (AOT) and an electrodynamic balance (EDB). The AOT allowed simultaneous determination of droplet size and refractive index at a particular RH through analysis of whispering gallery modes in the Raman spectra. This could then be converted into a radial GF. Kinetic measurements of the evaporative flux and equilibration of initially dilute droplets were made using the EDB at a well-defined RH. The mass flux equations of Kulmala et al. (Kulmala, Vesala, & Wagner, 1993) were employed to calculate the droplet water activity during evaporation, and thus deduce the hygroscopicity up to water activities approaching saturation. Initial focus was on compounds with O/C = 1, with the aim of determining how tightly constrained κ is for a fixed O/C ratio. The research was then expanded to look at compounds with a significantly higher and lower O/C to determine whether these were distinguishable from compounds with O/C = 1 on the basis of κ. Figure 1 shows an example of a GF measurement for the compound galactose.

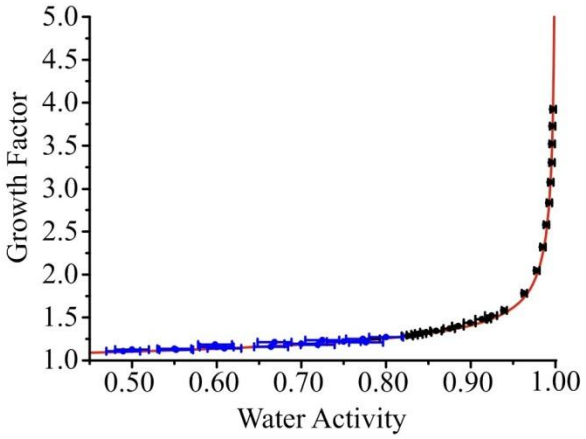

Figure 1. Experimental GF data for galactose from AOT (points below 0.8) and EDB (points above 0.8) compared to the AIOMFAC prediction (solid line).

In addition, published experimental data for κ were compiled and compared against O/C. The reported aerosol κ values include studies at subsaturated conditions and supersaturated conditions, single particle measurements and ensemble measurements, and a variety of experimental systems from field measurements to chamber SOA.

Experimental data and comparison with literature results strongly suggests the use of O/C as an indicator of κ should be more fully evaluated. O/C is a coarse parameter and ignores differences in chemical structure that may affect hygroscopicity.

This work is funded by the EPSRC and the NERC.

Duplissy, J., DeCarlo, P. F., Dommen, J., Alfarra, M. R., Metzger, a., Barmpadimos, I., Prevot, a. S. H., et al. (2011). *Atmospheric Chemistry and Physics*, *11*(3), 1155–1165. doi:10.5194/acp-11-1155-2011

Forster, P., Ramaswamy, V., Artaxo, P., Berntsen, T., Betts, R., Fahey, D. W., Haywood, J., et al. (2007). *Changes in Atmospheric Constituents and in Radiative Forcing*. *Change*. Cambridge University Press.

Kulmala, M., Vesala, T., & Wagner, P. E. (1993). *Proceedings of the Royal Society A: Mathematical, Physical and Engineering Sciences*, *441*(1913), 589–605. doi:10.1098/rspa.1993.0081

Petters, M. D., & Kreidenweis, S. M. (2007). *Atmospheric Chemistry and Physics*, *7*(8), 1961–1971. doi:10.5194/acp-7-1961-2007

Overview of the French contribution to the EMEP 2012-2013 summer and winter campaigns

V. Riffault[1], J.L. Jaffrezo[2], J. Sciare[3], K. Sellegri[4], S. Sauvage[1], V. Crenn[1], A. Waked[2], J.E. Petit[3,5], A. Colomb[4], S. Conil[6], J.L. Besombes[7], A. Setyan[1], E. Freney[4], T. Leonardis[1], N. Locoge[1], V. Gros[3], N. Bonnaire[3], R. Sarda-Estève[3], F. Dulac[3], M. Hervo[4], L. Chiappini[5], O. Favez[5], F. Gheusi[8], G. Athier[8], M. Mallet[8], T. Bourrianne[9], G. Roberts[9], N. Pascal[10], J. Descloitres[10]

[1]Mines Douai, CE, F-59508 Douai, France; [2]LGGE (Univ Grenoble / CNRS), F-38402 Saint-Martin d'Hères, France; [3]LSCE (CEA-CNRS-UVSQ), F-91190 Gif/Yvette, France; [4]LaMP (UPB-CNRS-OPGC), F-63171, Aubière, France; [5]INERIS, F-60550 Verneuil-en-Halatte, France; [6]ANDRA-OPE, F-55290, Bure, France; [7]LCME (Univ Savoie), F-73376 Le Bourget du Lac, France; [8]OMP/LA (Univ Toulouse / CNRS), F-31400, Toulouse, France; [9]CNRM(Météo-France / CNRS), F-31057 Toulouse, France ; [10]ICARE (Univ Lille1), F-59655 Villeneuve d'Ascq, France

Keywords: Chemical speciation, source apportionment, vertical profile, precursor VOCs

Presenting author email: veronique.riffault@mines-douai.fr

The EMEP network aims at providing scientific support on atmospheric monitoring and modelling, emission inventories and projections, and integrated assessment modelling. To reach these objectives, it has encouraged long- and short-term measurement periods in order to improve the scientific knowledge on PM levels, sources and formation processes at the European scale.

Within this framework and in coordination with the existing ChArMEx French program and ACTRIS EU project, two intensive periods have been held between June 8 and July 12, 2012 for summer and January 11 to February 8, 2013 for winter. Five locations in France (cf. Figure 1) were equipped with various on-line and off-line instruments (cf. Table 1) aiming at measuring PM chemical and physical properties, as well as precursor gases (both organic and inorganic).

The main objectives of these two campaigns were to (i) provide a large quality controlled database of PM levels and chemical composition for sites under rural, mid-altitude, urban or marine influences during two contrasted seasons; (ii) measure simultaneously PM compounds and their precursors to better understand processes such as secondary organic aerosols (SOA) formation or condensation of semi-volatile species; (iii) assess the importance of vertical exchanges in the variability of PM ground levels, especially in case of dust events; (iv) determine PM sources and their relative contributions.

Preliminary results will be presented and discussed.

The authors acknowledge funding from the French Agency of Environment and Energy Management (ADEME grants 1262C0022 and 1262C0039), the MISTRALS/ChArMEx program, the EU-FP7 ACTRIS program, CTC-CORSiCA and the CaPPA project (ANR-10-LABX-005).

Figure 1. Map of the EMEP winter and summer campaign sites in France (Google Maps - ©2013 Google)

Table 1. List of the various measurements carried out at the 5 sites during the winter (W) and summer (S) campaigns.

	Sampling period	Cap Corse	OPE	Puy-de-Dôme	Revin	SIRTA
PM_{10} mass	< 1hr	S, W	S, W	S, W	S, W	
$PM_{2.5}$ mass	< 1hr		S, W		S, W	
PM_1 mass		S, W				S, W
PM_{10} speciation	≥ daily	S, W	S, W	S, W	S, W	S, W
$PM_{2.5}$ speciation	≥ daily	S, W	S, W			S, W
PM_1 speciation (AMS, ACSM)	< 1hr	S, W		W	S	S, W
Black Carbon	< 1 hr	S, W	W	S, W	S, W	S, W
Precursor (O)VOCs	≤ 6 hrs	S, W		S, W	S, W	
NMHCs / (O)VOCs	< 1 hr	S			W	S, W
NO_x, CO and O_3	< 1 hr	S, W	S, W	S, W	S, W	S, W
CO_2	< 1 hr			S, W	S, W	S, W
SO_2	< 1 hr			S, W	S	
NH_3	< 1 hr				S	S, W
Diff./scat. coef.	< 1 hr	S, W	W	S, W		S, W
Extinction, AOD	< 1 hr	S, W	W	S, W		
Size distribution	< 1 hr	S, W	S, W	S, W		S, W

Dry deposition velocity measurements onto urban surfaces using atmospheric beryllium 7: development of a methodology and results

P. Roupsard[1,2], D. Maro[1], A. Coppalle[2], V. Ruban[3], M. Rozet[1], M. Talbaut[2], and S. Percot[3]

[1]Laboratoire de Radioécologie de Cherbourg-Octeville (LRC), Institut de Radioprotection et de Sûreté Nucléaire, Cherbourg-Octeville, 50130, France
[2]COmplexe de Recherche Interprofessionnel en Aérothermochimie (CORIA), Saint-Etienne du Rouvray, 76801, France
[3]Institut Français des Sciences et Technologies des Transports, de l'Aménagement et des Réseaux (IFSTTAR) de Nantes, Bouguenais, 44341, France
Keywords: dry deposition velocity, urban areas, beryllium 7, atmospheric aerosol
Presenting author email: roupsardpierre@laposte.net

Context and objectives

During the Fukushima nuclear plant accident, dry deposition has contributed to transfer particulate radionuclides (Katata et al., 2011). However, only few data on dry deposition in urban environment exists in the literature and very little is known (Fowler *et al.* 2009). The dry deposition transfer is quantified with the deposition velocity V_d (m s^{-1}), ratio between the aerosol dry deposition flux F (particles m^{-2} s^{-1}) and the aerosol concentration in the air C (particles m^{-3}). V_d depends on aerosol and deposit surface characteristics, and on meteorological conditions. Beryllium 7 (^{7}Be) is a natural radionuclide that can be used as a tracer to quantify V_d of the accumulation mode of the atmospheric aerosol.

The aim of the study is to develop and acquire an experimental method to measure V_d with urban surfaces, and onto ^{7}Be as a tracer, and to measure associated meteorological parameters. Results will be analysed and compared to the data of the literature to put in evidence the principal physical phenomena of deposition on urban surfaces.

Material and method

The experimental device is set up in the suburban of Nantes (France). It is composed of an assembly support equipped with urban surfaces (vertical glass and cement facing; horizontal asphalt and synthetic grass; slate, tile and zinc angled at 30°) directly exposed to the atmospheric aerosol to sample its deposits and to measure deposition fluxes. A roller blind protect it against precipitations. A Partisol® samples atmospheric aerosol on filter to measure the concentration of atmospheric ^{7}Be. An ultrasonic anemometer measures the wind speed at 1 m from the assembly support. Meteorological parameters are measured with a meteorological station. Each experiment was carried out for one month to sample quantifiable ^{7}Be deposits. Experiments are led during 15 consecutive months. ^{7}Be is measured by gamma spectrometry at the LRC. Filters containing atmospheric aerosol are put in geometries (cylindrical boxes) and directly measured. ^{7}Be deposit on urban surfaces must be recovered by washing with an acidic solution and put in geometries (50 mL container) to be measured. A method is developed to make corrections on measured activities that are underestimated with the washing method.

Results and discussions

Fig.1 shows the results of experiment. They are in the same order of magnitude than those measured by Roed (1987) using Tchernobyl radionuclides as tracers. However, for glass and cement facing, deposition velocities are higher than those measured by Maro *et al.* (2010) for the same surfaces with a generated fluorescein aerosol on 1 hour duration.

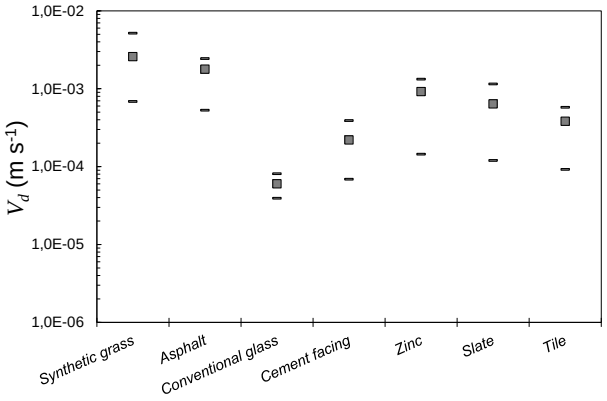

Fig. 1: V_d mean, minimum and maximum measured on each surface.

This highlights the role of additional physical phenomena on the long durations (1 month). The proposed hypothesis is the growing of atmospheric particles by water vapor condensation during dew episodes. Dry deposition velocities could be higher because of deposition rises by impaction and settling.

Conclusions

A measurement method of V_d using atmospheric ^{7}Be as a tracer has been developed. It permits to quantify V_d for real urban surfaces and to measure associated meteorological parameters. Results show differences in the order of magnitude between V_d measured on short duration expositions (~1 h) and on long duration expositions (~1 month). This involves an additional physical phenomenon contributing to the dry deposition on long durations. Further experiments will be necessary to explain differences between short and long durations. Particularly, continuous measurements of the atmospheric aerosol distribution will allow to verify the growing of particles and to measure their diameters during the dew episodes.

D. Fowler *et al.* (2009) *Atm. Env.* 43, 5193-5267.
G. Katata *et al.* (2011) *Jour. of Env. Rad.* 111, 2-12.
D. Maro et al. (2010) *Int. Aero. Conf*, Helsinki.
J. Roed (1987) *Rad. Prot. Dos.* 21, 33-36.

Seasonality of biological aerosol particles associated with African dust storms

Cristina Ruzene-Nespoli[1, 2], Janine Fröhlich-Nowoisky[1], T. Nunes[3], J. Cardoso[3, 4], C. Pio[3] & Ulrich Pöschl[1, 2]

[1]Multiphase Chemistry Department, Max Planck Institute for Chemistry, 55020, Mainz, Germany
[2]Institute of Geosciences, Johannes Gutenberg University, 55128, Mainz, Germany
[3]CESAM & Department of Environment, University of Aveiro, 3810-193, Aveiro, Portugal
[4]University of Cape Verde, Praia, 279, Santiago, Cabo Verde
Keywords: African dust, Bioaerosol, DNA
c.ruzene@mpic.de

There is a need to expand our knowledge of the diversity and biogeography of airborne microorganisms, since air connects all ecosystems at the Earth's surface. One of the most important phenomenon which can illustrate the role of the atmosphere as a dispersal mechanism for particulate matter is dust storms, that happen when the top soils from large deserts become airborne, and they can travel great distances through the atmosphere (Goudie and Middleton, 2001). More than half of the dust being transported in the atmosphere is believed to have originated from the Sahara-Sahel region in Africa (Kellog and Griffin, 2006). These dust storms are carrying microorganisms along with the mineral particles (Griffin, 2007).

Studies have shown that the global microbial taxa are not homogeneously distributed in the air, and the regional differences and how they come to be needs to be further understood (Fröhlich-Nowoisky *et al*, 2012). In order to better understand the relationship between microorganism transport and dust, the present study aims to seek for a rhythm in the airborne contents found in African dust events.

Air filter samples were collected between January 2011 and January 2012 in the Santiago Island from the Cape Verde archipelago. The sampling was done with a Hi-Vol with a PM10 head inlet and flow rate of 1,13 m^3min^{-1}.

Deoxyribonucleic acid (DNA) of filter sample aliquots were extracted, amplified, cloned and analysed as previously described (Fröhlich-Nowoisky *et al*, 2009). Primer pairs were used for targeting Fungi and Archaea.

Preliminary results show high species richness and seasonal cycles for different groups of Fungi and Archaea. In Archaea, there is a predominance of *Thaumarchaeota*, a recently defined phylum which contains all known ammonia-oxidizing Archaea (Stahl and de la Torre, 2012). Among *Euryarchaeota*, there are members of *Halobacteriales* and *Thermoplasmatales*, which are groups of extremophilic microorganisms. Although *Thaumarchaeota* are more diverse the whole year, the species richness for both phyla is highest in winter, which is the season with more dust storms, and lowest in spring.

For Fungi, *Basidiomycota* are slightly more diverse than *Ascomycota*. Members of the *Agaricomycetes* are predominant for *Basidiomycota*, with *Dothideomycetes* and *Sordariomycetes* appearing more often for *Ascomycota*. *Ascomycota* have higher species richness during summer and lower species richness during fall and winter, with a minimum in winter. *Basidiomycota* have a maximum of species richness in fall, with the lowest values observed during spring.

To expand the present data set, further results obtained from sequences that are still being analysed will be revealed.

Thanks for collaboration and support to M.O. Andreae, D. Jacob, N. Knothe, I. Müller, T. Pooya, the Max Planck Society (MPG), the LEC Geocycles in Mainz funded by the state Rheinland-Pfalz and the Portuguese Science Foundation through the project PTDD/AAC-CLI/100331/2008 (CV-Dust). J. Cardoso acknowledges the PhD grant SFRH-BD-6105-2009 from FCT.

Fröhlich-Nowoisky, J., Pickersgill, D.A., Després, V.R., & Pöschl U. (2009) *Proc. Natl Acad. Sci*. **106**, 12814-12819.

Fröhlich-Nowoisky, J., et al (2012) *Biogeosciences*, **9**, 1125–1136

Goudie, A.S. and Middleton, N.J. (2001) *Earth-Sci Rev* **56** (1–4), 179-204

Griffin, D.W. (2007) *Clin. Microbiol. Rev*. **20** (3), 459-477

Kellog, C.A. and Griffin D.W. (2006) *Trends Ecol Evol* **21** (11), 638-644

Stahl, D. A. and de la Torre, J. R. (2012) *Annu. Rev. Microbiol*. **66**, 83-101

Fluorescence based real-time measurements of atmospheric PBAP in urban environment

S. Saari[1], J.V. Niemi[2], T. Rönkkö[1], L. Pirjola[3], R. Hillamo[4], J. Keskinen[1]

[1]Department of Physics, Tampere University of Technology, P.O. Box 692, FI-33101 Tampere, Finland
[2]Helsinki Region Environmental Services Authority (HSY), P.O. Box 100, FI-00066 HSY, Finland
[3]Department of Technology, Metropolia University of Applied Science, Kalevankatu 43, FI-00180 Helsinki, Finland
[4]Air Quality, Finnish Meteorological Institute, Erik Palménin aukio 1, FI-00560 Helsinki, Finland

Keywords: fluorescence, bioaerosols, fungal spores, bacteria
Presenting author: sampo.saari@tut.fi

Primary Biogenic Aerosol Particles (PBAP) such as fungal spores and bacteria can act as CCN and IN in the atmosphere, so they have an impact on the global climate and precipitation. PBAP may contain living organisms, which can have various health effects for humans and animals. For these reasons, information on the concentration, size distribution, sources and types of PBAP are needed in various environments. Laser induced fluorescence (LIF) is a potential real-time method to detect PBAP. The LIF technique is selective for detecting biological molecules such as tryptophan, NADH and flavins that are present in bacterial cells and fungal spores. The focus on our previous studies was developing LIF based real time measurement technique for biological weapons detection (e.g. Manninen et al., 2009). The idea is processed to use similar measurement technique for atmospheric relevant fungal spores and bacteria. In recent studies, we found that airborne fungal spores and bacteria may have dissimilar fluorescence spectra, so it can be usable criteria in classification of atmospheric fungal spores and bacteria (Saari et al., 2013).

Our previous studies have focused on obtaining information of effective fluorescence measurement parameters of airborne fungal spores and bacteria that are the dominant in the PBAP number concentration fraction. There are still many problems to solve in LIF-based PBAP measurements. The fluorescence intensity from the aerosol particle depends mainly on the PBAP size and chemical composition but also on the instrumentation parameters. For these reasons, there is always a detection limit for smaller PBAP. So the particle size information is always necessary in the classification. We made parallel tests with the commercial UV-APS (TSI Corporation) and a self-made LIF-instrument called by BioScout. We found significant differences in counting efficiencies between the instruments for some common bacteria in laboratory conditions.

In this study, outdoor measurements were made with UV-APS and BioScout in urban environment during four time periods at winter, spring, summer and autumn. The results indicate that there are two dominant fluorescence particle modes during the measurement periods. We assume that the modes are mainly coming from fungal spores and bacteria. The concentrations and ratio of the fluorescent particle modes vary between the season periods. Sometimes there is strong diurnal variation in the fluorescent particle concentrations (Fig. 1). We found also that BioScout have much better fluorescent particle counting efficiency as compared to UV-APS. This is consistent with our laboratory results.

In conclusion, two LIF based instruments were tested in laboratory conditions and in urban environment. Preliminary results of outdoor measurements are promising. Real-time LIF technique seems to be suitable for atmospheric PBAP detection, but there are still many questions to answer and work to do. Investigation of the emission sources and transportation of PBAP needs meteorological data analysis and long term PBAP measurements with several instruments in various environments.

This work was supported by the Cluster for Energy and Environment (CLEEN Ltd) Measurement, Monitoring and Environmental Assessment (MMEA) Work package 4.5.2.

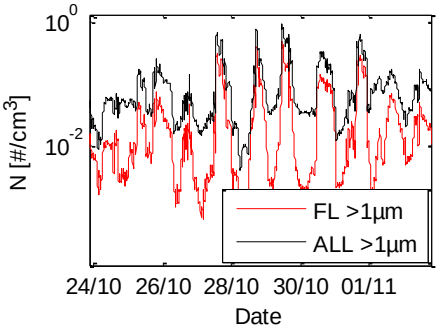

Fig. 1: Real-time data of the fluorescent and total particle concentrations measured by BioScout.

Manninen et al. (2009), Appl. Opt., 48, 4320

Saari et al. (2013), Accepted to Atm. Environment, DOI: 10.1016/j.atmosenv.2013.02.023

An observational study on air pollution conditions in two continuous haze periods in winter in Nanjing, China

Y.J. Zhang[1], L.L. Tang[2], H.L. Zhang[1] and L. Tang[1]

[1] Nanjing University of Information Science & Technology, Jiangsu Province 210044, P. R. China
[2] Jiangsu Environmental Monitoring Center, Jiangsu Province 210036, P. R. China
Keywords: Haze; Atmospheric particulate matter; Water-soluble ions; Pollution characteristics
Presenting author email: Yunj_mail@163.com

Two serious haze pollution courses occurred in Jiangsu Province, affected by the continuous haze weather conditions in the Central and East China in January 2013. According to the observed data from Jiangsu Environment Monitoring Center, the characteristics of particulate matter and gaseous pollutants these haze periods were analyzed. Results showed that the daily averaged mass concentrations of $PM_{2.5}$ were176-205 μg/m^3 as 5-6 times than the standards of EPA, and the maximum hourly value is 336 μg/m^3. Positive relationship between $PM_{2.5}$ and PM_{10} was found with correlation coefficients (R^2) as 0.87. Fine particles plays an important role in the two pollution process as $PM_{2.5}$ accounted for 70-86% of PM_{10}, The mass concentrations of SO_4^{2-}, NO_3^- and NH_4^+ exhibited higher values in submicron particles ($PM_{1.0}$) with the total mass concentrations of them accounting for 83% and 51% of those for $PM_{2.5}$. Meanwhile, the mass concentrations of $PM_{1.0}$ showed positive relationships with SO_4^{2-}, NO_3^- and NH_4^+, with the R^2 as 0.57, 0.65 and 0.73, respectively. While they exhibited worse correlations with $PM_{2.5}$ mass concentrations, indicating that these ions preferred to concentrate in the fine particles. A positive correlation between NH_4^+ with SO_4^{2-} and NO_3^- was found with R^2 as 0.8 and 0.85. The secondary aerosol obviously affected visibility. Positive relationship between black carton (BC) and visibility existed with R^2 as 0.31. BC make lower contribution to visibility when compared with the secondary aerosol which may be the key factors for the cause of the continuous haze weather conditions in the two periods.

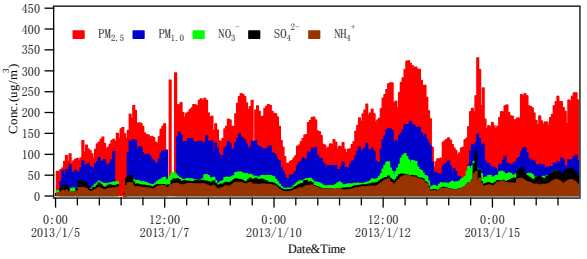

Figure 1. Time series of $PM_{2.5}$, $PM_{1.0}$, NO_3^-, SO_4^{2-}, and NH_4^+.

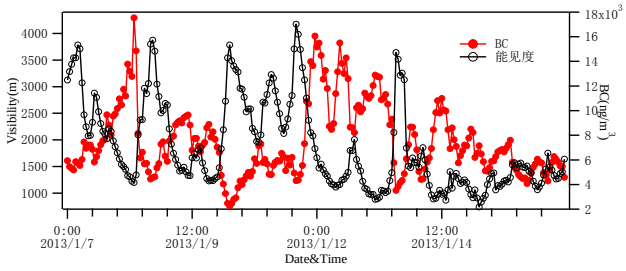

Figure 2. Time series of BC and visibility

This work was supported by the the High Education Natural Science Key Research of Jiangsu Province, China (Grant No. 11KJA170002)

José A. Morales, Danis Pirela. (1998) *Inorganic water soluble ions in atmospheric particles over Maracalibo Lake Basin in the western region of Venezuela* , Atmospheric Research. 46(3/4):307-320.

Peter K.K.Louies, Judith C.Chow. (2005) *$PM_{2.5}$ chemical composition in Hong Kong urban and regional variations*, Science of the Total Environment.338(3): 267-281.

Classification of Dust/Non-dust Particle from the Asian Dust Plumes and Retrieval of Microphysical Properties using Multiwavelength Raman Lidar System

S.K. Shin[1], Detelf Müller[2], Y.M. Noh[1], D.H. Shin[1], and K.H. Lee[3]

[1]School of Environmental Science & Engineering, Gwangju Institute of Science & Technology (GIST), Gwangju, 500-712, Korea
[2]Science System and Applications, Inc., NASA Langley Research Center, Hampton, VA23666, U. S. A.
[3]Department of Geoinformatics Engineering, Kyungil University, Gyungsan, Gyungsangbukdo, 712-701, Korea

Keywords: Lidar, Depolarization ratio, Asian dust, Single-scattering albedo
Presenting author email: skyun@gist.ac.kr

East Asia is one of the main source regions of aerosol pollution. It has been estimated that emission from industry and automobiles, dust emission from the large desert areas, and forest fire smoke in Siberia contribute to one-fourth to one-third of the total global emissions of the organic matter, soot, and dust (Ginoux *et al*., 2004). Dust storms that originate in the Taklamakan desert of China and the Gobi desert of Inner Mongolia occur frequently and are one major source of the dust emission in East Asia (Huang *et al*., 2005). Korea is located in the downwind area of the Asian continent and is significatly influenced by long-range transported dust in each spring season. Durinng transportthe dust particles could mix and react with other chemical components (e.g., SO_4^{2-}, NO_3^- and sea salt), which modify the optical and microphysical properties of the Asian dust.

In this study the particle depolarization ratio were retrieved from the observation with a multiwavelength Raman lidar at Gwangju, Korea (35.11˚N, 126.54˚E). The measurements were carried out on 24 February and 9 March 2004. Using the particle depolarization ratio, the non-dust particles were distinguished from the Asian dust plume, and the proportion of the non-dust particle to total dust plume was retrieved as shown in figure 1.

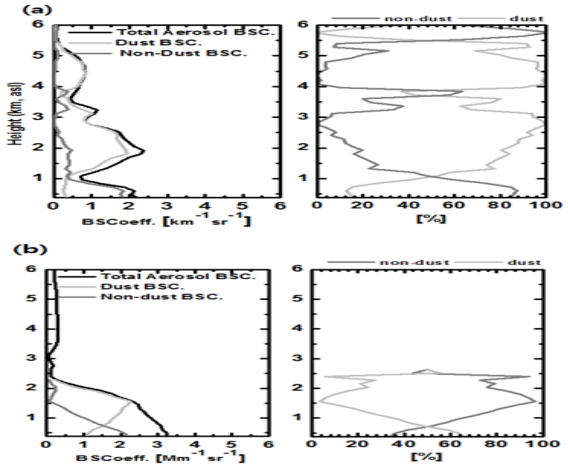

Figure 1. The vertical profiles of backscattering coefficient. The backscattering coefficient of total aerosol (black solid line), dust (light gray solid line) and non-dust particle (gray solid line) at 532 nm and the proportion of dust (gray color) and non-dust (light gray color) particle to the total aerosol (a) 24th Feb (b) 9th Mar

The calculated proportion of the non-dust particle was used for the retrieval of backscatter coefficients at 355, 532, and 1064nm and extinction coefficients at 355 and 532 nm of non-dust particles in the dust plume. Microphysical parameters of non-dust particles including single-scattering albedo at 532 nm were retrieved using retrieved optical values. The retrieved single-scattering albedo of non-dust particles was 0.92-0.95 below 1 km height and 0.82-0.91 above 1 km height on 24 February and 0.81±0.03 on 9 March 2004 as shown figure 2.

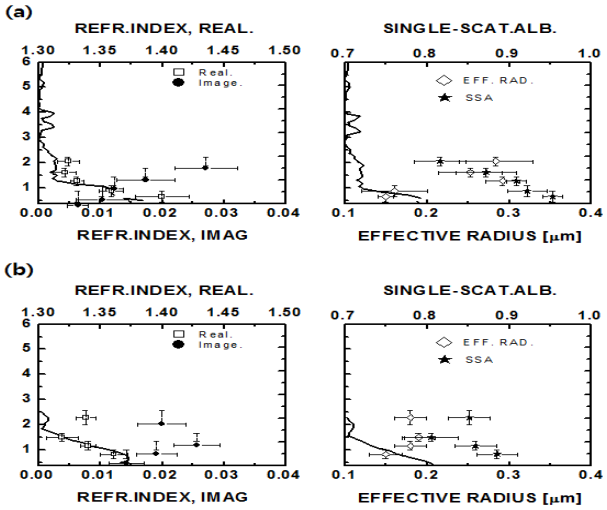

Figure 2. Microphysical parameters. Refractive index real part, Refractive index imaginary part, Particle effective radius and single scattering ableo

This work was funded by the CATER, Grant number 2012-7080 and Sungkyun Shin is supported by the Global Ph.D. Fellowship program which is sponsored by the National Research Foundation of Korea.

Ginoux, P., J.M.Prospero, O.Torres, and M.Chin (2004) Long term simulation of global dust distribution with the GOCART model: Correlation with North Atlantic Oscillation, *Environmental Modelling & Software*, **19**(2), 113-128.

Huang, J., P. Minnis, B. Lin, T. Wang, Y. Yi, Y. Hu, S. Sunmack, and K. Ayers (2005) Possible influences of Asian dust aerosols on cloud properties and radiative forcing ovserved from MODIS AND ceres, *Geophysical Research Letts*, **33**, L06824, doi:10.1029/2005GL024724.

Improvements to harmonize different soot measurement techniques in air quality monitoring networks

A. Schladitz[1], G. Löschau[1] and H.G. Kath[2]

[1]Saxon State Agency for Environment, Agriculture and Geology, Dresden, Saxony, 01326, Germany
[2]State Dept. for Environmental and Agricultural Operations in Saxony, Radebeul, Saxony, 01445, Germany
Keywords: Black carbon, Elemental carbon, Air quality guidelines
Presenting author email: alexander.schladitz@smul.sachsen.de

Measurements of soot particles in ambient air are depended on the definition of soot (Andreae and Gelencsér, 2006). While elemental carbon (EC) is analysed with thermal methods, black carbon (BC) is measured via optical methods by analysing the transmitted and reflected signal from a sample filter. So far, there exist intercomparison studies of BC and EC (e.g. Nordmann *et al.*, 2009) and between non-standardized measurement techniques for EC (Hitzenberger *et al.*, 2006). Up to now, intercomparison studies of BC and EC along different size fractions (PM_1, $PM_{2.5}$ and PM_{10}) for a longer time period (more than a year) are missing.

As a precaution to protect the human health and environment and in conjunction with new WHO air quality guidelines, BC and EC are simultaneously measured on certain hot spots within the Saxon air quality network (Dresden-Nord and Dresden-Winckelmannstr.). However, in the European air quality guideline 2008/50/EG neither a target value nor a limit value for EC or BC is included. Within the cross-border EU-project UltraSchwarz, BC is continuously measured and EC is measured every 6th day in Annaberg-Buchholz (Saxony; D) and Ústí nad Labem (Usti region, CZ). For consistency, BC is measured with a MAAP 5012 (Thermo Inc., Waltham, MA, USA) in all named sites downstream of a PM_1 - inlet and a membrane dryer in between. The membrane dryer guarantees that no measurement artefacts of BC on the deposited filter occur due to enhanced aerosol humidity. The relative humidity of the aerosol is monitored continuously and BC values with RH > 40% were disregarded. Sampling of EC occurs on quartz microfiber filters QFH 150 (Albet-Hahnemuehle, Dassel, D) downstream of a $PM_{2.5}$ - inlet for Annaberg-Buchholz and Ústí n. L. and a PM_1 - inlet for Dresden-Nord and Dresden-Winckelmannstr., respectively. EC is characterized by guideline VDI 2465 Part 1 using a carbon analyser (Ströhlein, Cuolomat 702).

Figure 1 shows a comparative measurement of BC (PM_1 – inlet) and EC (PM_1, $PM_{2.5}$ – inlet) at one site. Interestingly, both EC values do not differ significantly. Former measurements revealed that the EC mass fraction from traffic emissions is much smaller than $PM_{2.5}$, while the EC mass fraction originating from tire abrasion is larger than $PM_{2.5}$.

Figure 2 shows an intercomparison of BC and EC for all sites, partially with a different classification (ub = urban background, rs = roadside). All sites expect for Dresden-Winckelmannstr. show significant relation ($R^2 > 0.9$). A reason for the weak correlation for Dresden-Winckelmannstr. could be the less polluted season in summer 2012 with BC and EC values < 2µg/m^3 and a low daily variation. The measurement shall be repeated in the more polluted season.

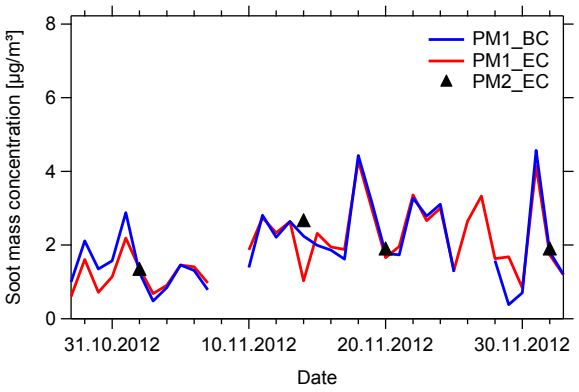

Figure 1: BC and EC time series for different size fractions for the site Annaberg-Buchholz.

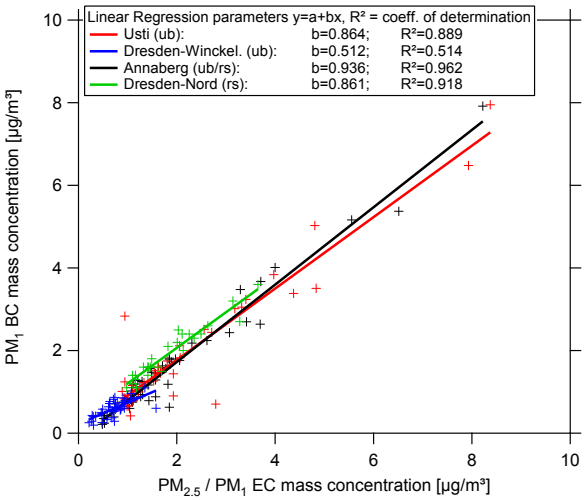

Figure 2: Intercomparison of BC and EC for different sites and classification (data from 1.1.2012 – 31.1.2013). For reasons of clarity the error bars were disregarded.

This work was co-financed by the European Regional Development Fund (ERDF). Many thanks to Helena Plachá and Mirosolav Bitter (both CHMU in Ústí) for providing the data for Ústí.

Andreae, M.O. and Gelencsér, A. (2006) *Atmos. Chem. Phys. 6,* 3131-3148.

Hitzenberger, R, Petzold, A. *et al.* (2006) *Environ. Sci. Technol. 40,* 6377-6383.

Nordmann, S., Birmili, W. *et al.* (2009) *Gefahrstoffe – Reinhaltung der Luft 69,* 469-474.

Single particle analysis of cloud residuals sampled at the research station Schneefernerhaus (2650 m) during ACRIDICON-Zugspitze 2012

S. Schmidt[1], J. Schneider[1], T. Klimach[1], S. Mertes[2], L.Schenk[2] and S. Borrmann[1, 3]

[1]Particle Chemistry Department, Max-Planck-Institute for Chemistry, 55128 Mainz, Germany
[2]Leibniz Institute for Tropospheric Research, Leipzig, Germany
[3]Institute for Atmospheric Physics, Johannes Gutenberg University, 55128 Mainz, Germany
Keywords: single particle analysis, cloud residuals, mass spectrometry
Presenting author email: susan.schmidt@mpic.de

During the ACRIDICON-Zugspitze campaign (17.09.2012 - 04.10.2012) at the research station Schneefernerhaus (German Alps, 2650 m a.s.l.) we investigated the chemical compositions of cloud residuals as well as the composition of the atmospheric background aerosol with a single particle mass spectrometer.

The cloud residuals were sampled with a counterflow virtual impactor (CVI; Mertes et al., 2005). During non-cloud periods this inlet was used as an aerosol-inlet to sample and analyse the background aerosol.

The chemical analysis of the cloud residuals and the background aerosol particles was done with the bipolar single particle mass spectrometer ALABAMA (Aircraft-based Laser Ablation Aerosol Mass Spectrometer) with a particle size range of 150 to 900 nm (Brands et al., 2011). Additionally the particle size was measured by an optical particle counter (OPC, Grimm 1.129) with a particle size range from 0.25 to 52 µm.

Over the whole time period about 3300 useable spectra were acquired during background aerosol measurements and about 5500 useable spectra of cloud residuals during cloud events. For further investigations only those spectra that have both polarities were used, in order to facilitate the assignment of these particles to distinct particle types. The evaluation of the data was done with the software package CRISP (Klimach et al., 2010) which contains three different sorting algorithms. This program allows for assignment for the mass spectra into different clusters that contain similar mass spectra. In this case the spectra were separated with the fuzzy c-means algorithm (Hinz et al., 1999).

The comparison of the chemical compositions of the cloud residuals and the particles of the background aerosol does not show any significant differences. This suggests that in the analysed size range all particles are activated as cloud droplets independent of their chemical composition. In both cases the main clusters contain particles with secondary inorganic compounds like sulphate and nitrate and potassium. For the cloud residuals this particle type represents 28% and for the background aerosol particles 24% of all investigated mass spectra.

Additionally, both the cloud residuals and the background aerosol particles show mainly particle types with secondary inorganic components internally mixed with organic compounds and/or carbon fragments.

The main difference between cloud residuals and background aerosol is that more particles containing lead were found in the cloud residuals (36 spectra in cloud residuals and only 3 in background aerosol). Whether the lead containing particles are preferably activated as cloud droplets or this finding is a result of different air mass origin has to be investigated.

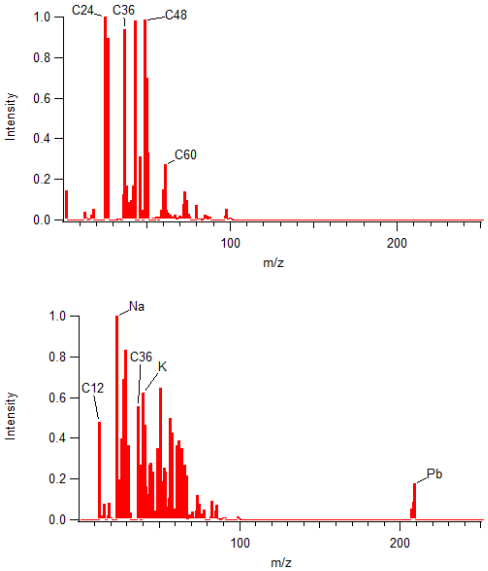

Fig. 1: Average spectra from the particle type which include lead of the background aerosol; above: anions, below: cations.

This work was supported by the DFG projects 1525 (INUIT), SPP 1294 (HALO) and the Max Planck Society (MPG).

Mertes, S., Lehmann, K., Nowak, A., Massling, A. and Wiedensohler, A. (2005). *Atmos. Environ.*, **39**, 4247-4256.

Brands, M., Kamphus, M., Böttger, T., Schneider, J., Drewnick, F., Roth, A., Curtius, J., Voigt, C., Borbon, A., Beekmann, M., Bourdon, A., Perrin, T. and Borrmann, S. (2011) *Aerosol Sci. Technol.*, **45**, 46-64.

Klimach, T., Drewnick, F., and Borrmann, S. (2010), International Aerosol Conference, Helsinki

Hinz, K.-P., Greweling, M., Drews, F., Spengler, B. (1999) *J Am Soc Mass Spectrom*, **10**, 648–660

In-situ single particle composition analysis of free tropospheric ice nuclei and ice residuals in mixed-phase clouds during INUIT-JFJ 2013

S. Schmidt[1], J. Schneider[1], T. Klimach[1], S. Mertes[2], L. Schenk[2], U. Kästner[2], F. Stratmann[2], U. Bundke[3], B. Nillius[3], F. Frank[3], J. Curtius[3] and S. Borrmann[1,4]
[1]Particle Chemistry Department, Max Planck Institute for Chemistry, 55128 Mainz, Germany
[2]Leibniz Institute for Tropospheric Research, 04318 Leipzig, Germany
[3]Institute for Atmospheric and Environmental Sciences, Goethe University, 60438 Frankfurt, Germany
[4]Institute for Atmospheric Physics, Johannes Gutenberg University, 55128 Mainz, Germany
Keywords: single particle analysis, ice nuclei, mass spectrometry
Presenting author email: susan.schmidt@mpic.de

During a field campaign at the High Alpine Research Station Jungfraujoch (JFJ, Swiss Alps, 3570 m a.s.l.) which was conducted in January/February 2013 in the framework of the research unit INUIT (Ice Nuclei research UnIT), we investigated the physico-chemical properties of ambient ice nuclei (IN) and ice particle residuals (IPR). By combining a pumped counterflow virtual impactor (PCVI) and online aerosol mass spectrometry, ice nuclei from ambient air, that were activated by an IN counter (FINCH) and pre-selected by the PCVI, were fed into an aerosol mass spectrometer and analyzed for their chemical composition, as well as for their microphysical properties. Additionally, ice crystals were sampled from ambient mixed-phase clouds by a unique Ice-CVI (Mertes et al, 2007) and their residues (IPR) were also analyzed in-situ by aerosol mass spectrometry.

Previous investigations conducted at the Jungfraujoch have shown that mineral dust particles dominate the ice particle residue number (Kamphus et al., 2010) but also black carbon was found to be enriched in these residual particles (Mertes et al., 2007; Cozic et al., 2008). The objective of the INUIT-JFJ 2013 campaign was to extend our understanding of ice formation beyond the previous findings with new instrumental techniques.

The chemical analysis of the IPR and IN was performed with the single particle mass spectrometer ALABAMA (Aircraft-based Laser Ablation Aerosol Mass Spectrometer) that covers a particle size range of 150 to 900 nm (Brands et al, 2011). Additionally, particle size was measured by an optical particle counter (OPC, Grimm 1.129) with a particle size range from 0.25 to 32 µm.

We acquired more than 600 mass spectra of IPR sampled by the Ice-CVI. The evaluation of the data will be done with the software package CRISP (Klimach et al., 2010). This program allows for the assignment of the mass spectra into different clusters that contain similar mass spectra. In this case the spectra will be sorted with the fuzzy c-means algorithm (Hinz et al. 1999).

The first preliminary analysis of the acquired IPR data shows that the most abundant particle type (17% of all mass spectra) has components of mineral dust like lithium (Li), sodium (Na), potassium (K), aluminum (Al), iron (Fe) but also organic compounds (Fig. 1). Another particle type (11% of all mass spectra) found in the IPR contains carbon fragments, organic compounds (OC), sodium, aluminum and potassium. These findings partially agree with the results from previous researches. After completion of the campaign, a more detailed analysis of the data will give further insights into the chemical nature of ice nuclei and ice particle residuals.

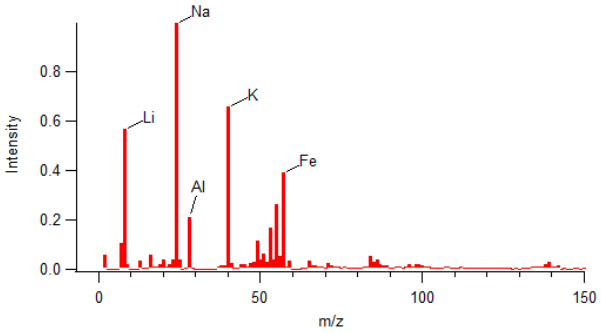

Fig. 1: Average mass spectrum of those mass spectra of ice residuals that were assigned to the largest cluster (17% of all spectra). The observed ions are characteristic for mineral dust.

This work was supported by the DFG projects 1525 (INUIT), SPP 1294 (HALO) and the Max Planck Society.

Mertes, S., Verheggen, B., Walter,S., Connolly,P., Ebert, M., Schneider, J., Bower, K. N., Cozic, J., Weinbruch, S., Baltensperger, U. and Weingartner, E. (2007) *Aerosol Sci. Technol.*, **41**, 848–864.

Kamphus, M., Ettner-Mahl, M., Klimach, T., Drewnick, F, Keller, L., Cziczo, D. J., Mertes, S., Borrmann, S. and Curtius, J. (2010) *Atmos. Chem. Phys.*, **10**, 8077–8095.

Cozic, J., Mertes, S., Verheggen, B., Cziczo, D. J., Gallavardin, S. J., Walter, S., Baltensperger, U. and Weingartner, E. (2008) *J. Geophys. Res.-Atmos.*, **113**, D15209.

Brands, M., Kamphus, M., Böttger, T., Schneider, J., Drewnick, F., Roth, A., Curtius, J., Voigt, C., Borbon, A., Beekmann, M., Bourdon, A., Perrin, T. and Borrmann, S. (2011) *Aerosol Sci. Technol.*, **45**, 46-64.

Klimach, T., Drewnick, F., and Borrmann, S. (2010), International Aerosol Conference, Helsinki

Hinz, K.-P., Greweling, M., Drews, F., Spengler, B. (1999) *J Am Soc Mass Spectrom*, **10**, 648–660.

New Homogeneous Ice Nucleation Results from Measurements at a Large Atmospheric Simulation Chamber

T. Schmitt, O. Möhler, D. Duft, M. Haarig, K. Höhler, A. Kiselev, I. Steinke and T. Leisner

Institute for Meteorology and Climate Research, Karlsruhe Institute of Technology, Hermann-von-Helmholtz-Platz 1, 76344 Eggenstein-Leopoldshafen, Germany
Keywords: cloud chamber, ice nucleation
Presenting author email: thea.schmitt@student.kit.edu

Phase transitions in clouds such as droplet formation by the condensation of water vapour or droplet freezing are in most cases heterogeneous processes triggered by aerosols. On the other hand, homogeneous ice nucleation without the participation of aerosols is an important process in deep convective systems, where almost pure water droplets are supercooled until homogeneous freezing occurs at temperatures below about 238 K.

A well cited theory which describes homogeneous ice nucleation was published by Pruppacher and Klett (1997). It is called classical nucleation theory and includes a number of uncertain parameters like the interface tension between the supercooled liquid and the ice phase or the activation energy. Therefore it is difficult to exactly formulate classical nucleation theory for a certain nucleating system like supercooled water drops. What is done instead is to fit classical nucleation theory formulations to experimental data, which also involve errors and uncertainties.

Here we present a reanalysis of droplet freezing experiments at the AIDA (Aerosol Interaction and Dynamics in the Atmosphere) cloud chamber at KIT, Karlsruhe, Germany, which follows experimental methods described by Benz *et al* (2005) who already published first homogeneous ice nucleation rates in supercooled water droplets derived from measurements at the AIDA facility.

At the large aerosol and cloud chamber AIDA the interaction between aerosol particles and clouds is being investigated. The facility operates under atmospherically relevant conditions within a wide range of temperature, pressure and humidity, whereby investigations of both tropospheric mixed-phase clouds and cirrus clouds can be realised. By controlled adiabatic expansions the ascent of an air parcel can be simulated. In order to investigate homogeneous freezing, sulphuric acid seed aerosol is typically injected into the chamber (Figure 1). By starting the expansion the gas temperature decreases and therefore the relative humidity rises whereby water condenses at the sulphuric acid droplets. They then grow until they are almost pure water drops. First ice particles appear at lower temperatures by homogeneous freezing. The ice particles then rapidly grow in size at the expense of the remaining droplets (Wegener-Bergeron-Findeisen process) with the result that at the end of the experiment only ice particles are left inside the chamber.

During these expansions, the aerosols, droplets and ice particles are monitored by a number of instruments. For the calculation of homogeneous ice nucleation rates the measurements of an optical particle counter (welas, PALAS GmbH) are used. The

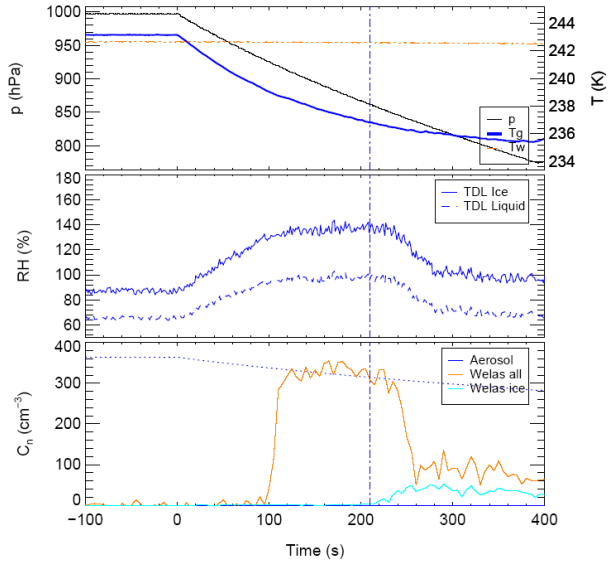

Figure 1. Data time series of a typical AIDA homogeneous droplet freezing experiment.

instrument detects the size of the resulting droplets and the number concentration of droplets and ice particles during the expansion. With these values homogeneous ice nucleation rates in supercooled water droplets can be calculated.

On the base of the new and improved data set we hope to achieve a more accurate fit of classical nucleation theory parameters. In addition, these new homogeneous ice nucleation results from the AIDA cloud chamber facility will be compared with homogeneous ice nucleation rates derived from other experiments like the cold stage where a droplet ensemble can be examined (Di Natale, 2012) or the Paul trap where single droplets can be studied by levitating them in an electrodynamic balance (Duft and Leisner, 2004; Rzesanke *et al*, 2012).

Benz, S., Megahed, K., Möhler, O., Saathoff, H., Wagner, R. and Schurath, U. (2005) *JPPA* **176**, 208-217.

Duft, D. and Leisner, T. (2004) *Atmos. Chem. Phys.* **4,** 1997-2000.

Di Natale, S. (2012) *Diploma Thesis – University of Heidelberg, Germany*.

Pruppacher, H.R. and Klett, J. (1997) *Microphysics of Clouds and Precipitation*, Kluwer Academic Publishers.

Rzesanke, D., Nadolny, J., Duft, D., Müller, R., Kiselev, A. and Leisner, T. (2012) *PCCP* **14,** 9359–9363.

Processing of ambient aerosols during fog events

A.Chakraborty[1], T.Gupta[1, 2] and S.N.Tripathi[1, 2]

[1]Department of Civil Engineering, IIT Kanpur, Kanpur, Uttar Pradesh, 208016, India
[2]Center for Environmental Science and Engineering, IIT Kanpur, Kanpur, Uttar Pradesh, 208016, India
Keywords: Fog processing, O/C, acidity.
Presenting author email: snt@iitk.ac.in

Fog is a major processing and removal agent of ambient aerosols. Enhanced secondary organic aerosol (SOA) production has been reported during fog events and there is a growing understanding that SOA formed via this aqueous processing can contribute significantly to ambient aerosol loading apart from traditional gaseous SOA.

The present study which was carried out during winter of 2012-13 in a heavily polluted city of Kanpur situated in Indo-Gangetic plane of India, focuses on identification and quantification of this aqueous processing of the ambient aerosols by natural fog. Although many smog chamber studies have been carried out to understand this aqueous processing and formation of SOA but often these studies were carried out in conditions not representative of complex ambient system and since very few ambient studies were reported till now so there is a need to evaluate what is happening in real ambient condition to properly understand this complex process.

During this campaign from 24 Nov, 2012 to 10 January, 2013, 12 fog events were captured from 20 Dec to 10 January and termed as foggy period while remaining as non foggy period. Foggy period typically showed very high RH and low temperatures than non foggy period with the highest RH (~95%) and lowest temperature (~3°C) occurring during actual fog events. We had deployed an array of instruments during this campaign for real time measurement of aerosol physicochemical properties – High Resolution Time of Flight Aerosol Mass Spectrometer (HR-ToF-AMS) for measurement of size resolved chemical composition of non refractory submicron aerosol, Scanning Mobility Particle Sizer (SMPS) for size distribution of submicron aerosol, Cloud Combination Probe (CCP) to measure fog droplet size distribution and liquid water content (LWC), Cloud Condensation Nuclei counter (CCN) to measure droplet forming potential of ambient aerosols, PM1 sampler and fog water collector, Vaisala RH & T sensor. This is the first time AMS is used in India and to our knowledge AMS has never used so extensively in ambient foggy condition before.

Average aerosol loading during foggy period was 104±44 μg/m^3, much higher than that of non foggy period which was 70±43 μg/m^3, but during actual fog events the loading was lowered to 85±23 μg/m^3 indicating overall aerosol removal by fog. Overall aerosol composition during both the period was dominated by organics which constitutes about 70% of total AMS mass followed by Nitrate, but during foggy period Sulfate was found to be increased many fold.

AMS and SMPS measured aerosol mass compared well. An average aerosol density of 1.3 g/cc was assumed for conversion from SMPS measured number to mass based on the measured aerosol chemical composition of 70% organics and 30% inorganic. Droplet size distribution and LWC revealed that every fog events consists of multiple cycles of dense and thin periods with highest LWC as high as 0.160 g/m^3 and average droplet size of 25±4 μm during densest periods.

HR-ToF-AMS measured aerosol O:C ratio was also analyzed to understand the real time variation in ambient organic aerosol oxidation level. Noticeable differences for the diurnal average values of O:C ratio between foggy and non foggy period are found. Although in both the period diurnal O:C ratio was higher around noontime typically representing photochemical activity but during foggy period the days were mostly hazy with very little and weak Sunlight, so fog processed aerosol may have retained their already oxidized products. During foggy period, night to early morning O:C ratio was 0.54±0.05, higher than that of non foggy period 0.43±0.03, clearly indicating enhanced oxidation activity, despite the fact that oxidized organics are preferentially scavenged by fog. Biomass burning activity doesn't seem to contribute much during any of the period as m/z = 60, 73 signals of AMS spectra which are the markers of biomass burning aerosol, remain low and almost the same. To our knowledge this is the first reporting of real time evolution of ambient oxidation level under foggy condition. AMS also showed that mode size of all the species specially organics and sulphate had shifted to a higher diameter during foggy period an indication of aging and mass addition via secondary production.

During foggy period the acidity of ambient aerosol which is measured by H^+ concentration was almost twice as high as non foggy period, mainly due to enhanced sulphate production. Although during actual fog events the acidity was lowered because of enhanced removal of sulphate which normally associated with larger droplets. Total organics from both the period showed very good correlation with aerosol acidity.

Kaul, D.S., Gupta, T, Tripathi, S.N., Tare, V., Collett Jr. J.L. (2011), *Secondary organic aerosol: A comparison between foggy and nonfoggy days*, Environmental Science & Technology, 45(17), 7307-7313.

Ervens, B, Turpin, B.J, Weber R. J., (2011), *Secondary organic aerosol formation in cloud droplets and aqueous particles (aqSOA): a review of laboratory, field and model studies*, Atmos. Chem. Phys., 11, 11069–11102.

Comparison of mass size distribution of PM and ions in Prague and Vienna in winter and summer

J. Schwarz[1], N. Zíková[1] , P. Vodička[1], I. Ševčíková[1], J. Kugler[1], A. Wonaschuetz[2], R. Wagner[2], I. Aschauer[2], W. Ludwig[2], R. Haindl[2], G. Zecha[2], R. Hitzenberger[2] and V. Ždímal[1]

[1]Department of Aerosol and Laser Studies, Institute of Chemical Process Fundamentals, Prague, 16502, Czech Republic
[2]Faculty of Physics, University of Vienna, Vienna, 1090, Austria

Keywords: urban environment, mass size distribution, water soluble ions.
Presenting author email: schwarz@icpf.cas.cz

Aerosol mass size distribution is an important factor that influences aerosol behavior both on local and global levels. The content of water soluble ions is the most important factor controlling hygroscopicity of aerosol particles. Hygroscopicity influences the dependence of particle size on relative humidity and therefore it is a substantial parameter for particle deposition in lungs, particle – cloud interactions, aerosol optical effects etc. Therefore, the size distribution of PM and water soluble ions was studied in two Central European capitals – Prague and Vienna both in summer and winter.

The measurements were done at an urban background site (Suchdol) located in the residential area in NW suburbs of Prague on the campus of the Institute of Chemical Process Fundamentals (ICPF) at 285 m a.s.l. The road with traffic density 10-15000 car per day is located in about 200m from the site. The closest house is placed about 30 m from the site. The sampling point was about 4 m above ground, on the roof of a sampling container. The sampling period was from 27th June to 7th July 2012, and from 6th to 15th February 2013. 11 samples were obtained in summer and 9 in winter. Each sampling took 23 hours.

The Vienna urban site was located on the roof of Faculty of Physics about 35 m above ground, close to the inner court of the building. The building is located in downtown Vienna but the roads next to the building have low traffic densities. The Vienna sampling period was from 17th to 30th July 2012, and from 14th to 30th with 9 samples in summer and 12 in winter. Each sample in Vienna took 23 hours except the weekend samples. Those two samples took 71 hour each.

The instrument used for size selective sampling followed by ion chromatography analysis of samples was a small deposit area cascade impactor (SDI) that has 12 stages and 11 l/min flow rate. The cut diameters of the stages were 0.041, 0.087, 0.15, 0.23, 0.34, 0.52, 0.73, 0.99, 1.5, 2.4, 4.2, and 8.0 µm (Maenhaut et al. 1996). The samples were extracted using 30 min ultrasonic bath and 1 hour shaking and analyzed using Dionex 5000 system both for cations and anions in parallel.

PM mass size distributions were determined using a Berner rotational cascade impactor with a flow rate of 25 l/min and calculated cut diameters of the stages 0.016, 0,032, 0.065, 0.13, 0.25, 0.5, 1, 2, 4, 8 µm.

The results we obtained on mass size distributions of mass and water soluble ions exhibit common basic features of ambient aerosols in Central Europe. E.g., mass size distributions in winter were dominated by a fine mode (see an example in Fig. 1). Sulfates and ammonium were almost exclusively present in the fine mode, fine nitrates were mostly low in summer (see an example in Fig. 2) due to high summer temperatures, but they had always a distinct coarse mode. Normal size distributions of ammonium and sulfates were often almost identical in summer due to low nitrates.

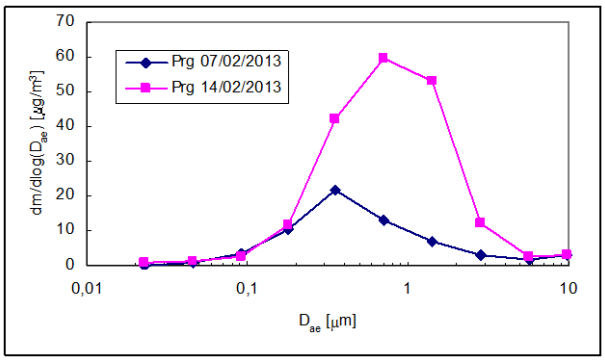

Fig. 1: An example of mass size distributions in Prague in winter

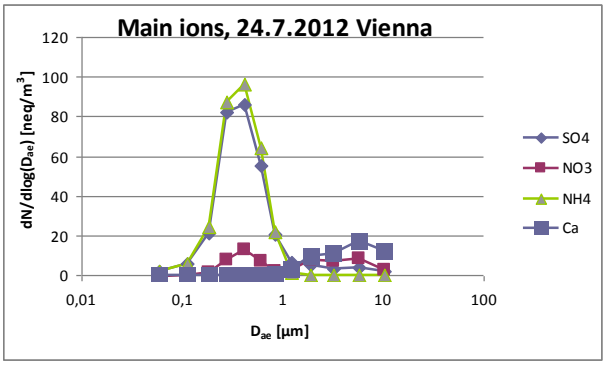

Fig. 2: An example of mass size distribution of ions in Vienna in summer.

This work was supported by the ÖAD, WTZ grant No. CZ 03/2012, the MEYS MOBILITY grant No. 7AMB12AT021, and the Czech Science Foundation grant No. P503/12/G147. We also thank to Prof. Willy Maenhaut for providing us with SDI impactors.

Maenhaut W., Hillamo R., Mäkela T., Jaffrezo J.-L., Bergin M.H., Davidson C.I., (1996)., *Nucl. Instrum. Methods B*, **109/110** 482-487

Characteristics of Local and Regional Nucleation Events at an Urban Background Site during Summer Period in Thessaloniki, Greece

D. Siakavaras[1], C. Samara[2], A. Kelessis[3], G. Biskos[1,4]

[1] Department of Environment, University of the Aegean, Mytilene 81100, Greece
[2]Department of Chemistry, Aristotle University of Thessaloniki, Thessaloniki 54124, Greece
[3]Environmental Department, Municipality of Thessaloniki, Paparigopoulou 7, Thessaloniki 54630, Greece
[4]Faculty of Applied Sciences, Delft University of Technology, Delft 2628-BL, The Netherlands

Keywords: PM, number size distribution, SMPS, nucleation events

Thessaloniki is a densely populated coastal city of northern Greece suffering from high concentrations of atmospheric particulate matter (PM). Previous studies have investigated the concentration levels, the chemical composition of PM, as well as the size distribution of particle mass concentrations and the relationship with PM mass, photochemical pollutants and meteorological parameters over the city (Voutsa *et al*., 2002; Petrakakis *et al*., 2007; Siakavaras *et al*., 2008; Terzi *et al*., 2010).

In this paper we report the characteristics of local and regional particle nucleation and growth events observed during the summer period. The measurements were carried out at Eptapyrgio: one of the urban background stations of the Municipality Air Quality network of Thessaloniki. A Scanning Mobility Particle Sizer (TSI, Model 3034) was employed to measure the size distributions of the particles having diameters in the range of 10-487 nm. An Integrating nephelometer (TSI, Model 3563) was also employed to measure the light scattering coefficient of the particles. $PM_{2.5}$ samples were collected on filters using a sequential sampler (Met One Instruments) for chemical characterization of the particles. Gaseous pollutants (CO, NO_x and O_3) and meteorological parameters (wind speed, wind direction, temperature and RH) were also recorded during the measurements. The experiments were conducted from 10 June to 20 July 2012.

Nucleation events were classified in 5 categories based on their intensity (Dal Maso *et al*., 2005). Almost 50% of the days exhibited new particle formation. More specifically, 11% of the days were classified as class Ia events, 16% as class Ib, and 21% as class II. Days that exhibited no clear particle formation patterns and thus were considered as undefined accounted for 34% of the total number of measurement days, whereas days that showed no events accounted for the rest 18%.

During the nucleation event of the 18th of June the apparent growth of the particles started locally at the lower detection limit (10 nm) at ca. 11.00 am and evolved until the end of the day to a particle size of 100 nm at a growth rate of 6.9 nm/h (cf. Fig. 1a).

At 7 days nucleation started at particle sizes around 20 nm. This is the case at the 19th of July where nucleation started at a remote site and particles were transported to the measuring site (Fig. 1b). Particles where detected at a size of 18 nm at 11:00 am and evolved until 15:00 pm to a size of 4 nm at a growth rate of 4.5 nm.

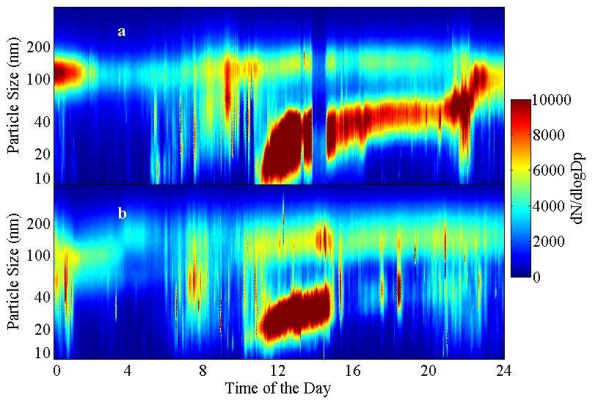

Figure 1. Typical number size distributions for a local particle formation and growth event on 18 June 2012 (a) and a regional particle formation and growth event on 19 July 2012 (b) at Eptapyrgio. On this day nucleation was transported to the site.

Acknowledgements
The SMPS used in this study was obtained through the AKMON 5 Project.
Research co-financed by the ESF and Greek national funds - Research Funding Program: Heracleitus II.
Research co-financed by Greece and the EU through operational program Education and Lifelong Learning of the NSRF - Research Funding ProgrammTHALES: Investing in knowledge society through the European Social Fund.

References

Voutsa, D., Samara, C., Kouimtzis, Th., Ochsenkuehn, K. (2002). *Atmospheric Environment*, 36, 4453-4462.

Siakavaras, D., Samara, C., Pilinis, C., Kelesis, A. *EAC2008, Thessaloniki, Greece, August 24-29, 2008 (*Abstract T02A043P).

Terzi, E., Argyropoulos, G., Bougatioti, A., Mihalopoulos, N., Nikolaou, K., Samara, C. (2010). *Atmospheric Environment*, 44, 2231-2239.

Petrakakis, M.J., Kelessis, A.G., Samara, C., Tzoumaka, P., Zoumakis, N.M., Iosifidis, E. CEMEPE 07, *Skiathos, June 24-28, 2007* (Proceedings pp 2471-2477).

Dal Maso,M., Kulmala, M., Riipinen, I., Wagner, R., Hussein, T., Aalto, P., Lehtinen, E.J (2005) Boreal Environment Research 10: 323-336.

MEASUREMENT CAPABILITIES OF THE POLAND-AOD NETWORK

A.Strzalkowska[1], P. Makuch[1], P. Pakszys[1], O. Zawadzka[2], P. Markuszewski[1],T. Zielinski[1], T. Petelski[1], K. M. Markowicz[2], I. Stachlewska[2], A. Ponczkowska[1], M. Wichorowski[1]
[1]Institute of Oceanology, Polish Academy of Science, Poland
[2]Institute of Geophysics, Faculty of Physics, University of Warsaw, Poland
Kaywords: POLAND-AOD, MICROTOPS, Volcano

The Poland-AOD research network was created in November 2011. The main purpose of this project are measurements and analysis of the optical properties of aerosols and radiative balance of the atmosphere. The network is composed of several laboratories such as the EUSAAR Sopot Station in the Institute of Oceanology Polish Academy of Sience, the University of Warsaw Radiative Transfer Laboratory, the Geophysical Obesrvatory in Belsk and the EUSAAR SolarAOT in Strzyzow. In spite of the fact that the network was officially established in November 2011, measurements were carried out under an unwritten cooperation at all four stations. The joint management of measurements gives a number of excellent results but the connection into one nationwide network offers many new opportunities.

The network was established to carry out work and develop climatology of the atmospheric aerosol optical properties and validation of inverse methods to determine the optical thickness and single scattering albedo from satellite data of MSG-9, as well as ground-based observations. Other tasks include modeling and experimental study of aerosol direct effect or transformation of the optical properties of aerosols based on contaminant transport models (NAAPS, GEM-AQ).

At each station measurements are made with the same equipment. The basic measuring devices are Multi-Filter-Rotating Shadowband Radiometer MFR-7 and Microtops photometers. Pyranometers and MFR-7 measure the radiation streams. The radiative balance at the upper boundary of the atmosphere is determined by the SEVIRI detector on satellite MSG-9. As one of the few networks POLAND-AOD makes measurements in the Baltic Sea. It is possible thanks to S/Y Oceania which belongs to IO PAS. During the research cruises measurements of the total scattering and back scattering coefficient are performed with use of the TSI Nephelometer. On S/Y Oceania scientists also uses AE-31/MAGEE Aethalometer to research concentration of soot and laser particle counter CSASP-100 and TSI Condensation Particle Counter for concentration and size distribution of aerosol particles.

Measurements are automatically collected from all stations of the network. Than the data are saved on a server located at the University of Warsaw Radiative Transfer Laboratory. The data are recorded on three levels. Level 1.0 is the raw data, at level 1.5 data are cloud-screened and at level 2.0 the data are quality-assured. All the research results are published on http://www.igf.fuw.edu.pl/meteo/stacja/PolandAODdata.php. The page is updated every minute.

In 2010 the European airspace was closed [1] because of the explosion of the Eyjafjöll volcano in Iceland. That gave an idea to measure optical properties of volcanic ash over Poland in these days. The observations were performed between 16 and 18 April at four Poland-AOD stations and in these case the measurements were not made only with Microtops sunphotometers. Instruments such as ceilometers and aerosol LIDARs also played a very important role. All analyses were supported with satellite data from MODIS, data analyses from AERONET and models such as FLEXOART or HYSPLIT. An indirect effect of volcanic aerosols on climate is through their influence on microphysical cloud properties [2]. That was the reason of combined LIDAR measurements with measurements which was made by the ceilometer.

Due to the presence of high cloud cover over the period between 16 and 18 April 2010 the remote sensing of the atmosphere over the region of central Europe was very difficult, especially on 16 April. AOD value ranged between 0.12 and 0.4 during the considered period and it was the highest on 16 April. Analyses of the optical properties of volcanic ash are difficult because they require knowledge about the particle size distribution, refractive index and particle shape. In order to simplify this problem uses the properties of desert dust particles according to the Optical Properties of Aerosol and Cloud Data Base [3].

1. IATA: Press Release, 2010. Volcano Crisis Cost Airlines $1.7 Billion in Revenue – IATA Urges Measures to Mitigate Impact: http://www.iata.org/pressroom/pr/Pages/2010-04-21-01.aspx, last access: 2 February 2011.
2. Durant, A. J., Shaw, R. A., Rose, W. I., Mi, Y., Ernst, G. G. J., 2008. Ice nucleation and overseeding of ice in volcanic clouds, J. Geophys. Res., **113**, D09206, doi:10.1029/2007JD009064.
3. Hess, M., Koepke, P., and Schult, I., 1998. Optical Properties of Aerosols and clouds: The software package OPAC, Bull. Am. Met. Soc., **79**, 831-844.

Aerosol characteristics during dust storm in Middle East and South-Western Asia

F. Subhan[1], K.Alam[1,2]

[1]Institute of Physics & Electronics, University of Peshawar, Peshawar,25120, Pakistan
[2]Higher education commission (HEC), Pakistan
Keywords: AOD, SSA, Radiative forcing, MODIS,AERONET.
Presenting author email: khanalamso@gmail.com

Aerosol optical and radiative properties were analyzed during dust storm in March, 2012 over Middle East and South-Western Asia using moderate resolution imaging Spectroradiometer (MODIS) and aerosol robotic network (AERONET) data. The aerosol optical depth (AOD) values were found maximum on 18th March in Kuwait, Bahrain, Qatar, and Saudi Arabia and were 4.948, 4.414, 4.283, and 4.999, respectively. The AOD values were also found maximum on 19th March in Oman, Arabian Sea, and Iran and were 4.552, 5, and 5, respectively. The dust storm spread over Pakistan and passed through Multan, Faisalabad, and Lahore. The maximum AOD values on 20th March were found to be 2.14, 2.63, and 2.66 over Multan, Faisalabad and Lahore, respectively. The aerosol volume size distributions were maximum during dusty days and minimum in non-dusty days in Lahore as shown in Figure.1.

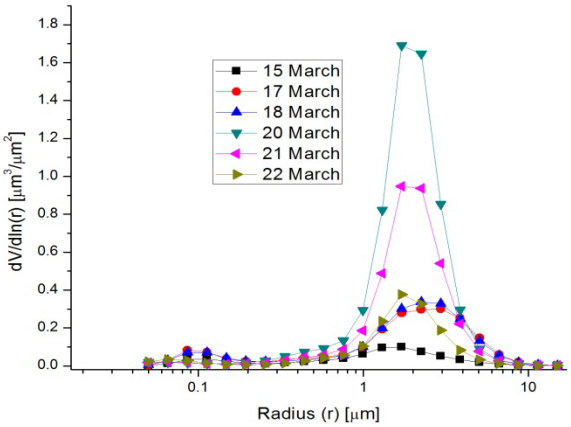

Figure.1. Aerosol volume size distribution during dust days (20-21 March) and non-dusty days (15,17,18,22 March)

The single scattering albedo (SSA) increases as wave length increases implying that SSA is wavelength dependent and increases rapidly with wavelength on the dusty days as compared non-dusty days. This rapid increase in SSA with wavelength revealed that dust particles were dominant and were of larger size as compared to other aerosols particles. The aerosol radiative forcing values at the surface and at top of atmosphere during dusty and non-dusty days were in the range of -64 Wm^{-2} to -260 Wm^{-2} (averaged -137±60 Wm^{-2}) and -20 Wm^{-2} to -105 Wm^{-2} (averaged -48±25 Wm^{-2}), respectively.

References

Alam, K., Trautmann, T., Blaschke, T., 2011a. Aerosol optical properties and radiative forcing over mega city Karachi. Atmospheric Research 101, 773-782.

Xia, X., Wang, P., Chen, H., Gouloub, P., Zhang, W., 2005. Ground-based remote sensing of aerosol optical properties over north China in spring. J. Remote Sens. 9, 429–437.

Zheng, Y., Liu, J., Wu, R., Li, Z., Wang, B., Tamio, T., 2008. Seasonal statistical characteristics of aerosol optical properties at a site near dust region in China. J.Geophys. Res. 113, D16205. doi:10.1029/2007JD009384.

Prasad, A.K., Singh, R.P., 2007. Changes in aerosol parameters during major dust storm events (2001-2005) over the Indo-Gangetic Plains using AERONET and MODIS data. Journal of Geophysical Research 112 (D09208). doi: 10.1029/ 2006JD007778.

Assessment of air pollution sources and implications for human health

Afrim SYLA, PhD Environment and Public health
University of Prishtina- Republic of Kosova
Tel. +377(0)44147473 ; E-mail: afrimsyla2002@yahoo.com

The present environmental situation in Mitrovica, put as in front of the responsibility to act more rationally towards nature and to be more responsible towards the protection of the environment for future generations. The protection lack of environment during the last ten years, as well as the conflict in Kosova as the origin of huge problems regarding present environmental situation in Mitrovica (Kosova). The city of Mitrovica, approcimately 40 km north of Prishtina, was the site of one the largest lead smelters in Europe, known as the Mitrovica Industrial Park.

Three potential sites have been identified by Environmental Deapartament, with the favoured site on the north bank of the Ibar at Bosniak Mahalla. However, a pilot soil survey (using portable XRF) by University of Prishtina at this site revealed very high metal levels (especially Pb) in the soils, and questions were therefore raised about the suitability of this site. Following discussions between Ministry of Environment ,University in Prishtina and Municipality, a series of objectives were identified relating to the three proposed development sites:

1. What are concentrations of Pb and other metals/metalloids in surface and sub-surface soils?

2. Are the Pb concentrations typical or atypical of soil Pb concentrations found elsewhere in Mitrovica city?

3. What is the bioaccessibility of soil Pb to the residents of Mitrovicë/a?

4. What is the source of the lead, and is the source still „active"?

Structural analysis of fine particles using a Time-of-Flight Secondary Ion Mass Spectrometer

A.Takami[1], N. Mayama[2,3], T. Sakamoto[3], K. Ohishi[3], S. Irei[1], A. Yoshino[4], S. Hatakeyama[4], K. Murano[5], Y. Sadanaga[6], H. Bandow[6], K. Misawa[2] and M. Fujii[2]

[1] National Institute for Environmental Studies, Tsukuba, Ibaraki 305-8506, Japan
[2]Tokyo Institute of Technology, Tokyo, [3]Kogakuin Univ., Tokyo, [4]Tokyo University of Agriculture and Technology, Tokyo, [5]Hosei Univ., Tokyo, [6]Osaka Prefecture Univ., Osaka, Japan
Keywords: Q-AMS, Fukue, long-range transport
Presenting author email: takamia@nies.go.jp

Rapid development in East Asian countries has brought the increase of emission of atmospheric pollutants (Ohara *et al.,* 2007). Gas and aerosol are transported from the Asian continent to the Pacific Ocean in the winter-spring by seasonal monsoon. Since the mixing state and chemical transformation of aerosol particles influence direct radiative forcing (Adachi *et al.,* 2010), individual particle analysis is important. Individual particles have been analyzed by electron probe microanalysis (EPMA) (Tomiyasu *et al.,* 1996), scanning electron microscopy (SEM) (Ault *et al.,* 2012) and transmission electron microscopy (TEM) (Adachi *et al.,* 2010). Recently, time-of-flight secondary ion mass spectrometry (TOF-SIMS) has been introduced to study the structure of aerosol particles (Sakamoto *et al.,* 2008). The TOF-SIMS can analyze the materials located inside the particles by the combination of FIB milling and repeated elemental mapping. We show the structure and chemical composition of fine aerosol particles with diameters of 1 μm collected in the East Asian region.

Sampling was performed at the National Institute of Environmental Studies (NIES) Fukue Atmospheric Observation site (Fukue site; 128.7E, 32.8N) in spring 2011. An Aerodyne quadrupole aerosol mass spectrometer (Q-AMS) was used for the continuous chemical analysis of aerosol. The TOF-SIMS sample was collected on the silicon substrate and was sent to Tokyo for the TOF-SIMS analysis.

Comparison of the Q-AMS measurement results with those of previous studies made at the same location (Takami *et al.* 2005) were similar, suggesting that the particle composition we observed is typical for this site.

Based on the results of TOF-SIMS, we classified the aerosol particles into three types: Type A, sulfate covered with Organic Matter (OM); Type B, soil-containing particles covered by sulfate and OM; Type C, BC and sulfate aggregates covered by OM (see Figure 1). As for Type B, soil was found inside the sulfate and OM was found on the outer surface. In Type C, BC was found at the edge and/or the surface of the sulfate, and formed BC-sulfate aggregates.

During the observation period, the relative abundances of Type A, B, and C particles were 55%, 20%, and 25%, respectively, while in Tokyo, they were 60%, 35%, and 5% (Table 1). More than half of the fine particles were light scattering, in Fukue and Tokyo. These results can be used for the revision and/or constraints of regional and global simulation for the radiative forcing.

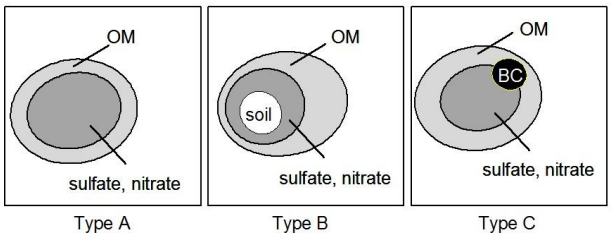

Figure 1 Schematics of the structures of fine particles of Types A to C

Table 1. The relative abundances of each type

	Type A (%)	Type B (%)	Type C(%)
Fukue	55	20	25
Tokyo	60	35	5

We greatly appreciate the support from GERF (B-1006, A-1101), MEXT-Shingakujutsu (ASEPH), and JST-SIRCP

Adachi, K., Chung,S.H., and Buseck, P.R. (2010), *J. Geophys. Res.*, *115*, D15206, doi:10.1029/ 2009 JD 012868.

Ault, A. P., Peters, T. M., Sawvel, E. J., Casuccio, G. S., Willis, R. D., Norris, G. A., and Grassian, V. H., (2012), *Environ. Sci. Technol.*, *46*(8), 4331−4339.

Ohara, T., Akimoto, H., Kurokawa. J, Horii, N., Yamaji, K., Yan, X., and Hayasaka, T. (2007), *Atmos. Chem. Phys.*, *7*(16), 4419–4444.

Sakamoto, T., Koizumi, M., Kawasaki, J., and Yamaguchi, J. (2008), *Appl. Surface Sci.*, *255*(4), 1617–1620.

Takami, A., Miyoshi, T., Shimono, S., and Hatakeyama, S., (2005), *Atmos. Environ.*, *39*(27), 4913–4924.

Tomiyasu, B., Arai, N, Koyama, H., Liu, G. L., Owari, M., and Nihei, Y. (1996), *Nippon Kagaku Kaishi, 5*, 500–507 (in Japanese).

Estimating PM2.5 in the Stockholm region from spaceborne AOT measurements

M. Tesche[1] and P. Glantz[1]

[1]Department for Applied Environmental Science, Stockholm University, Stockholm, Sweden
Keywords: PM2.5, aerosol optical thickness, air quality, remote sensing.
Presenting author email: matthias.tesche@itm.su.se

The aim of this study is to deduce surface PM2.5 for the region of Stockholm from satellite observations of aerosol optical thickness (AOT). Previous studies showed the potential for using aerosol observations from space for air-quality monitoring (e.g., Wang and Christopher, 2003; Hoff and Christopher, 2009 and references therein) — especially for tracking the pollution levels of in the air quality index. The present study is based on a previous work by Glantz *et al.* (2009). However, we now intended to obtain an AOT–PM2.5–relationship that is representative for the clean conditions that tend to prevail over the region of Stockholm. Note that it is yet to be explored if such methods can also be applied in a rather clean environment.

Here we use AOT at 555 nm from the MODIS collection 5 Atmosphere and Land product for MODIS–Terra (MOD04_L2, since 1999) and MODIS–Aqua (MYD04_L2, since 2002). AOT is provided with a spatial resolution (pixel size) of 10 km × 10 km. MODIS AOT was checked for reliability by means of a comparison to measurements carried out at the four long–term AERONET stations in Sweden: Gotland, Gustav Dalen Tower, Palgrunden, and SMHI. MODIS AOT was found to be well within the expected uncertainty range of $\pm 0.05 \pm 0.05 \times$AOT. It was also found that periods with AOT larger than 0.2 were scarce.

In the next step, the spaceborne AOT observations were related to surface measurements of PM2.5 at four in–situ measurement sites in the vicinity of Stockholm: Aspvreten (since 2000), Norr Malma (since 2005), Lilla Essingen (since 2005), and Uppsala (since 2007). These sites are representative for regional and urban background conditions. An AOT–to–PM2.5 relationship was obtained for cases ich which AOT values were available for at least 7 of the 9 pixels around a ground site. We use the binning approach suggested by Wang and Christopher (2003) to account for the wide spread in the data of both in–situ and MODIS observations. Furthermore, the AOT–to–PM2.5 relationship was obtained by using the median values in the respective bins of 0.05 AOT rather than the mean values. This approach reduces the impact of extreme values to the final outcome. Measurements of meteorological parameters (i.e., relative humidity, wind speed and direction) were available at the in–situ stations. Additional AOT–to–PM2.5 relationships were determined for cases in which the individual meteorological parameters showed values above and below their median values, respectively. These measurements were used to investigate possible effects of the meteorological situation on the median AOT–to–PM2.5 relationship and to properly assess the error of the PM2.5 retrieval. Note again that few cases occurred for which the PM2.5 concentration exceeded values of 30 μg m^{-3} or AOT was larger than 0.45. Hence, the obtained AOT–to–PM2.5 relationship is representative for relatively clean conditions.

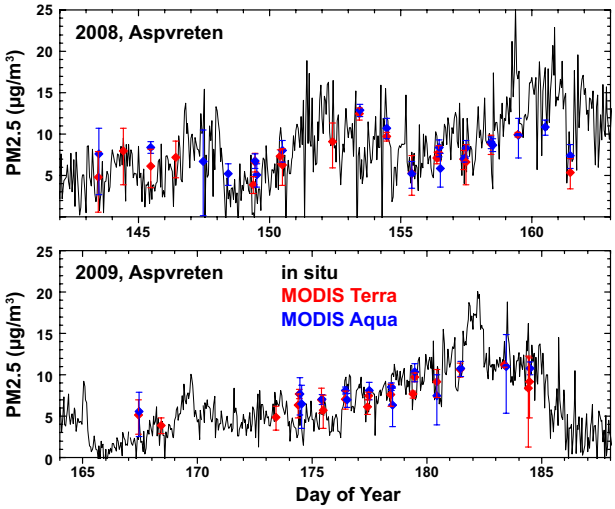

Figure 1: Retrieved (diamonds and error bars) and measured (black line) PM2.5 concentration at Aspvreten for selected time periods in 2008 and 2009.

Figure 1 presents PM2.5 time series for two selected periods in 2008 and 2009. PM2.5 as retrieved from MODIS observations agree with the surface measurements and follows the variation that occurred during the respective time periods.

Note that the AOT–to–PM2.5 relationship is established based on an assumption of homogeneous aerosol conditions within the planetary boundary layer (PBL) and an absence of elevated aerosol layers. While these conditions are widely given for the Stockholm region, future developments will focus on how seasonal differences in PBL development influence the retrieval of PM2.5 from satellite observations.

This work was supported by FORMAS under grant 216–2010–910.

Glantz *et al.* (2009) *Atmos. Environ.* **43**, 5838–5846.

Hoff, R. M. and Christopher S. A. (2009) *J. Air Waste Manag. Assoc.* **59**, 645–675.

Wang, J. and Christopher, S. A. (2003) *Geophys. Res. Lett.* **30**, doi:10.1029/2003GL018174.

Reconciling aerosol light extinction from ground-based in-situ measurements and active satellite remote sensing

M. Tesche[1], N. Rastak[1], P. Glantz[1], H.–C. Hansson[1], I. Riipinen[1], and R. Charlson[2]

[1]Department for Applied Environmental Science, Stockholm University, Stockholm, Sweden
[2]Department of Atmospheric Sciences, University of Washington, Seattle, WA 98195, USA
Keywords: aerosol extinction, hygroscopic growth, CALIPSO, Zeppelin station.
Presenting author email: matthias.tesche@itm.su.se

Aerosols play an important role in the Earth's climate system. This is especially relevant for the vulnerable and clean Arctic, where even slight changes in aerosol size or concentration can have large effects on cloudiness and the radiative budget. To assess aerosol microphysical and optical properties, in–situ measurements are performed at Mt. Zeppelin, Svalbard, since the early 1990s (Ström *et al.*, 2001). However, in–situ measurements are usually performed with dried aerosol samples whose particle size distribution, refractive index, or extinction coefficient can vary significantly during different ambient (i.e., humid) conditions. Arctic aerosols were also found to be highly sensitive to relative humidity (Zieger *et al.*, 2010). Microphysical models are used to transform the measured properties of the dried aerosol sample to values that are representative for ambient conditions. Such numbers are needed for a reliable assessment of aerosol optical properties.

In this study we try to reconcile particle light extinction coefficients derived from humidifying dry in–situ measurements at Zeppelin station and ambient observations with the lidar aboard the Cloud–Aerosol Lidar and Infrared Pathfinder Satellite Observations (CALIPSO) satellite (Winker *et al.*, 2009). The high overpass rate of polar–orbiting satellites over the Svalbard region favors a systematic comparison of continuous ground–based in–situ measurements and spaceborne lidar observations. Previous studies revealed that high correlation in aerosol properties can be expected for distances of up to 500 km over water (Kovacs 2006). However, for this study we only considered overpasses at distances of less than 360 km from the ground site at Svalbard.

The present study focuses on measurements performed in 2008. A comparison of ambient extinction coefficients measured by CALIPSO with humidified extinction coefficients from the in-situ measurements could be performed for 57 suitable cases — mostly during winter and spring. Clouds, low aerosol load, and a strong solar background (i.e., low signal–to–noise ratio in the spaceborne lidar measurements) inhibit comparisons during summer.

Figure 1 summarizes the findings of this study. On the whole, humidified extinction coefficients from ground-based in–situ measurements and ambient extinction coefficients from spaceborne lidar measurements were found to agree within a factor of one to five with a majority of the values not exceeding a factor of two. This is a surprisingly good finding when considering the efforts necessary to come up with comparable quantities. CALIPSO extinction coefficients are generally larger than the ones derived from the humidification of in–situ measurements. Is has been observed previously, that extinction coefficients measured with lidar are larger than the ones obtained from in–situ measurements (e.g., Masonis *et al.*, 2002).

In the future we will expand this study to the entire CALIPSO data set that currently spans six years.

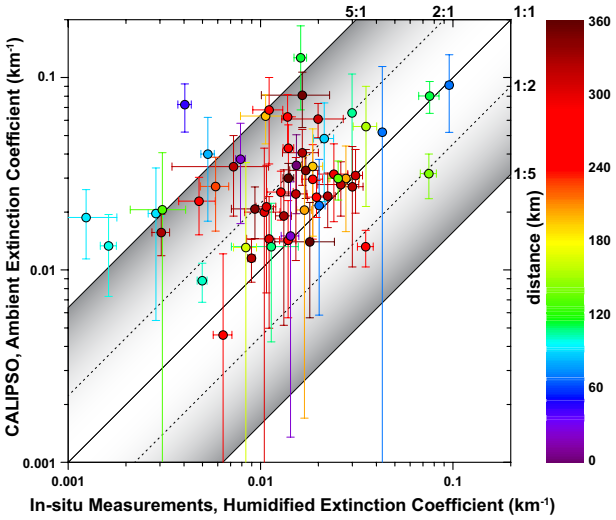

Figure 1: Comparison of the humidified extinction coefficient calculated from in–situ measurements at Zeppelin station with the ambient extinction coefficient extracted from CALIPSO overpasses for 57 suitable cases. The color coding describes the distance of the CALIPSO observation from the ground site. Error bars represent the standard deviation from averaging over 5 hourly nephelometer data points and 9 30–m CALIPSO height bins between 250 and 760 m, respectively. Ratios of 1:1, 1:2, and 1:5 are marked by solid and dashed lines as well as the shaded area.

Kovacs, T. (2006) *J. Geophys. Res.* **111**, 2006JD007349.
Masonis *et al.* (2002) *J. Geophys. Res.* **117 (D19)**, 8014.
Ström *et al.* (2001) *J. Phys. Chem. Earth.* **28**, 1181–1190.
Winker *et al.* (2009) *J. Atmos. Oceanic Technol.* **26**, 2310–2323.
Zieger *et al.* (2010) *Atmos. Chem. Phys.* **10**, 3875–389.

Investigating the Formation of H_2SO_4 from ion-induced Oxidation of SO_2

N.T. Tsona[1], N. Bork[1,2] and H. Vehkamäki[1]

[1]Department of Physics, University of Helsinki, Helsinki, 00014, Finland
[2]Department of Chemistry, University of Copenhagen, Copenhagen, 2100, Denmark
Keywords: Sulphuric acid, molecular clusters, ion-induced nucleation.
Presenting author email: narcisse.tsonatchinda@helsinki.fi

Atmospheric aerosols are very important in human life. They participate in the formation of cloud, acting as cloud condensation nuclei. Aerosols particles are either emitted directly to the atmosphere or produced by nucleation of gas-phase species. It is therefore fundamental to understand the formation of aerosols in order to predict climate. However, the mechanism of nucleation is not fully relatively understood.

Sulphuric acid (H_2SO_4) has been identified as an important precursor for the formation of atmospheric particles (Kulmala *et al* (2006)). It interacts strongly with bases, water, and various organics in the atmosphere and forms stable molecular clusters. Understanding the mechanism of nucleation is closely related to understanding the atmospheric production of H_2SO_4. H_2SO_4 is mostly from SO_2 oxidation by OH radical, catalysed by UV light. Recently, to complement the UV-induced mechanism, a new synthesis mechanism involving ions was found (Enghoff *et al* (2008)).

It was found that SO_2 reacts rapidly with e.g. O_2^-, O_3^-, and CO_3^- (Möhler *et al (*1992)) to form atmospherically relevant ions. Due to the low oxidation state of its sulfur atom, SO_2 is seemingly an important species in the production of ions relevant to aerosol science. Thereby, we have investigated the oxidation reaction of SO_2 by SO_4^-, detected in the atmosphere at relatively high concentration by Ehn *et al* (2010).

We used a density functional theory calculation to determine structures and formation energies of relevant species for our reactions. The reaction rates were determined using the transition state theory and all the calculations were performed at T=298.15 K and p= 1atm.

Results

Upon collision between SO_2 and SO_4^-, a $SO_2.SO_4^-$ cluster is formed and an oxidation subsequently occurs inside the cluster. The stable oxidation intermediate, $SO_3SO_3^-$, is formed with ca. 8 kcal/mol Gibbs free energy gain This means that the formation of $SO_3SO_3^-$ is a likely process at standard conditions. The energy gained by forming $SO_3SO_3^-$ might induce its decomposition into SO_3 and SO_3^-, but the decomposition reaction is endothermic by ca. 18 kcal/mol (Fig. 1). However, $SO_3SO_3^-$ is a long-lived species and may collide with abundant atmospheric species like O_2. The set of reactions

$$SO_4^-(H_2O)_{0\text{-}1} + SO_2 \rightarrow SO_3SO_3^-(H_2O)_{0\text{-}1}, \quad (R1)$$
$$SO_3SO_3^-(H_2O)_{0\text{-}1} + O_2 \rightarrow SO_5^-(H_2O)_{0\text{-}1} + SO_3, \quad (R2)$$

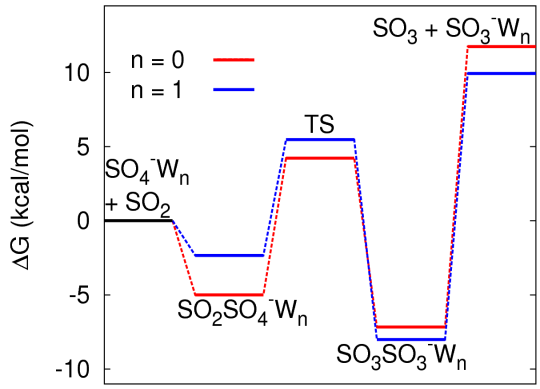

Figure 1. Free energy surface of SO_2 reaction with SO_4^-. The reaction forms a stable intermediate, $SO_3SO_3^-$, likely stable towards decomposition to SO_3 and SO_3^-. "TS" denotes transition state.

follows, where O_2 molecule induces evaporation of SO_3, while stabilizing SO_3^- as SO_5^-. The dehydrated products of reaction R2 is formed with ΔG=1.5 kcal/mol. The presence of water destabilizes the products by ca 3 kcal/mol. SO_3 easily hydrates in the atmosphere and is detected as H_2SO_4, while SO_5^-, detected in the atmosphere by Enh *et al* (2010) has been part of a complete study by Bork et al (2012).

Acknowledgments

This work was supported by Academy of Finland (LASTU Project No. 135054) and ERC Project No. 257360-MOCAPAF. We acknowledge the CSC IT Centre for Science in Espoo, Finland for computer time.

Kulmala, M., Lehtinen, K.E.J. and Laaksonen, A. (2006) *Atmos. Chem. Phys*. **6**, 787-793.

Enghoff, M.B. and Svensmark, H. (2008) *Atmos. Chem. Phys*. **8**, 4911-4923.

Möhler, O., Reiner, T. and Arnold, F. (1992) *J. Chem. Phys*. **97**, 8233-8239.

Ehn, M., Junninen, H., Petäjä, T., Kurtén, T., Kerminen, V.-M., Schobesberger, S., Manninen, H.E., Ortega, I.K., Vehkamäki, H., Kulmala M. and Worsnop, D.R. (2010). *Atmos. Chem. Phys*. **10**, 8513-8530.

Bork, N., Kurtén, T. and Vehkamäki, H. (2012) *Atmos. Chem. Phys. Discuss*. **12**, 30177–30201

Chemical characterization of aerosol particles in Évora: comparison between summer and winter campaigns

L.C. Tobias[1,2], N. Schiavon[2], K. Kandler[3], J. Mirão[2,4] and F. Wagner[1]

[1]Centro de Geofísica, Universidade de Évora, Évora, 7000-671, Portugal
[2]HERCULES Laboratory, Universidade de Évora, Évora, 7000-809, Portugal
[3]Institut für Angewandte Geowissenschaften, Technische Universität Darmstadt, 64287, Germany
[4]Centro de Química, Universidade de Évora, Évora, 7000-671, Portugal

Keywords: field campaign, aerosol chemistry, SEM-EDS, aerosol morphology
Presenting author email: lucia.nsvt@gmail.com

Introduction

Atmospheric aerosol particles play an important role in climate, air quality and human health.

In Portugal, extended time series on the chemistry and morphological parameters of atmospheric aerosol particles as well as on their seasonal dependency are still scarce and mostly confined to the North of the country.As part of a wider project on aerosol composition and distribution in Southwestern Iberia, in this study we compare aerosols collected in two intensive field measurement campaigns carried out in August 2011 and February 2012.

Experimental

In order to determine aerosol particle chemical and morphological properties, two sampling modes were adopted at the sampling site located on the roof of the Évora Geophysics Center:

- Active sampling:

Particles were collected on TEM grids by a cascade impactor and a vacuum pump with nominal particle diameter cut-offs at 1, 0.65, 0.45 and 0.25 µm. The samples were subsequently analysed by VP-SEM+EDS to obtain morphological and chemical compositional data.

- Passive sampling:

Particles were collected using a modified version of the aerosol passive sampler Type A “flat plates” by Ott and Peters (2008). The air could freely flow and particles were deposited by gravitation. The sampler was placed at the top of a university building about 15m above ground level. Sampling was performed weekly to account for the slow gravitational settling of particles.
Single particles automated analysis was performed using a HITACHI 3700N VP-SEM interfaced with a Bruker 5010 XFlash EDS and QUANTAX and automatic ESPRIT software.

The particles were classified into 9 chemical and mineralogical classes and into 4 morphological classes.

Results

Figure 1 shows an example of the relative % of the most abundant aerosol classes during two periods: 18-21 August 2011 and 14-21 February 2012. The relative amount of dust-related aerosols (quartz + silicates), increases generally with particle size. Dust aerosols seems to be more abundant in the larger grain-sizes and during the summer campaign, probably due to the incidence of desert storm episodes.

The sulphate concentrations are very different for the 2 set of samples in Fig. 1, with much higher % in summer suggesting a stronger sea salt contribution. It has to be noted that in winter campaign almost 50% of the smaller particles could not be attributed to one of the main chemical classes (Other). The majority of particles assigned to this *other class* did not display a EDS spectrum. On the other hand, the presence of organic and biological particles (with a low EDS signal also due to the C stub support) is to be expected if one takes into account the widespread use of wood as fuel for domestic heating and cooking is common in Évora especially during winter time.

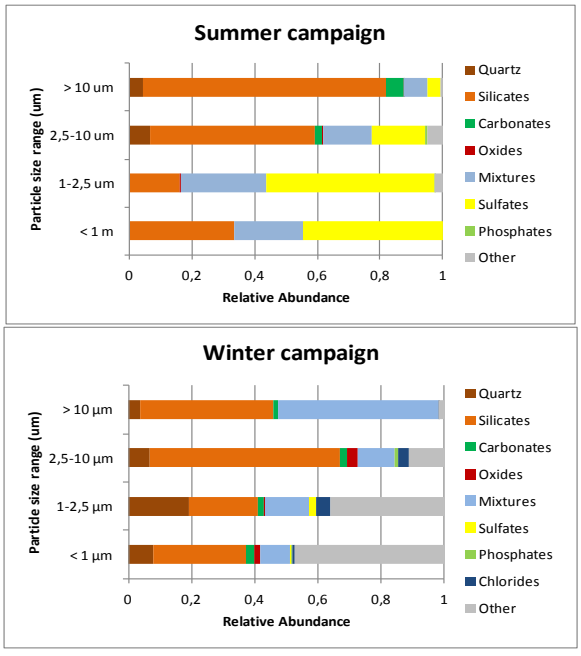

Figure1. Aerosol sampling periods: 18-21 August 2011 (top); 14-2 February 2012 (bottom)

This work was supported by the PTDC/AAC CLI/104925/2008 project from the Portuguese Foundation for Science and Technology.

„Aerosol-fingerprint" of Europe in the atmosphere of Debrecen, Hungary

Zsófia Török[1,2], Zsófia Kertész[1], Anikó Angyal[1], Enikő Furu[1,2] , Zoltán Szoboszlai[1], Zita Szikszai[1] and Ildikó Borbély-Kiss[1]

[1]Institute for Nuclear Research of the Hungarian Academy of Sciences, H-4026 Debrecen, Bem tér 18/c
[2]University of Debrecen, H-4032 Debrecen, Egyetem tér 1
Keywords: backward trajectory, source analysis
Presenting author email: torok.zsofia@atomki.mta.hu

Aerosol pollution is one of the main problems in the urban environment, because of the negative health and environmental impacted of particulate matter.

In cities, aerosol particles can arise locally (e.g. resuspended dust caused by traffic or soot from heating) or from distant sources (e.g. sea salt or Saharan dust). In this work we studied the possible distant source areas of the aerosol detected in Debrecen using backward-trajectory modelling.

In the center of Debrecen aerosol samples have been collected regulary in two size fractions: PM10-PM2.5 (particles with aerodynamic diameter between 2.5 and 10 μm) and PM2.5 (particles with aerodynamic diameter < 2.5μm) since 1993 twice a week. The aerosol concentration is measured by gravimetry and the elemental composition (for Z >13) is determined by Proton Induced X-ray Emission (PIXE) method at the macro-PIXE chamber in the IBA Laboratory of Atomki. By today the database contains more than 1200 sampling days and ~ 65.000 concentration data.

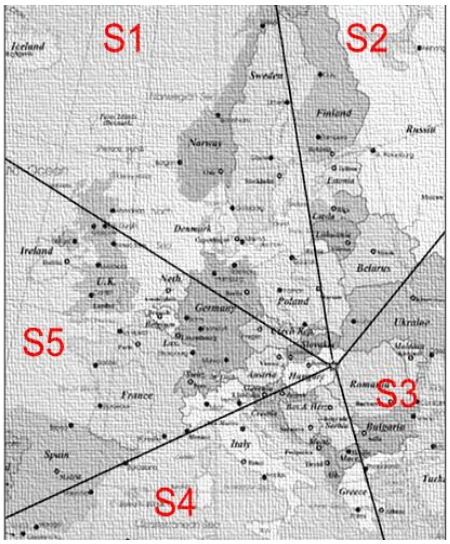

Figure1: Five sectors used to the classification the backward trajectory

The NOAA-HYSPLIT model was used to determine the spread of the aerosol particles. The backward trajectories were calculated for 72 hours periods at three different heights. We investigated what kind of aerosol composition is representative for the different European source areas. In a previous study (Borbély-Kiss *et al*, 1999) five sectors were assigned according to the most frequent wind directions (Fig1). Each trajectory has been classified to one sector. The origin of the air mass on high or low pollution levels were studied too. 513 days were found in the investigated period (1993-2006) when the sector was univocal.

Table1: Average concentration in the five sectors and the percentage contribution

	S1	S2	S3	S4	S5	Sum
events	89	58	127	88	151	513
PM10	30.9	29.8	35.7	42.5	28.8	33.3
PM2.5	18.1	16.9	19.6	23.2	17.0	18.9
>50 μg/m^3	23	15	39	42	40	159
% to sector	26%	26%	31%	48%	26%	

Table1 shows the number of events (row 1) when the body of air originated from the given sector and average aerosol concentration in both size fractions in μg/m^3 (row 2 and 3). The number of days when the measured PM10 concentration exceed the 24-h air quality limit (50 μg/m^3) are also included in the table. The ruling air mass trajctory directions are east-west. 70% of the high polution level episodes air masses originated from Southern and Eastern Europe.

Correlation analysis and receptor modelling (EPA PMF) were applyied to identify elemental fingerprints of the five sectors. This way we could separate local sources (for example road dust: high Mn and Pb content, bimass burning: K and Zn) from remote sources. In the case of NW Europe (S1) Al, Fe, Mn, Cl and Pb showed strong correlation with each other ($r > 0.7$, $p < 0.01$), which could be connected to iron mining and metallurgy. For NE Europe (S2) K, Si, Ca and Fe correlated with each other, which could be attributed to plastic industry. For SE (S3) Europe strong Br/Pb correlation were characteristics, which could aries from waste burners. In the case of Southern Europe (S4) sources attributed to Cr mining, mettallurgy and Saharan dust intrusions could be identified.

Borbély-Kiss I., Koltay E., Szabó Gy., Bozó L., Tar K. 1999. *Composition and sources of urban and rural atmospheric aerosol in Eastern Hungary*. Journal of Aerosol Science, 30, 369-391

Acknowledgement

This work was supported by the TÁMOP-4.2.2/B-10/1-2010-0024 project and co-financed by the European Union and the European Social Fund and the János Bolyai Research Scholarship of the Hungarian Academy of Sciences.

Measurements of black carbon using the Transmissometer

A.H. Tremper[1], D.C.Green[1] and G. Fuller[1]

[1]Environmental Research Group, King's College London, London, SE1 9NH, UK

Keywords: black carbon, elemental carbon, transmissometer, aethalometer
Presenting author email: anja.tremper@kcl.ac.uk

Quartz and teflon coated glass fibre filters were exposed in London as part of a PM_{10} mass measurement monitoring programme prior to the commencement of routine EC/OC measurements and prior to the implementation of the Low Emission Zone (LEZ). Analysis of these filters is designed to allow an assessment of tailpipe EC/BC emissions reductions brought about by the LEZ. The Transmissometer (Magee, 2007) offers a very cost effective method of measuring black carbon (BC) concentration on filter samples using a similar technique to that used in the Aethalometer (Magee, 2005). Various methods are available to correct aethalometer measurements for filter loading effects, (Virkkula et al., 2007; Park et al., 2010) but these methods do not directly apply to the transmissometer. Instead an empirical method was tested to correct for filter loading effects using the relationship between transmissometer BC and elemental carbon (EC) concentrations measured using a Sunset Labs Instrument.

Filters were exposed daily at the North Kensington (NK) urban background site, Marylebone Road (MY) traffic site and Earls Court Road (ECR) traffic site. After mass analysis, these filters were analysed using the Transmissometer. A subset of quartz filters, from NK and MY, were analysed for BC using the transmissometer before thermal analysis for EC by Sunset. These EC measurements were used to calculate the corrected transmissometer BC measurements with the generalised least squares method using XGenline (NPL, 2010). Various fitting methods of the calibration curve were tested. Subsequently time series of corrected BC measurements with a known uncertainty were produced to assess changes in the concentration due to the LEZ.

Two short time periods in 2006, during which thermal EC/OC measurements were available at KC and MY, were used to evaluate the transmissometer BC concentrations. Transmissometer BC from $PM_{2.5}$ filters and PM_{10} agreed well as most of the BC can be found in the smaller size fraction.

Comparing the transmissometer BC concentrations from the PM_{10} filters with the EC concentrations recorded by thermal analysis at MY, it is noticeable that the corrected BC is significantly lower than the thermal EC at higher concentrations (Fig. 1). This is not the case for NK, were concentrations are generally much lower (Fig. 2).

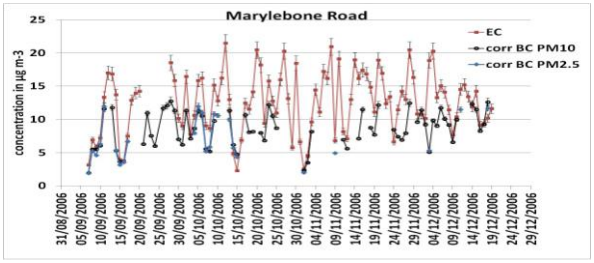

Figure 1: Conc. of thermal EC and corrected BC in PM_{10} and $PM_{2.5}$ filters at MY (all in µg m^{-3})

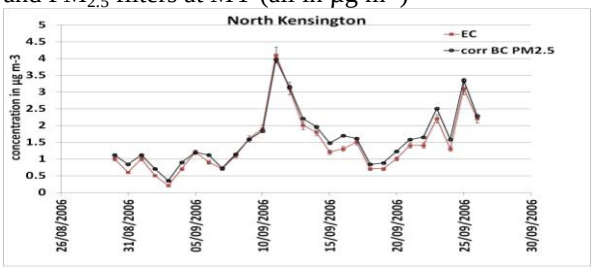

Figure 2: Conc. of thermal EC and corrected BC in PM_{10} and $PM_{2.5}$ filters at KC (all in µg m^{-3})

Overall the corrected transmissometer BC offers an opportunity to extend time series at sites with low EC concentrations – see Fig.3.

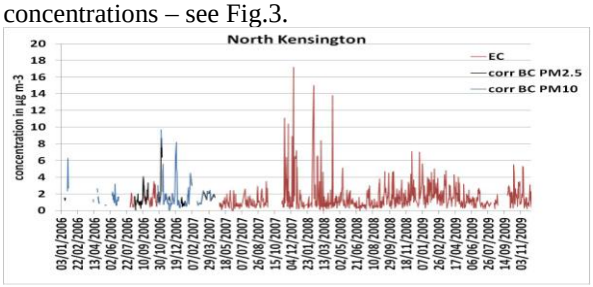

Figure 3: EC and corrected BC in PM_{10} and $PM_{2.5}$ filters at KC between 2006 and 2009 (all in µg m^{-3})

Thanks to TfL for financial support, Bureau Veritas and NPL for technical support. I would also like to thanks S. Sweeney, L. Clapp and C. Fitzgerald for help with the filter analysis.

Magee Scientific 2005. The Aethalometer ™ - Manual

Magee Scientific 2007. Dual-Wavelength Optical Transmissometer Data Acquisition System – Manual

NPL, 2010. http://www.npl.co.uk/mathematics-scientific-computing/mathematics-and-modelling-for-metrology/xgenline-8.1

Park, S.S et al 2010. ATMOS ENVIRON 44, 1449–1455.

Virkkula, et al. 2007. J AIR WASTE MA (1995), 57. 1214–1222

Effect of organics and their hygroscopicity on cloud condensation nuclei (CCN) activity

Deepika Bhattu and Sachchida Nand Tripathi*

Department of Civil Engineering, Indian Institute of Technology, Kanpur, Uttar Pradesh, 208016, India

Keywords: supersaturation, organics, hygroscopicity, size-resolved composition
*Presenting author email: snt@iitk.ac.in

Aerosols play a significant role in the Earth climate system directly by absorbing and scattering sunlight, and indirectly by acting as cloud condensation nuclei (CCN). Higher concentration of CCN in the air parcel results in small cloud droplets, thereby affecting the cloud radiative properties. This leads to reflection of incoming shortwave and cooling the Earth's surface (Twomey, 1974).

Aerosols are the complex mixture of organics, inorganics, BC and dust. The water uptake capacity of inorganics, single organic component are well understood and while the properties of their mixtures need further studies (Petters and Kreidenweis, 2007). Understanding the activation properties of the ambient aerosols need the size and mixing state resolved chemical composition, which is not possible with the present level of instrumentation.

Several studies examined the contribution of aerosol parameters like, size distribution and chemical composition or hygroscopicity, to CCN activity using Köhler theory. It has been found that performance of CCN closure study depends on how well the chemical composition mainly organics and mixing state of aerosols is treated. Various studies have tested different assumptions regarding mixing state of aerosols using chemical composition from AMS (both size resolved and bulk) (Cubsion et al., 2008). It appears that the closure ratio improves as the distance from the source region increases because the particles become more internally mixed and less size dependent.

We conducted measurements of CCN, aerosol size distribution and chemical composition at SS = 0.2-1% at the Indian Institute of Technology Kanpur, India, in November, 2012. The main goal of this study is to investigate the effect of organics and their hygroscopicity on cloud condensation nuclei activity. CCN closure study was carried out on the basis of size distribution measured through Scanning Mobility Particle Sizer (SMPS) and chemical composition from Aerodyne HR-ToF-AMS, using simple Köhler theory at five different supersaturations (0.2, 0.4, 0.6, 0.8, 1%). The size dependence of the chemical composition and the mixing state (internal and external) are accounted in various ways. During the sampling period, CCN concentration ranged from 1500-5000 #/cc at lower SS (0.2%) while at medium SS (0.4-0.6%) it ranges from 3000-15000 and at higher SS (0.8-1%) varies from 5000-20000. The total aerosol (CN) concentration varied from 7000 to 34000 #/cc. Diurnal variation in the activation fraction (CCN/CN) is observed with maxima in day time (1200-1800 hrs). In addition, both CCN and CN concentration decreased during day time due to expansion of boundary layer due to solar heating. Due to higher CCN loading, SS depletion correction has been applied throughout the sampling period (Lathem and Nenes, 2011).

Preliminary results show that differences in the $CCN_{predicted}$ and $CCN_{measured}$ decreases with the increase in SS. For example, closure ratio improved from 180 % to 50% as the SS increases from 0.2% to 1.0%, when aerosols were assumed to be internally mixed and composed of inorganics and insoluble organics. This can be attributed to less sensitivity of smaller sized particles to chemical composition. This over-prediction can be reduced by considering day time and night time aerosols separately during closure study. It has also been observed that O:C ratio increases from 0.3-0.6 during the day time due to photochemical activity and oxidation of organics, thus increasing the activation fraction. The effect of organics on CCN activity is examined using an effective hygroscopicity parameter through "κ-Köhler theory" (Petters and Kreidenweis, 2007).

This work is supported through a grant from Changing Water Cycle Programme of MoES, Govt. of India, and NERC, Govt. of U.K.

References:

Cubison M J, Ervens B, Feingold G, Docherty K S, Ulbrich I M, Shields L, Prather K, Hering S and Jimenez J L 2008 The influence of chemical composition and mixing state of Los Angeles urban aerosol on CCN number and cloud properties *Atmos. Chem. Phys.* **8** 5649-67

Lathem T L and Nenes A 2011 Water Vapor Depletion in the DMT Continuous-Flow CCN Chamber: Effects on Supersaturation and Droplet Growth *Aerosol Science and Technology* **45** 604-15

Petters M D and Kreidenweis S M 2007 A single parameter representation of hygroscopic growth and cloud condensation nucleus activity *Atmos. Chem. Phys.* **7** 1961-71

Twomey S 1974 Pollution and the planetary albedo *Atmospheric Environment (1967)* **8** 1251-6

Estimation of source apportionment using the UNMIX model of ambient $PM_{2.5}$ in Seoul area, Korea

Yeong-Jin Jeong, Tae-Ho Lee, and InJo Hwang
Department of Environmental Engineering, Daegu University, Gyeongsan, Gyeongbuk, 712-714, Korea

Keywords: air quality, $PM_{2.5}$, source apportionment, UNMIX, Seoul
Presenting author email: ihwang@daegu.ac.kr

Many countries recently have developed and carried out policies to control air pollutants, focusing their effort on establishing new environmental guidelines as well as in evaluating the pollution sources more accurately. Therefore, one of these efforts was to survey the physicochemical properties of atmospheric particulate matter (PM) and thereby, quantitatively understand to what extent the specific pollution sources affect the adjacent regional atmosphere (Yi and Hwang, 2013). The Seoul (capital of Korea) has severe air pollution problems, and a variety of governmental policies, such as expansion of the use of liquefied natural gas and low-sulfur fuels and movement of industrial sources out of the city, have been implemented to improve urban air quality. The objective of this study was to estimate the $PM_{2.5}$ composition at the sampling sites by surveying concentration trends after analyzing the mass concentration of $PM_{2.5}$ samples and the elements, ions, and carbon in $PM_{2.5}$. UNMIX was applied to identify the existing sources and apportionment of the PM mass to each source. These results suggest the possible role for maintain and manage ambient air quality of Seoul, and achieve reasonable air pollution strategies.

The ambient $PM_{2.5}$ samples were collected at 9 sampling sites (Hwagok, Guro, Banghak, Hyoje, Dongdaemun, Sinsa, Guui, Yongin, and Ui) in Seoul area. $PM_{2.5}$ samples were collected using Partisol 2300 (Thermo, USA) from September 2008 to March 2010. The samples were collected on Teflon, nylon, and quartz filters every 6 days. These filters were used for analysis of elemental, ionic species, and EC/OC by ICP, IC, and TOT method. The UNMIX model was used to develop source profiles and to estimate their mass contributions.

The five sources were identified as soil, secondary aerosol, vehicle/road dust, Ca related, and industry/oil/biomass burning. The average contributions of all the sources identified during the sampling periods were showed in Figure 1. The result of the UNMIX modeling showed that the source were apportioned by industry/oil/biomass burning 11.5 % (2.97 $\mu g/m^3$), Ca related 2.2 % (0.57 $\mu g/m^3$), vehicle/road dust 37.3 % (9.62 $\mu g/m^3$), secondary aerosol 39.5 % (10.20 $\mu g/m^3$), and soil 9.5 % (2.46 $\mu g/m^3$), respectively. Figure 2 shows comparison of source contributions between UNMIX and PMF model in the Hyoje sampling site. In the case of industry/oil/biomass burning and secondary aerosol source contributions of the PMF result showed slightly higher than the UNMIX result. On the other hand, in the case of vehicle/road dust and soil source contributions of the UNMIX result showed slightly higher than the PMF result.

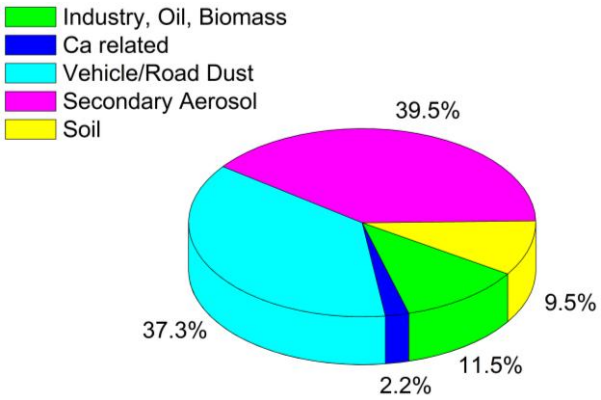

Figure 1. Average source contributions for the sampling periods at the Hyoje sampling site.

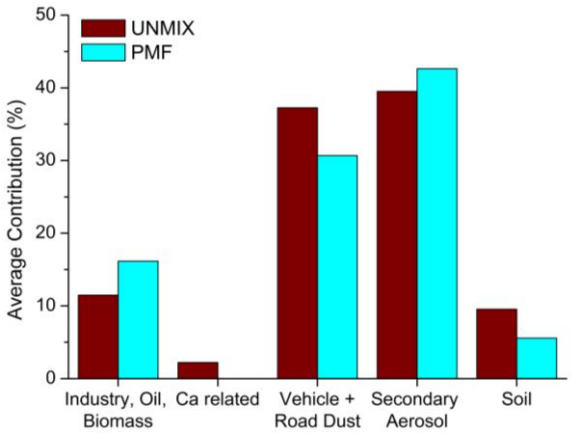

Figure 1. Comparison of source contributions between UNMIX and PMF in Hyoje sampling site.

This work was supported by Basic Science Research Program through the National Research Foundation of Korea (NRF) funded by the Ministry of Education, Science and Technology (grant No: 2012-0007782), and supported by National Institute of Environmental Research (NIER) under contract No. 2012-294.

Yi, S.M. and Hwang, I. (2013) Aerosol and Air Quality Research. (submitted).

Ionic composition and metal content of PM10 samples collected along longitudinal and latitudinal transects in the Norwegian and Greenland Seas during the AREX 2011 cruise.

R. Udisti[1], S. Becagli[1], E. Bolzacchini[2], G. Calzolai[3], M. Chiari[3], L. Ferrero[2], D. Frosini[1], M. Marconi[1], M.G. Perrone[2], G. Sangiorgi[2], M. Severi[1], R. Traversi[1], W. Walczowski[4], R. Zanini[1], T. Zielinski[4].

[1] Department of Chemistry, University of Florence, 50019 Sesto F.no (FI), Italy.
[2] DISAT, University of Milano-Bicocca, 20126 Milan, Italy.
[3]Dept. of Physics and Astronomy, University of Florence and INFN Florence, 50019 Sesto F.no (FI), Italy
[4] Institute of Oceanology, Polish Academy of Science, Sopot, Poland.

Keywords: Arctic aerosol, on-ship measurement, biogenic emissions, heavy metals
Presenting author email: udisti@unifi.it

The Arctic Glacial Sea is one of the world regions more affected by the impact of the present positive climate forcing. The consequent feedback processes, involving relevant variations of marine and coastal eco-systems (including large changes in extension and thickness of the annual and permanent sea ice and in the permafrost superficial structure) constitute a serious issue for the wild life and the human settlements at the high latitudes.

The atmospheric aerosol is one of the main components of the Earth climate system through the interaction of the particles with solar and Earth radiation, the cloud formation and the changes in superficial albedo. Although these effects are well known, large uncertainties affect not only their quantitative evaluation but also the sign of the variation (positive or negative climate forcings). This lack of knowledge especially affect the Polar Regions, were just a relative little number of monitoring stations is operative. Besides, data on the chemical composition of aerosol in the open sea are very scarce.

In order to contribute to fill this knowledge gap, an intensive sampling campaign was carried out in the sea area between Norway and Svalbard Islands (Norwegian and Greenland Seas) in the framework of the AREX 2011 oceanographic cruise aboard Oceania ship.

In the period June 20th – August 12th 2011, 79 12-h PM10 samples for ionic and metal composition (Teflon filters) and 42 24-h PM10 samples for Elemental and Organic Carbon fractions (EC and OC, respectively) on quartz filters were collected. The sampling devices (low volume sequential samplers with PM10 sampling heads) were located in a platform 7-m high over the ship deck in the bow section, in order to minimize the contamination risk from ship engine emissions. The very low values measured for heavy metals and EC fraction, possibly used as fuel combustion markers, suggest that the contamination levels could be considered negligible.

One half of each Teflon filter were analysed for inorganic and selected organic anions and inorganic cations by a three-ion chromatograph system. The remaining half was used for metal determination by SF-ICP-MS after mineralization with HNO_3 + H_2O_2 in microwave oven.

Here we report the spatial distribution of the most significant aerosol components along longitudinal (Tromso – Svalbard Islands) and latitudinal (east-to-west route in the Norwegian Sea and along the western side of the Svalbard Island) transects.

In particular, the atmospheric concentrations of secondary marine aerosol (sulphuric acid and methanesulphonic acids (MSA) from phytoplanktonic emissions) was plotted as a function of the ship position in order to attempt to figure out a possible relationship between biogenic aerosol and changes in the source strength as a function of time and marine area (figure 1).

From a temporal point of view, non-sea-salt sulphate and MSA show two sharp maxima in June, in phase one with each other, while lower contribution of biogenic emission are recorded in the filters collected in July. On the other hand, no clear trend along coastal to open-sea transects is evident. Higher MSA concentrations (up to 120 ng/m^3) were measured near the Norwegian coast, along the Tromso-Svalbard route, and in the south-west coastal areas of the Svalbard Island, while the lowest values (few ng/m^3) were found in the open-sea at north-west of the Islands

Spatial and temporal distribution of sea spray components (Na, Mg, chloride), N-cycle compounds (nitrate and ammonium salts), dust markers (Ca, Al, Fe, Mn, Ti) and selected heavy metals possibly coming from anthropic emissions were measured. C-cycle secondary aerosol components (OC fraction, light-chain carboxylic acids) were also determined in order to gain information on the possible contribution of the gas-to-particle conversion of volatile organic compounds (VOCs) in constituting a significant part of the aerosol formation nuclei.

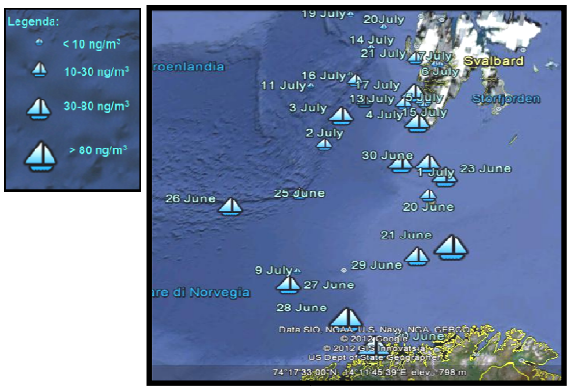

Figure 1. Spatial distribution of MSA in PM10 aerosol.

This work was supported by Italian Education, University and Research Ministry (MIUR) and by National Research Council (CNR-DTA) funds and facilities.

Project AEROLIT (Aerosol in Lithuania): Investigation of primary-secondary and regional-local contributions to particulate matter in the south-eastern Baltic region

V. Ulevicius[1], A.S.H. Prévôt [2], K. Plauškaitė[1], S. Byčenkienė[1], G. Mordas[1], V. Dudoitis[1], V. Remeikis[1], A. Garbaras[1], K. Kvietkus[1], I. Garbarienė[1], J. Dommen[2], J.G. Slowik[2], C. Bozzetti[2] and U. Baltensperger[2]

[1]Department of Environmental Research, Center for Physical Sciences and Technology, LT-02300 Vilnius, Lithuania
[2]Laboratory of Atmospheric Chemistry, Paul Scherrer Institut, Villigen, CH-5232, Switzerland
Keywords: aerosol concentration, source apportionment.
Presenting author email: ulevicv@klt.mii.lt

Atmospheric aerosols have critical effects on human health and the global radiation balance. The magnitude of these effects remains largely unknown due to uncertainties in carbonaceous aerosol sources, transformations, and atmospheric lifetime. **AEROLIT** will provide long-term, comprehensive measurements of carbonaceous aerosol composition at urban, rural, and coastal sites in Lithuania.

AEROLIT couples state-of-the-art measurements (aerosol mass spectra, stable isotope ratio measurements, and organic molecular markers analysis) with source apportionment factor analysis techniques using the multilinear engine to provide a quantitative assessment of the factors affecting Lithuanian air quality. Measurements will be simultaneously performed at coastal, rural, and urban sites. The **AEROLIT** project consists of five Work Packages (WPs) that will be completed over the study period (Fig. 1):

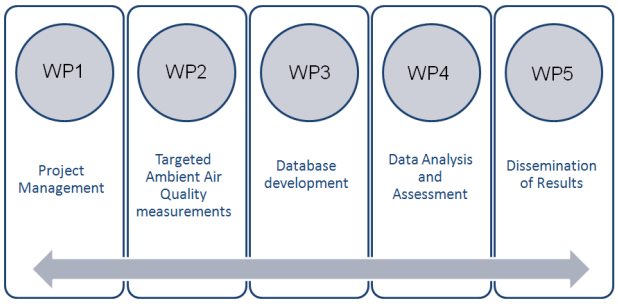

Figure 1. Research associated work plan.

The principal measurements to be performed are:
a) Long-term online aerosol mass spectrometry using an aerosol chemical speciation monitor (ACSM) and a quadrupole aerosol mass spectrometer (Q-AMS).
b) Long-term filter sampling with a High-Vol sampler at 3 sites: Offline analysis of aerosol collected on filters using high-resolution aerosol mass spectrometry (HR-AMS), the new compound-specific TAG-AMS (thermal desorption aerosol gas chromatography-AMS) technique (Williams *et al*, 2006) and isotope-ratio mass spectrometry (IR-MS).
c) Optical measurements of black carbon (BC) using a 7-wavelength aethalometer.
d) A subset of the filters collected in (b) will be analyzed for ^{14}C (modern/fossil carbon) and monosaccharide anhydrides (tracers for biomass combustion).

An example of the **AEROLIT** approach is given in Figure 2, where a pilot study of a biomass burning pollution event from long-range transported aerosols was investigated.

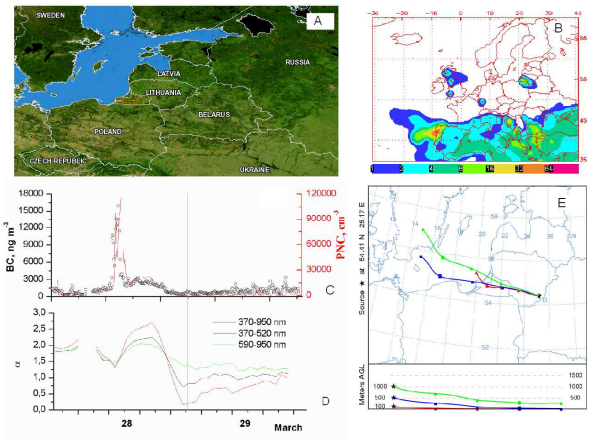

Figure 2. Active fires detected on 28-29 March, 2012 during high BC concentration event: (A) by the MODIS Rapid Response System, (B) NAAPS Smoke surface concentration (ng m^{-3}), (C,D) BC aerosol and particle number concentration and (E) 2-days air mass backward trajectories to Vilnius (at 100, 500 and 1000 m AGL) during the event of wildfires.

Previous results about aerosol source characterization in Lithuanian sites can be found in Garbariene *et al* (2012) and in Ulevicius *et al* (2010). **AEROLIT** brings together leading air quality and pollution researchers with the following goals:
• Identify and quantify the processes and sources governing spatial and temporal PM concentrations at urban, rural, and coastal locations in Lithuania.
• Classify and quantify carbonaceous aerosol in terms of emission mechanism (primary vs. secondary), source geography (local vs. regional vs. trans-national), and source/precursor class (natural vs. anthropogenic, modern vs. fossil carbon).
• Conduct targeted chemically resolved organic aerosol and related molecular-marker measurement campaigns in urban, rural and background sites for source apportionment.

This work was supported by the Lithuanian-Swiss cooperation programme ”Research and development“ project **AEROLIT** (Nr. CH-3-ŠMM-01/08).

Garbariene, I., Kvietkus, K., Šakalys, J., Ovadnevaitė, J. and Čeburnis, D. (2012) *J Atmos Chem* **69**, 159–174.
Ulevičius, V., Byčenkienė, S., Remeikis, V., Garbaras, A., Kecorius, S., Andriejauskienė, J., Jasinevičienė, D., Mocnik, G. (2010) *Atmospheric research* **98**, 190-200.
Williams, B. J., Goldstein, A. H., Kreisberg, N. M. and Hering, S. V. (2006) *Aerosol Sci. Tech* **40**, 627-638.

Air masses types over the remote Alborán Island

A.Valenzuela[1,2], F.J. Olmo[1,2], H. Lyamani[1,2], M.J. Granados Muñoz [1,2], J.L. Guerrero-Rascado[1,2], A. Quirantes[1], and L. Alados-Arboledas[1,2]

[1]Centro Andaluz de Medio Ambiente, Junta de Andalucía- Universidad de Granada, Avda. del Mediterráneo s/n, 18006-Granada, Spain.
[2]Departamento de Física Aplicada, Universidad de Granada, Avda. Fuentenueva s/n, 18071- Granada, Spain.
Keywords: aerosol optical properties, aerosol origin sources. remote island.

Presenting author email: avalenzuela@ugr.es

During the last decades an enormous effort has been done to determine the effects of aerosols on climate. However, due to their large spatial-temporal variability and the different mixtures between aerosol types, there are still significant uncertainties in understanding the aerosol optical and microphysical properties.

The aerosol optical properties in origin, as issued by the sources, are conditioned by the potential changes during the path of the air masses as well as by the local aerosol properties at the reception site. A possibility in order to minimize the effect of the local aerosol is placing the measuring stations in remote locations far from the potential influence of local aerosol sources. Measurements taken at small islands are valuable because local sources are generally negligible, and medium and long-range transport, together with aerosol aging processes, play a relevant role, thus providing information on aerosol properties over a relatively large scale.

Backward trajectory analysis is a widely used technique in order to relate the air masses origin with the aerosol optical properties at the receptor site (e.g. Pace et al., 2006).

In this work air masses over Alborán Island (35.95º N, 3.03º W) from June 2011 to January 2012 were analysed by means of back-trajectories using HYSPLIT model. The aerosol radiative properties have been classified taking into account sun-photometric measurements and the air mass history. The aim is to classify columnar aerosol properties according to the potential aerosol origin sources. The air masses classification method identifies as a potential aerosol source that region which the difference between the height of the air mass and the height of the boundary layer is minimum.

Optical and microphysical aerosol properties were simultaneously retrieved from sun-photometric measurements (CIMEL CE-318) according to the methodology described by Olmo et al. (2008). The instrument provides solar extinction measurements at 340, 380, 440, 670, 870 and 1020 nm, and sky radiance measurements at 440, 670, 870 and 1020 nm using the almucantar and principal plane configurations.

From the air masses classification three broad geographical sectors have been identified: Sector A (Mediterranean sea and Europe Centre), Sector B (North Africa), and Sector C (Atlantic Ocean and Iberian Peninsula).

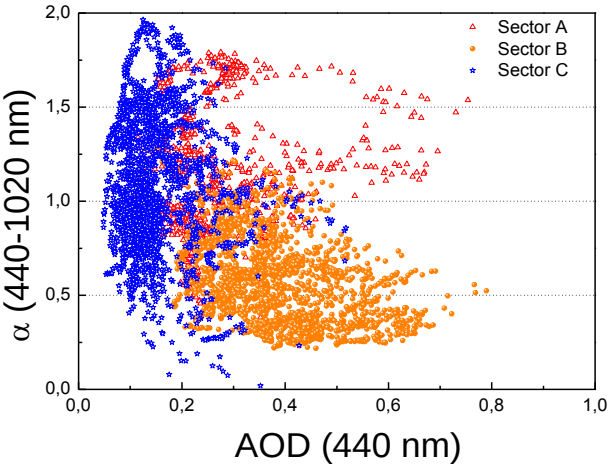

Figure 1. The Angstrom exponent (440-1020) versus AOD (440 nm) for each origin sector.

Figure 1 shows three main groups of particles corresponding to the three origin sectors. Although the values for sector B (African air mass) showed typical high aerosol optical depth (AOD) linked to low Angstrom exponent (α) (coarse particles) a small group of observations showed α values higher than 1, indicating also a contribution of fine particles during desert dust events. An important number of observations for sector C were concentrated in a range with AOD values below 0.2 and α value mainly concentrated in a region between 0.5–1.0 likely related to marine aerosol. The observations corresponding to the sector A contain points with AOD values in the range 0.2-0.8 and α mainly above 1, typical of fine mode aerosol from urban/industrial activities or biomass burning.

This work was supported by the Andalusia Regional Government through projects P08-RNM-3568 and P10-RNM-6299, by the Spanish Ministry of Science and Technology through projects CGL2010-18782, CSD2007-00067, CGL2011-13580-E/CLI and CGL2011-16124-E; and by EU through ACTRIS project (EU INFRA-2010-1.1.16-262254). We acknowledge the NOAA Air Resources Laboratory for the use of HYSPLIT model.

Pace, G., di Sarra, A., Meloni, D., Piacentino, S., Chamard, P. (2006). *Atmos. Chem. Phys*. **6**, 697-713.
Olmo, F.J., Quirantes, A., Lara, V., Lyamani, H., Alados-Arboledas, L. (2008). *J. Quant. Spectrosc. Radiat. Transfer*. **109**, 1504-1516.

A LUR model for NO_2 and BC to assess exposure of schoolchildren to traffic-related air pollution at their home address

Martine Van Poppel[1], Evi Dons[1,2], Luc Int Panis[1,2]

[1]VITO - Flemish Institute for Technological Research, 2400 Mol, Belgium
[2]Hasselt University, 3590 Diepenbeek, Belgium

Keywords: Black Carbon, NO_2, LUR, traffic.
Presenting author email: martine.vanpoppel@vito.be

To assess the health impact of traffic related air pollution on schoolchildren, the HEAPS study (Health Effects of Air Pollution in Antwerp Schools) was performed.
The HEAPS study comprises the biomonitoring of 130 children (aged 6-12) from 2 schools by measuring oxidative stress, inflammation and cardiovascular markers and simultaneous air quality monitoring.

To assess the exposure of the children, air quality measurements were performed at the school locations, at a selection of 40 home locations and while in transport. In addition the land use regression (LUR) technique was applied to model exposure to BC and NO_2 at all 130 home locations. BC and NO_2 measurements were performed at 8 home locations simultaneously during 5 consecutive weeks resulting in 40 home locations sampled. Monitoring was performed in two seasons: spring and autumn. NO_2 was monitored using diffusive sampling tubes resulting in a weekly average. BC was measured using µ-Aethalometer (AethLabs), resulting in 30 min time profiles and a weekly average. NO_2 was measured at 40 and an additional 13 locations simultaneously in each season. In addition, NO_2 and BC measurements were performed during the entire monitoring campaign at two school locations and at an urban location of the AQ monitoring network. The data of the last location were used to rescale BC and NO_2 concentrations that were measured consecutively.

Three categories of potential variables are included in the LUR: land use (CORINE land cover), traffic variables (e.g. traffic densities, road length, number of heavy duty vehicles), population density (addresses). To build the LUR model, the method as described by Henderson et al. (2007) was applied. For both pollutants a LUR model was set-up for spring, autumn and a yearly average.

Significant variables for both models (NO_2 and BC) in spring are traffic load (50m), heavy duty traffic (100 m) and road length (1km). At short distance (50 m and 100m), traffic characteristics are important for the variability of both pollutants. At a larger distance also the total number of roads affects the pollutants concentrations, probably as a proxy for urbanization. The BC model also includes the intensity at the nearest busy road (>10,000 vehicles) and the NO_2 model includes also nature with a negative estimate.

The LUR for autumn includes an additional variable 'number of address within 50 m'. This can be explained by additional sources of household heating, that are only relevant in the cold season.

Model validation was performed using leave-one-out cross-validation. Results for spring are presented in Table 1.
The paper will present the LUR results for spring, autumn and yearly average. Significant variables will be discussed and model validation will be presented.

Table 1: Results of model validation (spring)

	Conc. Modelled ($\mu g/m^3$)	Conc. Measured ($\mu g/m^3$)	r	IA	NMSE
BC	1.55	1.59	0.63	0.77	0.05
NO_2	28.1	28.2	0.90	0.94	0.01

Henderson S.B., Beckerman B., Jerrett M., and Brauer M., 2007. *Environmental Science and Technology* ***41****(7),* pp. 2422-2428.

Košetice Observatory – The Czech Background Aerosol Supersite

Váňa M.[1, 2], Čech J.[1], Holubová A.[1], Pavelka M.[2], Ondráček J.[3], Schwarz J.[3], Smolík J.[3], Zíková N.[3], Ždímal V.[3]

[1] Czech Hydrometeorological Institute, Košetice Observatory, 394 22 Košetice, Czech Republic
[2] Global Change Research Centre AS CR, Bělidla 984, 603 00 Brno, Czech Republic
[3] Institute of Chemical Process Fundamentals, AS CR, v.v.i., Prague, 165 02, Czech Republic

Keywords: atmospheric aerosols, background scale, ACTRIS, long-term monitoring

Presenting author email: milan.vana@chmi.cz

The Košetice observatory (49°35´ N, 15°05´E, 534 m a.s.l.) is operated by the Czech Hydrometeorological Institute (CHMI) and was established in 1988 as a station specialized in air quality monitoring at the background scale. The observatory is involved in GAW/WMO (Global Atmosphere Watch), EMEP/ECE (Co-operative Programme for Monitoring and Evaluation of Long-range Transmission of Air Pollutants in Europe) and ICP-IM (International Co-operative Programme on Integrated Monitoring).

The monitoring program includes meteorology, solar radiation, air chemistry, precipitation chemistry, hydrology, surface water chemistry and soil analysis. More detailed information is available in (Váňa *et a*l. 2007, 2009).

The basic measurements of atmospheric aerosols were implemented within the National Imission Network (operated by CHMI) since the start of the observatory. At the beginning, mass concentrations of total suspended particles (TSP) were monitored. In 1996, monitoring of PM_{10} concentrations started according to the European legislation. The recent studies have concluded that fine particles ($PM_{2.5}$) are more hazardous in terms of mortality on cardiopulmonary diseases and lung cancer (Pope et al., 2002). Measurement of $PM_{2.5}$ started at Košetice Observatory in 2004.

Thanks to its well selected location and long-term homogeneous data series, Košetice Observatory has been included into several European projects. In regards to atmospheric aerosols, the first of them was EUSAAR (European Supersites for Atmospheric Aerosol Research), an EU-funded I3 (Integrated Infrastructures Initiatives) project carried out in the FP6 framework of the specific research and technological development programme "Structuring the European Research Area - Support for Research Infrastructures" in the period 2006-2011. The EUSAAR aerosol activities are continuing within more widely composed EU FP7 project ACTRIS (Aerosols, Clouds, and Trace Gases Research Infrastructure Network).

Advanced aerosol measurements have been carried out in close co-operation with the Institute of Chemical Process Fundamentals (ICPF). Continuous sampling of dry particle number size distributions using a Scanning Mobility Particle Sizer (SMPS, TROPOS) started in 2008 with 5 min time resolution covering particle size range from 9 to 900 nm (Asmi et al., 2011). One year series of aerosol hygroscopicity data had been collected between 2008-2009 using a Humidity Tandem Differential Mobility Analyzer (HTDMA, ICPF) with one hour time resolution. $PM_{2.5}$ OC/EC measurement has been implemented since 2009 with 6 days sampling frequency on 2 quartz-fiber filters (Putaud et al., 2010). Since October 2011 (within ACTRIS), a carbon honeycomb denuder developed within EUSAAR had been installed upstream the filters. The OC/EC content in the samples has been determined by thermal-optical analysis at CHMI Central Laboratories in Prague-Libuš using the OC/EC Sunset Lab Dual Analyzer. Charring correction has been done by laser transmission monitoring.

Special attention to the climatological effects of atmospheric aerosols is devoted in The CzechGlobe project operated by Global Change Research Centre AS CR at the co-located station Košetice (ACTRIS) – Křešín u Pacova (ICOS). The measurements of optical properties of the atmospheric aerosol started in 2012 as the first of this type in the Czech Republic. The aerosol scattering coefficients at three wavelengths have been determined by an integrating nephelometer (TSI 3563). The aerosol absorption coefficients at seven wavelengths have been gathered using an aethalometer (AE-31, Magee). All parameters have been determined on dry aerosol particles, the measurement methods closely follow ACTRIS recommendations, and the results will be used for the extension of the Czech participation within ACTRIS.

The authors gratefully acknowledge funding from the European Union Seventh Framework Programme (FP7/2007-2013) under grant agreement n° 262254 and a project of Czech Science Foundation P209/11/1342. This work is an output of the CzechGlobe Centre that is being developed within the OP RDI and co-financed from EU funds and the State Budget of the Czech Republic (Project: CzechGlobe – Centre for Global Climate Change Impacts Studies, Reg. No. CZ.1.05/1.1.00/02.0073), of the National Infrastructure CzechCOS/ICOS (LM2010007) and institutional support (RVO:67179843).

Asmi A., Wiedensohler A., Laj P. et al. (2011). *Atmos. Chem. Phys.* **11**(11), 5505-5538.

Pope, CA; Burnett, RT; Thun, MJ; et al. (2002), *JAMA,* **287** (9), 1132-1141. DOI: 10.1001/jama.287.9.1132

Putaud J-P., Van Dingenen R., Alastuey A. et al. (2010) *Atmos. Environ.* **44**(10), 1308-1320.

Váňa M. et al. (2007, 2009) Kosetice Observatory – 20 years. Pt. 1 + 2, CHMI, Praha.

Váňa, M. et al. (2012) *P226 (SS01S1PO1) at EAC 2012*, Granada

Source apportionment of carbonaceous PM2.5 with ^{14}C analysis in Nagoya, Japan

F. Ikemori[1, 2] *, K. Honjyo[1], M. Yamagami[2], T. Nakamura[3]

[1] Graduate School of Environmental Studies, Nagoya University, Nagoya 464-8601, Japan
[2] Nagoya City Institute for Environmental Sciences, Nagoya 457-0841, Japan
[3] Center for Chronological Research, Nagoya University, Nagoya 464-8601, Japan
Keywords: radiocarbon, PM2.5, biomass carbon, fossil carbon.
Presenting author email: ikemori@nagoyakankaken.net

Radiocarbon (^{14}C) is a powerful tracer for estimating the source apportionment of carbonaceous compounds because ^{14}C can be used to discriminate between modern and fossil carbon. There are many studies of PM using ^{14}C in Japan, however studies with ^{14}C analysis for annual and long-range transport from Asian continent are few. We measured ^{14}C concentrations of total carbon (TC) in PM2.5 in Nagoya to investigate the source apportionment of carbonaceous compounds and the long-range transport from Asian continent.

Sampling of PM2.5 was conducted in Nagoya, Japan. Nagoya is located almost at the center of Japan (latitude 35°18'N, longitude 136°91'E), has a temperate climate (average temperature of 16.6 °C), over 2.2 million inhabitants and is one of the major cities in Japan. We carried out daily sampling of PM2.5 for 23.5 h using FRM-2000 from April 2003 to March 2004 at an urban site in Nagoya. 173 samples were collected for a year. Organic carbon (OC) and elemental carbon (EC) were analyzed by the IMPROVE thermal/optical reflectance (TOR) method with carbon analyzer (Sunset Lab). $^{14}C/^{12}C$ ratio was measured with an AMS ^{14}C system at Nagoya University. The samples for 3-11 days were pooled, because it required more than 1 mgC per 1 measurement in order to measure $^{14}C/^{12}C$ ratio with sufficient accuracy. Biomass carbon (BC) and fossil fuel carbon (FC) were calculated by the previous method (Takahashi *et al*, 2007).

The changes of pMC and OC/EC are shown in Fig. 1. Especially in spring, pMC and OC/EC show similar seasonal variations. It is suggested that the change of pMC is not influenced by primary sources (e.g. diesel, industry, etc.) but by other sources (e.g. secondary generation from volatile organic compounds (VOC), long-range transport, etc.).

The concentrations of FC and BC are shown in Fig. 2. BC concentration shows variations similar to OC in spring. Backward air mass trajectories were calculated during the sampling period in spring to identify the source region of high BC concentrations because the air mass flows from the Asian continent in spring. The air mass came from Siberia when OC and OC/EC have high values especially 5-1 and 6-1 (Fig. 2). However the result of 6-2 that has lower OC and BC concentration than 5-1 or 6-1 showed that the air mass came from various regions. In Siberia, large forest burning happened in 2003. High BC concentration in 5-1 and 6-1 is influenced by this forest burning in Siberia.

BC and FC show high concentrations in fall to winter. Some reports say that open burning of agricultural biomass and dry vegetation might be the dominant sources of biomass-derived aerosols. It is considered that biomass burning is important contributor to total carbon (TC) in fall to winter, because daily concentrations of K^+ which is a known tracer for biomass burning s how good correlation with BC. In addition, it is considered that fossil-origin carbon from primary sources is important contributor to TC, because daily concentrations of NO_3^-, NO_x and CO which are known the tracers for primary sources (e.g. diesel, industry, etc.) show good correlation with FC. The high BC and FC concentrations were due to atmospheric stability, because the velocity of the wind showed reverse variations for BC and FC.

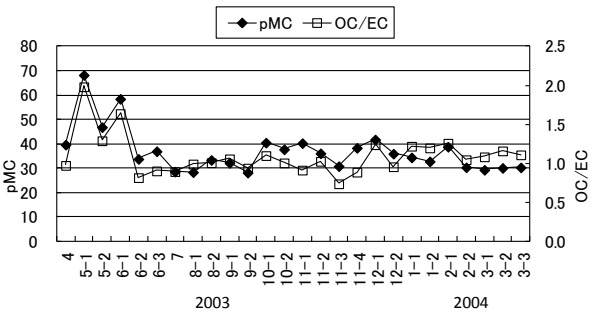

Figure 1. The changes of pMC to OC/EC.

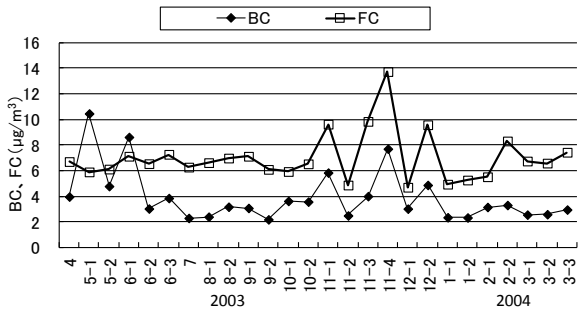

Figure 2. The variations of BC and FC concentration.

Takahashi, K., Hirabayashi, M., Tanabe, K., Shibata, Y., Nishikawa, M., Sakamoto, K., (2007) *Water, Air, Soil Pollut*. **185**, 305–310.

Biomass burning in the Amazon Region: Characterization of airborne particle-phase Polycyclic Aromatic Hydrocarbons

P.C. Vasconcellos[1], Nilmara de Oliveira Alves[2], Sofia Ellen da Silva Caumo[1], Paulo Artaxo[3], Sandra de Souza Hacon[4], Silvia Regina Batistuzzo de Medeiros[5]

[1]Instituto de Química, Universidade de São Paulo, 05509-000, Brazil
[2]Departamento de Bioquímica, Universidade Federal do Rio Grande do Norte, Natal, 59072-970, Brazil
[3]Instituto de Física, Universidade de São Paulo, 05509-000, Brazil
[4] Escola Nacional de Saúde Pública, Fundação Oswaldo Cruz, Rio de Janeiro, 21041-210, Brazil
Keywords: biomass burning, Brazilian Amazon, particulate matter, polycyclic aromatic hydrocarbons.
Presenting author email: perola@iq.usp.br

The Brazilian Amazon region has been intensively affected by deforestation and biomass burning, resulting in increased impacts on our climate and environment with adverse effects on health (Alves *et al*, 2011).

Moreover, studies have documented that one of the components that may be responsible for the observed health effects are organic particulate matter, mainly carcinogenic and/or mutagenic compounds such as polycyclic aromatic hydrocarbons (PAHs) (Boneta et al., 2009).

The objective this study was to identify and to quantify the PAHs in the particulate matter smaller than 10µm (PM_{10}) in filter samples collected in Porto Velho, located in the northern state of Rondonia, region of deforestation and human occupation in the Amazon.

The PM_{10} samples were collected during the dry season (July - October/2011) using high-volume sampler (Figure 1). Subsequently, the samples were extracted with dichloromethane and fractionated in different classes of organic compounds. The PAHs were analyzed by gas-chromatography-mass spectrometry.

Figure 1. The PM_{10} samples were collected using high-volume sampler in Porto Velho, Amazon region.

PM_{10} average mass concentration in the samples collected were 27.3 µg/m³ (Figure 2). The majority of the PM_{10} concentrations did not exceed the limit established by the World Health Organization (WHO) (50 µg/m³).

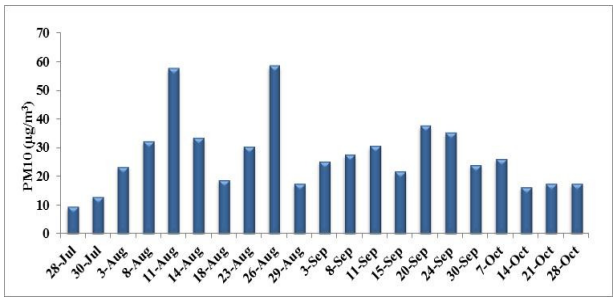

Figure 2. Concentrations of PM_{10} collected in Porto Velho.

The results showed that the anthracene, indene[1,2,3-c,d]pyrene and benzo[g,h,i]perylene were the most abundant compounds among those analyzed. Benzo[a]pyrene, a highly mutagenic and carcinogenic compound, has been identified (Figure 3).

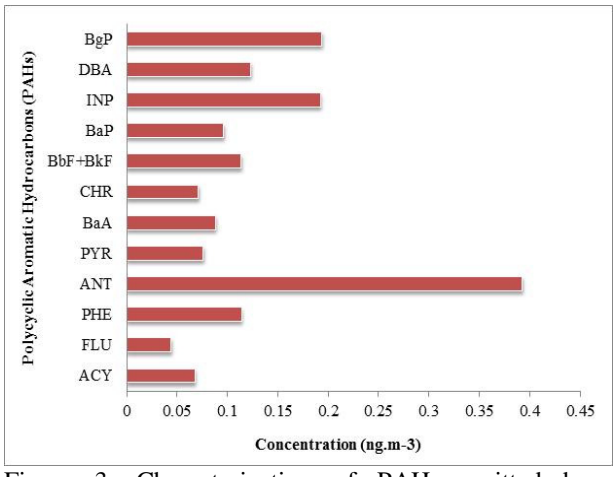

Figure 3. Characterization of PAHs emitted by biomass burning in Porto Velho.

This work was supported by MCT/CNPQ/INCT Process Nº 573797/2008-0 and MCT/CNPq Universal Process Nº 471033/2011-1. NOA is fellow from CNPq Process Nº141910/2010-0.

Alves, NO. et al. (2011) *Ecotoxicology and Environmental Safety*. 74, 1427-1433.

Boneta, S.et al. (2009) *Chemosphere*. 77:1030–4.

Optical and chemical characterization of biomass burning aerosols

J. Vasilescu, L. Marmureanu, A. Nemuc, C. Talianu, L. Belegante
National Institute of R&D for Optoelectronics, Magurele, Ilfov, RO 77125, Romania
Keywords: mass spectrometer, lidar, optical and chemical properties
Presenting author email: jeni@inoe.ro

The aim of this study is to characterize biomass burning organic aerosols (BBOA) detected during the EMEP summer campaign (07 June - 18 July 2012) at Magurele site (44.35 N, 26.03 E) near Bucharest, Romania, using collocated instruments.

Chemical composition and size resolved distribution of submicronic non-refractory aerosols at ground level have been evaluated using a C-TOF aerosol mass spectrometer (AMS) model (Allan et al, 2003). The long range transported aerosols have been studied using a multiwavelength Raman lidar system, which perform vertical measurements in the frame of EARLINET (Pappalardo, G., 2010) since 2008. The lidar system provides backscatter coefficients (1064, 532, 355 nm), extinction coefficients (532, 355 nm) and linear particle depolarization ratio (532 nm) of aerosols between 0.8 and 10 km altitude (Radu et al, 2010).

The long range transported aerosols cases were confirmed by Hysplit- Hybrid Single Particle Lagrangian Integrated Trajectory Mode (Draxler et al, 2012) and MODIS (Moderate Resolution Imaging Spectroradiometer) global fire maps.

Even though the instruments usually measure different air samples, AMS at the ground level and Lidar the vertical profile, on particular meteorological conditions the lofted layers sensed by lidar could be also detected by AMS after downward mixing. We identified 16 cases of biomass burning aerosols at ground level during this campaign. On 11th of July 2012 both AMS and lidar systems sensed BBOA. The air masses traveled from the West of Europe, where high density of forest fires has been showed by MODIS fire map.

The time series of 355 nm wavelength range corrected signal from lidar measurements show a distinct smoke layer at 2.5 km (Figure 1), which is mixing within the planetary boundary layer during the night of 11 July 2012. The plume, descending from 2.5 to 1.5 km, is characterized by extinction related Angstrom exponents (355/532 nm) between 2.2 and 1.7 and lidar ratios between 35 and 55, typical for smoke (Muller D. et al, 2005).

According to AMS measurements on 11 July 2012, main species at ground level are organics, nitrate, sulfate, and ammonium as can be observed in Figure 2. The organics concentrations represent around 40% from the total mass of the submicronic aerosols (Figure 2). The wood combustion marker *f60* values (ratio of m/z 60 to total organics) indicate the presence of BBOA (Cubison et al., 2011) after 18:00 UT, approximately 36 hours old. The age of BBOA was estimated by both *f44* (ratio of m/z 44 to total organics) and *f60* values and by Hysplit back trajectories. The smoke marker decreases by a factor of 2 between 18:00 and 14:00 next day, while the f44 increases from 0.15 to values around 0.25.

Using the synergy of AMS, lidar data and model the presence and age of BBOA was confirmed.

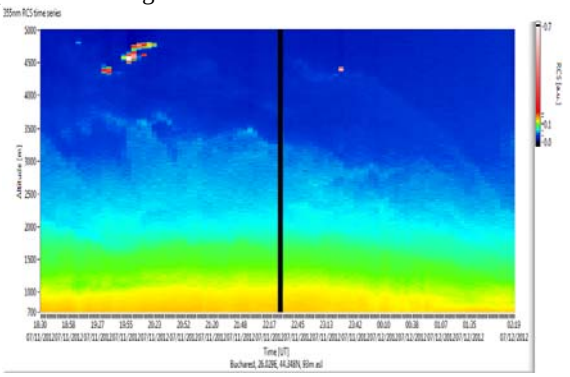

Figure 1. Vertical and temporal distribution of aerosol layers on 11th of July 2012 measured by the lidar

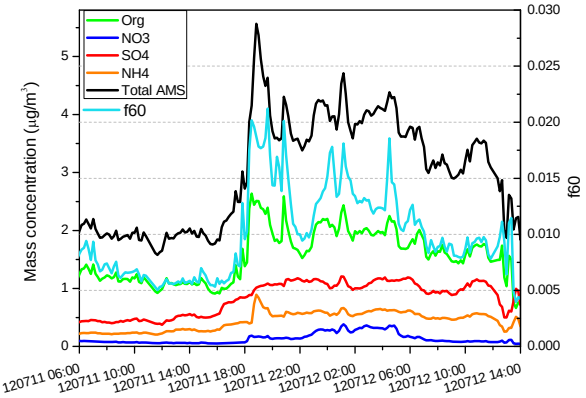

Figure 2. Time series of the mass concentrations of sulfate, nitrate, ammonium, organics and *f60* derived from AMS measurements on 11 of July 2012

This work was supported by a grant of the Romanian National Authority for Scientific Research, CNCS – UEFISCDI, PN-II-RU-PD-2011-3-0082, by Romanian-Swiss Research Programme, IZERZO_142146 / 1- AEROS and by the European Community's FP7-INFRASTRUCTURES-2010-1 under grant agreement number 382 262254 – ACTRIS.

Allan, J.D. et al, (2003), *J. Geophys. Res.* 108, 4091-4105
Cubison, M J et al, (2011), *Atmos. Chem. Phys.*, 11, 12049–12064
Draxler, R.R. and Rolph, G.D., (2012) HYSPLIT (HYbrid Single-Particle Lagrangian Integrated Trajectory) Model access via NOAA ARL READY Website
Muller, D. et al, (2005), *J. Geophys. Res.*, 110, D17201
Pappalardo, G. (2010), Feature article in *EARSeL Newsletter*, 82, 13-18
Radu, C et al, (2010), *J Optoelectron Adv Mat, 12*(1), 165-168

Chemical composition and hygroscopic properties of aerosol particles from Siberian boreal area.

S.Yu. Vasileva[1], G.N. Mironov[1], T.I. Rushkevich[1], S.S.Vlasenko[1], Xuguang Chi[2], A.V. Panov[3], M.O. Andreae[2], and E.F. Mikhailov[1,2]

[1]Department of Atmospheric Physics, St. Petersburg State University, St. Petersburg, 189216, Russia
[2]Max-Planck-Institute for Chemistry, Hahn-Meitner-Weg 1, D-55128 Mainz, Germany
[3]V.N. Sukachev Institute of Forest, Russian Academy of Science, 660036 Krasnoyarsk, Russia

Keywords: boreal aerosols, chemical composition, hygroscopic properties
Presenting author email: alfo4ka@rambler.ru

Organic aerosols (OA) along with the elemental carbon (EC) and inorganic ions strongly contribute to direct and indirect aerosol effects on climate. Boreal forests in Eurasia are a major source of primary organic aerosols (POA) directly emitted from the surface to the atmosphere and secondary organic aerosols (SOA) formed from gaseous precursors in the atmosphere. In order to evaluate and understand the influence of aerosols on climate change in the Artic and Northern Eurasia, long-term observations of the OC, EC and ion content of aerosols in the boreal zone are needed.

In this work we present continuous measurements from April 2010 to June 2012 conducted at Zotino Tall Tower Observatory in Central Siberia (ZOTTO, 60º N, 89º E), Russia . The quartz fiber filters were analyzed for organic and elemental carbon by thermal-optical instrument (SunSet lab.). The Nuclepore filters were analyzed for major anions and cations by ion chromatography (Dionex, ICS-1100). With help from high time resolution CO and light absorption results and HYSPLIT back trajectories calculations, the filter samples were separate to episode samples and non-episode samples.

The aerosols chemical composition were clearly different between episode and non-episode samples, and between winter and other three seasons. The winter episodes associated with elevated concentrations for most of species were usually related to anthropogenic pollution, the air masses during such episodes had passed over the central Siberian region around Omsk and Novosibirsk – a heavily industrialized area. During spring and fall, a number of samples exhibited high K+, and oxalate levels, indicating an impact from biomass burning. In addition a notable episode with extreme high Na, Cl, and Mg were observed for the samples collected between 20 to 24 December 2010, which may result from long range transport of sea salt.

In the aerosol chemical mass closure calculations, six aerosol types were considered. Organic matter (OM) contributed by far the most to the PM mass; it accounted for about 60-70% of the average PM mass. Followed by Secondary Inorganic Aerosols species (SO4, NH4, and NO3), more than 30% of PM mass. OM contribution to PM mass was lower in winter than that in the other three seasons, while EC, Ammonium and Nitrite show higher contribution in winter. The mean PM mass attribution to the different aerosol types Zotto during non-episodes periods were similar to those for the 2007 campaign at the forested site of Hyytiälä, Finland. EC and Nitrate were more important and Ammonium was clearly less important at Zotto, though.

Key issues are the hygroscopic growth of boreal aerosol particles and their activation as cloud condensation nuclei (CCN). Water soluble organic carbon compounds typically account for ~50% or more of total OC (Timonen, 2011) but their impact on aerosol water uptake and cloud formation are not fully characterized. In this study the mass-based hygroscopicity measurements under sub-saturated conditions at 5-99% RH (FDHA, Mikhailov et al., 2013) were used to characterize CCN and hygroscopic properties of the boreal aerosols. It was shown that aerosol water uptake is basically controlled by concentration of inorganic ions in the aged particles.

This work was supported by St. Petersburg state university under grant 11.38.650.2013 and Russian Foundation for Basic Research, under grant 12-05-00620.

E. Mikhailov et al., (2013), *Atmos. Chem. Phys*. **13**, 717-740.
W. Maenhaut, Wan Wang, and Xuguang Chi, Boreal environment research, (2011), **16**, 273-287.
A. Timonen, (2011), Finnish Meteorological Institute, Contributions No. 89, FMI-CONT-89, 76p.

Interpretation of Urban Particle-bound Polycyclic Aromatic Hydrocarbons Source Profiles of PMF with Known Site Specific Emission Characteristics

Eunhwa Jang[1,2], Mohamed S. Alam[1] and Roy M. Harrison[1,3]

[1]Division of Environmental Health & Risk Management, School of Geography, Earth & Environmental Sciences, University of Birmingham, Edgbaston, Birmingham, B15 2TT, United Kingdom
[2]Busan Metropolitan Institute of Health and Environment, MandeokDong, BukGu, Busan, 616-110, Republic of Korea
[3]Department of Environmental Sciences, Center of Excellence in Environmental Studies, King Abdulaziz University, PO Box 80203, Jeddah (21589), Saudi Arabia
Keywords: Positive Matrix Factorisation, particulate polycyclic aromatic hydrocarbons, site specific emission characteristics.
Presenting author email: EXJ101@bham.ac.uk

Measured concentrations of polycyclic aromatic hydrocarbons in urban air are the outputs of mixed emissions from various sources. Because of the carcinogenic and mutagenic properties of the inhalable size particulate PAHs, various methods for source apportionment have been reviewed to extract source specific profiles.

Positive Matrix Factorization has been widely used to apportion the source of pollutants recently, as one of the advanced receptor modelling tools. There are some difficulties to extract site representative profiles because of the uncertainties caused by transport and removal mechanisms between sources and receptors. However, the fact that there are similar extracted source profiles from different continental locations support the existence of source specific profiles (Christie et al., 2012).

Application of PCA to the UK PAH Network sites by Mari *et al* (2010) and Brown and Brown (2012) identified that urban PAH including benzo(a)pyrene was associated with metallurgical industry emissions, domestic solid fossil fuel combustion for heating, and traffic influence. However, common fuel usages between the domestic and industry sector sometimes make it difficult to separate the two specific source profiles and quantify each contribution.

An example of the results shown in Figure 1 is a decomposition of a known industry influenced urban particle-bound PAH dataset into an industry factor with sporadic emission, and a domestic combustion origin with notable seasonality. The latter profile strongly explained by cyclopenta(c,d)pyrene and anthanthrene, was consistent with a factor profile extracted from another dataset which domestic combustion is known to be prevalent.

Known local emission characteristics of combined PAH with seasonal variation made it possible to distinguish between domestic fuel combustion origin and industry influence. The largest contribution to the particle associated PAH and BaP was from traffic exhaust and solid fossil fuel combustion, respectively across UK urban areas.

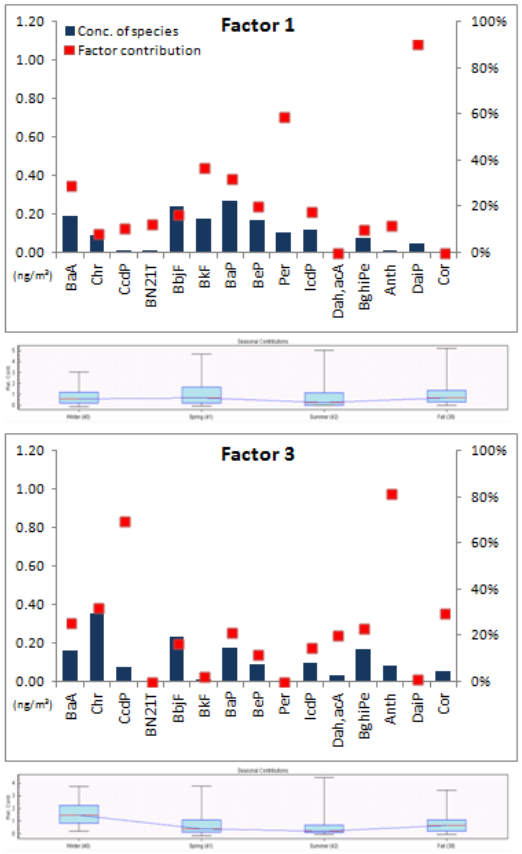

Figure 1. Extracted two factor profiles from known industry sites.

The authors acknowledge support from the Chevening Scholarship of Eunhwa Jang (KR/D/3/7/002/001/133, SEO/2267/1110) and U.K. Natural Environment Research Council.

Brown, A.S. and Brown, R.J.C. (2012). *Jour. Environ. Monitor.*, **14,** 2072-2082.

Christie, S., Raper, D., Lee, D.S., Williams, P.I., Rye, L., Blakey, S., Wilson, C.W., Lobo, P., Hagen, D. and Whitefield, P.D. (2012). *Environ. Sci. Technol.* **46,** 6393-6400.

Mari, M., Harrison, R.M., Schuhmacher, M., Domingo, J.L. and Pongpiachan, S. (2010). *Sci. Tot. Environ.* **408,** 2387-2393.

Water soluble ionic species of particulate matter in an urban road tunnel

M.S. Vieira-Filho[1], R. Astolfo[1], J.J. Pedrotti[2], A. Fornaro[1]

1- Dept. Atmospheric Sciences, University of São Paulo, IAG/USP, 05508-090, São Paulo, Brazil
2- Dept. Chemistry, University Presbiteriana Mackenzie, 01302-907, São Paulo, Brazil
Keywords: $PM_{2.5}$, ions, roadtunnel, urban.
Presenting author email: marcelovieira@model.iag.usp.br

The megacity of São Paulo is facing recurring problems regarding the degradation of air quality, with intense vehicular emissions accounting for a substantial part of this situation. The São Paulo vehicle fleet is quite diverse, containing old and new vehicles powered with gasol (gasoline with 20 - 25% ethanol), hydrated ethanol, CNG (compressed natural gas) and diesel. This fact, coupled with the changing fleet profile (addition of flex-fuel engines), increases the complexity of emissions and physical and chemical processes that involves aerosols.

In order to understand the limiting factors for the formation of aerosol in the atmosphere of São Paulo, in particular the participation of the major inorganic ionic species (sulfate, nitrate, ammonium and chloride), measurements campaigns were carried inside an urban road tunnel (Jânio Quadros) and in the surrounding region (Parque do Povo).

The campaign used two particle samplers (Tupiniquim - AFG model, and Partisol - automatic dichotomous model - Thermo Fischer), The samples were collected in May, 2011 with distinct sampling intervals, for the inner region the sampling period was divided into: (i) 8:00 to 14:00, (ii) 14:00 to 20:00, and (iii) 20:00 to 08:00 of the next day; and for the external region: (i) 08:00 to 20:00 and (ii) 20:00 to 08:00. Besides the particle samplers, two impinger systems for ammonia measurements were employed.

The soluble ions analysis of the fine and coarse particulate matter were performed by chromatographic system Methron 850, and ammonia measurements (in acid medium like ammonium ion) were performed using a flow injection system with gas diffusion and contactless conductivity detection (FIA-GD-C4D).

The results indicated that the median concentration of NH_3 inside the road tunnel (TJQ) was approximately four times higher than in the external region (PP). The mean concentration for the $PM_{2.5}$ major ions (SO_4^{2-}, NH_4^+, NO_3^-) were 2.42±1.45, 1.14±0.71, 0.80±0.52 μg m^{-3}, respectively, for the outside region and 3.27±1.76, 1.27±0.69, 0.76±0.53 μg m^{-3} for the road tunnel. The total mass concentration for fine particulate matter in the inner region was 41.2±10.8 μg m^{-3} and 29.2±17.9 μg m^{-3} for the PP region.

Regarding the representativeness of inorganic species, a simulation from the equilibrium model Isorropia II (Figure 1) attributes 20%, at least, of the total $PM_{2.5}$ mass for the samples collected in the surrounding region. Nonetheless, a maximum of 25% was attributed for the inner region. To verify the relation between the ionic species, a multiple regression analysis was calculated considering the NH_4^+ ion as a dependent variable and the major ionic species, temperature and relative humidity as independent variables. The regression indicated an increase of the adjusted determination coefficient by adding the chloride ion for the external region. However this increase is not observed for the road tunnel which indicates that ammonium ion has no association with this species in an environment with high sulfur oxides concentrations. A greater dependence of thermodynamic variables was observed in the road tunnel, whose slope coefficient for temperature was, β_T = -0.11, with significance level of 5% ($p < 0.05$).

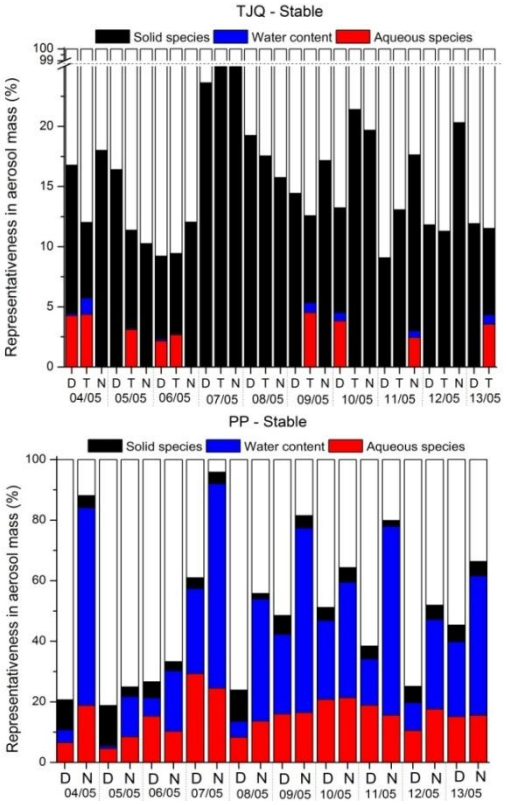

Figure 1. Distribution of solid and aqueous species and water content in the fine particulate matter. This simulation was performed using the ISORROPIA II equilibrium model for $PM_{2.5}$ sampled inside the Jânio Quadros road tunnel (upper graph - TJQ) and surrounding region (lower graph - PP).

The authors would like to thank greatly the resources devoted to this research by CAPES, FAPESP, CNPq and MackPesquisa.

R Core Team (2012). R: A language and environment for statistical computing. R Foundation for Statistical Computing, Vienna, Austria. ISBN 3-900051-07-0, URL:http://www.R-project.org/.

Determination of alkyl phenols in atmospheric aerosols by gas chromatography–ion trap mass spectrometry

M. Visentin, M.C. Pietrogrande,

Department of Chemical and Pharmaceutical Science, University of Ferrara, Ferrara, I44121, Italy
Keywords: biomass burning, wood combustion markers, GC/MS/MS analysis, PM chemical characterization
Presenting author email: vsnmrc@unife.it

In recent years there is increasing interest in atmospheric emissions from biomass burning, one of the largest sources of accumulation mode particles globally.

Specific molecular markers have been identified for tracing biomass combustion, in particular carbohydrates (predominately levoglucosan and other anydrosugars) produced by thermolysis of cellulose and hemicellulose and alkoxyphenols, as thermally decomposition products of lignin, one of the main components in wood. As the basic structure of lignin derives from p-coumaril, coniferyl and synapil alcohols, its burning releases in atmosphere molecules similar to their precursors, such as p-coumaric acid, vanillin, vanillic acid, acetovanillone ferulic acid, syringol, syringaldehyde, syringic acid and acetosyringone.

Different kinds of woods contain different percentage of the three monomers, so that their combustion releases different amounts of alkoxyphenols: diagnostic ratios of syringic/vanillic acids (S/V) and cinnamic/vanillic acids (C/V) have been proposed to identify emissions from specific plant tissue combustion, i.e., hard woods (oak, beech and walnut) or soft woods (conifers) and grass and soft plant tissues (Kuo *et al*, 2011).

GC–MS is the most widely applied technique for the characterization of organic aerosols since it provides multi-residue methodologies for the simultaneous analysis of several compounds with excellent separation efficiency, sensitivity and high number of species analyzed. Due to their high polarity, lignin phenols have to be converted into volatilizable and stable derivatives: trimethylsilyl derivatives are produced by using BSTFA (N,O-bis(trimethylsilyl)-trifluoroacetamide) as silylation reagent (Pietrogrande *et al*, 2011).

Due to small concentration of alkoxyphenols in environmental samples, very sensitive analytical methods like GC/MS/MS are needed. The present paper describes a gas chromatography tandem mass spectrometry method using an ion trap system, as a further development of the pervious GC/MS method (Pietrogrande *et al*, 2013), providing the low detection limits and the high reproducibility required by environmental monitoring.

All the compounds were monitored in multiple reaction mode (MRM). For each target analyte the precursor ion and collision-induced dissociation (CID) voltage were carefully selected to optimize CID efficiency to produce daughter ion(s) and minimize interference during the analysis. The MS detection conditions for each target compound are listed in Table 1.

Five-point calibration curves were prepared to quantify the target analytes in the concentration range of 0.2ngm^{-3} to 5ngm^{-3} using standard solutions. The limits of detection (LOD) of the proposed method were determined by three times the signal to noise ratio S/N (Table 1).

Table 1: MS/MS detection parameters for each target compound: precursor and parent ions. Comparison between sensitivity (LOD) of MS/MS and MS detection procedures.

Analyte	Precursor ion (*m/z*)	Parent ions (*m/z*)	MS/MS LOD (ngm^{-3})	MS (SIM) LOD (ngm^{-3})
Catechol	254	239, 166	0,76	1,24
Syringol	196	153, 181	0,51	0,94
Pyrogallol	239	133, 151, 211	0,45	3,53
Vanillic acid	267	223, 225	0,58	1,82
p-Coumaric acid	293	253, 255, 223	1,75	4,56
Syringic acid	297	243, 233, 219	0,57	3,26

As expected, compared to MS detection operating in the selected ion monitoring (SIM) mode, the MS/MS method is characterized by higher specificity and sensitivity due to the effective exclusion of interfering matrix compounds.

The applicability of the developed method to air quality monitoring was verified by application to $PM_{2.5}$ filters collected under different seasons (summer vs. winter) in different sampling sites (urban vs. rural) in the Emilia Romagna region (Northen Italy).

This work was financially supported by the “Supersito” project of the Regional Agency for Prevention and Environment of the Emilia-Romagna Region (ARPAER).

Kuo, L.J., Louchoan, P. and Herbert, B.E. (2011) *Chemosphere* **85**, 797-805.
Pietrogrande, M.C. and Bacco, D. (2011) *Ana.l Chim. Acta* **689**, 257–264.
Pietrogrande, M.C., Bacco D. and Chiereghin S. (2013) *Ana.l Bioana.l Chem.* **405,** 1095-1104.

Seasonal variations of organic carbon with different volatility at suburban site

Petr Vodička and Jaroslav Schwarz

Institute of Chemical Process Fundamentals of the AS CR, Prague, Czech Republic
Keywords: Organic carbon, OC fractions, Volatility, Ambient aerosol, Seasonal variations, Central Europe
Email: vodicka@icpf.cas.cz

The instrument for analysis of elemental and organic carbon (EC and OC) yields also additional information about volatility of individual OC fractions. Depending on the temperature protocol used, it is possible to distinguish and quantify pyrolitic carbon (PC) and OC1 to OC4 fractions (OC1 being the most and OC4 the least volatile one). This work characterizes diurnal trends of OC fractions at Prague suburban site during various seasons throughout the year.

Measurements of OC fractions were done by the field OC/EC analyzer (Sunset) provided with PM2.5 cyclone inlet. Sampling frequency was 2 hours. Thermal-optical analyses were performed by a modified EUSAAR2 protocol (Cavalli *et al*, 2010) that takes about 15 minutes. Fractions of organic carbon were taken in the following temperature ranges - OC1: <200°C, OC2: 200-300°C, OC3: 300-450°C and OC4: 450-640°C. OC_{total} = OC1+OC2+OC3+OC4+PC. One year data series was collected at Prague-Suchdol urban background station (50°7'36.473" N, 14°23'5.513" E, 277 m ASL) between September 2009 and August 2010. Over 3400 measurements were carried out for each OC fraction in this work.

In many studies published so far, various sources of carbonaceous particles had been mentioned during summer and winter seasons (e.g. Aurela *et al*, 2011). While in winter there is a significant impact of household heating, the influence of secondary OC of both anthropogenic and biogenic origin prevails in summer. Results of this study are in-line with these findings.

The highest concentrations of the most volatile OC1 fraction were found during wintertime (Fig. 1) with diurnal afternoon minima in all seasons. However, after looking at diurnal variations of $OC1/OC_{total}$ ratios during all seasons (Fig. 2), there is well visible the largest proportion of OC1 fraction during summer afternoons, and it corresponds to formation of secondary organic aerosols (SOA). Therefore, it can be assumed that the important part of summer suburban afternoon SOA is formed mainly by the most volatile components of OC. Other OC fractions were studied by a similar way as OC1 fraction and preliminary conclusions from one year measurements of individual OC fractions at Prague-Suchdol site show the following:

- The suburban environment is mainly the source of the most volatile OC1 fraction (especially during the night). It implies that the OC1 fraction is main part of anthropogenic emissions in wintertime and, in contrast to the less volatile fractions (OC2, OC3), it is also most affected by the thinner boundary layer.
- Secondary organic aerosols are the most probable summer source of OC1 fraction being formed mainly during afternoon hours.
- During interpretation of results it is necessary to pay attention to temperature profile of used protocol. For example, OC2 has both the lowest temperature step and absolute concentrations.

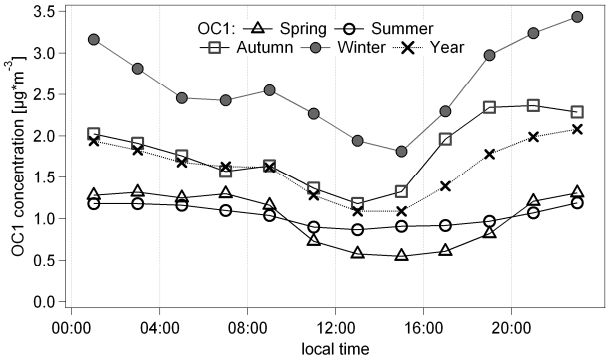

Fig.1. Diurnal cycles of OC1 concentrations averaged according to seasons.

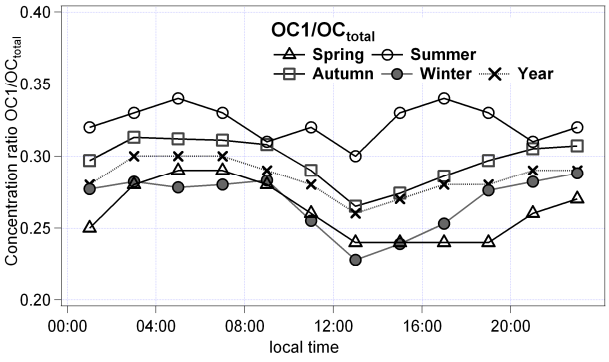

Fig.2. Diurnal variations of $OC1/OC_{total}$ ratio averaged according to seasons.

The authors of this work gratefully acknowledge a support by the Grant Agency of the Czech Republic under grant P209/11/1342.

Cavalli, F., Viana, M., Yttri, K. E., Genberg, J. and Putaud, J.-P. (2010) *Atmos. Meas. Tech.*, **3**, 79-89.

Aurela, M., Saarikoski, S., Timonen, H., Aalto, P., Keronen, P., Saarnio, K., Teinilä, K., Kulmala, M., Hillamo, R. (2011) *Atmospheric Environment* 45, 1394-1401.

Ionic composition of PM_{10} and $PM_{2.5}$ in the area of Thessaloniki, Northern Greece - Estimation of secondary inorganic aerosols and sea spray contribution

D. Voutsa[1], C.Samara[1], E. Manoli[1], E. Gounari[1], D. Lazarou[1], P. Tzoumaka[2]

[1]Aristotle University of Thessaloniki, Department of Chemistry,
Environmental Pollution Control Laboratory, University Campus, 54124 Thessaloniki, Greece
[2]Environmental Department, Municipality of Thessaloniki, Paparigopoulou 7, Thessaloniki 54630, Greece

Keywords: ionic constituents; PM10/PM2.5; secondary ionic aerosol; sea spray
Presenting author email: dvoutsa@chem.auth.gr

Ionic constituents represent a significant component of atmospheric particles (Putaud et al., 2010). Thessaloniki, Greece (40°62´E, 22°95´N) is a densely populated city suffering from high concentrations of airborne particulate matter. Previous studies at urban sites of the city indicated that ionic species were major components of PM_{10} (Voutsa et al., 2002; Terzi et al., 2010). However, there, there are no data available for PM2.5 fraction.

The aim of the present study was to investigate the ionic composition of both PM_{10} and $PM_{2.5}$ in the Major Area of Thessaloniki, Northern Greece. For this purpose, PM_{10} and $PM_{2.5}$ fractions were collected from an urban-traffic (UT) and an urban-background (UB) site. At both sites, PM_{10} and $PM_{2.5}$ samples were concurrently collected during the warm and the cold months of the year (July-Sept 2011 and Febr-April 2012). Sampling was carried out according to EN12341 and EN14907 using Low Volume Samplers operating at constant flow rate 2.3 m^3/h. PM_{10} and $PM_{2.5}$ fractions were collected on Φ 47 mm Teflon filters (Zefluor^{TM} membranes, Pall 2μm). Each sampling had a 24-h duration starting at 00:00. Ionic chromatography has been employed for the determination of water soluble ions (NO_3^-, SO_4^{2-}, Cl^-, Na^+, NH_4^+, K^+, Mg^{2+}, Ca^{2+}).

The average concentrations of ions associated with PM_{10} and $PM_{2.5}$ are shown in Fig. 1.

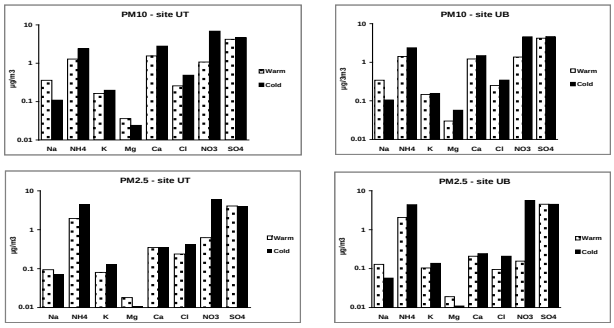

Figure 1. Average concentrations of ions associated with PM10 and PM2.5 at two sampling sites

The PM_{10} fractions of ions were almost similar at the two sampling sites. The $PM_{2.5}$ fractions of Ca^{2+}, Cl^- and NO_3^- (in summer) were higher at the UT site. Mg^{2+} and Ca^{2+} were mainly associated with the coarse fraction whereas NO_3^- and SO_4^{2-} with the fine fraction. Higher concentrations of NO_3^-, NH_4^+ and Cl^- were observed during winter. This trend is probably due to higher NO_x emissions during winter as well as to loss of nitrate or chloride ammonium during summertime. Moreover, K^+ exhibited higher concentrations during winter probably due to emissions from the increasing residential wood burning in the area.

Average contributions of ionic species to total PM_{10} mass were 25% at UT and 32% at UB. The corresponding contributions to total $PM_{2.5}$ mass were 30% and 43% at UT and UB, respectively. Sulfate was the predominant PM_{10} ionic constituent, followed by NO_3^-, Ca^{2+} and NH_4^+. The main ion in $PM_{2.5}$ was also SO_4^{2-}, followed by NH_4^+, NO_3^- and Ca^{2+}.

Secondary inorganic aerosol (SIA) calculated as the sum of non-sea salt of SO_4^{2-}, NO_3^- and NH_4^+ exhibited similar concentrations (~10% μg/m^3) at both sites. This may indicate common origin and removal processes, suggesting that SIA dynamics are more linked to regional processes than to local sources. The average contributions of SIA to $PM_{2.5}$ mass were 35% at UT *vs.* 45 % at UB. The corresponding contribution to PM10 mass was 20% at UT *vs.* 29% at UB. At both sites the concentration of SIA was almost two folds higher in winter. Similar SIA concentrations and temporal variation was also reported by other investigators (EEA, 2012; Squizzato et al., 2012). The sulfur oxidation ratio (SOR) showed that sulfate is photochemically oxidized in the atmosphere from its precursor SO_2. The nitrogen oxidation ratio exhibited higher values at the UB in cold period suggesting favorable conditions for gas conversion processes.

The marine contribution was calculated as the sum of Na^+ concentration and sea salt fractions of Cl^-, Mg^{2+}, K^+,Ca^{2+}, and SO_4^{2-}. The sea spray contribution to particulate matter on a mass basis was low (<2%) similar to the reported values from other Mediterranean coastal areas (Querol et al., 2008; Terzi et al., 2010; Eleftheriadis et al., 2011). The low $PM_{2.5}/PM_{10}$ ratio of sea spray showed the predominant coarse grain size of marine constituents.

References

EEA (2012). Report No4/2012, Copenhagen.
Eleftheriadis, K. et al. (2011). Proceedings EAC2011, Manchester, 4-9 September.
Querol, X. et al. (2008). *Atmos. Environ.*, **42**, 3964-3979.
Putaud, J.-P. et al. (2010). *Atmos. Environ.*, **44**, 1308-1320.
Terzi, E. et al. (2010). *Atmos. Environ.*, **44**, 2231-2239.
Squizzato, S. et al. (2012). *Atmos. Chem. Phys. Discuss.*, **12**, 16377-16406.
Voutsa, D. et al (2002). *Atmos. Environ.*, **36**, 4453-4462.

Aknowledgements

This work was supported by the European Community (LIFE + Environment Policy and Governance).

One year analysis of sedimentation samples at Évora, Portugal

F. Wagner[1], L. Tobias[2], K. Kandler[3], N. Schiavon[1,2], and J. Mirão[1,2]

[1]Centro de Geofísica, Universidade de Évora, Évora, 7000-671, Portugal
[2]HERCULES – Herança Cultural, Estudos e Salvaguarda, Universidade de Évora, Portugal
[3]Institut für Angewandte Geowissenschaften, Technische Universität Darmstadt, 64287, Germany

Keywords: aerosol mineralogy, aerosol chemistry, sedimentation sampling.
Presenting author email: frankwagner@uevora.pt

Data and Methods

Aerosol particles were investigated at the Geophysics Center of Evora (CGE, 38.57°N, 7.91°W, 290 m a.s.l.) for more than 1 year. The sampling period was usually 1 week. The particulate matter was collected on Aluminium stubs coated with carbon adhesives inserted into a modified version of the aerosol passive sampler Type A "flat plates" by Ott and Peters (2008).

The elemental analysis was done using an HITACHI VP-SEM interfaced with a Bruker EDS QUANTAX automatic ESPRIT software as well as FEI QUANTA 200 FEG. The conditions for SEM were as follows: 20 kV accelerating voltage; 10 mm working distance; 120 mA emission current; 70 mA probe current.

About 1000 particles were analysed for each sample and particle size and elemental composition was determined. Based on a set of rules the elemental composition of each particle was transformed into 8 chemical classes. Additional the particles were separated into 3 classes according to their size.

Trajectories were calculated with the HYSPLIT model (Draxler and Hess, 1998) in order to support the interpretation of the data. 10 days backward trajectories were calculated between 500 m a.s.l. and the top of the boundary layer, with a vertical spacing of 100 m and for every hour. Subsequently the location of the points along the trajectory path which are inside the boundary layer were determined and a source region (e.g. Africa, Europa, Atlantic Ocean) was assigned.

Results

Figure one shows the time series of the 8 chemical classes for the largest sampled particles (2.5 – 10 µm). Over the whole period silicates were predominant with an abundance of about 50%. Sulfates vary over time between almost 0% and 30%.

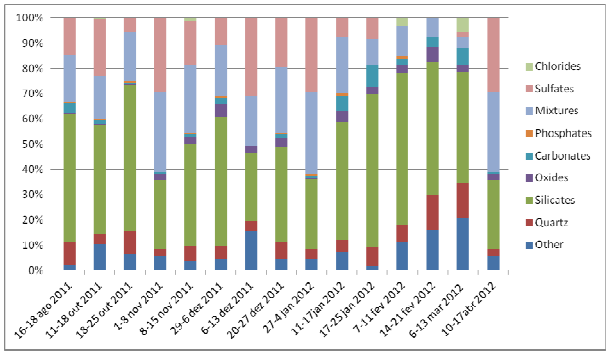

Figure 1. Time series for the chemical composition of deposited particles with diameters between 2.5 and 10 µm.

Acknowledgement

This work was supported by Fundação para a Ciencia e a Technologia and Compete.

References

Draxler, R.R., and G.D. Hess (1998) An overview of the HYSPLIT_4 modeling system of trajectories, dispersion, and deposition. *Aust. Meteor. Mag.*, 47, 295-308.

Ott, D.K., Peters, T. (2008) A Shelter to Protect a Passive Sampler for Coarse Particulate Matter, PM10-2.5. *Aerosol Sci. Technol.* 42, 299-309

Identification of parameters influencing the variability of particle number size distributions in Europe - a multi-site study

Clemens von Bismarck-Osten[1], Stephan Weber[1]

[1] Institute of Geoecology, Climatology and Environmental Meteorology, Technische Universität Braunschweig, Langer Kamp 19c, 38106 Braunschweig, Germany
Keywords: number size distribution, cluster, multiple regression, prediction
Author email: c.von-bismarck-osten@tu-bs.de, s.weber@tu-bs.de,

Three years of aerosol measurements from four European cities were analysed to identify and quantify the parameters influencing the particle number size distribution (NSD) at different measurement sites (Copenhagen, Helsinki, Leipzig, London). A 'triple-site' approach was established with data from a roadside, an urban background and a rural measurement station, which were available for each city. The NSD measurements were conducted over a diameter size range of 8 to 700 nm.

Average hourly total number concentrations varied between 3.300 cm^{-3} (Copenhagen rural) and 23,000 cm^{-3} (London roadside). Highest variability on the diurnal course was found for the roadside sites and on the seasonal course for the rural sites.

A first identification of the influencing parameters was found using correlation analysis pointing out wind speed, wind direction, temperature, shortwave downward solar radiation, daytime and season as most dominating factors. These were then quantified using a multiple linear regression approach with a partially non-linear treatment of input data documenting the highest influence for daytime (45%) followed by wind direction (18%), season (12%), wind speed (11%), temperature (8%) and solar radiation (6%) on average.

The variation of influence between the different cities are analysed and discussed. Subsequently NSDs were modelled using the regression approach in order to verify how well the parameters are capable of 'explaining' the actual NSD, showing best performance for roadside NSD with correlation coefficients between 0.65 and 0.8 (average COD of around 0.2 to 0.3, Fig.1) and with correlation coefficients of 0.5 to 0.6 only limited performance for the rural sites (COD of around 0.3 to 0.4 on average).

Finally the data was classified into a limited number of characteristic cluster size distributions using unsupervised and semi-supervised cluster analysis approaches. After a first source assignment of each cluster (e.g. on the basis of daytime and seasonal occurrence, wind sector, mean diameter or total number concentrations) the main information about the influence of the local (meteorological) conditions on the particle number size distribution can be derived. This way the main connections and interactions between the ambient environment and particles are reduced and compressed to a manageable minimum which makes it easier for a near-future forecasting of particle number size distributions.

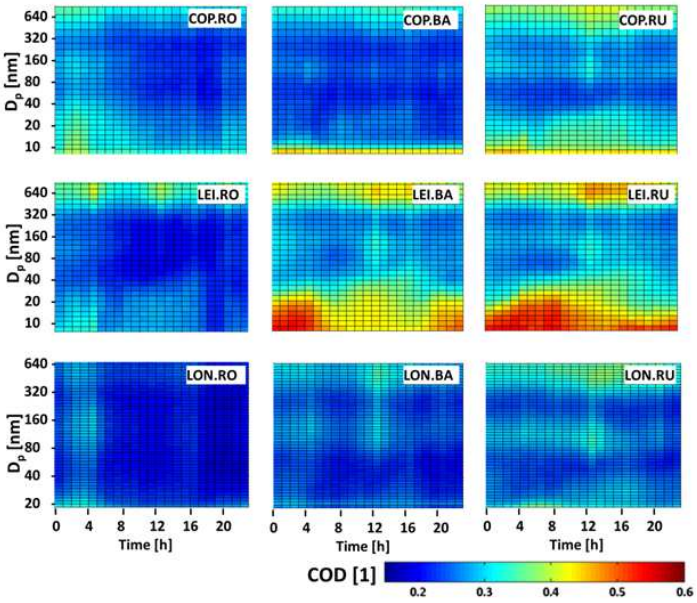

Fig.1: *Coefficient of Divergence (COD) for comparison of modelled and measured number size distribution. The smallest values indicate the highest conformity at a specific daytime and per particle size; the highest values indicate heterogeneous conditions. RO represents the roadside measurement site, BA the urban background and RU the rural site within Copenhagen (COP), Leipzig (LEI) and London (LON).*

Acknowledgements:

We would like to thank the respective institutions and personnel providing data and advice for this study. Wolfram Birmili (*Leibniz Institute of Tropospheric Research)*, Andreas Massling and Matthias Ketzel *(Arhus University)* are specifically acknowledged.

Vertical aerosol stratification above the Caribbean Sea near Barbados

B. Wehner[1], F. Ditas[1], H. Wex[1], I. Serikov[2], A. Wiedensohler[1], and H. Siebert[1]

[1]Leibniz Institute for Tropospheric Research (TROPOS), 04318 Leipzig, Germany
[2]Max-Planck-Institute for Meteorology, 20146 Hamburg, Germany
Keywords: aerosol layers, aerosol profiles.
Presenting author email: birgit@tropos.de

Shallow cumulus clouds are widespread in the trade wind regions and play an important role for the vertical transport of moisture, momentum, and heat as well as for the earth's radiation budget. The influence of aerosol particles on the formation and life cycle of these clouds is controversially discussed in the literature.

Therefore, one major topic of the CARRIBA (**C**loud, **A**erosol, **R**adiation, and Tu**R**bulence in the trade w**I**nd regime over **BA**rbados) campaigns in November 2010 and April 2011 was to investigate the temporal and spatial variability of aerosol particles near the Caribbean Island Barbados (Siebert et al., 2012). More than 30 research flights with the helicopter-borne platform ACTOS have been performed in that region.

For measuring the total particle number concentration a commercial CPC (model 3762, TSI Inc., St. Paul, USA) has been implemented on ACTOS to measure the total particle number concentration N with a time resolution of 1 s. The aerosol particle number size distribution (PNSD) from 6 nm to 2.5 µm was measured using an SMPS (designed by TROPOS) and an OPC (Model 1.129, Grimm Aerosol Technik, Ainring, Germany) with a time resolution of 120 s. Furthermore, ACTOS contains various instruments to measure cloud properties and thermodynamic parameters, such as temperature, humidity and 3D-wind vector. Continuous measurements of a Raman-Lidar located at Deebles Point at the East Coast of Barbados were also used to detect distinct aerosol layers.

Results

Figure 1 shows the profile of potential temperature Θ, specific humidity r and particle number concentration N measured on April 18, 2011. In the well-mixed sub-cloud layer (SCL < 500 m) Θ, r, and N are nearly constant. Above that height N increases slightly except for a short dip due to a cloud contact in around 700 m. Between 800 and 1200 m N reaches its maximum of this profile of ~ 1000 cm^{-3} and decreases above to values between 400 and 600 cm^{-3}. Above the SCL, the profile of N can be divided into strongly separated aerosol layers: e.g. Layer 1 from 800 to 1200 m and Layer 2 from 1200 to 1700 m.

Figure 2 shows PNSDs measured below 500 m (SCL), in Layer 1 (800 – 1200 m), and Layer 2 (1200 – 1700 m). The shape of the individual PNSDs is similar but the number concentration is highest in Layer 1 corresponding to the profile of N.

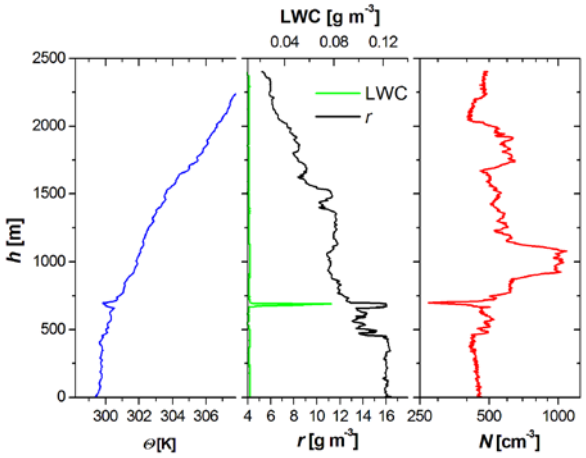

Figure 1. Vertical profiles of potential temperature Θ, specific humidity r and particle number concentration N measured on April 18, 2011 by ACTOS.

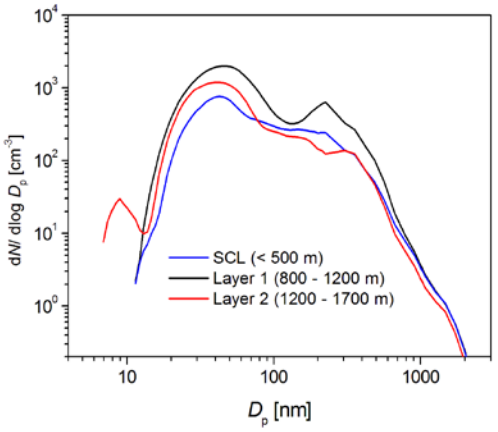

Figure 2. Particle number size distributions in selected layers: SCL (below 500 m), Layer 1, and Layer 2 on April 18, 2011.

The existence of such narrow aerosol layers has been observed on several days throughout the campaign. Obviously there are no efficient mixing processes to balance such concentration gradients immediately. The continuous Lidar data will be used to detect aerosol layers during the day and may give some information about their optical properties.

This work was supported by the Deutsche Forschungsgemeinschaft (SI 1534/3-1 and WE 1900/18-1).

Siebert, H., et al. (2012), The fine-scale structure of the trade wind regime over Barbados - An introduction to the CARRIBA project -, *Atmos. Chem. Phys. Discuss.*, *12*, 28609 - 28660.

Methods and limits of unipolar charged aerosol inversion

Z.N. Wei[1], L. Knobel[1], H.-J. Schmid[1]

[1]Chair of Particle Technology, University of Paderborn, Paderborn, Germany
Keywords: inversion, unipolar charger, electrical mobility, particle number size distribution
Presenting author email: zhongning.wei@uni-paderborn.de

The Scanning Mobility Particle Sizer (SMPS) is in widespread use for measuring the airborne particle size distributions and concentration which is electrical mobility based sizing techniques. In such a device the particles are classified according to the electric mobility. As a result after investigations an electrical particle mobility distribution is giving. But multiple charges per particle can result in particles of two different diameters but having the same electrical mobility. Therefore it is impossible or not easy to get the particle number size distribution directly. Thus the methods of conversion from electrical mobility particle distribution to particle size distribution are used extensively.

A NanoScan SMPS will be used for analytic unipolar charged nanoparticles. A patented unipolar charger charges more nanoparticles than bipolar charger, in other words, the bipolar charger has a lower charging efficiency, e.g., as pointed out in Wiedensohler (1988), over 90% of 10 nm particles would be neutral and could not be efficiently. Compared to the bipolar charging has the unipolar charging a higher charging efficiency (Tippayawong et al., 2011). Additionally the unipolar charger eliminates the need for radioactive material, which has less health risks and more regulations.

In a NanoScan a conditioner will be used in order to remove larger particles which could not be measured. Thus an electrical mobility particle distribution for the rest particles will be given by the TSI software. The measured mobility particle distribution for particles which are probably to have multiple charges and which can result in particles of two different diameters but having the same electrical mobility must be corrected and then the conversion from electrical mobility particle distribution to particle size distribution will be with the inversion routines calculated. But by the unipolar charger is the correction method encountered to limit, e.g. a lower resolution, lack of accuracy information for the larger particles. So we need to analysis and determine limits of the resolution and the size limit. And then these limits will be expected and quantified.

Furthermore we present the theory of a data inversion algorithm for the SMPS measurement. As pointed out in Stratmann et al. (1996), to convert from particle mobility distribution into particle size distribution, i.e. to calculate the number concentration of particles in size bin, a linear equation has to be solved. Where, the number of mobility bins, the number concentration in mobility and size bins and the probability of the particles to carry *n* elementary charges (or the charge number per particle) must be known. Namely the particle number size distribution will be calculated from the raw data, the measured electrical particle mobility. This method is called multiply charged inversion. If the unipolar charge distribution is principally known, it will be possible to obtain the particle number size distribution. The idea of this numeric method is under the assumption with a given number of sampling points of this particle number size distribution.

Wiedensohler, A. (1988). *An Approximation of the Bipolar Charge Distribution for Particles in the Submicron Size Range*. Jounal. Aerosol Science.

TSI, *Application Note SMPS-005.*

Stratmann, F., Wiedensohler A. (1996) *A New Data Inversion algorithm for DMPS-Measurements,* Institute for Tropospheric Research, Leipzig.

Intra, P., Tippayawong, N. (2011) *An Overview of Unipolar Charger Developments for Nanoparticle Charging*, Aerosol and air Quality Research.

Pfeifer, S., Müller, T., Wiedensohler A. (2012) *Enhanced multiple charge inversion algorithm for mobility size spectrometers,* Institute for Tropospheric Research, Leipzig.

Alpha radioactive aerosols behavior in the ground atmosphere

V.S. Yakovleva[1], M.S. Cherepnev[1], I.I. Ippolitov[2], P.M. Nagorsky[2], S.V. Smirnov[2], A.V. Vukolov[1]

[1]Department of Applied Physics, Tomsk Polytechnic University, Tomsk, 634050, Russian Federation
[2]Department of Climatic System, Institute of Monitoring of Climatic and Ecological System (IMCES) SB RAS, Tomsk, 634050, Russian Federation
Keywords: alpha, beta, radioactivity, aerosol, atmosphere, monitoring, detector.
Presenting author email: vsyakovleva@tpu.ru

Investigation of behavior of environmental background radioactivity (aerosols and gases) is one of the main tasks when solving problems of low dose effects. It also useful for investigation of electrical properties of atmosphere and climate global change forecasting, because of air radioactive aerosols and gases and their balance regulate the surface layer of atmospheric plasma. The main purpose of this work was to investigate temporal and spatial dynamics of α-radioactive aerosols in the ground atmosphere. The general distinctions of this investigation are: 1) synchronous measurements of characteristics of α- and β-radiation fields and volumetric activity of atmospheric radionuclides (radon isotopes and their aerosol decay products (DPs)) at one point; 2) parallel measurements at different heights up to 35 m; and 3) high time resolution of data series. Such approach allowed getting more informative data to reach the purpose of the work.

The long-term experiment was performed at Tomsk Observatory of Radioactivity and Ionizing Radiation (TORIR). Instrumental equipment included: scintillation detectors of α- and β-radiation (ATOMTEX, Republic of Belarus) installed at series of heights (0.1; 1; 5; 10; 25 and 35 m); radon isotopes and DPs radiometers (EQF 3200, SARAD, Germany; RRA-01-03, Russia; Ramon-01, Kazakhstan) and automated devices for radon (RFD) and thoron (TFD) flux densities measurements (Fig. 1). In order to determine the degree of external factors influence the monitoring of meteorological, actinometrical and atmospheric-electrical values was performed via automated information measuring system.

In accordance with simplify radon and PDs transport model (only turbulent diffusion) in air the vertical distribution of their concentrations follows exponential law and decrease with height. Results of experiment with help of scintillation α-detectors showed inverse dependence (Fig. 2), i.e. increasing of α-radioactive aerosols concentration with height.

The results of numerical simulation of radon isotopes and their DPs transport in ground atmosphere with using complex model (turbulent diffusion, moving under the influence of vertical wind, removal by gravity and precipitation) showed that turbulent diffusion coefficient and vertical component of wind velocity are the most important factors, which influence vertical aerosols distribution. But only when wind blows upwards (from ground surface) we can observe such inverse situation in vertical distribution of radioactive aerosols.

Because of α-active aerosol (radon isotopes and DPs) concentration is direct (by radioactive complex decay low) related with β-active aerosol concentration (DPs), the experimental check of vertical distribution for β-radioactivity in air was also applied. The results (Fig. 2) revealed different dependences of flux density from height for α- and β-radioactivity in air.

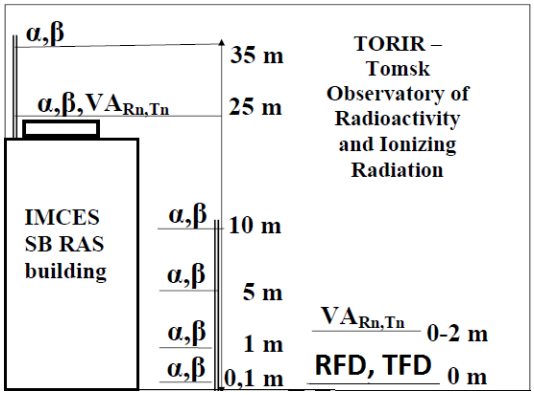

Figure 1. The scheme of experiment in Tomsk

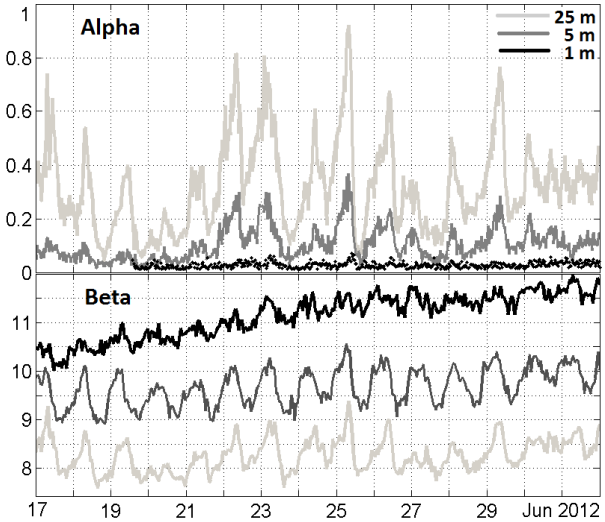

Figure 2. Temporal dynamics of α- and β-radiation flux densities in units of $m^{-2}s^{-1}$ at different heights

Detail discussion of behavior of α-radioactive aerosols in ground atmosphere during 2011–2013 and influencing factors are presented in the report.

This work was supported by RF Analytical departmental target program “Development of higher school scientific potential” under grant № 2.1.1/13707.

The role of condensable vapours in atmospheric new particle growth and shrinkage

L.-H. Young[1], P.-S. Cheng[1], Y.-J. Liou[1], S.-H. Lee[2], V.P. Kanawade[2] and T.-C. Hsiao[3]

[1]Department of Occupational Safety and Health, China Medical University, Taichung City, Taichung, 40402, Taiwan
[2]College of Public Health, Kent State University, Kent, OH, 44240, USA
[3]Graduate Institute of Environmental Engineering, National Central University, Jhongli City, Taoyuan, 32001, Taiwan
Keywords: nucleation, shrinkage, evaporation, semi-volatile.
Presenting author email: lhy@mail.cmu.edu.tw

New particle formation (NPF) is a key process that increases the number of aerosols in the atmosphere. It is characterized by a sudden burst of new particles of a few nanometres and subsequent growth to sizes of tens of nanometres. The latter growth is commonly considered as an irreversible process. However, particle shrinkage can occur due to the evaporation of the condensed species if the involved processes are reversible (Zhang *et al.*, 2012). To date, there are only a few observations of new particle shrinkage and thus still poorly understood.

In a multi-site NPF study in subtropical central Taiwan (Young *et al.*, 2012; Young *et al.*, 2013), 10-1000 nm particle number size distributions were measured with SMPS (GRIMM Model 5.500) in an urban (U), coastal (C), mountain (M) and downwind (D) area. The sampling campaigns were conducted during a cold and a warm season. Among the identified 14 NPF events, there were five particle shrinkage events during which the grown particles shrank back to sizes of ~10 nm, thereby creating a unique "arch-like" shape in the size distribution contour plot (Figure 1). The new particle growth and shrinkage rates (GR and SR), and their corresponding condensable vapour (C_v) and H_2SO_4 proxy (P) concentrations, and particle volume loss (VL) were estimated.

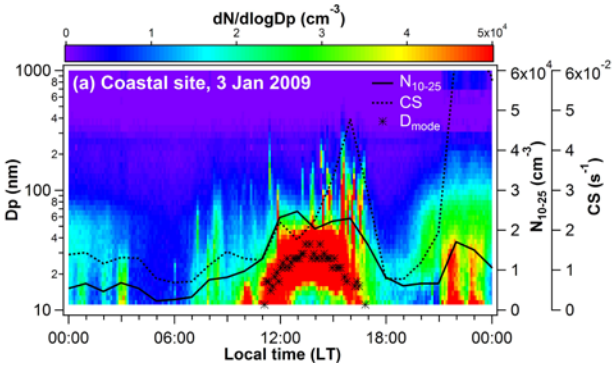

Figure 1. An example of new particle growth and shrinkage observed on the 3 January 2009.

Table 1 shows the GR, SR and GR-to-SR ratio, while Table 2 gives the C, P and VL for the five particle shrinkage events. As shown, the GR ranged from 7.4 to 17.3 nm hr^{-1}, whereas the SR ranged from 5.1 to 7.6 nm hr^{-1}. The SR-to-GR ratios were all above 0.44 indicating the SR were slower than the GR. The C of 1.69-6.59×10^8 cm^{-3} were required to explain the particle growth, whereas the P of 1.72-7.79×10^7 cm^{-3} were estimated to be produced under the observed atmospheric conditions. The P-to-C ratios were all below 0.22, suggesting that H_2SO_4 alone were not sufficient for the new particle growth. The VL on the 3 January 2009 and the 7 September 2010 were above 90%, indicating near complete evaporation. On the remaining three days, the VL were between 18% to 38%. These results clearly show that a notable fraction of the prior condensed chemical species evaporated from the particle phase to the gas phase. Bzdek *et al.* (2012) recently showed that sulfate contributed to 41-46% new particle growth, whereas NO_3^-, NH_4^+ and organics contributed to the remaining 54-59% growth. In particular, some of the latter chemical species are known to be semi-volatile and, as such, they have the potentials to evaporate off the new particles under favorable conditions.

Table 1. Growth rate (GR), shrinkage rate (SR) and SR-to-GR ratio during the new particle shrinkage events.

Date	Site	GR (nm hr^{-1})	SR (nm hr^{-1})	SR/GR
1/3/09	C	7.8	5.1	0.66
8/12/10	U	10.7	5.6	0.52
8/16/10	U	17.3	6.9	0.40
9/5/10	D	15.4	7.1	0.42
9/7/10	D	7.4	7.6	1.02

Table 2. Condensable vapour (C_v), H_2SO_4 proxy (P) concentrations, P-to-C ratio and particle volume loss (VL) during the new particle shrinkage events.

Date	Site	C (10^8 cm^{-3})	P (10^7 cm^{-3})	P/C	VL (%)
1/3/09	C	1.93	2.46	0.13	100
8/12/10	U	3.09	4.92	0.16	24
8/16/10	U	5.00	-	-	18
9/5/10	D	4.51	3.94	0.09	38
9/7/10	D	1.70	3.73	0.22	90

This work was supported by the Taiwan National Science Council under NSC 100-2628-E-039-001-MY3.

Bzdek, B.R., Zordan, C.A., Pennington, M.R. *et al.* (2012) *Environ. Sci. Technol.* **46**, 4365-4373.
Young, L.-H., Wang, Y.-T., Hsu, H.-C. *et al.* (2012) *Sci. Total Environ.* **425**, 135-145.
Young, L.-H., Lee, S.-H., Kanawade, V.J. *et al.* (2013) *Atmos. Chem. Phys.* **13**, 547-564.
Zhang, R., Khalizov, A., Wang, L., Hu, M. and Xu, W. (2012) *Chem. Rev.* **112**, 1957-2011.

Evolution of *n*-Alkanes in PM samples collected in São Paulo, Brazil (2000-2010)

P.C. Vasconcellos[1], Sofia Caumo[1] and J.B. De Andrade[2]

[1]Departmento de Química, Universidade de São Paulo, 05509-000, Brazil
[2]Departmento de Química Geral e Inorgânica, Universidade Federal da Bahia, Salvador, 40170-290, Brazil
Keywords: organic aerosols, n-alkanes in the atmosphere, biomass burning emissions, vehicular emissions
Presenting author email: perola@iq.usp.br

N-alkanes determination is interesting to study the origin and fate of atmospheric aerosols (Alves, 2008). They are ubiquitous in urban, continental or marine samples. They can be derived from both biogenic and anthropogenic sources which can be differentiated based on their *n*-alkanes distribution. Their relatively low reactivity and volatility make them interesting tracers of both atmospheric transport and particle origin.

Samples were collected for over ten years (from 2000 to 2010). All measurements were done in the campus of the University of São Paulo (SPA) using high-volume sampler (PM_{10}) and in 2000, total suspended particles (TSP). Samples collected during winter time (2000, 2002, 2003 2008, 2010) were collected in intensive campaigns (n=10-15 samples, in each campaign). Two extensive sampling (all over the year) were done collecting 26 samples (2001-2002) and 33 samples (2003-2004), those collected every 15 days. In the total, over 150 samples were analyzed.
Winter samples (Figure 1) were collected aiming to study the period with strong events of air pollution. Total *n*-alkanes concentrations presented variations ranging from 32 ng m^{-3} (PM_{10}, 2003) to 103 ng m^{-3} (TSP, 2002).

Colder and drier months (June to September) favored the pollutants accumulation. Besides, biomass burning plumes are often observed arriving of the vicinities from May to November to this site.

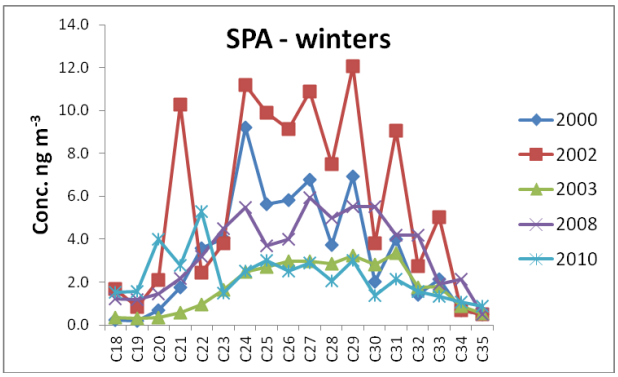

Figure 1. *N*-alkanes concentrations in the samples collected in the wintertime.

The relative contribution of biogenic emissions is assessed by wax normal alkanes index (Figure 2). In the average, considering all samples, the anthropogenic sources (biomass burning) were responsible for over 80% of these *n*-alkanes (higher than C_{25}) emissions.
The carbon preference index (CPI), a diagnostic parameter close to 1 indicated also the strong contribution of anthropogenic contaminants in PM coming from vehicular emissions (Vasconcellos *et al*, 2011).

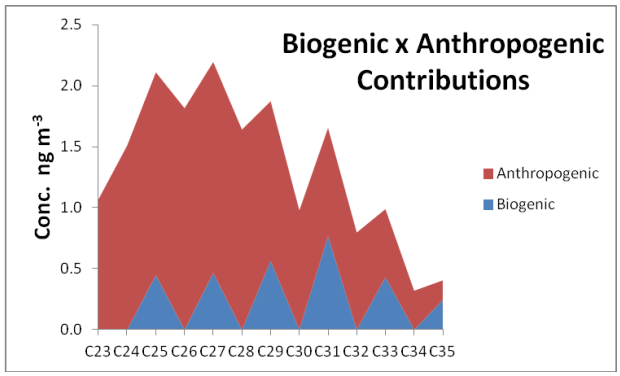

Figure 2. Relative contributions of the sources of *n*-alkanes.

In the extensive campaign (2003, Figure 3) where samples were collected all over the year, samples collected during the summer and fall campaigns presented the highest concentrations, differently of particulate matter concnetrations (higher in the wintertime).

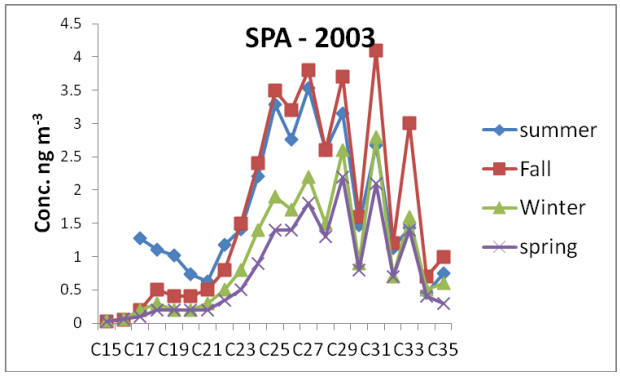

Figure 3. *N*-alkanes concentrations of the samples collected in the extensive campaign (2003).

In general *n*-alkanes lower than C_{25} (anthropogenic emission) were less abundant than those higher, emitted by biogenic (tropical vegetation) and by anthropogenic sources (sugarcane burning).

This work was supported by INCT – Energia e Ambiente and by NUANCE project (FAPESP).

Alves, C. (2008) *Ann. Bras.Acad. Sci.*80, 21-82.
Vasconcellos, P.C. et al. (2011) *Atmos. Environ.* 45, 5770-5777.

Comparison of particle number size distributions in three Central European capital cities

N. Zíková[1], T. Borsós[2], D. Řimnáčová[1], J. Smolík[1], Z. Wagner[3], T. Weidinger[4], J. Burkart[5,6], G. Steiner[5,7], G. Reischl[5], R. Hitzenberger[5], J. Schwarz[1], I. Salma[2] and V. Ždímal[1]

[1]Department of Aerosol and Laser Studies, Institute of Chemical Process Fundamentals, Prague, 16502, Czech Republic
[2]Institute of Chemistry, Eötvös University, Budapest, H-1117, Hungary
[3]E. Hála Laboratory of Thermodynamics, Institute of Chemical Process Fundamentals, Prague, 16502, Czech Republic
[4]Department of Meteorology, Eötvös University, Budapest, H-1117, Hungary
[5]Faculty of Physics, University of Vienna, Vienna, 1090, Austria
[6]Institute of Mountain Risk Engineering, University of Natural Resources & Life Sciences, Vienna, 1190, Austria
[7]Department of Physics, Division of Atmospheric Sciences, University of Helsinki, FI-00014, Finland

Keywords: urban environment, diurnal variation, number size distribution, new particle formation.
Presenting author email: zikova@icpf.cas.cz

Health aspects of ultrafine aerosol particles in urban environment have been studied extensively in recent years (Salma *et al.*, 2011; Putaud *et al.*, 2010; Qian *et al.*, 2007 etc.). Three main sources of the ultrafine particles have been defined – traffic, biomass burning, and atmospheric nucleation. However, the diurnal changes in intensities of individual sources are of considerable extent, similarly to the scale of variations in particle number concentrations due to meteorological phenomena.

In order to quantify the variability in all the aspects mentioned above, to reveal differences and similarities, as well as common or specific features, we compared different properties of particle number size distributions in three cities (Budapest, Prague and Vienna) that belong to the same region, type of climate, and are of comparable size. The three cities are situated in Central Europe in a relatively narrow band oriented in parallel with one of the prevailing wind directions that is NW in the region.

Number size distributions of atmospheric aerosol particles were determined over the mobility diameter range from 10 to 1000 nm in each of the three capitals for a one-year-long period. We derived and compared particle number concentrations in various size fractions, their diurnal and seasonal variations, and frequencies of new particle formation events.

Annual median particle number concentrations for Budapest, Prague and Vienna were 10.6×10^3, 7.3×10^3, and 8.0×10^3 #/cm^3, respectively. Differences may be related to the different pollution levels of the cities, and/or to the different measurement environments and local conditions (Borsos et al., 2012).

Furthermore, it has been found that contributions of the cumulative concentrations of particles smaller than 100 nm in diameter to the total number concentration were 80%, 84% and 74% for Budapest, Prague and Vienna, respectively. Thus, in each of the cities, the particles under 100 nm contribute decisively to the total number concentrations.

Diurnal variations of submicron particles larger than 100 nm, exhibited similar shape for all the cities (Fig. 1). The diurnal pattern with a peak at about 8 AM and another maximum at about 9 PM was related to the time-activity pattern of inhabitants and regional influences (traffic, heating etc.).

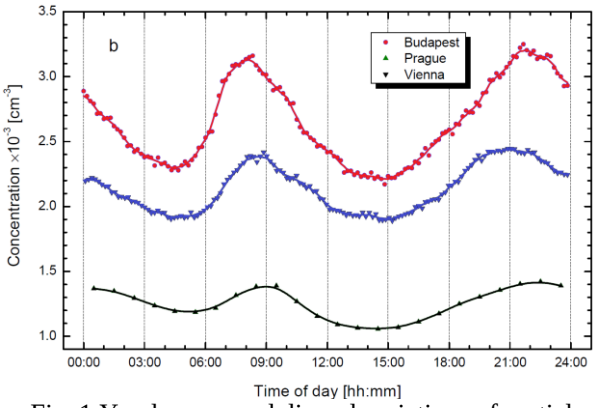

Fig. 1 Yearly averaged diurnal variations of particle number concentrations in Budapest, Vienna and Prague (particles between 100 and 1000 nm in diameter).

The structure of the diurnal variation for ultrafine particles (smaller than 100 nm in diameter) was similar to those in sizes between 100 and 1000 nm with an exception related to the position of the second peak. That peak was shifted from late evening to afternoon. This can be due to daily cycling in meteorological parameters, due to the character of the measurement site, and mainly due to the presence of new particle formation and subsequent growth in urban environments.

Financial support by a bilateral project between Hungary and Czech Republic, by the Hungarian Scientific Research Fund (K84091), by the Czech Science Foundation (CSF P209/11/1342), and by the Austrian Science Fund (FWF, P19515-N20) is appreciated. Authors thank Czech Hydrometeorological Institute, the Viennese Environmental Department, and the Austrian Central Institute for Meteorology and Geodynamics (ZAMG) for providing the meteorological and air quality data.

Borsós T., Řimnáčová D., Ždímal V., Smolík J. *et al.* (2012), *Sci. Tot. Environ.* **433**:418–426.
Qian S, Sakurai H, McMurry PH. (2007) *Atmos Environ*. **41**:4119–27.
Putaud J-P, Van Dingenen R, Alastuey A, *et al.* (2010) *Atmos Environ*. **44**:1308–20.
Salma I, Borsós T, Weidinger T, Aalto P, Hussein T, *et al*. (2011) *Atmos Chem Phys*,**11**:1339–53.

CCN activation of insoluble silica aerosols mixed with soluble pollutants

M. Dalirian[1], H. Keskinen[2], P. Miettinen[2], A. Virtanen[2], A. Laaksonen[2] and I. Riipinen[1]

[1] Department of Applied Environmental Science (ITM) and Bert Bolin Centre for Climate research, Stockholm University, Stockholm, Sweden
[2] Department of Applied Physics, University of Eastern Finland, Kuopio, Finland
Keywords: silica, coating, CCN activation
Presenting author email: Maryam.dalirian@itm.su.se

Insoluble particles, e.g. mineral dust, silica and soot, can act as CCN if they acquire some deliquescent material. Extensive data and theories on CCN activation of completely soluble and insoluble particles exist but the CCN activation of coated particles has been investigated less. In this study laboratory measurements were conducted on CCN activation of insoluble silica particles coated with soluble species. The experimental results were compared to the theoretical calculations using the framework introduced by Kumar *et al.* (2011b).

Measurements

Particles with insoluble core and soluble coating were generated and analyzed in this study. Fumed silica was used as the insoluble particle. Three different kinds of species were used as soluble coatings: ammonium sulphate, sucrose and a protein (bovine serum albumin known as BSA). The fractions of soluble species were 5%, 10% and 25% of total particulate mass in the original aqueous solution, which was atomized and dried to yield the mixed particles. Particle number distribution measurements were conducted using a scanning mobility particle sizer (SMPS). Size-resolved CCN activity was carried out using the Scanning Mobility CCN Analysis (SMCA) and the structure of atomized particles from aqueous suspension was defined by transmission electron microscopy (TEM).

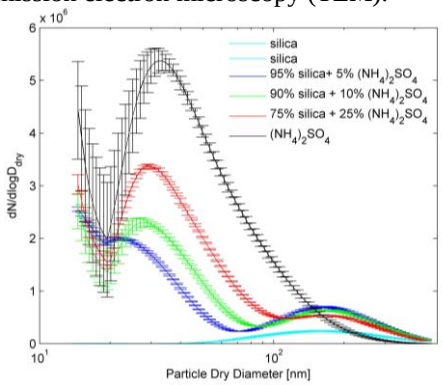

Figure 1: SMPS data for number size distributions of silica particles coated with $(NH_4)_2SO_4$.

Theory

κ-Köhler theory (Petters & Kreidenweis, 2007) was used to estimate the critical supersaturation of soluble particles. Critical supersaturation of pure silica particles, on the other hand, were calculated using the FHH adsorption theory (Sorjamaa and Laaksonen, 2007; Kumar *et al.*, 2009 & 2011a). For mixed soluble and insoluble particles a shell-and-core model (Kumar *et al.*, 2011b) was used in the calculations.

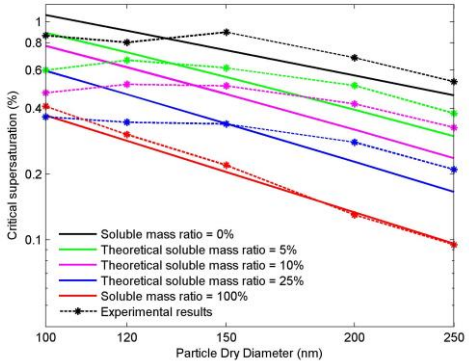

Figure 2: Calculated and experimental critical supersaturations for silica + sucrose particles

Conclusions

Pure and mixed particles of silica and soluble compounds (AS, sucrose and BSA) were generated. Morphology of silica and BSA agglomerates changed with particle size, while $(NH_4)_2SO_4$ and sucrose were spherical. The mixed particles resembled pure silica agglomerates. For pure soluble components the results were in good agreement with k-Köhler theory and for pure silica reasonable agreement was observed with adsorption theory, but deviation from the size-dependence was observed. The reason of these deviations could be e.g. uncertainty in the adsorption parameters and the effect of changing particle morphology with size. Mixed particles had reasonable agreement with the framework by Kumar et al., but shell-core model failed to reproduce the size-dependence of the CCN activation, probably due to the complex particle morphology.

Financial support from CRAICC and Vetenskapsrådet is gratefully acknowledged.

Kumar, P., Sokolik, I. N., and Nenes, A., (2011a), *Atmos. Chem. Phys*., 11, 3527.
Kumar, P., Sokolik, I. N., and Nenes, A., (2011b), *Atmos. Chem. Phys.*, 11, 8661.
Petters, M. D. and Kreidenweis, S. M. (2007), *Atmos. Chem. Phys*., 7, 1961.
Sorjamaa, R. and Laaksonen, A. (2007). *Atmos. Chem. Phys*., 7, 6175.

Measurements During The South American Biomass Burning Analysis (SAMBBA) Field Experiment

J. D. Allan[1,2], W. T. Morgan[1], P. I. Williams[1,2], M. Flynn[1], E. Darbyshire[1], A. Hodgson[1], B. T. Johnson[3], J. M. Haywood[3,4], S. Freitas[5], K. Longo[5], P. Artaxo[6] and H. Coe[1]

[1]School of Earth, Atmospheric & Environmental Sciences, University of Manchester, UK
[2]National Centre for Atmospheric Science, University of Manchester, UK
[3]The Met Office, Exeter, UK
[4]College of Engineering, Mathematics & Physical Sciences, University of Exeter, UK
[5]National Institute for Space Research (INPE), São José dos Campos, Brazil
[6]University of São Paulo, Brazil
Keywords: Wildfires, Amazon, AMS, Biomass
Presenting author email: james.allan@manchester.ac.uk

Biomass burning represents one of the largest sources of particulate matter in the atmosphere and can significantly perturb local air quality, meteorology and the earth's radiative balance (Bond et al., in press). Due to the relatively short atmospheric lifetimes, these effects are most acutely felt on regional scales and can have a significant effect on quality of life and the hydrological cycle. However, many of its predicted effects are very poorly constrained. The lifetime and properties of these aerosols are strongly dependent on their composition and injection height, which are turn are highly dependent on the burn conditions.

The South American Biomass Burning Analysis (SAMBBA) field campaign took place in Brazil in September and October 2012, towards the end of the dry season when biomass burning is typically at its peak. This was a collaborative project between a number of UK and Brazilian institutes and featured a comprehensive suite of state-of-the-art instruments on board the UK Facility for Airborne Atmospheric Measurements (FAAM) BAe-146 large research aircraft, based in Porto Velho, in the state of Rondonia. Aerosol instrumentation included an Aerodyne Aerosol Mass Spectrometer (AMS), Single Particle Soot Photometer (SP2), Scanning Mobility Particle Sizer (SMPS), Particle Soot Absorption Photometer (PSAP), Cloud Condensation Nuclei Counter (CCN), Passive Cavity Aerosol Spectrometer Probe (PCASP) and Nephelometers. In conjunction with other measurements, such as inorganic gases, VOCs, optical spectrometers, lidar and dropsondes, a comprehensive characterisation of the composition and dynamics of smoke plumes could be obtained, which can in turn be used to inform and validate models that attempt to simulate the emissions and impacts of these fires based on satellite data.

During the campaign, 19 sorties were performed and a number of different fires were characterised, along with regional hazes, background aerosols (in both the boundary layer and free troposphere) and 'clean' areas dominated by biogenic emissions. Very different aerosol compositions were found depending on the exact burn conditions. As an example, flight B737 sampled a large forest fire in a remote area of Rondonia, which was principally smouldering in nature, whereas B742 sampled fires in an agricultural area of Tocantins, which were principally flaming. The B742 case showed a larger mass concentration of black carbon (up to 50 µg m^{-3} instead of 5 µg m^{-3}), whereas organic matter concentrations were similar (up to 5 mg m^{-3}). Relationships were also found between different fractional mass spectral markers commonly used in the AMS, specifically *f*44 (oxygenated organics) and *f*60 (anhydrous sugars such as levoglucosan). The relationship between these markers changed between the two cases, although these were both within the range of previously published works (figure 1).

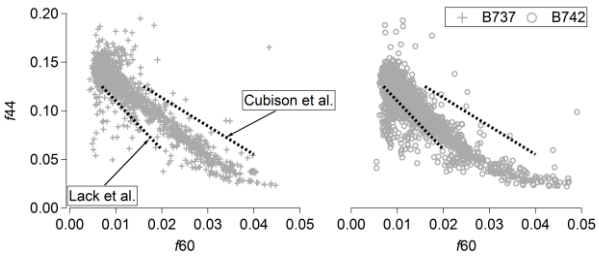

Figure 1: Relationship between *f*44 and *f*60 for a smouldering wildfire (B737) and flaming agricultural fires (B742). The dotted lines correspond to the relationships reported by Lack et al. (2012) and Cubison et al. (2011)

Further results from this campaign will be presented and discussed, quantifying the properties of aerosols under the various conditions. As well as differences in the plume characteristics with burn type, also of interest are the transformations during plume age. The intended applications of these data (e.g. to modelling activities) will also be discussed.

Bond et al.: *J. Geophys. Res. –Atmos.*, doi: 10.1002/jgrd.50171, in press.
Cubison et al.: *Atmos. Chem. Phys.*, 11, 12049-12064, doi:10.5194/acp-11-12049-2011, 2011.
Lack et al.: *Atmos. Chem. Phys.*, 13, 2415-2422, doi:10.5194/acp-13-2415-2013, 2013.

Characteristics of new particle formation events in Hungarian background air at K-puszta, 2008-2012

Zs. Bécsi[1], Á. Molnár[2], K. Imre[2] and P. P. Aalto[3]

[1]Department of Earth and Environmental Sciences, University of Pannonia, Veszprém, P.O. Box 158, H-8201, Hungary
[2]MTA-PE Air Chemistry Research Group, University of Pannonia, Veszprém, P.O. Box 158, H-8201, Hungary
[3]Department of Physics, University of Helsinki, Helsinki, P.O. Box 64, FI-00014, Finland
Keywords: aerosol, formation, growth, seasonality.
Presenting author email: becsi.zsuzsanna@gmail.com

Fine aerosol particles have been studied in the last years due to their important role in several atmospheric processes and effects on climate and human health. New particle formation events are observed all over the world both in polluted and clean, background air. Similarly, in Hungary NPF events can be detected in polluted cities like Budapest (Salma *et al* (2011), Borsós *et al* (2012)) as well as in rural air at K-puszta (Yli-Juuti *et al* (2009)). Our former results showed that at K-puszta new particle formation (NPF) can be frequently observed, the number of NPF events peaked in spring and autumn (September) per each year.

In this work we summarize our results on the particle formation at K-puszta station between Nov. 2008 and Dec. 2012. The size distribution of the particles between 3-800 nm is evaluated. On the basis of DMPS spectra the classification of particle formation events is carried out according to the recommendations of Yli-Juuti *et al* (2009). The event classification is studied with respect to the seasonal variation and the frequency of the particle formation event types (event, non-event and unclassified) is also discussed.

Figure 1. Event classification statistics (2012), K-puszta.

Generally, our four year statistics on new particle formation (NPF) shows that winter is the most inactive period. In contrast the number of NPF events was found to be the highest in spring and in autumn as presented for 2012 (Figure 1). As a consequence of the above-mentioned seasonal variation of the NPF events, the frequency of the nucleation mode (3-25 nm) was the highest during spring and autumn (Figure 2). On the other hand, in winter the accumulation mode (100-800 nm) showed the highest, while in spring and summer the lowest frequency. This seasonality is also shown by the "typical" seasonal number size distributions. This means that in spring the freshly formed particles, while in winter the aged particles characterize the aerosol size distribution.

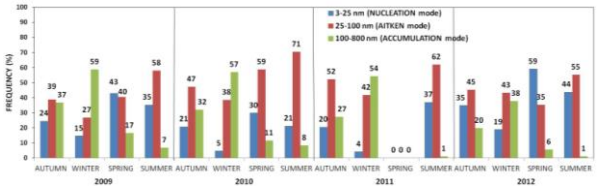

Figure 2. The seasonal frequency of the maximum concentrations in different particle modes (2009-2012).

The growth rate (GR) of the freshly formed particles is also calculated (Hirsikko *et al* (2005), Yli-Juuti *et al* (2009)). Our results on four-year data showed the high variability of particle GR with no significant seasonal variation at K-puszta. The rates were estimated between a few and 14 $nmhr^{-1}$ except some days with higher GR (between 16.5-18.41 $nmhr^{-1}$). The average GR was 5.85 $nmhr^{-1}$. On the other hand, the formation intensity of new nucleation mode particles (smaller than 25 nm) is also estimated. The calculation is based on the method considering the change of the particle number concentration in each size modes per unit time. The average formation rate for 10 nm particle size range was found between 0.33-46.31 particles $cm^{-3}sec^{-1}$.

The research leading to these results has received funding from the European Union Seventh Framework Programme (FP7/2007-2013) under grant agreement n° [262254], [ACTRIS]; and TÁMOP-4.2.2.A-11/1/KONV-2012-0064 (The project is realized with the support of the European Union, with the co-funding of the European Social Fund).

Salma, I., Borsós, T., Weidinger, T., Aalto, P., Hussein, T., Dal Maso, M. and Kulmala, M. (2011) *Atmos. Chem. Phys*., **11**, 1339–1353.

Borsós, T., Řimnáčová, D., Ždímal, V., Smolík, J., Wagner, Z., Weidinger, T., Burkart, J., Steiner, G., Reischl, G., Hitzenberger, R., Schwarz, J., Salma, I. (2012) *Sci. Total Environ.* **433,** 418–426.

Yli-Juuti, T., Riipinen, I., Aalto, P.P., Nieminen, T., Maenhaut, W., Janssens, I.A., Claeys, M., Salma, I., Ocskay, R., Hoffer, A., Imre, K. and Kulmala, M. (2009) *Boreal Env. Res.* **14**, 683-698.

Hirsikko, A., Laakso, L., Hõrrak, U., Aalto, P., Kerminen, V.-M. and Kulmala, M. (2005) *Boreal Env. Res.* **10**, 357-369.

Long-term observations of carbonaceous aerosols and related gaseous emissions near a crude-oil plant in South Italy

M. Calvello[1,2], M. Lovallo[4], F. Esposito[3] , L. Mangiamele[4], G. Pavese[1]

[1] CNR-IMAA, C. da S. Loya, 85050, Tito Scalo (PZ), Italy
[2] OAVDA, via Vittorio Emanuele II, 85052, Marsico Nuovo (PZ), Italy
[3] DIFA- Università della Basilicata, C. da Macchia Romana, 85100, Potenza, Italy
[4] ARPAB, Via della Fisica C/D, 85100, Potenza, Italy
Keywords: Carbonaceous aerosol, organic emissions, time series
Presenting author email: mariarosaria.calvello@imaa.cnr.it

A two-year dataset of almost continuous Black Carbon (BC) content measurements by a Magee AE31 7-wavelenghts aethalometer (370 to 950 nm) near a crude oil pre-treatment plant in South Italy (Agri Valley, 40.33°N, 15.92° E, 582 m a.s.l) has been analyzed. Since 1996 an intense crude-oil extraction together with a pre-treatment activity has been carried out at the site with continuous and controlled combustion processes and smoke emissions.

A suitably implemented algorithm has been applied to the aethalometer data in order to analyse absorption coefficient spectral dependence and to reduce the error in UVPM detection (Esposito *et al.*, 2012). BC and UVPM data have been compared to some organic compounds concentrations (Benzene, Toluene, Methane, Non-Methane Hydrocarbons) routinely measured at the same site and for the same period by ARPAB (Basilicata region environmental protection agency).

Recurrent trends have been searched for on a wide temporal scale (two-years diurnal cycles/ seasonal pattern, summer and winter) by applying the statistical Lomb-Scargle periodogram technique to the entire data-set. This is a powerful technique to be applied for frequency analysis of not equally-spaced data to obtain reconstructed spectra on both seasonal and annual basis (Hocke *et al*., 2009). These spectra can be considered as representative of background emissions to be compared with much intense emissions taking place in shorter periods (few days to few weeks) during the year (Pavese *et al*., 2012).

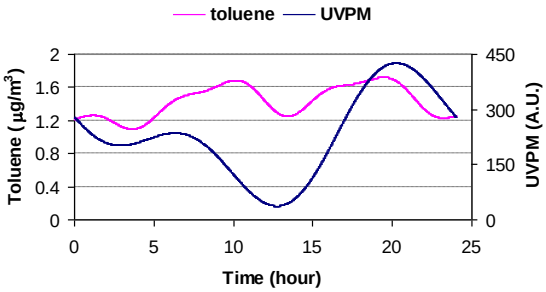

Figure 1: Reconstructed spectra of toluene and UVPM "typical day" as obtained by Lomb-Scargle periodogram for the two-year database.

As an example, reconstructed spectra of toluene and UVPM "typical day" from two-years concentrations data are shown in Figure 1. The differences observed can suggest different dynamics in aerosol formation and/or in adsorption processes onto atmospheric particles.

On the contrary, considering an episode of intense emissions (March, 8th- 19th 2011), UVPM and toluene time behaviours show similar patterns, as reported in Figure 2, highlighting the necessity to study emissions on different time-scales.

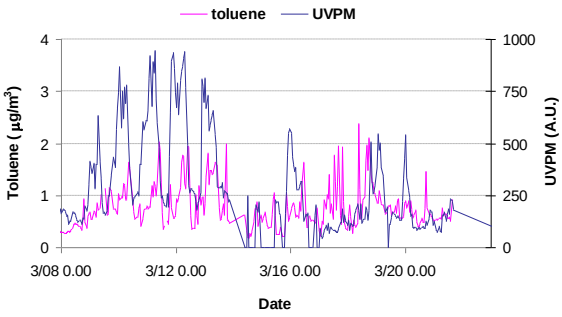

Figure 2: Temporal variation of toluene concentrations and UVPM hourly mean values for the period march 8th - 19th 2011.

To complete this study, an analysis of meteo-climatic parameters such as solar radiation, wind intensity and prevalent direction, has been carried out to verify if and when these parameters contribute to a major/minor agreement among combustion products time patterns.

This work was supported by "Osservatorio Ambientale della Val d'Agri" in the framework of the project "Integrated model for environmental matrix" and by ARPAB.

Esposito, F., Calvello, M., and Pavese, G. (2012). *Atmos. Meas. Tech. Discuss*., 5, 1003-1027

Hocke, K., and Kämpfer N. (2009). *Atmos. Chem. Phys.*, 9, 4197–4206.

Pavese, G., Calvello, M., Esposito, F., (2012). *Aerosol and air quality research*, 12, 1146-1156, 2012.

Wood-burning emissions within a continuous-flow photooxidation reactor: Soot-Particle Aerosol Mass Spectrometer characterization

J. C. Corbin[1], A. Keller[2], H. Butscher[2], B. Sierau[1], U. Lohmann[1], and A. A. Mensah[1]

[1]Institute for Atmosphere and Climate Science, ETH Zürich, Universitätstrasse 16, 8092 Zürich, Switzerland.
[2]Institute of Aerosol and Sensor Technology, FHNW, Klosterzelgstrasse 2, 5210 Windisch, Switzerland.

Keywords: wood-burning, photooxidation, AMS, SP-AMS
Presenting author email: joel.corbin@env.ethz.ch

Wood-burning stoves, used worldwide for heating and cooking, can be an important atmospheric source of primary and secondary aerosols. Current legislation restricts only the primary aerosol emissions of such stoves, which include primary organic aerosol particles (POA), ash, and soot. Such legislation neglects the potential formation of secondary organic aerosol (SOA), which may nucleate or condense after the atmospheric oxidation of volatile organic compounds. For example, smog chamber photooxidation experiments have observed wood-burning SOA concentrations up to four times higher than the corresponding POA emissions (Grieshop et al., 2009; Heringa et al., 2011).

To characterize the SOA-formation potential of wood-burning stoves and similar emissions, Keller and Burtscher (2012) have developed a continuous-flow photooxidation reactor for monitoring potential SOA in real-time. The short residence time (seconds) of this chamber allows the time-resolved measurement of potential SOA. However, the small chamber also necessitates higher-than-ambient irradiation conditions.

Here, we present results from high-resolution Aerosol Mass Spectrometer (AMS) and Soot-Particle AMS (SP-AMS) analysis of wood-stove emissions under three different conditions: filtered and photooxidized ("SOA"), unfiltered and photooxidized ("OxPOA"), and unfiltered emissions ("POA").

Figure 1 shows the increase in aerosol oxidation after photooxidation, as measured by the AMS. The figure shows the difference of the normalized SOA and POA organic mass spectra, averaged over multiple burns. High-resolution analysis has been used to identify organic species as C_xH_y (*green*), $C_xH_yO_{z=1}$ (*purple*), or $C_xH_yO_{z>1}$ (*pink*). However, data are presented on a unit-mass scale for clarity. As shown, the relative intensity of CO_x ions was higher for SOA, whereas C_xH_y was higher for POA. The pie charts (inset) summarize all three cases, showing $C_xH_yO_z$ increasing and C_xH_y decreasing, from left to right. For POA, the contribution of hydrocarbons C_xH_y was more than double that of SOA. Also, SOA contained more $C_xH_yO_{z>1}$ relative to OxPOA. Elemental analysis indicated that the shift of H:C and O:C ratios due to oxidation was comparable to, but significantly greater than, observations in Mexico City (Heald et al., 2010).

In these experiments, refractory species (those involatile below 600 °C) were also characterized with an SP-AMS laser equipped on the same AMS. High-resolution SP-AMS analysis yielded similar results to the AMS, with the major spectral change due only to pure-carbon ions (C_x). Detailed AMS and SP-AMS results will be presented and compared.

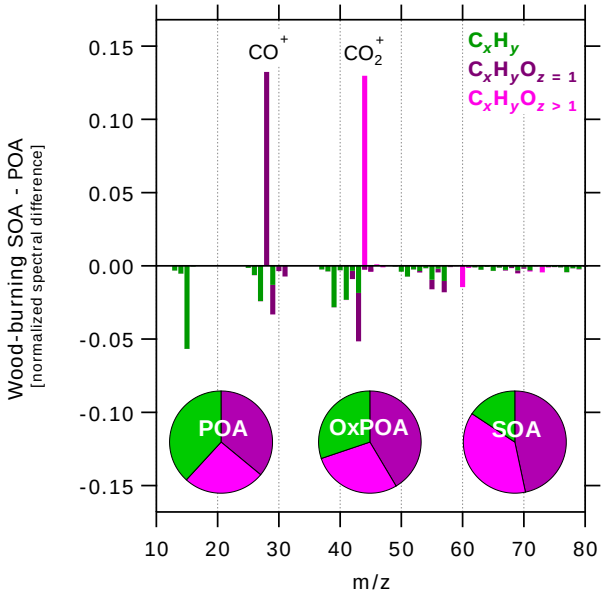

Figure 1. AMS difference mass spectrum for wood-stove SOA minus POA. Inset: pie charts of the organic composition for the three cases.

This work was supported by the Swiss National Fund, Swiss Federal Office for Energy, Swiss Federal Office for the Environment, and the IMBALANCE project of the ETH Zürich.

Grieshop, A.P., J.M. Logue, N.M. Donahue and A.L. Robinson (2009). Atmos. Chem. Phys., 9, 1263-1277. *doi:10.5194/acp-9-1263-2009*

Heringa, M.F., P.F. DeCarlo, R. Chirico, T. Tritscher, J. Dommen, E. Weingartner, R. Richter, G. Wehrle, A.S.H. Prévôt, U. Baltensperger (2011). Atmos. Chem. Phys., 11, 5945-5957. *doi:10.5194/acp-11-5945-2011*

Heald, C.L., J.H. Kroll, J.L. Jimenez, K.S. Docherty, P.F. DeCarlo, A.C. Aiken, Q. Chen, S.T. Martin, D.K. Farmer, P. Artaxo (2010). Geophys. Res. Lett., 37, L08803, *doi:10.1029/2010GL042737*

Keller and Burtscher (2012). J. Aerosol. Sci., 49, 9-20. *doi:10.1016/j.jaerosci.2012.02.007*

Variations of levels of atmospheric electrical and meteorological parameters and natural radioactivity in response to heavy smog due to forest fires

M.S. Cherepnev[1], A.V. Vukolov[1], I.I. Ippolitov[2], M.V. Kabanov[2], P.M. Nagorsky[2], Yu.A. Phalagov[3], S.V. Smirnov[2] and V.S. Yakovleva[1]

[1]Department of Applied Physics, Tomsk Polytechnic University, Tomsk, 634050, Russian Federation
[2]Institute of Monitoring of Climatic and Ecological System SB RAS, Tomsk, 634050, Russian Federation
[3]Institute of Atmospheric Optics, SB RAS, Tomsk, 634050, Russian Federation
Keywords: forest fires, aerosol, light ions, radioactivity.
Presenting author email: maxcherepnev@gmail.com

Extreme weather conditions created in summer in the European part of Russia in 2002 and 2010 and in Siberia in 2004 and 2012 due to forest fires led to the large number of forest and peat fires accompanied by extreme smoke of atmosphere.

Tropospheric aerosol together with greenhouse gases is an important climate-making factor influencing the radiation balance of the Earth. An important mechanism of variations of atmosphere electrical parameters (electric intensity E and polar conductivities $\lambda_{\pm}$) is the change in the number of light ions that are the main charge carriers due to their outflow onto the atmospheric aerosol. Decrease in the number of light ions in their outflow onto aerosol particles should lead to a decrease of $\lambda_{\pm}$ and to an increase of electric field intensity E. Ionization of air molecules in the atmosphere surface layer takes place mainly due to the natural radioactivity.

Based on a joint analysis of the variations of ionizing radiation levels (α-, β-, γ-background) in the atmosphere at heights of 5, 10 m and 25 m and depths of 0.1, 0.2, 0.5 and 1 m in the soil, meteorological and atmospheric electrical parameters in the summer smog due to summer forest fires in Siberia (2012) it was found that an increase of intensively smokiness and related with it decrease of visual range (S_m, Fig. 1, panel 1) and fall of solar radiation flux (I, panel 2) in the visible and UV ranges is followed by a decrease of λ_+ (panel 3) and the level of α-background radiation (panel 4). The clear dependence of β-, γ-background radiation level (panel 5) on S_m was not found.

Analysis of observation data of atmospheric electrical parameters during periods with maximal smog aerosol concentrations in the urban atmosphere surface layer due to long-term forest fires allowed for the first time to find out the effect of daily inversions of the electric field intensity with a changing range of 300 V/m and more in the daytime, of -300 V/m at night (panel 6). The observed effect of daily variations of the electric field in the atmosphere surface layer differs from the known effects by that it was detected in the smog conditions when forest fires covering large areas often for a long time in many regions. The proposed interpretation of this effect does not contradict the well-known diffusion-kinetic model of the ion charge aerosol.

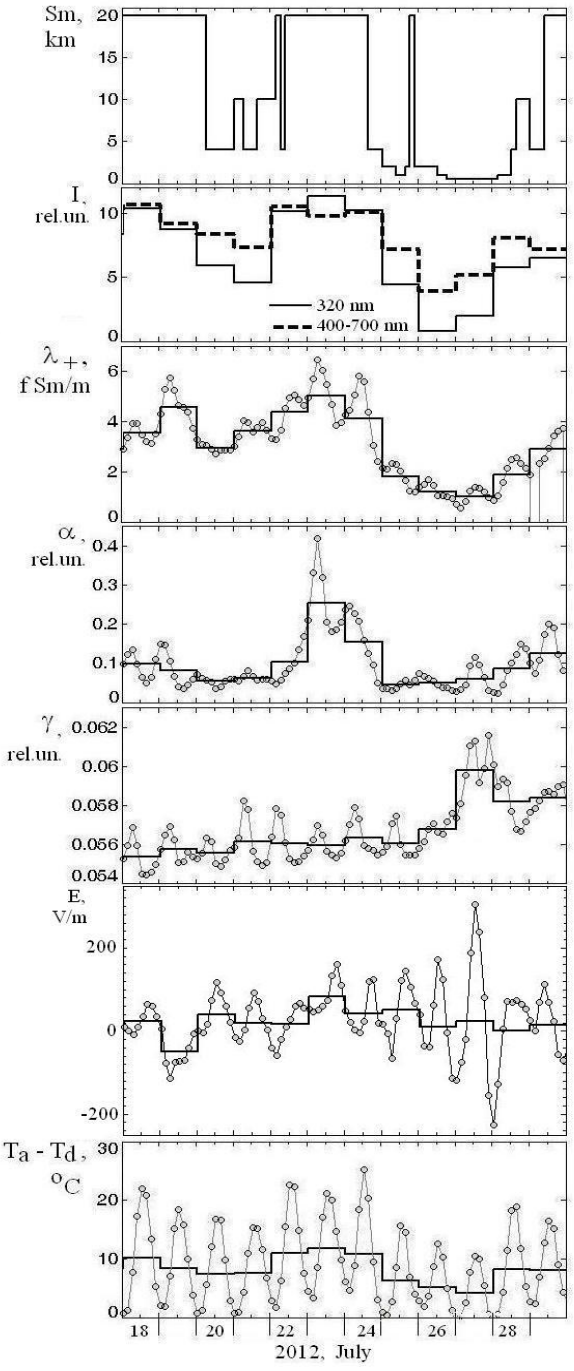

Figure 1. Variations of α-, γ-radiation components and meteorological quantities (S_m, I, λ_+, E, T_a -T_d) during the smog due to summer forest fires

Road tunnels - particle properties, wet and dry conditions

S. Janhäll[1], M. Gustafsson[1], S. Abbasi[2], G. Blomqvist[1], A. Gudmundsson[3], C. Johansson[4,5], M. Norman[5], U. Olofsson[2], B. Sjövall[5]

[1]VTI - Swedish National Road and Transport Research Institute, Linköping, SE 581 95, Sweden
[2] KTH Machine Design, Stockholm, SE 100 44, Sweden
[3]Division of Ergonomics and Aerosol Technology, Lund University, Lund, SE 221 00, Sweden
[4]Department of Applied Environmental Science, Stockholm University, Stockholm, SE 106 91, Sweden
[5] Stockholm Environment and Health Administration, SLB-analysis, Stockholm, SE 104 20, Sweden

Keywords: particle, tunnel, road, traffic
Presenting author email: sara.janhall@vti.se

Particulate air pollution in traffic tunnels is often very high due to high emissions and restricted air exchange (e.g. Gëller *et al.*, 2005). Road traffic tunnels have both exhaust and non-exhaust particle sources such as tires, pavement and brakes. In tunnel environments the emissions of ultrafine particles would decrease due to high levels of particle surface area for deposition (Janhäll *et al.*, 2012).

In an on-going research project, airborne particles in one road and one railroad tunnel (Gustafsson *et al*, these proceedings) are characterized regarding concentrations, size distributions and elemental composition in relation to traffic. This abstract show initial project results for the road traffic tunnel, with the aim to characterise and identify the main particle sources to be able to suggest abatement measures.

Particle properties were studied during campaigns in the Söderledstunneln (road tunnel in central Stockholm). The measurements were performed in a small room adjacent to the tunnel and with the inlets mounted within the tunnel from drilled holes, while the road dust load was measured directly at the road surface when the tunnel was closed for maintenance. Dust sampling was made with the VTI wet dust sampler (Jonsson *et al.*, 2008, Blomqvist *et al.*, these proceedings).

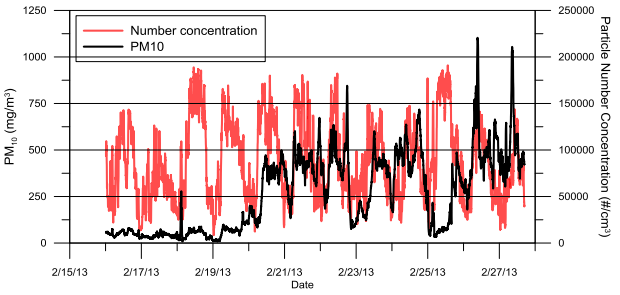

Figure 1.The concentrations of PM_{10} and particle number show the onset of abrasion particle suspension.

Figure 1 shows concentration of PM_{10} and of particle number. Around the 20th of February PM_{10} increase due to drying up of the road surface in the tunnel, while the particle number concentrations are not affected. The size distribution in the size range between 0.5 and 20 µm is shown in Figure 2, where it is clear that the wet conditions give a less pronounced peak as well as very much lower concentrations. Directly before the campaign started, also during wet conditions, samples of the road dust load showed very large levels as compared to road dust load at the surface roads in the same area.

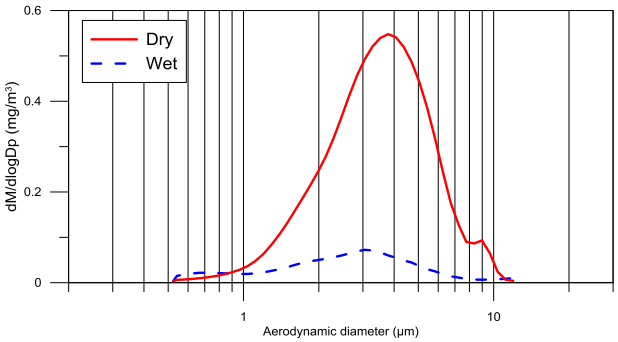

Figure 2. Particle mass size distribution averaged over the first, wet part of the campaign and over the second, dry part of the campaign, respectively.

Further work will describe differences between road and railroad tunnel particle emissions, size resolved particle composition, source apportionment and abatement strategies.

This work was supported by the BVFF; a research program financed Swedish Transport Administration, The Royal Institute of Technology, KTH, and the Swedish National Road and Transport Research Institute, VTI.

Gëller MD, Sardar SB, Phuleria H, Fine PM, Sioutas C. (2005) *Environmental Science and Technology*; **39**: 8653-8663.

Janhäll, S., Molnar, P., Hallquist, M. (2012): *J.Environ. Monit.*, **14**, 2488

Jonsson, P., Blomqvist, G., Gustafsson, M. (2008): *7th Int. Symp. Snow Removal and Ice Control Techn., Transportation Research Circular*, **E-C126**, 102-111

Winter particulate matter (PM10) sources for an Austrian-Slovenian border region.

M. Kistler[1], E.C. Cetintas[1], H. Bauer[1,†] and A. Kasper-Giebl[1]

[1]Institute of Chemical Technologies and Analytics, Vienna University of Technology, Vienna, A1060, Austria
Keywords: local PM10, carbonaceous aerosol.
Presenting author email: magdalena.kistler@tuwien.ac.at

Air pollution by particulate matter derived from biomass burning is recognized as a worldwide problem and is considered from the point of view of scientists and politicians, respectively. Many European regions have difficulties with keeping the internationally, nationally or locally defined limit values. Emission sources may cause pollution across the borders, what makes one-sided reduction policies inefficient. This is true also for residential burning particles, as observed e.g., in Aosta Valley (IT, FR, CH, Finardi *et al.,* 2002).

The following study was set by local authorities of South Austria and North Slovenia in order to develop efficient methods to improve the local air quality. The scientific goal was to obtain a detailed chemical characterization of collected particulate matter, information about its sources and the optimization of methods for assessment of source contributions.

Particulate matter sampling was conducted at four urban and three background stations in Carinthia (AT), South Styria (AT) and Maribor region (SI). PM10 was collected between 29.01.2011 and 28.02.2011 daily (24h), on quartz fibre filters (Pallflex, 150mm), using high volume samplers (~700m³). The particle mass was determined gravimetrically.

Circular filter aliquots (with 10mm diameter) were used for the determination of carbon parameters (organic carbon, OC and elemental carbon, EC) with a thermal-optical method (*Sunset OCEC Aerosol Lab Analyser*), using a EUSAAR2 temperature protocol (Cavalli *et al.,* 2009). Inorganic ions and sugars were analysed using ion chromatography (*Dionex*) with conductivity (ions) or pulsed amperometric detection (saccharides). For this purpose 3 to 5 filter aliquots (10mm) were eluted with extra pure Milli-Q (resistance 18.2 MΩ) water (anions, sugars) or with 12 mM methane sulphonic acid (cations).

HULIS (humic like substances) were determined with a TU Vienna derived method (Limbeck *et al.*, 2005) comprising an NDIR analysis of CO_2 evolved from combustion of water- and alkali-extract treated with appropriate solid phase extraction.

Selected elements including Al were analysed using X-Ray Fluorescence.

Aerosol water content was assessed with thermo-gravimetric method in which the loss of weight of a filter aliquot heated to 100°C in a thermo-balance under nitrogen atmosphere and kept at this temperature for 5 minutes is equivalent to the aerosol H_2O.

Source analysis was performed using a simple macro-tracer approach, describing up to nine main aerosol sources (Puxbaum *et al.,* 2005). This model involves anhydrosugars: levoglucosan and mannosan as specific tracers for wood burning (Schmidl *et al*., 2008, 2011, own unpublished data).

Except for the rural background station in Styria the short-term PM10 threshold value was exceeded between 17 and 20 times during the measurement period. The average PM10 concentration observed for urban sampling points was 60 µg/m³.

The contribution of biomass burning was lowest in the rural background in Styria (22%), and accounted up to 40% in Carinthia (urban background), being the most relevant local PM10 source. Similar significance was observed for secondary inorganic aerosols (ammonium sulphates and nitrates): between 29% (Carinthia, urban traffic) to 48% (Styria rural background). Traffic near locations were characterized by a higher impact of fossil fuel emissions (expected mainly from Diesel engines), mineral dust (carbonates and silicates) and de-icing salt (both from the re-suspension). On the other hand a higher amount of organic secondary aerosols was found at background measurement sites.

This work was conducted with samples collected within the INTERREG IVA SI-AT PMinter project conducted through the Municipality of Klagenfurt, Municipality of Maribor and Styrian Government, in cooperation with Provintial Government of Carinthia, Public Health Institute Maribor, TU Graz and the University of Maribor. Lab work by C. Ramirez Santa Cruz L. Sampaio Cordeiro Wagner, E. Schriener (Institute of Chem. Technologies and Analytics) and S. Lüftl from Institute of Material Science and Technology is gratefully acknowledged.

Cavalli, F., Viana, M., Yttri, K.E., Genberg, J., Putaud, J-P., (2009). *Atmos. Meas. Tech. Discuss.,* **2,** 2321–2345.

Finardi, S., Agnesod, G., Brusasca, G., Calori, G., Nanni, A., Pession, G., Tinarelli, G., Zublena, M., (2002). *Proc. 8th Int. Conf. on Harmonisation within Atmospheric Dispersion Modelling for Regulatory Purposes,* Sofia, Bulgaria.

Limbeck., A., Handler, M., Neuberger, B., Klatzer, B., Puxbaum, H., (2005). *Anal. Chem.,* **77,** 7288-7293.

Puxbaum, H., Kasper-Giebl, A., Bauer., H., (2005). *Conf.: Chemistry, Transport and Impact of Atmospheric Pollutants with Focus on Fine Particles*, Andechs, Germany.

Schmidl, C., Marr, I., Caseiro, A., Kotianova, P., Berner, A., Bauer, H., Kasper-Giebl, A., Puxbaum, H., (2008). *Atmos. Environ.,* **42**, 126-141.

Schmidl, C., Luisser, M., Paouvas, E., Lasselberger, L., Rzaca, M., Ramirez-Santa Cruz, C., Handler, M., Peng, G., Bauer, H, Puxbaum, H., (2011). *Atmos. Environ.,* **45**, 7443-7454.

Assessment of emission sources in an industrial area using instrumental and biomonitoring techniques

J.Lage[1], S.M.Almeida[1], M.A. Reis[1], P.C. Chaves[1], M.C. Freitas[1], T. Ribeiro[1], S. Garcia[2], J.P. Faria[3], B.G. Fernández[3], H.Th. Wolterbeek[4]

[1]URSN, IST-CTN, Instituto Superior Técnico, Universidade Técnica de Lisboa, Sacavém, 2686-953, Portugal
[2]Instituto de Soldadura e Qualidade, Portugal; [3] Global R&D – ArcelorMittal, Spain;
[4] Delft University of Technology, The Netherlands
Keywords: PM_{10}, biomonitors, source apportionment, industry.
Presenting author email: joanalage@ctn.ist.utl.pt

The objective of this study was to assess the air quality and the contribution of emission sources in the vicinity of an industrial area placed in the North of Spain, which is affected by a steelwork, a cement factory and a power plant. For that complementary tools were used:

1) Metal concentrations were mapped in the surroundings of the industrial area using passive biomonitors;

2) Geographic Information System was used to evaluate the relations between the spatial distribution of the elements, contamination factors, land use and topography and to identify the sources and processes associated with the pollutants' formation;

3) PM_{10} was sampled in the industrial area and a temporal database of aerosol species was built to evaluate the seasonal variations of metal concentrations;

4) Receptor models were used to identify and quantify the contributions of the industrial operations to metal concentration in the local ambient air.

The spatial distribution of the chemical elements assessed by the biomonitors showed an increase of Al, Ca, Cl, Cu, Fe, I, Mn, Na, Sb and V in the industrial area. Elements associated with the soil also presented increased concentrations in this area probably due to re-suspension caused by the heavy traffic of trucks (Fig.1).

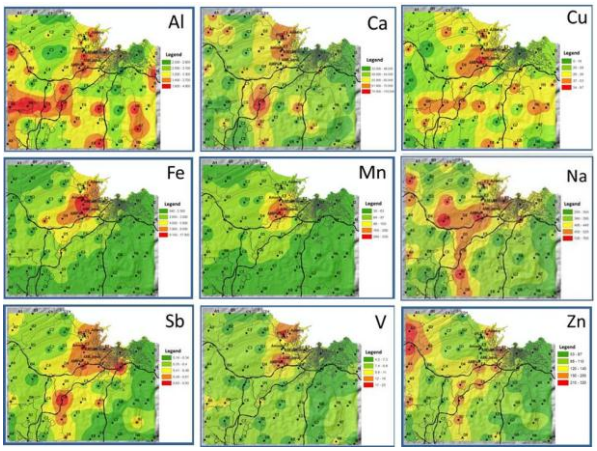

Figure 1. Spatial distribution of the Al, Ca, Cu, Fe, Mn, Na, Sb, V and Zn concentrations measured in the exposed biomonitores.

PMF applied to the PM_{10} compounds identified 7 emission sources. The first source clearly reflected the sea-spray composition, having high shares of Cl and Na, and contributed on average to 22% of the PM_{10} mass. The second source, which contributed on average to 11% of the total PM_{10} mass, was mainly composed of As, Cr, Cu, Ni, Pb, Sb and Zn and was attributed to mixed combustion processes and traffic. The third source contained high percentages of NH_4^+ that derives from gas to particle conversion processes. The contribution of this factor to PM_{10} mass was on average 12%. The fourth factor is made of Br and contributed for 1.8% of the total PM_{10} mass. The fifth source is dominated by NO_3^- and SO_4^{2-} and contributed on average for 19% of the PM_{10} mass concentration. The sixth source carries high percentages of Al, Ca, La, Si, Ti and V and account for 14% of the PM_{10}. These are the major constituents of soil and point out the fingerprint of mineral dust. The seventh factor was associated with steel production as it is defined by Fe and Mn. This source accounted for 21% of PM_{10} mass concentration (Fig.2).

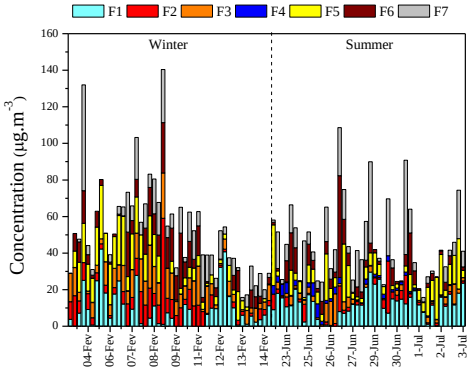

Figure 2. Source contribution for PM_{10} total mass concentration time series (µg.m^3).

This work showed that the use of complementary tools is essential in the assessment of the air quality. Atmospheric particles are usually measured instrumentally. However, particles sampling and characterization is necessarily performed by a limited number of sampling stations due to the associated high costs. As a result, vast areas are not covered by any monitoring system. Therefore, in one hand biomonitoring offers unique advantages - the ability to perform high-density sampling at any spatial scale at low cost and the measurement of a wide range of pollutants. In the other hand, instrumental measurements inform about the absolute air concentrations and the temporal trend of the pollutants.

This work was supported by the Portuguese "Fundação para a Ciência e Tecnologia" under the J. Lage PhD fellowship SFRH/BD/79084/2011. The research leading to these results has received funding from the European Community's Research Fund for Coal and Steel (RFCS) under grant agreement no RFSR-CT-2009-00029.

Relationship between oxidation level and optical properties of secondary organic aerosol

A. T. Lambe[1,2], C. D. Cappa[3], P. Massoli[2], T. B. Onasch[1,2], S. D. Forestieri[3], A. T. Martin[1], M. J. Cummings[1], D. R. Croasdale[1], W. H. Brune[4], D. R. Worsnop[2], P. Davidovits[1]

[1]Chemistry Department, Boston College, Chestnut Hill, Massachusetts, 02467, U.S.
[2]Aerodyne Research, Inc., Billerica, Massachusetts, 01801, U.S.
[3]Department of Civil and Environmental Engineering, University of California - Davis, Davis, California, 95616, U.S.
[4]Department of Meteorology and Atmospheric Sciences, The Pennsylvania State University, University Park, Pennsylvania, 16802, U.S.

Keywords: SOA, oxidative aging, optical properties, aerosol mass spectrometry.

Presenting author email: lambe@aerodyne.com

Brown carbon (BrC), which may include secondary organic aerosol (SOA), can be a significant climate-forcing agent via its optical absorption properties. However, the overall contribution of SOA to BrC remains poorly understood. Here, correlations between oxidation level and optical properties of SOA are examined. SOA was generated in a flow reactor in the absence of NO_x by OH oxidation of gas-phase precursors used as surrogates for anthropogenic (naphthalene, tricyclo[5.2.1.$0^{2,6}$]decane [JP-10]), biomass burning (guaiacol), and biogenic (α-pinene) emissions. SOA chemical composition was characterized with a time-of-flight aerosol mass spectrometer. The mass spectra yielded oxygen-to-carbon (O/C) ratios, used as a measurable surrogate for SOA oxidation level, that ranged from 0.29 to 1.29.

SOA mass-specific absorption cross sections (MAC) and refractive indices were calculated from real-time cavity ring-down photoacoustic spectrometry (CRD-PAS) measurements at 405 and 532 nm and from UV-Vis spectrometry measurements of methanol extracts of filter-collected particles (300 to 600 nm). At 405 nm, SOA MAC values and imaginary refractive indices ranged from $<$0.001 to 0.088 $m^2\ g^{-1}$ and 1.9×10^{-4} to 3.6×10^{-3}, respectively, increasing with SOA oxidation level. SOA light absorption decreased with increasing wavelength, leading to negligible absorption at 532 nm. Real refractive indices (n) of SOA at 405 nm ranged from 1.45 to 1.66 and for a given precursor changed at a rate of $\Delta(n)/\Delta(O/C)$ = -0.055 to -0.11. Comparison with literature studies suggests that under typical polluted conditions the effect of NO_x on SOA absorption is small. SOA may contribute significantly to atmospheric BrC, with the magnitude dependent on both precursor and oxidation level.

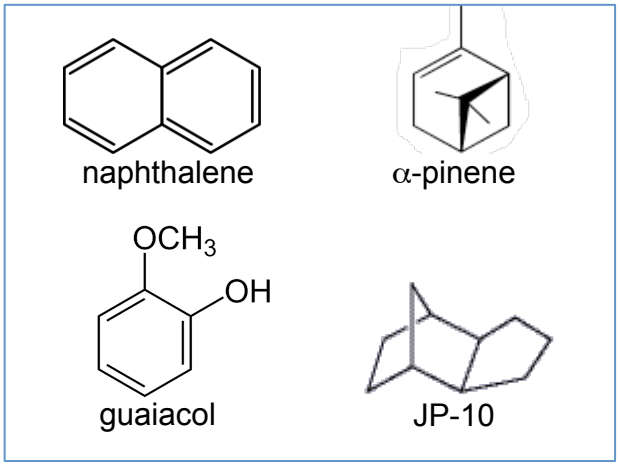

Figure 1: Molecular structures of SOA precursors used in this work.

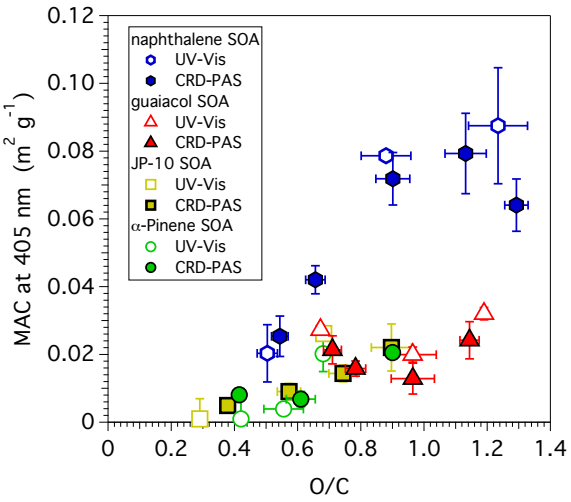

Figure 2: Mass-specific absorption cross sections (MAC) of SOA obtained at λ = 405 nm as a function of O/C ratio. MAC values are calculated from CRD-PAS and UV-Vis spectrometer measurements.

This research was supported by the Office of Science (BER), Department of Energy (Atmospheric Science Program) grants No. DE-SC0006980 and DE-FG02-05ER63995, and the Atmospheric Chemistry Program of the National Science Foundation grants No. ATM-0854916 and AGS-0904292 to Boston College and Aerodyne Research, Inc., ATM-0837913 to UC Davis, and and AGS-0855135 to Pennsylvania State University.

Cappa, C. D., Che, D. L., Kessler, S. H., Kroll, J. H., and Wilson, K. R. (2011) *J. Geophys. Res.*, **116**, D15204.

Lack, D. A., Lovejoy, E. R., Baynard, T., Pettersson, A., and Ravishankara, A. R. (2006) *Aerosol Sc. & Tech.*, **40**, 697–708.

Lambe, A. T., Ahern, A. T., Williams, L. R., Slowik, J. G., Wong, J. P. S., Abbatt, J. P. D., Brune, W. H., Ng, N. L., Wright, J. P., Croasdale, D. R., Worsnop, D. R., Davidovits, P., and Onasch, T. B. (2011) *Atmos. Meas. Tech.*, **4**, 445–461.

Updyke, K. M., Nguyen, T. B., and Nizkorodov, S. A. (2012) *Atmos. Environ.*, *63*, 22–31.

Zhong, M. and Jang, M. (2011) *Atmos. Environ.*, **45**, 4263–4271.

Observations on atmospheric electricity and aerosol-cloud interactions

Hanna E. Manninen[1,2], Hannes Tammet[1], Antti Mäkelä[3], Jussi Haapalainen[3], Sander Mirme[1], Tuomo Nieminen[2,4], Alessandro Franchin[2], Tuukka Petäjä[2], Markku Kulmala[2], and Urmas Hõrrak[1]

[1]Institute of Physics, University of Tartu, Ülikooli 18, 50090 Tartu, Estonia
[2]Department of Physics, P.O. Box 64, 00014 University of Helsinki, Finland
[3]Finnish Meteorological Institute, P.O. Box 503, 00101 Helsinki, Finland
[4]Helsinki Institute of Physics, P.O. Box 64, 00014 University of Helsinki, Finland
Keywords: atmospheric electricity, small ions, earth's electric field, lightning, aerosol-cloud interactions.
Presenting author email: hanna.manninen@helsinki.fi

Atmospheric ions play an important role in the fair weather electricity. Atmosphere's fair weather condition concerns the electric field and the electric current in the air as well as the air conductivity. On the other hand, atmospheric ions are important for Earth's climate, due to their potential role in secondary aerosol formation. This can lead to increased number of cloud condensation nuclei (CCN), which in turn can change the cloud properties. Our aim is to quantify the connections between these two important roles of air ions based on field observations and existing data archives.

When studying atmospheric electricity, the air ions are essential. Small ions, or charged molecular clusters, carry electric currents in the atmosphere. These small ions are continuously present, and their lifetime in lower atmosphere is about one minute. It's essential to find out a connection between the production rate of cluster ions, ion-ion recombination, and ion-aerosol attachment, and their ambient concentrations, in order to understand electrical properties of air istelf.

Currently, there's an intensive discussion about the connection between the atmospheric electricity and climate change. Recently, changes in atmosphere's electric properties caught new interest, as a possible connection between ionizing galactic cosmic rays, cloud cover and climatic effects was suggested (Carslaw, Harrison and Kirkby, 2002; Kirkby et al. 2011). The most significant factor of uncertainty in climate research is caused by atmospheric aerosols, especially due to small particle effects. Secondary formation of new particles through a process of gas-to-particle conversion, beginning with a few gas molecules colliding to form a cluster of 1-2 nm in diameter, is believed to be the dominant source of aerosol particles in the atmosphere. Some studies suggest that the contribution of air ions is important or even dominant to secondary aerosol formation, whereas other studies show that their role is negligible.

We studied the interactions between atmospheric electricity (air conductivity, electric field, and ambient concentartion of small ions), aerosol particles, and cloud properties. In other words, the correlations and trends in atmospheric ionization, electricity, aerosols, and CCN properties were studied. Most of the work here is based on analysis of already existing data archives, and some new measurements are established as a part of already existing measurement networks. The electrical properties of the atmosphere have been measured over a century now, whereas the longest continuous time series of aerosol particle data available is little over decade old. Tammet (2009) has collected a dataset, which comprises the measurements of atmospheric electric field, positive and negative conductivities, air ion concentrations, and accompanying meteorological measurements at 13 stations, including 7 stations of the former World Data Centre network on Atmospheric Electricity at the Main Geophysical Observatory, St. Petersburg, Russia.

The ongoing field observations of atmospheric aerosols are mainly performed at Hyytiälä SMEAR site, Southern Finland (Station for Measuring Ecosystem-Atmosphere Relations). Hyytiälä provides extensive dataset of measured aerosol particle (physical, chemical, and optical) properties, external and radon radiation, CCN properties, trace gases, meteorological parameters, different flux measurements (micrometeorology), and forest ecology observations. The atmosphere's electricity is measured with the air ion spectrometers (Manninen et al. 2010) to determine air conductivity and with the electric field mills, which measures the strength of atmospheric electric field. The plan is to extend the measurements of atmospheric electricity to the Finnish Meteorological Institute (FMI) site at Pallas, Northern Finland, and to SMEAR site at Järvselja, Estonia. Hyytiälä and Pallas stations are part of ACTRIS (Aerosols, Clouds, and Trace gases Research InfraStructure Network) and GAW (Global Atmosphere Watch) networks.

The lightning activity and ion concentration was also investigated. The lightning flash counter data for Hyytiälä, Pallas, and Järvseljä is collected by FMI. The systematic ground lightning observations are performed with eight ground-based sensors in Finland. The Norwegian, Swedish, and Estonian sensors have been integrated, completing the coverage up to the whole Nordic countries.

The support by the Finnish Cultural Foundation and the Academy of Finland Centre of Excellence program (project no. 1118615) are gratefully acknowledged.

Carslaw K. S., Harrison R. G., and Kirkby J. (2002) *Science* **298**, 1732-1736.
Kirkby J. et al. (2011) *Nature* **476**, 429-433.
Manninen et al. (2010) *Atmos. Chem. and Phys.* **10**, 7907-7927.
Tammet H. (2009) *Atmospheric Research* **91**, 194-200.

Effect of local pollutant sources on aerosol-cloud interactions at Puijo measurement station

H. Portin[1,2], A. Leskinen[1], A. Kortelainen[2], L. Hao[2], P. Miettinen[2], A. Jaatinen[2], , S. Romakkaniemi[2], A. Laaksonen[2,3], K.E.J. Lehtinen[1,2] and M. Komppula[1]

[1]Finnish Meteorological Institute, Kuopio Unit, P.O.Box 1627, FI-70211, Kuopio, Finland
[2]University of Eastern Finland, Department of Applied Physics, P.O.Box 1627, FI-70211, Kuopio, Finland
[3]Finnish Meteorological Institute, Research and Development, P.O.Box 503, FI-00101 Helsinki, Finland
Keywords: atmospheric aerosols, cloud droplet activation, aerosol-cloud interactions, chemical composition.
Presenting author email: harri.portin@fmi.fi

Puijo measurement station has provided continuous data on aerosol-cloud interactions since summer 2006 (Leskinen *et al* 2009). The station is located on top of the Puijo observation tower (306 m a.s.l, 224 m above the surrounding lake level) near the town of Kuopio, Finland. The station is covered by cloud about 15 % of the time, offering perfect conditions for aerosol-cloud interaction studies. With a special inlet setup (total and interstitial inlets) activated and non-activated particles can be measured separately. Continuous twin-inlet measurements include aerosol size distribution (twin-DMPS, 7-800 nm), scattering and absorption. Other continuous measurements include cloud droplet number and size distribution and weather parameters.

We also arrange intensive measurement campaigns every autumn (Puijo Cloud Experiment, PuCE) when the occurrence of clouds is the highest. During these campaigns, extra measurement devices have included aerosol mass spectrometer (AMS), cloud condensation nuclei counter and Hygroscopic Tandem Differential Mobility Analyzer. The AMS has been connected to the twin-inlet system¸ providing data about the chemical composition of activated and non-activated particles (Hao *et al* 2013).

In our current work, we have been analyzing results from PuCE 2010 and 2011 campaigns. During these campaigns, a total of 39 cloud events took place, with a total of 156 hours of in-cloud data. The aim of the research has been the identification of the possible effect of local pollutant sources on aerosol-cloud interactions. The tower is surrounded by residential areas and traffic routes in north, east and south, whereas in west and northwest there aren't any significant sources. Also, two important point sources exist within a few kilometres from the tower, a paper mill and a heating plant.

An example of a cloud event, during which it was possible to pinpoint the effect of local sources, took place on 22.-23.10., 2011. There were several periods with different particle population properties, which also affected the cloud properties to some extent. Here, three of these periods are chosen for a closer inspection.

During the clean period (22.10. 22:00-23.10. 5:45), wind direction was from north and northwest with low total particle and accumulation mode concentrations (fig. 1a). Between 5:45-6:15 on 23.10. wind direction was from northeast where the paper mill is located. Total particle concentration was still low but a pronounced accumulation mode was present. Particle chemical composition during this period was dominated by SO_4 and NH_4. When wind direction shifted to south (23.10. 9:45-13:00), a plume from the heating plant hit the tower. Elevated particle concentration was observed, with a distinguishable accumulation mode, consisting almost entirely of SO_4.

During the pollutant episodes, the size of activated particles was larger when compared to the clean period (fig. 1b). In clean conditions, as small as 100 nm particles activated, whereas during the polluted periods the average diameter for activation was larger. During the paper mill plume, droplet concentration was higher (240 cm^{-3}) with a smaller average droplet diameter (10.9 µm) when compared to the clean period (138 cm^{-3}, 12.2 µm). Unfortunately the cloud droplet probe was frozen during the heating plant plume.

As a conclusion, it is evident that local pollutant sources affect aerosol-cloud interactions. However, it is too early to say if this is only caused by the elevated number concentrations or if the different chemical composition also plays a role. Also, how often these periods take place requires more research and data from forthcoming campaigns.

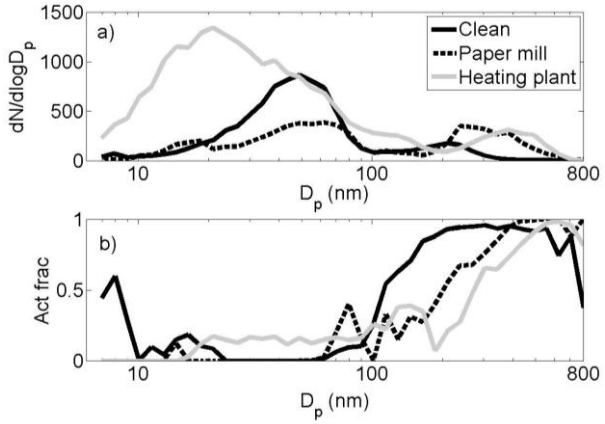

Figure 1. a) Total particle size distributions and b) particle activated fractions vs. size for the different periods during a cloud event on 22.-23.10.2011.

Hao, L., Romakkaniemi, S., Kortelainen, A., Jaatinen, A., Portin, H., Miettinen, P., Komppula, M., Leskinen, A., Virtanen, A., Smith, J., Sueper, D., Worsnop, D., Lehtinen, K.E.J. and Laaksonen, A. (2013). *Environ. Sci. Technol.*, In press.

Leskinen, A., Portin, H., Komppula, M., Miettinen, P., Arola, A., Lihavainen, H., Hatakka, J., Laaksonen, A. and Lehtinen, K.E.J. (2009). *Boreal Env. Res.*, **14**, 576-590.

Intercomparison of sulphuric acid measurements and neutral cluster composition in the lower free troposphere

L. Rondo[1], M. Simon[1], H. Junninen [2], J. Duplisy[2], A. Praplan[2], A. Adamov[2], A. Kürten[1], M. Sipilä[2], F. Bianchi[3], J. Tröstl[3], E. Weingartner[3], U. Baltensperger[3], M. Kulmala[2] and J. Curtius[1]

[1]Institute for Atmospheric and Environmental Sciences, University of Frankfurt, 60438 Frankfurt, Germany
[2]Department of Physics, University of Helsinki, 00014 Helsinki, Finland
[3]Laboratory of Atmospheric Chemistry, Paul Scherrer Institute, 5232 Villigen PSI, Switzerland

Keywords: Neutral sulphuric acid nucleation, new particle formation, Jungfraujoch

Aerosol nucleation from trace vapours is a ubiquitous process in the Earth's atmosphere and has been observed at many different places (Kulmala et al., 2004). It is thought that sulphuric acid is a key species in the formation process of small clusters and particles. A correlation between the particle formation rate and the concentration of sulphuric has been frequently observed during ground-level field campaigns. However, data coverage on the sulphuric acid concentrations at higher altitudes is relatively scarce, although, these regions are very important on a global scale. In addition, it is not clear if and what other compounds (besides water) are participating in the formation of aerosol particles in these regions.

During January and February 2013 the **Nu**cleation, **Cl**oud and **A**erosol **C**haracterization **E**xperiment (NUCLACE) took place at the high alpine research station Jungfraujoch (JFJ) in Switzerland. The JJF station is located at 3580 meters altitude and mainly influenced by free tropospheric air during this time of the year. One of the goals of the NUCLACE campaign was to investigate the role of ions on the formation of new particles. However, in this study we focus on the measurement of the sulfuric acid concentration as well as on the detection of neutral clusters and their composition with state-of-the-art instruments.

For this purpose, two Chemical Ionization Atmospheric Pressure interface Time-Of-Flight Mass Spectrometers (CI-APi-TOFs) were used (Jokinen et al., 2012). Within the inlets of both instruments nitrate primary ions are generated which can ionize neutral sulphuric acid and clusters through a proton transfer reaction or by clustering. The primary and the product ions are detected with a high resolution time of flight mass spectrometer. The combination of these two techniques allows low detection limits (at ppq levels) and the identification of ion species through their exact mass. Although both CI-APi-TOF instruments have the same principle they differ in the design of their ion source. The CI-APi-TOF from the University of Frankfurt utilizes a corona discharge needle (Kürten et al., 2011) while the CI-APi-TOF from the University of Helsinki (Jokinen et al., 2012) utilizes a soft x-ray ion source. In addition, the geometry of the ion drift regions and the inlet geometries differ slightly. Additionally, the operation of the CI-APi-TOFs at JFJ turned out to be challenging due to the low pressure and strong temperature variations inside the building where the instruments were located. Therefore, an intercomparison of the two instruments is important (see figure 1). Furthermore, it turned out that an on-site calibration needed to be performed to take into account the conditions at the measurement site. For this, a calibration unit similar to the one described by Kürten et al. (2012) has been brought to JFJ. With this set-up a known concentration of H_2SO_4 can be generated and measured by one CI-APi-TOF at a time.

We will report on the overall comparison of the two CI-APi-TOFs with respect to the sulfuric acid monomer concentrations. In addition, the instruments will be compared regarding the detection of different neutral clusters. Details about the calibration will also be presented.

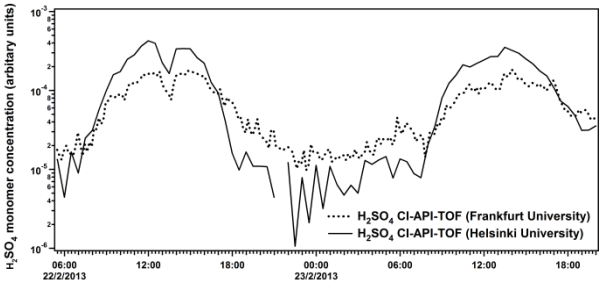

Figure 1. Observed diurnal variation of the sulphuric acid concentration measured by the two CI-APi-TOFs from Frankfurt and Helsinki.

We thank the International Foundation High Altitude Research Stations Jungfraujoch and Gornergrat (HFSJG), which made it possible to carry out the experiments at the JFJ. Also, we thank tofTools team for their support.

Kulmala, M., *et al*., (2004) J. Aerosol Sci., **35**, 143–176.
Jokinen, T., *et al* (2012) *Atmos. Chem. Phys.*,***12***, *4117-4125*
Kürten, A., *et al* (2011) *Atmos. Meas. Tech*., **4**, 437–443,
Kürten, A., *et al* (2012) *J. Phys. Chem. A*, 116 (**24**), 6375–6386

Air mass back trajectories and dry atmospheric aerosol mass size distributions in Prague

J. Schwarz[1], L. Štefancová[1] , W. Maenhaut[2], J. Smolík[1], W. Ždímal[1]

[1]Department of Aerosol and Laser Studies, Institute of Chemical Process Fundamentals AS CR, Prague, CZ-16502, Czech Republic
[2]Department of Analytical Chemistry, Ghent University, Gent, BE-9000, Belgium
Keywords: mass size distribution, air mass back trajectories, water soluble ions
Presenting author email: schwarz@icpf.cas.cz

Ambient aerosol size distribution is an important factor influencing aerosol behavior and properties including particle deposition in lungs and aerosol influence on clouds. Both influences are also driven by aerosol hygroscopicity. Cascade impactors used for size resolved determination of chemical composition suffer from changes of ambient RH during sampling. Due to this factor the same particle might be deposited at different impactor stage when it is sampled at noon at 40% RH or in the early morning at 99% RH. Therefore, we used a diffusional aerosol dryer and a 7-stage modified Berner low pressure impactor with a back-up filter (Štefancová et al., 2011) during the heating (shown as "winter" and non-heating season (shown as "summer") campaigns in 2008. The samples were analyzed for water-soluble ions (Cl^-, SO_4^{2-}, NO_3^-, Na^+, NH_4^+, K^+, Mg^{2+}, Ca^{2+}) and water-soluble organic carbon as a main species that influence aerosol hygroscopicity. Due to the drying, the aerosol size distributions were not influenced by the daily variability of ambient relative humidity.

The results cover the measurements from both campaigns (11 "winter" sampling days and 10 "summer" sampling days). The aerosols sampled on individual days were classified based on the connected air mass back trajectories into three classes: sea-influenced aerosol (SIA), continental aerosol (CA), and mixed aerosol (MA) for samples of intermediate origin.

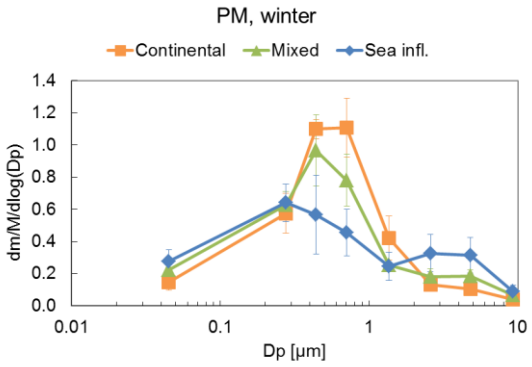

Fig. 1. Average normalized mass size distributions for the PM in the continental, mixed, and sea influenced aerosol samples of the winter campaign.

The differences between CA and SIA were substantial both when looking at the normalized mass size distributions of the particulate matter (PM, Fig. 1) and of the individual species (see an example for SO_4^{2-} in the summer in Fig. 2) and when taking into account

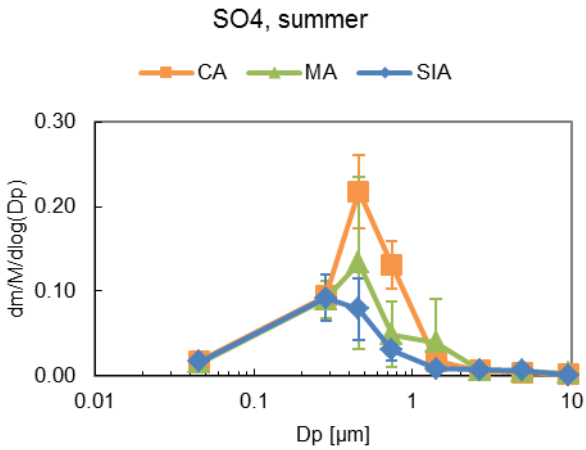

Fig. 2. Average normalized mass size distributions for the PM in the continental, mixed, and sea influenced aerosol samples of the summer campaign.

the absolute concentrations in the fine and coarse size fractions. The shift in the position of fine mode maxima could be explained by the prevailing influence of condensation or droplet mode formation of the accumulation mode particles (Hering and Friedlander, 1982). However, relative humidity profiles along the air mass trajectories could not explain the differences in size distributions in this way. Therefore another reason leading to explanation of the described differences (Schwarz et al., 2012) should be taken into account. As the first hypothesis, we suggest that the differences in average SO_2 concentration fields above Europe could explain our observations if the SO_2 concentration above Western Europe was so low that the diffusional limitation of SO_2 transport into droplets becomes important. This would change size dependence of sulphate formation rate from volume proportional to surface proportional.

This work was supported by the Czech Science Foundation under grant No. P209/11/1342.

Hering, S.V. and Fiedlander, S.K. (1982) *Atmos. Environ.* **16**, 2647–2656.

Štefancová, L., Schwarz, J., Mäkelä, T., Hillamo, R. and Smolík, J. (2011) *Aerosol Sci. Technol.*, **45**, 88-100.

Schwarz, J.; Štefancová, L.; Maenhaut, W., Smolík J. and Ždímal V.: (2012) *Sci. Tot. Environ.* **437**, 348-362.

Blue sky over the Ruhr – a review of the effectiveness of more than 50 years of air quality measures in Germany

S. Wurzler, H. Hebbinghaus, P. Bruckmann, J. Friesel, U. Pfeffer

North Rhine Westphalian State Agency for Nature, Environment and Consumer Protection, Recklinghausen, Germany
Keywords: air quality
Presenting author email: sabine.wurzler@lanuv.nrw.de

In January and February 2013, the poor air quality in many major cities in parts of Asia, such as Peking and Delhi, made headlines worldwide. The high concentrations of air pollutants and the accompanying pictures and effects look very familiar to those, who lived in the area Rhine Ruhr during the fifties and sixties. Notable was, e. g., the smog episode in December 1962, leading to an increase of mortality by 30 %. This drastically increased number of deaths owing to poor air quality made very apparent that something had to be done.

Already the year 1961 marked a turning point in German air quality planning, because of a notable speech of the subsequent chancellor, Willy Brandt, who demanded a change in politics concerning air quality with the catch phrase of blue sky over the Ruhr area. This was the first time that someone so prominently focussed on the combination of air quality, health effects and social justice, turning smoking stacks into something more than just a sign for economic success.

While this single talk did not mean an immediate change in politics and public awareness, it was a popular vision from which future activities could build. These activities included monitoring air quality as well as measures for emission reduction. The awareness of air quality as a challenging problem has grown in the public since then. Now, the blue sky is again visible over the Ruhr area, at least on sunny days. The European Commission has declared the year 2013 as the year of air quality. When comparing today's air quality in Europe to the situation in the past and to the present situation in Asia, this might seem a bit exaggerated at the first glance. But is this true? Are all problems already solved? Therefore, we review the past, present and possible future activities in Germany and Europe and their results for air quality. It can be seen, that the work on clean air includes some success stories. As an example, figure 1 shows the SO_2 concentration in the area Rhine Ruhr from 1964 till 2011. The TSP and PM10 trend from 1968 to 2011 can be seen in figure 2. These figures well illustrate the success stories of air quality measures – as well as some less favourable measures. It can be seen that the general trend shows a clear decrease in SO_2, PM10, and TSP concentrations. Measures like dust separation in industrial facilities, substituting solid fuels in space heating as well as the structural change in the Ruhr area all led to a reduction of SO_2, PM10, and TSP, while the policy of high stacks only led to a change in distribution, causing acidification and eutrophication in ecosystems. Particularly the desulphurisation of power plants since 1977 enhanced the decrease and it can be stated that today the concentrations of SO_2 in Germany are no longer problematic with respect to human health.

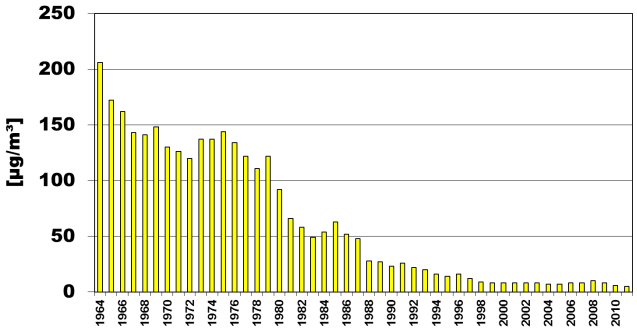

Fig. 1: Trend of annual average SO_2 concentrations in µg/m³ in the area Rhine Ruhr from 1964 to 2011. The highest concentrations correspond to values above 200 µg/m³, the lowest are below 10 µg/m³

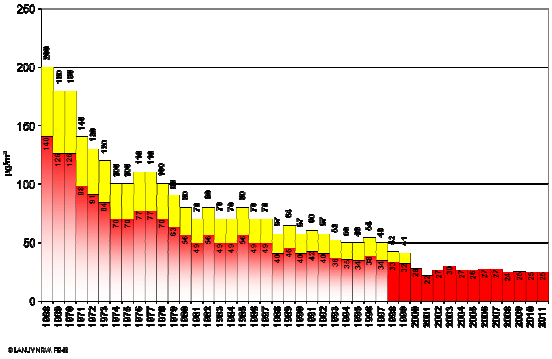

Fig. 2: Trend of annual average total suspended particle (TSP, yellow bars) and PM10 (red bars) concentrations in µg/m³ in the area Rhine Ruhr from 1968 to 2011. The highest concentrations correspond to values above 200 µg/m³, the lowest are below 50 µg/m³

But despite all advances, there are still problems to face. E. g., the high amount of road traffic is a main source for high NO_2 concentrations in cities. The number of PM10 exceedance days is still occasionally too high. Another challenge is the preservation of nature protection areas that can be adversely affected by high depositions of nitrogen, acid, or heavy metals.

Our presentation will give an overview of the last 50 years' challenges, success stories and memorable events as well as a reflection on current and future challenges in the area of air quality planning.

Tuesday, September 3, 2013

Plenary lecture: Primary Biological Atmospheric Aerosols by Ruprecht Jaenicke

Primary Biological Atmospheric Aerosols

Ruprecht Jaenicke
Institute for Physics of the Atmosphere
University Mainz / Germany

"Quantitative PCR and microscopy revealed that viable bacterial cells represented on average around 20% of the total particles in the 0.25 to 1 µm diameter range … suggesting that bacteria represent an important and underestimated fraction of micrometer-sized atmospheric aerosols". (DeLeon-Rodriguez, *et al*, 2013) Even if that statement covers only a certain situation and a certain part of the troposphere, it clearly shows that primary biological aerosol particles are a major fraction of the atmospheric aerosol.

While most primary particles of the atmospheric aerosol (maritime, mineral, etc) have sources limited to certain regions of the world, like the oceans, the deserts, etc, the primary biological aerosol particles (PBAP) are produced from all available surfaces of the world. The continental biosphere (leaves, animals, dead subjects) is a source for primary biological particles. Since the oceans are full of biological (dead and alive) material, each ejected sea spray particle contains biological material. Rock varnish may contain considerable amounts of organic material which sometimes may be responsible for the gel-like or lacquer-like appearance of the surface. The grey or black films may sometimes consist predominantly of dry cyanobacteria.

Partition	Global emissions (Tg yr^{-1})	Size range	References
PBAP	<10 (dominated by plant debris and fungal spores)	diameter: 4 µm for fungal spores; diameter not specified for plant debris	Winiwarter *et al* (2009)[1]
Biogenic	56 (0-90)	diameter <1 µm	IPCC (2001)[1]
PBAP	78 (includes only bacteria, fungal spores and pollen)	PM_{30}	Hoose *et al* (2010a)[1]
PBAP	186	split equally into the two coarse size fractions: 2.5-5 and 5-10 µm (PM_{10})	Mahowald *et al* (2008)[1]
PBAP	296 (includes only bacteria, fungal spores and pollen)	diameters as above	Jacobson and Streets, (2009)[1]
PBAP	~1000 (includes cellular fragments)	Total	Jaenicke (2005)[1]
Sea Spray	3340	Total	Penner et al (2001)
Mineral (Soil) Dust	2150	Total	Penner et al (2001)
Biomass Burning	54	0-2 µm	Penner et al (2001)

[1] Després et al (2012)

Rocks outside of deserts often are also covered by a varnish. Parts of biological soil crusts can also be ablated from desert surfaces and all these particles may contribute to the content of biological material in dust transported over long distances during storms (Despres et al 2012). In addition recent studies in Japan suggest that numerous culturable bacteria are transported with Asian dust over the East China Sea from the arid and semi-arid regions of Asia.

In the last years much research effort had been directed to the role of biological particles as ice nuclei and in forming clouds and rain. It is well known, that biological material acts much earlier (in term of freezing) then mineral (inorganic) material. So the cryosphere (deposited precipitation) is full of biological material. Resuspension of ice crystals then might add to the primary biological atmospheric aerosols.

Atmospheric biological particles have also an impact on hygiene and could cause adverse respiratory effects on humans.

The Table gives an impression about the source strength estimates published so far on global sources of primary biological particles. The other sources Sea Spray, Mineral Dust, Biomass Burning are given for comparison. That Table shows clearly, what an important fraction of the Atmospheric Aerosol the Primary Biological Particles are.

Selected references so far:

DeLeon-Rodriguez, N. *et al*. (2013) Microbiome of the upper troposphere: Species composition and prevalence, effects of tropical storms, and atmospheric implications. Proceedings of the National Academy of Sciences. www.pnas.org/cgi/doi/10.1073/pnas.1212089110

Després, V.R. *et al* (2012) Primary Biological Aerosol Particles in the Atmosphere: A Review. Tellus B, **64**, 015598, DOI: 10.3402/tellusb.v64i0.15598

Penner, J. E. *et al* (2001) Aerosols, their direct and indirect effects. In: *The scientific basis. Contribution of working group I to the third assessment report of the intergovernmental panel on climate change* (eds. Houghton, J. T., Y. Ding, D. J. Griggs, M. Noguer, P. J. van der Linden *et al).*, Cambridge, UK and New York, NY, USA, 289-348.

Tuesday, September 3, 2013

Session: Atmospheric Aerosols, *Carbonaceous aerosols*

Recommendations for the interpretation of "black carbon" measurements

Andreas Petzold[1], John A. Ogren[2], and the members of GAW SAG Aerosol

[1] Forschungszentrum Jülich GmbH, Institut für Energie- und Klimaforschung IEK-8, 52425 Jülich, Germany
[2] NOAA/ESRL Global Monitoring Division, Boulder, CO 80305, USA

Keywords: Black carbon, elemental carbon, air quality, monitoring.
Presenting author email: a.petzold@fz-juelich.de

Although black carbon (BC) is one of the key atmospheric particulate components driving climate change and air quality, there is no agreement on the terminology that considers all aspects of specific properties, definitions, measurement methods, and related uncertainties. Following Bond et al. (2013), who deserve credit for synthesizing BC definitions for the first time, BC is characterized by the following distinct properties: (1) it strongly absorbs visible light; (2) it is refractory with a volatilization temperature near 4000K; (3) it is insoluble in water and in the other components of the atmospheric aerosol; and (4) it consists of aggregates of small carbon spherules of < 10 to approx. 50 nm in diameter. In order to include distinct microstructure features, the authors add a fifth property saying that (5) it contains a high fraction of graphite-like sp2–bonded C atoms; see Table 1 for details.

There is much ambiguity in the scientific literature of measurements and numerical models that refer to BC with different names and based on different properties of the particles, with no clear definition of the terms. In consideration of the inadequate definitions available in the literature, and in order to overcome this unsatisfying situation, the authors propose a consistent terminology which is built along material properties.

The term “black carbon” (BC) is considered a useful qualitative description when referring to light-absorbing carbonaceous substances in atmospheric aerosol. In the absence of a method for uniquely determining the mass of BC, the term "BC" should be used as a qualitative and descriptive term when referring generally to material that shares some of the characteristics of BC in particular its carbonaceous composition combined with its light-absorbing properties. For quantitative applications the term requires clarification of the underlying determination:

- Equivalent black carbon (EBC) should be used instead of BC for data derived from optical absorption methods. It is recommended to report the optical measurements primarily as light absorption coefficient, and secondarily as EBC, together with a suitable mass absorption coefficient (MAC) for the conversion of light absorption coefficient into mass concentration.
- Refractory black carbon (rBC) should be used instead of BC for measurements derived from laser incandescence methods.
- Elemental carbon (EC) should be used instead of BC for data derived from methods that are specific to the carbon content of carbonaceous matter (evolved carbon, aerosol mass spectrometry, Raman spectroscopy).
- Soot is a useful qualitative description when referring to particles formed from incomplete combustion. This term is appropriate to and widely used in the research field on the formation of carbonaceous particles in combustion processes and on the emission of particulate matter from combustion sources.

Table 1. Properties defining Black Carbon

Property	Characteristics
Microstructure	graphitic-like structure containing a high fraction of sp^2-bonded carbon atoms
Morphology	aggregates consisting of small carbon spherules of < 10 to approx. 50 nm in diameter
Thermal stability	refractory material with a volatilization temperature near 4000K, gasification is possible only by oxidation which starts at temperatures above 340°C
Solubility	insoluble in organic solvents, in water, and in the other components of the atmospheric aerosol
Light absorption	uniformly absorbing in the spectral range of visible light with MAC(550 nm) > 5 m^2g^{-1} for freshly produced particles; characterized by a significant, non-zero and wavelength-independent imaginary part of the refractive index over the visible and near-visible spectral regions

The coherent terminology proposed here reflects the widespread origin of BC data and permits a consistent reporting of data in the scientific literature that were generated by similar methods. In order to support this effort authors of research papers are requested to clearly state means of calibration and conversion as metadata with any published values.

GAW SAG Aerosol members:
John A. Ogren (Chairman), Urs Baltensperger, Angela Benedetti, Markus Fiebig, Thomas Holzer-Popp, Stefan Kinne, Paolo Laj, Shao-Meng Li, Gelsomina Pappalardo, Andreas Petzold, Nobuo Sugimoto, Christoph Wehrli, Alfred Wiedensohler, Xiao-Ye Zhang.

SAG website: http://gaw.tropos.de/index.html

References
Bond, T.C., et al. (2013) *J. Geophys. Res.*, in press, doi: 10.1002/jgrd.50171.

Comparability of methods to measure black and elemental carbon in two European urban areas - site and seasonal similarities and differences

R. Hitzenberger[1], J. Schwarz[2], I. Aschauer[1], R. Haindl[1], W. Ludwig[1], R Wagner[1], A. Wonaschuetz[1], G. Zecha[1], I. Ševčíková[2], P. Vodička[2] , N. Zíková[2] , and V. Ždímal[2]
[1]Faculty of Physics, University of Vienna, Vienna, 1090, Austria
[2]Department of Aerosol and Laser Studies, Institute of Chemical Process Fundamentals, Prague, 16502, Czech Republic
Keywords: carbonaceous aerosols, atmospheric aerosols, measurement techniques
Presenting author email: regina.hitzenberger@univie.ac.at

Black (BC) and elemental carbon (EC) originate from incomplete combustion of carbonaceous fuels and are important constituents of atmospheric aerosols because of their optical and climatic effects (Jacobson 2005) and their possible health effects (Kim *et al.* 2003). Despite intensive efforts over the last decades, no standard measurement technique has been identified. In this presentation, we use the term BC for data obtained by optical methods, and EC for those obtained by thermal methods.

The study is focussed on an intercomparison of various measurement methods for BC and EC in two Central European cities (Prague, Czech Republic, and Vienna, Austria) which are rather similar in geographical features (total area covered, hilly surroundings, river, building density and characteristics) and have similarities and differences with regard to aerosol sources (in particular sources of black / elemental carbon). In earlier studies in Vienna under summer (Hitzenberger *et al.* 2006) and winter conditions (Reisinger *et al.* 2008) we found different conversion factors for BC and EC measured with different methods for the seasons.

The goal of the current study is to investigate whether similar conversion factors are applicable at the sites and whether the conversion factors obtained earlier (i.e. ca. 10 years ago) for Vienna are still valid or whether changing source conditions have resulted in shifts of the carbonaceous fractions of the aerosol that would require a new set of conversion factors.

For this goal, we performed two back-to-back campaigns in the two cities. The summer campaign was performed first in Prague (June 25 - July 9, 2012) and then in Vienna (July 16 – 30, 2012). The winter campaign was performed in Vienna (Jan. 14 – 30, 2013) and subsequently in Prague (Feb. 4 – 16, 2013).

In both campaigns, BC concentrations were measured on-line with a Multi Angle Absorption Photometer (MAAP) and a Micro-Aethalometer. For Prague, also data from a semi-continuous Sunset Analyzer (NIOSH and EUSAAR II protocols) are available. Off-line measurements of BC and brown carbon (BrC) were also performed using the modified integrating sphere technique capable to separate BC and BrC (Wonaschuetz *et* al 2009). EC concentrations were measured off-line using a Sunset analyzer. In addition to the EC / BC measurements, number size distributions and mass size distributions of the total aerosol were obtained and later analyzed for major ions as well as for black carbon (usually attributable to Diesel traffic) and brown carbon (usually attributable to wood combustion).

First results from the summer study on the intercomparability of the different methods of EC and BC determination show that as expected, the methods are rather well comparable under summer conditions, which agrees well with the earlier study in Vienna. The campaign averages seem to be rather different (e.g. in Vienna, the highest average EC concentration - 1.5 µg/m³ - was measured with the Aethalometer and the lowest - 0.5 µg/m³ - with the Sunset analyzer, transmission correction), but if the data variation is considered, these differences are not significant. Similar results were found for the Prague campaign. The influence of biomass smoke in summer in Prague is sometimes visible also in the BrC data, and is mostly absent in the Vienna summer data (BrC concentrations seldom were found to be above the detection limit). The full results of the intercomparison study will be the focus of this presentation.

This work was supported by the ÖAD, WTZ grant No. CZ 03/2012, the MEYS MOBILITY grant No. 7AMB12AT021, and the Czech Science Foundation grant No. P209/11/1342..

Hitzenberger, R., Petzold, A., Bauer, H, ,Ctyroky, P., Pouresmaeil, P., Laskus, L. and Puxbaum H. (2006) *Environ. Sci. Technol*. **40**, 6377-6383.

Jacobson, M. Z. (2005) *J. Geophys. Res.* **110**, Doi: 10.1029/2004JD005888.

Kim, H. J., Liu, X. D., Kobayashi, T., Kohyama, T., Wen, F. Q., Romberger, D. J., Conner, H., Gilmour, P. S., Donaldson, K., MacNee, W., Rennard, S. I. (2003) *Am. J. Respiratory cell Molec. Biology* **28**, 111-121.

Reisinger, P., Wonaschütz, A., Hitzenberger R., Petzold, A., Bauer, H., Jankowski, N., Puxbaum, H., Chi, X. and Maenhaut W. (2008*) Environ. Sci. Technol*. **42**, 884 – 889.

Wonaschütz, A., Hitzenberger, R., Bauer, H., Pouresmaeil, P., Klatzer, B., Caseiro, A. and Puxbaum H. (2009) *Environ. Sci. Technol*., **43**, 1141-1146.

Seasonal variations of black carbon physical properties influenced by different sources in London urban environment

Dantong Liu[1], James Allan[1,2], Michael Flynn[1], Dominique Young[1], Hugh Coe[1] and Martin Gallagher[1]

[1]Centre for Atmospheric Science, University of Manchester, Manchester, UK, M13 9PL
[2]National Centre for Atmospheric Science, University of Manchester, Manchester, UK
Key Words: Black carbon, Sources, Physical properties, Coating
Presenting author email: Dantong.liu@manchester.ac.uk

A recent comprehensive assessment of the contribution by black carbon aerosol (BC) to total climate determined it to be +1.1 W m^{-2}, and is deemed to be the second most important human emission in terms of its climate-forcing in the present-day atmosphere [Bond et al., 2013]. One of the most important and fundamental constraints on modelling BC climate forcing is determining its source strength. BC can be emitted from different combustion related sectors, i.e. they are often classified as fossil fuels for transportation; biofuels for industrial and residential uses including solid unprocessed biofuel, and open burning of biomass. The motivation to treat the source-attributed BC separately is due to its complex physical properties being largely source dependent, such as the BC size, mixing state, optical and hygroscopic properties. The variety of BC physical properties from sources can lead to considerable variations and uncertainties when modelling the BC direct forcing effect on climate and also the indirect forcing due to their different behaviours when interacting with clouds.

In urban environments, the BC from diesel fuel such as vehicle emission has been widely reported and been incorporated in most of the regional models. Although a few studies have emphasized the importance of emissions from residential solid fuel burning (i.e. from wood burning and cooking) in UK winter time [Allan et al., 2010; Liu et al., 2011], the properties of BC associated with these sources and their differences compared to that from vehicle emissions have not been well characterized.

This study reports results of continuous BC measurements from the Clean Air for London (ClearfLo) campaign for two major intensive observation periods (IOPs) during 2012. Both IOPs lasted for four weeks and were conducted in winter (11st Jan.- 08th Feb.) and 2012 summer (18th Jul.-22nd Aug.) respectively, the latter being during the period of the London Olympic Games. The experimental site was located in the grounds of a school in North Kensington, which is representative of a typical London urban background environment. A long term source attribution study in London based on the positive matrix factorization (PMF) analysis of AMS data shows that London urban environment in winter is significantly influenced by the source of solid fuel burning, such as wood burning for residential heating. In contrast vehicle emissions almost form the only BC source in summer. In the present study physical properties of BC were characterized using a single particle soot photometer. By assuming a core-shell model of coated BC, the relative coating thickness of the aprticles, which is the entire BC particle size (D_p) divided by refractory BC core size (D_c) - D_p/D_c, was also determined using Mie theory.

The physical properties of BC exhibited seasonal differences, summarized in Figure 1. The winter experimental period in London was generally more polluted than summer, with almost twice the BC mass loading on average. Both summer and winter showed a morning rush hour peak of BC mass, whereas an additional evening peak showed in winter. The BC particles in winter, influenced by solid fuel burning, showed larger core size (geometric mean mass diameter D_{geo}170-205nm) than in summer (D_{geo}155-180nm). The summer BC, dominated by vehicle emissions, showed consistent core size distribution throughout the experiment without any diurnal variation, however an apparent diurnal trend of BC core size was observed when influenced by solid fuel burning. The winter-time BC showed significantly thicker coatings than in summer (as reflected by D_p/D_c). The thickest BC coatings in summer were observed between 14:00-15:00 corresponding with the maximum photochemical reactions; however the strongest mixing occurred at midnight in winter. The work we will also present a methodology using Mie calculations to estimate the mass absorption cross section (MAC) and the absorption enhancement due to the coating for different sources of BC and relate these to different photochemical ages.

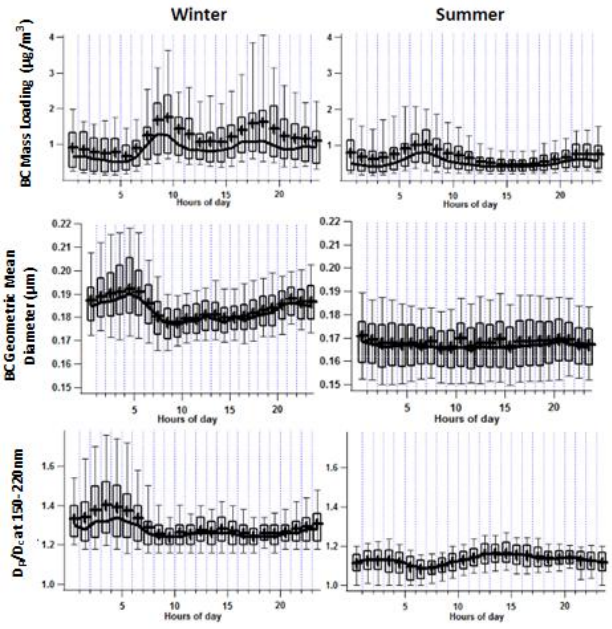

Figure 1. The diurnal trends of BC physical properties in winter and summer, from top panel to the bottom: BC mass loading, BC geometric mean diameter and D_p/D_c at 150-220nm

This work was supported by the UK Natural Environment Research Council under grants NE/H003150/1 and NE/H008136/1.

Bond T. C., S. J. Doherty et al. 2013: Bounding the role of black carbon in the climate system: A scientific assessment. *Journal of Geophysical Research: Atmospheres*. doi: 10.1002/jgrd.50171.

Allan, J. D., Williams, P. I. et al. 2010: Contributions from transport, solid fuel burning and cooking to primary organic aerosols in two UK cities, *Atmos. Chem. Phys.*, 10, 647–668.

Liu, D., Allan, J. et al. 2011: Carbonaceous aerosols contributed by traffic and solid fuel burning at a polluted rural site in Northwestern England, *Atmos. Chem. Phys.*, 11, 1603-1619.

Influence of vertical transport on the mixing state of black carbon at the high-alpine Jungfraujoch site

M. Gysel, M. Laborde, N. Bukowiecki, E. Hammer, P. Zieger, U. Baltensperger and E. Weingartner

Laboratory of Atmospheric Chemistry, Paul Scherrer Institute, 5232 Villigen PSI, Switzerland
Keywords: Black Carbon, Mixing State, Jungfraujoch, SP2
Presenting author email: martin.gysel@psi.ch

Atmospheric black carbon (BC) aerosol particles are mostly emitted by anthropogenic combustion processes. They are a concern due to their adverse effects on human health and their contribution to climate warming (Shindell *et al.*, 2012). Climate-relevant BC properties such as the mass absorption cross-section, cloud condensation nuclei activity and ice nuclei activity depend on the mixing state of BC. BC particles are often emitted with almost no coating and atmospheric aging processes such as condensation and coagulation result in acquisition of coatings with other aerosol components.

In this study we investigated the mixing state of BC particles observed at the high-alpine research station Jungfraujoch (3580 m asl) in the Swiss Alps. A single particle soot photometer (SP2; Schwarz *et al.*, 2006) was applied for quantitative detection of BC mass in individual particles using laser-induced incandescence. The coating thickness of BC particles is determined by comparison of the optical particle diameter (derived from the light scattering signal) with the BC core diameter (derived from the incandescence signal).

An example of the BC properties observed at the Jungfraujoch is shown in Fig. 1 for two days in summer 2010. The green shading indicates times when the Jungfraujoch was exposed to free tropospheric (FT) air, the pink shading indicates times with distinct influence from injections of the planetary boundary layer (PBL), and the grey shadings indicate local pollution from a snowcat. The arrival of PBL influence results in an increase of both BC particle number concentration (Fig. 1A) and BC mass concentration (Fig. 1B) by about one order of magnitude, while the number fraction of BC-containing particles (mass equiv. BC core diameter D_{MEV} > 70 nm) to purely scattering particles (optical diameter > 125 nm) remains unchanged (Fig. 1A). Fresh snowcat exhaust can be identified by a massive increase of BC-containing particles, while the concentration of purely scattering particles remains almost unaffected. Fig. 1C shows the median coating thickness ($\Delta_{coating}$) of BC cores with $D_{MEV} \approx 200$ nm. BC from the snowcat exhaust is uncoated within experimental uncertainty. A substantial coating thickness of $\Delta_{coating} \approx 60$ nm is observed for FT air and PBL influence results in a slight decrease of the coating thickness to $\Delta_{coating} \approx 40$ nm. The latter value is substantially larger than that of fresh pollutions in urban areas (e.g. Laborde *et al.*, 2012), thus indicating that the time scale for the acquisition of a substantial coating is shorter than the typical transport time from the BC source to the Jungfraujoch.

The whole data set covering 1.5 months will be used to investigate whether the coating thickness difference between FT air and PBL influenced air reported in Fig. 1 is generally representative. The influence of coating thickness variations on the mass absorption cross-section of the BC particles will also be addressed.

This work was supported by the Swiss National Science Foundation and the Swiss Global Atmosphere Watch program.

Laborde, M., Crippa, M., et al. (2012) *Atmos. Chem. Phys. Discuss.*, **12**, 25121–25180.

Schwarz, J. P., Gao, R. S., et al. (2006) *J. Geophys. Res.*, **111**, D16207.

Shindell, D., Kuylenstierna, J. C. I., et al. (2012) *Science*, **335**, 183-189.

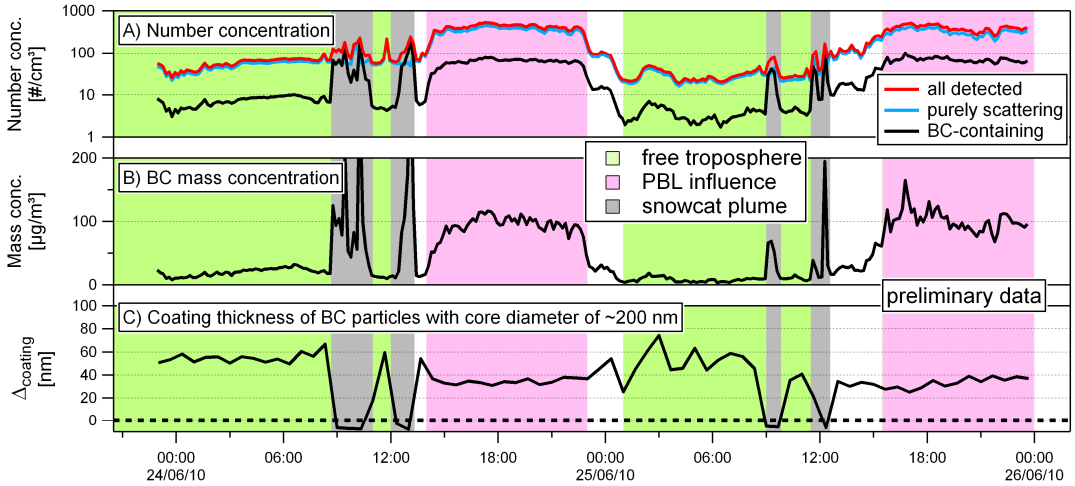

Figure 1: A) Number concentration of BC-containing, purely scattering and all detected particles, shown on a logarithmic scale. B) BC mass concentration. C) Coating thickness of the BC particles with non-BC aerosol components.

Fossil and non-fossil sources of OC and EC in Switzerland for winter-smog episodes

S. Szidat[1,2], P. Zotter[3], Y.L. Zhang[1,2,3], V.G. Ciobanu[3], L. Wacker[4], Baltensperger[3], and A.S.H. Prévôt[3]

[1]Department of Chemistry and Biochemistry, University of Bern, 3012 Berne, Switzerland
[2]Oeschger Centre for Climate Change Research, University of Bern, 3012 Berne, Switzerland
[3]Paul Scherrer Institute (PSI), 5232 Villigen-PSI, Switzerland
[4]Laboratory of Ion Beam Physics, ETH Zurich, 8093 Zurich, Switzerland

Keywords: Source apportionment, radiocarbon (^{14}C), carbonaceous particles, elemental carbon, organic carbon
Presenting author email: szidat@iac.unibe.ch

Persistent inversion conditions may occur in Switzerland in the plateau and in Alpine valleys during winter. Such winter-smog episodes may lead to high concentrations of particulate matter with an aerodynamic diameter <10 µm (PM_{10}) exceeding the legal daily limits of 50 µg/m^3 over several days to weeks. As such conditions may cause acute health effects, the emission sources of PM in general and of carbonaceous aerosols in particular are of special interest for these episodes. A substantial contribution of biomass burning was indicated in previous campaigns in Switzerland (Szidat 2009).

From winter 2007/2008 to winter 2011/2012, several stations of the Swiss federal and cantonal air monitoring programs provided quartz fibre filters for 5 days per winter (simultaneous collection for all stations) with high PM_{10} concentrations (Figure 1). Samples were analysed for major anions and cations as well as organic carbon (OC) and elemental carbon (EC) concentrations.

Figure 1. Map of the study. Stations marked in red participated only during one or two winters.

Fossil and non-fossil sources were apportioned for all filters by measurement of the long-lived radioisotope ^{14}C (radiocarbon) based on the fact that fossil materials are extinct in ^{14}C due to its age, where as fresh plants contain radiocarbon on the contemporary level (Szidat *et al.* 2006). ^{14}C analysis was performed on OC and EC separately, because both fractions typically originate from diverse sources with different fossil/non-fossil shares EC originates only from combustion of fossil-fuels and biomass burning. OC can be emitted as primary organic aerosol from biogenic sources, wood burning and fossil fuel combustion or can be formed in the atmosphere as secondary organic aerosol. In total, >500 individual ^{14}C determinations were conducted.

Special emphasis was laid upon an optimized isolation procedure for EC, as the ^{14}C value of this fraction directly reflects the biomass-burning contribution of the emissions. EC isolation was performed with the new protocol Swiss_4S, which combines steps of water extraction, combustion in oxygen and evaporation in helium for complete OC separation with online monitoring of the optical transmission (Zhang *et al.* 2012).

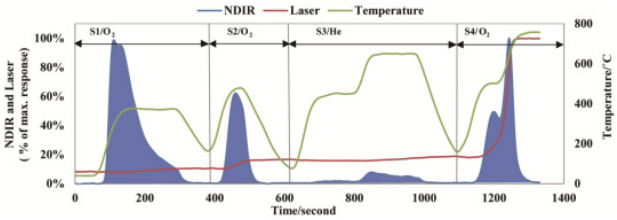

Figure 2. Thermogram based on the Swiss_4S protocol for isolation of EC for ^{14}C analysis (Zhang *et al.* 2012).

On the average, the non-fossil fractions of OC were larger than 75% for each station, which indicates that primary or secondary traffic emissions contributed only to a minor extent during the winter-smog episodes. This was even valid for the motorway (Reiden, Moleno) and kerbside stations (Bern), which demonstrates the importance of regionally mixed over local emissions. ^{14}C analysis of EC revealed that biomass burning contributed on the average by one to two thirds to the total burden of this carbonaceous aerosol fraction depending on the station characteristics: whereas traffic-related sites showed smaller proportions, dominating biomass-burning emissions were observed in Alpine valleys, where residential wood heating is common. In this work, we will present final results and discuss in detail the contribution of biomass burning for winter-smog episodes in Switzerland and its trend over the five years of the study.

This work was supported by the Swiss Federal Office for the Environment, the Swiss Cantons BS/BL, GR, SG, SO, TI, UR, VS and the Principality of Liechtenstein.

Szidat, S. *et al.* (2006). *J. Geophys. Res.* **111**, D07206.
Szidat, S. (2009). *Chimia* **63**, 157-61.
Zhang, Y. L. *et al.* (2012). *Atmos. Chem. Phys.* **12**, 10841-56.

Long-term variability of elemental and organic carbon in aerosols over Athens, Greece.

D. Paraskevopoulou[1,2], E. Liakakou[2], E. Gerasopoulos[2] and N. Mihalopoulos[1]

[1]Environmental and Analytical Chemical Division, Department of Chemistry, University of Crete, P.O. Box 2208, 71003 Heraklion, Greece
[2]Institute for Environmental Research and Sustainable Development, National Observatory of Athens, I. Metaxa and Vas. Pavlou, 15236, P. Penteli, Athens, Greece
Presenting author email: dparask@meteo.noa.gr

Atmospheric aerosol particles have direct impact on the climate of the earth through scattering and absorption of radiation. The carbonaceous fraction of particulate matter, which consists of elemental carbon (or black carbon) and a variety of organic compounds (organic carbon), plays a significant role on this climatic change and on public health, as well. Organic carbon is considered one of the main elements of aerosols that scatter radiation thus; the main component of particulate matter that absorbs light is elemental carbon.

Long-term (5-year) measurements of Elemental Carbon (EC) and Organic Carbon (OC) in atmospheric aerosols are presented here for the first time in the area of Athens, Greece. Furthermore, the seasonal variability of carbonaceous content has been studied, reflecting the effects of the on-going recession on the quality of the air.

To calculate the concentration of OC and EC, a total of 1500 samples have been collected using Dichotomous Partisol and Partisol FRM samplers on a 24hour basis, at Penteli's premises (National Observatory of Athens station: 38°3'N, 23°5'E, 527 m a.s.l) covering a 5 year period. All chemical analyses presented in this research, were conducted on the $PM_{2.5}$ fraction, since fine fraction of aerosols constitutes the major carrier of the studied air pollutants. The applied method for OC and EC measurements was described in detail by Theodosi *et al* 2010.

The daily concentrations and the seasonal cycle of organic and elemental carbon for the studied period, is presented in Fig.1a, and 1b, respectively. The levels of OC and EC concentrations appear to decrease from 2008 to 2010 while, since 2010 an increase is observed during the colder periods of the year. This could probably be attributed to the reduction of sources of air pollutants from 2008 to 2010 due to the beginning of the crisis in the economy while, since 2010 biomass burning seems to dominate in domestic heating, resulting in augmented carbonaceous aerosol production.

It can be observed that OC and EC present similar covariance during the studied period and their maximum values appear mostly on fall to winter season, as it was expected, since during this period of the year there is fuel combustion and domestic heating that mainly leads to production of elemental and organic carbon.

The whole period average estimated concentration for OC was 2.32 ± 1.29μg/m^3 and for EC was 0.54 ± 0.39μg/m^3. The average OC/EC ratio of the aforementioned in situ measurements was 6.17 while, the concentrations of OC and EC appeared to be well correlated (R^2=0.48).

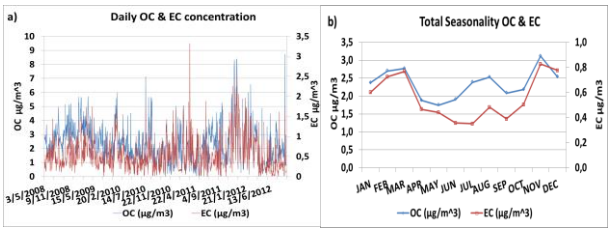

Figure 1 a. Daily OC and EC concentrations and b. Seasonal cycle of OC and EC concentrations at Penteli during the sampling period from 2008 until 2012.

The organic to elemental carbon ratio indicates that the organic carbon is mostly secondary. During colder period of the year additional sources like household heating contribute to the total carbon loadings. More importantly the type of domestic heating is considered a key parameter. As a consequence, it could be assumed that the deterioration of the air quality constitutes an additional side-effect of the years of recession in Greece.

Future studies will be focused on the correlation of OC and EC concentrations to ion concentration and optical properties of aerosols.

This research has been co-financed by the European Union (European Social Fund – ESF) and Greek national funds through the Operational Program "Education and Lifelong Learning" of the National Strategic Reference Framework (NSRF) - Research Funding Program: Heracleitus II. Investing in knowledge society through the European Social Fund.

Bougiatioti, A. Zarmpas, P. Koulouri, E. Antoniou, M. Theodosi, C. Kouvarakis, G. Saarikoski, S. Mäkelä, T. Hillamo R. Mihalopoulos, N. (2013) *Atm. Environ.* **64**, 251-262.

Sciare, J. Oikonomou, K. Favez, O. Liakakou, E. Markaki, Z. Cachier, H. and Mihalopoulos, N. (2008) *Atmos. Chem. Phys*. **8**, 5551–5563.

Theodosi, C. Im, U. Bougiatioti, A. Zarmpas, P. Yenigun, O. and Mihalopoulos, N. (2010) *Sci. Total Environ*. **408**, 2482-2491.

Influence of the traffic on the black carbon particle mass concentration and particle number size distribution in La Paz, Bolivia

A. Wiedensohler[1], K. Weinhold[1], M. Andrade[2], F. Velarde[2], I. Moreno[2], and F. Avila[2]

[1]Leibniz Institute for Tropospheric Research, Permoserstr. 15, 04318 Leipzig, Germany
[2]Laboratory for Atmospheric Physics, Department of Physics, University Mayor de San Andres, La Paz, Bolivia
Presenting author email: ali@tropos.de

Results from a intensive campaign carried in La Paz (16°30'13.83"S; 68° 7'45.56"W; 3580 m a.s.l.) Bolivia are presented on this work. Particle size distribution was measured using a Mobility Particle Size Spectrometer (following Wiedensohler et al.; 2012), whereas the particle mass concentration of black carbon (BC) was measured using a Multi Angle Absorption Photometer (MAAP). In addition meteorological parameters as well as CO concentration were collected. The instruments were set up at the Planetarium of University Mayor de San Andres, La Paz, Bolivia. The building is located beside a road with heavy traffic. Since La Paz is located in a valley reaching from approximately 3200 to 4000 m a.s.l., cars and trucks are operated on a high load when driving uphill.

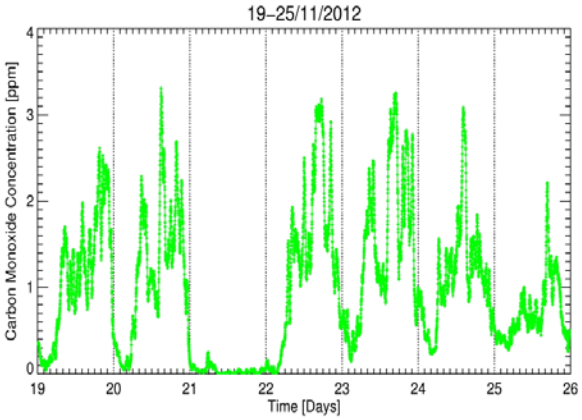

Figure 1: Carbon monoxide gas concentration for the week November 19 to 25, 2012.

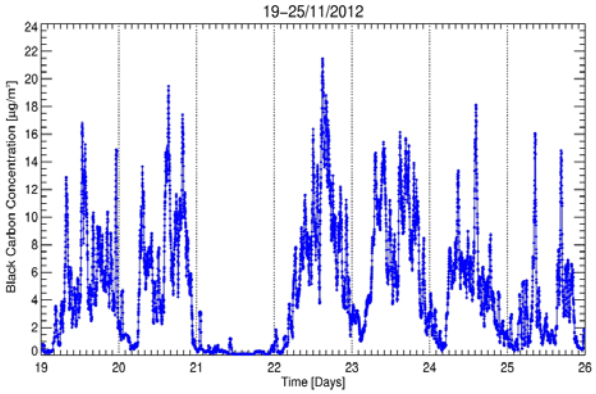

Figure 2: Black carbon particle mass concentration for the week November 19 to 25, 2012.

La Paz and El Alto (located at approximately 4000 m a.s.l.) are two of the major cities in the region. There are no other larger settlements in the surrounding. During November 21, 2012, the whole traffic was banned because of a national census in both cities, giving us the opportunity to study the influence of the traffic on the black carbon particle mass concentration, the particle number size distribution as well as the carbon monoxide gas concentration.

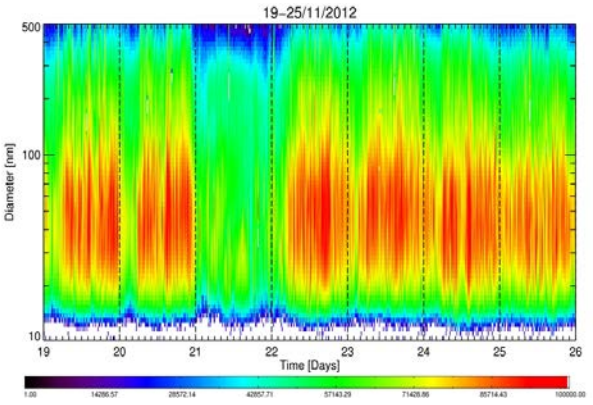

Figure 3: Particle number size distribution for the week November 19 to 25, 2012.

As seen from Figure 1, on November 21, 2012, the carbon monoxide gas concentration dropped to a value near Zero ppm from around 2ppm, during workdays November 19 -20 and 22-23, 2012. This indicated that due to the traffic ban, almost all sources of incomplete combustion have been switched-off. Figure 2 illustrates the same behavior for the BC particle mass concentration, meaning that BC was almost exclusively produced by the traffic. During regular working days, peaks of BC particle mass concentration were around 15 µg/m^3, whereas on November 21, 2012, the values were clearly below 1 µg/m^3. In Figure 3, a contour plot of the particle number size distribution of the week November 19 to 25, 2012 is shown. The red color illustrates high, whereas green and blues describe low particle number concentrations. Again, on November 21, the concentrations drop drastically, demonstration that the major fraction of the aerosol in the city of La Paz is produced by traffic.

Wiedensohler, A. et al. (2012). Mobility Particle Size Spectrometers: Harmonization of Technical Standards and Data Structure to Facilitate High Quality Long-term Observations of Atmospheric Particle Number Size Distributions. AMT 5, 657–685.

Long-term observations of carbonaceous aerosols and related gaseous emissions near a crude-oil plant in South Italy

M. Calvello[1,2], M. Lovallo[4], F. Esposito[3] , L. Mangiamele[4], G. Pavese[1]

[1] CNR-IMAA, C. da S. Loya, 85050, Tito Scalo (PZ), Italy
[2] OAVDA, via Vittorio Emanuele II, 85052, Marsico Nuovo (PZ), Italy
[3] DIFA- Università della Basilicata, C. da Macchia Romana, 85100, Potenza, Italy
[4] ARPAB, Via della Fisica C/D, 85100, Potenza, Italy
Keywords: Carbonaceous aerosol, organic emissions, time series
Presenting author email: mariarosaria.calvello@imaa.cnr.it

A two-year dataset of almost continuous Black Carbon (BC) content measurements by a Magee AE31 7-wavelenghts aethalometer (370 to 950 nm) near a crude oil pre-treatment plant in South Italy (Agri Valley, 40.33°N, 15.92° E, 582 m a.s.l) has been analyzed. Since 1996 an intense crude-oil extraction together with a pre-treatment activity has been carried out at the site with continuous and controlled combustion processes and smoke emissions.

A suitably implemented algorithm has been applied to the aethalometer data in order to analyse absorption coefficient spectral dependence and to reduce the error in UVPM detection (Esposito *et al.*, 2012). BC and UVPM data have been compared to some organic compounds concentrations (Benzene, Toluene, Methane, Non-Methane Hydrocarbons) routinely measured at the same site and for the same period by ARPAB (Basilicata region environmental protection agency).

Recurrent trends have been searched for on a wide temporal scale (two-years diurnal cycles/ seasonal pattern, summer and winter) by applying the statistical Lomb-Scargle periodogram technique to the entire data-set. This is a powerful technique to be applied for frequency analysis of not equally-spaced data to obtain reconstructed spectra on both seasonal and annual basis (Hocke *et al*., 2009). These spectra can be considered as representative of background emissions to be compared with much intense emissions taking place in shorter periods (few days to few weeks) during the year (Pavese *et al*., 2012).

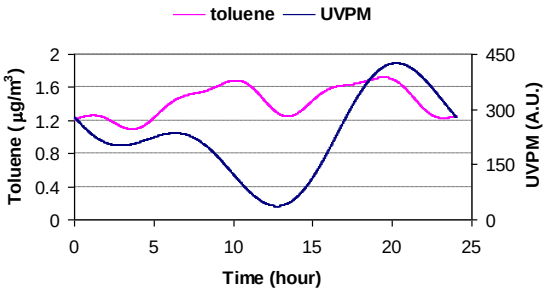

Figure 1: Reconstructed spectra of toluene and UVPM "typical day" as obtained by Lomb-Scargle periodogram for the two-year database.

As an example, reconstructed spectra of toluene and UVPM "typical day" from two-years concentrations data are shown in Figure 1. The differences observed can suggest different dynamics in aerosol formation and/or in adsorption processes onto atmospheric particles.

On the contrary, considering an episode of intense emissions (March, 8th- 19th 2011), UVPM and toluene time behaviours show similar patterns, as reported in Figure 2, highlighting the necessity to study emissions on different time-scales.

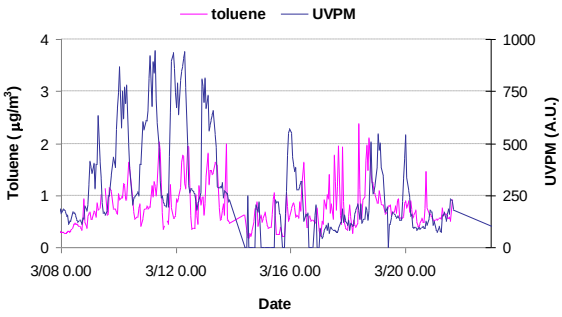

Figure 2: Temporal variation of toluene concentrations and UVPM hourly mean values for the period march 8th - 19th 2011.

To complete this study, an analysis of meteo-climatic parameters such as solar radiation, wind intensity and prevalent direction, has been carried out to verify if and when these parameters contribute to a major/minor agreement among combustion products time patterns.

This work was supported by "Osservatorio Ambientale della Val d'Agri" in the framework of the project "Integrated model for environmental matrix" and by ARPAB.

Esposito, F., Calvello, M., and Pavese, G. (2012). *Atmos. Meas. Tech. Discuss*., 5, 1003-1027

Hocke, K., and Kämpfer N. (2009). *Atmos. Chem. Phys.*, 9, 4197–4206.

Pavese, G., Calvello, M., Esposito, F., (2012). *Aerosol and air quality research*, 12, 1146-1156, 2012.

Tuesday, September 3, 2013

Session: Atmospheric Aerosols
New particle formation between ground and free troposphere

Secondary particle formation in Arctic Russia

E. Asmi[1], V. Kondratyev[2], D. Brus[1], H. Lihavainen[1], T. Laurila[1], M. Aurela[1], T. Uttal[3], V. Ivakhov[4] and A. Makshtas[5]

[1]Finnish Meteorological Institute, Helsinki, Finland
[2]Tiksi Hydrometeorological Service, Tiksi, Russia
3National Oceanic and Atmospheric Administration, Boulder, U.S.A
4Voeikov Main Geophysical Observatory, St. Petersburg, Russia
5Arctic and Antarctic Research Institute, St. Petersburg, Russia
Keywords: nucleation, growth, arctic, distribution.
Presenting author email: eija.asmi@fmi.fi

The Arctic and northern boreal regions of Eurasia are experiencing rapid environmental changes due to pressures by human activities. The Arctic environment is highly sensitive to changes in aerosol concentrations or composition, largely due to the high surface reflectance for the most part of the year. Secondary particle formation from atmospheric vapours is a mechanism, potentially affecting the aerosol particles, and the climate effects which follow, in these remote regions (e.g. Asmi et al., 2011). Direct measurements, especially in the Russian side of the Arctic, are though still lacking.

Tiksi meteorological observatory in northern Siberia (71°36´N; 128°53´E) on the shore of the Laptev Sea has been operating since 1930s. Recently, it was upgraded and joint in the network of the International Arctic Systems for Observing the Atmosphere (IASOA, www.IASOA.org), in the framework of the International Polar Year (IPY) Activity (#196) project. The project is run in collaboration between NOAA with the support of the NSF, Roshydromet (AARI and MGO units), government of the Republic of Sakha (Yakutia) and the FMI. FMI activities in Tiksi were initiated in summer 2010 and include aerosol size distribution measurements starting at 7 nm size. These are measured with a twin-DMPS system and here the data are used to pinpoint secondary particle formation events, as well as to tie them with meteorological and air mass properties.

In Figure 1, average concentration of nucleation mode (here: 7-25 nm) particles in each month is presented. It appears that the rise of sunlight in the month of March strongly assist secondary particle formation. With a snow covered ground in early spring, it is likely that the nucleating and condensing vapours are transported from longer distances. Another smaller peak in particle formation occurs in summer when local vegetation contributes as a source of vapours.

Analysis of air mass origin during the observed events supports the conclusions. During early spring, nucleation mode particles are increasingly seen in high Arctic air masses, while during summer, the small particles appear also in continental Siberian airflows.

A climate impact of the secondary particles is also studied. The preliminary results show that the particle growth rates are much higher in summer in comparison to other seasons, thereby allowing them to affect the climate more often. This is connected with vegetation sources of biogenic organic vapours, as seen with clear correlations with air mass origin and temperature (Fig. 2).

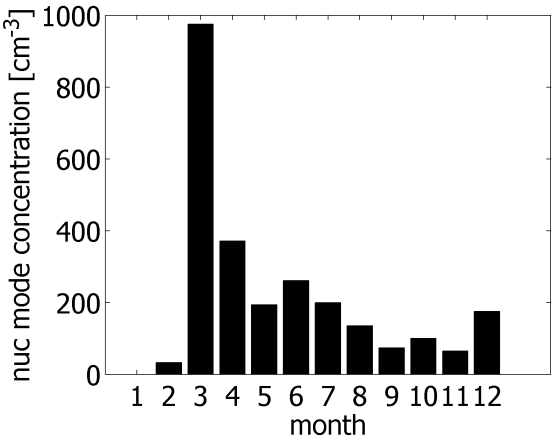

Figure 1. Average concentration of nucleation mode (7-25 nm) particles per each month.

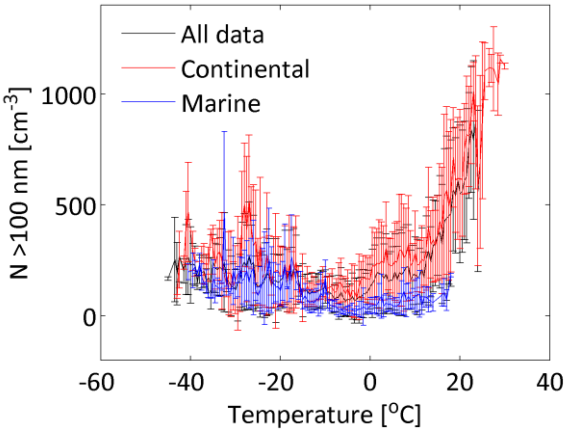

Figure 2. Accumulation mode (>100 nm) concentration as a function of temperature (black), and in continental (red) and marine (blue) air masses separately.

This research was supported by the Academy of Finland Center of Excellence program (project number 1118615).

Asmi, E., Kivekäs, N., Kerminen, V.-M., Komppula, M., Hyvärinen, A.-P., Hatakka, J., Viisanen, Y. and Lihavainen, H. (2011) *Atmos. Chem. Phys.* **11**, 12959-12972.

New Aerosol Particle formation in Amazonia

Matisāns M.[1], Tunved P.[1], Hamburger T.[1], Manninen H.E.[5], Backman J.[5], Rizzo L.[2], Artaxo P.[4], Riipinen I.[1], Swietlicki E.[3], Krejči R.[1], Kulmala M.[5]

[1]Department of Applied Environmental science, Stockholm University, Stockholm, 10691, Sweden
[2]Department of Earth and Exact Sciences, Federal University of São Paulo, São Paulo, Brazil
[3]Div. of Nuclear Physics, Dept. of Physics, Lund University, S-22100 Lund, Sweden
[4]Department of Applied Physics, Institute of Physics, University of São Paulo, São Paulo, Brazil
[5]Department of Physics, Helsinki University, Helsinki, Finland
Keywords: Nucleation, NPF, Amazonia, Particle growth, cluster analysis.
Presenting author email: modris.matisans@itm.su.se

Events of new particle formation (NPF) in tropical boundary layer followed by consecutive growth towards Aitken mode size range are sparse compared to mid- latitudes Kulmala et al. (2004). This is also the case for rainforest environment. More often short episodes of elevated ultra-fine and Aitken mode aerosol particle concentrations are observed their origin and the processes governing these episodes do however remain unclear. Based on observations performed in the Amazonian rainforest environment combined with statistical analysis we present a mechanism explaining the erratic appearance of ultra-fine aerosol in tropical boundary layer of the rainforest.

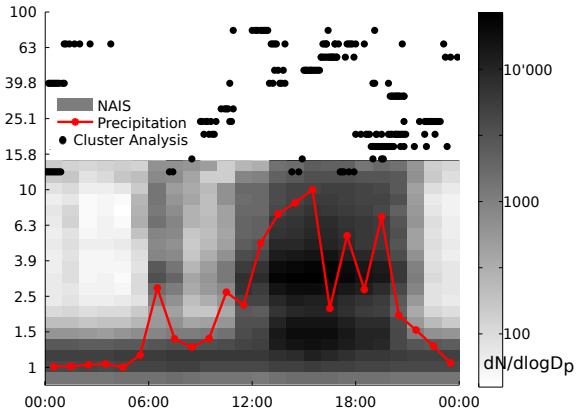

Figure 1: NAIS negative ion concentration 95th percentile diurnal pattern combined with cluster analysis method results (black dots). Mean values for precipitation are given in arbitrary units.

Abstract review

To observe any underlying ultra-fine particle processes we chose to look at the SMPS data and applied a statistical method based on kmeans cluster analysis technique. MacQueen (1967) has described kmeans cluster analysis in detail. Prior to our study cluster analysis has been implement in aerosol science for other purposes, such as principle meteorological component analysis in particle nucleation day classification (Hyvönen et al., 2005) and investigation of processes controlling the evolution of aerosol particle size distribution properties (Tunved et al., 2004). In this study we expand application of cluster analysis to a method that requires preliminary filtering and normalization of data. The introduced method allows for mining ultra fine particle statistics by analysing particle size distributions selectively.

Each scan was normalized to its maximum number concentration; thus, we are focusing on different shapes of particle size distributions instead of absolute number concentrations. Only size distributions having a local a maximum between 10 to 80 nm were considered further analysis. This was achieved by discarding size distributions whose second order derivative of number size distribution curve was greater than 0.

Diurnal occurrence cycle for the clusters reveals a pattern that we eventually compare to ion production by precipitation diurnal pattern. After ion production is stopped, 20 nm particle formation by self–coagulation estimates to 800 cm^{-3}.

Kulmala, M., Vehkamäki, H., Petäjä, T., Dal Maso, M., Lauri, A., Kerminen, V., Birmili, W., and McMurry, P. (2004) *Formation and growth rates of ultrafine atmospheric particles: a review of observations*, Journal of Aerosol Science, 35, 143âĂŞ176.

MacQueen, J. *Some methods for classification and analysis of multivariate observations* Proceedings of the fifth Berkeley symposium on mathematical statistics and probability vol. 1, p. 14, California, USA

Hyvönen, S., Junninen, H., Laakso, L., Dal Maso, M., Gronholm, T., Bonn, B., Keronen, P., Aalto, P., Hiltunen, V., Pohja, T., Launiainen, S., Hari, P., Mannila, H., and Kulmala, M. (2005) *A look at aerosol formation using data mining techniques*, Atmospheric Chemistry and Physics, 5, 3345–3356.

Tunved, P., Ström, J., Hansson, H., et al. (2004) *An investigation of processes controlling the evolution of the boundary layer aerosol size distribution properties at the Swedish background station Aspvreten*, Atmospheric Chemistry and Physics Discussions, 4, 4507–4543.

Formation and chemical properties of nano-sized particles in the lower free troposphere

J. Tröstl[1], J. Duplissy [2], F. Bianchi[1], L. Rondo[3], H. Junninen[2], A. Adamov[2], A.P. Praplan[2], C. Fuchs[1], J. Dommen[1], E. Weingartner[1] and U. Baltensperger[1]

[1]Laboratory of Atmospheric Chemistry, Paul Scherrer Institute, 5232 Villigen PSI, Switzerland
[2]Department of Physics, University of Helsinki, 00014 Helsinki, Finland
[3]Institute for Atmospheric and Environmental Sciences, University of Frankfurt, 60438 Frankfurt, Germany

Keywords: Aerosol Nucleation, Aerosol Growth, Charged Fraction, Jungfraujoch
Presenting author email: ernest.weingartner@psi.ch

Introduction

It is well known that atmospheric aerosols influence the Earth's climate directly by light scattering and indirectly by changing cloud properties. Atmospheric aerosols are either emitted directly to the atmosphere (primary sources such as sea spray, windblown dust, soot) or formed by gas-to-particle conversion (secondary sources such as nucleation). A recent study by Merikanto et al. (2009) indicates that up to 45% of **c**loud **c**ondensation **n**uclei (CCN) are formed by nucleation. Many nucleation events have been observed in the planetary boundary layer (e.g. Riipinen et al., 2007). However, only a few measurements have been carried out in the free troposphere (FT) (e.g. Weingartner et al., 1999; Boulon et al., 2010); hence our knowledge of aerosol nucleation in the FT is limited.

In January and February 2013 the **Nu**cleation, **Cl**oud and **A**erosol **C**haracterization **E**xperiment (NUCLACE) was conducted at the high alpine research station Jungfraujoch (JFJ) located in the lower FT at 3580 m asl. in the Swiss Alps. The goal was to characterize the properties of newly nucleated aerosol particles (i.e. their size, charge, nucleation and growth rates) and to understand their detailed formation mechanisms by measuring the prevailing precursor gas concentrations with state-of-the-art instrumentation.

Methods

For this purpose a nano scanning mobility particle sizer (nanoSMPS) and a condensation particle counter (CPC) were installed in the cupola of the Sphinx building on the JFJ. The nanoSMPS measured the number size distributions of particles with diameters D between 5 and 90 nm. The sampling was performed through the wall with a specific inlet (length = 40 cm, aerosol sampling flow 1 l/min, sampling line make up flow 8 l/min). The size spectra were corrected for CPC efficiency and diffusion losses in the sampling line. To avoid freezing of the inlet by supercooled cloud droplets a heating system was employed. An electrostatic precipitator was added to the sampling line to periodically remove all charged aerosols up to 120 nm. With this setup the total and neutral particle size distributions were measured with a time resolution of 200 s and the size dependent charged fraction was calculated.

In addition, two chemical ionization atmospheric pressure interface time of flight mass spectrometer (CI-APi-TOF, Jokinen et al 2012) were employed to measure neutral clusters in the gas phase, and two atmospheric pressure interface time of flight mass spectrometers (APi-TOF, Junninen 2010) measured the composition of charged clusters (positive and negative).

First Results

A number of nucleation events were observed. Nucleation mostly occurred at very low ambient temperatures (around -30°C) and was often related to the disappearance of clouds that were present at the station. Figure 1 shows such a typical nucleation event, where the particles grew to D = ~20 nm. This event shortly occurred after the clouds vanished around 12:00. Future data analysis will also include the measured precursor gas concentrations.

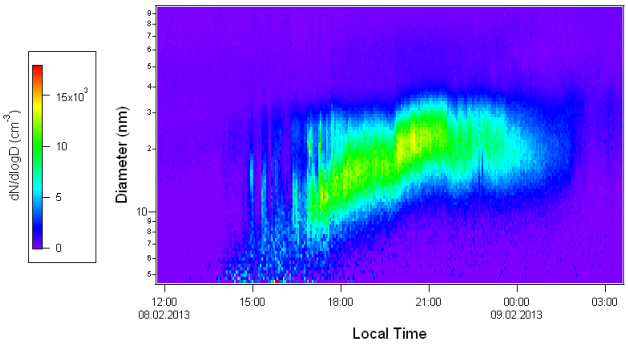

Figure 1. Evolution of particle number size distributions during a nucleation event in the free troposphere.

This work is supported by the EU Marie Curie Project "CLOUD-TRAIN" as well as the EU Infrastructure project ACTRIS. We thank the International Foundation High Altitude Research Stations Jungfraujoch and Gornergrat (HFSJG), which made it possible to carry out the experiments at the JFJ.

Boulon J. et al. (2010) *Atmos. Chem. Phys.* **10**, 9333-9349.
Jokinen, T. et al. (2012) *Atmos. Chem. Phys.* **12**, 4117-4125.
Junninen H. et al. (2010) *Atmos. Meas. Tech.* **3**, 1039-1053.
Merikanto J. et al. (2009) *Atmos. Chem. Phys.* **9**, 8601-8616.
Riipinen I. et al. (2007) *Atmos. Chem. Phys.* **7**, 1899–1914.
Weingartner E. et al. (1999) *J. Geophys. Res.* **104**, 26809-26820.

Enhancement in CCN concentrations during new particle formation events

Z.J. Wu[1], W. Birmili[1], L. Poulain[1], Z.B. Wang[1], A. Hamed[1,2], S. Henning[1], F. Stratmann[1], H. Herrmann[1], A. Wiedensohler[1]

[1]Leibniz Institute for Tropospheric Research (TROPOS), Leipzig, Germany

[2]Department of Applied Physics, University of Eastern Finland, P. O. Box 70211, Finland

Keywords: NPF, CCN, particle growth, organics

Presenting author email: wuzhijun@tropos.de

New particle formation (NPF) events are an important source of cloud condensation nuclei (CCN). However, the contribution of atmospheric NPF events to the global CCN budget remains the single largest uncertainty (Kerminen, et al., 2012). Therefore, information on mechanisms and the vapors responsible for NPF and growth would be needed for accurate prediction of CCN in order to realistically capture aerosol radiative effects. In our study, we investigate the effects of particle formation and growth and chemical ageing of pre-existing particles on CCN number concentration during the NPF events based on the observations made at a central Europe research station, Melpitz, Germany.

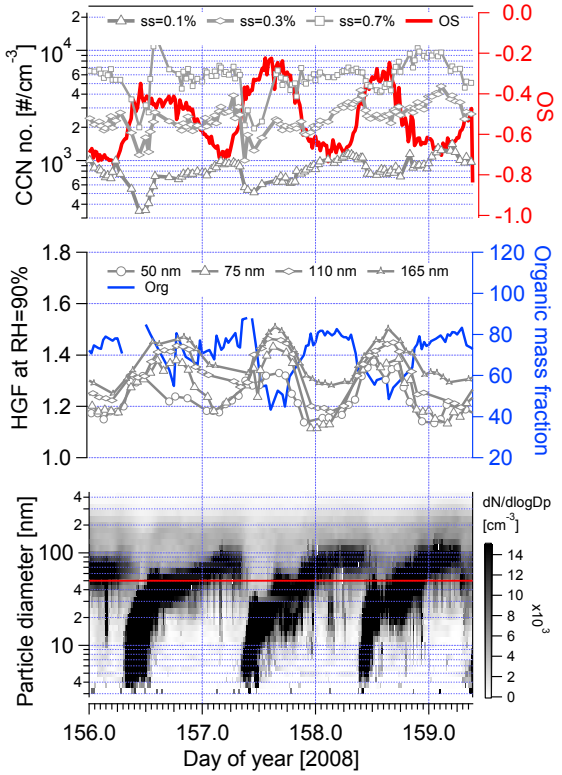

Fig. 1: Time series of different parameters during NPF events. The detail description is given in the text.

Investigations of the contribution of NPF on CCN concentrations are based on the size-resolved chemical composition (AMS), particle hygroscopic growth factor (HGF), particle number size distributions, sulfuric acid [H_2SO_4] and OH radical concentrations at Melpitz in 2008. The NPF bursts and continuous growth were continuously observed (Fig.1.). As a first step, the critical diameter (D_{crit}) at which 50% of the particles were activated was calculated from κ:

$$D_{crit} = \left(\frac{4A^3}{27\kappa \ln^2 S_C}\right)^{1/3}$$ (Petters and Kreidenweis, 2007)

Here, κ is calculated from size-resolved AMS data using the ZSR mixing rule.Secondly, the number concentration of potential CCN is derived by integrating the number size distribution of particles larger than D_{crit}. The oxidation state (OS) was calculated from AMS data according to Kroll et al, (2011) for the whole size range (PM1). The organic mass fraction was taken in the size range 50-200 nm (mobility diameter).

Comparing the increase of CCN number concentrations at the start time of the NPF bursts (B in table 1) and at the end time of NPF bursts (E in the table 1) shows that on average, the CCN number concentrations are enhanced by the factors of two between the beginnings and the end of NPF events. However, the increments are varied with varied super saturation values (SS). (See Table 1)

Table 1: Comparisons in CCN number concentrations (unit: /cm^3) before and after NPF events.

SS	0.1%		0.3%		0.7%	
DOY	B	E	B	E	B	E
157	419	913	1510	2696	2923	5982
158	542	1054	1313	3798	2298	6508
159	800	1277	2592	3651	4941	6794

As shown in Fig. 1, the HGF of 50-165 nm particles increased from 1.2 to 1.5 during NPF event. This is most likely due to that pre-existing particle gets aged quickly in a photochemically active environment associating with NPF. Both condensation of H_2SO_4 and aging of organic fraction (as indicating by increase in OS) could lead to increase in particle hygroscopicity. Correspondingly, their ability to act as CCN enhanced even though the NPF did not grow to CCN size during this timeframe. During nighttime, particles grew quickly due to condensation of organic vapors. At the same, the particle HGF declined significantly. As consequence, the ability of particles acting as CCN activity decreased significantly. Typically H_2SO_4 concentration is close zero during nighttime. Thus, the semi-volatile organic condensation plays a key role in particle growth. More organics condensed onto newly formed CCN-sized particles and higher supersaturations are needed to activate particles with the same size. This process weakened the contribution of NPF to CCN. But, the net effect leads to increase in CCN concentration, as listed in Table 1. More analysis for a longer-data set at Melpitz site, are ongoing and will be discussed in our presentation. *Petters, M.D. and Kreidenweis, S.M. (2007). Atmos.Chem. Phys., 7, 1961-1971.; Kerminen, et al., 2012, Atmos. Chem. Phys., 12, 12037-12059.; Kroll et al., 2011, Nature Chemistry 3,133–139.*

NanoShip: Are there any new particle formation events over the North Sea?

N. Kelbus[1,2], A. Massling[3], R. Lange[4], M. Fiebig[5], B. Henzing[6], M. Glasius[4], M. Bilde[4], Q. T. Nguyen[4], M. Moerman[6], G. de Leeuw[6,7,8], M. Dal Maso[7], Niku Kivekäs[2,8] and A. Kristensson[2]

[1]Dept. of Physical Geography and Ecosystem Sci., Lund University, P. O. Box 118, SE-221 00 Lund, Sweden
[2]Department of Physics, Lund University, P. O. Box 118, SE-221 00 Lund, Sweden
[3]Department of Environmental Science, Aarhus University, P. O. Box 358, DK-4000 Roskilde, Denmark
[4]Department of Chemistry, Aarhus University, Langelandsgade 140, DK-8000 Aarhus, Denmark
[5]Norwegian Institute for Air Research (NILU), NO-2007 Kjeller, Norway
[6]TNO, Princetonlaan 6, P.O.Box 80015, 3508TA Utrecht, the Netherlands
[7]Department of Physics, University of Helsinki, P. O. Box 64, FI-00014, Helsinki, Finland
[8]Finnish Meteorological Institute FMI, P.O. Box 503, FI-00101 Helsinki, Finland

Keywords: SMPS, DMPS, nucleation, shipping emissions
Presenting author email: natalia.kelbus@gmail.com

Over the continents, we are familiar with frequent formation of new nanometer-sized particles in the atmosphere, called "new particle formation" (NPF) (Kulmala et al., 2004). After subsequent condensation growth, the nanoparticles become large enough to be optically active and to impact on cloud formation, and thereby climate. In the marine boundary layer of pristine oceans, NPF events are not frequent (Pirjola et al., 2000). In the NanoShip project we investigate for the first time whether NPF events take place in a polluted marine boundary layer, like the North Sea considering ship traffic being the source for relevant precursors involved in the NPF.

During the NanoShip project, particle number size distribution measurements were carried out at a marine site (Høvsøre) at the Danish peninsula Jutland during 2012 to investigate the link between formation events and winds from the North Sea. Also archived data from the Norwegian and Dutch EUSAAR sites Birkenes and Cabauw were used to infer the appearance and frequency of formation events during conditions with winds from south-east and north-west, respectively.

We can infer where the formation of 1.5 nm diameter particles takes place by using the particle number size distribution data from Høvsøre and meteorological back trajectories according to the NanoMap method described by Johansson et al. (2012).

The NanoMap method can basically be described as follows (example): We hypothetically see that formation of 1.5 nm diameter particles is taking place between 10:00 and 12:00 am at Høvsøre, and that these particles grow to 30 nm in diameter after 7 to 9 hours. Hence, the 30 nm particles that we observe at Høvsøre in the evening have been formed 7 to 9 hours ago upwind of the site. With the back trajectories we trace the air back to when the particles were formed as 1.5 nm diameter particles somewhere over the North Sea.

In total, 82 days were classified according to the Dal Maso et al. (2005) classification, and during 41 % of these days there was a NPF event, and 17% of the days were a type 1 event. Only type 1 events were used in the NanoMap analysis. Figure 1 shows the location of particles with predicted diameters of 1.5 nm (preliminary results) from the NanoMap analysis for the 14 days with type 1 NPF events at Høvsøre.

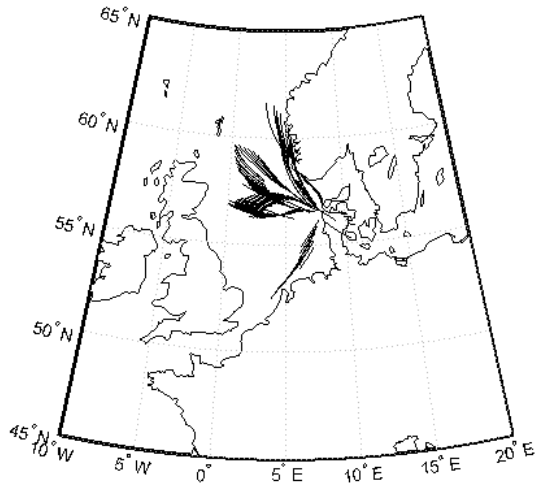

Figure 1. The location of new particle formation of 1.5 nm diameter particles (black lines) according to the NanoMap method and particle number size distribution data recorded at Høvsøre (56°27' E, 8°09' N, 2 m a.s.l).

We can conclude that NPF events are taking place frequently over the North Sea. The favourable conditions are preferably when we have cyclonic, low pressure air masses reaching the Danish marine site.

At the EAC conference, we intend to present in addition, an analysis of EMEP emission maps, aerosol condensation sinks, and if certain meteorological conditions or aerosol sources, like shipping are favouring the NPF over the North Sea.

This work was supported by the Swedish Research council FORMAS under grant 2010-850.

Johansson, M., et al. (2012) *Proceedings of the EAC 2012*, Grenada, September 2012, Spain.
Kulmala, M., et al. (2004) *Aer. Sci.*, **35**, 143-176.
Pirjola, L., et al. (2009) *J. Geoph. Res.*, ***105***, 26531-26546.

Onset of new particle formation in boundary layer

H. E. Manninen[1,2], S. Mirme[2], M. Ehn[1,3], K. Leino[1], S. Schobesberger[1], H. Junninen[1], E. Järvinen[1], J. Kangasluoma[1], T. Nieminen[1,4], R. Tillmann[3], F. Angelini[5], G. P. Gobbi[5], A. Mirme[2], S. Decesari[6], A. Wahner[3], T. Petäjä[1], D. R. Worsnop[1,7], F. Rohrer[3], T. F. Mentel[3] and M. Kulmala[1]

[1]Department of Physics, University of Helsinki, P.O. Box 64, 00014, Helsinki, Finland
[2]Institute of Physics, University of Tartu, Ülikooli 18, 50090, Tartu, Estonia
[3]Institute for Energy and Climate Research (IEK-8), Forschungszentrum Jülich, 52425 Jülich, Germany
[4]Helsinki Institute of Physics, P.O. Box 64, 00014 University of Helsinki, Finland
[5]Institute of Atmospheric Sciences and Climate, ISAC-CNR,
Via Fosso del Cavaliere 100, 00133, Rome, Italy
[6]Institute for Atmospheric Sciences and Climat, ISAC-CNR,
via Gobetti 101, 40129 Bologna, Italy
[7]Aerodyne Research Inc, Billerica, MA 01821, USA
Keywords: atmospheric aerosols, new particle formation, boundary layer, PEGASOS project.
Presenting author email: hanna.manninen@helsinki.fi

The planetary boundary layer (PBL) is chemically and physically the most dynamic part of the atmosphere as it has high loading of aerosol particles and their gaseous precursors. Secondary formation of atmospheric aerosol particles, so-called new particle formation (NPF), is believed to be the dominant source of aerosol particles in the atmosphere. Nucleation is a process of gas-to-particle conversion, beginning with a few gas molecules colliding to form a cluster of 1-2 nm in diameter (Kulmala et al. 2013). This first step of NPF is followed by the growth of the newly formed particles.

At this moment, the mechanisms of particle formation and the vapors participating in this process are not truly understood. Especially, in which part of the atmosphere the NPF takes place, is still an open question. To detect directly the very first steps of NPF in the atmosphere, we measured these chemical and physical processes within the PBL (altitudes up to 1 km). We used airborne Zeppelin measurements and ground based in-situ measurements. Using Zeppelin, we focused on the time of the development of the PBL from sunrise until noon to measure vertical profiles of aerosol particles and chemical compounds.

We have measured the vertical and the horizontal extension for NPF events using an instrumented airship, Zeppelin. The vertical profile measurements represent the particle and gas concentrations in the lower parts of the atmoshere: the residual layer, the nocturnal boundary layer, and the PBL. At the same time, the ground based measurements records present conditions in the surface layer. Horizontal, almost Lagrangian, experiments are possible as the airship drifts with the air mass.

The key instruments to measure the onset of NPF were Atmospheric Pressure interface Time-Of-Flight mass spectrometer (APi-TOF, Junninen et al. 2010), a Particle Size Magnifier (PSM, Vanhanen et al. 2011), and a Neutral cluster and Air Ion Spectrometer (NAIS, Mirme and Mirme, 2011). These instruments are able to measure particles at the size range ~1-2 nm where atmospheric nucleation and cluster activation takes place (Kulmala et al. 2013). The high time resolution of the instruments allowed us to observe the starting time of the NPF events. In addition, particle number size distributions from 1 nm to 1 µm, and concentration of NO, NO_x, O_3, CO, OH, HO_2, and lifetime of OH were measured, as well as meteorological parameters.

On June 2012, Zeppelin was measuring nucleation occuring in the Po Valley area, Nothern Italy, especially over the San Pietro Capofiume (SPC) field site. The newly formed particles were observed some hours after sunrise at ground level in SPC. The onset of NPF was usually observed onboard Zeppelin when it was measuring inside the rising mixed layer which is connected to the surface layer by effective vertical mixing. This observation suggests that the onset of NPF starts in the surface layer, and not in nocturnal boundary layer nor inside the residual layer. The newly formed, subsequently growing, particles were observed to be homogeneously distributed inside the mixed layer.

These measurements are part of the PEGASOS project which aims to quantify the magnitude of regional to global feedbacks between the atmospheric chemistry and physics, and thus quantify the changing climate. The Zeppelin flights are observing radicals, trace gases, and aerosols inside the lower troposphere over Europe. The main nucleation campaigns were performed in Po Valley (summer 2012), and Hyytiälä, Southern Finland (spring 2013). The results will support the numerical air-quality and climate modelling.

This research is supported by European Commission under the Framework Programme 7 (FP7-ENV-2010-265148), the Academy of Finland Centre of Excellence program (project no. 1118615) and the Finnish Cultural Foundation. The Zeppelin is accompanied by an international team of scientists and technicians who are all acknowledged.

Junninen H. et al. (2010) *Atmos. Meas. Tech.* **3**, 1039–1053.
Kulmala M. et al. (2013) *Science* **339**, 943–946.
Mirme S. and Mirme A. (2011) *Atmos. Meas. Tech. Discuss.*, **4**, 7405-7434.
Vanhanen J. et al. (2011) *Aerosol Sci. Tech.* **45**, 533–542.

Events of increased particle number concentrations around trade wind cumuli near Barbados

B. Wehner[1], F. Ditas[1], A. Wiedensohler[1] and H. Siebert[1]

[1]Leibniz Institute for Tropospheric Research (TROPOS), 04318 Leipzig, Germany
Keywords: new particle formation, clouds, ultrafine particles.
Presenting author email: birgit@tropos.de

Beside numerous measurements at ground-based stations, new particle formation has been occasionally observed in higher altitudes of the troposphere. However, such measurements are rare and thus the relevant processes and meteorological conditions under which particle formation and growth occur are still not completely understood.

In November 2010 and April 2011 the CARRIBA (**C**loud, **A**erosol, **R**adiation, and Tu**R**bulence in the trade w**I**nd regime over **BA**rbados) campaign (Siebert et al., 2012) has been performed to observe the role of aerosol particles within the life cycle of trade wind cumuli. During these campaigns more than 30 research flights using the helicopter-borne platform ACTOS (Airborne Cloud and Turbulence Observation System) have been done. For measuring aerosol particles a new FastCPC (Wehner et al., 2011) has been implemented on ACTOS to measure the total particle number concentration *N* with a time resolution of 10 Hz. The aerosol particle number size distribution from 6 nm to 2.5 µm was measured using an SMPS (designed by TROPOS) and an OPC (Model 1.129, Grimm Aerosol Technik, Ainring, Germany). Furthermore, ACTOS contains various instruments to measure cloud properties and thermodynamic parameters, such as temperature, humidity and wind vector.

Results & Discussion

The flight pattern of the individual flights started usually with a vertical profile over the sea east of the island of Barbados. After that ACTOS was usually carried to a field of shallow cumuli with typical cloud cover of 10 to 30%.

During individual flights, *N* was nearly constant around clouds about a few hundred cm^{-3}. During approximately 70 % of all flights one or more events with significantly increased (more than a factor of 5) values of *N* have been observed. These events were often connected to clouds, i.e. the number concentration increased close to cloud edges. However, in a few cases there was no cloud influence visible.

Figure 1 shows an example for increased particle number concentrations near cumulus clouds. The liquid water content (LWC) is used as cloud indicator. Here, the background value of *N* is around 300 cm^{-3}, while some peaks reach values above 4000 cm^{-3} near a cloud. Anthropogenic pollution as particle source can be excluded because the concentration of CO_2 did not show any increase in these regions.

Figure 1 shows no obvious correlation between specific humidity *r* or vertical wind speed *w* and observed increased particle number concentration. This is similar to most other cases and a more detailed analysis needs to be done.

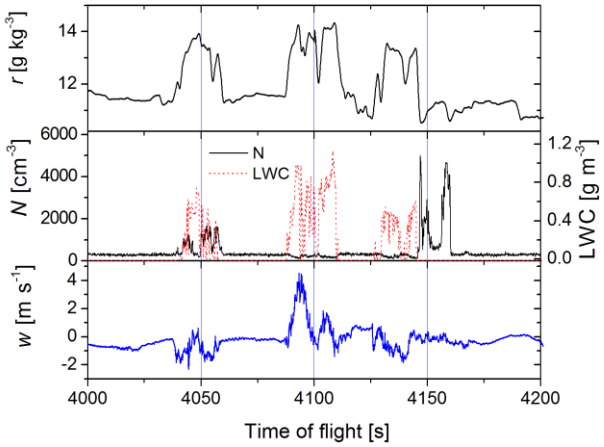

Figure 1. Time series of specific humidity *r*, total particle number concentration *N*, liquid water content LWC, and vertical wind speed *w*.

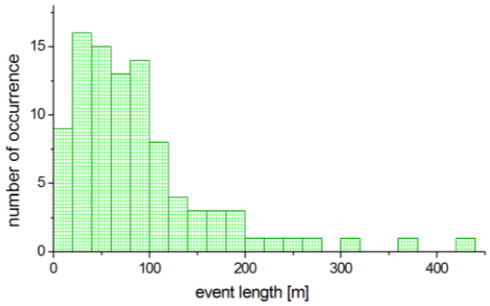

Figure 2. Length of events of increased *N*.

After a quality check, 95 events of increased particle number concentrations have been detected. Most of them occur close to cloud edges (~95%) others without any cloud nearby. More than 50% of them lasted between 1 and 5 s corresponding to a horizontal extension between 20 and 100 m. The detection of such small regions was possible due to the combination of the low true airspeed of 20 m/s and the fast measuring instrumentation. The implication of such particle bursts for further cloud development is not yet fully understood. In conclusion, the cloud system does not only act as a particle sink for CCN but also as a particle source. The relevance of new particle formation for the particle balance in general will be part of an on-going discussion.

This work was supported by the Deutsche Forschungsgemeinschaft (SI 1534/3-1 and WE 1900/18-1).

Siebert, H., et al. (2012), The fine-scale structure of the trade wind regime over Barbados - An introduction to the CARRIBA project -, *Atmos. Chem. Phys. Discuss.*, *12*, 28609 - 28660.

Wehner, B., et al.: Characterization of a new fast mixing type CPC and its application for atmospheric particle measurements, Atmos. Meas. Tech., 4, 822 - 833, 2011.

Characteristics of new particle formation events in Hungarian background air at K-puszta, 2008-2012

Zs. Bécsi[1], Á. Molnár[2], K. Imre[2] and P. P. Aalto[3]

[1]Department of Earth and Environmental Sciences, University of Pannonia, Veszprém, P.O. Box 158, H-8201, Hungary
[2]MTA-PE Air Chemistry Research Group, University of Pannonia, Veszprém, P.O. Box 158, H-8201, Hungary
[3]Department of Physics, University of Helsinki, Helsinki, P.O. Box 64, FI-00014, Finland
Keywords: aerosol, formation, growth, seasonality.
Presenting author email: becsi.zsuzsanna@gmail.com

Fine aerosol particles have been studied in the last years due to their important role in several atmospheric processes and effects on climate and human health. New particle formation events are observed all over the world both in polluted and clean, background air. Similarly, in Hungary NPF events can be detected in polluted cities like Budapest (Salma *et al* (2011), Borsós *et al* (2012)) as well as in rural air at K-puszta (Yli-Juuti *et al* (2009)). Our former results showed that at K-puszta new particle formation (NPF) can be frequently observed, the number of NPF events peaked in spring and autumn (September) per each year.

In this work we summarize our results on the particle formation at K-puszta station between Nov. 2008 and Dec. 2012. The size distribution of the particles between 3-800 nm is evaluated. On the basis of DMPS spectra the classification of particle formation events is carried out according to the recommendations of Yli-Juuti *et al* (2009). The event classification is studied with respect to the seasonal variation and the frequency of the particle formation event types (event, non-event and unclassified) is also discussed.

Figure 1. Event classification statistics (2012), K-puszta.

Generally, our four year statistics on new particle formation (NPF) shows that winter is the most inactive period. In contrast the number of NPF events was found to be the highest in spring and in autumn as presented for 2012 (Figure 1). As a consequence of the above-mentioned seasonal variation of the NPF events, the frequency of the nucleation mode (3-25 nm) was the highest during spring and autumn (Figure 2). On the other hand, in winter the accumulation mode (100-800 nm) showed the highest, while in spring and summer the lowest frequency. This seasonality is also shown by the "typical" seasonal number size distributions. This means that in spring the freshly formed particles, while in winter the aged particles characterize the aerosol size distribution.

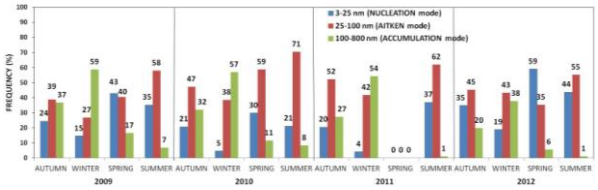

Figure 2. The seasonal frequency of the maximum concentrations in different particle modes (2009-2012).

The growth rate (GR) of the freshly formed particles is also calculated (Hirsikko *et al* (2005), Yli-Juuti *et al* (2009)). Our results on four-year data showed the high variability of particle GR with no significant seasonal variation at K-puszta. The rates were estimated between a few and 14 $nmhr^{-1}$ except some days with higher GR (between 16.5-18.41 $nmhr^{-1}$). The average GR was 5.85 $nmhr^{-1}$. On the other hand, the formation intensity of new nucleation mode particles (smaller than 25 nm) is also estimated. The calculation is based on the method considering the change of the particle number concentration in each size modes per unit time. The average formation rate for 10 nm particle size range was found between 0.33-46.31 particles $cm^{-3}sec^{-1}$.

The research leading to these results has received funding from the European Union Seventh Framework Programme (FP7/2007-2013) under grant agreement n° [262254], [ACTRIS]; and TÁMOP-4.2.2.A-11/1/KONV-2012-0064 (The project is realized with the support of the European Union, with the co-funding of the European Social Fund).

Salma, I., Borsós, T., Weidinger, T., Aalto, P., Hussein, T., Dal Maso, M. and Kulmala, M. (2011) *Atmos. Chem. Phys*., **11**, 1339–1353.

Borsós, T., Řimnáčová, D., Ždímal, V., Smolík, J., Wagner, Z., Weidinger, T., Burkart, J., Steiner, G., Reischl, G., Hitzenberger, R., Schwarz, J., Salma, I. (2012) *Sci. Total Environ.* **433,** 418–426.

Yli-Juuti, T., Riipinen, I., Aalto, P.P., Nieminen, T., Maenhaut, W., Janssens, I.A., Claeys, M., Salma, I., Ocskay, R., Hoffer, A., Imre, K. and Kulmala, M. (2009) *Boreal Env. Res.* **14**, 683-698.

Hirsikko, A., Laakso, L., Hõrrak, U., Aalto, P., Kerminen, V.-M. and Kulmala, M. (2005) *Boreal Env. Res.* **10**, 357-369.

Tuesday, September 3, 2013

Session: Aerosol Chemistry
Chemistry of organic aerosols 2

Novel smog chamber studies of wood burning emissions at low temperatures

E.A. Bruns[1], I. El Haddad[1], S.M. Platt[1], B. Temime-Roussel[2], D. Kilic,[1] Slowik, J.G.[1], A. Detournay[2], G. Močnik[3], N. Marchand[2], U. Baltensperger[1] and A.S.H. Prévôt[1]
[1]Laboratory of Atmospheric Chemistry, Paul Scherrer Institut, Villigen, 5232, Switzerland
[2]Laboratoire Chimie Provence, Equipe Instrumentation et Réactivité Atmosphérique, Universités d'Aix-Marseille-CNRS, UMR 6264, Marseille, 13331, France
[3]Aerosol d.o.o, Kamniška 41, 1000 Ljubljana, Slovenia
Keywords: wood burning, organic aerosol, black carbon, smog chamber.
Presenting author email: emily.bruns@psi.ch

Complete aerosol characterization is critical to understand aerosol influences on climate, air quality and health. Domestic wood burning is a significant source of atmospheric aerosols (Lanz et al., 2010), particularly in the winter, as it is a common heating method. Nevertheless, uncertainties remain in the magnitude and characteristics of wood burning emissions, including their chemical composition and optical properties.

In addition to directly emitted primary emissions, previous laboratory experiments have shown that oxidation of gas phase biomass emissions produces compounds with sufficiently low volatility to readily partition to the particles to form secondary organic aerosol (SOA). However, the total organic aerosol mass (OM) formed relative to black carbon (BC) tends to be lower than that observed in the atmosphere from biomass burning (Grieshop et al., 2009a,b; Heringa et al., 2011). This may be because previous laboratory studies were conducted at higher-than-ambient winter temperatures. This may affect both burner operation and gas/particle partitioning of semi-volatile organic aerosol, both of which may affect aerosol composition and loading.

We report results from experiments characterizing primary and secondary wood burning emissions performed at representative winter temperatures for the first time using a newly designed smog chamber capable of conducting photochemical experiments at low temperatures. Primary wood burning emissions were diluted to atmospherically-relevant concentrations (~5-120 μg/m^3) and injected into the chamber (7 m^3) using a heated inlet system. Formation and aging of secondary products was initiated by OH photochemistry. The effects of temperature and humidity were studied by performing experiments at 263 K and 288 K and at 50% and 90% relative humidity. The effect of wood loading in the stove was also studied.

Chemical composition and quantification of the non-refractory aerosol fraction was determined by high resolution aerosol mass spectrometry. Aethalometers were utilized with and without a thermal desorber to quantify BC and to examine the effects of organic coatings on BC optical properties. Measurements of gas phase species were made with a suite of instruments, including a proton transfer reaction mass spectrometer, to gain insight into the partitioning of compounds between the gas phase and particles with aging.

Conducting experiments at 263 K resulted in higher OM/BC ratios for the primary emissions (1.5-14) compared to experiments at 288 K (0.3-0.8) and better agreement with ambient measurements (OM/BC~7-19). (Szidat et al., 2006 and references within; Gianini et al., 2012). Also, lower temperatures enhanced the SOA/BC ratios. (Figure 1)

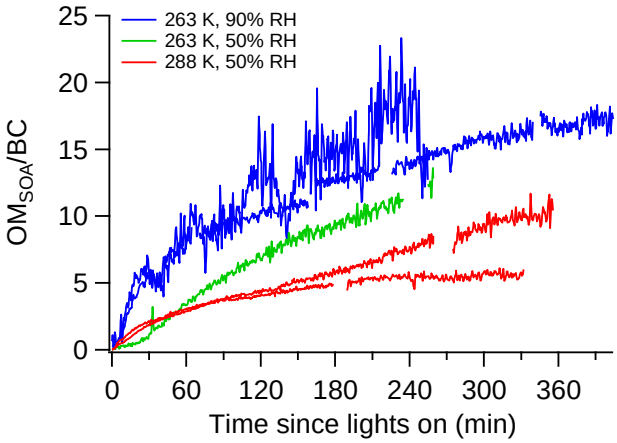

Figure 1. The ratio of SOA to BC during aging as a function of temperature and relative humidity.

These results are important in reconciling discrepancies between field and laboratory measurements. Total hydrocarbon and OH exposure will allow for consistent comparisons between experiments.

High fuel loading was found to generate significantly more polycyclic aromatic hydrocarbon (PAH) compared to average loadings and to produce considerable amounts of SOA after oxidative aging. As PAHs and their oxidation products are known to have deleterious effects on health, this is a significant finding to aid in the mitigation of negative wood burning impacts by improving burner operation protocols.

This work was supported by the PSI-FELLOW/COFUND program, the Competence Center Environment and Sustainability of the ETH Domain and the Swiss National Science Foundation.

Gianini, M.D.F., et al. (2012) *Atmos. Chem. Phys.* **54**, 149-158.
Grieshop, A.P., et al. (2009a) *Atmos. Chem. Phys.* **9**, 1263-1277.
Grieshop, A.P., et al. (2009b) *Atmos. Chem. Phys.* **9**, 2227-2240.
Heringa, M.F., et al. (2011) *Atmos. Chem. Phys.* **11**, 5945-5957.
Lanz, V.A., et al. (2010) *Atmos. Chem. Phys.* **10**, 10453-10471.
Szidat, S., et al. (2006) *J. Geophys. Res.* **111**.

Atmospheric reactivity of biomass burning emitted compounds: methoxyphenols OH rate constants and Secondary Organic Aerosol formation

A. Lauraguais[1,2], C. Coeur-Tourneur[1,2], A. Cassez[1,2], J.C.Wenger[3], A. Seydi[4], K. Deboudt[1,2], M. Fourmentin[1,2], and M. Choël[1,5]

[1] Université Lille Nord de FRANCE, Lille, Nord-Pas-de-Calais, 59000, France
[2] Laboratoire de Physico-Chimie de l'Atmosphère, Université du Littoral Côte d'Opale, Wimereux, 62930, France
[3] Department of Chemistry and Environmental Research Institute, University College Cork, Cork, Ireland
[4] University of Cheikh Anta Diop, Dakar, Sénégal
[5] LAboratoire de Spectrochimie Infrarouge et Raman, UMR CNRS 8516, Université Lille 1, Villeneuve d'Ascq Cedex, Nord-Pas-de-Calais, 59655, France.

Keywords: methoxyphenols, OH reaction, rate coefficient, SOA.
Presenting author email: amelie.lauraguais@univ-littoral.fr

Methoxyphenols are low molecular weight semi-volatile polar aromatic compounds produced from the pyrolysis of wood lignin.

The atmospheric reactivity of methoxyphenols (2-methoxyphenol or guaiacol, 3-methoxyphenol, 4-methoxyphenol, 2-methoxy-4-methylphenol and 2,6-dimethoxyphenol or syringol) with hydroxyl radical has been studied in a simulation chamber (8 m^3) at 294 ± 2 K, atmospheric pressure and dry conditions (RH < 1%).

Their OH rate coefficients, determined using the relative kinetic method, are summarized in table 1 together with their atmospheric lifetime. The atmospheric lifetime of methoxyphenols is around 2 hours, indicating that they are too reactive to be considered as stable tracers for wood smoke emissions.

In the discussion, the reactivity of methoxyphenols will be compared with other substituted aromatics and interpreted in relation to the type, number, and positions of the different substituents on the aromatic ring.

Table 1. Rate coefficients for methoxyphenol reaction with OH radicals (at 294 ± 2 K) and associated atmospheric lifetimes.

Compound	k_{OH} [a]	τ_{OH} [b]	Reference
2-methoxyphenol (guaiacol)	7.53 ± 0.41	2.3	Coeur *et al.* (2010)
3-methoxyphenol	9.80 ± 0.46	1.8	Coeur *et al.* (2010)
4-methoxyphenol	9.50 ± 0.55	1.8	Coeur *et al.* (2010)
2-methoxy-4-methylphenol	9.45 ± 0.59	1.8	Coeur *et al.* (2010)
2,6-dimethoxyphenol (syringol)	9.66 ± 1.11	1.8	Lauraguais *et al.* (2012)

[a] Units of 10^{-11} cm^3 $molecule^{-1}$ s^{-1}.
[b] Units of hour. $\tau_{OH} = 1/k_{OH}[OH]$, where 12 hour daily average [OH] = 1.6×10^6 molecule cm^{-3}.

Secondary organic aerosol formation from the OH reaction with guaiacol and syringol was also investigated under high NO_x conditions. The aerosol production was monitored using a SMPS (Scanning Mobility Particle Sizer). The SOA yields (Y) were determined as the ratio of the suspended aerosol mass corrected for wall losses (M_0) to the total reacted methoxyphenol concentration assuming a particle density of 1.4 g cm^{-3}. For guaiacol and syringol, particle formation was observed in the first few minutes of the reaction, with a very fast increase in the particle number concentration followed by a gradual decrease over the course of the experiment (Fig. 1).

The SOA yields were in the range 0.10-0.36 and 0.003-0.87 for syringol and guaiacol, respectively. Syringol SOA yields were lower than those of guaiacol, likely due to novel methoxy group chemistry that leads to early fragmentation in the gas-phase photooxidation (Yee *et al.*, 2013).

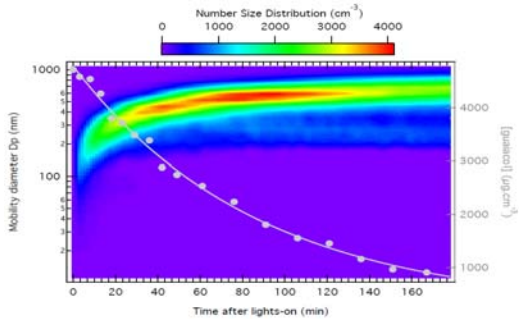

Figure 1. Typical concentration-time profiles for guaiacol and SOA (number-weighted size distribution) from a guaiacol/OH experiment.

SOA formed from the OH reaction with guaiacol have been characterized: 4-nitroguaiacol and 5-nitroguaiacol were clearly identified by GC/MS (Gas Chromatography/Mass Spectrometry), indicating that these compounds may be used as biomass burning aerosol tracers. Complementary analyses were also performed by Transmission (TEM) and Scanning (SEM) Electronic Microscopy: the corresponding pictures show that SOA are in an amorphous state which suggests the formation of oligomers.

This work was supported by the Research Institute of Industrial Environment (IRENI) and the Labex CaPPA (Chemical and Physical Properties of the Atmosphere).

Coeur-Tourneur C., Cassez A., Wenger J.C. (2010) *J. Phys. Chem.A* **114**, 11645-11650.

Lauraguais A., Coeur-Tourneur C., Cassez A., Seydi A. (2012) *Atmos. Environ.* **55**, 43-48.

Yee L.D., Kautzman K.E., Loza C.L., SChiling K.A., Coggon M.M., Chhabra P.S., Chan M.N. *et al* (2013) *Atmos. Chem. Phys. Disc.* **13**, 3485-3532.

Particle-bound Methoxyphenols and their atmospheric nitration products as wood combustion tracers

J. Orasche[1, 2, 3], J. Schnelle-Kreis[1], G. Abbaszade[1, 3], M. Elsasser[1, 2], R. Zimmermann[1, 2, 3]

[1]Joint Mass Spectrometry Centre, Comprehensive Molecular Analytics, Helmholtz Zentrum München, Germany
[2]Joint Mass Spectrometry Centre, Chair of Analytical Chemistry, University of Rostock, Germany
[3]HICE – Helmholtz Virtual Institute of Complex Molecular Systems in Environmental Health – www.hice-vi.eu

Keywords: Methoxyphenols, NO_3-radicals, wood smoke, particulate matter
Presenting author email: juergen.orasche@helmholtz-muenchen.de

In many countries all over the world generation of heating energy wood is still the major source for heating and cooking or has even started a renaissance, respectively. The application of wood is quite cheap but enforces environmental problems and health risks. This indicates, that the question of the linkage between Environment and Health, due to economical reasons, more and more becomes a question of the linkage between Energy and Health.

For elucidation and validation of air polluters, responsible sources must be well indicated by suitable source tracer compounds. Since most of the emitted compounds from wood combustion are highly degradable within the atmosphere, it is worth to examine their atmospheric reaction products, too. Therefore we investigated on methoxyphenols and their reaction products with NO_3-radicals. In a winter sampling campaign in the city of Augsburg, Germany, methoxyphenols and their related products were monitored by high resolution PM_1 filter sampling. By hourly filter changing 24 samples were collected a day. Filters were analyzed with a highly sensitive insitu-derivatization-thermal-desorption gas-chromatography time-of-flight-mass-spectrometry method (IDTD-GC-TOFMS) (Orasche et al. 2011). One step before methoxyphenols were well identified by emission measurements at different combustion conditions within a dilution sampling set-up (e. g. Orasche et al. 2013).

As described by Liu et al. (2012) for reaction chamber experiments a clear dependency of nitration products to NO_3-radicals can be observed. The NO_3 concentrations were related to the increasing NO_x-concentrations during the night time due to missing photo-oxidation-reactions. Figure 1 visualize this relationship between NO_2 and Hydroxynitrobenzene. The rise of concentrations takes place one to two hours later than increase of those of the precursors. Figure 2 shows the correlation between syringaldehyde and 2,6-Dimethoxynitrophenol. It indicates that an additional reaction pathway of syringaldehyde has to be discussed.

The results are indicating that in future source apportionment studies stable secondary organic aerosols (SOA) should be involved to avoid underestimation of specific sources. Moreover the health effects of compounds like the nitrated methoxyphenols have to be investigated carefully.

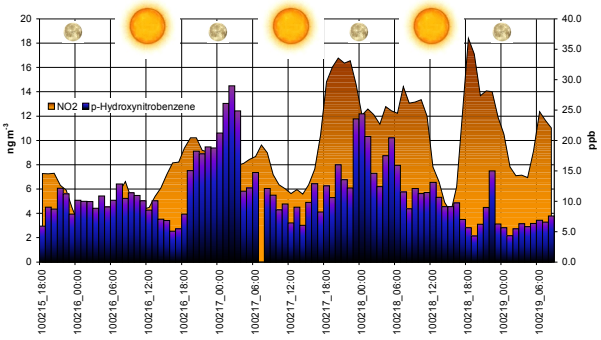

Figure 1. The relationship of p-Hydroxynitrobenzene and NO_2 during day- and night-time.

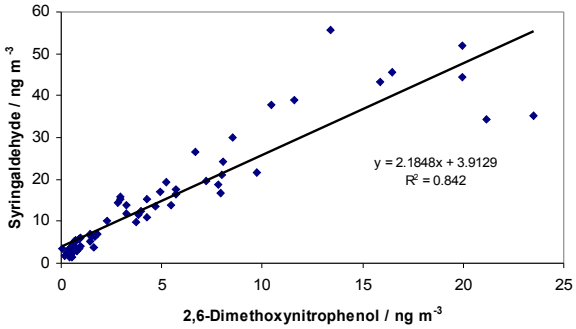

Figure 2. Correlation between Syringaldehyde and 2,6-Dimethoxynitrophenol.

This work was supported by the Helmholtz Virtual Institute of Complex Molecular Systems in Environmental Health (HICE).

Liu, C.; Zhang, P.; Wang, Y.; Yang, B.; Shu, J. In Environmental Science & Technology; American Chemical Society, 2012; Vol. 46, pp 13262-13269.

Orasche, J.; Schnelle-Kreis, J.; Abbaszade, G.; Zimmermann, R. Atmospheric Chemistry and Physics 2011, 11, 8977-8993.

Orasche, J.; Schnelle-Kreis, J.; Schön, C.; Hartmann, H.; Ruppert, H.; Arteaga-Salas, J. M.; Zimmermann, R. Energy & Fuels 2013, *Just accepted*.

Aqueous-phase photochemical oxidation and direct photolysis of vanillin as a model compound of methoxy-phenols from biomass burning

Yong Jie LI[1,#], Heidi H.Y. CHEUNG[1], Dan Dan HUANG[2], Wei Hong FAN[3], Liya E. YU[3], and Chak K. CHAN[1,2,*]

[1]Division of Environment, Hong Kong University of Science and Technology, Clear Water Bay, Hong Kong
[2]Dept. Chem. & Biomole. Eng., Hong Kong University of Science and Technology, Clear Water Bay, Hong Kong
[3]Division of Environmental Science and Engineering, National University of Singapore, Singapore
Keywords: aqueous-phase, SOA, vanillin, biomass.
[#]Presenting author email: lakeli@ust.hk; [*]Corresponding author email: keckchan@ust.hk

Aqueous-phase reactions of organic compounds are an important source of secondary organic aerosol (SOA) (Ervens 2011). Previous laboratory studies focused mostly on small aldehydes such as glyoxal (De Haan 2009; Tan 2009) as precursors, and recently on pinene oxidation products (Lee 2011).

Here we showed experimental results of aqueous-phase reactions of a semi-volatile and slightly water soluble methoxy-phenol from biomass burning, vanillin ($C_8H_8O_3$). Reactions were performed in a vessel (Lee 2011) with UV (254 nm) irradiation under two conditions: (1) photochemical oxidation with H_2O_2 as an OH radical source; and (2) direct photolysis without H_2O_2 added. Solution of the resulted products, as well as the ammonium sulfate added (Lee 2011), was atomized continuously and dried before on-line analyses. An Aerodyne High-resolution Time-of-Flight Aerosol Mass Spectrometer (HR-ToF-AMS) was used to measure the dried particle compositions, and a Hygroscopic Tandem Differential Mobility Analyzer (HTDMA) and a Cloud Condensation Nuclei counter (CCNc) were used to determine the particle growth factor and CCN activity respectively.

Prior to UV irradiation, most of vanillin evaporated to the gas phase during drying and gave negligible organic mass in particles (Figure 1, before time < 0 min). A large amount of SOA was formed and retained after reactions under both conditions, although products might be different under these two conditions according to HR-ToF-AMS characterization (Figure 1). Off-line analyses by liquid chromatography-mass spectrometry (LC-MS) and derivatization prior to gas chromatography-mass spectrometry (GC-MS) also confirmed that the product identities from these two conditions are different. Organic mass first increased rapidly and then decreased under condition (1), but kept increasing slowly under condition (2), as shown in Figure 1A and 1C, respectively. It was found that the degree of oxygenation of products from condition (1) first increased and then decreased, suggesting a competition between functionalization and fragmentation (Kroll 2009; Lee 2011), while it kept decreasing under condition (2). Hygroscopic behavior and CCN activity of ammonium sulfate decreased substantially with the organic products retained in the particles. The resolved growth factor of organics correlated with the increase of degree of oxygenation (O:C ratio) of organics formed.

Our results suggest that aqueous-phase reactions of methoxy-phenolic compounds from biomass burning can retain this portion of carbon mass in the particle phase even after extensive drying/dilution processes. This portion of carbon mass, once retained, significantly alters the particle hygroscopicity and CCN activity, which is not being considered in current climatic and visibility models.

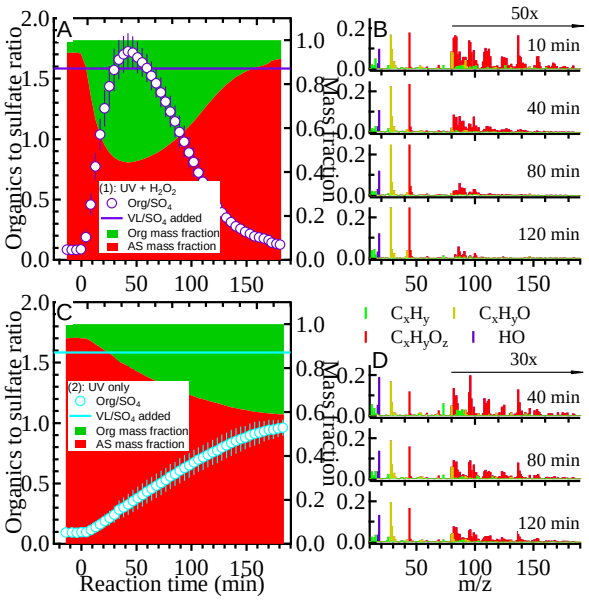

Figure 1. Changes of organic to sulfate ratio, organic mass fraction, and mass spectral feature during reactions under conditions (1) (A and B) and (2) (C and D).

This work was supported by the Research Grants Council (610909), the University Grants Committee (SEG-HKUST07) and the Environmental Conservation Funds (ECF) of Hong Kong (ECWW09EG04).

De Haan, Corrigan, Smith, Stroik, Turley, Lee, Tolbert, Jimenez, Cordova, and Ferrell, *Environ. Sci. Technol.*, 43, 2818-2824, 2009.

Ervens, Turpin, and Weber, *Atmos. Chem. Phys.*, 11, 11069-11102, 2011.

Kroll, Smith, Che, Kessler, Worsnop, and Wilson, *Phys. Chem. Chem. Phys.*, 11, 8005-8014, 2009.

Lee, Herckes, Leaitch, Macdonald, and Abbatt, *Geophys. Res. Lett.*, 38, L11805, doi: 11810.11029/12011gl047439, 2011.

Tan, Perri, Seitzinger, and Turpin, *Environ. Sci. Technol.*, 43, 8105-8112, 2009.

Secondary organic aerosol formation through aqueous phase photooxidation of aromatic compounds

Zoran Kitanovski[1], Irena Grgić[1], Alen Čusak[2] and Magda Claeys[3]

[1]Laboratory for Analytical Chemistry, National Institute of Chemistry, SI-1000 Ljubljana, Slovenia
[2]EN-FIST Center of Excellence, SI-1000 Ljubljana, Slovenia
[3]Department of Pharmaceutical Sciences, University of Antwerp, BE-2610 Antwerp, Belgium

Keywords: aqueous phase atmospheric chemistry, biomass burning aerosol, guaiacol, secondary organic aerosol
Presenting author email: irena.grgic@ki.si

Secondary organic aerosol (SOA) formed through the gas-phase oxidation of volatile organic compounds (VOCs) and further gas-to-particle partitioning cannot explain the gap between atmospheric observations and model predictions of organic aerosols (Heald *et al*., 2005). However, there is growing evidence that reactions in atmospheric waters may represent an additional and important source of SOA (Lim *et al*., 2010). Formation of low-volatility products in the aqueous phase has been observed during reactions of carbonyl and monoaromatic compounds found in the atmosphere (Ervens *et al*., 2011; Sun *et al*., 2010).

Monoaromatic compounds can be considered as a proxy for anthropogenic and biomass burning emissions. Methyl-nitrocatechols have been identified as an important class of SOA compounds from biomass burning and proposed as suitable tracers (Iinuma *et al.*, 2010; Kitanovski *et al*., 2012). In addition to nitro-catechols, other nitro-aromatics were determined in urban winter aerosols (Fig. 1), and constitute nearly 1% of the organic carbon (Kitanovski *et al*., 2012). A noticeable unknown peak consistent with a nitroguaiacol isomer was also detected in the latter study.

In the present study, the formation of SOA through aqueous-phase photooxidation (and nitration) of guaiacol (2-methoxyphenol), known to be emitted upon biomass burning, was studied. The main objectives were to chemical characterize the low-volatility products and examine their possible presence in ambient aerosols.

The aqueous phase reactions were performed in a thermostated reactor under well-defined experimental conditions. A solution of guaiacol was exposed to simulated sunlight (Xenon lamp, 300 W) in the presence of H_2O_2 (source of OH radicals) and NO_2^-. After isolation of the main reaction products by solid-phase extraction (SPE), their chemical structures were elucidated. To this aim, the SPE extract was first subjected to semi-preparative liquid chromatography, after which the main products were fractionated and isolated. Nuclear magnetic resonance spectroscopy (NMR) and liquid chromatography/negative ion electro-spray ionization tandem mass spectrometry (LC/(−)ESI-MS/MS) were used for structural elucidation.

The main products of guaiacol photooxidation and nitration are two nitroguaiacols (4-nitroguaiacol, 4NG; and 6-nitroguaiacol, 6NG) and one dinitroguaiacol (4,6-dinitroguaiacol, 4,6DNG). In addition, several minor phenolic oxidation products and oligomers of guaiacol and nitroguaiacol were formed. Using the isolated compounds as standards, several guaiacol products were identified in ambient PM10 from the city of Ljubljana (Slovenia) by means of LC/(−)ESI-MS/MS.

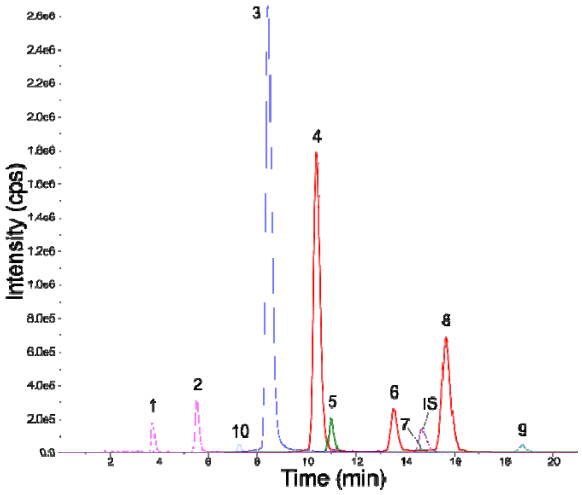

Figure 1. Selected reaction monitoring chromatograms for a winter sample (17/12/2010; PM_{10} mass conc. = 60 μg m^{-3}): 3NSA (**1**), 5NSA (**2**), 4NC (**3**), 4M5NC (**4**), 4NP (**5**), 3M6NC (**6**), 3M4NP (**7**), 3M5NC (**8**), 2M4NP (**9**), unknown nitroguaiacol (**10**), and picric acid (**IS**) (Kitanovski *et al.*, 2012).

This work was supported by the Slovenian Research Agency (Contract no. P1-0034-0104 and BI-BE/11-12-F-012).

Ervens, B., Turpin, B.J. and Weber, R.J. (2011) *Atmos. Chem. Phys.* **11**, 11069-11102.
Heald, C.L. *et al*. (2005) *Geophys. Res. Lett.* **32,** L18801.
Iinuma, Y., Böge, O., Gräfe, R. and Herrmann, H. (2010) *Environ. Sci. Technol*. **44**, 8453-8459.
Kitanovski, Z., Grgić, I., Vermeylen, R., Claeys, M. and Maenhaut, W. (2012) *J. Chromatogr. A* **1268,** 35-43.
Lim Y.B., Tan, Y., Perri, M.J., Seitzinger, S.P. and Turpin, B.J. (2010) *Atmos. Chem. Phys.* **10**, 10521-10539.
Sun, Y.L., Zhang, Q., Anastasio, C. and Sun, J. (2010) *Atmos. Chem. Phys.* **10**, 4809-4822.

Photosensitized reactions at the air-sea interface: a potential source of aerosol

R. Ciuraru, F. Bernard, S. Rossignol, L. Fine, C. George

Université de Lyon, Université Lyon 1, CNRS, UMR5256, IRCELYON, Institut de recherches sur la catalyse et l'environnement de Lyon, Villeurbanne, F-69626, France
FranceKeywords: multiphase chemistry, sea-surface microlayer, volatile organic compounds
Presenting author email: raluca.ciuraru@ircelyon.univ-lyon1.fr

The sea surface microlayer is the organic-enriched layer present at the air-sea interface which has different physical and chemical properties compared to subsurface waters. The chemical analysis of this microlayer is of great interest for many reasons including its major influence to reduce air–sea gas exchange by impeding molecular diffusion across the interface and by influencing the characteristics of water motion at the interface. Surface seawater contains a variety of substances which act as photosensitizers. They include components of the dissolved organic matter known also as humic acids. The sea surface microlayer is the primary recipient of the solar energy. Since the microlayer is enriched in chemicals and biota, a number of processes are likely to be more effective here than in the rest of the water column. These include changes in the chemical composition of the living cells of phytoplankton and the photodegradation of organic matter.

The focus of this study is to determine if the organic film acts as a hydrophobic barrier for the air-sea gas exchange and to identify and characterize the gaseous emissions and aerosol formation from the surface due to the photochemical processing of the sea surface microlayer. For this purpose, synthetic aqueous mixtures of NaCl, NaBr, NaI, photosensitizers (humic acids) containing an organic surfactant (hexanol, octanol, nonanoic acid) have been irradiated by means of a Xe lamp in a small Quartz cell. Potential gaseous products arising from this interfacial chemistry have been identified using a High Resolution Proton Transfer Reaction – Time of Flight Mass Spectrometer.

It has been observed that the presence of a thick organic film on the salt solutions reduces the transfer from the aqueous solution to the gas phase.

Experiments with an organic monolayer coverage at the air / interface led to the formation of a variety of gaseous aldehydes (heptanal, octanal, nonanal, nonenal), alkenes and –dienes (butene, 5-methyl-1, 4-hexadiene) . All these compounds were confirmed by GC/MS analysis. A formation of methylglyoxal and acetylacetone has also been detected. Surprisingly, isoprene formation was also observed under irradiation. Isoprene is being made possible by a specific chemistry occurring solely at the air/water interface and the corresponding mechanism will be presented.

Experiments were also performed with benzophenone, imidazole and 2-imidazolecarboxyaldehyde as photosensitizers and the results will be discussed.

Furthermore, experimental studies in a $2m^3$ multiphase atmospheric simulation chamber will be presented. In this experimental approach, natural or artificial sea water containing a surfactant and a photosensitizer can be irradiated by UV/VIS lamps. But this tool is especially designed to follow the aerosol formation potential of the above mentioned photosensitized reactions at the air/water interface.

Indeed, the photochemical processing of the microlayer will lead to the emission of a series of functionalized VOC which will be measured using a PTR-ToF MS and a GC/MS. The chemical processing of a large subset of these VOCs will lead to the formation of Secondary Organic Aerosols. The physical and chemical properties of these particles will be monitored and characterized by means of a SMPS and an Orbitrap LC/MS measurements.

These results highlight the presence of an undocumented chemistry at the air/water interface having a real potential of affecting the budget of VOCs and SOA loading in the marine boundary layer.

Black Carbon Containing Particles at a Rural Site Southeast of London: ClearfLo Winter IOP Detling Site

L. R. Williams[1], S. Herndon[1], J. Jayne[1], A. Freedman[1], B. Brooks[1], J. Franklin[1], P. Massoli[1], E. Fortner[1], P. Chhabra[1], M. Zahniser[1], H. Stark[1], T. Onasch[1], M. R. Canagaratna[1], D. R. Worsnop[1], F. Lopez-Hilfiker[2], C. Mohr[2], J. Thornton[2], N. L. Ng[3], L. Xu[3], W. B. Knighton[4], M. Dubey[5], A. Aiken[5], K. Gorkowski[5], S. Liu[5], T. Martin[6], R. Coulter[6], S. Visser[7], M. Furger[7], P. Zotter[7], and A. S. H. Prévôt[7]

[1]Aerodyne Research, Inc., Billerica, MA 01821, USA
[2]Department of Chemistry, University of Washington, Seattle, WA 98195, USA
[3]School of Earth and Atmospheric Sciences, Georgia Institute of Technology, Atlanta, GA, 30332, USA
[4]Department of Chemistry and Biochemistry, Montana State University, Bozeman, MT 59717, USA
[5]Earth and Environmental Sciences Division, Los Alamos National Laboratory, Los Alamos, NM, 87545, USA
[6]Environmental Science Division, Argonne National Laboratory, Argonne, IL 60439, USA
[7]Laboratory of Atmospheric Chemistry, Paul Scherrer Institute, Villigen PSI, Switzerland
Keywords: aerosol chemistry, atmospheric black carbon, urban aerosols
Presenting author email: Williams@aerodyne.com

Clean Air for London (ClearfLo) is a large, multidisciplinary study of the London urban atmosphere aimed at understanding the relationships between surface meteorology, gas-phase composition and particulate matter at a city street site, a city background site (away from local traffic sources) and at rural locations that sample the outflow from the London urban area. During the winter intensive (January to February, 2012) we deployed a suite of instruments at a rural site southeast of London in Detling, UK.

Data were collected through several co-located inlets mounted on a 9 m tower. Real-time particle instruments included an Aerodyne high-resolution time-of-flight mass spectrometer (HR-AMS), an Aerodyne soot particle mass spectrometer (SP-AMS), a multi-angle absorption photometer (MAAP), photo-acoustic soot spectrometers (PASS), a scanning mobility particle sizer (SMPS), cavity enhanced phase-shift particle extinction monitors (CAPS PMex), and a single particle soot photometer (SP2). Particle properties were measured with and without a thermal denuder (TD) in order to understand the effect of coatings on optical properties. Bulk particle chemistry was measured with filter samplers and a rotating drum impactor.

Gas phase measurements included air mass tracers (CO, CO_2, O_3, NO_x) and volatile organic compounds using a proton-transfer reaction mass spectrometer (PTR-MS). The micro-orifice volatilization impactor chemical ionization time-of-flight mass spectrometer (MOVI-CI-TOFMS), a recently developed chemical ionization instrument that measures organic acids in both the gas-phase and the particle-phase, was also deployed.

Over the course of the campaign, sampled air masses were of local (A249 motorway 200 m south of the site), regional (London to the northwest, industrial areas north of the site, or Maidstone city southwest of the site) or continental (mainland Europe) origin. Air mass origins were determined from back trajectories calculated by University of Leicester with the UK Met Office NAME dispersion model and from local wind speed and direction.

This talk will focus on black carbon containing particles measured at Detling. The SP-AMS instrument made in situ measurements of the chemical composition and size distributions of black carbon containing particles, both the black carbon component and any coatings. The mass spectra were analyzed with positive matrix factorization (PMF) yielding three factors. The first factor has dominant peaks at m/z 60 and 72, indicative of solid fuel burning. The second factor has a mass spectrum suggesting hydrocarbons, while the third factor has a mass spectrum associated with oxygenated organics and more aged aerosol particles. Figure 1 shows the time trends for the three factors. Time periods that are dominated by one factor are circled in blue and will be discussed in more detail. Connections between the chemical, microphysical, and optical properties of the aerosol particles in the different air masses will be presented.

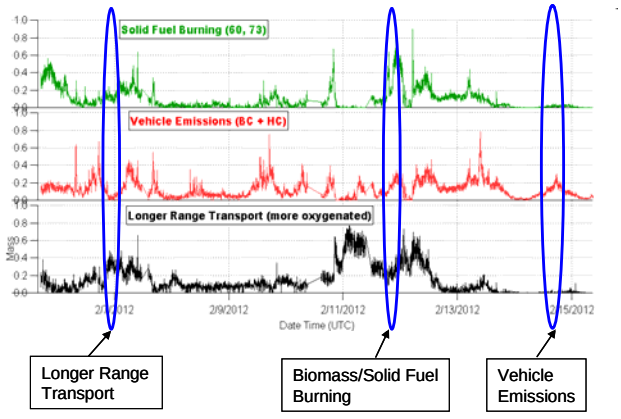

Figure 1. Time trends for PMF factors whose mass spectra suggest solid fuel burning, vehicle emissions and longer range transport sources.

Acknowledgements: This project was supported by the US Department of Energy Atmospheric System Research Program (Award No. DE-SC0006002) and the UK Natural Environment Research Council.

Contribution of Inorganic aerosols and trace gases due to biomass burning during cooking hours at a rural site in India

Sudha Singh*, Gyan Prakash Gupta, Bablu Kumar and U C Kulshrestha
School of Environmental Sciences, Jawaharlal Nehru University
New Delhi, INDIA
Keyword: aerosols, biomass burning, cooking
(*Email: sudha29jan@gmail.com)

Biomass burning is a major source of air pollution which emits a complex mixture of air pollutants in the form of gases and aerosols (Andreae and Merlet, 2001). These have significant impact on atmospheric chemistry, climate change, and human health. But due to lack of measurements across the globe especially from developing countries, aerosol budgets have large uncertainties. There are reports on their emissions from coal combustion and wood burning from USA and Europe but measurements are very limited from developing countries. In India, traditional cooking is still common which contributes large amount of such air pollutants. This study has been carried out as part of UNEP project `Surya' to report chemical characteristics of fine atmospheric aerosols collected during cooking hours in an indoor environment in a village.

Measurements were conducted to determine indoor air pollution due to burning of wood, dung cakes and agriculture residue in rural households in Khairatpur village which is located in district Sultanpur of Uttar Pradesh state of India. Aerosol samples along with gaseous species (NO_2, SO_2, and NH_3) were collected during December 2010-January 2011 by using handy sampler (Envirotech model APM 821) installed inside the house. The samples were collected on 8 hourly basis using Teflon filters. The water extract of these filters was analyzed for major anions (F^-, Cl^-, NO_3^-, SO_4^{2-}) and major cations (Na^+, NH_4^+, K^+, Ca^{2+} Mg^{2+}) by ion chromatography (Metrohm 883 Basic IC Plus).SO_2 was estimated by using ion chromatograph and NO_2 and NH_3 were estimated by using spectrophotometer.

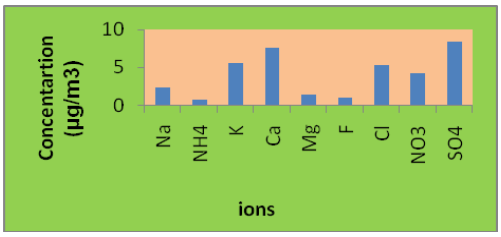

Fig.1 Concentrations (µg/m^3) of major ions during indoor cooking.

Fig.1 is the graphical representation of chemical composition of aerosol samples which indicates that SO_4^{2-} is dominant component followed by K^+, NO_3^-. SO_4^{2-} and Cl^-. Biomass burning is considered as a potential source of K^+ in air and its signature have been reported in Indian region (Kulshrestha et al., 2001). SO_4^{2-} which accounting for about 23% of the all components, is probably produced from the SO_2 emitted from biomass burning during cooking. SO_2 was recorded the highest among other gaseous species. Concentrations of gases are given in the Fig.2.

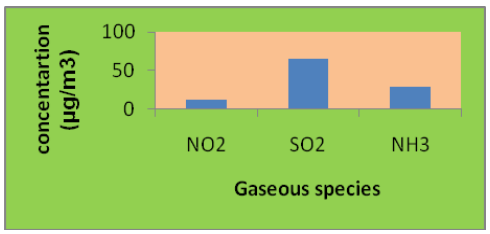

Fig.2 Concentration (µg/m^3) of trace gases during indoor cooking hours.

These findings indicated that a significant amount of aerosols as well as gases are contributed by biomass burning during traditional cooking process in rural India.

Acknowledgement: Authors sincerely thank RRC-UNEP-AIT, DST-PURSE, UGC and JNU for financial support.

References

Andreae, M.O., Merlet, P., 2001. *Emission of trace gases and aerosols from biomass burning*. Global Biogeochemical Cycles 15 (4), 955-966.

U C Kulshrestha, R Sekar, M Vairamani, Monika Jain, A K Sarkar, D C Parashar and A P Mitra. *Signatures of biomass burning over Indian Ocean during INDOEX*. IGAC Symposium, January 21-23, 2001, Bangkok, Thailand.

Tuesday, September 3, 2013

Session: Indoor and Working Place Aerosols
Workplace exposure

Nanoparticle Release from Dental Composites during Restoration Grinding and Polishing

Christof Asbach[1], Bryan Hellack[2], Bart Van Meerbeek[3], Marleen Peumans[3], Peter Hoet[4], Martin Wiemann[5], Thomas A.J. Kuhlbusch[2], Kirsten L. Van Landuyt[3]

[1] Air Quality & Filtration Unit, Institute of Energy and Environmental Technology, 47229 Duisburg, Germany

[2] Air Quality & Sustainable Nanotechnology Unit, Institute of Energy and Environmental Technology, 47229 Duisburg, Germany

[3] KU Leuven BIOMAT, Department of Oral Health Sciences & University Hospitals Leuven, KU Leuven (University of Leuven), B-3000 Leuven, Belgium

[4] Research Unit Experimental Toxicology, Center for Environmental and Health Research, KU Leuven (University of Leuven), B-3001 Leuven, Belgium

[5] IBE R&D gGmbH, 48149 Münster, Germany

Keywords: nanocomposite, dental material, nanoparticle exposure, nanoparticle release.
Presenting author email: asbach@iuta.de

Modern dental composite materials used for tooth restoration are made from a combination of polymer resin with e.g. SiO_2 or ZrO_2 filler particles. In order to be sufficiently strong to withstand chewing and to avoid excessive shrinkage of the composite during polymerization of the resin, the filler particle contents are high, usually >50vol%. While classic dental composites contained filler particles with sizes of several hundred nanometers up to micrometers, current materials typically also contain filler particles below 50nm. When contouring composite restorations using diamond burs, dentists often do not use water-cooling, such that filler particles are released directly into the airborne phase, leading to possible uptake via inhalation by both the dentist and the patient. It was shown in a previous study that release of nanoparticles during polishing or grinding of dental composites is generally possible (Van Landuyt *et al*., 2012). We here present a more thorough study which involved both the measurement of dentists' personal exposure as well as laboratory studies under defined conditions to characterize the particles released from a dental composite during grinding.

To characterize dentists' personal exposure, the number concentration, lung deposited surface area concentration and mean particle size were measured with a miniDiSC. The instrument was sampling through a flexible tube with its inlet placed in the breathing zone of the dentist. Simultaneously, a second miniDiSC instrument was placed approximately 5 m away to monitor particle background. Measurements were performed during extensive restorative/esthetic treatments with the so-called nano-composite Filtek Supreme XTE (3M ESPE), like veneering and total crown build-up of front teeth. Final contouring and finishing of the composite restorations was standardly performed by a diamond bur (roughness of 46-107 µm). Water-cooling and high-flow suctioning using the intra-oral vacuum suctioning device was only occasionally used, according to the standard procedures in the clinic.

The results clearly show that very high concentrations of particles are released during the various mechanical treatment steps of dental composites. The particle number concentrations in the breathing zone showed distinct peaks which could reach up to $>10^6$#/cm³. The concentration spikes usually coincided with a decrease in the mean particle size, indicating that nanoparticles have been released.

In order to better quantify the released material, laboratory measurements were conducted under defined conditions. Five different dental composites were investigated, including a so-called nano-composite (contains only nano-filler) and several (nano-)hybrid composites (contain both large filler and nano-filler particles). Dental composite blocks of defined sizes (17.4mm x 5.4mm x 1.6 mm) were prepared and ground with a rough bur (grain size 100µm), spinning at 200,000 rpm for approximately 2 minutes within an enclosure with low background concentration. The number size distributions of the airborne particles were measured with a Scanning Mobility Particle Sizer (SMPS) and particles sampled for consecutive analyses with an electrostatic precipitator (TSI NAS) with upstream unipolar charger. The investigations revealed that in all cases very high concentrations ($>10^6$ #/cm³) of mostly nanoscale particles were released, which agrees well with the personal exposure measurements. The median diameters of the size distributions during grinding of the different composites ranged from approximately 38 nm to 70 nm, but quickly increased afterwards due to coagulation.

SEM/EDX analyses of the collected samples showed that in some cases single nanoparticles were liberated from the matrix material. In addition the potency of the released material to produce reactive oxygen species (ROS) was measured by electron paramagnetic resonance spectroscopy in order to get an indication on whether the released material is potentially harmful. However, the results showed no increased activity of the material.

Results of the study will be presented and discussed particularly in view of occupational exposure and health risks of dentists.

Van Landuyt KL, Yoshihara K, Geebelen B, Peumans M, Godderis L, Hoet P, *et al*. (2012): Should we be concerned about composite (nano-)dust? *Dental materials : official publication of the Academy of Dental Materials.* **28**:1162-70

Micro and nanoparticles released from the thermal cutting of polystyrene foams and the associated isomerization of hexabromocyclododecane (HBCD) diastereomers

Y.-Y. Kuo[1,2], H. Zhang[3], A.C. Gerecke[1]* and J. Wang[1,2]*

[1]Empa, Swiss Federal Laboratories for Materials Science and Technology, Dübendorf CH-8600, Switzerland
[2] Institute of Environmental Engineering, ETH Zurich, Zurich CH-8093, Switzerland
[3] Dalian Institute of Chemical Physics, Chinese Academy of Sciences, Dalian 116023, China
Keywords: Emission Characterization, Indoor Air Pollution, Thermal Treatment, HBCD
Presenting author email: Yu-Ying.Kuo@empa.ch

Polystyrene foam is widely used as building insulation material, architectural model and packing material. Due to its tendency to depolymerize when exposed to fire temperatures, and to generate volatile products of high fuel values, flame retardant is required to meet fire safety regulation. Hexabromocyclododecane (HBCD) is currently the most important flame retardant to protect polystyrene against ignition. However, HBCD has been listed on the 2010 Environmental Protection Agency action plans due to the fulfilment of regulatory thresholds for a persistent organic pollutant (POP). Therefore, workplace exposure and environmental emission of HBCD should be avoided.

In this study, we investigated the co-release of aerosol particles and HBCD during the thermal cutting of expanded polystyrene foam (EPS) and extruded polystyrene foam (XPS). The generated particles were simultaneously measured by a fast mobility particle sizer (FMPS) and collected by a cascade impactor (NanoMoudi). Further chemical analysis was done by a LC-MS/MS after necessary concentration and purification. In the breathing zone of a cutting worker, the number concentration of aerosol particles was above 1×10^{12} particles m^{-3} in the surrounding of operating location in both of EPS and XPS tests. The air concentration of HBCD was more than 50 μg m^{-3}. Most of the released HBCD was partitioned into particles with an aerodynamic diameter at the nano-meter scale. The average concentrations of HBCD in these submicron particles generated from the thermal cutting of EPS and XPS were 13 times and 15 times higher than the concentrations in raw foams, respectively. (Zhang *et al*, 2012)

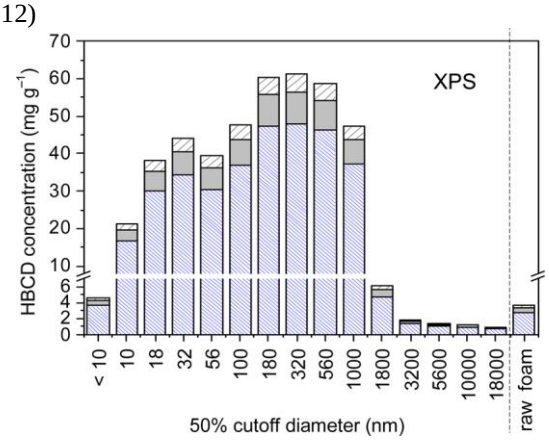

Figure 1. HBCD concentration in raw foams and in size separated particles from thermal cutting of XPS

In the meantime, HBCD underwent isomerization during this process, especially in tests of EPS form. The fraction of the more bio-accumulative α-HBCD increased remarkably, while the fraction of γ-HBCD decreased. The composition of HBCD diasteromers tended to resemble the ratio of thermal equilibrium reported by Peled *et al*. (1995) from the typical technical component. The fraction of HBCD diastereomers is independent from particle size but hugely influenced by the compartment.

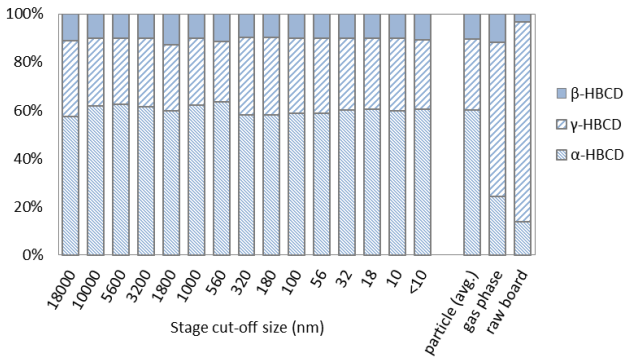

Figure 2. HBCD diastereomer fractions in different compartment and particle sizes in thermal cutting tests of EPS foam.

An occupational exposure assessment indicated that 7×10^7 particles and totally 20 μg of HBCD can deposit into the lung of the operating worker in 1 hour of working time. More than 70% of particles and 60% of HBCD of those would allocate in the alveolar region. This amount of HBCD is equivalent to the total intake of HBCD by an adult during 1−3 months in daily exposure. (Marvin *et al*, 2011)

Zhang, H., Kuo, Y.-Y., Gerecke, A. C. and Wang J. (2012) *Environ. Sci. Technol.* **46**, 10990-10996.

Peled, M., Scharia, R., and Sondock, D. (1995) *Advances in Organobromine Chemistry II* Elsevier Science, 92–99.

Marvin, C. H., Tomy, G. T., Armitage, J. M., Arnot, J. A., McCarty, L., Covaci, A. and Palace, V. (2011) *Environ. Sci. Technol.* **45**, 8613−8623.

Mixed dust exposure and health risk assessment in the ceramics industry

B. Moroni[1], D. Cappelletti[1], F. Scardazza[1], S. Becagli[2], R. Traversi[2], R. Udisti[2]

[1]Department of Civil and Environmental Engineering, University of Perugia, Perugia, 06123, Italy
[2]Department of Chemistry, University of Florence, Sesto Fiorentino, 50019, Italy
Keywords: electron microscopy, ICP-AES, mineralogy, bioavailable iron.
Presenting author email: b.moroni@tiscali.it

Health risk assessment in the ceramics industry traditionally rests upon crystalline silica toxicity and exposure levels (*e.g.*, NIOSH, 2002). Notwithstanding, workers in the ceramics factories may be exposed to a number of potential toxicants, including iron (Fubini and Fenoglio, 2007). Iron, which is a major element in the pastes of clay brick and pottery productions, has been shown to modulate quartz toxicity through enhancing or inhibitory effects depending on surface concentrations (Ghiazza *et al*, 2011). In this paper the nature and properties of quartz and Fe-bearing minerals in clay brick and pottery productions and the possible mutual interactions between them, have been evaluated by means of integrated individual particle characterisation-bulk chemical analyses of both the raw materials and the airborne dust particles.

Aerosol dust samples have been collected from different working stations in different clay brick and pottery factories in Umbria (Central Italy). Individual particle characterization has been performed by means of scanning electron microscopy (SEM) coupled with image analysis and EDS microanalysis (Moroni *et al* 2013). The bulk mineralogical composition has been determined by means of X-ray diffraction (XRD), while the concentration and the solubility degree of Fe in the bulk samples at both neutral (7.2) and acid pH (4.6) have been determined by inductively coupled plasma atomic emission spectrometry (ICP-AES). Distinctive technological features of toxicological interest have been also investigated by means of experimental firing tests on the pastes performed at 950°C (clay brick) and 1050°C (pottery) peak temperature.

Quartz morphology revealed similar grain size and surface morphology in both sectors, and lower values of the shape factor in the clay brick production. Mean values of the exposure doses for quartz in the clay brick and the pottery working environments were evaluated based on the grain size, leading to 84 and 93 $\mu g\ cm^{-2}$, respectively. These values greatly exceed the minimum dose (40 $\mu g\ cm^{-2}$) able to induce significant cytotoxic and inflammogenic effects on cell cultures (Ghiazza *et al.* 2011) although the particle mass concentrations in the factories be lower than the threshold limit value (0.025 $mg\ m^{-3}$). This fact suggests the necessity of employing surface area instead of gravimetric measurements when evaluating quartz occupational exposure.

The mineralogical composition of pastes is similar before firing, with just some more variability in the clay brick, and changes after firing in the pottery for remarkably higher amounts of the amorphous phase. The clay brick pastes, on turn, show lower total iron, and higher soluble iron contents in respect to the pottery pastes. The total iron amounts are mostly related to variable amounts of Fe-bearing clay minerals (mostly chlorite) and ores in the clay brick pastes. The soluble iron contents, on turn, depend on the amounts of the amorphous phase, as the thermal decomposition of Fe-rich silicates such as chlorite produces an amorphous phase which can retain iron and prevent hematite crystallization (Nodari *et al*, 2007). These facts point to the possible role of bioavailable soluble iron in modulating quartz toxicity in the airborne dust as a function of the composition of raw materials and the mineralogical-chemical evolution in the firing process.

Mean values of the Fe/Qz ratio have been estimated based on the values of iron and quartz concentrations in the samples, leading to the following results: $Fe/Qz_{clay\ brick}<0.03$; $Fe/Qz_{pottery} \sim 0.004$ The values obtained for clay brick are in the range of possible adverse health effect (Ghiazza *et al* 2011), while the values for pottery are too low to attain reliable interaction. Results support the evidence of higher incidence of silicosis in the clay brick division (Verdel *et al* 2006), although it should be better to consider the occurrence of mixed dust fibrogenetic processes rather than simple silicosis in this case (Mossman and Churg 1998). In the light of all these points, significant reduction of the health risk may be attained only after a deep examination of the properties and the exposure conditions of the whole materials even in the same working environment. Also, generalization of the results should be kept with caution and the situation be analysed case by case.

Fubini B. and Fenoglio I. (2007) *Elements* **3**, 407-414.

Ghiazza M., Scherbart A.M., Fenoglio I. et al. (2011) *Chem. Res. Toxicol*. **24,** 99–110.

Moroni B., Viti C. and Cappelletti D. (2013) *JESEE* doi:10.1038/jes.2013.3.

Mossman B.T. and Churg A. (1998) *Am. J. Resp. Crit. Car.* 157, 1666-1680.

NIOSH (2002) *Health effects of occupational exposure to respirable crystalline silica*, NIOSH Publ. No. 2002-129.

Nodari, L., Marcuz, E., Maritan, L., Mazzoli, C. and Russo U. (2007) *J. Eur. Ceram. Soc.* **27**, 4665-4673.

Verdel U., Incocciati E., Massera S. and Rughi D. (2006) *Proc. 24th A.I.D.I.I. Nat. Cong.*, 55-60.

A prototype of a new engineered nanoparticle monitoring device for workplaces: Device testing

J. Ruusunen[1], J. Leskinen[1], T. Torvela[1], M. Ihalainen[1,2], T. Karhunen[1], I. K. Koponen[3], V. Niemelä[4], A. Lähde[1] and J. Jokiniemi[1,5]

[1] University of Eastern Finland, Fine Particle and Aerosol Technology Laboratory, P.O.Box 1627, FI-70211, Kuopio, Finland
[2] PSI Paul Scherrer Institut, The Laboratory for Thermal-Hydraulics, CH-5232 Villigen PSI, Switzerland
[3]National Research Centre for the Working Environment, Lerso Parkallé 105, DK-2100 Copenhagen, Denmark
[4]Dekati Ltd., Osuusmyllynkatu 13, FIN-33700, Tampere, Finland
[5]VTT Technical Research Centre of Finland, P.O. Box 1000, 02044 VTT, Espoo, Finland
Keywords: nanoparticle, monitoring, workplace, LC-SAM.
Presenting author email: jarno.ruusunen@uef.fi

Occupational health risks related to workplace exposure to engineered nanoparticles (ENP) are still not well understood and there seems to be lack of instruments to measure of ENPs in the workplaces. On the market there are a few measurement devices for the ENP monitoring, such as the Nanoparticle surface area monitor (NSAM, model 3550, TSI, USA) (Asbach *et al*, 2009) and the Aerasense NanoMonitor (Philips, Netherlands). However, at workplaces there is still need for low-cost, easy to use and portable nanoparticle monitoring instruments. A prototype of a new engineered nanoparticle monitoring device (Dekati Low-Cost Surface Area Monitor LC-SAM, Dekati Ltd., Finland) based on escaping current technology has been built by Dekati Ltd in EU FP7 Nanodevice -project. In this study a prototype device was tested.

ENPs for the device testing were produced using Flame spray pyrolysis (FSP) (Karhunen *et al*, 2012) and Atmospheric pressure chemical vapour synthesis (APCVS) (Lähde *et al*, 2011). In addition, the aerosol generator (model 3076, TSI, USA) was used to produce ammonium sulfate ($(NH_4)_2SO_4$) and polystyrene latex (PSL) particles as reference materials, see Table 1.

The Scanning mobility particle sizer (SMPS, model 3080, TSI, USA), the NSAM, the Electrical low pressure impactor (ELPI and ELPI+, Dekati Ltd, Finland) and the Fast mobility particle sizer spectrometer (FMPS, model 3091, TSI, USA) were used to characterize the produced ENPs and the reference particles.

Material	GMD (nm)	c ($\cdot 10^4$/cm^3)
$(NH_4)_2SO_4$	40	6.9
PSL	74	1.0
Cu	98	5.7
LTO	193	5.1

Table 1. Materials used for testing, geometric mean diameter (GMD) and concentration (c) of the particles according to SMPS.

The produced ENPs were diluted with a porous tube diluter and an ejector diluter prior to sampling to achieve suitable sampling conditions. The Dekati LC-SAM was used in a small exposure chamber and the samples for the NSAM were taken from the same location.

The current I (fA) measured with the Dekati LC-SAM is relative to the active surface area of particles going through the device. For LTO ENPs the signal are presented in Figure 1a and the human lung-deposited surface area D (μm^2/cm^3) measured with the NSAM for LTO ENPs can be seen in Figure 1b. While the measuring principle of the Dekati LC-SAM and NSAM has some differences there was still a good agreement between the measured values.

As a conclusion, the Dekati LC-SAM has a good agreement between the measured values and the characteristic of the produced ENPs. Results indicated that tested device offer one alternative to measure workplace exposures for ENPs.

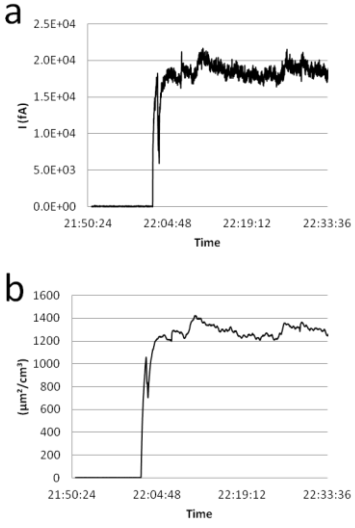

Figure 1. a) Current *I* (fA) of the Dekati LC-SAM and b) Lung deposition average *D* (μm²/cm³) of the NSAM.

The research leading to these results has received funding from the European Community's Seventh Framework Programme (FP7/2007-2013) under grant agreement n° 211464.

Asbach et al (2009) *J. Nanopart. Res.* **11**, 101-109
Karhunen, T. *et al* (2011) *ISRN Nanotechnology*. **2011**, article id 180821.
Lähde, A. *et al* (2011) *J. Nanopart. Res.* **13,** 3591-3598.

Occupational exposure to ultrafine particles – work place measurements

A.-K. Viitanen[1], A.J. Koivisto[1], T. Kanerva[2] and K. Hämeri[3]

[1]Finnish Institute of Occupational Health, Topeliuksenkatu 41 a A, FI-00250 Helsinki, Finland
[2]Finnish Institute of Occupational Health, Uimalankatu 1, FI-33540 Tampere, Finland
[3]Department of Physics, University of Helsinki, P.O. Box 64, FI-00014 Helsinki, Finland
Keywords: occupational health, ENP, ultrafine particles
Presenting author email: anna-kaisa.viitanen@ttl.fi

Ultrafine particles have been postulated to be one of the most expanding risks for occupational health (Brun et al. 2009). In work environment the employee may expose to ultrafine particles. These originate from unintentional sources, e.g. welding fumes and combustion particles, or they may be purposely manufactured process particles, such as engineered nanoparticles (ENPs) (e.g. Maynard et al. 2005).

Work environment airborne PM originates from outdoor air and indoor sources. Indoor sources may be separated by measuring size differentiated concentrations and following work processes (Koivisto et al. 2012). Representative data is still lacking in large scale, thus measurements in work places are seen important.

Methods

We are studying the number concentration of ultrafine particles in different working environments. The measurement setup used in workplace measurements is illustrated in Fig. 1.

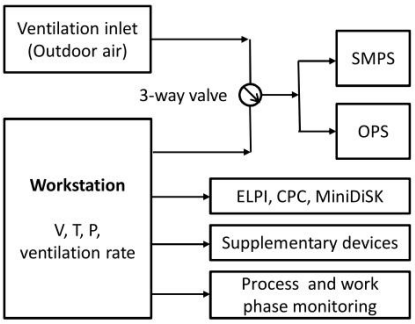

Figure 1. Measurement setup.

The exposure is defined from the work station and breathing zone. The ventilation inlet concentration defines the background. When measurements from ventilation inlet are not possible the outdoor air is measured instead where the penetration of the particles to indoors are defined with I/O measurements. For measuring number size distribution a Scanning mobility particle sizer (SMPS), Optical particle sizer (OPS), Condensation particle counter (CPC) and Electrical low pressure impactor (ELPI) are used. Personal exposure from the breathing zone is measured with MiniDiSC (Fierz et al. 2011). With this setup a particle size range of app. 3nm-10µm depending on application is achieved. Additionally other measurement devices are being used to produce supplementary information on measurements. This could be e.g. measurements of gas phase contaminants or collection of EM-samples. The work process is monitored and different processes during the working period are linked to the concentrations.

Results and Discussion

In this study the occupational exposure to fine and ultrafine particles in various working environments is measured. Fig 2. shows an example of the work place measurements. The total particle concentration and particle size distribution measured during one working day in an industrial factory handling nanodiamonds (ND) is shown. Based on the results the ND concentration during the handling process does not significantly differ from the ventilation inlet concentration (i.e. background). However, the personal exposure to large ND agglomerates may be seen. The workers inhalation exposure in this case was negligible due to proper use of respiratory protective equipment.

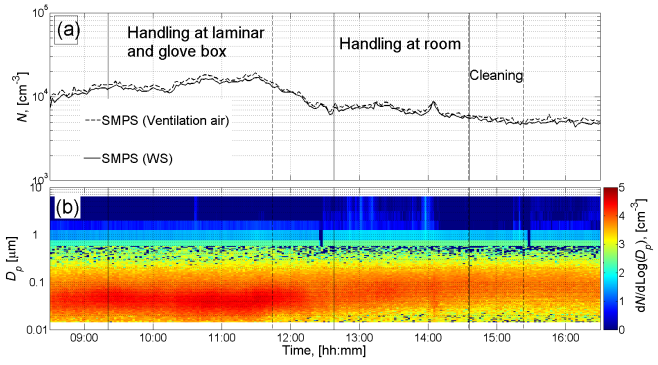

Figure 2. (a) Particle number concentration during a one day working period measured with SMPS from the work station (solid line) and ventilation inlet (dashed line). (b) Particle size distribution measured with SMPS and ELPI. Different work phases have been indicated into the figure with vertical lines.

Brun E. et al. (2009) European Risk Observatory Report 8. European Agency for Safety at Work. ISBN 978-98-9191-171-4.

Fierz, M., Houle, C., Steigmeier, P., Burtscer, H. (2011) Aerosol Sci. Tech. **45:1.**

Koivisto, A.J., Aromaa, M., Mäkelä, J.M., Pasanen, P., Hussein, T., Hämeri, K. (2012) ACSNano, **6:1195.**

Maynard, A.D. and Kuempel, E.D. (2005) J. Nanopart. Res. **7:687.**

The Use of Nuclepore Filter for Ambient and Workplace Nanoparticle Exposure Assessment

Sheng-Chieh Chen[1], Jing Wang[2,3], Heinz Fissan[4,5] and David Y.H. Pui[1]

[1]Particle Technology Laboratory, University of Minnesota, Minneapolis 55455, USA
[2]Institute of Environmental Engineering, ETH Zurich, Zurich, 8093, Switzerland
[3]Analytical Chemistry, EMPA, Dubendorf, 8600, Switzerland
[4]Institute of Energy and Environmental Technology (IUTA) e.V., 47229 Duisburg, Germany
[5]Center for Nanointegration Duisburg-Essen (CeNIDE), 47057 Duisburg, Germany

Keywords: exposure assessment, filter sampling, electron microscopy.
Presenting author email: jing.wang@ifu.baug.ethz.ch

Filter sampling followed by electron microscopy has long been used for measurement of airborne particles. The method provides direct measurement of the particle geometric size and morphology, which cannot be obtained from real-time instruments. The correlation between the particle concentrations on the filter surface and those in the air deserves careful investigation. In many applications, the collection filters are assumed to be absolute filters and the collected particle concentration is directly converted to the airborne concentration. This assumption is plausible if high efficiency filters are used. On the other hand, usage of high efficiency filters requires strong pumps and power consumption. This poses difficulty for field measurement and increasingly important personal sampling. If the collection filters cannot be assumed to be absolute filters, an accurate filtration model must be established to convert the particle concentration on the filter to the airborne concentration (Cyrs et al. 2010).

In the studies of ambient and workplace airborne particulate matters, the nanoparticles play more and more important roles. They may have specific properties, high local concentrations, and thus more severe effects on the environment and human health. Personal exposure assessment is attracting increasing interests because data under the real work conditions of the workers and that of residents living in the neighborhood of the plant can be obtained. The Nuclepore filters are often used for particle sampling due to their flat surface, which facilitate the microscopic analysis for the collected particles. We investigated the feasibility of Nuclepore filter collection with subsequent electron microscopy analysis to assess the nanoparticle exposure.

The pores of the Nuclepore filter are circular in cross section and the well-known capillary tube models were used for calculating the collection of particles (Spurny et al., 1969; Manton, 1978). We also proposed a modified model based on the Spurny model. We found that the inertia parameter, I (a function of medium and particle densities, filtration face velocity, filter porosity and pore diameter), should be used to determine the applicability of the models.

To search for a proper model, we studied the overall penetrations of three different spherical and cubic nanoparticles (PSL, Ag and NaCl), and three types of fractal particles (Ag open agglomerates and partly sintered aggregates, and soot aggloemrates), covering a wide range of particle sizes (20-800 nm) and densities (1.05-10.5 g/cm3), through Nuclepore filters with two different pore diameters (1 and 3 μm) and different face velocities (2-15 cm/s). The data of the overall penetration were in very good agreement with the properly applied models (Figure 1). A good agreement of filter surface collection between the validated model and the SEM analysis of this study (Figure 2) was obtained, indicating a correct nanoparticle number distribution in the air can be converted from the Nuclepore filter surface collection and this method can be applied for nanoparticle exposure assessment.

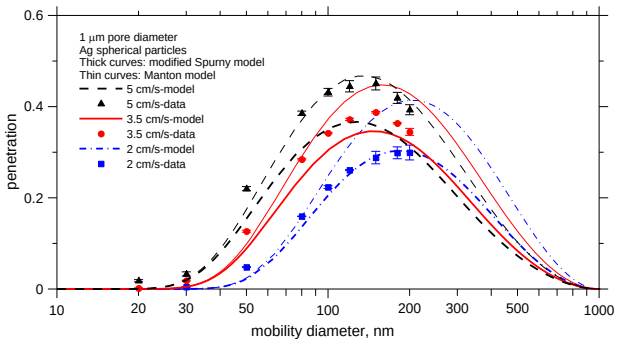

Figure 1. Comparison of Ag penetration in 1 μm filter between experiments and modified Spurny and Manton models at relatively low face velocities, 2-5 cm/s.

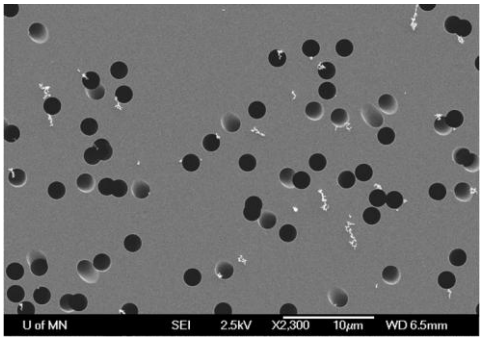

Figure 2. SEM image of soot agglomerates used in the penetration tests.

Cyrs, W.D., Boysen, D.A., Casuccio, G., Lersch, T., Peters, T.M., 2010. J. Aerosol Science 41, 655–664.
Spurny, K.R., Lodge, J.P., Frank, E.R., Sheesley, D.C., 1969. Environmental Science & Technology 3, 453–464.
Manton, M.J., 1978. Atmospheric Environment 12, 1669–1675.

Characterization and emission measurements of multi-walled carbon nanotube release during production

L. Ludvigsson[1,2], C. Isaxon[2], P. T. Nilsson[2], M. Hedmer[3], H. Tinnerberg[3] M. E. Messing[1], J Rissler[2], V. Skaug[4], A. Gudmundsson[2] M. Bohgard[2], J. Pagels[2]

[1]Solid State Physics, Lund University, SE-22100, Lund, Sweden
[2]Ergonomics and Aerosol Technology, Lund University, SE-22100, Lund, Sweden
[3]Occupational and Environmental Medicine, University Lund University Lund, SE-22100, Lund, Sweden
[4]National Institute of Occupational Health, PB 8149 Dep, 0033 Oslo, Norway
Presenting author email: Linus.Ludvigsson@ftf.lth.se

Keywords: Carbon nanotubes, emission measurement, SEM

The fields in which carbon nanotubes (CNTs) are found useful are rapidly growing, causing an increased demand worldwide. The industry is looking for ways to improve their production and thus increase the amount of CNTs being handled. This, together with the fear that exposure to CNT particles may cause similar health effects as asbestos (Donaldsson, 2006), create a need for accurate methods of emission assessments. We present results from field measurements performed using a range of techniques to assess emissions and exposure at a small-scale CNT producer that utilize the arc-discharge method for production of multi-walled CNTs.

Emissions and exposures when performing different work tasks in the production were examined including full-shift personal measurements. Samples of airborne particles were collected both in the emission zone and in the breathing zone of the workers. By using cyclones (BGI4L, BGI) respirable (cut-off 4µm aerodynamic diameter) dust fractions, were collected on polycarbonate (37 mm, 0.4 µm pores) filters. Particles were studied with Scanning Electron Microscopy (SEM) and online instruments were used both in the emission zone (<10cm from the source) and in the background (3 m from the closest known source). CNT containing particles were classified into 4 types displayed in figure 1. The size distribution of all measured particles in one sample is shown in figure 2.

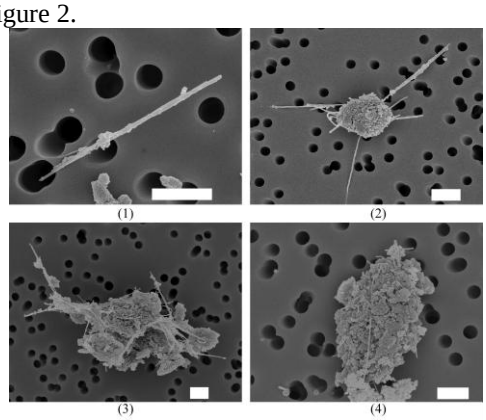

Figure 1 CNT particle types (1-4). The white scale bar equals 1 µm in each image.

Emissions of CNTs were detected in 9 out of 16 samples, with a CNT content of up to 11 CNT particles per cm^3. The CNT containing particles found in the respirable fraction did seldom exceed a length of 5 µm. Most of the CNT particles had dimensions larger than 1 µm, i. e. much larger than the mean particle diameter (0.2 µm)

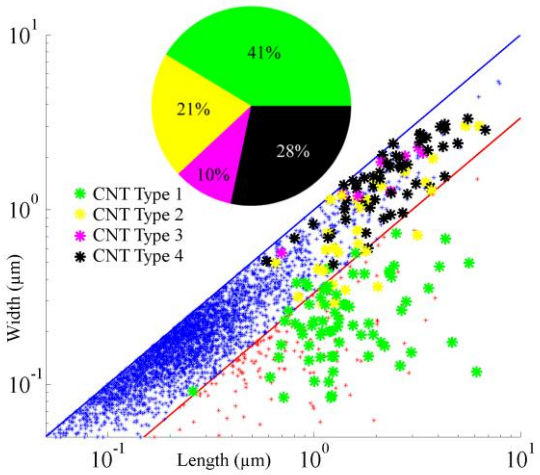

Figure 2 Distribution of measured particles in one sample, blue and red dots marks non-CNT containing particles. Particles between the blue and red line have an aspect ratio <3:1 and particles below the red line have an aspect ratio >3:1. The pie chart shows the distribution of the four different CNT types.

The combination of online instrumentation and SEM analysis contributed to clearly showed when emissions occur and what kind of particles that were emitted. The results show that several tasks in the production could cause workplace exposure.

This work was performed within the FAS centre METALUND and supported by the Swedish Council for Working Life and Social Research (FAS) and nmC@Lund

(REF) K. Donaldsson *et. al.* (2006) *Toxicological Sciences* 92(1), 5–22 (2006)

Particle characterization during abrasive treatment of composite material containing fibres by Cryo HRTEM

K.I. Lieke[1], M. Levin[1,2], K.A. Jensen[1] and I.K. Koponen[1]

[1]National Research Center for the Working Environment, 2100 Copenhagen, Denmark
[2]Department of Nanotechnology, Technical University of Denmark, 2800 Kgs. Lyngby, Denmark
Keywords: nano fibre composite, production emission, HRTEM, cryo.
Presenting author email: KirstenLieke@gmx.de

Composite material including nano particles and fibres is today used in production and sealing of surfaces. Highly stressed surfaces such as of cars, boats and light aircrafts need to provide properties that demand the use of new materials including nano fibres, that enhance stability. Manufacturing of these surfaces involves abrasive treatment, during which material is emitted. We characterized particles from treatment of composite material including nano fibres. Nano particles can have an adverse health effect (Donaldson et al., 2002) when inhaled by humans exposed to emissions during manufacturing and surface treatment.

Particles were collected using a micro intertial impactor set similar to the one described by Kandler (2009). Sampling was performed on 2 stages (upper cut off 0.89 µm and lower cut off 0.047 µm diameter) on Ni-TEM grids with Formvar carbon foil (Plano, Wetzlar, Germany).

Transmission electron microscopy (TEM) was used for analysis of particles on 12 samples from 6 tests in total. Overview and high-resolution (HR) microscopic images were recorded using a Tecnai T20 G2 (FEI, Eindhoven, the Netherlands) at the Center for Electron Nanoscopy, Technical University of Denmark, operating at 200kV. Due to beam sensitive material a nitrogen cooled cryo transfer holder (Gatan Inc. Ca. USA) was used to keep the sample below -80 degrees Celsius during analysis. It was accounted for possible beam damage and hydro carbon deposition by using low beam current densities and short acquisition time. Energy dispersive X-ray detection (EDS) was carried out on single particles using an Oxford 80mm silicon drift detector.

Scanning electron microscopy (SEM) was performed on samples collected from deposited material (powder) with a ESEM Quanta 200 FEG (FEI, Eindhoven, the Netherlands).

Online measurements with FMPS, ELPI, CPC and GRIMM dust monitor were conducted in parallel.

Particles in the size range from 40 nm up to 500 nm (average geometric diameter) were analysed and classified based on their structure, morphology, beam stability and chemical composition.

Particles originating from the composite proofed to be partly crystalline material (Figure 1). Few nanometer thin fibres were found in agglomerates of few hundred nanometers, parts of them sticking out of the bulk. Single fibers of 100 nm in width and several 100 nanometers in length were less abundant.

Ammonium sulfate, sodium chloride and soot particles that were found in high abundances on the substrates were classified as background particles. However, composite particles, as well as fibres were sometimes found internally mixed with background particles.

Particles revealed inhomogeneous composition and irregular shape and morphology. Size, surface area and density determination will be discussed for the different materials.

SEM investigations on deposited material revealed extreme charging of particles, especially of the fibrous material. Potential issues regarding the detection by instruments using electric mobility sizing will be critically discussed.

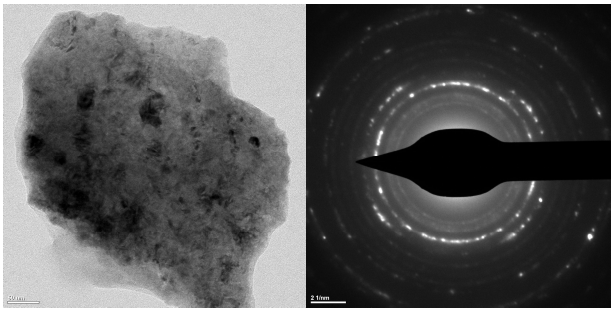

Figure 1. TEM bright field image (left) and diffraction pattern (right) of a nano particle originating from abrasive treatment of composite material.

The authors like to thank Signe Hjortkjær Hansen for technical support. We gratefully acknowledge excellent microscopy conditions at Center for Electron Nanosccopy (CEN), Technical University of Denmark and technical support by Wilhelmus Huyzer. This work was supported by the NanoSafetyCenter and Nanovalid.

Donaldson et al.,2002, Inflammation caused by particles and fibers, Inhalation tox. **9**, 5-27

Kandler, K., 2009. An aerosol sampler for single particle analysis. Presentation at the European Aerosol Conference 2009, Karlsruhe, Germany. Abstract T092A04.

Tuesday, September 3, 2013

Session: Instrumentation
Ambient aerosol instrumentation

Urban particulate matter monitoring on a mobile platform: a real time experiment on a long term scale

B. Moroni[1,2], E. Scocchera[1], A. Piazzalunga[3], M. G. Ranalli[4] , S. Castellini[5], and D. Cappelletti[2,5]

[1]DICA, Università di Perugia, Perugia, Italy
[2]Centro di Eccellenza SMAArt, Università di Perugia, Perugia, Italy
[3]DISAT, Università di Milano Bicocca, Milano, Italy
[4]Dipartimento di Economia, Finanza e Statistica, Università di Perugia, Perugia, Italy
[5]Dipartimento di Chimica, Biologia e Biotecnologie, Università di Perugia

Keywords: mobile platform, urban pollution, real time monitoring, traffic rates
Presenting author email: david.cappelletti@unipg.it

In this paper we propose an innovative approach to the study of urban pollution dynamics, with a particular emphasis to vehicular traffic and generated aerosols. In synthesis, a mobile monitoring platform has been developed exploiting the urban transport system in Perugia (Italy), called Minimetrò. It is based on a monorail train, exploiting a relatively high number of cabins (in average 20) driven by a wire rope continuously running at medium low speed (4-5 m/s) along a radial transect (~3 km, in approx. 20 minutes) over the city. The cabins travel on a monorail built 5 meters above the road level. The cabin path starts from a large suburban parking area, it crosses various heavy traffic roads and road crossings, passes through a park, climbs Perugia hill, and finally reaches the city center inside a terminal tunnel. All these features make the Minimetrò system a good mobile platform for real time investigation of the dynamics of formation and dispersion of pollutants in the urban area.

The basic idea has been to customize and integrate an Optical Particle Counter (OPC, 6 sec. resolution, 22 size classes) inside the cabin. To complement the information coming from the mobile station, two other fixed OPCs (FAI Instruments) have been installed at both ends of the Minimetrò line. Moreover the Minimetrò line passes at short distance (50 m) from the urban background and traffic monitoring stations of air quality. These provide hourly averaged O_3, NO_x, Benzene and CO concentrations, as well as 24h PM_{10} and $PM_{2.5}$ data records. In addition, the main weather parameters are recorded as well as a PBL stability monitor (FAI Instruments) has also been installed in this station. Finally, traffic rates are recorded continuously in two points along the Minimetrò line with a 5 minutes time resolution.

An example of aerosol data is shown in Figure 1, where the number concentration of coarse fraction particles (D_P>1 μm) is shown, for a particular day, as a function of the position along the path (*y* axis, in meters) and time of the day (*x* axis). The color code are number concentration of particles per volume of air. In this particular example the variable impact of a Saharan dust intrusion occurring in the late afternoon is evidenced in different areas of the city. In addition, higher particles concentrations (red areas in the graph) are observed near heavy traffic roads, which point to a role of particle resuspension.

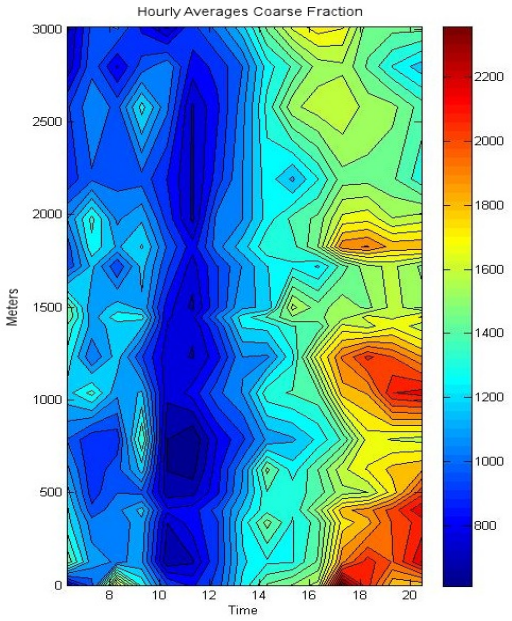

Figure 1 - Spatial – temporal distribution of coarse fraction particles recorded in date 20/10/2012.

The data acquisition started in September 2012 and will last one year. Ad-hoc statistical techniques are employed to fully exploit this large amount of information: functional data analysis can handle high frequency time series, while additive models can produce maps as those in Figure 1 and explain the contribution of covariates.

Special interest has been paid to the characterization of the aerosols in the underground paths of the Metro line in order to analyze the impact of degrading metal and rubber parts of the system. In this case the specific emission of the Metro system has been characterized, exploiting two HVS multistage impactors which allowed simultaneous samplings inside and outside the tunnel for metals and IPA size distributions. Moreover EC/OC ratios, black carbon as well as morphological a mineralogical assessments via electron microscopy on samples taken inside the tunnel have been used to integrate the mobile cabin data. Detailed results will be presented at the Conference.

A new aerosol conditioning system - Characterisation and first application

M. Laborde[1], B. Rosati[2] , P. Zieger[2], T. Petäjä[3], G. Kassell[4], D. Logan[4], E. Weingartner[2]

[1]AerosolConsultingML GmbH, Ennetbaden, Switzerland
[2]Laboratory of Atmospheric Chemistry, Paul Scherrer Institute, Villigen, Switzerland
[3]Department of Physics, University of Helsinki, Helsinki, Finland
[4]Ecotech Pty Ltd,Knoxfiled, Australia
Keywords: Hygroscopic growth, aerosol scattering, humidified nephelometer
Presenting author email: marie.laborde@aerosolconsulting.com

Aerosol particles are known to have the capability of taking up water. As a result, their optical properties (and especially their ability to scatter light) are altered and with it their direct impact on the Earth's radiative balance. Predicting the contribution of condensed water to light scattering remains however a challenge due to the fact that this highly depends on the particle dry size and chemical composition (i.e. the particles hygroscopicity). The relative humidity (RH) dependence of the particle light scattering coefficient $\sigma_{sp}\sigma_{sp}$) is therefore an important measure for climate forcing calculations but also needed for comparing in-situ with remote sensing measurements

This dependence is usually reported as *f(RH)* and is defined as in Eq. 1:

$$f(RH)_i = \frac{\sigma_{sp}(RH)_i}{\sigma_{sp}(RH)_{dry}}$$

Equation 1. Light scattering enhancement factor at a relative humidity

Several studies have successfully measured and modelled the ability of aerosol particles to take up water in various locations (Zieger et al., 2010) using a custom-built humidified nephelometer (WetNeph; Fierz-Schmidhauser et al., 2010). We present here the first results obtained with a newly commercially available aerosol conditioning system. A detailed characterization of this new instrument will soon be performed, including a comparison to the above mentioned custom built WetNeph. A first application in the field in Hyatiäla, Finland is also foreseen and will be presented.

The aerosol conditioning system used in this study (ACS 1000, Ecotech) allows for the humidity to be controlled within ±0.8% (Fig. 1) from ~40% to 90% RH. It is composed of a gore-tex humidifier, a nafion dryer and two integrating, polar nephelometers (Ecotech, Aurora 4000).

Figure 1: RH control of aerosol conditioning system ACS

The aerosol light scattering enhancement at 90% RH was measured (Fig. 2) for over a month in Melbourne, Australia. The figure shows the importance of the particles water uptake on their light scattering.

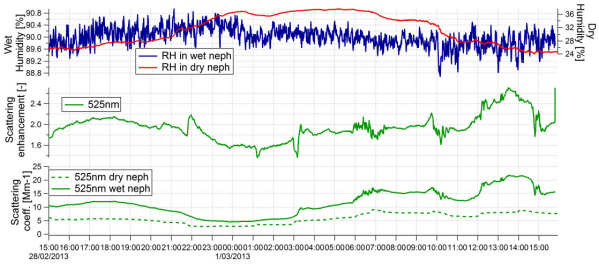

Figure 2: First application of the new humidified nephelometer

Zieger, P. et al. (2010), *Atmos. Chem. Phys.,* **10**, 3875-3890.

Fierz-Schmidhauser, R., et al. (2010) *Atmos. Meas. Tech.,* **3**, 39-50.

Particle number concentration monitor for atmospheric aerosols

L. Hillemann[1], A. Zschoppe[2]

[1]Institute of Process Engineering and Environmental Technology, TU Dresden, 01062 Dresden, Germany
[2]Topas GmbH, Oskar-Röder-Str. 12, 01237 Dresden, Germany
Keywords: particle number concentration monitor, atmospheric aerosol, corona-jet charger
Presenting author email: lars.hillemann@tu-dresden.de

The concentration of particle matter in ambient air is quantified in air quality monitoring networks. The classical mass-based methods are more and more completed by number-based methods. This enables to quantify the concentration of submicron particles, which especially show adverse health effects (Peters *et al*, 1997). For this purpose, an ultrafine particle monitor (UFPM) was designed and constructed to obtain particle number concentrations of atmospheric aerosols.

Fig. 1 shows a schematic diagram of the UFPM. The aerosol sample passes through a corona-jet charger, which charges all particles positively by diffusion charging. Subsequently, the charged particles are classified in a DMA due to their electrical mobility and quantified by a faraday cup aerosol electrometer. During a measurement with the UFPM the voltage in the DMA is increased from 0 to 10 kV in discrete steps within 10 min. The means of the electrical current, measured with the aerosol electrometer at every classifier voltage, are recorded in the vector **I**. The ranges of electrical mobility, corresponding to the classifier voltages, overlap by half its width. The captured range of particle mobility covers particle sizes from 20 to 720 nm in predefined size classes.

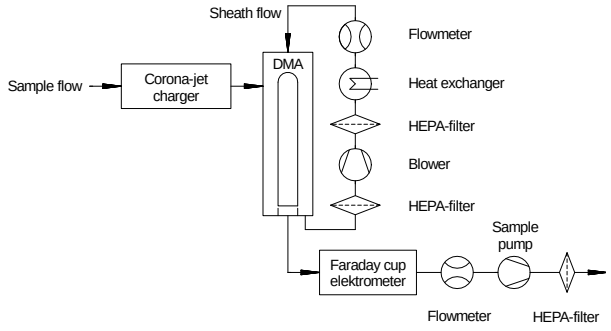

Figure 1: Schematic diagram of the ultrafine particle monitor (UFPM)

The data inversion delivers the connection between the measured electrical current **I** and the particle number concentration **C** by the charge distribution, the transfer function of the DMA and the inlet flow. These functions are summarized in the kernel matrix **K**.

$$\mathbf{I} = \mathbf{KC} \tag{1}$$

A data inversion algorithm, based on the Tikhonov-regularization, was implemented (Tikhonov, 1977).

A method was developed to calculate the kernel matrix from the data of comparison measurements with the UFPM and a reference mobility particle size spectrometer such as a scanning mobility particle sizer. In experimental comparisons, the number concentrations of laboratory and atmospheric aerosols measured by the UFPM were within a range of $\pm 20\,\%$ of the reference concentration determined by a SMPS. The distribution of the counting efficiency of the UFPM measured with atmospheric aerosol is shown as boxplot in Fig. 2. The counting efficiency is mainly between 0.8 and 1.2. The quartiles of the distribution of the counting efficiency of all size classes are between 0.81 and 1.02, the median varies between 0.90 and 0.93.

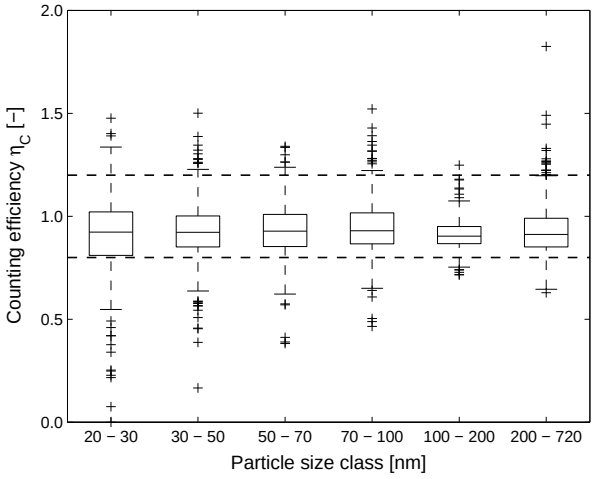

Figure 2: Counting efficiency of the UFPM for atmospheric aerosol

The UFPM is particulary designed to monitor atmospheric particle number concentration in air quality monitoring networks. The contribution will discuss the design and the function of the UFPM. It will focus on the data inversion and the method for the measurement of the kernel matrix data. Results of comparison measurements with the UFPM and a SMPS will be presented to confirm the good agreement of the UFPM to reference mobility particle size spectrometers.

Peters A. et al. (1997), *Am. J. Respir. Crit. Care Med.*, **155**, 1376-1383.

Tikhonov A. N. (1977) *Solutions of ill-posed Problems*, John Wiley & Sons, Hoboken.

A new visual expansion-type Condensation Particle Counter

B. Bühner, A. Wagner, A. Kürten and J. Curtius

Institute for Atmospheric and Environmental Sciences, Goethe University of Frankfurt, 60438 Frankfurt/M., Germany
Keywords: nanoparticles, instrumentation, CPC
Presenting author email: buehner@iau.uni-frankfurt,de

The particle number concentration is an important fundamental property of aerosol populations and is usually measured with Condensation Particle Counters (CPC). In these instruments nanometer-sized particles are magnified by condensational growth to sizes detectable by light within the range of the visual spectrum. This concept is applied in various commercial and custom-made setups (see McMurry, 2000, and references therein).

One approach for achieving the required super-saturation is realized in "expansion-type" CPCs through fast adiabatic expansion. Different methods have been applied for retrieving the number concentration of the particles after their activation and growth to micrometer-sized droplets. These automated methods usually rely either on the measurement of scattered or transmitted laser light after interaction with the droplet population (e.g. Kürten, 2005). Especially the reliable detection of low particle concentrations with such measurements can, however, be challenging because of noise or drifts in the measured light intensity.

We have developed a new expansion-type particle counter based on the visual detection of individual droplets. The design of the VIPER (Visual expansion-type Particle counter) utilizes a CCD camera and a fully automated image analysis based on a LabVIEW program. A section of the expansion chamber is illuminated by laser light. The laser beam is "shaped" by a cylindrical lens and defines – together with the chamber geometry – a thin optical volume which is used for the particle detection. A series of digital images is taken shortly after the adiabatic expansion and subsequently processed afterwards. The particles visible in the illuminated volume are counted autonomously by image analysis software.

This direct method of observation offers an absolute measurement of individual aerosol particles and is no longer dependent on the interpretation of intensity measurements. As single particles are individually detected rather than the optical properties of a particle ensemble, the result is basically unambiguous. Thus, the method can in principle be independent of calibration. However, the correct geometry of the illuminated volume and the loss of particles due to the expansion have to be taken into account.

The experimental setup of the VIPER is demonstrated to have a reliable performance under various experimental conditions in the laboratory and in the field. The particle size at which 50% of the particles are detected has been determined to be D_{p50} = 8nm (cut-off diameter) with detection of particles beginning at 3nm (using water as the working fluid).

The maximum concentration which can be measured accurately is around 4.4×10^5 cm^{-3}. The lowest measurable concentration is constrained by the counting statistics due to the rather small optical volume. Given this constraint a concentration of 2000 cm^{-3} would be measured with a statistical error of approx. 10 %.

The super-saturation achieved inside the measurement chamber can be controlled by the expansion ratio. Therefore, a thermal conditioning is not required which helps to keep the set-up simple. In addition to that, controlling the expansion ratio has further important advantages: (1) The super-saturation can quickly be adjusted between different expansions to set different lower cut-off sizes in subsequent measurements without time delay. (2) The whole setup can be made isothermal. This would allow the application of VIPER in low temperature environments. Thereby, the potential risk of evaporating particles before the measurement can be avoided.

Detailed instrument characterizations will be presented as well as side-by-side comparisons with other particle counters. We discuss the assessment of different working fluids and the performance of the VIPER CPC during field experiments.

McMurry, P.H. (2000) *Aerosol Science and Technology* **33**, 297–322.

Kürten, A., Curtius, J., Nillius, B. and Borrmann, S. (2005), *Aerosol Science and Technology* **39**/12, 1174 - 1183

Development of a high volume air-into-liquid aerosol collector for $PM_{2.5}$ and ultrafine particulate matter

Dongbin Wang[1], Payam Pakbin[1], Arian Saffari[1], James J Schauer[2] and Constantinos Sioutas[1]

[1]Department of Civil and Environmental Engineering, University of Southern California, Los Angeles, CA, 90089, USA
[2]Department of Civil and Environmental Engineering, University of Wisconsin, Madison, WI, 53718, USA
Keywords: aerosol collector, VACES, air-into-liquid.
Presenting author email: sioutas@usc.edu

A novel high volume aerosol sampler for $PM_{2.5}$ and ultrafine particulate matter (PM) was developed to collect ambient aerosols directly into a liquid phase, for application areas such as toxicity studies of PM as well as for direct chemical analysis of the collected suspension samples, thus overcoming limitations associated with the conventional filter samplers. This new collector was designed to be coupled with the USC Versatile Aerosol Concentration Enrichment System (VACES) technology described by Kim et al (2001), by integrating an inertial impactor to collect the super micron ambient aerosols after their condensational growth in the VACES, in the form of an aerosol suspension in liquid. The high-flow (200 LPM), low pressure drop (6.5 inches of water) impactor allows prolonged and unattended operation of the system.

Laboratory tests were conducted to evaluate the performance of the impactor. The collection efficiency of the inertial impactor was determined using monodisperse aerosols generated by atomizing suspensions of Polystyrene latex (PSL) particles (1, 1.5, 3 and 6μm) with a constant output nebulizer. Figure 1 presents the collection efficiency of the impactor as a function of particle aerodynamic diameter.

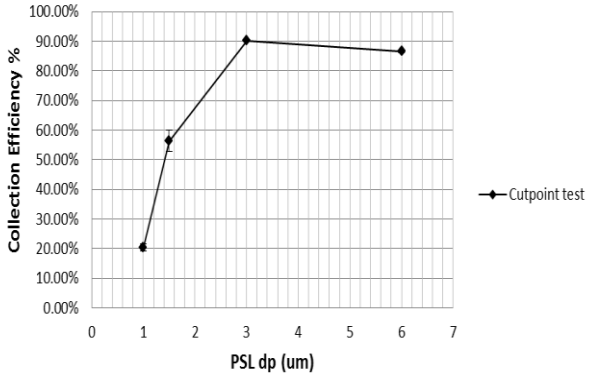

Figure 1. Collection efficiency curve of different PSL particles

Collection efficiency of the VACES-inertial impactor system was evaluated by testing different monodisperse PSL particles in sub-micron range: 42.5, 100, 300, 750nm and 1 μm, and polydisperse aerosols: glutaric acid and ammonium nitrate. The generated particles were first grown in the VACES prior to collection in the impactor. A fluorescence detector was used to measure the fluorescence signal of PSL particles on upstream and downstream filters and residual on the collector inlet and impaction walls, while mass concentration was measured by DustTrak upstream and downstream of the collector for polydisperse aerosols. Overall, the average collection efficiency of this collector was above 90%, as shown in Table 1.

Table 1. Collection efficiency of the new impactor

Aerosol	Efficiency	Inlet	Wall	Suspension
42.5nm	96.40%	4.53%	9.43%	82.44%
100nm	90.33%	2.11%	7.51%	80.71%
300nm	98.95%	1.17%	6.29%	91.49%
750nm	95.15%	2.87%	11.17%	81.10%
1 μm	99.08%	1.79%	9.30%	88.00%
glutaric acid	97.09%	-	-	-
ammonium nitrate	96.56%	-	-	-

Comparison of collection performance between the new impactor and the VACES/biosampler tandem was conducted using PSL particles of 300 and 750nm. Fluorescence signals of suspensions collected by these two samplers were measured and compared Results indicated that the aerosol collection performance was equivalent in both the impactor and biosampler.

Lastly, the whole system was deployed in the field and ambient $PM_{2.5}$ samples were collected both in the new collector and on filter substrates, similar to the test described by Daher et al (2011) to validate that the chemical compositions of suspension samples collected by the new impactor are equivalent to those on filter samples. This analysis is underway and results will be presented soon. Continuity test will be conducted to demonstrate the ability of prolonged and unattended operation.

Kim, S., P. A. Jaques, et al. (2001a). "Versatile aerosol concentration enrichment system (VACES) for simultaneous in vivo and in vitro evaluation of toxic effects of ultrafine, fine and coarse ambient particles - Part I: Development and laboratory characterization." Journal of Aerosol Science. 32(11): 1281-1297.

Daher, N., Z. Ning, et al. (2011). "Comparison of the Chemical and Oxidative Characteristics of Particulate Matter (PM) Collected by Different Methods: Filters, Impactors, and BioSamplers." *Aerosol Science and Technology*. **45**(11): 1294-1304.

Online Method for Size-Resolved Chemical Speciation of Nano-Particles

A. Wagner[1], A. Kürten[1], C. Fuchs[1,2], J. Hoker[1], J. Curtius[1]

[1]Institute for Atmospheric and Environmental Sciences, Goethe University, Frankfurt, 60438, Germany
[2]now at: Laboratory of Atmospheric Chemistry, Paul Scherrer Institut, Villigen, 5232, Switzerland
Keywords: nano-particles, instrumentation, mass spectrometry, nucleation.
Presenting author email: acwagner@iau.uni-frankfurt.de

The growth of aerosol particles originating from nucleation is an important atmospheric process. The availability of condensable vapors for this growth is a prerequisite for these particles to become cloud condensation nuclei (CCN). To determine the source and the mechanisms of the aerosol growth, the condensing vapors need to be chemically speciated. However, the chemical analysis of particles in the size range between 2 nm and 20 nm is an experimental challenge and there are only very few instruments which can perform such an analysis under atmospherically relevant conditions. The TD-CIMS (Thermal Desorption Chemical Ionisation Mass Spectrometer, Voisin et al. (2003)) is a unique instrument which is capable performing such measurements online and has already given important insights into some atmospheric processes leading to aerosol growth (e.g. Smith at al. (2010)). However, further studies are necessary, especially with respect to other environments and different particle sizes.

In this study, a new instrument is introduced which allows the size-resolved identification of the chemical composition of particles in the size range below 20 nm. The TD-DMA (Thermal Desorption Differential Mobility Analyzer) collects particles on a substrate and transfers them into the gas phase so that they can be analyzed with a mass spectrometer. The particles first pass through a DMA unit, so that only those with a selected size can reach the substrate. The substrate currently consists of a stainless steel wire to which HV can be applied in order to precipitate the particles. Once enough particles are collected, the substrate can be moved into the sample inlet of a chemical ionization mass spectrometer (CIMS). In this mode of operation the CIMS inlet line is flushed with ultrapure nitrogen and the wire is heated by electrical current which evaporates the particles into the clean carrier gas. This procedure ensures that on the one hand, only the particulate constituents will be analyzed and on the other hand they can reach concentrations which are high enough for chemical speciation.

The advantages of the TD-DMA are as follows: (1) The analysis is performed online. (2) The collection of particles is carried out size-resolved, as particles with different sizes likely have different chemical compositions. (3) The collection and evaporation unit is compact and can in principle be combined with different analyzing instruments. (4) The measurement time required for the particle evaporation is small compared to the overall measurement time. However, during the collection period the mass spectrometer can be used to measure the gas phase composition of the sample air. This feature allows obtaining a full picture of the processes occuring in the gas as well as the particulate phase with one single mass spectrometer.

Lab experiments with a tandem DMA setup have shown that the maximum transmission of the DMA unit is between 45% for 5 nm (see figure 1) and 60% for 15 nm. It could also be demonstrated that close to 100% of the size selected particles can be precipitated onto the substrate. Sulphuric acid particles 15 nm in diameter were successfully collected and subsequently evaporated in the inlet of a CIMS which showed signals characteristic for sulphuric acid.

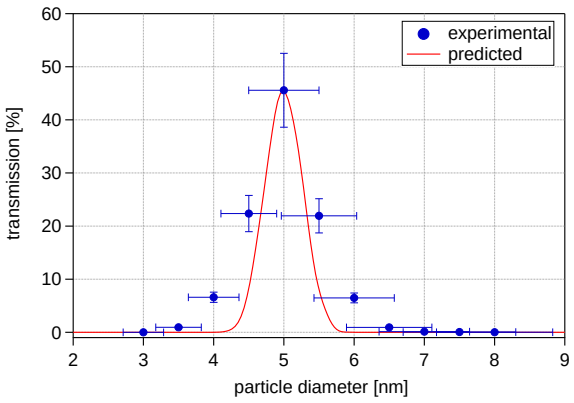

Figure 1: Experimental (blue) and predicted (red) transmission curve for particles with a diameter of 5 nm

The operational principle and the setup of the TD-DMA will be presented in detail. Results on the characterisation of the DMA transmission as well as first quantitative tests with respect to the collection and evaporation of different aerosol species will be discussed.

Voisin, D., Smith, J.N., Sakurai, H., McMurry, P.H. and Eisele, F.L. (2003) *Aerosol Sci. Technol.* **37**, 471-475.

Smith, J.N., Barsanti, K.C., Friedli, H.R., Ehn, M., Kulmala, M., Collins, D.R., Scheckman, J.H., Williams, B.J. and McMurry, P.H. (2010) *PNAS* **107**, 6634-6639.

Development of an automated total carbon analyzer for atmospheric aerosols

Y. Komazaki and Y. Kanaya

Research Institute for Global Change, Japan Agency for Marine-Earth Science and Technology, Yokohama, Kanagawa, 222-0037, Japan

Keywords: carbonaceous aerosol, automated analyser, intercomparison.
Presenting author email: komazaki-y@jamstec.go.jp

Introduction

Increasing attention is being paid to carbonaceous aerosols, a major component in $PM_{2.5}$, owing to the importance of its complex effects over various geographical scales, such as its effects on human health, haze, the hydrological cycle, and climate change. However, the sources, atmospheric processes, and impacts of carbonaceous aerosols are not well understood; moreover, uncertainties in measurement methods tend to be high owing to the complexity of the physical/chemical properties of carbonaceous aerosols as compared with the properties of other components (e.g., inorganic ions and minerals) of $PM_{2.5}$.

Thermal–optical analysis (TOA) is a popular method for determining aerosol EC and OC collected on quartz filters. However, the temperature protocol (e.g., IMPROVE, NIOSH) and optical detection (transmittance, reflectance) adopted in TOA strongly affect the separation of OC and EC.

EC and OC concentrations at Fukue Island in Japan were measured from November to December in 2012 in a short-term campaign using a semi-continuous TOA analyzer (Sunset Laboratory). However, the liquid-based calibrations of the instrument using two thermal protocols, namely IMPROVE-like and Total-Carbon (only in O_2/He mixture), showed a difference of ca. 30%.

The purpose of this study is to develop an automated semi-continuous total carbon (TC, TC = EC + OC) analyzer employing a thermal technique and to minimize the uncertainties in the measurement of carbonaceous aerosol.

Experiments, Results, and Discussions

Based on thermal desorption analysis, a semi-continuous automated analyzer for TC (TC_JA) was developed in this study. One-step heating in 2% O_2/He mixture up to 870 °C was employed to evolve carbonaceous compounds sampled on a quartz filter. TC concentrations were measured as CO_2 through a heated column with an oxidizing catalyst (MnO_2) using an NDIR CO_2 analyzer (LI-840A).

TC concentrations in Yokosuka, Japan, were measured using the semi-continuous carbon analyzer (Sunset Laboratory) and the TC analyzer developed in this study, and comparisons were conducted during the period from Sep 2012 to Feb 2013. A $PM_{2.5}$ sharp-cut cyclone (BGI) and a denuder (Sunset) were employed to remove any volatile organic compounds from the sample air.

Under almost the same thermal Total-Carbon protocols, the TC concentrations measured by the Sunset and newly developed instruments (TC_Sunset and TC_JA) were in good agreement, as shown in Figure 1. In the range below 4 μg/m^3, however, the TC_Sunset/TC_JA ratios were found to be concentration dependent, with higher ratios occurring in the lower concentration range. This result might indicate the better performance of the detection system as a result of the detector, theromogram data system (CDS plus, LAsoft), and/or gas dryer (Perma Pure) using Nafion membrane tubing, which continuously removes only water vapor from the gas streams.

In addition, TC_IMPROVE (OC + EC) measured using the Sunset analyzer was compared with the TC_JA. The concentrations with TC_IMPROVE tended to be higher than those of TC_JA (ca. 30% with a strong correlation). Identification of the exact origins of these differences is underway. These results will help to understand the differences in the liquid-based calibrations at Fukue.

We recommend that measurements by TOA should be undertaken using different protocols, such as IMPROVE-like and Total-Carbon protocols, for the accurate determination of EC and OC.

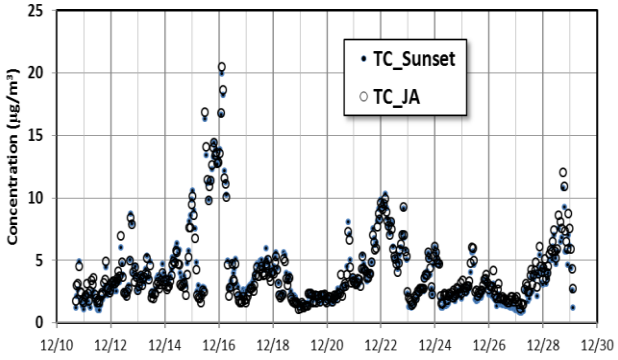

Figure 1 TC concentrations in Yokosuka, Japan, measured using the Sunset carbon analyzer and the TC analyzer developed in this study, Dec 2012

This work was supported by the Global Environment Research Fund (S-7, C-081, B-051) of the Ministry of the Environment, Japan.

Remotely operated PLUS-octocopter used as an aerosol measurement platform

P. Madl, C. Oberauer and F. Steinhäusler

Division of Physics and Biophysics, Department of Materials Engineering and Physics, PLUS University, Salzburg, A-5020, Austria
Keywords: unmanned aerial vehicle, flying aerosol measurement platform
Presenting author email: pierre.madl@sbg.ac.at

The herein presented design is part of the *BRIDGE* Concept Case Advanced Situation Awareness for proactive risk management. It will fill this gap by providing the user inter alia with real-time data on the extent of airborne pollution inventories.

One of the core-component is a manually controlled unmanned aerial vehicle (UAV), termed PLUS-Octocopter. As shown in Fig. 1, the system consists of a ground-station, a wireless communication link and the sensor-equipped flying platform. The latter houses 8 electric motors, Global Positioning System (GPS) for stabilized flying mode, two different cameras (visual (VIS) / infra-red (IR)) an onboard-computer and several solid state sensors (T, rH, p, β, γ) as well as a particle number counter (P_N) and a particle mass detector (P_M). Table 1 summarizes its core specifications:

Table 1. Technical specifications of the UAV.

UAV	Octocopter
Power supply	20Ah Li-polymer rechargeable batteries
Flying time	>15min, less at windy conditions
Weight	5 kg (incl. LiPo-pack)
add. payload	2.5 kg
Downlink	Radio-controlled @ 2.4 GHz
2D-sensors	2-servo-adjusted camera unit i) VIS camera (0.4 - 1 µm) i) IR-camera (7.5 - 13 µm)
1D-sensors	Atmospheric (T, rH, p) Radiation (β, γ) Particle mass (µg/m^3) Particle number conc. (1/cm^3) Gases (CO, CO_2, C_2H_6, CH_4, N_2O)
DPU	Win-OS ultra small PC
Flight rec.	120 GB shock resistant SSD
GPS	Flight control & auto-homing
Ground	
Downlink	Radio-controlled @ 2.4 GHz
Win-OS Laptop	Visualization of area (IR & VIS) and display of sensor data

UAV-Characteristics: Although the vehicle is controlled via the ground station, the onboard computer is used both as the data processing unit (DPU) for the control signals keeping the system airborne, as well as a flight recorder for logging flight-sensitive parameters; i.e. status of each cell within the LiPo-packs, GPS-data (location, altitude, flight path). At the same time the DPU-hub logs all the sensor data along with the VIS/IR-data streams. The up- and downlink system, which is likewise controlled via the DPU, is achieved using a commercially available high-power WLAN system operating in the 2.4 GHz-band. At any time, and at least at batteries in reserve capacity status, the UAV will be switched into GPS-guided automatic homing mode.

UAV-sensors: Apart from the 2-D-sensors and the standard atmospheric sniffers (see Table 1), the UAV features two aerosol sensors. The P_M-sensor detects mass-fractions <10µm with a sensitivity of <5ng (with the UAV grounded and slightly less in a stationary humming, airborne mode). The P_N-sensor records particle number concentration in three different size classes simultaneously (0.3, 2.5 and 10 µm). Both aerosol sensors require a data acquisition time of 10 sec, which translates into 6 readings per minute. A different set of sensors regard the solid-state pyroelectric sensors to detect gaseous substances. Their detection principle rests on the specific absorption bands in the IR-window in-between 3 to 5 µm (for the various gases listed in Table 1). The entire throughput of the sample air through the sensor-compartment is achieved via a miniature carbon-vein pump at a constant flow-rate of 5 L/min.

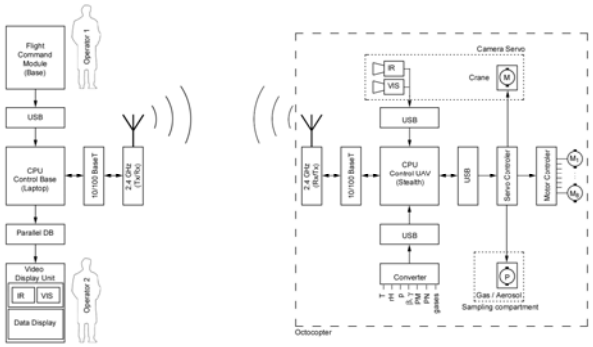

Figure 1. Schematic block diagram of the PLUS Octocopter-system, highlighting ground station and the UAV. *Legend*: Tx, Rx, Transmitter and receiver for the corresponding frequencies; M, Step-motor, M_1-M_8: lifting electric-motors; P, pump; VIS & IR, USB-compatible VIS and IR-camera units, CPU, Central processing unit; USB, Universal Serial Bus; Parallel DB, parallel Data Bus; 10/100BT, bidirectional Ethernet link; T, rH, p, β, γ, P_M, P_N, sensor compartment (see text).

Field of application: the above described system can be used for assisting incident commanders, fire-fighters, environmental air-quality monitoring at stacks, or other emission sources with limited access.

This work was partially supported by the 7th EU Framework Project No. 26.18.17. (BRIDGE).

Tuesday, September 3, 2013

Special Session: PMx
Source apportionment-intercomparisons and trends

European Intercomparison for Receptor Models Using a Synthetic Database

C.A. Belis[1], F. Karagulian[1], F. Amato[2,24], M. Almeida[3], G. Argyropoulos[4], P. Artaxo[5], M.C. Bove [6], D. Cesari[7], D. Contini[7], E. Diapouli[8], K. Eleftheriadis[8], I. El Haddad[9], R.M. Harrison[10], S. Hellebust[11], E. Jang[10], H. Jorquera[12], D. Mooibroek[13], S.Nava[14], J. K. Nøjgaard[15], M. Pandolfi[2], M.G. Perrone[16], A. Pietrodangelo[17], G. Pirovano[18], P. Pokorná[19], P.Prati[6], C. Samara[4], D. Saraga[8], A. Sfetsos[8], G. Valli[20], R. Vecchi[20], M. Vestenius[21], E. Yubero[22], P.K. Hopke[23]

[1]European Commission, Joint Research Centre, Institute for Environment and Sustainability - Ispra, 21027, Italy [2]Institute of Environmental Assessment and Water Research (IDAEA), Barcelona, 08034, Spain [3]High Technical Institute, Technical University of Lisbon, Lisbon, Portugal [4] Dept. of Chemistry, Aristotle University of Thessaloniki, University Campus, 54124, Thessaloniki, Greece [5]Intitute for Applied Physics, University of Sao Paulo, Sao Paulo, Brazil [6]Department of Physics, Università degli Studi di Genova and INFN-Genova, Genoa, Italy [7]Istituto di Scienze dell'Atmosfera e del Clima, ISAC-CNR, Lecce, 73100, Italy 16146, Italy [8]Environmental Research Laboratory NCSR Demokritos, Athens, 15310, Greece [9]Laboratory of Atmospheric Chemistry (LAC), Paul Scherrer Institut, Villigen, 5234, Switzerland [10]National Centre for Atmospheric Science, University of Birmingham, Birmingham, B15 2TT, UK [11]Chemistry Dept., University College Cork, Cork, Ireland [12]Dept of Chemical Engineering, Pontifical Catholic University of Chile, Santiago, Chile [13]National Institute of Public Health and the Environment, Bilthoven, The Netherlands [14]Department of Physics, Università degli Studi di Firenze and INFN-Firenze, Sesto Fiorentino, 50019, Italy [15]Department for Environmental Science, Aarhus University, Roskilde, 4000, Denmark [16]Department of Environmental Science, Università di Milano Bicocca, Milan, 20126, Italy [17]Institute for Atmospheric Pollution, National Research Council, Rome, Monterotondo Staz., 00016, Italy [18]RSE SpA 20134 Milano Italy [19]Faculty of Science, Charles University in Prague, 128 01 Prague 2, Prague, Czech Republic [20]Department of Physics, Università degli Studi di Milano and INFN, Milan, 20133, Italy [21]Finnish Meteorological Institute, Helsinki, FI-00101, Finland [22]Applied Physics Dept., Miguel Hernandez University, Elche Spain [23]Center for Air Resources Engineering and Science, Clarkson University, Potsdam, NY 13699-5708, USA [24]TNO, Built Environment and Geosciences, Dept Air Quality and Climate, 3508 Utrecht, The Netherlands

Keywords: intercomparison, source apportionment, receptor models, PM2.5, synthetic database
Presenting author email: claudio.belis@jrc.ec.europa.eu

Establishing to what extent a methodology for identifying pollution sources is appropriate for a specific purpose and expressing the reliability of the results quantitatively is complex.

In order to assess model performances and estimate their uncertainties, intercomparison exercises (IE) have been conducted within the framework of the JRC Initiative on Harmonization of Source Apportionment with Receptor Models (RM).

The present IE involved 20 expert groups from Europe and 2 from South America and was performed using a synthetic database (DB) developed on purpose.

The test DB consisted of 364 $PM_{2,5}$ daily samples including total mass and 38 inorganic and organic species deriving from a simulation of the CAMx PSAT tool for the calendar year 2005 and extracted for a cell corresponding to the city of Milan.

A total of 26 solutions obtained using the following model versions were reported for evaluation: EPA PMF 3.0 (12), EPA PMF 4.1 (1), EPA PMF 5.0 (1), PMF2 (3), EPA CMB 8.2 (4), EPA CMB ROBOTIC (1), FA MLR (1), COPREM (1) and ME-2 (1).

Participants provided the number and label of the identified sources, their contribution estimation (SCE) and uncertainty. In addition, the source/factor chemical profiles, the contribution of the sources to each species and the contribution of each source/factor in each sample were also reported.

Source/factors identified by participants were classified into 9 different source categories: biomass burning, traffic exhaust, road dust, sulphates, nitrates, crustal material, industry and secondary. An 85% of participants reported a number of source/factors close to the "true" number of sources in the synthetic database (±2).

The inclusion of every source/factor into a category was checked by comparing its chemical profile and time trend with all the other members of the same category and with the reference source. The SCEs of the different solutions were compared with the reference source contributions in the synthetic database using the z-score and z'-score indicators (ISO 5725-5) according to the methodology described by Karagulian & Belis, (2012).

More than 80% of the 200 assessed source/factor contribution estimations met the acceptability criterion when compared to the source contributions used in the creation of the synthetic database. Even though, these results are about 10% lower than those obtained in a previous intercomparison using real-world data, a quite satisfactory ability of RM to retrieve the "true" source contributions comes out from this IE.

Karagulian, F., and Belis, C. A., 2012. Enhancing Source Apportionment with Receptor Models to Foster the Air Quality Directive Implementation. International Journal of Environmental Pollution 50, 190-199.

Ten-year study of fine aerosol at Sde Boker, Israel: time trends, seasonal variation, correlations, and source areas for anthropogenic elements

W. Maenhaut[1,2], A. Karnieli[3] and M.O. Andreae[4]

[1]Department of Analytical Chemistry, Ghent University, Gent, BE-9000, Belgium
[2]Department of Pharmaceutical Sciences, University of Antwerp, Antwerpen, BE-2610, Belgium
[3]Remote Sensing Laboratory, Jacob Blaustein Institutes for Desert Research, Ben-Gurion University of the Negev, Sde Boker Campus 84990, Israel
[4]Biogeochemistry Department, Max Planck Institute for Chemistry, D-55020 Mainz, Germany
Keywords: fine aerosol, Negev desert, elements, source areas.
Presenting author email: willy.maenhaut@ugent.be

From January 1995 through December 2004 aerosol samples were collected with a Gent stacked filter unit sampler at Sde Boker, Israel. The samples were collected according to a 2-2-3 day schedule, which resulted in about 150 samples per year. The samples were analyzed for the particulate mass (PM) by weighing, for black carbon (BC) by a light reflectance technique, and for up to 46 elements by a combination of particle-induced X-ray emission (PIXE) and instrumental neutron activation analysis (INAA) (Maenhaut *et al.*, 2001). Here, we report on the fine (PM2) size fraction data for the PM, BC, and the following 9 anthropogenic elements S, V, Ni, Cu, Zn, As, Se, Sb, and Pb.

The annual medians of the PM, BC, and the 9 anthropogenic elements were examined for time trends. The largest changes over the 10-year period were found for S, Ni, Se, Sb, and Pb and they were -34%, -25%, -47%, +26%, and -40%, respectively. Substantial changes were also noted for the PM and Zn, i.e., of -18% and -12%, respectively, whereas no changes were noted for BC and the other elements. The decreases for S and the PM are consistent with those observed by Karnieli *et al.* (2009) for the July and August data from the same site.

The seasonal variation was also examined. The largest variation was seen for S, which exhibited 1.6 times larger concentrations in summer than in the other 3 seasons. As to the other elements, a similar seasonality was observed for As with 1.4 times enhanced concentrations in summer, and to a lesser extent also for the PM and Zn. That the PM follows S is not surprising as sulphate (estimated as 3 times S) accounted, on average, for 36% of the PM2 mass. For V, Ni, and Sb there was a clear tendency for lower concentrations in summer than in the other seasons. Pb exhibited its highest concentrations in fall and winter and virtually no seasonality was seen for BC, Cu, and Se.

S was substantially correlated with the PM ($r = 0.65$), whereas its correlation coefficients with BC and the 9 elements were all lower than 0.5. V and Ni were very highly correlated with each other ($r = 0.94$) and substantially ($0.5 < r < 0.7$) with BC, Sb, and Pb. The correlation between V and Ni, together with the average V/Ni ratio of 2.3±0.5 clearly point to heavy oil burning as the predominant source of both elements. Since BC at the site is thought to originate predominantly from the incomplete combustion of fossil fuels, it is not surprising to see that it is correlated with V and Ni. Cu was best correlated with BC ($r = 0.53$) and the correlation coefficients of Zn, As, and Se with the other elements, BC, and the PM were all lower than 0.5.

Trajectory statistics (Lupu and Maenhaut, 2002), using 10-day back trajectories with arrival at 300 m above ground, was applied to assess the source areas of the PM, BC, and the 9 elements. The trajectories came predominantly from the northwest, but there were seasonal differences in the transport pathways, with westerly ones becoming important in winter and northerly ones important in summer. The concentration field map for S is shown in Figure 1. It appears that the prevailing source region for S was southeastern Europe (i.e., Turkey, Bulgaria, Romania, Ukraine, and southern Russia). As had the southeastern part of European Russia as its prevailing source area, while the source picture for Zn was rather unclear. The other 6 anthropogenic elements and BC seemed to originate mainly from regional sources (i.e., Jordan, Syria, Iraq, and Saudi Arabia).

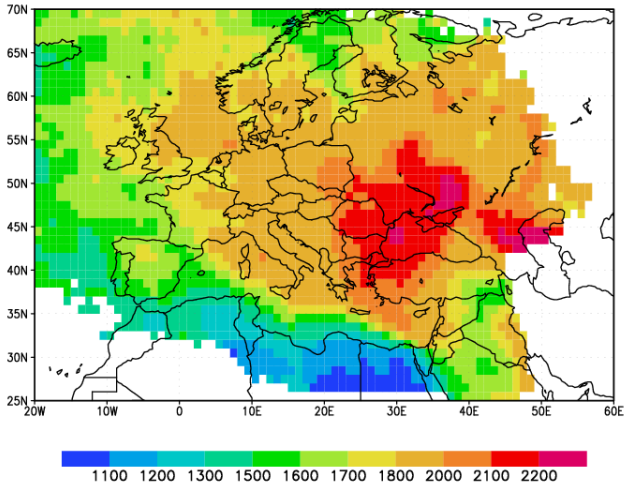

Figure 1. Fine S concentration field (ng/m^3, with the concentration scale shown at the bottom) as computed with trajectory statistics.

Karnieli, A., Derimian, Y., Indoitu, R., Panov, N., Levy, R.C., Remer, L.A., Maenhaut, W. and Holben, B.N. (2009) *J. Geophys. Res.* **114**, D00D19, doi:10.1029/2009JD011870.

Lupu, A and Maenhaut, W. (2002) *Atmos. Environ.* **36**, 5607-5618.

Maenhaut, W., Raes, N. and Wang, W. (2001) *Nucl. Instrum. Methods Phys. Res.* **B269**, 2693-2698.

Impact of international shipping on European air quality

M. Viana[1], A. Colette[2], J. van Aardenne[3], X. Querol[1], B. Degraeuwe[4], P. Hammingh[5] and I. de Vlieger[4]

[1] IDAEA-CSIC, 08034 Barcelona, Spain
[2] INERIS, France
[3] European Environment Agency, 1050 Copenhagen, Denmark
[4] VITO, 2400 Mol, Belgium
[5] PBL, 3720 Bilthoven, The Netherlands
Keywords: source apportionment, vessels, fossil fuel, human exposure.
Presenting author email: mar.viana@idaea.csic.es

Emissions from the marine transport sector contribute significantly to air pollution globally (Corbett & Fischbeck, 1997). Around 15% of global NOx and 5-8% of global SOx emissions are attributable to oceangoing ships (Eyring et al., 2005). Because nearly 70% of ship emissions are estimated to occur within 400 km of land, ships have the potential to contribute significantly to air quality degradation in coastal areas.

Shipping emissions are currently increasing, and even more so in the future due to the globalization of manufacturing processes and the increase of global-scale trade (USEPA, 2009). This increased flow of commercial ships into and out of ports does not only affect major ports, but also medium and small-scale ones. Although shipping contributes significantly to the international transportation sector, its emissions are not well quantified and are one of the least regulated anthropogenic sources.

In this context, the European Environment Agency initiated a project to investigate the current impact of the ship emissions on the ambient air levels of primary and secondary aerosols, and how the predicted future growth of ship traffic and the geographical expansion of waterways and ports, possibly combined with international regulations, will affect the atmospheric composition. In order to design and implement effective regulation to minimise environmental impacts of these emissions, detailed knowledge is necessary on their effects on climate and on their contribution to atmospheric pollution.

An in depth literature review was carried out focusing on the assessment of the impacts of shipping emissions and activities on urban air quality in coastal areas. The initial conclusion extracted from this review is that studies addressing this topic are relatively scarce, and that therefore there is a need to encourage this type of assessment in European coastal (and potentially, inland) areas. In particular, quantitative studies are especially scarce.

In addition to the literature review, the contribution of shipping activities to the degradation of European air quality and regional climate change was assessed by means of sensitivity chemistry transport simulations with the CHIMERE model based on the emission projections of the Global Energy Assessment.

The literature review evidenced that shipping emissions contribute to ambient PM levels in European coastal areas with 1-7% of PM_{10}, 1-14% of $PM_{2.5}$ (reaching a maximum of 20% in Genoa, Italy) and at least 11% of PM_1 (data for this size fraction available only for 1 location). Thus, it is evident that the impact of shipping activities increases with decreasing particle size. For the sake of comparison, contributions reported for non-European harbours (USA) were <5% of $PM_{2.5}$ in Los Angeles and 4-6% of $PM_{2.5}$ in Seattle. Spatially, shipping contributions to urban air quality degradation are higher in Mediterranean cities than in Atlantic coastal areas. However, it must be highlighted that results were obtained using different approaches and methodologies in the different regions, and thus may not be directly comparable.

The data available on gaseous pollutants is even more scarce than for PMx. Contributions from shipping to ambient NO_2 levels range between 7 and 24%, with the highest values being recorded in the Netherlands and Denmark. Increases in SO_2 concentrations were only reported in Sweden, as relative increases with respect to background concentrations and not in absolute terms.

Finally, current research evidences that shipping emissions impact not only the levels and composition of airborne particles and gaseous pollutants, but that they also may enhance new particle formation in urban areas and contribute to other forms of air quality degradation.

The modelling exercise evidenced that, to date, ships are responsible for about half of the NO_2 and SO_2 concentrations found over sea surface. In the future, SOx emissions are expected to be reduced, so that the contribution of ships to SO_2 over sea surface will decrease to about 1/3, whereas their contribution to absorbing BC will be higher than for the present-day.

In coastal areas, ships are responsible for about 7-8% of human exposure to particulate sulphate and 4% of the exposure to $PM_{2.5}$ and ozone peaks. The model results offer a good insight into the geographical variability of the impact, which is consistent with the estimates derived from ambient air monitoring.

This work was supported by the ETC/ACM, EEA and national projects CGL2011-26574 and CGL2010-19464.

Corbett & Fischbeck (1997) Science, (278) 823-824.
EEA (2013), EEA Technical Report.
Eyring, V et al. (2005) J. Geophys. Res., 110, D17305.
US-EPA (2009) EPA-420-R-09-007.
Riahi, K. et al. (2012) Global Energy Assessment: Toward a Sustainable Future.

Hourly elemental composition and source identification of fine and coarse particulate matter in the high polluted industrial area of Taranto (Italy)

F. Lucarelli[1], G. Calzolai[1], M. Chiari[1] and S.Nava[1]

[1]Department of Physics and Astronomy, University of Florence and National Institute of Nuclear Physics (INFN), Sesto Fiorentino (Florence), 50019, Italy

Keywords: PIXE, hourly composition, source apportionment, steel plant
Presenting author email: lucarelli@fi.infn.it

Taranto, an ancient Italian town lying on the Ionic Sea coast, is nowadays one of the most industrialized towns in the South of Italy. An industrial area, that includes the biggest steel plant of Europe, one of the biggest Italian refinery, a power plant and a big cement industry, is located in the northern suburbs of the town. During the last year pollution problems of this area have come under the spotlight and have become a very compelling issue for the policy makers.

In the frame of an extensive environmental investigation, promoted by the Italian Health Ministry, the ISPESL (Istituto Superiore per la Prevenzione e la Sicurezza del Lavoro) and the CNR (Consiglio Nazionale della Ricerca), aerosol samples were collected with high time resolution and analysed by PIXE. The project included two sampling campaigns (February–March and June 2004), in two different sites: Tamburi (site A in the following), an urban district in Taranto adjacent to the industrial area, and Statte (site B), a small town located 7 km N-NW of Taranto. Site A is a dense populated quarter subject to a heavy pollution flux; site B is located along the direction of prevalent winds from the industrial area.

The fine (< 2.5 μm) and coarse (2.5-10 μm) fractions of particulate matter were simultaneously collected in the two sampling sites by means of two ‘‘streaker’’ samplers (PIXE International Corporation). PIXE analyses were performed with a 3 MeV proton beam from the 3 MV Tandetron accelerator of the INFN-LABEC laboratory (Calzolai et al., 2006). These analyses allowed the assessment of the concentrations of several elements (Na, Mg, Al, Si, P, S, Cl, K, Ca, Ti, V, Cr, Mn, Fe, Ni, Cu, Zn, Br, Sr and Pb), including important industrial tracers, with hourly time resolution.

Although the vast majority of results in literature are limited to time resolution of the input samples of typically 12 or 24 h, most particulate emissions as well as their atmospheric transport and dilution processes change within a few hours and daily samples are not capable of tracking these rapid changes. Furthermore, source apportionment receptor models need a series of samples containing material from the same set of sources in differing proportions and increasing the time resolution of the measurements typically provides samples that have greater between-sample variability in the source contributions than samples integrated over longer time periods.

In this study the high time resolution of the adopted approach allowed us to follow in detail changes in the aerosol elemental composition due to both the time evolution of the industrial emissions and the time changes in meteorological conditions and thus transport pathways. Moreover, the location of the sampling sites, along the prevalent wind direction and in opposite position with respect to the industrial site, allowed us to follow the impact of the industrial plume as a function of wind direction.

The most significant feature of this data set is the presence of very high hourly concentrations of Fe (up to 15 μg/m^3 in the fine fraction and 12 μg/m^3 in the coarse one) and Mn (up to 170 ng/m^3 and 115 ng/m^3 in the fine and coarse fractions, respectively), which are typical tracers of steel smelter emissions. Their time trends are high correlated and show sharp peaks, typical of industrial emissions, which are in opposite phase in the two sampling sites (Fig. 1).

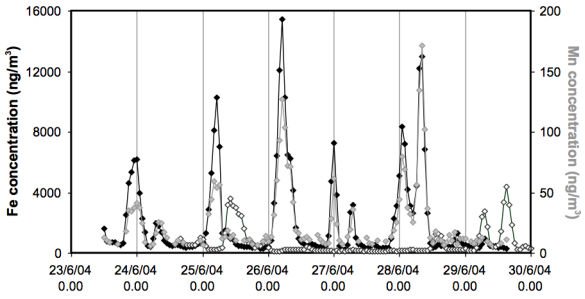

Figure 1. Hourly time trends of fine Fe (black) and fine Mn (white) in site A, and fine Fe (grey) in site B.

Positive Matrix Factorisation (PMF) has been applied to the data to assess the main aerosol sources, and in particular the impact of industrial emissions. Results of these analyses will be shown.

Calzolai, G., Chiari, M., Garcia-Orellana, I., Lucarelli, F., Migliori, A., Nava S., Taccetti, F. (2006), Nucl. Instr. and Meth. B 249, 584-587.

Source apportionment of size resolved particulate matter in European air pollution hot spot

P. Pokorná[1], J. Hovorka[1] and P.K. Hopke[2]

[1] Institute for Environmental Studies, Faculty of Science, Charles University in Prague, Benátská 2, 128 01, Prague 2, Czech Republic

[2]Center for Air Resources Engineering and Science, Clarkson University, Box 5708, Potsdam, NY 13699-5708, USA

Keywords: Hourly resolved aerosol elemental composition, DRUM, PMF.

Presenting author email: petra.karkulin@post.cz

The ambient aerosol source composition is particle size dependent (Dodd, 1991). Therefore, to improve the accuracy of aerosol source apportionment, size segregated aerosol measurement with high time resolution is required (Han, 2005; Peré-Trepat, 2007). The objective of presented study was to identify sources of size resolved ambient aerosols in industrial city Ostrava in Czech Republic, Central Europe.

Measurements were conducted from 26th Jan to 21st Feb 2012 in Ostrava city in the north-east part of the Czech Republic. The heavy industrialized city, accumulation of steel industry and coke plants, counts among the worst air quality region in EU.

A Davis Rotating-drum Uniform-size-cut Monitoring (DRUM) was used to sample with 1-h time resolution aerosol particles of aerodynamic diameter D_p for three size modes A (10 μm > Dp > 1.15 μm), B (1.15 μm > Dp > 0.34 μm) and C (0.34 μm > Dp > 0.1 μm). Aerosol masses were calculated from five minute data by Aerodynamic Particle Sizer, APS (3321, TSI) and Scanning mobility Particle Sizer, SMPS (3963, TSI). To evaluate middle-scale $PM_{2.5}$ variability in an urban airshed, $PM_{2.5}$ measurement by 7 laser photometers DustTrak, DT (8520, TSI) in a network arrangement was conducted. Complete meteorology wind speed (WS) wind direction (WD), temperature (T), relative humidity (RH), global radiation (GR), precipitation (P) were also concurrently recorded.

A bilinear receptor model, EPA PMF 4.2.0.0, was used to resolve the possible sources for 60 minutes mass integrates for three sizes m as measured by APS and SMPS and elemental composition for 28 elements sampled by 3DRUM analyzed by S-XRF.

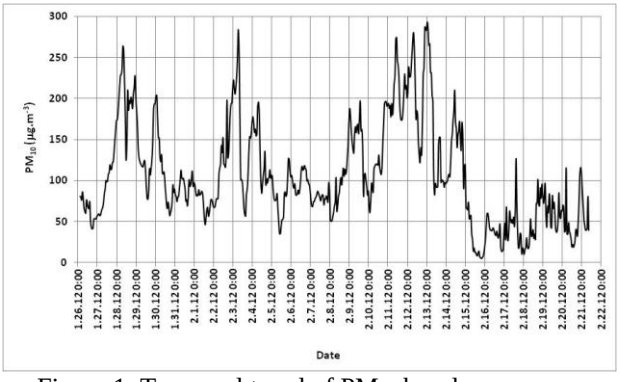

Figure 1. Temporal trend of PM_{10} hourly averages.

According to the different meteorological condition and PM_{10} levels the measuring campaign was separated into two periods, smog and after smog. The smog period characterized low T (median=-14.8 °C), WS (median=0.7 $m.s^{-1}$), WD prevailing from NE and high PM_{10} (median=108 $\mu g.m^{-3}$) lasted from 26th Jan to 14th Feb. The after smog period (15th – 21st Feb) was characterized by grow of T (median=-1.7 °C), WS (median=1.1 $m.s^{-1}$), WD prevailing from NW to SW and precipitation, which resulted in PM_{10} decrease (median=40.1 $\mu g.m^{-3}$) (Figure 1.). The median of three size fraction (A, B and C) during smog episode and after is quoted in the Table 1.

Table 1. The three fraction median value for smog and after smog episode in Ostrava 26th Jan-21st Feb 2012.

Size fraction	Smog	After smog
	median ($\mu g.m^{-3}$)	
A	22.1	11.5
B	39.1	10.8
C	47.6	15.4

The $PM_{2.5}$ inter-DT differences in the course of measurement were not statistically significant. We may conclude, that the monitoring station was well positioned and the measurements eligible at least for a middle scale of urban airshed.

The PMF resolved from five to six possible sources related to the size fraction. The sources of B and C fraction corresponded to each other from 83 % (5 sources from total number of 6 sources). The A fraction sources matched with the two fraction sources from 60 % (3 sources from total number of 5 sources). The antrophogenic sources industry, combustion and traffic (exhausted and nonexhausted emission) contributed most to PM_{10}.

This work was supported by the Grant Agency of the Czech Republic under the project GAP503/12/G147.

Dodd, J.A., Ondov, J.M., Tuncel, G., Dzubay, T.G., Stevens, R.K. (1991) *Environ. Sci. & Techol.* **25**, 890-903.

Han, J.S., Moon, K.J., Ryu, S.Y., Kim, Y.J., Perry, K.D. (2005) *Atmos. Environ.* **39**, 3113–3125.

Peré-Trepart, E., Kim, E., Paatero, P., Hopke, P.K. (2007) *Atmos. Environ.* **41**, 5921-5933.

A mass closure and source apportionment study on PM1 in Milan (Italy)

R. Vecchi[1], V. Bernardoni[1,2], M. Boretti[1], M. Elser[1,*], P. Fermo[2], A. Piazzalunga[3], R. Gonzalez Turrion[2] and G. Valli[1]

[1]Department of Physics, Università degli Studi di Milano & INFN, Milan, 20133, Italy
[2]Department of Chemistry, Università degli Studi di Milano, Milan, 20133, Italy
[3]Department of Environmental Science, University of Milano Bicocca, Milan, 20126, Italy
* now at Laboratory of Atmospheric Chemistry, Paul Scherrer Institut, Villigen ,5232, Switzerland

Keywords: PM1, chemical characterisation, ME-2
Presenting author email: roberta.vecchi@unimi.it

It is well known that the particle size plays a major role in determining the particle penetration in the respiratory system and therefore in threatening human health.

Despite this fact, data on PM1 composition and sources are still relatively rare. This work aimed at a detailed physical and chemical characterisation of PM1 to obtain the mass closure and to perform a source apportionment study using receptor modelling. Episodes with very high PM1 pollution levels were analysed in detail to identify processes/sources affecting this fine PM fraction.

Moreover, a critical comparison to the results obtained during the previous PM1 campaigns carried out by our group at the same location about 10 years ago (Vecchi et al. 2004; Vecchi et al., 2008) will be also shown.

PM1 was sampled at an urban background station in Milan, Italy, during winter 2011-2012. Milan is the greatest urban area in the Po Valley, a well-known hot-spot pollution area in Europe, especially during wintertime. Parallel PM1 sampling was carried out during daytime and nighttime (07-16, 19-04) on PTFE and quartz fibre filters using two low-volume samplers for a total of about 300 samples. Mass concentration was determined by the gravimetric technique and all the PM1 samples were chemically characterised for elements, inorganic ions, levoglucosan, EC/OC and water soluble organic compounds. BC determination was also carried out on both PTFE and quartz fibre filters by a polar photometer (Vecchi et al., 2010; Vecchi et al., 2012). Moreover, BC concentrations in PM1 were monitored with a 5 minute resolution by a MAAP. Ancillary information on atmospheric dispersion conditions was available by ^{222}Rn measurements and the main meteorological parameters (temperature, pressure, RH, solar radiation, wind speed and direction) were also monitored at the sampling site.

PM1 data were analysed by receptor modelling using Multilinear Engine ME-2 and 5 factors were identified. The most relevant contributions to PM1 were from ammonium nitrate and biomass burning (about 30% each) followed by ammonium sulphate (about 20%), traffic (about 15%) and industry (about 5%).

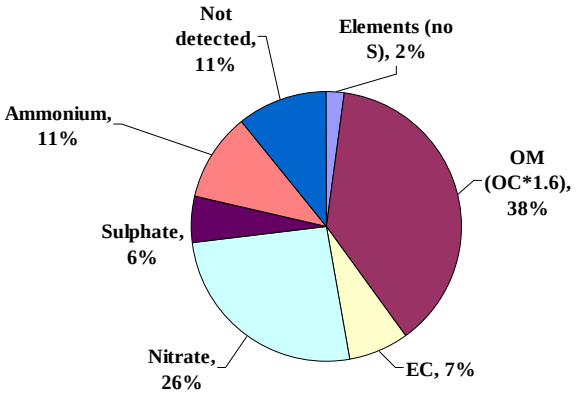

Figure 1. PM1 mass closure.

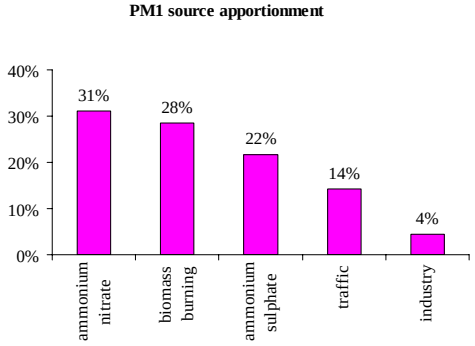

Figure 2. PM1 source apportionment.

References.

Vecchi, R., et al. (2004). Atmos. Environ. **38**, 4437–4446.

Vecchi, R., et al. (2008). Atmos. Environ. **42**, 2240–2253.

Vecchi, R., et al. (2010). *Abstract 11E2, International Aerosol Conference 2010*, Helsinki, August 29 - September 3, 2010.

Vecchi, R., et al. (2012). *Abstract, European Aerosol Conference 2012*, Granada, 2 – 7 September, 2012.

Performance of the Chemical Mass Balance Model with Various Traffic Profiles

Pallavi Pant[1], Jianxin Yin[1] and Roy M. Harrison[1, 2]

[1]School of Geography, Earth and Environmental Studies, University of Birmingham, Edgbaston, Birmingham, B15 2TT, UK
[2]Department of Environmental Sciences/Centre of Excellence in Environmental Studies, King Abdulaziz University, PO Box 80203, Jeddah (21589), Saudi Arabia
Keywords: source apportionment, traffic, particulate matter, source profiles.
Presenting author email: pxp024@bham.ac.uk

Road traffic is one of the key sources of particulate matter (PM) concentrations in urban areas, and a good understanding of the contribution of traffic emissions to PM mass is imperative for policy action. Receptor models such as the Chemical Mass Balance (CMB) and Positive Matrix Factorization (PMF) are routinely used for quantitative estimation of source contributions to PM. The CMB model, based on the principle of mass balance, requires locally-relevant profiles for reliable source contribution estimates (SCEs).

The aim of this study was to assess the response of the CMB-MM model to molecular marker profiles for traffic derived using different sampling approaches, i.e. dynamometer and twin-site sampling (Schauer *et al.*, 1996). The traffic estimates thus obtained were cross-compared using other proposed methods as described in Figure 1.

24-hour samples were collected using high-volume samplers at roadside, urban background and rural sites in Birmingham and London (UK) in 2007 and 2011 respectively. Chemical analysis was carried out using GC-MS as described in Yin *et al.* (2010).

Using ambient measurement-based molecular marker data from the roadside and background sites in London, a composite traffic profile for $PM_{2.5}$ OC was created. Based on previous studies and information about key sources in the area, a total of six profiles were used including vegetative detritus, wood combustion, coal combustion, natural gas, crustal dust and traffic (diesel, gasoline and smoking engine). Ambient data was analysed using the CMB8.2 software for attribution of $PM_{2.5}$ OC mass to different sources. The marker species for the sources were monitored using the MPIN matrix and cross-compared with other published studies and the r^2 and χ^2 were observed to be between 0.96-1.00 and 0.08- 3.00 respectively. $PM_{2.5}$ estimates were obtained using OC to $PM_{2.5}$ source conversion ratios previously published in Yin *et al.* (2010).

The model resolved the CMB mass reasonably well with both composite and dynamometer profiles with 88.8-117.1% of the $PM_{2.5}$ mass resolved across all datasets. In terms of resolution of the traffic source, while there was overall agreement between the SCEs from the different profiles, the t-stat values for the composite profile were consistently lower than the dynamometer profile runs. Comparisons with mass closure and the EC-tracer calculations lead to the conclusion that the composite profiles estimates the traffic source contribution better than the dynamometer profile. However, it is important to bear in mind that the traffic profiles generated using ambient data have higher uncertainties and the chemical species can be subject to oxidation in the atmosphere, both of which can impact upon the model output.

Analysis is currently underway to prepare traffic source profiles using tunnel data which will then be compared against twin-site profile and dynamometer profiles.

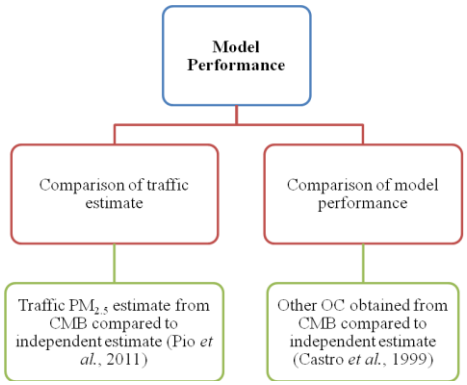

Figure 1: Assessment of model performance using independent estimates

Pallavi Pant gratefully acknowledges financial support from the University of Birmingham.

Schauer, J.J., Rogge, W.F., Hildemann, L.M., Mazurek, M.A., Cass, G.R. and Simoneit, B.R.T. (1996) *Atmos. Env.* **30**, 3837-3855.

Yan, B., Zheng, M., Hu, Y., Ding, X. et al. (2009) *Atmos. Env.* **43(12)**, 4287-4293.

Yin, J., Harrison, R.M., Chen, Q., Rutter, A. and Schauer, J.J. (2010) *Atmos. Env.* **44(6)**, 841-851.

PMF source apportionment for fine and coarse PM in Athens, Greece: Evolution of source contributions over the last decade

K. Eleftheriadis[1], E. Diapouli[1], A. Karanasiou[2], S. Vratolis[1], V. Vasilatou[1], M. Gini[1], D. Saraga[1], S. Pateraki[1], Th. Maggos[1]

[1] Institute of Nuclear & Radiological Sciences & Technology, Energy & Safety,
National Centre of Scientific Research "Demokritos", 15310 Ag. Paraskevi, Attiki, Greece
[2] Institute of Environmental Assessment and Water Research, Spanish Research Council, 08034 Barcelona, Spain
Keywords: $PM_{10}/PM_{2.5}$, source apportionment, PMF, source evolution.
Presenting author email: eleftheriadis@ipta.demokritos.gr

Particulate air pollution remains a significant environmental problem in big urban centres in Europe and around the world. The development of effective control policies calls for the identification of the main particulate matter (PM) sources, as well as the quantification of their contribution to elevated concentration levels. The city of Athens has been known to face severe air pollution problems due both to the presence of multiple particle sources and to the meteorological conditions and topography that promote pollutants build-up. The presence of significant natural sources further complicates the efforts to apply effective mitigation measures and to ensure compliance with air quality guidelines. The objective of the present work was to identify the major PM sources in the Athens area, quantify their relative contribution to coarse and fine particle concentrations and examine their evolution over the last decade.

Source apportionment by positive matrix factorization (PMF) analysis was performed on two $PM_{10}/PM_{2.5}$ datasets from 2002 and 2012. Both datasets covered warm and cold period. The 2002 measurement campaign included 24-hr gravimetric measurements from three urban residential sites. The collected teflon filters were analysed for a number of elements by electrothermal atomic absorption spectrometry (Cd, Pb, V, Ni, Mn, Cr, Cu, Fe and Al) and flame atomic absorption spectrometry (Ca, Mg, K and Na), as well as for major anions (Cl^-, NO_3^- and $SO4^{2-}$) by ion chromatography. In addition, black carbon (BC) data were obtained by means of an aethalometer (AE-9, Maggee Sci). The 2012 campaign was conducted at two urban background sites. 24-hr gravimetric measurements were performed with two different filter substrates (teflon and quartz) in order to allow for a more extensive chemical characterization of the aerosol fractions. Elemental composition was again quantified by electrothermal and flame atomic absorption spectrometry. Ionic species (Na^+, Mg^{2+}, Ca^{2+}, K^+, NH_4^+, SO_4^{2-}, NO_3^-, Cl^-) were quantified by ion chromatography, while elemental (EC) and organic (OC) carbon were also measured by thermal-optical methodology.

Two-dimensional Positive Matrix Factorisation (PMF) has been applied to each dataset. Details on input data preparation are provided in Karanasiou et al. (2009). Two PMF models were used, PMF2 (Version 4.2) and EPA PMF 3.0, and the obtained results were compared. Analysis was performed for different numbers of factors and the best solution was chosen based on goodness of fit parameters (Q value and the explained variation of the matrix F) as well as by examining the obtained factors profiles with respect to the possibility of associating them with specific source. In addition, multiple values of Fpeak (in the range -2.0 to 2.0) were examined in order to explore different rotations of the solutions.

In general the two models applied showed good agreement of results. Vehicular traffic was found the main contributor to fine particle concentrations, with marine aerosol also playing a major role. Fossil fuel combustion and traffic contributions were similar. Coarse particles concentrations seemed unaffected by all combustion-related sources and were attributed to a large extent to natural sources (sea salt, soil). (Figure 1)

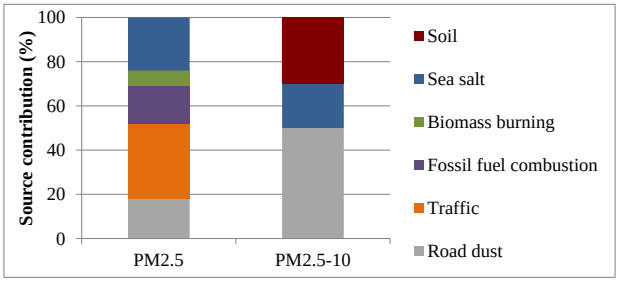

Figure 1. Relative contribution (%) of each source to PM concentration levels (Year 2002).

PMF analysis on the 2012 dataset is still in progress but initial results indicated a differentiation in PM source contributions over the last decade. This is also evident by the reduced concentration levels, attributed to a decrease in anthropogenic emissions either because of efficient mitigation measures (new-technology "cleaner" vehicles, traffic regulations etc.) and/or lower anthropogenic activity due to the financial crisis of the last two years. The final results are expected to provide an interesting insight into the present air pollution situation in the city and the potential "new" major contributors to the observed daily exceedances of air quality guidelines.

This work was supported by the European Commission LIFE+ Environment Policy and Governance programme.

Karanasiou, A.A., Siskos, P.A. and Eleftheriadis, K. (2009) *Atmos. Environ.* **43**, 3385–3395..

Tuesday, September 3, 2013

Session: Atmospheric Aerosols
New particle formation

Role of organics in particle nucleation as viewed from a positive ion spectrometer

F. Bianchi[1], J. Dommen[1], J. Tröstl[1], S. Schobesberger[2], H. Junninen[2], D.R. Worsnop[2,3], E. Weingartner[1], U. Baltensperger[1] and the CLOUD collaboration

[1]Laboratory of Atmospheric Chemistry, Paul Scherrer Institute, Villigen, 5232, Switzerland
[2]Department of Physics, University of Helsinki, FI-00014 Helsinki, Finland
[3]Aerodyne Research Inc., Billerica, Massachusetts 01821, USA
Nucleation, cluster, sulfuric acid, ions, mass spectrometry
Presenting author email: Josef.dommen@psi.ch

Formation of new particles from trace gases (nucleation) has been recognized as the main source of aerosols in the atmosphere. It is estimated that nucleation can be responsible for up to 50% of the total cloud condensation nuclei (CCN) concentration (Merikanto et al., 2009). However, the formation of new particles in the atmosphere is still a poorly understood process despite its importance. In recent years sulfuric acid (H_2SO_4) has emerged as the key player in atmospheric nucleation. In many field campaigns a good correlation between the concentration of H_2SO_4 and the rate of particle nucleation was found. Laboratory experiments have shown that binary H_2SO_4-H_2O homogeneous nucleation cannot explain the observations in many regions of the atmosphere. Ion-mediated nucleation (IMN) is discussed as a potential strong source of aerosol formation and as a mechanism of influence of cosmic rays on clouds and climate. Based on model simulations Yu et al. (2008) conclude that IMN is significant on a global scale. Thus, it is very important to determine which trace species participate in the first steps of the nucleation process and which mechanisms govern the nucleation.

Experiments were performed in the CLOUD chamber which allows the study of nucleation rates under highly controlled conditions of temperature, humidity and trace gas concentrations. This 26 m^3 stainless-steel chamber is equipped with state-of-the-art instruments can be exposed to a π^+ beam coming from CERN's proton synchrotron to simulate the effect of the galactic cosmic rays on the new particle formation process. On the other hand a 20kV/m electric clearing field can be engaged to enforce an ion-free environment.

We investigated new particle formation of sulfuric acid (H_2SO_4) in the presence of compounds such as ammonia, dimethylamine ($(CH_3)_2NH$), α-pinene ($C_{10}H_{16}$) and pinanediol ($C_{10}H_{18}O_2$). The nucleation process was induced either by ozonolysis of α-pinene or OH radical reactions produced by UV-photolysis of ozone or HONO.

Here we present results obtained with the atmospheric pressure interface time-of-flight mass spectrometer (APi-TOF, Tofwerk and Aerodyne Research) operated in the positive ion mode (Junninen et al., 2010). This instrument samples directly the ions present in the CLOUD chamber through a critical orifice and measures their mass-to-charge ratio at a resolution higher than 5000 Th/Th and a mass accuracy lower than 10 ppm. Due to the high resolution of the instrument the composition of the evolving positive charged clusters could be measured for the various systems: H_2SO_4–NH_3, H_2SO_4–DMA and H_2SO_4–oxidized organics (OxOrg). In the case of the H_2SO_4–NH_3 system we observed $(H_2SO_4)_n \cdot (NH_3)_{n+1} \cdot H^+$ positive ions for low *n* and one extra molecule of ammonia for higher *n*. In the presence of DMA ammonia was substituted by DMA but the composition and stoichiometry remained essentially the same. However, the time evolution of the cluster formation was quite different for the two systems. In the case of H_2SO_4–OxOrg clusters were found in the m/z range from 200 Th up to 1500 Th. Highly oxidized organic species were observed. In all those positively charged clusters, whose chemical composition could be identified, no H_2SO_4 was observed. These results with the positive ion spectra obtained in the laboratory will be compared to measurements in the ambient atmosphere during nucleation events.

We thank CERN for supporting CLOUD with important technical and financial resources, and for providing a particle beam from the CERN Proton Synchrotron. This research has received funding from the EC 7th Framework Programme (Marie Curie Initial Training Network "CLOUD-ITN" no. 215072, MC-ITN "CLOUD-TRAIN" no. 316662, and ERC-Advanced "ATMNUCLE" grant no. 227463), the German Federal Ministry of Education and Research (project nos. 01LK0902A and 01LK1222A), the Swiss National Science Foundation (project nos. 200020_135307 and 206620_130527), the Academy of Finland (Center of Excellence project no. 1118615), the Academy of Finland (135054, 133872, 251427, 139656, 139995, 137749, 141217, 141451), the Finnish Funding Agency for Technology and Innovation, the Nessling Foundation, the Austrian Science Fund (FWF; project no. P19546 and L593), the Portuguese Foundation for Science and Technology (project no. CERN/FP/116387/2010), the Swedish Research Council, Vetenskapsrådet (grant 2011-5120), the Presidium of the Russian Academy of Sciences and Russian Foundation for Basic Research (grants 08-02-91006-CERN and 12-02-91522-CERN), and the U.S. National Science Foundation (grants AGS1136479 and CHE1012293).

Junninen, H. et al. (2010) *Atmos. Meas. Tech.* **3**, 1039-1053.
Merikanto, J. et al. (2009) *Atmos. Chem. Phys.* **9**, 8601-8616.
Yu, F. et al. (2008) *Atmos. Chem. Phys.* **8**, 2537–2554.

Particle formation above natural and simulated salt lakes

K. A. Kamilli[1], J. Ofner[2], T. Sattler[3], T. Krause[3], C. Zetzsch[4], A. Held[1]

[1] Junior Professorship in Atmospheric Chemistry, University of Bayreuth, Germany
[2] Vienna University of Technology, Austria
[3] Institute of Earth Science, University of Heidelberg, Germany
[4] Atmospheric Chemistry Research Laboratory, University of Bayreuth, Germany
Keywords: New particle formation, Physical and chemical properties, Smog chamber experiments, Halogen-induced secondary organic aerosol.
Presenting author email: katharina.kamilli@uni-bayreuth.de

Western Australia was originally covered by natural eucalyptus forests, but land-use has changed considerably after large scale deforestation from 1950 to 1970. Thus, the ground-water level rose and brought dissolved salts and minerals to the surface. Nowadays, Western Australia is known for a great plenty of salt lakes with pH levels reaching from 2.5 to 7.1. The land is mainly used for wheat farming and livestock and becomes drier due to the lack of rain periods. One possible reason could be the formation of ultrafine particles from salt lakes, which increases the number of cloud condensation nuclei and thus potentially suppresses precipitation.

Several field campaigns have been conducted between 2006 and 2011 with car-based and airborne measurements, where new particle formation has been observed and has been related to the Western Australian salt lakes (Junkermann et al., 2009). To identify particle formation directly above the salt lakes, a 2.35 m³ PTFE chamber was set up above several lakes in 2012. Inside the chamber, photochemistry may take place whereas mixing through wind or advection of already existing particles is prevented. Salt lakes with a low pH level lead to strongly increased aerosol formation. In two chamber experiments also aerosol filter samples have been taken. The chemical analysis of the anions by ion chromatography showed a 8 to 17 times higher concentration of Cl^- than SO_4^{2-}. Thus, the particle formation seems to be influenced by halogens.

As salt lakes have been identified as a source for reactive halogen species (RHS; Buxmann et al., 2012) and RHS seem to interact with precursors of secondary organic aerosol (SOA), they could be producers of halogen induced secondary organic aerosol (XOA) (Ofner et al., 2012).

As reference experiments, laboratory based aerosol smog-chamber runs were performed to examine XOA formation under atmospheric conditions using simulated sunlight and the simplified chemical composition of a salt lake. The mixture included $FeSO_4$, NaCl and Na_2SO_4. After adding α-pinene to the simulated salt lake, a strong nucleation event began (Figure 1) in the absence of ozone comparable to the observed events in Western Australia in 2012. First results from the laboratory based aerosol smog-chamber experiments indicate a halogen-induced aerosol formation above Australian salt lakes. To validate this hypothesis, additional measurements above several salt lakes of Western Australia will be conducted in spring 2013 with combined physical and chemical investigations. The particle number size distribution will be recorded by a mobile DMPS system and for further chemical analysis filter and impactor samples will be taken.

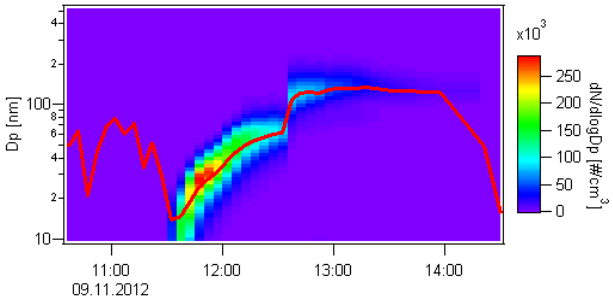

Figure 1. Contour plot with the geometric mean diameter (red) for an aerosol formation event above a simulated salt lake in a smog chamber experiment with simulated sunlight.

This work was funded by the German Research Foundation (DFG) under grants HE 5214/5-1 and ZE792/5-2.

Buxmann, J., Balzer, N., Bleicher, S., Platt, U., and Zetzsch, C.: Observations of bromine explosions in smog chamber experiments above a model salt pan, Int. J. Chem. Kinet., 44, 312-326, 2012.

Junkermann, W., Hacker, J., Lyons, T., and Nair, U.: Land use change suppresses precipitation, Atmos. Chem. Phys., 9, 6531–6539, 2009.

Ofner, J., Balzer, N., Buxmann, J., Grothe, H., Schmitt-Kopplin, Ph., Platt, U., and Zetzsch, C.: Halogenation processes of secondary organic aerosol and implications on halogen release mechanisms, Atmos. Chem. Phys., 12, 5787-5806, 2012.

Secondary aerosol formation from stress-induced biogenic emissions and possible climate feedbacks

Th. F. Mentel[1], E. Kleist[2], S. Andres[1], M. Dal Maso[1,4], Th. Hohaus[1], A. Kiendler-Scharr[1], Y. Rudich[5], M. Springer[1], R. Tillmann[1], R. Uerlings[2], A.Wahner[1], J. Wildt[2]

[1]Institut für Energie und Klimaforschung, IEK-8, Forschungszentrum Jülich, Germany
[2]Institut für Bio- und Geowissenschaften, IBG-2, Forschungszentrum Jülich, Germany
[3]Department of Physics, University of Helsinki, PO Box 48, 00014, Helsinki, Finland
[4]Dept. of Physics, Tampere University of Technology, 33101 Tampere, Finland
[5]Weizmann Institute of Science, Rehovot, 76100 Israel

Keywords: biogenic SOA , stress induced emissions, climate feedback

Presenting author email: a.kiendler-scharr@fz-juelich.de

Secondary organic aerosols (SOA) are an important component of tropospheric aerosols. A large fraction of secondary organic aerosols has biogenic sources. The contribution of monoterpenes (MT), isoprene, and sesquiterpenes (SQT) to BSOA formation after atmospheric oxidation are well known. Since aerosols play a role for climate by direct (light scattering and absorption) and indirect effects (cloud albedo, rain probability, cloud lifetime), SOA provides couplings between vegetation, air chemistry and climate. Currently these couplings are believed to provide overall a negative feedback (Kulmala et al., 2004, Goldstein et al., 2009).

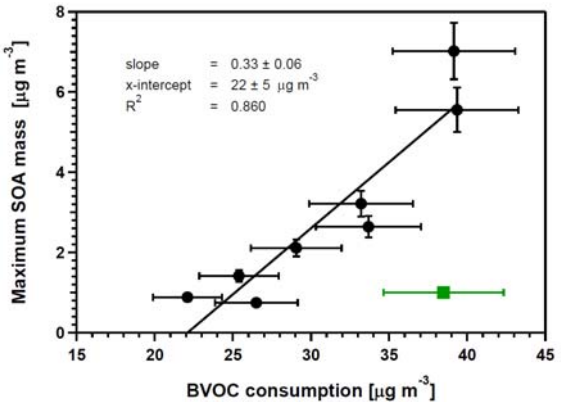

Figure 1, Maximum SOA mass versus consumption of C_{17}–BVOC dominated emissions. Black circles: data obtained at low contribution of GLV. Green square data point obtained on day 0 at high GLV emissions.

However, already SQT indicate that it is probably not sufficient to only consider the constitutive MT and isoprene emissions (Arneth and Niinemets, 2010). Plants tend to change emission patterns and strength, when they are facing stress (insect and pathogen attacks, heat, drought). Typical stress induced emissions are SQT, methylsalicylate (MeSa), and green leave volatiles (GLV). It is not unlikely, that fractions of forests always are exposed to biotic stress e.g. by insect or pathogen attacks, causing latent or episodic SIE emissions. On top heat or drought periods will modify the emissions. This would modify constitutive and SIE emissions episodically.

We determined the incremental mass yields of SOA formation from SIE caused by biotic stressors (Table 1). To simulate future climate effects we applied heat and drought on top. The experiments were performed with individual trees or small stands in the Jülich Plant Atmosphere Chamber JPAC (Mentel et al., ACPD 2013). Before the experiments trees were stored outside, near a forest, to simulate natural (stress) conditions. The trees were transferred to the JPAC for studies under controlled conditions (T, r.h.).

The SOA formation potential of SIE from common trees of Temperate and Boreal forests (Pine, Spruce, Birch, and Beech) were larger than those due to constitutive MT emissions: 17 ± 1% for SQT, 20 ± 3% for MeSa, and 30 ± 4% for C_{17}-BVOC.

Table 1. Incremental SOA yields for SIE and MT.

BVOC source	Action	Major BVOC	Mass yield
Boreal Stand	Aphids	SQT/MeSa	22 ± 2%
Diff. source		MeSa	20 ± 3%
Spruce	Aphids & heat	SQT	17 ± 1%
Temperate Stand	Aphids& drought	C_{17}-BVOC GLV	33 ± 6 %
Grey poplar	Ozone pulse	SQT/MeSa	20 ± 6%
Pine	None	MT 80%	5.3 ± 0.5%
Spruce	None	MT 90%	4.2 ± 0.7%
Diff. source		α-pinene	5.2 ± 0.5%
Holm oak	Heat	MT	6.0 ± 0.6%

In contrast to these SIE classes, GLV emissions have the potential to decrease SOA mass and number (Fig. 1), similar to isoprene (Kiendler-Scharr et al.,

Nanoparticle Growth Mechanisms During New Particle Formation

M.V. Johnston, B.R. Bzdek, A.J. Horan, J.W. DePalma

Department of Chemistry and Biochemistry, University of Delaware, Newark, Delaware, 19716, USA
Keywords: new particle formation, nucleation, nanoparticle composition, nano aerosol mass spectrometer
Presenting author email: mvj@udel.edu

Atmospheric new particle formation (NPF) is a key source of ambient ultrafine particles that may contribute substantially to the global production of cloud condensation nuclei (CCN). While NPF is driven by atmospheric nucleation, its impact on CCN concentration depends strongly on atmospheric growth mechanisms since the growth rate must exceed the loss rate due to scavenging in order for the particles to reach the CCN size range. We have made chemical composition measurements of 20 nm diameter particles during NPF in urban and remote locations using the Nano Aerosol Mass Spectrometer (NAMS). These measurements provide a quantitative assessment of important growth channels. We find several common features among NPF events in different locations and different times of year, and other features that are location/time specific. These features will be discussed in the context of our most recent field campaigns in the US and Europe.

With the improved time resolution of NAMS for these measurements (Pennington et. al, 2012), we are able to distinguish and quantify chemical species that are associated with nucleation vs. growth. At the onset of NPF (nucleation), we find that the composition of 20 nm particles changes even though the total aerosol mass concentration does not. These changes provide insight into the nucleation process since the chemical species that condense onto pre-existing "large" particles are likely to be similar to those that assist nucleation. In this regard, the species found to condense onto pre-existing particles during this time period include sulfuric acid, ammonia/amine and in some locations high O/C ratio carbonaceous matter. The change in nanoparticle composition coincides with an increase in the sulfuric acid gas phase concentration, which indicates the onset of NPF.

As the mode diameter increases and the aerosol mass concentration grows through the NAMS size range, other chemical species can increase relative to those involved in nucleation. While sulfuric acid condensation contributes to particle growth, it usually represents much less than half of the mass growth. The sulfur mole fraction determined by NAMS is taken as a quantitative measure of sulfate in the aerosol. (Bzdek et al., 2012) The sulfate mass fraction of growing particles (determined from NAMS measurements), along with the particle growth rate (determined from particle size measurements), can be used to back-calculate the gas phase sulfuric acid concentration. The sulfuric acid concentration calculated in this manner matches within experimental error the sulfuric acid concentration measured with a chemical ionization mass spectrometer, confirming that sulfuric acid uptake is collision limited.

During particle growth, the sulfur and nitrogen mole fractions are highly correlated, suggesting that cationic nitrogen (ammonia, amines) is taken into the particle to neutralize the condensing sulfuric acid. In some locations, the ratio of these two elements is such that sulfate in the particles is only partially neutralized (N/S<2). In other locations, sulfate appears to be completely neutralized (N/S>2).

We define "excess" nitrogen as N-2S where N is the nitrogen mole fraction and S is the sulfur mole fraction. We find that excess nitrogen is associated with particle *growth* but not *nucleation*. Excess nitrogen indicates that nitrate (either inorganic and/or organic) is an important growth species for NPF.

Carbonaceous matter is another important growth species. Depending on the location and time of year, the carbonaceous matter associated with particle growth can have an O/C ratio characteristic of fresh or slightly aged SOA.

Finally, we find that differences in the overall particle growth rate from one NPF event to another at a specific location and time of year are caused by variations in the growth rates of all major chemical species, not just one individual species.

References

Bzdek, B.R., Zordan, C.A., Pennington, M.R., Luther, G.W. and Johnston, M.V. *Environ. Sci. Technol.* (2012) **46**, 4365-4373.

Pennington, M.R. and Johnston, M.V. *Int. J. Mass Spectrom.* (2012) **311**, 64-71.

Comparative study of atmospheric particle formation using laboratory tools - COMPASS

T. S. Sun[1,2] and B. Bonn[2]

[1]Department of Geosciences, J.W. Goethe University, D-60438 Frankfurt/Main, Germany
[2]Biogeochemistry Department, Max-Planck-Institute for Chemistry, D-55128 Mainz, Germany
Keywords: nucleation, ambient aerosol, precursors.
Presenting author email: bonn@iau.uni-frankfurt.de

Abstract

A novel gas- and particle phase twin chamber has been constructed and tested for its use under real atmospheric conditions. It allows investigation of particle formation mechanisms as well as of the impact of certain parameters on the present conditions. It applies laboratory tools but uses ambient concentrations and conditions. In a first set of experiments particle formation in the urban area of Frankfurt have been conducted comparatively by either enhancing ozone in one of the chambers or by reducing the solar radiation intensity. Both parameters revealed significant effects on number and mass concentration resulting in a remarkable potential aerosol number and mass currently not produced. This has important implications for future emission budget calculations, local traffic and pollution strategies and for human health.

Introduction

New aerosol number and mass formation in the atmosphere includes a variety of precursor gases and processes with some of them known and intensively studies and others so far unknown or unexplained. This derives of the basic problem that there is currently no instrument that can accurately chemically analyse clusters and smallest particles in the ambient. However a notable fraction of these particles can affect human health and can grow to sizes beyond around 70 nm in diameter, at which it may act as cloud condensation nuclei and modifies the regional radiation budget. Because of this a better understanding of the chemistry and the controlling processes for the particles formation is required.

Methods

In order to bypass the analytical problem of small particle composition a novel twin chamber transparent to light was constructed. Both chambers consisted of ETFE foil, cylindrical in shape and acted as vertical laminar flow chambers with a total volume of 400 L and a residence time of (26.4±0.3) min. Both chambers were positioned in that way that they faced similar sunlight intensity and temperature and used the comparative method. Therefore one chamber was used as a reference (no. 2), while the conditions in the first one were modified to test the impact of certain parameters.

Experimental

First ambient experiments have been conducted at urban conditions (Campus Riedberg, Frankfurt/Main) during October and November. Intercomparison experiments using both chambers unmodified displayed no significant difference in the measurements of both chambers. Next, we enriched the present ozone level in chamber 2, while in a second period the second chamber was darkened to study the influence of OH chemistry.

Both parameters clearly displayed notable effects under urban conditions. Enhanced ozone (up to 70 ppb_v) increased both, i.e. particle number concentration and particle mass above 10 nm in diameter within 26 min residence time substantial (more than 40%, see Fig. 1). On the contrary, darkening of one of both chambers led to a decrease of number and mass concentration although temperature in the particular chamber was reduced due to the coverage with aluminium foil. Investigation of organic gases by proton transfer reaction-mass spectrometry revealed several potential candidates for precursors.

In total the new movable twin chamber displayed its functionality and capability to study ambient particle formation under different atmospheric conditions.

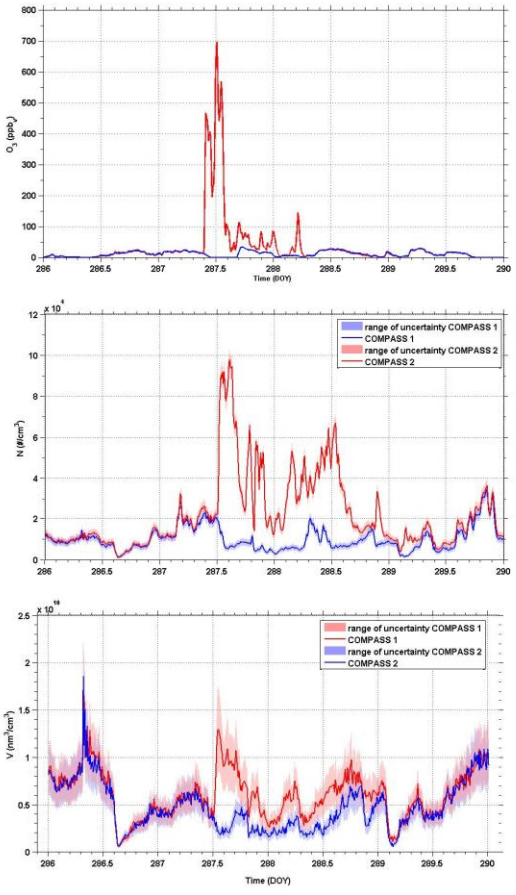

Figure 1. O_3 mixing ratio, particle number and volume concentration in both chambers during O_3-enrichment.

Estimating pre-existing aerosol effects on tropospheric aerosol production

M. Dal Maso[1], L. Liao[2], H. Vehkamäki[2], H.Korhonen[3], and K.E.J. Lehtinen[3]

[1]Tampere University of Technology, Dept. of Physics, PO Box 692, 33101 Tampere, Finland
[2]University of Helsinki, Department of Physics, PO Box 48, 00014, Helsinki, Finland
[3]Finnish Meteorological Institute, Kuopio Unit, P.O.Box 1627, 70211 Kuopio
Keywords: atmospheric aerosol, coagulation, new particle formation, modelling
Presenting author email: miikka.dalmaso@tut.fi

Understanding the source strength of tropospheric aerosol production is key to successfully predicting aerosol concentrations and their effect on human health and climate (Kulmala et al., 2004). Aerosol sources generally add aerosol particles or gas-phase aerosol precursors into atmospheric volumes already containing a significant number of pre-existing aerosol particles. This pre-existing aerosol acts as a sink for fresh aerosol particles as well as gaseous aerosol precursors.

Aerosol source processes are generally described as a source rate of aerosol particles into a given size range. Source rates from aerosol production processes such as combustion or secondary gas-to-particle conversion are often obtained in idealized conditions with no pre-existing aerosol present. Alternatively, the production rate is reported in context of realistic ambient concentrations but without characteristic information of the pre-existing aerosol.

The sink processes, caused by condensation and coagulation during the early steps of aerosol lifetime, can significantly alter the aerosol size distribution on timescales that are shorter than those implemented in conventional models predicting tropospheric aerosol concentrations. Parameterizations to take these effects already exist (eg. Lehtinen et al.,2007; Anttila et al, 2010), but they do not take into account effects caused by the size dependence of the particle growth (Vuollekoski et al., 2012) and the changes to the time dependence of the size distribution evolution caused by this.

In this study, we explore the different mechanisms that cause pre-existing aerosol to affect new aerosol sources. We use two models to study the effect of pre-extising aerosol on the source strength of atmospheric aerosol production processes. The molecular resolution model MOREAD, developed from the model by Lehtinen and Kulmala (2003), is used to quantify the effect of nanoparticle dynamics on the source rate of secondary nanoparticle production, and specially how these dynamics affect parameterizations of the formation rate of such particles. We also applied the 0d box model CHAMMO to study the carry-on effect of the pre-existing particles on the survival rate of particles to climatically significant sizes.

In addition to pure aerosol dynamics, pre-existing aerosol affects the particle formation process and the perceived dependencies on precursor vapors in the case of multiple chemical compound participating in the particle production. We studied the formation of secondary particles from sulphuric acid and VOC oxidation, and present results the describe particle formation dependencies in presence of sinks for nucleating and condensing vapours as well as additional sinks, such as dilution.

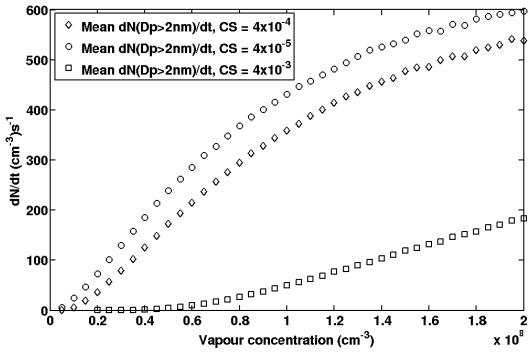

Figure 1: The perceived particle formation rate in a model aerosol with a prescribed formation rate of 1000 $cm^{-3}s^{-1}$ under varying background aerosol concentrations

Our model showed a strong influence of background aerosol on perceived particle formation rate even if the formation rate is technically derived very close to the actual formation size (see Fig. 1). The background aerosol is also key to the survival of fresh aerosol to CCN size; additionally, the relative chemical and condensation sink determine the dependency of particle formation rate on VOC precursor and oxidant concentration. We will illustrate these effects with field data, which shows clearly reduced particle formation activity with increasing background aerosol.

Anttila, T., et al: *J. Aerosol Sci.*, 41, 621–636, doi:10.1016/j.jaerosci.2010.04.008, 2010. 18783, 18785

Kulmala, M., et al: Formation and growth rates of ultrafine atmospheric particles: A review of observations *Aerosol Science* 35, 143-176, 2004

Lehtinen, K E J. and Kulmala, M. (2003): A model for particle formation and growth in the atmosphere with molecular resolution in size, *Atmos. Chem. Phys*., 3, 251-258

Lehtinen, K.E.J. et al: Estimating nucleation rates from apparent particle formation rates and vice versa: Revised formulation of the Kerminen–Kulmala equation *J. Aerosol. Sci* 38 (9), 988-994, 2007

Vuollekoski, H., et al: A numerical comparison of different methods for determining the particle formation rate *Atmos Chem Phys*, 12, 2289–2295, 2012

Intercomparison of sulphuric acid measurements and neutral cluster composition in the lower free troposphere

L. Rondo[1], M. Simon[1], H. Junninen [2], J. Duplisy[2], A. Praplan[2], A. Adamov[2], A. Kürten[1], M. Sipilä[2], F. Bianchi[3], J. Tröstl[3], E. Weingartner[3], U. Baltensperger[3], M. Kulmala[2] and J. Curtius[1]

[1]Institute for Atmospheric and Environmental Sciences, University of Frankfurt, 60438 Frankfurt, Germany
[2]Department of Physics, University of Helsinki, 00014 Helsinki, Finland
[3]Laboratory of Atmospheric Chemistry, Paul Scherrer Institute, 5232 Villigen PSI, Switzerland

Keywords: Neutral sulphuric acid nucleation, new particle formation, Jungfraujoch

Aerosol nucleation from trace vapours is a ubiquitous process in the Earth's atmosphere and has been observed at many different places (Kulmala et al., 2004). It is thought that sulphuric acid is a key species in the formation process of small clusters and particles. A correlation between the particle formation rate and the concentration of sulphuric has been frequently observed during ground-level field campaigns. However, data coverage on the sulphuric acid concentrations at higher altitudes is relatively scarce, although, these regions are very important on a global scale. In addition, it is not clear if and what other compounds (besides water) are participating in the formation of aerosol particles in these regions.

During January and February 2013 the **Nu**cleation, **Cl**oud and **A**erosol **C**haracterization **E**xperiment (NUCLACE) took place at the high alpine research station Jungfraujoch (JFJ) in Switzerland. The JJF station is located at 3580 meters altitude and mainly influenced by free tropospheric air during this time of the year. One of the goals of the NUCLACE campaign was to investigate the role of ions on the formation of new particles. However, in this study we focus on the measurement of the sulfuric acid concentration as well as on the detection of neutral clusters and their composition with state-of-the-art instruments.

For this purpose, two Chemical Ionization Atmospheric Pressure interface Time-Of-Flight Mass Spectrometers (CI-APi-TOFs) were used (Jokinen et al., 2012). Within the inlets of both instruments nitrate primary ions are generated which can ionize neutral sulphuric acid and clusters through a proton transfer reaction or by clustering. The primary and the product ions are detected with a high resolution time of flight mass spectrometer. The combination of these two techniques allows low detection limits (at ppq levels) and the identification of ion species through their exact mass. Although both CI-APi-TOF instruments have the same principle they differ in the design of their ion source. The CI-APi-TOF from the University of Frankfurt utilizes a corona discharge needle (Kürten et al., 2011) while the CI-APi-TOF from the University of Helsinki (Jokinen et al., 2012) utilizes a soft x-ray ion source. In addition, the geometry of the ion drift regions and the inlet geometries differ slightly. Additionally, the operation of the CI-APi-TOFs at JFJ turned out to be challenging due to the low pressure and strong temperature variations inside the building where the instruments were located. Therefore, an intercomparison of the two instruments is important (see figure 1). Furthermore, it turned out that an on-site calibration needed to be performed to take into account the conditions at the measurement site. For this, a calibration unit similar to the one described by Kürten et al. (2012) has been brought to JFJ. With this set-up a known concentration of H_2SO_4 can be generated and measured by one CI-APi-TOF at a time.

We will report on the overall comparison of the two CI-APi-TOFs with respect to the sulfuric acid monomer concentrations. In addition, the instruments will be compared regarding the detection of different neutral clusters. Details about the calibration will also be presented.

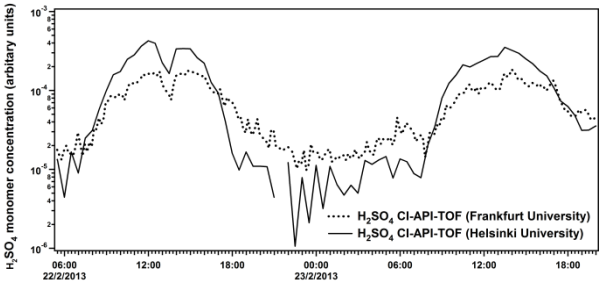

Figure 1. Observed diurnal variation of the sulphuric acid concentration measured by the two CI-APi-TOFs from Frankfurt and Helsinki.

We thank the International Foundation High Altitude Research Stations Jungfraujoch and Gornergrat (HFSJG), which made it possible to carry out the experiments at the JFJ. Also, we thank tofTools team for their support.

Kulmala, M., *et al*., (2004) J. Aerosol Sci., **35**, 143–176.
Jokinen, T., *et al* (2012) *Atmos. Chem. Phys.*,***12***, *4117-4125*
Kürten, A., *et al* (2011) *Atmos. Meas. Tech*., **4**, 437–443,
Kürten, A., *et al* (2012) *J. Phys. Chem. A*, 116 (**24**), 6375–6386

Tuesday, September 3, 2013

Session: Aerosol Modelling
Modelling aerosols in different environments

CFD prediction of the spatial distribution of particulate matter deposition indoors

J. Grau-Bové[1], L. Mazzei[2], M. Strlič[1]

[1]UCL Centre for Sustainable Heritage, University College London, WC1H 0NN, London, United Kingdom
[2]Department of Chemical Engineering, University College London, London, WC1E 7JE, United Kingdom
Keywords: particulate matter, indoor environment, CFD, eulerian particle transport
Presenting author email: josep.grau-bove.11@ucl.ac.uk

The development of mathematical models for aerosol transport and deposition in the size range $0.1\mu m$ - $10\mu m$, associated with atmospheric pollution, has been largely motivated by health and indoor comfort concerns. Consequently, the main interest of this models has been the prediction of particle concentration in the free volume of rooms, and they are typically validated with measurements of decay rates in the centre of an experimental chamber [1]. However, in some environments such as museums, archives or historic houses, in which valuable objects are on display, the main interest is not only to know the suspended particle concentration but, especially, to know the fate of these particles, i. e. the deposition rates and the spatial distribution of deposition. [2].

Model description

A model for particle transport and deposition has been implemented in a commercial CFD code. The disperse and continuous phases are resolved following an Eulerian-Eulerian approach. Since the Stokes number is well below 1, one-way coupling is assumed for the velocity fields. Following a comparison of turbulence models, the $k-\varepsilon$ has been chosen as the most suitable. The diffusive and convective terms of particle conservation equations have been modified to account for different phenomena. The diffusive term includes Brownian diffusion and turbulent diffusivity. The convective term adds a vertical component to the velocity field which describes gravitational settling. The semi-empirical deposition equations developed by Lai and Nazaroff [3], which are functions of the Schmidt number and require the wall shear stress as an input, have been implemented as boundary conditions for the particle concentration field. Their solution has been extended to surfaces with arbitrary face angles.

Validation

Since our main interest is in the spatial distribution of deposition, validation requires a comparison of the computational results with deposition values obtained at different points in a space. Published experiments offering data with such characteristics [4] have been simulated, and the numerical results have shown good agreement with experimental values. Figures 1 and 2, as an example, show the simulated distribution of deposition in the floor of a room after an accidental release of 5 g of particles with a normally distributed size, which corresponds with the reported experimental values. An on-going monitoring campaign involving monitoring of deposition and of suspended concentration will allow for validation of the model with a full-scale case study, enabling it to be used as a predictive tool for spatial distribution of deposition in indoor environments.

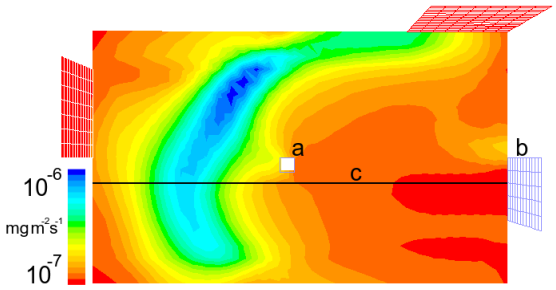

Figure 1: Instant deposition flux on the floor. t = 100 s, inlet velocity, v = 0.6 m/s, (a) is the particle inlet, which emits particles vertically, (b) is the air inlet and (c) is the line used to produce Figure 2.

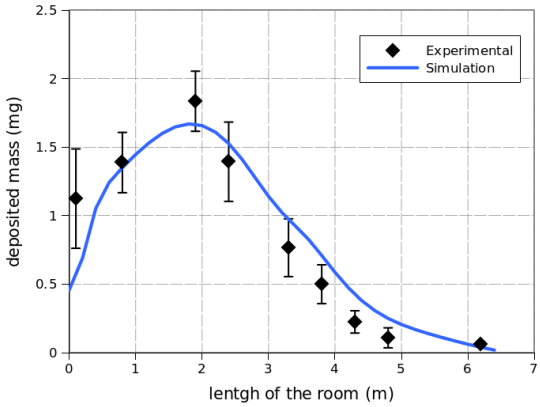

Figure 2: Experimental and simulated total deposited mass along the central line (c) 90 minutes after the release. Experimental values adapted from [2].

[1]S. Pakrer, J. Nelly (2010) *Journal of Aerosol Science.* **41(10)**, 921–934.
[2] J. Grau-Bové, M. Strlic (2013) Fine particulate matter in indoor cultural heritage. *Submitted to: Heritage Science* **31(4)**, 463–476.
[3] K. Lai, Alvin C. Nazaroff, William W.(2000) *Journal of Aerosol Science* **31(4)**, 463–476.
[4] Sajo E, Zhu H, Courtney JC. (2002) *Health Physics* **83(6)**, 871–883.

2009). Increased GLV emissions support positive feedback in case GLV emissions are related to heat, however exert a potential negative feedback when related to drought. Our results clearly indicate that different stress conditions can affect biogenic SOA production: Stress induced changes of BVOC emission patterns and strength strongly impact SOA formation causing increased (SQT, MeSa, C_{17}-BVOC) or decreased (GLV) SOA formation.

Results of our study indicate the importance of SIE for the existence of feedbacks between climate and vegetation via SOA formation. Biotic stress supports negative feedback and this may be effective already today. But heat and drought can turn the negative feedback proposed by Kulmala et al. (2004) and Goldstein et al. (2009) into a positive feedback in Temperate Forests dominated by *de-novo* emitters. Since it is likely that climate change will affect SIE from vegetation, SIE and their SOA formation potential have to be considered in future climate scenarios.

This work was supported by the integrated EU projects EUCAARI (Contract No. 036833-2) and PEGASOS (Contract No. 265307.). YR acknowledges support from the US-Israel bi-national science foundation (BSF) contract number 2008/146 and support by the Helen and Martin Kimmel Award for Innovative Investigation.

Arneth, A., and Niinemets, Ü. (2010) *Trends in Plant Science*, **15**, 118-125

Goldstein, A. H., Koven, C. D., Heald, C. L., and Fung, I. Y. (2009) *PNAS*, **106**, 8835-8840

Kiendler-Scharr, A., Wildt, J., Dal Maso, M., Hohaus, T., Kleist, E., Mentel, T. F., Tillmann, R., Uerlings, R., Schurr, U., and Wahner, A. (2009) *Nature*, **461**, 381-384

Kulmala, M., Suni, T., Lehtinen, K. E. J., Dal Maso, M., Boy, M., Reissell, A., Rannik, U., Aalto, P., Keronen, P., Hakola, H., Back, J. B., Hoffmann, T., Vesala, T., and Hari, P. (2004) Atmos. Chem. Phys., **4**, 557-562

Mentel, Th. F., Kleist, E., Andres, S., Dal Maso, M., Hohaus, Th., Kiendler-Scharr, A., Rudich, Y., Springer, M., Tillmann, R. Uerlings, R., Wahner, A., Wildt, J., (2013) Atmos. Chem. Phys. Disc. submitted

Correction of approximation errors with random forests applied to modelling of aerosol first indirect effect

A. Lipponen[1], V. Kolehmainen[1], S. Romakkaniemi[1] and H. Kokkola[2]

[1]Department of Applied Physics, University of Eastern Finland, P.O.Box 1672, FI-70211 Kuopio, Finland
[2]Finnish Meteorological Institute, Kuopio unit, P.O.Box 1627, FI-70211 Kuopio, Finland
Keywords: cloud, model, error, correction.
Presenting author email: Antti.Lipponen@uef.fi

In numerical simulations of atmospheric models, often a reduced model has to be used due to computation time or resource limitations. The use of a reduced model, however, induces errors to the simulation results. These errors are referred to as the approximation errors.

In this study, we consider the approximation errors caused by coarse discretizations of aerosol particle number and volume size distributions in a sectional aerosol model such as SALSA (Kokkola et al., 2008). We model the approximation error as an additive noise process in the simulation model and employ the random forest (Breiman, 2001) regression algorithm for constructing a computationally low cost predictor for the approximation error. In this way, the overall simulation problem is decomposed into two separate and computationally efficient simulation problems: solution of the reduced model and prediction of the approximation error realization. Given the trained random forest model, the accurate model can be approximated by the sum of the reduced model and the predicted approximation error realization.

The proposed approach is tested for handling the approximation errors due to a reduced coarse sectional representation of aerosol size distribution in the cloud droplet activation parameterization by Abdul-Razzak and Ghan (2002). Here a set of approximation error realizations between the accurate and reduced cloud droplet formation parametrizations is first constructed. Second, these approximation error realizations and the corresponding input variables of the parametrizations are used as the training data for the random forest algorithm and the random forest predictor is constructed and used in the simulations.

In this study, the approximative and sufficiently accurate parametrizations consisted of 7 and 70 size sections for the aerosol particle number and volume size distributions, respectively. The cloud droplet number concentration (CDNC) samples simulated with the accurate parametrization as functions of the CDNC samples computed both with the approximative and approximation error corrected parametrizations are shown in Figure 1. The mean squared and mean relative errors of the CDNC samples corresponding to the approximative and approximation error corrected parametrizations are shown in Table 1. The results show a significant improvement in the accuracy of the simulation compared to the conventional simulation with a reduced model. The approach proposed in this study is rather general and the extension of it to different physical simulation models is a straightforward task.

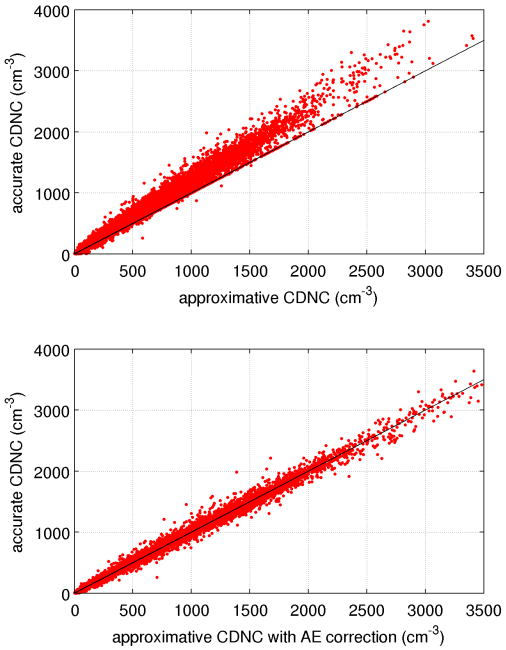

Figure 1. The cloud droplet number concentrations (CDNC) computed with the accurate parametrization as functions of approximative (up) and corrected (down) CDNC values. The solid black lines in the figures represent the identity lines.

Table 1. Mean squared errors and mean relative errors of the approximative and corrected CDNC values.

Parametrization	Mean squared error (cm^{-6})	Mean relative error (%)
Approximative	1.70×10^{4}	20.3
Approximation error corrected	1.27×10^{3}	8.4

This work was supported by the Academy of Finland (project 119270 and Centre of Excellence programs 1118615 and 250215) and by the strategic funding of the University of Eastern Finland.

Abdul-Razzak, H. and Ghan, S.J. (2002) *J. Geophys. Res.* **107**, doi:10.1029/2001JD000483.
Breiman, L. (2001) *Machine Learning* **45**, 5-32.
Kokkola, H., Korhonen, H., Lehtinen,, K.E.J., Makkonen, R., Asmi, A., Järvenoja, S., Anttila, T., Partanen, A.-I., Kulmala, M., Järvinen, H., Laaksonen, A., and Kerminen, V.-M. (2008) Atmos. Chem. Phys. 8, 2469-2483.

A simplified model to predict partitioning between the vapour and multiple condensed phases in mixed inorganic- organic aerosol particles

D. Topping[1,2], G. McFiggans[2] and M. Barley[2]

[1]National Centre for Atmospheric Science (NCAS), University of Manchester, Oxford Road, Manchester, UK.
[2] University of Manchester, Oxford Road, Manchester, UK
Keywords: aerosol particles, thermodynamics, .
Presenting author email: david.topping@manchester.ac.uk

Introduction

Knowledge of the physical state and morphology of internally mixed organic/inorganic aerosol particles is still largely uncertain (Song et al 2012). The wide range of concentrations and properties of organic compounds found within aerosol particles in the atmosphere suggest that liquid-liquid phase separation equilibrium ('LLE') might occur in certain ambient conditions. Predicting the equilibrium composition in multicomponent inorganic-organic aerosol particles using thermodynamic models has remained a challenge. Traditionally the most complex, and seemingly accurate, models rely on minimisation of the Gibbs energy of the system.

Currently available thermodynamic methods that account for partitioning between two liquid phases are computationally expensive and do not account for the vast number of organics expected to contribute to the condensed phase. Whilst empirical parameterisations based on organic:sulphate and O:C ratios have been constrained to specific systems (Bertram et al 2011), there is no general consensus on how to account for LLE across a broad range of scenarios. In this study, we reformulate the problem such that it can be solved using a robust and efficient iterative method and thus derive a generic simplified method for predicting coupled VLE and LLE in atmospheric aerosol particles. Comparisons with more complex benchmark models are made (figure 1) along with a discussion as the wider significance of LLE in relation to additional uncertainties in other properties.

Using the activity coefficient model AIOMFAC (Zuend et al 2008), partitioning coefficients between two liquid phases are derived based on the assumption of a continuum of forces that represent molecules that interact by London Dispersion forces (hydrocarbons) and molecules that interact by dipoles/hydrogen-bonding/electrostatic charges. Organics of atmospheric interest are assumed to form a continuum between H-bonding/dipole interactions at one extreme and purely London Dispersion forces at the other, so all these compounds partition between the two phases (assumed aqueous and hydrocarbon in this study). In this method the composition space is explored to discover the least miscible components (solvents) based on predictions from the AIOMFAC activity coefficient model.

Results

To test the applicability of the simplified model a set of coupled VLE-LLE partitioning calculations are compared with the results of Zuend et al (2010) for a system with an ammonium sulphate core and 4 organic compounds are multiple relative humidity (RH) (figure 1). Unrestricted with regards to the number of compounds used within the calculations, we then attempt to assess the potential importance of LLE in ambient aerosol using output from a gas phase degradation model with 2727 compounds. Here we use the results described by Barley et al (2010) in which the Master Chemical Mechanism was used to simulate the gas phase composition of air masses over multiple environments. The potential importance of LLE is discussed in relation to existing uncertainties in the properties of organic components.

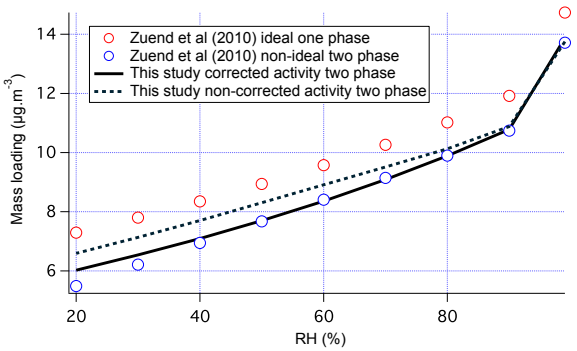

Figure 1. Mass loading of organics as a function of RH. A comparison with a benchmark thermodynamic framework of Zuend et al (2010).

This work was supported by the National Centre for Atmospheric Science (NCAS).

Barley, M. H., Topping, D., Lowe, D., Utembe, S., and McFiggans, G.: Atmos. Chem. Phys., 11, 13145-13159, doi:10.5194/acp-11-13145-2011, 2011.

Bertram, A. K., Martin, S. T., Hanna, S. J., Smith, M. L., Bodsworth, A., Chen, Q., Kuwata, M., Liu, A., You, Y., and Zorn, S. R.: Atmos. Chem. Phys., 11, 10995–11006, doi:10.5194/acp-11-10995-2011, 2011.

Song, M., Marcolli, C., Krieger, U. K., Zuend, A., and Peter, T.: Atmos. Chem. Phys., 12, 2691–2712, doi:10.5194/acp-12-2691- 2012, 2012.

Zuend, A., Marcolli, C., Luo, B. P., and Peter, T.: Atmos. Chem. Phys., 8, 4559–4593, doi:10.5194/acp- 8-4559-2008, 2008.

Zuend, A., Marcolli, C., Peter, T., and Seinfeld, J. H.: Atmos. Chem. Phys., 10, 7795–7820, doi:10.5194/acp- 10-7795-2010, 2010.

Wall losses of vapours distort yield calculations in SOA chamber experiments

H. Kokkola[1], P. Yli-Pirilä[2], H. Korhonen[1], M. Vesterinen[1], H. Keskinen[2], S. Romakkaniemi[2], L. Hao[2], J. Joutsensaari[2], D. Worsnop[3], A. Virtanen[2] and K. E. J. Lehtinen[1,2]

[1]Finnish Meteorological Institute, Kuopio Unit, 70211 Kuopio, Finland
[2]Department of Applied Physics, University of Eastern Finland, 70211 Kuopio, Finland
[3]Aerodyne Research Inc., Billerica, MA, 01821-3976, USA
Keywords: secondary organic aerosol, chamber measurements, aerosol modelling.
Presenting author email: kari.lehtinen@fmi.fi

Organic compounds can amount to 50% or more of atmospheric aerosol mass (Jimenez et al., 2009) and therefore have an important role in determining the climate and air quality effects of particulate matter. However, currently the contribution of secondary organic aerosol (SOA) formation both to aerosol total mass and particle growth from nucleation size to climatically relevant sizes is poorly understood (Riipinen et al., 2012). In this work, we shed some light on the formation of atmospheric SOA as we use well-constrained new particle formation experiments in a Teflon chamber together with aerosol microphysics modelling to demonstrate that low-volatile organic compounds formed in chamber studies may have gone undetected in previous experiments due to their very rapid partitioning onto chamber walls.

Our measurements were performed in a 4 m^3 Teflon chamber, in which three semi-volatile organic gases of distinctly different volatilities were injected. In the experiment, 20 ppb of these organic gases was repeatedly injected at 30 min intervals. Between the injections, a high-resolution proton transfer reaction mass spectrometer (PTR-TOF-MS) measured the gas-phase concentration of the compound and revealed that the equilibrium between the gas-phase and the chamber walls was reached within a few minutes of each injection. Such rapid equilibrium suggests that detection of very low-volatility compounds, which partition almost exclusively to chamber walls, is extremely difficult in chamber experiments and may therefore have gone unnoticed in several previous studies.

We tested this hypothesis further in a chamber experiment of α-pinene ozonolysis in the presence of an ammonium sulphate seed aerosol. In this experiment, new particle formation and subsequent growth of the nucleation mode was observed shortly after the injection of α-pinene and ozone. The formation of new particles indicates presence of gas phase compounds of very low volatility.

We attempted to simulate the observed growth with the aerosol microphysics model SALSA (Kokkola et al., 2009) by using the frequently used volatility bins and stoichiometric coefficients (Pathak et al., 2007) in the volatility basis set (VBS) framework, which have been derived from previous chamber studies. Using this set-up, the model was clearly unable to simulate the observed growth of the nucleation mode. To reproduce the growth of these small particles we optimized the values of stoichiometric coefficients for different volatility classes by minimizing the difference between the observed and modelled total number concentration in different particle size classes. The optimization resulted in approximately two orders of magnitude higher coefficient for the lowest volatility bins. When these optimized stoichiometric coefficients were applied in SALSA, the observed new particle growth event was reproduced with good fidelity as can be seen in Figure 1.

Our results indicate that very low-volatile organic compounds capable of contributing to nucleation mode growth form in the first-generation reactions of α-pinene oxidation. In previous chamber experiments these compounds have gone undetected because they are depleted to the chamber walls before being detected by measurement devices. Our findings call for new experimental approaches that can constrain the SOA formation yields in chambers in a more reliable way.

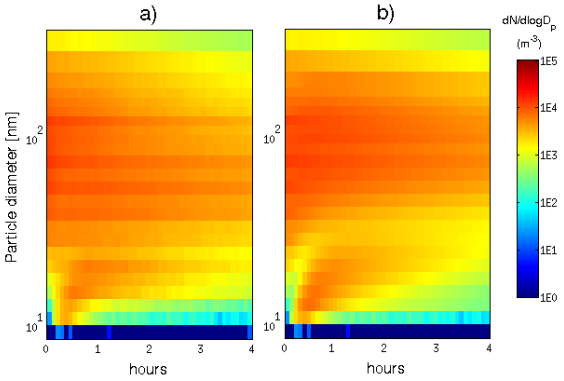

Figure 1. Measured (a) and modelled (b) growth of new particles in the presence of ammonium sulphate seed aerosol

This work was supported by the Maj and Thor Nessling Foundation (Project nr. 2012358), the Academy of Finland (no. 252908) and the strategic funding of the University of Eastern Finland.

Jimenez, J.L. et al. (2009) *Science*, **326** (5959), 1525-1529

Kokkola, H., et al. (2008) *Atmos. Chem. Phys.*, **8**, 2469-2483

Pathak, R. K., et al. (2007), *Atmos. Chem. Phys.*, **7**, 3811-3821

Riipinen, I., et al., (2012) *Nature. Geosci.*, **5**, 453-458

Numerical studies of aerosol activation behaviour in warm clouds compared to in-situ measurements at the high-alpine site Jungfraujoch

E. Hammer[1], C.R. Hoyle[1], B.P. Luo[2], M. Gysel[1], N. Bukowiecki[1], U. Lohmann[2], R. Vogt[3], C. Marcolli[2], T. Peter[2], U. Baltensperger[1] and E. Weingartner[1]

[1]Laboratory of Atmospheric Chemistry, Paul Scherrer Institut, 5232 Villigen PSI, Switzerland
[2]Institute for Atmospheric and Climate Science, ETH Zurich, 8092 Zurich, Switzerland
[3]Meteorology, Climatology and Remote Sensing, University of Basel, 4055 Basel, Switzerland
Keywords: Aerosol cloud interaction, CLACE, CCN, Modelling
Presenting author email: emanuel.hammer@psi.ch

Since 2000, 13 CLACE (Cloud and Aerosol Characterization Experiment) measurement campaigns have been performed at the High Altitude Research Station Jungfraujoch (JFJ, Switzerland, 3580 m asl). Of these, 5 focussed on the activation of aerosol to form warm clouds (i.e. liquid-phase). Additionally, comprehensive measurements of aerosol composition and physical properties have been performed at the Jungfraujoch since 1995. The Jungfraujoch is suitable for this purpose since it is in the free troposphere most of the time, and is also influenced by the continental air over Europe. Combined with the fact that the Jungfraujoch is within clouds for 40% of the time, this makes it an ideal site to study aerosol-cloud interactions.

In earlier studies, the cloud droplet activation of aerosol particles has been investigated by performing field measurements of activation (Henning et al., 2002). A recent study (Hammer et al., 2013) investigated the link between the measured cloud droplet number concentration and the cloud condensation nuclei (CCN) number concentrations that were derived from laboratory measurements. These measurements allowed a determination of the prevailing effective peak supersaturation ($SS_{eff.peak,\ retrieved}$) in ambient clouds, which was responsible for the activation of aerosol particles to cloud droplets.

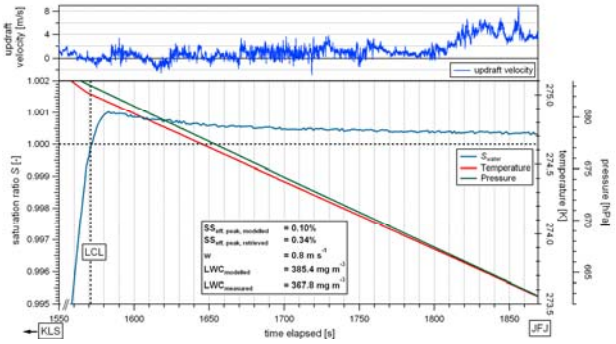

Figure 1. In the upper panel the measured updraft velocity is shown with a time resolution of 20 Hz. The lower panel shows an air parcel back trajectory for air masses starting at KLS and reaching the JFJ. The evolving saturation ratio (blue), temperature (red) and pressure (green) are shown (lower panel). LCL is the lifting condensation level.

The measured aerosol and cloud parameters such as activation diameter, cloud droplet number concentration and effective peak saturation were compared with values predicted by a cloud parcel model. The model, ZOMM (Zurich optical and microphysical model; Luo et al., 2003; Hoyle et al., 2005) simulates the microphysics of aerosols and cloud particles in air parcels including a fully kinetic calculation of water transfer between the gas and liquid phases. The model was initialised with conditions valid for the Kleine Scheidegg (KLS, 2061 m asl) which is located 4 km to the north of the JFJ, at lower altitude.

Figure 1 shows an example of a model simulation, following such an air parcel trajectory. All input parameters (dry aerosol size distribution, temperature, pressure, initial water vapour mixing ratio) were measured at the JFJ. The updraft velocity measured at the JFJ with an ultrasonic anemometer (Metek USA-1) is time-shifted so that it is time-synchronized with the predicted trajectory. It is expected that the air masses approaching the JFJ are experiencing turbulence, which can influence the temperature and thus the saturation ratio. The highest value on the trajectory of the saturation ratio is the maximum peak supersaturation ($SS_{eff.peak,modelled}$) which can be compared with the $SS_{eff.peak,retrieved}$. However, a difference between the predicted (0.10%) and retrieved (0.34%) value is evident. We will present possible explanations for this difference, including the effect of implementing a hygroscopicity parameter. In addition, sensitivity studies were carried out to assess the influence of turbulence on the $SS_{eff.peak,modelled}$.

This work was supported by MeteoSwiss in the framework of the Global Atmosphere Watch program. We thank the International Foundation High Altitude Research Station JFJ and Gornergrat for the opportunity to perform experiments on the Jungfraujoch.

Hammer, E. *et al.*, Aerosol activation behavior in liquid-phase clouds at the high-alpine site Jungfraujoch, Switzerland (3580 m asl), *to be submitted*

Henning, S., Weingartner, E., Schmidt, S., Wendisch, M., Gäggeler, H. W., Baltensperger, U. (2002), *Tellus B* **54**, 82-95.

Hoyle, C.R., B.P. Luo and T. Peter (2005), *Journal of the Atmospheric Sciences* **62**, 2568-2579.

Luo, B.P. *et al.* (2003), *Geophysical Research Letters* **30**.

Dependence of Aircraft Smoke Number on Black Carbon Size Distribution

M.E.J. Stettler[1], J.J. Swanson [1] and A.M. Boies[1]

[1]Department of Engineering, University of Cambridge, CB2 1PZ, United Kingdom
Keywords: combustion aerosols, aircraft emissions, soot generator, aerosol filtration.
Presenting author email: ms828@cam.ac.uk

Current methods used to estimate aircraft black carbon (BC) emissions for the purposes of air quality and climate impact studies rely on an outdated correlation and underestimate by a factor of 2-3. In this study, we show that the correlation between the BC mass concentration and smoke number is strongly dependent on the geometric mean of the particle size distribution. To test the correlation a new method to produce BC particles with a variable geometric mean diameter on the range 20-60 nm is employed to simulate BC particles emitted by aircraft gas turbine engines.

Aircraft engine exhaust is currently regulated on the basis of a filter smoke number (SN) – the observed change in reflectance of the filter after sampling a specified mass of exhaust. Estimates of aircraft BC emissions rely on an empirical correlation between SN and BC mass concentration (C_{BC}) derived using BC particles with geometric mean diameter (GMD) between 80-100 nm (Girling et al., 1990). Recent measurements of BC particles in aircraft exhaust have shown that aircraft soot can be characterized as having lognormal particle size distribution with a GMD between 20-40 nm (Kinsey et al., 2010).

A co-flow inverse diffusion flame provides a steady source of BC particles with variable GMD in the range 20-60 nm and geometric standard deviation between 1.5-1.7. The particle size distribution is characterised with a Scanning Mobility Particle Sizer (SMPS) and particle mass as a function of mobility diameter (d_m) is measured using a Centrifugal Particle Mass Analyser. Calculated BC mass concentrations are verified with gravimetric analysis. SN measurements are taken according to the standard aircraft test procedure (SAE, 1997). Correlations between SN and BC concentration are derived for 20, 30 and 60 nm GMD. Filtration efficiency of the specified SN filter as a function of d_m is measured.

In Fig. 1, the particle mass distributions for GMD~20 nm, GMD~30 nm and GMD~60 nm are superimposed on the filtration efficiency, indicating that filtration efficiency increases with d_m such that a smaller proportion of the BC mass is collected on the filter for a smaller GMD.

In Fig. 2 the correlation between SN and BC mass concentration is shown to be a function of d_m – for a smaller GMD a greater C_{BC} is required to produce the same SN, suggesting that current estimates underestimate aircraft BC mass emissions by up to a factor 2-3. These revised correlations improve estimates of aircraft BC emissions compared to measurements but do not account for uncertainty in the regulatory SNs.

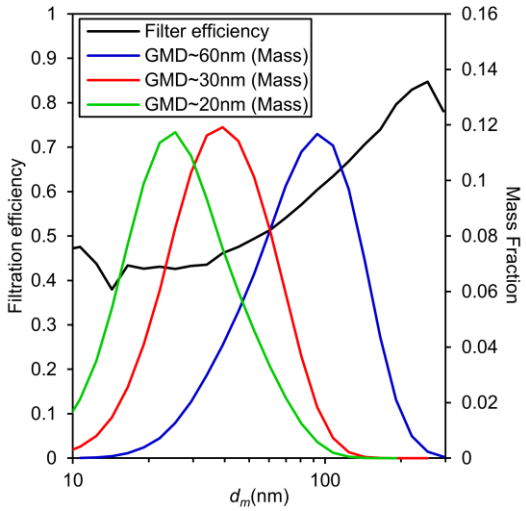

Figure 1. Filtration efficiency of the SN filter with mass distributions for GMD~20, GMD~30 and GMD~ 60 nm soot.

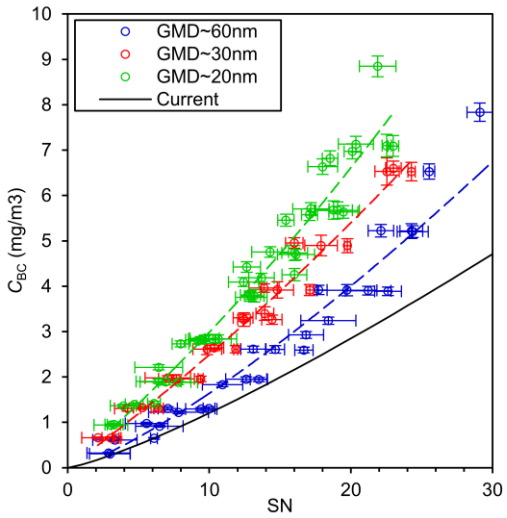

Figure 2. Correlation between C_{BC} and SN.

This work was supported by the UK Engineering and Physical Sciences Research Council (EP/H004505/1).

Girling, S.P., Hurley, C.D., Mitchell, J.P., Nichols, A.L., 1990. Aerosol Science and Technology 13, 8–19.

Kinsey, J.S., Dong, Y., Williams, D.C., Logan, R., 2010. Atmospheric Environment 44, 2147–2156.

SAE, 1997. Aerospace Recommended Practice 1179C Aircraft Gas Turbine Engine Exhaust Smoke Measurement, System.

Tuesday, September 3, 2013

Session: Combustion Aerosols
Combustion and industrial aerosols

Sulphuric Acid Aerosol Formation in Industrial Processes – Simulation and CPC measurement at a Pilot Plant

L.Brachert[1], S. Sinanis[1] and K. Schaber[1]

[1]Institute for Technical Thermodynamics and Refrigeration, Karlsruhe Institute of Technology, Karlsruhe, 76131, Germany

Keywords: Sulphuric Acid Aerosol, Coagulation, CPC, Homogeneous nucleation

Presenting author email: leonie.brachert@kit.edu

The formation of sulphuric acid aerosols is a phenomenon which emerges frequently in industrial processes. An important domain is for example the absorption-based flue gas cleaning in power plants (wet flue gas desulfurization). Problems such as corrosion and the occurrence of a distinct "blue plume" may arise due to the aerosol formation. The problem evolves in particular in the presence of $DeNO_X$-systems with selective catalytic reduction (SCR). The resulting aerosol droplets remain sub-micron even after coagulation and are difficult to precipitate.

The simulation tool AerCoDe has been developed at the Institute for Technical Thermodynamics and Refrigeration to predict aerosol formation initiated by heterogeneous (Wix, 2008) as well as homogeneous nucleation (Wix *et al*, 2010). In sulphuric acid – water systems homogeneous nucleation has to be considered. The reason for this is the occurrence of high supersaturations as a result of the extreme phase equilibrium of this binary system. The simulation yields high number concentrations up to 10^{10} 1/cm³ (Wix *et al*, 2010). The number concentration is slightly lower when the parameterisation of Vehkamäki et al (2003) is used to take the formation of hydrate clusters into account (Figure 1). The resulting number concentrations are high even for low inlet concentrations of H_2SO_4 combined with very small diameters (<20 nm) of the aerosol droplets.

Additional polydisperse coagulation calculations show the rapid decrease in number concentrations to 10^8 1/cm³. Due to the higher number concentrations and smaller droplets the coagulation has a larger influence on the number concentration for small sulphuric acid concentrations in the flue gas (Figure 1).

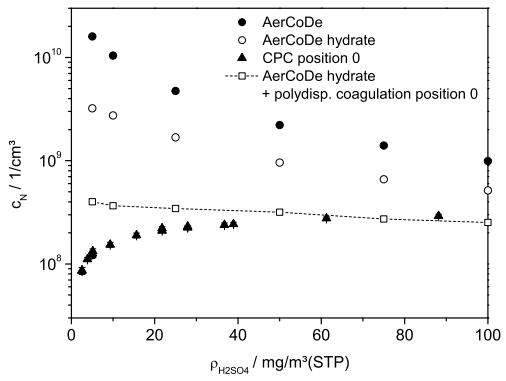

Figure 1 Total number concentrations in the absorption column outlet as a function of the H_2SO_4 inlet concentration. Simulation with AerCoDe and CPC measurements

The experiments at the pilot plant and the measurements with the condensational particle counter (CPC) confirm the high number concentrations in the order of magnitude of 10^8 1/cm³ (Figure1 and 2). At lower sulphuric acid concentrations remains a gap between simulations and experiments which can be explained partly by deposition and by the cut-off of the measurement device at smaller droplet sizes.

Experiments with varying number concentrations of soot particles in the pilot plant demonstrate the occurrence of homogeneous nucleation even in the presence of ~$5*10^6$ 1/cm³ foreign nuclei (compared to ~$2*10^4$ 1/cm³ in low soot mode). As a result, high number concentrations of sulphuric acid aerosol droplets with very small droplet diameters are present even at high soot concentrations.

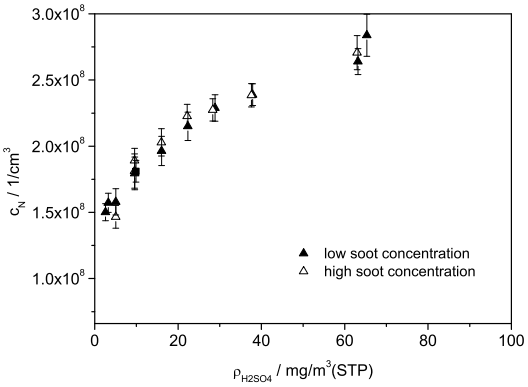

Figure 2 Total number concentrations in the absorption column outlet at low and high soot concentrations (CPC measurements)

This work was supported by the Deutsche Forschungsgesellschaft DFG under grant SCHA 524/19-1.

Vehkamäki, H.; Kulmala, M.; Lehtinen, K.E.J., (2003) *Environmental Science and Technology* **37**, 3392-3398

Wix, A., Brachert, L., Sinanis, S. and Schaber, K. (2010) *Journal of Aerosol Science* **41**, 1066-1079

Wix, A. (2008) *Fortschritt-Berichte VDI*, Reihe 3, Nr. **894** VDI-Verlag

Inactivation of Aerosolized Spores in Combustion Environments Using Filled Nano-composite Materials: Study with Two Surrogates of Bacillus Anthracis

S.A. Grinshpun[1], M. Yermakov[1], R. Indugula[1], X. He[1], T. Reponen[1], E. Dreizin[2], M. Schoenitz[2], S. Zhang[2], Y. Aly[2]

[1]Center for Health-Related Aerosol Studies, University of Cincinnati, Cincinnati, Ohio, USA
[2]Department of Chemical, Biological, and Pharmaceutical Engineering, New Jersey Institute of Technology, Newark, New Jersey, USA

Keywords: bioaerosol, combustion, viability, inactivation.
Presenting author email: sergey.grinshpun@uc.edu

Bio-threat agents may be aerosolized should a bio-weapon facility be accidentally or intentionally targeted. Some aerosolized microorganisms (e.g., bacterial spores) may survive the associated heat and chemical stresses and pose a major threat. Novel halogen-containing reactive materials (referred to as Filled Nano-composite Materials, FNM) are being developed with the added capability to inactivate viable microorganisms during their release to the atmosphere. A state-of-the-art laboratory facility was designed and built in our earlier efforts to evaluate the biocidal effects of heat and various compositions released during combustion.

The objective of this research was to determine the efficiency of combustion products of existing and newly-developed materials to inactivate aerosolized spores of two well-established surrogates of *Bacillus anthracis*: *Bacillus subtilis var. niger* (also referred to as *Bacillus atrophaeus* or BG spores) as well as *Bacillus thuringiensis* (Bt spores). The spores dispersed in dry air flow were exposed for sub-second time intervals to hydrocarbon flames seeded with different reactive powders. The bioaerosol particles interacted with the combustion products in a controlled high-temperature environment. The concentrations were determined for viable spores exposed to combustion (C_{exp}) and non-exposed spores ($C_{control}$); the ratio of $C_{control}/C_{exp}$ defined as Inactivation Factor (IF) was calculated for each tested reactive material and each of the two *Bacillus* species. The tests were performed with Al powder (dispersion = 3-4.5 μm) regarded as the reference material and two novel iodine-containing FNMs, Al·I_2 and Al·B·I_2, which release iodine when the base material (Al or Al·B) is melting in the powder combustion process.

The IF data are presented in Fig. 1 for BG and Bt exposed to combustion products at air temperatures of 192 to 210°C (above the iodine boiling point, 184°C). Both iodine-containing materials exhibited IFs higher than Al by two to three orders of magnitude, producing IF = 733 (Al·I_2) and 2,654 (Al·B·I_2) for BG and IF = 918 (Al·I_2) and 10,895 (Al·B·I_2) for Bt. The inactivation level provided by Al·B·I_2 was significantly higher than that of Al·I_2 for both species. The species effect on IF was statistically significant only for Al·B·I_2. Similar tests performed at exposure temperatures slightly below 184°C also showed an iodine-enhanced inactivation although generating much lower IF-levels (because only a small fraction of the released iodine remained in the gaseous phase in the exposure chamber). Overall, the results suggest a great biocidal potential of combustion products generated by the two tested iodine-containing FNMs.

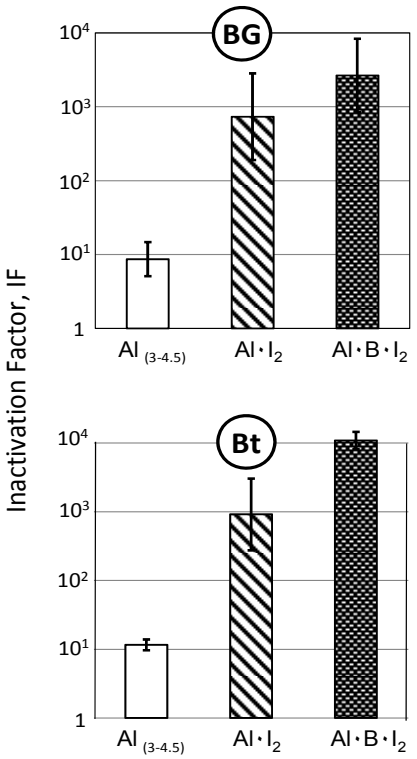

Figure 1. Inactivation factors for the aerosolized BG and Bt spores measured for $Al_{3\text{-}4.5}$ and two Al-based iodinated FNMs.

This study provided foundation for the hypothesis about a synergistic effect of dry heat and chemical products released during the FNM combustion. The heat-induced stress is considered as a tool to damage the spore protein coats and affect the spore outer membrane, cortex, and inner membrane, which, in turn, is expected to enhance the penetration of the "lethal" chemical products. This hypothesis is being tested in a separate investigation.

This research was funded by the U.S. Defense Threat Reduction Agency (DTRA). The authors extend their appreciation to Dr. Su Peiris of DTRA for her support and encouragement.

Size distribution and light scattering properties of standard test fire aerosols

Zs. Jurányi[1], S. Lauber[2] , A. Duric[2], M. Allemann[2], B. Schmid[2], M. Loepfe[1], and H. Burtscher[1]

[1]Institute of Aerosol and Sensor Technology, University of Applied Sciences Northwestern Switzerland, Windisch, CH-5210, Switzerland
[2]Siemens Schweiz AG, Building Technologies Division, International Headquarters, Gubelstrasse 22, Zug, CH-6300, Switzerland
Keywords: combustion aerosols, light scattering, size distribution, test fire.
Presenting author email: zsofia.juranyi@fhnw.ch

Introduction

Aerosol particles in smoke, produced by combustion processes, are widely used by fire alarm systems for early fire detection. Most existing smoke detectors belong to one of the two types: ionisation or photoelectric detectors. The photoelectric type detectors are taking over the market share from the ionization detectors because the ionization detectors use radioactive sources that lately get banned in many countries.

The detection of smoke in a photoelectric detector is based on the detection of the light scattered by the aerosol particles present in the smoke. In order to better understand and/or to improve the performance of the photoelectric detectors, the properties of the fire produced aerosol particles determining their optical scattering has to be measured.

Aerosol properties of 7 different standard EN54 test fires (see Table 1 for details about the fires) were measured in a fire laboratory. The particle number size distribution and it's time evolution were measured by a scanning mobility particle sizer (SMPS, TSI) and a white-light optical particle counter (WELAS digital 2000, Palas). The angular and time dependence of the differential scattering coefficient at 660 nm wavelength was measured by a home developed instrument: The aerosol is brought into a closed chamber where a laser diode illuminates the particles that can be found in the sampling volume. The scattered light is then detected simultaneously by avalanche photodiodes at 7 different angles.

Table 1. The different standard EN54 test fires

Name	Type of fire
TF1	flaming wood
TF2	smouldering wood
TF3	smouldering cotton
TF4	flaming polyurethane foam
TF5	flaming *n*-heptane with 5% toluene
TF6	flaming ethanol
TF8	flaming decalin

Results

Figure 1 shows the time evolution of the particle number size distribution for a flaming wood fire. Shortly after the ignition of the fire at 14:05 very small particles around 25 nm mobility diameter were formed. As the fire got larger, the previously mentioned mode disappeared suddenly, particles with a mean diameter around 150 nm became dominant and the particle number concentration has increased fast. At 14:13 the flame has died out, and therefore the concentration has started to decrease, however the width and the mean size of the size distribution has continued to increase.

Both the aerosol size distribution and scattering properties of the different fire types show a significant variability, e.g. the mean diameter of the number size distribution had values between 60 and 300 nm.

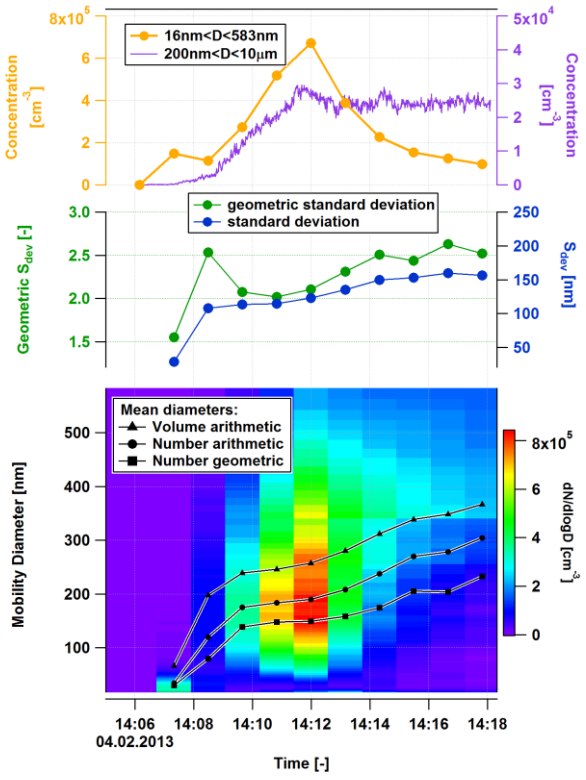

Figure 1. Size distribution properties for TF1 standard test fire

The overlapping size range between the mobility diameter and the optical diameter based size distribution measurement will be used to merge the two size distributions together. The angular light scattering will be compared to theory.

This work was supported by the Commission for Technology and Innovation (CTI) Switzerland.

On-site estimation of secondary organic aerosol production potential from wood burning appliances

A. Keller[1], J. C. Corbin[2], A. A. Mensah[2], B. Sierau[2], H. Burtscher[1]

[1]Institute for Aerosol and Sensor Technology, University of Applied Sciences Northwestern-Switzerland, 5210 Windisch, Switzerland

[2]Institute for Atmospheric and Climate Science, ETH Zurich, 8092 Zurich, Switzerland

Keywords: SOA (Second. Organic Aerosols), Wood Combustion, Emissions, Measurement (characterization).

Presenting author email: alejandro.keller@fhnw.ch

Organic aerosol (OA) can be the dominant component of ambient particulate matter (Szidat *et al.*, 2007). However, not all OA is present at the emission point. An important fraction, called secondary organic aerosol (SOA), forms after emitted organic gaseous carbon (OGC) undergoes atmospheric chemistry in a process that can take hours or even days to complete. Small combustion installations (SCI) that burn solid fuel produce important amounts of SOA (Grieshop *et al.*, 2009; Heringa *et al.*, 2011). Their SOA production potential depends, among other things, upon the type of technology and the operating conditions.

SOA is, thus, an important fraction of atmospheric PM that should be considered in emission control legislation. This poses a challenge for air quality regulatory agencies. Smog chamber experiments, for instance, are hardly appropriate for type approval testing or as a standard system for emissions control. We have tested a more compact solution: a continuous-flow reactor-tube with a residence time of only a few seconds. We will show that this setup is enough to oxidize OGC emissions from SCI and transform them into SOA, resulting in a SOA production potential between 0.01 and 1.28 g/Kg-CO_2 (Keller and Burtscher, 2012). These values depend upon the combustion phase and are comparable to previous published data from smog-chamber experiments. Changes in the dilution of the sample, tested up to a factor of 1:8, do not seem to influence the results. Field measurements show that larger automatic installations (e.g. boilers > 70kW) can achieve a very good combustion with no measurable OGC emissions and have, accordingly, no measurable SOA production potential either.

We will also present data from the chemical analysis of the resulting SOA by means of an Aerodyne aerosol mass spectrometer (AMS) run by ETH Zurich. This instrument shows that conditioning the emissions in our UV reactor results in a highly oxidized OA. The oxidation degree is higher than previously published data from field campaigns or smog chamber experiments (see, e.g., figure 1). This difference does not come into conflict with the purpose of our reactor. We do not want to predict an ambient outcome, which is influenced by atmospheric conditions and the contribution of other local sources. Instead, we want to provide a system that can estimate the maximum SOA production potential of wood burning appliances.

This research was supported by the Swiss Federal Office for Energy (SFOE), the Swiss Federal Office for the Environment (FOEN) and the IMBALANCE project of the Competence Center Environment and Sustainability (CCES) from the ETH Zurich and the Swiss National Fund (SNF).

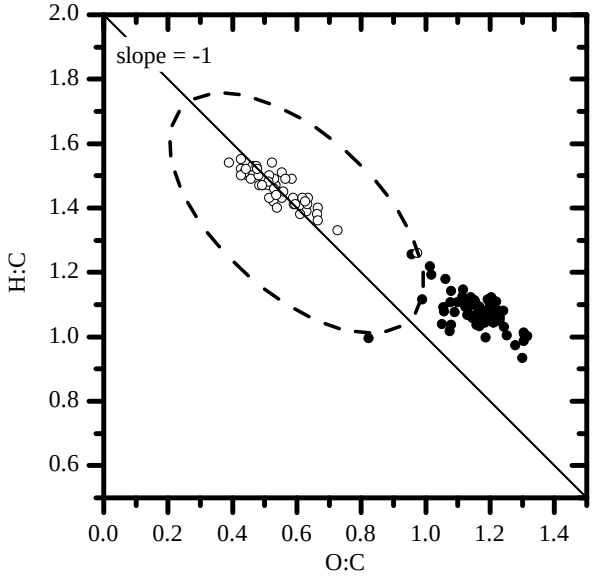

Figure 1: Van Krevelen diagrams of the elemental ratios of organic aerosol emitted during the warm combustion cycles of a log-wood stove measured by AMS run by ETH Zurich. Open circles represent the raw emissions whereas bullets represent the result of conditioning these emissions in the UV reactor tube. The dashed ellipse shows the area comprising ambient data from the MILAGRO C-130 aircraft campaign over and near Mexico City (Heald *et al.*, 2010).

Grieshop, A., Logue, J., Donahue, N., and Robinson, A. (2009). *Atmos. Chem. Phys.* **9**, 1263–1277.

Heald, C. L., Kroll, J. H., Jimenez, J. L., Docherty, K. S., DeCarlo, P. F., Aiken, A. C., Chen, Q., Martin, S. T., Farmer, D. K. and Artaxo, P. (2010) *Geophys. Res. Lett.* **37**, L08803, doi:10.1029/2010GL042737.

Heringa, M., DeCarlo, P., Chirico, R., Tritscher, T., Dommen, J., Weingartner, E., Richter, R., Wehrle, G., Prévôt, A., and Baltensperger, U. (2011). *Atmos. Chem. Phys.* **11**, 5945–5957.

Keller, A., Burtscher, H. (2012) *Aerosol Sci.* **49**, 9–20.

Szidat, S., Prévôt, A., Sandradewi, J., Alfarra, M., Synal, H.-A., Wacker, L., and Baltensperger, U. (2007). *Geophys. Res. Lett.* **34**, L05820.

Reference particles for toxicology studies of biomass combustion generated ash particles

T. Torvela[1], O. Uski[2], A. Lähde[1], J. Grigonyte[1], T. Karhunen[1], T. Koponen[1], M.-R. Hirvonen[2], J. Jokiniemi[1,3]

[1]Fine Particle and Aerosol Technology Laboratory, University of Eastern Finland, P.O. Box 1627, FI-70211 Kuopio, Finland
[2]Inhalation Toxicology Laboratory, University of Eastern Finland, P.O. Box 1627, FI-70211 Kuopio, Finland
[3]VTT Fine Particles, P.O. Box 1000, 02044 VTT Espoo, Finland
Keywords: biomass combustion, toxicology, nanoparticles, zinc
Presenting author email: tiina.torvela@uef.fi

The health risks of biomass combustion have been widely recognized (Mills *et al.*, 2009). However there is contradictory understanding of the factors that cause the adverse effects on human health. There is also a lack of knowledge regarding the relevant dose of particular pollutants causing the adverse health effects (Pope & Dockery, 2006).

In order to understand the toxicological responses, the properties of the exposing particles must be clearly defined. Pure substances or chemicals have been used in toxicological analyses as reference. However the size, crystallinity and solubility, for example, are major determinant factors for the toxicological response (Becker *et al.*, 2003). The properties of reference particles that are typically used in these studies differ, in general, from the ones of the pollutants. Therefore, it can be difficult to correlate toxicity of the references and the pollutants.

The ash of efficient combustion is mainly composed of alkali metal sulphates and chlorides, containing also various amounts of transition metal oxides such as ZnO (Sippula *et al.* 2009). The particle diameter is typically below 100 nm and thus fulfils the definition of nanoparticles (NPs, EC 2011). However, these efficient conditions are not typical for biomass combustion. In incomplete combustion condensed organic compounds are likely to participate in the particle formation. There are indications that organic compounds are capable of inducing radical alterations to the rheological behaviour, such as solubility, of the particles. Therefore the behaviour of the particles in contact with cells in a biological medium becomes more unpredictable.

In this study we have synthesized NPs containing ZnO, alkali salts and carbon in order to respond to the need for biomass combustion reference particles for toxicological studies. The NPs were designed to be similar in size, shape and chemical composition to the ash particles released from biomass combustion. Moreover, the physicochemical and rheological properties of the particles were characterised in order to identify the factors affecting their bioavailability. The effects on the cell viability of mice macrophage cells caused by the synthesized NPs were also evaluated.

The NPs were manufactured with chemical vapour synthesis (CVS, Moisala *et al.* 2006), using liquid Zn acetate dehydrate and alkali salts in water as a precursor solution. Purified air was used as carrier gas. The precursor was dispersed to gas with an ultrasonic atomizer and lead through a high-temperature (1000-1400°C) vertical flow reactor, and diluted rapidly with ambient temperature air to quench the chemical reactions. Particles were then analysed with on-line and off-line methods.

The resulting particles (Fig. 1) were characterised for size distribution, chemical composition, crystallinity, single particle morphology, thermal behaviour, surface properties, IR absorbance and rheological properties e.g. zeta potential and solubility. Cytotoxicity of the synthetic NPs was determined by a dose-response study which was carried out using mice RAW264.7 macrophage cells. The detected toxicological responses were compared to the real biomass combustion generated ash particle responses as described by Jalava *et al.* (2012).

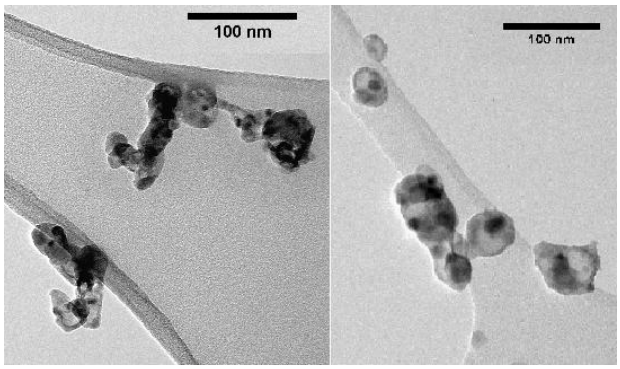

Figure 1. TEM images of ash particles released in biomass combustion (left figure), and ash–like NPs, synthesized with CVS process (right figure).

The research has received funding from the Helmholtz Institute, Germany under grant agreement n° AZ: 504500-ART0001, the University of Eastern Finland (NAMBER), and the non-profit foundation Suomen Luonnonvarain Tutkimussäätiö (Grant. no 1749/12).

Becker, S. *et al.* (2003). *Exp Lung Res* **29**:29-44.
Brunner, T.J. *et al*. (2006). *Environ Sci Technol* **40**: 4374-4381.
EC (2011). *Eur. Commission Official J.* L 257/38.
Jalava, P. *et al.* (2012). *Atmos. Environ.* **50**: 24-35.
Mills, N.L. *et al.* (2009). *Nature Clinical Practice Cardiovascular Medicine* **6**:36-44.
Moisala, A., *et al.* (2006). *Chem Eng Sci* **61**:4393-4402
Pope, C.A. 3rd and Dockery, D.W. (2006). *J Air Waste Manag Assoc* **56**:709-742.
Sippula, O. *et al.* (2009). *Atmos. Environ.* **43**, 4855-4864 (2009).

Study of fine particle emissions from small scale wood chips combustion boiler

A.Bologa[1], M. Ecker[2], H.-P. Rheinheimer[3], K.Woletz[1] and H.-R.Paur[1]

[1]Karlsruhe Institute of Technology, D-76344 Eggenstein - Leopoldshafen, Germany
[2]HDG-Bavaria GmbH; D- 84323 Massing, Germany
[3]CCA-Carola Clean Air GmbH, D-76344 Eggenstein – Leopoldshafen, Germany
Keywords: biomass combustion, fine particles, emission control, electrostatic precipitator.
Presenting author email: andrei.bologa@kit.edu

Wood combustion in small scale boilers is widely used for domestic heating. The boiler capacity, combustion conditions, fuel quality, etc. strongly influence on particle emissions from the facility. Due to progress of combustion technologies particle emissions from small scale wood combustion has decreased with respect to mass concentration. However, fine particles, which are associated with various diseases, still contribute significantly to the PM-burden in many cities, especially during winter heating period.

In Germany the Ordinance for Small Scale Combustion (1.BImSchV) regulates the level of particle emissions from biomass combustion facilities. According to the ordinance, starting from 01.01.2015, the particle mass concentration in the exhaust gas from modern small scale wood combustion boilers should be decreased from 100 mg/m_N^3 to 20 mg/m_N^3. So, a significant part of wood-fired boilers will require the improvement of combustion conditions and /or the use of the exhaust gas cleaning equipment.

The purpose of the current work is the study of fine particle emissions from small scale wood chips combustion boiler for different operation conditions and development of recommendations for enhancement of the efficiency of the gas cleaning equipment.

The long-term experimental studies were carried in the Karlsruhe Institute of Technology. The test facility consisted of a 100 kW wood chips boiler (Fa. HDG Bavaria) which was equipped with automatic system for fuel delivering into the combustion chamber. The wood-chips combustion boiler was tested during 2 measurements companies, every ca. 1000 h.

For control of fine particles emissions from the exhaust gases a novel form CAROLA© space charge electrostatic precipitators (ESP) were applied. The ESPs are designed by the CCA – Carola Clean Air GmbH.. The boiler and the electrostatic precipitators were operated in automatic non-stop regime.

The exhaust gas from the boiler was delivered into the test set-up gas duct which allowed the control of the operation conditions, such gas flow velocity and temperature, exhaust gas composition and particle mass concentration (measured by the corresponding equipment from Fa. Wöhler) and particle number concentration (measured by the Scanning Mobility particle Analyser (SMPS), Fa. TSI). Among the measurements, also the chemical analysis and the REM-analysis of the collected material were carried out.

The studies show that the exhaust gas composition strongly depends on the combustion stage and it is characterised by the increase of the CO concentration by the start-up and burn-out stages.

During the 1000 h of boiler operation round 100 gravimetric measurements were carried out. The analysis of the results shows that the exhaust gas temperature and the particle mass concentration strongly depend on the fuel quality, type of burnt material and wood humidity. With increase of humidity, particle mass concentration in the exhaust gas flow increases. Reduced particle emissions (round 50-60 mg/Nm³) correspond to the wood humidity ca. 12-14%. The increase of humidity up to 23-25% results in the increase of particle mass concentration in the exhaust gas up to 150 mg/Nm³.

The results of SMPS measurements show (fig.1) that the mean particle size is 160-180 nm. The aerosol is three-modal, what probably corresponds to different combustion condition stages in the boiler with automatic delivering of wood into the combustion chamber.

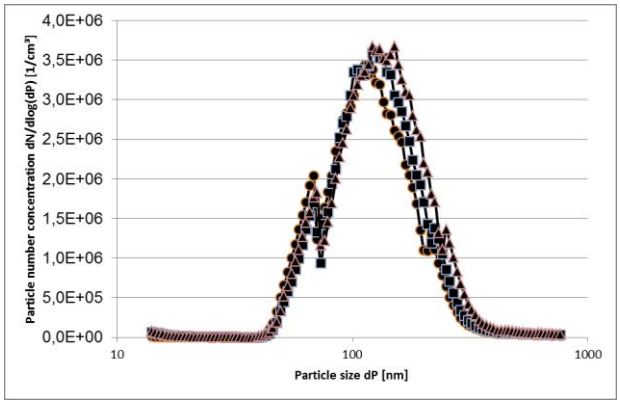

Figure 1. Example of particle size distribution in the exhaust gas flow, dilution factor 10

Among the discussion of the data of long-term observations of fine particle generation by wood combustion, the results of the reduction of fine emissions by the ESPs will be also presented. Detail results of the study of the electrostatic precipitators are the topic of the 2nd abstract presented by the EAC-2013.

The use of the novel ESP's strongly decreases particle mass and number concentration. The mass collection efficiency of the electrostatic precipitators is in-between 70% to 90% depending on combustion conditions.

Effects of severe congestion on PAH emissions from a heavy vehicle diesel engine

M. Vojtisek-Lom[1,2], M. Pechout[1], M. Mazač[1] and J.Topinka[3]

[1]Dept. of Vehicles and Engines, Technical Univ. of Liberec, 461 17 Liberec, Czech Republic
[2]Dept. of Mechanical Engineering, Czech Tech. University of Prague, 166 07 Prague, Czech Republic
[3]Institute of Experimental Medicine of the Czech Academy of Sciences, Prague, Czech Republic
Keywords: diesel engine, particulate matter, polyaromatic hydrocarbons, PAH, urban, congestion
Presenting author email: michal.vojtisek@tul.cz

Summary

The effects of severe congestion on heavy diesel particulate matter (PM) emissions were investigated in a laboratory experiment. Extended idling of a conventional diesel engine and subsequent operation at full load were found to produce higher levels of PM and polyaromatic hydrocarbons (PAH) and an order of magnitude higher levels of carcinogenic PAH compared to idling just after loaded operation and to stabilized operation at full load.

Introduction

Despite advances in engine technology, vehicular traffic remains to be one of the key sources of fine and ultrafine PM in urban air. This work investigates the effects of severe congestion, common for transit truck traffic in Prague and elsewhere, on PM emissions.

Experimental (see Fig. 1 for schematic)

A diesel engine (certified to 0.3 g/kWh PM) with a mechanical injection pump coupled to an engine dynamometer was run alternately at intermediate rpm and full load, and at idle rpm and 1-2% of rated power to simulate slow "creep". Raw exhaust was diluted at nominally 10:1 dilution ratio and sampled by a Hi-Vol sampler (EcoTech 3000) with a $PM_{2.5}$ impactor. A second Hi-Vol sampler was used to provide dilution air. Dilution ratio was verified by CO_2 concentrations measurements. Samples of PM taken on fluorocarbon coated and quartz filters were extracted and PAH content analysed by HPLC with fluorescence detection.

Results and Discussion

Emissions of benzo[a]pyrene, 7 carcinogenic PAH (cPAH) per US EPA (benzo[a]anthracene, chrysene, benzo[b]fluoranthene, benzo[k]fluoranthene, benzo[a]pyrene, dibenzo[a,h]anthracene, indeno[1,2,3-cd]pyrene), US EPA 16 PAH, and total particulate mass, expressed as mass per kg of fuel, are plotted in Fig. 2.

It appears that BaP and cPAH after tens of minutes of idling were an order of magnitude higher than during first several minutes following a higher load.

It also appears that BaP and cPAH during operation at full load were an order of magnitude higher during first several minutes after prolonged (one-hour) idling compared to "stabilized" operation at full load.

It thus seems that prolonged idling may substantially increase emissions of carcinogenic PAH not only during, but also after the idling episode.

Toxicity of extracts of particulate matter sampled from exhaust gases of heavy diesel vehicles under real-world urban operation is currently being evaluated.

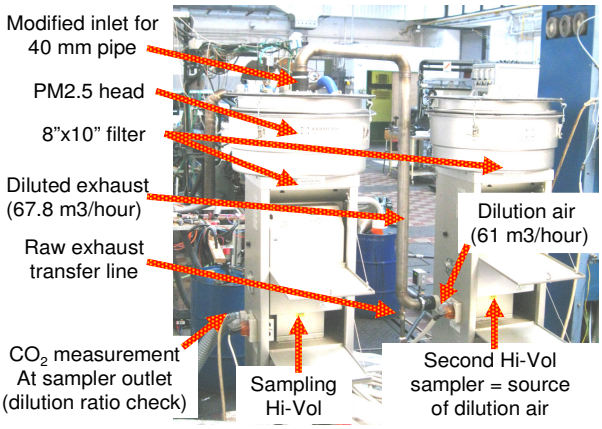

Fig. 1: Sampling setup

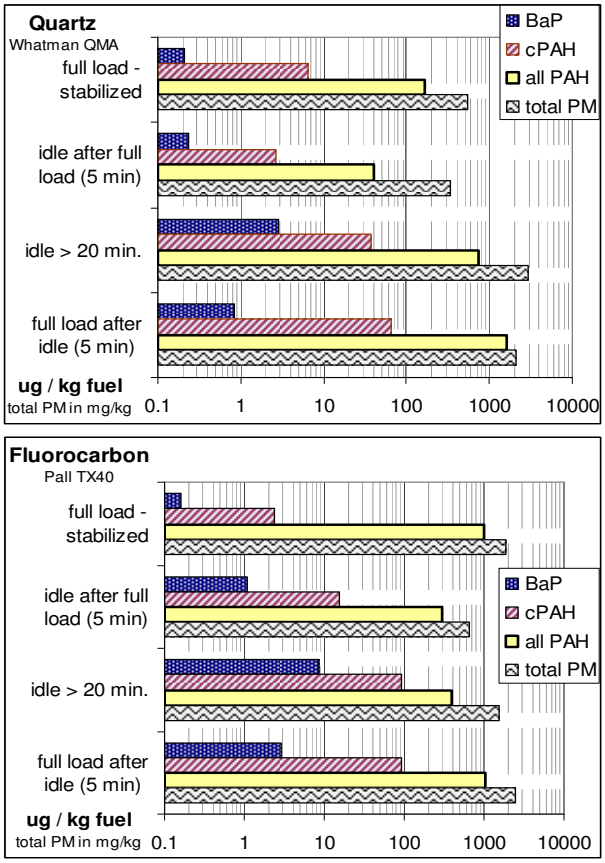

Figure 2: Benzo[a]pyrene, carcinogenic PAH and all PAH emissions in micrograms per kg of fuel

This work was supported by the EU LIFE+ project MEDETOX (LIFE10 ENV/CZ/651) and Czech Science Foundation Grant 13-01438S.

Tuesday, September 3, 2013

Session: PMx
Urban and regional PMx

EC/OC comparison exercise with same thermal protocols after temperature offsets correction

P. Panteliadis[1], T. Hafkenscheid[2], B. Cary[3] and W. Maenhaut[4]

[1]Department of Air quality, Public Health Service Amsterdam, 1018WT, The Netherlands
[2]National Institute for Public Health and the Environment, Bilthoven, The Netherlands
[3]Sunset Laboratory Inc., Tigard, Oregon, USA
[4]Department of Analytical Chemistry, Ghent University, Gent, BE-9000, Belgium
Keywords: Elemental Carbon, EUSAAR2, NIOSH, temperature offsets
Presenting author email: ppanteliadis@ggd.amsterdam.nl

The department of Air Quality of Public Health Service Amsterdam has been organizing laboratory comparison exercises for the past few years on thermal-optical elemental carbon / organic carbon (EC/OC) analysers. To our knowledge, all laboratory comparisons performed in Europe up to 2012 considered results derived from different protocols applied per participant, usually NIOSH (Birch & Cary, 1996) or EUSAAR2 (Cavalli et al., 2010), limiting comparability of the performance of each laboratory. The scope of the 2012 comparison exercise was to evaluate results based on an identical, to the extent possible, instrument set-up for all participants. By definition the same protocol should then be applied. Yet, the debate over NIOSH and EUSAAR2 is still ongoing in Europe and a selection of one out the two would have been complex. As an alternative, we decided for the use of both protocols by each participant, providing additional information that could point out possible differences between the two protocols.

Each protocol facilitates several thermal steps and instrument-specific deviations of the desired temperature can alter the sample treatment and bias the analysis result. Since the introduction of a temperature calibration kit by the analyser manufacturer (Sunset Laboratory Inc, OR, US) in early 2012 it is possible to overcome these deviations. All participants agreed on performing the calibration and compensating for the temperature offsets before the comparison exercise analysis.

A total of 20 1.5 cm^2 punches, derived from 5 PM sampled quartz filters, and two sucrose standard solutions were delivered to each of the 17 participants. Duplicate analyses per filter and triplicate per solution were performed applying each protocol. Next to the EC and OC concentrations, raw data and thermograms were provided and additional analysis factors were investigated, namely, split time, transit time, pyrolytic carbon, temperature offsets and thermal peaks distribution. All analyses were performed on transmittance mode (TOT) while the majority of participants also provided reflectance (TOR) results.

In the comparison of EUSAAR2 derived thermograms (Figure 1), notable differences were observed in peak distribution, especially after the 4th, suggesting possible pre-oxidation on a number of analysers. The split point separating EC from OC fell in a range of about 100 seconds. Similar observations were made on the respective NIOSH thermograms. Figure 2 shows all paired EC results for EUSAAR2 and NIOSH indicating that reported EC concentrations may vary for

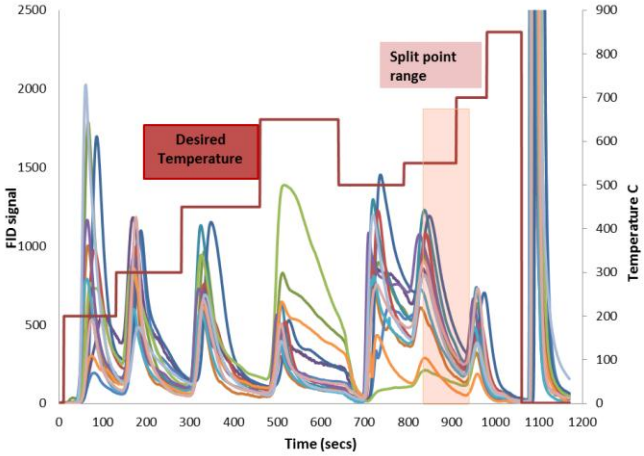

Figure 1. Thermograms of TOT ECOC analysis on PM loaded quartz filter, by EUSAAR2 for all participants.

the same filter in regard to the protocol applied. No differences were observed for total carbon (TC) where $TC_{NIOSH} = 0.99 \cdot TC_{EUSAAR2}$ (R^2=0.98) for loaded PM filters and $TC_{NIOSH} = 1.00 \cdot TC_{EUSAAR2}$ (R^2=0.98) for sucrose solutions was found.

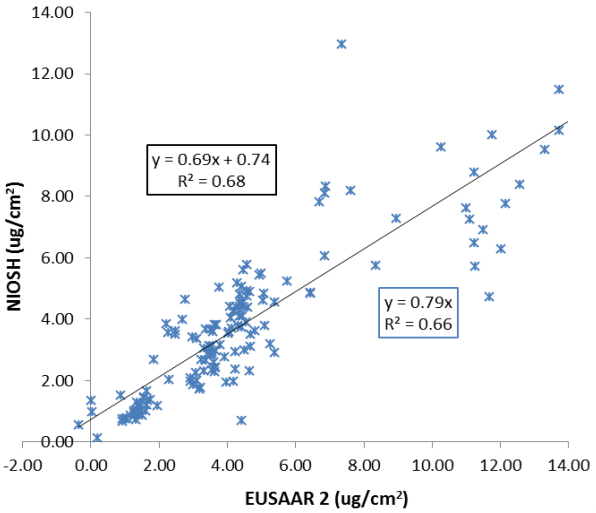

Figure 2. Comparison of EC concentrations by TOT EUSAAR2 and NIOSH on PM loaded quartz filters (N=150).

Birch, M.E. and Cary, R.C. (1996) *Aerosol Sci. Technol.* **25**, 221-241.

Cavalli, F., M. Viana, K. E. Yttri, J. Genberg and J.-P. Putaud (2010) *Atmos. Meas. Tech*. **3**, 79–89.

The fossil fraction of carbon in PM2.5: Variations on seasonal and diurnal time scales

U. Dusek[1], M. Monaco[1], A. Kappetijn[1], H. A. J. Meijer[2], S. Szidat[3], and T. Röckmann[1]

[1]IMAU, Utrecht University, Utrecht, the Netherlands
[2]Center for Isotope Research, Groningen University, Groningen, the Netherlands
[3]Department of Chemistry and Biochemistry, University of Berne, 3012, Switzerland

Keywords: organic carbon, elemental carbon, radiocarbon, 14C, fossil fuel, source apportionment, PM2.5
Presenting author email: u.dusekt@uu.nl

Measurement of the radioactive carbon isotope ^{14}C in aerosols can provide a direct estimate of the contribution of fossil fuel sources to aerosol carbon (e.g. Szidat et al., 2007). In aerosol science, measurements of $^{14}C/^{12}C$ ratios are usually reported as fraction modern ($F^{14}C$). The radiocarbon signature gives a clear distinction between 'modern' carbon sources ($F^{14}C$ around 1.1-1.2 for biomass burning and around 1.05 for biogenic secondary organic aerosol) and 'fossil' carbon sources ($F^{14}C$ =0 for primary and secondary formation from fossil fuel combustion). Due to the high cost of ^{14}C analyses very few long-term studies have been conducted to date. The data that will be presented offer a unique insight into the seasonal variation of source contributions to the carbonaceous aerosol in a highly industrialized region.

High volume filter samples of PM2.5 have been collected roughly twice per month from February 2011 – July 2012 at Cabauw, a rural location in the Netherlands surrounded by major urban centers and highways. This site is representative of regional background aerosol contamination in the Netherlands. We report measurements of $F^{14}C$ for total carbon (TC), organic carbon (OC), water insoluble OC (WIOC) and thermally refractory carbon (RC) as a proxy for elemental carbon.

The fraction modern of OC lies between 0.65 - 1 and shows only a moderate seasonal variation, with highest values in the spring and lowest values in the summer. EC is generally dominated by fossil carbon, but shows a distinct seasonal variation with higher contribution of modern sources from November – Mai. This contribution is normally attributed to wood combustion, see Figure 1, but this is questionable for the filter samples taken in spring. The modern contribution is low when air masses arrive from the ocean and high for air masses with European continental origin, pointing to a main source outside the Netherlands. Water soluble organic carbon is dominated by modern sources throughout the year.

For TC concentrations between 1.2 and 8 $\mu g/m^3$, f_m(TC) increases with TC concentration. A Keeling plot implies that synoptic scale variation in f_m(TC) are mainly due to a modern source, imposed on a regional background with a relatively high contribution from fossil sources. TC concentrations > 8 $\mu g/m^3$ are associated with pollution events and can have much higher fossil contributions.

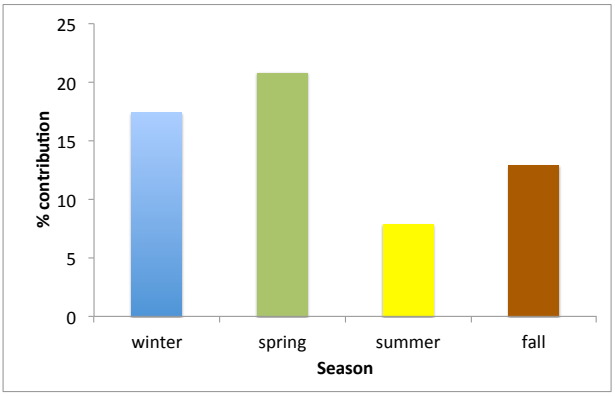

Figure 1. Contribution of biomass burning to refractory carbon in different seasons. Up to approximately 5% can be explained by not ideal separation of OC and RC

Measurements of diurnal variations in $F^{14}C$ can give an indication of the importance of regional emissions, such as traffic, or SOA production from biogenic emissions. For selected time periods during spring and summer 2012, we took separate day and night filter samples that were analyzed for ^{14}C in TC, OC, WIOC, and RC. In all carbon fractions the fossil contribution was higher in day time than in night time. This is consistent with the traffic density in the region, which is higher during day time (7 am to 7 pm) than during night time. Contrary to the synoptic scale variation dominated by modern carbon, the shorter term variations in the regional aerosol seem dominated by fossil sources. Condensation of semi-volatile carbon in the cooler night time might contribute to this trend.

Using a simple model, the contributions of fossil emissions, biomass burning, and biogenic emissions will be estimated for all carbon fractions. The seasonal variation in the source contributions will be presented and discussed.

This work was supported by the Netherlands Organization for Scientific Research (NWO, grant nr. ALW820.01.001).

Szidat, S., Prevot, A. S. H., Sandradewi, J., Alfarra, M. R., Synal, H.-A., Wacker, L., and Baltensperger, U., (2007) *Geophys. Res. Lett.,* **34**, L05820, doi:10.1029/2006GL028325.

Ultrafine particles at eight urban sites in Antwerp: instrument comparison and spatiotemporal variation in particle number concentration and size distribution

J. Staelens[1], E. Frijns[2], P. Berghmans[2], G.P.A. Kos[3], C. Matheeussen[1], P. Panteliadis[4], B. Bergmans[5], E.P. Weijers[3], K. Wyche[6] and E. Roekens[1]

[1]Department Air, Environment and Communication, Flemish Environment Agency (VMM), Antwerp, 2000, Belgium
[2]Flemish Institute for Technological Research (VITO), Mol, 2400, Belgium
[3]Environment & Energy Eng., Energy research Centre of the Netherlands (ECN), Petten, 1755ZG, the Netherlands
[4]Department of Air Quality, Public Health Service of Amsterdam, Amsterdam, 1000CE, the Netherlands
[5]Air Quality, Institut Scientifique de Service Public (ISSeP), Liège, 4000, Belgium
[6]Department of Chemistry, University of Leicester, Leicester, LE2 7TG, United Kingdom
Keywords: urban air quality, ultrafine particles, black carbon, number size distribution.
Presenting author email: j.staelens@vmm.be

Due to the short atmospheric lifetime of ultrafine particles (UFP) and their strong dependence on local sources, ambient particle number concentrations and size distributions may vary significantly on short spatial and temporal scales. Because UFP are a primary pollutant that is rapidly transformed by physicochemical processes (dispersion, coagulation, deposition, etc.) and emitted mainly by mobile sources, they show a very high spatial variation. The particle number concentration is known to be elevated near roads and to decrease with increasing distance to the road primarily as a result of dispersion. Therefore, UFP measurements at a single urban background air quality monitoring station may not be indicative of the actual exposure in the communities surrounding this station.

To address this problem and to more accurately estimate human exposure and subsequent health impacts of UFP, more intensive measurements on finer spatial scales are needed. Therefore, UFP measurements were carried out at eight urban background or hotspot sites in the city of Antwerp (Belgium).

UFP instrument comparison

As different types of UFP instruments were used, first a 3-week field comparison was carried out in January 2013. Four types of UFP instruments were involved: (i) a particle counter with water as condensation liquid (TSI-3783 or EPC, n = 5), (ii) a differential mobility analyzer with an electrometer and corona discharger to ionize the sampled aerosol (TSI-3031 or UFP monitor, n = 3), (iii) a scanning mobility particle size spectrometer (SMPS) with butanol condensation particle counter and a Kr-85 source (Grimm CPC-5420 with L-DMA, n = 3), and (iv) a second type of SMPS with a butanol particle counter and a Ni-83 source (TSI-3772 with L-DMA, n = 1).

All devices were set up in measuring stations or trailers at an urban background site next to a moderately busy road. The results indicate good comparability of the instruments per type of instrument. The particle number concentration measured by the five EPC instruments was strongly correlated ($R^2 > 0.98$). More particles were detected in the high inlet flow mode (3.0 L/min) than with a lower inlet flow (0.6 L/min). The number of instruments sampling from a single TSI sampling system influenced the results as well. Without inlet screen assembly the average number concentration by the EPC instruments differed less than 12% from each other.

For the three UFP monitors good correlation ($R^2 > 0.91$) was generally observed between the size-specific particle number concentrations, except for the highest size channel (>200 nm). For the lowest size channel (20-30 nm) the difference between the UFP monitors was up to 30%, but the total number concentration differed less than 10%. For the three Grimm SMPS devices there was a strong correlation ($R^2 > 0.95$) between the size-specific particle number concentrations and also the total number concentration (10-1094 nm) was very comparable, with a difference of on average less than 3%.

Spatiotemporal UFP variation

In February 2013, the UFP number concentrations and size distributions were simultaneously measured (i) at three sites with an increasing distance (10, 30 and 55 m) to a major traffic road and (ii) at four other urban sites in Antwerp. At each of these seven sites an EPC was set up together with a UFP monitor or an SMPS. To relate the UFP measurements to the local traffic conditions, traffic intensity was monitored at all sites. Diffusive samplers were used to monitor weekly NO_x concentrations. In the road gradient study also black carbon concentrations were measured.

The research questions of this 4-week study were (i) to determine the effects of a busy traffic road on particle number, size distribution, black carbon and NO_x concentrations into adjacent neighbourhoods, (ii) to determine the small-scale spatial variability of particle number concentration and size distribution within an urban area, (iii) to examine how this variation is affected by the site location (source vs. receptor), traffic intensity and meteorology, and (iv) to analyze particle number data with high time resolution in order to determine regional vs. local contributions to particle number levels.

This study is part of the Joaquin project (Joint Air Quality Initiative; www.joaquin.eu) that is supported by INTERREG IVB North-West Europe.

Long term trend and weekly cycles of PM_{10} in the Po valley

A. Bigi, G. Ghermandi

Department of Engineering "Enzo Ferrari", University of Modena and Reggio Emilia, Modena, I-41125, Italy
Keywords: long-term trend, PM_{10}, Po valley
alessandro.bigi@unimore.it

In order to assess changes and variability in daily PM_{10} concentration in the Po valley, 35 pluri-annual time-series have been analysed. Data have been collected at 35 different sampling sites within the Po valley, including both traffic and background sites, either urban, suburban or rural. The dataset comprise pollution data up to January 2012 acquired within the Regional Environmental Agency monitoring networks; all data are referred to actual sampling condition, as required by 2008/50/EC.

Series with at least 10 years of data have been tested for long term trends in the deseasonalised monthly means, in annual quantiles and in binned monthly concentration. In the former test data have been deseasonlised by STL (Cleveland *et al*, 1990) technique and temporal trend has been estimated *via* GLS model on the STL trend component. Trend significance has been estimated by model-based resampling. Trend for the 25th, 50th and 95th annual quantiles has been estimated by Theil-Sen method; significance of annual quantiles trend has been tested by non-parametric resampling. In order to assess a seasonal long term trend, PM_{10} daily concentration for each month have been binned by 15μg/m³ increments and the frequency of each bin in each month over the sampling period has been computed. The trend in these frequencies for each month have been estimated by Theil-Sen method and significance has been tested by non parametric bootstrap, similarly to annual quantiles.

Weekly pattern at each site have been estimated, in order to assess pollution condition and anthropogenic sources influence at each station. Weekly cycle has been investigated through the study of PM_{10} anomalies. Being the data highly non normal, the analysis of deviations used a Kruskal-Wallis test. The significance of the weekly cycle has been double checked by group deviations in 6- and 8-days-week, and performing a Kruskal-Wallis test for these series of anomalies. Also the weekend effect magnitude for each site has been computed, i.e. the difference between the mean PM_{10} anomaly of Saturday through Monday and the mean PM_{10} anomaly between Wednesday through Friday.

A cluster analysis has been applied in order to highlight stations sharing similar pollution conditions over the reference period. Clusters have been built by hierarchical method, computing the dissimilarity matrix by Euclidean distance and using Ward's method to aggregate the data.

Finally, at the sites where both $PM_{2.5}$ and PM_{10} are sampled, a comparison of the weekly patterns for the two pollutants has been performed.

Results

Here are some of the main findings of the study:

- most sites exhibited significant decreasing trends in monthly, annual and seasonal data
- decreasing trends can be high (up to ~4.5% / year)
- many decreasing trends are higher over the period 2002 - 2011 compared to 1998 - 2011
- most of the decrease is due to lower autumn-winter high concentrations
- a significant weekly cycle is present in almost all of the sites; consistent results are shown by the analysis of weekly cycle magnitude
- clustering is driven mostly by the geographical position than by site classification

Finally the study shows how multiple and proper analysis methods are necessary in order to assess the significance of a pattern on atmospheric pollutant data.

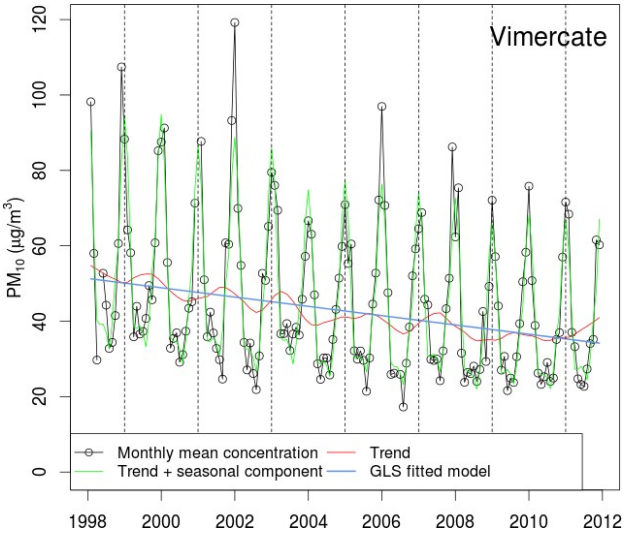

Figure 1. Deseasonalisation of monthly mean PM_{10} at Vimercate, along with GLS trend

Cleveland, R. B., Cleveland, W. S., McRae, J., and Terpenning, I. (1990) *J. Off. Stat.* **6**, 3–33

Fugitive particle emissions from steel making: source characteristics and local air quality impact investigated with a mobile laboratory

F. Drewnick[1], F. Freutel[1], S.-L. von der Weiden-Reinmüller[1], J. Fachinger[1] and S. Borrmann[1,2]

[1]Particle Chemistry Department, Max Planck Institute for Chemistry, Mainz, 55128, Germany
[2]Institute of Physics of the Atmosphere, Johannes Gutenberg University Mainz, Mainz, 55128, Germany
Keywords: steelworks emissions, source characteristics, pollutant mapping, mobile laboratory.
Presenting author email: frank.drewnick@mpic.de

Industrial stack emissions are largely regulated and therefore typically reasonably well known. However, much less is known on the characteristics and local impact of fugitive emissions which can originate from multiple sources in industrial facilities. The focus of this study is the investigation of fugitive particulate emissions from sources on integrated steel plants, both in terms of emission characteristics and of their impact onto the air quality in the area around such sites.

The highly time resolved measurements within this study were performed using the mobile aerosol research laboratory MoLa (Drewnick *et al.*, 2012). MoLa provides state-of-the-art instrumentation to determine aerosol number (d_p > 2.5 nm) and mass (PM_1, $PM_{2.5}$, PM_{10}) concentrations, particle size distributions (d_p = 6 nm – 32 µm) and chemical composition of the sub-micron aerosol. In addition several trace gases and all relevant meteorological variables are measured.

For determination of fugitive emission source characteristics, stationary measurements of the ambient aerosol were performed within the steelworks several tens to several hundred meters downwind of the individual facilities. The distribution of air pollutants in the vicinity of the plant and their impact onto local air quality were determined by applying a combination of stationary and mobile measurements, both downwind the steelworks and in the unpolluted background.

In order to extract the best possible information from the Aerodyne HR-ToF-AMS mass spectra different approaches have been used. In addition to the determination of the standard species, PMF was applied to separate the organic aerosol into fresh combustion-related and oxygenated (i.e. aged) fractions. Thorough analysis of the high-resolution mass spectra provided information on aerosol components like iron, rubidium and zinc halogenides as well as lead, all not included in the standard analysis procedure of the instrument.

Measurements downwind of blast furnaces, coke ovens, a BOS (basic oxygen steelmaking) plant, ore and coal stockyards and a vehicle movement area were used to determine the respective fugitive emission source characteristics. Due to the close proximity of multiple sources on an integrated steel plant, miniscule variations in wind directions can cause the advection of background air or of emissions from other sources to the measurement site, resulting in systematic biases in integrating measurements. Therefore, the combination of highly time-resolved wind and pollutant measurements is necessary to reliably determine the source contribution to the locally observed ambient aerosol.

A total of more than 1300 km of mobile measurements in the vicinity of two steel plants was performed to determine the concentration distributions for multiple aerosol and trace gas variables in the respective areas. After removal of data contaminated by local sources (e.g., vehicles in front of MoLa) pollutant concentrations along the driving tracks were calculated. Using an extrapolation and interpolation algorithm that accounts for the different transport characteristics parallel and perpendicular to the wind direction, two-dimensional distribution maps were calculated for every pollutant measured with MoLa (e.g., Fig. 1). For days where wind directions did not change strongly over the time of the measurement this procedure provided valuable information on the impact of the steelworks emissions onto the local air quality in the vicinity of the plant.

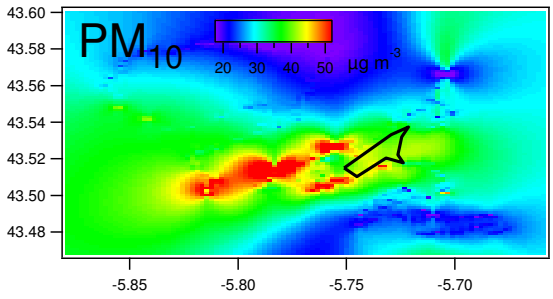

Figure 1. Distribution of PM_{10} in the vicinity of a steel plant. Two separate sources of PM_{10} on and near the steelworks (black framed area) can be distinguished.

Additional stationary measurements in the unpolluted background and within the emission plume were performed. These data were used to determine the background aerosol characteristics as well as the temporal variability of the steelworks impact onto various locations.

This work was supported by the European Community's Research Fund for Coal and Steel (RFCS) under grant agreement No° RFSR-CT-2009-00029.

Drewnick, F., Böttger, T., von der Weiden-Reinmüller, S.-L., Zorn, S.R., Klimach, T., Schneider, J., and Borrmann, S. (2012) *Atmos. Meas. Techn.* **5**, 1443-1457.

Elemental composition and potential toxicity of airborne particles at some urban schools

L. R. Crilley[1,2], G. A. Ayoko[1,2], E. Stelcer[3], D. D. Cohen[3] and L. Morawaska[1,2]

[1]International Laboratory for Air Quality and Health, Queensland University of Technology, Brisbane, QLD, 4001, Australia
[2]Institute of Health and Biomedical Innovation, Queensland University of Technology, Brisbane, QLD, 4059, Australia
[3]Institute for Environmental Research, Australian Nuclear Science and Technology Organisation, Sydney, NSW 2232, Australia.

Keywords: elemental composition, schools, vehicle emissions
Presenting author email: g.ayoko@qut.edu.au

Although both the size and chemical composition of ambient particles are important parameters in determining their toxicities, their relative contributions are unclear (Heal et al., 2012). Children are particularly at risk to the detrimental health effects that have been linked to long term exposure to airborne particles (See e.g. Ruckerl et al., 2011). However, there is currently limited understanding of the health effects in children due to long term exposure to airborne particles. Schools are locations within an urban environment where children experience significant exposure to vehicle emissions, and to date there is limited information assessing children's exposure at school. This study is a part of a large project aimed at gaining a holistic picture of the exposure of children to traffic related pollutants. In the current paper, results from the investigation of the elemental composition of airborne particle at urban schools are presented.

Airborne Particulate Matter (PM) with aerodynamic diameters equal to or less than 1.0 (PM_1) and equal to or less than 2.5 micrometer ($PM_{2.5}$) were collected in 25 schools in Brisbane, Australia. $PM_{2.5}$ and PM_1 samples were both collected for 24 hours (8am to 8am) for one week at each school. Filters were subsequently analysed by Ion Beam Analysis (IBA) for their elemental compositions at ANSTO. Twenty-one elements (Na, Al, Si, P, S, K, Ca, Ti, V, Cr, Mn, Fe, Co, Ni, Cu, Zn, Br, Sr, Cd and Pb) were analyzed. Gravimetric analysis was performed on preconditioned filters on a 5 point balance.

The gravimetric results revealed that the on average the PM_1 fraction made up 82 ± 18% of the $PM_{2.5}$ fraction by mass at the schools. Therefore the majority of the sampled particles were in the PM_1 fraction. In Figure 1 the average concentrations across all the school are given. Overall, elements with crustal origins such as Al, Si, K, Ca, Ti, Mn and Fe were found predominantly in the $PM_{2.5}$ fraction. Whereas elements that are more associated with anthropogenic emissions, such as Cr, Pb, Ni, V, Cu and Zn were found predominantly in the PM_1 fraction. Comparison to previous work at roadside location in Brisbane (Friend et al., 2011) revealed that Cr, Ni, Br and Pb had statistically significantly higher $PM_{2.5}$ concentrations at the schools than the roadside indicating an influence from school traffic and other anthropogenic sources.

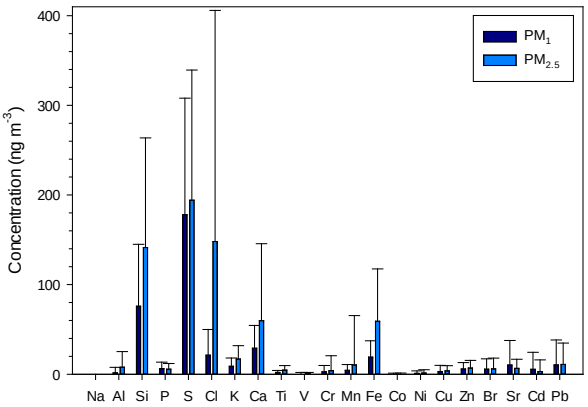

Figure 1: Average concentration of each element across all schools for the both size fractions. Error bars represent 1 standard deviation.

The more toxic heavy metals were found to be in the smaller particle sizes indicating that the PM_1 fraction may have greater detrimental health effects than the $PM_{2.5}$ fraction. Therefore, the results from this study point to PM_1 as a potentially better fraction to use when investigating the health effects of airborne particles. Further work is required to confirm this hypothesis.

Acknowledgements
This work was supported by the Australian Research Council, Department of Transport and Main Roads (DTMR) and Department of Education and Training (DET) through Linkage Grant LP0990134 while the elemental analysis was funded by AINSE grant 11097 . Our particular thanks go to Randall Fletcher (DTMR) and Andy Monk (DET) for their vision regarding the importance of this work. We would also like to thank all members of the UPTECH project, especially Dr Mandana Mazaheri.

References

Rückerl, R., Schneider, A., Breitner, S., Cyrys, J., Peters, A. *Inhal. Toxicol.* **2011**, 555-592.
Heal, M. R., Kumar, P., Harrison, R. M. *Chem. Soc. Rev.* **2012**, 6606-6630.
Friend, A. J., Ayoko, G. A. Stelcer, E. Cohen, D. *Environ. Chem.* **2011**, 569-580.

Characterisation of the aerosol sources in Brindisi (Italy) harbour area within the CESAPO project: an overview of the experimental results

D. Contini[1], D. Cesari[1], A. Donateo[1], A. Gambaro[2], A. Genga[3], G. Giovanelli[4], R. Giua[5], F.M. Grasso[1], E. Gregoris[6], P. Ielpo[1,7], S. Masieri[4], E. Merico[1], E. Morabito[2], A. Nocioni[5], T. Pastore[5], and M. Siciliano[3]

[1] Istituto di Scienze dell'Atmosfera e del Clima, ISAC-CNR, Lecce, 73100, Italy
[2] Dipartimento di Scienze Ambientali, Informatica e Statistica, Università ca' Foscari Venezia, Venezia, 30123, Italy
[3] Dipartimento di Scienze e Tecnologie Biologiche e Ambientali, Università del Salento, Lecce, 73100, Italy
[4] Istituto di Scienze dell'Atmosfera e del Clima, ISAC-CNR, Bologna, 40129, Italy
[5] Agenzia Regionale per la Prevenzione e la Protezione dell'Ambiente, ARPA Puglia, Bari, 70126, Italy
[6] Istituto per la Dinamica dei Processi Ambientali, IDPA-CNR, Venezia, 30123, Italy
[7] Istituto di Ricerca sulle Acque, IRSA-CNR, Bari, 70132, Italy
Keywords: ship emissions, source apportionment, PM2.5, number particle concentration.
Presenting author email: d.contini@isac.cnr.it

The harbour areas are economic centres and transport hubs, that bring together different transport modes (sea, road, railway transport) and, often, include relevant industrial activities. Emissions of ships and of harbour-related activities could have potential negative impact on air quality especially for fine and ultrafine atmospheric particles (Contini at al., 2011; Healy et al., 2010).

At the beginning of 2012 it was started the research project CESAPO (Contribution of Emission Sources on the Air quality of the POrt-cities in Greece and Italy), within the framework of Interreg Greece-Italy 2007/2013, having among its objectives the quantification of the contribution to atmospheric particles of emission sources in two important Mediterranean port-cities: Patra (Greece) and Brindisi (Italy) using state-of-the-art modelling and experimental approaches. Here, an overview of the experimental results obtained in Brindisi will be presented. The area studied is influenced by several emissions: an industrial area, three power plants, an airport and an harbour with a freight traffic and total goods movement that accounted for more than 9.5 million tons and over 520,000 passengers in 2011. Experimental activities in CESAPO were based on an intensive observation period (IOP) of 5 months (June-October 2012). During the IOP the data of 10 fixed monitoring stations (the regional network managed by ARPA Puglia) and those from two additional stations specifically installed during the project inside the harbour area were collected. A station was used to characterize the chemical composition of PM2.5 (metals, major water soluble ions and carbon content) and PAHs (in the gaseous and aerosol phases) and the other was devoted to high temporal resolution (1 second) measurements of PM2.5 mass, number concentrations of submicron particles and diurnal spatially integrated gaseous concentrations using a remote sensing DOAS system (Premuda et al., 2011).

Results of source apportionment based on PM2.5 composition, using the Positive Matrix Factorization (EPA PMF3.0), and on high temporal resolution measurements will be presented and compared with other harbour areas in Italy and Europe. Preliminary results indicate that average PM10 and PM2.5 concentrations in the harbour area are smaller than those observed in the urban area but SO_2 concentrations associated to oil combustion and shipping emissions were larger. The secondary non-sea-salt-sulphate was essentially ammonium sulphate and accounted for about 32% of PM2.5. The detailed contributions of ship traffic and of harbour activities (loading/unloading of ships) were analysed using high temporal resolution measurements. The two contributions appear to be of the same order of magnitude and sporadic in nature being due to numerous short concentrations peaks (durations variable between 10 and 100 minutes) in PM2.5 and in the number of sub-micron particles. An example of peaks to due ships is reported in Figure 1. These peaks were analysed using a statistical methodology that takes into account the wind direction and the actual ships traffic to quantitatively characterize the contribution of vessels traffic and of harbour activities.

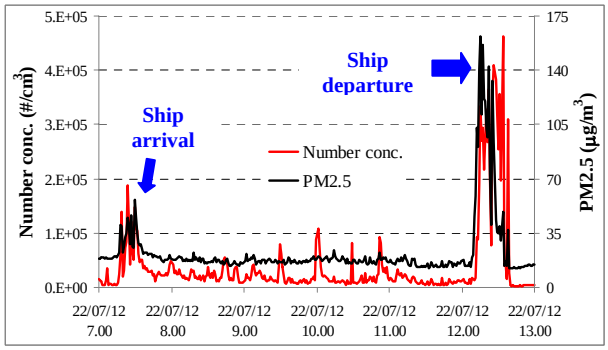

Figure 1. Example of ship emissions contribution to PM2.5 and number particle concentrations.

This work was supported by the Interreg Greece-Italy 2007-2013 program under grant I1.32.06.

Contini, D., Gambaro, A., Belosi, F., De Pieri, S., Cairns, W.R.L., Donateo, A., Zanotto, E., Citron, M. (2011) *J. Environ. Manage.* **92**, 2119-2129.

Healy, R.M., Helleburst, S., Kourtchev, I., Allanic, A., O'Connor, I.P., Bell, J.M., Healy, D.A., Sodeau, J.R., Wenger, J.C. (2010) *Atmos. Chem. Phys.* **10**, 9593-9613.

Premuda, M, Masieri, S., Kostadinov I., Bortoli, D., Petritoli A., Giovanelli, G. (2011) *Atmos. Environ.* **45**, 5212-5219.

Tuesday, September 3, 2013

Session: Aerosol-based Nanotechnology
Fabrication of nanostructured materials

Rapid synthesis of multi-layered & multi-functional polymer nanocomposite films

C.O. Blattmann, G.A. Sotiriou and S.E. Pratsinis

Particle Technology Laboratory, Department of Mechanical and Process Engineering
ETH Zurich, CH-8092 Zurich, Switzerland
Keywords: polymer nanocomposite, multi-functional, thin film.
Presenting author email: blattmac@student.ethz.ch

Polymer nanocomposites consist of a polymer matrix with nano-sized fillers. They may exhibit different properties than the pure polymer or a polymer with micron-sized fillers (Hagleitner, 2001). This change comes forth due to the unique material properties of nanoparticles as well as their increased specific surface area. An increase in mechanical durability (Camenzind, 2010), greater thermal stability (Kashiwagi, 2005) is common. Incorporation of superparamagnetic, plasmonic or phosphorescence properties is also possible by adjusting the filler material (Sotiriou, 2013). Agglomeration of the fillers, however, seriously hinders this task (Schulz, 2008). Nanocomposite homogeneity is achieved usually at the expense of lower filler loading even though fillers are surface functionalized prior to their embedding in the polymer (Suter, 2011). With this step their loading can be enhanced (e.g. up to 20%) while maintaining dispersion homogeneity (Schulz, 2008). This, however, increases the cost and complicates the processing.

Here a new route for synthesis of nanocomposite polymer films was invented. Superparamagnetic, phosphorescent and plasmonic polymer nanocomposites were made by directly depositing and integrating flame-made Fe_2O_3, Eu/Tb-doped Y_2O_3 and Ag nanoparticles, respectively, into a poly-methyl methacrylate (PMMA) matrix. Such properties allow the polymer film to serve as a sensor, actuator, display or electromagnetic shield (Sotiriou, 2013). Such a multitude of functionalities in one film is desired in miniaturized devices such as lab-on-a-chip (Suter, 2011).

The entire manufacturing procedure consists of dry synthesis of nanoparticles by flame-spray pyrolysis (Strobel, 2007) while directly depositing them on a cooled substrate and subsequently spin-coating with a polymer solution (Sotiriou, 2013). By varying the particle deposition parameters, *in-situ* flame annealing conditions and the spin-coating speed, the particle film thickness and filler loading (i.e. vol%) can be selected.

The nanoparticle loading in the polymer films is determined by thermogravimetric analysis. These loadings are higher than conventional methodologies without affecting film flexibility. Figure 1A shows the response of such a film to an external magnet. Imaging of this nanocomposite film by electron microscopy reveals a homogeneous layered particle distribution throughout the polymer (Figure 1B).

A free-standing thin flexible film (Fig. 1A) can be achieved by coating the deposition substrate with a sacrificial layer prior to manufacturing. Furthermore multi-layered structures with the same and/or different nanoparticles are easily achieved (Sotiriou, 2013). The substrate for deposition consists of a pre-existing polymer nanocomposite film. This allows one to easily incorporate sequentially additional functionalities.

Overall the multitude of polymer – nanoparticle combination possibilities achievable by scalable flame-spray pyrolysis (Strobel, 2007) and high filler fractions with homogeneous distribution distinguish the current nanocomposite synthesis technique.

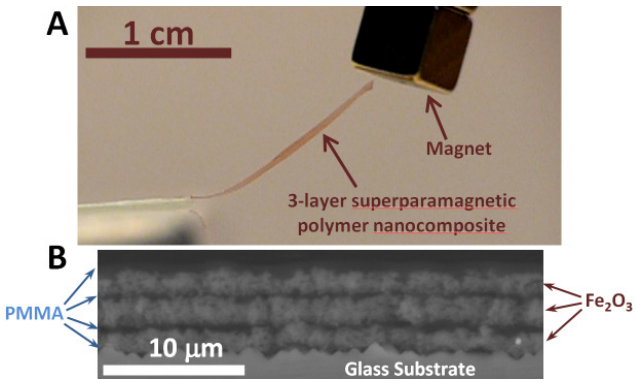

Figure 1. Magnetically-actuated multi-layer superparamagnetic nanocomposite film by a magnet at the top right (A). Vertical cut of that film showing the 3 homogeneous nanostructured layers of Fe_2O_3 (light grey) within the PMMA (dark grey) matrix (B).

Support by the Swiss National Science Foundation (No. 200020-126694) and the European Research Council under the European Union's Seventh Framework Programme (FP7/2007-2013)/ERC grant agreement n° 247283 is gratefully acknowledged.

Camenzind, A., Schweizer, T., Sztucki, M. and Pratsinis, S.E. (2010) *Polymer* **51**, 1796-1804.

Hagleitner, C., Hierlemann, A., Lange, D., Kummer, A., Kerness, N., Brand, O. and Baltes, H. (2001) *Nature* **414**, 293-296.

Kashiwagi, T., Du, F.M., Douglas, J.F., Winey, K.I., Harris, R.H. and Shields, J.R. (2005) *Nat. Mater.* **4**, 928-933.

Schulz, H., Schimmoeller, B., Pratsinis, S.E., Salz, U. and Bock, T. (2008) *J. Dent.* **36**, 579-587.

Sotiriou, G.A., Blattmann, C.O. and Pratsinis, S.E. (2013) *Adv. Funct. Mater.* **23**, 34-41.

Strobel, R. Pratsinis, S.E. (2007) *J. Mater. Chem.*, **17**, 4743 – 4756.

Suter, M., Ergeneman, O., Züricher, J., Moitzi, C., Pané, S., Rudin, T., Pratsinis, S.E., Nelson, B.J. and Hierold, C. (2011) *Sens. Actuators* **156**, 433-443.

Electrostatic charging during electrospray deposition of polymer granular coatings

Eszter Bodnár[1], Nikolas Sochorakis[1], Jordi Grifoll[1], Joan Rosell-Llompart[1,2]

[1]Chemical Engineering Department, Universitat Rovira i Virgili, Tarragona, E-43007, Spain
[2]Catalan Institution for Research and Advanced Studies (ICREA), Barcelona, E-08010, Spain
Keywords: electrospray; spray coating; polymer particles; electrostatic charging
Presenting author email: eszter.bodnar@urv.cat

Electrospray is a liquid atomization technique which has been applied to form thin coatings over solid substrates from a wide range of starting solutions (Jaworek, 2007). Highly charged droplets are formed, which repel each other, forming a spray which travels towards a collection electrode. When the droplets contain non-volatile solutes, either a continuous film or a granular coating made of dry residues can be collected.

The electrode configuration and the applied needle voltage (needed for a stable cone-jet mode) determine the electric field and the spray geometry, which in turn define the collection area of the film on the conductive substrate. Therefore, such films are generally considered to be uniform and to grow linearly with deposition time. However, in this study, we have noticed that granular polymer films grow wider during the deposition process.

We have studied the film growth dynamics and the degree of uniformity of the film thickness, as a function of factors which influence the rate of charge accumulation during coating, such as needle-plate separation and ambient relative humidity (RH).

The granular polymer films shown in Figure 1, for example, show radial variations not only in thickness but also in film morphology (size segregation of primary and satellite particles). At the 6.4 mm location, the buried layer of residues from satellite droplets (S) must have been collected earlier than the top layer of residues from primary droplets (P).

Figure 2 shows that these films grow wide faster at low than at high RH. We believe that electrostatic

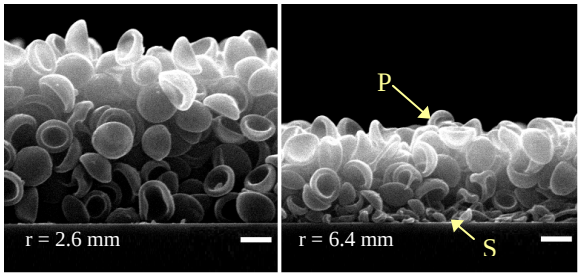

Figure 1. Cross section views by SEM of an ethyl cellulose granular film at different radial locations, collected at 10% RH. Scale bar 1 μm.

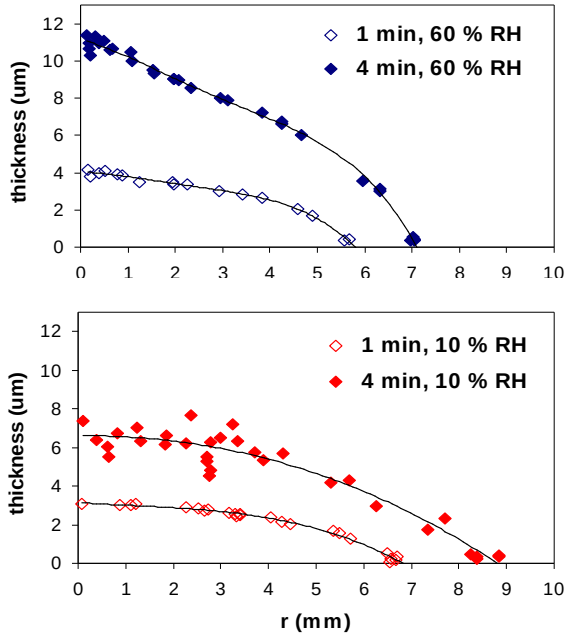

Figure 2. Thickness radial profiles of deposited ethyl cellulose films at fixed inter-electrode separation.

charges accumulate on the film during collection of polymer particles, and contribute a repulsive electric force (pointing towards the droplet emission zone) which acts to slow down the droplets and the dry particles that define the electrospray plume. As a result, the lifetime of the dry particles in the spray is increased, and the spray widens by electrostatic expansion before its particles reach the collector.

This model explains the observed trends of the radial profile of film thickness versus RH (Fig. 2) and inter-electrode separation (not shown here).

This research was funded by Ministerio de Educación y Ciencia (Spain) (CTQ2008-05758/PPQ and DPI2012-35687) and Generalitat de Catalunya (2009SGR-01529).

Jaworek, A. (2007) *J. Mater. Sci.*, **42** 266–297.

Towards deposition of single layer graphene by an electrospray ion-assisted method

L.B. Modesto-Lopez[1], O.V. Bilousov[2], J.M. Serres[2], J. Rosell-Llompart[3,4], J.J. Carvajal[2], and F. Díaz[2]

[1]Department of Environmental Science, University of Eastern Finland, Kuopio, P.O. Box 1627, FI-70211, Finland
[2]Física i Cristal·lografia de Materials and EMaS, Universitat Rovira i Virgili, Tarragona, Catalonia, E-43007, Spain
[3]Department of Chemical Engineering, Universitat Rovira i Virgili, Tarragona, Catalonia, E-43007, Spain
[4]Catalan Institution for Research and Advanced Studies (ICREA), Barcelona, Catalonia, E-08010, Spain
Keywords: graphene, electrospray, ion-assisted, thin-film.
Presenting author email: luis.modesto@uef.fi

The technological potential of graphene fosters studies on its deposition to form thin films on a variety of substrates (Blake *et al*, 2008). Spraying is a physical process extensively used to fabricate films and coatings because of its flexibility in the chemical composition of materials that can be deposited. Electrospray, a liquid atomization method that leads to highly charged, nearly monosized micro- and nano-droplets, has been applied to create thin films and coatings (Jaworek, 2007; Modesto-Lopez & Biswas, 2010). Because of its electrostatic control, electrospray deposition (ESD) results in a nearly 100 % deposition efficiency on conductive substrates.

Previously we have reported the deposition of multilayer graphene nanosheets onto silicon and quartz substrates using an electrospray ion-assisted (EIA) method (Modesto-Lopez *et al*, 2012; Uecker et al, 2010). The films comprised multilayered graphene and large agglomerates. In our EIA approach the ions facilitate the deposition of graphene onto dielectric substrates, which is otherwise difficult to achieve with conventional ESD. Films of varying thicknesses can be obtained by adjusting the deposition time and the concentration of graphene in the precursor suspension.

The objective of this study is to deposit single layer graphene films using the EIA method. We also investigate the relationships between coating morphology and EIA process parameters. Suspensions of commercial graphene flakes (Grupo Antolin, Spain) were diluted to 0.005 wt% in dymethylformamide, and were electrosprayed onto Si and quartz substrates. Electrospray was performed in the cone-jet mode. The films were characterized with atomic force microscopy (AFM) and micro-Raman spectroscopy. Figure 1a shows an AFM image of a film collected for 10 min onto Si from an electrospray operated at a liquid flow rate of ~1 µL/min. The film is comprised of relatively large graphene flakes of uniform thickness (clear areas) over the Si substrate (darker areas). Such thickness is approximately 1.1 nm as shown in the profile of Figure 1b, which corresponds to the green line in Figure 1a.

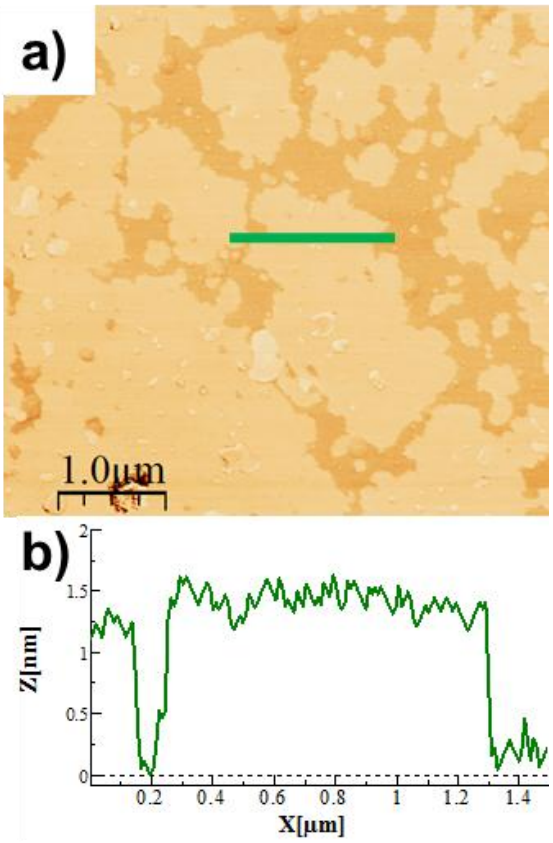

Figure 1. a) AFM phase image of a graphene thin film deposited for 10 min onto a Si substrate, b) cross-section profile from topographic image (green line shown in a)).

This work was supported by the Spanish Government (grants CTQ2008-05758/PPQ, DPI2012-35687, TEC2010-21574, and MAT2011-29255) and by the Catalan Government (grant 2009SGR-01529).

Blake, P., Brimicombe, P.D., Nair, R.R., Booth, T.J., Jiang, D., Schedin, F., Ponomarenko, L.A., Morozov, S.V. *et al.* (2008) *Nano Lett.*, **8(6)**, 1704-1708.

Modesto-Lopez, L.B., Bilousov, O.V., Carvajal, J.J., Diaz, F. and Rosell-Llompart, J. (2012) *Proc. European Aerosol Conference*.

Jaworek, A. (2007) *J. Mater. Sci.* **42(1)**: 266-297.

Modesto-Lopez, L. B., Biswas P. (2010) *J. Aerosol Sci.* **41**, 790-804.

Uecker, J.C., Tepper, G.C., and Rosell-Llompart, J. (2010) *Polymer* **51**, 5221-5228.

Large-Area Patterning of Three-dimensional Nanoparticle Structure Arrays via Ion Assisted Aerosol Lithography (IAAL) and Multi-tip Spark Discharge

K.-Y. Ha[1], H.-S. Choi[1], K.-N. Jung[1], K.-H. Han[1,2], J.-K. Lee[1], and M. Choi[1]

[1]Global Frontier Center for Multiscale Energy Systems, Division of WCU Multiscale Mechanical Design, School of Mechanical and Aerospace Engineering, Seoul National University, Seoul, 151-744, Korea
[2]Present address: Samsung Electronics, Gyeonggi-do 443-742, Korea.
Keywords: nanoparticle assembly, spark discharge generator, nanofabrication.
Presenting author email: hky0220@snu.ac.kr

A great deal of attention has been paid recently to the development of novel methods for fabricating nanoscale structures. In order to implement practical nanodevices using the unique features of nanostructures, large-area patterning technique is necessary. In particular, three-dimensional nanoparticle assembly method based on ion-assisted aerosol lithography (IAAL) has been reported (Kim et al. 2006, Lee et al. 2011, and Han et al. 2012) as an effective way to produce multi-dimensional assembly of nanoparticles in a parallel fashion at atmosphere.

For the case of the IAAL using a single-tip spark discharge generator, charged nanoparticles generated by spark discharge move along an electric field not by diffusion process. Thus, there exists the limitation of realizing large-area patterning along with precisely controllable uniformity. In this regard, the nanoparticles have to be injected over as wide an area as possible for the large-area patterning. We present here large-area fabrication of three-dimensional nanoparticle structure arrays using a multi-tip spark discharge generator based on the pin-to-plate type at atmospheric pressure (Figure 1).

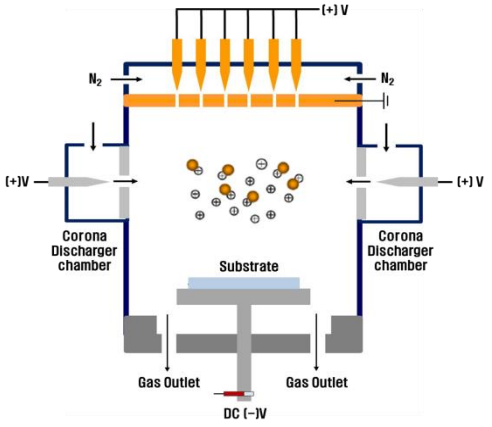

Figure1. Schematic of a multi-tip spark discharge generator

The interval and number of the tips in a multi-tip spark discharge generator are designed to minimize nanoparticle agglomeration and induce high concentration of nanoparticles. The distance between a plate and a sample is set to minimize losses of nanoparticles at the wall, as well as ensure uniformity of resulting nanostructures on a substrate.

With consideration of these conditions, large-area patterns of ordered nanostructures in the size of 50 by 50 square millimeter were fabricated on the substrate in a massive parallel way (Figure 2). In addition, the shape of the nanoparticle structures was variously controlled by changing the size of nanoparticles with the same prepattern formed on a substrate. Tuning the size of nanoparticles can be obtained by varying the parameters such as the electric circuit, the gap between pin to plate, and the flow-rate of nitrogen gas.

This large-area patterning technique using IAAL and multi-tip spark discharge generator will open the door to apply three-dimensional nanoparticle structures with a variety of shapes to diverse nanodevices including optoelectronics, sensing, and electronics.

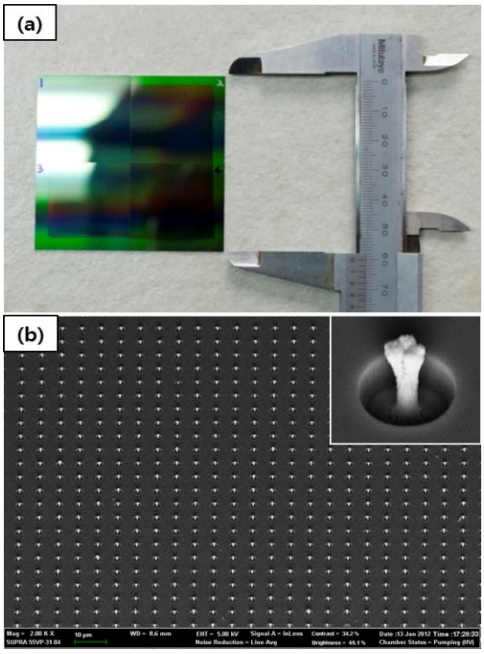

Figure2. (a) Actual image of the completed sample (b) SEM image of nanostructure array fabricated by a multi-tip spark discharge generator

This work was supported by the Global Frontier R&D Program on Center for Multiscale Energy System funded by the National Research Foundation under the Ministry of Education, Science and Technology, Korea (20110031567)

Kim *et al.*, (2006) *Nat. Nanotechnol.* **1**, 117-121.
Lee *et al.*, (2011) *Nano Lett.* **11**, 119-124.
Han *et al.*, (2012) *J. Aerosol Sci.* **52**, 80-88

Silver-decorated silica nanoparticles in a multilayered plasmonic structure

J. Harra[1], M. Zdanowicz[2], M. Virkki[2], A. Rantamäki[3], M. Honkanen[4], G. Genty[2], M. Kauranen[2], J. M. Mäkelä[1]

[1]Aerosol Physics Laboratory, Department of Physics, Tampere University of Technology, Tampere, Finland
[2]Optics Laboratory, Department of Physics, Tampere University of Technology, Tampere, Finland
[3]Optoelectronics Research Centre, Tampere University of Technology, Tampere, Finland
[4]Department of Materials Science, Tampere University of Technology, Tampere, Finland
Keywords: nanoparticle synthesis, silver, silicon dioxide, localized surface plasmon resonance.
Presenting author email: juha.harra@tut.fi

Introduction

Optical properties of noble metal nanoparticles, such as gold and silver, are dominated by coherent oscillations of conduction electrons, which give rise to localized surface plasmon resonances. The wavelength of the resonances depends on the particle size, shape and dielectric environment.

In our previous study (Harra *et al*, 2012), the plasmon resonance wavelength of spherical single-component silver particles was tuned by controlling their size (50–130 nm). Even though the coverage of the silver particles on the substrate was relatively low ($< 10\,\%$), the overlapping of the particles caused the extinction spectra of the prepared surface samples to broaden to longer wavelengths (> 500 nm).

In plasmonic applications, such as colored coatings and nonlinear optical materials, it is preferable to be able to tune the extinction while maintaining a narrow and well-defined resonance band. In this study, we demonstrate such control by using a multilayered structure consisting of silver-decorated silica nanoparticles.

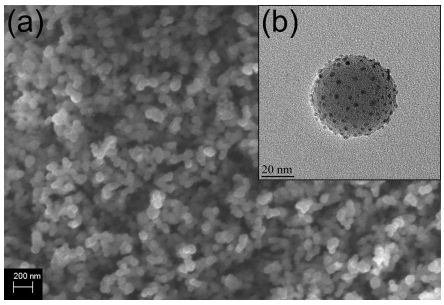

Figure 1: (a) An SEM image of the decorated particles on a glass substrate after a collection time of 30 min and (b) a TEM image of a single particle.

Experimental

Aerosol techniques were used to synthesize the silver-decorated silica nanoparticles. The synthesis process composed of chemical vapor synthesis of larger silica particles and their subsequent decoration with smaller silver particles by an evaporation–condensation method. A layer of decorated particles was deposited on a glass substrate and coated with a thin layer of glass by electron beam evaporation. This process was repeated several times in order to obtain a multilayered structure.

The synthesized particles were characterized with a scanning mobility particle sizer and a transmission electron microscope (TEM), whereas, the plasmonic glass samples were studied with a UV-VIS spectrophotometer and a scanning electron microscope (SEM).

Results and discussion

Figure 1a shows an SEM image of a glass substrate covered with a porous layer of nanoparticles after a collection time of 30 minutes. The individual particles consisted of approximately 50 nm silica spheres decorated with a few nanometer silver particles, as shown in a TEM image (Fig. 1b).

Figure 2 shows extinction spectra of the multilayered nanoparticle structures containing 1–4 layers. The plasmon resonance band, typical of silver at around a wavelength of 400 nm, remains well-defined and relatively narrow, while the extinction grows linearly as the number of layers increases. The inserts show how the yellow color of the multilayered samples intensifies as well.

This study shows that the dielectric silica in the decorated particles reduces unwanted contacts between metal particles, thus, a well-defined extinction spectrum can be maintained. In addition, multilayered structures can be used to improve the mechanical and chemical stability of the nanoparticles in plasmonic materials.

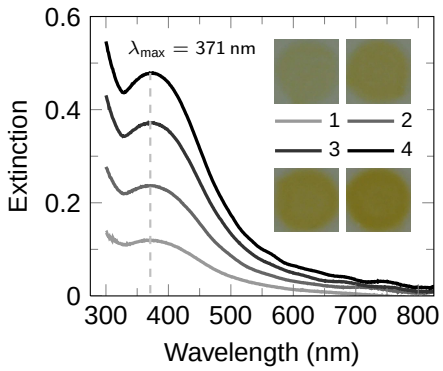

Figure 2: Extinction spectra of the multilayered nanoparticle structures with 1–4 layers. The inserts show photographs of the samples.

This work was supported by the Academy of Finland (decision 136080).

Harra, J., Mäkitalo, J., Siikanen, R., Virkki, M., Genty, G., Kobayashi, T., Kauranen, M. and Mäkelä, J. M. (2012) *J. Nanopart. Res.*, **14**, 870.

Aerosol synthesis of semiconductor nanowires

M. Heurlin[1], M.H. Magnusson[1,2], D. Lindgren[1], M. Ek[3], L.R. Wallenberg[3], L. Samuelson[1] and K. Deppert[1]

[1]Department of Physics, Lund University, Lund, 22100, Sweden
[2]Sol Voltaics AB, Ideon Science Park, Lund, 22370, Sweden
[3]Department of Chemistry, Lund University, Lund, 22100, Sweden
Keywords: aerotaxy, nanowire, semiconductor, nanostructure
Presenting author email: knut.deppert@ftf.lth.se

Semiconductor nanowires are key building blocks for the next generation of light-emitting diodes (Qian *et al*, 2005), solar cells (Wallentin et al, 2013) and batteries (Chan *et al*, 2008). To fabricate functional nanowire-based devices on an industrial scale requires an efficient methodology that enables the mass production of nanowires with perfect crystallinity, reproducible and controlled dimensions and material composition, and low cost. So far there have been no reports of reliable methods that can satisfy all of these requirements. Here we show how aerotaxy, an aerosol-based growth method (Deppert and Samuelson, 1996), can be used to grow nanowires continuously with controlled nanoscale dimensions, a high degree of crystallinity and at a remarkable growth rate.

In our aerotaxy approach, catalytic size-selected Au aerosol particles induce nucleation and growth of GaAs nanowires with a growth rate of about 1 micrometre per second, which is 20 to 1,000 times higher than previously reported for traditional, substrate-based growth of nanowires made of group III–V materials (Borgström *et al*, 2007, Joyce *et al*, 2009, Ramdani *et al*, 2010). We demonstrate that the method allows sensitive and reproducible control of the nanowire dimensions and shape—and, thus, controlled optical and electronic properties—through the variation of growth temperature, time and Au particle size. Photoluminescence measurements reveal that even as-grown nanowires have good optical properties and excellent spectral uniformity. Detailed transmission electron microscopy investigations show that our aerotaxy-grown nanowires form along one of the four equivalent 〈111〉B crystallographic directions in the zincblende unit cell, which is also the preferred growth direction for III–V nanowires seeded by Au particles on a single-crystal substrate. The reported continuous and potentially high-throughput method can be expected substantially to reduce the cost of producing high-quality nanowires and may enable the low-cost fabrication of nanowire-based devices on an industrial scale (Heurlin *et al*, 2012).

This work was performed within the Nanometer Structure Consortium at Lund University (nmC@LU) and supported by the Swedish Research Council, the Swedish Foundation for Strategic Research, the Knut and Alice Wallenberg Foundation and VINNOVA.

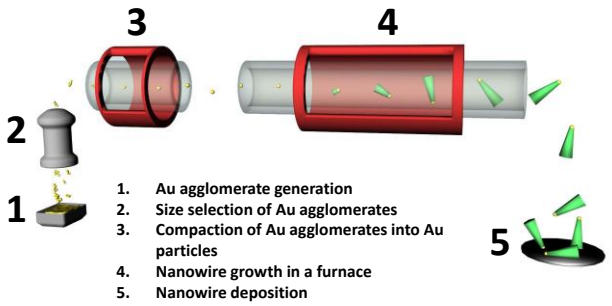

Figure 1. Schematic of the aerotaxy process.

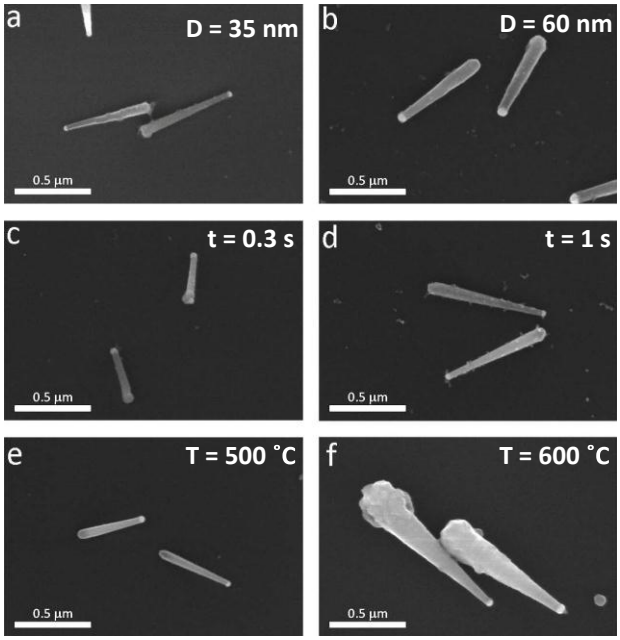

Figure 2: Snapshots of fabricated nanowires under different conditions.

Borgström, M.T., Immink, G., Ketelaars, B., Algra, R. and Bakkers, E.P.A.M. (2007) *Nature Nanotechnol.* **2**, 541–544.
Chan, C.K. *et al* (2008) *Nature Nanotechnol* **3**, 31–35.
Deppert, K. and Samuelson, L. (1996) *Appl. Phys. Lett.* **68**, 1409–1411.
Heurlin, M. *et al* (2012) *Nature.* **492**, 90-94.
Joyce, H.J. *et al* (2009) *Nano Lett.* **9**, 695–701.
Qian, F., Gradecak, S., Li, Y., Wen, C.-Y. and Lieber, C.M. (2005) *Nano Lett*. **5**, 2287–2291 (2005).
Ramdani, M.R. *et al* (2010) *Nano Lett.* **10**, 1836–1841.
Wallentin, J. *et al* (2013) *Science*, DOI:10.1126/science. 1230969

Dry deposition of electrosprayed liquid suspensions

S. Martin. B. Martinez-Vazquez, P.L. Garcia-Ybarra and J.L. Castillo

Dept. Fisica Matematica y de Fluidos, Facultad de Ciencias, UNED, 28040 Madrid, Spain
Keywords: Electrospray, Aerosol deposition; aerosol-based nanotechnology, polymeric fuel cell, catalytic layers
Presenting author email: jcastillo@ccia.uned.es

Granular materials formed by accumulation and adhesion of incoming aerosol particles acquire a morphological structure controlled by the form of the constitutive particles and by the way that these particles arrive and attach to the forming material (Garcia-Ybarra *et al*, 2012, Castillo *et al*, 2013).

Monte Carlo simulations of aerosol deposits (Rodriguez-Perez *et al*, 2005 and 2007) have shown the trends for controlling the deposit structure and indicated some ways to prepare granular materials from nanopowders with tailored morphology depending on their final use. A step forward in nanomaterial research consists in the performance of experimental studies that could confirm these theoretical predictions. Thus, an experimental set-up has been implemented to generate nanoparticles in a gas that are later on driven towards a collecting surface (Martin *et al*, 2012). In this study, a standard catalyst ink commonly used for preparing electrodes valuable for proton exchange membrane fuel cells (PEMFC) has been used (Martin *et al*, 2013).

The electrospray technique is used to generate nearly monodispersed sprays of small electrically charged droplets from this liquid suspension. In the electrospray cone-jet configuration (Martin *et al*, 2012) the jet breaks up forming a cloud of tiny droplets with a narrow distribution of droplet sizes. These charged droplets evaporate along their flight in the gas leaving dry charged nanoparticles which are driven by the electric field towards the collecting surface. The arriving nanoparticles accumulate on the collector plate forming a structured granular deposit.

The efficiency in the capture of the electrosprayed particles may be substantially improved if an opposite voltage, respect to the needle, is applied to the collector substrate. In this double polarization scheme, the electrospray cone-jet domain may be substantially enlarged by a proper selection of the voltage at the collecting plate and a noticeable increase in the flow rate range for electrospraying in the cone-jet mode can be achieved (Martin *et al*, 2011). Therefore, the double polarization can be used to control the electric field at the needle tip (which indeed is the key factor for achieving a stable cone-jet electrospray) as well as the electric field at the collecting plate.

In the case of low conductivity suspensions electrosprayed at moderate flow rates (♦ points in Fig.1) the deposit is formed by fractal-like structures composed by clusters (of a few catalyst particles each) arranged in a dendritic way. The dendritic arrangement of the catalyst clusters results in a highly porous deposit with an enhanced permeability and increased active surface. One may expect that all these morphological properties of the granular material may lead to high catalyst utilization when used as a catalyst layer. For larger flow rates (◊ points in Fig. 1) the deposit is formed by patched clusters of thousands of single particles. Moreover, compact deposits appear when the flow rate is large enough (□ and △ points in Fig.1). These compact deposits result from an incomplete evaporation of the droplets during their flight toward the substrate. The deposit is formed from wet suspensions with the ethanol evaporating later on.

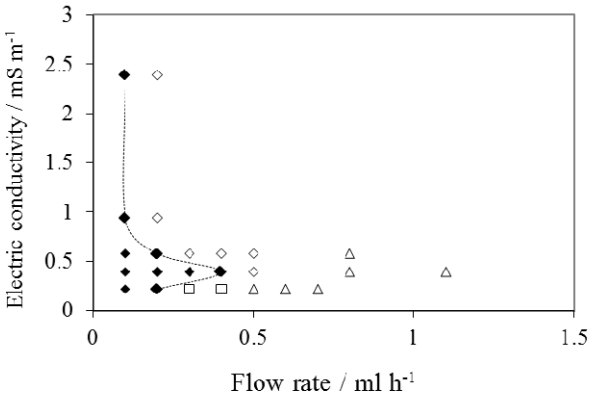

Figure 1. Phase diagram. Different types of deposit structure depending on the electric conductivity of the catalytic ink and on flow rate. Fractal-like deposits ♦, patched clusters ◊, and compact structures (□ and △).

This work has been supported by the Ministerio de Economía y Competitividad (Spain) under Grant ENE2011-26868 and Program Consolider-Ingenio 2010 (CSD2010-00011) and also by Comunidad de Madrid (Project HYSYCOMB, S2009ENE- 1597).

Castillo, J.L., Martin, S., Rodriguez-Perez, D., Perea, A. and Garcia-Ybarra, P. L. (2013) *KONA Powder and Particle J.*, submitted.

Garcia-Ybarra, P.L., Castillo, J.L. and Martin, S. (2012) Patent application no. P201200341.

Martin, S., Garcia-Ybarra, P.L. and Castillo, J.L. (2012) *J. Aerosol Sci.* **46**, 53-63

Martin, S., Martinez-Vazquez, B., Garcia-Ybarra P.L. and Castillo, J.L. (2013) J. Power Sources **229**, 179-184.

Rodriguez-Perez, D., Castillo, J.L. and Antoranz, J.C. (2005) *Physical Review E* **72**, 021403.

Rodriguez-Perez, D., Castillo, J.L. and Antoranz, J.C. (2007) *Physical Review E* **76**, 011407.

Tuesday, September 3, 2013

Poster session B,
Aerosol Chemistry, Posters B001 – B063

Organic Aerosol Formation Photoenhanced by the Formation of Secondary Photo-sensitizers in ageing Aerosols

Kifle Z. AREGAHEGN, Barbara NOZIÈRE and Christian GEORGE

Université de Lyon; université Lyon 1; CNRS, UMR5256, IRCELYON, Institut de recherches sur la catalyse et l'environnement de Lyon, Villeurbanne, F-69626, France
Keywords: aerosol growth, imidazole-2-carboxaldehyde, photosensitized reaction, autophotocatalysis
Presenting author email: kifle.aregahegn@ircelyon.univ-lyon1.fr

Humankind is facing a changing environment possibly due to anthropogenic stress on the atmosphere. In this context, aerosols play a key role by affecting the radiative climate forcing, hydrological cycle, and by their adverse effect on health (Harrison et al., 2000). The role of organic compounds in these processes is however still poorly understood because of their massive chemical complexity and numerous transformations. This is particularly true for Secondary Organic Aerosol (SOA), which are produced in the atmosphere by organic gases.

Traditionally, the driving forces for SOA growth is believed to be the partitioning onto aerosol seeds of condensable gases, either emitted primarily or resulting from the gas phase oxidation of organic gases (Volkamer et al. 2009). However, even the most up-to-date models based on such mechanisms cannot account for the SOA mass observed in the atmosphere, suggesting the existence of other, yet unknown formation processes. The present study shows experimental evidence that particulate phase chemistry produces photo-sensitizers that lead to photo-induced formation and growth of secondary organic aerosol in the near UV and the presence of volatile organic compounds (VOC) such as terpenes (Monge et al. 2012).

By means of an aerosol flow tube reactor equipped with Scanning Mobility Particle Sizer (SMPS) having Kr-85 source aerosol neutralizer, Differential Mobility Analyzer (DMA) and Condensation Particle Sizer (CPC), we identified that traces in the aerosol phase of glyoxal chemistry products, as is explained in Gallway et al., and Yu et al.,(Galloway et al. 2009; Yu et al. 2011), namely imidazole-2-carboxaldehyde (IC) is a strong photo-sensitizer when irradiated with near-UV. In the presence of volatile organic compounds such as terpenes, this chemistry leads to fast aerosol growth. (Aregahegn et al., submitted, 2013).

Furthermore, the influence of pH, type and concentration of VOCs, composition of seed particles, relative humidity and irradiation intensity on particle growth were studied.

SOA growth was favored with VOCs containing tertiary unsaturated carbons.Thus, Due to the presence of exocyclic and endocyclic unsaturated tertiary carbon, limonene was observed to lead to an efficient SOA formation and growth. This novel photo-sensitizer, IC, contributed to more than 30% of SOA growth in 19min irradiation time in the presence of terpenes in the system, depending linearly with the irradiation intensity. These results demonstrate that, upon ageing, organic aerosols can produce photo-sensitizers which auto-photo-catalyses their SOA growth.

Galloway, M. M., et al. (2009), *Atmos. Chem. Phys.*, 9, 3331-45.

Harrison, Roy M. and Yin, Jianxin (2000), *Sci. Total Environ.*, 249 (1–3), 85-101.

Monge, Maria Eugenia, et al. (2012), *Proc. Nat. Acad. Sci.*, 109 (18), 6840-44.

Volkamer, R., Ziemann, P. J., and Molina, M. J. (2009), *Atmos. Chem. Phys.*, 9 (6), 1907-28.

Yu, Ge, et al. (2011), *Environ. Sci. Technol.*, 45 (15), 6336-42.

H_2SO_4 formation from olefin ozonolysis in the presence of SO_2: Influence of water vapour content and temperature

T. Berndt[1], T. Jokinen[1,2], M. Sipilä[2], R. L. Mauldin III[2,3], H. Herrmann[1], F. Stratmann[1], H. Junninen[2], M. Kulmala[2]

[1]Leibniz Institute for Tropospheric Research, Leipzig, 04318, Germany
[2]Depatment of Physics, University of Helsinki, Helsinki, 00014, Finland
[3]University of Colorado, Boulder, Colorado, 80302, United States
Keywords: H_2SO_4, stabilized Criegee Intermediate, mass spectrometry
Presenting author email: berndt@tropos.de

For more than a decade the formation of new aerosol particles in the atmosphere has been the subject of intense studies in both, field and laboratory. H_2SO_4 was ascertained to play a central role in this process. A dominante pathway of H_2SO_4 generation represents the OH radical initiated oxidation of SO_2. Recently it was discovered that also other oxidants than OH radicals, very likely stabilized Criegee Intermediates (sCI), can significantly contribute to H_2SO_4 formation under atmospheric conditions (Mauldin *et. al.*, 2012). Criegee Intermediates originate from the reaction of ozone with unsaturated substances (olefins) and occur with different structures associated with a different chemical behaviour. Unfortunately, the formation yields of sCI as well as their chemical reactivity toward atmospheric trace gases (SO_2, acids, etc.) and water vapour are not well characterized and are, at least partly, subject of speculation. Welz *et. al.* (2012) reported on unexpectedly high rate coefficients of the reaction of CH_2OO with SO_2 and other trace gases. As a result from our laboratory, clearly lower rate coefficients for the reaction of a series of sCI with SO_2 have been measured (Berndt *et. al.*, 2012). Generally, there is a debate at the moment regarding the relevance of the sCI + SO_2 reaction in competition with the probably, much more important sCI + H_2O pathway.

This experimental study focuses on H_2SO_4 formation from the ozonolysis of tetra-methylethylene (TME) and trans-2-butene in the presence and absence of an OH radical scavenger at atmospheric pressure conducted in the temperature range of 278 - 343 K and a relative humidity of 8 - 60%. The experiments have been performed in a flow tube (IfT-LFT) for close to atmospheric reactant concentrations, [olefin] = (1 - 4)·10^{10} molecule cm^{-3}, [O_3] = 2·10^{11} molecule cm^{-3}. H_2SO_4 was detected by means of a high resolution mass spectrometer with a chemical ionization inlet, CI-APi-TOF, utilizing NO_3^- ions for chemical ionization (Jokinen *et. al.*, 2012). In the case of the ozonolysis of TME, additional H_2SO_4 formation in the presence of the OH radical scavenger showed no clear RH dependence. In the trans-2-butene system, however, distinct RH-dependent H_2SO_4 production was detected, see for instance figure 1. The observed effects point to the occurrence of two oxidants for SO_2 (beside OH radicals) with different chemical behaviour, probably the syn- and anti-conformers of acetaldehyde oxide.

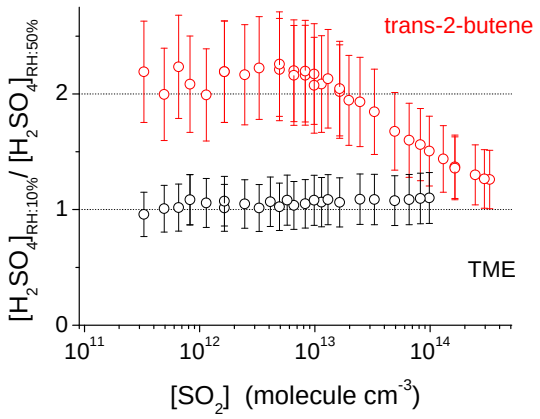

Figure 1: Ratio of measured H_2SO_4 at RH = 10 and 50 % as a function of SO_2 concentration, presence of an OH radical scavenger, 293 K.

Berndt, T., Jokinen, T., Mauldin III, R. L., Petäjä, T., Herrmann, H., Junninen, H., Paasonen, P., Worsnop, D. R., Sipilä, M., (2012), *J. Phys. Chem. Lett.*, 3, 2892-2896.

Jokinen, T., Sipilä, M., Junninen, H., Ehn, M., Lönn, G., Hakala, J., Petäjä, T., Mauldin III, R. L., Kulmala, M., and Worsnop, D. R., (2012), *Atmos. Chem. Phys.*, 12, 4117-4125, doi: 10.5194/acp-12-4117-2012.

Mauldin III, R. L., Berndt, T., Sipilä, M., Paasonen, P., Petäjä, T., Kim, S., Kúrten, T., Stratmann, F., Kerminen, V.-M., Kulmala, M., (2012), *Nature*, 488, 193–196, doi: 10.1038/nature11278.

Welz, O., Savee, J. D., Osborn, D. L., Vasu, S. S., Percival, C. J., Shallcross, D. E., Taatjes, C. A., (2012), *Science*, *335*, 204-207.

Development of a method to measure the $\delta^{13}C$ for OC and EC in PM

L. Bourcier[1,2] and B. Geypens[1]

[1]Institute for Reference materials and Measurements - Joint Research Centre - European Commission, 2440, Belgium
[2] Now at: CNR - Institute for Atmospheric Sciences and Climate, Via Gobetti 101, 40129 Bologna, Italy

Keywords: carbonaceous particles, source identification, isotopic ratio.
Presenting author email: l.bourcier@isac.cnr.it

Information on the atmospheric composition, from the local to the global scale, is of strategic value in particular for climate and air quality related studies. Stable isotope research for both compounds specific and bulk analysis finds its applications in various fields (Hoefs, 1987; Flanagan et al 2005). One of its applications is the source identification since the $^{13}C/^{12}C$ is highly dependent on its origin. This has been done by the study of the stable carbon isotopic composition ($^{13}C/^{12}C$) (Cachier et al 1989; Widory et al 2004; Ceburnis et al 2011).

In the literature, the simultaneous characterization of OC/EC and $\delta^{13}C$ is made with two different analyses (Huang et al 2006). Our objective is to develop a method to obtain in one single analysis the OC and EC concentrations and their isotopic ratios.

Methodology

The original reference method (EA-IRMS) has been modified by replacing the elemental analyser by a sunset lab. instrument. An extra reducing oven was installed in order to convert the NO_2 produced by the PM samples while heating the filter. In the following, the experimental set-up is designated as S-RT-IRMS.

The calibration of OC and EC is performed with known amount of sucrose, as usually used. For the isotopic ratio, since the standard VPDB is in very limited quantity, we used methionine to calibrate the analysis.

Two different temperature protocols have been used. The first one (Huang2006.par) has been adapted from Huang et al (2006). The second one (eusaar2.par) has been developed within the EUSAAR project (Cavalli et al 2010).

Results

Table 1. Mean $\delta^{13}C_{VPDB}$ (‰) and standard deviation of sucrose, methionine and graphite.

	EA-IRMS		S-RT-IRMS	
	powder	solution	Huang2006	Eusaar2
Sucr.	-25.67 ± 0.46	-25.82 ± 0.06	-25.08 ± 0.09	-25.02 ± 0.40
Meth.	-27.99*	-27.99 ± 0.10	-27.76 ± 0.17	-27.66 ± 0.25
Grap.	-16.34 ± 0.05		-16.25 ± 0.21	

* reference value

The isotopic ratios of pure compounds were measured with both reference method and the S-RT-IRMS (Table 1). There is a good agreement with both methods.

Some repeatability tests have been done. It appeared that the inhomogeneity of the filter creates a higher variability than the one due to the S-RT-IRMS.

Last, the analysis of real PM filters showed a good agreement (Table 2) between the reference method and our development.

Table 2. $\delta^{13}C$ of filters (eusaar2.par). The uncertainty is ± 0.27; value obtained from the repeatability tests.

	EA-IRMS	S-RT-IRMS
02/02/2012	-25.34 ‰	-25.55 ‰
23/01/2012	-26.60 ‰	-26.61 ‰
09/01/2012	-25.85‰	-25.93 ‰
27/01/2012	-26.35 ‰	-26.00 ‰
19/03/2012	-25.78 ‰	-25.85‰

Cachier, H. (1989) *Aer. Sci. Technol.* **10**, 379-385.
Cavalli, F., Viana, M., Yttri, K.E., Genberg, J. and Putaud, J.-P. (2010) *Atmos. Meas. Tech.* **3**, 79-89.
Ceburnis, D., Garbaras, A., Szidat, S., Rinaldi, M., Fahrni, S., Perron, N., Wacker, L., Leinert, S., Remeikis, V., Facchini, M.C., Prevot, A.S.H., Jennings, S.G., Ramonet, M. and O'Dowd, C.D. (2011) *Atmos. Chem. Phys.* **11**, 8593-8606.
Flanagan, L. B., Ehleringer, J. R. and Pataki, D. E. (2005) *Stable Isotopes and Biosphere Atmosphere Interactions: Process and Biological Controls*, Elsevier, Great Britain.
Hoefs, J. (1987) *Stable Isotope Geochemistry*, third ed. Springer-Verlag, Berlin, Germany.
Huang, L., Brook, J.R., Zhang, W., Li, S.M., Graham, L., Ernst, D., Chivulescu, A. and Lu, G. (2006) *Atmos. Environ.* **40**, 2690-2705.
Widory, R., Roy, S., Le Moullec, Y., Goupil, G., Cocherie, A. and Guerrot, C. (2004) *Atmos. Environ.* **38**, 953-961.

Secondary organic aerosol formation in the ozonolysis of biogenic volatile organic compounds performed in a laminar flow reactor

T. Braure[1,2], V. Riffault[1,2], A. Tomas[1,2], M. Duncianu[1,2], Y. Bedjanian[3] and P. Coddeville[1,2]

[1] Université Lille Nord de France, F-59000, Lille, France
[2] Mines Douai, CE, F-59508 Douai, France
[3]Institut de Combustion Aérothermique Réactivité et Environnement, F-45071, Orléans, France
Keywords: limonene, α-pinene, nucleation, aerosol yield.
Presenting author email: tristan.braure@mines-douai.fr

The oxidation of Biogenic Volatile Organic Compounds (BVOC) emitted by vegetation, such as monoterpenes ($C_{10}H_{16}$) or sesquiterpenes ($C_{15}H_{24}$) is an important source of Secondary Organic Aerosol (SOA). Because of their large global emissions and high reactivity with the major atmospheric oxidants (Atkinson and Arey, 2003) – and particularly with ozone (O_3) – they are believed to be the dominant contributors to global SOA formation (Kanakidou *et al*, 2005).

α-Pinene and limonene are two of the three most important BVOC emitted in the atmosphere (Griffin *et al*, 1999), with conifers as major sources (Geron *et al*, 2000, Pokorska *et al*, 2012). These two BVOC (especially limonene) are also emitted in indoor air by air fresheners and cleaning products such as kitchen cleaners and dishwashing detergents (Huang *et al*, 2011). It has been highlighted in previous studies that their reactions with ozone could produce SOA (Chen *et al*, 2011, Waring *et al*, 2011, Bernard *et al*, 2012) either in atmospheric or indoor environments, and could then lead to significant climate (Myhre *et al*, 2001) and health (Gaschen *et al*, 2010) effects.

In the present work, the ozonolysis reactions of limonene and α-pinene have been investigated at room temperature and atmospheric pressure using a laminar flow reactor newly developed in our laboratory (Figure 1, Duncianu *et al*, 2012), which allows the monitoring of the first steps of ozonolysis reactions (typically ~30 seconds to 5 minutes) providing complementary data to more widely performed smog chamber experiments.

The rate coefficients have been measured under pseudo first-order conditions in excess of the BVOC. The decay of ozone has been monitored with an O_3 analyser while BVOC concentrations have been determined using online sampling onto adsorbent cartridges followed by thermodesorption and subsequent analysis in a GC/FID-MS system. Specific experiments have been performed to identify and quantify both gas-phase and particulate products using a TD/GC/FID-MS system, a SMPS and a HR-ToF-AMS, respectively.

Results will be further discussed and compared to literature data.

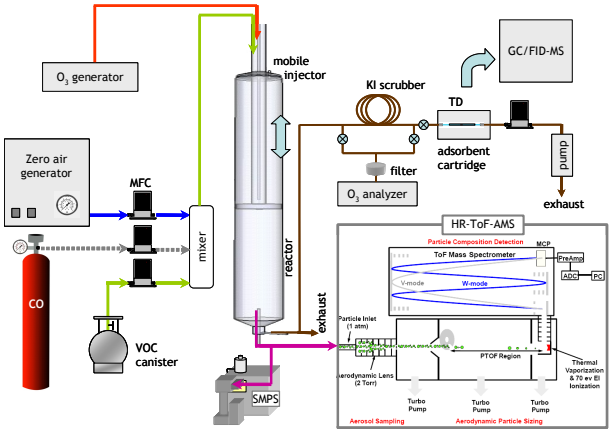

Figure 1. Schematic of the experimental setup and instrumentation (MFC: mass flow controller) (adapted from Duncianu *et al*, 2012).

Our laboratory participates in the Research Institute of Industrial Environment (IRENI) which is financed by the Communauté Urbaine de Dunkerque, the Nord-Pas de Calais Regional Council, the French Ministry of Education and Research, and European funds (FEDER). The CaPPA project (Chemical and Physical Properties of the Atmosphere) is funded by the French National Research Agency (ANR) through the PIA (Programme d'Investissements d'Avenir) under contract ANR-10-LABX-005. M. Duncianu and T. Braure are grateful for PhD scholarships from the Nord-Pas de Calais Regional Council and Armines.

Atkinson, R. and Arey, J. (2003) *Atm. Env.* **37**, S197-S219.
Bernard, F. *et al.* (2012) *J. Aer. Sci.* **43**, 14-30.
Chen, X. *et al.* (2011) *Env. Sci. Tech.* **45**, 276-282.
Duncianu, M. *et al.* (2012) *J. Phys. Chem. A* **116**, 6169-6179.
Gaschen, A. *et al.* (2010) *Env. Sci. Tech.* **44**, 1424-1430.
Geron, C. *et al.* (2000) *Atm. Env.* **34**, 1761-1781.
Griffin, R.J. *et al.* (1999) *Geophys. Res. Lett.* **26**, 2721-2724.
Huang, Y. *et al.* (2011) *Atm. Env.* **45**, 6191-6196.
Kanakidou, M. *et al.* (2005) *Atm. Chem. Phys.* **5**, 1053-1123.
Myhre, G. *et al.* (2001) *Atm. Env.* **35**, 2361-2373.
Pokorska, O. *et al.* (2012) *Atm. Env.* **59**, 501-508.
Waring, M.S. *et al.* (2011) *Atm. Env.* **45**, 4235-4242.

Geochemical anomalies in aerosol induced by mining and metallurgical activities in SW Spain

J. de la Rosa, A.M. Sánchez de la Campa, Y. González-Castanedo[1], R. Fernández Camacho[1], J. C.Fernández Caliani[1,] A. Alastuey[2], and X. Querol[2]

[1]Associate Unit CSIC-University of Huelva "Atmospheric Pollution", Center for Research in Sustainable Chemistry (CIQSO) University of Huelva, 21071, Huelva, Spain
[2]Institute of Environmental Assessment and Water Research (IDAEA-CSIC), Barcelona, Spain
Keywords: PM10, Cu-Smelter. Mining Waste, SW Spain.
Presenting author email: jesus@uhu.es

SW Spain, and more specifically the Iberian Pyrite Belt, has been an area of intense mining and metallurgy since Roman times to the present. In the nineteenth century, mineral extraction coexisted with a rudimentary smelters based on so-called "teleras": wood furnaces with polymetallic sulfides burning for weeks.

Anthropogenic emissions can influence negatively on air quality due to SO_2 "clouds" and toxic elements. Subsequently, large smelters were installed, implying an improvement compared to the "teleras", although affecting adversely the air quality of mining towns. In 1970, the 2nd Industrial Development Plan of Spain was developed in the city of Huelva, favoring the placement of a Cu smelter near the town. Today, this Cu smelter is the second most important of Europe, with a total production in 2011 of 247,000 tons of Cu cathodes.

Mining-industrial activity has been referred to explain the high cancer mortality suffered by this region of Spain (Abente Lopez et al., 2006), conforming a "cancer triangle" between the provinces of Cadiz, Seville and Huelva, with extensions towards Extremadura (Benach et al., 2003).

In this work, we present a geochemical study in PM10 during the years 2009 to 2011 in three sampling monitoring stations representative of the **mining area** (Nerva, Rio Tinto Mining District), **urban area with industrial influence** (Campus Universitario del Carmen, Huelva) and **rural background** (Matalascañas, near the Doñana National Park), in order to characterize: 1) the main geochemical anomalies of toxic elements, 2) seasonality, and 3) source contribution.

Normally, mining and smelting operations occur in the same place, and therefore, this study is a good opportunity to quantify the impact from and extension of mining waste resuspension (Sánchez de la Campa et al., 2011a), and compare them with those derived from the smelter (Alastuey et al., 2006; Sánchez de la Campa et al., 2011b) strategy of PM10 implies high volume captors at intervals between 1-2 times every week. The number of filters obtained in each sampling station was 208 at University Campus, 220 and 189 in Nerva (Riotinto Mining District) and Matalascañas (Doñana) respectively. Filters were weighing under standard conditions (T and RH), and they were digested with strong acid according Querol et al. (1996). Furthermore, part of the filter was used to obtain a lixiviated with degree MQ H2O. Subsequently, the samples were analyzed by ICP-MS, ICP-OES, IC and Ctotal Analyzer. The total mass analyzed is between 70-80%.

The results of this study confirm the geochemical anomalies in As, Se, Bi, Cd, and Pb at a Spanish point of view (Querol et al., 2008) and Andalusia (de la Rosa et al., 2010).

Chemical analysis of PM10 near Cu-smelter near Huelva city, demonstrate the important contribution of Cu + Zn + As + Cd + Pb + Sn + Bi in air (Fernández-Camacho et al. 2012). The main emission sources of As are the flash furnace (144 $\mu g/m^3$) and refining furnace (18.75 $\mu g/m^3$). The peak concentration corresponds to a grain size of these particles in the fine (<1 micron) and ultrafine fraction (<0.1 microns) in the flash furnace and the refining furnace, respectively.

We conclude that high temperatures of smelting processes can produce particles of toxic elements (eg As, Se, Bi, Cd and Pb) in the ultra-fine fraction, with high residence-time, allowing long-distance transport, compared with coarse particles derived from mining waste. Therefore, they can impact in ecological zones of high interest (eg Doñana National Park), away Industrial States.

This work was funded by the Project 2011-RNM7800: Department of Innovation Science and Enterprise, Andalusian Autonomous Government and the Project CGL2011-28025: Spanish Ministry of Science and Innovation (MINECO).

References

Alastuey A., et al., (2006) *JAWMA* **56**, 993-1006.
Benach J., et al. (2003) *Eur J Pub Health* **13**, 115-123.
de la Rosa J.D., et al., (2010) *Atm Env* **44**, 4595-4605.
Fernández-Camacho R., et al. (2012) *Atm Env* **61**, 507-517.
López-Abente G., et al. (2006) *BMC Pub Health* **6**, 17.
Querol X., et al. (1996) *Atm Env* **30**, 3557-72.
Querol X., et al. (2007) *Atm Env* **41**, 7219-31.
Sánchez de la Campa A.M., et al. (2011a) *Env Res* **111**, 1018-23.
Sánchez de la Campa, A.M. et al (2011b) *J. Environ. Monit.*, **13**, 1276-1287.

Synthesis and glass formation properties of compounds representative of low-volatility secondary organic aerosol particles

H. P. Dette[1], M. Qi[1], D. C. Schröder[1], A. Godt[1] and T. Koop[1]

[1]Faculty of Chemistry, Bielefeld University, Bielefeld, 33615, Germany
Keywords: SOA, glass formation, spray drying
Presenting author email: hans_peter.dette@uni-bielefeld.de

Secondary organic aerosol (SOA) particles arise from the atmospheric oxidation of volatile organic compounds (VOC). SOA particles consist of a myriad of organic compounds, but several key components have been identified (e.g. Hallquist et al., 2009). For example, in boreal forests α-pinene is one of the most important VOC precursors. Its gas-phase oxidation proceeds via pinonic acid, a semi-volatile compound, to the second-generation oxidation product 3-methylbutane-1,2,3-tricarboxylic acid (3-MBTCA, see Fig.1), a low-volatile compound found predominantly in the aerosol phase (Jimenez et al., 2009; Müller et al. ACP 2012). Not much is known, however, about the physico-chemical properties and the phase state of 3-MBCTA. This knowledge is particularly important, because it has been suggested recently that SOA particles in boreal forests may exist in a glassy, i.e. amorphous solid state at room temperature under dry conditions (Virtanen et al., 2010). An amorphous semi-solid or solid state of organic aerosol particles has important atmospheric implications such as delayed gas-to-aerosol partitioning (Shiraiwa and Seinfeld, 2012; Zelenyuk *et al*., 2012). However, the glass formation properties of key compounds of oxygenated organic aerosol such as 3-MBTCA have not been investigated until now. Here we describe the synthesis and physico-chemical characterization of 3-MBTCA.

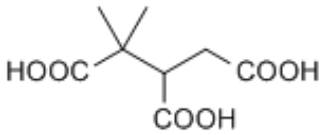

Fig.1: 3-MBTCA.

3-MBCTA was synthesized from methyl isobutyrate and dimethyl maleate in two steps with an overall yield of 78%. The compound was characterized by ^{1}H NMR and ^{13}C NMR spectroscopy, and mass spectrometry. The melting point of 3-MBTCA was found to be T_m = 426 K, in good agreement with literature data (Alder *et al.*, 1949). From knowledge of this T_m value a glass transition temperature of about T_g = 299 K has been predicted (Koop *et al.*, 2011). In the present study we were interested in confirming this value experimentally.

We have employed differential scanning calorimetry (DSC) to determine the temperature-dependent phase state behaviour of 3-MBCTA. In DSC experiments any substance has to be melted before it can be transferred into a glassy state. However, upon melting 3-MBTCA transformed into a lactone, implying that its T_g cannot be determined in the traditional way.

For this reason we have developed a novel spray diffusion drying technique in which a dilute aqueous solution of a water-soluble organic substance is atomized into aerosol particles that are then dried in several subsequent diffusion dryers. This drying may result in glass formation in each individual aerosol particle. The vitrified aerosol particles are then recollected in an impactor until enough mass has accumulated that their T_g can be determined by DSC.

The new technique has been tested using several reference compounds such as sugars or citric acid and the T_g values determined in this manner were in agreement with values obtained by previous methods. The experiments performed with 3-MBCTA show that its T_g is indeed above room-temperature supporting recent proposals of a glassy state of SOA particles. Such an amorphous solid state implies impedance of chemical reactions (Shiraiwa *et al.*, 2011) and the potential of such particles to act as ice nuclei at lower temperatures in the upper troposphere (Murray *et al.*, 2010).

References

Alder, K., Söll, H. and Söll, H. (1949) *Just. Lieb. Annal.Chem.* **565**, 73–99.

Hallquist, M., *et al*. (2009) *Atmos. Chem. Phys.* **9**, 5155–5236.

Jimenez, J. L.*, et al.* (2009) *Science*, **326**, 1525–9.

Koop, T., *et al.* (2011) *Phys. Chem. Chem. Phys.* **13**, 19238–55.

Müller, L., *et al.* (2012) *Atmos. Chem. Phys.* **12**, 1483–1496.

Murray, B. J., *et al*. (2010) *Nature Geosci.* **3**, 233–237.

Shiraiwa, M., Ammann, M., Koop, T. and Pöschl, U. (2011) *Proc. Natl. Acad. Sci.* **108**, 11003–11008.

Shiraiwa, M. and Seinfeld, J. H.(2012) *Geophys. Res. Lett.* **39**, L24801.

Virtanen, A., *et al.* (2010) *Nature* **467**, 824–827.

Zelenyuk, A., Imre, D., Beránek, J., Abramson, E., Wilson, J. and Shrivastava, M. (2012) *Environ. Sci. Technol.* **46**, 12459–12466.

PM formation processes in the urban atmosphere: comparison between South and North Italy

P.R. Dambruoso[1],G. de Gennaro[1], A. Di Gilio[1], P. Fermo[2], R.,Gonzalez Turion[3], A. Piazzalunga[3]

[1]Department of Chemistry, University of Bari, Bari, Puglia, via Orabona, 4, 70126, Italy
[2]Department of Inorganic, Metallorganic and Analytical Chemistry, University of Milan, Milan, via Celoria, 18, 20133 Milano, Italy
[3]Department of Chemistry, University of Milan-Bicocca, Milan, Piazza della Scienza, 3, 20126 Milano, *Italy*

HNO_3, HONO, PM formation processes, AIM 9000D
alessia.digilio@uniba.it

The determination of inorganic fraction in PM is very important to define the effective contribution of each source to fine PM. This fraction and the ions in particular, which constitute about 30-40% of total mass of PM2.5, can be used as markers of different sources. Moreover, time resolved information about ions and inorganic gases allow to study the chemical reactions and the chemical physical processes occurring in atmosphere. Nowadays, the disadvantages of this approach are the limited time resolution of the chemical characterization of PM filter samples and the simultaneous collection of inorganic gases concentrations data.

The AIM9000D is an automatic instrumentation that provides time-resolved direct measurements of anion and cation both in particulate (NO_3^-, SO_4^{2-}, Cl^-, NH_4^+, Na^+, K^+, Mg^{2+}, Ca^{2+}) and gases phases (such as HCl, HNO_3, HNO_2, SO_2 and NH_3) and it is an useful tool that allows to investigate the chemical process leading to the formation of ionic fraction of PM2.5 but also physical transformations and subsequent gas-particle partitioning of its semi-volatile inorganic constituents.

The main goal of this work was the study of PM formation processes using high time resolved information about ions and inorganic gases concentrations. For this purpose, two monitoring campaigns have been performed in Bari and in Milan. In particular, the first sampling campaign took place at the urban background station in the Campus of University of Bari from 1st to 20th October 2011, while the second one on the roof of the University of Milan from 6th June 2012 to 26th July 2012.

In this work the preliminary results about the nitrous (HONO) and nitric (HNO_3) acids concentrations in atmophere have been reported. The data analysis showed that nitrous acid concentrations were well correlated with NOx concentrations and humidity percentage both at Milan (for example only a few days in fig. 1) and Bari, confirming that etereogeneus reactions between NO_2 and H_2O on particle surface occurred (Stutz et al., 2004). Even if this reaction determines also the nitric acid formation, despite of Bari site, the nitrous and nitric acids hourly concentrations determined at Milan showed an uncorrelated behavior. Moreover, the hourly HONO concentrations peak between 06:00 and 08:00 am, during morning traffic rush hours. These findings suggested that HONO formation at Milan was probably due to the homogeneous recombination of the NO and OH radicals, that contributes to significant HONO amounts under conditions of elevated NO concentrations (Wong et al., 2011). However, this process competes with HONO photolysis occurring in the morning (Harrison et al., 1996; Carr et al., 2009), that determines a decrease of HONO concentrations in daytime.

As concern nitric acids, higher photoreactivity, more vehicular traffic emissions and atmospheric stability in Milan determined a photochemical production of HNO_3. The hourly mean concentrations of HNO_3 in fact, showed a clear daytime peak when high ozone concentrations were registered (fig 2a). On the contrary, the hourly concentrations of nitric acid were related to humidity percentage and NOx concentrations. In particular high concentrations were determined in the night hours between 3:00 and 6:00 a.m (fig.2b). This result suggested that the main formation process of HNO_3 in Bari was due to etereogenuos reaction occuring in the dark, between nitrate radical (NO_3) and water on particle surface (Spataro et al., 2013).

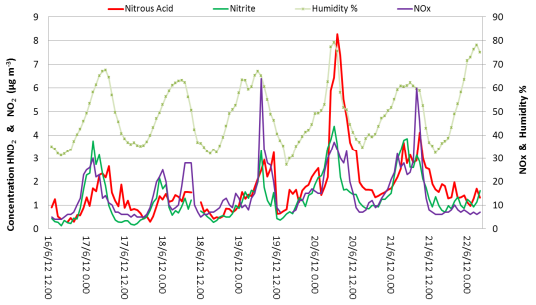

Fig. 1: Hourly concentrations of Nitrous acid, nitrogen oxides and nitrite with RH% determined at Milan

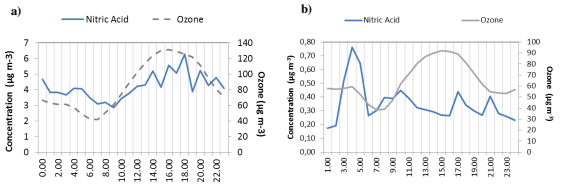

Fig. 2: Hourly trends of Ozone and Nitric acids concentrations at Milan (a) and Bari (b)

Reference

Carr et al., 2009. Science 324:336b.
Harrison et al.,1996. J Geophys Res 101:14429–39.
Spataro et al., 2013. Sci. Tot. Env. 447 210–224
Stutz et al., 2004. J Geophys Res 109:D03307.
Wong et al., 2011. Atmos Chem Phys 11:3595–609.

Formation mechanism and important implications of highly oxidized molecules (HOM) in the gas phase

M. Ehn[1,2], E. Kleist[3], H. Junninen[2], M. Sipilä[2], T. Petäjä[2], I. Pullinen[1], M. Springer[1], S. Andres[3], M. Rissanen[2], J. Kontkanen[2], S. Schobesberger[2], F. Rubach[1], R. Tillman[1], B. H. Lee[4], F. Lopez-Hilfiker[4], V.-M. Kerminen[2], M. Kulmala[2], D. R. Worsnop[2,5], J. Thornton[4,2], J. Wildt[3], T. F. Mentel[1]

[1] Institute for Energy and Climate Research (IEK-8), Forschungszentrum Jülich, 52425 Jülich, Germany
[2] Department of Physics, P.O. Box 64, 00014 University of Helsinki, Finland
[3] Institute of Bio- and Geosciences (IBG-2), Forschungszentrum Jülich, 52425 Jülich, Germany
[4] Department of Atmospheric Sciences, ATG Building, University of Washington, Seattle, WA 98195, USA
[5] Aerodyne Research, Inc., 45 Manning Road, Billerica, MA 01821, USA
Keywords: New particle formation, SOA, mass spectrometry, chamber studies
Presenting author email: mikael.ehn@helsinki.fi

It has been found that, on average, more than half of the atmospheric aerosol mass consists of organic compounds (Zhang *et al*, 2007). In most environments, the major part of the organic aerosol (OA) is of secondary origin (Jimenez *et al*, 2009) (SOA), meaning that it has been formed from oxidized organic molecules condensing onto pre-existing aerosol particles. The condensation and evaporation of organics to/from aerosol particles has been modeled with different methods, with varying success. The most generally used method being partitioning theory (Pankow, 1994), although this has also been found to be insufficient in some studies (e.g. Riipinen *et al*, 2011). Riipinen *et al* (2011) found that the growth of newly formed sub-100 nm particles could only be explained using a model where about half of the organic vapors condensed irreversibly, i.e. as though they were completely non-volatile.

Recently, Ehn *et al* (2012) reported on a new group of compounds detected in the gas phase that were much more oxidized than observed before, e.g. C_{10}-compunds with atomic O:C ratios up to unity. The compounds were detected both in the laboratory and ambient air, and are expected to have extremely low volatilities. Due to the lack of quantitative measurements, the implications of these highly oxidized molecules (HOM) on aerosol formation could not be determined. With the help of the newly developed instrumentation, we have been able to quantify the HOMs and their contribution to aerosol particle formation and growth.

A novel combination of mass spectrometers (PTRTOF, iodine CIMS, nitrate-CIMS) was deployed to monitor the gas phase oxidation of volatile organic compounds (VOCs) at the Jülich Plant Atmosphere Chamber (Mentel *et al*, 2009). The instruments provided high mass and time resolution data of volatile, semi-volatile, and low-volatility (HOM) compounds, which could be related to aerosol number and mass properties measured in parallel by an extensive suite of aerosol instrumentation. The main VOC studied was alpha-pinene.

Our results suggest a surprisingly high abundance of the HOMs, consequently suggesting a very important role in aerosol formation. Indeed, the HOMs under many conditions seemed to be the driving force in aerosol formation, both concerning particle number and mass, while semi-volatile species such as pinonic and pinic acid, although more abundant than the detected HOMs, were less important.

We propose that HOMs can explain the major part of the "non-volatile vapors" that Riipinen *et al* (2011) required to explain ambient observations in their model. The role of HOMs in nucleation and initial growth of newly formed particles, as well as their contribution to SOA mass yields will be discussed in more detail.

M. E. gratefully acknowledges financial support by the Emil Aaltonen foundation. This work was supported by the ERC Advanced Grant EU-FP7-ATMNUCLE (project no 227463), and by the Academy of Finland Center of Excellence program (project no 1118615).

Ehn, M. et al (2012) *Atmos. Chem. Phys*., 12, 5113-5127, doi:10.5194/acp-12-5113-2012.
Jimenez, J.L. et al (2009) *Science*, 326, 1525-1529.
Mentel, T. F. et al (2009) *Atmos. Chem. Phys*., 9, 4387-4406, doi:10.5194/acp- 9-4387-2009.
Pankow, J. F. (1994) *Atmos. Environ.*, 28, 185–188.
Riipinen, I. et al (2011), *Atmos. Chem. Phys***.**, 11, 3865-3878, DOI 10.5194/acp-11-3865-2011.
Zhang, Q. et al. (2007) *Geophys. Res. Lett*., 34, L13801, doi:10.1029/2007gl029979.

Noise as an indicator of traffic and ultrafine particles in Huelva city

I.M. Brito Cabeza[1], R. Fernández-Camacho[1], J.D. de la Rosa[1]

[1]Associate Unit CSIC-University of Huelva "Atmospheric Pollution", Center for Research in Sustainable Chemistry (CIQSO), University of Huelva, 21071, Huelva, Spain
Keywords: noise, ultrafine particles, vehicles.
Presenting author email: rocio.fernandez@dgeo.uhu.es

Noise caused by road traffic is one of the main environmental problems in many European urban areas. The noise associated to road traffic is a source of pollution. In urban environments, vehicle exhaust emissions are the major source of ultrafine particles (diameter smaller than 0.1 µm).

We present a study on noise as an indicator of traffic and ultrafine particles in Huelva city. The study is based on measurements of noise levels, number of particles coarser than 2.5 nm (PN), black carbon concentrations (BC), PM_{10} levels, gaseous pollutants concentrations and meteorological parameters monitored during 2009 in the University Campus monitoring station.

In order to identify the process contributing to ultrafine particles concentrations (PN), two components (PN1 and PN2) were segregated following the methodology of Rodríguez and Cuevas (2007). PN1 accounts for primary vehicle exhaust emissions and may also include compounds nucleating/condensing immediately after emission. PN2 accounts for new particle formation due to nucleation and rapid particle growth to detectable sizes.

The space-time evolution between PN and noise levels showed a high correlation suggesting the environmental noise is linked to traffic as a main source in urban areas. The decreasing in noise levels from working days to weekends is also observed.

During the winter season (Fig. 1A) a linear correlation between LAeq and PN1 (fresh vehicle exhaust emissions) was observed, with a value of the PN1 / LAeq slope of 720.32 particles / dB. During the summer season (Fig. 1B), an exponential relationship between PN1 and LAeq was observed, with a PN1 / LAeq slope value of $0.7469e^{0.1783}$ / dB.

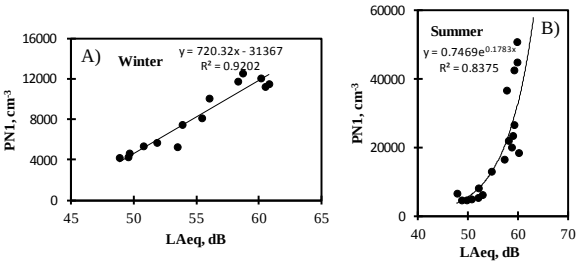

Figure 1. Hourly average values of PN1 vs. noise levels (LAeq) for every hour of the day during winter (A) and summer (B) during 2009 in the University Campus monitoring station.

A Principal Component Analysis (PCA) identified vehicle exhaust emissions as a main source. The association of noise levels in this factor suggests the road traffic as key factor in noise pollution.

According to the chemical composition of the particles and their influence on noise levels, this study points the high correlation between the noise levels and road dust elements. During the morning rush hours, especially on working days, high concentrations of crustal elements (Al, Fe) associated with pavement, brakes and tires were observed. Simultaneous increases in noise levels were registered, pointing the clear relationship between noise and vehicle exhaust emissions.

In order to quantify the relationship between PN1 and LAeq with road traffic intensity, PN1 and LAeq concentrations were averaged at 100 vehicles / hour intervals during peak rush hours in winter and summer mornings (Fig. 2). The results showed a high linear correlation with the number of vehicles / hour during the winter and summer mornings. From PN1 versus LAeq equations obtained in winter and summer, ultrafine particle concentrations related with traffic emissions have been calculated from noise data. Noise levels increases by 1 dB per 100 vehicles / hour. This is equivalent to 1000 particles per vehicle.

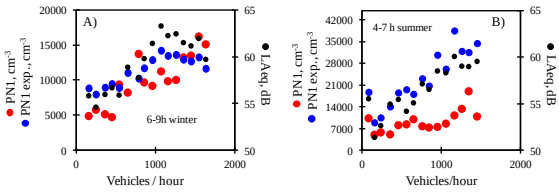

Figure 2. Hourly average values of PN1 and PN1 experimental particles and of LAeq vs. vehicles / hour on winter and summer mornings. Data were average at 100 vehicles / hour intervals.

This work was supported by the P11-RNM-7800 research project, Department of Environmental, Rural and Marine of the Andalusian Autonomous Government, the Eygema Company and the Council of Huelva.

Rodríguez, S., Cuevas, E. (2007) *J. Aerosol Sci.* **38**, 1207-1219.

Chemical characterization of PM2.5 belonging to a port city

A. Genga[1], M. Siciliano[1], D. Contini[2], D. Cesari[2]

[2]Dipartimento di Scienze e Tecnologie Biologiche e Ambientali, Università del Salento, Lecce, Apulia, 73100, Italy
[1]Istituto di Scienze dell'Atmosfera e del Clima, ISAC-CNR, Lecce, Apulia, 73100, Italy
Keywords: PM2.5, chemical characterization, port emission.
Presenting author email: alessandra.genga@unisalento.it

Air emissions from the maritime transport sector account for a significant portion of total emissions, affecting air quality, climate change and human health. The design and application of effective policy actions to abate such emissions require that air emissions and their geographic location be robustly estimated. (Contini at al., 2011; Miola et al., 2011)

At the beginning of 2012 it was started the research project CESAPO (Contribution of Emission Sources on the Air quality of the POrt-cities in Greece and Italy), within the framework of Interreg Italy-Greece 2007/2013. The general objective of the project is to quantify the contribution of emission sources to the air pollution of the port cities, giving more emphasis on the maritime transport and the activities within the harbour, and link the scientific outcomes with integrated proposed actions for sustainable urban development in the Mediterranean Region. In particular in this work the chemical characterization of PM2.5 is reported and the aim is to investigate the contribution of the emissions of ships and of the harbour to the particulate matter in Brindisi.

The experimental campaign was carried out every day from June to October 2012 and globally 148 PM2.5 samples were collected on quartz filters and 148 on Teflon membrane of 47 mm.

Soluble ionic species were determined on teflon filters via High Performance Ion Chromatography (HPIC, Dionex DX-500 System), for SO_4^{2-}, NO_3^-, NH_4^+, Cl^-, Na^+, K^+, Mg^{2+} and Ca^{2+} while the quartz filters were analysed via Graphite Furnace Atomic Absorption Spectroscopy (GF-AAS, Perkin Elmer Analyst 600 System) for determination of 8 elements (Ni, Cu, V, Mn, As, Pb, Cr, Sb) and by Inductively Coupled Plasma Atomic Emission Spectroscopy (ICP-AES, Varian Liberty 110 spectrometer) for 4 elements (Fe, Al, Zn and Ti). Each filter has been extracted in Milli-Q water: two successive extractions of 20 min in an ultrasonic bath have been used for a nearly complete recovery, with the renewal of the water at each step. In each of the 2 extraction steps 10 ml of Milli-Q water has been used. It has to be put in evidence that two extractions were sufficient to extract more than 98% of the measured ions. The extracted solutions have been analysed by HPIC for major ionic species. Anion determination has been performed by means of a Ion Pac ®AS14A column (Dionex) using 1.8 mM Na_2CO_3 /1.7 mM $NaHCO_3$ as eluent at 2 ml/min flow-rate and, for the detection, a conductivity system equipped with a ASRS ®-ULTRA suppression mode (Dionex). Cations determination has been performed by means of an Ion Pac ® CS12A column (Dionex) using 20 mN H_2SO_4 as eluent at 1 ml/min flow-rate and, for the detection, a conductivity system equipped with a CSRS ® -ULTRA suppres.(Contini et al., 2010)

The secondary non-sea-salt-sulphate was essentially ammonium sulphate and accounted for about 32% of PM2.5, while the metal concentration take into account 2-3 %.

The content of OC/EC has been carried out by the carbon analyzer (Sunset, USA).

Preliminary results of OC/EC concentration will be presented.

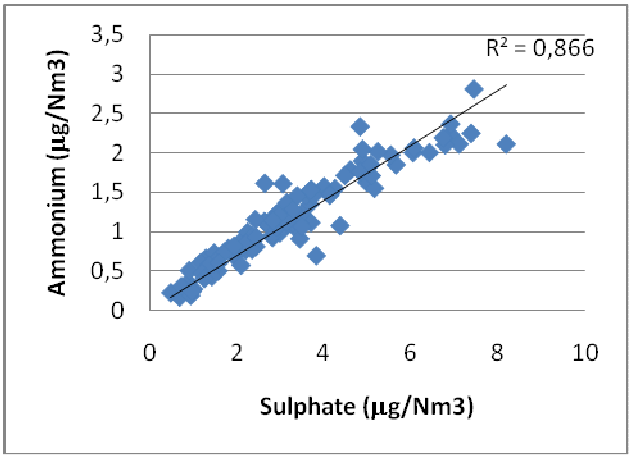

Figure 1. Secondary ammonium sulphate.

This work was supported by the Interreg Greece-Italy 2007-2013 program under grant I1.32.06.

Contini, D., Gambaro, A., Belosi, F., De Pieri, S., Cairns, W.R.L., Donateo, A., Zanotto, E., Citron, M. (2011) *J. Environ. Manage.* **92**, 2119-2129.

Miola A., Ciuffo B., (2011) *Atmosp. Environ.*, **45**, 2242-2251.

D. Contini, A. Genga, D. Cesari, M. Siciliano, A. Donateo, M. C. Bove, M. R. Guascito (2010) Atmosp. Res, **95**, 40-54.

Temperature dependence of nopinone partitioning coefficient in organic aerosol

B. Steitz[1], I. Gensch[1], T. Hohaus[2], H.Saathoff[3] and A. Kiendler-Scharr[1]

[1]Institut für Energie- und Klimaforschung, Troposphäre (IEK-8), Forschungszentrum Jülich GmbH, Jülich, Germany.
[2] Aerodyne Research, Inc., Billerica, Massachusetts, USA.
[3]Institute for Meteorology and Climate Research (IMK-AAF), Karlsruhe Institute of Technology, Karlsruhe, Germany.
Keywords: semi-volatile SOA
Presenting author email: i.gensch@fz-juelich.de

Secondary organic aerosol (SOA) represents a significant fraction of the total aerosol mass, thus strongly influencing aerosol properties. A detailed understanding of SOA formation from volatile organic compounds (VOCs) as well as the partitioning of the semi-volatile products between gas and particle phase is necessary to better predict the organic matter in the atmosphere. In this study, we present the experimentally determined partitioning coefficient of nopinone, a major oxidation product of β-pinene The observed temperature dependence of the partitioning coefficient is discussed.

Experiments studying the SOA formation from β-pinene ozonolysis were conducted in the temperature range between 243 K and 303 K at the AIDA chamber of the Karlsruhe Institute of Technology (KIT). During all β-pinene experiments, gas and particle phase concentration of the major reaction product, nopinone, was measured by combining an Aerosol Collection Module (ACM) with the high-resolution Proton Transfer Reaction-Time of Flight-Mass Spectrometer (PTR-ToF-MS). Alternate measurements of the nopinone concentration in gas phase only and particle phase only were used to calculate the partitioning coefficient of nopinone.

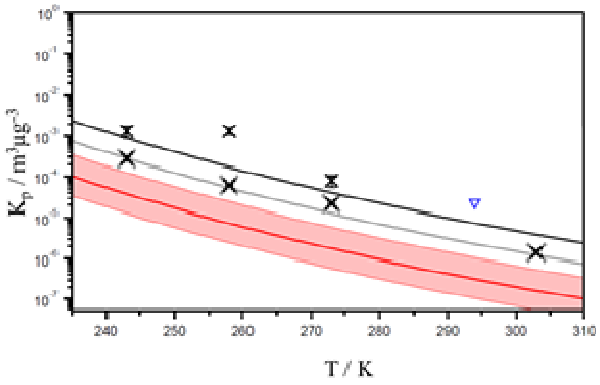

Figure 1: *Nopinone partitioning coefficient at different temperatures from measurements with PTR-ToF-MS and ACM (black crosses) as well as the temperature dependence fit (black line). Gray crosses mark the partitioning coefficient values derived from ACM measurements after additional nopinone injection. The gray line shows a fit to data points with added nopinone. The pink shaded area marks the range of theoretically determined partitioning coefficient following Jenkin, 2004. For this, an activity coefficient between 3 (lower limit) and 0.3 (upper limit of the pink area) is considered. The red line in the middle shows the partitioning coefficient temperature dependence for an activity coefficient of 1. The blue triangle shows the experimentally derived nopinone partitioning coefficient from Hohaus (2009).*

The partition coefficients experimentally determined at 243, 258, 273 and 303K , before and after an additional nopinone injection, are presented in Figure 1. Overall, the partitioning coefficient increases with decreasing temperatures. The experimental results are compared with calculations arising from studies on the gas-particle partitioning, based on the Pankow absorption model (Jenkin, 2004). These calculations were employed to fit the temperature dependence of nopinone partition coefficient to the experimental data sets. Using the activity coefficient as a free fitting parameter results in an activity coefficient of 0.042 ± 0.019. This is below the range of 0.3 - 3 that is typically assumed for activity coefficients in SOA formation (Seinfeld and Pankow, 2003).

The experimental partitioning coefficients determined in this study compare well with the value obtained by Hohaus (2009) and show a temperature dependence following the trend predicted by theory. Yet, they are up to two orders of magnitude higher than values calculated based on equilibrium partitioning assumptions. Possible reasons for this discrepancy will be discussed.

Hohaus, T. (2009) *Development of a new online method for compound specific measurementsof organic aerosols*, PhD Diss., Forschungszentrum Juelich.
Jenkin, M. E. (2004) *Atmos. Chem. Phys.* **4**, 1741-1757.
Seinfeld, J. H. and Pankow, J. F. (2003) *An. Rev. Phys. Chem.*, **54**, 121-140.

How did chemical composition of the Po Valley radiation fog change in the last twenty years?

L.Giulianelli[1], M.C. Facchini[1], S. Gilardoni[1], S. Decesari[1], M. Rinaldi[1], C. Carbone[1], M. Paglione[1], and S. Fuzzi[1]

[1] Institute for Atmospheric Science and Climate (ISAC), CNR, Bologna, Italy
Keywords: chemical composition, fog, multiphase chemistry, time series.
Presenting author email: l.giulianelli@isac.cnr.it

Radiation fog is formed by the steady cooling of air close to the ground where main emissions take place, and is characterized by strong atmospheric stability and low wind speed. Fog is an atmospheric multiphase system where water droplets, aerosol particles and gases interact. Gas to particle partitioning, chemical reactions in liquid phase or at the gas-liquid interface and scavenging of aerosol particles take place. The presence of fog has a relevant impact on atmospheric chemistry and air quality and by deposition it can affect the natural ecosystem and historical artifacts.

For these reasons it is important to have a detailed knowledge of the chemical composition of fog samples, especially in areas like the Po Valley (northern Italy) where fog episodes are very frequent during the fall-winter season. The Po Valley is a densely inhabited region characterized by numerous agricultural and industrial activities and intense vehicular traffic, making it one of the most polluted region in Europe. The interest in having a deeper knowledge about fog chemical composition goes back to the early eighties when the first fog samples were collected at the field station of San Pietro Capofiume, Fuzzi *et al*. (1983). The station is located in the south eastern part of the Po Valley between the cities of Bologna and Ferrara. Initially fog droplets were sampled occasionally. Starting from November 1989 up to now fog samples have been collected throughout the fall-winter season during each dense fog episode, Fuzzi *et al* (1992, 1996, 1997).

This allowed us to build a more than twenty years long database of chemical composition (NH_4^+, $SO_4^=$, NO_3^-, soluble organic compounds, etc.), pH, conductivity and liquid water content (LWC). The observation of this unique database showed a decreasing trend of conductivity and ionic strength, that is a lower content of ionic species in the fog droplets. Mean conductivity values range from 460 µS/cm in 1989/90 to 114 µS/cm in 2010/11. Analyzing the trend of the single ionic species, also the three major ions (NH_4^+, $SO_4^=$, NO_3^-) that alone represent up to 90% of the total ionic strength, decrease. Sulphate shows the highest relative decrease, as demonstrated by the negative trend of $SO_4^=/NO_3^-$ ratio. Ionic concentrations within each season are very variable: 0.03-27.87, 0.02-16.90, 0.04-25.04 µeq/l for NO_3^-, $SO_4^=$, NH_4^+ respectively. Trends are built using the seasonal volume weighted means for each species, in order to take into account the contribution of LWC and lifetime of each fog event. Also pH values are very variable, ranging from 2.44 to 8.83, but the annual trend calculated by the weighted means of each season shows an increase: fog droplets are less acidic now than 20 years ago. During the 90s mean pH values ranged from 3.7 to 4.7, while values ranged from 4.1 to 6.9 from 2000 to 2011. We suppose this is correlated with the decrease of sulphate. Not much is known about the role of organic compounds in fog droplets pH. Water soluble organic carbon (WSOC) analysis are available only from 1997 and the results do not show any correlation to pH. More detailed analysis of the organic fraction should be carried out to address this topic.

Having available such a long database allows to observe differences in fog chemical composition through the years and eventually relate them with emission changes. This could be useful to determine the effectiveness of past policies and could be helpful for future choices.

Fuzzi, S., Orsi, G. and Mariotti, M. (1983) *J. Aerosol Sci.* **14**, 2, 135-138.

Fuzzi, S., et al. (1992) *Tellus*, **44B**, 448-468.

Fuzzi, S., et al. (1996) *Atmos. Environ.* **30**, 201-213.

Fuzzi, S., Orsi, G., Bonforte, G., Zardini, B. and Franchini P.L. (1997) *Water, Air and Soli Pollut.* **93**, 383-394.

Speciation of metals in refinery emissions particles

Y. González-Castanedo[1], D. A. Sánchez Rodas[1,2], C. Ferrer[1] and J. de la Rosa[1]

[1]Associate Unit CSIC-University of Huelva "Atmospheric Pollution", Center for Research in Sustainable Chemistry (CIQSO), University of Huelva, 21071, Huelva, Spain
[2]Department of Chemistry and Science of Materials, Campus El Carmen, University of Huelva, 21071, Huelva, Spain
Keywords: speciation, refinery, metal, bioavailability.
Presenting author email: yolanda.gonzalez@dgeo.uhu.es

The Bay of Algeciras is a well documented industrial pollution hot spot, with relatively high concentrations of metals such us Ni, V, Cr and La in PM10 and PM2.5, being attributed to both industry (de la Rosa *et al.,* 2010) and shipping emissions (Pandolfi et *al.,* 2010). These metal releases inevitably impact on the local ecosystem and surroundings populations. They were identified in the cocktail of pollutants emanating from different emissions stacks from San Roque refinery complex located in the Bay of Algeciras by Sánchez de la Campa *et al.,* (2011). V and Ni are related to the refining of crude oil and processing of its downstream products in the petrochemical complex, while La is specifically used in the form of La-concentrates in zeolitic fluid catalytic cracking units (FCC) which crack heavier crude oil distillation fractions into lighter compounds (LPG) (Moreno *et al*., 2010).

The goal of this work is to evaluate the bioavailability of the main metal content emitted from refinery including V, Cr, Co, Mo, La, Ce and Pb, The study deals with the size distribution and chemical characterization of particulate matter emitted by the most polluting emissions stack in the refinery complex: sulpholane (V, Cr, Ni in particles with diameter < 0,33µm), HDS (V in particles with diameter < 10 µm, Cr and Ni in particles with diameter < 0,33µm, La 2-10µm) and FCC (Cr, Ni and La in particles with diameter 0,3-10 µm). For this aim, four steps Tessier sequential procedure modified by Fernández Espinosa *et al.,* (2006) was applied to airborne emissions refinery samples.

This speciation scheme determines the chemical form in which the metals are present: 1st step: soluble and exchangeable metals, 2nd step: carbonates, oxides and reducible metals, 3rd step: bound to organic matter, oxidizable and sulphidic metals and 4rd step: residual metals. The dissolved metals in the first matrix (H_20 Milli-Q) are the most potentially toxic for the human health. Moreover, the metal bioavailability was studied depend on size particles. Four cut off stage diameter (>17 µm, 5-14 µm, 0,67-1,3 µm, < 0,33µm) were used. The final solutions, obtained of each step extraction, were analyzed by ICP-MS.
Figure 1 show the metal extraction percentage obtained in H_20 Millli-Q matrix from FCC stack emissions samples.

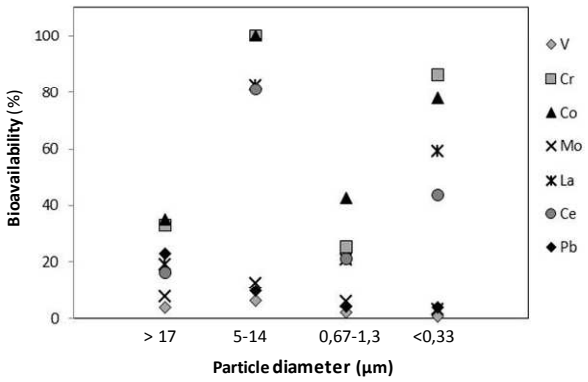

Figure 1.Bioavailability (%) vs. particle diameter (µm) from FCC particulate matter emissions.

V, Mo and Pb show a low extraction percentage (below 25%) of the soluble chemical forms in all the size particle modes. However, the rest of the elements present a different bioavailability depend on size distribution.
The great bioavailability of Cr (86), Co (78%) and La (59%) in the smallest particle mode (< 0,33 µm) is remarkable. Therefore, these metals can been considered hazardous pollutants to human health due to their high residence time and wide dispersion to be easily inhaled and assimilated by our organism.

This work was funded by the Projects 2007-RNM027329 and 2011-RNM7800: Department of Innovation Science and Enterprise, Andalusian Autonomous Government and the Project CGL2011-28025: Spanish Ministry of Science and Innovation (MINECO).

de la Rosa, J.D. et al., (2010) *Atmospheric Environment* **44**, 4595-4605.
Fernández Espinosa A.J. et al., (2006) *Inter. J. Environ. Anal. Chem*. **86**, 641-651.
Moreno, T. et al., (2008) *Environmental Science Technology*, **42**, 6502-6507.
Pandolfi, M. et al., (2011) *Environmental Science Pollution Research*, **18**, 260-269.
Sánchez de la Campa, A.M. et al (2011) *J. Environ. Monit.*, **13**, 1276-1287.

Thermal properties of secondary organic aerosols

A. Lutz, E. U. Emanuelsson, Å. K. Watne and M. Hallquist

Department of Chemistry and Molecular Biology, University of Gothenburg,
412 96 Gothenburg, Sweden
Keywords: Volatility, VTDMA, Volume Fraction Remaining
Presenting author email: Anna.Lutz@gu.se

Secondary Organic Aerosols (SOA) has a complex chemical composition and cannot easily be described in terms of vapour pressures or heat of vaporisation. Consequently several different volatility measures are used to describe their thermal properties. However, it is a challenge to clearly present and compare volatility data. To overcome this we have developed a method that makes it easy to compare volatilities and gain more information about the thermal properties of SOA.

Methods

The thermal properties of SOA can be obtained with a Volatility Tandem Differential Mobility Analyzer (VTDMA). The VTDMA measures how much size selected particles evaporate at a certain temperature.

The volatility of the particles can be presented in several different ways. Volume Fraction Remaining, VFR(T), is derived from the measured particle modal diameter (D_p) at a certain evaporation temperature T and nomalised to the selected diameter (D_{pRef}).

$$VFR(T)=(D_p/D_{pRef})^3$$

Typically, VFR(T) has been derived for several temperatures e.g. from 298 K up to 483 K. To obtain more information over the full range of evaporation temperatures, a sigmoidal curve was fitted to the full range of VFR data versus evaporation temperature.

$$VFR_T=VFR_{max}+\frac{(VFR_{min}-VFR_{max})}{1+\left(\frac{T_{position}}{T}\right)^{S_{VFR}}}$$

The slope factor S_{VFR} and $T_{position}$ define the shape and the mid-position of the curve. VFR_{max} and VFR_{min} define the boundaries of the highest and lowest VFRs, respectively. To more strictly define the most volatile and the non-volatile fraction, the equation was used to derive VFR_{298K} and VFR_{523K}. In addition, $T_{VFR0.5}$, the temperature where half of the particles volume is evaporated was calculated. $T_{VFR0.5}$ is a general measure of the volatility. The slope factor, $S_{VFR,}$ is a qualitative measure on the distribution of the volatility of the major components of the particles.

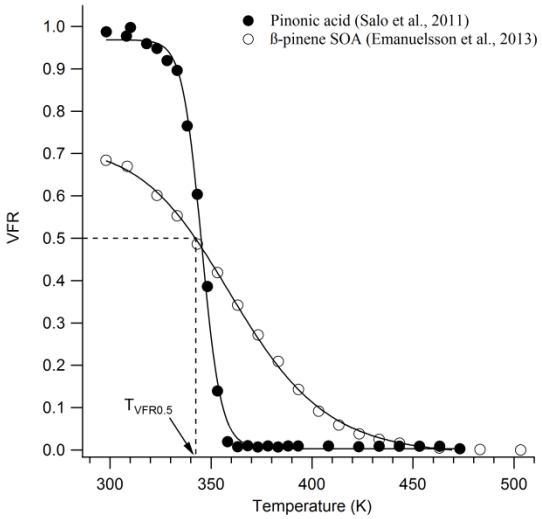

Figure 1. Pinonic acid and SOA from β-pinene charaterised over several evaporation temperatures.

In Figure 1, pure pinonic acid and SOA formed from ozonolysis of β-pinene are compared. A less steep slope (increased S_{VFR}) indicates a wider distribution of volatilities e. g. a more complex chemical composition. Pure pinonic acid (S_{VFR} = -72.4) has a steeper slope than the β-pinene SOA (S_{VFR} = -15.6). $T_{VFR0.5}$ for pure pinonic acid and β-pinene SOA was 342.2 K and 364.6 K, respectively.

Conclusions

The parameters $T_{VFR0.5}$ and S_{VFR} derived from the Sigmoidal fit have been shown to be valuable for comparing volatilities measured using a VTDMA instrument. An increase in $T_{VFR0.5}$ corresponds to less volatile aerosol particles and a decrease in S_{VFR} corresponds to a more complex volatility distribution.

The research presented is a contribution to the Swedish strategic research area ModElling the Regional and Global Earth system, MERGE. This work was supported by Formas (214-2010-1756) and the Swedish Research Council (80475101).

Salo, K. *et al.*, (2011). *Atmos Chem Phys*, **9**, 11055-11067.

Emanuelsson, E. *et al.*, (2013) Submitted to *J. Phys. Chem. A*

Diurnal variation of C_2-C_5 organosulfates detected during PEGASOS field campaign

Yoshiteru Iinuma, Laurent Poulain, Dominik van Pinxteren and Hartmut Herrmann

Leibniz-Institut für Troposphärenforschung (TROPOS), Leipizg, D-04318, Germany
Keywords: SOA, isoprene, methacrolein, glyoxal.
Presenting author email: yoshi@tropos.de

Recent studies have shown that isoprene and monoterpene originating organosulfates are present in the field and laboratory secondary organic aerosol (SOA) samples. The formation of organosulfates is suggested to involve the interaction of oxidation products of biogenic volatile organic compounds (VOCs) and sulfur containing species from anthropogenic sources, and suggested to be marker compounds for processed SOA (Hallquist, *et al.*, 2009). Although the mass fraction of organosulfates in total sulfate mass is typically smaller than 15% (Stone *et al.*, 2012; Hawkins *et al.*, 2010; Lukács *et al.*, 2009), the mechanisms provide an important means to form low volatile SOA compounds from oxygenated VOCs that are typically too volatile to form SOA.

In the present study, a series of isoprene originating organosulfates were analysed in ambient fine particle samples (PM1) that were collected during a PEGASOS (Pan-European Gas-Aerosol-Climate Interaction Study) field campaign in June and July 2012. The campaign was carried out at the San Pietro Capofiume in the North Eastern part of the Po Valley, Northern Italy. The sampling site is approximately 40 km away from Bologna and impacted by both anthropogenic and natural emissions from surrounding cites and agricultural fields. The PM1 samples were collected using a Digiel High-Volume sampler (Hagnau, Switzerland) twice a day (daytime, 9 a.m. to 9 p.m., and nighttime, 9 p.m. to 9 a.m.). The filter samples were extracted with methanol, evaporated to dryness under a gentle stream of nitrogen at 10°C, and reconstituted in 200 μL of methanol/H_2O solution (50/50, v/v). The extracts were analysed by Ultra Performance Liquid Chromatography coupled to Electrospray Ionisation Quadrupole Time-Of-Flight Mass Spectrometry (UPLC/(-)ESI-QTOFMS (Iinuma *et al.*, 2009).

A series of isoprene originating organosulfates were detected in the samples. These are *m/z* 153 (hydroxyacetone organosulfate, $C_3H_5O_5S^-$), 155 (glyoxal organosulfate, $C_2H_3O_6S^-$), 169 (methylglyoxal organosulfate, $C_3H_5O_6S^-$), 183 (methacrolein organosulfate, $C_4H_7O_6S^-$), 199 (methacrolein organosulfate, $C_4H_7O_7S^-$) and 215 (methyltetrol organosulfate, $C_5H_{11}O_7S^-$). Figure 1 shows a time series of these compounds. Owing to lack of authentic standard compounds, only the signal intensities are compared in this study. In general, the intensities of these signals were higher in the daytime samples than in the nighttime samples, indicating that the formation of these compounds involves the photochemical oxidation.

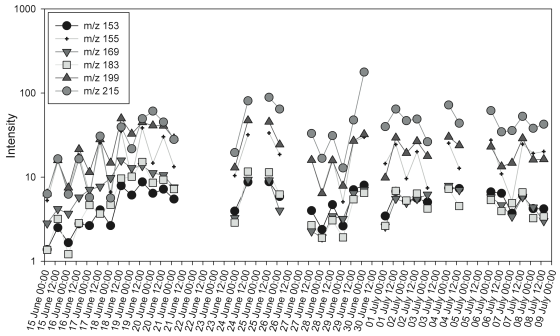

Figure 1. Time series of isoprene originating organosulfates detected in this study.

Table 1 summarises the correlation coefficients determined for the detected organosulfates. Although statistically significant correlations were obtained between all the compounds, the *m/z* 215 compound showed somewhat weaker correlations than the others, which may be related to the formation mechanisms of the *m/z* 215 compound.

Table 1. Correlation coefficients between detected organosulfate compounds

	m/z 153	*m/z 155*	*m/z 169*	*m/z 183*	*m/z 199*	*m/z 215*
m/z 153	1.00					
m/z 155	0.78	1.00				
m/z 169	0.64	0.55	1.00			
m/z 183	0.83	0.70	0.83	1.00		
m/z 199	0.86	0.82	0.84	0.91	1.00	
m/z 215	0.72	0.64	0.24	0.48	0.57	1.00

This work was supported by EU FP7 IP PEGASOS (FP7-ENV-2010/265148).

Hallquist, M., et al. (2009) *Atmos. Chem. Phys.* **9(14)**, 5155-5236.

Hawkins, L. N., Russell, L. M., Covert, D. S., Quinn, P. K., and Bates, T. S. (2010) *J. Geophys. Res.*, [Atmos.], **115**, Doi 10.1029/2009jd013276.

Iinuma, Y., Boge, O., Kahnt, A., and Herrmann, H. (2009) *Phys Chem Chem Phys* **11(36)**, 7985-7997.

Lukács, H., Gelencsér, A., Hoffer, A., Kiss, G., Horváth, K., and Hartyáni, Z. (2009) *Atmos. Chem. Phys.* 9(1), 231-238.

Stone, E. A., Yang, L. M., Yu, L. Y. E. and Rupakheti, M. (2012) *Atmos. Environ.* **47**, 323-329, doi 10.1016/J.Atmosenv.2011.10.058.

Reactivity of chlorine radical on palmitic acid particles: kinetic measurements and products identification

M. Mendez[1], R. Ciuraru[1], N. Visez[1] and D. Petitprez[1]

[1] Physicochimie des Processus de Combustion et de l'Atmosphère (PC2A) UMR CNRS 8522 Université Lille 1, F-59655, Villeneuve d'Ascq, France

Keywords: multiphase-chemistry, oxidation, radical.
Presenting author email: maxence.mendez@gmail.com

Recent studies have revealed that the concentration of organic matter in marine environments exhibits a seasonal behaviour, dominating the chemical composition of ultrafine particulate matter (PM_1) during periods of high biological activity. Chemical analyses of organic compounds sampled from this interfacial layer have allowed to identify mostly fatty acid (C12-C18) compounds (Marty, Saliot et al. 1979). Heterogeneous chemistry involving particulate matter is mainly initiated by surface reactions with gas-phase radicals thus playing a significant role in the chemical evolution of such species. Therefore heterogeneous reactions of this kind should also be considered along with radical reactions in the homogeneous gas-phase, in order to gain an accurate description of the key chemical pathways of the atmosphere and the global oxidant budget. Although the OH radical is the primary daytime oxidant, halogen atoms may also significantly participate in oxidation processes, especially in the marine boundary layer where Cl atoms are mainly generated from the photolysis of active chlorine species and their concentrations can be up to 10^6 atom.cm^{-3} (Spicer, Chapman et al. 1998)

In an attempt to better understand the heterogeneous oxidation of particulate organic compounds, reactions between Cl atoms and palmitic acid (PA) have been performed in our laboratory within an Aerosol Flow Tube (AFT) where fine particles generated by homogeneous condensation of PA vapours are introduced with Cl_2 as an oxidant precursor. Cl atoms are generated by photolysis of the molecular chlorine using UV lamps surrounding the reactor. Uptake coefficient has been determined by monitoring the decay of PA by GC/MS analysis as a function of the chlorine exposure. Experiments have been conducted with and without O_2. Identification of the reaction products in the condensed phase have been performed by GC/MS analyses.

The heterogeneous reactivity experiments performed without O_2 lead to the determination of $\gamma = 14 \pm 5$ and reveal that: (1) an important secondary chemistry involves Cl_2; (2) monochlorinated and polychlorinated compounds are formed (from $PACl_1$ to $PACl_4$ detected). Although, the PA particles are solid, the whole PA matter can notwithstanding be consumed. In the presence of oxygen, the reaction is still leaded by secondary chemistry but the propagation chain length is smaller than in absence of O_2 because there is no regeneration of $Cl^{\cdot}$ and lead to an uptake coefficient $\gamma = 3 \pm 1$ obtained from the figure 1.

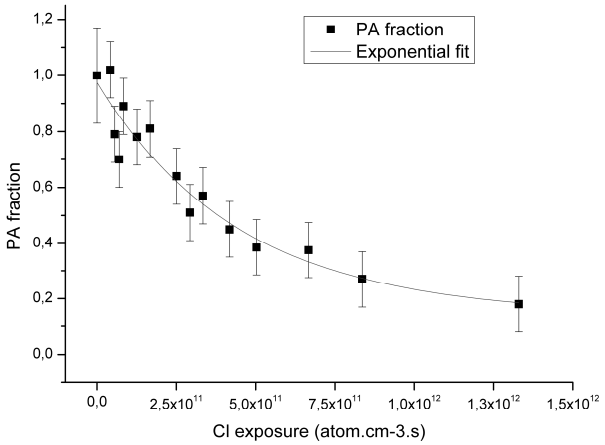

Figure 1. Experimental data (squares) and exponential fit (line) of PA decay as function of chlorine exposure in presence of O_2.

Results coming from experiments realized with O_2 allow us to observe products relevant with the detected compounds in the tropospheric particulate matter. We have observed the formation of HCl, CO and CO_2 in the gas-phase, while, in the particulate phase, oxocarboxylic acids (OXA) and dicarboxylic acids (DCA) are identified by GC/MS. Formation of alcohols and monocarboxylic acids are also suspected.

Finally, we have highlighted that there is a significant fragmentation and functionalization of the fatty acids by oxidation initiated by radicals. This leads to the volatilization of oxygenated low-molecular weighted organic compounds in the atmosphere and the formation of OXA and DCA in the condensed phase, species which have been indentified in particulate matter sampled in a large number of environmental conditions (urban, costal, remote marine, remote continental) (Mkoma and Kawamura 2013). Further research is needed to evaluate whether the functionalization of the primary organic matter and the formation of more polar compounds in the particle lead to the modification of the hygroscopicity of the particle.

Marty, J. C., A. Saliot, et al. (1979). J. Geophys. Res. **84**(C9): 5707-5716.

Mkoma, S. L. and K. Kawamura (2013). Atmos. Chem. Phys. **13**(4): 2235-2251.

Spicer, C. W., E. G. Chapman, et al. (1998). Nature **394**(6691): 353-356.

Characterization and interaction between bacterial community and chemical composition of Particulate Matter in two areas of Po Valley

E. Innocente[1], G. Rampazzo[1], S. Squizzato[1], V. Bertolini[2], A. Franzetti[2],I. Gandolfi[2], G. Bestetti[2]

[1]Department of Environmental Sciences, Informatics and Statistics - University Ca' Foscari, Venice, 30123, Italy
[2]Department of Earth and Environmental Sciences (DISAT) - University of Milano-Bicocca, Milan, Italy
Keywords: PM_x, bioaerosol, chemical composition
Presenting author email: elena.innocente@unive.it

At present many of studies are focused on chemical composition, source apportionment, and health effect of atmospheric particulate matter (Pope and Dockery, 2006, Heinrich et al., 2012).
Recently, there is an increasing attention on the bioaerosol and on the characterization of the bacterial population associated to particulate matter especially due to the presence of endotoxins and pathogenic bacteria that are of great concern for their potential harmful effects (Mueller- Annelin et al., 2004, Peccia et al., 2008).
However the relationship between chemical composition and biological fraction has been poorly investigated. Therefore the aim of this study is to disclose a connection between those different approach of aerosols study.

Sampling sites were located in two different areas of the Po Valley, the most industrialized and urbanized area of Italy. Three sites were located in the Venice area, a coastal site influenced by the presence of the lagoon and industries, in the eastern part of the Po Valley. The last one is located in Milan a polluted area in the middle of the Valley.

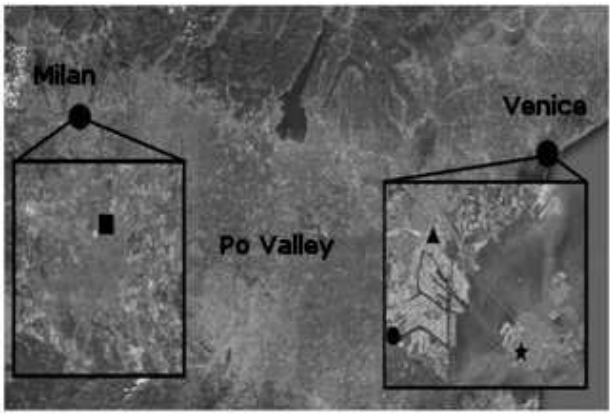

Figure 1. Sampling site location.

PM_{10} and total suspended particulate (TSP) samples were collected on quartz fiber filters (Ø 100 and 150 mm) using high volume samplers durind 24-hours sampling events distributed along five seasonal periods in 2011 and 2012 (April 2011, July 2011, October 2011, January 2012, March-April 2012) to evaluate seasonal variability.
Meteorological parameters were also collected during the sampling campaign

The filters were cut in two portions for the analyses.
The first part was used for the microbiological analyses: DNA was extracted from the quartz fiber filters and the bacterial hypervariable region V5-V6 of gene 16S rRNA was amplified with barcoded primers to study the bacterial community composition in sampling areas.
The second part was further spliced in two parts and used for chemical analyses:

- water soluble inorganic ions (WSIIs) were extracted by ultrasonic method and analyzed by ion chromatography (Na^+, NH_4^+, K^+ Mg^{2+}, Ca^{2+}, F^-, Cl^-, NO_3^-, SO_4^{2-}) (Squizzato et al, 2012).
- the second part was digested by microwave assessed digestion and elements (Al, Fe, Ca, Mg, K, S, Ti, Cr, Ni, Mn, V, Zn, Cu, Ba, As, Ag, Cd, Pb, Sb, Co) were analyzed by ICP-MS and ICP-OES.

The relationship between chemical composition, bacterial community and meteorological parameters will be investigated by statistical methods. The correlation between cytotoxic elements in air particulate matter that can affect bacterial taxon composition, and other elements or ions that can enhance or reduce bacterial concentration will be particularly considered.

The species composition of bacterial communities and their correlation with seasons and meteorological conditions (e.g. wind speed and direction, temperature) will be also investigated.

Heinrich, J., Thiering, E., Rzehak, P., Krämer, U., Hochadel, M., Rauchfuss, K.M., Gehring, U., Wichmann, H. (2013) *Occup. Environ. Med.* 2013;**70**, 179–186.

Mueller-Anneling, L., Avol E., Peters, J.M., Thorne, P.S. (2004). *Environ. Health Perspect.* **112**, 583–588.

Peccia, J., Milton, D. K., Reponen, T., Hill, J., (2008). *Environ. Sci. Technol.*, **42 (13)**, 4631–4637.

Pope III, C.A., Dockery, D.W., (2006). *J. Air Waste Manage. Assoc.* **56**, 709–742.

Squizzato, S., Masiol, M., Innocente, E., Pecorari, E., Rampazzo, G., Pavoni, B., 2012., *J. Aerosol. Sci.* **46**, 64–76.

Raman Microspectriscopic Identification and Characterization of Individual Airborne Volcanic Ash Particles

N. P. Ivleva[1], S. Huckele[1], B., Weinzierl[2], C., Haisch[1], T., Baumann[1], R., Niessner[1]

[1]Technische Universität München (TUM), Institute of Hydrochemistry, Chair for Analytical Chemistry, Marchioninistr. 17, Munich, D-81377, Germany
[2]Deutsches Zentrum für Luft- und Raumfahrt (DLR), Institut für Physik der Atmosphäre, Oberpfaffenhofen, D-82234, Germany
Keywords: volcanic ash, particle identification, characterization, Raman Microspectroscopy (RM)
Presenting author email: Natalia.Ivleva@ch.tum.de

Volcanic eruptions can have significant impact on climate, public health and air traffic safety. During the eruption of the volcano Eyjafjalla in Iceland (63.63° N, 19.62° W, 1666 m a.s.l) in April/May 2010, volcanic ash (VA) plumes were ejected into the atmosphere up to 9 km a.s.l. (Sigmundsson *et al.* 2010) and distributed over Europe, which ceased air traffic in 23 European countries for several weeks. Different methods for the analysis of chemical composition and structure of VA were applied during the last three years (Gasteiger *et al.* 2011; Gislason *et al.* 2011; Schumann *et al.* 2011; Weber *et al.* 2012), however, to our best knowledge, no work concerning identification and/or characterization of individual airborne VA particles from Eyjafjalla (or from other volcanoes) using Raman Microspectroscopy (RM) was published. RM, which is based on the effect of an inelastic light scattering by molecules, provides fingerprint spectra and allows non-destructive distinction of a wide range of chemical substances in air particulate matter with the spatial resolution of an optical microscope (Ivleva *et al.* 2007).

Samples of fresh and aged airborne VA particles suitable for single-particle RM analysis were collected during aircraft research flights (Schumann *et al.* 2011), operated by "Deutsches Zentrum für Luft- und Raumfahrt" (DLR) on May 2th (from Keflavik to Stornoway; top part of the fresh plume over the North Atlantic) and May 18th (aged ash plume survey over Germany and North Sea). In addition, aerosol samples were collected at ground level in an urban setting at the Institute of Hydrochemistry in Munich (TUM), using the Electrical Low Pressure Impactor (ELPI). Furthermore, volcanic ash particles taken at the ground near the eruption (June, 2010) and basaltic rock were studied by RM. Particle size and morphology, Raman patterns (revealing mineral composition and structure), and the particle stability with respect to the laser beam intensity were taken into account. We analyzed similarities between Eyjafjalla VA particles, collected at the different sampling sites, and compared them with the spectra of more than forty glassy and crystalline minerals (SpecID, Horiba Scientific) by applying cluster analysis (CA), in order to achieve information on structure and composition of volcanic ash.

Figure 1 shows representative VA particles from fresh (fp) and aged (ap) plumes, the corresponding Raman spectra, and spectra of some reference compounds. The fp and ap VA particles are brownish and can change color and shape when they melt in the focus of the intense excitation laser beam. The particles exhibit similar spectral pattern with relatively broad bands near 310, 390, 415, 540, and 720 cm^{-1}, suggesting the presence of different minerals with rather disordered crystalline structure (Ivleva *et al.* 2013). A very broad band, which extends from ca. 200 cm^{-1} to ca. 700 cm^{-1}, is typical for glassy structures, such as SiO_2 glasses. We can assume a complex structure of VA particles, where different mineral phases are embedded in glassy matrix. Slight differences in the spectra of fresh and aged VA particles suggest variable proportions of the different minerals, partial precipitation, or chemical aging of VA during the transport. In addition, soot, sodium nitrate and titanium dioxide particles were found in aged plumes and particular matter sampled on ground level, indicating anthropogenic influence. These results show that RM is indeed an effective method for identification and chemical characterization of individual airborne volcanic particles.

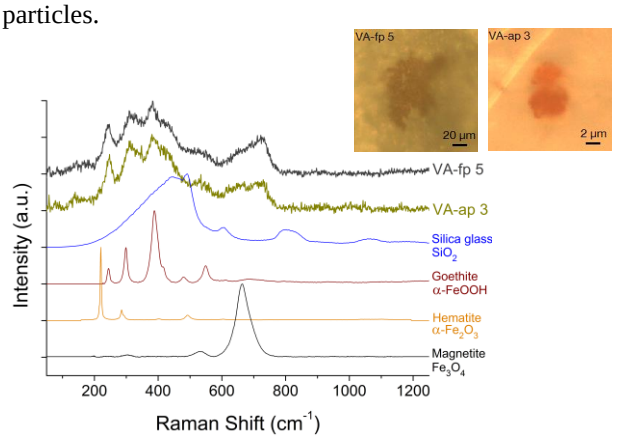

Figure 1. Optical microscope images of VA particles from fresh (fp) and aged (ap) plumes, corresponding spectra of VA and reference compounds.

Gasteiger, J., Gross, S., Freudenthaler, V., Wiegner, M. (2011) *Atmos. Chem. Phys.* **11**, 2209-2223.
Gislason, S. R., Hassenkam, T., Nedel, S., Bovet, N., Eiriksdottir, E. S., Alfredsson, H. A., Hem, C. P., *et al.* (2011) *Proc. Natl. Acad. Sci. U. S. A.* **108**, 7307-7312, S7307/7301-S7307/7303.
Ivleva, N. P., Huckele, S., Weinzierl, B., Niessner, R., Haisch, C., Baumann, T. (2013) *Anal. Bioanal. Chem.*, submitted.
Ivleva, N. P., McKeon, U., Niessner, R., Pöschl, U. (2007) *Aerosol Sci. Technol.* **41**, 655-671.
Schumann, U., Weinzierl, B., Reitebuch, O., Schlager, H., Minikin, A., Forster, C., Baumann, R., *et al.* (2011) *Atmos. Chem. Phys.* **11**, 2245-2279.
Sigmundsson, F., Hreinsdottir, S., Hooper, A., Arnadottir, T., Pedersen, R., Roberts, M. J., Oskarsson, N., *et al.* (2010) *Nature* **468**, 426-430.
Weber, K., Eliasson, J., Vogel, A., Fischer, C., Pohl, T., van Haren, G., Meier, M., *et al.* (2012) *Atmos. Environ.* **48**, 9-21.

On the oxidation of gaseous iodine at elevated temperatures

T. Kärkelä[1], J. Holm[2], A. Auvinen[1], C. Ekberg[2] and J.K. Jokiniemi[1,3]

[1]VTT Technical Research Centre of Finland, Emission Control, Espoo, FI-02044 VTT, Finland
[2]Chalmers University of Technology, Nuclear Chemistry, Göteborg, SE-41296, Sweden
[3]University of Eastern Finland, Environmental Science, Kuopio, FI-70211, Finland
Keywords: iodine, ozone, radiation
Presenting author email: Teemu.Karkela@vtt.fi

The aim in this study was to examine the oxidation of gaseous inorganic and organic iodine when exposed to gaseous ozone and UV (c-type) radiation. The experiments were conducted with EXSI-CONT (EXperimental Studies on Iodine chemistry – CONTainment) facility. Gaseous iodine was exposed to UV radiation with a radiation wavelength maximum at 185 nm, which is able to generate ozone (O_3) from air efficiently. Additional ozone was produced with an ozone generator. The oxygen to nitrogen ratio and the humidity of the carrier gas was varied in the tests as well. The experiments were conducted at 50 °C, 90 °C and 120 °C. The residence time of the gas flow inside the facility was varied from 1.75 s to 7 s.

The formation and growth of the iodine containing aerosol particles was characterised online with Scanning Mobility Particle Sizer (SMPS), Electrical Low Pressure Impactor (ELPI), Condensation Particle Counter (CPC) and Tapered Element Oscillating Microbalance (TEOM) devices. During the tests the speciation of gaseous reaction products was measured using Fourier Transform Infra-Red analyser (FTIR). After the tests, the concentration of gaseous and particulate iodine fractions was quantified with Inductively Coupled Plasma Mass Spectrometry (ICP-MS). The size, morphology and elemental composition of particles was also analysed using Scanning Electron Microscopy coupled with Energy-Dispersive X-ray spectroscopy (SEM-EDX).

The formation of reaction products was very fast when gaseous iodine was exposed to UV radiation or ozone. The diameter of the formed iodine oxide particles, measured in the gas phase, ranged from dozens to a few hundred of nanometres. The colour of iodine oxide particles formed at 100 °C, and then collected on a plane filter, was observed to be light/yellow. The particles were most likely a mixture of I_2O_4 (diiodine tetroxide) and I_2O_5 (diiodine pentoxide). The formation of I_2O_5 is expected to be the dominant reaction at dry conditions when temperature exceeds 100°C. When the samples were exposed to air, they reacted with the humidity and their colour changed to purple/dark brown. This reaction was very fast, because the diameter of the particles was very small. The uptake of humidity decomposed the IOx particles to iodic acid (HIO_3) and elemental iodine (I_2) (Dählie, 1964b; Chase, 1996). The diameter and mass concentration of particles increased when the residence time, relative humidity, radiation intensity, ozone concentration or the temperature of the facility were increased. A model on the oxidation of elemental iodine was derived.

The formation of gaseous reaction products was studied as well. The most important detected species, resulting from the decomposition of gaseous CH_3I, were methanol (CH_3OH) and formaldehyde (CH_2O). When the concentration of ozone was very high, significant formation of secondary gaseous reaction products was observed, e.g. formic acid (CH_2O_2) and methyl formiate ($HCOOCH_3$).

When the coolant of fuel in a nuclear power plant (NPP) is lost, the melting of overheated fuel rods will take place. As a consequence, the vaporized fission products (FPs) are transported through the primary circuit of nuclear reactor and released through a break in the circuit into the gas phase of containment building. There FPs, such as gaseous iodine, are exposed to air radiolysis products as well as to the radiation - such as alpha, beta, gamma and X-ray - itself. This may lead to oxidation of gaseous iodine and subsequent formation of iodine containing aerosol particles. As radiotoxic iodine constitutes one of the major hazards of the possible source term (e.g. Fukushima Daiichi nuclear accident), it is of interest to understand the behavior of iodine in the conditions of severe accident.

This work was supported by the SAFIR2010, SAFIR2014 and NKS-R programs.

Dählie, G. and Kjekshus, A. (1964b) *Acta Chemica Scandinavica* **18(1)**, 144–56.
Chase, M. W. (1996) *Journal of Physical and Chemical Reference Data* **25(5)**, 1297–1340.

Hygroscopicity of nucleated nanoparticles in the presence of sulfuric acid and organics

Jaeseok Kim[1], Helmi Keskinen[1], Petri Vaattovaara[1], Pasi Miettinene[1], Jorma Joutsensaari[1], Annele Virtanen[1], and CLOUD collaboration

[1]Department of Applied Physics, University of Eastern Finland, Kuopio campus, 70211 Kuopio, Finland
Keywords: Hygroscopicity, nanoparticles, CLOUD, nano-HTDMA
Presenting author email: jaeseok.kim@uef.fi

Atmospheric aerosols are emitted from natural and anthropogenic sources (i.e., primary aerosols) and are generated by gas-to-particle conversion processes (i.e., secondary aerosols). They influence Earth's climate change either by scattering and absorbing incoming sunlight or by acting as cloud condensation nuclei for cloud formation. In addition, they can cause adverse human heath effect and participate in various heterogeneous reactions with vapours in the atmosphere. Especially, hygroscopicity, the ability of water uptake by particles, is important properties to indirectly estimate chemical composition in particles. In this study, we focus on hygroscopicity of nucleated nanoparticles (10, 15, and 20 nm) produced by CLOUD (Cosmic Leaving Outdoor Droplets) experiments at CERN (Kirkby et al 2011).

A nano-tandem differential mobility analyzer (nano-TDMA) was applied to measure hygroscopicity of nanoparticles in the presence of sulfuric acid and organics during CLOUD 7 experiment. Generated particles inside CLOUD chamber were dried and then particles having certain size were selected with differential mobility analyzer (DMA). The selected particles were introduced into aerosol humidifier. Relative humidity in the humidifier was around 90%. Size distibution of humidified particles were determined with another DMA and condensation particle counter (CPC; TSI 3785).

In this way, we can determine hygroscopic growth factor (HGF) that is the ratio of geometric mean diameter (GMD) of size dependent nanoparticles at humidified condition to that at dry condition. And hygroscopic parameter κ can be derived from Petters and Kreidenweis (2007) with following equation:

$$\kappa = \left(HGF^3 - 1\right) \cdot \left[\frac{1}{S} \cdot \exp\left(\frac{4\sigma_w M_w}{RT\rho_w d_{dry} HGF}\right) - 1\right]$$

where S, σ_w, M_w, ρ_w, R, and T are saturation ratio, water surface tension at room temperature, molecular weight of water, density of liquid water, ideal gas constant, and room temperature, respectively. Also the organic volume fraction (ε_o) in the selected nanoparticles was calculated assuming two compounds consisting of organic and inorganic sulfates (Keskinen et al 2012)

$$\varepsilon_O = \frac{\kappa - \kappa_i}{\kappa_o - \kappa_i}$$

where κ is measured values, κ_o, κ_i are the hygroscopicity parameter for organic and inorganic sulfate, respectively.

The hygroscopicity of nanoparticles in the presence of sulfuric acid and organics with OH scavenger was smaller than those without OH scavenger in the chamber regardless of experimental conditions. It indicates that hygroscopicity of nanoparticles is enhanced by OH oxidant.

We would like to thank CERN for supporting CLOUD with important technical and financial resources, and for providing a particle beam from the CERN Proton Synchrotron. This research has received funding from the EC Seventh Framework Programme (Marie Curie Initial Training Network "CLOUD-ITN" no. 215072, MC-ITN "CLOUD-TRAIN" no. 316662, and ERC-Advanced "ATMNUCLE" grant no. 227463), the German Federal Ministry of Education and Research (project nos. 01LK0902A and 01LK1222A), the Swiss National Science Foundation (project nos. 200020_135307 and 206620_130527), the Academy of Finland (Center of Excellence project no. 1118615), the Academy of Finland (135054, 133872, 251427, 139656, 139995, 137749, 141217, 141451), the Finnish Funding Agency for Technology and Innovation, the Nessling Foundation, the Austrian Science Fund (FWF; project no. P19546 and L593), the Portuguese Foundation for Science and Technology (project no. CERN/FP/116387/ 2010), the Swedish Research Council, Vetenskapsrådet (grant 2011-5120), the Presidium of the Russian Academy of Sciences and Russian Foundation for Basic Research (grants 08-02-91006-CERN and 12-02-91522-CERN), and the U.S. National Science Foundation (grants AGS1136479 and CHE1012293).

Kirkby, J., Curtius, J., Almeida, J., Dunne, E., Duplissy, J. et al. (2011) Nature 476, 429–433.

Petters, M.D. and Kreidenweis, S.M. (2007) Atomos. Chem. Phys 7, 1961-1971.

Keskinen, H., Virtanen, A., Joutsensaari, J., Tsagkogeorgas, G., Duplissy, J. et al (2012) Atmos. Chem. Phys. Discuss. 12, 31071-31105.

Characterization of particulate matter in Kraków, Poland.

M. Kistler[1], L. Samek[2], K. Styszko[3], K. Szramowiat[3], L.Furman[2], M. Gerhardus[1] and A. Kasper-Giebl[1]

[1]Institute of Chemical Technologies and Analytics, Vienna University of Technology, Vienna, A1060, Austria
[2]Faculty of Physics and Applied Computer Science, AGH University of Science and Technology, Kraków, 30-059, Poland
[3]Department of Coal Chemistry and Environmental Sciences, AGH University of Science and Technology, Kraków, 30-059, Poland
Keywords: aerosols, Poland, benzo(a)pyrene, Hg(p).
Presenting author email: magdalena.kistler@tuwien.ac.at

Airborne particulate matter poses a significant problem in South Poland. Kraków is classified at the eighth place among 575 most PM2.5-polluted cities and at the 145th place among 1100 most PM10-polluted cities listed in the WHO ranking (WHO, 2013). According to its basin location the city often suffers under temperature inversion causing high pollution periods. Continuous air quality monitoring and several studies conducted already in the region showed that residential solid fuel combustion and traffic have a dominant influence on particulate matter burden (e.g., Larsen *et al*., 2007), being responsible for increased concentration of toxic and noxious chemicals. However, the available information is not persuasive enough to become a catalyst for efficient policies reducing the emissions and lowering the human exposure to hazardous substances.

The current study combines two sampling campaigns (February 2011 – PM10 and February 2013 – PM10 and PM2.5). Particulate matter was collected in the centre of Krakow (Aleja Mickiewicza, AGH, University of Science and Technology) with low volume samplers operated with daily (24h) intervals. Quartz fibre filters (Pall, 47mm) were used for sampling, field blanks were collected.

Particulate matter mass was measured gravimetrically under stable humidity and temperature conditions. Circular aliquots were punched out of the filters in order to conduct chemical analyses. Analytes and the respective aerosol sources are listed in Table 1.

Table 1. Characteristic sources their chemical fingerprints and analytical methods.

Source	Component group	Method
Combustion	EC, OC	Thermal-optical
RWC, BA	Saccharides	HPAE PAD
SA	Inorganic anions	HPAE CD
SA	Inorganic cations	HPCE CD
Combustion	PAHs	GC-MS
Combustion, Industry	Selected elements	XRF
Combustion, Industry	Particulate Hg	CV-AAS

RWC = residential wood combustion, BA = biological aerosol, SA = secondary aerosol, EC = elemental carbon, OC = organic carbon, PAHs = polycyclic aromatic hydrocarbons

The aim of the study is to chemically characterize PM10 and PM2.5 as well as to quantify aerosol sources being locally relevant. The comparison of two winter periods will help to assess the pollutants which were not reduced over a period of two years.

The source apportionment method used for Kraków is based on the macro-tracer model derived in Austria (Puxbaum *et al*., 2005). This model is taking advantage of the existence of source specific compounds and stability of their relations in emission and ambient air.

The winter PM10 concentrations observed during the sampling period in winter 2011 exceeded constantly the admissible threshold of 50 µg/m³. The similar trend is expected for 2013, as no powerful reduction measures have been applied in the city since that time.

In 2011 the highest mass contribution was found for carbonaceous aerosols (50%), followed by inorganic secondary aerosols (30%). Levoglucosan (anhydrous saccharide used to assess residential wood burning impact) concentrations did not exceed 1% of PM10. Analysed PAHs contributed only 0.1% to PM10 mass, but benzo(a)pyrene (BaP) concentrations were around 10 ng/m³ (being 10 times higher than the annual limit value). Residential coal combustion is expected to be the most prominent BaP source.

This work is an ongoing cooperation between Vienna University of Technology and AGH University of Science and Technology, Kraków. We acknowledge the work of students of both institutions involved in the study. Work was financially supported by the International Atomic Energy Agency (project RER/1/008), the Polish Ministry of Science and Higher Education grants for Scientific Research and KICCoalGas “Development of a Coal Gasification Technology for High Efficiency Fuel and Power Production”.

Larsen, B. R., Juninnen, H., Astorga, C., Cancelinha, J., Douglas, K., Duvalle, R., Jiménez , J., Niedziele , J., Paradiz , B., Rey, M., Stanczyk, K., Tsakovski, S., Viana, M., Wåhlin, P. (2007) *Geophysical Research Abstracts*, **9**, EGU.

Puxbaum, H., Kasper-Giebl, A., Bauer., H., (2005). *Chemistry, Transport and Impact of Atmospheric Pollutants with Focus on Fine Particles*, Andechs, Germany.

WHO (2013). Available on-line: http://www.who.int/phe/health_topics/outdoorair/databases/en/index.html, accessed on 25.02.2013.

Molecular composition of PM2.5 aerosols from Cork Harbour, Ireland using ultrahigh resolution mass spectrometry

I. Kourtchev[1], I.P. O'Connor[2], S. Fuller[1], K. Kristenen[3], W. Maenhaut[4,5], J.C. Wenger[2], J.R. Sodeau[2], M. Glasius[3], and M.Kalberer[1]

[1]Department of Chemistry, University of Cambridge, Cambridge, CB2 1EW, UK
[2]Department of Chemistry and Environmental Research Institute, University College Cork, Cork, Ireland
[3]Department of Chemistry, Aarhus University, Aarhus, DK-8000, Denmark
[4]Dept. of Pharmaceutical Sciences, University of Antwerp (UA), Universiteitsplein 1, 2610 Antwerpen, Belgium
[5]Department of Analytical Chemistry, Ghent University, Krijgslaan 281, S12, B-9000 Gent, Belgium

Keywords: SOA, Ultra-High Resolution Mass Spectrometry, Molecular composition.

Presenting author email: ink22@cam.ac.uk

Aerosol particles have a profound effect on the radiative balance of the atmosphere and human health (Kanakidou et al., 2005). Organic compounds are important constituents of fine particulate matter in the troposphere; however, due to the complexity of the aerosol matrix, their comprehensive analysis at a molecular level is a long standing issue. In this study, we applied direct infusion nano-electrospray (nanoESI) ultrahigh resolution mass spectrometry (UHR-MS), which allows the determination of hundreds of individual constituents at once (Nizkorodov et al., 2011), for the analysis of ten$PM_{2.5}$ aerosol samples collected from Tivoli Industrial and Dock Estate (Cork, Ireland) during 9-17 September, 2011.

All aerosol samples were analysed for organic carbon (OC) and elemental carbon (EC) using a thermal optical transmittance (TOT) technique. Depending on the OC load of the aerosol sample, a portion of the filter was extracted in methanol, filtered, and reduced by volume to approximately 100 μL. The extracts were analysed using an LTQ Orbitrap Velos MS fitted with a chip-based electrospray ion source, TriVersa NanoMate®. The mass spectra were recorded in negative mode over the mass ranges *m/z* 100-650 and 150-900 with a mass resolving power of 100,000 (m/Δm) at *m/z* 400. Background peaks were subsequently eliminated by subtraction of peaks present in blank samples. The remaining peaks were assigned probable empirical formulae applying several conservative rules and constraints (e.g., valence rule, double bond equivalent, isotopic ratios) and assuming that ions contain only ^{12}C, ^{13}C, ^{1}H, ^{16}O, ^{14}N, ^{32}S, and ^{34}S. In addition, selected samples were screened for organic acids and organosulphates using liquid chromatography LC/ESI-qTOF MS.

Depending on the sample, 400-640 elemental formulae were identified using direct infusion UHR-MS and attributed to organic species with molecular weights below 450 Da. The assigned formulae were grouped into four subgroups: CHO, CHOS, CHON and CHONS with CHO (average 63% of the total formulae) being the most frequently apportioned subgroup, followed by CHON (25%), CHOS (9%), and CHONS (3%). A rather large number of identified organonitrates indicates anthropogenic influence on the aerosol composition at Tivoli Industrial and Dock Estate site. O/C and H/C ratios of the aerosols were on average 0.45 and 1.3, respectively and remained constant throughout the sampling period.

Kendrick Mass Defect and Van Krevelen approaches were used to identify compound classes and mass distributions of the detected species. A very high number of aromatic like compounds that typically have low H/C ($\leq$1.0) and O/C ratios (($\leq$0.5) and aliphatic compounds with high H/C ratios ($\geq$1.5) and low O/C ratios ($\leq$0.5) were observed in all samples. These findings suggest that the sampling site is affected by both anthropogenic and biogenic activities. The majority of the species had carbon oxidation state (OSc) between – 1.5 and +1 with 20 or less carbon atoms, suggesting that they are semi- and low-volatile organic compounds corresponding to both 'fresh' and 'aged' aerosol produced by multistep oxidation reactions. A very large fraction of ions had OSc<-1 that is characteristic for primary biomass burning aerosol, indicating that even during summer burning of domestic fuel material is important.

LC/MS analysis of the aerosol samples allowed identification of a few dicarboxylic acids and organosulphates which possibly originated from combined anthropogenic and biogenic sources.The results of this work demonstrate that the studied site is a very complex environment affected by a variety of industrial and domestic activities and natural sources, which is reflected by the unique aerosol composition representing many emission sources.

The work at the University of Cambridge was supported by a Marie Curie Intra-European fellowship (project # 254319).

Kanakidou, M., Seinfeld, J. H., Pandis, Barnes, I., Dentener, F. J., Facchini, M. C., van Dingenen, R., Ervens, B., Nenes, A., Nielsen, C. J., Swietlicki, E., Putaud, J. P., et al. (2005). *Atmos. Chem. Phys.*, **5**, 1053-1123.

Nizkorodov, S.A., Laskin, J., and Laskin, A. (2011). *Phys. Chem. Chem. Phys.*, **13**, 3612-3629.

New experimental tools for characterization of nucleation and reactivity in small aerosols

J. Lengyel[1,2], M. Fárník[1], P. Slavíček[2] and T. Zeuch[3]

[1]J. Heyrovský Institute of Physical Chemistry, Academy of Science of the Czech Republic, Prague, Czech Republic
[2]Department of Physical Chemistry, Institute of Chemical Technology, Prague, Czech Republic
[3]Institut für Physikalische Chemie, Georg-August-Universität, Göttingen, Germany

Keywords: nitric acid, solvated electron, mass spectrometry, nucleation.
Presenting author email: jozef.lengyel@jh-inst.cas.cz

The study of atmospheric aerosols attracts a considerable attention because of its influence on atmospheric chemistry and climate. Perhaps the most famous example is the ozone hole where the polar stratospheric clouds play a key role in the ozone depletion process (Finlayson-Pitts and Pitts, 2000). The atmospheric aerosol particle generation starts with growing of small aerosols and ice nanoparticles via nucleation and uptake of various atmospheric molecules on these particles. Therefore the uptake processes have recently been investigated in our laboratory (Lengyel, Kočišek *et al*, 2012). The dissolution of water with hygroscopic species such as H_2SO_4 and HNO_3 substantially speeds up the aggregation leading to the homogeneous heteromolecular nucleation of clouds in troposphere and stratosphere.

There are several experimental methods based on mass spectrometric techniques that can provide comprehensive information on the chemical composition, size, morphology and phase of aerosols (Laskin *et al*, 2012, Kolb and Worsnop, 2012). In the presented work, the nucleation of mixed nitric acid/ water aerosols is investigated by two different mass spectrometric techniques providing complementary information. In both experiments the small aerosol particles were produced by supersonic expansion of saturated nitric acid vapor seeded in buffer gas, and mass spectra were investigated by a reflectron time of flight mass spectrometer. The aerosols were ionized by electrons in one case, while sodium doping followed by UV photoionization was implemented in the other experiment.

This unique combination of both techniques (shown in fig. 1) reveals that only aerosols containing at least one acid molecule are generated, i.e. the acid molecule serves as the nucleation centre in the expansion. The experiments also suggest that at least four water molecules are needed for HNO_3 acidic dissociation. The small aerosols are undoubtedly generated, as proved by electron ionization; however, they are not detected by the Na doping due to a fast charge-transfer reaction between the Na atom and HNO_3. It was also confirmed by the *ab initio* calculations. These points to limitations of the Na doping recently advocated as a general method for atmospheric aerosol detection. On the other hand, the combination of the two methods introduces a tool for detecting molecules with sizable electron affinity in aerosols (Lengyel, Pysanenko *et al*, 2012).

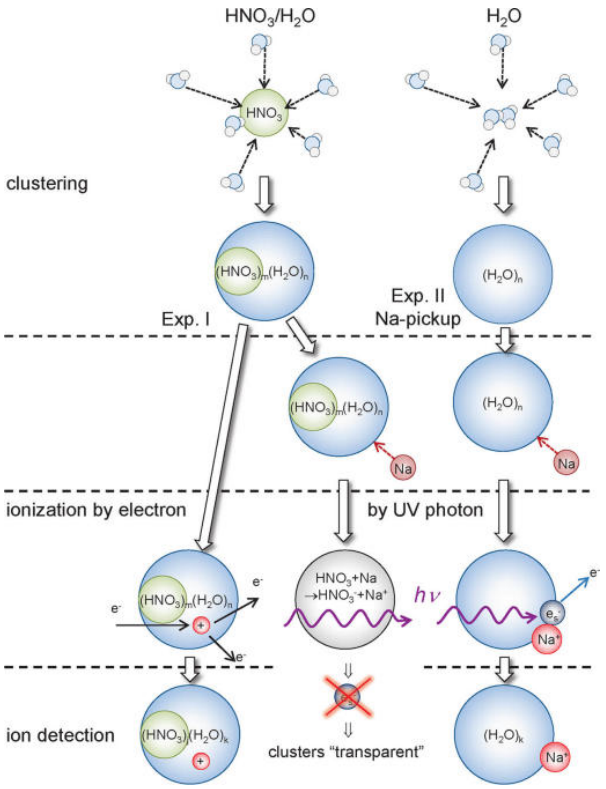

Figure 1. Schematic illustration of processes observed in the present aerosol experiments

This work was supported by the Grant Agency of the Czech Republic under grants P208/11/0161 and 203/09/0422.

Finlayson-Pitts, B. J., Pitts, J. N. (2000) *Chemistry of the upper and lower atmosphere*, Academic Press, San Diego.

Kolb, C. E., Worsnop, D. R. (2012) *Annu. Rev. Phys. Chem.* **63**, 471-491.

Laskin, A., Laskin, J. and Nizkorodov, S. A. (2012) *Environ. Chem.* **9**, 163-189.

Lengyel, J., Kočišek, J., Poterya, V., Pysanenko, A., Svrčková, P., Fárník, M., Zaouris, D. K. and Fedor, J. (2012) *J. Chem. Phys.* **137**, 034304.

Lengyel, J., Pysanenko, A., Kočišek, J., Poterya, V., Pradzynski, C. C., Zeuch, T., Slavíček, P. and Fárník, M. (2012) *J. Phys. Chem. Lett.* **3**, 3096-3101.

NOx Effects on Secondary Organic Aerosol Formation of Biogenic and Anthropogenic Organic Gases

J.H. Park[1], K.M. Jung[1], W.G. Woo[1], W.K. Jo[1], and H.J. Lim[1]

[1]Department of Environmental Engineering, Kyungpook National University, Daegu, 702-701, South Korea
Keywords: secondary organic aerosol, NO_x effect, biogenic organic, anthropogenic organic.
Presenting author email: hjlim@knu.ac.kr

Organic aerosol consists of a large fraction of atmospheric fine aerosol and shows important roles in climate change, visibility degradation, adverse public health (Pöschl, 2005). NO_x is strongly associated with secondary organic aerosol (SOA) formation in atmospheric photochemical reactions (Kroll and Seinfeld, 2008). NO_x effects are crucial in clear understanding of SOA formation and reliable SOA prediction. In this study, NO_x effects were investigated for biogenic and anthropogenic reactive organic gases (ROGs) as a function of ROG/NO_x and NO_2/NO_x ratios. α-Pinene and d-limonene were examined as a representative of biogenic ROGs. Toluene and m-xylene were selected as a representative of anthropogenic ROGs.

An indoor smog chamber with 7.5 m^3 Teflon bag was used in the photochemical SOA formation. SOA formations were conducted by photochemical reaction in the absence of seed particles at dry condition (<5% RH) of room temperature (~25℃). Hydrogen peroxide was used as OH radical source in the OH radical initiated SOA formation reactions. The photochemical reaction was began by irradiating the reaction mixture of ROG, NO_x, and H_2O_2.

d-Limonene with 2 double bond showed much higher SOA yields of 12.0%-88.4% relative to 4.3%-43.2% of α-pinene with a double bond. SOA yields were ranged from 2.8%-9.4% and 1.1%-13.3% for toluene and m-xylene, respectively. The wide span of SOA yield was influenced by ROG/NO_x ratio and NO_2/NO_x ratio. At both low and high NO_2/NO_x ratios, SOA yield peaked at ROG/NO_x ratio around 0.77 and 1.10 for α-pinene and d-limonene, respectively. It decreased at lower and higher ROG/NO_x ratios with abrupt decrease below the critical ROG/NO_x ratio. For d-limonene, decreasing NO_2/NO_x ratio significantly suppressed SOA formation at both low and mid ROG/NO_x ratios. In case of α-pinene, the effect of NO_2/NO_x ratio was negligible at mid ROG/NO_x ratio, whereas it elevated SOA yield at high NO_2/NO_x ratio of low ROG/NO_x ratio. It was more substantial for d-limonene at low ROG/NO_x ratio. Discrepancies in the NO_x effects are largely affected by the number and position of double bond of α -pinene and d-limonene. SOA yield peaked at ROG/NO_x ratio of 9.5% and 13.3% for toluene and m-xylene, respectively. Toluene exhibited significantly enhanced SOA formation at higher NO_2/NO_x ratio, whereas m-xylene showed minimal influence of NO_2/NO_x ratio.

NO_x effects might be caused by the contribution of reaction route of alkyl peroxy radicals and the resultant volatility distribution of products. Reaction of unsaturated intermediates from ring cleavage reaction with O_3 could also affect the NO_x effect. Time-dependent growth and yield curves were effectively used in the mechanistic understanding of SOA formation. Figure 1 and 2 show time-dependent growth curves of toluene and m-xylene at different ROG/NO_x and NO_2/NO_x ratios..

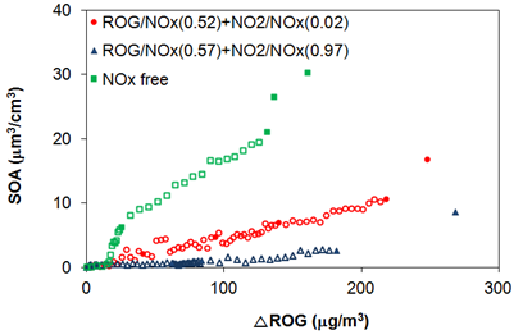

Figure 1. Time-dependent growth curves of toluene as a function of ROG/NO_x and NO_2/NO_x ratios.

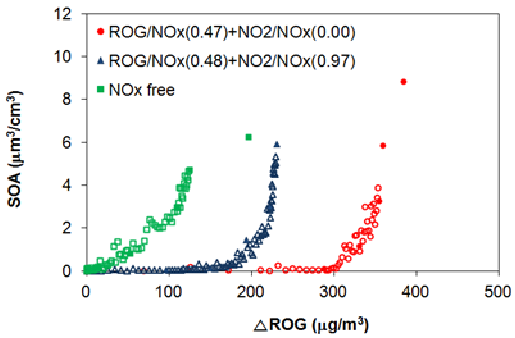

Figure 2. Time-dependent growth curves of m-xylene as a function of ROG/NO_x and NO_2/NO_x ratios.

This work was supported by the National Research Foundation of Korea (NRF) grant funded by the Korea government (MEST) (No. 2011-01350000).

Pöschl, U. (2005) Atmospheric Aerosols: composition, transformation, climate and health effects, *Angew. Chem. Int. Ed.*, 44, 7520 – 7540.

Kroll, J.H. and Seinfeld, J.H. (2008) Chemistry of secondary organic aerosol: Formation and evolution of low-volatility organics in the atmosphere, *Atmos. Environ.*, 42, 3593–3624.

Temporal trends in the atmospheric concentration of selected metals in the PM10 aerosol collected in March-September 2010 at Ny-Ålesund (Svalbard Islands)

M. Malandrino[1], A. Giacomino[1], O. Abollino[1], S. Becagli[2], D. Frosini[2], M. Severi[2], R. Traversi[2], R. Udisti[2]

[1]Department of Chemistry, University of Turin, Torino, Piedmont, 10125, Italy
[2]Department of Chemistry, University of Florence, Sesto Fiorentino, Tuscany, 50019, Italy
Keywords: PM_{10}, Ny Ålesund, metals.
Presenting author email: mery.malandrino@unito.it

The study of the size-distribution and chemical composition of the atmospheric particulate is a topic of ever-increasing interest for the scientific community, since the aerosol was found to have a remarkable effect on both the health of living organisms and, at a larger scale, on the ongoing climate changes.

The Arctic regions, owing to their distinctive environmental properties, are showing to be the first areas affected by the present climatic variations. In this scenario, the study of the chemical composition of atmospheric particulate matter in the polar areas is important to understand the feedback processes between the climate forcing and the environmental responses. For this aim, it is important to know the areas of origin of the atmospheric particulate present in the Arctic regions and the processes that caused its formation.

In this study, the concentrations of main and trace metals in the PM_{10} collected at Ny-Ålesund (Svalbard Islands) during the spring and summer 2010 campaign was determined. From the results obtained it can be concluded that both local and continental sources influence the composition of the Arctic atmospheric particulate matter. Indeed, Svalbard Islands are affected by aerosols coming from the continental areas of North America, North Europe and Asia by long range transport processes, especially occurring in early spring. This seasonal pattern is evident in the PM10 temporal profiles of the majority of the chemical components of the atmospheric particulate, that show higher atmospheric concentrations in March-April.

In the PM_{10} samples collected during the 2010 campaign at Ny Alesund, Na, K, Ca, Al, Zn and Fe are the metals showing the highest concentrations (at ng/m^3 level), while the other elements are present at lower concentrations (few pg/m^3). The enrichment factors, calculated considering Fe as crustal reference, are higher than 100 for Zn, Mo, As, Cd, Hg, Pb and Na, pointing out their different origin (anthropic and sea spray sources). The chemometric investigation on the experimental results shows an evident separation between spring and summer Arctic PM_{10} samples. Principal Component Analysis evidences a strong correlation among Al, Mn, Ti and Fe, as expected for metals mainly coming from crustal sources (both from local inputs and long-range transport). A correlation among As, Cu, Hg, K, Na and Pb is evident. As, Cu, Hg and Pb could be attributed to long range transport of pollutants from anthropized areas in North America and Northern Europe. The correlation with Na and K, markers of sea spray aerosol, could be attributed to common transport processes over large seawater regions. Another PCA factor includes Cr, Ni and V. This factor could be related to emissions from fossil fuel, coal and heavy oil combustion processes.

Among the trace elements, Rare Earth Elements (REEs) deserve a particular relevance because their concentrations, or better their concentration ratios, can be used as fingerprints of continental sources of dust. The rare earth elements have the typical saw-toothed trend with lanthanides having even atomic number in greater amount than those having odd atomic number and a decreasing trend from La to Lu.

PM10 samples show a strong seasonal pattern. All the REEs show very low concentrations in March-April, while their atmospheric load significantly increases in late spring-summer (Figure 1).

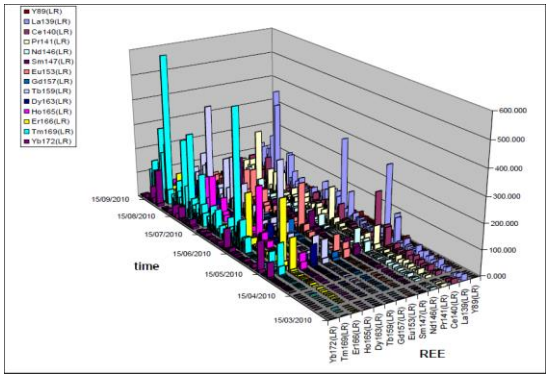

Figure 1. Temporal profile of REEs in NyA PM10.

This evidence could be explained by the higher contribution of local source, more intense after snow melting, with respect to the long-range transport inputs. The different sources can be shown by the temporal trend of the ratio between light-REEs (LREEs: from La to Sm) and heavy-REEs (HREEs: from Eu to Yb). In early spring, the LRREs/HREEs ratio is very high (up to 14 in the late April). Such ratio is much lower (around a background value of 3) in the remaining period, with two exceptions: in early July and in late August. An increasing trend is shown in the fall samples. High LRREs/HREEs ratios should be related to long range transport of dust, more frequent in early spring and occasionally occurring in other periods, while low LRREs/HREEs ratios could attributed to local sources.

This work was supported by Italian Education, University and Research Ministry (MIUR) and by National Research Council (CNR) funds and facilities.

Within-city variability as a tool for source apportionment of trace elements. Application to the Barcelona metropolitan area

M.C. Minguillón[1], M. Cirach[2], G. Hoek[3], B. Brunekreef[3], M. Nieuwenhuijsen[2] and X. Querol[1]

[1]Institute of Environmental Assessment and Water Research (IDAEA), CSIC, Barcelona, 08034, Spain
[2]Centre for Research in Environmental Epidemiology (CREAL), Barcelona, 08003, Spain
[3]Institute for Risk Assessment Sciences and Julius Center for Health Sciences and Primary Care, University Medical Center Utrecht, Utrecht University, Utrecht, 3508TD, The Netherlands
Keywords: metals, sources, Barcelona, urban.
Presenting author email: mariacruz.minguillon@idaea.csic.es

Trace and major elements concentrations in PM_{10} and $PM_{2.5}$ were measured at 20 sites spread in the Barcelona metropolitan area (6 urban background sites, 13 road traffic sites and 1 rural background site). Three 2-week samples per site and size fraction were collected during 2009 using low volume samplers, adding a total of 120 samples. Additionally, a reference site was instrumented similar to the other sites and was used for seasonal correction of the data. Collected samples were analyzed for elemental composition using Energy Dispersive X-ray fluorescence (XRF). The work was performed as part of the ESCAPE project, which aims to investigate long-term effects on human health of exposure to air pollution in Europe.

Elements were found in concentrations within the usual range in Spanish urban areas (Querol et al., 2008). Some elements, such as Al, Na, Ni, S and V were recorded in higher concentrations during the warm period (spring+summer) with respect to the cold period (autumn+winter). Al is associated with mineral matter, which is higher during the warm season due to enhanced soil resuspension due to drier conditions. Na is associated with sea salt, with a typical higher contribution in summer. Ni and V are associated with fueloil combustion, with a contribution typically higher during the warm season. S is assumed to be present as sulphate, higher in summer and lower in winter due to its temperature-dependent particle-gas equilibrium.

Elements found in higher concentration at the traffic sites were: Ba, Cr, Cu, Fe, Mn, Pb, Sn, and Zn, which can then be attributed to the influence of road traffic (including road dust resuspension). On the contrary, some other elements did not show any significant difference between traffic sites and urban background sites, indicating a more regional behaviour: Al, Ca, Cl, K, Mg, Na, Ni, P, Rb, S, Si, Sr, and V.

Some spatial variability, not related to the type of site, was observed for some elements. Thus, Cl and Na concentrations were higher at the sites close to the coastal line, whereas concentrations diminished with increasing distance to the coast, evidencing the sea spray origin of these two species. Ni and V concentrations were highest at the site closest to the port, pointing to the influence of the ship emissions on the ambient concentrations of these two elements (Figure 1 shows average V concentrations as an example). The spatial variation of some other elements needs to be further investigated to be able to conclude on a specific origin.

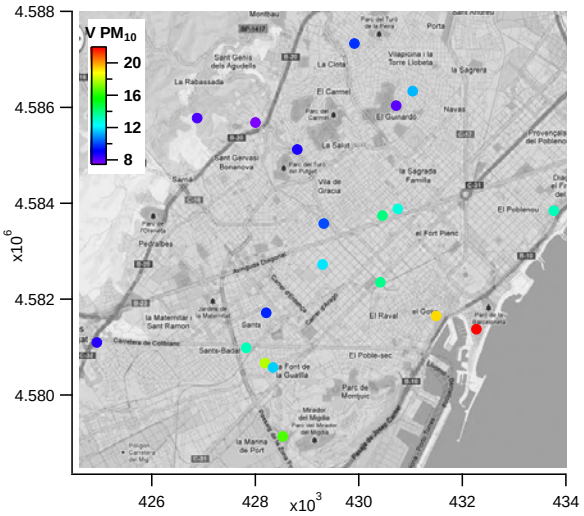

Figure 1. Average vanadium concentrations in PM_{10} at the Barcelona sites during 2009.

On average, the SiO_2/Al_2O_3 ratio was 3.4 in $PM_{2.5}$ and 3.6 in PM_{10}, ranging from 3.0 to 3.7 in $PM_{2.5}$ and from 3.3 to 3.9 in PM_{10} as averages for each of the sites. No significant differences were found for different type of sites indicating that the sources affecting the urban background sites, the traffic sites and the regional background site are either the same or they have the same SiO_2/Al_2O_3 ratio. This experimental ratio will be very useful for future studies, since SiO_2 concentrations had to be estimated based on Al_2O_3 concentrations in several air quality studies, due to the impossibility of analyzing SiO_2 in quartz fibre filters.

This work was funded by the ESCAPE project (European Union's Seventh Framework Programme), and the Generalitat de Catalunya 2009 SGR8. M.C.Minguillón was funded by the JAE-Doc CSIC program, co-funded by the European Social Fund (ESF).

Querol, X., Alastuey, A., Moreno, T., et al. (2008). *Atmos. Environ.* **42**, 3964-3979.

Real time chemical characterization of fine particulate matter in a Spanish regional background site

M.C. Minguillón[1], A. Ripoll[1] , N. Pérez[1], X. Querol[1] and A. Alastuey[1]

[1]Institute of Environmental Assessment and Water Research (IDAEA-CSIC), Barcelona, 08034, Spain
Keywords: ACSM, regional background, organics, chemical composition.
Presenting author email: mariacruz.minguillon@idaea.csic.es

Ambient aerosols have adverse effects on human health, and affect climate, ecosystems, crops, and regional visibility. Fine particulate matter (PM_1, particles with an aerodynamic diameter <1 µm) contains substantial fractions of carbonaceous aerosols and inorganic compounds. Carbonaceous aerosols comprise organic compounds, collectively referred to as organic aerosol (OA), elemental carbon (EC), and carbonates (from mineral dust), although the latter is negligible in submicron aerosol. It is necessary to know the sources of submicron aerosols to design strategies aimed at mitigating their effects. Known sources of carbonaceous aerosols are biomass, biofuel, and waste burning, residential heating, cooking, fossil-fuel combustion (including road traffic emissions), and biogenic emissions.

A forested regional background site located in northeast Spain, 50 km away from Barcelona, was chosen for the present study: Montseny (MSY, 41°46'46"N 02°21'29"E, 720 m a.s.l.). MSY is part of the Aerosols, Clouds, and Trace gases Research InfraStructure (ACTRIS) Network (http://www.actris.net). The Western Mediterranean Basin presents unique atmospheric dynamics regulated by complex climatic and orographic effects which control the concentration, composition and transport of PM. In general, in summertime, local circulation dominates the atmospheric dynamics, favouring the regional accumulation of pollutants and the stratification of polluted air masses. In winter, the inflow of clean Atlantic air masses favours the reduction of pollution levels. However, under anticyclonic conditions, pollution from the coast and valleys is accumulated due to thermal inversions persisting for a few days, and local upslope breezes can bring polluted air masses from the valley towards rural mountainous areas (Pérez et al., 2008).

An Aerosol Chemical Speciation Monitor (ACSM, Aerodyne Research Inc.) was deployed at MSY in June 2012 and sampling is planned to continue for a whole year, according to the ACTRIS schedule, in which a high number of European regional sites will deploy an ACSM for this time period. The ACSM measures non-refractory submicron aerosol distinguishing OA, nitrate, sulphate, ammonium and chloride (Ng et al., 2011). The ACSM was set to measure with a time resolution of approximately 30 min. Mass calibration of the ACSM was carried out regularly by determining the instrument response factor to a known ammonium nitrate calibration aerosol. Moreover, the sulphate response factor was calculated using a known ammonium sulphate calibration aerosol right after an ammonium nitrate calibration, and hence knowing the ammonium response factor. Positive Matrix Factorization (PMF), and complementarily Multilinear Engine (ME2), of the organic mass spectral data matrix will be carried out, providing information on different sources or types of the OA, such as hydrocarbon-like OA (HOA, a surrogate of road traffic emissions), biomass burning OA (BBOA), and oxygenated OA (OOA, a surrogate for secondary OA). A preliminary analysis of the dataset already showed the possibility to identify such sources, and also to distinguish between two separate OOA with different degrees of oxidation.

Additional measurements (complementary to the ACSM dataset) are: a) real time black carbon concentrations, measured by a Multi Angle Absorption Photometer (MAAP) with a PM_{10} inlet, b) 24h PM_1 samples collected on quartz fibre filters using high volume samplers with a PM_1 impactor inlet, c) real time PM_1 concentrations, measured by an optical laser spectrometer (GRIMM 1107) and corrected with the factors obtained by comparison with 'in situ' simultaneous gravimetric measurements. The 24h PM_1 samples are analyzed offline for organic matter, nitrate, sulphate, ammonium and chloride, among other components, which will be compared to the ACSM dataset.

This work was supported by ACTRIS (7th framework programme), GRACCIE (project CSD2007-00067), VAMOS (project CGL2010-19464/CLI), and Generalitat de Catalunya 2009 SGR8. M.C. Minguillón was funded by JAE-Doc CSIC program, co-funded by the European Social Fund (ESF).

Ng, N.L., Herndon, S.C., Trimborn, A., Canagaratna, M.R., Croteau, P.L., Onasch, T.B., Sueper, D., Worsnop, D.R., Zhang, Q., Sun, Y.L. and Jayne, J.T. (2011) *Aerosol Sci. Technol.* **45**, 770-784.

Pérez, N., Pey, J., Castillo, S., Viana, M., Alastuey, A., and Querol, X. (2008) *Sci. Total Environ.* **407**, 527-540.

Vertical profiles and seasonal variation of aerosol particles in the PBL upon Ny Ålesund (Svalbard Islands): electron microscopy vs geochemical records

B. Moroni[1], S. Becagli[2], E. Bolzacchini[3], M. Busetto[4], L. Ferrero[3], D. Frosini[2], C. Lanconelli[4], A. Lupi[4], M. Mazzola[4], R. Traversi[2], R.Udisti[2], V. Vitale[4] and D. Cappelletti[1]

[1]DICA and Centro di Eccellenza SMAArt, University of Perugia, Perugia, 06123, Italy
[2]Department of Chemistry, University of Florence, Sesto Fiorentino, 50019, Italy
[3]POLARIS research centre, DISAT, University of Milano-Bicocca, Piazza della Scienza 1, Milano, 20126, Italy
[4]Institute of Atmospheric Science and Climate, Via Gobetti 1010, Bologna, 40129, Italy
Keywords: SEM-EDS, mineral chemistry, particle size and shape, local vs long range sources.
Presenting author email: b.moroni@tiscali.it

Studies on the nature, properties and seasonal variability of aerosols in the polar regions are a critical point in the definition of the sources, atmospheric reactions and transport processes on these regions. They are, on turn, main aspects in the assessment of the direct climate forcing due to polar aerosols on the regional and global scales for climate changes modelling (IPCC 2007).

In order to achieve these goals, two sampling/measurement campaigns were performed during spring/summer 2011 and 2012 in the framework of the PRIN (Progetti di Rilevante Interesse Nazionale) 2009 "ARCTICA" project. Size-segregated particle samplings were carried out at the Gruvebadet observatory, about 1 km South-West the Ny Alesund village (Svalbard Islands) both at ground level (about 50 m a.s.l.) and along vertical profiles (up to ~ 1,000 m a.g.l.). In this latter case a tethered balloon was employed. Particles were collected on polycarbonate filters using a four-stage DEKATI sampler (cut-off diameters D_p: < 1μm, 1-2.5 μm, 2.5-10 μm and > 10 μm) at ground level, and a two-stage miniaturized Sioutas SKC cascade impactor (cut-off diameters D_p: < 1 μm and > 1 μm) in the balloon samplings. Individual particle size, morphology and chemical composition were investigated by scanning electron microscopy coupled with energy dispersive microanalysis (SEM-EDS). The elemental atomic ratios were calculated and then compared with those of pure minerals and phases to obtain distinct particle classes.

Silicates (quartz, feldspars, micas, pyroxenes, amphiboles, clay minerals), carbonates (calcite, dolomite), metal particles (Fe, Ti, mixed Fe-Cr-Ni, Cu oxides), sulfate (gypsum, alkali-sulfates) and chloride (halite and sylvite) salts are the main particle groups in the samples. Except for Cu metal oxides, they are all from soil (silicates, carbonates, Fe, Ti and mixed metal particles) and from sea spray (sulfate, chloride) natural sources. In particular, compositional data of evaporites suggest the co-precipitation in cold conditions.

Seasonal trends of the type, size and relative abundance of the mineral phases along the vertical profiles are evidenced. In spring, in particular, < 1 μm fine grained chloride salts are the main aerosol component at ground level in the case of north wind circulation (clear sky, medium to dry conditions), while 1 μm < D_p< 2.5 μm fine grained silicates are the prevailing phase component at some height (~ 250 m a.s.l.) in the PBL for south wind circulation (cloudy, wet conditions). An abrupt decrease of the total amount of airborne particles is observed in summer, along with a significant increase of marine particles larger than 1 μm at every altitude in the PBL. Remarkable differences in the mineral chemistry of silicates are also observed in the transition from spring to summer. In particular, the general enrichment of feldspars, chain-like silicates (various pyroxene and amphibole types) and Ti oxide (titanite) suggest a local provenance from granitoid source rocks widely outcropping in the western margin of the Svalbard archipelago, that is in good accordance with seasonal deglaciation in the area. In the meanwhile the general decrease of carbonates and sheet-like silicates follows the decrease of long range transport phenomena from Siberia. This is likely due to the northerly position of the Arctic front in this season (Law and Stohl, 2007) which prevents long range atmospheric circulation from Europe and Russia leading to almost local patterns of aerosol deposition, along with local deglaciation.

Results of OPC measurements, bulk chemical analyses and back trajectory calculations confirm this typical seasonal trend. The REE patterns, in particular, reveal a change of the Eu anomaly from negative to positive values, along with a general enrichment of HREEs in the summer season. This is in good accordance with the higher amount of intermediate-acidic chain silicates (*e.g.*, hornblende) in the aerosols during summer. Detailed examination and comparison with the mineralogical associations and parageneses of the surrounding basement regions will provide further evidence to these studies.

In conclusion, SEM methods revealed distinct distributions of number, size and geochemical properties of different particles classes in the aerosols. They reflect distinct behaviours and spatial/temporal evolution of the constituent particles, along with the common occurrence of dust inputs from regional to long range sources. All these features have to be taken into account when approaching the modelling of atmospheric processes in a such complex environment.

This work was supported by Italian Education, University and Research Ministry (MIUR) and by National Research Council (CNR) funds and facilities.

IPCC 2007 - Intergovernmental Panel on Climate Change 2007 Report.
Law K. and Stohl A. (2007) *Science* **315**, 1537-1540.

Secondary organic aerosols (SOA) chemical characterization employing simulated NMR spectra of model compositions.

M. Paglione[1], F. Moretti[2], E. Tagliavini[2], E. Finessi[1*], M. C. Facchini[1] and S. Decesari[1]

[1] Institute of Atmospheric Sciences and Climate, National Research Council, Bologna, I-40129, Italy;
[2]Department of Chemical Physics, University of Bologna, Bologna, I-40100, Italy;
[*]now at Department of Chemistry, University of York, Heslington, York, YO10 5DD, UK.

Keywords: SOA, H-NMR, MCM
Presenting author email: m.paglione@isac.cnr.it

Secondary organic aerosol (SOA) accounts for a significant fraction of ambient particulate matter and a detailed knowledge of the formation, properties and transformation of SOA is therefore required to evaluate its impact on atmospheric processes, climate and human health (Hallquist et al., 2009). Elucidation of the chemical and physical processes underlying SOA formation has been pursued using various experimental and modeling approaches of different degree of complexity. Most employed methods rely on the definition of volatility classes for the constituents of SOA as a function of precursor types and oxidation conditions. This kind of information can be achieved relatively easily in laboratory experiments and their application to field conditions is based on the hypothesis that the actual chemical processes involved in SOA formation occur at the same manner in smog chambers and in real ambient aerosol particles. In order to cope with the real complexity of the system, explicit gas-phase chemical models coupled to gas/particle partitioning models have been formulated (e.g., Johnson et al., 2006), Explicit chemistry models are much more complex and contain many more uncertain parameters then the approaches based on volatility distributions, but in turn, they can be constrained by the observations not only for total organic aerosol concentrations but also in respect to the actual chemical composition. For this reason, efforts aimed to identify good diagnostics extracted from chemical observations of ambient and laboratory SOA is a promising tool to reduce the uncertainty in SOA formation models in an effective way. In this context, molecular markers can provide unambiguous information of the occurrence of specific SOA types in ambient air, but their use as diagnostics for SOA composition is limited by the fact that molecular speciation methods show limited analytical recovery. Functional group methods have the clear advantage of targeting integral properties of the organic complex mixtures. In other words, molecular complexity can be reduced to a relatively small number of functionalities. The main caveat of functional group spectroscopic methods is that the individual techniques exhibit very different sensitivities to specific organic structures and that the spectra always present large peak overlaps. To cope with such complexity, *simulated* spectra can be generated starting from the modeled chemical composition so that models and observations can be compared directly using the spectral data.

This study examines the use of simulated H-NMR spectra as diagnostics for models of biogenic and anthropogenic SOA formation. Spectral fingerprints for selected SOA systems – ozonolysis and photooxidation of alpha-pinene and photooxidation of 1,3,5-trimethylbenzene (TMB) – were recorded for samples of SOA collected during reaction chamber experiments. The simulation of H-NMR spectra starting from model compositions was carried out using ACD-Labs algorithms tested against their ability to reproduce the spectra of standard compounds, including molecules possessing a complex stereochemistry like the oxidation products of alpha-pinene. Simulated spectra were recorded for model mixtures comprising compounds derived from literature studies of GC/MS and LC/MS characterization, as well as compounds expected to occur in SOA based on explicit gas-phase chemistry models for alpha-pinene and TMB. In particular, a set of chemical species from the Master Chemical Mechanism (MCM) was selected, based on simple assumptions about their expected volatility, to account for the uncharacterized fraction of SOA.

The results show that compounds bearing double bonds were very unlikely to occur in both alpha-pinene and TMB SOA samples. The analysis provides also candidate basic structures for the SOA fraction uncharacterized at the molecular level. These findings indicate that H-NMR spectroscopy can be used as a new, useful diagnostic tool for SOA formation models including explicit chemistry.

Camredon, M., et al. (2010), *Distribution of gaseous and particulate organic composition during dark α -pinene ozonolysis,* Atmos. Chem. Phys., 10, 2893-2917.

Hallquist, M. et al. (2009), *The formation, properties and impact of secondary organic aerosol: current and emerging issues*, Atmos. Chem. Phys., 9, 5155-5236, doi:10.5194/acp-9-5155-2009.

Johnson, D. et al. (2006), *Simulating regional scale secondary organic aerosol formation during the TORCH 2003 campaign in the southern UK,* Atmos. Chem. Phys., 6, 403-418.

On the enigma of new particle formation in the atmosphere

T.-E. Parts, A. Luts, K. Komsaare, M. Noppel, and U. Hõrrak

Institute of Physics, University of Tartu, Ülikooli 18, 50090 Tartu, Estonia
Keywords: aerosol chemistry, aerosol spectrometry, mass spectrometry, water clusters
Presenting author email: tiia-ene.parts@ut.ee

It is still an enigma of atmospheric science how aerosol particles are formed at the molecular level although scientists have peeled away layer after layer of this mystery by developing new techniques to observe smaller and smaller particles (Andreae, 2013; Kulmala *et al.,* 2013). It is interesting that in the Amazon rainforest new particle formation (NPF) almost never occurs (Pöhlker *et al.,* 2012). Can it be related to potential role of high humidity, besides the effects of the molecules, such as acids, amines and organics? Also, the mystery of the chemical processes that lead from volatile organic gases to organic aerosols in the atmosphere should be unravelled (Andreae, 2013).

We use an advanced method to investigate the formation of aerosol particles starting from gas phase reactions including trace gases and ions in the laboratory conditions (Luts *et al.,* 2011, Parts *et al.,* 2012). Particularly, we study the effect of enhanced humidity. We produce new air ions by a radioactive ^{241}Am and trace their evolution within the age interval from few tenths of a second (young ions) up to few ten seconds (old ions). The changes in size and mass distributions of ions are investigated concurrently by means of two instruments: 1) air ion spectrometer (AIS, Airel Ltd) and 2) mass spectrometer (MS, Sciex API-300).

The behaviour of the air ions obviously depends on the particular chemical composition of the air.

Mass spectra of negative air ions show that the enhanced concentration of water has no effect on the set of the abundant MS peaks, but changes their relative intensity. This effect is especially noticeable in the case of young negative ions. Old ions undergo insignificant modification of the mass spectra (Luts *et al.,* 2011). In several cases, we observed *m/z* at 89, 125, 179, and 269, which are in a good correspondence with the masses of water clusters $OH^-(H_2O)_4$, $OH^-(H_2O)_6$, $OH^-(H_2O)_9$, $OH^-(H_2O)_{14}$. Even though the existence of such clusters remains questionable and needs to be proved.

The AIS spectra of negative ions demonstrate that variations in the concentration of water vapour have effect both upon young and old negative ions. More water vapour induces more large young ions, but less large old ions, when to compare with the background spectra of young and old ions, respectively. This can be interpreted as smaller clusters are more stable and the size distribution of negative ions depends on the age and water vapour concentration. The AIS spectra of positive ions is also affected by changes in water concentration, but the modifications are weaker.

Mass spectra of positive air ion consist of a large number of peaks (Fig. 1). Positively charged clusters are larger than dominant negative clusters. Contrary to negative ions, high water vapour concentration altered the set of abundant MS peaks what complicates the interpretation of results. The observed at *m/z* 378(379), 408 and 436 peaks could be related to known stable water clusters $(H_2O)_{21}$, but this proposal should be proved later.

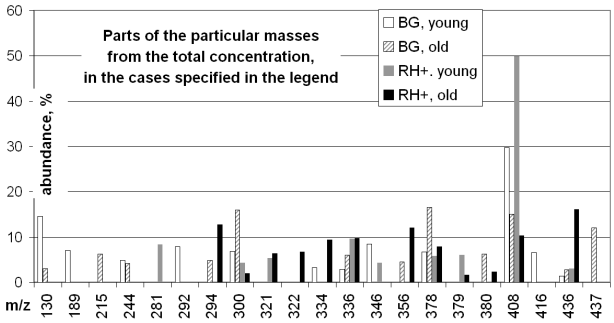

Figure 1. Positive air ions mass distribution at different relative humidity (BG – background ions, RH – relative humidity).

In the Amazon rainforest (Pöhlker *et al*., 2012), the concentration of water vapour is high. Polar oxidized volatile organic compounds (VOCs) and other biogenic emission can react with water and lead to secondary organic aerosol particles. Water should play an important role in these processes and could be a reason why NPF is not observed. Unravelling the enigma of water properties (*eg* clusters formation and stability) could be a key to understand new particle formation in the atmosphere.

This work was supported by he Estonian Science Foundation grants 8342, 8806 and by the research project SF0180043s08 of Tartu University.

Andreae, M. O. (2013) *Science* **339**, 911-912.
Kulmala, M. *et al* (2013) *Science* **339**, 943-946.
Luts, A. *et al* (2011) *J. Aerosol Sci.* **42**, 820-838.
Parts, T. *et al* (2012) *Proc. 2012 European Aerosol Conf*., Granada, Spain, 2nd-9th September. www.eac2012.com/EAC2012Book/files/1157.pdf
Pöhlker, C. *et al* (2012) *Science,* **337**, 1075-1078.

Experimental studies of the formation of cluster ions formed by corona discharge in an atmosphere containing SO_2, NH_3, and H_2O

Preben Hvelplund[1], Jens Olaf Pepke Pedersen[2], Kristian Støchkel[1], Martin B. Enghoff[2], Theo Kurtén[3]

[1]Department of Physics and Astronomy, Aarhus University, Ny Munkegade 120, DK 8000 Aarhus C, Denmark.
[2]National Space Institute, Technical University of Denmark, Elektrovej, bldg.. 327, DK 2800 Kgs. Lyngby, Denmark
[3]Department of Chemistry, University of Helsinki, P.O. Box 55, FI 00014 Finland,
Keywords: Corona discharge; cluster formation; sulfuric acid
Presenting author email: jopp@space.dtu.dk

We report on studies of ion induced nucleation in a corona discharge taking place in an atmosphere containing SO_2, NH_3, and H_2O at standard temperature and pressure. Positive ions such as $H_3O^+(H_2O)_n$, $NH_4^+(H_2O)_n$, and $H^+(H_2SO_4)(H_2O)_n$ and negative ions such as $HSO_5^-(H_2O)_n$, $SO_4^-(H_2O)_n$, $HSO_4^-(H_2O)_n$ and $NO_3^-(H_2O)_n$ have been recorded. Large values of n (> 100) were observed and the experiment indicates the existence of even larger water clusters. In contrast, only clusters with a maximum of 2 sulfuric acid molecules were observed. Fragmentation studies also revealed that the negative ion HSO_5^-, which has been observed in many studies, in our experiments is contaminated by $O_2^-(HNO_3)(H_2O)$ ions, and this may also have been the case in other experiments. Finally an ion with *m/z* = 232 (where *m* is the cluster mass in amu and *z* the charge state), capable of attaching H_2O-molecules was observed and studied by fragmentation.

Experiments

The ions are formed by corona discharge in the laboratory atmosphere, where gases such as SO_2, NH_3, and H_2O could be added to the discharge region. The corona ionizer discharge needle is placed inside a flow reactor, which is attached to the inlet capillary that interface the discharge region to the mass spectrometer. The flow reactor was kept at room temperature and the gas pressure was around 1 atm. The discharge gas was introduced to the flow reactor by flowing synthetic air.

The corona voltage was held between 2 and 3 kV, the tube lens potential was 60 V and the heated capillary temperature was normally held at room temperature. Measurements were done with both positive and negative voltages applied to the discharge needle (relative to the capillary inlet) in order to extract both positive and negative ions. The ions were accelerated by an electrostatic potential of 50 kV. The precursor ions were mass selected with a bending magnet and passed through a 3-cm long gas cell with entrance and exit apertures of 1 and 3 mm diameter containing neon as target gas. The product ions exiting the cell were analyzed according to their *m/z*-value, by scanning the voltage of the electrostatic hemispherical analyzer and fragmentation spectra were obtained in so called mass-analyzed ion kinetic energy spectra (MIKE) spectra.

Mass spectra showing the distribution of ions produced in the ion source were obtained by scanning the magnet with no target gas in the target cell and using a fixed analyzer voltage that was related to the acceleration voltage.

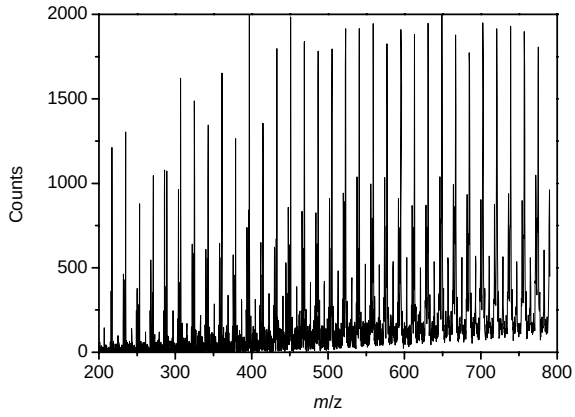

Figure 1. Positive ion *m/z* spectrum.

Figure 1 shows an example of the observed distributions. The largest peaks (around 2000 counts) can be identified as $H_3O^+(H_2O)_n$, with n going from 1 to 38. The largest observed clusters with n=38 is not an upper limit for the cluster size but corresponds to the *m/z*-value, where the scans were stopped, and it is likely that even larger clusters exist at our experimental conditions. The series with peaks at one mass unit less than the previous series (around 1000 counts) can be identified as $NH_4^+(H_2O)_n$. The series with intensities around 500 counts relates to $H^+(H_2SO_4)(H_2O)_n$.

For the negative ions we also observe the existence of clusters with a very large number of water molecules (n>100) and our results also indicate that only experimental limitations constrain us from observing even larger clusters. The large clusters are built around a single core ion containing sulfur or NO_3.

Hvelplund, P., Pedersen, J.O.P., Støchkel, K., Enghoff, M.B., and Kurtén, T. (2013) *Int. J. Mass. Spectrom. (submitted).*

Poster B032, PAHs and ALKs in the Arctic (Svalbard Island) aerosol: results from the AREX2011 oceanographic campaign
By E. Bolzacchini, L. Ferrero, F. Marazzi, A. Molinelli, M. G. Perrone, G. Sangiorgi, S. Becagli, R. Traversi, R. Udisti, W. Walczowski, T. Zielinski

File is damaged

Chemical characterization of polar organic markers in PM 2.5 during an intensive campaign of Supersito Project in Po Valley (Italy)

M.C. Pietrogrande[1], M. Visentin[1], D. Bacco[1], S. Ferrari[2], V. Poluzzi[2]

[1]Department of Chemical and Pharmaceutical Science, University of Ferrara, Ferrara, I44121, Italy
[2] Emilia-Romagna Regional Agency for Protection and Environment, Bologna, I-40138 Italy
Keywords: PM2.5 chemical composition, intensive campaigns, Po Valley (Italy,) polar organic markers
Presenting author email: mpc@unife.it

The composition and seasonal variations of a wide range of water-soluble organic compounds (WSOCs) were determined in the atmospheric aerosol in Emilia-Romagna region (Northern Italy), as a part of the "Supersito" Project (http://www.arpa.emr.it/supersito/). The present study is focused on dicarboxylic acids, sugars and methoxyphenols, as chemical tracers giving valuable information for elucidating sources, processes and pathways of organics in the atmosphere.

$PM_{2.5}$ filters were collected in two intensive field campaigns in winter 2011 (November 14th to December 6th) and summer 2012 (June 13rd to July 10th). The investigated sites were two locations representing an urban background station of Bologna city, a great urban centre in Northern Italy, and a rural site (about 30 Km north-east of Bologna in the Po Valley) representing an agricultural and remote region.

An analytical protocol, including solvent extraction and derivatization reaction, has been properly optimized to permit the simultaneous analysis of 48 target WSOCs, including 18 dicarboxylic acids, 17 sugars and 13 methoxyphenols (Pietrogrande *et al*, 2011; Pietrogrande *et al*, 2013). The developed method provided rapid and accurate quantification of WSOCs with low detection limits ($\leq 1 ngm^{-3}$) and good reproducibility (RSD%$\leq$11%) useful for aerosol monitoring.

The developed method was applied for chemical characterization of different classes of WSOCs in the $PM_{2.5}$ filters collected in both the seasons in urban and rural sites (mean values of total concentrations of acids, sugars and phenols are reported in Table 1).

Table 1. Mean concentration values of total acids, sugars and phenols and levoglucosan in $PM_{2.5}$ filters collected in winter and summer in urban and rural sites.

Analytes	Winter		Summer	
	Urban ngm^{-3}	Rural ngm^{-3}	Urban ngm^{-3}	Rural ngm^{-3}
Total acids	272	301	n.d.	0.5
Total sugars	1263	1135	6.7	43
Levoglucosan	1028	918	2.2	5.4
Total phenols	13.3	9.7	0.0	0.5

In general, data similarities indicate the regional nature of the primary sources and atmospheric processes affecting the $PM_{2.5}$ composition that seems weakly influenced by local emission sources.

In all seasons the most abundant compound is levoglucosan, as the major by-product from biomass burning, suggesting that this is the major source of aerosol, accordingly with values measured in other Italian cities (Piazzalunga, 2011). In addition to levoglucosan, less abundant degradation products from biopolymers (e.g. galactosan and mannosan from cellulose, methoxyphenols from lignin) were quantified as useful tools for identifying combustion sources: the data obtained in both the seasons are diagnostic for wood combustion with a predominant contribution of hardwood fuel.

As expected, a pronounced season pattern of dicarboxylic acids was observed, with higher winter concentrations compared with summer: this is a consequence of the higher anthropogenic emissions in the cold season combined with winter atmospheric conditions in the investigated area that are characterized by low mixing heights and possible formation of inversion layers (Balducci, 2010).

Some biogenic sugars were quantified, as indicators of primary emissions from the terrestrial biomass (plant detritus, airborne microbes, spores of lichens and fungi). The relative contribution of such sugars is higher in summer compared with winter closely reflecting the higher sugar production and utilization by the ecosystem as well as the enhanced agricultural activity in the hot season.

The distribution profiles and the diagnostic ratios of the target WSOCs provided relevant information for estimating the contribution of primary emission sources (power plants, vehicular circulation, biomass burning) associated with secondary constituents from both biogenic and anthropogenic precursors.

This research was conducted as part of the "Supersito" Project, which was supported and financed by Emilia-Romagna Region and Regional Agency for Prevention and Environment under Deliberation Regional Government n. 428/10.

Pietrogrande, M.C. and Bacco, D. (2011) *Ana.l Chim. Acta* **689**, 257–264.
Pietrogrande, M.C., Bacco D. and Chiereghin S. (2013) *Anal Bioanal. Chem.* **405,** 1095-1104.
Piazzalunga, A., C. Belis, C., Bernardoni, V., Cazzuli, O., Fermo, P., Valli, G., Vecchi, R. (2011) *Atmos. Environ*. 45, 6642-6649
Balducci, C. and Cucinato, A. (2010) 44,652-659.

Photodissociation dynamics of CF_2Cl_2 molecule in aerosol particles

V. Poterya, A. Pysanenko, J. Lengyel, P. Svrčková, J. Kočišek and M. Fárník

J. Heyrovský Intsitute of Physical Chemistry, ASCR, Dolejškova3, Prague 8, 18223, Czech Republic
Keywords: ozone depletion, photochemistry, caging.
Presenting author email: viktoriya.poterya@jh-inst.cas.cz

The chlorofluorocarbons (CFCs) are extremely inert compounds which decay only in the upper stratosphere after absorption of high energy solar radiation. The decomposition pathway can lead to formation of reactive Cl radicals which triggers the ozone depletion cycle. One of the crucial questions for stratospheric chemistry is how is the photodissociation dynamics of these species influenced by the aerosol particles in the stratosphere? The polar stratospheric cloud (PSC) particles can adsorb CFCs and change their photochemistry.

To investigate this effect, we have studied the UV photodissociation of CF_2Cl_2 (CFC-12) molecule in molecular beam experiment: first we study the photodissociation of an isolated molecule, then simulate the influence of the solvent by the simplest archetype solvent species, i.e. rare gas atoms in Ar and Xe clusters, and finally we will investigate the CFC photodissociation on ice nanoparticles.

We have overlapped the molecular beam with two laser beams. The photodissociation was studied at 193 nm, and $Cl(^2P_{3/2})$ and $Cl^*(^2P_{1/2})$ fragments were ionized using (2+1) REMPI schemes around 235 nm. The ionic products were guided onto position sensitive 2D detector by velocity mapping electrode configuration. From the images recorded by a CCD camera complete 3D information about the fragment velocities can be obtained.

The Cl-fragments images of are shown in Fig. 1: (a) corresponds to the photodissociation of isolated molecule, and (b) originates from CF_2Cl_2 in clusters. The circular edges in both images correspond to the fast Cl fragment, while the central bright spot in (b) corresponds to Cl atoms with near zero kinetic energy due to the cluster *caging effect*.

The graph below the images shows the corresponding Cl-fragment kinetic energy distributions (KEDs). These results resolve a discrepancy from the previous CF_2Cl_2 molecule photodissociation studies (Baum 1993, and Yen 1993). The presence of the slow Cl fragments in the spectra points to the secondary dissociation of CF_2Cl fragment radical. Our measurements show that more than one Cl atom can be released per one UV-photon from a CF_2Cl_2 molecule, and also that a Cl_2 molecule can be released instead. In addition all these fragments can be trapped by cage effect if the photodissociation happens on PSC particles. All these conclusions can have significant consequences for stratospheric ozone modelling.

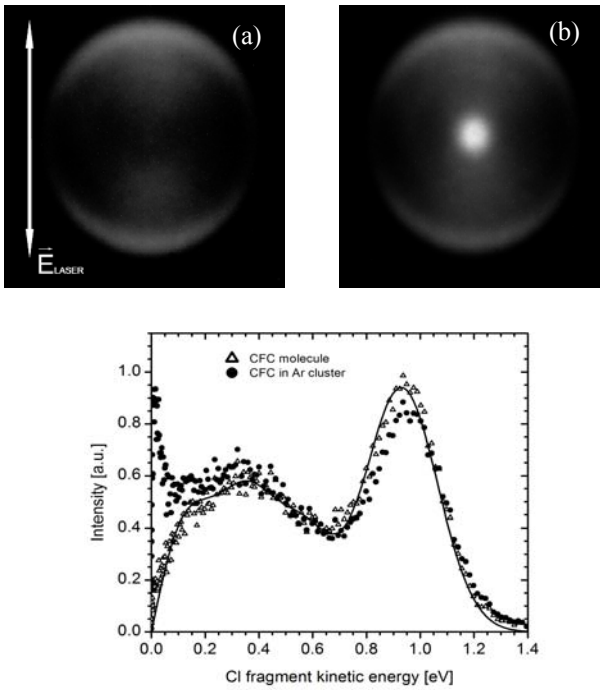

Figure 1. Images of Cl atoms from photolysis of (a) CFC-12 molecules and (b) CFC in Ar clusters, together with corresponding velocity distributions (bottom).

This work was supported by the Grant Agency of the Czech Republic under grants P208/11/0161 and 203/09/0422.

Baum, G., Huber, J. R. (1993) *Chem. Phys. Lett.* **20**, 261.
Yen, M., Johnson, P. M., White, M. G. (1993) *J. Chem. Phys.* **99**, 126.

Kinetic Measurements in Acoustically Levitated Terpene Droplets

K. Rastogi[1], C. Yuan[1], R. Willoughby[1], S. Almabrok[1] and C. Pfrang[1]
[1]Department of Chemistry, University of Reading, P.O.Box 224. Reading, RG6 6AD, UK
Keywords: Acoustic Levitation, Raman, Kinetics, Alpha-pinene.
Corresponding author email: k.rastogi@pgr.reading.ac.uk

Raman Acoustic Levitation (RAL) was employed for chemical analysis of the behaviour of selected terpenes. The ageing of droplets of terpenes such as α-pinene was analysed in the presence of the bath gases nitrogen, oxygen and ozone. Changes in the chemical composition of the levitated droplets was followed as a function of time.

Volatile Organic Compounds (VOCs) play an important role in atmospheric chemistry[1]. Vegetation is a key source of VOCs[2]. These biogenic VOCs include isoprene and a variety of terpenes. α-Pinene is one of the major terpene components and has received considerable attention[3]. Individual droplets of organic compounds can be studied by techniques such as acoustic (ultrasonic) levitation[4]. For the Raman Acoustic Levitation (RAL) studies presented here we combined ultrasonic levitation with Raman microscopy (see Fig. 1).

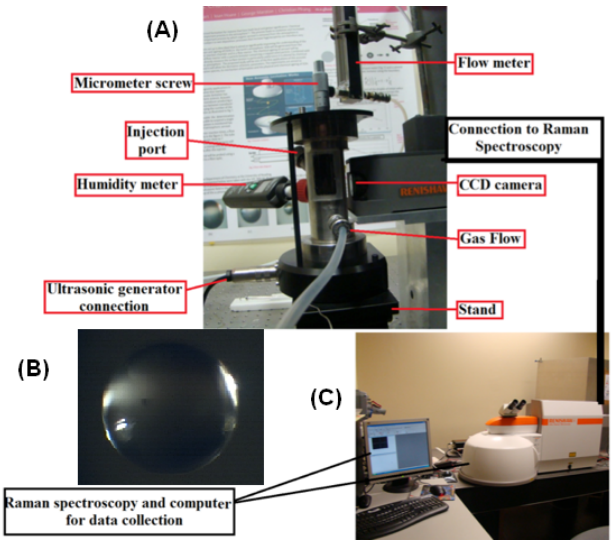

Fig. 1 (a & c) depict the levitation system coupled to a Raman microscope; and (b) shows an image of a levitated α-pinene droplet in nitrogen.

Fig. 1 (b) illustrates an acoustically levitated α-pinene droplet and Fig. 2 displays the corresponding Raman spectra. An unexpected oxidation peak appeared both in nitrogen and oxygen at room temperature and 80% relative humidity (RH) as shown in Fig. 2 (b).

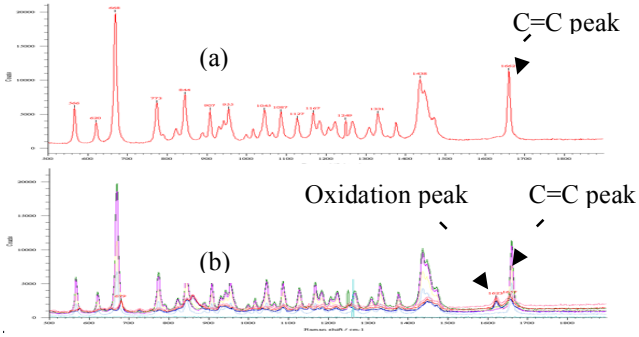

Fig. 2 Full range Raman spectra for a levitated α-pinene droplet (initial diameter: 0.99 mm) under N_2 and 80% RH for (a) $t = 0$ and (b) $t = 7.5$ min.

The appearance of the oxidation peak has been investigated under both wet and dry conditions in nitrogen and oxygen environments.

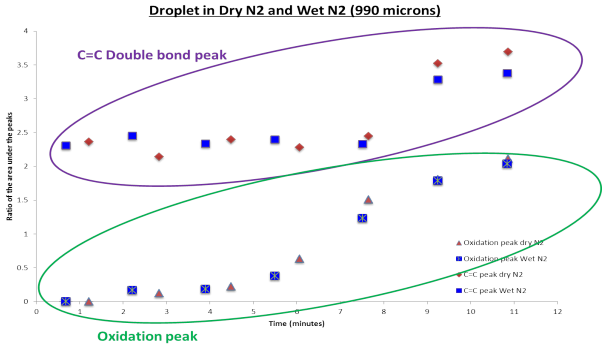

Fig. 3 Measurements of relative peak areas in the Raman spectra as a function of time for levitated α-pinene droplets in N_2 (the peak areas are normalised to an inert peak at ca. 1086 cm^{-1}).

From Fig. 3 it becomes apparent that the oxidation peak is observed even under nitrogen gas, and no significant difference is seen for dry and wet conditions. To further investigate this unexpected effect, detailed analysis is currently being carried out at Reading.

References

1. F. Fehsenfeld, J. Calvert, R. Fall, P. Goldan, A. B. Guenther, C. N. Hewitt, B. Lamb, S. Liu, M. Trainer, H. Westberg and P. Zimmerman, *Global Biogeochemical Cycles*, 1992, **6**, 389.
2. V. Isidorov, J. Jaroszynska, T. Sacharewicz and E. Piroznikow, *Atmospheric Environment*, 1999, **33**, 4739.
3. S. Juuti, J. Arey and R. Atkinson, *Journal of Geophysical Research: Atmospheres*, 1990, **95**, 7515.
4. R. Tuckermann, L. Puskar, M. Zavabeti, R. Sekine and D. McNaughton, *Analytical and Bioanalytical Chemistry*, 2009, **394**, 1433.

Gas phase sampling and determination of carbonyl compounds in ship diesel emissions: Differences between light fuel oil and heavy fuel oil operation

Ahmed A. Reda[1,2,5], G. Abbaszade[1,5], J. Lintelmann[1,5], H. Harndorf [1,5], R. Rabe[3,4], O. Sippula[3,2,5], T. Streibel[2,5], J. Schnelle-Kreis[1,5] and R. Zimmermann[1,2,5]

1-Joint Mass Spectrometry Centre, Comprehensive Molecular Analytics, Helmholtz Zentrum München, Germany
2-Joint Mass Spectrometry Centre, Chair of Analytical Chemistry, University of Rostock, Germany
3- Department of Environmental Science, University of Eastern Finland, Kuopio, Finland
4-Faculty of mechanical engineering and marine technology, University of Rostock, Germany
5- HICE – Helmholtz Virtual Institute of Complex Molecular Systems in Environmental Health, www.hice-vi.eu
Keywords: Ship emission, Carbonyl compounds, DNPH
Presenting author email: ahmed.reda@helmholtz-muenchen.de

Ship or marine transportation represents major conduit of international trade, and during the last decade the numbers of ships started to rise very quickly due to the development and globalization of the markets and also as cheap way for goods transportation because of this increment there has been growing awareness of the environmental impacts of maritime transport special on the ports or coastal regions[1]. Ship emission estimates diverge widely for all chemical compounds in both particles and gases phase and based on current hypotheses that reactive organic compounds in particle as well as in gas phase of aerosols are particularly relevant the Helmholtz Virtual Institute of Complex Molecular Systems in Environmental Health (HICE)[2]. Gas phase containing different categories of organic compounds and on these categories are carbonyl compounds (CCs) which have received increased attention recently due to their important role in ground-level ozone formation and health effects [3].

A measurement campaign was conducted by the Helmholtz Virtual Institute of Complex Molecular Systems in Environmental Health (HICE) at the University of Rostock to investigate the characteristics of the emitted primary aerosols and their effects on lung epithelial cells. A set of state-of-the art online instrumentation measuring gases, size distribution and chemical composition were used in conjunction with the cell exposure system (Air-Liquid-Interface). Heavy Fuel Oil (HFO 180) and Distillate fuel (EN 590) were used as fuels in a one cylinder ship diesel engine operated at different loads according to ISO 8187-4 E2 for emission testing.

Our work involved sampling off CCs with two different sampling methods, commercial high sample volume DNPH cartridges and impingers almost the same as in CARB 430 method. Both sampling methods depending on derivatization with 2,4-Dinitrophenylhydrazine DNPH in acidic media. The derivatization adducts were analyzed by High Performance Liquid Chromatography with Diode Array Detector (HPLC-DAD) and by Gas Chromatography Mass Spectroscopy (GC-MS). An enhanced HPLC method was applied using a chromatography modeling software program called DryLab. The method was capable to separate and quantify 23 carbonyl compounds with correlation coefficient R^2 (0.9978) for formaldehyde till (0.9989) for decanal, the detection range for most carbonyls start from (10-1000ng) for formaldehyde and (10-500 ng) for decanal.

The GC-MS method show a good separation and detection for twenty CCs with correlation coefficient R^2 (0.9984) for formaldehyde till (0.9995) for decanal, the detection range were (0.10-15ng) for formaldehyde till (5-50ng) for decanal.

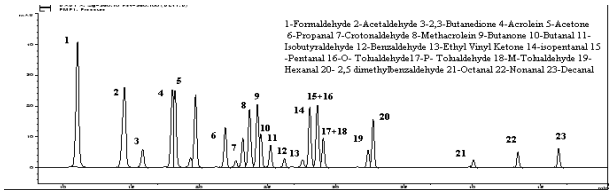

Figure (1) Separation of CCs-DNPH hydrozone by HPLC

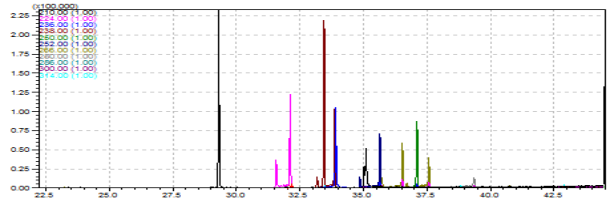

Figure (2) Separation of CCs-DNPH hydrozone by GC-MS

Real samples were collected with different sampling conditions, concerning engine loads, dilution ratios, sampling periods and fuel types. The first results for the CCs show that emissions from the heavy fuel oil usage contained more carbonyl compound than CCs from light fuel oil operation. The samples from HFO also contains a higher percentage of low molecular weight CCs with respect to the higher molecular weight CCs.

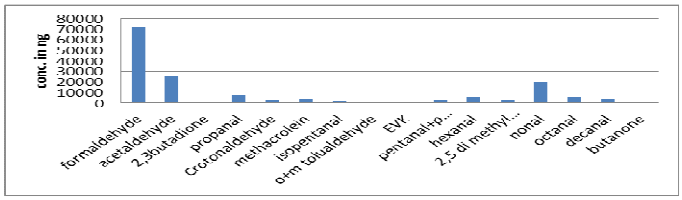

Figure (3) Carbonyl compounds in ship diesel emission (heavy fuel oil operation-HFO) given in ng/m^3

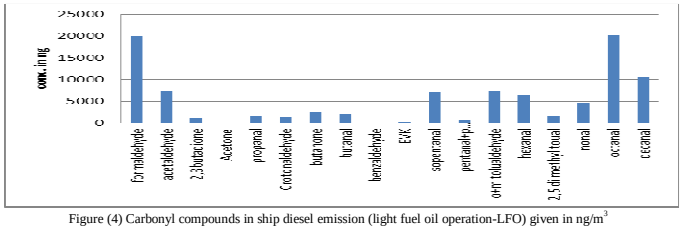

Figure (4) Carbonyl compounds in ship diesel emission (light fuel oil operation-LFO) given in ng/m^3

1-Apollonia Miola, Biagio Ciuffo' (2011) Atmospheric Environment 45 2242-2251.

2- Helmholtz Virtual Institute of Complex Molecular Systems in Environmental Health, HICE (www.hice-vi.eu).

3- Seco, R., Peñuelas, J., Filellaet, (2007). Atmospheric Environment 41 (12), 2477e2499.

Regional scale oxidation of organic aerosol observed through HR-ToF-AMS measurements at Mt. Cimone (2165 m asl), Italy

M. Rinaldi[1], S. Gilardoni[1], S. Decesari[1], S. Fuzzi[1], S. Ferrari[2], V. Poluzzi[2] and M.C. Facchini[1]

[1]Institute of Atmospheric Sciences and Climate, National Research Council, Bologna, 40129, Italy
[2]Centro Tematico Regionale Aree Urbane, Arpa Emilia-Romagna, Bologna, 40138, Italy
Keywords: organic aerosol, aerosol ageing, aerosol chemistry, AMS.
Presenting author email: m.rinaldi@isac.cnr.it

High resolution time of flight aerosol mass spectrometer (HR-ToF-AMS) measurements have been performed, for the first time, at Mt. Cimone GAW station (44°12' N, 10°42' E, 2165 m asl) from 11 June to 9 July 2012, under the framework of the EU project PEGASOS and the Emilia-Romagna Region project SUPERSITO.

Mt. Cimone (44°12' N, 10°42' E, 2165 m asl) is the highest peak of the Northern Apennines and dominates the highly populated and heavily polluted Po Valley region.

Observed average concentrations (and mass contributions) of the main AMS species during the campaign were 2.8±2.4 μg m^{-3} (63%), 0.92±0.60 μg m^{-3} (20%), 0.33±0.46 μg m^{-3} (7%) and 0.41±0.33 μg m^{-3} (9%) for organics, sulphate, nitrate and ammonium, respectively, assuming a composition dependent collection efficiency (Middlebrook *et al.*, 2012), for an average reconstructed non refractory PM1 mass of 4.5±3.4 μg m^{-3}.

All the main AMS species presented a clear diurnal cycle with higher concentrations during the day and lower during the night, as a result of the planetary boundary layer (PBL) dynamics. During the night the site is well above the shallow residual layer, therefore in the free troposphere, and unconnected to the Po Valley aerosol sources. On the contrary, during the day, the site is inside the PBL and affected by the underlying aerosol sources.

The peculiar character of the site allows the investigation of organic aerosol (OA) ageing occurring at regional scale over the Po Valley. In fact, particles sampled during the day are representative of the early stages of aerosol atmospheric oxidation, comprising processed primary OA and secondary OA formed in the Po Valley basin. During the night, the aerosol sampled at Mt. Cimone is representative of more processed conditions, as the free troposphere contains aerosols with an age from several hours (transported during the day from the underlying valley) to days (transported during previous PBL evolution cycles).

To investigate the OA oxidation, based on the specific humidity (SH) as a tracer of the PBL evolution, we classified as PBL-influenced the samples collected between 12:00 and 18:00 LT, free troposphere (FT) the samples collected between 22:00 and 05:00 LT and transition (TR) all the samples collected in between.

Elemental analysis performed with high resolution mass spectra (Aiken *et al.*, 2007), revealed average H/C ratios of 1.38±0.04, 1.32±0.06 and 1.28±0.06 for PBL, TR and FT samples, respectively, while the O/C ratios were 0.54±0.04, 0.59±0.06 and 0.62±0.06 for PBL, TR and FT samples. Consequently, the OM/OC ratio passed from 1.83±0.05 in PBL, through 1.90±0.08 in TR, to 1.94±0.08 in FT samples.

These results evidence the progressive oxidation of OAs over the Po Valley basin, from few hours after their emission/formation to one or more days of atmospheric processing. On a Van Krevelen space, the data produce a slope of ~ –1, suggesting that the observed regional scale oxidation processes occur mainly through the addition of carboxylic functional groups (Heald *et al.*, 2010).

This is further confirmed by the analysis of the HR mass fragments, showing that, from PBL to FT samples, the average contribution of fragments containing carbon, hydrogen and more than one oxygen atom (CHO>1) passes from 25% to 33%, while both CH and CHO fragments decrease their contribution.

Further analysis of the dataset is currently ongoing to investigate the contribution of organo-sulphates and organo-nitrates as a function of the aerosol ageing.

Concluding, high time resolution online measurements performed at Mt. Cimone GAW station, thanks to the peculiar location of the site, are ideal to investigate and characterize the atmospheric processing of organic aerosols occurring over the Po Valley basin.

This work was supported by the EU FP7 PEGASOS project (FP7-ENV-2010/265148) and by the Emilia-Romagna Region project SUPERSITO (DGR 428/10).

Aiken, A.C., DeCarlo, P.F. and Jimenez, J.L. (2007) *Analytical Chemistry* **79**, 8350-8358.

Heald, C. L., Kroll, J. H., Jimenez, J. L., Docherty, K. S., Decarlo, P. F., Aiken, A. C., Chen, Q., Martin, S. T., Farmer, D. K. and Artaxo, P. (2010) *Geophys. Res. Lett.* **37**, L08803.

Middlebrook, A.M., Bahreini, R., Jimenez, J.L. and Canagaratna M.R. (2012) *Aerosol Science and Technology* **46**, 258–271.

Investigation of the oxidation mechanism of limonene photosensitized by imidazole-2-carboxaldehyde and leading to aerosol growth

S. Rossignol, L. Tinel, K. Aregahegn, L. Fine, B. Nozière and C. George

Université de Lyon, Université Lyon 1, CNRS, UMR5256, IRCELYON, Institut de recherches sur la catalyse et l'environnement de Lyon, Villeurbanne, F-69626, France
Keywords: imidazole-2-carboxaldehyde, photosensitized reaction, aerosol growth, limonene.
Presenting author email: stephanie.rossignol@ircelyon.univ-lyon1.fr

Recent studies have revealed the significant formation of light absorbing materials, including imidazole and its derivatives, in aqueous aerosol mimics in the presence of both ammonium sulphate and glyoxal (Galloway et al. 2009; Nozière et al. 2009; Yu et al. 2011; Kampf et al. 2012). Besides the potential impact on radiative properties of secondary organic aerosols, our team has shown that imidazole-2-carboxaldehyde (IC) can act as a photosensitizer, initiating aerosols growth in the presence of gaseous limonene and UV/visible light (Aregahegn et al., abstract submitted to the EAC 2013).

This work focuses on the characterisation of the chemical mechanism leading to this aerosols growth, and on the major products identification.

The molecular composition of organic/aqueous solutions exposed to UV/visible light and containing IC and limonene is followed in time by HR-ESI-MS in positive and negative modes. Limonene consumption is followed by HPLC-UV.

HR-ESI-MS and UPLC-HR-ESI-MS analyses are performed in parallel on IC/ammonium sulphate aerosols exposed to gaseous limonene and UV/visible light during flow tube experiments and collected onto Teflon filters subsequently solvent extracted.

In addition,, the lifetime of the triplet state of IC in aqueous/organic solutions in the presence of different terpenes is measured by means of photolysis experiments and compared in order to explain the first steps of the photosensitized reaction.

First HR-ESI-MS results of the irradiation of organic solutions containing IC and limonene, show the formation of the major "traditional" limonene oxidation products (e.g., coming from gas phase limonene ozonolysis, Leungsakul et al. 2005): limononaldehyde, keto-limononaldehyde, limonic acid, limononic acid ... Hundreds of other oxygenated species are however detected, typically with a number of carbon atoms ranging from 4 to 20 and with O/C ratios ranging from 0.2 to 0.7. Monomers and dimers of limonene oxidation products are observed but species with lower carbon numbers than monomeric compounds are predominant. Moreover, and surprisingly, the production rates of all products tend to increase with reaction time and the limonene consumption presents an apparent linearity. These preliminary findings would suggest, under our experimental conditions, an oxidation mechanism initiated by a relatively slow photosensitized process (e.g., electron transfer from limonene to the triplet state of IC, which formation is confirmed by laser photolysis experiments), followed by an increase of radicals in the solution leading to an extended limonene oxidation. The UV radiation, and/or the low concentration of reactants, are susceptible in our context to limit the formation of oligomers (Bateman et al. 2011) and promote fragmentation pathways.

Alongside, the preliminary results of the analysis of IC/ammonium sulphate aerosols exposed to both limonene and UV light in flow tube experiments confirm the presence of limonene oxidation products and, in the same time, confirm that the observed aerosol growth is due to limonene multiphase oxidation reactions initiated by a photochemical mechanism linked to the presence of IC.

Through this elucidation of the photosensitized oxidation mechanism of limonene by IC, this study attempts to provide a new insight in how light activated chemical reactions at the gas/aerosol interface can be of atmospheric significance and, potentially, of overall environment relevance, at other air/condensed phase surfaces, such as air/water interfaces.

Bateman, A. P., Nizkorodov, S. A., Laskin, J., et al. (2011) *Phys. Chem. Chem. Phys.* **13**(26) 12199-12212.

Galloway, M. M., Chhabra, P. S., Chan, A. W. H., et al. (2009) *Atmos. Chem. Phys.* **9**(10) 3331-3345.

Kampf, C. J., Jakob, R. and Hoffmann, T. (2012). *Atmos. Chem. Phys.* **12**(14) 6323-6333.

Leungsakul, S., Jaoui, M. and Kamens, R. M. (2005) *Environ. Sci. Technol.* **39**(24) 9583-9594.

Nozière, B., Dziedzic, P. and Córdova, A. (2009) J. Phys. Chem. **113**, 231-237

Yu, G., Bayer, A. R., Galloway, M. M., et al. (2011) *Environ. Sci. Technol.* **45**(15) 6336-6342.

Impact on Air Quality operations cleaning and inspection of Natural Gas pipelines in Central Mexico

L.M. Rodríguez, A.M. Sánchez de la Campa and J.D. de la Rosa

Associate Unit CSIC-UHU "Atmospheric Pollution". Center for Research in Sustainable Chemistry (CIQSO), University of Huelva, Campus El Carmen E21071 Huelva, Spain
Keywords: PLITTH, Natural Gas, Air quality, HYSPLIT.
Presenting author email: luismanuel.rodriguez@alu.uhu.es

Methane anthropogenic emissions are generated by the production of oil and natural gas leaks (Finlayson-Pitts & Pitts, 2000). The main processes impacting on the atmosphere are transport and storage of natural gas, including fugitive emissions in pipeline derived from the maintenance activities (USEPA, 1996). The Cleaning/ Inspection Process of Oil Pipelines (PLITTH), is a preventative maintenance procedure used to monitor the mechanical integrity of the pipelines, which requires natural gas emission to the atmosphere. In 2011, 69 PLITTH in central Mexico were performed.

In this work, Hybrid Single Particle Lagrangian Integrated Trajectory (HYSPLIT, Draxler and Rolph, 2003) model has been used to predict transport and dispersion of PLITTH emissions. The results showed that Air Quality of Metropolitan Area of Mexico (ZMVM) can be modify in least 12 of the analyzed events in 2011. The impact of PLITTH contaminant in ZMVM is showed in Figure 1 using PM10.

One of the main important episodes of impact occur on 11th January 2011, in which the Metropolitan Environmental Commission (CAM) of the ZMVM, activated the Atmospheric Environmental Contingency Program on 11th - 12th January by high PM_{10} values recorded at station XALOSTOC (XAL) to Northwest of the ZMVM. The high levels obtained were favored by a high pressure system coupled to the emissions for the PLITTH, and dominant local wind of W, NW and SW.

A solid residual of PLITTH was analyzed using Inductively Coupled Plasma (ICP-MS). 48 toxic potentially elements, among which Pb, Zn, Sr, Cr and lesser proportion of Mo, Cu, Sn, Nb were characterized. During PLITTH, several of toxic elements can be incorporated into the atmosphere as particulate material along with methane and its derivatives, and can impact negatively on air quality of urban areas densely populated.

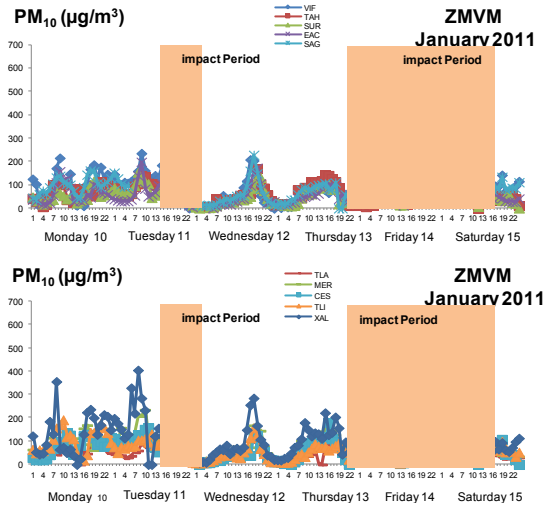

Figure 1. Emission of PLITTH on January 11, 2011 at 13:47 pm and its impact on the monitoring stations of the ZMVM.

In conclusion, approximately 82% of PLITTH impacts were developed at cities or states, most of which have not air quality networks, making difficult to assess the impact on the population and the environment.

Draxler and Rolph, 2003. NOAA *Air Resources Laboratory*, Silver Spring, MD.

Finlayson-Pitts Barbara J., Pitts Jr James N. (2000), *Chemistry of the Upper and Lower Atmosphere*, Academic Press.

United States Environmental Protection Agency (USEPA) (1996), *Methane Emissions from the Natural Gas Industry*, Volume 6: Vented and Combustion Source Summary.

Characterization of fine particles in the near-field of a metallurgy plant: Overview of the NANO-INDUS project

A. Setyan[1,2], P. Flament[1,2], N. Locoge[1,3], K. Deboudt[1,2], V. Riffault[1,3], L. Y. Alleman[1,3], C. Schoemaecker[1,4], J. Arndt[5], P. Augustin[1,2], F. Blond[6], F. Cazier[1,7], H. Delbarre[1,2], D. Dewaele[1,7], P. Dewalle[1,4], M. Fourmentin[1,2], P. Genevray[1,7], R. Healy[5], P. Le Louer[8], T. Leonardis[1,3], H. Marris[1,2], S. Mbengue[1,3] and J. Wenger[5]

[1]Université Lille Nord de France, 59000 Lille, France.
[2]Laboratoire de Physico-Chimie de l'Atmosphère, EA 4493-Université du Littoral Côte d'Opale, 59140 Dunkerque, France.
[3]Mines Douai, CE, 59508 Douai, France.
[4]Laboratoire de Physico-Chimie des Processus de Combustion et de l'Atmosphère, UMR CNRS-Lille1 8522, 59655 Villeneuve d'Ascq, France.
[5]Department of Chemistry and Environmental Research Institute, University College Cork, Cork, Ireland.
[6]Glencore Manganèse France SAS, 59792 Grande Synthe, France.
[7]Centre Commun de Mesures, Université du Littoral Côte d'Opale, 59140 Dunkerque, France.
[8]LECES, CS 25843, 57078 Metz CEDEX 03, France.

Keywords: industrial aerosols, aerosol chemistry, organics, heavy metals.
Presenting author email: ari.setyan@gmail.com

Industrial areas can be a significant source of particulate pollution and companies are therefore required to measure the particle concentration emitted from stacks. However, the physico-chemical properties of the particles leaving an industrial area are often poorly characterized and there is little information on the evolution of the plume between the source and the surrounding areas. Moreover, air quality monitoring stations are usually located away from industrial areas, because they are not considered as representative. The aim of the NANO-INDUS project was to study the evolution of the physico-chemical properties of industrial fine particles over a short-range distance, before they reach surrounding urban areas. First, measurements were performed directly at the stacks of a plant manufacturing iron-manganese alloy near Dunkirk, France. Then, an intensive field campaign was undertaken at a site located close (<1 km) to the stacks (Figure 1).

Preliminary results obtained during the intensive field campaign are presented here. The concentration of non-refractory submicron particles (NR-PM_1) was 10.2 $\mu g \cdot m^{-3}$ on average during this study. Particles were dominated by inorganic species (67% of the total mass), with organics accounting for 33%. The concentrations of several metallic species (Fe, Mn, V, Cu) were higher than those typically observed at urban environments, and their presence is likely related to industrial activities. However, the concentration and chemical composition of fine particles were subject to dynamic variations, even during periods with constant wind direction. This observation could be due to atmospheric turbulence or to variable emission rates from the plant. The organic fraction was highly oxidized (average O/C ratio = 0.52), which was not expected for this kind of site influenced by industrial and urban emissions. Thus, the sampling site might also be influenced by long-range transport of particles and precursor volatile organic compounds (VOCs), leading to secondary organic aerosol (SOA) formation. The comparison between different air masses shows significant differences in terms of particle concentration, chemical composition and size distribution. Under air masses coming from the industrial area, the particle and gas (CO, CO_2, NO_x, SO_2) concentrations were much higher than during periods dominated by urban or marine emissions. Moreover, the mass size distribution was dominated by submicron particles during periods subject to industrial emissions.

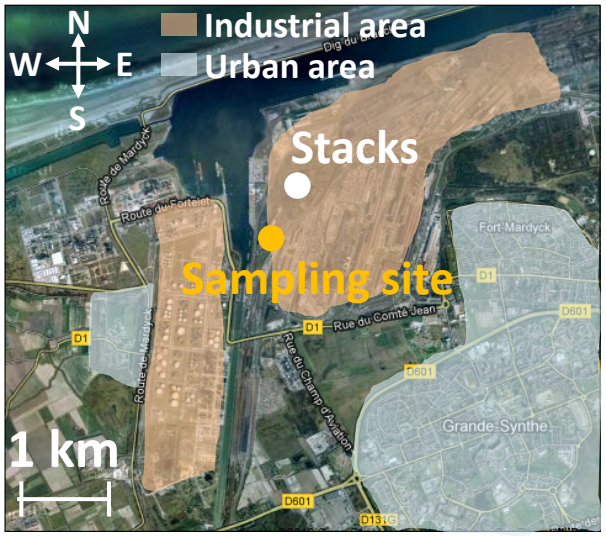

Figure 1. Map of the industrial area of Dunkirk, with the locations of the sampling site and the stacks of the metallurgy plant

The NANO-INDUS project was supported by the French Environment and Energy Management Agency (ADEME) under grant N° 11-81-C0089.

Organic aerosol: distribution between fog water and interstitial air - a report for two mountainous sites in Germany

S. Schüttauf[1], J. Matschullat[1], F. Zimmermann[1], D. van Pinxteren[2] and H. Herrmann[2]

[1]Interdisziplinary Environmental Research Centre, technical University Bergakademie Freiberg, Freiberg, Sachsen, 09599, Germany
[2]Chemistry Department, Leibnitz Institute for Troposheric Research, Leipzig, Sachsen, 04318, Germany
Keywords: fog water, interstitial aerosol, dicarboxylic acids, SOA
email: Stephanie.schuettauf@ioez.tu-freiberg.de

Aerosols are in the focus of current research because of their potential impact on humans and ecosystemic health. They may cause cardiovascular and neurodegenerative diseases and are in charge of oxidative stress. The toxicological effect of organic aerosols depends on their reactivity, influenced by their composition. In this context, fog and cloud water are important media. Due to its special microstructure, fog enables chemical reactions that do not exist in the gas phase. Long residence times near ground level support such chemical reactions. Furthermore, fog and cloud water are media for particle reformation. Hence, fog and cloud water considerably influence aerosols, their composition and properties in the atmosphere.

To date there is a demand in understanding transformation processes of organic compounds by fog and cloud water. We report measurements of the chemical composition of fog and interstitial aerosol samples from a) Zinnwald-Georgenfeld, 877 m a.s.l., eastern Erzgebirge, and b) Fichtelberg, 1,214 m a.s.l., highest elevation of the German Erzgebirge. The Erzgebirge was chosen because of a periodic occurrence of long-distance air mass transport, charged with high pollution concentrations. The most important source for these pollutants is the highly industrialized Northern Bohemian Basin (200–300 m a.s.l.) with a major concentration of Czech Republic's lignite power plants, petrochemical and heavy industry. Furthermore, the sampling site is characterized by a high frequency of fog events.

Passive string collectors were used to sample fog water, as described in Lange *et al.* (2003). Interstitial aerosol was collected using an aerosol sampler, based on impaction principles, and operating with quartz fiber filters. We determined the concentration of major ions, trace metals and carbonaceous material next to pH-values and electrical conductivity. TOC (OC/EC), carboxylic acids, sugar and sugar derivatives, and nitrophenols were in focus of the organic analysis.

Fog waters, characterized by a pH of 4 and an electrical conductivity of 130 µS cm^{-1} (mean values), showed an inorganic composition dominated by sulfate, nitrate and ammonium. Thereby, Zinnwald is the more polluted site; Fichtelberg is much less influenced by air pollution. Main trace elements are Fe, Al, Zn and Pb.

Within the organic fraction of fog water 22 "substituted"carboxylic acids (C5-C10) were determined, belonging to six different groups (aliphatic monocarboxylic acids (MCA), functionalized aliphatic MCA; aromatic and nitro-aromatic MCA, aliphatic dicarboxylic acids (DCA), functionalized aliphatic DCA, and aromatic DCA). Zinnwald was dominated by levulinic, benzoic, adipic and 7-oxoocatanoic acid (0.98 µmol L^{-1}, 0.25 µmol L^{-1}, 0.15 µmol L^{-1}, 0.09 µmol L^{-1}). Fichtelberg showed the highest concentrations for 2-isopropylmalic, azelaic and suberic acid (0.08 µmol L^{-1}, 0.06 µmol L^{-1}, 0.05 µmol L^{-1}). Furthermore, 8 short-chain carboxylic acids (C1-C4, oxalate, malonate, formiate, malate, succinate, glutarate, acetate and glycolate) were determined at both sites. For the interstitial aerosol, three different short-chain acids were found: oxalate (12.9 ng/m³), malonate (5.8 ng/m³) and succinate (2.9 ng/m³). The differences between the liquid and the interstitial phase were significant. There is enrichment in the fog water with a factor of 2 (oxalate), 6 (malonate) and 10 (succinate) (Figure 1).

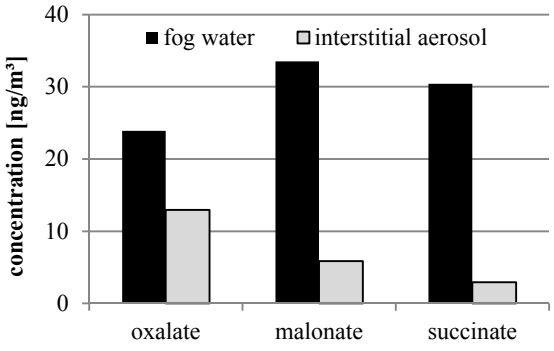

Figure 1. Concentration of carboxylic acids/salts in fog water and in interstitial aerosol.

Possible explanations for the observations could be photochemical processes, different phase distributions of the carboxylic species (in relation to the fog/interstitial phase) and the long residence time of fog concerning to increased process intensities

However, there must be further research to improve our understanding of transformation processes of organic compounds by fog and cloud water. This needs further investigation.

References

Lange, C.A., Matschullat, J., Zimmermann, F., Sterzik, G., Wienhaus, O. (2003) Fog frequency and chemical composition of fog water – a relevant contribution to atmospheric deposition in the eastern Erzgebirge, Germany. *Atmos Environ,* **39,** 3731-3739

Modelling the multiphase chemical processing of aerosol constituents in orographic hill cap clouds during HCCT-2010

A. Tilgner, P. Bräuer, R. Wolke and H. Herrmann

Leibniz Institute for Tropospheric Research (TROPOS), Permoserstr. 15, Leipzig, 04318, Germany

Keywords: multiphase chemistry, aerosol modelling, aerosol cloud interaction
tilgner@tropos.de

Tropospheric clouds and deliquescent aerosol particles are a complex multiphase and multi-component environment with simultaneously occurring gas and aqueous phase chemical transformations. Such aqueous phase chemical processes in cloud droplets are expected to proceed very efficient on short timescales and hence they are able to alter the chemical aerosol composition and the deduced physical properties on a global scale. Besides the physico-chemical aerosol processing, chemical aerosol-cloud interactions have significant effects on the whole multiphase oxidation budget.

In order to improve the still limited understanding of the aerosol-cloud interactions, Lagrangian-type field experiments, where an orographic cloud is used as a natural flow-through reactor, are used for studying such processes in more detail. In Sept./Oct. 2010, the Lagrangian-type cloud passage experiment HCCT-2010 (Hill Cap Cloud Thuringia 2010) was conducted at Mt. Schmücke in Thuringia, Germany to study aerosol cloud interactions (see Figure 1). As known from former cloud passage experiments, particularly associated model investigations (see e.g. Tilgner et al., 2005) including comparisons of model results with observations have considerably contributed to the interpretation of the measured field data.

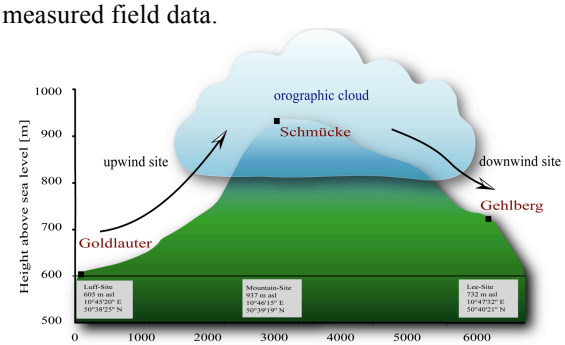

Figure 1. Schematic representation of the campaign area of the cloud passage experiment HCCT-2010.

In the present study, the parcel model SPACCIM (SPectral Aerosol Cloud Chemistry Interaction Model, Wolke et al., 2005) was applied to investigate the effects of multiphase chemical processing of tropospheric aerosol particles and trace gases resulting from a passage through an orographic cloud at Mt. Schmücke (Germany) during HCCT-2010. The applied model combines a complex microphysical and a detailed multiphase chemistry model with 11381 gas phase and over 3700 aqueous phase reactions. The chemical multiphase mechanism (MCMv3.1 (Master Chemical Mechanism; Saunders et al., 2003)/ CAPRAM3.7 (Chemical Aqueous Phase RAdical Mechanism, modified following Herrmann et al., 2005)) incorporates a detailed near-explicit description of the inorganic and organic multiphase chemistry based on time-dependent size-resolved aerosol/cloud spectra. The measured physical and chemical data at the upwind site provided the basis for the model initialisation under real environmental conditions.

SPACCIM simulations have been carried out for few cloud events, which provided appropriate meteorological and overflow conditions fulfilling the cloud passage experiment requirements. Model results of the cloud passage simulation have been compared with experimental cloud water composition data at Mt. Schmücke (summit site) as well as gas and aerosol measurements at the downwind site in order to interpret the experimental data and to evaluate the model results. To this end, detailed analyses of the chemical multiphase system have been performed including chemical source and sink studies with special emphasis on radical and non-radical oxidants as well as important organic and inorganic chemical subsystems. For the first time, modelled interstitial gas phase in-cloud HO_x radical concentrations were compared with in-cloud measurements. Moreover, a central objective of the study was to assess in-cloud oxidations of important C2 and C3 organic compounds. Total organic mass increases after the cloud passage of about 200 ng m^{-3} were modelled. Comparisons between modelled and measured concentrations have revealed good agreements for various measured cloud water constituents. However for organic compounds with low water solubilities measurements have shown considerably higher concentrations than the model results indicating an enrichment in the cloud droplets.

This work was supported by the German Research Foundation (DFG, He 3086/15-1).

References

Herrmann, H. et al. (2005) *Atmos. Environ.* **39** (23-24), 4351-4363.

Saunders, S. M. et al. (2003) *Atmos. Chem. Phys.*, **3**, 161-180.

Tilgner, A. et al. (2005) *Atmos. Environ.* **39** (23-24), 4389-4401.

Wolke, R. et al. (2005) *Atmos. Environ.* **39** (23-24), 4375-4388.

Mass distribution of elements among four fractions of suspended dust in Zabrze, Poland.

W. Rogula-Kozłowska, K. Klejnowski, P. Rogula-Kopiec, B. Błaszczak, M. Mathews, S. Szopa

Institute of Environmental Engineering, Polish Academy of Sciences, 34 M. Skłodowska Curie St., 41-819 Zabrze, Poland

Keywords: PM1, EDXRF, size-resolved elemental composition, Silesia.

email: wioletta@ipis.zabrze.pl

Despite the increasing number of studies concerning determination of concentrations and elemental composition of, especially the fine dust, the existing amount of relevant information and data on these subjects is noticeably insufficient, i.a. in the Eastern Europe area. Knowledge about the chemical composition, including the elemental composition of, particularly the submicron dust in Poland, is very limited. The aim of this study was to determine and compare the elemental composition of four fractions of suspended dust in an urban area, characteristic for the Upper-Silesian Agglomeration in terms of the exposure of its population.

Diurnal samples of the four dust fractions (PM_1, $PM_{1\text{-}2.5}$, $PM_{2.5\text{-}10}$ and $PM_{10\text{-}40}$) were collected for eight months (January-August) in Zabrze with the use of a DEKATI-PM10 cascade impactor. The elemental composition of PM samples was determined by means of energy dispersive X-ray fluorescence (Epsilon 5, PANalytical Inc., Rogula-Kozłowska et al. 2013).

Average concentrations in the winter – heating season (January-April) and average concentrations in the summer – non-heating season (May-August) of 35 elements bound to each of the four examined fractions of dust were calculated. Additionally the influence of anthropogenic sources on the concentrations of elements bound to each PM fraction was estimated based on the analysis of so called enrichment factors (EF, Fig. 1), and the strength of linear relationships (Pearson's linear correlation coefficients) between each pair of elements were investigated – separately for fine and coarse dust.

The highest concentrations in Zabrze were observed for nonmetals – sulfur and chlorine, and their concentrations were significantly lower in the summer than in the winter–heating, season. Both elements – S and Cl – were concentrated mainly in the finest particles. Their share in the coarse dust, even in the summer season, was small. The concentrations of both sulfur and chlorine in the air of Zabrze are determined by anthropogenic sources.

Si, Al and Fe, Mg, K, Ca and Ti, Sr, Rb in the air of Zabrze consist a group of elements of a typically crustal origin. In Zabrze concentrations of these elements, regardless of the fraction of dust to which they are bound, are determined by natural sources. This conclusion is confirmed by small seasonal variations in concentrations of these elements or cases, in which concentrations of the elements are higher in the summer than in the winter season.

A significant portion of mass of crustal elements, particularly Al, Si and Fe, was concentrated in the coarse dust fractions. However, thorough analysis of mass distribution of these components among the dust fractions indicates that some of them – K, Ca, Mg, Rb, Sr, can be additionally emitted from anthropogenic sources. It particularly concerns the fraction bound to fine dust and the winter-heating season. The estimated contribution of soil matter to the mass of TSP is about 6.8 and 9.7 % in the winter and summer season, respectively. The share of soil matter in PM_1 is one half smaller.

Concentrations of the remaining metals in most cases did not exceed 100 $ng \cdot m^{-3}$ (except for Mn, Zn, Ge, Sb, La) and usually varied seasonally – were higher in the winter season. Co, Cu, Zn, Pb and As were concentrated mainly in fine dust, while V, Mn, Co, Cr, Ni, Ag, Cd and Ba were mostly bound to coarse dust. It was assumed that the first group, present in higher concentrations as components bound to fine dust, are mainly of anthropogenic origin and are closely associated with combustion processes. The remaining elements, especially in the winter, originate partly from combustion processes, but resuspension of road dust is the source of the majority of their mass.

The largest contributors to the levels of elements bound to fine dust in Zabrze are the sources of emission including burning of fossil fuels, biomass, waste and liquid fuels in domestic furnaces and car engines. Also the possible influence of industrial sources was identified. Concentrations of elements in coarse dust are determined by resuspension of soil and road dust, and to a lesser extent, by municipal emission.

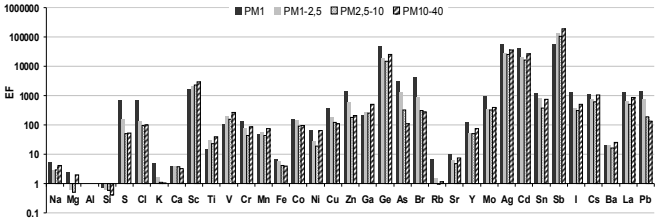

Figure 1. Average values of *EF* for PM_1-, $PM_{1\text{-}2.5}$-, $PM_{2.5\text{-}10}$- and $PM_{10\text{-}40}$-related elements in Zabrze in the period: January-August

This work was partially supported by the grant No. N N523 564038 from the Polish Ministry of Science and Higher Education.

Rogula-Kozłowska, W., Błaszczak, B., Szopa, S., Klejnowski, K., Sówka, I., Zwoździak, A., Jabłońska, M., Mathews, B. (2013) Environ. Monit. Assess., 185, 581-601.

Thermal properties of SOA from Ozone and OH induced oxidation of terpenes

J. Westerlund[1], Å.K. Watne[1], Å. M. Hallquist[2] and M. Hallquist[1]

[1]Atmospheric science, Department of Chemistry and Molecular Biology, University of Gothenburg, 412 96, Gothenburg, Sweden
[2]IVL Swedish Environmental Research Institute Ltd, Box 5302, 400 15, Gothenburg, Sweden
Keywords: Second organic aerosol, Aerosol chemistry, Volatility, Oxidation.
Presenting author email: jonathan.westerlund@chem.gu.se

Introduction

Secondary Organic Aerosols (SOA) constitutes a major fraction of atmospheric particles and they have an important impact on the climate by scattering and absorption of solar radiation. SOA have both direct and indirect climate effects where the latter is the least understood. Key steps yet to understand and quantify are formation, properties and transformation of SOA where knowledge today is poor (Hallquist et al., 2009).

Oxidation of four terpenes was studied with respect to both ozone and OH chemistry with a focus on thermal properties on the SOA formed.

Method

Four terpenes were oxidised in two separate flow through systems where ozone and OH chemistry was separated (figure 1). OH was studied in a Potential Aerosol Mass (PAM) chamber. PAM is defined as the maximum aerosol mass that can be produced from precursor gases (Kang et al., 2007). Ozone chemistry was studied in the laminar flow reactor GFROST (Gothenburg – Flow-tube Reactor for Oxidation Studies at low Temperatures) which is described elsewhere (Jonsson et al., 2008).

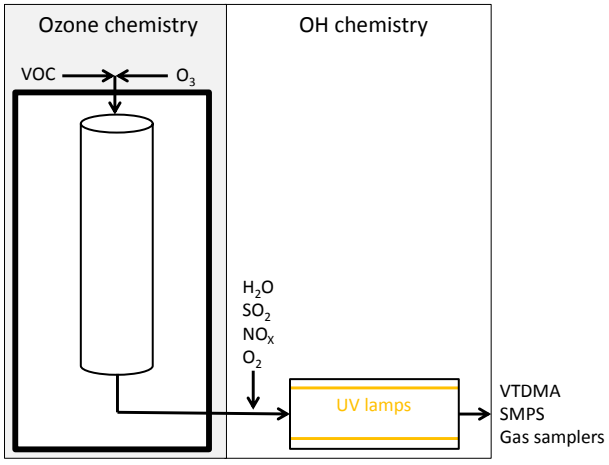

Figure 1. Set-up used to separate OH-chemistry (PAM-chamber) and Ozone chemistry (Laminar flow tube GFROST)

Low VOC levels were selected and high oxidation levels to simulate a few hours of ozone chemistry and 2 – 7 days of OH chemistry. The experiments were performed in room temperature and at atmospheric pressure.

Thermal properties of the SOA formed were studied with a Volatility Tandem Mobility Analyser (VTDMA). Oxidation of SO_2 was used to determine OH concentration using a T100U SO_2 analyzer (Teledyne). NOx was selectively used to further simulate atmospheric conditions measured with a CLD 700 AL (Eco physics). Ozone was continuously measured with a 49C ozone analyser (Thermo environmental instruments inc.).

Results

Limonene, α-pinene, Δ-carene and β-pinene were oxidized in a number of experiments. The oxidant first attacking the VOC determine to a great extend the characteristics of the aerosol produced, both regarding number, mass and thermal properties. However, a terpene initially oxidised only with ozone will with additional OH oxidation become more volatile. This is presumably because of gas phase oxidation allowing more semi-volatile material to condense into the aerosol phase.

The PAM chamber has been coupled to a previously well studied laminar flow tube and VTDMA system. The PAM-chamber was thoroughly evaluated regarding e.g. temperature and OH concentration.

The authors acknowledge Leif Marsteen at NILU for the the logging program CLL used for the SO_2-analyzer.

Hallquist, M., et al. (2009), *Atmos. Chem. Phys.* **9**, 5155-5236

Jonsson, Å. M., Hallquist, M. and Ljungström, E. (2008), *Environ. Sci. Technol.* **42**, 16, 5938-5944

Kang, E., Root, M. J., Toohey, D. W. and Brune, W. H. (2007), *Atmos. Chem. Phys.* **7**, 5727-5744

Microstructural changes on the carbon functional groups of individual aerosol particles from cooking activities during photochemical oxidation

E. Coz[1], I. El Haddad[2], S. Platt[2], J. G. Slowik[2], A. S. H. Prévôt[2], S. Steimer[3,4], G. Grzinic[3,5], M. Lampimäki[3], B. Artíñano[1] and M. Ammann[3]

[1]Department of the Environment, CIEMAT, Madrid, ES-28040, Spain
[2]Laboratory of Atmospheric Chemistry, PSI, Villigen-PSI, CH-5232, Switzerland
[3]Laboratory of Radiochemistry and Environmental Chemistry, PSI, Villigen-PSI, CH-5232, Switzerland
[4]IACETH, ETH Zurich, Zurich, CH-8092, Switzerland
[5]Department of Chemistry and Biochemistry, University of Bern, Bern, CH-3012, Switzerland

Keywords: organic aerosols, cooking activities, photochemistry, microstructure.
Presenting author email: esther.coz@ciemat.es

Cooking emissions are a major contributor to indoor and outdoor $PM_{2.5}$ organic aerosols (Mohr et al., 2012). Understanding the changes in behaviour and properties of these emissions with atmospheric processing is crucial to quantify their effects on climate and to design effective abatement strategies. Nevertheless, very little is known about the microstructural properties and the effects of atmospheric processing thereon, properties undoubtedly related with the optical and hygroscopic properties determinant on assessing the effects of aerosols on climate change.

The present study aimed at the characterization of the chemical heterogeneities and changes in the internal microstructure of individual aerosol particles from different cooking activities. The major goal was to establish a relation between changes in the carbon functional groups and photochemical aging in laboratory generated aerosol particles, not only identifying the different groups but the spatial distribution within the individual particle structure.

The aging experiments were conducted in the PSI mobile smog chamber (Platt et al., 2012) with grilled chicken/NOx/hν and boiled vegetables/NOx/hν, as testing systems for the cooking emissions. Two different samples were collected during the experiment timeline, from primary and aged emissions, to be subsequently analyzed by STXM/NEXAFS at the PolLux beamline of the PSI SLS (Raabe et al., 2008). Complementary high-resolution SEM analyses were conducted to complete the microstructural study.

Results corroborated that cooking activities emit a variety of organic compounds that behave very differently during atmospheric processing from source to source and type of activity. This is also evidenced by changes in the particle structure. Vegetable boiling produced a wide range of primary organic structures not present when the emission is highly aged. These differences stressed the complexity in the interpretation of the results. In addition, no typical aged features were found on the NEXAFS spectra of the particles. In the case of the grilled meat, a major contribution of unsaturated moieties was found in particles from the slightly aged samples. The unsaturated groups seem to be the nuclei of the later condensed groups forming coatings of different thicknesses (Fig. 1). This was consistent with the results from the AMS analysis. This novel information is especially interesting for the improvement of the radiative transfer and CCN (Cloud Condensation Nuclei) activity estimations that include a core-to-shell particle model in climate change studies.

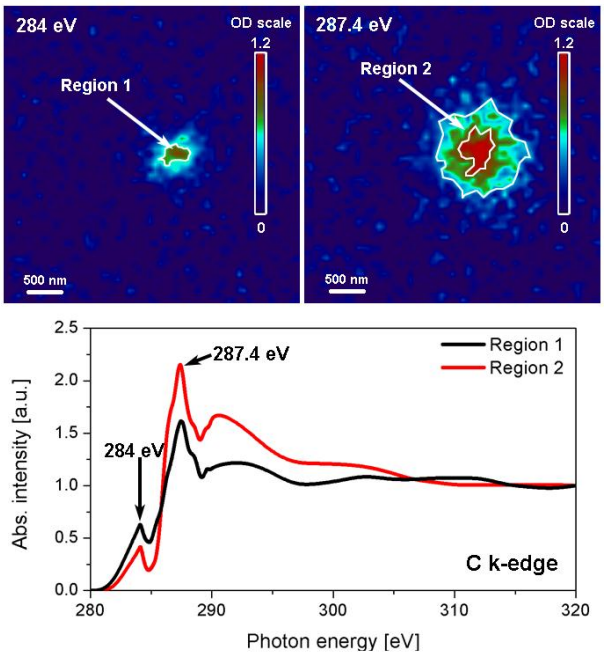

Figure 1. Top: Optical density (O.D.) images of a particle from the meat-cooking sample measured at 284.0 eV (quinone-C) and 287.4 eV (aromatic/aliphatic-C) (Hopkins et al., 2007). Bottom: C K- edge spectra of the regions 1 and 2 from the same particle.

We would like to acknowledge B. Watts and J. Raabe for their technical support at the Pollux beamline. This work is supported by the EU FP7 project PEGASOS, the SNSF through the short stay IZK0Z2_142687, the MICROSOL project (CGL2011-27020), and the AEROCLIMA project (CIVP16A1811) by Fundación Ramón Areces. The SEM analyses were conducted at the National Center for Electron Microscopy (UCM, Madrid, Spain).

Hopkins et al. (2007), *Aerosol Sci.* **38**, 573 - 591
Mohr et al. (2012) *Atmos. Chem. Phys.* **12**, 1649-1665.
Platt et al. (2012) *Atmos. Chem. Phys. Discuss.* **12**, 28343-28383.
Raabe, J. et al. (2008) *Rev. Sci. Instrum.* **79**, 113704.

Automatic hourly measurements of hydrocarbons (C2-C11) in Metropolitan Area of Sao Paulo: Spring campaign

P.A. Dominutti[1], T. Nogueira[1,] A. Fornaro[1]and M. F. Andrade[1]

[1]Department of Atmospheric Sciences, University of São Paulo, IAG/USP, São Paulo, 05508-090, Brazil
Keywords: Ozone precursors, NMHCs, sampling, urban air pollution
Presenting author email: pamela@model.iag.usp.br

A large variety of volatile non-methane hydrocarbons (NMHC) is found in the atmosphere. These species have a key role in the formation of tropospheric ozone. Ozone represents one of the main atmospheric pollutants in the Metropolitan Area of Sao Paulo (MASP). In this region, its concentration exceeds the national air quality standards (80 ppb/hour) for several days of the year.

In order to characterize emission fonts and to establish the behaviour pattern for some atmospheric NMHC, a campaign was carried out in MASP, during the Spring of 2012. The sampling point is located in a west region of MASP, inside the University of São Paulo Campus, surrounded by important avenues, with intense vehicular traffic (trucks, buses and light vehicles).

The ozone precursors automated measurement from Perkin Elmer® system is based on: 1) a Thermal Desorber (TD) fitted with an air sampler accessory, in which the dried sample is concentrated in an electrically cooled sorbent trap (−30 °C) in the TD. In a second stage, the concentrated sample is desorbed by rapid heating at a rate of 40 °C s^{-1} up to 325 °C, maintained for 6 min, and transferred by a helium (6.0) carrier flow into the chromatographic system. 2) A Clarus 500 gas chromatography with two columns and two flame ionization detectors (FID). Operation was optimized for systematic measurement of more than 50 NMHC (C2–C11) every hour. Ambient air samples were collected during the spring season period (2012), which are of main interest for local ozone episodes in the area.

The most abundant compounds were trans-2 hexene, toluene, ethane, ethylene, p-xylene, 2,3-dimethyl-butane and 1,2,4-trimethyl-benzene, which are related with a greater photochemical ozone potential formation following the MIR reactivity scale of Carter (Carter, 2010). These results are in agreement to the ones found in other NMHC long-term campaigns.

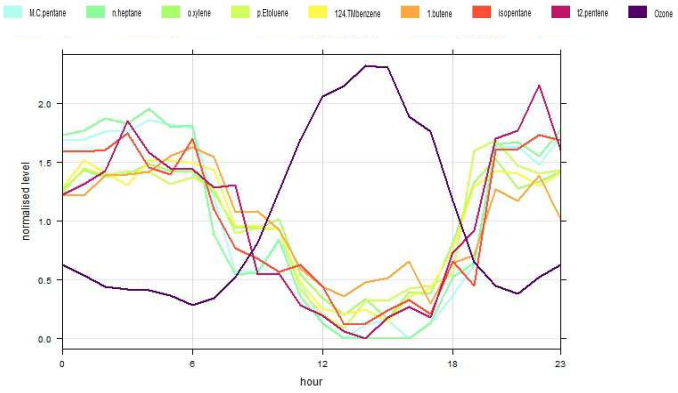

Figure 2. Evolution of the hourly average pattern of some selected NMHC and Ozone (normalized)

Statistical correlation analysis classified the data into groups with similar characteristics and infers possible emission sources of each group. In addition, Factor Analysis was applied to the base data determining descriptive factors that allow us to find specific tracers for different emissions fonts in this area of São Paulo city. The matrices of Figure 1 show a high correlation between aromatic compounds, and a negative correlation of some of them with the ozone. The hourly time average evolution can be seen in Figure 2. As can be observed, most of the compounds follow a similar pattern, which is inversed to the compared ozone daily pattern.

The authors would like to thank for the data supported by CETESB and for the financial support of CAPES, FAPESP, CNPq and INAIRA

Carter (2010) *Updated maximum incremental reactivity scale and hydrocarbon bin reactivities for regulatory applications*. University of California, Riverside.

R Core Team (2012). R: A language and environment for statistical computing. R Found. for Statistical Computing, ISBN 3-900051-07-0.

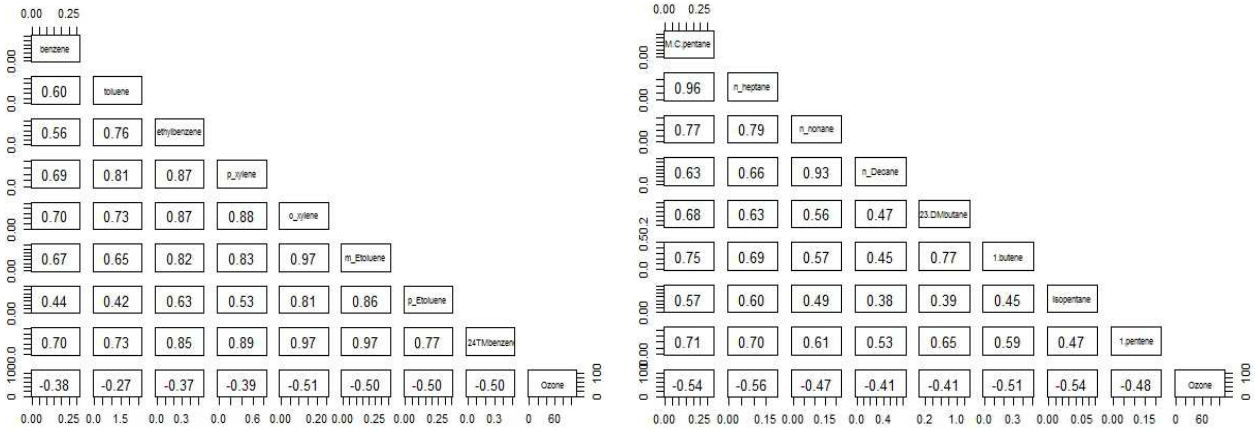

Figure 1. Correlation matrices of some NMHC and Ozone

Chemical composition of PM_{10} and PM_1 at a remote mountain site in NE of Spain

A. Ripoll[1], M.C. Minguillon[1], J. Pey[1,2], X. Querol[1] and A. Alastuey[1]

[1] Institute of Environmental Assessment and Water Research (IDAEA-CSIC), Barcelona, 08034, Spain
[2]Aix-Marseille Université, CNRS, LCE FRE 3416, Marseille, 13331, France
Keywords: tropospheric aerosols, continental background, PM_1, chemical composition
Presenting author email: anna.ripoll@idaea.csic.es

Chemical composition of particulate matter (PM) was determined at Montsec (MSC, NE of Spain, 42º 3' N; 0º 44' W) remote site, to investigate variability of tropospheric aerosols speciation and to quantify sources of aerosols in a continental background environment. This work summarizes results on partitioning and variability of major and trace components in PM_{10} and PM_1.

24h PM_{10} and PM_1 samples were collected at a ratio of 1 sample out of 4 days, on quartz fibre filters using high-volume samplers (MCV CAV-A/MSb).

Overall, 371 (Nov 2009-Dec 2012) and 221 (Mar 2011-Dec 2012) samples of PM_{10} and PM_1, respectively, were collected. PM concentrations were determined by standard gravimetric procedures. Samples were treated following the methodology from Querol *et al* (2001) for the determination of the major and trace elements concentrations. In addition to the routine measurements, intensive campaigns were performed during Mar-Apr 2011, Jul-Aug 2011, Jan-Feb 2012, and Jun-Jul 2012.

Low average concentrations of PM, which are typical of remote sites, were recorded. The lowest PM concentrations were measured in winter (7.6 µg m^{-3} and 6.5 µg m^{-3} for PM_{10} and PM_1 respectively) because during this season MSC is frequently above the planetary boundary layer (PBL) and is mainly influenced by long-range-transported particles. On the contrary, the highest concentrations were measured during summer (15.0 µg m^{-3} for PM_{10} and 10.2 µg m^{-3} for PM_1) due to the recirculation processes that accumulate regional pollutants (Figure 1) and to the frequent impact of Saharan dust outbreaks.

The chemical components were grouped as:

- Mineral matter (MM: sum of components typically found in rock-forming minerals, including Al_2O_3, SiO_2, CO_3^{-2}, Ca, Fe, K and Mg)
- Sea Spray (SS: sum of Cl^- and Na^+)
- Secondary inorganic species were treated individually (sulphate: SO4, nitrate: NO3, ammonium: NH4)
- Organic matter (OM, calculated from the organic carbon (OC) as 2.2*OC) and elemental carbon (EC)
- Trace elements (TE: sum of Li, Be, V, Ni, Ti, Cu, Zn, As, Cr, Mn, Co, Ga, Se, Rb, Sr, Cd, Sn, Sb, Ba, La, Ce, , Hf, Ta, TI, Pb, P, Bi, Th, and U).

The percentage of each species with respect to the total mass was very similar in summer and in winter for both size fractions (Figure 1), except for SO4 and NO3. SO4 concentrations were higher in summer and lower in winter, opposite to NO3 concentrations, due their different sources and gas to particle equilibrium. Also, in summer, a higher contribution of coarse MM was evidenced due to the frequent impact of Saharan dust events and to the wind-induced soil resuspension.

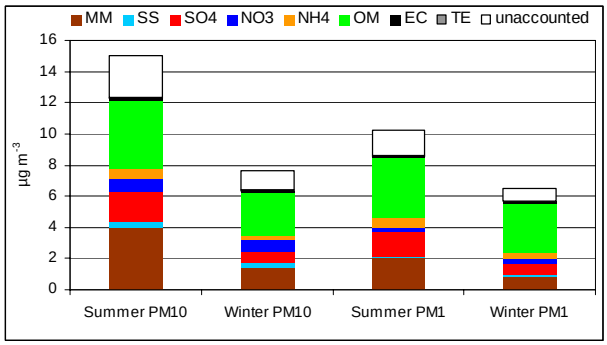

Figure 1. MM, SS, SO4, NO3, NH4, OM, EC and TE summer and winter mean concentrations for PM_{10} and PM_1 at MSC site.

MM, SS, NO3, and TE were mainly in the coarse fraction, whereas SO4, NH4, OM and EC were principally fine (Figure 2).

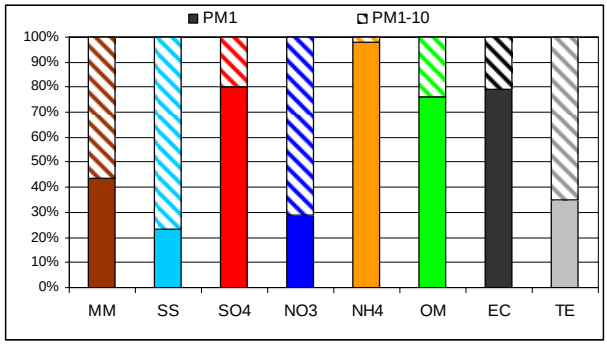

Figure 2. Mean PM_1 and PM_{1-10} proportion (%) of PM_{10}.

Chemical composition of PM will be interpreted as a function of meteorological scenarios, and source apportionment will be estimated by receptor models.

This work was supported by the MICINN (Spanish Ministry of Science and Innovation) and FEDER funds under the project CARIATI (CGL2008-06294/CLI). M.C.M. was funded by JAE-Doc CSIC, co-funded by the European Social Fund (ESF).

Querol, X., Alastuey, A., Rodriguez, S., Plana, F., Mantilla, E., and Ruiz, C.R., (2001) *Atmos. Environ.*, **35**, 845-858.

Profiles and seasonal-distribution of PAH and *n*-alkanes in the urban atmosphere of Elche, Spain

J. Gil-Moltó, N. Galindo, M. Varea and C. Chofre

Department of Physics, Miguel Hernández University, Avda. de la Universidad s/n, 03202, Elche, Spain
Keywords: PM, PAH, alkanes, size distribution, seasonal distribution.
Presenting author email: j.gil@umh.es

Particle-bound PAHs and *n*-alkanes have been widely studied since the organic fraction of atmospheric particulate matter (PM) was considered as a complex mixture of hundreds of different compounds. These two families of pollutants have received special attention due to PAH mutagenic and/or carcinogenic properties and because of the relatively high concentrations of aliphatic hydrocarbon found in most of the studied areas.

Organic compounds can be found in both the coarse (>2.5 μm) and the fine (<2.5 μm) fractions of atmospheric PM, although the higher concentrations are usually associated to the fine fraction (Sicre *et al* 1987), which is also the most dangerous one because it can reach the human lung alveoli (Gerde *et al,* 1991).

PM1, PM2.5 and PM10 samples were collected, from November 2008 until July 2009, for simultaneous 24-hourperiods on the roof of a 15 m height building at the Miguel Hernández University by means of low volume samplers (2.3 m^3/h) on teflon-impregnated glass-fibre filters. Seventeen PAHs and twenty seven *n*-alkanes from C16 to C40, plus the branched alkanes pristine and phytane were analysed by thermal desorption coupled with gas chromatography-mass spectrometry (TD-GC-MS) (Gil-Moltó *et al,* 2009).

Mean concentrations of the sum of all PAHs and hydrocarbons studied (TPAH and THC, respectively) for the spring-summer (SS) and autumn-winter (AW) seasons, along with the concentrations of hydrocarbons with odd and even carbon number, are shown in Table 1.

Table 1. Mean concentrations during the study period.

Compound	Season	PM1 (ng/m^3)	PM2.5 (ng/m^3)	PM10 (ng/m^3)
TPAH	SS	0.42	0.56	0.57
	AW	1.03	1.42	1.44
THC	SS	9.71	11.96	17.14
	AW	13.02	19.31	19.42
HCeven	SS	4.05	5.10	5.88
	AW	5.45	8.07	8.04
HCodd	SS	5.62	6.84	11.22
	AW	7.50	11.07	11.35

Around 70 % of PAHs were associated to the PM1 fraction, and almost the rest were found in the PM2.5-1 one. As expected, PAHs were predominantly associated to the submicron fraction, making this fraction more toxic for human health. In fact, all PAHs were found linked to particles below 2.5 μm.

Benzo(b)fluoranthene and its homologue benzo(k)fluoranthene, two PAH strongly associated to vehicular emissions, were the most abundant PAH in all the fractions, followed by chrysene, usually related to incomplete combustion or pyrolysis of coal and crude oil, as well as home heating.

No statistical differences were found in PAH profiles in PM1 and PM2.5, pointing to common sources for all PAHs in these two fractions.

Hydrocarbon particle content presented different profiles depending not only on the size fraction, but also on season of the year. In general, the higher *n*-alkane concentrations were observed during the cold season, although their size distributions were different from those obtained for the warm period. During the spring-summer period, around 30% of the total *n*-alkanes were associated to the PM10-2.5 fraction, and practically the rest (56%) was in the PM1 one. Meanwhile, when temperatures decreased, 69% of the THC were found in PM1 and 30% in PM2.5-1. Therefore, a clear shift of *n*-alkane towards the submicron fraction is observed.

The values of the carbon preference index (CPI) (between 1.3 and 1.9) and percentages of total wax *n*-alkanes (%WNA) were calculated. WNA values for PM1, PM2.5 and PM10 are shown in Figure 1, along with the concentrations of *n*-alkanes in PM1 for the two seasons.

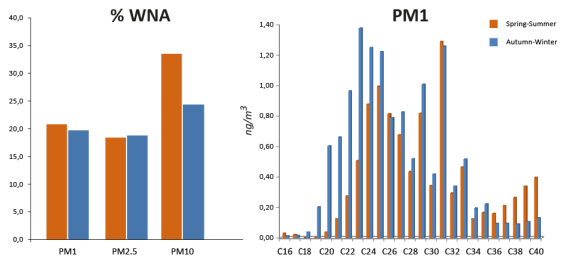

Figure 1. Percentage of Plant Wax and PM1 *n*-alkane concentrations during the study period.

C_{max}, CPI and % WNA suggest a mixture of anthropogenic and biogenic origins for *n*-alkanes, with an increase of biogenic emissions during the spring-summer period. Wax *n*-alkanes from plants significantly contributed to the total content of *n*-alkanes PM10, especially during the war season.

This work was supported by the Ministerio de Educación y Ciencia under the CGL2007-63326 (DAPASE).

Gerde, P., Medinsky, M. A. and Bond, J. A. (1991) *Toxicol. Appl. Pharm.* **107**, 239-252.

Gil–Moltó, J., Varea, M., Galindo, N. and Crespo, J. (2009) *J. Chromatogr. A* **1216**, 1285-1289.

Sicre, M. A., Marty, J. C., Saliot, A., Aparicio, X., Grimalt, J. and Albaiges, J. (1987) *Atmos. Environ.* **21**, 2247-2259.

Organic and elemental carbon in the surroundings of a cement complex in southeastern Spain

E. Yubero[1], N. Galindo[1], S. Nava[2], M. Chiari[2], J. Nicolás[1], G. Calzolai[2], F. Lucarelli[2] and J. Crespo[1]

[1]Department of Physics, Miguel Hernández University, Avda. Universidad, 03202, Elche, Spain
[2]Department of Physics, University of Florence and INFN, via Sansone 1, I-50019, Sesto Fiorentino, Italy
Keywords: carbonaceous aerosols, PM2.5, PM10, OC-to-EC ratio.
Presenting author email: eyubero@umh.es

Carbonaceous species are major components of atmospheric particulate matter (PM) and directly affect human health and the environment. The carbonaceous fraction of PM consists of elemental carbon (EC) and organic carbon (OC), which includes thousands of organic compounds. In this work, we present OC and EC concentrations in both PM2.5 and PM10 daily samples collected at a suburban location close to a cement complex in southeastern Spain. The samples were gathered every four days from September 2005 to August 2006. Details of the sampling campaign and the characteristics of the sampling site are given in Galindo *et al* (2011). OC and EC concentrations were obtained at INFN of Florence with a Sunset Laboratory Thermal-Optical Carbon Aerosol analyser using the NIOSH protocol.

Annual average concentrations of PM and carbonaceous species during the study period are presented in Table 1. OC concentrations were obtained by subtracting the carbon carbonate (CC) - calculated from the anion deficit (Galindo *et al*, 2011) - from the organic carbon content obtained from the thermal-optical analysis.

Table 1. Annual mean concentrations (μg/m^3) of PM, OC and EC in PM2.5 and PM10.

Fraction	PM	OC	EC
PM2.5	18.0±7.6	2.3±1.2	1.0±0.5
PM10	40.5±17.5	2.6±1.4	1.1±0.6

Annual mean OC and EC concentrations were generally lower than those measured at urban stations in the Mediterranean basin and Europe, but higher than those found at rural locations (Pio *et al*, 2011). OC was the main constituent of total carbon (TC = EC + OC), both in PM2.5 and PM10, contributing approximately 70%. This percentage is very similar to that obtained by Viana *et al* (2006) in Barcelona.

As expected, the contribution of TC to the average PM2.5 mass concentration was significant (20±9%) and only sulphate accounted for a higher proportion of the PM2.5 mass (26±9%). In PM10, TC contributed only 10±4% to the annual mean concentration.

Figure 1 shows monthly variations of OC and EC concentrations and the OC/EC ratio for PM2.5. Similar results were found for the PM10 fraction. OC levels were maxima in winter and minima during spring and summer, with a winter/summer ratio of 1.5 for PM2.5 and 1.8 for PM10. This seasonal pattern was caused by the lower atmospheric dispersion conditions and the shift of the gas-particle equilibrium to particulate phase during winter. EC concentrations showed limited monthly variations probably because of the relatively constant flow of traffic in the area surrounding the sampling site.

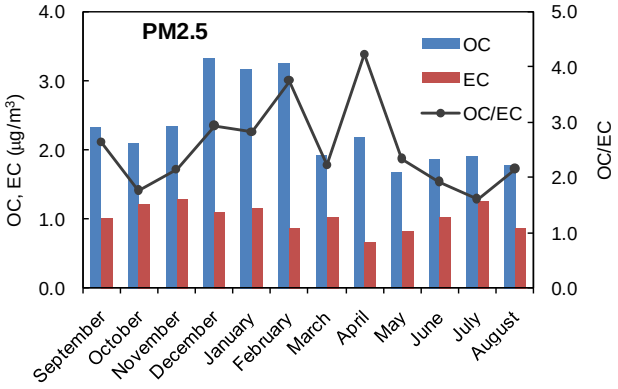

Figure 1. Monthly OC and EC concentrations and OC/EC ratio.

Annual average OC/EC ratios were 2.5±1.3 and 2.5±1.6 for PM2.5 and PM10, respectively. These values fell within the range reported for other European urban and industrial locations (Pio *et al*, 2011), although a different seasonal variation was observed. At our sampling site, the lowest OC/EC ratios were obtained in summer (Figure 1), suggesting a high contribution of semi-volatile organic compounds in comparison with non-volatile organics. This assumption was supported by the significant negative correlation obtained between monthly average OC concentrations and temperature in both PM2.5 and PM10 ($r > 0.78$).

This work was partially supported by the Spanish Ministry of Science and Innovation under the CGL2009-08036 (PASSE) and CGL2012-39623-C02-2 (PRISMA) projects.

Galindo, N., Yubero, E., Nicolás, J.F., Crespo, J., Pastor, C., Carratalá, A and Santacatalina, M. (2011) Atmos. Environ. 45, 2043-2049.

Pio, C., Cerqueira, M., Harrison, R.M., Nunes, T., Mirante, F., Alves, C., Oliveira, C., Sánchez de la Campa, A., Artíñano, B. and Matos, M. (2011). *Atmos. Environ.* **45**, 6121-3132.

Viana, M., Chi, X., Maenhaut, W., Querol, X., Alastuey, A., Mikuška, P. and Večeřa, Z. (2006). *Atmos. Environ.* **40**, 2180-2193.

ATD-GC-MS method for characterization and quantification of organic compounds associated to gunshot particles

R. Magnusson[1], L. Hägglund[1], S. Hedenstierna[2] and H. Wingfors[1]

[1]FOI Swedish Defence Research Agency, CBRN Defence and Security, Umeå, SE-901 82, Sweden
[2]FOI Swedish Defence Research Agency, Department of Energetic Materials, Tumba, SE-147 25, Sweden
Keywords: ATD-GC-MS, oxy-PAH, gunshot particles, SRM 1649b.
Presenting author email: roger.magnusson@foi.se

Numerous studies have shown that military and civil use of lead containing ammunitions is associated to severe environmental and health considerations i.e. high blood levels. This has led to the development of lead-free ammunition however these replacement products have been associated to other health implications such as respiratory irritation, asthma, fever and nausea. Emissions from shooting with small calibre ammunition makes up of a complex mixture of gases and particles. For instance, polycyclic aromatic hydrocarbons (PAHs) that are known to have mutagenic properties have been identified in emissions from small calibre rifles using nitro-based propellants (Moxnes *et al*, 2013). It has further been shown that respirable particles in the size range 0.29-0.57 µm from shooting were associated to higher mutagenic activity as compared to larger particle fractions (Palmer, 1994). The aim of this work was to develop a rapid method for quantitative chemical analysis of mutagenic and toxic organic compounds (PAHs and oxy-PAHs) associated to particles and to apply the method in a study of gunshot particles from lead free ammunition. Two standard reference materials, SRM1649b (urban dust) and SRM 1650b (diesel particulate matter) were used for method validation and comparison.

In a 0.7 m^3 test chamber an assault rifle (AK5C) was mounted and three single shots of lead-free ammunition were fired through remote control. Particles were sampled on glassfiber filters (GFF, Ø25 mm) with a flow of 1.0 l/min for 15 minutes. Particles were also monitored with Electrical Low Pressure Impactor (ELPI) and a medium-volume particle sampler (pre-weighed PTFE-filters) to monitor dynamic properties and accurate mass concentrations, respectively.

Table 1. Measured PAH and oxy-PAH concentrations in SRM 1649b (urban dust) and in gunshot particles.

	1649b Certified (mg/kg)	1649b Measured (mg/kg)	Gunshot Measured (mg/kg)
Pyr	4.78±0.03	4.6±0.6	20±1.6
BaA	2.09±0.05	2.0±0.4	4.0±0.3
BaP	2.47±0.17	2.0±0.2	4.6±0.5
A-9,10-dione	1.9*	1.3±0.2	0.47±0.04
BdeA-7-one	4.1*	5.8±0.4	3.0±0.3
BaA-7,12-dione	5.9*	5.0±0.4	0.44±0.05

*Average of results published by Albinet *et al* (2006) and Layshock (2010)

The GFFs were placed in empty metal sampling tubes and PM-bound organics were analysed using automated thermal desorption coupled with gas chromatography-mass spectrometry (ATD-GC-MS), desorption at 300 °C with a helium flow of 50 ml/min for 5 minutes. Fifteen PAHs and sixteen oxy-PAHs were individually quantified. Furthermore, the particles were analysed for metal content using inductively-coupled plasma mass spectrometry (ICP-MS)

Substantial amounts of particles were emitted (~30 mg/shot) of which the vast majority were smaller than 4 µm. As expected, cupper and zink were the dominating elemental species. Table 1 shows the results for some PAHs and oxy-PAHs in SRM 1649 (urban dust) and in gunshot particles. Generally the PAH content in the gunshot particles were higher than in SRM 1649b while the opposite was seen for oxy-PAHs. Monitoring the particle characteristics with ELPI over time revealed that the size distribution was skewed towards fine and ultrafine particles as demonstrated in figure 1 resembling a typical combustion pattern. We hypothesize that the late appearance of larger particles (>948 nm at ~4 min) is a result of agglomeration and condensation processes.

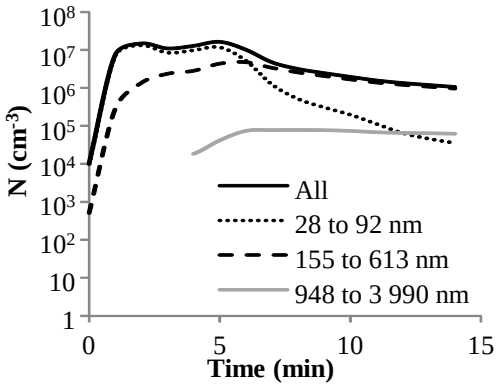

Figure 1. Dynamic properties of small particles emitted from fire arms in the test chamber (ELPI data).

This work was funded by the Swedish Ministry of Defence and Swedish Armed Forces.

Moxnes J. F., Jensen T. L., Smestad E., Unneberg E. and Dullum O. (2013) *Propellants Explos. Pyrotech*., in press, published online 25 OCT 2012, DOI: 10.1002/prep.201200021.

Palmer W. G., Andrews A. W., Mellini D., Terra J. A., Hoffmann F. J., Hoke S. H. (1994) *J. Toxicol. Environ. Health* **43**, 423–433.

Differences between inorganic ion concentrations in an urban and a remote background station

E. Yubero[1], J.F. Nicolás[1], N. Galindo[1], R. Soler1, J. Crespo[1]
[1]Department of Physics, Miguel Hernández University, Avda. Universidad, 03202, Elche, Spain
Keywords: PM1, Inorganic ions, Regional sulphate background, remote stations
Presenting author email: eyubero@umh.es

Two different locations were chosen for the present study. The first location is the city centre of Elche (235,000 inhabitants), approximately 12 km from the Spanish Mediterranean coast. The sampling point is situated in a busy canyon street with a lot of traffic. The device was placed 3 m above ground level on the first floor of a City Hall building. The other location is at the top of the Aitana mountain range (38°38'56.50"N, 0°15'55.23"W, ▲1558 amsl.). It is located approximately 60km from the city of Elche and 20 km from the Mediterranean coast in an east westerly direction. Twenty-four hour PM1 samples were collected approximately every three days from February to October 2012 using a low volume sampler (2.3m/h). The set of samples (around 168 samples in each site) collected was analysed for inorganic ions in our facilities at the Miguel Hernandez University with Dionex chromatographs with the method described by Nicolas et al. (2009).

Period mean, seasonal averages and daily maximum and minimum concentration values are presented from both sites during the study period (Table 1 and 2), for the main inorganic ions. From all the ions analyzed, only those with a high percentage of data above the mdl have been chosen for this study.

Table 1. Statistics and seasonal evolution of main inorganic ions in Aitana (μg/m^3)

	NO_3^-	SO_4^{2-}	$C_2O_4^{2-}$	NH_4^+
Mean	0.11	0.87	0.07	0.33
%<mdl	26	2	2	8
Std. Dev.	0.16	0.64	0.05	0.26
Max	1.17	3.16	0.35	1.44
Min	0.02	0.02	0.0002	0.01
Summer	0.05	1.20	0.08	0.44
Autumn	0.25	0.66	0.11	0.16
Winter	0.18	0.45	0.04	0.19
Spring	0.09	1.02	0.07	0.39

As can be seen, Aitana ion concentration is very low for all the ions. The highest concentration was found for the sulphate ion, with higher concentrations during spring and summer than in winter due to a higher photochemical activity. In contrast, nitrate levels were very low during the entire study. The levels in summer are negligible, being higher during winter and autumn. This is due to the thermal decomposition of ammonium nitrate at high temperatures. The nitrate concentrations measured in the Aitana station are remarkably low, despite being located close to important cities such as Benidorm (a coastal city which is highly populated during summer months, is located less than 20km away). Ammonium ion concentrations are also remarkable, showing a high correlation with the sulphate ion concentrations. This highlights the presence of ammonium sulphate. This compound and the organic matter are the main constituents of the PM1 Aitana aerosol.

Table 2. Statistics and seasonal evolution of main inorganic ions in Elche (μg/m^3)

	NO_3^-	SO_4^{2-}	$C_2O_4^{2-}$	NH_4^+
Mean	0.48	1.99	0.15	0.77
%<mdl	2	0	5	0
Std. Dev.	0.88	1.47	0.07	0.65
Max	8.66	10.42	0.49	4.51
Min	0.07	0.22	0.04	0.05
Summer	0.18	2.60	0.17	0.88
Autumn	0.47	1.62	0.12	0.59
Winter	0.53	1.83	0.15	0.71
Spring	0.26	2.32	0.16	0.88

In table 2, the same results are present for the urban traffic station ions in Elche. The ions with higher concentrations are sulphate and ammonium. On the contrary the presence of nitrate is not negligible in this station, showing a higher concentration in winter. The correlation between sulphate and ammonium ions is high, especially during the summer months whereas during winter, the presence of ammonium nitrate is observed during high atmospheric stability episodes. Potassium ion is also measured in the urban city but without a clear origin and seasonal evolution.

This work was supported by the Spanish Ministry of Science and Innovation under the CGL2009-08036 (PASSE) project and by the Spanish Ministry of Economy and Competitivity under the CGL2012-39623-C02-02 (PRISMA-AITANA) project. We would like to thank the military area (EVA nº 5) for its assistance in this work.

J. F. Nicolás, N. Galindo, E. Yubero, C. Pastor, R. Esclapez, J. Crespo (2009), *Aerosol inorganic ions in a semiarid region on the southeastern Spanish Mediterranean coast*. Water Air Soil Pollut, 201 pp. 149–159

Knudsen Cell measurements applied for the study of gaseous precursors and chemical process acting in aerosol formation for the RADES (RAdiological Dispersion Events Set-up) set-up.

F.G. Di Lemma[1, 2], J.Y. Colle[2], and R.J.M. Konings[1, 2]

[1]Department of Radiation, Radionuclides & Reactors, Faculty of Applied Physics, Delft University of Technology, Delft, 2629JB, The Netherlands.
[2]European Commission, DG Joint Research Centre, Institute for Transuranium Elements, P.O. Box 2340, D-76125, Karlsruhe, Germany.
Keywords: Nuclear aerosols, Accident, Aerosol characterization, Precursors.
Presenting author email: fidelma.DI-LEMMA@ec.europa.eu

Characterization of the aerosols formed during accidents and sabotages involving nuclear and radioactive material, is of main importance for the radiological risk assessment. The quantification and characterization of the source term (which includes the aerosols, but also the gaseous species released) is in fact the input for calculation of the extension and level of contamination, following events in which radioactivity is released in the environment. Furthermore the chemical composition of the release is essential to calculate the health risk for the population concerned (radiotoxicity). As reported by Molecke "These data are the input for follow-on modeling studies to quantify respirable hazards, associated radiological risk assessments, vulnerability assessments, and potential cask physical protection design modifications." (Molecke *et al*. (2006)).

A novel experimental set up RADES (as described in detail by Di Lemma et al. (2012)) has been developed for the study of the aerosol released from RDE's (Radiological Dispersion Events); in this poster the aerosol characterization of particles produced during RDE's involving nuclear fuel will be presented. Tests were conducted on simulated nuclear fuel, consisting of non-radioactive samples: they were composed of a ZrO_2 matrix simulating UO_2, doped with chemicals which simulate fission products. The RADES set-up permits to create aerosol in controlled condition (gaseous atmosphere and pressure), to collect them and to perform then post-analyses on these (such as chemical and elemental composition, as well as size distribution). In order to better understand the chemical processes occurring in the RADES set-up, which influence the final composition of the aerosols and so their radiotoxicity, the measurements have been linked with a Knudsen Effusion Mass Spectrometer (KEMS) measurement. By the KEMS in fact we are able to measure and analyse the behaviour of the partial vapour pressure over the simulated fuel in equilibrium conditions and in function of the temperature. From these data we could infer the composition of the vapour created from the simulated fuel, which can represent further the vapour precursor of the aerosols. These data are then confronted with the data from ICP-MS, RAMAN and SEM-EDX analyses performed on the aerosol created and collected in the RADES set-up, which give information on the elements present in the final formed aerosol and their chemical composition. These studies may permit to understand the chemical reaction of the initial vapour with the environment in the RADES set-up, though it must be realised that the operating conditions of the two instrumentations are very different. In the RADES set-up the sample is heated to very high temperature (up to 4500 K) with very fast transients (tenths of ms) in atmospheric condition, while the KEMS operates "in vacuum", in equilibrium conditions. This will may permit on the other hand to analyse the different vaporization processes occurring in different conditions, and permit to understand how the vaporization/condensation processes in the RADES relate to the aerosol formation in non-equilibrium conditions.

This work is supported by the 7th Framework Program of the European Commission.

Di Lemma F.G., Colle J.Y., Thiele H. and Konings R.J.M. (2012) *Proc. of European Aerosol Conference 2012*, European Aerosol Conference Handbook.

Molecke, M.A, Brockmann, J.E., Lucero D.A. et al. (2006) 47th Annual Meeting of the INNM.

ATD-GC-MS method for characterization and quantification of organic compounds associated to gunshot particles

R. Magnusson[1], L. Hägglund[1], S. Hedenstierna[2] and H. Wingfors[1]

[1]FOI Swedish Defence Research Agency, CBRN Defence and Security, Umeå, SE-901 82, Sweden
[2]FOI Swedish Defence Research Agency, Department of Energetic Materials, Tumba, SE-147 25, Sweden
Keywords: ATD-GC-MS, oxy-PAH, gunshot particles, SRM 1649b.
Presenting author email: roger.magnusson@foi.se

Numerous studies have shown that military and civil use of lead containing ammunitions is associated to severe environmental and health considerations i.e. high blood levels. This has led to the development of lead-free ammunition however these replacement products have been associated to other health implications such as respiratory irritation, asthma, fever and nausea. Emissions from shooting with small calibre ammunition makes up of a complex mixture of gases and particles. For instance, polycyclic aromatic hydrocarbons (PAHs) that are known to have mutagenic properties have been identified in emissions from small calibre rifles using nitro-based propellants (Moxnes *et al*, 2013). It has further been shown that respirable particles in the size range 0.29-0.57 µm from shooting were associated to higher mutagenic activity as compared to larger particle fractions (Palmer, 1994). The aim of this work was to develop a rapid method for quantitative chemical analysis of mutagenic and toxic organic compounds (PAHs and oxy-PAHs) associated to particles and to apply the method in a study of gunshot particles from lead free ammunition. Two standard reference materials, SRM1649b (urban dust) and SRM 1650b (diesel particulate matter) were used for method validation and comparison.

In a 0.7 m^3 test chamber an assault rifle (AK5C) was mounted and three single shots of lead-free ammunition were fired through remote control. Particles were sampled on glassfiber filters (GFF, Ø25 mm) with a flow of 1.0 l/min for 15 minutes. Particles were also monitored with Electrical Low Pressure Impactor (ELPI) and a medium-volume particle sampler (pre-weighed PTFE-filters) to monitor dynamic properties and accurate mass concentrations, respectively.

Table 1. Measured PAH and oxy-PAH concentrations in SRM 1649b (urban dust) and in gunshot particles.

	1649b Certified (mg/kg)	1649b Measured (mg/kg)	Gunshot Measured (mg/kg)
Pyr	4.78±0.03	4.6±0.6	20±1.6
BaA	2.09±0.05	2.0±0.4	4.0±0.3
BaP	2.47±0.17	2.0±0.2	4.6±0.5
A-9,10-dione	1.9*	1.3±0.2	0.47±0.04
BdeA-7-one	4.1*	5.8±0.4	3.0±0.3
BaA-7,12-dione	5.9*	5.0±0.4	0.44±0.05

*Average of results published by Albinet *et al* (2006) and Layshock (2010)

The GFFs were placed in empty metal sampling tubes and PM-bound organics were analysed using automated thermal desorption coupled with gas chromatography-mass spectrometry (ATD-GC-MS), desorption at 300 °C with a helium flow of 50 ml/min for 5 minutes. Fifteen PAHs and sixteen oxy-PAHs were individually quantified. Furthermore, the particles were analysed for metal content using inductively-coupled plasma mass spectrometry (ICP-MS)

Substantial amounts of particles were emitted (~30 mg/shot) of which the vast majority were smaller than 4 µm. As expected, cupper and zink were the dominating elemental species. Table 1 shows the results for some PAHs and oxy-PAHs in SRM 1649 (urban dust) and in gunshot particles. Generally the PAH content in the gunshot particles were higher than in SRM 1649b while the opposite was seen for oxy-PAHs. Monitoring the particle characteristics with ELPI over time revealed that the size distribution was skewed towards fine and ultrafine particles as demonstrated in figure 1 resembling a typical combustion pattern. We hypothesize that the late appearance of larger particles (>948 nm at ~4 min) is a result of agglomeration and condensation processes.

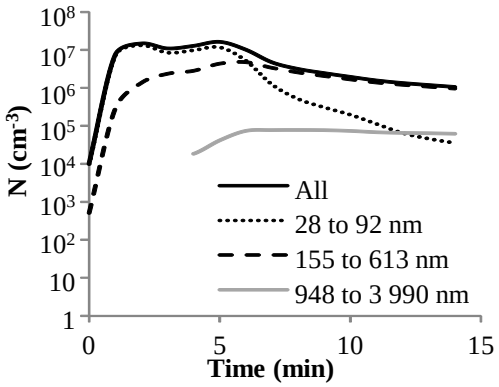

Figure 1. Dynamic properties of small particles emitted from fire arms in the test chamber (ELPI data).

This work was funded by the Swedish Ministry of Defence and Swedish Armed Forces.

Moxnes J. F., Jensen T. L., Smestad E., Unneberg E. and Dullum O. (2013) *Propellants Explos. Pyrotech*., in press, published online 25 OCT 2012, DOI: 10.1002/prep.201200021.

Palmer W. G., Andrews A. W., Mellini D., Terra J. A., Hoffmann F. J., Hoke S. H. (1994) *J. Toxicol. Environ. Health* **43**, 423–433.

Saturation vapour pressures of subcooled liquid oxodicarboxylic acids

I. Crljenica [1,6], T. Yli-Juuti [2], A.A. Zardini [3,4], J. Julin [1,6], M. Bilde [5], I. Riipinen [1,6]

[1]Department of Applied Environmental Science (ITM), Stockholm University, 10691 Stockholm, Sweden
[2]Department of Physics, University of Helsinki, P.O. Box 64, 00014 Helsinki, Finland
[3]Department of Chemistry, University of Copenhagen, Universitetsparken 5, 2100 Copenhagen, Denmark
[4]Institute for Energy and Transport, Sustainable Transport Unit, European Commission Joint Research Centre, 21027 Ispra, Italy
[5]Department of Chemistry, Aarhus University, Langelandsgade 140, 8000 Aarhus, Denmark
[6]Bert Bolin Centre for Climate Research, Stockholm University, 10691 Stockholm, Sweden
Keywords: saturation vapour pressure, organic acids, group contribution methods, evaporation.
Presenting author email: ivica.crljenica@itm.su.se

Atmospheric aerosols contain a significant mass fraction of organic particles which are composed of a large number of compounds with varying and poorly known physical properties (Jimenez *et al*, 2009). In this study we estimate the saturation vapour pressure of low volatility organic compounds present in the atmosphere by interpreting the evaporation experiments of oxodicarboxylic acid aqueous solution droplets at ambient temperature. The modelling of evaporation is done with a two-compartment binary mass transport model including group contribution methods parametrizations for the physical properties of the organic acids.

The experimental data (particle diameter vs. time) were obtained from a TDMA system including a controlled-humidity isothermal laminar flow reactor (Bilde *et al*, 2003). The evaporation was modelled with a two-compartment (the liquid bulk of the aerosol particle and the gaseous surroundings) binary mass transport model with fixed relative humidity and temperature, and dynamic activity coefficients (Riipinen *et al*, 2006). The accommodation coefficients were set to unity. A dilution parameter for oxodicarboxylic acid had to be introduced into the model to account for the uncertainty in the gas phase concentrations of the evaporating compounds. The physical properties of pure liquid organic acids used in the model were estimated through group contribution methods (Poling *et al*, 2007). Activity coefficients, for organic acid and water, were calculated using the UNIFAC Dortmund method (Jakob *et al*, 2006). Density of pure liquid organic acids was predicted by the GCVOL-OL-60 method (Ihmels *et al*, 2003). Surface tension at room temperature was estimated with the GC-MG method (Conte *et al*, 2008). Diffusion coefficients were calculated using the Fuller *et al*. method (Poling *et al*, 2007). The physical properties of water were calculated by the appropriate methods (Poling *et al*, 2007). The physical properties of the binary mixture were calculated as a mass weighted average for density, and as mole weighted average for surface tension. The comparison between the experimental data and the model results, assessed through the method of least squares, gave us the value for the saturation vapour pressure of the organic acid.

Figure 1 shows a typical measurement dataset for 2-oxoglutaric acid together with the best modelled evaporation curve with the subcooled liquid saturation vapour pressure of $2.61 \cdot 10^{-5}$ Pa. This value can be compared with $3.2 \cdot 10^{-5}$ Pa for the measured saturation vapour pressure of solid oxoglutaric acid (Frosch *et al*, 2010), or with $80 \cdot 10^{-5}$ Pa for the subcooled liquid glutaric acid determined from measurements by using a model similar to the one we used (Koponen *et al*, 2007), or $93 \pm 27 \cdot 10^{-5}$ Pa for the measured saturation vapour pressure of subcooled liquid glutaric acid (Soonsin *et al*, 2010).

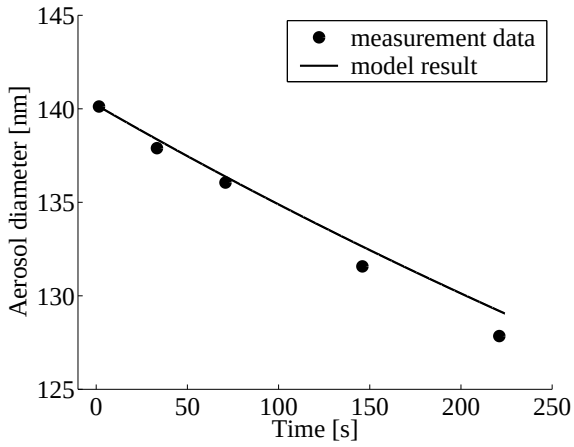

Figure 1. Modelled evaporation curve (line) and the measurements (points) for 2-oxoglutaric acid (relative humidity 40%, long residence time of 222s).

This work was supported by the ERC Grant 278277 ATMOGAIN. We acknowledge the Nordic Center of Excellence CRAICC.

Bilde *et al.* (2003) *En. Sci. Tech.* **37**, 1371-1378.
Conte *et al.* (2008) *Ind. Eng. Chem. Res.* **47**, 7940-7954.
Frosch *et al.* (2010) *Atmos. Chem. Phys.* **10**, 5873-5890.
Ihmels *et al.* (2003) *Ind. Eng. Chem. Res.* **42**, 408-412.
Jakob *et al.* (2006) *Ind. Eng. Chem. Res.* **45**, 7924-7933.
Jimenez *et al.* (2009) *Science* **326**, 1525-1529.
Koponen *et al.* (2007) *En. Sci. Tech.* **41**, 3926-3933.
Poling *et al.* (2007) *The Properties of Gases and Liquids (Fifth Edition)*, McGraw-Hill Education.
Riipinen *et al.* (2006) *Atmos. Res.* **82**, 579-590.
Soonsin *et al.* (2010) *Atmos. Chem. Phys.* **10**, 11753-11767.

Flow tube analysis of the chemical composition of freshly nucleated secondary organic aerosol particles

S. G. Gonser[1], C. Berberich[1] and A. Held[1]

[1] Junior Professorship in Atmospheric Chemistry, University of Bayreuth, 95440 Bayreuth, Germany
Keywords: Aerosol mass spectrometry, Nucleation mode, SOA, Chemical composition.
Presenting author email: stefan.gonser@uni-bayreuth.de

An aerosol mass spectrometer for particles with diameters below 30 nm called the Chemical Analyzer for Charged Ultrafine Particles (CAChUP) has been developed. The instrument was designed to study the chemical composition of freshly nucleated secondary aerosol particles.

CAChUP consists of a custom-built aerosol sizing and collection unit coupled to a time-of-flight mass spectrometer (TOF-MS). The aerosol sizing and collection unit is composed of three major parts: (1) a unipolar aerosol charger, based on corona discharge from carbon fibres (e.g. Han *et al*, 2008), with an extrinsic charging efficiency of 32 % for 20 nm particles; (2) a compact radial differential mobility analyser (Zhang *et al,* 1995) for particle size separation in the diameter range from 1 nm to 100 nm (geometric standard deviation of 1.09); and (3) an electrostatic precipitator where the aerosol is collected on a high-voltage biased metal filament, while a nitrogen counterflow protects the sample from contamination. After collection, the aerosol sample is thermally desorbed, and the resulting gas sample is transferred to a Tofwerk CTOF mass spectrometer for chemical analysis.

First characterization experiments in the laboratory have been successfully conducted by means of a laminar flow tube. In the flow tube, secondary organic aerosol particles (SOA) have been produced from dark ozonolysis of gas phase alpha-pinene. Particles with a diameter of 25 nm were separated from the aerosol population in the flow tube and analysed for their molecular composition.

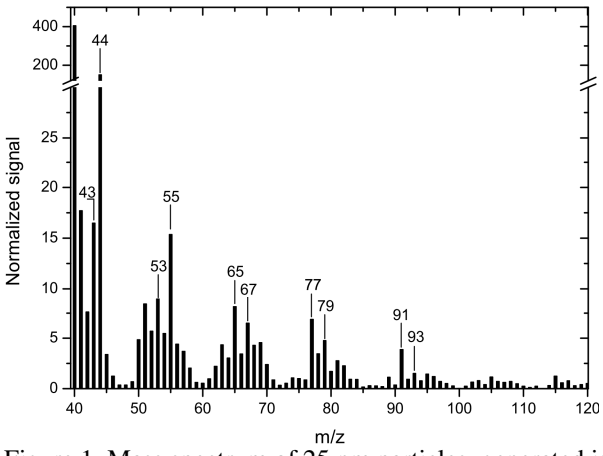

Figure 1. Mass spectrum of 25 nm particles, generated in a laminar flow tube from dark ozonolysis of alpha-pinene.

A particle mass spectrum of a one hour collection period is presented in Fig. 1. The mass spectrum compares well with previous measurements of SOA from alpha-pinene ozonolysis (e.g. Shilling *et al*, 2009).

Further experiments regarding the chemical composition of SOA during growth will be presented. For this purpose particles are generated from ozonolysis of different individual terpenes and their mixtures in the laminar flow tube. The flow tube is designed to set the reaction time of terpenes and ozone between a few seconds up to several minutes, thus resulting in the production of particles of differing sizes and ages. Flow tube experiments allow the collection of one distinct particle diameter for an extended time period, and therefore, a sufficiently large aerosol mass is available for analysis even when extremely small particle diameters (< 10 nm) are to be analysed. The aim of this study is to investigate the evolution of the chemical composition of freshly formed secondary aerosol particles.

This work is funded by the Deutsche Forschungsgemeinschaft (DFG) under grant DFG HE 5214/3-1.

Han, B., Kim, H. J., Kim, Y. J. and Sioutas, C. (2008) *Aerosol Sci. Technol.* **42**, 793-800.

Shilling, J. E., Chen, Q., King, S. M., Rosenoern, T., Kroll, J. H., Worsnop, D. R., DeCarlo, P. F., Aiken, A. C., Sueper, D., Jimenez, J. L., and Martin, S. T. (2009) *Atmos. Chem. Phys.* **9,** 771–782.

Zhang, S. H., Akutsu, Y., Russell, L. M., Flagan, R. C. and Seinfeld, J. H. (1995) *Aerosol Sci. Technol.* **23**, 357-372.

Secondary organic aerosol production potential from diesel and gasoline vehicle exhaust under different ambient conditions

S.M. Pieber[1], S.M. Platt[1], I. El Haddad[1], A.A. Zardini[2], R. Suarez-Bertoa[2], J.G. Slowik[1], R.J. Huang[1], S. Hellebust[3], B. Temime-roussel[3], N. Marchand[3], L. Drinovec[4], G. Mocnik[4], U. Baltensperger[1], C. Astorga[2] and A.S.H. Prévôt[1]

[1]Laboratory of Atmospheric Chemistry, Paul Scherrer Institute, Villigen, CH-5232, Switzerland
[2]Instiute for Energy and Transport, Sustainable Transport Unit, EC Joint Research Centre, Ispra, I-21027, Italy
[3]Laboratoire Chimie Environment, Aix Marseille Université, Marseille, F-13 331, France
[4]Aerosol d.o.o., SI-1000 Ljubljana, Slovenia

Keywords: secondary organic aerosol (SOA), smog chamber, vehicle emissions, AMS
Presenting author email: simone.pieber@psi.ch, corresponding author email: andre.prevot@psi.ch

Organic aerosol (OA) is a major fraction of the submicron aerosol known to influence climate and to adversely affect health. OA consists of directly emitted primary OA (POA), and "secondary" OA (SOA), formed in-situ in the atmosphere via the reaction of volatile precursors. Vehicle exhaust is already a known source of POA and likely contributes to SOA in urban areas (Robinson *et al.*, 2007; Weikamp *et al.* 2007). However, the magnitude of this contribution is unknown.

The secondary organic aerosol production potential (SAPP) of vehicle exhaust has recently been estimated by (i) analyzing ambient data from urban areas combined with fuel consumption data (Bahreini *et al.*, 2012), or (ii) by examining the chemical composition of raw fuels (Gentner *et al.*, 2012). Contradictory and thus somewhat controversial results in the relative SAPP of diesel vs. gasoline vehicle exhaust were observed.

Experimental data from smog chamber studies can provide quantitative measurements of the relative SAPP of different fuels and vehicle types, and elucidate the impact of variable ambient conditions. This information is crucial for our understanding of vehicular pollution and formulation of emission control strategies.

Therefore, we studied the SAPP of passenger cars and trucks as a function of fuel type (gasoline, diesel) at different temperatures (T 22 vs. -7°C) and relative humidity (RH ~40 vs. ~90%). Vehicle exhaust was sampled at the tailpipe during regulatory driving cycles on chassis dynamometers (European Joint Research Centre Ispra, Italy), diluted (200 – 400x) and introduced into the PSI mobile smog chamber (Platt *et al.* 2012) via a heated tube (150 °C). OA was quantified with a high-resolution time-of-flight aerosol mass spectrometer. Black carbon was measured using aethalometers. Volatile organic compounds (VOCs) were analysed with a high resolution proton-transfer time-of-flight mass spectrometer. Gas-phase monitors were used to quantify CO, CO_2, CH_4, total hydrocarbons, NH_3 and other gases in the chamber. Emission factors (EFs, e.g. g per kg fuel) were calculated from a carbon mass balance.

We found that the vehicle emissions and SAPP are significantly affected by temperature and RH: doubling the RH in the chamber resulted in a 3-fold higher SOA EF (*Figure 1*). Primary and secondary aerosol emissions from diesel and gasoline vehicles will be compared at different temperature and RH.

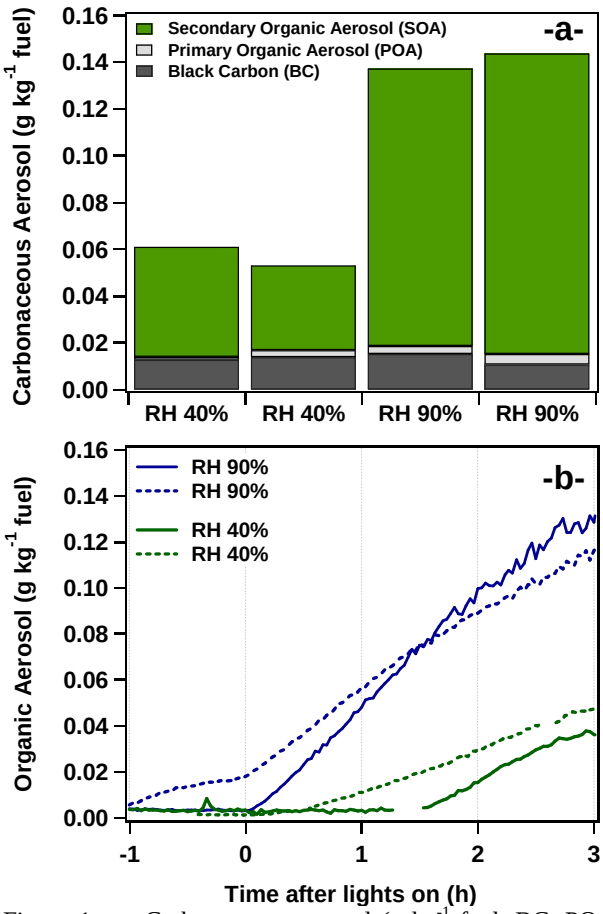

Figure 1. -a- Carbonaceous aerosol (g kg^{-1} fuel, BC, POA and SOA) from a Euro 5 gasoline car. -b- Temporal evolution of the OA formation in the smog chamber at similar OH exposure but different relative humidity (RH).

This work was supported by the Swiss Federal Office for the Environment and the Swiss Federal Roads Office. The test bench operation was financed by the EU. We thank U. Manfredi, M. Sculati, F. Muehlberger, M. Cadario and R. Richter for their expert technical assistance.

Bahreini, R., *et al.* (2012) *Geophys. Res. Lett.* **39**, L06805.
Gentner, D.R. *et al.* (2012) *PNAS* **109**, 18318.
Platt, S.M., *et al.* (2013) *Atmos. Phy. Chem. Discuss.* **12**, 28343.
Robinson, A.L., *et al.* (2007) *Science* **315**, 1259.
Weitkamp, E.A., *et al.* (2007) *Environ. Sci. Technol.* **41**, 6969.

Synthesis of Ag triangular nanoplates protected by glutathione and their interaction of hemoglobin

N.Kinoshita, T. Ito, N. Nishida, H. Tanaka

Institute of Science and Engineering, Chuo Univ. 1-13-27 Kasuga, Bunkyo-ku, Tokyo, 112-8551, Japan

Keywords: Ag nanoplate, hemoglobin,

Presenting author email: kinokino23@gmail.com

Ag trianglular nanoplates have attracted much attention because of their unique structure. On the other hand blood proteins such hemoglobin (Hb) are the major biomolecule in lives and the major target of many kinds of medicines, viruses, metal ions, *etc*. Consequently, the fundamental understanding of the conformational behavior of these proteins interacted with nanoplates is of critical importance in a protein-metallic conjugates system. In this study, we synthesized Ag triangular nanoplates protected by glutathione (Ag:SG nanoplate) [1], and analyzed the conformational change of Hb interacted with nanoplates

Ag:PVP nanoplates were synthesized by photoreduction of $AgNO_3$ with PVP . The obtained nanoplates were mixed and stirred with glutathione. After 20 hours stirring, the formed precipitation was rinsed by ethanol, and was re-dispersed into water. The products were characterized by UV-vis absorption spectroscopy, scanning transmission electron microscopy (STEM), circle dichroism (CD) spectroscopy and X–ray photoelectron spectroscopy (XPS). Afterwards, this solution was mixed with 1 mL of hemoglobin solution. The obtained products were characterized by the same analysis methods.

Ag:SG nanoplates showed characteristic Cotton effects in the CD spectrum which were induced by SPR of nanoplates. This indicates that new chiroptical properties were induced by the adsorption of chiral molecules in the achiral nanoplates. In other words, chiral electromagnetic currents are generated inside the metal nanoplates by the presence of GSH molecules as chiral chromophores. The UV-vis absorption spectra for Ag:SG nanoplates agreed well with those for typical triangular nanoplates. Therefore, the shape of nanoplates is not affected by the present substitution process. This is also confirmed by STEM image. Chemical shifts of the binding energy observed upon XPS analysis revealed that GSH molecules attached to Ag nanoplates in the S-Ag bond and that PVP of Ag nanoplates is largely removed thought substitution reactions with GSH.

As shown in Figure 1, three peaks pointed by arrows are observed at 400, 700 and 1100 nm for the nanoplates with Hb. These peaks can be ascribed as hemoglobin, truncated nanoplates, and triangular nanoplates, respectively. When absorbances of these peaks are compared with nanoplates without Hb as shown in Figure 1, the decrease of the 1100 nm peak is larger than that of the 700 nm peak. This indicates that reactivity of triangular nanoplates is higher than that of truncated ones. In fact, truncated nanoplates were dominantly observed for Ag:SG nanoplates with Hb in STEM images.

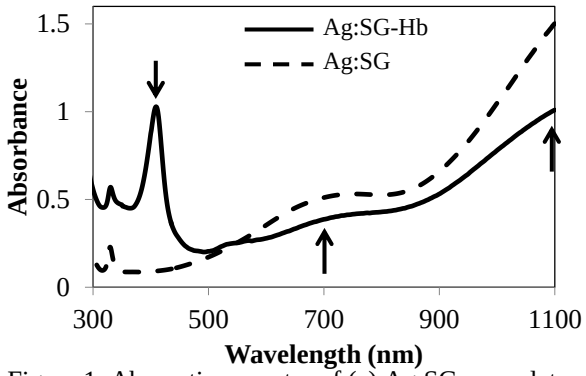

Figure 1. Absorption spectra of (a) Ag:SG nanoplates with Hb and (b) Ag:SG nanoplates without Hb

[1] N. Nishida, Y. Kojima, and H. Tanaka, (2012) *Chem. Lett.* **41,** 926-928

First Steps in Atmospheric Particle Formation

J. Fedor[2], J. Lengyel[1], J. Kocisek[1], V. Poterya[1], A. Pysanenko[1], P. Svrčková[1], M. Fárník[1]

[1]J. Heyrovský Institute of Physical Chemistry v.v.i., Academy of Sciences of the Czech Republic, Dolejškova 3, 18223 Prague, Czech Republic
[2]Department of Chemistry, University of Fribourg, Chemin du Musee 9, CH-1700 Fribourg, Switzerland
Keywords: cluster, polar stratospheric cloud, heterogeneous chemistry, cross section
Presenting author email: kocisek@jh-inst.cas.cz

We present here the results of combined experimental and molecular dynamics (MD) computational study of pickup of atmospheric molecules on water nanoparticles (clusters). These could be viewed as the precursors for the larger atmospheric particles – aerosols and ices.

First we focused on adsorption of H_2O, NO, and NO_2 molecules on large pure water clusters. Clusters with mean size 260 or 430 water molecules were prepared in the water vapor expansion into the vacuum. Skimmed beam passed through pickup chamber, where the gas of interest was introduced. After pickup the cluster speed distribution was measured using pseudorandom chopper technique. The pickup cross section was then estimated on the basis of the speed variation with the pickup cell pressure. Details can be found in current publication Lengyel *et al.* (2012). Fig. 1 represents the comparison between measured cross section and geometrical cross section for cluster. We can see that cross section for water adsorption is more than 2 times the expected value.

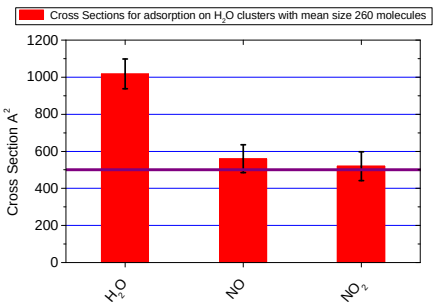

Figure 1. *Comparison of measured sticking cross section values with geometrical cross section (purple line).*

Except the particle growth, adsorption on ice particles is important prerequisite of heterogeneous chemistry in atmospheres. Independent of the reaction, the most important step is the reactant adsorption on the particle. Cross section is than fundamental characteristics of the adsorption process. In present study it was measured for several species relevant for atmospheric chemistry, mainly halocarbons, but also HCl, HBr, methane or alcohols. All show significant divergence from the geometrical cross section predictions.

We employ MD simulations to understand the observation. At first MD simulations were used to confirm the suitability of the experimental method. The most important assumption during the estimation of adsorption cross section is that only sticking collisions lead to nonstochastic momentum transfer between cluster and gas in the pickup cell. Demonstration of this fact can be seen on Fig. 2. Additionally, by fitting the step function like showed on Fig.2 to the data from MD simulation we estimated sticking cross section values in good agreement with experiment. Supported by agreement we try to illuminate the physical processes behind the CS discrepancies. Fitting the MD model interaction potential between the cluster and impacting molecule we obtained r^{-3} potential dependence. The long range potential can lead to significantly higher cross section in comparison to Van der Waals interaction r^{-6}, which is usually neglected.

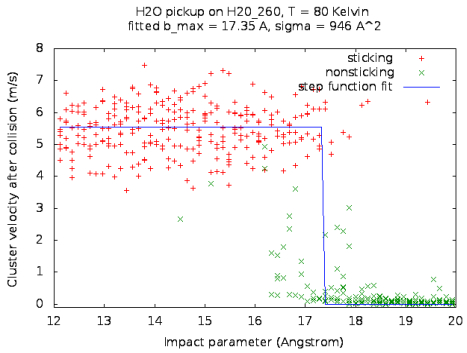

Figure 2. *Effect of sticking + and nonsticking x collisions on the change in the cluster velocity after collision, together with step function fit modelling the measured cross section value.*

The study shows that the formation of PSCs can be significantly faster than expected. Also the sticking probability of various heterogeneous chemistry precursors differ significantly from the expected values, what can have impact on the future ozone level predictions. More important it shows us that neutral-neutral interaction in the case of large particles can have long range character and needs more detailed exploration.

This work was supported by GACR grants Nr. KJB400400902 and 203/09/0422. J.K. acknowledges the support of FP7 ITN grant ICONIC No. 238 671.

Lengyel J., Kočišek J., Poterya V., Pysanenko A., Svrčková P., Fárník M., Zaouris D.K., Fedor J. (2012) *Journal of Chemical Physics* 137(3), 034304

Interaction of gas-born Ag nanoparticles with DNAs of salmon testes

M. Shibata, N. Nishida, H. Tanaka

Institute of Science and Engineering, Chuo Univ. 1-13-27 Kasuga, Bunkyo-ku, Tokyo, 112-8551, Japan
Keywords: Ag nanoparticle, gas born, DNA, salmon testes
Presenting author email: tef.ts2525@gmail.com

Ag nanoparticles are widely used nowadays in the daily products because they are believed as safe and functional, but their actual affection for biomaterials such as DNAs has not been well known yet. In this study, we have investigated interaction of gas-born Ag nanoparticles with DNAs of salmon testes by using gas-liquid transport method recently developed [1].

Ag nanoparticles were produced by gas aggregation method heated at 1100 ^{o}C with N_2 gas flow at 2.0 slm, and were directly blowing into DNA dispersion for 24 h; the DNA dispersion was prepared by mixing of 1.0 mg of salmon testes DNA with 200 mL of pure water. The obtained dispersion was analyzed using scanning transmission electron microscope (BF-STEM), absorption spectrum, circular dichroism (CD) spectroscopy and fluorescence spectroscopy. Diameter of the produced nanoparticles was estimated to be 8 nm at this condition from STEM images for specimen collected by electro-deposition of nanoparticles onto collodion-coated Cu grid.

Figure 1 shows that absorption spectrum of salmon-testes DNA dispersion after blowing of 8 nm Ag nanoparticles for 24 h. The peak at 260 and 410 nm are ascribed to DNA and Ag nanoparticles. Appearance of the 410 nm peak indicates that Ag nanoparticles were effectively taken into dispersion. In fact, when the dispersion was observed by STEM images, extensive amount of nanoparticles was observed. In addition, diameter and shape of these nanoparticles were the almost same as those for the gas-born Ag nanoparticles themselves. It is worthy to note that the observed absorbance was much higher than that reported previously [1]. This indicates that DNAs were highly probable to be worked as effective collector of gas-born nanoparticles.

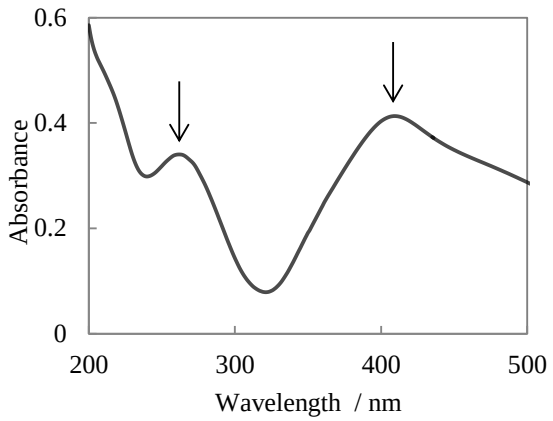

Figure 1. Absorption spectrum of dispersion of salmon-testes DNAs after blowing of gas-born Ag nanoparticles with 8 nm in diameter for 24 h.

In CD spectrum, peak profiles due to Cotton effects for B-form DNA were found to be completely changed for the dispersion after blowing. This indicates that introduction of Ag nanoparticles into dispersion causes conformational change of DNAs. Additionally, when ethidium bromide known as intercalater of double strand of DNA was used as chromophor, distinct decrease of fluorescence was observed for the dispersion after blowing. This indicates that DNA structure was effectively affected by Ag nanoparticles.

[1] N. Hashimoto, N. Nishida, H. Murayama, and H. Tanaka, (2011) Chem. Lett. 40, 144-146.

Regional modelling of the tropospheric multiphase system using COSMO-MUSCAT: Sensitivity on detail of cloud microphysics and chemical mechanism

R. Schrödner[1], A. Tilgner[1] and R. Wolke[1]

[1]Institute for Tropospheric Research, Leipzig, 04318, Germany
Keywords: Aerosol cloud interaction, Multiphase chemistry, Modelling (regional), Cloud microphysics.
Presenting author email: roland.schroedner@tropos.de

Clouds play a major role in the atmosphere due to their influence on the Earth's radiative budget, on the hydrologic cycle and on the tropospheric chemical composition (e.g. Ramanathan et al., 2001). Cloud lifetime is driven by the dynamics of the atmosphere at the synoptic scale and, in close interaction, by microphysical processes (e.g. nucleation of cloud droplets and ice crystals, condensation and evaporation, collision/coalescence processes, freezing, sedimentation of hydrometeor) on the small scale.

These processes depend on the chemical composition of particles and cloud droplets. In addition, microphysical processes redistribute chemicals among the various reservoirs: gaseous, particulate, liquid and ice phases. Clouds favor the development of "multiphase chemistry" since they are an ideal reaction medium for this: (1) clouds support very efficient photochemical processes inside droplets; (2) certain homogeneous chemical reactions within clouds can be usually faster than the equivalent reactions in the gas phase, and reactions such as those involving ionic species, can be important; (3) finally, interactions between the aqueous and solid phase can contribute additionally to chemical processes in clouds (for example dissolution of soluble particulate species). The evaluation of multiphase chemistry versus overall tropospheric chemistry and its role in the Earth's radiative budget is challenging since microphysical and chemical processes occurring at different time scales within clouds are still poorly known.

The model system COSMO-MUSCAT consists of MUSCAT (Wolke et al., 2004a) and the forecast model of the German Weather Service (DWD) COSMO (Schättler et al., 2008). Both models are coupled online. MUSCAT was extended to consider cloud-chemical processes (chemical aqueous phase reactions and phase transfer processes) on the regional scale replacing the former aqueous phase parameterization.

Based on the increasing kinetic and mechanistic knowledge on chemical aqueous phase reactions in the last two decades, advanced aqueous phase chemical mechanisms such as the Chemical Aqueous Phase Radical Mechanism (CAPRAM) are continuously developed (Tilgner and Herrmann, 2010). CAPRAM is an almost explicit mechanism which describes relevant chemical aqueous-phase conversions of both inorganic and organic compounds. A reduced version of the mechanism, applicable for 3D chemistry transport models was created (Deguillaume et al., 2009).

With the advanced model system, sensitivity-studies have been conducted for urban and remote cases. The comparison of different chemical mechanisms have revealed agreements but also interesting differences for important chemical subsystems e.g. in the modeled multiphase HO_x budget and pH whereas more simple mechanism (without organics) lead to less acidic cloud droplets than CAPRAM. Investigation of reaction fluxes show that this is mostly due to organic acidification in CAPRAM. The difference in pH leads consequently to different regimes for e.g. the S(IV)-oxidation. A simple size-resolved microphysical scheme was introduced which shows the different chemical behavior of the droplet-size-bins.

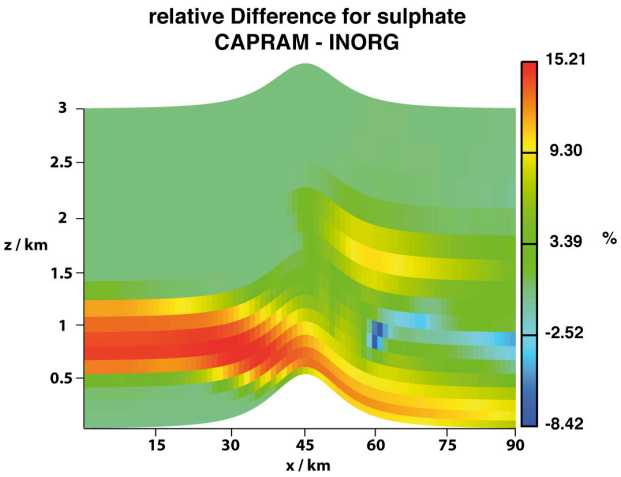

Figure 1. Height profile in x-direction of the simulated mass of S(VI) simulated with CAPRAM compared to the run with simple inorganic chemistry. The cloud is located left of the mountain (red and yellow area). Species stream in from the left-hand side.

This work was supported by the Deutsche Bundesstiftung Umwelt (DBU).

Deguillaume, L., et al. (2010), *Journal of Atmospheric Chemistry*, *64*(1), 1-35.

Ramanathan, V., Crutzen, P. J., Kiehl, J. T. and Rosenfeld, D. (2001) *Science*. 294, 2119 - 2124

Schättler, U., Doms, G. and Schraff, C. (2008): *A Description of the Nonhydrostatic Regional COSMO-Model Part VII: User's Guide.*

Tilgner, A. and Herrmann, H. (2010) *Atmospheric Environment*, *44*(40), 5415-5422

Wolke, R., Knoth, O., Hellmuth, O., Schröder, W. and Renner, E. (2004a) *Parallel computing: Software technology, algorithms, architectures and applications*, 363-370

Extinction characteristics of SOA formed following the photolysis of 2-nitrophenol: A broadband study in the near-ultraviolet

E. M. Wilson[1, 2], J.C.Wenger[1, 2], D. S. Venables[1, 2]

[1] Department of Chemistry, University College Cork, Cork, Ireland
[2] Environmental Research Institute, University College Cork, Cork, Ireland

Keywords: Optical properties, 2-nitrophenol, IBBCEAS, secondary organic aerosol
Presenting author email: eoin.wilson@umail.ucc.ie

The contribution of atmospheric aerosols is a large source of uncertainty in our understanding of radiative forcing. Although scattering of light by particles is well known, recent research has shown that particulate absorption can be important in the near-UV (Jacobsen 1998). There have been few studies of the optical properties of secondary organic aerosol (SOA) in the near-UV region. The aim of this study is to characterise the aerosol optical properties of SOA formed from the photolysis of 2-nitrophenol.

Nitrophenols are an important class of aromatic hydrocarbons that are of concern because of their carcinogenic and phytotoxic properties (Harrison et al, 2005). The largest sources of these compounds are anthropogenic and they have been found in air, cloud, soil, fog and snow samples. 2-nitrophenol is a particularly important nitrophenol compound in the troposphere. It is a gas phase precursor of nitrous acid, HONO, and thus an indirect source of the atmospheric oxidant OH.

We have recently developed and demonstrated an incoherent broadband cavity enhanced absorption spectroscopy (IBBCEAS) system for studying the near-UV optical properties of aerosols (Chen et al., 2011; Wilson et al, 2012). The system is connected across a 4 m^3 atmospheric simulation chamber in the Centre for Research into Atmospheric Chemistry at University College Cork. Uniquely, the system gives real time, in situ measurements of the aerosol extinction across a continuous spectral region from 320-405 nm.

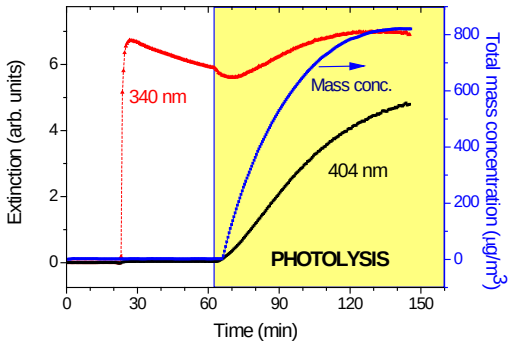

Figure 1. Time profile of aerosol mass concentration (blue) and sample extinction at 340 nm (red) and 404 nm (black) during SOA formation. Gas phase 2-nitrophenol was introduced at 22 minutes and photolysis began at 62 minutes.

In a series of experiments, gas phase 2-nitrophenol was introduced into the chamber and subsequently photolysed. SOA was formed promptly and in high yields upon illuminating the chamber. The extinction across the chamber increased rapidly when the chamber lights were on and coincided with aerosol formation (Fig. 1). Off-line filter samples were taken to study the absorption characteristics of the particles in solution, allowing us to compare on-line and off-line techniques. The extinction due to aerosol was investigated under a variety of different experimental conditions. These included the presence of an OH scavenger, changes in relative humidity, and the presence of ammonium sulphate seed particles. The influence of NO_2 on suppressing the aerosol particle yield was also studied. An analysis of the extinction spectra is used to propose a possible mechanistic pathway for the photolysis of 2-nitrophenol.

We gratefully acknowledge financial support from Science Foundation Ireland through grant 11/RFP/GEO3200.

References:

Chen, J., Wenger, J. S., Venables, D. S. (2011) *J. Phys. Chem. A*, **115**, 12235–12242

Harrison, M. A. J., Barra, S., Borghesi, D., Vione, D., Arsene, C., Olariu, R. L. (2005) Atmos. Environ. 2005, 39, 231–248.

Jacobsen, M. Z. J. Geophys. Res., 103, D9, 10,593-10,604, 1998.

Wilson, E. M., Chen, J., Varma, R. V., Wenger, J. S., Venables, D. S. Proc. Int. Rad. Symp. 2012 (in press)

Changes of aerosol properties during the ozonolysis of unsaturated carboxylic acids in the absence and presence of oxygen

[1]C. Keunecke, [2]M. Beck, [2]T. Hoffmann, [1]T. Zeuch

[1]Institut für Physikalische Chemie, Georg-August-Universität Göttingen, Göttingen, 37077, Germany
[2]Institut für Anorganische und Analytische Chemie, Johannes Guttenberg-Universität, Mainz, 55128, Germany

Keywords: SOA, Ozone, Alkene oxidation, Organic acids
Presenting author email: tzeuch1@gwdg.de

In the past decades large efforts have been made in laboratory studies to elucidate the secondary organic aerosol (SOA) formation mechanism. Critical issues have been studied such as reaction product formation and the influence of relative humidity, temperature, presence of additional organic matter and seed aerosol. However, the mechanism of organic nucleation is still not fully understood. Consequently significant uncertainty remains in closing the gap between laboratory experiments, theoretical predictions, nucleation rates and particle growth rates observed in field studies. In a recent study we could show that (besides volatility considerations of detected reaction products) SOA formation during alkene ozonolysis experiments depends also on kinetic parameters and is strongly linked to intermediate species like peroxy radicals (Wolf *et al*., 2009, 2011).

In order to allow for a controlled reaction chamber filling and minimized aerosol wall losses during laboratory SOA experiments (e.g. a large reaction volume to surface ratio), we apply a 64 L stationary reaction cell with ozone / alkene premixing chambers, FTIR spectroscopy for gas phase species analysis and a SMPS system for measuring particle size distributions in the submicron size range. With this type of reactor design we achieve a well controlled mixing within two seconds which defines a precise starting point of the chemical reaction and allows a controlled variation of process parameters including reaction pressure (Wolf et al. 2011). The particles produced in these experiments were sampled on a filter. For the product analysis we employed liquid chromatography/mass spectrometry (LC/ESI-MS). With this combined approach the influence of reaction conditions like absence and presence of oxygen or pressure on gas phase chemistry and aerosol composition is elucidated.

Fig. 1 shows that the presence of various amounts of oxygen in the reactive mixture strongly influences the observed particle number concentrations during the ozonolysis of methacrylic and butenoic acid. For O_2 partial pressures below 1 mbar a significant increase of particle numbers is observed for both carboxylic acids. The mass spectrometric analysis of the aerosol composition for the experiment with butenoic acid revealed that the highest mass fraction (*m/z* > 230) was not present in experiments in the absence of O_2 where higher (!) aerosol yields were observed in terms of particle number concentration and mass. An increased yield of a product with *m/z* 205 was found in the nitrogen atmosphere experiment.

The influence of oxygen in ozonolysis experiments is related to secondary oxidation steps. In the vinylhydroperoxide pathway the Criegee intermediate (CI) decomposes forming OH radicals and an alkyl radical R, which reacts with O_2 to RO_2, a peroxy radical. In the case of the two acids under study the addition O_2 to the larger CI leads to highly oxidized intermediates. On average they tend to decompose into products with increased volatility compared to the experiment in nitrogen. However, the influence of peroxy chemistry on the build-up of compounds with low volatility is reflected in the presence of the highest mass fraction (*m/z* > 230) in the synthetic air experiments with butenoic acid.

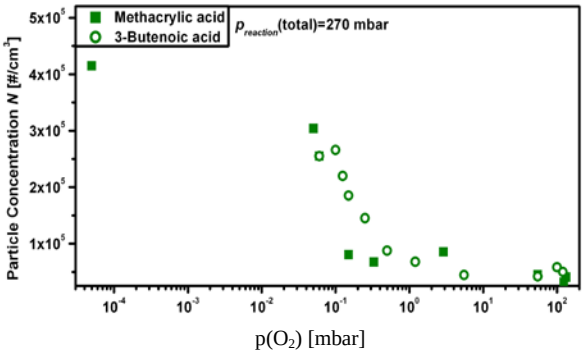

Figure 2. This figure illustrates the dependence of the total particle concentration on the amount of oxygen in the reactive mixture. Constant quantities of reactants were converted: $p_{0,\ acid}$=5 Pa, $p_{0,\ ozone}$=0.1 Pa for 3-Butenoic acid, $p_{0,\ ozone}$=0.2 Pa for Methacrylic acid.

J. L. Wolf, M. A. Suhm, and T. Zeuch, *Ang. Chem. Int. Ed.*, **48** (2009), 2231.
J. L. Wolf, S. Richters, J. Pecher, and T. Zeuch, *Phys. Chem. Chem. Phys.*, **13** (2011) 10952.

Tuesday, September 3, 2013

Poster session B,
Aerosol Modelling, Posters B064 – B125

Long-Term Variability of Terrestrial, Terpenoid BVOC Emissions in the Last Millennium

Juan C Acosta[1], Hamish Struthers[1], Eduardo Zorita[2], Annica ML Ekman[3], Alex Guenther[4] and Ilona Riipinen[1]

[1]Applied Environmental Science, Stockholm University , Stockholm, Sweden.
[2]Institute for Coastal Research, Helmholtz-Zentrum Geesthacht, Geesthacht, Germany.
[3]Department of Meteorology, Stockholm University, Stockholm, Sweden.
[4]Atmospheric Chemistry Division, NCAR Earth System Laboratory, Boulder, CO, USA
Keywords: BVOCs, Paleoclimate, Isoprene, Monoterpenes.
Presenting author email: juan.acostanavarro@helsinki.fi

Natural vegetation emits large amounts of volatile organic compounds into the atmosphere. Estimates of the total global source of biogenic volatile organic compounds (BVOCs) in the past millennium range between 1050 and 1100 Tg yr-1 (Adams et al. 2001). BVOCs have multiple impacts on atmospheric chemistry, they alter the concentrations of tropospheric aerosol in continental regions, and affect ozone formation and the oxidizing capacity of the troposphere (Seinfeld & Pandis, 2006). Organic compounds constitute 20-90% of the submicron aerosol mass, depending on location. Most of this contribution is secondary, meaning that the emitted VOCs are oxidized in the atmosphere followed by gas-to-particle conversion of the oxidation products (Jimenez et al., 2009). BVOCs emitted by vegetation are the dominant source of secondary organic aerosol (SOA) in the atmosphere (Guenther et al., 1995). Estimates of the present-day organic aerosol budgets are improving rapidly, but it is unclear how the organic aerosol fraction has evolved in the past. Such information is, however, needed for accurate estimates on the climate forcing caused by aerosols. Understanding the factors that have governed BVOC emissions in the past is a prerequisite for completing this task.

We evaluated the variability of global fluxes of isoprene, monoterpenes and sesquiterpenes over the last millennium using the Model of Emissions of Gases and Aerosols from Nature (MEGAN) (Guenther et al., 2006). MEGAN estimates the emission activity of BVOCs using meteorological conditions and vegetation as input. The model is driven off-line using fields from an Earth System Model millennium simulations (Jungclaus et al. 2010) and reconstructions of the global changes of terrestrial vegetation (Kaplan et al., 2010). We found that compared to preindustrial times (1000-1800 A.D.), global isoprene emissions have decreased 8%, monoterpenes emissions have increased 10% and sesquiterpenes emissions have increased 15% during the time period 1950-1990 A.D.. The results suggest that the variation of isoprene emissions is governed by land-use changes, while monoterpenenes and sesquiterpenes variations are dominated by climate variability.

Adams, J.M. (2001). Chemosphere - Global Change Science, 3, 73-91
Seinfeld, J.H. and Pandis, S. N. (2006). Atmospheric Chemistry and Physics . Wiley, New York
Jimenez, J. L. et al. (2009). Science, 326, 1525-1529
Guenther, A. et al. (1995). J. Geophys. Res., 100, 8873-8892
Guenther, A et al. (2006). Atmospheric Chemistry and Physics, 6:3181–3210
Jungclaus, J. H. et al. (2010). Climate of the Past, 6:723–737
Kaplan, J. O. et al (2010). The Holocene 21(5), 775-791

Applications of Multiple Regression Analysis to estimate Aerosol Optical Depth over the Arabian Gulf

F.M. Al-Kandari, H.K. Al-Jassar and K.S. Rao

Department of Physics, University of Kuwait, Khaldiya, Kuwait, 13060, Kuwait
Keywords: Aerosol Optical depth, multiple regression analysis, sun photometer, AERONET.
Presenting author email: fatma.alkandri@gmail.com

A statistical model is built to predict the value of aerosol optical depth at 500 nm (AOT 500) from most effective climate parameters. Seasonal data of the Arabian Gulf is used in this study.

The season division is set accordingly to a comprehensive study for weather parameters from May 2009 till May 2010 in conjunction with Aerosol data. These data sets are obtained from ground based measurements of three gulf AERONET sites, Kuwait University, Kuwait, (29.32N, 47.97^{o}E at elevation of 42 meters), Solar Village, Riyadh, (24.91^{o}N, 46.41^{o}E at elevation of 764 meters) and Dhadnah, AlFujairah (25.51^{o}N, 56.327^{o}E at elevation of 81 meters).

New criteria are set for selecting hourly aerosol measurements from the sun photometers according to weather conditions. All hourly readings are with sky clearance $\leq$ 6, humidity (RH) < 83%. If the registered humidity at time of measurements is > 60% and accompanied with rain or rain droplets, then the hourly readings are omitted. The condition for selecting data is summarized as follows:

RH $\geq$ 60 + W2, where (W2 $\geq$ 80)

W2 is a scale measure for weather stability and indication for drizzles and rain.

A correlation value of 0.8 is found between regression standardized predicted values of AOT 500 with the observed values. The prediction of the statistical model shows accuracy near 82% of the observed data , This may be related to the climate nature of Arabian Peninsula, in which most the days during the year are clear from clouds.

The approach to test for errors in model created by step-wise regression is to assess the model against a set of data that was not used to create the model (Mark and Goldberg, 2001).

The AERONET Synergy tool and the Hybrid Single-Particle Lagrangian Integrated Trajectory (HYSPLIT, Draxler and Hess, 1998) together demonstrate the origin and the intensity of desert dust storms. Their results support the prediction model.

The regression equation for spring season in Kuwait yields:

τ_{500}= -1.205α - 0.ΔT – 7.7*10^{-5} visibility + 0.22 WVC + 0.024 *air pressure + 0.053* wind speed.

Where τ_{500} is aerosol optical depth at 500nm, α is the Angstrom exponent obtained from 500nm and 870nm wave lengths , ΔT is the absolute difference between maximum and minimum temperature per day in C^{0} and WVC is the water vapour content.

Residuals for the difference between the predicted value of AOT & the actual mean value = 0. Also most values fall between -2 to 2. The regression standardized residual histogram (Figure 1) is symmetric which means no outliers are found except in small range (less than 1% of data).A plot of expected cumulative probability versus observed cumulative probability (P-P plot) shows normal residuals distribution around line fit graph (Figure 2).

The same standards are applied on all seasons for Kuwait, Solar Village & Dhadnah.

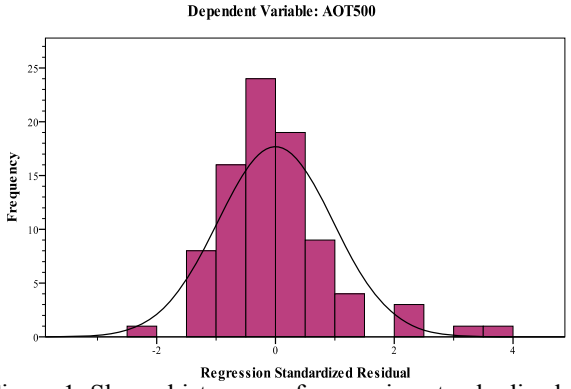

Figure 1: Shows histogram of regression standardized residual.

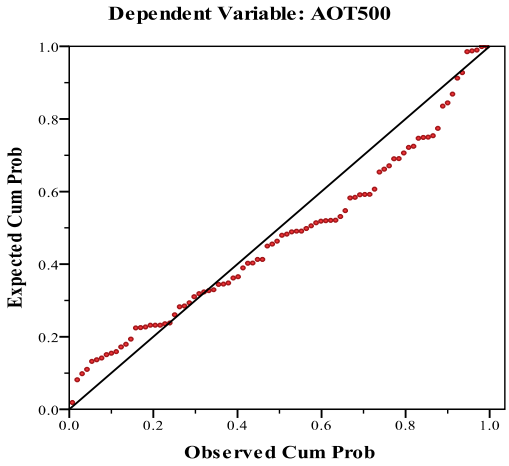

Figure 2: Shows normal P-P plot of regression standardized residual.

This work was supported by The Research Administration Department of Kuwait University, under Project Code: SP02/09.We are grateful to the principal investigators of the Gulf AERONET sites, Naif Al-Abbadi (Solar Village) and Brent Holben (Dhadnah), all the sites staff and the responsible Institutions in Saudi Arabia and United Arab of Emirates for their efforts in maintaining AERONET Data.

Draxler, R. R. and G. D. Hess (1998) *An Overview of the Hysplit_4 Modeling System for Trajectories, Dispersion, and Deposition*, Aust. Met. Mag., 47, 295-308.

Mark, J. and Goldberg, N. (2001). *The Appraisal Journal, Multiple Regression Analysis and Mass Assessment: Rev. Lett. Jan. 89-109.*

Simulation of ice nucleation in a parcel model

C. Anquetil-Deck[1], C. Hoose[1] and P. Conolly[2]

[1]Institute for Meteorology and Climate Research, Karlsruhe Institute of Technology, Eggenstein-Leopoldshafen, 76344, Germany
[2]School of Earth, Atmospheric and Environmental Science, University of Manchester, Manchester, M13 9PL, United Kingdom
Keywords: aerosol, parcel model, ice nucleation, active-site density

Presenting author email: candy.anquetil-deck@kit.edu

The effect of different aerosol (mineral dust, bacteria and soot) acting as immersion ice nuclei is investigated using ACPIM (Aerosol–Cloud Precipitation Interaction Model) (Connolly *et al* (2009)).

ACPIM is a powerful tool which can be used in two different ways. This box model can be, either, driven by experimental data (experiments carried out at the AIDA cloud chamber facility) or used as an air parcel in order to examine different ice nucleation parameterizations under specific conditions.

This adiabatic air parcel model was employed for the simulation of a convective cloud. In a first step, immersion freezing is described based on Diehl and Wurzler's parameterization (Diehl and Wurzler (2010)). The effect of each aerosol is studied individually and the results were compared to the ones in Diehl and Wurzler (2010).

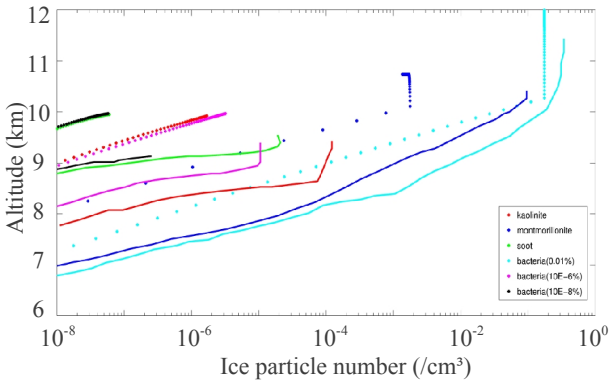

Figure 1. Comparison between ACPIM (dots) and data from Diehl and Wurzler (2010).

The study with mineral dust aerosol is then extended using Niemand *et al.* 's parameterization (Niemand *et al* (2012)), which was derived form laboratory studies in AIDA and is an extension of surface site density approach suggested by Connolly *et al* (2009).

Then, the effect of two aerosols acting simultaneously is investigated; introducing Hummel *et al.* 's parameterization for biological aerosols (Hummel *et al* (2013)) :

$$f_{in} = f_{max}\left(1 - \exp\left(-A_p * n_s(T)\right)\right)$$

With an empirically fitted ice nucleation active site density n_s based on AIDA measurements of Pseudomonas syringae bacteria (Oehm *et al* (2013)).

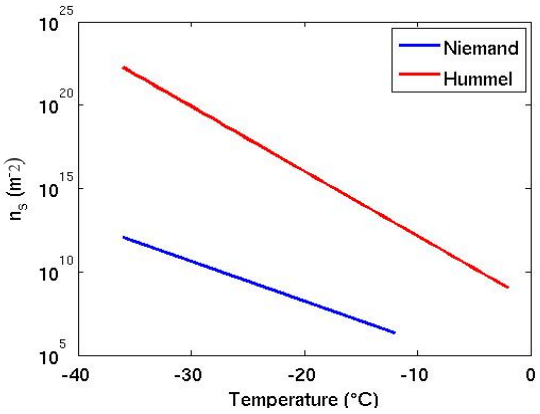

Figure 2. Immersion freezing parameterizations from (Niemand *et al* (2012) and Hummel *et al* (2013))

This research was funded by the Helmholtz Association through the President's Initiative and Networking Fund.

Connolly, P. J., Möhler O., Field P. R., Saathoff H., Burgess, R., Choularton, T. and Gallagher, M. (2009) Atmos. Chem. Phys., **9**, 2805-2824

Diehl, K. and Wurzler, S. (2010) Atmos. Env. **44**, 4622-4628

Niemand, M., Möhler, O., Vogel B., Vogel, H., Hoose, C., Connolly, P., Klein, H., Bingemer, H., DeMott, P., Skrotzki, J. and Leisner T. (2012) J. Atmos. Sci. **69**, 3077-3092

Hummel, M. *et al.* (2013) In preparation

Oehm, C. *et al.* (2013) In preparation

Modelling amazonian biomass burning aerosol using WRF-Chem

S. Archer-Nicholls[1], D. Lowe[1], W. Morgan[1], G. McFiggans[1]

[1]Centre for Atmospheric Science, University of Manchester, Manchester, M13 9PL, United Kingdom
Keywords: WRF-Chem, Biomass Burning Aerosol.
Presenting author email: scott.archer-nicholls-2@postgrad.manchester.ac.uk

Aerosols constitute some of the largest uncertainties in climate forcings in current models. Biomass burning aerosols (BBA) can make up a large proportion of the aerosol population. However, concentrations of BBA vary widely depending on season and location. In the Amazon dry season concentrations as high as 10,000 cm^{-3} have been observed (Roberts *et al.*, 2003). With their high proportion of black carbon, BBA are known to be strongly absorbing, with SSA close to the boundary between being net absorbers and scatterers, meaning the net radiative forcing can be uncertain (Forster *et al.*, 2007). Nonetheless, BBA can impact greatly on local weather and climate due to their optical properties and ability to act as CCN, influencing clouds in the region.

The South AMerican Biomass Burning and Analysis (SAMBBA) consortium is an international research project consisting of seven British Universities, UK Met Office, University of Sao Paulo and INPE (Brazilian Space Agency). It has been set up to investigate the sources, properties and impacts of BBA from the Amazon on the regional and global scale. SAMBBA consists of both an extensive measurement and modelling campaign. The measurement campaign consisted of a series of research flights using the modified FAAM BAE-146, carried out in September and October 2012 in Brazilian Amazonia. Detailed measurements profiling the chemical and aerosol content of the background Amazonian troposphere and within biomass burning plumes were taken.

The modelling component of the consortium is organised as a hierarchy of models, acting over a range of scales, from global to cloud resolving. The Weather Research and Forecasting Model with Chemistry (WRF-Chem) has been applied at the regional scale (25 km horizontal grid spacing, with nests for particular case studies run at 5 km) to investigate how BBA are emitted and processed in the atmosphere.

WRF-Chem is a fully-coupled, "online" regional climate model with fully consistent meteorological and air quality components, each using the same transport, grid spacing and timestep (Grell *et al.*, 2005). A parameterisation has been developed that calculates the injection height of biomass burning aerosols into the upper atmosphere, based on land-use and the fire source strength and size (Frietas *et al.* 2007). This has been integrated into WRF-Chem and used in the past to simulate biomass-burning events in Canada (Grell *et al.*, 2011)). Currently the biomass burning emissions this scheme is designed to work with are only compatible with bulk GOCART and the MADE/SORGAM modal aerosol schemes. We are modifying the scheme to function using MOSAIC sectional aerosol (Zaver *et al.*, 2008), in order to better resolve the size distribution of BBA.

We will be presenting preliminary model results for the SAMBBA campaigns. The vertical and horizontal distribution of the BBA in the model will be evaluated and size distribution of new and aged BBA assessed. Early comparisons between WRF-Chem results and aircraft measurements for particular case studies will be will also be shown and the implications discussed.

This work is supported by the Nature Environment Research Council (NERC) as part of the SAMBBA project under grant NE/J010073/1.

Freitas, S. R., Longo, K. M., Chatfield, R., Latham, D., Dias, M. A. F. Silva, Andreae, M. O., Prins, E., Unesp, F. E. G. (2007) *Atmos. Chem. Phys.*, **7**, 3385-3398.

Forster, P., Ramaswamy, V. , Artaxo, P., Berntsen, T., Betts, R., Fahey, D.W., Haywood, J., Lean, J., Lowe, D.C., Myhre, G., Nganga, J., Prinn, R., Raga, G., Schulz, M., and Van Dorland, R. (2007). *Contribution of Working Group I to the Fourth Assessment Report of the Intergovernmental Panel on Climate Change*, Cambridge University Press, Cambridge, United Kingdom and New York, NY, USA

Grell, G. A., Peckham, S. E., Schmitz, R., McKeen, S. A., Frost, G., Skamarock, W. C., and Eder, B. (2005). *Atmos. Env.*, **39**, 6957–6975, doi:10.1016/j.atmosenv.2005.04.027

Grell, G., Freitas, S. R., Stuefer, M., Fast, J. (2011). *Atmos. Chem. Phys.*, **11**, 5289–5303, doi:doi:10.5194/acp-11-5289-2011

Roberts, G. C., Nenes, A., Seinfeld, J. H., Andreae, M. O. (2003). *J. Geophys. Res.*, *108*(**D2**), 4062, doi:10.1029/2001JD000985

Zaveri, R. A., Easter, R. C., Fast, J. D., and Peters, L. K. (2008). *J. Geophys. Res.*, **113**, doi:10.1029/2007JD008782

Modeling the chemical and radiative effects of aerosol during the wildfires of 2007 in Greece

E. Athanasopoulou[1], D. Rieger[2], C. Walter[2], H. Vogel[2], B. Vogel[2] and E. Gerasopoulos[1]

[1] Institute for Environmental Research and Sustainable Development, National Observatory of Athens, Greece
[2]Institute for Meteorology and Climate Research, Karlsruhe Institute of Technology (KIT), Germany
Keywords: radiative effects, aerosol chemistry, online coupled atmospheric model, COSMO-ART.
Presenting author email: eathana@meteo.noa.gr

The 2007 wildfires in Peloponnese were the most destructive in the modern history of Greece. The important fire tracers (gaseous and particulate phase) and aerosol radiative forcing are studied with the chemistry transport model COSMO-ART (Vogel et al., 2009).

Simulations are performed between August 15 and September 13 with a horizontal resolution of 2.8 km and a vertical extent up to 20 km. The anthropogenic emission database used is the TNO/MACC (Kuenen et al. 2011). Fires are represented as hourly emission rates of gaseous (e.g. Nitrogen Oxides, NO_x, speciated non-methane hydrocarbons, NMHC) and carbonaceous aerosol species (TC). The data processed and used are retrieved from the GFED, Version 3 (van der Werf et al., 2010; Mu et al., 2010). In order to quantify the effect of wildfires on air quality and radiation, the change in the concentrations of primary (TC and NO_x), secondary (Ozone, O_3) produced species, and radiation was calculated as the difference between the standard run and a scenario excluding fire emissions (Fig. 1).

First, it is shown that the wild fires affect an area extending more than 500 km downwind the fire spots, around 3.6 km agl in the vertical over the fire spots, and up to 4.5 km asl in distances greater than 150 km downwind (not shown), during a period of 13 days. During this event, fires shape the 80% of ground TC over Messenia, which results being 27 times higher than TC values during the rest of the month. The presence of NO_x determines whether the oxidation leads to O3 production or loss. Indeed, the burnt area acts as an urban zone for O_3, which at the very high ambient NO_x conditions that occur over the fire spots O_3 is destroyed, whereas downwind fires O_3 is accumulated due to the lower NO_x levels. The same effect appears also in the vertical, where O_3 changes become positive at around 300m height agl. Fires contribute to O_3 exceedances (daily value of 60 ppb) at the area with positive O_3 changes (daily value of 70 ppb).

The change in aerosol profiles and chemical composition due to the fires affects the net radiative flux by -10 Wm^{-2} at the surface over the fire spots and by 1-2.5 Wm^{-2} downwind. This leads to a decrease of the temperature over land and an increase over water. The contribution of the different aerosol species and the different feedback on the atmosphere over land and water will be presented during the conference.

Recently, the direct heat input of forest fires is also implemented in COSMO-ART through the fire radiative power, acquired from GFED. The aim was to compare its effect on air temperature, with the aforementioned temperature changes. Results towards this direction will be presented during the conference.

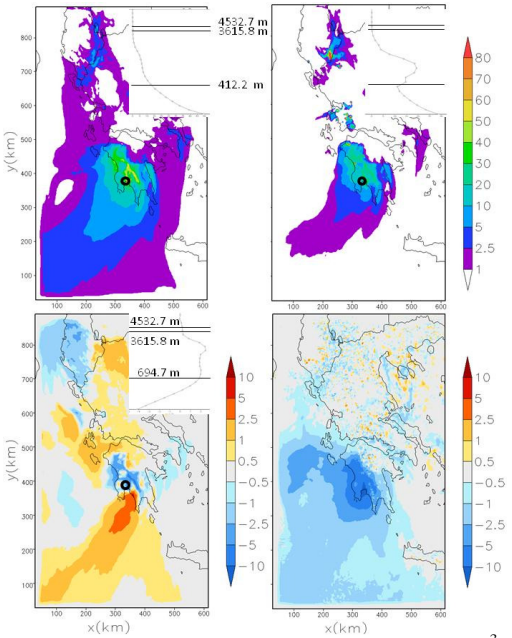

Figure 1. Spatial distribution of: (a) of TC (μgm^{-3}) averaged up to 412 m agl, (b) NO_x (μgm^{-3}) averaged up to 412 m agl, (c) O_3 (ppb) averaged up to 695 m agl and (d) total surface radiative forcing (Wm^{-2}), during the wildfires in Peloponnese, Greece (22 August – 02 September 2007). Embedded lie the vertical concentration profiles over the site marked in the map.

Part of this work, has received funding from the EU project CLIMRUN (FP7-ENV-2010-265192). E. Gerasopoulos would like to acknowledge the XENIOS (NSRF/Co-operation) Project & the Navarino Environ. Observatory for the experimental data to be used.

Baldauf M, Seifert A, Forstner J, Majewski D, Raschendorfer M, Reinhardt T (2011) *Mon Wea Rev*. doi:10.1175/MWR-D-10-05013.1 (e-view).

Kuenen J, Denier van der Gon H, Visschedijk A, van der Brugh H (2011). *TNO-report-060-UT-00588*.

Vogel, B., Vogel, H., Baumer, D., Bangert, M., Lundgren, K., Rinke, R. And Stanelle T. (2009) *Atmos. Chem. Phys*. 9, 8661–8680.

van der Werf, G.R., Randerson, J.T., Giglio, L., et. al. (2010). *Atmos. Chem. Phys.*, 10, 11707-11735.

Mu, M., Randerson, J.T. van der Werf, G.R. et. al. (2010), *J. Geophys. Res.-Atmos*.,116: D24303.

Model simulations on the effects of deposition freezing in convective clouds

K. Diehl and S.K. Mitra

Institute of Atmospheric Physics, University of Mainz, 55099 Mainz, Germany
Keywords: Deposition freezing, air parcel model
Presenting author email: kdiehl@uni-mainz.de

For detailed investigations of cloud microphysical processes adiabatic parcel models with entrainment are often employed. The air parcel model of Diehl *et al.* (2006) represents a spectral bin model which explicitly solves the microphysical equations. The initiation of the ice phase is parameterized and describes the effects of different types of ice nuclei (mineral dust, soot, biological particles) in immersion and contact modes. Results indicated that certain aerosol types significantly alter cloud microphysics (Diehl *et al.*, 2006).

In the present study a parameterization of deposition freezing has been developed on the basis of the outcome of experiments (Ardon-Dryer and Levin, 2012; Danielczok and Bingemer, 2012). These were performed with the vapor diffusion chamber FRIDGE (Bingemer et al., 2012) for atmospheric particles and two types of mineral dust. The parameterization equations give the fraction of activated ice nuclei in dependence of ice supersaturation.

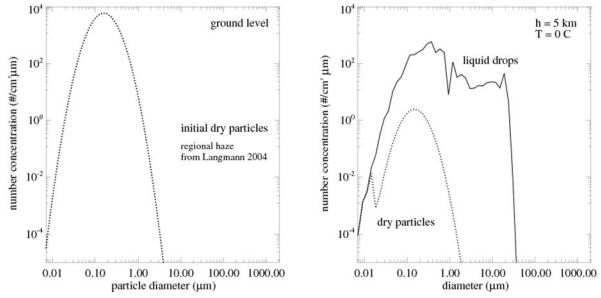

Figure 1. Initial particle number size distribution and liquid drop and interstitial particle size distributions.

The model has been initiated by a dry aerosol particle number size distribution (Figure 1, left panel) and by a temperature difference of 1.5K between parcel and environment. During the air parcel rise, aerosol particles are activated as drops due to their size and soluble fraction. Additional particles are mixed in by entrainment. Thus, interstitial aerosol particles are available during the ascent of the parcel which may serve as deposition ice nuclei (Figure 1, right panel).

In dependence of the available dry particles and the ice supersaturation, the number of ice particles formed by deposition freezing has been calculated. Potential deposition ice nuclei have to exceed the critical germ size dependant on temperature and ice supersaturation to become active. Threshold values of temperature and ice supersaturation have been set based on measurements. Cases with atmospheric particles and mineral dust have been simulated. Simulations with biological particles will also be included.

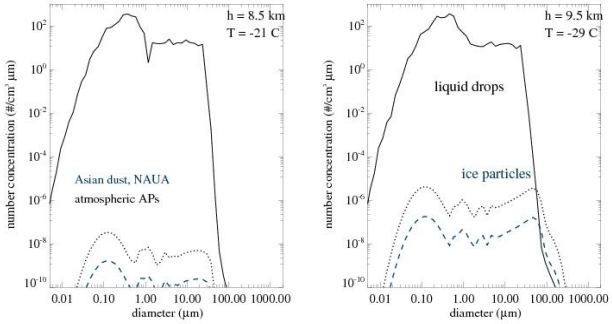

Figure 2. Development of number concentrations of liquid drops and ice particles with height for two cases.

Figure 2 shows the development of the number concentration of liquid drops and ice particles with increasing altitude and corresponding decreasing temperature. Example cases are Asian dust and atmospheric particles. At –21°C deposition freezing has set in. In comparison to the number concentration of liquid drops, only a small fraction of ice is produced. The spectrum shows a maximum at 0.15 µm and smaller maxima at larger sizes. This indicates that firstly, as primary ice formation, very small ice particles are formed due to the size of the involved particles. Afterwards, these pristine ice particles serve as nuclei for secondary ice formation, i.e. by collisions with supercooled liquid drops. This process produces ice particles of larger sizes which are further growing by the deposition of water vapor and by riming. At the end of the air parcel rise at –29°C, still a mixed-phase cloud is present with only a small ice fraction.

In comparison to immersion and contact freezing where larger sizes are preferred (Diehl *et al.*, 2006) the importance of deposition freezing in clouds lies in the formation of pristine ice particles which extend the ice particle spectra towards smaller sizes and affect secondary ice formation. Model simulations with coupled freezing in all three modes will demonstrate the competition of the different processes.

This work is part of the research group INUIT and is supported by the Deutsche Forschungsgemeinschaft under grant DI 1539/1-1.

Ardon-Dryer, K., and Levin, Z. (2012) Pers. Comm.
Danielczok, A., and Bingemer, H. (2012) Pers. Comm.
Bingemer, H., et al. (2012) *Atmos. Chem. Phys.,* **12,** 857-867.
Diehl, K., et al. (2006) *J. Geophys. Res.,* **111,** D07202, doi:10.1029/2005JD005884.
Langmann, B. (2004) Pers. Comm.

On blow-up in some mathematical models related to phase transitions and turbulence

E.I. Galakhov[1] and O.A. Salieva[2]

[1]Department of Mathematical Analysis and Theory of Functions, Peoples' Friendship University of Russia, Moscow, 117198, Russia
[2]Department of Applied Mathematics, Moscow State Technological University "Stankin", Moscow, 127994, Russia
Keywords: phase transitions, turbulence, blow-up.
Presenting author email: galakhov@rambler. ru

Introduction

Phase transitions and turbulence in the atmosphere have a great impact on distribution and dynamics of aerosols (Badger et al., 2006; Meneguz and Reeks, 2011).

Mathematical models of these phenomena are described by differential equations whose solutions (or their derivatives) tend to infinity as the time or other variables approach some finite values (Savin et al., 2006). This situation is known as *blow-up*. Therefore, determining conditions for blow-up and estimating blow-up time is an important theoretical and applied problem.

Recently, S. Pohozaev developed the nonlinear capacity method, which allows establish blow-up conditions for a broad range of problems (Pohozaev, 2009).

In the present work, the nonlinear capacity method is adapted to the case of operators with coefficients that tend to infinity near some unbounded sets, for example, straight lines or planes in the 3-dimensional space.

Assumptions

Let $S \subset R^n$ be a closed unbounded set. Take $\varepsilon > 0, x \in R^n$. Denote $\rho(x)$=dist(x,S) and $S^\varepsilon = \{x \in R^n : \rho(x) < \varepsilon\}$.

Let there exist positive constants α, c_1, c_2, ε_0, and R_0 such that for each $\varepsilon \in (0, \varepsilon_0)$ and $R>R_0$ there hold inequalities

$$c_1 \varepsilon^\alpha R^{n-\alpha} \le \mu(S^\varepsilon \cap B_R(0)) \le c_2 \varepsilon^\alpha R^{n-\alpha}, \quad (1)$$

where $B_R(0) = \{x \in R^n : | x | < R\}$.

Remark 1. Condition (1) on S is natural for a whole class of aforementioned sets.

Main Results

For the sake of definiteness, the results are formulated in a special case, namely for the evolutional inequality

$$u_t - \Delta u \ge u^q \rho^{-\alpha}(x) \quad (x \in R^n \setminus S, t \in R_+) \quad (2)$$

with initial conditions

$$u(x,0) = u_0(x) \quad (x \in R^n \setminus S). \quad (3)$$

The initial function $u_0(x)$ is assumed to satisfy the estimate

$$u_0(x) \ge c \, | x |^\lambda \, \rho^\mu(x) \quad (x \in R^n \setminus S) \quad (4)$$

with some constants $c>0$, $\lambda, \mu \in R$.

Remark 2. Condition (4) imposes limitations on the growth of initial functions as $|x| \to \infty$ and $\rho(x) \to 0$, which is natural in applications.

A typical result concerning inequality (2) can be formulated as follows.

Theorem. *Suppose that S satisfies* (1). *Let* $q > 1$, *and let* u_0 *satisfy* (4) *with* $\alpha > \max\{(\mu - \lambda)(q-1) + 2, 0\}$.

Then any solution of the Cauchy problem (2), (3) *blows up in finite time.*

Remark 3. Similarly, sufficient conditions for blow-up are established for other classes of differential inequalities such as:

- Semilinear and quasilinear elliptic inequalities.
- Elliptic inequalities with gradient terms.
- More general evolutional differential inequalities, etc.

Future Prospects

- To estimate blow-up time in terms of known data.
- To develop numerical simulation of blow-up for the class of problems under investigation.

This work was supported by the Russian Foundation for Basic Research under grants 11-01-00348a and 11-01-12018-ofi-m-2011.

Badger, C.L., George, I., Griffiths, P. T., Braban, C. F., Cox, R. A. and Abbatt, J. P. D. (2006) *Atmos. Chem. Phys.* **6**, 755–768.

Meneguz, E. and Reeks, M.W. (2011) *J. Fluid Mech.* **686**, 338-351.

Pohozaev, S. (2009) *Milan J. Math.* **77**, 127–150.

Savin, V. O., Sciunzi, B. and Valdinoci, E. (2006) *Memoirs AMS* **182**, 1-144.

Modeling of optical properties sea-salt aerosol in the surface layer of the marine and coastal atmosphere

G. A. Kaloshin

V.E. Zuev Institute of Atmospheric Optics Rus. Acad. Sci., Siberian Branch, Tomsk, 634055, Russia
Keywords: aerosol extinction, Mie scattering, wind mode, fetch.
Presenting author email: gkaloshin@iao.ru

A microphysical model for the surface layer of marine and coastal atmospheric aerosols that is based on long-term observations of size distributions for 0.01–100 μm particles in different geographic sites is presented. The fundamental feature of the model is parameterization of amplitudes and widths for aerosol modes of the aerosol size distribution function (ASDF) as the functions of the fetch and the wind speed. The ASDF shape and its dependence on meteorological parameters, the altitudes above sea level (H), the fetch (X), the wind speed (U) and the relative humidity (RH) is investigated. The spectral profiles of the aerosol extinction coefficients calculated using the MaexPro (Marine Aerosol Extinction Profiles) are in good agreement with the observation data and the numerical results obtained from avalable aerosol models. Moreover, the MaexPro was found to be an accurate and a reliable instrument for investigation of the optical properties of atmospheric aerosols.

The particle size distribution dN/dr of the coastal aerosol microphysical model, in the range of the particle radii 0.01–100 μm, may be expressed as the sum of four modified lognormal functions, (Piazzola, Kaloshin, 2005; Kaloshin G., Grishin I., 2011) similar to the models NAM and ANAM:

$$\frac{dN}{dr} = \sum_{i=1}^{4} \frac{A_i}{f} \exp\left\{ -C_i \left(\ln\left(\frac{r}{f r_{0i}} \right)^2 \right) \right\} \quad (1)$$

where: r_{01} = 0.03, r_{02} = 0.24, r_{03} = 2, r_{04} = 10 μm; f is represents the humidity growth factor; Ai is denotes the amplitude of the ith mode; Ci is is the width of the ith mode. The selected particle size of 0.01 – 100 μm is due to the special attention given to the wavelength band of 0.2 - 14 μm, where the aerosol extinction is of great practical interest.

Having obtained the aerosol size distribution and the refraction index, we next calculate the aerosol extinction σ(λ) value by means of the classical Mie solution, assuming the aerosol particles are spherically shaped (Boren, Huffman. 1983).

The aerosol substance is a combination of the following materials: a dry substance, sea salt and water as listed in Table 1.

Table 1. Comparison between theoretical predictions and experimental measurements.

Mode	Materials	The mode size, μm	References
1	Insoluble	0.03	Shettle, Fenn (1979)
2	Soluble	0.24	Volz (1972)
3	Salt + water	2	Shettle (1979)
4	Salt + water	10	Hale, Query (1973)

In the model MaexPro, the real and imaginary parts of the complex optical index for the components of the aerosol particle substance have been taken from the empirical results as shown by (Volz, 1972) by means of an extrapolation in the wavelength band 0.2 – 14 μm, sampled at the interval Δλ = 0.001 μm.

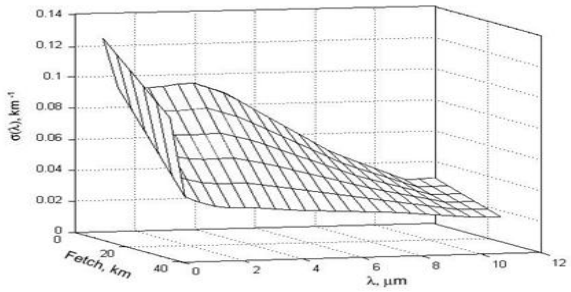

Figure 1. The spectral aerosol extinction coefficient σ(λ) vs. fetch X: H = 20 m, RH = 75%, U = 3.3 m/s.

Figure 1 shows how significant the dependence of the extinction spectra on the fetch parameter is. It is clear that at small values of the fetch (3-10 km) the extinction spectra decline steeply; this is typical for coastal aerosol. With increasing fetch, the extinction spectra become almost uniform as expected for marine aerosols, which means that in the coastal environment the fetch can be used in the same way as the air mass parameter (Gathman and A.M. van Eijk, 1998).

Based on the comparison with the observations, we conclude that the MaexPro is capable to realistically describe the impact of several different factors, such as meteorological parameters, the geometrical features of the shoreline and the wind mode. The calculation results are in agreement with the observation data at changing meteorological parameters obtained in different geographic sites by different authors.

Boren, C.F., D.R. Huffman. (1983). NY: Wiley.
Gathman S.G., van Eijk. Proc. SPIE 3433, 41-52 (1998).
Hale G.M., M.R.Query. (1973). Appl. Opt. 12: 555–563.
KaloshinG., GrishinI.(2011).Atm.-Ocean.49(2),112-120.
Piazzola J., Kaloshin G. (2005). J. Aerosol Science, 36(3), 341-359.
Shettle, E.P., R.W. Fenn. (1979). Report No. AFGL-TR-79-0214.
Volz F.E. (1972). Appl. Opt., 11, 755-759.

Coupled chemical mechanism and sectional aerosol developments within WRF-Chem

D. Lowe[1], S. Archer-Nicholls[1], S. Utembe[1,2], D. Topping[1,3], M. Barley[1], R. Zaveri[4], G. McFiggans[1]

[1]Centre for Atmospheric Science, University of Manchester, Manchester, M13 9PL, United Kingdom
[2]Earth Sciences, The University of Melbourne, Victoria, Australia
[3]National Centre for Atmospheric Science, University of Manchester, Manchester, M13 9PL, United Kingdom
[4]Pacific Northwest National Laboratory, Richland, Washington, USA
Keywords: NOx, Modelling, Multiphase, SOA
Presenting author email: douglas.lowe@manchester.ac.uk

Aerosol particles play an integral part in the chemistry of the atmosphere — by acting as reaction surfaces for heterogeneous chemistry, as chemical sources, and by removing components through scavenging and dry deposition. They also influence the climate, directly through radiative scattering and adsorption, and indirectly through influencing cloud formation by acting as cloud condensation nuclei. In order to improve our understanding of how aerosols have these effects they have been included, with varying degrees of detail, in global and regional atmospheric models.

The mesoscale Weather Research and Forecasting (WRF) meteorological model (http://www.wrf-model.org; Skamarock et al., 2005) has been expanded to create the WRF-chem model (Grell et al., 2005), which simulates gas-phase chemical and aerosol microphysical processes on-line with the meteorological fields, allowing explicit coupling between the processes. A variety of gas-phase chemical schemes and aerosol mechanisms are available and the modular setup of WRF-chem allows different gas-chemistry and aerosol modules to be evaluated and compared using the same chemical emissions and meteorology input data (c.f. Fast et al., 2006). Here we present developments made to WRF-chem with the aim to improve the representation of gaseous and condensed-phase processes for use within, and to address the scientific objectives of, the NERC funded RONOCO and VOCALS-UK consortium projects.

We have extended the gas-phase chemistry options by adding the CRIv2 (Common Representative Intermediates, version 2) gas-phase scheme (Watson et al., 2008). This is derived from the Master Chemical Mechanism, and enables improved modelling of organic gas-phase chemistry, which is important in reproducing ozone and the volatile organic compound (VOC) budgets.

The MOSAIC aerosol module (Zaveri et al., 2008) has been extended with the addition of organic aerosol components, comprising of 2 involatile, and 13 semi-volatile, organic compounds (Barley et al., 2011). Non-ideal interactions between these compounds in the condensed-phase, which change the individual component vapour pressures, are calculated using the PD-FiTE method (Topping et al., 2012). The partitioning organic components have been chosen using MCM box-model studies to select the greatest contributing components to organic aerosol mass. These have been linked either to related CRIv2 compounds or, where no suitable compounds exist, related to the concentrations of surrogate compounds through numerical fits.

Sea-spray aerosol source terms have been updated following the work of Fuentes et al. (2010; 2011). This extends the source term down to smaller particle sizes and connects the source term to the biogenic activity of the ocean, allowing the representation of the influence of the organic content on particle formation. Also included is a size-resolved primary organic fraction to the sea-spray emissions, assumed involatile.

Night-time NOx chemistry and aerosol formation is governed by the heterogeneous uptake of N_2O_5 on aerosol particles. We have incorporated the parameterisation of Bertram and Thornton (2009) into the MOSAIC sectional aerosol module to represent this process. This converts N_2O_5 to aerosol nitrate and $ClNO_2$, with composition dependent uptake coefficients and branching ratios.

This work was conducted as part of the RONOCO (ROle of Nighttime chemistry in controlling the Oxidising Capacity of the atmOsphere) (NERC grant: NE/F004656/1) and VOCALS-UK (Vamos Ocean Cloud Atmosphere Land Study) (NE/F019874/1) projects.

Barley, M. H., Topping, D., Lowe, D., Utembe, S., and McFiggans, G. (2011). *Atmos. Chem. Phys.*, **11**, 13145–13159

Bertram, T. H., and Thornton, J. A. (2009). *Atmos. Chem. Phys.*, **9**, 8351–8363

Fast, J. D., Gustafson, W. I., Easter, R. C., Zaveri, R. A., Barnard, J. C., Chapman, E. G., Grell, G. A., and Peckham, S. E. (2006). *J. Geophys. Res.*, **111**, 1–29, doi:10.1029/2005JD006721

Fuentes, E., Coe, H., Green, D., de Leeuw, G., and McFiggans, G. (2010). *Atmos. Chem. Phys.*, **10**, 9295–9317

Fuentes, E., Coe, H., Green, D., and McFiggans, G. (2011). *Atmos. Chem. Phys.*, **11**, 2585–2602

Grell, G. A., Peckham, S. E., Schmitz, R., McKeen, S. A., Frost, G., Skamarock, W. C., and Eder, B. (2005). *Atmos. Env.*, **39**, 6957–6975, doi:10.1016/j.atmosenv.2005.04.027

Skamarock, W. C., Klemp, J. B., Dudhia, J., Gill, D. O., Barker, M., Wang, W., and Powers, J. G. (2005). *NCAR Tech. Note, NCAR/TN-468+STR*

Topping, D., Lowe, D., and McFiggans, G. (2012). *Geosci. Model Dev.*, **5**, 1–13

Watson, L. A., Shallcross, D. E., Utembe, S. R., and Jenkin, M. E. (2008). *Atmos. Env.*, **42**, 7196–7204, doi:10.1016/jatmosenv.2008.07.034

Zaveri, R. A., Easter, R. C., Fast, J. D., and Peters, L. K. (2008). *J. Geophys. Res.*, **113**, doi:10.1029/2007JD008782

WRF CHEM in the marine environment

E.Miklos[1], D.Martin[1] and C.D.O'Dowd[1]

[1]School of Physics and Center for Climate and Air Pollution Studies,
Ryan Institute for Environmental, Marine and Energy Research, National University of Ireland, Galway
Keywords: WRF-CHEM, sea salt
Presenting author email: e.miklos1@nuigalway.ie

WRF-CHEM is the Weather Research and Forecasting (WRF) model coupled with Chemistry (Grell et al., 2005). The model simulates the emission, transport, mixing, and chemical transformation of trace gases and aerosols simultaneously with the meteorology. From a northern European perspective the contribution of sea salt to particular matter concentrations can be significant especially in coastal areas and the predictive ability of air quality models to forecast ambient sea salt levels is important for the effective management of air quality.

In this work we evaluate the performance of the WRF-CHEM model to forecast sea salt levels with particular emphasis on the Irish domain. Coarse and accumulation mode sea salt are determined using the parameterisation of Gong (2003) with fluxes calculated as a function of wind speed (based on the semi empirical paramaterisation of Monahan et al., 1986).
These fluxes are distributed in 4 size bins (1 sub-micron and 3 super micron). Simulations are performed for a winter and summer month in order to elucidate any seasonal bias in the parameterisation deployed.

For effective evaluation and validation a provisional assessment of the model performance with regard to meteorological indicators has been undertaken. These initial simulations have been centred over a European domain at a resolution of 50 x 50km and focus on November 2009.

Shown below in Figure 1 is the agreement between forecasts and observations for monthly averaged cumulative precipitation. Given the significant impact of wet deposition as a loss mechanism for ambient sea salt the ability to forecast accurately precipitation will have a significant bearing on the accuracy of the forecast.

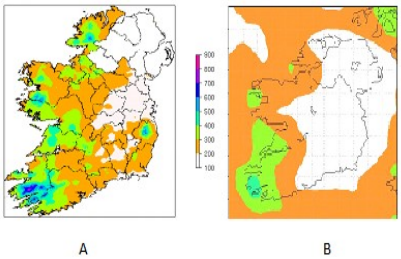

Figure 1. Observed monthly precipitation (A) 1km x 1km (Met Eireann) and modelled precipitation (B) 50 km x 50km (WRF) for November 2009.

Shown in Figure 2 is the agreement between modelled and measured wind direction over the same period from a measurement site in Iberian Peninsula (40.8000° N, 0.5167° E). There is also a high degree of correlation with wind speed (R>0.8).

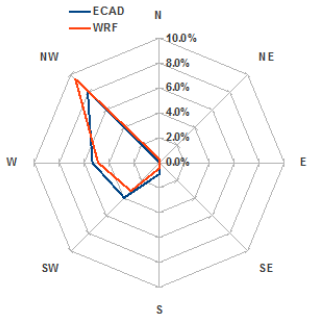

Figure 2. Observed monthly measured (ECAD) and modelled (WRF) wind direction for November 2009.

A more complete evaluation is currently being undertaken. Results for simulations will be evaluated against high resolution aerosol mass spectrometer speciated sub micron sea salt measurements as well as available speciated PM10 and PM2.5 filter measurements across a range of sites.

This work was supported by RH5250.

Gong, S.L. (2003), *A parametrization pf sea-salt aerosol source function for sub-and super-micron particles*, Global Biogeochem Cy, **17** (4), 1097, doi:10.1029/2003gb002079

Grell, G.A., Peckham, S.E., Schmitz, R., McKeen, S.A., Frost, G., Skamarock, W.C. and Eder, B. (2005) *Fully coupled online chemistry within the WRF model*, Atmos. Environ. **39**, 957-6976

Monahan, E.C., Spiel, E.d., and Davidson, K.L. (1986) *A model of marine aerosol generation via whitecaps and wave disruption*, 167-174 pp., Reidel, Dordrecht

3D modeling of open-pored foams regarding particle deposition from aerosols

K. Schmidt, A. Hellmann, S. Ripperger

Chair of Particle Process Engineering, Technical University Kaiserslautern, Kaiserslautern, 67663, Germany
Keywords: foam, aerosol, deposition, simulation.
Presenting author email: kilian.schmidt@mv.uni-kl.de

Open-pored foams are highly porous and permeable materials, which are suited for a wide range of technical applications and also for particle filtration amongst others. The description of their complex spatial structure by characterizing parameters like porosity, pore diameter and link diameter is a simplification, which limits the prediction capability of models based on these parameters (Clark, 2009).

However, by using 3D pore structure models for the computation of the permeability or particle fraction deposition rates from fluids, the spatial structure of the open-pored foam is completely comprised. The 3D pore structure model can be obtained either by tomography or be generated by some algorithm (Redenbach, 2011). In both cases, at first a voxel model is obtained (i.e. a 3D pixel image). Thus, when a polyhedron mesh based flow and particle deposition simulation should be applied, the polyhedron mesh must be generated first (Skibinski, 2012).

In the presented work, tomographical open-pored foam models as well as models generated by a novel universal algorithm are used to compute air flow and NaCl aerosol deposition at a series of different open-pored foam materials. One of these is shown in Figure 1. Here, flow and particle computations are conducted directly on the voxel models, s.t. the polyhedron mesh generation step is avoided. The preparation of the models as well as the flow and particle computations are carried out with the in-house development DNSlab. The simulation results are then compared to measurements which have also been conducted by the authors. The simulated and measured particle fraction deposition rates show a very good agreement. The results for the material shown in Figure 1 are depicted in Figure 2.

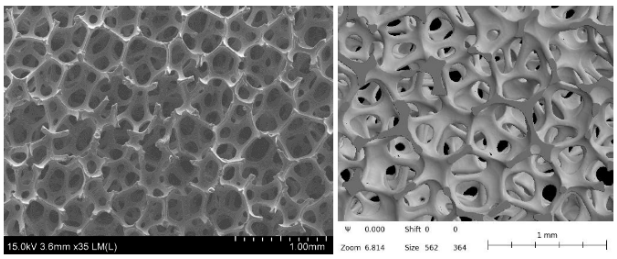

Figure 1. Real structure (left) and generated model (right) of an examined open-pored foam.

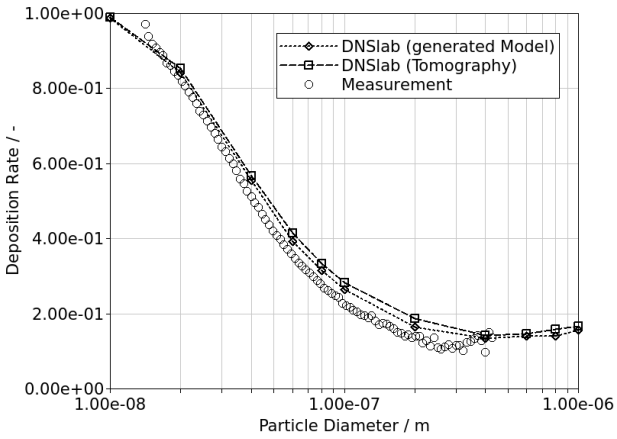

Figure 2. Comparison of NaCl particle fraction deposition rates from experiment and simulation with generated model and tomography for the open-pored foam material shown in Figure 1. The sample thickness is 16 mm, the aerosol flow rate is 0.055 m/s.

Clark, P., Koehler, K. A., Volckens, J. (2009) *Aerosol Science* **40**, 563-572

Redenbach, C., Wirjadi, O., Rief, S., Wiegmann, A. (2011) *Advanced engineering materials* **13/3**, 171-177

Skibinski, J., Wejrzanowski, T., Szumbarski, J., Kurzydlowski, K. J. (2012) *Advances in Fluid Mechanics* **IX**, 109-118

Modelling the impact of mineral dust on air quality in Beijing during a dust event

S. Schrader[1,3], B. Vogel[2], H. Vogel[2], K. Schäfer[3], R. R. Shen[3], R. Forkel[3], P. Suppan[3], G. Tang[4], Y. Wang[4], S. Norra[1]

[1]Institute of Geography and Geoecology, Karlsruhe Institute of Technology (KIT), 76128 Karlsruhe, Germany
[2]Institute of Meteorology and Climate Research – Department of Troposphere Research (IMK-TRO), Karlsruhe Institute of Technology (KIT), 76344 Eggenstein-Leopoldshafen, Germany
[3]Institute of Meteorology and Climate Research – Department of Atmospheric Environmental Research (IMK-IFU), Karlsruhe Institute of Technology (KIT), 82467 Garmisch-Partenkirchen, Germany
Institute of Atmospheric Physics (IAP) - State Key Laboratory of Atmospheric Boundary Layer Physics and Atmospheric Chemistry (LAPC), Chinese Academy of Sciences (CAS), Beijing, China

Keywords: Modelling (regional), Asian dust, air pollution, megacity

Presenting author email: stefanie.schrader@kit.edu

Sand- and dust storms frequently occur in spring in Northern China causing very high geogenic particle mass concentrations in the atmosphere in the source regions (Wu *et al*., 2009). These dust particles can be also transported over long distances towards the highly urbanized areas of Eastern China. In megacities like Beijing, the anthropogenic and geogenic aerosol loading can lead to severe reduction of air quality and and visibility as well as harm the human health (Schleicher *et al*., 2010; Chen *et al*., 2011). Moreover the aerosol has impact on the state of the atmosphere altering radiative fluxes and cloud formation processes (Bangert *et al*., 2012). Still, a lack of information exists about the mixing of mineral dust in the urban atmosphere.

To investigate the contribution of mineral dust to the urban air quality of the Greater Beijing area and its impact on the state of the atmosphere the comprehensive online coupled model system COSMO-ART (Vogel *et al.*, 2009) has been set up for Northern China. COSMO-ART consists of the meteorological weather forecast model COSMO of the German Weather Service (DWD) and ART for the treatment of aerosols and reactive trace gases. The mineral dust module of COSMO-ART allows the online coupled calculation of mineral dust mass and number concentrations and their interactions with the physical parameters of the atmosphere. The model domain covers whole Northern China which allows the investigation of the influence of mineral dust from all Chinese desert areas to the aerosol loading in Beijing atmosphere. COSMO-ART is set up with 40 vertical levels and a horizontal resolution of 28 km x 28 km.

The simulated mineral dust and anthropogenic PM_{10} and $PM_{2.5}$ concentrations are compared to PM_{10} and $PM_{2.5}$ measurement data from ground based stations. Measurements are conducted by LAPC in the Greater Beijing area (Xin *et al*., 2012). The meteorological data for model and measurement comparison are taken from WMO meteorological stations. Additional information about the spatial distribution and aerosol types are available from CALIPSO lidar data.

COSMO-ART is applied for the Asian dust storm event that hit Beijing on April 30th in 2011 lasting for about one day. Several meteorological stations in the Greater Beijing area reported blowing sand, widespread dust conditions and strong wind speeds from north-western directions. Visibility in this area dropped down to 1 km due to the high aerosol loading in the atmosphere. Observed PM_{10} and $PM_{2.5}$ concentrations of all stations showed a sudden steep peak of up to 1250 µg/m³ and 350 µg/m³, respectively. COSMO-ART is able to simulate the timing and level of this peak quite well. This confirms that the high particle concentrations observed in Beijing during this episode are of geogenic origin brought into the city area from dust sources north-west of Beijing (Gobi desert mainly). Additional information about the spatial distribution of the mineral dust is taken from CALIPSO lidar data. It shows that there is a mixing of the mineral dust particles with anthropogenic pollutants in the urban atmosphere of Beijing.

This work is partly funded by the Graduate School for Climate and Environment (GRACE) of KIT and the KIT Centre for Climate and Environment.

Bangert, M., Nenes, A., Vogel, B., Vogel, H., Barahona, D., Karydis, V., Kumar, P., Kottmeier, C. and Blahak, U. (2012) *Atmos. Chem. Phys*., 12, 4045-4063

Huang, K., Zhuang, G., Lin, Y., Li, J., Sun, Y., Zhang, W. and Fu, J. S. (2010) *J. Geophys. Res*., 115, D00K16.

Schleicher, N., Norra, S., Chai, F., Chen, Y., Wang, S., Stüben, D. (2010) *J. Environ. Monit.*, 12, 434-441.

Vogel, B., Vogel, H., Bäumer, D., Bangert, M., Lundgren, K., Rinke, R. and Stanelle, T. (2009) *Atmos. Chem. Phys.*, 9, 8661-8680.

Wu, Z. J., Cheng, Y. F., Hu, M., Wehner, B., Sugimoto, N. and Wiedensohler, A. (2009) *Atmos. Chem. Phys*., 9, 6915-6932.

Xin, J., Wang, Y., Wang, L., Tang, G., Sun, Y., Pan, Y. and Ji, D. (2012) *Adv. Atmos. Sci*., 29, 1330-1342.

The model of propagation of acoustic signal on water surface with precipitated aerosol particles

L.A. Uvarova[1, 2], V.V. Zabolotin[1], I.V. Krivenko[3] and T.V. Kazarova[2]

[1]Department of Applied Mathematics, Moscow State University of Technology "STANKIN", 127994, Russia
[3] Department of Physics, Tver State University of Technology, 170026, Russia
[2]Department of Ecology, Moscow State Academy of Water Transport, Moscow, 117105, Russia
Keywords: aerosol particles, precipitation, electromagnetic field, acoustic signal
Presenting author email: uvarova_la@rambler.ru

It is well known that one of main mechanism of the atmospheric purification is the precipitation of aerosol particles. The precipitation takes place both on forests, cities, *etc* and on seas and other reservoirs. What's more, a heterogeneous on composition of atmospheric precipitation takes place as a result of atmospheric migration of chemical elements. For example, the content of several metals (copper, nickel, cadmium and other) in aerosol particles increases at the transition from continental territories to coastal territories and to seas (reservoirs).

The precipitation of aerosol particles on surface of reservoirs carries out in turn to the change of the water properties. Consequently, it carries out to change of the main properties which are connected with propagation of signal of different nature. The precipitation depends on particles sizes. The large aerosol particles precipitate by gravitation soon. More small particles can fly for a long time. Consequently, such particles can spread radioactive dash.

The investigation of the propagation of signals in water with new the surface properties may be carry out with the using of electromagnetic radiation.

In given work we considered the following model problem. The collective of spherical particles was situated on the surface of the liquid (water). The water surface was modelled by two ways: 1) the plane; 2) the wave surface corresponded with the solutions of the KdV equation (the breather and the cnoidal waves). In second case the displacement of the particles relatively to position on the plane takes place. The interaction of the Gaussian beam of the electromagnetic wave with the water surface without disperse particles and with disperse particles was considered. On the basis of the Mie theory were determined the internal electromagnetic field of disperse particles and absorbed energy. After the determination of the energy it is possible to find the heat source for the determination the temperature of particles and the medium (water in given case). The heat source q_i is defined on the base of an electrodynamics problem decision: $q_i = 4\pi n_{ri} n_{pi} \left|\vec{E}\right|^2 I / n_m \lambda$, where n_{ri} and n_{pi} are indexes of refraction and absorption coefficient of the matter of the particle *j* accordingly, $\left|\vec{E}\right|^2$ is the square of the amplitude of the electric vector, *I* is the intensity of the initiative radiation, n_m is the index of environment refraction, λ is an electromagnetic initiative radiation wave length. In this case when particle is nearby other particle we use the theory of group presentation for the determination of the absorbed energy (Uvarova *et al*, 2006). The determined energy permits to calculate the temperature *T* of particles on the basis of the heat non-stationary equation. Further we considered the change of the pressure and, consequently, the propagation of the acoustic signal. The solution of the given problem we carried out by the finite element method and some analytical results.

The carried out calculation were shown that the disperse layer on the surface of the liquid affects on the character of the propagated acoustic signals.

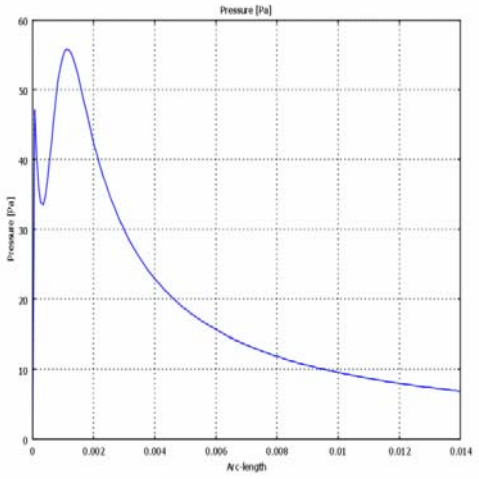

On figures are represented the example of the solution for the pressure (on axis OY) from product of distance *x* on angle in radian (on axis OX) in water with small particles of aluminium, the power of laser radiation is 10^8Wt/m^2. The carried out calculation were shown that for different metal particles the propagation of the acoustic signal depends from the geometry of the system, substance of particle and physical property of the medium. For example, the peak of acoustic signal for iron particles appears more than for aluminium ones. Consequently, the exchange in system "atmosphere – water basin" can carry out to the change of properties of surface layer, velocity and other physical characteristics of the propagated signals.

Acknowledgement

This work was supported by the Russian Fund for Basic Research (Grant No. 12-01-00874-a).

Uvarova L.F., Krivenko I.V., Smirnova M.A. (2006) *Chemical Engineering Transactions*, **10**, .251-256.

Airport emissions characterized by multivariate nonlinear time series models

G. Valotto[1], C. Varin[1], C Gaetan[1], E. Pecorari[1], G. Rampazzo[1], D. Bassano[2], S. Sollecito[2], E. Rampado[3]

[1]Department of Environmental Science Informatics and Statistics, University Ca' Foscari, Dorsoduro 2137, I-30123 Venezia, Italy
[2]SAVE S.p.A., Marco Polo Venice airport viale G. Galilei 30/1, I-30173 Tessera-Venezia, Italy
[3]Ente Zona Industriale di Porto Marghera, via dell'Elettricità 39, I-30175 Porto Marghera-Venezia, Italy
Keywords: airport emission, nonlinear time series models
Presenting author email: valotto@unive.it

Aviation activities are included in the Community Scheme of Allowances of Greenhouse Gases by the 2008/101/CE Directive of European Parliament and the Council of December 19th, 2008, amending the 2003/87/EC Directive. The airport major emission sources are aircraft engines fuelled by petroleum products, activities directly related to the passengers and luggage movements, as well as the airport structure operations (heating, fuel storage, etc.).

Ca' Foscari University in collaboration with SAVE S.p.A. and Ente Zona Industriale (EZI) has been studying the "Marco Polo" airport (45°30'40''N, 12°20'38''E – Tessera, Venice - Italy) emissions since June 2009, by monitoring the main atmospheric variables, and the major pollutants concentration revealed in the study area. Specifically, the chemical species monitored every hour are: PM_{10}, SO_2, O_3, NO, NO_X, NO_2, CO, methane and non-methane hydrocarbons, while meteorological variables sampled are wind speed and direction, solar radiation intensity, precipitation rate, and temperature. The sampling site (a parking area near the airstrip – site 1 highlighted in yellow in figure 1) was chosen estimating the main fallout points of aircraft emissions below 1000 m and neglecting the other sources. This estimation was achieved by processing the air traffic data provided by SAVE SpA, using a Lagrangian model SPRAY (Tinarelli et al., 1994) that is part of the SCAIMAR modelling system, managed by EZI. The study of airport pollutants dispersion in the Venice area is extremely important because: i) Marco Polo air traffic is among the highest in Italy and ii) the airport is located near the Venice lagoon, a complex and delicate ecosystem.

Multivariate nonlinear time series models are developed in order to study the dynamic interaction of monitored pollutants as a function of weather conditions and to give useful information for the characterization of airport emission contribution.

Results show that near the study area there are several sources of monitored pollutants (some of these are highlighted in red in figure 1), and that the airport is not the dominant one.

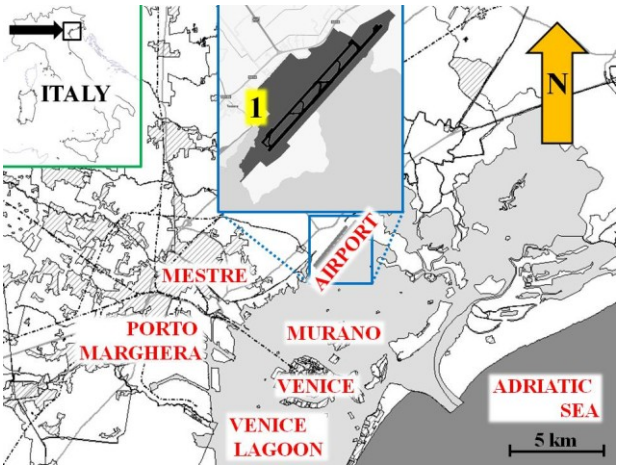

Figure 1. "Marco Polo" Airport location near Venice lagoon and sampling point

References

Tinarelli G., Anfossi D., Brusasca G., Ferrero E., Giostra U., Morselli M.G., Moussafir J., Tampieri F., Trombetti F. (1994). Lagrangian particle simulation of tracer dispersion in the Lee of a schematic two-dimensional hill. Journal of Applied Meteorology, 33, pp. 744–756.

Photophoresis of fractal-like aerosol particles: physical model and methodical approaches

M.V. Vasiljeva*, S.A. Beresnev, L.B. Kochneva and V.I. Gryazin

Ural Federal University, Ekaterinburg, 620083, Russia
Keywords: fundamental aerosol physics, stratospheric aerosols, photophoresis, soot aerosol
Presenting author email*: mary_ru@mail.ru

A unilaterally irradiated particle in a rarefied gas is affected by the photophoretic force. This force is of a radiometric nature and is the result of gas molecules interaction with the non-uniformly heated particle surface. To solve a photophoresis problem it is necessary to consider electromagnetic radiation absorbed by the particle (the electrodynamic part of the problem) and to calculate the photophoretic force and velocity (the gas-kinetic part). The possible applications of radiometric photophoresis in gases are rather extensive: particle transport in combustion environments, photophoretic separation of particles, photophoretic trapping, photophoretic velocimetry, photophoretic effects in optical tweezers, various astrophysical and meteorological applications.

Nowadays, the kinetic theory of photophoresis for spherical homogeneous particles developed by Beresnev *et al* (1993) has found confirmation in experiment for a complete set of determining parameters. In particular, on its basis it has been predicted that well-known radiometric photophoresis can be the significant mechanism of vertical transport for absorbing soot-like particles in the stratosphere (Beresnev *et al*, 2011; Beresnev *et al*, 2012). On the other hand, the most part of soot atmospheric particles have a fractal-like structure. From here it is necessary to expect changes of thermal-physics and optical characteristics of these particles in comparison with homogeneous spheres. Besides, the quantitative changes in photophoretic velocities of such particles are possible also. From here follows the necessity of new microphysical and optical models for fractal-like soot particles.

The rich information of such kind contains in laboratory photophoretic experiments with fractal-like soot particles (Karasev *et al*, 2004). It has been shown, that fractal-like soot particles demonstrate confidently the longitidunal photophoretic motion in the field of directed laser irradiation.

Comparison of theory for homogeneous spheres (Beresnev *et al*, 1993) gives the good agreement with experiment at unexpectedly high heat-conductivity coefficient for soot particles. Optical characteristics for fractal-like particles, apparently, insignificantly differ from similar characteristics for homogeneous spheres. It is possible to approximate with good accuracy the mobility radius of these particles R_m by radius of gyration R_g of the aggregate.

The sufficient information for new photophoretic model development are the fractal dimension of particles D_f and general characteristics for primary particles in aggregate (Fig. 1).

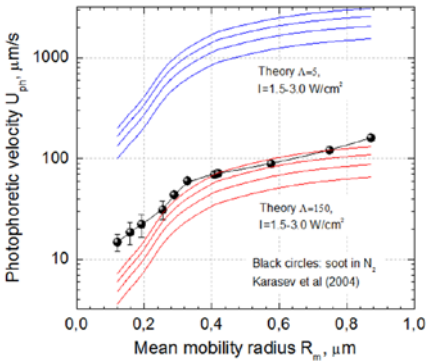

Figure 1. Comparison of measured photophoretic velocity for fractal-like soot aggregates with D_f =1.8 (Karasev *et al*, 2004) with theoretical predictions for spheres (Beresnev *et al*, 1993).

The principal propositions of new offered model are:

1. It is useful to keep the mathematical formalism used in model of homogeneous spheres (the general solution of fractal-like particle problem is extremely difficult).
2. For thermal-physics characteristics of fractal-like particles the model for estimation of effective heat conductivity of nanocomposites and nanofluids is used (e.g., Evans *et al*, 2008).
3. For calculations of optical characteristics for fractal-like particles it is possible to use methods of effective medium approximations (e.g., Chylek *et al*, 1988).
4. The determined above characteristics are used in gas-kinetic calculations for photophoretic force and velocity, where Knudsen number is determined on radius of gyration of aggregate R_g. Reliability and accuracy of suggested model is necessary to estimate by comparison with adequate experimental and theoretical data.

This work was supported by the Ministry of Education and Science of the Russian Federation (research project implemented by leading scientist at Russian institution of higher education, agreement No.11.G34.31.0064).

Beresnev, S.A., Kochneva, L.B., Zhuravleva, T.B. and Firsov, K.M. (2012) *Atmos. Oceanic Opt.* **25(4)**, 286-291.

Beresnev, S.A., Kochneva, L.B., Zakharon, V.I. and Gribanov, K.G. (2011) *Atmos. Oceanic Opt.* **24(7)**, 597-600 (in Russian).

Beresnev, S.A., Chernyak, V.G. and Fomyagin, G.A. (1993) *Phys. Fluids A* **5(8)**, 2043-2052.

Karasev, V.V., Ivanova, N.A., Sadykova, A.R. et al. (2004) *J. Aerosol Sci.* **35(3)**, 363-381.

Evans, W., Prasher, R., Fish, J. et al. (2008) *Int. J. Heat Mass Transfer* **51**, 1431-1438.

Chylek, P., Srivastava, V., Pinnick, R.G. and Wang R.T. (1988) *Appl. Opt.* **27(12)**, 2396-2404.

Modelling the chemically speciated $PM_{2.5}$ over the French Northern region using the WRF-Chem system coupled to EMEP and regional emission inventories.

M. Mendez[1], V. Fèvre-Nollet[1], P. Lebègue[1], D. Petitprez[1], N. Visez[1] and R. Borge[2]

[1] Physico-Chimie des Processus de Combustion et de l'atmosphère, PC2A, UMR 8522 CNRS/Lille 1, Université Lille1, Villeneuve d'Ascq, F-59655, France

[2] Department of Chemical and Environmental Engineering, Technical University of Madrid (UPM), c/ Jose Gutierrez Abascal 2, 28006 Madrid, Spain

Keywords: emission, inventory, modelling, composition.
Presenting author email: maxence.mendez@gmail.com

Introduction The lack of information about aerosol chemical and physical properties in modelling systems is a critical step to enhance the emission reduction policies and the knowledge about aerosol impacts over radiative forcing and health.

A data processing system, the European Emission Adaptation SYstem for WRF-Chem model (EASYWRF-Chem) has been developed to generate chemical information compatible with the WRF-Chem requirements from any emission inventory based on CORINAIR. EASYWRF-Chem has been created mixing SMOKE data and CORINAIR methodologies. The emission generation system created allows the use of low (EMEP) and highly (Regional) detailed emission inventories and has been tested on the WRF-Chem model.

Methodology Using the RADM2 or RACM mechanism, we converted "emission species" into "model species" using the SAPRC methodology. An aerosol chemical speciation profile processing completes EASYWRF-Chem. Coming from the adaptation of US EPA $PM_{2.5}$ profiles (Borge et al., 2008), those data separate the unspeciated $PM_{2.5}$ emission into five chemical families: sulphate, nitrate, elemental carbon, organic aerosol and unspeciated aerosol.

The WRF-Chem has been implemented on a European area with high resolution domains. Since $PM_{2.5}$ speciation modelling has never been evaluated over Europe with detailed emission inventories and with a high resolution modelling system, we statistically compared the simulated aerosol concentrations with measurements in order to evaluate the general performance of the modelling system and the chemical speciation of anthropogenic particles at regional scale.

The five chemical families have been quantified during four measurements campaigns in two sites over the French northern region. It included winter and summer measurements using a High Resolution – Time of Flight – Aerosol Mass Spectrometer (HR-ToF-AMS). This instrument provides hourly resolved PM_1 concentrations over the same chemical families.

Meteorology, gas phase chemistry and particle phase composition has been evaluated simultaneously.

Results Finally, it reveals that EASYWRF-Chem simulations respectively overestimate the PM_{10} concentrations of +30% and +4% for summer and winter periods. The statistical analysis of $PM_{2.5}$ concentrations shows that, in summer, WRF-Chem overestimates them of +1% while, in winter, the concentrations are underestimated of -14%.

Particulate organic matter concentrations in $PM_{2.5}$ are underestimated but hourly variations of concentrations are well simulated.

Sulphates concentrations are not correlated to the observed concentrations, the average concentration is underestimated.

Nitrates concentrations are overestimated by a factor of two but variations are fairly well represented. Ammonium particulate matter is well represented.

Black Carbon (BC) measurements reveal that EASYWRF-Chem forecast performance is higher in winter than during summer when BC concentrations are very low.

Borge, R., Lumbreras, J., and Rodríguez, E.: Development of a high-resolution emission inventory for Spain using the SMOKE modelling system: A case study for the years 2000 and 2010, Environmental Modelling & Software, 23, 1026-1044, 10.1016/j.envsoft.2007.11.002, 2008.

Black carbon and particle number emission factors of different vehicle types measured in real driving conditions

I. Ježek[1], D. Westherdal[2], G. Močnik[1]

[1]Aerosol d.o.o., Ljubljana, Slovenia
[2]Cornell University, Ithaca, NY 14853, USA
Keywords: emission factors, cars, diesel emissions.
Presenting author email: irena.jezek@aerosol.si

For estimating emissions from on road mobile sources models multiply the activity of the source to its emission factor. The activity of a vehicle fleet is monitored by traffic counters which can report the number of different types of vehicles passing one site and sometimes also their speed. To determine emission factors for a vehicle fleet is more difficult due to the large number of vehicles with different engines and different exhaust treatment systems. Not only the versatility of engines and exhaust treatments, the amount of pollutants vehicles emit depends also on the vehicles maintenance, quality of fuel, traffic fluency, driving regime, topography, and weather. Usually emission factors for individual vehicles are measured with dynamometers. These tests are good for studying the influence of fuel type, additives, acceleration, engine type, temperature, dilution... but are expensive, time consuming and measure emissions of only few vehicles supposedly representative for the whole vehicle fleet. Studies have shown that few individual vehicles can contribute significantly to the fleet emissions, much more than the average vehicle in the fleet, and measurements of large number of vehicles are desired (eg. Kirchstetter, 1999 and Wang, 2011).

We measured emission factors of individual vehicles in real driving conditions by chasing them on European highways and regional roads similar as Wang (2011). We did not measure only heavy duty vehicles and busses but also light duty vehicles and cars, for which no similar studies have been performed so far. We measured concentrations of black carbon (Aethalometer AE33), particle number concentration (FMPS) and CO2 (Carbocap 343). We developed a methodology for calculating time evolution of the emission factors, with which we can evaluate individual vehicles EF while accelerating and while constant driving as shown on figure 1. We measured approximately 250 different vehicles.

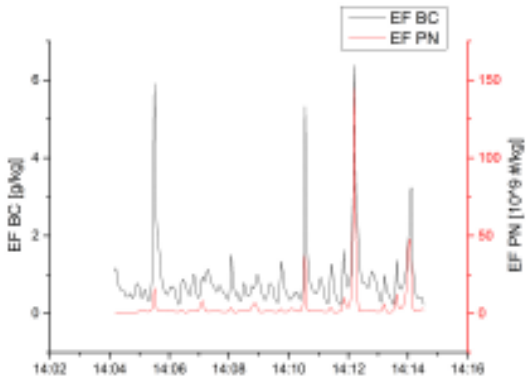

Figure 1 Time evolving emission factors for black carbon (EF BC) and particle number (EF PN).

Operation is in part financed by the European Union, European Social Fund.

Kirchstetter, T.W., Harley, A., Kreisberg, N.M., Stolzenburg, M.R., Hering, S.V., (1999) *On-road measurement of fine particle and nitrogen oxide emissions from light- and heavy-duty motor vehicles.* Atmosphric Environment 33, 2955–2968.

Wang, X., Westerdahl, D., Wo, Y., Pan, X., Zhang, K. M., (2011) *On-road emission factor distributions of individual diesel vehicles in and around Beijing, China*; Atmospheric Environment 45, 503-51.

Modelled and measured aerosol hygroscopicity for aerosol corrosion prevention and energy saving in green data center designing

Luca Ferrero[1], Giorgia Sangiorgi[1], Maria Grazia Perrone[1], Marco Moscatelli[1], Luca D'Angelo[1], Grazia Rovelli[1], Alberto Ariatta[2], Redy Truccolo[2], Ezio Bolzacchini[1]

[1]Department of Earht and Environmental Sciences, University of Milano-Bicocca, P.zza della Scienza 1, 20126 Milano, Italy.
[2]ARIATTA Engeneering Systems, Via Elba 12, 20144, Milano, Italy.
Keywords: E-AIM Model, Deliquescence Relative Humidity, Aerosol Chamber, Energy Efficiency, CO_2, green computing
Presenting author email: luca.ferrero@unimib.it

Industrial data centers (DC) are responsible for a large global electricity usage (~27% in Western Europe) mainly due to their cooling systems (35-50% of energy consumption) (Shehabi et al., 2008). Air conditioning (AC) costs could be reduced using a Direct Free Cooling (DFC) system which uses outside air to directly cool the information technology (IT). However this approach involves the risk to introduce outdoor aerosol which can become electrically conductive if the surrounding air reaches the aerosol Deliquescence Relative Humidity (DRH) thus causing bridging and corrosion that can damage the IT (ASHRAE, 2011; Shehabi et al., 2008).

Data Center Site

This study was conducted in Italy at Sannazzaro de' Burgondi (SdB, Po Valley), to specifically optimize the DFC (thermodynamic limits and indoor aerosol levels) of a DC, at the design, for the Italian Oil and Gas Company (ENI) (5200 m^2 of IT installed, 30 MW; $8*10^6$ m^3 h^{-1} of cooling air; www.eni.com/green-data-center/it_IT/pages/home.shtml) (Ferrero et al., 2013). The main aim was to design a DFC avoiding to reach the aerosol DRH: this increase the DC energy efficiency, whilst at the same time preventing aerosol corrosion.

Thus, Spring (24/03/2010-19/04/2010) and summer (10/06/2010-10/07/2010) campaigns were conducted at SdB to measure aerosol properties and meteorological parameters.

Experimental

PM_1 and $PM_{2.5}$ were sampled (4 hours; FAI-Hydra sampler; 2.3 m^3 h^{-1}, PTFE filters, Ø=47 mm) and chemically analyzed by means of ion chromatography (IC, Dionex ICS-90 and ICS-2000). The aerosol chemistry was used as an input parameter to calculate the aerosol DRH, using the Extended-Aerosol Inorganic Model (E-AIM; a state-of-the-art thermodynamic model for the H^+-NH_4^+-SO_4^{2-}-NO_3^--carboxylic acids-H_2O aerosol system Clegg et al., 1998; Pathak et al., 2004). The aerosol number size distribution was monitored through an Optical Particle Counter Tandem system ($TOPC_s$: 2 Grimm *1.107 "Environcheck"*; 31 size classes, from 0.25 µm up to 32 µm) allowing to asses the aerosol pollution level at the location of the GDC-ENI. $TOPC_s$ "wet" and "dry" data were compared allowing to the reconstruction of the hygroscopicity curve (Khlystov et al., 2005) to be compared with results estimated via E-AIM. Moreover an Aerosol Exposure Chamber (AEC; 1 m^3) had been specifically designed for studying the aerosol hygroscopicity by means of conductivity measurements as a function of the relative humidity: PM samples were housed over special PTFE supports, provided with a pair of electrodes each and conductivity measurements were carried out using the Hewlett-Packard 3421A acquisition module, while a T and RH were monitored using LSI-Lastem sensors. 1% RH step were obtaind by means of a evaporation unit filled with ultrapure, Milli-Q, water. Measurements were conducted at 25°C, the IT cooling set-point within the GCD-ENI.

Main Results

The E-AIM model was applied to each PM_x sample to estimate the DRH values. The average DRH for PM_1 was 61.2±1.1% (spring), and 68.4±1.4% (summer), while in the case of $PM_{2.5}$ it was 60.8±0.7% (spring) and 62.4±0.9% (summer). Lower DRH values during spring reflected the influence of aerosol chemistry: NO_3^- was predominant during spring (17-20% of PM_x mass), while SO_4^{2-} during summer (10-18% of PM_x mass); NH_4^+ remain fairly constant during both campaigns (4-7% in both cases). The obtained E-AIM output were validated using $TOPC_s$ and experimental AEC data. R^2 between $TOPC_s$ and E-AIM were 0.97 and 0.85 for PM_1, in spring and summer, and were 0.98 and 0.95, for $PM_{2.5}$, respectively.

Moreover, the AEC was used to measure, at 25°C, the aerosol hygroscopicity of a 15 $PM_{2.5}$ subset sample with the aim to validate if the E-AIM model. Considering the whole $PM_{2.5}$ subset, the averaged DRH estimated via E-AIM was 62.8±2.0% in keeping with the values measured using the AEC: 61.2±1.5%.

Therefore, E-AIM DRH_s values were used to optimize the DFC operating cycle: all the averaged DRH_s were found to be slightly higher than 60% allowing to choose 60% of RH as the upper limit for the DFC operating cycle to prevent a corrosive effects of the aerosol.

Thus, the energy consumption of the GDC-ENI was estimated considering, on annual basis, the total time when outdoor thermodynamic conditions allowed DFC operation. An annual energy saving of 81% was found, compared to traditional AC data centers: 7.4 MWh for 1 kW of installed IT and 221 GWh for the entire GDC-ENI. In terms of environment savings, t of CO_2 not emitted were estimated considering a CO_2 emission factor of 362 gCO_2 kWh^{-1} (European Environment Agency, EEA: http://www.eea.europa.eu/). Results evidenced an emission savings for each kW of IT: 2.7 t of CO_2 (80 kt the entire GDC-ENI), compared to traditional AC data centers.

References

ASHRAE. 2011 *Gaseous and particulate contamination guidelines for data centers*. Whitepaper.

Ferrero L. et al. 2013. Env. Sci. Tech., *submitted*.

Clegg S.L. et al. 1998. J. Phys. Chem. A, 102, 2137-2154.

Khlystov A. et al. 2005. J. Geophys. Res., 110, doi:10.1029/2004JD004651.

Pathak R.K. et al. 2004. Atmos. Environ., 38, 2965–2974.

Shehabi A. et al. 2008. Atmos. Environ., 42, 5978–5990.

The role of organic condensation on ultrafine particle growth during nucleation events

D. Patoulias [1], I. Riipinen[2], and S.N. Pandis[1,3]

[1]Department of Chemical Engineering, University of Patras, Patras, Greece
[2] Department of Applied Environmental Science & Bert Bolin Centre for Climate Research, Stockholm University, SE-11418, Stockholm, Sweden
[3]Department of Chemical Engineering, Carnegie Mellon University, Pittsburgh, PA 15213, USA
Keywords: DMAN, ternary nucleation, aerosol nucleation and growth, modeling
Presenting author email: davidpat@chemeng.upatras.gr

New particles are introduced in the atmosphere by direct emission from a variety of sources and nucleation (in-situ formation). These ultrafine particles can grow to larger sizes and become cloud condensation nuclei (CCN) affecting cloud droplet concentrations, cloud reflectivity and lifetime. This indirect effect of aerosols on climate is thus perturbing the energy balance of the planet (Twomey, 1974; Albrecht, 1989).

In this work, we applied an updated box model version of the Dynamic Model for Aerosol Nucleation (Jung et al., 2006) in order to simulate the nucleation and subsequent growth in a remote continental location, Hyytiala, Finland. The individual effects of various processes and parameters on aerosol growth were quantified. DMAN uses the Two-Moment Aerosol Sectional algorithm (Adams and Seinfeld, 2002) to track both aerosol number and mass concentration using a sectional approach. The model describes both coagulation and condensation (sulfate, ammonium, organics, etc.) by using the TOMAS algorithm. Our approach combines the SAPRC-99 mechanism for the simulation of gas-phase chemistry, and the 1-D the volatility basis set framework (VBS) for secondary organic aerosol formation and OA chemical aging.

The surface energy of the condensing organics has as a significant effect on the ultrafine particle rate. For a typical spring nucleation episode, an increase of the assumed surface energy results in a decrease of the particle number concentration above 3 nm (N_3) but it increases the number concentration above 100 nm (N_{100}). On the other hand the different parameterizations of the secondary OA chemical aging have a small effect on N_3 but can have a major effect on N_{100}.

Fig. 1 shows a comparison of predicted vs. observed size distribution for 6 May 2008 at Hyytiala. The model reproduces the observed onset of nucleation and the qualitative features of the event. The particle growth is reproduced well with the new particles reaching a diameter of around 50 nm. The nucleation starts at 9.00 am and these new particles grow during the day. The predicted composition of the newly formed particles is shown at Fig 1c. During the nucleation event from 9.00 to 13:00, the new particles consist of sulfate, ammonium and low volatility SOA. After the end of the nucleation, these new particles continue to grow mainly due to the condensation of the semi-volatile SOA. At the end of the day, the new particles consist mainly of organics (95%).

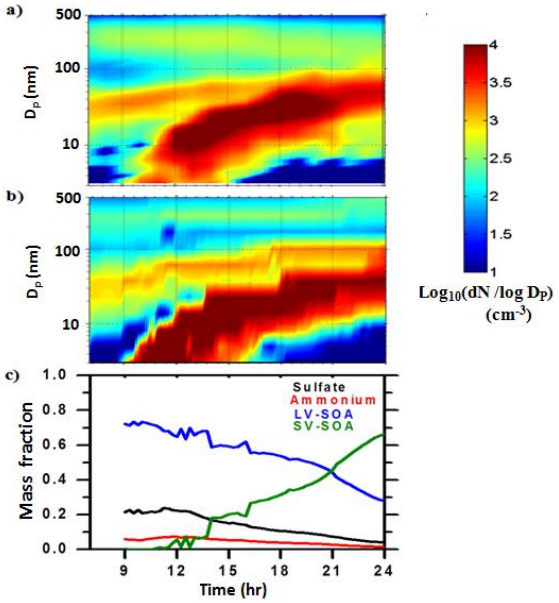

Figure 1. Comparison of (a) measured and (b) predicted dry size distribution as a function of time for 6 May 2008 at Hyytiala. Particle number concentration (z-axis) is plotted against time of day (x-axis) and particle diameter (y-axis). (c) Predicted composition of new particles during the growth.

The simulation suggests that while sulfuric acid plays an important role of nucleation of new particles, it is not responsible for most of their growth, a finding consistent with the analysis of field observations in the site. In contrast, the low-volatility SOA components represent 75% of the new particle mass during the event and 30% at the end of the day. The semivolatile-SOA produced upon oxidation of biogenic volatile organic compounds (BVOCs) is a key player for the later stages of growth.

Adams, P. J., and J. H. Seinfeld (2002) Predicting global aerosol size distributions in general circulation models, J. Geophys. Res., 107, 4370.

Albrecht, B. A.: Aerosols, cloud microphysics, and fractional cloudiness, Science, 245, 1227–1230, 1989.

Jung, J., P. J. Adams, and S. N. Pandis (2006), Simulating the size distribution and chemical composition of ultrafine particles during nucleation events, Atmos. Environ., 40, 2248–2259.

Twomey, S.: Pollution and the Planetary Albedo, Atmos. Environ., 8, 1251–1256, 1974.

Computational modeling of aerosol formation and evolution using OpenFOAM®

E. M. A Frederix[1], A. K. Kuczaj[3], M. Nordlund[3], C. Winkelmann[3], B. J. Geurts[1,2]

[1]Department of Applied Mathematics, University of Twente, Enschede, 7500 AE, The Netherlands
[2]Department of Applied Physics, Eindhoven University of Technology, Eindhoven, 5300 MB, The Netherlands
[3]Philip Morris International R&D, Philip Morris Products SA, Neuchâtel, 2000, Switzerland
Keywords: Nucleation, numerics, modeling, LFDC.
Presenting author email: e.m.a.frederix@utwente.nl

In the process of single-species homogeneous vapor condensation into aerosol, surface is created between liquid and vapor. The energy of formation of such surface limits the condensation of vapor from a supersaturated state. Nucleation, the mechanism of generation of embryo sites, or nuclei, on which vapor is able to condense, is an important process. Developing an understanding of this process is important, as it may lead to a considerable contribution to many engineering problems, as well as atmospheric and environmental science. In this work, we present an OpenFOAM®-based numerical simulation tool, which is capable of predicting aerosol formation using a two-moment representation of the aerosol and classical nucleation theory. We aim at developing a flexible utility, which enables researchers interested in various aerosol production-related applications to quickly study concepts like aerosol nucleation, condensation, diffusion and transport.

The general convection-diffusion-reaction equations for species vapor mass fraction Y, aerosol droplet number concentration N (first moment) and aerosol mass fraction Z (second moment) in an Eulerian framework are given with:

$$\partial_t(\rho Y) + \partial_j(u_j \rho Y) = \partial_j(D\partial_j(\rho Y)) - S_{v\to l} \quad (1a)$$
$$\partial_t(\rho Z) + \partial_j(u_j \rho Z) = S_{v\to l} \quad (1b)$$
$$\partial_t N + \partial_j(u_j N) = J_N - J_C \quad (1c)$$

with carrier fluid density ρ, velocity field u_j, vapor diffusivity D and droplet coalescence rate J_C. The source term $S_{v\to l}$ associated with the transfer from vapor to liquid is governed by two contributions: that of nucleation, S_{nuc}, and that of evaporation or condensation, S_{e-c}. The nucleation mass flow rate is specified as the mass of a critical cluster, multiplied by the nucleation rate J_N. A critical cluster is defined as a kernel of condensed molecules with a probability for growing into a droplet equal to the probability for dispersing into individual molecules again. The nucleation rate for a vapor is given by classical nucleation theory, and strongly depends on the saturation. Transport equations (1) contain multi-scale physics. The typical time scales of diffusion and convection are orders of magnitude larger than those of nucleation or condensation. The formation of critical clusters is relatively fast. It is clear that the formation of aerosol droplets should numerically be resolved at the smallest time scale, in order to yield an accurate result.

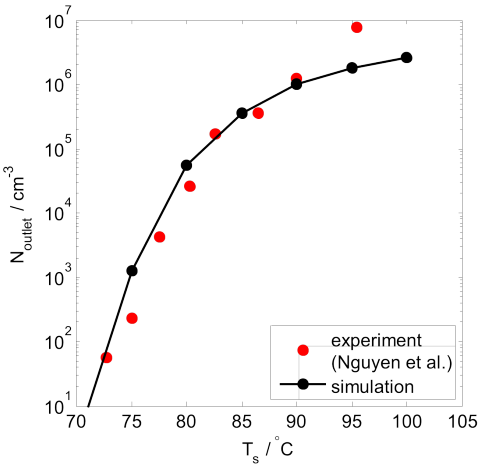

Figure 1: Aerosol droplet number density at pipe outlet as a function of saturator temperature T_s.

We compare our numerical approach with the results of physical experiments, each using a laminar flow diffusion chamber (LFDC), (Nguyen *et al*, 1987; Lihavainen and Viisanen, 2001; Hämeri and Kulmala, 1996) with different species and/or carrier gasses. Figure 1 shows a good agreement between experimental and numerical results for the aerosol droplet number density N as a function of saturator temperature T_s, with dibutylphthalate (DBP) as saturated vapor.

The development of the OpenFOAM®-based simulation tool is a stepping stone towards a more comprehensive multi-species model. We aim at developing a robust numerical approach which is capable of determining the composition and size of the critical cluster and its subsequent evolution. Moreover, we will extend the presented two-moment approach with a third moment, taking into account the width of the droplet size distribution of the aerosol.

The research described in this article was supported by Philip Morris Products S.A. and the authors wish to thank Philip Morris Products S.A. for their financial support.

Lihavainen, H. and Viisanen, Y. (2001) J. Phys. Chem. B, **105**, 11619–11629.

Hämeri, K. and Kulmala, M. (1996) J. Chem.Phys. **105**, 7696–7704

Nguyen, H.V., Okuyama, K., Mimura, T., Kousaka, Y., Flagan, R.C., and Seinfeld, J.H. (1987) J. Colloid Interf. Sci. **119**, 491–504.

Modeling of long-term particle formation and growth in the planetary boundary layer

L. Zhou[1,2], M. Boy[1], T. Nieminen[1], D. Mogensen[1], S. Smolander[1], and Markku Kulmala[1]

[1]Department of Physics, University of Helsinki, P. O. Box 48, 00014 Helsinki, Finland
[2]Department of Forest Science, University of Helsinki, P.O. Box 27, 00014 Helsinki, Finland
Keywords: boundary layer modeling, particle formation and growth, aerosol dynamics
Presenting author email: luxi.zhou@helsinki.fi

Natural and anthropogenic aerosols may have a great impact on climate as they can directly interact with solar radiation and indirectly affect the Earth's radiation balance and precipitation by modifying clouds. In order to quantify the direct and indirect effect, we must understand the complex processes that connect an aerosol particle to a cloud droplet. However, while modern measurement techniques are able to detect particle sizes down to nanometre all the way from ground up to the stratosphere, the data does not serve for all of our needs for understanding the processes. Hence we will demonstrate a modelling approach to investigate the complex processes of aerosols in the planetary boundary layer (PBL) over the boreal forest.

SOSAA (model to **S**imulate the concentration of **O**rganic vapours, **S**ulphuric **A**cid, and **A**erosol) was developed by adding an aerosol dynamics model UHMA (Korhonen, 2004) to an exiting chemistry – transport column model SOSA (Boy, 2011). It was constructed to study the emissions, transport, chemistry, as well as aerosols in the PBL. Up to our knowledge, it is the first column model existing in the world with detailed chemistry and aerosol dynamics. Thanks to the parallel computing, the model can be used to study the aerosol processes in the PBL for a few days up to a year with high vertical resolution. As a first application of the model, we present new particle formation study of the year 2010 in a Finnish boreal forest site, Hyytiälä, Finland, where the Station to Measure Ecosystem Atmosphere Relation (SMEAR II) is located (Hari and Kulmala, 2005). Chemistry in the model is validated against the measurements from the HUMPPA-COPEC campaign, which was conducted at SMEAR II during summer 2010 (Williams, 2011).

We tested kinetic nucleation (Weber, 1997) and organic nucleation (Kulmala and Kerminen, 2008) theory. Kinetic nucleation theory states that the nucleation rate is proportional to the square of ambient sulfuric acid concentration. Organic nucleation theory assumes that both sulfuric acid and organics are taking part in the nucleation, although the detailed knowledge about the participating compound is not achieved up today. In the simulations, the nucleating organics are the first stable reaction products from monoterpenes oxidized by hydroxide (OH).

Simulation results show that organic nucleation theory generally gives better prediction in nucleation rates compared to organic nucleation theory. The agreement is relatively well in spring time compared to autumn and winter. One reason could be that emissions were underestimated in autumn and winter. We include the first stable oxidation products from the oxidation of monoterpenes as the organic condensing vapors. Even though the growth of particles in the model suffers from the uncertainties in organic chemistry and the missing knowledge of physical properties of organic compounds. In Figure 1, we see that the model is able to predict the number concentrations of particles between 25 and 100 nm sufficiently good. In general, the model captures 10 out of 11 observed event days in 2010.

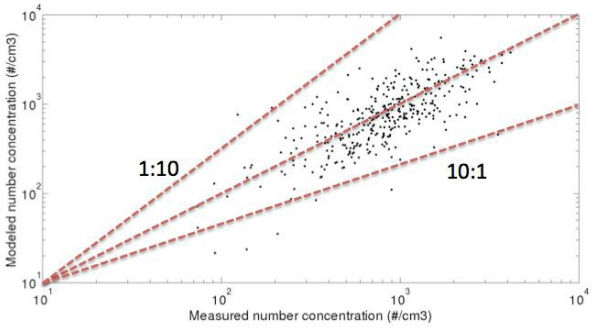

Figure 1.Scatter plot of measured number concentrations of particles between 25 and 100nm against simulated.

The finacial support by Helsinki University Centre for Environment (HENVI), the Academy of Finland Centre of Excellence program (project no. 1118615), and the European Commission 6th Framework program project EUCAARI is gratefully acknowledged.

Boy, M., Sogachev, A., Lauros, J., Zhou, L. and Smolander, S. (2011) *Atmos. Chem. Phys.* **11**, 43-51.

Korhonen, H., Lehtinen, K. E. J. and Kulmala, M. (2004) *Atmos. Chem. Phys.* **4**, 757-771.

Hari, P. and Kulmala, M. (2005) *Boreal Environ. Res.* **10** , 357-369.

Williams, J. et al. (2011) *Atmos. Chem. Phys.* **11**, 10599-10618.

Weber, R. J. et al. (1997) *J. Geophys. Res.* **102** , 4375-4385.

Kulmala, M. and Kerminen, V.-M. (2008) *Atmos.Res.* **90**, 132-150.

Long range transport and chemical transformation of aerosols over the Aegean Sea during a recent Etesian period

E. Athanasopoulou[1], A. Protonotariou[1], E. Bossioli[1], J. Allan[2], A. Dandou[1], G. Papangelis[1], H. Coe[2], A. Bacak[2], J. Kalogiros[3], N. Mihalopoulos[4], G. Biskos[5] and M. Tombrou[1]

[1]Department of Applied Physics, National and Kapodistrian University of Athens, Athens 15784, Greece
[2]School of Earth, Atmosphere and Environmental Sciences, University of Manchester M13 9PL, UK
[3]Institute for Environmental Research and Sustainable Development, National Observatory of Athens 15236, Greece
[4] Department of Chemistry, University of Crete, Heraklion 71003, Greece
[5]Department of Environment, University of Aegean, Mytilene 81100, Greece
Keywords: Aerosol chemistry, SOA, Aegean Sea, PMCAMx.
Presenting author email: eathana@phys.uoa.gr

The region of the Aegean Sea is a cross road of air masses from anthropogenic and natural pollution sources, thus an ideal natural laboratory to study the interaction of gaseous species with atmospheric particles. The period of interest (28 August–10 September, 2011) corresponds to the most common synoptic situation during summer ('Etesians': strong NE winds) that transports air masses form central and E. Europe. Under these conditions, which are also characterized by a strong photochemical activity, the interaction of gaseous pollutants and aerosol particles from local maritime (ships and sea surface) and distant sources can enhance the formation of secondary aerosols (namely $NaNO_3$ and SOA) (Mihalopoulos, 2007).

The aerosol model used for this study is an updated version of PMCAMx that couples SAPRC with ISORROPIA II and VBS modules for gaseous, inorganic and organic aerosol chemistry, respectively (Fountoukis et al., 2011). Aerosols are represented by a detailed aerosol composition (K^+, Ca^{2+}, Mg^{2+}, NH_4^+, Na^+, SO_4^{2-}, NO_3, Cl^-, H_2O, EC, and OC: primary, oxidized primary, anthropogenic & biogenic secondary), distributed over 10 size bins in the diameter range 0.04-40μm.

Air quality simulations are offline coupled with the WRF/ARW model (Skamarock et al., 2005), applied over Europe. A nested simulation over Greece with a high-resolution grid (6x6km) provides the meteorological fields and a detailed boundary layer structure. Emission inputs cover all important sources: industry, transport, forest activity, as well as sea-salt aerosol and road/soil dust, calculated online with meteorology (Athanasopoulou et al., 2008; 2010).

Long-range transport of air masses is handled (as boundary conditions) through simulations during the same period by the global model GEOS-CHEM v8-03-01 nested (0.5x0.67deg) over Europe (Protonotariou et al., 2012). Sensitivity simulations reveal the role of gaseous and fine particles transported from the Balkans. Special focus is given on SOA formation (Fig. 1), because increased summer VOCs emissions from the north are transported and age over the Aegean.

These simulations are directly comparable with aerosol measurements performed during the same period (Tombrou et al., 2012) at two ground stations (on the islands of Crete and Lemnos) and with an airborne platform (BAe146-FAAM aircraft).

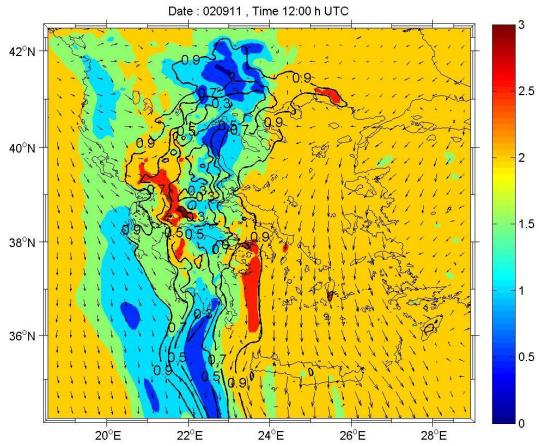

Figure 1. PMCAMx predictions for hourly ground SOA concentrations (μgm^{-3}) over Greece. Vectors show WRF/ARW predictions for U_{10}. Isolines represent the long-range transported SOA fraction.

This work is funded by the project AERAS-EtS (within the framework of the Action "Supporting Postdoctoral Researchers" of the Operational Program "Education and Lifelong Learning", co-financed by the European Social Fund (ESF) and the Greek State). Experimental data are available from the AEGEAN_GAME2 project funded under a EUFAR EC Project (227159). E. Athanasopoulou thanks C. Fountoukis and S. N. Pandis for use of the updated PMCAMx code.

Athanasopoulou E., Tombrou, M. Pandis. S.N., Russell A. (2008) *Atmos. Chem. Phys*., **8**, 5755–5769.
Athanasopoulou E., Tombrou M., Russell, A. Et al (2010) *J. Geophys. Res.* **115**, D17301.
Fountoukis C., Racherla P.N., Denier H.A.C. et al. (2011) *Atmos. Phys. Chem.* **11**, 10331–10347.
Mihalopoulos N. (2007) *Regional Climate Variability and its Impacts in the Mediterranean Area*, Springer.
Protonotariou A., Bossioli E., Tombrou M. et al (2012) ISBN 978-3-642-29171-5, *Springer Heidelberg New York Dordrecht London*.
Skamarock, W.C. and Eder, B. (2005) *Atmos. Environ*. **39(37)**, 6957–6975.
Tombrou M., Bossioli E., Kalogiros Y. et al. (2012) ISBN 978-3-642-29171-5, *Springer Heidelberg New York Dordrecht London*.

On the influence of WRF schemes in reconstructing the Planetary Boundary Layer height in the Po Valley

A. Balzarini[1], M. Moscatelli[2], F. Angelini[3], L. Ferrero[2], G. Pirovano[1], G.M. Riva[1], E. Bolzacchini[2]

[1]RSE S.p.A., via Rubattino 54, 20134 Milano, Italy
[2] POLARIS research center, Department of Earth and Environmental Sciences, University of Milano-Bicocca, Piazza della Scienza 1, 20126 Milano, Italy
[3] ENEA/UTAPRAD-DIM, via Enrico Fermi 45, 00044 Frascati, Italy, formerly at CNR/ISAC, via del fosso del cavaliere 100, 00133 Roma, Italy
Keywords: planetary boundary layer, WRF meteorological model, vertical profile, lidar
Presenting author email: alessandra.balzarini@rse-web.it

The reconstruction of Planetary Boundary Layer (PBL) is one of the most important issues in air quality simulations, since its depth affects ground concentrations of primary and secondary pollutants. This is particularly the case in basin valleys where weak circulation conditions often limit PBL heights to the first hundred meters above ground level (Ferrero *et al.*, 2010). A typical example of these conditions is represented by the densely populated area of the Po valley in Northern Italy.

In order to assess the skill of the WRF meteorological model in reproducing PBL structure and evolution in the peculiar area of the Po valley, a sensitivity test has been conducted by comparing experimental data and different model simulations.

Five PBL modelling schemes (ACM2, MRF, MYJ, YSU and UWMT) have been selected for the analysis and compared to particle vertical profiles by balloon soundings as well as to data collected by meteorological balloons and Lidar (Light Detection and Ranging) measurements.

Experimental measures were collected in the urban area of Milan, in the middle of the Po valley, by means of a tethered balloon equipped with an optical particle counter and a meteorological station as well as by a Lidar instrument. PBL height was derived in both cases using a gradient method (Ferrero *et al.*, 2010; Angelini *et al.*, 2009). Additionally, meteorological soundings of Milano Linate airport were considered too. The availability of this set of highly specialized experimental data represented an unprecedented opportunity for model evaluation over Northern Italy.

WRF has been applied for July 2007 and February 2008 over three nested domains, with the last one focused on the Po valley area, having a spatial resolution of 5 km. Initial and boundary conditions were obtained from the ECMWF analysis fields. Only the 5 km domain was compared to observations.

Comparisons have been done in terms of vertical profiles, temporal variation and statistical indexes. As an example, Figure 1 shows the hourly trend of the five schemes and observations for February 11th, 2008.

Results indicate substantial differences among the five schemes, and between these and observations. Table 1 reported model performances for both summer 2007 and winter 2008. The schemes generally overestimate PBL height, but the best performances are clearly related to YSU and UWMT parameterizations.

For each scheme the main parameterizations are discussed as well as their effects on PBL and meteorological fields reconstruction.

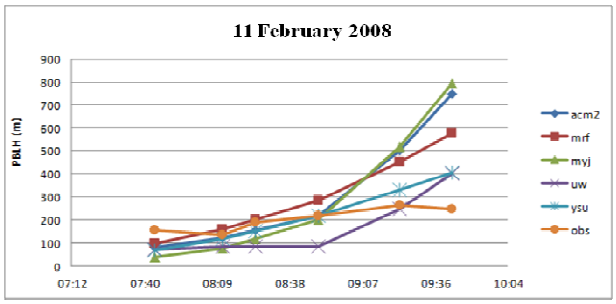

Figure 1. Hourly trend of PBL height in Milan for February 11th, 2008. The figure shows the five parameterizations as well as the observed data by balloon sounding.

Table 1. BIAS index for the five schemes in both July 2007 and February 2008.

	ACM2 (m)	MRF (m)	MYJ (m)	YSU (m)	UWMT (m)
July 2007	198.49	180.33	219.52	113.08	39.26
February 2008	132.67	134.12	118.27	40.98	-19.68

References

Angelini, F., Barnaba, F., Landi, T. C., Caporaso, L., Gobbi, G. P. (2009) *Radiation Protection Dosimetry* **137**, 275-279.

Ferrero, L., Perrone, M. G., Petraccone, S., Sangiorgi, G., Ferrini, B. S., Lo Porto, C., Lazzati, Z., Cocchi, D., Bruno, F., Greco, F., Riccio, A., Bolzacchini, E. (2010) *Atmos. Chem. Phys.* **10**, 3915–3932.

Multicomponent aerosol modelling with detailed chemical species

A. Rusanen[1], M. Boy[1], S. Smolander[1], D. Mogensen[1], P. Roldin[2] and E. Hermansson [2, 3]

[1]Department of Physics, University of Helsinki, Helsinki, P.O. Box 48 FI-00014, Finland
[2]Division of Nuclear Physics, Department of Physics, Lund university, P.O. Box 118 SE-221 00, Lund, Sweden
[3]Centre for Environmental and Climate Research, Lund university, P.O. Box 118 SE-221 00, Lund, Sweden

Keywords: aerosol dynamics, organic aerosols, aerosol modelling
Presenting author email: michael.boy@helsinki.fi

A modelling study by Merikanto et al. (2009) showed that on a global average, about half of all Cloud Condensation Nuclei (CCN) originated from secondary organic aerosols. Yu and Luo (2009) claimed that secondary particles even dominate the number abundance in most parts of the troposphere (>80%). However, other studies suggest that the effect of new particle formation on CCN numbers, even with artificially enhanced SOA formation, remains modest (Pierce et al., 2008). Up to today, a complete understanding about which compounds are responsible for the formation of thermodynamic stable clusters and their growth to CCN size is not completely achieved.

The growth plays a crucial role and the mechanism widely used in regional and synoptic models is the two-dimensional volatility basis set (VBS, Donahue et al., 2011). This code employs saturation mass concentration of organic compounds and the oxygen content to describe volatility, mixing thermodynamics, and chemical evolution of organic aerosols. It has the advantage that explicit knowledge of the condensing organic species and their thermodynamic properties are not required. However, depending on the set of different reaction rates in the code it tends to over- or underestimate the simulated SOA mass.

In this study we have applied the zero-dimensional version of the model MALTE, and present the first results of simulations with measurements from the SMEAR II station in Hyytiälä, Southern Finland. We use explicit chemical species as the condensable vapours, to see if this increases our understanding of what compounds are responsible for the growth of the newly formed particles, and what effects does the use of an explicit chemistry module have on the aerosol aging in the atmosphere.

MALTE-BOX includes chemistry, emissions and aerosol dynamics. Thus it can be used to model situations that can be approximated as well mixed. Formerly all organics were classified into two classes in the aerosol module. We modified the model to use the actual chemical species as the condensing vapours. For this, the physical properties of the compounds need to be predicted. Unfortunately measurements are not available in all cases. Necessary properties were estimated based on molecular structure. There are several ways to do this (Poling et al., 2001). The method described in (Girolami, 1994) was used to predict the liquid phase density and the diffusion volume of the compounds was evaluated based on the method by Fuller et al. (1966). Saturation vapour pressures were predicted with the method presented in Nannoolal et al. (2008).

We applied MALTE-BOX to measurements made at the SMEAR II station. The measured and predicted particle compositions of the newly formed and aged particles will be presented.

This research was supported by the Academy of Finland Centre of Excellence program (project number 1118 615).

Donahue, N. M., Epstein, S. A., Pandis, S. N., & Robinson, A. L. (2011) A two-dimensional volatility basis set: 1. organic-aerosol mixing thermodynamics, *Atmos. Chem. Phys., 11(7), 3303-3318.*

Fuller, E.N., P.D. Schettler, and J.C. Giddings (1966): A New Method For Prediction Of Binary Gas-Phase Diffusion Coefficients, *Industrial And Engineering Chemistry, 58 (5):19.*

Girolami, G. (1994) A Simple "Back of the Envelope" Method for Estimating the Densities and Molecular Volumes of Liquids and Solids, *Journal of Chemical Education, Vol. 71, Issue 11, 962.*

Merikanto, J., Spracklen, D. V., Mann, G. W., Pickering, S. J., and Carslaw, K. S. (2009) Impact of nucleation on global CCN, *Atmos. Chem. Phys., 9, 8601–8616.*

Nannoolal, Y., Rarey, J., and Ramjugernath, D. (2008) Estimation of pure component properties-Part 3. Estimation of the vapor pressure of non-electrolyte organic compounds via group contributions and group interactions, *Fluid Phase Equilibria, 269, 117 -133.*

Pierce, J. R., Engelhart, G. J., Hildebrandt, L., Weitkamp, E. A., Pathak, R. K., Donahue, N. M., Robinson, A. L., Adams, P. J., and Pandis, S. N. (2008) Constraining particle evolution from wall losses, coagulation, and condensation-evaporation in smogchamber experiments: Optimal estimation based on size distribution measurements, *Aerosol Sci. Technol., 42, 1001–1015.*

Poling, B.E., Prauznitz, J.M and O'Connel J.P, (2001) The properties of gases and liquids, 5th ed., *McGraw- Hill, New York.*

Yu, F. and Luo, G. (2009) Simulation of particle size distribution with a global aerosol model: contribution of nucleation to aerosol and CCN number concentrations, *Atmos. Chem. Phys., 9, 7691– 7710.*

Phenomenological modelling of particle resuspension on bubbling PMMA.

S. Delcour[1, 2], F.-X. Ouf[1], N. Azema[2], A. Coppalle[3], J.Yon[3], L. Ferry[2], F. Gensdarmes[1], J.-M. Lopez-Cuesta[2]
[1]Institut de Radioprotection et de Sûreté Nucléaire (IRSN), PSN-RES, SCA, LPMA, Gif-Sur-Yvette, 91192, France.
[2]Ecole des Mines d'Alès, Centre des Matériaux (CMGD)-Pôle Matériaux Polymères Avancés
6 Avenue de Clavières, 30319 Alès Cedex, France.
[3]UMR 6614 CORIA, INSA de Rouen, Avenue de l'université, B.P. 8, Saint-Etienne du Rouvray, 76801, France
Keywords : resuspension, fire, PMMA, bubble.
Presenting author email: simon.delcour@irsn.fr

Along the nuclear fuel industrial process, radioactive materials are handled in confined glove boxes, which retain a surface contamination by radioactive solid particles. Evaluating the potential release of radioactive particles in case of a fire occurring in a nuclear facility is of critical interest for nuclear safety studies. Several experiments have been conducted in order to gather reference data for these studies, highlighting a specific behaviour of PMMA, namely a flash of emission. This flash is often related to the bubbling of PMMA, but so far no experimental proof has been obtained to support this allegation.

A previous study proposed an empirical correlation between the incoming heat flux and the onset of the flash (Ouf *et al.*, 2013). One can note that this correlation fits with the time to reach a surface temperature of 275°C, which is the starting temperature for thermal degradation of PMMA, according to thermo-gravimetric analysis. At 275°C, the depolymerisation process starts, yielding monomer molecules (Methyl methacrylate – MMA). MMA's boiling temperature is around 100°C, so the pyrolysis products are overheated and will immediately nucleate into bubbles. This observation supports the previous assumption but a more detailed investigation is required.

An experimental study of the bubbling of PMMA is conducted to gather specific data on the bubbling, in order to validate a theoretical model. Three pristine PMMA samples are exposed to a heat flux of 45 kW/m^2, using a radiant panel (modified cone calorimeter), for durations of 40, 50 and 60 seconds and then quenched in water to stop the thermal degradation. X-ray tomography is then performed on the bubble layer and a three dimensional reconstruction is performed before analysing the bubble layer's microstructure.

Bubble size distribution (volume equivalent diameter) and size-to-depth profiles are obtained for all three samples (see figure 1 for the 60 s sample).

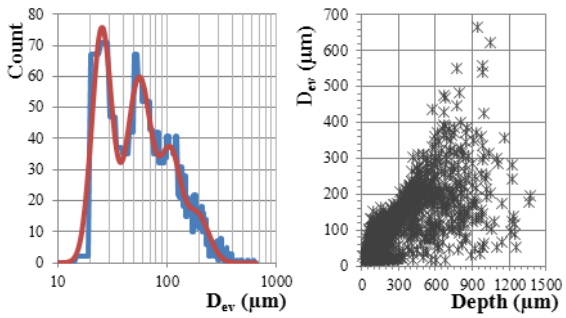

Figure 1. Bubbles size distribution and size-to-depth profiles inside PMMA exposed during 60 s to 45 kW/m^2

An increase in mean size with depth is observed with all three samples. This indicates that the bubbling-induced resuspension is mostly caused by the large amount of small (< 200 µm) bubbles that burst in the early phase of thermal degradation; probably because of their higher internal pressure.

A physical model of resuspension of a solid particle by a bursting bubble is proposed (see figure 2), based on the pressure difference between the bubble and the atmosphere.

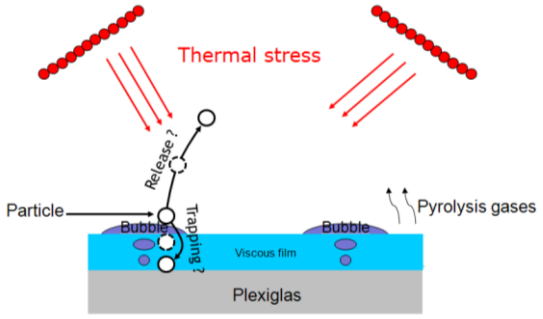

Figure 2. Modelling of the bubble-induced resuspension

This pressure difference is obtained using the ThermaKin code (Stoliarov and Lyon, 2008) to obtain a full thermal model of the polymer sample, including the effects of degradation; the pressure difference is then computed using the Laplace law with a model of surface tension. Effects of drag and inertia are taken into account in a one-dimensional, mechanical model. This model is then refined to include the surface density of the particle deposit and the bubble bursting frequency to obtain a value for the flux of particles. No hypothesis is made on the nature of the particle, allowing us to investigate radioactive particles (PuO_2).

Further developments of this model will include the effects of gravitational and thermal migration (Soret effect) of the particles inside the viscous film of polymer. These phenomena will tend to trap the particles and block their release, acting oppositely to the bubbling.

The authors wish to express their deepest thanks to Dr B. Fayard from NOVITOM for her assistance in the reconstruction of X-ray tomography data.

Ouf, F.-X., Delcour, S., Azema, N., Coppalle, A., Ferry, L., Gensdarmes, F., Lopez-Cuesta, J.-M., Niang, A., Pontreau, S. and Yon, J. (2013) J. Hazardous Materials, http://dx.doi.org/10.1016/j.hazmat.2013.01.060

Stoliarov, S. and Lyon, R. (2008) *Thermo-Kinetic Model of Burning*, DOT/FAA/AR-TN08/17.

Ageing of Sodium Combustion Aerosols: a Theoretical and Experimental Study

E. Mathé[1,2], M.P. Kissane[1] and D. Petitprez[2]

[1]Institut de Radioprotection et de Sûreté Nucléaire (IRSN/PSN), Cadarache, 13115 Saint Paul-Lez-Durance, France
[2]Laboratoire de Physico-Chimie des Processus de Combustion et de l'Atmosphère (PC2A), UMR 8522 CNRS-Lille1,Université de Lille 1, 59655 Villeneuve d'Ascq, France
Keywords: aerosols, sodium, simulation, experiment.
Presenting author email: emmanuel.mathe@irsn.fr

In the context of the Generation IV initiative (www.gen-4.org) and, more immediately, the strategic choice France may make in the coming years regarding development of nuclear power, sodium-leak accidents in sodium-cooled fast-neutron reactor (SFR) facilities are the subject of renewed interest. The objective here is to model the aerosol contamination produced by a sodium fire in the containment during a SFR severe accident.

Assuming that an accident has occurred, it has previously been shown that the mass of oxide aerosols produced by a sodium spray fire can involve more than 60% of the ejected sodium (Mathé and Kissane, 2012). We are now interested in the physicochemical transformations of the sodium oxide aerosols since their toxicity diminishes as they age.

Theoretical Study

Sodium oxide aerosols produced inside the containment would consume ambient water vapour and carbon dioxide forming hydroxide, carbonate and bicarbonate species probably as successive concentric layers on the aerosols.

A single layer-transformation model exists (Cooper, 1980) but the theoretical approach used (diffusion in a porous medium) has not been validated.

Based on this model, a numerical simulation of the aerosol transformation for a realistic case was made. For a 1.8s spray fire producing 1t of sodium oxide aerosols in a containment with a relative humidity of 5%, we obtain the results of Figure 1.

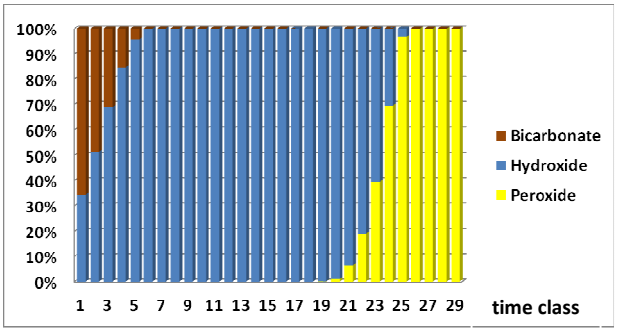

Figure 1. Evolution of the final composition of sodium aerosols for each injection-time class.

The first aerosols injected are highly transformed into bicarbonate until exhaustion of the carbon dioxide at which point the hydroxide prevails. Then, once the water vapour is fully consumed, the oxide aerosols can no longer evolve chemically.

To validate this simulation we require gas diffusion coefficients in the different aerosol layers (taken here from Cooper, 1980). Analytical data being essentially nonexistent, we undertook an experiment to measure the different diffusion coefficients.

Experimental Study

To calculate the diffusion coefficients, we could measure the kinetics of gases consumed during the transformation of a given quantity of sodium oxide aerosol. The problem is that the gas consumption rate is too fast to measure. Instead, we developed experiments using thin pellets of sodium oxide and hydroxide. The different diffusion coefficients can be derived from the gas consumption rates and other experimental parameters.

First, we make the sodium oxide or hydroxide pellets in an inert preparation glove box and then we allow them to react in a second glove box with different atmospheres, i.e., specific water vapour and carbon dioxide concentrations.

H_2O and CO_2 consumption will be monitored versus the exposure time by conventional gas probes. Formation of O_2 will also be detected using an IR tuneable-diode laser spectroscopy technique. Kinetic parameters and diffusion coefficients will be calculated by fitting the experimental data to a model describing the chemical mechanisms (R1, R2 and R3).

$$2\ Na_2O_2 + 2\ H_2O \rightarrow 4\ NaOH + O_2 \qquad (R1)$$

$$2\ NaOH + CO_2 \rightarrow Na_2CO_3 + H_2O \qquad (R2)$$

$$Na_2CO_3 + CO_2 + H_2O \rightarrow 2\ NaHCO_3 \qquad (R3)$$

The experimental results and Cooper's model will be compared: either a readjustment of Cooper's model will suffice or a new model will be developed.

This work is financially supported by the 7th Framework project JASMIN (contract 295803).

Cooper, D.W. (1980) *Prediction of the Rates of Chemical Transformation of Sodium Fire Aerosols*, US NRC report NUREG/CR-1724.

Mathé, E. and Kissane, M.P. (2012) *Modélisation de la Production d'Aérosols par la Combustion de Sodium*, CFA 20121, 25-26 janvier 2012, Paris, ASFERA.

A modeling study of regional sources contributing to atmospheric $PM_{2.5}$ of Taiwan

Tu-Fu Chen[1], Wen-Yinn Lin[2], Ken-Hui Chang[1,*]

[1] Department and Graduate School of Safety Health and Environmental Engineering, National Yunlin University of Science and Technology, Yunlin 64002, Taiwan.

[2] Institute of Environmental Engineering and Management, National Taipei University of Technology, Taipei City 10608, Taiwan.

Keywords: long range transport, East Asia, $PM_{2.5}$ composition

Presenting author email: changken@yuntech.edu.tw

The effect of transboundary long range transport (LRT) on the areas located at downstream of large emission source is play a major role to air quality (Shimadera et al., 2009; Koo et al., 2008; Wang, 2005). Air pollutants emitted in East Asia were increasing for past ten years because of rapid economic growth (Ohara et al., 2007). The atmospheric $PM_{2.5}$ of Taiwan, located at downstream of East Asia's continental outflow, should be affected significantly by the other countries in East Asia.

Taiwan EPA announced a new strict air quality standard for $PM_{2.5}$ in 2012. To meet the standard, Taiwan has to implement a number of proper control strategies, which is determined for various regional and local sources by a series of studies. The study is subjected to explore the relative importance of various regional sources for atmospheric $PM_{2.5}$ in Taiwan. MM5/CMAQ was adopted to simulate air quality of East Asia and Taiwan by a configuration of three-level nested domains shown in Figure 1. Four emission scenarios were designed to simulate and assess the contribution of various regional sources for 2007 including Taiwan-self source, direct and indirect effects of LRT by East Asia source, as well as background concentration of East Asia. The four scenarios are (a) base case (BS): all sources of Taiwan and the other countries are considered; (b) zero East Asia case (ZE): Taiwan sources are considered only without East Asia sources; (c) zero Taiwan case (ZT): East Asia sources are considered only without Taiwan sources; and (d) all zero case (ZA): all sources of Taiwan and the other countries are not considered.

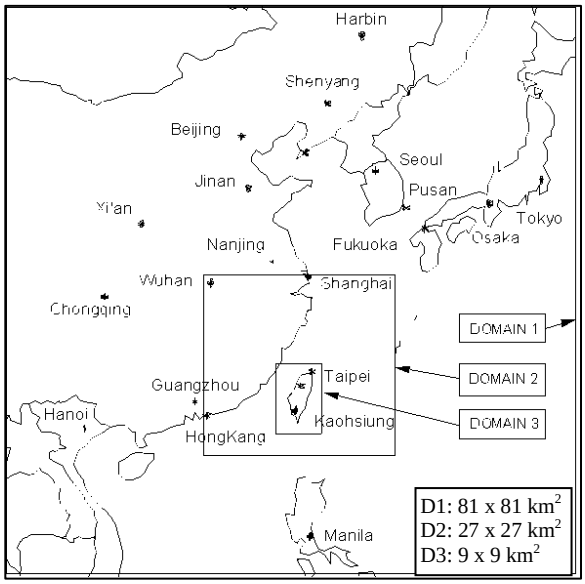

Fig. 1 Configuration of three-level nested domains.

The simulation and analysis results shown in Table 1 indicate that Taiwan-self sources contribute a highest ratio of 60% to Taiwan's atmospheric $PM_{2.5}$ in 2007, LRT of East Asia's sources contribute a second ratio of 37% (27% and 9% for direct and indirect effects), and background of East Asia contribute the rest of 3%. It also indicates that the effects of LRT are almost higher than 40% for all seasons except summer with 14% only.

The indirect effect of LRT means that the precursors are transported from the other countries to Taiwan and reacted with the precursors emitted in Taiwan to form $PM_{2.5}$. Therefore, the indirect effect of LRT is controllable for Taiwan in contrast of uncontrollable direct effect of LRT. The contribution ratio of various regional sources to secondary $PM_{2.5}$ is shown on Table 2. The direct LRT effect for sulfate is as high as 57%, while that for nitrate is 7% only. Thus, the sulfate consisted in $PM_{2.5}$ is difficult to be reduced by SO_2 emission reduction in Taiwan, however, the nitrate is relative easy to be controlled by NOx emission reduction in Taiwan.

Tab. 1 Contribution ratio of regional sources for atmospheric $PM_{2.5}$ of Taiwan in 2007 (%)

	Taiwan-self	LRT of East Asia		Background of East Asia
		direct	indirect	
Spring	56.9	30.1	10.2	2.8
Summer	81.0	8.8	5.8	4.3
Fall	57.7	29.0	9.9	3.4
Winter	57.5	30.5	9.8	2.3
Whole year	60.3	27.3	9.4	3.0

Tab. 2 Contribution ratio of regional sources for secondary $PM_{2.5}$ of Taiwan in 2007 (%)

	Taiwan-self	LRT of East Asia		Background of East Asia
		direct	indirect	
SO_4^{2-}	31.9	56.8	6.0	5.2
NO_3^-	57.5	6.9	35.6	0.0
NH_4^+	43.2	32.4	24.2	0.2
SOA	73.8	10.2	16.0	0.0
Secondary $PM_{2.5}$	44.6	34.5	18.6	2.3

Wang, K.Y., J. Geophys. Res., 110, D07306 (2005).

Ohara, T., H. Akimoto, J. Kurokawa, N. Horii, K. Yamaji, X. Yan, T. Hayasaka, Atmos. Chem. Phys., 4419-4444 (2007).

Koo, Y.S., S.T. Kim, H.Y. Yun, J.S. Han, J.Y. Lee, K.H. Kim, E.C. Jeon, 2008, Atmos. Res., 90, 264-271.

Shimadera, H., K.L. Shrestha, A. Kondo, A. Kaga, Y. Inoue, 2008, J. Environ. Sci., 20(7), 838-845.

The Contribution of Local and Regional Sources to Particulate Matter in European Megacities

K. Skyllakou[1.2] , A.G. Megaritis[1,2] C. Fountoukis[2], B. N. Murphy[3], P. E. Haralabidis[4] and S.N. Pandis[1,2,3]

[1]Department of Chemical Engineering, University of Patras, 26500, Patras, Greece
[2]Institute of Chemical Engineering Sciences (FORTH/ICE-HT), 26504, Patras, Greece
[3]Department of Environment, University of the Aegean, University Hill, 81100, Mytilene, Greece
[4]Department of Chemical Engineering, Carnegie Mellon University, Pittsburgh, PA 15213, USA
Keywords: PSAT, Emissions Sources, Contributions, $PM_{2.5}$
Presenting author email: ksakousti@chemeng.upatras.gr

The ongoing urbanization over the past decade has led to an increasing number of Megacities around the world, now hosting more than half of the world's population These large urban centers are substantial sources of anthropogenic pollutants having adverse effects on human health, visibility and ecosystems. In order to improve air quality in those urban areas we need to quantify the fraction of the pollution originating from local and regional sources and to determine the response of the system to emission controls. Three-dimensional chemical transport models (CTMs) are well suited to help address these source receptor questions since they model all the necessary processes that impact air pollution concentrations and transport in the domain.

In this study we applied PMCAMx (Fountoukis et al., 2011) a three dimensional CTM over Europe to study the influence that emissions in large European urban areas (e.g. Paris, London, Po Valley) might have on the concentration of the major $PM_{2.5}$ components during a summer and a winter period. We combined PMCAMx with the Particulate Source Apportionment Technology (PSAT) (Wagstrom et al., 2011) which directly computes the contribution of different emission areas or source types. The contributions of local, medium, and long range transport and different source categories (e.g., transport, fires, etc.) were quantified.

Local emission sources are predicted to have a significant effect on primary pollutant levels, like Elemental Carbon (EC) while secondary pollutants concentrations are dominated by sources outside major urban areas like Paris. The impact of local sources is high for EC (up to 60%) for both periods. Sulphur dioxide-sources located more than 500 km away from Paris account for 70% of the concentration of $PM_{2.5}$ sulphate in Paris during summer and almost 50% during the simulated winter period. SOA mid-range sources (from 100 km up to 500 km away from Paris) play the most important role in Paris SOA-concentrations with their summer contribution being around 70% and their winter around 60%.

The PSAT results were compared with those of an "annihilation" scenario zeroing out all anthropogenic emissions over an urban area. The results of these simulations suggest that the two methods, despite the non-linearity of the corresponding processes for secondary aerosol formation, are in good agreement with each other (Figure 2). PSAT is a lot more computationally efficient.

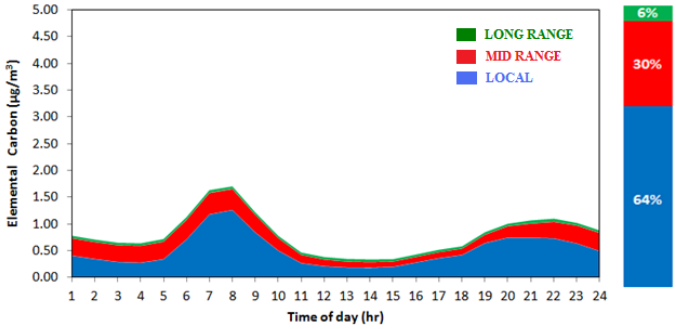

Figure 1. Hourly variation of Elemental Carbon and the contributions from each source for the center of the Paris during summer.

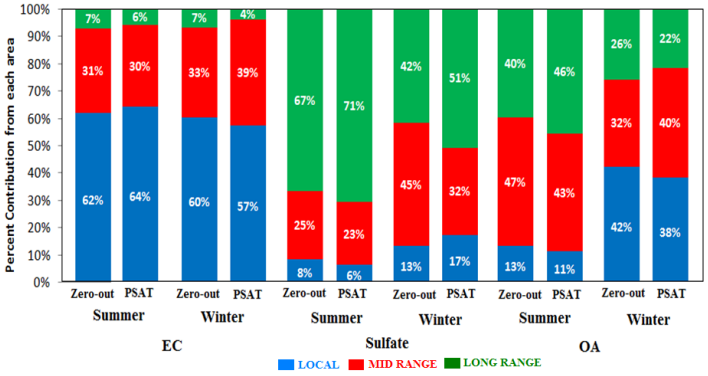

Figure 2. Contribution from each area for EC , sulphate and OA for the two methods for both periods.

Acknowledgement:
This work was funded by the European Commission 7th Framework Program project MEGAPOLI.

Refrences

Fountoukis C., Racherla P. N., Denier van der Gon H. A. C., Polymeneas P., Charalampidis P. E., Pilinis C., Wiedensohler A., Dall'Osto M., O'Dowd C., and S. N. Pandis: *Evaluation of a three-dimensional chemical transport model (PMCAMx) in the European domain during the EUCAARI May 2008 campaign, Atmos. Chem. Phys., 11, 10331-10347, 2011*

Wagstrom K., Spyros N. Pandis: *Contribution of long range transport to local fine particulate matter concerns, Atmos. Environ., 45, 2730-2735, 2011b.*

Transport of aerosol particles from the Fukushima accident

G. Lujanienė[1], S. Byčenkienė[1], P.P. Povinec[2]

[1] Department of Environmental Research, SRI Center for Physical Sciences and Technology, Vilnius, Lithuania,
[2] Faculty of Mathematics, Physics and Informatics, Comenius University, Bratislava, Slovakia
Keywords: Fukushima accident; radionuclides; aerosol transport
Presenting author email: lujaniene@ar.fi.lt

Measurements of activity concentrations of ^{131}I; ^{129m}Te, ^{132}Te, ^{134}Cs; ^{136}Cs, ^{137}Cs in aerosol were carried out in daily samples after the Fukushima accident during the period of March – April, 2011 in Vilnius.

The ground level air samples were collected on the outskirts of Vilnius (54°42'N, 25°30'E). FPP-15 filters made of chlorinated polyvinyl chloride (~ 1 m^2 surface) were exposed at the height of 1 m above the ground. High volume samplers with flow rates (2400 m^3 h^{-1} - 6000 m^3 h^{-1}) were operated. The sampling was carried out continuously. The activity concentrations of gamma-emitters were measured in 12 or 24 h samples by gamma-ray spectrometry using a HPGe detector (relative efficiency of 42 %, resolution of 1.9 keV at 1.33 MeV). The combined uncertainty of measurements by gamma-spectrometry was better than ± 7 % (k = 2).

The radiochemical analyses of Am and Pu were performed on monthly samples (total volume ~ 2.0x10^{6}m^3) of aerosol ashes (~ 30 g). The applied radioanalytical procedures are described in detail by Lujanienė (2011). The measurements of Pu and Am isotopes deposited on stainless-steel discs were carried out with the Alphaquattro (Silena) spectrometer. Accuracy and precision of analysis were tested using reference materials IAEA-135, NIST SRM No 4350B and 4357, as well as in intercomparison exercises, organized by the Risø National Laboratory (Denmark), and the National Physical Laboratory (UK). The precision of Pu and Am measurements was better than ±8 % and ±10%, respectively (k = 2).

Three-dimensional 13-day backward trajectories of air masses that reached Vilnius at 850 hPa and 700 hPa height were calculated employing the Hybrid Single-Particle Lagrangian Integrated Trajectory (Draxler & Rolph, 2011). A meso-scale chemical transport model system (EURAD, http://www.eurad.uni-koeln.de) was used to evaluate the wet and dry deposition of particulate ^{137}Cs, and a potential dispersion of the radioactive cloud after a nuclear accident for three levels

The measured activity concentrations at the site of investigation resulted from a long-range air mass transport and arrival time following downward air mass transport and meteorology (Lujanienė et al., 2012). The activity concentrations of ^{131}I and ^{137}Cs ranged from 2 μBq m^{-3} to 3800 μBq m^{-3} and from 0.2 μBq m^{-3} to 1070 μBq m^{-3}, respectively. In addition to ^{131}I, ^{134}Cs and ^{137}Cs ^{132}I, ^{132}Te, ^{129}Te, ^{129m}Te and ^{136}Cs were detected in the aerosol filters as well. Variations in activity ratios of ^{131}I/^{137}Cs, ^{132}Te/^{129m}Te, ^{134}Cs/^{137}Cs and ^{137}Cs/^{136}Cs were observed. They were mainly due to the decay of the short-lived isotopes (e.g. ^{129m}Te, ^{131}I, ^{136}Cs) while an increase in ^{134}Cs/^{137}Cs was explained by the presence of the Chernobyl-derived ^{137}Cs in the environment. An increase in the activity ratio was observed whereas the highest activity ratio (1 ± 0.05) was found in the most active sample collected on 4 April. Contrary to the ^{134}Cs/^{137}Cs ratio the maxima of ^{131}I/^{137}Cs ratios did not coincide with ^{137}Cs or ^{131}I activities. It was found that different behavior of highly volatile ^{131}I and ^{137}Cs resulted in enrichment of ground level aerosol particles by ^{131}I with respect to ^{137}Cs. Simulated activity concentrations of ^{137}Cs attached to aerosol particles for the Vilnius site reasonably agreed with measured activities in aerosol samples during the Fukushima accident (Lujanienė et al., 2013).

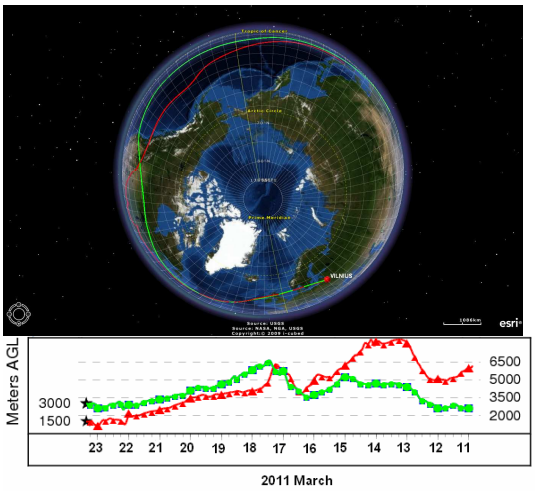

Figure 1. Backward trajectories of air-mass transport ending on 23 March, 2011 in Vilnius.

The activity concentration of actinides measured in the integrated sample collected in March–April, 2011 showed a small contribution of Pu with unusual activity and atom ratios indicating the presence of the spent fuel of different origin than that of the Chernobyl accident (Lujanienė et al., 2012).

Lujanienė, G. (2011) *Proc. Int. Sym. on Isotopes in Hydrology, Marine Ecosystems, and Climate Change Studies. Monaco, IAEA* (in press).

Draxler, R.R., Rolph, G.D., (2011) NOAA *Air Resources Laboratory, Silver Spring, MD, USA.* http://ready.arl.noaa.gov/HYSPLIT.php

Lujanienė, G., Byčenkienė, S., Povinec, P.P., Gera, M. (2012) *J. Environ. Radioact.* **114**, 71-80.

Lujanienė G., Byčenkienė S., Povinec P.P. (2013) *Appl. Radiat. Isot.* (in press).

Cs, Am and Pu isotopes in the atmosphere: source terms and tracer studies

G. Lujanienė[1], D. Valiulis[1], S. Byčenkienė[1], J. Šakalys[1], P.P. Povinec[2]

[1] Department of Environmental Research, SRI Center for Physical Sciences and Technology, Vilnius, Lithuania,
[2] Faculty of Mathematics, Physics and Informatics, Comenius University, Bratislava, Slovakia
Keywords: Pu isotopes; Global fallout; Chernobyl accident; Fukushima accident
Presenting author email: lujaniene@ar.fi.lt

Anthropogenic radionuclides introduced into the atmosphere from various sources have been applied as tools for investigation of contaminant behavior and transport phenomena in the atmosphere. Recent developments in analytical techniques such as gamma-spectrometry and mass spectrometry of long-lived radionuclides have enabled to study atmospheric processes and transport of Saharan, North America and China desert dust. Specifically Pu isotopes have been representing a new tool for investigation of atmospheric processes in Europe, North America and in Asia.

^{137}Cs, ^{241}Am and Pu isotopes in aerosol samples collected at Preila background and Vilnius sampling stations during 1993–2011 were analyzed with special emphasis on better understanding of different sources with characteristic signatures observed at a given site. ^{239,240}Pu monthly activity concentrations in Vilnius ranged from 0.9 to 300 nBq/m^3 (mean value of 13.4 nBq/m^3) and well correlated with amount of total suspended particles, mineral dust and Al concentrations, however, no correlation with PM_{10} was found. The highest ^{239,240}Pu activity within the 1995–2011 record with the ^{240}Pu/^{239}Pu atom ratio close to the Chernobyl value was found in 1995, and it was attributed to the transport of "hot" particles from the areas contaminated after the Chernobyl accident. The ^{137}Cs/^{239,240}Pu ratios varied from 80 to 2500.

The results from long-term measurements of ^{240}Pu/^{239}Pu atom ratios showed a bimodal frequency distribution with median values of 0.195 and 0.253, indicating two main sources contributing to the Pu activities at the Vilnius sampling station (Lujanienė et al., 2012 a). The first mode with the median value of 0.195 (from 0.155 to 0.215) corresponds to the global fallout ratio of ~ 0.17–0.19 characteristic for the Northern Hemisphere (Kelley et al., 1999). The second mode showed the median value of 0.253 (from 0.225 to 0.285) which could be attributed to the nuclear reactor Pu with characteristic ^{240}Pu/^{239}Pu atom ratio of 0.23–0.67 (Warneke et al., 2002).

Three-day backward trajectories of air-masses for 4 selected sectors for three arrival heights: 20, 500 and 1000 m AGL were modeled to assess the transport of aerosol particles to the Vilnius sampling station in 1997–2001 and 2005–2006. A weak correlation between the ^{137}Cs activity concentration in daily samples and height (r = 0.28 (20 m), 0.32 (500 m), and 0.31 (1000 m) in 1997–2001, and for 2005–2006 (r = 0.41 (20 m), 0.49 (500 m), and 0.49 (1000 m)) was found for the Chernobyl sector, while for other sectors no correlation was observed (Lujanienė et al., 2012 b).

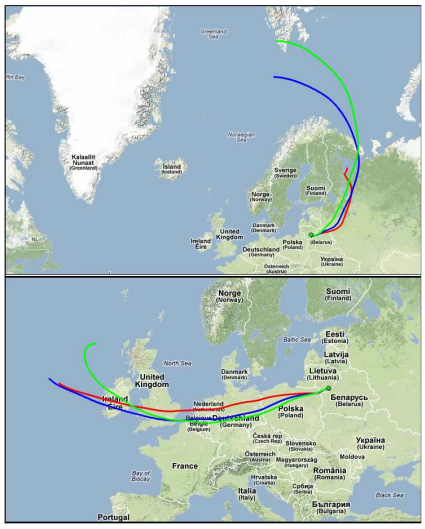

Figure 1. An example of air-mass backward trajectories ending at Vilnius sampling site.

The ^{240}Pu/^{239}Pu ratio in monthly samples and corresponding trajectories (n = 1069) were analyzed. A weak negative correlation (-0.37) of the ^{240}Pu/^{239}Pu atom ratio with transport direction was found for the Siberian region. By contrast to the North–East sector (Figure 1), the ^{240}Pu/^{239}Pu ratio showed a weak positive correlation of 0.46 (significance level of correlation p > 0.99) with the number of trajectories arriving from the Arctic and the Baltic region. This implies that particles with higher ^{240}Pu/^{239}Pu ratios (up to 0.295) tend to be transported from the North–West while no correlation with the Chernobyl region was observed. Measurements carried out during the Fukushima accident showed a negligible impact of this source with Pu activities by four orders of magnitude lower as compared to the Chernobyl accident (Lujanienė et al., 2012 a, b). In spite of the low detected activities, these observations are important for tracer studies for the assessment of transport of various pollutants, for investigation of atmospheric circulation and validation of existing models for future use.

Kelley J.M., Bond L.A., Beasley T.M. (1999) *Sci. Total Environ.* **238,** 483–500.

Lujanienė, G., Valiulis, D., Byčenkienė, S., Šakalys, J., Povinec, P.P. (2012 a) *Atmos. Environ.* **61**, 419-427.

Lujanienė, G., Byčenkienė, S., Povinec, P.P., Gera, M. (2012 b) *J. Environ. Radioact.* **114**, 71-80.

Warneke T., Croudace I.W., Warwick P.E., Taylor R.N. (2002) *Earth Planet. Sci. Lett.* **203**, 1047–1057.

Comparison of the results of two air quality models in the simulation of a turbo gas cogeneration plant PM emissions

P. Ugolini[1], A.Trentini[1], G.Bonafé[1] and V.Poluzzi[1]

[1]Agency for Prevention and Environment of Emilia-Romagna region, Bologna, I-40138, Italy
Keywords: advanced Gaussian model, Lagrangian particle model, correlation, energy plant.
Presenting author email: atrentini@arpa.emr.it

The aim of this study is to compare the outputs of two different models for estimating PM pollutant concentrations caused by a turbo gas cogeneration plant emissions.

The models used are:

- ADMS-Urban, an advanced quasi-Gaussian model, developed by CERC,
- LAPMOD, a lagrangian particle model, developed by Enviroware srl.

The ADMS-Urban (version 3.0) used in this study is an advanced Gaussian dispersion model with a normal Gaussian distribution in stable and neutral conditions, in which the vertical dispersion is approximated by two different Gaussian distributions in a convective boundary layer. Furthermore, ADMS applies up-to-date physics using parameterisations of the boundary layer structure based on the Monin–Obukhov length and the boundary layer height.

Lapmod is a three-dimensional dispersion model that simulate fall out of pollutant emissions by releasing a large number particle for each source at each time step and following their motion. Particles motion is the resulting effect of the mean wind field and the turbulent diffusion. The particles random walk induced by turbulence is Markovian.

The study has been carried out for a domain that contains Imola (Italy), a medium town (68862 inhabitant) where a combined cycle gas turbine (CCGT), coupled with district heating, has been built. The plant, located in urban area, has a capacity of up to 80 Megawatts of electricity and 80 Megawatts of thermal energy.

The emissions of CCGT plant has been considered as point sources.

Emission rates have been structured in Lapmod by implementing an hour by hour release file from continuous monitoring system data of CCGT. In Adms–Urban an hour by hour temporal variation in total emissions has been calculated from the same data of the continuous monitoring system.

Meteorological input data, for the referring year (2010), has been obtained:

- by CALMET, a mass consistent meteorological pre processor, for Adms-Urban;
- by LAMA (assimilation cycle of the operational meteorological model COSMO-I7) downscaled with a mass consistent high resolution processor CACHI (Cosmo Analysis Calmet-High-resolution-Integrated), for Lapmod.

A grid point over Imola of CALMET domain has been used for the meteo-dataset for Adms-Urban, whilst a 3D meteo dataset has been built for Lapmod.

Output concentrations estimated by both models have been calculated according to a long-term simulation, in which the concentrations have been estimated on the nodes of a grid, formed by 30x30 points, with a 200 meters path, covering the whole 6x6 km^2 domain.

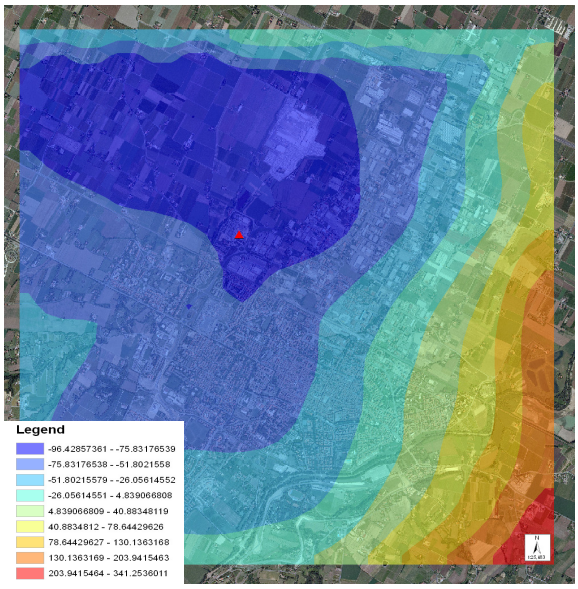

Figure 1. Normalized differences between ADMS Urban and Lapmod

In the map are presented the differences normalized between the two models. Interpretation of the results will be discussed.

G. Bonafe, M. Deserti, S. Jongen, E. Minguzzi, and M. Stortini. Validation of the meteorological input for air quality simulations in Northern Italy. In C. Borrego and E. Renner, editors, *Developments in Environmental Sciences,* volume 6, pages 795-797. Elsevier, 2007.

CERC, (2001). *ADMS-Urban: Urban Air Quality Management System. User Guide. Version 3.0* CERC Limited, Cambridge.

Bellasio R. e R. Bianconi (2012) *The LAPMOD modelling system for simulating atmospheric pollution in complex orography (in Italian). Ingegneria Ambientale*, vol. XLI, n. 6, 492-500.

On an influence of a temperature jump on a molecular heat flow which is taken away from a surface of strongly heated solid spherical aerosol particle

E.R.Shchukin[1], L.A.Uvarova[2], N.V.Malay[3], Z.L.Shulimanova[1]

[1] Institute for High Temperature RAS, Moscow, 125412, Russia
[2] Department of Applied Mathematics, Moscow State University of Technology "STANKIN", Moscow, 127994, Russia
[3] Belgorod State University, Belgorod, 308015, Russia
Keywords: particles, heating, temperature jump
Presenting author email: uvarova_la@rambler.ru

In zones of laser radiation passage through aerosols (Bennet, U.S.) at their enlightenment, diagnostics and combustion aerosol particles strongly heated by the radiation can considerably influence on a temperature distribution inside the aerosol.

Theoretically the estimation of this influence can be carried out, knowing the formulas, allowing to estimate a value of molecular heat flows which are taken away from the surface of heated particles. Formulas found earlier (Shchukin.E.R.) allow to estimate a value of molecular heat flows without an influence of the gas temperature jump (Loyalka,S.K.) near the particle's surface.

Authors of the report in the quasi-stationary approach, taking into account the temperature jump , carried out a mathematical modeling of the molecular heat exchange process of the motionless solid highly thermal conductive spherical aerosol particle with the surface Knudsen number Kn < 0.3 and the gaseous environment in the one component gas with temperature $T_{e\infty}$ and pressure p_∞ The surface temperature of the particle is $T_p >> T_{e\infty}$. The particle's radius is sufficiently small in order to neglect an influence of a gravitational convection on the heat transport. The thermal conductivity coefficient of the gas κ_e depends on the gas temperature T_e by a power law: $\kappa_e = \kappa_{e\infty} t_e^{\omega}$, where $t_e = T_e / T_{e\infty}$.

The T_e distribution is described by the boundary problem (1) in the considered conditions in the environment of the particle

$$\frac{d}{dr} r^2 \kappa_e \frac{dT_e}{dr} = 0,$$

$$\Delta T_{es} = -c_T \lambda \left. \frac{dT_e}{dr} \right|_{r=R}, \quad T_{es} = T_e\big|_{r=R},$$

$$T_e\big|_{r\to\infty} = T_{e\infty}, \qquad (1)$$

where r is the radial coordinate, T_{es} is the value of the gas temperature interpolated from the volume, $\Delta T_{es} = T_p - T_{es}$ - is the gas temperature jump at the surface of the particle, c_T is a coefficient of the temperature jump, λ -is the mean free path of the gas molecules at the temperature T_e. The following analytic expression for a dimensionless temperature t_e was obtained in the process of the solution of (1):

$$t_e = \left[1 + (R/r)\left(t_{es}^{1+\omega} - 1\right)\right]^{1/(1+\omega)}, \; t_{es} = t_p - \Delta t_{es},$$

$$\Delta t_{es} = \left(A_1 - \sqrt{A_1^2 - 4A_0A_2}\right)\Big/ 2A_2, \qquad (2)$$

where $\varepsilon = (c_T/(1+\omega))(\lambda_\infty / R)$, $\lambda_\infty = \lambda$ at $T_e = T_{e\infty}$, $A_0 = \varepsilon\left(t_p^2 - t_p^{1-\omega}\right)$,

$$A_1 = \left[1 + \varepsilon\left(2t_p - (1-\omega)t_p^{-\omega}\right)\right],$$

$$A_2 = \varepsilon\left[2 + \omega(1-\omega)t_p^{-(1+\omega)}\right]/2.$$

An expression for the molecular stream $Q_T^{(M)}$ taken away from the surface of the particle was found with a help of (2), and is equal to

$$Q_T^{(M)} = 4\pi R \kappa_{e\infty} T_{e\infty} f_T^{(M)},$$

$$f_T^{(M)} = \left(t_{es}^{1+\omega} - 1\right)/(1+\omega). \qquad (3)$$

A numerical analysis carried out with a help of (2), (3) has shown, in particular, that the increase in temperature of the surface of the particle can lead to noticeable monotonous increase of the gas temperature jump and strong increase of the molecular heat flow near the surface of moderately large aerosol particles.

References

Bennet,U.S. and Rosasco, G.I. (1978) J. Appl. Phys. **49**,N2, 640-647.

Shchukin, E.R. (2001) In mathematical Modeling Problems, Methods, Applications(Edited by Uvarova L.A. et.al.) Kluver Academic, Plenum Publishers, New York, 255-267.

Loyalka,S.K. and Sielvert,C.E. (1978) Phys. Fluids. **21**, N5, 854-855.

A novel method to determine the growth rate of a growing particle mode

T. Anttila[1], J. Leppä[1] and H. Lihavainen[1]

[1]Finnish Meteorological Institute, P.O. Box 503, 00101 Helsinki, Finland
Keywords: aerosol dynamics, new particle formation
Presenting author email: tatu.anttila@fmi.fi

Atmospheric new particle formation (NPF) events are characterized by appearance of particles at the lowest measured diameter range and subsequent emergence of a growing mode which can often be visualized as a "banana" (Fig. 1). These events have atmospheric relevance as they provide a potentially large source of particles that act as seeds for cloud droplets. A key parameter associated with this phenomenon is the growth rate (GR) of a newly-formed aerosol mode as it contains information on the mechanisms underlying atmospheric NPF events and provides constraints for numerical models simulating NPF (Yli-Juuti *et al.*, 2011). Several methods for determining GR have been developed, but obtaining accurate size- and time-resolved data on GR can still be challenging with the current methods.

Here we propose a method for determining the growth that is based on calculating the count mean diameter CMD over a certain size interval [$d_{min}(t)$, $d_{max}(t)$], and using the following relation:

$$\mathrm{GR}(t) = \frac{\mathrm{d}}{\mathrm{d}t}\mathrm{CMD}(t) = \frac{\mathrm{d}}{\mathrm{d}t}\left(\frac{\int_{d_{\min}(t)}^{d_{\max}(t)} n(d_\mathrm{p}) d_\mathrm{p} \mathrm{d}d_\mathrm{p}}{\int_{d_{\min}(t)}^{d_{\max}(t)} n(d_\mathrm{p}) \mathrm{d}d_\mathrm{p}} \right) \quad (1)$$

where d_p is the particle diameter and $n(d_p)$ is the particle number size distribution. In practice, GR is obtained through numerical differentiation and integrals are replaced by sums.

Two main challenges in applying equation (1) are: how to determine parameters d_{min} and d_{max}, and how to eliminate "noise" that arises from numerical differentiation of CMD together with "noise" in the original size distribution data? We approached the former issue by first calculating the diameter corresponding to the peak concentration in the growing mode as a function of time, $d_{peak}(t)$. A log-normal fit was then performed around d_{peak} which yields the geometric standard deviation of the mode as a function of time, $\sigma_g(t)$. Finally, the following relations were used: $d_{min}(t) = d_{peak}(t)/(\sigma_g(t)\times\alpha)$, and $d_{max}(t) = d_{peak}(t)\times(\sigma_g(t)\times\alpha)$. Here α is a free dimensionless parameter that, together with σ_g, determines the size range over which CMD is calculated. Regarding the latter issue, GR was calculated numerically with finite differences, and the resulting time series was then smoothed using an algorithm described by Stickel (2010).

The approach was evaluated against NPF events generated with an aerosol dynamic model (Anttila *et al.*, 2010), where GR was held constant. To imitate atmospheric data, particle concentrations were perturbed by ±10%. Such comparison is illustrated in Figures 1 and 2. As can be seen, after a growing mode has emerged, the smoothed GR tracks the correct GR accurately despite the fact that non-smoothed GR contains significant amount of noise.

Systematic study on the performance of the method will be presented later, and the feasibility of the method in interpreting atmospheric and laboratory data will be investigated.

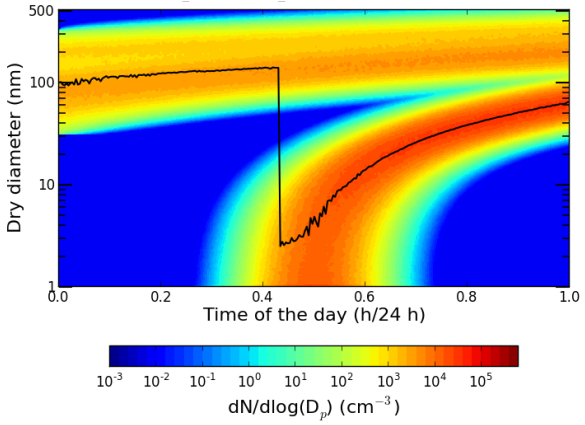

Figure 1. Time evolution of a particle size distribution and CMD (black line).

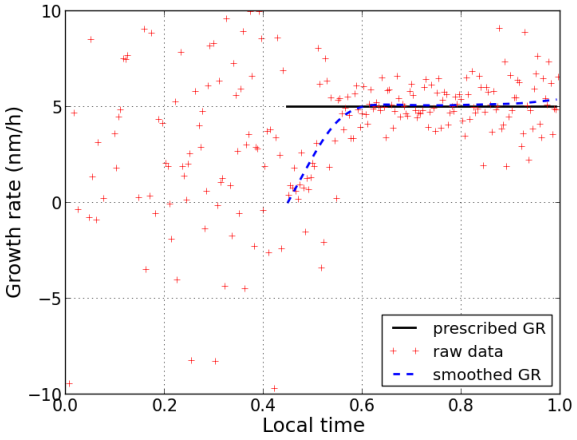

Figure 2. Various growth rates (see legend) during the simulation depicted in Figure1.

This work was supported by the Academy of Finland Center of Excellence program (project number 1118615).

Anttila, T., Kerminen, V.-M., and Lehtinen, K. (2010). *J. Aerosol Sci.* **41**, 621-636.

Stickel, J. (2010). *Comp. Chem. Eng.* **34**, 467-475.

Yli-Juuti et al. (2011). *Atmos. Chem. Phys.* **11**, 11865-12886.

Determination of geometrical length of airborne carbon nanotubes by filtration method

Y.K. Bahk[1, 2] and J. Wang[1, 2]

[1]Institute of Environmental Engineering, ETH Zurich, Zurich, 8093, Switzerland
[2]Analytical Chemistry, EMPA, Dubendorf, 8600, Switzerland
Keywords: carbon nanotube, filtration, electron microscopy, mobility diameter.
Presenting author email: ykbahk@ifu.baug.ethz.ch

The geometrical length of carbon nanotubes (CNTs) is of significant importance and this study aims at its fast determination. We evaluated a method to determine the geometrical length of CNTs by electrical mobility classification (Kim et al. 2007) and developed the filtration based method. The measurement was carried out in air and the suitable generation method for airborne CNTs from liquid suspensions was investigated, followed by a proper control of the CNT dispersion degree by changing the CNT concentration in the liquid suspension. Airborne CNTs were generated by an atomizer, classified by a differential mobility analyzer (DMA) and characterized by electron microscopy. The CNT geometrical lengths measured by electron microscopy served as the basis for comparison with the other methods. Two theoretical models (Lall and Friedlander, 2006 and Li et al., 2012) for elongated particles were investigated and the comparison showed good agreement. This provided an approach to determine the CNT length by the combination of mobility measurement and model calculation. The other developed method, which employed a filtration model with uniform screens, showed comparable results with the CNT lengths as obtained from the electron microscopy.

Figure 1 shows a schematic of CNT filtration measurement system, which consists of an airborne CNT generation system, a size classification system and penetration measurement system. A Collison type atomizer was used to generate airborne CNTs. The multi walled carbon nanotubes (MWCNTs) from the generator were passed through a diffusion dryer to ensure that liquid vapors were removed. In order to classify the generated airborne CNTs, a DMA (TSI 3081) was used. The mobility size distribution was obtained by using the scanning mobility particle sizer (SMPS). In order to control the degree of CNT dispersion, the concentration of CNTs in the suspensions was varied and the resulting size distributions of aerosolized CNTs were measured.

Single dispersed airborne CNTs were collected on silicon substrates, by using a nanometer aerosol sampler (TSI 3089), for SEM analysis sample preparation purposes. A large number of DMA-classified airborne MWCNTs were collected and their lengths were measured from the SEM images. The length distribution of MWCNTs was fitted to a lognormal distribution and mean lengths of MWCNTs were obtained. The obtained geometrical lengths were compared with models provided by Li et al. (2012) and Lall and Friedlander (2006). The lengths were also compared with calculated lengths by the filtration method, which included the particle capture mechanisms (Wang et al. 2011a, b). The results are shown in Figure 2 and comparison with our SEM results showed that the models give satisfactory results.

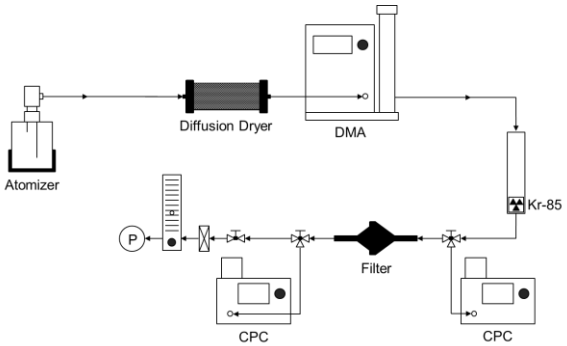

Figure 1. Experimental system for CNT filtration tests.

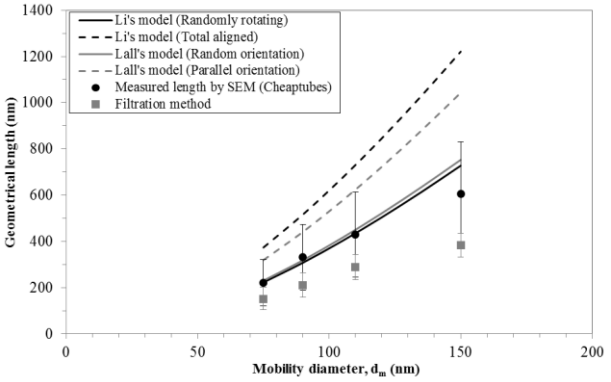

Figure 2. Comparison between the measured geometrical length of CNTs by SEM analysis and obtained length of CNTs by model calculations.

Kim, S. H., Mulholland, G. W. and Zachariah, M. R. (2007) Journal of Aerosol Science, 38, 823-842.
Lall, A. A. and Friedlander, S. K. (2006) 37(3), 260-271.
Li, M., Mulholland, G. W. and Zachariah, M. R. (2012) Aerosol Sci. Tech., 46, 1035-1044.
Wang, J., Kim, S. C. and Pui, D. Y. H. (2011a) Aerosol Sci. Tech., 45(3), 443-452.
Wang, J., Kim, S. C. and Pui, D. Y. H. (2011b) Journal of Nanoparticle Research, 13, 4565-4573.

Modelling of aerosol optical properties with CHIMERE and OPAC and validation with Brewer and Cimel measurements at Brussels, Belgium

V. De Bock[1], A. Delcloo[1], A. Mangold[1] and H. De Backer[1]

[1]Observations Department, Royal Meteorological Institute of Belgium, Brussels, B-1180, Belgium
Keywords: AOD, Chemical Transport Model, OPAC.
Presenting author email: Veerle.DeBock@meteo.be

The current UV forecasting model of the Royal Meteorological Institute of Belgium uses climatological monthly Aerosol Optical Depth (AOD) values in order to forecast the UV index for today, tomorrow and the day after tomorrow. In order to improve the UV forecasts, it would be interesting if we were able to reliably predict the AOD for those days, instead of using climatology. Therefore we are investigating the possibility of combining a Chemical Transport Model (CTM), with the OPAC (Optical Properties of Aerosols and Clouds; Hess et al., 1998) software package to model AOD values.

The CTM we use is CHIMERE, a chemical transport model for the prediction and simulation of air quality (http://www.lmd.polytechnique.fr/chimere/, Vautard *et al.* 2001) that provides the chemical composition of aerosol particles up to a height of 5.5km, with data for Brussels going back to 1990. The model is forced by the meteorological fields of European Centre for Medium-range Weather Forecast's ERA-INTERIM reanalysis. The emissions are taken from the EMEP database (Vestreng, 2003). The chemical mechanism used is MELCHIOR (Derognat *et al*. 2003). To be able to use the CHIMERE output as input for the OPAC software package, some alterations (e.g. change of units from µg/m³ to particles/cm³, redefinition of aerosol classes) had to be made.

The OPAC software package provides optical properties in the solar and terrestrial spectral range of atmospheric particulate matter. The optical properties are calculated on the basis of the microphysical data (size distribution and spectral refractive index) under the assumption of spherical particles in case of aerosols. Data are given for up to 61 wavelengths between 0.25 and 40 µm and up to 8 values of relative humidity.

In this research, we are interested in the modeled AOD values at 300, 350 and 500nm since we can validate the modeled optical properties with measured data at those wavelengths from the Brewer spectrophotometer and the Cimel sunphotometer located in Brussels. This will also allow us to gain more knowledge on the optical properties within the UV spectral range where there are still many uncertainties concerning the behavior of aerosol optical properties. Previous research has shown that it is possible to retrieve the AOD using both the direct sun measurements (at 306, 310, 313, 316 and 320nm) as the sun scan measurements (at 340nm) of the Brewer spectrophotometer (Cheymol & De Backer, 2003; De Bock *et al*., 2010). Also the AOD measurements of the collocated Cimel sunphotometer (at 340 and 500 nm) will be used as input for the validation of the model. This poster will present the first results of the comparison of modeled and measured AOD values for Uccle, Belgium.

This work was supported by the Belgian Science Policy under the project AGACC II contract SD/CS/07A. We also thank Christian Hermans of the Belgian Institute for Space Aeronomy, PI for the AERONET sunphotometer in Brussels.

Cheymol, A. and De Backer, H. (2003) *J. Geophys. Res*. **108**, 4800.

De Bock, V., De Backer, H., Mangold, A. and Delcloo, A. (2010) *Atmos. Meas. Tech.*, **3**, 1577-1588.

Derognat, C., Beekmann, M., Schmidt, H., Vautard, R., Martin, D. and Neininger B. (2003) *J. Geophys. Res*., ESQUIF special section.

Hess, M., Koepke, P. and Schult, I. (1998), *Bulletin of the American Meteorological Society*, **79(5)**, 831-844

Vautard, R., Beekmann, M., Roux, J. and Gombert, D. (2001), *Atmos. Env*. **35**, 2449-2461.

Vestreng, 2003 Review and revision of Emission data reported to CLRTAP, EMEP status Report.

Modelling of air quality : number of particles

S. Deschamps[1], K. N. Sartelet[1], F. Freutel[2]

[1]CEREA, Joint Laboratory École des Ponts ParisTech/EDF R&D, Université Paris-Est, 77455 Marne-la-Vallée, France
[2]Particle Chemistry Department, Max Planck Institute for Chemistry, D-55128 Mainz, Germany
Keywords: Aerosol, air quality model, Number concentration.
Presenting author email: stephanie.deschamps@cerea.enpc.fr

Although ongoing air quality regulations only apply to particle mass, the number of particles may also has a negative impact on human health. Therefore it is essential that air quality models simulate both particle mass and number, and that simulations represent well the measured concentrations in the atmosphere. Particle mass is regulated for particles with aerodynamic diameters less than 2.5 and 10 µm ($PM_{2.5}$ and PM_{10}). Ultra fine particles, which have diameters less than 0.1 µm, usually have low mass concentrations, but high number concentrations.

The Polyphemus air quality modelling system is modified in order to simulate as accurately as possible both particle mass and number. The modelling of particle number has to include some processes which are not essential to the modelling of particle mass, such as nucleation and the Kelvin effect, which allows to consider the curvature of particles for condensation/evaporation. Furthermore, a numerical algorithm that accurately represent the evolution of both number and mass concentrations of particles (*Devilliers et al*, 2013) for condensation/evaporation is implemented.

Table 1: Comparisons of simulated mass concentrations to BDQA measurements ($\bar{o}$ represent measured concentrations and $\bar{c}$ simulated concentrations. MFB is the mean fractional bias and MFE the mean fractional error).

	$\bar{o}$ ($\mu g.m^{-3}$)	$\bar{c}$ ($\mu g.m^{-3}$)	MFB (%)	MFE (%)
$PM_{2.5}$	13.6	10.8	-16.8	39.6
PM_{10}	25.7	12.8	-60	63.9

The model is evaluated for both mass and number concentrations by comparisons to measurements performed during the "MEGAPOLI" campaign in July 2009 in the Paris metropolitan area.

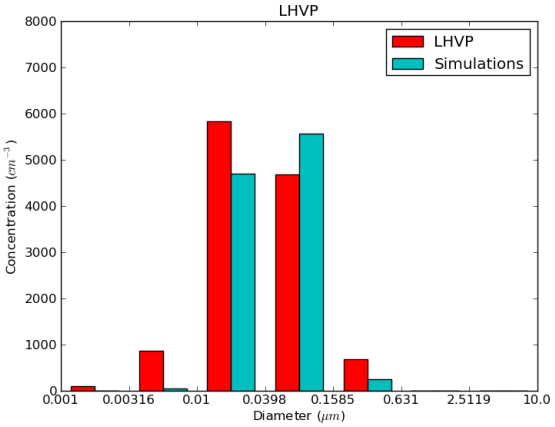

Figure 1: Comparison between simulated and measured number concentrations at LHVP (Laboratoire d'Hygiène de la Ville de Paris).

The authors would like to thank Maik Merkel, Alfred Wiedensohler (Leibniz Institute for Tropospheric Research) and Evangelia Kostenidou (FORTH Institute) for providing aerosol number concentration measurements.

Devilliers, M., Debry, E., Sartelet K. N., Seigneur, C. (2013), *A new algorithm to solve condensation/evaporation for ultra fine, fine and coarse particles*, Journal of Aerosol Science, **55**, 116–136.

Influence of the geometry of the aerosol conducting system on the deposition of particles from inhalable aerosols on cellular surfaces in vitro

C. Brodbeck[1], D. Ritter[2], J. Knebel[2]

[1]Department of Simulation Engineering, Fraunhofer Institute for Algorithms and Scientific Computing, Sankt Augustin, 53754, Germany
[2]Department of In vitro and Mechanistic Toxicology, Fraunhofer Institute of Toxicology and Experimental Medicine, Hannover, 30625, Germany
Keywords: aerosol, in vitro, particle deposition, computational simulation of fluids (CFD).
Presenting author email: carsten.brodbeck@scai.fraunhofer.de

Within the last decade the air liquid interphase (ALI) cell culture technology became the state-of-the-art method for in-vitro testing of airborne substances. Cells are cultured on microporous membranes and thereby get efficiently into contact with the test atmosphere while being supplied with nutrients and being humidified from the basal side of the membrane. Biological models like cell lines from the human lung or complex *ex vivo* models like precision cut lung slices (PCLS) can be applied. Sensitivity and relevance of the basic technique for use with chemical gases were demonstrated in round-robin prevalidation studies in Germany including laboratories from Fraunhofer, academia and governmental institutions (BfR and BAuA). However, especially for the application of this basic technology on the testing of a broader range of airborne materials like droplet and particle aerosols, there is still no general scientific consensus on the question of the most suitable exposure design. Concepts including complex physical phenomenons like electrostatic deposition of particles or thermophoresis have been introduced to address specific scientific questions. To develop a concept for a more general application of the ALI culture technology for all kinds of airborne materials in the long run, this study aimed in a first step at the characterization of the influence of the aerosol conduction system on the particle deposition by the use of computational fluid dynamics (CFD).

In the CFD simulation models applied within the scope of this project the fluid air is treated as an incompressible continuum in an Euler frame of reference and as a laminar flow. The particles are regarded as solid spheres of different size in a Lagrangian frame of reference. As the particles are dispersed and the portion of volume is rather small in the continuous phase the influence of the dispersed phase on the continuous phase is neglected. The particles exhibit inertia and are exposed to drag, pressure and gravity forces. The particle diameters are defined by a cumulative distribution function. Due to the result of a simulation of an experimental setup, it could be shown that particles do not cover the border areas of the tubes, when they are reaching the cell culture device. Because of this the injection distribution of particles for partial models omitted areas close to the tube walls. The behaviour of particles which hit or touch a wall was defined as “stuck”, so that these particles were removed from the flow field and were accumulated on the wall for visual and numerical evaluation. For the simulations the CFD software STAR-CCM+[3] was applied.

Concerning the deposition behaviour of the particles on the cell culture membrane, several geometries were investigated. All geometries had a 180° deflection of the flow in common, but other geometrical details like the inlet nozzle design were modified and simulated in order to increase and smooth the deposition rate. However the deposition rate showed a very robust behaviour, as the resulting differences encountered were rather small. Two geometries showed a smoother but also a lower deposition rate at the same time. The other geometries with partially exceeding designs were fairly equivalent. Due to the partially submicronic size of the particles, it is now planned to proceed with simulations accounting for brownian motion and thermophoresis applying temperature gradients. As STAR-CCM+ does not support the above described effects, FLUENT[4] will be applied for these simulations. Thus it is the aim by accounting for these effects in the numerical simulations to investigate if one of the geometrical structures is predominant.

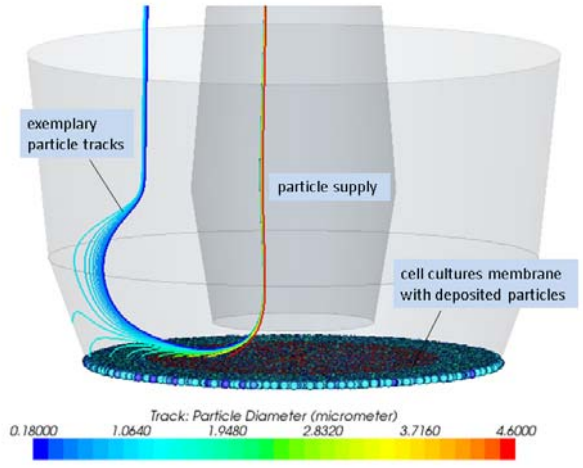

Figure 1: CFD of particle deposition on cell culture membrane with STAR-CCM+

[3]STAR-CCM+ is registered trademark of CD-adapco
[4]FLUENT is registered trademark of ANSYS, Inc.

Comparison of the atmospheric Chemistry Transport Model COSMO-MUSCAT with experimentally determined aerosol parameters

C. Engler[1], R. Wolke[1], W. Birmili[1], and A. Wiedensohler[1]

[1]Leibniz-Institute for Tropospheric Research, Permoserstraße 15, 04318 Leipzig, Germany
Keywords: atmospheric modeling, size distributions, model validation
e-mail: christa.engler@tropos.de

The chemistry-transport model system COSMO-MUSCAT was used for a detailed observation-model comparison. The model system consist of the online coupled code of the operational forecast model COSMO (Schättler et al., 2009) and the chemistry-transport model MUSCAT (Wolke et al., 2012). For the description of the particle size distributions, an extended version of the modal aerosol model M7 (Vignati at al., 2004) was used.

Experimentally determined particle number size distributions from the GUAN-Network in Germany (Birmili et al., 2009) were used for the comparison of a spring episode in 2009. In the beginning, very low pollutant concentrations were observed due to north-westerly advection. Afterwards a stable high pressure system leaded to accumulation and thus high pollutant concentrations. The flow changed to westerly and back to a stable high pressure system above the considered area resulting in dilution and again accumulation of pollutants. In the end of the episode, very low pollutant concentrations due to zonal advection of maritime air.

The total mass and chemical composition of PM_{10} and PM_1 (regarded as representative for the accumulation mode) was compared at one location. The mass of PM_{10} was significantly underestimated; the mass of PM_1 was in better agreement with the observed data. The sulphate concentration was in good agreement for both, PM_{10} and PM_1. Nitrate was underestimated in PM_{10} and overestimated in PM_1. Ammonium was slightly underestimated in PM_{10}, but rather overestimated in PM_1. The sea salt concentration was significantly too high, whereas the dust concentration was significantly too low for both, PM_{10} and PM_1. Table 1 shows the correlation coefficients and the relative deviation between the model and the experimental data for a subset of parameters.

Parameter	R^2	Mean deviation (relative)
N_{accu}	0.13	2.7
$D_{p,accu}$	0.07	1.2
PM_{10} (24h)	0.75	0.44
sulfate (PM_{10})	0.61	0.77
nitrate (PM_{10})	0.82	0.74
ammonium (PM_{10})	0.69	0.58

Table 1. Comparison between model simulations and experimental data in Melpitz, Germany.

The physical aerosol parameters were compared for the accumulation mode, since there were only scarce observations of the coarse mode available and modeling of the Aitken mode appeared difficult. The comparison included three stations, which showed more or less the same features. The particle volume was underestimated in the model, but temporal trends were represented well. The simulated number concentration was in the correct order of magnitude but decreased over the period of concern. This is probably due to too large deposition processes or because of too less emissions. This has to be investigated further.

In order to compare the particle diameter, the measured particle number size distributions were fitted with mostly three log-normal modes with the same sigma as used in the model. The comparison resulted in the particle diameter being also in the right order of magnitude but more or less uniform, in contrast to the observations. It tended to be overestimated. Figure 1 shows an example of the comparison of the accumulation mode particle diameter at one out of three stations.

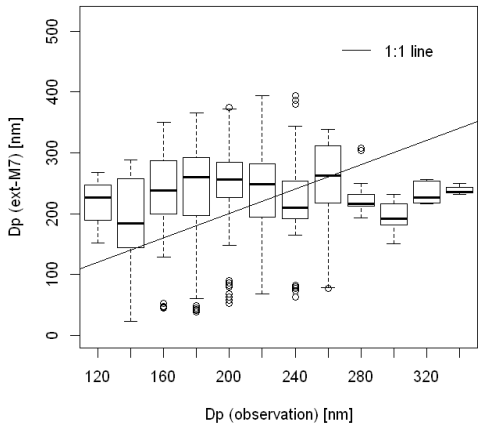

Figure 1. Comparison of experimentally determined and simulated particle diameter in the accumulation mode in Melpitz, Germany.

This work was supported by the German Federal Environmental Foundation (DBU).

Birmili, W., Weinhold, K., Nordmann, S. et al. (2009) *Gefahrst. – Reinhaltg. Luft.* **69**, 137-145.

Schättler U., Doms, G. and Schraff C. (2009) *Deutscher Wetterdienst*, www.cosmo-model.org.

Vignati, E., Wilson, J. and Stier, P. (2004) *J. Geophys. Res.* **109**, D22202. doi:10.1029/2003JD004485.

Wolke, R., Schröder, W., Schrödner, R. and Renner, E. (2012) *Atmos. Env.* **53**, 110-130.

Year-round modelling study on particle formation a South African savannah

R. Gierens[1], L. Laakso[1,2,3], V. Vakkari[1], L. Zhou[1], D. Mogensen[1], J.P. Beukes[3], P.G. Van Zyl[3], and M. Boy[1]

[1]Department of Physics, Division of Atmospheric Sciences, University of Helsinki, Helsinki, 00014, Finland
[2]Finnish Meteorological Institute, Research and Development, P.O. BOX 503, FI-00101, Finland
[3]School of Physical and Chemical Sciences, North-West University, Potchefstroom, South Africa
Keywords: aerosol modelling, particle formation and growth, boundary layer, South African savannah.
Presenting author email: rosa.gierens@helsinki.fi

Africa is one of the less studied continents in respect to atmospheric aerosols. In this study measurements from a savannah environment in South Africa were used to model new particle formation and growth for a full year.

The measurements utilized in this study were done at the Welgelund measurement station, a savannah site in northern South Africa, approximately 100 km west of Johannesburg. The site has very few local pollutant sources, but pollutant plumes from metropolitan and industrial areas are oberved frequently, as well as clean air advected from areas with little antropogenic sources. Measurements in the region have shown a high frequency of particle formation (Vakkari *et al*, 2013): on another savannah site 69% of days observed showed a clear nucleation event (Figure 1). The measurements include meteorological variables (temperature, relative humidity, wind speed and direction, precipitation, vertical temperature gradient, and radiation), trace gas concentrations (SO_2, NO_x, CO, and O_3), flux measurements (H_2O, CO_2, and sensible heat), soil measurements (moisture and heat at differemt dephts), aerosol number size distribution, and concentrations of volatile organic compounds (VOC). The observational data was used for input and comparisons with the simulations. More information about the station can be found at http://www.welgegund.org/.

SOSA (Model to Simulate the concentrations of Organic vapours and Sulphuric Acid) is a one-dimensional model, which includes modules for boundary layer meteorology, emissions from the canopy and chemical processes (Boy *et al,* 2011). For this work a further developed version of the model was used, which also includes aerosol dynamics simulated with UHMA (University of Helsinki Multicomponent aerosol model). UHMA focuses on new particle formation and growth (Korhonen *et al*, 2004), and thereby SOSA is well suited to study these phenomena. Boundary layer meteorology and plant-atmosphere interactions are solved by SCADIS (Scalar Distribution). The emissions of monoterpenes and other organic vapours from the canopy are calculated with MEGAN (Model of Emissions of Gases and Aerosols from Nature). The chemistry is calculated using the Kinetic PreProcessor (KPP), and chemical reaction equations are from the Master Chemical Mechanism (http://mcm.leeds.ac.uk/MCM/).

In this work we simulated a full year to be able to study the different air masses on the site as well as seasonal variations in particle formation. The period from February 2011 to February 2012 was chosen. The frequent n events and particle growth was evaluated in detail. This work will present new model results to give a better understanding on the new particle formation process in South-Africa and discuss the reasons for high frequency of nucleation episodes observed.

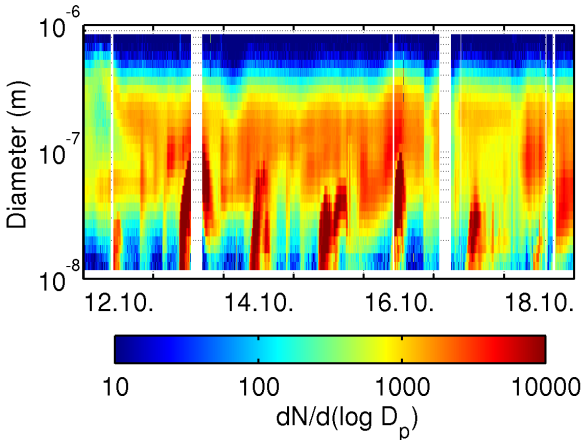

Figure 1. Observed size distribution on savannah show a high frequency of nucleation events. Measurements were done in Botsalano in October 2007.

This work was supported by the Finnish Center of Excellence program, and for computational resources CSC – IT Center for Science Ltd is gratefully acknowledged.

Boy, M., Sogachev, A., Lauros, J., Zhou, L., Guenther, A. and Smolander, S. (2011) SOSA - a new model to simulate the concentrations of organic vapours and sulphuric acid inside the ABL - Part I: Model description and initial evaluation, Atmos. Chem. Phys. **11**, 43-51.

Korhonen, H., Lehtinen, K. E. J., and Kulmala, M. (2004) Atmos. Chem. Phys. , **4**, 471.

V. Vakkari, J. P. Beukes, H. Laakso, D. Mabaso, J. J. Pienaar, M. Kulmala, and L. Laakso (2013) Long-term observations of aerosol size distributions in semi-clean and polluted savannah in South Africa, Atmos. Chem. Phys., **13**, 1751-1770.

Binary aerosol droplet formation

X. Z. Zhen[1], H.-J. Schmid[1]

[1]Chair for Particle Technology, University of Paderborn, Paderborn, 33098, Germany
Keywords: PBE, Monte Carlo, binary aerosol formation, SLS
Presenting author email: xinze.zhen@uni-paderborn.de

One of our main goals in this work is to study the evolution of the aerosol drop size distribution and the droplet concentration distribution from the water/glycerol vapour mixture. A theoretical analysis of binary droplet formation from a water/glycerol vapour mixture has been performed using a “1.5”-dimensional population balance model to simulate the evolution of the aerosol drop size distribution as well as the mean droplet concentration. The simulation includes the relevant mechanisms nucleation, condensation, evaporation and coagulation.

The simulation model was developed and implemented in the commercial solver PARSIVAL. The self-adaptive numerical algorithms in PARSIVAL are based on the Galerkin h-p (h-p: Variable grid - variable order) method and a temporal discretization of Roth’s type (Wulkow et al., 2001).

As expected, from these simulation results it can be seen that nucleation and condensation are strongly affected by the supersaturation. The properties of the droplets are investigated at different vapor compositions. At a higher glycerol concentration in the vapor despite higher nucleation rates larger droplet sizes evolve compared to low glycerol vapor pressure. The evolution of the mean droplets composition starts from almost pure glycerol, is then reduced quickly, passes a minimum before, finally increasing again towards equilibrium composition. Furthermore, the final mean droplet size depends on the mass of vapor at a constant vapor composition of water/glycerol.

The influence of the mechanisms in determining the droplet size is an important focus. At the beginning of the process, aerosol nucleation is playing a dominant role, with rather small droplet growth rates. Later on, the condensation process becomes more and more important and due to the increasing number of droplets and growing particle surface the condensing mass increases rapidly and the mean droplet size significantly increases. The coagulation process is becoming significant even later than the condensation. With severe reduction of the number of droplets coagulation leads to an even faster growth of droplet sizes.

However traditional dynamic simulation methods are at a disadvantage when modeling more than one internal variable, whereas. Monte Carlo methods easily can be extended to a multidimensional case. Monte Carlo simulation is based on the use of a particle ensemble representative for the whole system in order to calculate the properties of the system. Here we use event-driven Monte Carlo algorithm with a stepwise constant-volume method formulated for simultaneous nucleation, condensation and coagulation (Maisels et al., 2004). By using event driven time evolution, the problem of choosing a correct time step is removed. The accuracy of the Monte Carlo solver depends on the number of simulation particles. The droplet number changes according to the chosen mechanism. At each step of the simulation a mechanism is selected with a probability that is directly calculated with the rate of the three processes. The nucleation and coagulation processes result in increases or decreases of the drop concentration, respectively. However, condensation results in surface growth but does not effect the total drop number concentration. When the droplet number in the simulation volume increases or decreases by a factor of two of its initial value, the simulation volume is halved or doubled, respectively.

A systematic validation of the Monte Carlo algorithm with respect to simulation parameters (ensemble size, integration step size etc.) will be presented. Subsequently, a comparison of droplet size distributions and droplet composition resulting from Monte-Carlo and 1.5D-population balance, respectively, will be given. Furthermore, a parameter study using the Monte Carlo technique shows impressively the advantage of this new algorithm.

When nanoparticles are present in a moving fluid, they will be transported by the fluid. Nanoparticles can move in and out of fluid parcels and their location will differ from those of the fluid parcels due to random/Brownian motion. Thus, in future studies a method which allows combing Monte-Carlo based PBE modeling with CFD model will be developed (Kruis et al,. 2012).

The measurement of the particle size of the aerosol is by light scattering. A liquid mixture of glycerol and water is evaporated by heating and then condensed by cooling, thus the aerosol is produced. The experimental procedure used for the formation is designed and built. For the measurements a goniometer with a He-Ne laser is selected. Before measurement of the aerosol many preparation measurements are carried out to check the converted structure. Subsequently, the measurements with different parameters can be performed. Finally, the scattering intensity of the droplets is evaluated and compared with the theoretical values. Thus, the size of the particles is determined.

Wulkow, M., Gerstlauer, A., P. and Nieken, U. (2001) *Chem. Eng. Sci.* **56**, 2575-2588.

Maisels, A., Kruis, F.E. and Fissan, H. (2004) *Chem. Eng. Sci.* **59**, 2231-2239.

Kruis, F.E., Wei, J., v. d. Zwaag, T. and Haep. S. (2012) *Chem. Eng. Sci.* **70**, 109-120

Modelling the fine and coarse fraction of heavy metals in high resolution Spanish domains

M.A. González[1] and M. G. Vivanco[1]

[1]Environment Department, CIEMAT, Madrid, 28040, Spain
Keywords: air quality modeling, heavy metals, particulate matter, air pollution
Presenting author email: mangeles.gonzalez@ciemat.es

Heavy metals are present in the atmosphere in particulate form. These particles, emitted by natural and anthropogenic sources, can cause damages in ecosystems and human health, via inhalation and ingestion. Size particle is an important factor to take into account since the fine fraction can be easily incorporated in organisms, affecting lungs and alveolus. Although metals are generally considered to be present in the fine fraction, some studies based on PM10, PM2.5 and PM1 measurements recorded in Spain (Ferández-Camacho *et al*, 2012; Querol *et al*, 2008) indicate the presence of some metals also in the coarse fraction, as it is the case of Cu and Zn. Monitoring heavy metals is important because they are legislated by European Directives 2008/50/CE and 2004/107/CE. These Directives sets an annual limit value of 500 ng/m3 for Pb, and annual target levels for As (6 ng/m^3), Cd (5 ng/m^3) and Ni (20 ng/m^3). For the other metals (Cr, Cu, Zn and Se), no Directive regulating annual limit or target values is currently established.

Air quality modelling is an important tool for simulating air pollutants.. The CHIMERE is a eulerian air quality model extensively used for different air quality management activities. Metals, such as Cd, Pb, As, Ni,, Cu, Cr, Zn and Se, have been recently included in this model in a special version, developed by the CIEMAT modelling group. Some studies have been recently published, showing the model performance for these metals in Spain and Europe (Vivanco *et al*, 2011; González *et al*, 2012). In those studies all the metals were considered to be emitted in the fine fraction, and were treated as fine inert particles during all the processes. A new step in CHIMERE metal modelling has been given, taking into account a fine (<2.5 micrometres) and a coarse (2.5-10 micrometres) fraction. This preliminary version was applied to simulated two high-resolution domains, centered in conflictive areas in Spain, with high levels of heavy metals pollution (Barcelona and Huelva). These areas were selected by taking into account one previous modelling study (Vivanco *et al*, 2011). Some results and the evaluation of the model performance will be presented

Vivanco, M.G., M.A. González, I. Palomino, J.L. Garrido, X. Querol, B. Bessagnet, J. de la Rosa and A.M. Sánchez de la Campa (2011). *Modelling Arsenic, Lead, Cadmium and Nickel Ambient Air Concentrations in Spain,* ICCSA 2011, 243-246, International Conference on Computational Science and Its Applications.

González, M.A., M.G. Vivanco, I. Palomino, J.L. Garrido, M. Santiago, B. Bessagnet (2012). *Modelling Some Heavy Metals Air Concentration in Europe.* Water, Air & Soil Pollution **223**, 8, 5227-5242.

Fernández-Camacho, R., S. Rodríguez, J. de la Rosa, A.M. Sánchez de la Campa, A. Alastuey, X. Querol, Y. González-Castanedo, I. Garcia-Orellana, S. Nava (2012). *Ultrafine particle and !ne trace metal (As, Cd, Cu, Pb and Zn) pollution episodesinduced by industrial emissions in Huelva, SW Spain.* Atmospheric Environment, **61**, 507-517.

Querol, X., A. Alastuey, T. Moreno, M.M. Viana, S. Castillo, J. Pey, S. Rodríguez, B. Artiñano, P. Salvador, M. Sánchez, S. Garcia Dos Santos, M.D. Herce Garraleta, R. Fernandez-Patier, S. Moreno-Grau, L. Negral, M.C. Minguillón, E. Monfort, M.J. Sanz, R. Palomo-Marín, E. Pinilla-Gil, E. Cuevas, J. de la Rosa, A. Sánchez de la Campa, *Spatial and temporal variations in airborne particulate matter (PM10 and PM2.5) across Spain 1999–2005* (2008), Atmospheric Environment, **42**, 17, 3964-3979.

Measurement and 3D Simulation of NaCl aerosol deposition on electrically charged microfibers

A. Hellmann, K. Schmidt, M. Pitz, S. Ripperger

Chair of Particle Process Engineering, Kaiserslautern University of Technology, Kaiserslautern, Rhineland-Palatinate, 67663, Germany
Keywords: Filtration, Simulation, Electret, Aerosol
Presenting author email: albert.hellmann@mv.uni-kl.de

An important effect influencing the deposition of aerosols especially on electret microfibers is electrostatic. E.g., electret fibres are used in particle filters for respiratory protection or inside air cabin filters. Measurement and simulation techniques for electrostatic forces respectively charges still need to be investigated. Charge quantity and distribution inside microporous media are usually unknown and can additionally change the charge continuously.

At the modelling of particle deposition based on a single fiber approach, the electrical field is taken into account only in a basic way to such a degree that the interaction of the electrical field induced by several adjacent charged fibers is neglected.

Measurements and 3D simulations of particle deposition on electret microfibres have been carried out. The filtration efficiency for submicron particles can be measured by Scanning Mobility Particle Sizer (SMPS).

The measurement and evaluation of the filtration efficiency for submicron particles is technically extensive, time-consuming and the influence of electrostatic is hard to estimate. Therefore, direct numerical simulation is applied to get deeper insight into the occurring effects. For a 3D model of the distribution of charged fibres e.g. spotted or bipolar the airflow and the electric field are computed directly at high resolution as shown in figure 1 and 2. The trajectory of each single particle driven by flow, electric field and diffusion is computed, as well as the deposition of the particle at the fibre surface.

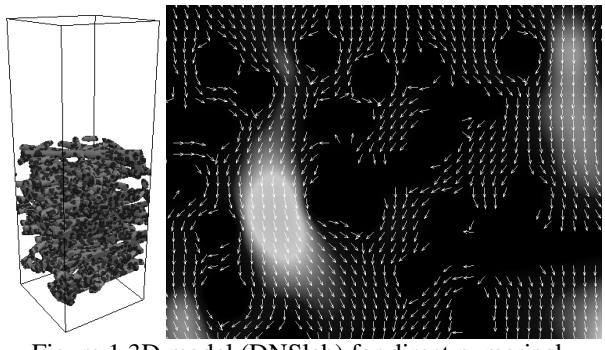

Figure 1 3D model (DNSlab) for direct numerical simulation (left) and a 2D slice of a computed flow field around defines fibre area.

In this contribution the results of measurements and 3D simulations for the aerosol fraction deposition rates at a collection of electrically charged and discharged microfibers will be presented and compared.

Figure 2 Example of a generated spotted charged fibre media.

This work is supported by the Institute for Occupational Safety and Health of the German Social Accident Insurance (IFA).

Löffler F., Dietrich H., Flatt W., *Staubabscheidung mit Schlauchfiltern und Taschenfiltern*, Vieweg, 1984

Breidenbach A., Schmidt F., *Efficiency of Electret Cabin Air Filters using different Test Aerosols*, Filtech 2011 Wiesbaden, proceedings II, pp. 349 to 356

Hellmann, A.; Schmidt, K.; Ripperger, S.; Thelen, C; Möhlmann, C., *Bestimmung der Abscheidewirkung von faserförmigen Filtermedien gegenüber ultrafeinen Partikeln*, Gefahrstoffe - Reinhaltung der Luft 72 Nr. 11/12, S. 484-488, 2012

Schmidt, K., Rief, S., Wiegmann, A., Ripperger, S., *Microstructure Modeling and Simulation of Nanoparticle Deposition*, World Congress on Particle Technology 6, Nürnberg, 2010

Black carbon and organic carbon in Finland: Measurements vs. model

A.I. Hienola, J.-P. Pietikäinen, D. O'Donnell, K. Saarnio and A. Laaksonen

Finnish Meteorological Institute, Erik Palmenin aukio 1, FI-00101 Helsinki, Finland

Keywords: black carbon, organic carbon, global model.
Presenting author email: anca.hienola@fmi.fi

Measurements of black carbon (BC) and organic carbon (OC) surface concentrations at four locations in Finland have been analyzed and compared to the results of the global model ECHAM5-HAM2 (Stier *et al.* (2005), Zhang *et al* (2012)).

OC and BC concentrations were measured with 3-h time resolution using semi-continuous thermal-optical OC/EC Field Analyzers (Sunset Laboratory Inc., Portland, OR). BC was determined optically and total carbon concentration thermally. The concentration of OC was obtained by subtracting the BC concentration from the total carbon concentration. The measurements were conducted during various time periods during 2010-2011 at Helsinki (urban site, Sept. 2010-Dec. 2011), Oulanka (remote site, July-Dec. 2011), Virolahti (SE Finland, Russian border 6 km to the east and E18 highway 5 km to the north, Sept. 2010-Dec. 2011) and Utö (a small island about 60 km from the Finnish SW coast, July-Dec. 2011).

Three versions of the global model ECHAM5-HAM2 were used in this study: ECHAM5-HAM2 with emissions from AEROCOM 2000 (henceforth called ECHAM), ECHAM with the secondary organic aerosol scheme of O'Donnell *et al.* (2011) (ECHAM-DOD), and ECHAM5-HAM2 with new anthropogenic emission dataset for BC, OC and sulfur dioxide (SO_2) derived from the GAINS model output (Kupiainen and Klimont (2007)) with updated ship emissions and newly introduced aviation emissions (ECHAM-GAINS). The models have been run for 2010 and 2011.

At all four sites the models underestimated the measurements up to a factor of 3 for both BC and OC – depending on the location.

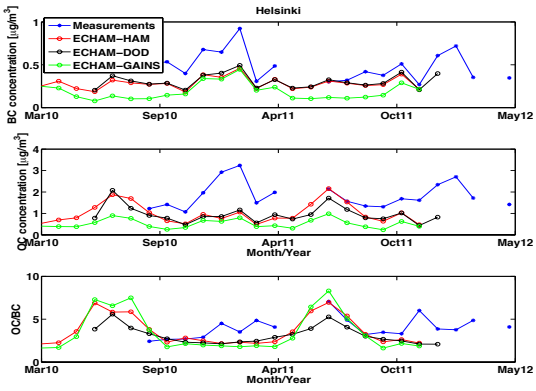

Figure 1. Median BC and OC concentrations and their ratios for Helsinki site.

The best results were obtained by ECHAM-DOD, which was slightly, but not significantly better than ECHAM, while ECHAM-GAINS introduced even a higher difference. Figure 1 presents the BC and OC median concentrations and their ratios for Helsinki, where BC is underestimated by a factor of 2 or less by ECHAM and ECHAM-DOD, and by a factor of 3 by ECHAM-GAINS.

We considered the behaviour of OC to BC ratios, as they can be used as approximate indicator of the potential radiative effects of individual source categories, based on an assumption that OC will reflect light and induce a negative radiative forcing effect in the atmosphere, and that BC will absorb light and induce a positive forcing effect.

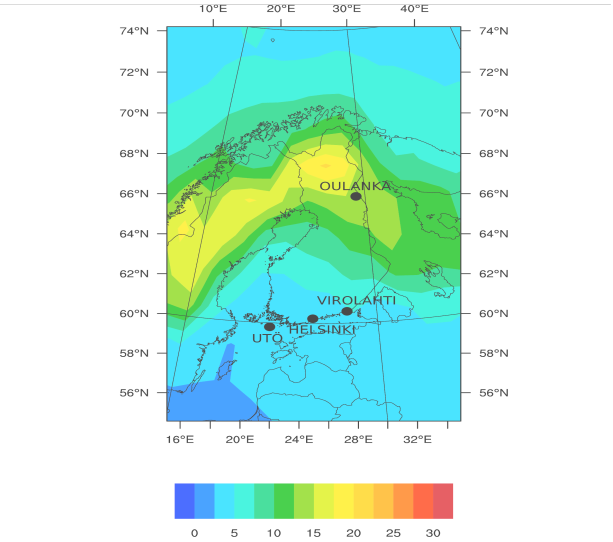

Figure 2. Spatial distribution of the yearly average of OC/BC for 2010. The black dots represent the locations of the measurement stations.

It is known that high OC/BC ratios are due primarily to very small BC concentrations. Figure 2 presents the modeled spatial distribution of yearly averaged OC/BC, showing that Northern Finland is dominated by high concentrations of OC, while in the Southern part the BC is the main driving force.

Stier et al. (2005) *Atmos. Chem. Phys.*, 5, 1125-1156.
Zhang et al. (2012) *Atmos. Chem. Phys.*, 12, 8911-8949
O'Donnell et al. (2011) *Atmos. Chem. Phys.*, 11, 8635-8659
Kupiainen and Klimont (2007) Atm. Env., 41, 2156-2170

Modelling aerosol agglomeration using molecular dynamics methodology

G. Inci[1], A. Kronenburg[1]

[1]Institute for Combustion Technology, University of Stuttgart, Herdweg 51, 70174 Stuttgart, Germany
Keywords: agglomeration, MD, fractal dimension.
Presenting author email: gizem.inci@itv.uni-stuttgart.de

In this study, we investigate the dynamic behaviour and morphologies of the aerosol aggregates in the free molecular ($Kn \gg 1$) and transition ($Kn \approx 1$) regimes. We model the formation and growth of the aerosol aggregates using the molecular dynamics (MD) simulation software ESPRESSO (Arnold, 2013). During the simulations, the binding agents are created between the collided particles in order to irreversibly adhere the collided particles and construct aggregates such that the particles remain fixed at the first contact point and do not rearrange their positions. The random motion of the Brownian particles is simulated by solving the Langevin equations of motion. We use the Langevin thermostat in ESPRESSO (for details please see (Arnold, 2013)). At each time step, all particles are subjected to a random and a frictional force. These two forces satisfy the fluctuation-dissipation theorem and balance each other. The Langevin equation for the i-th particle is then given by

$$m\dot{u}_i(t) = -\gamma u_i(t) F_C + W_i(t), \qquad (1)$$

where F_C are conservative forces, γ is the friction coefficient between the primary particles and surrounding fluid, u_i is the velocity of the i-th particle and $W_i(t)$ is Einstein's white noise term, which is a Gaussian random source.

The exact modeling of the friction coefficient depends on the Knudsen number, $Kn = 2l_{fluid}/d_p$. In the continuum regime, the well known Stokes law applies. However, in the free molecular regime, a slip velocity between the particle and the surrounding fluid exists. The friction coefficient will be lower than the Stokes law would predict, and the so-called Cunningham correction, C_C needs to be introduced (Chen, 1984),

In this work, the simulations are carried out with a system consisting of 1250 spherical particles suspended in motionless air. Particles are randomly placed in a cubic box with periodic boundary conditions for all sides. The particle interactions are taken to be a Lennard-Jones intermolecular potential assuming all primary particles have the same (known) diameter. For the purpose of illustration, we consider 3 different cases; (i) d_p=100nm and T_{air}=300K, (ii) d_p=50nm and T_{air}=300K, and (iii) d_p=50nm and T_{air}=1200K.

The morphology of the aggregates is quantified by using fractal dimensions, D_f. The agglomeration methodology prevents restructuring during the simulation and fractal aggregates are obtained. Moreover, it is found that the fractal dimensions of the aggregates with more than 10 particles obey the power law.

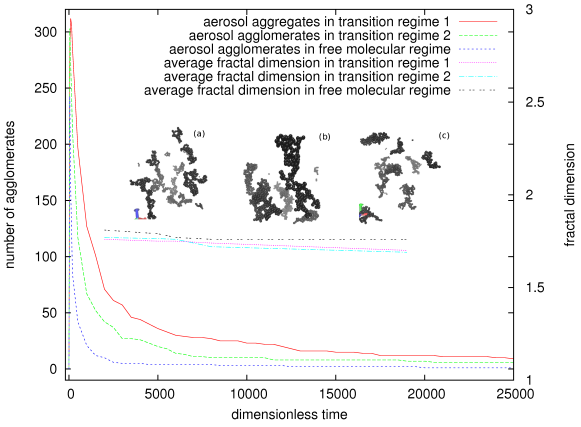

Figure 1: Evolution of aerosol aggregates, change of fractal dimension and aggregates (a) in the transition regime Kn=1, (b) in the transition regime Kn=2, and (c) in the free molecular regime.

Figure 1 shows that the fractal dimensions of the aggregates decrease as the aggregates grow in both transition and free molecular regimes. In the free molecular regime, a regime encountered for example at high temperatures, particles move fast, therefore the collision probability is high. Aggregate growth is more rapid in the free molecular regime than in the transition regime, however, aggregates that are formed in the free molecular regime are more compact. The average fractal dimensions of the aerosol aggregates at different times but possesing similar aggregate distributions are $D_f = 1.69$ and $D_f = 1.7$ in the transition regime ($Kn = 1$, $Kn = 2$) and $D_f = 1.81$ in the free molecular regime. These results agree well with other numerical and experimental studies, and the typical aggregates as shown in the inlet of Fig. 1 stronlgy resemble in shape and structure real aggregates of e.g. soot (Flagan, 1993). Further studies will investigate the aggregate dynamics in different flow fields ranging from simple shear flows to fully turbulent flows.

This work is supported by the DFG as part of the Collaborative Research Center (SFB) 716.

Arnold, A., Lenz, O., Kesselheim, S., Weeber, R., Fahrenberger, F., Roehm, D., Kosovan, P., and Holm, C. (2013) *Springer*.

Lee, K.W. and Chen, H. (1984) *Aerosol Science and Technology* **3**, 327–334.

Roak, S.N., Flagan, R.C. and Nguyen, H.V. (1993) *Aerosol Science and Technology* **18**, 25–47.

Identification of atmospheric $PM_{2.5}$ sources using Non-negative Matrix Factorization modeling in urban-industrial mixed environments

A. Kfoury[1,2], F. Ledoux[1,2], A. Limem[1,3], G. Delmaire[1,3], G. Roussel[1,3], D. Courcot[1,2,*]

[1]Université Lille Nord de France, F-59000 Lille, France
[2]Université du Littoral Côte d'Opale, UCEIV EA4492, F-59140 Dunkerque, France
[3]Université du Littoral Côte d'Opale, LISIC EA4491, F-62228 Calais, France
Keywords: $PM_{2.5}$, receptor modeling, ICP-MS, source apportionment.
Author email: dominique.courcot@univ-littoral.fr

Receptor modeling constitutes a complementary method added to chemical analysis, which are essential to reveal the nature of PM sources. Between the different available modeling algorithms, many types of receptor models like multivariate models and positive matrix factorization (PMF) developed by Paatero (Paatero et *al.*, 1993) provide a flexible approach that can effectively use the information content of chemical data, and has been used worldwide as a credible modeling method (Pandolfi et *al.*, 2008).

Many problems can be encountered when using receptor modeling, the most important one of which is the identification of closely related sources such as "crustal dust" and "traffic resuspended soil dust" for example (Viana et *al.*, 2008).

In order to resolve this problem, constraints must be included in the calculations in order to increase the sensitivity of the model on certain characteristics considered exclusive to each of the sources. Our non-negative matrix factorization is a new method that allows the use of measurement uncertainties as well as constraints in the calculations (Delmaire et *al*., 2010).

Our model calculates the profile (F) and contribution (G) matrices using the following equation:

$$X = \mathbf{GF} + E$$

Equation 1. Matrix factorization equation (X: observation matrix; E: error)

Furthermore, it optimizes the calculations by minimizing the error between estimated and observed values:

$$\{G, F\} = \arg\min_{G,F} \sum_{i=1}^{n} \sum_{j=1}^{m} \left(x_{ij} - (GF)_{ij}\right)^2$$

Equation 2. Minimizing the error between estimated and observed values

The constraints are acquired from the *a priori* knowledge on the sources under study. This information is available through literature reviewing or direct source samples' analysis.

Furthermore, the constraints can be included in two forms: equality and inequality. When applied, the first forces the calculations to consider a specific value of a chemical element in a profile, whereas the inequality constraint gives an order of abundance to each element between the different sources profiles.

Recent studies have showed that the use of receptor modeling that includes measurement uncertainties as well as constraints gave reliable results in the study of particulate pollution source apportionment (Viana et *al.*, 2008), especially when using chemical data representing the composition of PM collected from pollution mixed environments.

This method has been applied in our study using data on $PM_{2.5}$ samples collected in three medium sized cities subjected to a mixture of emission sources and located in northern France, a region in which PM limit values are exceeded regularly. $PM_{2.5}$ samples were taken from the sites during two sampling campaigns realized in winter 2010 and spring 2011, then analyzed for major and trace elements, major ions and total carbon contents. The data were modeled using NMF and the results allowed us to identify site specific and regional profiles.

The application of the NMF using the chemical data acquired from the analysis of about 350 $PM_{2.5}$ samples allowed us to identify 9 to 11 sources of PM pollution as well as their contributions depending on the sampling sites. Finally, the reconstructed concentrations obtained using NMF estimated values proved to be well correlated to the observed ones attained by direct chemical analysis.

The UCEIV laboratory contributes in the work of the Institut de Recherche en Environnement Industriel (IRENI), which is financed by the Communauté Urbaine de Dunkerque, the Région Nord Pas-de-Calais, the Ministère de l'Enseignement Supérieur et de la Recherche, the CNRS and European Regional Development Fund (ERDF).

Delmaire, G., Roussel, G., Hleis, D., Ledoux, F. (2010) *Journal Europeen des Systemes Automatises* **44**, 547-566

Paatero, P., Tapper, U. (1993). *Chemometrics and Intelligent Laboratory Systems* **18**, 183–194.

Pandolfi M, Viana M., Minguillo´n M.C., Querol X., Alastuey A., Amato F., Celades I., Escrig E., Monfort E. (2008). *Atmospheric Environment* **42**, 9007-9017.

Viana M., T.A.J. Kuhlbusch T.A.J., X. Querol X., Alastuey A., Harrison R.M., Hopke P.K., Winiwarter W., Vallius M., Szidat S., Prévôt A.S.H., Hueglin C., Bloemen H., Wåhlin P., Vecchi R., Miranda A.I., Kasper-Giebl A., Maenhaut W., Hitzenberger R., 2008, *Aerosol Science* **39**, 827–849.

Mathematical study of penetration efficiency of aerosol particles for human breathing with protective facemask

I.T. Mukhametzanov, S.K. Zaripov, A.K. Gilfanov
Kazan Federal University, Kazan, Russia, 420008

Keywords: facemask, human inhalability, porous layer, CFD
Presenting author email: ilnar@front.ru

The results of numerical investigations of penetration efficiencies of aerosol particles through a protection field and through faceseal leakage for human breathing with protective facemasks are presented.

Filtering facepiece particulate facemasks are widely used to reduce inhalation exposure to airborne particles that may be associated with negative health effects. The protection level of facemasks is defined by the percentage of ambient particles penetrating inside the protection device. In a real situation, there are two ways of particle penetration: the expected way through a facemask porous medium and through the faceseal leakage. It is impossible to provide zero size of faceseal leakage for real facemasks. Due to large aerodynamic drag of porous medium the air and particles will move to the faceseal leakage. The experimental studies of two particle pathways showed that the penetration efficiency of the faceseal leakage can be considerable (Grinshpun, 2009). It means that the use of these protection devices will not provide the needed level of protection from airborne particles of infectious nature.

As a human head model an idealized spherical body with suction through a circular orifice is taken. It was shown in previous investigations than the human inhalation fraction can be described by the aspiration efficiency of an idealized spherical sampler. A thin porous layer is located before the suction orifice to simulate the facemask. The mathematical model includes the fluid flow and particle motion equations. To describe the air flow through the facemask the porous medium model is applied within the porous layer. The equations are numerically solved by a CFD code, FLUENT. The trajectories of aerosol particles are calculated in the found velocity field.

The example of particle trajectories with a diameter of 20 μm near the facemask before the suction orifice of a spherical body is shown in fig.1. Some particles penetrate through the faceseal leakage. The dependence of the ratio *P* of particle flux through leakage to particle flux to protective mask on diameter of particle at various permeabilities *k* is shown in fig.2. Depending on the permeability of the porous layer and the leakage size the part of particles that penetrates through leakage can be considerable.

The parametrical studies of the dependencies of the penetration efficiencies as a function of permeability of the protection device, particle size, faceseal leakage size and wind velocity are made. The mathematical model and the obtained results can be used in optimization of the geometrical and physical properties of facemasks to eliminate or minimize the particle penetration outside the protection field.

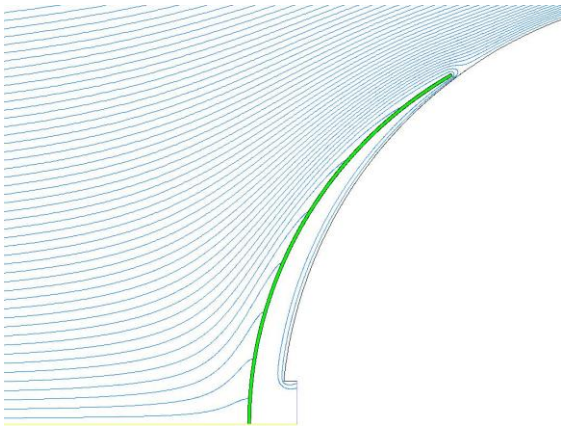

Fig.1. The trajectories of aerosol particles

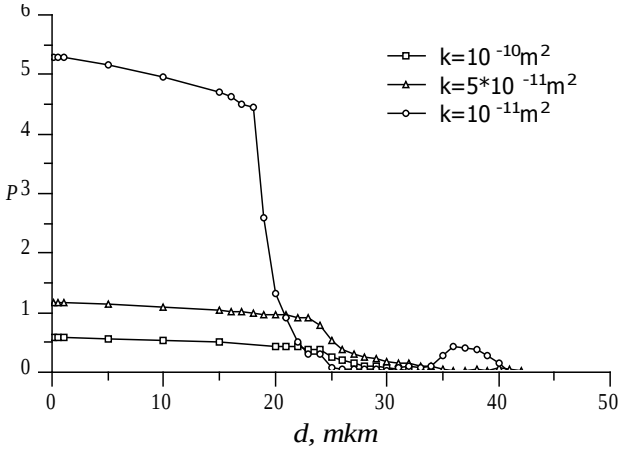

Fig.2. *P* is a particle diameter function

The work was supported by the RFBR (grants № 12-01-00333, 12-07-00007).

REFERENCES

Grinshpun S. et al, (2009) J. of Occupational and Environmental Hygiene, **6**, 593-603.

Diagrams for drift acceleration of inclusion in acoustic field.

D.A. Gubaidullin, P.P. Osipov

Institute of Mechanical Engineering of Russian Academy of Sciences. Kazan, Tatarstan, 420011, Russia
Keywords: particle drift, forces in acoustic fields.
Presenting author email: petro300@rambler.ru

Inclusion (elastic or rigid particle, bubble) in acoustic field is subject to the action of various forces: Stokes, Oseen type forces, Archimedes, added mass, Basset and other less studied forces. Oscillations of fluid may cause a drift of inclusion. This effect is widely used in wave technologies of separation and coagulation. Inclusion drift acceleration in standing wave with fluid velocity $v_1 = U_0 \sin kx \sin \omega t$ depends on the wave number k, frequency ω, amplitude U_0, density of fluid ρ_1, elasticity of fluid, as well as on inclusion density ρ_2, elasticity, location, relaxation time τ_v, surface tension between inclusion and fluid.

Numerous investigations on inclusion drift problem have been done in the last three decades. Various formulas for drift acceleration were obtained. Recently a new approach to the drift problem was developed in (1. Gubaidullin D.A., Ossipov P.P. 2011). The model of drift of compressible inclusion in compressible fluid at low Reynolds number taking into account Stokes force, added mass and Archimedes forces and surface tension was investigated analytically. Method of small parameter and Van-der-Pole was used. This approach is based on decomposition of inclusion motion into slow and fast parts (evolution and oscillation). Obtained in this work formula for drift acceleration and coordinates ρ_1/ρ_2, $(\omega\tau_v)^2$ were laid to the base of diagram for drift direction. This diagram covers all possible frequencies of standing wave, and all relative inclusion densities. Diagram shows existence of threshold curves, dividing the drift regimes into several groups. In each group the drift of inclusion is directed to the nodes or antinodes of standing wave. The further step in better understanding and systematizing the inclusion drift problem in standing wave was done in (2. Gubaidullin D.A., Ossipov P.P. 2013). The drift of incompressible inclusion at different Reynolds and Strouhal numbers under influence of viscosity, added mass and Archimedes forces was investigated numerically. The diagram of drift direction with coordinates $D = 3\rho_1/(\rho_1 + 2\rho_2)$-density parameter, $\mu_p^2 = \{1 + [\omega\tau_v(1 + 0.5\,\rho_1/\rho_2)]^2\}^{-1}$ - squared entrainment coefficient, was introduced. The existence of threshold curves in diagram, dividing all drift regimes into several groups was revealed. The threshold curves for different Reynolds and Strouhal numbers were computed. It was shown that with increasing Reynolds and Strouhal numbers the threshold value of squared entrainment coefficient decreases significantly. In (3. Gubaidullin D.A., Ossipov P.P. 2013) the direction of drift of incompressible particle in acoustic resonator with periodic weak shock wave was studied numerically. The impact of main hydrodynamic forces on drift direction was investigated. Simulations revealed the existence of threshold value of particle radius which divides drift regimes in two groups with opposite drift directions.

The main result of above mentioned articles was development of diagrams for drift direction. The further step in better understanding of drift problem is introduction of diagrams for drift acceleration instead of those for drift direction. They are mush more informative, because depict the level curves for dimensionless drift acceleration. The 0-level curves correspond to the threshold curves in diagrams for drift direction. In Figure 1 the diagram for drift acceleration of incompressible inclusion in compressible fluid is presented. There are two threshold curves, dividing all regimes into three regions. Numbers depict the drift acceleration. The grayed regions correspond to drift towards the nodes, white- corresponds to drift towards the antinodes.

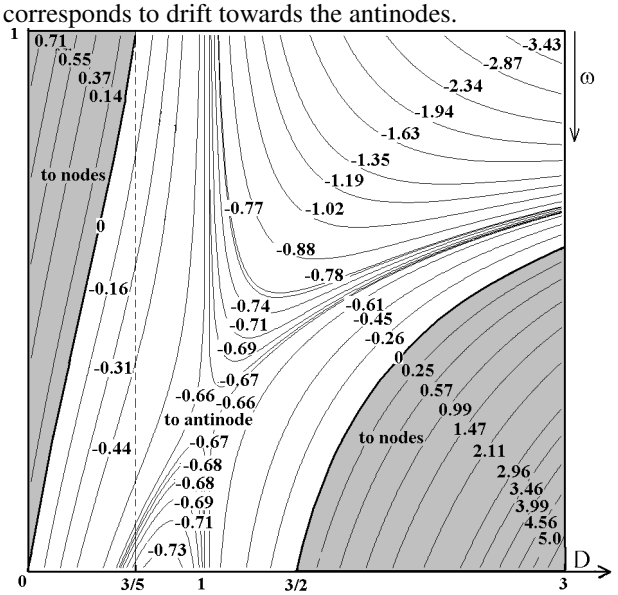

Figure 1. Diagram for drift acceleration.

In present work different models of inclusion drift and corresponding diagrams of acceleration are presented and analysed.

This work was supported by RFFR (Grant № 10-01-00098).

1. Gubaidullin D.A., Ossipov P.P. (2011) J. Eng. Phys. Thermophysics. 84 (2), 270–283.
2. Gubaidullin D.A., Ossipov P.P. (2013) J. Eng. Phys. Thermophysics. 86 (1) 50–58.
3. Gubaidullin D.A., Ossipov P.P. (2013) J. Applied Math. and Computation. 219 (2013) 4535–4544.

Comparison of two airports emissions and pollutants dispersion in urban areas

E. Pecorari[1], G. Valotto[1], S Squizzato[1], G. Rampazzo[1], D. Bassano[2], S. Sollecito[2], E. Rampado[3]

[1]Department of Environmental Science Informatics and Statistics, University Ca' Foscari, Dorsoduro 2137, I-30123 Venezia, Italy
[2]SAVE S.p.A., Marco Polo Venice airport Viale G. Galilei 30/1, I-30173 Tessera-Venezia, Italy
[3]Ente Zona Industriale di Porto Marghera, via dell'Elettricità 39, I-30175 Porto Marghera-Venezia, Italy
Keywords: airport emission, atmospheric modelling
Presenting author email: eliana.pecorari@unive.it

Since 2009, a collaboration between Ca' Foscari University of Venice, SAVE S.p.A., AerTre S.p.A. and Ente della Zona Industriale di Porto Marhera (EZI) has started to study the emissions of the "Marco Polo" and "A. Canova" airports. The sites are set near two big urban areas: respectively Venice and Treviso.

Despite the proximity (~28 km), the two sites are characterized by different environmental and atmospheric conditions and emission sources. In Venice, several studies have been conducted to estimate air pollutants dispersion and concentrations (Pecorari et al., 2013; Squizzato et al., 2012) mainly considering short time period of analysis. Otherwise, Treviso has not been studied yet and it is characterized by very high pollution phenomena.

Figure 1 shows the sampling sites location. The first is located inside the "Marco Polo" airport (45°30'40''N, 12°20'38''E – Tessera, Venice - Italy), on the border of the Venice Lagoon that is a complex and sensitive ecosystem. The second one is located near Treviso (45°41'03''N, 12°05'15''E – Treviso – Italy), one of the most important city in the Veneto Region.

Figure 1. 'Marco Polo' and 'Antonio Canova' airports location.

Both the sites are situated in the North-Eastern part of Italy between the Po Valley (that is recognized as one of the most polluted area in Europe) and the Adriatic Sea. In this area the two airports represent a strategic point from the touristic and the commercial point of view. Unfortunately, their location, near to several emission sources, can be sensitive respect to air pollution causing direct and indirect contributions.

In order to better assess airport contribution a parallel monitoring campaign has been developed in the two airports and a lagrangian model, SPRAY (Tinarelli et al., 1994), has been used to estimate aircraft pollutant dispersion area.

Results have been correlated to the meteorological conditions and to the local emission sources scenario that characterizes the two urban sites. Modelled data have been compared with measurements in order to check aircraft emission fall out in the area. All the data have been used to compare the two airports impact on the respective urban area.

In order to check Venice airport impact on local urban area a specific case have been studied in this site during 2009. An eulerian photochemical model have been applied in order to assess the interaction among the several emission sources and to check Marco Polo airport contribution. Predicted data showed good performance of the model for all the area and aircraft contribution appears scarce respect to the other sources. High level reached is strongly connected with the presence of a heavy-traffic road near the Venice airport. In this view, a road transport modellization have been conducted to compare traffic impact respect to airport emissions. The strong pollutant peaks seems to concur with traffic jams.

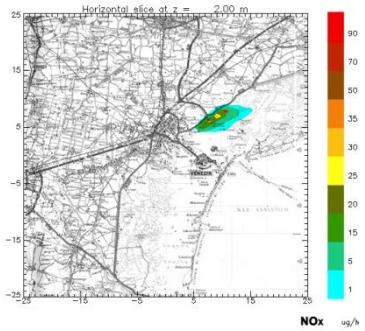

Figure 2. Road traffic dispersion near Treviso airport.

References:

Tinarelli, G., Anfossi, D., Brusasca, G., Ferrero, E., Giostra, U., Morselli, M.G., Moussafir, J., Tampieri, F. and Trombetti F. (1994) J. Appl. Meteorol. 33, 744–756.

Pecorari, E., Squizzato, S., Masiol, M., Radice, P., Pavoni, B. and Rampazzo G. (2013) Sci. Total Environ. 443, 681-691.

Squizzato, S., Masiol, M., Brunelli, A., Pistollato, S., Tarabotti, E., Rampazzo, G. and Pavoni, B. (2013) Atmos. Chem. Phys. 13, 1927-1939.

A methodology to assess occupational exposure to MNMs by modelling

M. Pilou[1], T. Oroz[2], C. Vaquero Moralejo[3], P. Neofytou[1] and C. Housiadas[1]

[1]Thermal-Hydraulic Analysis & Multiphase Flows Laboratory, INRAESTES,
NCSR "Demokritos", Ag.Paraskevi, Attiki, 15310, Greece
[2]Navarrean Nanoproduct Technology, TECNAN , Los Arcos, Navarra, 31210, Spain
[3]Manufacturing Engineering Department, Industrial Systems Unit, Tecnalia Research and Innovation,
Miñano, Àlava, 01510, Spain
Keywords: CFD modelling, occupational exposure, MNPs
Presenting author email: pilou@ipta.demokritos.gr

Despite the toxicological effects of certain construction and industry related manufactured nanomaterials (MNMs) (Lee *et al*, 2010) and the subsequent human exposure from their dispersion according to certain working situations (van Broekhuizen *et al*, 2011) there is a lack of modelling efforts towards understanding the relevant dispersion aspects and estimating the internal doses for workers.

In the present work different computational models, both in-house and commercial, are integrated in a single methodology in order to estimate occupational exposure to MNMs by inhalation.

In particular, the following three steps describe the modelling process. First, air velocity, pressure and temperature fields are calculated using the commercial computational fluid dynamics (CFD) package ANSYS CFX. The k-ε model is employed for turbulence modelling.

In the second step, the obtained airflow field is used to determine the dispersion of MNMs in space using the CFD-based in-house code of Pilou *et al* (2011). This is a three dimensional, fully Eulerian, mechanistic model that incorporates the effects of particle convection, Brownian and turbulent diffusion, and thermophoresis, as well as the effects of particles inertia and gravitational settling.

In the third and final step, the one dimensional, Eulerian, mechanistic model of Mitsakou *et al* (2006) is used for calculation of particle transport and deposition in the human respiratory tract. In particular, the concentration of particles at the breathing zone of the workers, obtained in the previous step, is the input to the model, and as a result the internal dose of MNMs in the different regions of the human lung is obtained.

The developed methodology is used in order to estimate occupational exposure to MNMs by inhalation in a realistic environment. In particular, we demonstrate the capabilities of the integrated model by determining the deposition of particles in the respiratory tract of workers in a MNMs production and handling site. Results of air flow field and particle distribution in the production site as well as internal doses of inhaled MNMs for the workers at different working stations will be given.

Overall, to the authors' opinion, the proposed integrated methodology could serve as a valuable support decision tool in order to minimize the risks of occupational exposure to potentially harmful MNMs.

This work is supported by project SCAFFOLD under Project No. 280535 of the European Commission.

van Broekhuizen, P., van Broekhuizen, F., Cornelissen, R. and Reijnders, L. (2011) *J Nanopart Res*, **13**, 447–462

Lee, J., Mahendra, S. and Alvarez, PJJ. (2010) *ACS Nano*, **4**, 3580-3590.

Mitsakou, C., Helmis, C. and Housiadas, C. (2005) *J Aerosol Sci*, **36**, 75-94.

Pilou, M., Tsangaris, S., Neofytou, P., Housiadas, C. and Drossinos, Y. (2011) *Aerosol Sci Tech*, **45**, 1376-1387.

The charging of amine containing clusters using protonated acetone

K. Ruusuvuori[1], P. Hietala[1], O. Kupiainen[1], T. Kurtén[2] and H. Vehkamäki[1]

[1]Division of Atmospheric Sciences, Department of Physics, P.O.Box 64, FI-00014 University of Helsinki, Finland
[2]Laboratory of Physical Chemistry, Department of Chemistry, University of Helsinki, P.O. BOX 55, FI-00014, Finland
Keywords: Nucleation, modelling, acetone, amines.
Presenting author email: kai.ruusuvuori@helsinki.fi

Nucleation is one of many important atmospheric processes. While the initial steps of atmospheric new particle formation generally require sulfuric acid (Sipilä *et al*, 2010), it is typically not enough to explain observations by itself. This means that some other condensing vapours are needed. The role of amines in this new particle formation has been the subject of recent studies and it has been suggested that they may play an important role, at least in the lower atmosphere (Kirkby *et al* 2011, Petäjä *et al*, 2011).

Our aim is to study if protonated acetone (monomers and dimers) can be successfully used to charge amine containing clusters with and without sulphuric acid. Understanding the possible reaction pathways will give us important insight on amine measurements performed using an acetone based Chemical Ionization Atmospheric Pressure interface Time-Of-Flight mass spectrometer (CI-APi-TOF).

The quantum chemical calculations are performed using standard off-the-shelf quantum chemistry programs such as Gaussian 09 and Turbomole (version 6.3.1). Geometries, standard enthalpies (eg. at 298.15 K and 1 bar), Gibbs free energies of formation and evaporation rates for clusters are obtained as described in the paper by Ortega *et al* (2012).

Initial results suggest that the use of protonated acetone in the charging of amine containing clusters is viable. Data analysis concerning the concentrations of different cluster types before and after charging is still ongoing.

We thank the CSC – IT Center for Science Ltd. for computer time and technical assistance. We also thank Dr. Mikael Ehn for his assistance. The financial support by the Academy of Finland (Centre of Excellence program Project No. 1118615 and LASTU program project number 135054) and ERC StG 257360-MOCAPAF is gratefully acknowledged.

Sipilä, M., Berndt, T., Petäjä, T., Brus, D., Vanhanen, J., Stratmann, F., Patokoski, J., Mauldin III, R. L., Hyvärinen, A.-P., Lihavainen, H. and Kulmala, M. (2010) *Science* **327**, 1243–1246.

Kirkby, J., Curtius, J., Almeida, J., Dunne, E., Duplissy, J., Ehrhart, S., Franchin, A., Gagné, S., Ickes, L., Kürten, A., Kupc, A., Metzger, A., Riccobono, F., Rondo, L., Schobesberger, S., Tsagkogeorgas, G., Wimmer, D., Amorim, A., Bianchi, F., Breitenlechner, M., David, A., Dommen, J., Downard, A., Ehn, M., Flagan, R. C., Haider, S., Hansel, A., Hauser, D., Jud, W., Junninen, H., Kreissl, F., Kvashin, A., Laaksonen, A., Lehtipalo, K., Lima, J., Lovejoy, E. R., Makhmutov, V., Mathot, S., Mikkilä, J., Minginette, P., Mogo, S., Nieminen, T., Onnela, A., Pereira, P., Petäjä, T., Schnitzhofer, R., Seinfeld, J. H., Sipilä, M., Stozhkov, Y., Stratmann, F., Tome, A., Vanhanen, J., Viisanen, Y., Vrtala, A., Wagner, P. E., Walther, H., Weingartner, E., Wex, H., Winkler, P. M., Carslaw, K. S., Worsnop, D. R., Baltensperger, U. and Kulmala, M. (2011) *Nature* **476**, 429–433.

Petäjä, T., Sipilä, M., Paasonen, P., Nieminen, T., Kurtén, T., Ortega, I. K., Stratmann, F., Vehkamäki, H., Berndt, T. and Kulmala, M. (2011) *Phys. Rev. Lett.* **106**, 228302.

Ortega, I. K., Kupiainen, O., Kurtén, T., Olenius, T., Wilkman, O., McGrath, M. J., Loukonen, V. and Vehkamäki, H. (2012) *Atmos. Chem. Phys* **12**, 225-235.

Influence of the inlet particle diameter distribution on the experimental determination of cyclone collection efficiency

B. Sagot and J. Giardi

[1]Thermo-Fluids Laboratory, ESTACA, 92300, Levallois-Perret, France
Keywords: cyclone separator, collection efficiency, particle diameter distribution.
Presenting author email: benoit.sagot@estaca.fr

The aim of this experimental study is to investigate the influence on a cyclone collection efficiency determination of the inlet particle diameter distribution. The internal diameter of the cyclone has been fixed to a given value of 30 mm, which is a typical size of these devices when they are used for the separation of oil mist from blow-by gases, in internal combustion engines. To reproduce the flow rates and temperature operating conditions (80°C) of combustion engines, we developed a temperature controlled flow bench, with a polydisperse aerosol generator producing engine oil droplets with diameter in a 0.3-10 µm range.

Measurements of the aerosol particle concentrations upstream and downstream of the cyclone permitted the determination of the particle collection efficiency, with flow rates ranging from 56 to 262 Nl/min which are typical operating conditions. During this study, we observed classically that for any given value of the flow rate, the collection efficiency increases with the particle diameter, to reach a value close to 100%. While in most of the practical applications, this grade-efficiency curve takes a smooth "S" shape, with low values of the collection efficiency for small particle diameters, we observed however that a minimum in the grade-efficiency curve exists for high values of the flow rate, with an increase of the collection efficiency for low values of the particle diameter. Such experimental results have already been observed by Abrahamson and Allen (1986), and the shape of the curve is described as a "tail" by Hoffmann & Stein (2002). The aim of this experimental study is to investigate the influence of the particle load on the grade efficiency curve, and particularly on the intensity of the "tail" for small diameter particles.

As an illustration, for a fixed flow rate with a given value of 100 Nl/min, and a fixed particle mass load of 125 mg/m³, we changed the oil in the aerosol generator, and the corresponding measurements of the collection efficiency are reported in figure 1, together with the dimensionless particle number distribution dN/N. As observed, the aerosol generated with engine oil is composed with a fraction of large particles significantly higher than for DEHS, and measurements obtained with DEHS demonstrate a high reduction of the "tail" in the collection efficiency curve observed for small particles with diameter below 1 µm.

These measurements seem to confirm the explanation proposed by Cortés & Gil (2007) who suggested that this tail could be attributed to a swept of the small particles by the larger particles inside the vortex: when we modify the particle number distribution with an increase in the fraction of small particles, the collection efficiency of the fine particles reduces, suggesting that the entrainment mechanism has been reduced.

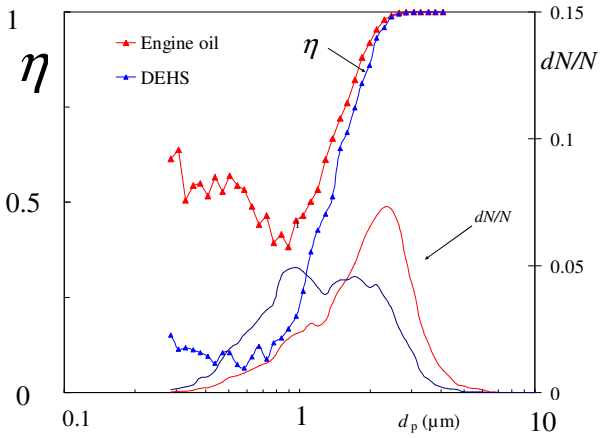

Figure 1. Collection efficiency measurements, for a fixed flow rate of 100 Nl/min..

To further investigate the influence of the inlet particle diameter distribution on the collection efficiency, we used different cyclones, associated in series, to cut the large diameter particles from the inlet distribution.

We observed a significant reduction in the "tail", by removing from the distribution the large particles. These measurement results will be detailed in the submitted paper. This result suggests that the collection efficiency of cyclones should be carried out with polydisperse aerosols, and with particle-size distributions that correspond to real-life conditions of use of the cyclone.

Abrahansen, J. and Allen, R. W. K. (1986) The efficiency of conventional return-flow cyclones at high temperatures. *American Institute of Chemical Engineers Journa*l **99**, 31-43.

Cortés, C. and Gil, A. (2007) Modeling the gas and particle flow inside cyclone separators. *Progress in Energy and Combustion Science* **33**, 409-452.

Hoffmann, A. C. and Stein, L. E. (2002) *Gas Cyclones and Swirl Tubes. Principles, Design and Operation*, Springer, New York.

Novel informatics software for automated individual aerosol component property predictions and complex ensemble predictions – an online community facility

D. Topping[1,3], M. Bane[2], M. Barley[3], D. Lowe[3], R. Pinning[2] and G. McFiggans[3]
[1]National Centre for Atmospheric Science, University of Manchester, Manchester, UK
[2]IT Services, University of Manchester, Manchester, UK
[3]Centre for Atmospheric Science, University of Manchester, Manchester, UK
Keywords: Aerosol modeling, Organic aerosols, Informatics.
Presenting author email: david.topping@manchester.ac.uk

Introduction:
Atmospheric aerosols are known to be an important yet highly uncertain component of the earth's climate and air quality (Solomon et al 2007). Owing to the complexity and diversity of atmospheric aerosol components, quantification of the properties that determine their highly uncertain climatic and human health impacts requires the development of novel technological applications. Inorganic material is restricted to a few well-understood compounds. However, organic material can comprise many thousands, as yet largely unidentified, compounds with a vast range of properties.

We must be able to predict however many thousands of components can exist in particulate matter. Predicting the evolution of aerosol requires calculating the distribution of all components between the gas and aerosol phase. This requires knowledge of all component vapour pressures and other thermodynamic properties. The many thousands of individual aerosol components ensure that explicit manual calculation of these properties is laborious and time- consuming. The emergence of explicit automatic mechanism generation techniques (Aumont, 2005; Jenkin, 2003) including up to many millions of individual gas phase products as aerosol precursors renders the process impossible and automation is necessary.

It can require significant resource to develop methods for automating these processes, but also to develop efficient numerical frameworks that drive the complex calculations. In this presentation we showcase development and application of a new online facility that combines benchmark aerosol models with open source informatics software to provide a new community service.

The model system:
The facility is written in python, a high-level language is widely used as a scripting language for web applications. It supports both fixed-point and floating-point numeric calculations, string manipulation and facilities for structures and multi-dimensional arrays. It is distributed under a permissive free software license and is available for all major operating systems, which will enable our software to be highly portable. Also, a PYTHON interface has been developed for the chemical informatics software of our choice (Open Babel) as described by O'Boyle et al (2008).
The SMILES chemical informatics syntax is used to automate extraction of molecular substructure information from individual compound identifiers (figure 1). Commonly employed in commercial and public software, it can be imported by most molecular editors and has a wide base of software support and extensive theoretical backing (www.daylight.com).

We will demonstrate the need for developing libraries that capture all functionality of compounds expected in the atmosphere, a problem that occurs in other available online services used by the community.

Example applications:
Important uncertainties are in those parameters which dictate the aerosol water content and gas / aerosol partitioning. To this end we will demonstrate the use of this facility to calculate fundamental properties, such as pure component vapour pressures, for an unlimited set of compounds. Absorptive partitioning simulations carried out on the facility will demonstrate the ability to predict secondary organic aerosol loading and composition using output from complex gas phase degradation mechanisms. Specifically we will use output from the Master Chemical Mechanism (MCM Jenkin (2003)) to simulate the detailed composition of aerosol in multiple scenarios.

Future outlook:
The facility is also designed to act as a springboard for collaborative purposes, the inclusion of specific visualization techniques enabling the modeling and measurement community to directly compare outputs from models and instruments. In addition we will present progress on using GPGPUs (General purpose graphical processing units) to obtain large increases in computational performance on the complex models hosted on the website. This is an exciting area of research and is already being explored for chemical models that are often heavily reduced to reduce numerical complexity.

This work is supported by the National Centre for Atmospheric Science (NCAS), NERC grant NE/H002588/1 and NERC grant NE/J013471/1.

Aumont, B., Szopa, S., and Madronich, S. Atmos. Chem. Phys., 5, 2497-2517, (2005).
Jenkin, M. E., Saunders, S. M., Wagner, V., and Pilling, M. J.: Atmospheric Chemistry and Physics, 3, 181-193, (2003).
O'Boyle,N.M. Morley, C., and Hutchison, G. R.: Chem. Cent. J., 2, 1–7. (2008).
Solomon, S., Qin, D., Manning, M., Chen, Z., Marquis, M., Averyt, K. B., Tignor, M., and Miller, H. L., IPCC: Climate change 2007

Modeling global secondary organic aerosol formation and growth: Integrating the volatility basis set into the EMAC chemistry climate model

A.P. Tsimpidi[1], V.A. Karydis[1], S.N. Pandis[2,3] and J. Lelieveld[1,4]

[1]Max Planck Institute for Chemistry, Mainz, 55128, Germany
[2]Department of Chemical Engineering, University of Patras, Patras, Greece
[3]Department of Chemical Engineering, Carnegie Mellon University, Pittsburgh, PA 15213, USA
[4]Energy, environment and water research Center, Cyprus Institute, Nicosia, 1645, Cyprus

Keywords: Organic Aerosols, Chemistry Climate Models, Volatility Basis Set, Secondary Organic Aerosols.
Presenting author email: a.tsimpidi@mpic.de

Organic compounds are an important constituent of atmospheric particulates. Depending on the region it contributes 20 to 90% to the total submicron particulate mass (Zhang et al., 2007). However, organic aerosol sources, atmospheric processing, and removal are very uncertain. This study aims to improve the description of organic aerosols suitable for large-scale modelling, making use of recent developments based on laboratory and field measurements. The volatility basis set, VBS (Tsimpidi et al., 2010;Lane et al., 2008), a computationally efficient framework for the description of organic aerosol partitioning and chemical aging, is implemented in the ECHAM/MESSy Atmospheric Chemistry (EMAC) model (Jöckel et al., 2006) to simulate secondary organic aerosol (SOA) formation. SOA formation from monoterpenes, sesquiterpenes, isoprene, and anthropogenic precursors will be estimated, respectively. The new OA module suggests that the semi-volatile products of the VOC oxidation reactions are grouped by their effective saturation concentration into four aerosol species. The aerosol yields used for the production of the four SOA species were measured during recent smog chamber experiments and are also given in Table 1. This four-product set was suggested by Lane et al. (2008) as being satisfactory for the representation of biogenic and anthropogenic organic matter for urban and regional pollution modeling. The new OA module also assumes that the semi-volatile organics in the gas phase continue to react with the OH radical. These chemical reactions can lead to continued SOA formation even after complete precursor consumption and may become a major source of SOA (Murphy and Pandis, 2009;Tsimpidi et al., 2010). Different assumptions regarding the water solubility of secondary organic gas, the temperature sensitivity of SOA, and the chemical aging of anthropogenic SOA by gas-phase reaction with the hydroxyl radical, have been explored. The new organic aerosol module is tested in long-term simulations covering the years 2005-2008. Model predictions with and without SOA aging are compared with data from the European Monitoring and Evaluation Programme (EMEP), the Clean Air Status and Trends Network (CASTNet), the Acid Deposition Monitoring Network in East Asia (EANET), as well as with results from the global aerosol mass spectrometer (AMS) dataset (Zhang et al., 2007). The possibility of high anthropogenic SOA production rates, that may challenge the assumption that anthropogenic volatile organic compounds are SOA precursors of minor importance on a global scale, will be investigated.

Table 1. SOA yield scenarios using a four-product basis set with saturation concentrations of 1, 10, 100, and 1000μg m^{-3} at 298 K.

SOA precursors	SOA Yields (μg m^{-3}/μg m^{-3})			
	1	10	100	1000
Higher Alkenes	-	-	0.3	-
Terminal Alkenes	0.005	0.009	0.060	0.225
Internal Alkenes	0.023	0.044	0.129	0.375
Toluene	0.011	0.257	0.750	0.964
Xylene	0.075	0.3	0.375	0.525
Monoteprenes	0.107	0.092	0.359	0.600
Sesquiterpenes	0.075	0.150	0.750	0.900
Isoprene	0.009	0.030	0.015	0.000

References

Jöckel, P., Tost, H., Pozzer, A., Bruehl, C., Buchholz, J., Ganzeveld, L., Hoor, P., Kerkweg, A., Lawrence, M. G., Sander, R., Steil, B., Stiller, G., Tanarhte, M., Taraborrelli, D., Van Aardenne, J., and Lelieveld, J. (2006) *Atmos. Chem. Phys.*, 6, 5067-5104.

Lane, T. E., Donahue, N. M., and Pandis, S. N. (2008) *Atmos. Environ.*, 42, 7439-7451.

Murphy, B. N., and Pandis, S. N. (2009) *Environ. Sci. & Tech.*, 43, 4722-4728.

Tsimpidi, A. P., Karydis, V. A., Zavala, M., Lei, W., Molina, L., Ulbrich, I. M., Jimenez, J. L., and Pandis, S. N. (2010) *Atmos. Chem. Phys.*, 10, 525-546, 2010.

Zhang, Q., Jimenez, J. L., Canagaratna, M. R., Allan, J. D., Coe, H., Ulbrich, I., Alfarra, M. R., Takami, A., Middlebrook, A. M., Sun, Y. L., Dzepina, K., Dunlea, E., Docherty, K., DeCarlo, P. F., Salcedo, D., Onasch, T., Jayne, J. T., Miyoshi, T., Shimono, A., Hatakeyama, S., Takegawa, N., Kondo, Y., Schneider, J., Drewnick, F., Borrmann, S., Weimer, S., Demerjian, K., Williams, P., Bower, K., Bahreini, R., Cottrell, L., Griffin, R. J., Rautiainen, J., Sun, J. Y., Zhang, Y. M., and Worsnop, D. R. (2007) *Geoph. Res.h Let.*, 34, L13801.

Source apportionment of $PM_{2.5}$ concentrations: comparison of source-oriented and receptor-oriented techniques

G. Pirovano[1], C. Colombi[2], G. Lonati[3], A. Balzarini[1] and G.M. Riva[1]

[1] RSE Spa, via Rubattino 54 - 20134 Milano, Italy
[2] ARPA Lombardia Settore Monitoraggi Ambientali, via Juvara 22 – 20129 Milano, Italy
[3]DICA Politecnico di Milano, P.za L. da Vinci 32 – 20133 Milano, Italy
Keywords: source apportionment, chemistry transport models, receptor models, Po valley.
Presenting author email: guido.pirovano@rse-web.it

Airborne particulate matter is a complex mixture of both primary and secondary compounds, produced by several kinds of anthropogenic and natural sources, as well as by various chemical and physical processes in the atmosphere. Thus, the development of effective air quality policies requires a thorough knowledge of the role played by the different emission sources. Broadly speaking, both source-oriented and receptor-oriented approach can be applied for source apportionment (SA), to estimate these different contributions.

This work compares the SA results produced by two implementations of these approaches for $PM_{2.5}$ in the Po valley (Northern Italy), selected as case study due to its very critical conditions, with frequent exceedances of the air quality standards. Receptor modelling analysis has been performed using the Chemical Mass Balance model version 8.2 (U.S. E.P.A., 2004), fed with local source profiles (Colombi et al. 2010). $PM_{2.5}$ composition data were derived from a multi-year field campaign covering 2003-2007 (PARFIL Project). Source oriented analysis has been performed by means of the CAMx chemistry transport model, that implements PSAT (Yarwood et al., 2004), a powerful source apportionment algorithm. CAMx model was implemented for the calendar year 2005 over a 5 km resolution domain covering the whole Po valley. A set of 28 source categories was tracked including: road transport sector split according to the fuel, residential heating, energy production and agriculture. CMB source profiles were used as $PM_{2.5}$ emission speciation profiles by CAMx.

SA results from CMB and CAMx model at different receptors located at both urban and rural sites are presented and issues related to the comparison methodology are discussed. As an example, Figure 1 shows the results obtained for an urban receptor site in Milan for the winter season. $PM_{2.5}$ mass concentrations reconstructed by CMB was very close to the observed one, while CAMX partially underestimated it (-15%) CAMx results showed contributions to the $PM_{2.5}$ winter mean of 27% from road transport, 12% from biomass domestic heating, 52% from secondary sources; corresponding CMB results were 46% for road transport, 7% for biomass heating, 44% for secondary sources.

General conclusions stemming from the comparison of SA results at the different sites were:

- CAMx tends to underestimate the $PM_{2.5}$ observed mass concentration more than CMB; such discrepancy seems mainly related to a missing primary $PM_{2.5}$ fraction than to the accuracy in the modelling of the secondary fraction.
- Both models showed a better agreement in winter than in summer, suggesting that on low concentration conditions SA results are less reliable than on polluted situations.

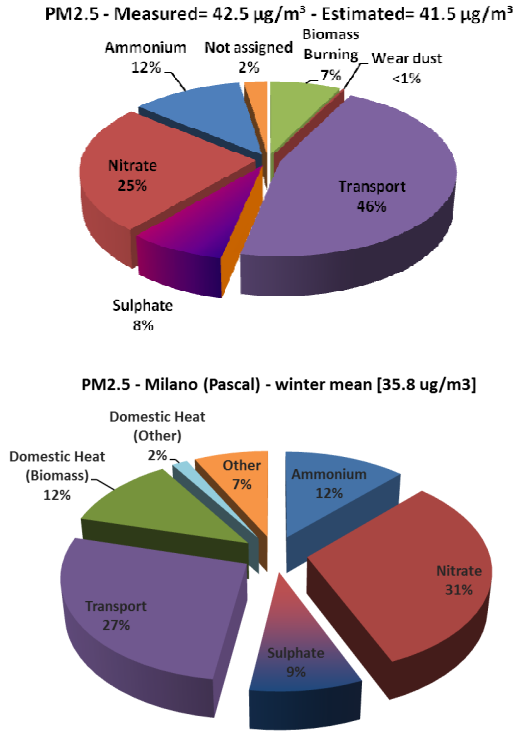

Figure 1. Comparison of PM2.5 source apportionment results at Milan receptor obtained by CMB (top) and CAMx/PSAT (bottom) for the winter season.

ENVIRON (2011) *CAMx User's Guide Version 5.4.* ENVIRON International Corporation, Novato, CA.

Yarwood, G., Morris, R.E., Wilson, G.M., (2004) *Proceedings of the 27th NATO/ CCMS conference*. Springer Verlag.

U.S. E.P.A., 2004. EPA-*CMB8.2 Users Manual*. EPA-452/R-04-011,

Colombi C., Gianelle V., Belis C., Larsen B, (2010) *Chem. Eng. Transactions*, Vol. 22.

Periodic changes in the parameters of finite coagulating systems with sources and sinks at steady state regime approach

V.A. Zagaynov[1], A. Maslov[1], A.A.Lushnikov[1], I.E. Agranovski[1,2], A.B. Leontyev[1], Yu.G. Biryukov[1]

[1] Karpov Institute of Physical Chemistry, Vorontsovo Pole 10, Moscow, 105064, Russia
[2] Griffith School of Engineering, Griffith University, Brisbane, 4111 QLD, Australia
Keywords: aerosol system oscillations, nucleation
Presenting author email: zagaynov@cc.nifhi.ac.ru

As is known, finite coagulating systems with sources and sinks could reach steady state regimes. At the stage, when a system is approaching such regime, its parameters are not necessarily change smoothly; some periodic changes (McGrow, and Saunders (1984), Badger, and Dryden (1939)) could occur along the transition period. Smoluchowski equation could be written to account for these fluctuations:

$$\frac{\partial c_1}{\partial t} = I - \sum_{n=1}^{G} K_{1n} c_1 c_n , \qquad (1)$$

$$\frac{\partial c_g}{\partial t} = \frac{1}{2}\sum_{n=1}^{g} K_{n,g-n} c_n c_{g-n} - c_g \sum_{n=1}^{G} K_{g,n} c_n , \qquad (2)$$

where c_g – particle concentration, $K_{g,n}$ – frequency of collisions of particles consisting g and n monomers with resulting formation of particle with $(g+n)$ monomers, I – speed of monomer supply from the source to the atmosphere per unit of time and unit of volume, and G is a maximum particle size produced in the system.

Particles larger than G are removed from the system and do not further participate in the system evolution. Some stationary particle size distribution is possible in such systems. If $G \to \infty$, time required to reach such distribution becomes indefinitely long. Direct integration of this system of differential equations provides the results clearly showing parameters' oscillations during steady state regime approach. Detailed information about periodic changes may be obtained by asymptotic properties of the equation system. To this end let us linearize the system near steady state point and find eigen values of the matrix. Its real parts give damping decrement of time dependence curve and image parts give oscillation frequencies, which linear combination shows deviations of time dependence from asymptotic line.

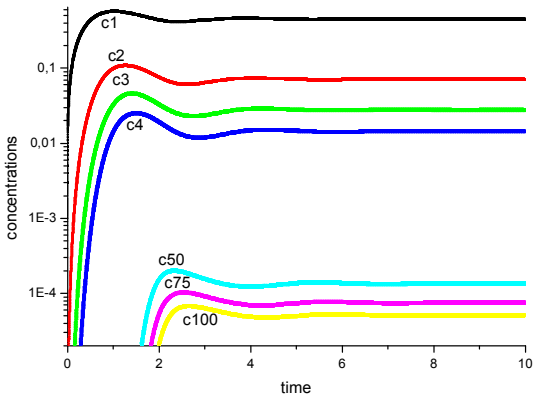

Figure 1. Oscillations of concentration of particles consisting of different numbers of monomers c_1 – c_4 and c_{50} –c_{100} (superscripts represent numbers of monomers) for $K_{ij}=i+j$; G =100 and dimensionless time.

The method was applied to equation system (1). Such estimates were made for model nuclei ($K_{ij}=1$; $K_{ij}=i+j$) and free molecular regime.

The results demonstrated that complex solutions of the abovementioned algebraic equations correspond to oscillation attenuation and frequencies, which are observed in solutions of the corresponding differential equation.

To extend the suggested approach enabling it to cover larger sizes, a model with coincidence of linear and logarithmic size scales has been built. This procedure was proven to be capable of modeling real processes occurring in the atmosphere.

McGrow, R. and Saunders J. H. (1984). *Aerosol Sci. Tech.* **4**, 367 – 380.
Badger, T.H.M. and Dryden, I.G.C. (1939). *Trans. Faraday Soc.* **35**, 607.

Efficiency of inertial capture of aerosol particles by porous fiber in cylinder array

[1]S.K. Zaripov, [2]O.V. Grigorieva, [1]S.A. Soloviev
[1]Kazan Federal University, Kazan, Russia
[2]Kazan State Power University, Kazan, Russia

Keywords: inertial capture, capture efficiency, porous cylinder, CFD
Presenting author email: shamil.zaripov@kpfu.ru

The problem of motion of aerosol particles in the air flow through periodic arrays of porous cylinders is numerically solved. The efficiency of inertial capture of particles is studied by varying the parameters of porous cylinders and the dispersed phase.

Problem of the motion of dispersed flow in porous structures is of practical importance due to their applications in air purification devices. The possibility of using porous bodies as elements of porous structures was discussed in Kirsh (2007).

A two-dimensional flow of an incompressible gas with suspended aerosol particles in the flow through an array of porous cylinders with radius r_c is considered. In the assumption that the particle concentration is small, the influence of the dispersed phase on the air flow is neglected. The air motion around the cylinder and in the porous area is described by the equations (Bhattacharyya et.al., 2006):

$$\nabla \bar{u} = 0 \qquad (1)$$

$$\varepsilon^{-2} \rho \bar{u} \nabla \bar{u} = -\nabla p + \frac{\mu}{\varepsilon} \Delta \bar{u} - b \frac{\mu}{k} \bar{u} \qquad (2)$$

where $\bar{u}$ is the gas velocity, μ and ρ are the dynamic viscosity and air density, p is the pressure, ε is the porosity, k is the permeability of the porous medium. The parameter b equals to zero outside the cylinder and to one inside the cylinder. The gas velocity $\bar{u}$ averaged over the volume of pore space is related to the flow rate, $\bar{u}_f$, by $\bar{u} = \varepsilon \bar{u}_f$.

On the left boundary of the periodic computational domain the free-stream velocity U_0 is given. On the right outer boundary the zero pressure is given. Centerline of the computational domain both outside and inside the porous cylinder corresponds to symmetry conditions. Equations of the carrier phase motion (1-2) are solved by the finite volume method using a CFD code, FLUENT. The flow field was also described analytically using the Kuwabara cell model for porous cylinder (Stechkina, 1979, Kirsh, 2007). The equations of motion of suspended particles are numerically integrated in the obtained velocity field. The particulate flow is characterized by the dimensionless parameters: the Reynolds number $\mathrm{Re} = \rho U_\infty 2r_c / \mu$ (U_∞ – velocity of the undisturbed flow), the Darcy number $\mathrm{Da} = k / r_c^2$, the Stokes number $\mathrm{St} = U_\infty / r_c \tau$ (τ – the relaxation time of a particle).

To calculate the capture efficiency E_e the particle trajectories are traced outside the porous cylinder. The value E_e is calculated as the ratio of the number n_d of particles, which reached the surface, to the total number n_t of started particles: $E_e = n_d / n_t$. The dependencies of E_e on the Stokes number at given values of solidity α=1-ε=0.05 and various Darcy numbers, obtained on the base of numerical and analytical fluid flow models, are presented in fig.1. Lines 1,3,5 and 2,4,6 correspond to the numerical and Kuwabara models. Lines 1-2,3-4,5-6 correspond to Da=0,10^{-2}, 10^{-1}. In the absence of the gas flow through the cylinder (solid cylinder) the efficiency of inertial deposition decreases to zero at the finite Stokes number. For the porous cylinder, at sufficiently small values of St the value E_e remains finite. An increase of the Darcy number leads to a noticeable growth of the value E_e, for example, for the cylinder with the Darcy number Da=0.1 the value E_e is equal ~0.17 at St=0.1. The dependencies of E_e(St) at Da=0.1 for α=0,0.01,0.05 are shown in fig.2. The value E_e is larger at small St for larger α.

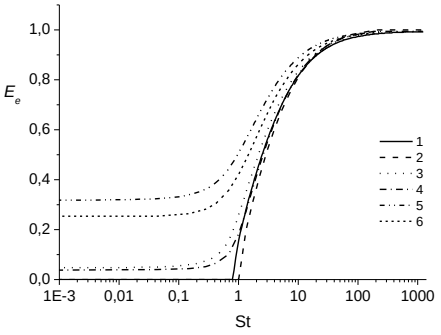

Fig. 1.

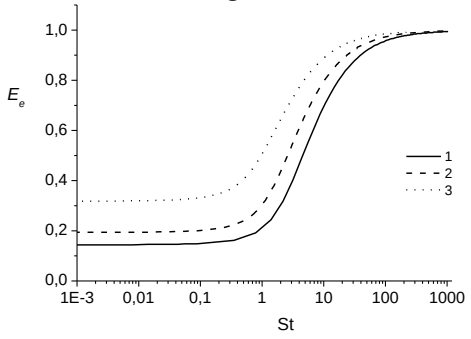

Fig. 2.

The work was supported by the RFBR (grants № 12-01-00333, 12-07-00007).

REFERENCES

Bhattacharyya S., Dhinakaran S., Khalili A. **(**2006) *Chemical Engineering Science*, **61**, 4451–4461.

Kirsh V.A. (2007) *Separation and Purification Technology*, **58**, 288–294.

Stechkina I.B. (1979) Izv.AN USSR, Fluid Mechanics, **6**, 122-124 (in Russian).

Tuesday, September 3, 2013

Poster session B,
Aerosol-based Nanotechnology, Posters B126 – B166

Direct Transfer of Aerosol Particles into Liquid Suspensions

C. Anderlohr[1], K. Schaber[1]

[1]Institute for Technical Thermodynamics and Refrigeration, Karlsruhe Institute of Technology, Karlsruhe, 76131, Germany
Keywords: Silica, Stabilization, Wet-Electrostatic-Precipitation, Flame-Synthesis, Suspension
Presenting author email: christopher.anderlohr@kit.edu

Nanoparticles produced by gas phase processes are usually precipitated in (baghouse-) filters forming a more or less agglomerated powder.

However, in many cases the final application of these particles is not as a powder but as a liquid suspension, i.e. printable electronics, heterogeneous catalysis, paints etc. This necessitates the dispersion of the particles into a liquid before use.

In this work the direct transfer of SiO_2 nanoparticles generated by a lab scale flame reactor into aqueous suspensions by means of a wet electrostatic precipitator (WESP) and particle stabilization in the liquid are studied.

Wet electrostatic precipitation is an energy efficient possibility for gas cleaning with high removal efficiencies. WESPs are employed in numerous industrial applications, i.e. the control of acid mist, the precipitation of sticky or high resistivity aerosol particles, or when fire hazard is an issue. Recently, there have also been approaches of using WESPs for emission control of diesel particulate matter from stationary diesel generators (Saiyasitpanich, 2007).

Different from dry type electrostatic precipitators, particles collected on the precipitation electrode are not removed by intermittent rapping, but are washed off by a liquid flushing the electrode. In the common processes the precipitated particles are usually removed from the flushing liquid before it is redistributed onto the collection electrodes (Parker, 1997). The aim of this study, rather than extracting the particles from the liquid, is to produce a stable suspension of product particles, which can be used directly for its later application.

The aerosol particles produced in the gas phase in our setup exhibit little to no agglomeration. Thus, if the single particles can be precipitated directly into the liquid, no additional energy for dispersion and deagglomeration is necessary in order to create a stable suspension. Thus the particle size distribution (PSD) should be preserved during the transfer.

During the experiments the PSDs in the liquid suspension are measured by Photon Correlation Spectroscopy (PCS) as well as with the novel Liquid Nanoparticle Sizer (LNS) technique by TSI. These data are compared to the SMPS-measurements of the aerosol size distributions. It is shown that direct particle transfer into suspensions with merely minor changes to the PSD is possible (Fig. 1). These suspensions can be stable for several weeks before exhibiting any signs of degradation.

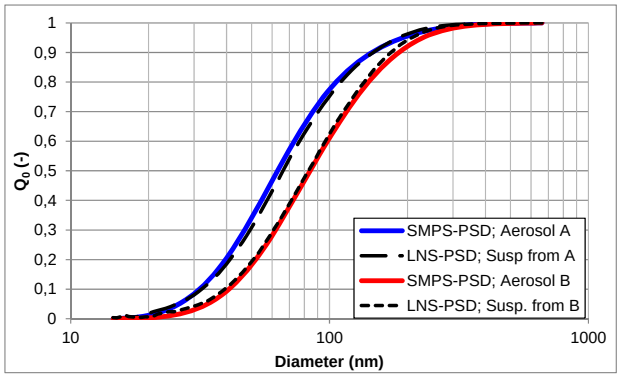

Figure 1: LNS-PSDs of SiO_2 nanoparticles in liquid suspension with the SMPS-PSDs of the corresponding aerosols before precipitation.

For possible industrial application it is desirable to produce suspensions with a high solid content. In order to achieve high particle concentrations, the suspension is recirculated in the WESP. The influences of residence time and concentration are studied (Fig. 2).
Furthermore, the effects of pH-value, salt concentration and stabilizing agents in the circulated liquid on stabilization are investigated.

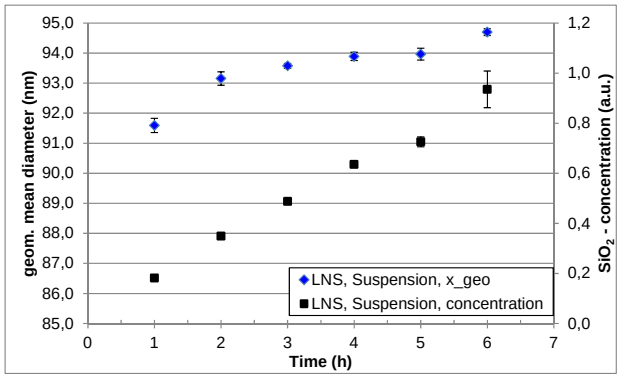

Figure 2: Progression of geom. mean diameter and particle concentration over time, during precipitation in the WESP.

Parker, K. (1997) *Applied Electrostatic Precipitation*, Blackie Academic & Professional, Great Britain.
Saiyasitpanich, P. (2007) *Journal of Electrostatics.* **65**, 618-624.

Dependency of particle size on filtration mechanisms of nanofiber web

Hyun-Jin Choi[1,3], Sang Bum Kim[1], Sung Hyun Kim[3] and Myong-Hwa Lee[2,*]

[1]Green Process and Material R&D Group, Korea Institute of Industrial Technology, Cheonan-si, Chungnam 331-822, Republic of Korea
[2]Energy System R&D Group, Korea Institute of Industrial Technology, Cheonan-si, Chungnam 331-822, Republic of Korea
[3]Department of Chemical and Biological Engineering, Korea University, Seoul 136-701, Republic of Korea
Keywords: nanofiber, polyurethane, diffusion, interception
Presenting author email: choihj@kitech.re.kr

Aerosol filtration, especially fibrous filtration is quite useful in various industrial fields such as air cleaning and particle sampling due to its simple structure and low cost. Conventional filtration theory reveals that filtration efficiency can be improved by decreasing fiber diameter. Finer fibers lead higher collection efficiency of particle due to diffusion and interception (Hinds, 1999). Therefore, many researchers made efforts to fabricate nanofibers with various methods in order to use filter media.

In the recent years, a good alternative to fabricate nanofibers is electrospinning, which has received considerable attention, due to its simplicity and applicability (Yun *et al*, 2010). Various polymers have been successfully used in the fabrication of nanofibers by electrospinning for past few years. However, electrospun filter media using polyurethane which has excellent mechanical properties (tensile strength, durability, elasticity and water insolubility) (Sheikh *et al*, 2011) were not challenged yet. In addition, it is necessary to investigate the filtration performance of ultrafine particles and collection mechanisms of electrospun filter media. Therefore, polyurethane nanofibers were prepared by electrospinning and the effect of processing parameters such as polymer concentration, electric field and tip to collector distance on fiber morphology were investigated in this study. Furthermore, the filtration performance of ultrafine particles and collection mechanisms were examined.

We found that the fiber formation and morphology is extremely influenced by polymer concentration, electric field and less influenced by tip to collector distance. We could make nanofibers with 100~200 nm in diameter at polymer concentration of 10 wt%, electric field of 1.43 kv/cm and tip to collector distance of 7cm. Based on the above results, the electrospun filter media was prepared and Figure 1 shows their morphology and fiber size distribution.

The fabricated filter media had minimum collection efficiency at the particle size of 80 nm. In general, conventional filter media has minimum collection efficiency at the particle size range of 100 nm to 300 nm. However, the MPPS (Most Penetration Particle Size) for the filter media was shifted to smaller particle size which is likely to have electrostatic attraction such as electret filter.

In addition, we derived the single fiber efficiency of an electrospun filter using a log-penetration equation and plotted as a function of Peclet number. As a result, interception was a significant mechanism in nanofiber filtration for ultrafine particles. This study shows that electrospinning is an effective method for the fabrication of nanofiber filter which has high filtration performance due to electrostatic force.

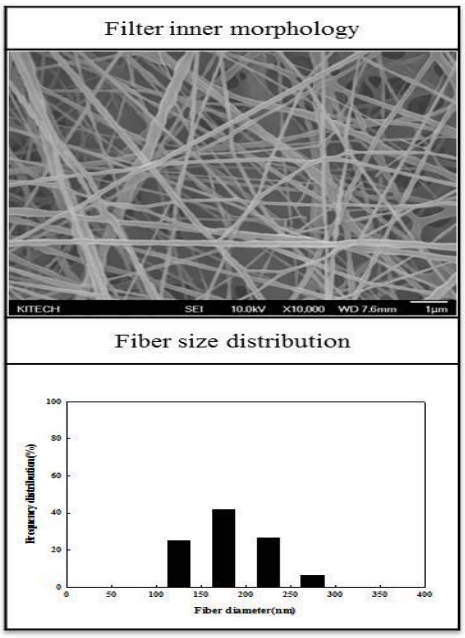

Figure 1. Filter inner morphology and fiber size distribution of electrospun filter media.

This research was financially supported by the eco-innovation project, Republic of Korea (project no.20120001102)

Hinds, W.C. (1999) *Aerosol Technology. Second ed.* Wiley

Yun, K.M., Suryamas, A.B., Iskandar, F., Bao, L., Niinuma, H. and Okuyama, K. (2010) *Sep. Purif. Technol*. **75**, 340-345

Sheikh, F.A., Kanjwal, M.A., Saran, S., Chung, W-.J. and Kim, H. (2011) *Appl. Surf. Sci*. **257**, 3020-3026.

Aerosol Synthesized Porous Catalytic Particles for Emission Control Applications

G. Kastrinaki[1,4], M. Kostoglou[3] and A.G. Konstandopoulos[1,2]

[1]Aerosol &Particle Technology Laboratory, CERTH/CPERI, Thessaloniki, P.O. Box 60361, 57001, Greece
[2] Department of Chemical Engineering, Aristotle University, Thessaloniki, PO. Box 1517, 54006, Greece
[3] Department of Chemistry, Aristotle University, Thessaloniki, PO. Box 1517, 54006, Greece
[4] Department of Mechanical Engineering, University of W. Macedonia, Kozani, 50100, Greece

Keywords: porous particles, aerosol spray pyrolysis
Presenting author email: georgiak@cperi.certh.gr

In automotive emission control applications one is targeting the oxidation of hydrocarbons (HC) and carbon monoxide (CO) towards non toxic gases carbon dioxide (CO_2) and water (H_2O), In addition oxidation of nitrogen monoxide NO to nitrogen dioxide (NO_2) is often desired, before any final nitrogen oxides (NO_x) reduction, since NO_2 plays important role in Diesel Particulate Filter (DPF) regeneration and Selective Catalytic Reduction (SCR) reactions. Gas oxidation (NO, HC, CO) is facilitated by catalytic materials, mainly Platinum (Pt) Group Metals, that are dispersed on a high surface area oxide material (support) such as silica, alumina etc, .

The goal of this work is to employ Aerosol Spray Pyrolysis (ASP) (Karadimitra et al, 2001). for the one-step synthesis of catalytic systems (Pt on oxide particles). The small size of aerosol particles would increase the catalyst surface area while the one-step synthesis would enhance the productivity of the process. In ASP, a solution of metal precursors is atomized into fine droplets, which undergo evaporation of the solvent and precipitation of the dissolved material, which upon further thermal treatment is converted to the oxide form of the metal precursors. The control of the different synthesis parameters such as the precursor material and its concentration, the solvent type, temperature, flow rate and post treatment determine the particle characteristics and generation of porous nanoparticles has been already reported (Lorentzou et al, 2011).

In the present work Pt loaded porous silica and alumina nanoparticles (with a 200 nm mean particle size) at different Pt loadings have been synthesized and characterized for their catalytic oxidation activity.

The catalytic particles were tested in a fixed bed reactor system with respect to their catalytic activity for NO oxidation to NO_2 as well as for C_2H_4 oxidation in a feed stream of $10\%O_2$ in N_2. The evaluation was performed in the presence and absence of HCs in order to also assess inhibition effects. A theoretical model was also developed and was shown to describe satisfactorily the experimental data at moderate levels of conversion, while when mass transfer limitations were included in the model, the agreement with the experimental data over the entire conversion range was excellent.

Figure 1 provides a representative result for the oxidation of C_2H_4 on some of the catalytic nanoparticles produced (consisting of Pt/porous alumina). For oxidation comparison, Pt impregnated in commercially sourced alumina procured under similar experimental conditions is also shown. The aerosol-based catalyst has a significantly higher activity which is attributed to a combination of higher surface area and dispersion, currently under investigation.

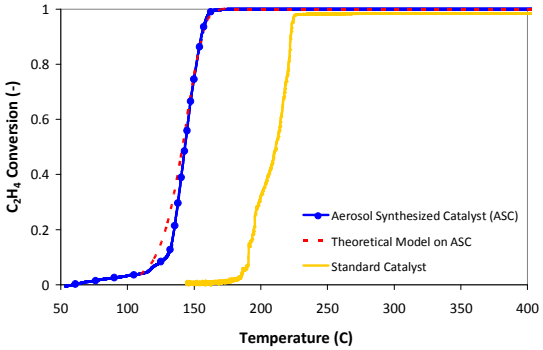

Figure 1. C_2H_4 oxidation on aerosol-based and commercially procured materials at the same Pt load.

The current work demonstrates the potential of aerosol-synthesized porous nanoparticle catalysts for automotive emission control applications. Work is continuing with the scaling-up of the production process of the porous catalytic nanoparticles and their incorporation into monolithic reactors for testing under realistic exhaust conditions on engines.

Lorentzou S., Kastrinaki G., Pagkoura C., Konstandopoulos A.G. (2011), *Nanoscience and Nanotechnology Letters*, 3, **5**, 697-704.

Karadimitra K., Papaioannou E., Konstandopoulos A.G (2001), *J. Aerosol Sci*., **32**, Suppl. 1, S233-234.

Aerosol nanoparticles captured into colloids by using an electrospray cloud as a filter

M. Valenti[1], G. Biskos[1], A. Kourmouli[1] and A. Schmidt-Ott[1]

[1] Chemical Engineering, Delft University of Technology, Delft, 2628 BL, The Netherlands
Keywords: Electrospray, Nanoparticles, Colloids, Spark-discharge aerosol generator.
Presenting author email: M.valenti@tudelft.nl

Engineered nanoparticles (ENPs) have remarkable size-dependent properties which make them great candidates for applications in novel materials for catalysis, electronics, optical devices, as well as in the pharmaceutical industry (e.g. drug delivery carriers).

An elegant way for producing well-defined ENPs is by using various aerosol-based techniques (e.g., spark discharge, flame synthesis, etc.). However, many applications require the nanoparticles to be embedded in specific liquids. An intermediate step is therefore required for getting the ENPs from a gaseous to a liquid medium.

Single size colloids, synthesized mainly by chemical reductions, have been extensively studied. However, these reduction methodologies often leave appreciable amounts of residual ions in solution. For applications where these residual ions are counterproductive, a different methodology must be used to ensure a predetermined purity in the single size colloid.

This work introduces a way of capturing well-defined aerosol particles in liquid solvents using the electrospray (ES) technique. Although we demonstrate the performance of the system for metal particles generated from the spark discharge, and use an ethanol/water mixture as a solvent, the technique can be used for ENPs produced from any aerosol-based technique and with a wide range of solvents.

Methodology

Metal nanoparticles having diameters from 1 to 100 nm are produced in N_2 with a spark-discharge aerosol generator (Schwyn et al., 1988, Tabrizi et al., 2008). The particles are then passed through a Differential Mobility Analyzer (DMA) to select particles of a very narrow mobility range. The mono-dispersed aerosol coming out of the DMA, are then neutralized and passed through the ES filter. The highly charged liquid micro-droplets in the ES filter, that capture the ENPs, are collected in a reservoir.

Preliminary results

In order to prove that indeed particles in this size range (1-100 nm) can be captured with an ES cloud, we sent a neutralized poly-dispersed gold aerosol (1-100 nm) directly to the ES filter (ethanol droplets) and measured its capture efficiency (Figure 1.) by counting the nanoparticles that survive the ES cloud with an scanning mobility particle sizer (SMPS; see Figure 2.). Positive filter efficiencies were measured throughout the full nanoparticle size range.

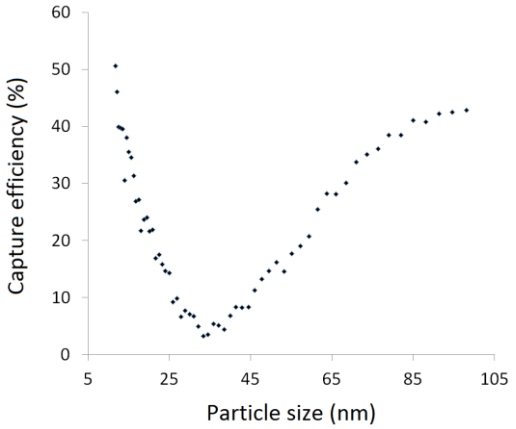

Figure 1. Capturing efficiency of aerosol nanoparticles by an ES filter.

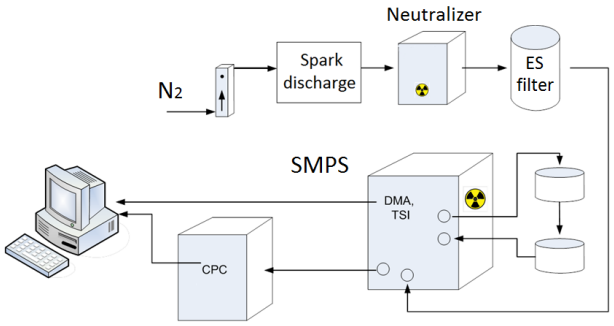

Figure 2. Experimental set-up used to measure the capturing efficiency shown in figure 1.

Conclusions

Gas phase metal nanoparticles within the size range of 1-100 nm can be captured into a colloidal suspension by using an ES filter. The methodology described above could be used to produce well-defined single size colloids with virtually no ion impurities.

Further work has to be made to maximize the capture efficiency of the filter via the ES parameters (e.g. droplet charge, number of droplets, etc).

Schwyn, S., Garwin, E. & Schmidt-Ott, A., *J. Aerosol Sci.*, 19(5), 639-642 (1998).

Tabrizi, N.S., Ullmann M., Vons V. A., Lafont U., Schmidt-Ott, A, *J. Nanopart. Res.*, 11(2), 315-332 (2008).

The measurement of nanoparticle deposition efficiency in the lungs of Wistar rats

Svetlana G. Matveeva,[1] Anatoly M. Baklanov,[1] Tatyana G. Tolstikova,[2] Sergey W. Ankow[2]

[1] *Institute of Chemical Kinetics and Combustion, Novosibirsk, 630090, Russia*

[2] *Institute of Organic Chemistry, Novosibirsk, 630090, Russia*

svetlana.matveeva@kinetics.nsc.ru

The nanoaerosol drug delivery to a patient is used now for the treatment of both respiratory and systemic diseases. Lung-deposited dose depends on the particle deposition efficiency, which in turn is function of the size. The aim of present work was experimental definition of dependence of nanoparticle deposition efficiency from the diameter in the rat's respiratory tract. The basic idea of the experiment was to determine the depletion of aerosol due to rats breathing.

The inhalation scheme (Fig.1) includes a flow aerosol generator, four glass boxes for rats, filter, diluter and aerosol spectrometer. The horizontal evaporation–condensation aerosol generator was made of a molybdenum glass tube with an outer heater. Air flow was supplied to the inlet of the generator. The original substances (nisoldipin or sodium chloride) were put to the hot zone inside the tube. The saturated vapor was formed inside the generator. The temperature dropped down at the outlet of the heated zone resulting in vapor supersaturation. Then there was the homogeneous nucleation. The final aerosol was admitted into the nose-only exposure glass chambers. Each chamber contained one rat during the experiment. The laboratory Wistar rats were used. The aerosol depletion due to rats breathing was determined by comparing the substance particle concentration at the outlet of loaded and unloaded consecutive chambers. The aerosol concentration and size distribution were measured with the aerosol spectrometer. This aerosol spectrometer consists of an automatic diffusion battery, condensation chamber, and photoelectric counter.

Nanoparticle deposition efficiency (Fig.2) was calculated via the following formula [1], [2]:

$$\varepsilon = \frac{F}{f * V_T} * [1 - (\frac{n}{n_0})^{\frac{1}{N}}]$$, where

ε - deposition efficiency, F - flow rate, f - average rat breathing frequency, V_T - tidal volume, n – number concentration of loaded chambers, n_0 - number concentration of unloaded chambers, N – number of chambers.

Using the NOE chambers, the rats lung deposition efficiency was evaluated as a function of the particle diameter changing from about unity at d = 5 nm to about 0.3 at d = 100 nm. Deposition efficiency was not depend on the type of material, but only on the size.

Financial support for this work was provided by the Siberian Branch of Russian Academy of Sciences (SBRAS): Interdisciplinary Integration Project No.3 and SBRAS-Taiwan Collaboration Project No.7; RFBR project No. 11-08-01204-a and the cooperation Agreement between CNR (Italian National Research Council) and RAS (Russian Academy of Science) years 2011-2013.

1. Andrei A. Onischuk et al. // J. of Aerosol Med. And Pulmonary Drug Delivery. 2008. V.21. № 2.

2. Andrei A. Onischuk et al. // J. of Aerosol Med. And Pulmonary Drug Delivery. 2009. V.22. № 1.

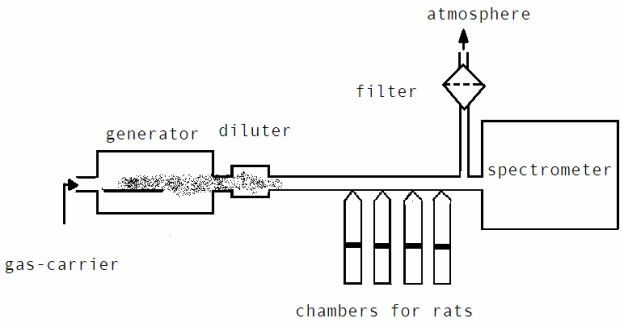

Fig. 1. Experimental setup.

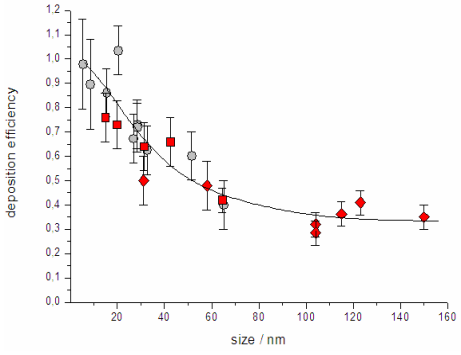

Fig. 3. Deposition efficiency from the size.

Experimental study of homogeneous nucleation from the antimony supersaturated vapor

O.V. Borovkova[1,2], A.M. Baklanov[1], S.V. Vosel[1,2], F. B. Baimasheva[1,2]

[1]Institute of Chemical Kinetics and Combustion, SB RAS, Novosibirsk, 630090, Russia
[2]Novosibirsk State University, Novosibirsk, 630090, Russia
Keywords: homogeneous nucleation, antimony, surface tension
Presenting author email: borovkova@kinetics.nsc.ru

Thermodynamic properties of an interface can be completely determined by the surface tension. Recently, it became clear that the surface tension σ of nanoscale droplets might significantly differ from that for the flat surface. Therefore, both to understand and to predict processes such as homogeneous nucleation, the solubility of nanoparticles and similar ones, it is necessary to determine the value of the surface tension of nanoscale droplets. In the case of critical nucleus, which are typical nanoscale droplets, this can be done by the evaluation from the experimentally measured rate of the nucleation from supersaturated vapor (Vosel, 2012).

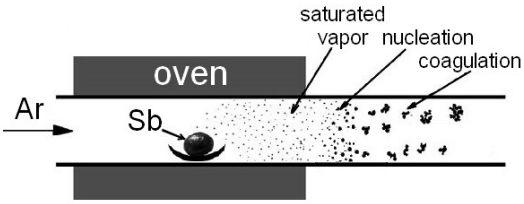

Figure 1. Experimental setup.

This work is devoted to the experimental study of homogeneous nucleation from Sb vapor in a laminar flow diffusion chamber (Fig. 1). The flow diffusion chamber consisted of a quartz tube with an outer heater. A piece of Sb was put inside the heated zone to generate the saturated vapor. Argon flux was supplied to the inlet of the tube. At the outlet of the heated zone the temperature decreased resulting in the vapor supersaturation and nucleation. The particle size and number concentration at the outlet of chamber were measured by the automatic diffusion battery coupled with a condensation nucleus counter.

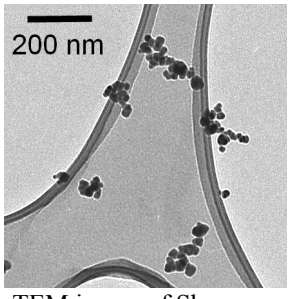

Figure 2. TEM image of Sb nanoparticles.

The morphology of the outlet particles was studied using JEOL-JEM 100SX TEM. The aggregates consisting of small primary particles originated from critical nuclei were observed (Fig. 2). The aggregate size, concentration and fractal dimension were studied as a function of heating temperature as well as size and number of the primary particles per aggregate.

"The supersaturation cut-off" method was used to find the approximate dimensions of the nucleation zone (Fig. 3). The metal grid was put inside the tube perpendicularly to the flow. The decrease in the outlet particles concentration was observed while changing the position of the grid within the nucleation zone. Therefore, the approximate nucleation volume was estimated.

The number of particles formed in the nucleation zone can be determined using the outlet aerosol concentration and mean number of the primary particles per aggregate. As in our conditions temperature inside the oven was below the melting temperature of antimony, coalescence doesn't take place. Thus, it's possible to determine the quantity of critical nuclei in nucleation zone with high precision.

Based on the experimental results nucleation parameters have been obtained. At nucleation temperature of 350 K the typical nucleation rate was found to be $1.7 \cdot 10^{10}$ $cm^{-3}s^{-1}$.

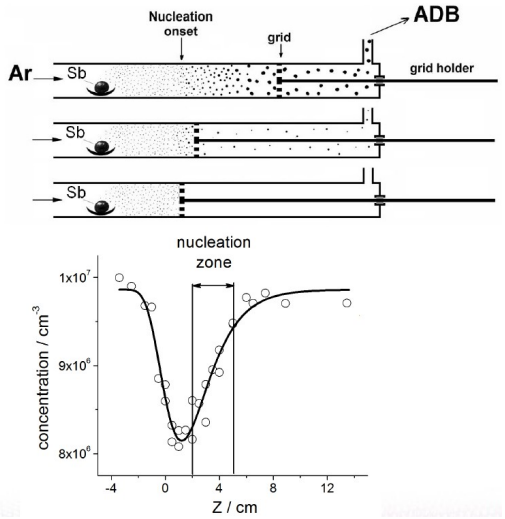

Figure 3. Experimental setup for the "supersaturation cut-off" method and the outlet particle concentration vs. the grid position.

This work was supported by RFBR (project №11-08-01204-a).

Vosel S.V., Onischuk A.A., Purtov P.A., Tolstikova T.G., (2012) *Aerosols Handbook: Measurement, Dosimetry, and Health Effects*, CRC Press.

Dustiness testing of engineered nanomaterials based on ZrO_2 by vortex shaker method

E. Jankowska[1], P. Sobiech[1], J. Łukaszewska[1], O. Witschger[2], S. Bau[2] and B. Bianchi[2]

[1]Department of Chemical, Aerosol and Biological Hazards, Central Institute for Labour Protection - National Research Institute (CIOP-PIB), Warsaw, 00-701, Poland
[2] Laboratoire de Métrologie des Aérosols, Institut National de Recherche et de Sécurité (INRS), F-54519, Vandoeuvre, France
Keywords: nanomaterials, nano-objects, dustiness, vortex shaker.
Presenting author email: eljan@ciop.pl

Information about dustiness of engineered nanomaterials is very important during the design and the realize of many industrial processes. This information is also very essential for evaluation, controlling and minimize exposure workers to nano-objects. Dustiness determined with gravimetric method is not appropriate to the evaluation of workers exposure since parameters which characterized of nano-objects emission are mainly number concentration and size distribution.

The aim of the investigation was to determined number concentrations of nano-objects emitted when generated nanomaterials with vortex shaker method (Witschger, et al., 2011). This results can reflected of dustiness of nanomaterials. Investigations were done for 3 engineered nanomaterials based on zirconium oxide: pure zirconium oxide (ZrO_2) and stabilized by calcium (ZrO_2+8%CaO) or yttria (ZrO_2+8%Y_2O_3). Those nanomaterials are available from NanoAmor. Test-stand showing equipment for aerosol generation (vortex genius 3) and getting of respirable fraction of nano-objects (cyclone of GK 2.69) is presented on Figure 1.

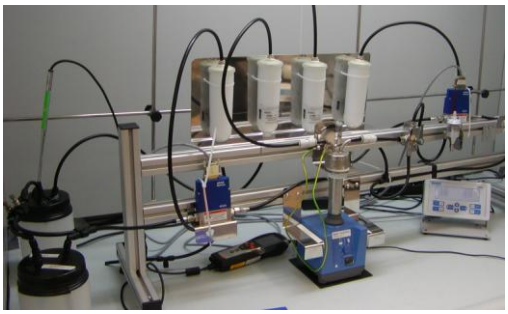

Figure 1. Test-stand for generation of resbirable fraction of nano-objects from nanomaterials (vortex shaker method).

Total number concentrations of particles with diameter 0.01-8.14μm were measured with Electrical Low Pressure Impactor ELPI+ with flowrate 9.91dm^3/min. Results of investigation are shown on Figure 2. Received data indicated that from investigated nanomaterials pure zirconium oxide (ZrO_2) was characterized highest emission of nano-objects, with possibility of staying them by the longer time in the air. For the time up to 1000s from starting of ZrO_2 generation total concentrations of particles varied between 5700-8500#/cm^3 and after 3000-3500s were ca. 2000-3000#/cm^3. Another tendency of changes concentrations during generations were observed for zirconium oxide stabilized by calcium (ZrO_2+8%CaO) or yttria (ZrO_2+8%Y_2O_3). For them pikes of concentrations were visible ca. 150s after starting nanomaterials generations, ca. 4700#/cm^3 for ZrO_2+8%CaO and ca. 5800#/cm^3 for ZrO_2+8%Y_2O_3. About 700s after starting generations of ZrO_2+8%CaO or ZrO_2+8%Y_2O_3 concentrations achieved ca. 500#/cm^3 for ZrO_2+8%CaO and ca. 2100#/cm^3 for ZrO_2+8%Y_2O_3.

It can be concluded that zirconium oxide stabilized by calcium (ZrO_2+8%CaO) or yttria (ZrO_2+8%Y_2O_3) are less dusty than pure zirconium oxide (ZrO_2).

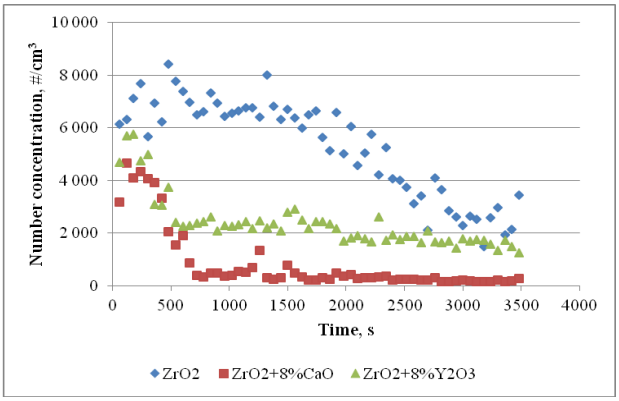

Figure 2. Total number concentration of particles 0.01-8.14μm obtained during generation of nanomaterials (ZrO_2, ZrO_2+8%CaO, ZrO_2+8%Y_2O_3) with vortex shaker method.

Currently are carried out standardization works (CEN) in the field of "Workplace atmospheres - Measurement of dustiness of bulk nanomaterials". One from the developed methods is vortex shaker method. Participants of the project: INRS (leader), CIOP-PIB, HSL, IGF, NRCWE and TNO.

This study was prepared on the basis of the results of project 04.A.18 carried out within of the NP "Safety and working conditions improvement", funded in the years 2011-2013 by the Ministry of Labour and Social Policy. Main co-ordinator CIOP-PIB.

Witschger, O et al. (2011) *DUSTINANO: A PEROSH Initiative Towards a Harmonized Approach for Evaluating the Dustiness of Nanopowders.* On Fifth International Symposium on Nanotechnology – Occupational and Environmental Health, August 9-12, 2011 Boston, MA, USA.

An effort towards understanding the sources of impurities in generating nanoparticles via liquid-phase methods

E.M. Faghihi, L. Morawska and C. He

International Laboratory for Air Quality and Health (ILAQH), Queensland University of Technology (QUT), Brisbane, Australia

Keywords: nanoparticles, aerosolisation, impurities.

Contact email address: e.majdfaghihi@qut.edu.au

Introduction: Generating nano-sized materials of a controlled size and chemical composition is essential for the manufacturing of materials with enhanced properties on an industrial scale, as well as for research purposes, such as toxicological studies. Among the generation methods for airborne nanoparticles (also known as aerosolisation methods), liquid-phase techniques have been widely applied due to the simplicity of their use and their high particle production rate. The use of a collison nebulizer is one such technique, in which the atomisation takes place as a result of the liquid being sucked into the air stream and injected toward the inner walls of the nebulizer reservoir via nozzles, before the solution is dispersed. Despite the above-mentioned benefits, this method also falls victim to various sources of impurities (Knight and Petrucci 2003; W. LaFranchi, Knight et al. 2003). Since these impurities can affect the characterization of the generated nanoparticles, it is crucial to understand and minimize their effect.

This study aims to quantify the impurities and determine their sources through the physical characterization of nebulized water nanoparticles.

Methods: We designed an experiment in which different metrics of the nebulized water nanoparticles, including size, number concentration and volatility, were assessed. Deionised (DI) water was chosen for this study because the size distribution of the nebulized particles measured by a Scanning Mobility Particle Sizer (SMPS) confirmed that this water carried the least level of impurities compared to the two other pure water types available (distilled and HPLC-grade water).

Firstly, the residues from the nebulizer reservoir and nozzle were studied as a potential source of contaminants. For this purpose, the reservoir and the nozzle were washed with DI water several times and sonicated for ten minutes to determine if this could reduce the impurities.

To investigate the role of the volatile organic content of nebulized DI water nanoparticles in determining the level of impurity, we designed a second experiment in which a thermodenuder was used to study the effect of temperature on the size distribution and number concentration of the nebulized water particles. To do so, a Condensation Particle Counter (CPC) and a SMPS were used to measure the number concentration and size distribution of the particles before and after they passed through the thermodenuder.

Results: Comparison of the size distributions, both before and after the washing and sonicating of the nebulizer, showed a decrease in the median diameter (from 22 to 17 nm) and number concentration (from 1.52e4 to 6.1e3 particles/cm^3) of the impurities.

In the second experiment, an incremental increase in temperature from 25 ˚C to 260 ˚C led to a decrease in number concentration, as a result of the evaporation of small water particles. However, not all of the particles evaporated, even at high temperatures. According to Figure 1, although both total number concentration and mode diameter of the nebulized water particles decreased due to the high temperature (from 963 to 508 p/cm^3 and from 42.9 to 37.2 nm, respectively), it can also be seen that a number of these particles were not volatile organic particles and did not evaporate.

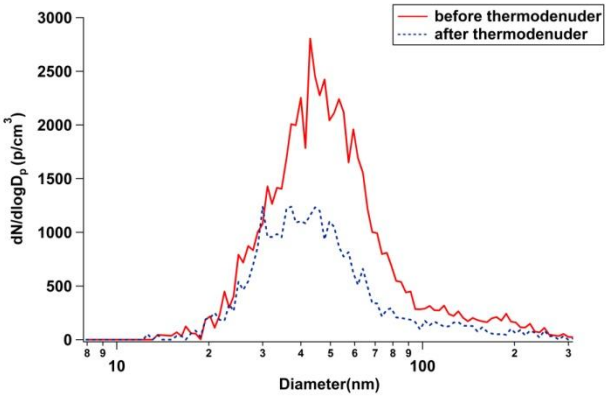

Figure 1- Size distribution measured before and after the thermodenuder at 200 ˚C

Conclusions: The results confirmed that not all of the impurities were volatile organics stemming from the nebulized water. The other possible sources of contaminants were residues inside the nebulizer, which could be removed by washing and sonicating the nebulizer reservoir and nozzle (in this case, a 23% decrease in size and 60% decrease in total number concentration) and also leaching from the inner walls of the container used to keep and carry the DI water.

Knight, M. and G. A. Petrucci (2003). "Study of Residual Particle Concentrations Generated by the Ultrasonic Nebulization of Deionized Water Stored in Different Container Types." Analytical Chemistry **75**(17): 4486-4492.

W. LaFranchi, B., Knight, M. et al. (2003). "Leaching as a source of residual particles from nebulization of deionized water." Journal of Aerosol Science **34**(11): 1589-1594.

New measurement system for PM and ultrafine particles

J. Spielvogel, M. Weiß

Palas GmbH, Karlsruhe, 76229, Germany
Keywords: aerosol instrumentation, particle sizer, nanoparticles, number concentration
Presenting author email: spielvogel@palas.de

According to a recently published report by the European Environment Agency about one third of Europe's population in cities is exposed to excessive concentrations of particulate matter (PM). These people are also exposed to high concentrations of ultrafine particles caused for example by traffic and heating.

We will present a new measurement system that can measure the number concentration and size distribution of airborne particles from 8 nm to 18 µm. In addition, it also reports simultaneously different PM-fractions such as PM-1, PM-2.5 and PM-10. With a time resolution of 5 minutes it can further capture dynamic changes in the aerosol distribution caused for example by rush hour traffic in the morning and afternoon.

The measurement system combines a scanning mobility particle sizer in which the working fluid to condense the particles can be chosen to be water or butanol with a continuous ambient air quality monitoring system. In the latter a polychromatic light source is used to illuminate aerosol particles as they pass through the optical sensing volume. The scattered light of each individual particle is then detected with a photomultiplier.

The system is operated through a touchscreen with intuitive graphical user interface and integrated data logger. Data can be easily viewed on the screen or later extensively evaluated through the included software.

We will show and discuss selected measurements in which the additional information of particle size distribution helps to interpret the PM-data and also facilitates source apportionment.

Nanoparticles generation modes of the multi-spark discharge generator

A.A. Efimov[1], V.V. Ivanov[1,2,3], I.V. Beketov[3] and I.A. Volkov[1,2]

[1]Moscow Institute of Physics and Technology, Dolgoprudnyi, Moscow region, 141700, Russian Federation
[2]RUSNANO Metrology Center, LLC, Moscow, 117036, Russian Federation
[3]Institute of Electrophysics, Russian Academy of Sciences, Ural Branch, Ekaterinburg, 620016, Russian Federation

Keywords: spark discharge, nanoparticle production, diffusion aerosol spectrometer.

Presenting author email: newaldan@gmail.com

Production of nanoparticles is an urgent task, due to the high needs of industry in the materials with unique physical-chemical properties for creation of new devices and products on their basis. The unique physical and chemical properties of nanoparticles are caused by surface and quantum size effects.

Although there are many methods to produce nanoparticles, we have chosen the method of spark discharge as a highly scalable and versatile method for the production the nanoparticles of metal and semiconductor materials, Tabrizi *et al* (2009). In this work, we have built and tested the spark discharge generator (SDG) with three spark gaps connected in series, Figure 1.

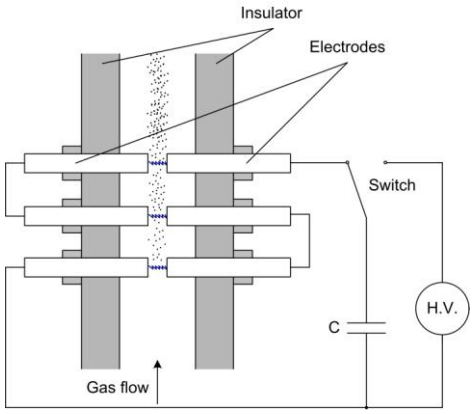

Figure 1. Schematic of the spark discharge generator.

Series connection of many spark gaps in the SDG in comparison with one-spark case allows generating larger quantities of aerosol nanoparticles with stable particles size distribution. The high voltage power supply HV was used to charge the capacitors in a voltage range from 0 to 5 kV. In the experiments we used capacitors varied in the range since 0.1 uF to 0.5 uF. Electrodes, between which the spark occurred, were made in the form of cylinders of about 100 mm in length and of 5 mm in diameter. The titanium and aluminum electrodes were used in the experiments. Air flow was regulated in the range from 0 to 160 l/min. Maximum frequency of the discharge pulses was 10 Hz.

According to literature most of the works regarding measurements of particle size distribution of aerosol particles generated by SDG was performed with a scanning mobility particle sizer (SMPS). However the SMPS can limit the accuracy of measurements particle size distributions because the particles generated by the SDG may be nonspherical. Moreover due to the small particle size there will be an error in charging efficiency. In order to avoid these factors, we used a different method of measuring the aerosol nanoparticles. The particle size distribution was measured using diffusion aerosol spectrometer DAS (model 2702, «AeroNanoTech» LLC, Russia). Its method of measurement is based on analysis the coefficients of particles penetration through a section of the diffusion battery, Julanov *et al* (2002).

During the experiment the influence of the SDG operating parameters on the particle size distribution was determined. Operating parameters of the SDG were: charging voltage (U), spark frequency (f), capacity (C), gas flow rate (Q) and electrode material (Me). A typical example of the measured distributions are shown on Figure 2.

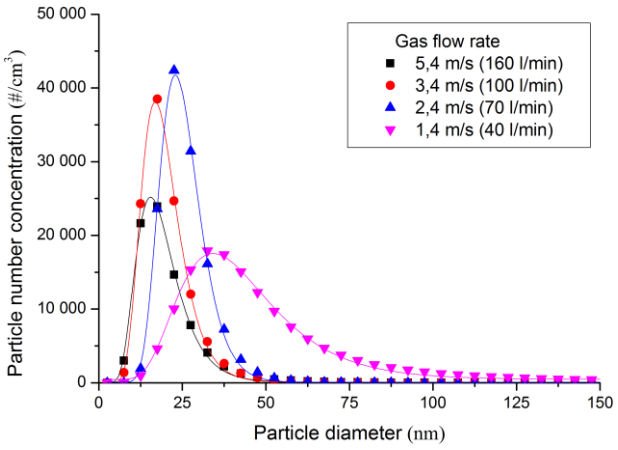

Figure 2. Effect of gas flow rate on the particle size distribution measured with DAS 2702 (titanium electrodes; C = 0.33 uF; U = 2.0 kV and f = 0.5 Hz).

Tabrizi, N.S., Ullmann, M., Vons, V.A., Lafont, U., Schmidt-Ott, A. (2009) Generation of nanoparticles by spark discharge, *Journal of Nanoparticle Research*, 11 (2), pp. 315-332

Julanov, Yu.V., Lushnikov, A.A., Zagaynov, V.A. (2002) Diffusion aerosol spectrometer, *Atmospheric Research*, 62 (3-4), pp. 295-302

Size Controlled Synthesis of Spherical Nanoparticles by Spark Discharge

J. Feng, A. Maisser, T. Pfeiffer, G. Biskos and A. Schmidt-Ott

Department of Chemical Engineering, Delft University of Technology, Delft, Julianalaan 138, 2628 BL, Netherlands
Keywords: Primary nanoparticles, Spark discharge, Synthesis.

Spark discharge electrode ablation which was described firstly by Schwyn *et al* (1998) is a versatile method of nanoparticle production with a narrow size distribution. A spark generator basically consists of a pair of electrodes whereby repeated spark discharges take place over a gap within a mm range. Each spark generates a vapour cloud which condenses into nanoparticles. Meanwhile, an inert gas flow continuously flushes the gap for cooling and dilution. Spark generators are widely used in modern laboratories, and efforts are currently underway to scale up the process to achieve industrial production rates. Agglomerates are generated in most cases and thus lead to an agglomerate diameter, which are expected to overcome since the primary particle diameter is usually advantageous to control the properties of the product and individual sphere-like (primary) particles are required in various applications. Schwyn *et al* (1988) and Tabrizi *et al* (2009) have demonstrated that sufficient dilution can avoid agglomeration in the spark process.

In the present paper, we have systematically investigated the influence of process parameters on primary particle size. The ability to control the primary particle size of nanostructured materials is essential since it is a key variable in many thermal, mechanical and optical properties. Our present results are based on gold nanoparticles.

The inert gas dilutes and cools the vapour which forms the particles. In this work, parameters to be set are the repetition frequency *f*, the electrode gap distance *d*, the flow rate *Q* and the energy *E* provided per spark. The latter two parameters (*Q*, *E*) are expected to be of great importance as they directly influence the concentration and temperature in the vapour condensation process. A Scanning Mobility Particle Sizer system is applied to obtain the modal particle diameter. Different dilution rates lead to different sizes of spherical particle formation (Fig. 1). The inserts show electron micrographs with different parameters, indicating that particles smaller than ca. 5 nm have coalesced to form sphere-like shapes. According to the work of Koch *et al* (1990), it can be concluded that for particles larger than 5 nm $\tau_{coalescence} > \tau_{collision}$ is valid for the characteristic times for coalescence and collision. Spark energy also tunes the particle size shown in Figure 2. This is expected, since the energy of the spark directly influences the amount of material evaporated with relation to $\tau_{collision}$ as well as the temperature history, which controls $\tau_{coalescence}$. Under the conditions applied, the size of primary particles is reproducible and variable between 2.7 and 5 nm. Smaller particle sizes can be achieved, which can be decreased to the single atom (Peineke, 2009). Larger round particles can be produced by inducing coalescence of agglomerates by heating the aerosol stream (Kruis, 1998). The present progress has shown the potential to effectively control the size of primary particle in the spark generation process.

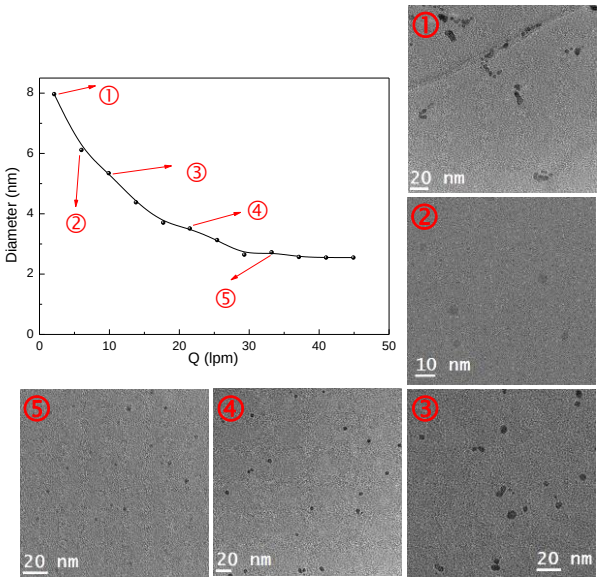

Figure 1. Particle diameter vs. flow rate (*E*=0.2623 mJ/spark, Spark duration=4 μs).

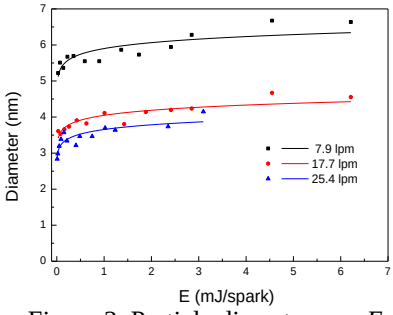

Figure 2. Particle diameters vs. *E*.

This work was supported by European Commission 7th Framework Program under grant agreement No. 280765 (BUONAPART-E).

Schwyn, S., Garwin, E. and Schmidt-Ott, A. (1988) *J. Aerosol Sci.* **19**, 639-642.

Tabrizi, N.S., Ullmann, M., Vons, V.A., Lafont, U. and Schmidt-Ott, A. (2009) *J. Nanopart. Res.* **11**, 315-332.

Koch, W. and Friedlander, S.K. (1990) *J. Colloid. Interf. Sci.* **140**, 419-427.

Peineke C., Attoui, M., Robles, R., Reber, A.C., Khanna, S.N. and Schmidt-Ott, A. (2009) *J. Aerosol Sci*. **40**, 423-430.

Kruis, F.E., Nielsch, K., Fissan, H., Rellinghaus, B. and Wassermann, E.F. (1998) *J. Appl. Phys. Lett.* **73**, 547-549.

Fluid-Particle Dynamics of Nanoparticle Synthesis in Flame Spray Reactors

A.J. Gröhn, S.E. Pratsinis and K. Wegner

Department of Mechanical and Process Engineering, Swiss Federal Institute of Technology (ETH), Zurich, CH-8092, Switzerland

Keywords: Particle Dynamics, Computational Fluid Dynamics, Flame Synthesis.

Presenting author email: arto.groehn@plt.mavt.ethz.ch

Introduction

Flame spray pyrolysis (FSP; Mädler et al., 2002) has been shown a versatile and economic process for nanoparticle production (Wegner et al., 2011). It relies on inexpensive metal-containing liquid precursors, which are atomized by a dispersion gas and ignited to form a spray flame. Following spray droplet evaporation and precursor conversion nanoparticles grow by nucleation, coagulation, sintering and/or surface growth. Fundamental understanding of the complex interactions between these mechanisms is required for transfer of the current laboratory batch process to continuous manufacturing scale (Gröhn et al., 2012).

The objective of this work is the development of a computational fluid-particle dynamics model covering all important process steps to assist reactor operation, optimization and scale-up. The model is performance-tested and validated for the example of zirconia (ZrO_2) nanoparticle production.

Method

Spray, fluid, combustion and aerosol dynamics are integrated in a computational fluid dynamics (CFD) solver to predict product zirconia nanoparticle properties without adjustable parameters or need of experimental input data. By assuming immediate particle formation on precursor oxidation and a self-preserving particle size distribution a robust and computationally feasible description of the process could be constructed (Gröhn et al., 2011). In order to obtain insight into the FSP process for scale-up the model is extended to include both laboratory- and pilot-scale reactor geometries.

Fourier-transform infrared spectroscopy, Phase-doppler anemometry and nanoparticle sampling in-situ the flame are employed for characterizing the temperature, velocity and particle growth profiles of the flame reactor and are used for validation of the computational code (Gröhn et al., 2012).

Results and Discussion

Figure 1 shows simulated primary particle diameters compared with the measurements for 3, 5 and 7 l/min dispersion O_2 and 4 ml/min 0.5 M Zr precursor flow. The predicted primary particle size is strongly influenced by the description of zirconia sintering as revealed by comparing three literature expressions for the solid-state diffusion coefficient, showing that an adequate description of sintering is required for the development of accurate aerosol synthesis models.

Parametric simulations with the CFD model revealed that nanoparticle production rate can be increased without affecting the primary particle size by maintaining constant precursor to dispersion gas flow. Successful scale-up using such method was demonstrated with experiments.

A simple and robust model describing flame spray synthesis of zirconia nanoparticles has been developed that does not rely on experimental input data and is well suited for process design, reactor optimization and scale-up of the widely-used FSP process for synthesis of a broad spectrum of nanostructured materials.

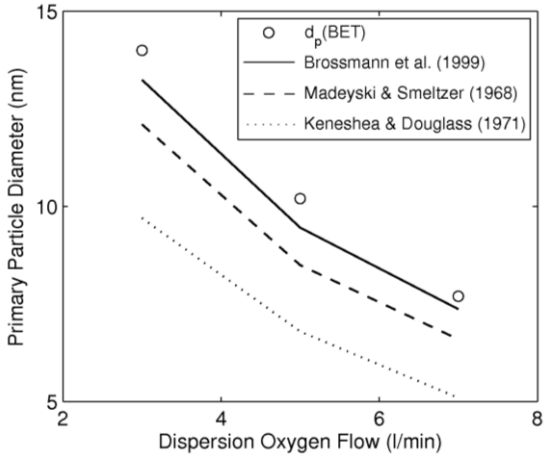

Figure 1. Effect of sintering rate on the predicted primary particle diameters for 4 ml/min of 0.5 M Zr precursor. Grain boundary diffusivity of Brossmann et al. (1999) gave best agreement with experiments.

The research leading to these results has received funding from the European Community's Seventh Framework Programme (FP7 / 2007-2013) under grant agreement n° 228885.

Brossmann, U., Wurschum, R., Sodervall, U. and Schaefer, H.E. (1999), J. Appl. Phys. 85, 7646 - 7654.

Gröhn, A.J., Buesser, B., Jokiniemi, J.K. and Pratsinis, S.E. (2011), Ind. Eng. Chem. Res. 50, 3159 - 3168.

Gröhn, A.J., Pratsinis, S.E., and Wegner, K. (2012), Chem. Eng. J. 191, 491 - 502.

Keneshea, F.J. and Douglass, D.L. (1971), Oxid. Met. 3, 1 - 14.

Madeyski, A. and Smeltzer, W.W. (1968), Mater. Res. Bull. 3, 369 - 375.

Mädler, L., Kammler, H.K., Mueller, R. and Pratsinis, S.E. (2002), J. Aerosol Sci. 33, 369 - 389.

Wegner, K., Schimmoeller, B., Thiebaut, B., Fernandez, C. and Rao, T.N. (2011), KONA Powder and Particle. 29, 251 - 265.

Generation of Mn oxides nanoparticles

P. Mikuška[1], Z. Večeřa[1], B. Dočekal[1] and P. Moravec[2]

[1]Institute of Analytical Chemistry of the AS CR, v.v.i., Brno, CZ-60200, Czech Republic
[2]Institute of Chemical Process Fundamentals of the AS CR, v.v.i., Prague, CZ-16502, Czech Republic
Keywords: Manganese oxides nanoparticles, inhalation, synthesis
Presenting author email: mikuska@iach.cz

The nano scale objects are created within a wide range of anthropogenic processes including welding procedures. Welding produces high amounts of fumes containing manganese oxides nanoparticles (MnONPs). Several recent epidemiologic studies describe occupational exposure ranges of approximately 0.01–5 mg/m^3 Mn in fumes. An accumulation of Mn in lung, liver, and olfactory bulb after acute inhalation exposures is confirmed, but data emerge from animal studies ongoing days maximally two weeks.

Due to an absence of suitable instrumentation for the inhalation and production of MnONPs, there are no studies to concern of long lasting inhalation experiments (months) with chronic concentration of MnONPs.

An inhalation chamber for the whole body exposure studies of small animals to nanoparticles under strictly controlled experimental conditions was constructed recently (Večeřa *et al*, 2012). The inhalation chamber allows long-term inhalation experiments with up to four discrete groups of small animals. The inhalation chamber was tested for leakage of nanoparticles by means of manganese oxides nanoparticles (MnONPs).

Manganese oxides nanoparticles (MnONPs) were synthesized continuously in a vertical hot wall tube flow reactor using thermal decomposition of metal organic precursor manganese(II)acetylacetonate at temperature 850°C in the presence of 30 vol. % of oxygen. The vapors of manganese(II)acetylacetonate were generated from solid form in front of the reactor in saturator at temperature 140-170°C and after that released vapours were transported by nitrogen (flow rate 0.5 l/min) into the reactor. The total flow rate of nitrogen/oxygen mixture throught the flow reactor was 2 l/min. At the outlet of the reactor, MnONPs transported in nitrogen/oxygen mixture were mixed with air (1 l/min). The concentration (1-3×10^7 particles/cm^3) as well as the size (7-50 nm) of produced nanoparticles (Mn_xO_y) was stable for at least a few weeks.

The concentration and size of generated nanoparticles were measured by SMPS (TSI, model 3936L72).

To establish chemical composition, the generated nanoparticles were sampled on cellulose nitrate membrane filters (Millipore, porosity 1.2 μm), the filters were digested in acids in microwave device and content of Mn in extracts was analysed using an AAS (AAnalyst 600 Perkin-Elmer). Content of Mn in NPs collected on cellulose filters was in the range 67-79%, which indicates that generated nanoparticles are composed of mixture of two Mn oxides, Mn_2O_3 (i.e., 69.6% Mn) and MnO (i.e., 77.4% Mn).

For morphology study, the nanoparticles were sampled on cellulose nitrate membrane filters, silver membrane filters and/or deposited onto cupreous TEM grids by electrostatic collection using a Nanometer aerosol sampler (TSI, model 3089) and analysed by a scanning emission microscopy and a transmission emission microscopy.

We suppose that MnONPs are produced as single nanoparticles, however, we identified on filters also larger aggregates. The primary generated MnONPs have shape of sphere with diameter in the range several nm – tens nm.

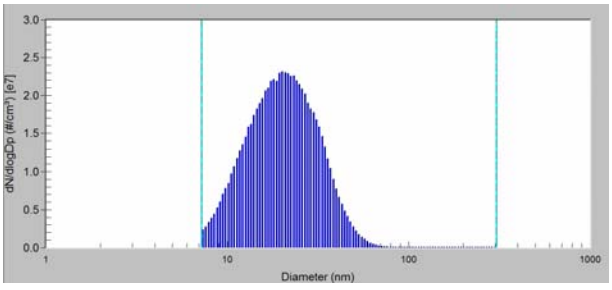

Figure 1. Size distribution of generated Manganese oxides nanoparticles

This work was supported by an Institutional research plan of the Institute of Analytical Chemistry of the Academy of Sciences of the Czech Republic, v.v.i., No. RVO: 68081715 and by the Grant Agency of the Czech Republic under grant P503/11/2315.

Večeřa Z., Mikuška P. (2012), *Sborník 13. konference České aerosolové společnosti*, Třeboň, Česká Republika, 25.-26.10.2012, str. 43-46.

Synthesis of N-modified TiO_2 nano powder by plasma spray for visible light photocatalysis

C.H. Tsai[1], Y.M. Kuo[2], Y.I. Tsai[3], L.C.Wang[4] and Y.F. Wang[5]

[1]Department of Chemical and Materials Engineering, National Kaohsiung University of Applied Sciences, Kaohsiung, Taiwan
[2]Department of Safety Health and Environmental Engineering, Chung Hwa University of Medical Technology, Tainan, Taiwan
[3]Department of Environmental Resources Management, Chia Nan University of Pharmacy and Science, Tainan, Taiwan
[4]Department of Civil Engineering and Engineering Informatics, Cheng Shiu University, Kaohsiung, Taiwan
[5]Department of Bioenvironmental Engineering, Chung Yuan Christian University, Chung-Li, Taiwan

Keywords: Synthesis, Discharge, Titania, Modification.
Presenting author email: chtsai@cc.kuas.edu.tw

Nano particles of N-modified TiO_2 photocatalyst for visible light catalysis have great potential application on the environmental and energy industry (Chen *et al*., 2007). The preparation for the titania-based visible light photocatalyst usually are carried out by liquid phase synthesis, while with the drawbacks, including long reaction time (1-24 hr), residual carbon matter, and high cost of precursors. Rapid gas phase synthesis of titania is not easily for control of operating condition and size distribution. Moreover, the modification of titania need be performed via multiple stages.

In this study, a clear and transparent $H_2O/TiCl_4$ solution was sprayed as nano aerosols into the reactor for rapid (< 1 sec) thermal synthesizing N-modified TiO_2 ($TiO_{2-x}N_x$) particles by using an atmospheric-pressure microwave plasma torch. The continue microwave plasma system was assembled by a commercially available magnetron (National Electronics YJ-1600, 2.45 GHz) with maximum stationary power of 5 kW. A quartz tube are intersected the waveguide (ASTEX WR340) and the resonator perpendicularly. The powders were collected by 14-stage impactors (MOUDI).

The experimental conditions are as follows: inlet $H_2O/TiCl_4$ molar ratio = 8, the applied power = 900 W, and the inlet $NH_3/N_2/O_2$ molar ratio = 0.5/13.5/1.5.

In order to avoid blocking the atomizer, the precursors must be in the form of a clear and transparent liquid. Moreover, the clean solution reduces the amount of Cl atoms in the feedstock or N-TiO_2. The results show that at an initial $H_2O/TiCl_4$ volume ratio of 8, the final stock solution with a $[Ti^{4+}]$ concentration of 1.14 M and a Ti/Cl atomic ratio of 0.9 is clear and transparent. Yellow ($Ti(OH)_xCl_{4-x}$) or white ($Ti(OH)_4$) was found for other $H_2O/TiCl_4$ volume ratios via the following reaction (Ritala *et al*., 1993):

$$TiCl_4 + H_2O \rightarrow Ti(OH)_xCl_{4-x} + xHCl \quad 0 \leqq x \leqq 4$$

The mass-fractionated particle samples were collected by 14-stage impactors (MOUDI). The results showed that the most of particles (in number) were in 5-10 nm stage impactor, reaching 97.8% of total particle number. Though the most of the mass was contributed by particles in the size of 0.54-6.2 μm, reaching 63.6% of the total mass (Table 1).

The photographs of powders show that the spherical TiO_2 with a primary particle of about 10 nm was found, and the secondary particles were aggregated by the primary particles. In addition, the XRD patterns show that the structural characteristics of powders were mainly anatase crystallization.

Elemental analysis by EDS shows that N atoms were doped in TiO_2. Chemical bonding analysis by XPS confirms the N-doping. The N_{1S} peak could be fitted to three line shapes with binding energies at 395.8, 399.1, and 401.5 eV. These different binding energy peaks are fitted to N^{1+} at 395.8 eV, N^{2+} at 399.1 eV and N^{3+} at 401.5 eV, respectively.

UV-Visible absorption spectrum was used to confirm the red shift of band gap for N-TiO_2. The photocatalytic efficiency of unmodified and N-doped TiO_2 is consistent with commercial P25 powders for the duration of UV-light degradation. By visible light degradation, the conversion of methylene blue is much higher for N-doped TiO_2 than P25, indicating that by using MW plasma torch for producing N-modified, nano TiO_2 powders is an excellent approach.

Table 1. Size distribution of N-TiO_2 powders prepared by $NH_3/N_2/O_2$ MW plasma

Size distribution, μm	Medium size Dp, μm	TiO_2 particles no. percentage n', %	TiO_2 mass percentage, M',%
0.005~0.01	**0.008**	**97.77**	3.06
0.01~0.018	**0.014**	**1.812**	0.37
0.018~0.032	0.025	0.32286	0.37
0.54~1	0.770	0.000463	**15.72**
1~1.8	1.400	0.000115	**23.51**
1.8~2.5	2.150	0.000009	**6.62**
2.5~6.2	4.350	0.000003	**17.71**
6.2~10	8.100	0.000000	12.54

This work was supported by the National Council of Taiwan for its financial support under grants NSC 100-2221-E-151-004-MY2.

Chen, C., Bai, H., Chein, H., Chen, T. M. (2007), *Aerosol Sci. Technol.*, **41**, 1018-1028.
Ritala, M., Leskela, M., Nykanen, E., Soininen, P. and Niinisto, L. (1993), *Thin Solid Films*, **225**, 288-295.

Experimental study of homogeneous nucleation from the sulfur supersaturated vapor: Evaluation of the surface tension of critical nucleus.

S.V. Valiulin[1], S.V. Vosel[1,2], A.A. Onischuk[1,2], V.V. Karasev[1]

[1]Institute of Chemical Kinetics and Combustion, Novosibirsk, 630090, Russia
[2]Novosibirsk State University, Novosibirsk, 630090, Russia
Key words: homogeneous nucleation, sulfur, critical nucleus, surface tension
Presenting author email: valiulin@kinetics.nsc.ru

The surface curvature dependence of surface tension is a central problem in the surface thermodynamics. There are many theoretical contributions in the literature where the surface tension $\sigma(R_s)$ of a small drop was calculated as a function of its radius R_s. It is hardly possible to measure directly the curvature dependence of surface tension. However, the nucleation rate is a function of surface tension and therefore experimentally measured parameters of the homogeneous nucleation (rate, temperature, supersaturation) can be used to determine $\sigma(R_s)$. In a work [1] new formula for the nucleation rate was proposed. This formula is based on the Kusaka's theory, the theory of Reiss accounting the translational movement of the mass center of the drop, and Frenkel's kinetic theory of liquids. Thus we have a rigorous formula accounting both the $\sigma(R_s)$ dependence and translation-rotation correction factor which allows us to calculate the dependence of the surface tension on radius from the experimental nucleation rate.

In present work the homogeneous nucleation of sulfur supersaturated vapor is studied in a laminar flow nucleation chamber. The experimental setup is shown in Fig. 1. The concentration of outcoming aerosol particles is analyzed by an Automatic Diffusion Battery coupled with a condensation nucleus counter. The rate of sulfur evaporation from crucible and rate of sulfur wall deposition is measured by direct weighing of the wall deposits and crucible. The axial and radial temperature profiles are measured by a thermocouple. The radial profiles of sulfur vapor concentration and supersaturation are determined solving the mass transfer equation. Based on the rigorous formula and experimental data the surface tension of sulfur critical nuclei resulting from the nucleation has been calculated. The surface tension $\sigma(R_s)$ of the sulfur critical nucleus is found to be 72.5 ± 1.1 dyne/cm for the radius of the surface of tension $R_s \approx 10.6$ Å at temperature 312 – 319 K. The value of $\sigma(R_s)$ proved to be 5 % higher than the surface tension of a flat surface.

The "supersaturation cut-off" method for to find approximate confines of the nucleation zone was developed. The idea of this method is in inserting a stainless steel grid inside the nucleation region. The vapor to grid deposition results in the suppression of nucleation downflow which is observed as a decrease of outlet aerosol concentration. The outlet concentration vs. axial grid position curve has a dip which gives approximate confines of the nucleation zone. It was shown that the "supersaturation cut-off" method was in a good agreement with the calculations of the nucleation region, Fig. 2.

Financial support for this work was provided by the Siberian Branch of Russian Academy of Sciences (SBRAS): Interdisciplinary Integration Project No. 3 and SBRAS-Taiwan Collaboration Project No. 7; RFBR project no. 11-08-01204-a and the cooperation Agreement between CNR (Italian National Research Council) and RAS (Russian Academy of Science) years 2011-2013.

1. *Vosel S.V., Onischuk A.A., Purtov P.A., Tolstikova T.G.* // In: Aerosols Handbook: Measurement, Dosimetry, and Health Effects / Ed. by Ruser L.S., Harley N.H. London – New York – Washington: CRC Press, 2012.

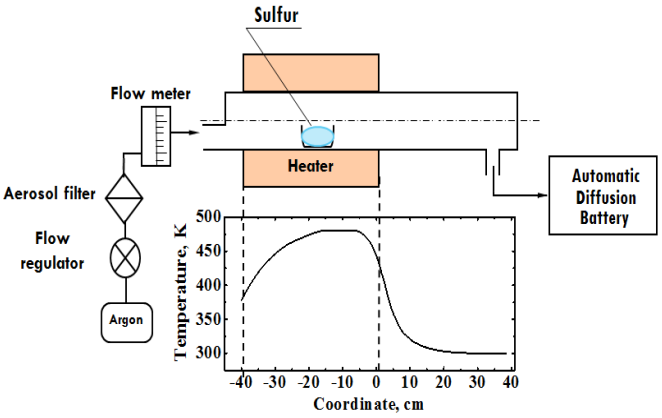

Figure 1. The schematic of experimental setup.

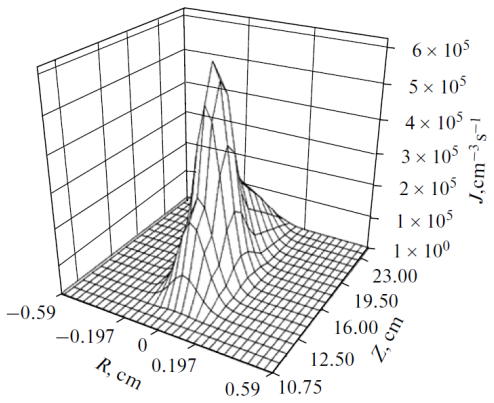

Figure 2. Calculated field of nucleation rate.

Cu-Ni spark discharge nanoparticles from alloy feedstock of varied composition

M. Wagner[1] and M. Seipenbusch[1]

[1]Institute for Mechanical Process Engineering and Mechanics (MVM), Karlsruhe Institute of Technology, Karlsruhe, D-76131, Germany

Keywords: Generation of nanoparticles; nanoparticles, composition; spark discharge
Presenting author email: moritz.wagner@kit.edu

Since its inception by (Schwyn et al 1988), spark discharging has been applied to produce particles from a broad range of electrode materials, both pure metals and semiconductors. The method's ability to produce particles from arbitrary conducting feedstock material and therefore its versatility is one of its advantages.

Recently, particle size distributions and evaporation rates for a number of pure metallic and semiconductor electrode materials were determined by (Tabrizi et al 2009a, Vons et al 2011). Furthermore, it was shown that the spark discharge method may be used to produce bimetallic particles by employing electrodes made of two different materials or using alloyed or sintered electrodes (Tabrizi et al 2009b).

The variance in composition of the resulting particles is reported to be much higher when using electrodes of two different materials in comparison to alloyed electrodes. The average composition may be controlled by discharge characteristics to some extent when using two electrodes of different composition. However, since the average composition of particles from alloyed electrodes is known to be close to the feedstock composition, the use of alloyed or sintered electrodes appears to be the most promising route towards reliable production of bimetallic nanoparticles.

In this study, nanoparticles were produced using alloyed copper/nickel electrodes of varying composition. Copper and nickel were chosen as primary metals as these elements are known to produce homogenous alloys, i.e. they only form a single solid phase. Both materials, as well as their alloys, exhibit a face-centred cubic crystal structure with similar lattice constants.

Particle production was conducted using a spark discharge generator (c.f. Fig. 1) with conventional RCL-circuit (C=15 nF) and nitrogen as carrier gas The major part of the setup was evacuated and purged with nitrogen (purity 5.0) prior to production. Residual oxygen content in the inert gas was reduced by means of a gas purifier. The produced particles were collected in powder form after precipitation on a surface filter element. Samples were deposited on TEM grids by means of a dedicated low pressure impactor. Fig. 2. depicts the setup used in this investigation.

Mean particle composition was investigated using several techniques including ICP-OES, while STEM-EDX was used to determine the elemental distribution inside the produced nanoparticle agglomerates. Particle morphology and size was characterized by TEM while production rate was measured gravimetrically.

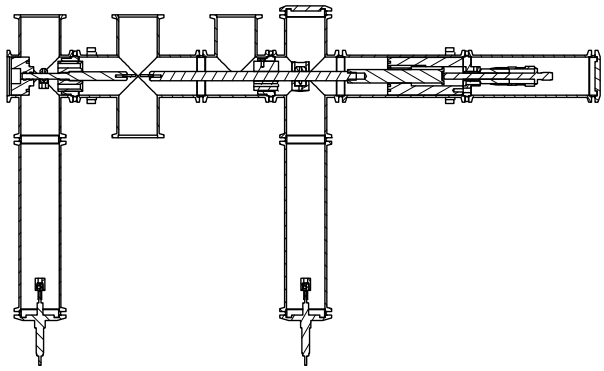

Figure 1. Cross-section of the employed spark discharge generator

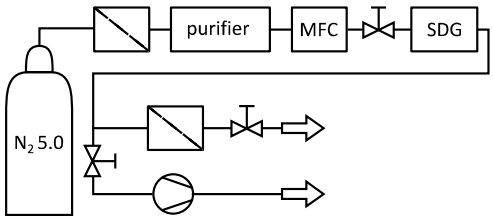

Figure 2. Schematic of the setup

The research leading to these results has received funding from the European Union's Seventh Framework Programme under Grant Agreement No. 280765 (BUONAPART-E).

Schwyn, S., Garwin, E. & Schmidt-Ott, A. (1988). Aerosol generation by spark discharge. *Journal of Aerosol Science* **19**, 639–642.

Tabrizi, N., Ullmann, M., Vons, V., Lafont, U. & Schmidt-Ott, A (2009a). Generation of nanoparticles by spark discharge. *Journal of Nanoparticle Research* **11**, 315–332.

Tabrizi, N., Xu, Q., van der Pers, N., Lafont, U. & Schmidt-Ott, A. (2009b). Synthesis of mixed metallic nanoparticles by spark discharge. *Journal of Nanoparticle Research* **11**, 1209–1218.

Vons, V., de Smet, L., Munao, D., Evirgen, A., Kelder, E., Schmidt-Ott, A. (2011). Silicon nanoparticles produced by spark discharge. *Journal of Nanoparticle Research* **13**, 4867–4879.

Simulation of the flow field in a nanoparticle synthesis spray flame reactor including a particle coating process

C. Weise, I. Wlokas and A. Kempf

Institute for Combustion and Gas Dynamics, Chair for Fluid Dynamics, University of Duisburg-Essen, Germany
and CeNIDE, Center for NanoIntegration and CCSS, Center for Computational Sciences and Simulation
Keywords: nanoparticle synthesis, CFD, spray flame, coating.
Presenting author email: claudia.weise.ivg@uni-due.de

Nanoparticles are widely used in consumer products, industrial applications and in the energy industry.

For the aerosol synthesis of nanoparticles, spray flame reactors are commonly used which enable high production rates of particles with different properties and structures. A liquid precursor-solution is injected into the reactor, atomized, evaporated and ignited, forming a self-sustaining spray flame. The nanoparticles are formed inside the flame through nucleation and condensation and increase due to growth, agglomeration and aggregation. Further downstream, the core-shell structured particles are coated continuously by injection of a secondary precursor (Teleki et al., 2008).

The efficiency of the particle production and the quality of the products depend on the thermodynamic state, the precursor and the particle residence time in the different zones of the reactor (Kammler et al., 2001, Teleki et al., 2009). The control and optimization of the synthesis process therefore requires knowledge of these parameters, which can be obtained from computational fluid dynamics (CFD). Figure 1 shows an example of the temperature distribution inside a spray flame reactor calculated with CFD and the stages of the process.

In this work, CFD simulations were used to investigate variations of process parameters and reactor geometry in order to find the best operating conditions. The investigated reactor (Hardt et al., 2011) is applied for synthesis of Silica (SiO_2) coated Titania (TiO_2) particles from Titanium-tetraisopropoxide (TTIP).

The calculations were performed in two stages: in the first stage, the spray flame was simulated in order to determine the shape and the quantity of the heat source in direct vicinity of the burner. The spray was modelled with an Euler-Lagrangian approach using a two-way coupling of flow and droplets considering the evaporation process. The turbulence was modelled using the k-epsilon closure and the combustion using the Eddy Dissipation approach.

For the second stage, the complete reactor including the coating nozzle was calculated using a simplified heat release model. This simplification enabled the simulation of a large number of geometry variants at acceptable cost. The dispersed particle phase was described using an Eulerian approach and the particle dynamics were modelled with a method of moments using a locally monodisperse particle size distribution (Kruis et al., 1993). The quality of the mixing in the coating zone was determined from the ratio of particle number concentration and secondary precursor concentration. This is a simplified estimate that does not consider the joint PDF of particle and precursor concentration. The transport equations for the dispersed phase and the population balance model were implemented in the framework of the open source CFD software OpenFOAM.

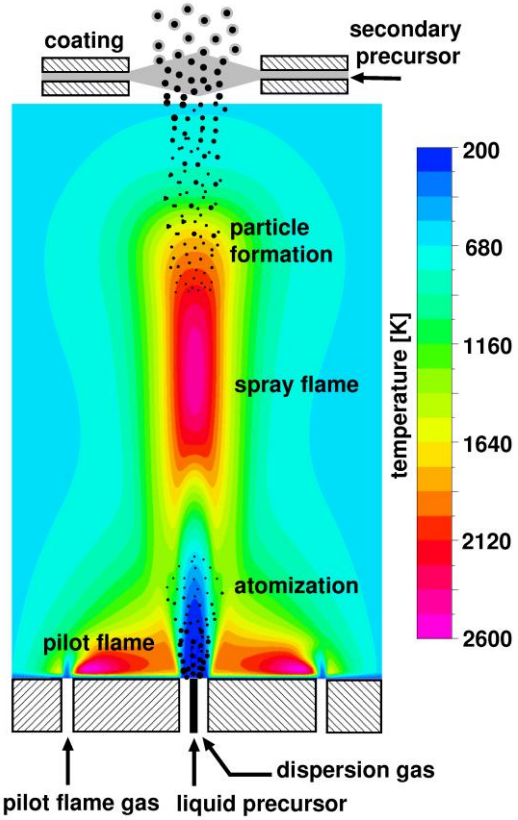

Figure 1: Temperature distribution and illustration of the particle production process inside a spray flame reactor.

Teleki, A., M.C. Heine, F. Krumeich, M.K. Akhtar, and S.E. Pratsinis (2008), *Langmuir*, 24, 12553-12558.

Kammler, H. K., L. Mädler, S. E. Pratsinis (2001), *Chemie Ingenieur Technik*, 73, 6, 708.

Teleki A., B. Buesser, M.C. Heine, F. Krumeich, M.K. Akhtar, S.E. Pratsinis (2009), *Industrial & Engineering Chemistry Research*, 48, 1, 85-92.

Hardt, S., A. Hamid, C. Weise, I. Wlokas, H. Wiggers and C. Schulz (2011), *Experimental and Numerical Investigation of Flame Spray assisted TiO2 Synthesis from Titaniumtetraisopropoxide*, 5th European Combustion Meeting, Cardiff.

Kruis, F.E., K.A. Kusters, S.E. Pratsinis (1993), *Aerosol Science and Technology*, 19, 4, 514-526.

Emission spectroscopic investigation of the spark discharge used for Cu nanoparticle production

A. Kohut[1], A. Metzinger[2], G. Galbács[2], L. Ludvigsson[3], B.O. Meuller[3], M.E. Messing[3], Zs. Márton[4], K. Deppert[3], and Zs. Geretovszky[1]

[1]Department of Optics and Quantum Electronics, University of Szeged, 6720 Szeged, Hungary
[2]Department of Inorganic and Analytical Chemistry, University of Szeged, 6720 Szeged, Hungary
[3]Department of Physics, Lund University, Lund, 22100, Sweden
[4]Department of Environmental Physics and Laser Spectroscopy, University of Pécs, 7624 Pécs, Hungary
Keywords: nanoparticles, spark discharge generator, spectroscopy
Presenting author email: linus.ludvigsson@ftf.lth.se

Copper nanoparticles (NPs) were generated by means of a spark discharge ignited between two copper electrodes in a flowing N_2 environment. The electrodes were powered by the simplest bipolar, capacitor charging layout. In these spark discharge generators (SDG) the particle formation is driven by the local melting and evaporation of the electrode material under the impact of the spark plasma followed by adiabatic expansion.

In order to obtain fundamental information on the NP formation process in an SDG, we carried out extensive time-resolved emission spectroscopic measurements of the electrode gap. To this end, a high sensitivity light collecting spectrometer system consisting of an Echelle spectrograph equipped with an intensified CCD detector (Andor Mechelle 5000 + Andor iStar 734-18F-03) was added to the SDG setup. Spatially integrated light was collected in a direction perpendicular to the electrodes' axis, via an optical fiber. Spectrometer operation was triggered from a passive high voltage probe (Tektronix P6015A) connected to the anode. The electro-optical setup allowed for the collection of the 300-800 nm spectral and 100 ns – 15 µs temporal ranges with an overall time delay of 95 ns and time resolution of 100 ns. Each spectrum was measured on separate sparks and 11 spectra were averaged at each delay.

The acquired emission spectra indicated the presence of atomic and ionized nitrogen (N^{2+}, N^+, N) and copper (Cu, Cu^+) species in the spark gap. N_2 and N_2^+ bands were not detected in the studied temporal window. Fig. 1 shows that after the ignition of the discharge, the emission of doubly ionized nitrogen peaks first at very early times (ca. 100 ns), followed by the emission from ionized nitrogen (at around 1 µs) already in a broader distribution. Emission from the atomic species of the electrode material and gas environment starts later and lasts significantly longer (10-12 µs in duration).

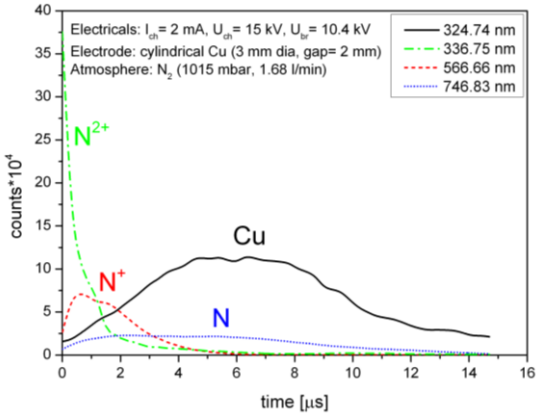

Figure 1. Temporal evolution of the emission of the species detected in the spark discharge.

We also collected time-resolved electrical data on the spark plasma, with the goal of exploring the influence of the settings at the capacitor charger (charging voltage and current) on the plasma and particle characteristics. The data in the present system in a N_2 environment clearly indicate that *i)* as long as the charging voltage is equal or higher than the breakdown voltage, the charging voltage has no influence on the plasma characteristics, *ii)* the charging current can not only influence the discharge frequency, but also the breakdown voltage and hence also the electrode material evaporation. These observations were also supported by the spectroscopic and particle characterization data, which will be discussed in detail in our presentation. For example, an increasing charging current decreased the breakdown voltage, indicated by a decrease in the intensity of all observed emission lines (equivalent with a drop in the number concentration of the related species in the discharge gap).

This work was supported by the European Union´s Seventh Framework Program (EU FP7) under Grant Agreement No. 280765 (BUONAPART-E) and by the TÁMOP programme of Hungary (No. 4.2.2.A-11/1/KONV-2012-0060).

Characterization of Carbon Nano-Particles from the Clad of Nuclear Fuel in HTGR with Inherent Safety (I) - Qualitative Analysis

H. Nishida[1], G. Iwanaka[1], H. Takano[1] and M. Itoh[1]

[1]Department of Chemical Engineering and Materials Science, Doshisha University, Kyoto 610-0321 JAPAN
Keywords: nuclear aerosol, nano-carbon particles, HTGR, inherent safety.
Presenting author email: dum0748@mail4.doshisha.ac.jp

High Temperature Gas-cooled Reactor (HTGR) with the absolute inherent safety is one of the Generation-III+ (Gen-III+) and -IV (Gen-IV) nuclear reactors. The absolute inherent safety means safety self-shutdown system inherency without any support from outside even in the case of electric power loss and/or mechanical breaks of the core control system of the reactor. The inherent safety of the reactor is ensured by the specific nuclear core design and the heat exchange system with He Gas. Although thus high inherent safety and wide industrial applicability using its very high temperature operation were installed even in the Gen-II HTGR, such types of nuclear reactor were not adopted for commercial nuclear power plants because of the higher costs both for construction and running than the current light water nuclear reactors as used in Fukushima and all others.

After the accident on 3.11 at the site-**I** of Fukushima, Topco, the situations drastically shifted from economics to safety in worldwide, and the new HTGR based on the thorium cycle will be emerging as a new solution on the several arguments concerning future energy safety. In HTGR, carbon graphite and He are used for the moderator and nuclear clad and the coolant, respectively. The inherency works well to prevent the meltdown of the nuclear core, however, the loss of cooling accident (LOCA) may cause severe radioactive contamination by the radio-activated carbon particles in the coolant generated from the carbon of the moderator and nuclear clad.

In this research, several characteristics of such carbon nano-particles were examined for the particles thus generated under very high temperature from the same type of carbon graphite used in HTGR for the designing an inline particle removal system of the primary cooling system in Gen-III+HTGR.

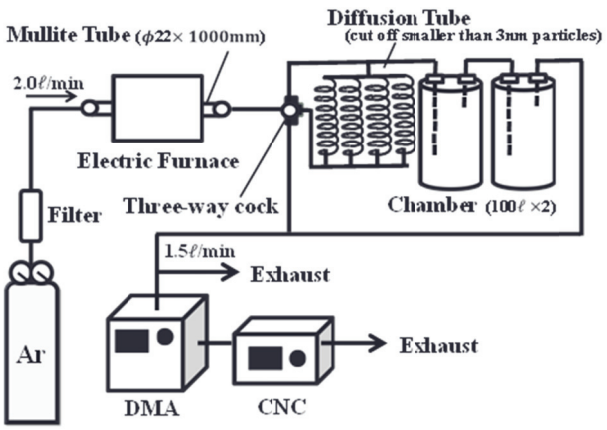

Fig. 1 The schematic diagram of experimental apparatus.

In the particle generation, two mechanisms were assumed: nucleation process after the sublimation of carbon and fragmentation of carbon graphite by thermal shock under very high temperature. **Figure 1** shows the schematics of experimental apparatus. Three alternating sampling paths were installed: (a) direct path, (b) particle growth one in chambers after via diffusion tube (3nm cut) and (c) simple particle growth one in the plenum chambers. The particles were measured by a CNC with DMA (TSI). To prevent the electric breakdown in DMA by carrier gas, Ar was applied as the gas instead of He. Ar was flowed into a Mullite™ tube heated at 1470K with the rate of 2.0ℓ/min. Carbon three pebbles (ϕ10mm, Toyo Tanso) made of IG-110 carbon, the same type of carbon used in HTGR and PBMR (Sumita, et al, 2006), were set at the center of the Mullite tube.

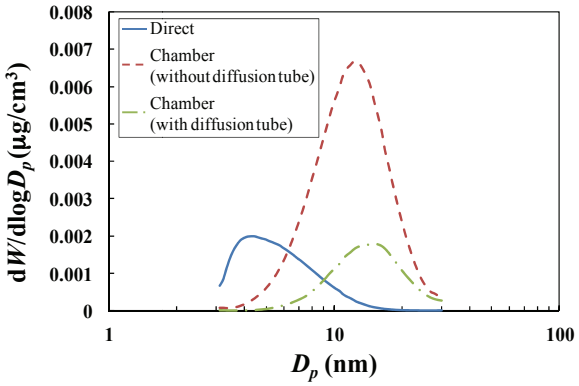

Fig. 2 Moving averaged mass size distributions of generated from carbon pebble heated at 1470K.

Figure 2 shows the mass concentration distribution of the three alternating paths; the data were modified with the moving averaged method of 5 points to avoid unconditional ambiguities. The total mass of carbon particles of the paths were (a) 5.771μg/cm^3, (b) 10.76μg/cm^3 (c) 47.13μg/cm^3. The mass of (b) and (c) became larger than that of (a). It was because the carbon vapor and the particles smaller than the sensing range of CNC (3nm) grew up to the range after condensation and coagulation in the chambers (residence time: 5000s). The mass difference of the two cases through chambers shows the true mass of the vapor and the small particles. From the comparison of the three mass data, it was made clear that major mass fraction of the particles was the fragmentation rather than the nucleation via sublimation, and the design of particle removal system should be focused in the mechanism of around 10nm in diameter.

Sumita, J. et al., (2006) JAEA-Technology, **48** (1), 1-19.

Synthesis and characterization of calcium oxide based particles for CO_2 adsorption applications

K.G. Sakellariou[1, 2], G. Kastrinaki[1,3], G. Karagiannakis[1] and A.G. Konstandopoulos[1,2]

[1]Aerosol & Particle Technology Laboratory, CERTH/CPERI, Thessaloniki, P.O. Box 60361, 57001, Greece
[2] Department of Chemical Engineering, Aristotle University, Thessaloniki, PO. Box 1517, 54006, Greece
[3] Department of Mechanical Engineering, University of W. Macedonia, Kozani, 50100, Greece

Keywords: calcium oxide particles, CO_2 capture, aerosol spray pyrolysis.
Presenting author email: ksakella@cperi.certh.gr

It is generally accepted that the significant increase in atmospheric carbon dioxide (CO_2) concentration is strongly linked to the greenhouse effect. Therefore, CO_2 capture and storage or utilization have emerged as critical research areas that require the development of inexpensive materials with large and stable CO_2 adsorption capacity.

Calcium-based sorbents constitute a group of materials that are promising for CO_2 storage applications (Choi et al, 2009). Calcium Oxide (CaO), also known as quicklime, is a widely used and inexpensive chemical compound. It is manufactured by thermal decomposition of abundant materials (e.g. limestone or chalk), which mainly consist of $CaCO_3$. CaO, among other uses, is also a promising candidate for CO_2 capture from fossil-fuel based power plants (Schaube et al, 2011).

CO_2 capture and release, with the aid of CaO, is based on a carbonation-calcination reaction cycle at high temperatures, as described by the following scheme:

$$CaO_{(solid)} + CO_2 \xrightarrow{\sim 700^\circ C} CaCO_{3(solid)} \quad \Delta H^\circ_{298} = -178 \text{ kJ/mol} \quad (1)$$

$$CaCO_{3(solid)} \xrightarrow{\sim 900^\circ C} CaO_{(solid)} + CO_2 \quad \Delta H^\circ_{298} = +178 \text{ kJ/mol} \quad (2)$$

The aim of the current study was to prepare CaO-based materials with higher surface area than commercial materials and also to exhibit structural and morphological stability at high temperatures and in particular during the aforementioned two-step process (Eq. (1)-(2)).

To this respect, CaO-based, as well as composite calcium oxide particles were synthesized by Aerosol Spray Pyrolysis (ASP) (Karadimitra et al, 2001) and by Liquid Phase Self-propagating High temperature Synthesis (LPSHS) methods. In ASP, a precursor solution is atomized into fine droplets, which act as micro-reactors undergoing evaporation of the solvent and precipitation of the reacting material. In LPSHS the total precursor amount is processed in a single reactor and involves gradual solvent evaporation which, in the presence of a fuel, results to a combustion reaction.

The effect of the synthesis method and of the precursor materials utilized in each case was studied in order to comparatively identify the obtained particles morphologies and their preliminary performance in the aforementioned CO_2 capture and release scheme.

The materials morphology was examined by Transmission and Scanning Electron Microscopy (TEM & SEM), showing a nearly spherical morphology for the ASP-synthesized particles (Fig. 1) and irregularly shaped, open-structure particles for the LPSHS-synthesized materials.

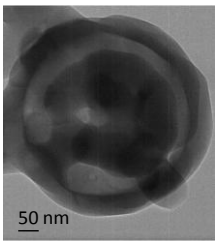

Figure 1. TEM image of $CaO/Ca_{12}A_{l4}O_{33}$ particle by ASP.

CaO-based materials were also structurally characterized by X-Ray Diffraction (XRD). It was indicated that $Ca_{12}A_{l4}O_{33}$ was the predominant phase in the ASP-particles, while the $Ca_3Al_2O_6$ phase was identified as the main compound in the LPSHS samples.

Surface area and pore size measurements were conducted by BET analysis. The materials had a surface area in the range of 3-10 m^2/g, depending on the process synthesis conditions with the ASP-prepared powders exhibiting higher surface area than the LPSHS-synthesized particles (Table 1).

Table 1. Comparison of the surface area of the ASP and LPSHS-obtained particles.

Method	BET (m2/g)
ASP	10.57
LPSHS	3.02

The CO_2 adsorption capacity was evaluated by Thermogravimetric Analysis (TGA), as well as with the aid of fixed bed reactor experiments.

Choi S., Drese J.H., Jones C.W. (2009), *Chem. Sus. Chem.*, **2**, 796 – 854.

Schaube F., Wörner A., Tamme R. (2011), *J. Sol. En. Eng.*, **133**, 031006-1 – 031006-7.

Karadimitra K., Papaioannou E., Konstandopoulos A.G (2001), *J. Aerosol Sci.*, **32**, Suppl. 1, S233-234.

Detection of Airborne Carbon Nanotubes via Embedded Nickel Catalysts in Quasi-Real Time

N. Neubauer[1] and G. Kasper[1]

[1]Karlsruhe Institute of Technology (KIT), Institute for Mechanical Process Engineering and Mechanics, Karlsruhe, 76131, Germany
Keywords: carbon nanotubes, nickel, CAAM, quasi-real time
Presenting author email: nicole.neubauer@kit.edu

Workers involved in the production and handling of carbon nanotubes (CNT) are likely to be at a high exposure risk. As CNT are supposed to be harmful to human health, their detection in the workplace air is highly desirable. In a recent publication (Neubauer et al., 2011) we introduced a new measurement technique for the material-specific detection of catalytically active nanoparticles (e.g. nickel) with a high sensitivity. Based on this concept we have developed a compact and portable laboratory prototype which we call the Catalytic Activity Aerosol Monitor (CAAM; Figure 1, left side) (Neubauer et al., 2013). In this study, this new type of detector is investigated with respect to its capability to detect airborne CNT aerosols via embedded nickel catalysts.

Experimental

As a catalyst for the generation of CNT, a nickel aerosol was produced by spark discharge. The addition of acetylene and hydrogen at 600°C led to an on-line formation of CNT by aerosol chemical vapour deposition (aerosol-CVD). For the detection by the CAAM, defined volumes of both the CNT and the nickel aerosol were sampled onto filters. After sampling was completed, pre-mixed and pre-heated gaseous reaction educts were added initiating a catalytic reaction. As model reactions for the detection of CNT via embedded nickel catalysts, the hydrogenation and the oxidation of CO were chosen. The composition of the reaction gases was measured by an IR sensor, hereby providing a measure for the catalytic activity of the nickel particles. In addition, both the nickel and the CNT aerosol were characterized by electrical mobility spectrometry, electron microscopy (TEM) and thermogravimetry.

Results

Electron microscopy analysis resulted in a median primary particle size of 3.5 nm for the nickel nanoparticles. They are arranged in agglomerates with a mode of the mobility equivalent diameter of 74 nm. Figure 1 (right side) shows a TEM image of CNT with embedded nickel catalyst nanoparticles.

While the mass of the pure nickel particles was stable during thermogravimetry (20-950°C), the CNT evaporated at a temperature of 420°C. However, this temperature is higher than the required reaction temperature of 350°C for both the CO-hydrogenation and the CO-oxidation. With this the CNT did not evaporate during CAAM analysis.

The catalytic experiments showed a proportional dependence of the catalytic activity on the sampled volume for the pure nickel nanoparticles. As no catalytic signal could be detected for the CNT aerosols, the embedded nickel nanoparticles seemed to be not accessible for catalysis. However, if the CNT were burnt away in an intermediate step by adding a mixture of oxygen and nitrogen at 500°C to the sampled CNT, the nickel nanoparticles could be detected again by the CAAM.

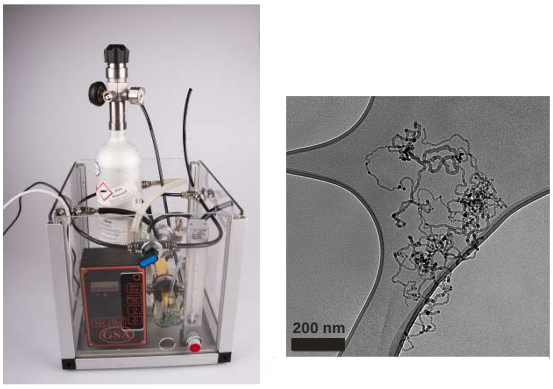

Figure 1. Left side: Catalytic Activity Aerosol Monitor (CAAM), Right side: TEM image of CNT with embedded nickel catalyst nanoparticles

Conclusion

An intermediate step of CNT burning between aerosol sampling and the catalytic reaction enables the detection of formerly embedded catalyst nickel nanoparticles by the CAAM. With this, the CAAM technique also allows the detection of CNT aerosols in workplace air in quasi-real time.

References

Neubauer N, Weis F, Binder A, Seipenbusch M and Kasper G. (2011) *Journal of Physics: Conference Series 304 (1)*

Neubauer N, Seipenbusch M and Kasper G. (2013) *Annals of Occupational Hygiene (accepted)*

The research leading to these results has received funding from the European Commission's Seventh Framework Programme (FP7/2007-2013) under grant agreement n° 211464-2 (Nanodevice).

Acute respiratory response on workers exposure to nanoparticles in different occupational settings

I. Szadkowska-Stańczyk, S. Bujak-Pietrek, and U. Mikołajczyk

Department of Environmental Health Hazards, Nofer Institute of Occupational Medicine, Lodz, , 91-348, Poland
Keywords: nanoparticles, pulmonary function, occupational exposure
Presenting author email: irenasta@imp.lodz.p

Introduction

Information about the risk of nanotechnology and its influence for human health is still out of our knowledge. Scientific study results on the route of exposure, and further penetration of nanoparticles into different tissues and organs are very limited. The respiratory system seems to be main routes which nanoparticles emitted into the environment can get into the body and easily achieve the smallest bronchi and alveoli.

Number of workers involved with nanotechnology is still increasing. Occupational exposure to nanoparticles concerning the workers engaged directly in manufacture or processing of nanomaterials, but also the people using these nano-products for the production of other goods as well as the consumers.

Epidemiological study have shown that exposure to airborne nanoparticles is correlated with adverse health effects, particularly increased pulmonary and cardiovascular responses.

Aim:

The aim of this study was to analyse nanoparticle exposure in different occupational settings and its effects on cross-shift changes in workers respiratory airflow.

Methods:

The nanoparticles exposure assessment included determination the number concentration of nanoparticles (CPC TSI model 3007-2) and the surface area concentration of particles potentially deposited in alveolar (A) and tracheo-bronchial (TB) region of lungs (AeroTrak 9000 TSI).

Cross-shift spirometric measurements were performed using portable spirometer and changes in FEV1 (ΔFEV1) were calculated.

The workposts under measurements were:

- abrasion of textile coating containing nano-Ag and nano-Cu
- manual plastering and grinding of mortar containing nano-SiO2
- abrasion test of dental materials with nanoparticles
- manual abrasion of dental components with nanoparticles

Results:

The number concentration of released particles ranged from 1500 p/cm3 during manual abrasion of dental components to 20000 p/cm3 during plastering and grinding of mortar. Similar situation concerned the surface area concentration. The highest value of surface area concentration of particles in A and TB region were observed during manual plastering and grinding of mortar and there were respectively 65,2 µm2/cm3(A) and 14,1 µm2/cm3(TB).

Analysis of FEV1 values before and after work-shift showed decrease of this parameter in most workers under study. There was observed slight correlation between number concentration of released nano-sized particles and FEV 1 decrease.

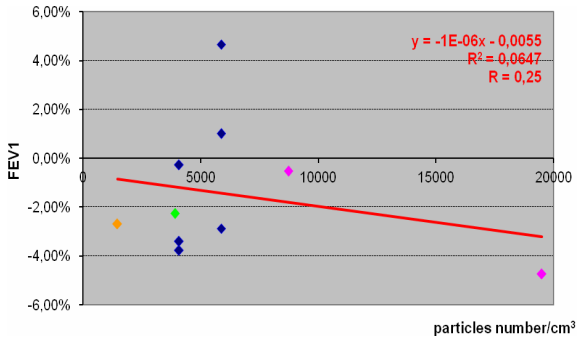

Figure 1. Relationship between the number concentration of nanoparticles and spirometric parameters changes

Slight correlation was observed also between surface area concentration and cross-shift declines in FEV1.

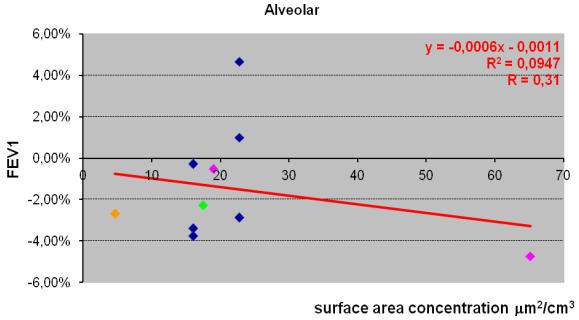

Figure 2. Relationship between the surface area concentration of particles potentially deposited in A region and spirometric parameters changes

Conclusion:

Our results suggest that exposure to nanoparticles released in different processes could be considered as a factor influencing the activity of the respiratory system and further studies should be done to prove this relationship.

This work was supported under grant agreement nr 5052/B/P01/2010/38.

Testing particulate matter toxicity via *in vitro* methods: what should be tested?

A.J. Wlodarczyk[1], K.A. BéruBé[1]

[1]School of Biosciences, Cardiff University, Museum Avenue, Cardiff CF10 3AX, Wales, UK
Keywords: particulate matter, nanoparticles, cytotoxicity, reactive oxygen species
Presenting author email: annajuliawlodarczyk@gmail.com

Unlike other toxic substances, usually of a known chemical formula, air particulate matter (PM) is a mixture of solid and liquid particles. The most frequently used tests are *in vitro* in nature and examine 'cell viability' following 24-hour exposure to PM. In most cases, PM induces sub-toxic viability responses but other key cell functions are not detected.

The aim of this study was to compare the toxicity profiles of engineered NPs: zinc oxide (ZnO), crystalline form of silicon oxide (SiO_2), and nickel (Ni), which are frequently present in ambient air pollution. Three different assays (acellular and cellular) were chosen to test PM biological targets: (1) plasmid scission assay – detecting DNA damage (indicative of the ability to produce reactive oxygen species; ROS; Figure 1); (2) haemolysis assay – informing about red blood cells (RBCs) membranes integrity; (3) proliferation assay inspected on HUVEC (human umbilical vein endothelial cells) at 24, 48 and 72 hours post-exposure to NPs.

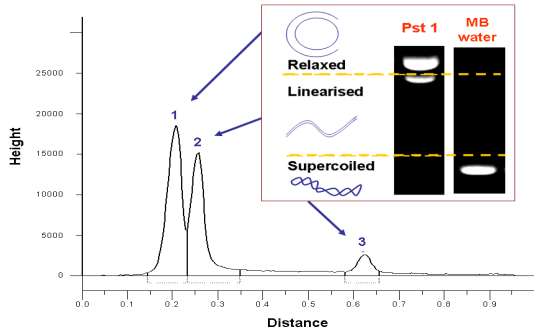

Figure 1. Identification and quantification of plasmid X174 RF DNA isoforms. ROS converts 'supercoiled' (undamaged) into 'relaxed' and 'linearized' isoforms.

DNA damage was observed at a dose of 1 µg/ml for ZnO and Ni NPs. Severe damage (90%) was caused by Ni NPs at a dose of 1 mg/ml. Silica particles caused no damage over the dose range (Figure 2).

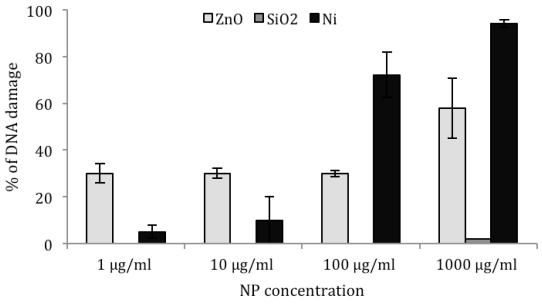

Figure 2. NPs impact on plasmid DNA.

Only SiO_2 NPs caused leakage of haemoglobin from RBCs (Figure 3).

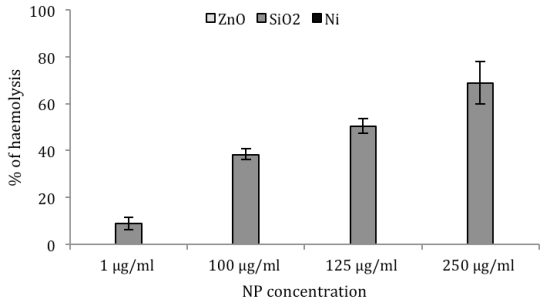

Figure 3. NPs disruption of RBCs membranes.

Results from proliferation assay showed that the most toxic NPs were ZnO, at a dose of 50 µg/cm^2, killing nearly all cells after 24 hours. The same dose of Ni NPs decreased the number of cells by 50% and significantly reduced cell proliferation in the second and third days of incubation. In contrast, SiO_2 NPs caused no change in cell viability after 24 hours of incubation. However, after 48 and 72 hours, proliferation was inhibited by 40% and 50%, respectively.

Concluding, exposure to NPs, which constitute PM, causes multi-factorial biological responses that may only be detected through a panel of bioassays that target key biological responses. For example, metal NPs (Zn, Ni) induce DNA damage and exert immediate endothelial cell death, whereas only crystalline quartz disrupts membrane integrity and its effect on cell proliferation could be seen in long-term exposure. Therefore, toxic effects of PM may be multi-directional, as different components of PM may influence different properties of a cell.

This work was supported by Doctus - Malopolski Scholarship Fund for PhD students co-funded by the European Social Fund, and PhD research project N N404 102 639

Wlodarczyk, A.J. (2012) (2012) *The influence of particulate matter nanoparticles on bronchial epithelium and vascular endothelium - new mechanisms of adverse health effects of industrial air pollution,* PhD dissertation, Jagiellonian University, Cracow, Poland

The impact of zinc oxide nanoparticles on metabolic activity in the cells of respiratory and reproductive system

L. Zapór

Central Institute for Labour Protection - National Research Institute, Czerniakowska 16, 00-701 Warsaw, Poland
Keywords: bioavailability, oxidative stress, zinc oxide nanoparticles.
Presenting author email: lizap@ciop.pl

Because of expanding application of zinc oxide nanoparticles (ZnO-NPs) for industrial purposes, unintended human exposure in the work environment is highly probable, hence an evaluation of potential toxicity of ZnO-NPs is necessary. It is reasonable it more, that toxicological data on the toxicity of ZnO-NPs are inconclusive. The aim of this study was to assess the impact of ZnO-NPs on reactive oxygen species (ROS) formation in the cells of respiratory and reproductive system depending on the particle size of ZnO-NPs.

Toxicity of different sizes of ZnO particles, i.e., ZnO nanopowders (ZnO<50 nm; ZnO<100 nm particle size), microsized metallic ZnO powder (ZnO-micro) and stabilized commercially dispersion of ZnO<100 nm was evaluated on four cellular lines: Chinese hamster ovary cells (CHO), mouse testicular Sertoli cells (15P-1), human pulmonary cancer cells (A549) and mouse macrophage cells (RAW264.7) after 24-hour exposure. ZnO-NPs were characterized in terms of particle morphology by scanning electron microscopy (SEM) and particle size distribution by dynamic light scattering (DLS) methods.

The effect of ZnO-NPs on cell viability, metabolic activity, lipid peroxidation, generation of intracellular ROS and total oxidative and antioxidative capacity of cells was studied. Additionally bioavailability of zinc [Zn^{2+}] for cells was assessed by proton induced X-ray emission analysis (PIXE).

The SEM and DLS methods confirmed that there was a size difference between the ZnO-NPs, but there was strong tendency to aggregation of particles. All tested ZnO-NPs induced a dose-related negative effect on cell viability and caused oxidative metabolism disturbance assessed on the basis of lipid peroxidation (Fig. 1), intracellular ROS generation and total oxidative/antioxidative capacity of cells. It is worth noting that increase in total oxidative status of cells was observed at concentrations lower than cytotoxic doses. These results suggest that the toxicity of ZnO-NPs is caused by elevated oxidative stress.

The results of toxicity correspond well with the results of bioavailability of zinc oxide particles. The zinc oxide particles forming aggregates were weakly available for the cells so less toxic (Fig.2).

Conclusion: Determination of the physicochemical parameters of the nanoparticles is of fundamental importance in exposure assessment, since the physical properties (particle size distribution, state of aggregation) affect the toxic potency of nanomaterials. The phenomenon of aggregation of nanoparticles may be conducive working environment because it reduces their bioavailability and toxicity.

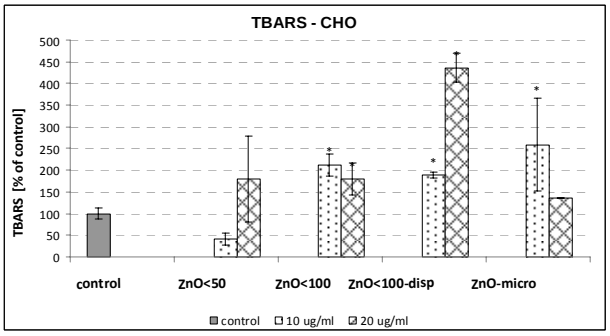

Figure 1. A comparison the effect of ZnO-NPs on lipid peroxidation in CHO cells. Cells were treated with 10, and 20 ug/ml ZnO for 24 h and controls received culture medium only. The thiobarbituric acid assay (TBARS) was used to detect lipid peroxidation. Results expressed as % of control. Each bar represents an average value ± S.D. of at least three independent experiments.

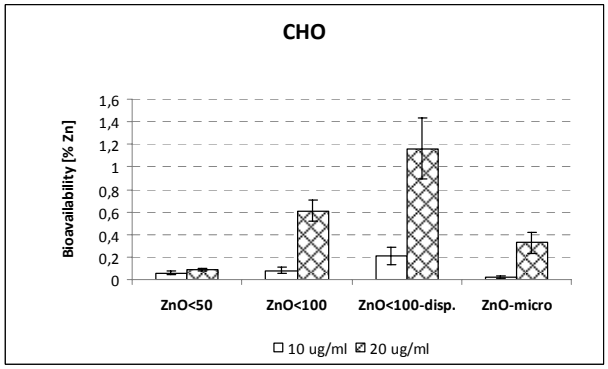

Figure 2. A comparison the bioavailability of Zn[2+] in CHO cells exposed to equimolar concentrations of ZnO-NPs compared to the concentration of Zn[2+] in the solution [%]. Each bar represents an average value ± S.D. from at least three experiments

Acknowledgement: This publication has been based on the results of a research task carried out within the scope of the second stage of the National Programme “Improvement of safety and working conditions” partly supported in 2011–2013 — within the scope of research and development — by the Ministry of Science and Higher Education/National Centre for Research and Development.

A new device for continuous unattended measurements of UFP

M. Pesch[1], H. Grimm[2], R. Albrecht[3], A. Edfelder[4],

Grimm Aerosol Technik GmbH & Co. KG, 83404 Ainring, Germany
Keywords: Ultrafine Particles, UFP, Environmental CPC, Network, semi volatile components (SVC)
Presenting author email: mp@grimm-aerosol.com

Although ultrafine particles account only for a little share in the total mass concentration, they are under a cloud of being harmful to health (Wichman und Peters, 2000). For this reason an additional monitoring of this particle fractions´ exposure is absolutely necessary. First steps of continuous measurements of ultra fine particles have already been realized in our systems like the Grimm 665 Wide Range Aerosol Spectrometer. Due to the temporal resolution of the integrated mobility spectrometer (SMPS) as well as its comparatively high costs it is unsuitable for an area-wide monitoring of the total particle concentration. A more competitive alternative for measuring the particle exposure in the nanometer range and simultaneously having a high temporal resolution of 1 second is a our special environmental Condensation Particle Counter (CPC).

We present a new system (465 UFP) which is based upon the Grimm CPC 5.4 product line, and is absolutely qualified for continuous measurements of the particle exposure in the nanometer range. The device is performed for long term unattended measurements, e.g. in measurements networks or at hot spots (Figure 1).

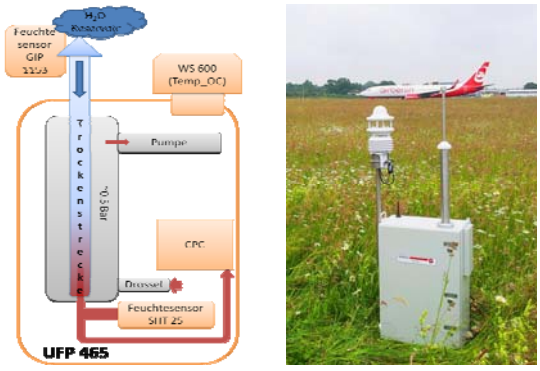

Figure 1: Schematic assembly of the 465 UFP (left) as well as a field measurement at the airport Hamburg (right)

Count efficiency, dryer performances and particle losses in the inlet pipe have been characterized comprehensively and comply by now with the already existing recommendations of the standard working group CEN/TC 264/WG 32 for an environmental CPC.

On the basis of field measurements next to the runway and the A1 (German Autobahn 1) near Osnabrück the impressive performance as well as further fields of application of the 465 UFP will be introduced and discussed.

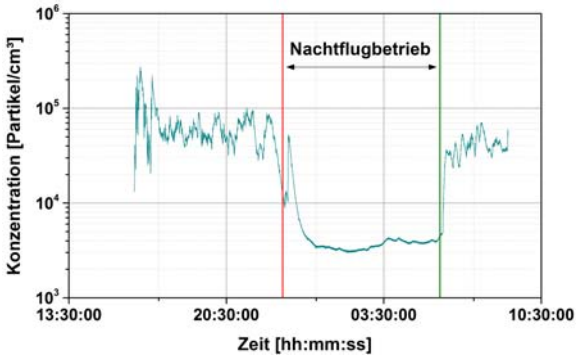

Figure 2: Temporal development of the particle exposure next to the runway of the airport Hamburg.

H. E. Wichmann und A. Peters (2000), Epidemiological evidence of the effects of ultrafine particle exposure, *Philosophical Transactions of the Royal Society of London, Series a, Mathematical Physical and Engineering Sciences*, 358 (1775): 2751 _ 2768, 2000.

Portable device for simultaneous measurements of Nano particles and it agglomerations at workplaces

H. Grimm[1], M. Pesch[2], M. Richter[3], A. Comouth[4]

Grimm Aerosol Technik GmbH & Co. KG, 83404 Ainring, Germany
Keywords: aerosol instruments, Nano particles, particle size distributions, work place measurements
Presenting author email: mp@grimm-aerosol.com

Measurements of particle size distributions for Nano particles and particles in the µ-meter size range generally requires a combination of separated devices as SMPS and optical particle counters (OPC) or aerodynamic particle sizers (APS). Especially the SMPS is complex, quite heavy and not always easy to use. This technique generally needs a radioactive source as Kr85 or AM241 for a well defined charging equilibrium of the aerosols that reduces flexibility at workplaces.

The company GRIMM developed in the frame of the EU founded Project NANODEVICE a new compact and portable device that consists of an electrical and an optical aerosol sensor. The device allows the simultaneous measurements of Nano particles and it agglomerations: it allows particle size detections between 10 nm and 25 µm with 42 size channels. The time resolution of one complete scan is 1 minute. The system is compact, easy to use and does not need any consumables. A radioactive source is not required.

Figures 1 and 2 demonstrate measurements that have been carried out at workplaces. The objective of the measurements shown is number, size and mass of particles caused by soldering processes.

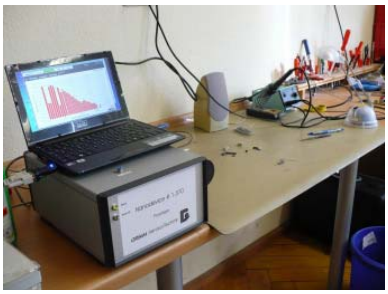

Figure 1: Measurements at workplaces, determination of background concentration

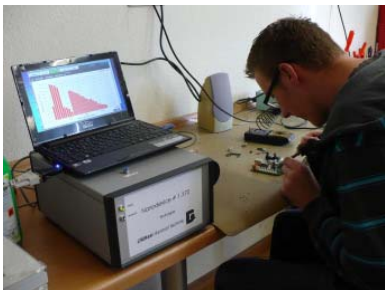

Figure 2: Measurements at workplaces, determination of all particles caused by soldering

An example measurement results is shown in figures 3 and 4. The soldering process has caused a high increase of very small Nano particles. These particles are mainly caused by condensation processes of volatile components: Figure 3 shows that during soldering between 15:28 and 15:29 total concentration of Nano particles exceeded concentrations of 350,000 particles/cm³ whereas the background concentration was less than 10,000 particles/cm³. The size distribution has shown that these particles are mainly in the range of 15 nm to 20 nm.

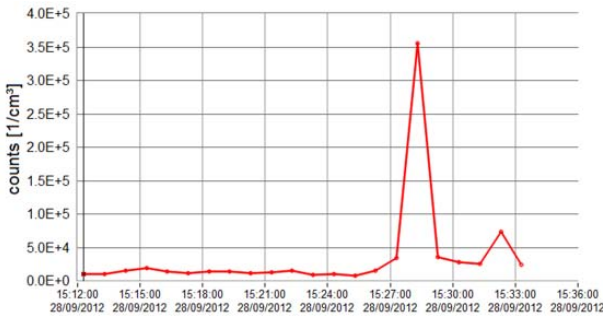

Figure 3: Number concentration of particles during soldering

An interesting point is the distribution of particle masses during soldering. The mass is determined by the particles caused by the soldering process size range from 15 nm to 40 nm but also by particles larger than 2 µm (figure 4). These large particles have been formed by agglomeration processes of primary Nano sized particles. A small amount was also caused by the background concentration.

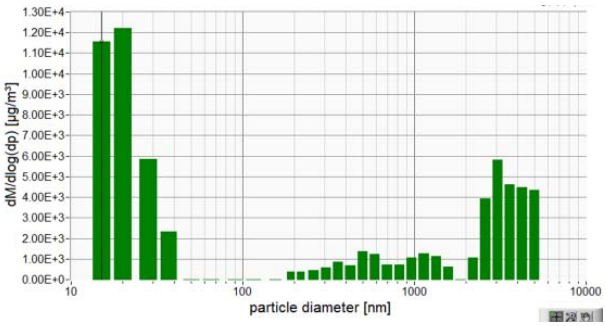

Figure 4: Mass distribution of particles during soldering

Combustion of CNT-containing composite materials in a laboratory scale incinerator

A.M. Todea[1], B. Stahlmecke[1], C. Asbach[1] and T.A.J Kuhlbusch[1, 2]

[1] Air Quality & Sustainable Nanotechnology, Institute of Energy and Environmental Technology (IUTA), Duisburg, 47229, Germany

[2] CENIDE, Center for Nanointegration Duisburg-Essen, 47057, Duisburg, Germany

Keywords: composite, CNT, incineration, emission.

Presenting author email: tky@iuta.de

Currently, there is growing interest in industry for nanoparticles and nanocomposites due to their wide range of applications. Since a large amount of the composite materials will finally be incinerated once their functional life has come to an end, it is important to know whether municipal waste incinerators have the ability to completely remove the additives from the flue gases or solid residues (slag), thus avoiding their emission to the environment.

An increasing number of experimental and commercial composite materials use carbon nanotubes (CNTs) in order to improve material properties like electrical conductivity or mechanical strength. The aim of the study presented here was to investigate whether CNTs may be released under the simulated conditions in a municipal waste incinerator due to incomplete combustion as part of the (fly) ash or slag. The operating parameters were chosen in order to fulfill the minimum requirements for municipal waste incinerators set forth in the 17th Ordinance on the Implementation of the Federal Immission Control Act ("17th BImSchV").

To simulate a municipal waste incinerator in the lab, two tube furnaces (Carbolite, models CTF 12/65/550 and TZF 12/65/550) were used in series, connected with a quartz glass tube. A ceramic crucible was used as sample container and means of transport of the composite material in the first furnace. While the first furnace was used to mimic the incineration of the composite material, the second furnace was used to simulate thermal after treatment of the exhaust gases. A primary air flow (compressed air with 21 % oxygen content, 14 l/min) was fed to the quartz tube from the entrance of the first furnace. A secondary air flow (7 l/min) was added to the second furnace to maintain the minimum legal requirements regarding the minimal O_2 concentration of 6 % and the 2 s residence time at 850 °C for thermal after treatment.

Three different composite materials, i. e. polycarbonate (PC), polyamide (PA) and polyethylene (PE) with different CNT amounts (0 wt%, 5 wt% and 7.5 wt%, Baytubes C150P® with a typical diameter of approximately 20 nm – 30 nm and a typical length after post-production treatment below 5 µm) were investigated. The particle size distribution in the exhaust gas that resulted during incineration of the composite materials was measured using a Fast Mobility Particle Sizer (FMPS, Model 3091, TSI Inc). Furthermore, the released fragments were electrostatically sampled with a Nanometer Aerosol Sampler (NAS, Model 3089, TSI Inc) and analysed using scanning electron microscopy (SEM, JEOL 7500F). The oxygen content was measured with 1 s time resolution towards the end of the second furnace together with other gas components using a multi component gas analyzer (NGA 2000 MLT 5).

The particle size distributions were comparable for all materials, with count median diameters (CMD) in the range 113 nm to 132 nm and total number concentrations in the range 1.07×10^7 #/cm³ to 2.11×10^7 #/cm³ (Table 1). The composite materials with different amounts of CNTs showed slightly lower number concentrations and larger CMD.

Table 1. Measured total number concentration and count median diameter (CMD) of the particle size distribution along with standard deviations.

Material (10 reruns for each material)	Conc. (#/cm^3) $\times10^6$	SD	CMD (nm)	SD
PC no CNT	21.1	1.4	131	0.8
PC + 5% CNT	14.8	2.1	132	1.1
PC + 7.5% CNT	15.9	1.8	132	1.1
PA no CNT	18.3	1.1	113	1.5
PA + 5% CNT	10.7	1.6	127	1.7
PA + 7.5% CNT	10.7	1.9	124	2.5
PE no CNT	19.9	3.4	121	4.1
PE + 5% CNT	15.1	2.7	128	1.2
PE + 7.5% CNT	15.5	1.9	128	1.7

The FMPS results showed no indication for largely different number size distributions for materials with and without CNTs. Also the SEM images of the NAS samples did not show any evidence for airborne free CNTs. Considering that the flue gases from an incinerator get filtered before they are released into the atmosphere, it can be concluded that a release of CNT from municipal waste incinerators into the atmosphere is rather unlikely.

This work has been conducted within the CarboSafe project that has received funding (Grant No. 03X0043D) from the German Federal Ministry for Education and Research (BMBF) as part of the InnoCNT initiative.

17th BImSchV, (2003) *Siebzehnte Verordnung zur Durchführung des Bundes-Immissionsschutzgesetzes (Verordnung über die Verbrennung und die Mitverbrennung von Abfällen, in der Fassung der Bekanntmachung vom 14.08.2003*, BGBI. I S. 1633.

Characterization of Polyamide Nanofiber Media for Aerosol Filtration Applications

J. Matulevicius, L. Kliucininkas, D. Martuzevicius

Department of Environmental Engineering, Kaunas University of Technology, Radvilenu pl. 19, LT-50254 Kaunas, Lithuania

Keywords: Filter media, nanofiber, air filtration, electrospinning

Presenting author email: jonas.matulevicius@gmail.com

Introduction

The aim of the study was to form polyamide (PA) nanofiber media with properties suitable for air filtration applications. In order to develop filter media with suitable characteristics authors have performed series of experiments with polyamide 6 and polyamide 6/6. Polyamide is strong, somewhat flexible material that can take small impacts and resist some pressure while being bent.

The electrospinning method was applied to form nano fiber media. The electrospinning parameters, such as voltage, tip to collector distance, and collection time were investigated.

The comparative characterization of PA fibers was focused on fiber size, solidity of the fibers and thickness of filter media. All these characteristics are important to achieve high filtration efficiency and reduce pressure drop.

Experimental

The homogeneous solutions were obtained by dissolving PA 6 and PA 6/6 pellets in several systems of solvents: formic acid, formic acid/acetic acid 3/2 (v/v), and formic acid/dichloromethane 3/1 (v/v). The solutions were sprayed by syringe pump (LSP01-1A, Longerpumps, PRC) with a syringe needle of internal diameter of 0.7 mm. Electrospun fibers were collected on a vertically positioned cylindrical collector coated with aluminium foil and rotating at a linear speed of 150 cm/min.

The morphology, diameter, and thickness of the PA fibers and media were investigated by using scanning electron microscope (Hitachi S-4800, Japan) and atomic force microscopy (Asylum Research MFP-3D,USA). The basis weight was defined using ultra-microbalances (UYA 3Y, Poland). The solidity of the fibers was calculated from the experimental data.

Results

The range of electrospinning parameters and characteristic values of the filter media are presented in Table 1. The relationships between the solution concentration and fiber diameter (Fig. 1) show that both PA 6 and PA 6/6 follow similar trends of increasing diameters with increasing concentrations of polymers. The minimal fiber diameter of 60 nm was observed for PA 6/6.

It was found that collection time and tip-to-collector distance are the major parameters of electrospinning that have effect on the characteristics of nanofiber media. Basis weight and thickness characterize solidity of the media and have direct influence on the filtration parameters. We noticed that due to the lower length of polymer chain PA 6 tended to form spider-net structure. Spider-net (ultrafine fibers) was formed between the regular fibers and increased surface to volume ratio of filter media. At the same time it contributed to a higher mechanical strength of the filter media.

.

Table 1. The parameters of electrospinning and characteristic values of fiber media $\left(\frac{\min \div \max}{median}\right)$

El-spinning parameters	Concentration, % w/v	Voltage, kV	Distance, cm	Collection time, min
PA 6/6	$\left(\frac{8 \div 14}{11}\right)$	$\left(\frac{12 \div 20}{16}\right)$	$\left(\frac{6 \div 12}{9}\right)$	$\left(\frac{5 \div 20}{10.5}\right)$
PA 6	$\left(\frac{20 \div 28}{24}\right)$	$\left(\frac{12 \div 20}{16}\right)$	$\left(\frac{6 \div 12}{9}\right)$	$\left(\frac{5 \div 20}{10.5}\right)$
Filter media	**Diameter, nm**	**Basis weight, g/m^2**	**Solidity**	**Thickness, µm**
PA 6/6	$\left(\frac{60 \div 376}{218}\right)$	$\left(\frac{0.12 \div 1.16}{0.64}\right)$	$\left(\frac{0.01 \div 0.17}{0.09}\right)$	$\left(\frac{1.3 \div 8.4}{4.85}\right)$
PA 6	$\left(\frac{99 \div 234}{166.5}\right)$	$\left(\frac{0.11 \div 1.07}{0.59}\right)$	$\left(\frac{0.01 \div 0.164}{0.087}\right)$	$\left(\frac{1.2 \div 7.9}{4.55}\right)$

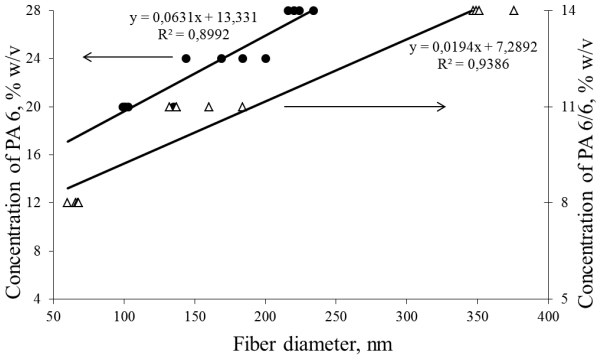

Figure 1. Relationships between the concentrations of PA 6 and PA 6/6 solutions and fiber diameters

The current study provides prerequisites for PA nanofiber media to be used in air filtration applications.

Sublimation growth of 3C-SiC in induction heating of preceramic Si-C nanoparticles

M. Miettinen[1], J. Hokkinen[2] , T. Karhunen[1], T. Torvela[1], U. Tapper[2], J. Jokiniemi[1,2] and A. Lähde[1]

[1]Department of Environmental Science, University of Eastern Finland, Kuopio, 70211, Finland
[2]Fine Particles Team, Technical Research Center of Finland, Espoo, 02044 VTT, Finland
Keywords: Si-C nanoparticles, induction heating, sublimation growth, 3C-SiC
Presenting author email: mirella.miettinen@uef.fi

Cubic 3C-SiC is unique compared to hexagonal polytypes of SiC, because of its isotropic physical properties, higher electron mobility and lower density of the near interface traps in e.g. SiO_2/3C-SiC system. Furthermore, 3C-SiC is the only polytype that grows on silicon and is shown to be a suitable substrate for the growth of graphene.

Poor availability of good quality bulk 3C-SiC seeds and substrates hinder the development of 3C-SiC technology. Cubic silicon carbide occurs spontaneously in the range of 1500-2000 °C, in both a solution and a chemical vapour deposition (CVD) route (Chaussende *et al*, 2008). However, stabilization of 3C-SiC nucleation is a challenge, because several parameters influence the polytype nucleation and growth (e.g. temperature, Si/C ratio, supersaturation, vapour composition, substrate properties). Because 3C-SiC is a metastable form, a solid-state 3C to 6H transition is usually encountered at temperatures above 2000 °C.

In this work sublimation growth of 3C-SiC in controlled induction heating of previously reported preceramic silicon-carbon nanoparticles (Miettinen *et al* 2011) under argon flow at atmospheric pressure was studied. A wide range of induction temperatures from 1900 ºC up to 2600 ºC was used to allow 3C-SiC nucleation to occur, and to follow up solid-state transition from 3C- to 6H-SiC at temperatures above 2000 °C.

An X-Ray diffraction (XRD) analysis was done after induction heating of the precursors. Additionally, thermal gravimetric analysis (TGA) was conducted to study thermal stability of the formed SiC crystals and to remove free carbon. Scanning electron microscopy (SEM) and dispersive Raman spectroscopy analyses were performed both after induction heating and after TGA treatment.

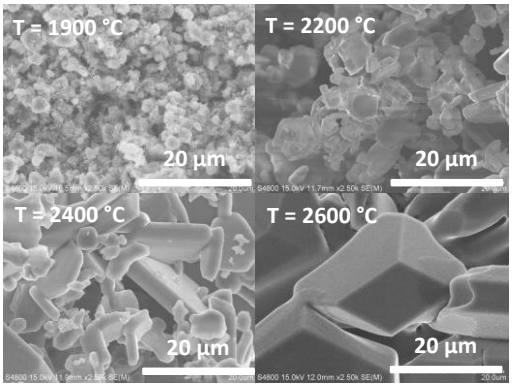

Figure 1.The SEM micrographs of TGA treated SiC crystals formed at different induction temperatures

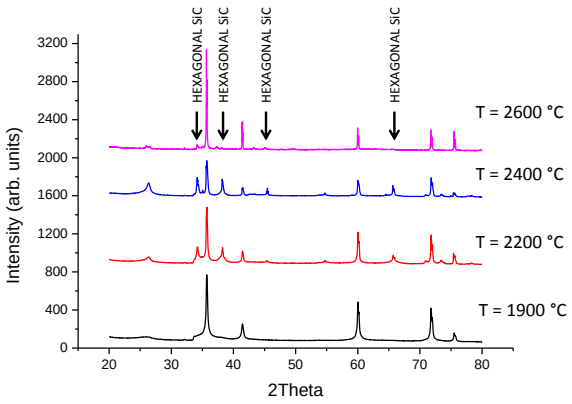

Figure 2. The XRD patterns of SiC crystals formed at different induction temperatures

SEM micrographs (Fig. 2) prove that large crystals were grown during the process. Crystal size increased with increasing induction temperature. At the highest induction temperature complete dissociation of the precursor silicon-carbon particles occurred and long SiC rods were grown on the exit of the crucible, while material left in the crucible was carbon.

XRD analysis reveal that SiC crystals consisted of several polytypes. Peaks related to cubic 3C-SiC (PDF 04-002-9070, ICDD) and hexagonal 6H-SiC (PDF 04-010-5698, ICDD) crystal structures matched with the sample spectrum in all the cases (Fig. 2). However, the spectra contained regions that could not be interpreted entirely with the 3C and 6H-SiC reference patterns. Consequently, it was obvious that also higher order hexagonal (e.g. 69R-SiC and 84R-SiC) polytypes existed in our crystals, except at induction temperature of 2600 ^{o}C, where only peaks of 3C- and 6H-SiC were detected.

As a conclusion, induction heating of synthetic Si-C nanoparticles at temperatures between 1900 and 2600 °C led to growth of large polycrystals of SiC. 3C-SiC was dominant at the lowest (~74 w-%) and at the highest (~91 w-%) induction temperature, where complete dissociation of the precursor silicon-carbon particles occurred. Solid-state transition from 3C- to 6H-SiC started below 2000 °C and was almost completed at induction temperature of 2400 °C. Lower induction temperature and longer growth period is needed for growth of larger 3C-SiC crystals.

Supported by the strategic funding of the University of Eastern Finland under the NAMBER spearhead project.

Chaussende, D. *et al* (2008) *J. Crystal Growth* ***310***,*976-981.*
Miettinen, M. *et al* (2011) *J. Nanopart. Res.* ***13***,*4631-4645.*

Generation of Pb/PbO_x nanoparticles for inhalation experiments

P. Moravec, J. Smolík, J. Ondráček, P. Vodička and R. Fajgar

Institute of Chemical Process Fundamentals AS CR, v.v.i., Prague, 16502, Czech Republic
Keywords: evaporation/condensation, externally heated tube reactor, MOCVD, nanoparticle generation.
Presenting author email: moravec@icpf.cas.cz

Health aspects of nanoparticles (NP′s) on living beings are considered to be important. However, the real data of the impact of NP′s inhalation are rather rare. A study of allocation of MnO_x nanoparticles in organs of laboratory animals in inhalation chamber was presented by Večeřa and Mikuška (2012). For these experiments a source of continual generation of nanoparticles in duration of days or even weeks and in appropriate concentration is necessary. In this work a study of continual generation of Pb/PbO_x nanoparticles in hot wall tube reactor are presented.

NP′s were synthesized in an externally heated tube flow reactor with i. d. 25 mm and length of heated zone 1 m. Three methods of NP′s generation were tested: i) thermal decomposition of lead bis(2,2,6,6,-tetramethyl-3-5heptanedionate) (PbTHD2) in inert atmosphere (pyrolysis), ii) thermal decomposition of PbTHD2 in oxidizing atmosphere (10 vol. % O_2, oxidation), iii) evaporation/condensation of metallic Pb. Particle production was studied in dependence on reactor temperature (T_R), precursor concentration (P_{PbTHD2} or P_{Pb}), and reactor flow rate (Q_R). The particle production was monitored by scanning mobility particle sizer (SMPS, TSI model 3936L75) and samples for particle characterization were deposited onto TEM grids using nanometer aerosol sampler (NAS, TSI model 3089) and on Sterlitech Ag filters. Particle characteristics were studied by transmission/scanning electron microscopy (TEM/SEM), energy dispersive spectroscopy (EDS), atomic mass spectroscopy (AMS), elemental carbon organic carbon (ECOC), X-ray diffractometry (XRD) and X-ray photoelectron spectrometry (XPS).

Production of NP′s by pyrolysis was stable at reactor temperature up to 550 °C with number concentration above $1.5 \cdot 10^7$ #/cm^3. With increasing T_R NP′s concentration at the reactor outlet decreases possibly due to deposition on the reactor wall. Size of primary particles specified by TEM was in the range from 5 to 15 nm. The content of Pb in samples determined by AMS varied between 46 and 61 mass %. ECOC analysis detected no EC and 22 mass % of OC. NP′s generated by oxidation have higher content of Pb (84 mass %) and almost zero content of both EC and OC. However, number concentration of generated particles was lower ($\leq 1.1 \cdot 10^7$ #/cm^3 at T_R 480 °C) and with increasing T_R the production of NP′s decreased rapidly. By evaporation/condensation method the production of NP′s was performed at T_R ranging from 840 to 860 °C. Number concentration of generated particles was above $1.5 \cdot 10^7$ #/cm^3 and mean particle/cluster size was between 20 and 30 nm (Figure 1) and the content of Pb in the samples was 80 mass %. XRD analysis (performed with a lag of about three weeks) showed diffraction pattern of hydrocerussite ($Pb_3(CO_3)_2(OH)_2$, PDF 00-013-0131), which indicates that Pb NP′s are not long-term stable in the air and react with oxygen, CO_2 and air humidity. XPS analysis showed that lead is present in NP′s in bonds Pb-O.

From the three tested methods the evaporation/condensation of metallic Pb seems to be the most suitable for long lasting inhalation experiments due to its simplicity, unambiguous mechanism of NP′s formation and well defined composition. Even so, NP′s can change their composition during the lag between their formation and inhalation.

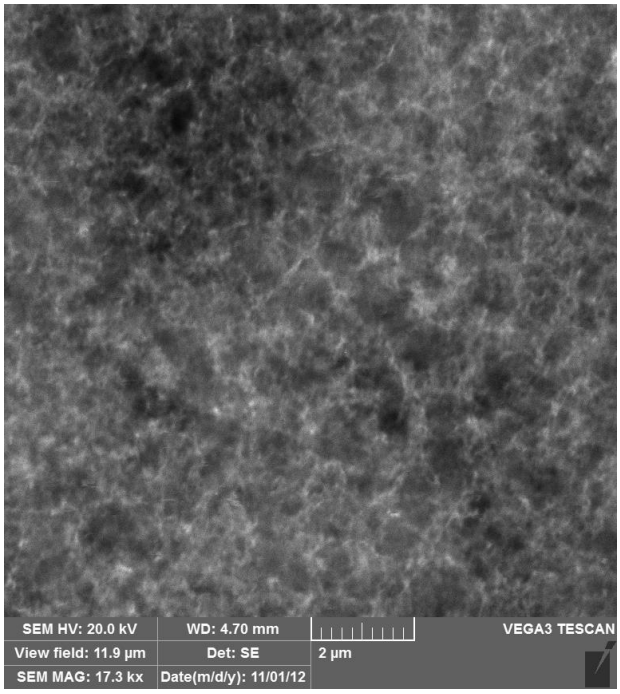

Figure 1. SEM image of NP′s generated by evaporation/condensation of metallic Pb at T_R=860 °C, Q_R=1000 cm^3/min.

This work was supported by the Grant Agency of the Czech Republic under grants P503/11/2315 and P503/12/G147. XPS analyses were performed by Dr. Josef Zemek, Institute of Physics AS CR, v.v.i., AMS analyses by MSc. Ludmila Soukupová, ICPF AS CR, v.v.i. and XRD analyses by Dr. Roman Skála, Geological Institute AS CR, v.v.i.

Večeřa, Z., and Mikuška, P. (2012) *Proc. 13th An. Conf. of the Czech Aerosol Soc., October 2012, Třeboň*.

Batch-to-batch reproducibility - a challenge for safety assessment and regulation

H.-R. Paur[1], C. Adelhelm[1], S. Diabaté[1], J. Forsgren[4], E. Mahon[2], S. Mülhopt[1], J. P. Bagaria[3], V. Puntes[3], R. Schneider[1], C. Weiss[1], T. Wilkins, Y. Jiang[5]

[1]Institute for Technical Chemistry, Karlsruhe Institute of Technology, 76021 Karlsruhe, Germany
[2]University College Dublin (UCD, CBNI) , Dublin, Ireland
[2]University College Dublin (UCD, CBNI) , Dublin, Ireland
[3]Institute Català de Nanotecnologia, Bellaterra (Barcelona), Spain
[4]Uppsala University, Department of Engineering sciences, Uppsala, Sweden
[5]University of Leeds, Leeds, UK

Keywords: nanoparticles, quality, characterization
Presenting author email: muelhopt@kit.edu

For the safety assessment of nanoparticles reference materials of highest quality are required in sufficient quantities to the laboratories performing the tests. During physico- chemical and biochemical tests variability of the results for different batches is observed. The reasons for this variability are not yet clear. They may depend among other reasons on the variability of the physical properties and chemical composition of the tested particles, their dispersion in media and the exposure conditions. Without assuring the quality of reference materials the safety assessment and subsequent regulation of nanomaterials may face on-going discussion and legal challenge.

The identification of potential sources of variability of nanoparticles and their reduction is therefore an important task. As a first step towards this goal OECD proposed parameters for nanoparticle batches have been measured in the QualityNano project. These batches were prepared under carefully controlled conditions to relate the synthesis conditions with the measured results. The variability observed and the methods used will be discussed in more detail.

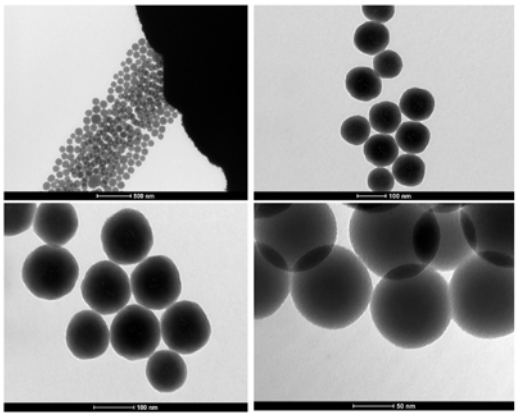

Figure 1. TEM images of silica nanoparticles SilNP003 produced by Stöber synthesis

Preliminary conclusions are drawn based on this work and on previous studies:

- Depending on the synthesis conditions the size distributions of the particle batches vary significantly.
- The size distributions of particles from liquid phase synthesis are narrow, however partial agglomeration is observed.
- Materials from flame synthesis are mostly aggregated and have broader size distributions.
- The batches produced by liquid phase synthesis are partly contaminated by low concentrations of metals (e.g. Cu).
- Particles from flame synthesis have a higher chemical purity, than the ones produced by Stöber synthesis.

With respect to the methods applied for measurement of the particle batches it is concluded:

- As the particles are frequently agglomerated or even aggregated the particle size distributions should be measured by several methods such as DLS and/or SMPS/electrospray and HR-TEM.
- The size distribution and crystallinity of the primary particles in agglomerates and aggregates should be characterized by HRTEM/SEM.
- ICP-MS is a valuable tool to identify variability of particle batches due to contamination by trace metals.
- The particle properties must be considered in the design and the interpretation of bioassays with respect to particle protein interaction, which may change the biological responses.
- The agglomeration of nanoparticles in culture media may lead to a partial sedimentation of the particles, which makes the dose determination difficult. To determine the applied dose the exposure at the air-liquid interface is the method of choice.

To reduce the variability of test results it is advised to set physico-chemical characterisation of all used particle batches by representative TEM images, DLS and ICP-MS. Only by identification and exclusion of particle batches of questionable quality this challenge for safety assessment and regulation will be met.

Acknowledgement:
This work was part of the infrastructure QualityNano: the European Union-funded infrastructure for Quality in nanomaterials safety testing. http://www.qualitynano.eu/

Contrasting manufactured nano objects emitted during maintenance of common particle generators with originally synthesized particles

P.T. Nilsson[1], L. Ludvigsson[2], J. Rissler[1], M. E. Messing[2], C. Isaxon[1], A. C. Eriksson[1], M. Hedmer[3], H. Tinnerberg[3], K. Deppert[2], A. Gudmundsson[1] and J. Pagels[1]
[1]Ergonomics and Aerosol Technology, Lund University, P.O. Box 118, SE-22100, Lund, Sweden
[2]Solid State Physics, Lund University, P.O. Box 118, SE-22100, Lund, Sweden
[3]Occupational and Environmental Medicine, Lund University, SE-22100, Lund, Sweden
Keywords: agglomerates, exposure, lung deposition, AMS
Presenting author email: patrik.nilsson@design.lth.se

The production of engineered nanoparticles is rapidly growing and thus is the risk for unintentional human exposure increasing.

Workplace exposure measurements during handling of nanomaterials were recently reviewed (Kuhlbusch, 2011). Often production processes are monitored for emissions of manufactured nano objects (MNOs) in the particle size range <1µm. Less studied processes are cleaning and maintenance of particle synthesizing equipment.

In this work we characterized particle emissions during maintenance of common particle generators (a Spark Discharge Generator, SDG, and a High Temperature furnace, HT) and contrasted them to the originally synthesized particles, which we denote "*as-produced*". Both generators were operated upstream a sintering furnace, which was used to process the particles to a near-spherical shape.

Online characterization of as-produced particles, from the synthesizing process, was carried out with a Scanning Mobility Particle Sizer (SMPS) and filter sampling for analysis with transmission electron microscopy. The sampling during the emission measurements was carried out close to the expected emission zone by using an Aerodynamic Particle Sizer (APS, 3321, TSI Inc.) and a Condensation particle counter (P-trak, 8525, TSI inc.) for particle number concentration. Filters for scanning electron microscopy (SEM) analysis were collected. In addition a Laser Vaporization Aerosol Mass Spectrometer (LV-AMS, Aerodyne Inc.) was used for highly time-resolved chemical identification of both the as-produced and emitted particles.

The emissions in terms of mass and surface area were dominated by particles >1µm. SEM analysis revealed that the particles were highly agglomerated and were consisting of nanometer sized structures, figure 1.

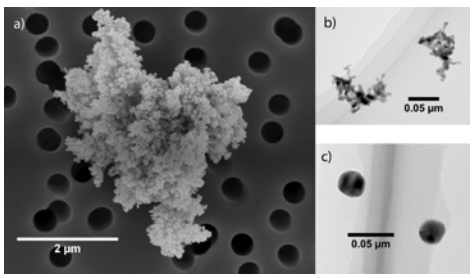

Figure 1. a) Typical emitted agglomerate with nanostructures related to sintered particles. b) Aggregates formed by the SDG. c) Sintered particles

The chemical identification of the emitted particles showed that they were dominated by the metal elements used during the particle synthesis sessions prior to the maintenance. The nano meter structures, of which the agglomerates consisted, could in terms of size and shape, be related to both the originally as-produced aggregates and the sintered particles.

By considering the geometric mean diameters of the as-produced (~0.03 µm) and of the emitted (1.8 µm) particles it is evident that they, respectively, overlap with the lower and the upper maxima of the pulmonary deposition curve (Multiple Path Particle Dosimetry, MPPD), figure 2.

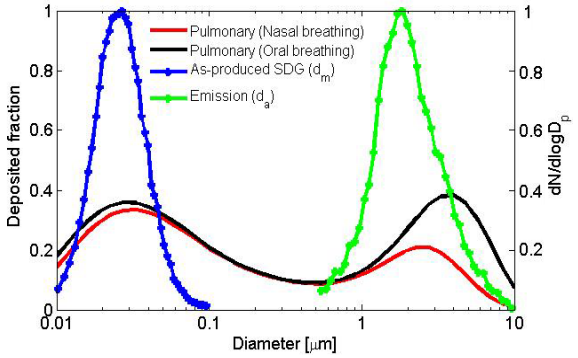

Figure 2. Two pulmonary deposition curves (MPPD) shown together with typical particle number size distributions (normalized) of as-produced particles and emitted particles during maintenance of the generators.

The fate of the emitted "*super-agglomerates*" after deposition in the lung fluid is unknown. If only kept together by van der Waals forces de-agglomeration is possible and thus the emitted agglomerates may have the same possible effects as free as-produced nanoparticles. This work shows the importance of including measurements of particles >1µm in assessments of emissions and exposure to manufactured nano objects since the agglomerates contribute significantly to the total emitted particle surface area, a key factor in particle toxicology.

This work was supported by the Consortium for Aerosol Science and Technology (CAST), by the Nanometer Structure Consortium at Lund University (nmC@LU), the Swedish research council FAS and the FAS-centre METALUND

Kuhlbusch, T., Asbach C., Fissan H., Gohler D. and Stintz, M. (2011) *Particle and Fibre Toxicology*, **8**

Fragmentation of Nanoparticle Agglomerates by Collisions in Supersonic Flows

Yoshiki Okada, Nao Oshio, Keiichi Oda, and Masaki Yabuhana

Graduate School of Science and Engineering, Kansai University,
3-3-35 Yamate-cho, Suita-shi, Osaka 564-8680, Japan
Keywords: Fragmentation, Nanoparticle agglomerates, Supersonic flow, Collision
Presenting author email: yokada@kansai-u.ac.jp

A major difficulty in making and handling nanoparticles is their tendency to agglomerate due to van der Waal forces and to form large fractal structures. In the present study, we investigated the deagglomeration of nanoparticles caused by collisions of nanoparticle agglomerates with a vibrating metal plate as well as a fixed metal plate, and the counter-collision of two supersonic flows containing agglomerated particles. Our deagglomeration experiments were carried out under several different conditions using silica nanoparticle agglomerates.

Silica particles (sicastar®, avg. dia. 80 nm; Micromod Partikeltechnologie, Germany) dispersed in methanol were used as the test particles. The liquid sample was atomized by a nebulizer with a N_2 gas expansion flow. The aerosol gas, after passing on a ^{241}Am plate for ionization of the particles, was introduced into a differential mobility analyzer (DMA). The agglomerated silica particles (approx. 150 nm in dia.) which were classified by the DMA were introduced into the collision system at 99.7 kPa. We used two kinds of collision systems: (a) the collision of agglomerates in a flow with a metal plate (as shown in Fig. 1a) and (b) the counter-collision of two supersonic flows containing agglomerates (as shown in Fig. 1b).The resulting degree of deagglomeration of nanoparticles was evaluated by a TEM analysis of the particles after the collision.

Figure 2a shows the distribution of the number of primary silica particles composing the respective agglomerates after the collision of the agglomerates in a sonic flow with a vibrating plate in the collision system shown in Fig. 1a. Compared with the distribution observed in the case of the collision with the fixed plate, we found that the deagglomeration with the vibrating plate was much more successful than that with the fixed plate. We believe that the vibration of the plate is very effective for the deagglomeration of nanoparticles because the vibration of the collision plate enhances the bounce of the fragments formed by the collision. The collision fragments bounced off of the vibrating plate and were deposited on the TEM grid, while the fragments stuck to the fixed collision plate.

Figure 2b shows the distribution of the number of primary silica particles composing the respective agglomerates after the collision of the agglomerates in the two opposed supersonic flows (Fig. 1b). The data shown in Fig. 2b indicate that the proportion of the non-agglomerated particles was as high as approximately 73% and the deagglomeration was achieved without any fusion of agglomerates. The results of the experiments revealed that the collision of agglomerates with a plate generates the problem of particles remaining on the metal plate even under low-collision velocity, and the counter-collision of two supersonic flows containing agglomerated particles induces a highly efficient fragmentation of agglomerates.

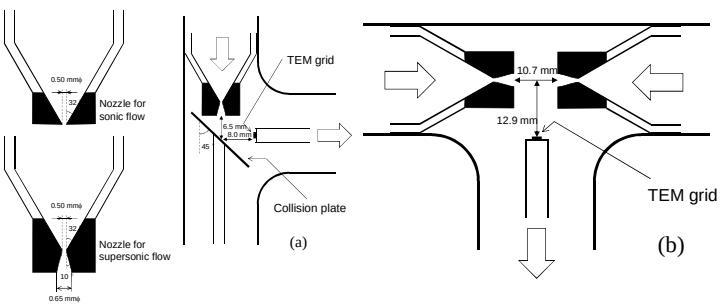

Fig. 1 Schematic diagram of the collision systems

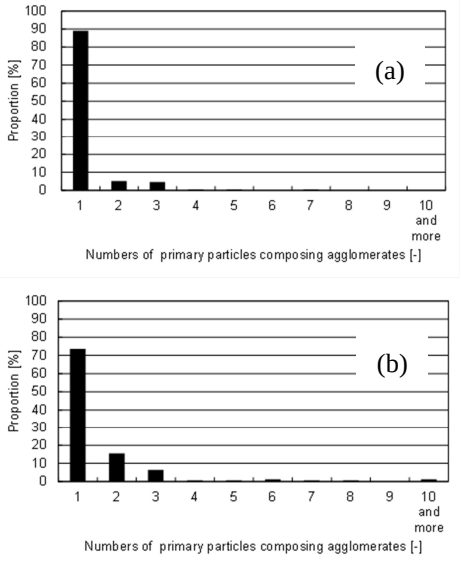

Fig. 2 Distributions of the number of primary silica particles composing the respective agglomerates after the collisions

High-throughput multi-jet electrospinning for two fluids using a coaxial grooved nozzle

Inyong Park[1], Woojin kim[1] and Sang Soo Kim[1]

Aerosol and Particle Technology Laboratory, School of Mechanical, Aerospace & Systems Engineering, Korea Advanced Institute of Science and Technology, Guseong-dong, Yuseong-gu, Republic of Korea
Keywords: Multi-jet electrospinning, Coaxial grooved nozzle, Polymeric nanofiber, High-throughput
Presenting author email: inyongpark@kaist.ac.kr

Electrospinning is a simple and versatile technique for fabricating nanofibers and fibrous mats, capable of producing continuous nanofibers with various types of surface morphology. Because of its numerous advantages, the procedure has been widely employed with variety of polymers in various applications. To increase the throughput, we have introduced coaxial grooved nozzles. (Fig.1) By using a coaxial grooved nozzle and two fluids, including polyethylene oxide (PEO), we are able to achieve stable multi-jet operation and relatively high throughput. The multi-jets are initiated by the multi-jet mode of the inner fluid, and share the total flow rate of the polymer solution. We have investigated the operating conditions for various flow rate combinations of two fluids.

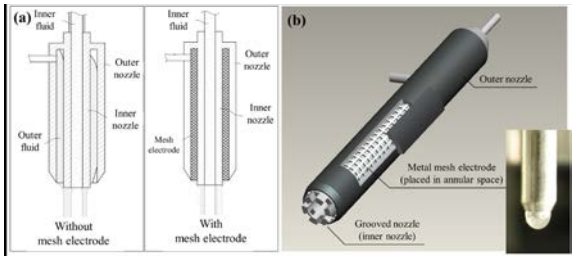

Figure 1. Schematics coaxial grooved nozzle.

The formation mechanism of multi-jet electrospinning with two fluids is described as follows. In previous research on electrospray, we observed that when the applied voltage reached a certain onset voltage, multi-jets became anchored in the grooves of the nozzle tip. In electrospinning, a single jet is similarly divided into multi-jets by the splitting of the electrified inner jet. In general, multi-jets can be formed from a polymer jet alone, but in the present case, it would be difficult to achieve because of the relatively high flow rates. To summarize the mechanism of multi-jet electrospinning for two fluids, the two liquids create two fluid layers, and the charged inner fluid is subjected to a repulsive force as it enters the functional domain of the multi-jet mode. This force is directly transferred in the outward direction along the two fluid layers. The exterior of the single jet becomes extremely unstable, and finally the two-layered jet divides into thinner multi-jets. To find the optimized number of multi-jets and flow rate of the inner fluid, we examined jet formation while adjusting the flow rate of the inner fluid. When the polymer solution was fed at 6 ml/h, three jets appeared at the tip of the nozzle for voltages close to 25 kV. When three jets formed, fiber deposition was observed on the collector. One or two multi-jets proved to be insufficient. In these cases, polymer solution was delivered to the collector, and fibers were not formed. This result shows that for fiber deposition to occur, the single jet must be divided into an adequate number of thinner multi-jets. As the flow rate of the polymer solution increased, the number of multi-jets required for stable operation also increased. In the 6-ml/h case, three jets were sufficient for stable operation, whereas in the 14-ml/h case, five jets were necessary for stable operation. When the flow rate of the inner fluid was inadequate, the additional jet was not formed. However when the flow rate of the inner fluid was excessive, there was interference between the inner fluid and the electrospun multi-jets, and the jets became intermittent. Using these results, we determined the optimized flow rate conditions. The results are summarized in Figure 2.

$Q_{ethanol}$	Q_{PEO}	1 jet	2 jets	3 jets	4 jets	5jets
0 ml/h	6 ml/h	12.5 kV	-	-	-	-
1 ml/h	6 ml/h	10.3 kV	15.7 kV	23.1 kV	-	-
2 ml/h	6 ml/h	5.5 kV	15.1 kV	21.3 kV	-	-
3 ml/h	6 ml/h	4.0 kV	14.0 kV	17.1 kV	21.8 kV	-
$Q_{ethanol}$	Q_{PEO}	1 jet	2 jets	3 jets	4 jets	5jets
1 ml/h	8 ml/h	8.0 kV	16.8 kV	21.5 kV	22.6 kV	-
2 ml/h	8 ml/h	7.2 kV	15.6 kV	20.4 kV	24.4 kV	-
3 ml/h	8 ml/h	6.0 kV	15.2 kV	20.3 kV	23.2kV	-
4 ml/h	8 ml/h	5.8 kV	15.1 kV	20.5 kV	-	-
$Q_{ethanol}$	Q_{PEO}	1 jet	2 jets	3 jets	4 jets	5jets
2 ml/h	10 ml/h	7.6 kV	18.3 kV	23.4 kV	-	-
3 ml/h	10 ml/h	7.1 kV	17.2 kV	18.5 kV	20.5 kV	23.9 kV
4 ml/h	10 ml/h	5.1 kV	16.3 kV	18.3 kV	19.5 kV	-
5 ml/h	10 ml/h	5.2 kV	16.9 kV	20.1 kV	21.8 kV	-
$Q_{ethanol}$	Q_{PEO}	1 jet	2 jets	3 jets	4 jets	5jets
3 ml/h	12 ml/h	7.8 kV	16.4 kV	18.4 kV	23.4 kV	-
4 ml/h	12 ml/h	7.5 kV	13.3 kV	20.4 kV	22.4 kV	24.0 kV
5 ml/h	12 ml/h	5.5 kV	15.1 kV	20.5 kV	22.4 kV	-
$Q_{ethanol}$	Q_{PEO}	1 jet	2 jets	3 jets	4 jets	5jets
4 ml/h	14 ml/h	7.5 kV	15.3 kV	20.9 kV	22.5 kV	23.8 kV
5 ml/h	14 ml/h	7.3 kV	15.2 kV	21.3 kV	23.2 kV	24.7 kV

Direct deposition
Unstable multi-jet
Stable multi-jet

Figure 2. Operating conditions for multi-jet electrospinning.

The morphology of the resulting nanofibers is uniform without bead formation. The fibers have an average diameter of about 350 nm.

This research was supported by Basic Science Research Program through the National Research Foundation of Korea(NRF) funded by the Ministry of Education, Science and Technology (2012-0009248)

Doshi, J., Reneker, DH., (1995) *J Electrost.*, 35, 151–6.
Demir, MM., Yilgor, I., Yilgor, E. and Erman, B. (2002) *Polymer*,43, 3303–9.

Impact of size and concentration on the particle charging properties of an annular DBD

M. Pesch[1], H. Grimm[2], T. Külz[3], M. Richter[4], R. Albrecht[5]

Grimm Aerosol Technik GmbH & Co. KG, Dorfstraße 9, 83404 Ainring, Germany
Keywords: DBD, neutralizer, charge distribution
Presenting author email: MP@grimm-aerosol.com

Many scientific and industrial applications such as electrostatic precipitation, neutralization or electrostatic measurement techniques require the charging of aerosol particles (Kwon et al., 2006). Especially for the widely used scanning mobility particle sizers (SMPS) a well defined charge distribution is essential in order to transfer the electrical mobility spectrum into a meaningful size distribution. For this purpose usually diffusion chargers are applied in which the collision between bipolar ions and particles lead to an equilibrium particle charge distribution (Fuchs, 1963). In most cases radioactive sources like ^{241}Am, ^{85}Kr or ^{210}Po are applied for the generation of bipolar ions in reasonable concentrations. However legal restrictions complicate and often even prohibit the use of radioactive sources. Another efficient way of particle charging without legal restrictions is the use of gas discharge neutralizers. Beside corona chargers the use of dielectric barrier discharges for aerosol particle charging was reported (Borra, 2005, Byeon et al., 2008). The aim of this work is to specify a commercially available annular dielectric barrier discharger (aDBD) regarding charging properties as function of particle size and concentration.

Therefore we investigated the particle losses and charge distribution induced by the aDBD as well as the deviation between electrical mobility spectra of polydisperse aerosols neutralized with an aDBD and ^{241}Am source respectively. The aDBD was operated with a peak to peak voltage of 7.4kV and a frequency of about 20 kHz as well as a sample flow rate of 0.3 lpm. The particle background induced by the aDBD was measured to be below 100 cm^{-3}. Size distributions and particle concentrations were measured between 10 nm and 950 nm using a differential mobility analyzer (Grimm, l-DMA) and condensation particle counter (Grimm CPC, 5.416). Diesel soot, DEHS and NaCl particles were applied at concentrations between 1x10^4 cm^{-3} and 3.5x10^6 cm^{-3}. While DEHS and NaCl particles were suspended in air using an atomizer (Grimm, 7.821) diesel soot particles were directly supplied by a common diesel motor.

Figure 1 compares the SMPS mobility spectra resulting from ^{241}Am and aDBD neutralized NaCl aerosol particles. We observed a very good agreement to size at low concentrations and for large particles. However for small particles and at high concentrations significant differences occur. Below 90 nm mobility equivalent diameter we observe an increasingly reduced particle concentration compared to ^{241}Am with decreasing diameter. These differences mainly arise due to electro-collection on an additional electrode which assures a stable plasma operation.

Between 90 nm and 950 nm the size distributions are in good agreement for total number concentrations below 2x10^4 cm^{-3}. Higher concentrations induce an increasing deviation which however is constant for the entire size range. This deviation as function of the total number concentration can be approximated by a pseudo voigt profile which may be applied in order to correct SMPS measurements under high concentrations.

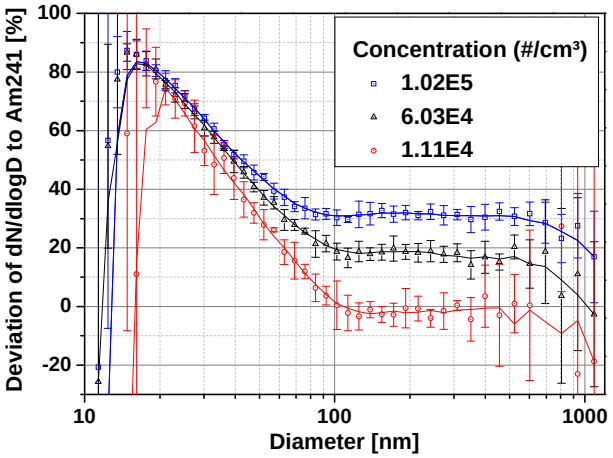

Figure 1: Deviation of a NaCl electrical mobility spectrum measured with an SMPS-aDBD combination to an Am241 neutralizer as function of particle size and concentration. Error bars represent the 95% confidence interval out of 5 measurements.

In this contribution we present the impact of particle concentration and size on the charging properties of the Grimm aDBD neutralizer and discuss the contribution of particle losses and charge distribution on the observed deviations to ^{241}Am

Fuchs, N. A. (1963) *Geofisica Pura Appl.*, **56**, 185–193
S.B. Kwon et al. (2006) *J. Aerosol Science* **37,** 483–499
Borra JP (2005) *J. Phys. D : Appl. Phys* **39**, 19-54
Byeon J H et al. (2008) *J. Aerosol Science* **39** 460-466

Positioning of nano-sized noble metal aerosols in an organic light-emitting diode for enhanced quantum efficiency

H.-K Sung[1], J.-C. Lee[2], J.-K. Lee[1], C. Kim[2], and M. Choi[1]

[1]Global Frontier Center for Multiscale Energy Systems, School of Mechanical and Aerospace Engineering, Seoul National University, 151-744, Korea
[2]Program in Nano Science and Technology, Graduate School of Convergence Science and Technology, Seoul National University, Seoul 151-742, Republic of Korea
Keywords: nanoparticles, nanodevice, organic light-emitting diode
Presenting author email: hksung@snu.ac.kr

We report a method of incorporating aerosol gold nanoparticles (Au NPs) into an organic layer without any damage to the surrounding organic materials and its application to fabricating an Au NP-embedded organic light-emitting diode (OLED) for enhanced external quantum efficiency (EQE).

An Au NP layer has been successfully incorporated in the middle of organic layer by means of aerosol method adopting a dry and low-temperature process. This has enabled us to investigate the influence of the position of an Au NP layer on the performance of a fluorescence OLED. Here, four distances (d = 10, 20, 30 and 40 nm) of the Au NP layer away from the emissive layer were tested.

The structure of the Au NP-embedded OLED was ITO/NPB (50 − d nm)/Au NPs/NPB (d nm)/Alq3 (50 nm)/LiF (0.5 nm)/Al (100 nm). To fabricate the Au NP-embedded OLEDs, substrates were moved between a vacuum thermal evaporator and a homemade electrostatic precipitator (ESP) installed inside a nitrogen (N_2) glovebox. The ESP was connected to a homemade spark discharge generator (SDG) so that Au NPs generated by the SDG were led to the ESP by a N_2 carrier gas and collected on the substrate on which an organic layer was previously deposited by vacuum thermal evaporation (VTE). We adopted pin-to-plate configuration for the SDG (Han, 2012), and the geometric mean diameter and the geometric standard deviation of the Au NPs were measured as 6.0 nm and 1.43, respectively. The surface coverage density of the Au NP layer was found to be 1900 particles per μm^2 on average. In addition, for comparison, various Au NP layers were fabricated with a conventional vacuum thermal evaporation method at d = 20 nm by changing the deposition rate and thickness.

Figure 1 shows that the Au NP layers were formed well inside the NPB layers by either the SDG-ESP or VTE. However, a few Au NPs were observed to penetrate into the bottom organic layer when VTE was used, which was not observed when the SDG-ESP was used.

Figure 2 shows the external quantum efficiency-current density (*EQE-J*) characteristics. It is noted that all the Au NP-embedded OLEDs fabricated by VTE exhibited poor EQE compared to the reference device, while those by the SDG-ESP showed larger EQE than the reference device. Interestingly, the EQE was enhanced most when the Au NP layer was located at d = 20 nm (increased 37 %) among the Au NP-embedded OLEDs fabricated by the SDG-ESP. It was attributed to hole trapping into the Au NPs. According to the position of the positively charged Au NPs due to the trapped holes, the charge balance and the exciton formation rate improved competitively, and, consequently, the EQE was maximized for the device with d = 20 nm.

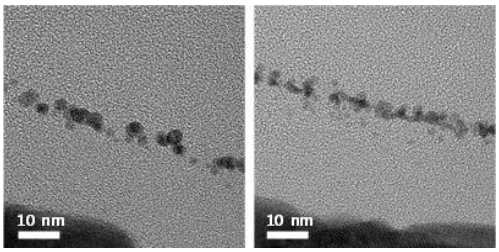

Figure 1. Cross-sectional TEM images of the OLEDs incorporating the Au NPs fabricated using the SDG-ESP (left) and VTE (right).

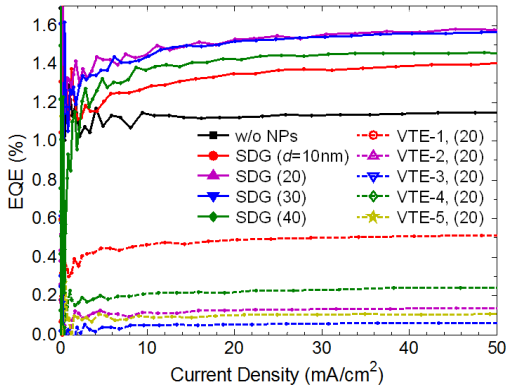

Figure 2. *EQE-J* characteristics of the OLEDs without Au NPs, with the Au NP layer fabricated using the SDG-ESP with different values of d, and with the Au NP layer introduced at d = 20 nm fabricated using VTE with different deposition rates and thicknesses.

This work was done by financial support from the Global Frontier Centre for Multiscale Energy Systems supported by the Korean Ministry of Science and Technology.

Han, K., Kim, W., Yu, J., Lee, J., Lee, H., Gyu Woo, C., Choi, M. (2012) *J. Aerosol Sci.* **52**, 80-88.

Tuesday, September 3, 2013

Poster session B,
Combustion Aerosols, Posters B167 – B241

Penetration of Combustion Aerosol Particles through an N95 FFR Respirator Filter

S.A. Grinshpun, X. He, J.Y. Kim, T. Reponen

Center for Health-Related Aerosol Studies, University of Cincinnati, Cincinnati, Ohio, USA

Keywords: filter, respirator, combustion aerosol
Presenting author email: sergey.grinshpun@uc.edu

Smoke generated from a fire consists primarily of ultrafine particles.[1] Exposure to combustion aerosols may cause various adverse health outcomes, including respiratory problems and impairment of cardiovascular function.[2-4] The Filtering Facepiece Respirators (FFRs), including N95-certified ones [filter efficiency ≥95%, i.e. penetration <5%, according to the National Institute for Occupational Safety and Health (NIOSH)] are commonly used for protecting the wearers from various aerosol exposures, including smoke. The filter performance of these respirators is usually determined using conventional aerosol challenges such as charge-equilibrated NaCl particles.[5] However, it has not been examined how well the data obtained with these challenges represent the actual protection offered by an N95 FFR filter against combustion aerosols.

The objective of this study was to evaluate the penetration of combustion particles of different sizes through an N95 FFR filter under different flow rates and exposure time conditions and compare the data to the corresponding penetration values obtained using the charge-equilibrated NaCl particles. The study was carried out using the University of Cincinnati's Respirator Evaluation Facility. The tested N95 FFRs were fully sealed on a breathing manikin and challenged with a specific aerosol being evaluated. First, we used NaCl particles generated by a Particle Generator (TSI Inc.) and passed through a Kr^{85} particle equilibrator. A constant inhalation flow (Q = 15, 30, 55, and 85 L/min) was established, and the aerosol concentrations inside (C_{in}) and outside (C_{out}) of the respirator were measured size-selectively with a Nanoparticle Spectrometer (PMS Inc.) at time points of 0, 30, 60 and 90 minutes. The filter penetration was calculated as C_{in}/C_{out}. Second, the same respirator was exposed to one of the three combustion aerosols generated by burning a specific material being tested. The experiments were performed with plastic, wood and paper. The first measurement (time t=0) was conducted after 15 minutes of active burning to allow the aerosol system to stabilize.

The experimental results showed that penetration curves produced with both NaCl and combustion aerosols did not change dramatically during the 90-min exposure period. Additionally, the most penetrating particle size (MPPS) for both NaCl and combustion aerosols was found to be in a range from 30 to 40 nm, suggesting that the MPPS was not significantly affected by the characteristics of a challenge aerosol.

It was found that the combustion particles might penetrate the respirator filter more readily than the NaCl challenge particles. This was especially pronounced for plastic aerosol with a particle sizes below 100 nm. Under some conditions, the penetration exceeded 5%, which is not expected for an N95 respirator filter. This finding can be partially attributed to the influence of highly charged combustion particles on the pre-charged filter media fibers, which may inhibit the efficiency of the filter. The other explanation involves the combustion-originated vapors that may condense on the electret filter material and thus affect its properties.

Overall, the results suggest that the performance data obtained with the well-established NaCl aerosol challenge may not accurately predict (and rather overestimate) the protection level provided by the N95 respirator filters against combustion aerosol particles.

The outcomes of this pilot study call for a more extensive investigation of the interaction between the combustion aerosol particles and different filter materials using a study design that is capable of accounting for various aerosol properties and filter characteristics. The data will be useful in an effort to enhance the present NIOSH respirator testing and certification program.

This research was funded by the NIOSH Targeted Research Training Program and Pilot Research Project Training Program (University of Cincinnati, Education and Research Center, Grant T42/OH008432-07). The authors also acknowledge support from the U.S. Defense Threat Reduction Agency (DTRA).

REFERENCES:

1. Baxter, C.S., C.S. Ross, T. Fabian, J.L. Borgerson, J. Shawon, P.D. Gandhi et al.: Ultrafine Particle Exposure During Fire Suppression-Is It an Important Contributory Factor for Coronary Heart Disease in Firefighters? J. Occup. Environ. Med. 52(8): 791-796 (2010).
2. Peters, A., H.E. Wichmann, T. Tuch, J. Heinrich, and J. Heyder: Respiratory Effects are Associated with the Number of Ultrafine Particles. Am. J. Respir. Crit. Care Med. 155(4): 1376-1383 (1997).
3. Schwartz, J., D.W. Dockery, and L.M. Neas: Is Daily Mortality Associated Specifically with Fine Particles? J. Air Waste Manag. Assoc. 46(10): 927-939 (1996).
4. Timonen, K.L., E. Vanninen, J. de Hartog, A. Ibald-Mulli, B. Brunekreef, D.R. Gold et al.: Effects of Ultrafine and Fine Particulate and Gaseous air Pollution on Cardiac Autonomic Control in Subjects with Coronary Artery Disease: The ULTRA Study. J. Expos. Sci. Environ. Epidemiol. 16(4): 332-341 (2005).
5. NIOSH. National Institute for Occupational Safety and Health. US DHHS, Public Health Service. "Respiratory Protective Devices; Final Rules and Notices" Federal Register 60:110, pp 30335-30393 1995.

Selective catalytic reduction nitrogen oxides with methane over nanosized CuO supported on Al_2O_3. Part 1. Materials structural characterization

Chang-Mao Hung[1], Mu-Hsing Kuo[2], Shui-Jen Chen[3], Wei-Bang Lin[4] and Wen-Liang Lai[5]

[1]Department of Vehicle Engineering, Yung-Ta Institute of Technology and Commerce, 316 Chung-Shan Road, Linlo, Pingtung 909, Taiwan, Republic of China.
[2]School of Health Information Science, University of Victoria, B.C., Canada.
[3]Department of Environmental Science and Engineering, National Pingtung University of Science and Technology, 1 Shuefu Road, Neipu, Pingtung 912, Taiwan, Republic of China.
[4]Department of Mechanical Engineering, Chinese Military Academy, Fenshan, Kaohsiung 830, Taiwan, Republic of China.
[5]Department of Environmental Science and Occupational Safety and Hygiene, Tajen University, 20 Wei-Shin Road, Yanpu Shiang, Pingtung 907, Taiwan, Republic of China.
Keywords: selective catalytic reduction, nitrogen oxides, nanosized Cu/γ-Al_2O_3 catalyst.
Presenting author email: hungcm1031@gmail.com

Nitrogen oxides (NO_x) are one of the most toxic components, and are increasingly attracting the attention of stringent environmental emission regulations in Taiwan. The primary sources of NO_x ($NO+NO_2+N_2O$), including several stationary industrial fossil fuel high temperature combustion processes and automobile exhaust sources, are of concern because these pollutants are significant precursors to acidic precipitation, which may acidification of the aquatic and terrestrial systems, and because the pollutants react in the atmosphere to generate ozone and photochemical smog. Therefore, in an environmental point of view, the removal and control of NO_x emission from industrial waste streams are important. The selective catalytic reduction (SCR) of NO in a stream to molecular nitrogen and water is one method for solving problems of nitrogen oxides pollution. Moreover, copper-containing catalysts are active in a wider range of reactions of transformation of NO with respect to other catalytic systems. Hence, this work considers the SCR of NO by hydrocarbons (HC-SCR) using methane as a reducing agent over CuO supported on Al_2O_3 in a tubular fixed-bed reactor (TFBR) at temperatures from 623-1023 K in the presence of oxygen was studied. A nanosized CuO/γ-Al_2O_3 catalyst was prepared by incipient wetness impregnation approach of copper nitrate and γ-alumina support. The catalysts were characterized using TEM and FTIR. Figure 1 presents the textural characteristics of the nanosized Cu/γ-Al_2O_3 catalyst. These crystal phases may be responsible for the high activity of the catalysts. Figure 2 compares the FTIR spectra on the nanosized Cu/γ-Al_2O_3 catalysts, and also confirms the presence of the CuO-like phase on the surface of the nanoscale Cu/γ-Al_2O_3 catalyst. It reveals that the peaks associated with the CuO-like phase on the framework are associated with a peak at around 1400 cm^{-1}. Therefore, the highly catalytic activity of the nanosized Cu/γ-Al_2O_3 catalyst system in reduction NO with CH_4 may be explained by the reversible redox behavior of CuO-Al_2O_3 couples in promoting the functional mechanism.

Figure 1. TEM photograph of the fresh nanosized Cu/γ-Al_2O_3 catalyst.

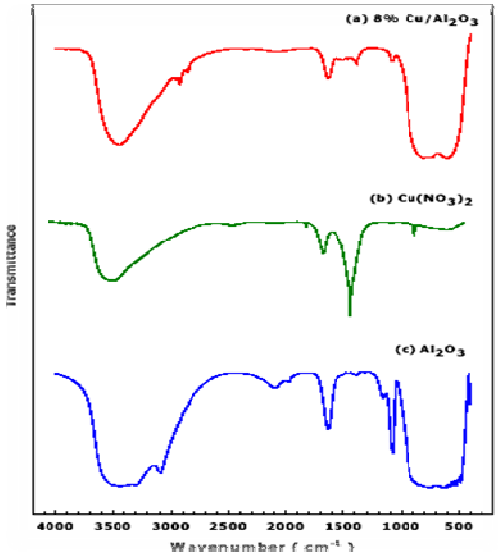

Figure 2. FTIR pattern of fresh nanosized Cu/γ-Al_2O_3 catalyst.

Selective catalytic reduction nitrogen oxides with methane over nanosized CuO supported on Al_2O_3. Part 2. Catalytic activity and mechanism study

Chang-Mao Hung[1], Mu-Hsing Kuo[2], Shui-Jen Chen[3], Wei-Bang Lin[4] and Wen-Liang Lai[5]

[1]Department of Vehicle Engineering, Yung-Ta Institute of Technology and Commerce, 316 Chung-Shan Road, Linlo, Pingtung 909, Taiwan, Republic of China.
[2]School of Health Information Science, University of Victoria, B.C., Canada.
[3]Department of Environmental Science and Engineering, National Pingtung University of Science and Technology, 1 Shuefu Road, Neipu, Pingtung 912, Taiwan, Republic of China.
[4]Department of Mechanical Engineering, Chinese Military Academy, Fenshan, Kaohsiung 830, Taiwan, Republic of China.
[5]Department of Environmental Science and Occupational Safety and Hygiene, Tajen University, 20 Wei-Shin Road, Yanpu Shiang, Pingtung 907, Taiwan, Republic of China.
Keywords: selective catalytic reduction, nitrogen oxides, nanosized Cu/γ-Al_2O_3 catalyst.
Presenting author email: hungcm1031@gmail.com

NO_x is a toxic inorganic gas with a pungent odor under ambient conditions, and is potentially harmful to public health. Moreover, it is known, various technologies have been explored for the reducing NO_x emissions can be classified as wet or dry processes. The use of wet-scrubbing agents to adsorb NO_x enables alkali in water or hydrogen peroxide to be used as the liquid for capturing NO_x. Besides, complete biological treatment systems have been extensively investigated and implemented. Recently, selective catalytic reduction (SCR) and selective non-catalytic reduction (SNCR) have been established to increase the effectiveness of advanced reduction processes technology using dedicated catalysts, which potentially shorten the reaction times of reduction, and allow it to proceed under milder operating conditions. Supported copper oxides were found to have the high activity among the tested transition metal oxides for the reduction of NO. Hence, the catalytic process of NO_x in a stream to N_2 and H_2O is one method for solving problems of NO_x pollution. This work considers the reduction of NO from by SCR over nanosized Cu/γ-Al_2O_3 catalyst at temperatures between 623 and 1023 K. A nanosized Cu/γ-Al_2O_3 catalyst was prepared by incipient wetness impregnation approach of copper nitrate and γ-alumina support, which were different in the loading of copper. The catalysts were characterized using UV-Vis. Figure 1 presents the effect of copper loading on the conversion of γ-Al_2O_3 at various temperatures. The figure indicates that the maximum activity increases with copper loading in the range of 2 to 8%, and the reaction conditions strongly affect the relationship between the activity of the catalyst and copper content. The lower loadings may offer few active sites and thus showed lower activities. Thus, in this study 8% nanosized Cu/γ-Al_2O_3 catalyst was selected as optimal in the following. Figure 2 shows the bands in the ranges of 300-350 nm and 700-900 nm and were attributed to the $Cu^{2+} - O_2^-$ electronic transition species and the d-d transitions of Cu^{2+} in an octahedral environment with Oh symmetry, respectively.

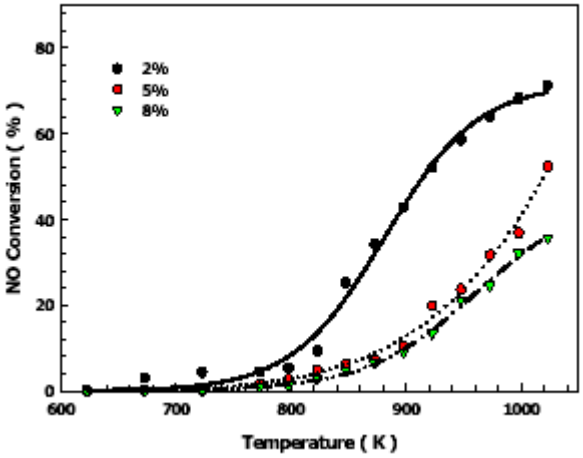

Figure 1. Effect of various copper loading on the nanosized Cu/γ-Al_2O_3 catalyst for the conversion of NO with CH_4. Test conditions : 600 ppm NO in He, 600 ppm CH_4 in He, O_2 = 2%, GHSV = 108000 ml/h-g.

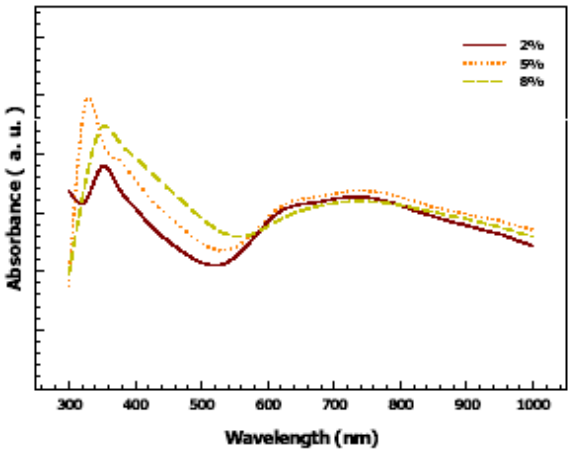

Figure 2. UV-Vis pattern of the various copper loading on the nanosized Cu/γ-Al_2O_3 catalyst.

Selective catalytic reduction nitrogen oxides with methane over nanosized CuO supported on Al_2O_3. Part 3. Reaction kinetic behavior study

Chang-Mao Hung[1], Mu-Hsing Kuo[2], Shui-Jen Chen[3], Wei-Bang Lin[4] and Wen-Liang Lai[5]

[1]Department of Vehicle Engineering, Yung-Ta Institute of Technology and Commerce, 316 Chung-Shan Road, Linlo, Pingtung 909, Taiwan, Republic of China.
[2]School of Health Information Science, University of Victoria, B.C., Canada.
[3]Department of Environmental Science and Engineering, National Pingtung University of Science and Technology, 1 Shuefu Road, Neipu, Pingtung 912, Taiwan, Republic of China.
[4]Department of Mechanical Engineering, Chinese Military Academy, Fenshan, Kaohsiung 830, Taiwan, Republic of China.
[5]Department of Environmental Science and Occupational Safety and Hygiene, Tajen University, 20 Wei-Shin Road, Yanpu Shiang, Pingtung 907, Taiwan, Republic of China.
Keywords: nitrogen oxides, nanosized Cu/γ-Al_2O_3 catalyst, kinetic model.
Presenting author email: hungcm1031@gmail.com

The primary sources of NO_x, including several stationary industrial fossil fuel high temperature combustion processes and automobile exhaust sources, are of concern because these pollutants are significant precursors to acidic precipitation, which may acidification of the aquatic and terrestrial systems, and because the pollutants react in the atmosphere to generate ozone and photochemical smog. Moreover, the kinetic behavior of NO reduction with catalysis can be accounted by using the rate expression of the kinetic model. Kinetic parameters are also developed on the basis of the differential reactor data in this study. The adsorptive and catalytic behavior of a catalyst is strongly influenced by the capacity and texture of its exterior surface. Figure 1 presents the XRD patterns on the nanosized Cu/γ-Al_2O_3 catalysts, verifying the presence of CuO phases of the nanosized Cu/γ-Al_2O_3 catalyst. Dominant CuO diffraction peaks appeared near 2θ=35.5, 38.8, 48.7, 61.4, and 68.0° for a catalyst. As reported in the previous work established that CuO is the most active phase. However, under reduction conditions over the nanosized Cu/γ-Al_2O_3 catalyst, the oxidation state of copper may vary between Cu^{2+} and Cu^{+}, which might also govern the efficiency of the deNO reaction. Figure 2 compares the ATR-FTIR spectra on the catalysts, and also confirms the presence of the CuO-like phase on the surface of the nanosized Cu/γ-Al_2O_3 catalyst. It reveals that the peaks associated with the CuO-like phase on the framework are associated with a peak at around 2348 cm^{-1}. Therefore, the highly catalytic activity of the catalyst system in reduction NO with methane may be explained by the reversible redox behavior of CuO-Al_2O_3 couples in promoting the functional mechanism. Moreover, a kinetic rate expression was developed to describe the data over the range of conditions investigated. Furthermore, correlation equations in the form of Arrhenius's law are derived from experimental data to predict the destruction efficiencies of NO from the temperatures and residence period in a catalytic process. A Langmuir-Hinshelwood model incorporating a first-order reaction appears to adequately represent the NO reduction, which shows fairly good agreements with experimental data. This kinetic model is appropriate for oxygen presence and high concentrations of NO.

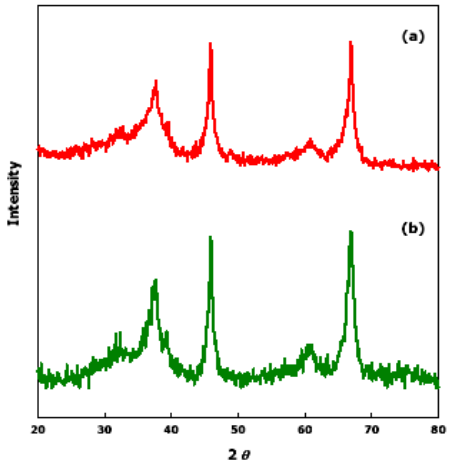

Figure 1. XRD pattern of the nanosized Cu/γ-Al_2O_3 catalyst. (a) fresh, (b) after activity test.

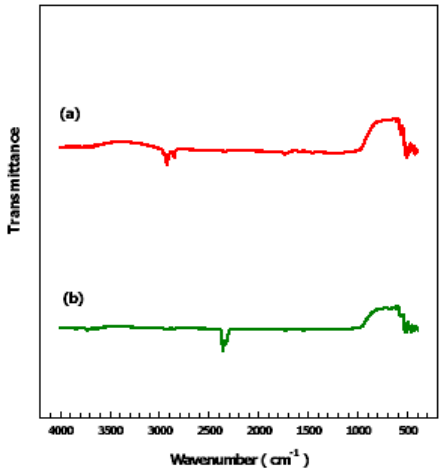

Figure 2. ATR-FTIR pattern of the nanosized Cu/γ-Al_2O_3 catalyst. (a) fresh, (b) after activity test.

Characterization of aerosols emitted during the incineration of nanocomposites

G. Ounoughene[1, 2], O. Le Bihan[3], C. Chivas-Joly[4], C. Longuet[5], A. Joubert[2], C. Motzkus[4], D. Venditti[6], S. Durécu[6], B. Debray[3], J-M. Lopez-Cuesta[5], and L. Le Coq[2]

[1]ADEME, 20 avenue du Grésillé, Angers, 49004, France
[2]LUNAM, Ecole des Mines de Nantes, GEPEA, CNRS, UMR 6144, 4 rue Alfred Kastler, Nantes, 44307, France
[3]INERIS, Parc Technologique Alata, Verneuil-en-Halatte, 60550, France
[4]LNE, 29 Avenue Roger Hennequin, Trappes, 78197, France
[5]Ecole des Mines d'Alès – Centre des Matériaux C2MA, 6 Avenue de Clavières, Alès, 30319, France
[6]TREDI - Séché Global Solutions, 9 Av. Forêt de Haye, Vandoeuvre-lès-Nancy, 54505, France
Keywords: nanocomposites, nanoparticles, incineration, aerosols.
Presenting author email: ghania.ounoughene@mines-nantes.fr

End-of-life nanocomposites are likely to undergo disposal through thermal treatment like incineration. Data from literature indicate that nanocomposites present specific behaviours according to the conditions of thermal treatment [1]. It is thus relevant to understand the mechanisms of emission and thermal degradation of nanocomposites under incineration conditions. Thence, the characterization of the effluents during the incineration of nanocomposites, collected downstream the incinerator furnace (or even upstream the flue-gas cleaning systems), provides an insight in the "nanosafety" of this technology [2], useful to cope with nanowastes (wastes containing nanomaterials).

At a lab-scale, the emission mechanisms and the thermal degradation mechanisms were determined using various devices: a microcalorimeter PCFC and a fire propagation apparatus (FPA Tewarson) coupled with a Fourier Transformed InfraRed (FTIR); as well as a modified tubular furnace (Fig. 1) coupled with a gas analyser. Conditions of thermal degradation implemented in those laboratory devices were accurately characterized by evaluating and controlling (whenever possible) the key operational parameters that govern an incineration process, *i.e.* chiefly: temperature, residence time, air-excess and turbulence.

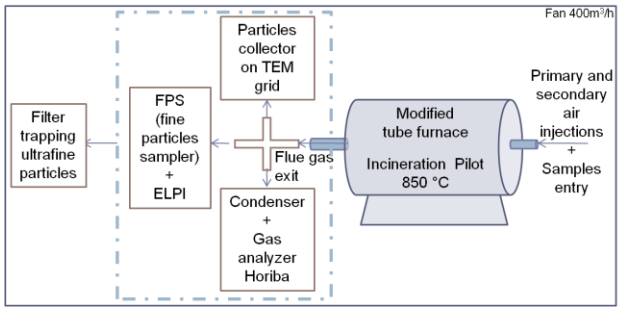

Figure 1. Incineration Pilot - Schematic diagram of the experimental device.

This study reports particularly on the composition and microstructure of the aerosols produced during combustion tests. The size distribution of particles contained in the flue-gas was determined using an Electrical Low Pressure Impactor (ELPI) coupled with combustion devices and the morphology was determined using TEM observation (transmission electronic microscopy) via a MPS (mini-particle-sampler) [3]. Our tests were performed on specimens of nanocomposites incorporating different mineral fillers (like sepiolite and halloysite nanoclays) and neat polymer matrices.

The characterization of the combustion aerosols from the small-scale thermal degradation of nanocomposites is a first step for determining nano-objects potentially released during incineration process.

References

[1] Motzkus C., Chivas-Joly C., Guillaume E., Ducourtieux S., Saragoza L., Lesenechal D., Macé T., Lopez-Cuesta J-M., Longuet C. (2012), *Aerosols emitted by the combustion of polymers containing nanoparticles*, J Nanopart Res, 14, 1-17

[2] Tran D.T., Ounoughene G., Fleury D., Venditti D., Durecu S., Joubert A., Fiany E., Meunier T., Le Bihan O. and Le Coq L. (2012) *The NANOFlueGas Project: characterization of nanoparticulate emissions from the incineration of wastes containing manufactured nanomaterials*, International conference on safe production and use of nanomaterials, Nanosafe 2012, 13-15 november 2012, Grenoble

[3] R'mili B., Le Bihan O., Dutouquet C., Aguerre-Chariol O., Frejafon E. (2013) *Particle Sampling by TEM Grid Filtration,* Aerosol Science and Technology (accepted for publication)

Particle Emission from the Aircraft Engine Testing Cycles

J.J. Rodríguez-Maroto[1], V. Archilla[2], D. Sanz-Rivera[1], E. Rojas-García[1], M. Pujadas[1], J.L. Mosquera[1], D. Mercader[2], A. Gonzalez[2] (ISDEFE), A. Jimenez[2], J. Mena[2], A. Entero[2] (ISDEFE), J.M. Fernández-Mainez[1] and J.C. Bezares[1]

[1] Department of Environment, CIEMAT, Av.. Complutense 40, 28040 Madrid, Spain
[2] Turbojet Test Centre, Ctra. Torrejón-Ajalvir, km 4, 28850 Torrejón de Ardoz, Spain
Keywords: aircraft, engines, turbofan, emission, particles, PM, turbojet testbed, combustion
Presenting author email: jesus.maroto@ciemat.es

Emissions from aircraft engines and their potential influence on local and global environmental concerns have become the subject of intensive study by scientists. Environmental problems to be considered in relation to these emissions could include: climate change and local and regional air pollution due to volatile organic compounds (VOC) such as UHC, and particulate matter (PM) emissions. The particles emitted can affect in a local area to: public health, agriculture production and ecosystems, buildings and infrastructure.

The aircraft engines are tested in modern test bed, for the purpose of studying and developing new generation engines (higher power/efficiency ratios, and less contamination). One of the most advanced installations in the world for testing aircraft engines with a thrust of up to 140,000 pounds is the Turbojet Test Centre, TTC/INTA. In the tests performed in TTC emissions from engine are expelled through a duct (detuner) up to exit stack. Previously the hot gas from engine is mixed with air sucked from the test cell, resulting in a natural dilution.

During a series of aircraft engine tests carried out in TTC the PM emission to the atmosphere have been monitored. A particle sample was continuously extracted from stack and its concentration and size distribution were simultaneously measurement using a Scanning Mobility Particle Sizer (SMPS) and a Condensation Particle Counter (CPC), after 100:1 dilution by two ejector diluters.

The results showed that in the measurement point the variations in the properties of the particle sample were sensitive enough to the changes in engine power, so that the measures were able to reflect transients of the test cycle without time offset. It can be seen that particle concentration varies in a way opposite to the engine power applied, while particle size distribution mode, median or geometric mean increase with increasing power (figure 1).

Usually smoke number increases with higher engine power output (EPA, 1978), the same as the particle mass (Hagen, 2006; Herndon, 2006). However, the contrary effect has been found when measured away from engine exit (Miake-Lye, 2009). Some studies have reported a decrease in particle concentration with increasing engine power beyond the stage point of the engine (EASA, 2012).

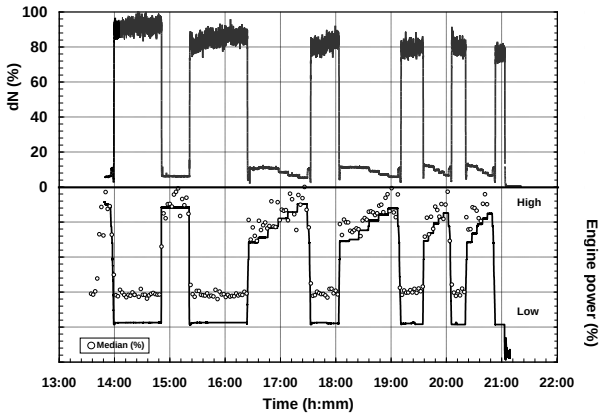

Figure1. Engine power, concentration and median diameter of particle vs. test time.

Regarding particle size distribution, it was found to be bimodal; modes of nuclei (20-30 nm) and accumulation (60-70 nm). The concentration of the nucleus mode was always higher than the accumulation one. When the engine power increased, the accumulation mode resulted to be dominant and nucleus were not significant, while if it decreased the main mode was the nucleus one, in agreement with other studies, (Whitefield, 2006; EASA, 2011; EASA, 2012; Lobo, 2011), in which smaller particles are found at lower engine power output, all of them measured in test beds and next to airport courses.

This work was supported by INTA and CIEMAT into Framework Agreement for collaboration, to make TTC/INTA a Strategic Platform to allow assessment of the environmental impact.

EPA, (1978). *Air Pollutant Emission Factors for Military and Civil Aircraft*, EPA-450/3-78-117
Hagen, D.E. et al (2006). *TAC, Oxford U.K., 247-251.*
Herndon et al (2006), *TAC , Oxford U.K.,252-255.*
Lobo, P. et al, (2011) *En. Sci. Technol.* ***45****, 10744-10749.*
EASA, (2011), *SAMPLE II*. Final report.p103
EASA, (2012), *SAMPLE III - SC02*. Final report.78 -82.
Miake-Lye, R.C. et al (2009), *TAC-2 Aachen-Maastricht 26-32*
Whitefield, P.D. et al, (2006), *TAC, Oxford U.K.,95-100.*

Gas-droplet flows in fire safety engineering

K.N. Volkov[1] and V.N. Emelyanov[2]

[1]Faculty of Science, Engineering and Computing, Kingston University, London, SW15 3DW, United Kingdom
[2]Faculty of Power Engineering, Baltic State Technical University, Saint Petersburg, 190005, Russia
Keywords: combustion aerosols, droplets, multiphase processes, aerosol fundamentals, CFD.
Presenting author email: k.volkov@kingston.ac.uk

Interaction of laser pulse with gas-droplet mixtures plays an important role in different applications including environmental monitoring of high-risk industrial objects and enclosed spaces, and laser ignition of volumetric explosion for application to fire mitigation. For the optimization of technological processes and for keeping the environment free from droplets, a detailed knowledge of the interaction of laser pulse with individual droplets is necessary. The physical and mathematical models of optical breakdown on individual droplet and up-to-date numerical methodology for computer modeling are developed, and laser-induced breakdown on liquid droplet is studied.

A chain of processes leading to explosion and optical breakdown of individual droplet was developed (Figure 1). These processes depend on optical properties of droplet and ratio of droplet radius to radius of laser spot.

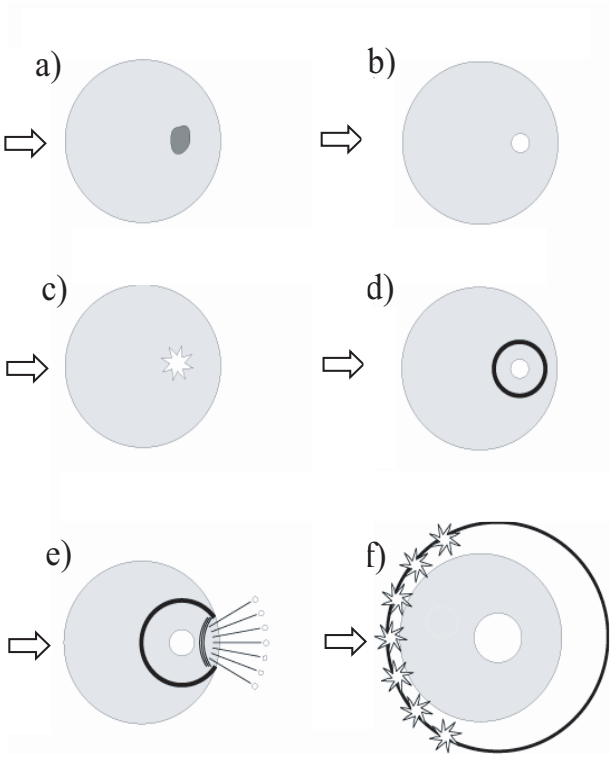

Figure 1. Optical breakdown on liquid droplet.

The laser radiation focuses inside a droplet near its shadow side (fragment a). In this region, overheating conditions arise, and liquid is in meta-stable state in which its temperature exceeds the temperature of saturated vapour at given temperature. Internal vapour cavity is formed, and liquid boils off in this cavity (fragment b). Increase in pressure in the vapour cavity creates conditions for internal micro-breakdown. Free electrons are generated as a result of isothermal ionization. It leads to collisions of electrons with ions and atoms and electron–electron collisions. Internal micro-plasma spot is appeared and absorbs laser radiation (fragment c). Further increase in pressure in the vapour cavity forms shock wave expanding inside droplet (fragment d). Expansion of shock wave induces thermal ionization of surrounding gas on shock wave front (fragment e). Free electrons that have appeared on shock wave front induce chain mechanism of breakdown, receiving their energy due to reverse drag effect (fragment f). The cascade ionization process is significant at high pressure and longer laser pulse because under these conditions, electron-atom or electron-ion collisions have sufficient time to occur during the laser pulse.

Sub-models describe heating, evaporation, appearance of free electrons due to thermal ionisation on front of shock wave, development of electron avalanche due to reverse drag effect. Heating model is based on solution of unsteady heat diffusive equation. To compute optical properties of particle (e.g., absorption efficiency of laser radiation), semi-empirical data are used. The equations describing electron avalanche include the equation of heating of vapor aureole of particle due to electron–atom collisions, the equation of warming-up of electrons, the ionization kinetic equation of vapor as a result of electron impact, and the equation of particle mass. The plasma is considered as an ideal gas. The Euler equations are used for the simulation of gas dynamical processes in the droplet. A simple model of one-step chemical reaction is used in order to reproduce combustion of individual droplet.

The time of optical breakdown is a result of the competition between 3 factors: (i) time of heating a droplet to the temperature of explosive transformation (at low pulse energy, the large droplets do not have enough time for being heated, and the small droplets exchange heat intensively with the surrounding), (ii) intensity of the shock wave contributing to the thermal ionization of vapour (for massive droplets, the intensity of shock wave is low), (iii) time of development of an electron avalanche. Increase in droplet radius leads to increase in time of droplet heating and decrease in degree of ionization. No electron avalanche develops at low intensity of laser pulse, and threshold value of optical breakdown increases.

The nanofraction of fly ashes in Swiss waste incineration plants (WIP) and the respective modelled contributions of engineered nanomaterials (ENM)

Jelena Buha[1,2], N. Müller[3], B. Nowack[3], A. Ulrich[1] and J. Wang[1,2]

[1]Analytical Chemistry Laboratory, Empa, Dubendorf, 8600, Switzerland
[2]Institute of Environmental Engineering, ETH Zurich, Zurich, 8093, Switzerland
[3]Technology and Society Laboratory, Empa, St. Gallen, 9014, Switzerland
Keywords: ENM, fly ashes, WIP, nanofraction
Presenting author email: jelena.buha@empa.ch

In the past, waste incineration processes had been identified as an important source of ultrafine air pollutants, implying necessary treatment systems for exhaust air. Today, these systems are able to remove around 99.99% of all ultrafine particles as measured in the Swiss waste incineration plants (Burtscher et al. 2002). However, studies investigating the size distribution of fly ash from waste incineration plants so far focused on micro-sized particles only (Cobo et al. 2009).

This study aims at identifying the nano sized fraction (by particle weight and number), and characterize physical and chemical properties of fly ash from waste, wood and sludge incineration in Switzerland. Samples from five different waste incineration plants were pre-fractionated, aerosolized and then analysed with a scanning mobility particle sizer (SMPS) and aerodynamic particle sizer (APS) for the accurate size determination. First results show that a large number fraction of all particles are smaller than 2 µm - while this fraction accounts for only a small part of the total weight.

Additionally, we assess the contribution of ENM to the nanoparticulate fraction of the generated ash. In general, little is known about the behaviour of ENM at the interface from the technosphere to the ecosphere. Previous modelling of ENM flows to the environment revealed that significant amounts enter the waste stream and therefore waste incineration plants and landfills. In order to model the flows of ENM during waste incineration and landfilling by including a more detailed description of the different processes and considering ENM-specific transformation reactions, a novel model was generated (Mueller et al. 2013). It allows a quantitative prediction of expected ENM flows to waste incineration processes. Four substances were modelled: nano-TiO_2, nano-ZnO, nano-Ag and carbon nanotube (CNT). These ENM are representative for commonly used materials and products, illustrating a variety of ENM with different behaviours. The modelling was performed for Switzerland where almost 100% of the municipal waste and sewage sludge are burned. The mass-based modelling showed that the major ENM flows go from the waste incineration plant to the landfill as bottom ash. All other flows within the system boundary (e.g. with the fly ash) were predicted to be about one magnitude smaller than the bottom ash flow. Example for one of the substances modelled (TiO_2) is shown in Figure 1.

Comparing these numbers to the total amount of fly ash produced in Switzerland, ENM amount to only a small fraction of the nano-sized fly ash even in the unlikely case that all ENM survive the incineration process unchanged. It is thus highlighted that the majority of the nanoparticles in fly ash is combustion generated. The results of the modelling show that waste incineration can have a strong influence on some ENM but that still the majority of the ENM-mass is expected to end up in landfills.

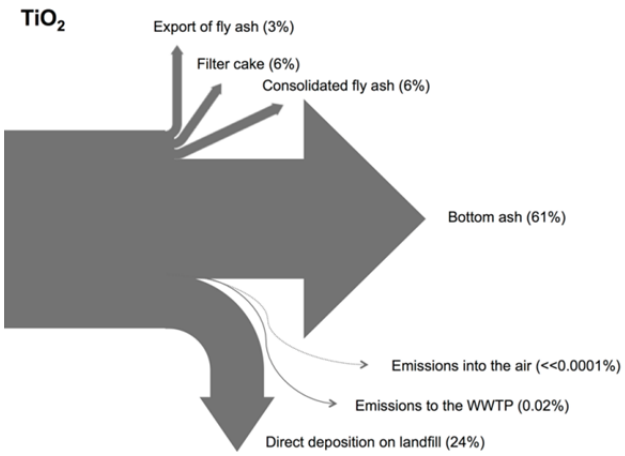

Figure 1: Waste disposal as input-output system for the ENM (TiO_2). Flows are shown in % of the total flow that enters the landfill (WWTP-waste water treatment plant).

This work was supported by the Swiss Federal Office for the Environment (FOEN).

Burtscher, H.; Zürcher, M.; Kasper, A.; Brunner, M. (2002) *Proc. Int. ETH Conf. on Nanoparticle Measurement, Mayer, A., Ed. BUWAL*, **52**.

Cobo, M.; Gálvez, A.; Conesa, J. A.; Montes de Correa, C. (2009) *Journal of Hazardous Materials*, **168**, 1223–1232.

Mueller, N. C.; Buha, J.; Wang, J.; Ulrich, A.; Nowack, B. (2013) *Environmental Science: Processes & Impacts*, **15**, 251-259.

Tandem-DMA measurements of gases and particles in large-scale biomass combustion and gasification

Dan Gall[1], Mohit Pushp[2], Camilla Forsman[1], Kent O. Davidsson[2], Mattias Hallquist[1] and Jan B. C. Pettersson[1]

[1]Department of Chemistry and Molecular Biology, Atmospheric Science, University of Gothenburg, SE-412 96, Göteborg, Sweden
[2]SP Technical Research Institute of Sweden
Keywords: combustion, gasification, tar, tandem-DMA
Presenting author email: dan.gall@gu.se

Large-scale conversion of biomass may be used to produce heat, electricity and transport fuels, and it may thereby help limit our current dependence on fossil fuels. Industrial-scale combustion of biofuels has a number of challenges related to the heterogeneity, moisture and ash content of the feedstock, which may result in slagging and corrosion problems and reduced conversion efficiency. The alternative method of gasification of biomass provides a gas mixture, often referred to a synthesis gas, which may subsequently be transformed into methanol or methane in a catalytic process. Several gasification concepts are currently being researched and common problems relate to the unwanted production of tar components and the poisoning of catalysts by ash elements.

The further optimization of industrial combustion and gasification processes requires the development of methods that reliably and with high time-resolution measure the aerosol composition. On-line methods are of particular interest because of their use in process optimization, and as warning systems for high concentrations of unwanted components.

Here we present results from experiments where a volatility tandem differential mobility analyzer (VTDMA) was used to characterize particles and condensable components in combustion and gasification applications. Combustion studies where performed in a 12 MW_{th} circulating fluidized bed boiler (CFB) at Chalmers University of Technology (Davidsson *et al.*, 2007). Aerosol was sampled after the exit of the primary cyclone of the CFB at a gas temperature of 800 °C. Similar experiments were carried out at a 4 MW_{th} gasifier at Chalmers by sampling of the raw gas after the gasifier unit at an approximate temperature of 750 °C.

A sampling probe was used to extract gas from the reactors and the overall measurement strategy was to rapidly dilute and quench the hot sampled gas by mixing with an inert gas flow. The dilution results in rapid cooling of the gas and condensation of condensable components on existing particles, or nucleation of new particles. Different probe designs were evaluated with respect to sampling efficiency and effects of wall losses.

A narrow particle size range was selected by a DMA run in re-circulating mode with either air or nitrogen for combustion and gasification, respectively. The size-selected particles were directed through an oven that was ramped between room temperature and 800 °C, and the size distribution after the oven was characterized with a scanning mobility particle sizer (SMPS).

Figure 1 shows typical SMPS size distributions obtained for different oven temperatures when sampling from the CFB combustion boiler during feeding with wood chips. The size-selected particles begin to evaporate above 500 °C, which is consistent with a major KCl fraction in the detected particles. Size distributions measured at different oven temperatures were used to produce thermograms that display the remaining particle fraction as a function of temperature. Thermograms for selected compounds were also characterized under laboratory conditions, and the results were used to identify major aerosol components in the hot-gas experiments. Corresponding gasification studies were carried out with emphasis on the characterization of tar and inorganic compounds.

The studies confirm that the VTDMA method can be used to characterize both particles and condensable gases in combustion and gasification, and the potential of the method for industrial applications is discussed.

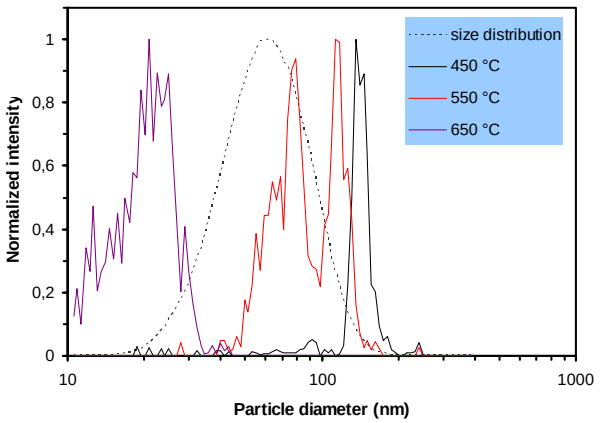

Figure 1. Normalized number size distributions obtained during combustion of wood chips in a 10 MW_{th} CFB: total particle size distribution (dotted line), and distributions measured with pre-selected 150 nm particles using the VTDMA setup at three different temperatures (solid lines).

This work was supported by the Swedish Energy Agency. We acknowledge the assistance from personnel at Chalmers University of Technology during the experiments.

Davidsson, K. O., Åmand, L. E., Leckner, B., Kovacevik, B., Svane, M., Hagström, M., Pettersson, J. B. C., Pettersson, J., Asteman, H., Svensson, J. E., Johansson, L. G. (2007) *Energy Fuels* **21**, 71-81.

Condensing Heat Exchanger for Fine Particle Precipitation and Efficient Heat Recovery in Small Scale Wood Combustion

J.Grigonyte[1], O.Sippula[1], I. Nuutinen[1], T. Koponen[1], H. Lamberg[1], T. Kaivosoja[1] and J. Jokiniemi[1,2]

[1]Department of Environmental Science, Univ. of Eastern Finland, P.O. Box 1627, FI-70211 Kuopio, Finland
[2]VTT Technical Research Centre of Finland, P.O. Box 1000, FI-02044 VTT, Espoo, Finland
Keywords: condensing heat exchanger, fine particle, wood combustion, thermophoresis.
Presenting author email: julija.grigonyte@uef.fi

The wood pellet is an alternative energy source suitable for use at various large scale as well as domestic pellet stoves. The main negative side in this type of biomass usage during combustion process is the fine particle (PM1 defined as a particles with median aerodynamic diameter $d_a \leq 1$ µm) and gaseous emissions. Therefore it is important to develop low emission biomass combustion devices. The aim of this work was to study the potential of condensing heat exchanger (CHX) for simultaneous fine particle precipitation and efficient heat recovery.

Experiments with a condensing heat exchanger were performed for optimal fine particle precipitation. The heat exchanger was operated in two different modes: floor heating and high temperature heating with incoming and outcoming water temperatures of 24,1 – 25,7 ˚C and 54,3 – 57,5 ˚C, respectively. Reference measurements were carried out with a conventional tube heat exchanger.

The condensing heat exchanger was installed in the combustion reactor which consists of a 40 kW solid fuel burner and a ceramic insulated combustion chamber. The CHX was equipped with water scrubbing system to keep the heat exchanger walls clean. The temperatures of a flue gas and water upstream and downstream the CHX were monitored continuously as well as pressure drop over the CHX. The flue gas composition was analyzed with FTIR (Gasmet) and single gas analyzers (ABB) which continuously were measured CO2, CO, O2 and NOx. The condensate which was collected in the bottom of CHX was weighed and later on analyzed for the content of inorganic compounds.

Before particle measurement the sample air flow was diluted by a porous tube – ejector dilution system (dilution ratio 23 - 32). After dilution sample was divided by the different instruments. PM1 fraction particles were collected by the pre cut – off impactors. The filters were weighed and analyzed for OC, EC and inorganic compounds. Particle number size and mass size distributions were determined by ELPI (Dekati), DLPI (Dekati) and SMPS (TSI).

During the experiments the air to fuel ratio ranged from 1,9 to 2,3 at floor heating mode and 1,7 to 2,0 at high temperature heating mode. The CO, organic carbon (OC) and elemental carbon (EC) in all measured cases were very low, showing nearly complete combustion conditions. The PM1 were mainly composed of K, Na, SO_4^{2-}, Cl^- and Zn. The condensate analysis showed a similar chemical composition as shown for the particle emissions.

The average of PM1 emissions is presented in Figure 1. Summarizing, the experimental set up with CHX generated 32 % lower PM1 emissions in the high temperature heating case and 36 % of PM1 lower emissions in floor heating case compared to the reference boiler case. The results showed that the thermal efficiency in floor heating mode reached over 100 %, due to released heat by water condensation. The usage of the scrubber increased the PM1 emissions in comparison to the CHX operated without scrubber. The heat exchanger thermodynamics and fine particle desposition was also simulated with a computational model. Theoretically CHX was predicted to have PM1 precipitation of 56 and 50 % in floor and high temperature heating modes, respectively, based on thermophoretic and diffusiophoretic forces. The reference boiler was simulated to have a PM1 precipitation of 19 %. Thus, the experimental findings between the conventional reference boiler and the CHX were in good agreement with the simulations.

The results indicate that a condensing heat exchanger in small scale biomass-fired boilers can be designed for fine particle reduction with simultaneous high thermal efficiency. The tested system is especially suitable for floor heating operation and for moist fuels, for example wood chips.

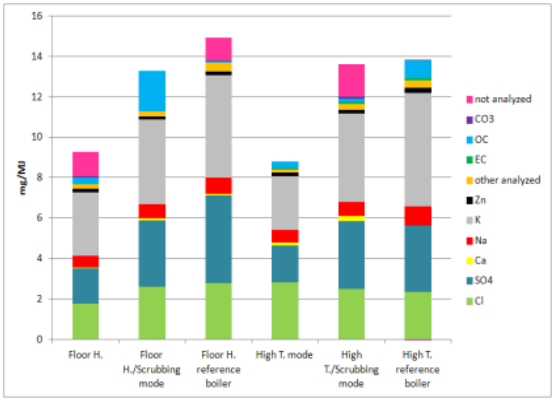

Figure 1. PM1 emissions and their chemical composition downstream the CHX and conventional reference boiler.

The authors thank the Finnish Funding Agency for Technology and Innovation, the strategic funding of the University of Eastern Finland (Sustainable Bioenergy, Climate Change and Health) and Fortum Foundation for financial support.

Effect on pore size distribution on filtration performance of ceramic filter media

Jeong-Uk Kim[1], Hyun-Jin Choi[2,3], Sung Hyun Kim[3] and Myong-Hwa Lee[1, *]

[1]Energy System R&D Group, Korea Institute of Industrial Technology, Cheonan-si, Chungnam 331-822, Republic of Korea
[2]Green Process and Material R&D Group, Korea Institute of Industrial Technology, Cheonan-si, Chungnam 331-822, Republic of Korea
[3]Department of Chemical and Biological Engineering, Korea University, Seoul 136-701, Republic of Korea
Keywords: ceramic filter, pore size distribution, filtration, pressure drop
Presenting author email: jeonguk00@kitech.re.kr

Either ceramic or metallic filter is generally used in order to remove a particle-laden flue gas with high temperature. However, ceramic filter is more relevant to be applied to extremely high temperature region. So far, it has been tested in both lab-scale and pilot scale experiments. Especially, a SiC ceramic filter has a high oxidation resistance, thermal expansion coefficient, corrosion resistance, thermal conductivity and excellent mechanical properties (Li *et al.*, 2011).

The selection of manufacturing components(ceramic materials, binders and sintering promoting agents) as well as their mixing ratio are very important in manufacturing ceramic filter media. Furthermore, pore size distribution of produced filter media is critical to determine the collection performance. Flue gas from combustion facilities will pass easily through the filter media when its porosity and pore size are large, resulting in low pressure drop and low collection efficiency (Ohzawa et al., 1998, De Freitas et al., 2006).

The purpose of this work is to investigate how the porosity and pore size distribution affect the filter performance of a ceramic filter. We prepared circular type ceramic filters with 47mm in diameter and 2.54mm in thickness which have different SiC powder distributions(SiC powder size : 25 ㎛, 100 ㎛, 200 ㎛).

The physical properties of produced filter media were shown in Table 1.

Table 1. Physical properties of produced ceramic filters.

SiC powder size [㎛]	Porosity [%]	Pressure drop [mmH_2O]
25	43.31	100
100	45.59	8
200	46.35	4

Pressure drop was measured at the face velocity of 1m/min. It was found that the pressure drop was decreased with increasing SiC powder size and porosity. The collection efficiencies of ceramic filters were plotted as a function of particle diameter in Figure 1. As powder size used in manufacturing filter media increased, the collection efficiency was decreased. We could obtain ceramic filter media with high collection efficiency by introducing SiC powders with 25 ㎛ in diameter.

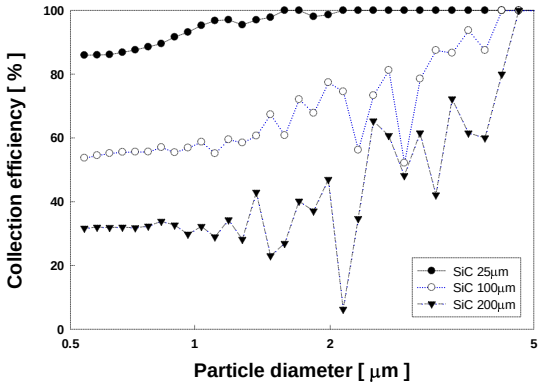

Figure 1. Dust collection efficiency as a function of particle diameter (face velocity=1 m/min).

This research was financially supported by the Eco-innovation project, Republic of Korea (Project No. 20120001102)

Li, J., Lin, H., Li, J. (2011) *J. European Ceram. Soc.* 31, 825-831
Ohzawa, Y., Nomura, K., Sugiyama, K. (1998) *Mater. Sci. Eng*. A255, 33-38.
De Freitas, N., Goncalves, j., Innocentini, M. and Coury, J. (2006) *J. Hazard. Mater.* B136 747-756

Characterizing physical properties of aerosol particles in a bubbling fluidized bed boiler

H. Kuuluvainen[1], P. Karjalainen[1], J. Maunula[2], J. Kauppinen[3], M. Räsänen[3], R. Taipale[3], P. Vainikka[3], J. Roppo[2], J. Keskinen[1], T. Rönkkö[1]

[1]Department of Physics, Tampere University of Technology, Tampere, Finland
[2]Metso Power, Tampere, Finland
[3]VTT Technical Research Center of Finland, Jyväskylä, Finland
Keywords: fluidized bed boiler, fly ash, biomass burning, waste incineration
Presenting author email: heino.kuuluvainen@tut.fi

Introduction

The utilization of biomass and waste in energy production has increased significantly in recent years. Unfortunately, burning of biomass and waste incineration lead to various ash related problems in power plants. The most well-known problem is the high temperature corrosion of superheaters in a boiler induced by alkali chloride deposition (Nielsen et al., 2000). Altogether, the increased utilisation of biomass fuels and different waste fuels has led to an increased need to study the combustion process and to develop fuel additives against corrosion.

In this study, aerosol measured from a bubbling fluidized bed (BFB) boiler is characterized. The work is based on a previously developed sampling system and the chemical characterization of flue gas particles (e.g. Vainikka et al., 2011). The main purpose of this study is to broaden the analysis of aerosol particles measured with this sampling system and to monitor the effect of ferric sulphate as fuel additive on the aerosol. So far, the chemical composition of flue gas particles has been studied in many different cases, but the physical properties have not been characterized at all. In this study, aerosol size distributions and the physical structure of particles, including particle density and morphology, are considered.

Experimental

The experiments were carried out at a co-incineration plant. During the experiments, four different fuel mixtures, including different amounts of SRF (solid recovered fuel), bark, sludge and peat, were used. The sample was taken either from the superheater or from the 2nd pass of the boiler. The sampling system consists of an air-cooled sampling probe, two ejector diluters and two cyclones with a 10 µm cut-size.

For measuring aerosol size distributions, two parallel scanning mobility particle sizers (SMPS) were used. In addition, there was a TEM collector and an electrical low pressure impactor (ELPI), with which the sample could be led straight to the inlet or through a differential particle sizer (DMA). The latter case enabled a measurement of monodisperse aerosol and different particle sizes with the ELPI. Comparing the mobility diameter calculated from the DMA settings and the aerodynamic diameter calculated from the ELPI data, the effective density of the particles could be defined.

Results

The aerosol size distribution measurements showed that particles in the sub-500 nm size range mainly form two modes. The smaller mode exists with higher concentrations at the superheater but is also seen at the 2nd pass of the boiler. The larger mode is more stable and the concentrations are closer to each other at different measurement locations. According to the effective density measurements, the density of the smaller mode is around $1.4\,\mathrm{g/cm^3}$. The larger mode has much higher density and it seems to obey core-shell like density as a function of particle size.

The results indicate that the larger mode exists already in the boiler. In the dilution, gas phase components condense on the existing particles and form new particles through nucleation. This results in a new mode of particles, referred before as the smaller mode, and core-shell structures in the larger mode. The effect of ferric sulphate as fuel additive is seen in decreased particle concentration especially in the smaller mode. Also the density values of these particles are slightly lower.

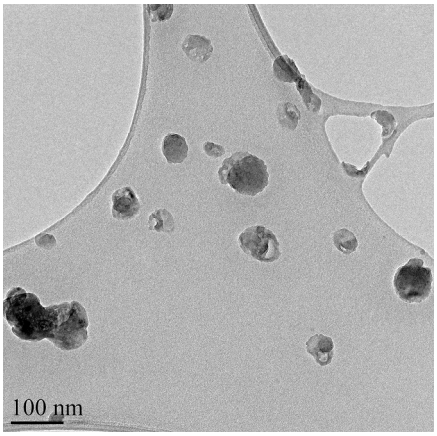

Figure 1: A TEM image of some collected particles.

Nielsen, H. P., Frandsen, F. J., Dam-Johansen, K., Baxter, L. L. (2000) *Prog. Energy Combust. Sci.* 26 (3), 283–298.

Vainikka, P., Enestam, S., Silvennoinen, J., Taipale, R., Yrjas, P., Frantsi, A., Hannula, J., Hupa, M. (2011) *Fuel* 90 (3), 1101–1112.

Diagnostics of burning tungsten particles by two-color imaging pyrometry

S.G. Orlovskaya, F.F. Karimova and M.S. Shkoropado

Department of Thermal Physics, Odessa National I.I. Mechnikov's University, Odessa, 65009, Ukraine
Keywords: temperature, imaging, tungsten, particle
Presenting author email: svetor@rambler.ru

It is necessary to measure moving particles temperature for diagnostics of high temperature processes: plasma spraying (Fauchais, 2004), metal and coal particles combustion and so on.

The most appropriate non-contact diagnostics method of moving objects is spectral ratio pyrometry (Avila, 2012). So we use imaging pyrometry to define temperature histories of burning tungsten particles in-flight. The metal sparks are formed by tungsten rod pressing against a corundum grindstone. They are registered by digital camera through rotating stroboscope type disk. The image of the particle trajectory looks like set of streaks (Figure 1a).

Optical diagnostics of such sparks is not simple because tungsten glows rather dimly at temperatures below 1500 K. So to obtain sufficiently high signal to noise ratio we have to use relatively wide spectral bands. The built-in filters of Canon 350d have appropriate characteristics with half-width about 100 nm.

So we use the ratio of red (R) and green (G) channels signals S_R/S_G to determine burning particles temperature. The well known expression derived from Wien's formula isn't applicable for temperature calculation in this case. So we have to modify the traditional method of spectral ratio pyrometry to define color temperature of glowing particles.

We calibrate relative response of Canon 350d color channels by radiation of a platinum filament (20 cm length, 300 mcm diameter), heated electrically. The glowing platinum filament is imaged in raw format, and simultaneously its brightness temperature T_b is measured in the central zone by disappearing filament pyrometer. Then we calculate a true temperature value T_r according the well-known equation:

$$\frac{1}{T_r} = \frac{1}{T_b} + \frac{\lambda}{C_2} \ln \varepsilon(\lambda, T)$$

here: C_2 = 1.4388 m·K, λ=0.65 mcm, ε (0.65,T)≈ 0.3.

The raw files are converted into tiff format and are processed by use Image Processing Toolbox MatLab 7.0. Firstly a rectangular region is cropped in the central zone. The signals in R and G channels are filtrated, averaged over selected area and then their ratio is calculated. This procedure is fulfilled for various values of heating current. In so way the empirical dependence $S_R/S_G=f(T)$ is obtained. After that the images of tungsten sparks streaks are processed in the same way to determine temperature histories of hot moving particles. It is found that tungsten particles temperatures not exceed 1370÷1420 K and drop quickly. A formula for calculating a particle burning time is very simple: $t_b=n/v$, here n – a number of streaks along its trajectory; v – a stroboscope rotation frequency, c^{-1}. The particles burning times in cold air vary in range 0.04÷0.07 c. There are presented successive steps of temperature definition in Figure 1.

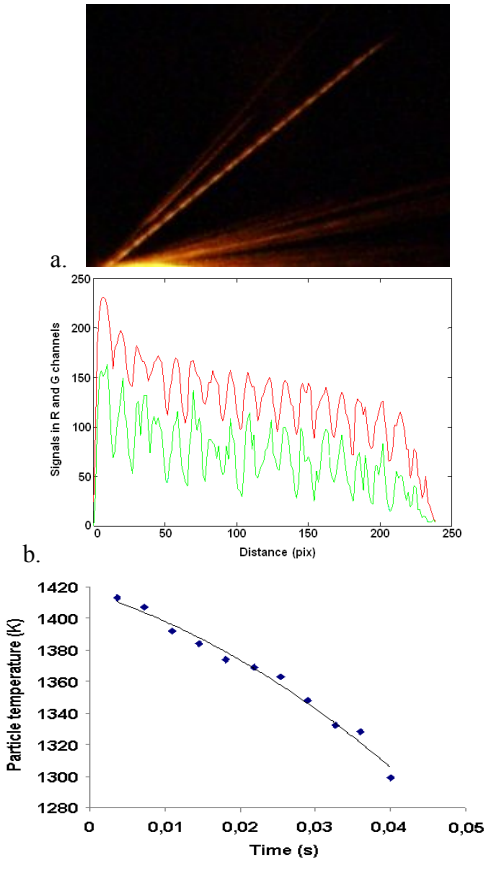

Figure 1. The particle streaks (a); the profiles of R and G values (b); temperature history of tungsten particle (c).

Thus the elaborated technique of two-color imaging pyrometry is applicable for diagnostics of hot moving particles.

Fauchais, P. (2004) *J. Phys. D: Appl. Phys.* **37,** R86–R108.

Avila M., and oth. (2012) *Industrial Combustion,* Article Number 201201.

Fate of hazardous elements from biomass burned in stoves and boilers

Torben Seidel & Hans Ruppert

Dept. of Sedimentology and Environmental Geology, Geoscience Center, Goettingen University, Goldschmidtstrasse 3, D-37077 Goettingen, Germany
Keywords: biomass burning, emission, concentration, fluxes, heavy metals
Presenting author email: tseidel1@gwdg.de

Biomass burning as an alternative energy supplier may play an essential future role due to the sighted reduction of the greenhouse gas effect, the shortage of fossil energy sources and the striving autonomy from fossil fuels. The growing contribution of biomass burning may have adverse effects such as higher emissions of harmful inorganic and organic substances in contrast to fossil fuels such as oil and gas.

Especially for in - house facilities burning biomass reliable measurements of concentrations and fluxes of heavy metals in the flue gas are lacking. For a reliable reconstruction of element fluxes and for input/output balances, the originating ashes such as grate ash, heat exchanger ash and fly ash are collected.

In the ideal case the amount of an element contained in the fuel should be identical with the combined element amounts in the different ash fractions. Systematic burning experiments with wood and straw in boilers reveal that significant amounts of heavy metals such as the environmentally and health relevant elements Cr, Co, Ni, Cu, Zn, Mo, Cd, Sn, Sb, Tl, and Pb are missing illustrated as the recovery rate of these elements (Fig. 1).

This suggests that they either leave the chimney as molecules or ultrafine particles or that they “disappear” in the refractory lining material. The volatile property of these elements can be affirmed by a crucial lower presence in others than fly ashes.

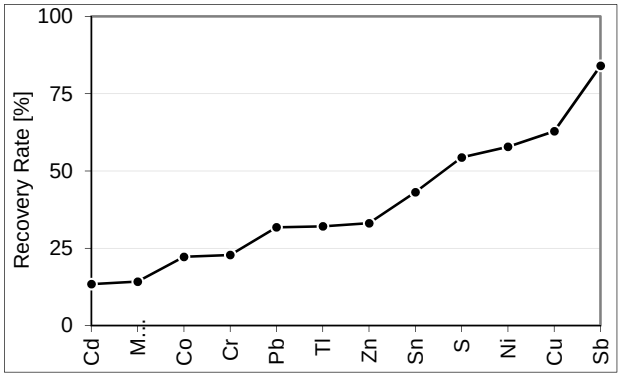

Fig. 1: Recovery rate (%) of elements by burning wood-chips in a 30 kW boiler (combined element amounts in grate ash, internal heat exchanger ash and fly ash divided by the element amounts contained in the wood chips).

We tested if elements pass the filter by percolating the air behind the filter through absorption solutions of HNO_3-HCl-H_2O and HNO_3-H_2O_2-H_2O respectively (VDI-guideline 3868). The measured concentrations are close to the detection limit and by far below the expected concentrations (Table 1). This means a leaving of this missing amount of these elements through the chimney can be suspended.

Tab. 1: Expected element concentration in the absorption solution determined from the balance calculations (Fig. 1) and measured element concentration in the absorption solution.

Element	Expected concentration [ppm]	HNO_3 + HCl	H_2O_2 + HNO_3
S	5,04	<0,02	<0,3
Cr	0,172	<0,002	<0,01
Co	0,06288	<0,00006	<0,0001
Ni	0,058	<0,004	<0,008
Cu	0,085	<0,006	<0,007
Zn	1,55	<0,002	<0,002
Mo	0,0092	<0,0002	<0,0003
Cd	0,03189	<0,00001	<0,00002
Sn	0,0019	<0,0002	<0,0002
Sb	0,0001	<0,0002	<0,0002
Tl	0,002560	<0,000002	<0,000002
Pb	0,039	<0,006	<0,02

The second explanation for the low recovery rate could be fixation by refractory lining materials such as chamotte. First experiments of a part of the refractory lining material from the roof of a stove show a large potential to act as a sink. The concentration in the unaffected material after correction with the fuel is still high and nearly unvaried and it shows that it is possible to store large element amounts in this material. The enrichment of some elements may be facilitated by the large open porosity (>20%) of this material and may explain in part small recovery rates. But very high extraction efficiencies would be necessary to remove appreciable amounts of these elements from the flue gas. For example: about 80% of Cd released during wood burning should be stored in the lining. Also the requirements on such a material can make a difference, e.g. the lining material of a boiler seems to have a lower retention potential for emitted elements.

Tab. 2: Calculation of the potential of the refractory lining of a stove with beech wood - log as fuel to act as a sink.

	Cd	Zn	Tl	Pb	Bi	Sb
Used baffle [ppm]	1,07	167	1,28	89,7	1,22	2,49
Content in the baffle [mg][1)]	6,42	996	7,68	538,2	7,32	14,9
Beech wood - log [ppm]	0,05	3,58	0,0015	0,1	0,0005	0,0024
Content in the burned beech wood - log [mg][2)]	1	716	0,3	20	0,1	0,48
Content [mg] in the baffle after subtraction of the content added by the fuel.	5,42	280	7,38	518,2	7,22	13,46
Concentration [ppm] of the baffle without potential content supply by the fuel	0,9	46,7	1,23	86,4	1,20	2,24

[1)] Weight of the baffle: ~6 kg

[2)] Mass of burned beech wood - log until dismounting of the baffle: 200 kg.

To assess the environmental impact of a furnace, flux calculations for elements are much more relevant than listing of simple concentration data. In addition, only element fluxes enable the comparison of emissions from different furnaces and fuels under different burning conditions, etc. But the fate of elements with low recovery rates has to be ascertained (retention in refractory lining material, contamination of the fuel, unknown sinks in the flue gas path).

Biomass Combustion in Stoves – Influence on Emissions and Toxic Potential of Particles

C. Schön[1] and H. Hartmann[1], J. Gerth[2]

[1] Technology and Support Centre in the Centre of Excellence for Renewable Resources, Schulgasse 18, 94315 Straubing, Germany
[2] Technical University Hamburg-Harburg, Eißendorfer Str. 40 (N), 21073 Hamburg, Germany
Keywords: wood stoves, biomass combustion, particle emissions, toxic potential.
Presenting author email: claudia.schoen@tfz.bayern.de

Wood stoves are widely used and can emit high fractions of gaseous and particulate matter (PME) depending on several impacts such as wood log size, fuel mass loaded per batch, moisture content and fuel type. From the obtained results recommendations for fuel properties and reloading strategies are given.

Measurements were performed using two different chimney stoves and one tiled stove insert. One of the chimney stoves used was suitable for coal combustion. All stoves were fired usually with beech wood which was prepared as cuboid-shaped test fuels in accordance to the Norwegian test standard NS 3058. The log size of the test fuel shape was varied between 5x5 cm, 7x7 cm and 9x9 cm. The fuel load applied ranged between 30 and 167 % based on the nominal heat output of the stoves using the medium sized logs with 7x7 cm. Measurements on particle and gaseous emissions were performed. The combustion test stand was equipped with a parallel sampling of particles from a diluted and undiluted flue gas in order to allow the identification of excessive particle emissions due to condensation of hydrocarbons for all test trials. The collected particle emission from the diluted flue gas were further chemically analysed for e. g. polycyclic aromatic hydrocarbons (PAH).

The determined PAH values were used for the estimation of the toxic equivalents (TEQ) of the emitted PM based on the weighing factors of the different 16 EPA PAH using the proposal of the DFG since different PAH have different health risk potentials. During the measurements gaseous emissions such as CO and organic gaseous carbon (OGC) as well as particle emission in the undiluted (hot) and diluted (cooled) flue gas were also determined.

The PME measurement in the diluted flue gas (samples taken at temperatures below 50°C) clearly shows more pronounced effects on combustion conditions compared to PME measurement done in the hot (undiluted) flue gas as it is typically done for type testing. But if PAHs are also considered in this comparison some differences are observed.

For example the mass loaded per batch was varied for 3 combustion appliances. For all furnaces there was a good agreement on the PME trend from low load to an overload. With respect PME only, one could also conclude that the second chimney stove performs better than the first chimney stove, see Figure 1. But if PAH-emissions are considered the opposite conclusion can be drawn. Figure 2 shows that chimney stove 2 causes a higher toxic potential (TEQ) at low load and at overload compared to the first chimney stove.

Such investigations were also performed with variable fuel moisture contents (spruce and beech wood) using chimney stove 1. In addition, results shall also be presented for several other fuels which were burnt in all three appliances including wood and pure bark briquettes.

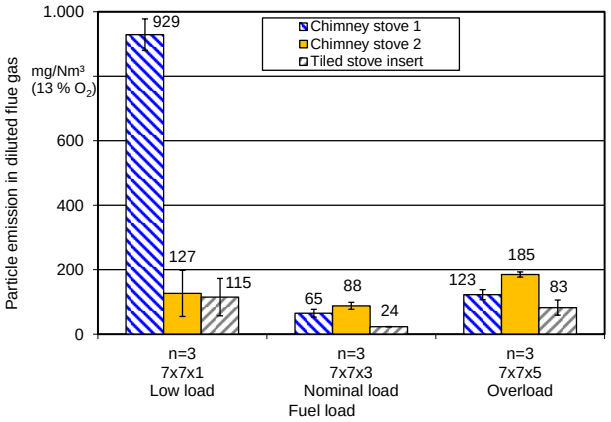

Figure 1. Influence of fuel mass loaded per batch on PM emissions determined in the diluted flue from 3 different appliances (fuel used: beech wood logs

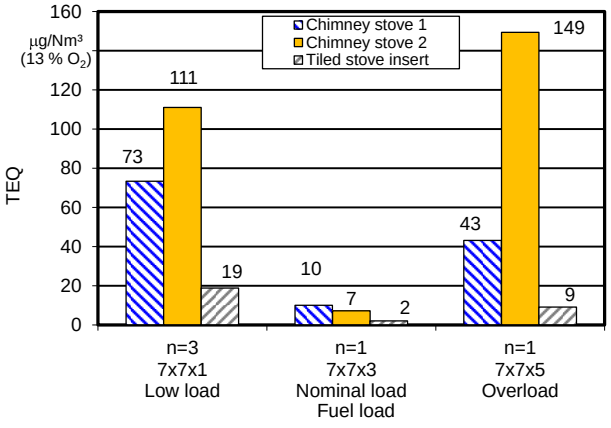

Figure 2. Influence of fuel mass loaded per batch on PAH emission, expressed as toxic potential (TEQ), from 3 different appliances (fuel used: beech wood logs).

The research was funded by the German Federal Ministry for the Environment, Nature Conversion and Nuclear Safety (BMU).

Ultrafine particulate matter emissions from a gasoline direct injection engine

B. R'Mili[1], A. Boréave[1], W.Y. Hernandez[1], M.N. Tsampas[1], N. Charbonnel[1], L. Retailleau-Mevel[1], B. D'Anna[1], P. Vernoux[1], M. Leblanc[2], S. Zinola[2], S. Raux[2]

[1]Université de Lyon, Institut de Recherches sur la Catalyse et l'Environnement de Lyon, UMR 5256, CNRS, Université Claude Bernard Lyon 1, 2 avenue A. Einstein, 69626 Villeurbanne, France

[2]IFP Energies nouvelles - Direction Techniques d'Applications Energétiques, Etablissement de Lyon, Rond-point de l'échangeur de Solaize - BP 3, 69360 Solaize - France

Keywords: Ultrafine Particulates, Gasoline Particulate Filter, Gasoline Direct injection, Three-Way Converter

Presenting author email: badr.rmili@ircelyon.univ-lyon1.fr

Epidemiological studies have linked exposure to particles matter less than 2.5 microns in diameter ($PM_{2.5}$) with adverse health (cardiovascular or pulmonary diseases that would cause premature death). The contribution of the transport sector to the total concentration of $PM_{2.5}$ in the ambient air is 12% [1]. This value represents an average which likely is higher in areas near emission sources (i.e. urban area). PM abatement in exhausts of gasoline direct injection (GDI) engines, which aims to improve fuel efficiency, will be necessary due to the strengthening of the European legislations. GDI engines offer a number of opportunities for improving fuel efficiency, such as reducing pumping losses, charge air cooling, and downsizing when turbocharged [2]. However, direct injection of fuel into the engine cylinder is susceptible to incomplete fuel evaporation and to fuel impingement on piston and cylinder walls, both of which lead to combustion of liquid fuel and, consequently, to PM emissions increase [3]. Gasoline Particulate Filters (GPF) are currently developed to mechanically filter the soot particles emitted by GDI engines. The particle sizes in this case are typically smaller in comparison with diesel engines [4].

Ultrafine particulate (UFP) matter (1-40 nm) emissions from a GDI engine (1.6 L) were characterized as a function of the engine operating regime in terms of particle numbers and size distributions. Exhaust gas samples were analyzed upstream and downstream a three-way converter (TWC), as well as downstream a GPF, i.e. at the exhaust outlet. UFPs were analyzed with a Scanning Mobility Particle Sizer equipped with a dielectric barrier discharge, a differential mobility analyzer (176 channels) to classify the PM size range that enters into a Faraday-Cup Electrometer (FCE) to count the charged particulates (SMPS+E, Grimm). After a two stage dilution (realized by FPS4000, DEKATI), the sampled aerosol was analyzed in the range 1 to 38 nm. SMPS+E data were compared with those of a SMPS (TSI, model 3080, PM size range 3-150 nm) and a DMS (Differential Mobility Spectrometer, Cambustion, PM size range analysis 5-1000 nm). In addition, the fraction of the elemental carbon in PM was estimated with a Multi-Angle Absorption Photometer (MAAP, Thermo Scientific, model 5012). UFPs with diameters lower than 20 nm was detected upstream the TWC. UFPs total concentrations were high, in the range 2 – 20 10^{14} part/m^3 depending on the engine load. UFPs size distributions were found to be bimodal with mean diameters around 2-3 nm and 10 nm, respectively. The impact of TWC on UFP concentration and size was significant since a large part of UFPs, lower than 10 nm, was removed. Furthermore, the overall UFPs number was divided by one order of magnitude. The filtering efficiency for UFPs of the GPF was found to be high since no UFPs was detectable using the SMPS+E downstream the GPF (Fig. 1). These results will be discussed in relation with PM analysis in the range 5 – 200 nm, carbon elemental concentration as well as gas pollutant emissions.

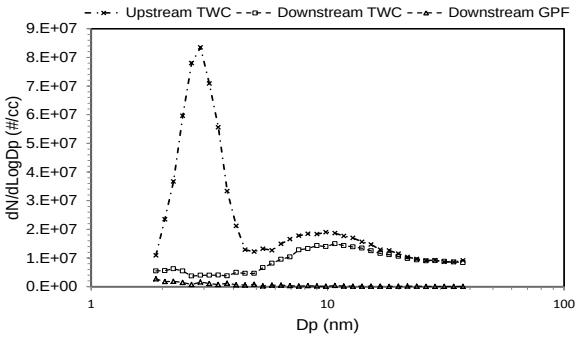

Figure 1: UFPs size distributions at 2500 rpm/ 13 bar. Dilution ratio= 6.

The authors would like to thank the "Agence National de la Recherche (ANR)" for the financial support of the TRIPTIC-H project (N°ANR-11-VPTT-003-05).

[1] WHO, 2006a: Health risks of particulate matter from long-range transboundary air pollution. WHO report E88189, WHO Regional Office for Europe, Copenhagen, Denmark.

[2] J. Yi, S. Wooldridge, G. Coulson, J. Hilditch, C.O. Lyer, P. Moilanen, G. Papaioannou, D. Reich, M. Shelby, B. VanDer-Wege, C. Weaver, Z. Xu, G. Davis, B. Hinds, A. Schamel, SAE Technical Paper. 2009-01-1494 (2009).

[3] S. J. Harris, M. M. Maricq, Aerosol Science 32 (2001) 749.

[4] M.M. Maricq, Combustion and Flame. 159 (2012) 170.

Fractional cabin air recirculation: A simple and robust way to reduce PM exposure for passengers

Heejung Jung[1,2] and Michael Grady[1,2]

[1]Department of Mechanical Engineering, University of California, Riverside, CA 92521, U.S.A.
[2]College of Engineering-Center for Environmental Research and Technology (CE-CERT), University of California, Riverside, CA92507, U.S.A.
Keywords: vehicle cabin air quality
Presenting author email: heejung@engr.ucr.edu

A vehicle cabin provides a unique environment in which passengers are confined during their ride. Current vehicle HVAC systems are optimized to reduce the dust concentration and noise coming from roadway while maintaining comfortable temperature and humidity for passengers. On roadways, in-cabin exposures to ultrafine particles have been shown to be 10 times higher than ambient levels and contribute to approximately 50% of total daily ultrafine particle exposure among Los Angeles commuters (Zhu et al, 2007; Fruin et al. 2008). These results can apply to most of urban areas where high traffic volume exists. The high exposure at the above studies is because air on the roadway is entrained into the vehicle cabin. Scientists found cabin air-recirculation can reduce particle concentrations in the vehicle cabin significantly and effectively. However, their findings could not be applied to the cars in the market because of the simultaneous increase of CO_2 concentrations in the cabin.

This study (Jung 2013, Grady and Jung 2013) proposes continuous fractional recirculation of cabin air (as opposed to full recirculation and off/off control) to suppress increase of cabin CO_2 concentrations while taking advantages of air recirculation. The study showed cabin CO_2 concentration is determined by the balance between source strength and vehicle body leakage rate. This balance is influenced by multiple parameters: vehicle speed, cabin volume, fan speed and number of passengers. The study demonstrated to control cabin CO_2 concentrations at certain target level by adjusting opening of the recirculation door angle. This method is a cost effective way of maintaining clean air quality of the cabin and can be applicable to new cars.

Figure 1 shows comparison of CO_2 concentrations between mathematical model equations and experimental data during full recirculation mode at two different fan speeds while the vehicle is at constant speed of 21 km/h. The model predicts extremely well the time evolution of CO_2 concentrations.

Figure 2 shows a possible control strategy of cabin CO_2 concentration at a certain target concentration level. Upon the choice of recirculation mode the fraction of recirculation changes to control the cabin CO_2 concentration within the target range. For this example we chose rather high concentration (2000 ppm) as a target concentration to expect some energy saving from vehicle thermal management perspective as well.

Overall the presentation includes results and discussion from 1) feasibility test: proof-of-concept, 2) characterization of vehicle HVAC system, 3) influence of vehicle speed, 4) input parameters to control cabin CO_2 concentration, and 5) mathematical modelling.

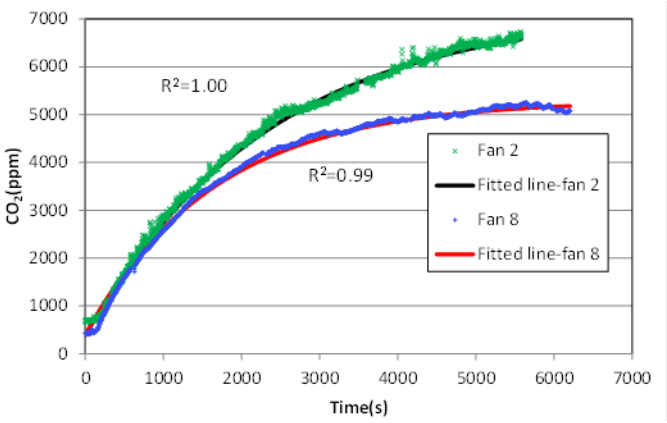

Figure 1 Evolution of cabin CO_2 concentration during full recirculation mode. The vehicle was at constant speed of 21 km/h. Green and blue markers show experimental data and black and red solid lines show fitted lines for fan speed 2 and 8, respectively

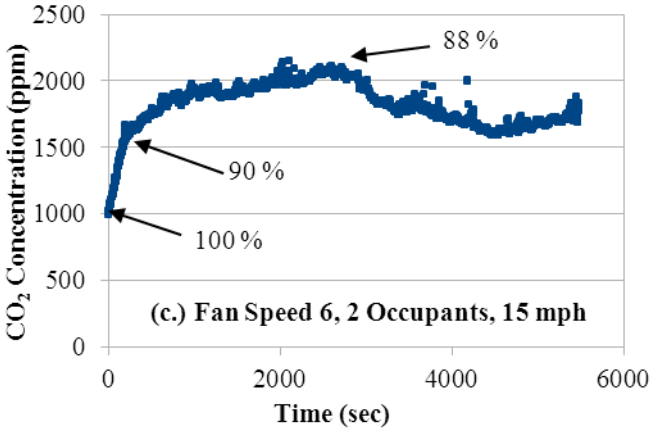

Figure 2 Feasibility test to control cabin CO_2 concentration at a certain target level, at 15 mph and fan speed 6 with two passengers. Percentage indicates degree of recirculation.

This work was supported by Hyundai-Kia motors.

Zhu, Y. F. et al., 2007, Environmental Science & Technology 41(7): 2138-2145.
Fruin, S. et al., 2008, Atmospheric Environment 42(2): 207-219.
Jung, H. (2013) SAE Technical Paper, 2013-01-1497.
Grady, M., Jung, H. (2013) SAE Technical Paper, 2013-01-1494.

Particle emissions of a heavy duty diesel engine fuelled with fossil diesel and hydrotreated vegetable oil

P. Karjalainen[1], J. Heikkilä[1], T. Rönkkö[1], M. Happonen[1], F. Mylläri[1], L. Pirjola[2], T. Lähde[2], D. Rothe[3] and J. Keskinen[1]

[1]Department of Physics, Tampere University of Technology, Tampere, Finland
[2]Department of Technology, Metropolia University of Applied Sciences, Helsinki, Finland
[3]MAN Truck & Bus AG, EMRE - Engine Research Exhaust Aftertreatment, Nuremberg, Germany
Keywords: diesel exhaust particles, biodiesel, hydrotreated vegetable oil.
Presenting author email: panu.karjalainen@tut.fi

Diesel exhaust emissions are a major concern for light and heavy duty vehicles due to adverse health and environmental effects. As well as increasing the air pollution components, e.g. NO_x, SO_x and PM, in the densely populated areas, diesel vehicles emit a vast amount of CO_2. One way to reduce the net CO_2 emissions is to increase the amount of bio components in the fuel. By changing the chemical and physical structure of the fuel, the exhaust emission nanoparticles and other pollution components may also change.

Hydrotreated vegetable oil (HVO) is one of renewable diesel fuels (Kuronen *et al.* 2007). The blending percentage of HVO to fossil fuel can vary between 0–100%. According to the review study of Hartikka *et al.* 2012, by using HVO (compared to fossil diesel), emissions of every regulated component were reduced on average in 14 Euro IV heavy duty vehicles. NOx, PM, CO and HC emissions were reduced by 8%, 34%, 25% and 26%, respectively, and also CO_2 emission was reduced by 4% due to larger H/C ratio in HVO compared to fossil diesel. HVO has also been observed to reduce soot particle number emissions compared to fossil fuel while the structure and oxidation properties of the particles were unaffected which indicates that similar particle filters can be used (Happonen *et al.* 2010).

In this study, particle emissions of a Euro IV truck engine were studied on an engine dynamometer. Test fuels were 100% fossil diesel fuel, complying with the EN590 standard, and 100% HVO fuel. The particle size distributions were measured with two ELPIs (Electrical low pressure impactor, Dekati), two EEPSs (Engine exhaust particle sizer, TSI), an SMPS (Scanning mobility particle sizer, TSI) and a Nano-SMPS. Particle number concentration was also measured with a UCPC (Ultrafine condensation particle counter, TSI). The exhaust sampling was conducted with two dilution systems. A double ejector dilution (DED) was used for one ELPI, while the exhaust sample for all the other instruments was diluted with a porous tube diluter (PTD). Also a thermodenuder (TD) was applied after the PTD sampling to remove the semivolatile particle fraction.

Nonvolatile particle emission factors measured with the ELPI after DED are shown in Figure 1. The emission factor is calculated from particle number and CO_2 concentrations which were measured from the same location of the sampling system. Overall, the particle number emissions are lower with HVO fuel compared to fossil fuel; differences are especially remarkable at the ESC points 7, 9 and 11 where the engine runs at low load. The particle number concentrations measured with different instruments were in very good correlation which increases the reliability of the results. Somewhat unexpectedly the nucleation mode was absent at all of the engine load conditions with both fuels. Size distributions, as well as concentrations, were similar with and without the TD consisting solely of soot particles.

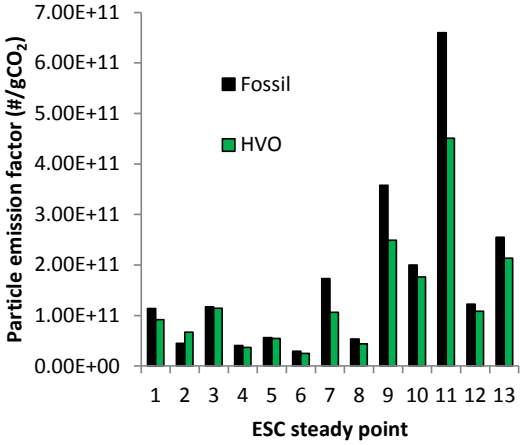

Figure 1. Solid particle engine-out number emission factors with a fossil diesel fuel and hydrotreated vegetable oil (HVO) at different ESC cycle steady test points. Particle concentrations were measured with the ELPI behind the DED sampling

The study was conducted in the TREAM projects supported by the Finnish Funding Agency for Technology and Innovation (Tekes), Neste Oil Oyj, Ecocat Oy, AGCO Power and Nanol Technologies.

Kuronen, M. *et al.* (2007). *SAE Technical Paper Series 2007-01-4031.*
Hartikka, T. *et al.* (2012). *SAE Techical Paper Series 2012-01-1585.*
Happonen, M. *et al.* (2010). *Fuel 89, 4008—4013.*

Particle number and size distribution of Euro 5 and Euro 6 passenger cars at 22°C and -7°C

F. Riccobono[1], U. Manfredi[1] and G. Martini[1]

[1]European Commission, Joint Research Centre, Ispra, 21027, Italy
Keywords: combustion, nucleation, filtration, legislation.
Presenting author email: francesco.riccobono@jrc.ec.europa.eu

The European introduction of particle number limits on the emissions of diesel passenger cars (September 2011 for type approval tests) led to the installation of highly efficient diesel particle filters (DPF) on all Euro 5 and Euro 6 compression ignition cars. Currently the assessment of the particle number is regulated according to the Particle Measurement Programme (PMP) developed by the Working Party on Pollution and Energy of the United Nations ECE. The PMP protocol was developed to complement the well-established particulate mass measurement, it consists of measuring the particle number after two dilution steps and a thermal treatment of the sample, in order to remove the volatile particles and reproducibly counts only the non-volatile particles with a diameter larger than 23 nm. This protocol proved to be a robust and sensitive method to discriminate between high and low efficiency DPFs. Due to diffusion mechanism the filter efficiency increases with the decrease of particle's diameter, thus regulating non-volatile particles with diameters larger than 23 nm allowed to effectively regulate all the soot particles from DPF equipped diesel cars. However the absence of a filtration system could lead to the emissions of non-volatile particles with diameters smaller than 23 nm.

The introduction of the particulate number limit for gasoline cars is envisaged for 2017. Among the different engine types the Gasoline Direct Injection (G-DI) cars have demonstrated the fastest market penetration in the last decade and the latest scenarios predict a share of G-DI in new registered gasoline vehicles in Europe that reaches 50% in 2015. The reason for such a strong market penetration lies in the lower fuel consumption of the G-DI vehicles compared to port fuel injection gasoline vehicles. The drawback of the G-DI technology is the elevated particle number emissions. Literature data show that G-DI particle number emissions exceed the diesel standard by 5 to 25 times.

We assessed the non-volatile particle number concentration and the size distribution of the particulate emissions from an array of different diesel and gasoline passenger cars including diesel DPF equipped cars, G-DI, Port Fuel Injection and flexy-fuel gasoline cars. We performed experiments under regulated (New European Driving Cycle) and unregulated conditions at 22°C and at -7°C.

The measurement of the non-volatile fraction of particles has been performed with two different commercially available PMP systems with PMP compliant Condensation Particle Counters (CPC, 50% detection efficiency at 23 nm). We evaluated the ability of the PMP procedure to capture the non-volatile fraction G-DI emitted particles under different experimental conditions and with the use of Condensation Particle Counters with a detection efficiency of 50% of 10 and 4.5 nm. We also measured the concentration of all the particles larger than 3.5 nm with a Condensation Particle Counter with a 50% detection efficiency of 3.5 nm. Moreover we estimated the effect of re-nucleated particles downstream of the evaporation tube of the PMP system varying the dilution ratio of the second stage of dilution.

Figure 1 shows the real time emission rates of particles measured with two different CPCs over the New European Driving Cycle (NEDC): a PMP compliant system and a total counter.

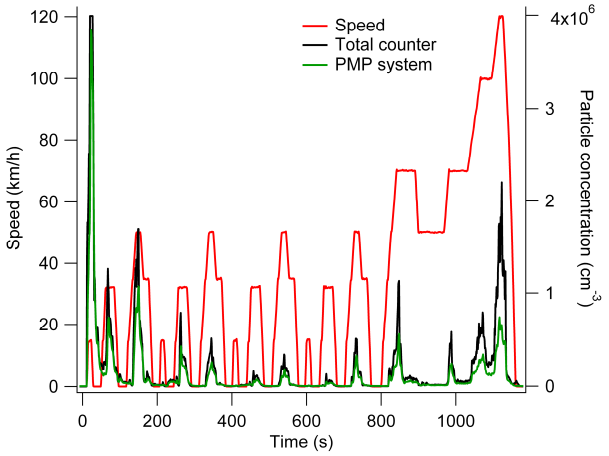

Figure 1. Real time emission rates measured with a total counter (TSI 3025, d50 CPC = 3.5 nm) CPC and a PMP compliant system (d50 CPC = 23 nm).

We have assessed the effect of the cell temperature on particle number emission rates and on the size distribution of the emitted particles over the NEDC cycle and steady state engine load conditions.
The comparison between the different vehicles will be presented and the differences between the measured particle concentrations will be discussed.

Andersson J., Giechaskiel B., Muñoz-Bueno R., Sandback E. and Dilara P. (2007). Particle Measurement Programme (PMP) Light-Duty Inter-Laboratory Correlation Exercise (ILCE_LD) Final Report. EUR 22775 EN.

Giechaskiel B., Cresnoverh M., Jörgl H. and Bergmann A. (2010). Calibration and Accuracy of a Particle Number Measurement System. *Measurement Science and Technology*, **21,** 045102.

Investigations on the removal of volatile components from diesel exhaust

B. Kiwull, J. C. Wolf and R. Niessner

Chair for Analytical Chemistry, Technical University of Munich, Marchioninistr. 17, 81377, Munich, Germany
Keywords: Diesel exhaust, volatile particles, particle number measurement.
Presenting author email: bettina.kiwull@mytum.de

Fine and especially ultrafine particles are considered to be harmful for human health (Oberdörster, 1995). As diesel-powered vehicles are a significant source for particles in this size range, it is important to limit and consequently reduce the emissions caused by their exhaust. Unfortunately, the well-tried attempt to confine the emissions based on the mass sampled on a filter turned out to be ineffective for fine particles and low particle concentrations (Matter, 1999). For this reason a new limit which is based on the particle number, was established within the European Union in 2011 (EU 566/2011).

Additionally to the number limit a new measurement procedure was introduced. It suggests the quantification of the particles with a condensation nucleus counter (CNC). It furthermore instructs a removal of volatile particles from the exhaust gas before quantification of the solid residue (figure 1). One crucial point of this measurement procedure is that the volatiles have to be removed completely from the exhaust gas to ensure reproducible and accurate results.

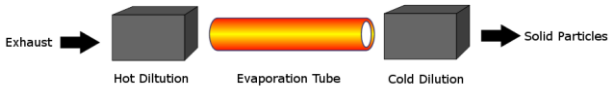

Figure 1. Scheme of the evaporation tube.

Subject of our research is to investigate different apparatus applied for the separation of volatile particles from exhaust gas in terms of their removal efficiency and capacity. To simplify the investigations, a model aerosol is used to mimic real exhaust gas. It consists of spark discharge soot coated with n-hexadecane respectively sulphuric acid particles suspended in dry particle free air.

At present there are three volatile particle remover types (VPR) known in literature: evaporation tube, thermodenuder and catalytic stripper (Giechaskiel, 2011). Our investigations started with the evaporation tube (ET). Within this device the exhaust is heated (evaporation of the volatiles) and consequently diluted (prevent recondensation).

To examine the removal efficiency, soot particles of different size were coated with a 1-nm layer of hexadecane and subsequently heated in the ET (figure 2). It can be seen that the counting efficiency of a CPC is increasing if a coating is present on the particle. This means that incomplete removal leads to changes in the detected particle number. After removal of the volatile component the counting efficiency is again on the same level as uncoated soot (soot reference). Thus it can be said that a complete removal of n-hexadecane is possible with the evaporation tube.

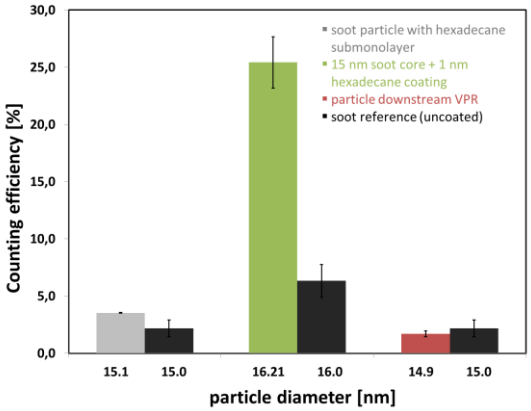

Figure 2. CPC counting efficiency of spark discharge soot (uncoated, coated with n-hexadecane and thermally treated).

Further experiments are conducted considering volatile exhaust components which are not as easy to remove as n-hexadecane. Catalytic stripper and thermal denuder are investigated in an analogous manner.

Oberdörster G., Gelein R., Ferin J., Weiss B. (1995), *Inhalation Toxicology* **7**, 111-124.

Matter U., Siegmann H., Burtscher H. (1999), Environ. *Sci. Technol.* **33**, 1946-1952.

Giechaskiel B., Mamakos A., Andersson J., Dilara P., Martini G., Schindler W, Bergmann A. (2011), *Aerosol Sci.Technol.* **46**, 719-749.

Commission Regulation (EU) No.566/2011

Effects of severe congestion on PAH emissions from a heavy vehicle diesel engine

M. Vojtisek-Lom[1,2], M. Pechout[1], M. Mazač[1] and J.Topinka[3]

[1]Dept. of Vehicles and Engines, Technical Univ. of Liberec, 461 17 Liberec, Czech Republic
[2]Dept. of Mechanical Engineering, Czech Tech. University of Prague, 166 07 Prague, Czech Republic
[3]Institute of Experimental Medicine of the Czech Academy of Sciences, Prague, Czech Republic
Keywords: diesel engine, particulate matter, polyaromatic hydrocarbons, PAH, urban, congestion
Presenting author email: michal.vojtisek@tul.cz

Summary

The effects of severe congestion on heavy diesel particulate matter (PM) emissions were investigated in a laboratory experiment. Extended idling of a conventional diesel engine and subsequent operation at full load were found to produce higher levels of PM and polyaromatic hydrocarbons (PAH) and an order of magnitude higher levels of carcinogenic PAH compared to idling just after loaded operation and to stabilized operation at full load.

Introduction

Despite advances in engine technology, vehicular traffic remains to be one of the key sources of fine and ultrafine PM in urban air. This work investigates the effects of severe congestion, common for transit truck traffic in Prague and elsewhere, on PM emissions.

Experimental (see Fig. 1 for schematic)

A diesel engine (certified to 0.3 g/kWh PM) with a mechanical injection pump coupled to an engine dynamometer was run alternately at intermediate rpm and full load, and at idle rpm and 1-2% of rated power to simulate slow "creep". Raw exhaust was diluted at nominally 10:1 dilution ratio and sampled by a Hi-Vol sampler (EcoTech 3000) with a $PM_{2.5}$ impactor. A second Hi-Vol sampler was used to provide dilution air. Dilution ratio was verified by CO_2 concentrations measurements. Samples of PM taken on fluorocarbon coated and quartz filters were extracted and PAH content analysed by HPLC with fluorescence detection.

Results and Discussion

Emissions of benzo[a]pyrene, 7 carcinogenic PAH (cPAH) per US EPA (benzo[a]anthracene, chrysene, benzo[b]fluoranthene, benzo[k]fluoranthene, benzo[a]pyrene, dibenzo[a,h]anthracene, indeno[1,2,3-cd]pyrene), US EPA 16 PAH, and total particulate mass, expressed as mass per kg of fuel, are plotted in Fig. 2.

It appears that BaP and cPAH after tens of minutes of idling were an order of magnitude higher than during first several minutes following a higher load.

It also appears that BaP and cPAH during operation at full load were an order of magnitude higher during first several minutes after prolonged (one-hour) idling compared to "stabilized" operation at full load.

It thus seems that prolonged idling may substantially increase emissions of carcinogenic PAH not only during, but also after the idling episode.

Toxicity of extracts of particulate matter sampled from exhaust gases of heavy diesel vehicles under real-world urban operation is currently being evaluated.

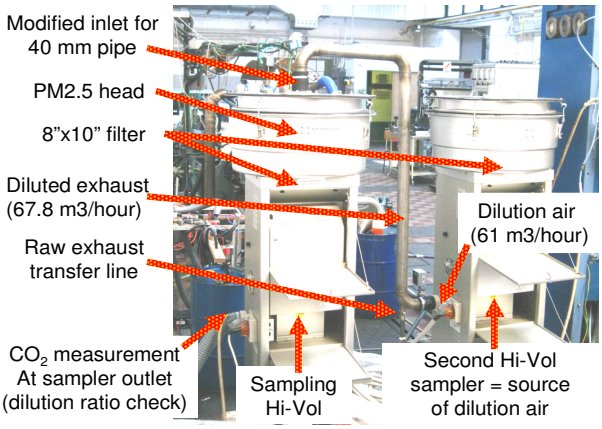

Fig. 1: Sampling setup

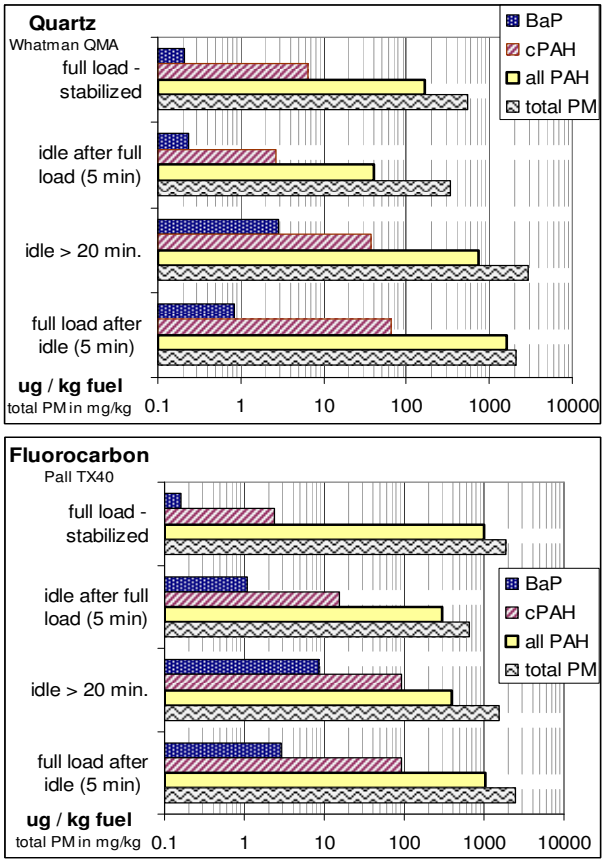

Figure 2: Benzo[a]pyrene, carcinogenic PAH and all PAH emissions in micrograms per kg of fuel

This work was supported by the EU LIFE+ project MEDETOX (LIFE10 ENV/CZ/651) and Czech Science Foundation Grant 13-01438S.

Emissions of gases and $PM_{2.5}$ during combustion of wood logs in a stove or a fireplace

V. Martins[1], A.I. Calvo[1], C. Alves[1], T. Nunes[1], R. Hillamo[2], K. Teinilä[2], M. Duarte[1], L. Mendes[1] and L.A.C. Tarelho[1]

[1]Centre for Environmental and Marine Studies, Department of Environment and Planning, University of Aveiro, Aveiro, 3810-193, Portugal
[2]Finnish Meteorological Institute, Erik Palmenin aukio 1 FIN-00560, Helsinki, Finland
Keywords: biomass, domestic combustion, flue gas, organic tracers, $PM_{2.5}$
Presenting author email: celia.alvest@ua.pt

Combustion gases from biomass burning in domestic equipments has been recognised as a significant emission source of air pollutants (McDonald *et al.*, 2000). It is responsible for large impacts on air quality, as well as significant potential effects on public health and global climate change (Bølling *et al.*, 2009; Hellén *et al.*, 2008).

The aim of the current study was to characterise the emissions of residential wood combustion. Logs of threes common in Spain (*Quercus pyrenaica*, *Populus nigra* and *Fagus sylvatica*) were burned in two different combustion appliances, a fireplace and a woodstove. Measurements were carried out at the biomass combustion facility of the University of Aveiro (Portugal). During each combustion experiment, which lasted between 60 and 90 minutes, about 2.0 kg of wood were burned. Three or four combustion experiments were performed for each biomass type. The flue gas composition was monitored continuously in the exhaust ducts of both burning appliances. Total hydrocarbons (THC) and carbon oxides (CO_2 and CO) were measured using automatic analysers with flame ionisation and non-dispersive infrared detectors, respectively. Particulate matter with aerodynamic diameter below 2.5 µm ($PM_{2.5}$) was sampled in a dilution tunnel under isokinetic conditions, onto quartz fibre filters, using a low volume sampler. Filters were analysed by a thermal-optical transmission method in order to obtain the elemental and organic carbon (EC and OC) content. Furthermore, levoglucosan, mannosan, and galactosan, commonly used as tracers for biomass burning, were determined by high-performance anion-exchange chromatography with electrospray ionisation mass spectrometry detection (Saarnio *et al*., 2010).

The flue gas composition and emission rate of some compounds varied widely depending on fuel type, characteristics of the combustion equipment, and operating conditions. Generally, CO, CO_2, THC and $PM_{2.5}$ emissions from the fireplace were higher than those observed for the woodstove (Table 1). In an open fire, the large quantity of bypass air leads to high heat losses in the flue gases. The very high air flow through the fireplace also increases the total smoke emission by lowering the flame temperature and sweeping away unburned fuel gases before they can be heated to their ignition temperature. The carbonaceous matter represented 73-85% of the particulate mass emitted, regardless of species burned and combustion appliances. This carbonaceous content was dominated by OC. The EC mass fractions in particles emitted from the woodstove were substantially higher than those of the fireplace, whereas the opposite was observed for OC.

Table 1. Emission factors (g kg^{-1} biomass burned, dry basis).

		Q. pyrenaica	*P. nigra*	*F. sylvatica*
Fireplace	$PM_{2.5}$	12.5±4.1	14.0±5.1	5.8±1.3
	OC	9.0±3.0	10.5±3.4	3.9±0.9
	EC	0.60±0.09	0.79±0.19	0.43±0.23
	Levogl.	1.02±0.45	0.66±0.24	0.35±0.02
	Mann.	0.052±0.020	0.061±0.022	0.023±0.003
	Galact.	0.094±0.034	0.035±0.011	0.022±0.002
	CO_2	1618±83	1765±179	1749±92
	CO	86.0±14.1	115.8±11.7	74.4±6.7
	THC	24.7±6.3	27.8±4.8	13.7±2.1
Woodstove	$PM_{2.5}$	13.3±3.8	4.4±1.4	2.8±0.7
	OC	9.1±2.7	2.9±1.1	1.6±0.5
	EC	0.90±0.20	0.88±0.05	0.43±0.13
	Levogl.	1.09±0.17	0.21±0.15	0.20±0.05
	Mann.	0.056±0.012	0.014±0.009	0.013±0.007
	Galact.	0.105±0.013	0.011±0.009	0.013±0.007
	CO_2	1415±136	1879±29	1748±59
	CO	95.6±7.8	84.1±4.9	54.9±3.9
	THC	23.2±1.2	8.6±2.2	5.2±0.9

The mean levoglucosan mass fractions in $PM_{2.5}$ emitted by the two combustion equipments were very similar. The anhydrosugar yields from the combustion of *Q. pyrenaica*, *P. nigra* and *F. Sylvatica* represented around 8, 5 and 6-7% of the $PM_{2.5}$ weight, respectively. Percentages always lower than 1% were obtained for the levoglucosan stereoisomers. Anhydrosugar emissions were strongly enhanced during the start-up phase and decrease progressively until the glowing combustion phase.

This work was supported by the Portuguese Science Foundation (FCT) through the project BIOEMI, PTDC/AMB/65706/2006. Ana I. Calvo acknowledges the posdoc grant SFRH/BPD/64810/2009 from FCT.

Bølling *et al.* (2009) *Part. Fibre Toxicol*. **6**, doi:10.1186/1743-8977-6-29.
Hellén *et al.* (2008) *Sci. Total Environ*. **393**, 283-290.
McDonald *et al.* (2000) *Environ. Sci. Technol*. **34**, 2080-2091.
Saarnio *et al*. (2010) *Anal. Bioanal. Chem*. **398**, 2253–2264.

Combustion of forest residues in a bubbling fluidised bed: characterisation of particulate matter emissions

A.I. Calvo[1], L.A.C. Tarelho[1], E.R. Teixeira[1], R. Modolo[2], C. Alves[1], T. Nunes[1], M. Duarte[1], E. Coz[3], D. Custódio[1], A. Castro[4], B. Artiñano[3], R. Fraile[4]

[1]Centre for Environmental and Marine Studies (CESAM), Department of Environment and Planning, University of Aveiro, 3810-193 Aveiro, Portugal
[2]Department Civil Engineering/CICECO, University of Aveiro, 3810-193 Aveiro, Portugal
[3]Centre for Energy, Environment and Technology Research (CIEMAT), Madrid, Spain
[4]Department of Physics, IMARENAB University of León, 24071 León, Spain
Keywords: aerosols, biomass waste, bottom ash, fluidised bed
Presenting author email: celia.alves@ua.pt

The use of biomass as fuel is taken an increasing interest regarding industrial heat and power production. Linked to this demand for bioenergy production, the volume of industrial ashes will increase, turning the efficient management of these products into an important challenge. Fluidised bed combustors (FBC) have been identified as one of the most appropriated technologies for converting biomass into thermal energy due to their inherent advantages of low process temperatures, isothermal operating conditions, and fuel flexibility. During biomass combustion in FBC two main types of ashes are produced: the bottom bed ashes and the fly ashes. Knowledge about the characteristics of these ashes is important in order to evaluate appropriate management solutions. However, biomass combustion is a source of particulate matter with a significant impact, not only on public health and on the environment, but also affecting the performance of the heat recovery equipment (economic impact).

In this study, particulate emissions (fly ashes) from the combustion of forest biomass residues resulting from eucalyptus felling for the cellulose industry were studied. These forest biomass residues were air dried, chopped and sieved in order to obtain particles in the size range of 1-5 mm. The combustion experiments were conducted in a pilot-scale bubbling fluidised bed combustor (BFBC) (Tarelho *et al.*, 2011). During biomass combustion in the BFBC, a bottom bed treated (sieved, 0.25-1.00 mm, and water leached) and recycled from an industrial bubbling fluidised bed using forest biomass residues as fuel was taken as bed material. The goal was to evaluate the effect of recycling a fraction of bottom bed in industrial FBC, taking into consideration its particular characteristics (Tarelho *et al.*, 2012). During the biomass combustion experiments in the pilot scale BFBC, the flue gas passed through a cyclone separator to minimise particle emissions into the atmosphere.

In order to characterise the fly ash particles in the flue gas, two different sampling systems were used: i) a low volume instrument to collect $PM_{2.5}$ onto quartz filters directly from the inlet and outlet cyclone ducts and ii) a Venturi system that allows to sample the combustion flue gas directly from the inlet duct of the cyclone by using dry filtered compressed air. Two different instruments used this flue gas flow for particle sampling: i) an optical counter for the continuous monitoring of particle size distributions, and ii) a Gent PM_{10} stacked filter unit sampler using polycarbonate filters (0.2 µm pore size) for later Scanning Electron Microscopy (SEM) analyses.

After $PM_{2.5}$ mass determination by gravimetric analysis, small punches from the loaded quartz filters were analysed by several techniques: i) ion chromatography was used for determining water-soluble inorganic ions, ii) the carbonate mass fractions were obtained by acidification of samples with phosphoric acid, and iii) a thermal-optical transmission technique was used for organic and elemental carbon determination, after removal of carbonates by exposing the filters to HCl vapour and neutralisation of the HCl excess with NaOH.

$PM_{2.5}$ concentrations of 139±5 mg m^{-3} and 105±13 mg m^{-3} were observed before and after de cyclone, respectively. Total carbon (OC+EC) constitutes less than 10% of the $PM_{2.5}$ mass at both sampling points. OC/EC ratios of 1.9±0.6 and 1.1±0.4 were registered before and after the cyclone. K^+ and Cl^- were the dominant water-soluble inorganic ions. Almost 20% (w/w) of the particulate matter emitted is constituted by carbonates. This fact was confirmed by FE-SEM that showed that filters were loaded of submicrometric calcium enriched minerals, salts, and biogenic and soot particles. A bimodal size distribution was found.

This work was supported by the Portuguese Science Foundation (FCT) through the projects PTDC/AAC-AMB/098112/2008 (Bias-to-soil) and PTDC/AMB/65706/2006 (BIOEMI). The electron microscopy was conducted at CNME-UCM through the AEROCLIMA project CIVP16A1811 (Fundación Ramón Areces). Ana I. Calvo acknowledges the posdoc grant SFRH/BPD/64810/2009 from FCT.

Tarelho, L.A.C., Neves, D.S.F., Matos, M.A.A. (2011). *Biomass Bioenergy* **35**, 1511-1523.

Tarelho, L.A.C., Teixeira, E.R., Silva, D.F.R., Modolo, R.C.E. (2012). *Proceedings of ASH 2012*, Stockholm (Sweden), January 25-27.

Prospecting analysis of soot for post-fire investigation

A. Bellivier[1], M. Meneceur[1] and H. Bazin[1]

[1]Department of Physical Measure and Fire Sciences , Laboratoire Central de la Préfecture de Police
39bis rue de Dantzig, 75015 Paris, France

Keywords: post-fire investigation, soot, analysis.
Presenting author email: axel.bellivier@interieur.gouv.fr

Motivation

The aim of post-fire investigation is to extract information from a fire scene to determine the origin and cause of the fire. Most traces and clues are, however, partially or completely destroyed by fire and intervention of fire-fighters. The problem is to find a source of information. The soot is particularly interesting because it is a record of the history of the fire. How to decode this information? How link the soot to his original material?

The objective of this study is to explore different analysis devices and to evaluate the information that each one can provide for the investigation.

Few studies have been found earlier, the most interesting seems to be Pinorini *et al* (1994).

Protocol

Based on a reference soot, obtained in laboratory from a methane / ethylene flame (M / E soot; 5.0 mg), various analytical devices are used to determine an analysis protocol.

The following analytical devices were used: liquid chromatography coupled with a fluorescence detector (HPLC), gas chromatography coupled to a mass spectrometer (GC-MS) and thermogravimetric analysis (TGA).

Soot analysis

This protocol is then applied to two soot obtained in the laboratory: acetylene soot (A soot, 5.0 mg) and polystyrene soot (2 samples: PS1 and PS2 soot; both 5.1 mg).

The results of HPLC allows to quantify PAHs masses. And phenanthrene, fluoranthene, pyrene, benzo (a) pyrene and indeno (1,2,3-cd) pyrene seems to differentiate materials (Figure 1). The total mass of PAH for each samples is highly variable: 16,14 µg for M/E soot; 0.580 µg for A soot; 94.53 µg for PS1 and 106.11 µg for PS2.

The results of GC-MS allows to find qualitatively other PAHs such as naphthalene, acenaphthylene or phenylnaphthalene. The presence of phenanthrene and pyrene, quantified by HPLC, were confirmed by GC-MS.

The results of the ATG are operated according to the method of Jiang *et al* (2011). The results are presented in Table 1. We distinguish significant differences between the different samples. The two polystyrene soot are in the same range.

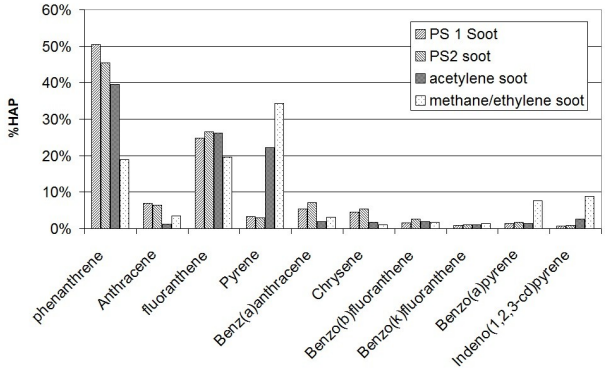

Figure 1. Percentage Distribution of PAHs after HPLC analysis.

Table 1. Organic carbon (OC) and elemental (EC) obtained by TGA analysis.

	M/E soot	A soot	PS1 soot	PS2 soot
EC	79.12	93.76	68.29	70.68
OC	20.46	02.42	30.43	28.05
Other	00.42	03.83	01.28	01.28

Conclusion

Devices used have provided lots of information to differentiate soot. The TGA is a technique particularly attractive since it provides information on the composition of soot (percentage of elemental carbon and organic carbon). GC-MS can see all the compounds unlike HPLC. However, it should be interesting with a quantitative GC-MS. It has also been observed that these results were linked to each other, especially OC rate with HAP mass.

In terms of the investigation, soot seem to offer many different features. We now come to relate them to their original material. This will rebuild the progress of the fire.

M. Jiang, Y. Wu, G. Lin, L. Xu, Z. Chen, F. Fu, *Pyrolysis and thermal-oxidation characterization of organic carbon and black carbon aerosols*, **2011**, Sci. Total. Environ., 409(20), pp. 4449-55.

Pinorini, M. T., Lennard, C. J., Margot, E, Dustin, I., and Furrer, E, *Soot As an Indicator in Fire Investigations: Physical and Chemical Analyses*, Journal of Forensic Sciences, JFSCA, Vol. 39, No. 4, **July 1994**, pp. 933-973.

Nanoparticles Emissions from Pottery Manufacturing

A.Voliotis[1], S. Bezantakos[1,2], M. Giamarelou[1], G. Biskos[1,3]

[1]Department of Environment, University of Aegean, Mytilene 81100, Greece
[2]ERL, Inst. of Nuclear Tech. & Rad. Protection, NCSR Demokritos, 15310 Ag.Paraskevi, Attiki, Greece
[3]Faculty of Applied Sciences, Delft University of Technology, Delft 2628-BL, The Netherlands

Keywords: Aerosol, Ceramics, Nanoparticles, Pottery
Presenting author email: bezantakos@env.aegean.gr

Airborne nanoparticles emitted from craftsmanship and industrial processes can have toxic effects upon human health (Brunekreef & Holgate, 2002). A good example of such craftsmanship, which in many places is embedded in local tradition, is pottery where high temperatures are required to fire the ceramics for producing the final products. Although the potential risk of nanoparticle emissions from industrial fabrication of ceramics has been addressed (cf. Minguillón *et al*., 2007), measurements of the exposure for small/medium-size traditional potteries have not been assessed to the best of our knowledge.

In this paper we report measurements of airborne particles emitted from firing ceramics in a small-sized pottery on Lesvos island in Greece. Size distributions of particles having diameters from 10.4 to 469.8 nm were recorded using a Scanning Mobility Particle Sizer (SMPS; TSI Model 3034). Particles having diameter > 300 nm were also measured using an Optical Particle Counter (OPC; Grimm Model 1.108). For all the measurements, air was sampled through a 6-m long copper tube (ID = 6.35 mm) with a sampling rate of 2 lpm. The inlet of the tube was placed 1 m above the furnace exhaust.

During the pottery fabrication process, hand-made ceramics are at first fired for half a day before the paintwork and glaze are applied. Then they are fired again for almost the same time to stabilize the surface of the pottery. In both firing processes, the furnace temperature rises almost linearly from ambient temperature to 980°C over a period of 11 hours. Repeated measurements were conducted for both firing processes, i.e. with unpainted/unglazed and with painted/glazed ceramics, over a period of one month.

Fig.1 shows the evolution of the size distributions of the particles during two characteristic runs of the oven. In the first run (Fig. 1a) ceramics fired without paint and glaze, whereas in the second run (Fig. 1b) they were painted and glazed. In both cases an increase in the concentration of particles smaller than 40 nm is observed after the 5th hour of the firing process, when the temperature of the furnace was about 580°C. Interestingly, the concentrations of the particles sub-40 nm particles emitted from the painted/glazed pottery is more than double when compared to those of the unpainted/unglazed ceramics. This difference is not observed only between the 5th and 6th hour after the firing process started, but also for the entire duration of the experiment. In the first run for example, the maximum total number concentration was observed 10.5 hours after the initiation of the furnace was switched on, reaching 7×10^5 particles per cm^3. In the second run, the highest concentration was 1.8×10^6, and was observed 9.5 hours after the start of the firing process. In both cases the temperature of the furnace was between 920 and 970 °C.

The systematic difference in the concentration of the emitted nanoparticles between the two runs indicates that the paints and glazes applied on the ceramics give off material for nanoparticle formation. Because the materials used for the paints and the glaze contain toxic compounds (e.g., organics and heavy metals), these are very likely to be present also on the emitted nanoparticles. Given that the size of the particles is in the range that can allow penetration to the deepest part of the respiratory system, it is therefore mandatory to measure their chemical composition in order to fully assess their potential effects upon human health.

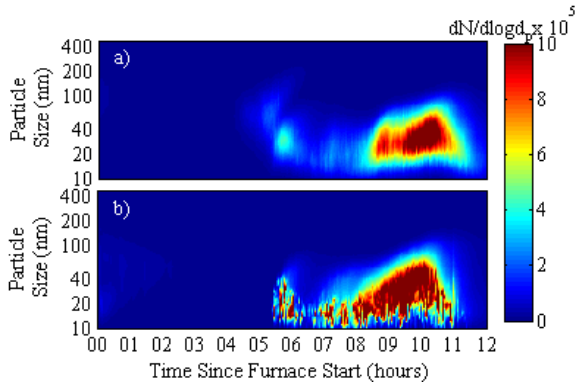

Figure 1. Evolution of the particle size distributions recorded during firing of (a) unpainted and unglazed ceramics, and (b) painted and glazed ceramics.

References

Brunekreef B., Holgate S. T. (2002). *The Lancet*, 360, 1233-1242.

de la Campa, A.M.S., de la Rosa,J.D., Gonzales-Castanedo, Y., Frenadez-Camacho R., Alastuey A., Querol X., Pio C. (2010). *Atmospheric Research*, 96, 633–644.

Minguillón M. C., Querol X., Alastuey A., Monfort E., Mantilla E., Sanz M. J., Sanz F., Roig A., Renau A., Felis C., Miró J. V., Artíñano B. (2007). *Science of the Total Environment*, 372, 382–396.

Wildfires in North Spain: Smoke aerosol and its radiative effects

A. Castro[1], E. Alonso-Blanco[2], A.I. Calvo[3], V. Pont[4], M. Mallet[4], C. Alves[3], R. Fraile[1]

[1]Department of Physics, IMARENAB University of León, 24071 León, Spain
[2]Centre for Energy, Environment and Technology Research (CIEMAT), Madrid, Spain
[3]Centre for Environmental and Marine Studies (CESAM), Department of Environment and Planning, University of Aveiro, Aveiro, 3810-193, Portugal
[4]Laboratoire d'Aérologie, OMP, Université de Toulouse III, CNRS, UPS, Toulouse, France
Keywords: aerosols, radiative forcing, size distribution, wildfires
Presenting author email: acasi@unileon.es

Wildfires constitute a major source of concern since they are responsible for important economic, human and environmental losses. They are a relevant source of aerosol particles and trace gases, with important impacts on several aspects: human health, visibility, biogeochemical cycles, atmospheric chemistry and global and regional climate. Wildfires change significantly chemical, optical and radiative characteristics of aerosol particles. Linked to these emissions, solar irradiance at the top and at the bottom of the atmosphere results affected, causing important effects on regional conditions of the climate system (Chubarova et al., 2012). At present, radiative direct forcing of wildfires continues to be at a medium to low level of scientific understanding (IPCC, 2007).

Several authors have pointed out that changes in climate will propitiate a considerable increase in fire intensity, frequency and area burned. Hence, a complete characterisation of forest fire emissions and their effects is of great interest. Furthermore, it is important to keep in mind that transport processes play a crucial role, as these events not only have a local impact, but they also have consequences at thousands of kilometres from the source.

On 19th August 2012 a forest fire occurred in the district of Castrocontrigo (León, Spain) (42° 10′ 58″ N, 6° 11′ 18″ W) in the southwest of the province of León and lasted for 10 days. A vast area was affected, including several districts. The land that was burnt (117.24 km^2) included shrub (11.69 km^2) and wooded land (105.55 km^2). Furthermore, another forest fire occurred in Cubo de Benavente (Zamora, Spain) (42° 07′ 25″ N, 6° 09′ 47″ W) affecting a total of 8.24 km^2 between 18th and 20th August 2012. The effects of these wildfires were rapidly noticeable in the city of León (42° 35′ 59″ N, 5° 34′ 18″ W, 840 m asl), located at around 60 km and 100 km, respectively, from the points where the wildfires started. Thus, mainly on 19-21 August, a thick haze from these fire events covered the city, limiting visibility. The presence in the air of large amount of ash and cinder and a significant particle deposition onto cars, land, buildings, etc., was observed. There was also a large red/pink halo around the sun, which caused a partial darkness in the city, uncommon during daylight hours.

A sampling campaign was carried out in the city of León during August 2012. A laser spectrometer PCASP-X was used for measuring particles from 0.1 µm to 10 µm. This optical counter was calibrated with latex particles with a refractive index of 1.58 –0.0i. To retrieve the exact number concentration versus exact size, the raw size bins were corrected using a program based on Mie Theory implemented with a computer code developed by Bohren and Huffman (1983). Additional measurements that were carried out *in situ* included temperature at surface level, and direction and speed of surface wind. The short-wave radiative forcing (SW) was studied using the Radiative Transference Model (RTM) GAME (Global Atmospheric Model) (Dubuisson et al 2004).

Using the data collected in the city of León, this study aims to analyse the aerosol properties and their radiative effects during the wildfires occurring in Castrocontrigo and Cubo de Benavente to compare the smoke aerosol with the characteristics of the atmosphere before and after the fire events.

An appropriate understanding of the emissions from wildfires and their radiative effects is needed in order to quantify the atmospheric impacts of these events (they likely affect regional atmospheric stability, heating rates, surface temperatures, cloud formation, and precipitation) and to provide input data for local/regional climate modelling.

This study was supported by the Spanish Ministry of Science and Innovation (Grant TEC2010-19241-C02-01). Elisabeth Alonso and Ana I. Calvo acknowledge the pre-doctoral (CGL2010-1777 from the Spanish Ministry Science and Innovation) and posdoc (SFRH/BPD/64810/ 2009 from FCT) grants, respectively.

Bohren, C. F., and D. R. Huffman (1983), Absorption and Scattering of Light by Small Particles, 544 pp., Wiley, New York.

Chubarova, N., Nezval', Y., Sviridenkov, M., Smirnov, A., and Slutsker, I. (2012) *Atmos. Meas. Tech.*, **5**, 557–568.

Dubuisson, P., Dessailly, D., Vesperini, M. and Frouin, R. (2004) *J. Geophys. Res.* **109**, D19106.

IPCC, Intergovernmental Panel on Climate Change (2007), Climate Change 2007: The Physical Basis of Climate Change. J. T. Houghton et al., Cambridge Univ. Press, New York.

Influence of biodiesel-to-diesel addition on major ions and trace elements in fine particulate matter exhausted by a diesel engine

G. O. da Rocha[1,4,*], J. V. S. Santos[1,2], A. C. D. Regis[1], L. Tormen[3], A. L. N. Guarieiro [1,4], J. D. S. da Silva[1], A. J. Curtis[3,4] and J.B. de Andrade[1,4].

[1]Institute of Chemistry, Universidade Federal da Bahia, 40170-290, Salvador-BA, Brazil
[2]Instituto Federal de Educação, Ciência e Tecnologia Baiano, 45995-000, Teixeira de Freitas-BA, Brazil
[3]Department of Chemistry, Universidade Federal de Santa Catarina, 88040-090, Florianópolis-SC, Brazil
[4] INCT for Energy & Environment, 40170-290, Salvador-BA, Brazil
Keywords: particulate matter, major ions, trace elements and biodiesel.
Presenting author email: giseleor@ufba.br

Due to increasing environmental awareness, the decline of petroleum resources and also the rising price of fossil diesel, alternative fuels such as biodiesel are increasingly discussed in many countries around the world (Guarieiro *et al* 2008). Even though the general interest in biofuels as alternatives to petroleum diesel has increased, few studies have been conducted to characterize the chemical composition of fine particles emitted from diesel engines fueled with biodiesel blends.

Fine particles ($PM_{2.5}$) were collected with a diesel engine (Agrale, model M85, 10 HP) coupled to a steady-state dynamometer for sample collection. The emission measurement system was operated based on the constant volume (CVS) principle, and a dilution tunnel (6 m x 120 mm i.d.) was used to dilute the engine exhaust with filtered and scrubbed ambient air. Experiments were run with speed rate at 1800 rpm, operating in a stationary mode and load of 1 kW. Three different fuels were used, in regard to the quantity of biodiesel added (B4, B50, and B100) to fossil diesel. The collection of samples was done by a $PM_{2.5}$ cyclone inlet attached to a holder with a PTFE filter (47 mm d. x 1 µm pore size). Afterwards, major ions analysis (F^-, Cl^-, NO_3^-, SO_4^-, PO_4^{3-}, lactate, formate, succinate, oxalate, Na^+, K^+, NH_4^+, Mg^{2+}, and Ca^{2+}) was done by an ion chromatograph with conductivity detection as well as trace elements analysis (Mn, Fe, Cu, Zn, Ba, Pb, and Cr) was carried out by ICP-MS.

When increasing the amount of biodiesel in the tested fuels there was an increase in fuel consumption. In relation to B4, the use of B50 and B100 caused a rise of 14 % and 20 % of the fuel consumption, respectively. On the other hand, the addition of biodiesel causes a decrease in the emitted $PM_{2.5}$ mass. This reduction is 16 % (B50) and 20 % (B100). This reduction is probably due to a more complete combustion of biodiesel than diesel.

Results of major ions and metals are expressed as emission rate of each species amount in relation to the mass of burnt fuel (Fig. 1). Regarding emission rates for the elements (Fig. 1a), the result can be divided into two groups: one made of the elements that have reduced their emissions with the addition of biodiesel (Mn, Fe, Cu, Zn and Pb) and other group formed by those elements who emission was increased with the addition of biodiesel (Cr and Ba). In the second group, the increases were 89% (Ba) and 90% (Cr) for B100 in comparison with B4.

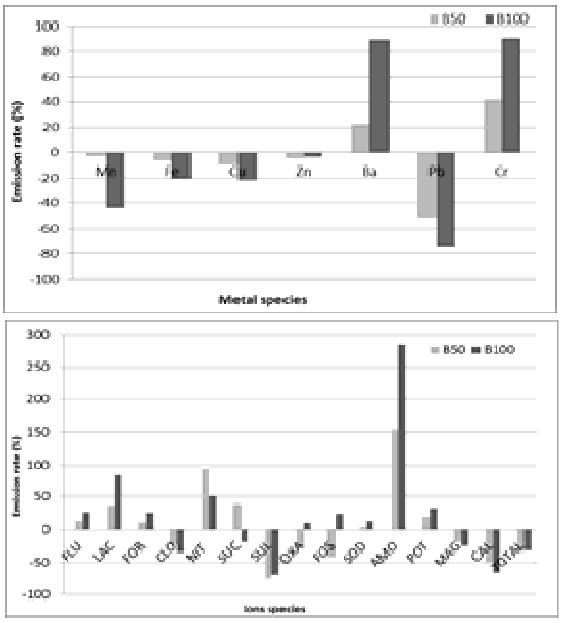

(a)

(b)

Figure 1. Emission rate (%) for (a) trace elements and (b) major ions in $PM_{2.5}$ emitted by B50 and B100 blends in relation to B4.

When considering total ions (Fig. 1b) similar reductions (30 %) were observed for both B50 and B100. Depending on the fuel used, a rise is observed in emission rate for NH_4^+ (284 %), lactate (85%), K^+ (33 %), formate (27 %), Na^+ (27%) and F^- (13 %). In turn, SO_4^{2-} (69 %), Ca^{2+} (66 %), Mg^{2+} (35 %), and Cl^- (25 %) emission rates were reduced when more biodiesel is added to fossil diesel. Finally, some ions such as succinate, oxalate and PO_4^{3-} were eventually decreased or increased among B50 and B100 fuels, not showing a clear trend. Our results suggest that emissions from biodiesel might be a good fuel choice in terms of $PM_{2.5}$, some major ions (SO_4^{2-}, Ca^{2+}, Mg^{2+}, and Cl^-) and trace elements (Mn, Fe, Cu, Zn, and Pb) but not for the all species studied. Perhaps, addition of a lower amount of biodiesel to diesel may promote benefices in both environmental and human health concerns.

This work was supported by PETROBRÁS, FAPESB, CAPES, CNPq, INCT for Energy & Environment.

Guarieiro, L.L.N., Pereira, P.A.P., Torres, E.A., da Rocha, G.O., de Andrade, J.B. (2008) *Atmos. Environ.* **42**, 8211-8218.

Effective density of particulate matter emitted from aircraft gas turbine engine sources

L. Durdina[1, 2], B. Brem[1, 2], M. Abegglen[3], B. Sierau[3] and J. Wang[1, 2]

[1]Air Quality and Particle Research Group, Empa, Dübendorf, CH-8600, Switzerland
[2]Institute of Environmental Engineering (IfU), ETH Zürich, Zürich, CH-8093, Switzerland
[3]Institute for Atmospheric and Climate Science (IACETH), ETH Zürich, Zürich, CH-8092, Switzerland
Keywords: effective density, particle mass, aircraft, exhaust
Presenting author email: lukas.durdina@empa.ch

Growing air travel and airport operations pose potential hazards both for local air quality and global climate. The study of physical and chemical properties of aviation-produced PM advances our understanding of its behaviour and potential negative effects. Recent research has been also motivated by the prepared legislation for PM emissions from aircraft gas turbine engines.

Particle effective density establishes the relationship between mobility size and aerodynamic size. It is also required for conversion of size distributions to mass distributions. Several studies have focused on determination of effective density of combustion aerosols (*e.g.* Park *et al*, 2003).

This study presents initial results of effective density measurements of aircraft gas turbine PM using Centrifugal particle mass analyzer (CPMA, Cambustion). Only particles in a narrow range of mass-to-charge ratio penetrate the CPMA (Olfert *et al*, 2005).

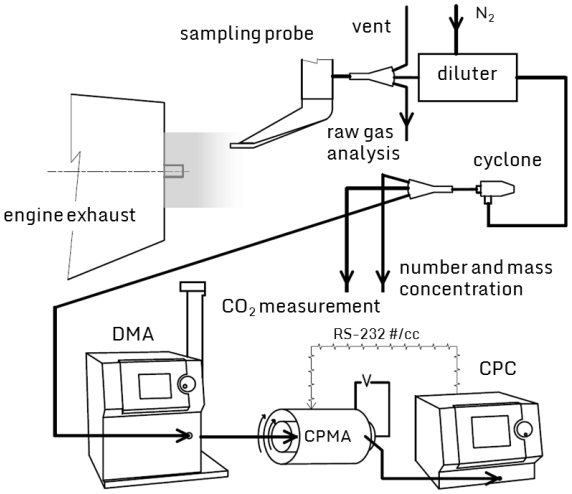

Figure 1. Schematic of the experimental setup.

Experiments were performed in an aircraft engine test cell at SR Technics, Zurich airport. Schematic of the system and experimental setup for particle effective density measurement is seen in Fig. 1.

Particles were sampled from the diluted particle transfer line of the PM sampling system at 1.5 l/min. They were passed through a radioactive charge neutralizer and then classified in a differential mobility analyzer (DMA, Model 3080, TSI Inc.) by mobility diameter. The DMA was set on 10 l/min sheath flow. Aerosol then entered the CPMA where the particles were classified by mass. Exiting particles of the CPMA were counted by a condensation particle counter (CPC, Model 3775, TSI Inc.).

Two CPMA-DMA-CPC setups were run in parallel with the aim to obtain particle mass data for more particle sizes during the limited time of one engine test point. The selected particle sizes lied in the range of highest number concentration of the engine PM. Effective density was then calculated as the mode of the particle mass distribution divided by the volume of the mobility-equivalent spherical particle.

Effective density results from a CFM56-5B series engine are presented in Fig 2. The engine test cycle consisted of a series of power conditions defined by the turbine inlet temperature T3 and engine rotational speed.

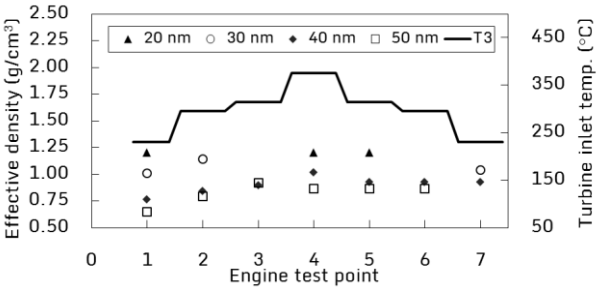

Figure 2. Effective density of particles for individual engine test points and mobility diameters.

A decreasing particle effective density with increasing size was observed due to the structural nature of fractal agglomerate (Fig. 2). Particle effective density was found to be in the range of 0.65 - 1.25 g/cm^3. An increase of effective density with engine speed can be observed especially for 40 and 50 nm particles. However, with decreasing engine power in the second half of the engine test effective density did not return to previous values. In order to investigate whether this finding is related to engine warm-up or fits within the measurement uncertainty, more tests are required.

Due to transient nature of the emitted PM (short test point duration) an experimental setup allowing faster measurement is needed and currently under investigation.

This work is sponsored by the Swiss Federal Office of Civil Aviation (BAZL). We thank SR Technics for the use of their facilities.

Park, K., Cao, F., Kittelson, D.B. and McMurry, P.H. (2003) *Environ. Sci. Technol*. **37**, 577-583

Olfert, J.S. and Collings, N. (2005) *J. Aer. Sci.* **36**, 1338-1352.

Particulate matter generated by heating/cooking plants in traditional homes of Mt. Everest region in central southern Himalaya (Nepal)

P. Fermo[1], A. Piazzalunga[1], R. Gonzalez[1], D. Comunian[1], G. Tartari[2], F. Salerno[2], G. Viviano[2], P. Ielpo[3,4], S. Di Sabatino[5], S. Bhochhibhoya[6], R.K. Maskey [6]

[1]Department of Chemistry, University of Milan , 20133, Milan, Italy
[2] Water Research Institute, National Research Council, 20861, Brugherio, Italy
[3] Water Research Institute, National Research Council, 70132, Bari, Italy
[4] Institute of Atmospheric sciences and Climate, National Research Council, 73100, Lecce, Italy
[5] DiSTeBA Department, University of Salento, 73100, Lecce, Italy
[6]Department of Civil and Geomatics Engineering, Kathmandu University, Dhulikhel Kavre, Nepal

Keywords: indoor PM, Black Carbon, biomass burning, levoglucosan,
Presenting author email: paola.fermo@unimi.it

Atmospheric aerosol affect Earth's radiative budget and atmospheric air quality and represents a risks to human health. Recent studies have demonstrated that in the Himalayan region aerosol components such as soot, sulfates, organics, dust, contribute to the formation of "Atmospheric Brown Clouds (ABC)" and important sources in this region are represented by combustion of biofuels used in cooking and heating, agricultural residue burning and forest fires (Vadrevu et al., 2012).

In particular Black Carbon (BC) emitted from biomass burning can significantly alter the radiative balance by absorbing solar radiation and causing atmospheric heating, while BC deposited on snow and ice can significantly reduce the surface albedo, hasten melt, and trigger albedo feedback (Lau et al., 2008).

Although the importance of biomass burning in the Himalayan region is well recognized, precise data are lacking and only recently efforts have been made to assess the contribution of this source to aerosol (Vadrevu et al., 2012).

In the traditional households of Mt. Everest region, fuelwood, kerosene and animal dung constitute the main energy sources used for cooking, space heating and lighting. The kitchens are equipped mainly with open fireplaces for cooking lacking of a chimney and contributing to PM emission (Salerno et al., 2010).

Aim of the present study is to characterize the chemical composition of particulate matter (PM) generated indoor from the combustion of different fuels and to assess how this source can affects outdoor PM composition.

For this purpose Sagarmatha (Everest) National Park and Buffer Zone (SNPBZ) in Nepal is the main case study, due to the abundance of information available about the local socio-ecological system. A preliminary sampling campaign has been carried out during June 2012 in order to collect PM depositions inside traditional households located in four villages (Phakding, Namche Bazar, Tukla, Pangboche).

For each village three homes equipped with traditional stoves have been selected. The kind of fuel (different types of wood, kerosene, yak dung) burnt in each open fireplaces was also known. Outdoor PM depositions have been also collected in the vicinity of each house.

PM samples have been characterized from the chemical point of view as concerns major ions, OC (Organic Carbon), EC (Elemental Carbon), levoglucosan, TOC (Total Organic Carbon) and PAHs. In fact since it has been demonstrated that wood burning contribute to PAHs emission, these specific substances will be analyze. PAHs are also of great interest as regards indoors pollution since this class of compounds, is recognized as carcinogen by IARC.

The estimation of wood burning contribution to PM can be achieved through the quantification of a specific tracer, i.e. levoglucosan (Piazzalunga et al., 2011).

The macro-tracer approach will be applied using weighed emission factors selected taking into account the kind of wood burnt in SNPBZ.

On the base of all the compositional data acquired it'll be investigated the reliability to apply the receptor models to the data set for the source apportionment study.

These preliminary results will be helpful in order to program a more complete campaign during which PM2.5 samples will be collected both indoor and outdoor.

Vadrevu, K. P.et al. (2012) Atmos. Environ., **47**, 241-251.

Lau, K.M. et al. (2008) Bulletin of the American Meteorological Society, **89**, 369-383.

Salerno, F. et al. (2010), Mountain Research and Develop., **30**, 113-126.

Piazzalunga A. et al. (2011) Atmos. Environ., **45**,6642-6649.

New CO_2 Mitigation Process with Diesel Dynamo Power Plant Associated by Optimized Aerosol Driven Technique

K. Fukamizu[1], H. Takano[1] and M. Itoh[1]

[1]Department of Chemical Engineering and Materials Science, Doshisha University
Kyo-Tanabe, Kyoto 610-0321 JAPAN
Keywords: aerosol driven technique, CO_2, De-NOx, DCC.
Presenting author email: dum0705@mail4.doshisha.ac.jp

The replacement of current steam power plants to high efficient diesel-combined cycle (DCC) power plants is very practical way for the mitigation of CO_2 emission from power sector; it will be possible to attain 50 million ton/year emission reduction of CO_2, i.e., a half of the target value liable to Japan if the following problem can be overcome.

The high thermal efficiency in DCC is due to its high operation temperature. There additional NO_X emitted (about 5g/kWh)) at high temperature combustion is discharged to the atmosphere, and the development of highly energy effective De-NOx process is the most important to attain the CO_2 mitigation project based on the replacement. In the previous study (Yamamoto, 2010), the De-NO_X efficiency using our Aerosol Driven Technique (ADT) (Azuma, 2008) was 14.4g/kWh, and was insufficient for the target value (20g/kWh; it means 12% reduction of emitted CO_2 from power sector based on current steam power plants) of De-NO_X efficiency. The objective of this research is to fulfil the critical value with the optimization of ADT from the viewpoint of the selection of most effective foreign particle diameter.

The experimental setup for the ADT De-NO_X process was similar to that by Yamamoto (2010); NO_X was converted into NH_4NO_3 with NH_3 radical by the non-thermal plasma technique. Initial NO_X concentration in the reaction chamber was set at 800 ppmv (NO: 80, NO_2: 720). Relative humidity in the chamber was kept more than 95%. O_3 was generated with a corona discharger. NO_X concentration was measured with combustion gas analysers (NO: TSI CA6030, NO_2: TSI CA6040). DOP particles for the ADT were generated with a Rapaport-Weinstock type aerosol generator; the applied diameters of the foreign particles were 0.08, 0.10, 0.12, 0.13, 0.15 and 0.24 μm.

The removal efficiency was the most important parameter for this De-NO_X process, and it was defined as

$$RE_{NO_X} = \frac{dW - dW_{ini}}{E} \times \frac{M_{NO_X}}{M_{AN}} \times \frac{60}{t} \times \frac{Q}{Q_{col}} \qquad (1)$$

where dW is the collected particles weight by cascade impactor (QCM), dW_{ini} is the initial weight of the foreign DOP particles, M_{NOx} and M_{AN} are the molar weights of NOx and NH_4NO_3 respectively, t is the collected time, Q_{col} is the flow rate of the QCM (2.4ℓ/min).

Table 1 shows the NO_X concentration at the outlet of the De-NO_X experimental system with ADT (heterogeneous nucleation of NH_4NO_3 particles) and without ADT (homogeneous one). It showed that the NO_X concentration reduced about 10% installing ADT. **Table 2** and **Fig.1** show the importance of the selection of foreign particle diameter for the removal efficiency of NO_X. Especially, $D_{g,final}$, the final diameter of grown NH_4NO_3 particles generated via homogeneous nucleation, was very small, and the resultant RE_{NOX} became so small comparing to the heterogeneous one.

Table 1 De-NOx efficacy by ADT in this experiment

	Initial C_{NOX} (ppmv)	C_{NOX} (ppmv)
Without ADT	800	257
With ADT	800	166

Table 2 Final particle diameter, collected NH_4NO_3 mass and removal efficiency with and without ADT

Initial D_g (μm)	$D_{g,final}$ (μm)	$\frac{dW}{}$ ($\times 10^{-5}$mg/cm^3)	RE_{NOX}
Without ADT	0.08	2.5	4.2
With ADT	0.26	6.9	17.6

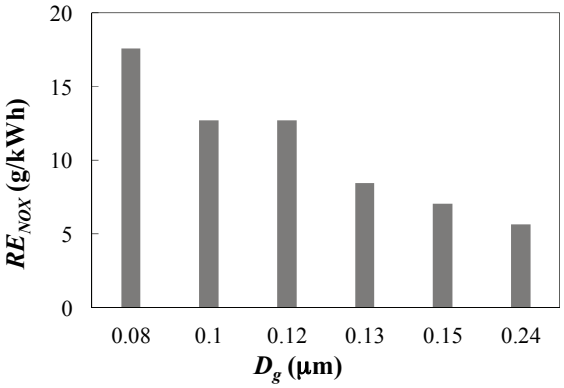

Fig. 1 Relationship between removal efficiency and initial diameter of foreign particles for ADT.

By the optimization of ADT process with most effective foreign particles, the removal efficiency could be revised up to 17.6g/kWh from 14.4g/kWh, and it will not be so difficult to attain the target value (20g/kWh) of this process by further optimization of ADT.

Yamamoto, R., Takano, H. and Itoh, M. (2010) *Abstract Book of IAC2010,* P3W56.

Azuma, D., Takano, H. and Itoh, M. (2008) *Proc. ICOPS 2008*, 2P61.

Investigating the aethalometer model to estimate black carbon and airborne particles from wood burning

G. W. Fuller [(1)]
MRC HPA Centre for Environment and Health, King's College London, London, SE1 9NH, UK
Presenting author email: gary.fuller@kcl.ac.uk

Introduction

Although air pollution from wood burning is a recognised problem in the Scandinavian and Alpine areas there is a risk that the European Union commitment to obtain 20% energy from renewable sources is leading to a return to urban wood combustion. New evidence of urban wood burning is emerging from studies in London, Paris, Berlin (Fuller et al 2013) and with member states of the European Union committed to obtain 20% of their energy requirements from renewable sources by 2020, increased wood burning is inevitable.

Quantification of PM from wood burning through the filter based measurement of tracers such as anhydrous sugars produced from the charring of cellulose (mainly levoglucosan) and fine potassium is both expensive and has poor time resolution. The aethalometer (Magee Scientific) offers an alternative method to assess PM_{10} from wood smoke based on its different optical absorption characteristics compared with black carbon; notably increased absorption in the UV wavelength compared to IR which can be used to apportion black carbon (BC) between fossil fuel and wood burning and to provide a tracer for PM from wood burning (Sandradewi et al., 2008).

The aethalometer method for tracing of wood burning PM is subject the assumed values of the angstrom coefficients for fossil fuels (αff) and wood burning (αwb). However, the sensitivity of the wood burning tracer, B_{abs} wb (370), to assumptions of αff and αwb have not been fully explored.

Measurement methods

Aethalometer (2λ) and Sunset EC/OC measurements were undertaken in London, UK, from 2008 to 2011 along with two short term (~40 day) levoglucosan measurement campaigns during winter 2009 and 2010.

Results and discussion

By varying αff and αwb by 10% from the commonly used values of αff =1.0 and αwb = 2.0 it was found that mean B_{abs} wb (370) in London was more sensitive to changes in αff (+20% at αff =0.9 and -26% at αff = 1.1) than it was to changes in αwb (-10% at αwb = 2.2 and +16% at αwb = 2.2).

Having two independent methods to measure wood burning PM, provided further opportunities to conduct sensitivity testing and to assess the validity of the athelometer method. Using αff =1.0 and αwb = 2.0, correlations (r^2) between levoglucosan and B_{abs} (370) wb were good (0.79) and this did not vary when αwb was varied between 1.8 and 2.2. The magnitude of the levoglucosan and B_{abs} (370) wb cannot be usefully used test variations in αff and αwb since both require the applications of further factors before an estimate of PM mass concentration can be obtained, however, zero concentrations of both tracers should occur at the same time. Although zero measurements were not present in the dataset, the regression intercept of levoglucosan on Babs (370) wb should be zero if the methods are consistent. Figure 1 shows how the reduced major axis regression intercept varied as αff was varied between 0.2 and 1.3. It was found that an intercept of zero was only possible at a αff value of 0.96, consistent with the literature estimates. At this value the intercept became insensitive to variations in αwb. Looking at this test in another way, the derivation of a value of αff; a physical property of ambient aerosol of 0.96, consistent with literature estimates contributes to the validity of the athealometer method to trace wood burning PM. Figure 1 also shows the effect of a varying αff on the magnitude of Babs (370) wb, with αwb between 1.8 and 2.2. It can be seen that the sensitivity of B_{abs} (370) wb to changes in αwb were fairly constant for values αff < 1 but it became insensitive to changes in αwb as the athelometer model broke down and produced large negative intercepts with values of αff above 1.2.

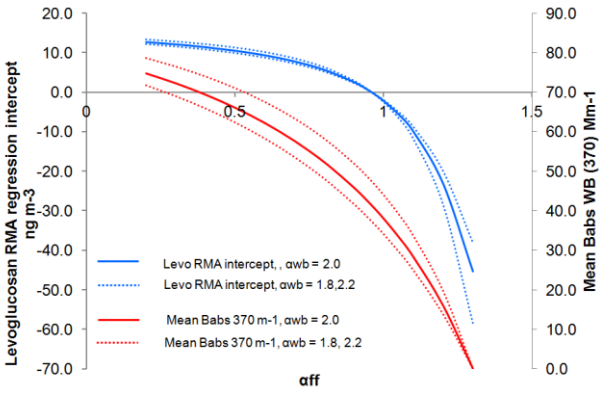

Figure 1 Regression intercept as a function αff (black line). Grey line shows B_{abs} (370) wb, with αwb between 1.8 and 2.2.

References

Fuller et al 2013. Atmos Env 68 (2013) 295–296
Sandradewi et al., 2008. Environ. Sci. Technol. 2008, 42, 3316–3323.

Thanks to Karl Espen Yttri, NILU, Norway for levoglucosan measurements.

Reduction of PAHs emitted from a generator fuelled by waste-edible-oil-biodiesel with acetone and isopropyl alcohol addition

Jen-Hsiung Tsai[1], Shui-Jen Chen[1,*], Wen-Yinn Lin[2], Kuo-Lin Huang[1], Chih-Chung Lin[1] and Yung-Shun Chen[1]

[1]Department of Environmental Science and Engineering, National Pingtung University of Science and Technology, Pingtung County, Nei Pu, 91201, Taiwan
[2]Institute of Environmental Engineering and Management, National Taipei University of Technology, Taipei City, 10608, Taiwan
Keywords: PAHs, waste-edible-oil-biodiesel, acetone, isopropyl alcohol.
Presenting author email: chensj@mail.npust.edu.tw

Diesel engine exhaust has been official classed by the International Agency for Research on Cancer (IARC) as carcinogenic to humans (Group 1) in June 2012 (IARC, 2012), and has been concerned worldwide for its adverse health effects. Diesel exhaust particles (DEPs) mainly consist of carbon particles, ash, SOFs (soluble organic fractions), and sulfur-containing compounds. Accordingly, the PAHs on the DEPs comprise mostly carbon particles, ash, and SOFs (Ning and Sioutas, 2010). The US EPA designated 16 non-substituent PAHs as major pollutants, and eight of these (BaA, BeP, CHR, BbF, BkF, IND, DBA and BghiP) are notable for their carcinogenic characteristics (Menzie *et al.*, 1992). Some report showed that adding an oxygen agent, such as ethanol or acetone or biodiesel, to pure petroleum diesel can improve engine fuel combustion efficiency and reduce the emissions of CO, HC, PM, and PAHs (Lin *et al.*, 2010; Tsai *et al.*, 2010; Lee *et al.*, 2011), and lower the biotoxicity of diesel particulate matter (DPM) (Tsai *et al.*, 2011; Tsai *et al.*, 2012). A type of blended fuel with biodiesel and solvent addition into fossil diesel has been proposed and it is called "Biodieselhol". In this study, a combination of acetone, isopropyl alcohol, and waste-edible-oil-biodiesel was added to conventional fossil diesel to investigate the PAH emission characteristics of a biodieselhol-fueled diesel engine generator and the feasibility of using the blended fuels as alternative fuels for diesel engines.

Different blended fuels were tested at the stable energy output (110 V/60 Hz, 1800 rpm) of a generator under varying engine loadings. The tested biodieselhols consisted of pure diesel oil (D100) with 1−3 vol. % pure acetone (denoted as A), 1−70 vol. % waste-edible-oil-biodiesel (denoted as W), and 1 vol. % pure isopropyl alcohol (the stabilizer, denoted as P). An auto-detector flow sampling system equipped with quartz fiber filters was installed on the downstream side of the diesel generator exhaust to determine suspended particles and particulate phase PAHs. Gas phase PAHs were collected by two connected cartridges (filled with XAD-16 resins).

Figure 1 shows that, regardless of the percentages of waste-edible-oil-biodiesel, acetone, and isopropyl alcohol, replacing D100 with biodieselhol reduced the emissions of Total-PAHs by 6.13–42.5% (average, 24.1%) and emissions of Total-BaP_{eq} by 16.6–74.8% (average, 53.2%)) from the diesel engine generator. Among these tested fuels, the one with waste-edible-oil-biodiesel = 20% exhibited the best emission reductions of Total-PAHs (average 41.3%) and Total-BaP_{eq} (average 72.0%). When the percentages of waste-edible-oil-biodiesel in fuel were less than 20%, the increase of waste-edible-oil-biodiesel in fuel could obtain more reduction in Total-PAHs and Total-BaP_{eq} emission. Although, in blends with percentage of waste-edible-oil-biodiesel higher than 20% (i.e., W30D70, W30A1P1D68, W30A2P1D67, W30A3P1D66, W50D50, and W70D30), the concentrations of emitted Total-PAHs and Total-BaP_{eq} increased with waste-edible-oil-biodiesel addition percentage, the concentrations of emitted Total-PAHs and Total-BaP_{eq} were still less than that using fossil diesel as the fuel, at waste-edible-oil-biodiesel ≤ 70%.

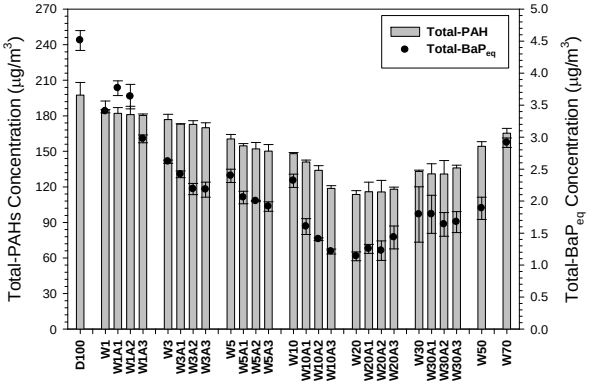

Figure 1. Total-PAHs and Total-BaP_{eq} emitted from the generator fuelled by biodieselhols.

This work was supported by the National Science Council of the Republic of China, Taiwan, under Contract No. NSC 100-2221-E-020-004-MY3.

IARC (2012) *Press Release*, available at: http://www.iarc.fr/en/media-centre/pr/2012/pdfs/pr213_E.pdf

Lee, W.J., Liu, Y.C., Mwangi, F.K., Chen, W.H., Lin, S.L., Fukushima, Y., Liao, C.N. and Wang, L.C. (2011) *Energy* **36**, 5591–5599

Lin, S.L., Lee, W.J., Lee, C.F. and Chen S.J. (2010) *Energy Fuels* **24**, 4522–4533.

Menzie, C.A., Potocki, B.B. and Santodonato, J. (1992) *Environ. Sci. Technol.* **26**, 1278–1284.

Ning, Z. and Sioutas, C. (2010). *Aerosol Air Qual. Res.* **10**, 43–58.

Tsai, J.H., Chen, S.J., Huang, K.L., Lin, T.C., Chaung, H.C., Chiu, C.H., Chiu, J.Y., Lin, C.C. and Tsai, P.Y. (2012) *Aerosol Air Qual. Res.* **12**, 843–855.

Tsai, J.H., Chen, S.J., Huang, K.L., Lin, Y.C., Lee, W.J., Lin, C.C. and Lin, W.Y. (2010) *J. Hazard. Mater.* **179**, 237–243.

Tsai, J.H., Huang, K.L., Chiu, C.H., Lin, C.C., Kuo, W.C., Lin, W.Y., Chaung, H.C., Yang,T.H. and Chen, S.J. (2011) *Aerosol Air Qual. Res.* **11**, 822–836.

Cytotoxicity of exhaust emissions from a generator fuelled by waste-edible-oil-biodiesel with acetone and isopropyl alcohol addition

Jen-Hsiung Tsai[1], Shui-Jen Chen[1,*], Kuo-Lin Huang[1], Wen-Yinn Lin[2], Yi-Chu Huang[1], Te-San Chen[1], Hso-Chi Chaung[3] and Tsai-Yun Wu[1]

[1]Department of Environmental Science and Engineering, National Pingtung University of Science and Technology, Pingtung County, Nei Pu, 91201, Taiwan
[2]Institute of Environmental Engineering and Management, National Taipei University of Technology, Taipei City, 10608, Taiwan
[3]Department of Veterinary Medicine, National Pingtung University of Science and Technology, Pingtung County, Nei Pu, 91201, Taiwan
Keywords: waste-edible-oil-biodiesel, cytotoxicity, acetone, diesel generator.
Presenting author email: chensj@mail.npust.edu.tw

Exhaust fumes from diesel engines may cause cancers, according to a panel of experts working for the International Agency for Research on Cancer (IARC) (IARC, 2012). To alleviate the environment impacts and adverse health effects from diesel exhausts, although the mechanical design of diesel engines has been improved and catalytic converters have been installed, the fuel used by diesel engines is also a critical factor which influences the compositions of particle and gas pollutants emitted by diesel engines. Lin *et al.* (2010) and Lee *et al.* (2011) reported that diesel engines using blended fuels (bio-fuels; blends of diesels, biodiesels, and alcohols) could reduce the emissions of total-PAHs and total-BaP_{eq}. Although the use of blended fuels may significantly reduce emissions from diesel engines, it is necessary to evaluate the potential cytotoxicity of diesel exhausts and their effects on health when using bio-fuels.

In this study, the combination of 1−3 vol. % pure acetone (denoted as A), 1 vol. % pure isopropyl alcohol (the stabilizer, denoted as P), and 1−20 vol. % waste-edible-oil-biodiesel (denoted as W) addition into conventional fossil diesel (D100) was tested. Different blended fuels were tested at the stable energy output (110 V/60 Hz, 1800 rpm) of a generator under varying engine loadings. An auto-detector flow sampling system equipped with quartz fiber filters and two connected cartridges (filled with XAD-16 resins) were used to collect particulate phase and gas phase PAHs, respectively. Each sample was extracted in a *Soxhlet* extractor using a mixed solvent (n-hexane and dichloromethane 1:1 vol/vol) for 24 hr. Subsequently, human male macrophage/monocyte cell strains (U937) were exposed to various extract samples for 24 hours after various organic solvents had been replaced by DMSO (dimethyl sulfoxide). The MTT (3-(4,5-dimethyl-thiazol-2-yl)-2,5-diphenyltetrazolium bromide) assay was adopted to analyze the cell viability rates of various extracts of diesel exhaust emissions (DEEs).

Figure 1 shows the cytotoxicity (cell death rate (CDR)) of DEEs from the diesel-engine generator fuelled with various biofuel blends. Among these tested fuels, using various bio-fuels in place of D100 could reduce the CDR of DEEs' organic solvent extracts by 4.89–57.6% (average, 21.9%). Rgardless of the percentages of added waste-edible-oil-biodiesel, acetone, and isopropyl alcohol, the CDR value decreased with increasing percentage of biofuel blends; in particular, W20 had the best cytotoxicity reductions (57.6%). When the addition percentage of waste-edible-oil-biodiesel was less than 5%, the cytotoxicity of DEEs decreased as the addition percentage of acetone increased; however, an opposite trend was observed at waste-edible-oil-biodiesel addition ≥ 5%. Nevertheless, the values of cytotoxicity were still less than that using fossil diesel as the fuel, at waste-edible-oil-biodiesel ≥ 5%. The above results suggest that the blended fuel (fossil diesel with waste-edible-oil-biodiesel, acetone, and isopropyl alcohol addition) may be used as an alternative fuel to petroleum diesel to reduce the hazards of emissions from diesel engines to human health.

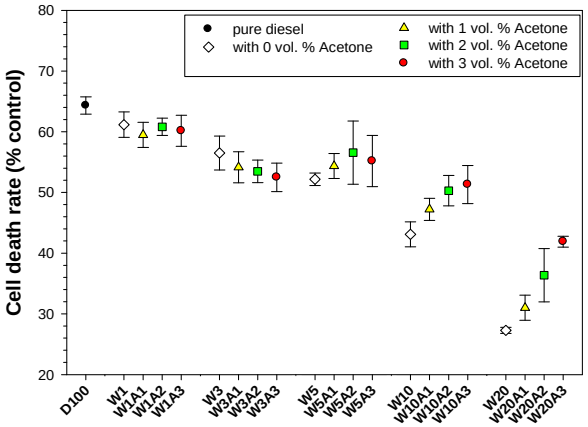

Figure 1. Cytotoxicity (cell death rate) of DEEs from the diesel-engine generator fuelled with biofuels.

This work was supported by the National Science Council of the Republic of China, Taiwan, under Contract No. NSC 100-2221-E-020-004-MY3.

IARC (2012) *Press Release*, available at: http://www.iarc.fr/en/media-centre/pr/2012/pdfs/pr213_E.pdf

Lee, W.J., Liu, Y.C., Mwangi, F.K., Chen, W.H., Lin, S.L., Fukushima, Y., Liao, C.N. and Wang, L.C. (2011) *Energy* **36**, 5591–5599

Lin, S.L., Lee, W.J., Lee, C.F. and Chen S.J. (2010) *Energy Fuels* **24**, 4522–4533.

Characteristics of SO_2 removal by using $CaCO_3$ sorbent particle in an oxy-PC combustion system

Seongha Jeong[1], Kang Soo Lee[1], Sang In Keel[2], Jin Han Yun[2], and Sang Soo Kim[1]

[1]Department of Mechanical Engineering, Korea Advanced Institute of Science and Technology, Daejeon, Republic of Korea
[2]Environmental Systems Research Division, Korea Institute of Machinery and Materials, Daejeon, Republic of Korea
Keywords: Oxy-PC Combustion System, Calcium Carbonate, sulfur dioxide, desulfurization
Presenting author email: jeongsh@kaist.ac.kr

CCS (CO_2 capture and storage) is the technology which can directly reduce the emission of greenhouse gases. oxy-PC combustion system (which is one of the CCS capture technology) has advantages over other systems because it is economical and recovers the CO_2 with high purity. in oxy-PC combustion, flue-gas recirculation creates an atmosphere that is primarily CO_2 with a small amount of O_2. Therefore, the phenomena of sorbent particles in an oxy atmosphere are different compared with those in an air atmosphere.

SO_2 removal experiments by using $CaCO_3$ sorbent particle was performed in a drop tube furnace experimental setup in air atmosphere and oxy-PC atmosphere.

To estimate the effect of temperature in a reactor on a particle behavior and SO_2 removal characteristics, experiments were conducted by varying a temperature 800-1100°C. Reaction time in a reactor was set to 2 sec. As seen in Fig. 1, SO_2 removal efficiency increased with temperature rise in an air atmosphere, while it had maximum value between 900-1000°C in an oxy-PC atmosphere. in general, adsorption became enhanced as the temperature increased. However, in an oxy-PC atmosphere, the degree of adsorption showed the maximum value due to the significant sintering effect. Furthermore, decomposition phenomenon of the adsorbed SO_2 from the sorbent particle accelerated the decline of the SO_2 removal efficiency.

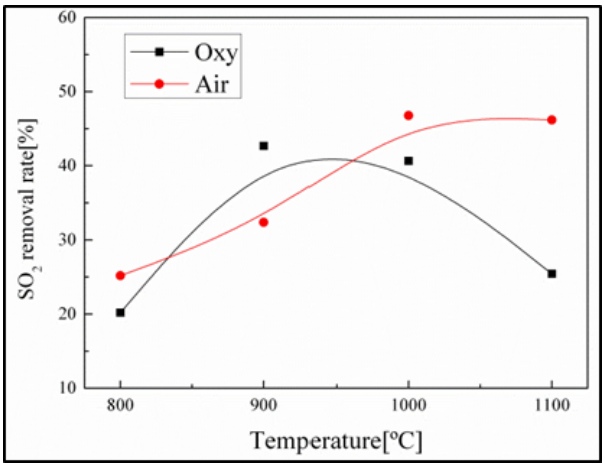

Figure 1. SO_2 removal rates by varying a temperature in air and oxy-PC atmospheres, respectively.

To estimate the effect of reaction time in a reactor on a particle behavior and SO_2 removal characteristics, experiments were conducted by varying a reaction time 1.0-2.0 sec. Temperature in a reactor was set to 1000°C. Figure 2 shows the SO_2 removal efficiencies by varying a reaction time in an air and oxy-PC atmospheres, respectively. As seen in Fig. 2, SO_2 removal efficiency showed the same level within the experimental conditions in an air atmosphere, while it increased until the reaction time of 2 sec. It was attributed to CO_2 partial pressure in an oxy-PC atmosphere. In an oxy-PC atmosphere, calcination was delayed due to the higher CO_2 partial pressure in a surrounding medium. Thus, it takes long time to make the sufficient SO_2 adsorption in an oxy-PC atmosphere.

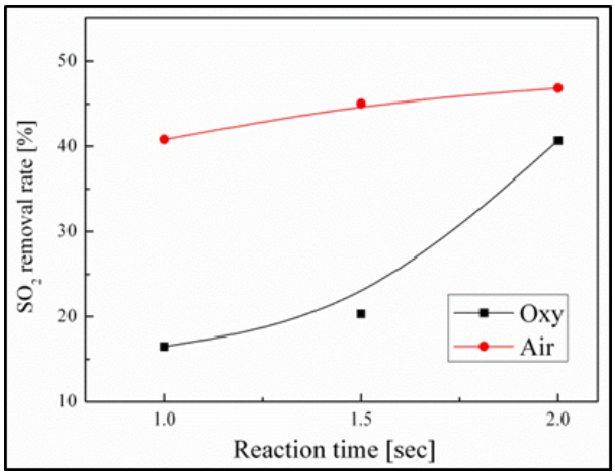

Figure 2. SO_2 removal rates by varying a reaction time in air and oxy-PC atmospheres, respectively.

This work was supported by Energy Resources Technology Development Project of the Korea Energy Management Corporation and by EEWS research program.

C. Chen et al., "Mechanism of Highly Efficient In-Furnace Desulfurization by Limestone under O_2/CO_2 Coal combustion atmosphere", Ind. Eng. Chem. Res., Vol. 45, pp. 5078-5085 (2006).

Liu H., Katagiri S., Kaneko U., & Okazaki K., “Sulfation behavior of limestone under high CO2 concentration in O_2/CO_2 coal combustion”, Fuel 79, 945-953 (2000)

Dry absorption of SO_2 with hydrated lime in spout-bed circulating dry scrubber system

Young-Ok Park[1], Seong-Min Cheon[1,2] and Yong-Ha Kim[3]

[1]Clean Fuel Research Group, Korea Institute of Energy Research, Deajeon, 305-343, Korea
[2]Department of Chemical Engineering, Sogang University, Seoul, 121-742, Korea
[3]Department of Chemical Engineering, Pukyong National University, Busan, 608-739, Korea

Keywords: hydrated lime, circulating dry scrubber system, SO_2 removal, semi-dry reactor, mean particle size of hydrated lime
Presenting author email: yhkim@pknu.ac.kr

Different technologies have been developed for acid gas removal in emission from waste incineration, coal combustion and ore sinter process. The post-combustion acid gas removal technologies have been widely incorporated in the operation of large coal power plants in order to achieve the regulations of SO_2 and NOx mainly. These technologies are based on the use of sorbents, usually calcitic sorbents, such as $CaCO_3$, CaO in the desulfurization processes at high and medium temperatures, and hydrated lime in low temperature processes[1-2].

The methods of dry scrubbing and dry additive injection into furnace were emerged in the last decade including isolated moistening of absorbents (being a mixture of reaction products and fresh reactant), in such a way that it keeps the propertied of dry powder (having not more than 12 mass % of water). This method mitigates sticking of solids to apparatus walls and corrosion is minimized and the board use of carbon steel in apparatus manufacturing made possible. In the semi dry technologies that are mainly the subject of this paper, binding of acid gases goes mostly in water solution according to the reactions[3]:

$$Ca(OH)_2 + SO_2 \rightarrow CaSO_3 \cdot 1/2H_2O + 1/2H_2O$$

$$Ca(OH)_2 + SO_3 \rightarrow CaSO_4 \cdot 1/2H_2O + 1/2H_2O$$

$$Ca(OH)_2 + SO_2 + H2O + 1/2O2 \rightarrow CaSO_4 \cdot 2H_2O$$

$$CaSO_3 \cdot 1/2H_2O + 1/2O_2 \rightarrow CaSO_4 \cdot 1/2H_2O$$

$$Ca(OH)_2 + CO_2 \rightarrow CaCO_3 + H_2O$$

$$Ca(OH)_2 + 2HCl \rightarrow CaCl_2 + 2H_2O$$

$$Ca(OH)_2 + 2HF \rightarrow CaF_2 + 2H_2O$$

Actually have appeared some type of so called dry calcium desulfurization methods in which absorption takes place on the moistened surface of sorbent. Their common advantage is simple construction of reactor in which the main process of SO2 bonding takes place as well as taking off desulfurization product in form of powder separated from clean gas in the conventional filtering equipment.

The spout-bed dry scrubber system was developed as a dry technology that would work for a wide range of plants which was able to treat all the important flue gas pollutants like SOx, HCl and HF as well as fine particulates. This system has the high chemical and physical heat and mass transfer rates of a circulating spout-bed system and used for the elimination of the pollutants. A diagram of the demo-scale spout-bed dry scrubber system which tested at the sinter process of steel making factory is presented in Figure 1. This sinter flue gas is taken from the duct of downstream of the sinter plant. The sinter flue gas flows into the spout-bed reactor via a gas distributing bottom. In the spout-bed reactor the flue gas gets in turbulent contact with absorbent so that pollutants like SO_2, SO_3 and HCl are removed in a high extent. Due to high velocities are discharged at the head of the reactor and separated in the directly adjoining bag filter.

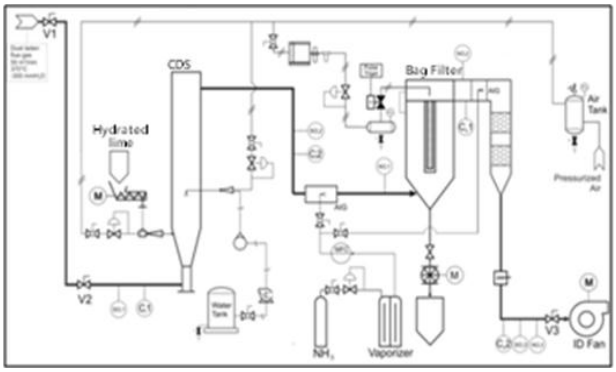

Figure 1. Flow diagram of the demo-scale spout-bed circulating dry scrubber system.

The aim of the present research is to remove of SO_2 in flowing sinter flue gas using the demo-scale spout-bed circulating dry scrubber. The effect of different properties of hydrated lime as absorbents was investigated with operating variables such as Ca/S molar ratio, mean particle size and surface area of hydrated lime and superficial gas velocity. The physical properties of 3-type of hydrated lime is given the Table 1.

Table 1 physical properties of 3-type of adsorbents

Sample	*C-1*	*C-2*	*C-3*
Surface area, m^2/g	40.4	37.4	46.5
Pore volume, cm^3/g	0.207	0.184	0.227
Mea particle size, μm	6.8	7.2	6.3

The volumetric flow rates of the demo-scale reactor vary from 2,000 to 3,000 Nm^3/hr. Their SO_2 control efficiency was in the range of 85% to 96%.

This work was supported in part of the Industrial Related Project grant funded by the Korea Institute of Energy Research.

[1] R. Martinelli, T.R. Goots, P.S. Nolan, in Proceedings of the 1993 SO_2 Control Symposium, Vol.3, Boston, 1993.
[2] G.R. Offen, M.W. McElroy, JAPCA 37, 968, 1987.
[3] A. Licata, W. Schuettenhelm, in Proceedings of 9th Annual North America Waste to Energy Conference, ASME 2001.

Real-time chemical composition analysis of particle emissions from woodchip combustion

A. Kortelainen[1], J. Joutsensaari[1] , P. Tiitta[2] , A. Jaatinen[1] , P. Miettinen[1] , L. Hao[1] , J. Leskinen[2] , A. Virén[2] , T. Torvela[2] , J. Tissari[2] , J. Jokiniemi[2], D. R. Worsnop[1,3,4] , A. Laaksonen[1,3] and A. Virtanen[1]

[1] Department of Applied physics, University of Eastern Finland, Kuopio, 70211, Finland.
[2] Department of Environmental Science, University of Eastern Finland, Kuopio, 70211, Finland.
[3]Finnish Meteorological Institute, Climate change, Helsinki, 00101, Finland.
[4]Aerodyne Research Inc., Billerica, MA, 01821, USA.
Keywords: aerosol, combustion, chemical composition
Presenting author email: aki-matti.kortelainen@uef.fi

Residential wood combustion (RWC) produces high amounts of gaseous and particulate emissions into atmosphere. RWC for heat production has been and will assessed to be one of the major sources of fine particle mass emissions as use of fossil fuels is predicted to be reduced in the future. Composition of crucial particulate emissions in wood combustion, ash, inorganic compounds, polycyclic aromatic hydrocarbons (PAH), alkali metals, elemental (soot) and organic carbon are depending on the combustion conditions (Tissari, 2008). Therefore it is important to study the variation of particulate emissions chemical composition during different burning processes.

In recent studies, the chemical composition of particulate emissions from residential wood combustion has been analyzed from the collected filter samples. However, conventional methods have poor temporal information from aerosol composition in rapidly changing circumstances. In this work aerosol chemical composition in near real-time from efficient to poor combustion conditions emissions of 40 kW grate fired burner was measured by Aerodyne high-resolution time-of-flight AMS (HR-ToF-AMS) (DeCarlo, 2006).

Table 1. Average mass concentrations and standard deviations (std) of compounds during and outside of gaseous CO peaks in poor combustion.

Compoud	During peak, mass loading ($\mu g/m^3$)	Outside of the peak, mass loading ($\mu g/m^3$)
HOA	1.9 ± 1.5	0.5 ± 1.0
LV-OOA	3.2 ± 2.0	0.7 ± 0.5
Aromatic	3.7 ± 3.7	7.1 ± 5.1
PAH^{2+}	7.6 ± 10.0	0.4 ± 0.4
PAH	8.6 ± 14.0	0.6 ± 0.5

It was found that particulate PAH compounds are formed during the constantly occurring short-period CO peaks shown in figure 1 and table 1, when combustion conditions changed temporarily because of grate movements of the burner. Organic species were split by positive matrix factorization (PMF) method (Ulbrich, 2009) into LV-OOA (Low-Volatile, highly Oxidized Organic Aerosol), HOA (Hydrocarbon-like Organic Aerosol), PAH and Aromatic factor. It was found that particulate PAHs split into once and doubly charged ion fragments in the instrument (Table 1). Aromatic factor was mainly composed of one aromatic ring containing species, for example C_6H_5, and it was in the background throughout the combustion experiment in incomplete combustion circumstances. Hence it was noticed that aromatic ring containing organic species split into two factors where one ring containing species were in aromatic factor and several ring containing species were in PAHs. LV-OOA was likely oxalic acid, composed of $CO2^+$, CO^+ and water ion fragments. Sulfate was originated from inorganic salts and was mainly in the background in the medium circumstances that were in between efficient and poor, combustion conditions.

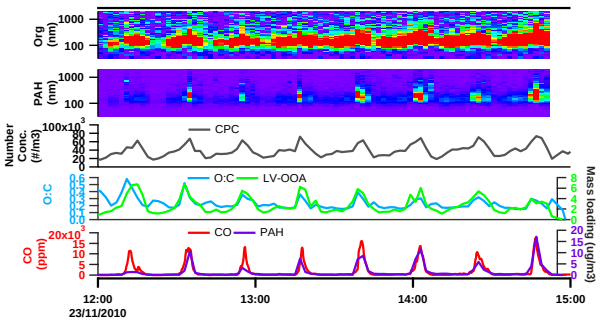

Figure 1. AMS organics and PAH size-resolved mass concentrations, CPC number concentration, O:C ratio, LV-OOA, gaseous CO and PAH double charge factor vs time during poor combustion.

The financial support by the Academy of Finland Centre of Excellence program (project no 1118615) and ERA-NET Bioenergy BioHealth project is gratefully acknowledged.

DeCarlo, P.F., J.R. Kimmel, A. Trimborn, M.J. Northway, J.T. Jayne, A.C. Aiken, M. Gonin, K. Fuhrer, T. Horvath, K. Docherty, D.R. Worsnop, and J.L. Jimenez, (2006) *Analytical Chemistry*, **78**:8281-8289.

Tissari, J. Lyyränen, J. Hytönen, K., Sippula, O., Tapper, U., Frey, A., Saarnio, K, Pennanen, A. S., Hillamo, R., Salonen, R. O., Hirvonen, M. –R. and Jokiniemi, J., (2008) *Atmospheric Environment*, **42**, 7862-7873.

Ulbrich, I.M. , Canagaratna, M.R., Zhang, Q., Worsnop, D.R., and Jimenez J.L. (2009) *Atmospheric Chemistry and Physics* , **9**(9), 2891-2918.

Ash behaviour and emission formation in co-combustion of wood and two agricultural fuels

M. Kortelainen[1], J. Tissari[1], T. Torvela[1], T. Karhunen[1], H. Lamberg[1], I. Nuutinen[1], O. Sippula[1] and J. Jokiniemi[1,2]

[1]Department of Environmental Science, University of Eastern Finland, Fine Particle and Aerosol Technology Laboratory, P.O. Box 1627 FI-70211 Kuopio, Finland
[2]VTT Technical Research Centre of Finland, P.O. Box 1000, FI-02044 VTT, Espoo, Finland
Keywords: biomass combustion, co-combustion, agricultural fuel, ash.
Presenting author email: Miika.Kortelainent@uef.fi

Utilizing annual biomass in heat and energy production is an interesting option considering the reduction of CO_2 emissions. Typically, volumes of agricultural residues are too low for large-scale utilisation, but local small-scale combustion is considered as a cost-effective solution. Combustion of field biomass would be one possibility for countries that have limited availability of woody biomass and large yield of agricultural residues.

The drawback of field biomass is high concentration of potassium, chlorine and sulphur, which may cause high mass emissions of PM and formation of corrosive deposits on heat exchanger surfaces. It is known that chemical composition of the fuel has a strong effect on the release of alkali metals (Tissari et al., 2008). Vaporized alkali metals form alkali sulphates and chlorides, which condense and form fine particles. Understanding the behaviour of ash forming elements in combustion is important considering the emissions, fouling of the combustion device and sintering of ash, as well as utilization of the ashes (fertilizers, soil enrichment).

In this work, the fine ash (PM_1) and bottom ash compositions were studied in co-combustion of wood chips with reed canary grass and wood chips with straw. The mixing ratio of wood chips and reed canary grass (WC+RCG) was 78/22 (wt %) respectively. With wood chips and straw (WC+S) two batches were mixed at proportions of 67/33 and 77.5/22.5 (wood chips/straw, wt %). All fuels were analysed for moisture and ash content, heating values and ash-forming elements.

The burner utilised in the experiment was a 40 kW moving step-grate stoker burner. Further details of combustion reactor are presented by Kettunen et al. (2011).

Gaseous compounds (NO_X, O_2, SO_2, CO, CO_2) were measured from undiluted flue gas with FTIR. For particle sampling flue gas was diluted in two steps. First dilution was done with a porous tube diluter (PRD) and further dilution with an ejector diluter (ED). The average total dilution ratio (DR) varied between 32 and 46. Particle size distribution was measured from diluted sample with an electric low pressure impactor (ELPI). PM_1 samples were collected on Teflon filters. Concentrations of organic, elemental and carbonate carbon (OC, EC and CO_3) were analysed from quartz filters positioned after pre-impactor (1 µm). Samples were also taken for TEM-EDS and XRD analyses.

Primary combustion air was fed through the grate and secondary combustion air from the top of the burner (approx. 13 cm above grate). Combustion air flows were measured continuously with hot-wire sensors.

Co-combustion of wood chips and reed canary grass produced similar fine fly ash emission levels than burning pure wood whips. The PM_1 emissions varied between 17 and 24 mg/MJ, whereas good combustion of wood chips produced emissions between 12 and 22 mg/MJ. The fine fly ash emissions from co-combustion of wood chips and straw on the other hand were 7.5 to 18-fold compared to wood combustion. In addition, the EC emission increased significantly due to lower combustion efficiency caused by the high ash content and inhomogeneous fuel quality.

Reed canary grass had slightly lower release percentage of potassium in fly ash, but clearly higher release of chlorine compared to straw, where Cl is released as HCl in gas phase. Also bottom ash retention percentage of potassium was higher in reed canary grass combustion. Molar ratio of K/Cl in fuel was observed to have negative correlation with SO_4^{2-} in fly ash as well as total fine fly ash emission.

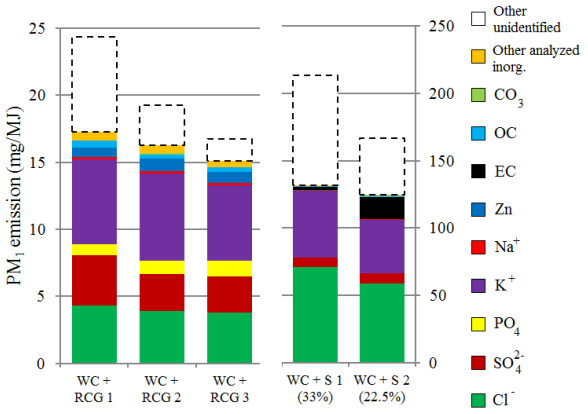

Figure 1. PM_1 emissions and their composition (notice the tenfold scale in straw co-combustion).

In this experiment reed canary grass turned out to be more suitable fuel for co-combustion with wood chips than straw.

The authors thank the Finnish Funding Agency for Technology and Innovation and the strategic funding of the University of Eastern Finland (Sustainable Bioenergy, Climate Change and Health) for financial support.

Tissari, J., Sippula, O., Kouki, J., Vuorio, K. and Jokiniemi, J. (2008) *Energy Fuels,* **22**, 2033–2042.

Kettunen, T., Kortelainen, M., Sippula, O., Nuutinen, I., Lamberg, H. and Jokiniemi, J. (2011) *European Aerosol Conference.* Manchester, United Kingdom.

Characteristics of the particulate matter from road tunnel environment

R. Licbinsky[1], J. Huzlik[1], J. Faimon[2] and K. Kreislova[3]

[1]Division of Transport Infrastructure and Environment, Transport Research Centre, Brno, 636 00, Czech Republic
[2]Department of Geological Sciences, Masaryk University, Brno 611 37, Czech Republic
[3]SVUOM Ltd., Prague, 170 00, Czech Republic

Keywords: particulate matter, traffic, road tunnel, size distribution.
Presenting author email: roman.licbinsky@cdv.cz

Presently, traffic represents one of the most significant sources of air pollution. Vehicle combustion itself emits fine and ultrafine particulate matter fractions (PM) (Morawska and Zhang, 2002). Besides, PM originates by abrasion of vehicle parts (tires, break-shoe lining, clutch lining etc.), corrosion of vehicle body or supporting equipment (crash barriers, traffic signs), and by resuspension of dust from road or maintenance materials (Colvile *et al.*, 2001). The road tunnel environment is a suitable site for characteristics of the traffic-related emissions (Sanchez-Ccoyllo *et al.*, 2009) and particle size distribution (Handler *et al.*, 2008).

PM sampling campaigns were performed in the Mrázovka city road tunnel that is the component of an internal city ring in Prague. This tunnel is 1,260 m long with driving directions placed in the separate tubes each with two lanes. In 2011, the traffic intensity in the studied tunnel part was 23,000 vehicles per 24 hours, 96 % of which were passenger cars. The PM_{10} and $PM_{2.5}$ fractions were sampled on nitrocellulose filters using Leckel MVS6 devices during 24 hours and the PM concentrations were determine by subsequent gravimetric analysis (Mettler-Toledo MX5/A). The Environcheck 107 device was used for a continual monitoring of particle size distribution. The monitoring was performed during one-week sampling campaigns. The variability in different seasons was studied especially in relation to winter road maintenance. The traffic intensity was calculated from a camera security system.

The results demonstrated the dominant share of coarse particles ($PM_{2.5-10}$) during all monitoring campaigns covering in average 72 % - 76 % of PM_{10}. These low differences indicate the same source of particles during all campaigns. Nevertheless, the fluctuation of coarse particles in time is evident from particle size distribution measurements. The highest portion of coarse particles in PM_{10} was determined in working days especially in morning and afternoon rush hours. However, very weaek correlation was found between the traffic intensity and the concentration of $PM_{2.5-10}$ particle fraction (R^2 ~ 0.22 – 0.28). The reason of the higher shares of coarse particle fraction during the rush hours could be a resuspension of the road dust from pavement and from surfaces next to the road and turbulent air flow due to moving vehicles.

The concentrations of fine particles ($PM_{2.5}$) that are produced mostly by a fuel combustion in vehicles engines indicate also some fluctuation in time with a local maximum during the morning rush hours. These fluctuations are very small compared to those of coarse particles. The stronger positive correlation was found between the $PM_{2.5}$ concentrations and the traffic intensity at spring sampling campaign (R^2 ranges between 0.25 and 0.5).

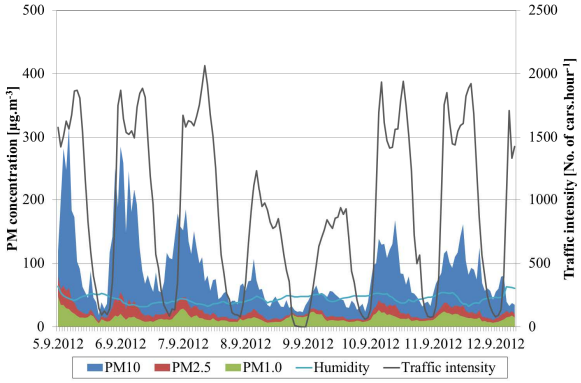

Figure 1. Particle size distribution and traffic intensity.

The PM_{10} and $PM_{2.5}$ samples were analyzed for 20 selected elements to characterise their chemical composition. Al and Ca were determined in the highest concentrations in both analysed fractions. Cu was found as the most common heavy metal in both fractions. In contrast, Pb and Ni concentrations were the lowest among the heavy metals. Trace element concentrations were very low (order of units of nanograms) including Pt concentrations near or below the detection limit of ICP-MS technique.

This work was supported by the Technology Agency of the Czech Republic under the project No TA01031043 “Quantification of specific pollution effect on materials and corrosion protection in tunnels”.

Colvile, R.N., Hutchinson, E.J., Mindell, J.S. and Warren, R.F. (2001) *Atmos. Environ.* **35**, 1537-1565.
Morawska, L. and Zhang, J. (2002) *Chemosphere.* **49**, 1045 – 1058.
Handler M., Puls C., Zbiral J., Marr I., Puxbaum H. and Limbeck A. (2008) Atmos. Environ. **42**, 2173–2186.
Sanchez-Ccoyllo O.R., Ynoue R.Y., Martins L.D., Astolfo R., Miranda R.M., Freitas E.D., Borges A.S., Fornaro A., Freitas H., Moreira A. and Andrade M.F. (2009) *Environ. Monit. Assess.* **149**, 241–249.

On the relation between aerodynamic and mobility diameter distributions for aggregates consisting of few monomers

A. Melas[1,2,3], M. Kostoglou[4], P. Baltzopoulou[1], Y. Drossinos[3] and A.G. Konstandopoulos[1,2]

[1]Aerosol & Particle Technology Laboratory, CPERI/CERTH, P.O. Box 60361, 57001, Thessaloniki, Greece
[2] Dept. of Chemical Engineering, Aristotle University, P.O. Box 1517, 54006, Thessaloniki, Greece
[3] European Commission, Joint Research Centre, Ispra (VA), 21027, Italy
[4] Div. of Chemical Technology, Dept. of Chemistry, Aristotle University, Thessaloniki, 54124, Greece
Keywords: aggregate structure, mobility radius, aerodynamic radius.
Presenting author email: admelas@auth.gr

Combined measurements of electrical-mobility-based (measured by Scanning Mobility Particle Sizer, SMPS) and aerodynamic-diameter-based (measured by Electrical Low Pressure Impactor, ELPI) distributions are typically employed to study the morphology of soot aggregates produced by diesel engines. This approach is used to calculate the aggregate's effective density, ρ_{eff} (Virtanen *et al.*, 2004). The effective density can be correlated to the particle morphology assuming specific morphology descriptors. For well-defined isotropic fractal aggregates the appropriate descriptor is the fractal dimension. In this way the size-dependence of the fractal dimension can be estimated (Konstandopoulos *et al.*, 2004, Baltzopoulou *et al.,* 2012).

In some cases, such as diesel soot and flame soot (Di Stasio *et al.*, 2002), the aggregates consist of a relatively small number of monomers or exhibit specific (non-random) anisotropic structures. In these cases the concept of effective density is under question and the exploitation of the aerodynamic and the mobility diameter distributions cannot be made without incorporating knowledge on the structure of the aggregates.

From a fundamental point of view, ELPI gives the aggregate distribution with respect to the variable f/m (where f is the friction factor and m is the particle mass). The mobility analyzer (SMPS) gives the distribution with respect to f. The inverse problem of determining the structure of the aggregates for these distributions is difficult to be solved. Therefore, the direct problem of determining the two distributions for given structures is evaluated. In particular, the cases of the well-defined structures (e.g. linear aggregates) and of oligomers (3-5mers) are studied.

For given distributions of these particles the mobility and aerodynamic radius distributions were constructed and compared. The mobility radius (R_m) in the continuum regime was calculated as suggested by Isella and Drossinos (2011) who related it to the molecule-aggregate collision rate. By calculating the steady-state molecular diffusive flux over the aggregate surface we determine the collision rate. This method is expanded to the transition regime by changing the boundary conditions. While in the continuum regime the fluid density on the surface is zero, in the transition regime it depends on a constant α(Kn) which depends on the Knudsen number. The aerodynamic radius is related to the mobility via the effective density, $R^2_{ae}=\rho_{eff} R^2_m/\rho_o$, where ρ_o is the unit density (1g/cm^3).

Figure 1 presents the mobility and the aerodynamic radii of trimers in the continuum regime against the trimer angle, a morphological descriptor of the spatial arrangement of the three monomers. The trimer angle (θ_{213}) is specified by two intersecting lines passing through the center of the central monomer (2) and the center of the two (1, 3) monomers pairwise touching it. These results combined with similar calculations in the transition regime provide a complete approach for the extraction of information on particle size and morphology.

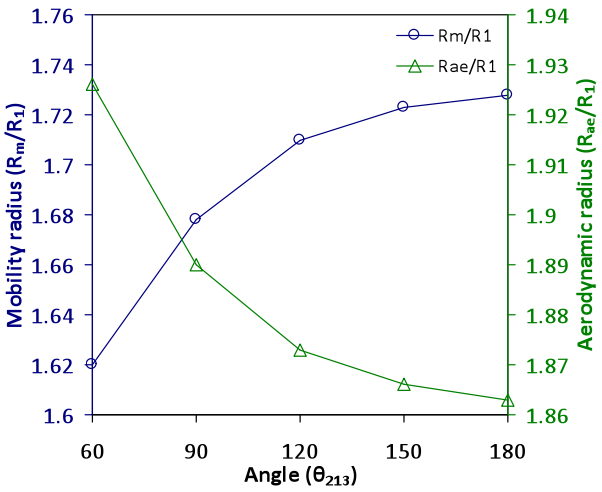

Figure 1. The mobility (R_m) and the aerodynamic radius (R_{ae}) of 3-mers against the trimer angle in the continuum regime.

Virtanen A., Ristimaki J. & Keskinen J. (2004) *Aerosol Sci. Technol.*, **38**, 437.

Konstandopoulos A.G., Boudouris, D., Baltzopoulou P.K., Papaioannou E. (2004) *8th ETH Conference on Combustion Generated Particles*, August 16-18, Zurich, Switzerland.

P. Baltzopoulou, E. Papaioannou, M. Kostoglou, A.G. Konstandopoulos. (2012) *European Aerosol Conference EAC 2012*, EAC-2012-P074, September 2-7, Granada, Spain.

Di Stasio, S., Konstandopoulos, A.G. and Kostoglou, M. (2002) *J. Colloid Interface Sci.,* **247**, 33.

L. Isella and Y. Drossinos (2011), *J. Colloid Interface Sci.*. **356**, 505

Immunomodulatory effects of short-term exposure to fine particulate matter from smog episode in Ostrava region: *in vitro* study

T. Brzicová[1], I. Lochman[2] P. Danihelka[1], A. Lochmanová[3], K. Lach[2] and V. Mička[2]

[1]VŠB – Technical University of Ostrava, Ostrava, 700 30, Czech Republic
[2]Department of Immunology and Allergology, Institute of Public Health Ostrava, Ostrava, 702 00, Czech Republic
[3]Faculty of Medicine of Ostrava, University of Ostrava, Ostrava, 703 00, Czech Republic

Keywords: $PM_{2.5}$, Health Effects, Immunological Assays, Ostrava Region
Presenting author email: tana.brzicova@vsb.cz

Many efforts were devoted to reduce air pollution in industrialized countries during the past few decades in response to findings that heavily polluted air is significantly associated with increased morbidity and mortality of exposed population (Pope et al., 1992; Dockery et al., 1993). However, despite these attempts, there are still many regions, where extended presence of air pollution sources hampers to achieve air pollution levels considered to be without significant adverse impact on human health.

An example of such a region, where limit values for PM_{10} and $PM_{2.5}$ recommended by WHO guidelines, as well as national legislative limits, are regularly exceeded, is the Ostrava region. The Ostrava region is located in the northeast of the Czech Republic and represents an area with one of the most polluted air in Europe. This undesirable state is caused by geomorphological and meteorological conditions of the Ostrava basin in combination with various and numerous air pollution sources. Temperature inversion occurring during the winter season further contributes to the accumulation of air pollutants by constraining their dispersion. Under inversion conditions, concentrations of $PM_{2.5}$ can achieve few hundreds $\mu g/m^3$.

Thus, population in Ostrava is exposed to high concentrations of airborne particles with diverse sizes and chemical compositions. Other pollutants present in the air can bind to the particle surface and together, they form a "chemical cocktail", a multicomponent mixture whose adverse health effects are difficult to predict or estimate from measurement of PM concentrations in the air. Data from epidemiology studies suggest the adverse health impact on the local population and shortened life expectancy associated with heavy pollution by airborne particles (Tomášková *et al*., 2007).

The precise mechanisms of how inhaled airborne particles exert their adverse health effects remain still unclear. However, recent research suggests the crucial role of the immune system in the development, as well as in the worsening of many serious pulmonary and cardiovascular disorders (Seaton *et al*., 1999; Li *et al*., 2008).

The presented study was aimed at *in vitro* evaluating of potential harmful health effects of a fine particulate matter sample ($PM_{2.5}$) mediated through changes in various types of the immune response. The tested particle sample was collected during a smog episode in Ostrava-Radvanice and represents real airborne particulate matter to which the population in the Ostrava region is exposed during inversion situations. Using four *in vitro* immunological assays, we evaluated the changes in selected parameters of the immune response (reactive oxygen species generation, allergenic properties, T-lymphocyte proliferation, selected cytokine release), which could serve as markers of non-specific adverse action of particulate matter on human health.

Even if certain immunomodulatory effects of airborne particles were observed, changes in evaluated immune response parameters were not significant to prove impact on the immune cells´ functions of healthy persons during short-term exposure. Obtained data indeed cannot exclude health risks of long-term exposure to airborne particles, especially for individuals with genetic predisposition to certain diseases or already existing disease.

This study emphasizes the *in vitro* assessment of complex effects of airborne particles in conditions similar to actual ones in an organism exposed to particle polluted air.

This work was supported by the project INEF CZ.1.05/2.1.00/01.0036.

Dockery, D.W., Pope, III, C.A., Xu, X., Spengler, J.D., Ware, J.H., Fay, M.E., Ferris, B.G. Jr., Speizer, F.E. (1993) *New Engl. J. Med.* **329**, 1753-1759.
Li, N., Xia, T., Nel, A.E. (2008) *Free Radic. Biol. Med.* **44**, 1689-1699.
Pope, III, C.A., Schwartz, J., Ransom, M.R. (1992) *Arch. Environ. Health*. **4**7, 211-217.
Seaton, A., Soutar, A., Crawford, V., Elton, R., McNerlan, S., Cherrie, J., Watt, M., Agius, R., Stout, R. (1999) *Thorax*. **54**(11), 1027-1032.
Tomášková, H., Tomášek, I., Šlachtová, H., Šebáková, H. (2011) *Hygiena*. **56**(1), 5-10.

PAH, PCDD/F and HCB emissions from residential wood combustion

K. Mõts[1, 2], M. Maasikmets[1, 3], E. Teinemaa[1], K. Vainumäe[1], L. Lehes[1], T. Arumäe[1], V. Kimmel[3]

[1]Estonian Environmental Research Centre (EERC), Marja 4d, 10617 Tallinn, Estonia; [2]Tallinn University of Technology (TUT), Institute of Chemical and Materials Technology, Ehitajate tee 5, 19086 Tallinn; [3]Estonian University of Life Science (EULC), Institute of Agricultural and Environmental Sciences, Kreutzwaldi 5, 51014 Tartu, Estonia

Keywords: PAH, wood combustion, stoves

Presenting author email: krista.mots@klab.ee

Incomplete combustion of organic material in the presence of chlorine causes the formation of chlorinated organic by-products, such as polychlorinated dibenzo-p-dioxins (PCDDs), polychlorinated dibenzofurans (PCDFs), polychlorinated biphenyls (PCBs), and hexachlorobenzene (HCB) (Hedman et al., 2006). Residential wood combustion (RWC) in woodstoves and fireplaces is estimated to account for 78% of PAH, 53% of PCDD/F and 70% of HCB emissions in Estonia in 2010 (Kohv et al., 2012). These estimates are subject to large uncertainty as emission factors (EF) used in this inventory are derived from one general study and may not be representative for Estonia and used EF as are not dependent from the type of combustion equipment.

The combination of dispersion modelling and measurement campaigns in different areas is useful tool to validate emission databases for residential heating. Therefore emission and ambient air measurements were performed and EF were validated through combination of ambient measurement campaigns and dispersion modelling.

Emission measurements were conducted at three different combustion facilities: a masonry stove, a cooking stove and a fireplace, as those combustion facilities are typically used in Estonian households. Measurements were carried out in EERC stove test laboratory. Conifer and hardwood logwood with different humidity were used. Each log batch was weighed, heating value was measured and the relative humidity (RH) of each log was measured. PAH, PCDD/F and HCB samples were collected from the hot flue gas, with an Eva dioxin sampler (Metlab) into filter, XAD adsorbent and pre-afterwash liquid. Samples were taken through an insulated, externally heated (180 °C) sample line. Samples were taken during the whole burning process (up to 4 hours, including start-up phase). Samples were analysed with the GC/HRMS. Simultaneously gas samples (O_2, SO_2, NO, NO_2, CO, CO_2, VOCs), temperature (°C), RH (%) and gas flow (m/s) were measured during the whole burning process. Samples for the gas analyses were taken through an insulated, externally heated (180 °C) sample line and through the filter units to the gas analyser (Testo 360, Testo AG).

Ambient air measurements were conducted at the RWC area in Tallinn, Estonia. A high volume sampler DHA-80 (Digitel) was used to collect PM10 and PM2.5 samples for subsequent chemical analysis. PM10 and PM2.5 samples were analysed regarding the PAH, PCDD/F and HCB with the GC/HRMS. Simultaneously gas samples (O_2, SO_2, NO, NO_2, CO, NMVOC, O_3) and meteorological parameters were measured during the whole measurement campaign.

The emission database for RWC for Tallinn was created based on house types from Estonian 2012 census data and EF obtained in current study. The dispersion modelling of emissions of RWC were carried out using ensemble of three local scale dispersion models (two Gaussian and one Eulerian dispersion model). Modelled levels of PAH, PCDD/F and HCB were compared against results of ambient air measurement campaigns.

Results

Highest PAH EF were measured at the cooking stove, which was more than 4 times higher compared to the masonry stove. PCDD/F EF in the fireplace are ca 46 times higher compared to the masonry and the cooking stove. HCB EF are 2 times higher in the cooking stove compared to the other combustion facilities. Taken into account that the combustion equipment type and other relevant flue gas and wood parameters (temperature, RH) play an important role in PAH, PCDD/F, HCB formation, this should be considered in further emission inventories.

The combination of dispersion modelling and measurement technique was used for validation of EF for RWC. Good agreement in certain areas between measured and modelled results was found.

This work was supported by the Estonian Ministry of Environment and Estonian Science Foundation project BioAtmos.

Hedman, B., Näslund, M. & Marklund, S. (2006). Emission of PCDD/F, PCB, and HCB from Combustion of Firewood and Pellets in Residential Stoves and Boilers. *Environmental Science & Technology*, **40**(16), 4968-4975.

Kohv, N., Heintalu, H., Mandel, E. & Link, A. (2012). Estonian Informative Inventory Report 1990-2010.

Toxicological Responses to Ozone Aging of Aerosols from Small-scale Biomass Combustion

E. Z. Nordin[1], O. Uski[2], R. Nyström[3], P. Jalava[2], J. Genberg[4], A. C. Eriksson[4], C. Bergvall[5], R. Westerholm[5] C. Boman[3], J. Jokiniemi[6], J. Pagels[1], and M.-R. Hirvonen[2]

[1]Ergonomics and Aerosol Technology, Lund University, P.O. Box 118, SE-22100, Lund, Sweden
[2] National Institute for Health and Welfare, Kuopio, Finland
[3]Thermochemical Energy Technology Laboratory, Umeå University, SE-901 87, Umeå, Sweden
[4]Nuclear Physics, Lund University, P.O. Box 118, SE-22100, Lund, Sweden
[5]Dept. of Analytical Chemistry, Stockholm University, Svante Arrhenius väg 16, SE-10691 Stockholm, Sweden
[6] University of Eastern Finland, Department of Environmental Sciences,, Kuopio, Finland

Keywords: biomass combustion, aging, toxicology, PAHs,
Corresponding authors email: erik.nordin@design.lth.se

Small scale wood combustion for domestic heating and energy production is being regarded as a climate friendly alternative to fossil fuel combustion. Inefficient wood combustion emits elevated levels of aerosol particles and has therefore been recognized as a potential health threat, partly due to high content of polycyclic aromatic hydrocarbons (PAHs), of which several are rated as carcinogenic. When emitted to the ambient air the wood smoke aerosol is subjected to atmospheric aging, a process which physically and chemically transforms the aerosol, Kocbach Bølling et al (2009) states that more research is needed about health effects from aging of biomass combustion aerosol. The aim of this project was to investigate the toxicological response from fresh and aged biomass burning aerosol and link that to atmospheric transformation due to ozone aging and chemical composition of the aerosol.

A conventional wood stove was used in the study, operated in two modes, normal firing procedure at nominal load (NOM) and adjusted sooty procedure which gave a more incomplete combustion (denoted wood smoke, WS) (two experiments of each). To study the toxicological effects of aging a new method was developed, which allowed us to use the same batch of wood smoke aerosol for both studies of fresh and aged aerosol. The emissions were diluted and sampled to a 15.3 m^3 reaction chamber (Nyström et al., 2013). The emissions were characterized using online techniques (TEOM and SMPS), PUF + filters (gas and particulate PAHs), OC/EC filter sampling and gas monitors (NO_x and CO). For the toxicological studies filters were collected using a Dekati gravimetric impactor (DGI), the collected filters were also analyzed for PAHs, metals and ions. After characterization and filter sampling of the fresh aerosol about 1000 ppb of ozone was added and the aged aerosol was characterized in the same way as the fresh aerosol. By using aerosol from the same wood smoke batch, differences in chemical and physical characteristics between fresh and aged aerosol is avoided.

$PM_{1.0}$ from the DGI filters was used for the toxicological studies. The filters from each experimental situation were pooled together and the aerosol was extracted using an ultrasonic bath and methanol. The toxicological analysis was performed on mouse RAW264.7 macrophages using four different doses (15, 50, 150 and 300 mg ml^{-1}) and blank exposure and consisted of cell cycle analysis and cell viability tests (flow cytometry total DNA content analysis), inflammatory markers (cytokine TNF-α and chemokine MIP-2) and genotoxicity (Comet Assay).

The chemical composition of the aerosol from the four experimental situations is shown in table 1. The relative content of K, Cl and SO_4 was about four times higher for the more efficient NOM mode than for the WS mode. Only a minor increase in relative OC content was detected when aging the aerosol from the WS mode, the OC content decreased in the NOM case. This indicates that the aging process does not cause significant condensation of organic material on the soot cores. The relative particulate PAHs content measured on the DGI filters decreased from 0.39 % to 0.18 % when the WS mode aerosol was aged, which is an indication that the ozone aging induces surface reactions.

Table 1, Chemical composition of fresh and aged aerosol.

Experimental situation	OC (%)	EC (%)	NO_3 (%)	Zn (%)	K+Cl+ SO_4 (%)
WS-fresh	49.3	47.4	0.7	0.2	2.1
WS-aged	52.4	41.8	3.1	0.2	1.3
NOM-fresh	14.8	73.6	0.8	0,7	8.2
NOM-aged	6.2	78.6	6.2	0,8	6.8

Fresh WS mode particles were significantly more cytotoxic than the particles from the NOM mode. Ozone aging increased the cytotoxicity for both combustion modes. Fresh WS mode particles caused increased inflammatory responses compared to fresh NOM mode particles. The inflammatory responses was increased when the cells was exposed to aged NOM mode particles, compared to fresh. This effect could not be seen for the WS mode aerosol. All aerosol samples induced genotoxic responses higher than the control level. Due to the low viability of the cells exposed to the highest dose of fresh and aged WS mode aerosol, the samples could not be analyzed for genotoxicity. Aged aerosol from the WS mode gave by far the greatest genotoxic response.

The newly developed method was successful and made it possible to investigate the toxicity of fresh and aged biomass combustion emissions from two combustion situations, as well as characterizing the aerosol. The toxicity of aerosol from biomass combustion is affected by the combustion conditions and atmospheric aging. Aging of aerosol from incomplete combustion increases the DNA damage response compared to fresh samples of aerosol from the same combustion batch.

References:
Kocbach Bølling A. et al., (2009) Part Fibre Toxicol, **6**, 29.
Nyström R. et al., (2013) Conference proceeding submitted to EAC
Acknowledgements: This work was supported by the ERA-NET project Biohealth through the Swedish Energy Agency and the Swedish research council FORMAS.

Fourier-transform-ion-cyclotron-resonance mass spectrometry with laser-desorption-ionization of primary ship diesel exhaust particles

C. Rüger[1], T. Schwemer[1,3], M. Sklorz[1,2,3], R. Zimmermann[1,2,3]

[1]Joint Mass Spectrometry Centre / Chair of Analytical Chemistry, University of Rostock, 18051 Rostock, Germany
[2]Joint Mass Spectrometry Centre, Cooperation Group Comprehensive Molecular Analytics, Helmholtz Zentrum München, Ingolstädter Landstr. 1, 85764 Neuherberg, Germany
[3]HICE – Helmholtz Virtual Institute of Complex Molecular Systems in Environmental Health – Aerosols and Health, www.hice-vi.eu

Keywords: ship diesel emissions, LDI, high resolution mass spectrometry, soot
Presenting author email: christopher.rueger@uni-rostock.de

Introduction

Negative effects on the health caused by combustion aerosols are known since a long time. One of the most underestimated sources are ship diesel emissions. The comprehensive chemical characterization of organic compounds in the particulate matter is the key for a deeper understanding of biological health effects.

The chemical composition of ship diesel combustion aerosol is poorly investigated. Due to the extreme high complexity of combustion aerosols high resolution mass spectrometry using laser-desorption-ionization is one promising tool for revealing components with the same molecular mass and assigning molecular sum formulas.

Experimental Section

The samples were taken during a measurement campaign at the Faculty of Mechanical Engineering and Marine Technology at University Rostock. The experiments were performed at a four-stroke one cylinder ship diesel engine with three liter cylinder capacity driven with heavy fuel oil (HFO) and light fuel oil (LFO) at different loads.

Exhaust gas was diluted by clean air and particles were collected by impaction on aluminum or stainless steel foils. Size classes of the applied low pressure impactor ranged from 30 nm up to 10 µm. Time traces were collected using a rotating drum impactor with cutpoints of 0.1 µm, 1 µm and 10 µm, respectively.

The measurements were carried out with a solariX Fourier-transform-ion-cyclotron-resonance mass spectrometer (Bruker Daltonik GmbH, Bremen, Germany) equipped with a 7 Tesla superconducting magnet. The setup was used without further modification except of a self-made MALDI-Target to position the impactor foils directly in the ion source. The third harmonic of a Neodymium-YAG laser (355 nm) was used with moderate laser strength of 30 up to 70 % and various foci. Mass resolution was set to about 300˙000 @ m/z = 400.

Results and Discussion

The laser-desorption-ionization (LDI) mass spectra obtained show two types of ionized species: radical cations and protonated species. Most abundant are $CH^{\bullet+}$, $CHO^{\bullet+}$ and $CNH^{\bullet+}$ class compounds, in accordance to the results of Cho et al. (2012).

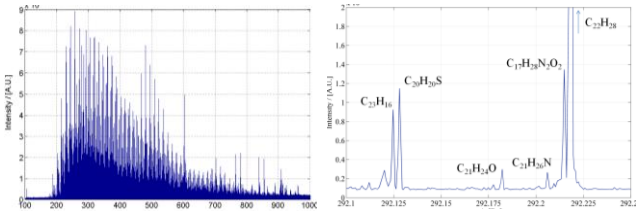

Figure 1: Broadband mass spectrum (left) and a blow up of m/z = 292.1 to 292.2 (right) of HFO-combustion particles sampled by ELPI obtained by (+) laser-desorption-ionization mass spectrometry

Direct LDI-measurements of the HFO feed indicates that the majority of the signals refer to products of incomplete combustion. Additionally, differences in the intensity of individual species and some new compounds were identified in the aerosol.

The high resolution mass spectrometry allows the determination of exact sum formula; thereby the signals can be assigned to alkylated, nitro- and oxo-PAH-species as well as to low abundant sulfur containing molecules. Because of the ionization method no aliphatic compounds were found.

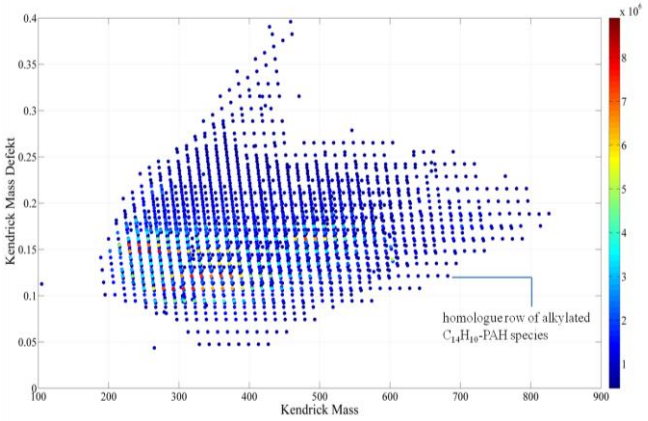

Figure 2: Kendrick Plot observed from HFO sample by (+) laser-desorption-ionization

Acknowledgements

This work was supported by the University Rostock and the Helmholtz Virtual Institute of Complex Molecular Systems in Environmental Health (HICE).

Cho, Y., Witt, M., Kim, Y. H., Kim, S. (2012) *analytical chemistry*, **84**, 8587 - 8594

Removal Characteristics of Iron Particles by Ceramic Candle Filters and the Effect of the flue Gas Inlet Configuration in Particulate Collectors

Y. O. Park, N. Hasolli

Clean Fuel Department, Korea Institute of Energy Research, Daejeon, Korea
Keywords: new steelmaking process, ceramic candle filter, dust load, iron slurry, high temperature and high pressure
Presenting author email: yopark@kier.re.kr

Traditional de-dusting systems in new steel making industry are a wet scrubber system including the slurry treatment system in addition to the particulate removal facility[1]. The iron slurry, as a by-product of the process, can be further processed to reach the dry status after which it can be pressed in compact iron briquettes for recycling purpose. In addition the high temperature flue gas through the system can decrease the flue gas temperature.

In order to eliminate the iron slurry from the system a dry type iron particulate removal system allows high particulate removal efficiency with no additional downstream facility for slurry treatment. High temperature and high pressure iron particulate laden flue gas treatment is done by applying ceramic candle filters which can remove particle load with high efficiency and can endure extreme operating conditions. Removal of collected particles from the outer surface of ceramic filters is done by high pressure air injection the candles with high pressurized air, driven in counter flow to flue gas stream. Based on the dust load the ceramic candle filters are pulsed frequently. Due to accumulated dust on the outer surface, the pressure drop increases consequently until pressure drop of filter cleaning start is reached. In order to reduce the dust load facing the ceramic candle filter, a new concept of centrifugal separator was introduced at the lower part of the collector. This configuration of the inlet duct was compared with the traditional direct inlet. The combination of cyclone and bag filters was studied in the reference[2-3]. In their study the authors reported a significant decrease of dust load inside the lower part of separator prior to reaching the filter bags. We expect that the dust load will reduce and the pulsing of the ceramic filter candles will be less frequent thus extending the life span of ceramic filters.

Table 1. Experimental conditions

Test filter: Silicon-carbide ceramic filter		
Filtration area,	m^2	0.294
Filtration velocity,	m/min	0.5 ~ 1.0
Inlet dust concentration,	g/m^3	20.0
Pulse-jet air pressure,	kg_f/cm^2	5.0
Pulse duration,	msec	100
Pulsing DP,	mmH_2O	250

Test set-up consists of the following operational units: heaters, ceramic filter chamber with lower part, dust hopper, dust feeder, air pulsing unit, flow controller, compressor unit, data acquisition unit, particle concentration measurement device and control panel. Dust feeder was operating under high pressure and at controlled feeding rates. Pulsing of the filter candle was initiated automatically after the pressure drop (DP) has reached the setting terminal pressure drop value (250 mmH_2O). Data of the residual pressure drop and the pressure drop evolution were collected automatically using data acquisition unit. Particle concentration was measured at the inlet and outlet of the filter chamber and the particle collection efficiency calculated.

The results show that when the unit is operated with the cyclone part the pulsing interval was increased. The increase of pulsing interval was proven to be dependent on the filtration velocity. The higher the velocity the greater was the difference between two configurations of the inlet duct. Also we could observe a significant decrease of residual pressure drop when the unit was operated with the cyclone part installed, as shown in Figure 1.

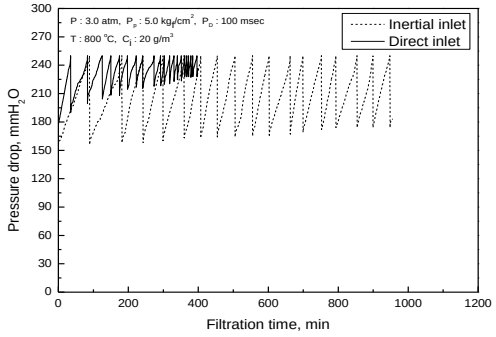

Figure 1. Comparison between two inlet duct configurations and the impact on the pressure drop.

The effect of the presence of cyclone part on the iron particle removal efficiency was observed. For the configuration with cyclone part, the overall collection efficiency increased above the value 99.99% for filtration velocities 0.5, 0.8 and 1.0 m/min.

[1] I.O Lee, M.K. Shin, M. Cho, H.G. Kim and H.G. Lee. (2002), Energy and Pollutants Reducing Technologies in New Ironmaking Processes at POSSCO, ISIJ International, 42, S33-S37.

[2] Kim, S.D., Park, Y.O. and Kang Y. (2004). Performance comparison of the CYBAGFILTER® and existing bag filter, Journal of Korean Society for Atmospheric Environment, 20(6), 739~748.

[3] Kim, S.D. Son, J.E., Park, Y.O., Cheong D.K. and Kang Y. (2004). Characteristics of flow field and particulate trajectories in bag filter with centrifugal force application, Korean Chem. Eng. Res., 42(3), 318~325.

Chemical profile of wood burning $PM_{2.5}$ and PM_1 in the two largest cities of Greece, Athens and Thessaloniki

St. Pateraki[1], Th. Maggos[1], D.A. Sarigiannis[2], M. Kermenidou[2], S.K. Karakitsios[2],V.D. Assimakopoulos[3], A. Zagkos[4] and D.N. Asimakopoulos[4]

[1]Environmental Research Laboratory/ I.N.RA.S.T.E.S., NCSR 'Demokritos', Athens, 15310, Greece
[2]Department of Chemical Engineering, Aristotle University of Thessaloniki, Thessaloniki, 54124, Greece
[3]Institute for Environmental Research and Sustainable Development, National Observatory of Athens, Athens, 15236, Greece
[4]Department of Applied Physics, Faculty of Physics, University of Athens, 15784, Athens, Greece

Keywords: wood burning, fine particles, chemical composition, meteorology
Presenting author email: stella@ipta.demokritos.gr

Particulate Matter (PM) is one of the most challenging environmental issues due to its well established impact on human health, air quality and global climate change. The current interest of scientific and regulatory communities is moving to finer PM fractions ($PM_{2.5}$ and PM_1), as a consequence of their relevant implications on the human health; they can remain in suspension much longer than coarse particles and they can penetrate more deeply into the human respiratory tract, elucidating early biological responses (Amodio et al. (2010)).

Wood combustion and various other forms of biomass burning have clearly been indicated as major contributors to ambient aerosol levels. Especially during periods of low vertical mixing due to stagnant weather conditions, the effects on both local air quality and human health can be considerable. In the industrialized world, including North America, Europe and the Far East, wood is burned in fireplaces and wood stoves for different purposes, including pleasure, heating, and cooking (Wang et al. (2005)). The increasing cost of oil and natural gas has been an important factor driving the increased usage of wood for heating and cooking purposes and resulting in increased PM burden of exposure.

In line with such scientific demands, the experimental set-up and the data analysis of the specific work allow the retrieval of information on the wood burning fine particles. The main objective of this study is the investigation of the influence of the residential wood-combustion emissions on the configuration of the PM profile, both mass and composition. Taking into consideration the complexity of the aerosols character, simultaneous measurements of both $PM_{2.5}$ and PM_1 fractions took place at different types of environment, in the two largest cities of Greece, Athens and Thessaloniki. The monitoring stations were selected carefully, representing urban background, suburban - industrialized and urban-traffic locations. Chemical characterization with respect to ionic and carbonaceous species was also carried out on the collected samples. The particle mass concentration determination was conducted gravimetrically according to EN 12341. The water-soluble ions (Cl^-, NO_3^-, SO_4^{2-}, NH_4^+, K^+, Mg^{2+}, Ca^{2+}) were detected using suppressed ion chromatography (IC), while the carbon elements (OC (organic carbon), EC (elemental carbon)) were determined with the use of a carbon analyser (Sunset Lab, USA). Beyond these, levoglucosan was used as a tracer of biomass burning (Belis et al. (2013)), using a GS-MS (Agilent, USA) analysis. The 2-months fieldwork took place during the winter period of 2013.

The acquired data will be evaluated in order to illustrate intra/inter-site differences accounting for the role of the type of the environment on the wood burning $PM_{2.5}$ and PM_1 profile. In an attempt to estimate the contribution of the emissions from the wood combustion, the obtained PM characteristics will be compared with those reported from previous works at the same locations. Focusing on the changes in the prevailing atmospheric circulation patterns (mesoscale/ synoptic), a possible link with the meteorology will be attempted. Finally, a mass closure study of the available chemical species in conjunction with the observed PM mass concentration will be also presented.

The first results at Thessaloniki showed that days with very low temperature (below 6-7 ^{0}C) and wind speed values were characterized by elevated PM concentrations, up to 98 and 92 μg/m^3 for $PM_{2.5}$ and PM_1 respectively. Furthermore, ambient levoglucosan reaching concentrations up to 4 mg/m^3 and being positively correlated (especially for the urban background station) to $PM_{2.5}$ and PM_1, verified the extensive use of biomass burning. During higher temperature days (above 11-12^{0}C) biomass burning was reduced, leading to lower values of the pollutants. Interestingly, the spatial PM differentiation between the traffic and the urban background atmosphere was not so prominent, owing to the prevalence of the residential heating emissions. Finally, daily $PM_{2.5}$ and PM_1 load is significantly increased (up to 50%), being compared to previous years. Since traffic volume is reduced and the related input to air pollution is lower, the respective contribution of residential heating (and more specifically biomass burning) is now dominant.

Amodio, M. et al. (2010) *Atmos. Res.* **98,** 207–218
Belis, CA. et al. (2013) *Atmos. Environ.* **69**, 94-108
Wang, H. et al. (2005) *Atmos. Environ.* **39**, 5865–5875

Emissions of volatile organic compounds from ritual burning practices

Shamsh Pervez[1]*, Rajan Chakrabarty[2], Barbara Zielinska[2], Shippi Dewangan[1]

[1]School of Studies in Chemistry
Pt. Ravishankar Shukla University, Raipur- 492010 (C.G.)

[2]Division of Atmospheric Sciences
Desert Research Institute, Reno, NV, USA, 89512

*Presenting author email- shamshp@yahoo.co.in.;shamshpervez@gmail.com; Tel.: +91-9425242455

Worshipping activity is a customary practice related with many religions and cultures in various Asian countries, including India. Smoke from burning in religious and ritual places produces a large number of health-damaging and carcinogenic air pollutants include volatile organic compounds (VOCs) such as formaldehyde, benzene, 1, 3 butadiene, styrene, etc. This study evaluates real-world VOC's emission conditions in contrast to other studies that examined emissions from specific types of incense or biomass material. Sampling was conducted at four different religious places in Raipur city, District Raipur, Chhattisgarh, India: 1) Hindu Temples, 2) Muslim Graveyards (Holy shrines), 3) Buddhist Temples,4) Marriage Ceremony. Concentrations of selected VOC's, Respirable Particulate Matter (RPM, aerodynamic diameter <5 µm), carbon dioxide (CO_2), and carbon monoxide (CO) were sampled from the smoke plumes. The Emission Factor (EF) has been determined by:

$$EF_j\ (g.kg^{-1}) = \frac{\triangle C_j \text{ X } 1000\ (g.kg^{-1}) \text{ X } C_{Fraction}}{(\triangle CO_2\text{-C} + \triangle CO\text{-C} + \triangle THC\text{-C} + \triangle PM\text{-C})}$$

EF_i= Emission Factor of pollutant x in $g.kg^{-1}$
$\triangle C_i$= background-corrected concentration of pollutant x in $mg.m^{-3}$
$\triangle CO_2$-C = mass fraction of C in CO_2 in $mg.m^{-3}$

$\triangle$CO-C = mass fraction of C in CO in $mg.m^{-3}$

$\triangle$THC-C = mass fraction of C in total hydrocarbon in $mg.m^{-3}$

$\triangle$PM-C = mass fraction of C in particulate matter in $mg.m^{-3}$
$C_{Fraction}$ = carbon content in dry material

Benzene has shown highest emission factor (EF) among selected volatile organic compounds in all places. All the selected religious and ritual venues have shown different pattern of VOC EF's compared to laboratory based controlled chamber studies.

Table: Emission Factor ($g.kg^{-1}$) of measured gaseous pollutants and respirable particulate matter for Indian different religious based burning activities

Species / Sites	CO_2	CO	RPM
Marriage Ceremony	2711.70±274.49	190.36±23.76	47.38±5.90
Muslim Graveyards	352.20±6.38	78.78±11.82	30.69±2.64
Buddhist Temple	1240.98±159.88	213.39±26.94	33.09±2.76
Hindu Temple	687.57±98.78	1.72±0.23	18.12±2.05

This work is supported by Department of Science and Technology, Govt of India and DRI, Reno, NV.

Akagi, S. K., Yokelson, R. J., et al. 2011.Emission factors for open and domestic biomass burning for use in atmospheric models. Atmos. Chem. phys.11, 4039-4072.

Andreae, M. O., Merlet, P.2001. Emission of trace gases and aerosols from biomass burning. Global Biogeo. Cycles.15(4), 955-966.

Particle and gas phase distribution of toxic metals during biomass combustion

D. Pudasainee, H.-R. Paur, A. Bologa and H. Seifert

Institute of Technical Chemistry (ITC), Karlsruhe Institute of Technology (KIT)
Hermann-von-Helmholtz-Platz 1, 76344 Eggenstein-Leopoldshafen, Germany
Keywords: biomass combustion, CAROLA-ESP, mercury, metals emission
Presenting author email: deepak.pudasainee@itc-tab.fzk.de

Combustion of biomass releases several pollutants: particle, NOx, SOx, metals etc., of health and environmental concerns (Williams et al., 2012). Since fine particulates are associated with increased mortality, cardiovascular diseases and impact on climate, it is necessary to control such emission. CAROLA- electrostatic precipitator (ESP) was developed at Karlsruhe Institute of Technology, Germany to control fine particles from biomass combustion in small scale units (Bologa et al., 2012). Biomass contains trace concentration of metals which are released into the environment during combustion. Particle bound metals usually are removed in dry type particle removal system, however, gas form are not. So knowing the distribution of metals has an important implication in its removal within the pollution control devices and fate in the environment. In this paper, particle and gas phase distribution of selected toxic heavy metals (Cd, Cr, Pb and Hg) from biomass combustion and their behavior is presented. Flue gas was sampled simultaneously at the inlet and outlet of CAROLA- ESP according to US EPA method 29. Particulate and gaseous samples were collected to measure selected heavy metals emission concentration and distribution in flue gas, temperature ranging from 160 to 203 ^{0}C. Heavy metals concentrations were determined using Inductively Coupled Plasma Mass Spectroscopy.

In combustion flue gas, particle concentration ranged 55.5 to 173.9 mg/Nm^3 and 13.0 to 23.9 mg/Nm^3 at the inlet and outlet of CAROLA- ESP, respectively. Particle removal efficiency of CAROLA- ESP ranged 64 to 86%. Heavy metals were more enriched in fly ash than bottom ash. This is in agreement with the earlier studies (e.g. Narodoslawsky and Obernberger, 1996).

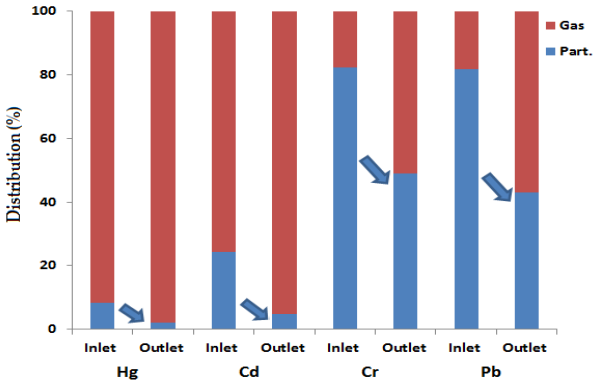

Figure 1. Metals distribution into particle and gas phase in flue gas at the inlet and outlet of CAROLA-ESP.

Metals concentrations in flue gas at the inlet CAROLA- ESP were 0.45 µg/Nm^3 (Cd), 0.63 µg/Nm^3 (Hg), 1.69 µg/Nm^3 (Cr) and 3.75 µg/Nm^3 (Pb). Similarly, metals concentration in flue gas at outlet CAROLA- ESP were 0.22 µg/Nm^3 (Cd), 0.52 µg/Nm^3 (Hg), 0.61 µg/Nm^3 (Cr) and 1.13 µg/Nm^3 (Pb). This corresponds to metals removal in CAROLA- ESP from 16.9 to 69.9%. Metals distribution into particle and gas phase in flue gas is presented in Figure 1. Cr and Pb were mainly distributed in particulate form. On the other hand, Hg and Cd were distributed mainly in gas form. Passing through the CAROLA- ESP 78.3 to 90.4% of particulate bound metals were removed. So at the outlet, gaseous form metals were dominant.

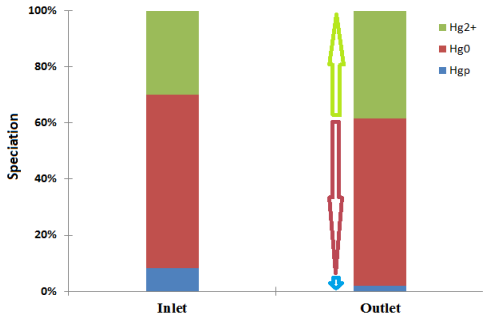

Figure 2. Hg speciation variation in flue gas at the inlet and outlet of CAROLA- ESP.

At the inlet of CAROLA- ESP, 92% Hg was speciated into gaseous form and 8% as Hg_p (Figure 2). Passing through the CAROLA- ESP, particulate bound Hg was significantly removed (78.5%), however, overall removal of Hg was low (16.9%). Hg^0 decreased and Hg^{2+} increased due to possible interaction with oxidants in flue gas, mainly HCl. Metal distribution into gas and particle form during combustion is a complex phenomenon primarily dependent on initial metals concentration in fuel, availability of oxygen and chloride, combustion temperature, flue gas residence time etc. More data in controlled conditions are required to explain the distribution of metals during biomass combustion and efficiently control them.

Bologa, A., Paur, H.R., Seifert, H. And Woletz, K. (2012) Manag Environ Qual Int J **23**(1), 36–55.

Narodoslawsky, M., Obernberger, I. (1996) *J. Hazard. Mater.* **50** (2-3), 157-168.

Williams, A., Jones, J.M., Ma, L., Pourkashanian, M. (2012). *Prog. Energy Combust. Sci.* **38** 113-137.

Laboratory particle-phase emissions from sugarcane burning: chemical and mutagenicity characterization

E. R. Dias[1], K. F. Souza[1], D. A. Morales[2], F. Kummrow[3],
G. A. Umbuzeiro[2], L. R. F. Carvalho[1*]

[1] Institute of Chemistry, University of São Paulo, São Paulo, São Paulo, 05513-970, Brazil
[2] Faculty of Technology, State University of Campinas, Limeira, São Paulo, 13484-332, Brazil.
[3]Federal University of São Paulo, Diadema, São Paulo, 09972-270, Brazil.
Keywords: sugarcane burning, PAH, oxy-PAH, nitro-PAH.
*Presenting author email: lrfdcarv@iq.usp.br

Open burning of biomass is a common method for agricultural residue disposal and represents a considerable source of pollutants in the atmosphere. Although there are economic and practical benefits, the environmental and health risks of this activity need to be fairly recognized. Pollutants in smoke from agricultural burning include, among others, semi volatile organic compounds, present in solid and gas phases, such as polycyclic aromatic hydrocarbons (PAHs), which have carcinogenic and mutagenic properties to humans.

In Brazil, sugarcane is a predominant crop in the Southeastern region, especially in the state of São Paulo, whose currently production responds for 62% of the Brazilian entire production. Areas under the influence of sugarcane burning have presented higher mutagenic activity in comparison to urban areas (Umbuzeiro *et al*, 2008).

The objectives of this study were: (i) to assess PAHs, nitro-PAHs and oxy-PAHs emission levels from the burning of sugarcane straw; (ii) to determine the emission factors of the identified target compounds; (iii) to assess the mutagenic activity of fractionated organic extracts and (iv) to compare the identified compounds levels with the mutagenic responses in the *Salmonella*/microsome assay (White, 2002).

Smoke particulate matter from sugarcane subjected to laboratory burning was sampled by low volume air filtration on quartz fiber filters covered with Teflon. The polycyclic aromatic hydrocarbons (PAHs), nitro-PAHs and oxy-PAHs present were analyzed by GC-MS. PAH and nitro-PAH show to be only minor components and the target nitro-PAHs were undetected under the analytical conditions used. In contrast, the target oxy-PAH compounds (9-fluorenone = 9-Flu, 9,10-anthraquinone = 9,10-Ant and 1,9-benzo[10]anthrone = Bzo) were found at relatively high concentrations in each individual fraction.

This is the first report of emission factors for the PAHs and oxy-PAHs (Table 1) in the sugarcane burning. The emission factors ranged from 0.19 to 0.90 μg Kg^{-1} for PAH compounds (results of a single combined extract) and 6.1 to 10.5 μg Kg^{-1} for oxy-PAH compounds (average of ten results corresponding to the individual extracts).

Table 1. Emission factors (μg Kg^{-1}) of oxy-PAH compounds in particles from sugarcane burning.

Emission factor, ( ) = RSD in %		
9-Flu	9,10-Ant	Bzo
6.1(42.1)	10.5 (50.1)	10.1 (36.6)

The concentration of the target oxy-PAH compounds in smoke aerosols in the ten experiments performed were highly variable, as it depends on the combustion conditions.

The most mutagenic fractions in the *Salmonella*/microsome assay were the oxy ones (Figure 1). Unsubstituted PAHs are present at concentrations below of the sensitivity of the *Salmonella*/microsome microsuspension assay performed with the highly sensitive strain YG5161.

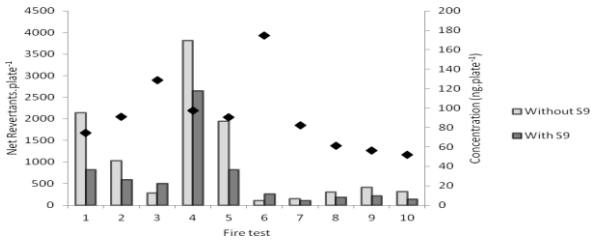

Figure 1. Mutagenicity of the oxy-PAH extracts in the Salmonella/microsome microsuspension assay with YG1041 with and without S9 expressed in net revertants per plate in comparison with the sum of the concentrations of the three oxy-PAH identified in the extracts (9-Flu, 9,10-Ant, Bzo) per plate.

This work has been supported in part by grants from FAPESP, Fundação de Amparo à Pesquisa de São Paulo (Project 08/58073-5).

Umbuzeiro, G.A., Franco, A., Magalhães, D., Castro, V.F.J., Kummrow, F., Rech, C.M., Carvalho, L.R.F. Vasconcellos, P.C. (2008) Environ. Mol. Mutagen. **49** (4) 249–255.

White, P.A. Mutat. Res. (2002) **515** (1-2) 85–98.

Characterisation of different soot types regarding morphology and black carbon content

H. Saathoff, A. Comouth, B. Altstädter, C. Linke, A. Kiselev, and K.-H. Naumann

Institute for Meteorology and Climate Research, Karlsruhe Institute of Technology, Hermann-von-Helmholtz-Platz 1, 76344 Eggenstein-Leopoldshafen, Germany
Keywords: soot, black and organic carbon, morphology
Presenting author email: harald.saathoff@kit.edu

Soot particles are besides mineral dust the major absorbing atmospheric aerosols and model calculations suggest that black carbon (BC) may be the second strongest contributor to global warming (Jacobson, 2001). Furthermore, adverse health effects are attributed to fine aerosol particles which are dominated by soot particles especially in urban areas (Laden et al. 2000). During their atmospheric lifetime of several days soot particles undergo changes in their morphology, hygroscopicity, and optical properties with profound implications for their potential impact on human health and climate forcing (Zhang et al., 2008). To determine the relevant soot concentrations and properties in the atmosphere soot characterisation techniques like the single particle soot photometer (SP2) gain increasing importance (Laborde et al., 2012). The aim of this work is a characterisation of soot particles of different composition with different measurement techniques to quantify their measurement capabilities.

Therefore we studied the dynamic behaviour of soot from a propane burner (mini CAST) and a spark generator (GfG, Palas) in a 3.7 m^3 steel vessel for time periods of typically 8 hours. Size distributions were measured with differential mobility analysers (SMPS, TSI, 3071 & 3080) in the size range between 14 and 820 nm. On the basis of the measured initial particle size distribution and particle number concentration (CPC, TSI, 3025, 3022) model calculations were done using the aerosol model COSIMA (Naumann, 2003), a computer program simulating the dynamics of fractal aerosols (Wentzel et al., 2003). The soot particles were characterised regarding their single particle mass with an aerosol particle mass analyser (APM 3601, Kanomax) and regarding their black carbon content with a single particle soot photometer (SP2, DMT). Both instruments were operated in tandem with a differential mobility analyser (DMA, TSI 3080). Furthermore, filter samples of the soot particles were analysed with an environmental scanning electron microscop (ESEM) on their morphology and by thermal treatment (VDI 2565-2) on their elemental and organic carbon content.

Figure 1 shows the evolution of the effective density of propane burner soot particles for different mobility sizes over 8 hours. The particle number decreased in this time from $1.6*10^5$ cm^{-3} to $1.7*10^4$ cm^{-3}. The monomers of the soot aggregates had a mean size of (32±7) nm and an organic carbon content of (4±3) %. The gas mixture burned in the mini CAST burner had a carbon to oxygen atom ratio of 0.29, hence close to the stoichiometric ratio for burning propane. The fractal dimension (D_f) of the soot aggregates was estimated to D_f = (1.99±0.1) from the experimental data which agrees with the value D_f = (1.90±0.1) determined by comparison of the aerosol dynamic model with the measured particle mass concentration, size, and number evolution within the experimental error. The particle mass concentrations determined by the APM show average deviations of less than 3% with the BC concentrations measured by the SP2 instrument for particle sizes of 200 nm and larger. For particle sizes between 140-90 nm these deviations increase to 20-35%.

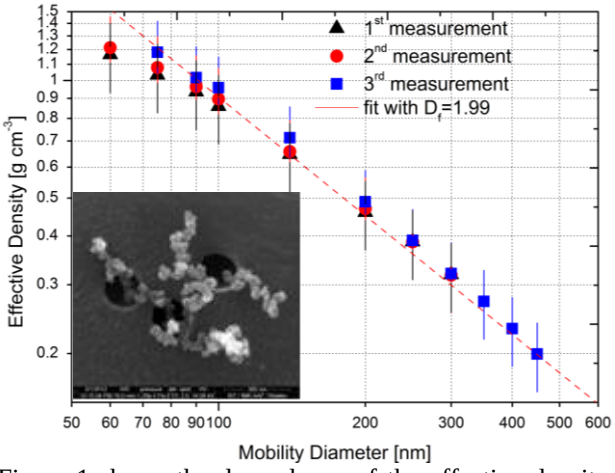

Figure 1 shows the dependence of the effective density of propane burner (CAST) soot on the particle mobility diameter for three subsequent measurements over a time period of 8 hours in a dynamically evolving soot aerosol. A typical soot aggregate is shown as an ESEM micrograph.

This paper discusses the characteristic properties of propane burner soot with organic carbon fractions between 4 and 60 % and compares the results of the APM-DMA analysis with the results of the SP2 measurements and the model calculations.

Jacobson, M. Z. (2001) *Nature* **409**, 695-697.
Laborde et al., (2012) Atmos. Meas. Tech. **5**, 3077-3097.
Laden, F., Neas, L.M., Dockery, D.W., Schwartz, J. (2000) *Environ. Health Perspect*. **108**, 941-947.
Naumann, K.-H. (2003) *J. Aerosol Sci.* **34**, 1371-1397.
Wentzel, M., Gorzawski, H., Naumann, K.-H., Saathoff, H., Weinbruch, S. (2003) *J. Aerosol Sci.* **34**, 1347-1370.
Zhang, R., Khalizov, A.F., Pagels, J., Zhang, D., Xue, H., and McMurry, P.H. (2008) *Proc. Natl. Acad. Sci. USA* **105**, 10291–10296.

Characterization of indoor and outdoor aerosol during extreme pollution events from winter heating in single-family home districts

I. Stasiulaitienė[1], E. Krugly[1], L. Kliučininkas[1], T. Prasauskas[1], M. Tichonovas[1], A. Garbaras[2] and D. Martuzevičius[1]

[1]Department of Environmental Engineering, Kaunas University of Technology, Kaunas, Lithuania
[2]State scientific research institute Center for Physical Sciences and Technology, Institute of Physics, Vilnius, Lithuania
Keywords: PM, PSD, Indoor/Outdoor, combustion, PAH.
Presenting author email: inga.stasiulaitiene@ktu.lt

Introduction

Heating systems based on solid fuel are the most popular in single family home districts of Nordic countries. Wood-based biomass is mostly used fuel. At the same time in countries of lower income, other types of fuels such as coal, or even uncontrolled fuels such as calorific fraction of household waste are being incinerated. Combustion of the above mentioned fuels in small scale devices result in broad spectra of pollutants emitted, including particulate matter, VOCs, PAHs and other products of incomplete combustion. High density of this type point sources cause extreme concentrations of pollutants in ambient air, especially in the events of unfavorable meteorological conditions. Indoor air is also affected to a higher extent, although there is little data on I/O levels of aerosol concentration during such events.

The aim of this research was to characterize aerosol particles during peak pollution events in residential area of single family houses.

Methods

Concentration of outdoor and indoor air aerosol particles was measured in residential area of Kaunas city, Lithuania. Measurements were performed in January, 2013. The sampling site was located in the centre of city, which in turn is situated in the river valley. Entire district was occupied with private houses (years built 1950-1970) that have individual heating systems based centralized natural gas, biomass or fossil fuel burning.

Measurements of outdoor aerosol PSD were performed using ELPI+ (Dekati Ltd., Finland). Gravimetric $PM_{2.5}$ mass concentration was determined by PEM 10 lpm (MSP Corp., USA) samplers and $PM_{2.5}$ 16.7 lpm cyclones (BGI Inc., USA) on 25 and 37 mm Tissuquartz filters (Pall, USA), respectively. Subsequently, these filters were analyzed for stable carbon isotopes and anhydrous sugars. TSP (25 mm GF/A filters) samplers and XAD-2 (SKC Inc., USA) sorbent tubes were used for particulate and vapour phase PAH sampling. Measurement devices were placed on the second floor balcony, at 6 meters height.

Indoor samplers were placed in the second floor uninhabited room. Pumps of samplers were placed separately in another room. Measurement of indoor aerosol PSD was performed by MOUDI 110 30 lpm (MSP Corp. USA). Particles were collected on raw aluminum foil. Real time particle distribution and trend was obtained with OPC Handheld 3016IAQ (Lighthouse Inc., USA). Similar PM sampling techniques were used for indoor PM sampling for subsequent analyses of stable carbon isotopes, anhydrous sugars as well as gaseous and particle-bound PAHs.

Ambient temperature, relative humidity, CO and CO_2 concentrations were measured by IAQ-Calc meters (TSI Inc, USA). Average temperature during sampling period: outdoors -12 °C, indoors - +16 °C.

Results

During the sampling campaign, several extreme pollution events were registered, with PM2,5 concentrations reaching above 200 μm/m^3. Out of these periods, size distribution data of one hour was extracted to plot PSD presented in Figure 1. It represents evening pollution episode at 10 pm, when the emissions were the strongest. Based on number concentration, particle size distribution was bimodal with modes at 0.0165 μm ($121 \cdot 10^4$, #/cm^3) and 0.154 μm ($6.51 \cdot 10^4$, #/cm^3). The measured PSD is very similar to reported in literature in urban areas highly influenced by biomass combustion emissions. At the same time, the nucleation mode was present, indicating freshly-emitted combustion aerosol. According volume concentration particle size distribution was unimodal with mode at 0.944 μm (2580 μm^3/ cm^3), with an increase in nano particle range.

Substantial relationship between outdoor and indoor particle concentrations was observed, showing significant contribution of combustion particles to indoor air. Tracer chemical analyses revealed that a possible mix of fuels contributing to aerosol concentrations, possibly including biomass, coal, calorific fraction of waste.

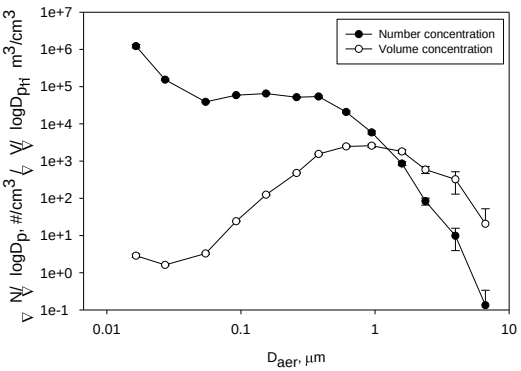

Figure 1. PSD of outdoor air aerosol during peak pollution event.

This work was supported by Research Council of Lithuania under grant "Pollution Control in Biomass Combustion: from Pollutant Formation to Human Exposure (BioMassPoll), project No. ATE05/2012.

Verifying modified EAD (MEAD) used in measuring metal fume nanoparticle and charactering its exposure concentration during gas metal arc and flux cored arc welding processes

P.J. Tsai[1,2], Y.F. Wang[1]

[1] Department of Occupational Safety and Health, College of Public Health, China Medical University and Hospital, 91, Hsueh-Shih Road, Taichung 40402, Taiwan
[2] Department of Environmental and Occupational Health, Medical College, National Cheng Kung University, 138, Sheng-Li Rd., Tainan 70428, Taiwan
Keywords: MEAD, nanoparticle, welding, metal fume.
Presenting author email: pjtsai100@cmu.edu.tw

The whole study was conducted to verify the suitability of MEAD on measuring metal fumes with high dielectric constant properties and characterize metal fume nanoparticle exposure by using the MEAD during gas metal arc and flux cored arc welding processes.
Results show that the concentrations estimated for the TB and A region, the results obtained from the NSAM for the testing welding processes quite comparable to those corresponding values obtained from MEAD (Figure 1). Considering both NSAM and MEAD sharing the same measuring principles, comparable results obtained from both instruments could be theoretically expectable. After normalization, no significant difference can be found between the results obtained from SMPS and MEAD (Figure 2). It is concluded that the obtained MEAD results are suitable for assessing metal fume nanoparticle exposures. Table 1 shows the size distributions of fume nanoparticles obtained from welding processes within current intensity 120A measured by the MEAD. From the tested welding operation conditions, a uni-modal was found for fume nanoparticles emitted from the selected welding processes. The CMD increase with the current intensity, it could be mainly explained by the higher arc temperature. By comparing the results shown in Table 2 and Table 3, significant differences can be found in the fractions of nanoparticles deposited on each of the three regions while different exposure metrics were adopted. Our results clearly indicate the importance for simultaneously predicting both the surface area and number concentrations of nanoparticles deposited on different regions of the respiratory tract for fume nanoparticle exposure assessments.

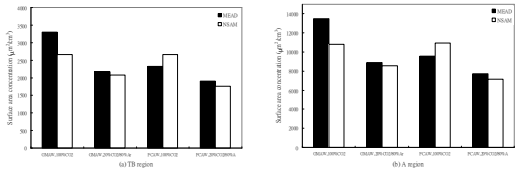

Figure 1. Confirmations of nanoparticles deposited on (a) TB region and (b) A region for data derived from MEAD and NSAM measured results.

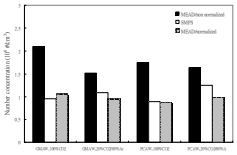

Figure 2. Comparing number concentrations obtained from SMPS with that from MEAD (a) non-normalized (b) after being normalized.

Table 1. Size distributions of fume nanoparticles (1－1000 nm) obtained from the testing welding processes were measured by MEAD.

welding condition		Number-based size distribution (nm)	
welding type/electrode	shield gas	CMD (rang)	σ_g
GMAW/KM 56	100%CO_2	124 (100 - 158)	1.70
	20%CO_2/80%Ar	117 (110 - 124)	1.81
FCAW/KFX 71T	100%CO_2	127 (116 - 133)	1.82
	20%CO_2/80%Ar	116 (110 - 120)	1.81

Table 2. Estimated number concentrations (10^6 #/cm^3) of fume nanoparticles deposited in the H, TB, and A regions of the respiratory tract for data obtained from the testing welding process.

welding condition		total deposited	H	TB	A
welding type/electrode	shield gas	concentration	Fraction(%)	Fraction(%)	Fraction(%)
GMAW/KM 56	100%CO_2	2.07±0.458	19	16	65
	20%CO_2/80%Ar	1.51±0.095	19	16	65
FCAW/KFX 71T	100%CO_2	1.69±0.207	18	17	65
	20%CO_2/80%Ar	1.61±0.155	17	17	66

Table 3. Estimated surface area concentrations (10^4 $\mu m^2/cm^3$) of fume nanoparticles deposited in the H, TB, and A regions of the respiratory tract for data from the testing welding process.

welding condition		total deposited	H	TB	A
welding type/electrode	shield gas	concentration	Fraction(%)	Fraction(%)	Fraction(%)
GMAW/KM 56	100%CO_2	2.42±0.810	29	14	57
	20%CO_2/80%Ar	1.62±0.132	32	13	55
FCAW/KFX 71T	100%CO_2	1.74±0.270	32	13	55
	20%CO_2/80%Ar	1.35±0.132	29	14	57

Wang, Y.F., Tsai, P.J., Chen, C.W., Chen, D.R., Hsu, D.J. (2010) Using a modified electrical aerosol detector (MEAD) to predict nanoparticle exposures to different regions of the respiratory tract for workers in a carbon black manufacturing industry. Environ. Sci. Tech. 44, 6767–6774.

Wang, Y.F., Tsai, P.J., Chen, C.W., Dai, Y.T. (2011) Size distributions and exposure concentrations of nanoparticles associated with the emissions of oil mists from fastener manufacturing processes. Journal of Hazardous Materials. 198, 182–187.

Particle size distributions of PAHs in workplace atmospheres and their exposure concentrations to workers in a steal and iron manufacturing factory

Y.F. Wang[1], P.J. Tsai[1,2]

[1] Department of Occupational Safety and Health, College of Public Health, China Medical University and Hospital, 91, Hsueh-Shih Road, Taichung 40402, Taiwan
[2] Department of Environmental and Occupational Health, Medical College, National Cheng Kung University, 138, Sheng-Li Rd., Tainan 70428, Taiwan
Keywords: steal and iron manufacturing, PAHs, particle size distribution.
Presenting author email: sakuray66@gmail.com

The objective of this study was set out to characterize size distributions of polycyclic aromatic hydrocarbons (PAHs) in three workplace atmospheres of the electric arc furnace, ladle and metalluray in a steal and iron manufacturing factory and to assess their exposures to workers when they are on maintenance and on activity, respectively. Particle size segregating samplings were conducted on the workplace atmospheres of the three selected industrial processes by using the modified Marple 8-stage cascade impactor (*m*-Marple).

We found that mass median aerodynamic diameter (MMAD) of the fine mode and coarse mode fell to the range 0.222–1.57 μm and 16.1–22.7 μm on maintenance, respectively (Table 1). The MMAD of the fine mode and coarse mode fell to the range 0.373–2.35 μm and 26.1–31.3 μm on activity, respectively (Table 2).

Personal inhalable PAHs samplings on maintenance were conducted on workers in the three selected working area revealed their exposure levels as: ladle workers (6918 ng/m^3) > metalluray workers (5818 ng/m^3) > electric arc furnace workers (3361 ng/m^3). On activity, their exposure levels were the same trend as: ladle workers (8294 ng/m^3) > metalluray workers (6700 ng/m^3) > electric arc furnace workers (5369 ng/m^3) (Table 3). Our results clearly suggest that appropriate control measures should be taken by the steal and iron manufacturing factory, particularly for the abatement of PAHs exposure concentrations of the inhalable fraction.

The fractions of inhaled particles deposited to different regions of the respiratory tracts found that the alveolar region was consistently higher than both head and tracheobronchial regions in all three studied exposure working area (Table 4). The above results clearly indicated that most PAHs generated from the steal and iron manufacturing process might be able to reach the deep lung (i.e., the alveolar region).

Table 1 Particle size distributions of the selected sampling areas on maintenance in steal and iron manufacturing workplaces.

area	stastics	Fine mode			Coarse mode		
		Mean	Min	Max	Mean	Min	Max
Electric arc furnace	MMAD	1.04	0.904	1.08	20.6	17.8	26.0
	GSD	1.58	1.20	3.50	2.55	2.27	3.50
	Fraction (%)	7.21	6.28	12.3	92.8	87.7	93.7
Ladle	MMAD	1.57	0.197	2.82	22.7	15.8	35.8
	GSD	3.08	1.61	3.50	3.02	1.70	3.16
	Fraction (%)	5.70	2.76	7.08	94.3	92.9	97.2
Metalluray	MMAD	0.222	0.198	0.514	16.1	10.3	24.6
	GSD	2.80	2.60	3.50	2.26	1.98	3.50
	Fraction (%)	23.9	11.4	26.3	76.1	73.7	88.6

Table 2 Particle size distributions of the selected sampling areas on activity in steal and iron manufacturing workplaces.

area	stastics	Fine mode			Coarse mode		
		Mean	Min	Max	Mean	Min	Max
Electric arc furnace	MMAD	2.35	0.700	3.12	31.3	26.3	35.2
	GSD	2.57	1.36	3.25	3.44	2.65	3.50
	Fraction (%)	10.2	2.00	15.8	89.8	84.2	98.0
Ladle	MMAD	0.575	0.152	0.829	26.1	23.6	32.7
	GSD	1.51	1.20	2.95	2.56	2.14	3.17
	Fraction (%)	1.60	0.432	2.22	98.4	97.8	99.6
Metalluray	MMAD	0.373	0.100	0.537	27.6	21.3	30.5
	GSD	1.91	1.20	3.50	2.85	2.47	3.50
	Fraction (%)	12.5	8.01	17.2	87.5	0.778	92.0

Table 3 Estimated the concentrations and fraction of PAHs exposed to different regions of the respiratory tract for workers of the selected working areas.

Area	work situation	Conc (ng/m^3)	Inh/total (%)	Thorac/total (%)	Resp/total (%)
Electric arc furnace	maintenance	3,361	84.0	65.4	48.5
	activity	5,369	86.4	71.3	57.8
Ladle	maintenance	6,918	83.5	64.9	49.4
	activity	8,294	81.4	60.8	42.0
Metalluray	maintenance	5,818	79.4	60.1	50.1
	activity	6,700	77.9	52.2	32.3

Table 4 The fraction of PAHs deposited in different respiratory tract on maintenance and activity for workers of the selected working areas.

Area	work situation	Head (%)	TB* (%)	AL** (%)
Electric arc furnace	maintenance	22.1	20.1	57.8
	activity	17.5	15.6	66.9
Ladle	maintenance	22.3	18.5	59.2
	activity	25.3	23.1	51.6
Metalluray	maintenance	24.3	12.6	63.0
	activity	32.9	25.6	41.4

* TB：Trachea bronchial；** AL：Alveolar

Tsai, P.J., Shieh, H.Y., Lee, W.J., Lai, S.O. (2002) Characterization of PAHs in the atmosphere of carbon black manufacturing workplaces. Journal of Hazardous Materials. A91, 25–42.

Chen, M.R., Tsai, P.J., Chang, C.C., Shih, T.S., Lee, W.J., Liao, P.C. (2007) Particle size distributions of oil mists in workplace atmospheres and their exposure concentrations to workers in a fastener manufacturing industry. Journal of Hazardous Materials. 146, 393–398.

Comprehensive analysis of anthropogenic aerosol using automated classification for GCxGC-TOF analysis

B. A. Weggler[1,2], J. Orasche[1,2], T. Gröger[1,2], R. Zimmermann [1,2]

[1]Joint Mass Spectrometry Centre, Rostock University(Analyt. Chem.) & Helmholtz Zentrum München (HMGU/CMA), Germany (D)

[2]HICE - Helmholtz Virtual Institute of Complex Molecular Systems ind Environmental Health - Aerosol and Health, www.hice-vi.eu

Keywords: comprehensive, automated classification,

Presenting author email: benedikt.weggler@helmholtz-muenchen.de

The Virtual Helmholtz Institute (HICE) addresses the health effects of anthropogenic combustion processes. This is performed by means of a joint comprehensive characterization of the chemical and physical properties of the investigated combustion aerosol as well as the biological effects on cell cultures with high-end innovative methods. With targeted analyses based on chromatography and mass spectrometry a wide range of important analytes could be quantified. (Lintelmann, 2010; Orasche, 2011) However, the complexity of combustion aerosols exceeds the capacities of such targeted methods and instrumentation by far. Comprehensive two dimensional gas Chromatography is a very promising tool to extend the number of accessible analytes even further.

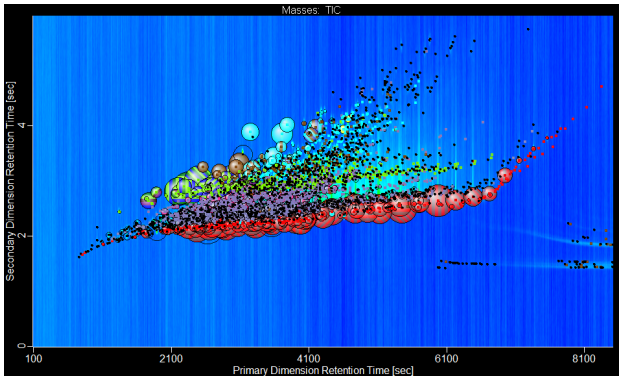

Figure 1: Bubble plot of an urban aerosol sample obtained after using the developed scripting. The different colors indicate several substance classes.

Comprehensive two-dimensional gas chromatography time-of-flight mass spectrometry: Automated Classification and Non-targeted automated comparison of semi-volatile organic compounds

Multidimensional Gas-Chromatography is well suited for the comprehensive characterization of complex sample compositions. However, the huge amount of data reveals also some drawback of the technique. This is the difficult and troublesome evaluation of the obtained data. Not at least because of this disadvantage the multidimensional gas-chromatography is little used in the field of aerosol science (Welthagen, 2003).

Nevertheless, aerosols represent complex mixtures of substances and therefore GCxGCc should be most suited for analyzing. The first approach focuses on a semi-quantitative comparison of substance classes. Current attempts for an automated classification of substance classes are being made in order to simplify the data evaluation. Most commercial available data processing software, e.g. from LECO, had embedded features to use customized algorithms for classification (Vogt, 2007; Welthagen, 2005). These classification algorithms are based on knowledge based rules. Within the scope of the HICE project advanced scripting rules for the comprehensive analysis of semi volatile organic compounds were developed and applied to compare the chemical composition of particulate matter from different combustion sources.

The enhanced separation power of GCxGC combined with state-of-the-art deconvolution technologie offers also the opportunity to align and compare thousands of jet not identifies peaks semi-quantitatively on a molecular level.

References

Lintelmann (2010) *A liquid chromatography-athmospheric pressure photoionization tandem mass spectrometric method for the determination of azaarenes in athmospheric particulate matter*, J. Chromatogr. A 2010

Orasche (2011) *In situ derivatization thermal desorption GC-TOFMS for direct analysis of particel-bound non polar and polar organic species*. Atmos. CHem. Phys 2011

Welthagen (2003) *Search criteria and rules for comprehensive two-dimensional gas chromatography-time-of-flight mass spectrometry analysis of airborne particulate matter*, J. Chromatogr. 2003

Vogt (2007) *Automated compound classification for ambient aerosol sample separation using comprehensive two-dimensional gas cromatography time-of-flight mass spectrometry*, J. Chromatogr. 2007

Welthagen (2005) *Application of direct thermal desorption gas chromatography and comprehensive two-dimensional gas chromatography coupled to time of flight mass spectrometry for analysis of organic compounds in ambient aerosol particles*, J. of Sep. Sci. 2005

Physical and chemical characterisation of PM emissions from in-operation ship engines

Moldanová, J.[1], Fridell, E.[1], Winnes, H., Boman, J.[2], Tishkova, V.[3], Demirdjian, B.[4], Joulie, S.[3], Bladt, H.[5], Ivaleva, N., P.[5]

[1] IVL, Swedish Environmental Research Institute, Box 53021, 400 14 Gothenburg, Sweden
[2] Department of chemistry and molecular biology, Atmospheric science, University of Gothenburg, SE-412 96, Gothenburg, Sweden
[3] CEMES/CNRS, 29 rue Jeanne Marvig BP 94347, 31055, Toulouse Cedex 4, France
[4] Aix-Marseille Univ., CNRS, CINaM UMR 7325, 13288, Marseille, France
[5] Chair for Analytical Chemistry, Institute of Hydrochemistry, Technische Universität München, 813 77 Munich, Germany

Keywords: Ship emissions, PM, PM composition, emission measurements.

Emissions of particulate matter (PM) from shipping contribute significantly to the anthropogenic burden of PM. The environmental effects of PM from shipping include negative impact on human health through increased concentrations of particles in many coastal areas and harbour cities and the climate impact. The chemical composition and physical properties of PM vary with type of fuel burned, type of engine and engine operation mode.

In this paper a number of parameters describing emission factors (EFs) of particulate matter from ship engines were investigated during 2 on-board measurement campaigns for 3 different engines and 3 different types of fuels. The measured EFs for PM mass were in the range 0.3 to 2.7 g/kg-fuel with lowest values for emissions from combustion of marine gas oil (MGO) and the highest for heavy fuel oil (HFO). The emission factors for particle numbers EF(PN) in the range 5x1015 - 1 x1017 #/kg-fuel were found, the number concentration was dominated by particles in the ultrafine mode and c.a. 2/3 of particles were non-volatile. The PM mass was dominated by particles in accumulation mode.

Main metal elements in case of HFO exhaust PM were V, Ni, Fe, Ca and Zn, in case of MGO Ca, Zn and P. V and Ni were typical tracers of HFO while Ca, Zn and P are tracers of the lubricant oil. EC makes up 10-38% of the PM mass, there were not found large differences between HFO and MGO fuels. EC and ash elements make up 23-40% of the PM mass. Organic matter makes-up 25-60% of the PM. The measured EF(OC) were 0.59 ± 0.15 g/kg-fuel for HFO and 0.22 ± 0.01 g/kg-fuel for MGO. The measured EF(SO42-) were low, c.a. 100-200 mg/kg-fuel for HFO with 1% FSC, 70-85 mg/kg-fuel for HFO with 0.5% FSC and 3-6 mg/kg-fuel for MGO. This corresponds to 0.2-0.7% and 0.01-0.02% of fuel S converted to PM sulphate for HFO and MGO, respectively.

The (scanning) transmission electron microscopy (TEM and STEM) images of the collected PM have shown different types of particles. The maps of elements obtained from STEM showed heterogeneous composition of primary soot particles with respect to the trace metals and sulphur. Composition of the char-mineral particles indicates that species like CaSO4, CaO and/or CaCO3, SiO2 and/or Al2SiO5, V2O5 and Fe3O4 may be present; the last two were also confirmed by analyses of FTIR spectra of the PM samples. The Temperature Programmed Oxidation (TPO) of PM from the ship exhaust samples showed higher soot oxidation reactivity compared to automotive diesel soot, PM from the HFO exhaust is more reactive than PM from the MGO exhaust. This higher oxidation reactivity could be explained by high content of catalytically active contaminants; in particular in the HFO exhaust PM for which the ED XRF analyses showed high content of V, Ni and S.

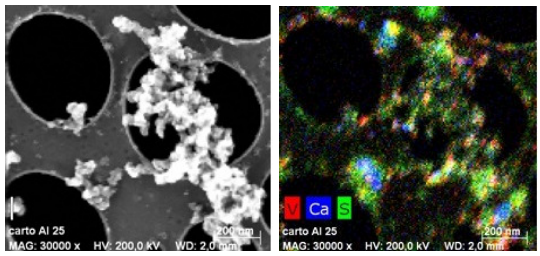

Figure 1. STEM image of an agglomerate of soot-type particles in ship exhaust (left) and their elemental composition map of V, Ca and S (right).

The data obtained during the experiments add information on emission factors for both gaseous and PM-bound compounds from ship engines using different fuels and under different engine load conditions. Observed variability of the EFs illustrates uncertainties of these emission factors as a result of measurement uncertainties, influences from trace components of fuels and lubricants and from differences between individual engines.

This work was a part of EU FP7 project TRANSPHORM (no: 243406). IVL foundation, Stenaline and Deutsche Forschungsgemeinschaft (DFG) are gratefully acknowledged for additional financial support.

Exposure to airborne (1→3)-β-D-glucans during metalworking processes

M. Cyprowski, A. Lawniczek-Walczyk and R.L. Górny

Department of Chemical, Aerosol, and Biological Hazards, Central Institute for Labour Protection – National Research Institute, Warsaw, 00-701, Poland
Keywords: (1→3)-β-D-glucans, occupational exposure, metalworking processes, size distribution
Presenting author email: macyp@ciop.pl

During different machining operations, the metalworking fluids (MWF) can be biodeteriorated by fungi. Their propagules can be released into the air with MWF droplets. Whereas the occurrence of fungal spores in such working environment is relatively well controlled, the presence of (1→3)-β-D-glucans and occupational exposure to these immunotoxic components of fungal cell wall have so far been slightly recognized (Cyprowski *et al*, 2011). The aim of this study was to assess an exposure to airborne (1→3)-β-D-glucans released into the air during metalworking processes.

All aerosol measurements were carried out at work sites (L1-4) as well as in indoor and outdoor backgrounds (to control an influence of internal, i.e. within factory, and external, i.e. atmospheric, sources of microbial emission, respectively). The MWF aerosol measurements were performed near 4 metal-processing machines (1 grinder, 3 lathes), in which water-based MWF was used. For determination of (1→3)-β-D-glucans, the air samples were collected using 8-stage cascade impactor with 0.4/0.7/1.1/2.1/3.3/4.7/5.8/9 µm cut sizes. During 30-minute sampling at a flow rate of 28.3 l/min, the particles of each size range were separated onto 81-mm glass-fiber filters with a pore size of 1.0 µm. The glucan analysis was performed using Glucatell® test. Additionally, the concentrations of airborne culturable fungi were carried out using 6-stage Andersen impactor. Bioaerosol samples were collected on glass Petri dishes filled with malt extract agar. The sampling time was 5 minutes at a flow rate of 28.3 l/min. All isolated species were taxonomically identified.

The concentrations of glucans and fungi at studied sampling points are presented in Table 1. The highest glucan levels were found at work site L1 (grinder) – 6.64 ng/m^3, and the lowest at L2 (center lathe) – 3.02 ng/m^3. The concentrations of airborne culturable fungi were low, reaching maximally 367 CFU/m^3 at work site L1.

Table 1. Concentrations of airborne (1→3)-β-D-glucans and fungi at metalworking factory.

Work site (machine) or background	(1→3)-β-D-glucans [ng/m^3]	Fungi [CFU/m^3]
L1 (grinder)	6.64	367
L2 (center lathe)	3.02	154
L3 (center lathe)	4.88	84
L4 (NC lathe)	4.02	98
Indoor background	7.74	21
Outdoor background	16.1	77

The qualitative analysis of airborne mycoflora showed a dominance of *Acremonium*, *Penicillium*, and *Aspergillus* genera. There were no significant correlations between the concentrations of glucans and fungi.

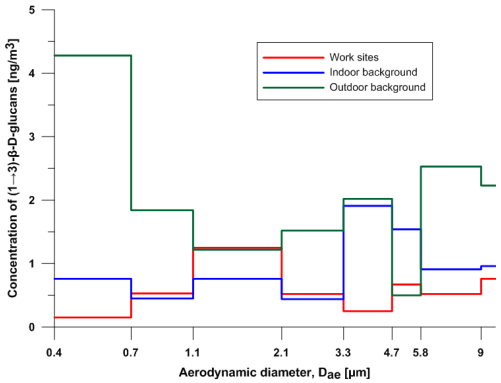

Figure 1. Size distribution of (1→3)-β-D-glucans in the air at metalworking factory.

The concentrations of (1→3)-β-D-glucans in MWF aerosol fractions showed large variability between the studied particulate size ranges as well as sampling sites (Kruskal-Wallis test: in both cases $p<0.05$) – see Figure 1. Based on the results it can be stated, that glucans are carried in the air mainly by MWF particles with aerodynamic diameter of 1.1-2.1 µm. The glucan concentrations are lower in this particle size range, if such MWF emission does not exist. In this case, the main glucan carriers are either small fragments (less than 0.7 µm in diameter), or single fungal spores or their aggregates (greater than 5.8 µm). Due to the half-life of airborne particles in 1.1-2.1 µm size range from a few to several hours, their mechanical elimination from the environment contaminated with MWF seems to be a simple and effective removal method. From the viewpoint of worker's exposure to airborne glucans, the use of personal protective masks with a suitable particle capture efficiency in this range should effectively reduce the risk of adverse health outcomes.

This work was funded by the Polish Ministry of Labour and Social Policy from the Multiannual Program "Improvement of safety and working conditions (2011–2013)" under grant no. III.B.01.

Cyprowski, M., Sowiak, M. and Szadkowska-Stanczyk, I. (2011). *Aerobiologia* **27**, 345-351.

Nanoparticle release from nanostructured powders during low- and high-energetic dry dispersing processes

D. Göhler and M. Stintz

Research Group Mechanical Process Engineering, Institute of Process Engineering and Environmental Technology, Technische Universität Dresden, 01062 Dresden, Germany
Keywords: nanoparticle release, exposure, nanostructured powders, powder dispersing.
Presenting author email: daniel.goehler@tu-dresden.de

Possible risk of substances to health, safety and environment depends on the coexistence of material toxicity and material exposure (NRC, 1983). The steadily increasing production, processing and use of nanomaterials necessitate thus an extended risk assessment taking into account the material's dispersing state. In this context, systematic dispersing studies on nanomaterials in laboratory can provide basic information about the ability and the quantity of nanoparticle release into the air (Kuhlbusch *et al.*, 2011).

Nanostructured powders (e.g. nano-pigments, powder flow agents) constitute the origin for the fabrication of many products and were thus the subject of several nanoparticle release studies (Kuhlbusch *et al.*, 2011). Performed laboratory investigations on nanostructured powders can roughly be classified according to the applied dispersing energy input into three treatment procedures: drop down procedures (e.g. Jensen *et al.*, 2009), fluidized bed methods (e.g. Maynard, 2002) and high energy dispersing (e.g. Stahlmecke *et al.*, 2009).

Up to now, no single method exists to characterize the particle release from nanostructured powders due to different treatment processes, i.e. every method simulates one typical handling procedure (e.g. refilling, emptying). Moreover, existing devices were mostly optimized for one kind of powder (e.g. fluidized bed methods for fibrous powders like carbon nanotubes). Current technical solutions have often the disadvantage of changing fundamental powder properties, like the mixing state or the bulk density. Improper combination with measurement instruments, as often observed in the literature, can lead to considerable artifacts in measured concentrations and particle size distributions.

To estimate the quantity range of (nano)-particle release into air from nanostructured powders (pigments, pyrogenic silica, titanium dioxide, zeolites) in accordance with ISO/TS 12025:2012, a low-energetic and a high-energetic dry dispersing procedure were used for aerosolization. The latter one based on the dispersing process within a rotating brush generator (Model RBG 1000, Palas GmbH, Germany) operated with dispersion cover A at a dispersing pressure of 3.5 bar (relative flow velocity of 100 $m \cdot s^{-1}$), a volumetric powder flow of 25.7 $mm^3 \cdot min^{-1}$ and a rotational steel brush frequency of 1210 min^{-1}. In the absence of suitable commercial aerosol generators that produce steady-state particle number concentrations and particle size distributions from various powders at weak dispersing energy input for SMPS-analyses, a dispersing device based on a linear-driven notch and a stainless steel capillary tube was developed (Göhler et al., 2010) and operated at volumetric powder flow rate of 30 $mm^3 \cdot min^{-1}$ and a relative flow velocity of 24.4 $m \cdot s^{-1}$.

For the purpose of cross-process comparability, the measured data were expressed as fractional numbers of released particles and related to the treated sample mass. Release data were determined not only for the nanoscale, but also for the submicrometre and micrometre size range, to characterize completely the simulated release scenarios. Results on the analyzed nanostructured powders showed, that the methodology is appropriate for (nano)-particle release analyses.

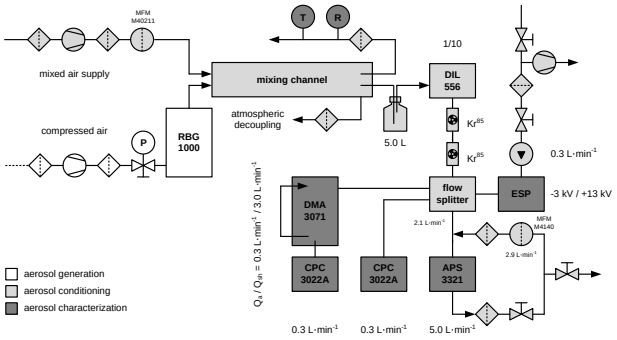

Figure 1: Schematic diagram of the operated experimental setup for high-energetic dry powder dispersion

The presentation will give detailed information on the experimental conditions, the performed evaluation of the measurement data and results of different nanostructured powders that were analyzed. Moreover, the presentation will discuss release data for further investigations on the (nano)-particle release into the air from powdered materials.

Göhler, D., Hillemann, L., Vorbau, M., Stintz, M. and Barthel, H. (2010) *Proc. 6th World Congress on Part. Technol.*

Jensen, K., Koponen, I., Clausen, P. and Schneider, T. (2009) *J. Nanopart. Res.* **11**(1), 133-146.

Kuhlbusch, T.A.J., Asbach, C., Fissan, H., Göhler, D. and Stintz, M. (2011) *Part. Fibre Toxicol.* **8**: 22.

NRC (1983) National Academic Press, Washington DC, 1983.

Maynard, A. (2002) *Ann. Occup. Hyg.* **46**(S1), 197-202.

Schneider, T. and Jensen, K. A. (2008) *Ann. Occup. Hyg.* **52**(1), 23-34.

Stahlmecke, B.; Wagener, S.; Asbach, C.; Kaminski, H.; Fissan, H. and Kuhlbusch, T. A. J. (2009) *J. Nanopart. Res.* **11**(7), 1625-1635.

Characterization of Carbon Nano-Particles from the Clad of Nuclear Fuel in HTGR with Inherent Safety(II) –Quantitative Analysis

G. Iwanaka[1], H. Nishida[1], H. Takano[1] and M. Itoh[1]

[1]Department of Chemical Engineering and Materials Science, Doshisha University
Kyo-Tanabe, Kyoto 610-0321 JAPAN
Keywords: nuclear aerosol, carbon mass balance, HTGR, inherent safety.
Presenting author email: dum0721@mail4.doshisha.ac.jp

The carbon nano-particles generated in the He coolant of High Temperature Gas Reactor will be radio-activated by the irradiation of neutrons in nuclear reactor core, and they will cause severe radioactive contamination in the case of LOCA even in HTGR with inherent safety. In the previous experiment (Nishida, et al., 2013), a qualitative analysis of the carbon nano-particles generated from IG-110 carbon pebble, the nuclear fuel clad, was reported concerning the R&D on a passive removal system in the primary cooling system of HTGR or PBMR.

In this report, more quantitative analysis of the carbon nano-particles was carried out associated with SEM analysis on the morphological change of surface of IC-110 carbon plate and carbon pebble before and after the heating to make clear the generation mechanism.

Setup of the experimental system was same to that of Nishida, et al. (2013). The morphological change of the carbon surface was observed with SEM. Decrease of mass of the carbons due to the *worn-down* caused by heating was measured with an electronic force balance. The surface change of the carbon pebble is shown in **Fig.1**. The pictures were taken without any tilt, and lower acceleration voltage (3kV) was applied to avoid giving extra damage on the surface.

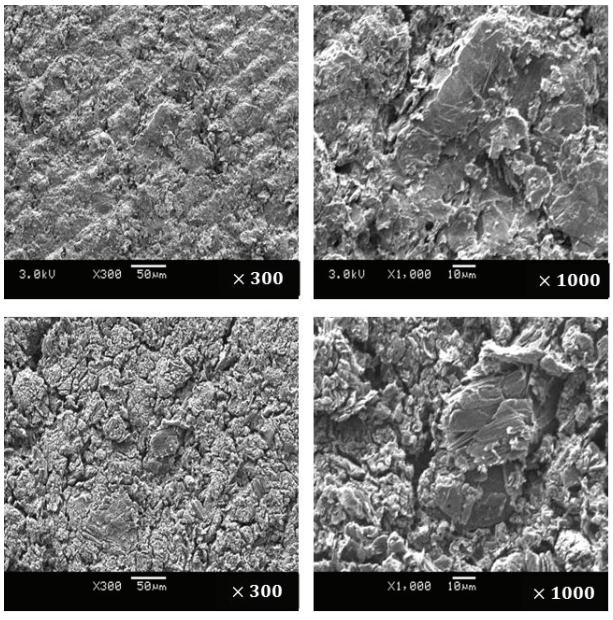

Fig.1 SEM pictures of carbon pebble (IG-110). Heating temperature was 1400K, and the pictures (upper two: before heating, lower two: after heating) were taken from the top view.

Figure 2 shows the same type of SEM picture for the carbon plate. In both cases, the roughness of the surface in lower magnification scale looked like to be smooth after heating. However, in higher one, clacking of the surface was observed clearly, especially in the plate. Sublimation of carbon will make the surface smooth, and the fragmentation or microscopic breaking due to heat shock will produce such type of clacking.

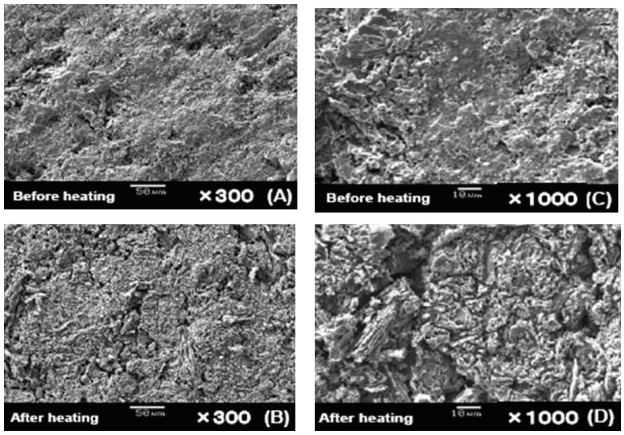

Fig.2 SEM pictures of carbon plate (IG-110). Conditions were same to Fig.1.

After 72 hours heating in the electric furnace at 1400K with continuous flowing of Ar gas, the average mass differences of carbon pebble and carbon plate by sublimation and/or fragmentation were 0.0383 g (4.11%) and 0.0089 g (5.1%), respectively. The mass of carbon vaporized from the carbon pebble set at continuous flow field of Ar gas was estimated theoretically to be 0.00797 g (less than 20% of the experimental value for mass reduction), and the difference between the experimental and the theoretical one will be the mass of generated fragments breaking from the pebble surface.

As shown in the qualitative analysis (Nishida, et al., 2013), the same conclusion was obtained that the major mechanism of carbon nano-particles generation in high temperature was not the homogeneous nucleation following the sublimation but the fragmentation caused by abrupt thermal shock. It provides us a clear design concept to R&D of the passive removal system in the primary cooling system of HTGR or PBMR, i.e., the main target diameter for reduction is about 10nm.

Nishida, H., Iwanaka, G., Takano, H. and Itoh, M. (2013) *Abstract of EAC2013 (This Abstract)*

Risk assessment of airborne engineered nanomaterials

A. J. Koivisto[1], A.-K. Viitanen[1], T. Hussein[2], T. Kanerva[1], T. Tuomi[1], H. Stockmann-Juvala[1], K. Hämeri[2]

[1]Nanosafety Research Centre, Finnish Institute of Occupational Health, Helsinki, Topeliuksenkatu 41 a A, FI-00250, Finland

[2]Department of Physics, University of Helsinki, Helsinki, PO Box 64, FI-00014, Finland

Keywords: nanomaterial, exposure, dose, risk.

Presenting author email: joonas.koivisto@ttl.fi

Introduction

Risk is defined as the probability that the exposure to a hazard will lead to adverse health effect. In work environment, indoor air may contain pollution from various sources which potential toxicities may differ significantly. Such exposure scenario may occur in production and use of engineered nanomaterials (ENMs). This is because ENMs have been shown to be potentially more toxic for human health than for example incidentally emitted background particles (BPs). Thus, in risk assessment, exposure should be examined separately for ENMs and BPs.

Methods

We measured ENM exposure concentrations and defined inhaled doses in three different workplaces: NP synthesis (Koivisto *et al.*, 2012a), packing of nanoscale titanium dioxide (Koivisto *et al.*, 2012b), and handling of nanodiamonds (to be published). Risk was estimated by using recommended occupational exposure limits (RELs) for nanomaterials and by using inhaled dose and extrapolated dose-biological response from mice to humans (Reagan-Shaw *et al.*, 2008).

Results

Figure 1 shows an example how a worker was exposed in TiO_2 ENM in packing process. During pouring processes, the TiO_2 concentration was 450 cm^{-3} and 1.5 mg m^{-3}. The calculated inhaled TiO_2 dose during 10 minute exposure was 36×10^6 particles with a mass dose of 310 μg. Calculated estimate showed that 89% of the TiO_2 particles were deposited in head-airways.

The RELs for TiO_2 ENM is either 40 000 cm^{-3} (IFA 2012) or 0.3 mg m^{-3} (NIOSH 2011) as time-weighted average concentrations for up to 10 h per day during a 40-h work week. Thus, here the RELs in mass concentration was exceeded only momentarily. Lindberg *et al* (2012) showed that TiO_2 particles do not cause genotoxic effects at retained dose of 84 μg in mice, which human equivalent dose would be 20 mg in human lungs. Thus, there should not be a risk for genotoxic effects in this case.

Discussion and conclusions

This study shows an example how to estimate the risk from measured exposure concentrations and doses respectively by using RELs or dose-biological responses.

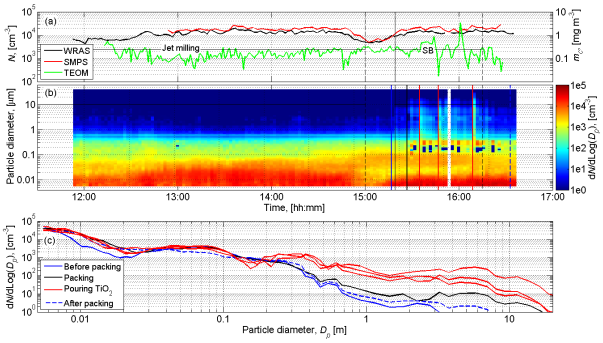

Figure 1: Particle concentrations during jet milling and packing of TiO_2: (a) shows the particle and mass concentration time series, (b) shows the particle size distribution time series, and (c) shows the selected particle size distributions which are plotted with the respective line color and style in (b).

This work was supported by the Graduate School in Environmental Health (SYTYKE).

Koivisto, A.J.,Aromaa, M., Mäkelä, J.M., Pasanen, P., Hussein, T. and Hämeri, K. (2012a). *ACS Nano* **6**, 1195–1203.

Koivisto, A.J., Lyyränen, J., Auvinen, A., Vanhala, E., Hämeri, K., Tuomi, T., Jokiniemi, J. (2012b). *Inhal. Toxicol.* **24**, 839–849.

Reagan-Shaw, S., Nihal, M., Ahmad, N. (2008). *FASEB J.* **22**, 659–661.

Lindberg, H.K., Falck, G.C.-M., Catalán, J., Koivisto, A.J., Suhonen, S., Järventaus, H., Rossi, E.M., Nykäsenoja, H., Peltonen, Y., Morenoc, C., Alenius, H., Tuomi, T., Savolainen, K.M., Norppa, H. (2012). *Mutat. Res.* **745**, 58–64.

IFA (2010). http://www.dguv.de/ifa/en/fac/nanopartikel/beurteilungsmassstaebe/index.jsp.

NIOSH (2011). NIOSH publication No. 2011–160.

Stability of nanoparticle agglomerates in flames
First results of investigations on the release during waste incineration

I.-M. Liesen[1], W. Baumann[1], M. Hauser[1], H. Mätzing[1], H.-R. Paur[1], H. Seifert[1]

[1]Institute for Technical Chemistry, Karlsruhe Institute of Technology, 76021 Karlsruhe, Germany
Keywords: aerosol, waste combustion, deagglomeration, SMPS, ELPI, ICP MS
Presenting author email: inge-maria.liesen@kit.edu

Background:

Currently, several nanostructured materials are applied widely in products sold to customers, but there is a lack of information about what happens to engineered nanoparticles during waste incineration.

The focus of the project is the thermal stability of engineered nanoparticle agglomerates in flames.

The objective of the fundamental investigation is to identify the influence of thermal energy to the stability of nanoparticle agglomerates. These findings are implemented in an experiment at a pilot scale incineration plant (BRENDA).

Material and methods:

Laboratory experiments:

A dispersion of engineered nanoparticles is atomized by a two-component jet using air. For flame investigations the aerosol is introduced into the fresh gas of a propane flame. The flame is a laminar premixed flame which is not insulated by a sheath air stream, so that oxygen has the possibility to diffuse into the flame. The aerosol size distribution is measured before and after flame ignition, far downstream of the flame front (T ≈200 °C).

In the experiments, different metal oxides (titanium dioxide, silica, cerium oxide and zinc oxide) are investigated.

Pilot plant experiments:

To test the behavior of engineered nanoparticles in waste incineration plants, a nanoparticle dispersion will be introduced into the pilot incineration plant BRENDA which consists of a combustion chamber with steam boiler and flue gas cleaning. Measurements will be realized for detecting the introduced nanoparticles in the afterburning chamber, behind the boiler and in the stack. The results will give information about the release of nanoparticles during the incineration process.

Measurement technique:

The size distribution is measured by scanning mobility particle sizer SMPS+C (Grimm, Austria) which uses the electrical mobility as equivalent diameter. Comparative measurements are done with an Electrical Low Pressure Impactor ELPI+ (DEKATI, Finland) using the aerodynamic equivalent diameter. The results in the laboratory are verified by Transmission Electron Microscopy (TEM). For detecting the introduced nanoparticles in the pilot plant the mass concentration is determined using the Dekati Low Pressure Impactor DLPI (DEKATI, Finland). Then the impactor stages are chemically analyzed by inductively coupled plasma mass spectrometry ICP MS recovering the introduced substance.

Results:

First results of the laboratory experiments show that the size distribution is influenced by the flame.

An example is given in figure 1, where a cerium dioxide aerosol at flame conditions and without flame is shown. The plotted particle size distribution is measured with SMPS+C (Grimm, Austria). At room temperature (without flame ignition), the measured modal diameter is about 60 nm at a total concentration of $2*10^5$ particles per cm³ and a size distribution width of log σ_g = 0,3. After flame ignition, the modal diameter decreased to 23 nm and the total concentration increased to $5*10^6$ particles per cm³ with a size distribution width of log σ_g = 0,2.

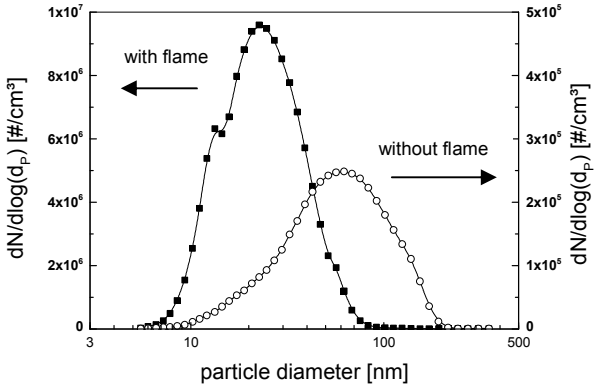

Figure 1: Comparison of the size distribution of a cerium oxide before and after flame ignition.

References:

Paur, H-R.; Baumann W.; Mätzing, H.; Seifert, H. (2005): *Formation of nanoparticles in flames; measurement by particle mass spectrometry and numerical simulation.* Nanotechnology 16 (7), S. 354.

Mätzing, H.; Baumann, W.; Bockhorn, H.; Paur, H-R.; Seifert, H. (2012): *Detection of electrically charged soot particles in laminar premixed flames.* Combustion and Flame 159 (3), S. 1082–1089.

Tuesday, September 3, 2013

Poster session B,
Reserve posters B223 – B237

Uptake of N_2O_5 to citric acid aerosol particles

G. Gržinić[1,2], T. Bartels-Rausch[1] A. Türler[2], and M. Ammann[1]

[1] Laboratory of Radiochemistry and Environmental Chemistry, Paul Scherrer Institute, Villigen, 5232, Switzerland
[2]Department of Chemistry and Biochemistry, University of Bern, Bern, Switzerland, 3012, Switzerland
Keywords: N_2O_5, ozone budget, nitrogen oxides, uptake coefficient.
Presenting author email: markus.ammann@psi.ch

Dinitrogen pentoxide is a significant reactive intermediate in the night time chemistry of nitrogen oxides, serving as a major NO_x sink by heterogeneous hydrolysis on aerosol surfaces. It can influence tropospheric ozone production and therefore the oxidative capacity of the atmosphere (Chang et al., 2011).

We used the short-lived radioactive tracer ^{13}N (Ammann, 2001) in conjunction with an aerosol flow tube reactor in order to study N_2O_5 uptake kinetics on aerosol particles. ^{13}NO was mixed with non labeled NO and O_3 in a first flow reactor, where N_2O_5 is synthesized under dry conditions. The N_2O_5 flow is then admitted into the aerosol flow reactor together with the aerosol flow containing deliquesced citric acid particles generated by ultrasonic nebulisation and conditioned to the relative humidity of interest. Movable inlets allow varying the length of the aerosol flow tube. Behind the reactor a Scanning Mobility Particle Sizer (SMPS) system is used to characterize the aerosol. The remaining gas exiting the reactor is passed through a parallel plate diffusion denuder system for selective separation of gaseous species and a particle filter to trap the particles. Activity of the ^{13}N labeled species can be monitored via scintillation counters placed on the denuder plates and the particle filter, respectively.

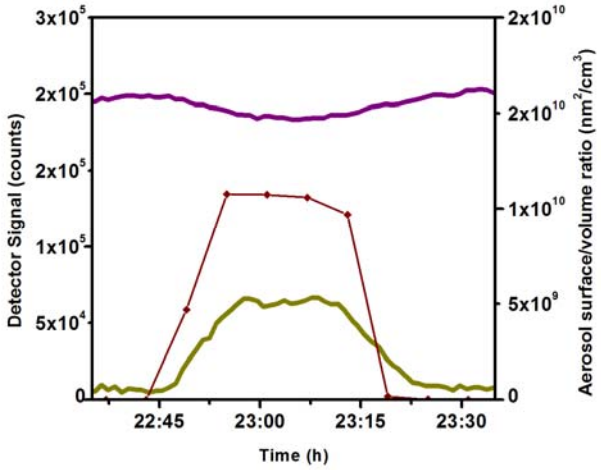

Figure 1. Gas phase N_2O_5 (solid magenta), particulate N (solid green, magnified by a factor of 10), and aerosol surface area (red) to volume ratio during an uptake experiment.

Fig. 1 shows data from a typical experiment with citric acid aerosol, where the loss of N_2O_5 from the gas phase is accompanied by an increase in particulate nitrate. Figure 2, shows a set of measurements conducted at a relative humidity of 62 %, at a fixed reaction time of around one minute, and at varying aerosol surface to volume ratio, along with a simple first-order fit (Vlasenko et al., 2006).

The preliminary results obtained have shown that the uptake coefficient increases with humidity from $1.65\pm0.3x10^{-3}$ (~27% RH) to $1.25\pm0.3x10^{-2}$ (45% RH) and $2.00\pm0.3x10^{-2}$ (61.5% RH). This is comparable to some polycarboxylic acids (like malonic acid), but higher than some others (Ammann et al., 2012). The increase is likely related to the increasing amount of water associated with citric acid at higher humidity that promotes hydrolysis of N_2O_5.

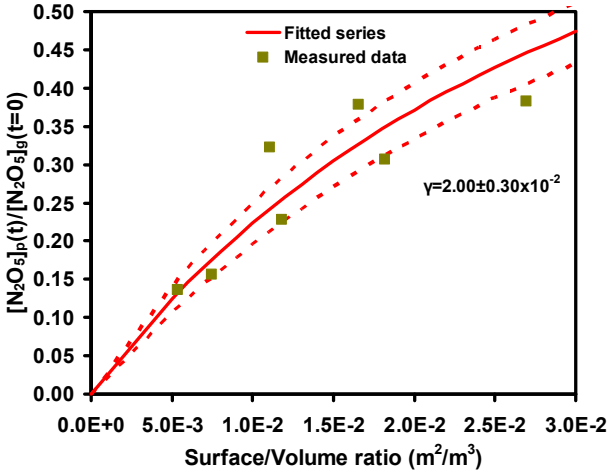

Figure 2. Data set collected using citric acid aerosol at 61.5% RH. Green squares represent measured data points while the red curve is a fit to the data according to the kinetic model, with the dotted curve showing the error range

This work is supported by the Swiss National Science Foundation (grant no. 130175).

Chang, W.L., Bhave, P.V., Brown, S.S., Riemer, N., Stutz, J., & Dabdub, D. (2011). *Aerosol Science and Technology,* **45**, 665-695.

Ammann, M. (2001). *Radiochim. Acta,* **89**, 831-838.

Vlasenko, A., Sjogren, S., Weingartner, E., Stemmler, K., Gäggeler, H.W., & Ammann, M. (2006). *Atmos. Chem. Phys.,* **6**, 2147-2160.

Ammann, M., Cox, R.A., Crowley, J.N., Jenkin, M.E., Mellouki, A., Rossi, M.J., Troe, J., & Wallington, T.J. (2012). *Atmos. Chem. Phys. Discuss.,* **12**, 32109-32472.

Pressure dependency of ozonolysis product formation of α-pinene focusing on low volatile compounds such as organic acids and dimeric compounds

M. Beck[1], C. Keunecke[2], T. Zeuch[2] and T. Hoffmann[1]

[1]Institut für Anorganische und Analytische Chemie, Johannes Gutenberg-Universität Mainz, Mainz, 55128, Germany
[2]Institut für Physikalische Chemie, Georg-August-Universität Göttingen, Göttingen, 37077, Germany

Keywords: SOA, ozone, monoterpene oxidation, organic acids.
Presenting author email: hoffmant@uni-mainz.de

Secondary organic aerosols (SOA) are important for air quality and the global climate. Therefore, a better understanding of formation mechanism, growth, sources and also quantity of SOA is necessary. Today many details concerning these aspects are unknown.

SOA is formed by volatile organic compounds (VOCs) oxidized by ozone, OH- and NO_3-radicals in the atmosphere. The products of these oxidations have different kinds of functional groups (e.g. acid- and aldehyde-groups). Thus the volatility of the compounds decreases and nucleation or condensation on existing particles occurs. As monoterpenes are an important part of VOCs, the atmospheric oxidation is of high interest in aerosol research. α-Pinene is a very common monoterpene and therefore an often used model substance for mechanistic studies (Müller *et al.* 2009).

Besides oxidation products with monomeric structure, such as pinic acid for example, dimers were found in SOA. The formation of these is discussed intensively. Various reactions in the gas- and/or particle phase are possible. The dimers of α-pinene are of high interest due to the quantity of this terpene in the atmosphere. A lot of research hereby is focused on the compounds with the molecular mass 358 and 368. For the former very different formation pathways and chemical structures are suggested in the literature. These two dimers are of special interest because they were also observed in environmental samples. Therefore the possibility of using them as marker substances for various atmospheric conditions is discussed. A much higher number of dimeric compounds can be detected in atmospheric simulation chambers. This is due to the higher concentration of monoterpene and ozone used especially in mechanistic studies (Kundu *et al.* 2012).

Ozonolysis of α-pinene in the reaction chamber at the University of Göttingen, which can be operated at reduced pressures, is used to get more information about the formation process. This spheric reaction cell has a volume of 64 L with ozone and alkene premixing chambers, which allow well-controlled reactant mixing within two seconds. A FTIR- spectrometer for gas phase species analysis and a SMPS system for measuring particle size distributions and mass are attached to the chamber (Wolf *et al.* 2011). The aerosol particles were sampled on filters after the reaction in the chamber was finished (typically after five minutes) and the chamber was filled to ambient pressure. A methanol-water-solution was used for extraction of the filters. RP-HPLC-ESI-IT/MS^n was used for analysis.

Experiments were performed at three different reaction pressures (10, 20 and 460 mbar) with almost identically concentrations of ozone (5 ppm at 1 bar) and excess α-pinene. In general lower pressure yields lower particle number concentrations and smaller aerosol masses.

Therefore, the samples of the high pressure experiments at 460 mbar were used to identify the ozonolysis products. The often reported monomeric products such as terpenylic acid, pinic acid and hydroxypinonic acid were detected. About twenty dimeric compounds with a mass-to-charge ratio (m/z) between 300 and 400 were observed including the above mentioned dimers 358 and 368. For most of these dimers no confirmed or even suggested chemical structures are available in the literature. The MS/MS-experiments showed for the majority of the dimers a fragment with m/z 185 like pinic acid. Therefore, it is assumed that most of these compounds contain a pinic acid analogue or a closely related chemical structure.

The analysis of the filter samples confirmed a decreasing yield with decreasing reaction pressure for most of the compounds. Due to the lack of authentic standards for almost all substances only a semi-quantitative analysis was performed by comparison of the peak area. A roughly classification in six groups was performed (as shown in table 1).

The strong influence of pressure on the relative yields of SOA components seems to be related to the presence and absence of stabilized Criegee intermediates and different degrees of chemical activation of other intermediate species at high and low pressures. After further analysis the results are expected to provide constraints for suggested dimer formation mechanisms.

Table 1. Classification of pressure dependency. 100% represents the product yield at 460 mbar.

Group	1	2a	2	2b	3	4
10 mbar	< 1%	< 1%	1-3%	3-10%	3-25%	>50%
20 mbar	< 5%	5-20%	5-20%	5-20%	20-50%	>50%

L. Müller, M.C. Reinnig, H. Hayen, T. Hoffmann, *Rapid Commun. Mass Spectrom.*, **23** (2009) 971
S. Kundu, R. Fisseha, A.L. Putman, T. A. Rahn, and L. R. Mazzoleni, Atmos. Chem. Phys., **12** (2012) 5523
J. L. Wolf, S. Richters, J. Pecher, and T. Zeuch, *Phys. Chem. Chem. Phys.*, **13** (2011) 10952.

Dry deposition of electrosprayed liquid suspensions

S. Martin. B. Martinez-Vazquez, P.L. Garcia-Ybarra and J.L. Castillo

Dept. Fisica Matematica y de Fluidos, Facultad de Ciencias, UNED, 28040 Madrid, Spain
Keywords: Electrospray, Aerosol deposition; aerosol-based nanotechnology, polymeric fuel cell, catalytic layers
Presenting author email: jcastillo@ccia.uned.es

Granular materials formed by accumulation and adhesion of incoming aerosol particles acquire a morphological structure controlled by the form of the constitutive particles and by the way that these particles arrive and attach to the forming material (Garcia-Ybarra *et al*, 2012, Castillo *et al*, 2013).

Monte Carlo simulations of aerosol deposits (Rodriguez-Perez *et al*, 2005 and 2007) have shown the trends for controlling the deposit structure and indicated some ways to prepare granular materials from nanopowders with tailored morphology depending on their final use. A step forward in nanomaterial research consists in the performance of experimental studies that could confirm these theoretical predictions. Thus, an experimental set-up has been implemented to generate nanoparticles in a gas that are later on driven towards a collecting surface (Martin *et al*, 2012). In this study, a standard catalyst ink commonly used for preparing electrodes valuable for proton exchange membrane fuel cells (PEMFC) has been used (Martin *et al*, 2013).

The electrospray technique is used to generate nearly monodispersed sprays of small electrically charged droplets from this liquid suspension. In the electrospray cone-jet configuration (Martin *et al*, 2012) the jet breaks up forming a cloud of tiny droplets with a narrow distribution of droplet sizes. These charged droplets evaporate along their flight in the gas leaving dry charged nanoparticles which are driven by the electric field towards the collecting surface. The arriving nanoparticles accumulate on the collector plate forming a structured granular deposit.

The efficiency in the capture of the electrosprayed particles may be substantially improved if an opposite voltage, respect to the needle, is applied to the collector substrate. In this double polarization scheme, the electrospray cone-jet domain may be substantially enlarged by a proper selection of the voltage at the collecting plate and a noticeable increase in the flow rate range for electrospraying in the cone-jet mode can be achieved (Martin *et al*, 2011). Therefore, the double polarization can be used to control the electric field at the needle tip (which indeed is the key factor for achieving a stable cone-jet electrospray) as well as the electric field at the collecting plate.

In the case of low conductivity suspensions electrosprayed at moderate flow rates (♦ points in Fig.1) the deposit is formed by fractal-like structures composed by clusters (of a few catalyst particles each) arranged in a dendritic way. The dendritic arrangement of the catalyst clusters results in a highly porous deposit with an enhanced permeability and increased active surface. One may expect that all these morphological properties of the granular material may lead to high catalyst utilization when used as a catalyst layer. For larger flow rates (◊ points in Fig. 1) the deposit is formed by patched clusters of thousands of single particles. Moreover, compact deposits appear when the flow rate is large enough (□ and △ points in Fig.1). These compact deposits result from an incomplete evaporation of the droplets during their flight toward the substrate. The deposit is formed from wet suspensions with the ethanol evaporating later on.

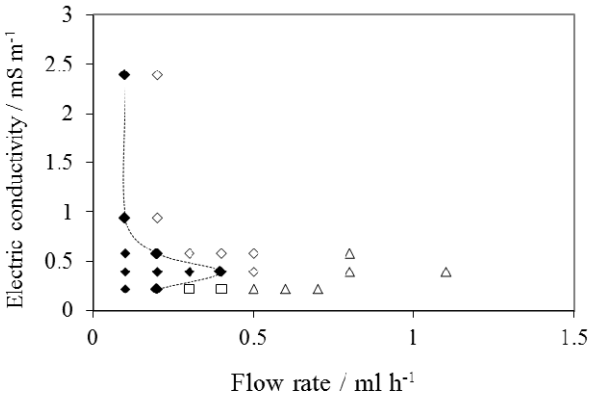

Figure 1. Phase diagram. Different types of deposit structure depending on the electric conductivity of the catalytic ink and on flow rate. Fractal-like deposits ♦, patched clusters ◊, and compact structures (□ and △).

This work has been supported by the Ministerio de Economía y Competitividad (Spain) under Grant ENE2011-26868 and Program Consolider-Ingenio 2010 (CSD2010-00011) and also by Comunidad de Madrid (Project HYSYCOMB, S2009ENE- 1597).

Castillo, J.L., Martin, S., Rodriguez-Perez, D., Perea, A. and Garcia-Ybarra, P. L. (2013) *KONA Powder and Particle J.*, submitted.

Garcia-Ybarra, P.L., Castillo, J.L. and Martin, S. (2012) Patent application no. P201200341.

Martin, S., Garcia-Ybarra, P.L. and Castillo, J.L. (2012) *J. Aerosol Sci.* **46**, 53-63

Martin, S., Martinez-Vazquez, B., Garcia-Ybarra P.L. and Castillo, J.L. (2013) J. Power Sources **229**, 179-184.

Rodriguez-Perez, D., Castillo, J.L. and Antoranz, J.C. (2005) *Physical Review E* **72**, 021403.

Rodriguez-Perez, D., Castillo, J.L. and Antoranz, J.C. (2007) *Physical Review E* **76**, 011407.

Quantitative single particle mass spectrometry with the Aerodyne aerosol mass spectrometer: development of a new classification algorithm and application to field data

F. Freutel[1], F. Drewnick[1], J. Schneider[1], T. Klimach[1], and S. Borrmann[1,2]

[1]Particle Chemistry Department, Max Planck Institute for Chemistry, 55128 Mainz, Germany
[2]Institute of Atmospheric Physics, Johannes Gutenberg University Mainz, 55128 Mainz, Germany
Keywords: single particle aerosol mass spectrometry, classification algorithm, MEGAPOLI.
Presenting author email: fr.freutel@mpic.de

Single particle mass spectrometry using laser desorption / ionization instruments is well established; however, this method is typically not capable of providing quantitative information about the chemical composition of the individual particles. Efficient single particle mass spectrometry using the Aerodyne aerosol mass spectrometer (AMS) has become possible with the introduction of the light scattering probe by Cross *et al* (2009). Here, the particles are flash vaporized on a hot surface and ionized by electron impact ionization. This method provides reproducible fragmentation patterns of individual chemical species, and therefore enables quantification of different, non-refractory chemical compounds within the single particles (diameters ~300 - 1000 nm).

So far, published cluster algorithms like principal component analysis (Cross *et al*, 2009) or k-means clustering (Liu *et al*, 2012) have been used for the analysis of AMS single particle data. In these studies quantitative information on the content of different aerosol species has been acquired separately by using the same procedures as applied to AMS ensemble mass spectra. No unambiguous method was used yet to both quantify the contents of organic and inorganic species and to identify and separate different organic species within single particles.

Here, we present the development, laboratory validation, and field application of a new method for AMS single particle analysis, which provides both quantitative information about the contents of different organic and inorganic species within single particles and classification of particles into different particle types.

In a first step the single particle mass spectra are compared to reference mass spectra for typical particle components (i.e., NH_4NO_3, $(NH_4)_2SO_4$, glucose as biomass (burning) proxy, oleic acid as cooking proxy, oxygenated organic aerosol OOA from ambient measurements, and gasoline engine exhaust). To obtain quantitative information on the content of these components in the particles, the corresponding mass spectra are subtracted proportionately from the single particle mass spectra. Depending on the components found in every single particle it is assigned to a certain particle type. This approach allows an unambiguous detection of different species within the single particle mass spectra, and, unlike clustering algorithms, does not depend on the specific dataset analyzed.

In laboratory measurements this method was tested and validated. Species in laboratory-generated single particle mass spectra are reasonably well identified and separated, as long as sufficient signal is available.

The new single particle analysis method was applied successfully to AMS data acquired during field measurements which took place in July 2009 in Paris within the MEGAPOLI project. About 90% out of ~26,000 single particle mass spectra have successfully been classified according to their composition (Fig. 1). Particles originating from primary emissions (i.e. cooking and traffic) are found to be externally mixed with internally mixed particles of OOA, nitrate and sulphate. Only for a small fraction of particles, mixtures of different organic species or organics other than OOA with inorganics were found ("mixed organics" in Fig. 1).

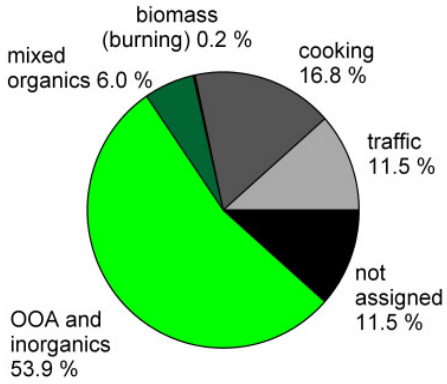

Figure 1. Classification of the AMS single particle mass spectra acquired during the MEGAPOLI campaign.

Comparison of averaged single particle composition with results from ensemble measurements showed good agreement. In addition to direct information about aerosol mixing state and consequently potential particle sources, this method provides valuable data on absolute concentrations of certain species within individual particles and their temporal variations.

We thank E.S. Cross, D. Sueper, T.B. Onasch, and J. Kimmel for providing the basic data analysis and the data acquisition software, respectively.

Cross, E.S., Onasch, T.B., Canagaratna, M., Jayne, J.T., Kimmel, J., Yu, X.-Y., Alexander, M.L., Worsnop, D.R., and Davidovits, P. (2009) *Atmos. Chem. Phys.* **9**, 7769-7793.

Liu, S., Russell, L.M., Sueper, D.T., and Onasch, T.B. (2012) *Atmos. Meas. Tech. Discuss.* **5**, 3047-3077.

Smoke particle morphology for different fire types determined by equivalent ratio tube furnace method

Jaehark Goo

Department of Fire Protection and Safety, Woosuk University,
Samnye-eup, Wanju-gun, Jeonbuk 565-701, South Korea
Keywords: tube furnace, smoke, particles, morphology.
Presenting author email: jaygoo@woosuk.ac.kr

The adverse health effects of smoke are associated with the inhalation of smoke particles, and depend on the amount and location of their deposition within the respiratory tract. The characteristics of the penetration and deposition of smoke aerosols into the lungs that determine the adverse health effects are related to the morphology and the size distribution of smoke particles (Hertzberg and Blomqvist, 2003).

Most cases of smoke inhalation involve smoke from compartment fires, and the time-varying size distribution of the smoke particles is an important factor in lung deposition. Several researchers measured the size distributions of smoke particles generated in typical test fires, but the information derived about the morphology of smoke particles was insufficient for examining lung deposition (Hertzberg and Blomqvist, 2003; Blomqvist *et al*, 2007). Recently, Goo (2012) calculated the development of the size distribution of smoke particles in a compartment fire using an analytical method.

The present work investigates the morphology of smoke particles for different fire types, in order to determine the initial conditions for calculations related to the development of particles in a compartment fire. The steady-state tube furnace method given in ISO/TS 19700 (2009) is used for the generation of smoke particles. The size distribution of the particles is measured for different fire types using a cascade impactor, and the morphology of the particles for each stage of the impactor is analyzed using transmission electron microscope (TEM).

The tube furnace used has a maximum set temperature of 1,100 ^{o}C, a 600-mm heating zone, and a total length of 700 mm (AHI Co. Ltd.). The quartz tube of the furnace has an inlet length of 900 mm and an outlet length of 85 mm. The outer diameter of the tube is 48.0 mm, and the wall thickness is 1.5 mm. Strip specimens or pellets are spread in a quartz sample boat over a length of 800 mm at a loading density of 25 mg/mm. An induction motor (DKM, 9IDG3-200FP) is used for introducing the sample into the quartz tube with a typical advance rate of 40 mm/min. Primary air is introduced into the quartz tube with a maximum flow rate of 20 L/min using an mass flow controller (MFC: KOFLOC, 3660) and a readout (MJT, MR300).

The mixing chamber is made of 5-mm-thick polystyrene and 1-mm-thick stainless steel plates, with the inner dimensions of 310 mm (depth) × 310 mm (width) × 340 mm (height). Secondary air is introduced into the mixing chamber with a total flow rate of 50 L/min with the primary air using a flow meter (KFM, PA-20).

Table 1. Test conditions.

Stage	1	2	3	4
T (^{o}C)	350	650	650	825
Qp (L/min)	2	-	-	-
Equ. ratio (ø)	-	< 0.75	2	2

The furnace temperature (T) and the flow rates of primary air (Qp) are changed for each fire type, as shown in the Table 1. TEM (HITACHI, H-7650) is used to examine the morphology of the particles (Figure 1) by collecting smoke particles on the TEM Grid (TedPella, 01800-F) from the mixing chamber through the impactor, with a flow rate of 1 L/min controlled by the MFC. Typical materials, such as polyethylene, PVC, polyprophylene, polyurethane, and wood, etc. are used for the experiment.

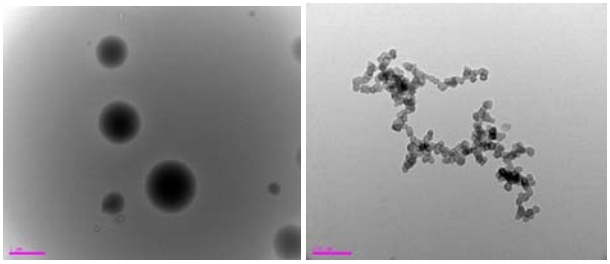

Figure 1. Typical TEM images of wood smoke for stage 1 (left, 2 μm scale), and stage 2 (right, 200 nm scale)

This work was supported by the National Research Foundation of Korea (NRF-2012R1A1A2006711).

Blomqvist, P., Hertzberg T., Tuovinen H., Arrhenius K. and Rosell L. (2007) Detailed determination of smoke gas contents using a small-scale controlled equivalence ratio tube furnace method, Fire and Materials 31, 495-521.

Goo, Jaehark (2012) Development of the size distribution of smoke particles in a compartment fire, Fire Safety Journal 47, 46–53.

Hertzberg, T. and Blomqvist P. (2003) Particles from fires – a screening of common materials found in buildings, Fire and Materials 27, 295-314.

ISO/TS 19700, (2006) Controlled equivalence ratio method for the determination of hazardous components of fire effluents.

Industrial by-products as precursors for gas-phase nanoparticle synthesis

T. Karhunen[1], A. Lähde[1], T. Torvela[1], J. Jokiniemi[1,2]

[1]Fine Particle and Aerosol Technology Laboratory, University of Eastern Finland, Kuopio, 70211, Finland
[2]Fine Particles Team, Technical Research Center of Finland, Espoo, 02044 VTT, Finland
Keywords: $LiFePO_4$, CVS, phase composition.
Presenting author email: tommi.karhunen@uef.fi

The structure of global energy supply is changing rapidly towards sustainable energy solutions. However, all forms of sustainable and intermittent energy production (e.g. wind power, photovoltaics) and sustainable transportation (e.g. hybrid and full electric vehicles) require excellent energy storage systems in order to increase their effectiveness (Hall and Bain, 2008).

Li-ion secondary cells are one of the most advanced battery energy storage systems currently available due to their high energy density (Du Pasquier *et al*, 2003). One of the main obstacles in their wide scale adoption, however, is the high cost of such batteries.

This obstacle can be overcome, firstly, by increasing the operational life time of the batteries. $LiFePO_4$ is a very promising electrode material for achieving this. In proper combination with an conductive additive it can be used to make Li-ion batteries that can undergo at least 1000 charge/discharge cycles without significant degradation in performance (Song *et al*, 2011). Furthermore, $LiFePO_4$ and its precursors are environmentally friendly.

Secondly, the cost of the precursor materials can be reduced by utilising alternative sources, such as industrial by-products. At least iron and phosphorus are available in the industrial waste streams. Utilising these streams will also reduce the environmental impact of the production.

Lastly, the synthesis process itself can be optimised. Gas-phase processes are highly material and energy efficient routes for synthesis of nanoparticles with controlled composition and particle size. With the proper selection of the process environment the waste streams can also be easily utilised in these processes.

In this paper we present a gas-phase method for the synthesis of LiFePO4 nanoparticles utilising industrial waste stream of FeSO4·7H2O. The precursors were dissolved in water and atomized using an ultrasonic nebuliser. The produced droplets were then carried to the heated zone of the reactor. Experiments were carried out at temperatures between 200 and 1000 °C in atmospheres with varying reduction potentials. The aerosol exiting the heated zone was rapidly cooled with a large volume of dilution gas (air or N2) at ambient temperature.

With increasing temperature the particles became more solid with increasing fraction of $LiFePO_4$ (Figure 1). Increasing the reducing potential of the synthesis atmosphere increases the ratio of the Pnma-to-Cmcm polymorphs of $LiFePO_4$ (Figure 2). The effects of temperature, precursor composition and process atmosphere on the product composition will be presented.

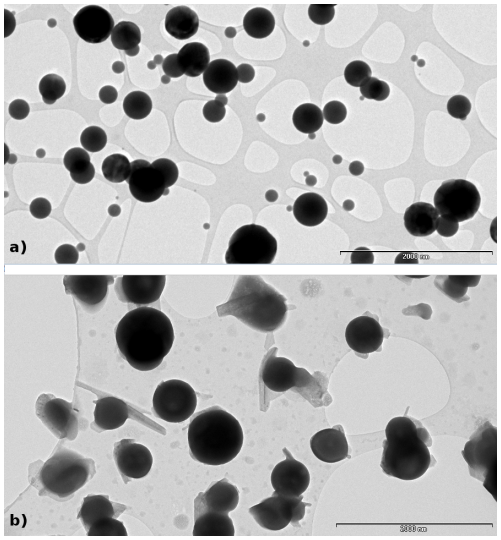

Figure 1: TEM images of $LiFePO_4$ samples synthesised at (a) 800 °C and (b) 600 °C.

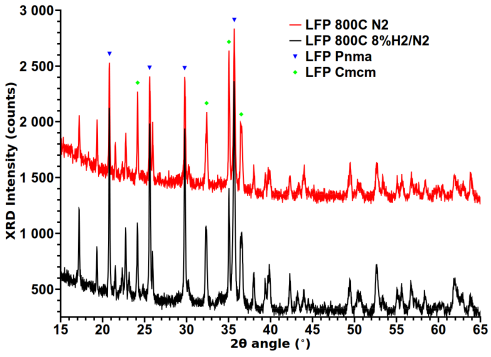

Figure 2: XRD diffractiograms of $LiFePO_4$ samples synthesised in N2 (red) and 8%H2/N2 (black).

This work was supported by Foundation for Research of Natural Resources in Finland (grant 1749/12), the Fortum Foundation (grant 12-072), and the strategic funding of the University of Eastern Finland (NAMBER spearhead project).

Hall, P. J. and Bain E. J. (2008) *Energy Policy* **36**, 4352–4355.

du Pasquier, A., Plitz, I., Menocal, S. and Amatucci, G. (2003) *J. Power Sources* **115** (1), 171–178.

Song, M.-K., Park, S., Alamgir, F. M., Cho, J., Liu, M. (2011) *Mat. Sci. Eng. R* **72**, 203–252.

Dilution affects particle properties originating from residential biomass combustion

H. Lamberg[1], T. Kaivosoja[1], J. Leskinen[1], M. Kortelainen[1], A. Viren[1], H. Koponen[1], V. Tiihonen[1], M. Miettinen[1], J. Pyykönen[2], J. Jokiniemi[1,2] and J. Tissari[1]

[1]Department of Environmental Science, University of Eastern Finland, Fine Particle and Aerosol Technology Laboratory, P.O. Box 1627, FI-70211 Kuopio, Finland
[2] VTT, Technical Research Centre of Finland, Fine Particles, P.O. Box 1000, FI-02044 VTT, Espoo, Finland
Keywords: dilution, biomass combustion, sampling.
Presenting author email: heikki.lamberg@uef.fi

Residential biomass combustion is known to be a significant source of particulate matter (PM) in regions where it is in common use. Sampling of fine particles from residential combustion appliances is of great significance because of a need to create standards for particulate emission measurements. Small-scale biomass combustion sources often emit fine particles that contain substantial amounts of organic compounds that condense at relatively low temperatures. Sampling procedures, such as temperature control and dilution ratio (DR), are known to affect sampled particles, especially as concerns their organic constituent (Lipsky et al. 2006). The aim of this study was to identify the effect of DR on fine particles, and to study the use of porous tube diluter in this type of measurements.

Batch combustion appliance with simple combustion technology, a sauna stove, was used in the experiments. Sampling of flue gases was done with a setup of porous tube and ejector diluters (Tissari et al. 2007). Three different DRs, 15, 40 and 115, were used. DRs were controlled with simultaneous CO_2 concentration measurements in the flue gas and in the diluted sample gas. Two similar dilution and sampling systems were operated during each measurement at different DRs. This ensured that the samples were comparable even if the combustion process varied slightly between each individual experiment, which is often present in batch-combustion process.

Overall, only a minor effect of DR on sampled PM mass was observed in the experiments. As expected, the smallest DR seemed to lead to the highest PM mass. While the total PM mass remained rather constant, a large variation as a function of DR was observed in measured particulate form PAH content, in the studied combustion conditions. The total particulate PAH at DR 15 was 1.8-fold to 2.9-fold compared to DRs 40 and 115, respectively (Fig. 1). The PAH/PM_1 ratio decreased from 9.4% to 5.8% and 2.5%, while DR increased from 15 to 40 and 115. The effect of DR was the largest for light PAH compounds. Heavy PAH species have most likely condensed prior to sampling. The fact that their measured concentrations scaled very well with DRs indicated that the porous tube diluter worked in a reliable way.

Computational fluid dynamics (CFD) modelling was used to obtain a better understanding of flows and losses inside the porous tube diluter. The studies identified the tip of the porous tube nozzle as the critical region for condensable organic vapour and fine particle losses. Right at the tip, the porous flow does not provide protection. Overall, only minor sampling losses are predicted for typical small-scale biomass combustion conditions. Model considerations of dynamics involved in gas-to-particle conversions indicate that the residence times in the diluter are sufficient for equilibrium, provided that no chemical reactions are involved. This is the case for PAH compounds that are the same in the gaseous and condensed forms. Indeed, vapour pressures seem to provide sufficient explanation of the observed trends in PAH contents.

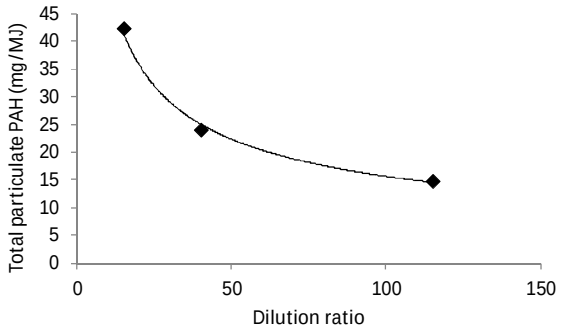

Figure 1. The effect of dilution ratio on total particulate PAH.

The porous tube diluter worked in a consistent and reliable way in the measurements. The experiments indicate that, even in cases where total PM emissions only show weak DR dependence, particulate properties may still be significantly affected by DR. This is especially true of health effect studies. The samples have large variation in their PAH contents, and consequently, possibly in their health effects as well.

This work is part of the ERA-NET joined project EN-PME-TEST. The work at UEF and VTT is funded by the Finnish Funding Agency for Technology and Innovation (TEKES). This work was further supported in part by the strategic funding of the University of Eastern Finland for project Sustainable Bioenergy, Climate change and Health (SUBI).

Lipsky, E.M. and Robinson, A.L. (2006). *Environ. Sci. Technol.* **40**, 155–162.
Tissari, J., Hytönen, K., Lyyränen, J., Jokiniemi, J. (2007). *Atmos. Environ.* **41**, 8330–8344.

A novel set-up for source characterization and human exposures of biomass combustion aerosols

R. Nyström[1], E. Z. Nordin[2], J. H. Pagels[2] A. Blomberg[3], T. Sandström[3] and C. Boman[1]

[1]Thermochemical Energy Conversion Laboratory, Department of Applied Physics and Electronics, Umeå University, SE-901 87 Umeå, Sweden
[2]Ergonomics and Aerosol Technology, Lund University, SE-221 00 Lund, Sweden
[3]Dept. of Public Health and Clinical Medicine, Division of Medicine, Umeå University, SE-901 87 Umeå, Sweden

Keywords: biomass combustion, aerosol chamber, controlled human exposure, health effects
Corresponding author: robin.nystrom@umu.se

Emissions from biomass combustion are a major source of indoor and outdoor air pollution, and are estimated to cause millions of premature deaths worldwide annually. Pollution from different biomass combustion sources are a complex and varying mixture of gases and particles, strongly dependent on fuel, technology and operation [Kocbach *et al*, 2009]. Although adverse respiratory effects have been associated with "wood smoke" in epidemiological and controlled exposure studies, important information concerning biomass combustion aerosols is still missing. Examples of such areas are; cardiovascular effects, underlying biological pathways and importance of different aerosol particle properties. A chamber set-up built for controlled human exposures gives unique opportunities to directly relate specific exposure conditions to different short term (acute) respiratory and cardiovascular responses in humans.

The objective of this project was therefore to describe and evaluate a novel chamber set-up for studies of health effects of biomass combustion aerosols using controlled human exposures. In this paper we discuss the biomass combustion aerosol exposure set-up including aspects of; *i)* combustion systems, *ii)* aerosol dilution, *iii)* chamber design and function, and *iv)* exposure data from the first recently performed campaign.

The exposure set-up is located in connection to the combustion laboratory within the Thermochemical Energy Conversion Laboratory (TEC-Lab) at Umeå University. The facility includes several combustion technologies to be used for different aerosol generation purposes such as human exposures and/or other aerosol experimental research. For example, traditional wood log stoves, modern wood pellet boilers using different burner technologies, a fluidized bed reactor and novel grate fired reactors for controlled generation of different kinds of biomass aerosols, are available.

Different flue gas/aerosol dilution systems are available, e.g. ejector dilutors (ED) and porous tube dilutors (PTD). In the first exposure campaign, a three step dilution system with filtered air at ambient temperature was used including a first PTD (~1:10), followed by an ED (~1:6) and a final counter-current flow injection in the main HEPA filtered air flow that enters the chamber.

The chamber is 15.3 m^3 (2.7 x 2.4 x 2.4 m) with a small ante-chamber with interior surfaces made of stainless steel/aluminium, except for 2.4 m^2 observation glass window facing a control room. The set-up is designed for air exchange rates of 2-10 times per hour. CO, NO_x and total hydrocarbons as well as temperature and relative humidity are continuously monitored. Particle mass concentration is measured by a TEOM equipped with a PM_1 pre-cyclone and an integrated filter sampler. Particle mobility size distribution and number concentration are measured with a SMPS system. In addition, several different filter and impactor sampling lines are applied for off-line chemical characterization including, e.g. carbon fractions (OC/EC), PAH/oxy-PAH and inorganic alkali and trace metals, as well as toxicological (*in-vitro*) characterization.

A first human exposure study in the new set-up was performed to elucidate acute airway inflammatory responses and cardiovascular effects after exposure to emissions from incomplete wood log combustion. A common Nordic wood stove was used with a special adjusted combustion approach to generate incomplete (soot-rich) conditions in a repeatable manner for the exposure campaign. The target PM_1 mass concentration in the chamber was 300 $\mu g/m^3$ thus in line with a previous experimental wood smoke study [Sehlstedt *et al*, 2011] and several diesel engine exhaust studies performed by the Umeå group and collaborators. Fourteen healthy non-smoking subjects were successfully exposed to diluted wood smoke (PM_1 314±38 $\mu g/m^3$) or filtered air for three hours in a randomized, double-blind crossover study. The EC/TC (total carbon) ratio was 0.72 ± 0.08, and it was estimated that the total PM consisted of approximately 38% soot, 24% organics and 38% inorganics.

Aspects of chamber function (e.g. flow profiles and mixing conditions) as well as aerosol dynamic effects (e.g. coagulation and wall losses) at different chamber conditions are presently under evaluation and will be discussed. Accordingly, the new and novel set-up for biomass combustion aerosol generation, characterization and health effect studies has successfully been established and so far used in one human exposure study and one aerosol ageing and toxicology study (Nordin *et al*., EAC 2013).

The work was supported by the Swedish Energy Agency within the ERA-NET Bioenergy project *Biohealth* and the strategic funding by Umeå University´s young researcher award (C Boman).

Kocbach Bølling, A., Pagels, J., Yttri, K.-E., Barregard, L., Sällsten, G., Schwarze, P.E., Boman, C. (2009) *Part Fibre Toxicol*. **6**:29.

Sehlstedt, M., Dove, R., Boman, C., Mudway, I.S., Pagels, J., Swietlicki, E., Löndahl, J., Westerholm, R., Bosson, J., Barath, S., Behndig, A.F., Pourazar, J., Sandström, T., Blomberg, A. (2010) Part Fibre Toxicol **7**:21.

Synthesis of tailored organic-inorganic nanostructures by charge controlled coagulation

S. Sigmund[1], E. Akgün[2], J. Meyer[1], M. Wörner[2] and G. Kasper[1]

[1]Institute of Mechanical Process Engineering and Mechanics, Karlsruhe Institute of Technology, 76131 Karlsruhe, Germany
[2]Institute of Process Engineering in Life Science, Karlsruhe Institute of Technology, 76131 Karlsruhe, Germany
Keywords: Composite nanoparticles, electrostatic particle coating
Presenting author email: stephanie.sigmund@kit.edu

Based on charge controlled coagulation between monomer droplets and core particles, precisely tailored nano-composites, consisting of polymer coated core particles are synthesised.

Continuous polymer coatings do mainly have protective properties. Depending on the shell morphology, a highly sensitive or reactive core particle can be protected from uncontrolled reactions or can be completely encapsulated from ambiance. At the same time a tailored polymer shell can be employed to realize a controlled core particle reaction. By influencing the shell thickness, it is possible to directly modify release kinetics of an active core substance. Therefore, a simple method to control the shell thickness of the generated particle systems is strongly desired.

We will present such a method of controlled coating with enclosed polymer layers. Usually hybrid nanostructures are generated in liquid phase processes (Nabhi et al.). However, aerosol processes offer certain advantages, such as high product purity etc. In our case, by means of attractive interactions between gasborne, electrically charged core particles and inversely charged monomer droplets, selective agglomeration is enforced. At the same time repulsive forces interact between charges of the same polarity. Hence agglomeration among core particles or droplets respectively, is kinetically inhibited. The principle of selective agglomeration between inversely charged droplets or particles is not new (Borra et al., Maisels et al.), but processes taking advantage of selective agglomeration to generate coating structures are rare. Once particles collide with droplets, these will wet the particle surface completely to form an enclosed shell. This shell is polymerized afterwards. Thereby, assuming that one droplet wets one core particle, the droplet size determines the shell thickness. Hence a polymeric shell onto a core particle of the desired thickness can be generated by producing monomer droplets of a definite size.

To do experimental studies on the generation of tailored hybrid nanoparticles, monodisperse silica particles with 150 nm in diameter were chosen as model core particles. Silica particles are brought into gas phase by spraying an aqueous particle suspension and subsequent drying. The charging step takes place in a corona charger. By applying positive high voltage potential, core particles gain multiple positive charges during this charging step. Monomer droplets are generated by atomizing a solution, consisting of butyl acrylate and photo initiator. Subsequently monomer droplets of the desired droplet size are classified in a DMA at constant voltage. These monodisperse droplets were charged in a second corona charger but with inverse, thus negative polarity. Core and coating material aerosols were mixed in number ratio of 1:1 to achieve coagulation of one droplet with one core particle and therefore to minimize the occurrence of multiple or uncoated core particles. The mixed aerosol is passed through a residence time volume to ensure coagulation and core particle wetting. The homogeneous monomer coating is then directly photo polymerized by irradiation with UV light to form a solid, polymeric shell. To provide coating evidence, the size increase of the core particle size due to the polymer shell is measured in a conventional tandem DMA setup. Supplementary the hybrid particles are analysed visually via transmission electron micrographs.

Shell thickness measurements for several droplet sizes, by tandem DMA and visual analysis will be presented. Those measurements were compared with theoretical calculated shell thickness, from droplet size. The experimentally determined shell thicknesses agreed well with theoretically expected values.

This project is part of the JointLab IP3, a joint initiative of KIT and BASF. Financial support by the ministry of science, research and the arts of Baden-Württemberg (Az. 33-729.61-3) is gratefully acknowledged.

Borra, J.P., Camelot D., Chou K.L., Kooyman P.J., Marijnissen J.C.M., Scarlett B. (1999). *Bipolar coagulation for powder production: Micro-mixing inside droplets. Journal of Aerosol Science, 30, 945.*

Nabih, N., Landfester, K., Taden, A.,(2011). *Water-Based Inorganic/Polymer Hybrid Particles Prepared Via a Multiple Minieemulsion Process.* Journal of Polymer Science Part A, Polymer Chemistry, 49, 5019.

Maisels, A., Kruis, F.E., Fissan, H., Rellinghaus, B., Zähres, H.(2000) *Synthesis of Tailored Composite Nanoparticles in the Gas Phase.* Applied Physics Letters, 77, 4431

Contribution of Inorganic aerosols and trace gases due to biomass burning during cooking hours at a rural site in India

Sudha Singh*, Gyan Prakash Gupta, Bablu Kumar and U C Kulshrestha
School of Environmental Sciences, Jawaharlal Nehru University
New Delhi, INDIA
Keyword: aerosols, biomass burning, cooking
(*Email: sudha29jan@gmail.com)

Biomass burning is a major source of air pollution which emits a complex mixture of air pollutants in the form of gases and aerosols (Andreae and Merlet, 2001). These have significant impact on atmospheric chemistry, climate change, and human health. But due to lack of measurements across the globe especially from developing countries, aerosol budgets have large uncertainties. There are reports on their emissions from coal combustion and wood burning from USA and Europe but measurements are very limited from developing countries. In India, traditional cooking is still common which contributes large amount of such air pollutants. This study has been carried out as part of UNEP project `Surya' to report chemical characteristics of fine atmospheric aerosols collected during cooking hours in an indoor environment in a village.

Measurements were conducted to determine indoor air pollution due to burning of wood, dung cakes and agriculture residue in rural households in Khairatpur village which is located in district Sultanpur of Uttar Pradesh state of India. Aerosol samples along with gaseous species (NO_2, SO_2, and NH_3) were collected during December 2010-January 2011 by using handy sampler (Envirotech model APM 821) installed inside the house. The samples were collected on 8 hourly basis using Teflon filters. The water extract of these filters was analyzed for major anions (F^-, Cl^-, NO_3^-, SO_4^{2-}) and major cations (Na^+, NH_4^+, K^+, Ca^{2+} Mg^{2+}) by ion chromatography (Metrohm 883 Basic IC Plus).SO_2 was estimated by using ion chromatograph and NO_2 and NH_3 were estimated by using spectrophotometer.

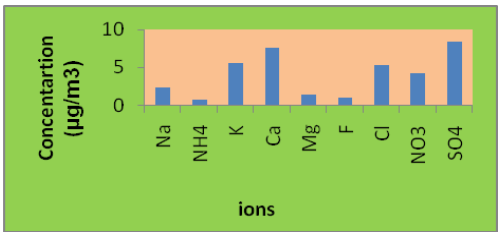

Fig.1 Concentrations (µg/m^3) of major ions during indoor cooking.

Fig.1 is the graphical representation of chemical composition of aerosol samples which indicates that SO_4^{2-} is dominant component followed by K^+, NO_3^-. SO_4^{2-} and Cl^-. Biomass burning is considered as a potential source of K^+ in air and its signature have been reported in Indian region (Kulshrestha et al., 2001). SO_4^{2-} which accounting for about 23% of the all components, is probably produced from the SO_2 emitted from biomass burning during cooking. SO_2 was recorded the highest among other gaseous species. Concentrations of gases are given in the Fig.2.

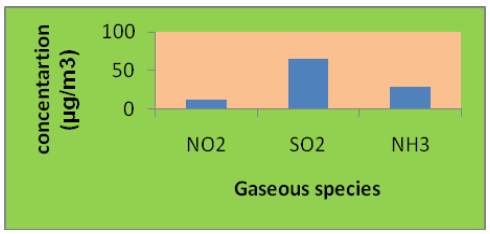

Fig.2 Concentration (µg/m^3) of trace gases during indoor cooking hours.

These findings indicated that a significant amount of aerosols as well as gases are contributed by biomass burning during traditional cooking process in rural India.

Acknowledgement: Authors sincerely thank RRC-UNEP-AIT, DST-PURSE, UGC and JNU for financial support.

References

Andreae, M.O., Merlet, P., 2001. *Emission of trace gases and aerosols from biomass burning*. Global Biogeochemical Cycles 15 (4), 955-966.

U C Kulshrestha, R Sekar, M Vairamani, Monika Jain, A K Sarkar, D C Parashar and A P Mitra. *Signatures of biomass burning over Indian Ocean during INDOEX*. IGAC Symposium, January 21-23, 2001, Bangkok, Thailand.

Dependence of Aircraft Smoke Number on Black Carbon Size Distribution

M.E.J. Stettler[1], J.J. Swanson [1] and A.M. Boies[1]

[1]Department of Engineering, University of Cambridge, CB2 1PZ, United Kingdom
Keywords: combustion aerosols, aircraft emissions, soot generator, aerosol filtration.
Presenting author email: ms828@cam.ac.uk

Current methods used to estimate aircraft black carbon (BC) emissions for the purposes of air quality and climate impact studies rely on an outdated correlation and underestimate by a factor of 2-3. In this study, we show that the correlation between the BC mass concentration and smoke number is strongly dependent on the geometric mean of the particle size distribution. To test the correlation a new method to produce BC particles with a variable geometric mean diameter on the range 20-60 nm is employed to simulate BC particles emitted by aircraft gas turbine engines.

Aircraft engine exhaust is currently regulated on the basis of a filter smoke number (SN) – the observed change in reflectance of the filter after sampling a specified mass of exhaust. Estimates of aircraft BC emissions rely on an empirical correlation between SN and BC mass concentration (C_{BC}) derived using BC particles with geometric mean diameter (GMD) between 80-100 nm (Girling et al., 1990). Recent measurements of BC particles in aircraft exhaust have shown that aircraft soot can be characterized as having lognormal particle size distribution with a GMD between 20-40 nm (Kinsey et al., 2010).

A co-flow inverse diffusion flame provides a steady source of BC particles with variable GMD in the range 20-60 nm and geometric standard deviation between 1.5-1.7. The particle size distribution is characterised with a Scanning Mobility Particle Sizer (SMPS) and particle mass as a function of mobility diameter (d_m) is measured using a Centrifugal Particle Mass Analyser. Calculated BC mass concentrations are verified with gravimetric analysis. SN measurements are taken according to the standard aircraft test procedure (SAE, 1997). Correlations between SN and BC concentration are derived for 20, 30 and 60 nm GMD. Filtration efficiency of the specified SN filter as a function of d_m is measured.

In Fig. 1, the particle mass distributions for GMD~20 nm, GMD~30 nm and GMD~60 nm are superimposed on the filtration efficiency, indicating that filtration efficiency increases with d_m such that a smaller proportion of the BC mass is collected on the filter for a smaller GMD.

In Fig. 2 the correlation between SN and BC mass concentration is shown to be a function of d_m – for a smaller GMD a greater C_{BC} is required to produce the same SN, suggesting that current estimates underestimate aircraft BC mass emissions by up to a factor 2-3. These revised correlations improve estimates of aircraft BC emissions compared to measurements but do not account for uncertainty in the regulatory SNs.

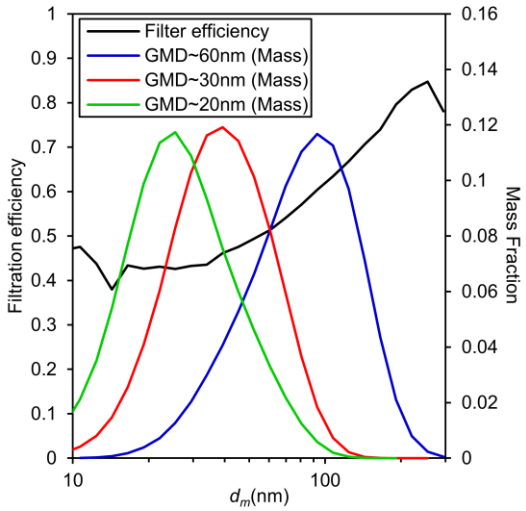

Figure 1. Filtration efficiency of the SN filter with mass distributions for GMD~20, GMD~30 and GMD~ 60 nm soot.

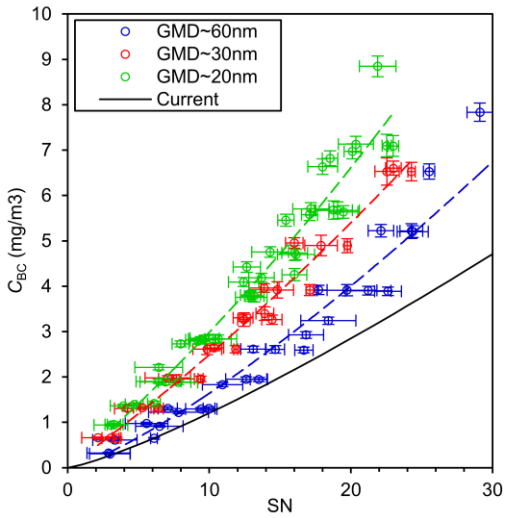

Figure 2. Correlation between C_{BC} and SN.

This work was supported by the UK Engineering and Physical Sciences Research Council (EP/H004505/1).

Girling, S.P., Hurley, C.D., Mitchell, J.P., Nichols, A.L., 1990. Aerosol Science and Technology 13, 8–19.

Kinsey, J.S., Dong, Y., Williams, D.C., Logan, R., 2010. Atmospheric Environment 44, 2147–2156.

SAE, 1997. Aerospace Recommended Practice 1179C Aircraft Gas Turbine Engine Exhaust Smoke Measurement, System.

Characterisation of solid and semi-volatile gas-turbine particulate matter using a catalytic stripper

J.J. Swanson[1], T.J. Johnson[2], J.S. Olfert[2], M.P. Johnson[3], P.I. Williams[4,5], G.J. Smallwood[6] and A.M. Boies[1]

[1]Department of Engineering, University of Cambridge, Cambridge, CB2 1PZ, UK
[2]Department of Mechanical Engineering, University of Alberta, Edmonton, Alberta, T6G 2G8, Canada
[3]Rolls-Royce plc, Derby DE24 8BJ, UK
[4]National Centre for Atmospheric Science, University of Manchester, Manchester, M13 9PL, UK
[5]SEAES, University of Manchester, Manchester, M13 9PL, UK
[6]NRC Canada, Ottawa, Ontario K1A 0R6, Canada
Keywords: EC/OC, aerosol, exhaust, CPMA
Presenting author email: js2011@cam.ac.uk

Gas turbine particulate matter (GTPM) consists of solid and semi-volatile particles that originate from partially oxidised fuel and lubricating oils. Many techniques are available for measurement of particle number, size, and mass. However, often the volatile nature of these particles is not measured *a priori*. Advanced techniques are designed to respond to particles of a specific volatility or composition (such as solid, elemental carbon) but there are known cross-sensitivities. Catalytic stripper[1] (CS) technology provides an alternative method to aid in further elucidating the composition of an aerosol. A CS contains an oxidising catalyst that is used to fully remove the semi-volatile hydrocarbon particles and vapors in an exhaust gas stream. In this way, remaining particles are operationally defined as "solid."

The primary objective of this study was to measure the solid and semi-volatile fractions present in GTPM using a catalytic stripper specifically designed for the "Sample III " program that aimed to support SAE E-31 in drafting the Aerospace Recommended Practice (ARP) on the measurement of aircraft engine non-volatile particulate matter (nvPM) number emissions[2]. GTPM was generated by a GE CFM56-5B4-2P engine (120 kN, 27000 lb) with a dual annular combustor (DAC) is designed to minimise emissions, especially of NO_x, by optimising combustion for the different engine power modes and flight phases. Operating conditions were chosen to provide combinations of different levels of solid and semi-volatile material at modest power levels, thus minimising fuel consumption and allowing for more extensive testing.

Fig. 1 shows the sampling apparatus with raw gas turbine exhaust being sampled using 16 m transfer line heated to 160°C that is compliant with current regulations and a manifold to distribute the aerosol.

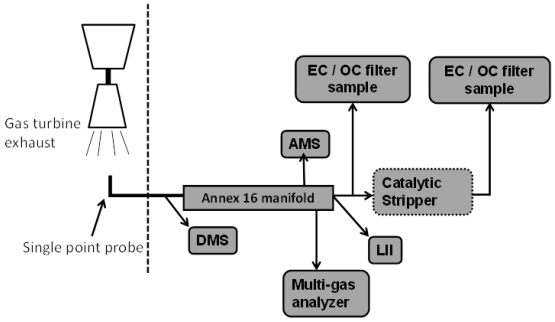

Figure 1. GTPM measurement apparatus for raw exhaust.

The primary evaluation metric reported on here is the EUSAAR "EC/OC" protocol that is used to define the concentration of elemental carbon. EC results were compared with laser induced incandescence (LII), which directly measures a related quantity, namely "black carbon." The EC/OC method also classifies the amount of (semi-volatile) organic carbon present, and therefore enables estimates of the semi-volatile faction. Results are also compared with both gas analysis and an alternative method particle measurement, the centrifugal particle mass analyser (CPMA) used with and without a CS.

Fig. 2 shows results of EC/OC analysis upstream and downstream of the CS for various engine power conditions. Results upstream the CS show that the elemental carbon fraction of the PM varies from ~10% to 90%, whereas downstream the CS there is only elemental carbon. Thus, for all turbine conditions the CS removes all OC, which allows for parallel measurement of the solid fraction using any typical aerosol instrument.

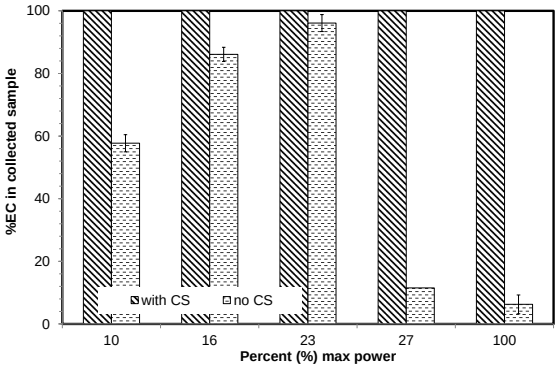

Figure 2. EC/OC results showing %EC in each sample collected up and downstream of the CS.

This work was supported by the UK Engineering and Physical Sciences Research Council (EP/H004505/1) and EASA Contract No: EASA.2010.FC10, Specific Contract Sample III - SC02.

[1]Swanson, J.; Kittelson, D. (2010). Evaluation of Thermal Denuder and Catalytic Stripper Methods for Solid Particle Measurements. *J. Aerosol Science*, 41:12, 1113 – 1122.

[2]Crayford, A.; Johnson, M. SAMPLE III: Contribution to aircraft engine PM certification requirement and standard. Second Specific Contract– Final Report. *EASA.2010.FC.10 Specific Contract No: SC02*.

Impact of biogenic emissions on $PM_{2.5}$ concentration over Europe

E. Tagaris, R.E.P. Sotiropoulou, N. Gounaris, S. Andronopoulos and D. Vlachogiannis

Environmental Research Laboratory, NCSR Demokritos, Aghia Paraskevi Attikis, 15310 Athens, Greece
Keywords: biogenic emissions, particulate matter, Europe
Presenting author email: tagaris@ipta.demokritos.gr

Natural and biogenic emissions are contributing to atmospheric pollution in addition to anthropogenic emissions. Over 90% of the total Volatile Organic Compounds (VOCs) entering the atmosphere are biogenic (Greenberg et al., 1999), having an important role in regulating the atmospheric composition. The impact of both anthropogenic and biogenic emissions on air quality is very important, as only the anthropogenic part can be influenced by abatement measures. Curci et al. (2009) estimated that biogenic VOC emissions increased on average summer daily ozone maxima over Europe by 5% (2.5 ppbv) using the CHIMERE chemistry-transport model. Sartelet et al. (2012) using the Polyphemus air quality modeling platform estimated that ozone decreased by 10-11% on average over Europe (locally up to 35%) while secondary organic aerosols decreased by 72-88% when removing biogenic emissions. The objective of this study is to estimate the effect of biogenic emissions on $PM_{2.5}$ concentration and chemical composition over Europe.

Meteorological fields are derived using the Penn State/NCAR Mesoscale Model (MM5) (Grell et al., 1994).

Emissions are processed by the Sparse Matrix Operator Kernel Emissions (SMOKE v2.6) Modeling System (http://www.smoke-model.org). The TNO gridded anthropogenic emissions inventory for the year 2006 over Europe in a 0.1 × 0.1 degrees resolution (ftp://neptunus.tno.nl) is used. The Biogenic Emission Inventory System, version 3 (BEIS3) is used for processing biogenic source emissions (http://www.epa.gov/asmdnerl/biogen.html) using the USGS gridded land use data in 1 Km resolution (http://edc2.usgs.gov/glcc/glcc.php).

The Community Multiscale Air Quality (CMAQ v 4.7) Modeling System with the Carbon Bond mechanism (CB05) (http://www.camx.com/publ/pdfs/CB05_Final_Report_120805.pdf) is used for the regional air quality modeling (177 × 217 grid cells of 35 km × 35 km, with 14 vertical layers) (Byun et al., 2006).

$PM_{2.5}$ concentrations are simulated with and without biogenic emissions for July, 2006. The effect of the addition of biogenic emissions to anthropogenic ones is computed to reduce the average monthly mean $PM_{2.5}$ concentration over European land by 2% with both positive and negative responses regionally (Fig. 1). The addition of biogenic emissions increases the average monthly mean organic carbon concentration by 14% (Fig. 2) and decreases the monthly mean inorganic component concentrations (SO_4: -6%, NO_3: -4%, and NH_4: -6% on average) due to the reduction in oxidant levels (OH: -30% on average). However, regional changes in inorganic concentrations with both positive and negative responses are simulated.

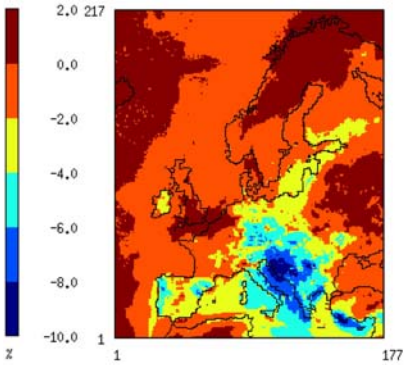

Fig. 1: Average change in $PM_{2.5}$ concentration (%) for July 2006 when biogenic emissions are added to anthropogenic emissions

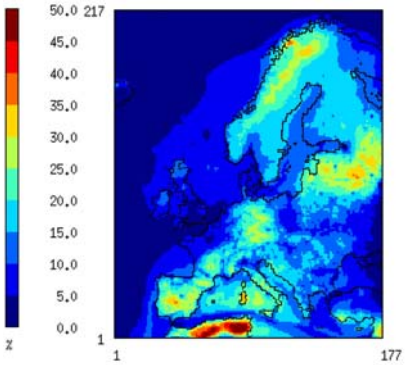

Fig. 2: Average change in OC concentration (%) for July 2006 when biogenic emissions are added to anthropogenic emissions

This work was supported by the National Strategic Reference Framework (NSRF) 2007-2013 grand No 09SYN-31-667.

Byun, D. W., and K. L. Schere (2006), *Appl. Mech. Rev.*, **59**, 51–77.

Curci, et al., (2009), *Atmos. Environ.*, **43**, 1444–1455.

Grell, G., et al. (1994), *Tech. Note NCAR/TN-398+STR*, Natl.Cent. for Atmos. Res., Boulder, Colo.

Greenberg, et al. (1999), *Atmos. Environ.*, **33**, 855– 867.

Sartelet et al. (2012), *Atmos. Environ.*, **53**, 131-141.

Climate and biofuels in Brazil

H. Vuollekoski[1], R. Makkonen[2], A. Asmi[1], R. Hillamo[3], T. Petäjä[1] and M. Kulmala[1]

[1]Department of Physics, University of Helsinki, Helsinki, 00014, Finland
[2]Department of Geosciences, University of Oslo, Oslo, 0371, Norway
[3]Finnish Meteorological Institute, Helsinki, 00560, Finland
Keywords: biofuels, climate, global modeling.
Presenting author email: henri.vuollekoski@helsinki.fi

Introduction

Biofuels represent a renewable source of energy that may increase the energy independence and economic well being of nations, as well as help reduce the net greenhouse gas emissions. These are some of the reasons why the usage of biofuels especially in transport is increasing rapidly. However, while this replacement of fossil fuels may decrease the net carbon dioxide emissions, the growing demand of biofuels may have consequences related to e.g. human health, agriculture and climate.

One example of such nation is Brazil, which has had a pro-biofuel regulatory environment already since 1975, and is the current world-leader in terms of vehicles running on sugarcane ethanol. If Brazil manages to replace all its consumption of fossil fuels by biofuels in the near future, what kind of climatic implications would this conversion potentially have? The transition would require significant agricultural changes to enhance sugarcane production, and these plantations would likely replace currently forested regions. The current methods of harvesting sugarcane often involve burning, which causes serious air pollution in certain regions (Lara *et al.*, 2005). Also, the primary emissions caused by combustion of ethanol fuel differ from those of traditional gasoline. The scope of our research is limited to the aforementioned effects, although a more realistic scenario would likely include the likely socio-economic side effects.

The land area of Brazil accounts for less than 6% of the global land surface. With this in mind, we try to identify the potential global climatic effects of the Brazilian transition to biofuels. We approach this question with global climate modeling.

Methods

All modeling in this study has been performed with the ECHAM5.5-HAM2 (Zhang *et al.*, 2012), which is a general circulation model that includes parameterizations for the effects of aerosols on climate. The sensitivity studies implemented so far have been executed by replacing the characteristic size of emissions due to fossil fuel combustion, according to current estimates (Stier *et al.*, 2005), in a region covering Brazil, while leaving rest of the world as it was. This change in size of the emitted particles is based on experimental laboratory studies on car engines.

Preliminary results

The first sensitivity study consisted of a 5.5-year control run and an otherwise identical run but with emissions in smaller size over Brazil. The results indicate significant increase in Aitken mode particles on surface level over Brazil, but this is likely due to the mass-based emission scenario. There is also a slight increase in the concentration of cloud condensation nuclei, but this and other effects may be attributed to noise.

We therefore conducted a similar set of runs for duration of 20 years. These suggest small changes in total cloud cover (see Figure 1), but more detailed analysis has to be carried out before conclusions.

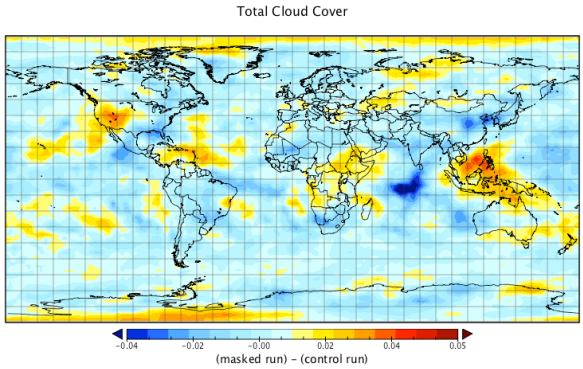

Figure 1. The difference in total cloud cover in a 20-year-long sensitivity test.

We acknowledge funding from "The effects of intensive bio-fuel production and use on regional air quality and global climate, BIOFUSE" (Academy of Finland, project 133603).
We thank Dr. Topi Rönkkö from Tampere University of Technology for technical consultation.
Risto Makkonen acknowledges funding from the CRAICC project.

Lara, L., Artaxo, P., Martinelli, L., et al. (2005) *Atmos. Env.*, **39** (26), 4627–4637.
Zhang, K., O'Donnell, D., Kazil, J., et al. (2012) *Atmos. Chem. Phys.*, **12** (19), 8911–8949.
Stier, P., Feichter, J., Kinne, S., et al. (2005) *Atmos. Chem. Phys.*, **5**, 1125–1156.

Wednesday, September 4, 2013

Plenary lecture: The Dynamics of Indoor Aerosol: what is important, where, when and why?
By Lidia Morawska

The Dynamics of Indoor Aerosol: what is important, where, when and why?

Lidia Morawska

Recent 'Global Burden of Disease' studies have provided quantitative evidence of the significant role indoor and outdoor aerosols play as human health risk factors. Tobacco smoke, including second hand smoke, household air pollution from solid fuels or ambient particulate matter are among the top risks, leading to lower life expectancy around the world. At the same time, theories behind the basic processes driving aerosol dynamics are reasonably well established and have good mathematical description. There are also various types of well established modelling approaches available, including those based on balance equations, CFD or Monte Carlo modelling, and they have been employed in many research projects to date, in order to gain insight into the nature of indoor aerosol dynamics. Numerous experimental studies have also quantified the relevant parameters of indoor environments and indoor air.

Has this science of indoor aerosols been used in urban planning and building design to reduce the risks posed by indoor aerosols? Have we extended existing skills in the numerical computation of aerosol dynamics or aerosol spatial distribution towards indoor particle formation processes? Or instead, are we shifting to personal exposure assessment? This presentation will explore these and other contemporary challenges in relation to indoor aerosol research and its application.

Wednesday, September 4, 2013

Session: Atmospheric Aerosols
Physico-chemical properties and transport

Unmanned Aircraft Aerosol Sampling: Improvements in Capabilities and Sample Analyses

C.F. Cahill[1,2], G.W. Walker[1], T.A. Cahill[3]. C.R. Iceman[2] and D.E. Barnes[3]

[1]Geophysical Institute, University of Alaska Fairbanks, Fairbanks, Alaska, 99775, USA
[2]Department of Chemistry and Biochemistry, University of Alaska Fairbanks, Fairbanks, Alaska, 99775, USA
[3]DELTA Group, University of California, Davis, California, 95616, USA
Keywords: unmanned aircraft, wildfire smoke
Presenting author email: cfcahill@alaska.edu

The use of unmanned aircraft systems (UAS) to collect atmospheric aerosol samples is gaining popularity. However, limitations on access to airspace, the number of aircraft allowed to fly simultaneously in a small area, and the sensitivity of aerosol analyses have prevented UAS from being used to their full potential. The University of Alaska has been working on resolving these issues so UAS can be used effectively in atmospheric aerosol sampling studies. This abstract details recent experiences with flying multiple manned and unmanned aircraft simultaneously during a wildfire study in Florida, USA, in fall 2012 and some improvements in sample analysis that will improve scientists' ability to analyze the small amounts of mass collected during UAS aerosol sampling.

The Prescribed Fire Combustion and Atmospheric Dynamics Research Experiment (Rx-CADRE) conducted in late October through early November, 2013, at Eglin Air Force Base in Florida, demonstrated that four UAS and two manned aircraft could be deployed simultaneously to monitor the smoke plume and burning behaviour of a series of prescribed fires from three to 400 ha in area (Figure 1). An Aeryon Scout, two G2Rs, and a Boeing ScanEagle were deployed at 20 m, 200 m, 215 m, and 500 m above the fire, respectively. The Aeryon Scout was used to map the fuels available to burn before and after the fire, so the concentration of smoke particles emitted from the fires could be related to the fuels consumed by the fires and emission factors could be determined. The black carbon and particulate matter measurements collected by an Aethlabs AE52 aethalometer on the ScanEagle will confirm the efficiency of the burn as observed by the thermal cameras on the UASs and the highly aerosol equipped manned aircraft that followed the smoke plume. These measurements are being compared with the VIIRS and MODIS satellite sensor overpasses to establish aerosol thresholds for these sensors.

One of the challenges with an experiment such as Rx-CADRE is the limited amount of aerosol that may be collected by a UAS's instruments during a small fire or if the UAS is above the primary smoke plume. The trade-off has always been that it requires a longer UAS dwell time over an area to get the aerosol concentration and composition over a specific spot versus the ability to map large regions using a UAS. Scientists from the University of Alaska Fairbanks, the University of California, Davis, and Arizona State University are using the Stanford Synchrotron Radiation Lightsource (SSRL) to overcome these limitations. The high flux and energy range of polarized x-rays and ultraviolet light provided by SSRL is allowing the analysis of very small spots (0.5 mm by 1.0 mm) of aerosol collected on a filter or impaction media with very high sensitivity. This overcomes the problem of not having enough particle mass to analyze collected during the UAV's flight over a specific region. The high energy light from SSRL also allows us to excite heavy elements such as uranium while filtering out the far higher x-ray counts from lighter elements that would mask the heavy elements' signatures under normal conditions. This 'filtered white beam' technique greatly increases the sensitivity for the heavier elements of interest to health professionals and pollution experts. The Rx-CADRE samples provide an excellent example of what can be done with time-resolved samples collected by a UAS.

The combination of the successful use of multiple UASs and the improved analysis of aerosols collected by the UASs will allow for UASs to be used effectively in future vertically and spatially-resolved aerosol studies.

Figure 1. This photograph shows the fire behavior and smoke emitted from one of the Rx-CADRE burns as observed using thermal cameras from a Boeing ScanEagle flying at 500 m.

This work was supported by the National Aeronautics and Space Administration (NASA) under grant NNX11AQ27A, the Japanese Aerospace Exploration Agency (JAXA) under the IARC-JAXA Arctic Research Project, and the Army Research Laboratory under grant W911NF-12-2-0068.

Aerosol mass spectrometry on a Zeppelin NT in the planetary boundary layer

F. Rubach[1], A. Trimborn[2], T.F. Mentel[1], A. Wahner[1] and the PEGASOS 2012 Zeppelin Team
[1]Institute for Energy and Climate 8: Troposphere (IEK-8), Forschungszentrum Jülich GmbH, 52425 Jülich, Germany
[2]AeroMegt GmbH, 40723 Hilden, Germany
Keywords: Aerosol mass spectrometry, Airborne measurements, Planetary Boundary Layer.
Presenting author email: f.rubach@fz-juelich.de

The airship Zeppelin NT is an airborne platform capable of flying at low speed throughout the entire planetary boundary layer (PBL). Equipped with a high scientific payload of more than 1 ton, the Zeppelin is an ideal platform to study regional processes in the lowest layers of the atmosphere with high spatial resolution. Here, we will focus on secondary aerosols

Atmospheric aerosols are medium long lived and are of particular interest due to their influence on the global radiation budget. Measurements on board the Zeppelin NT can serve to separate processes of local production from transport processes.

For aerosol measurements on the Zeppelin NT, a High-Resolution Time-of-Flight Aerosol Mass spectrometer (DeCarlo *et al*, 2006) was adapted to the requirements of the an airborne platform. A weight reduction of over 20 % compared to the commercial instrument was achieved, while space occupation and footprint were each reduced by over 25 %. The instrument is now certified to withstand an emergency landing scenario with forces of over 4 kN acting on it.

Within the PEGASOS project (Pan European Gas-AeroSOl-climate interaction Study), the instrument took part in 10 measurement flights over the course of seven weeks. Three flights were starting from Rotterdam, NL, seven flights were starting from Ozzano, IT near Bologna in the Po Valley. Flight patterns included vertical profiles to study the dynamics of the PBL and cross sections through regions of interest to shed light on local production and transport processes.

Exemplary, data obtained during such cross sections on 21 June 2012 were used in conjunction with backward trajectories calculated using the HYSPLIT web-interface (Draxler and Hess, 1997) with meteorological data from GDAS (Parrish and Derber, 1992) to estimate the aerosol production rate of the Po Valley as a source region (see Fig. 1). The aerosol production rate found for nitrate aerosol was the highest, followed by the organic aerosol formation rate. Sulfate aerosol exhibited a low formation rate.

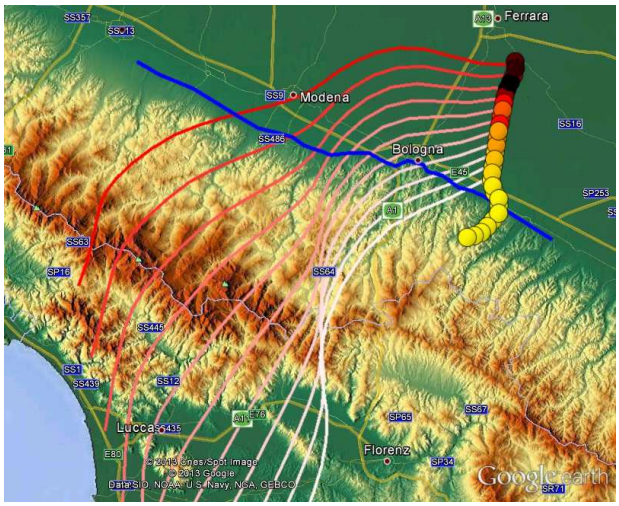

Figure 1. Comparison between nitrate aerosol mass concentration and air mass residence time in Po Valley, IT. Darker dot colours correspond to higher nitrate mass concentration. The highest values were observed crossing the trajectory with the longest residence time in the Po Valley.

The new instrument was operated successfully on nine out of ten measurement days under at times harsh conditions with ambient temperatures of up to 40°C and relative humidities of up to 90 %.

New insights into the aerosol chemical composition as a function of height were gained from regional sections as well as vertical profiles. Furthermore, a new method to elucidate the functionalization of organic aerosol was developed.

These findings will be presented in detail.

The PEGASOS project is funded by the European Commission under the Framework Programme 7 (FP7-ENV-2010-265148).

DeCarlo, P.F. *et al* (2006), *Anal. Chem.*, **78**, 8281-8289.
Draxler, R. R., and G. D. Hess (1997), *NOAA Tech. Memo. ERL ARL-224*, NOAA, Silver Spring, Md.
Parrish, D. F. and Derber, J. C. (1992), *Monthly Weather Rev.*, **120**, 1747-1763

Classification of aerosol size distributions observed at a tropical high altitude station

T. Hamburger[1], M. Matisāns[1], J. Ström[1], P. Tunved[1], G. Hoschild[2], J. Gross[2], S. Calderon[3], P. Hoffmann[3], T. Schmeissner[4] and R. Krejci[1,5]

[1]Department of Applied Environmental Science (ITM), Stockholm University, Stockholm, 106 91, Sweden
[2] Karlsruhe Institute of Technology, Institute for Meteorology and Climate Research (ASF), 76344 Eggenstein-Leopoldshafen, Germany
[3]Universidad de Los Andes, Merida 5101, Venezuela
[4]Leibniz Institute for Tropospheric Research (TROPOS), 04318 Leipzig, Germany
[5]Division of Atmospheric Sciences Department of Physics, University of Helsinki, FI 00014 Helsinki, Finland

Keywords: aerosol measurement, biomass burning, size distribution, tropospheric aerosols.
Presenting author email: thomas.hamburger@itm.su.se

The tropics comprise an important source region of aerosol particles. However, long-term measurements of aerosol properties in the tropical free troposphere are sparse. Aerosol measurements were conducted between March 2007 and May 2009 at the Pico Espejo Atmospheric Research Station Alexander von Humboldt (Schmeissner et al, 2011). The Pico Espejo (8.51° N, 71.05° W, 4765 m a.s.l.) is located on the top of the mountain ridge of the Andes close to the city of Mérida, Venezuela (Figure 1).

Particle number concentration, size distribution, volatility and light absorption were observed at the high altitude research station. The aerosol instrumentation contained a Particle Soot Absorption Photometer (PSAP) and a Differential Mobility Particle Sizer (DMPS). Particle number concentrations were measured using Condensation Particle Counters (CPC). A thermodenuder was used to heat the sampled aerosol to 300°C.

The Venezuelan savannah spreads out east of the Venezuelan Andes, i.e. upwind the observation site. The savannah region comprises a wide area of potential biomass burning land during the dry season, December-April (Morales et al., 1990). The boundary layer air masses which are affected by biomass burning reach the high altitude station during daytime due to shallow convection and uplift of air masses along the mountain slope.

The special location of the observation site allows for observations of different air mass types during the wet and dry season. Air masses within the lower free troposphere (LFT) and the boundary layer (BL) were observed. The interactions and mixing at the boundary layers between the different air masses could be studied.

Observed aerosol number size distributions were grouped and classified by using cluster analysis (Dorling et al., 1992). Prior to the clustering, each observation was normalised to its maximum number concentration. Hence, the observations were clustered according to the shape of the size distribution. This procedure allows for investigating the source types and processes leading to the respective shapes rather than examining the source strength which controls the number concentration.

Figure 1 shows the resulting clusters and their average number size distributions. The size distributions are ordered clockwise according to their skewness starting from the top left corner with dominating accumulation mode towards dominating Aitken mode. Size distributions which indicate new particle formation were dominantly observed at the transition from the lower free troposphere to the boundary layer at noon time during the dry season. The dry season was also dominated by size distributions exhibiting high aerosol mass compared to the wet season.

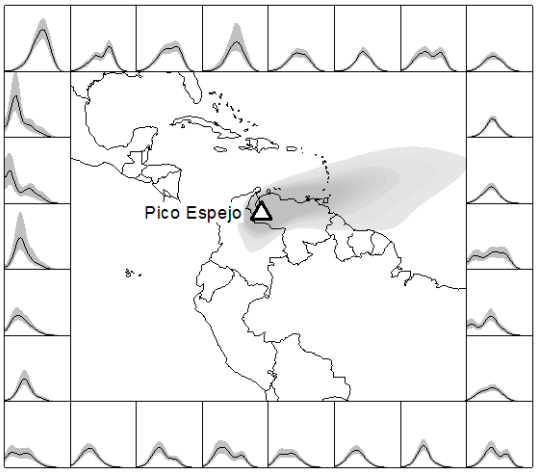

Figure 1. Clustered size distributions (25th-75th percentile and median). The grey shade in the map indicates possible source regions based on 5-day back trajectories.

Further analysis of statistics on observed meteorological parameters and particle properties allowed for insight into occurring aerosol processes and air mass types for each cluster.

This work has been funded by Swedish Research Council (VR) and Swedish International Development Cooperation Agency (SIDA).

Dorling, S. R., et al. (1992) *Atmospheric Environment* **26A**, 2575-2581.
Morales, J. A., et al. (1990) *Atmospheric Environment* **24A**, 407-414.
Schmeissner, T, et al. (2011) *Atmos. Chem. Phys.* **11**, 3319-3332.

Chemical composition (ions and selected metals) of size-segregated aerosol samples collected at Ny Alesund (Svalbard Island - Norway) during the 2010 and 2011 summer campaigns.

S. Becagli[1], M. Busetto[2], G. Calzolai[3], D. Cappelletti[4], D. Frosini[1], F. Lucarelli[3], A. Lupi[2], M. Mazzola[2], B. Moroni[4], S. Nava[3], M. Severi[1], R. Traversi[1], A. Viola[5], V. Vitale[2], R. Udisti[1]

[1] Department of Chemistry, University of Florence, 50019 Sesto F.no (FI), Italy.
[2] CNR-ISAC, 40129 Bologna, Italy.
[3]Dept. of Physics and Astronomy, University of Florence and INFN Florence, 50019 Sesto F.no (FI), Italy
[4]DICA and SMAArt, University of Perugia, Perugia, 06125, Italy
[5] CNR-ISAC, 00133 Roma, Italy.

Keywords: Arctic aerosol, chemical composition, Ny Alesund, seasonal pattern
Presenting author email: udisti@unifi.it

The atmospheric aerosol plays a relevant role in the complex feedback processes between environmental conditions and climatic changes because of the scattering and absorption processes of the solar radiation and its contribution in the hydrological cycle by promoting the cloud formation. IPCC 2007 report shows very large uncertainties in sign and intensity of the climate forcing induced by the atmospheric particulate. For instance, the black carbon particles act as positive forcings because light absorption processes prevail. On the contrary, liquid droplets of sulphuric acid exert a negative forcing due to the prevalent scattering effect on the incoming solar radiation. Such effects are even more complex in the polar regions, where the high superficial albedo can play a higher scattering than aerosol particle or cloud surface. In this case, the presence of aerosol or cloud coverage represents a positive climate forcing. Finally, a reliable evaluation of the climatic effect of the aerosol particles in the Polar Region is hindered by an incomplete spatial coverage of the monitoring sites.

In order to improve our knowledge on the size distribution and chemical composition of the Arctic aerosol, since 2010 an observatory was installed at Ny Alesund (78.6 °N, 11.6 °E), Svalbard Islands.

During two summer (March-September) campaigns (2010 and 2011), several hundred samples were collected by different devices: PM10 sequential samplers (on Teflon filters for inorganic components and quarttz filters for organic compounds), 4-stage (>10, 10-2.5, 2.5-1, < 1 um) and 12-stage (> 10 um to 0.040 um) Dekati impactors (for ions, metals and elements analysis), and medium-volume PM10 collector (for trace metals content). Aerosol samplings were carried out with a temporal resolution from 1 to 4 days and were coupled with continuous size distribution measurements by a Scanning Mobility Particle Sizer (SMPS), working in the range 6 - 500 nm, and an Aerodynamic Particle Sizer (APS), able to count the atmospheric particulate in the range 0.5 – 20 um. The two instruments were synchronized in order to obtain a unique spectrum of 106 size-classes in the range 6 nm –20 um every 10 minutes.

Aerosol filters were analysed by Ion Chromatography (inorganic anions and cations and selected organic anions), ICP-AES and ICP-MS (selected metals, including Rare Earth Elements), PIXE (elemental composition) and thermo-optical SUNSET analyser (EC and OC fractions).

Here we report temporal profiles of the most significant chemical components, used as markers of emission sources and/or transport processes. Particular attention was spent in depicting the seasonal (spring-fall) trend of the main components of the bio-geo-chemical cycles of sulphur (sea salt sulphate, non-sea-salt sulphate, methanesulphonic acid), nitrogen (nitrate and ammonium salt) and carbon (short-chain carboxylic acids, OC fraction). Besides, the measurements of the EC fraction can be used in assessing the relationship between the optical effect of the black carbon particles (measured by absorption techniques) and the actual content of elemental carbon in size-segregated particles.

Figure 1 shows the temporal trends of four relevant components of the secondary aerosol in the daily PM10 samples in March-September 2010. Sulphate, ammonium and oxalate show the input of long-range transport of polluted air masses from continental areas occurring in the early spring. On the contrary, MSA profile points out the higher biogenic emissions of marine biogenic sources in late spring-early summer.

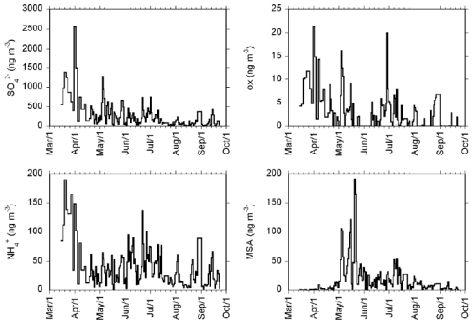

Figure 1. Temporal trends of selected markers in PM10.

The chemical composition has been compared with the high-resolution particle size-distribution, meteo conditions and back-trajectory reconstruction to better understand the effect of changes in source intensity and transport processes. Besides, a multivariate statical analysis based on a receptor model (Positive Matrix Factorization and Absolute Principal Components Analysis) was applied to the data set for source apportionment analysis.

This work was supported by Italian Education, University and Research Ministry (MIUR) and by National Research Council (CNR-DTA) funds and facilities.

Sub-micrometer non-refractory aerosol composition and their sources at Welgegund in the southern African grassland region

Tiitta, P.[1,2], Vakkari, V.[5], Josipovic, M.[1], Croteau, P.[6], Beukes, P.[1], Van Zyl, P.[1], Venter, A.[1], Jaars, K.[1], Pienaar, J.[1], Ng, S.[8], Canagaratna, M.[6], Jayne, J.[6], Kerminen, V. [4], Kulmala, M.[5], Laaksonen, A. [3,4], Jokiniemi, J. [2,7], Worsnop, D.[5,6] and Laakso, L.[1,5]

[1]School of Physical and Chemical Sciences, NWU, 2520 Potchefstroom, South Africa
[2] Department of Environmental Sciences, University of Eastern Finland, P.O.Box 1627, FI-70211 Kuopio, Finland
[3] Department of Applied Physics, University of Eastern Finland, P.O.Box 1627, FI-70211 Kuopio, Finland
[4]Finnish Meteorological Institute, P.O. Box 503, 00101 Finland
[5]Department of Physics, University of Helsinki, P.O. Box 64, 00014 Finland
[6]Aerodyne Research Inc., 45 Manning Road, Billerica, MA 01821-3976, Massachusetts, USA
[7]VTT technical Research Centre of Finland, Fine Particles, P.O.Box 1000, FI-02044, Espoo, Finland
[8]School of Chemical and Biomolecular Engineering and School of Earth and Atmospheric Sciences, Georgia Institute of Technology, Atlanta, Georgia, USA

Keywords: submicron particles, aerosol mass spectrometry, aerosol chemistry, organic aerosols, nitrate
Presenting author email: petri.tiitta@uef.fi

In this study we present the first long-term high time resolution aerosol chemical composition measurements in southern Africa.

The Welgegund measurement site, with a wide range of atmospheric aerosol and gas, as well as meteorological observations (Beukes *et al.*, 2013; www.welgegund.org) is located approximately 100 km south-west of the Johannesburg-Pretoria conurbation (population over 10 million), in South Africa (26°34'10"S, 26°56'21"E, 1480 m.asl). There are only a few local pollution sources close to the measurement site. It is frequently over-passed by air masses with pollution plumes from the highly populated megacity and major industrialized regions in the interior of South Africa. There are also clean air intrusions from a clean western sector.

The submicron chemical composition was measured by using a Aerosol Chemical Speciation Monitor (ACSM, Ng *et al.*, 2011). Positive matrix factorization (PMF) was also applied to characterize the sources and transformation of organic aerosols (OA) in the atmosphere. Air mass history was investigated using back trajectories (HYSPLIT). Our results provide an overview of the chemical composition of submicron species in southern Africa during wet and dry seasons. Insights into the sources and atmospheric processing of organics aerosols near the megacity area of Johannesburg are also obtained.

The high biomass burning organic aerosol (BBOA) and nitrate (NO_3^-) concentrations observed when air-masses over passed the megacity (MC) region (Figure 1) indicate the large amount of emissions from combustion processes in the densely populated megacity region. These emissions characterized mainly from traffic and household combustion (domestic burning of biomass for heating and cooking). However, the highest BBOA concentrations (up to 40 μg/m^3) were observed during the dry season, strongly and frequently impacted by to savannah fires and adverse meteorological conditions over the interior of South Africa (see Swap *et al.*, 2003).

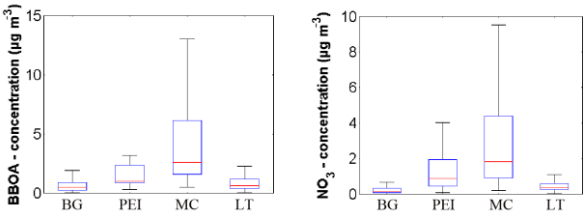

Figure 1. Average biomass burning organic aerosol (BBOA) and nitrate (NO_3^-) concentrations during the dry season calculated for four source regions, i.e background without major sources (BG), petrochemical industry (PEI), megacity (MC) and long-range transport regions (LT). The box plot indicates the 25th and 75th percentiles and the line within the box marks the median. Whiskers show 5 th and 95th percentiles.

This work was supported by the Academy of Finland (project number 132640**)** and the Saastamoinen foundation.

Beukes, J.P., Vakkari, V., van Zyl, P.G., Venter, A.D., Josipovic, M., Jaars, K., Tiitta, P., Kulmala, M., Worsnop, D. Pienaar, J.J., Järvinen, E., Chellapermal, R., Ignatius, K., Maalick, Z., Cesnulyte, V., Ripamonti, G., Laban, T.L., Skrabalova, L., du Toit, M., Virkkula, A., and Laakso, L., Source region characterization of the South African interior, in prepartion to be submitted to ACPD, 2013.

Ng, N., Herndon, S., Trimborn, A., Canagaratna, M., Croteau, P., Onasch, T., Sueper, D., Worsnop, D., Zhang, Q., Sun, Y., Jayne, J. (2011) *Aerosol Sci. Tech.*, 45(7), 780-794.

Swap, R., Annegarn, H., Suttles, J., King, M., Platnick, S., Privette, J. and Scholes, R. (2003). Africa burning: A thematic analysis of the Southern African Regional Science Initiative (SAFARI 2000). *J. Geophys. Res*. 108, 8465. DOI: 10.1029/2003JD 003747.

Chemical composition of the 300°C refractory fraction of the atmospheric aerosol at the Central European station Melpitz, Germany

L. Poulain[1], W. Birmili[1], F. Canonaco[2], M. Crippa[2], Z.J. Wu[1], S. Nordmann[1], G. Spindler[1], A.S.H. Prévôt[2], A. Wiedensohler[1] and H. Herrmann[1]

[1] Leibniz-Institute for Tropospheric Research (TROPOS), Permoserstr. 15, 04318 Leipzig, Germany
[2] Paul Scherrer Institute (PSI), Villigen, Switzerland
Keywords: volatility, AMS, chemical composition.
Presenting author email: poulain@tropos.de

The volatilization of the atmospheric aerosol leaves so-called refractory particle cores containing material that is non-volatile at the given temperature. In the fine particle mode (particle diameter < 1 µm), this refractory material can be mainly associated with soot particles and low-volatile organics, and occasionally to a smaller fraction with sea salt and mineral dust. The carbonaceous materials have in common that they are responsible for effects as different as atmospheric light absorption (black carbon, BC), and adverse effects upon human health (toxic compounds attached to diesel soot). In consequence, there is a significant interest to describe the carbonaceous particle mass fraction in functional detail, and characterize the existing methodologies for their continuous monitoring in the atmosphere.

This work analyses the refractory atmospheric aerosol fraction at the regional Central European research site Melpitz (Germany). The experimental methods combine a mobility particle size spectrometer (3-800 nm) in conjunction with a thermodenuder working at 300°C (residence time of 0.8 – 1 s), a multi-angle absorption photometer (MAAP), and an aerosol mass spectrometer (AMS) during two intensive field campaigns (May-June 2008 and February-March 2009). As a first result, we detected refractory volume fractions of 11±3 % (2008) and 17±8 % (2009) in the atmospheric aerosol. In both periods, BC was in close linear correlation with the refractory fraction, but was not sufficient to quantitatively explain the refractory particle mass concentration.

Based on the assumption that BC is not altered by the heating process, the refractory particle mass fraction was explained by black carbon and a refractory organic aerosol (ROA) contribution estimated as a fraction of the Low-Volatility Oxygenated Organic Aerosol (LV-OOA); the latter was identified from AMS data by factor analysis. Although carbonaceous compounds dominated the refractory particle mass fraction for most of the observation time, a cross-sensitivity of partially volatile marine aerosol particles could be seen in Atlantic air masses during February-March 2009. These particles were originally in the super-µm range, but moved into the submicrometer range after volatilization. In summary, after correction from the supermicrometer artifact for each period, our results confirm that the volatilization of the atmospheric aerosol in a thermodenuder at 300°C leaves not only major fractions of black carbon (47% and 59% of the estimated refractory mass for the 2008 and 2009 campaigns, respectively), Figure 1, but also of organic compounds (53% and 41% of the estimated refractory mass for the 2008 and 2009 campaigns respectively).

The present work shows that organics were more volatile in summer than in winter, which emphasizes the influence of different organic sources as well as differences in the organic aerosol behavior in the atmosphere (e.g. secondary organic aerosol formation and/or aging processes). Different sources of uncertainty and factors influencing the present estimation will be presented. Furthermore, recommendations are proposed for future long-term observations using a thermodenuder.

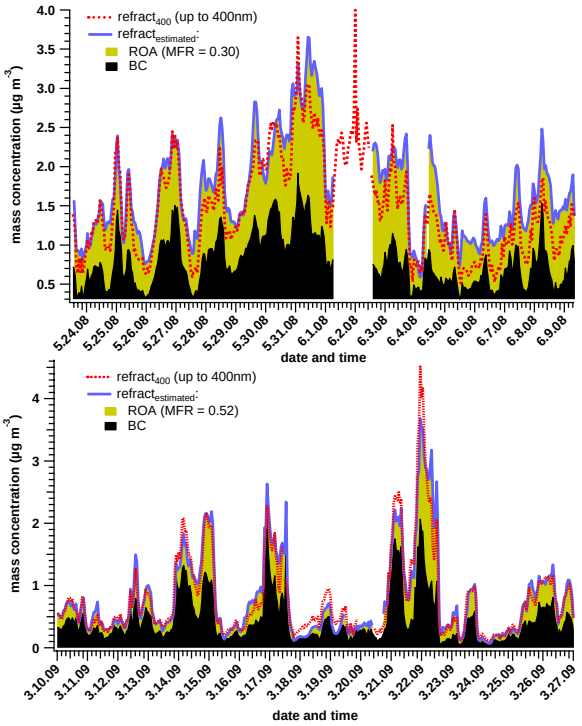

Figure 1: Time series of the measured (red line) and estimated (blue line) refractory mass concentration for late spring 2008 (top) and early spring 2009 (bottom). Contributions of BC and Refractory organic aerosol (ROA) are also included.

This work was supported by the German Federal Environment Agency grants No 35103031, 35101038, UFOPLAN grand No 370343200, and the Swiss Federal Office for the Environment.

Seasonal and spatial variation of PM_1 organic tracers in densely populated Mediterranean urban areas: Barcelona vs. Madrid

B.L. van Drooge[1], M.Fontal[1], N.Bravo[1], P.Fernandez[1], M.A.Fernández[2], J.Muñoz-Arnanz[2], B.Jiménez[2], J.O.Grimalt[1]

[1]Dpt. Environmental Chemistry. Institute of Environmental Assessment and Water Research (IDÆA), CSIC. Jordi Girona, 18. 08034 Barcelona, Spain.
[2]Dpt. Instrumental Analysis and Environmental Chemistry. Institute of Organic Chemistry (IQOG), CSIC. Juan de la Cierva, 3. 28006 Madrid, Spain.

Keywords: organic aerosol, biogenic SOC, biomass burning, urban aerosol
Presenting author email: barend.vandrooge@idaea.csic.es

A comprehensive PM1 aerosol characterization was conducted within the AEROTRANS project. About 100 organic tracer compounds were analyzed in PM_1 filter extracts that were sampled from 2010 to 2012 in busy streets in the urban centres of Madrid (700 m.asl) and Barcelona (20 m.asl) (Spain), at ground-level and at 40 m.agl (N=57). Both urban areas have intensive traffic and a Mediterranean climate, although Madrid is continental and Barcelona is coastal. Summer and winter season was sampled, as well as night- and daytime, in order to distinguish possible seasonal and diurnal variation in organic tracer composition and concentrations.

Primary organic tracers for traffic and dust were 2 times higher at ground-level, with a daytime maximum, and generally 2 times higher concentrations in winter.

No significant differences were observed between ground-level and altitude measurements for secondary organic carbon (SOC) tracers, from biogenic origin (isoprene and pinene) and anthropogenic origin, suggesting that many of these products are related to regional air mass circulation and relatively stable in the urban atmosphere. However, relationships between specific biogenic tracers could be explained by the abundance of oxidants in the urban atmosphere, such as the relationship between isoprene SOCs and NOx (Figure 1). The biogenic SOC concentrations were about 10 times higher in summer than in winter. Largest differences were observed for isoprene SOC tracers (Figure 2).

Organic tracers for biomass burning increased by a factor of ~7 in both sites during the winter. There was more discrepancy in the concentration between ground-level and altitude, suggesting the presence of local sources or less atmospheric stability for these compounds. However, the good correlations between biomass tracers from different 'families' (e.g. acids and saccharides) suggested that nearby sources were responsible for this variation. A summer-time 2012 PM-event in Barcelona was directly linked to the impact of a sever wild-fire 100 km to the north of the city. All biomass organic tracers increase a factor ~100 in the 12-hour sample, while levels 'normalized' to background concentrations in the sample afterwards.

Despite the different geographical locations (continental vs. coastal), Madrid and Barcelona exhibit very similar compositions and concentrations of organic tracers for biogenic and anthropogenic SOC as well as for biomass burning. Larger differences were observed for primary organics, such as primary sugars and fatty acids (figure 2.) which were all higher in Barcelona and could be related to more humid atmosphere of Barcelona compared to Madrid.

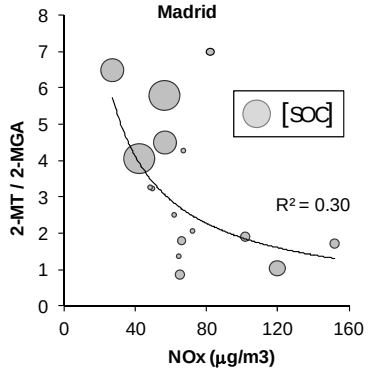

Figure 1. 2-methyltetrols-to-2-methylglyceric acid ratios vs. NOx concentrations in Madrid in relation with isoprene SOC.

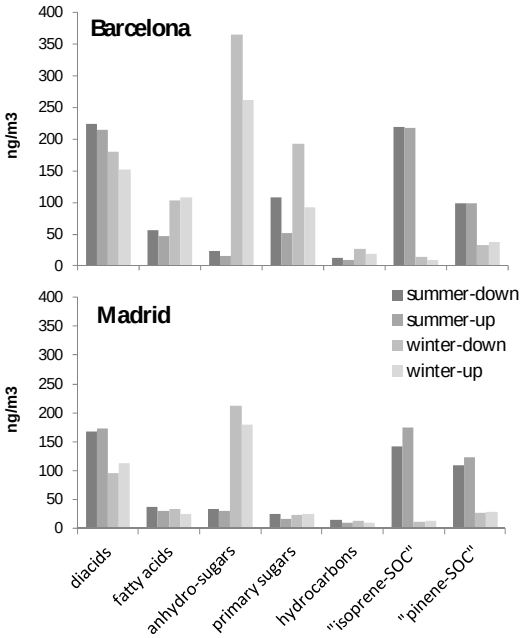

Figure 1. Concentrations of organic tracers in PM1 from Barcelona and Madrid sampled at ground-level (down) and 40 m.agl (up).

This work was supported by the Spanish Ministry of Economy under grant CTQ2009-14777-C02-01 and CTQ2009-14777-C02-02

Winter particulate matter (PM10) sources for an Austrian-Slovenian border region.

M. Kistler[1], E.C. Cetintas[1], H. Bauer[1,†] and A. Kasper-Giebl[1]

[1]Institute of Chemical Technologies and Analytics, Vienna University of Technology, Vienna, A1060, Austria
Keywords: local PM10, carbonaceous aerosol.
Presenting author email: magdalena.kistler@tuwien.ac.at

Air pollution by particulate matter derived from biomass burning is recognized as a worldwide problem and is considered from the point of view of scientists and politicians, respectively. Many European regions have difficulties with keeping the internationally, nationally or locally defined limit values. Emission sources may cause pollution across the borders, what makes one-sided reduction policies inefficient. This is true also for residential burning particles, as observed e.g., in Aosta Valley (IT, FR, CH, Finardi *et al.,* 2002).

The following study was set by local authorities of South Austria and North Slovenia in order to develop efficient methods to improve the local air quality. The scientific goal was to obtain a detailed chemical characterization of collected particulate matter, information about its sources and the optimization of methods for assessment of source contributions.

Particulate matter sampling was conducted at four urban and three background stations in Carinthia (AT), South Styria (AT) and Maribor region (SI). PM10 was collected between 29.01.2011 and 28.02.2011 daily (24h), on quartz fibre filters (Pallflex, 150mm), using high volume samplers (~700m³). The particle mass was determined gravimetrically.

Circular filter aliquots (with 10mm diameter) were used for the determination of carbon parameters (organic carbon, OC and elemental carbon, EC) with a thermal-optical method (*Sunset OCEC Aerosol Lab Analyser*), using a EUSAAR2 temperature protocol (Cavalli *et al.,* 2009). Inorganic ions and sugars were analysed using ion chromatography (*Dionex*) with conductivity (ions) or pulsed amperometric detection (saccharides). For this purpose 3 to 5 filter aliquots (10mm) were eluted with extra pure Milli-Q (resistance 18.2 MΩ) water (anions, sugars) or with 12 mM methane sulphonic acid (cations).

HULIS (humic like substances) were determined with a TU Vienna derived method (Limbeck *et al.*, 2005) comprising an NDIR analysis of CO_2 evolved from combustion of water- and alkali-extract treated with appropriate solid phase extraction.

Selected elements including Al were analysed using X-Ray Fluorescence.

Aerosol water content was assessed with thermo-gravimetric method in which the loss of weight of a filter aliquot heated to 100°C in a thermo-balance under nitrogen atmosphere and kept at this temperature for 5 minutes is equivalent to the aerosol H_2O.

Source analysis was performed using a simple macro-tracer approach, describing up to nine main aerosol sources (Puxbaum *et al.,* 2005). This model involves anhydrosugars: levoglucosan and mannosan as specific tracers for wood burning (Schmidl *et al*., 2008, 2011, own unpublished data).

Except for the rural background station in Styria the short-term PM10 threshold value was exceeded between 17 and 20 times during the measurement period. The average PM10 concentration observed for urban sampling points was 60 µg/m³.

The contribution of biomass burning was lowest in the rural background in Styria (22%), and accounted up to 40% in Carinthia (urban background), being the most relevant local PM10 source. Similar significance was observed for secondary inorganic aerosols (ammonium sulphates and nitrates): between 29% (Carinthia, urban traffic) to 48% (Styria rural background). Traffic near locations were characterized by a higher impact of fossil fuel emissions (expected mainly from Diesel engines), mineral dust (carbonates and silicates) and de-icing salt (both from the re-suspension). On the other hand a higher amount of organic secondary aerosols was found at background measurement sites.

This work was conducted with samples collected within the INTERREG IVA SI-AT PMinter project conducted through the Municipality of Klagenfurt, Municipality of Maribor and Styrian Government, in cooperation with Provintial Government of Carinthia, Public Health Institute Maribor, TU Graz and the University of Maribor. Lab work by C. Ramirez Santa Cruz L. Sampaio Cordeiro Wagner, E. Schriener (Institute of Chem. Technologies and Analytics) and S. Lüftl from Institute of Material Science and Technology is gratefully acknowledged.

Cavalli, F., Viana, M., Yttri, K.E., Genberg, J., Putaud, J-P., (2009). *Atmos. Meas. Tech. Discuss.,* **2,** 2321–2345.

Finardi, S., Agnesod, G., Brusasca, G., Calori, G., Nanni, A., Pession, G., Tinarelli, G., Zublena, M., (2002). *Proc. 8th Int. Conf. on Harmonisation within Atmospheric Dispersion Modelling for Regulatory Purposes,* Sofia, Bulgaria.

Limbeck., A., Handler, M., Neuberger, B., Klatzer, B., Puxbaum, H., (2005). *Anal. Chem.,* **77,** 7288-7293.

Puxbaum, H., Kasper-Giebl, A., Bauer., H., (2005). *Conf.: Chemistry, Transport and Impact of Atmospheric Pollutants with Focus on Fine Particles*, Andechs, Germany.

Schmidl, C., Marr, I., Caseiro, A., Kotianova, P., Berner, A., Bauer, H., Kasper-Giebl, A., Puxbaum, H., (2008). *Atmos. Environ.,* **42**, 126-141.

Schmidl, C., Luisser, M., Paouvas, E., Lasselberger, L., Rzaca, M., Ramirez-Santa Cruz, C., Handler, M., Peng, G., Bauer, H, Puxbaum, H., (2011). *Atmos. Environ.,* **45**, 7443-7454.

Wednesday, September 4, 2013

Session: Atmospheric Aerosols,
Urban aerosols-from particle counts to chemical compostion

Nanoparticle emissions from road vehicles in Asian and European cities and allied health implications

Prashant Kumar[1, 2], Roy M. Harrison[3, 4]

[1]Department of Civil and Environmental Engineering, Faculty of Engineering and Physical Sciences (FEPS), University of Surrey, Guildford GU2 7XH, United Kingdom
[2]Environmental Flow (EnFlo) Research Centre, FEPS, University of Surrey, Guildford GU2 7XH, United Kingdom
[3]Division of Environmental Health & Risk Management, School of Geography, Earth & Environmental Sciences, University of Birmingham, Edgbaston, Birmingham B15 2TT, United Kingdom
[4]Also at: Centre of Excellence in Environmental Studies, King Abdulaziz University, PO Box 80203, Jeddah (21589) Saudi Arabia
Keywords: Nanoparticles, Pollution, Emissions, Exposure.
Presenting author email: P.Kumar@surrey.ac.uk

Epidemiological evidence has accumulated in recent years to demonstrate the association between human health effects and exposure to airborne nanoparticles (referring here to those below 300 nm since these contribute over 99% of total particle number concentrations, PNCs, in ambient environments). Vehicles can add up to 90% of total PNCs in polluted cities where vehicle numbers are increasing, as is likely to be the case with the nanoparticle emissions and hence the exposure of urban dwellers (Kumar *et al*., 2013).

This work examines the nanoparticle emissions from road vehicles in Asian and European urban environments, the levels of ambient and roadside PNCs, discusses the elementary reasons for the differences in PNC levels, and analyses the health impacts. About 45 sampling locations in 30 European cities are evaluated (Kumar *et al*., 2012). As summarised in Figure 1, the average PNCs at the roadside and urban background sites were found to be $3.82\pm3.25 \times 10^4$ cm^{-3} and $1.63\pm0.82 \times 10^4$ cm^{-3}, respectively. A sample review of PNCs in Asian environments was conducted which, as expected, showed notably higher PNCs than those found in European environments.

Preliminary estimates of total particle number emissions from road vehicles in Delhi were made in current and future years (Kumar *et al*., 2011). The results revealed the typical characteristics of traffic emissions and exposure in typical Asian cities, highlighting the largest contribution from the heavy duty vehicles, followed by passenger cars, to total particle number emissions despite their modest contribution to vehicle kilometres travelled. The introduction of zero sulphur motor fuels in Europe is having a beneficial impact upon airborne nanoparticle concentrations, and the use of diesel particle filters should further improve the situation in the more developed countries, but problems will remain for many years to come, especially in the less developed world.

PK and RMH gratefully acknowledge the support received from collaborators (Profs. Lidia Morawska, Mukesh Khare, Rex Britter, Prateek Sharma, and Drs. B.R. Gurjar, Suresh Jain, and A.S. Nagpure) at various stages of this research.

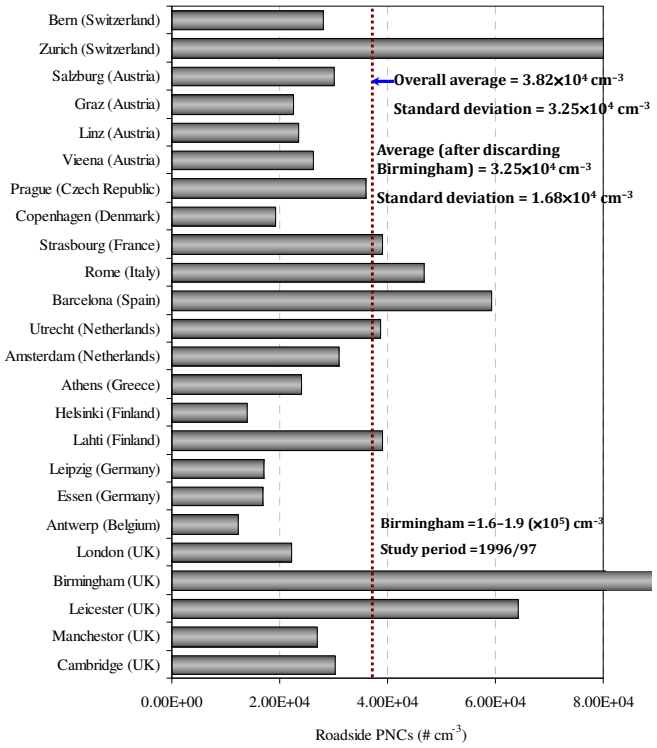

Figure 1. Typical roadside average PNCs at various locations in European cities (source: Kumar *et al*., 2012).

Kumar, P., Gurjar, B.R., Nagpure, A. and Harrison, R.M. (2011) Preliminary estimates of particle number emissions from road vehicles in megacity Delhi and associated health impacts. *Environ. Sci. Technol.* **45,** 5514-5521.

Kumar, P., Morawska, L. and Harrison, R.M. (2012) Nanoparticles in European cities and associated health impacts. *In: The Handbook of Environmental Chemistry: Air Quality in Europe* (Springer-Verlag Berlin Heidelberg; Viana, M. Eds), pp. 1-27.

Kumar, P., Jain, S., Gurjar, B.R., Sharma, P., Khare, M., Morawska, L. and Britter, R. (2013) Can a "Blue Sky" return to Indian megacities? *Atmos. Environ.* doi: 10.1016/j.atmosenv.2013.01.055, In Press.

Long-term Variations of Particle Sources in Beijing, China

J. Gu[1, 2], S. Breitner[1], A. Schneider[1], M. Hu[3], Z.J Wu[3, 4], Z.B Wang[3, 4], A. Wiedensohler[4], B. Wehner[4], U. Franck[5], J. Soentgen[2], A. Peters[1] and J. Cyrys[1, 2]

[1]Institute of Epidemiology II, Helmholtz Zentrum München, Neuherberg, 86754, Germany
[2]Environment Science Center, University of Augsburg, Augsburg, 86159, Germany
[3]State Key Joint Laboratory of Environmental Simulation and Pollution Control, Peking University, Beijing, 100871, China
[4]Department Aerosol and Clouds, Leibniz Institute for Tropospheric Research, Leipzig, 04318, Germany
[5]Core Facility Studies, Helmholtz Centre for Environmental Research – UFZ, Leipzig, 04318, Germany
Keywords: particle size distribution, source apportionment, Olympic, Beijing.
Presenting author email: jianwei.gu@physik.uni-augsburg.de

Studies have shown that ultrafine particles (UFP, often expressed in particle number concentrations, PNC) have adverse health effects independently from particulate mass (Delfino *et al*., 2005). Beijing, the home of about 20 million people, is one of the most air polluted cities. To improve the air quality during the 2008 Summer Olympics, Beijing had strove to cut the emissions. As already reported, air quality during the Game period (Aug 8-24, 2008) was improved, e.g., levels of particulate mass, chemical composition and gaseous pollutants (Wang *et al*., 2010; Schleicher *et al*., 2012). However, it is still not clear whether the observed decrease was caused by the introduced measures or by meteorological conditions. The aims of this study are to evaluate the long-term variations in source contribution to particle levels in Beijing by means of Positive Matrix Factorization (US EPA PMF 3.0), and to study the reductions of PNC in summer 2008.

Particle number size distribution data (PNSD) covering the size range of 3 nm to 10 µm was obtained by a combination of Dual Mobility Particle Size Spectrometer (TROPOS-type TDMPS) and Aerodynamic Particle Size Spectrometer (TSI APS model 3321). The data was collected at an urban background monitoring site located on the campus of Peking University, Beijing between March 2004 and December 2008.

Seven factors were obtained from the source apportionment analysis and were associated with nucleation, growth of new particles, traffic emissions, combustion emissions, secondary aerosols, long range transported dust and coarse particles. Factor particle volume concentration (PVC) was calculated from PNC assuming spherical shape of particles.

Table 1 shows the factor PNC and PVC from 2005-2008. Figure 1 presents the factor contributions to PNC in four years. Highest PNC was found in 2005 (27317 cm^{-3}). The lowest PNC were observed in 2008 and 2006 (20057 and 21173 cm^{-3}, respectively), a decrease of ~23% compared with 2005. A consistent decrease in combustion factor from 2005 to 2008 was observed. The other factors, with their highest levels observed in 2005, didn't show consistent increasing or decreasing trends.

High particle volume concentrations were found in 2007 (131.0 $\mu m^3\ cm^{-3}$), followed by 2005 (124.5 $\mu m^3\ cm^{-3}$). Lower PVC were found in 2006 and 2008 (105.7 and 109.3 $\mu m^3\ cm^{-3}$, respectively), which was mainly due to low concentrations of combustion factor and secondary aerosols factor. Long-range dust factor showed an increasing trend from 2005 to 2008.

Table 1. Factor PNC and PVC in 2005-2008 (factors with marginal contributions to PNC/PVC are omitted).

PNC (cm^{-3})	2005	2006	2007*	2008
Nucleation	3079	1823	1714	2376
Growth of new particles	5578	4224	5006	4681
Traffic	11256	8528	10113	9124
Combustion	6463	5924	5918	4124
Sum	27317	21173	23761	21057
PVC ($\mu m^3\ cm^{-3}$)	2005	2006	2007	2008
Combustion	39.6	36.3	43.1	30.0
Secondary aerosols	38.7	25.8	39.2	27.9
Long-range dust	17.1	24.4	26.1	26.8
Coarse particles	23.4	14.9	16.8	19.3
Sum	124.5	105.7	131.0	109.3

*the year 2007 has data coverage of 34% only.

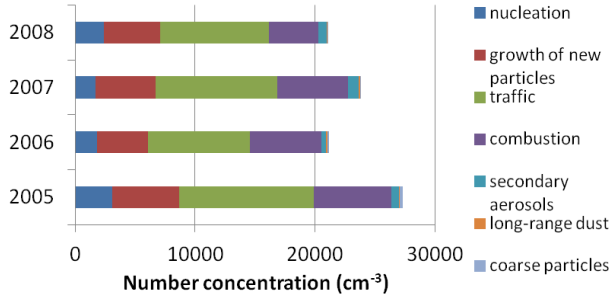

Figure 1. Factor contributions to PNC in 2005-2008.

Analysis on the summer 2008 to study if the meteorology further influenced the PSD factors during the Olympic Game period is already ongoing and will be presented at the conference.

Delfino, R., Sioutas, C., Malik, S. (2005) *Environ Health Perspect.* **113**, 934–46.
Wang, T., Nie, W., Gao, J., Xue, L., et al. (2010) *Atmos Chem Phys*. **10**, 7603-7615.
Schleicher, N., Norra, S., Chen, Y., Chai, F., Wang, S. (2012) *Sci Total Environ*. **427-428**, 146-158.

Road tunnels - particle properties, wet and dry conditions

S. Janhäll[1], M. Gustafsson[1], S. Abbasi[2], G. Blomqvist[1], A. Gudmundsson[3], C. Johansson[4,5], M. Norman[5], U. Olofsson[2], B. Sjövall[5]

[1]VTI - Swedish National Road and Transport Research Institute, Linköping, SE 581 95, Sweden
[2] KTH Machine Design, Stockholm, SE 100 44, Sweden
[3]Division of Ergonomics and Aerosol Technology, Lund University, Lund, SE 221 00, Sweden
[4]Department of Applied Environmental Science, Stockholm University, Stockholm, SE 106 91, Sweden
[5] Stockholm Environment and Health Administration, SLB-analysis, Stockholm, SE 104 20, Sweden

Keywords: particle, tunnel, road, traffic
Presenting author email: sara.janhall@vti.se

Particulate air pollution in traffic tunnels is often very high due to high emissions and restricted air exchange (e.g. Gëller *et al.*, 2005). Road traffic tunnels have both exhaust and non-exhaust particle sources such as tires, pavement and brakes. In tunnel environments the emissions of ultrafine particles would decrease due to high levels of particle surface area for deposition (Janhäll *et al.*, 2012).

In an on-going research project, airborne particles in one road and one railroad tunnel (Gustafsson *et al*, these proceedings) are characterized regarding concentrations, size distributions and elemental composition in relation to traffic. This abstract show initial project results for the road traffic tunnel, with the aim to characterise and identify the main particle sources to be able to suggest abatement measures.

Particle properties were studied during campaigns in the Söderledstunneln (road tunnel in central Stockholm). The measurements were performed in a small room adjacent to the tunnel and with the inlets mounted within the tunnel from drilled holes, while the road dust load was measured directly at the road surface when the tunnel was closed for maintenance. Dust sampling was made with the VTI wet dust sampler (Jonsson *et al.*, 2008, Blomqvist *et al.*, these proceedings).

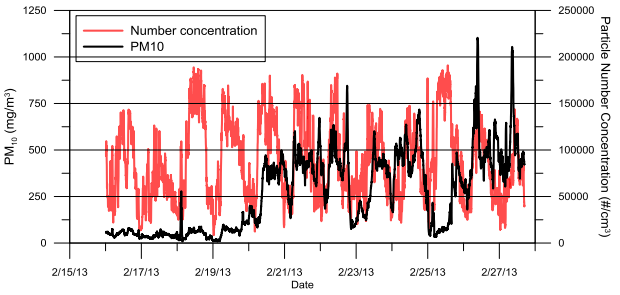

Figure 1.The concentrations of PM_{10} and particle number show the onset of abrasion particle suspension.

Figure 1 shows concentration of PM_{10} and of particle number. Around the 20th of February PM_{10} increase due to drying up of the road surface in the tunnel, while the particle number concentrations are not affected. The size distribution in the size range between 0.5 and 20 µm is shown in Figure 2, where it is clear that the wet conditions give a less pronounced peak as well as very much lower concentrations. Directly before the campaign started, also during wet conditions, samples of the road dust load showed very large levels as compared to road dust load at the surface roads in the same area.

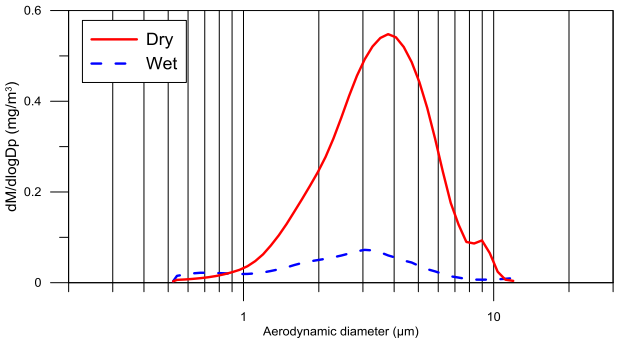

Figure 2. Particle mass size distribution averaged over the first, wet part of the campaign and over the second, dry part of the campaign, respectively.

Further work will describe differences between road and railroad tunnel particle emissions, size resolved particle composition, source apportionment and abatement strategies.

This work was supported by the BVFF; a research program financed Swedish Transport Administration, The Royal Institute of Technology, KTH, and the Swedish National Road and Transport Research Institute, VTI.

Gëller MD, Sardar SB, Phuleria H, Fine PM, Sioutas C. (2005) *Environmental Science and Technology*; **39**: 8653-8663.

Janhäll, S., Molnar, P., Hallquist, M. (2012): *J.Environ. Monit.*, **14**, 2488

Jonsson, P., Blomqvist, G., Gustafsson, M. (2008): *7th Int. Symp. Snow Removal and Ice Control Techn., Transportation Research Circular*, **E-C126**, 102-111

Particle Number Size Distribution Statistics at Urban and Suburban Background and Remote Sites in Greece during Summer

S. Vratolis[1], M. Gini[1], D. Siakavaras[2], S. Bezantakos[1,2], I. Stavroulas[4], N. Kalivitis[4], E. Kostenidou[5], E. Louvaris[5], G. Biskos[2,3], N. Mihalopoulos[4], S. Pandis[5,6], C. Pilinis[2], K. Eleftheriadis[1]

[1]Institute of Nuclear & Radiological Sciences & Technology, Energy & Safety, National Centre of Scientific Research "Demokritos", 15310 Ag. Paraskevi, Attiki, Greece
[2]Dept. of Environment, University of the Aegean, Mytilene, 81100, Greece
[3]Faculty of Applied Sciences, Delft University of Technology, Delft, 2628-BL, The Netherlands
[4]Institute of Chemical Engineering, ICE-HT, Patras, 26504, Greece
[5]Environmental Chemical Processes Laboratory, Dept. of Chemistry, University of Crete, Heraklion, 71003, Greece
[6]Depts. of Chemical Engineering & Engineering & Public Policy, Carnegie Mellon University, Pittsburgh, PA, U.S.A

Keywords: Aerosol Number concentration, MeanParticle size, Modal analysis, 24h variability
Presenting author email: vratolis@ipta.demokritos.gr

The number size distributions of sub-micrometer aerosol particles in the environment display a statistically significant modal structure (van Dingenen et al., 2004). This structure depends on a number of factors such as local atmospheric conditions, density and type of emissions as well as a number of atmospheric processes. A series of intensive campaigns were conducted over several sites in Greece during the summer of 2012, and the particle number concentrations as well as the respective size distributions were measured by means of Scanning Mobility Particle Sizers (SMPSs). After statistical analysis, preliminary results from the measured number size distributions are presented in Table 1 for four sites including two suburban background sites in Athens and Patras, one urban background site in Thessaloniki and the Mediterranean remote site of Finokalia in Crete. The highest median concentration is observed in Athens and the lowest at the remote station of Finokalia in Crete. Patras display the highest variability in the observed values followed by Thessaloniki in terms of min and max values. The relatively low median values observed at the Thessaloniki site are investigated further with respect to other particle size distribution metrics.

The size distributions were assumed to be reproduced by a sum of lognormal modes, each characterized by a geometric mean size $D_{pgi,}$ a standard deviation σ_{gi} and a particle number N_i. Least square fitting iterative analysis was performed on datasets by means of a modified algorithm based on the work of Hussein et al. (2005). The maximum number of log-normal modes was set to three and the algorithm was allowed to reduce that number to one, provided a better or equivalent fit was reached. Results were grouped on 3 types of modes generally attributed to Nucleation, Aitken and Accumulation modes, with each type allowed to appear in a small or larger size fraction (indicated by 1 or 2) within the boundaries of these modes. Results for the GAW site in Athens are displayed in Fig. 1. Higher variability in the mean concentration range during the 24-hour cycle is observed for the Nucleation and Aitken modes, but not for the accumulation mode. This is partly explained by the formation and transport mechanisms known to govern the occurrence of smaller ultrafine particles.

Table 1: Summary of partcle number concnetrations observed at different sites in Greece.

N [cm^{-3}]	Median (x 10^3)	Min (x 10^3)	Max (x 10^3)	Std (x 10^3)
Athens	6.16	1.88	27.12	4.79
Patras	4.27	0.96	456.28	12.61
Thessaloniki	3.52	0.48	132.02	2.66
Finokalia	3.13	1.06	9.33	1.02

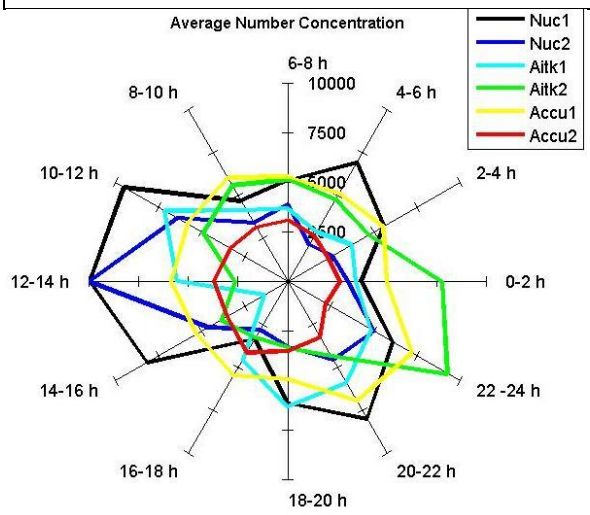

Fig. 1. Statistics of the average concnetrations for 2 hour periods observed over the 24hour daily cycle during the summer of 2012 at the Demokritos GAW suburban background station.

Acknowledgement:
This research was co-financed by Greece and the European Union through the education and lifelong learning operational program Thales: "Sources and physicochemical properties of fine and ultrafine aerosol particles that affect the regional climate of Greece".

References

R. van Dingenen , et al (2004). *Atmos. Environ*, 38, 2561-2577
Hussein, T., et al., (2005) Boreal Environment Research, 10, 337–355.

Highly time- and size-resolved measurements of trace elements in London during ClearfLo

S. Visser[1], M. Furger[1], U. Flechsig[2], K. Appel[3], R. Dressler[4], P. Zotter[1], J.G. Slowik[1], A.S.H. Prevot[1], U. Baltensperger[1]

[1] Laboratory of Atmospheric Chemistry, Paul Scherrer Institute, Villigen PSI, Switzerland
[2] Swiss Light Source, Paul Scherrer Institute, Villigen PSI, Switzerland
[3] DESY Photon Science, Hamburg, Germany
[4] Laboratory of Radiochemistry and Environmental Chemistry, Paul Scherrer Institute, Villigen PSI, Switzerland
Keywords: trace elements, XRF, PM and source apportionment, urban aerosol
Presenting author email: suzanne.visser@psi.ch

The identification and quantification of particle sources has long proven challenging due to the complex composition of ambient aerosol. Measurements of trace elements provide uniquely source-specific information; e.g. barium and copper are emitted by traffic sources, while vanadium and nickel are linked to heavy oil combustion. The power of source apportionment by trace elemental analysis is greatly enhanced by simultaneous measurements of complementary aerosol species. Optimization of trace elemental data requires measurements with sufficient temporal resolution to distinguish sources with different characteristic diurnal patterns such as traffic and sea salt, while size-resolved measurements can help resolve different source classes with similar composition, e.g. iron from resuspension appears in $PM_{10-2.5}$ while brake wear processes appear in PM_1. Here we present highly time- and size-resolved measurements of trace elements as part of the ClearfLo (Clean Air for London) 2012 field campaign, a multinational collaborative effort to investigate boundary layer pollution in and around London, UK.

Sampling was performed at several sites in and around London during two Intensive Observation Periods (IOPs) in 2012. During the winter IOP (11 Jan. to 8 Feb.) particulate matter was sampled at a site with heavy traffic (Marylebone Road, MR) and an urban background site (North Kensington, NK) in London, and at a rural site in Detling, southeast of London. Summer sampling took place at the two London sites from 18 July till 22 August, a period which included the Olympic Games. Rotating drum impactors (RDIs) collected particles in three size bins ($PM_{10-2.5}$, $PM_{2.5-1.0}$ and $PM_{1.0-0.1}$) with a high time resolution of 2 h, instead of more common 24 h sampling times (Bukowiecki et al., 2005). The elemental composition of the samples was analysed by synchrotron radiation induced X-ray fluorescence spectrometry (SR-XRF) at the Swiss Light Source (SLS, Paul Scherrer Institute, CH) and at HASYLAB (Deutsches Elektronen-Synchrotron, DE). The RDI SR-XRF setup provides quantification of elements with atomic number 11 (sodium) to 82 (lead) with a detection limit on the order of a few pg (Richard et al., 2010).

Figure 1 shows the median diurnal variations of selected elements in $PM_{10-2.5}$ (ng m^{-3}) during the winter IOP. The rush hour peaks for iron (Fe) and barium (Ba) (top panel) are commonly observed in a street canyon with stop-and-go traffic. Ba is typically related to brake wear (e.g. Furusjö et al., 2007) and elevated concentrations are thus likely at such a site (Ba at NK was below detection limit). Elevated concentrations during daytime for mineral dust elements like aluminium (Al) and calcium (Ca) (centre panel) occur from continuous resuspension at MR. NK shows lower levels due to dilution of air during transport from the traffic to the urban background site. Rather constant values were observed for e.g. sodium (Na) and magnesium (Mg) (bottom panel). These sea salt elements are likely advected throughout the day, but the elevated values at MR indicate local emissions as well. Correlations with e.g. black carbon, nitrogen oxides and meteorological conditions will enhance the source separation of the trace elements.

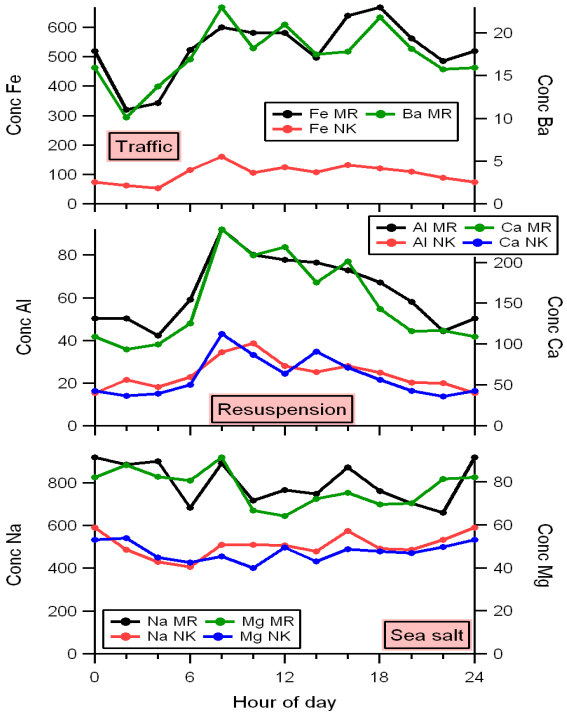

Figure 1. Median diurnal variations of $PM_{10-2.5}$ trace elements (ng m^{-3}) separated into three suggested source categories for a heavy traffic (MR) and an urban background (NK) site during ClearfLo 2012, winter IOP.

This work was funded by the ClearfLo project (NERC grant NE/H00324X/1), the SNF (grant 200021_132467 /1) and the European Community's Seventh Framework Programme (FP7/2007-2013, grant n°312284).

Bukowiecki, N. et al. (2005) *Environ. Sci. Technol.* **39**, 5754-5762
Furusjö, E. et al. (2007) *Sci. Total Environ.* **387**, 206-219
Richard, A. et al. (2010) *Atmos. Meas. Tech.* **3**, 1473-1485

Exposure of schoolchildren to traffic-related air pollution: the HEAPS study

Martine Van Poppel[1], Evi Dons[1,2], Luc Int Panis[1,2], S. De Prins[1], G. Koppen[1], Christina Matheeussen[3], Patrick Berghmans[1]

[1]VITO - Flemish Institute for Technological Research, 2400 Mol, Belgium
[2]Hasselt University, 3590 Diepenbeek, Belgium
[3]Flemish Environment Agency, 2000 Antwerp, Belgium

Keywords: Black Carbon, NO_2, UFP, traffic.
Presenting author email: martine.vanpoppel@vito.be

To assess the health impact of traffic related air pollution on schoolchildren, the HEAPS study (Health Effects of Air Pollution in Antwerp Schools) was performed.
The HEAPS study comprises the biomonitoring of 130 children (aged 6-12) from 2 schools by measuring oxidative stress, inflammation and cardiovascular markers and simultaneous air quality monitoring.

To assess the exposure of the children, air quality measurements were performed at the two schools, at a selection of 40 home locations and while in transport. One of the schools was located next to a busy road of 20,000 vehicles/day (School 2), the other school was located at an urban background (School 1). The schools were located in the same urban area. Measurements were performed in two seasons: in spring (May – June 2011) and in autumn (November – December 2011).
This paper discusses the air quality measurements at the school locations.

BC, EC, NOx, PM and UFP were measured at the playground of both schools. Also traffic counts were performed at each of the school locations. At school 2, measurements were also performed at the street side and at the windows of 7 classes to assess the spatial variability within the school area. In addition, NO_2 and BC measurements were performed during the entire monitoring campaign at an urban location of the AQ monitoring network.
Nitric oxides were measured using a mobile platform (Airpointer, Recordum) comprising a Chemiluminescent technique for measuring NO and NO_2. UFP number concentrations were measured using CPC (TSI type 3783, 3786 and 3787) and Nanocheck (Grimm). Size distribution was measured using SMPS (TSI). $PM_{2.5}$ mass concentration measurements were performed using a low volume filter sampler (Partisol, Thermo). Selected filters were subsequently analyzed for EC/OC using TOT (Thermo Optical Transmission, Sunset) technique. PM fractions (PM_{10}, $PM_{2.5}$, PM_1) were measured using a Grimm optical counter (model 1.108). In addition, NO_2 was monitored using diffusive sampling tubes and BC was measured using µ-Aethalometers (AethLabs); these techniques were used at the home locations because they can be easily deployed at 10 (or more) locations simultaneously. The measurements at the school were used to assess exposure at school and to compare the different measurement techniques and correlation between pollutants and traffic.

The results showed similar concentrations at the playground of both schools, despite the difference in traffic. However at school 2, increased concentrations were measured at the street side showing up to 2 times higher concentrations of BC in spring, as compared to the concentrations measured at the playground of the school. UFP, EC were increased by 70% in spring.
Higher concentrations were observed in autumn compared to springtime, however a slightly different behaviour was observed for different pollutants. A good correlation was found between UFP concentrations and BC or NO_2. Pollutants showed good correlation with traffic counts, whereas the correlation was better if only heavy duty vehicles were considered.

This paper will further discuss the seasonal variability of UFP, BC and NO_2 at school locations, the correlation between pollutants and spatial variability.

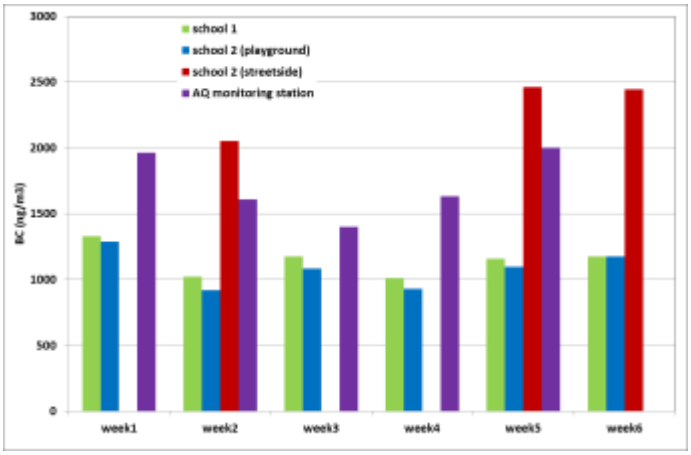

Figure 1. BC concentrations at school 1, school 2 (playground), school 2 (street side) and urban AQ monitoring station, measured in spring

Acknowledgement: the study was financed by the Flemish Environment Agency (VMM), the Flemish Administration of Environment, Nature and Energy (LNE), and the Flemish Agency for Care and Health (VZG)

Aerosol particles from smoking, cooking, and various pyrotechnical devices: laboratory characterization and detection in a football stadium

P. Faber[1], F. Drewnick[1] and S. Borrmann[1,2]

[1]Particle Chemistry Department, Max Planck Institute for Chemistry, D-55128 Mainz, Germany
[2]Institute for Atmospheric Physics, Johannes Gutenberg University, D-55128 Mainz, Germany
Keywords: HR-ToF-AMS, aerosol particles, emission source, football stadium
Presenting author email: peter.faber@mpic.de

Little is known about the chemical and physical characteristics of particles from less abundant anthropogenic aerosol sources (Zhang et al., 2011) such as those associated with football stadiums. Nevertheless, locally and temporally these sources can have a significant impact on the ambient aerosol and thus potentially on human health.

Several anthropogenic emission sources of aerosol particles that are typically found in football stadiums were therefore addressed in combined field and laboratory studies by using a set of modern online instruments for real-time measurements of particle, trace gas, and meteorological parameters (Drewnick et al., 2012). A high-resolution time-of-flight aerosol mass spectrometer (HR-ToF-AMS) provided online data on the chemical composition of the non-refractory PM_1.

The field campaign took place in a German football stadium (*Coface-Arena*, Mainz) during an official *Bundesliga* (German football league) match on 20th April 2012. The mass concentration of the organic aerosol fraction was elevated on average by a factor of almost 6 during the football match event (10.7 ± 7.6 µg m^{-3}) compared to background levels (1.9 ± 0.5 µg m^{-3}). Highly time-resolved online data on the organic aerosol explored a temporal structure that could be clearly related to the local activities reflecting different phases of the match. Additionally, the organic mass size distribution during the football match revealed considerable contributions of freshly emitted particles. Contrary to that, mass concentrations and size distributions of the inorganic non-refractory PM_1 components (NH_4, NO_3, SO_4, Chl) were not significantly different from background measurements. Positive matrix factorization (PMF) established cigarette-smoking organic aerosol (CSOA) and cooking organic aerosol (COA) as the dominating fractions of the submicron organic particulate matter in the stadium during the match. Here we present the high-resolution mass spectra as well as the elemental ratios (OM:OC, O:C, H:C, N:C) of both factors. Furthermore, we compare the strength and the temporal evolution of these emissions concerning different phases of the football match event (Figure 1). All species that were elevated during the match reached their initial background levels within one hour after the match had finished.

Laboratory measurements of various specific aerosols were performed to support the analysis of the field data. These measurements include the characterization of emissions from deep-frying of French fries and from sausage cooking, from cigarette smoking, from different pyrotechnical devices (fireworks, hand flares, color smoke bombs), and from laboratory-generated metal-containing aerosols. Although no aerosols from pyrotechnical devices could be detected in the field measurement, we estimated their potential influence on the local air quality by calculating emission factors based on laboratory data. In addition to information on the physical and chemical characteristics of the related aerosols, the laboratory measurements provided a large number of standard spectra that have not been available so far for HR-AMS ambient aerosol analyses.

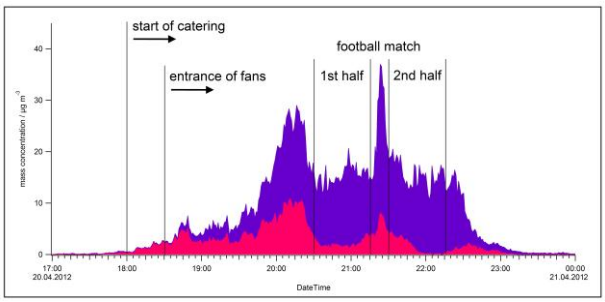

Figure 1. Temporal evolution of cooking organic aerosol (pink) and cigarette-smoking organic aerosol (purple) within a football stadium reflecting different phases of the match.

Although HR-AMS mass spectra of most investigated aerosols within this study were dominated by organics, the emissions from fireworks and hand flares explored distinct contributions of inorganic species and metal compounds. Here we present laboratory studies for a set of non-refractory metal chlorides that enable the quantitation of these compounds by the HR-ToF-AMS in ambient measurements for the first time.

Thomas Böttger and the Coface Arena team are gratefully acknowledged for technical support.

Drewnick, F., Böttger, T., von der Weiden-Reinmüller, S.-L., Zorn, S.R., Klimach, T., Schneider, J., Borrmann, S. (2012). *Atm. Meas. Tech*. **5**, 1443-1457.

Zhang, Q., Jimenez, J.L., Canagaratna, M.R., Ulbrich, I.M., Ng, N.L., Worsnop, D.R., Sun, Y. (2011). *Anal. Bioanal. Chem*. **401**, 3045-3067.

Wednesday, September 4, 2013

Session: Aerosol Modelling,
Modelling atmospheric aerosols

Linking climate change and air quality over Europe: Effects on aerosol concentrations

A.G. Megaritis[1,2], C. Fountoukis[2], and S.N. Pandis[1,2,3]

[1] Department of Chemical Engineering, University of Patras, Patras, Greece
[2]Institute of Chemical Engineering Sciences (ICEHT), Foundation for Research & Technology-Hellas (FORTH), Patras, Greece
[3]Department of Chemical Engineering, Carnegie Mellon University, Pittsburgh, PA 15213, USA
Keywords: PMCAMx, $PM_{2.5}$ concentrations, climate change, air quality
Presenting author email: athmegaritis@chemeng.upatras.gr

Atmospheric particulate matter, a major constituent of air pollution, in high concentrations could have detrimental effects on human health, as well as on visibility and ecosystems (Seinfeld and Pandis, 2006). Concentrations of PM are strongly influenced by meteorology, but when designing air quality strategies it has been traditionally assumed that climate will remain constant. However, climate change over the next decades is expected to be significant (IPCC, 2007) and may impact local and regional PM levels. Determining how PM concentrations change as climate changes is an important step toward estimating future air quality, as it may allow air quality policy planners to relax the assumption of constant climate and meteorology.

In this study we applied PMCAMx (Fountoukis et al., 2011), a three dimensional chemical transport model, in Europe, in order to quantify the individual effects of various meteorological parameters on particulate matter less than 2.5 μm ($PM_{2.5}$). The modeling domain covers a 5400×5832 km^2 region in Europe with a 36×36 km resolution grid and 14 vertical layers extending up to ~6 km in height.

Our simulations covered 2 periods representative of different seasons to examine also the seasonal dependence of the air quality. In addition to a base case scenario for each simulation period, a suite of perturbations in various meteorological factors, such as temperature, wind speed, were imposed to determine the sensitivities of $PM_{2.5}$ concentrations and composition to these parameters.

Fig. 1 shows the predicted average $PM_{2.5}$ changes to various meteorological perturbations over Europe. $PM_{2.5}$ concentrations have on average a negative response to temperature increase in both periods (-31 ng m^{-3} K^{-1} during summer and -60 ng m^{-3} K^{-1} in the winter). Temperature decreased average nitrate (up to 30%) and organic levels (up to 10%), and increased sulfate (up to 10%), during both periods.

The expected changes on wind speed, precipitation rate and absolute humidity are predicted to be as significant as temperature changes. Decreases of wind speed led to changes in advection and transport resulting in average increases in $PM_{2.5}$ concentrations in both periods of 34 ng m^{-3} $\%^{-1}$ during summer and 32 ng m^{-3} $\%^{-1}$ in the winter. $PM_{2.5}$ concentrations decreased with increasing precipitation rate in both periods (12 ng m^{-3} $\%^{-1}$ during summer and 10.9 ng m^{-3} $\%^{-1}$ in the winter), due mainly to changes on $PM_{2.5}$ wet deposition (up to 10%). Increases in absolute humidity led to significant changes on semi-volatile aerosol partitioning (up to 20%) and $PM_{2.5}$ dry deposition (up to 50%), while the predicted $PM_{2.5}$ concentrations changes are driven largely by increases in nitrate (up to 30% during summer) and decreases in sulfate (up to 10% in the winter).

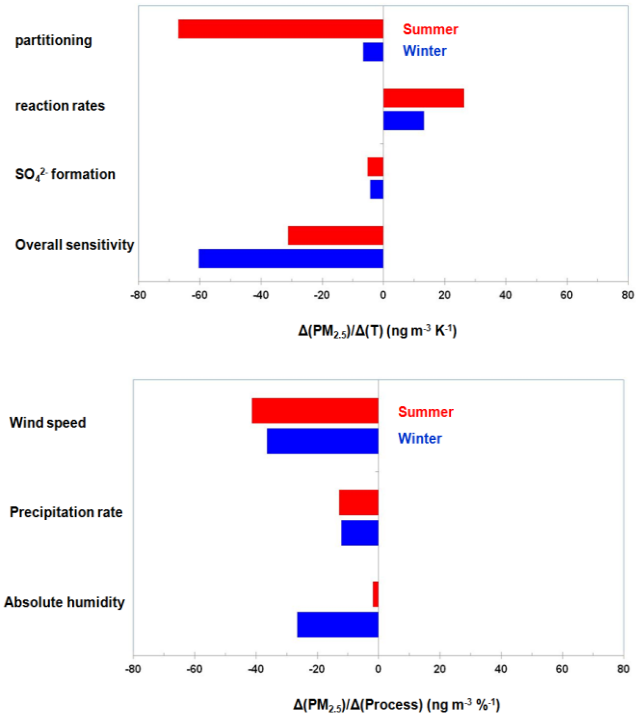

Figure 1. Predicted average $PM_{2.5}$ sensitivities to (a) temperature changes (ng m^{-3} K^{-1}), and (b) other meteorological perturbations (ng m^{-3} $\%^{-1}$), during summer and winter.

This work was funded by the European Community's 7th Framework Programme EU project PEGASOS (contract 265307).

Fountoukis, C., et al. (2011) Evaluation of a three-dimensional chemical transport model (PMCAMx) in the European domain during the EUCAARI May 2008 campaign, *Atmos. Chem. Phys.*, 11, 10331–10347.

Seinfeld, J. H., and Pandis, S. N. (2006) *Atmospheric chemistry and physics: From air pollution to climate change*, 2nd ed.; John Wiley and Sons, Hoboken, NJ.

Particle Number Concentrations over Europe in 2030: The Role of Emissions and New particle Formation

L. Ahlm[1], J. Julin[1], C. Fountoukis[2], S.N. Pandis[2,3,4], and I. Riipinen[1]

[1]Department of Applied Environmental Science (ITM), Stockholm University, Stockholm, Sweden
[2]Institute of Chemical Engineering Sciences, Foundation for Research and Technology Hellas (ICEHT/FORTH), Patras, Greece
[3]Department of Chemical Engineering, Carnegie Mellon University, Pittsburgh, USA
[4]Department of Chemical Engineering, University of Patras, Patras, Greece
Keywords: number concentration, scenarios, nucleation, emissions
Presenting author email: lars.ahlm@itm.su.se

The aerosol particle number concentration is a key parameter when estimating impacts of aerosol particles on climate and human health. Aerosol particles may be emitted directly (primary particles) or form in the atmosphere by homogeneous nucleation (secondary particles).

We use a three-dimensional chemical transport model with detailed microphysics, PMCAMx-UF, to simulate particle number concentrations over Europe in the year 2030, by applying emission scenarios (Amann et al., 2012) for trace gases and primary aerosols focusing on a photochemically active period. The emission scenarios include anthropogenic sulphur dioxide, ammonia, nitrogen oxides, and primary aerosol particles with a diameter less than 2.5 µm ($PM_{2.5}$) (Table 1). We test three different emission scenarios: a Baseline scenario assuming full implementation of existing air pollution control legislation in the European Union; a Maximum Technically Feasible Reduction (MTFR) scenario exploring to what extent emissions could be further reduced through full application of available technical measures; and a Maximum Control Efforts (MCE) scenario exploring the ultimate emission reductions that could be achieved through rapid decarbonisation, application of all available air pollution control technologies, and a change of diets to include less meat.

Table 1. Percentage change in emissions over Europe 2005-2030 (Amann et al., 2012).

	SO_2	NH_3	$PM_{2.5}$	NO_x
Baseline	-73	0	-38	-66
MTFR	-82	-30	-69	-75
MCE	-85	-40	-74	-90

Figure 1a shows the predicted percentage change in total particle number concentration (N_{tot}) over Europe from applying the baseline emission scenario in PMCAMx-UF. In general, a reduction of 40-70% in N_{tot} is predicted over continental Europe, resulting from the reduced emissons (Table 1). However, in some local areas, Figure 1a indicates enhanced total particle number concentrations. Since $PM_{2.5}$ emissions have been reduced, these locally enhanced concentrations must be associated with increasing new particle formation due to a reduced condensation sink following from the reduction in concentrations of primary particles. For particles larger than 100 nm (N_{100}) (Figure 1b), concentrations are predicted to decrease all over Europe; reductions of 60-80% are predicted over southeastern Europe, while reductions of 30-60% are predicted over most other parts of Europe.

The predicted decrease in N_{tot} is mainly a result of reduced new particle formation due to the expected reduction in SO_2 emissions, and the predicted decrease in N_{100} is a result of both decreasing condensational growth and reduced primary aerosol emissions. Sensitivity tests reveal that a reduction in SO_2 emissions is far more efficient than any other emission reduction investigated in reducing N_{tot}. For N_{100}, emission reductions of both SO_2 and $PM_{2.5}$ contribute significantly to the reduced concentration. The predicted reductions in both N_{tot} and N_{100} in this study will likely reduce both the aerosol direct and indirect effects, and limit the damaging effects of aerosol particles on human health in Europe.

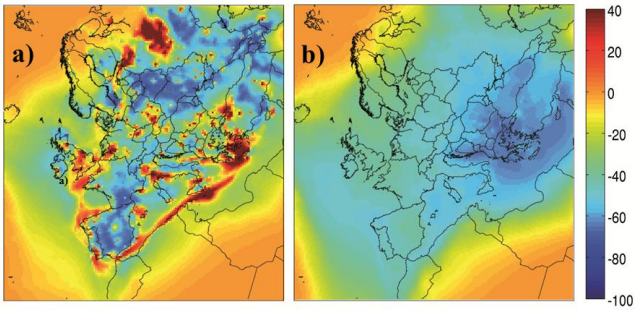

Figure 1. Mean percentage change in particle number concentration between 2008 and 2030 according to the baseline scenario for N_{tot} (a) and N_{100} (b).

This project was supported by the European Research Council (ERC) ATMOGAIN (No 278277), the FP7 project PEGASOS (No. 265148), and the Bert Bolin Centre for Climate Research (BBCC).

Amann, M., Borken-Kleefeld, J., Cofala, J., Heyes, C., Klimont, Z., Rafaj, P., Purohit, P., Schöpp, W., and Winiwarter, W. (2012) *Future emissions of air pollutants in Europe. Current legislation baseline and the scope for further reductions*, IIASA, TSAP Report #1, Version 1.0.

Predictions of aerosol extinction coefficients over Greece by means of a new modular software system

P. E. Charalampidis (Haralabidis)[1,2], C. Pilinis[1] , C. Fountoukis[2], A. Panagiotopoulou[2,3] and S. N. Pandis[3,4]
[1]Department of Environment, University of the Aegean, University Hill, 81100, Mytilene, Greece
[2]Institute of Chemical Engineering Sciences, (ICEHT/FORTH), Patras, Greece
[3]Department of Chemical Engineering, University of Patras, Patras, Greece
[4]Department of Chemical Engineering, Carnegie Mellon University, Pittsburgh, PA 15213, USA
Keywords: Air-quality, AOD, PMCAMx, Greece.
Presenting author P. E. Charalampidis (Haralabidis): pharala@env.aegean.gr

Atmospheric aerosols interact with electromagnetic radiation by scattering and absorbing solar radiation. By utilizing plausible assumptions about the aerosol microphysical state, it is possible to estimate the aerosol extinction coefficient, for a given aerosol size distribution and chemical composition, using either Mie-theory or semiempirical approximations (Roy *et al.*, 2007). A valuable source of data for calculating the aerosol optical properties are three-dimensional Chemical Transport Models (CTMs). The PMCAMx-2008 (Fountoukis *et al.*, 2011) CTM, provides vertical profiles of the aerosol size composition distributions at high spatial and temporal resolutions.

Air quality models are typically validated using available surface measurements of the various ambient aerosol properties (Vijayaraghavan *et al.*, 2008), including scattering measurements provided by nephelometers. These measurements, although highly accurate, are spatially sparse and not representative of the columnar aerosol optical properties. The aerosol Optical Depth (AOD) is a property of the total atmospheric column, directly proportional to the vertical distribution of the aerosol extinction coefficient. Local retrievals of AOD are made available by the AERONET network (Holben *et al.*, 1998) on a regular basis. Furthermore the use of satellites facilitates more complete special coverage.

In this study we present results from a new modular software system (AtmOpt), specifically developed to investigate the aerosol optical properties over Greece, using output data from the PMACAMx-2008 model and the WRF weather model. This code can also incorporate ground level measurements along with data provided by the AERONET and the MODIS satellite instruments, in order to provide automated evaluation of the performance of the PMCAMx-2008 model.

In order to create the necessary data pool we performed a number of PMCAMx-2008 and WRF runs. Details of these simulations can be found elsewhere in the literature (Fountoukis *et al.*, 2011). The WRF and PMCAMx-2008 model simulations provided detailed aerosol size composition distributions and Relative Humidities (RH) over Greece. These datasets are forwarded to the AtmOpt system. Extinctions calculations are performed either directly by application of Mie theory, or by using the "reconstructed mass-extinction" (RM) method (Roy *et al.*, 2007). An example of the simulated AOD values, attributed to PM2.5 and estimated by Mie theory is presented in Figure 1.

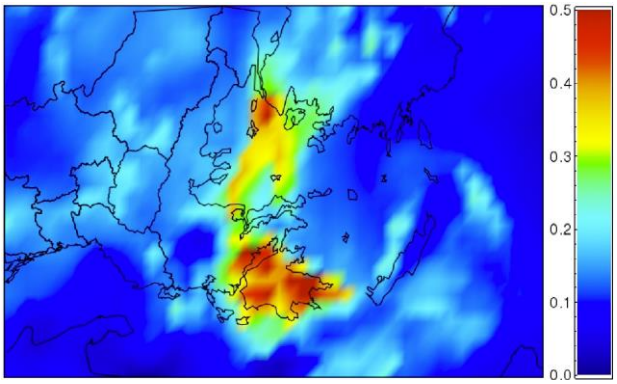

Figure 1. Simulated PM2.5 AOD over Greece using the PMCAMx-2008 output (May 14th 2008 at 9:00 UTC).

By utilizing the AtmOpt system we are able to model the aerosol optical properties. We will present a detailed and novel analysis of the various aspects of the aerosol optical state over Greece including contributions by various chemical species and assess the performance of the PMCAMx-2008 model. For this purpose we take advantage of the AERONET excellent temporal resolution and the MODIS high spatial coverage, along with the wealth of data (e.g. Angstrom exponents, cloud screening, quality assurance indicators etc.) provided by these remote sensing instruments.

This research has been co-financed by the European Union (European Social Fund – ESF) and Greek national funds through the Operational Program "Education and Lifelong Learning" of the National Strategic Reference Framework (NSRF) - Research Funding Program: THALES. Investing in knowledge society through the European Social Fund.

Fountoukis, C., Racherla, P. N., Denier van der Gon, H. A. C., Polymeneas, P., Charalampidis, P. E., Pilinis, C., Wiedensohler, A., Dall'Osto, M., O'Dowd, C. and Pandis, S. N. (2011) *Atmos. Chem. Phys.* **11**, 10331–10347.

Holben, B. N., et al. (1998) *Remote Sens. Environ.* **66**, 1– 16.

Roy, B., Mathur, R., Gilliland, A. B. and Howard, S. C. (2007) *J. Geophys. Res.* **112**, D14301.

Vijayaraghavan, K., Snell, H. and Seigneur, C. (2008) *Environ. Sci. Technol.* **42**, 8187-8192.

Mitigation of Arctic warming by controlling European black carbon emissions (MACEB): modelling results

J.-P. Pietikäinen[1], K. Kupiainen[2,3], Z. Klimont[2], A.-P. Hyvärinen[1], A. Laaksonen[1], H. Lihavainen[1]

[1]Finnish Meteorological Institute, Helsinki, 00101, Finland
[2]International Institute for Applied Systems Analysis, Laxenburg, A-2361, Austria
[3]Finnish Environment Institute SYKE, Helsinki, 00251, Finland
Keywords: modelling, black carbon, arctic climate
Presenting author email: Joni-Pekka.Pietikainen@fmi.fi

Black carbon (BC) is a light absorbing aerosol formed in incomplete combustion of biofuel, fossil fuels and biomass. Besides the absorption, BC particles influence on the radiation balance by deposition on snow and decreasing the snow albedo. This leads to heating and as a result the snow cover melts. Artic areas, for example, have already suffered from the global warming and different methods to protect these areas are being studied.

One of the main goals of MACEB project is to find the best approach to mitigate the warming of Arctic climate by different black carbon emission reductions. To achive this goal, several model simulations are conducted with the global aerosol-climate model ECHAM5-HAM2 (Stier *et al* (2005), Zhang *et al* (2012)). We implemented a new anthropogenic emission dataset for BC, organic carbon (OC) and sulfur dioxide (SO_2) which all have been derived from the GAINS model output (operated by the International Institute for Applied Systems Analysis, IIASA). In addition, we have updated the ship emissions (OC, BC and SO_2) and introduced aviation emissions (BC).

A series of different simulations have been carried on with different emission scenarios using both freely running, and nudged model. We have chosen the year 2005 to be the reference year and done scenario simulations for the years 2020 and 2030. The different scenarios used in this study are called CLEC, CLECC, BCadd and MTFR. CLEC and CLECC scenarios include all presently agreed policies affecting air pollutant emissions, but CLECC is further designed to keep the total forcing due to long-lived greenhouse gases at 450ppm CO_2-eqv level by the end of the century via CO_2 mitigation measures mostly targeting the energy production and industrial sectors. BCadd scenario includes a portfolio of most important measures that could yield the largest reductions in radiative forcing from short-lived climate forcers (SLCFs) at the global scale in 2030. Measures with a relatively small net impact or increase in radiative forcing have been excluded from this portfolio. MTFR implements the maximum reduction potential of aerosol and SO_2 emissions with currently available technologies. In addition to these scenarios, we study the influence of Finland's and EU's (EU-27 countries) emissions on Arctic climate by removing the BC and OC emissions from these areas.

Figures 1 and 2 show how the BC burden changes between normal simulation and CLEC 2020 scenario (in nudged mode). Within the CLEC scenario the reduction of BC is clearly seen in Europe. The burden seems to increase mostly in Africa, Middle-East and India. It is important to notice that although the reductions works in Europe, the polar region might still be influenced by a positive bias (please note the different units in Figs. 1 and 2). It is known that Arctic region is an area of clean air so even a relatively small increment in BC concentration might lead to noticeable changes in the regional climate. One of the biggest uncertainties is how much will the deposited BC influence on the snow albedo. Based on our results the Arctic area will be under more BC concentrated air masses already in 2020, if the scenario for the current European legislation with the Climate Policy is used.

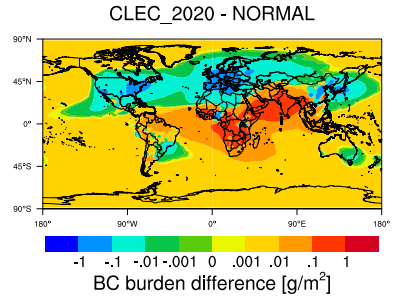

Figure 1: BC burden difference between CLEC 2020 scenario and current climate.

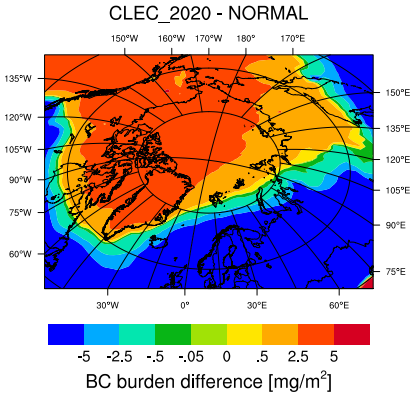

Figure 2: Same as in Fig. 1, but for Arctic area (different units).

During the conference we will present the rest of our results in more details and show how well the different reduction methods actually work for the Arctic region.

This work was supported by the EU Life+ project (LIFE09 ENV/FI/000572 MACEB).

Stier et al. (2005) *Atmos. Chem. Phys.*, 5, 1125-1156.
Zhang et al. (2012) *Atmos. Chem. Phys.*, 12, 8911-8949.

Modeling biogenic secondary organic aerosol formation in the subarctic

E. Hermansson[1,2], P. Roldin[1,2], A. Rusanen[3], D. Mogensen[3], S. Madronich[4], A. Hodzic[4], E. Swietlicki[1,2] and M. Boy[3]

[1]Department of Physics, Lund University, Lund, SE-221 00, Sweden
[2]Centre for Environmental and Climate Research, Lund University, Lund, SE-221 00, Lund, Sweden
[3]Department of Physics, University of Helsinki, Helsinki, FI-000 14, Finland
[4]National Center for Atmospheric Research, Boulder, Colorado, 80307, USA
Keywords: Biogenic secondary organic aerosol, ADCHEM, MCMv3.2.
Presenting author email: emilie.hermansson@nuclear.lu.se

Biogenic volatile organic carbon (BVOC) compounds, such as α-pinene, are emitted by the vegetation and oxidized in the atmosphere to form less volatile compounds. These compounds can take part in the formation and growth of secondary organic aerosols (SOA) and thus increase the aerosol load and also the concentration of cloud condensation nuclei which will affect climate.

We have modeled the formation and growth of secondary particles along an air mass trajectory over the northern European boreal forest and compared the results with size distribution measurements from three stations the air mass passes close to (Abisko, Pallas and Värriö).

The model used is an updated version of the aerosol dynamic and particle phase chemistry module from the ADCHEM model (Roldin *et al*, 2011), coupled with the Master Chemical Mechanism version 3.2 (Jenkin *et al*, 1997; Sanders *et al*, 2003). The emission of BVOC (represented by α-pinene in our model) is estimated using a method described in Tunved *et al* (2006). The model then considers the gas-to-particle partitioning of the 42 most important oxidation products. Liquid saturation vapor pressures of each oxidation product are decided by using the method proposed by Nannoolal *et al* (2008).

During the first 54 hours of the trajectory, the air mass is over the Atlantic Ocean, while it spends the remaining hours over land where the particle mass starts increasing (see Figure 1). The modeled growth is mainly caused by organic gas-to-particle conversion and seems to be a bit slower than the measured growth. Despite this, the model seems to be able to handle SOA formation relatively well at realistic BVOC-emissions and low primary particle concentration.

These are preliminary results which will be analyzed further and compared to results achieved by the model MALTE-BOX (Boy *et al*, 2012) which uses the University of Helsinki Multicomponent Aerosol model, UHMA (Korhonen *et al*, 2004). To test how well MCMv3.2 can describe the gas phase oxidation, a fully explicit gas phase oxidation scheme, called GECKO-A (Aumont *et al*, 2005), will also be applied.

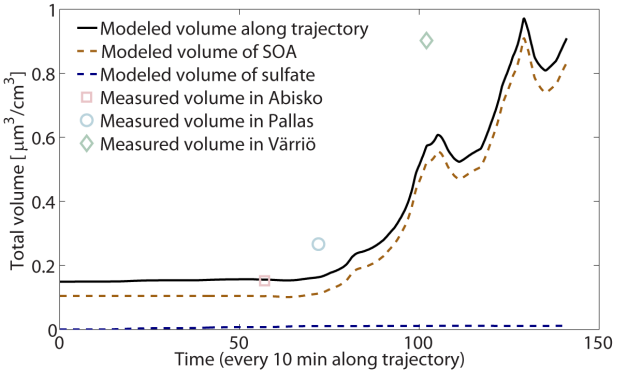

Figure 1. The solid line represents the total modeled particle volume along the trajectory, which consist mostly of SOA (dashed brown line) but also a small fraction of sulfate (dashed blue line). The modeled results are compared to size distribution measurements.

Aumont, B., Szopa, S. and Madronich, S. (2005) *Atmos. Chem. Phys.* **5**, 2497-2517.

Boy, M., Mogensen, D., Smolander, S., Zhou, L., Nieminen, T., Paasonen, P., Plass-Dülmer, C., Sipilä, M., Petäjä, T., Mauldin, L., Berresheim, H. and Kulmala, M. (2012) *Atmos. Chem. Phys. Discuss.* **12**, 27693-27736.

Jenkin, M.E., Sanders, S.M. and Pilling, M.J. (1997) *Atmos. Environ.* **31**, 81-104.

Korhonen, H., Lehtinen, K.E.J and Kulmala, M. (2004) *Atmos. Chem. Phys.* **4**, 757-771.

Nannoolal, Y., Rarey, J. and Ramjugermath, D. (2008) *Fluid Phase Equilibria* **269**, 117-133.

Roldin, P., Swietlicki, E., Schurgers, G., Arneth, A. Lehtinen, K.E.J., Boy, M. and Kulmala, M. (2011) *Atmos. Chem. Phys.* **11**, 5867-5896.

Sanders, S.M., Jenkin, M.E., Derwent, R.G. and Pilling, M.J. (2003) *Atmos. Chem. Phys.* **3**, 161-180.

Tunved, P., Hansson, H.C., Kerminen, V.M., Ström, J., Dal Maso, M., Lihavainen, H., Viisanen, Y., Aalto, P.P., Komppula, M. and Kulmala, M. (2006) *Science* **312**, 261-263.

Taking the step from bulk to size-segregated aerosol description: Modelling of size distributions with the EMEP/MSC-W model

M. Karl[1] and S. Tsyro[2]

[1] Norwegian Institute for Air Research, NILU, Kjeller, NO-2027, Norway.
[2] Norwegian Meteorological Institute, met.no, Oslo, NO-0313, Norway
Keywords: Atmospheric chemistry transport model, Particle number climatology, Aerosol dynamics
Presenting author email: svetlana.tsyro@met.no

Knowledge of the size distribution of atmospheric aerosols in the submicron size range is essential for estimation of aerosol climate effects and also health implications. Concerning effects on Earth's radiative balance, aerosol extinction of short and long wave radiation and interaction with clouds depends on their size. On the other hand, growing evidences suggest increased health effect from transport-related particles, in particular ultrafine ones (e.g. Oberdörster, 2001; Krzyzanowski et al., 2005). Ultrafine particles contribute negligibly in currently regulated PM_{10} and $PM_{2.5}$ mass and should be described in terms of number density.

The EMEP/MSC-W model (Simpson et al., 2012) is an atmospheric chemistry transport model, calculating photo-chemistry and PM on regional to global scale. It is flexible with respect to the choice of projection and horizontal resolution (tested for between 4x4 km and 1x1° grid), and has 20 vertical layers up to 100 hPa. The standard model deals with bulk aerosol mass, distinguishing fine and coarse particles.

Table 1. Median particle number concentrations in the size range 30 - 50 nm and 50 - 500 nm. Observed values adopted from Asmi et al. (2011).

Site	N_{30-50} obs. (#/cm^3)	N_{30-50} model (#/cm^3)	N_{50-500} obs. (#/cm^3)	N_{50-500} model (#/cm^3)
Birkenes	156	296	511	121
Aspvreten	284	241	1081	132
SMEAR	223	239	878	115
Pallas	89	97	205	37
K-Puszta	697	592	3120	375
Melpitz	860	434	2327	275
Kosetice	700	460	3194	265
Waldhof	878	413	2434	263
Cabauw	1914	889	3387	554
Finokalia	220	660	1345	625
Ispra	1341	1032	4448	598
Mace Head	105	364	241	199

Recently, aerosol dynamics of the sectional aerosol model MAFOR (Karl et al., 2011; http://mafor.nilu.no) have been implemented in the EMEP model to simulate size-resolved particle number and mass concentrations. In this work, 16 size sections were used to represent the aerosol size distribution from 1 nm to 10 µm. The new approach consistently solves the time evolution of the particle number and mass concentration distribution using the fixed sectional method in a robust manner on a 3-D atmospheric grid.

We present European maps of size-resolved aerosol and evaluate the model ability to reproduce observed particle size distributions. First comparison of modelled number concentration in the sizes of 30 - 50 nm (N_{30-50}) and 50 - 500 nm (N_{50-500}) to observational data (2008-2009) published by Asmi et al. (2011), summarized in Table 1, revealed reasonable agreement for most remote sites and esp. for the ultrafine fraction, whereas N_{50-500} was underestimated by the model. The discrepancies are partly associated with uncertainties in the particle emission data, but are also due to currently deficient treatment of processes: better descriptions of particle deposition and of particle growth due to condensation of inorganic and organic vapours, are expected to improve the model's predictive capabilities.

Modelled size distribution at Birkenes, Ispra and K-Puszta for winter and summer are shown in Figure 1. The shape of the size distributions has little variability among the sites, probably due to the use of a uniform particle emission spectrum for entire Europe. Increased nucleation of sulphuric acid led to higher numbers of nucleation mode particles in summer.

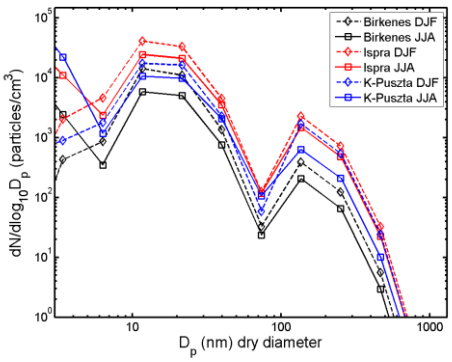

Figure 1. Modelled number size distribution in winter (DJF) and summer (JJA) at various sites in Europe.

This work was partly supported within the EC seventh framework project (no. 243406) TRANSPHORM.

Asmi, A., Wiedensohler, A., Laj, P., Fjaeraa, A.-M., Sellegri, K., Birmili, W., and co-authors (2011), *Atmos. Chem. Phys.*, **11**, 5505-5538.

Karl, M., A. Gross, C. Leck, and Pirjola, L. (2011), *Tellus*, **63B**, 1001-1025.

Oberdörster, G. (2001), *Int. Archives of Occupational and Environmental Health*, **74** (1), 1-8.

Krzyzanowski et al., 2005. WHO, ISBN 92-890-1373-7.

Simpson, D., Benedictow, A., Berge, H., Bergström, R., Emberson, L. D., Fagerli, H., and co-authors (2012), *Atmos. Chem. Phys.*, **12**, 7825-7865.

Contribution of primary emissions, secondary organic aerosol and nucleation on global aerosol number concentrations in NorESM

R. Makkonen[1], Ø. Seland[2], A. Kirkevåg[2], T. Iversen[1,2] and J.E. Kristjánsson[1]

[1]Department of Geosciences, University of Oslo, Oslo, N-0316, Norway
[2]Norwegian Meteorological Institute, Oslo, N-0313, Norway
Keywords: nucleation, SOA, NorESM.
Presenting author email: risto.makkonen@geo.uio.no

Atmospheric aerosol number concentrations are sensitive to new particle formation (Makkonen et al., 2009) and primary emissions (Reddington et al., 2011). Some agreement between observations and global simulations of aerosol number can be found (Spracklen et al., 2010), but significant uncertainties still persist in aerosol and precursor emissions, as well as relevant processes.

Here, the Norwegian Earth System Model (NorESM, Kirkevåg et al. 2013) is used to model aerosol number concentrations. We model biogenic secondary organic aerosol (SOA) formation from monoterpene oxidation products. 50 % of the monoterpene ozonolysis product are assumed to contribute to the growth of nucleated particles, rest of the SOA is modeled as particles with an initial diameter of 80 nm. Binary sulfuric acid-water nucleation is active throughout the atmosphere, while activation-type nucleation is included in the boundary layer.

We have run the model with two sets of prescribed black carbon (BC) emission diameter for fossil fuel (24 and 48 nm), as well as with and without nucleation or SOA formation. We analyse the corresponding changes in the total aerosol number concentrations and contributions from the externally mixed aerosol modes (Fig. 1). We also show the sensitivity of cloud droplet number concentrations and aerosol indirect effect to the selected parameters.

In a simulation without nucleation, decreasing the BC emission size from 48 to 24 nm increases the global aerosol number concentration by 360 cm^{-3} (60 %). However, the concentration increase is smaller in magnitude (270 cm^{-3}) when nucleation is included in the model: the increased number of BC particles acts as a sink for both small nuclei and sulfuric acid.

Turning on nucleation has a significant effect on aerosol number. The increase in number concentration is 560 cm^{-3} (470 cm^{-3}) when BC emission size is set to 48 nm (24 nm). SOA formation increases number concentrations by 15-30 % globally, depending on BC size. SOA formation actually decreases the nucleation rates (by increasing the condensation and coagulation sinks), but nuclei survival probabilities are increased due to more rapid particle growth. The particle number increase due to SOA formation is ~75% smaller if nucleation is not accounted for. SOA formation also increases the cloud droplet number concentration (CDNC) by 5 % globally.

Even increased aerosol number concentrations might lead to decreased concentrations of cloud condensation nuclei. When using a smaller size for BC, CNDC is decreased by ~1 %. Despite doubling the total aerosol number concentration, turning on nucleation can decrease CDNC by almost 5 %. Decrease in CDNC can be due to e.g. increased competition of sulfuric acid condensation, leading to slower growth rates.

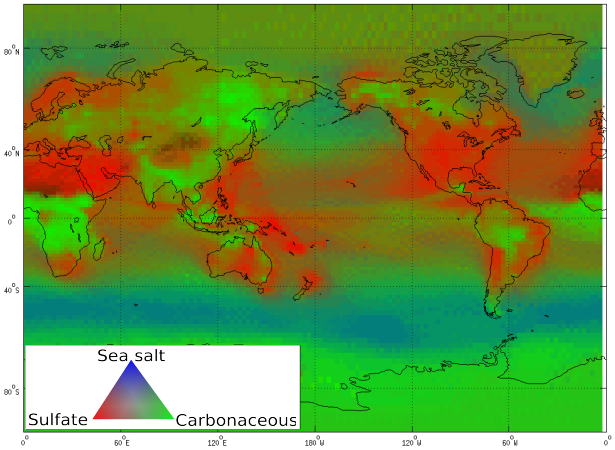

Figure 1. Relative contribution of sulfate (red), black and organic carbon (green) and sea salt (blue) to aerosol number concentration based on 5-year simulation.

The financial support by CRAICC is gratefully acknowledged.

Kirkevåg, A. et al. (2013) *Geosci. Model Dev.*, **6**, 207-244.
Makkonen, R. et al. (2009) *Atmos. Chem. Phys.*, **9**, 1747-1766.
Reddington, C.L. et al. (2011), *Atmos. Chem. Phys.*, **11**, 12007-12036.
Spracklen, D. et al. (2010) *Atmos. Chem. Phys.*, **10**, 4775-4793.

Climate and biofuels in Brazil

H. Vuollekoski[1], R. Makkonen[2], A. Asmi[1], R. Hillamo[3], T. Petäjä[1] and M. Kulmala[1]

[1]Department of Physics, University of Helsinki, Helsinki, 00014, Finland
[2]Department of Geosciences, University of Oslo, Oslo, 0371, Norway
[3]Finnish Meteorological Institute, Helsinki, 00560, Finland
Keywords: biofuels, climate, global modeling.
Presenting author email: henri.vuollekoski@helsinki.fi

Introduction

Biofuels represent a renewable source of energy that may increase the energy independence and economic well being of nations, as well as help reduce the net greenhouse gas emissions. These are some of the reasons why the usage of biofuels especially in transport is increasing rapidly. However, while this replacement of fossil fuels may decrease the net carbon dioxide emissions, the growing demand of biofuels may have consequences related to e.g. human health, agriculture and climate.

One example of such nation is Brazil, which has had a pro-biofuel regulatory environment already since 1975, and is the current world-leader in terms of vehicles running on sugarcane ethanol. If Brazil manages to replace all its consumption of fossil fuels by biofuels in the near future, what kind of climatic implications would this conversion potentially have? The transition would require significant agricultural changes to enhance sugarcane production, and these plantations would likely replace currently forested regions. The current methods of harvesting sugarcane often involve burning, which causes serious air pollution in certain regions (Lara *et al.*, 2005). Also, the primary emissions caused by combustion of ethanol fuel differ from those of traditional gasoline. The scope of our research is limited to the aforementioned effects, although a more realistic scenario would likely include the likely socio-economic side effects.

The land area of Brazil accounts for less than 6% of the global land surface. With this in mind, we try to identify the potential global climatic effects of the Brazilian transition to biofuels. We approach this question with global climate modeling.

Methods

All modeling in this study has been performed with the ECHAM5.5-HAM2 (Zhang *et al.*, 2012), which is a general circulation model that includes parameterizations for the effects of aerosols on climate. The sensitivity studies implemented so far have been executed by replacing the characteristic size of emissions due to fossil fuel combustion, according to current estimates (Stier *et al.*, 2005), in a region covering Brazil, while leaving rest of the world as it was. This change in size of the emitted particles is based on experimental laboratory studies on car engines.

Preliminary results

The first sensitivity study consisted of a 5.5-year control run and an otherwise identical run but with emissions in smaller size over Brazil. The results indicate significant increase in Aitken mode particles on surface level over Brazil, but this is likely due to the mass-based emission scenario. There is also a slight increase in the concentration of cloud condensation nuclei, but this and other effects may be attributed to noise.

We therefore conducted a similar set of runs for duration of 20 years. These suggest small changes in total cloud cover (see Figure 1), but more detailed analysis has to be carried out before conclusions.

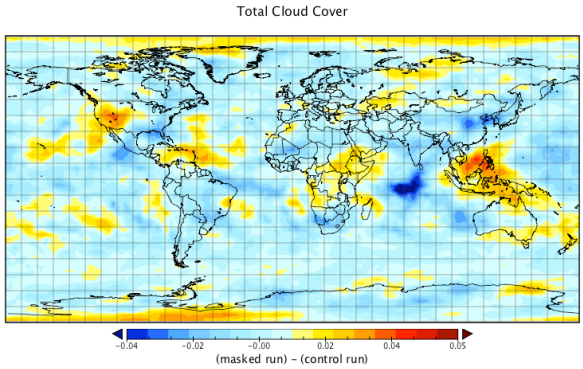

Figure 1. The difference in total cloud cover in a 20-year-long sensitivity test.

We acknowledge funding from "The effects of intensive bio-fuel production and use on regional air quality and global climate, BIOFUSE" (Academy of Finland, project 133603).
We thank Dr. Topi Rönkkö from Tampere University of Technology for technical consultation.
Risto Makkonen acknowledges funding from the CRAICC project.

Lara, L., Artaxo, P., Martinelli, L., et al. (2005) *Atmos. Env.*, **39** (26), 4627–4637.
Zhang, K., O'Donnell, D., Kazil, J., et al. (2012) *Atmos. Chem. Phys.*, **12** (19), 8911–8949.
Stier, P., Feichter, J., Kinne, S., et al. (2005) *Atmos. Chem. Phys.*, **5**, 1125–1156.

Wednesday, September 4, 2013

Session: Indoor and Working Place Aerosols
Chemistry / Instrumentation

The Effects of Mainstream and Sidestream Environmental Tobacco Smoke Composition for Enhanced Condensational Droplet Growth by Water Vapor

X. Tang[1,3], Z. Zheng[2,3], H. S. Jung[2,3], A. Asa-Awuku[1,3]

[1]Department of Chemical and Environmental Engineering, University of California, Riverside, California, 92521, USA
[2]Department of Mechanical Engineering, University of California, Riverside, California, 92521, USA
[3]Center for Environmental Research and Technology (CE-CERT), University of California, Riverside, California, 92507, USA

Keywords: hygroscopicity, water-uptake, aerosol, droplets

Presenting author email: akua@engr.ucr.edu

Adverse health effects from particulate matter (PM) are caused by the deposition of particles in the respiratory tract during inhalation. The water vapor uptake by hygroscopic particulate components can alter dry particle size and deposition efficiencies (Londahl et al. 2009). Therefore, the dose and deposition site of these aerosols are influenced by the growth of the particles. Relative humidity in the lung is estimated at 99.5% RH (Anselm et al. 1990), and more recent work has calculated instantaneous values in the supersaturated range (up to 104% RH) (up tp 104% RH;Varghese and Gangamma 2009; Longest et al. 2010). At large RH, enhanced condensational growth (ECG) may occur, droplets may form (Longest et al. 2010) and dry particles will effectively behave as cloud condensation nuclei (CCN) within the respiratory system. The following study explores the aerosol composition of inhaled cigarette smoke in relation to ECG and CCN properties.

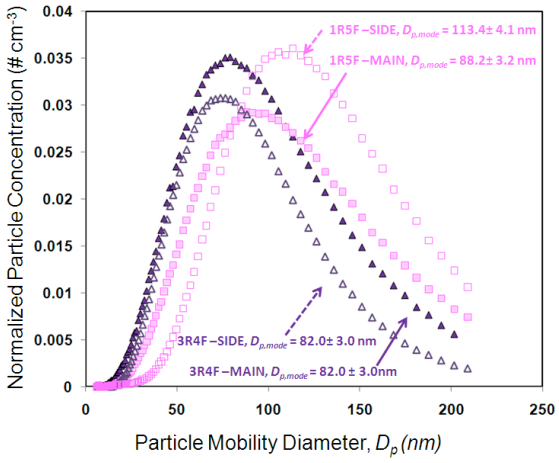

Figure 1. Particle Size distributions from mainstream and sidestream ETS. 1R5F cigarettes form particles of larger modes in both mainstream and sidestream ETS.

Although tobacco smoke is well known for its adverse health effects, the hygroscopicity and droplet growth properties have not been thoroughly explored. In this study, cigarette smoke is further characterized and several state-of-art analysis techniques are applied to understand the effects of particle hygroscopicty on particle deposition. Two types of research cigarettes are tested using a Walton Smoking Machine and two kinds of smoke are produced during smoking: main stream and side stream. In addition to tar-like-materials, tobacco smoke contains soluble organic materials that influence particle water uptake and droplet formation during inhalation. Online and offline analysis are combined to analyze the aerosol phase of cigarette smoke. The two types of cigarettes produce aerosols of similar hygroscopicity (κ_{eff}~0.15) in main and side stream smoke. The elemental composition and oxidation state of cigarette smoke is examined with high resolution data analysis by an Aerodyne High Resolution (HR) Time-of-Flight Aerosol Mass Spectrometer (HR-ToF-AMS). The oxygen-to-carbon ratio from HR data suggests that more oxidized components are present in mainstream smoke. Water soluble organic carbon is characterized by offline filter measurements, as well as elemental carbon/ organic carbon (EC/OC). EC/OC measurement shows that the majority of particles in both main and side stream smokes are organic compounds. Despite of diverse physical compositions of tested cigarettes, main and side

Table 1: Aerosol activation and average single-parameter hygroscopicity data

Type	stream	$\kappa_{eff,\,avg}$
1R5F	main	0.15 ± 0.01
	side	0.15 ± 0.01
3R4F	main	0.15 ± 0.01
	side	0.15 ± 0.02

This works was supported by the National Science Foundation Proposal (grant #1032388).

Londahl, J., Massling, A., Swietlicki, E., Brauner, E. V., Ketzel, M., Pagels, J. and Loft, S. (2009). *Environ Sci Technol* **43**:4659-4664.

Anselm, A., Heibel, T., Gebhart, J. and Ferron, G. (1990). *J Aerosol Sci* **21**:S427-S430.

Longest, P. W., McLeskey, J. T. and Hindle, M. (2010).. *Aerosol Sci Tech* **44**:473-483.

Varghese, S. K. and Gangamma, S. (2009). *Inhal Toxicol* **21**:619-630.

A study on SVOC aerosol evaporation and its possible implications on workplace sampling

G.C. Dragan[1,2], E. Karg[1], D. Breuer[3], M. Blaskowitz[3], H. Nordsieck[4], J. Schnelle-Kreis[1] and R. Zimmermann[1,2]

[1]Joint Mass Spectrometry Centre, Cooperation Group Comprehensive Molecular Analytics, Helmholtz Zentrum München, Ingolstädter Landstr. 1, 85764 Neuherberg, Germany
[2]Joint Mass Spectrometry Centre, Chair of Analytical Chemistry, University of Rostock, Dr.-Lorenz-Weg 1, 18059 Rostock, Germany
[3]Institute for Occupational Safety and Health, German Social Accident Insurance (IFA), Alte Heerstr. 111, 53757 Sankt Augustin, Germany
[4]bifa Environmental Institute, Am Mittleren Moos 46, 86167 Augsburg, Germany
Keywords: SVOC aerosol, particle evaporation, evaporative losses, computational model
Presenting author email: constantin.dragan@helmholtz-muenchen.de

Aerosols of Semi-Volatile Organic Compound (SVOC) origin represent a big challenge to industrial hygienists due to toxicological and sampling issues. Especially problematic is the sampling of hazardous semi-volatiles that appear in both particulate and gaseous phases in the workplace (oil mists, PAHs, alkanolamines, inorganic acids, etc) (Breuer 1999). More attention has to be given to these dynamic aerosol systems as the particle-vapour distribution is considerably depending on the sampling conditions. Thus the real-phase distribution can be shifted by evaporating particles or condensing vapour.

Due to the fact that *off-line* filter-adsorber sampling setup can induce artefacts when measuring SVOC aerosols, we investigated a new *on-line* alternative to filter sampling that can accurately distinguish between vapour and particle mass.

The *on-line* approach to analyse SVOC aerosols was to account for the total mass (TM) with a Flame Ionization Detector (FID) coupled with a heated transfer line. The particle mass (PM) was calculated from the particle diameter measured using an optical white light particle sizer, while the vapour mass (VM) was calculated as the difference between the measured total and particulate mass (VM=TM-PM).

In order to study SVOC particle evaporation an experimental apparatus comprising of a Sinclair-La Mer aerosol generator, a flow tube and the above mentioned aerosol sampling system was set up inside a temperature controlled chamber. Several n-alkane (C_{14} to C_{20}) monodisperse aerosols were generated with various particle diameters, diluted with particle free nitrogen and monitored for particle evaporation losses.

Fig. 1 shows 1, 1.5 and 2 µm hexadecane particles evaporation in the flow tube. Continuous lines represent the initial particle size distribution (PSD), while the dotted lines represent the PSD after additional 3 seconds of residence time. The experimental data were also compared to a diffusion based theoretical computational model. The experimental and model data were found to be in a good agreement for the flow tube experiments (results will be shown in the presentation).

Comparisons between the developed *on-line* method and the *off-line* filter-adsorber sampling method were done for n-alkanes of different volatilities and particle mass loads. The *off-line* samplers comprise of a glass fibre filter for the separation of the particle phase and XAD2 adsorber for the quantification of the remaining vapours.

Our results confirm that the *off-line* method can be biased for SVOC aerosol measurement. The only comparable result that is independent of sampling method is for TM. The *off-line* method systematically returns lower PM and higher VM values (Fig. 2), a clear indication for particle evaporation. This effect is also expected to influence the workplace risk assessment, with the particle-vapour distribution being influenced by the sampling conditions. The amount of evaporated aerosol is difficult to predict as it is influenced by several parameters like gas phase saturation, droplet diameter, substance volatility and sampling temperature.

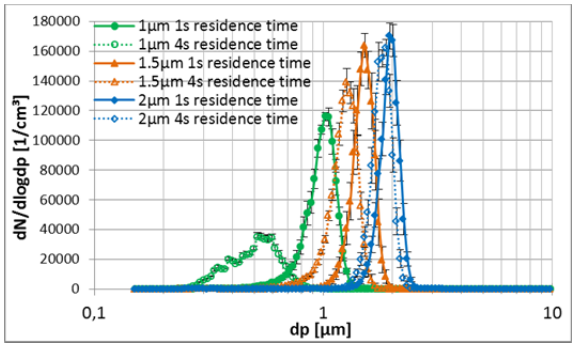

Figure 1. Evaporation of hexadecane particles

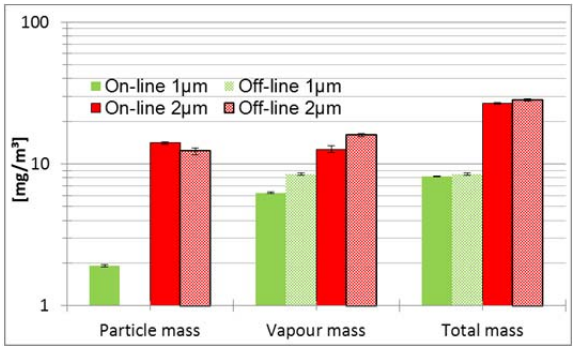

Figure 2. Comparison between *on-line* and *off-line* measurements for hexadecane 1 and 2 µm data.

This work is supported by the German Social Accident Insurance (DGUV), research contract FP299.
The health effects of organic compounds in aerosols are currently investigated in the framework of the Helmholtz Virtual Institute of Complex Molecular Systems in Environmental Health, HICE (www.hice-vi.eu).

Breuer, D. (1999). "Measurement of vapour–aerosol mixtures." J. Environ. Monit.(1): 299-305.

Household products and indoor air quality: emission, reactivity and by-products in both gaseous and particulate phases

A. Mêmе[1], M. Nicolas[2], L. Chiappini[3], C. Rio[3], J. Nicolle[1], S. Rossignol[3] and B. D'Anna[1]

[1]Institut de Recherches sur la Catalyse et l'Environnement de Lyon (IRCELYON), University Claude Bernard Lyon 1, Lyon, Rhône-Alpes, France
[2] Centre Scientifique et Technique du Bâtiment (CSTB), Grenoble, Isère, France
[3]Institut National de l'Environnement Industriel et des Risques (INERIS), Verneuil-en-Halatte, Oise, France

Keywords: domestic activity, cleaning products, primary emissions, secondary emissions.
Presenting author email: aurelie.meme@ircelyon.univ-lyon1.fr

In western countries, where people spend most of their time in confined areas, indoor air quality is recognized as a public health issue. Among multiple indoor air pollution sources (building materials, furniture, heating) the use of housecleaning products is still poorly characterized.

It is well known that limonene, a good Secondary Organic Aerosols (SOAs) precursor towards ozonolysis (Chen and Hopke, 2010), is widely employed in scented products such as freshener and household cleaners (Nazaroff and Weschler, 2004). Besides, indoor ozone levels can be high enough to initiate gas phase chemistry (Weschler, 2000) and possibly to lead to the formation of indoor secondary products which may be of health concern. Investigations are therefore necessary to characterize the chemical composition of particles and gases formed during housecleaning use and to evaluate real population exposure.

The ADOQ project (Activités DOmestiques et Qualité de l'air intérieur) aims at identifying and quantifying VOCs, SVOCs and particles emitted and/or secondarily formed consequently to the use of housecleaning products. In the frame of this project, emissions of 54 housecleaning products representative of domestic activities have been characterized using an emission test chamber. The housecleaning products displaying the most intense VOCs emission (particularly limonene) have been selected and tested in real indoor conditions inside the experimental house MARIA (Maison Automatisée pour des Recherches Innovantes sur l'Air).

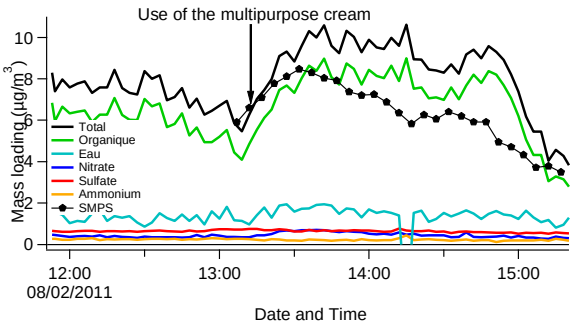

Figure 1. On-line particles mass loading evolution using an AMS and a SMPS and the chemical speciation as a function of time upon application of the surface cleaning cream.

For each housecleaning product physical characterisation of particles (mass, size and number distribution evolution which enabled the observation of nucleation events) has been performed. Chemical speciation of both gas and particulate phases was achieved using TD-GC-MS techniques (Rossignol et al., 2012). Some cleaning products have been extensively studied using an Aerosol Mass Spectrometer Aerodyne, allowing on-line and in-situ analysis of particulate matter below 1µm. Application of a surface cleaning cream, shown in Figure 1, suggests its relevant contribution to the total organic loading of PM_1 (with an increase from 6 to 10 µg/m^3).

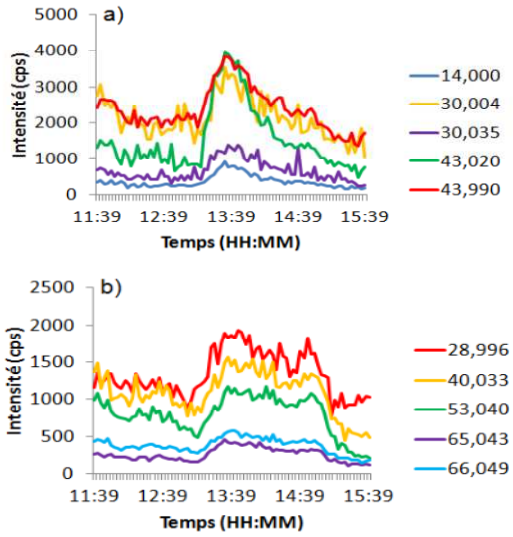

Figure 2. On-line ion fragments associated to (a) "primary-type" time evolution and (b) "secondary-type" time evolution behaviour.

The AMS further indicates different time evolution for the identified ion fragments, as shown in Figure 2.

Finally, comparison between on-line and off-line techniques confirms the importance of secondary aerosol formation when high limonene amount are present.

Nazaroff W.W. and Weschler C.J., 2004. *Atmospheric Environment*, **38**, 2841-2865.
Chen, X. and Hopke, P.K. (2010) *Indoor Air* **20**, 320 328.
Weschler, C.J. (2000) *Indoor Air* **10**, 269–288.

Personal monitor for engineered nanoparticles using a MEMS cantilever balance

S. Merzsch[1], H.S. Wasisto[1], I. Kirsch[2], A. Waag, E. Peiner[1] and E. Uhde[2]

[1] Institute of Semiconductor Technology (IHT), TU Braunschweig, Braunschweig, Germany
[2]Dept. Material Analysis and Indoor Chemistry, Fraunhofer WKI, Braunschweig, Germany
Keywords: Engineered nanoparticles, personal sampler, MEMS.
Presenting author email: erik.uhde@wki.fraunhofer.de

Nanomaterials as additives have become common in the production of consumer goods and building materials. The range of application extends from daily live products like cosmetics or wall paints to special uses in high performance coatings, glues. The volume of production exceeds several 10,000 t per year (Hendren *et al*, 2011) for the nanomaterials in most widespread use. Engineered nanomaterials can thus no longer be regarded as a sparely used research object, but have become a type of industrial raw material among others.

Therefore, the production environment, where large amounts of nanomaterials are handled and substantial exposure is possible, monitoring of the air quality is an important issue in respect to further use of this technology. A demand for personal monitors to assess the exposure of workers towards these particles undoubtedly exists (Tsai *et al*, 2011). Simple collection of the particles on filters or impactors offers an affordable solution to this, but requires complex laboratory analysis and cannot provide timely warning in case of increased concentrations in the surrounding environment. Therefore a direct-reading instrument would be more suitable for this purpose. Unlike a conventional particle counter, such a device must be small and lightweight, and the sensor and the electronics must be simple enough to allow a mass production at low costs.

A MEMS (micro-electromechanical system) based approach was proposed to weigh extremely small particles. This concept was developed further to design a particle detector for use in personal monitors. A joint project (NANOEXPO) examines the possibility of using piezoelectrically and thermally excited cantilevers as sensors for ultrafine particles. The project team developed and currently tests a small personal dosimeter-like sampler that collects and weighs ultrafine particles over a work shift.

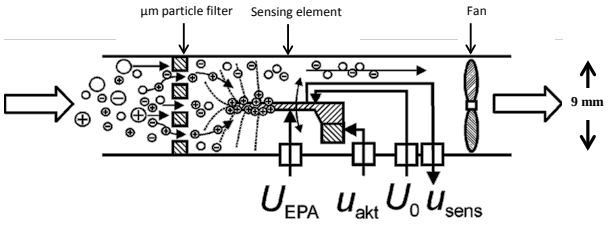

Figure 1. Schematic of the sampler. U_{EPA} is the collection voltage (-480 V)

The sampler consists of a flow channel (Fig. 1) with a coarse-particle pre-filter, the sensing cantilever and a micro-fan to force air through the channel. Sub-micrometer particles are trapped on the cantilever by electrophoresis or thermophoresis (depending on the selected sampling head, Fig 2), the resonant frequency change of the loaded cantilever is then used to determine the mass of the collected particles. The device uses a variable loading phase of 1 – 15 min and reaches a typical detection limit of < 1 µg/m³. The personal sampler is validated in environmental test chambers against test aerosols generated from technical nano-particles (SiO_2, carbon, TiO_2, Ag, and PTFE).

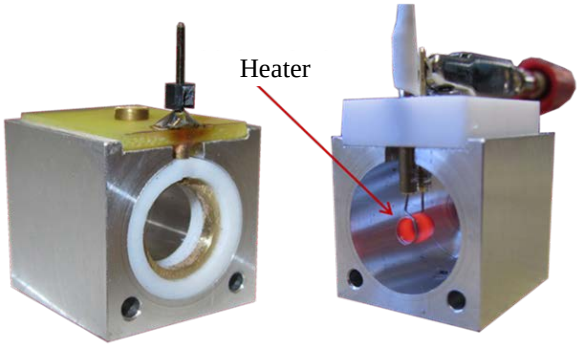

Figure 2. Electrophoretic (left) and thermophoretic (right) sampling head of the personal monitor.

At the current development stage the microbalance-detector prototypes show a mass-sensitivity sufficient to allow for 15-minute measurement cycles if the (preferred) second resonant mode is used for sensing. A mass resolution below 1 ng can be reached under typical indoor conditions, and the cross-sensitivity in regard to environmental changes (especially high humidity, temperature changes) is in an acceptable range. Since mass resolution can be improved with smaller cantilevers, but the particle collection efficiency mostly scales with the cantilever surface area, modification of the cantilever surface is currently evaluated to further increase the sensitivity of the sensor.

The authors greatly acknowledge funding by the German Federal Ministry of Education and Research (BMBF) under grant no. 03X0098A/B.

Hendren CO, Mesnard X, Dröge J, Wiesner MR, (2011) *Environ. Sci. Technol.* 45 (7), 2562-2569

Tsai CJ, Huang CY, Chen SC, Ho CE, Huang CH, Chen CW, Chang CP, Tsai SJ, Ellenbecker MJ, (2011) *J. Nanopart. Res*. 13, 4161-4172

Test of indoor air cleaners

B. Mølgaard[1], A.J. Koivisto[2], T. Hussein[1] and K. Hämeri[1]

[1]Department of Physics, University of Helsinki, FI-00014, University of Helsinki, Finland
[2]Finnish Institute of Occupational Health, FI-00250, Helsinki, Finland

Keywords: Indoor aerosol, Air cleaning

Clean indoor air is important for human health and well-being. Clean air is usually be obtained by reduction of indoor air pollutant sources and by ensuring sufficient ventilation. However, the outdoor air is not always clean, so often the incoming air is cleaned by filtration. Air cleaning devices may also be placed in the indoor environment.

We have tested five commercially available air cleaning devices which are all designed to remove aerosol particles from the indoor air. Cleaning of coarse particles is good for removing pollen, mould, and dust particles, cleaning of fine particles for removing long-range transported particles, and cleaning of ultra-fine particles for removing particles from local combustion and many indoor sources.

We tested air cleaners from five producers: Electrolux, IQAir, Elixair, Plymovent, and LightAir. The device from LightAir was an electrostatic precipitator with the ion flow on the outside of the device. All the others used fans to suck the air through some filters, and in one case also through an electrostatic precipitator. These were tested, one by one, in a room with a ventilation rate of 0.6 air changes/hour. The incoming air was first filtered and then an aerosol generator injected particles into it. The incoming aerosol and the aerosol in the room were monitored with a Scanning Mobility Particle Sizer (SMPS) and an Optical Particle sizer (OPS). Two fans in the room ensured that the air was well mixed. Each experiment lasted about 24 h. In the beginning the aerosol generator was on while the air cleaner was off. Then after 160 min the air cleaner was turned on and the particle concentration decreased until it reached a steady-state. A few hours before the end of the experiment the aerosol generator was turned off. Then the particle concentration decreased rapidly. Similar studies have considered this fast decay only (Zuraimi *et al* 2011; Kim *et al* 2013), but by utilising a longer data time series we reduced the uncertainties of our results.

The number size distribution in the chamber is described by the balance equation (assuming no indoor sources)

$$\frac{dN_i}{dt} = N_{vent,i}\lambda - N_i(\lambda + \beta_i + \gamma_i) + J_{coag,i}$$

where N_i is the number concentration of particles in size class i in the chamber, $N_{vent,i}$ is the corresponding concentration for the incoming aerosol, λ is the ventilation rate, β_i and γ_i are respectively the deposition and cleaning rates for particles of size class i, and $J_{coag,i}$ is the change rate due to coagulation.

We used the measured number size distribution data to estimate λ, β_i, and γ_i. This is possible because we measured periods with and without the air cleaners, and with and without incoming particles. By multiplying the cleaning rate with the room volume we obtained the Clean Air Delivery Rate (CADR) which is a standard measure of air cleaner performance.

For most of the air cleaners the CADR size dependence is small for particles smaller than 600 nm, and for supermicron particles the CADR was somewhat higher. The LightAir device was an exception. This was expected because of a different method for cleaning the air. The obtained CADR fit well with the information from the producers.

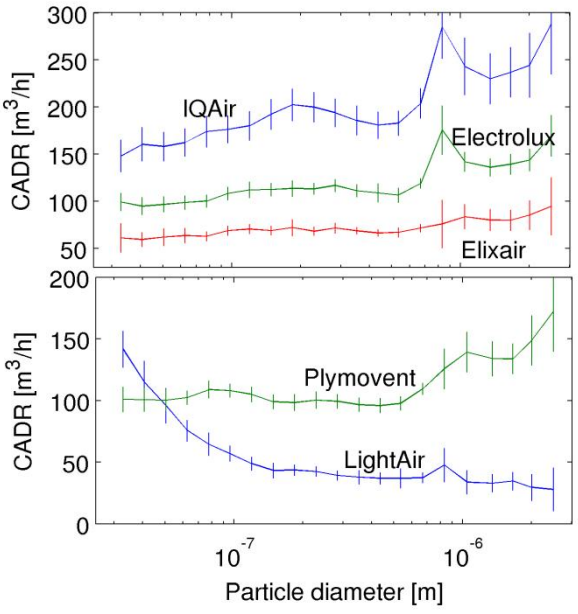

Figure 1. Size-resolved Clean Air Delivery Rates.

Zuraimi, M.S., Nilsson, G.J., Magee, R.J. (2011) *Build. Environ.* **46**, 2512-2519.
Kim, H.J., Han, B., Kim, Y.J., Jeong, C.S., Lee, S.H. (2013). *Build. Environ.* **60**, 272-279.

Use of portable particle counters for the assessment of residential exposure to indoor-generated particles

A.Wierzbicka[1], G. Bekö[2], J. Toftum[2] and G. Clausen[2]

[1]Ergonomics and Aerosol Technology, Lund University, P.O. Box 118, SE-221 00 Lund, Sweden
[2]International Centre for Indoor Environment and Energy, Dept. of Civil Engineering, Technical University of Denmark, 2800-Lyngby, Denmark

Keywords: portable particle counters, indoor sources, residential exposure
Presenting author email: aneta.wierzbicka@design.lth.se

Contribution of indoor sources of particles to personal exposure has not been fully assessed nor understood. Ambient and non-ambient origin of particles present in indoor environments with their site specificity and intermittent nature do not make the assessment easy. In the past large and noisy instruments requiring operator attendance prevented measurements in indoor environments on large scale. Data available on indoor particle number concentrations originate from measurements conducted in a few residences. So far three published studies addressed indoor source contribution to residential exposure, the amount of residences covered range between 1 to 7 (Bhangar et al., 2011; Mullen et. al., 2011, Wallace and Ott, 2011)

The aim of this study was to evaluate the suitability of portable particle counters for the assessment of the indoor sources contribution to residential particle exposure.

Measurements were conducted in 56 residences in Copenhagen for about 45h during weekdays of the 2011/2012 winter season. Three NanoTracers (Philips Aerasense) were used for particle number concentration measurements in the size range between 10 and 300 nm. Participants filled in a detailed activity logbook for identification of time spent at home, identification of indoor sources and subsequent estimation of the contribution of indoor sources to residential particle exposure. The instruments were purchased directly before the commencement of the measurements thus were manufacturer's calibrated. Their performance in measuring particle concentration was assesed against a Scanning Mobility Particle Sizer (SMPS 3934, TSI Inc.) at the end of the measurement period in a chamber experiments conducted in the Aerosol Laboratory at Lund University. Particles from three typical indoor sources (candle, cigarette smoke, incense) were used for comparisons.

Results from the chamber experiments showed that for the tested indoor sources 1-hour average NanoTracer-to-SMPS number concentration ratios were between 0.73 and 1.03 for the three instruments, indicating that the NanoTracers tend to underestimate the number concentrations. The obtained results can be compared to results of Asbach et al. (2012) who reported Nanotracers' accuracy of ± 30% for measuring number concentrations of sodium chloride, di-ethyl-hexyl-sebacate and soot particles. On two occasions in our chamber experiments one Nanotracer showed 43% lower concentration during incense burning while another showed 53% higher concentrations during cigarette smoke, compared to SMPS. There was no trend suggesting that any of the instruments would measure different results in a consistent manner. Thus, no correction factor was applied to the measured data.

Based on the time resolved particle number concentrations and the detailed activity logbooks, indoor sources were identified and their contribution to the daily residential exposure was estimated. On average, indoor sources accounted for 65% of the daily residential exposure. When the contribution from candle burning, the dominant indoor particle source, was excluded, the indoor sources accounted for 50%. These values are comparable to the results from 7 California residences (Bhangar et al., 2011) where indoor sources accounted on average for 59% of the residential exposure.

Even if the accuracy of the NanoTracers is ± 30%, their small size, battery and silent operation make them an interesting alternative for measurements in indoor environments, where minimal disturbance for the occupants is crucial. They allow conducting time resolved particle number measurements in a relatively large study population, that can give a unique insight into important part of personal exposure i.e. residential exposure. Results from the measurements in 56 Danish residences proved that these instruments can be used for estimation of residential exposure to indoor-generated particles. The results point out that contribution of indoor sources can be significant and should be considered in the health effects assessments. However the use of these portable instruments requires regular comparisons of their performance against other particle counters as well as their cross-comparisons (if several are used).

This study was part of the Centre for Indoor Air and Health in Dwellings (CISBO) study, which has been initiated and supported by the REALDANIA foundation. This work was further supported by VINNOVA - Swedish Governmental Agency for Innovation Systems, FAS - Swedish Council for Working Life and Social Research and AFA Insurance.

Asbach, C., et. al., 2012. Annals of Occupational Hygiene, 56:606-621.
Bhangar, S., et al., 2011. Indoor Air, **21**, 132-144.
Mullen, N.A., et al., 2011. Atmospheric Environment, **45**, 7574-7582.
Wallace, L., Ott, W. 2011. Journal of Exposure Science and Environmental Epidemiology, **21**, 20-30.

Chemical composition of hookah smoke derived aerosol measured with an Aerosol Chemical Speciation Monitor

P.L. Croteau[1], J.T. Jayne[1], D.R. Worsnop[1], T. Oh[2], C. DeForest Hauser [2]
[1]Center for Aerosol and Cloud Chemistry, Aerodyne Research, Inc., Billerica, MA, 02067, USA
[2]Department of Chemistry, Davidson College, Davidson, NC, 28035, USA
Keywords: chemical composition, health effects, tobacco, aerosol mass spectrometry
Presenting author email: croteau@aerodyne.com

Hookah (also known as narghile, shisha, and hubble-bubble) smoking originated in India during the 15th century and has since spread to various Middle Eastern and Mediterranean regions as well as western countries, including the United States where there has recently been a dramatic increase in its prevalence (Eisenberg et al., 2008). In a hookah, as users inhale, air is drawn over charcoal which indirectly combusts the tobacco. The mixture of charcoal and tobacco smoke is then drawn through water and to the user. The tobacco smoked with a hookah is often sweetened with, for instance, molasses. While smoke from cigarettes has been relatively well characterized, little is known about the chemical composition of hookah smoke aerosol, which is expected to be different due to the different method of combustion, the water filtration, the added influence of the charcoal, and the presence of sweeteners in the tobacco.

Here we present on-line aerosol chemical composition measurements of hookah smoke using the recently developed Aerodyne Aerosol Chemical Speciation Monitor (ACSM). The ACSM samples the air through a 100 µm orifice into an aerodynamic focusing lens where particles are focused into a beam which is transmitted through a vacuum system to a tungsten surface that is heated to 600ºC. The particles are vaporized and the resulting gases along with the remaining air are ionized with electron impact and detected with a small quadrupole mass spectrometer. The particle-only mass spectrum is determined by switching an automated 3-way valve between whole air and filtered air and taking the difference of the filtered and unfiltered mass spectra (Ng, et al., 2011).

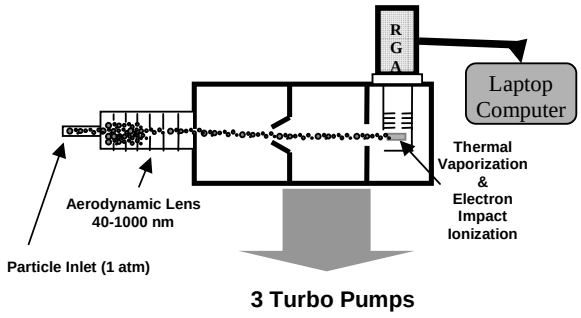

Figure 1: A diagram of the aerosol chemical speciation monitor

Previous studies of the particle phase of hookah smoke aerosol are quite limited and have relied on off-line techniques to examine total particle mass, individual compounds or classes of compounds (such as nicotine, polycyclic aromatic hydrocarbons, or aldehydes), or tar (nicotine-free dry particulate matter) extracted from filters (Shihadeh, 2005). This study is the first to measure bulk chemical composition of hookah smoke particles using an on-line technique.

This work was funded by the Davidson Research Initiative. Development of the ACSM has been supported by EPA SBIR Grant EP-D-05-057 and DOE SBIR Grant DE-SC0001673.

Eisenberg, T., Ward, K.D., Smith-Simone, S., Maziac, W. (2008), J. Adolecent Health, 42(5), 526-529.

Ng, N., Herndon, S., Trimborn, A., Canagaratna, M., Croteau, P., Onasch, T., Sueper, D., Worsnop, D., Zhang, Q., Sun, Y., Jayne, J. (2011) *Aerosol Sci. Tech.*, 45(7), 780-794.

Shihadeh, A., Saleh, R. (2005), *Food Chem. Toxicol.*, **43**(5), 655-661.

An experimental approach to measure particle deposition in large circular ventilation ducts

G. Da[1], E. Géhin[1], M. Ben-Othmane[2], M. Havet[3], C. Solliec[4], C.Motzkus[1]

[1]CERTES, Université Paris-Est, Créteil, 94010, France
[2]Clauger, Brignais, 69530, France
[3]Umr GEPEA, Oniris, 44322, Nantes, France
[4]Umr GEPEA, Ecole des Mines de Nantes, 44300, Nantes, France
Keywords: Bio-aerosol, Particle deposition, Ventilation ducts, Food-industries.
Presenting author email: guillaume.da@u-pec.fr

This study was a part of the French project CleanAirNet, which aimed at producing new knowledge, models and techniques to help controlling the safety of the food products, through a better control of aerosol particle (bioaerosols) transport and deposition in the ventilation networks of the food industry. A small body of experimental literature has been reported on large ventilation ducts (Sippola, 2004). The purpose of this paper was to investigate particle deposition experiments in large circular ducts for fully developed turbulent flow.

An experimental setup (called MIDAS) was designed in a laboratory to validate a theoretically based model predicting particle deposition velocities for fully developed turbulent flow in an horizontal with circular cross-section (Ben Othmane, 2010).

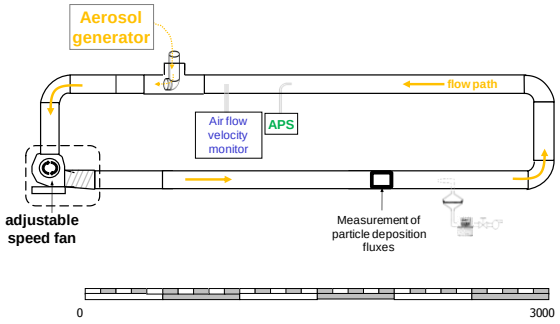

Figure 1. The experimental bench to investigate particle deposition velocity.

The experimental bench proposed in this study included a ventilation system, a monodisperse fluorescent aerosol generation system (VOAG, TSI), and direct-reading instruments to monitor the following parameters in real time: air-velocity, temperature, relative humidity, particle aerodynamic diameter (APS, TSI). The deposition of particles mass onto different surface orientations (with respect to gravity) was calculated by wiping the fluorescent particles and subsequently by measuring their concentrations by spectrofluorometry (FluoroMax, HORIBA). The particle mass deposited on filter was also determined by fluorescent techniques.

Experiments conducted at (5.0 ± 0.3) m/s in the circular duct system (160 mm in diameter, Reynolds number of 5.3×10^5) showed great stability for the generation of particles with nominal size of (0.92 ± 0.01) (2.12 ± 0.03), (3.47 ± 0.03) and (6.02 ± 0.11) µm; with trials lasted for 72, 4, 3 and 1 hour respectively.

The fluorescent technique allowed measuring deposited mass particle down to ($4.8\text{x}10^{-11}$ ± $1.1\text{x}10^{-11}$) kg. The deposition velocities obtained with 6 µm particles showed maximum uncertainty and variability of 35% and 26% respectively.

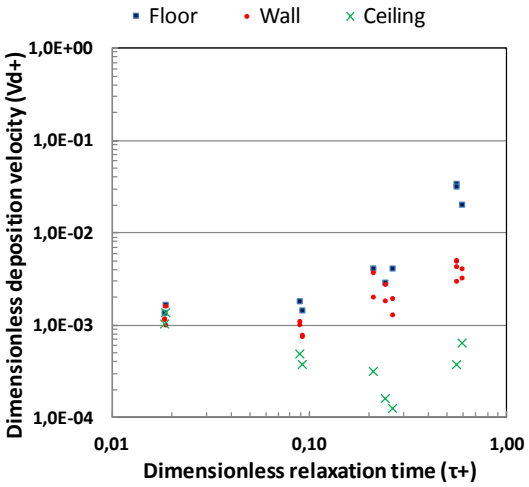

Figure 2. The influence of surface orientation in the circular duct, on dimensionless velocity.

The measured dimensionless deposition velocity showed the influence of the surface orientation (floor, wall and ceiling), in which a clear effect of the particle diameter is demonstrated. The experimental approach proposed in this study can be used to validate models on particle deposition in ventilation ducts from food factories, by considering large circular sections, turbulent flows, and thermal gradients for thermophoresis.

This work was supported by the French National Research Agency under the project CleanAirNet: “Hygienic design of ventilation duct networks in food factories”.

Ben Othmane, M., Havet, M., Géhin, E. and Solliec, C. (2010) *Aerosol Sci. Technol.* **44**, 775-784.
Sippola, M.R. and Nazaroff, W.W. (2004) *Aerosol Sci. Technol.* **38**, 12.

Wednesday, September 4, 2013

Session: Aerosol-based Nanotechnology, *Nanoparticle synthesis in the gas phase*

Anti-agglomeration of spark discharge generated aerosols via unipolar air ions

Kyu-Tae Park, Massoud Massoudi Farid and Jungho Hwang

Department of Mechanical Engineering, Yonsei University, Seoul, 120-749, South Korea
Keywords: spark discharge, agglomeration, charged particle, moment method.
Presenting author email: GT@yonsei.ac.kr

This paper reports the effect of air ion on reducing agglomeration of metal aerosol particles generated from homogeneous spark discharge. For air ion generation, a carbon fiber ionizer was located right above the spark channel formed between two metal electrodes. Once the air ions were generated, they were directly delivered to the particles and charged the particles.

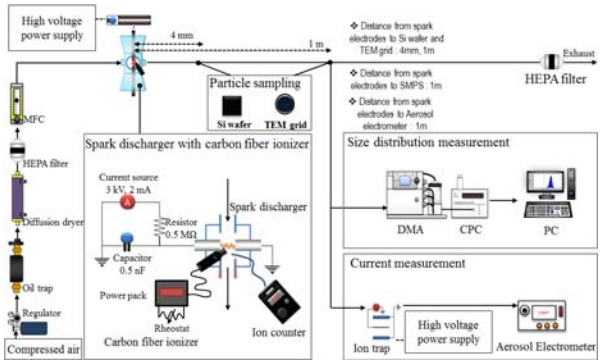

Figure 1. Schematic of experimental setup

In this study, a theoretical approach was carried out to predict the particle size distribution with time. For this purpose, the Brownian coagulation theory between charged particles was connected with the moment method. The particle size distribution was characterized by the scanning mobility particle sizer (SMPS) system and compared with the theoretically determined size distribution where results of current measurement, and transmission electron microscopy (TEM), and scanning electron microscopy (SEM) were used (Figure 1).

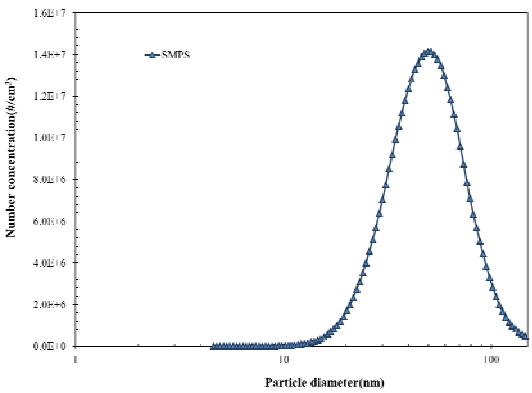

Figure 2. Size distribution of spark generated particles

Experimental results were in good agreement with calculations by the moment method. The particle size right after the spark generation was about 4 nm. Then, the size increased to 50nm at 1m downstream (residence time of 1.76sec) from the spark channel owing to Brownian agglomeration, when there were no air ions injected (Figure 2).

However, with the injection of air ions (ion concentration : particle concentration = 10 : 1), the size of particles was reduced to be around 10 nm due to the repulsive force between unipolarly charged particles with an average charge number of 0.39 (Figure 3).

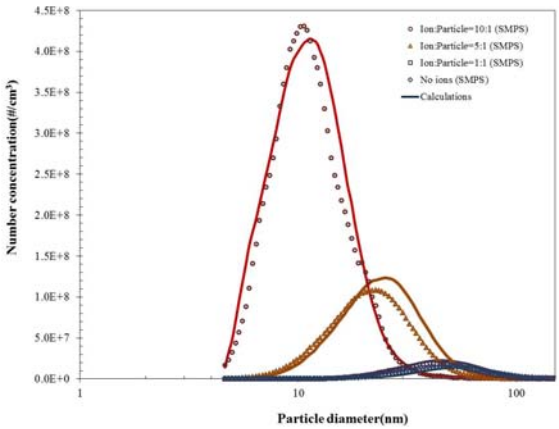

Figure 3. Effect of air ions on particle size distribution

This research was supported by Future-based Technology Development Program (Green Nano Technology Development Program) through the National Research Foundation of Korea (NRF) funded by the Ministry of Education, Science and Technology (grant number 2011-0030206)..

Tabrizi, N.S., Xu, Q., van der Pers, N.M., Schmidt-Ott, A. (2010). Generation of mixed metallic nanoparticles from immiscible metals by spark discharge. *Journal of Nanoparticle Research*, 12, 247-259..

Schwyn, S., Garwin, E., & Schmidt-Ott, A. (1988). Aerosol generation by spark discharge. *Journal of Aerosol Science*, 19, 639–642.

Borra, J.-P. (2006). Nucleation and aerosol processing in atmospheric pressure electrical discharges: Powders production, coatings and filtration. *Journal of Physics* D, 39, R19–R54.

A Controlled Spark Generator for Increased Nanoparticle Production

T.V. Pfeiffer[1], P. Keijzer[2] and A. Schmidt-Ott[1]

[1]Department of Chemical Engineering, Delft University of Technology, Delft, 2628 BL, the Netherlands
[2]Electrical and Mechanical Support Division, Delft University of Technology, 2628 CD, the Netherlands
Keywords: Spark discharge, gas phase synthesis of nanoparticles, scale up.
Presenting author email: t.v.pfeiffer@tudelft.nl

Spark generators allow the production of high purity nanoparticles, without the need for precursors or solvents. The particles form through ablation of target electrodes by repetitive sparks of constant energy. Current spark generators still follow the original design (Schwyn, 1988), and give poor production rates on the order of 1 mg/hour per electrode pair. An important limiting factor is the repetition rate of the sparks: above ~300 Hz the well-defined spark regime transitions to a chaotic, quasi-continuous discharge. Here, we present a novel approach to increase the production rate, by increasing the repetition rate with constant spark energy.

The distinguishing feature of spark discharge is the short, high intensity oscillating capacitive discharge. This results in high temperatures (10^4 K) and fast quench rates (>10^7 K/s), allowing unique phases to be produced. Up to ~300 Hz, the production rate of a spark generator is proportional to the repetition rate (Helsper, 1993). However, suitable capacitor charging power supplies for higher repetition rates are expensive. Regardless of the power source, residual space charge from a previous spark lowers the gas breakdown voltage at higher frequencies, giving erratic behaviour and strong variations in spark energy. To properly scale up the production rate of a spark generator, constant spark energy has to be maintained also at higher repetition rates

To achieve this we decoupled the charging and discharging cycles of the spark generator circuit, as schematically shown in figure 1. The capacitor is charged while the gap is disconnected (S_2 open), which allows the spark energy to be set without causing premature breakdown in the gap. The spark is initiated by connecting the fully charged capacitor to the spark gap (S_1 open, S_2 closed). Repetition rate, spark energy and gap spacing can be set independent of gas properties and each other, which is a significant improvement over the standard design. The upper repetition rate of this method is limited only by the duration of the spark, ~100 kHz for a typical <10 µs spark.

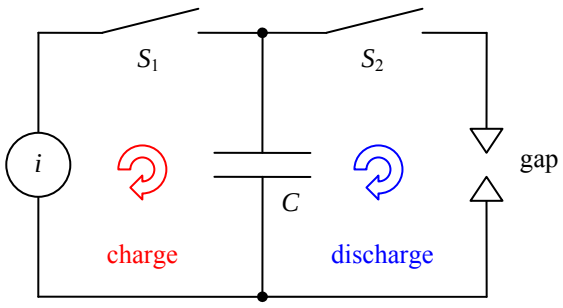

Figure 1. New spark generator concept

On the concept of figure 1, a 1.25 kW prototype was developed and built based on readily available 1.5kV IGBTs (Insulated Gate Bipolar Transistor). The prototype provides up to 50mJ sparks with an upper repetition rate of 25 kHz. Ar and He were used as quench gases. Large gas flows of 100-1000 SLM, in closed loop configuration to limit gas consumption, are necessary to prevent melting of the electrodes at power inputs >~250W. Niobium electrodes were used because of the high melting point of Nb. The impurities in commercial grade gas result in Nb_2O_5 as product (XRD).

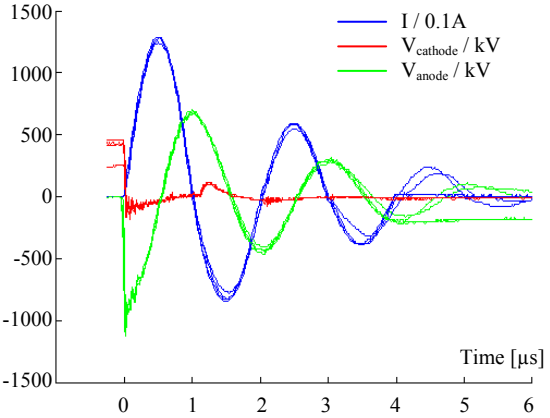

Figure 2. Oscilloscope traces of 9 consecutive 1.2 kV, 32 mJ sparks at a 6.6 kHz repetition rate.

The discharges show the familiar RLC-like oscillations with resonance frequencies around 1 MHz. TEM shows the characteristic fractal-like agglomerates of spark generated nanoparticles, with primary particles of 6 nm (σ_g = 1.6). For Nb, the yield (mass per energy) at high repetition rates is identical to that in the classic system at low repetition rates (Tabrizi, 2009). Mass output scales linearly even at repetition rates well above 1 kHz. We conclude that the production of nanoparticles by spark discharge has been successfully scaled up by two orders of magnitude, while retaining the well-defined, repetitive identical sparks.

Work funded by Agentschap NL, grant EOS-LT07052.

Helsper, C., Mölter W., Löffler F., Wadenpohl C., Kaufmann S., and Wenninger G. (1993) *Atmospheric Environment A.* **27** 1271-1275.

Schwyn, S., Garwin E. and Schmidt-Ott, A. (1988) *Journal of Aerosol Science* **19,** 639-642.

Tabrizi, N. S., Ullmann, M., Vons, V. A., Lafont, U. and Schmidt-Ott. A. (2009) *Journal of. Nanoparticle Research.* **11**, 315-332.

Experimental study on the transition from spark to arc discharge with respect to nanoparticle production

E. Hontañón[1], J.M. Palomares[2], M. Stein[1], X. Guo[3], R. Engeln[2], H. Nirschl[3] and F.E. Kruis[1]

[1]Institute for Technology of Nanostructures, University of Duisburg-Essen, Duisburg, 47057-Germany
[2]Department of Applied Physics, Eindhoven University of Technology, Eindhoven, 600MB-The Netherlands
[3]Institute for Mechanical Process Engineering and Mechanics, Karlsruhe Institute of Technology, Karlsruhe, 76131-Germany

Keywords: spark discharge, glow discharge, arc discharge, mass output rate.
Presenting author email: esther.hontanon@uni-due.de

Due to their unique properties and multiple applications in optical, magnetic, thermal, electrical, biological sensor devices, textiles, cosmetics and medicine, metal nanoparticles are beginning to be widely manufactured and used. This work is aimed to investigate the production of metal nanoparticles by atmospheric plasma synthesis, from the electrical discharge between two electrodes in an inert gas atmosphere.

The setup uses an optimized single unit (OSU) consisting of a cylindrical chamber with multiple ports through which the electrodes are inserted, the gas enters and the aerosol exits the chamber (Stein et al., 2013). The whole system is vacuum tight (<10^{-5} mbar). The electrodes lay vertically facing each other within a certain distance and the gas flows upwards coaxially around the electrodes. The consumable electrode is a copper rod and the gas is ultrapure nitrogen. The OSU is powered by a high voltage (HV) power supply (Technix) in parallel with a capacitance box (30 nF). Two HV (+10 kV) power supplies allow reaching charging currents of up to 150 mA and 1.5 A respectively. Currents of up to 200 A are delivered by a Tig welding machine (Klimag 210P) operating at low voltage (<30 V). An extensive series of experiments were conducted in order to assess the dependence of the aerosol mass flow rate and particle size distribution on the applied current (1 mA-50 A) and the gas flow rate (5-50 slm). The mass flow rate and the particle size distribution of the copper aerosols were measured online by means of TEOM and SMPS. Also, the mass output rate was determined by gravimetric analysis of aerosol samples collected onto filters; copper particles were then analyzed by SWAXS and TEM. The V-I characteristic of the discharge and the optical emission spectrum of the plasma (Cu/N_2) were measured online too.

The mass output rate is displayed as a function of the charging current in Fig. 1. Three main discharge regimes with distinct V-I characteristics and emission spectra were identified in the experiments: spark discharge, glow discharge and arc discharge. At a current of about 10 A the copper rod melts and, then, a graphite crucible is used to hold the molten copper. A mass output rate of 2 $g \cdot h^{-1}$ was attained by arc discharge at a current of nearly 45 A. The parameters of the particle size distribution of the copper aerosols are listed in Table 1. In general, the geometric mean diameter d_g and the particle number concentration N increase as current increases, consistently with the increase in the mass output rate. Also, d_g decreases with increasing gas flow rate. The geometric standard deviation σ_g varies between 1.4 and 1.7 with increasing current and depends weakly on gas flow rate.

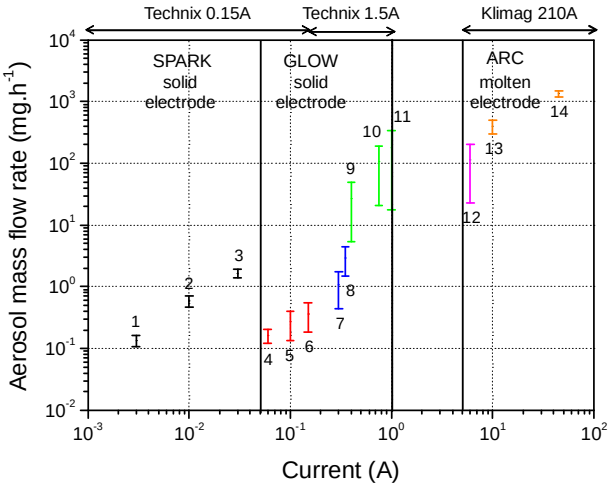

Figure 1. Mass output rate of copper nanoparticles generated by electrical discharges.

Table 1. Particle size distribution of copper nanoparticles generated by electrical discharges.

Glow discharge (solid rod)					
Fig.1	q (slm)	I (mA)	d_g (nm)	σ_g	N (cm^{-3})
4	10	60	16.7	1.35	7.0×10^6
5	10	100	17.7	1.40	1.0×10^7
6	10	150	18.2	1.35	1.2×10^7
7	10	300	20.1	1.53	3.0×10^7
8	10	350	27.4	1.53	3.9×10^7
9	20	400	41.3	1.63	6.6×10^7
10	20	750	49.0	1.67	1.4×10^8
11	20	1000	50.7	1.57	2.4×10^8
Arc discharge (solid rod)					
Fig.1	q (slm)	I (A)	d_g (nm)	σ_g	N (cm^{-3})
12	20	6	53.9	1.73	9.6×10^7
Arc discharge (molten pool)					
Fig.1	q (slm)	I (A)	d_g (nm)	σ_g	N (cm^{-3})
13	20	15	61.5	1.71	1.6×10^8
14	20	45	94.7	1.60	5.2×10^8

This work was supported by the European Union´s Seventh Framework Program (EU FP7) under Grant Agreement No. 280765 (BUONAPART-E).

Stein, M., Kiesler, D., Kruis, F.E. (2013) *J. Nanopart. Res.* 15:1400.

Enclosed Flame Spray Pyrolysis: Control of Product Particle Characteristics by the Air Entrainment

O. Waser[1], and S.E. Pratsinis[1]

[1]Department of Mechanical and Process Engineering, ETH Zurich, 8092, Switzerland
Keywords: CuO, quenching, coagulation, structure control
Presenting author email: oliver.waser@ptl.mavt.ethz.ch

Synthesis of functional nanoparticles requires more and more refined production processes. Enclosing the scalable flame spray pyrolysis (FSP) process facilitates synthesis of a number of sophisticated nanomaterials (Strobel and Pratsinis 2007). That way, for example, it is possible to make metallic nanoparticles (Athanassiou *et al* 2006), coat nanoparticles with thin silica (Teleki *et al* 2008) or carbon layers (Waser *et al* 2011) and control the $FeO/Fe_3O_4/Fe_2O_3$ particle phase composition (Strobel and Pratsinis 2009).

In-situ coating or functionalizing such particles' surface with SiO_2 requires a conveyed aerosol stream for efficient precursor utilization and hermetic coating (Teleki *et al* 2008). Such conditions can be achieved in tube-enclosed FSP configurations where for in-situ carbon coating of $LiFePO_4$, both, oxygen control and conveyed aerosol are required (Waser *et al* 2011).

Primary particle size is another important aspect of functional nanoparticles and its control by FSP settings (including precursor solution composition and burner configuration) is well established. The underlying mechanism for this size variation lies in controlling the temperature history of the particles (Pratsinis 1998) and droplet/particle concentration of the respective flames (Strobel and Pratsinis 2007). So tube-enclosed flame configurations lead to larger product particles compared to open FSP at equal flame conditions (Strobel and Pratsinis 2009) as air entrainment and heat losses can be limited substantially. So there are further opportunities for size and composition that still remain unexplored.

Here we investigate the primary particle size and structure of CuO nanoparticles made in a tube enclosed FSP configuration as a function of entrained air a) flow rate, b) radial velocity and c) preheating temperature. The air is thereby supplied through a ring gap of variable height at the FSP surface level. The resulting particles were analyzed by X-ray diffraction (XRD), nitrogen adsorption (BET), transmission electron microscopy (TEM) as well as differential mobility analyzers (DMA) and aerosol particle mass (APM) analysis to determine the aerosol particle structure.

The entrained air flow rate plays a key role in nanoparticle synthesis in tube-enclosed FSP: The product primary particle size decreases from about 40 to 10 nm (d_{BET}) with increasing air flow rate from 0 to 300 L/min at constant flame settings and thus constant production rate (Fig. 1, circles). Also the CuO crystallite size (d_{XRD}) follows the same trend indicating formation of monocrystalline nanoparticles (Fig. 1, squares).

By supplying higher air flow rates into the tube than an open flame would naturally entrain (≥ 300 L/min), even smaller primary particles can be obtained than in open configuration (open symbols in Fig. 1). This is a result of more efficient cooling and dilution of the freshly formed aerosol in these over-ventilated flames that reduce particle growth by coagulation and sintering.

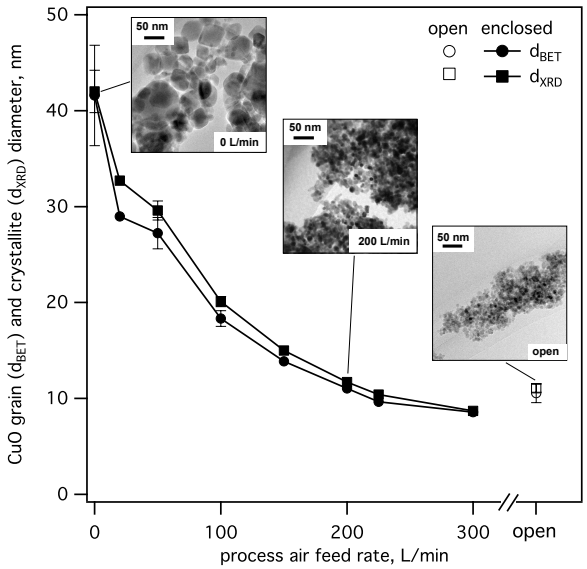

Figure 1. The CuO grain (d_{BET}, circles) and crystallite sizes (d_{XRD}, squares) decrease with increasing entrained air feed rate allowing precise primary particle size control at constant production rate and even smaller particle sizes than with open-FSP due to more efficient flame quenching.

The research leading to these results has received funding from the European Research Council under the European Union's Seventh Framework Programme (*FP7/2007-2013)* / ERC *grant agreement* n° 247283.

Athanassiou, E. K., Grass, R. N. and Stark, W. J. (2006) *Nanotechnology* **17.** 1668-1673.

Pratsinis, S. E. (1998) *Prog Energ Combust* **24.** 197-219.

Strobel, R. and Pratsinis, S. E. (2007) *J. Mater. Chem.* **17.** 4743-4756.

Strobel, R. and Pratsinis, S. E. (2009) *Adv Powder Technol* **20.** 190-194.

Teleki, A., Heine, M. C., Krumeich, F., Akhtar, M. K. and Pratsinis, S. E. (2008) *Langmuir* **24.** 12553-12558.

Waser, O., Buchel, R., Hintennach, A., Novák, P. and Pratsinis, S. E. (2011) *J. Aerosol. Sci.* **42.** 657-667.

Flame spray synthesis of amorphous Indium-Zinc Oxide (IZO) nanoparticles and their electrical and optical properties - towards an application in field effect transistors

D. Kilian[1], S. Polster[2], M.P.M. Jank[2,3], L. Frey[2,3] and W. Peukert[1]

[1]Institute of Particle Technology, University of Erlangen, Erlangen, Bavaria, 91058, Germany
[2]Chair of Electron Devices, University of Erlangen, Erlangen, Bavaria, 91058, Germany
[3]Fraunhofer Institute for Integrated Systems and Device Technology, Erlangen, Bavaria, 91058, Germany

Keywords: flame spray pyrolysis, amorphous nanoparticles, mixed oxides, electronics
Presenting author email: daniel.kilian@lfg.fau.de.

As Flame Spray Pyrolysis (FSP) provides the possibility to mix a broad range of elements at the precursor stage it is one of the most suitable processes for designing new nanomaterials with tailor-made properties, e.g. needed for semiconductors.

One promising material class are amorphous transparent oxide semiconductors (AOS) based on ZnO for transparent (flexible) thin-film transistors (Nomura et al, 2004). The addition of indium, gallium or aluminium influences the band gap, defect density and amorphous state in a distinct composition range. The synthesis of AOS is often carried out by sputtering techniques, providing high device mobilities (Li et al., 2012) but also requiring costly vacuum equipment. Solution based routes like sol-gel processes are used but amorphous films are often not achieved (Lee, 2005). As FSP provides very short residence times, easy precursor mixing and the synthesis can be executed under atmospheric pressure it is a suitable and cost-effective process for the synthesis of AOS. In previous work (Height et al, 2006) the addition of Indium between 1 to 10 at.% to ZnO precursor led to ZnO nanorods, showing the influence of Indium on the morphology. To the best of our knowledge this is the only FSP-based synthesis of In-ZnO.

In this abstract we present our first results regarding the characterization of flame-made indium-zinc oxide nanoparticles towards an application as active layer in field effect transistors. The precursor composition is varied beginning with pure ethanolic zinc acetyl acetonate solution. The molar indium content is increased from 0.167, 0.348, 0.545 and 0.762 to pure ethanolic indium acetyl acetonate solution. The particles are collected by a filter unit and primary particle size, crystallinity and optical properties are analyzed by SEM, TEM, XRD, gas sorption and spectroscopic methods (PL, UV-VIS-NIR).

Table 1 and Figure 1a show basic results derived from XRD analysis of the final product as function of initial indium content in the precursor solution.

Table 1. Phase structure as function of indium content

mol. In content	phase composition
0.0	crystalline ZnO
0.167	mixed phase ZnO/In_2O_3
0.348	mixed phase ZnO/In_2O_3
0.545	amorphous/nanocrystalline
0.762	mixed phase ZnO/In_2O_3
1.0	crystalline In_2O_3

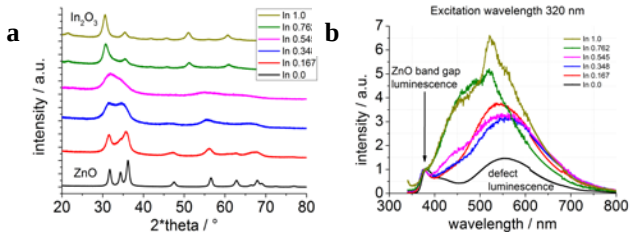

Figure 1. a) XRD patterns of the flame-made product powder. b) PL spectra of the product powder normalized to the intrinsic ZnO band gap emission at ~ 376 nm.

It can be seen, that FSP synthesis is suitable to control the phase composition by the indium content. The most promising composition for an application in flexible devices is a molar indium content of around 0.545. Since defects in the material play a major role in electronic applications regarding the charge carrier mobility and density the PL spectra of the product is depicted in Figure 1b. With increasing indium content the defect luminescence between 400 nm and 800 nm is increasing for the mixed oxide systems. This result can be explained by the increasing amorphous character with indium addition up to 0.545 mol % and is in good agreement with the XRD patterns. Furthermore, UV-VIS spectroscopy shows a shift in the absorption edge indicating the influence of the composition on the band gap (not shown here).

Based on these results and our experience in the fabrication of field effect transistors from nanoparticulate ZnO (Walther et al., 2010) we are convinced that In-ZnO is a very promising material for further improvement of the electronic device performance.

Nomura, K. et al. (2004) *Nature* **432**, 488 – 492.

Li, M. et al. (2012) *Jap. J. Appl. Physics* **51**, 1 - 5.

Lee, S.M. et al. (2005) *Thin Solid Films* **484**, 184 – 187

Height, M.J. et al. (2006) *Chem. Mater.* **18**, 572 – 578

Walther, S., Polster S. et al. (2010) *J. Vac. Sci. Technol. B* **29,** 1 - 6.

Parametric study of iron and iron-oxide nanoparticle synthesis via Aerosol Spray Pyrolysis

G. Kastrinaki[1,3], S. Lorentzou[1], G. Karagiannakis[1] and A.G. Konstandopoulos[1,2]

[1]Aerosol &Particle Technology Laboratory, CERTH/CPERI, Thessaloniki, P.O. Box 60361, 57001, Greece
[2] Department of Chemical Engineering, Aristotle University, Thessaloniki, PO. Box 1517, 54006, Greece
[3] Department of Mechanical Engineering, University of W. Macedonia, Kozani, 50100, Greece

Keywords: iron nanoparticles, aerosol spray pyrolysis
Presenting author email:souzana@cperi.certh.gr

Emerging markets for energy (Karagiannakis et al, 2011), biomarker and magnetic data storage applications, drive the need for the production of iron and iron oxide based particles via continuous and scalable techniques. Aerosol synthesis routes have the advantage of being continuous, relatively simple and industrially-scalable techniques. More specifically, Aerosol Spray Pyrolysis (ASP) is a one-step, flexible and efficient method for the synthesis of tailor made nanoparticles (NP) (Karadimitra et al, 2001; Lorentzou et al, 2011).

In the current study, we examine the effect of different synthesis parameters such as the precursor material and its concentration, the solvent type, temperature, carrier gas, flow rate and exposure to different gases after synthesis on iron and iron oxide nanoparticle characteristics, such as morphology, crystallinity, mean particle size and composition. . The precursor materials used were commercial as well as appropriately purified precursors obtained from a low - cost mill-scale industrial by-product, in order to synthesize particles that could be used in a multitude of relevant applications.

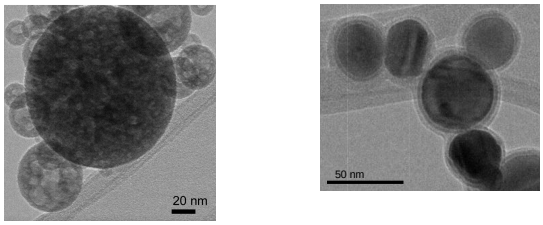

A b

Figure 1:TEM image of (a) iron oxide particles from $Fe(NO_3)_3$ precursor (b) iron particles from industrial by-product derived precursor.

The synthesized particles have been post-characterized with Transmission Electron Microscopy (TEM), X-Ray Diffraction (XRD) and Energy Dispersive X-Ray Spectroscopy (EDS), in order to correlate synthesis parameters to resulting particle crystal structure and morphological characteristics. Particle crystallinity depends on the synthesis temperature, the residence time in the reactor and the temperature gradient applied after the aerosol spray generation. The different particle morphologies (such as dense, porous or core-shell) are determined largely by the composition of the precursor solution (type of iron salt, solvent, concentration) and carrier gas composition (O_2, N_2, H_2, etc). Knowledge obtained by the previous study was applied to synthesize iron nanoparticles from a low cost industrial by-product, normally treated as a waste.

The synthesized particles from different precursor concentrations (0.002-0.2M) were characterized on line with a Scanning Mobility Particle Sizer (SMPS) to study the effect of precursor concentration on particle size.

Particles made from a $Fe(NO_3)_3$ solution were studied under different carrier gases and were subjected to different reducing post treatments in order to obtain iron nanoparticle formation. Four different conditions with respect to the carrier gas were studied and were evaluated, with a representative result shown in Figure 2.

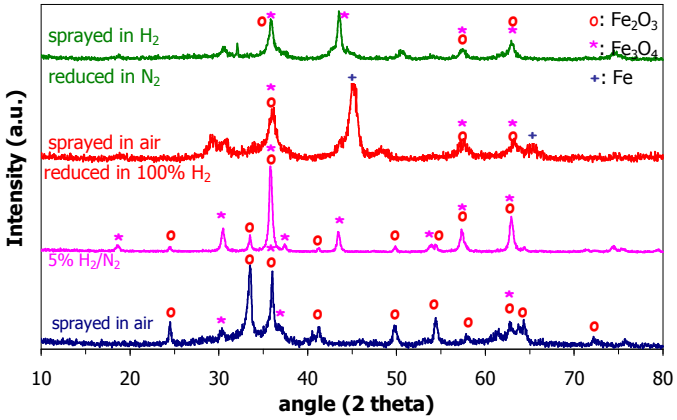

Figure 2. XRD patterns of ASP particles under different spraying and post treatment gas environments.

Aerosol Spray Pyrolysis is a flexible and promising technology for the production of various iron-based crystal structures and morphologies by controlling the parameters of the synthesis process.

Karadimitra K., Papaioannou E., Konstandopoulos A.G (2001), *J. Aerosol Sci*., **32**, Suppl. 1, S233-234.

Karagiannakis G., Mandilas C., Konstandopoulos A., Beatrice C., Lazzaro M., Rispoli N., Pastor J.V., Ros E., Molina S., (2011) *SAE Int. J. Fuels Lubr.* 4, **2** , 282-297

Lorentzou S., Kastrinaki G., Pagkoura C., Konstandopoulos A.G. (2011), *Nanoscience and Nanotechnology Letters*, 3, **5**, 697-704.

Aerosol synthesis of silicon germanium hybrid and alloy nanoparticles

C. Mehringer[1], B. Butz[2], E. Spiecker[2] and W. Peukert[1]

[1]Institute of Particle Technology, Friedrich-Alexander-University Erlangen-Nuremberg, Cauerstr. 4, 91058 Erlangen, Germany
[2]Center for Nanoanalysis and Electron Microscopy (CENEM), Friedrich-Alexander-University Erlangen-Nuremberg, Cauerstr. 6, 91058 Erlangen, Germany
Keywords: nanoparticles, material synthesis, silicon, germanium.
Presenting author email: christian.mehringer@lfg.fau.de

Nanocrystalline germanium (Ge) and silicon (Si), as well as the GeSi alloy are promising materials for the application in printable electronics. Dispersed in organic liquids and deposited as thin functional film the nanocrystals (NCs) can be utilized in electronics, optoelectronics or photovoltaics. The synthesis of freestanding NCs is challenging and can for example be achieved in a nonthermal plasma reactor (Pi and Kortshagen, 2009). We report on our progress in synthesizing Si and GeSi NCs in a reactor system utilizing two consecutive hot-wall reactors.

The setup allows to produce silicon nanoparticles (NPs), GeSi alloy NPs and anisotropic hybrid particles from Ge and Si (Ge@Si NPs). The first reactor stage (HWR I) can be used for Si NP synthesis via monosilane (SiH_4) pyrolysis in Argon carrier gas. GeSi alloy particles of variable composition are produced by feeding SiH_4 and monogermane (GeH_4) into the reactor simultaneously in varying ratios. After the first reactor stage the aerosol is quenched by additional argon. Prior to the second reactor stage (HWR II) GeH_4 can be fed into the system. As a consequence, Ge growth at the NPs from the first stage (e.g. Si NPs) takes place at temperatures of 700°C to 900°C. At the reactor exit the aerosol is quenched by nitrogen. The particles are collected with a membrane filter or sampled via a low pressure impactor by deposition on TEM grids or silicon wafers.

Figure 1 shows SEM images of Ge@Si NPs. GeSi-700-b is synthesized at 700 °C, GeSi-600-c at 600 °C in HWR II. Ge appears bright due to its higher density compared to silicon (dark material). It is observed, that at lower temperature the Ge grows in several patches, while at higher temperatures predominantly one patch is observed at the Si NP surface.

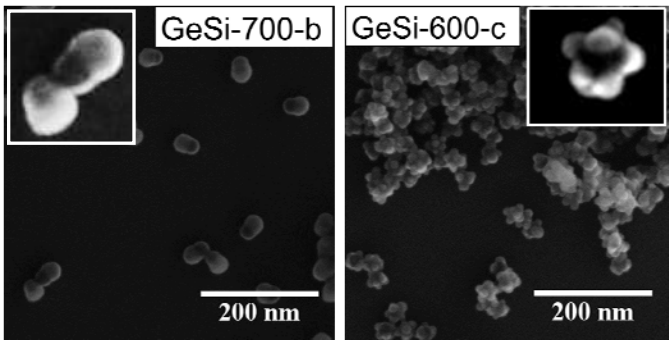

Figure 1. STEM image of Ge@Si NPs. Insets show higher magnification

This is explained by differences in surface diffusion. At higher temperatures higher diffusion leads to decreasing surface supersaturation of Ge on the SiNP surface in a zone around a Ge patch, thus supressing nucleation of further patches. At lower temperatures surface diffusion is lower and several patches can nucleate (Markov, 1971).

Figure 2 shows a high resolution TEM image of exemplary GeSi alloy particles. They are spherical and monocrystalline. Their mean size is 26 nm with a geometric standard deviation (GSD) of 1.25. They are composed of 1.3 at% Si and 97.7 at% Ge, as XRD and EDX measurements show in good agreement. Since Ge and Si are fully miscible over the whole composition range, particles of every composition are accessible by varying the ratio of GeH_4 and SiH_4 in the precursor feed.

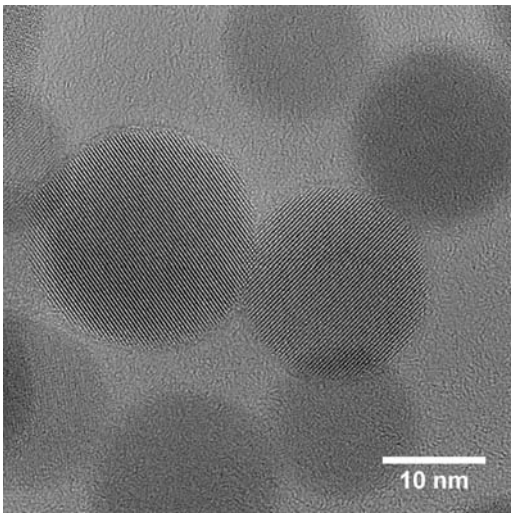

Figure 2. HRTEM image of GeSi alloy NPs

The progress on the synthesis of the germanium-silicon hybrid particles will be demonstrated, regarding the influence of the process parameters on their morphology, composition and growth. Furthermore the tailoring of GeSi alloy nanoparticle morphology and composition as function of process parameters mentioned above will be demonstrated.

This work was supported by the German Research Council (DFG) and the Cluster of Excellence “Engineering of Advanced Materials” (EAM).

Pi, X. D.; Kortshagen, U. Nanotechnology. 2009, 20 (29), 295602.
Markov, I. Thin Solid Films. 1971, 8 (4), 281–292.

Parametric study of iron and iron-oxide nanoparticle synthesis via Aerosol Spray Pyrolysis

G. Kastrinaki[1,3], S. Lorentzou[1], G. Karagiannakis[1] and A.G. Konstandopoulos[1,2]

[1]Aerosol &Particle Technology Laboratory, CERTH/CPERI, Thessaloniki, P.O. Box 60361, 57001, Greece
[2] Department of Chemical Engineering, Aristotle University, Thessaloniki, PO. Box 1517, 54006, Greece
[3] Department of Mechanical Engineering, University of W. Macedonia, Kozani, 50100, Greece

Keywords: iron nanoparticles, aerosol spray pyrolysis
Presenting author email:souzana@cperi.certh.gr

Emerging markets for energy (Karagiannakis et al, 2011), biomarker and magnetic data storage applications, drive the need for the production of iron and iron oxide based particles via continuous and scalable techniques. Aerosol synthesis routes have the advantage of being continuous, relatively simple and industrially-scalable techniques. More specifically, Aerosol Spray Pyrolysis (ASP) is a one-step, flexible and efficient method for the synthesis of tailor made nanoparticles (NP) (Karadimitra et al, 2001; Lorentzou et al, 2011).

In the current study, we examine the effect of different synthesis parameters such as the precursor material and its concentration, the solvent type, temperature, carrier gas, flow rate and exposure to different gases after synthesis on iron and iron oxide nanoparticle characteristics, such as morphology, crystallinity, mean particle size and composition. . The precursor materials used were commercial as well as appropriately purified precursors obtained from a low - cost mill-scale industrial by-product, in order to synthesize particles that could be used in a multitude of relevant applications.

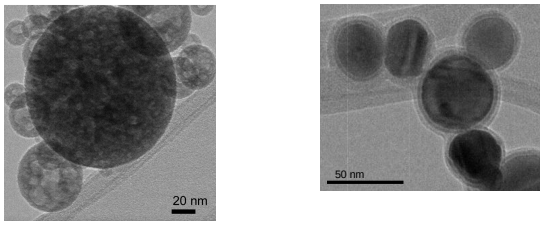

A b

Figure 1:TEM image of (a) iron oxide particles from $Fe(NO_3)_3$ precursor (b) iron particles from industrial by-product derived precursor.

The synthesized particles have been post-characterized with Transmission Electron Microscopy (TEM), X-Ray Diffraction (XRD) and Energy Dispersive X-Ray Spectroscopy (EDS), in order to correlate synthesis parameters to resulting particle crystal structure and morphological characteristics. Particle crystallinity depends on the synthesis temperature, the residence time in the reactor and the temperature gradient applied after the aerosol spray generation. The different particle morphologies (such as dense, porous or core-shell) are determined largely by the composition of the precursor solution (type of iron salt, solvent, concentration) and carrier gas composition (O_2, N_2, H_2, etc). Knowledge obtained by the previous study was applied to synthesize iron nanoparticles from a low cost industrial by-product, normally treated as a waste.

The synthesized particles from different precursor concentrations (0.002-0.2M) were characterized on line with a Scanning Mobility Particle Sizer (SMPS) to study the effect of precursor concentration on particle size.

Particles made from a $Fe(NO_3)_3$ solution were studied under different carrier gases and were subjected to different reducing post treatments in order to obtain iron nanoparticle formation. Four different conditions with respect to the carrier gas were studied and were evaluated, with a representative result shown in Figure 2.

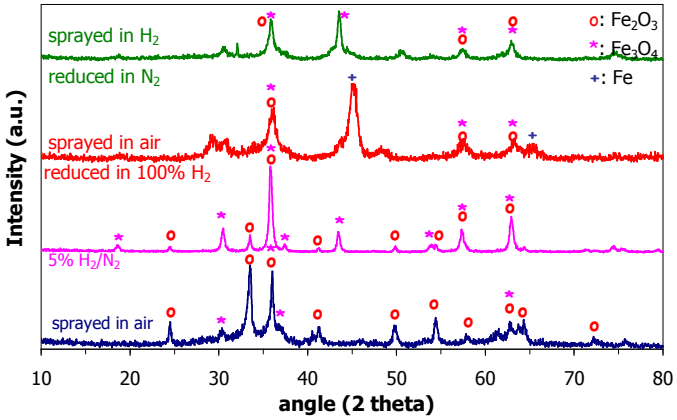

Figure 2. XRD patterns of ASP particles under different spraying and post treatment gas environments.

Aerosol Spray Pyrolysis is a flexible and promising technology for the production of various iron-based crystal structures and morphologies by controlling the parameters of the synthesis process.

Karadimitra K., Papaioannou E., Konstandopoulos A.G (2001), *J. Aerosol Sci*., **32**, Suppl. 1, S233-234.

Karagiannakis G., Mandilas C., Konstandopoulos A., Beatrice C., Lazzaro M., Rispoli N., Pastor J.V., Ros E., Molina S., (2011) *SAE Int. J. Fuels Lubr.* 4, **2** , 282-297

Lorentzou S., Kastrinaki G., Pagkoura C., Konstandopoulos A.G. (2011), *Nanoscience and Nanotechnology Letters*, 3, **5**, 697-704.

Synthesis of tailored organic-inorganic nanostructures by charge controlled coagulation

S. Sigmund[1], E. Akgün[2], J. Meyer[1], M. Wörner[2] and G. Kasper[1]

[1]Institute of Mechanical Process Engineering and Mechanics, Karlsruhe Institute of Technology, 76131 Karlsruhe, Germany
[2]Institute of Process Engineering in Life Science, Karlsruhe Institute of Technology, 76131 Karlsruhe, Germany
Keywords: Composite nanoparticles, electrostatic particle coating
Presenting author email: stephanie.sigmund@kit.edu

Based on charge controlled coagulation between monomer droplets and core particles, precisely tailored nano-composites, consisting of polymer coated core particles are synthesised.

Continuous polymer coatings do mainly have protective properties. Depending on the shell morphology, a highly sensitive or reactive core particle can be protected from uncontrolled reactions or can be completely encapsulated from ambiance. At the same time a tailored polymer shell can be employed to realize a controlled core particle reaction. By influencing the shell thickness, it is possible to directly modify release kinetics of an active core substance. Therefore, a simple method to control the shell thickness of the generated particle systems is strongly desired.

We will present such a method of controlled coating with enclosed polymer layers. Usually hybrid nanostructures are generated in liquid phase processes (Nabhi et al.). However, aerosol processes offer certain advantages, such as high product purity etc. In our case, by means of attractive interactions between gasborne, electrically charged core particles and inversely charged monomer droplets, selective agglomeration is enforced. At the same time repulsive forces interact between charges of the same polarity. Hence agglomeration among core particles or droplets respectively, is kinetically inhibited. The principle of selective agglomeration between inversely charged droplets or particles is not new (Borra et al., Maisels et al.), but processes taking advantage of selective agglomeration to generate coating structures are rare. Once particles collide with droplets, these will wet the particle surface completely to form an enclosed shell. This shell is polymerized afterwards. Thereby, assuming that one droplet wets one core particle, the droplet size determines the shell thickness. Hence a polymeric shell onto a core particle of the desired thickness can be generated by producing monomer droplets of a definite size.

To do experimental studies on the generation of tailored hybrid nanoparticles, monodisperse silica particles with 150 nm in diameter were chosen as model core particles. Silica particles are brought into gas phase by spraying an aqueous particle suspension and subsequent drying. The charging step takes place in a corona charger. By applying positive high voltage potential, core particles gain multiple positive charges during this charging step. Monomer droplets are generated by atomizing a solution, consisting of butyl acrylate and photo initiator. Subsequently monomer droplets of the desired droplet size are classified in a DMA at constant voltage. These monodisperse droplets were charged in a second corona charger but with inverse, thus negative polarity. Core and coating material aerosols were mixed in number ratio of 1:1 to achieve coagulation of one droplet with one core particle and therefore to minimize the occurrence of multiple or uncoated core particles. The mixed aerosol is passed through a residence time volume to ensure coagulation and core particle wetting. The homogeneous monomer coating is then directly photo polymerized by irradiation with UV light to form a solid, polymeric shell. To provide coating evidence, the size increase of the core particle size due to the polymer shell is measured in a conventional tandem DMA setup. Supplementary the hybrid particles are analysed visually via transmission electron micrographs.

Shell thickness measurements for several droplet sizes, by tandem DMA and visual analysis will be presented. Those measurements were compared with theoretical calculated shell thickness, from droplet size. The experimentally determined shell thicknesses agreed well with theoretically expected values.

This project is part of the JointLab IP3, a joint initiative of KIT and BASF. Financial support by the ministry of science, research and the arts of Baden-Württemberg (Az. 33-729.61-3) is gratefully acknowledged.

Borra, J.P., Camelot D., Chou K.L., Kooyman P.J., Marijnissen J.C.M., Scarlett B. (1999). *Bipolar coagulation for powder production: Micro-mixing inside droplets. Journal of Aerosol Science, 30, 945.*

Nabih, N., Landfester, K., Taden, A.,(2011). *Water-Based Inorganic/Polymer Hybrid Particles Prepared Via a Multiple Minieemulsion Process.* Journal of Polymer Science Part A, Polymer Chemistry, 49, 5019.

Maisels, A., Kruis, F.E., Fissan, H., Rellinghaus, B., Zähres, H.(2000) *Synthesis of Tailored Composite Nanoparticles in the Gas Phase.* Applied Physics Letters, 77, 4431

Wednesday, September 4, 2013

Special Session: Particle-Lung Interactions, *Bioaerosols and health*

Daily values of bio-aerosols relevant in allergy: the biological exposome

J.T.M. Buters[1,2], I. Weichenmeier[1,2], G. Pusch[1,2], E. Bartusel[1,2], D. Kupresanin[1,2], H. Behrendt[2], C. Schmidt-Weber[1,2]

[1] ZAUM, Center of Allergy & Environment, Helmholtz Centrum München and Technische Universität München, Munich, Germany
[2] Christine Kuehne Center for Allergy Research and Education (CK-CARE), Kuehne Foundation, Munich, Germany

Keywords: Allergens, Endotoxin, pollen, molds spores
Presenting author email: buters@lrz.tum.de

Allergies have been increasing steadily since decades and an end to this increase is not in sight. Currently about 20% of European citizens (about 80 million individuals) suffer from one kind of allergic disease like asthma or hay fever [1]. Much of the disease is driven by biological exposure, currently badly described.

Methods Pollen and molds were measured with the classic Hirst type volumetric sampler, allergens and bacteria by a Chemvol high-volume cascade impactor equipped with the stages PM>10µm, 10µm>PM>2.5µm, 2.5µm>PM>0.12µm and 0.12µm>PM>0. Quantitative analysis for pollen and mold spores was done microscopically, allergens were determined by ELISA and bacteria by the novel recombinant Factor c (rFc) endotoxin assay. Daily samples were taken at two locations: Davos, Switzerland (1500m a.s.l.) and Munich, Germany (510m a.s.l.).

Results Bacteria, although generally about 0.4-1µm in size were >50% detected in the fraction of air containing large particle (PM>10µm). Little was found in the smaller particulate fractions. The same was true for the pollen, allergens and molds. Molds peaked in mid summer, not autumn. Although pollen were the sole source of allergens, they differed up to 10-fold with allergen count showing that pollen vary substantially in their allergen release capacity. Bio-exposome in Davos was >66% of the exposure compared to Munich, i.e. substantial. The only exception were birch pollen counts, which were much lower in Davos (15% of Munich).

Conclusions The biological components of ambient air are predominantly detected in the >PM10µm fraction, the fraction commonly ignored in air quality measurements. Mountain air might be clean, but with ample biological components relevant for allergy.

[1] Ring J, Akdis C, Behrendt H, Lauener RP, Schappi G, Akdis M, et al. Davos declaration: Allergy as a global problem. *Allergy* 2012;67:141-143.

Airborne influenza virus survival in the air environment

O.Pyankov[1,2], O.Pyankova[2], E.V. Usachev[1] and I.E. Agranovski[1]

[1]Griffith School of Engineering, Griffith University, Brisbane, 4111 QLD, Australia
[2]State Research Centre of Virology and Biotechnology "Vector", Koltsovo, Novosibirsk region, 630559, Russia
Keywords: Virus inactivation, personal sampler, influenza virus.
Presenting author email: i.agranovski@griffith.edu.au

Recent interest towards investigations in the area of airborne virus behavior was ignited by a number of respiratory infection outbreak events, including Avian and Swine Influenza and SARS virus spread in various countries causing substantial social and economic damages. A significant number of corresponding papers have been published in the first decade of this century. The main research effort was focused on identification of virus transmission routs, exposure effects, transmission dynamics, monitoring methods and techniques, and rapid detection of targeted pathogens in the ambient air. This paper reports results on time related inactivation of pathogenic influenza strains in the ambient air under controlled laboratory conditions involving a range of influenza virus strains obtained in various countries.

A laboratory setup used in this project is shown in Fig 1. A virus containing suspension was aerosolized into an aerosol chamber by a nebulizer (BGI, Inc., USA). A rotating aerosol chamber was used to ensure minimal aerosol settlement under action of gravitation.

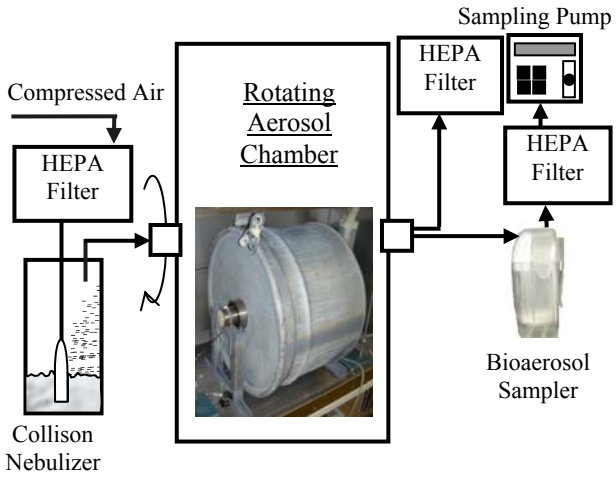

Figure 1. Laboratory setup

Three personal bioaerosol samples each charged with 50 ml of collecting liquid were used for monitoring viable virus concentration at 0, 15, 30, 60 and 90 min after virus aerosolization enabling determination of time related virus inactivation. A modified Hank's solution, consisted of Hank's solution containing 2% volumetric of inactivated bovine serum, 100 U/mL of penicillin and 100 μg/mL of streptomycin was used as the samplers' collection liquid for all experiments. Six viral strains including A/CALIFORNIA/04/2009 (H1N1), A/Moscow /225/2009(H1N1), /Chicken/Kurgan/05/2005(H5N1), A/Chicken/Suzdalka/Nov-11/2005(H5N1), A/Chicken/ Crimea/08/2005(H5N1) and A/AICHI/ 2/68(N3H2) were used in the experiments.

The results obtained for H1N1 and H5N1 strains show close trend with regards to inactivation in the ambient air; rapid inactivation of approximately 60% of microorganisms over the first 30 minutes with following inactivation at much slower rate over the remaining 60 minutes of experiment. A different picture was observed for the H3N2 strain, which demonstrated much higher robustness compared to other subtypes; even after 90 minutes, around 50% of viral particles were still alive. Based on quite substantial number of experimental repeats some generalized conclusions could be made. The most important is based on a fact that two subtypes of influenza virus, which recently caused pandemics demonstrate very similar inactivation behavior in aerosol form. The results of this research could be directly used in health and epidemiological studies, modeling of HVAC systems, microbiological studies and many others.

It should also be noticed that rotating aerosol chamber was found to be very useful device for time related investigations of airborne microorganisms' behavior. It allowed keeping them in the air for quite substantial time periods with relatively low gravitational losses.

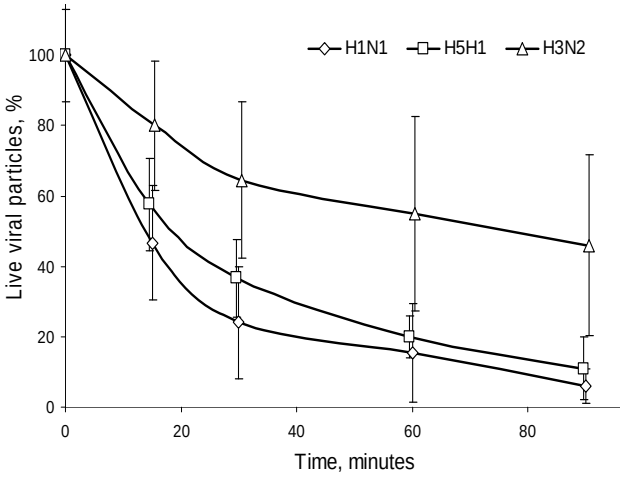

Figure 2. Inactivation of various strains of Influenza virus in the ambient air

Agranovski et al. (2005). *J.Aerosol Sci*. **36**, 609-617.
Pyankov, O.V., Pyankova, O. and Agranovski, I.E. (2012). *J. Aerosol Sci*. **53**, 21 - 28.

Toxicological effects of the particulate emissions from diesel engines and wood combustion are affected by used technology

P.I. Jalava[1], M.S. Happo[1], T. Brunner[2], I. Obernberger[2], T. Murtonen[3], P. Aakko-Saksa[3], J. Mäki-Paakkanen[4], J. Jokiniemi[1,3] and M-R. Hirvonen[1,4]

[1]University of Eastern Finland, Department of Environmental Science, FI-70211, Kuopio, Finland
[2]Graz University of Technology, Bioenergy 2020+, Graz, Austria.
[3] VTT Technical Research Centre of Finland, Fine Particles, FI-02044 VTT, Espoo, Finland
[4]National Institute for Health and Welfare, Department of Environmental Health, FI-70701, Kuopio, Finland
Keywords: Health effects of aerosols, Biofuels, Particulate matter, Toxicology

Particulate air pollution is one of the major public health concerns worldwide. Emissions from traffic and energy production are among the most important sources of these harmful particles. Especially residential wood combustion has increased in the same time as other emissions e.g. from traffic have been decreasing. The combustion emissions are associated with a large variety of adverse health effects, including both cardiac and respiratory symptoms. Recently IARC declared diesel engine emission to be carcinogenic to human but the biomass combustion emissions do not have the same status yet. This decision concerning diesel engine emissions is based mostly on the data from very old technologies. However, the engines have gone through significant improvements during recent years but the development of small scale combustion has been much slower.

We have investigated several modern and old technology heating appliances as well as different diesel engine types for the physicochemical and toxicological properties of the emitted particulate matter (PM). The studies included three types of diesel engines, Euro 2 small industrial engine, a large Euro IV truck engine and CNG powered bus. The conventional diesel fuel (EN590), rapeseed methyl ester (RME) and hydrotreated vegetable oil (HVO) was used as fuels in the two former and the catalyst aftertreatment was applied. Biomass furnaces were old and modern technology logwood boilers, old and new technology stoves and wood chip and pellet burning boilers. Particulate samples (Dp<1µm) for both toxicological and chemical characterization were collected from the diluted emissions. RAW 264.7 macrophage cell line was exposed to the particulate samples for 24h. Inflammatory parameters, TNFα and chemokine MIP-2 were analyzed. Cytotoxicity was analyzed with MTT assay and flow cytometric methods (PI exclusion and cell cycle analysis). Genotoxicity was determined with comet assay and intracellular oxidative species were detected in flow cytometric analyses of DCF oxidation. There were large differences in the magnitude of the toxicological responses. Old technology biomass combustion samples were up to 30 times more potent inducers of genotoxic responses than the modern technologies. The results from the engines were not as drastic but they revealed up to 8-fold differences in genotoxicity, respectively. The magnitude of the toxicological responses was generally slightly higher by the biomass combustion samples than the engine emission samples.

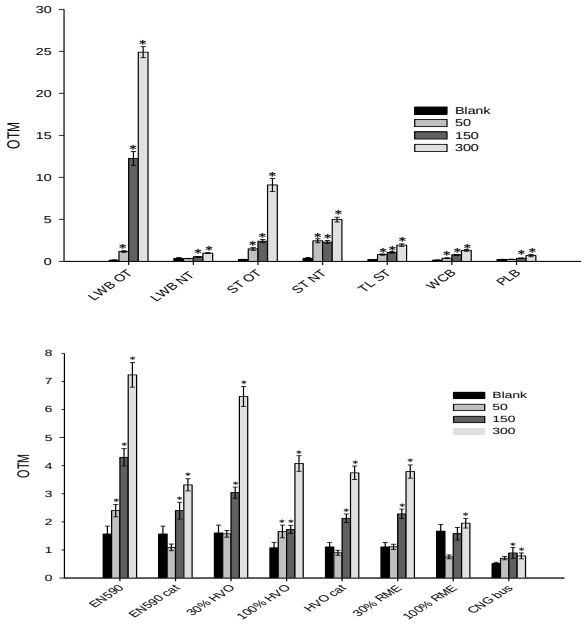

Genotoxicity assessed with comet assay after 24h exposure to PM_1 emission samples from different situations. Bars show blank and three doses (50, 150 and 300µg/ml) ± SEM. Upper figure presents the results from biomass combustion whereas the lower figure is for the engine emissions.

The old technologies had in most cases larger emissions than the technologically developed alternatives. This emphasizes the differences between the samples. The modern technologies can be considered less harmful than the old, but also the emissions from modern technologies can cause harmful effects. From the toxicological perspective the emissions from at least the old technology biomass combustion should not be considered as less harmful than the emissions from the engines.

Jalava PI, Tapanainen M., Kuuspalo K, et al. (2010) *Inhal. Toxicol.* **22** (S2) 48-58.
Jalava PI., Happo M, Kelz J, et al. (2012a). *Atmos. Environ.* **50**: 24-35.
Jalava P.I., Aakko-Saksa P., Murtonen T., et al. (2012b). *Part. Fibre Toxicol.* 9: 37.
Uski O., Happo M.S., Jalava P.I et al. (2012). *Inhal. Toxicol.* **24 14**: 952-965.
Happo MS, Uski O, Jalava PI, et al. (2013). *Sci. Total Environ.* **443:** 256-266.

Long-term effects of repeated exposure to fine and ultrafine particles on lung epithelial cells and fibroblasts.

L. Boublil[1], M.C. Borot[1], L. Martinon[2], J. Sciare[3], A. Baeza-Squiban[1]

[1] Unit of Fonctional and Adaptive Biology, University Paris Diderot, Lab Molecular and Cellular Responses to Xenobiotics, EAC CNRS 4413, 75205 Paris Cedex 13, France.
[2] Laboratory of study of inhaled particles, Mairie de Paris, 75013 Paris, France
[3] Laboratory of climate and environment sciences, CEA-CNRS, Centre de Saclay, 91190 Gif sur Yvette cedex, France
Keywords: atmospheric particles, airway remodeling, differentiation, inflammation
Presenting author email: baeza@univ-paris-diderot.fr

Chronic exposure to particulate matter (PM) is suspected to exacerbate chronic inflammatory diseases such as asthma characterized by an airway remodeling. This remodeling affects the different tissues constituting the airway walls and especially bronchial cells that produce more mucus and fibroblasts that proliferate. However the underlying mechanisms are far to be understood. In this context, to better understand the long term effects of PM, we developed an experimental strategy using primary culture of human bronchial epithelial repeatedly exposed to PM to investigate whether particles could contribute to airway remodeling by inducing sustained inflammation and mucus secretion. Moreover we investigated whether the epithelial secretions induced by particle exposure could have a proliferative effect on lung fibroblasts

Particles were sampled in Paris with 13 stages Dekati impactors in order to collect coarse (10-1µm), fine (1-0.1µm) and ultrafine (<0.1µm) particles. Their effect was observed on primary cultures of normal human bronchial epithelial cells (NHBE) grown at an air-liquid interface in two compartments chambers (Transwell). After four 48 hrs-spaced treatments of 4 hrs from 1 to 10 µg/cm², the evolution of the pro-inflammatory response, the epithelium differentiation and the fate of particles were studied during the 5 following weeks. Moreover, we investigated whether the epithelial secretome could have a mitogenic effect on fibroblasts using two different approaches: cell counting of fibroblasts were performed either when grown in presence of conditioned media (basal media from untreated or PM-treated cells) or when co-cultured with epithelial cells treated or not with fine PM.

Ultrastructural observations revealed that particles were still present in the bronchial epithelium 5 weeks after treatments. Such particles likely represent the insoluble core of the particles as we supposed that organic compounds have been metabolized. Indeed, we observed an increased expression of cytochrome P450 1A1, a xenobiotic metabolizing enzyme involved in organic compounds metabolism, in fine and ultrafine PM-treated cultures. CYP1A1 was highly dose-dependently overexpressed during particle treatment and return to basal level two weeks after the end of the treatments. GM-CSF and IL-6, two biomarkers of a pro-inflammatory response, are slightly but significantly released after each treatment but maintained and increased (for IL-6) and up to 6 weeks. Amphiregulin (a growth factor of the EGF Receptor ligand family involved in the pro-inflammatory response and mucus release (Ramgolam *et al.*, 2012, Val *et al.*, 2012)) was released after each treatment but decreased after the end of the treatments. The number of cells expressing MUC5AC, an important mucin in bronchia, was increased in fine and ultrafine PM-treated cultures.

The proliferation of fibroblasts was increased when exposed to conditioned media from fine PM-treated cells recovered during the 4-treatment period and not by conditioned media from fine PM-treated cells recovered after the treatment period. This proliferation was inhibited when conditioned media were used in presence of an antibody directed against EGF receptor suggesting that EGFR ligands such as amphiregulin were responsible for this mitogenic effect. The proliferation of fibroblasts was also increased when they were co-cultured with epithelial cells treated with fine PM.

Our results demonstrated that bronchial epithelial cells repeatedly exposed to urban fine and ultrafine particles exhibited a sustained pro-inflammatory response, evolved towards a mucous phenotype and produced mediators involved in fibroblast proliferation. Altogether these data suggest that PM could favor the airway remodeling.

This work was supported by the National Agency for Research ANR under grant CESA 009 02, project “Megatox”.

Ramgolam K, Hamel R, Rumelhard M, Marano F, Baeza-Squiban A. (2012) *Arch Toxicol.* **86**:1537-46.
Val S, Belade E, George I., Boczkowski J, Baeza-Squiban A. (2012) *Arch Toxicol.* **86**:1851-9.

Exposure and harm to combustion-derived particles: searching for biomarkers

K. A. BéruBé[1,4], I. A. Guschina[1], A. J. Wlodarcyzk[1,4], Z. Prytherch[1], T. Jones[2,3], E. Karg[3,4], O. Sippula[3,4], H. Harndorf[4,5] , R. Rabe[4,5], T. Streibel[3,4] and R. Zimmermann[3,4]

[1]School of Biosciences, Cardiff University, Cardiff, Wales, CF10 3AX, UK
[2]School of Earth Sciences, Cardiff University, Cardiff, Wales, CF10 3AT, UK
[3] Joint Mass Spectrometry Centre, Rostock University (Analytical Chemistry) and Helmholtz Zentrum München (CMA), Germany
[4] HICE – Helmholtz Virtual Institute of Complex Molecular Systems in Environmental Health-Aerosols and Health, www.hice-vi.eu
[5] University of Rostock, Chair of Piston Machines and Internal Combustion Engines, Germany

Keywords: combustion particles, reactive organic compounds, phospholipids, fatty acids, biomarkers.
Presenting author email: berube@cardiff.ac.uk

The human lung is the portal of entry for ambient particulate matter (PM) from combustion-derived (CD) processes (e.g. diesel and shipping exhausts and wood burning). Over a 24 hour period a person will inhale 20m^3 of air resulting in deposition of particles on the epithelial surface of the lung. It has been well-established that exposure to CDPM (Figure 1) causes increased risk for cardiopulmonary diseases and exacerbation of pre-existing diseases.

The physicochemical properties of size, surface area and presence of transition metals have been implicated as drivers of the oxidative capacity of CDPM. However, the precise role of reactive organic compounds (ROC) in ambient aerosols, present either in the gas phase or the particle phase or in both phases, have not been fully-investigated for their relevance in the induction of the observed adverse health effects.

Oxidation of fatty acids linked to the cell membrane phospholipids leads to many metabolites that have been used as markers of the process. Such metabolites have long been considered to be involved in two possibly inter-related processes: cell/tissue damage and signalling. As one approach to resolve the role played by ROCs, their effects on fatty acid and lipid metabolism in human lung tissues will be studied in detail by using the standard biochemical techniques and lipidomics.

When addressing the toxicity of inhalation hazards such as CDPM, there is a need for a model system that resembles the human lung. In our *in vitro* exposure studies, normal human bronchial epithelial (NHBE) cells were grown at the air-liquid interface (ALI) using filter-well technology (Prytherch *et al* 2011), to create an *in vivo*-like 3-dimensional lung model (Figure 2). This model is a fully-differentiated, pseudo-stratified, muco-ciliary epithelium containing basal, serous, Clara, goblet and ciliated cells.

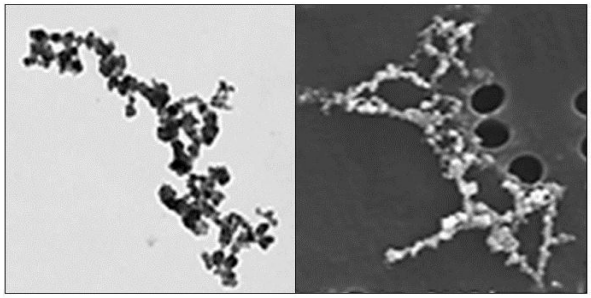

Figure 1. Transmission (left) and scanning (right) electron micrographs of CDPM.

NHBE cells were exposed to the following categories of CDPM at a dose of 152µg/cm^2: carbon black (CB; negative control; Monarch 120, Cabot UK; DQ12 quartz (positive control), shipping diesel engine PM (light fuel oil - LFO) and heavy fuel oil -HFO) collected during a HICE campaign for investigation of health effects of shipping diesel emissions at Rostock University. Following exposure (24 hours), tissue integrity (i.e. transepithelial electrical resistance (TEER); Figure 3) was measured to reveal CB and DQ12 reduced TEER by 19% and 56%, whereas both shipping diesel aerosols (H/LFO) induced about 74% disruption of tissue integrity (Figure 3).

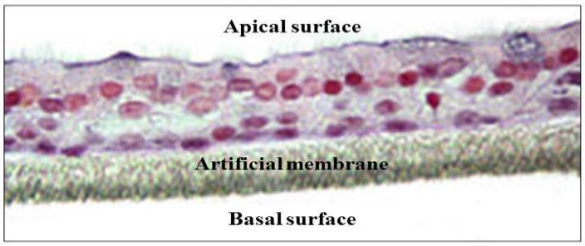

Figure 2. Light microscopy image of NHBE model (Haematoxylin & Eosin stained).

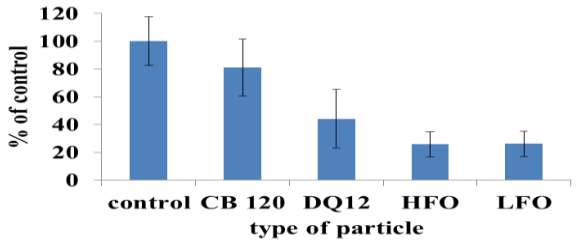

Figure 3. TEER readings for CDPM-exposed cells.

The fatty acid profiles were also affected post-exposure to CDPM. Data indicated that total fatty acid profiles demonstrated changes in ratios between saturated and unsaturated fatty acids. Levels of some polyunsaturated fatty acids, e.g. arachidonic acid (C20:4n-6), which is a precursor to production of pro-inflammatory mediators, slightly increased as a result of this exposure. Further work, applying both functional phospholipid and mediator lipidomics, will allow us to reveal mechanisms behind the changes observed, as well identifying biomarkers of cell damage by specific CDPM ROCs.

Prytherch, Z., Job, C., Marshall, H., Oreffo, V., Foster, M. and BéruBé, K.A. (2011) *Macro. Bios.* **11,** 1467–77.

This work was supported by HICE (www.hice-vi.eu).

Studying the causes of health effects of combustion-derived aerosols in the framework of the Virtual Helmholtz Institute HICE: First results on ship diesel and wood combustion aerosols

R.Zimmermann[1,11], T.G.Dittmar[2,11], T.Kanashova[2,11], J.Buters[3,11], S.Öder[3,11], H.Paur[4,11], C.Schlager[4], S.Mülhopt[4], M.Dilger[4,11], C.Weiß[4,11], S.Diabate[4], H.Harndorf[5,11], B Stengel[5,11], R. Rabe[5], M.-R.Hirvonen[6,11], J.Jokiniemi[6,11], T. Torvela[6], K.Hiller[7,11], S.C.Sapccariu[7,11], K.A.BeruBe[8,11], A.J.Wlodarcyzk[8,11], O.Sippula[1,6,11], B.Michalke[9], T.Krebs[10,11], M.Kelbg[5,11], J.Tiggesbäumker[5,11], T.Streibel[1], E.Karg[1], S.Scholtes[1,11], J.Schnelle-Kreis[1], J.Lintelmann[1], M.Sklorz[1], M. Arteaga Salas[1,11], S. Klingbeil[1,11], J.Orasche[1], P.Richthammer[1], L. Müller[1,11], M. Elsasser[1], A.Rheda[1], B.Werner[1,11], J.Passig[1,11], T. Gröger[1], G.Abbaszade[1], C.Radischat[1,11]

[1]Joint Mass Spectrometry Centre, Rostock University (Analyt. Chem.)&Helmholtz Zentrum München (HMGU/CMA),Germany (D); [2]MDC, Berlin, D; [3]ZAUM, Technical University Munich, D; [4]KIT (ITC/ITG), Karlsruhe, D; [5] University of Rostock (Inst. of Piston Machines & Int. Combust. Engines and Inst. of Physics), D; [6]University Eastern Finland-Kuopio; [7]Uni Luxemburg; [8]Cardiff University, UK; [9]HMGU, D; [10]Vitrocell GmbH, Waldkirch, D; [11]HICE – Helmholtz Virtual Institute of Complex Molecular Systems in Environmental Health-Aerosols and Health, www.hice-vi.eu

Presenting author email: ralf.zimmermann@helmholtz-muenchen.de *or* ralf.zimmermann@uni-rostock.de

Keywords: ship diesel/wood combustion, chemical/physical characterization, cell exposure, health effects

The Virtual Helmholtz Institute HICE addresses the health effects of anthropogenic combustion processes. This is performed by means of a joint comprehensive characterization of the chemical & physical properties of the investigated combustion aerosols as well as the biological effects on cell cultures with high-end innovative methods. The data is jointly analyzed. Human alveolar basal epithelial cells (A549, BEAS2B etc.) are air-liquid interface exposed (ALI) to the diluted combustion aerosols (dilution 10-100x) and subsequently are toxicologically and molecular-biologically characterized. In addition to classical toxicological methods the RNA-transcription, protein expression and metabolite profile-changes are studied (transcriptomics, proteomics and metabolomics). By using stable isotope labeling technologies (^{13}C-glucose for metabolomics; ^{2}H-lysine for proteomics-SILAC) a very high sensitivity and accuracy for detection of molecular-biological effects is achieved at sub-tox.-effect dose levels. Aerosols from wood combustion and ship diesel engine (heavy/ light fuel oil) have been already investigated; other sources (car, truck) are currently studied. The main objectives of HICE are: i) a better understanding of the health effects mechanisms & early response effects as well as identification of health relevant parameters in aerosol, ii) investigation of the effects of organic compounds in gas/particles phase and elucidation of potential synergistic effects between gas phase compounds and particles, iii) studying the effects of the transition from fossil to bio fuels. Based on the "Karlsruhe exposure system" (KIT) a new mobile ALI exposition system was built (HICE-ALI). Furthermore, a mobile S2-biological laboratory was set up for the HICE-measurement campaigns. First experiments were performed at a wood combustion test facility (KIT) and at a research ship diesel engine which is operable with both, light and heavy fuel oil (L/HFO, U Rostock). The characterization of the aerosols includes a comprehensive chemical and physical profiling (GC-MS, LC-MS, FT-IR, ICP-MS, SMPS, AMS, ELPI, PTR, TEM). The ship diesel exhaust contains soot aggregates (Fig. 1), associated with organic and inorganic compounds. Furthermore two innovative photo ionization mass spectrometers (SPI-MS and REMPI-TOFMS were applied for on-line detection of polycyclic aromatics (PAH) and other species in the exhaust gases, showing that partly high gas phase concentrations of health relevant compounds are observable. In Fig. 2(left) the effect of wood combustion and ship diesel PM on the protein expression of ALI-exposed A549 cells is depicted. Filtered aerosol (gas phase) is used as reference for the isotope labeling based method (SILAC). Therefore the effect of the wood combustion and shipping diesel PM can be directly compared. The ship diesel aerosol causes a broader distribution in the observed fold changes (log2), i.e. more proteins are significantly up- or down-regulated in case of shipping diesel aerosol-exposure. This corresponds to a stronger biological effect if compared to wood combustion aerosol exposure. First metabolic results support this finding. The chemical analysis results on the wood combustion and ship diesel PM (Fig.2, right) depict more PAH/oxidized PAH but less of some transition metals (V, Fe) in the wood combustion case. Interestingly, higher alkylated PAH are more abundant in shipping PM. The results suggest that PAH/Oxy-PAH may be less relevant for PM effects on A549 alveolar basal epithelial cells. The influence of transition metals and alkylated PAH needs to be further investigated.

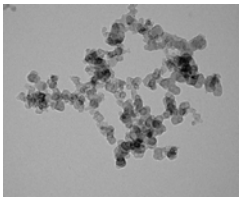

Figure 1) Ship diesel soot (TEM microphotograph)

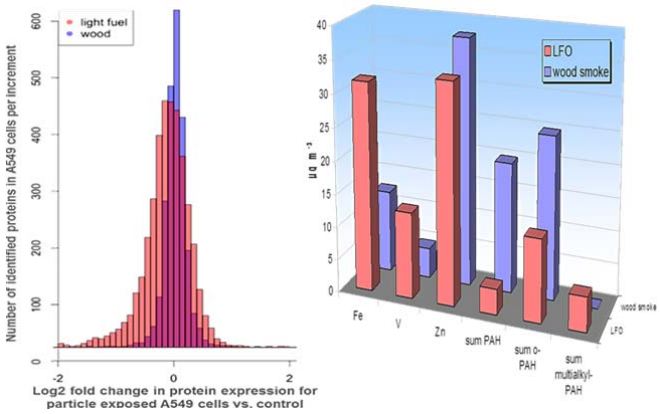

Figure 2 left) SILAC-proteomic results, showing the number of detected proteins as a function of the log2 fold change induced by wood and ship diesel PM. right) Chemical analysis of the PM.

This work/HICE (www.hice-vi.eu) is supported by the Helmholtz association (HGF).

Aerosol Deposition Measurement in the Model of Human Lungs using Positron Emission Tomography

F. Lizal[1], J. Jedelsky[1], J. Adam[2,3], M. Belka[1], and M. Jicha[1]

[1]Brno University of Technology, Faculty of Mechanical Engineering, Energy Institute, 61669 Brno, Czech Republic
[2] UJVRez a.s., Division of Radiopharmaceuticals, 250 68 Husinec-Rez, Czech Republic
[3] Masaryk Memorial Cancer Institute, 656 53 Brno, Czech Republic
Keywords: aerosol deposition, human lungs, positron emission tomography.
Presenting author email: lizal@fme.vutbr.cz

The ability to deliver the exact amount of aerosolized medication to the specific region of lungs is the cornerstone of effective inhalation therapy of both lung and systemic diseases. Targeted inhalation of medication is termed successful if at least 50% of inhaled aerosol deposit in the desired region (Zeman *et al* 2010). However, current inhalation devices reach only the level of 30% deposition in conducting airways that are the target region in the treatment of asthma, chronic obstructive pulmonary disease, or cystic fibrosis (Heyder, 2004, Zeman *et al* 2010). To achieve more effective targeted delivery of aerosolized medication further experiments are to be performed and analysed.

We employed Positron Emission Tomography (PET) for the measurement of aerosol deposition in a realistic model (Fig. 1) of human lungs (Lizal *et al* 2012a). PET is a commonly used method in the nuclear medicine. The method is based on a detection of a pair of simultaneously emitted annihilation photons moving in opposite directions as a result of positron – electron interaction after the positron emission decay of a suitable radioisotope. In our case the liquid aerosol particles from di(2-ethylhexyl) sebacate (DEHS) were generated by the condensation monodisperse aerosol generator (CMAG) and labeled with fluorine-18 as a radioactive tracer. (Lizal *et al* 2012b).

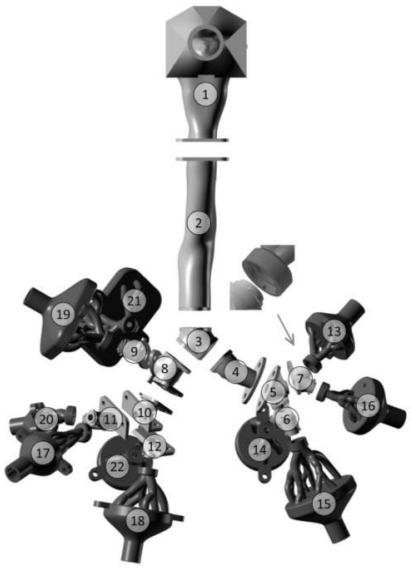

Figure 1. The realistic model of human lungs

Aerosol deposition was measured for two sizes of particles (2.5 μm and 4.3 μm) and for three different inhalation flowrates (15, 30 and 60 L/min). The radioactive aerosol particles were led to the model and non-depositing particles were collected by output filters following each of the model outputs.

Deposition characteristics were calculated from the radioactivity of the deposited aerosol measured by PET. *Deposition efficiency* (Fig. 2) is a ratio of the number of particles deposited in a given segment to the number of particles entering the segment.

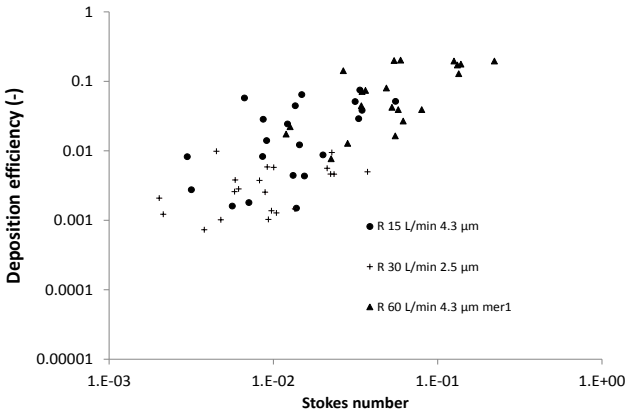

Figure 2. Deposition efficiency in the realistic model.

The results proved correlation of deposition efficiency with Stokes number, which means that the main deposition mechanism is inertial impaction. As a next task the methodology for tagging the solid aerosol particles with radioactive tracer will be developed and deposition of porous and fiber aerosols will be measured.

This work was supported by the Czech Science Foundation under the grant P105/11/1339, and by the project FSI-S-11-6. Frantisek Lizal was supported by the project CZ.1.07/2.3.00/30.0039 of Brno University of Technology.

Heyder, J. (2004) *Proc Am Thorac Soc*, **Vol. 1**, 315-320.
Lizal, F., Elcner, J., Hopke, P. K., Jedelsky, J., and Jicha, M. (2012a) *Proc. IMechE Part H-Journal of Engineering in Medicine* **226** (H3), 197-207.
Lizal, F., Jedelsky, J., Adam, J., Belka, M., Jicha, M. (2012b). *Proc. Int. Conf. Experimental Fluid Mechanics 2012*. Technical University of Liberec.
Zeman, K. L., Wu, J. H. and Bennett, W. D. (2010) *Journal of Aerosol Medicine and Pulmonary Drug Delivery* **23** (6), 363-369.

Thursday, September 5, 2013

Plenary lecture: Nucleation of vapours-molecular content of critical clusters and activation of nanoparticles

By Paul E. Wagner and P.M. Winkler

Nucleation of vapours - molecular content of critical clusters and activation of nanoparticles

P.E. Wagner and P.M. Winkler

Fakultät für Physik, Universität Wien, 1090 Vienna, Austria
Keywords: nucleation, molecular cluster, Kelvin equation, condensation particle counter.
Presenting author email: paul.wagner@univie.ac.at

During the last years considerable advances in the study of gas to liquid phase transitions were achieved. Experiments on particle new formation have been extended down to molecular sizes (Winkler *et al.* 2008). Measurements of critical cluster sizes were performed pointing directly to the key step in the phase transition (Winkler *et al.* 2012). Atmospheric observations have demonstrated particle formation by nucleation to be a frequent phenomenon in the global atmosphere (Kulmala and Kerminen 2008). Wang *et al.* (2012) have pointed out that the initial growth of freshly nucleated small molecular clusters in the atmosphere can be described by heterogeneous nucleation. Despite of recent progress, however, nucleation processes are still among the least understood phenomena in aerosol science.

In this presentation we are providing an overview over some recent studies of nucleation and condensation processes at the Vienna expansion chamber system (Wagner *et al.* 2003).

New particle formation by homogeneous or by heterogeneous nucleation generally proceeds via molecular clusters of critical size, beyond which molecular clusters are likely to grow further to form new particles. Accordingly, critical clusters can be considered as the starting point of the nucleation process. The radius r^* of a critical cluster is related to the saturation ratio S and temperature T of a condensable vapour by

$$r^* = \frac{2\sigma M}{\rho RT \cdot \ln S} \quad \text{(Kelvin equation)},$$

where σ, ρ and M are surface tension, density and molar mass of the condensing liquid, respectively. This relation has been derived under the idealizing assumptions of the classical nucleation theory and its range of applicability needs to be tested experimentally. Under quite general assumptions Oxtoby and Kashchiev (1994) have derived the relation

$$\Delta N^* \cong \left(\frac{\partial \ln J}{\partial \ln S} \right)_T \quad \text{(nucleation theorem)},$$

which allows to approximately determine the (excess) molecular content ΔN^* of a critical cluster from the slope of experimental nucleation rate J vs saturation ratio S curves in a log-log plot. Recently Vehkamäki *et al.* (2007) have reformulated this theorem for application to heterogeneous nucleation. Possible limitations of the validity of the nucleation theorem have recently been discussed by Vehkamäki *et al.* (2012).

Homogeneous nucleation experiments (Strey *et al.* 1994) have provided information on the sizes of critical clusters down to diameters of about 2nm in satisfactory agreement with the Kelvin equation.

Experiments on heterogeneous nucleation in n-propanol vapour by Winkler *et al.* 2008 allowed for the first time to bridge the scale from molecular clusters to nanoparticles. For charged seed particles an enhancement of heterogeneous nucleation and a significant sign preference were observed. The onset vapour supersaturations required for activation of charged and of uncharged nanoparticles were found to be well below the Kelvin prediction. As a consequence the term "Kelvin diameter" needs to be critically reconsidered and the fundamental detection range of Condensation Particle Counters is extended to smaller particle diameters.

Recently we performed experiments on heterogeneous nucleation on single ion molecules (Winkler *et al.* 2012). By means of the nucleation theorem we obtained critical cluster diameters strongly exceeding the diameter of the seed molecules, but in satisfactory agreement with the Kelvin-Thomson equation.

In experiments on the temperature dependence of heterogeneous nucleation (Schobesberger *et al.* 2010; Kupc *et al.* 2013) we surprisingly observed unexpected temperature trends for certain combinations of particle and vapour compositions. This seems to be evidence for strong molecular-scale interactions at the seed particle surface (McGraw *et al.* 2012).

This work was supported by the EC Seventh Framework Programme under the grant agreement no. 215072 (Marie Curie Initial Training Network "CLOUD-ITN") and by the Austrian Science Fund under project no. P19546 and L593.

Kulmala, M., Kerminen, V.-M. (2008) *Atmos. Res.* **90**, 132 (2008).
Kupc, A. *et al.* (2013) *Aerosol Sci. Technol.*, submitted.
McGraw, R. L., Wang, J., Kuang, C. (2012) *Aerosol Sci. Technol.* **46**, 1053.
Oxtoby, D. W., Kashchiev, D. (1994) *J. Chem. Phys.* **100**, 7665.
Schobesberger, S. *et al.* (2010) *ChemPhysChem* **11**, 3874.
Strey, R., Wagner, P. E., Viisanen, Y. (1994) *J. Phys. Chem.* **98**, 7748.
Vehkamäki, H. *et al.* (2007) *J. Chem. Phys.* **126**, 174707
Vehkamäki, H. *et al.* (2012) *J. Chem. Phys.* **136**, 094107
Wagner, P. E., *et al* (2003) *Phys. Rev. E* **67**, 021605.
Wang, J., McGraw, R. L., Kuang, C. (2012) *Atmos. Chem. Phys. Discuss.* **12**, 22813.
Winkler, P. M. *et al*. (2008) *Science* **319**, 1374.
Winkler, P. M. *et al*. (2012) *Phys. Rev. Lett.* **108**, 085701

Thursday, September 5, 2013

Session: Atmospheric Aerosols
Aerosol cloud interaction

Evaporation and condensation of semivolatile aerosol compounds in the DMT-CCN counter

S. Romakkaniemi[1], A. Jaatinen[1], A. Laaksonen[1,2], A. Nenes[3,4], and T. Raatikainen[2,3]

[1]Department of Applied Physics, University of Eastern Finland, Kuopio, P.O.Box 70211, Finland
[2]Finnish Meteorological Institute, Climate Change, Helsinki, Finland
[3]School of Earth and Atmospheric Sciences, Georgia Institute of Technology, Atlanta, Georgia, USA
[4]School of Chemical and Biomolecular Engineering, Georgia Institute of Technology, Atlanta, Georgia, USA
Keywords: semivolatile aerosol, CCN, CCN counter.
Presenting author email: sami.romakkaniemi@uef.fi

Atmospheric aerosol particles are composed of large variety of chemical compounds with different vapour pressures affecting the partitioning between aerosol and gas phase. Some of these can be considered to be nonvolatile meaning their vapor pressure is so low that in practice they are always found from the particle phase. Other group of compounds found from particles is semivolatile. Depending on the conditions, like temperature and relative humidity, these compounds may exist in the gas, liquid or solid particle phase. This has to be taken into account both to fully address the effect of semivolatiles on indirect and indirect aerosol forcing, and also in the experiments when hygroscopicity and CCN activity of aerosol particles are addressed.

In this study the effect of inorganic semivolatile aerosol compounds on CCN activity of aerosol particles is studied by using computational model for DMT-CCN counter (Roberts and Nenes 2005), cloud parcel model for condensation kinetics and experiments to quantify the modeled results. Concentrations of water vapour and semivolatiles as well as aerosol trajectories in the CCN-column are calculated by a computational fluid dynamics model (Raatikainen *et al*. 2012). These trajectories and vapor concentrations were then used as an input for cloud parcel model (Romakkaniemi *et al.* 2005) to simulate condensation kinetics of water and semivolatiles between aerosol particles and the gas phase. From these results the smallest particle size able to activate in different supersaturations was determined. This size is called as a critical particle diameter. From measurements this is determined as a particle size where 50% of particles activated in the CCN counter.

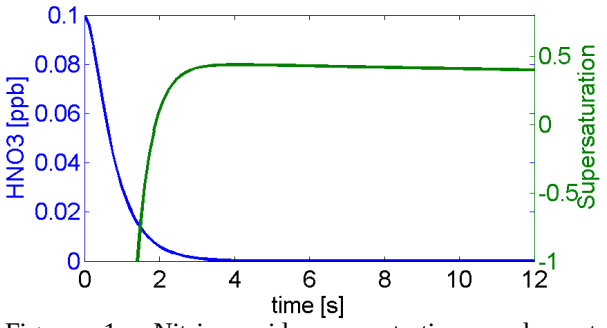

Figure 1: Nitric acid concentration and water supersaturation in the CCN column as a function of time in the column.

In the experimental and modeling setup the dried ammonium nitrate particles are taken into CCN column in the CCN counter. Beyond being the source for water, wetted walls in the CCN column act as a perfect sink for gas phase ammonia and nitric acid. Thus their gas phase concentration (Figure 1) is quickly decreased in the centerline of sample flow in the direction of flow. Depending on the gas phase concentration of nitric acid and ammonia, they start condense on particles or evaporate from particles as soon as the aerosol will become liquid solution.

Table 1. Comparison between modelling and experimental results for the critical aerosol particle diameters in different supersaturations.

Supersaturation	Meas Dc [nm]	Mod Dc [nm]	Mod Dc [nm] no evap.
0.2	84	91	80
0.3	71	75	62
0.4	62	65	51
0.6	53	54	40
0.8	47	48	33

As can be seen from the results presented in Table 1, the modelled and measured critical diameters agree nicely when evaporation is taken into account. Thus the model is able to accurately predict the evaporation of nitric and ammonia from aerosol particles before the maximum supersaturation is reached. Based on these results evaporation of semivolatile aerosol compounds can lead to underestimation of aerosol CCN activity.

This study has been supported by the Academy of Finland Center of Excellence program (project number 1118615) and by the strategic funding of the University of Eastern Finland.

Raatikainen, T., Moore, R. H., Lathem, T. L., and Nenes, A. (2012) *Atmos. Chem. Phys*., **12**, 4227-4243.
Roberts, G. C. and Nenes, A. (2005) *Aerosol Sci. Tech.*, **39**, 206–221.
Romakkaniemi, S., Kokkola, H., and Laaksonen A. (2005) *J. Geophys. Res. (Atmos)*, **110**:D15202

Long-term hygroscopic properties of ambient aerosol in a boreal environment, as measured by the size-resolved Cloud Condensation Nuclei counter (CCNc)

M. Paramonov[1], M. Äijälä[1], P.P. Aalto[1], A. Asmi[1], N. Prisle[1], V.-M. Kerminen[1], M. Kulmala[1] and T. Petäjä[1]

[1]Department of Physics, University of Helsinki, PO Box 64, FI-00014, Helsinki, Finland
Keywords: CCN activation, cloud, critical diameter, hygroscopicity.
Presenting author email: mikhail.paramonov@helsinki.fi

Ambient aerosol CCN and hygroscopic properties were measured with a size-segregated CCNc in a boreal environment of Southern Finland at the SMEAR II station. The instrumental setup operated at five levels of supersaturation S covering a range from 0.1% to 1%, and measured particles with a size range of 20–300 nm. The instrument has been operating since February 2009, and a total of 29 non-consecutive months of measurement data are presented.

Critical diameter D_c was calculated for each activation spectrum as a mid-point of the fitted sigmoid curve, i.e. 50% of particles activated. For each pair of D_c and S, hygroscopicity parameter κ was calculated according to the EH1 Köhler model using Eq. A30 in Rose *et al*. (2008). The surface tension of pure water of 0.072 J m^{-2} was assumed. No normalisation of activation spectra took place prior to the curve fitting; therefore, discussion below concerns only the CCN-active fraction of the ambient aerosol.

The median D_c and κ for the whole dataset in this study are reported at 75 nm and 0.22, respectively. The median κ shows that aerosol in the boreal environment of Southern Finland is less hygroscopic than the global continental and European continental averages, as presented by Pringle *et al*. (2010), most likely due to a presence of a large organic fraction within the aerosol. The aerosol is, however, more hygroscopic than ambient aerosol in an Amazon rainforest, the European high alpine site or the mountainous forest (Fig. 1). The Figure also reveals that the rate of change of κ with size at the SMEAR II station is higher than in three other locations, indicating differences in the species of condensing material and the oxidation and aging processes.

A month of CCNc data was analysed in parallel with aerosol mass spectrometer (AMS) measurements in order to determine the effect of atmospheric refractory species on κ. A negative correlation was observed between κ and the organic mass fraction, and a positive correlation was found between κ and sulphate and ammonia species, logically following the behaviour of these species in the atmosphere with respect to their affinity for water.

The biogenic emissions in the boreal environment of Southern Finland make ambient aerosol of >100 nm in diameter less hygroscopic in the spring and summer time, compared to other seasons – the seasonal variation of D_c needed for CCN activation is important to remember when estimating CCN concentrations from aerosol particle number measurements. The participation of biogenic emissions in photochemical reactions is responsible for introducing a diurnal pattern in the behaviour of aerosol hygroscopicity in the spring and summer for particles ~50 nm in diameter. The diminished photochemistry, temperature and biogenic activity in autumn and winter result both in the highest seasonal hygroscopicity of larger ambient aerosol and in the absence of the diurnal trend of D_c and κ for particles of any size.

No distinct effect of atmospheric new particle formation (NPF) on D_c and κ was observed. Ambient aerosol was found to be internally mixed in the summer, and externally mixed during the rest of the year.

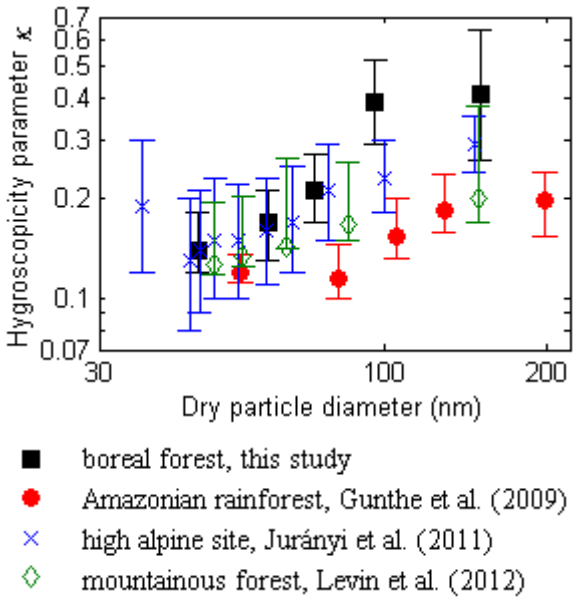

Figure 1. Relationship between particle dry size (taken as D_c) and κ for several studies. Shown are the median values, with error bars being 25th and 75th percentiles (for Gunthe *et al*. (2009) percentiles estimated from the original publication).

This work was supported by the Maj and Tor Nessling Foundation projects nr. 2010143, 2012443 and 2013325. The authors are thankful to Dr. Ezra Levin and Anthony Prenni for a timely provision of some additional data.

Gunthe, S.S. *et al*. (2009) *Atmos. Chem. Phys.* **9**, 7551-7575.
Jyrányi, Z. *et al*. (2011). *J. Geophys. Res.*, **116**, D10204.
Levin, E.J.T. *et al*. (2012). *J. Geophys. Res.*, **117**, D06201.
Pringle, K.J. *et al*. (2010) *Atmos. Chem. Phys.* **10**, 5241-5255.
Rose, D. *et al*. (2008) *Atmos. Chem. Phys.* **8**, 1153-1179.

Mass spectrometric analysis of cloud droplet residuals in different orographic clouds

J. Schneider[1] and S. Mertes[2]

[1]Particle Chemistry Department, Max Planck Institute for Chemistry, Mainz, 55128, Germany
[2]Leibniz Institute for Tropospheric Research, 04318 Leipzig, Germany
Keywords: aerosol-cloud interaction, aerosol mass spectrometry, cloud chemistry
Presenting author email: johannes.schneider@mpic.de

We conducted in-situ mass spectrometric analysis of cloud droplet residuals from orographic clouds on several mountain research sites: On the central German mountain Schmücke (10°46'15"E, 50°39'19"N, 937 m a.s.l.) during the project HCCT, 2010, on the Puerto Rican mountain Pico del Este (65°45'33"W, 18°16'07"N, 1039 m a.s.l.) during the project PRADACS, 2011, and on the German alpine mountain Zugspitze (10°59'11" E, 47°25'16"N, 2650 m a.s.l.), during the project ACRIDICON-Zugspitze, 2012. Cloud droplets with diameters larger than 5 µm were sampled by a counterflow virtual impactor (CVI, Mertes et al., 2005) that evaporates the cloud water after sampling, and the submicrometer residual particles were analyzed by means of a compact time-of-flight aerosol mass spectrometer (C-ToF-AMS, Drewnick et al., 2005) that included also a light scattering module for single particle analysis. Additional measurements included size distribution and number concentration of the cloud droplets and the residual particles, cloud liquid water content (LWC), as well as interstitial and out-of-cloud aerosol particle composition, number and size.

The measurement sites represent different cloud regimes: Continental European orographic clouds (on a low mountain range during HCCT and on a high alpine mountain during ACRIDICON) and Caribbean trade wind orographic clouds (PRADACS). The different geographical locations are reflected in the composition of the background aerosol particles as well as in the composition of the cloud residuals: While the marine aerosol measured at Puerto Rico is dominated by sulfate (Fig. 1a), the continental aerosol at the Central German mountain Schmücke (Fig. 1b) is dominated by organics, as well as at the high mountain station at the Zugspitze (Fig. 1c), the latter being rather unexpected.

Interestingly, the cloud residual analysis show similar features in both cases: the fractions of nitrate and organics are enhanced in the cloud residuals compared to the out-of-cloud aerosol, and also a significant amount of chloride is detected in the cloud residuals, but not in the out-of-cloud aerosol.

The enhanced nitrate fraction is most likely due to uptake of gas-phase nitric acid by the cloud droplets. The enhanced chloride content can be explained by cloud processing of sea salt (NaCl) particles by reaction with H_2SO_4 and NH_3 to NH_4Cl which can be detected by the AMS. Interestingly this feature is not only observed in the marine aerosol at Puerto Rico but also at the high continental mountain site Zugspitze. At the lower continental site Schmücke the chloride and nitrate enhancements are much smaller.

This presentation will also discuss the single particle analysis that gives insight into the mixing state of the aerosol particles and cloud droplet residuals.

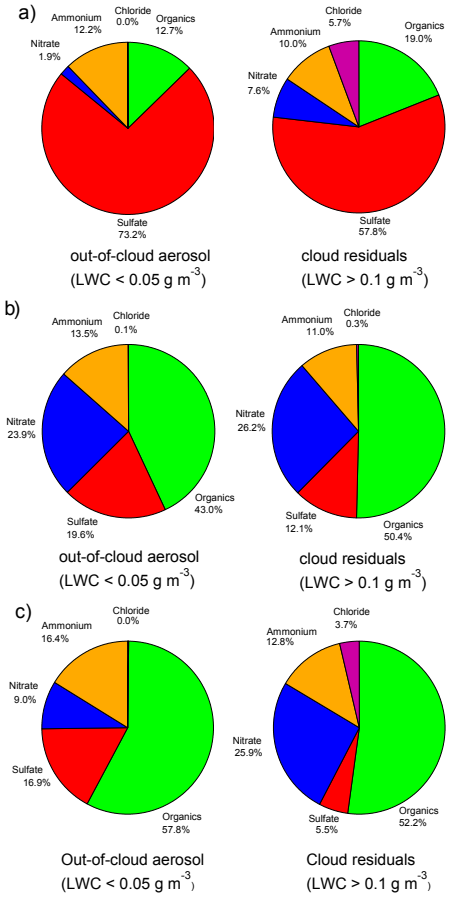

Figure 1. Average composition of aerosol particles measured out of clouds (left) and of cloud residuals (right) during: a) PRACDAS (Pico del Este, Puerto Rico); b) HCCT (Schmücke, Germany); c) ACRIDICON (Zugspitze, Germany).

This work was supported by the DFG SPP 1294 “HALO” (ACRIDICON, PRADACS) and the Max Planck Society (HCCT).

Mertes, S., Lehmann, K., Nowak, A., Massling, A. and Wiedensohler, A. (2005). *Atmos. Environ.*, **39**, 4247-4256.

Drewnick, F., Hings, S., DeCarlo, P., Jayne, J. T., Gonin, M., Fuhrer, K., Weimer, S., Jimenez, J. L., Demerjian, K. L., Borrmann, S., and Worsnop, D. R. (2005). *Aerosol Sci. Technol.*, **39**, 637–658.

What controls cloud droplet number concentration of trade wind cumuli?

F. Ditas[1], B. Wehner[1], H. Siebert[1], T. Schmeißner[1], M. Simmel[1], H. Wex[1] and A. Wiedensohler[1]

[1]Leibniz Institute for Tropospheric Research (TROPOS), 04318 Leipzig, Germany
Keywords: aerosol-cloud-interaction, activation, trade wind cumuli
Presenting author email: ditas@tropos.de

Aerosol and cloud microphysical properties of trade wind cumuli were determined during the CARRIBA (Clouds, Aerosol, Radiation, and tuRbulence in the trade wInd regime over BArbados) experiment in November 2010 and April 2011. Measurements were performed with the helicopter-borne measurement platform ACTOS (Airborne Cloud Turbulence Observation System, Siebert et al., 2006) with high temporal and spatial resolution. For detailed information about the aerosol instrumentation the reader is referred to Ditas et al. (2012).

This study deals with the statistical analysis of aerosol-cloud-interactions of 730 individual clouds measured during 11 research flights under comparable meteorological conditions. The analysis provides information on the number concentration of activated particles (N_{act}), activation diameter ($D_{p,\ act}$) and critical supersaturation (S_{crit}). The calculation of N_{act} is based on the comparison of total particle number concentration outside of clouds and the interstitial particle number concentration inside clouds. This method is validated against cloud droplet number concentration data (N_d). Activation diameter and critical supersaturation are derived using the measured particle number size distribution and Köhler theory.

Furthermore, the cloud microphysical parcel model of Simmel and Wurzler (2006) is applied to compare to observed N_{act} and to calculate flight-averaged CCN (cloud condensation nuclei) concentration for a fixed updraft. An updraft of 2 m s^{-1} was used for the data shown here ($N_{CCN,\ 2\ m\ s\text{-}1}$), representing typical updraft velocities observed during the campaign.

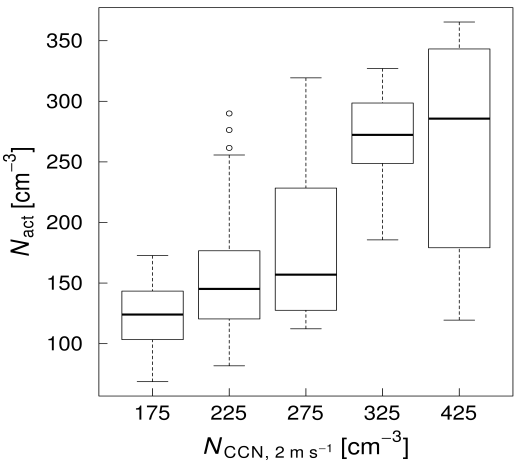

Fig. 1. Boxplot of number of activated particles versus the CCN concentration calculated for a fixed updraft of 2 m s^{-1}. Boxes cover 50% and error bars 75% of the observed data which are grouped into bins of 50 cm^{-3}. Horizontal line inside boxes denote the median, single circles denote outliers.

Figure 1 shows a boxplot of N_{act} versus $N_{CCN,\ 2\ m\ s\text{-}1}$ for 239 more active clouds (selected under consideration of vertical wind velocity and adiabatic liquid water content). The median N_{act} indicates a positive trend for increasing $N_{CCN,\ 2\ m\ s\text{-}1}$. This emphasizes a strong influence of the available aerosol on the observed number concentration of activated particles.

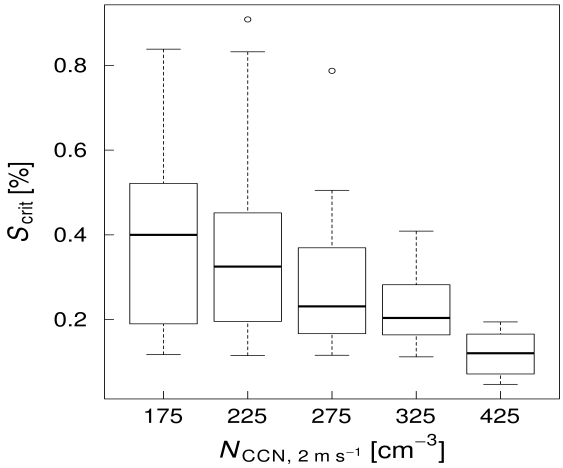

Fig. 2. Boxplot of derived critical supersaturation versus the CCN concentration calculated for a fixed updraft of 2 m s^{-1}. The chart design is similar to Figure 1.

In Fig. 2, the relationship between S_{crit} and $N_{CCN,\ 2\ m\ s\text{-}1}$ is investigated. The median S_{crit} and upper error bars feature a decrease for increasing $N_{CCN,\ 2\ m\ s\text{-}1}$. This effect results from the faster redistribution of water vapor in cases of higher CCN or cloud droplet concentration (N_d indirectly proportional to phase relaxation time). Hence, the highest critical supersaturation values on the order of 0.8% are derived for the lowest aerosol concentration.

Finally, to decide which parameters control the cloud droplet number concentration, the susceptibility of N_{act} to $N_{CCN,\ 2\ m\ s\text{-}1}$ and the measured vertical wind velocity (w) was investigated. Concentrating on one flight (with constant aerosol number size distribution), a variation of w highly influences N_{act}. However, taking into account the results of all flights, the flight to flight variability of $N_{CCN,\ 2\ m\ s\text{-}1}$ overrules the variability in N_{act} caused by w. Hence, the amount of available aerosol is dominating the number concentration of activated particles and cloud droplet number concentration, respectively.

We thank the CIMH (Caribbean Institute for Meteorology and Hydrology), Horizon Helicopters, enviscope GmbH, and Barbados Concorde Experience. This project was funded by DFG-grant SI 1534/3-1 and the TROPOS.

Ditas, F., R.A. Shaw, H. Siebert, M. Simmel, B. Wehner, and A. Wiedensohler (2012). *Aerosols-cloud microphysics-thermodynamics-turbulence: evaluating supersaturation in a marine stratocumulus cloud. Atmos. Chem. and Phys.*, 12(5), pp. 2459–2468.

Siebert, H., H. Franke, K. Lehmann, R. Maser, E. W. Saw, D. Schell, R. A. Shaw, and M. Wendisch (2006). *Probing Fine-Scale Dynamics and Microphysics of Clouds with Helicopter-Borne Measurements, Bull. Amer. Met. Soc.*, 87, 1727 – 1738.

Simmel, M. and Wurzler, S. (2006). *Condensation and activation in sectional cloud microphysical models. Atmos. Res.*, 80(2-3), pp. 218–236.

Size-dependent aerosol activation properties measured in radiation and stratus lowering fog during the ParisFog 2012/13 field campaign

E. Hammer[1], J. Hofer[1], M. Gysel[1], G. Roberts[3,4], N. Bukowiecki[1], J.C. Dupont[2], F. Burnet[3], M. Haeffelin[2], U. Baltensperger[1] & E. Weingartner[1]

[1]Laboratory of Atmospheric Chemistry, Paul Scherrer Institut, 5232 Villigen PSI, Switzerland
[2]LMD, IPSL, Ecole Polytechnique, Palaiseau, France
[3]CNRS-GAME/Meteo France, 42 av. Gaspard Coriolis, 31057 Toulouse, France
[4]Scripps Institution of Oceanography, 9300 Gilman Dr., La Jolla CA 92093, USA
Keywords: Aerosol cloud interaction, CCN.
Presenting author email: emanuel.hammer@psi.ch

Fog causes tremendous hazards in road traffic, maritime navigation, as well as in air traffic and railway traffic. There is a great demand, e.g. from airports, for more reliable fog forecasts to prevent such accidents. Improved fog forecasts require a better understanding of the numerous complex mechanisms during the fog life cycle.

During winter 2012/13 a field campaign called ParisFog aiming on fog research has taken place at SIRTA (Site Instrumental de Recherche par Télédétection Atmosphérique). SIRTA is about 20 km south of Paris in a semi-urban environment. It hosts active and passive remote sensing instruments to continuously quantify cloud and aerosol properties, as well as key atmospheric parameters (Haeffelin et al., 2005).

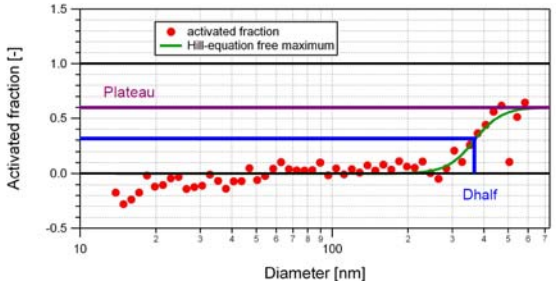

Figure 1. Activated fraction with a hill-equation fit for an hourly average.

From October 2012 to January 2013 a scanning mobility particle sizer (SMPS) has been installed at SIRTA to measure the particle number size distribution. The device has been connected to a switching valve that switched between the total and the interstitial inlet. The total inlet was heated. Thus, all particles can be measured including the fog residuals, since the water evaporates from the fog droplets and leaves the dry residual particles behind. On the interstitial inlet system an aerodynamic size discriminator was attached. The cut-off size was 1 µm. This inlet samples only the non-activated aerosols, as the aerosols larger than 1 µm are expected to be activated to cloud droplets. To monitor and quantify fog events a particle volume monitor (PVM-100; Gerber, 1991) has been installed which measured the liquid water content and the effective radius of the fog droplets.

For the selected fog events, based on the PVM-100 data, the activated fraction has been calculated which is defined as (Verheggen et al., 2007):

$$F_N(D_p) = \frac{(N_{tot}(D_p) - N_{int}(D_p))}{N_{tot}(D_p)} \qquad (1)$$

Where $N_{tot}(D_p)$ is the number concentration of the total particles with diameter D_p and $N_{int}(D_p)$ is the number concentration of the interstitial aerosols with diameter D_p. Figure 1 shows an example for an hourly average on the 10/10/2012 05:30 where D_{half} has been retrieved as the middle between the lowest (i.e. 0) and highest plateau value.

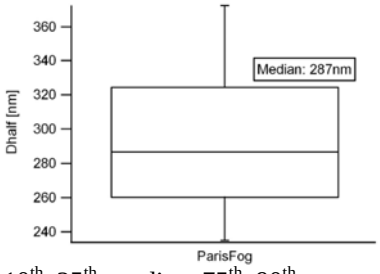

Figure 2. 10th, 25th, median, 75th, 90th percentiles of the activation diameters (D_{half}) for all classified fog events during ParisFog2012/13.

It has been observed that the activation plateau is quite often below 1 with a considerable fluctuation within the different fog events. This is likely due to entrainment of drier air into the fog.

The median of the activation diameters (D_{half}) during the 10 fog events ranges from 252 nm to 400 nm (see Figure 2). The median over all fog events is 287 nm.

Gerber, H. (1991) *Journal of the Atmospheric Sciences* **48**, 2569-2588.

Haeffelin, M. (2005) *et al.*, *Annales Geophysicae* **23**, 253-275.

Verheggen, B., Cozic, J., Weingartner, E., Bower, K., Mertes, S., Connolly, P., Gallagher, M., Flynn, Choularton, T., Baltensperger, U. (2007) *Journal of Geophysical Research-Atmospheres* **112**, D23202.

Assessment of cloud maximum supersaturation by size-resolved CCN measurements

M. Krüger[1], D. Rose[1], Y. Cheng[1], H. Su[1], C. Pöhlker[1], J. Schneider[1], S. Schmidt[1], T. Klimach[1], S. Mertes[2], M. O. Andreae[1], U.Pöschl[1]

[1]Max Planck Institute for Chemistry, 55020 Mainz, Germany
[2]Leibniz Institute for Tropospheric Research, Leipzig, Germany
Keyword: CCN, aerosol-cloud interactions.
Presenting author email: m.kruger@mpic.de

Cloud condensation nuclei (CCN) measurements determine the fraction of aerosol particles that act as condensation nuclei when exposed to supersaturated conditions. During a cloud event, a certain fraction of the CCN has already been activated to droplets depending on the maximum supersaturation that was recently present in the cloud. Thus, CCN measurements during single cloud events are strongly affected by the maximum supersaturation in the cloud. The present work aims to assess the maximum supersaturation in single cloud events.

CCN measurements were conducted during the ACRIDICON-Zugspitze campaign (17.09.2012 - 04.10.2012) at the research station Schneefernerhaus (German Alps, 2650 m a.s.l.). Size-resolved CCN spectra of the non-activated aerosol particles of a cloud (separated by an interstitial inlet) were measured by a combination of a differential mobility analyzer (DMA), a condensation particle counter (CPC) and a CCN counter built by Droplet Measurement Technologies (DMT) (e.g., Rose et al., 2008; Rose et al., 2011).

During a cloud event, no CCN were detected by the instrument for small supersaturations. Only when the supersaturation in the CCN counter was increased above a certain level, these aerosol particles were activated and the activation curve was similar to the activation curve for aerosol particles without cloud (Fig.1). The aerosol particles sampled during no-cloud conditions activate at significantly lower defined supersaturations in the CCN counter than the interstitial aerosol particles during cloud.

The highest supersaturation level during a cloud event at which no interstitial particles were activated in the CCN counter can be regarded as a lower limit for the maximum supersaturation of the cloud ($S_{max,l}$). The lowest supersaturation level where activation could be observed in the CCN counter can be regarded as an upper limit for the maximum supersaturation of the cloud ($S_{max,u}$).

Figure 1 shows the activation curve of 170 nm particles for cloud and no-cloud conditions at different supersaturations in the CCN counter. It gives an impression of the specific maximum supersaturation of the measured cloud event which is between $S_{max,l}$ and $S_{max,u}$. The observed cloud events during the campaign show maximum supersaturations in the range of 0.07% to 0.39%.

This is in agreement with liquid water content (LWC) measurements showing higher cloud maximum supersaturations with higher LWC.

We will compare the CCN spectra with data from mass spectrometer measurements and STXM measurements to derive the chemical composition of the CCN. Especially the influence of organic compounds on the CCN activation is currently of interest (e.g., Topping and McFiggans, 2012).

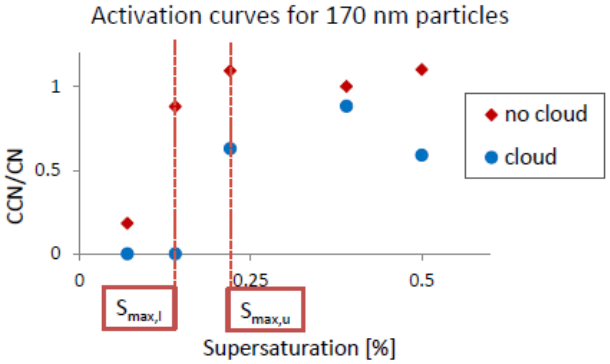

Fig. 1: Comparison of the activation curves for 170 nm aerosol particles at different supersaturations in the CCN counter, for cloud and no-cloud conditions during a single cloud event. In this case $S_{max,l}$ is 0.14% and $S_{max,u}$ is 0.22%.

This work has been supported by the DFG projects SPP 1294 (HALO) and the Max Planck Society (MPG).

Rose, D., S. S. Gunthe, E. Mikhailov, G. P. Frank, U.Dusek,M. O. Andreae, and U. Pöschl: Calibration and measurement uncertainties of a continuous-flow cloud condensation nuclei counter (DMT-CCNC): CCN activation of ammonium sulfate and sodium chloride aerosol particles in theory and experiment, Atmos. Chem. Phys., 8, 1153 – 1179, 2008.

Rose, D., Gunthe, S. S., Su, H., Garland, R. M., Yang, H., Berghof, M., Cheng, Y. F., Wehner, B., Achtert, P., Nowak, A., Wiedensohler, A., Takegawa, N., Kondo, Y., Hu, M., Zhang, Y., Andreae, M. O., and Pöschl, U.: Cloud condensation nuclei in polluted air and biomass burning smoke near the mega-city Guangzhou, China – Part 2: Size-resolved aerosol chemical composition, diurnal cycles, and externally mixed weakly CCN-active soot particles, Atmospheric Chemistry and Physics, 11, 2817-2836, 2011

Topping, D. O. and G. McFiggans: Tight coupling of particle size, number and composition in atmospheric cloud droplet activation, Atmos. Chem. Phys., 12, 3253–3260, 2012.

Comprehensive Investigations on the Ice Nucleation Efficiency of Natural Soil Dust Samples

K. Höhler[1], I. Steinke[1], D. Cziczo[2], A. Danielczok[3], F. Frank[3], S. Garimella[2], O. Möhler[1], M. Raddatz[4], M. Schnaiter[1], O. Stetzer[5], and E. Toprak[1] (alphabetically ordered after I.S.)

[1]Institute for Meteorology and Climate Research, Karlsruhe Institute of Technology (KIT), Germany
[2]Dept. of Earth, Atmospheric and Planetary Sciences, Massachusetts Institute of Technology, Cambridge, USA
[3]Institute for Atmospheric and Environmental Sciences, Goethe-University Frankfurt, Germany
[4]Leibniz Institute for Tropospheric Research, Leipzig, Germany
[5]Institute for Atmospheric and Climate Science, ETH Zürich, Switzerland
Keywords: nucleation, ice, cloud, soil
Presenting author email: Kristina.Hoehler@KIT.edu

Soil dust is a complex mixture of different minerals and organic material. Aerosols of this material are fed into the atmosphere by a variety of processes, such as e. g. tillage activities. Their role in climate processes is not yet completely understood and especially the ability to induce heterogeneous ice nucleation might be an important factor for their influence on earth's radiative budget.

For the investigation of aerosol ice nucleation ability, a broad range of instruments is currently being used, each constrained by its specific design. Also, especially for inartificial samples, discrepancies in findings by different methods might be due to sample variances and / or differences in aerosol preparation from the bulk sample.

To benefit from a comprehensive investigation of identical aerosol, a range of ice nucleation instruments participated in the campaign IN-19, which was held at the AIDA (Aerosol Interaction and Dynamics in the Atmosphere) facility in July 2012. Here, we used the AIDA cloud simulation chamber (Steinke *et al.* (2011)), the ice nucleation static diffusion chamber FRIDGE (Bingemer *et al.* (2012)), the continuous flow diffusion chambers PINC (Chou *et al.* (2011)) and SPIN (MIT), and the ice nucleation chamber FINCH (Bundke *et al.* (2008)) to learn about the heterogeneous nucleation behaviour of selected soil samples.

By combination of these methods, we have been able to investigate the same aerosol over a broad range of temperatures and humidities. Also, by sampling aerosol from a separate Aerosol Preparation Chamber (APC) using a Maxi-Differential Mobility Analyzer (Maxi-DMA) (Raddatz *et al.* (2013)), size selective measurements have been realized.

We here present findings made for soil sampled in northern Germany and in Argentina. Those samples have been selected due to their comparably high content of biological material. The bacterial activity of the aerosol in the AIDA chamber has been characterized with the WIBS instrument (Toprak and Schnaiter (2013)) prior to the cloud expansion experiment. We find that compared to desert dust aerosol, which shows significantly lower bacterial activity than the samples under investigation, enhanced ice nucleation ability in the immersion mode is observed.

In first comparisons, the data measured by the various instruments complement each other nicely. E.g. FRIDGE results correlate with AIDA measurements with respect to the minimum temperature required for efficient deposition mode nucleation, as is shown in Figure 1.

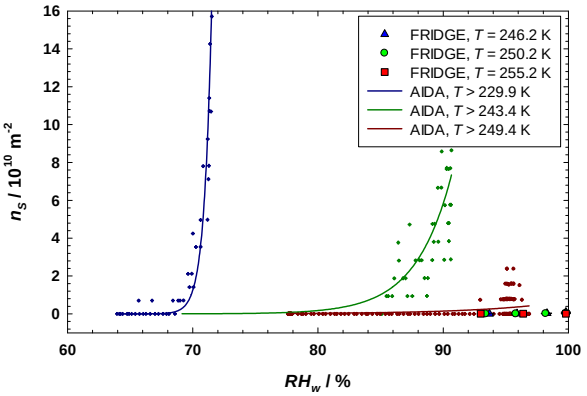

Figure 1. Ice active surface site densities n_S (number of ice crystals per surface area) measured with AIDA and FRIDGE at relative humidities RH_w below water saturation

We currently further compile the information gathered with the various instruments to achieve a complete picture on the heterogeneous ice nucleation ability of the soil dust samples under investigation. We will discuss the benefits and shortcomings of the individual instruments to complete our understanding and will further analyse the role of biological content in the nucleation behaviour.

This work was supported by the DFG HALO SPP 1294 (contract number MOEH 668/1-2) and by EUROCHAMP2 (Transnational Access Activity E2-2012-05-14-0075.)

Chou, C. et al. (2011), *Atmos. Chem. Phys.* **11**, 4725-4738.
Bingemer, H. et al. (2012) *Atmos. Chem. Phys.* **12**, 857-867.
Bundke, U. et al. (2008) *Atmos. Res.* **90**, 180-186.
Raddatz, M. et al. (2013), *AIP Conf. Proc.*, in press.
Steinke, I. et al. (2011) *Atmos. Chem. Phys.* **11**, 12945-12958.
Toprak, E. and Schnaiter, M. (2013) *Atmos. Chem. Phys.* **13**, 225-243.

Effect of local pollutant sources on aerosol-cloud interactions at Puijo measurement station

H. Portin[1,2], A. Leskinen[1], A. Kortelainen[2], L. Hao[2], P. Miettinen[2], A. Jaatinen[2], , S. Romakkaniemi[2], A. Laaksonen[2,3], K.E.J. Lehtinen[1,2] and M. Komppula[1]

[1]Finnish Meteorological Institute, Kuopio Unit, P.O.Box 1627, FI-70211, Kuopio, Finland
[2]University of Eastern Finland, Department of Applied Physics, P.O.Box 1627, FI-70211, Kuopio, Finland
[3]Finnish Meteorological Institute, Research and Development, P.O.Box 503, FI-00101 Helsinki, Finland
Keywords: atmospheric aerosols, cloud droplet activation, aerosol-cloud interactions, chemical composition.
Presenting author email: harri.portin@fmi.fi

Puijo measurement station has provided continuous data on aerosol-cloud interactions since summer 2006 (Leskinen *et al* 2009). The station is located on top of the Puijo observation tower (306 m a.s.l, 224 m above the surrounding lake level) near the town of Kuopio, Finland. The station is covered by cloud about 15 % of the time, offering perfect conditions for aerosol-cloud interaction studies. With a special inlet setup (total and interstitial inlets) activated and non-activated particles can be measured separately. Continuous twin-inlet measurements include aerosol size distribution (twin-DMPS, 7-800 nm), scattering and absorption. Other continuous measurements include cloud droplet number and size distribution and weather parameters.

We also arrange intensive measurement campaigns every autumn (Puijo Cloud Experiment, PuCE) when the occurrence of clouds is the highest. During these campaigns, extra measurement devices have included aerosol mass spectrometer (AMS), cloud condensation nuclei counter and Hygroscopic Tandem Differential Mobility Analyzer. The AMS has been connected to the twin-inlet system¸ providing data about the chemical composition of activated and non-activated particles (Hao *et al* 2013).

In our current work, we have been analyzing results from PuCE 2010 and 2011 campaigns. During these campaigns, a total of 39 cloud events took place, with a total of 156 hours of in-cloud data. The aim of the research has been the identification of the possible effect of local pollutant sources on aerosol-cloud interactions. The tower is surrounded by residential areas and traffic routes in north, east and south, whereas in west and northwest there aren't any significant sources. Also, two important point sources exist within a few kilometres from the tower, a paper mill and a heating plant.

An example of a cloud event, during which it was possible to pinpoint the effect of local sources, took place on 22.-23.10., 2011. There were several periods with different particle population properties, which also affected the cloud properties to some extent. Here, three of these periods are chosen for a closer inspection.

During the clean period (22.10. 22:00-23.10. 5:45), wind direction was from north and northwest with low total particle and accumulation mode concentrations (fig. 1a). Between 5:45-6:15 on 23.10. wind direction was from northeast where the paper mill is located. Total particle concentration was still low but a pronounced accumulation mode was present. Particle chemical composition during this period was dominated by SO_4 and NH_4. When wind direction shifted to south (23.10. 9:45-13:00), a plume from the heating plant hit the tower. Elevated particle concentration was observed, with a distinguishable accumulation mode, consisting almost entirely of SO_4.

During the pollutant episodes, the size of activated particles was larger when compared to the clean period (fig. 1b). In clean conditions, as small as 100 nm particles activated, whereas during the polluted periods the average diameter for activation was larger. During the paper mill plume, droplet concentration was higher (240 cm^{-3}) with a smaller average droplet diameter (10.9 µm) when compared to the clean period (138 cm^{-3}, 12.2 µm). Unfortunately the cloud droplet probe was frozen during the heating plant plume.

As a conclusion, it is evident that local pollutant sources affect aerosol-cloud interactions. However, it is too early to say if this is only caused by the elevated number concentrations or if the different chemical composition also plays a role. Also, how often these periods take place requires more research and data from forthcoming campaigns.

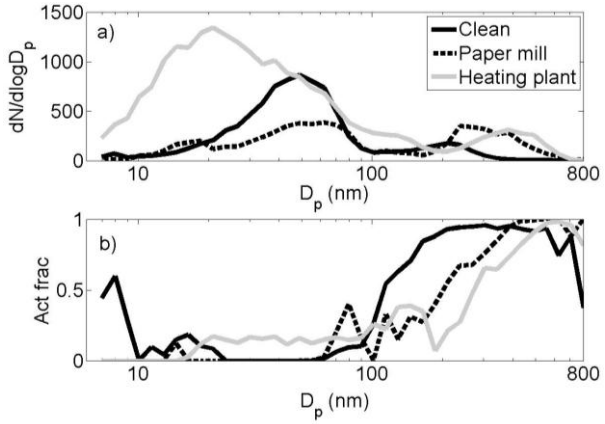

Figure 1. a) Total particle size distributions and b) particle activated fractions vs. size for the different periods during a cloud event on 22.-23.10.2011.

Hao, L., Romakkaniemi, S., Kortelainen, A., Jaatinen, A., Portin, H., Miettinen, P., Komppula, M., Leskinen, A., Virtanen, A., Smith, J., Sueper, D., Worsnop, D., Lehtinen, K.E.J. and Laaksonen, A. (2013). *Environ. Sci. Technol.*, In press.

Leskinen, A., Portin, H., Komppula, M., Miettinen, P., Arola, A., Lihavainen, H., Hatakka, J., Laaksonen, A. and Lehtinen, K.E.J. (2009). *Boreal Env. Res.*, **14**, 576-590.

Thursday, September 5, 2013

Session: Atmospheric Aerosols,
Turbulent exchange, transport and transformation

Natural surfactants promote the uptake of soot-particles in aerosols

T. Hede[1], C. Leck[1], L. Sun[2], Y. Tu[2] and H. Ågren[2]

[1] Department of Meteorology, Stockholm University, S-106 91 Stockholm, Sweden.

[2] Department of Theoretical Chemistry, Royal Institute of Technology, S-106 91 Stockholm, Sweden.
Keywords: molecular dynamics, soot, surfactant, aggregate
Presenting author email: hede@misu.su.se

The effects of light absorbing carbon particles (soot) are amongst the most uncertain, and they are also considered to cause climate warming on the same order of magnitude as anthropogenic carbon dioxide. This study contributes to the understanding of the potential for transformation of the surface character of soot from hydrophobic to hydrophilic. We use molecular dynamics simulations to show how natural surfactants facilitate solubilization of fluoranthene, which we use as a model compound for soot, in nano-sized water clusters.

The aim if the study is to explore whether natural surfactants can increase the water-solubility for soot or BC in airborne aerosol particles. Such surfactants can be found among the secondary organic aerosols (SOA) (Grieshop et al., 2009). Cis-pinonic acid (CPA) is a secondary organic oxidation product of α-pinene evaporated from trees (O´Dowd et al., 2002).

CPA is amphiphilic with surfactant properties (Li et al., 2010). In a previous study (Hede et al., 2011) we showed that CPA is able to form aggregates inside nanosized particles. The nanoaerosols that we have simulated here are 8.6 nm in diameter and consist of 10000 water molecules together with a number of organic molecules. Fluoranthene, which is a polycyclic aromatic hydrocarbon (PAH) abundant in soot, is like other PAHs emitted from incomplete combustion from various sources such as diesel engines (Maricq, 2007).

Fig. 1 shows how one fluoranthene molecule is solubilized in an aggregate inside the nanoaerosol (red square).

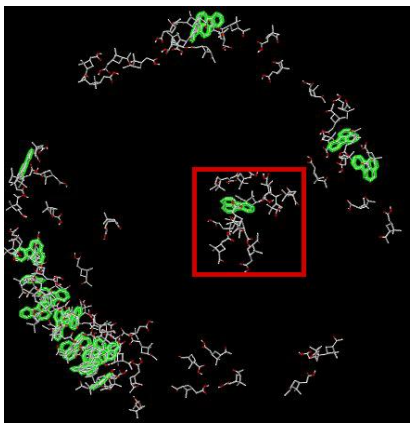

Figure 1. Fluoranthene solubilized at the surface and in an aggregate (red square). Water molecules removed for clarity

The rest of the fluoranthene molecules are solubilized at the surface. The radial number density (RND) plot for the system of 81 CPA and 27 Fluoranthene molecules is shown in Fig. 2. As we can see, the CPA and fluoranthene molecules are found at almost the same radial distance, namely in the aggregate or at the surface.

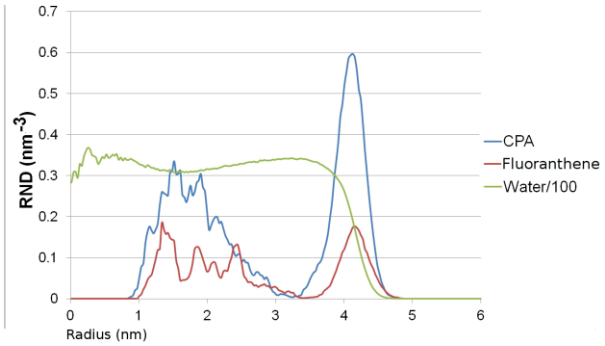

Figure 2. RND for CPA, fluoranthene and water.

The solubilization of fluoranthene in the aggregates and at the surface promoted by the natural surfactant CPA shows that the uptake of hydrophobic material such as soot is facilitated by SOA in the nanoaerosols. This may also change the light absorbing properties (Schnaiter et al., 2003).

Grieshop, AP., Donahue, NM. and Robinson, AL. (2009) *Atmos. Chem. Phys.* **9**, 2227–2240.

Hede, T., Li, X., Leck, C., Tu, Y. and Ågren, H. (2011) *Atmos. Chem. Phys.*, **11**, 6549-6557, doi:10.5194/acp-11-6549-2011

Li, X., Hede, T., Tu, Y., Leck, C. and Ågren, H. (2010) *J. Phys. Chem. Lett.*, **1 (4)**, 769–773, doi: 10.1021/jz9004784

Maricq, MM. (2007) *J. Aerosol Sci.*, **38**, 1079 – 1118.

O´Dowd, CD., Aalto, P., Hämeri, K., Kulmala, M. and Hoffmann, T. (2002) *Nature*, **416**, 497-498.

Schnaiter, M., Horvath, H., Möhler, O., Naumann, KH., Saathoff, H. and Schöck, OW. (2003) *Aersol Sci.*, **34**, 1421-1444.

Annual cycle of Background Aerosol at Troll Station, Antarctica

M. Fiebig[1], D. Hirdman[2], C.R. Lunder[3], J.A. Ogren[4], and A. Stohl[1]

[1]Department for Atmospheric and Climate Research, Norwegian Institute for Air Research, Kjeller, Norway
[2]Centre for Environmental and Climate Research (CEC), Lund University, Lund, Sweden
[3]Monitoring and Information Technology Department, Norwegian Institute for Air Research, Kjeller, Norway
[4]Earth System Research Laboratory / GMD, National Oceanic and Atmospheric Administration, Boulder (CO), USA
Keywords: Antarctic aerosol, Troll atmospheric observatory, aerosol annual cycle.
Presenting author email: Markus.Fiebig@nilu.no

The aerosol monitoring program at Troll Antarctic atmospheric observatory (Queen Maud Land, 72°01′S, 2°32′E, 1309 m a.s.l.) includes the aerosol scattering coefficient at 450, 550, and 700 nm (TSI 3563 nephelometer) and the particle number size distribution (0.03 µm < Dp < 0.8 µm, Differential Mobility Particle Sizer, DMPS) (Hansen *et al.*, 2009). The time series of both instruments, collected since Feb. 2007 (see Figure 1), show a distinct annual cycle of the aerosol properties associated with background air masses, i.e. those not corresponding to peaks of any origin. Comparison of the aerosol scattering coefficient measured by nephelometer and calculated from the DMPS measurements by Mie-theory assuming an (NH4)2SO4 composition show a correlation coefficient of ~0.8, confirming a common origin of both annual cycles. The same annual cycle in background aerosol scattering coefficient as found at Troll can be detected in corresponding data collected at South Pole atmospheric observatory. This shows that that the annual cycle of Antarctic background aerosol properties is a large scale phenomenon.

Using the Lagrangian transport model FLEXPART and ground-level ozone data collected at Troll, it is demonstrated that the air masses associated with background aerosol loadings at Troll originate from the upper troposphere / lower stratosphere UT/LS) region and descend over the Antarctic continent. Further, the aerosol property annual cycle includes a cycle of total aerosol particle volume. FLEXPART is used also to calculate the integral solar irradiance the background air masses received prior to arriving at Troll. It is demonstrated that the observed annual cycle in Antarctic background aerosol properties is consistent with the assumption of a production of aerosol volume in Antarctic UT/LS air that is limited by solar irradiance, i.e. photochemical production.

The observed annual cycle in Antarctic UT/LS aerosol is suggested as benchmark test for natural aerosol processes for climate models in order to improve the distinction between natural and anthropogenic aerosol.

This work was supported by the Norwegian Research Council under grant 208436/F40 and by the Norwegian Polar Institute under grant 2011/70/13/KH/ls.

Fiebig, M. et al. (2013): Annual cycle of Antarctic Background Aerosol: A Window Into the Upper Troposphere / Lower Stratosphere, *Atmos Chem. Phys.*, in prep.

Hansen, G. et al. (2009): Polar Res. **28**(3), 353–363

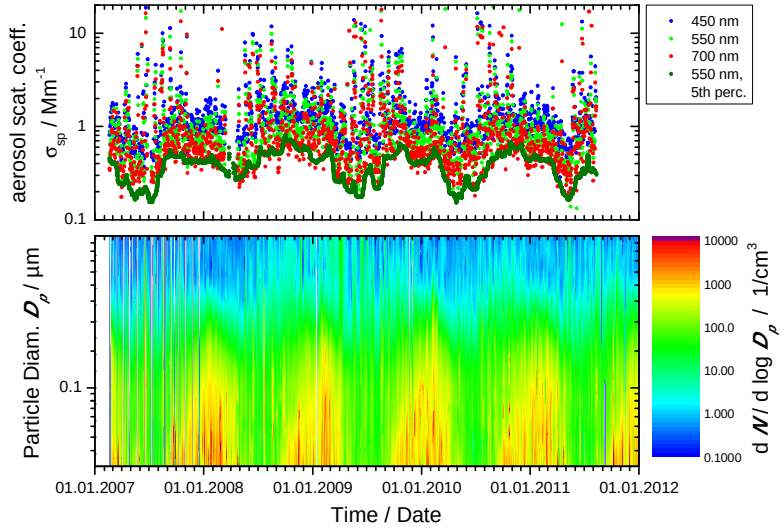

Figure 1: Troll 2007 - 2011 time series of aerosol scattering coefficient (450, 550, 700~nm, daily averages, upper panel) and particle number size distribution (PNSD, lower panel). Upper panel also contains time series of the 550~nm aerosol scattering coefficient running 4 week 5th percentile (dark green) to underline the background annual cycle. The PNSD is plotted as colour contour surface plot time series.

Monitoring ship emissions with continuous onshore SMPS measurements

N. Kivekäs[1], R. Lange[2], A. Massling[3], Q.T. Nguyen[2] M. Glasius[2] and A. Kristensson[1]

[1]Department of Physics, Lund University, Lund, 22100, Sweden
[2]Department of Chemistry, Aarhus University, Aarhus, 8000, Denmark
[3]Department of Environmental Science, Aarhus University, Roskilde, 4000, Denmark

Keywords: ship traffic, emissions, SMPS, background.
Presenting author email: niku.kivekas@nuclear.lu.se

The accumulated emissions from ship traffic are cooling the climate mainly due to reduced methane lifetime caused by NOx emissions and also due to the direct and indirect climate effects of the particles emitted. There is, however, a lot of uncertainty in the magnitude of this cooling effect. According to our knowledge there are no long data series of detected aged ship emissions that are dispersed wider in the atmosphere.

Therefore, we measured the particle number size distribution at a background site approximately 35 km downwind of a heavy trafficked ship lane, representative of roughly 1-3 hours aged ship plumes. The site Høvsøre (56°27' E, 8°09' N, 2m a.s.l) is positioned on the western coast of Jutland peninsula in Denmark. It is located in flat terrain approximately 1.8 km inland from the shoreline. The measurements were conducted using a Scanning Mobility Particle Sizer (SMPS), covering particle diameter range 12 - 500 nm. The measurement period was from March 9th to July 23rd 2012.

We also studied air mass back trajectories (Draxler and Hess, 1998) arriving at the site. During 28% of the measurement days the air had constantly arrived from the sea and passed over the ship lane in last couple of hours. These days were examined further.

During most of these days we observed a large number of clear short-duration peaks above the background particle number concentration (Figure 1). During occurrence of the peaks the number concentration increased typically by several thousand particles cm^{-3}, but during some days with very low background particle concentration the increase was only some hundreds of particles cm^{-3}. The peaks were assumed to be formed by emissions from individual ships on the ship lane. The peak diameters (in dN/dlogD_p above background level) were typically at 40-50 nm and a weakly elevated accumulation mode concentrations were observed. When particle size distributions were converted to dV/dlogD_p, the peak diameters increased to 60-80 nm, and a second mode was often found with peak diameter around 200 nm. Counting statistics for the larger particles were not sufficient for calculating the relative contribution of the second peak to the total particulate volume in the plume.

These peaks were compared to reported emissions from individual ships near Gothenburg harbor (Jonsson *et al*., 2011). The number concentrations at Høvsøre were found to be two orders of magnitude lower than in Gothenburg, which was expected because of the longer transport time and therefore much stronger dilution of the plume at Høvsøre. The peak diameters observed at Høvsøre were also slightly higher than those at Gothenburg, indicating further growth of the particles in the plume during aging.

The number of separable peaks per day was usually 20-40 (Figure 1), which is clearly less than the average number of ships per day (about 100) on that ship route. This indicates that we are missing a large number of ships on any given day. Potential reasons for this could be 1) coinciding peaks; 2) stronger dilution of the plumes originating from the further edge of the ship lane; 3) some of the plumes pass over our measurement site at higher altitude or 4) a fraction of the ships are not emitting enough particles to be identified at Høvsøre.

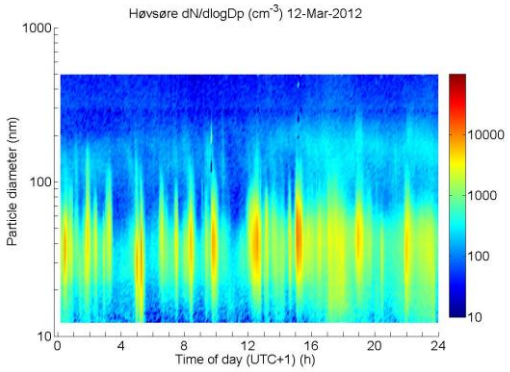

Figure 1. The particle number size distribution at March 13th, 2012 at Høvsøre. Ship plumes are seen as elevated number concentrations at sub-100nm size range.

Already at this stage of the research we can conclude that we do observe a lot of plumes from individual ships at approximately 35 km distance to the ship. These plumes should represent the aging of ship induced emissions, as well as their climate impact better than emissions measured on a ship itself or in near vicinity of one. We can also conclude that we are unable to observe plumes from every individual ship.

The next stage of the research is to use automatic ship identification system to connect the plumes to individual ships, and to investigate the effect of different meteorological parameters and background particle concentrations on the plume peaks. More results on these issues are expected before the EAC 2013 conference.

This work was supported by the Nordic research and innovation initiative CRAICC (Cryosphere-atmosphere interactions in a changing Arctic climate).

Draxler, R. R. and Hess, G. (1998), *Australian Meteorological Magazine* **210**, 295-308.
Jonsson, Å. M., Westerlund, J. and Hallquist, M. (2011) *Geophys. Res. Lett.* **38**, doi:10.1029/2011GL047672.

Analysis of particle size distribution changes between three measurement sites in Northern Scandinavia

R. Väänänen[1], E.-M. Kyrö[1], T. Nieminen[1,2], N. Kivekäs[3,4], H. Junninen[1], A. Virkkula[1,3], M. Dal Maso[1,5], H. Lihavainen[3], Y. Viisanen[3], B. Svenningsson[4], T. Holst[6], A. Arneth[7], P.P. Aalto[1], M. Kulmala[1], V.-M. Kerminen[1]

[1]University of Helsinki, Department of Physics, Helsinki, 00014 University of Helsinki, Finland
[2]Helsinki Institute of Physics, P.O. Box 64, 00014 University of Helsinki, Finland
[3]Finnish Meteorological Institute, Climate Change Unit, 00101 Helsinki, Finland
[4]Lund University, Department of Physics, Lund, 22100 Lund, Sweden
[5]Tampere University of Technology, Dept. of Physics, PO Box 692, 33101 Tampere, Finland
[6]Department of Physical Geography and Ecosystems Science, Sölvegatan 12, 223 62 Lund, Sweden
[7]Karlsruher Institute of Technology, Instute of Meteorology and Climate Research/Atmospheric Environmental Research (IMK-IFU), Kreuzeckbahnstr. 19, 82467 Garmisch-Partenkirchen, German

Keywords: Aerosol, air-mass-transport
Presenting author email: riikka.vaananen@helsinki.fi

Atmospheric particles have a complex role in the warming of the high northern latitudes: Black carbon both in air and on snow enhances the warming (Law and Stohl 2007, Flanner *et al*. 2009), whereas biogenic secondary aerosols have a cooling effect via their cloud interactions (Kulmala *et al*, 2004).

We combined the aerosol size distribution data observed at three measurements with calculated air mass trajectory data (Draxler & Hess, 1998) to deepen the understand of aerosol particle dynamics when air masses travel several hundreds of kilometres above the boreal forest zone in Northern Scandinavia.

The measurement sites are situated along a line from east to west on latitudes 67-68 °N. Two of the three measurement stations, Värriö SMEAR I station and Pallas GAW station, are situated in Finland, and the third one, Abisko, is in Sweden, near the border of Norway. The distance between Abisko and Värriö is 440 km. Abisko is located next to the Scandinavian mountains and 70 km from the Atlantic Ocean. Its surroundings is dominated by subarctic mires, birch forest and mountain tundra. Värriö and Pallas are surrounded by boreal forest. The Pallas station is situated above the tree line.

The aerosol size distribution data was measured between Aug-2005 and Dec-2007. In Abisko there was a Scanning Mobility Particle Sizer with a cut-off size of 10 nm, and in Pallas and Värriö there were Differential Mobility Particle Sizers with cut-off sizes of 7 nm and 3 nm, respectively. Abisko data was from several campaigns, and it covered c. half of the analyzed period.

We used three methods to analyze the aerosol dynamics. First, the days were classified to new particle formation (NPF) event days, non event days, and undefined days, and the NPF events were analyzed according to a schema created by Dal Maso *et al* (2005).

Secondly, we analyzed the aerosol size distributions as a function the corresponding air mass had been above the continental. This broadened the analysis made by Tunved *et al* (2006). We compared the apparent growths of particle diameters, their accumulated masses, number concentrations and condensation sinks.

Third approach was to study the changes in size distributions when the airmass analysis showed that same air mass was passed two measurement stations. To get comparable initial states, the size distributions at the upwind station were clustered. We analyzed the dynamics of each these clusters.

Our results showed (Väänänen *et al*, submitted), that during the growing season, the Aitken-mode particles grew at an apparent rate of around 1 nm/h or less when air masses travelled hundreds of kilometres. This rate was found to be several times smaller than the average growth rate during the new particle formation event. This indicates that the condensational growth has an important effect in the regional-scale air masses also when the evident nucleation is not observed.

The financial support by the Academy of Finland Centre of Excellence program (project no 1118615) and the Nordic Centre of Excellence CRAICC are gratefully acknowledged.

Dal Maso, M., Kulmala, M., Riipinen, I., Wagner, R., Hussein, T., Aalto, P.P. & Lehtinen, K.E.J. (2005) *Boreal Env. Research*, vol. 10, no. 5, pp. 323-336.

Draxler, R.R. & Hess, G. (1998) *Australian Meteorological Magazine*, vol. 47, no. 4, pp. 295.

Flanner, M., Zender, C., Hess, P., Mahowald, N., Painter, T., Ramanathan, V. & Rasch, P. (2009) *Atmos.Chem.Phys*, vol. 9, no. 7, pp. 2481-2497.

Kulmala, M., Suni, T., Lehtinen, K., Dal Maso, M., Boy, M., Reissell, A., Rannik, Ü., Aalto, P., Keronen, P. & Hakola, H. (2004) *Atmospheric Chemistry and Physics*, vol. 4, no. 2, pp. 557-562.

Law, K.S. & Stohl, A. (2007) Science, vol. 315, no. 5818, pp. 1537-1540.

Tunved, P., Hansson, H.C., Kerminen, V.M., Ström, J., Maso, M.D., Lihavainen, H., Viisanen, Y., Aalto, P., Komppula, M. & Kulmala, M. (2006), *Science*, vol. 312, no. 5771, pp. 261.

Väänänen R. et al. submitted to Atm. Chem. Phys. Discuss. 2013

Airborne measurements of aerosol particle physical, optical and chemical properties in Finland

E. Asmi[1], D. Brus[1], S. Carbone[1], R. Hillamo[1], J. Hatakka[1], T. Laurila[1], H. Lihavainen[1], E. Rouhe[2], S. Saarikoski[1] and Y. Viisanen[1]

[1]Finnish Meteorological Institute, Erik Palménin aukio 1, P.O. Box 503, FI-00101, Helsinki, Finland
[2]Department of Radio Science and Engineering, Aalto University, P.O. Box 13000, FI-00076 Aalto, Finland
Keywords: airplane, profiles, chemistry, number.
Presenting author email: eija.asmi@fmi.fi

Because the climate effects depend on the composition and quantities of the total atmospheric column, there is a strong demand for the vertical measurements of the important climate forcers, such as aerosol particles. Therefore, a new measurement platform, equipped with instrumentation for atmospheric aerosol particle characterization, as well as for greenhouse gas and trace gas concentration measurements, was constructed in Finland. For the first time, this was used in summer 2012 to study the profiles of the atmospheric constituents over the southern Finland and the Baltic Sea. Here, the measurement concept is introduced, and a brief overview of first results with some examples is given.

An airplane used is a modified Short Skyvan SC-7 research airplane, which is a non-pressurized twin-engine turbo-propeller aircraft with a maximum operating distance of 1370 km. On board on first flights were instruments for aerosol chemical and physical characterization: a Soot Particle-Aerosol Mass Spectrometer (SP-AMS, Aerodyne Research Inc., USA) for fast high resolution particle chemical characterization, a 3-wl nephelometer model 3563 (TSI Inc., St. Paul, Minnesota, USA) for particle scattering measurements, a continuous-flow stream wise thermal-gradient cloud condensation nuclei counter (DMT-CCNC) model CCN-100 (Droplet Measurement Technologies, Inc., DMT, USA) for CCN total number measurements at fixed supersaturation of 0.34 % and two condensation particle counters (CNC) model 3010 (TSI Inc., St. Paul, Minnesota, USA). The CCN, one CNC, and SP-AMS were operated behind the Constant Pressure Inlet (CPI, DMT, USA), set to 650 mbar. Concentrations of carbon dioxide (CO2), methane (CH4) and water vapour (H2O) were measured using a Picarro G1301-m (Picarro, Inc. Sunnyvale, CA USA), using near-infrared lasers and Cavity Ring-Down Spectroscopy, and specifically designed for airplane measurements. Sample was drawn trough a BMI Isokinetic Inlet System (Model 1200, Brechtel Manufacturing Inc., USA), equipped with anti-icing system, pitot tube, and temperature and pressure sensors. Position and speed were taken from the airplane system MIDG II INS/GPS.

As an example of the results obtained, we present the CCN and CN profiles over land (Fig 1a), where near 3 km altitude a layer of small particles was present, indicating secondary particle formation taking place. Below this altitude, at around 2 km height, a sudden increase of nitrate, accompanied with an increase of ammonia, was detected. We interpret this as an indication of strong anthropogenic signal at this layer, showing simultaneously an interesting case of nitrate partitioning in aerosol phase with the decreasing temperature and humidity, as suggested e.g. by Morino et al., 2006.

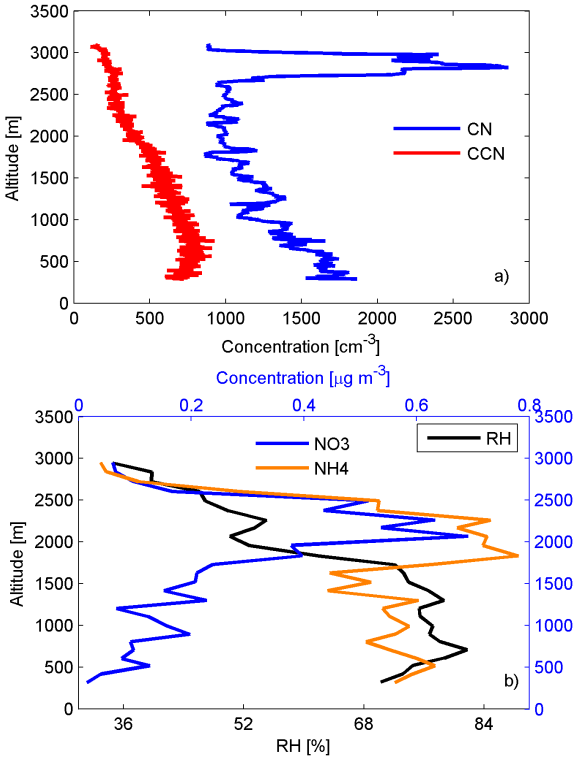

Figure 1. a) Total (CN) and CCN particle number concentration and b) relative humidity (black) and nitrate (blue) and ammonia (orange) concentrations, as measured during the first ascent over land with an altitude presented in y-axis.

This work was supported by the Measurement, Monitoring and Environmental Assessment (MMEA) and by the Academy of Finland Center of Excellence (project number 1118615) programs.

Morino, Y., Kondo, Y., Takegawa, N., Miyazaki, Y., Kita, K., Komazaki, Y., Fukuda, M., Miyakawa, T., Moteki, N. and Worsnop, D.R. (2006) *J. Geophys. Res.* **111**, D15215, doi:10.1029/2005JD006887.

Annual measurement of size resolved particle fluxes in an urban environment

M.J. Deventer[1], O. Klemm[1] and F. Grießbaum[1,2]

[1]Climatology Working Group, University of Münster, 48149 Münster, Germany
[2]now at LI-COR Biosciences GmbH, Bad Homburg 61352, Germany
Keywords: urban flux, size-segregated aerosols, optical particle counter, eddy covariance
Julian.Deventer@uni-muenster.de

The turbulent exchange of aerosol particles between the urban boundary layer and the urban surface has been studied from March 2012 to March 2013. The scope of this experiment is to investigate and quantify the contributions of particles of various size classes (diameter range 0.6 µm < Dm < 10 µm) to total urban particle fluxes, and to study their seasonal variability. The data was collected on a radio tower of 62 m height within the urban area of Münster, a medium sized city (ca. 290 000 inhabitants) in northwest Germany. The combination of two fast optical particle counters (UHSAS and PCASP-X2, manufactured by Droplet Measurement Technologies, Boulder, Colorado (USA)) and three-dimensional wind measurement with an ultrasonic anemometer enabled us to calculate particle number fluxes for 16 size bins using the eddy covariance method.

Previous source apportionment studies found that a considerable portion of Münster's particle mass originates from distant sources (Gietl and Klemm, 2009). Furthermore, a first size-resolved particle flux study, using an electrical low-pressure impactor (ELPI) with the disjunct eddy covariance technique, observed a co-occurrence of positive (upward) number fluxes with negative (downward) mass fluxes (Schmidt and Klemm, 2008). These results are in good agreement with the direct EC-measurements, taken with 2 fast OPCs in the spring of 2011 (Deventer *et al.* 2011). The authors describe a tipping point between bi-directional particle fluxes at 168 ± 20 nm. Until now, negative particle fluxes were rarely reported for urban areas in the literature (Martin et al. 2009). Thus a long-term study can yield valuable information on how frequent such fluxes occur. Furthermore, the annual data set enables us to search for seasonal patterns in particle concentrations and fluxes as a function of particle size and to identify driving factors (e.g. turbulence development) for deposition fluxes.

The results reveal that particle concentrations as well as the particle fluxes exhibit a pronounced seasonality. Highest concentrations were observed during the winter months, whereas the lowest concentrations were sampled in the early summer. Furthermore, the average daily patterns differ notably: For winter days, we observed high concentrations for particles with diameters Dm up to 160 nm throughout the whole day. During spring and summer days the concentrations in this size range significantly decrease between 12:00 and 20:00, when turbulence tends to be well developed. Later in the evening, when turbulent transport ceases, the concentrations rise again.

Total particle number fluxes (0.6 µm < Dm < 10 µm) reach the highest values during the winter, peaking around $3 \cdot 10^7$ # m^{-2} s^{-1}. Summerly number fluxes are notably smaller. However, in this period, we frequently observed negative (deposition) fluxes for particles with diameters > 170 nm, whereas during the winter most of the fluxes for the entire size range were positive. The downward directed flux of particles within the accumulation- and coarse modes (diameter > 0.17 µm) during summer leads to a co-occurrence of a negative total mass flux, peaking at -0.2 µg m^{-2} s^{-1}.

The presentation will further analyse the above reported patterns and expand on topics like relevant time scales, correlations with turbulence characteristics, energy- and greenhouse gas fluxes as well as the impact of different flux source regions.

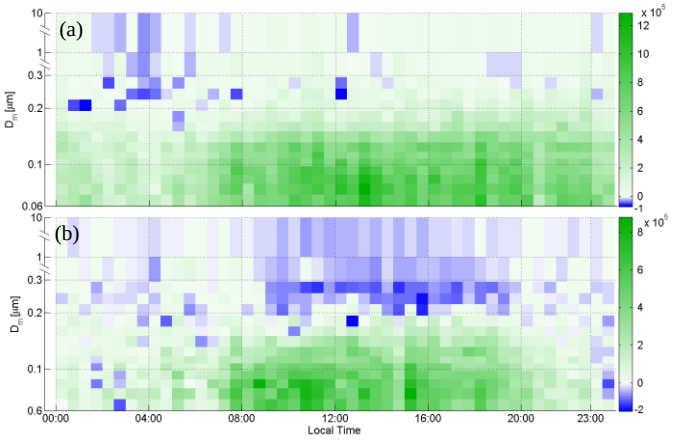

Figure 1. Averaged daily number fluxes for (a) december and (b) august. Colouring symbolizes number fluxes [# m^{-2} s^{-1}], normalized by dlog(D_m) .

This work is supported by the Deutsche Forschungsgemeinschaft (DFG) under grant KL 623 / 12-1.

Deventer, M.J., Griessbaum, F., and Klemm, O. (2011) *Abstract 10D3, European Aerosol Conference 2011, 4-9 Sept, Manchester (UK).*

Gietl, J.K. and Klemm, O. (2009) *Aerosol Science & Tech.* **43**, 828–837.

Martin, C.L., Logley, I.D., Dorsey, J.R., Thomas, R.M., Gallagher, M.W. and Nemitz, E. (2009) *Atmos. Environ.* **43**, 4714–4721.

Schmidt, A. and Klemm, O. (2008) *Atmos. Chem. Phys.* **8(24)**, 7405–7417.

New methods to quantify the contributions of rainout, washout and dry deposition to the total deposition flux of atmospheric aerosol on horizontal urban surfaces

P. Laguionie[1], D. Maro[1], P. Roupsard[1], S. Percot[1], L. Solier[1], V. Ruban[2], M. Rozet[1], D. Hébert[1] and O. Connan[1]

[1]Institut de Radioprotection et de Sûreté Nucléaire (IRSN), PRP-ENV/SERIS/LRC, Cherbourg-Octeville, 50130, France

[2]Institut Français des Sciences et Technologies des Transports, de l'Aménagement et des Réseaux (IFSTTAR), GER7, Bouguenais, 44344, France

Keywords: deposition flux, dry deposition, washout, rainout.

Presenting author email: philippe.laguionie@irsn.fr

In the event of accidental or chronic atmospheric pollution, knowing the total deposition flux of atmospheric aerosol is fundamental to estimate risks for the population and the environment. Deposition flux differs between rural and urban area as the latter has higher surface roughness and type heterogeneities. Although urban areas are continuously growing both in terms of spatial coverage and number of inhabitants, urban aerosol deposition flux remains poorly studied. More urban data sets are now needed as underlined by the scientific community (Fowler *et al.*, 2009; National Research Council, 2012) and is the focus of this study.

The total deposition flux of atmospheric aerosol is made of both dry and wet contributions. Pollutant wet deposition occurs through either washout or rainout processes, which respectively correspond to below-cloud and in-cloud aerosol particle scavenging by the rain droplets. For the first time, this study estimates the respective weighting of these three deposition processes over urban substrates. Data are based on natural radioactive Beryllium-7 (^{7}Be) submicron aerosol tracer. ^{7}Be (53.2-day half-life) comes from cosmic ray spallation in the upper atmosphere. Therefore, ^{7}Be is naturally present in the environment and representative of the atmospheric aerosol accumulation mode.

Experiments were conducted in the suburban area of Nantes (65 km², 282 000 inhabitants) in France, between 9/9/2010 and 1/12/2011. The method developed by Roupsard *et al.* (2012) was used to determine the dry deposition flux over horizontal urban substrates such as asphalt. The rainout and washout components of the wet deposition were estimated using a new method that will be presented during the conference. Overall this method requires (1) monthly-integrated data of ^{7}Be concentration in rainwater at ground level and in atmospheric aerosol particle sampled by Partisol^{TM}, (2) scavenging coefficients for ^{7}Be aerosol particle size as a function of rainfall intensity (Laguionie *et al*, 2011), (3) local atmospheric ^{7}Be reload rate, and (4) meteorological parameters.

Over 13-month average, rainout, washout and dry deposition contributed to respectively 72±21%, 12±10% and 16±13% of the total deposition flux of atmospheric aerosol on horizontal surfaces (Figure 1), with meteorological conditions representative of oceanic climate. The rainout contribution was dominant due to ^{7}Be stratospheric origin. The rainout process intra-annual variability was linked to seasonal changes in both rainfall and ^{7}Be production rate. In terms of washout process, intra-annual change was due to monthly-variations in both rainfall duration (as the scavenging process mainly occurs at the onset of the rainfall) and 7Be atmospheric reloading during dry periods. Washout and dry deposition contribution temporal variations both depend on ^{7}Be concentration within the atmospheric boundary layer and may display similar trend over given periods.

These results will be further discussed during the conference.

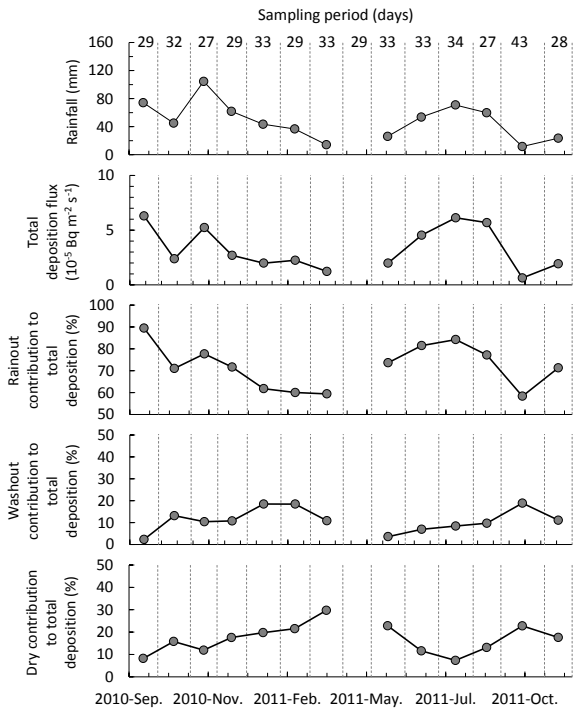

Figure 1. Rainfall and contribution of rainout, washout and dry deposition to total deposition flux in time.

This work was supported by the French National Research Agency (INOGEV research program) and the French Institute of Radioprotection and Nuclear Safety.

Fowler, D. *et al.* (2009) *Atm. Env.* **43**, 5193-5267.

Laguionie, P. *et al.* (2011) *Proc. European Aerosol Conference*, 4-9 Sept., Manchester, UK.

National Research Council (2012) *Urban Meteorology, Forecasting, Monitoring, and Meeting User' Needs*, The National Academic Press, Washington, D.C.

Roupsard, P. *et al.* (2012) *Proc. European Aerosol Conference*, 2-7 Sept, Granada, Spain.

Air mass back trajectories and dry atmospheric aerosol mass size distributions in Prague

J. Schwarz[1], L. Štefancová[1] , W. Maenhaut[2], J. Smolík[1], W. Ždímal[1]

[1]Department of Aerosol and Laser Studies, Institute of Chemical Process Fundamentals AS CR, Prague, CZ-16502, Czech Republic
[2]Department of Analytical Chemistry, Ghent University, Gent, BE-9000, Belgium
Keywords: mass size distribution, air mass back trajectories, water soluble ions
Presenting author email: schwarz@icpf.cas.cz

Ambient aerosol size distribution is an important factor influencing aerosol behavior and properties including particle deposition in lungs and aerosol influence on clouds. Both influences are also driven by aerosol hygroscopicity. Cascade impactors used for size resolved determination of chemical composition suffer from changes of ambient RH during sampling. Due to this factor the same particle might be deposited at different impactor stage when it is sampled at noon at 40% RH or in the early morning at 99% RH. Therefore, we used a diffusional aerosol dryer and a 7-stage modified Berner low pressure impactor with a back-up filter (Štefancová et al., 2011) during the heating (shown as "winter" and non-heating season (shown as "summer") campaigns in 2008. The samples were analyzed for water-soluble ions (Cl^-, SO_4^{2-}, NO_3^-, Na^+, NH_4^+, K^+, Mg^{2+}, Ca^{2+}) and water-soluble organic carbon as a main species that influence aerosol hygroscopicity. Due to the drying, the aerosol size distributions were not influenced by the daily variability of ambient relative humidity.

The results cover the measurements from both campaigns (11 "winter" sampling days and 10 "summer" sampling days). The aerosols sampled on individual days were classified based on the connected air mass back trajectories into three classes: sea-influenced aerosol (SIA), continental aerosol (CA), and mixed aerosol (MA) for samples of intermediate origin.

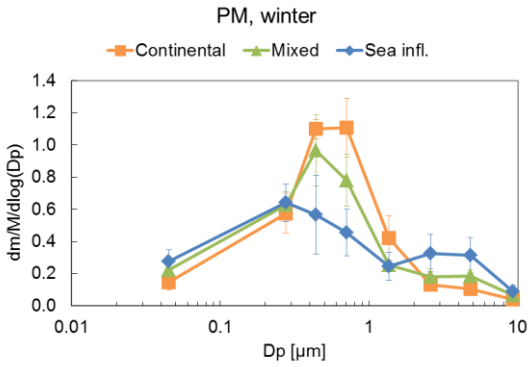

Fig. 1. Average normalized mass size distributions for the PM in the continental, mixed, and sea influenced aerosol samples of the winter campaign.

The differences between CA and SIA were substantial both when looking at the normalized mass size distributions of the particulate matter (PM, Fig. 1) and of the individual species (see an example for SO_4^{2-} in the summer in Fig. 2) and when taking into account

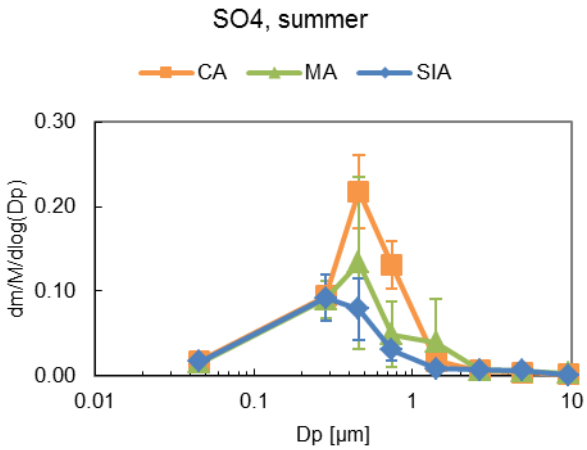

Fig. 2. Average normalized mass size distributions for the PM in the continental, mixed, and sea influenced aerosol samples of the summer campaign.

the absolute concentrations in the fine and coarse size fractions. The shift in the position of fine mode maxima could be explained by the prevailing influence of condensation or droplet mode formation of the accumulation mode particles (Hering and Friedlander, 1982). However, relative humidity profiles along the air mass trajectories could not explain the differences in size distributions in this way. Therefore another reason leading to explanation of the described differences (Schwarz et al., 2012) should be taken into account. As the first hypothesis, we suggest that the differences in average SO_2 concentration fields above Europe could explain our observations if the SO_2 concentration above Western Europe was so low that the diffusional limitation of SO_2 transport into droplets becomes important. This would change size dependence of sulphate formation rate from volume proportional to surface proportional.

This work was supported by the Czech Science Foundation under grant No. P209/11/1342.

Hering, S.V. and Fiedlander, S.K. (1982) *Atmos. Environ.* **16**, 2647–2656.
Štefancová, L., Schwarz, J., Mäkelä, T., Hillamo, R. and Smolík, J. (2011) *Aerosol Sci. Technol.*, **45**, 88-100.
Schwarz, J.; Štefancová, L.; Maenhaut, W., Smolík J. and Ždímal V.: (2012) *Sci. Tot. Environ.* **437**, 348-362.

Thursday, September 5, 2013

Session: Combustion Aerosols,
Engines related emissions

Oxidation reactivity of (bio)diesel generated soot

H. Bladt, N. P. Ivleva and R. Niessner

Chair for Analytical Chemistry, Technische Universität München, Munich, 81377, Germany
Keywords: automotive soot, temperature-programmed oxidation, Raman microspectroscopy.
Presenting author email: bladt@tum.de

Soot oxidation reactivity is an essential parameter in automotive industry for optimizing engine parameters and designing exhaust aftertreatment systems. The more reactive a soot type is towards oxidation, the less energy is needed for the regeneration of a diesel particle filter. Under certain conditions it is even possible to continuously regenerate the particle filter at exhaust gas temperature (continuous regenerating trap CRT). Thus, for the development of an efficient exhaust aftertreatment system it is important to determine the optimal conditions and understand the underlying mechanisms of soot oxidation.

Additionally, there has been only little fundamental research on the impact of the use of biodiesel on soot oxidation reactivity. As the EU obligates the increment of the blending quota of biofuel to fossil fuel to up to 10 % until 2020 by the guideline 2009/28/EG, it is essential to study the impacts of parameters like blending quota of biodiesel to fossil diesel and engine parameters on soot structure and soot oxidation reactivity.

We study soot oxidation reactivity by temperature-programmed oxidation (TPO, setup see Figure 1), which models the soot oxidation in a common diesel exhaust aftertreatment system. The soot-loaded filter sample is exposed to a gas flow at rising temperature from 373 to 973 K at a heating rate of 5 K min^{-1}. The gas flow simulates real exhaust composition and may contain besides O_2 and N_2 also other gases such as NO_2 and H_2O. The combustion emissions are monitored in dependence of applied temperature to the soot sample by FTIR spectrometry.

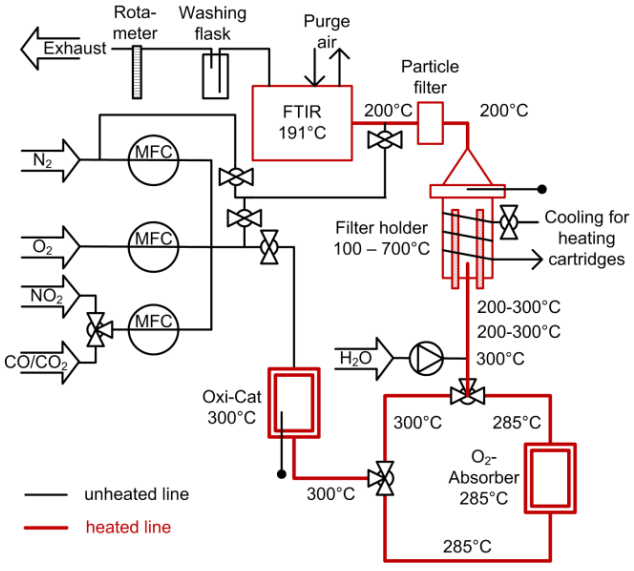

Figure 1. Scheme of TPO test bench.

By means of TPO, we studied the impact of different exhaust gas mixtures containing O_2, H_2O and/or NO_2 on soot oxidation reactivity. Figure 2 shows the emission profiles of CO and CO_2 of commercial Printex XE2 soot (Degussa) in dependence of temperature and applied gas mixture. The temperature of maximum emission T_{max} can be used as criterion for soot oxidation reactivity (see Figure 2). It can be clearly demonstrated that NO_2 and H_2O are strongly increasing soot oxidation reactivity by shifting T_{max} towards lower temperatures.

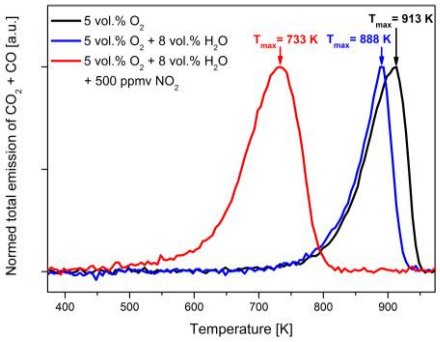

Figure 2. TPO emission profiles of Printex XE2 soot analyzed under different oxidative conditions.

Raman microspectroscopy (RM) is furthermore applied to characterize the soot structure. RM is an established tool for the analysis of structural differences in the disordered (represented by Raman D band) and graphitic soot domains (represented by Raman G band) between different soot samples (Ivleva et al., 2007). Furthermore, the Raman spectra of soot exhibit a unique feature as the spectra of one sample differ in position and relative intensity of the D band when analyzed at different laser excitation wavelengths due to the dispersive character of the D band in soot spectra.

Final aim of this study is to analyze the soot oxidation reactivity by TPO under different conditions and correlate the TPO data with the structural information given by RM. Among others, a rapid and non-destructive method for the evaluation of the oxidation reactivity of biofuel generated soot by RM shall be established based on the method of multiwavelength Raman microspectroscopy (MWRM) for fossil fuel developed by Schmid *et al.* (2011).

This work is supported by Forschungsvereinigung Verbrennungskraftmaschinen (FVV e.V.) and Fachagentur Nachwachsende Rohstoffe (FNR e.V.).

N. P. Ivleva, U. McKeon, R. Niessner, U. Pöschl (2007) *Aerosol Sci. Technol.* **41**, 655-671.

J. Schmid, B. Grob, R. Niessner, N. P. Ivleva (2011) *Anal. Chem.* **83**, 1173-1179.

Can scooter emissions dominate urban organic aerosol?

I. El Haddad[1], S. M. Platt[1], A. A. Zardini[2], J.G. Slowik[1], M. Clairotte[2], C. Astorga[2], P. Barmet[1], R, Chirico[3], J. Dommen[1], U. Baltensperger[1], and A. S. H. Prévôt[1]

[1]Laboratory of Atmospheric Chemistry, Paul Scherrer Institute (PSI), Villigen, CH-5232, Switzerland
[2]Institute for Energy and transport, Sustainable Transport Unit, EC Joint Research Centre, 21027 Ispra, Italy
[3]Italian National Agency for New Technologies, Energy and Sustainable Economic Development (ENEA), FIS-LAS, Via E. Fermi 45, 00044 Frascati, Italy

Keywords: scooters, smog chamber, primary organic aerosol, secondary organic aerosol.

Presenting author email: imad.el-haddad@psi.ch

In urban areas, where the health impact of pollutants increases due to higher population density, traffic is a major source of ambient organic aerosol (OA). A significant fraction of OA from traffic is secondary, produced via the reaction of exhaust precursor gases with atmospheric oxidants. Secondary OA (SOA) has not been systematically assessed for different vehicles and driving conditions and thus its relative importance compared to directly emitted, primary OA (POA) is unknown, hindering the design of effective vehicle emissions regulations.

2-stroke (2S) scooters are inexpensive and convenient and as such are a popular means of transportation globally, particularly in Asia (e.g. 6% in Thailand vs. <1% in Europe, Klaassen et al. 2005). European regulations for scooters are less stringent than for other vehicles and thus primary particulate emissions from 2S engines are estimated to be much higher. Furthermore, current estimates suggest scooters may emit more volatile organic compounds (VOCs) than all other vehicles combined in Europe by 2020 (Geivanidis et al., 2008), implying that scooters dominate SOA production from traffic emissions. Thus assessing the effects of scooters on public health requires consideration of both POA, and SOA production.

Here, we quantify POA emission factors (EF, mg kg^{-1}_{fuel}) and potential SOA EFs from 2S scooters, and the effect of using aromatic free fuel instead of standard gasoline thereon. During the tests, Euro 1 and Euro 2 2S scooters were run in idle or simulated low power conditions. Emissions from a Euro 2 2S scooter were also sampled during regulatory driving cycles (ECE47) on a chassis dynamometer.

Vehicle exhaust was introduced into smog chambers, where POA emission and SOA production were quantified using a high-resolution time-of-flight aerosol mass spectrometer (HR-ToF-AMS). A high resolution proton transfer time-of-flight mass spectrometer (PTR-ToF-MS) was used to investigate volatile organic compounds and a suite of instruments was utilized to quantify CO, CO_2, O_3, NO_X and total hydrocarbons.

We show that the oxidation of VOCs in the exhaust emissions of 2S scooters produce significant SOA, exceeding by up to an order of magnitude POA emissions (see Figure 1). By monitoring the decay of VOC precursors, we show that SOA formation from 2S scooter emissions essentially stems from the condensation of aromatic oxidation products. Further, we demonstrate that replacing the standard gasoline with an aromatic-free fuel mitigates SOA production (Figure 1), underlining the major role of aromatic compounds from 2S exhaust on SOA production. POA and potential SOA EFs determined here from 2S scooters will be presented and compared with EF from other vehicles, including 4-stroke scooters, gasoline cars and diesel cars to assess the contributions of 2S scooters in urban atmospheres.

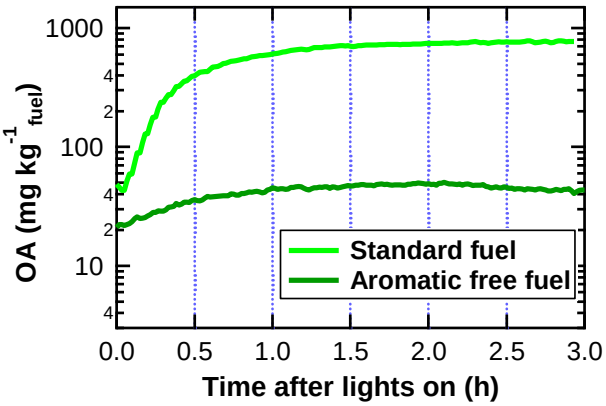

Figure 1. POA+potential SOA emission factors from a Euro 2 2-stroke scooter filled with standard gasoline and with aromatic free fuel, during the ECE47 driving cycle.

This work was funded by the Swiss Federal Office for the Environment (FOEN) and the Federal Roads Office (FEDRO). The test bench operation was financed by the European Union, European Social Fund. We thank Mirco Sculati, Franz Muehlberger, Maurino, Cadario and Rene Richter for their excellent technical assistance.

Geivanidis, S., Ntziachristos, L., Samaras, Z., Xanthopoulos, A., Heinz, S., & Bugsel, B. (2008) *Arisotle University Thessaloniki, Thessaloniki*.

Klaassen, G., Berglund, C., and Wagner, F. (2005) International Institute for Applied Systems Analysis (IIASA), Laxenburg, Austria.

Transformation of Black Carbon Aerosol in the Atmosphere – Observations from Smog Chamber Studies and Ambient Air

J.H. Pagels[1], A.C. Eriksson[2], J. Rissler[1], E.Z. Nordin[1], C. Wittbom[2], P.T. Nilsson[1], A. Kristensson[2], P. Roldin[2], B. Svenningsson[2] and E. Swietlicki[2]

[1]Ergonomics and Aerosol Technology, Lund University, Lund, SE-22100, Sweden
[2]Division of Nuclear Physics, Lund University, Lund, SE-22100, Sweden
Keywords: soot transformation, BC, SP-AMS, DMA-APM, smog chamber
Presenting author email: Joakim.pagels@design.lth.se

Atmospheric processing of soot ultimately leads to transformation of the agglomerated soot structure to close to spherical particles with an embedded elemental carbon core. These processes affect health and climate relevant (e.g. optics and cloud formation) and properties but the dynamics and time scales of the processes are poorly known (Zhang et al. 2008). The vacuum aerodynamic size distribution measured with the Soot Particle Aerosol Mass Spectrometer (SP-AMS) is a powerful tool to separate fresh and aged soot. In this work we investigated the transformation of diesel soot in detail in a smog chamber and contrast these results with recent street side and rural background measurements.

The composition of the soot core, its coatings and vacuum aerodynamic size distribution (Dva) was analyzed with an SP-AMS (Aerodyne Research). The soot morphology and size dependent condensed mass fraction was investigated using a Differential Mobility Analyzer-Thermal Denuder-Aerosol Particle Mass Analyzer (DMA-TD-APM) combined with TEM.

Controlled experiments were first carried out in a 6 m^3 Teflon (FEP) smog chamber using black lights to initiate OH-chemistry. Diesel exhaust from an idling Euro II light duty vehicle was injected using a heated inlet. Varying concentrations of the anthropogenic SOA precursors toluene and m-xylene were added to the smog to investigate different degrees of aging. Soot transformation time scales are calculated based on the secondary aerosol mass flux to the particle phase in the chamber. Atmospheric background measurements were carried out at the Vavihill supersite in south Sweden. Urban street-side measurements were carried out in downtown Copenhagen adjacent to a busy street (60 km south-west of the background site).

During condensation of SOA, the effective density increased from low values typical for fresh diesel agglomerates towards 1.4 g/cm^3 and the dynamic shape factor decreased towards 1.0, which showed that the soot agglomerates had been transformed to essentially spherical particles. The results have been summarized in a parameterization of the dependence of particle morphology (dynamic shape factor and effective density) on the condensed mass fraction and particle size during aging in the smog chamber. Humidifying the particles from the smog chamber to 90% RH using a hygroscopic tandem DMA, showed that uptake of water vapor leads to progressed compaction of the soot core.

Vacuum aerodynamic sizes of soot particles detected with the SP-AMS increased from about 100 nm up to about 400 nm when the organic fraction increased from about 10% to 95% with aging in the chamber. This was due to the dual effects of increased volume and more compact shape leading to increased Dva (figure 1).

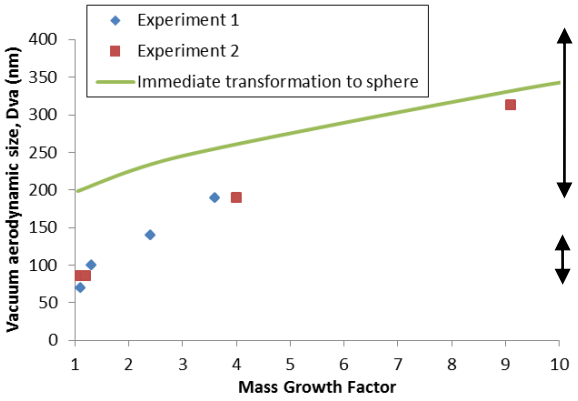

Figure 1. Mass median Dva vs mass growth factor measured in the smog chamber. To illustrate the large impact of particle morphology on the Dva, calculated results assuming immediate transformation to spheres are given for comparison. Arrows indicate the range of the two modes of soot containing particles at street side measurements.

In the street side measurements two main particle types were found, more massive particles with effective densities of about 1.4 g/cm^3 nearly independent of particle size (interpreted as long range transport) and less massive particles with effective density decreasing with size. The SP-AMS showed one mode consistent with fresh agglomerated soot (Dva~100 nm) and another mode of larger soot containing particles.

At the background station at eastern wind directions, the more massive particles strongly dominated, while during south-western winds there was in addition a mode of less massive particles with effective densities equal to or higher than for fresh diesel soot, indicative of urban influence from the Copenhagen-Malmö metropolitan area (population: 2.6 Million).

We have shown that the combination of the SP-AMS and DMA-TD-APM is a powerful tool to investigate soot transformation in various environments. The vacuum aerodynamic size distribution measured with SP-AMS is a powerful tool in separating fresh and aged soot on a quantitative mass basis. However, more information is needed to investigate the transformation of soot from other sources such as biomass combustion.

This work was financed by the Swedish research council FORMAS, grant nbr. 2010-1678

Zhang, Khalizov, Pagels et al. (2008) PNAS 30, 10291

Effect of atmospheric ageing on volatility and ROS of biodiesel exhaust nano-particles

Pourkhesalian, A.[1], Stevanovic, S.[1], Rahman, M.[1], Wang, H. [1], Mallet, M.[1], Pham, X. P. [2],Masri, A.[2], Brown, R.[1], Ristovski, Z.D.[1]

[1] ILAQH & BERF, Science and Engineering Faculty, Queensland University of Technology, Brisbane, 4000, Australia
[2] School of Aerospace, Mechanical and Mechatronic Engineering, The University of Sidney, Sidney, 2006, Australia
Keywords: Diesel particulate matter, aging, ROS.
Presenting author email: alimohammad.pourkhesalian@qut.edu.au

Generally, the magnitude of pollutant emissions from diesel engines is ultimately coupled to the structure of fuel molecules. The presence of oxygen, level of unsaturation and the carbon chain length of respective molecules influence the combustion chemistry. It is speculated that increased oxygen content in the fuel may lead to the increased oxidative potential (Stevanovic, S. 2013). Also, upon the exposure to UV and ozone in the atmosphere, the chemical composition of the exhaust is changed. The presence of an oxidant and UV is triggering the cascade of photochemical reactions as well as the partitioning of semi-volatile compounds between the gas and particle phase. To gain an insight into the relationship between the molecular structures of the esters, their volatile organic content and the potential toxicity of diesel exhaust particulate matter, measurements were conducted on a modern common rail diesel engine. This research also investigates the contribution of atmospheric conditions on the transfer of semi-volatile fraction of diesel exhaust from the gas phase to the particle phase and the extent to which semi-volatile compounds (SVOCs) are related to the oxidative potential, expressed through the concentration of reactive oxygen species (ROS) (Stevanovic, S. 2013).

Methodology: A Cummins diesel engine runs on blends of four methyl ester biodiesels and conventional diesel on a variety of operating conditions. The exhaust produced by the engine passes through a multi-stage dilution system followed by a flow through reactor by which ageing process is induced. A Volatility Tandem Differential Mobility Analyser (VTDMA) measures the change in volatile content of particles. A profluorescent nitroxide molecular probe (bis(phenylethynyl) anthracene-nitroxide; BPEAnit) (Stevanovic, S. 2013) is used for assessing the oxidative potential of particles (i.e. potential of particles to induce oxidative stress).

Results and discussion: Figure 1 shows the volatility of 60nm particles from the 50% blends of four metyl-esters and diesel fuel. Overall, the organic content of the particles in all blends has increased after ageing. As the oxidative potential is related not only to the organic content but also to the portion of the oxidised organic fraction of PM (Stevanovic, S. 2013), particles are more potentially toxic after being exposed to oxidative agents i.e. ozone and UV light.

The results of VTDMA measurement are in good correlation with the oxidative potential measured by BPEAnit. It shows that in almost all cases, the oxidative potential of the particle phase increases after being exposed to ozone and UV light. It is also evident that there is a correlation between the level of saturation of the fuel and the organic content of the particles where the most saturated fuel produces the most volatile particles. In addition, the volatility of aged particles produced by saturated fuels increases more than those produced by less saturated blends.

The presented research shows that biodiesel, compared to the commercial diesel, emits more volatile particles with higher ROS concentrations, and interestingly, the matter is deteriorating over time as diesel exhaust is aged in the atmosphere. Also, an increase in organic fraction upon aging indicated that the greater amount of SVOCs is present after the combustion of biofuels. Since the organic fraction is tied to the oxidative capacity of particles, those particles produced by bio-diesel are likely to be more harmful than those produced by commercial diesel. Overall, the ROS measurements confirm the mentioned hypothesis.
It also sheds a light onto new aspects of particulate emissions that should be taken into account when establishing relevant metrics for health implications of emissions from various future fuels. While the common belief is in favour of a movement from conventional fuels to those extracted from animals and plants, findings of this research may argue the latter notation.

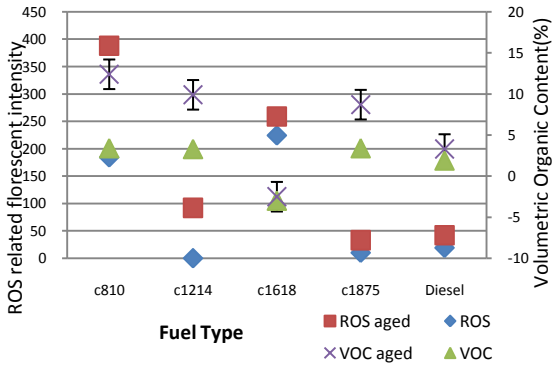

Figure 1. The change in volatile content of particles and ROS of particles before after ageing process

References:

1."The influence of oxygenated organic aerosols (OOA) on the oxidative potential of diesel and biodiesel particulate matter" Authors: Stevanovic, S.; Miljevic, B.; Surawski, N.; Fairfull-Smith, K.; Bottle, S.; Brown, R.; Ristovski, Z. Manuscript ID: es-2013-007433, Submitted to ES&T.

Real-world nanoparticle emissions of passenger cars and heavy duty diesel vehicles

T. Rönkkö[1], L. Pirjola[2], P. Karjalainen[1], S. Saari[1] and J. Keskinen[1]

[1]Department of Physics, Tampere University of Technology, P.O. Box 692, FIN-33101,Tampere, Finland
[2]Department of Technology, Metropolia University of Applied Sciences, Helsinki, Finland
Keywords: exhaust particles, vehicle emissions, on-road measurements, nucleation mode.
Presenting author email: topi.ronkko@tut.fi

Vehicle exhaust has been frequently reported to contain nanoparticles which differ from soot particles by their chemical composition, physical characteristics and formation mechanisms. These nanoparticles are usually seen in exhaust particle size distribution as a separate mode, frequently called *nucleation mode*. Mixing, dilution and cooling of vehicle exhaust are in a critical role in nanoparticle emission formation i.e. the initial formation of the nanoparticles and the condensation of semivolatile exhaust compounds on the existing nanoparticles can take place during those processes. Typically the exhaust particle studies have been conducted in laboratory conditions, where the exhaust dilution does not equal exactly the real-world process, especially from the viewpoint of the nanoparticle formation. Due to that, the knowledge of real exhaust emissions and e.g. the human exposure on vehicle emissions require studies conducted on road and in real-world driving and exhaust dilution conditions.

The development of the nucleation mode and local dilution ratio within the vehicle exhaust was reviewed and the findings of studies comparing real-world and dynamometer measurements were analysed (Keskinen and Rönkkö, 2010). A series of on-road exhaust measurements were conducted, focusing on the exhaust nanoparticle emissions and the effects of vehicle technologies on those emissions. Measurements were conducted for passenger cars and heavy duty diesel trucks equipped with different exhaust after-treatment devices. Particle measurements were performed exploiting the "Sniffer" laboratory vehicle (Pirjola et al. 2004) equipped with two SMPSs, an ELPI, a CPC, a thermodenuder and gas analyzers for CO_2, CO and NO_x. In addition, the data related to driving parameters and weather conditions was collected.

Exhaust nanoparticle observations have been frequently connected to fuel and lubricant oil sulphur levels. On the other hand, the particle formation has been explained by nucleation of sulphuric acid and water during cooling dilution of exhaust in the atmosphere. However, nanoparticles seem to be an essential part of real particle emissions also when the fuel sulphur level is low, in our measurements below 10 ppm. The exhaust plume nanoparticles form at low dilution ratios ≤ 10 or even before the dilution process in high temperature conditions. Anyway, nanoparticle mode (or nucleation mode) seems to be fully developed at a dilution ratio of approximately 100. In regard to driving conditions, especially the transients of engine load were observed to be in important role in emission formation. In addition, exhaust after-treatment affect the nanoparticles; e.g. the use of a partial diesel particle filter, here the combination of a diesel oxidation catalyst (DOC) and a particle oxidation catalyst (POC), decreased significantly the real-world nanoparticle emissions of heavy duty diesel truck (Figure 1).

The effect of the DOC+POC on exhaust plume nanoparticles is a qualitative example of a correlation between real-world nanoparticle emissions and emission studies conducted in the laboratory conditions; e.g. Heikkilä et al. (2009) reported similar effects for a DOC+POC system. In addition, the review indicated that the trends in the vehicle exhaust nanoparticle formation, including those caused by differences in vehicle speed and engine load, engine and after-treatment technology and fuel and lubricant formulation can be mimicked in laboratory conditions. However, laboratory studies of vehicle exhaust nanoparticles require proper exhaust sampling and dilution methods and comparisons with real-world studies.

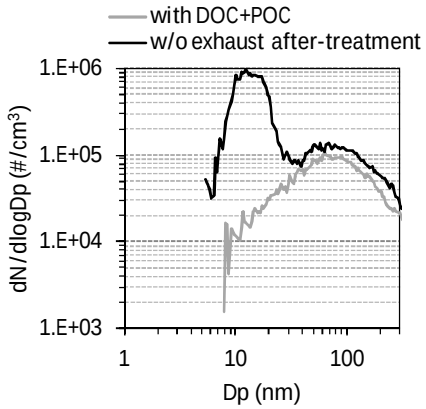

Figure 1. Real-world particle size distributions measured from exhaust plume of heavy duty diesel truck equipped with partial diesel particle filter and without exhaust after-treatment. Measurement was conducted at medium engine load conditions.

Studies were conducted in the REAL-EM and TREAM projects supported by The Finnish Funding Agency for Technology and Innovation (Tekes), Neste Oil Oyj, Ecocat Oy, AGCO Power and Nanol Technologies.

Heikkilä, J. *et al*. (2009). *J. Air & Waste Manage. Assoc.* **59**:1148–1154

Keskinen and Rönkkö (2010), *J. Air & Waste Manage. Assoc*. **60**, 1245–1255.

Pirjola et al. (2004), *Atmospheric Environment*, **38**, 3625-3635.

Chemical composition of particulate and gas emissions from a 4-stroke marine diesel engine operated with heavy and distillate fuel oils

O. Sippula[1,2,5], B. Stengel[3,5], M. Sklorz[1,5], T. Streibel[1,5], R. Rabe[3,5], H. Harndorf[3,5], J. Orasche[1,5], J. Lintelmann[1,5], B. Michalke[4], G. Abbaszade[1,5], C. Radischat[1,5], J. Schnelle-Kreis[1,5], R. Zimmermann[1,5]

[1]Joint Mass Spectrometry Centre / Chair of Analytical Chemistry, University of Rostock, 18051 Rostock, Germany / Cooperation Group Comprehensive Molecular Analytics, Helmholtz Zentrum München, 85764 Neuherberg, Germany
[2]Department of Environmental Science, University of Eastern Finland, Kuopio, FI-70101, Finland
[3] Fakultät für Maschinenbau und Schiffstechnik Lehrstuhl für Kolbenmaschinen und Verbrennungsmotoren, Albert-Einstein-Str. 2, Universität Rostock, 18059 Rostock, Germany
[4]Analytical Biogeochemistry Helmholtz Zentrum München, Ingolstädter Landstr. 1, 85764 Neuherberg, Germany
[5]HICE – Helmholtz Virtual Institute of Complex Molecular Systems in Environmental Health – Aerosols and Health, www.hice-vi.eu

Keywords: Diesel engine, Ship emissions, PAH, Soot
Presenting author email: olli.sippula@uef.fi

Exhaust emissions from ships are known to generate high amounts of particulate and gaseous pollutants which have environmental, health and climate effects. Especially the use of heavy fuel oils may generate high amounts of harmful aerosol emissions into the environment. However, the chemical composition of these emissions it is still relatively poorly known.

Experiments with a 4-stroke single cylinder (80 kW nominal power) research engine with a common rail injection system were conducted in the engine laboratory at the University of Rostock. The structure of the engine represents a typical medium speed ship diesel engine. The engine was operated with distillate fuel ("DF", EN590) and a heavy fuel oil ("HFO 350", 2.7 % sulphur) with nominal speed (1500 rpm) and engine loads ranging from "idle" to 100 %. In addition, early and late injection points were used in the engine, representing "low-soot" and "low-NOx" operations.

The flue gas was analysed for O_2, CO_2, CO, NO_X, SO_2 and THC with single gas analyzers (AVL CEB II). The volatile and semivolatile organic species were measured online with a resonance enhanced multiphoton-ionization time-of-flight mass spectrometer (REMPI-TOF-MS) and a proton transfer reaction mass spectrometer (PTR-MS, Ionicon). Particulate samples from the engine exhaust were collected on quartz fiber filters in steady-state conditions applying a diluting sampling system (AVL Smart Sampler).

The filter samples were analysed for inorganic species (ICP-MS), a number of PAHs, oxy-PAHs, hopanes (Thermal desorption GC-TOF-MS), Azaarenes and 1-nitropyrene (LC-FD) and for organic (OC) and elemental carbon (EC) (thermal-optical analysis, DRI). The carbon analysis was coupled with a time-of-flight mass spectrometer with both single photon ionization (SPI, 118 nm) and resonance enhanced multiphoton ionization (REMPI, 266 nm) in order to analyse molecular compositions of the organic fractions, as described by Grabowsky et al. (2011).

The PM emissions, in the load range of 25-100 %, were between 154-236 mg/kWh with DF and 728-1902 mg/kWh with HFO. The low load conditions generated clearly higher emissions up to several grams per kWh. The particles contained substantial organic material fractions, with OC/EC ratios varying between 2 and 22 depending on the engine operational conditions. The EC and inorganic (metals + sulphate) fractions varied in the ranges 2-29 % and 3-23 %, respectively. The emissions from HFO contained significant amounts of V and Ni, released from the fuel as well as sulphuric acid. Emissions with both fuels contained Ca, originating mainly from the lubrication oil. The thermal desorption GC-MS included quantification of 11 PAHs, 17 oxy-PAHs and 11 hopanes with clearly higher emission from HFO than DF. Furthermore, 9 different Azaarenes were quantified from the HFO samples, while for DF their concentrations were below the quantification limit. The REMPI-TOF-MS showed high amounts of alkylated PAHs in the PM of both fuels, with the most distinct difference the high amounts of alkylated chrysenes in the HFO emissions. A comparison of direct fuel analysis and PM emission analysis by REMPI revealed similar patterns indicating that the aromatic emissions (e.g. PAHs) are mainly present already in the fuel.

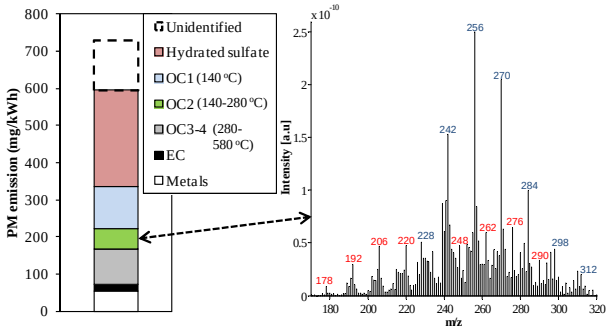

Figure 1. PM chemical composition and REMPI analysis from the OC2 fraction when operated with HFO and 50% load.

The chemical characteristics of emissions in altogether 15 operational conditions with 2 different fuels were analysed. The emissions were generally clearly higher from HFO than from DF, with the exception of EC emissions which were on a similar level with both of the fuels.

This work was supported by the Helmholtz Virtual Institute of Complex Molecular Systems in Environmental Health (HICE) and the Academy of Finland.

Grabowsky, J., Streibel, T., Sklorz, M., Chow, J.C., Watson, J.G., Mamakos, A. and Zimmermann, R. (2011) *Anal. Bioanal. Chem.* **401**, 3153-3164.

Effects of secondary organic aerosols from gasoline exhaust on healthy and diseased respiratory epithelia

M. Krapf[1], L. Künzi[2], N. Daher[3], J. Dommen[1], S. Schneider[2], N. Jeannet[2], S. Platt[1], J. G. Slowik[1], A. S. H. Prévôt[1], M. Kalberer[4], C. Sioutas[3], U. Baltensperger[1] and M. Geiser[2]

[1]Laboratory of Atmospheric Chemistry, Paul Scherrer Institute, Villigen, 5232, Switzerland
[2]Institute of Anatomy, University of Bern, Bern, 3012, Switzerland
[3]Department of Civil and Environmental Engineering, University of Southern California, Los Angeles, 90089, California, United States of America
[4]Department of Chemistry, University of Cambridge, Cambridge, CB2 1EW, United Kingdom
Keywords: secondary organic aerosols, SOA, gasoline exhaust, health effects
Presenting author email: manuel.krapf@psi.ch

Gasoline exhaust is a major anthropogenic source of atmospheric particles (Bahreini, 2012) and potentially contributes to respiratory diseases from inhalation exposure. Individuals with pre-existing lung diseases are more vulnerable than healthy people.

The aim of this study was to investigate acute responses of cultured respiratory epithelium cells after exposure to photochemically aged aerosols from gasoline exhaust using advanced technologies from aerosol science and in-vitro toxicology.

To achieve this aim, exhaust of a gasoline car (EURO 5 standard) was diluted and injected into a smog chamber consisting of a 27 m^3 fluorinated ethylene propylene bag suspended in a temperature-controlled enclosure, resulting in aerosol concentrations of typically 10-30 μg m^{-3} before and 100-250 μg m^{-3} after aging. A combination of instruments monitoring gas- as well as particle phase allowed precise measurements of several parameters. These included chamber temperature, relative humidity, oxides of nitrogen, ozone, total hydrocarbon, black carbon, as well as the total particle number and volume concentration. In addition an aerosol mass spectrometer was used to monitor chemical composition during the aerosol aging process.

After injection of exhaust and homogenisation/equilibration of the chamber, secondary organic aerosol (SOA) was produced through photochemical processes initiated by irradiation with artificial sunlight (4 xenon arc lamps and 80 blacklights). Then, the aged aerosol was transferred from the smog chamber through a versatile aerosol concentration enrichment system (VACES) (Wang, 2013) into an aerosol deposition chamber (Mertes, 2013). By enriching particle concentrations up to a factor of 50, the dose of particles deposited on cell cultures could be varied over a broad range.

The total particle concentration was permanently measured after the enrichment system. Harmful gases were removed using a charcoal denuder and SOA was deposited out of a continuous air-flow (0.6 L/min) simultaneously on 12 individual cell cultures through electrostatic deposition. The conditions in the aerosol deposition chamber were continuously recorded and could be adjusted to a relative humidity of 85-95 % and a temperature of 37 °C. Therefore, particle-cell interactions could be simulated at physiological conditions while minimizing stress on the cell cultures. A detailed knowledge of particle deposition characteristics on the cell cultures allowed evaluating reliable dose-response relationships (Mertes, 2013).

Re-differentiated human bronchial epithelia (HBE) cultured at an established air-liquid interface and the bronchial cell line BEAS-2B were exposed to the aerosol for 2 hours. Biological endpoint tests determined the dose-response relationships in the exposed cells. Several tests were performed including (i) necrotic cell death assessed by release of lactate dehydrogenase from damaged cells, (ii) induction of apoptosis by activation of caspase-3, (iii) inflammatory responses by expression and release of inflammatory mediators and (iv) oxidative stress by induction of mRNA synthesis of respective markers.

Results demonstrate cytotoxicity as well as inflammatory responses of HBE and BEAS-2B cells after exposure to SOA from gasoline exhaust. Different responses of cell cultures from a donor with lung disease were observed compared to HBE from a healthy donor. In addition, there is evidence for substantial differences between responses of BEAS-2B cells and HBE cells after aerosol exposure, which challenges the use of cell lines to study effects of inhaled particles in vitro.

The combination of aerosol science and in-vitro toxicology technologies provides a highly realistic and reproducible system for testing toxicity of environmental aerosols and determining dose-response relationships.

This work was supported by the Swiss National Science Foundation (CR3213-140851).
Special acknowledgements go to the University of Southern California (USC) Viterbi School of Engineering.

Bahreini, R., et al. (2012), *Geophys. Res. Lett.*, *39*(6), L06805.
Wang, D., et al. (2013), *Aerosol Sci. Technol.*, *47*(3), 231-238.
Mertes, P., et al. (2013), *J Aerosol Med Pulm D*, DOI: 10.1089/jamp.2012.0985, *in press.*

Characterisation of solid and semi-volatile gas-turbine particulate matter using a catalytic stripper

J.J. Swanson[1], T.J. Johnson[2], J.S. Olfert[2], M.P. Johnson[3], P.I. Williams[4,5], G.J. Smallwood[6] and A.M. Boies[1]

[1]Department of Engineering, University of Cambridge, Cambridge, CB2 1PZ, UK
[2]Department of Mechanical Engineering, University of Alberta, Edmonton, Alberta, T6G 2G8, Canada
[3]Rolls-Royce plc, Derby DE24 8BJ, UK
[4]National Centre for Atmospheric Science, University of Manchester, Manchester, M13 9PL, UK
[5]SEAES, University of Manchester, Manchester, M13 9PL, UK
[6]NRC Canada, Ottawa, Ontario K1A 0R6, Canada
Keywords: EC/OC, aerosol, exhaust, CPMA
Presenting author email: js2011@cam.ac.uk

Gas turbine particulate matter (GTPM) consists of solid and semi-volatile particles that originate from partially oxidised fuel and lubricating oils. Many techniques are available for measurement of particle number, size, and mass. However, often the volatile nature of these particles is not measured *a priori*. Advanced techniques are designed to respond to particles of a specific volatility or composition (such as solid, elemental carbon) but there are known cross-sensitivities. Catalytic stripper[1] (CS) technology provides an alternative method to aid in further elucidating the composition of an aerosol. A CS contains an oxidising catalyst that is used to fully remove the semi-volatile hydrocarbon particles and vapors in an exhaust gas stream. In this way, remaining particles are operationally defined as "solid."

The primary objective of this study was to measure the solid and semi-volatile fractions present in GTPM using a catalytic stripper specifically designed for the "Sample III " program that aimed to support SAE E-31 in drafting the Aerospace Recommended Practice (ARP) on the measurement of aircraft engine non-volatile particulate matter (nvPM) number emissions[2]. GTPM was generated by a GE CFM56-5B4-2P engine (120 kN, 27000 lb) with a dual annular combustor (DAC) is designed to minimise emissions, especially of NO_x, by optimising combustion for the different engine power modes and flight phases. Operating conditions were chosen to provide combinations of different levels of solid and semi-volatile material at modest power levels, thus minimising fuel consumption and allowing for more extensive testing.

Fig. 1 shows the sampling apparatus with raw gas turbine exhaust being sampled using 16 m transfer line heated to 160°C that is compliant with current regulations and a manifold to distribute the aerosol.

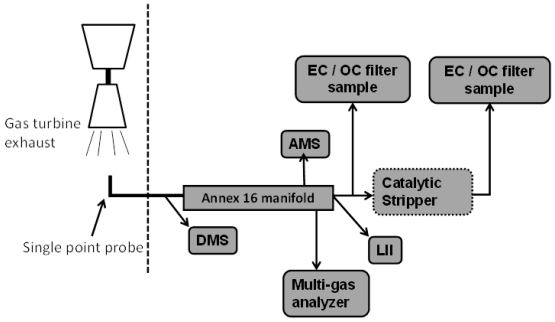

Figure 1. GTPM measurement apparatus for raw exhaust.

The primary evaluation metric reported on here is the EUSAAR "EC/OC" protocol that is used to define the concentration of elemental carbon. EC results were compared with laser induced incandescence (LII), which directly measures a related quantity, namely "black carbon." The EC/OC method also classifies the amount of (semi-volatile) organic carbon present, and therefore enables estimates of the semi-volatile faction. Results are also compared with both gas analysis and an alternative method particle measurement, the centrifugal particle mass analyser (CPMA) used with and without a CS.

Fig. 2 shows results of EC/OC analysis upstream and downstream of the CS for various engine power conditions. Results upstream the CS show that the elemental carbon fraction of the PM varies from ~10% to 90%, whereas downstream the CS there is only elemental carbon. Thus, for all turbine conditions the CS removes all OC, which allows for parallel measurement of the solid fraction using any typical aerosol instrument.

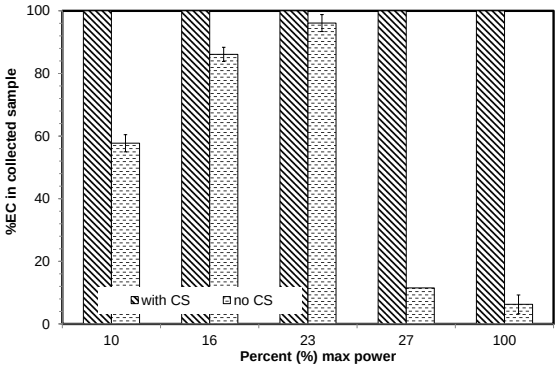

Figure 2. EC/OC results showing %EC in each sample collected up and downstream of the CS.

This work was supported by the UK Engineering and Physical Sciences Research Council (EP/H004505/1) and EASA Contract No: EASA.2010.FC10, Specific Contract Sample III - SC02.

[1]Swanson, J.; Kittelson, D. (2010). Evaluation of Thermal Denuder and Catalytic Stripper Methods for Solid Particle Measurements. *J. Aerosol Science*, 41:12, 1113 – 1122.

[2]Crayford, A.; Johnson, M. SAMPLE III: Contribution to aircraft engine PM certification requirement and standard. Second Specific Contract– Final Report. *EASA.2010.FC.10 Specific Contract No: SC02*.

Thursday, September 5, 2013

Session: Electrical Effects, *Electrical effects*

Effects of induced gas flow on electrospray dynamics

A.K. Arumugham[1], Jordi Grifoll[1] and Joan Rosell-Llompart [1,2]

[1]Departament d'Enginyeria Química, Universitat Rovira i Virgili, Tarragona, 43007, Spain
[2]ICREA (Catalan Institution for Research and Advanced Studies), Barcelona, 08010, Spain
Keywords: electrospray, numerical simulation, induced gas flow, spray dynamics.
Presenting author email: ajithkumar.arumugham@urv.cat

Electrosprays are constituted of highly charged micro drops created by the action of electrostatic forces. Because these aerosol particles move with a net velocity relative to the surrounding gas, their reactive drag force on the gas causes the gas to flow. We are investigating the extent to which this gas motion influences electrospray droplet evaporation and vapor concentration, as well as the electrospray dynamics.

Considering non volatile sprays initially, we have devised a numerical scheme based on the vorticity-streamfunction method to describe the Eulerian gas flow dynamics, which is coupled to a Lagrangian particle dynamics model (Grifoll and Rosell-Llompart, 2012). The body force for the gas flow field is the reactive drag force on gas due to droplet motion. A final steady state system configuration is obtained iteratively through a series of coupled time-averaged pseudo-steady state solutions in both frameworks. With a limited number of realizations of the particle dynamics, it is necessary to use a filtering scheme that smoothly distributes the force per unit volume created by the relative movement between the 'point droplets' and the gas (Apte *et al*, 2008).

Results

We have applied this methodology to the well characterized experimental system of Tang and Gomez (1994). Figure 1 shows two snapshots of the simulated spray, one assuming still ambient gas and the other of complete gas-spray simulation under the influence of induced gas motion, including gas streamlines. The droplets produce a prominent flux about spray axis, ensued from an axial acceleration. A similar flow pattern has been reported in simulations of wind induced by corona discharges (Zhao and Adamiak, 2005). In addition, the induced gas flow produces a reduction in the plume width, which is also reflected in the radial distribution of number density shown in Figure 2. This effect is due to a reduction of the (Lagrangian) time available to the cloud for expanding under the action of electrostatic repulsion forces between the droplets. Figure 2 also shows that inclusion of induced air flow in the simulations leads to more accurate agreement with the experimental number density profiles.

Acknowledgements

Ministerio de Educación y Ciencia (Spain), projects CTQ2008-05758/PPQ and DPI2012-35687. Generalitat de Catalunya, ref. 2009SGR-01529. A.K.A. acknowledges a Universitat Rovira i Virgili scholarship.

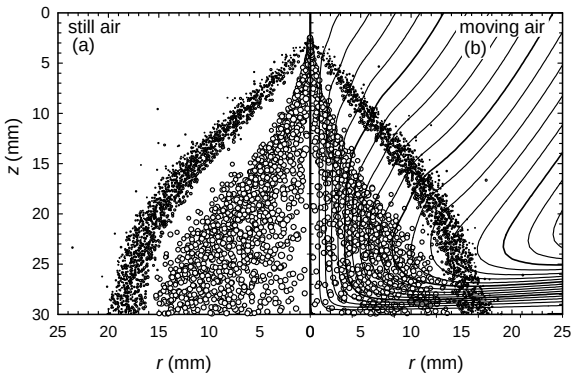

Figure 1. Snapshots of simulated spray considering still ambient gas, and induced gas flow

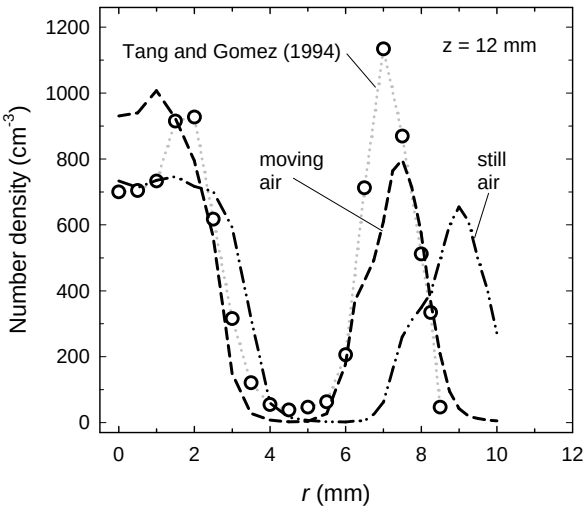

Figure 2. Radial distribution of droplet number density in comparison with experimental data

References

Apte, S.V., Mahesh, K., and Lundgren, T. (2008) *Int. J. Multiphase Flow* **34**, 260-271.

Grifoll, J. and Rosell-Llompart, J. (2012) *J. Aer. Sci.* **47**, 78-93.

Tang, K. and Gomez, A. (1994) *Phys. Fluids* **6(7)**, 2317-2332.

Zhao, L. and Adamiak, K. (2005) *J. Electrostat.* **63**, 337-350.

Reduction of fine particle emissions from small scale wood chips combustion boiler by use of compact electrostatic precipitator

A.Bologa[1], M. Ecker[2], H.-P. Rheinheimer[3], K.Woletz[1] and H.-R.Paur[1]

[1]Karlsruhe Institute of Technology, D-76344 Eggenstein - Leopoldshafen, Germany
[2]HDG-Bavaria GmbH; D- 84323 Massing, Germany
[3]CCA-Carola Clean Air GmbH, D-76344 Eggenstein – Leopoldshafen, Germany
Keywords: biomass combustion, fine particles, emission control, electrostatic precipitator.
Presenting author email: andrei.bologa@kit.edu

Wood combustion in small scale combustion facilities is responsible for emissions of fine particles which are associated with various diseases. The chemical composition of generated particles, their size distribution, number and mass concentration strongly depends on combustion conditions, fuel quality and varies from the design of the combustion device. Fine particles emissions are strongly associated with increased mortality and cardiovascular diseases, so there is an increasing need for reduction of particle emissions into the atmosphere.

The purpose of the current work is the study of the reduction of fine particle emissions from the small scale wood chips combustion boiler by use of the novel form space charge electrostatic precipitator. The long-term experimental studies (over 1000 h) were carried in the Karlsruhe Institute of Technology. The test facility consisted of a 100 kW wood chips boiler (Fa. HDG Bavaria). For control of fine particles emissions from the exhaust gases a novel form CAROLA© space charge electrostatic precipitators (ESP) were applied. The ESPs are designed by the CCA – Carola Clean Air GmbH.

The exhaust gas from the boiler was delivered into the ESPs. During the tests the gas flow velocity and temperature, exhaust gas composition and particle mass concentration (measured by the corresponding equipment from Fa. Wöhler) and particle number concentration (measured by the Scanning Mobility particle Analyser (SMPS), Fa. TSI) were controlled. Among this were measured current-voltage characteristics of the electrostatic precipitators for different operation conditions, power consumption for corona discharge and total power consumption of the ESP, including the cleaning of the ionizer and collector stages. By the long-term measurements were also defined particle mass and fractional collection efficiencies of the ESPs and the stability of operation was observed.

The compact pilot electrostatic precipitator (fig.1) consists on grounded housing with high voltage ionizer and two grounded brush-electrode collectors. Particles are charged in the DC negative polarity corona discharge and further charged particles are precipitated in the brush-electrodes under the influence of space charged effects. At the test facility the precipitators are operated at gas temperatures up to 200 °C and gas flow rate up to 150 m³/h. The maximum value of applied voltage is 20 kV with operation corona current round 1 mA depending on particle number concentration and exhaust gas composition. The size of the precipitator (LxWxH) is 750x360x920 mm.

The use of new approaches to the design of the high voltage insulator and the system for isolator protection, effective cleaning of the ionizer and collector stages ensures stable operation of the ESP by different combustion conditions.

Figure 1. CAROLA electrostatic precipitator

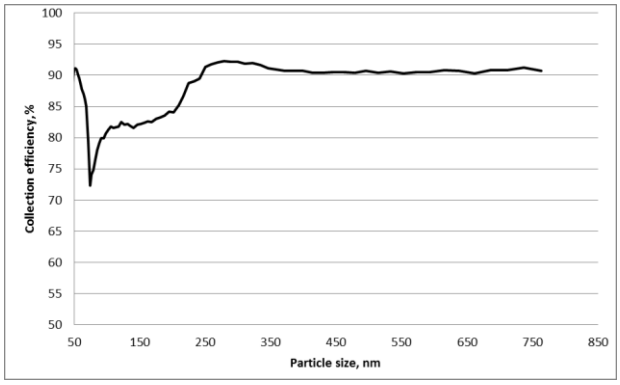

Figure 2 Fractional collection efficiency of the pilot electrostatic precipitator

The long-term observation of the simultaneous operation of the wood combustion boiler and the ESP has shown that the precipitator does not disturb the operation of the boiler.

The use of novel ESP's decreases particle mass and number concentration. The mass collection efficiency of the electrostatic precipitators is in-between 70% to 90% depending on combustion conditions.

The fractional collection efficiency for particles with size 100-250 nm is in-between 80% and 90%, increasing >90% for particles larger than 250 nm (fig.2).

The formation of solid charged aerosol particles at the destruction of metal bodies and bodies of other materials

A.B. Vatazhin, D.A. Golentsov, V.A. Likhter

Central Institute of Aviation Motors (CIAM), Moscow, 11116, Russia
Keywords: body electrization, charged aerosols.
vatazhin@ciam.ru

Now in CIAM the important electric effect is under investigation. The effect consists in formation of an electric charge on solid particles, formed at the destruction of bodies (the elements of technical devices) of various materials (metals, dielectric and composites).

Registration of such charged particles, which are carried out from the device with gasdynamic flow, provides the possibilities of electrostatic diagnostics of the beginning and development of process of a body destruction. The efficiency of such diagnostics directly depends on the knowledge of a sign of the charge of particles arising at destruction. It demands carrying out of special experimental and theoretical researches.

A number of experimental researches on electrostatic diagnostics on laboratory installations and on aviation engines was carried out. The laboratory installation included the equipment for tearing of bodies on which the destruction of cores or plates was carried out. The tearing place was blown by an air stream. In tearing the particles (solid aerosol fragments) arose which were taken down by the stream. The specially located antenna registered an electric signal from these particles. Their size of the particles was estimated on registration of integrated characteristics of light scattered by the formed particles under small angles and was considered to be about 50-100 microns.

In the researches the fundamental result earlier received by us was confirmed. The particles formed at the destruction of metal bodies are positively charged. Their total charge was appeared to proportional to the tensile strength of the material and to a square of the characteristic size of a body (e.g. the plate thickness, Vatazhin et al, 2003, Golentsov et al, 2012). The new results by definition of the sign of the charge of the particles formed in tearing of "non-standard" metal samples were obtained (the plates with holes, the bodies with the cavities filled with other particles). The interesting effect was found out: the particles arising at destruction of the body and the particles before being in the cavity in it are charged opposite.

The research of the formation of the charged ice particles was carried out in being covered with ice of elements of aviation engines. At work of the modelling turbine on not operational mode there was a temperature drop of the gas stream. It led to covering with ice of the turbine elements. At turbine operation, the ice particles broke from the turbine elements and were taken out from the turbine by the air stream. On an exit of the turbine the special antenna was fixed that registered the flight of the charged ice particles by it. On fig. 1 the registered signal is shown. Each peak represents the flight of the charged ice group. The analysis of signals was shown

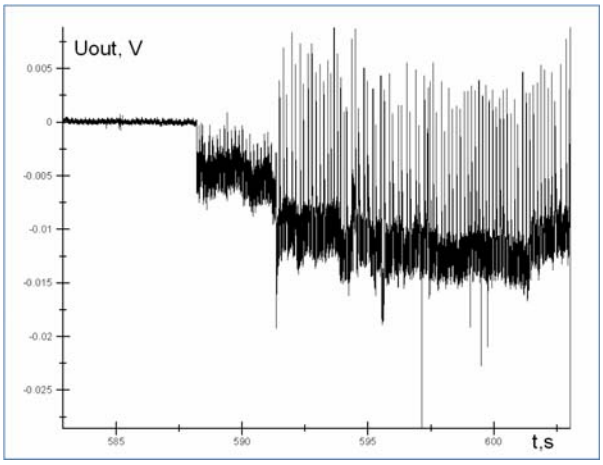

Figure 1. The electrostatic antenna signal in frosting-up of the modelling turbine elements

that, unlike the particles arising at destruction of metal bodies, the charge of ice particles is negative. So it allows to assume that dielectric particles are charged negatively, unlike the metal ones. It proves to be true also in modelling experiments on tearing of dielectric samples of plastic.

The conclusion. On the basis of the researches of the formation of the solid aerosol particles in destructing of bodies of various materials, the method of electrostatic diagnostics of abnormal conditions of engine and power devices with air flow channel is improved. The examples of successful detection of abnormal operation state of aviation engines were shown.

This work was supported by the Russian Foundation for Basic Research (project No. 11-01-00349-a).

Vatazhin A.B. *et al.* (2003) *Fluid Dynamics*. **38**, 1, 69-77.

Golentsov D.A. *et al*. (2012) *Measurements world.* **5**, 52-58.

Generation of negative ion mobility standards using tetra-alkyl ammonium halide salts

G. Steiner[1,2], J. Kangasluoma[1], M. Breitenlechner[2], E. Canaval[2], M. Sipilä[1], A. Hansel[2], M. Kulmala[1]

[1] Department of Physics, Division of Atmospheric Sciences, University of Helsinki, P.O. Box 64, 00014, Finland
[2] Institute of Ion Physics and Applied Physics, University of Innsbruck, 6020 Innsbruck, Austria
Keywords: Ion clusters, Ion mobility, DMA, electrospray
Presenting author email: gerhard.steiner@helsinki.fi

Tetra alkyl halide salts, dissolved in high grade alcohols as reviewed by Ude & Fernández de la Mora (2005) have proven to be very good candidates for the generation of positively charged, well defined molecular clusters. Definitely, it can be said, that the possibility of the generation of ion mobility standards has opened the doors for new ways of generating test/model aerosols for laboratory experiments and for instrument calibration.
In positive mode, the mobility distribution of tetra-alkyl ammonium halide salts yields a unique pattern of peaks, associated with stable cluster species of the form $A^+(AB)_n$, where "A" denotes the tetra-alkyl ammonium ion (monomer) and "AB" the neutral tetra-alkyl ammonium halide molecule.

In this work, tetra alkyl ammonium halide salts are used to generate the negatively charged counterpart-clusters of the positive mobility standards. Accordingly, the cluster can be described in the form $A^-(AB)_n$, where "A" denotes the negatively charged halide ion, and "AB" again the neutral tetra-alkyl ammonium halide molecule, as observed by Kangasluoma et al. (2013).

The negatively charged clusters are produced by means of an electrospray generator (ES). The version used in this study is a slightly modified version of the design presented by Rosell-Llompart and Fernández de la Mora (1994). The redesign features an improved observation of the interior of the electrospray chamber with an inbuilt LED light source and an optical system with a high resolution microscope camera (3 mega pixel). The mobility analysis of the ion clusters was performed with a newly developed high resolution mobility analyzer (UDMA; Steiner et al. 2010), running in a closed-loop configuration to avoid unwanted contaminations.

For the preliminary experiments, four different tetra-alkyl halide salts where used:

- tetra-ethyl ammonium chloride (TEACl)
- tetra-butyl ammonium iodide (TBAI)
- tetra-pentyl ammonium iodide (TPAI)
- tetra-heptyl ammonium bromide (THABr)

For TBAI, TPAI and THABr, spectroscopy grade methanol was chosen as solvent liquid, TEACl was dissolved in spectroscopy grade acetonitrile. For every substance, a base-solution of 1mMol/L was made. If necessary, the base solution was further diluted to increase the signal intensity of the clusters. Carrier gases where purified compressed air or synthetic air from a gas cylinder.

The results displayed in Figure 1 show sharp peaks for every substance, associated to the dimer and trimer clusters of the negatively charged tetra-alkyl halides. Since the ES is operated at relatively high voltages between 3 to 4kV, ions originating from a corona discharge on the tip of the capillary are observed. Therefore, unfortunately no mobility/size peak of the monomer clusters (the negative halide ion) can be separated.

For future experiments, it is planned to setup the high resolution UDMA in series to a mass spectrometer, for a mass-to-charge analysis and chemical identification of the generated molecular ion clusters.

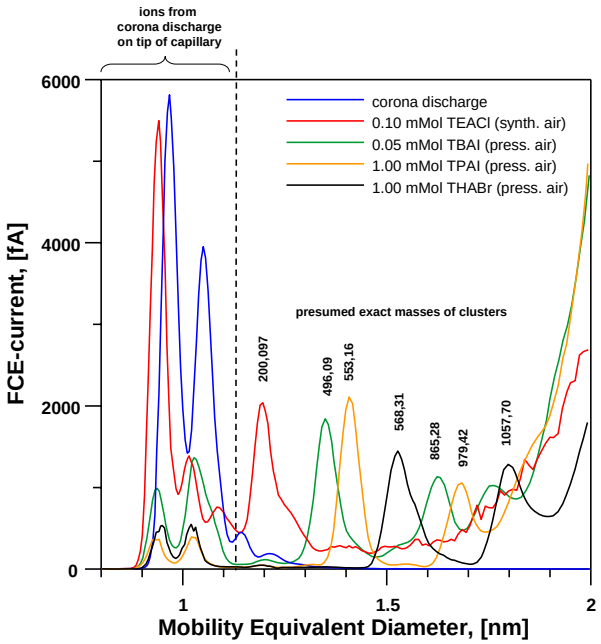

Figure 1: Size spectra of various the tetra-alkyl ammonium halide salts in negative electrospray mode.

Ude S. and Ferández de la Mora J. (2005). *Journal of Aerosol Science, 36, 1224-1237*

Kangasluoma, J., Junninen, Lehtipalo K., Mikkilä, J., Vanhanen J., Attoui, M., Sipilä M., Worsnop, D., Kulmala, M. & Petäjä, T. (2013) *Aerosol Science and Technology, DOI: 10.1080/02786826.2013.773393*

Rosell-Llompart J. and Fernández de la Mora, J (1994). *Journal of Aerosol Science, 25, 6, 1093-1119*

Steiner G., Attoui M., Wimmer D. and Reischl, G.P. (2010). *Aerosol Science and Technology, 44: 4, 308 – 315*

A New Effective Unipolar Charger for Calibration and Validation of Commercial Particle Number Measurement Systems

B. Grob[1], R. Niessner[1]

[1]Chair for Analytical Chemistry, Technical University of Munich, Munich, 81377, Germany
Keywords: particle charging, particle counting, CPC calibration
Presenting author email: benedikt.grob@mytum.de

The cancer-causing effects as well the influence on the climate is a well known problem of diesel soot particles. Therefore the European Union forces the car manufacturers with the current and upcoming emission standards Euro 5b and 6 to limit the emitted particle number of the diesel engines.

So far the industry is using a complex sample preconditioning system for removing the volatile particles and to dilute the aerosol. The non-volatile particles are counted afterwords by a Condensation Particle Counter. The hole system has to be calibrated by the manufacturers as well be validated during the operation due to altering effects. Therefore a system is necessary, which produces a highly reproducible aerosol and a suitable counter as a reference. The regulations dictates that the CPCs have to have their cut-off at 23 nm and a counting efficiency of 90 % at an electrical mobility diameter of 41 nm.

To validate such a particle counting system a spark discharge soot generator can be used together with a differential mobility analyzer and an electrometer as reference counter. To provide a sufficient high number of charged particles as well as to avoid of the commonly used Krypton-85 bipolar charger, due to security issues, an efficient, cheap and stable charger is needed. For this reason we developed a new unipolar charger based on the indirect photoelectric diffusion charging of aerosol particles published by Bucholski and Niessner (1991).

The charger consists of an elliptically grooved, electrically grounded alumina block. In one focus of the ellipse an UV lamp ($\lambda = 254$ nm) is fixed to focus the photons on the surface of a non-porous, non-graphitized carbon rod in the second focus. The rod is covered by a quartz glass tube, where the aerosol gets sucked through. Inside of the tube a grounded metal grid is fixed to apply a weak electrical field. Due to the photoelectrical effect electrons get emitted from the surface of the rod and create ions by attachment processes with the oxygen molecules in the mixing air. Due to diffusion the electrons can collide with the aerosol particles and charge them in the usual way.

This method seems to be very stable over a long time period and shows no performance loss because of the totally chemical inert surface of the rod. Beside this fact the charging efficiency shows up to be sufficient high for a practical use. Together with a spark discharge generator, DMA and an electrometer a reproducable calibration and validation system for commercial particle number measurement systems can be provided.

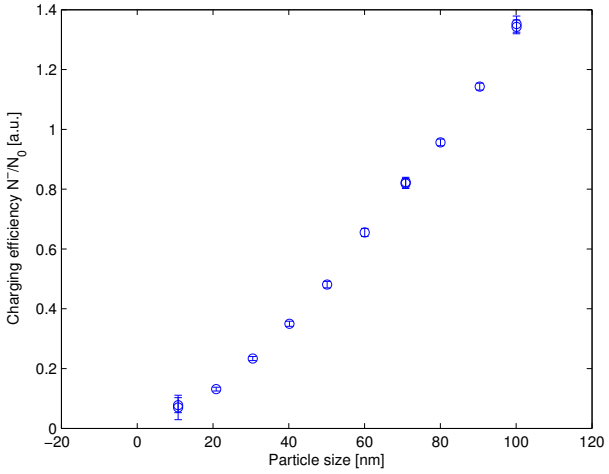

Figure 1: The size dependency of the charging efficiency of the indirect photoelectric diffusion charger for a spark discharge aerosol (GFG 1000, Palas, Germany).

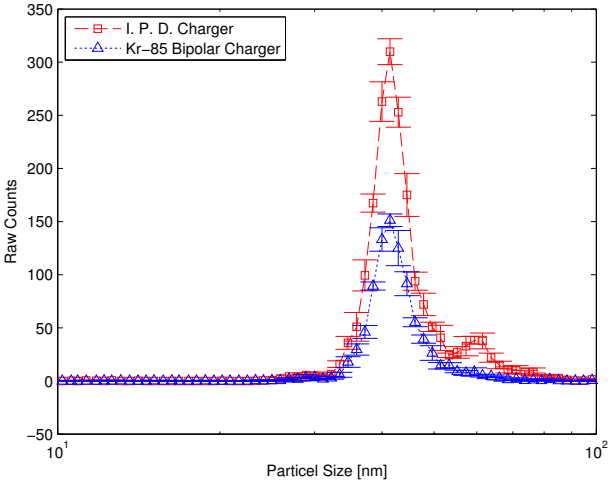

Figure 2: A comparison between the indirect photoelectric diffusion charger and a new Kr-85 bipolar charger (350 MBq) for a 41 nm spark discharge aerosol measured by a SMPS.

Bucholski, A., Niessner, R. (1991) *Journal of Aerosol Science* **22**, 111–115.

The Unipolar Charging Rate and Bipolar Charge Distribution for Nonspherical Particles

Ranganathan Gopalakrishnan[1] & Christopher J. Hogan Jr.[1]

[1]Department of Mechanical Engineering, University of Minnesota, Minneapolis, Minnesota, 55455, USA
Keywords: Diffusion Charging, Aggregates & Agglomerates, Nonspherical particles
Presenting author email: hogan@me.umn.edu

The charging of particles via collisions with ions (diffusion charging) is an integral step in many nanoparticle characterization systems and control technologies. Considerable prior effort has hence been devoted to the determination the diffusion charging rate, i.e. the rate at which ions collide with and transfer charge to particles. With knowledge of this rate, both the increase in net charge on particles in unipolar ion environments, and the steady-state charge distribution on particles in bipolar ion environments can be determined. However, prior analyses are limited to spherical particles; for non-spherical particles, the diffusion charging rate and steady-state charge distributions remain unknown, leaving ambiguities in all electrostatic based analyses of non-spherical particles. Motived by this issue, we have utilized a combination of Brownian dynamics and molecular dynamics simulations to examine (1) the collision rate between particles of arbitrary shape and ions, and (2) the steady state charge distribution on arbitrary shaped particles in the presence of realistic ion populations (with mass and diffusion coefficient distributions determined by tandem differential mobility analysis-mass spectrometry). Results for both of these simulations are provided in this presentation.

In unipolar charging, the collision kernel, which defines the collision rate between particles and ions of known number concentrations, is parameterized by the dimensionless collision kernel H for all shapes, and depends upon the diffusive Knudsen number, Kn_D, the ratio of the ion mean persistence path to a well-defined particle length scale. This particle length scale is a combination of the orientation averaged projected area PA and the Smoluchowski radius R_s of the particle. In the continuum ($Kn_D \rightarrow 0$) and free molecular ($Kn_D \rightarrow \infty$) regimes, the dimensional collision kernel collapses to a particle geometry independent function, expressed in terms of Ψ_E and Ψ_I, the potential energy to thermal energy ratios for the Coulomb and image potentials, respectively. Dimensionlessly, these functions lead to $H = 4\pi Kn_D^2$ as $Kn_D \rightarrow 0$ and $H = (8\pi)^{1/2} Kn_D$ as $Kn_D \rightarrow \infty$. In the transition regime (finite Kn_D), as shown in Figure 1 the dimensionless collision kernel is shown to be geometry independent for conducting particles, depending only on a suitably defined Kn_D.

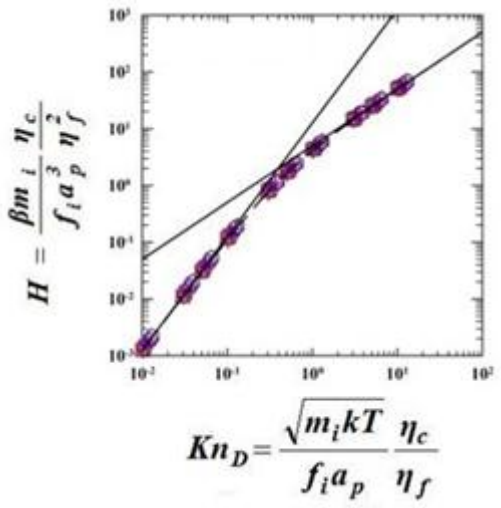

Figure 1. The dimensionless collision kernel, H, as a function of the diffusive Knudsen number, Kn_D, determined from Brownian dynamics calculations of particle charging by unipolar ions. Plotted points represent results for particles of varying geometry and varying number of charges, yet all collapse to a single dimensionless curve. The solid lines shown represent the $Kn_D \rightarrow 0$ and $Kn_D \rightarrow \infty$ limiting expressions.

To study bipolar charging, a Brownian dynamics method is also employed, but which circumvents ion-particle collision rate calculation while still enabling determination of the steady state charge distribution on non-spherical aerosol particles. BD calculations are performed using both monodisperse and measured polydisperse ion properties under atmospheric pressure, room temperature conditions. In the examination of non-spherical particles (aggregates, linear chains and cylinders), two models are employed: (1). accumulated charge distributes itself along particle surfaces, and (2). accumulated charge is immobile. Independent of model, it is found that particles having a Projected Area (PA) to diffusion based surface area (πR_s^2) ratio close to unity have similar bipolar charge distributions to spheres sphere of the same mobility diameter. However, model specific behavior is observed for highly non-spherical particles ($PA/\pi R_s^2 < 0.5$). With distributed charge, highly non-spherical particles acquire more charges than an equivalent mobility sphere in the sub 100 nm range, yet acquire less charge than spheres in the submicrometer range. Conversely with immobile charges, non-spherical particles are found to be more charged than equivalent mobility diameter spheres in both the nano- and submicrometer size ranges.

Bipolar diffusion charging of aerosol nanoparticles by means of AC-corona discharge and soft X-ray devices

P. Kallinger[1] and W.W. Szymanski[1]

[1]Faculty of Physics, University of Vienna, Boltzmanngasse 5, Vienna, 1090, Austria
Keywords: bipolar charging, soft X-ray, AC corona discharge, nanoparticles
Presenting author email: peter.kallinger@univie.ac.at

An essential requirement for most handling and measuring techniques of aerosol nanoparticles is their predictable charge condition. Until recently radioactive sources (α- or β-ray emitters) were used for this purpose. Due to safety issues and increasingly strict regulations for the usage of radioactive materials there is a need for a suitable substitute.

Here we study the charging probability of aerosol nanoparticles using two different bipolar, non-radioactive charging devices – the AC corona discharge based "Electrical Ionizer" (Model 1090, MSP Inc.) and the soft X-ray based "Advanced Aerosol Neutralizer" (Model 3087, TSI Inc.). The measurements were performed with a tandem DMA arrangement as shown in Fig. 1. Monodisperse unipolar mainly singly charged sucrose particles were produced in the size range of 5 – 40 nm using an electrospray aerosol generator with a subsequent classifier DMA operating at a constant voltage. These aerosol particles were then routed through the particular charger in question into the analyzer DMA-CPC system by which the electrical mobility distribution of the particles exiting the investigated charger was measured. Both DMAs were operating at the same polarity. Additionally, a second CPC was placed in front of the investigated charger to observe possible particle concentration fluctuations and to consider it during data evaluation. The aerosol flow rate through a charger could be changed by adding particle free air to the aerosol after the classifier DMA and was varied in the range between 0.6 and 5.0 liters per minute.

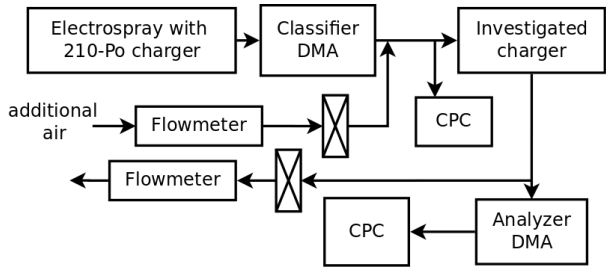

Figure 1. Schematics of the experimental setup.

With the investigated charger turned off no ions were produced and the charge condition of particles remained unchanged. In this case the distribution of charged particles entering the analyzer DMA was the same as the distribution of the particles leaving the classifier DMA (in an ideal case all particles were singly charged) resulting in the measurement of the total particle fraction by the analyzer DMA. Alternatively, when the charger was turned on the aerosol particles were expected to reach a charge equilibrium (Fuchs, 1963, Wiedensohler, 1988) in the charger and consequently only the charged fraction was measured by the analyzer DMA. These data was used to calculate the charging probability (N_charged/N_total) shown in Fig. 2. First results show a good agreement with the predicted charge distribution, with a deviation for the Electrical Ionizer below 10 nm in diameter. However, it has to be stated that the indicated limit for operation of this charger is at a diameter of 10 nm. Further measurements with different nanoparticles are in progress.

Moreover, for both of the investigated chargers also the long-term performance was studied operating the chargers for > 36 h and continuously scanning the charged particle distribution with the analyzer DMA. Results of investigations in progress will be reported.

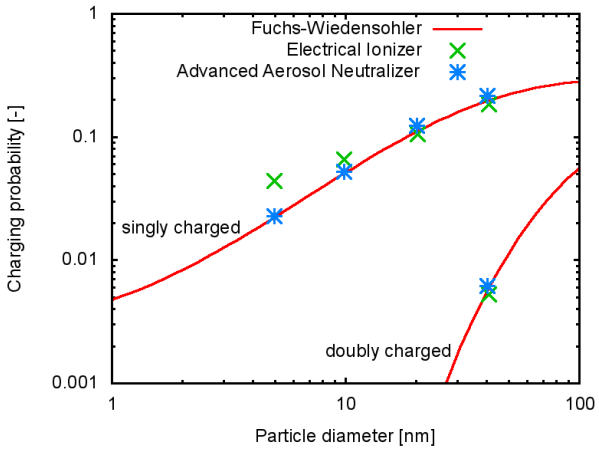

Figure 2. Comparison of the measured charging probability of negatively charged sucrose particles at a flow rate of 1.5 lpm with the Wiedensohler approximation to the model by Fuchs (1963). (Note that the lower size limit for the "Electrical Ionizer" given by the manufacturer is 10 nm).

This work was supported by the Austrian Science Foundation (FWF), Project Nr. TRP29.

Fuchs, N.A. (1963) *Geofis. Pura Appl.* **56**, 185-193.
Wiedensohler, A. (1988) *J. Aerosol Sci.* **19**, 387-389.

Diurnal variation of small and large ion concentrations in an urban location

E.R. Jayaratne, X. Ling and L. Morawska

International Laboratory for Air Quality and Health. Institute of Health and Biomedical Innovation.
Queensland University of Technology. Brisbane 4000. Australia.
Keywords: ions, particles, attachment, charged aerosols
Presenting author email: r.jayaratne@qut.edu.au

A Neutral cluster and Air Ion Spectrometer (NAIS) was used to monitor the concentration of airborne ions on 258 full days between Nov 2011 and Dec 2012 in Brisbane, Australia. The air was sampled from outside a window on the sixth floor of a building close to the city centre, approximately 100 m away from a busy freeway. The NAIS detects all ions and charged particles smaller than 42 nm. It was operated in a 4 min measurement cycle, with ion data recorded at 10 s intervals over 2 min during each cycle. The data were analysed to derive the diurnal variation of small, large and total ion concentrations in the environment. We adapt the definition of Horrak et al (2000) and classify small ions as molecular clusters smaller than 1.6 nm and large ions as charged particles larger than this size.

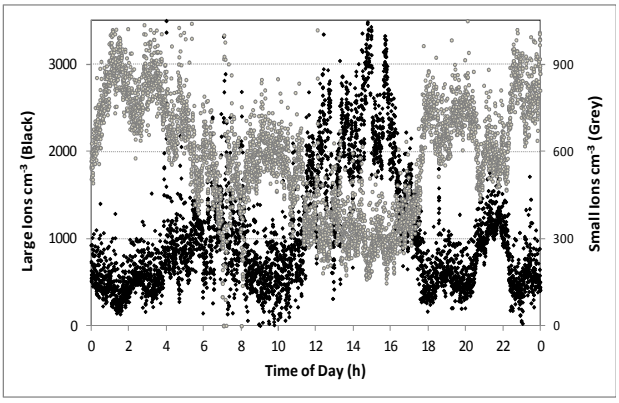

Figure 1: Diurnal variation of large and small ion concentrations on 3 February 2012 in Brisbane.

Fig 1 shows the large and small ion concentrations on a typical day. The large ion concentration generally peaked during the middle of the day, especially when there was secondary particle formation due to nucleation of organic precursors from motor vehicle emissions. On this day, a condensation particle counter showed a particle number concentration (PNC) of about 2 x 10^4 cm^{-3} between 12h and 14h. It is well known that small ions rapidly attach to particles in the air. There is an apparent negative correlation between the large and small ion concentrations in Fig 1. The maximum small ion and minimum large ion concentrations generally occurred between midnight and 4 am when the air was relatively clean (PNC of about $3x10^3$ cm^{-3}), while the maximum large ion and minimum small ion concentrations were observed soon after mid day when the PNC was a maximum (1-$3x10^4$ cm^{-3}).

Fig 2 shows the mean hourly total ion concentrations over the entire measurement period. The error bars show the corresponding standard deviations. The total ion concentration was fairly constant between $1x10^3$ and $2x10^3$ cm^{-3} right through the night and showed maximum concentrations of between $3x10^3$ and $4x10^3$ cm^{-3} shortly after mid day.

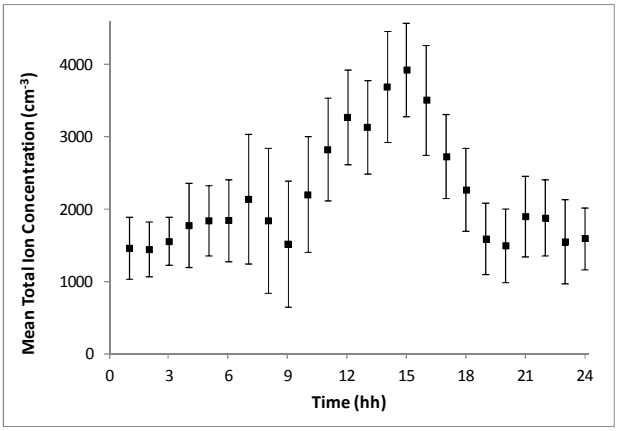

Figure 2: Mean hourly values of the total ion concentration with standard deviations.

The health effects of ions and charged particles are still largely unknown. Some studies have shown that, during inhalation, charged particles are more likely to be deposited in the human lungs than similarly sized uncharged particles (Cohen et al, 1998). While there have been several reports of small ion concentrations in urban environments (Retalis et al, 2009, Ling et al, 2010), there have not been many similar studies dealing with large ions and charged particles (Hirssiko et al, 2007, 2011). We believe that this is the first study of charged particles in an urban environment in the Southern Hemisphere.

Cohen, B.S., Xiong, J.Q., Fang, C., Li, W. (1998) *Health Physics*. 74, 554-560.
Hirsikko, A., Juuti, T.Y, et al (2007) *Boreal Environ Res.* 12, 295-310.
Hirsikko, A., Nieminen, T., et al. (2011) *Atmos Chem Phys.*, 11, 267-798.
Horrak, U., Salm, J., Tammet, H. (2000) *J Geophys Res.* 105(D7), 9291-9302.
Ling, X., Jayaratne, E.R., Morawska, L. (2010) *Atmos Environ*. 44, 2186-2193.
Retalis, A., Nastos, P., Retalis, D. (2009) *Atmos Res*. 91, 219-228.

Thursday, September 5, 2013

Session: Fundamentals
Nucleation theory and experiments

Nucleation in the Presence of Background Aerosol

Charles Clement

15 Witan Way, Wantage, Oxon OX12 9EU, U.K.
Keywords: condensation, nucleation, aerosol formation
Presenting author email: charles.clement@btinternet.com

When condensable molecules are being produced, either by chemical reactions or cooling, it is important to know whether they will all condense on existing aerosol or form a new aerosol by nucleation. For example, ultrafine particles in the workplace can be highly injurious to health. The suppression of nucleation by existing aerosol is well known in the atmosphere, and is well illustrated by an analysis of a complete set of Finnish forest nucleation data observed in 1996 and 1997 (Clement *et al* 2001). Here we point out physical situations and processes where this suppression does not necessarily occur

In a homogeneous atmosphere where condensable molecules are being produced by chemical reactions, the level of supersaturation reached is always limited by condensation on, and coagulation of tiny nuclei with, existing aerosol. As the level is inversely proportional to the removal rate onto existing aerosol, suppression of nucleation is guaranteed for large amounts of existing aerosol. In situations where supersaturation is produced by cooling a vapour-gas mixture, particularly those involving mixing with another mixture, motion of vapour and aerosol takes place. Differences in their motion can lead to large local differences in amount of aerosol present and consequent supersaturation. It was previously pointed out (Clement and Mather 2005), that the observed presence of a small-sized sulphuric acid aerosol in a volcanic plume initially containing a large amount of large-sized aerosol could be attributed to this effect. The acid vapour diffuses into the surrounding air at a much greater rate than large aerosol particles so that nucleation is possible.

Very similar situations must have arisen in the many experiments performed by Buckle and collaborators (see Buckle and Marwella (1987) and references therein) who evaporated heated metals into gas flows to produce aerosols. The geometry is shown in Fig.1 where the metallic vapour diffuses into a laminar gas flow (Mg and Pb into argon in Buckle and Mawella (1987)). Observed size distributions of aerosol are often very wide and sometimes have two peaks, interpreted as arising from nucleation of both liquid droplets and solid particles. The continuing nucleation after the initial aerosol is formed will arise because the aerosol is carried upwards with the flow whereas the vapour continues to diffuse horizontally into virgin gas.

The experiments cannot be interpreted by the theory given in Buckle (1986) because of its essentially one-dimensional nature. All the mass current including both vapour and aerosol is moving in the same direction so that the aerosol will inhibit new nucleation. Instead, continuing nucleation uninhibited by aerosol already produced will give rise to a very wide size distribution which may, if the freezing point temperature is crossed be concentrated into two peaks for liquid and solid nuclei. Detailed analysis of the experimental results of Buckle requires two-dimensional calculations of heat and mass transfer.

The cooling of vapour-gas mixtures by turbulent mixing or in turbulent flows at cooled walls is another area where even considerable amounts of aerosol may not prevent nucleation. The basic reason is that rapid flows can produce large temperature differences across small distances, for example across a boundary layer at a wall. The consequent large temperature gradient can produce a large supersaturation in a small layer of width δ. A criterion (Clement 1987) for the amount of aerosol needed to prevent this is

$$[\, 4\pi N \langle R \rangle \,]^{1/2} \delta >> 1,$$

where N is the aerosol number concentration with mean radius $\langle R \rangle$.

The consequence of this criterion is that the onset of turbulence in flow through cooling tubes increases the likelihood of nucleation occurring. In general higher levels of turbulence will lead to smaller boundary layer distances and more nucleation.

Where many vapours are present, the lack of nucleation suppression can lead to a variety of aerosols being formed, and a nuclear example is discussed.

Buckle, E.R. and Mawella, K.J.A. (1987) *J. Aerosol Science*, 18, 139-146.

Buckle, E.R. (1986) *Proc.Roy.Soc.London* A406 227-261.

Clement, C.F. (1987) AERE TP1223.

Clement, C. F., Pirjola, L., dal Maso, M., Makela, J.M. and Kulmala, M. (2001) *J. Aerosol Science*, 32, 217-236.

Clement, C.F. and Mather, T.A. (2005) Abstracts of the European Aerosol Conference ed. W. Maenhaut p178

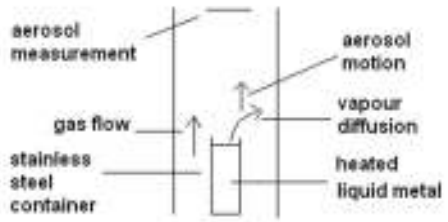

Fig. 1. Buckle apparatus for aerosol production.

Numerical Investigation of the Effect of Hydrodynamic Mixing on Droplet Nucleation and Growth

A. O. Alshaarawi, G. Scribano, K. Zhou, A. Attili, F. Bisetti

Clean Combustion Research Center, King Abdullah University of Science and Technology, Thuwal, 23955-6900, Kingdom of Saudi Arabia

Keywords: Quadrature Method of Moments, CFD, aerosol transport, mixing

Presenting author email: amjad.shaarawi@kaust.edu.sa

Aerosol flows are relevant in several applications of practical importance. These include soot formation in flames, material synthesis in flow reactors, crystallization and precipitation in the chemical and pharmaceutical industries, spray combustion and various environmental applications.

The understanding of aerosol systems in spatially homogeneous configurations has reached a mature stage, but in practice, aerosol processes and particles formation take place in highly inhomogeneous turbulent flows. By nature of turbulence, the flow is characterized by a wide range of length and time scales in the momentum, temperature, and concentration fields. Aerosol processes, such as nucleation, droplet growth by condensation (heterogeneous nucleation) and coagulation, are strongly non-linear and depend on the local vapor concentration and temperature. Moreover, aerosol processes depend on residence times and history effects. Thus, the study of aerosol flows is challenging and very little previous work exists on this topic.

In the current study, the dynamics of the nucleation and growth of di-butyl-phthalate (DBP) droplets are simulated in a counterflow configuration, i.e. a laboratory laminar stagnation flow. This experiment is chosen in order to introduce a tractable hydrodynamic residence time interacting with the time scales of aerosol processes. A counterflow flow setup consists of two opposed nozzles blowing streams towards each other. One stream is cold nitrogen and the other is hot nitrogen saturated with DBP vapor (saturation ratio $S = 1$). Near the stagnation plane (where cooling by mixing takes place), nano-size droplets of DBP nucleate and grow due to heterogeneous nucleation.

The flow field is simulated using a stream-function formulation. The GDE of the particle size distribution (PSD) is integrated to obtain transport equations for moments. The Quadrature Method of Moments (QMOM) is used for closure. Moments are transported using a second-order upwind scheme in space and an adaptive variable-order scheme in time. Homogeneous nucleation is described by classical Becker-Döring theory and heterogeneous nucleation is modelled using the generalized Mason's formula.

A wide range of hydrodynamic residence times is investigated (residence time is defined as the the ratio of the distance separating the two nozzles to the inlet velocity L/u_0). Two regimes are identified as shown in Figure 1. At short residence times, vapor consumption is neglected and increasing the residence time produces more particles (higher average number density). We refere to this regime as the nucleation regime. After a critical residence time is exceeded, vapor consumption becomes important. In this regime (the condensation regime) increasing the residence time consumes more vapor and thus produces less average particle number density.

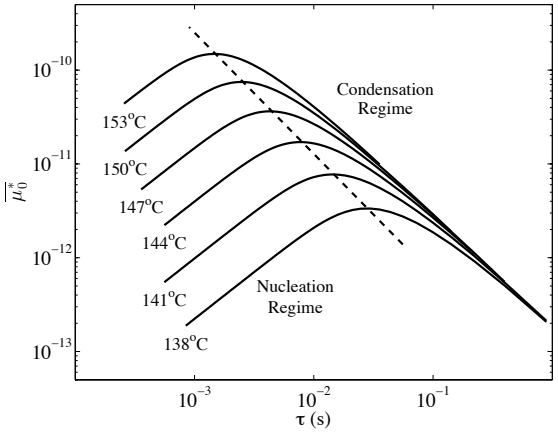

Figure 1: Dimensionless average number density ($\overline{\mu_0^*} = \int \mu_0(x)dx/\mu_r$) vs. the residence time ($\tau = L/u_0$), where $\mu_0(x)$ is the number density and μ_r is maximum possible number density. L is half the separation between the two nozzles and u_0 is the velocity at the inlets. The cold inlet is fixed at 0°C. Curves are labeled with the value of the temperature of the hot stream. The dashed line connects the maximum values, separating the nucleation and the condensation regimes.

In the nucleation regime, the average volume fraction grows at a constant rate with residence time. Once the condensation regime is reached, the average volume fraction reaches a saturation level and the rate at which it increases starts to vanish.

Coagulation was shown to have a negligible effect on the number density distribution in both regimes under the considered conditions.

These conclusions agree with the experimental observations by Okuyama *et al.* (1987).

Okuyama, K., Kousaka, Y., Warren, D., Flagan, R., and Seinfeld, J. (1987) Homogeneous nucleation by continuous mixing of high temperature vapor with room temperature gas. *Aerosol Sci. and Tech.*, 6(1):15-27.

Effect of Surface Energy Evolution on Particle Nucleation under GASP Conditions

D.E. Rosner[1] and M. Arias-Zugasti[2]

[1]Department of Chemical and Environmental Engineering, Yale University, New Haven, CT, 06520–8286, USA
[2]Departmento de Física Matemática y de Fluidos, UNED, Madrid, Apdo 60141, 28080, Spain
Keywords: GASP, particle nucleation rate, surface energy, particle nucleation size.
Presenting author email: maz@dfmf.uned.es

We address here the problem of particle nucleation and growth under so-called: Gas-Anti-Solvent-Precipitation (GASP) conditions. This complex environment is of considerable interest in many current technologies. In the pharmaceutical industry, which motivated the present work, GASP is used to produce the controlled precipitation of an Active Pharmaceutical Ingredient (API) from an organic solvent often sprayed into compressed CO2. Of vital importance is the ability to predict and control the size distribution of the nucleated particles, with the usual goal of producing narrow distributions of ultrafine particles to facilitate rapid dissolution when administered. Our theoretical model is illustrated using the system: phenanthrene [as API-surrogate] precipitated from liquid toluene using CO2 as anti-solvent at ca. 60 bar and 298K) .Our preliminary results demonstrate the need to account for the time evolution of not only the supersaturation (as was already known) but also the surface energy of the particle/fluid interface (usually not considered).

In our well-mixed single droplet theoretical model we consider the time evolution of particle nucleation- and condensation-growth-rates, fully coupled to the evolving environmental conditions associated with CO2 uptake and solution volume change. Particle nucleation rates are conveniently approximated using Classical Nucleation Theory (CNT), and single particle growth rates are based on a kinetic model including Gibbs-Kelvin(-Ostwald) curvature corrections for recently born particles. However, the numerical method used to solve the Population Balance Equation governing the particle number density distribution function (NDDF) is not restricted to any particular choice of rate laws for nucleation or growth, nor does it presume or restrict the mathematical form of the NDDF. Our model identifies the dependence of the characteristic particle size and nucleation/growth time scales of the problem as a function of the control parameters in the isobaric/isothermal GASP environment (mainly pressure level and initial API under-saturation). Besides revealing the relevant dimensionless numbers that govern the performance of such systems, we demonstrate the importance of *surface energy evolution* (SEE) in determining the critical nucleation size, and the associated nucleation rate, in this variable composition "carrier fluid". Our model also reveals the effects of SEE on the finally observed particle NDDF. In this regard, we find that a non-monotonic time evolution of the critical nucleation size can give rise to multi-modal size distribution functions, without the need to involve physical processes other than particle nucleation. Our results also show that, for the system under consideration (phenanthrene precipitated from a micron size toluene solution using CO2 as anti-solvent) typical particle growth times are orders of magnitude longer than the corresponding characteristic nucleation times. Hence, in this case post-nucleation particle growth introduces only a small correction, and the finally observed precipitated particle NDDF basically betrays the integrated time history of the critical nucleus size convoluted with ln(supersaturation). As a corollary, controlling the time evolution of the critical nucleus size (via both effective surface energy and supersaturation) enables NDDF-control, which in some cases can even yield (normally undesirable) multimodal API particle populations.

This work was supported by Industrial Affiliates of the Sol Reaction Engineering (SRE-) Research Group at Yale, Yale ChE graduate alumni and the School of Engineering and Applied Science. MAZ also wishes to acknowledge the support of Ministerio de Ciencia e Innovación (#CSD2010-00011 and #ENE2011-26868) and Comunidad de Madrid (#S2009/ENE-1597) at UNED (Madrid).

Debenedetti, P.G. (1990) *AIChE J.* **36**, 1289-1298.

Dixon, D.J. and Johnston, K.P. (1991) *AIChE J.* **37**, 1441-1449.

Girifalco L.A. and Good R.J. (1957) *Journal of Phys. Chem.* **61**, 904-909.

Martin A. and Cocero, M.J., (2008) "Micronization Processes with Supercritical Fluids: Fundamentals and Mechanisms", *Advanced Drug Delivery Reviews*, **60**, 339-350

A heterogeneous nucleation theory with explicit account of vapor adsorption

A. Laaksonen[1,2]

[1]Finnish Meteorological Institute, Helsinki, Finland
[2]Department of Applied Physics, University of Eastern Finland, Kuopio, Finland
Keywords: Heterogeneous nucleation, Adsorption, Water vapour
Presenting author email: ari.laaksonen@fmi.fi

In the classical picture of heterogeneous nucleation, spherical liquid caps appear on a surface at supersaturated conditions, and if these caps are larger than so called critical size, they grow spontaneously, whereas smaller caps will evaporate. In reality, vapor adsorption takes place already at subsaturated conditions, and depending on the substrate-vapor interactions, the adsorbed layer may consist of clusters centered on so called active sites. The extent of adsorption can be calculated using adsorption isotherms which give the average adsorption layer thickness as a function of vapor saturation ratio, provided that adsorption constants (characterizing the substrate-vapor interactions) are known. Here I propose a new theory that combines adsorption and heterogeneous nucleation so that it can be used to calculate both the adsorption layer thickness at subsaturated conditions, as well as the onset supersaturation for nucleation.

Consider spherical liquid caps with a contact angle Φ forming on a flat surface. The average number of monolayers in the liquid cap is denoted by $\Theta = (V/a)/d_v$, where V and a are the liquid cap volume, and its area of contact with the substrate, respectively, and d_v is the diameter of the vapor molecule (calculated assuming spherical shape). The adsorption is described using the FHH (Frenkel-Halsey-Hill) isotherm given by

$$\ln(S) = \frac{-A'}{\Theta_{av}^{B'}}$$

where S denotes the vapor saturation ratio, Θ_{av} is the average number of monolayers ($\Theta_{av} = \Theta Na/a_{tot}$) with N and a_{tot} the number of liquid caps on the substrate and the total surface area of the substrate, respectively, and A' and B' are adsorption parameters. The FHH equation describes adsorption equilibrium for the whole surface. With a single spherical cap, the curvature of the cap influences the equilibrium, and we can write

$$\ln(S) = \frac{-A}{\Theta^{B}} + \frac{2\sigma v}{kTR}$$

where σ is surface tension, v is volume of the condensed molecule, k is the Boltzmann constant, T is temperature, and R is radius of the spherical liquid cap. The radius can be expressed using the contact angle and the number of monolayers to rewrite the above equation as

$$\ln(S) = \frac{-A}{\Theta^{B}} + \frac{2\sigma v f(\Phi)}{3kTd_v\Theta}$$

where $f(\Phi)$ is a function of the contact angle only. If S is plotted as a function of Θ, it will show a maximum at some value above 1. The maximum denotes the critical supersaturation, at which point the spherical liquid caps will start growing spontaneously due to vapor condensation. In order to find the critical cap layer thickness Θ^* and the critical saturation ratio S^*, the derivative of $\ln(S)$ with respect to Θ is set to zero, giving

$$\Theta^* = \left(\frac{2\sigma v f(\Phi)}{3kTd_v AB}\right)^{1/(1-B)}$$

and

$$S^* = \exp\left(\frac{-A}{\Theta^{*B}}\right)\exp\left(\frac{2\sigma v f(\Phi)}{3kTd_v\Theta^*}\right)$$

Fig. 1 shows a comparison between the present theory and classical heterogeneous nucleation theory for gas-liquid nucleation of water on flat surfaces.

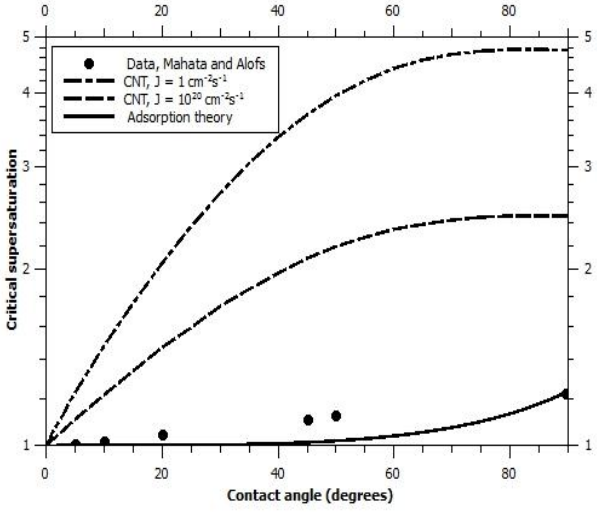

Figure 1. Critical supersaturation as a function of contact angle predicted with the current theory using A =3, B = 2 (solid line) and classical heterogeneous nucleation theory (J = 1 $cm^{-2}s^{-1}$; dashed line; J = 10^{20} $cm^{-2}s^{-1}$, dash-dotted line), and experimental data by Mahata and Alofs (J. Atmos. Sci. 32, 116, 1975) (circles).

Heterogeneous Nucleation on Nanometer and Sub-Nanometer Sized Charged Atomic Clusters

K. Barmpounis[1], A. Maisser[1], M.B. Attoui[2], G. Biskos[1] and A. Schmidt-Ott[1]

[1] Chemical Engineering, Delft University of Technology, Delft, 2628 BL, Netherlands
[2] University Paris Est Creteil, University Paris-Diderot, LISA, UMR CNRS, Paris, France
Keywords: Heterogeneous nucleation, charge effect, atomic clusters
Presenting author email: k.barmpounis@tudelft.nl

Condensation of vapour molecules on nanoparticles and clusters plays a crucial role in a number of industrial and environmental processes.

An important factor affecting vapour condensation on nanoparticles in the nanometer range is their charge (Wilson, 1897, Nadykto *et al*, 2003). The presence of charge creates an electric field in the vicinity of the particles that lowers the free energy barrier required for nucleation. As a result charged clusters can be activated at lower supersaturation levels than the neutral.

Although theory can predict this difference in the nucleation process for charged and neutral particles, it is not yet fully understood why positive particles require higher supersaturation level than negative particles in order to become activated.

Heterogeneous nucleation studies can be performed with the use of a Condensation Particle Counter (CPC). This instrument is commonly used as an aerosol nanoparticle detector, providing concentration measurements. It relies on the condensation of vapour molecules on to the particle surface, by creating a supersaturated environment from which particles pass through. This leads to the formation of a liquid droplet around the particle, large enough to be detected optically.

In this study, we report measurements of the detection efficiency of a commercial ultrafine butanol based CPC (3025, TSI, Inc., St. Paul, MN), in the sub 3 nm singly charged particles range.

The experimental setup for measuring the detection efficiency consisted of a spark discharge generator (SDG), a half-mini DMA (M. Attoui *et al.*, 2013) an aerosol electrometer and the CPC.

The SDG has been used to generate small singly self-charged silver atomic clusters, of 5 atoms or less. The generation and production of these small clusters will be presented in another abstract for the EAC 2013.

The CPC was operated at increased temperature difference between saturator and condenser, in order to improve the detection efficiency for small sub-nanometer particles. The operation of a boosted-CPC can be found in literature (Kuang et al.2011). As shown in Fig.1, the boosted CPC is capable of detecting sub-nanometer sized atomic clusters.

A clear alternating trend is observed, as the cluster size decreases. For clusters of inverse mobility (1/Z) larger than ~ 0.8 Vs/cm^2, presence of negative charge shows higher detection efficiency than positive one. Meanwhile, for clusters of 1/Z< 0.8 Vs/cm^2, the trend is reversed. Moreover, very small positive clusters are activated with the same efficiency, regardless of the decreasing size. This comes in contrast with the classical theory of heterogeneous nucleation, in which nucleation rate should decrease with decreasing particle size.

The ability of negative particles, with sizes larger than ~1 nm, to activate at a lower supersaturation has been observed elsewhere (Winkler *et al.*, 2008). A possible explanation for this phenomenon involves the ion-dipole molecule interaction. Non-symmetrical polar molecules will orientate on the particle surface according to the particle polarity. This leads to a difference in the structure of positive and negative nucleating embryos.

In such small cluster sizes, it is expected that a thermodynamic approach of nucleation will not be sufficient to interpret experimental data. Indeed, a theory involving a quantum description of the cluster dynamics seems to be more accurately approaching the nucleation process, for small sub 3nm atomic clusters (Nadykto *et al*, 2006).

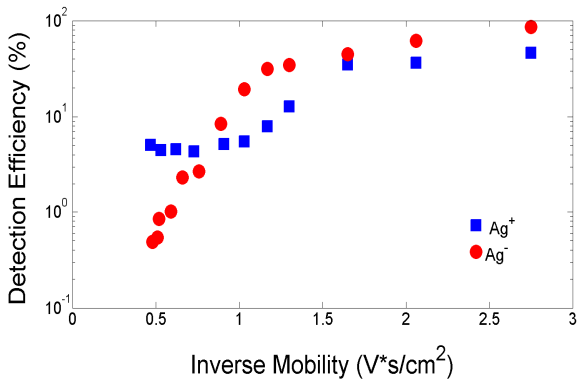

Figure 1. Measured detection efficiency of positive and negative atomic clusters suspended in N_2.

Wilson, C.T.R., (1897), *Phil.Trans.Roy.Soc*, A189,265

Nadykto,A.B, Yu F., (2003), *J.Geophys.Res.*, 108(D23),4717

Attoui, M., Paragano, J. Cuevas, Fernandez de la Mora, J. (2013) *Aerosol Science and Technology*, DOI:10.1080/02786826.2013.764966

C.Kuang, M.Chen, P.H.McMurry, J. Wang, (2012), *Aerosol Science and Technology,*46:309-315

Winkler,P.,M., Steiner, G., Vrtala, A., Vehkamaki, H., Noppel, M., Lehtinen, K.E.J., Reischl, G.P., Wagner, P.E., Kulmala, M. (2008), *Science*, 319, 1374-1377

Nadykto,A.,Natsheh A.,Yu F., Mikkelsen K., Ruuskanen J.,(2006) *Phy.Rev.Let,*96.

Heterogeneous nucleation of sulfur vapor on tungsten oxide and NaCl nanoparticles: Determination of the radius and the contact angle of critical nucleus.

S.V. Valiulin[1], V.V. Karasev[1], S.V. Vosel[1,2], A.A. Onischuk[1,2], A.M. Baklanov[1]

[1]Institute of Chemical Kinetics and Combustion SB RAS, Novosibirsk, 630090, Russia
[2]Novosibirsk State University, Novosibirsk, 630090, Russia
Key words: heterogeneous nucleation, sulfur, critical nucleus, contact angle
Presenting author email: valiulin@kinetics.nsc.ru

The heterogeneous nucleation plays an important role in the atmospheric processes, in the condensation particle counters and can be used to generate composite nanomaterials. Heterogeneous nucleation depends on the surface property of the seed particles. If surface of the seed particle is not perfectly wettable, critical nucleus with radius r and contact angle Θ is formed on the surface of particle.

In this work we describe the method of determination of the radius and the contact angle of the critical nucleus that formed on the surface of the seed nanoparticles during heterogeneous nucleation in the flow chamber. The experimental setup is shown in Fig. 1. It consists of three main parts [1]: the particle generator, the flow nucleation chamber and an Automatic diffusion battery (ADB) coupled with a condensation nucleus counter to measure aerosol size distribution and particle number concentration. Two different types of seed particles (tungsten oxide and NaCl) were used in the experiments. The particles were obtained by evaporation of sample material in the crucible (located in the high-temperature zone) followed by vapor condensation in the flow. Particle size distributions are well described by log-normal law. For tungsten oxide particles: geometric mean diameter d_g = 7.8, geometric standard deviation σ_g = 1.45, for NaCl: d_g = 7.3 nm, σ_g = 1.45.

The flow of argon with seed particles enter in the nucleation chamber where the heterogeneous nucleation takes place. Fig. 2. shows the size distributions of the incoming seed particles (solid line) and the particles at the outlet of chamber (after the heterogeneous nucleation). One can see that size distribution at the output is bimodal. One of these modes (left) is a part of the spectrum of original particles which is smaller than the size required for the start of heterogeneous nucleation. The second mode (right) is formed by particles on which critical nucleus were generated followed by condensation growth. During the experiments we varied the vapor pressure of sulfur at the unchanged size distribution of seed nanoparticles. The axial and radial temperature profiles were measured by a thermocouple. The radial profiles of sulfur vapor concentration and supersaturation were determined by solving the mass transfer equation.

Next, we used the Fletcher`s formula for the rate of heterogeneous nucleation with pre-exponential factor, offered by us. Free parameter in this formula is the contact angle of the critical nucleus on the surface of seed particle. For each experiment, we have found a contact angle that give good agreement with experimental data (part of enlarged particles) As a result, we obtained the dependence between the contact angle of lenticular critical nucleus and the radius of maternal seed particle (Fig. 3, triangles - tungsten oxide particle, rings - NaCl particle). Thus, we have a monotonically increasing dependence between the contact angle of critical nucleus and the size of the maternal seed particle. Qualitatively, this is consistent with the dependence results [2, 3], where the heterogeneous nucleation of n-nonane and n-propanol on the surface of tungsten oxide and silver seed nanoparticles was studied. By using the process of condensation growth in the flow of sulfur vapor, we have prepared samples of submicron droplets of sulfur at the surface of formvar substrate (Fig. 4). This specimen was shaded through deposition of silver in a vacuum evaporator at the angle of 15^0 to the specimen surface. This makes it possible to determine the height (thickness) of sulfur lenticular particles. As a result, it was calculated that the contact angle for a range of droplet sizes 100 – 300 nm amounts to 63 ± 6 ^{0}. In addition, in [4] provided data on the contact angles of the sub-millimeter droplets of sulfur on a silicon substrate (58 ± 2^0) and teflon (82 ± 2^0). Based on above data, it can be assumed, that the contact angles for macro-droplets of sulfur on tungsten oxide and sodium chloride are higher than for nano-sized range. In this case, applying the approach, developed in [2, 5], we can conclude that the line tension of studied sulfur critical nuclei is negative. Our nearest plan is to obtain the missing experimental data, which will give a more reliable description of the studied process.

Financial support for this work was provided by the Siberian Branch of Russian Academy of Sciences (SBRAS): Interdisciplinary Integration Project No. 3 and SBRAS-Taiwan Collaboration Project No. 7; RFBR project no. 11-08-01204-a.

[1] *S.V. Valiulin, V.V. Karasev et al.* // Atmospheric and Oceanic Optics V. 25. (2012) P. 451.
[2] *A.I. Hienola et al.* // J. Chem. Phys. 126, (2007) P. 094705.
[3] *P.M. Winkler et al.* / Atmospheric Research 90 (2008) P. 187.
[4] *K. Terpilowski et al.* // J. Colloid Interface Sci. 319 (2008) P. 514.
[5] *M. Lazaridis* // J. Colloid Interface Sci. 155 (1993) P. 386

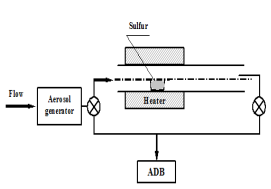

Fig 1.

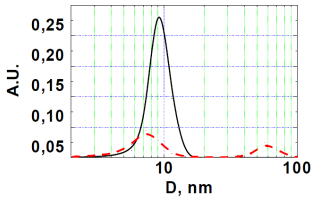

Fig 2.

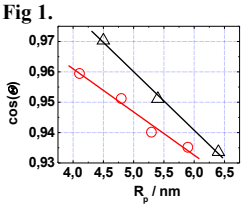

Fig 3.

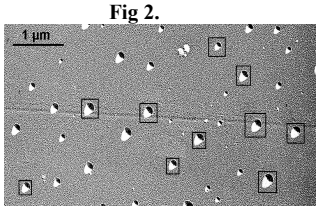

Fig 4.

A 19m deep well – a downward thermal diffusion cloud chamber?

R.F. Holub[1], P.K.Hopke[1], J. Hovorka[2], P. Otahal[3] and V. Zdimal[4]

[1]Department of Chemical Engineering, CARES, Clarkson University, Potsdam, NY, 13699, USA
[2]Institute for Environmental Studies, Faculty of Science, Charles University in Prague, Albertov 6, 128 43 Prague 2, Czech Republic
[3]National Institute for Nuclear, Chemical and Biological Protection, Nuclear Department, Kamenna 71, Milin, 262 31, Czech Republic
[4] Department of Aerosols and Laser Studies, Institute of Chemical Process Fundamentals, AS CR, Prague, 165 02, Czech Republic

Keywords: heterogeneous nucleation, thermal gradient, droplets formation, composition of CN.
Presenting author: Phil Hopke email: phopke@clarkson.edu

An unusual phenomenon, first observed on a clear summer day after several rainy days, were droplets constantly hitting the water surface in a 19 m deep and 2.4 m diameter water well. This droplet formation was occurring during the night as well. Since the droplet formation was near continuous, we called it “the eternal rain”. The water well is about 230 years old and located in the Benedictine monastery in Broumov, Czech Republic.

A series of measurements, listed below, starting at the top opening of the well, all the way down in steps of 0.5 m, were made. The ambient temperature at the top of the well varied between (in the second half of August) 15 to 30ºC. The temperature at the bottom of the well was constant at about 8ºC. The decrease in temperature was gradual, except the last few meters, when it was practically constant. The wall surface temperature basically followed the observed air temperatures.

CO_2 varied between around 450 ppm at the top to 2600 ppm at the bottom. The change in concentration occurred between 6 to 10 m depth. O_3 varied between 90 ug/m^3 at the top and about 12 ug/m^3 at the bottom. The sudden change occurred within the first 3 m of the depth.

The CN concentration, measured by UCPC 3025A, and by P-trak (both of TSI, Inc.) showed a depth dependence similar to ozone. At the top, the concentration was about 16000/cm^3, while at 8 m about 3000/cm3. The difference between UCPC and P-trak gives concentration of 3-20 nm. The concentration of 3-20 nm at the bottom several meters is constant, around 1000/cm^3.

In an attempt to describe the mechanism causing the observed flux of droplets falling to the bottom of the well, we expected that the well behaves as a natural Thermal Diffusion Cloud Chamber in a downward regime (e.g. Katz and Ostermier, 1967). In that case, we neglect any convective fluxes in the well and the main mechanism of water vapour transport is molecular diffusion driven by concentration gradient between the upper boundary of the well and almost isothermal water surface at the bottom. At the same time, the heat transport between the warmer top of the well and its colder bottom is driven by heat conduction in the water vapour – air mixture. These coupled transport processes lead to almost linear vertical profiles of both temperature and partial vapour pressure of water. Because the equilibrium vapour pressure of water is an exponential function of temperature, water vapour in the well may become supersaturated with maximum supersaturation located in the lowest third of the well.

Taking into account the temperatures at the well opening and at its bottom, preliminary calculations showed that the supersaturation at its maximum would not be sufficient for homogeneous nucleation of water. In the most extreme case with highest outside temperatures, the supersaturation might have reached a limit for an observable nucleation on air ions. However, at the presence of almost any heterogeneous particle moving downward the well space, this particle would easily serve as a condensation nuclei providing surface for water condensation. Due to a long condensation path and taking into account fast condensational growth in supersaturated water vapour, the grown droplets might have easily grown to sizes of hundreds of micrometers or larger and be observed as macroscopic droplets hitting the water surface at the well bottom.

The question remains concerning the nature of particles serving as CN. It is not clear whether these nuclei enter the well from above as the ambient aerosol particles, or there is some inherent source of particles inside the well. As was shown in measurements in isolated caves and a mine (Holub et al., 1999, and Holub et al., 2001), aerosol particles in the size range 3-200 nm have been observed there without coming from outdoors. These aerosols have been also measured routinely by earth scientists as a prospecting tool for locating hidden deposits (Cao et al., 2009). Similarly, Kristiansson et al. (1990) used entails digging a hole about 1 m^3 volume in the ground, placing a collector inside (for istance, a Transmission Electron Microscopy grid), and then measuring, after 45 days of exposure, the size and composition of the nanoparticles collected on the grid. The compositions reflected minerals deep below the collectors, and not of the outdoor aerosols.

Cao, J.J., Hu R.Z., Liang Z.R., Peng Z.L., (2009) *J. Geochem. Exploration* **101**, 247-253.

Holub, R.F., Reimer, G.M., Hopke, P.K., Hovorka, J., Krcmar, B., Smrz, P.K., (1999) *J. Aerosol Sci.*,**30**, Suppl.1, S111-112.

Holub, R.F., Hovorka, J., Reimer, G.M., Honeyman, B.D., Hopke, P.K. and Smrz, P.K., (2001) *J. Aerosol Sci.*, 34, S61-62.

Katz, J. L., Ostermier, B. J. (1967), *J. Chem. Phys.* **47**, 478.

Kristiansson, K., Malmqvist, L. Persson, W., (1990) *Endeavor (New Series)* **14**, 28-33.

Free energy barrier in the growth of sulfuric acid clusters

T. Olenius[1], O. Kupiainen[1], I.K. Ortega[1] and H. Vehkamäki[1]

[1]Department of Physics, University of Helsinki, Helsinki, FI-00014, Finland
Keywords: sulfuric acid, molecular clusters, modeling, new particle formation
Presenting author email: tinja.olenius@helsinki.fi

Formation of secondary atmospheric particles begins with the clustering of gas phase molecules into small molecular clusters, which can grow by colliding with gas molecules and each other. As experimental observation of the smallest clusters is extremely difficult, theoretical methods provide necessary tools to study the properties of these clusters.

We have used first principles quantum chemistry combined with a dynamic model to study the kinetics of sets of small clusters containing either sulfuric acid (H_2SO_4) and ammonia (NH_3) or sulfuric acid and dimethylamine (DMA, $(CH_3)_2NH$) molecules. The model (Atmospheric Cluster Dynamics Code; McGrath *et al*, 2012) solves the steady-state of the system considering all possible collision and evaporation processes. Collision rates are calculated as in the kinetic gas theory, and evaporation rates are derived from quantum chemical Gibbs free energy of formation of the clusters (Ortega *et al*, 2012). We included in the simulations clusters containing in principle up to four acid and four base molecules for DMA; for ammonia, the behavior of the system was not as straightforward as for DMA and therefore the set was extended to include clusters with up to five acids and five bases in order to better understand the system. Both sets were studied with and without electrically charged clusters.

We performed the simulations in atmospherically relevant conditions. The base concentration was fixed by setting a constant base monomer concentration, whereas the acid concentration was set by fixing the sum of all neutral clusters containing one acid and any number of base molecules, as the instrument for measuring the acid concentration (CIMS; Chemical Ionization Mass Spectrometer) is likely to detect also these clusters as acid monomers. We tracked the main clustering pathways in each system and converted the quantum chemical Gibbs free energies of formation of the growing clusters to the acid and base concentrations used in the simulations.

Figure 1 shows the Gibbs free energy of formation of the growing clusters as a function of growth step in the studied systems. In the system with sulfuric acid and ammonia, there are energy barriers in the main growth pathways both in the electrically neutral and ionic systems. Charged clusters dominate the clustering routes in the ionic system by growing out as negative or positive cluster ions and forming neutral clusters by recombination. In the acid-DMA system the growth along the most significant pathways is barrierless and occurs via electrically neutral clusters also when ions are present.

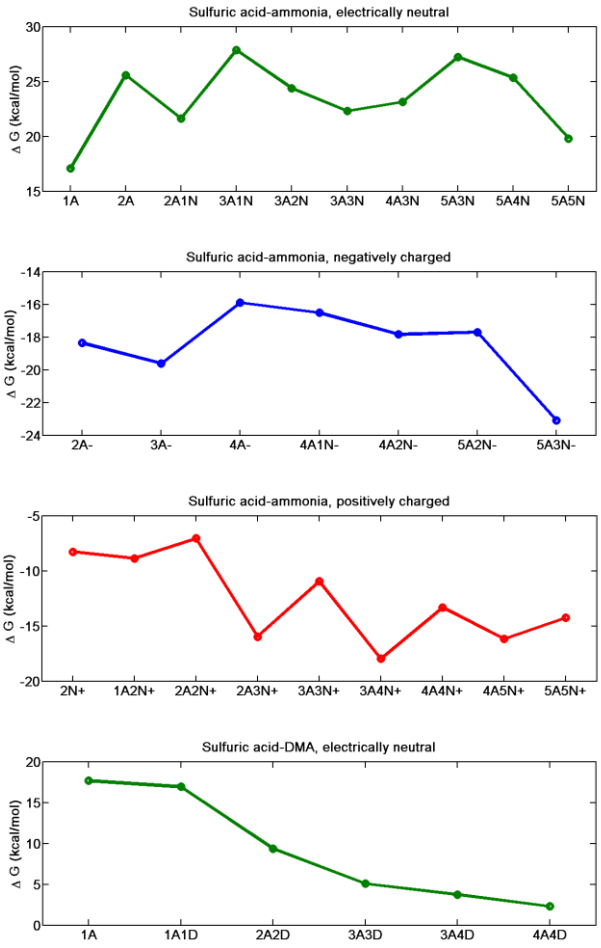

Figure 1. Gibbs free energy of formation as a function of growth step along the most significant growth routes in the sulfuric acid-ammonia and sulfuric acid-DMA systems at T=5 °C, $[H_2SO_4]=10^6$ cm^{-3} and $[NH_3]$=100 ppt or [DMA]=1 ppt. For ammonia, both electrically neutral and charged growth routes are shown; for DMA, only the neutral route is shown as the contribution of ions is insignificant. Acid, ammonia and DMA molecules are denoted with A, N, and D, respectively.

This work was supported by FP7-MOCAPAF project No 257360, FP7-ATMNUCLE project No 227463, Väisälä Foundation and Academy of Finland. The authors thank CSC- IT Center for Science in Espoo, Finland for the computing time.

McGrath, M.J. *et al* (2012) *Atmos. Chem. Phys.* **12**, 2345-2355.

Ortega, I.K. *et al* (2012) *Atmos. Chem. Phys.* **12**, 225-235.

Thursday, September 5, 2013

Session: Aerosol Chemistry,
Heterogeneous chemistry of aerosol

Heterogeneous reaction of sulphur dioxide on Eyjafjallajökull's volcanic ash from the 2010 eruption

Yoan Dupart[1], Laurence Burel,[1] Pierre Delichere,[1] Christian Geoage,[1] and Barbara D'Anna [1]
[1] Université de Lyon, Lyon; Université Lyon 1; CNRS, UMR5256, IRCELYON, Institut de recherches sur la catalyse et l'environnement de Lyon, , 2 avenue Albert Einstein, F-69626, Villeurbanne, France

Keywords: volcanic ash, photochemistry, sulphur oxide uptake, sulphate
Presenting author email: barbara.danna@ircelyon.univ-lyon1.fr

Volcanic eruptions may induce important climatic and weather modifications. When volcanic ashes are emitted into the atmosphere they can travel for several weeks according to their size distribution and altitude of the ashes emission.

The Eyjafjallajökull eruption, between April 14th and May 23th, is considered as a medium-size eruption with injection of the ashes plume at relative low altitude (troposphere). However, ash was widely dispersed because of upper-level winds that advected the plume over the UK and continental Europe, as well as into the translattalntic flight routes.

During volcanic eruptions high amounts of SO_2 were injected into the atmosphere (from 50 to 200 ppbv) [1]. Previous literature showed that SO_2 could be convert into sulfate on mineral dust surfaces under dark conditions [2]. Sor far no conversion of SO_2 has been studied with real volcanic ashes and under day conditions (light exposure). The present study focuses on SO_2 kinetics on real Eyjafjallajökull's ash samples, collected the 20th of April 2010 at Seljavellir.

The kinetics was investigated using a flow-tube set up at atmospheric pressure and simulating atmospheric conditions. The ashes were deposited on a horizontal cylindrical coated-wall flow tube reactor surrounded by 5 fluorescent lamps (emission from 320-420 nm, λ_{max}=365nm). The kinetic studies revealed that the under UV-A irradiation conversion of SO_2 into sulphates is enhanced on these ash samples (as shown in figure 1 below).

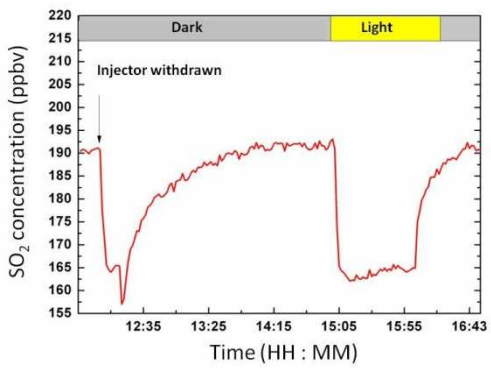

Figure 1. Uptake of SO_2 under darkness and weak UV-A irradiation on Eyjafjallajökull's ash sample.

Moreover chemical analyses as, Ion Chromatography (IC) and Scanning Electron Microscopy (SEM) coupled to energy dispersion spectrometry (EDS) were performed on volcanic ashes before and after exposition to gaseous SO_2. X-ray photoelectron spectroscopy (XPS) and ion chromatography (IC) analyses confirmed an enhanced SO_2 uptake under irradiation with conversion of SO_2 to sulphate. Beside SEM-EDS analysis suggested that the conversion takes place systematically on iron oxide site.

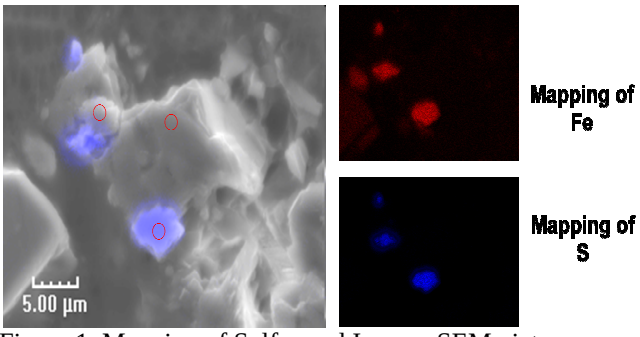

Figure 1. Mapping of Sulfur and Iron on SEM picture.

By combining kinetics and chemical analyses a new reaction mechanism for SO_2 conversion on volcanic ashes under light conditions is proposed.

Self, S., M. Widdowson, T. Thordarson, and A. E. Jay (2006), *Earth Planet. Sci. Lett.*, *248*(1-2), 518-532.

Zhang, X. Y., G. S. Zhuang, J. M. Chen, Y. Wang, X. Wang, Z. S. An, and P. Zhang (2006), *J. Phys. Chem. B*, **110**(25), 12588-12596.

Estimating amorphous deliquescence time scales of SOA from biogenic and anthropogenic precursors: Implications for heterogeneous ice nucleation on glassy aerosols.

T. Berkemeier[1,2], M. Shiraiwa[2,3], U. Pöschl[2] and T. Koop[1]

[1]Faculty of Chemistry, Bielefeld University, Bielefeld, 33615, Germany
[2]Multiphase Chemistry Department, Max-Planck-Institute for Chemistry, Mainz, 55128, Germany
[3]Division of Chemistry and Chemical Engineering, California Institute of Technology, Pasadena, CA91125, USA
Keywords: SOA, glassy state, diffusion, ice nucleation
Presenting author email: t.berkemeier@mpic.de

Recently, secondary organic aerosol (SOA) particles have been found to exhibit a highly viscous, amorphous state under atmospherically relevant conditions (Virtanen *et al*., 2010). Implications of such a glassy state are retardation of chemical reactions (Shiraiwa *et al*. 2011), incomplete gas-to-particle partitioning of semi-volatile constituents (Zelenyuk *et al*., 2012), and suppressed ice nucleation (Murray *et al*., 2008).

The actual phase state of SOA particles depends on several influencing factors such as composition, temperature and relative humidity. SOA comprises a multitude of complex mixtures of very different chemical substances. Typically, SOA is classified by precursor material (Hallquist *et al.*, 2009) and studies have shown that SOA from these classes exhibit differences in phase state under otherwise similar conditions (Saukko *et al*., 2012).

In atmospheric updrafts, which represent an important cloud formation mechanism, these particles may also deviate from humidification equilibrium, i.e. the agreement between ambient relative humidity and water activity inside the particle may not be established (Fig. 1). The degree of this temporal delay is governed by the rate of humidification, the particle size and the diffusivity of water inside the glassy organic particle matrix, which in turn depends on chemical composition, water content, and temperature.

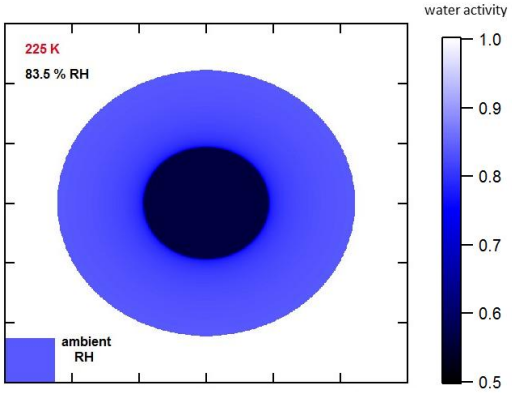

Figure 1. Partial deliquescence during an updraft simulation: While the surface is already liquid, the particle core remains glassy.

As recent studies have shown, glassy SOA particles may act as heterogeneous ice nuclei at low temperature (e.g. Murray *et al*., 2010). This new ice nucleation pathway might help explaining inconsistencies between measured and predicted relative humidities in the tropopause region.

Here we show how the delayed deliquescence of SOA particles can be quantified for several types of SOA and their surrogates by applying a kinetic flux model (Shiraiwa *et al*., 2012). Accompanying this model, we employ a novel methodology to estimate diffusivities from readily available glass transition and hygroscopic growth data. Using this approach we established a set of best guesses of these well-studied input parameters to investigate characteristic differences in low-temperature amorphous deliquescence between different SOA precursor classes and important surrogates, such as citric acid and sucrose.

Based on these parameterizations, we studied how the SOA particles' phase states and velocities of the respective deliquescence processes affect the particles' ice nucleation ability at low temperatures. These model simulations can be used to estimate upper temperature boundaries below which heterogeneous ice nucleation of glassy aerosols may occur as a function of humidification rates and particle size. A comparison between SOA from different precursors shows that this new ice nucleation pathway is more relevant for anthropogenic than for biogenic precursors.

References

Hallquist, M. *et al*. (2009) *Atmos. Chem. Phys.* **9**, 5155.
Murray, B. J. (2008) *Atmos. Chem. Phys.* **8**, 5423.
Murray, B. J. *et al*. (2010) *Nature Geosci.* **3**, 233.
Saukko, E. *et al*. (2012) *Atmos. Chem. Phys*. **12**, 7517.
Shiraiwa, M., Ammann, M., Koop, T. and Pöschl, U. (2011) *Proc. Natl. Acad. Sci.* **108**, 11003.
Shiraiwa, M., Pfrang, C., Koop, T. and Pöschl, U. (2012) *Atmos. Chem. Phys.* **12**, 2777.
Virtanen, A. *et al.* (2010) *Nature* **467**, 824.
Zelenyuk, A. *et al*. (2012) *Environ. Sci. Technol.* **46**, 12459.
Zobrist, B. *et al*. (2011) *Phys. Chem. Chem. Phys.* **13**, 3514.

Surfactants in cloud activation: do they matter?

B. Mølgaard[1], J. Hong[1], M. Paramonov[1], T. Yli-Juuti[1], N.L. Prisle[1]

[1]Department of Physics, Division of Atmospheric Science, University of Helsinki, Helsinki, 00014, Finland
Keywords: surfactants, surface tension, surface partitioning, CCN.
Presenting author email: nonne.prisle@helsinki.fi

It has been recognized for nearly two decades that the surface tension of aqueous aerosols will play a critical role in governing their cloud forming abilities (Shulman, 1996) and that surface active compounds with the potential to substantially decrease surface tension are indeed present in atmospheric aerosols (Facchini, 1999).

Decreased surface tension at the point of droplet activation is readily anticipated from standard Köhler theory to enhance cloud condensation nucleus (CCN) potential. Increased CCN activity may in turn influence the aerosol indirect climate effects via cloud droplet numbers and sizes, and hence cloud albedo and life time. This makes surfactant components an alluring unicorn for reconciling measurements with predictions of atmospheric CCN.

Nevertheless, after a good many studies of surfactant CCN activity and several important insights as to the influences of surface activity on droplet activation thermodynamics, the overall impact of surface active aerosol components on CCN activity and large scale aerosol climate effects remains ambiguous. In some cases, enhanced aerosol CCN activity has been rationalized with considerations of reduced aqueous surface tension by surface active organic components (Asa-Awuku, 2008), whereas other studies have shown that the overall effect of surfactants on CCN activation is nearly negligible (Prisle, 2011).

Many different factors contribute to this bothersome dilemma. We highlight some of these and the mechanisms by which studies of CCN activity are impacted. The first question is what the surface tension of aerosols actually *is*? It cannot be measured directly. Surfactants accumulate at the aqueous surface and the resulting partitioning of dissolved material between bulk and surface phases may deplete the bulk in small droplets with large surface areas. This can affect the surface tension and thus the curvature effect on equilibrium vapour pressure of activating droplets, and may greatly change the solute effect (Sorjamaa, 2004).

When you want to model the global effects of surfactants in atmospheric aerosols, detailed process level descriptions are too complex to be readily implemented in large-scale frameworks (Kokkola, 2006). Furthermore, the non-linearity of surfactant effects in activation thermodynamics challenges attempts to parameterize process level mechanisms over an aerosol population of different sizes and compositions (Prisle, 2011, and references herein).

A number of recent studies measure and parameterize surface tensions of atmospherically relevant aqueous systems as functions of varying composition. Such surface tension measurements and parameterizations are essential for including surface tension effects in modelling of droplet activation. Still, it is futile to ever hope of getting a comprehensive description of surface tensions over the entire range of aqueous mixing states found in atmospheric aerosols. The surface tension of solutions comprising known atmospheric surfactants has been seen to respond to mixing with other solutes in ways that are not readily anticipated. Surface tension measurements may frequently have been performed for mixing states not representative of atmospheric aerosols, thus decreasing the usefulness of the derived parameterizations. Furthermore, the first studies of global climate effects resulting from surfactant CCN activity points to the need for great caution when representing the ensemble of surface active organic aerosol by simple proxy systems (Prisle, 2012a).

It was recently shown that atmospheric surfactants are not chemically inert, but rather may participate in chemical reactions in the aqueous surface. Such reactions may consequently alter the surface composition and properties, and may even occur without corresponding changes in the bulk solution taking place (Prisle, 2012b).

We revisit results from previous studies of aqueous surface tensions for atmospherically relevant aerosol mixtures and their effects on predicted CCN activity. We wish to guide and focus future efforts targeting effects of surface active atmospheric aerosol, such as for which aqueous systems, and in particular which compositions and concentrations, to measure surface tensions. We explore simple frameworks within which to assess implications of measured surface tensions for CCN activity of aqueous aerosols, ultimately to make recommendations for the treatment of the different properties of surfactants in large scale modelling of aerosol climate effects.

This work was funded by the Finnish Academy of Science.

Asa-Awuku, A., *et al.* (2008). *Atmos. Chem. Phys.*, **8**, 799-812.

Facchini, M.C., *et al.* (1999). *Nature*, **401**, 257-259.

Kokkola, H., *et al.* (2006). *Geophys. Res. Lett.*, **33**, L10816.

Prisle, N.L., *et al.* (2011). *Atmos. Chem. Phys.*, **11**, 4073-4083.

Prisle, N.L., *et al.* (2012a). *Geophys. Res. Lett.*, **39**, L05802.

Prisle, N.L., *et al.* (2012b). *Atmos. Chem. Phys.*, **12**, 12227-12242.

Shulman, M., *et al.* (1996). *Geophys. Res. Lett.*, **23**, 277-280.

Sorjamaa, R., *et al.* (2004). *Atmos. Chem. Phys.*, **4**, 2107-2117.

Gas-particle partitioning of atmospheric aerosols: Interplay of physical state, non-ideal mixing and morphology

Manabu Shiraiwa[1], Andreas Zuend[1], Allan K. Bertram[2], and John H. Seinfeld[1]

[1] Division of Chemistry and Chemical Engineering, California Institute of Technology, Pasadena, CA91125, USA
[2] Department of Chemistry, University of British Columbia, Vancouver, BC, V6T 1Z1, Canada
Keywords: secondary organic aerosol, amorphous semi-solid, non-ideality, hygroscopic growth
Presenting author email: shiraiwa@caltech.edu

Atmospheric aerosols, comprising organic compounds and inorganic salts, play a key role in air quality and climate. Mounting evidence exists that these particles frequently exhibit phase separation into predominantly organic and aqueous electrolyte-rich phases (*You et al.*, 2012). As well, the presence of amorphous semi-solid or glassy particle phases has been established (*Virtanen et al.*, 2010; *Koop et al.*, 2011). Using the canonical system of ammonium sulfate mixed with organics from the ozone oxidation of α-pinene, we illustrate theoretically the interplay of physical state, non-ideality, and particle morphology affecting aerosol mass concentration and the characteristic timescale of gas-particle mass transfer.

The state-of-the-art thermodynamic model AIOMFAC (Aerosol Inorganic-Organic Mixtures Functional groups Activity Coefficients; *Zuend et al.*, 2008; 2011) is used to investigate the effect of phase separation on secondary organic aerosol formation. We demonstrate that phase separation can significantly affect hygroscopic growth and gas-particle partitioning (particle mass and chemical composition).

It is generally assumed that VOC oxidation products rapidly adopt gas-aerosol equilibrium. Here we estimate the equilibration timescale of SOA gas-particle partitioning using a state-of-the-art kinetic flux model (kinetic multi-layer model of gas-particle interaction in aerosol and clouds; *Shiraiwa et al.*, 2012). Equilibration timescale is found to be of order seconds to minutes for partitioning of relatively high volatility organic compounds into liquid particles, thereby adhering to equilibrium gas-particle partitioning. However, equilibration timescale increases to hours or days for organic aerosol associated with semi-solid particles, low volatility, large particle size, and low mass loadings (Fig. 1). Instantaneous equilibrium partitioning may lead to substantial overestimation of particle mass concentration and underestimation of gas-phase concentration (*Shiraiwa & Seinfeld*, 2012).

Moreover, we demonstrate that semi-solid or glassy phases may kinetically inhibit the hygroscopic growth especially under low relative humidity and temperature. Thus, the interplay of physical state, non-ideal mixing and morphology have significant implications for the interpretation of laboratory data and the development of improved atmospheric air quality and climate models.

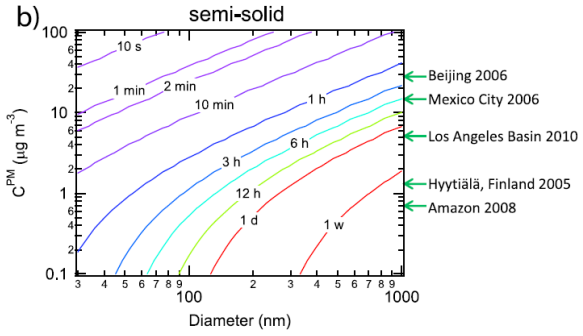

Figure 1. Equilibration timescale of SOA partitioning SVOC (C^* = 10 μg m^{-3}) in (b) semi-solid (bulk diffusivity D_b = 10^{-15} cm^{-2} s^{-1}) matrix as functions of particle diameter (nm) and mass concentration of pre-existing particles. Ambient organic mass concentrations are indicated (*Shiraiwa & Seinfeld*, 2012).

This work was funded by US National Science Foundation grant AGS-1057183. MS was supported by the Japan Society for the Promotion of Science (JSPS) Postdoctoral Fellowship for Research Abroad.

T. Koop, J. Bookhold, M. Shiraiwa and U. Pöschl, *Phys. Chem. Chem. Phys.*, 2011, **13**, 19238-19255.
M. Shiraiwa, C. Pfrang, T. Koop and U. Pöschl, *Atmos. Chem. Phys.*, 2012, **12**, 2777-2794.
M. Shiraiwa and J. H. Seinfeld, *Geophys. Res. Lett.*, 2012, **39**, L24801.
A. Virtanen, et al., *Nature*, 2010, **467**, 824-827.
Y. You, et al., *Proc Natl Acad Sci USA*, 2012, **109**, 13188-13193.
A. Zuend, C. Marcolli, B. P. Luo and T. Peter, *Atmos. Chem. Phys.*, 2008, **8**, 4559-4593.
A. Zuend, C. Marcolli, A. M. Booth, D. M. Lienhard, V. Soonsin, U. K. Krieger, D. O. Topping, G. McFiggans, T. Peter and J. H. Seinfeld, *Atmos. Chem. Phys.*, 2011, **11**, 9155-9206.

Role of organic and inorganic salts in atmospheric nanoparticle growth: a modelling study

T. Yli-Juuti[1], K. Barsanti[2], L. Hildebrandt Ruiz[3,4], A.-J. Kieloaho[1], U. Makkonen[5], T. Petäjä[1], T. Ruuskanen[1], M. Kulmala[1] and I. Riipinen[6]

[1]Department of Physics, University of Helsinki, Helsinki, FI-00014, Finland
[2]Department of Civil & Environmental Engineering, Portland State University, Portland, OR, 97201, USA
[3]Atmospheric Chemistry Division, National Center for Atmospheric Research, Boulder, CO, 80305, USA
[4]Now at: McKetta Department of Chemical Engineering, The University of Texas at Austin, Austin, TX, USA
[5]Finnish Meteorological Institute, Helsinki, FI-00101, Finland
[6]Department of Applied Environmental Science and Bert Bolin Center for Climate Research, Stockholm University, Stockholm, 10691, Sweden
Keywords: particle growth, aerosol chemistry, new particle formation, organic aerosol.
Presenting author email: taina.yli-juuti@helsinki.fi

New particle formation, i.e. formation of new nanometer sized particles from gas phase precursors and their subsequent growth towards larger sizes, is a significant source of aerosol particles in many atmospheric environments. Condensational growth is a critical step on the way of these nanoparticles to climate forcers, and growth rate of particles determines to a large extend their survivor probability to cloud condensation nuclei sizes. Large fraction of the condensational growth of atmospheric nanoparticles is due to organic vapors, but not all the vapors and processes related to their condensation are identified yet (Riipinen et al., 2012). In order to grow the nanoparticles, the compounds need to either be low-volatile or transferred into low-volatile substances through particle phase processes. Existence of semi-volatile organic acids and amines in nanoparticles has suggested that particle phase salt formation may play an important role in nanoparticle growth (Smith et al., 2010).

In this study we used particle growth model MABNAG (Model for Acid-Base Chemistry in Nanoparticle Growth) to study the importance of salt formation on nanoparticle growth. We focused on the effect of salt formation on condensation of organic acids and the relative roles of ammonia and amines for particles of 3-20 nm in diameter. MABNAG is a condensational particle growth model for monodisperse aqueous particles where particle phase acid dissociation and base protonation are accounted for. The model is based on bulk thermodynamics and utilizes Extended Aerosol Inorganic Model (E-AIM; Clegg et al. 1992; Clegg and Seinfeld, 2006) for calculating the particle phase chemistry. MABNAG predicts the particle size and composition evolution in time based on gas phase concentrations of vapors and initial particle size and composition. In this study, modelled system included five vapors: sulfuric acid, ammonia, an organic acid, an amine and water. When calculating the condensation of vapors, both size and composition dependence is taken in to account for the equilibrium vapor pressures.

At typical boreal forest conditions the model predicted the effect of dissociation, and thereby salt formation, to be small for the condensation of organic acid. As most of the growth was due to condensation of the organic acid, salt formation affected the particle growth rates only little The relative roles of the two bases were rather similar at all particle sizes between 3-20 nm, and depended on their relative gas phase concentrations, while the absolute contribution of the bases increased with particle size. At base-rich conditions (amine conc. > 10^9 cm^{-3} / ammonia conc. > 10^{10} cm^{-3}) significant fraction of the organic acid was predicted to dissociate which further increased the particle growth rate. In all cases, all the amine and ammonia was predicted to protonate in particle phase – indicating the importance of salt formation for the condensation of the bases.

Comparison of MABNAG to a quantum chemistry based modelling approach on salt formation in nanoparticles during the growth (Riipinen et al., 2012) revealed a difference between the two approaches in predictions for condensation of amines. Further study is thus needed on the applicability of bulk thermodynamics (used in MABNAG) in the nanoparticle size range.

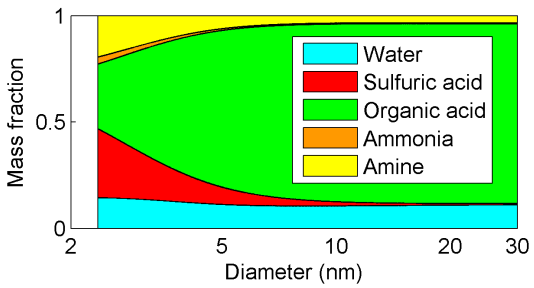

Figure 1. Predicted mass fractions at typical ambient conditions at boreal forest site Hyytiälä.

This research was supported by the Academy of Finland Center of Excellence program (project No. 1118615), ACCC Doctoral Programme (project No. 129663), Vetenskapsrådet (project No. 2011-5120), European Research Council Grant ATMOGAIN (No. 278277), and US DOE Grant (No. DE-SC0006861).

Riipinen, I. et al. (2012) *Nature Geoscience* **5**, 453-458.
Smith, J. N. et al. (2010) *PNAS* **107**, 6634-6639.
Clegg, S. L. et al. (1992) *J. Phys. Chem.* **96**, 9470-9479.
Clegg, S. L. and Seinfeld, J. H. (2006) *J. Phys. Chem. A* **110**, 5692-5717.

Secondary organic aerosol production potential from diesel and gasoline vehicle exhaust under different ambient conditions

S.M. Pieber[1], S.M. Platt[1], I. El Haddad[1], A.A. Zardini[2], R. Suarez-Bertoa[2], J.G. Slowik[1], R.J. Huang[1], S. Hellebust[3], B. Temime-roussel[3], N. Marchand[3], L. Drinovec[4], G. Mocnik[4], U. Baltensperger[1], C. Astorga[2] and A.S.H. Prévôt[1]

[1]Laboratory of Atmospheric Chemistry, Paul Scherrer Institute, Villigen, CH-5232, Switzerland
[2]Instiute for Energy and Transport, Sustainable Transport Unit, EC Joint Research Centre, Ispra, I-21027, Italy
[3]Laboratoire Chimie Environment, Aix Marseille Université, Marseille, F-13 331, France
[4]Aerosol d.o.o., SI-1000 Ljubljana, Slovenia

Keywords: secondary organic aerosol (SOA), smog chamber, vehicle emissions, AMS
Presenting author email: simone.pieber@psi.ch, corresponding author email: andre.prevot@psi.ch

Organic aerosol (OA) is a major fraction of the submicron aerosol known to influence climate and to adversely affect health. OA consists of directly emitted primary OA (POA), and "secondary" OA (SOA), formed in-situ in the atmosphere via the reaction of volatile precursors. Vehicle exhaust is already a known source of POA and likely contributes to SOA in urban areas (Robinson *et al.*, 2007; Weikamp *et al.* 2007). However, the magnitude of this contribution is unknown.

The secondary organic aerosol production potential (SAPP) of vehicle exhaust has recently been estimated by (i) analyzing ambient data from urban areas combined with fuel consumption data (Bahreini *et al.*, 2012), or (ii) by examining the chemical composition of raw fuels (Gentner *et al.*, 2012). Contradictory and thus somewhat controversial results in the relative SAPP of diesel vs. gasoline vehicle exhaust were observed.

Experimental data from smog chamber studies can provide quantitative measurements of the relative SAPP of different fuels and vehicle types, and elucidate the impact of variable ambient conditions. This information is crucial for our understanding of vehicular pollution and formulation of emission control strategies.

Therefore, we studied the SAPP of passenger cars and trucks as a function of fuel type (gasoline, diesel) at different temperatures (T 22 vs. -7°C) and relative humidity (RH ~40 vs. ~90%). Vehicle exhaust was sampled at the tailpipe during regulatory driving cycles on chassis dynamometers (European Joint Research Centre Ispra, Italy), diluted (200 – 400x) and introduced into the PSI mobile smog chamber (Platt *et al.* 2012) via a heated tube (150 °C). OA was quantified with a high-resolution time-of-flight aerosol mass spectrometer. Black carbon was measured using aethalometers. Volatile organic compounds (VOCs) were analysed with a high resolution proton-transfer time-of-flight mass spectrometer. Gas-phase monitors were used to quantify CO, CO_2, CH_4, total hydrocarbons, NH_3 and other gases in the chamber. Emission factors (EFs, e.g. g per kg fuel) were calculated from a carbon mass balance.

We found that the vehicle emissions and SAPP are significantly affected by temperature and RH: doubling the RH in the chamber resulted in a 3-fold higher SOA EF (*Figure 1*). Primary and secondary aerosol emissions from diesel and gasoline vehicles will be compared at different temperature and RH.

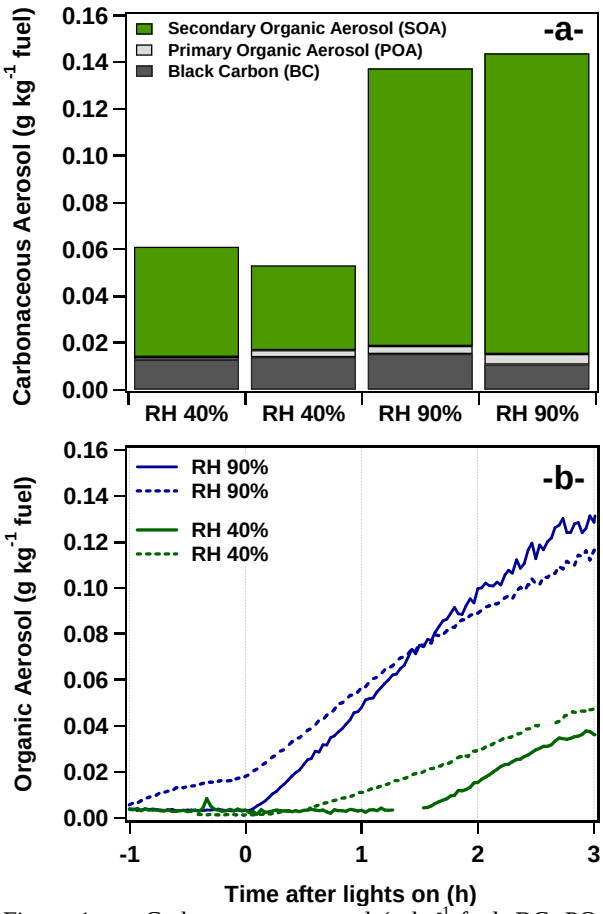

Figure 1. -a- Carbonaceous aerosol (g kg^{-1} fuel, BC, POA and SOA) from a Euro 5 gasoline car. -b- Temporal evolution of the OA formation in the smog chamber at similar OH exposure but different relative humidity (RH).

This work was supported by the Swiss Federal Office for the Environment and the Swiss Federal Roads Office. The test bench operation was financed by the EU. We thank U. Manfredi, M. Sculati, F. Muehlberger, M. Cadario and R. Richter for their expert technical assistance.

Bahreini, R., *et al.* (2012) *Geophys. Res. Lett.* **39**, L06805.
Gentner, D.R. *et al.* (2012) *PNAS* **109**, 18318.
Platt, S.M., *et al.* (2013) *Atmos. Phy. Chem. Discuss.* **12**, 28343.
Robinson, A.L., *et al.* (2007) *Science* **315**, 1259.
Weitkamp, E.A., *et al.* (2007) *Environ. Sci. Technol.* **41**, 6969.

Uptake of N_2O_5 to citric acid aerosol particles

G. Gržinić[1,2], T. Bartels-Rausch[1] A. Türler[2], and M. Ammann[1]

[1] Laboratory of Radiochemistry and Environmental Chemistry, Paul Scherrer Institute, Villigen, 5232, Switzerland
[2]Department of Chemistry and Biochemistry, University of Bern, Bern, Switzerland, 3012, Switzerland
Keywords: N_2O_5, ozone budget, nitrogen oxides, uptake coefficient.
Presenting author email: markus.ammann@psi.ch

Dinitrogen pentoxide is a significant reactive intermediate in the night time chemistry of nitrogen oxides, serving as a major NO_x sink by heterogeneous hydrolysis on aerosol surfaces. It can influence tropospheric ozone production and therefore the oxidative capacity of the atmosphere (Chang et al., 2011).

We used the short-lived radioactive tracer ^{13}N (Ammann, 2001) in conjunction with an aerosol flow tube reactor in order to study N_2O_5 uptake kinetics on aerosol particles. ^{13}NO was mixed with non labeled NO and O_3 in a first flow reactor, where N_2O_5 is synthesized under dry conditions. The N_2O_5 flow is then admitted into the aerosol flow reactor together with the aerosol flow containing deliquesced citric acid particles generated by ultrasonic nebulisation and conditioned to the relative humidity of interest. Movable inlets allow varying the length of the aerosol flow tube. Behind the reactor a Scanning Mobility Particle Sizer (SMPS) system is used to characterize the aerosol. The remaining gas exiting the reactor is passed through a parallel plate diffusion denuder system for selective separation of gaseous species and a particle filter to trap the particles. Activity of the ^{13}N labeled species can be monitored via scintillation counters placed on the denuder plates and the particle filter, respectively.

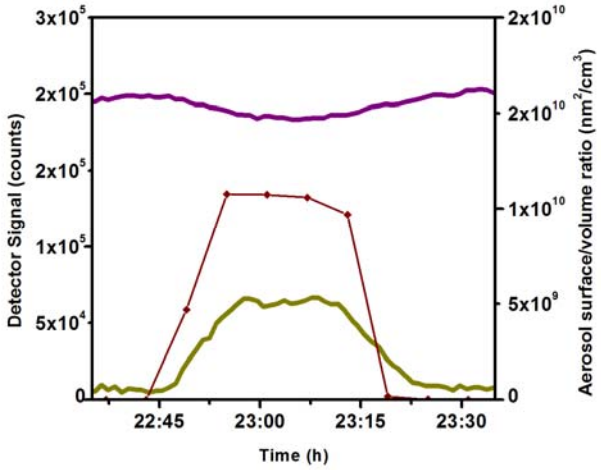

Figure 1. Gas phase N_2O_5 (solid magenta), particulate N (solid green, magnified by a factor of 10), and aerosol surface area (red) to volume ratio during an uptake experiment.

Fig. 1 shows data from a typical experiment with citric acid aerosol, where the loss of N_2O_5 from the gas phase is accompanied by an increase in particulate nitrate. Figure 2, shows a set of measurements conducted at a relative humidity of 62 %, at a fixed reaction time of around one minute, and at varying aerosol surface to volume ratio, along with a simple first-order fit (Vlasenko et al., 2006).

The preliminary results obtained have shown that the uptake coefficient increases with humidity from $1.65\pm0.3x10^{-3}$ (~27% RH) to $1.25\pm0.3x10^{-2}$ (45% RH) and $2.00\pm0.3x10^{-2}$ (61.5% RH). This is comparable to some polycarboxylic acids (like malonic acid), but higher than some others (Ammann et al., 2012). The increase is likely related to the increasing amount of water associated with citric acid at higher humidity that promotes hydrolysis of N_2O_5.

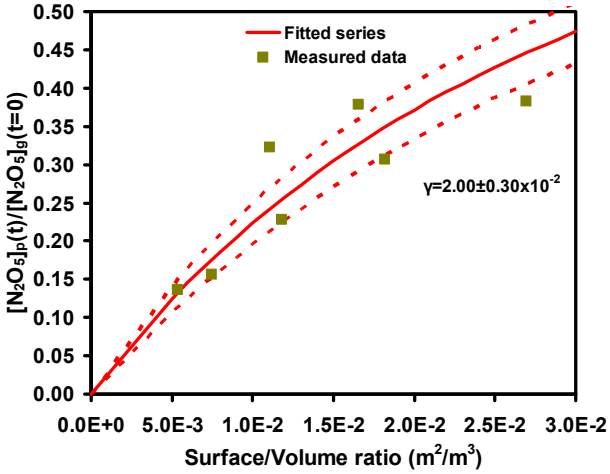

Figure 2. Data set collected using citric acid aerosol at 61.5% RH. Green squares represent measured data points while the red curve is a fit to the data according to the kinetic model, with the dotted curve showing the error range

This work is supported by the Swiss National Science Foundation (grant no. 130175).

Chang, W.L., Bhave, P.V., Brown, S.S., Riemer, N., Stutz, J., & Dabdub, D. (2011). *Aerosol Science and Technology,* **45**, 665-695.

Ammann, M. (2001). *Radiochim. Acta,* **89**, 831-838.

Vlasenko, A., Sjogren, S., Weingartner, E., Stemmler, K., Gäggeler, H.W., & Ammann, M. (2006). *Atmos. Chem. Phys.,* **6**, 2147-2160.

Ammann, M., Cox, R.A., Crowley, J.N., Jenkin, M.E., Mellouki, A., Rossi, M.J., Troe, J., & Wallington, T.J. (2012). *Atmos. Chem. Phys. Discuss.,* **12**, 32109-32472.

Thursday, September 5, 2013

Session: PMx, *Source-specific emissions of carbonaceous aerosol from combustion processes*

Thermal/Optical Analysis of Major Elements (C, H, N, S, and O) for Particles from Different Emission Sources

X.L. Wang, J.A. Robles, X.F. Yang, L.-W.A. Chen, J.C. Chow, and J.G. Watson

Desert Research Institute, 2215 Raggio Pkwy, Reno, NV, USA
Keywords: organic carbon, elemental carbon, emission, source.
Presenting author email: xwang@dri.edu

Atmospheric carbonaceous aerosols are related to adverse effects on the Earth's radiation balance, human health, visibility degradation, and material damage. Characteristic chemical information is needed for carbonaceous particles to assess their source, property, and impact. Thermal evolution methods quantify organic and elemental carbon (OC and EC, respectively) collected on filters by heating the sample at different temperatures under different oxidizing conditions. For example, the widely used IMPROVE_A protocol (Chow *et al*, 2007) measures eight carbon fractions (4 OC + 3 EC + OP [pyrolyzed OC]). Measurement of these thermally-resolved OC and EC fractions in aerosol emissions from gasoline- and diesel-powered vehicles enhances the ability of receptor models to discriminate between these sources (Watson et al., 1994). Carbon fraction alone are usually not sufficent to differentiate sources. Due to the complex nature of carbonaceous particles, standard chemical analysis techniques such as gas chromatography-mass spectrometry (GC/MS) typically identifies less than 30% of total organic matter (OM). New technologies, such as the particle into liquid sampler (PILS), thermal desorption aerosol GC/MS (TAG)-Flame Ionization Detector (FID), and aerosol mass spectrometers, are fast developing and perfecting for in situ identification and quantification of organic compounds in aerosols (Hallquist *et al*, 2009).

While there is tremendous complexity of carbonaceous aerosols at the molecular level, they are composed of only a few main elements (e.g., C, H, N, S, and O). Independent measurement of these elements provides new tools to study these aerosols. A Thermal Elemental Analyzer (TEA) has been developed to analyze C, H, N, S, and O on filter samples using a thermal/optical method adapted from the DRI Model 2001 Thermal/Optical Carbon Analyzer. A small punch (~0.5 cm^2) from a quartz-fiber filter sample is heated in programmed heating steps, e.g., following the IMPROVE_A protocol. Carbonaceous and other materials are volatilized, pyrolyzed, and combusted to gas phase compounds under either an inert ultrapure He atmosphere at lower temperatures (< ~600 °C) or a mixture of 98% He and 2% O_2 atmosphere at higher temperatures (> ~600 °C). C, H, N, and S are determined by the Pregl-Dumas method, where evolved gaseous species are oxidized in a high temperature (~900 °C) CHNS reactor containing oxidizing agents to convert organic components to CO_2, H_2O, NO_x/N_2, and SO_2. The oxidation products are measured by a quadrupole mass selective detector (MSD). Quantification of O is based on the Unterzaucher method in which O is converted to CO in the O reactor, consisting of a nickel-coated carbon reactant. CO is then oxidized to CO_2 using metal oxides and is quantified by a nondispersive infrared (NDIR) sensor. Calibration of the TEA with chemicals of known quantities of C, H, N, S, and O shows that the signal and element quantity have excellent linearity. Figure 1 shows an example of the thermogram from an aerosol sample collected at the Fresno supersite. Thermally separated CHNSO fractions of particles from several sources, including gasoline- and diesel-powered vehicle exhausts, wood smoke, industrial stacks, and ship emissions, as well as ambient aerosols will be presented.

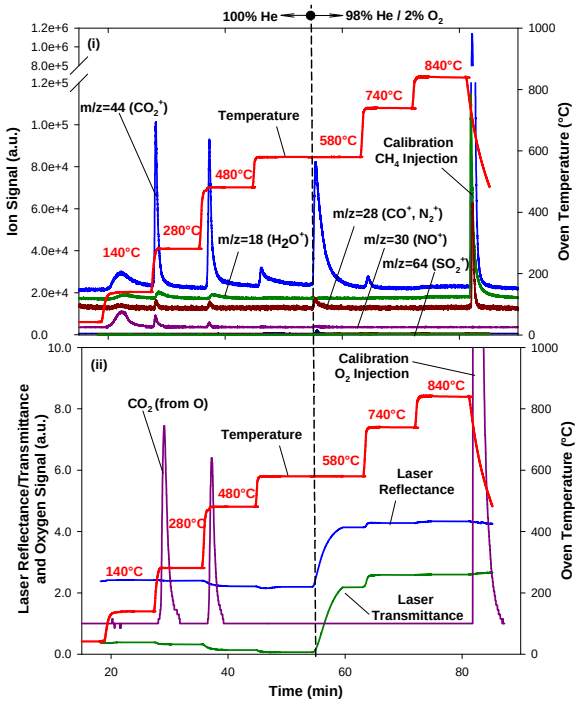

Figure 1. Thermogram of CHNS (top panel) and O and optical signal (bottom panel) for an ambient aerosol sample from Fresno, CA.

This work was supported in part by the U.S. National Park Service (C2350000894) and National Science Foundation (CHE1214163).

Chow, J.C., Watson, J.G., Chen, L.-W.A., Chang, M.C.O., Robinson, N.F., Trimble, D. and Kohl, S.D. (2007) *J. Air Waste Manage. Assoc.*, **57**(9), 1014-1023.

Hallquist, M. *et al* (2009) *Atmos. Chem. Phys.*, **9**(14), 5155-5236.

Assessing the Wintertime Contribution of Biomass Smoke to Organic Aerosol at 15 Sites in Switzerland by Analysing Filter Samples Using Aerosol Mass Spectrometry

K. R. Dällenbach[1], I. El-Haddad[1], P. Zotter[1], J. Slowik[1], F. Canonaco[1], V. G. Ciobanu[1,2], A. Piazzalunga[3], P. Fermo[4], U. Baltensperger[1], S. Szidat[2], A. S. H. Prévôt[1]

[1]Laboratory of Atmospheric Chemistry, Paul Scherrer Institute, CH-5232 Villigen, Switzerland
[2]Department of Chemistry & Biochemistry, University of Berne, CH-3012 Berne, Switzerland
[3]University of Milano Bicocca, Department of Environmental Science, 20126 Milano, Italy
[4]University of Milan, Department of Chemistry, 20133, Milan, Italy

Keywords: Aerosol mass spectrometer, Source apportionment, Biomass burning
Presenting author email: kaspar.daellenbach@psi.ch

In winter, domestic wood burning yields high concentrations of organic aerosol (OA) in the alpine regions and urban areas such as Grenoble, Zurich and Milano (Lanz et al. 2010; Piazzalunga et al. 2011). Biomass burning contributes on the order of 15% of submicron OA even in the megacity of Paris (Crippa et al. 2013). Due to the carcinogenic potential of biogenic smoke, it is crucial to examine its contribution and sources in different regions in order to design effective mitigation strategies. Such an analysis requires measurements capable of quantitatively distinguishing OA sources, distributed over a broad spatial scale and with sufficient spatial density to elucidate regional differences.

Aerosol mass spectrometer (AMS, Aerodyne) measurements of OA and subsequent application of positive matrix factorization (PMF) have proven capable of quantifying the biomass burning fraction (BBOA), even within a mixed aerosol containing other primary sources such as traffic (hydrocarbon-like OA, HOA), and secondary oxygenated OA (OOA), formed in-situ in the atmosphere via the oxidation of volatile organic compound precursors (e.g. Lanz et al. 2007). However, the cost and complex maintenance required by this instrument makes impractical its systematic long-term deployment at sufficient sites to determine regional characteristics. To overcome these limitations, we have developed a method for the analysis of conventional aerosol filter samples using high-resolution AMS measurements. Such samples are relatively easy and inexpensive to collect and store, and are already routinely collected at many air quality stations.

The analysis method consists of water extraction of the particulate material from quartz filters and subsequent atomization of the resulting solutions into the AMS. The extraction efficiency is estimated as ~80% and the mass spectra obtained by this methodology are very similar to the corresponding on-line measurements considering different settings (e.g. different sites and different seasons).

We present here the first application of this technique to filter samples collected during 2 consecutive winters (2008 and 2009) at 15 stations in Switzerland with different exposure characteristics (including a complete yearly cycle for one of the stations). Data are analysed with the multilinear engine ME-2 (Paatero 1999), with a toolkit for Igor, which allows to constrain certain sources when running a PMF, and combined with other measurements, including organic and elemental carbon (OC/EC), ions, levoglucosan (marker for biomass burning), and radiocarbon content (^{14}C), to provide an improved estimation of the biomass smoke contribution to OA (Figure 1). BBOA contribution and emission profiles at different stations will be discussed and related to the prevailing meteorological and combustion conditions.

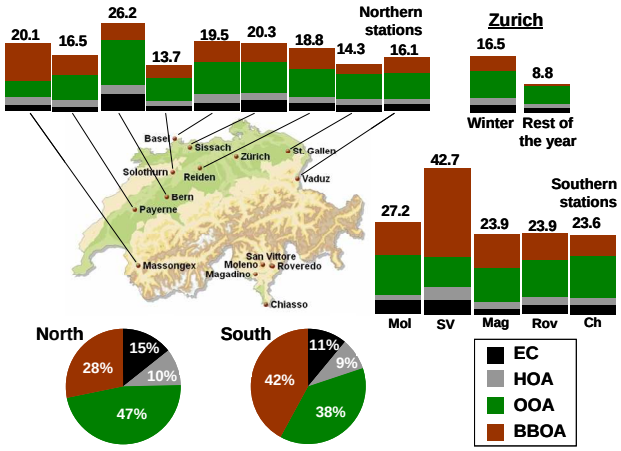

Figure 1: PMF applied to off-line AMS measurements presenting the average contributions of EC, HOA, BBOA and OOA at 15 different sites in Switzerland. The comparison shows that the BBOA contribution is two times higher in the southern part of Switzerland, presumably related to less efficient burning conditions in this region.

This work was supported by the Swiss Federal office for the Environment and the Swiss National Science Foundation.

Crippa, M. et al. (2013) Atmos. Chem. Phys., **13**, 961-981.
Lanz, V et al. (2007) Atmos. Chem. Phys., **7**, 1503-1522.
Lanz, V. et al. (2010) Atmos. Chem. Phys., **10**, 10453-10471.
Paatero, P. (1999), J. Comp. Graph. Stat., 8, 854-888.
Piazzalunga, A et al. (2011) Atmos. Env., **45**, 6642-6649

Carbonaceous Aerosols Emitted from Light-Duty Vehicles Operating on Ethanol Fuel Blends

M.D. Hays[1], R. Baldauf[1,2], B.J. George[1], J. Schmid[1], R. Snow[1], T. Long[1] and W. Preston[3],

[1]U.S. Environmental Protection Agency, Office of Research and Development, RTP, NC, 27711, USA
[2] U.S. Environmental Protection Agency, Office of Transportation and Air Quality, Ann Arbor, MI, 48105, USA
[3]ARCADIS U.S., RTP, NC 27711

Keywords: fine particle matter, organic carbon, elemental carbon, organic markers
Presenting author email: hays.michael@epa.gov

In the United States and elsewhere ethanol is being used as a renewable fuel in motor vehicles in an effort to reduce greenhouse gases and dependence on imported oil. Air pollution is among the many environmental and public health concerns associated with increased ethanol use in vehicles. *Jacobson* [2007] showed for the U.S. market that full conversion to e85 ([85% ethanol, 15% gasoline]—the maximum standard blend used in modern dual fuel vehicles—from 100% gasoline may cause excess morbidity and mortality risk. Higher ozone, peroxy acetal nitrate (PAN), and volatile carbonyl concentrations in urban air are associated with ethanol fuel combustion in vehicles. Of the studies examining combustion emissions from light-duty vehicles (LDVs) operating on ethanol-gasoline blends, the vast majority characterize air toxics (e.g., benzene, 1,3-butadiene, acetaldehyde, and formaldehyde), criteria pollutants (e.g., CO, NOx, particulate matter [PM], and O_3), or greenhouse gases[*Graham et al.*, 2008; *Yoon and Lee*, 2011]. Fewer examine the PM composition despite its climate relevancy, toxicological importance, and use in regulatory-based air quality and predictive dispersion models.

This study aims to examine carbonaceous aerosol emissions from three Tier 2-certified 2008 model year LDVs burning e0, e10, and e85 fuel blends at -7°C and 24°C. The LDVs were tested on an electric chasis dynamometer using the LA-92 Urban Driving Cycle (UDC). Exhaust was collected from a dilution tunnel and constant volume sampling system. Chemical analysis of fine particle matter ($PM_{2.5}$) was the main focus of the study and was conducted using thermal-optical transmission (TOT) and thermal extraction (TE)-gas chromatography-mass spectrometry (GC-MS) techniques. Statistical regression models were applied to log-scaled measurements to assess relationships with the covariates of temperature, fuel type, and UDC phase.

UDC phase-integrated organic carbon (OC) and elemental carbon (EC) emissions factors varied from 30 to 618 µg/km and from 1 to 2748 µg/km, respectively. Figure 1 shows the log-transformed OC and EC data. UDC phase 1 and the -7°C cell temperature produce significantly higher carbonaceous aerosol emissions, and the relatively low OC/EC ratios are an interesting feature of these data.

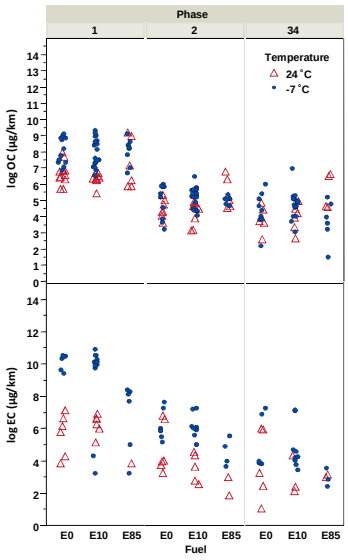

Figure 1. Fine aerosol OC and EC emissions (µg/km) from LDVs burning e0, e10, and e85 at -7°C and 24°C.

Historically, the OC and EC proportions in PM emissions from LDVs have varied rather substantially. In the U.S. emissions database (SPECIATE), OC (50.3% ± 40.3%) is significantly (p > 0.0001) higher than EC (30.7% ± 23.3%). The present LDV emissions study has produced higher mean pooled EC (60% ± 30%) likely due to the aggressive nature of the LA-92 UDC. Further analysis regarding the implications of these results will be provided. In addition, more on the exhaustive semivolatile organic compound (SVOC) analysis, including the polycyclic aromatic hydrocarbon (PAH), hopane and sterane marker, and saturated hydrocarbon emissions factors will be discussed.

Graham, L. A., S. L. Belisle, and C.-L. Baas (2008) *Atmos. Environ. 42*(19), 4498-4516.
Jacobson, M. Z. (2007), *Environ. Sci. Technol.*, *41*(11), 4150-4157.
Yoon, S. H., and C. S. Lee (2011) *Energy & Fuels*, *25*(8), 3484-3492.

Emissions of a GDI vehicle operating with different composition engine oils

L. Pirjola[1,2], T. Lähde[1], A. Malinen[1], J. Heikkilä[3], P. Karjalainen[3], T. Rönkkö[3], K. Kulmala[4] and J. Keskinen[3]

[1]Department of Technology, Metropolia University of Applied Sciences, P.O. Box 4021, FI-00180 Helsinki, Finland
[2]Department of Physics, University of Helsinki, P.O. Box 64, FI-00014 Helsinki, Finland
[3]Department of Physics, Aerosol Physics Laboratory, Tampere University of Technology, P.O. Box 692, FI-33101 Tampere, Finland
[4]Neste Oil Oyj, P.O. Box 95, FI-00095 Neste Oil, Finland
Keywords: gasoline exhaust, size distributions, lubricants, metals.
Presenting author email: liisa.pirjola@metropolia.fi, liisa.pirjola@helsinki.fi

Diesel engines produce more particulate matter than their gasoline counterparts. However, the gasoline direct injection (GDI) spark ignition-type engines have been shown to emit solid particles in concentrations comparable to common direct injection compression ignition diesel engines. Metals from lubricant oil or fuel have been found to increase the particle number concentration in the below 20 nm size range and even change the soot characteristics at high metal concentrations (e.g. Gidney *et al*, 2010). Furthermore, Cheun *et el* (2010) reported that the PM-induced toxic activity of vehicular exhaust is strongly associated with tracers of lube oil emission, such as Zn, P, Ca and hopanes suggesting that incomplete combustion of lube oil plays a significant role in the exposure and health.

In this work (Pirjola *et al*, 2013), we compare the exhaust emissions of a EURO V passenger car AUDI 1.8 TFSI equipped with a three-way catalyst and used standard gasoline fuel (FSC<10 ppm) but five different synthetic engine oils (Oil1-Oil5) filling the viscosity grade requirement of SAE 5W-30. The measurements were performed at a chassis dynamometer over the New European Driving Cycle (NEDC) as well as over three steady state cycles. Exhaust sampling and dilution for particle measurements was conducted using a porous tube diluter, an ageing chamber and a secondary diluter. Number concentration and number size distribution of particles larger than 3 nm were measured by Nano-SMPS, SMPS, CPC and ELPI, and a thermodenuder was used to study particle volatility characteristics. Diluted NOx and CO_2 concentration were measured; for dilution ratio also raw CO_2 concentration was measured.

Furthermore, exhaust particle measurements were performed also on road with two of the engine oils (Oil1 and Oil4). A mobile laboratory van Sniffer (Pirjola *et al*, 2004) equipped with the same instrumentation chased AUDI at a distance of 10 m.

During the steady state tests particle size distributions were bimodal. The smaller mode was peaking at below 20 nm and the larger mode at 60-70 nm with all oils; however, the concentrations varied from oil to oil, and were inversely proportional to the engine load. Figure 1 shows that the total number concentration, measured by the ELPI, was lowest with Oil4 for all engine loads. Oil4 possessed smallest calsium and zink concentrations whereas sulphur concentration was smallest in Oil3 followed by Oil4.

During the NEDC tests the highest exhaust particle concentrations were observed in speed transients. Especially during the highest wheel speed mode and the final deceleration, high number of particles below 20 nm was measured with Oil1 and Oil2. These particles were highly volatile, indicating that their formation takes place when the exhaust aerosol was cooled in the diluter. On-road tests supported the results obtained in the laboratory for both Oil1 and Oil4.

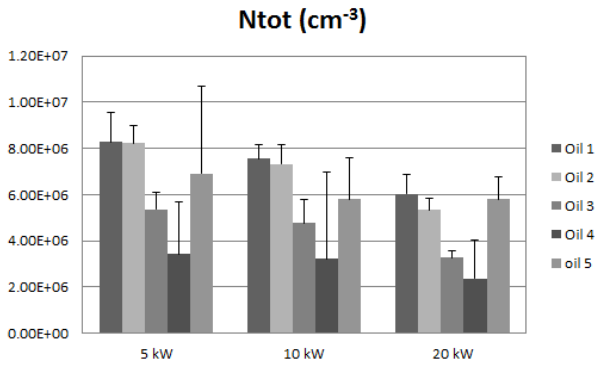

Figure 1. Averaged total particle number concentrations along with standard deviations for different lubricant oils during three steady state conditions. Concentrations have been calculated to raw exhaust concentrations.

This work was part of the TREAM project funded by Ecocat Oy, Neste Oil Oyj, AGCO Power, Oy Nanol Technologies Ab and Tekes (the Finnish Funding Agency for Technology and Innovation).

Cheung, K.L., Ntziachristos, L., Tzamkiozis, T., Schaueer, J.J., Samaras, Z, Moore, K.F., Sioutas, C. (2010) *Aerosol Sci. Technol.* **44**,500-513.

Gidney, J.T., Twigg, M.V., Kittelson, D.B. (2010) *Environ. Sci. Technol.* **44**, 2562-2569.

Pirjola L., Parviainen H., Hussein T., Valli A., Hämeri K., Aalto P., Virtanen A., Keskinen J., Pakkanen T., Mäkelä T., Hillamo R (2004). *Atmos. Environ.* **38**, 3625-3635.

Pirjola, L., et al. (2013). Manuscript in preparation.

Biodiesel with controlled physicochemical properties, a means to further reduce diesel engine particle emissions

[1]M. M. Rahman, [2]A.M. Pourkhesalian, [2]S. Stevanovic, [2] M.J. Islam, [3]H. Wang, [3]B. Miljevic, [3]P. Phamxuan, [3]R.J. Brown, [3]A. Masri, [3]Z.D. Ristovski

[1]Department of Chemistry Physics and Mechanical Engineering, Queensland University of Technology (QUT), Brisbane, QLD-4001, Australia
[2]School of Aerospace, Mechanical and Mechatronic Engineering, The University Sydney, NSW-2006, Australia
Keywords: Biodiesel, Fuel properties, Particle emission, Diesel engine
Presenting author e-mail: m1.rahman@student.qut.edu.au

The issue of particle emissions from diesel engines is still a matter of concern due its deleterious effects both on human health and environment(Ristovski et al., 2012). Recently, International Agency for Research on Cancer (IARC) inclusion of diesel engine exhaust particles as carcinogenic to human health added a new margin on it. Apart from the use of after treatment technology, biodiesel is also considered as potential way to reduce particle emission alongside with other emissions(Xue, Grift, & Hansen, 2011). Global biodiesel production is still reasonably small compared to its counterpart fossil diesel, but even this small amount comes from a wide variety of feed stocks. Contrary to fossil diesel, the important physicochemical properties of biodiesel vary among different feed stocks(Hoekman, Broch, Robbins, Ceniceros, & Natarajan, 2012).

Keeping in mind the aforementioned circumstances, the aim of this study is to investigate the effect of biodiesel physical properties and chemical composition on particle emissions alongside with engine performance. Four biodiesels with controlled chemical composition and a low sulfur diesel fuel were used in a common rail turbocharged diesel engine. It was observed that biodiesel with shorter carbon chain length and higher degree of saturation can reduce particle emissions significantly. With the increase of carbon chain length and degree of unsaturation in biodiesel, particle emissions increase. The percent of fuel bound oxygen in biodiesel plays a major role in reducing the particle emissions. As shown in Figure 1. We observed strong correlation between both particle number (PN) and particle mass (PM) emissions with weight percentage of oxygen in the fuel. Increase of oxygen content to 10%, in the fuel, can reduce PM2.5 emissions 60% and PN almost by an order of magnitude.

Apart from the oxygen content and chemical structure of fatty acid methyl ester (FAME) in biodiesel, particle emission also fairly correlated with some of the physical properties of biodiesel. Among them viscosity, iodine value and saponification value are prominent.

Biodiesel also influenced particles size resulting in smaller count median diameter (CMD) of particles than particles from petro-diesel in scanning mobility particle sizer (SMPS) measurement. Among the biodiesels a similar trend as to PN and PM was observed for particle size as well. It was also found that the biodiesel produced less PM and PN resulted in a smaller CMD of particles.

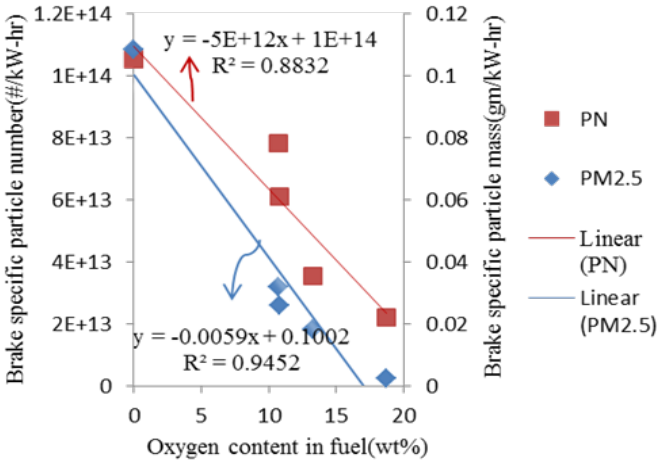

Figure1. : Variation in PN and PM with fuel bound oxygen content

The reduction of particle size for biodiesel was further revealed in Nano aerosol surface area monitor, where the overall surface area of particles from biodiesel was reasonably lower than the particles from petroleum diesel.

Hoekman, S. K., Broch, A., Robbins, C., Ceniceros, E., & Natarajan, M. (2012). Review of biodiesel composition, properties, and specifications. *Renewable and Sustainable Energy Reviews*, *16*(1), 143-169.

Ristovski, Z. D., Miljevic, B., Surawski, N. C., Morawska, L., Fong, K. M., Goh, F., & Yang, I. A. (2012). Respiratory health effects of diesel particulate matter. *Respirology*, *17*(2), 201-212.

Xue, J., Grift, T. E., & Hansen, A. C. (2011). Effect of biodiesel on engine performances and emissions. *Renewable and Sustainable Energy Reviews*, *15*(2), 1098-1116.

Preliminary measurement results on aerosol emission from materials combustion

M. Targosz*, C. Chivas-Joly, L. Saragoza, C. Motzkus, F. Gaie-Levrel

LNE, 29 Avenue Roger Hennequin, 78197 Trappes Cedex, France
Keywords: aerosol measurements, cone calorimeter, fibres emission, smoke release
Presenting author e-mail: marta-malgorzata.targosz@lne.fr

Introduction

The use of composite materials for aeronautical and naval applications becomes widespread nowadays. Due to their specific properties, composites have the potential to reduce the mass of vehicles (and thus fuel consumption) and contribute to the improvement of some other characteristics like mechanical strength and stiffness. Generalization of the use of composite materials in transportation should also reduce its environmental impact by decreasing CO_2 emissions.

However, one of the main problem of using composite materials is their behavior in case of fire, including post-crash fires. At higher temperatures, the organic matrix of composites decomposes with gaseous species and aerosols release, which toxicity aspects are still unknown. For that reason, the assessment of potential health and environmental impacts caused by the dispersion of solid and gaseous degradation products from aeronautical materials in a post-crash fire is essential.

This research project intends to understand and characterize the production of aerosols and gases from the combustion of composite materials as well as to model their dispersion into the atmosphere, based on experimental and numerical results.

Experimental setup

The fire behavior, qualitative and quantitative production of aerosol and gaseous species will be determined by using a Cone Calorimeter (CC) coupled with a set of metrological devices (Figure 1) as Dekati Low Pressure Impactor (DLPI), Dilutor L7 (hot stage dilution), Dilutor VKL10 (cold stage dilution), Condensation Particle Counter (CPC 3022), Aerodynamic Particle Sizer (APS 3321), and Scanning Mobility Particle Sizer (SMPS 3080). The morphology of aerosol particles collected on each DLPI stage will be analyzed by Scanning Electron Microscopy (SEM).

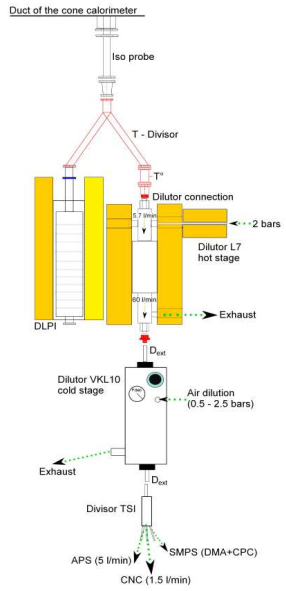

Fig.1. Experimental layout.

First results

The fire behaviour of various structural aircraft and naval composites under defined combustion conditions (75kW/m^2) has been studied in order to select materials characterized by the shortest burnthrough time, the highest level of damages, the highest yield of smoke release and the presence of volatile soot and fibers. A preliminary analysis of gaseous and solid combustion products for two selected composite materials was performed. The number of particles generated over time during combustion of MAT4 and MAT7 (epoxy resin/carbon fibers and epoxy resin/unidirectional carbon fibers, respectively) in two experiments performed for both materials, are shown in Figure 2.

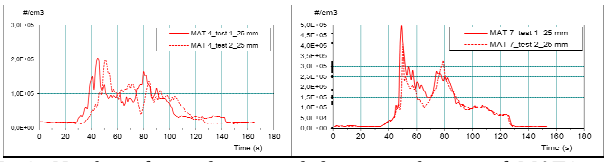

Fig.2. Number of particles emitted during combustion of MAT4 and MAT7, sample size 25x25 mm.

The SEM pictures presented in Figure 3 show the morphology of collected soot particles in the 6th and 10th DLPI stage during combustion of nanocomposite MAT4.

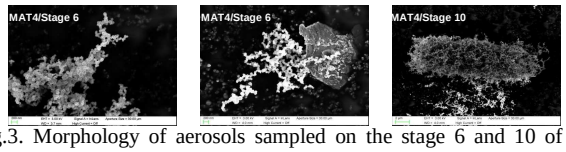

Fig.3. Morphology of aerosols sampled on the stage 6 and 10 of the DLPI during MAT4 combustion.

Conclusions

Smoke production during combustion of structural composites is related to the burnthrough test, applied fire conditions, and specifically by the presence of fibers and the nature of polymer materials. The preliminary SEM observations of the aerosol surfaces helped to identify several visible fibers depending on the composite composition. The soot particles morphology seems be different between the DLPI stages for both tested materials.

Acknowledgement

The present work was performed as a part of the DACOFEU research project within the cooperation of S. Le Névé (DGA-Aeronautical Systems), J. Gutierrez (DCNS Research), P. Boschet (EUROCOPTER) and G. Leroy (INERIS). The precious help of Prof. José-Marie Lopez-Cuesta is gratefully acknowledged.

References

Chivas-Joly, C. et al. (2010), *Influence of carbon nanotubes on fire behavior and on decomposition products of thermoplastic polymers*, Interflam 12th International Conference on Fire Science and Engineering, Nottingham, UK.

Motzkus, C. et al. (2012), *Journal of Nanoparticles Research* 14:1-17.

Office of Aviation Research Washington, (1998), D. C., *Health Hazards of Combustion Products From Aircraft Composite Materials*, Springfield, USA.

Atmospheric tar balls: primary droplets from biomass burning?

Á. Tóth[1], A. Hoffer[2], I. Nyírő-Kósa[2], M. Pósfai[1], and A. Gelencsér[1, 2]

[1] Department of Earth and Environmental Sciences, University of Pannonia, Veszprém, P.O. Box 158, H-8201, Hungary
[2] MTA-PE Air Chemistry Group of the Hungarian Academy of Sciences, University of Pannonia, Veszprém, P.O. Box 158, H-8201, Hungary
Keywords: tar ball, formation mechanism, primary emission, biomass burning.
Presenting author email: ubul.toth@gmail.com

Biomass burning is a globally important source of anthropogenic carbonaceous aerosol. Atmospheric tar balls occur in large numbers in relatively fresh biomass burning plumes (Pósfai *et al* 2003). These particles can be easily recognized by transmission electron microscopy (TEM) by their shape and composition. In contrast to other spherical aerosol types such as sulphates the amorphous, spherical tar ball particles are stable and do not volatilize under the electron beam. These particles differ from soot particles as well, since they do not contain a microstructure of concentric graphene-like layers. Due to their absorption properties tar ball particles have an important role in the Earth's radiation budget (Alexander *et al* 2008). These particles typically occur externally mixed with other particles in the atmosphere. According to elemental analyses of individual particles, tar balls consist mostly of carbon, with a minor amount of oxygen and may contain only traces of sulphur, potassium, chlorine and silicon. The average C/O molar ratio is about 10 (Pósfai, *et al* 2004).

It has been hypothesized that tar ball particles form in secondary processes from pyrolysis products in the atmosphere (Pósfai, *et al* 2004). However, these particles are homogenous, they do not contain an internal core and form a distinct group of particles with diameters up to 500 nm. On the basis of these features we now hypothesize that tar ball particles are ejected as droplets of tar, produced during the pyrolysis and are emitted from inside the vascular tissues and other pores of the burnt plants.

In this study we carried out a laboratory experiment to produce tar ball particles under conditions simulating the hypothesized formation mechanism but with the total exclusion of flame or fire. A closed all-glass apparatus was constructed in which droplets were generated from tar-water emulsion by bubbling purified air or nitrogen through it. The droplets were passed through a heated zone at 450 ^{o}C to simulate thermal processes occurring in the fire zone. Then the airflow was cooled and dried with excess dry air and the particles were collected on grids for TEM analysis.

The tar-water emulsions used in the experiments were prepared previously by dry distillation of various plants (e.g. needles of *Pinus ponderosa* and logs of Turkey oak).

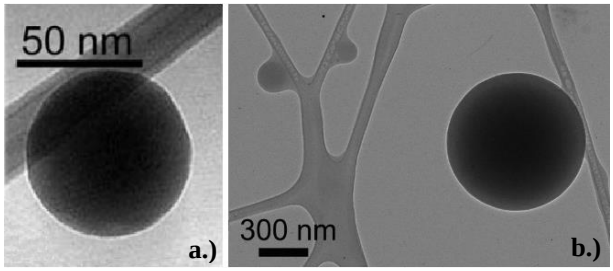

Figure 1. Bright-field TEM images of (**a.**) atmospheric tar ball (Pósfai *et al.*, 2004); (**b.**) laboratory-generated tar ball.

The morphology and elemental compositions of the particles were studied using TEM with energy-dispersive X-ray spectrometry (EDS). The generated particles were perfectly spherical and similarly to atmospheric tar ball particles, they were homogeneous (did not contain a condensation core) as it can be seen in *Figure 1b*. The C/O molar ratio of the laboratory-generated tar ball particles were also in the range reported for atmospheric tar balls. Our results imply that the suggested primary mechanism may be a feasible pathway of tar ball formation in biomass burning, but further studies are clearly warranted.

Present work was published in the frame of the project ***TÁMOP-4.2.2.A-11/1/KONV-2012-0064***. The project is realized with the support of the European Union, with the co-funding of European Social Fund.

Alexander, D. T. L., P. A. Crozier, J. R. Anderson, (2008), Brown Carbon Spheres In East Asian Outflow and Their Optical Properties, *Science*, **321**, 833.

Pósfai, M., R. Simonics, J. Li, P. V. Hobbs, and P. R. Buseck (2003), Individual aerosol particles from biomass burning in southern Africa, 1, Compositions and size distributions of carbonaceous particles, *J. Geophys. Res.*, **108** (D13), 8483.

Pósfai, M., A. Gelencsér, R. Simonics, K. Arató, J. Li, P. V. Hobbs, and P. R. Buseck (2004), Atmospheric tar balls: Particles from biomass and biofuel burning, *J. Geophys. Res.*, **109**, (D06213).

Thursday, September 5, 2013

Session: Particle-Lung Interactions, *Exposure and dosimetry*

Hygroscopic Particle Deposition Model for Rat Lungs

G.A. Ferron[1], S. Upadhyay[2], R. Zimmermann[3] and E. Karg[1]

[1]Cooperation Group "Comprehensive Molecular Analytics", Helmholtz Zentrum, 85758 München, Germany
[2]Department of Environmental and Occupational Health, University of Pittsburgh, Pittsburgh, PA 15219-3130, USA
[3]Department of Analytical and Technical Chemistry, University of Rostock, 18051 Rostock, Germany
Keywords: Rat, regional lung deposition, hygroscopic substances.
Presenting author email: karg@helmholtz-muenchen.de

During inhalation, particles are transported into the lungs and partitionally deposited. By computer models, the cumulated number, surface area or mass of the deposited particles can be calculated and related to body mass, lung surface area or cell number as a deposited dose parameter. Model calculations are a repeatedly used to estimate the deposited dose.

Usually, particle properties like sedimentation**,** diffusion and impaction are taken als the basic mechanisms for model calculations. A computer model was developed for the human airways (Ferron *et al.,* 1988) which additionally considers the hygroscopicity of the inhaled particles. This model was tested and adjusted using measured human deposition data for both non-hygroacopic and hygroscopic particles. It could be shown that there were notable differences compared to non-hygroscopic particle model calculations.

For inhalation studies, rodents are frequently used as test subjects. Here we present a model of the deposition of hygroscopic aerosol particles in the rat airways.

Table 1. The maximum and minimum ratio of the total lung deposition of a salt (drug) and a non-hygroscopic material (with a density of 1 g cm^{-3}) with the same initial dry particle size.

Substance	Max. ratio	Min. ratio
NaCl	3.28	0.57
CoCl2.6H2O	2.44	0.63
ZnSO4.7H2O	2.13	0.70
Histamine-dihydrochloride	1.86	0.65
carbenicillin-disodium	1.53	0.70
atropine sulfate	1.5	0.76

In a first step, a model for the deposition of non-hygroscopic particles in the rat lungs was derived from the human model (Schmid *et al*., 2008). As no data have been available for hygroscopic rat lung deposition, the hygroscopic model was scaled from human to rat lung conditions by physical assumptions. The lung structure of Weibel (1963) was used for the human, while the rodent airways are taken from the model of Yeh et al. (1979).

The changes by hygroscopicity are expressed as the ratio of the diameter achieved by hygroscopic growth and the initially dry particle diameter. Ratios from 0.57 to 3.28 were calculated for materials listed in Table 1 for particle diameters between 0.02 and 5 µm. The corresponding changes for human airways were higher (0.62 and 3.43), what can be explained by the smaller residence time of aerosol particles in the rat airways.

The shift of deposition curves compared to the ones for non-hygroscopic particles is nearly proportional to the growth factor (defined as the ratio of the particle size at humid and totally dry conditions). The growth factor can be calculated from a salt's physical properties for a known humidiy. It therefore can be used to estimate the deposition of an arbitrary hygroscopic material using the growth factors and deposition curves presented from the model.

As a conclusion, the hygroscopic properties of salts and drugs substancially influence the lung deposition in rodents and should therefore be considered in lung deposition modeling. The growth factor of a salt or drug can be used to estimate irs deposition.

This study is accepted for publication in J. Aerosol Med Pulmon Drug Delivery.

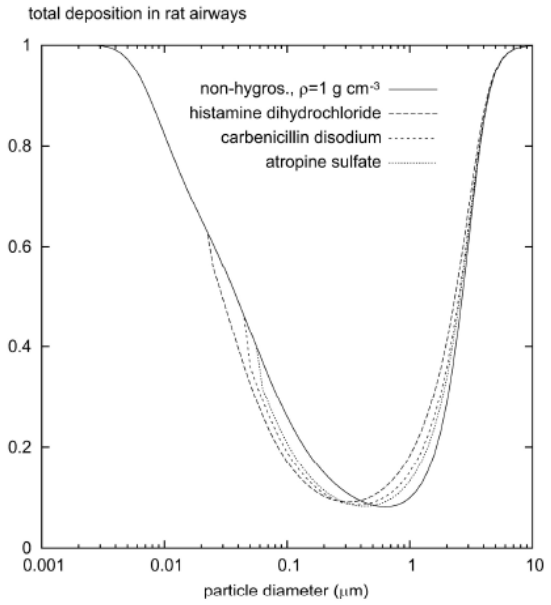

Figure 1. Total deposition in the rat lungs for non-hygroscopic particles and different drugs (Table 1).

Ferron GA, *et al.* (1988). J Aerosol Sci. **19**, 343-363 & 611-631.

Schmid O, *et al.* (2008). J Aerosol Med Pulmon Drug Delivery. 326, 291-307.

Weibel ER (1963). Morphometry of the human lung. Academic Press, New York.

Yeh HC, *et al.* (1979). Anat. Rec. 195, 483-492.

Uptake of $PM_{2.5}$ mass by respiratory tract region and particle size: Hypothetical estimates for the FINRISK Cohort, Helsinki, Finland

Hänninen O[1], Sorjamaa R[1], Lipponen P[1], Kangas L[2], Karppinen A[2], Yli-Tuomi T[1]

[1]National Institute for Health and Welfare (THL), Department of Environmental Health, Kuopio, P.O. Box 95, Finland
[2] Finnish Meteorological Institute, Helsinki, Finland

Keywords: $PM_{2.5}$, particle size dependent processes, infiltration, lung deposition
Presenting author email: otto.hanninen@thl.fi

Particle size distribution is known to affect the lung deposition. However, particle size distribution modification by infiltration has not been evaluated.

The aim of this work is to use realistic spatial and hypothetical particle size distributions in Helsinki to estimate the contribution of local tailpipe, resuspension, and long-range transported particles to the human uptakes by respiratory tract regions.

Methods. Outdoor $PM_{2.5}$ concentrations were estimated for 5700 residential locations of FINRISK cohort members in 2010 using CAR-FMI dispersion model accounting for traffic sources and background concentrations observed at Luukki station. Particle source information (tailpipe, resuspension, background) was used to estimate hypothetical lognormal source-specific particle size distributions. Unimodal lognormal size distributions were created using literature (Kleeman *et al*., 2000, Hussein *et al*., 2005, 2008) for the traffic sources. Observed monthly average size distributions at the SMEAR II Hyytiälä rural background station (DMPS+APS) were used for the regional component (Figure 1). Previously developed and evaluated particle size specific mass-balance model was used to estimate the changes in the particle size distributions by infiltration (Hänninen *et al*., 2004, 2012). ICRP 1994 model was then used to calculate the hypothetical respiratory tract uptakes assuming that the subjects spent the whole year indoors at home.

Results. Particle mass uptake was dominated by accumulation mode particles in the alveolar region, followed by same particle size range in the bronchiole and then resuspension (Dp 1-2.5 µm) particles in the alveolar region (Figure 2). When looking at particle mass, ultrafines do not dominate uptakes even in the alveolar region. Accumulation mode particles have an order of magnitude higher contribution to alveolar uptakes when ignoring times spent in traffic. Accumulation mode particles may act as carriers of ultrafines and enhance their uptake in the alveolar region. Similar findings were recently presented by Zhang *et al*., (2012) for PAHs.

This work has been supported by EU Contract FP7-ENV-2009-1-243406 (TRANSPHORM), and Academy of Finland Contract 133792 (PM Sizex).

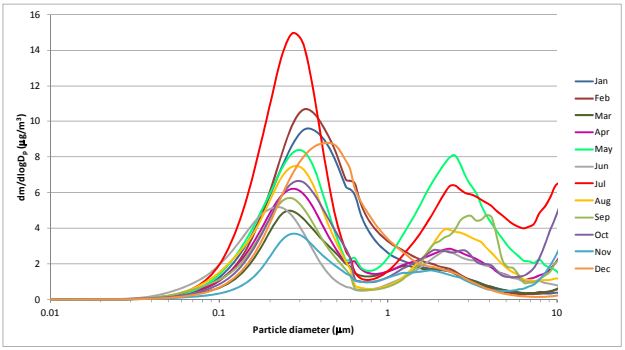

Figure 1. Monthly particle mass distributions from SMEAR II station located in Hyytiälä, Finland, 2010.

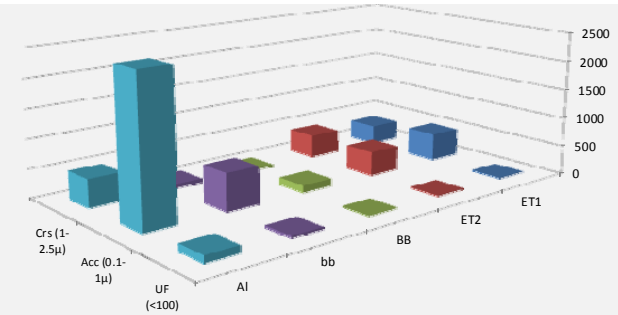

Figure 2. Annual PM mass uptake (µg) by respiratory tract region (x-axis) and particle size category (z-axis).

Hänninen, O., Lebret, E., Ilacqua, V., Katsouyanni, K., Künzli, N., Srám, R.J. and Jantunen, M. (2004) *Atm.Env.* **38**, 6411 – 6423.

Hänninen, O., Sorjamaa, R., Pekkanen, J., Lanki, T. and Cyrys, J. (2012) *Proc. Of Congress on Air Quality*, Athens, Greece.

Hussein, T., Hämeri, K., Aalto, P.P., Paatero, P., and Kulmala, M., 2005. Modal structure and spatial-temporal variations of urban and suburban aerosols in Helsinki-Finland. *Atm. Env*. **39**, 1655-1668.

Hussein, T., Johansson, C., Karlsson, H., and Hansson, H.-C., 2008. Factors affecting non-tailpipe aerosol particle emissions from paved roads: On-road measurements in Stockholm, Sweden. *Atm. Env*. **42**, 688-702.

Kleeman, M. J., Schauer, J. J., and Cass, G. R., 2000. Size and composition of fine particulate matter emitted from motor vehicles. Environ. Sci & Tech. **34**, 1132-1142.

Zhang, K., Zhang, B.-Z., Li, S.-M., Wong, C. and Zeng, E.Y. (2012) *Sci. Tot. Env.* **431**: 245-251.

Exposure to Particulate Matter and Pulmonary Function Status of Traffic wardens in Two Selected Local Government Areas in South-Western Nigeria.

Godson R.E.E Ana (PhD)[1], Oluseye J. Olamijulo (MPH)[1]

[1]Department of Environmental Health Sciences,
Faculty of Public Health, College of Medicine,
University of Ibadan, Ibadan, Nigeria.
Key Words: Particulate matter, pulmonary function, urban communities, Ibadan

Presenting author email: johnette07@yahoo.com

Abstract

Vehicular emissions are a complex mix of pollutants. Although data on road traffic emissions are available in Nigeria, information as regards the personal exposure of traffic wardens to particulate matter is lacking. We determined the levels of particulate matter and then assess its effect on the pulmonary function of traffic wardens.

Ibadan North and Northeast Local Government Areas were purposely selected for this descriptive cross-sectional study. Concentration of particulate matter was measured using personal respirable dust sampler model APM 801 within 30cm range of the traffic wardens' nasal region and values were compared with WHO guideline limit. Measurements were done in the morning (6am-8am), afternoon (12pm-2pm) and evening (4pm-6pm). A calibrated spirometer was used to determine the Force Expiratory Volume in 1 second (FEV_1) of traffic wardens. Data were analyzed using descriptive statistics, t-test and Pearson correlation test at P = 0.05.

The mean concentration of particulate matter recorded in the afternoon was 28.1± 11.5µg/m^3. This value exceeded the WHO guideline limit for particulate matter (25µg/m^3). The peak concentration of particulate matter (49.01µg/m^3) was obtained in the evening. There was a significant difference between the actual $FEV_1$of the Traffic wardens (2.21±0.71L) and their expected FEV_1 (4.01±0.57L). A significant negative correlation was observed between particulate matter and the actual FEV_1 of Traffic wardens (r = - 0.6).

Traffic wardens are highly vulnerable to respiratory impairment due their exposure to particulate matter at concentrations that exceed WHO guideline limit. The use of nose mask and regular health check up is recommended.

Dynamics of highly concentrated, fresh aerosols during inhalation

L. Pichelstorfer and W. Hofmann

Department of Materials Research and Physics, University of Salzburg, 5020 Salzburg, Austria
Keywords: Coagulation, phase transition, heat/vapour transport
Presenting author email: Lukas.Pichelstorfer@sbg.ac.at

To assess health risks due to aerosol exposure, information on local particle as well as vapour deposition is crucial. Airborne particles that contain volatile substances are, in terms of mass transport, permanently interacting with the surrounding gas phase. Therefore, reducing aerosol dynamics to particle-particle interaction is not appropriate in many cases. While coagulation is basically a function of particle number and shape of the size distribution, phase transition also strongly depends on energy balances and composition of particle and vapour.

To simulate aerosol dynamics of a fresh and highly concentrated aerosol within the human respiratory system, we assumed that the incoming aerosol is in thermodynamic equilibrium with its surrounding. This assumption is necessary to assess the initial microscopic particle composition. Then aerosol dynamics, including coagulation, heat and vapour transport between the particulate and the vapour phase, and between the system boundary and the vapour phase, as well as phase transition, were computed. The effects of coagulation and phase transition as well as the superposition of both processes on the initial particle size distribution are depicted in figure 1, where phase transition implicitly shows the effect of heat and vapour transfer on the aerosol.

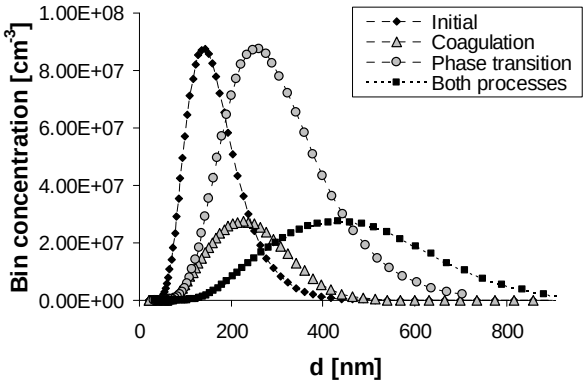

Figure 1: The influence of coagulation and phase transition on the initial particle size distribution.

As an example, we chose to simulate the evolution of a cigarette smoke particle size distribution measured by Ingebrethsen (2011). Further inputs are experimentally determined particle and vapour composition (Davies and Vaught, 2003; Lipowicz and Piadé, 2003). The initial particle size distribution has a concentration of 1.54 x 10^9 particles per cm^3. Its shape is lognormal with an average particle diameter of 150 nm and a geometric standard deviation of 1.44. Initial vapour humidity was assumed to be 75% in case of water and 7.9% in case of nicotine. Based on these assumptions initial water and nicotine fractions were computed for the particulate phase as a function of particle diameter.

The most important effect in the oral region is coagulation. Within a puffing period of 2 s and a subsequent 1 s breath hold, particles below 100 nm are almost reduced to zero, whereas particles larger than 250 nm are newly formed. Furthermore, the total particle concentration is reduced by about 70% from 1.54 x 10^9 cm^{-3} to 5.2 x 10^9 cm^{-3}.

Phase change strongly depends on the speed of water vapour transport from the system wall towards the vapour and on the removal of latent heat which is produced by condensation of water vapour on the particle surface. In the present simulation, phase change effects coagulation by a) reducing the diffusivity of the particles and by b) widening the particle size distribution. The reduced diffusivity is caused by the increasing particle diameter. This reduces thermal coagulation which was found to be the biggest contributor to total coagulation. On the other hand, phase transition widens the size distribution since the growth factor increases with increasing particle diameter. This has a positive effect on the thermal coagulation rate. The simulated net change of coagulation by phase transition is in the order of a few percent of the initial particle concentration.

Note that coagulation, phase transition and heat and vapour transport show strong interactions. Coagulation affects phase transition by changing particle composition particle number and the shape of the size distribution. Phase transition strongly depends on the supply of condensable vapour and the removal of latent heat. Heat and vapour transport also determines whether and where volatile substances are deposited.

This aerosol dynamics model, which in principle can be incorporated into any deposition model, will be implemented into the stochastic deposition model IDEAL (Koblinger and Hofmann, 1990), considering dilution, deposition, coagulation and phase transition.

Davies, H.M., and Vaught, A. (2003) *The Reference Cigarette*. KentuckyTobacco Research & Development Center, Lexington, KY, 2003

Ingebrethsen, B.J., Alderman, S.L., and Ademe, B. (2011) *Aerosol Sci. Technol*. **45:12**, 1422-1428.

Koblinger, L. and Hofmann, W. (1990) *J. Aerosol Sci.* **21**, 661-674.

Lipowicz, P.J., and Piadé, J.J. (2004) *J. Aerosol Sci*. **35**, 33-45.

Mechanistic exposure assessment of ultrafine PM

D.A. Sarigiannis[1,2], Z. Samaras[3], E. Vouitsis[3], S. Karakitsios[1] and V. Kalaitzis[1]

[1]Department of Chemical Engineering, Aristotle University of Thessaloniki, Thessaloniki, 54124, Greece
[2]Centre for Research and Technology Hellas (CE.R.T.H.), Thessaloniki, 57001, Greece
[3]Department of Mechanical Engineering, Aristotle University of Thessaloniki, University Campus, 54124, Thessaloniki, Greece
Keywords: PM number distribution, PM exposure, lung deposition.
Presenting author email: denis@eng.auth.gr

Exposure to PM is linked to various acute and long-term health effects; however the lack of in depth understanding of the mechanisms of toxicity obfuscates targeted risk assessment possibly resulting in overly conservative risk management. To better understand the etiology of the association between PM air pollution and human disease, a better understanding of the actual exposure to different PM size fractions and the relevance of deposition and toxicity mechanisms to the observed health outcomes is needed. The above elucidate the need to use more informative PM exposure metrics taking into account not only the overall mass concentration, but also the corresponding Particle Number Count (PNC), as a descriptor of the size distribution of airborne particles.

The study includes a set of Ultra Fine Particles (UFP) measurements and exposure modeling including deposition across human respiratory tract (HRT). The UFP measurements were carried out in two urban sites in the city of Thessaloniki (traffic and an urban background one). In both sites, fixed monitoring stations of the regulatory monitoring network exist, providing average daily data for PM10 and PM2.5. PM concentration data comprise the input for a detailed exposure model which incorporates the dependence of inhalation rate on type of activity. The output of the exposure model is the input for the HRT Multiple-Path Particle Dosimetry (MPPD) model, which is used to estimate the deposition distribution of particles of different aerodynamic diameters.

The annual $PM_{10}/PM_{2.5}$ concentrations for the two stations are 54/38 μg/m^3 (traffic station) and 33/23 μg/m^3 (background station) respectively. Although the $PM_{10}/PM_{2.5}$ ratio between the two sites does not differ substantially, the differences are much larger when it comes to PNC (77149 and 32459 particles/cm^3) – the corresponding UPFs mass concentration at the traffic and the background station is estimated equal to 5.9 and 2.4 μg/m^3 respectively. Averaging the data from all measurements, the geometric mean diameter (GMD) for the traffic site is equal to 35.7 (sd 1.76) nm, while for the background site the corresponding value is equal to 44.7 (sd 1.99) nm. GMD intra-day variability is wider for the urban site, fluctuating between 32.4 to 50.6 nm (Figure 1). This variation is inversely correlated to traffic intensity; the higher the intensity of traffic (and consequently, traffic emissions), the smaller are the UFPs. The urban background monitoring station is located in such a way so as the sampled air is well mixed, allowing the smaller particles to be subjected to processes such as nucleation and hydroscopic growth.

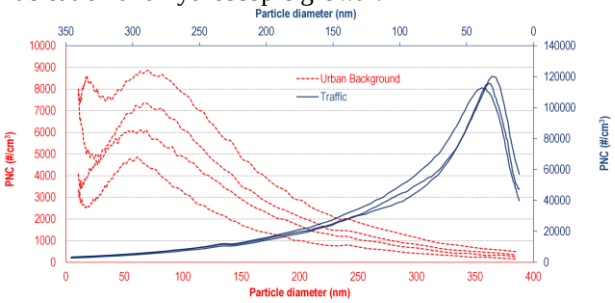

Figure 1. Typical particle count number distributions during peak hours.

To capture the implications of these dynamic processes for the overall UFP exposure, an exposure scenario was built (exposure for 2 hours per day, 5 days per week). This is very important, since different size particles tend to deposit at different fractions along the respiratory tract. The results indicated that exposure between the two measurements sites correspond to significantly different HRT deposition patterns, especially with respect to the lower respiratory tract, the overall deposition is almost four times higher at the traffic site vs. the urban background site (25.4 and 7 μg deposited respectively). This variation is reflected neither in the overall UFP PNC, nor in the PM10 and PM2.5 mass concentrations, which are monitored daily in the respective sites (Figure 2).

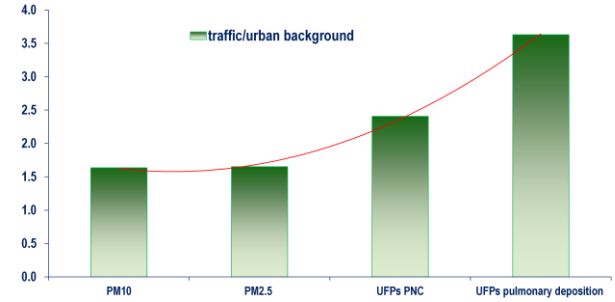

Figure 2. Non-linearity characterizing different PM exposure metrics.

The differences identified above, pose the question to what extent, the currently used concentration-response functions associating coarse and fine PM to mortality and morbidity reflect properly the causal association between actual exposure and health effects.

Using cloud motion for fast, efficient and realistic *in vitro* delivery of inhaled drugs to pulmonary cells

A.G. Lenz[1], D. Cei[1,3], M. Schmidmeir[1], N. Pfister[1], G. Burgstaller[1], B. Lentner[1], O. Eickelberg[1,2], T. Stoeger[1], S. Meiners[1], and O. Schmid[1]

Comprehensive Pneumology Center (CPC-M), [1]Institute of Lung Biology and Disease, Helmholtz Zentrum München, 85764 Neuherberg, Germany and [2]University Hospital of the Ludwig Maximilians University (LMU), Member of the German Center for Lung Research (DZL), Munich, Germany
[3]Research Center E.Piaggio, University of Pisa, Pisa, Italy

Keywords: pulmonary drug delivery to cells, air-liquid interface, cloud effects
Presenting author email: otmar.schmid@helmholtz-muenchen.de

Chronic lung diseases such as chronic obstructive pulmonary disease, lung cancer, and asthma are the second leading cause of death worldwide (WHO). Currently, there is no causal cure for any of these diseases. Hence, research in this field is expected to intensify significantly in the upcoming years. In addition, recent technological advances in inhalation technology have provided highly efficient, breath-controlled inhalation devices which are making inhaled drugs increasingly more attractive not only for the treatment of lung disease, but also for non-invasive systemic drug delivery. However, the preclinical development of aerosolized drugs for inhalation therapy is hampered by the lack of easy-to-use and yet efficient *in vitro* methods for aerosol-to-cell drug delivery.

Our study describes an innovative droplet-to-cell delivery system for Air-Liquid Interface Cell Exposure (ALICE-CLOUD), which utilizes the principles of cloud physics to close this gap (Lenz et al., 2009). The ALICE-CLOUD is designed for preclinical testing of aerosolized liquids/drugs at physiologically realistic (air-liquid interface) cell culture conditions. The underlying principle of cloud motion and the physical performance of the system are described. As a biological proof-of-concept study we apply this technology to test the inflammatory efficacy of aerosolized Bortezomib - a FDA-approved proteasome inhibitor for systemic cancer treatment – which has not been used for inhalation therapy, yet.

An aqueous fluoresceine solution was used to characterize the physical performance of the ALICE-CLOUD. Figure 1 shows that nebulization of 200 µl of aqueous fluoresceine (5 µg/ml) with an AeronebPro vibrating membrane nebulizer (MMD ~ 5µm; Aerogen Inc.) is completed within 180 s, where 95% of the final (asymptotic) dose is delivered already 100 s after initiating nebulization. In this period of time 88+/-12% (95% CL) of the nebulized liquid is deposited onto the bottom plate of the ALICE-CLOUD, where a standard multi-well plate for cell culturing is placed (here: 6-well plate with transwell insert for air-liquid interface cell cultures). This corresponds to a cell delivery efficiency of 19% (6-well insert) due to limited cell coverage in standard multi-well plates. The dose variability between different transwell inserts is <15% (95% CL) and the aerosol-to-cell delivery rate is 0.5 µl drug per cm^2 cell area per minute.

In a biological proof-of-concept study we stimulated human alveolar lung cells (A549) with TNF-α to induce an inflammatory response (here: 8-fold activation of the IL- promoter after 24h). Simultaneous application of a single dose of aerosolized Bortezomib with the ALICE-CLOUD reduced proteasome activity by up to 80% without impairing cell viability (WST-1 and LDH assays). A significant reduction of the IL-8 level and hence a therapeutic effect was observed after nebulising 200 µl of >100µM Bortezomib solution. Comparative dose-response measurements using submerged cell cultures and non-nebulized Bortezomib revealed that the cell-specific efficacy of nebulized and non-nebulized Bortezomib is similar.

The ALICE-CLOUD technology is a compact, efficient and simple to operate system for screening for inhalation drugs. Our data suggest that Bortezomib can be aerosolized without loss of efficacy to mediate potent anti-inflammatory effects on a human lung cells. Hence, Bortezomib is a promising candidate drug for inhalation therapy.

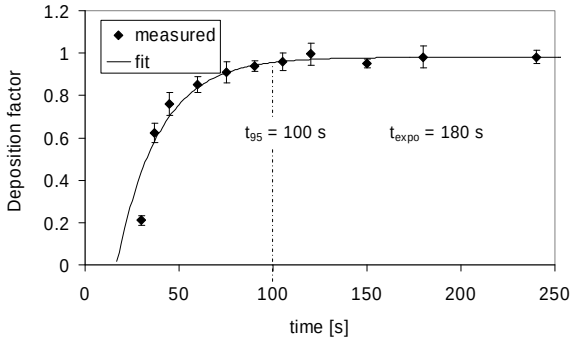

Figure 1. Time course of aerosol deposition onto cells in the ALICE-CLOUD (unity corresponds to 100% of the invested liquid is evenly distributed onto the bottom plate of the ALICE-CLOUD)

This study was supported by the German Federal Ministry of Education and Research within the Leading-Edge Cluster “m4 – Personalized Medicine” in Munich.

Lenz, A.G., Karg, E., Lentner, B., Dittrich, V., Brandenberger, C., Rothen-Rutishauser, B., Schulz, H., Ferron, G. A., Schmid, O., *Part. Fibre Toxicol.* , 32, doi:10.1186/1743-8977-6-32, 2009

Release of fine particles from birch pollen grains following impaction

N. Visez[1], M. Choël[2], G. Loubert[1], G. Chassard[1], D. Petitprez[1]

[1]PhysicoChimie des Processus de Combustion et de l'Atmosphère, UMR 8522 CNRS Université Lille 1, Villeneuve d'Ascq, 59655, France
[2]Laboratoire de Spectrochimie Infrarouge et Raman, UMR 8516 CNRS Université Lille 1, Villeneuve d'Ascq, 59655, France
Keywords: Birch pollen, Ozone, Asthma, Granule.
Presenting author email: nicolas.visez@univ-lille1.fr

Dispersion of pollen allergens in the fine (ie. respirable) particle fraction is a major concern for allergenic asthma. Release of cytoplasmic particles may occur through hydration or germination of the pollen (Schäppi *et al*, 1997). Moreover, air pollution has been shown to facilitate pollen rupture (Motta *et al*, 2006). In this work, we have investigated rupture of the pollen and subsequent release of cytoplasmic particles following a mechanical stress generated with a PM_{10} impactor.

Experimental conditions. Birch pollen grains (ca. 20 µm) were aerosolized in the laboratory into a synthetic air flow of 10 $L.min^{-1}$ and sent into an impactor (Dekati) equipped solely with a PM_{10} stage. Particle size distributions were measured at the outlet of the impactor with an Aerosol Particle Sizer (TSI 3321). Impaction tests were also done with pollen grains artificially polluted with 3 ppm of ozone for 4 hours. Particle size distributions were normalised to show an equal number of pollen grains at 17 µm. All experiments were done in triplicate. For the purpose of FEG-SEM imaging, experiments were done with PM_{10} and PM_1 stages. Particles impacted were collected onto adhesive conductive carbon tapes for investigation of structural damage of the grains.

Results. Comparison of size distributions for native pollen and impacted pollen shows formation of an aerosol composed of fine particles with two size modes centred at 0.7 and 2.0 µm (figure 1). Formation of those particles was surprisingly smaller with ozone-polluted pollen. Pollen has been probably dried by the flow of synthetic air during the ozone exposure suggesting a role of the water content of the grain.

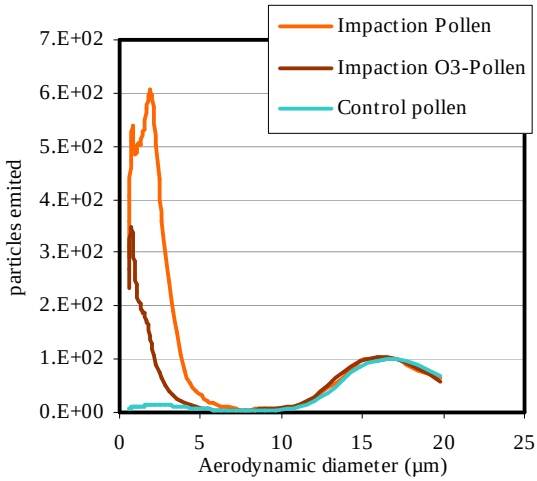

Figure 1. Normalised particle size distributions measured for aerosolized pollen (control run) and for pollen impaction (O_3-polluted or not).

Morphological examination of the sampling on PM_{10} stage by SEM revealed that a number of birch pollens were broken (figure 2). Small particles of micrometric size and ovoid shape were observed in PM_1 fraction (not shown).

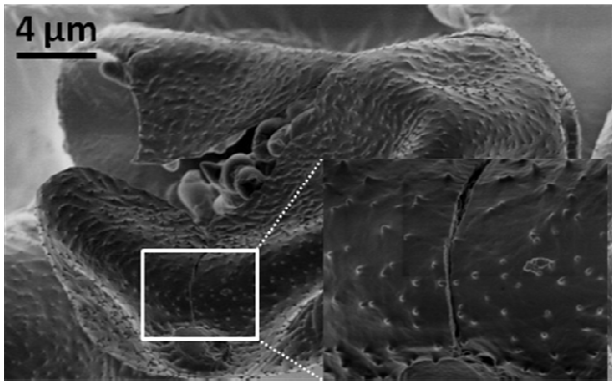

Figure 2. SEM image of a damaged pollen grain exhibiting a large fracture enabling the release of cytoplasmic granules. Insert: enlarged view of a crack in the exine.

Conclusion. Our results show that impaction on a solid surface at wind speed of about 3 $m.s^{-1}$ can induce birch pollen grain rupture. To the best of our knowledge, we gave evidence for the first time of a new mechanism for the release of respirable particles from birch pollen directly in an aerosol phase. Mechanical rupture may occur for pollen through wind transportation but also during pollen sampling by impaction. This latter is of particular importance for an artefact-free detection of allergens on fine particles by use of a multi-stage cascade impactor.

This work was supported by Région Nord Pas-de-Calais, Ministère de l'Enseignement Supérieur et de la Recherche, CNRS, Université Lille 1, European Regional Development Fund (ERDF) and IRENI (Institut de Recherche en ENvironnement Industriel).

Motta, A., Marliere, M., Peltre, G., Sterenberg, P., Lacroix, G. (2006). *Int. Arch. Allergy Immunol.*, 139, 294-298.

Schäppi, G.F., Taylor, P.E., Staff, I.A., Suphioglu, C., Knox, R.B. (1997). *Sex. Plant Reprod.*, 10, 315-323.

Thursday, September 5, 2013

Special Session: Combustion Aerosols, *Composition and health effects*

Chemical Properties of Combustion Aerosols: An Overview

M.D. Hays[1]

[1]U.S. Environmental Protection Agency, Office of Research and Development, RTP, NC, 27711, USA

Keywords: fine particle matter, organic carbon, black carbon, organic markers
Presenting author email: hays.michael@epa.gov

A wide variety of pyrogenic and anthropogenic sources emit fine aerosols to the atmosphere. The physical and chemical properties of these aerosols are of interest due to their influence on climate, human health, and visibility.

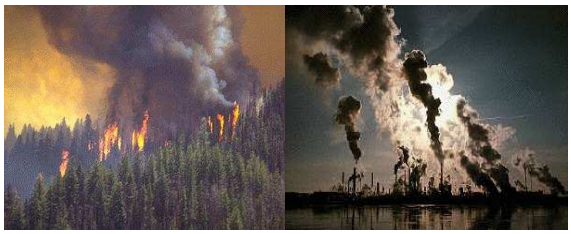

Figure 1. Two combustion source types: Biomass burning and industrial-based.

Aerosol chemical composition is remarkably complex. Combustion aerosols can comprise tens of thousands of organic compounds, refractory carbon, metals, cations, anions, salts, and other inorganic phases and substituents [*Hays et al.*, 2004]. Aerosol organic matter normally contains semivolatile material that partitions between the gas-, liquid-, and particle-phases, a process controlled by dynamic equilibrium or interfacial mass transfer considerations. Volatile and semivolatile gas-phase organic matter can undergo photo-oxidation in the atmosphere, creating particle nuclei or growing particles further via condensation. This diverse chemistry and processing of combustion emissions aerosols produces distinct particle morphology and nanostructure that is heterogeneous, which in turn contributes to the optical properties, aerodynamic nature, and thus fate and transport of these aerosols [*Hays and VanderWal*, 2007].

Exhaustive determination of the complex chemical nature of combustion aerosols requires utilizing a series of advanced analytical techniques. *The focus of this talk is the analytical measurements that have evolved in the aerosol and combustion science community for reliably measuring chemical composition.* The use of both real-time and laboratory-based instrumentation will be covered. What will be shown is how real-time particle instrumentation has improved our ability to monitor: (i) transient combustion events; (ii) single black carbon (BC) particles; (iii) the extent of volatile organic mass coating BC, and (iv) organic composition at low aerosol mass. Photoacoustic spectroscopy, laser incandescence methods, and mass spectroscopy-based applications central to aerosol investigations are topics of interest.

In addition, the benefits and disadvantages of off-line laboratory techniques will be considered with regard to combustion aerosol composition. The use of X-ray fluorescence spectroscopy (XRF) and inductively coupled plasma-mass spectroscopy (ICP-MS) for metals will be included together with the high-vacuum electron microscopy techniques that are capable of not only measuring heterogeneous micro- and nano-structure (Figure 2) but of also detecting metal inclusions in combustion soot mixtures.

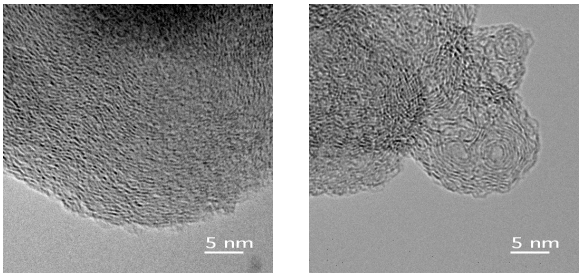

Figure 2. High-resolution transmission electron microscopy (HR-TEM) of oil boiler soot (left) and aircraft engine soot (right).

Finally, the application of liquid and gas chromatography (LC and GC) for the identification of novel organic markers in biomass burning and anthropogenic aerosols will explored. In specific, the use of two dimensional GC methods and hyphenated MS techniques for identifying organic nitrogen compounds will be further considered [*Ma and Hays*, 2008; *Samy et al.*, 2011]. The effects of sampling methods on detection limits and organic analyte concentration measurements will be discussed as well.

Hays, M. D., N. Smith, and Y. Dong (2004) *J. Geophys. Res.*, *109, D16*, D16S04.

Hays, M. D., and R. L. VanderWal (2007) *Energy Fuels*, *21*(2), 801-811.

Ma, Y., and M. D. Hays (2008), *J. Chrom. A*, *1200*(2), 228-234.

Samy, S., J. Robinson, and M.D. Hays (2011), *Anal Bioanal Chem*, *401*(10), 3103-3113.

Chemical, physical and toxicological properties of biomass combustion aerosols

M-R. Hirvonen[1,2], J. Jokiniemi[1,3]

[1]University of Eastern Finland, Department of Environmental Science, FI-70211, Kuopio, Finland
[2]National Institute for Health and Welfare, Department of Environmental Health, FI-70701, Kuopio, Finland
[3] VTT Technical Research Centre of Finland, Fine Particles, FI-02044 VTT, Espoo, Finland
Keywords: Biomass combustion, Particulate matter
Presenting author email: Maija-Riitta.Hirvonen@uef.fi and Jorma.Jokiniemi@uef.fi

Combustion emissions from traffic (e.g. Janssen et al. 2002), energy production with coal and oil (e.g. Clancy et al. 2002) and heating with wood (e.g. Schreuder et al. 2006) have emerged as the main sources behind the adverse health effects. The causality between physico-chemical characteristics and toxicological properties of particulate emissions from the heating appliances, engine types and fuels are poorly understood. In search for the key components and properties of biomass combustion emissions that cause the observed health related toxicological responses, we have used multidisciplinary experimental approach. Particulate emissions from modern new and old technology combustion appliances, combustion conditions and fuels were investigated for their physicochemical and health related toxicological properties. PM_1 samples were collected from different modern and old technology heating appliance emissions using Dekati Gravimetric Impactor (DGI) after porous tube diluter (PRD). Thereafter, the samples were weighed and extracted with methanol for subsequent toxicological and chemical analyses.

Gaseous emissions were measured with FTIR (Gasmet technologies) from the stack. PM_1 samples were collected for OC/EC analyses with filter holders (Gelman Sciences 2220) from diluted flue gas. Particle emissions were measured with on-line measurement instruments: ELPI (Dekati), SMPS (TSI) and TEOM (Thermo Scientific).

In *in vivo* studies, healthy C57BL/6J mice were intratracheally exposed dose and time dependent manner. After the exposure, bronchoalveolar lavage fluid (BALF) was assayed for indicators of inflammation, cytotoxicity and genotoxicity. In *in vitro* studies, the mouse RAW 264.7 macrophages or human lung epithelial cell line A549, were exposed to different doses of PM_1 samples for time. Thereafter, inflammatory, cytotoxic and genotoxic markers were detected as well as changes in the cell cycle.

The fine particles from wood-fired combustion were composed mainly of ash (alkali), condensed organic material and soot. The principal factors of ash particle emissions were attributed to combustion temperature affecting the mass of volatilised ash, cooling rate of exhaust gas and composition of fuel affecting on elements released (K, Na, S, Cl, Zn, Pb, Ca…). The organic fraction was low in continuous burning and it can be reduced also in batch combustion by controlling the location of air injection and mixing in the burning chamber.

In general the highest emissions were in incomplete combustions situations like firing phase and smouldering combustion and lowest in the continuous burning of wood chips and pellet. In the batch burning the average PM1 emission was about 100 mg/MJ, in the effective devices about 50 mg/MJ. In the continuous burning PM1 emission was 5 – 30 mg/MJ. The number emissions were 10^{13} – 10^{14} #/MJ and did not correlate with other emission compounds. The particle average size varied between 80 to 200 nm. The size distributions were usually unimodal and shape of particles were agglomerates, covered by organic material in incomplete situations.

Most of the PM samples from the studied appliances caused dose dependent increase in at least some of the toxicological parameters in the exposed cells. Emissions from old technology appliances with incomplete combustion were in most cases more potent inducers of toxicological responses than those from the new technology appliances with more complete combustion. However, the results indicated that also the modern wood combustion appliances and optimal burning conditions may emit particles evoking high cytotoxicity and clear cell cycle arrest. Moreover, all the studied combustion particles caused DNA damage both in the mouse and in the human cell line, but the magnitude of the response was largely different between the samples. These genotoxic responses were associated with increased PAH levels, but there seem to be also other species of organic matter and metals in PM harboring toxicological potential both *in vitro* and *in vivo*. It is noteworthy that the old technology appliances had larger mass emissions than the new technology appliances, which emphasizes the differences. Thus, the promotion and supporting of technologies that ensure efficient and complete combustion and avoid high soot and PAH combustion sequences is motivated of both public health and climate impact reasons.

This study was supported by the Academy of Finland, the Finnish Funding Agency for Technology and Innovation, industry and strategic funding of the University of Eastern Finland for project sustainable bioenergy, climate change and health.

Biological effects of ship diesel exposure on human bronchial epithelial cells – effects of gas phase vs. particle phase of different fuels at the air liquid interface -

S. Oeder[1,6], O. Sippula[2,3,6], B. Stengel[4,6], R. Rabe[4], H. Harndorf[4,6], H. Paur[5,6], C. Schlager[5], E. Karg[2], T. Streibel[2,6], C. Schmidt-Weber[1], R. Zimmermann[2,6], J.T.M. Buters[1,6]

[1] ZAUM- Center of Allergy and Environment, TUM/Helmholtz Zentrum München, Germany, D; [2] Joint Mass Spectrometry Centre, Rostock University (Analyt. Chem.)&Helmholtz Zentrum München (HMGU/CMA), D; [3] Department of Environmental Science, University of Estern Finland, Kuopio, Fi; [4] University of Rostock, Inst. of Piston Machines & Int. Combust. Engines and Inst. of Physics, D; [5] KIT (ITC/ITG), Karlsruhe, D; [6] HICE – Helmholtz Virtual Institute of Complex Molecular Systems in Environmental Health-Aerosols and Health, www.hice-vi.eu

Keywords: ship diesel, toxicity, health, air-liquid interface.

Introduction: Combustion aerosols cause a wide range of health effects and influence the pathophysiology of many diseases. The Virtual Helmholtz Institute HICE addresses the health effects of anthropogenic combustion processes. This is performed by means comprehensive characterization of the chemical and physical properties of combustion aerosols as well as the biological effects on cell cultures. To get a comprehensive picture of how these health effects are influenced, the entity of metabolic pathways has to be analyzed. Metabolism strongly depends on metabolic active enzymes and other proteins. The availability of these proteins is determined by the expression of the respective gene. Therefore gene expression represents one first step in regulation of metabolism. As gene expression is highly influancable by environmental agents, we studied within HICE the transcriptome (entity of gene transcripts) of bronchial epithelial cells that were directly exposed to combustion aerosols at the air-liquid interface.

Methods: Within the ship diesel sampling campaign in Rostock, Germany, human immortilized bronchial epithelial cells (BEAS-2B) where exposed to the complete combustion aerosol (including particles) and to the gas phase of the combustion aerosol alone (filtered aerosol). The aerosol was generated in a ship engine being operated with light and heavy fuel oil (LFO and HFO). Cells were exposed in the "HICE exposure system" at the air-liquid interface for 4 hours to clean air diluted exhaust (1:40 for LFO and 1:100 for HFO). Subsequently cells were lysed and frozen. RNA extraction was conducted using Rneasy columns (Qiagen). RNA quantity was measured by UV/VIS spectrophotometry (Nanodrop, Qiagen) and RNA integrity was assessed after electrophoretic separation (Bioanalyzer, Agilent). Whole transcriptome analysis was performed on Sure Print G3 human gene expression microarrays using single color Cy3 labeling (Agilent). Statistics on transcriptome data and pathway analysis were done using GeneSpring software (Agilent).

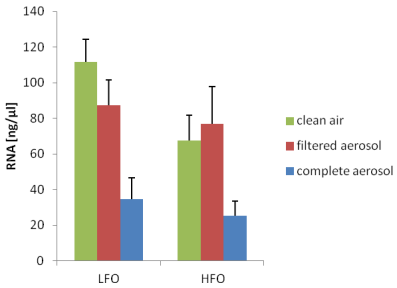

Figure 1. RNA yield after ship diesel exposure

Results: Exposure to the combustion aerosol caused clear decrease in total RNA, indicating cellular toxicity of LFO. Though higher diluted, HFO caused the same toxic effect compared to LFO. Especially changed were genes that code for proteins that are necessary for translation of RNA into proteins (cytoplasmic ribosomal proteins), for proteins of the energy metabolism (electron transport chain and oxidative phosphorylation), for cellular signal transduction (G-protein coupled receptors), for phase I and phase II enzymes of xenobiotic metabolism (cytochrome P450, phase-1-functionalization of compounds, metapathway biotransformation), for proteins of immunomodulatory interactions and for blood clotting. For most of the genes regulation was much stronger after exposure to the complete combustion aerosol than to the gas phase of the aerosol alone.

Conclusion: Ship diesel combustion aerosol increased the general activity status of the bronchial epithelium (translational activity, energy metabolism) and induced specific cellular signaling. The induction of xenobiotic metabolism indicates the presence of organic compounds and increases the risk of an activation of these substances into toxic metabolites. Further health hazard stems from the induction of blood clotting. These effects seem to be caused by the particles or by substances that are attached to the combustion particle cores, because the gas phase alone had much weaker effects.

This work and HICE (www.hice-vi.eu) is supported by the Impulse and Networking funds of the Helmholtz association (HGF) and by CK-CARE.

Health relevant compounds in wood combustion and ship diesel aerosols: Evaluation of the toxicity due to polycyclic aromatic hydrocarbons

J.Orasche[1, 13], T.G.Dittmar[2, 13], T.Kanashova[2, 13], J.Buters[3, 13], S.Öder[3, 13], H.Paur[4, 13], C.Schlager[4], S.Mülhopt[4], M.Dilger[4, 13], C.Weiß[4, 13], S.Diabate[4], H.Harndorf[5, 13], B.Stengel[5, 13], R.Rabe[5], K.Hiller[7, 13], S.C.Sapccariu[7, 13], K.A.BeruBe[8, 13], A.J.Wlodarcyzk[8, 13], O.Sippula[1, 6, 13], J. Jokiniemi[6, 11, 13], M.-R. Hirvonen[6, 12, 13], B.Michalke[9], T.Krebs[10, 13], M.Kelbg[5, 13], J.Tiggesbäumker[5, 13], T. Streibel[1], E.Karg[1], G.Abbaszade[1], S.Scholtes[1, 13], J.Schnelle-Kreis[1], J.Lintelmann[1], M.Sklorz[1], M.Arteaga Salas[1, 13], S.Klingbeil[1, 13], P.Richthammer[1, 13], L.Müller[1, 13], M.Elsasser[1], A.Rheda[1], B.Werner[1, 13], J.Passig[1, 13], T. Gröger[1, 13], C.Radischat[1, 13], R.Zimmermann[1, 13]

[1]Joint Mass Spectrometry Centre, Rostock University (Analyt. Chem.) & Helmholtz Zentrum München (CMA), D; [2]MDC, Berlin, D; [3]ZAUM, Technical University Munich, D; [4]KIT (ITC/ITG), Karlsruhe, D; [5]University of Rostock (Inst. of Piston Machines & Inst. Combust. Engines and Inst. of Physics), D; [6]University Eastern Finland-Kuopio; [7]Uni. Luxemburg; [8]Cardiff University, UK; [9]Helmholtz Zentrum München (BGC), D; [10]Vitrocell GmbH, Tübingen, D; [11]VTT Technical Research Centre of Finland; [12]National Institute for Health and Welfare, Kuopio, Finland; [13]HICE Helmholtz Virtual Institute of Complex Molecular Systems in Environmental Health - Aerosols and Health, www.hice-vi.eu

Keywords: toxicity equivalent, PAH, ship-engine emissions, wood combustion
Presenting author email: juergen.orasche@helmholtz-muenchen.de

A globalization of trade is responsible for a steady increase of navigation on the seven seas. The ship engines are suitable to be operated with heavy fuel oil (HFO). HFO, more or less the residual of oil refining, contains high amounts of heavy metals and polycyclic aromatic hydrocarbons (PAH). The coastal regions are highly impacted by the emissions from shipping lanes near the coast and the use of HFO. In contrast, inner continental regions in Europe are suffering from wood combustion (WC) emissions. In Germany the consumption of wood for residential heating increased within eight years more than twice.

The Virtual Helmholtz Institute HICE addresses the health effects of anthropogenic combustion processes. This is performed by means comprehensive characterization of the chemical & physical properties of combustion aerosols as well as the biological effects on cell cultures. Here, for comparison of different combustion sources, PAH-related toxicity equivalents (TEQ) were calculated. It is based on the proposal of the German Research Foundation (DFG) that the health risk is proportional summarised by different PAH with different health risk potentials (Greim, 2008). PAH were weighted by their carcinogenic, mutagenic and gen-activating effects due to formation of toxic metabolites.

Experiments with a 4-stroke research engine were conducted at the University of Rostock. Emissions from a simple constructed log wood stove were collected at the KIT, Karlsruhe. Although the emissions of particle-bound PAH showed differences in pattern the total amounts emitted by WC and HFO-operated engines were comparable (figure 1). The emissions from one large cargo ship (up-scaled results) equates around 400 single-family houses heated with a log wood stove (figure 2) regarding TEQs. When referring these results to the energy output of the different energy sources it can be postulated that log wood stoves affect the human health about thirty-times more than ships operated with HFO. Moreover, cargo ships could be a comparative eco-friendly means of transportation, assuming that engines are operated with diesel-like light fuel oil (LFO).

Nevertheless, harmful carbonaceous contents of PM as well as hazardous heavy metals can still be found within the emissions of LFO-operated engines. Compared with WC higher alkylated PAH are highly expressed within ship engine emissions, whereas Methylpyrenes (ship engine: 4.1 µg m^{-3}, WC: 3.9 µg m^{-3}) and Methylchrysenes (ship engine: 0.68 µg m^{-3}, WC: 0.57 µg m^{-3}) were found to have similar concentrations.

On the other hand dimethylated pyrenes were found only in emissions from the ship engine with concentrations of 3.9 µg m^{-3} when applying LFO.

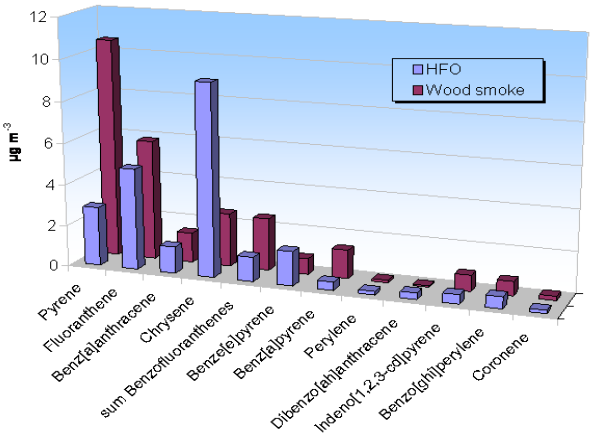

Figure 1. Particle-bound PAH – a comparison of wood smoke and HFO-operated ship engine exhaust.

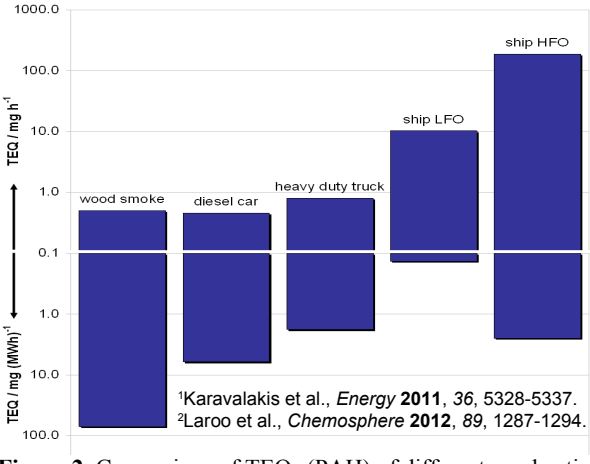

Figure 2. Comparison of TEQs (PAH) of different combustion sources, related to time and energy output, respectively.

This work/HICE (www.hice-vi.eu) is supported by the Helmholtz association (HGF).

Greim, et al.: Gesundheitsschädliche Arbeitsstoffe - Toxikologisch-arbeitsmedizinische Begründungen von MAK-Werten und Einstufungen, Wiley, 2008.

Air-liquid interface exposure systems for the assessment of toxicity of combustion aerosols

H.-R. Paur[1], S. Mülhopt[1], M. Dilger[2,3], C. Schlager[1], T. Krebs[4], R. Zimmermann[3], S. Diabaté[2], C. Weiss[2]

[1]Institute for Technical Chemistry, Karlsruhe Institute of Technology, 76021 Karlsruhe, Germany
[2]Institute of Toxicology and Genetics, Karlsruhe Institute of Technology, 76021 Karlsruhe, Germany
[3]HICE – Helmholtz Virtual Institute of Complex Molecular Systems in Environmental Health – Aerosols and Health, www.hice-vi.eu
[4]VITROCELL Systems GmbH, 79183 Waldkirch, Germany

Keywords: Exposure, Health effects of aerosols, Human lung cells, Combustion aerosols
Presenting author email: paur@kit.edu

Despite numerous efforts to reduce the ambient air concentrations of fine particles by improved combustion and filter technologies, the health effects due to inhalation of ultrafine particles are still the most important problem in environmental health. Besides the combustion of fossil fuels the increasing combustion of wood in domestic stoves and boilers may even increase the fine particle burden.

The on-line characterization of physico-chemical properties of combustion derived particles has progressed by application of novel particle sizers and mass spectrometry. The assessment of health effects is still conducted by epidemiology or costly animal experiments. Characterization of biological effects of ultrafine particles to human cells by in-vitro studies, with particle extracts induces numerous artifacts during sampling, extraction, dose determination and biological testing, all of which renders the results derived hardly reproducible. The application of air-liquid interface exposure of human lungs cells to characterize the biological effects of combustion aerosols will avoid many of the pitfalls of the previous method [1].

Experimental

For the reproducible assessment of lung toxicity of airborne particle emissions from combustion processes the Karlsruhe Exposure System was developed as described in detail before [2]. In this fully automatic system cell cultures (A549, BEAS-2B) grown on porous membrane inserts, which are in contact with nutrient medium, are exposed directly to diluted aerosol from combustion sources.

To reduce sampling and filter artefacts the system is interfaced to the off gas duct by means of a porous tube diluter. The aerosol passes through the size selective inlet to exclude the particles size fraction above 2.5 µm. In the conditioning reactor the gas is humidified by steam injection. By metallic sampling probes the gas samples are drawn into the air-liquid interface modules (Vitrocell systems) by a vacuum pump. For each of the 18 exposure positions the flow rate is measured by a mass flow controller. All exposure parameters such as temperatures and flow rates are recorded by a Lab View data acquisition system.

Figure 1. HICE exposure system for air-liquid interface exposure of human lung cells towards combustion derived particle emissions

To estimate the deposited particles mass calibration experiments with fluorescent nanoparticles are conducted prior to the exposure.

First results from the exposure of A549 human lung epithelial cells will be reported.

Acknowledgement:
This work was supported by the Helmholtz Association within the virtual institute HICE. Further Information: www.hice-vi.eu

References:

[1] Paur, H.-R., Cassee, F. R., Teeguarden, J., Fissan, H., Diabate, S., Aufderheide, M., Kreyling, W. G., et al. (2011). *Journal of Aerosol Science*, 42(10), 668–692. doi:10.1016/j.jaerosci.2011.06.005

[2] Paur, H.R., Mülhopt, S., Diabaté, S., Weiss, C. (2008) *Journal für Verbraucherschutz und Lebensmittelsicherheit*, 3, 319-329

Oxidative potential of particulate matter in a major urban environment

Frank J Kelly, Ben Barratt, Cathryn Tonne and Ian Mudway

MRC-HPA Centre for Environment & Health, King's College London, 150 Stamford Street, London, SE1 9NH, UK
Keywords: Particulate matter, oxidative potential, lung, toxicity
Presenting author email: frank.kelly@kcl.ac.uk

Oxidative potential (OP) is a novel metric that reflects one aspect of the toxicity of ambient particulate matter (Kelly, 2003). By augmenting measurements of the physical and chemical characteristics or particulate matter with this metric, we hope to gain a greater understanding of which components are driving its health effects and which emissions sources require most urgent remedial action. The assimilation of a unique long-term dataset of two indicators of OP across a large urban area allowed us to relate variations in toxicity with meteorological conditions and emission sources.

A database of particulate matter OP from 16 monitoring sites across London over the period 2000 to 2006 was constructed. The oxidative burden associated with collected PM was assessed by measuring the oxidative depletion of antioxidants within a synthetic human respiratory tract lining fluid (RTLF) model (Ayres et al, 2008). This method reports two metrics of oxidative activity; glutathione oxidation ('OP^{GSH}') and ascorbate oxidation ('OP^{AA}'). A aggregation method was used to produce an uninterrupted 'London background' OP time series with weekly resolution utilising results from the six available urban background monitoring sites. Spearman's rank correlation coefficients were produced to show relationships between weekly mean background OP^{AA} and OP^{GSH} per unit mass and per unit volume and various pollutant and meteorological explanatory variables.

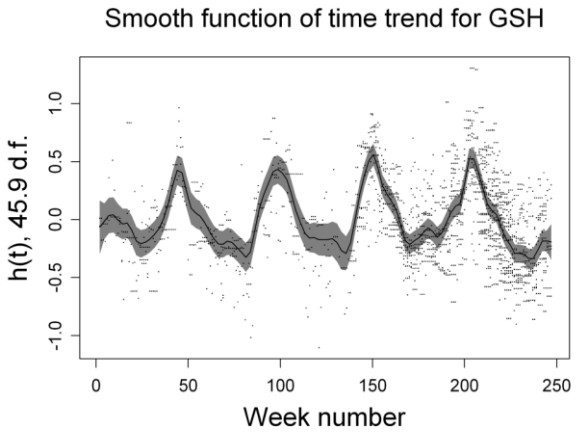

Figure 1. Plot of time trend for GSH OP. The shaded regions and points display pointwise standard errors (including uncertainty about the overall mean) and partial residuals, respectively.

OP^{GSH} exhibited behavior typical of a primary urban pollutant, with peaks in activity coinciding with the lowest mean incoming solar radiation rates (r_s=-0.68) and troughs during the summer months. The correspondingly close relationship between OP^{GSH} and NO_X (r_s=0.46) was an indication that both pollutants are strongly influenced by dispersion rates of local vehicle emissions. There was no correlation between London background PM_{10} and OP^{GSH} (r_s=-0.06), indicating that PM_{10} composition is more important than PM_{10} mass in relation to oxidative activity. There was evidence of peaks in OP^{AA} concentrations during large secondary particulate episodes and the correlation factor for OP^{AA} and rural PM_{10} was higher than any other metric (r_s=0.29). This suggested that regional-scale sources including secondary particulate mass have a greater role in determining OP^{AA} activity. No clear overall trend was apparent in OP^{AA} over the seven year period, but there was evidence of an increasing trend in peak winter time OP^{GSH}.

As far as we are aware this is the first long time series of OP measurements across an urban area. The two OP metrics demonstrated contrasting characteristics and relationships with other pollutants and meteorology. The OP^{GSH} metric provided evidence that each unit of PM_{10} mass has greater oxidative activity during the autumn and winter months than during the summer. The OP^{AA} metric showed a more complex variation but suggested that particle activity may increase during secondary episodes. Neither metric was correlated with particulate mass. This study demonstrated a strong link between primary traffic related pollutants and particle oxidative toxicity.

This work was supported by Heath Effects Institute (USA) and the Medical Research Council (UK).

Kelly FJ. (2003) *Occup Envir Med* 60: 612-616.

Ayres J G, Borm P, Cassee F R, Castranova V, Donaldson K, Ghio A, Harrison R M, Hider R, Kelly FJ, Kooter I M. (2008) *Inhalation Toxicology*, 20:75-9

A novel set-up for source characterization and human exposures of biomass combustion aerosols

R. Nyström[1], E. Z. Nordin[2], J. H. Pagels[2] A. Blomberg[3], T. Sandström[3] and C. Boman[1]

[1]Thermochemical Energy Conversion Laboratory, Department of Applied Physics and Electronics, Umeå University, SE-901 87 Umeå, Sweden
[2]Ergonomics and Aerosol Technology, Lund University, SE-221 00 Lund, Sweden
[3]Dept. of Public Health and Clinical Medicine, Division of Medicine, Umeå University, SE-901 87 Umeå, Sweden

Keywords: biomass combustion, aerosol chamber, controlled human exposure, health effects
Corresponding author: robin.nystrom@umu.se

Emissions from biomass combustion are a major source of indoor and outdoor air pollution, and are estimated to cause millions of premature deaths worldwide annually. Pollution from different biomass combustion sources are a complex and varying mixture of gases and particles, strongly dependent on fuel, technology and operation [Kocbach *et al*, 2009]. Although adverse respiratory effects have been associated with "wood smoke" in epidemiological and controlled exposure studies, important information concerning biomass combustion aerosols is still missing. Examples of such areas are; cardiovascular effects, underlying biological pathways and importance of different aerosol particle properties. A chamber set-up built for controlled human exposures gives unique opportunities to directly relate specific exposure conditions to different short term (acute) respiratory and cardiovascular responses in humans.

The objective of this project was therefore to describe and evaluate a novel chamber set-up for studies of health effects of biomass combustion aerosols using controlled human exposures. In this paper we discuss the biomass combustion aerosol exposure set-up including aspects of; *i)* combustion systems, *ii)* aerosol dilution, *iii)* chamber design and function, and *iv)* exposure data from the first recently performed campaign.

The exposure set-up is located in connection to the combustion laboratory within the Thermochemical Energy Conversion Laboratory (TEC-Lab) at Umeå University. The facility includes several combustion technologies to be used for different aerosol generation purposes such as human exposures and/or other aerosol experimental research. For example, traditional wood log stoves, modern wood pellet boilers using different burner technologies, a fluidized bed reactor and novel grate fired reactors for controlled generation of different kinds of biomass aerosols, are available.

Different flue gas/aerosol dilution systems are available, e.g. ejector dilutors (ED) and porous tube dilutors (PTD). In the first exposure campaign, a three step dilution system with filtered air at ambient temperature was used including a first PTD (~1:10), followed by an ED (~1:6) and a final counter-current flow injection in the main HEPA filtered air flow that enters the chamber.

The chamber is 15.3 m^3 (2.7 x 2.4 x 2.4 m) with a small ante-chamber with interior surfaces made of stainless steel/aluminium, except for 2.4 m^2 observation glass window facing a control room. The set-up is designed for air exchange rates of 2-10 times per hour. CO, NO_x and total hydrocarbons as well as temperature and relative humidity are continuously monitored. Particle mass concentration is measured by a TEOM equipped with a PM_1 pre-cyclone and an integrated filter sampler. Particle mobility size distribution and number concentration are measured with a SMPS system. In addition, several different filter and impactor sampling lines are applied for off-line chemical characterization including, e.g. carbon fractions (OC/EC), PAH/oxy-PAH and inorganic alkali and trace metals, as well as toxicological (*in-vitro*) characterization.

A first human exposure study in the new set-up was performed to elucidate acute airway inflammatory responses and cardiovascular effects after exposure to emissions from incomplete wood log combustion. A common Nordic wood stove was used with a special adjusted combustion approach to generate incomplete (soot-rich) conditions in a repeatable manner for the exposure campaign. The target PM_1 mass concentration in the chamber was 300 $\mu g/m^3$ thus in line with a previous experimental wood smoke study [Sehlstedt *et al*, 2011] and several diesel engine exhaust studies performed by the Umeå group and collaborators. Fourteen healthy non-smoking subjects were successfully exposed to diluted wood smoke (PM_1 314±38 $\mu g/m^3$) or filtered air for three hours in a randomized, double-blind crossover study. The EC/TC (total carbon) ratio was 0.72 ± 0.08, and it was estimated that the total PM consisted of approximately 38% soot, 24% organics and 38% inorganics.

Aspects of chamber function (e.g. flow profiles and mixing conditions) as well as aerosol dynamic effects (e.g. coagulation and wall losses) at different chamber conditions are presently under evaluation and will be discussed. Accordingly, the new and novel set-up for biomass combustion aerosol generation, characterization and health effect studies has successfully been established and so far used in one human exposure study and one aerosol ageing and toxicology study (Nordin *et al*., EAC 2013).

The work was supported by the Swedish Energy Agency within the ERA-NET Bioenergy project *Biohealth* and the strategic funding by Umeå University´s young researcher award (C Boman).

Kocbach Bølling, A., Pagels, J., Yttri, K.-E., Barregard, L., Sällsten, G., Schwarze, P.E., Boman, C. (2009) *Part Fibre Toxicol*. **6**:29.

Sehlstedt, M., Dove, R., Boman, C., Mudway, I.S., Pagels, J., Swietlicki, E., Löndahl, J., Westerholm, R., Bosson, J., Barath, S., Behndig, A.F., Pourazar, J., Sandström, T., Blomberg, A. (2010) Part Fibre Toxicol **7**:21.

Thursday, September 5, 2013

Session: Atmospheric Aerosols,
Biomass burning and bioaerosols

Particle characterisation during biomass burning events in Tasmania, Australia

F. Reisen[1], C.P. Meyer[1], M.D. Keywood[1] and S. Crumeyrolle[2]

[1]Centre for Australian Weather and Climate Research, CSIRO Marine and Atmospheric Research, Aspendale, Victoria 3195, Australia
[2]NASA Langley Research Centre, Hampton, Virginia, 23681, USA
Keywords: prescribed burning, levoglucosan, residential wood burning, biomass.
Presenting author email: Fabienne.Reisen@csiro.au

Regional pollution from biomass burning has become an issue of public concern in Tasmania. Smoke plumes are frequently visible at large distance, and when ground-level smoke concentrations cause discomfort or trigger acute health responses, the events are vividly remembered. Current public perception is that smoke produced by regeneration burning is the principal cause of pollution events and a significant risk to health. To date there are few data on these events.

In order to assess the seasonal air quality in the Huon Valley in southern Tasmania, we monitored fine ($PM_{2.5}$) and coarse (PM_{10}) particle concentrations and their chemical composition between March 2009 and September 2010 at two locations, Geeveston, an urban site and Grove, a rural site. Additionally an intensive campaign was carried out during the regeneration burning season in March and April 2010 during which microphysical and chemical properties of the aerosol were measured at Geeveston.

PM concentrations were substantially elevated both in autumn and winter at Geeveston compared to Grove, indicating that PM concentrations were primarily influenced by localised sources rather than by regional pollution. The measured elevated concentrations of levoglucosan, a unique tracer for wood smoke, confirmed that biomass burning was a significant source of $PM_{2.5}$ concentrations. Although the intensity of emissions from prescribed burns and residential woodheaters was similar, emissions from residential woodheaters were the largest source of $PM_{2.5}$, with a contribution of 80% to the ambient $PM_{2.5}$ load compared to an 11% contribution from prescribed burns.

In background air, the size-resolved mass distributions were typical of a non-polluted atmosphere in which sea-salt was the major source of coarse mode particles, and secondary particles (represented here by non-sea salt sulphate), were the major components of the fine particle mode (Figure 1, left). During the main smoke plume event, we observed high content of levoglucosan and organic carbon and the size distribution spectrum was dominated by a single mode around 1.5 µm (Figure 1, right).

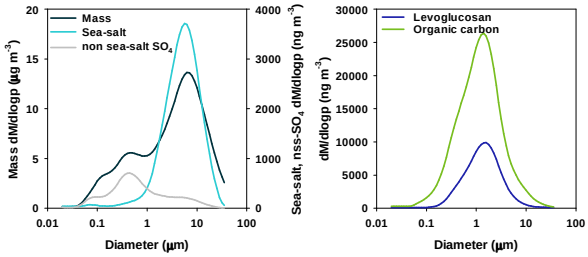

Figure 1. Size resolved chemical composition of background air (left) and smoke event (right)

We also observed contrasting characteristics of clean and smoke impacted air in the size-resolved particle concentrations. In clean background air, particle number concentrations were low, with size mode ranging between 20 and 100 nm. During the severe smoke event, the mode was substantially larger and particle growth was clearly evident increasing from 93 nm to about 157 nm in 12 h at a growth rate of 5.3 nm h^{-1} (Figure 2) Particle growth can be caused by condensation of either organic gases or water onto particles, however, because the condensation sink for water vapour during this event is extremely high (40 s^{-1}) compared to the monthly average (2 s^{-1}), we can conclude that the growth observed here is due mainly to humidity and that the smoke in this event was relatively fresh.

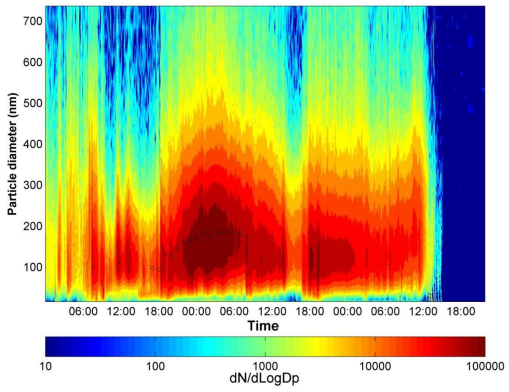

Figure 2. Size distribution of aerosol particles measured with the SMPS during severe smoke event.

This work was jointly funded by Forestry Tasmania and CSIRO Marine and Atmospheric Research under Contract 25/6/2009.

Biomass burning layers measured during the Deep Convective Clouds and Chemistry experiment (DC3) with an airborne Single Particle Soot Photometer (SP2)

K. Heimerl[1], B. Weinzierl[1,2], A. Minikin[1], D. Sauer[2,1], D. Fütterer[1], M. Lichtenstern[1], H. Schlager[1], J. P. Schwarz[3], M. Z. Markovic[3], A. E. Perring[3], D. W. Fahey[4], and H. Huntrieser[1]

[1] Institut für Physik der Atmosphäre, Deutsches Zentrum für Luft- und Raumfahrt (DLR), Oberpfaffenhofen, Germany.
[2] Ludwig-Maximilians-Universität München (LMU), Meteorologisches Institut, München, Germany.
[3] Cooperative Institute for Research in Environmental Sciences (CIRES), University of Colorado, Boulder/CO, USA.
[4] Chemical Sciences Division, Earth System Research Laboratory, NOAA, Boulder/CO, USA.
Keywords: biomass burning aerosol, single particle soot photometer, DC3.
Presenting author email: Katharina.Heimerl@dlr.de

The Deep Convective Clouds and Chemistry (DC3) experiment was conducted in the central and eastern U.S. in the summer of 2012, investigating the role of thunderstorms in physical and chemical processes and their influence on the upper troposphere. Both ground-based and airborne measurements were performed, with radar, lightning and meteorological observations on the ground and three research aircraft, the NCAR GV, the NASA DC8 and the DLR (German Aerospace Center) Falcon. This presentation shows measurements made with a Single Particle Soot Photometer (SP2) mainly focusing on the instrument mounted on the DLR Falcon, data from the SP2 instrument on the DC8 are included for comparison.

The Falcon instrumentation comprised various instruments for in-situ measurements of trace gases and aerosols. Measured trace gas species were NO, CO, O_3, CO_2, CH_4, SO_2, and volatile organic compounds. The range of aerosol in-situ instruments included optical particle counters for size distributions in different size ranges (UHSAS-A, FSSP-300, FSSP-100, PCASP-100X and Sky-OPC 1.129), a multi-channel CPC system for total and non-volatile particle concentrations and, for absorbing particles, a three-wavelength PSAP and a Single Particle Soot Photometer (SP2), measuring the refractory black carbon (rBC) mass. Being a strongly absorbing product of combustion processes, rBC influences the global radiation budget depending on its highly variable concentration.

The DLR Falcon made measurements during 13 local flights based at the Salina/KS airport and during the transfer from Germany to the U.S. and back. Aside from thunderstorm measurements, biomass burning layers were detected almost during every flight, as the summer of 2012 was one of the worst wildfire seasons on record in the continental U.S. A biomass burning layer was also sampled during a wing-by-wing intercomparison flight between the DLR-Falcon and the NASA-DC8, providing a good opportunity to compare the two different SP2 instruments in a biomass burning plume.

In the middle troposphere, where the biomass burning layers with highest rBC mass concentrations were found, the rBC mass concentrations spanned four orders of magnitude (Figure 1). Most biomass burning layers measured during the local flights were observed between 3 and 8 km, although some layers were observed at 11 km during the transfer flights over North America and Greenland (not shown in this figure). The most prominent layers, originating from New Mexico wildfires, were found at 7 km, on June 11th 2012 (Little Bear wildfire), and between 3 and 6 km on May 29th and 30th of 2012 (Whitewater-Baldy wildfire).

rBC mass concentrations as high as 2 µg/m³ were detected in some plumes. All biomass burning plumes showed higher fractions of rBC cores with thick coatings than found in the boundary layer. However, a plume found at 11 km over Newfoundland during back transfer showed also a high fraction of thinly coated particles, while the median diameter of rBC particles in this plume was lower than found in other biomass burning plumes or the boundary layer.

This presentation will give an overview of the different biomass burning layers measured at various altitudes and distances from the wildfire. To address sources and characteristics of the various plumes, back trajectories and microphysical properties of the particles in the plumes will be presented.

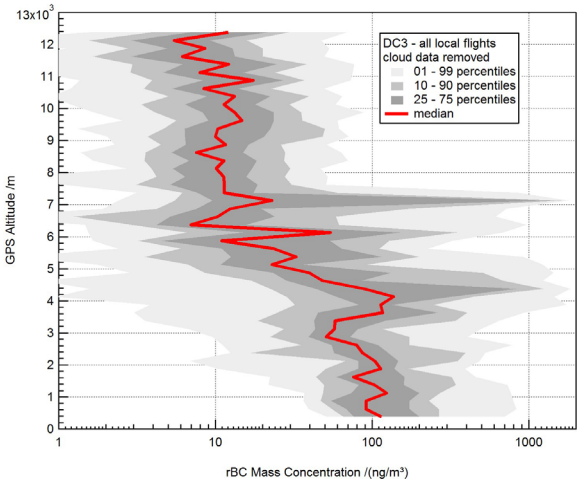

Figure 1: Median profile and percentiles of all rBC measurements outside clouds during DC3 local Falcon flights

Acknowledgements:
This work has been funded by the Helmholtz Association under grant number VH-NG-606 (Helmholtz-Hochschul-Nachwuchsforschergruppe AerCARE). We thank the DC3 Science Team and DLR Flight Operations for their great support.

Primary particles and marker compounds from wood combustion in household stoves

M. Maasikmets[1, 2], E. Teinemaa[1], K. Vainumäe[1], L. Parts[1], L. Lehes[1], T. Arumäe[1], V. Kimmel[2]

[1]Estonian Environmental Research Centre (EERC), Marja 4d, 10617Tallinn, Estonia; [2]Estonian University of Life Science (EULC), Institute of Agricultural and Environmental Sciences, Kreutzwaldi 5, 51014 Tartu, Estonia
Keywords: primary particles, wood combustion, stoves, marker compounds
Presenting author email: marek.maasikmets@klab.ee

Biomass combustion is a major global source of fine particulate matter (PM) in the atmosphere with significant impacts on regional air quality, visibility, ecosystems, human health, and global climate (Hobbs, 1997). Once released to the atmosphere, biomass smoke is mixed with the particulate matter emitted from many other natural and anthropogenic pollution sources, in many cases becoming difficult to recognize and quantify (Simoneit et al., 1999). In Estonia wood and wood chips account > 90% of the fuel used for residential heating (Loosaar et al., 2008). Source apportionment studies as well as emission inventories depend on reliable data about emission sources. There is, however, lack of information concerning the characterisation of particulate emissions from small scale biomass combustion systems in North-East Europe. Molecular markers have been used extensively in source apportionment studies and to evaluate the transport, transformation, and fate of atmospheric species (Engling et al., 2006).

Three different combustion facilities were tested: a masonry stove, a cooking stove and a fireplace, as those combustion facilities are typically used in Estonian households. Measurements were carried out in EERC stove test laboratory and they included both filter sampling (PM10, PM2.5, PM1, PM<1) and online methods. Conifer and hardwood logwood with different humidity was used. Each log batch was weighed, heating value was measured and the RH of each log was measured separately. All samples were taken from the hot flue gas. For the particle measurements Dekati® PM10 Impactor (10 l/min, Dekati Ltd) was used. The Dekati® PM10 Impactor classifies airborne particles into four size fractions (PM10, PM2.5, PM1, PM<1). Samples were taken through an insulated, externally heated (up to 180 °C) sample line. Samples were taken during the start-up phase (up to 20 min) and during the constant flaming process (up to 30 min). For the removal of larger particles the Dekati® Cyclone (10 l/min, Dekati Ltd.) with the nominal cutpoint D50 10 µm, was used. From the filter samples organic carbon (OC), elemental carbon (EC), levoglucosan and ionic composition (Na^+, K^+, Ca^{2+}, Mg^{2+}, $NH4^+$, $SO4^{2-}$, Cl^-) were analysed. The organic (OC) and elemental carbon (EC) fractions were determined from quartz filter samples with a thermal optical method using a carbon analyzer constructed by Sunset Laboratories (Model-3 Semi-Continuous OC-EC Field Analyzer, Sunset Laboratory). The analyses were performed according to the NIOSH method 5040. Levoglucosane was detected with the gas chromatograph-mass spectrometry (GC-MS) after chemical derivatization. Ionic composition of the particles fractions were analyzed by ion chromatography (Dionex DX2000 and DX2100). Simultaneously gas samples (O_2, SO_2, NO, NO_2, CO, CO_2, VOC), temperature (°C), relative humidity (%) and gas flow (m/s) were measured during the whole burning process. Samples for the gas analyses were taken through an insulated, externally heated (up to 180 °C) sample line and through the filter units to the gas analyser (Testo 360, Testo AG).

Results

OC and levoglucosane content in smaller PM fractions was higher. The average levoglucosane content in PM10 fraction was in average 50.083 µg per filter and in PM<1 fraction in average 1127.400 µg per filter. Potassium content in PM10 fraction was smaller compared with other PM fractions. Taken into account that the combustion equipment type and other relevant flue gas and wood parameters (temperature, RH, heating value) play an important role in PMx and marker compound formation, this should be considered in further emission inventories.

This work was supported by the Estonian MoE and by the Estonian Science Foundation project BioAtmos.

Engling, G., Carrico, C. M., Kreidenweis, S. M., Collett Jr, J. L., Day, D. E., Malm, W. C., Lincoln, E., Min Hao, W., Iinuma, Y. & Herrmann, H. (2006). Determination of levoglucosan in biomass combustion aerosol by high-performance anion-exchange chromatography with pulsed amperometric detection. *Atmospheric Environment*, **40, Supplement 2**(0), 299-311.

Hobbs, P. V., Reid, J.S., Kotchenruther, R.A., Ferek, R.J., Weiss, R. (1997). Direct radiative forcing by smoke from biomass burning. *Science of The Total Environment*, **275**, 1776-1778.

Loosaar, J., Kask, Ü., Kask, L., Parve, T. & Link, S. (2008). Hinnang eramute kütmisest välisõhku eralduvate saasteainete heitkoguste kohta Eestis (in Estonian). *Contract no 7082*.

Simoneit, B. R. T., Schauer, J. J., Nolte, C. G., Oros, D. R., Elias, V. O., Fraser, M. P., Rogge, W. F. & Cass, G. R. (1999). Levoglucosan, a tracer for cellulose in biomass burning and atmospheric particles. *Atmospheric Environment*, **33**(2), 173-182.

The comparison of long-term changes in the bioerosol components in Southwestern Siberia in the near-ground atmospheric layer and at the altitudes of 500 - 7000 m

A.S. Safatov[1], G.A. Buryak[1], V.A. Vechkanov[1], I.S. Andreeva[1], S.T. Olkin[1], I.K. Reznikova[1], V.M. Generalov[1], M.Yu. Arshinov[2], B.D. Belan[2], D.V. Simonenkov[2] and G.N. Tolmachev[2]

[1]FSRI State Research Center of Virology and Biotechnology "Vector", Novosibirsk Region, 630559, Koltsovo, Russia
[2]Institute of Atmospheric Optics, SB RAS, 634055, Tomsk, Russian Federation
Keywords: atmospheric aerosol, bioaerosol, microorganisms, long term trend.
Presenting author email: safatov@vector.nsc.ru

Since 1999, the authors have been monitoring the biological components of atmospheric aerosol in Southwestern Siberia by both ground sampling and aircraft probing of the atmosphere (Arshinov *et al.*, 2010). The purpose of this work is to analyze the data obtained during 14 years and to reveal the differences between the near-ground and high-altitude concentrations of biological components of atmospheric aerosols in the region.

Ground-based measurements were conducted at the site of FSRI SRC "Vector" located in the vicinity of Novosibirsk for 1 day (4 samples) in the middle of each month. Samples were collected into impingers (1.5 m^3) to detect viable microorganisms and on fiber filters (9 m^3) for chemical analysis of samples. Altitude samples were collected on a day during the last ten days of each month at successive altitudes of 7000, 5500, 4000, 3000, 2000, 1500, 1000 and 500 m using an aircraft laboratory Tupolev-134 (Belan *et al.*, 2011) on the same impingers (volume sample of 0.5 m^3) and filters (sample volume of about 2 m^3).

The concentration of culturable microorganisms in the samples was determined by culturing methods, and the species they belonged to were determined by molecular biological methods (Safatov *et al.*, 2010). The concentrations of the total protein, the main elements and ions in the samples were determined by methods described in Safatov *et al*. (2010).

Figures 1 and 2 present the changes in the concentrations of culturable microorganisms and the total protein in the atmosphere of Southwestern Siberia averaged over all the measurements performed during a calendar year. As follows from the presented data, the concentrations of culturable microorganisms in the near-ground atmospheric layer and on the average at the altitudes of 500-7000 m are close to each other. The concentration of the total protein in the near-ground atmospheric layer is considerably **lower** than that at the altitudes of 500 – 7000 m. The observed fact can be explained by a more essential contribution of remote bioaerosol sources as compared to local ones into the observed concentrations.

The concentrations of both the total protein and culturable microorganisms showed downward trends during the observation period. The concentrations of viable microorganisms decreased by approximately 10 times both in the near-ground layer and at the altitudes of 500- 7000 m. The total protein concentration in the near-ground layer remains practically unchanged, and that in the layer at the altitudes of 500 – 7000 m decreases by approximately 2.5 times. An intra-year trend is revealed in these concentrations against the background of a decrease: the maximal value (in the warm period of the year) was greater than the minimal one (in the cold period of the year) by approximately 2 times for the total protein and by approximately 10 times for culturable microorganisms.

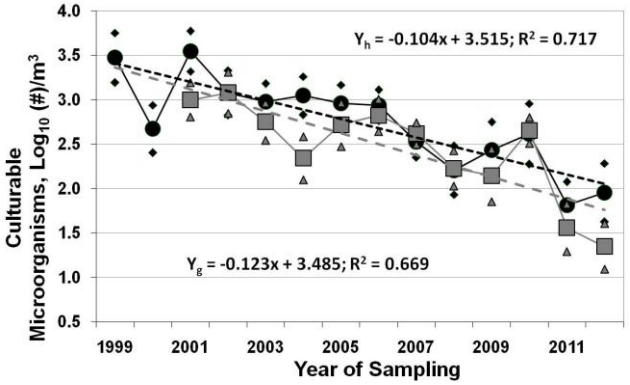

Figure 1. Annual average concentrations of culturable microorganisms in the near-ground layer (grey, g) and in the layer at the altitudes of 500- 7000 m (black, h). The average and mean-square values are given.

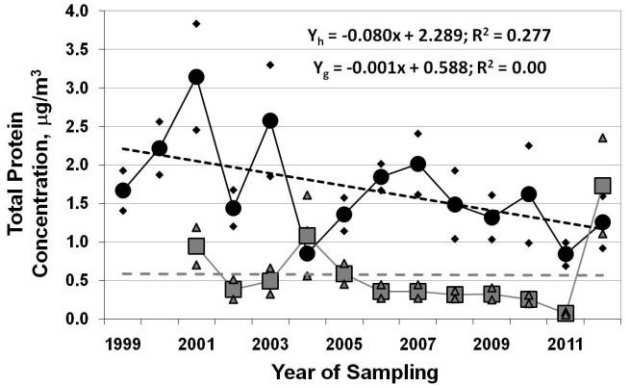

Figure 2. The same for total protein.

This work was partially supported by the SB RAS Integrated Project under grant 35-2012.

Arshinov, M.Yu. *et al.* (2010) *Atmos. Oceanic Optics*, **22**, 950–957.

Belan B.D. *et al.* (2011) *Atmos. Oceanic Optics*, **24**, 805–816.

Safatov A.S. *et al.* (2010) In: Aerosol – Science and Technology. /Ed. I. Agranovski. Wiley-VCH, 407-454.

Filtration and inactivation of aerosolized bacteriophage MS2 with air ions and electric field

Junho Hyun[1], Yun-Haeng Joe[2] and Jungho Hwang[1,2]

[1]Graduate Program of Clean Technology, Yonsei University, Seoul, 120749, South Korea
[2]Department of Mechanical Engineering, Yonsei University, Seoul, 120749, South Korea
Keywords: air ion, virus inactivation,
Presenting author email: junhohyun@yonsei.ac.kr

Particles of biological origin, such as bacteria, viruses, fungi, and pollen as well as their fragments that are present in air are referred to as bioaerosols. Bioaerosols can cause serious health hazards when they contaminate a human environment. Influenza virus, severe acute respiratory syndrome (SARS) virus, and the threat of avian and swine flu are natural examples illustrating the profound, everyday impacts of bioaerosols on public health. Filtration is one of the most common methods of removing airborne particulates. It has been applied various situations from personal facepiece respirators to central heating, ventilation, and air-conditioning (HVAC) system of buildings because filtration can archive high removal efficiency of aerosol particles still simple and economical. However, indoor bioaerosols accumulate in large quantities on the filters, where they are able to multiply under certain conditions, especially if high amounts of moisture are present on the filters. Moreover, the organic or inorganic materials deposited on the filter media after air filtration contribute to microbial growth. This inevitably leads to decreased filter efficacy and, probably, to deterioration of the filters and the eventual release of microorganisms.

To inactivate aerosolized microorganism, there are various controlling technologies for this contaminant, including air ions, chemical treatment, photocatalytic oxidation, Ultraviolet Germicidal Irradiation (UVGI) and dielectric barrier discharge. Especially the carbon fiber ionizer, with an ion emission tip consisting of a bundle of micron-sized carbon fibers, produced stable unipolar or bipolar ions in sufficiently high concentrations without generating particulate matter or ozone. Each fiber was supplied with a high voltage, and ions were emitted from the ends of the fiber.

Electrostatic particle capture enhances conventional mechanical filtration mechanisms in the submicron size range without increasing the pressure drop. Electret filter which made of charged filter fiber is widely used because of its high performance yet low pressure drop. Some studied the electrified filter collector coupled with external electrical field and some studied air ionizer to discharge the particles. In Park *et al* (2011) the increase in efficiency (the difference between efficiency with and without ionizers) with ionization gradually decreased as the particle size increased, as has been reported by filtration studies that demonstrated that the increase in efficiency with electrostatic force decreased as the particle size increased. The size of our test virus, bacteriophage MS2, is found 27 nm which would highly affected by electrostatic force.

In this work, we studied the viability of air ions and electric field to virus deposited onto a medium filter. First we discharged aerosolized virus with unipolar ions then deposited onto a medium filter. Electric field was applied to filter for enhancing filtration efficiency. We used MS2 bacteriophage, a 27 nm tailless non-enveloped icosahedral RNA-coliphage, relatively stable against environmental stress, has been used in the past as a simulant of most mammalian viruses, and it is known as an indicator for enteric viruses. After deposition, filter was exposured to unipolar or bipolar ions.

This research was supported by Korean Ministry of Environment as “The Eco-Innovation project”(402-111-005)

Park J.H., Yoon K.Y. and Hwang J. (2011) *Build. Environ.* **41**, 935–943.

Measurements During The South American Biomass Burning Analysis (SAMBBA) Field Experiment

J. D. Allan[1,2], W. T. Morgan[1], P. I. Williams[1,2], M. Flynn[1], E. Darbyshire[1], A. Hodgson[1], B. T. Johnson[3], J. M. Haywood[3,4], S. Freitas[5], K. Longo[5], P. Artaxo[6] and H. Coe[1]

[1]School of Earth, Atmospheric & Environmental Sciences, University of Manchester, UK
[2]National Centre for Atmospheric Science, University of Manchester, UK
[3]The Met Office, Exeter, UK
[4]College of Engineering, Mathematics & Physical Sciences, University of Exeter, UK
[5]National Institute for Space Research (INPE), São José dos Campos, Brazil
[6]University of São Paulo, Brazil
Keywords: Wildfires, Amazon, AMS, Biomass
Presenting author email: james.allan@manchester.ac.uk

Biomass burning represents one of the largest sources of particulate matter in the atmosphere and can significantly perturb local air quality, meteorology and the earth's radiative balance (Bond et al., in press). Due to the relatively short atmospheric lifetimes, these effects are most acutely felt on regional scales and can have a significant effect on quality of life and the hydrological cycle. However, many of its predicted effects are very poorly constrained. The lifetime and properties of these aerosols are strongly dependent on their composition and injection height, which are turn are highly dependent on the burn conditions.

The South American Biomass Burning Analysis (SAMBBA) field campaign took place in Brazil in September and October 2012, towards the end of the dry season when biomass burning is typically at its peak. This was a collaborative project between a number of UK and Brazilian institutes and featured a comprehensive suite of state-of-the-art instruments on board the UK Facility for Airborne Atmospheric Measurements (FAAM) BAe-146 large research aircraft, based in Porto Velho, in the state of Rondonia. Aerosol instrumentation included an Aerodyne Aerosol Mass Spectrometer (AMS), Single Particle Soot Photometer (SP2), Scanning Mobility Particle Sizer (SMPS), Particle Soot Absorption Photometer (PSAP), Cloud Condensation Nuclei Counter (CCN), Passive Cavity Aerosol Spectrometer Probe (PCASP) and Nephelometers. In conjunction with other measurements, such as inorganic gases, VOCs, optical spectrometers, lidar and dropsondes, a comprehensive characterisation of the composition and dynamics of smoke plumes could be obtained, which can in turn be used to inform and validate models that attempt to simulate the emissions and impacts of these fires based on satellite data.

During the campaign, 19 sorties were performed and a number of different fires were characterised, along with regional hazes, background aerosols (in both the boundary layer and free troposphere) and 'clean' areas dominated by biogenic emissions. Very different aerosol compositions were found depending on the exact burn conditions. As an example, flight B737 sampled a large forest fire in a remote area of Rondonia, which was principally smouldering in nature, whereas B742 sampled fires in an agricultural area of Tocantins, which were principally flaming. The B742 case showed a larger mass concentration of black carbon (up to 50 µg m^{-3} instead of 5 µg m^{-3}), whereas organic matter concentrations were similar (up to 5 mg m^{-3}). Relationships were also found between different fractional mass spectral markers commonly used in the AMS, specifically *f*44 (oxygenated organics) and *f*60 (anhydrous sugars such as levoglucosan). The relationship between these markers changed between the two cases, although these were both within the range of previously published works (figure 1).

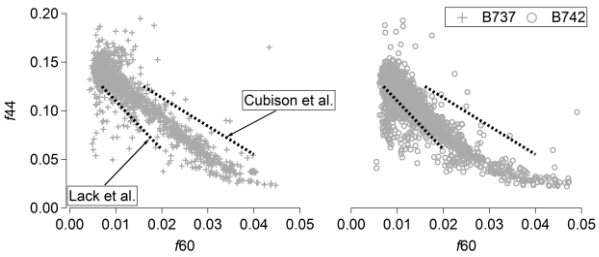

Figure 1: Relationship between *f*44 and *f*60 for a smouldering wildfire (B737) and flaming agricultural fires (B742). The dotted lines correspond to the relationships reported by Lack et al. (2012) and Cubison et al. (2011)

Further results from this campaign will be presented and discussed, quantifying the properties of aerosols under the various conditions. As well as differences in the plume characteristics with burn type, also of interest are the transformations during plume age. The intended applications of these data (e.g. to modelling activities) will also be discussed.

Bond et al.: *J. Geophys. Res. –Atmos.*, doi: 10.1002/jgrd.50171, in press.
Cubison et al.: *Atmos. Chem. Phys.*, 11, 12049-12064, doi:10.5194/acp-11-12049-2011, 2011.
Lack et al.: *Atmos. Chem. Phys.*, 13, 2415-2422, doi:10.5194/acp-13-2415-2013, 2013.

Thursday, September 5, 2013

Special Session: Aerosol Modelling, Atmospheric Aerosols, *European Year of Air Quality 2013*

Experimental and modeling analyses of emission measurements for a heavy-duty diesel bus: the comparison between on-road and in-lab methods

Y. Jason Wang[1], Zheming Tong[1], Topi Rönkkö[2], Jorma Keskinen[2], Liisa Pirjola[3], K. Max Zhang[1]

[1]Sibley School of Mechanical and Aerospace Engineering, Cornell University, Ithaca, NY, 14850, USA

[2]Department of Physics, Tampere University of Technology, Tampere, FI-33101, Finland

[3]Department of Technology, Metropolia University of Applied Sciences, Helsinki, FI-00180, Finland

Keywords: emission inventory, particle sampling, dilution, design

Presenting author email: yw365@cornell.edu

The development of emission inventories relies on the emission testing. On-road chasing method can capture the real world vehicle emissions and establish a link between the atmospheric dilution and the undiluted exhaust; while the in-lab chassis dynamometer measurements are widely used for regulatory purposes because tests are made under well-controlled conditions (Rönkkö et al, 2006). However, the differences between the on-road and in-lab methods have not been well studied; meanwhile, experimental and modeling results have indicated that particle emission measurements are sensitive to how dilution is conducted (Lipsky et al, 2005; Wang et al, 2013; Rönkkö et al, 2006). The objective of this study is to investigate the impact of on-road and in-lab transport and transformation of aerosol particles on particulate emissions through experimental and modeling analyses.

For the on-road method, the turbulent flow field in the wake of a scaled diesel bus is studied in a wind tunnel using Particle image velocimetry (PIV) method and the numerical Large-eddy Simulation model. Aerosol dynamics in this diluting exhaust plume is simulated by a turbulent reacting flow model (CTAG) and evaluated by the corresponding on-road experiments (Ronkko et al, 2006). For the in-lab method, the turbulent flow field and aerosol dynamics inside a two-stage dilution system (a porous diluter followed by an ageing chamber and a Dekati ejector diluter) are modeled by CTAG and evaluated by in-lab experiments.

In the on-road chasing environment, strongly affected by vehicle-induced turbulence, the shape of the exhaust plume is changing rapidly in the wake of the vehicle and nucleation takes place in the near-wake region (Figure 1). The maximum nucleation rates occur in the areas where the gradients of sulfuric acid, temperature, relative humidity and dilution are the steepest. Combined with sensitivity studies, the crucial parameters, e.g., the locations of the sampling inlet, the chasing distances, the direction and velocity of ambient wind are investigated to provide implications for the future on-road chasing emission measurements.

The approach of in-lab experiments is based on exhaust sampling and dilution method developed in "Particulates" program of EU. In that method, the exhaust is mixing rapidly with the dilution air inside the porous diluter and near the entrance of the ageing chamber. Then the flow transforms to laminar inside the ageing chamber. The mixture is further diluted inside the ejector diluter, where the supersonic flow is achieved at the orifice. It is found that the formation of new particles can occur in the porous diluter and near the entrance of the ageing chamber. Particle size distributions (PSDs) show adequate agreement between experiments and CTAG (Figure 2). The discrepancy between on-road and in-lab PSDs is due to 1) different dilution parameters, e.g., temperature and relative humidity of dilution air (Line 4 v.s. Line 5); 2) the intensity of the dilution process (Line 2 v.s. Line 5), i.e., the dilution rate, as introduced in Wang et al (2013), since within the first few seconds (where nucleation is the strongest), the on-road dilution ratio can achieve up to 1000 in the wake of the diesel bus, while for the in-lab system, the dilution ratio is maintained at ~96 (12×8).

A thorough understanding of these two methods is important for the ongoing effort to define a standardized sampling methodology for characterizing emissions from vehicles, especially with diesel engines.

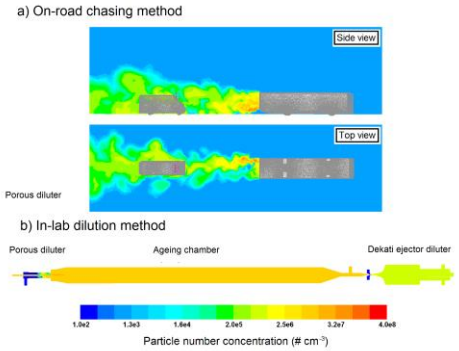

Figure 1. Instantaneous distributions of particle number concentration on-road and in-lab for driving condition 7.

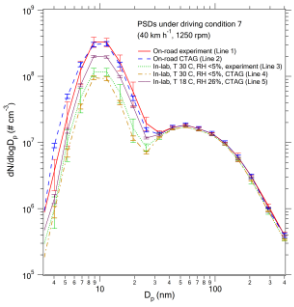

Figure 2. Comparisons of PSDs (measurements v.s. CTAG) under on-road and in-lab methods for driving condition 7.

This work is supported by the USEPA under grant R834561.

Lipsky, E., and Robinson, A. (2005) *Aerosol Sci. Technol.* **39(6)**, 542-553.

Rönkkö, T., Virtanen, A., Vaaraslahti, K., Keskinen, J., Pirjola, L., Lappi, M. (2006) *Atmos. Environ.* **40(16)**, 2893-2901.

Wang, Y., Yang, B., Lipsky, E., Robinson, A., Zhang, K. (2013) *Environ. Sci. Technol.* **47(2)**, 889-898.

Source apportionment of sub-micron particles in the urban background by Positive Matrix Factorization

H. Yu[1], U. Quass[1], H. Kaminski[1] and T. A. J. Kuhlbusch[1, 2]

[1]Air Quality & Sustainable Nanotechnology Unit, Institute for Energy and Environmental Technology (IUTA e.V.), 47229 Duisburg, Germany

[2]CENIDE, Center for Nanointegration Duisburg-Essen, 47057 Duisburg, Germany

Keywords: source apportionment, particle number size distribution, positive matrix factorization.

Presenting author email: quass@iuta.de

Atmospheric particles are regulated and monitored by a lot of countries as they are strongly associated with poor visibility and adverse health effects. Presently, these regulations are focused on particle mass concentrations. However, other particle metrics, like particle number concentration (PNC) or particle surface concentration, (both dominated by submicron particles) are discussed to be better correlated to some health endpoints than mass concentration, especially for cardiovascular diseases, as was also observed in some epidemiological studies [Atkinson et al., 2010; Breitner et al., 2011]. As a result, there is an ongoing discussion if sub-micron particle metrics should also be subjected to regulation in ambient air [ETH, 2012].

The presented study was started on this background to obtain more detailed source information on particle number concentrations by using particle number size distribution data along with some extra measurements from daily monitoring.

The measurements were conducted at a joined urban background measurement site of IUTA and the State Agency for Nature, Environment and Consumer Protection of North Rhine Westphalia (LANUV) in Mülheim Styrum, Germany. This site is influenced by traffic emission from a motorway in northern directions. The main wind direction is from the southwest. Measurement data for a three-year period from March, 2009 to February, 2012 was selected for further evaluation. Following metrics were determined: number size distribution (14.1 - 736.5 nm), lung-deposited particle surface concentration (LDS), PM_1 (starting from March, 2011), PM_{10} and NOx. Data for PM_{10}, NOx and for meteorological conditions were provided by LANUV.

All data were rigorously evaluated prior to processing. The time resolution of the data was averaged to two-hourly values and the particle size classes were reduced to 16 channels per decade to facilitate the source apportionment analysis. Further, following size classes were used as additional PMF variables: total number concentration (Total), number concentration for ultra fine particles (UFP, <100nm) and number concentration for the particles larger than 100nm (FP).

The receptor model EPA PMF 3.0 was chosen for this study as this software has been successfully applied to similar dataset in a previous study [Gu et al., 2011]. Among all the results from this model, the seven-factor result was considered to be the most robust and plausible based on factor composition, diurnal patterns and conditional probability function (CPF) diagrams of wind direction influence. The identified source groups and their averaged contributions to some source-indicative variables are shown in Table 1.

Table 1 Contributions of resolved factors (%)

Short name	NOx $\mu g\ m^{-3}$	UFP cm^{-3}	FP cm^{-3}	Total cm^{-3}	LDS $\mu m^2 cm^{-3}$	PM_{10} $\mu g\ m^{-3}$
Nucleation	1.3	15.0	0.9	12.9	~0*	0.6
Secondary	19.6	1.6	10.3	2.9	9.1	24.5
Dust	4.9	0.8	3.6	1.2	3.5	16.2
Background	3.1	0.8	31.1	5.2	17.4	32.8
Fresh Gasoline	17.7	36.4	5.4	31.9	16.2	8.2
Aged Gasoline	21.0	33.1	4.7	28.8	21.7	10.1
Diesel	32.4	12.4	43.8	17.1	32.1	7.5

The results show that traffic factors appear to be the major contributors for total and UFP particle number concentrations, while the nucleation factor and the other factors have moderate or low contributions to them. The three distinguished traffic related factors resemble corresponding emission particle size distribution profiles and have typical diurnal patterns. However, without support by chemical analyses, interpretations of factor characteristics may imply considerable uncertainty due to the absence of selective or unique tracer compounds.

LANUV is acknowledged for partially funding the measurement campaign and providing meteorological data along with some daily monitoring data for this study.

Atkinson, R.W., Fuller, G.W., Anderson, H.R., Harrison, R.M. and Armstrong, B. (2010) *Epidemiology (21): 501-511*.

Breitner, S., Liu, L., Cyrys, J., Brüske, I., Franck, U., Schlink, U., Leitte, A.M., Herbarth, O., Wiedensohler, A., Wehner, B., Hu, M., Pan, X.-C., Wichmann, H.-E. and Peters, A. (2011) *Science of the Total Environment 409(24):5196-5204.*

ETH Conference on Combustion Generated Nano-particles, 2012. *Focus Event "How to regulate ambient nanoparticles", 27. June. 2012, Zürich*.

Gu, J., Pitz, M., Schnelle-Kreis, J., Diemer, J., Reller, A., Zimmermann, R., Soentgen, J., Stoelzel, M., Wichmann, H.-E., Peters, A. and Cyrys, J. (2011) *Atmospheric Environment 45, 1849-1857.*

Air quality in a Mediterranean city-port: Particulate matter source apportionment using the WRF-CAMx modeling system

A. Poupkou[1], N. Liora[2], A. Karagiannidis[1], T. Giannaros[2], D. Melas[2], A. Argiriou[1]

[1]Department of Physics, University of Patras, Patras, 26500, Greece
[2]Department of Physics, Aristotle University of Thessaloniki, Thessaloniki, 54124, Greece
Keywords: source apportionment, maritime emissions, CAMx, Patras.
Presenting author email: poupkou@auth.gr

During the last decades, there has been an increasing urbanization pressure on the Mediterranean port-cities with impacts not only on the economic growth but also on the environment. The main objective of this study is the quantification of the contribution of pollutant emission sources to the air pollution in the city-port of Patras in Greece. More emphasis is given on the contribution of the maritime transport and the activities within the harbor area.

A modeling system is used that consists of the mesoscale meteorological model WRF and the photochemical model CAMx. Source apportionment is performed for the particulate matter (PM). Observational data are also used in order to identify the meteorological conditions that favor the increased PM concentrations.

The modeling system is applied over a 10km resolution grid that covers the Balkan Peninsula and a 2km grid that spans over Patras. Summer and winter simulation periods are examined in order to account for different meteorological conditions in the study area. The chemical boundary conditions are taken from the IFS-MOZART global modeling system.

The emission model MOSESS (Markakis *et al* 2009) has been applied in order to compile a spatially (2km resolution) and temporally resolved inventory for CO, NOx, SO2, NH3, NMVOCs, PM10 and PM2.5 emissions from anthropogenic sources (central heating, industries, road and non-road vehicles etc.) on the basis of the European scale emission inventory for the year 2007 of The Netherlands Organisation (Kuenen *et al* 2011). Emphasis is given on the estimation of pollutant emissions from the various activities inside the area of the harbor (stockpiles, unloading processes, harbor machineries etc) as well as from the maritime transport (cargo, passenger ships etc) on the basis of activity data provided by the Patras Port Authority (Figure 1).

Natural emissions of PM10, PM2.5 and biogenic NMVOCs are calculated employing the NEMO model (Poupkou *et al* 2010). NEMO can quantify hourly emission rates for sea salt, windblown dust and biogenic NMVOCs driven by the meteorology of WRF.

The CAMx model is extended to include the tool Particulate Source Apportioning Technology (PSAT) in order to provide PM source apportionment among specific source categories. The emission sources to be apportioned for Patras are the following:
1) Maritime and Harbor activities, 2) Road traffic, 3) Central heating, 4) Industries, 5) Soil (windblown dust) and 6) Vegetation (biogenic NMVOCs).

PM is a key pollutant in the urban atmosphere of Patras. The work presented will try, with the aid of a high resolution pollutant emission inventory and modeling system, to provide some insight on the issue of PM pollution in Patras (in relation also with the presence of the port) in order to allow the policy makers to develop effective control strategies for the atmospheric pollution.

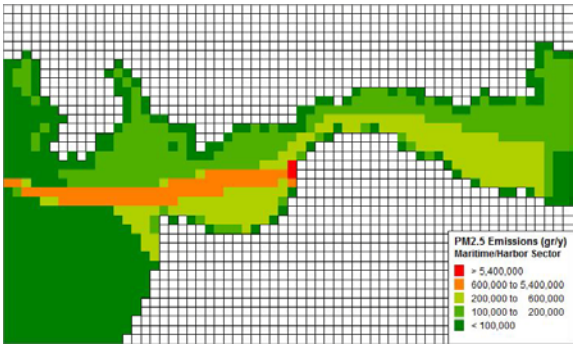

Figure 1. Annual PM2.5 maritime/harbor emissions in the Patras modeling domain.

This work is financed by the European Territorial Cooperation Programme Greece-Italy 2007-2013 project CESAPO, co-financed by the European Union (ERDF) and by National Funds of Greece and Italy. We would like to thank for the IFS-MOZART data provided in the framework of the EU FP7 project "Monitoring Atmospheric Composition and Climate Interim Implementation" (Grant agreement no: 283576).

Kuenen, J., van der Gon, H. D., Visschedijk, A., Dröge, R. and van Gijlswijk, R. (2011) *MACC European emission inventory for the years 2003-2007*, The Netherlands Organisation.

Markakis, K., Poupkou, A., Katragkou, E., Giannaros, T. and Melas. D. (2009) *2009 GEIA-ACCENT Conference, Emissions of gases and aerosols, Progress and modeling needs*.

Poupkou, A., Giannaros, T., Markakis, K. Kioutsioukis, I., Curci, G., Melas, D., and Zerefos, C. (2010) *Environ Modell Softw* **25**, 1845-1856.

Size specific distribution of the atmospheric particulate persistent organic pollutants (POPs) on a seasonal scale

Céline Degrendele[1], Krzysztof Okonski[1], Lisa Melymuk[1], Linda Landlová[1], Petr Kukučka[1] and Jana Klánová[1]
[1]Research Centre for Toxic Compounds in the Environment, Faculty of Science, Masaryk University, Kamenice 5/753, 625 00 Brno, Czech Republic
Keywords: POPs, particle-bound, size distribution, seasonal variation
Presenting author email: degrendele@recetox.muni.cz

Persistent organic pollutants (POPs) such as polychlorinated biphenyls (PCBs), polybrominated diphenyl ethers (PBDEs), perfluorinated compounds (PFCs), organochlorine pesticides (OCPs), polychlorinated dibenzo-p-dioxins and dibenzofurans (PCDD/Fs) and novel brominated flame retardants (nBFRs) are of high interest due to their persistence and accumulation in the environment and to their possible toxicity.

Seasonal particle size fraction distributions have been investigated for a wide range of POPs, ranging from pollutants banned under the Stockholm Convention to current-use flame retardants. Recent studies have suggested that better characterization of the size-distribution of the particulate POPs is useful for two reasons. First, it improves our understanding of the transport of those compounds from emission sources to remote areas, and second, it permits better characterization of the potential human exposure to POPs via inhalation.

Weekly atmospheric samples from urban and semi-rural sites in the Czech Republic were collected between October 2009 and October 2010 using a high volume air sampler equipped with a cascade impactor (separating particles into 6 size fractions: <0.49 µm; 0.49-0.95 µm; 0.95-1.5 µm; 1.5-3.0 µm; 3.0-7.2 µm; 7.2-10 µm). Individual samples of each fraction were combined into 4 composite seasonal samples.

Target analyte concentrations (PCBs, PBDEs, dioxin-like PCBs, nBFRs, PFCs, OCPs, CUPs (current use pesticides) and PCDD/Fs) were quantified using automatic solvent extraction, fractionation techniques and GC-MS or LC-MS instrumental analysis.

The data suggest that proximity to primary sources drives particulate POPs concentrations, as the concentrations measured at the urban site were significantly higher than those measured at the semi-rural site for combustion or consumer products-related pollutants (Figures 1 and 2). Concentrations measured for different pesticides were higher at the semi-rural site and higher during warm seasons, while PAHs, PCDD/Fs and PBDEs concentrations were higher in cold seasons.

Most of the target compounds were associated with the two finest particle size fractions (<0.49 µm, 0.49-0.95 µm), together accounting for more than 50% of the particle-bound POPs (Figures 1 and 2).

In summer, lower-molecular weight compounds were distributed more evenly amongst size fractions, which may suggest volatilization and redistribution of POPs amongst aerosols at warmer temperatures. Generally, the proportion of finest particles was higher at the urban site than at the semi-urban site. The distribution of size-specific particulate POPs has shown to be strongly related to local and seasonal sources and influenced by the temperature changes.

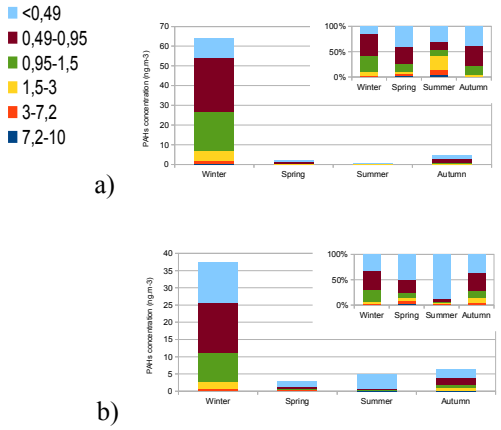

Figure 1: Seasonal size distribution of ΣPAHs at Telnice (a) and Kotlařska (b)

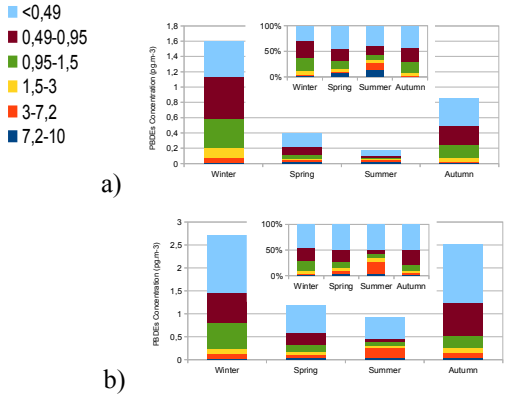

Figure 2: Seasonal size distribution of ΣPBDEs at Telnice (a) and Kotlařska (b)

Modelling multiphase night-time processes with WRF-Chem

D. Lowe[1], S. Archer-Nicholls[1], W. Morgan[1], S. Utembe[1,2], G. McFiggans[1]

[1]Centre for Atmospheric Science, University of Manchester, Manchester, M13 9PL, United Kingdom
[2]Earth Sciences, The University of Melbourne, Victoria, Australia
Keywords: NOx, Modelling, Multiphase, Nighttime
Presenting author email: douglas.lowe@manchester.ac.uk

Aerosol particles play an integral part in the chemistry of the atmosphere — by acting as reaction surfaces for heterogeneous chemistry, as chemical sources, and by removing components through scavenging and dry deposition. They have an important influence on the lifetime of the nitrate radical (NO_3), which is the dominant oxidant in the nocturnal atmosphere. NO_3 and NO_2 are in thermal equilibrium with N_2O_5, which acts as a reservoir species for NO_3. However N_2O_5 also provides an important loss pathway for NOx by conversion to HNO_3 via heterogeneous reactions on aerosol particles, the rates of which are dependent on aerosol composition, relative humidity and temperature (Allan et al., 1999, Davis et al., 2008; Bertram & Thornton, 2009). In order to properly predict the oxidative capacity of the nocturnal atmosphere we must understand the influence of aerosols on gas-phase chemistry.

This study uses the WRF-Chem regional atmospheric chemistry model (Grell et al., 2005; Fast et al., 2006), with the MOSAIC sectional aerosol module (Zaveri et al., 2008). We have added the CRIMech gas phase chemistry scheme (Watson et al., 2008) to WRF-Chem using the KPP interface, and coupled it to the MOSAIC sectional aerosol module. In addition we have modified MOSAIC to include the heterogeneous uptake of N_2O_5 (Bertram & Thornton, 2009). The details of these, and other, developments made to WRF-Chem are covered in a companion presentation.

Anthropogenic emissions have been calculated using the NAEI (naei.defra.gov.uk) and TNO (Denier van der Gon et al., 2010) emission databases, with diurnal and weekly cycles superimposed. Biogenic emissions are calculated online within WRF-Chem, based on USGS land-use categorisation. The meteorological fields are initialised with, and bounded by, ECMWF ERA Interim data (Dee et al., 2011) Radiative feedback from the aerosol fields is allowed to influence the meteorology. Chemical boundary conditions are taken from MOZART global model data (Emmons et al., 2010).

Three chemical scenarios are considered: a base case with full N_2O_5 heterogeneous chemistry; N_2O_5 heterogenous chemistry without the chloride ion pathway; and no N_2O_5 heterogeneous chemistry. For each scenario we have run the model over a 15km resolution grid covering NW Europe for the period 10–30th July 2010. A second domain, covering England and the North Sea at a resolution of 5km, has also been run for selected dates during this period for more detailed comparisons with aircraft measurement data.

We will present an analysis of the effects of N_2O_5 heterogeneous chemistry on: i) night-time gas-phase NOx chemistry; ii) the regional distribution of aerosol composition; iii) the relative day-time and night-time contributions to nitrate aerosol and of the relative contribution of the hydrolysis and chloride channels to the effects.

This work was conducted as part of the RONOCO (ROle of Nighttime chemistry in controlling the Oxidising Capacity of the atmOsphere) (NERC grant: NE/F004656/1) project .

Allan, B. J., Carslaw, N., Coe, H., Burgess, R. A., and Plane, J. M. C. (1999). *J. Atmos. Chem.*, **33**, 129–154

Bertram, T. H., and Thornton, J. A. (2009). *Atmos. Chem. Phys.*, **9**, 8351–8363

Davies, J. M., Bhave, P. V., and Foley, K. M. (2008). *Atmos. Chem. Phys.*, **8**, 5295–5311

Dee, D. P., et al. (2011). *Q. J. R. Meteorol. Sci.*, **137**, 553–597, doi:10.1002/qj.828

Denier van der Gon, H. A. C., Visschedijk, A., van der Brugh, H., and Dröge, R. (2010). TNO report: *TNO-034-UT-2010-01895_RPT-ML*, Utrecht

Emmons, L. K., et al. (2010). *Geosci. Model Dev.*, **3**, 43–67, doi:10.5194/gmd-3-43-3010

Evans, M. J., and Jacob, D. J. (2005). *Geophys. Res. Lett.*, **32**, L09813, doi:10.1029/2005GL022469

Fast, J. D., Gustafson, W. I., Easter, R. C., Zaveri, R. A., Barnard, J. C., Chapman, E. G., Grell, G. A., and Peckham, S. E. (2006). *J. Geophys. Res.*, **111**, 1–29, doi:10.1029/2005JD006721

Grell, G. A., Peckham, S. E., Schmitz, R., McKeen, S. A., Frost, G., Skamarock, W. C., and Eder, B. (2005). *Atmos. Env.*, **39**, 6957–6975, doi:10.1016/j.atmosenv.2005.04.027

Watson, L. A., Shallcross, D. E., Utembe, S. R., and Jenkin, M. E. (2008). *Atmos. Env.*, **42**, 7196–7204, doi:10.1016/jatmosenv.2008.07.034

Zaveri, R. A., Easter, R. C., Fast, J. D., and Peters, L. K. (2008). *J. Geophys. Res.*, **113**, doi:10.1029/2007JD008782

Air quality modeling of mega cities in Yangtze River Delta region

L.L Tang[1,2], B. Zhu[2], Y.J. Zhang[2] and L. Tang[2]

[1] The Center of Jiangsu Environmental Monitoring, Nanjing, 210036, China
[2] Jiangsu Key Laboratory of Atmospheric Environment Monitoring and Pollution Control, Nanjing University of Information Science & Technology, Nanjing, 210044, China
Keywords: Yangtze River Delta, Air pollution, CMAQ, contribution ratio.
Presenting author email: lili.tang@nuist.edu.cn

Recently with the development of industry and population growth in Yangtze River Delta (YRD) region, air pollutants emitted by human activities have risen dramatically. Air pollutants emitted by mega cities in Yangtze River Delta mainly include: SO_2, NOx, CO, VOCs and aerosol. Both VOCs and NOx play critical roles during O_3 formation in the troposphere. A better understanding of the relationship between O_3 precursors (VOCs, NOx) and O_3 formations in Yangtze River Delta region is one of the critical pre-required information to develop effective O_3 control strategies. A third generation air quality model Models-3/CMAQ developed by U.S. Environmental Protection Agency are used to study the combined pollution in YRD region.

In this paper we verified the simulation results and found that the simulation results of O_3 SO_2 and NO_2 are in agreement with experiment results. The mean correlation coefficient and mean normalized bias and mean agreement index are 0.96, 7.26% and 0.92 separately. Mean agreement index of SO_2 is 0.62. Mean correlation coefficient and mean agreement index are 0.66 and 0.67 separately. Simulation results of PM10 are somewhat lower than experiment results. However, the trend of simulation results is consistent with the observation data. The lifetime of SO_2 and NO_x are too short to long-range transport. High concentration of NO in urban area leads to ozone loss. The highest mean ozone concentration appeared in spring and lowest in winter, this phenomenon is correlated with O_3 production rate and surrounding transportation. High O_3 concentrations were associated with the occurrence of high-pressure systems. Wind field convergence is beneficial to air pollutant accumulation.

In this study we closed the emission of NOx and VOCs in January and July 2008, to test the contribution of O_3 and it's precursors (VOCs, NOx) from surrounding places. The mean contribution rate of NOx, VOCs and O_3 in January are 9.5%, 38.9% and 125.1%, separately. NOx and VOCs mainly comes from north-west direction of YRD region. O_3 mainly came from south-east direction of YRD region. During winter YRD is an ozone net loss region. The mean contribution rate of NOx, VOCs and O_3 in July are 7.7%, 51.4% and 94.4%. During summer monsoon brought NOx form northern part of Zhejiang Province. VOCs mainly came from mountain area in south-west direction of YRD. Ozone form land around YRD is more than from ocean.

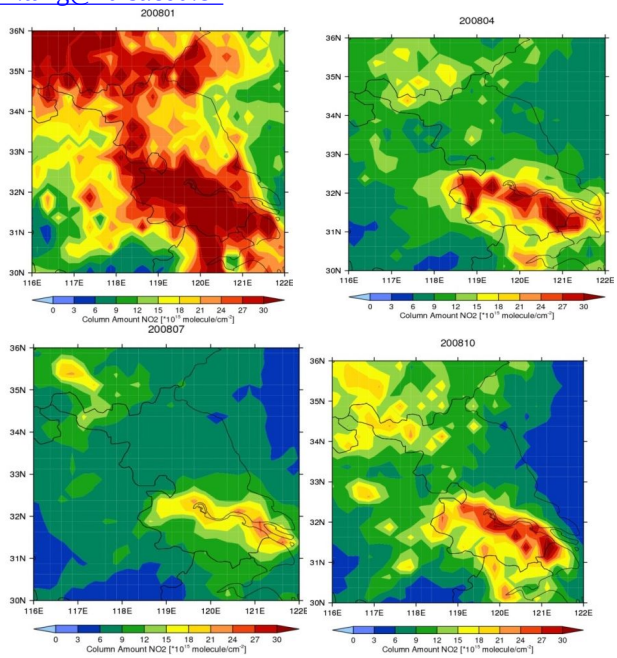

Figure 1. Concentrations distribution of NO_2 in the atmosphere of Yangtze River Delta region during different seasons

This work was supported by the High Education Natural Science Key Research of Jiangsu Province, China (Grant No.11KJA170002)

Reference

1. Zhang, Q., Zhao, C., Tie, X., Wei, Q., Li, G., Li, C., (2006). *Atmos. Environ*. 40: 4513–4527.
2. Draxler R R, Hess G D. (1998). Aust. Meteor. Mag., 47: 295-308.
3. Tie, X., Chandra, S., Ziemke, J.R., Granier, Claire, Brasseur, G., (2006). J. Atmos. Chem. doi:10.1007/s10874-006-9045-7
4. Bin Zhu, Hajime Akimoto, Zifa Wang, *et al*.（2004） *J.Geophysical Research Letters*, 31, 7104-7108.

Thursday, September 5, 2013

Poster session C

Electrical effects, Posters C001 - C009

Incineration of the diesel particulate matter using the dielectric barrier discharge on the electrostatic precipitator

Y. Ehara[1], M. Kobayashi[1], H. Muramatsu[2], A. Zukeran[2], H. Kawakami[3] and T. Inui[3]

[1]Dep. of Electrical and Electronic Engineering, Tokyo City University, Tokyo, 158-8557, Japan
[2]Dep. of Electronic & Electrical Engineering, Kanagawa Institute of Technology, Kanagawa, 243-0292, Japan
[3]Dept. of Road Systems Engineering, Fuji Electric Co., Ltd, Tokyo, 191-8502, Japan

Keywords: electrostatic precipitator, dielectric barrier discharge, particulate matters.
Email: yehara@tcu.ac.jp

The particulate matters (PMs) emitted from marine diesel engine exhaust during the combustion process have low resistivity and extremely small in the range of 70-120nm. These particles cause a various human health and environment impacts. After MARPOL 73/78 Annex VI entered into force on 1st of July 2010, shipping-induced NOx and SOx, PM emissions are regulated stricter.

This research has been developed an after treatment system for removal of particulate matter (PM) emissions from a diesel engine. The PM was collected by electrostatic precipitator (ESP) using a high-frequency dielectric barrier discharge (DBD). In the DBD, the air is activated by discharge and produces ozone, oxygen radical and nitrogen radical. Therefore, the diesel particulates are oxidized and incinerated under low temperature condition.

A diesel engine generator, displacement volume of 435cc, using light oil was used. The particle size-dependent number densities before and after the ESP was determined by the Scanning Mobility Particle Sizer (SMPS, Model 3034) for the particle size ranged 20-800 nm and the particle counter (PC, Rion KC-01E) for the particle size of 300-5,000nm, respectively. The gas velocity was 13m/s. The ESP using DBD were composed by a parallel plate electrode. Both electrodes were covered by the dielectric glass plate. The discharge gap length was 3.5mm. The discharge power was measured by Lissajous method.

Particle-size dependent collection efficiency as a function of the discharge power of 5-20W was shown in Figure 1. The collection efficiency of large particles is higher than that of small particles. The collection efficiency increased with increasing the discharge power. The maximum collection efficiency was 22% at particle size of 3,200nm with 5W discharge power. The maximum collection efficiency was 68% at particle size of 1,400nm with 5W discharge power.

Figures 2 (a)-(b) show the pictures of the dielectric glass after 60min operation by DBD. In the discharge power of 5W, the dielectric glass surface has a lot of soot compared with 20W. However, the collection efficiency of high discharge power is higher than that of low discharge power as shown in Figure 1. It was clear that the collected particles were incinerated with ozone generated by DBD. The ESP using DBD has high potential especially for highly concentrated marine diesel engine emission control.

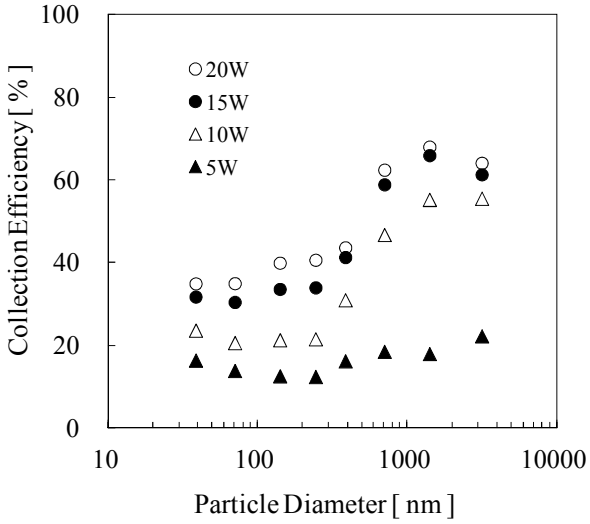

Figure 1. Particle-size dependent collection efficiency as a function of the discharge power of 5-20 W.

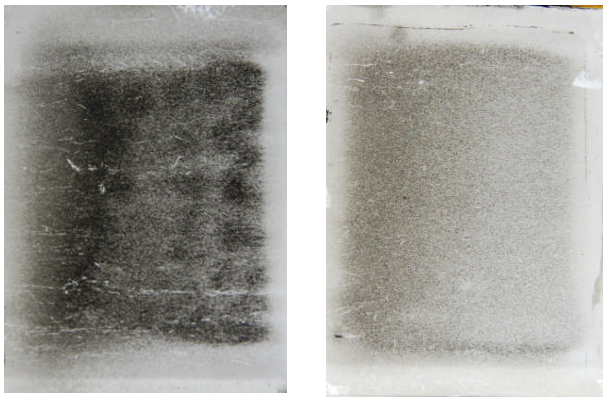

(a) 5 W (b) 20 W

Figure 2. The picture of the dielectric glass after 60 min ESP operation.

This work was supported by the Grant-in-Aid for Scientific Research (B) of the Japanese Society for the Promotion of Science.

Yoshiyasu Ehara, et al. (2012) *Proc. 8th Int. Symp. on Non-Thermal/Thermal Plasma*

Manipulation of aerosol particles with nonlinear polarizability

K.V. Generalov[1], D.V Korneev[1], V.M. Generalov[1], M.V. Kruchinina[2], B.N. Zaycev[1]
[1] Federal Budgete Research Institution «The State Research Center of Virology and Biotechnology "VECTOR"», Koltsovo, Novosibirsk region, 630559, Russia

[2] Federal Budget Research Institution Research Institute of Internal Medicine, Siberian Branch of the Russian Academy of Medical Sciences, 175/1 Boris Bogatkov str., Novosibirsk, Novosibirsk Region, 630089, Russia
Keywords: particle, polarizability, dielectrophoresis, nonlinear
Presenting author email: gkv@vector.nsc.ru

In the non-uniform alternating electric field (NAEF), the redistribution of electric charges and polarization take place, and the induced dipole moment is formed within the entire volume of the particle (including bacteria, cells, viruses and nanoparticles). From the theoretical point of view, linear and nonlinear charge redistribution reflects the peculiarities of the dynamics of electric charge motion over the entire volume of the particle. Anyway, this is due to the physical and chemical properties and inhomogeneity of all its structures such as the walls, core and capsid. It should be noted that each of them has also significant differences in electrical properties, the dielectric constant, capacitance, conductivity and water content. In the non-uniform electric field, the dipole particle is affected by the time-averaged force vector, which causes its forward motion (Hughes, 2003).

$$\langle \vec{F}_p \rangle = \langle 2 \cdot \pi \cdot \varepsilon_{cp} \cdot \varepsilon_o \cdot r_p^3 \cdot [\frac{\varepsilon_p - \varepsilon_{cp}}{\varepsilon_p + 2 \cdot \varepsilon_{cp}}] \cdot \nabla E_{cp}^2 \rangle \quad (1)$$

where: ε_{cp} ~1, is the dielectric constant of air;
ε_0 is the dielectric constant;
ε_p is the dielectric constant of the particle;
r_p is radius of the particle;
∇E_{cp}^2 is the gradient of the square of the electric field of air.

Expression (1) represents the polarizability of a_p particle in an expanded form

$$\alpha_p = 4 \cdot \pi \cdot r_p^3 \cdot \varepsilon_{cp} \cdot \frac{\varepsilon_p - \varepsilon_{cp}}{\varepsilon_p + 2 \cdot \varepsilon_{cp}} \quad (2)$$

Two forces emerge as a result of the interaction of the induced dipole moment of each particle with the voltage gradient of the electric field. The first force causes forward motion of the particle to the nearest electrode where the gradient of the square of the electric field is maximal. The second force determined by the vector product of the induced dipole moment and the gradient of the square of the electric field that makes it rotate around its own axis. It is well known that the dielectric constant ε_p of a substance (particle) depends on the frequency of the external electric field (Physical …., 1991). The frequency dependence of the difference ε_p - ε_{cp} will have a significant impact on the behavior and translational velocity of the particle to the nearest electrode. Our own simulations performed in water showed that particles were rotating around their own axis with a frequency greater than 1 Hz in NAEF, which is indicative of the non-linear polarization effect. All this results in pronounced, individual characteristics of their behavior in NAEF, Foto 1. The force acting on the particle with a relative permittivity $\varepsilon_p \sim 2 \cdot \varepsilon_{cp}$ close to 1 (which is typical for air) is negligible. The force acting on the particle with a relative permittivity hundreds or even thousands of times greater than 1 $\varepsilon_p \sim 10^{(2 \div 3)} \cdot \varepsilon_{cp}$ increases proportionally. The list of materials with similar properties is very long (Physical …, 1991). Thus, this opens new opportunities to manipulate aerosol particles based on subtle differences related to their dielectric constant and nonlinear polarizability.

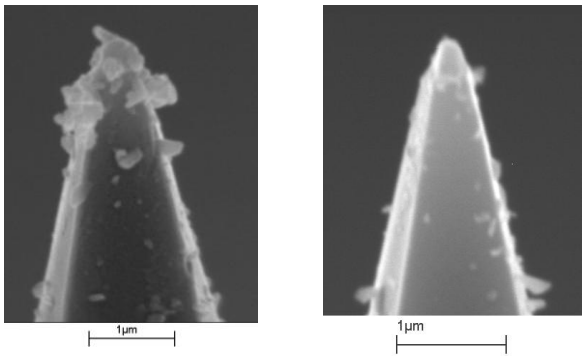

a) b)

Foto 1. Vaccinia virus on an electrode.
a) – probe after exposure in viral suspension with voltage; b) – probe after exposure in viral suspension with no voltage.

The study was supported by The Ministry of education and science of Russian Federation, project 8041.

Hughes M.P. (2003). Nanoelectromechanics in Engineering and biology. Boca Raton, London, New York, Washington, D.C.: CRC PRESS Boca Raton, 320 p.

Physical quantities. Handbook. (1991). Grigor'eva I.S., Meilikhova E.Z. (Eds.) Moscow: Energoatomizdat. 1232 p. (in Russian).

An ESP nanoparticle generator

C.W. Lin[1], W.Y. Lin[2], T.C. Hisao[3], Y.M. Kuo[4] and C.C. Chen[1]

[1]Institute of Occupational Medicine and Industrial Hygiene, National Taiwan University, Taipei, Taiwan
[2]Institute of Environmental Planning and Management, National Taipei University of Technology, Taipei, Taiwan
[3] Graduate Institute of Environmental Engineering, National Central University, Jhongli City, Taoyuan, Taiwan
[4]Department of Occupational Safety and Health, Chung-Hwa University of Medical Technology, Tainan, Taiwan
Keywords: nanoparticle generator, corona discharge, ozone, electrode
Presenting author email: ccchen@ntu.edu.tw

Electrostatic precipitators (ESPs) are devices commonly used to remove charged particles in gas by electrostatic force. It is characterized by high collection efficiency, low pressure drop and low maintenance requirements (Mizuno, 2000). These devices originally designed for dust collection was found to generate particles under specific operating conditions. The transition from electrostatic precipitation to nanoparticle generation has been thoroughly investigated (Lin et al., 2012). This unique feature was utilized in the present study to develop a nanoparticle generator based on corona discharge.

A lab-scale wire-plate type positive corona discharger was built for characterizing the aerosol emission from this ESP nanoparticle generator, as shown in Figure 1. Environmental contaminants were removed by HEPA filter, active charcoal and silica gel. Gold, tungsten, molybdenum, and stainless steel were used as the electrode to study the material dependency. Gas temperature was controlled by a feedback heater. A positive direct current power supply was employed to energize the corona discharger. A scanning mobility particle sizer with a nano differential mobility analyzer was employed to measure the aerosol number concentration and size distribution. Ozone concentration was monitored by using an ozone analyzer. The sampling locations of SMPS and ozone analyzer were 20 and 15 cm downstream the corona discharger, respectively. The major operating parameters included electrode diameter, electrode spacing, air velocity, air temperature, applied voltage and current.

Sputtering on the corona discharger was the principal mechanism of aerosol generation. Aerosol concentration increased with increasing electric field strength when the applied voltage was higher than the onset voltage, and decreased rapidly when the electric field strength exceeded a specific value. The maximum aerosol concentration occurred when the electric field strength was around 8.2, 9.8, and 11.2 kV for electrode diameter of 0.1, 0.2 and 0.3 mm, respectively. The smaller discharge electrode diameter generated more aerosol particles, but lower ozone concentration when compared to larger electrode diameter. The differences in aerosol concentration due to the change of electric field strength decreased with increasing electrode diameter, because the mean kinetic energy was more uniform in the larger electrode. Electrode materials did not affect the I-V curve but the aerosol generation rate and the ozone concentration were clearly material-dependent. Gold was chosen as the discharge electrode because of stable and high sputtering yield.

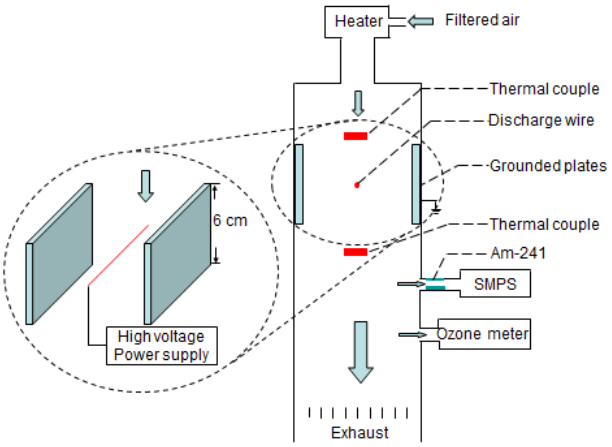

Figure 1. Schematic diagram of the experimental setup.

This work was supported by the National Science Council of Taiwan through grant NSC 99-2221-E-002 -069 -MY3.

Lin, C.W., S.H. Huang, Y.M. Kuo, K.N. Chang, C.S. Wu and C.C. Chen (2012), *Journal of Aerosol Science* 51: 57-65.
Mizuno, A. (2000). IEEE Transactions 7, 615-624.

Experimental study of a louvered electrostatic precipitator

C. W. Lin[1], S.H. Huang, W. Y. Lin[2], T. C. Hisao[3], Y. M. Kuo[4] and C. C. Chen[1]

[1]Institute of Occupational Medicine and Industrial Hygiene, National Taiwan University, Taipei, Taiwan
[2]Institute of Environmental Planning and Management, National Taipei University of Technology, Taipei Taiwan.
[3]Gradutate Institute of Environmental Engineering, National Central University, Jhongli City, Taoyuan, Taiwan
[4]Department of Occupational Safety and Helath, Chung-Hwa University of Medical Technology, Tainan, Taiwan
Keywords: Electrostatic precipitator, louver, energy consumption, window
Presenting author email: ccchen@ntu.edu.tw

Due to global warming, many countries are committed to reducing carbon emissions by increasing the efficiency of energy use. The drawbacks of air conditioners include high energy consumption and increased level of indoor pollutants trapped in a relatively sealed home. General ventilation increases the indoor air temperatures by expose to radiant energy (sunlight). The louvered window can reduce indoor temperature by blocking radiant energy and the ESP structure similar to the louvered window (Hatamipour and Abedi, 2008). The main purpose of the present study was to design and characterize a louvered electrostatic precipitator (ESP) that can reduce the aerosol concentration coming in from outdoors and block radiant energy at the same time, while permitting natural ventilation.

A lab-scale louvered ESP was built to carry out the aerosol filtration test, as shown in Figure 1. The discharge wire was made of stainless steel with a diameter of 0.3 mm. Particle number concentration and size distribution were obtained in the power on and power off modes. These data were then employed to evaluate the aerosol penetration of the ESP. The particle size distribution and ozone concentration were recorded by APS, SMPS and Ozone meter. The major operating parameters include the length of the collection plate, the filtration velocity and the flow rate through the ESP unit, the position of the discharge wire and the louver angle. The energy quality index considers both aerosol penetration and energy consumption was used to evaluate the louver ESP performance.

The results showed that the louver adjustment significantly affected the ESP performance. The discharge wire should be positioned in the middle to provide optimal ESP performance, although moving around the electrode did not significantly change the energy consumption and ozone generation. The collection plates with excessive length were proven to be ineffective. The wire-to-plate distance decreased with increasing louver angle. The louver adjustments resulted in changes of the effective collection area, electric field strength and air velocity. The field strength should be as low as possible to obtain a high energy quality index. For a given energy consumption, the energy quality index was not significantly affected by the louver angle. This phenomenon was due to a trade-off between the electric field strength and the effective collection area. Therefore, all aerosol penetration curves showed within a narrow band.

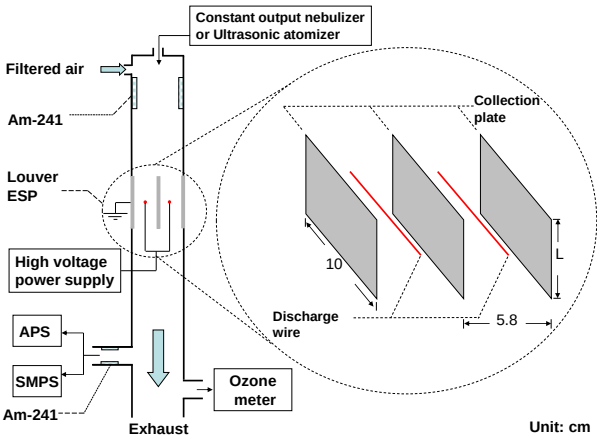

Fig 1. Schematic diagram of the experimental setup.

This work was supported by the National Science Council of Taiwan through grant NSC 99-2221-E-002-069-MY3.

Hatamipour, M.S. and Abedi, A., (2008). *Energy Conversion and Management*, 49(8): 2317-2323.

Open Channel Electrospray System

Joon Sang Kang, Jae Hee Jung and Gwi- Nam Bae

Center for Environment, Health and Welfare Research, Korea Institute of Science and Technology (KIST),
Hwarang-ro 14-gil 5 Seongbuk-gu, Seoul, Republic of Korea

Keywords: Electrohydrodynamic, Multi-jet, high throughput, monodisperse
Presenting author email:022698@kist.re.kr

Although there are a lot of positive characteristics of the electrospray system, the system is restricted in many area because of the low flow rate. The electrospray system is related to the scaling laws relating the diameter of the electrosprayed droplet, d, and the flow rate, Q. With $d \sim Q^{1/3}$ or $d \sim Q^{1/2}$, the flow rate becomes very low for smaller droplets (Ganan-Galvo *et al.*, 1997; Fernandez de la Mora & Locertales, 1993). Therefore, increasing the droplet productivity at the micro/nano droplet level is difficult.

In order to overcome this drawback, we employed new electrospray nozzle that has multiple holes arrayed on the side of the nozzle. In particular, the working fluid was divided among the holes and ran along an open channel on the outer wall of the nozzle. From the nozzle configuration, we achieved the desired monodispersity of the generated droplets and positional stability

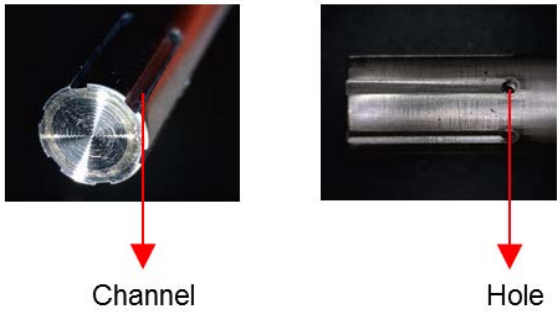

Figure 1. Pictures of nozzle

Figure 1 shows the pictures of nozzle in the present study. The primary difference of the nozzle in the present study compared to a conventional nozzle was that the nozzle exit was welded shut, and the working fluid was emitted through multiple holes arrayed on the side of the nozzle. The nozzle was made by stainless steel, and the outer diameter of the nozzle was 6.4 mm. Six holes (0.8 mm diameter) were evenly spaced on the side of the nozzle. To eliminate the positional instability of the multi-jet mode, an open channel was introduced from each hole to the tip of the nozzle.

Figure 2 (a) and (b) show that the difference in multi-jet formation depending on various experimental conditions, which demonstrate that an increased electric potential led to a much shorter liquid meniscus and that each jet was focused toward the open channel, as clearly shown in the Fig. 2 (c) and (d). Previous study reported that the number of jets rose with increasing electrical potential in the multi-jet mode (Duby *et al.*, 2006). However, in the present nozzle system, the number of jets was increased up to a maximum of 18 jets with increasing electric potential, but further increases in the electric potential decreased the number of jets down to 12.

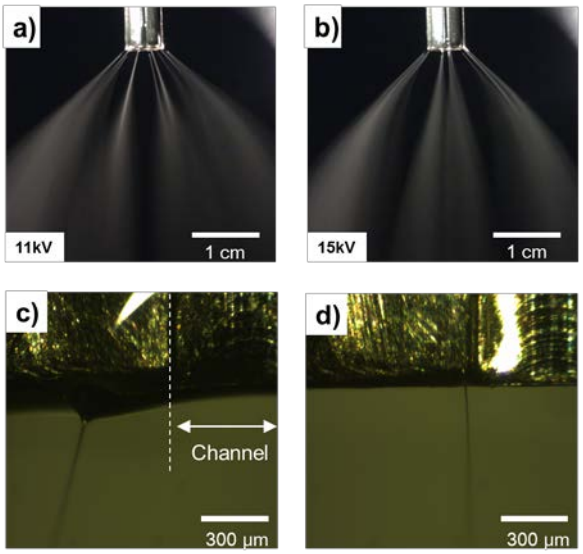

Figure 2. Picture of the various operational modes of the electrospray, with magnified views (Q = 60 ml/h)

This work was supported by the the Converging Research Center funded by Ministry of education, Science and Technology (2012K001370)

Duby, M., Deng, W., Kim, K., Gomez, T., and Gomez, A. (2006). Stabilization of monodisperse electrosprays in the multi-jet mode via electric field enhancement, *J.Aerosol Sci.*, **37**, 306-322.

Fernandez de la Mora, J., and Locertales, I. G., (1993). The current emitted by highly conducting Taylor cones, *J. Fluid Mech.*, **260**, 155-184.

Ganan-Calvo, A. M., Davila, J., and Barrero, A. (1997). Current and droplet size in the electrospraying of liquids. Scaling law, *J. Aerosol Sci.*, **28**, 249-275.

Effect of aperture rate on improving collection efficiency in hole-type electrostatic precipitator

H.Kawakami[1], A.Osako[2], Y.Watanabe[2], Y.Ehara[2], Y.Nitta[3], A.Zukeran[3], T.Inui[1]

[1]Dept. of Road Systems Engineering, Fuji Electric Co., Ltd., Toyo, 191-8502, Japan
[2]Dept. of Electrical & Electronic Engineering, Tokyo City University, Tokyo, 158-8557, Japan
[3]Dept. of Electronic & Electrical Engineering, Kanagawa Institute of Technology, Kanagawa, 243-0292, Japan
Keywords: electrostatic precipitator, collection efficiency, re-entrainment, marine diesel
Presenting author email:kawakami-hitomi@fujielectric.co.jp

The exhaust gases included the particulate matter (PM) emitted from marine diesels may cause the serious problem of pollution on the coast. Electrostatic precipitators (ESPs) have been used to decontaminate polluted exhaust gases emitted from industrial plants, etc.. However, the collection of low resistivity particles, such as PM emitted from marine diesel, is known to be difficult to precipitate.

In this study, the new hole-type ESP, which has hole-punched ground electrode, was developed to overcome the re-entrainment and increase the collection efficiency. We investigated the effect of the aperture rate of the hole-punched electrode on improving the collection efficiency.

The electrode structure of hole-type ESP is shown in Figure 1. The hole-type ESP consists of the grounding case, multiple hole-punched inner ground electrode and the high voltage center electrode. The hole diameter is 1 mm and the aperture rate is between 22.6 to 40.2% on the hole-punched ground electrode. The upstream and downstream portions of the space between the hole-punched ground electrode and the grounding case are closed. The flue gas is connected to the upstream portion between the high voltage center electrode and the hole-punched ground electrode (H.Kawakami, 2012). PM was emitted from the diesel engine (Yanmer, YDG200A-5E, 200cc), the gas velocity in the ESP is 1.5 m/s. DC -8 kV was applied to the high voltage center electrode, and the discharge current was 0.5 mA. The particle number concentrations are measured using the scanning mobility particle sizer (SMPS, TSI, Model 3080) and the particle counter (RION, KC-01E) after hot dilution.

The particle size distribution is shown in Figure 2. The gas temperatures were 130 ^{o}C, the high voltage was not applied to ESP. The particle size distributions have a peak at 70 nm of the particle diameter. It is clear that the ultra-fine particles, which are extremely harmful to human health, are included in the exhaust gas.

The collection efficiency as a function of particle diameter for various aperture rates at 1mm of hole-punched diameter is shown in Figure 3. The result at plate ground electrode, which does not have hole-punch, is also indicated in Figure 3. The collection efficiency between 20 to 1000 nm is approximately 80 % at plate ground electrode. The collection efficiency lager than 1000 nm decreases with increasing the particle diameter due to particle re-entrainment (A. Zukeran, 1999). The collection efficiency between 20 to 1000 nm increases with decreasing the aperture rate. The collection efficiencies lager than 1000 nm are significantly improved in comparison with that at plate ground electrode. This result indicates the effect of preventing particle re-entrainment in the hole-type ESP. The collection characteristics at high gas velocity, which is between 10 to 30 m/s, will be investigated in the future.

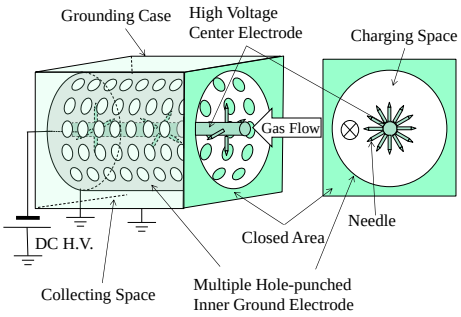

Figure 1. The electrode structure of hole-type ESP

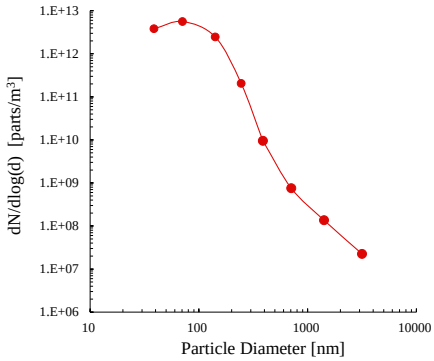

Figure 2. The particle size distribution.

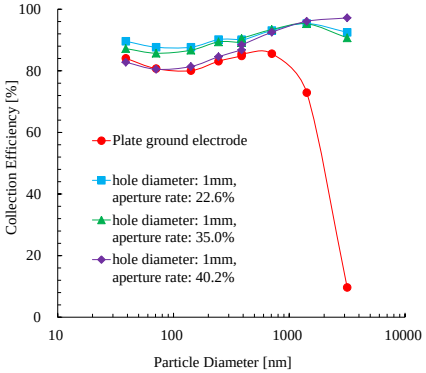

Figure 3. The collection efficiency as a function of particle diameter for various aperture rate.

H.Kawakami *et al* (2012) *International Journal of Plasma Environmental Science & Technology*, 6, 2, 104-110

A. Zukeran *et al* (1999) *IEEE Trans. on Ind. Appl*. 35, 2, 346-351

The Effect of Surface Charge on Characteristics of Fibrous Membrane

Yu-Rou Jhong[1], Hsin-Ying Lin[1], Sheng-Kai Chan[1], Tsung-Ming Tu[1], Yu-Chih Cheng[1], Yuan-Yi Chang[1], Chun-Wan Chen[2], Wen-Yinn Lin[1,*]

[1]Institute of Environmental Engineering and Management, National Taipei University of Technology, Taipei City 10608, Taiwan.
[2]Institute of Occupational Safety and Health, New Taipei City 22143, Taiwan.
Keywords: fibers; electrostatic; pressure drop
Presenting author email: wylin@ntut.edu.tw

Electrostatic attraction is a kind of basic mechanisms by which an aerosol particle can be collected onto a fiber (Hinds, 1999). Charged fibers can greatly enhance filter collection. Basing on electrostatic mechanisms, a filter can achieve specified collection efficiency at a lower packing density and thereby lower resistances to gas flow in the filter. This can achieve high removal efficiency without a large pressure drop (Nifuku *et al.*, 2001). In spite of many studies have been researching on the surface charge of fiber affects the filtration properties by theoretical simulation; few have been carried out on the experimental result. The objective of this study was to investigate the filtration properties of electrostatic filter.

In this study, an electrospinning system was set up. It was applied to produce fibrous membranes. The filtration test system was shown in figure 1. Fibrous membranes, made of PMMA, were tested to investigate the aerosol filtration characteristics of fabric filters while challenged with polydisperse NaCl particles. A constant output atomizer was used to generate particles. Besides, the aerosol concentrations and size distributions were measured by using an SMPS. The fiber diameter of test fibrous membranes was including 490, 1100, 2040, and 4052 nm. And then the applied voltage of fibrous membranes electrified was 12 kV by using corona discharge.

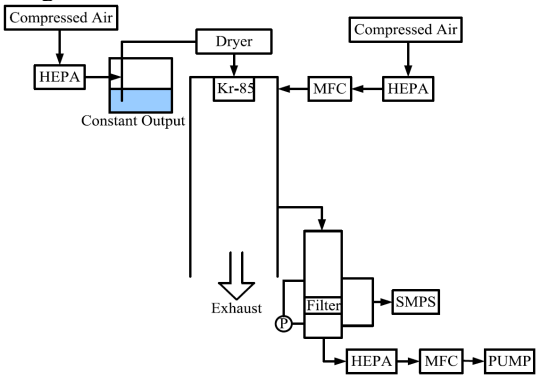

Figure 1. Schematic diagram of test system

The consequence of this study suggested that the morphology of the fibers was smooth and bead-free, which was photographed by scanning electron microscope (SEM), and shown in figure 2.

On the pressure drop test of different fiber diameter fibrous membranes, the effect of various filtration velocities on pressure drop was shown on figure 3. The pressure drop of fibrous membranes was increased as the filtration velocity increased and as the fiber diameter decreased.

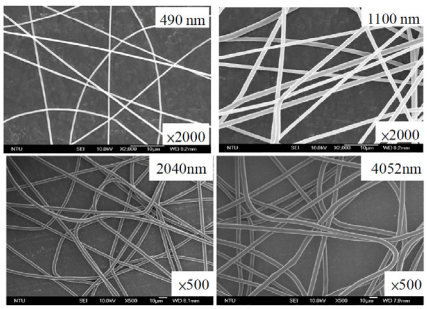

Figure 2. The morphology of fibers (SEM)

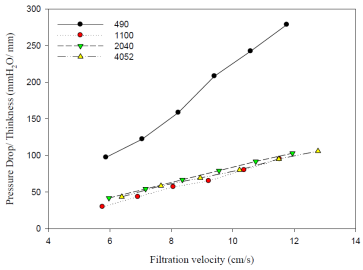

Figure 3. The effect of various filtration velocities on pressure drop

Penetration results of fibrous membranes shown in figure 4. The results suggested that the penetration increased with decreasing the fiber diameter of fibrous membranes.

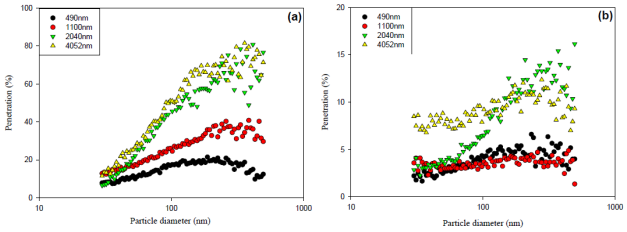

Figure 4 Penetration of fibrous membranes (a) Uncharged (b) Charged

Besides, as using electrostatic fibrous membranes, the penetration was significantly reduced. The filter quality could be improved by installing electrostatic fibrous membranes.

William-C Hinds, (1999), "Aerosol Technology," *New York: WILEY-INTERSCIENCE*.

Nifuku, M. Zhou, Y. Kisie, A. Kobayashi, T. Katoh, H. (2001) "Charging characteristics for electret filter materials," *Journal of Electrostatics*, Vol. 51-52, pp. 200-205.

Characterization of an ion jet unipolar electrical aerosol diffusion charger

Wen-Yinn Lin[1,*], Ken-Hui Chang[2], Chih-Chieh Chen[3], Shao-Hao Lu[1], Yuan-Yi Chang[1], and Jin-Yuan Syu[1]

[1] Institute of Environmental Engineering and Management, National Taipei University of Technology, Taipei City 10608, Taiwan.

[2]Department and Graduate School of Safety Health and Environment Engineering, National Yunlin University of Science and Technology, Yunlin 64002, Taiwan.

[3]Institute of Occupational Medicine and Industrial Hygiene, National Taiwan University, Taipei City 10055, Taiwan.

Keywords: nanoparticle, unipolar electrical, diffusion

Presenting author email: wylin@ntut.edu.tw

In aerosol physical mechanics, the electrostatic force is one of the most important effects (Hinds, 1999). Charging of nanoparticle is an important project of study within some different areas such as aerosol measure, ultra-fine particle control and material synthesis. Particularly, nanoparticle is difficult to be charged with field charging alone. In the case of relatively large particles, bipolar chargers are sufficiently efficient and produce a more or less well known equilibrium charge distribution. If the particle size is smaller, the charged particles with ions of opposite polarity becomes neutral particles (i.e. neutralization) (Alonso et al., 2006). A simple method is passed a unipolar ion cloud without electrical field from the DC corona discharge. Loss of charged particles is avoided if the aerosol flow passes a cloud of unipolar ions (Marquard et al., 2006). Therefore, this study focuses on the investigation of nanoparticle charge for a unipolar electrical aerosol diffusion charger, especially paying attention to the particle loss and the average number of elementary charges.

In this study, an ion jet unipolar electrical aerosol diffusion charger test system was set up, which is shown in figure 1. There are three main parts of this study: monodisperse aerosol generator system, charge chamber, and measurement system. A constant output atomizer was used to generate particles. The differential mobility analyzer (DMA) is widely used to generate monodisperse aerosol. Besides, the aerosol concentration was measured with an SMPS and the number of elementary charges was calculated with an aerosol electrometer.

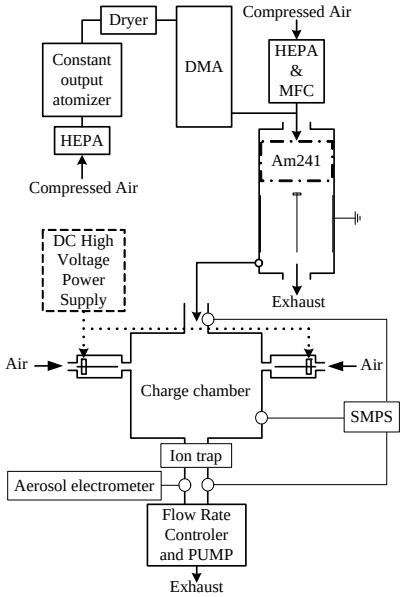

Figure 1. Schematic diagram of test system.

The result of figure 2 shows that the average number of elementary charges increased if particle size and jet flow rate becomes larger. In addition, there is no electric field loss in this charger. Just only has the charged loss (figure 3) which is calculated with $\eta_e = 1-\exp[-(24\kappa)^{1/3}]$. The charged loss was increased as the particle size increased. Beyond that, the concentration of particles is diluted with the jet flow of unipolar electrical aerosol diffusion charger (figure 4) irrespective of the size of particles.

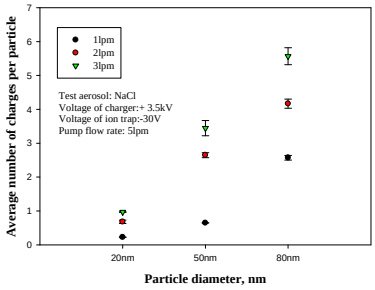

Figure 2. The average number of elementary charges of three different monodisperse particles.

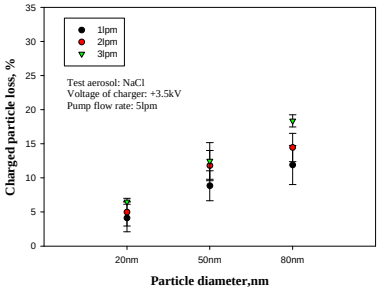

Figure 3. The charged particle loss of three different monodisperse particles.

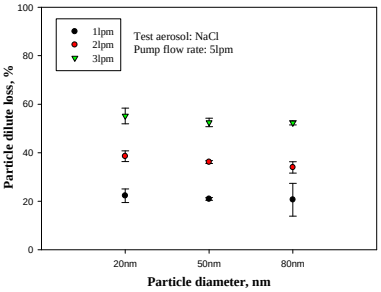

Figure 4. The diluted loss of three different monodisperse particles.

William-C Hinds, (1999), "Aerosol Technology," *New York: WILEY-INTERSCIENCE*.

Alonso, M. Martin, M.I. and Alguacil, F.J. (2006) *Journal of Electrostatics*, Vol.64:3-4, pp.203–214.

Marquard, A. Meyer, J. and Kasper, G. (2006) *Journal of Aerosol Science*, Vol.37:9, pp.1069–1080.

SO_2 Reduction by water condensation for marine diesel

A.Zukeran[1], K.Ninomiya[1], Y.Ehara[2], K.Yasumoto[3], H.Kawakami[3], T.Inui[3]

[1]Dept. of Electronic & Electrical Engineering, Kanagawa Institute of Technology, Kanagawa, 243-0292, Japan
[2]Dept. of Electrical & Electronic Engineering, Tokyo City University, Tokyo, 158-8557, Japan
[3]Dept. of Road Systems Engineering, Fuji Electric Co., Ltd., Toyo, 191-8502, Japan
Keywords: electrostatic precipitator, SO_2, marine diesel, condensation
Presenting author email:zukeran-akinori@ele.kanagawa-it.ac.jp

The exhaust gases emitted from marine diesel may cause the serious problem of pollution on the coast. Therefore, it has been regulated in MARPOL Treaty 73/78 Annex VI of IMO Air Pollution Control since 2005. The reductions of SOx, NOx and PM using plasma and chemical technologies have been investigated (Masuda, 1988, Yamamoto, 2002)

In this study, reduction of SO_2 for marine diesel was investigated using the electrostatic precipitator (ESP) with the heat exchanger. The experiments were carried out to reduce SO_2 due to condensation of water in the exhausted gas.

The schematic diagram of the experimental system is shown in Figure 1. The experimental system consists of the diesel engine (Denyo, DA-3100SS-IV, 400cc), the heat exchanger and the ESP. The exhausted gas at 180 ^oC of the temperature is cooled to 20 ^oC, and generated mist particles due to water condensation in the heat exchanger. The mist particles are collected in the ESP. The particle number concentrations are measured upstream and downstream the heat exchanger using the scanning mobility particle sizer (SMPS, TSI, 3936NL76) after hot dilution. SO_2 concentrations also measured by the SO_2 monitor using UV fluorescence (HORIBA, APSA-370) after hot dilution.

The particle size distribution downstream the heat exchanger for various gas temperatures is shown in Figure 2. The gas temperatures were regulated by the flow rate of the refrigerant. The particle size distributions have a peak at 70 nm of the particle diameter. The peak values between 120 to 50 ^oC are almost the same. However, the peak value increases with decreasing the gas temperature between 40 to 20 ^oC. In this experiment, the condensation water was sampled under 40 ^oC of the temperature. Therefore, this cause is the condensation due to cooling the gas temperature.

The SO_2 concentration and De-SO_2 rate as a function of the gas temperature is shown in Figure 3. The SO_2 concentration decreases with decreasing the gas temperature, and the De-SO_2 rate increases with decreasing the gas temperature. This result indicates that the SO_2 concentration in the exhausted gas emitted from marine engine is reduced due to decreasing the gas temperature using the heat exchanger. This cause is considered that SO_2 are absorbed to the condensation water.

As a result, it is indicated that SO_2 concentration decreases with decreasing the exhausted gas temperature due to the condensation. The collection of mist particles absorbed SO_2 will be investigated in the future.

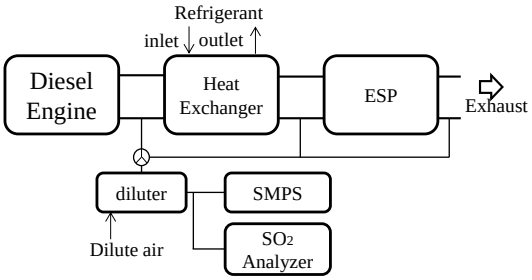

Figure 1. The schematic diagram of experimental system.

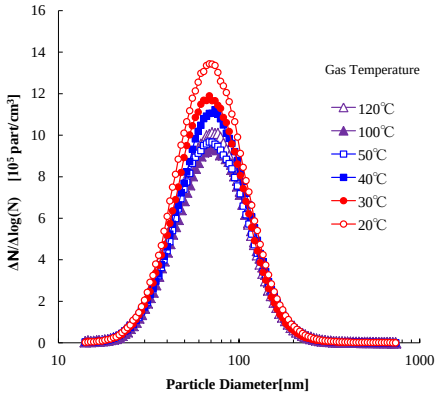

Figure 2. The particle size distribution downstream the heat exchanger as a function of the gas temperature.

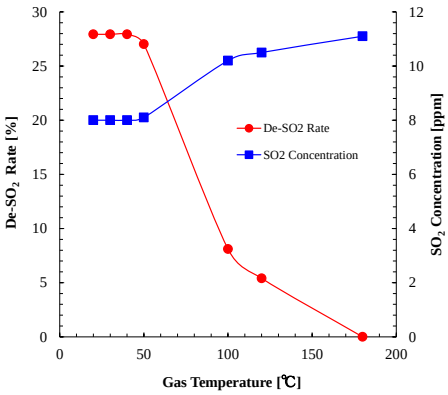

Figure 3. The De-SO_2 and SO_2 concentration as a function of the gas temperature.

This work was supported by a Grant-in-Aid for Scientific Research (B), No. 24360361, from the Japan Society for the Promotion of Science.

T.Urabe, Y.Wu, M.Ono, S.Masuda (1988) *Journal of the Institute of electrostatics Japan*, 12, 5, 354-359
T.Yamamoto, M.Okubo, T.Nagaoka, K.Hayakawa (2002) *IEEE Trans. on Ind. Appl.* 38, 5, 1168-1173

Thursday, September 5, 2013

Poster session C

Fundamentals, Posters C010 – C043

Modifications to the bipolar charging theory for spherical particles

J.L. de La Verpillière[1], J.J. Swanson[1], A.M. Boies[1]

[1]Department of Engineering, University of Cambridge, Cambridge, UK, CB2 1PZ
Keywords: electrical mobility, Fuchs charging theory, neutraliser, unsteady state.
Presenting author email: jean.delaverpilliere@student.ecp.fr

In many cases, measurement of particle size and concentration depends on the knowledge of the distribution of charges they have acquired, either naturally or from a neutraliser. Since the use of radioactive materials such as ^{85}Kr is often a constraining factor in the lab, alternative commercial charging devices, relying on soft X-ray or AC corona discharge for ionization, have recently been developed. As shown on Fig. 1, it has been previously experimentally demonstrated that such variations in neutralization techniques lead to different charging characteristics (Swanson et al., 2012). Direct measurement showed that different neutralisers produce ions with different electrical mobility distributions, but the standard Fuchs charging theory failed to explain the observed charge distribution discrepancies between the neutralisers, even when the known mobility was used as an input.

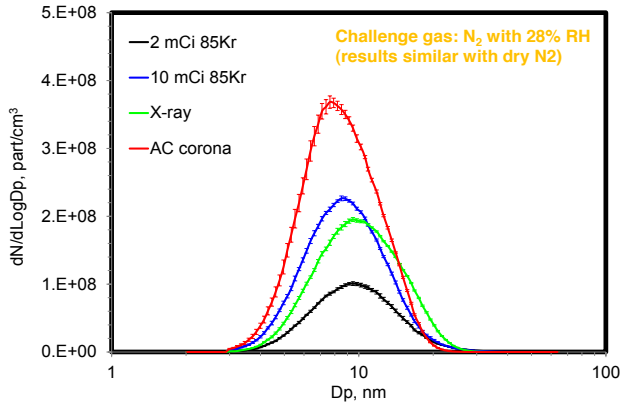

Figure 1. Inverted size distributions measured with an SMPS using 4 different neutralisers. Source particles are spherical silver particles.

In Fuchs theory, it is assumed that spherical particles interact with a cloud of bipolar ions of known and uniform characteristics in terms of mass, electrical mobility, and ratio of positive to negative ions (Fuchs, 1963). This steady state assumption is a useful closure relation that enables a rapid calculation of the charging state. Subsequent to this model, others such as Alonso and Alguacil (2003) have developed the theory to account for non-steady effects. They showed that in the case of a cylindrical charger with an alpha particles source on the wall, the unsteady effects of diffusion losses tend to make the extrinsic efficiency of the neutraliser smaller than its experimentally measured charging probability. On the other hand, the attraction between a given ion and a given particle is described by the ion-aerosol attachment coefficients. So far the effect of electrical mobility on the derivation of the attachment coefficients has only been investigated by varying the mean ion mobility in the model. The objective of this work is to investigate two modifications to the existing bipolar charging theory in order to improve the understanding of the mechanisms responsible for charging inside three commercially available neutralisers.

The first modification is to consider that steady state is not reached within the neutraliser due to ions diffusion losses to the neutraliser wall, as a result, the ion properties are no longer considered uniform along the neutraliser. Transport equations for particles of each polarity and for ions are derived from charge conservation equations, and solved using a forward numerical method. Alonso and Alguacil's (2003) model is therefore extended to neutralisers of more complex geometries, relying on different ionizing sources (beta particles and soft X-rays). Multiple charging has also been implemented into the model.

The second modification is related to the derivation of the ion-aerosol attachment coefficients. It is well known that ions of a wide mobility range are generated within a neutraliser. Ion mobility was therefore not treated as a discrete parameter, but as a stochastic variable. It was then possible to identify which kinds of ions actually control the charging process. Calculated results show that ions with a very high mobility generally have a higher overall charging activity than ions with a smaller mobility, despite the latter having a higher concentration.

Results of the numerical simulations are compared to the experimental trends to determine whether the physical explanations used to justify the theoretical modifications actually reduce the discrepancies observed between neutralisers. Our numerical simulations confirm that in all cases, unsteady effects are more important for very small particles, which has been observed experimentally. Ion electrical mobility has a significant impact on the ion-aerosol attachment coefficients and therefore influences the final particle charge distribution.

Fuchs, N. A. (1963) *Pure and Applied Geophysics*, 56, 185-93.

Swanson, J.J, de La Verpillière, J.L., Boies, A.M. (2012) *European Aerosol Conference.*

Alonso, M., Alguacil, F.J. (2003) *Aerosol Science, 34,* 1647-1664.

Restructuring of Aggregates and their Primary Particle Size Distribution during Sintering

M.L. Eggersdorfer and S.E. Pratsinis

Department of Mechanical and Process Engineering, ETH Zurich, CH-8092 Zürich, Switzerland

Keywords: Fractal-like Structure, Grain Boundary, Simulation, Sintering.
Presenting author email: meggers@ptl.mavt.ethz.ch

Particle suspensions and films often exhibit unique properties that depend on particle size distribution, like the opacity of titania pigments, the color of quantum dot or plasmonic nanoparticle suspensions and the superparamagnetism of iron oxide nanoparticles to name a few. Typically a narrow size distribution facilitates harvesting these effects from paints to solar cells, bio sensors and light emitting devices.

Aerosol processes allow rapid and scalable production of nanoparticles over a wide range of sizes. In such processes, however, particles grow typically by Brownian coagulation that places a lower limit to the width of the size distribution, the so-called self-preserving size distribution with a geometric standard deviation of about 1.45. Such a constraint would limit aerosol-made particles in applications requiring narrow size distributions. Furthermore, when primary particles (PP) with different high temperature residence time histories (e.g. from different reactor streamlines or reaction rates) are mixed, fractal-like particles with quite polydisperse PP size distributions (PPSD) are obtained. This polydispersity, however, can be reduced by PP sintering that proceeds inversely proportional to particle size, similar to condensation that is routinely used in generation of monodisperse aerosols.

Sintering can lead to a narrower PPSD than their parent aggregates. The narrowest PPSD was obtained when TiO_2 aggregates were produced by $TiCl_4$ or titanium isopropoxide oxidation followed by coagulation and sintering (Heine and Pratsinis, 2007). This was observed also with flame-made ZnO nanocrystalline aggregates exhibiting a blueshift of their absorption spectrum with decreasing ZnO crystallite size from about 8 to 1.5 nm (Mädler et al., 2002). A narrow crystal size distribution is required for this quantum-size effect.

During sintering of aggregates of polydisperse PP, restructuring takes place, the average PP size increases and the PPSD narrows affecting particle performance in a number of applications (Fig. 1, Eggersdorfer and Pratsinis, 2013). Here, aggregate sintering by viscous flow (Eggersdorfer et al., 2011), lattice and grain boundary diffusion (Eggersdorfer et al., 2012) is simulated by multiparticle discrete element methods focusing on PP growth dynamics and elucidating the restructuring of aggregates during their coalescence. The effect of initial PPSD and sintering mechanisms on the evolution of PP polydispersity and surface area mean diameter are presented. Each sintering mechanism results in a distinct evolution of PPSD but quite similar growth in average PP diameter. Grain boundary diffusion has the strongest impact among all sintering mechanisms and rapidly results in the narrowest PPSD as it has the strongest dependence on PP size. During sintering of aggregates with initially monodisperse PPs, the PPSD goes through a maximum width before narrowing again as PPs coalesce. A power law holds between projected aggregate surface area and number of PPs regardless of sintering mechanism and initial PP polydispersity. This law can be readily used in aerosol reactor design and for characterization of aggregates independent of material composition, initial PP polydispersity and sintering mechanism.

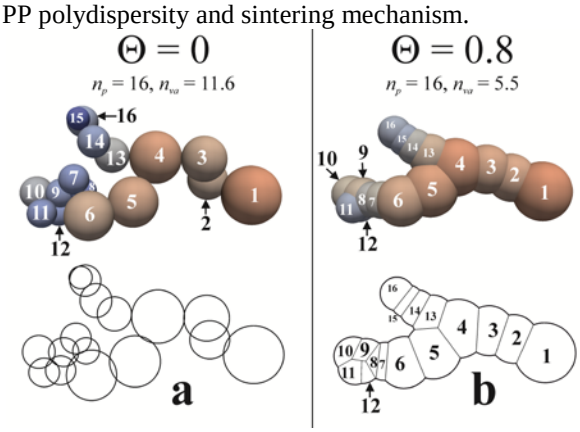

Figure 1. The geometric standard deviation σ_g of PP size distribution for a) agglomerates and b) aggregates is calculated with the diameters d of their constituent PPs at dimensionless time Θ. The sinter neck or grain boundaries between neighboring particles are sketched with thin lines. For aggregates, the d represents the maximum extension of the PP or crystal size (truncated sphere). The number of PPs, n_p, remains constant while the average PP number, n_{va}, decreases during sintering due to the decreasing surface area of the aggregate.

Financial support by ETH Research Grant (ETHIIRA) ETH-11 09-1 and the European Research Council under the European Union's Seventh Framework Programme (FP7/2007-2013)/ERC grant agreement n° 247283 is gratefully acknowledged.

Eggersdorfer, M.L., Kadau, D., Herrmann, H.J. and Pratsinis, S.E. (2011) *Langmuir* **27**, 6358-6367.

Eggersdorfer, M.L., Kadau, D., Herrmann, H.J. and Pratsinis, S.E. (2012) *J. Aerosol Sci.* **46**, 7-19.

Eggersdorfer, M.L., Pratsinis, S.E. (2013) *AIChE J.* in press.

Heine, M.C. and Pratsinis, S.E. (2007) *J. Aerosol Sci.* **38**, 17-38.

Mädler, L., Stark, W.J. and Pratsinis S.E. (2002) *J. App. Phys.* **92**, 6537-6540.

Acoustic waves in vapour-gas mixtures with polydispersed particles and droplets

Yu.V. Fedorov, D.A. Gubaidullin and D.D. Gubaidullina

Institute of Mechanics and Engineering, Russian Academy of Sciences, Kazan, Tatarstan, 420111, Russia
Keywords: acoustic waves, phase transformations
Presenting author email: yurafedorov89@gmail.com

The propagation of small disturbances in two-component gas-vapour mixtures with polydispersed particles and drops in the presence of phase transitions is studied. A mathematical model is proposed, the dispersion relation is obtained. The effect of the droplet and particle polydispersity on the dispersion and dissipation of small disturbances is analysed.

Fig. 1 illustrate the effect of polydispersity of droplets and particles on the form of the decrement of attenuation on the wavelength on the nondimensional oscillation frequency $\Omega_{5,3} = \omega\tau_{va}^{(5,3)}$, where $\tau_{va}^{(5,3)}$ is the velocity relaxation time, $a_{5,3}$ is average radii Gubaidullin and Nigmatulin (2000). The calculations were performed using the dispersion equation Gubaidullin and Fedorov (2012) and the dispersion relation for the case of monodispersed droplets and particles Gubaidullin *et al* (2011). A mixture of ait with water vapour, water droplets and particles of ash was considered. The relative mass contents of droplets of water m_a and ash particles m_b we will take equal to 0.3. The pressure of the carrier phase $p_1 = 0.1$ MPa, temperature $T_0 = 271$ K. The radii of the droplets and particles were set as follows: curve *1* - $a = 10^{-4}$, $b = 10^{-6}$ m, curve *2* - $a = 10^{-5}$, $b = 10^{-7}$ m, curve *3* - $a \in [10^{-5}, 10^{-4}]$, $b \in [10^{-7}, 10^{-6}]$ m. Curve *1* is built on the monodispersed theory with maximum radii from the range, curve *2* is calculated on the monodispersed theory with minimum radii from the range, curve *3* – on polydispersed theory. Distribution functions of droplets and particles sizes: $N_0(a) = a^{-3}$, $N_0(b) = b^{-3}$.

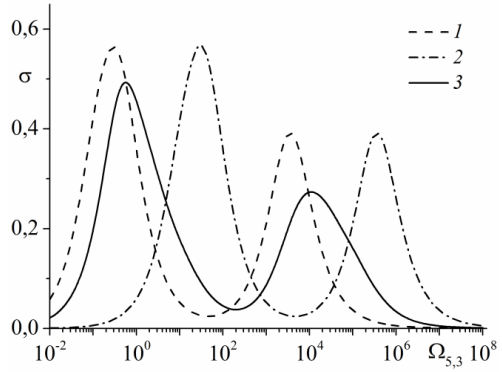

Figure 1. Dependences of the attenuation decrement on dimensionless oscillation frequency

The presence of the two fractions in the mixture leads to the occurrence of two local maxima in the dependences the attenuation decrement per wavelength. Since in real fogs droplets and particles are mainly polydispersed, then, as it seen from fig. 1, the attenuation is not so strong comparably with calculations with monodispersed droplets and particles. It should be noted that the polydispersity, as well as the distribution functions of dispersed phases of sizes, substantially affect the dynamics of wave propagation.

There are experimental data Cole and Dobbins (1971) on the attenuation decrement in the wavelength in the particular case "vapour-gas-droplet" mixture without particles ($m_b = 0$). The radius of the droplets ranged from 10^{-6} up to 10^{-5} m. Three groups of the experimental points correspond to the three experiments carried out at different mass content of drops, and different temperatures (different concentration of vapour in the gas phase):

1 - $T_0 = 281$ K, $m_a = 0.0076$, $k_V = 0.012$

2 - $T_0 = 276$ K, $m_a = 0.0039$, $k_V = 0.008$

3 - $T_0 = 271$ K, $m_a = 0.0038$, $k_V = 0.006$

Note that because of the complexity of the experiment there is a large spread of experimental data 10-15%. In fig. 2 $\omega\tau$ - the dimensionless oscillation frequency, where $\tau = 3\tau_{va}^{(3,1)} / (2m_a)$.

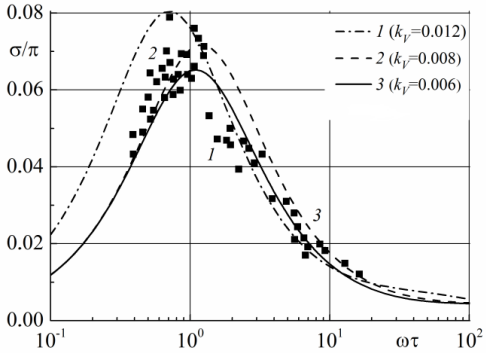

Figure 2. This is a comparison between theory and experimental data.

Overall, there is good agreement between theory and experiment.

Gubaidullin, D.A. and Nigmatulin, R.I. (2000) *Int. J. of Multiphase Flow*. **26**, 207-228.

Gubaidullin, D.A. and Fedorov Yu.V. (2012) *Fluid Dynamics*. **47**, 593-600.

Gubaidullin, D.A., Nikiforov A.A. and Utkina E.A. *Fluid Dynamics*. **46**, 72-79.

Cole, J.E. and Dobbins, R.A. (1971) *J. Atm. Sci.* **28**. 202-209.

Multiscale design of aerosol synthesis of materials: Effect of structure on TiO_2 & SiO_2 particle growth by coagulation and sintering

E. Goudeli, M.L. Eggersdorfer and S.E. Pratsinis

Department of Mechanical and Process Engineering, ETH Zurich, CH-8092 Zurich, Switzerland
Keywords: aggregate, fractal dimension, sintering, molecular dynamics.
Presenting author email: goudeli@ptl.mavt.ethz.ch

Multiscale design of aerosol reactors for synthesis of nanomaterials includes continuum, mesoscale, molecular dynamics and quantum mechanics models spanning 10 - 15 orders of magnitude in length and time, respectively. Quantum mechanics account for the electronic structure of matter determining the interatomic potentials in molecular dynamic (MD) models for accurate estimation of sintering and crystallization rates. For example, Figure 1 shows how MD models reveal the dominance of surface diffusion in sintering of TiO_2 nanoaerosols by monitoring the lattice plane evolution (Buesser, 2011). Mesoscale models provide the transport properties and coagulation rate of multiparticle structures; Continuum models describe the effect of process variables on product particle size & morphology at various process temperatures and residence times (Buesser, 2012).

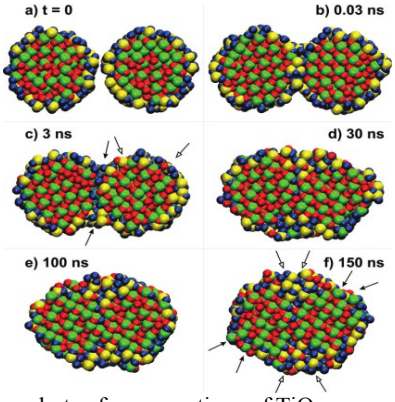

Figure 1. Snapshots of cross sections of TiO_2 nanoparticles with Ti and O ions initially (t= 0 ns) green and red (bulk ions) or yellow and blue (surface ions), respectively, at a) t= 0, b) 0.03, c) 3, d) 30, e) 100, and f) 150 ns (Buesser *et al.*, 2011).

Here the effect of the rapidly evolving structure (fractal dimension, D_f) of TiO_2 & SiO_2 particles made by coagulation and sintering is explored on their primary particle and collision diameters. This is done over their process synthesis parameter space (Tsantilis, 2004; Gass, 2006) by intefacing MD, mesocale (Eggersdorfer, 2012) & continuum models (Kruis, 1993). Structure is important as it affects particle transport, conductivity & scattering. Continuum models, however, typically assume a spherical or fractal-like shape at constant D_f neglecting the effect of evolving structure on particle growth dynamics and final particle properties (Kruis, 1993). Notable exceptions are those of Xiong and Pratsinis (1993) and Artelt *et al.* (2003) who had interpolated D_f at an arbitrary rate or slope from that of full coalescence to that of non-coalescing agglomerates.

The time-evolution of primary and agglomerate particle diameter and morphology are investigated, accounting for simultaneous coagulation and sintering as well as for the D_f evolution from mesoscale simulations (Eggersdorfer et al., 2012) with the characteristic sintering time of rutile titania (Fig. 1) from MD simulations (Buesser *et al.* 2011). The D_f varies from 3 (full coalescence) to 1.8 (non-coalescing agglomerates by cluster-cluster agglomeration) and its effect on soft & hard agglomerate and primary particle diameters is monitored at various maximum temperatures, T_{max} cooling rates, CR and precursor mole fraction, ϕ.

Accounting for the change in D_f hardly affects the primary particle, d_p, and collision, d_c, diameters, even though it affects the transient evolution of d_c (Fig. 2). In contrast, the evolution of D_f seems to have a profound effect on the hard-agglomerate diameter, the agglomerate diameter, d_{cH}, at the end of particle sintering (Grass et al., 2006) especially at low maximum temperatures and high cooling rates.

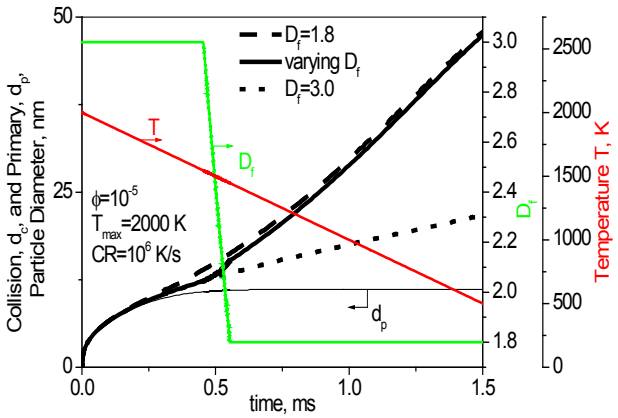

Figure 2. Evolution of the agglomerate collision, d_c (bold, black solid line), and primary particle diameters, d_p (thin black solid line), with variable D_f (green line) at non-isothermal conditions (red line). The evolution of d_c is compared to simulations with constant D_f = 1.8 (dashed line) and 3 (dotted line).

Artelt, C., Schmid, H.J. and Peukert, W. (2003) *J. Aerosol Sci.* **34**, 511-534

Buesser, B., and Pratsinis, S.E. (2012) *Annu. Rev. Chem. Biomol. Eng.*, **3**, 103-127

Buesser, B., Gröhn, A.J. and Pratsinis, S.E. (2011) *J. Phys. Chemistry C* **115**, 11030-11035

Eggersdorfer, M.L., Kadau, D., Herrmann, H.J. and Pratsinis, S.E. (2012) *J. Aerosol Sci.*, **46**, 7-19

Grass, R.N., Tsantilis S. and Pratsinis, S.E. (2006) *AIChE J.*, **52**, 1318-1325

Kruis, F. E., Kusters, K. A., Pratsinis, S.E. and Scarlett, B. (1993) *Aerosol Sci. Technol.* **19**, 514-526

Xiong, Y., and Pratsinis, S.E. (1993). *J. Aerosol Sci.* **24**, 283-300.

Dynamics of aerosols and particles at nonlinear oscillations in tubes

D.A. Gubaidullin, R.G. Zaripov and L.A. Tkachenko

Institute of Mechanics and Engineering, Kazan Science Center, Russian Academy of Sciences, Kazan, 420111, Russia
Keywords: aerosol, coagulation, deposition, particles, oscillations.
Presenting author email: damirgubaidullin@gmail.com

In the present work, longitudinal oscillations of an aerosol of different initial number concentration and dynamics of particles is considered in tubes of different length with various geometry on the end near to resonant frequencies.

Experimental investigations oscillations of an aerosol were carried out for different length of tubes in a shock-wave and shock-free modes near to subharmonic and natural resonances. Di-ethyl-hexyl-sebacate $C_{26}H_{50}O_4$ was used as the working fluid to generate aerosol. The majority of droplets have the geometric diameter 0.863 μm. Number concentration of drops for all experiments monotonously decreases with time and with growth of the excitation frequency. In the case of a closed tube, this process is defined by the coagulation of aerosol and deposition of droplets on the tube walls. In an open tube, the discharge of aerosol to the environment is observed in addition to the coagulation of aerosol and deposition of droplets on the tube walls. The dependence of the time of coagulation of aerosol on the excitation frequency likewise exhibits a nonmonotonic pattern with a maximum and a minimum when passing the resonance. It is established, that presence of a flange slows down process of a coagulation of an aerosol. Reduction of internal diameter of a flange results in increase in the time of coagulation. In so doing, the time of coagulation of aerosol in the case of an open tube is reduced by a factor of two and more compared to the time of coagulation in a closed tube. Nonlinear dependence of the time of coagulation of droplets is established at nonlinear oscillations of an aerosol in a tube from initial number concentration of an aerosol. It has been found that a decrease in the tube length and increase oscillation intensity results in a decrease in the time of coagulation of aerosol. It is shown, that with increase of intensity of the oscillations, the caused increase of amplitude, time of coagulation and deposition of an aerosol decreases. For the closed tube this dependence has nonlinear character, and for an open tube - almost linear. It is revealed that in a shock-free mode (for small amplitudes of displacement piston) time of coagulation and deposition aerosol in the closed tube in 2-4 times, and time of a clarification of an in an open tube at 6-12 time lower, than at natural deposition.

The numerical modeling of a drift of the solid spherical particles were in a suspension in a nonlinear wave field of the closed tube and open flat channel at excitation of oscillations of a gas column on three first fundamental frequencies is executed. These researches have been carried out about use of model of a single particle and with application of model of interpenetrating continuums. It is obtained, that easy particles drift under an operation of acoustical current, and heavy are displaced under an action of wave pressure. In result easy and heavy particles concentrate in different areas of the resonator: easy are displaced to antinodes of a standing wave of velocity, heavy – to nodes. Depending on a steepness of a wave front of compression, the same particles can behave as easy at small nonlinearity, or as heavy at steep enough fast-head wave front. Drift of heavy particles in the open channel proceeds in two stages. The first quickly proceeding stage is connected to the mechanism of drift due to asymmetry of a wave, and the second with drift under action of developed acoustic stream. Influence of radius of particles on distribution of temperature and average density of a disperse phase along an axis of the channel is revealed.

Dynamics of a single particle with various physical and geometrical parameters is experimentally investigated at the longitudinal oscillations gas in tubes. Along an axis of a tube the particle moves from the closed (open) end to the piston, near to a wall – to the return side, making longitudinal oscillations with increase in the oscillations swing that is caused by acoustic streaming. In a radial direction, the oscillating particle moves from an axis to a wall of the tube up to a boundary point. Outside of a tube, the particle moves from the open end to an exterior wave field practically without oscillations with nonlinear increase of coordinate from time. It is revealed, that the increase in lengths of a tube and excitation frequency of gas in up to - resonant modes gives in growth of an oscillations swing of a particle and increase of its average velocity. Nonmonotonic character for dependence of oscillations swing and average velocity of a spherical particle from excitation frequency of gas is detected. At approach to a resonance oscillations swing and average velocity are incremented, attain the maximum value on a resonance frequency and decrease behind a resonance. Effect of a weight and diameter of a particle on its oscillations swing and average velocity is investigated. Shift of a curve maximum for dependence of a particle average velocity from oscillation frequency aside magnifications of frequency is shown at increase of a weight or diameter of a particle.

This work was supported by the Russian Fund of Foundation Investigation under grant 13-01-00135 and within the framework of the Federal target program "Scientific and scientific and pedagogical shots of innovative Russia for 2009-2013" (project №14.B37.21.0644).

De-agglomeration and bounce of the iron oxide agglomerates due to the impaction

M. Ihalainen[1,2], T. Lind[1], T. Torvela[2], J. Ruusunen[2], A. Lähde[2], P. Tiitta[2] and J. Jokiniemi[2,3]

[1]PSI Paul Scherrer Institut, The Laboratory for Thermal-Hydraulics, CH-5232 Villigen PSI, Switzerland
[2]Fine Particle and Aerosol Technology Laboratory, Department of Environmental Science, University of Eastern Finland, P.O. Box 1627, FI-70211 Kuopio, Finland
[3]VTT Technical Research Centre of Finland, Fine Particles, P.O. Box 1602, 02044 VTT, Espoo, Finland
Keywords: inertial impaction, deagglomeration, bouncing.
Presenting author email: mika.ihalainen@uef.fi

The impaction behaviour of aerosol particles has applications in fields such as powder processing, nuclear safety, and health research. To be able to understand better how agglomerates adhere to surface, bounce, and de-agglomerate, both the de-agglomeration and bounce have to be monitored simultaneously. For this purpose a method to study impaction behaviour was developed described by Ihalainen *et al*. (2012). This method is applied here to evaluate the de-agglomeration and bounce of the iron oxides particles impacting at varying velocities onto impaction plate covered with aluminium foil.

Iron nanoparticle agglomerates with two different oxidation states were produced using an atmospheric pressure chemical vapour synthesis (APCVS) method (Lähde *et al*., 2011). Iron pentacarbonyl was applied as a precursor material and two different oxidation conditions (0.05 v-% and 21 v-% of oxygen) were applied.

The impaction of the iron oxide agglomerates was studied with the following method (Ihalainen *et al*. 2012). The agglomerates were first size classified with a Differential Mobility Analyzer (DMA) to obtain monodisperse number size distribution of the agglomerates. Then the agglomerates were impacted onto an impaction plate located in a single stage Micro Uniform Deposit Impactor (MOUDI). On that impaction plate, there was also a Transmission Electron Microscope (TEM) grid for the offline analysis of the impacted particles. The bounced particles were collected into a low pressure sampling chamber located downstream of the MOUDI. Both a Scanning Mobility Particle Sizer (SMPS) and Transmission Electron Microscopy were used to analyze the bounced particles. Estimations for the mass concentrations before and after the impaction in aerosol phase were obtained using the SMPS data. An Aerosol Particle Mass (APM) analyzer was utilized in combination with the SMPS to evaluate the size dependent effective density of the agglomerates.

The geometric mean diameter (GMD) of the bounced particles showed similar trend in the both oxidizing cases (Fig. 1). At the lowest pressure difference over the jet plate of the impactor, the particle size was near 200 nm. As the pressure difference increased, which means that the impaction velocity will increased, the GMD value decreased to a value of about 100 nm in both cases. At higher pressure differences, i.e. higher impaction velocities, there was more kinetic energy available for the de-agglomeration thus leading to smaller fragment size.

The mass fraction of the de-agglomerated and bounced particles, are shown in Fig. 2. It describes the ratio of the mass concentration of the bounced and de-agglomerated particles to those before the impaction. It was found that the bounce fraction was the lowest at the slowest impaction velocities and the highest when the impaction velocity reached its maximum value. In addition, not all the particles de-agglomerated during the impaction process but some of the agglomerates bounced intact in both cases. On overall, the change in oxidation conditions did not affect significantly on the fragment size or mass fraction of the bounced particles. Further analysis will be carried out to characterize the properties of the particles, such as the primary particle size.

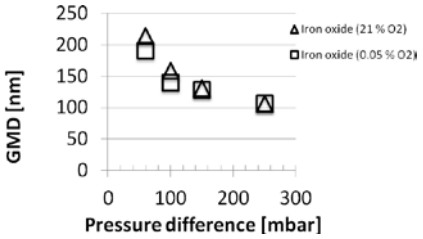

Figure 1. Geometric mean diameter (GMD) of the bounced particles measured with a SMPS.

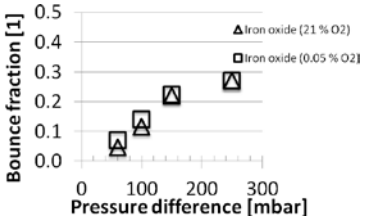

Figure 2. Mass based fraction of de-agglomerated and bounced particles.

This work was carried out in support of the international ARTIST II program which is acknowledged for funding this work. The authors express their gratitude to those members of the Laboratory for Thermal-Hydraulics at PSI and of the Fine Particle and Aerosol Technology Laboratory at the University of Eastern Finland that participated in the experimental work and construction of the facility.

Ihalainen, M., Lind, T., Torvela, T., Lehtinen, K.E.J. and Jokiniemi, J. (2012) *Aerosol Sci. Technol.* **46:9,** 990-1001.

Lähde, A., Kokkonen, N., Karttunen, A., Jääskeläinen, S., Tapper, U., Pakkanen, T.A., Jokiniemi, J (2011) *J. Nanopart. Res.* **13,** 3591-3598.

Propagation of acoustic disturbances in N-fractional gas-liquid systems

D.A. Gubaidullin, A.A. Nikiforov, E.A. Teregulova and R.N. Gafiyatov

Institute of Mechanics and Engineering, Kazan Science Center, Russian Academy of Sciences, Kazan, 420111, Russia
Keywords: aerosol, waves, damping, heat and mass transfer.
Presenting author email: anikiforov1@yandex.ru

To-date, a large interest is the study of wave dynamics of dispersed media. A significant number of works on acoustics gas-liquid systems devoted to theoretical study of harmonic disturbances. Various problems of acoustics, gas mixtures and mixtures of liquids with bubbles of gas is considered in the well-known monograph (Nigmatulin, 1989). In the monograph (Temkin, 2005) the short review of results on research of acoustic disturbances in monodisperse gas-suspensions without phase transformations is given. In (Kandula, 2010) comparison of nonlinear and linear theories for the description of dispersion and sound dissipation in the diluted suspensions is carried out. In (Gubaidullin and Nikiforov, 2010) presented results of a theoretical study of propagation of acoustic disturbances in two-phase mixtures of liquids with vapor and gas bubbles for the cases of plane, spherical, and cylindrical waves. The propagation of acoustic waves in two-fraction mixtures of gas with vapor, droplets and solid particles of different materials and sizes in the presence of phase transitions is investigated in (Gubaidullin *et al*, 2011). In (Gubaidullin *et al*, 2012) investigated the dynamics of the weak perturbations in two-fraction mixtures of the liquid with vapor–gas and gas bubbles of different sizes and compositions taking into account the phase transformations in one of the fractions.

In this work propagation of acoustic waves in N-fractional mixtures of gas-liquid systems (gas with drops or liquid with gas bubbles, when the dispersed phase is presented by the inclusions of N different materials and sizes) is investigated. The mathematical models is presented, the dispersion relations and a wave equations are received and dispersion curves are calculated.

As an example on the received dispersion relation, dispersive curves for a three-fractional mix of air with particles of sand, ice and soot are calculated. In figures 1 dependence of decrement of attenuation on wavelength from the nondimensional oscillation frequency for a three-fractional mix of air with particles of sand of radius $r_a = 10^{-6}$ m and mass concentration $m_a = 0.05$, ice of radius of $r_b = 10^{-5}$ m and mass concentration $m_b = 0.1$ and soot of radius of $r_c = 8 \cdot 10^{-6}$ m with the various mass concentration (solid line $m_c = 0.15$, dash line $m_c = 0.35$, dash dot line $m_c = 0.55$) are shown. It is visible that with increase in the mass concentration of soot particles dissipation of waves grows. Decrement of attenuation on wavelength with increasing mass concentration of the soot particles increases not the entire range of nondimensional oscillation frequency. In this case, the decrement of attenuation increases less than in monodisperse gas suspension at the same the growth the mass concentration of the dispersed phase. As shown in figure 1, the difference between the size and thermophysical parameters of particles of each of fractions leads to emergence of three inflection curves for dependence of decrement of attenuation on wavelength in the frequency range inversely proportional to typical relaxation times of the phase velocity $\omega\tau_{va}$, $\omega\tau_{vb}$ and $\omega\tau_{vc} = 1$, here τ_{vj} is the relaxation time of phase velocities (Gubaidullin *et al*, 2011).

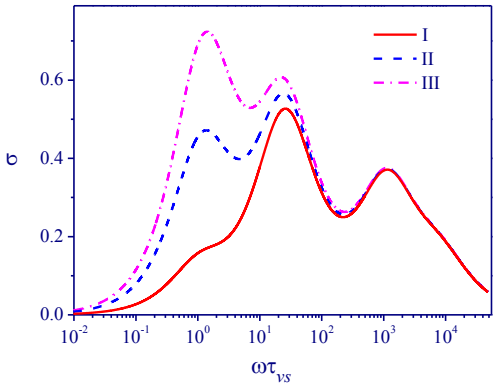

Figure 1. Dependence of decrement of attenuation on wavelength from the nondimensional oscillation frequency.

This work was supported by the Russian Fund of Foundation Investigation under grant 13-01-00135 and within the framework of the Federal target program "Scientific and scientific and pedagogical shots of innovative Russia for 2009-2013" (project №14.B37.21.0644).

Nigmatulin, R.I. (1989) *Dynamics of Multiphase Media*, Washington: Hemisphere.

Temkin, S. (2005) *Suspension acoustics: An introduction to the physics of suspension*, Cambridge University Press.

Kandula, M. (2010) *Journal of the Acoustical Society of America*, **127**(3), EL115-EL120.

Gubaidullin, D.A., Nikiforov, A.A. (2010) *High Temperature*, **48**(2), 170-175.

Gubaidullin D.A., Nikiforov A.A., Utkina E.A. (2011) *Fluid Dynamics*, **46**(1), 72-79.

Gubaidullin, D.A., Nikifirov, A.A., Gafiyatov, R.N. (2012) *High Temperature*, **50**(2), 250-254.

Experimental investigation dynamics of aerosols at oscillations in tubes in a no shock-wave mode

D.A. Gubaidullin, R.G. Zaripov and L.A. Tkachenko

Institute of Mechanics and Engineering, Kazan Science Center, Russian Academy of Sciences, Kazan, 420111, Russia
Keywords: aerosol, coagulation, deposition, oscillations, experiment.
Presenting author email: luda_tkachenko@inbox.ru

Research wave dynamics in heterogeneous media near to resonance frequencies represents significant interest. One of ways on suppression of aerosols, it is especial in the closed volumes, acoustical coagulation and their deposition is. Results on acoustical coagulation and deposition of drops or particles of aerosols are in detail given in monographies (Mednikov, 1965; Temkin, 2005). Behaviour of an aerosol at their non-linear oscillations in tubes in basic were investigated in a shock-wave process near to resonance frequencies (Gulyaev and Kuznetsov, 1963; Temkin, 1970; Shuster *et al*., 2002; Gubaidullin *et al*., 2004). No shock-wave process when losses on walls become essential is insufficiently investigated. The purpose of the present work is studying features of coagulation and deposition of an aerosol in the closed and open tubes in a no shock-wave process on the first natural frequency.

The longitudinal established oscillations of an aerosol in a quartz tube in length of $L = 1.06$ m and a internal diameter of $2R = 0.0365$ m were generated by the flat piston. It was set in motion by vibrostand TV51075 (TIRA). Frequency and amplitude sine wave oscillations were set and controlled by means of program module SineVIEW, established on a computer, by means of the piezoelectric accelerometer and controller. The system of measurement of pressure of gas consisted of the pressure sensor, placed near to the piston, three-channel bridge amplifier of a voltage and digital oscillograph. For measurement of transparence the measuring complex consisting of the laser with wave length of 630 nm which was a light source and digital luxmeter was used. The ray of light passed perpendicularly axes of a tube through its middle and got in the centre of the sensor. The data from a luxmeter moved on a computer and were handled. Di-ethyl-hexyl-sebacate $C_{26}H_{50}O_4$ was used as the working fluid to generate aerosol. Aerosol with diameter 0.863 μm was created by means of the Atomizer Aerosol Generator.

The dependences of numerical concentration of drops of an aerosol on time are obtained at different importance of amplitude of displacement of the piston on an observable resonance frequency $\nu_1^* = 160.7$ Hz for closed tube and $\nu_1^* = 78.6$ Hz for open tube. The monotonic process of the decrease in concentration with time includes mainly the coagulation of aerosol droplets, their deposition on the tube walls, and the unsteady discharge of aerosol from the open end of the tube in the form of a pulsating jet. Is accepted, that time of variation of concentration is the time of a coagulation and a deposition of an aerosol in closed tube and the time of clearing of the aerosol in open tube. It is shown, that with increase of intensity of the oscillations, the caused increase of amplitude, time of coagulation and deposition and time of clearing of an aerosol decreases. The nonmonotonic pattern of the dependence of the time of coagulation and deposition and time of clearing on the frequency of excitation with a minimal value at resonance is observed (figure 1). It is found that the time of coagulation and deposition aerosol in the closed tube by 2-4 times and time of clearing aerosol in an open tube by 6-12 times lower than at natural depositing.

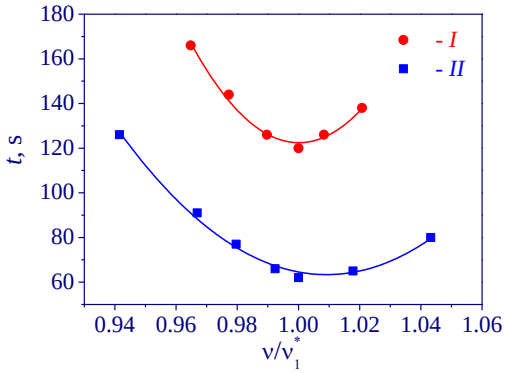

Figure 1. Dependence of time of coagulation and deposition (*I*) and time of clearing (*II*) of an aerosol on frequency of excitation for amplitude of displacement of the piston $l = 0.3$ mm. Line – polynomial approximation.

This work was supported by the Russian Fund of Foundation Investigation under grant 13-01-00135 and within the framework of the Federal target program "Scientific and scientific and pedagogical shots of innovative Russia for 2009-2013" (project №14.B37.21.0644).

Mednikov, P.E. (1965) *Acoustic Coagulation and Precipitation of Aerosols*, New York: Consultant Bureau.

Temkin, S. (2005) *Suspension Acoustics: An Introduction to the Physics of Suspensions*, New York: Cambridge University Press.

Gulyaev, A.I and Kuznetsov, V.N. (1963) *Sov. Phys. Acoust.* **8**, 236–238.

Temkin, S. (1970) *Phys. Fluids*, **13**, 1639–1641.

Shuster, K., Fichman, M, Goldshtein, A. and Gutfinger,C. (2002) *Physic Fluids*, **14**(5), 1802–1805.

Gubaidullin, D.A., Zaripov, R.G., Galiullin, R.G., Galiullina, E.R. and Tkachenko, L.A. (2004) *High Temperature*, **42**(5), 794–802.

Calculation of deposition on fibrous filters due to impaction – critical trajectories

S. J. Dunnett[1] and C. F. Clement[2]

[1]Department of Aeronautical and Automotive Engineering, Loughborough University, Loughborough, Leics. LE11 3TU, U.K.
[2]15 Witan Way, Wantage, Oxon, OX12 9EU, U.K.
Keywords: fibrous filter, filtration, numerical simulation, particle deposition
Presenting author email: s.j.dunnett@lboro.ac.uk

Introduction

Fibrous filters are routinely used to remove particles from the air. The filters consist of numerous fibres arranged in such a way that they are mostly perpendicular to the air flow through it. The packing fraction of such filters is generally small enabling the modelling of filter performance to be undertaken using single fibre theory. When the filters are in use particles collect on the fibres and are removed from the air. The deposit collected on the fibres affects the air flow through the filter and hence the subsequent deposit of particles. To date we have a fairly good understanding of the performance of fibrous filters at the start of their lives when no deposit is collected. However the feedback effects of the deposit upon the filter performance are less well understood. The aim of the present work is to consider this feedback effects for particles of the size for which impaction is the main mechanism of deposition. In particular an efficient mathematical technique has been developed to determine the particle trajectories that separate the impacting and non-impacting particles.

Numerical model and procedure

A numerical model has been developed previously, Dunnett and Clement (2012), which investigates the performance of fibrous filters in the early stages of particle loading. In the model the Boundary Element Method is used to determine the flow field around a single fibre containing deposit. The neighbouring fibres are taken into account in the model by the application of the boundary conditions. The deposit collected on the fibre is assumed to form a smooth porous layer and the flow through the porous layer is assumed to be modelled by Darcy's law. The model has been used to consider the deposition of particles due to diffusion and interception. In this work we are extending the work to consider particles for which impaction is the main mechanism of deposition. This is the case for Stokes numbers, St ≥1 where $\mathrm{St} = \frac{d_p^2 \rho_p U_0 C}{18 \mu d_f}$ d_p, d_f are the particle and fibre diameters, ρ_p the particle density, C the Cunningham correction factor, μ the air viscosity and U_0 the flow velocity away from the fibre.

For impaction, critical trajectories exist which define the region from which particles will deposit on the fibre. These trajectories are tangential to the fibre surface at impact, see Figure 1. Away from the fibre particles are initially moving with the flow in the x direction with velocity $u = U_0$ and the problem of finding the critical trajectory reduces to that of finding the distance from the axis, y_0, for a trajectory to reach the appropriate tangential boundary condition on the fibre surface. This reduces to solving the differential equations for a trajectory which satisfy a particular boundary condition.

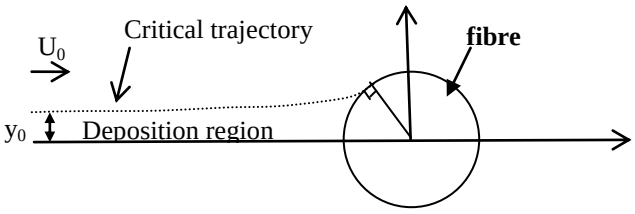

Figure 1. Critical trajectory

It has been found that the critical trajectories can be found in an efficient manner adopting an iterative procedure of solving the differential equations based on a modification of Newton's method. This results in a reduction in the numerical simulations needed to determine the region of deposition on the fibre surface and the filter efficiency. The procedure can be adopted for clean fibres and also for fibres that contain a porous layer of deposit.

As the deposit collects on the fibre it forms a surface on the face of the fibre facing the flow which grows with time. The critical trajectories define the outer edge of that surface.

In the work presented here we will investigate the deposition surface formed on the fibres for various situations of concern in filtration. The results will be compared with available experimental data.

References

Dunnett, S.J. and Clement, C.F. (2012) J. Aerosol Sci. 53, 85-99

Study of filtration performances of fibrous media: comparison between flat and industrial-geometry prototypes filters

L.F. González[1,2], A. Joubert[1], Y. Andrès[1], C. Delahaye[2], N. Berthelot[2], X. Chaucherie[2], L. Le Coq[1]

[1] LUNAM, Ecole des Mines de Nantes, GEPEA-CNRS UMR 6144, Nantes, 44307, France
[2] Veolia Environnement Recherche et Innovation VERI, Limay, 78520, France
Keywords: filtration performances, fibrous filters, aerosols filtration
Presenting author email: laurence.le-coq@mines-nantes.fr

In recent years, great consideration has been paid to indoor air quality (IAQ) and its influence on health of buildings occupants, especially because people in industrial countries stay almost 80% of their time in enclosed spaces (Gustavsson, 2010). Ventilation systems contribute to IAQ supplying fresh air, limiting outdoor pollutants and evacuating indoor contaminants such as aerosols. Air cleaning technologies are often coupled with ventilation systems for improving IAQ such as filtration with fibrous media for particles removal from air. Filtration performances of fibrous media have been studied basically in laboratory using flat filters (Novick et al., 1992; Walsh, 1996). Nevertheless, filters in Air Handling Units (AHU) have different geometries to optimize the efficiency to pressure drop ratio such as bag and pleated filters. A lack of knowledge is remaining about evolution of performances during clogging of this type of filters regarding pressure drop and efficiencies. Time of life of these filters is uncertain and they are replaced periodically without estimation about their performances.

The aim of this study is to predict the performances variation of industrial filters during clogging in comparison with flat filters. This could help to understand aerosols behaviour on fibrous filters with different geometries typically used in AHU having into account their efficiency and pressure drop which could be extrapolated to an economic point of view.

First of all, a laboratory-scale Air Handling Unit AHU has been developed to realize the clogging of filters with solid aerosols. It is a closed-loop vent through which air can be continuously circulated at controlled and regulated temperature (T) and relative humidity (RH). Symmetric velocity profiles were found upstream of the filter. Prototypes filters of different efficiencies (G4 to F9 according to European standard EN13779) and industrial geometries (bag and pleated filters) are tested at a characteristic air filtration velocity of real AHU (0.1-0.9 $m.s^{-1}$). Filters performances during the clogging are estimated with particles counting upstream and downstream of the filter (optical particle counter PALAS Welas) as well as pressure drop is monitored.

Two typical industrial geometries and materials of filters used in AHU, as well as flat filters, are studied: fibre glass-bag filters and cotton/polyester-pleated filters (Table 1). Aluminium oxide (Al_2O_3) commercial dust was selected to clog the filters because of its size distribution close to PM10 ambient urban aerosols.

A dust generator RBG1000 PALAS is used for particles dispersion into the pilot at average concentration of 30.000 particles/cm^3 (10^5 µg/m^3). Particle size distribution has been determined: number size distribution is d_{50}= 0.5 µm and d_{90}=2.5 µm, mass size distribution is $d_{50=}$3.8 µm and d_{90}=7 µm.

Table 1. Prototype filters

	Efficiency/ Geometry	Material	Filtration velocity (m/s)
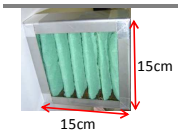	G4/ pleated	Cotton+ polyester fibres	0.9
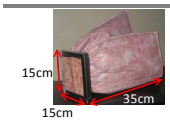	F7 / 2 bags	Glass fibre	0.4
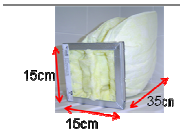	F9 / 2 bags	Glass fibre	0.4

Changes in pressure drop and efficiency during clogging of the different filters are compared according to the mass of particles retained on filters. Comparisons allow evaluating the influence of filters geometry on the change in performances during time.

This work was supported by Veolia Environnement Research & Innovation (VERI) in collaboration with the Ecole des Mines de Nantes.

Gustavsson, J. (2010). *Air filtration in HVAC systems*. Brussels: REHVA.

Novick, V. J., Monson, P. R., & Ellison, P. E. (1992). The effect of solid particle mass loading on the pressure drop of HEPA filters. *Journal of Aerosol Science, 23*(6), 657-665.

Walsh, D. C. (1996). Recent advances in the understanding of fibrous filter behaviour under solid particle load. *Filtration & Separation, 33*(6), 501-506.

Degradation of glass fiber filter media exposed to acidic and alkaline contaminants

Myong-Hwa Lee[1, *], Jeong-Uk Kim[1] and Eunsol Kim[2]
[1]Energy System R&D Group, Korea Institute of Industrial Technology, Cheonan-si, Chungnam 331-822, Republic of Korea
[2]Dept. of Physics, The State University of New York , Albany, 1400 Washington Ave., Albany, NY 12222, USA
Keywords: degradation, glass fiber filter, tensile strength, elongation
Presenting author email: myonghwa@kitech.re.kr

Bag house system is usually used to remove particulate matters in flue gas discharged from various combustion facilities. Bag filter installed in a bag house is the most important component to determine the performance of a system. However, the filters are frequently exposed to acidic and alkaline contaminants in flue gas. Therefore, the filament fibers might be degraded by leaching of metallic cations (e.g. Na^+ ions) due to acidic and basic environments.

Bagherpour *et al.* (2009) have shown that the environmental factors would accelerate the rate of thermal degradation during working and storage years.

However, most of previous studies on the degradation are focused on fabricated materials of the reinforcement fibers in a chemical environment (Wei *et al.*, 2010). There are seldom studies about the degradation mechanisms of bag filter media.

In this study, we made an effort to figure out the degradation mechanisms of a glass fiber filter (Teflon B finished glass) exposed to acidic and basic chemicals. The concentration of exposed acid and base (5, 10, 20, 30 wt%) and exposure time (12, 24, 36, 48, 60 hrs) were chosen as effective parameters. The weight loss, tensile strength and elongation were investigated to observe the effects of chemical exposure.

Figure 1 illustrates the weight loss of the glass fiber filter by HCl treatment. As shown in the figure, the weight loss was high at 12 hr exposure under 5% HCl concentration and it maintained plateau. However, the weight loss kept decreasing with exposure time in other conditions.

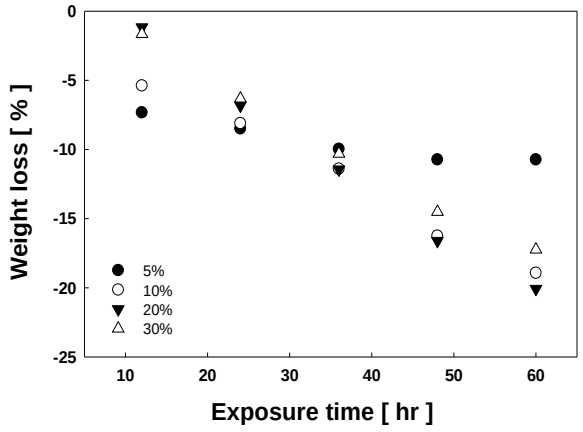

Fig. 1 Weight loss of glass fiber filter by HCl treatment.

Figure 2 shows the weight loss of the glass fiber filter by NaOH treatment. We found that there was no change in weight loss by NaOH exposure.

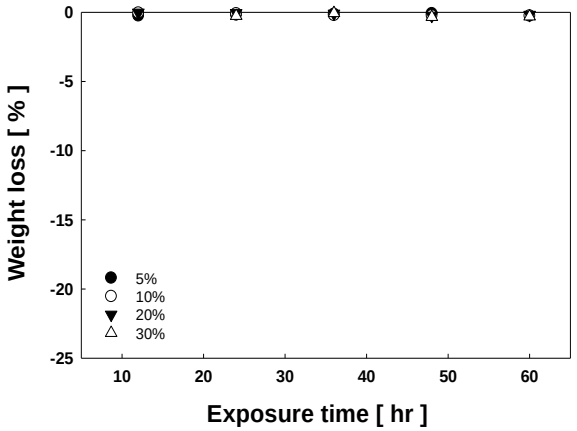

Fig. 2 Weight loss of glass fiber filter by NaOH treatment.

This work was financially supported by the KITECH R&D Program (Project No. EO-13-0010).

Bagherpour, S., Bagheri, R. and Saatchi, A. (2009) Mater. Des. 30, 271-274
Wei, B., Cao, H., Song, S. (2010) Mater. Des. 31, 4244-4250.

Filtration characteristics of air filter loaded with differently charged particles

H.S. Park

Climate Change Research Division, Korea Institute of Energy Research, Daejeon, 305-343, South Korea
Keywords: filtration, loading, particle charge.
Presenting author email: phs@kier.re.kr

Once a new air filter is applied to an air purification process, the filter becomes loaded with dust particles. Thus, the study on the particle loading characteristics of air filter is very essential in order to understand the real filtration phenomena during filter use. In this study, the effect of particle and filter charge on the particle loading property of air filter was investigated.

Charged filter and uncharged filter prepared by discharging the charged filter by isopropyl alcohol were used as test samples, and three types of particle having different charge states were supplied to filters tested. Fig. 1 is a schematic diagram of filter test apparatus. As a filter is continuously loaded with particles, the pressure drop of the filter was monitored and collection efficiency was calculated by periodically measuring particle concentrations at upstream and downstream of filter.

For neutralized particles there was a big difference in areal mass loading rates between charged and uncharged filters due to the very small amount of particle charge, on the other hand the difference was diminished for atomized particle and finally almost vanished for corona charged particles. As shown in Fig. 2, the pressure drop of filter loaded with corona charged particles was only half of those for neutralized and atomized particles at the same areal mass loading because of the porous structure of particle deposit formed on filter fibers (Fig.3), caused by the repulsive forces between particles.

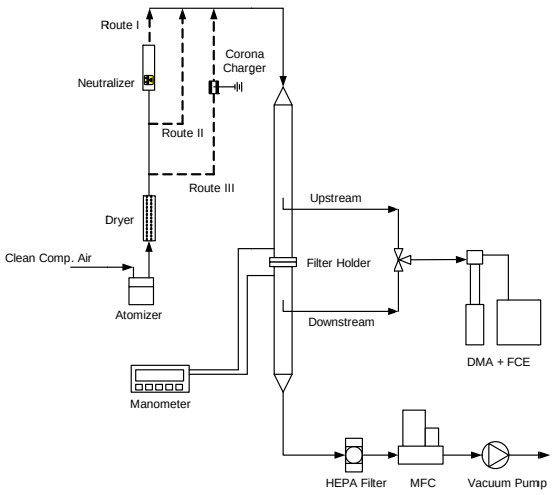

Figure 1. Schematic diagram of filter test apparatus used in this study.

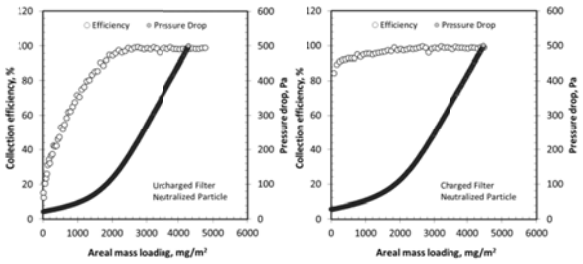

(a) neutralized particle

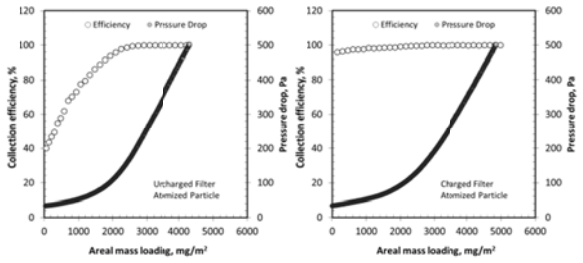

(b) atomized particle

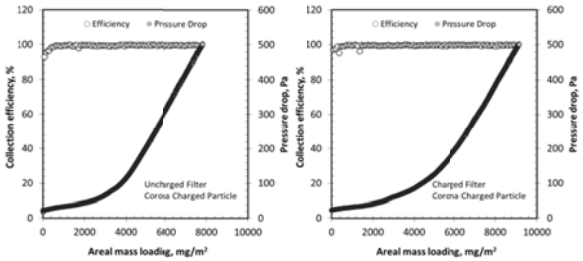

(c) corona charged particle

Figure 2. Collection efficiency and pressure drop of air filter loaded with differently charged particles.

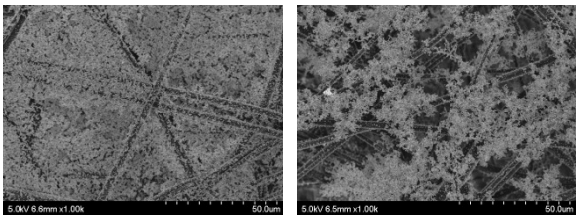

(a) neutralized (b) corona charged

Figure 3. Deposition patterns of particles on electrically charged filter.

This study was supported by the Converging Research Center Program through the National Research Foundation of Korea (NRF) funded by the Ministry of Education, Science and Technology.

Influence of particle and filter charge on collection efficiency of air filters in an externally applied electric field

H.S. Park

Climate Change Research Division, Korea Institute of Energy Research, Daejeon, 305-343, South Korea
Keywords: filter, electric field, charge.
Presenting author email: phs@kier.re.kr

Electrostatic forces have been widely used for enhancing the performance of air filters. Particle charge, filter charge, and external electric field can raise filtration efficiency without any increase of pressure drop of filter. Charged filters have very high initial collection efficiency, but the filter charge gradually loses its effect as particles are captured on filter fibers (Walsh and Stenhouse, 1997). Applying an electric field across filter media can be an alternative method to overcome the drawback of charged filters, even though it has several limitations to extend its application. In this work, the effectiveness of electric field applied to air filters was experimentally examined.

Three different filter media were used for test, as listed in Table 1. Filter A is an electrically charged filter provided by a company. Filter A has a 3-layer structure, and its middle layer is composed of polypropylene fibers of 2~10 μm in diameter. Filter B is prepared by immersing Filter A into isopropanol and drying. This is general process to get rid of filter charge. Thus, Filter B can be accepted as non-charge filter. Filter C is a commercial micro-glassfiber filter (Type A/E, Pall Corp.). NaCl particles as test aerosol are generated via an atomizer and diffusion dryer. Aerosol neutralizer was used for bipolar charging of particles, which is denoted as 'neutralized particle'. 'uncharged particle' was supplied to filter by removing charged particles from 'neutralized particle' via an electrostatic precipitator. Electric field was formed across filter media using two metal meshes as electrodes between which an electric potential of (-)1000 V was applied. The filtration velocity was fixed at 5.3 cm/s through this study.

Table 1. Fundamental properties of tested filter media.

sample	filter charge	fiber material
Filter A	charged	polypropylene
Filter B	IPA treated	polypropylene
Filter C	as received	glass fiber

As can be seen in Fig. 1, Filter A shows the minimum efficiency of 80% for 70 nm neutralized particles, while approximately 70% efficiency for 150nm uncharged particle. The effect of external electric field was very little for Filter A. From the results for the non-charge Filter B, it can be known that Filter B has no charge and the dominant electrostatic force acting on neutralized particles is Coulombic force due to the particle charge and external electric field. Filter C is a highly efficient filter media whose minimum efficiency is over 96%, thus external electric field made only little difference in filter efficiency. Additionally, there was no significant effect of electric forces on collection efficiency for the particles smaller than 50 nm in diameter under experimental conditions of this work.

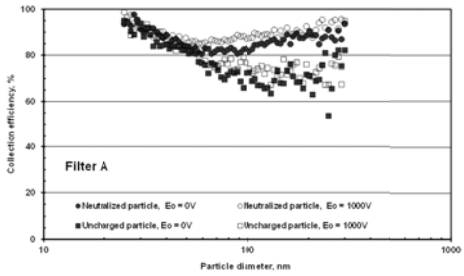

(a) Filter A

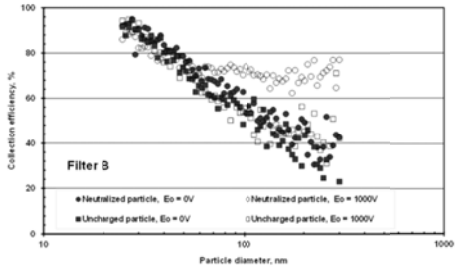

(b) Filter B

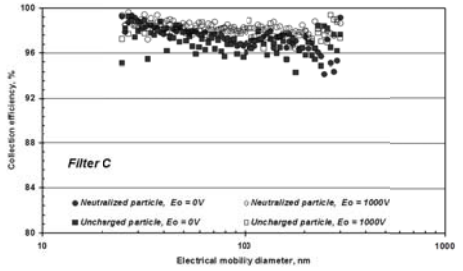

(c) Filter C

Figure 1. Collection efficiency of tested filters for NaCl particles under various electrostatic conditions.

This study was supported by the Converging Research Center Program through the National Research Foundation of Korea (NRF) funded by the Ministry of Education, Science and Technology.

Walsh, D.C. and Stenhouse, J.I.T. (1997) *J. Aerosol Sci.*, **28**, 307-321.

The analytical description of the dynamics of the impurity redistribution in the composite particles by coagulation

D.V. Tsaplin, V.N. Piskunov

Russian Federal Nuclear Center – VNIIEF; Sarov, Nizhni Novgorod region, 607190, Russia
Keywords: aerosol formation, coagulation, composite particles, analytical solutions
Presenting author email: tsaplindv@mail.ru

The description of the composite particles formation consisting of mixture of different materials is important for many practical problems, such as the analysis of accidental releases in atmosphere, the description of multiphase processes in chemical reactors and others. The programs developed for the numerical simulation of these processes require optimization of computational methods and verification. For these purposes it is convenient to use the solutions of the kinetics equations for composite particles in concise form (impurity integrated) (Piskunov, 2013). This report focuses on the new results on the development of this approach.

Statement of the problem. The complete kinetic equation for two-component system has the form (Lushnikov, 1976; Piskunov, 2013):

$$\frac{\partial C}{\partial t}=\frac{1}{2}\int_0^g\int_0^\alpha K(g-s,\alpha-\beta;s,\beta)C(g-s,\alpha-\beta)C(s,\beta)ds\,d\beta$$

$$-C(g,\alpha)\int_0^\infty\int_0^\infty K(g,\alpha;s,\beta)C(s,\beta)ds\,d\beta\equiv S\left(C,g,\alpha,t\right) \qquad (1)$$

where $C(g,\alpha,t)$ is the concentration of particles containing at time t the total mass g and the impurity mass α, $K(g,\alpha;s,\beta)$ are coagulation coefficients.

In the concise description the one component (impurity) is taken integrally by using the zero $n(g,t)$ and the first $m(g,t)$ moments of entire spectrum (Simons, 1981; Piskunov et al., 1997):

$$n(g,t)=\int_0^\infty C(g,\alpha,t)d\alpha\,;\quad m(g,t)=\int_0^\infty \alpha C(g,\alpha,t)d\alpha \qquad (2)$$

The ratio $m(g,t)/gn(g,t)$ determines the average impurity mass in a particle. In the concise description the equation (1) is replaced by the following chain of equations:

$$\partial_t n=\frac{1}{2}\int_0^g K(g-s,s)n(g-s)n(s)ds-n(g)\int_0^\infty K(g,s)n(s)ds\,, \qquad (3)$$

$$\partial_t m=\int_0^g K(g-s,s)n(g-s)m(s)ds-m(g)\int_0^\infty K(g,s)n(s)ds\,. \qquad (4)$$

Analytical solutions. The general analytical solution of the kinetic equation (1) for the additive kernel $K(g_1,g_2)=K_0(g_1+g_2)=K_0(x_1+y_1+x_2+y_2)$ (where x and y are the mass of the individual components, and $g=x+y$) was obtained by Fernandez-Diaz and Gomez-Garcia (2007). In the case of the exponential initial distribution

$$C(x,y,t=0)=ab\mathrm{e}^{-ax-by}=ab\theta(g-\alpha)\mathrm{e}^{-ag-(b-a)\alpha}=C_0(g,\alpha) \qquad (5)$$

(a, b are parameters; $\theta(g)=0$, if $g<0$ and $\theta(g)=1$, if $g>0$, and $\alpha=y$) this solution is:

$$C(g,\alpha,\tau)=\theta(g-\alpha)ab(1-\tau)\mathrm{e}^{-\left(a+\frac{ab\tau}{a+b}\right)g-(b-a)\alpha}\sum_{k=0}^{\infty}\frac{\left(\dfrac{a^2b^2\tau g\alpha(g-\alpha)}{a+b}\right)^k}{(k+1)!(k!)^2} \qquad (6)$$

where $\tau=1-\exp\left(-(a+b)K_0t/ab\right)$ is the dimensionless time. Integrating the solution (5) we find the expressions for the values $n(g,t)$ and $m(g,t)$ that can also be obtained by solving the system of equations (3-4):

$$n=\frac{1-\tau}{g\sqrt{\tau}}\mathrm{e}^{-ag(1+\tau)}I_1(2g\alpha\sqrt{\tau})\,;\ m=\frac{a(1-\tau)}{b-a}\mathrm{e}^{-ag(1+\tau)}I_0(2g\alpha\sqrt{\tau})\,, \qquad (7)$$

where I_0 and I_1 are the modified Bessel functions of the first kind.

Relaxation to the uniform distribution. The dynamics of the impurity redistribution in the composite particles with time is important for practical problems. In (Piskunov, 2013) a large number of analytical solutions were obtained for the initial particle spectra in which the relative mass of the impurity is uniformly distributed by size. The general results of the stability of the uniform distribution of the impurity were formulated and were proved. In the case of the non-uniform initial distribution of impurity we express its mass concentration $m_1(g,t)$ through the mass concentration for uniform distribution $m_0(g,t)=gn_0(g,t)$ and we introduce the quantity $\eta(g,t)$ that takes into account the difference between the two cases:

$$m_1(g,t)=m_0(g,t)\left[1+\eta(g,t)\right] \qquad (8)$$

Substituting this expression into equation (4) and using (3) in the case of the constant kernel $K(x,y)=K_0$ and the exponential distribution $n_0(g,t)=(N^2/M)\mathrm{e}^{-gN/M}$ (where $N=N_0/(1+K_0N_0t/2)$ and M are total number and mass concentrations) we obtain the solution for $\eta(g,t)$:

$$\eta(g,\tau)=\eta_0(g)\exp(-N_0\tau g/M)+$$
$$+\frac{N_0\tau g}{M}\int_0^1 y\eta_0\left(gy\right)\mathrm{e}^{-\frac{N_0\tau g}{M}y}\left(2+\frac{N_0\tau g}{M}(1-y)\right)dy, \qquad (9)$$

where $\tau=1-N/N_0$ is the dimensionless time. This solution allows to define the asymptotic behavior for $\eta(g,t)$. For example, for $\eta_0(g)=A\mathrm{e}^{ag}$ with parameters A, a ($a<N_0/M$) we obtain that at $g\to\infty$ and $t\to\infty$:

$$\eta(g,\tau)\approx A\Big/\left(1-aM/N_0\right)^2=\mathrm{const}\,, \qquad (10)$$

i.e. the non-uniform initial distribution of impurity at large times becomes the uniform one for a large part of the spectrum of composite particles (except for the small g). Moreover, the relaxation time coincides with the coagulation time.

Fernandez-Diaz, J.M. and Gomez-Garcia, G.J. (2007) *Europhys. Lett.,* **78**, 56002.

Lushnikov, A. (1976) *J. Colloid Interf. Sci.* **54**, 94–101.

Piskunov, V.N. (2013) *Physica D,* in press.

Piskunov, V.N. et al. (1997) *J. Aerosol Sci.*, **28** (7), 1215–1231.

Simons, S. (1981) *Annals of Nuclear Energy*, **8**, 287–294.

Detection of the negative thermophoresis phenomenon in microgravity experiments

A.A. Vedernikov[1] , S.A. Beresnev[2] and A.V. Markovich[1]

[1]Université Libre de Bruxelles, Brussels, B-1050, Belgium
[2]Ural Federal University, Ekaterinburg, 620083, Russia
Keywords: aerosol dynamics, thermophoresis, microgravity, accommodation coefficient
Presenting author email: Sergey.Beresnev@usu.ru

Thermophoresis (motion of particles due to temperature gradient in a gas) is a subject of many-year experimental and theoretical investigations of great significance for fundamental and applied aerosol physics.

Substantial improvement of accuracy and sensitivity due to diminishing convective effects is possible to get in microgravity conditions performing experiments in drop towers, in parabolic airplane flights, or onboard the orbital space station. Microgravity conditions are the most advantageous, if not the only suitable for decisive experiments in tackling the problem of "negative thermophoresis", i.e. predicted for high-conductivity aerosol particles at small Knudsen numbers motion in the direction of temperature gradient and not against as for the traditional thermophoresis. Among recent researches in this area we will note the attempt to detect this phenomenon in the experiments with model macroparticles (Ventura *et al*, 2012) and new theoretical results for negative thermophoretic force for high-conducting particles (Takata and Hattori, 2012).

According to theoretical analysis the thermophoretic force and velocity are very sensitive to the variation of energy accommodation coefficient α_E. The value of α_E governs the magnitude of the heat flux normal to the surface, which, in its turn, controls the competition of oppositely directed thermal creep and thermal stress gas flow near the particle surface so that the thermophoretic velocity can be positive even for high-conductivity particles at very small Kn numbers. Experimental analysis of negative thermophoresis thus splits into two tasks: 1) testing which theories are adequate – those taking into account the thermal stress slip or without it and 2) which model most accurately takes into account peculiarities of these phenomena.

Experiments were performed at Bremen Drop Tower (Germany) with 4.7 s duration of high quality microgravity (better than 10^{-5}g). We used two types of particles *a*) high heat conductivity ($\Lambda = \lambda_p/\lambda_g$ =20500) polydisperse copper spherical particles with mean diameter of 74 μm and *b*) low conductivity ($\Lambda = 1.8$) hollow glass spheres with about the same particle size distribution. Particles were injected separately into the cubic cell filled with nitrogen at normal pressure with four windows for stereoscopic observation in back illumination. The gradient was created by a heated wire in the cell center. Velocities were analyzed for the particles, for which three-dimensional trajectories were identified. Radial components of particle velocities were related to the thermophoretic motion. Previous results (Vedernikov *et al* (2008) and Beresnev *et al* (2008)) are here completed with the analysis of motion of low conductivity particles and detailed three-dimensional simulation of residual convective motion.

Typical velocities of low conductivity particles were around 0.3-0.5 mm/s depending on their distance from the wire and showed excellent agreement with the theory of Brock (1962). Velocities of copper particles appeared to be 30-50 times lower under the same conditions. Reduced thermophoretic velocities of copper particles are presented on Fig. 1 after refinement on residual convective motion.

These results meet predictions of gas-kinetic theories that take into account the thermal stress slip flow. As for the second task mentioned at the beginning, the experiments were still not sensitive enough to define the sign of the motion and relate it to a particular set of accommodation coefficients.

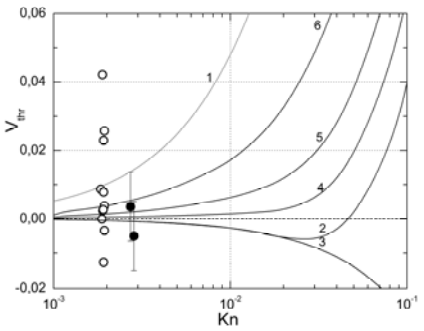

Figure 1. The dimensionless thermophoretic velocity V_{thr} for copper particles. Microgravity experiments: black circles stand for particles close to the wire where negative thermophoresis is dominant; open circles stand for particles far from the wire where dominates residual convection. Theory: 1 – Brock (1962); 2-6 – Beresnev et al (1995): 2 – calculations and 3 – asymptotic solution at $\alpha_\tau = \alpha_E = 1.0$; 4 – calculations at $\alpha_\tau = 1.0;\ \alpha_E = 0.95$; 5 – at $\alpha_\tau = 1.0;\ \alpha_E = 0.90$; 6 – at $\alpha_\tau = 1.0;\ \alpha_E = 0.80$.

ESA PRODEX Program, Belgian Federal Science Policy Office and Bremen Drop Tower Operation and Service Company ZARM FABmbH (Germany) are greatly acknowledged for their support.

Beresnev, S.A., Vedernikov, A.A. and Markovich, A.V. (2008) *Atmos. Oceanic Opt.* **21(7)**, 508-513.

Takata, S. and Hattori, M. (2012). *AIP Conf. Proc.* **1501**, 59-66.

Vedernikov, A., Beresnev S. and Markovich A. (2008) *J. Jap. Soc. Micrograv. Appl.* **25**, 267-272.

Ventura, A., Ketsdever, A., Webb, R. *et al*. (2012) *AIP Conf. Proc.* **1501**, 727-734.

Contribution to the study of particle resuspension kinetics during thermal degradation of polymers.

S. Delcour[1, 2], F.-X. Ouf[1], N. Azema[2], A. Coppalle[3], J.Yon[3], L. Ferry[2], F. Gensdarmes[1], J.-M. Lopez-Cuesta[2]
[1]Institut de Radioprotection et de Sûreté Nucléaire (IRSN), PSN-RES, SCA, LPMA, Gif-Sur-Yvette, 91192, France.
[2]Ecole des Mines d'Alès, Centre des Matériaux (C2MA)-Pôle Matériaux Polymères Avancés
6 Avenue de Clavières, 30319 Alès Cedex, France.
[3]UMR 6614 CORIA, INSA de Rouen, Avenue de l'université, B.P. 8, Saint-Etienne du Rouvray, 76801, France
Keywords: resuspension, fire, polymers.
Presenting author email: simon.delcour@irsn.fr

In the nuclear industry, solid radioactive powders are manufactured, handled and treated in a confined way using glove boxes mainly composed of PolyMethyl MethAcrylate (PMMA) or PolyCarbonate (PC) sheets. The handling of such radioactive material may contaminate the inner walls of glove boxes and this surface contamination by particles may be released in case of accidental situation such as a fire. Therefore, in order to quantify the toxicological and environmental impact of a fire occurring in a nuclear facility, it is necessary to be able to predict the emission rate of radioactive aerosols in the event of such accidental situation. Given the complexity of using radioactive particles in fire experiments, alumina oxide (Al_2O_3) is used as a thermally stable (same as PuO_2) surrogate to investigate the effect of particle size. A theoretical model is being developed to help the identification of specific criterion for the choice of the surrogate.

The experimental setup is composed of a mass loss cone calorimeter modified for aerosol sampling. It is composed of a conical radiative heater which allows applying heat fluxes ranging from 10 to 100 kW/m^2 at the surface of the sample placed on a weighing cell. Soot and alumina oxide aerosol released are sampled using an isokinetic probe and filter holders on cellulose acetate membrane. The release fraction (ratio between emitted and initially available mass of contaminant aerosols) of surrogate aerosols deposited on sheets of PMMA and PC is determined by ICP-MS as a function of the size distribution of aerosol (Al_2O_3 with respectively 0.7 µm and 3.6 µm for geometrical diameter) and incident heat flux (from 25-35 kW/m^2 for pyrolysis to 45-50 kW/m^2 for auto-ignition). Further details could be found in Ouf *et al.* (2013).

Experimental results are reported on the resuspension of particles deposited on polymer samples representative of glove boxes used in the nuclear industry, under thermal degradation. A parametric study was carried out on the effects of heat flux, air flow rate, fuel type and particle size. Small-scale experiments were conducted on 10x10 cm² PMMA and PC samples covered with aluminium oxide particles. It was observed for both polymer (fuel) samples that heat flux has no effect on the airborne release fraction (ARF), whereas particle size is a significant parameter. In the case of the PMMA sample, ARF values for 0.7 and 3.6 µm diameter particles range from 12.2% (+/- 6.2%) to 2.1% (+/- 0.6%), respectively, whereas the respective values for the PC sample range from 3.2% (+/- 0.8%) to 6.9% (+/- 3.9%). As the particle diameter increases, a significant decrease in particle release is observed for the PMMA sample, whereas an increase is observed for the PC sample (see figure 1).

Furthermore, a peak airborne release rate is observed during the first instants of PMMA exposure to thermal stress. An empirical relationship has been proposed between the duration of this peak release (DT_{flash}) and the external heat flux (see figure 2). This relationship also fits the time to reach a surface temperature of 275°C.

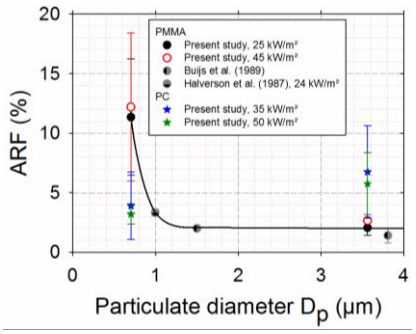

Figure 1. Evolution of ARF for alumina particles deposited on horizontal PMMA and PC sheets

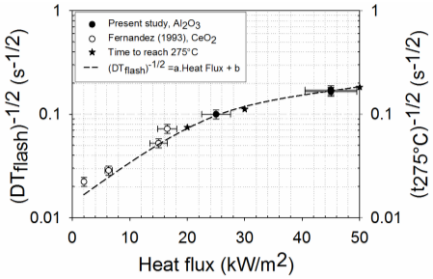

Figure 2. Evolution of duration of peak release as a function of heat flux for PMMA

Buijs, K., Chavanne de Dalmassy, B. and Pickering, S. (1989) *J. Nucl. Mater.***166**, 199-207.

Halverson, M., Ballinger, M. and Dennis, G. (1987) Combustion aerosols formed during burning of radioactively contaminated materials. Experimental results, NUREG/CR 4736. PNL-5999.

Ouf, F.-X., Delcour, S., Azema, N., Coppalle, A., Ferry, L., Gensdarmes, F., Lopez-Cuesta, J.-M., Niang, A., Pontreau, S. and Yon, J. (2013) *J. Hazardous Materials*, http://dx.doi.org/10.1016/j.jhazmat.2013.01.060

Fernandez, Y., Experimental study on release of radioactive aerosols during the thermal degradation of contaminated organic materials present in nuclear installation, *In French*. PhD Thesis, Université de Savoie. Rapport CEA-R-5663 (1993).

Determining the mass accommodation coefficient of dicarboxylic acids using molecular dynamics simulations

Jan Julin[1] and Ilona Riipinen[1]

[1]Department of Applied Environmental Science and Bert Bolin Centre for Climate Research, SE-10691 Stockholm, Stockholm University, Sweden.

Keywords: mass accommodation, fundamental aerosol physics, adipic acid, molecular dynamics.

Presenting author email: jan.julin@itm.su.se

The ability of an atmospheric aerosol particle to uptake gas phase molecules arriving on the aerosol surface will limit the rate of the condensational growth of the particles, and thus control their growth from the nanoscale to climate-relevant sizes. The fraction of the incoming molecules that remain with the condensed phase is given by the mass accommodation coefficient α_m. This coefficient can be defined either as a surface accommodation coefficient, where any molecule that is not directly scattered back to the gas phase is counted as accommodated, or as a bulk accommodation coefficient, where it is necessary for a molecule to cross the surface into the bulk before it is considered accommodated (Kolb *et al.* 2010). Experiments have suggested that the mass accommodation coefficients of various dicarboxylic acids on surfaces consisting of the same species are far from unity (Saleh *et al.* 2012). Technically these experimental values are evaporation coefficients, but the value of the evaporation coefficient is in general assumed to be identical with the condensation, or mass accommodation, coefficient. In this work we have performed molecular dynamics (MD) simulations of the mass accommodation of adipic acid, as well as other dicarboxylic acids, on solid surfaces corresponding to the experimental conditions.

The MD simulations were performed using the GROMACS software (Hess *et al*. 2008), and the OPLS-AA potential (Kaminski *et al.* 2001) was used to model the acid molecules. The simulation setup consists of a slab of 1000 acid molecules, located in the middle of an elongated simulation box, and incoming molecules that are "shot" toward the surface (close-up seen in Fig. 1). The simulation temperature was T=313.15 K, which corresponds to the thermodenuder temperature in the experiments of Saleh *et al.* (2012).

To create the slab, the molecules were initially placed in a cubic simulation box at a higher temperature (i.e. a liquid temperature). After initial equilibration, the system was cooled through simulated annealing to the desired temperature. Finally, following a short constant pressure simulation at the lower temperature, the system was allowed to equilibrate for several nanoseconds. Only after this step the simulation box was elongated in the *z*-direction.

The mass accommodation simulations consisted of creating incoming molecules at both sides of the slab, with the starting configurations for the slab taken at fixed intervals from slab-only simulations. The incoming molecules were added to the box so that the atom closest to the surface was approximately 1.5 nm away from the surface. The molecules were placed at random *x*,*y*-coordinates, with various orientations. Their initial velocities were assigned from the Maxwell-Boltzmann distribution corresponding to the desired temperature, but always pointing at the center of the surface. The mass accommodation coefficient is determined by classifying the fates of the incoming molecules when they arrive at the surface.

Preliminary results for adipic acid show that when treating α_m as a surface accommodation coefficient we have $\alpha_m \approx 1$, that is, we find that the vast majority of incoming molecules do not scatter. On the other hand, the bulk accommodation coefficient determined from the data is going to differ from unity quite noticeably, as the solid state of the slab efficiently hinders the incoming molecules from crossing the surface into the bulk within the simulation time.

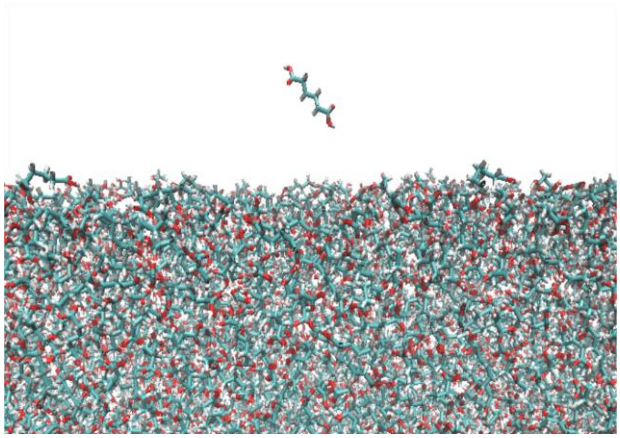

Figure 1. A snapshot of an adipic acid molecule arriving at an adipic acid surface.

This work was supported by the European Research Council grant ATMOGAIN (No. 278277). Computational resources were provided by PDC Center for high performance computing.

Kolb, C. E. *et al.* (2010). *Atm. Chem. Phys.* **10**, 10561-10605.

Saleh, R., Khlystov, A., and Shihadeh, A. (2012). *Aerosol Sci. Tech.* **46**, 22.

Hess, B., Kutzner, C., van der Spoel, D., and Lindahl, E. (2008). *J. Chem. Theory Comp.* **4**, 435-477.

Kaminski, G. A., Friesner, R. A., Tirado-Rives, J., and Jorgensen W. L. (2001). *J. Phys. Chem. B* **105**, 6474.

Size dependence of incorporation of gas molecules into aerosol nanoparticles

V.V. Levdansky[1], J. Smolík[2], V. Ždímal[2] and P. Moravec[2]

[1]A.V. Luikov Heat and Mass Transfer Institute NASB, 15 P. Brovka Str., 220072 Minsk, Belarus
[2]Institute of Chemical Process Fundamentals AS CR, v.v.i., Rozvojova 135, 165 02 Prague 6, Czech Republic
Keywords: aerosol, nanoparticles, size effect.
Presenting author email: vlev5@yahoo.com

The influence of size effects on the physicochemical transformations and transfer phenomena in the heterogeneous systems with nanoobjects attracts increasing attention of researchers. These problems are of interest for nanotechnology and atmospheric physics. Size effects can influence the cohesive energy as well as the activation energies of vacancy formation and diffusion of atoms in the nanoscale particles (Vanithakumari and Nanda, 2008). Phase transitions in aerosol systems with nanoscale particles (clusters) also depend on the nanoparticle size (Levdansky *et al*., 2010). Hear we discuss the size dependence of the mass accommodation coefficient in the aerosol system with nanoparticles.

The equation for the mass accommodation coefficient γ can be written as (Hanson, 1997; Crowley *et al*., 2010)

$$\gamma = \frac{\alpha_s k_{abs}}{k_{des} + k_{abs}}, \qquad (1)$$

where α_s is the sticking coefficient, k_{abs} is the rate constant for absorption, k_{des} is the rate constant for desorption.

The sticking coefficient α_s is related to the rate constant for adsorption k_{ads} (Hanson, 1997). The values of k_{ads}, k_{des}, k_{abs} in the general case depend on the nanoparticle size due to the size dependence of adsorption and desorption of molecules (Murzin, 2009) and absorption of adsorbed molecules (Levdansky *et al.*, 2009). The melting temperature and surface tension also depend on the nanoparticle size (Rekhviashvili and Kishtikova, 2006). Taking into account the above-mentioned, we can write the following equation for the mass accommodation coefficient for the nanoparticle γ_p:

$$\gamma_p = \frac{4}{v} \frac{k_{ads,\infty} \exp\left(-\frac{4\alpha_{ads}\lambda\omega}{d}\right) k_{abs,\infty} \exp\left(\frac{4\psi\delta}{d}\right)}{k_{des,\infty} \exp\left[\frac{4(1-\alpha_{ads})\lambda\omega}{d}\right] + k_{abs,\infty} \exp\left(\frac{4\psi\delta}{d}\right)}, \qquad (2)$$

where v is the mean thermal velocity of gas molecules, $k_{ads,\infty}$, $k_{des,\infty}$, $k_{abs,\infty}$ are respectively the rate constants for adsorption, desorption and absorption for bulk matter, α_{ads} is the Polanyi parameter for the adsorption rate constant (Murzin, 2009), d is the particle diameter, δ is the Tolman length (it is assumed that $d >> \delta$), $\lambda = \sigma_\infty V_m/(RT)$, $\psi = Q_{abs,\infty}/(RT)$, $\omega = 1 - 4\delta/d$, σ_∞ is the surface tension for bulk matter, V_m is the molar volume of the substance forming the nanoparticle, R is the gas constant, T is the temperature, $Q_{abs,\infty}$ is the activation energy for the transition of molecules from the adsorption state to the absorption state for bulk matter.

Let us consider the limiting case when $k_{des} >> k_{abs}$. Figure 1 shows the dependence $\gamma^* = \gamma_p/\gamma_\infty$, where γ_∞ is the mass accommodation coefficient for bulk matter, on the dimensionless diameter of the nanoparticle $d^* = d/\delta$ at different values of the parameters ψ and $\varphi = \sigma_\infty V_m/(Q_{abs,\infty}\delta)$. It is seen that γ^* increases with a decrease in d^* and φ and with an increase in ψ.

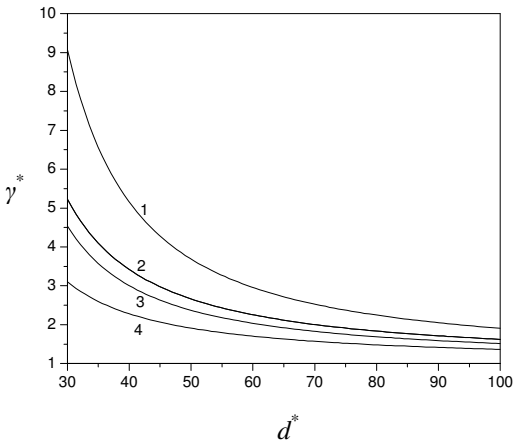

Figure 1. Dependence of γ^* on d^*; 1, 2: $\varphi = 0.2$; 3, 4: $\varphi = 0.5$; 1, 3. $\psi = 20$; 2, 4: $\psi = 15$.

This work was supported by GAAVCR project IAA200760905.

Crowley, J.N., Ammann, M., Cox, R.A., Hynes, R.G., Jenkin, M.E., Mellouki, A., Rossi, M.J., Troe, J. and Wallington, T.J. (2010) *Atmos. Chem. Phys*. **10**, 9059-9223.

Hanson, D.R. (1997) *J. Phys. Chem.* B **101**, 4998-5001.

Levdansky, V.V., Smolik, J. and Moravec, P. (2009) *Aerosol Air Qual. Res.* **9**, 257-265.

Levdansky, V.V., Smolik, J. and Moravec, P. (2010) *Int. Commun. Heat Mass Transfer* **37**, 593-595.

Murzin, D.Yu. (2009) *Chem. Eng. Sci.* **64**, 1046-1052.

Rekhviashvili, S.Sh. and Kishtikova, E.V. (2006) *Tech. Phys. Lett.* **32**, 439-441.

Vanithakumari, S.C. and Nanda, K.K. (2008) *Phys. Lett.* A **372**, 6930-6934.

Influence of size effect on chemical reactions on surface of aerosol nanoparticles

V.V. Levdansky[1], J. Smolík[2], V. Ždímal[2] and P. Moravec[2]

[1]A.V. Luikov Heat and Mass Transfer Institute NASB, 15 P. Brovka Str., 220072 Minsk, Belarus
[2]Institute of Chemical Process Fundamentals AS CR, v.v.i., Rozvojova 135, 165 02 Prague 6, Czech Republic
Keywords: aerosol, nanoparticles, chemical reaction.
Presenting author email: vlev5@yahoo.com

Chemical reactions in aerosol systems are paramount for a number of processes occurring in the atmosphere and in various areas of chemical technology. In the case of the nanoscale aerosol particles the particle size can influence the rate of a chemical reaction on the nanoparticle surface.

The nanoparticle size can affect the activation energy of a chemical reaction (Lu and Meng, 2010) as well as the Langmuir constant for adsorption of the reactant molecules (Murzin, 2009). A decrease in the activation energy of a chemical reaction with a reduction in the nanoparticle size leads to an increase in the reactive uptake coefficient. A decrease in the Langmuir adsorption constant with a reduction in the nanoparticle size can reduce the reactive uptake coefficient. Here we consider the joint influence of the mentioned factors on the reactive uptake coefficient for the Eley-Rideal mechanism of a chemical reaction on the nanoparticle surface.

The reactive uptake coefficient γ_r for the Eley-Rideal mechanism of a chemical reaction is given by (Crowley *et al.*, 2010)

$$\gamma_r = \alpha_r \theta_B , \qquad (1)$$

where α_r is the elementary reaction probability in the collision of the gas phase reactant molecule A with the adsorbed reactant molecule B, θ_B is the surface coverage related to adsorption of molecules of the component B (for simplicity, we neglect here adsorption of molecules of the component A and the reaction product).

Taking into account the Langmuir model for adsorption and the size dependence of the Langmuir adsorption constant (Murzin, 2009), the activation energy of a chemical reaction (Lu and Meng, 2010) as well as the melting temperature and surface tension (Rekhviashvili and Kishtikova, 2006), the value of γ_r for the nanoparticle (γ_{rp}) can be written as

$$\gamma_{rp} = \alpha_{r\infty} \exp\left(\frac{4E_{r\infty}\delta}{RTd}\right)\frac{P_B K_{B\infty}\exp(-\xi)}{1+P_B K_{B\infty}\exp(-\xi)} . \qquad (2)$$

Here $\alpha_{r\infty}$ is the value of α_r without considering the size effect, d is the particle diameter, δ is the Tolman length (it is assumed that $d >> \delta$), $E_{r\infty}$ is the activation energy of a chemical reaction on the surface of bulk matter, R is the gas constant, T is the temperature, P_B is the partial pressure of the component B in a gas phase, $K_{B\infty}$ is the Langmuir adsorption constant for adsorption of the component B on the surface of bulk matter, the value of ξ is given by

$$\xi = \frac{4\sigma_\infty V_m}{dRT}\left(1-\frac{4\delta}{d}\right), \qquad (3)$$

where σ_∞ is the surface tension for bulk matter, V_m is the molar volume of a substance forming the nanoparticle.

Figure 1 shows the dependence of $\gamma^* = \gamma_{rp}/\gamma_{r\infty}$, where $\gamma_{r\infty}$ is the reactive uptake coefficient for bulk matter, on the dimensionless diameter $d^* = d/\delta$ at $P_B K_{B\infty}\exp(-\xi) << 1$, $\sigma_\infty V_m/(E_{r\infty}\delta) = 0.2$ and different values of the parameter $\psi = E_{r\infty}/(RT)$. It is seen that γ^* increases with a decrease in d^* and with a rise in ψ.

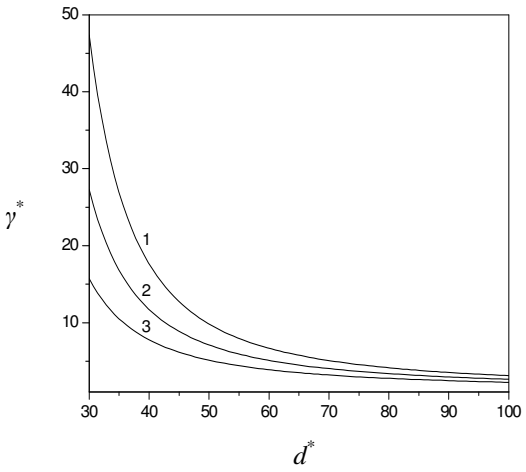

Figure 1. Dependence of γ^* on d^*; 1: $\psi = 35$, 2: $\psi = 30$, 3: $\psi = 25$.

This work was supported by GAAVCR project IAA200760905.

Crowley, J.N., Ammann, M., Cox, R.A., Hynes, R.G., Jenkin, M.E., Mellouki, A., Rossi, M.J., Troe, J. and Wallington, T.J. (2010) *Atmos. Chem. Phys.* **10**, 9059-9223.

Lu, H.M. and Meng, X.K. (2010) *J. Phys. Chem.* C **114**, 1534-1538.

Murzin, D.Yu. (2009) *Chem. Eng. Sci.* **64**, 1046-1052.

Rekhviashvili, S.Sh. and Kishtikova, E.V. (2006) *Tech. Phys. Lett.* **32**, 439-441.

Evolution of Size and Temperature of Droplets in the Process of Bulk Condensation

N.M. Kortsenshteyn[1], A.K. Yastrebov[2]

[1]G.M. Krzhizhanovsky Power Engineering Institute, Moscow, Russia
[2]Department of Low Temperatures, Moscow Power Engineering Institute, Moscow, Russia
Keywords: bulk condensation, kinetic equation
Presenting author email: ars48@yandex.ru

In various studies of bulk condensation temperature of droplets is often assumed to be equal to temperature of gaseous phase or to saturation temperature at vapor pressure. We compared results which have been obtained with use of these assumptions and in general formulation (Korstenshteyn and Yastrebov, 2012). However we assumed that all droplets have the same temperature, but the equation of heat balance for a single droplet shows that its temperature depends on its size. In this work we consider temperature distribution of droplets in the process of bulk condensation.

We proposed the modification of the kinetic equation for distribution function of droplets. This modification does not require the assumption of equality of all droplets' temperature. The distribution function is defined as derivative of droplets' number by their radius and temperature. The modified kinetic equation is written as follows:

$$\frac{\partial f}{\partial t}+\frac{\partial\left(\dot{r}f\right)}{\partial r}+\frac{\partial\left(\dot{T}f\right)}{\partial T}=\frac{I}{\rho}\delta\left(r-r_{cr}\right)\delta\left(T-T_s\right) \qquad (1)$$

Here f is the distribution function of droplet sizes and temperatures, r is the droplet radius, $\dot{r}$ is the droplet growth rate, $\dot{T}$ is the rate of variation of droplet's temperature, I is the nucleation rate, ρ is the density of two-phase mixture, δ is the delta function, r_{cr} is the critical droplet radius, and T_s is the saturation temperature. The rate of variation of droplet's temperature can be found as follows:

$$\dot{T}=3\frac{\left(L-C_{pm}\left(T-T_m\right)\right)\rho'\dot{r}-q}{\rho'C'r} \qquad (2)$$

Here L is phase transition heat, ρ' and C' are density and specific heat of liquid, C_{pm} and T_m are specific heat and temperature of gaseous phase, and q is interphase heat flux. This formula was obtained from the equation of heat balance for a single droplet. There is droplet's temperature T_0 for which value of $\dot{T}$ is equal to zero. In this case all the heat released at condensation on the surface of droplet is transferred to the gaseous phase. For free molecular regime both growth rate and interphase heat flux do not depend on droplet's size, so the temperature T_0 is the same for all droplets.

Testing of proposed modification was carried out for the problem of condensational relaxation at instantaneous creation of supersaturated state. We considered the mixture of cesium (vapor) and argon (non-condensable gas). This mixture was taken as example of free molecular regime of droplets' condensational growth. The initial temperature of mixture was 560 K, the partial pressure of vapor was 10 times higher than saturation pressure at this temperature.

We obtained results of numerical solution with and without taking into account temperature distribution of droplets. These results are almost identical because temperature of most of the droplets is close to the average one. The value of $\dot{T}$ is inversely proportional to the size of droplets. The size of newly formed droplets is equal to the critical one which is very small at initial supersaturation ratio at beginning of relaxation. The rate of temperature variation is very high for newly formed droplets, and their temperature becomes equal to T_0 within a very short time (about 10^{-8} s). So results obtained with use of the same temperature of all droplets should be close to ones obtained with use of the modified kinetic equation. Example of temperature distribution function f_T is shown in Figure 1. This function is defined as integral of the distribution function of droplet sizes and temperatures by droplet size. It can be seen that number of droplets with temperature between T_0 and T_s is very small in comparison with number of droplets with temperature T_0, so their influence on the average temperature of droplets can be neglected. The problem of condensational relaxation can be solved with use of the same temperature of all droplets. Our numerical results confirm the efficiency of the proposed modification of the kinetic equation.

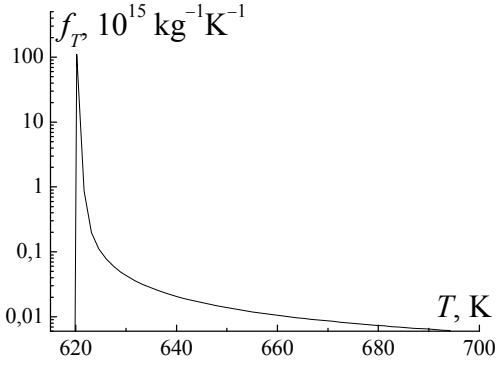

Figure 1. Example of temperature distribution function.

The paper was prepared as part of work under the grant of the President of the Russian Federation MK-6180.2012.8 for young scientists and the grant of the Russian Foundation for Basic Research 13-08-00962.

Kortsenshteyn, N.M., and Yastrebov, A.K. (2012), *Int. J. Heat Mass Tran.* **55**, 1133-1140.

Nucleation near critical supersaturation

Z. Kožíšek[1], P. Demo[1]

[1]Institute of Physics, Academy of Sciences of the Czech Republic, Cukrovarnická 10, 162 00 Prague 6, Czech Republic
Keywords: nucleation, critical supersaturation
Presenting author email: kozisek@fzu.cz

Nuclei of a new phase are formed due to fluctuations. Small sub-critical nuclei have tendency to dissolve, but supercritical ones grow to microscopic sizes. The critical supersaturation is the threshold limit when no amount of new stable phase is detected. This quantity has important technological aspect. The critical supersaturation depends on the used detectable method, on the system under consideration, and on the volume of a parent phase (Kashchiev, 2011).

For the sake of simplicity we will consider homogeneous nucleation of vapor. (Nevertheless, our approach can be easily generalized to formation of crystallites from a liquid phase.) Katz (1970) introduced the critical supersaturation as the supersaturation at a rate of nucleation of one nucleus $\mathrm{cm}^{-3}\ \mathrm{s}^{-1}$. This is quite good approximation for nucleation of droplets from supersaturated vapor, but the use of this approximation to a liquid-solid phase transition is disputable. That is why we selected (Kožíšek *et al*, 2011) the critical supersaturation as the value at which one supercritical nucleus, formed by a certain number of molecules, is formed. The critical supersaturation was determined from $F_i = 1$, where F_i denotes the number of nuclei in unit volume formed by i molecules, and i was set to 1000. It is clear that the critical supersaturation depends on its definition (Kashchiev, 2000).

At supersaturation near its critical value a certain maximum nucleus size is reached and larger nuclei are not formed due to decreasing number density of nuclei as a function of size. The aim of this work is to determine how the maximum size of nuclei depends on the supersaturation.

We have numerically solved the kinetic equations describing homogeneous nucleation of ethanol droplets from supersaturated vapor – for details see Kožíšek and Demo (2009). In this work we have chosen the temperature T = 260 K. If we use the Katz definition $J^S = 1\ \mathrm{cm}^{-3}\mathrm{s}^{-1}$ (Katz, 1970), where J^S denotes the stationary nucleation rate, the critical supersaturation $S^* = 2.4249$, the critical size $i^* = 143$ and $F_{i^*} = 0.03$. The maximum size of formed nucleus is 80, *i.e.* $F_{80} = 1$ at the stationary state. No supercritical droplets are formed.

As the supersaturation increases, the maximum size of nuclei increases. We have determined the maximum radius of formed nucleus r_{max} (from the size distribution of nuclei F), for two cases: (i) one nucleus is formed within cubic meter (squares in Fig. 1) and (ii) cubic decimeter (circles in Fig. 1). Maximum radius of nucleus, r_{max}, increases with supersaturation, S, and at the same supersaturation r_{max} increases with the volume.

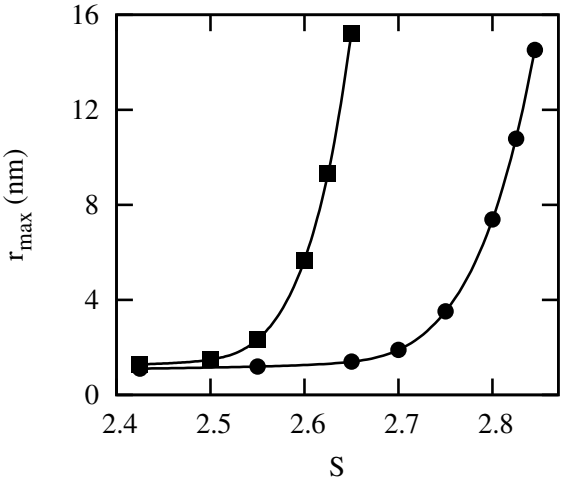

Figure 1: Maximum radius of nucleus, r_{max}, formed in cubic meter (squares) and cubic decimeter (circles) as a function of supersaturation S.

According to the Katz (1970) definition of critical supersaturation ($J^S = 1\ \mathrm{cm}^{-3}\,\mathrm{s}^{-1}$), S^* does not depend on the volume. On the other hand the highest supersaturation, at which the supersaturated vapor remains in metastable phase and no new phase evolves, depends on the volume of the system under consideration. As the supersaturation increases the growth of droplets up to microscopic sizes occurs after overcoming of some supersaturation level.

This work was supported by the Czech Science Foundation under Project no. P108/12/0891.

Kashchiev, D. (2011) *J. Chem. Phys.* **134**, 196102.
Katz, J. L. (1970) *J. Stat. Phys.* **2**, 137-146.
Kožíšek, Z., Sato K., Ueno S. and Demo, P. (2011) *J. Chem. Phys.* **134**, 094508.
Kashchiev, D. (2000) *Nucleation: Basic Theory With Applications*, Butterworth– Heinemann, Oxford.
Kožíšek, P. and Demo, P. (2009) *J. Aerosol. Sci.* **40**, 44-54 and 802-806.

Heterogeneous nucleation on partially wettable charged conducting seed particle

M. Noppel[1], H. Vehkamäki[2], P. M. Winkler[3], M. Kulmala[2], P. E. Wagner[3]

[1]Institute of Physics, University of Tartu, 18 Ülikooli St., 50090 Tartu, Estonia
[2]Department of Physical Sciences, University of Helsinki, P.O. Box 64, 00014 University of Helsinki, Finland
[3]Fakultät für Physik, Universität Wien, Boltzmanngasse 5, A-1090 Wien, Austria
Keywords: heterogeneous nucleation, charged seed particle, thermodynamics, consistent formalism.
Presenting author email: madis.noppel@ut.ee

The currently widely used model for ion-induced nucleation assumes complete spherical symmetry of the system, implying that the seed ion is immediately surrounded by the condensing liquid from all sides. This theory, although giving a rough picture of the observed behaviour, fails to fully reproduce experiments.

We apply a thermodynamically consistent formalism (Nishioka and Kusaka, 1992; Debenedetti and Reiss, 1998) to calculate the reversible work needed to form a dielectric liquid nucleus of a new phase on a charged insoluble conducting sphere within a uniform macroscopic one- or multicomponent mother phase. Compared with widely used ion-induced nucleation theory we take a step further and treat more realistic geometries, where a cap-shaped liquid cluster forms on the surface of the seed particle. The spherical symmetry is lost. We consider the formation energy of an embryo constrained to have fixed volume and shape. The bulk and surface phases of constrained embryo and its environment are in thermodynamic equilibrium, but not necessarily with each other. Electrostatic energy of the system is found as an energy that is required to carry electric charge from infinity to a seed particle or, alternatively, the energy of electrostatic field generated by this charging process. At charging the seed is either bare or has a constrained embryo on it. We limit ourselves to a linear relationship between dielectric displacement and electric field strength.

In nucleation theory a real system is replaced with a hypothetical system where bulk properties differently from the real system preserve their values up to dividing surfaces between bulk phases. Usually certain location of diving surfaces (e.g. surfaces of tension) and values of coefficients like the coefficients of surface and line tensions are chosen so that free energies of hypothetical and real systems coincide. In the neutral case differences in energy densities of systems occur only in transition zones. We assume that the location of dividing surfaces assures also that the difference in total electrostatic energies evoked by differences in dielectric properties of real and hypothetical systems can be ignored. Unlike neutral system, in the charged systems the difference in electrostatic energy densities manifest itself over the entire extent of systems. This makes the introduction of excess quantities more complicated. We show that the assumption concerning the coincidence of electrostatic energies is valid with a relative uncertainty of the order of the ratio of the width of transition zone between bulk phases to the size of an embryo. We take into account also the possibility that the molecules in the surface layers can be spontaneously permanently polarized, and introduce the surface and line excess polarizations. The surface excess polarization is the electrical potential difference of a hypothetical system through the double layer charge distribution at the dividing surface. The line excess polarization describes the effect of seed particle charge and the polarization of triple line zone on the line tension. This excess quantity is proportional to the charge of the seed and it is additional to the line tension of uncharged system.

The expression of the formation energy of a constrained embryo is varied and the extremity condition for a critical embryo found. The equalities of chemical potentials of each species between the nucleus and the vapour represent the conditions of chemical equilibrium. The generalized Young equation that relates contact angle with surface tensions, surface excess polarizations and line tension containing also the electrical contribution from triple line excess polarization expresses the condition of mechanical equilibrium at three-phase contact line. The generalized Laplace equation gives the condition of mechanical equilibrium at vapour-liquid interface: it relates generalized pressures in neighbouring bulk phases at an interface with surface tension, excess surface polarization and dielectric displacements in neighbouring phases with two principal radii of surface curvature and curvatures of equipotential surfaces in neighbouring phases at that point. We re-express also the generalized Laplace equation as a partial differential equation, which, along with electrostatic Laplace equations for bulk phases, determines the shape of a nucleus. Finally, we derive expressions that are suitable for calculations of the size and composition of a critical nucleus (generalized version of the classical Kelvin-Thomson equation).

This work was supported by the Estonian Science Foundation (Grant 8806), the Estonian Research Council Targeted Financing Project (SF0180043s08) and Academy of Finland (Project number 1127372, Center of Excellence program project number 1118615, LASTU program project number 135054), ERC Starting grant 257360-MOCAPAF

Nishioka, K. and Kusaka, I. (1992) *J. Chem. Phys*. **96**, 5370-5376.
Debenedetti, P. G. and Reiss, H. (1998) *J. Chem. Phys*. **108**, 5498- 5505.

The Role of Highly Oxidized Organics in New Particle Formation

I.K. Ortega and H. Vehkamäki

Department of Physics, University of Helsinki, Post Office Box 64, FI-00014, Helsinki, Finland.
Keywords: Highly oxidized organics, cluster formation, quantum chemistry, sulfuric acid.
Presenting author email: ismael.ortegacolomer@helsinki.fi

Atmospheric new particle is an important source of aerosols and cloud condensation nuclei (Merikanto et al. 2009). Is known that sulfuric acid plays a key role in this phenomenon (Sipila et al 2010). On the other hand, typical atmospheric concentrations of sulfuric acid and water can not explain the observed new particle formation rates, thus some additional compound/s able to enhance the formation of particles are needed.

Organic acids produced by oxidation of volatile organic compounds (VOCs) have been proposed as key compounds in new-particle formation as well. However, there is no consensus about the participation of these compounds in new-particle formation; some studies conclude that these oxidized VOC are just involved in particle growth (Laaksonen et al. 2008), while other studies state that they are involved in the very first steps of new-particle formation but not in growth (Zhang et al. 2009).

In the present work we have used quantum chemical methods (Ortega et al 2012) to calculate the formation free energies of clusters formed by sulfuric acid and different organic acids (OxdOrg). We used ACDC (McGrath et al. 2012) model to estimate the effect of organic acids in new particle formation. We have chosen three oxidation products of alpha-pinene with increasing O:C ratio, namely Pinonic acid (PA), 7-Hydroxy-pinonic acid (HPA) and 3-Metyl-1,2,3-butane-tricarboxilyc acid (MBTA).

Results

Figure 1 shows the dependence of simulated formation rates with sulfuric acid concentration for the three different organic acids considered in this study. The simulations include only neutral clusters. We simulated the formation rates at 278K, and assuming a concentration of 1pptv for the OxdOrg.

Formation rates obtained using PA or HPA are 10 – 12 orders of magnitude smaller than the ones observed in Hyytiälä. On the other hand, the same amount of MBTA produced formation rates close to the observed ones. These preliminary results indicate that highly oxidized organic compounds may play a key role in atmospheric new particle formation.

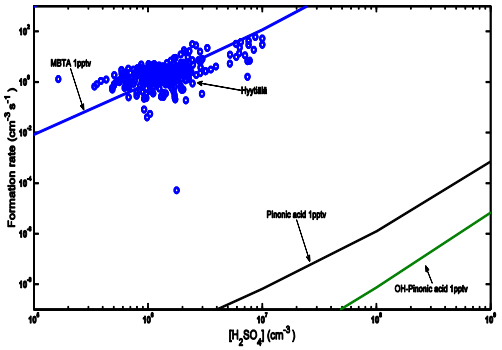

Figure 1. Formation rate versus sulfuric acid concentration. ACDC simulations correspond to 1 pptv of organic acid at 278K and includes only neutral clusters. Blue circles correspond to data measured in Hyytiälä field station, blue line correspond MBTA simulations, black line correspond to PA simulations and Green line correspond to HPA simulations.

We acknowledge the Academy of Finland (CoE Project No. 1118615, LASTU Project No. 135054), the Nessling Foundation, ERC Project Nos. 257360-MOCAPAF and 27463-ATMNUCLE for funding. We thank the CSC Centre for Scientific Computing in Espoo, Finland for computer time, and the CLOUD team for helpful discussions.

Merikanto, J., Spracklen, D.V., Mann, G.W., Pickering S.J., Carslaw, K.S. (2009) *Atmos.Chem.Phys.* **9**, 8601-8616.

Sipilä, M., et al. (2010) *Science*, **327,** 1243-1246.

Laaksonen, A., et al. (2008) *Atmos. Chem. Phys.* **8**, 2657 - 2665.

Zhang, R., et al. (2009) *Proc. Natl. Acad. Sci.* **106**, 17650- 17654.

Ortega, I.K. et al. (2012) *Atmos. Chem. Phys.* **12**, 225-235.

McGrath M.L. et al. (2012) *Atmos. Chem. Phys.* **12**, 2345-2355.

Linking Neutral and Charged Sulfuric Acid - Ammonia and Sulfuric Acid - Dimethylamine Clusters

I. K. Ortega[1], O. Kupiainen[1], T. Olenius[1], V. Loukonen[1], T. Kurtén[2] and H. Vehkamäki[1]

[1]Department of Physics, University of Helsinki, Post Office Box 64, FI-00014, Helsinki, Finland.
[2]Department of Chemistry, University of Helsinki, Post Office Box 55, FI-00014, Helsinki, Finland.

Keywords: Amines, Ionic clusters, cluster formation, quantum chemistry.
Presenting author email: ismael.ortegacolomer@helsinki.fi

New-particle formation is an important source of aerosols and cloud condensation nuclei in the atmosphere (Merikanto et al. 2009). But, despite its importance, the process is still poorly understood. The main problem about understanding new-particle formation is the size of the nucleating clusters. They are formed by only few molecules, and they have diameters close to 1 nm. Therefore they are well below present detection limits if they are electrically neutral. Very recent developments in cutting-edge high-resolution mass spectroscopy (APi-TOF instrument) are starting to permit the unambiguous chemical characterization of charged atmospheric clusters from molecular scale upward (Junninen et al. 2010). However, these experiments alone yield no information on the neutral clusters. A charger can be included before the mass spectrometer (e.g. CI-APi-TOF), but depending on the charging mechanism used in the instruments, some cluster types may not be charged, others may be broken up and others may be chemically completely altered by the process.

We have used quantum chemical calculations (Ortega et al. 2012) to calculate the evaporation rates of charged sulfuric acid-ammonia and sulfuric acid–DMA clusters. Figures 1 and 2 compare the evaporation rates of neutral clusters (Ortega et al. 2012) with the evaporation rates of the corresponding charged clusters and the evaporation rates of the most stable charged clusters.

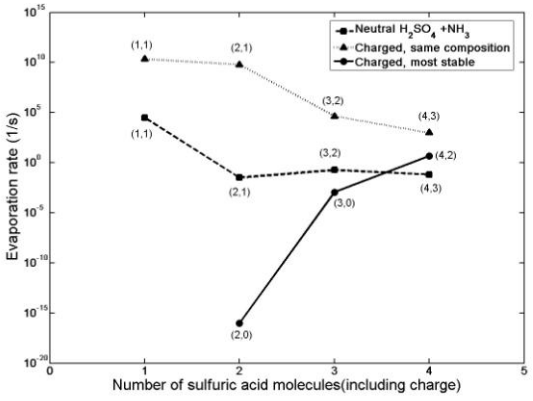

Figure 1. Evaporation rates of ammonia containing clusters.

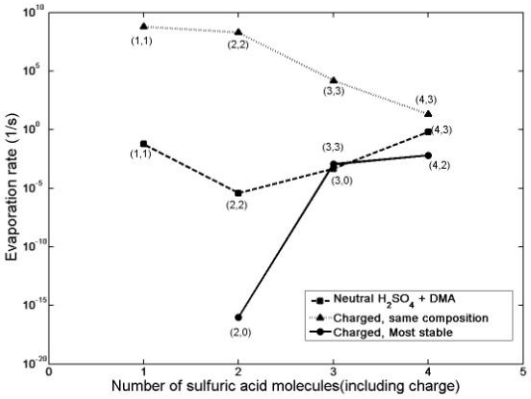

Figure 2. Evaporation rates of DMA containing clusters.

We found that ammonia and DMA molecules will evaporate from small negatively charged sulfuric acid clusters. Ammonia will evaporate from clusters with three or less sulfuric acid molecules and DMAwill evaporate from clusters with two or less sulfuric acid molecules. This shows how, although small neutral clusters containing base molecules are stable, they will lose the base molecules when charged and be detected as charged pure sulfuric acid clusters. These results can explain why small charged ammonia clusters were not observed by APi-TOF during the CLOUD experiment (Kirkby et al. 2011).

We acknowledge the Academy of Finland (CoE Project No. 1118615, LASTU Project No. 135054), the Nessling Foundation, the Väisälä Foundation and ERC Project Nos. 257360- MOCAPAF and 27463-ATMNUCLE for funding. We thank the CSC Centre for Scientific Computing in Espoo, Finland for computer time, and the CLOUD team for helpful discussions.

Merikanto, J., et al. (2009) *Atmos.Chem.Phys.* **9**, 8601-8616.
Junninen, H., et al., (2010) *Atmos. Meas. Tech.* **3,** 1039 - 1053.
Ortega, I.K., et al. (2012) *Atmos. Chem. Phys*. **12**, 225-235.
Kirkby, J., et al. (2011), *Nature.* **476,** 429 – 433.

Determination of Nanoparticles Surface Tension from Experimental Data on Homogeneous Nucleation of Ibuprofen Vapors

A.V. Samodurov[1,2], A.M. Baklanov[2], S.V. Vosel[1,2]

[1]Novosibirsk State University, Novosibirsk, 630090, Russia
[2]Laboratory of Nanoparticles, Institute of Chemical Kinetics and Combustion SB RAS, Novosibirsk, 630090, Russia
Keywords: nanoparticles, homogenous nucleation, ibuprofen.
Presenting author email: samodurovav@gmail.com

Introduction

Past years of investigations have shown that properties of nanoscaled matter can dramatically differ from that of a bulk matter. The thermodynamic properties of interphase boundary layer can be fully characterised by the state function called surface tension, σ. In Gibbs rigorous theory surface tension is the function of curvature radius. Therefore, the information of surface tension dependence on nanoparticle radius R is very important when investigating colloid systems (i.e. processes of formation, aging, stability). Unfortunately, it is not easy to measure nanoparticle surface tension in direct experiments. However, it is possible to estimate surface tension of nanoparticles by the means of i.e. MD simulations, but only for simple systems (for example, LJ fluids). On the other hand the homogeneous nucleation rate is a function of surface tension. Therefore experimentally determined homogeneous nucleation parameters (nucleation rate, temperature, supersaturation ratio) can be used for $\sigma(R)$ dependence evaluation. Recently a new rigorous formula for homogeneous nucleation rate has appeared (Vosel *et al*, 2009). This formula takes into account not only the dependence σ on nanoparticle radius but also translation-rotation movement of a critical nucleus.

The goal of this work was to determine homogeneous nucleation parameters for ibuprofen (popular NSAID), and to determine critical nuclei surface tension.

Methods

In our experiments we utilized laminar flow horizontal nucleation chamber. It consisted of a quartz tube with an external cylindrical heater. An inert carrier gas (argon, 99.999% purity) entered the chamber and passed through heated zone of the tube. A crucible with a ibuprofen racemate (Aldrich) was located in the maximum inner temperature zone of the heated area. During typical experiment the substance evaporated from the crucible. A gas flow containing ibuprofen unsaturated vapors entered a cool zone of the chamber. As gas cooled vapors became saturated first, then supersaturation ratio increased and homogeneous nucleation occurred in some area of the chamber. New formed critical nuclei grew fast due to vapor condensation on them.

The number concentration and average diameter of aerosol particles at the exit of the chamber were measured by automatic diffusion battery (ADB). In order to obtain the approximate location of nucleation zone a new "supersaturation cut-off" technique was used. 3D supersaturation and temperature profiles inside the chamber were obtained through experiments as well as computer simulations. Experimental data was used to calculate homogeneous nucleation rate. Then using the rigorous formula (Vosel *et al,* 2009) surface of tension of critical nuclei was obtained as well as their radius R.

Results

It was found that the surface tension of 1.6 nm radius ibuprofen critical nuclei is about 1.06 times larger than surface tension of bulk ibuprofen ($24.38 \cdot 10^{-3}$ N/m at the temperature of nucleation). This results correspond to temperature of nucleation equals to 318K, supersaturation ratio 11 and homogeneous nucleation rate 10^7 $cm^{-3}s^{-1}$. Critical nucleus of 1.6 nm radius contains approximately 36 ibuprofen molecules.

Financial support for this work was provided by Russian Federation for Basic Research (RFBR) Project No. 11-08-01204-a, and joint research project between SB RAS and NSC Taiwan 2011–2013.

Vosel S.V., Onischuk A.A., Purtov P.A. (2009) *J. Chem. Phys.* **131**, 204508-1.

Systematic correlation between aerodynamic shape factor and optical properties

S. Pfeifer[1], T. Mueller[1] and A. Wiedensohler[1]

[1]Leibniz Institute for Tropospheric Research, Leipzig, 04318, Germany
Keywords: non-sphericity, aerodynamic shape factor, optical properties.
Presenting author email: pfeifer@tropos.de

There are many scientific researches of the influence of non-spherical aerosol particles to optical properties and fluid dynamics. Either for the optics or the fluid dynamics exist semi-theoretical approaches up to complex numerical simulations.

To obtain an physically consistent, plausible approach, we have to consider the morphology entirely, e.g. an optical closure with an particle number size distribution measured with an aerodynamic based instrument. When an aerodynamic shape factor is used to correct the size distribution, using Mie theory to calculate optical properties of this particle population must be critically questioned.

Because simulations of optical properties for arbitrary shaped particles (especially discrete dipole approximation) need a lot of numerical power, we have to find an useful but simple optical shape factor. Simultaneously, to further simplify the fact of particle morphology, we have to analyse the correlation between this optical shape factor and the aerodynamic shape factor. This would lead to a simple but useful approach to consider the manifold influence of the particle morphology.

Numerical simulations

In a first step, numerical simulations were accomplished for a moderate number of particle shapes, from simple ellipsoids, cylinders, cuboids (prolate and oblate) up to realistic looking arbitrary shaped particles.

To calculate the aerodynamic shape factor, we used a modified version of “stkSolver” (Fernandez, 2006). The results of some characteristic shapes, such as a cube or cylinders, are in a good agreement with values from literature.

Depending on the particle shape the optical properties were calculated using T-Matrix method (MIESCHKA, Rother, 2009) or DDA (ADDA, Yurkin & Hoekstra, 2011). The maximum simulated size parameter was 30, which is a moderate value to investigate the influence of particles morphology to coarse mode particles (lowest super micron range).

Results

With a focus on the systematic deviations for dust events, the primary aim is to investigate the influence of particle shape to the scattering coefficients. For all particle shapes, the scattering coefficients were calculated using fictive log normal distributed particle populations with a mean size parameter from 0.3 to 10.

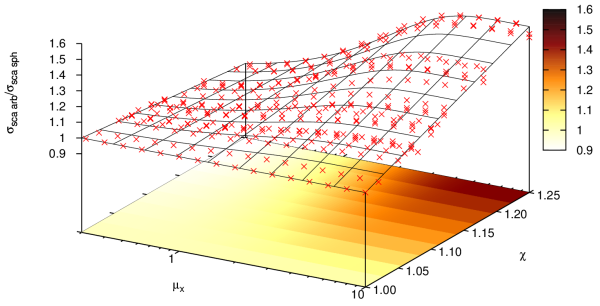

Figure 1. 2D scattering plot of the signal increase for the scattering coefficient of the arbitrary shaped particle to the volume equivalent sphere as a function of the mean size parameter μ_x and the aerodynamic shape factor χ.

The numerical results show a good correlation of the aerodynamic shape factor and the increase of the scattering coefficients relative to the volume equivalent sphere for all particle shapes and mean size parameters larger than approx. 3. Smaller particles act like the volume equivalent sphere, independently of their morphology.

This surprising result is based on the fact that larger particles scale with their geometrical cross section in contrast to smaller particles, which scale with the volume (Pollack & Cuzzi, 1979). In general, for non spherical particles the ratio of orientation averaged cross section equivalent diameter to the volume equivalent diameter increases. The aerodynamic shape factor itself can also be approximated using inter alia these both diameters (Leith, 1997), which leads to this positive correlation. As a consequence, the aerodynamic shape factor seems to be already sufficient to estimate the signal increase of the scattering coefficient for non spherical particle.

Fernandez, C. R. (2006), stkSolver v1.0, *http://software.ihpc.a-star.edu.sg/projects/stkSolver/stkSolver.php.*

Rother, T. (2009), Electromagnetic Wave Scattering on Nonspherical Particles: Basic Methodology and Simulations. *Springer Berlin Heidelberg, 1st edition.*

Yurkin, M. A. and Hoekstra (2011), A. G., *Journal of Quantitative Spectroscopy and Radiative Transfer, 112(13):2234–2247.*

Pollack, J. B. and Cuzzi, J. N. (1997), *Journal of Atmospheric Science 37:868-881.*

Leith, D. (1997) Drag on Nonspherical Objects, *Aerosol Science and Technology, 6:153-161.*

Experiments on neutral cluster generation and detection below 2 nm size

J. Kangasluoma[1], H. Junninen[1], M. Sipilä[1], M. Kulmala[1], and T. Petäjä[1]

[1] Faculty of Physics, Department of Atmospheric Sciences, University of Helsinki, P.O. Box 64, 00014, Finland
Keywords: cluster, aerosol generation, CPC.
Presenting author email: juha.kangasluoma@helsinki.fi

The research of atmospheric nucleation has gone down to sizes of individual molecules and molecular clusters which have led to development of new instruments capable of detecting single molecules and clusters down to 1 nm. Airmodus particle size magnifier (PSM, Vanhanen et al 2011) has been successfully applied to chamber and ambient measurements (Kulmala et al. 2013, Kirkby et al. 2011), however, to convert the signal of the instrument to absolute cluster and particle concentrations remains extremely difficult due to the varying response of the PSM to ions of different chemical composition and sample carrier gas conditions as we have shown in our previous study (Kangasluoma et al. 2013). In addition to this, one not answered and studied question due to its difficulty is: what is the PSM response to neutral clusters in the sub 2 nm sizes?

To study this problem we utilized the aerosol generation method used in Kangasluoma et al. (2013). Briefly, ammonium sulphate is evaporated to grade 5.0 cryo nitrogen, cooled down to prevent growth, charged with a ^{241}Am source and finally the sample is size classified with Herrmann type high resolution differential mobility analyzer (Herrmann et al. 2000). After size classification, we neutralized the negatively charged aerosol by transporting positive charger ions to the sample flow with an electric field against a flow of nitrogen. Measuring the sample then by mass spectrometer or another DMA, a quite constant neutralization efficiency of about 18 % was observed. The fact that ion-ion collisions occurred was expected, but the question, what the neutralized sample was remains open.

To get the first hints what happened in the collision, we used the PSM as detector with varying detection efficiency. In contrary to normal PSM operation mode we altered the saturator temperature instead of the saturator flow to keep the flow dynamics constant. Electrometer was also used in parallel with the PSM to monitor that the total concentration stayed constant, and we tested that the PSM did not detect the ions pushed to the sample flow even with the highest detection efficiency.

The results are presented in figure 1. Blue dots represent the detection efficiency of the "normal" negative ammonium sulphate with diameter of 1.7 nm and the data is normalized to reach unity as the detection did not increase in the highest saturator temperatures. The rest of the data is scaled with the same factor. When the neutralizer is switched on, the PSM detects negative clusters plus the neutral clusters (Ne+N). This is shown by red dots. It is immediately seen that with lower detection efficiency the PSM detects less Ne+N than completely charged sample. When the temperature is increased, the PSM detects the opposite: more Ne+N than completely charged. With charger on and ion filter at the PSM inlet we measured only the completely neutral sample which is given by black dots. This was to verify that we actually generate neutral clusters. By assuming that 18 % of the charged aerosol is neutralized (multiplying electrometer concentration by 0.18 and comparing that to neutral concentration), we get the green dots which show that when the PSM detection efficiency is increased enough, all neutralized sample is detected as double counts. In other experiments we found that by still further increasing the detection efficiency, neutralized clusters might be detected as triple counts. So far we are not able to explain the results in any other way than that the ion-ion collision breaks the charged ammonium sulphate cluster apart and both, or all, resulting neutral clusters are observed when PSM detection efficiency is increased. As we have no method to characterize the neutral clusters, we cannot conclude anything about the detection efficiency of the neutrals compared to the charged clusters. This study however shows that ion-ion collision might lead to something else than recombination and is under further study. Ultimately the objective of these studies is to give complete detection efficiency curve for neutral cluster detection of the PSM.

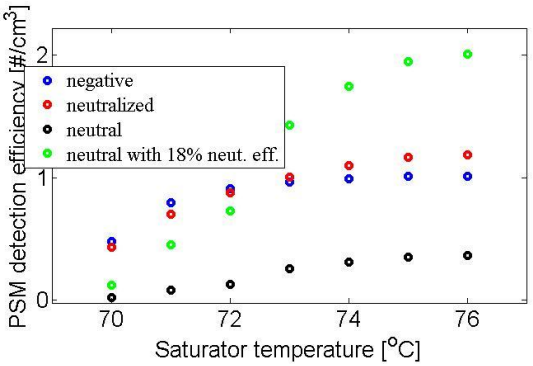

Figure 1. Scaled PSM detection efficiencies as a function of saturator temperature for negative 1.7 nm ammonium sulphate. Explanation of the data is given in the text.

Herrmann, et al. (2000). *Abstract AAAR Conference*, 15B5.

Kangasluoma et al., (2013). Aerosol Sci. Technol. in press

Kirkby, J. *et al.* (2011) *Nature* **476**, 429-433.

Kulmala, M. *et al* (2013). *Science*, **22**, 911-912.

Vanhanen, J. *et al.* (2011) *Aerosol Sci.Tech.* **4**, 533-542.

A method to determine the size distribution of recombination products from atmospheric measurements

Jenni Kontkanen[1], Tuomo Nieminen[1,2], Hanna E. Manninen[1], Katrianne Lehtipalo[1,3], Veli-Matti Kerminen[1], Kari E. J. Lehtinen[4], and Markku Kulmala[1]

[1]Department of Physics, University of Helsinki, Finland
[2]Helsinki Institute of Physics, Helsinki, Finland
[3]Airmodus Oy, Helsinki, Finland
[4]Department of Applied Physics, University of Eastern Finland, and Finnish Meteorological Institute, Kuopio, Finland
Keywords: ion-ion recombination, clusters, ions, new particle formation
Presenting author email: veli-matti.kerminen@helsinki.fi

Ion-ion recombination is a process where a neutral cluster is formed in a collision between two oppositely charged clusters. Based on atmospheric measurements, recombination has been estimated to have only a minor role in new particle formation in boreal forest (Kulmala *et al*., 2007; 2013). However, some model studies propose that recombination could be more important than indicated by the measurements (Yu and Turco 2008). In this work we present the method developed by Kontkanen *et al*. (2013) to determine the size distribution of recombination products from atmospheric measurements. We also apply the method to data measured in Hyytiälä, Finland.

The concentration of recombination products N_{rec} in a size range *i* can be estimated from the equation:

$$\frac{dN_{rec,i}}{dt} = \lambda_i \alpha \sum_{j,k} r_{jk} N_j^+ N_k^- - CoagS_i N_{rec,i} . \qquad (1)$$

Here λ_i denotes the fraction of stable recombination products and α is the ion-ion recombination coefficient. N_j^+ and N_k^- refer to the concentrations of positive and negative ions in the size ranges *j* and *k*, and r_{jk} tells which fraction of the recombination products formed in their collisions end up in the size class *i.* $CoagS_i$ denotes the coagulation sink. Hence, Eq. (1) includes the terms representing the production of neutral clusters in collisions between two oppositely charged ions and the loss of them due to coagulation. The sources and sinks of neutral clusters due to charging, condensational growth and break-ups of larger clusters are neglected. In steady state Eq. (1) can be written as

$$N_{rec,i} = \frac{\lambda_i \alpha \sum_{j,k} r_{jk} N_j^+ N_k^-}{CoagS_i} . \qquad (2)$$

The production rate of recombination products to a size range *i* can be obtained from ion mobility distributions measured with the NAIS (Neutral cluster and Air Ion Spectrometer; Manninen *et al*. 2009). First, we may convert the mobility ranges of NAIS channels to mass ranges. Thereafter, we can calculate the masses of recombination products formed in collisions between ions from different channels. Finally, we may convert the masses of recombination products to mobility diameters and thus determine the production rate of recombination products to the examined size range *i*.

In earlier studies the fraction of stable recombination products, λ_i, has been assumed to equal unity. However, we can estimate the maximum value for the coefficient, $\lambda_{max,i}$, from measurements. This can be done by stating that the concentration of recombination products in a size range *i* cannot exceed the concentration of all neutral clusters, which can be obtained by subtracting ion concentration from the total concentration.

To asses the role of recombination in the dynamics of sub-2nm clusters, we applied our method to data measured in Hyytiälä, Finland, during spring 2011. The total cluster concentration in six sub-2nm size classes was measured with the PSM (Particle Size Magnifier; Vanhanen et al., 2011) and ion concentration in the same size classes was measured with the NAIS.

The production rate and the concentration of recombination products were calculated for six sub-2nm size classes (0.9–1.1 nm, 1.1–1.3 nm, 1.3–1.5 nm, 1.5–1.7 nm, 1.7–1.9 nm, and 1.9–2.1 nm). The median production rates of recombination products were observed to vary between 2×10^{-3} cm^{-3} s^{-1} and 8×10^{-2} cm^{-3}s^{-1} in these size classes. The median concentrations of recombination products varied between 2 cm^{-3} and 33 cm^{-3}. Both the production rate and the concentration of recombination products were lowest in the smallest (0.9–1.1 nm) and the largest (1.9–2.1 nm) size classes, and highest in the size classes between them.

The fraction of recombination products of all neutral clusters was also examined. The fraction was lowest in the smallest size class, in which the median fraction was 7×10^{-4}. In other size classes the median fraction was between 0.04 and 0.11. Thus, it seems that on average only a small proportion of all neutral clusters in Hyytiälä are formed in ion-ion recombination. This result is in agreement with the findings of earlier studies estimating the concentration of recombination products from atmospheric measurements.

This work was supported by Finnish Centre of Excellence (FCoE), Cryosphere-Atmosphere Interactions in a Changing Arctic Climate (CRAICC), and European Research Council (ERC).

Kontkanen J. *et al*. (2013) in preparation.
Kulmala M. *et al*. (2007) *Science* **318**, 89–92.
Kulmala M. *et al*. (2013) *Science* **339**, 943–946.
Manninen H. E. *et al*. (2009) *Boreal Environ. Res*. **14**, 591–605.
Vanhanen J. *et al*. (2011) *Aerosol Sci. Tech.* **45**, 533–542.
Yu F. and Turco R. (2008) *Atmos. Chem. Phys*. **8**, 6085–6102

Generation of sub-Nanometer Atomic Clusters in the Aerosol Phase using Spark Discharge Generation (SDG)

A. Maisser[1], K. Barmpounis[1], M.B. Attoui[2], G. Biskos[1] and A. Schmidt-Ott[1]

[1] Chemical Engineering, Delft University of Technology, Delft, 2628 BL, Netherlands
[2]University Paris Est Creteil, University Paris-Diderot, LISA, UMR CNRS, Paris, France

Keywords: atomic clusters, sub-nanometer, spark discharge, high resolution differential mobility analysis.
Presenting author email: a.maisser@tudelft.nl

Spark discharge generation (SDG) is a method to generate highly-pure singly-charged metallic particles of various sizes. Recent studies have shown that this method is also capable of producing atomic clusters, consisting of less than 5 atoms per cluster. The production rates of these small clusters are potentially sufficiently high to enable applications for e.g. catalysis or synthesis of materials with tailored properties. Since their properties depend on the number of atoms, controlling the cluster size can influence the electronic, optical, structural and chemical characteristics of a cluster.

A custom-made SDG operated at low spark energies with a high dilution flow, in order to quench the formation of bigger particles, was employed to generate the atomic clusters. The electrical mobility was measured usinga high-flow/high-resolution differential mobility analyser (Attoui *et al*., 2012, half mini DMA, NanoEngineering corp., FL, USA). To increase the measuring precision and to keep the purity of the aerosol constant along the whole setup the sheath flow in the DMA was recirculating. Three gases (nitrogen, helium and argon) of different purity have been used, in order to investigate the effect of trace oxygen molecules to the atomic cluster production process.

The DMA was first calibrated using electrical mobility standards of bromide ions.

As shown in Fig. 1 the inverse mobility distributions show several distinct peaks for positive as well as for negative clusters. Each peak corresponds to clusters consisting of different number of single silver atoms. The corresponding number of atoms of positive atomic clusters has been identified by comparing the measured electrical mobility with experimental values of silver clusters collision cross-sections reported by Weis *et al*. (2002). The collision cross section scales linearly with the inverse electrical mobility.

The agreement between the mobilities measured in our study and those reported in literature,is within the experimental uncertainty as shown in Fig. 2.The peaks in the spectra shown in Fig.1 correspond to atomic clusters with n=1,2,3, and 5 number of atoms.

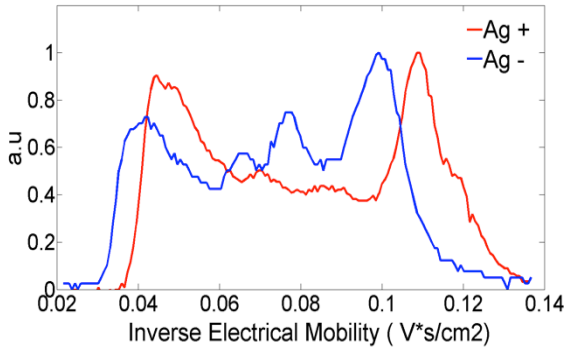

Figure 1. Inverse mobility distribution of positive and negative atomic clusters produced in He gas.

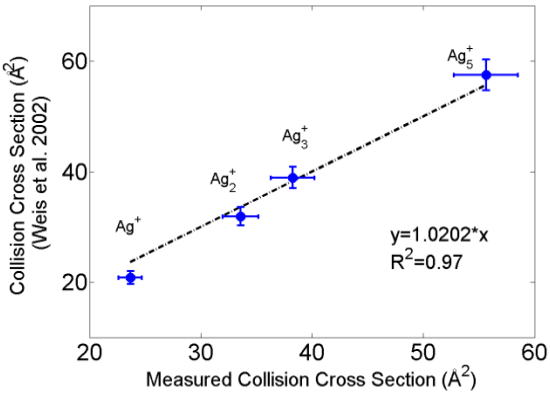

Figure 2. Comparison of the collision cross sections of Ag atomic clusters measurementsin this study and by Weis *et al.* 2002.

Attoui, M., Paragano, J. Cuevas, Fernandez de la Mora, J. (2013) *Aerosol Science and Technology*, DOI:10.1080/02786826.2013.764966

Weis, P, Bierweiler, T, Gilb, S, Kappes, M.M. (2002)*Phys. Rev. Lett.* **355**, 355-364.

Calculation of dynamic properties of fractal aggregates in the transition regime.

A.D. Melas[1 2], A.G. Konstandopoulos[1 3], L. Isella[4] and Y. Drossinos[2]
[1]Department of Chemical Engineering, Aristotle University, 50006 Thessaloniki, Greece
[2]European Commission, Joint Research Centre, 21027 Ispra (VA), Italy
[3]Aerosol & Particle Technology Laboratory, CERTH/CPERI, P.O. Box 60361, 57001 Thessaloniki, Greece
[4]European Commission, DG Energy, L-2530, Luxemburg
Keywords: collision rate, friction coefficient, mobility radius.
Presenting author email: Anastasios.Melas@jrc.ec.europa.eu

The dynamic properties of spherical particles depend on the relation between their primary particles size (R_1) and the gas mean free path (λ). In the transition regime, when R_1 is comparable to the gas mean free path λ, the friction coefficient can be calculated from the creeping-flow Stokes expression divided with a correction factor called Cunningham factor ($C(Kn)$).

$$f_N = \frac{6\pi\mu R_h(0)}{C(Kn)} = 6\pi\mu R_h(Kn). \qquad (1)$$

where μ is the dynamic fluid viscosity, R_h the hydrodynamic radius, and Kn the Knudsen number ($Kn = \lambda/R_1$). The calculation of $C(Kn)$ can be done by the following empirical expression $C(Kn) = 1 + AKn$, where $A = \alpha + \beta exp(-\gamma/Kn)$. The values of α, β, γ depend on the fraction of molecules diffusely reflected and the size of the monomers used to fit experimental data. While for a monomer the calculation of the Cunningham factor is trivial, for more complicated structures few results are reported in the literature. The reason is that in general the Knudsen number maybe defined in term of characteristic length scale L; for a monomer $L = R_1$, while for a more complex structure it is difficult to specify it. Dahneke (1982) suggested the use of an adjusted sphere radius which has the same $C(Kn)$ as the non-spherical structure would have had. He provides values of Kn_a for straight chains with the fraction of molecules diffusely reflected 0.93. The calculation of Kn_a is very important as it allows the calculation of many parameters in the transition regime like the mobility radius (R_m), the dynamic shape factor (χ_N) and the effective density (ρ_{eff}).

Isella and Drossinos (2010) introduced an approximate method for friction coefficient calculations in the continuum regime, where it is related to the ratio of molecular collision rates of a N-particle structure (K_N) to a monomer's. In the continuum regime by solving a diffusion equation with the appropriate boundary conditions (Dirichlet boundary conditions) we can calculate the R_h and the f_N. We extend this method in the transition regime by solving the steady-state molecular diffusion equation with a Robin boundary condition. Far away from the aggregate we have $\rho = 1$ while on the aggregate surface $\rho(R_1) = \alpha(Kn)(\mathrm{d}\rho/\mathrm{d}r) \mid R_1$. Our basic claim is that

$$C_1(Kn_a) = C_N(Kn) = \frac{f_N(0)}{f_N(Kn)} = \frac{K_N(0)}{K_N(Kn)}. \qquad (2)$$

The factor α defines a virtual boundary inside a monomer in the transition regime where the collision rate equals the one in the continuum regime. Hence, from the analytical solution of the diffusion equation, we obtain $\alpha(Kn)/R_1 = C(Kn) - 1$. From the above $\alpha(Kn)$ depends only on the flow regime and the fraction of gas molecules diffusely reflected.

An alternative method that we used for the Kn_a calculation is the interpolation between the two limiting cases, the continuum regime ($Kn = 0$) and the free molecular regime ($Kn = \infty$). The calculation of Kn_a is done by (Zhang et al. 2012),

$$Kn_a = \frac{\lambda\pi R_m(0)}{PA} \qquad (3)$$

where PA is the projected area of an aggregate. In the free molecular regime it equals the mobility radius squared times π.

We use both methods for the friction calculations in the transition regime. We validate the methods by calculating $C(Kn_a)$ of straight chains and by comparing them with the results of Dahneke. The good agreement suggests that both methods can be used for friction calculations of structures with $d_f \neq 1$ in the transition regime .

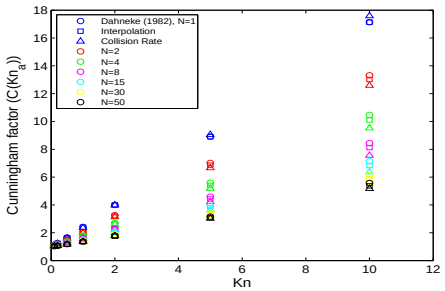

Figure 1: Comparison between $C(Kn_a)$ calculated by Dahneke and by our two different methods.

This work was supported by the European Commission Doctoral Fellowship (ADM).

B. Dahneke (1982), Aerosol Sci. Technol. **1**, 179.
L. Isella, Y. Drossinos (2011), J. Colloid Interface Sci. **356**, 505.
C. Zhang, T. Thajudeen, C. Larriba, T. E. Schwartzentruber, C. J. Hogan, Aerosol Sci. Technol. **46** (2012) 1065.

Analysis of the Current Models of Aerosol Dry Deposition

V.N.Piskunov

Russian Federal Nuclear Center – VNIIEF; Sarov, Nizhni Novgorod region, 607190, Russia

Keywords: aerosol, dry deposition, rough surfaces, theoretical models, comparison with experimental data

Presenting author email: piskunov@vniief.ru

Lately, the models of dry deposition of aerosols on rough surfaces have been developed intensively. The following three models will be considered.

Z-W model (Zhao and Wu, 2006) is based on a rigorous treatment of walk and directed motion of particles in the boundary layer. The lower boundary is defined by the empirical interpretation of the experiments.

S-P model (Piskunov, 2009) is based on the empirical generalization of experimental results? obtained Sehmel in 1973-1980 and review of (Slinn, 1978). The model agrees with analytical solutions for smooth surfaces.

H-S model (Hussein et al, 2012) integrates the results of (Zhao and Wu, 2006) and considers not only the roughness height K, but also the distance in between L. The corrections are referred to the weakly inhomogeneous ones with $K/L < 0.082$!! At $K/L > 0.082$ it agrees with Z-W model.

Further, the three models will be compared, the conclusion will be drawn concerning their completeness and the ways of dry deposition model development will be suggested.

1. The direct comparison of H-S and S-P under experimental conditions of Hussein et al (2009)

In figures: across – the particle diameters, vertically – the deposition velocities.

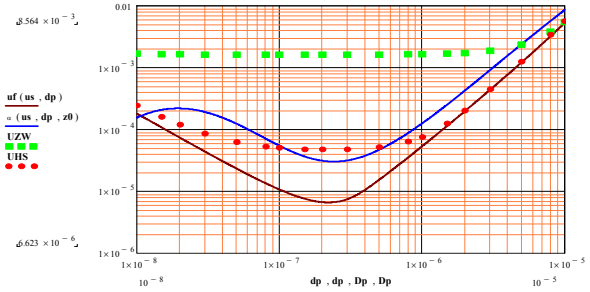

Figure 1 – Data for rough wall plaster (u^* = 0.1 m/s; K = 380-542 μm; K/L = 0.08169)

The difference between the blue curve (S-P model) and the red dots (H-S model) is less than two and ranges between the spread of the experimental data (they are not given here, since they are graphically given in Hussein et al (2009).

2. Data counting (Roupsard et al, 2013)

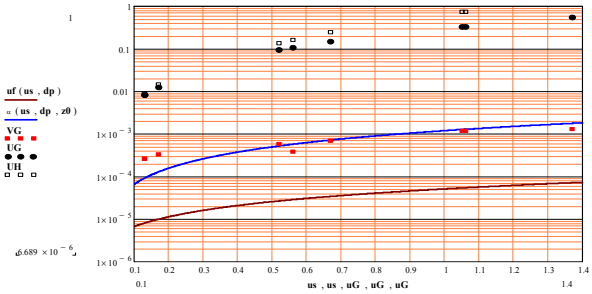

Figure 2 – Data for sinthetic grass ($0.1 \le u^* \le 1.5$ m/s; d_p = 0. 2 μm; K = 4 400 μm; $K/L \sim 1$)

The results speak for themselves.

3. Data counting (Slinn, 1978)

From the calculations it follows that for u^*>0.1m/s works well only model S-P. Apparently, H-S and Z-W models overestimate the deposition velocities due to the extremely large values of the form-factor $F = K - e$.

4. Discussion of results

It is obvious from the whole comparison of computations and three groups of experiments that the completely adequate model of dry deposition has not been developed at this time. S-P model is more general for all the environmental conditions, though its empirical character is more adapted to the atmospheric problems and surfaces of high roughness. H-S and Z-W are more adapted to the flows in ventilation pipes with low roughness and friction velocities. H-S model extends Z-W model for inhomogeneous surfaces with $K/L <$ 0.082, and agrees with Z-W model for the ordinary surfaces. On the strength of all the evidence author would prefer S-P model.

Conclusions

1. Currently, the problem of theoretical prediction of aerosol deposition velocities on a rough surface can hardly be solved.

2. The statement of (Hussein et al, 2012), that S-P model overestimates the experimental data is not true. For weakly inhomogeneous surfaces, both models are equivalent. For ordinary surfaces with $K/L \sim 1$ S-P works much better.

3. At this stage author suggest using the semi-empirical S-P model for practical purposes in various cases.

4. For rigorous approaches author suggest analysis and application of the results of Macdonald (2000) for the form-factor F evaluation.

5. Apparently, the integration of theoreticians and experimentalists efforts is more effective to make a coordinated plan of experimental works.

References

Hussein, T., Kubincova, L., Dohanyosova, P., Hruska, A., Dzumbova, L., Hemerka, J., et al. (2009) *Build. Environ.*, **44**,:2056–2063.

Hussein, T., Smolik, J, Kerminen, V., and Kulmala, M. (2012) *Aerosol Science and Technology* **46**, 44–59.

Macdonald, R.W. (2000) *Boundary-Layer Meteorology* **97**, 25–45.

Piskunov, V. (2009) *Aerosol Science* **40**, 664—679.

Roupsard, P., Amielh, M., Maro, D., Coppalle, A., Branger, H., Connan, O., Laguionie, P., He´bert, D., and Talbaut, M.. (2013) *Journal of Aerosol Science* **55**, 12–24.

Slinn, W.G.N. (1978) *Nuclear Safety*, **19(2)**, 205–219.

Zhao, B., and Wu, J. (2006) *Atmospheric Environment* **40**, 6918–6927.

Thursday, September 5, 2013

Poster session C

Instrumentation, Posters C044 – C083

Comparisons of Rman- and WALI-derived aerosol optical properties during HyMeX

M-L. Boytard[1,2], P. Royer[2], P. Chazette[1], J. Totems[1], X. Shang[1], and F. Marnas[1]

[1]Laboratoire des Sciences du Climat et de l'Environnement, CEA-CNRS-UVSQ, 91191 Gif-sur-Yvette Cedex, France
[2]LEOSPHERE, 76 rue de Monceau, 75008 Paris, France
Keywords: aerosol, Raman lidar, R-Man$_{510}$, HyMeX
Presenting author email: mai-lan.boytard@lsce.ipsl.fr

As to confront the increasing need of more accuracy and continuity in both the surveillance of pollution and the climate forecasting lidars have developed considerably. The Raman lidars have the advantage of giving the extinction and backscatter coefficients without any assumption or synergy with another instrument (e.g. Whiteman et al., 1992). LSCE and LEOSPHERE Company developed a new prototype of portable N_2-Raman lidar for the study of the low and middle troposphere (Royer et al., 2010). Such system was used in the framework of the MEGAPOLI European program and for the survey of volcanic ashes (Chazette et al., 2011). It gave rise to the new Raman lidar R-Man$_{510}$ developed and recently commercialized by LEOSPHERE Company and WALI (Water-vapor and Aerosol LIdar) developed by LSCE. The comparison between those two would allow the validation of the first one.

Both lidars were deployed during the HyMeX (Hydrological cycle in Mediterranean EXperiment) campaign, in autumn 2012 in Menorca. This campaign aimed at understanding the climatic phenomena and improving the meteorological forecasts of extreme events over the Western Mediterranean region. This area is particularly interesting for it diversity of aerosols coming from maritime, Saharan dust and/or anthropogenic sources. Hence, the measurements performed during the HyMeX campaign prove to be a good support for the comparison between both lidars. They allow retrieving and comparing aerosol optical properties (extinction coefficient, aerosol optical depth, depolarization ratio) derived from the lidars.

R-Man$_{510}$	WALI
Reception channels	
Elastic // 355 nm Elastic ⊥ 355 nm N_2-Raman 387 nm	Elastic total 355 nm Elastic ⊥ 355 nm N_2-Raman 387 nm
Reception diameters	
15 cm	
Full overlap	
~300 m	
Vertical sampling	
1.5 m 7.5 m	0.75 m (analog) 15 m (photon counting)
Vertical resolution	
~30 m	

Table 1: R-Man$_{510}$ and WALI technical characteristics

The main technical characteristics of these two eye-safe lidars are given in Table 1. WALI and R-Man$_{510}$ have different optical designs for the separation of polarizations. The main other differences are the pulse repetition frequency and the emitted energy that are in favor of the reference instrument WALI, mainly during daytime.

Figure 1 illustrates the matching between the extinction coefficients and the volume depolarization ratios (VDR) derived from the lidars. These measurements have been acquired during a dust event coming from Saharan desert. These non-spherical mineral particles are highlighted by high depolarization ratio and can be observed up to 5 km above mean sea level.

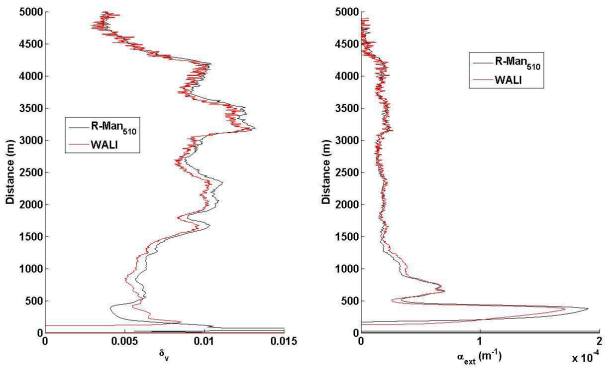

Figure 1. Vertical profiles of both the volume depolarisation ratio δ_v (left panel) and the aerosol extinction coefficient α_{ext} (right panel), October 5th 2012 between 0h and 1h.

Various atmospheric conditions have been observed during the campaign (dust events, clean maritime, cirrus clouds…). This will give the opportunity to evaluate daytime and nighttime performances of the R-Man$_{510}$ compared to the research lidar WALI.

This work was supported by the French Agence Nationale de la Recherche (ANR), the French space agency (CNES) and the Commissariat à l'Energie Atomique (CEA).

Chazette, P. et al. (2011), *J. Geophys. Res.*, **117**, D00U14, doi:10.1029/2011JD015755.
Royer, P., Chazette, P., Lardier, M., and Sauvage, L. (2010), *Atmos. Environ.*, **45**, 7487-7495.
Whiteman, D.N., Melfi, S.H., and Ferrare, R.A. (1992), *Appl. Opt.*, **31**, 3068-3082.

Determining effective density of nanostructured particles by tandem electrical mobility and mass measurement (tandem DMA/APM): application to thermal spraying fumes

S. Bau[1], A. Charvet[2], D. Bémer[1] and D. Thomas[2]

[1]Institut National de Recherche et Sécurité (INRS), Vandœuvre les Nancy, F-54519, France
[2]Laboratory of Reactions and Chemical Engineering (LRGP), University of Lorraine – CNRS, Nancy, F-54000, France
Keywords: airborne nanostructured particle, effective density, fractal dimension, particle mass analyzer.
Presenting author email: sebastien.bau@inrs.fr

Thermal spraying is a surface treatment process which makes it possible to deposit different types of material on various substrates. This process generates large quantities of fumes, composed mainly of primary particles with diameters below 100 nm (Bémer *et al.*, 2010), as shown in Figure 1.

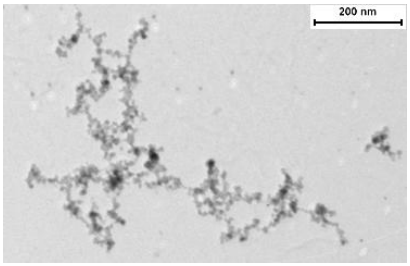

Figure 1. TEM picture of nanostructured particles produced by thermal spraying of a Zn/Al mixture.

To assess occupational exposure, the behaviour of the nanostructured particles produced must be better described and understood. This remains a challenge. Particle effective density is among the parameters of interest, mainly due to its role in particle deposition in the human respiratory tract (ICRP, 1994). In addition, it is required to determine the relationship between equivalent diameters and to convert number distributions to mass distributions (Mc Murry *et al.*, 2002).

Specific instrumentation is required to determine the effective density of airborne nanoparticles as this property cannot be measured directly. Various methods have been proposed to manage this issue, such as measuring electrical mobility and aerodynamic diameters (tandem DMA/ELPI) of the same nanostructured particles (e.g. Van Gulijk *et al.*, 2004; Virtanen *et al.*, 2004).

In this study, we used tandem DMA/APM (e.g. Mc Murry *et al.*, 2002; Ku *et al.*, 2006). Briefly, this setup is based on particle selection according to their electrical mobility using a Differential Mobility Analyzer (DMA, TSI model 3080) and subsequent mass selection in a Particle Mass Analyzer (APM, Kanomax model 3601). The number concentration of airborne particles was monitored by a Condensation Particle Counter (CPC, Grimm model 5.403), while their electrical charge was measured with an aerosol electrometer (TSI, model 3068B).

In addition to particle effective density, the fractal dimension and the number of primary particles making up agglomerates were determined. These data were compared to values calculated based on Lall & Friedlander's theory (Lall & Friedlander, 2006).

Preliminary investigations carried out on airborne silver nanoparticles produced by spark discharge were performed. Results indicated that different rotation speed / optimum voltage doublets give rise to a similar effective density for particles of a given electrical mobility diameter. In addition, the raw curve from which optimal voltage is derived was found to be larger for high rotation speeds.

The protocol was then applied to nanostructured particles emitted during thermal spraying of a Zn/Al mixture onto a surface. How their effective density evolves according to particle size is shown in Figure 2.

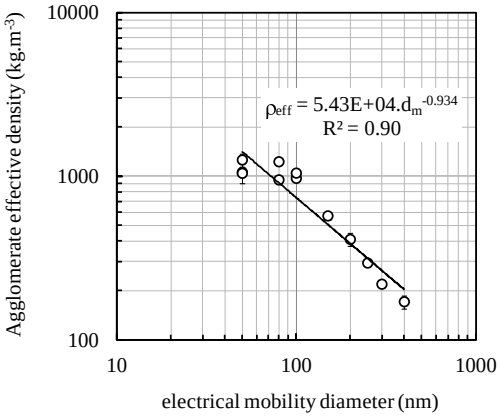

Figure 2. Effective density of nanostructured particles generated by thermal spraying of a Zn/Al mixture as a function of their electrical mobility diameter.

Bémer D., Régnier R., Subra I., Sutter B., Leclerc M.T. and Morele Y. (2010) *Ann. Occup. Hyg.* **54**, 607-614.

ICRP (1994) *Publication 66: Human respiratory tract model for radiological protection*, Oxford: Pergamon.

Ku B.K., Emery M.S., Maynard A.D., Stolzenburg M.R. and Mc Murry P.H. (2006) *Nanotechnol.* **17**, 3613-3621.

Lall A.A. and Friedlander S.K. (2006) *J. Aerosol Sci.* **37**, 260-271.

Mc Murry P.H., Wang X., Park K. and Ehara K. (2002) *Aerosol Sci. Technol*. **36**, 227-238.

Van Gulijk C., Marijnissen J.C.M., Makkee M., Moulijn J.A. and Schmidt-Ott A. (2004) *J. Aerosol Sci.* **35**, 633-655.

Virtanen A., Ristimäki J. And Keskinen J. (2004) *Aerosol Sci. Technol.* **38**, 437-446.

Direct analysis of secondary organic aerosol using atmospheric-pressure glow discharge mass spectrometry

M. Brüggemann and T. Hoffmann

Institute of Inorganic and Analytical Chemistry, Johannes Gutenberg University, Mainz, Germany

Keywords: Instrumentation/chemical char., SOA (Second. Organic Aerosols), Ambient Mass Spectrometry.
Presenting author email: brueggemann@uni-mainz.de

Secondary organic aerosol (SOA) is formed when oxidation products of volatile organic compounds undergo gas-to-particle conversions. It accounts for a substantial fraction of ambient tropospheric aerosol and has implications on the earth's climate and human health. However, the characterization of the chemical composition and chemical transformations remain a major challenge in aerosol research and are bound to big uncertainties (Hoffmann *et al.*, 2011).

Today the Aerosol Mass Spectrometer (AMS) is probably the most common technique to obtain chemical and size-resolved information about sub-micron aerosol particles. It uses, however, an electron impact ion source, which is a hard ionization technique and leads to many fragmentations. Therefore, it is not possible with this instrument to monitor single organic compounds, which can serve as marker compounds for anthropogenic activities, wild fires or natural atmospheric conditions (Lanz *et al.*, 2010).

Addressing these technical drawbacks of the AMS and further questions concerning the chemical composition of SOA, we are developing a method to use atmospheric-pressure glow discharge mass spectrometry for the on- and offline analysis of SOA. Here we present the first application of the recently introduced flowing atmospheric-pressure afterglow (FAPA) ion source (Shelley *et al.*, 2011) for the chemical characterization of laboratory-generated SOA. The ion source is used for the offline analysis of SOA particles collected on PTFE-coated filters as well as the online analysis of SOA gas and particle phase.

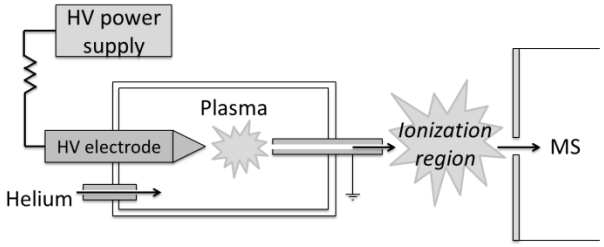

Figure 1. Schematic of the flowing atmospheric-pressure afterglow ion source combined with mass spectrometry.

The FAPA source is based on a Helium glow discharge plasma at atmospheric pressure, which is maintained between two electrodes in a ceramic discharge cell. Since one of the electrodes is a capillary, excited Helium atoms and other reagent ions can exit the discharge cell and ionize analyte molecules in front of the source (fig. 1). This very soft ionization technique offers the possibility to obtain mass spectra with very little fragmentation (fig. 2). Additionally, the ion source can operate already at relatively low temperatures of about 50 °C, thus enabling the analysis even of very thermolabile substances in SOA.

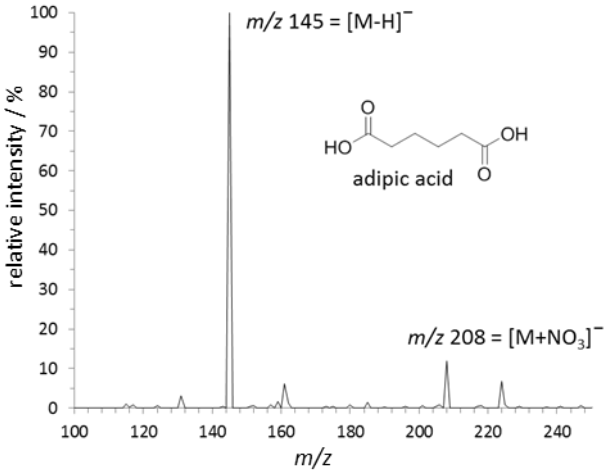

Figure 2. Mass spectrum of adipic acid in negative mode; the deprotonated molecular ion at *m/z* 145 is the most abundant signal, at *m/z* 208 a weak signal of the nitrate adduct is observed.

For all experiments SOA was produced from the ozonolysis of terpenes under dark and dry conditions. For offline experiments particulate matter was collected on PTFE-coated quartz filters and the collected particles were analyzed by desorption/ionization with the FAPA-MS. For online measurements the reaction chamber was directly connected to the ionization region of the FAPA-MS.

This work was supported by the Max Planck Graduate Center with the Johannes Gutenberg University.

Hoffmann, T., Huang, R.-J. and Kalberer, M. (2011) *Anal. Chem.* **83**, 4649-4664.

Lanz, V. A., Prévôt, A. S. H., Alfarra, M. R., Weimer, S., Mohr, C., DeCarlo, P. F., Gianini, M. F. D., Hueglin, C., Schneider, J., Favez, O., D'Anna, B., George, C., Baltensperger, U. (2010) *Atmos. Chem. Phys.* **10**, 10453-10471.

Shelley, J. T., Wiley, J. S. and Hieftje, G. M. (2011) *Anal. Chem.* **83**, 5741-5748.

AEROSOLS DETECTION AND RANGING: FAST LASER IMAGING OPTICAL EMISSION SPECTROSCOPY (DARLIOES)

Strat MITACHI[1], Marius Mihai CAZACU[1], Adrian TIMOFTE[1, 2], Dan DIMITRIU[1], Silviu GURLUI[1]

1 "Alexandru Ioan Cuza" University of Iasi, Faculty of Physics, Atmosphere Optics, Spectroscopy and Lasers Laboratory, 11 Carol I Blvd., 700506 Iasi, Romania
[2] National Meteorological Administration, Regional Forecast Center Bacau, 1 Cuza Voda Str., 600274 Bacau, Romania
Keyword: aerosols, LIDAR, fast-imaging-spectroscopy, optical-emission-spectroscopy (OES)
Presenting author email: sgurlui@uaic.ro

Depending on the space-time chemical composition, sources type activity or process, meteorological conditions, air pollutants (both organic and inorganic compounds), generally the air pollution causes significant damage to human health and environment and dramatically influencing the climate changes. These pollutants may include some of the following well known chemical compounds: sulphur dioxide, ozone, carbon dioxide, volatile organic compounds, hydrogen sulphide, particulate matter, carbon monoxide, toxic air contaminants (mercury, lead, etc) but their contributions in the time-scale atmosphere dynamics are far from fully understood as following discussed details.

As a complementary approach to the satellite measurement spectral data, ground based instruments as Sunphotometer, Radiometer, DOAS, LIDAR & DIAL, mass-spectroscopy & shadowgraphy - laser matter desorption, in a variety of configurations are extensively developed and some of these must be improved even to obtain UV-IR image – remote investigated ice nucleation layer-atmospheric pattern, as following will be proposed in this paper.

Moreover, in order to better understanding the fundamental of some critical physico-chemical transformation of the atmosphere compounds but also for applications point of view, we propose a new LIDAR power instrument DARLIOES as is shown in Fig. 1.

This instrument is able to capture fast plume airborne image (2ns gate time) and may used to investigate in real time several chemical compound behaviour at a given point of the free atmosphere. Some advantahge of the proposed instrument may summarized as following: time-space resolved temperature and humidity profiles (Raman scattering of oxygen 353 nm & 354 nm; real-time monitoring tool to measure concentration of sulphur dioxide injected in the troposphere from the volcanic eruption ash, water profiles and their dynamics, acid rain, chemical transformation/physical properties; DIAL H_2O and SO_2; UV fluorescence using the two stronger absorption emission lines of 218.9 nm and 220.8 nm, respectively; water vibrational Raman scattering at 407 nm; ice nucleation variability, physical and chemical impact, the influence upon the mixed-phase cloud; dust mineralogical composition dynamics influences upon the ice nucleation; Raman scattering of oxygen - 353 nm & 354nm; fast ICCD imagery (IR spectrum) of ice nucleation pattern clouds; studies of the ice nucleation and propagation in plants; detection and characterization of carcinogenic BaP or PAH compounds adsorbed on the soot in a given smoke plume, bacterial and fungal spores, biogenic aerosols generally that have the potential to fluorescence; UV fluorescence of PAH {Benzo(ghi)perylene Excitation (Ex-301 nm/ Emission Em-420 nm); Naphthalene (Ex-275 nm/ Em-325 nm); Anthracene (Ex-255 nm/Em-375 nm); Pyrene (Ex-270 nm/ Em-420 nm), etc).

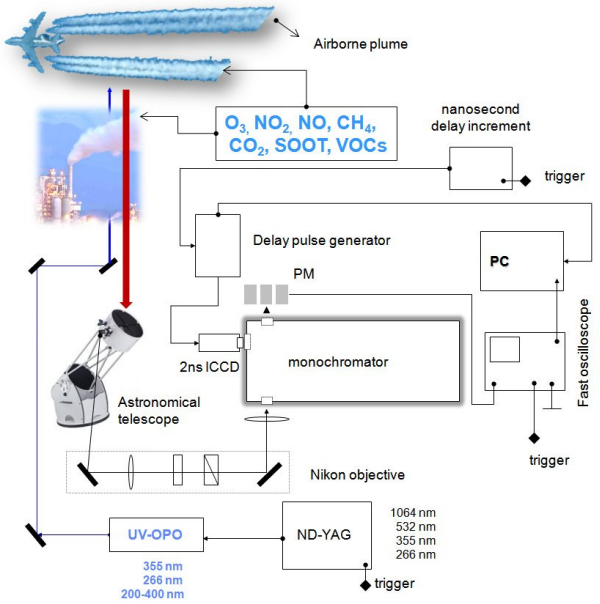

Fig. 1. DARLIOES equipment, experimental set-up. UV-OPO pulsed laser combined with high resolution spectroscopy and fast ICCD camera make available different spectroscopy real time diagnosis tools.

P. Hairston, Ho J, F. Quant, (1997), *Laser-induced fluorescence and Raman scattering for real time measurement of suspended particulate matter*, J Aerosol Sci.; 28(3):471-82

Dengxin Hua, et al., (2007), *Daytime Temperature Profiling of Planetary Boundary Layer with Ultraviolet Rotational Raman Lidar*, Jpn. J. Appl. Phys. 46 5849

S. Gurlui, M. Agop, P. Nica, M. Ziskind, C. Focsa, (2008), *Experimental and Theoretical Investigations of a Laser Produced Aluminum Plasma*, Phys. Rev. E, 78, 026405

Kärcher, B. and T. Koop, (2005), The role of organic aerosols in homogeneous ice formation. Atmos. Chem. Phys. 5 (3), 703-714.

Measurement of solid particle concentration is aided by catalytic stripper technology

J. J. Swanson and H.-J. Schulz

Catalytic Instruments GmbH, Lug ins Land 53, 83024 Rosenheim, Germany
Keywords: semi-volatile, new instrumentation, exhaust
Presenting author email: jacob.swanson@gmail.com

Diesel, locomotive, and gas turbine exhaust contains a complex mixture of solid particles and semi-volatile material that is found in both the particle and the vapor phase. Physical and chemical characterization of these exhaust aerosols in the environment enables a better understanding of potential health effects, effectiveness of alternative combustion technologies and emission control devices, and also the impact of new fuel and lubricant formulations on emissions. To reflect the growing consensus that solid, elemental carbon is a relevant metric and to force the use of diesel particulate filters, Euro 5b regulations introduced a protocol for measuring the solid particle number concentration for particles larger than 23 nm. Similarly, the aerospace SAE E-31 program aims to develop a methodology to measure solid particle mass and number concentration in gas turbine exhaust.

While the aforementioned efforts are generally successful, issues remain with regards to the standard heated tube approach ("evaporation tube" or "thermal denuder") for separating solid and semi-volatile material due to the formation of artifacts that manifest as incomplete evaporation and/or vapor renucleation. An alternative to this is the catalytic stripper (CS)[1], which has the potential to allow reliable extension of solid particle methods to a lower size range in the absence of artifacts.

The objectives of this paper are two-fold. First, recent advances in CS technology that have been presented in successful "demonstration studies" are discussed. These include 1) design of a miniature CS[2], 2) laboratory validation of a CS when challenged with very high concentrations of semi-volatile hydrocarbon and sulfuric acid aerosols[3], and 3) performance of the CS compared to other methods[3]. While demonstration studies have validated the technology, standardizing the approach is the next step to move forward. Thus, the second objective is to describe current efforts to improve both the design of the catalytic element and choice of components as well as methods used for evaluation.

The CS geometry is fixed though the choice of cell density and physical dimensions. For a fixed geometry, the operating temperature and flowrate dictate performance, although performance needs may vary depending on application. Fig. 1 shows typical solid particle loss curves for a CS operating at 1.5 l/min and 350°C. Design parameters for the CS reflect a balance between solid particle loss, flowrate, residence time, operating temperature, and vapor removal. Fig. 1 shows how the removal of tetracontane vapor increases at the expense of decreased penetration of solid material – this effect is magnified for the smallest particles.

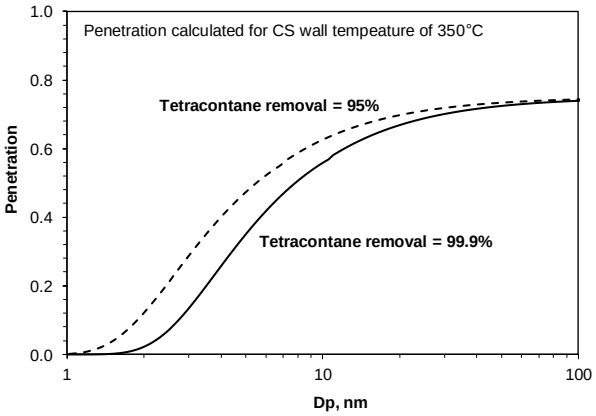

Figure 1 Typical solid particle loss curves (including diffusion and thermophoresis) for CS designed to remove 95% and 99.9% of tetracontane ($C_{40}H_{82}$).

Fig. 2 shows a cross-sectional view of a typical catalytic element including heating, insulation, and the catalytic material.

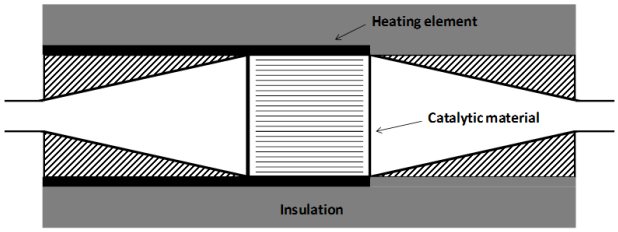

Figure 2 Schematic of catalytic element. Aerosol flow is from left to right.

Overall, results show CS technology is a robust means to separate solid and semi-volatile material. The combination of CS technology and any traditional particle instrument can then be used to provide a real-time measure of solid particle number, size, surface area, or mass concentration. Further to this, the standardization of catalytic element design and performance evaluation techniques provides a basic platform for the design for new aerosol instrumentation.

[1]Abdul-Khalek, I.S.; Kittelson, D.B. (1995). Real time measurement of volatile and solid exhaust particles using a catalytic stripper. *Society of Automotive Engineers*, 950236.

[2]Swanson, J., Kittelson, D., Giechaskiel, B., Bergmann, A. et al., (2013). A Miniature Catalytic Stripper for Particles Less Than 23 Nanometers. *SAE Int. J. Fuels Lubr.* 6 (2), doi:10.4271/2013-01-1570.

[3]Swanson, J.; Kittelson, D. (2010). Evaluation of Thermal Denuder and Catalytic Stripper Methods for Solid Particle Measurements. *J. Aerosol Science*, 41:12, 1113 – 1122.

A new Instrument to Observe Contact Freezing of Single Supercooled Levitated Water Droplets

H.-J. Tong[1], F.D. Pope[2] and M. Kalberer[1]

[1]University of Cambridge, Lensfield Road, Cambridge, CB2 1EW, UK
[2]School of Geography, Earth and Environmental Sciences, University of Birmingham, Edgbaston, Birmingham B15 2TT, UK
Keywords: contact freezing, ice nucleation, single droplet, electrodynamic balance.
Presenting author email: ht326@cam.ac.uk

Freezing of liquid water droplets is one of the most important processes that influences cloud behavior and ultimately the climate; however ice nucleation processes are at present poorly understood. It is difficult to distinguish the important parameters that affect the different mechanisms of freezing and this causes great uncertainty.

Contact freezing has been observed at temperatures greater than -20 °C (Bunker, 2012). This is significantly higher than the homogenous freezing temperature of approximately -38 °C. In addition to temperature, the activity of ice nuclei (IN), in the contact mode, depends upon: the morphology, composition and the size of the IN (Hoose, 2012).

Recent laboratory results for contact freezing are mainly based upon studies which use droplets deposited upon substrates. The efficiency of the contact freezing mode for single suspended droplets is unknown. This technique will allow for measurement of IN efficiencies without the potential bias caused by substrate contact nucleation.

In the present study a new electrodynamic balance (EDB) with cylindrical electrodes was designed and built. A schematic diagram of the instrument is shown in Figure 1. The EDB can trap single 5~100 μm diameter water droplets. The core geometrical structure of the EDB cell, including the electrodes, was described previously (Christian, 2009). Droplets can be injected into EDB cell at ~2 m s^{-1}. 0~1000 V AC are applied to the upper electrode and 0~1000 V AC coupled with 0~10 V DC are applied to the lower electrode to trap the water droplets.

After a charged droplet is trapped, a 532 nm laser is used to illuminate the trapped droplet. Two cameras are used to locate and size the trapped droplet.

Initial experiments are investigating IN composed of mineral particles. The IN collides with the supercooled droplet that is levitated in the EDB cell. A DMA will be used to obtain monodisperse IN particles which are subsequently neutralized through use of an electrofilter. The EDB can be cooled to -40 °C by the particle flow passing through a liquid nitrogen dewar.

Two optical particle counters (OPC) will be used to count the number of IN before and after collisions with the supercooled droplet. The OPC can detect 350~1000 nm particles at frequency of 100s Hz. The contact freezing efficiency of the IN is determined by comparing the difference in number concentration of the particles above and below the supercooled droplet.

We will present the contact freezing efficiency of mineral dust particles and a compare the results with other non-contact free techniques.

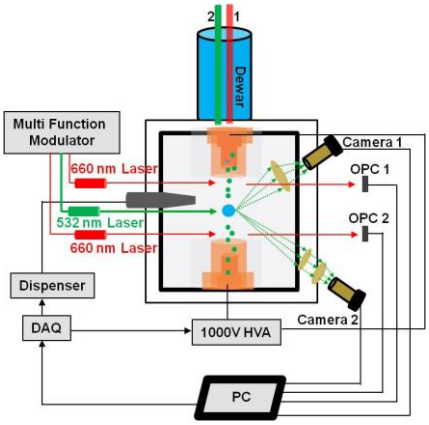

Figure 1. The low temperature EDB system. Camera 1 is for droplet location. Camera 2 is for Mie scattering detection. OPC 1 and OPC 2 are optical particle counters. DAQ is a data acquisition box. In tube 1 the aerosol is introduced through inner electrode into the EDB. Tube 2 is for sheath gas flowing between inner and outer electrode to obtain additional and uniform cooling in the EDB.

Bunker, K. W., China, S., Mazzoleni, C., Kostinski, A. and Cantrell, W. (2012) *Atmos. Chem. Phys. Discuss.*, 12, 20291-20309.

Christian, H., Wills, J. B., Reid, J. P., Tschudi, T. and Tropea, C. (2009) *Phys. Chem. Chem. Phys.* 11, 9720-9728.

Hoose, C. and Möhler, O. (2012) *Atmos. Chem. Phys.*, 12, 9817-9854.

On-board study of nano- and micrometer-particle characteristics of a running electric train

S. Abbasi[1], U. Olofsson[1], T. Tritscher[2] T. Krinke[2]

[1]Department of Machine design, Royal Institute of technology (KTH), Stockholm, 100 44, Sweden
[2]TSI GmbH, Particle Instruments, Aachen 52068, Germany

Keywords: non-exhaust, railway, size-distribution,
Presenting author email: torsten.tritscher@tsi.com

Currently, the high concentration of particles in the enclosed environment such as railway tunnels and subway stations raised worries among researchers dealing with air quality (Abbasi *et al*, 2012, 2013). Although studying particle characteristics in rail traffic started in 1909, effective action has yet to be taken because of lack of relevant knowledge.

In this study for the first time an Alstom X-60 EMUs was instrumented by two sets of Optical Particle Sizers (OPS), TSI model 3330 and a NanoScan Scanning Mobility Particle Sizer (SMPS), TSI model 3910. The train was operated back-and-forth in a 86-km route between Älvjö and Uppsala stations in Swedish inter-city tracks over the course of 2 days.

Two sampling points were designated underneath of train compartment to represent both background and railway-source based particles (*e.g.* wheel-rail contact, braking materials, and concrete sleepers). Two other sampling points were designated inside the cabin compartment. All of sampling points were connected to OPS and Nanoscan SMPS (Fig. 1).

These characteristics were integrated with the train operational conditions from automatic train control (ATC) and Train control and management system (MSTC) data. According to this study, the dominant peaks of nano- and micrometer-particles were highly dependent on different environments such as tunnels, bridges, urban high-traffic and low-traffic area as well as different operational conditions such as acceleration and deceleration.

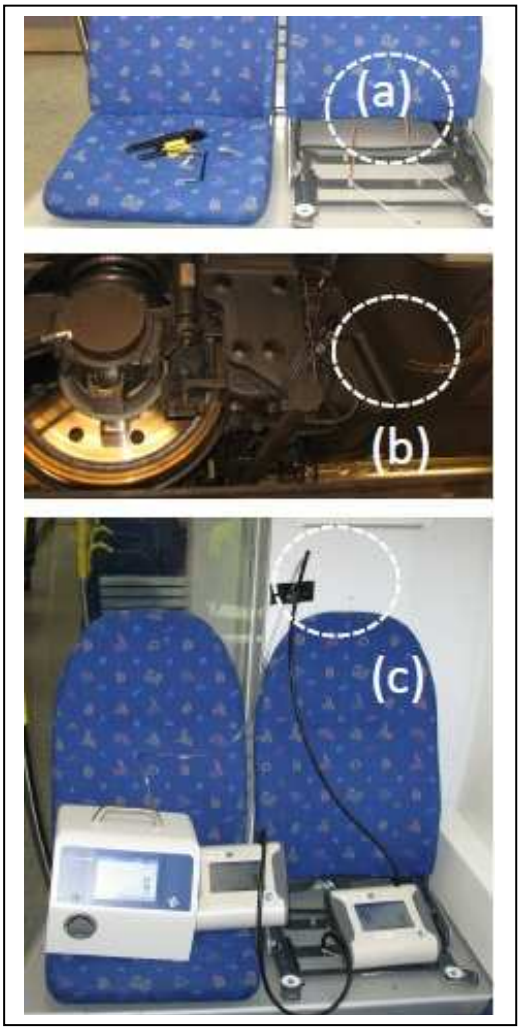

Fig 1. Sampling points set-up: (a) Head of copper tubes insides compartment; (b)Tail of copper tubes underneath of compartment and near bogie; (c) Sampling tubes inside compartment

This work was supported by KTH Railway group.

Abbasi, S., A. Jansson, U. Olofsson, and U. Sellgren. (2012). *Crit. Rev. Environ. Sci. Technol* http://dx.doi.org/10.1080/10643389.2012.685348

Abbasi, S., U., Sellgren, U. Olofsson, (2013) *Aerosol and Air quality research.*

A new device for the investigation of nucleation, dynamic growth and surface properties of single ice crystals

J. Voigtländer[1], C. Chou[2], H. Bieligk[1], T. Clauss[1], P. Herenz[1] , D. Niedermeier[1], J.Z. Ulanowski[2], F. Stratmann[1]

[1]Leibniz Institute for Tropospheric Research, Leipzig, Germany
[2]Science & Technology Research Institute, University of Hertfordshire, UK
Keywords: ice nucleation, dynamic growth, optical properties, ice particle, laminar flow tube
Presenting author email: jensv@tropos.de

Because a) the nucleation and growth of atmospheric ice particles is of great importance for both, weather and climate on earth, and b) the knowledge considering the influence of ice particle surface properties on the radiative properties of clouds is still sparse, we developed a new device to investigate nucleation, dynamic growth and light scattering properties of a fixed ice crystal in dependence on the prevailing thermodynamic conditions. The instrument is based on our experiences with the laminar flow tube chamber LACIS (Leipzig Aerosol Cloud Interaction Simulator, Stratmann et al., 2004). Connected to the flow tube is a SID3-type (Small Ice Detector, Kaye et al., 2008) instrument. This instrument, called LISA (Leipzig Ice Scattering Apparatus), has been additionally equipped with an optical microscope. A single ice nucleus (IN) with a dry size of 2-5 micrometer is attached to a thin glass fiber and positioned within the optical measuring volume of LISA. The fixed particle is exposed to the thermodynamically controlled air flow, exiting the flow tube. Two mass flow controllers adjusting a dry and a humidified gas flow are applied to control both, the temperature and the saturation ratio. The thermodynamic conditions in the experiments were characterized using a) computational fluid dynamics (CFD) calculations, b) temperature and dew-point measurements, and c) evaluation of droplet and ice particle growth data. Dependent on both, temperature and saturation ratio, ice nucleation and ice particle growth/shrinkage occur and can be studied. Thereby, the optical microscope allows a time dependent visualization of the particle/ice crystal (Fig. 1a), and the LISA instrument is applied to obtain 2-D light scattering patterns (Fig. 1b). Both devices together allow to investigate the influence of thermodynamic conditions on ice particle growth, the particle shape and its surface properties.

In first experiments we could show the feasibility of the setup to investigate droplet activation, as well as ice particle nucleation and growth. We successfully performed condensation freezing and deposition nucleation experiments considering kaolinite and Snowmax™ (Johnson Controls Snow, Colorado, USA) particles. Thereby, we could prove that different temperatures and saturation ratios result in different growth rates and ice crystal shapes, but also in different surface properties. Examplarily, Fig. 2 shows the time dependent evolution of ice particle size and relative surface roughness (0 – smooth, 1 – rough) calculated from the LISA data. In general, comparing simple ice particles (like single columns) with more complex crystals (such as dendrites), the surface roughness value is larger for the latter ones. But in the experiments we also found that, regarding one single ice crystal, the surface roughness can be also modified by (small) variations of the prevailing thermodynamic conditions. Thereby, the surface roughness tend to increase for growing, and to decrease for shrinking ice particles. We could also prove that these findings are independent of the absolute particle size (Fig. 2). Further investigations and data evaluation are ongoing.

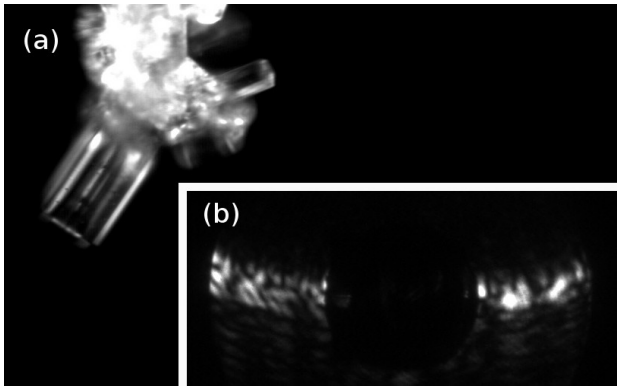

Figure 1. Example for a microscope picture of ice crystals growing over the fibre (a) and the corresponding scattering pattern measured with LISA (b).

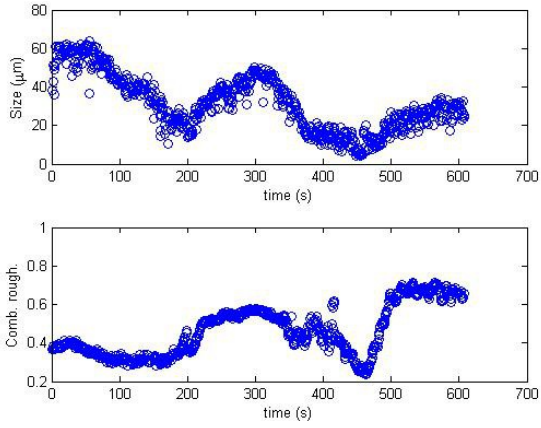

Figure 2. Example for the time dependent evolution of ice particle size and combined surface roughness.

Kaye, P., Hirst, E., Greenaway, R., Ulanowski, Z., Hesse, E., DeMott, P., Saunders, C., Conolly, P. (2008): Classifying atmospheric ice crystals by spatial light scattering, *Optics Letters*, **33**, 1545-1547.

Stratmann, F., Kiselev, A., Wurzler, S., Wendisch, M., Heintzenberg, J., Charlson, R. J., Diehl, K., Wex, H., Schmidt, S. (2004): Laboratory studies and numerical simulations of cloud droplet formation under realistic supersaturation conditions., *J. Atmos. Ocean. Tech.*, **21**, 876–887.

A real-time analyzing and weighing system

D. Weidauer[1], C. Bey[1] , F. Freyer[1] and N. Derenda[1]

[1]Comde-Derenda GmbH, Kieler Str. 9, 14532 Stahnsdorf, Germany
Keywords: X-ray analysis, gravimetric, scattered light photometer, robotic.
Presenting author email: weidauer@comde.de

Gravimetric measurement is the reference method for determination of particulate matter in ambient air (EN 12341), (EN 14907). This method requires sample intervals as long as 24 h and conditioning phases as long as 48 h before a precise result can be obtained. Once the mass of a loaded filter disk has been determined to a satisfactory precision, the disk can be processed further by methods such as chemical analysis, laser spectroscopy or X-ray analysis. This entire process chain, including scheduling and transport, can easily take a week or longer until all results are available.

The authors present a setup that combines (a) aerosol sampling on filters with (b) a scattered light photometer, (c) a sub-microgram balance, (d) an X-ray fluorescence spectrometer and (e) an X-ray diffractometer in a complete, self-contained system. The workflow is handled by a robotic system implementing a workflow optimised for quick preliminary and early final results. The operating concept of this setup includes the following interactions between the contained instruments:

(i) The scattered light photometer provides highly time-resolved data about the aerosol concentration. As well as being capable of providing this data online, it can be used to determine the minimum required sampling time for the filter disk currently placed in the suction line. In cases of high concentration, the filter collects a significant mass in a relative short time interval, so the filter could be changed and processed earlier than according to the standard time intervals.

(ii) The advantage of the scattered light photometer data is its time resolution and real-time availability. However, the photometer signals are not only dependent on the concentration and size distribution, but also on the particles' colour and brightness. It is therefore an attractive option to post-calibrate photometric data by the results of gravimetry as soon as the latter are available.

(iii) Weighing a filter disk requires conditioning for a defined humidity. The robotic system however allows repetitive weighing during the conditioning phase, providing information about the hygroscopicity of the collected dust. The final result after the legally required conditioning time may already be estimated after a fraction of that time. The precision of this estimate will increase with the number of weighing processes the robotic system can accommodate in this period.

(iv) X-ray fluorescence spectroscopy provides information about the elementary composition of the sampled dust. This is a standard method e.g. for detection of heavy metals. The difficult quantitative analysis can be supported by the results of the gravimetric measurements.

(v) X-ray fluorescence provides elementary composition only. Crystalline phases however can be distinguished by X-ray diffraction, providing valuable information complementary to the element analysis.

(vi) The analysis of X-Ray diffraction spectra has undergone significant development in the last years by applying modern computational methods as well as fundamental has been made providing large reference databases (Grazulis, Lutterotti *et al* 2001). However, blind analysis of X-ray diffraction spectra without any advance information is very difficult and may result in ambiguous results (Madsen, Scarlett *et al* 2001, 2002), especially if the sample consists of several, even if very few, phases, and especially when the phases of particular interest constitute only a minor part of the composition. Results of X-ray fluorescence analysis are therefore valuable complementary information for the analysis of X-ray diffraction spectra.

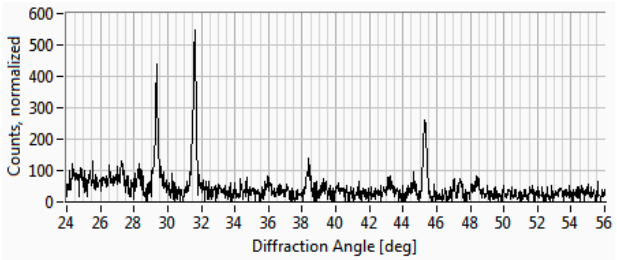

Figure 1. XRD spectrum, acquisition time 30 min. Aluminium cast facility, sampling duration 12 h, daytime, mass on filter 16 mg.

Figure 1. shows first data obtained with the system presented on the conference. That system is a demonstration to study beneficial interactions between these combined instruments. The system is at the same time one example configuration of a modular system with robotic handling. The combination with a suction line makes it field-usable, however, there may be few applications that justify placing such significant capital expenditure in a field spot.

This work was supported by grants of Land Brandenburg, Germany, 2011-2013.

Grazulis, S., Chateigner, D., Downs, R., Yokochi, A., Quirós, M., Lutterotti, L. *J. Appl. Cryst.* **42**, 726-729

Madsen, I., Scarlett, N., Cranswick, L., et al. (2001) *J. Appl. Cryst.* **34**, 409-426

Scarlett, N., Madsen, I., Cranswick, L., et al. (2002) *J. Appl. Cryst.* **35**, 383-400

Review of the field experiments on the transfer of pollution in urban areas in 1979 and 2003.

Yu.S. Balashov, V.N. Piskunov

Russian Federal Nuclear Center
All-Russian Research Institute Of Experimental Physics

Keywords: urban pollution, field experiments, tracer, model evaluation
Presenting author email: balashov.yu@gmail.com

Rather extensive material on full-scale field experiments in urban areas has been accumulated so far. On the researches a large number of articles have already been presented in the print and electronic media. Despite this fact, there is a shortage of original raw data of the specific experiments, with detailed descriptions of the experiments and the original statements of emissions. But these data are urgently needed for the validation and verification of modern models of pollution transport in the city.

This article presents eight best-known full-scale field experiments mostly in a real urban environment, which were held in the period from 1979 to 2003

1. .**Copenhagen** (1978-1979, sulfur-hexafluoride), (Gryning and Lyck, 1984, 2002)
2. **Indianapolis**, (1985, sulfur-hexafluoride), (Murray and Bowne, 1988)
3. **St. Louis**, (1968, SO2), (McElroy and Pooler, 1968)
4. **Lillestrom (**1987, Lillestrom (near Oslo), sulfur-hexafluoride), (Sivertsen and Bohler, 1985)
5. **URBAN/VTMX** (2000, Salt Lake City, sulfur-hexafluoride)
6. **MUST** (2001, Dugway Proving Grounds, sulfur-hexafluoride) (Biltoft, 2001, Biltoft et al., 2002)
7. **BUBBLE** (2002, Bazel, sulfur-hexafluoride), (Gryning et al., 2003)
8. **JU03** (2003, Oklahoma City, sulfur-hexafluoride).

For each experience, the following information provides a brief places, experimental setup, the equipment, the conditions of the sampling and other peculiarities of individual studies. In addition, for some experiments, the sources specified to obtain more information up to the real-time data gained from the individual sensors.

This work will be useful as an overview to inform the scientific community as well as for the revision and analysis of the results for subsequent application in the models

Biltoft, C.A., (2001): Customer report for Mock Urban Setting Test. Report No. WDTC-FR-01-121, U.S. Army Dugway Proving Ground, Dugway, UT.

Biltoft, C.A., Yee, E. and Jones, C.D., (2002): Overview of the Mock Urban Setting Test (MUST). Proceedings of the Fourth Symposium on the Urban Environment. May 20-24, Norfolk, VA.

Gryning, S.E., and Lyck, E., (1984): Atmospheric dispersion from elevated sources in an urban area: comparison between tracer experiments and model calculations. *Journal of Climate and Applied Meteorology*, Vol. 23:651-660.

Gryning, S.E., and Lyck, E., (2002): The Copenhagen Tracer Experiments: Reporting of Measurements. Risø-R-1054(rev.1)(EN), Riso National Laboratory, Roskilde, Denmark, 75 pages.http://www.risoe.dk/rispubl/VEA/veapdf/ris-r-1054_rev1.pdf

Gryning, S-E., E. Batchvarova, M. W. Rotach, A. Christen and R. Vogt, (2003): Roof-level SF6 tracer experiments in the city of Basel. Draft Summary 72 pages. http://www.unibas.ch/geo/mcr/Projects/BUBBLE/index.htm

Murray, D.R., and Bowne, N.E., (1988) *Urban Power Plant Plume Studies*, EPRI Report No. EA-5468, Research Project 2736-1, Electric Power Research Institute, Palo Alto, CA.

McElroy, J.L. and Pooler, F., (1968): *St. Louis Dispersion Study Volume I – Instrumentation, Procedures and Data Tablulations; Volume II-Analysis*. National Air Pollution Control Administration. Publication Number AP-53. U.S. Department of Health Education and Welfare, Arlington, VA, Volume I 352 pages, and Volume II 51 pages.

McElroy, J.L. and Pooler, F., (1968): *St. Louis Dispersion Study Volume I – Instrumentation, Procedures and Data Tablulations; Volume II-Analysis*. National Air Pollution Control Administration. Publication Number AP-53. U.S. Department of Health Education and Welfare, Arlington, VA, Volume I 352 pages, and Volume II 51 pages.

Sivertsen, B., and Bohler, T., (1985): *Verification of Dispersion Estimates Using Tracer Data*. NILU Report TR 19/85, The Norwegian Institute for Air Research, Kjeller, Norway.

VTMX webpage http://www.eol.ucar.edu/isf/projects/vtmx/

Comparing particle number size distributions and number concentrations for airborne nanoparticles measured by SMPS, FMPS and UWCPC

S. Bau[1], V. Hase[2], P. Danihelka[2] and O. Witschger[1]

[1]Institut National de Recherche et Sécurité (INRS), Vandœuvre les Nancy, F-54519, France
[2]Technical University of Ostrava, Ostrava-Poruba, CZ-708 00, Czech Republic
Keywords: airborne nanoparticle, number size distribution, real-time instruments, electrical mobility diameter.
Presenting author email: sebastien.bau@inrs.fr

Nanomaterials hold great promise in fields as wide-ranging as health, food, energy, materials, and transport. Nanomaterials research and development is therefore very active, and the economic stakes are high. However, questions have also been raised related to the health risks associated with these substances. As they become more widely used, it is probable that occupational exposure through inhalation will increase. Hence, it is important to be able to measure these particles (Maynard *et al.,* 2006) to better describe and understand their behaviour.

This study aimed at comparing a number of instruments measuring airborne nanoparticles. Similar intercomparison studies have been performed previously (Leskinen *et al.*, 2012; Kaminski *et al.*, 2013), revealing acceptable discrepancies between results for different devices. However, we believe it is important to extend these comparisons by using different aerosols.

In this study, we simultaneously measured particle number size distributions using a Scanning Mobility Particle Sizer (SMPS, Grimm, composed of a Differential Mobility Analyzer DMA Vienna Type and a Condensation Particle Counter CPC model 5.403) and a Fast Mobility Particle Sizer (FMPS, TSI model 3091). The total number concentration was monitored with an Ultrafine Water-based Condensation Particle Counter (UWCPC, TSI model 3786). A Nanotracer (Aerasense, Philips, discontinued) was also placed in the experimental setup.

The CAIMAN facility (Jacoby *et al.*, 2011) was used to produce spherical silver nanoparticles and fractal-like nanostructured carbon agglomerates by spark-discharge, as shown in Figure 1.

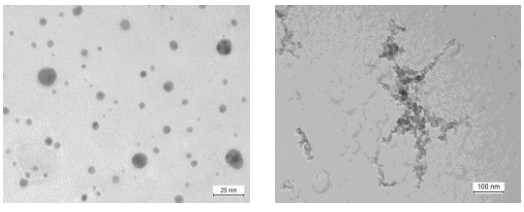

Figure 1. TEM picture of nanoparticles produced by the CAIMAN facility (left: silver, right: carbon).

Modal diameters of the particles produced ranged from 29 to 83 nm for silver, and from 25 to 153 nm for carbon. SMPS data for carbon particles were corrected according to Lall & Friedlander's theory (Lall & Friedlander, 2006), with an input primary particle diameter of 16 nm. Data relative to particle sizes are presented in Figure 2, where SMPS data are taken as the reference values.

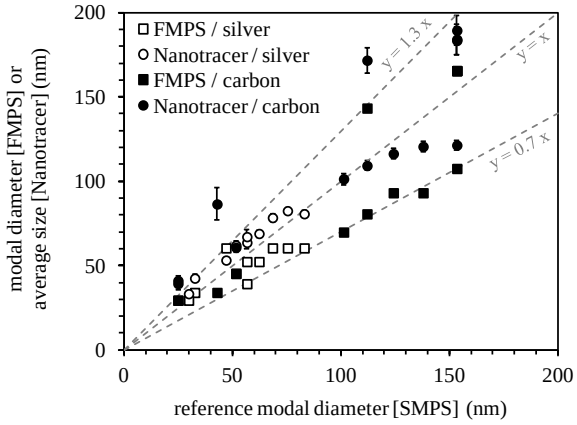

Figure 2. Comparison of particle sizes measured by the different instruments for the two test aerosols.

Relative discrepancies between FMPS measurements and reference were roughly ±30% for both silver and carbon nanoparticles. Average sizes measured by the Nanotracer correlated well with those returned by the reference system for silver particles (0% to 30% relative discrepancies), while for carbon nanoparticles, relative discrepancies were between -20% and 65%.

Number concentrations for the different devices were compared to the reference measurement from UWCPC. Concentrations measured by SMPS were half the reference value for silver particles, whatever the particle number size distribution and total concentration. The behavior of other devices and the influence of aerosol characteristics will be discussed.

Jacoby J., Bau S. and Witschger O. (2011) *J. Phys. Conf. Ser.*, **304**, 012014.

Kaminski H., Kuhlbusch T.A.J., Rath S., Götz U., Sprenger M., Wels D., Polloczek J., Bachmann V., Dziurowitz N., Kiesling H.J., Schwiegelsohn A., Monz C., Dahmann D. and Asbach C. (2013) *J. Aerosol Sci.*, in press.

Lall A.A. and Friedlander S.K. (2006) *J. Aerosol Sci.* **37**, 260-271.

Leskinen J., Joutsensaari J., Lyyränen J., Koivisto J., Ruusunen J., Järvelä M., Tuomi T., Hämeri K., Auvinen A. and Jokiniemi J. (2012) *J. Nanopart. Res.* **14**, 718-733.

Maynard A.D., Aitken R.J., Butz T., Colvin V., Donaldson K., Oberdörster G., Philbert M.A., Ryan J., Seaton A., Stone V., Tinkle S.S., Tran L., Walker H.J. and Warheit D. (2006) *Nature* **444**: 267-269.

UFP measurement: comparison of commercial equipments using different measuring principles

B. Bergmans[1], F. Lenartz[1], J. Mertens[2], N. Faniel[2] and T. Krinke[3]

[1]Department of Air Quality, Institut Scientifique de Service Public (ISSeP), Liege, 40000, Belgium
[2] Sustainable Process Technology, LABORELEC (GDF SUEZ), Linkebeek, Brussels, 1630, Belgium
[3]TSI, Aachen, 52058, Germany
Keywords: UFP, SMPS, ELPI, TSI3031
Presenting author email: b.bergmans@issep.be

Particulate matter (PM) is known to cause adverse health effects when inhaled. Currently, air quality standards are in force for PM_{10} and $PM_{2.5}$. However, epidemiological and toxicological studies suggest that the driving characteristics for health effects are more related to the sub-micron particles (Pope and Dockery 2006). Their measurements should thus be promoted and not only episodically. Therefore, a lot of monitoring networks are developing ultrafine particles (UFP) measurements.

As the monitoring of UFP is neither regulated yet by a European directive nor normalized, major variations exist between measurement principles and commercial equipments available on the market.

Only a few comparisons between instruments are available in the literature (Ji Ping Shi et al., 1999 - B. Wehner et al. 2007) and these are generally limited to two instruments carried out in lab conditions. A technical standard should be prepared soon by CEN/TC264/WG32, but has not yet started. In a joint measurement campaign ISSeP, TSI and LABORELEC investigated different commercial equipments. Results obtained for some of them are presented in this paper.

Instruments deployed were a scanning mobility particle sizer (SMPS 7-850 nm), an ultrafine particle monitor (TSI3031 20-800 nm) and an electrical low pressure impactor (ELPI$^+$ 6nm–10µm). The measures were carried out during 3 winter months at different locations including 2 traffic stations, 1 urban background station and 1 urban station. All instruments were installed using the same sampling line and aerosol was dried so that relative humidity remains below 40%.

Typical time series recorded by the three instruments at a traffic location (Herstal, BE) are presented in figure1 and Pearson correlations obtained on full period are in table 1

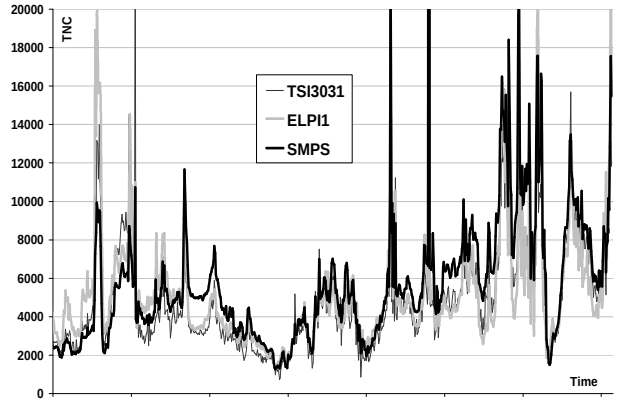

Figure 1: Typical recorded time series

Table 1: Pearson correlation between instruments

<20nm	SMPS	TSI3031	ELPI+	100-200nm	SMPS	TSI3031	ELPI+
SMPS	1	NA	0.56	SMPS	1	0.91	0.79
TSI3031	-	1	NA	TSI3031	-	1	0.87
ELPI+	-	-	1	ELPI+	-	-	1
20-50nm	SMPS	TSI3031	ELPI+	200-800nm	SMPS	TSI3031	ELPI+
SMPS	1	0.92	0.89	SMPS	1	0.61	0.84
TSI3031	-	1	0.95	TSI3031	-	1	0.53
ELPI+	-	-	1	ELPI+	-	-	1
50-100nm	SMPS	TSI3031	ELPI+	20-800 nm	SMPS	TSI3031	ELPI+
SMPS	1	0.95	0.93	SMPS	1	0.92	0.92
TSI3031	-	1	0.95	TSI3031	-	1	0.98
ELPI+	-	-	1	ELPI+	-	-	1

TSI3031 seems not to be in phase for its biggest channel (200-800 nm), nevertheless the impact of this class size on total number is not so high and other instruments (scattering) are available for this size range.

ELPI seems to overestimate the smallest channel (< 20 nm), but the true cut off is not clear as the yield of the corona charger depend on the particle/droplet size. We also expect possible overestimation of the correction algorithm and an impact of the diffusion losses.

The pros and cons of each type of instruments are discussed in the study. Trueness and reproducibility is not the only aspect for a monitoring network: robustness, compatibility with other instruments, equipment cost and maintenance, training of personal, compatibility with all measurement sites should also be taken into account.

Table 2: Summary of pros and cons of each instrument

	Cost	Maintenance	Training	Trueness	urban	Rural
SMPS	−−−	−−−	−−−	+++	+++	+++
TSI3031	−−	−	−	++	++	?
ELPI+	−−	−−	−−−	++	++	?

SMPS, TSI3031 and ELPI$^+$ seem to be good candidates for continuous monitoring of UFP. Each instrument has advantages and disadvantages. Further tests in rural areas are already planned to get results at low concentration.

This work was partly executed within the InterReg IV A project PM_Lab. ISSeP also acknowledges financial support of the Walloon Region.

Pope C.A. and Dockery D.W. (2006). Health Effects of Fine Particulate Air Pollution: Lines that Connect J. Air & Waste Manage. Assoc. 56:709–742

Ji Ping Shi, A.A. Khan, Roy M. Harrison
Meas. of UFP conc. and size distribution in the urban atmosphere. Sc. of the Total Environment, 235:51-64

B. Wehner et al. (2007).
Ultrafine particles: Comparisons UFP 330 / DMPS UFIPOLNET - UFP in Urban air – Dresden.

Comparison among un-denuder filter based, denuder filter pack and continuous techniques for inorganic artefact assessment

P. R. Dambruoso[1], G. de Gennaro[1], A. Di Gilio[1], P. Fermo[4], R. Filardi[1], A. Piazzalunga[2], R. Gonzalez Turion[2], R. Vecchi[3].

[1]Department of Chemistry, University of Bari, Bari, Puglia, via Orabona, 4, 70126, Italy
[2]Department of Chemistry, University of Milan-Bicocca, Milan, Piazza della Scienza, 3, 20126 Milano, Italy
[3]Department of Physics, University of Milan, Milan, via Celoria, 18, 20133 Milano, Italy
[4]Department of Inorganic, Metallorganic and Analytical Chemistry, University of Milan, Milan, via Celoria, 18, 20133 Milano, Italy

Inorganic sampling artefact, nitrite, nitrate, PM2,5, AIM 9000D
alessia.digilio@uniba.it

The particulate matter consists of thousands of chemical species characterized by several physical and chemical properties. Sulphate, nitrate and ammonium are the main components of the inorganic fraction and account for 30-40% of total mass of PM2.5 (Minguillóna et al., 2012).

Traditionally in measuring the ambient concentrations of aerosols, water-soluble inorganic fraction of PM are determined by filter-based method. This method has several shortcomings such as labor intensity, lengthy analysis time, poor resolution time and the sampling artefacts. The most studied sampling artefact regards the nitrate content determined on filter. PM2.5 nitrate concentrations, in fact, can result overestimated due to the absorption of gas-phase nitric acid on the filter, and underestimated due to the evaporation of ammonium nitrate collected on filter during the sample collection (Vecchi et al., 2009). The most rigorous methods recommended by United States Environmental Protection Agency (USEPA Compendium Method IO-4.2) for avoiding gas/aerosol artefacts is the use of diffusion denuders and a filter pack. These denuders first denude the air stream of condensable gases and then sample the aerosols with a filter pack that can collect both the aerosol and any volatilized products from it. Nowadays semi-continuous instruments that provide data of PM ionic component have been developed. Among the most modern automated systems equipped with denuders, the Ambient Ion Monitor AIM 9000D (by URG&Co) has been used for this work. The AIM is a real-time analytical instrument capable of simultaneous sampling and measurements of water-soluble PM2.5 constituents and ion gas precursors.

In this study, in order to assess the inorganic artifact and the AIM performance for avoiding them, the results obtained measuring nitrate and nitrite determined by an un-denuded filter based sampler, a denuder filter-pack sampler and a semi-continuous system have been reported.

The preliminary results analysis highlighted a noticeable difference in nitrate and nitrite amount determined on 24h filters and on three 8h filters samples simultaneously; especially for nitrite concentration when lower NOx and higher Ozone concentrations were registered (for example in fig. 1 are reported only few days). Moreover, as shown in figure 2, the nitrate concentrations determined by AIM showed a good correlation with those determined by the rigorous artefact free methods based on denuder filter pack sampler. However in specific days, the particulate nitrate concentrations determined by AIM result unexpectedly lower than those determined by denuder filter pack method. In these days, characterized by higher ozone concentrations, the particulate nitrite concentrations on filter for denuder filter pack methods were very lower than those determined by AIM and usually not determined. These findings suggested a possible oxidation of nitrite to nitrate on filter during PM collection (Yu et al., 2005). Therefore, this reaction probably determines another important artefact in nitrate determination on filter. Finally, these results showed also the potentiality of the automatic instrument in nitrate artefact free measurements and taking into account the user-friendliness and lower time and cost consumption, AIM could be an useful tool for an accurate determination of PM ionic composition.

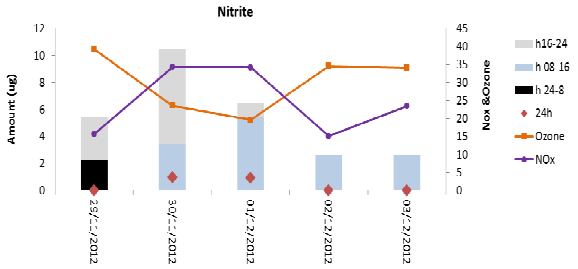

Fig. 1: Comparison among nitrate amount determined on 24 and 8 hours filters. NOx and Ozone concentrations behavior

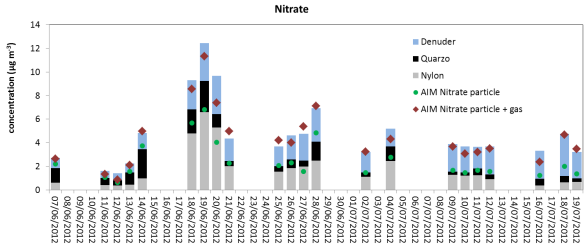

Fig. 2: Comparison between nitrate concentrations determined by denuder filter pack method and by AIM

Vecchi, R. et al., 2009. Atm. Env. 43 (2009) 1713–1720.
Minguillóna, M.C., et al. 2012. Sci.Tot.Env.427–428: 191–202
Yu et al., 2005. J. Air & Waste Manag. Ass. 55, 1100–1110.

Comparison of On-line and Off-line methods for the quantification of particle bound Reactive Oxygen Species

S.J. Fuller[1], F.P.H. Wragg[1] and M. Kalberer[1]

[1]Department of Chemistry, University of Cambridge, Cambridge, Cambridgeshire, CB2 1EW, UK
Keywords: SOA, ROS, Instrumentation.
Presenting author email: sjf53@cam.ac.uk

Aerosol particles have long been associated with adverse health effects in the population. However links between the organic particle fraction and health effects are still poorly understood. It is thought that reactive oxygen species (ROS) present in organic aerosol can cause the observed health effects. There have been many filter collection studies that use adapted biological acellular assays to study the oxidative reactivity of ambient and laboratory generated aerosol. The most popular of which uses the fluorescence probe DCFH due to it's reactivity to a large range of ROS. Due to the reactive nature of ROS efforts have been made to automate the aerosol sampling and analysis process to reduce the time between collection and analysis associated with filter collection, which reduces decomposition of reactive species, and which allows for higher time resolution measurements (Venkatachari and Hopke, 2008). As yet however, there has been no direct comparison between the off-line filter collection methods and on-line automated systems.

In this study on-line and off-line methods were compared by measuring the ROS reactivity of oxidized oleic acid aerosol, a frequently used organic aerosol model system. For online measurements, particles were collected and continuously extracted on a wetted hydrophilic filter (Takeuchi et al., 2005). The particle collector samples air at up to 5 litres per minute and collects particles larger than an aerodynamic diameter of 50 nm with greater than 95% efficiency. The particles are continuously collected and extracted into a solution of horseradish peroxidase (HRP) (0.5 units per ml) that allows immediate reaction of ROS on collection and minimizes any reactive losses of ROS before analysis. The concentration of ROS is characterised following subsequent reaction of the oxidised HRP with DCFH (5 µM) for 10 minutes at 40°C, yielding the fluorescent product DCF in the continuous flow set-up. The concentration of DCF is measured using fluorescence spectroscopy in a flow-through cell and calibrated to ROS concentration with hydrogen peroxide. With a sampling rate of 5 lpm the detection limit of the system is approximately 10 nMoles of hydrogen peroxides per cubic meter of air.

For offline measurements the oxidized oleic acid aerosol particles were collected on a Teflon filter. The filters were collected for a range of times from 1 min to 15 min before extraction in water. The aqueous extract (0.8 ml) was combined with DCFH (1ml, 10 µM, 20 % PBS) and HRP solutions (0.2 ml, 5 units ml^{-1}) and measured with the same fluorescence technique as used in the online measurements.

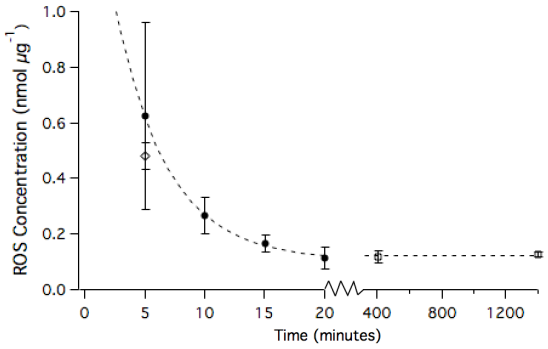

Figure 1. ROS concentration of oxidized oleic acid particles against time between particle collection and analysis. Comparison between online (diamond) and offline (circles) method.

On-line results show a linear relationship between aerosol concentrations and ROS concentrations with a gradient of 0.48 nmol ROS μg^{-1} particle mass. Figure 1 shows the combined results from the online and offline study with the time axis showing the time between start of sample collection and analysis for the offline samples. The ROS concentration determined with the online method is indicated by the open diamond symbol (at 0.48 nmol ROS μg^{-1}). Particles analyzed and collected with the offline method (filled and open circles) showed comparable values only when collected for a very short time (ca. 1min) followed by immediate analysis with ROS concentrations of 0.62 ± 0.33 nmol ROS μg^{-1}. However after a 15-minute delay time between particle collection and analysis the ROS concentration fell by a factor of up to five to 0.12 ± 0.04 nmol ROS μg^{-1}. When the filters were stored in the dark and reanalysed several hours later (open circles), there was no further decrease in the ROS activity (open circles, Figure 1) suggesting the presence of two different types of ROS in the particle.

Thus on-line methods are able to quantify also very short-lived ROS where as off-line studies are not able to capture the most reactive, and potentially the most health-relevant, fraction of particle bound ROS. This study suggests that particle bound ROS off-line studies are likely to greatly underestimate particle bound ROS activity.

M. Takeuchi, S.M.R. Ullah, P.K. Dasgupta, D.R. Collins and A. Williams, *Analytical Chemistry* **77**(2005), pp. 8031-8040.

P. Venkatachari and P.K. Hopke, *Aerosol Science and Technology* **42**(2008), pp. 629-635.

Inter-comparison of size distribution measurements in cloud expansion studies

E. Järvinen[1], M. Schnaiter[1], P. Vochezer[1], K. Höhler[1], N. Hiranuma[1] and O. Möhler[1]

[1]Institute for Meteorology and Climate Research, Karlsruhe Institute of Technology (KIT), Karlsruhe, Germany
Keywords: optical instrumentation, size distribution, PPD, welas.
Presenting author email: emma.jaervinen@kit.edu

In cloud expansion studies, the size distribution of droplets and/or ice particles is measured using optical particle counters (welas, Benz et al. (2005)). In addition, other instruments are in addition able to distinguish the particle phase by the forward scattering from particles (PPD) or by backscattering linear depolarisation ratio (SIMONE, Schnaiter et al. (2012)). The method of retrieving the size information from the measured spectra varies, but is usually based on Mie scattering of liquid droplets. As result we get the equivalent forward, side or backward scattering diameter of measured droplets based on the instrument used.

It is not established, what instrumentation is optimal for getting the most accurate information from size distribution in expansion chamber experiments. In our work we compare and evaluate the quality of size distributions retrieved from optical measurements from welas and from PPD. Based on our inter-comparison, we discuss the validation and weaknesses of both instruments and give recommendation on how to measure droplet and ice distributions.

The experimental results presented here were conducted in the AIDA (Aerosol Interaction and Dynamics in the Atmosphere) cloud chamber (i.e. Möhler et al. (2003)) during the INUIT-3 campaign. As test particles we used polydisperse Snomax and Illite dust aerosol or monodisperse Snomax and Illite dust aerosol combined with sulphuric acid. The starting temperatures of the experiments varied from 268 K to 246 K.

Figure 1 shows one expansion experiment run from the campaign. The pumping of the chamber was started at the time 0 seconds. When the temperature dropped to 243 Kelvins at around 80 seconds, we observed the formation of droplets by an increase in particle diameter measured by welas and PPD. The droplet formation is also seen in the increase of forward and backward scattering measured by SIMONE. At around 400 seconds after the pumping was started, ice particle formation was iniated. This was detected simultaneously by an increase of the depolarization ratio measured by SIMONE and the particle counters welas and PPD. The size range of droplets given by welas and PPD are comparable, but the ice particles detected by PPD seem to be smaller than those detected by welas. In addition, according to PPD the ice particles are growing straight from droplet mode, while in welas measurements a gap between droplet mode and ice mode is observed. This relates to different angular ranges that are used for interpretation of the scattering from the ice particles. The welas is measuring close to 90° scattering angle where ice particles show enhanced scattering compared to droplets of the same volume. Freezing of a droplet already leads to a sudden increase of the measured optical size.

In future work we want to compare the statistics of both size distributions during the times when just droplets or ice particles are present. We will compare the size distributions measured for Snowmax particles and Illite particles. Here, our goal is to determine how well the sizing works for different used aerosol types and for spherical droplets compared to non-spherical ice particles. As shown in fig. 1, we expect differences in the ice particle size distribution measured with welas and PPD, but for droplets both should agree.

The final step in our work is to reconstruct the depolarization ratios measured with SIMONE by using the size distributions measured with PPD and welas fitting the Mie-theory to those size distributions assuming single shape for the particles. By comparing the modelled depolarisation ratios to the measured ones, we are able to know if it is possible to have closure for one or both instruments to measure the size distribution.

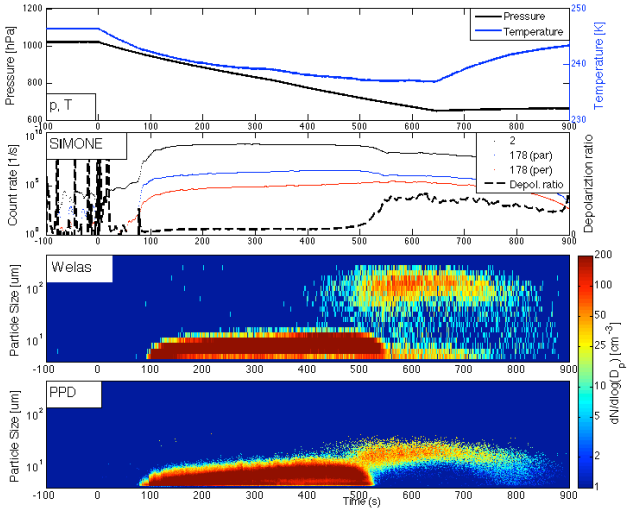

Figure 1. Pressure and temperature, SIMONE forwards scattering, backward scattering and depolarization ratio and the size distribution plots from welas and PPD during one expansion experiment.

Benz, S., Megahed, K., Möhler, O., Saathoff, H., Wagner, R. and Schurath, U. (2005) *J. Photochem. Photobiol.* A **176** 208–217.

Möhler, O., Stetzer, O., Schaefers, S., Linke, C., Schnaiter, M., Tiede, R., Saathoff, H., Krämer, M., Mangold, A., Budz, P., Zink, P., Schreiner, J., Mauersberger, K., Haag, W., Kärcher, B., and Schurath, U. Atmos. Chem. Phys. **3**, 211-223 (2003).

Schnaiter ,M., Büttner, S., Möhler, O., Skrotzki, J., Vragel, M., Wagner, R. (2012) *Atmos. Chem. Phys.* **12**,10465–84.

Validating SMPS-measured size distribution of double-mode spherical Silica nanoparticles by Transmission Electron Microscope (TEM)

E.M. Faghihi, L. Morawska, G. Johnson and T. Bostrom

International Laboratory for Air Quality and Health (ILAQH), Queensland University of Technology (QUT), Brisbane, Australia

Keywords: nanoparticles, size distribution, characterization.

Contact email address: e.majdfaghihi@qut.edu.au

Introduction: A nanoparticles size is one of their key physical characteristics that can affect their fate in a human's respiratory tract (in case of inhalation) and also in the environment. Hence, measuring the size distribution of nanoparticles is absolutely essential and contributes greatly to their characterization. For years, Scanning Mobility Particle Sizers (SMPS), which rely on measuring the electrical mobility diameter of particles, have been used as one of the most reliable real-time instruments for the size distribution measurement of nanoparticles. Despite its benefits, this instrument has some drawbacks, including equivalency problems for non-spherical particles (i.e. assuming a non-spherical particle is equal to a spherical particle of diameter *d* due to the same electrical mobility), as well as limitations in terms of its use in workplaces, because of its large size and the complexity of its operation (Kuhlbusch T, Asbach C et al. 2011).

In this study, we aimed to evaluate the performance of the SMPS in measuring the size distribution of double-mode silica particles, by comparing the results with the size distribution calculated from the analysis of TEM images.

Methods: A water-based colloidal suspension containing two populations of silica particles with different sizes was aerosolized using a nebulizer. The aerosol flow passed through a diffusion dryer and was divided into two separate flows: one to the SMPS for on-line size distribution measurement and the other to the electrostatic precipitator with a Formvar-Carbon coated cupper TEM grid inside for particle deposition.

30 SMPS scans were generated (3 days, 10 each) to verify the repeatability and reproducibility of the results. TEM imaging was done by a JOEL 2100 instrument and the particles dimensions were measured using *ImageJ v1.45k* analysis software. The measured diameter range of the Klebosol particles was divided into several *bins* and the number of particles in each bin was counted and used to calculate the size distribution.

Results: Figure 1 presents the size distribution of silica particles measured by the SMPS. As shown, there are several peaks in the graph but not all of them are related to silica particles. They represent solute residues (#1), doubly charged particles (#2) and finally, particle clusters (#3). However, both silica particle populations were also detected by SMPS and are circled in the figure (peaks of interest).

The average mean diameter/GSD measured by the SMPS, for the first and second population of silica particles were (45.1 nm/1.077 nm) and (82.2 nm/1.071 nm), respectively. Table 1 summarizes the results of size distribution measurement using TEM images.

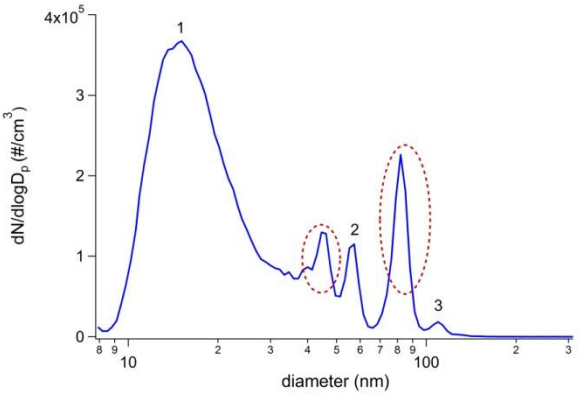

Figure 1. Size distribution of silica particles; SMPS results

Table 1. TEM analysis results

Population	*Size range (nm)*	*Mean diameter (nm)*	*GSD (nm)*	*Number of particles*	*Aspect ratio*
First	31.7-58	42.9	5.38	37	1.055
Second	58.1-89.5	78.9	5.96	68	1.041

According to the results, there is a difference between the mean diameters derived from the SMPS and TEM (5% for the first population and 4% for the second), which could be due to the sampling methods, the use of a neutralizer in the SMPS or statistical errors caused by the insufficient number of particles analyzed using the TEM method.

Conclusions: Despite the minor discrepancy mentioned above, the SMPS results showed a high level of accuracy in measuring the size distribution of double-mode spherical nanoparticles. However, the results might differ for non-spherical particles of a more complicated morphology, since they might have unknown orientations in the SMPS classifier which could result in measurement inaccuracy.

Kuhlbusch T, Asbach C, et al. (2011). "Nanoparticle exposure at nanotechnology workplaces: a review." Particle and Fibre Toxicology **8**(22): provisional version.

Application and recalibration of a GRIMM spectrometer in the monitoring of Sahara dust

C. Pio[1], J. Cardoso[1], T. Nunes[1], C. Alves[1], M. Cerqueira[1], S.M. Almeida[2], M. Almeida-Silva[2], M.C. Freitas[2]

[1]CESAM & Department of Environment, University of Aveiro, Portugal
[2]ITN, Instituto Superior Tecnico, Portugal
Presenting author email: casimiro@ua.pt

Optical Aerosol Spectrometers are relatively inexpensive devices employed in the measurement of aerosol concentrations with basis on the univocal relation between particle size and its light scattering properties. Optical Aerosol spectrometers are only sufficiently sensitive to particle size ranges above 200 nm, being specially adapted to measure coarse aerosols such as dust and sea salt spray.

A GRIMM optical aerosol spectrometer, model EDM164, was deployed for monitoring, during one year, the atmospheric aerosol in Cape Verde, region periodically subject to important Sahara dust intrusions. The device was pre-calibrated at the factory with Poly Styrene Latex (PSL) particles. With the GRIMM, numeric size distributions between 0.25 and 32 um, in 31 size bins, were determined as 5 minutes averages along 2011. In parallel the aerosol was co-collected with PM2.5 and PM10 samplers and concentrations determined gravimetrically after 1-2 days of sampling. In a number of occasions parallel sampling was performed also with impactors, for mass size distribution evaluation.

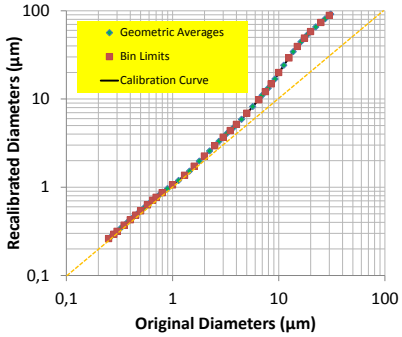

Figure 1- Recalculation of GRIMM particle size diameters using Mie theory, for dust particles having refractive index= 1.53-0.005i.

Using predictable aerosol particles density the GRIMM number concentrations were transformed into mass concentrations. These were intercompared with PM gravimetric concentrations, taking into account PM head inlet cutting characteristics and probable particle dynamic shape factors. While for $PM_{2.5}$ results were comparable, (GRIM=0.83*GRAV+0.58; R^2=0.99), for PM_{10} GRIMM concentrations were in average only 58% of the gravimetric measurements (GRIM=0.58*GRAV +1.3; R^2=0.96).

A possible cause for the results discrepancy are the different shapes and optical characteristics of the PSL aerosol used at factory calibration (Refractive Index RI=1.59) and the Sahara dust that has a brownish colour and therefore an imaginary RI component. The GRIMM calibration curve was re-calculated for Sahara type dust particles having refractive indexes in accordance with Kandler et al., (2007), by using the Mie theory adapted to the GRIMM optical geometry (software kindly provided by Thomas Mueller, Leipzig). The GRIMM recalculated values for the size distribution adapted to Sahara dust characteristics resulted in a much better agreement with gravimetric PM10 measurements (Fig. 2).

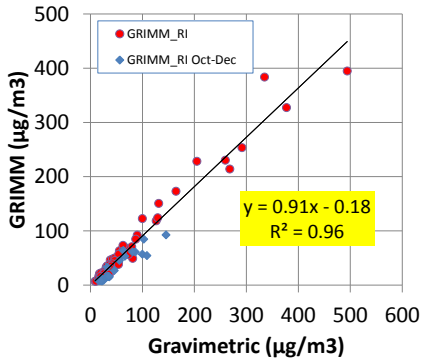

Figure 2- GRIMM and gravimetric PM10 measurement comparison, after recalibration

As seen in Figure 1 RI based recalibration has effects for size ranges above 1-2 um and becomes quite large for particles above 10 um. As result size distributions obtained with recalibrated GRIMM data present a quite high peak for particles larger than 10 um (see example in Figure 3) which does not seem expectable taking into account literature information and the size cut-off of GRIMM inlet.

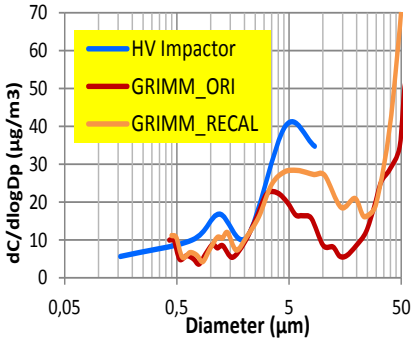

Figure 3- Comparison of mass size distribution obtained with the GRIMM and the impactor

Acknowledgement: This work was funded by the Portuguese Science Foundation (FCT) through the project PTDD/AAC-CLI/100331/2008. J. Cardoso acknowledges the PhD grant SFRH-BD-6105-2009 from FCT.

References: Kandler et al. (2007) *Atmos. Environ.*, **41**, 8058–8074

Description of the aerosol size distribution of the atmosphere during a Saharan dust intrusion over South Spain with airborne and ground based instrumentation: AMISOC

N. Seoane-Vieira[1], J. Andrey-Andrés[2], M. Sorribas[3], A. Corrales Sierra[4], R. González-Armengod[1], M. Gil[2], B. de la Morena[5], B. Marqués[4].

[1]Laboratorio de Telemedida e Instrumentación, Área de Ensayos en Vuelo y Armamento (AEVA), Instituto Nacional de Técnica Aeroespacial (INTA), 28850 Torrejón de Ardoz, Madrid, Spain

[2]Área de Investigación e Instrumentación Atmosférica (AIIA), Instituto Nacional de Técnica Aeroespacial (INTA), 28850 Torrejón de Ardoz, Madrid, Spain

[3] Andalusian Center for Enviromental Research, University of Granada, 18006 Granada, Spain

[4]Plataformas Aéreas de Investigación (PAI), Subdirección General de Experimentación y Certificación Instituto Nacional de Técnica Aeroespacial (INTA), 28850 Torrejón de Ardoz, Madrid, Spain

[5]Estación de Sondeos Atmosféricos El Arenosillo (ARN) Instituto Nacional de Técnica Aeroespacial (INTA) 21130 Mazagón - Moguer - Huelva

Keywords: Aerosol instrumentation, Airborne measurement, Saharan dust.

Presenting author email: nevesseoane@gmail.com

The occurrence of Saharan dust intrusions over the Iberian Peninsula as primary source of atmospheric aerosols is well known but there is not much information on the vertical profiles of the particles size distribution by airborne instrumentation. This work aims to the improvement of knowledge about it, as well as, to compare ground based and airborne measurements. On the other hand, the representativeness of surface measurements will also be analyzed.

The AMISOC campaign (Puentedura et al., 2012) was carried out in May and June 2012. This campaign combined ground based and aero-transported instrumentation aiming to measure aerosols in the presence and absence of a Saharan dust outbreak. AMISOC (Atmospheric MInor Species relevant to the Ozone Chemistry at both sides of the jet) is a research project funded by a Spanish R&D program.

Measurements were taken in South Spain: “El Arenosillo” sounding Station (ARN) (37.1N, 6.7W in Huelva). Selected dates for the campaign were chosen based on an atmospheric dust alert system using information from different models (DREAM, MAAPS, and SKIRON). Dates 31 May and 1 June 2012 were representative of Saharan dust intrusion while 13 June 2012 was representative of no dust.

The characterization of the vertical profiles of several atmospheric parameters was done by the use of CAPS (Cloud, Aerosol and Precipitation Spectrometer) atmospheric probe (Droplet Measurements Technology, Boulder, CO). The CAPS probe measures temperature, pressure, relative humidity, liquid water content, aircraft velocity and altitude, aerosol particle and cloud hydrometeor size distributions and other miscellaneous data. In this work we have used the measurement of CAS instrument; an OPC ranges particles from 0.5-50 µm. This probe was installed on the Spanish National Aerospace Technique Institute (INTA) CASA C-212 atmospheric research aircraft. Additionally, from “El Arenosillo”, dry ambient sub-micron size distribution within (0.55-1) µm and super-micron size distribution within (1-10) µm were monitored by an Aerodynamic Particle Sizer (APS) (TSI Mod. 3321).

Atmospheric profiles, with or without Saharan dust, were characterized by the particle number concentrations in several particle sizes and thermodynamic profiles. Figure 1 shows the vertical profile during a desert dust day (31/05/2012) of the temperature and relative humidity (left side) and the particle number size distribution (right side)

The Saharan dust intrusion analyzed in this work took place under the presence of clouds at about 5 km and 6 km height (see Figure 1). This cloud condition has allowed exploring the interactions of cloud droplets with Saharan dust aerosols.

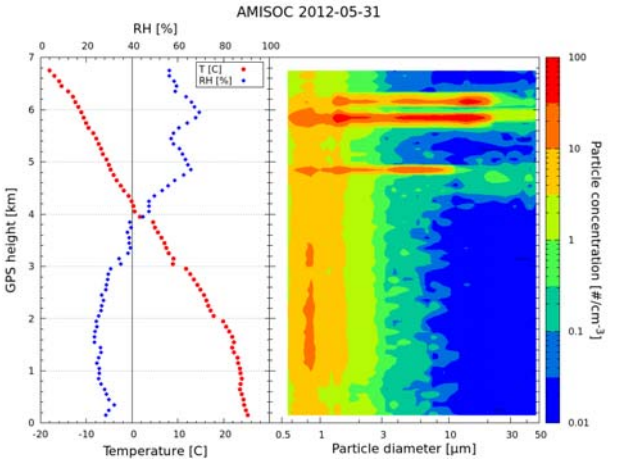

Figure 1: On the left side shows temperature and humidity profile from CAPS probe and in the right side vertical profile of the number particle size distribution of a dusty day.

References:

Puentedura, O et al., 2012. AMISOC 2012: Multi-instrument campaign for assessment of trace gas-aerosol interaction. European Aerosol Conference, Granada, Spain.

Acknowledgments This work is supported by the Spanish Ministry for Research and Innovation (MINECO) under grant CGL2011-24891 (project AMISOC) and the Andalusian Regional Government through TASTESOS project (P10-RNM-6299). The authors of this study are grateful to the CLAEX unit of the Spanish Air Force for operating the C-212.

Model 3088 Advanced Aerosol Neutralizer: Comparisons with Previous Generation

J.H. Scheckman, S. Elzey, J.E. Farnsworth, Horn, H-G. and B. Osmondson

TSI Incorporated, Shoreview, Minnesota, 55126, USA
Keywords: neutralizer, particle charge, soft X-ray, SMPS
Presenting author email: jacob.scheckman@tsi.com

Charge neutralization is a necessary and important step for many aerosol instruments and techniques. Particle sizing by differential mobility analysis, for example, relies on sample particles having a well-defined, known charge state. Traditionally, radioactive neutralizers have been used to generate bipolar ions which interact with particles by diffusion, and bring the particle population to a known, bipolar charge distribution.

Recently, low-energy soft X-ray neutralizers have been employed as an alternative to radioactive sources (Shimada *et al*, 2002; Lee *et al*, 2005). The soft X-rays ionize the air molecules, creating bipolar ions which bring the particles that they interact with to a Fuchs distribution consistent with radioactive sources such as americium-241.

Presented here are side-by-side comparisons between the previous (Model 3087) and new (Model 3088) generations of TSI's Advanced Aerosol Neutralizer. The new model features neutralizer performance consistent with the previous generation along with enhanced usability. Further, it offers full integration into the new TSI Model 3082 Electrostatic Classifier (Farnsworth, *et al*, 2013).

Radiation output from the soft x-Ray source was measured directly and was consistent between the models. Particle losses and particle generation were characterized across the full flow range of the instrument with agreement between the models.

Figure 1 shows several examples of particle size distributions comparing the SMPS response using the different neutralizers. This comparison was extended to the full flow and concentration range of the neutralizers and showed consistent performance from the previous generation to the new generation of Advanced Aerosol Neutralizer.

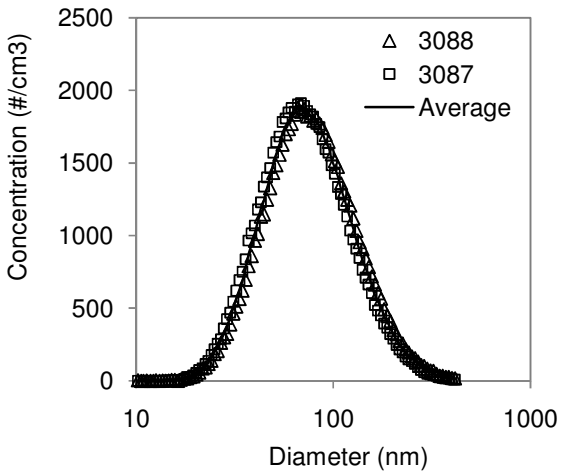

Figure 1. Comparison of SMPS response with Model 3087 and new Model 3088 Advanced Aerosol Neutralizer

Farnsworth, J.E., Quant, F., Horn, H.G., Osmondson, B. and Caldow, R. (2013) *Proc. Of Euro. Aerosol Conf.* In Preparation.

Lee, H. M., Soo Kim, C., Shimada, M., and Okuyama, K. (2005). *Journal of Aerosol Science*, **36**(7), 813–829.

Shimada, M., Han, B., Okuyama, K., and Otani, Y. (2002). *Journal of Chemical Engineering of Japan*, **35**(8), 786–793.

Black carbon measurements in snow with the single particle soot photometer

J. Svensson[1], D. Brus[1], A.-P. Hyvärinen[1], H. Lihavainen[1]
[1]Climate Change Unit, Finnish Meteorological Institute, Helsinki, PO.Box 503, 00101 Finland.
Keywords: Black Carbon, Snow albedo, Single particle soot photometer
Presenting author email: jonas.svensson@fmi.fi

Quantifying light-absorbing impurities in snow is a critical parameter needed to evaluate snow reflectance. The presence of light-absorbing particles, such as black carbon (BC), significantly lowers the albedo, and contributes to earlier melting of the snow pack (e.g. Flanner et al., 2007).

At present, there are mainly three different techniques used to measure BC in snow. Two methods collect the particles on filters for analyses with optical and thermal-optical methods. The third and newest developed technique does not utilize filters, instead it uses the single particle soot photometer (SP2) to quantify the BC mass concentration through laser-induced incandescence (McConnell et al., 2007). An additional benefit of using the SP2 is that the size distribution of the BC particles can be derived unlike the case in the other two filter based methods.

Due to the SP2's nature of measuring ambient aerosol, the need to aerosolize the BC particles in the melted snow introduces additional uncertainties in the measurements. This is system set-up dependent and an initial assessment has been done (Schwarz et al., 2012). There is still a great need, however, to deepen our understanding of these measurements. In this study we used an empirical approach similar to that used by Schwartz et al. (2012), in which particles in liquid were nebulized and thereafter measured with the SP2.

Polystyrene latex spheres (PSL) of know concentrations with diameters of 100, 202, 304, 360, 498, 802, and 1112 nm were used to determine the efficiency of the ultrasonic nebulizer (U5000AT+, Cetac) utilized to aerosolize the particles in the liquid. The efficiency at which particles were nebulized and detected by the SP2 was shown to be dependent of the peristaltic flow supplying the nebulizer. The flows with the greatest efficiency were determined to be in the range of 0.02-0.04 mL/min, where the average efficiency for all sizes was 0.04. Each PSL's size efficiency in this flow range is shown in figure 1.From this figure it can be noted that there is a reduction in efficiency of particles with a size greater than 800 nm.

The efficiency that different BC sizes were nebulized was also investigated. This was achieved through a DMPS, where certain sizes of BC particles were selected from a solution of Aquadag (a standard BC material used to calibrate the SP2). These measurements revealed an average efficiency of 0.4 for BC particles in the size range 100-600 nm. Gravimetric BC samples were then measured to observe the response of our measurement set-up. Using the efficiency for the PSL's and the BC sizes we were able to get the corresponding BC concentration of the gravimetric samples (fig. 2). This figure shows PSL's overestimate while the BC size correction underestimates.

Utilizing this measurement approach will be done for snow samples collected in Arctic Scandinavia, 2013, and a comparison with the established OC/EC method for measuring EC in snow will also be carried out before the EAC.

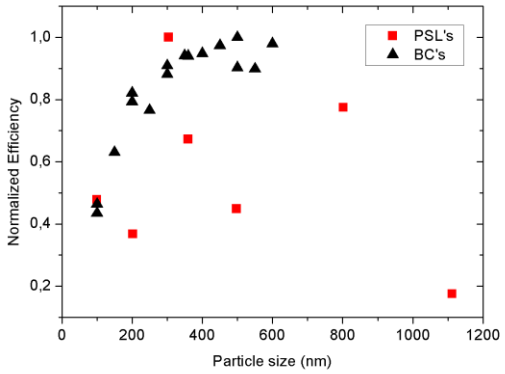

Figure 1. Normalized efficiency for PSL's and selected BC sizes.

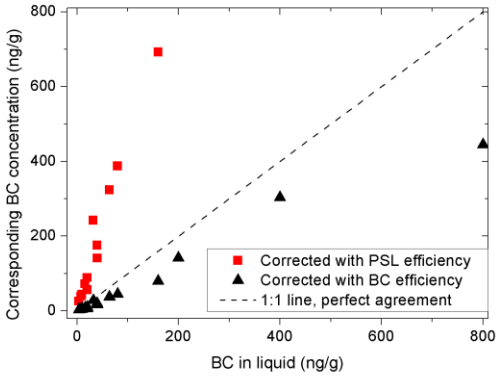

Figure 2. Analyzed gravimetric samples and their corrected BC concentration using the efficiencies from the PSL's (red points) and BC sizes (black points).

This was supported by the Nordic Top-level Research Initiative (TRI) *Cryosphere-Atmosphere Interactions in a Changing Arctic Climate* (CRAICC), the Academy of Finland through the Finnish Centre of Excellence in Physics, Chemistry, Biology and Meteorology of Atmospheric Composition and Climate Change (program number 1118615), Arctic Absorbing Aerosols and Albedo of Snow (project number 3162), and LIFE09 ENV/FI/000572 MACEB.

Flanner et al. (2007) *J. Geophys. Res.*, **112**, D11202
McConnell et al. (2007) *Science*, **317**, 1381-1384.
Schwarz et al. (2012) *Atmos. Meas. Tech.* **5**, 2581-2592.

RADES (RAdiological Dispersion Events Set-up) set-up and result from the characterization of the aerosol from simulated RDE´s (Radiological Dispersion Events).

F.G. Di Lemma[1, 2], J.Y. Colle[2], Thiele H. [2], Ernsteberg M. [2] and R.J.M. Konings[1, 2]

[1]Department of Radiation, Radionuclides & Reactors, Faculty of Applied Physics, Delft University of Technology, Delft, 2629JB, The Netherlands.
[2]European Commission, DG Joint Research Centre, Institute for Transuranium Elements, P.O. Box 2340, D-76125, Karlsruhe, Germany.
Keywords: Instrumentation, Radioactive aerosols, Aerosol characterization, SEM/EDX.
Presenting author email: fidelma.DI-LEMMA@ec.europa.eu

Evaluation of the source term, which means to perform a quantitative analysis of the radioactive release (including both the description and quantification of the gaseous species and aerosol particles release), is of main importance for risk assessment and emergency response in case of accident or sabotage involving nuclear material or radioactive sources. Many codes (such as ARGOS, RODOS, HOTSPOT) are available to evaluate the extension and levels of contaminated area after a radioactive releases. These codes need however of a quantitative assessment of the source term as input for their calculation.

A new experimental set-up (RADES) for the characterization of aerosol formation has been developed, to support the need of a better understanding of the source term related to RDE's with experimental data. In our experimental set-up we simulate RDE's by applying different thermal transients to sample materials. These materials have been chosen because they are widely used in commercial applications, such as nuclear medicine, sterilisation, or nuclear energy. Thermal transients are applied by a Nd:YAG continuous wave laser emitting at 1064 nm. The power of the laser is control in our experiment through a PID controller (Proportional, Integral, Derivate controller), the set point of the controller has been set to a quasi square temperature pulse. The created vapour forms aerosols by condensation in a cooler controlled environment; these aerosols are then collected by different systems (MOUDI impactor or MILLIPORE filters) for post analyses (e.g. size distribution, chemical and elemental composition). Techniques applied included SEM/EDX, ICP-MS, RAMAN.

In this presentation the results from the test performed on Co, CsCl, CsI and simulated nuclear fuel (consisting of a ZrO_2 matrix doped with chemicals simulating fission products BaO, Pd, CsI) will be presented, also the influence of different gases (Ar and ambient Air) on the aerosol formation will be shown. The results from the chemical analysis (ICP-MS and SEM/EDX) on the aerosols will be presented during the talk. For what concern the SEM analysis similarity in size distribution and form of the agglomerates was observed between the aerosol Co and ZrO_2 and between CsCl and CsI. The former show the formation of two types of aerosols: spherical individual particles with a diameter >1 μm and "string" structures formed by particles in the range of 50-300 nm. Influence of the chosen atmosphere was strongly shown for the Co and could be related to difference between the vapour pressure of metallic and oxidized Co. The salts (CsCl and CsI) on the other hand present as well a similar behaviour, showing particles of a mean bigger diameter and tendency to created spherical and independent particles. Strong coagulation phenomena were seen when the power applied was higher and high releases were observed.

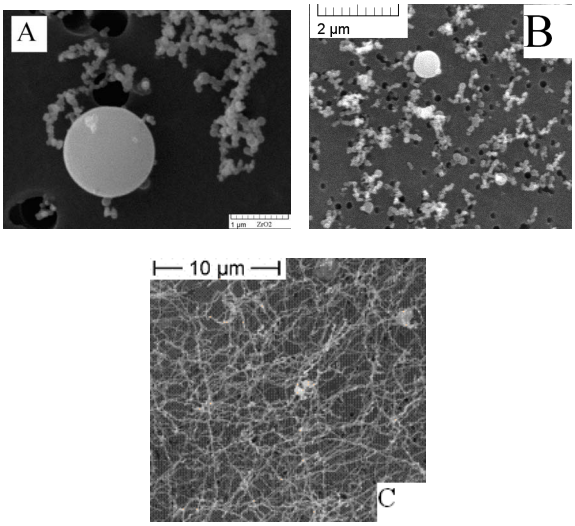

Figure 1. Example of aerosols collected from A) ZrO_2 B) and C) Co, showing similarity in size and form; Co aerosol where formed B) in air atmosphere and C) in Ar atmosphere, showing the influence of the atmosphere in particles agglomeration phenomena.

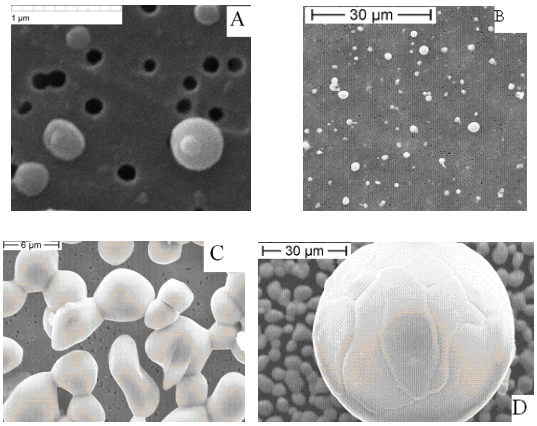

Figure 2. Example of aerosols collected for CsI, showing A) and B) spherical individual aerosols; C) and D) strong coagulation phenomena.

This work is supported by the 7th Framework Program of the European Commission.

A laboratory evaluation of four commercial particle sizers under several aerosol types

G.C. Dragan[1,2], J. Schnelle-Kreis[1,3], E. Karg[1,3] and R. Zimmermann[1,2,3]

[1]Joint Mass Spectrometry Centre, Cooperation Group Comprehensive Molecular Analytics, Helmholtz Zentrum München, Ingolstädter Landstr. 1, 85764 Neuherberg, Germany
[2]Joint Mass Spectrometry Centre, Chair of Analytical Chemistry, University of Rostock, Dr.-Lorenz-Weg 1, 18059 Rostock, Germany
[3]HICE – Helmholtz Virtual Institute of Complex Molecular Systems in Environmental Health – Aerosols and Health, www.hice-vi.eu
Keywords: particle sizing, aerosol spectrometer
Presenting author email: constantin.dragan@helmholtz-muenchen.de

Epidemiological studies have consistently shown an association between particulate air pollution and respiratory disease (Seaton et al., 1995). Therefore, aerosol monitoring has an important role in determining possible exposure events and eventual health risks related to hazardous particle inhalation.

Optical particle counters (OPC) and time-of-flight particle sizers are often used for determining size resolved particulate mass concentration for ambient and workplace measurements. As particle sizers are usually calibrated to accurately measure polystyrene latex (PSL) test particles, more information is needed regarding their ability to sample oil mist or ambient aerosols. Sampling of aerosols with different optical properties and densities compared to PSL particles can lead to errors in particle sizing and particle mass calculation.

The goal of this study was to evaluate the performance of four commercial particle sizers for oil mist, PSL and ambient aerosols. Sizing as well as counting efficiency was evaluated for several aerosol particle diameters and number concentrations. The particle sizers evaluated in this study were: a Palas Welas 3000 optical aerosol spectrometer, Grimm 1.108 and 1.109 optical portable aerosol spectrometers (PAS) and a TSI 3321 time-of-flight aerodynamic particle sizer (APS).

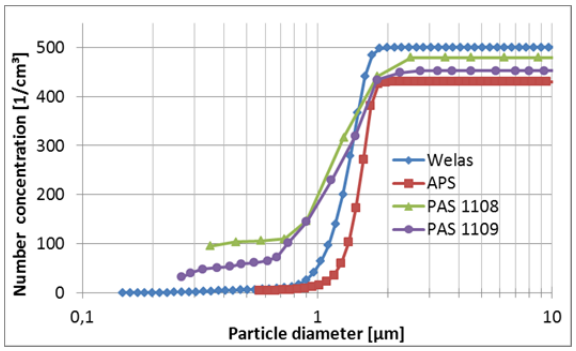

Figure 1. Summed particle number concentration of 4 particle sizers for hexadecane aerosol

An experimental facility was set up in order to test the performance of the four selected commercial particle sizers. The experimental facility is comprised of an aerosol generator, a dilution and mixing unit, a flow tube to allow the aerosol to stabilise and a TSI 3708 flow splitter to provide a representative sample for every particle sizer. Two different aerosol generators were used during the measurements. Hexadecane and octadecane particles were generated using a Topas SLG 270 condensation generator, while certified PSL particle standards were generated with a Topas ATM 220 nebuliser.

The results show that the tested devices often show different results, depending on aerosol type, particle size and number concentration. Significant differences were observed for ambient aerosol (Fig. 3), mainly due to the very different efficiency of the spectrometers to count particles smaller than 0,5 µm.

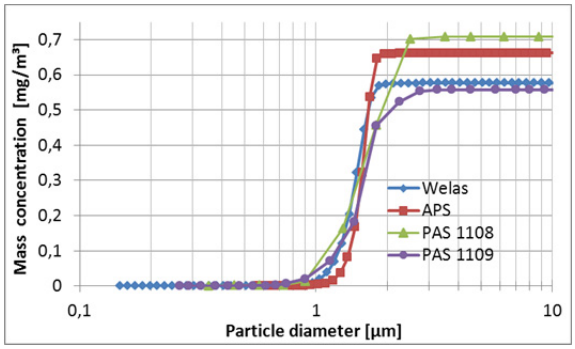

Figure 2. Summed particle mass concentration of 4 particle sizers for hexadecane aerosol

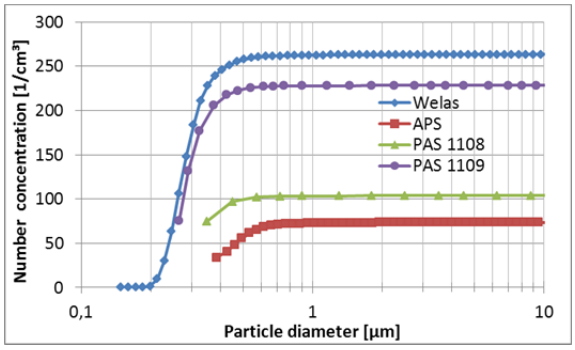

Figure 3. Summed particle number concentration of 4 particle sizers for ambient aerosol

This work is supported by the German Social Accident Insurance (DGUV), research contract FP299.
The health effects of organic compounds in aerosols are currently investigated in the framework of the Helmholtz Virtual Institute of Complex Molecular Systems in Environmental Health, HICE (www.hice-vi.eu).

Seaton, A., D. Godden, et al. (1995). "Particulate air pollution and acute health effects." The Lancet **345**(8943): 176-178.

On-line Diagnostics for Particle Size in Nanoparticle Manufacturing

A.J. Gröhn, M.L. Eggersdorfer, S.E. Pratsinis and K. Wegner

Department of Mechanical and Process Engineering, Swiss Federal Institute of Technology (ETH), Zurich, CH-8092, Switzerland

Keywords: Aerosol Sampling, On-line Characterization, Agglomerate Structure.

Presenting author email: arto.groehn@plt.mavt.ethz.ch

Introduction

Real-time aerosol characterization is not only important for airborne pollutants but also for monitoring of continuous aerosol processes, such as the production of engineered nanoparticles. For instance, the primary particle and agglomerate sizes often govern particle properties and must be controlled in a narrow range in order to achieve certain product performance. Flame aerosol reactors that dominate the field in terms of throughput, cost and versatility have production rates up to 1 ton per hour. Here, real-time online diagnostics for particle size can assist process control, assuring production quality and resulting in significant cost savings.

Sampling these production streams, however, is all but trivial. Particle concentrations are as high as 10^{18} #/kg_{gas}, requiring an enormous dilution of the aerosol to quench particle growth processes. The probe has to withstand temperatures up to ~1500 K and possibly corrosive environments. For this reason, mostly ex-situ methods have been used to determine particle size and morphology.

Here, an in-situ method for real-time determination of average agglomerate mass, volume, mobility and structure along with the constituent primary particle size is presented. It is performance-tested in continuous lab- and pilot-scale production lines for nanoparticles made by flame spray pyrolysis (FSP; Mädler et al., 2002).

Method

Flame synthesis of zirconia nanoparticles at rates up to 2 kg/h is used as a test system. A sampling probe for continuous extraction of the hot and highly concentrated aerosol was designed and constructed. Immediate dilution with adjustable cooling air flow rate allows effective suppression of coagulation. This enables in addition to continuous and real-time process monitoring direct measurement of the primary and agglomerate particle growth dynamics.

Online characterization of the fractal-like particles is achieved by combining a differential mobility analyser (DMA) with an aerosol particle mass analyser (APM) and applying a power-law correlation to derive average primary particle size as proposed by Eggersdorfer et al. (2012).

Results of the in-situ measurements are compared against off-line particle size characterization as well as predictions of a computational fluid dynamics (CFD)-based process model interfacing spray, fluid, combustion and aerosol dynamics (Gröhn et al., 2011, 2012).

Results and Discussion

Figure 1 presents how process simulations (Gröhn et al., 2012) show an increase in the agglomerate size and degree of aggregation for increasing precursor concentration consistent with experimental data at 4 ml/min precursor feed and dispersion O_2 flow of 5 l/min. Also the onset of soft-agglomerate formation can be determined from simulations. More detailed sampling at different radial and axial positions in the FSP reactor are to be conducted for improved model validation. Already good quantitative agreement is attained between the filter samples, CFD predictions and on-line sampling.

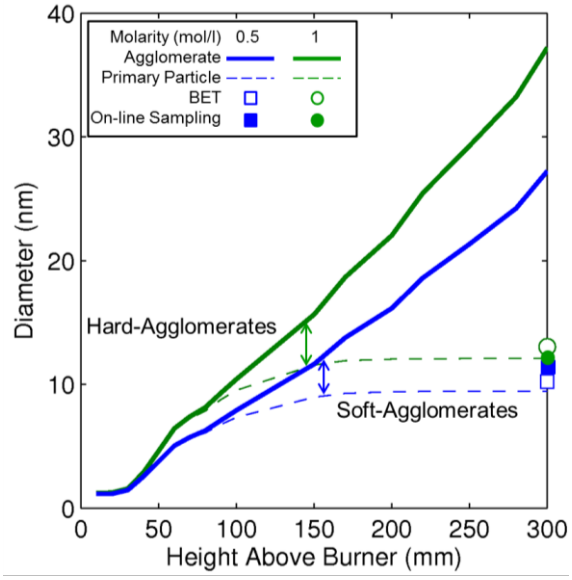

Figure 1. Predicted evolution of primary particle and agglomerate collision diameters for 4 ml/min of 0.5 and 1 M Zr precursor. Initiation of soft-agglomerate formation is indicated with arrows.

The research leading to these results has received funding from the European Community's Seventh Framework Programme (FP7 / 2007-2013) under grant agreement n° 228885.

Eggersdorfer, M.L., Gröhn, A.J., Sorensen, C.M., McMurry, P.H. and Pratsinis, S.E. (2012), J. Colloid. Interface Sci. 387, 12 - 23.

Gröhn, A.J., Buesser, B., Jokiniemi, J.K. and Pratsinis, S.E. (2011), Ind. Eng. Chem. Res. 50, 3159 - 3168.

Gröhn, A.J., Pratsinis, S.E., and Wegner, K. (2012), Chem. Eng. J. 191, 491 - 502.

Mädler, L., Kammler, H.K., Mueller, R. and Pratsinis, S.E. (2002), J. Aerosol Sci. 33, 369 - 389.

XPS analysis of size-segregated aerosol collected in an urban background site in Lecce (Italy)

M. R. Guascito[1], P. Ielpo[2,3], D. Cesari[2], A. Genga[1], C. Malitesta[1], D. Chirizzi[4], D. Contini[2]

[1]Dipartimento di Scienze e Tecnologie Biologiche e Ambientali, Università del Salento, Lecce, Apulia, 73100, Italy
[2]Istituto di Scienze dell'Atmosfera e del Clima, ISAC-CNR, Lecce, Apulia, 73100, Italy
[3]Istituto di Ricerca Sulle Acque, IRSA-CNR, Bari, Apulia, 70132, Italy
[4]Dipartimento di Beni Culturali, Università del Salento, Lecce, Apulia, 73100, Italy

Keywords: XPSanalysis, size-segregated aerosol, MOUDI
Presenting author email: mrachele.guascito@unisalento.it

Surface chemical composition plays an important role in determining the optical properties of aerosol and its reactivity. Therefore, the determination of surface composition of atmospheric aerosol is an important task because the surface of particles is involved in particle growth/shrink and it may contain chemical species potentially toxic (Klejnowski et al. 2012). Moreover, surface chemistry is dependent on particle size and it is an important feature that may shed light on particulate origin, its reactivity and participation in heterogeneous reactions thus influencing the oxidation state, elemental composition, the formation of functional groups on the surface and the radiative properties that determine the climatic effects (Clarke and Kapustin, 2010). There are many methods and instruments available for studying different properties of the surface of airborne Particulate Matter (PM), ranging from morphology to elemental composition (Coury and Dillner, 2008). X-ray Photoelectron Spectroscopy (XPS) for the chemical surface analysis of PM is not yet a routine method in aerosol characterisation. Nonetheless, in the last years the interest towards the application of this has rapidly grown (Vander Wal et al. 2011). One of the main advantages of XPS relies on the possible identification, in terms of quantification and chemical speciation, of all the elements (except H and He) present on particle surface and segregated in ~10-15 nm depth.

In this work we present an XPS surface study of different size fractions of atmospheric particles. Samples were collected in a background site in Lecce (SE of Italy) in modality "size-segregated", using a 10 stages impactor (MOUDI II, 120R) with rotating collection plates having an inlet with a nominal cut-off at 18 µm and 10 stages with a 50% efficiency cut-off at 10, 5.6, 3.2, 1.8, 1.0, 0.56, 0.32, 0.18, 0.10 and 0.056 µm. The collection substrates were Al foils (47 mm in diameter) and only a fraction of collected samples were examined by XPS (size 10 mm x 7mm). The other part of the samples were analyzed by high-performance ion chromatography HPIC (Dionex DX600), for determining the content of the main soluble ions, and by catalytic combustion analysis and NDIR detection (Shimadzu TOC-5050 Analyzer) for water soluble organic (WSOC) and inorganic (WSIC) carbon, in the bulk of collected particles. Elemental % (concentrations > 0.1-1%) surface chemical composition was determined for each size fraction with particular attention to S (SO_4^{2-}), Na^+, N (NH_4^+, NO_3^- , organic nitrogen) and Cl^-. Detailed analysis of C1s XPS spectra allowed to distinguish oxygen-containing groups such as carbonylic, carboxylic, and carbonate groups (e.g. Figure1). In some cases different hybridisation carbon states Csp2/Csp3 associated to different bonds, probably produced during particle formation, were also discriminated. The average mass size distribution of collected aerosol showed a bimodal shape with an accumulation mode (centred at 0.35 µm) and a coarse mode (centred at 4.5 µm). This work will aim at the systematic evaluation of surface chemical composition of particles of different sizes in order to put in evidence the differences in the surface composition of the two aerosol modes. Further, surface composition will be compared to the water soluble chemical components observed in the bulk of collected aerosol.

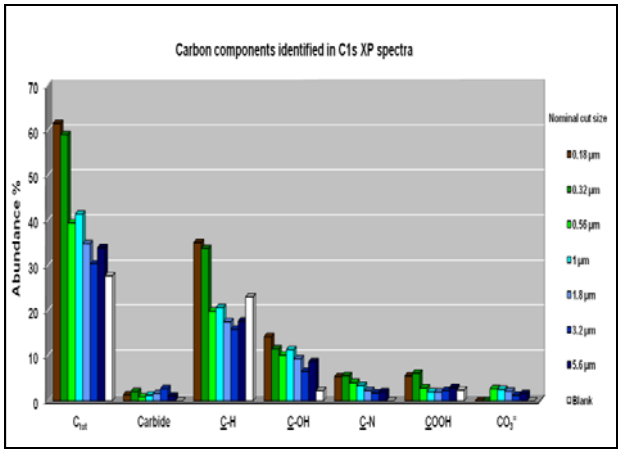

Figure 1. Size-segregated distribution of carbon components identified in C1s XP spectra. The indicated diameters are the geometric mean diameters of the stage analysed.

This study was performed with the financial support of the regional research network AITECH (Applied Innovation Technologies for Diagnosis and Conservation of Built Heritage).

Clarke A. and Kapustin V., (2010). *Science,* **329**, 1489-1492.

Coury C., Dillner A. M. (2008). *Atmospheric Environment*, **42**, 5923– 5932.

Klejnowski K., Pastuszka J.S., Rogula-Kozłowska W., Talik E., Krasa A., (2012) *Bull. Environ. Contam. Toxicol.*, **88**, 255-259.

Vander Wal R. L., Bryg V. M., Hays M. D. (2011). *Analytical Chemistry,* **83,** 1924–1930.

Characterization of filter materials for aerosol research – size resolved penetration

J. Ondráček, N. Zíková and V. Ždímal

Department of Aerosol and Laser Studies, Institute of Chemical Process Fundamentals, AS CR, v.v.i., Prague 6, 165 02, Czech Republic

Keywords: size resolved penetration, "aerosol" filters, "home-made" filter tester.

Presenting author email: ondracek@icpf.cas.cz

Generally, various types of filtration material can be met in many moments of everyday life (air filtration in offices and cars; personal, medical and military respirators, etc.). In aerosol science the filtration material is used for aerosol sampling (sampling heads) as well as for production of clean particle-free air (HEPA filters). Therefore it is necessary to know the size resolved penetration (counterpart of filtration efficiency) of these materials for various reasons (ventilation standards, medical care, military purposes, scientific concerns).

Information available from filter manufactures, a background of a decision on which filter to use for the specific purposes, is usually not detailed enough. The description, if available at all, typically includes characteristics like filter type, thickness, wettability, air resistance, gravimetric extractables and porosity (Millipore, 2001). However, the only information concerning aerosol particles' penetration is the total penetration of di-octylphalate (DOP) or paraffin oil. These measurements are based on very well-known standards (NIOSH or EN) describing how to perform the testing of filter efficiency, such as EN 1822 for HEPA and ULPA filters; EN 143 and 149 for respirators.

Unfortunately all these standardized tests bring several issues. First of all, the filters are challenged with polydisperse aerosols with given Count Median Diameter (CMD) positioned close to the Most Penetrating Particle Size (MPPS), assumed to be at 300 nm in diameter. Moreover, these tests measure only overall penetration giving no information about the real MPPS that is often shifted towards smaller diameters. It also means that the standard omits the fact that penetration is a function of particle size. Secondly, the measurements are usually performed using optical particle counters, OPCs, having their lower detection limit as high as 100 nm. Thirdly, one of the solutions prescribed in the EN 1822 for the aerosol generations, is sodium chloride, NaCl. Shape of these particles (cubical shape for NaCl) does not fully comply with the commonly used theoretical assumption in aerosol science – spherical particles (e.g. when we select monodisperse particles in the DMA).

Therefore, taking into account all the previously mentioned issues, the results of such an analysis based on standardized methods give only limited information about penetration of tested filter material. Considering both importance of filters for ongoing aerosol research and unsatisfactory description of filters filtration efficiency, aim of this work is to define size dependent penetration through filter material of the most often used filters in aerosol research.

In order to obtain detailed size resolved penetration of filtration materials used for aerosol research, we have developed our own filter testing system. Our filter tester (LACP, ICPF) consists of four main parts. They can be listed as follows (in the sequence as the air flows through the instrument): aerosol generator, particle size separator, filter holder and two particle detectors.

The studied filter materials were divided into four groups according to the used materials: cellulose filters, Teflon membrane filters, fiber filters (both glass and quartz fibers) and polycarbonate filters. All the tested filters are commercially available and widely used (such as Whatman, Millipore and Pall).

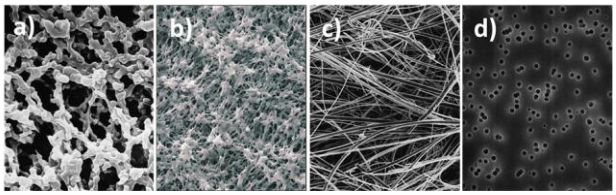

Figure 1. SEM pictures of a) mixed cellulose ester filter, b) PFTE (Teflo) filter, c) glass fiber filter, and d) polycarbonate filter.

Testing of various filter materials proved the functionality, good precision and reproducibility of a home-made filter tester. The measurements of penetration for standard commercial filter materials might be useful for many scientists and other users working with these materials. The comparison of penetrations for different types of filtration materials showed wide variety of penetration curves, MPPS and the maximum penetration. This study also confirmed our initial doubts about the standard filter efficiency testing method, regarding the used testing material, setting of MPPS and measuring only the total penetration of polydisperse aerosol. Therefore, such a study could serve also as a basis for improvements in the filter efficiency standard method, which seems to give insufficient and in some perspectives limited or even misleading information.

This work was supported by the Ministry of Interior of the CR under grant No. VF2010201513.
Authors would like to thank also to Prof. Holub from Clarkson University for a long-term loan of one UCPC, and to Mr. Š. Rychlík from the CHMI for providing some of the filter materials.

Millipore, (2001). *Glass Fiber Filters*, data sheet.

Data Merging of Size Distributions from Electrical Mobility and Optical Measurements

T. Tritscher[1], A.F. Zerrath[2], S. Elzey[2] and H. S. Han[2]

[1]TSI GmbH, Particle Instruments, Aachen, 52068, Germany
[2]TSI Inc., Shoreview, MN, 55116, USA
Keywords: SMPS, OPS, Particle number size distribution, Refractive index, Nanoparticle.
Presenting author email: torsten.tritscher@tsi.com

The measurement of size, concentration, and potential exposure to nanomaterials has received increasing attention during the last years. Nanoparticles are present in ambient air as well as in indoor or laboratory environments. A key parameter for the characterization of particles is their size distribution and number concentration.

The TSI Scanning Mobility Particle Sizer (SMPS) is well established, also used as a reference and is able to cover the range from 2.5 nm to 1 µm. Recently, a small, portable and easy to handle version of the SMPS was introduced to the market: the NanoScan SMPS, TSI model 3910 (Elzey *et al*. 2012). A Radial Differential Mobility Analyzer classifies the particles, which are then individually counted by an integrated, isopropanol-based Condensation Particle Counter (CPC). Number size distributions in the range from 10 to 420 nm can be obtained in 13 channels.

The size range of both SMPS systems can be extended to coarse particles with an additional compact instrument: the Optical Particle Sizer (OPS), TSI model 3330. The OPS is able to provide number size distributions in the range from 300 nm to 10 µm with 16 freely adjustable channels. This optical sizing method reports an optical particle diameter, which is often different from the electrical mobility diameter measured by the SMPS technique.

TSI DataMerge software is able to merge SMPS data with size distributions from aerodynamic diameter measurements from an Aerodynamic Particle Sizer (APS). DeCarlo *et al*. (2004) also reported on combining mobility and aerodynamic diameter.

We present here a next-generation data merging tool for optical diameter and electrical mobility diameter. This software module is the first approach to merge the data from the two different sizers to compile a single data set describing the particle size distribution from 10 nm to 10 µm. This software tool is user friendly and easy to use. It also allows reviewing and averaging data from SMPS, NanoScan SMPS and/or OPS. More importantly, when merging the OPS and SMPS/NanoScan distributions, the software can take the aerosol optical properties into account by automatically determining the aerosol effective refractive index.

Figure 1 shows an example for ambient measurements from NanoScan SMPS and OPS on the top panel and the resulting composite fit on the bottom panel. The merging procedure is more or less challenging depending on the particle type, concentration and distribution. The software allows several pre-settings, data averaging and adjustments. The curve fitting algorithm uses up to 3 modes of lognormal distribution function to curve fit the data.

The presentation will show different merged data sets and merged options to demonstrate their impact on the composite fit accuracy.

DeCarlo, P.F., Slowik, J.G., Worsnop, D.R., Davidovits, P. and Jimenez, J.L. (2004), *Aerosol Science and Technology* 38, 12, 1185-1205

Elzey, S., Caldow, R., Johnson, J.P., Grose, M., Morell, S. and Jensen, D. (2012), *EAC 2012 proceedings*, WG08S2O06

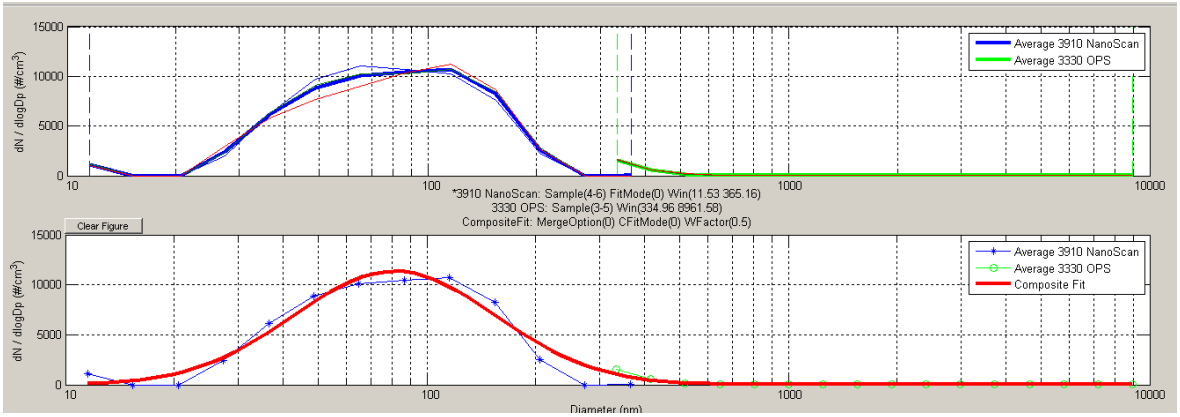

Figure 1. Top panel: Ambient data from NanoScan SMPS 3910 (blue bold line) und OPS 3330 (green bold line), thin lines represent the individual scans. Bottom panel: Fitted size distribution (red bold line) from 10 nm to 10 µm.

Tandem of Differential Mobility Analyzer and Centrifugal Particle Mass Analyzer: application to hygroscopic growth of aerosol particles

S.S.Vlasenko[1], E.F.Mikhailov[1]

[1]Department of Atmospheric Physics, St. Petersburg State University, St. Petersburg, 198504, Russia
Keywords: hygroscopic growth, DMA, CPMA
Presenting author email: Sergey.Vlasenko@paloma.spbu.ru

The interaction of atmospheric aerosol particles with water vapor is a crucial factor in determining their aerodynamic size and optical properties and hence their atmospheric lifetime, radiative forcing effects, height distribution etc. The prevalent technique to study hygroscopic behavior of aerosol particles is based on using a tandem of hygroscopic differential mobility analyzers (HTDMA) which enables to follow the particles mobility diameter as function of relative humidity, so the water uptake by aerosols has to be calculated by indirect way with some uncertainty due to lack information about particle shape and density.

In this study we introduce the approach to hygroscopic growth research based on direct particle mass measurements using centrifugal particle mass analyzer (CPMA, Cambustion Ltd). The mass-based measuring technique is more preferable to describe water uptake of aerosol using thermodynamic or parametric models (Mikhailov *et al,* 2013).

Ammonium sulfate (AS) particles were used as a test object. A 0.01wt% AS solution was dispersed by TSI atomizer (Model 3076). The polydisperse aerosol was dried to below 10%RH by passing through a diffusion dryer and entered the DMA (TSI 3080 with X-rays aerosol neutralizer TSI 3087). The resulting monodisperse particles (mobility diameter 100 nm) then passed through a series of one (hydration mode) or two (dehydration mode) single-tube Nafion humidity exchangers. One Nafion humidity exchangers was filled with water to guarantee aerosol exposure to high (>95%) RH, another was blown through with air at controlled RH. The humidified aerosol particles passed through CPMA operating in scanning mode and reckoned by water-based condensation particle counter (TSI model 3787). A combination of scanning CPMA with CPC gives particle mass distribution (Olfert and Collings, 2005).

In hydration mode monodisperse aerosol passed only through air-conditioned humidity exchanger with increasing RH in discrete steps from 5% to 95%. At every stable RH level a mass spectrum of humidified aerosol was measured by CPMA (cycle duration about 10 min). The hygroscopic mass growth factor (G_m) was determined as ratio of modal particle mass at given RH to modal particle mass at dry condition (<10%RH). Figure 1 shows mass growth factors plotted against relative humidity (open circles). The obtained results are in good agreement with the FDHA measurements (dashed line) (Mikhailov et al., 2013) which used here as reference data. Particularly in the CPMA experiments AS particles exhibited deliquescence transition at RH=80±2% .

Upon dehydration monodisperse particles after DMA firstly passed through water-filled humidity exchanger and then entered air-conditioned humidity exchanger with step-down RH. The measuring procedure was the same as in hydration mode.

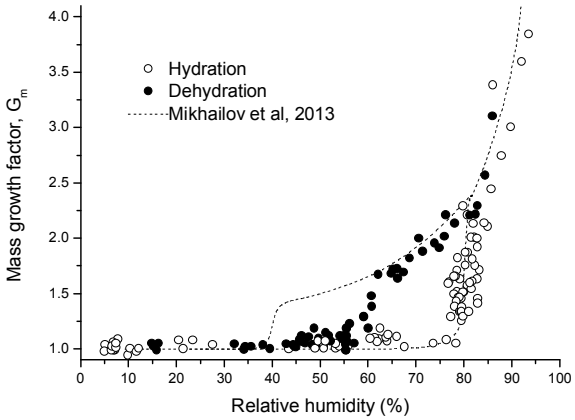

Figure 1. Hygroscopic growth of ammonium sulfate particles measured by tandem of DMA-CPMA.

The obtained data plotted in figure 1. (closed circles). Obviously efflorescence of AS solution droplets in CPMA experiments occurs at RH=61±2% that is much higher than efflorescence RH in FDHA or HTDMA experiments. The observable discrepancy may be due to some impurities in AS solution or due to partial coagulation inside CPMA.

Nevertheless the described technique appears to be promising for *in situ* measurements of hygroscopic properties of aerosol particles.

This work was supported by geosciences research centre of St. Petersburg State University "Geomodel" and Russian Foundation for Basic Research under grants 11-05-00945 and 12-05-00620.

E. Mikhailov, S. Vlasenko, D. Rose, and U. Pöschl (2013) *Atmos. Chem. Phys*. **13**, 717–740.

J.Olfert and N.Collings (2005) *Journal of Aerosol Science,* **36**, 1338-1352.

Steady-state mass-mobility measurements of cigarette smoke using a CPMA

T.J. Johnson[1], R. Cabot[2], C. Treacy[2], C. Dickens[2], J. McAughey[2], C. U. Yurteri[2], J.P.R. Symonds[3] and J.S. Olfert[1]

[1]Department of Mechanical Engineering, University of Alberta, Edmonton, Alberta, T6G 2G8, Canada
[2]British American Tobacco, Regent's Park Road, Millbrook, Southampton, SO15 8TL, U.K.
[3]Cambustion Ltd., J6 The Paddocks, 347 Cherry Hinton Road, Cambridge, CB1 8DH, U.K.
Keywords: CPMA, Tobacco smoke, Density.
Presenting author email: Caner_Yurteri@bat.com

Tobacco smoke is a dynamic formation of gaseous and particulate material. The density of particulate phase can change due to evaporation - condensation and alter its mass and mobility. Therefore these aerosol characteristics are important for modelling lung deposition or smoke particle transport in air. The mass and mobility of cigarette smoke particles was measured using a Centrifugal Particle Mass Analyzer (CPMA) and Differential Mobility Analyzer (DMA).

The experimental setup, shown in Figure 1, placed a DMA and Condensation Particle Counter (CPC) upstream of a CPMA. The DMA selected the particles based on electrical mobility, while the upstream CPC accounted for the particle concentration decreasing in the bag over time. The CPMA then further classified the particles by mass-to-charge ratio. By stepping the CPMA through the particle mass range and counting the number of classified particles with the downstream CPC the mass-classified concentration peak was determined for the set DMA mobility size.

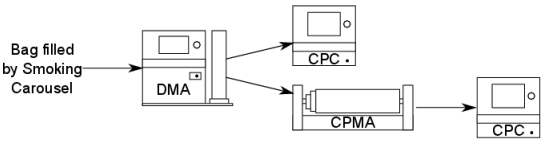

Figure 1. Experimental setup of DMA-CPMA-CPC system.

Due to the scanning nature of the DMA-CPMA-CPC set-up, only steady-state measurements could be completed. Since smoking is not a steady-state process, smoke was produced using an ISO smoking routine on a smoking carousel and collected in a Tedlar bag. The effective density measured using this experimental setup is shown in Figure 2.

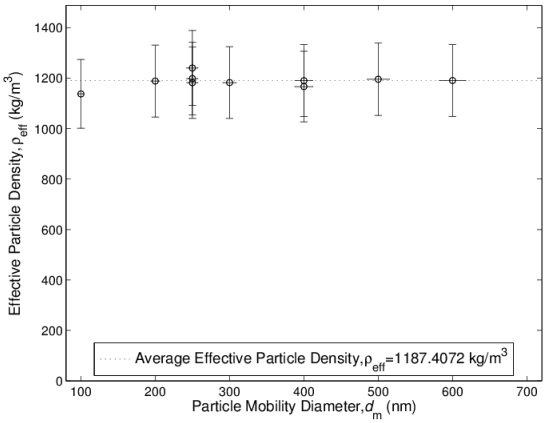

Figure 2. Effective density of cigarette smoke measured using a DMA-CPMA-CPC system.

The effective density is constant over the measured mobility size range and has a mean value of 1190±140 kg/m^3. Using a Millikan cell Lipowicz (1988) measured the effective density of smoke particles in the 1.1 to 1.5 µm diameter range to be 1100±20 kg/m^3.

The effects of the initial particle concentration and smoke aging time on the effective particle density are shown in Figure 3.

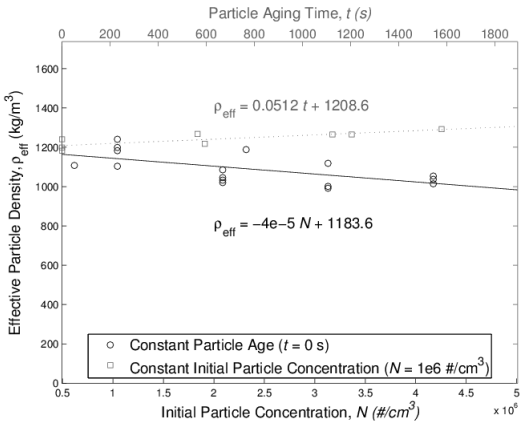

Figure 3. Effects of initial particle concentration and aging time on effective density of 250 nm particles.

Aging the particles caused the effective density to increase slightly, with every 1000 seconds of aging increasing the effective density on average by 4.3% compared to fresh smoke. This increase could be due to the volatility of the smoke causing lighter components of the particle to evaporate over time. Conversely, increasing the initial particle concentration in the bag caused the effective density of fresh smoke to decrease. A 10^6 particle per cm^3 increase in initial particle concentration caused a 3.3% decrease in the effective density. During the bag filling process, the evaporation of volatile material is sensitive to the initial particle concentration. Therefore, as the initial particle concentration increased or more volatile material evaporated during the filling process, the vapour pressure in the bag increased, slowing the evaporation rate of the volatile components. However the effects of aging and initial particle concentration are relatively small and within the uncertainty of the instruments.

This work was supported by British American Tobacco.

Lipowicz, P. J. (1988). Determination of cigarette smoke particle density from mass and mobility measurements in a Millikan cell, *Journal of Aerosol Science*, **19**, 587–589.

Assessment of Voltage Shift in Tandem DMAs by Brownian Particle Trajectory Simulation

M.Alonso[1], F.J. Alguacil[1], J.P. Santos[2] and V. Gómez[3]

[1]Centro Nacional de Investigaciones Metalúrgicas (CENIM-CSIC), Madrid, Spain
[2]Instituto de Física Aplicada (IFA-CSIC), Madrid, Spain
[3]Instituto de Nanociencia de Aragón (INA), Zaragoza, Spain
Keywords: Tandem DMA, voltage shift, Brownian particle trajectory
Presenting author email: malonso@cenim.csic.es

Past experimental works have shown that when two geometrically identical differential mobility analyzers operating under the same conditions are connected in series, in such a manner that the particles classified by the first unit are fed to the second one (tandem DMA), the peak voltage at which particles are classified in the second instrument may substantially differ from the fixed voltage applied to the first DMA.

Voltage shifts only appear when the aerosol particles have a very high mobility. When these particles are present at sufficiently large concentrations, the additional space-charge electric field created by the unipolarly charged particles migrating between the DMA electrodes may be of the same order of magnitude as the applied field, in which case, the simple Knutson-Whitby relationship between mobility and voltage ceases to be valid.

The voltage shift phenomenon may even arise when the aerosol concentration is not large. In this case, the strong Brownian motion of the particles leads to the appearance, in the classified aerosol stream, of particles with mobility outside the theoretical range. Figure 1 illustrates this point. Suppose that the actual mobility distribution of the original aerosol is given by the curve shown, and that the voltage applied to the first DMA is such that the theoretical peak mobility of the classified particles is Z_1. Clearly, there are no particles with such mobility within the aerosol population; however, due to diffusion broadening of the transfer function, some particles in the tail of the mobility distribution will appear in the classification stream. If these particles are subsequently fed to the second DMA and the voltage is scanned, it will be found that the peak voltage corresponds to a mobility $Z_2 < Z_1$, where, in contrast with Z_1, Z_2 is a "real" mobility, i.e. particles with that mobility do exist in the original aerosol.

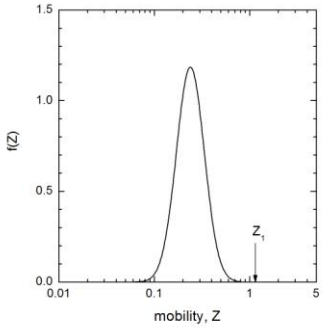

Figure 1. Particle Mobility distribution at DMA-1 inlet.

Numerical simulations of voltage shifts in tandem DMAs have been carried out, based on the calculation of the trajectories of Brownian particles under the applied electric field. The simulation starts by considering a log-normal mobility distribution for the original aerosol, and calculating the corresponding mobility distribution of the classified aerosol when a fixed voltage V_1 is applied to DMA-1 (the mobility Z_1 corresponding to this voltage is calculated with the well-known Knutson-Whitby relation). The aerosol having the thus calculated distribution is then reclassified in DMA-2. The voltage applied to the second unit is scanned, and the program calculates the total number of particles classified at each voltage. From this distribution, the mean voltage $<V_2>$ is calculated and transformed into its corresponding mobility Z_2. The illustrative results shown in Figure 2 were obtained using TSI short-column DMAs (length = 11.11 cm) operated at Q_a/Q_c=2/20.

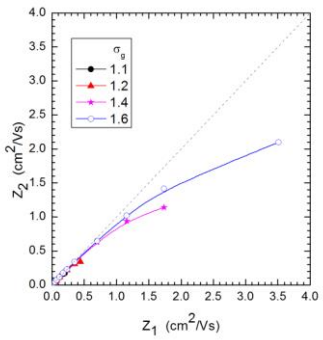

Figure 2. Peak mobility as measured from DMA-2 vs nominal mobility of particles classified by DMA-1. Log-normal particle size distribution at DMA-1 inlet, with D_{pg} = 5 nm, and σ_g as stated in the legend.

Quite large deviations between Z_1 and Z_2 can be observed in this example. It demonstrates the need to be cautious when using a DMA to withdraw very small particles, especially when their size falls within the tail of the distribution.

A final observation: In the example of Figure 1, we assumed that the aerosol mobility distribution was already known. In practice, this distribution is not known. We could then apply a certain voltage to DMA-1 and obtain a stream of particles with nominal mobility Z_1 (say, 3.5 cm^2/Vs), and we might believe that we are really producing particles with such a high mobility. According to Figure 2, the actual mobility of these particles is much smaller, about 2.1 cm^2/Vs, typical of negative air ions.

Instrumental optimization of the compact laser mass spectrometer LAMPAS 3 for on-line single particle analysis under various field conditions

K.-P. Hinz[1], A. Fendt[1] and B. Spengler[1]

[1]Institute of Inorganic and Analytical Chemistry, Justus Liebig University Giessen, Giessen, D-35392, Germany

Keywords: Aerosol mass spectrometry, Atmospheric aerosols, Chemical composition, Single particle analysis

Presenting author email: klaus-peter.hinz@uni-giessen.de

During the last two decades the development of mass spectrometric systems resulted in a variety of instruments for elemental analysis, bio-chemical investigations or control and identification of dangerous substances in the environment. In aerosol science online mass spectrometric instrumentation is often used to characterize particle ensembles or single particles without prior sampling and sample transportation. Transportable instruments of this type can be operated directly at sites of interest provide for a fast chemical and physical in situ characterization of individual particles combined with a high level of specificity. During the last few years the reduction of the size of such mass spectrometric instrumentation was one major requirement to make them accessible for new application fields such as quality control, public safety and clinical diagnostics (Hinz et al., 2011).

The compact mobile laser mass spectrometer LAMPAS 3 (19" rack, 150 cm in height) was developed with improved instrumental parameters and options for a user-friendly long-term operation. The highly robust instrument is designed for operation under field conditions and can be easily transported. Aerosol particles are introduced into the instrument through a differentially pumped inlet system. Inside the mass spectrometer particles are optically detected by two continuous laser beams. Particle size is determined using their size-dependent velocity. Afterwards, an actively triggered UV laser evaporates and ionizes the detected particles. The generated ions are analysed with a bipolar time-of-flight mass spectrometer.

During optimization of the LAMPAS 3 system several instrumental features (voltage settings, delayed ion extraction, use of reflectron time-of-flight analysers, laser beam attenuation) were integrated to significantly improve mass resolving power and mass accuracy. An improved quality of results is also observed, using enhanced statistical classification and interpretation of data.

Several measurements were performed under laboratory and field conditions (e.g. on Jungfraujoch 2013) to optimize the instrumental parameters of the LAMPAS 3 system. Particles of various ambient origins and standard particles such as polystyrene latex spheres, salt particles and mineral particles were used to characterize the instrumental performance.

Results of the instrumental optimization and applications will be presented. E.g., spectra detected at the challenging site of Jungfraujoch at an altitude of 3580 m asl showed characteristic signal patterns of mineral and carbonaceous particles as well as mixtures of these particle types with secondary components such as ammonium, nitrate and sulphate. The aim of these investigations was, among others, the characterization of ice nuclei and of background aerosol in the lower troposphere for a better understanding of cloud formation and their influence on earth climate.

Instrumental improvements and optimization of the LAMPAS 3 results in an analytical system suitable for aerosol characterization under various conditions and requirements. In the future, the compact laser mass spectrometer LAMPAS 3 will offer the possibility of advanced in situ particle identification in various application fields.

This work was supported by the Deutsche Forschungsgemeinschaft (DFG), Germany, Grant No. HI 857/4-1, and the research program "Landes-Offensive zur Entwicklung Wissenschaftlich-oekonomischer Exzellenz - LOEWE", research focus "AmbiProbe", state of Hesse, Germany.

Hinz, K.-P.; Gelhausen, E.; Schäfer, K. C.; Takats, Z.; Spengler, B. (2011) Anal. Bioanal. Chem. **401,** 3165-3172.

Multi-Element Scanning Thermal Analysis (MESTA) of Aerosols and Nano-Carbon Particles

Y.P. Hsieh[1], G. Bugna[1] and K. Robertson[2]

[1]Center for Water and Air Quality, Florida A&M Univeristy, Tallahassee, Florida, 32307, USA
[2]Tall Timbers Research Station, Tallahassee, Florida, USA
Keywords: Biomass burning, MESTA, thermogram, PM.
Presenting author email: yhsieh@famu.edu

A rapid and sensitive method for the chemical analysis of aerosols is highly desirable because aerosol samples are usually small, heterogeneous and easily contaminable. We report here the development of a multi-elemental scanning thermal analysis (MESTA) that can quickly and sensitively analyze aerosols with little or no pretreatment. Basically, the MESTA heats up a sample from ambient to 800 ^{o}C at a given heating rate and under a given atmosphere. The volatile during the heating is carried by a carrier gas to a high-temperature oxygenated quartz tube (1100 ^{o}C) where the C, N, S and H contents are oxidized to their respective oxides and detected by the respective detectors. The result of a MESTA is a C, N, S and H thermogram of a sample, which reveals the chemical/thermal character of the compounds in a sample. Since 2007, MESTA has been successfully applied to the analysis of aerosols, nano-carbons, and black carbons in environmental samples. MESTA can differentiate organic and inorganic forms of C, N and S rapidly and sensitively without pretreatment. It provides ample chemical signatures for the characterization and identification of aerosols. Present here are the MESTA results of aerosols from ambient air, forest fires and animal farms and nano-carbon samples. Aerosols of ambient air are enriched with low-temperature volatile N and S components, which are absorbed ammonia and organic sulfur, respectively. Forest fire emitted aerosols are lacking the low-temperature N and S components but enriched with more thermally stable (>350 ^{o}C) compounds. MESTA can not only differentiate sources of aerosols between biomass burning and ambient air, it can discern the aerosols produced from different combustion phases of a fire (smoldering or flaming or mixed). MESTA has also been used to examine the chemical/thermal properties of nano-carbons after oxidation or chemical processes. This study shows that MESTA may be a promising technique for analyzing aerosol and nano-crbon particles for management and research purposes.

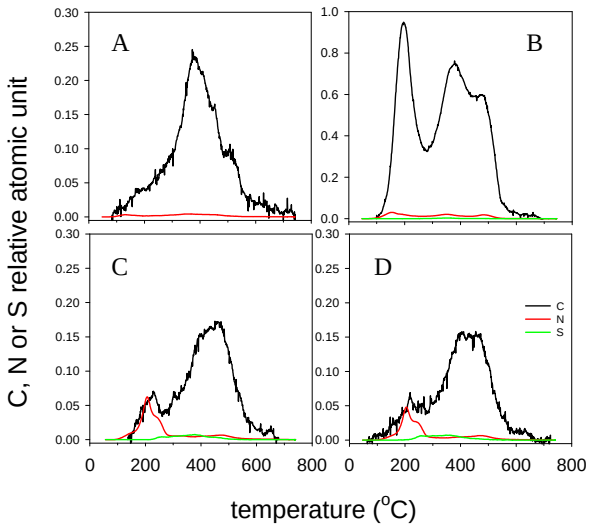

Figure 1. MESTA thermograms of PM2.5 collected at the burning (A), 14 hours after the burning (B), 58 h after the burning (C) and 148 h after burning (D).

This work was supported by a National Science Foundation/Atmospheric Chemistry Grant #0962970 to YP Hsieh, K. Robertson and G. Bugna.

References

Hsieh, Y.P., (2007) *J. AOAC International* 90:54-59

Hsieh, Y.P., Bugna, G. and Robertson, K. (2010) *Proceedings of the 24th Tall Timbers Fire Ecology Conference* pp 73-78.

Das, O., Wang, Y and Hsieh, Y.P. (2010) *Organic Chemistry* 41:263-269

Hiseh, Y.P. and Bugna, G. (2008) *Org. Geochem.* 39:1562-1571

Study on particle capture characteristics and numerical analysis for impaction sizer

C-H Huang, C-J Wu, Y-Y Chang

Department of Environmental Engineering and Health, Yuanpei University, 30015 Hsinchu, Taiwan

Keywords: impaction sizer, particle capture efficiency, Stokes number
Presenting author email: chhuang@mail.ypu.edu.tw

Design, testing and evaluation of an impaction sizer are very important for fine particles sampling in the atmosphere. Studies have pointed out that substrate coated with grease in the impaction sizer can maintain its capture particulate characteristics. However, the loaded particulate was accumulated on the grease substrate under long-time heavy loading conditions. Another foam impaction sizer has been applied to the study of fine particles sampling. The foam impaction sizer has the characteristics of reducing particulate rebound effect and of higher particulate loadings. However, its particulate capture efficiency curve does not follow the steep theoretical curve. The particle capture efficiencies of foam impaction sizer with larger porosity and thickness was found to be higher than those with smaller thickness and porosity.

In this study, the particle capture characteristics of an impaction sizer were studied experimentally first. Oleic acid particles were generated as liquid particles by utilizing an ultrasonic atomizing nozzle. An aerodynamic particle sizer was used to measure the aerosol number concentrations at the inlet and outlet of the foam impaction sizer installed in the lower section of the test chamber to determine the particle collection efficiency. Foam substrate was used as the collection substrates of impaction sizer with thicknesses of 3 mm and foam porosity of 100 ppi.

The flow field in the foam impaction sizer was then simulated by solving the Navier-Stokes equations in the cylindrical coordinate. The governing equation was discretized by means of the finite volume method. After obtaining the flow field, the particle equations of motion were solved numerically to obtained particle trajectories in the foam impaction sizer.

Fig. 1 shows the particle capture efficiencies of foam impaction sizer with jet diameter of 0.72 cm at the flow rate of 15 LPM as the rate of jet diameter to distance between jet and collection substrate equals 1. The particle capture efficiencies of foam impaction sizer increase as the square root of Stokes number increased. Results show that the particle capture efficiencies of foam impaction sizer for solid particles are similar with those for liquid particles. It indicates that particle bounce is insignificant for the foam impaction sizer as the particle loading in light condition. This study will perform the numerical calculations of the particle capture efficiencies for a novel foam impaction sizer. This study will also evaluate experimentally the particle capture efficiencies of the novel foam impaction sizer for different conditions.

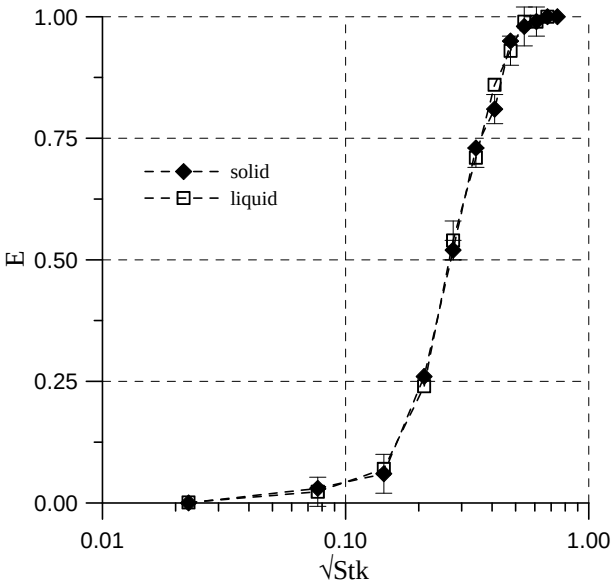

Fig. 1 Particle capture efficiency of foam impaction sizer.

Consistency of Long-term Black Carbon Trends from Thermal and Optical Measurements in the U.S. IMPROVE Network

L.-W.A. Chen[1], J.C. Chow[1], J.G. Watson[1] and B.A. Schichtel[2]

[1]Division of Atmospheric Sciences, Desert Research Institute, Reno, Nevada, 89512, USA
[2]Cooperative Institute for Research in the Atmosphere, Colorado State University, Fort Collins, Colorado, 80523, USA
Keywords: visibility, EC, absorption, reflectance
Presenting author email: antony@dri.edu

Decreasing trends of black carbon (BC), also termed elemental carbon (EC) as determined by thermal/optical analysis, have been reported at the U.S. IMPROVE (Interagency Monitoring of PROtected Visual Environments) network from 1990 to 2004 (Murphy *et al*, 2011), consistent with the phase-in of cleaner engines, residential biomass burning technologies, and prescribed burning practices. BC trends for the past decade (2000–2009) are examined in this study due to an upgrade of IMPROVE carbon instruments and the thermal/optical analysis protocol since 2005.

The IMPROVE thermal/optical reflectance (TOR) method separates BC from organic carbon (OC) on filter samples by temperature-dependent volatilization and oxidation. A fraction of OC chars in the inert atmosphere, as evidenced by decreases in light (632.8 nm He/Ne laser) reflected from the aerosol deposit on the filter surface, is continuously monitored during the analysis and corrected from BC measurements (Chen *et al*, 2004). The 2005 carbon instrument upgrade led to a transition from the IMPROVE to IMPROVE_A protocol (Chow *et al*, 2007). The new protocol does not change the temperatures plateaus but rather reflected the "actual" analysis temperatures that had been implemented since the inception of the IMPROVE network. It also enables simultaneous monitoring of filter reflectance and transmittance without changing the reflectance measurement configuration.

Optical measurements designed for charring correction provide alternatives for quantifying BC abundances on filters. Filter attenuation using reflected light (τ_R) is defined as

$$\tau_R = -\ln(R/R_0) \qquad (1)$$

where R and R_0 are the reflected light intensity of particle-laden (prior to carbon analysis) and blank (after carbon analysis) filter, respectively. τ_R is an independent measure of light absorption coefficient (b_{abs}) as well as BC on the filter (e.g., Janssen *et al*, 2011). Digital thermograms of > 83 000 IMPROVE samples acquired by 24-h sampling on every third day from 2000 through 2009 were reprocessed to obtain the τ_R values. The 65 sites with the longest records and highest data recovery rates are used for this analysis (Chen *et al*, 2012). They represented 25 U.S. geographic regions.

The changes in regression coefficients between BC and τ_R before and after 2005 were first examined with a dummy-variable approach (Gujarati, 1970), and relationships between BC measured from the two periods were established (Chen *et al*, 2012). The variability is shown to be within ±10% in general. Larger deviations occur for high or low extreme BC levels.

BC and τ_R trends were further assessed using a nonparametric Mann-Kendall (M-K) test. M-K statistics yield Sen's slope (Burn and Hag Elnur, 2002) and its p-value and confidence intervals. BC and τ_R show universal decreasing trends across the U.S. The BC and τ_R trends are well correlated (Figure 1), with national average downward rates (relative to the 2000–2004 baseline medians) of 4.5 % yr^{-1} for BC and 4.1 % yr^{-1} for τ_R. The consistency between BC and τ_R measurements adds to the weight of evidence that BC reductions are real rather than an artifact of changes to the measurement process. At the current rate of progress, the goal of the U.S. Regional Haze Rule for BC should be met by the 2064 deadline.

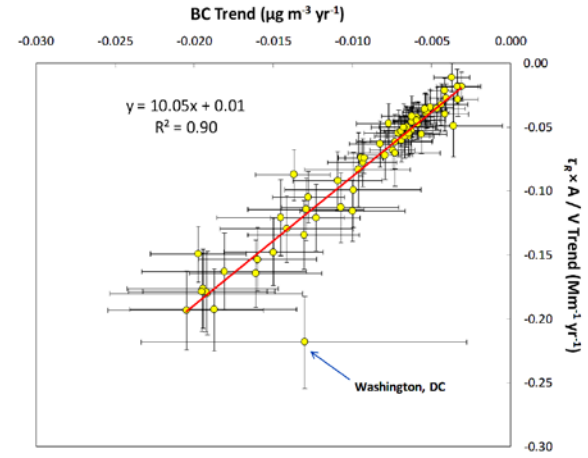

Fig. 1. A comparison of BC and τ_R trends for 65 IMPROVE sites during 2000–2009. The unit of slope is $m^2\ g^{-1}$, corresponding to mass specific absorption of BC.

This work was supported by the U.S. National Park Service (C2350000894) and U.S. Environmental Protection Agency (T2350086187).

Burn, D.H. and Hag Elnur, M.A. (2002) *J. Hydrol.*, **255**, 107-122.

Chen, L.-W.A., Chow, J.C., Watson, J.G., Moosmüller, H. and Arnott, W.P. (2004) *J. Aerosol Sci.*, **35**(6), 765-780.

Chen, L.-W.A., Chow, J.C., Watson, J.G. and Schichtel, B.A. (2012) *Atmos. Meas. Tech.*, **5**, 2329-2338.

Chow, J.C., and *et al* (2007) *J. Air Waste Manage. Assoc.*, **57**(9), 1014-1023.

Gujarati, D. (1970) *Amer. Stat.*, **24**, 18-22.

Janssen, N.A.H., and *et al* (2011) *Environ. Health Perspect.*, **119**, 1691-1699.

Murphy, D.M., and *et al* (2011) *Atmos. Chem. Phys.*, **11**, 4679-4686.

Airspace Dimension Test (ADT) – A novel technique for diagnosis of chronic obstructive pulmonary disease with nanoparticles

Jonas Jakobsson[1], John Kumlin[1], Johan Hedlund[1], Per Wollmer[2], Jakob Löndahl[1]

[1]Division of Aerosol Technology (EAT), Lund Institute of Technology, 221 00, Lund, Sweden
[2]Dept. of Clinical Sciences Malmö, Lund University, 205 02, Malmö, Sweden
Keywords: Lung deposition, nano particles, COPD, emphysema.
Presenting author email: Jonas.Jakobsson@design.lth.se

Introduction

Chronic Obstructive Pulmonary Disease (COPD) is one of the most common causes of death worldwide and is projected to increase to the third leading cause of death by 2030, depending on smoking habits, air pollution and demographic changes in many countries (Murray et al, 1997).

An early diagnosis is crucial to the outcome for the patient but current methods lack in precision.

It has been theoretically and experimentally shown that lung deposition of nanoparticles differ between healthy human subjects and COPD patients. This makes it plausible that lung deposition could be used as a diagnostic technique for COPD and emphysema (Löndahl et al., 2012).

The objective of this study was to develop and characterize a novel technique, named airspace dimension test (ADT), for lung diagnosis with inhaled nanoparticles.

Methods

An instrument was constructed to perform measurements of lung deposition of nanoparticles in human subjects over a single breath.

A well-controlled aerosol of polystyrene nanosphere particles with a narrow size distribution is generated. The aerosol is diluted with clean air to a concentration around 2000 particles/cm^3.

The subject inhales the aerosol with a vital capacity manoeuvre, holds breath for a determined period of time and then exhales into a sample collector. The particle concentration of the inhaled and exhaled aerosol is measured by a condensation particle counter (CPC). The exhaled aerosol is compared to the inhaled aerosol and the deposition fraction (DF) is calculated.

The sensitivity, precision and resolution of the technique was characterized by measurements with varying particle sizes and breath hold times in a small group of healthy subjects.

Results

DF increased with increasing particle size and decreasing breath hold time as could be expected for particles in the diffusion dominated size regime. The observed data agrees with adjusted simulations using a semi empirical lung deposition model. (Figure 1). Figure 1 shows how the DF depends on the inhaled particle size and the dwelling time in the lungs of a human subject.

The standard deviation for three consecutive measurements with 50 nm particles on the same volunteer was found to be 0.35%, while the intersubject variability was 3.3%. Thus, the instrument has sufficient precision to differentiate between individuals.

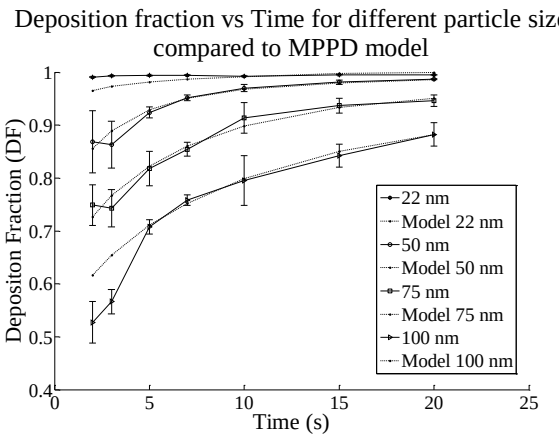

Figure 1. Lung deposition fraction depends on the inhaled particle size and breathing pattern.

Conclusions

The instrument shows both sensitivity and precision. Because lung deposition of nanoparticles (<100 nm) is controlled mainly by diffusion, a process depending on particle size, time and distances, it seems likely that the measurements reflect the geometrical airway dimensions of the lung. The observed data supports this.

ADT measurements are expected to yield information similar to that of a MRI examination of the lungs, using hyperpolarized ^{3}He, but at a fraction of the cost and with minimal discomfort for the subject.

Hopefully this technology can provide a valuable contribution to the diagnosis of COPD and emphysema in a near future.

We gratefully acknowledge The Swedish Research Council (project 621-2011-3560), the Crafoord foundation and the Swedish heart and lung foundation for financial support.

Murray, C. J. L. & Lopez, A. D. (1997), *Alternative projections of mortality and disability by cause 1990-2020: Global burden of disease study. Lancet*, 349**,** 1498-1504.

Löndahl J, Swietlicki W, Rissler J, Bengtsson A, Boman C, Blomberg A, Sandström T. (2012), *Experimental Determination of Diesel Combustion Particles in Patients with Chronic Obstructive Pulmonary Disease.* Particle and Fibre Toxicology 2012, 9:30

Remotely operated PLUS-octocopter used as an aerosol measurement platform

P. Madl, C. Oberauer and F. Steinhäusler

Division of Physics and Biophysics, Department of Materials Engineering and Physics, PLUS University, Salzburg, A-5020, Austria
Keywords: unmanned aerial vehicle, flying aerosol measurement platform
Presenting author email: pierre.madl@sbg.ac.at

The herein presented design is part of the *BRIDGE* Concept Case Advanced Situation Awareness for proactive risk management. It will fill this gap by providing the user inter alia with real-time data on the extent of airborne pollution inventories.

One of the core-component is a manually controlled unmanned aerial vehicle (UAV), termed PLUS-Octocopter. As shown in Fig. 1, the system consists of a ground-station, a wireless communication link and the sensor-equipped flying platform. The latter houses 8 electric motors, Global Positioning System (GPS) for stabilized flying mode, two different cameras (visual (VIS) / infra-red (IR)) an onboard-computer and several solid state sensors (T, rH, p, β, γ) as well as a particle number counter (P_N) and a particle mass detector (P_M). Table 1 summarizes its core specifications:

Table 1. Technical specifications of the UAV.

UAV	Octocopter
Power supply	20Ah Li-polymer rechargeable batteries
Flying time	>15min, less at windy conditions
Weight	5 kg (incl. LiPo-pack)
add. payload	2.5 kg
Downlink	Radio-controlled @ 2.4 GHz
2D-sensors	2-servo-adjusted camera unit i) VIS camera (0.4 - 1 µm) i) IR-camera (7.5 - 13 µm)
1D-sensors	Atmospheric (T, rH, p) Radiation (β, γ) Particle mass (µg/m^3) Particle number conc. (1/cm^3) Gases (CO, CO_2, C_2H_6, CH_4, N_2O)
DPU	Win-OS ultra small PC
Flight rec.	120 GB shock resistant SSD
GPS	Flight control & auto-homing
Ground	
Downlink	Radio-controlled @ 2.4 GHz
Win-OS Laptop	Visualization of area (IR & VIS) and display of sensor data

UAV-Characteristics: Although the vehicle is controlled via the ground station, the onboard computer is used both as the data processing unit (DPU) for the control signals keeping the system airborne, as well as a flight recorder for logging flight-sensitive parameters; i.e. status of each cell within the LiPo-packs, GPS-data (location, altitude, flight path). At the same time the DPU-hub logs all the sensor data along with the VIS/IR-data streams. The up- and downlink system, which is likewise controlled via the DPU, is achieved using a commercially available high-power WLAN system operating in the 2.4 GHz-band. At any time, and at least at batteries in reserve capacity status, the UAV will be switched into GPS-guided automatic homing mode.

UAV-sensors: Apart from the 2-D-sensors and the standard atmospheric sniffers (see Table 1), the UAV features two aerosol sensors. The P_M-sensor detects mass-fractions <10µm with a sensitivity of <5ng (with the UAV grounded and slightly less in a stationary humming, airborne mode). The P_N-sensor records particle number concentration in three different size classes simultaneously (0.3, 2.5 and 10 µm). Both aerosol sensors require a data acquisition time of 10 sec, which translates into 6 readings per minute. A different set of sensors regard the solid-state pyroelectric sensors to detect gaseous substances. Their detection principle rests on the specific absorption bands in the IR-window in-between 3 to 5 µm (for the various gases listed in Table 1). The entire throughput of the sample air through the sensor-compartment is achieved via a miniature carbon-vein pump at a constant flow-rate of 5 L/min.

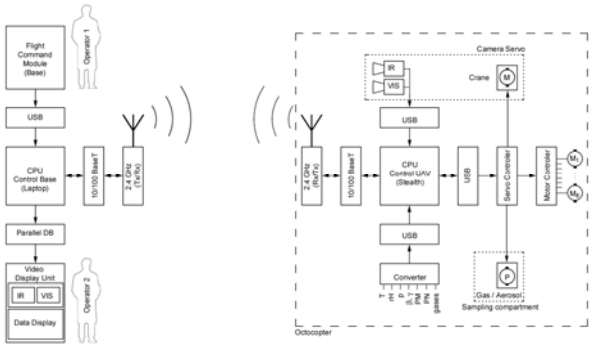

Figure 1. Schematic block diagram of the PLUS Octocopter-system, highlighting ground station and the UAV. *Legend*: Tx, Rx, Transmitter and receiver for the corresponding frequencies; M, Step-motor, M_1-M_8: lifting electric-motors; P, pump; VIS & IR, USB-compatible VIS and IR-camera units, CPU, Central processing unit; USB, Universal Serial Bus; Parallel DB, parallel Data Bus; 10/100BT, bidirectional Ethernet link; T, rH, p, β, γ, P_M, P_N, sensor compartment (see text).

Field of application: the above described system can be used for assisting incident commanders, fire-fighters, environmental air-quality monitoring at stacks, or other emission sources with limited access.

This work was partially supported by the 7th EU Framework Project No. 26.18.17. (BRIDGE).

A CAPS-Based Single Scattering Albedo Monitor

T. B. Onasch, P. Massoli, P.L. Kebabian and A. Freedman

Center for Sensor Systems and Technologies, Aerodyne Research, Inc., Billerica, MA 01821 U.S.A.
Keywords: aerosol, single scattering albedo, extinction, nephelometer.
Presenting author email: onasch@aerodyne.com

We present data detailing the performance of a particle single scattering albedo (SSA) monitor that incorporates both a CAPS (Cavity Attenuated Phase Shift)-based optical extinction measurement [Massoli, et al., 2010] and an inverse nephelometer in the same measurement volume. Since an absolute extinction measurement is provided, the scattering channel can be calibrated with any non-absorbing particle (e.g., a PSL) or gas (other than air). The monitor demonstrates noise levels of less than 1 Mm^{-1} (1σ, 1 s) in both channels while providing 1 s response time (10-90%).

The aerosol extinction measurement is identical to that of the CAPS PM_{ex} monitor. However, the middle portion of the optical path incorporates a 10 cm i.d. sphere. The sphere walls are coated with Avian-D paint which provides a water-proof surface with >98% diffuse reflectance over the visible light range. Within the sphere region, the aerosol flow is contained within a transparent tube to prevent the particles from contaminating the sphere.

As with all instruments employing a nephelometer to measure scattering, the CAPS PM_{SSA} demonstrates a measurement bias as a function of particle size. The larger the particle, the more the differential scattering cross section grows in the forward and backward directions at the expense of sideways scattering. As there must be apertures for the probe light to enter and leave the measurement volume, less scattered light is thus captured for large particles compared to smaller ones. This 'truncation' error was measured using PSLs of varying diameter by measuring the apparent SSA compared to a value of unity expected for the non-absorbing particles. Virtually no truncation error is measured out to a diameter of ~500 nm. (See Fig. 1.) The response falls to 90% at 1 micron and to 80% at 2..5 micron diameter. While this level of error is not insignificant at large particle diameters, it is substantially smaller than commercially available nephelometers.

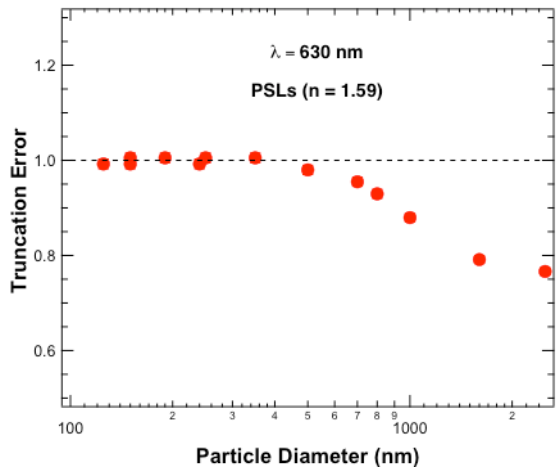

Fig. 1 Truncation error of CAPS PM_{SSA} at 630 nm measured using non-absorbing PSLs.

We have tested the CAPS PM_{SSA} monitor extensively in the laboratory. For example, SSA measurements of nascent and organic and sulfuric acid coated soot particles using a CAPS PM_{SSA} at 630 nm and a cavity ring down-based extinction monitor coupled to a photoacoustic particle absorption spectrometer at 532 nm, courtesy of C. Cappa, U.C. Davis, showed excellent agreement between the two over a wide range of SSA values. (See Figure 2.) The soot particles were generated using a methane diffusion flame, coated via gas-to-particle condensation, and size selected at 350 nm mobility diameter, small enough to eliminate the effects of scattering truncation.

The CAPS PM_{SSA} monitor can be operated in any wavelength region compatible with the availability of high reflectivity mirrors, LEDs and photomultiplier tube (PMT) photocathodes. At present, the available wavelength band is restricted to the 400-700 nm region because of the lack of suitable high reflectivity mirrors in the UV and of photocathode mateials in the near-IR.

This work was supported by the Atmospheric System Research program of the U.S. Department of Energy.

Massoli, P. Kebabian, P., Onasch, T, Hills, F. and Freedman, A. (2010) Aerosol. Sci. Technol. **44**:428–435

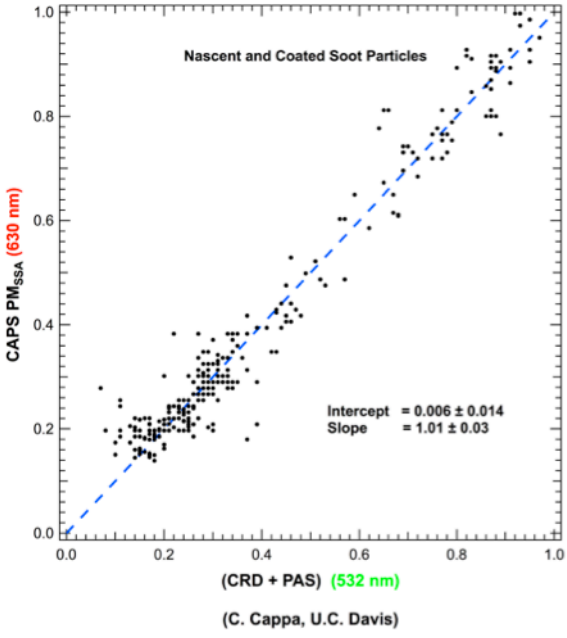

Figure 2. Comparison of measured SSA using CAPS PM_{SSA} (630 nm) and CRD Extinction+Photoacoustic Absorption Spectrometer (courtesy of C. Cappa, U.C. Davis) operating at 532 nm.

Performance Enhancements to TSI Water-based Condensation Particle Counters

J.H. Scheckman, S. Morell and F. Quant

TSI Incorporated, Shoreview, Minnesota, 55126, USA
Keywords: CPC, water-based CPC
Presenting author email: jacob.scheckman@tsi.com

Condensation particle technology has been a core aerosol measurement technique for many years (McMurry, 2000). Traditionally, butanol has been used as the "working fluid" in the condensation particle counter (CPC). More recently, water-based CPC's (WCPC) have been developed (Hering *et al.*, 2005), and used in nearly all CPC applications including standalone operations such as ambient monitoring as well as in multi-component systems such as SMPS.

Several enhancements to TSI's WCPC's have been implemented including flow system modifications, mechanical changes and firmware adjustments. These changes were made in order to improve long term reliability and ease of maintenance. Mitigation was added against rare flooding events as well as to enable complete flooding recoverability without permanent damage or requiring repair or recalibration. Mechanical changes to the inlet assembly allow for easier removal/replacement of the growth tube wick.

Small modifications to the WCPC engine resulted in a more consistent signal at high concentrations, and improved linearity as concentration approaches $1x10^6$ p/cm^3. (Model 3783 Environmental Particle Counter) Figure 1 shows an example comparison of the old design compared to the new design.

Additionally experiments are presented in which flooding was induced in properly functioning WCPC's with this new design. Figure 2 shows concentration data measured with a TSI Model 3783 WCPC sampling ambient laboratory aerosol while 10mL of water is injected (twice) directly into the inlet with a syringe. During the injection, the CPC concentration drops to zero as a steady jet of water flows through the optics. This is followed by a short spike in indicated concentration as the stream becomes intermittent, after which the concentration almost immediately recovers to its steady value. In additional experiments, we show that pulse height also returns to its steady-state value after recovery from an induced flooding event.

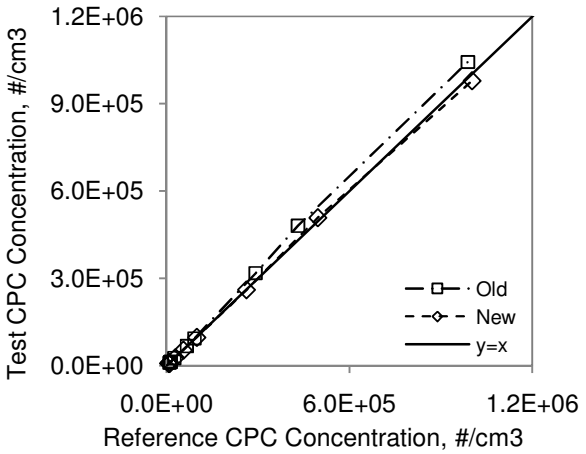

Figure 1. Comparison of linearity in Model 3783 Environmental Particle Counter with Old and New design.

Hering, S. V, Stolzenburg, M. R., Quant, F. R., O'Berreit, D. R., & Keady, P. B. (2005). *Aerosol Science and Technology*, 39(7), 659–672.

McMurry, P. H. (2000). *Aerosol Science and Technology*, 33(4), 297–322.

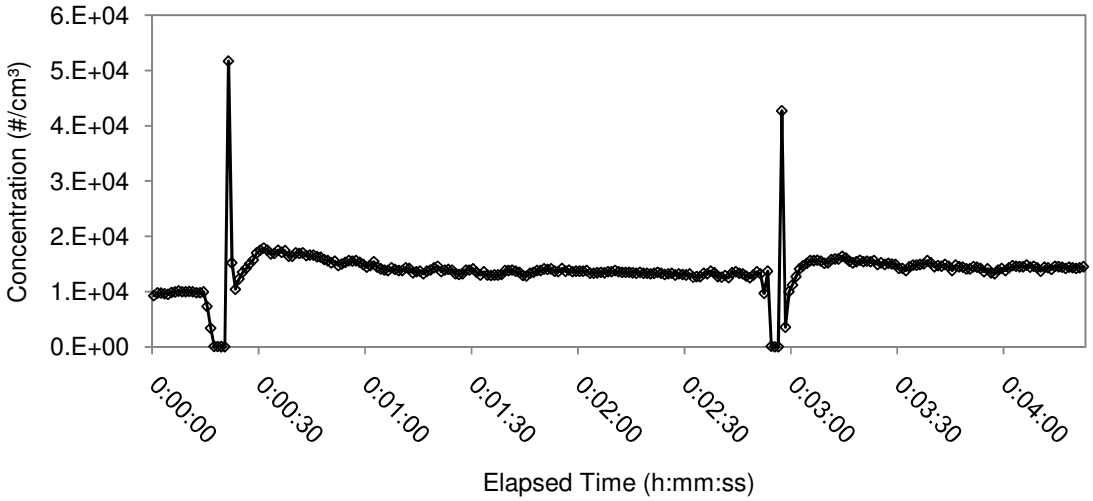

Evaluation and development of Scanning Flow CCN Analysis

C. Wittbom[1], B. Svenningsson[1], S. Sjogren[1], E. Swietlicki[1]
[1]Department of Physics, Lund University, P.O. Box 118 SE 221 00, Lund, Sweden
Keywords: CCNC, SFCA, critical supersaturation.
Presenting author email: cerina.wittbom@nuclear.lu.se

Atmospheric aerosols influence the climate and hydrological cycle of Earth by acting as cloud condensation nuclei (CCN). The ability of aerosol particles, to act as CCN, depends on the particle size and chemical composition as well as the ambient water vapour supersaturation (SS). Köhler theory (Köhler 1936) is commonly used to predict and describe the ability of the particles to activate into cloud droplets. However, the activation of complex mixtures of particles in ambient air is not fully explained nor understood by theory. There is a demand for better temporal and supersaturation resolution for ambient measurements as well as in laboratory experiments. A more rapid and continuous technique would enable measurements of e.g. small samples, fast processes, or a better understanding of a rapidly ageing aerosol. For regional and global measurement networks a standardization of measurement procedure and techniques at different sampling sites are of great importance.

Here, the Continuous-Flow Streamwise Thermal-Gradient Cloud Condensation Nuclei Counter (CCNC, DMT-100), a commercial instrument, has been evaluated when running the instrument in an altered mode of operation. By scanning the flow in the instrument, while maintaining a constant pressure and temperature gradient through the instrument column, rapid and continuous measurements are made possible. Moore and Nenes (2009) introduced the Scanning Flow CCN Analysis (SFCA), with a detailed description of the measurement procedure accompanied by results from both laboratory and ambient measurements. They also present a comparison between the former, "conventional" stepwise-ΔT way of operation with the new mode with scanning flow. However, there are still uncertainties of how to operate the CCNC in SFCA mode for long-term measurements. This evaluation of the SFCA is part of the EU FP7 ACTRIS Infrastructure project (www.actris.net) and is the first step towards a standardization of CCN measurements with high temporal and supersaturation resolution within the European network.

To induce a supersaturation change in the "conventional" operation mode, the flow is kept constant, while the temperature gradient is varied in a stepwise way. Due to the slow temperature stabilization, measurement of whole supersaturation spectra is time consuming. By adding a small software change to the robust and well-established hardware of the CCNC, the flow is instead varied through the column in a controlled manner, while the streamwise temperature gradient (ΔT) and pressure is maintained constant. The flow rate in the chamber is varying in a scan cycle, where the flow increases/decreases linearly, as well as a shortly kept constant at maximum/minimum flow rates. When calibrating the instrument the flow and the corresponding activated fraction of the particles generate a supersaturation curve with a "critical flow rate", Q_{50}. From knowledge of the particle dry diameter and chemical composition Q_{50} is translated to a critical supersaturation (SS_c) using Köhler theory. Hence, every instantaneous flow rate corresponds to a critical supersaturation. However, the calibration curves are specific for the chosen ΔT, scan time and pressure.

SFCA enables measurements of many supersaturation spectra during a short time period, allowing a better temporal resolution (Fig.1) and also smaller samples are needed. The inlet temperature can be kept closer to ambient conditions and therefore minimizing biases from volatilization of semi-volatile compounds in the instrument.

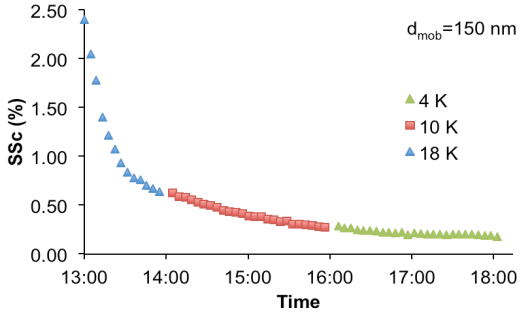

Figure 1. Results of measurements using SFCA for the ageing process of diesel soot agglomerates (mobility diameter 150 nm). SFCA entails high temporal resolution of the CCN spectra. The shift of ΔT makes it possible to cover the whole aging process.

To fully cover the supersaturation spectra of ambient air, a three-step change of the temperature gradient (ΔT = 4, 10, and 18 K) has been introduced (Fig.1). For better resolution and more reliable data of the activation step we recommend an optimal scan cycle of 5 min. To keep the aerosol sample flow rate at constant, a second flow has been introduced, mirroring the flow in the CCNC.

Laboratory experiments of calibration substances such as ammonium sulphate and sucrose, with good repeatability, has been performed. SFCA has also been used for measurements of soot agglomerates during ageing processes (Fig.1) and for other organic mixtures.

This work was supported by ACTRIS.

Moore, R. & Nenes, A. (2009) *Aerosol Sci. & Tech.* 43:1192-1207.
Köhler, H. (1936). *The Nucleus in and Growth of Hygroscopic Droplets,* Trans. Faraday Soc. 1152.

Generation and growth of aerosol particles on nucleus of radioactive decays

V.A. Zagaynov[1,2], N.A. Klyachin[2], N.P. Kalashnikov[2], A.A.Lushnikov[1], I.E. Agranovski[1,3], and Yu.G. Biruykov[1]

[1] Karpov Institute of Physical Chemistry, Vorontsovo Pole 10, Moscow, 105064, Russia
[2] Moscow Engineering Physics Institute, Kashirskoe shosse 31, Moscow, 115409, Russia
[3] Griffith School of Engineering, Griffith University, Brisbane, 4111 QLD, Australia
Keywords: Radioactive aerosol, ion nuclei.
Presenting author email: zagaynov@cc.nifhi.ac.ru

Aerosol particles could grow on charged ions nuclei. Such nuclei could be produced by different processes occurring in a gas phase, including chemical and photo-chemical reactions and radioactive decay. In particular, appearance of ions in the gas phase could be related to alpha, beta and gamma radiation. Moreover, it is common belief that radiation, both natural and anthropogenic, is the main contributor of ions to the atmosphere. It was shown (Freidlander, 2000) that presence of oversaturated vapor does not always ensures particle growth on charged ions. The reason is based on a fact that, according to the classic theory of nucleation, there is a Coulomb's barrier exists for charged nuclei, preventing small particle growth up to the point where substantial oversaturation is reached. Considering that the size of the critical cluster is small (few dozens of molecules), the surface tension could not be considered, as almost all molecules are located on the surface. In this situation, a kinetic approach ought to be used to describe the mechanism of the particle growth on charged ions.

Cloud (Wilson) chambers and diffusion chambers are commonly used for detecting ionizing radiation by visualised particle growth on the ion nuclei produced by radioactive decay. Diffusion chambers have some important advantages as (1) they are self cleaning from alien nuclei, (2) allow identifying a nature of radioactive particle, and (3) could operate continuously. Figure 1 shows some traces of radioactive decay products.

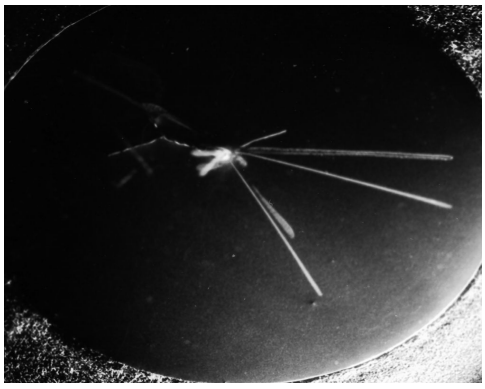

Figure 1. Decay of ^{239}Pu observed by diffusion chamber

Similar process is used for growth of clusters and nanoparticles in CNCs, where ions could also act as nuclei for particle growth. On this basis, the Diffusion Aerosol Spectrometer (DAS) equipped with CNC could be used for measuring particles grown on both ion and molecular cluster nuclei. To distinct these types of particles, it is crucial to separate ones produced on ion nuclei and carrying its charge from others which acquired charge as the result of collision with gas ions. Let c_0 be a concentration of light ions, c_n - concentration of particles containing n molecules, ion concentration - c_{in} , a rate of ion generation in a unit of volume per unit of time - I, rate of collision of ions carrying k and n molecules - α_{kn} , and velocity of collision of neutral particles containing n molecules and light ions is K_{1n} . Then, the following equations could be written to describe rates of variation of concentrations of light ions and particles:

$$\frac{\partial c_{i1}}{\partial t} = I - \alpha_{11} c_{i1}^2 - \sum_n^G \alpha_{1n} c_{i1} c_{in} - \sum_n K_{1n} c_{i1} c_n , \quad (1)$$

$$\frac{\partial c_{in}}{\partial t} = K_{1n} c_{i1} c_n - \alpha_{1n} c_{i1} c_{in} , \quad (2)$$

Solving these equations enables determining of concentrations of neutral particles, unity charged particles and light ions. In a case of stationary regime, the left hand side of equations could be taken as 0 and $c_{i1} >> c_{in}$ and $c_{i1} >> c_n$. Then, for these conditions, Eq. (2) provides the following relation $\frac{c_{in}}{c_n} = \frac{K_{1n}}{\alpha_{1n}}$. For small particles causing main interest, K_{1n} and α_{1n} could be taken from Lushnikov and Kulmala (2004):

$$\alpha(a) = \frac{4\pi D l_c}{1 - e^{-\frac{l_c}{R(a)}}} , \quad (3)$$

where D - diffusion coefficient, $l_c = \frac{e^2}{kT}$ - Coulomb's distance of interaction, $R(a) = \frac{4D}{v_T}$, e - electron charge, k - Boltzmann's constant, and v_T is a rate of heat motion.

Concentrations of charged and neutral particles were experimentally obtained with the aid of a condenser placed at the entry to the DAS. The results enabled to separately identify concentrations of charged and neutral particles. Additional experiments with radioactive sources with different power enabled to identify a rate of atmospheric particle generation.

S. Friedlander. (2000). *Smoke, Dust, and Haze Fundamental of Aerosol Dynamics*, Oxford University Press

A.A. Lushnikov and M. Kulmala. (2004). *Phys. Rev. E.* **70**, 046413

Thursday, September 5, 2013

Poster session C

Particle-Lung Interactions, Posters C084 – C098

Biological response in lung cells by brake dust from a novel set-up to generate one source wear particles

S. Abbasi[1], B. Ekstrand-Hammarström[2], U. Bergström[2], A. Bucht[2,3], U. Olofsson[1], U. Sellgren[1], A. Jansson[4]

[1]Department of Machine design, Royal Institute of technology (KTH), Stockholm, 100 44, Sweden
[2]Division of CBRN Defence and Security, Swedish Defence Research Agency (FOI), Umeå, 901 82, Sweden
[3]Deptartment of Public Health and Clinical Medicine, Umeå University Hospital, Umeå, 901 89, Sweden
[4]Department of Applied Environmental Science, Stockholm University, Stockholm, 106 91, Sweden

Keywords: airborne particles, wear, brake pads, toxicity, IL-8

Recent legislation has resulted in reduced emission of combustion particles from vehicles and therefore the relative contribution of wear particles on the PM levels has increased. Although scientific research on airborne wear-based particles started in 1909, there is neither legislation that controls the generation of wear-based particles nor approved method to study one source-based wear particles (Abbasi *et al*, 2012). The chemical composition of brake pads differs in different vehicles and in addition, the PM generated from these will differ depending on operational conditions (*e.g.* speed, brake pressure and temperature.) Here the aim was to generate PM from a cast iron brake disc and low metallic (LM) brake pad using different cycles/temperatures and study if their potential to induce inflammatory response in a lung epithelial cell line.

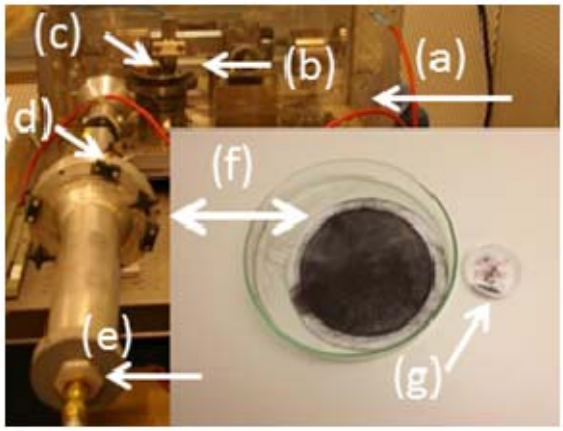

Fig. 1. The experimental set-up to generate particles from braking material, (a) a tribometer in a sealed chamber, (b) square shaped pin from car brake pad, (c) rotating disc from brake disc, (d) filter holder, (e) connection to vacuum pump, (f) filters with deposited particles, (g) collected particles.

Particle generation: Fig. 1 shows the set-up used in this study to generate wear particles from brake pads. In this set-up, the mechanism to blow clean air into an enclosed tribometer (a) monitoring the particle characteristics was akin to work of Olofsson *et al.* to study particles from bearing (2009). However, the 60-mm-diameter discs (c) from cast iron brake disc and the 20-mm-squared shape pins (b) from LM brake pad were used in this study. The dead weight was 100 N and the rotational speed was 3000 rpm. Particles deposited on filter surface (f) were mechanically removed and kept in a glass container (g). *Inflammatory response*: To investigate how cells in respiratory epithelium react to PM from cast iron brake disc and LM brake pads human alveolar type II cells (A549) were exposed to increasing levels of PM. After 24 hours of exposure of PM extracted from the filters, a significant and dose-dependent increase of production of reactive oxygen species and interleukin-8 was observed in the A549 cells. The data indicate that PM from filter 101may be more potent in inducing the biological response.

Here we have demonstrated that the conditions during generation of PM from braking materials have an impact on the response on oxidative stress and inflammatory response in lung epithelial cells.

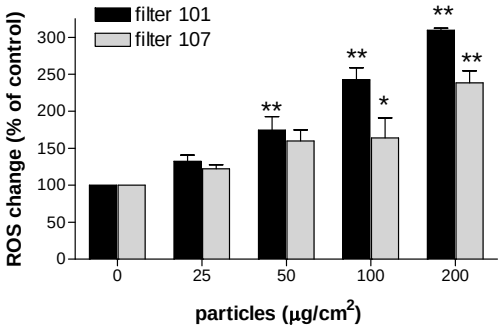

Fig. 2. Production of reactive oxygen species (ROS) in the human lung epithelial A549 after 24 hours of exposure to particles generated from car brake pads. Particles from both filters induce a dose dependent increase of ROS as compared to control.

Altogether, our novel set up for generating single source particles can be used to generate PM under realistic. conditions. These PM can then be used to elucidate the relationship between choice of material, and driving behaviour, for the detrimental health effects of PM from individual sources.

This work was supported by: Swedish Defence Research Agency (FOI) and Royal Institute of Technology (KTH).

Abbasi, S., Jansson, A., Olofsson, U., and Sellgren, U.. (2012) *Crit. Rev. Environ. Sci. Technol.* http://dx.doi.org/10.1080/10643389.2012.685348

Olofsson, U., Olander, L., and Jansson, A. (2009) *J. Tribol.*, 131, 1-4

A multiculture cell exposure chamber for the assessment of airborne and engineered nanoparticles effects on health

A. Asimakopoulou[1], E. Daskalos[1], N. Lewinski[2], E. Papaioannou[1], A.G. Konstandopoulos[1,3]

[1]Aerosol and Particle Technology Laboratory, CPERI/CERTH, P.O. Box 60361, 57001, Greece
[2] Institut universitaire romand de Santé au Travail, IST, Rue du Bugnon 21, 1011, Lausanne, Switzerland
[3]Department of Chemical Engineering, Aristotle University, Thessaloniki, Greece
Keywords: cell exposure chamber, dose control, airborne nanoparticles, engineered nanoparticles, health effects.
Presenting author email: asimak@cperi.certh.gr

In order to study the various health influencing parameters related to engineered nanoparticles as well as to soot emitted by Diesel engines, there is an urgent need for appropriate sampling devices and methods for *in vitro* cell exposure studies that simulate the respiratory system and facilitate associated biological and toxicological tests.

The objective of the present work was the further advancement of a Multiculture Exposure Chamber (MEC) (initially developed in Papaioannou *et al*, see also Asimakopoulou *et al*, 2011) into a dose-controlled system for efficient delivery of nanoparticles to cells (Figure 1). It was validated with various types of nanoparticles (Diesel engine soot aggregates, SiO_2 nanoparticles) and with state-of-the-art nanoparticle measurement instrumentation to assess the local deposition of nanoparticles on the cell cultures.

Figure 1. The upgraded Multiculture Exposure Chamber (MEC).

The dose of nanoparticles to which cell cultures are being exposed was evaluated in the normal operation of the *in vitro* cell culture exposure chamber based on measurements of the size specific nanoparticle collection efficiency of a cell-free device. The average nanoparticle deposition efficiency in the MEC is approximately 82%.

A high degree of flow homogeneity has been observed with flow visualization tests, while further design modifications in the future will provide perfect flow distribution similar to that of the Papaioannou *et al* MEC version.

The nanoparticle deposition was demonstrated by Transmission Electron Microscopy (TEM). TEM grids were placed in the 6-well plate inserts both in empty wells and in wells containing double-distilled water. The overall picture of the TEM grids used in our experiments reveal that soot particles reach the entire exposed MEC space. Further validation studies of particle transport in the MEC are performed employing Computational Fluid Dynamics (CFD).

In-use testing of the dose-controlled cell exposure system was performed by exposing A549 lung cell cultures to fluorescently labelled SiO_2 nanoparticles. Deposition of the nanoparticles on the cell cultures was demonstrated by visualization of the nanoparticle fluorescence in the cell cultures following exposure (Figure 2). The potential of the deposited nanoparticles to generate reactive oxygen species (ROS) (e.g. free radicals and peroxides) was also monitored, thus expressing the oxidative stress of the cells, which can cause extensive cellular and/or DNA damage. The efficient delivery of nanoparticles as well as the homogeneity in particle deposition among the 6-well plate inserts was demonstrated by fluorescence microscopy.

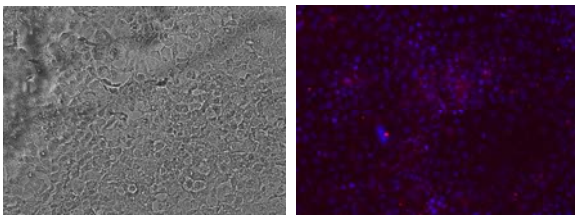

(a) (b)

Figure 2. Microscope images of A549 cells exposed to Fluoprobe532 labeled SiO_2 nanoparticles. Magnification = 200x, Blue = nuclei (DAPI), Red = nanoparticles (Fluoprobe532).

Papaioannou E., Konstandopoulos A.G., Morin J.P. and Preterre D., (2006) *SAE Tech. Paper* No. **2006-01-1075 (SP-2024)**, 389-399.

Asimakopoulou, A., Daskalos, E., Lewinski, N., Riediker, M., Papaioannou, E. and Konstandopoulos, A.G. (2011) *J. Phys.: Conf. Series*, **304**(1), 012005.

Effect of flow rate on fiber deposition in the model of human lungs

M. Bělka[1], F. Lízal[1], M. Jicha[1], J. Jedelsky[1]

[1]Department of Thermodynamics and Environmental Engineering, Faculty of Mechanical Engineering, Brno University of Technology, Brno 616 69, Czech Republic
Keywords: fiber deposition, respiratory airways, optical microscopy, image analysis
Presenting author email: y107099@stud.fme.vutbr.cz

Long exposure and inhalation of fibers can have very harmful effects on human health, because they resist the pulmonary clearance mechanisms, penetrate deep into the human lungs and retain there. The toxicity of fibers depends on their size characteristics, e.g. length and diameter, and on their biopersistence. Asbestos were definitely banned in 2005 and after that they were replaced mainly by man-made vitreous fibers (MMVF). MMVF include glass, rock, wool or ceramic fibers. They are widely used nowadays, which motivates comprehensive research on this topic.

Glass wool fibers with diameter of 1 μm were used in this study. Generated fibers were classified in a classifier, their average length was 10 μm. Classified fibers were mixed with air in a dilutor and delivered into a realistic model of the human lungs (Figure 1.). The model consisted of oral cavity and respiratory airways up to the 7th generation of branching. Different flow rates were tested (30 and 50 LPM). Glass fibers, which passed through the model, deposited on the output filters. The model has 10 outputs therefore there were 10 output filters. Ten flow meters were situated behind the output filters to regulate the air flow generated by the air pump. More details about experimental setup were published by Wang et al (2005).

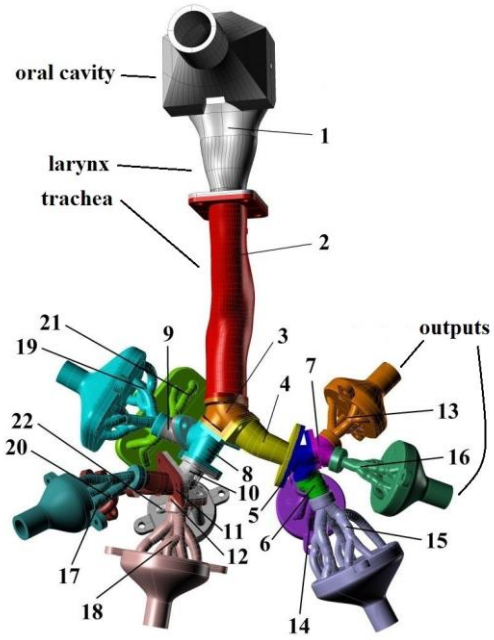

Figure 1. Realistic model of the human lungs with the segment labels

The experiment was run for four hours and the output filters were changed every 30 min. The model was disassembled after the experiment. Every segment of the model was rinsed with isopropanol and resulting solution was filtered using vacuum filtration unit. The filters were then dried and both the filters from the model and output filters were made transparent by acetone vapours.

New method was developed to analyse the filters with fibers, which replaced the method following the NIOSH 7400 methodology. Our method is based on an image analysis. Images of the filters are captured by high definition camera attached to an optical microscope. Images are analysed and fibers are counted by in-house software. Unfortunately, filters from the model could not have been analysed automatically as they contained too many impurities.

Deposition efficiency was calculated afterwards. It is the ratio of number of fibers entering the segment and number of fibers deposited in the segment. The results of the experiment are represented in Figure 2. The deposition efficiency increased with decreasing airway diameter, but over 95 % of fibres got through the model and deposited on the output filters anyway. This agrees with the theory, that fibres can follow the air flow in the lungs and penetrate into lower respiratory airways and therefore induce some health hazards. Deposition efficiency increases with increase in flow rate.

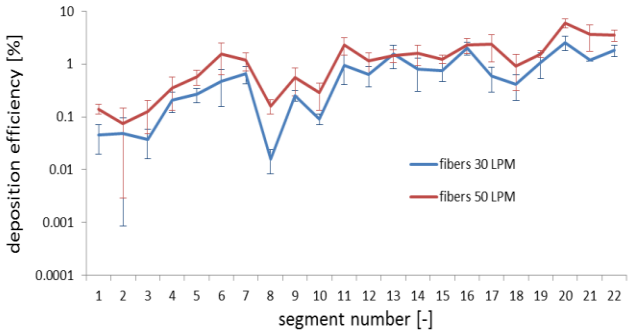

Figure 2. Deposition efficiency in the model

The authors are grateful to Philip K. Hopke from CARES, Clarkson University, NY, USA for his support and kind help. This work was supported by Czech Grant Agency under the grant P105/11/1339 and by the project FSI-S-11-6.

Wang Z., Hopke P. K., Baron P. A. et al (2005), *Aerosol Science and Technology* **39**(11), 1056-1063

A portable device to measure puffing behaviour and tobacco smoke exposure

C. Graham[1], S.Slayford[1]

[1]British American Tobacco, Group R&D, Southampton, SO15 8TL, UK
Keywords: tobacco smoke, puffing behaviour, optical tar
Presenting author email: carl_graham@bat.com

Standardised machine methods to measure cigarettes have been developed to routinely measure cigarette smoke yields (ISO 3308:2000). While this methodology allows products to be compared it is not indicative of how smokers use a product. Therefore, to provide more accurate measurements of the levels of smoke to which smokers are exposed, it is necessary to measure their puffing behaviour (topography). Since 2002, British American Tobacco (BAT) has used the Smoking Analyser 7 (SA7, BAT/C-Matic Systems) to measure a smoker's puffing topography and optical tar in real time. Optical tar is an estimate of Nicotine Free Dry Particulate Matter (NFDPM) or tar, based on light obscuration from the smoke aerosol.

The SA7 can only be used in a central location, due to its need for a trained operator. Under these conditions smokers' behaviour may be altered. We have therefore developed a portable, handheld version named the Portable Smoking Analyser (PSA). This records puffing behaviour (flow, volume, duration and interval), by measuring the pressure drop across the device, and optical tar per puff, again by light obscuration, against a gravimetric calibration.

The PSA was tested using a two stage approach; the first stage evaluated the accuracy and precision of the PSA in recording machine-generated flow rates and volumes, while the second stage used pre-recorded human puffing profiles.

During stage one, a series of flow rates were drawn through the PSA using a Smoking Cycle Simulator (Cambustion, Cambridge UK) with a mass flow meter (TSI, High Wycombe UK) in-line to record the flow rate generated. Figure 1 shows a comparison of the flow rates recorded by the PSA compared to the mass flow meter.

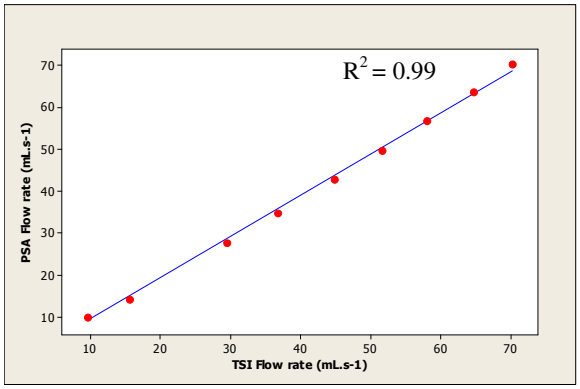

Figure 1 - PSA recorded flow rate against TSI mass flow meter flow rate

There was no significant difference between the flow rates recorded by the PSA and those recorded by the TSI flow meter (p=0.909, range 10 - 70 mLs^{-1}, RSD ± 1.5%).

The accuracy and precision of volumes was also assessed using a glass syringe to draw air through the PSA. A calibrated soap bubble flow meter was placed in-line to record the volumes drawn. There was no significant difference between the measured volumes (p=0.922, range 20 -100 mL, RSD ± 1.3%).

In stage 2, a prototype smoke machine, LM4X (Borgwaldt, Hamburg Germany) was used to replicate human puffing profiles, previously collected using the SA7, with the PSA re-recording the profiles. The PSA recorded volumes were then evaluated against the volumes from the SA7. The PSA volumes were not statistically different to the SA7 volumes (p=0.910, range 14 - 121 mL, RSD ± 2.3%).

During stage 2 Cambridge Filter Pads (CFP) were place behind the PSA to collect the smoke particulate matter from the cigarette. These CFPs were then analysed for nicotine and water by gas chromatography, allowing calculation of NFDPM. The correlation between the optical tar estimate from the PSA and NFDPM is shown in Figure 2. There was no significant difference between the optical tar estimate and the NFDPM (p=0.535, range 0.3 – 38.8mg).

.

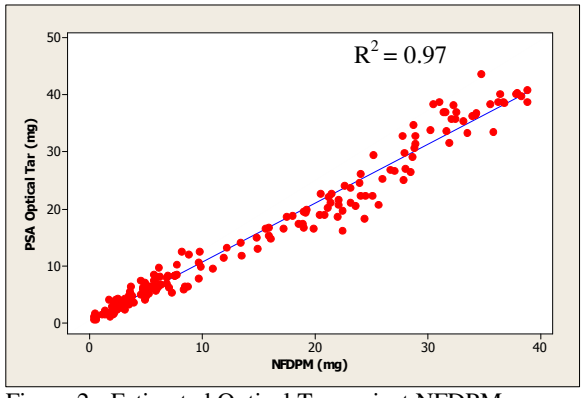

Figure 2 - Estimated Optical Tar against NFDPM

Based on these data, the PSA has been shown to be an accurate and precise device for measuring puffing topography and estimating NFDPM.

In vivo measurements of nanometer-sized particle deposition in the nasal cavities of Taiwanese adults

D.J. Hsu and C.W. Lee

Department of Safety, Health and Environmental Engineering, National Kaohsiung First University of Science and Technology, Kaohsiung 811, Taiwan
Keywords: Deposition efficiency, Nasal cavity, Nano-particles.
Presenting author email: hsuderjen@nkfust.edu.tw

Numerous studies on the removal efficiency of inhaled particles in the nasal region have been performed in the past decades, by using either replicate casts or human volunteers (Hsu and Chuang, 2012). Many empirical equations were also developed to characterize the deposition efficiency in this region. However, most of those studies were primarily based on a limited number of white male subjects (Kim and Hu, 2006). Kesavanathan and Swift (1998) pointed out that nasal anatomic and dimensional factor are important in determining the amount of deposition in the nasal passage and that particle deposition data from a demographically diverse group is important. An anthropometric study in Taiwan indicated that Taiwanese have a shorter craniofacial depth (i.e., distance between glabella and occiput) and longer craniofacial width (i.e., distance between two tragi) than Americans (Yu et al., 1996). Another US study suggested that Chinese workers have shorter face length, longer face width and smaller nose protrusion than Americans (Du et al., 2008). These differences in facial features are likely to affect the anatomical structure of the upper respiratory tract and, consequently, the characteristics of particle deposition in this region between the two ethnic groups. Thus, the experimental data of particle deposition in the respiratory tract reported previously will be less applicable to the Asians if the nasal particle deposition is different between two ethnic groups.

15 Taiwanese adults (subjects A~O, 9 males and 6 females) were recruited to participate in the measurements of nasal deposition efficiency of particles ranging from 14 to 500 nm. The human respiratory flow rates of 5, 10, 15, and 20 LPM were used to represent different human workload. Particle size and number concentrations were measured by a Scanning Mobility Particle Sizer (SMPS) (TSI Inc., Shoreview, MN, USA). The nasal passage cross-sectional area as a function of distance from the nostril of each subject was measured by an otolaryngologist using an acoustic rhinometer (Eccovision, Hood Laboratories, Pembroke, MA, USA). The minimum cross-sectional area (A_{min}) and volume of nasal cavity were determined from the measurements.

The results showed the deposition efficiency decreased with the increasing flow rate, and this trend conforms with the published data. No significant difference was found in the deposition efficiency of male and female subjects. The efficiency obtained from the Taiwanese adults was higher than the current available data which were mainly obtained from the white male subjects. This trend between the two ethnic groups is opposite to that found in the micrometer-sized particles (Hsu and Chuang, 2012). Additionally, subjects A and N were found to have a relatively large difference in the minimum nasal cross-sectional area, while subjects D and K had the smallest difference in this parameter. Figure 1 shows the deposition efficiency as a function of particle size for the subjects A, D, K and N at respiratory flow rate of 10 liters per minute . As shown in the figure, the data from subjects D and K collapse into a single curve, while subjects A and N had apparently different efficiencies. This supports what was noted by Cheng (2003): that the minimum cross-sectional area is the critical dimension in determining the nasal deposition efficiency.

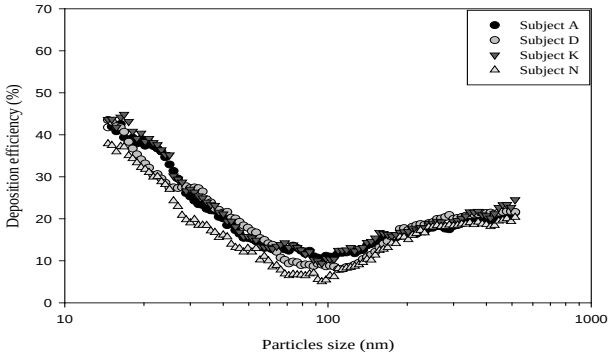

Figure 1. Comparison of nasal particle deposition efficiency of subjects A, D, K and N.

This work was financially supported by the National Science Council, Taiwan under NSC101-2221-E-327-017.

Cheng, Y. S. (2003). *AerosolSci. Technol.* 37:659–671.

Du, L., Zhuang, Z., Guan, H., Xing, J., Tang, X., Wang, L., Wang, Z., Wang, H., Liu, Y., Su, W., Benson, S., Gallagher, S., Viscusi, D. and Chen, W. (2008) *Ann. Occup. Hyg.* 52, 773-782.

Hsu, D.J. and Chuang M.H. (2012) *Aerosol Sci. Technol.* 46, 631-638.

Kesavanathan, J. and Swift, D.L. (1998) *Aerosol Sci. Technol.* 28, 457-463.

Kim, C., and Hu, S.C. (2006) *J. Appl. Physiol.* 101, 401-412.

Yu, C.Y., Yeh, W.Y., Yang, Y.X., and Chang, P.H. (1996) *J.Occup. Safety Health* (in Chinese). 4, 31-46.

Role of size and composition of traffic and wood burning aerosols in the molecular responses induced in airway epithelial and pulmonary artery endothelial cells.

L. Boublil[2×], M. Lisbonne-Autissier[1×], M. Thierry-Mieg[1], M. Leroux[2], J.P. Savineau[1], L. Martinon[3], J. Sciare[4], K. Andreau[2], A. Baeza-Squiban[2××] and I. Baudrimont[1××]

[1] CRCTB, INSERM U1045, Univ Bordeaux Segalen, F-33076 Bordeaux, France

[2] Laboratory of Molecular and Cellular Responses to Xenobiotics, Univ Paris Diderot, Paris Cedex, France

[3] Laboratory of study of inhaled particles, Mairie de Paris, 75013 Paris, France

[4] Laboratory of climate and environment sciences, CEA-CNRS, Centre de Saclay, 91190 Gif sur Yvette cedex, France

[×] These authors contributed equally to the work, [××] These authors contributed equally to the work

Keywords: Urban particles, oxidative stress, inflammation, xenobiotic metabolism.

Presenting author email: isabelle.baudrimont@u-bordeaux2.fr

Introduction

Exposure to particulate pollution is suspected to be involved in cardio-respiratory and cardiovascular health effects. Urban populations living in megacities highly impacted by traffic are particularly vulnerable and more susceptible to develop diseases such as bronchopulmonary cancers, asthma and chronic obstructive pulmonary disease…). After inhalation, the finest particles could accumulate into the respiratory tract, cross the epithelial barrier and reach the systemic circulation where they could exert their deleterious effects on the cardiovascular system by direct interaction with the vascular endothelium. The respiratory tract is the first target of inhaled particles and endothelial cells, which line the inner surface of blood arteries, can have direct contact with the finest particles. Effects on endothelial cells can also be indirect resulting from secretions produced by epithelial cells in response to PM exposure and to different pollutants adsorbed on particles. Experimental studies have shown that lung inflammation seems to be the main short term effect to an acute particle exposure. However, the underlying biological mechanisms and the role of particle physico-chemical characteristics are still misunderstood.

The aim of this study is to evaluate (i) the direct toxicity of different urban PM size-fraction on human bronchial epithelial cells (16-HBE) and on pulmonary artery endothelial cells (HPAEC) (ii) the indirect activation of HPAEC after exposure to PM-induced 16-HBE epithelial secretions (iii) the relative sensitivity of these cells after exposure to the same PM size fraction.

Methods

Coarse, fine and ultrafine particles were sampled in Paris at specific periods of the day when they show high concentrations in combustion aerosols (traffic diesel emissions-TR and domestic heating with wood burning-WB). After recovery of particles from sampling filters, the two cellular models were directly exposed to the different size fractions from 1 to 10µg/cm², non cytotoxic concentrations Different endpoints were studied (i) production of reactive oxygen species by a fluorescent probe (H_2DCF-DA) (ii) pro-inflammatory response by measuring the release of various cytokines (IL-6, IL-8) by ELISA (iii) gene expression involved in these oxidative and inflammatory responses (Heme oxygenase-1-HO-1, IL-6, IL-8, GM-CSF, amphiregulin-AR), gene expression involved in xenobiotic metabolizing enzyme (CYP1A1, a predictive biomarker of polyaromatic hydrocarbon (PAH) bioavailability, NADPH quinone oxidoreductase NQO-1), by qPCR. In addition HPAEC were exposed for 24h to epithelial conditioned medium: culture medium from epithelial cells exposed or not for 24h to PM.

Results

Our results show similarities of response between the 2 target cells. Indeed a significant correlation was observed between 16-HBE and HPAEC cells for the CYP1A1 expression. It suggests that, in these cells, the PAH show a good bioavailability and induce the metabolism pathways of the organic compounds as also strengthened by a significant correlation for NQO-1 expression in both cell types. For the pro-inflammatory response, a significant correlation is observed between 16-HBE and HPAEC if we take into account the GM-CSF for the epithelial cells (a quite sensitive pro-inflammatory biomarker for these cells) and the IL-6 for endothelial cells (great sensitivity of IL-6 in these cells). Interestingly, endothelial cells were more sensitive to PM as compared to epithelial cells.

Whatever the cell type and the site of sampling, we observed a strongest reactivity of urban ultrafine and fine fractions as compared to the coarse fraction. No clear difference of toxicity was observed between traffic and wood burning aerosols suggesting that whatever the source of combustion the main short-term effect of an acute PM exposure is a pro-inflammatory response mediated through oxidative stress.

Moreover we provide evidence of an indirect pro-inflammatory response of HPAEC cells. When they are exposed to fine PM-induced epithelial secretions, they exhibited an increased IL-6 release. It suggests that epithelial mediators and/or soluble components of PM present in the conditioned medium were responsible for this pro-inflammatory effect.

Conclusion

Our results show that combustion (traffic and wood-burning) particles and especially the finest one can elicit a pro-inflammatory and oxidative response in both epithelial and endothelial cells and thus present a respiratory and cardiovascular disease risk.

This work was supported by the National Agency for Research ANR under grant CESA 009 02, project “Megatox”.

In vitro efficiency measurements of the deposition of pMDI generated aerosols in a realistic central airway geometry

A. Kerekes, A. Nagy, M. Veres, D. Oszetzky, A. Czitrovszky,
Institute for Solid State Physics and Optics, Wigner Research Centre for Physics of the H.A.S.,
Budapest 1121, Hungary
Keywords: In vitro, deposition, pMDI, Raman spectroscopy,
Presenting author email: kerekes.attila@wigner.mta.hu

The deposition efficiency of the different inhaled pharmaceutical products in the targeted region of the human respiratory tract is often presented as the results of an in vivo measurement (Newmana, 2006). The drawback is that these results have generally poor resolution and the factors affecting the deposition are not adequately controlled. Consequently, we could get an integrated view of the particle deposition but the in vivo methods are inappropriate for performing deeper analysis of the effects of every individual parameter which is involved in the total deposition process.

If we intend to investigate all the parameters which can influence the deposition process – like the MMAD (mass median aerodynamical diameter) of the inhaler generated aerosol cloud or the initial velocity of the drog particles, the geometry of the actual human airway tract, the breathing waveform of the investigated person, but we could mention the enviromental temperature also etc. – then the implementation of an in vitro experiment would be a good choice for reaching our goals. The amount of the particles that were sucked through the hollow airway model and deposited on the inner surface can be measured by different methods. The ratio of the deposited particles in the targeted area and the particles that were introduced into the human respiratory tract model can be measured in several ways. One way is the preparation of radioactive seeding particles. The intensity of the radiation emitted from the target area is proportional to the concentration of the deposited seeding particles on the investigated surface (Heenan, 2004). Another method is to rinse the deposited particles and measure the concentration of the solution we prepared. These methods are quite cumbersome if we would like to perform a large number of deposition experiments in the same research infrastructure.

In case of in vitro deposition experiments in human airways the Raman or fluorescence spectroscopy has been used relatively infrequently although these methods are suitable for direct detection of the active substance of the inhaled drogs. The reason for this contradiction is the pure scattered Raman intensity from the sample in these types of measurements. The detectation volume, which is determinated by the diameter of the excitation beam and the parameters of the sensing optics, can be increased limitedly. The particle concentration on the investigated surface area is usually not enough for Raman spectroscopy measurements. An other problem is the scaling of the detected signal by one or two order of magnitude, because usually there is not enough scattered Raman intensity.

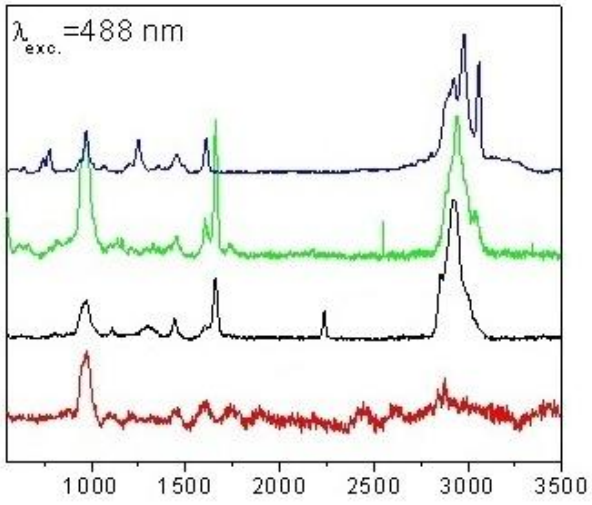

Figure 1. Raman spectra of four different metered dose inhaler. The peaks of the active ingredients are well-defined.

We designed and developed an experimental layout for measuring the efficiency of the inhaled drug deposition by Raman spectroscopy in a human respiratory airway model made by rapid prototyping based on CT image series. The complete system contains a pulmonary waveform generator which is able to increase the correlation between the in vivo and the in vitro measurements. The digital version of the respiratory model is suitable for the comparision of the results by CFD (computational fluid dynamics) simulation technics.

This work was supported by the National Research Agency under grant KTIA_AIK_12-1-2012-0019.

S. Newmana, A. Salmona, R. Naveb, A. Drollmannb (2006) *Respiratory Medicine Volume 100, Issue 3, Pages 375–384*

A.F. Heenan, W.H. Finlay, B. Grgic, A. Pollard, P.K.P. Burnell (2004) *Journal of Aerosol Science* **35,** 1013-1023

Aerosol Deposition Measurement in the Model of Human Lungs using Positron Emission Tomography

F. Lizal[1], J. Jedelsky[1], J. Adam[2,3], M. Belka[1], and M. Jicha[1]

[1]Brno University of Technology, Faculty of Mechanical Engineering, Energy Institute, 61669 Brno, Czech Republic
[2] UJVRez a.s., Division of Radiopharmaceuticals, 250 68 Husinec-Rez, Czech Republic
[3] Masaryk Memorial Cancer Institute, 656 53 Brno, Czech Republic
Keywords: aerosol deposition, human lungs, positron emission tomography.
Presenting author email: lizal@fme.vutbr.cz

The ability to deliver the exact amount of aerosolized medication to the specific region of lungs is the cornerstone of effective inhalation therapy of both lung and systemic diseases. Targeted inhalation of medication is termed successful if at least 50% of inhaled aerosol deposit in the desired region (Zeman *et al* 2010). However, current inhalation devices reach only the level of 30% deposition in conducting airways that are the target region in the treatment of asthma, chronic obstructive pulmonary disease, or cystic fibrosis (Heyder, 2004, Zeman *et al* 2010). To achieve more effective targeted delivery of aerosolized medication further experiments are to be performed and analysed.

We employed Positron Emission Tomography (PET) for the measurement of aerosol deposition in a realistic model (Fig. 1) of human lungs (Lizal *et al* 2012a). PET is a commonly used method in the nuclear medicine. The method is based on a detection of a pair of simultaneously emitted annihilation photons moving in opposite directions as a result of positron – electron interaction after the positron emission decay of a suitable radioisotope. In our case the liquid aerosol particles from di(2-ethylhexyl) sebacate (DEHS) were generated by the condensation monodisperse aerosol generator (CMAG) and labeled with fluorine-18 as a radioactive tracer. (Lizal *et al* 2012b).

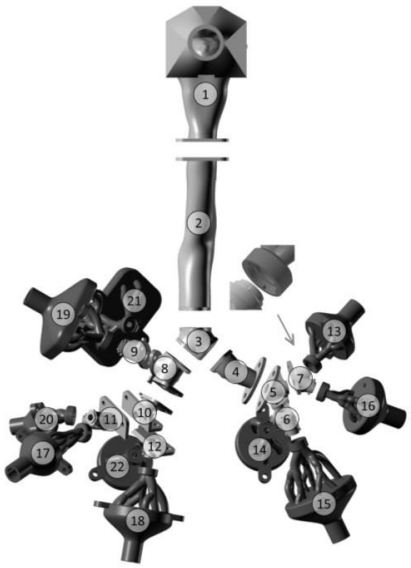

Figure 1. The realistic model of human lungs

Aerosol deposition was measured for two sizes of particles (2.5 μm and 4.3 μm) and for three different inhalation flowrates (15, 30 and 60 L/min). The radioactive aerosol particles were led to the model and non-depositing particles were collected by output filters following each of the model outputs.

Deposition characteristics were calculated from the radioactivity of the deposited aerosol measured by PET. *Deposition efficiency* (Fig. 2) is a ratio of the number of particles deposited in a given segment to the number of particles entering the segment.

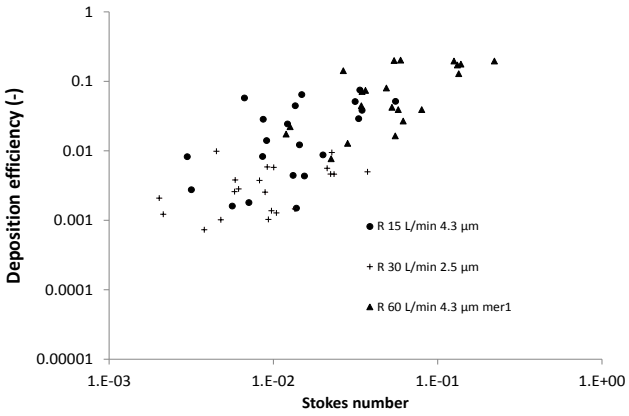

Figure 2. Deposition efficiency in the realistic model.

The results proved correlation of deposition efficiency with Stokes number, which means that the main deposition mechanism is inertial impaction. As a next task the methodology for tagging the solid aerosol particles with radioactive tracer will be developed and deposition of porous and fiber aerosols will be measured.

This work was supported by the Czech Science Foundation under the grant P105/11/1339, and by the project FSI-S-11-6. Frantisek Lizal was supported by the project CZ.1.07/2.3.00/30.0039 of Brno University of Technology.

Heyder, J. (2004) *Proc Am Thorac Soc*, **Vol. 1**, 315-320.
Lizal, F., Elcner, J., Hopke, P. K., Jedelsky, J., and Jicha, M. (2012a) *Proc. IMechE Part H-Journal of Engineering in Medicine* **226** (H3), 197-207.
Lizal, F., Jedelsky, J., Adam, J., Belka, M., Jicha, M. (2012b). *Proc. Int. Conf. Experimental Fluid Mechanics 2012*. Technical University of Liberec.
Zeman, K. L., Wu, J. H. and Bennett, W. D. (2010) *Journal of Aerosol Medicine and Pulmonary Drug Delivery* **23** (6), 363-369.

Airspace dimension test (ADT) with nanoparticles for identification of patients with respiratory disease

Jakob Löndahl[1], Jonas Jakobsson[1], Tobias Andersson[2], Per Wollmer[2]

[1]Division of Aerosol Technology (EAT), Lund Institute of Technology, 221 00, Lund, Sweden
[2]Dept. of Clinical Sciences Malmö, Lund University, 205 02, Malmö, Sweden
Keywords: Lung deposition, nano particles, COPD, emphysema.
Presenting author email: jakob.londahl@design.lth.se

An early diagnosis of respiratory disease is important for a good treatment of patients. However, many respiratory conditions are difficult to identify only based on basic spirometry and alternative tools may be both expensive and include unwanted exposure to radiation (e.g. X-ray computed tomography, CT). Thus, there is a need for cheap and easy methods to measure the structure of the lung – especially for the pulmonary region.

The objective of this work is to evaluate a novel method named airspace dimension test (ADT) in a group of healthy volunteers and patients with respiratory disease.

Methods

An instrument has been constructed for measurement of lung deposition of nanoparticles over a single breath (Jacobson et al., 2013). Subjects, wearing a nose clip, inhale low concentrations of nanoparticles (<10000 cm^{-3}) through a mouthpiece. The lung deposited fraction of nanoparticles is measured over a single breath hold for air exhaled from the pulmonary region. The total time for a measurement is about 60 s. The measurement was repeated three times for each subject.

Deposition measurements were carried out for 26 healthy volunteers and 20 patients with varying degree of respiratory disease. Of the patients, 6 were normal as measured with common spirometry, 7 were mild obstructive and 7 had obstruction or emphysema.

Results

Figure 1 illustrates the deposition fraction of 50 nm particles for the subjects. Mean values were 0.98 in the normal, 0.96 in the probably normal, 0.94 in the mild obstructive and 0.92 in the obstruction/emphysema group. There is a significant difference between the healthy group and patients.

From a clinical perspective, the most interesting comparison is between the groups classified as normal and “probably normal”. In the group “probably normal”, there was no conclusive evidence of airflow limitation at spirometry, but according to the ADT measurements they may have early stages of lung disease.

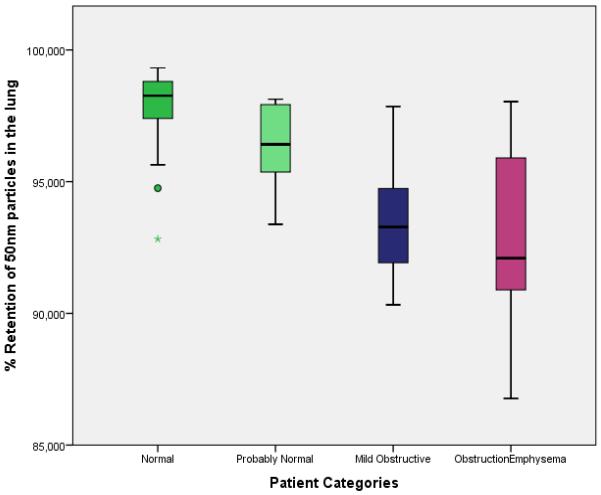

Figure 1: The result of measurements on 20 healthy volunteers (normal) and 26 patients with varying degree of respiratory disease.

Conclusions

The preliminary results indicate that ADT data show differences between various types of respiratory disease. Because of the low cost and limited time needed for measurement and analysis (typically less than 4 minutes in total), the method could be used on patients with just suspected lung disease. Thus, it could be valuable to discover disease at an early stage.

We believe that the ADT measurements provide information on the dimensions of the peripheral airspaces and alveolar volumes. The test may then be a fast and cheap alternative to more time consuming and expensive methods such as CT and MRI with hyperpolarized ^{3}He. However, comparison with these methods remains to be carried out.

We gratefully acknowledge The Swedish Research Council (project 621-2011-3560), the Crafoord foundation and the Swedish heart and lung foundation for financial support.

Jakobsson, J., Kumlin, J., Hedlund, J., Wollmer, P. Löndahl, J. (2013) submitted to *European aerosol conference 2013*

Experimental investigation of the transport and deposition of ambient aerosols in the human airways

A. Nagy, A. Kerekes, A. Czitrovszky

Institute for Solid State Physics and Optics, Wigner Research Centre for Physics of the H.A.S, Budapest 1121, Hungary

Keywords: particle deposition, experimental system.
Presenting author email: nagy.attila@wigner.mta.hu

Contamination of the atmosphere especially in large cities and in many workplaces leads to growing risks to human health - smog alerts and excess of the limits are more frequently occur. The most common diseases that lead to the most work loss are respiratory diseases - allergic respiratory symptoms are now considered endemic. There is a growing number of asthma and COPD.

The investigation of the transport and deposition of inhaled aerosols in human airways is a rather difficult task with "in vivo" methods. The various imaging techniques are capable of formulating certain statements regarding the respiratory deposition of particles, but in many cases their application raises ethical issues due to the required radiation dose, their resolution is not sufficient and the equipments are expensive. These reasons provided the driving force of "in vitro" studies and the development of various simulation techniques.

The aim of this study is the experimental investigation of the transport and deposition of ambient detrimental or toxic aerosols in human airways with contact- and perturbation-free laser optical measurement methods. These investigations provide essential information on detrimental health effects of ambient aerosols, which depends on the spatial distribution of the deposition. (Salma et al. 2002, Balásházy et al. 2003)

The experimental research was carried out using laser light scattering measurement techniques (particle counting, laser Doppler velocimetry) and Raman-luminescence-spectroscopy. Hollow realistic lung models were produced by 3D rapid prototyping technique in 1:1 size and geometry based on CT image series of human airways. Breathing was forced by a programmable and controllable breathing simulator, specially developed for this research. (Kerekes et al. 2009, 2012)

Laboratory tests were carried out with the developed complex measuring system using generated well defined particles and compared the results with computer simulations based on numerical CFD codes.

After the laboratory tests experimental data were obtained by the system using in-door air.

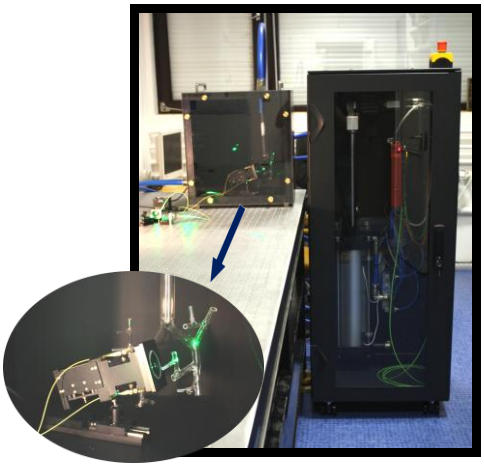

Figure 1. Experimental setup.

This work was supported by the National Research Agency under grant KTIA_AIK_12-1-2012-0019 and TéT_10-1-2011-0725.

A. Kerekes, A. Nagy, A. Czitrovszky, Experimental air flow and deposition studies with hollow bronchial airway models, Journal of Aerosol Medicine and Pulmonary Drug Delivery 22(2)., pp.175-176., (2009)

A. Kerekes, A. Nagy, A. Czitrovszky, Theoretical and experimental investigation of aerosol deposition in realistic human airway model, European Aerosol Conference EAC2012, Sept. 2-7. Granada, Spain, A-WG06S1P30, P253, 1094. (2012) http://www.eac2012.com/EAC2012Book/3.html

Salma I, Balásházy I, Winkler-Heil R, Hofmann W, Záray Gy; Effect of particle mass size distribution on the deposition of aerosols in the human respiratory system; J AEROSOL SCI; 33: 119-132; (2002)

Balásházy I, Hofmann W, Heistracher T; Local particle deposition patterns may play a key role in the development of lung cancer J APPL PHYSIOL 94, 1719-1725 (2003).

Coincidental study of inhalation and intratracheal instillation for hazard assessment of nanoparticles

T. Oyabu[1], Y. Morimoto[1], M. Horie[1], Y. Yoshiura[1], M. Shimada[2], M. Kubo[2], BW. Lee[1], T. Okada[1] and T. Myojo[1]

[1]Institute of Industrial Ecological Sciences, University of Occupational and Environmental Health, Japan. Kitakyushu, 807-8555, Japan
[2]Department of Chemical Engineering, Hiroshima University, Higashi-hiroshima, 739-8527, Japan
Keywords: nanoparticles, hazard assessment, inhalation, intratracheal instillation
Presenting author email: toyabu@med.uoeh-u.ac.jp

For assessing the inhalation toxicity of nanoparticles, inhalation study and intratracheal instillation study were generally performed. Although inhalation study is gold standard as we all known, it takes much time and effort. Instead, many intratracheal instillation studies were performed which has advantage of being able to assess several materials in a short time. However there are not enough evidences that the data in the intratracheal instillation studies reflect the harmful effect of chemicals. Therefore, in this research, we performed an intrtaracheal instillation study and an inhalation study of the same material, nickel oxide nanoparticle, at almost the same dose to rat lung and compared the results of the two methods.

Inhalation study: Male Fisher 344 rats were exposed to NiO nanoparticles at 3 concentrations, 0, 1.65 $\pm$0.20 and 0.32$\pm$0.07 mg/m^3 for 4 weeks. At 3 days, 1, 3 months after the inhalation, each 10 rats of both groups were dissected.

Intratracheal instillation study: 0, 0.2 mg, 1 mg of NiO nanoparticle suspended in 0.4 ml distilled water were intratracheally instilled into Fischer 344 male rat's lung. At 3 days, 1 week, 1, 3, 6, 12 months after the instillation, each 10 rats were dissected.

After collecting broncho-alveolar lavage, dissected lungs from each 5 rats of all groups were used for determination of NiO amounts in lungs. Lungs were acid-digested with microwave and the Ni concentration in completely digested solution was determined by ICP-AES. And some part of bronchoalveolar lavage fluid (BALF) was used for NiO determination. And the number of PMN was also counted in BALF.

The determined amounts of NiO in rat lungs of all groups at 3 days after the treatment are shown in Table. The amounts of NiO in lung at 3 days after the inhalation were almost the same with that at 3 days after 0.2 mg instillation.

Lung weight and the number of PMN in BALF are also shown in Figure 1 and 2. Lung weights and the PMN number of two inhalation groups and two instillation groups increased compared with control groups. Lung weight and PMN in BALF of both high concentration-inhalation group and 0.2 mg instillation group, in which NiO amounts in lung are the same, increased similarly although the time difference exists.

Our results suggested that both inhalation study and instillation study show the similar inflammation at almost same lung dose. Further research is continued.

Table NiO amounts in rat lung

	NiO amount in lung (μg)
Inhalation:	
Low concentration	40 ± 2.4
High concentration	132 ± 9.9
Intratracheal instillation	
0.2 mg instillation	136 ± 6.5
1 mg instillation	738 ± 50

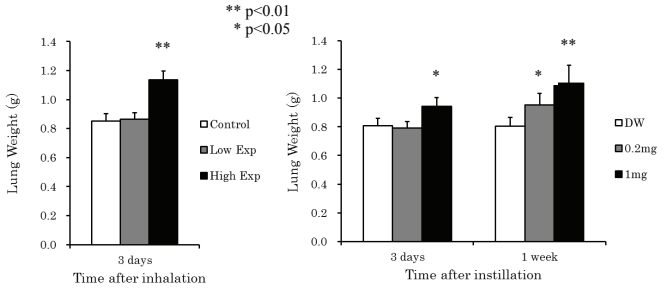

Figure 1. Lung weight of the two methods.

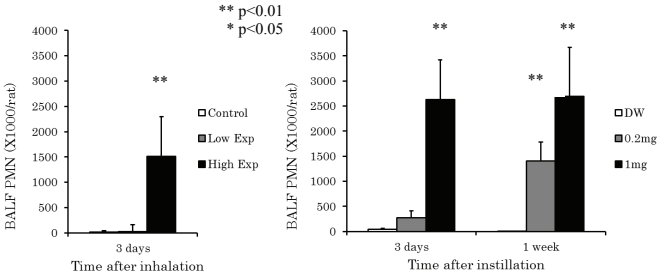

Figure 2. PMN in BALF of the two methods.

This work is on the research program of "Development of innovative methodology for safety assessment of industrial nanomaterials" supported by Ministry of Economy, Trade and Industry (METI) of Japan.

HEAPS study design: Health Effects of Air Pollution in Antwerp Schools

Evi Dons[1,2], Martine Van Poppel[1], S. De Prins[1], Luc Int Panis[1,2], G. Koppen[1]

[1]VITO - Flemish Institute for Technological Research, 2400 Mol, Belgium
[2]Hasselt University, 3590 Diepenbeek, Belgium

Keywords: Black Carbon, UFP, traffic, health effects.
Presenting author email: martine.vanpoppel@vito.be

The HEAPS study (Health Effects of Air Pollution in Antwerp Schools) was set up to evaluate the health impact of traffic related air pollution on school children. Two research goals were defined in this study:
(i) To evaluate which health effects can be measured in children in relation to traffic-related pollutants in their everyday surroundings.
(ii) To evaluate which traffic-related parameters are best for estimating exposures which may cause possible health effects.

The study set-up comprises two main parts: air pollution exposure assessment and health monitoring (Figure 1). Subtasks involved fixed and mobile air quality measurements, land use regression modelling, health assessment through questionnaires and non-invasive biomarker measurements. In this poster, the study design of the HEAPS project is discussed, and data are represented to provide evidence that the study design was appropriate.

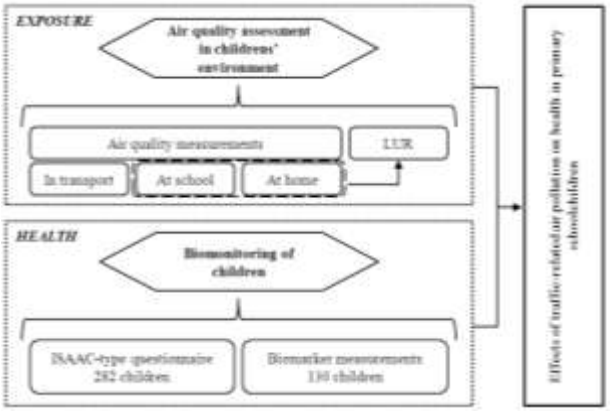

Figure 1. Study design of HEAPS

Air pollution exposure assessment

Air quality was monitored in two seasons, spring and autumn 2011, in 2 schools, at approximately 50 home locations and in transport (Table 1). The first school is located next to a quiet no-through road in the vicinity of a public park. The second school is situated next to a major road (>20,000veh/day). Air quality measurements were done in the playground at both schools, and at the street side for the school next to the busy road. Home measurements were done at selected home locations, at building facades or on street lighting at a height of 2-3m. Mobile measurements in two dominant transport modes per school were performed. Air pollution measurements were translated into exposure estimates in different time frames: a time frame to evaluate acute health effects, a time frame to assess subacute effects, and a time frame that considers long term health effects. UFP, PM, BC, NOx, and O_3 concentrations measured at school the day before and on the day of medical examination were used for assessing acute health effects. To determine medium term exposure, personal exposure was estimated using modeled BC and NO_2 concentrations from a land use regression (LUR) model. Time-activity patterns of children were taken into account by stratifying between exposure at home and at school. Transport from and to school is included as an additional micro-environment although these short trips were proven to be only of minor importance in aggregated exposure. Long term exposure was estimated at the home location using LUR models. Personal NO_2 samplers were carried by the children during 1 week.

Pollutant	School	Home	Transport
$PM_{2.5}$ mass, filter (EC, OC)	X		
NO_2	X	X	
Particle number	X		X
Black carbon	X	X	X
PM factions, particle number	X		
NO, NO_2, NO_x, O_3	X		

Table 1. Overview of measured pollutants in different microenvironments.

Health monitoring

Health assessment consisted of a medical examination, non-invasive collection of biological matrices and oxidative stress, inflammation and cardiovascular biomarkers, and questionnaires. 130 children (aged 6-12) from 2 schools were selected for participation. Medical examinations were carried out in all 130 children in both spring and autumn of 2011, simultaneous with the air quality measurements. ISAAC-type questionnaires were distributed amongst all children attending one of the schools.

Acknowledgement: the study was financed by the Flemish Environment Agency (VMM), the Flemish Administration of Environment, Nature and Energy (LNE), and the Flemish Agency for Care and Health (VZG).

Differential uptake kinetics of nitrogen dioxide on various pollen grains

N. Visez[1], G. Chassard[1], S. Gosselin[1], M. Choël[2], D. Petitprez[1]

[1]PhysicoChimie des Processus de Combustion et de l'Atmosphère, UMR 8522 CNRS Université Lille 1, Villeneuve d'Ascq, 59655, France
[2]Laboratoire de Spectrochimie Infrarouge et Raman, UMR 8516 CNRS Université Lille 1, Villeneuve d'Ascq, 59655, France
Keywords: uptake coefficient, allergy, pollution.
Presenting author email: nicolas.visez@univ-lille1.fr

The effects of gaseous pollutants on pollen structure, viability and allergenicity have been widely studied for many pollen species (cf. references for reviews). Despite such extensive works, there is no information available to compare the effects of pollutants between the pollen species. In this study, we used a chemical kinetic approach to compare the potential sensitiveness of pollen of different species to a NO_2 exposure.

Methods. Experiments were performed with desiccated pollens of birch, timothy grass and cypress and with freshly collected birch pollen. Those materials were exposed for 10 minutes to 5,000 ppmv of NO_2 in a closed cell. The gas phase concentration of the pollutant was measured online by FTIR spectroscopy. In a typical experiment, the NO_2 concentration in the cell decreased with different rates depending on the pollen nature and on the quantity of pollen exposed.

After exposure, pollen grains were deposited onto adhesive tape and surface analysis was carried out using a ToF-SIMS instrument with a pulsed Bi_3^+ primary ion beam (25 keV, 0.25 pA).

Results. For all pollen species, the uptake of NO_2 was fast as shown in figure 1. No reaction products have been detected in the gas phase by means of FTIR spectroscopy. For a fixed mass of pollen (about 65 mg), the following first order kinetic constants have been measured for desiccated pollens:

$k(\text{cypress})=0.0045\ s^{-1}$
$k(\text{timothy grass})=0.0021\ s^{-1}$
$k(\text{birch})=0.0007\ s^{-1}$

For the same experimental conditions, these values indicated for example that the NO_2 concentration decreases six times more rapidly in the presence of cypress pollen compared to birch.

Experiments with birch pollen, stored under desiccated conditions and freshly harvested, demonstrated that pollen freshness increased by a factor of two the kinetic of NO_2 uptake. Exposure done with pollen more or less dried have shown an increase of uptake with a higher water content of the pollen. As a result, we suggest that the observed increase with fresh pollen is explainable by higher water content.

Concerning ToF-SIMS analysis, two fragments were observed with higher intensities in the mass spectra of polluted pollens: m/z=46 (NO_2^-) and m/z=62 (NO_3^-), compared to the mass spectra of untreated pollen. Formation of HNO_3 by the reaction of NO_2 with water has probably occurred on the pollen surface. This confirmed the role of water in surface reactivity.

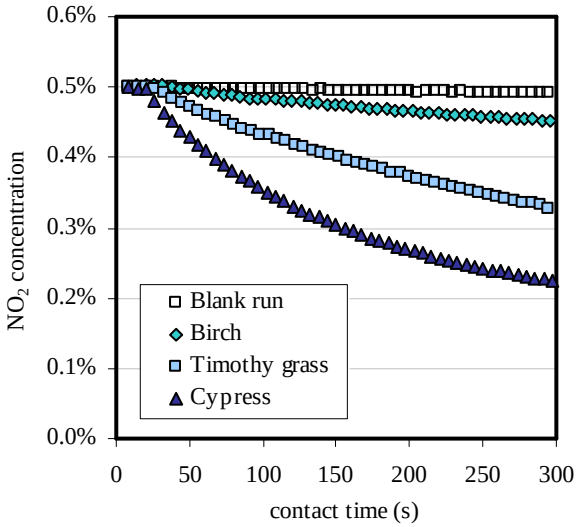

Figure 1. Decrease of NO_2 concentration for different species of pollen exposed (about 65 mg).

Conclusions. According to our experimental data, it is clear that pollen from different species have different behaviour regarding the uptake of NO_2. The sensitiveness of pollen to NO_2 is decreasing in the following manner: cypress > timothy grass > birch.

Fresh pollen appears to be much more sensitive to pollutants than desiccated one. Following reaction with NO_2, acidification of the pollen surface is expected with the possible formation of HNO_3.

This work was supported by the Région Nord Pas-de-Calais, the Ministère de l'Enseignement Supérieur et de la Recherche, CNRS, Université Lille 1, European Regional Development Fund (ERDF) and IRENI, Institut de Recherche en ENvironnement Industriel.

Bartra, J., Mullol, J., del Cuvillo, A., Dávila, F., 2007. J Investig Allergol Clin Immunol, 17, 3-8.
Kim, H., Bernstein, J.A., 2009. Current Allergy and Asthma Reports, 9, 128-133.
Riedl, M.A., 2008. Current Allergy and Asthma Reports, 8, 139-146.

Characterisation of an analysis system used to quantify health-relevant reactive oxygen species (ROS) in atmospheric aerosol particles

F.P.H. Wragg, S.J. Fuller and M. Kalberer

Department of Chemistry, University of Cambridge, Cambridge, CB2 1EW, UK
Keywords: DCFH fluorescence probe, reactive oxygen species, oxidative stress, organic aerosol
Presenting author email: francis.wragg@atm.ch.cam.ac.uk

The adverse health effects associated with ambient aerosol particles have been well documented in epidemiological studies, and further supported with biological cell culture studies. There is a widely accepted association between ambient aerosol particle levels and cardiovascular or respiratory based hospital admission/mortality rates. However, due to the large variability in ambient particulate matter, it is still unknown which physical or chemical properties are responsible for these negative health effects.

Previous studies highlight reactive oxygen species (ROS) in organic particulate matter as being a potential major cause. Many of these studies have used the fluorescence probe 2-7 dichlorofluorescein (DCFH), in combination with horseradish peroxidase (HRP), to quantify particle-bound ROS, but the reaction mechanism and kinetics of the assay itself has not been clarified to a great degree of detail (Venkatachari & Hopke 2008). This lack of detailed understanding leads to various assumptions having to be made in order to interpret the results obtained.

To characterize the DCFH/HRP assay with model compounds for atmospheric particle components, varying concentrations (0.9 ml, 0.0 - 1.0 μM) of different ROS were combined with the DCFH (1 ml, 10 μM, 20 % PBS) and HRP (0.1 ml, 10 units ml^{-1}) solution. The fluorescence measurements were taken during a 15 minute reaction time using a 4-way cuvette holder maintained at 41°C.

HRP interacts with DCFH via two alternative cycles: the peroxidase cycle – whereby the HRP ground state is oxidized by peroxide and subsequently reduced by DCFH to give the fluorescent product DCF; and the oxidase cycle – HRP is reduced by DCFH, then oxidized back to its ground state by oxygen (Berglund et al. 2002). The peroxidase cycle provides two moles of fluorescent product DCF per mole of HRP used, and provides a steeper gradient of fluorescence intensity over time.

Figure 1 shows the increase in fluorescence over time of the DCFH/HRP assay both with, and without, a ROS present. Two distinct phases are clearly visible in the reactivity of the assay. The oxidase-cycle phase, causing a background fluorescence gradient in both runs, is due to exposure of the assay to ambient oxygen levels within the lab air. The steeper peroxidase-cycle phase is unique to the sample with ROS (peracetic acid) present. Peracetic acid reacts in the aqueous system to give H_2O_2, as shown in Figure 2.

This data suggests that the DCFH/HRP assay is specific to H_2O_2. When considering the oxidative ability of different reactants, rather than measuring reactivity of each individual species, it measures the sum conversion into H_2O_2/reactive radicals. This further strengthens the validity of using DCFH/HRP to determine potential health impacts of particle-bound ROS, because its reactivity is specific to the very species suspected of causing oxidative stress/inflammation within an aqueous human lung environment.

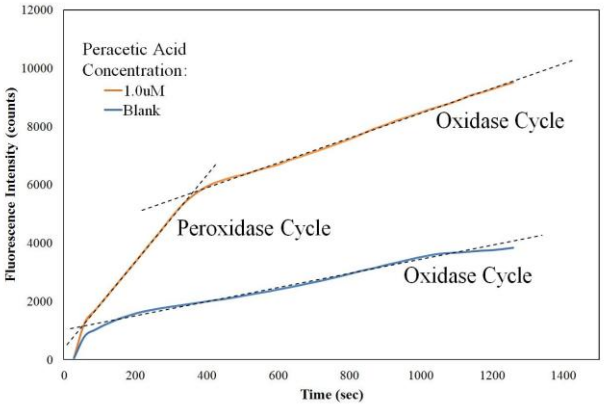

Figure 1. Fluorescence vs time plot of the DCFH/HRP assay with and without peracetic acid present.

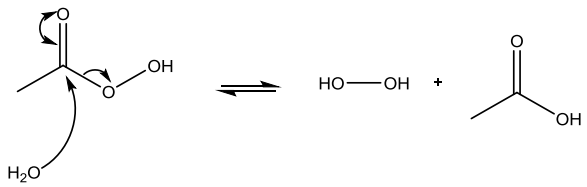

Figure 2. Equilibrium between peracetic acid and H_2O_2 in an aqueous environment.

This work was supported by the European Research Council, Project 279405.

Venkatachari, P. & Hopke, P. K., *Aerosol Science and Technology*, **42**, 629–635 (2008)
Berglund, G. I. *et al,. Nature*, **417**, 463–8 (2002)

Analysing biological activity of dust from moisture damaged buildings: Relation of microbial components with toxicity

K. Huttunen[1], J. Tirkkonen[1], E. Krop[2], M. Täubel[3], J. Pekkanen[3], A. Hyvärinen[3], D. Heederik[2], J.-P. Zock[4] and M.-R. Hirvonen[1, 3]

[1]Department of Environmental Science, University of Eastern Finland, Kuopio, FI-70211, Finland
[2]Institute for Risk Assessment Sciences, Utrecht University, Utrecht, 3508, The Netherlands
[2]Department of Environmental Health, National Institute for Health and Welfare, Kuopio, FI-70701, Finland
[4]Centre for Research in Environmental Epidemiology (CREAL), Barcelona, E-08003, Spain
Keywords: bioaerosols, inflammation, toxicity, dust.
Presenting author email: kati.huttunen@uef.fi

Moisture damages in buildings occur frequently all around the world. Exposure to a moisture damaged environment has been associated with increased occurence of respiratory infections and upper respiratory tract symptoms, cough, wheeze and dyspnoea (WHO 2009). Available moisture in building materials enables the growth of micro-organisms, resulting in potential exposure to spores, spore fragments, secondary metabolites and cellular components of microbes.

Collecting settled dust is a way to get an integrated sample of particles that once were airborne. The sampling time extends typically over several weeks, which improves the representativeness of the sample compared to short time sampling. However, settled dust lacks both the gaseous phase and the smallest, non-settling particles present in indoor air. The aim of this study was to compare the concentration of microbial components in settled dust samples with toxicity and inflammatory responses caused by exposure to the dust in a cell culture model.

Methods

Dust samples were collected from moisture- and mold damaged schools (n=14) and reference schools (n = 11) in Spain, The Netherlands and Finland. Settled dust was collected to cardboard boxes for 8 weeks, the sample was vacuumed on a filter, suspended in a dilution buffer, and stored frozen. Before exposure experiments, the samples from each school were pooled together, filtered to remove the largest particles, aliquotted and frozen again. The concentrations of ergosterol and endotoxin were measured with GC-MS-MS (Lappalainen *et al* 2008) and Limulus assay (Jacobs *et al* 2012), respectively.

A mouse macrophage cell line (RAW264.7) was exposed to four doses of dust suspension for 24 hours. The viability of the exposed cells was analysed by measuring the function of the mitochondria [3-(4,5-Dimethylthiazol-2-yl)-2,5-diphenyltetrazolium bromide (MTT)-test] and permeability of the cell membrane [propidiumiodide (PI) –staining] (Markkanen *et al* 2008). The concentrations of proinflammatory mediators [nitric oxide (NO), tumor necrosis factor (TNF)α, interleukin (IL)-6 and macrophage inflammatory protein (MIP)2] were analysed from the cell culture medium (Huttunen *et al* 2003).

The concentration of microbial components in dust correlated significantly with both toxicity and the ability to induce inflammatory responses (Table 1). Interestingly, the correlation between toxicity and ergosterol was strongest among the samples collected from damaged schools, whereas the correlation between toxicity and endotoxin was strongest within the reference schools. However, associations between microbial components and dust levels should be considered simultaneously in further analyses.

Table 1. Spearman correlation between concentrations of microbial components and biological activity of the settled dust samples collected form moisture damaged and reference schools in three European countries.

Toxicity	Endotoxin	Ergosterol
MTT-test	-0,836*	-0,724*
PI-exclusion	0,808*	0,734*
Inflammatory response		
NO	0,841*	0,731*
IL-6	0,857*	0,792*
TNF	0,848*	0,788*
MIP2	0,833*	0,768*

This work was supported by the European commission FP7 under grant 211488: HITEA (Health Effects of Indoor Pollutants: Integrating microbial, toxicological and epidemiological approaches)

Huttunen, K., Hyvärinen, A., Nevalainen, A., Komulainen, H. and Hirvonen, M.-R. (2003) *Environ.. Health Perspect.* **111**, 85-92.

Lappalainen, M.H., Roponen, M., Nevalainen, A., Laine, O. and Pekkanen, J. (2008) *Clin. Exp. Allergy* **38**, 1483-1492.

Markkanen P. (Penttinen P.), Pelkonen J., Tapanainen M., Mäki-Paakkanen J., Jalava P.I., Hirvonen M.-R. (2008) *Inhal. Toxicol.* **21**, 857-867.

Jacobs, J. H., Krop, E. J. M., de Wind, S., Spithoven, J. and Heederik, D. J. J. (2012) *Eur. Respir. J.,* PMID 23100494

WHO (2009) *WHO quidelines for indoor air quality: dampness and mould.* WHO Regional Office for Europe.

Environmental monitoring to inform built environments vulnerability to airborne disease transmission

Z.A.Nasir[1], L.Campos[1], M. Canales[1], L.Ciric[1] and I. Colbeck[2]

[1]Department of Civil, Environmental and Geomatic Engineering, University College London, WC1E 6BT, UK
[2]School of Biological Sciences, University of Essex, Colchester, Essex, CO4 3SQ, UK
Keywords: Air Health, Particles, CO_2, Offices.
Presenting author email: Z.nasar@ucl.ac.uk

In the 21st century, environmental heath in the built environment is central to public health. The way we design, construct, use and manage indoor environments can have substantial impact on our wellbeing. Of the wide range of indoor air contaminants, infectious agents are of the greatest concern due to their potential to cause huge damage to global public health. In recent years we have witnessed the emergence of new diseases (e.g. influenza H1N1 and SARS) and their potential to cause wide spread disease in societies across the globe. The uncertainty about when a pandemic may occur and the unpredictability of its severity leave no option but to prepare in advance. A range of environmental factors can enhance the probability of disease transmission in built environments. These include: prolonged exposure to infectious individuals/sources in small enclosed spaces, inadequate ventilation, and recirculation of contaminated air. Therefore, there is an urgent need to develop practical tools to assess the relative risk that built environments pose in infection transmission.

The present study aims to highlight the use of environmental monitoring as a tool to assess air health in built environments and to inform their vulnerability to airborne disease transmission. Measurements were carried to monitor the number concentration of particles in 6 different sizes (Lighthouse laser particle counter, 5016), CO_2, temperature, relative humidity (IAQ4 – BW Technologies) and airborne culturable bacteria (Andersen 6 stage sampler) in a mechanically ventilated office during October 2012 under two different scenarios: ventilation system off and on. The floor area and volume of the office was 28 m^2 and 80 m^3, respectively, and it had five work stations.

The summary of results presented in Figure 1 and Table 1 clearly shows the impact of poor ventilation on the concentration of airborne bacteria, particles in all the size ranges and CO_2.

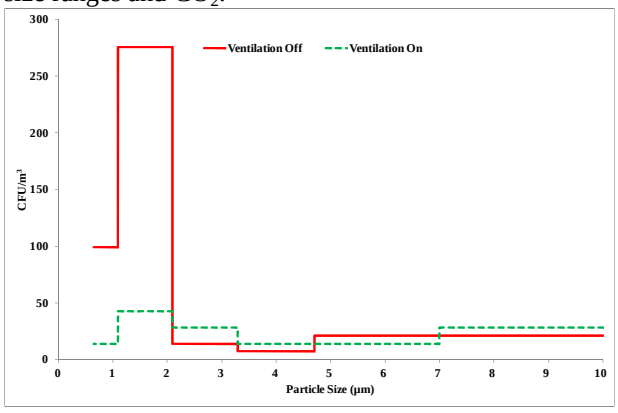

Figure1.Size distribution of culturable airborne bacteria

Table 1. Hourly average number concentration of particles and CO_2 in a mechanically ventilated office

NUMBER CONCENTRATION (#/m³)				
	Ventilation OFF		***Ventilation ON***	
	Mean	**SD**	**Mean**	**SD**
Day Time (8.00 – 19.00)				
0.5 µm	8,804,986	7,511,997	265,594	112,764
0.7 µm	1,459,121	1,226,868	86,991	36,838
1.0 µm	358,566	160,785	79,104	38,742
3 µm	41,176	28,699	21,853	13,339
5 µm	5,525	5,078	4,059	2,501
10 µm	2,802	3,890	2,009	1,605
Night Time (20.00 – 07.00)				
0.5 µm	10,370,265	6,179,079	220,588	158,489
0.7 µm	1,792,998	1,203,352	69,081	40,972
1.0 µm	388,301	228,027	42,505	28,374
3 µm	16,898	17,953	3,851	4,511
5 µm	995	2,123	445	813
10 µm	212	602	120	227
CO_2 (PPM)				
Overall	783	325	529	139
Day	1,005	297	626	127
Night	534	83	420	26

Inadequate supply of outdoor air relative to occupant density resulted in the accumulation of particles and CO_2 in the office air. It also impacted greatly on relative humidity. (49-63% during ventilation system off and 35-46% during ventilation system on). It is evident that in the presence of an infectious source in this built environment the occupants' risk of exposure will be enhanced under an inadequate ventilation scenario. It is important to highlight that very often the need for ventilation is governed by psychological and physiological needs of the occupants and the current guidelines and codes proposed by different organizations on indoor air quality in work places are focused on thermal comfort and odour removal rather than preventing infection transmission.

Environmental monitoring of airborne particles and CO_2 can play a pivotal role in evaluating air health in built environments and identifying ill/malfunctioning elements. This can assist in the design of venue and scenario specific mitigation strategies to reduce vulnerability of the built environment to airborne infection transmission.

This study was funded by the Engineering and Physical Science Research Council, United Kingdom, grant reference EP/G029881/1

Air concentration of ultra-fine particles released from the Diesel engines

S. Bujak-Pietrek, U. Mikołajczyk, and I. Szadkowska-Stańczyk

Department of Environmental Health Hazards, Nofer Institute of Occupational Medicine, Lodz, 91-348, Poland
Keywords: diesel exhaust particles, occupational exposure
Presenting author email: ulmik@imp.lodz.pl

Introduction

Diesel engines exhaust are a multi-component mixtures of various chemical compounds formed by incomplete combustion of diesel fuel and its pollution. They are a significant source of ultra-fine particles, with sizes ranged in tens to hundreds of nanometers, which contaminate living and working environment. Ultra-fine particles in diesel exhaust can be inhaled and easily transported to the alveoli. Occupational exposure to ultra-fine particles released from diesel engines concerning the workers serving the vehicles and devices with engines of this type. This group can include operators of excavators, cranes, forklifts, etc., bus depot workers, auto mechanics, railway workers.

Aim:

The aim of this project was the assessment of number, surface area and mass concentration of the particles less than 1000 nanometer in the workpost air during Diesel engine activity.

Methods:

Condensation Particle Counter (TSI model 3007-2) was used to determine the number of particles in a given volume of air in the 10-1000 nm range (in particles/cm3 - p/cm3). AeroTrak 9000 (TSI) was used to determine the surface area concentration of particles potentially deposited in the tracheo-bronchial (TB) and alveolar (A) region of lungs in the 10-1000 nm (in $\mu m^2/cm^3$). DustTrak (TSI, model 8534) was used to estimate the size segregated mass concentration (PM1, PM2,5, respirable, PM10 and total dust)

Following workposts were under measurements:

- bus repair workshop
- daily bus service depot

Air samples were taken by 16 minutes, with 2 minutes time intervals, at the height 1,5 m from the ground. Sampling strategy included the measurement before, during and after activity. Background was measured in the room without the source of Diesel exhaust particles.

Results:

The value of the particle number concentration observed in the bus repair workshop was increased from 7761 particles/cm^3 before diesel engines were working to the value of 16842 particles/cm^3 during engine operation. In the daily bus service depot this values were respectively 47998 particles/cm^3 before and 145094 particles/cm^3 during analysed activity. In the room without a source of emissions concentration was 7653 particles/cm^3.

Surface area concentration before the work shift in bus repair workshop were 246,4 $\mu m^2/cm^3$ for A region and 65,5 $\mu m^2/cm^3$ for TB. During the work shift, when the Diesel engines were turned on, the surface area concentration was 757,0 m^2/cm^3 for particles potentially deposited in A region, while in the region TB the value was 172 $\mu m^2/cm^3$. The background values were at the level of 35,0 $\mu m^2/cm^3$ (A) and 7,9 $\mu m^2/cm^3$ (TB) .

Before the work in daily service depot started, the surface area concentration was 121,9 $\mu m^2/cm^3$ for A region and 49,3 $\mu m^2/cm^3$ for TB. During the passage the busses by daily service hall surface area concentration was respectively 488,3 $\mu m^2/cm^3$ and 131,7. $\mu m^2/cm^3$ for A and TB region. In the control room, these values were as follows: A – 31,0 $\mu m^2/cm^3$, TB – 6,2 $\mu m^2/cm^3$.

Prior to starting the work shift the total mass concentration of the aerosol was 0,29 mg/m^3 in the workshop and 0,16 mg/m^3 in the daily service depot. While the engine of buses were turned on, mass concentrations on these workposts were 1,03 mg/m^3 (workshop) and 0,63 mg/m^3 (daily service) The background values were at a level of 0,05 mg/m^3 and 0,09 mg/m^3.

Conclusion:

- The number concentration of ultra-fine particles emitted from a diesel engine in the bus workshop was 22-fold higher and 3-fold higher in the daily service depot compared with the state before starting the engine
- During engine operation was observed 3 - 4- fold increase of the surface area concentration of the particles deposited in both the alveolar and tracheo-bronchial region
- Mass concentration of particles emitted during the process increased 3,5 - 4.times depending on the workpost.

Increase in number concentration and in particular surface area concentration of particles deposited in A region should be considered as a potential cause of respiratory disorders. Further studies of this issue are necessary.

This work was supported under grant agreement nr 5052/B/P01/2010/38.

Workers exposure to carbon black dust containing nano-sized particles.

U. Mikołajczyk, S. Bujak-Pietrek and I. Szadkowska-Stańczyk

[1]Department of Environmental Health Hazards, Nofer Institute of Occupational Medicine, 91-348 Lodz, Poland
Keywords: carbon black, nanoparticles, occupational exposure,
Presenting author email: ulmik@imp.lodz.pl

Aim of communication

Carbon black is a material the most commonly used in the rubber industry, but also as black pigment in inks, toners, paints and plastics. This material is highly formed of almost pure carbon. This is the most commonly used nanomaterial - the size of individual particles of carbon black is ranged from 20 nm to 100 nm, depending on the type of carbon black. The diameter of aggregates formed by the carbon black particles is ranged from 50 nm - 600 nm. In selected researched was shown that inhalation of carbon black can cause the changes in the respiratory system if exposed workers. The aim of present study was to assess the number, surface area and mass concentration, of ultra-fine particles during the pouring and packing of carbon black.

Methods

The measurements were carried out at the carbon black plant before the work shift, during the pouring and packing of material and after the work.
Following devices were used during the measurement cycle:

- Condensation Particle Counter (TSI model 3007-2) - to determine the number of particles concentrations
- AeroTrak 9000 (TSI) – to determine the surface area concentrations of the particles potentially deposited in the alveolar (A) and tracheo-bronchial (TB) region of lungs
- DustTrak (TSI model 8534) - to determine size segregated mass fraction

Air samples were collected for 16 minutes each sample at a height of 1.5 m from the ground in the breathing zone of workers.

Results

The average concentration of ultra-fine particle number found during the pouring and packing of carbon black was 14203 particles/cm^3 and increased by 37.5% compared to the concentration before the start of the analysed process. The surface area concentration of the particles, potentially deposited in the region A was 223 μm^2/cm^3 during the activity and increased by 21.6% compared to the concentration before. In the case of TB fraction the values were 78.8 μm^2/cm^3 during the work and 10.4% of the increase before it begins. Total mass concentration of the particles was 1.45 mg/m^3 during the analysed process, and before the activity this value was 0.11 mg/m^3, which indicates an increase of 7.6%.

Conclusions

- Number concentration of particles smaller than 1000 nm released in the process under study was more than 2 - fold higher compared to the value before the activity.
- The surface area concentration of the particles was 5-fold higher in the case of particles possibly deposited in a region A, and 9 - fold higher the TB region.
- Mass concentration of particles released during the activities of packing and pouring of carbon black was 13-fold higher than before the work shift. `
- Pouring and packaging carbon black associated with significant increase in mass, number and surface area of particles and should be considered as a potential harmful factor

The nano-sized particles are important factor in exposure assessment of workers involved in the process of pouring and packing of carbon black.

In the analysed process the increase in the parameters characterizing the carbon black dust was observed.

Acknowledgements: This work was supported under the grant agreement nr 5052/B/P01/2010/38.

Tests of the personal respiratory protective equipment using radioactive aerosols

P.Otahal[1], J.Vosahlik[1] and I.Burian[1]

[1]National Institute for Nuclear, Chemical and Biological Protection, Nuclear Department, Kamenna 71, Milin, 262 31, Czech Republic

Keywords: radioactive aerosol, respiratory protection, radon, filtration efficiency.

Presenting author email: otahal@sujchbo.cz

Personal respiratory protective equipment (RPE) should satisfy at least the requirements of the European Standards. Non-radioactive aerosol particles are used in standard testing process for RPE. The presented paper describes alternative methods to test the protection level of RPE using radioactive aerosol particles.

Aerosol particles are sampled from Radon-Aerosol Chamber (RAC) which volume is 10 m^3. Nebulized salt crystals (size mode: 30 nm – 200 nm) and condensed carnauba wax (size mode 200 nm – 350 nm) are the main sources of aerosol particles. Aerosol particles are contaminated by radon daughter products. The standard concentration of radon for RPE testing is between 50 – 200 $kBq \cdot m^{-3}$.

Simplified diagram (Figure 1) presents the main principle of configuration for RPE material testing:

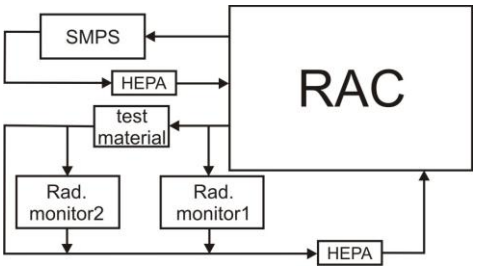

Figure 1. Simplified diagram of RPE material testing

In the upper part of Fig.1 it is possible to see aerosol measuring branch which controls parameters - concentration, geometric mean of diameter, GSD etc. by Scanning Mobility Particle Seizer 3936 (TSI).
In the lower part two equipment for radioactive aerosols measurement are demonstrated – one (1) characterized state before RPE, the left part (2) state behind „filtering“ by RPE. The ratio of results (2/1) represents an estimation of penetration at known velocity of air stream and known aerosol diameter. The volume of samples which are taken from RAC are negligible compared to the total volume of testing chamber. Radioactive contamination is determined by alpha spectrometer 7401 VR (Canberra).

Results and Discussion

This method was applied for testing RPE materials of personal protective equipment (filtering efficiency FFP3 and FFP2) and of medical masks. For each RPE there were five samples cut out, which were gradually tested. Each of the sample was tested at various flow rates.

The following figures 2 and 3 present the results of the best and the worst materials considering their penetration.

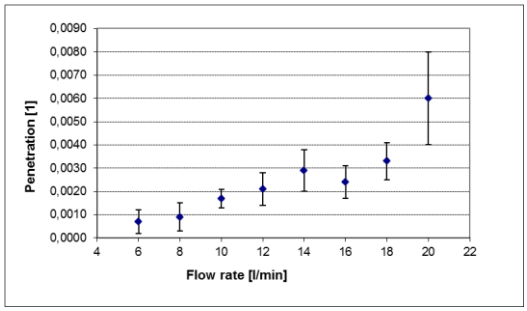

Figure 2 The dependence of penetration to flow rate for material class FFP3 (size mode 350 nm, GSD 1,4)

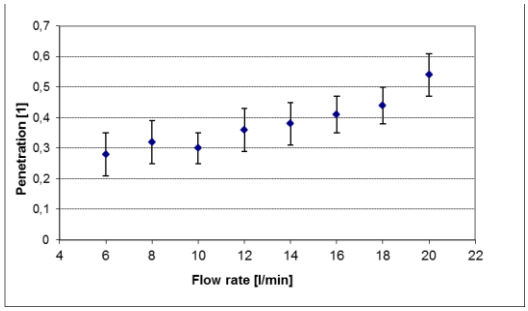

Figure 3. The dependence of penetration to flow rate for medical drape (size mode 320 nm, GSD 1,5)

Conclusion

Presented method allows the determination of penetration of aerosols particles for various types of materials forming RPE. Due to relative simplicity and large dynamical range of the measurements of radioactive contamination, this method seems to be more accurate mainly for materials with low degree of penetration.

This work was supported by project VF 20110201513 of Ministry of the Interior of the Czech Republic.

Burian I., Otahal P., Vosahlik J., Pilecka E. (2011): Czech primary radon measurement equipment, Radiation Protection Dosimetry, Vol 145, No. 2-3, pp. 333-336

Verification of airflow patterns and leakage of contaminants from fume cupboard

T. Jankowski
Department of Chemical, Aerosol and Biological Hazards, Central Institute for Labour Protection – National Research Institute, 00-701 Warsaw, Poland
Keywords: trace gases, fume hood, dust, ventilation
Presenting author email: tojan@ciop.pl

One of the most important safety devices in a laboratory is the properly functioning fume cupboard. In the fume cupboard, hazardous chemicals released from experiments are drawn away from the worker and exhausted by fans. The performance of a fume cupboard is determined by a complex interaction of factors from the working chamber, the exhaust system, fume cupboard location, system indicators and operational parameters. The test methods used to judge the performance of a fume cupboard may include face velocity test, flow visualization and tracer gas test.

This article presents results of tests of influence of changes of airflow patterns and face velocities on the performance of different fume cupboards under given conditions and environment of use.

Table 1. Operational and measuring parameters.

Flow rate [m^3/h]	Face velocity [m/s]	Robustness [-]	Efficiency [%]
250	0.04	6	92.48
366	0.14	3	97.70
582	0.23	9	94.26
742	0.07	1	82.03

As a result, average values of the statement of volume of air flow in the exhaust duct, the face velocity, the robustness and the air exchange rate examined, it was found that the increase in the suction flow rate does not guarantee the increase of face velocity of fume cupboards and thereby increase its robustness level and the efficiency (Table 1). An important parameter in this case is also a way of making the fume cupboard and shaping the airflow patterns in and around the fume cupboard.

Figure 1. Local and gross smoke visualisation.

Flow visualization tests demonstrate detailed flow patterns in different regions of the cupboard to qualitatively support the experimental results of the tracer gas measurements (Fig.1).

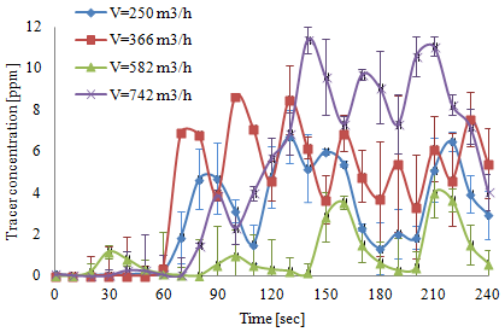

Figure 2. Distribution of SF_6 at robustness tests.

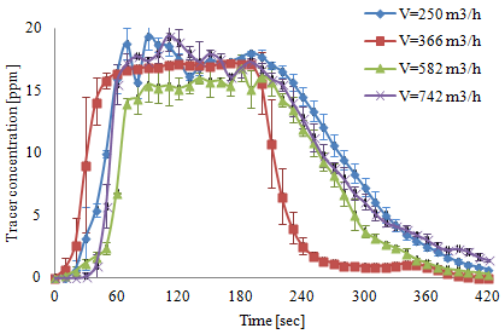

Figure 3. SF_6 distribution at purge measurements.

The overall concentration trend of contaminants along the face of the fume cupboard is obtained experimentally. Figure 2 and 3 shows the variability of concentration of SF_6 across the sash opening.

The airflow patterns and performance of the laboratory fume cupboard are closely correlated. The source position, geometric features and presence of an operator are important to the laboratory fume hood performance. The performance of the cupboard is strongly influenced by the ventilation system and other features of the laboratory in which it is installed.

This paper has been prepared on the basis of the results of task 04.A.09 carried out within the National Programme “Improvement of safety and working conditions” partly supported in 2011-2013 within the scope of state services by the Ministry of Labour and Social Policy. The CIOP-PIB is the Programme's main co-ordinator.

Chen, J-K. (2012) *Ind. Health*, **50**, 103–114.

Effect of air exchange rate on the removal of aerosol in a test chamber

T. Prasauskas[1], L. Gagyte[2], A. Jurelionis[2], D. Ciuzas[1], E. Krugly[1], L. Seduikyte[3] and D. Martuzevicius[1]

[1]Department of Environmental Engineering, Kaunas University of Technology, Kaunas, Lithuania
[2]Department of Geotechnical Engineering, Kaunas University of Technology, Kaunas, Lithuania
[3]Department of Graphics Drawing, Kaunas University of Technology, Kaunas, Lithuania
Keywords: indoor aerosol, ventilation, air exchange rate, chamber
Presenting author email: tadas.prasauskas@ktu.lt

Introduction

Various air distribution methods are used in rooms in order to ensure good indoor air quality (IAQ) and removal of particles from the zones occupied by people. It is known that air movement contributes to transmission and spread of infectious disease and the proficient ventilation systems may provide a solution to sufficient IAQ.

It is important to develop an understanding of aerosol dispersion in the room under various air exchange rates and air distribution methods. In this study, we have analysed behaviour of aerosol under various ventilation rates and regimes.

Methods

A room-imitating test chamber (floor area 13 m^2, volume 32.5 m^3) equipped with two air supply and two air disposal units in the ceiling was used during the experiment. Two distribution methods – one-way and four-way mixing – of pre-filtered and conditioned air were employed at four air change rates (1, 2, 3, and 4 h^{-1}).

A solution of 10% sodium chloride (NaCl) was periodically dispersed by a nebulizer (model MRE CN24 3–Jet Collison Nebulizer, BGI Inc., Waltham, MA, USA) and dried by mixing it with air (v/v ratio of 1:5). Aerosol particle charge was reduced to equilibrium by a corona charger before supplying it to the chamber. The aerosol was fed at a height of 1.1 m in the air supply side for 1 s at a flowrate of 36 lpm. Peak $PNC_{2.5}$ reached 3500 - 5100 cm^{-3}.

Real-time particle size distribution (PSD) measurements were performed using an Optical Particle Counter (OPC) (model HANDHELD 3016 IAQ, Lighthouse worldwide solutions, Fremont, CA, USA). Aerosol concentration was measured at 1.8 m above the ground representing human breathing zone. The OPC was positioned below the air disposal device in order to reflect the dynamics of aerosol to be removed from the chamber.

Results

The aerosol concentration was fluctuating rapidly in the chamber, showing substantial turbulence in the air movement, although air velocity was maintained below 0.1 m/s. Fig. 1a) presents normalized particle concentrations in case of one-way mixing air supply, at four levels of air exchange rates. It is evident that with increasing air exchange rate, the particles were transported to the exhaust more rapidly (peak concentration occurring ~30 s later in case of 1 h^{-1} vs. 4 h^{-1}). Moreover, in cases of 1 and 2 h^{-1}, the aerosol concentration remained at elevated levels after 5 minutes, showing ineffective removal of particles.

In case of four-way mixing, aerosol dispersion pattern was distinctively different. Air exchange ratio did not seem to have a prevailing effect on $PNC_{2.5}$ close to the exhaust. Moreover, high air exchange rates seemed to disperse particles in the entire volume of the chamber, slowing the overall removal rate. At the same time, four way mixing may be effective tool to immediately reduce particle concentration at the point of generation.

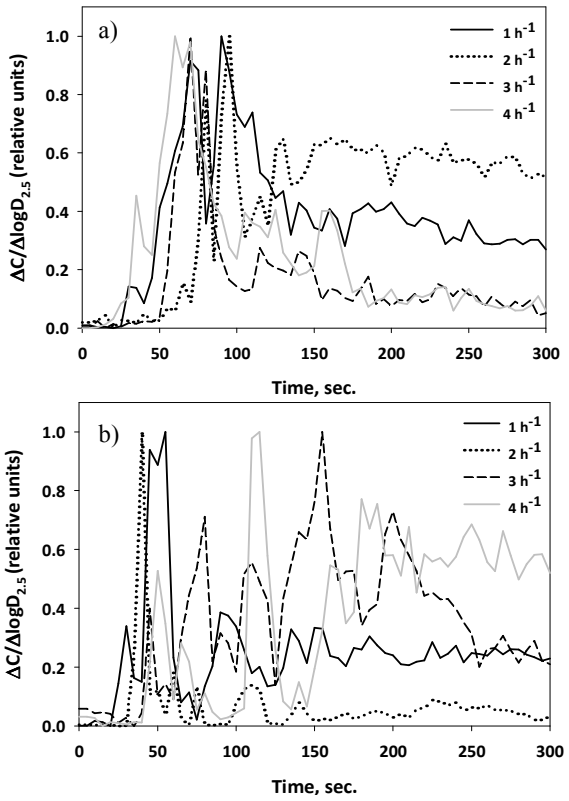

Figure 1. Variation of PNC2.5 (5 sec average) over time under various air exchange rates at a) one way mixing air supply and b) four-way mixing air supply.

This study was supported by European Social Fund under the Global Grant Scheme (Project "Air Quality Management in Low Energy Homes", No. VP1-3.1-ŠMM-07-K-02-075).

Coarse and fine particulate emissions from drilling activity

Farhad Azarmi[1], Prashant Kumar[1, 2] and Mike Mulheron[1]

[1] Division of Civil, Chemical and Environmental Engineering, Faculty of Engineering and Physical Sciences (FEPS), University of Surrey, Guildford GU2 7XH, United Kingdom[2]
[2]Environmental Flow (EnFlo) Research Centre, FEPS, University of Surrey, Guildford GU2 7XH, United Kingdom
Keywords: PM, drilling, emission factor, concrete.
Presenting author email: f.azarmi@surrey.ac.uk

Building-related activities such as drilling, cutting and mixing of concrete have the potential to generate coarse (PM_{10}, i.e. those below ≤10 µm) and fine ($PM_{2.5}$, i.e. those below ≤2.5 µm) particle dust. However, there are still limited numbers of studies currently available which can provide a good account of the release of particulate matter (PM) from a variety of building activities (Kumar *et al.*, 2012c). This gap indicates a need to understand the emission characteristics of various construction activities. One such activity, which is carried out in abundance at construction sites, is 'drilling'. Past work indicate that the drilling process can also generate both the coarse and fine particles that can become available for inhalation by the site workers (Balout et al., 2007).

The aim of this work is to investigate the release of coarse and fine particle dust during the concrete drilling and estimate the emission factors (EF) of PM_{10}, $PM_{2.5}$ and PM_1 dust. The knowledge of the PM concentrations is important for the exposure assessment of the people working on sites and investigating dispersion into the surrounding built environment. The key results of such a work could help establishing the EFs of various building activities, such as drilling of concrete slabs in this particular case, besides providing useful inputs to the environmental regulations and development of guidelines for construction industry.

A GRIMM portable aerosol spectrometer (model 1.109; Peters *et al.*, 2006) was used to measure PM_{10}, $PM_{2.5}$ and PM_1 concentrations during the drilling of concrete slab. The measurements were taken close to the source (i.e. 1 m). Nimbus handheld drill was used for drilling purpose. The drill was hallow from inside, and contained the external and internal diameters as 0.091 and 0.083 m, respectively.

Table 1 presents the summary of results obtained. Figure 1 shows the concentrations of PM_{10}, $PM_{2.5}$ and PM_1 during the drilling activity as well as before and after the drilling (representing background concentrations). Figure 1 shows a clear increase in PM concentrations during the drilling compared with pre– and post– background concentrations. The peak values during the drilling were noted as 7.62×10^4 µg/m^3, 6.78×10^3 µg/m^3 and 6.15×10^2 µg/m^3 for PM_{10}, $PM_{2.5}$ and PM_1, respectively. These were ~1650, 450 and 110 times over the background concentrations of PM_{10}, $PM_{2.5}$ and PM_1, respectively. Largest differences between the PM_{10} concentrations clearly indicate that the drilling activity produced majority of particles in coarse size range, followed by the fine particles (i.e. $PM_{2.5}$ and PM_1). The emission factors (EF) were derived using the measured concentrations. These were estimated to be in the range of 0.002 to 0.057 µg/s for the different types of PM dust (see Table 1). The results presented here are preliminary, based on a short experimental campaign. Detailed experiments are planned to substantiate these findings and develop EFs for various other building activities. Availability of such EFs can greatly help in the development of emission inventories from construction sites.

Table 1. Summary of PM concentrations and the EFs.

	Background (µg/m^3)	During activity (µg/m^3)	EF (µg/s)
PM_{10} (Av±SD)	46.3±50.3	20399±20357	0.057
$PM_{2.5}$ (Av±SD)	13.8± 4.2	923±1636	0.025
PM_1 (Av±SD)	5.56± 0.77	105±131	0.002

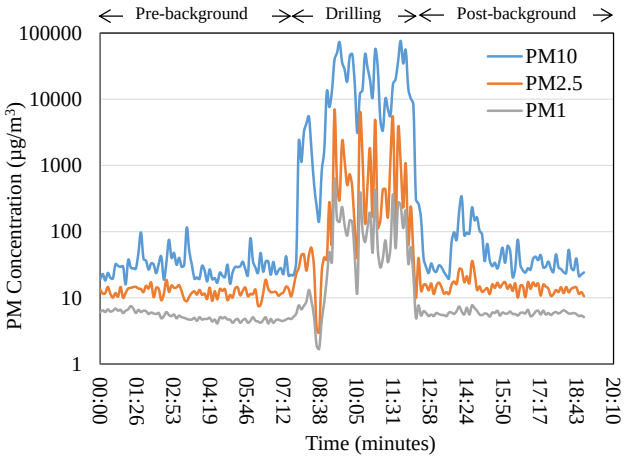

Figure 1. PM_{10}, $PM_{2.5}$ and PM_1 concentrations over time.

Balout, B., Songmene, V., Masounave, J., 2007. An experimental study of dust Generation during dry drilling of pre-Cooled and pre-Heated workpiece materials. *Journal of Manufacturing Processes* 9, 23-34.

Kumar, P., Mulheron, M., Som, C., 2012. Release of ultrafine particles from three simulated building processes. *Journal of Nanoparticle Research* 14, 1-14.

Peters T.M., Ott, D., O'Shaughnessy, P.T., 2006. Comparison of the Grimm 1.108 and 1.109 portable aerosol spectrometer to the TSI 3321 aerodynamic particle sizer for dry particles. *Annals of Occupational Hygiene* 50, 843-850.

Particle concentrations and radon equilibrium ratios in an occupied auditorium

I. Bilska[1], M.R. Dudzinska[1], K. Kozak[2], J. Mazur[2] and B. Polednik[1]

[1]Faculty of Environmental Engineering , Lublin University of Technology, Lublin, 20-618, Poland
[2] Institute of Nuclear Physics PAN, Krakow, 31-342, Poland
Keywords: particle concentration, radon progeny, indoor air quality.
Presenting author's email: i.bilska@wis.pol.lublin.pl

Indoor air quality is mostly assessed on the basis of its thermal parameters, chemical components and aerosol concentrations. These factors significantly affect the subjective comfort. Radon (^{222}Rn) concentration levels are also very important (Kozak et al., 2012). This sensible imperceptible radioactive gas and its radioactive solid decay products can pose harmful health effects (Machaj and Urbański, 2004).

The aim of the study was to determine aerosol particle, radon and radon decay product concentrations in occupied and unoccupied auditorium.

Measurements were conducted in air-conditioned auditorium of Environmental Engineering Faculty in Lublin University of Technology. The room can accommodate up to 200 people. It is equipped with a system to control indoor air parameters e.g. relative humidity, temperature and CO_2 concentration.

Continuous measurements of radon (^{222}Rn) concentrations (conducted with students' presence and their absence) were performed with the use of AlphaGUARD PQ2000 (Genitron). Concentrations of radon decay products were measured using EQF3220 (SARAD). DUSTRAK DRX 8533, OPS 3330 and P-Trak 8525 (TSI Inc.) were used to measure indoor particle mass and number concentrations.

Figure 1 shows radon, its decay product concentration changes and values of equilibrium ratio in the occupied and unoccupied auditorium. The equilibrium ratio (ER) was calculated from the following Equation :

$$ER = \frac{EEC_{Rn}}{C_{Rn}} \qquad (1)$$

where EEC_{Rn} is effective equivalent concentration of short-lived radon decay products (Bq/m^3) and C_{Rn} is radon concentration (Bq/m^3).

It is observed that radon and its decay products concentrations and ER values were significantly depended on the students' presence and the air exchanged rate in the monitored auditorium.

Figure 2 shows the relation between radon and aerosol particle concentrations.

The obtained results confirm the importance of the aerosol particle concentrations and the air exchange rates in the assessments and evaluations of the indoor air quality. The results also indicated the significance of such parameters while decreasing the radon-related health risk in air-conditioned premises.

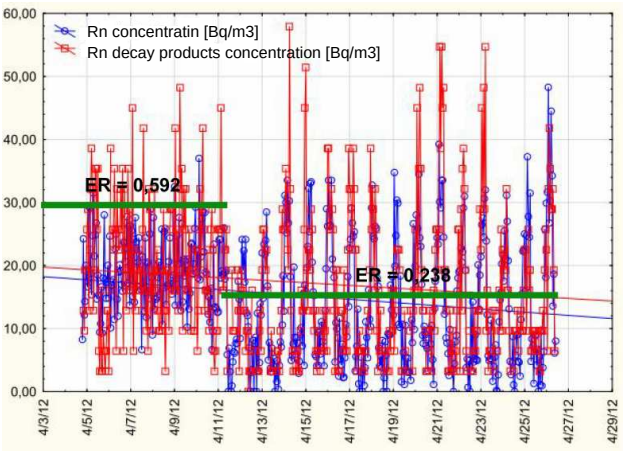

Figure 1. Radon equilibrium ratio values in occupied and unoccupied auditorium.

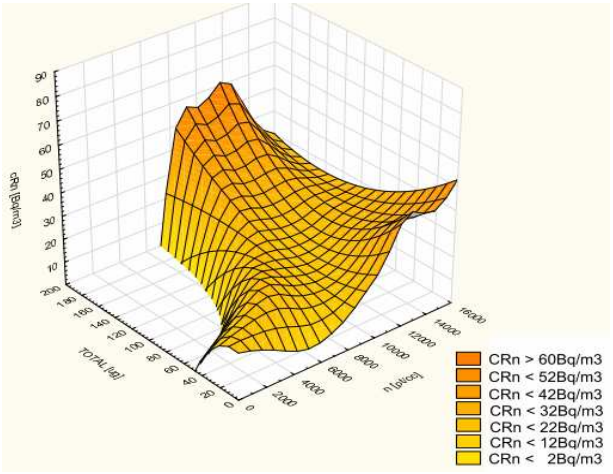

Figure 2. Radon concentration vs. particle mass and number concentrations.

This work was supported by the research program PB 7454/B/T02/2011/40.

Kozak K., Dudzińska M. R., Mazur J., Połednik B., Grzadziel D. (2012) *Radon exposures in premises in the Lublin region, eastern Poland*, Healthy Buildings 2012.

Machaj B. and Urbański P. (2004) Influence of aerosol concentration and multivariate processing on the indication of radon progeny concentration in air, *Nukleonika*, **49(3)**, 123-129.

Assessment of fungal aerosol in different type of residential buildings located in the city free of flood

K. Bródka, M. Sowiak, M. Wojtania, A. Kozajda and I. Szadkowska-Stańczyk

Department of Environmental Health Hazards, Nofer Institute of Occupational Medicine, 91-348 Lodz, Poland
Keywords: fungi, dwellings, air contamination
Presenting author email: kbrodka@imp.lodz.pl

In the indoor air of residential buildings even located in areas free of flood can find many species of fungi mainly of the genera: *Aspergillus, Cladosporium*, *Penicillium*, *Fusarium*. Their sources are: outdoor air, spores and fragments of mycelium present in the settled dust, in flowerpots, carpets but also fungi growing on various types of building and finishing materials. Structural elements, the type of used material and the age of the building can effect on the colonization and growth of fungi. Conditions conducive to the occurrence of fungi in buildings can appear both during build and later during their exploitation (bad ventilation, new tight windows, lack of rooms airing, activities in home like cooking, etc.). Fungi can be both an infectious and allergic agents, and longer exposure to this kind of microorganisms can cause serious respiratory diseases.

Aim: The aim of this study was to assess the contamination of dwellings indoor air by fungi in different type of residential buildings.

Materials and Methods: In a large city (over a half million inhabitants) which was free of flood in the last century 700 dwellings located in different types of buildings were randomly selected. Among dwellings residents questionnaire study was conducted and information describing building and dwelling were collected. Air samples for assessment of the levels of fungi were collected from 60 dwellings in three type of buildings (block of flats n=36, old tenement house n=17 and detached house n=7) during summer and winter. The air was sampled for 24 hours using pump and a measuring head filled with a filter. After the sampling the filters were transported to the laboratory where the biological material was eluted and series of 10-fold dilutions was made. To determine the total number of fungi plates with Malt Extract Agar containing chloramphenicol and streptomycin were used. The plates were incubated at 25°C for 7 to 10 days. Identification of fungi was carried out according to standard diagnostic techniques and procedures. The presence of five allergenic to human genera (*Penicillium*, *Aspergillus*, *Cladosporium*, *Alternaria*, *Stachybotrys*) were studied. Among the *Aspergillus* genus the fungi of *Aspergillus fumigatus* species were determined. Geometric means of fungi concentrations in the dwellings location in different type of buildings were analyzed.

Results: Concentrations GM, (ranges) of airborne fungi in blocks of flats, tenement houses and detached houses in summer were $6.96x10^1$ cfu/m^3 ($1.04x10^1$ – $1.17x10^3$), $1.03x10^2$ cfu/m^3 ($2.39x10^1$ – $4.93x10^2$), $1.62x10^2$ cfu/m^3 ($1.8x10^1$ – $5.83x10^2$) and in winter $3.62x10^1$ cfu/m^3 (3.23 - $1.7x10^3$), $2.29x10^2$ cfu/m^3 ($2.18x10^1$ – $6.73x10^3$), $3.34x10^1$ cfu/m^3 (2.5 – $2.33x10^3$), respectively. In summer significantly higher concentrations of fungi were found in blocks of flats and detached houses than in tenement houses ($p<0.05$). The highest mean concentration of fungi in winter was in tenement houses and the lowest in the blocks of flats ($p<0.001$). In two cases only (in tenement houses) the concentrations of fungi exceeded the Polish reference limit value for the home environment ($5.0x10^3$ cfu/m^3, Górny, 2004). In collected samples isolated fungi of the genus *Stachybotrys* were not found. The allergenic genera of fungi in blocks, tenement houses and detached houses in summer constituted 59.0%, 67.8% and 78.1% and in winter 86.5%, 94.7% and 88.5% of all isolated fungi respectively. Qualitative analysis showed that in summer the largest percentage of fungi of the *Penicillium* genus were found in dwellings located in the blocks of flats and detached houses, in winter in those types of buildings the fungi of the *Aspergillus* genus were the most numerous. In tenements the reversed trend was observed. In all types of buildings, both in summer and in winter the fungi of the species *Aspergillus fumigatus* which were qualified to the second biosafety categories according to the classification BSL (biosafety levels) were isolated (de Hoog, 1996).

Conclusions: 1. The type of building significantly modified the concentration of airborne fungi in dwellings but only in winter season The highest mean concentration of fungi was found in old tenement houses. **2.** Only in a few cases the level of fungi exceeded the reference limit values. **3.** Among identified microorganisms, fungi of *Aspergillus fumigatus* which are in BSL-2 according to the classification BSL were found. **4.** Share of allergenic fungi was much higher in winter than in summer.

The project was carried out under grant 1754/B/P01/2010/39

References:

Górny, R.L. (2004) *PiMOŚP* **3**, 17-39 [in Polish]
de Hoog, G.S. (1996) *Mycoses* **39**, 407-417

Indoor air in child homes related to selected home characteristic.

M. Sowiak, K. Bródka, A. Kozajda, M. Wojtania and I. Szadkowska-Stańczyk

Department of Environmental Health Hazards, Nofer Institute of Occupational Medicine, Lodz, 91-348, Poland
Keywords: airborne fungi, home environment.
Presenting author email: kbrodka@imp.lodz.pl

In most countries around the world, people spend more than 80% of their time indoors, out of which a large part in their homes (Klepeis et. al., 2001). In the case of children and elderly people, this time is even longer. Thus, people breathe air which is mostly the air inside those dwellings. Therefore, the concentration of various pollutants in the air of homes has become an important factor in the individual exposure of most people, including children. Among the indoor air pollutants fungi are especially important. Indoor exposure to certain fungal genera is a risk factor for upper respiratory symptoms (cough, wheeze), asthma and allergy in both adults and children (Garrett et. al., 1998). The level of air pollution by fungi in homes is influenced by many different factors, including behavior and lifestyle of the inhabitants, construction and the finishing the rooms and the state of maintenance. Due to the multitude of factors affecting indoor air quality of dwellings, there is still a need for research in this direction.

The aim of this study was to assess the contamination of indoor air by fungi in child homes related to selected home characteristic (type of room and type of floor).

Materials and methods: Mycological analysis was carried out in 50 Polish dwellings, where up two-year old children were living, and outside buildings (background). All dwellings were located in urban agglomeration. In each child home the samples were taken in two rooms - in living room (LR) and in child room (CHR) - or in one room, when it was common for activities of adults and child (LCHR). The air samples were collected directly on Petri plates with Malt Extract Agar medium (5-10 min., air flow 20 l/min.) using Burkard Air Sampler. All samples were incubated 5 days in 30°C temperature. The quantitative and qualitative analysis of fungi were performed using the standard microbiological procedures. Qualitative identification of fungi was conducted to the level of five allergenic to human and most common in indoor air genera: *Penicillium, Aspergillus, Cladosporium, Alternaria* and *Stachybotrys.*

Results: The geometric mean of airborne fungi concentrations indoor child homes was $5.13x10^1$ cfu/m^3 (range: 2.5 – $5.31x10^2$ cfu/m^3) and outdoor was $9.32x10^1$ cfu/m^3 (range: $1.50x10^1$ cfu/m^3 – $3.87x10^2$ cfu/m^3). The concentration of fungi in the air of any dwelling did not exceed the reference value for the home environment ($5.0x10^3$ cfu/m^3, Górny, 2004).

Concentrations of airborne fungi in the CHR amounted to on average $4.38x10^1$ cfu/m^3 and was slightly lower than in the LR (GM=$5.79x10^1$ cfu/m^3) and the LCHR (GM=$5.78x10^1$ cfu/m^3). The levels of fungi concentration in the air in various types of rooms did not differ significantly (p>0.05). Taking into account the type of floor the lowest geometric mean of airborne fungi concentrations was observed in a room where the floor was covered with carpet or carpet lining ($3.18x10^1$ cfu/m^3). The geometric mean of airborne fungi concentrations in rooms with smooth floor (floor covered with panels, parquet or terracotta) and with mixed floor (panels or parquet with rug or carpet) was similar and amounted to $5.24x10^1$ cfu/m^3 and $5.56x10^1$ cfu/m^3, respectively. Statistical analysis showed that the type of floor had no significant influence on the level of fungi concentration in the air of child homes (p>0.05). In any of the examined dwellings were detected airborne fungi of the genus *Stachybotrys.* Allergenic fungi of the genera *Penicillium, Aspergillus, Cladosporium* and *Alternaria* constituted on average in the indoor air of child homes and in outdoor air 65.63% and 47.54% of all fungal aerosol, respectively. Indoor and outdoor air was dominated by *Penicillium* genus with average 42.11% and 20.74% share, respectively. In 40% of indoor air samples was present *Aspergillus fumigatus* species qualified to the 2 class of biological agents potentially hazardous for people according to the BSL classification (de Hoog, 1996).

Conclusions: 1. The concentrations of airborne fungi indoor child homes were low and did not exceed the Polish reference value for the home environment ($5.0x10^3$ cfu/m^3, Górny, 2004). **2.** Type of room and type of floor in the homes of children did not modify significantly the concentration of fungi in indoor air. **3.** Mycological pollution of indoor air in dwellings was associated most with the presence of fungi allergenic to humans. **4.** Among identified airborne fungi in child homes, was present *Aspergillus fumigatus* species qualified to the 2 class of hazard (BSL classification).

This study was carried out under grant EOG/PNRF-218-AI-1/07 from Polish-Norwegian research Fund.

References:

Garrett, M.H., Rayment, P.R., Hooper, M.A., Abramson, M.J. and Hooper, B.M. (1998) *Clin. Exp. Allergy*, **28**, 459-467.

Klepeis, N.E., Nelson, W.C., Ott, W.R., Robinson, J.P., Tsang, A.M., Switzer, P., Behar, J.V., Hern, S.C. and Engelmann, W.H. (2001) *JESEE* **11**, 231–252

Górny, R. L. (2004) *PiMOŚP* **3**(41), 17-39 [in Polish].

de Hoog, G.S. (1996) *Mycoses*, **39**, 407-417

Indoor particles collected passively in urban and rural primary schools of Portugal

N. Canha[1], S.M. Almeida[1], M.C. Freitas[1], H.T. Wolterbeek[2]

[1] URSN, IST/ITN, Instituto Superior Técnico, Universidade Técnica de Lisboa
Polo de Loures - Campus Tecnológico e Nuclear, E.N. 10, 2686-953 Sacavém, Portugal
[2]Department of Radiation, Radionuclides and Reactors, Faculty of Applied Sciences, Delft University of Technology, Mekelweg 15, 2629 JB Delft, The Netherlands
Keywords: indoor particles, primary schools, chemical composition, passive methodology.
Presenting author email: nunocanha@ctn.ist.utl.pt

Over the last decade, several studies have been conducted to assess the indoor air quality in schools since its importance concerning health, performance and attendance of students have been demonstrated. In fact, children spend most of their time in indoor environments which conducts to a higher exposure to indoor pollutants than outdoor ones. By the other hand, children breathe higher volumes of air relative to their body weights and have a lower capacity to deal with toxic chemicals, which consequently enhances their susceptibility to potential health consequences due to the indoor air contaminants.

This study focuses on the application of a new passive methodology to collect particulate matter in classrooms of primary schools since there are some disadvantages of active samplers, such as: 1) the need of expensive equipment and additional accessories (power supply, air-flow meters and pump); 2) interference with the activities of the classrooms, due to the noise of the equipments; and 3) not convenient or feasible for use in remote areas or to do a simultaneous sampling on a great number of sites.

A passive sampling methodology was applied to collect particulate matter (PM) in classrooms of urban and rural primary schools. Shortly, particles were collected by passive deposition in polycarbonate filters exposed inside the classrooms. The sampling was carried out for 1 year, which allowed to study the seasonal variability of the particles, concerning their masses and chemical content.

Figure 1. Location of the studied primary schools in the urban (left) and rural (right) clusters.

The chemical characterization of the collected particles was conducted to assess the soluble ions content (by ion chromatography and atomic absorption spectrometry) and their elemental composition (by instrumental neutron activation analysis). To identify main polluting sources, correlations between parameters and enrichment factors were studied.

Autumn revealed the higher particle masses concentration among all seasons.

Table 1. Mean values of the particles concentration collected in the studied primary schools over the sampling seasons.

	Particles Concentration (µg.day^{-1}.cm^{2})	
Season	Urban	Rural
Autumn	1.54 ± 0.74	n.a.
Winter	1.49 ± 0.58	1.35 ± 0.73
Spring	1.05 ± 0.38	1.22 ± 0.32
Summer	0.27 ± 0.20	0.14 ± 0.14

The major element in the collected particles was calcium, representing 59 to 64% of the analyzed mass of the particles inside the urban classrooms when the students were attending. In the rural cluster, calcium remained the major component but with a slight lower contribution to the overall particles composition (42 to 29%).

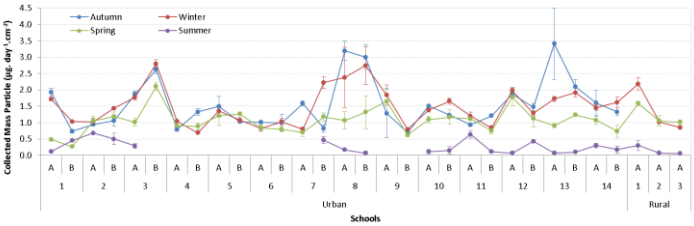

Figure 1. Seasonal variability of particles concentration over the studied clusters.

The calcium source was the chalk used in the blackboards of the classrooms since a strong correlation between Ca^{2+} and SO_4^{2-} was found. Soil re-suspension, traffic and other anthropogenic emission sources could be identified. Enrichment of the particles with Br, Ca, Zn and Sb was found in the urban cluster while in the rural cluster it was found enrichment for the same elements, except for Ca. The comparison between the results of the schools from both clusters allowed to identify classrooms with higher particles concentrations that can indicate potential indoor air quality problems (reflected by an indoor accumulation of pollutants).

This work was supported by the Fundação para a Ciência e a Tecnologia (FCT; Portugal) under research contract PTDC/SAU-ESA/65597/2006. N. Canha thanks FCT for his PhD grant (SFRH/BD/72272/2010).

Canha, N., Freitas, M.C., Almeida, S.M., Almeida, M., Ribeiro, M., Galinha, C., Wolterbeek, H.Th. (2010) J. Radioanal. Nucl. Chem. 286 (2): 495-500.

Almeida, S.M., Canha, N., Silva, A., Freitas, M.C., Pegas, P., Alves, C., Evtyugina, M., Pio, C.A. (2011) Atmos. Environ. 45: 7594-7599.

Filtration of an ultrafine aerosol produced by thermal spraying using a granular bed

D. Bémer[1], Y. Morele[1], I. Subra[1], A.Charvet[2], D. Thomas[2]

[1] Institut National de Recherche et Sécurité (INRS), rue du Morvan, 54519 Vandoeuvre, France
[2] Laboratoire de Réaction et Génie des Procédés, UMR 7274 Université de Lorraine/CNRS, 1 rue Grandville, 54000 Nancy, France
Keywords : granular bed, ultrafine particle, thermal spraying
Presenting author email: denis.bemer@inrs.fr

Industrial filtering installations currently experience major problems associated with the treatment of the ultrafine particles produced by thermal spraying processes due to their high clogging properties (Bémer *et al*, 2013).

Granular beds allow ultrafine particles to be collected, by different mechanisms like brownian diffusion, (Ozis *et al*, 2004), electrostatic forces (Tardos *et al*, 1983), etc. The performance of granular beds have formed the subject of numerous studies, but mainly based on their initial state characterisation. However, variation in their performance characteristics during clogging (Kuo *et al*, 2010), i.e. based on particle accumulation within the bed, has been much less studied, especially in the submicronic particle size range. The aim of this study is to establish the variation in filtration efficiency and pressure drop ΔP of a granular bed during clogging by an ultrafine aerosol generated by an electric arc-based metal thermal spray gun (Zn/Al wire), and to evaluate the performance of a technique of ΔP regeneration by shocks .

The studied aerosol is characterised by a number concentration of 7.10^8 cm^{-3} and a mass concentration of 90 $mg.m^{-3}$ and a mean aerodynamic mass diameter of 110 nm (Elpi measurement, Dekati^R).

The experimental set-up, consists of a tubular granular bed 39 mm diameter, composed of three stages 11 mm long, followed by a 10.5 cm long stage. Each stage, supported by a metal grid, is filled with 0.695 mm diameter glass beads with a bed packing fraction of 0.615.The mass of glass beads was 21 g per stage and 200 g for the last one. Each stage was fitted with static pressure outlets for monitoring the pressure drop during clogging. The particle-laden air is supplied from the top of the column at a flowrate of 5 $l.min^{-1}$. At the end of the clogging phase, a series of shocks was applied at a frequency of 50 Hz to the outside wall of the first stage using a small vibrating device.

The evolution of ΔP of the three stages (11 mm long) during four clogging/unclogging cycles is presented in Fig.1. Stage 1 gradually clogs and its efficiency increases, thereby reducing the particle flow to the lower stages 2 and 3, and curtailing the increase in ΔP. This experiment shows that particle accumulation mainly occurs within the first centimetre of the column, which mainly controls the ΔP within the whole system during clogging.

The granular bed mass efficiency E, defined by the ratio of the mass retained by the mass entering the column was 97.5 % ± 0.4 from the first to the fourth cycle.

As it can be seen in Fig.1, the ΔP of the three stages recovers its initial value after unclogging. The shocks technique experimented in this study appears really promising but should be tested with more clogging/unclogging cycles for validation purposes. Furthermore, checking that the unclogging process does not lead to particle emission as often observed in pulse-jet cleaning of filter media should also be undertaken.

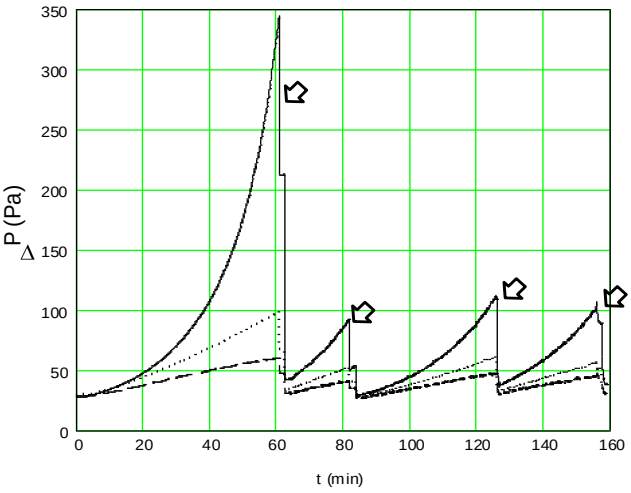

Figure 1. ΔP variation of the three 11 mm long stages during four clogging/unclogging cycles. — stage 1, …. stage 2, ---- stage 3.

Bémer, D., Régnier, R., Morele, Y. et al. (2013). Study of clogging and cleaning cycles of a pleated cartridge filter used in a thermal spraying process to filter ultrafine particles. *Powder Technology*, **234**, 1-6.

Kuo, Y-M., Huang S-H., Lin, W-Y. et al. (2010). Filtration and loading characteristics of granular bed filters. *J. Aerosol Sci.* **41**, 223-229.

Ozis, F., Singh, M., Devinny, J., Sioutas, C., (2004). Removal of ultrafine and fine particulate matter from air by a granular bed filter., *J. Waste Manage. Assoc*., **54,** 935-940.

Tardos, G., Pfeffer, R., Peters, M., Sweeney, T., (1983). Filtration of airborne dust in a triboelectrically charged fluidized bed, *Ind. & Eng. Chem. Fundam*., **22**(4), 445-453.

Physical parameters of powders and release of aerosol

P. Görner[1], R. Wrobel[1], M. Knider[2], A. Boivin[1], F. Clerc[1]

[1]INRS Department of Pollutants Metrology, Laboratory of Aerosol Metrology, 54500 Vandœuvre, France
[2]University of Henri Poincaré, Institute of Technology, 54300 Lunéville, France
Keywords: aerosol, dustiness, powder.
Presenting author email: peter.gorner@inrs.fr

Handling of bulk materials in the workplace can be a major source of release of airborne particles into the atmosphere. Worker exposure to such created ambient aerosols brings a risk of undesirable health effects. The ratio of mass of aerosolized particles to mass of handled powder in controlled conditions gives a dustiness index [$mg.kg^{-1}$].

The goal of this study was to correlate the measured dustiness indices with some physical parameters of powders, such as particle-size distribution, flowability and floodability. These parameters are currently used in connection with industrial conveying of bulk materials and transportation of powders since they often contribute significantly to ambient aerosol concentration in the workplace

Dustiness can be measured using several methods developed in different laboratories. Our choice was to use a method able to measure dustiness indices in three health-related aerosol fractions: inhalable, thoracic and alveolar. A standardized rotating drum (John Fish Holdings, UK) was used to measure dustiness. The method of Coulter-Counter (Coultronics®, US) was used to measure particle-size distribution, and the Powder Tester PT-S (Hozokawa Micron Corp., J) to measure mechanical properties of bulk materials.

Firstly, we assessed the variation of fused alumina dustiness as a function of particle-size. Two alumina powders, one fine (Aloxite 50, mass median diameter MMD=5.35 µm) and another coarser (Aloxite 125, MMD=11.15 µm) were mixed in several proportions and the dustiness of the mixtures measured.

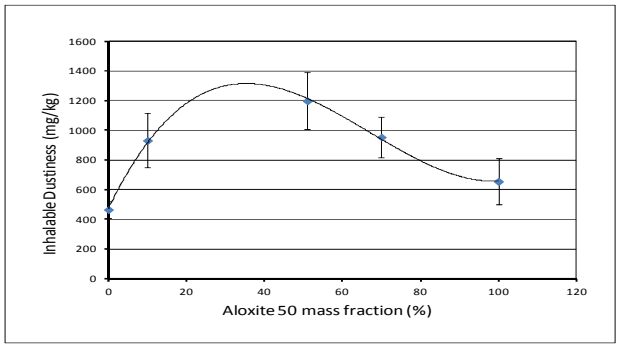

Figure 1 shows variation in inhalable dustiness index as a function of Aloxite 50 content in the mixture

It can be seen from Figure 1 that the finer material has a higher dustiness index than the coarser one but the maximum dustiness corresponds to the mixture with about 35% of coarser material. The mechanism of aerosol release during the powder handling involves both, fine and coarse particles: while fine particles have a higher propensity to be airborne, coarse particles bring the energy necessary to break inter-particle cohesion forces during handling. (Görner et al, 1989).

Several mechanical properties of powder materials have been defined in the literature: Angle of Repose, Angle of Fall, Bulk Density, Compressibility, Cohesiveness, Dispersibility, etc. After measuring them, we did not find a correlation between dustiness and these parameters. But we have found a relationship between dustiness and flowability or floodability. Both flowability and floodability are characteristics made up of several of the above-mentioned parameters and they characterize transport behavior of a powder.

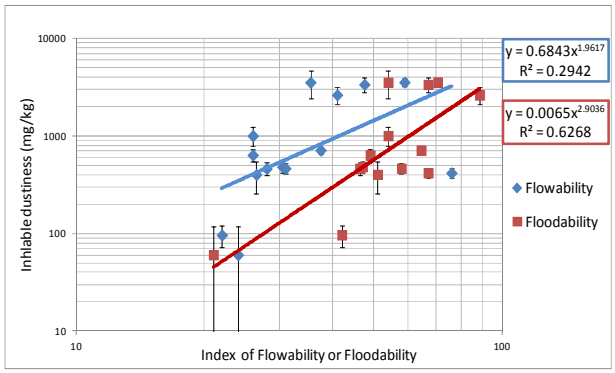

Figure 2 shows a relationship between inhalable dustiness and flowability or floodability of different powders

Figure 2 shows an approximately linear increase in dustiness with increasing flowability or floodability. Bulk materials with good conveying properties are dustier. It was also found (not shown here) that dustiness of coarser materials is better correlated with flowability while dustiness of finer materials is better correlated with floodability. All of these correlations were not statistically significant, probably due to the small number of experimental measurements.

In conclusion we can state that even when dustiness is connected to other physical parameters of bulk powders, it would be rather hazardous to estimate a dustiness potential from them. Dustiness index, if required, should be measured separately.

Görner, P., Pich, J. (1989) Generalized Theory of Dispersion Forces, *J. Aerosol Sci*. **20**. 735-747.

PM_{10} and $PM_{2.5}$ air pollution in Chinese village homes in the Xuanwei region

Fengxia Li[1,2*], Jürgen Schnelle-Kreis[1], Gülcin Abbaszade[1], Bernhard Michalke[3], Ralf Zimmermann[1,2], Jing Wang[4], Shao Longyi[4]

[1]Joint Mass Spectrometry Centre, Cooperation Group Comprehensive Molecular Analytics, Helmholtz Zentrum München, Ingolstädter Landstr. 1, 85764 Neuherberg, Germany
[2]Joint Mass Spectrometry Centre / Chair of Analytical Chemistry, University of Rostock, 18051 Rostock, Germany
[3] Analytical Biogeochemistry Helmholtz Zentrum München, Ingolstädter Landstr. 1, 85764 Neuherberg, Germany
[4] China University Mining & Technology Beijing, Dept Resources & Earth Sci, Beijing 100083, Peoples R China
Keywords: Xuanwei, indoor air pollution, particulate matter, PAHs
Presenting author email: Fengxia.li@helmholtz-muenchen.de

Objective: Xuanwei is a county in the northeast of Yunnan province, China. It is rich in coal resources and well known for the high morbidity and mortality caused by lung cancer in some places in this region. Previous studies indicated that this high lung cancer mortality could not be attributed to smoking or occupational exposure. Instead, it was highly associated with indoor air pollution (Lv et al., 2009). High level of particulate matter (PM_{10}) and toxic organic compound, such as polycyclic aromatic hydrocarbon (PAHs) from coal or wood combustion in the unvented fire pit, was suggested to be the reason for the high lung cancer morbidity and mortality (the highest mortality in china among none-smoking women) in these places. Recently, high concentration of quartz present in the coal has also been proposed to be involved in the cancer development. In spite of many studies, none of them can fully explain the high lung cancer rate in this area. The objective of this study is investigation of the present status of the particulate matter and chemical compound pollution after stove improvement, and what could be the possible difference regarding the indoor particulate matter composition between villages with high and low cancer rate in Xuanwei.

Methods: Seven PM_{10} and 3 corresponding $PM_{2.5}$ samples were taken in four houses in Hutou village with high lung cancer rate, and two houses in Xize village and one house in Luoshui village with low cancer rate in Xuanwei. Organic molecular markers, including PAHs, alkylated PAHs, and biomass burning tracer substances, in these samples were simultaneously analyzed by in-situ derivatisation thermal desorption gas chromatography coupled with time of flight mass spectrometry (IDTD–GC–TOFMS). Elements were determined by inductively coupled plasma mass spectrometry (ICP-MS). Elemental and organic carbon component (EC/OC) was analyzed by thermal-optical analysis IMPROVE-A protocol.

Results: As can be seen from Table 1, our result indicates that the indoor air pollution due to PM and PAHs is somehow alleviated with the ventilation of chimney, yet it is still problematic. As for Benzo[a]pyrene (BaP), it is much higher than the Chinese national standard (GB/T18883-2002) 1.0 $ng.m^{-3}$ with regard to daily average. The other PAHs levels, which are not included in the standard, are also very high. We also found that there was relatively low $PM_{2.5}$ fraction in the PM_{10} (29%, 55% and 32% in Hutou, Luoshui and Xize, respectively), as well as even lower percentages of PAHs in $PM_{2.5}$ (21% ±9%, 18% ±3% and 24%±4% in Hutou, Luoshui and Xize, respectively) as well as some elements of extremely low percentages in $PM_{2.5}$ in Hutou. This indicates that the re-suspended particulate matter plays an important role in the indoor air pollution in these rooms. The alkylated-PAHs are detected to be higher than or comparable to their mother PAHs in different samples from Hutou and Luoshui, where coal is burned in fire-pit or stand stove. However, few types of alkylated PAHs and lower ratio compared to the mother PAHs are detected in Xize village, where wood is burned in different stove, as is shown in fig 1. Biomass tracer compounds are found to abundantly exist in samples from Xize, where wood is burned.

Table 1. PM_{10} and BaP concentration comparison of our measurement with data from literature

Study	Our study			Study 1		Study 2		Study 3	Study 4	
Ventilation	Vented			Unvented		Unvented	Vented	Vented	Unvented	Vented
Region	Hutou	Xize	Luoshui	Laibin	Luoshui	Xuanwei	Xuanwei	Xuanwei, Fuyuan	Xuanwei	Xuanwei
BaP	92	105	87	679.7	437.6	1660	250	95.7	901.3	143.0
PM_{10}	355	227	401			2080	710		1600	500

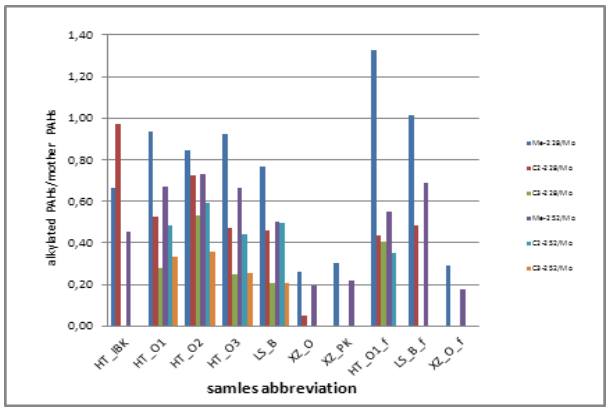

Fig 1. Ratios of alkylated PAHs to their mother PAHs. Me-228/Mo, C2-228/Mo, C3-228/Mo refer to the ratio of Methylated, two carbons or three carbons alkylated PAHs to their mother PAHs with molecular weight of 228. The same for PAHs molecular weight 252.

Lv, J., Xu, R., Wu, G., Zhang, Q., Li, Y., Wang, P., Liao, C., Liu, J., Jiang, G., Wei, F. (2009) *Indoor and outdoor air pollution of polycyclic aromatic hydrocarbons (PAHs) in Xuanwei and Fuyuan, China*, Journal of Environmental Monitoring.

Indoor particle load caused by burning of different types of candles and incense

C. Heuck[1], S. A. Hofmann[1], A. Hubach[1], J. Mehlhorn[1], S. Titel[1], K. Wissmüller[1], K. A. Kamilli[1], S. G. Gonser[1], A. Held[1]

[1]Junior Professorship in Atmospheric Chemistry, University of Bayreuth, Bayreuth Center of Ecology and Environmental Research, 95440 Bayreuth, Germany

Keywords: particle load, indoor, candles, incense.

Presenting author email: christine.heuck@gmx.de

Burning candles and incense emit considerable numbers of particles, including harmful substances like benzo(a)pyrene (Wallace, 2000). Most studies on this issue were conducted in small test chambers in laboratories (e. g. Lau *et al.*, 1997; Fine *et al.*, 1999), so there is still a lack of information on particle emission under true-to-life conditions.

In this study the increase of detectable particle load in an interior room by burning candles and incenses was investigated. Therefore, tea lights, paraffin candles and beeswax candles were lighted up in a furnished and previously aerated interior room and extinguished after one hour of burning. Total particle number concentration was measured with a condensation particle counter and particle size distribution (diameter 0.3 – 10 μm) with an optical particle spectrometer. Particles were also collected on quartz filters and afterwards analysed by temperature-programmed pyrolysis mass spectroscopy. This procedure was repeated for incense sticks and incense cones, but duration of these experiments was adapted to individual combustion times of the sticks/cones.

Mean total particle number concentration during combustion was highest for the beeswax candle ($4.6 \cdot 10^5 \pm 2.0 \cdot 10^4$ cm^{-3}), followed by tea light ($3 \cdot 10^5 \pm 8.4 \cdot 10^4$ cm^{-3}) and paraffin candle ($2.3 \cdot 10^5 \pm 4.7 \cdot 10^4$ cm^{-3}) (Figure 1A). Emission of larger particles (0.3 – 10 μm) for all candles increased sharply after extinguishing though the particle number concentration was lowest for the tea light (Figure 1B). Even though the mean total particle emissions of the incense sticks and cones were lower than for candles, they reached considerably high concentration maxima ($1 \cdot 10^6$ cm^{-3} and $5.8 \cdot 10^5$ cm^{-3}) (Figure 2A). The incense stick emitted much more particles of larger sizes than the incense cone (Figure 2B). With PM_1/PM_{10} ratios between 0.91 (incense stick) and 0.99 (incense cone and tea light) fine particles contributed most to total particle mass. For pyrolysis, a distinct m/z difference of 14 amu probably implies the stepwise release of CH_2 groups from organic compounds. The fraction of low-volatile compounds of the tea light was much lower than for all other combustion articles.

The investigations of this study showed that candles and incense differ considerably in their emission schemes. New aspects on indoor particle pollution and hazards to health caused by these popular decoration articles were explored.

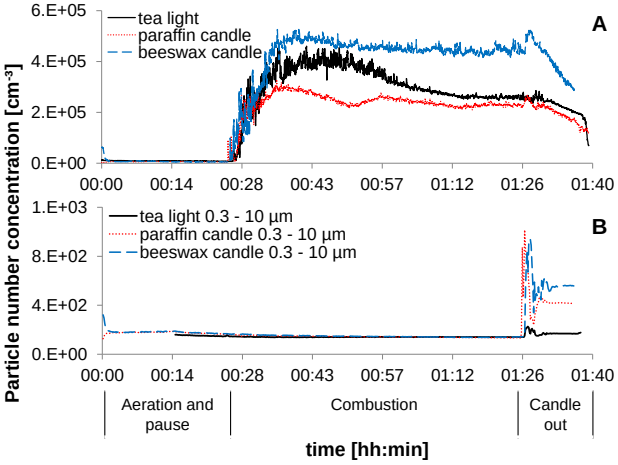

Figure 1: Total particle number concentration (A) and number concentration of particles 0.3 – 10 μm (B) during burning of tea light, paraffin and beeswax candle.

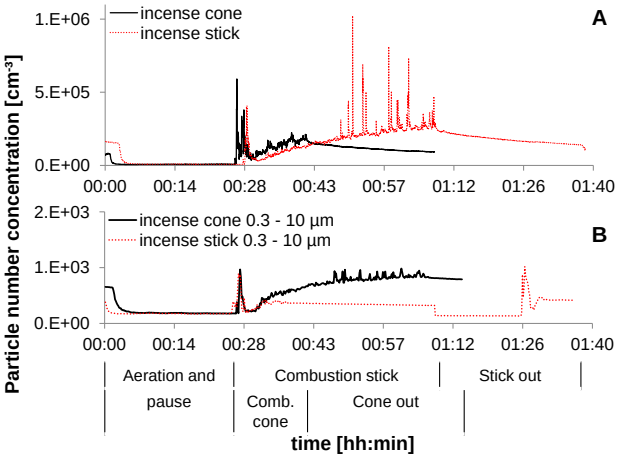

Figure 2: Total particle number concentration (A) and number concentration of particles 0.3 – 10 μm (B) during burning of incense cones and sticks.

Fine, P., Cass, G. and Simoneit, B. R. T. (1999) *Environ. Sci. Technol.* **33**, 2352–2362.

Lau, C., Fiedler, H., Hutzinger, O., Schwind, K.-H. and Hosseinpour, J. (1997) *Chemosphere* **34**, 1623–1630.

Wallace, L. (2000) *Appl. Occup. Environ. Hyg.* **15(1)**, 39–47.

Influence of food surface area on $PM_{2.5}$ and particle number concentration during frying

M. Amouei Torkmahalleh, Y. Zhao, P.K. Hopke, A. Rossner and A.R. Ferro

Center for Air Resources Engineering and Science, Clarkson University, Potsdam, NY, 13699, USA

Keywords: frying, $PM_{2.5}$, food, surface area

Presenting author email: phopke@clarkson.edu

Introduction

The primary sources of indoor aerosols in a home are cooking and tobacco smoking (Hussein et al., 2006). Among cooking activities, frying or stir-frying have been found to be responsible for the highest particle emissions. See and Balasubramanian (2006) showed that frying compared to steaming and boiling leads to greater increase in the particle concentration. Lee et al. (2001) also found that stir-frying was a larger source of particle emissions when compared with other cooking methods. Torkmahalleh et al. (2012 and 2013) showed that cooking oils with high smoke temperature (i.e, soybean and canola oils) and additive such as sea salt, table salt and black pepper can profoundly decrease the level of $PM_{2.5}$ and particle number concentration, at certain temperature. The aim of this study is to investigate the effect of food surface area and mass during frying on $PM_{2.5}$ and particle number concentration.

Materials and Method

The experiments were conducted in an operating laboratory hood. The details of the experimental procedure were given by Torkmahalleh et al. (2012a). The experiments were conducted using tofu and soybean oil. The lab hood is separated into two sections side to side. In one section, a 1L beaker containing 200 ml of soybean oil together with a piece of tofu fully immerged in the oil was heated on a hot plate. The beaker then was moved to the other side of hood for monitoring when the oil reached around 205°C. The first particle measurement was at 185±1°C for each set of experiments since adding tofu accelerated the decrease of the oil temperature. The main variables in this experiment were the total surface area and total mass of tofu, which means that the total surface area and mass of tofu varied among three sets of experiment. Each set was replicated five times. Particle emissions were monitored approximately 0.35 m above the oil surface. After each replicate, the beaker was washed with a soap solution and rinsed with distilled water to remove any oil between experiments. A TSI (St. Paul, MN) DustTrak with a $PM_{2.5}$ inlet was used to estimate the mass concentration of particles emitted during the experiments. The sampling time for these instruments was set to 1 minute. Particle number and size distribution ranging from 10 nm to 500 nm were monitored by a MSP (Shoreview, MN) wide range particle spectrometer (WPS), for which the sampling time for each scan was set to 2 minutes.

Results and Discussion

Figure 1 shows particle mass concentrations of heating pure soybean oil and frying soybean oil together with tofu with different surface areas and masses. There are no major changes observed by adding tofu with the smaller surface area and mass values. Thus, the tofu with a relatively small size does not influence particle mass concentration substantially. However, compared to the $PM_{2.5}$ concentration from pure soybean oil only, tofu with total surface area of 108 cm^2 and mass of 75 g increases the particle mass concentration by 10 times at 185°C to around 22 mg/m^3. This result could be attributed to the large amount of vapor released from frying tofu with a large surface area. The particle mass emissions from frying pure oil and tofu decreased with decreasing temperature.

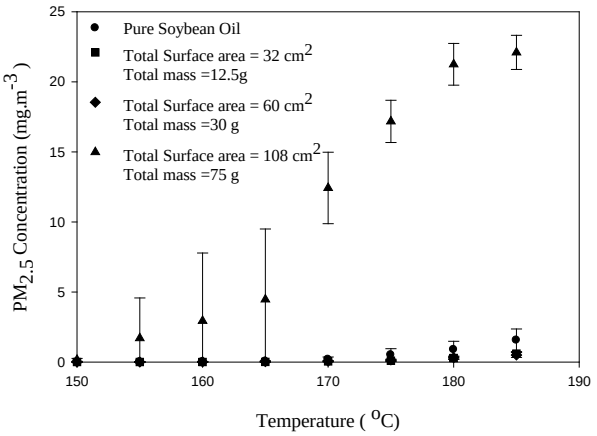

Figure 1. Mean and standard deviation of $PM_{2.5}$ concentration against temperature for soybean oil together with tofu

References

Hussein, T., Glytsos, T., Ondracek, J., Dohanyosova, P., Zdimal, V., Hameri, K., Lazaridis, M., Smolik, J., Kulmala, M., (2006) Atmos. Environ., 40, 4285–4307.

See, S.W., Balasubramanian, R., (2006) Aerosol Air Qual. Res. 6, 82–92.

Lee, S., Li, W., Chan, L. (2001) Sci. Total Environ., 279, 181–193.

Torkmahalleh, M. A., Goldasteh, I., Zhao, Y., Udochu, N. M., Rossner, A., Hopke, P.K. and Ferro, A.R. (2012) Indoor Air. 22, 483-491.

Air Quality in London Paddington Train Station

U. Chong[1], J.J. Swanson[1] and A.M. Boies[1]

[1]Department of Engineering, Trumpington Street University of Cambridge, Cambridge, CB2 1PZ, UK
Keywords: Indoor and Working Place Aerosols, Combustion Aerosols, Aerosol Modelling
Presenting author email: uc211@cam.ac.uk

Exposure to airborne particles from diesel railcars and locomotives in semi-enclosed train stations could present a major health risk for frequent travellers and station employees. While the EU and UK government have recently enacted PM emissions standards on rail traction diesel engines, these regulations only apply to engines that are post-2006 type approved (EU 2004). PM concentrations inside semi-enclosed environments are not regulated by EU air quality standards that apply to outdoor air quality. This presents a strong motivation to evaluate the air quality and emissions inside a station that has diesel trains, such as London Paddington.

Paddington Station is the 8th busiest train station in Great Britain (ORR 2010). Train schedule data indicate that approximately 70% of journeys in Paddington are diesel fuelled. In the context of Paddington, the goals of this study are (a) to quantify the indoor air quality and diesel emissions and (b) to assess the impacts of diesel train emissions on air quality. The methodology of this study is based upon a theoretical air quality model and an experimental measurement campaign.

In the measurement campaign, PM mass was measured at 5 locations using TSI AM510 monitors. Particle size distributions and number concentrations were measured at 2 locations using a TSI CPC and SMPS. Measurements were taken with and without a catalytic stripper to quantify the semi-volatile content of PM. Air samples were also collected on filters for analysis of metals, ions, and elemental/organic carbon (EC/OC) particle composition. Real time measurements of CO_2, NO_x, and SO_2 were also measured at the same 2 locations. Using anemometers, wind speed and direction data were collected at the 2 largest openings into the station so that a simplified mixed box model of particle mass concentrations in the station could be derived.

A theoretical mixed box model was developed based upon Nazaroff (2004) and solved with Euler's method. The model calculated particle mass concentration as a function of indoor emissions rate, natural ventilation, and air leak infiltration. Idle and acceleration emissions factors were developed for train types and traffic schedules specific to Paddington station. Natural ventilation was calculated from an air flow rate that was measured at the 2 largest openings in the building. Air leak infiltration was calculated based upon Gowri et al. (2009).

Measured results include total particle number, mass, and size distribution. Generally, results showed that respirable PM concentrations in the station were similar to concentrations on a typical London roadside (Marylebone Road). However, during some peak rush hours, concentrations of PM and NO_2 exceeded outdoor EU limits. EC/OC measurements shown in Fig. 1 indicate that the organic fraction of PM depend on the location in the station with highest concentrations near Praed Ramp, furthest from the trains. Similar conclusions drawn from concentration metrics are also discussed in the presentation.

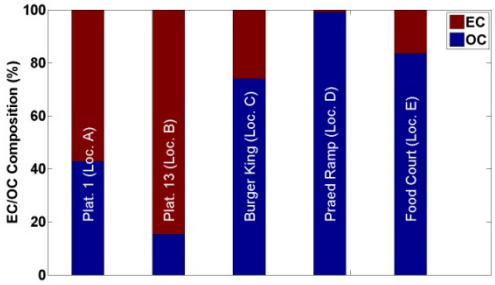

Figure 1: EC/OC ratio variation by location

Modelled PM concentrations tracked closely with measured concentrations. The results from 1 day of analysis (Thursday) are shown in Fig. 2.

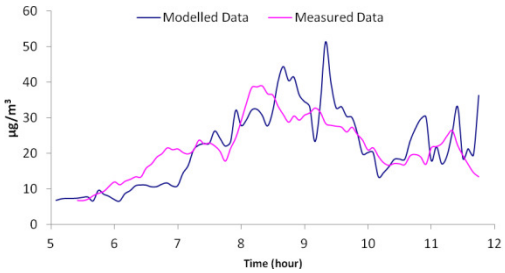

Figure 2: Modelled versus measured PM concentrations

The coefficient of determination between modelled and measured results was R^2=0.24. The daily averaged modelled concentration was also calculated to be within 2% of the measured concentration.

The measured PM mass concentrations in the station are close to London roadside levels. Speciation measurements show that diesel trains constitute a significant portion of PM. A mixed box model was developed to simulate PM mass concentrations. Further research could result in a more precise mixed box model that can assess the air quality impact of emissions abatement technologies on the diesel trains in the context of impending rail traction emissions regulations.

EU (2004) *Directive 2004/26/EC of the European Parliament and of the Council*. Official Journal of the European Union L-146.

Gowri, K.; Winiarski, D.; Jamagin, R. (2009) *Infiltration Modeling Guidelines for Commercial Building Energy Analysis*. US Department of Energy Report PNNL-18898.

Nazaroff, W.W. (2004) Indoor Particle Dynamics. *Indoor Air*. 14: 175-183.

ORR (2010) *2009-2010 Station Usage Report and Data*. UK Office of Rail Regulation.

This work is supported by the EPSRC and Schiff Foundation.

Source characterisation and estimation of daily residential exposure to ultrafine particles

C. Isaxon[1], A. Wierzbicka[1], E.Z. Nordin[1], A. Dahl[1], G. Wieslander[2], M. Bohgard[1]

[1]Department of Ergonomics and Aerosol Technology, University of Lund, Lund, Sweden
[2]Department of Occupational and Environmental Medicine, Uppsala University, Uppsala, Sweden
Keywords: exposure, emissions, ultrafines, sources.
Presenting author email: Christina.isaxon@design.lth.se

Humans, at least in the industrialized part of the world, spend a large part of their lives in their homes, and are hereby subjected to various indoor generated airborne particles, which often dominate the particle concentrations (Wierzbicka, 2008). Most of our knowledge concerning particles of indoor origin and their potential health effects is derived from epidemiological studies based on measurements of outdoor particles. These particles are considered to be the background exposure indoors. There is a need to further investigate the contribution from human activities to concentrations in indoor environments.

The aim of this study has been to characterize the air quality in residential dwellings, identify sources of indoor particles (<300 nm) on the basis of residential activities, quantify their source strength and from measurements and detailed log books estimate daily residential exposure levels (concentration*hours per day).

For seven consecutive days, time resolved stationary measurements were conducted in randomly selected homes (N=42) in the urban area of Lund in southern Sweden. Number concentrations, and mean diameter of particles <300 nm were monitored with Discmini (University of Applied Sciences, Windisch, CH) and Nanotracer (Philips Aerasense). Since a majority of particles generated by indoor activities are smaller than 100 nm, results from the Nanotracer and Discmini could be considered as good approximations of ultrafine particles. The accuracy of both the Nanotracer and Discmini are ±30% (Asbach et. al., 2012). All measurements were made during off-pollen season (October-April). The instruments were placed centrally in the dwelling, but not in, or close to, the kitchen. CO_2 data was collected, by a custom-made instrument from Technical University of Denmark, DTU, and used to calculate air exchange rates based on the ASTM standard (2002). The habitants filled in detailed activity log books, and reported when they were present or absent in the dwelling.

A data classification was carried out by sorting the data into two categories: occupancy time (at least one person present in the home) and non-occupancy time. Occupancy time occurred during an average of 77 % of the measurement period. Activities occurred on average 33 % of the occupancy time. Average concentration of particles (<300 nm) during occupancy time was 49000±64000 cm^{-3}, and during non-occupancy time 6000±4000 cm^{-3}. The origins of elevated concentrations were identified using the activity logs. Several of the concentration peaks were results of a combination of two or more particle generating activities. 13 different single activities could however be identified as contributing significantly to the indoor air particle concentration (Figure 1). Cooking activities (boiling, frying, oven, microwave oven, toaster, and their combinations) and candle burning were shown to be the major particle sources, contributing to 31 and 26 % of the daily residential exposure, respectively.

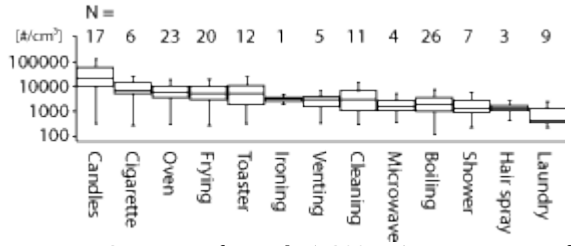

Figure 1. Summary of particle (<300 nm) concentrations from various indoor sources. Box plots denote minimum values, 1st quartile, median, 3rd quartile and maximum values. N is the number of events the calculations are based on.

Source strengths could be estimated for 8 of the 13 activities, using the method described by Wierzbicka (2008). The particle source strengths ranged from $1 \cdot 10^{12}$ to $8 \cdot 10^{13}$ min^{-1}.

The average daily residential exposure was estimated to 399000 cm^{-3}h/d, the same range as in Californian homes as reported by Bhangar et al (2011). Indoor activities contributed to 86 % of the daily residential exposure, while the background (outdoor generated) particles contributed to 14%.

Most particles generated by indoor activities are small (<300), and have the potential to be deposited deep in the respiratory system. A major part of the daily residential exposure has its origin in human activities, thus these should be considered in personal exposure assessment and their potential health effects should be evaluated. Time resolved data and activity logs are important tools to assess the contribution of various activities to the overall residential exposure.

Acknowledgements:
The Swedish Research Council Formas and Vinnova - Swedish Governmental Agency for Innovation Systems

References:

Asbach, C., Kaminski, H., Von Barany, D. Kuhlbusch, T.A.J., Monz, C., Dziurowitz, N., Pelzer, J., Vossen, K., Berlin, K., Dietrich, S., Gotz, U., Kiesling, H.J., Schierl, R., Dahmann, D. 2012. Comparability of Portable Nanoparticle Exposure Monitors. Annals of Occupational Hygiene, 56:606-621.

Bhangar S., Mullen N.A., Hering S.V., Kreisberg N.M., Nazaroff W.W. 2011. Ultrafine particle concentrations and exposures in seven residences in northern California. Indoor Air 21:132-144

Wierzbicka A. 2008. What are the characteristics of airborne particles that we are exposed to? Focus on indoor environments and emissions from biomass fired district heating. Doctoral thesis. Lund University, Sweden.

VOC and particle emissions from a household cleaning product

A.W. Nørgaard, J.D. Kudal, I.K. Koponen, and P. Wolkoff

National Research Centre for the Working Environment, 2100, Copenhagen, Denmark
Keywords: Terpene-ozone reactions, indoor VOCs, secondary organic aerosols, mass spectrometry
Presenting author email: awn@nrcwe.dk

Common household cleaning products (HHCP) may contain chemicals that affect human respiratory health (Zock *et al*. 2010). Both volatile organic compounds (VOCs) and aerosolized chemicals emitted from spray cleaning products, are of concern. The phase of the VOCs, i.e. gaseous versus aerosols, is important due to the different deposition mechanisms in the respiratory system. Thus, we followed the emissions of VOCs and the evolution of freshly nucleated aerosol particles from a common HHCP. In series of near- realistic user scenarios HHCP (20 to 40 g) was applied to a steel surface (1-2 m^2) inside a walk-in exposure chamber (20.3 m^3) that simulates indoor conditions with either low (10 ppb) or high ozone (45 ppb) levels. The air exchange rate was: 0.6 ± 0.1 h^{-1}, temperature: 22 ± 2 °C, and relative humidity: 50 ±15 %. VOCs were measured by 1.) Sampling on Tenax TA adsorbent tubes and analyzed by thermal desorption-gas chromatography/mass spectrometry (TD-GC/MS) and 2.) Real time monitoring by atmospheric sampling Townsend discharge ionization (triple quad) mass spectrometry (ASTDI-MS) according to (Nøjgaard *et al*. 2007). Carbonyl compounds, such as formaldehyde, were sampled on 2,4-dinitro phenylhydrazine (DNPH) cartridges followed by liquid extraction and analysis by liquid chromatography with UV detection. Particles were measured by: 1.) Fast mobility particle sizer (FMPS), 2.) Electrical low pressure impactor (ELPI), 3.) Condensation particle counter (CPC), and 4.) Particle surface area monitor (NSAM).

The HHCP contains several terpenes (fragrances) with limonene as the most abundant. Limonene rapidly undergoes ozone-initiated reactions, to produce a host of oxygenated products (Calogirou *et al.* 1999). These products are of concern, since they are suspected to adversely affect the indoor air quality; further, secondary organic aerosols (SOA) are formed, e.g. (Vartiainen *et al*. 2006).

Preliminary results

A maximum gas phase limonene concentration about 350 μg/m^3 (63 ppb) was reached within the first 30 min upon application of 40 g HHCP at low ozone conditions. At high ozone conditions, well-known limonene oxidation products such as 3-isopropenyl-6-oxo-heptanal (IPOH) and 6-methyl-5-heptene-2-one (6-MHO) were observed in relatively constant concentrations for the first 100 min, see Figure 1. Hereafter, they decreased together with the limonene concentration. Similar trends were observed in real-time by ASTDI-MS.

Elevated concentration of small particles between 6 and 10 nm was observed immediately after application of the HHCP. Within two minutes, the small particle mode peaked around 30 nm and the number concentration increased from 500 to 9e5 #/cm^{-3}. In the beginning of the condensational growth, the mean diameter of the particles was 5.6 nm. After 120 minutes, the particle mean diameter increased to 110 nm.

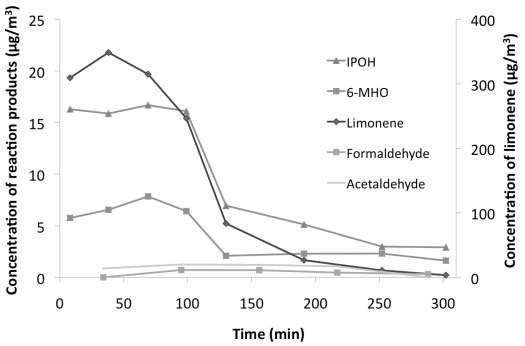

Figure 1. Ozone-initiated gas phase concentrations of limonene and some of its products measure by TD-GC/MS.

Support was obtained from the project "OFFICAIR" (On the reduction of health effects from combined exposure to indoor air pollutants in modern offices) funded by the European Union 7th Framework (Agreement 265267) under the Theme: ENV.2010.1.2.2-1.

Calogirou, A., Larsen, B.R., Kotzias, D. (1999) *Atmos. Environ.* **33**, 1423-1439.

Nøjgaard, J. K., Larsen, K., Wolkoff, P. (2007) *Int. J. Mass Spectrom.* **260**, 49-56.

Vartiainen, E., Kulmala, M., Ruuskanen, J., Taipale, R., Rinne, J., Vehkamäki, H. (2006) *Atmos. Environ.* **40**, 7882-7892.

Zock, J. P., Vizcaya, D., Le Moual, N. (2010) *Curr. Opin. Allergy and Clin. Immunol.* **10**, 114-120.

Radon progeny particle concentration changes in an air-conditioned auditorium

B. Polednik[1], M.R. Dudzinska[1], K. Kozak[2], J. Mazur[2] and D. Grzadziel[2]

[1]Faculty of Environmental Engineering , Lublin University of Technology, Lublin, 20-618, Poland
[2] Institute of Nuclear Physics PAN, Krakow, 31-342, Poland
Keywords: radon, decay products, aerosol particles, auditorium.
Presenting author email: b.polednik@wis.pol.lublin.pl

Radon (Rn) and its progeny (Prog.) constitute harmful pollutants present in the indoor environment. Apart from ionizing radiation, solid heavy metal radon progeny may also have adverse health effects (Duffus, 2002). Until now the research related to the indoor radon concentrations was carried out mainly in naturally ventilated unoccupied premises (Mostafa *et al.,* 2011).

This study provides detailed data on the Rn, Prog. aerosol particle concentration, and the indoor air parameter changes in the occupied and unoccupied air-conditioned auditorium at Lublin University of Technology in Lublin, Poland.

The concentrations of radon and its decay products were measured with the use of AlphaGUARD PQ2000 PRO (Genitron) and EQF3220 (SARAD). The particle mass (PM) and number (PN) concentrations were continuously determined by means of the Dust Trak DRX model 8533 and P-Trak model 8525 (TSI Inc.), respectively. The indoor air parameters were measured using a system Almemo 5690-2M (Ahlborn).

Figure 1 shows not only changes of the concentrations of Rn and Prog. but also of the indoor air parameters in the unoccupied auditorium, when the AC was switched off (AC off) as well as during the classes with students' presence. The AC was switched on during the day and switched off during the night (AC on/off). Higher average Rn and Prog. concentrations were recorded in the auditorium with AC off. The average PN concentrations were the same in both ventilation modes. A positive correlation ($p<0.001$) has been observed between the Rn concentration and the PN and PM_1 concentrations during the AC on/off mode. A negative correlation has been observed for the Prog. concentration and the indoor air temperature and CO_2 concentration in the AC off mode. The obtained results confirm the importance of the indoor air parameters during the assessment of the radiation hazards related to the presence of radon in air-conditioned premises.

This work was supported by the Polish Ministry of Science and Higher Education under the grant 7454/B/T02/2011/40.

Duffus J.H. (2002) Heavy metals a meaningless term? *Pure and Applied Chemistry*, **74**, 793-807.

Mostafa A.M.A., Tamaki K., Moriizumi J., Yamazawa H., and Iida T. (2011) The weather dependence of particle size distribution of indoor radioactive aerosol associated with radon decay products. *Radiat. Prot. Dosimetry*, **146(1-3)**, 19-22.

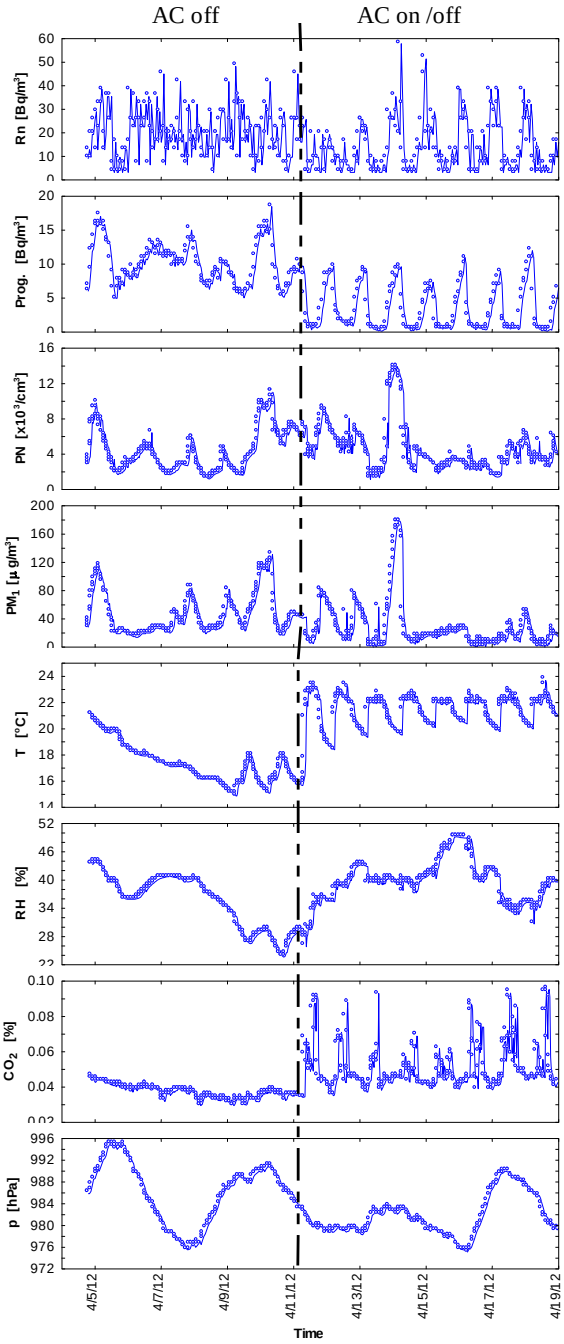

Figure 1. Time series of the concentrations of radon (Rn) and its decay products (Prog.), ultrafine particle number (PN) and mass (PM_1) concentrations, indoor air temperature (T), relative humidity (RH), CO_2 concentration and air pressure (p) changes in the auditorium during the AC off and AC on/off mode.

Exposure to indoor air pollutants during physical activity in gymnasiums

C.A. Ramos[1], S. M. Almeida[1], H. T. Wolterbeek[2]

[1] IST/ITN, Instituto Superior Técnico, Universidade Técnica de Lisboa, Estrada Nacional 10, 2686-953 Sacavém, Portugal;
[2] Faculty of Applied Sciences, Department of Radiation, Radionuclides and Reactors, Section RIH (Radiation and Isotopes in Health), Technical University of Delft, Delft, The Netherlands.
Presenting author email: carla.ramos@ctn.ist.utl.pt
Keywords: indoor, gymnasiums, assessment

Physical activity has become a social need among people, and is clearly proved that exercise is a way to prevent all-cause and cardiovascular-related death, diabetes mellitus and obesity. However, athletes and the common individual can be at risk when they are practicing exercise in polluted environments due the fact that 1) the ventilation rates increase and the quantity of pollutants inhaled increase proportionally; 2) most of the air is inhaled through mouth, bypassing the normal nasal mechanisms for filtration of large particles and 3) the increased airflow velocity carries pollutants deeper in to the respiratory tract[1]. Due to these facts, research in the field of indoor and outdoor air quality while practice exercise is important to improve the scientific knowledge and the implementation of best practices/recommendations for people who workout.

Firstly, measurements of the indoor pollutants PM_{10}, CO_2, CO, H_2CO, VOCs and O_3 was made in 15 gymnasiums in Lisbon in order to get a general perception of IAQ in this setting. After this, three gyms were selected to perform a deep analysis during one week in each one. Measurements were performed during the occupation time, in the studios and in the bodybuilding room, in order to recognize daily patterns and identify pollutant sources.

PM was measured in the indoor of the gyms 1) with a direct reading equipment (Lighthouse 3016) with five different granulometries (PM_{10-5}, $PM_{5-2.5}$, $PM_{2.5-1}$, $PM_{1-0.5}$, $PM_{0.5-0.3}$) and 2) with a medium volume sampler (MVS6 Leckel) using teflon filters. Simultaneously, in outdoor was used a Partisol 2000 with teflon filters. Particle mass concentration was determined by gravimetry with a Mettler Toledo microbalance (UMT5). Filters were weighed before and after sampling in a humidity and temperature controlled room. Elemental analysis of PM_{10} sampled in the filters was performed by using Neutron Activation Analysis in Portuguese Research Reactor.

Figure 1shows that PM_{10} concentrations were different between gyms and spaces. The outdoor concentrations presented a great contribution in the PM_{10} indoor concentrations of gym 2. PM continuous measurements indicated that the concentrations increase when the spaces are occupied during classes, mostly in the coarse fraction (PM_{10-5} µm and PM_{5-10} µm).

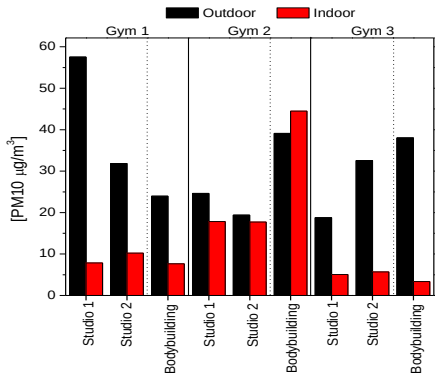

Figure 1. Concentrations indoor and outdoor measured in the spaces of the gyms

CO_2 concentrations presented very high values during physical activity. Table 1 show the maximum and the average values measured in the studios while physical activities classes were performed.

Table 1. Maximum and average CO_2 concentrations measured indoor during classes

		Maximum (mg/m^3)	Average (mg/m^3)
Gym 1	Studio 1	2738	1844
	Studio 2	2917	2118
Gym 2	Studio 1	3001	1997
	Studio 2	2200	1381
Gym 3	Studio 1	2219	963
	Studio 2	1652	1125

In addition to the pollutants assessment, a physiological analysis (respiratory frequency, heart rate, minute ventilation) was performed to the gym users during the physical activity, in order to establish the personal exposure to the measured air pollutants.

Results presented a strong support to the importance of the implementation of actions that will improve the air quality in sport facilities. It is crucial to improve the HVAC system maintenance, ventilation rates and occupants behaviour in order to potentiate the sport benefits.

The author is gratefully acknowledge to all gyms that collaborate, to Dr. Amádis Santos of EFACEC, to Dr.ª Célia Alves and Dr.ª Teresa Nunes of Aveiro University and to ESTeSL, and also to Fundação para a Ciência e Tecnologia (FCT) for the PhD Grant - SFRH/BD/79277/2011.

[1] Carlisle, A., & Sharp, N. (2001). *Br J Sports Med* , **35**, 214-222.

Investigation of particulate matter from wave soldering processes at a printed circuit board manufacturing company

Z. Szoboszlai[1], Zs. Kertész[1], Z. Szikszai[1], A. Angyal[1], E. Furu[1,3], Zs. Török[1,3], L. Daróczi[2] and Á.Z. Kiss[1]

[1]Institute for Nuclear Research, Hungarian Academy of Sciences (ATOMKI), Debrecen, H-4001, P.O Box 51., Hungary
[2] Department of Solid State Physics, University of Debrecen, Debrecen, H-4010, P.O. Box 2., Hungary
[3]University of Debrecen, Debrecen, H-4032, Egyetem tér 1, Hungary
Keywords: wave soldering, workplace aerosol, PIXE, single particle analysis.
Presenting author email: szoboszlai.zoltan@atomki.mta.hu

It is well known that the electronics products industry has exposed workers to high doses of metals. Several studies have reported that the inhalation of metal dust and fumes is associated with adverse health effects such as metal fume fever and other respiratory diseases.

In this study, our aim was to investigate indoor aerosol particles in a working environment where the soldering and testing of different kinds of printed circuit boards (PCB) and other electronic components takes place (Szoboszlai, 2012). Wave soldering is one of the main processes used for attaching metal components to the board during the manufacturing of PCBs. (The name is derived from the use of waves of molten solder. The constituents of the solder alloy are dependent on the type of wave solder e.g. leaded (Sn–Pb) or lead free wave solder (Sn–Ag–Cu–Sb)).

Aerosol samples were collected in a large working hall where approximately 100 people worked. Two 48-h long sampling campaigns were carried out. One was in October 2008 and the other was in May 2009. A two-stage sampler with Nuclepore polycarbonate filters of 8 μm and 0.4 μm pore diameter was used to collect the $PM_{2.5}$ and $PM_{2.5-10}$ size fractions separately. In addition, a ten-stage PIXE International cascade impactor was used to provide size resolved samples in the following ten fractions >16, 16-8, 8-4, 4-2, 2-1, 1-0.5, 0.5-0.25, 0.25-0.12, 0.12-0.06 and <0.06 μm aerodynamic diameter. Aerosol samples were collected in the following sites: next to 2 wave solders (in one of them unleaded and in the other leaded melt was used), below a supply air ventilator and close to a location named “store of hazardous materials”.

The elemental compositions (for $Z \geq 13$) of the bulk samples were measured by PIXE analytical method in the IBA Laboratory of ATOMKI. Additional information concerning the characteristics of the aerosol particles was drawn from individual particle analysis by scanning nuclear microscopy and SEM.

In this study, we have showed that the manufacturing of the PCBs is associated with aerosol emissions. Based on the elemental ratios and correlations, size distribution data and single particle analysis, the creation processes and the indoor sources were identified, e.g. soldering, fluxing, etching and cleaning. The concentration of PM and the elemental components increased at the wave solders. The main constituents of the leaded and the unleaded melt were recognized in the indoor aerosols. Flux-related (Zn, Cl), and etching-related (Fe, Cl) elemental compositions were also identified.

The PM concentrations measured indoors were higher in 2008 than in 2009. The differences between the two sampling periods could be attributed to the change in technology and working schedule. From 2008 to 2009 most of the leaded wave solders were put out of operation, which could be detected through the decrease in lead concentration.

It was confirmed that relative to the outdoor atmosphere inside the working hall the air was clean due to supply air ventilators and the low indoor emission rate. Although the concentrations of Pb were less than the limit value of the WHO, there was a maximum in the fine mode in the mass size distributions of Pb and other metals Ag, Cu, Zn (Fig. 1.). Based on the stochastic lung model calculations, the majority of the observed elements are deposited in the extrathoracic regions. These calculations showed higher deposition probability for Pb in the acinar region than for particles of natural origin.

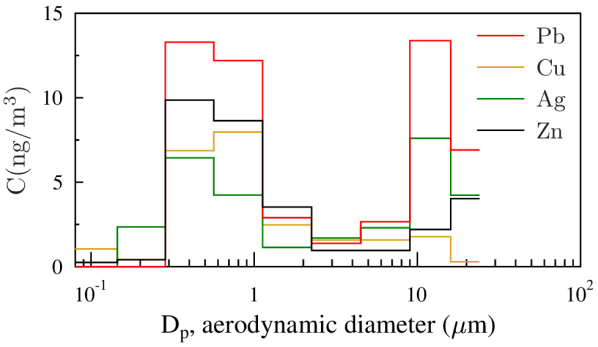

Figure 1. Mass size distribution of Pb, Cu, Ag and Zn elements (sampled in the workplace in 2008).

Z. Szoboszlai, Zs. Kertész, Z. Szikszai, A. Angyal, E. Furu, Zs. Török, L. Daróczi, Á.Z. Kiss (2012) *Journal of Hazardous Materials* **203**, 308-316.

Acknowledgement
This work was supported by the TÁMOP-4.2.2/B-10/1-2010-0024 project and co-financed by the European Union and the European Social Fund. This study was carried out in the frame of the János Bolyai Research Scholarship of the Hungarian Academy of Sciences.

Comparative study of indoor aerosols collected at educational institutions: kindergarten, elementary school, and secondary grammar school.

Z. Szoboszlai[1], E. Furu[1,2], A. Angyal[1], Zs. Török[1,2] and Zs. Kertész[1]

[1]Institute for Nuclear Research, Hungarian Academy of Sciences (ATOMKI), Debrecen, H-4001, P.O Box 51., Hungary
[2]University of Debrecen, Debrecen, H-4032, Egyetem tér 1, Hungary
Keywords: school aerosol, children exposure, elemental composition, PIXE.
Presenting author email: szoboszlai.zoltan@atomki.mta.hu

In Hungary everybody is required to attend to a sort of educational institution between 6 and 18 years of age. This means that an average schoolchild is in a limited space at least six to eight hours a day. It is well known that the exposure to particulate matter (PM) during school-age, when children are in their growing stage, can have lifelong adverse effects on their health. Because of these facts, it is particularly important to better investigate the air parameters of scholastic environments.

The goal of the present study is to characterize and compare the concentration, elemental composition and mass size distribution of particle matter sampled in a heating and non-heating season in three educational institutes in the centre of Debrecen, Hungary. Two schools (a primary and a secondary grammar) and a kindergarten were selected. The sampling campaigns were carried out during teaching ours i.e. from 8 am to 4-6 pm in the following microenvironments: different classrooms, school yards, gymnasiums, a computer lab, a chemical lab, a director's office and a so-called salt-room. Outdoor aerosol collection was carried out at the same time in the yards of the institutions.

The elemental compositions of the samples were measured by particle induced X-ray emission (PIXE) method in the IBA Laboratory of ATOMKI. Macro-PIXE was used to determine the elemental composition (for $Z \geq 13$) and elemental mass size distributions of bulk samples. Moreover single particle analysis was performed with micro-PIXE and scanning electron microscopy (SEM) at the ATOMKI. On the basis of the obtained data, the total and regional deposition efficiencies of the different types of particles within the human respiratory system were also calculated by using a stochastic lung deposition model.

In our previous study (Szoboszlai, 2011), carried out in a heating season (2009/2010) in the three educational institutions, we found high concentration of coarse aerosols and showed that the concentration increased in the lower educational levels. In the non-heating season (2010), we found that the concentrations followed the trend which was observed in the heating season ($C_{kindergarden.} > C_{primary\ school} > C_{secondary\ school}$) but the amount of the PM concentration was lower than in the heating season (Fig. 1.). We also found that the concentrations of coarse aerosols were higher inside the institutions than in outdoor in the non-heating season. On the basis of elemental concentration, we observed that most part of the PM mass inside the institutions is originated from the crust and transported from outdoors through the windows and foot transport in all seasons. Minor part of the PM is derived from local indoor sources, such as detergents, chalk, building materials, magnesia powder, and chemical reactions from the chemistry laboratory.

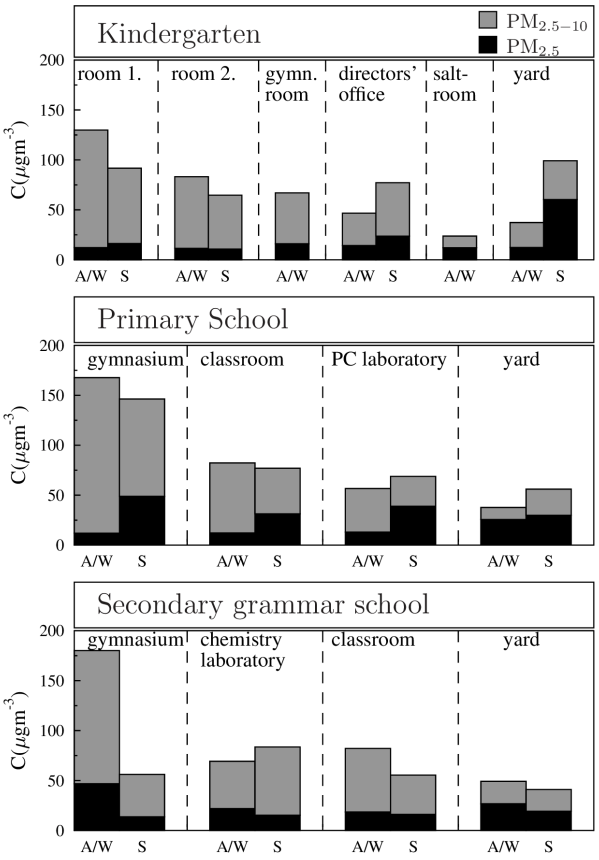

Figure 1. $PM_{2.5}$ and $PM_{2.5-10}$ average concentrations in 3 educational institutions of Debrecen. (A/W= autumn/winter, S=summer)

Szoboszlai Z., Furu E., Angyal A., Szikszai Z., Kertész Zs. (2011), *X-ray Spectrometry* **40:(3)** 176-180.

Acknowledgement
This work was supported by the TÁMOP-4.2.2/B-10/1-2010-0024 project and co-financed by the European Union and the European Social Fund. This study was carried out in the frame of the János Bolyai Research Scholarship of the Hungarian Academy of Sciences.

Seasonal behavior of indoor and outdoor PAHs in different microenvironments of Rome, Italy

M.P. Gatto [1], A. Gordiani [1], P. Romagnoli [2], C. Balducci [2], M. Perilli [2], A. Cecinato [2], M. Gherardi [1]

[1]Department of Occupational Hygiene, Research Sector, INAIL Research (Italian Workers' Compensation Authority), Monte Porzio Catone, Rome, 00040, Italy
[2]Institute of Atmospheric Pollution Research, National Research Council, Monterotondo Stazione RM, 00015, Italy

Keywords: particle-bound PAHs, carcinogenic PAHs, indoor microenvironments,

mp.gatto@inail.it

Among Persistent Organic Pollutants (POP), Polycyclic Aromatic Hydrocarbons (PAHs) are a class of complex organic chemicals of increasing concern for their occurrence in the environment. They are ubiquitous in ambient air and have been identified as carcinogenic, benzo[a]pyrene (B[a]P), and some of them as probably and possibly carcinogenic. PAHs can be found in the atmosphere in both gaseous and particulate forms ($PM_{2.5}$ and PM_{10}) depending on their volatility which is governed by their chemical structure. The best known PAH is the benzo[a]pyrene (B[a]P). To identify and to quantify population exposure among children and elderly people to PAHs content in particulate matter in highly urbanized areas and to assess the impact on human health, in order to support environmental policy and regulation in this field, EXPAH project has proposed an integrated approach based on measurements and modeling techniques (http://www.ispesl.it/expah/).

In the frame of this Life+ EXPAH project, particle-bound PAHs were monitored in the urban area of Rome in order to assess the actual human exposure in different living/working places (microenvironments).

The method was based on $PM_{2.5}$ active sampling at low volume conditions on PTFE filters and GC/MS determination of non-volatile PAH congeners, characterized by higher carcinogenic and mutagenic potencies. According to the experimental design, two seasonal in-field campaigns (summer and winter) were performed by sampling both indoor and outdoor living/working microenvironments.

In each seasonal campaign, 17 locations were monitored including six schools, two offices and nine houses. The study was focused on seven "carcinogenic" PAHs (benz[a]anthracene, benzo[b]fluoranthene, benzo[j]fluoranthene, benzo[k]fluoranthene, benzo[a]pyrene, indeno[1,2,3-cd]pyrene and dibenz[a,h]anthracene) and a mutagenic congener (benzo[ghi]perylene).

Results

Large differences between winter and summer indoor and outdoor PAH's values were found in the city of Rome (see Fig. 1). During the winter in-field campaign (December 2011-March 2012), the target PAHs ranged from 6.0 to 7.4 ng/m^3 (indoor), and 8.4 to 13.2 ng/m^3 (outdoor). The typical indoor/outdoor ratio was ca. 0.7. During the summer campaigns (lasted from May to July 2012), the target PAHs ranged 0.40÷1.35 ng/m^3 (indoor), and 0.62÷1.52 ng/m^3 (outdoor). Heating and biomass burning during winter were presumably responsible of this finding.

The winter values were well above the guideline value for BaP (1 ng/m^3) whereas the summer values were well below. During the winter the average BaP detected indoor ranged from 0.94 (offices) to 1.14 (schools) ng/m^3, and the respective outdoor values ranged from 1.4 and 2.0 ng/m^3; during the summer BaP ranged from 0.04 to 0.15 ng/m^3 (indoor) and 0.06 to 0.19 ng/m^3 (outdoor).

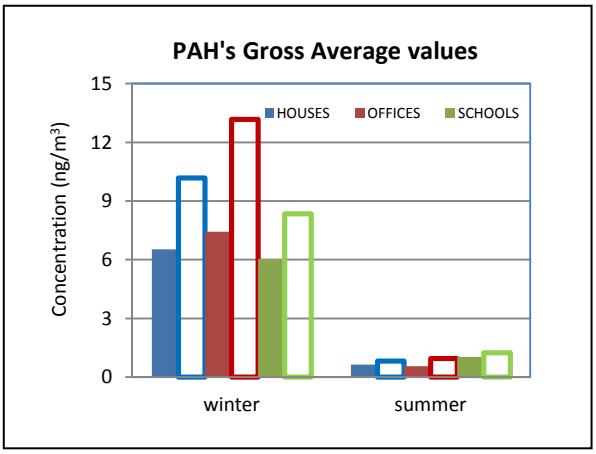

Fig. 1. Total PAHs in the investigated microenvironments: full bars refer to Indoor; empty bars refer to Outdoor

According to results, in the principal life environments humans seem to be exposed to PAH levels similar to those typical of outdoor air. In winter, these level can exceed the guideline values of ambient air quality.

Acknowledgment
This investigation is supported by EC LIFE+ Environmental Health Program.

Indoor/outdoor ratio and percent distribution behaviours of PAHs in Rome, Italy

P.Romagnoli [1], C.Balducci [1], M.Perilli[1], A.Cecinato [1], M.Gherardi [2], M.P.Gatto [2]

[1]Institute of Atmospheric Pollution Research, National Research Council, Monterotondo Stazione, Rome, 00015, Italy
[2]Department of Occupational Hygiene, Research Sector, INAIL Research (Italian Workers' Compensation Authority), Monte PorzioCatone, Rome, 00040, Italy
Keywors: PAHs, indoor pollution, indoor/outdoor penetration ratio, molecular markers
Presenting author e-mail: romagnoli@iia.cnr.it

In the frame of the Life+ EXPAH project, PAHs were monitored to assess the exposition experienced by population to airborne toxicants. Measurements were carried out both indoors and outdoors at schools, homes and offices. Two weeks in-field campaigns were made from late November 2011 up to July 2012 in Rome.

Our concern was focused on carcino-genic/mutagenic PAHs (benz[a]anthracene BaA, benzo[b/j/k]fluoranthenes BbjkF, benzo[a]pyrene BaP, indeno[1,2,3-cd]pyrene IP, dibenz[a,h]anthracene DBA and benzo[ghi]perylene), as well as on perylene PE and benzo[e]pyrene BeP.

The method for PAHs monitoring in the airborne particulates was optimized for indoor environments using low-volume sampling and daily sample gathering (weekly frequency). Besides neat concentrations, attention was paid to two topics, namely:

- the indoor/outdoor concentration ratio; and
- the percent profile of PAH congeners investigated.

Indeed, pollution is not restricted to open air; on the contrary, air toxicants not only can move to indoors but also can be released by indigenous sources like heating, cooking, and tobacco smoking. The blend of sources can change dramatically and PAH composition is influenced by air reactivity. Thus, this study could provide suitable insights on source impact and nature.

Results

Table 1 shows the average indoor/outdoor concentration ratios observed at the target sites.They were <1.0 but higher than expected supposing outdoor sources as predominant. All ratios were higher in the warm season suggesting a lower impact of indigenous sources and/or reduced penetration of pollutants from outdoors. As for percent distribution, differences were observed site to site and with the season; e.g., the BbjF/BkF ratio and the relative abundances of BPs and PE were highly influenced by year time (see Fig. 1).

Table 1. Average indoor/outdoor concentration ratios observed in this study (Rome, 2011-12)

	winter	summer
houses	0.64	0.79
offices	0.56	0.59
schools	0.72	0.84
Mean value	*0.64*	*0.74*

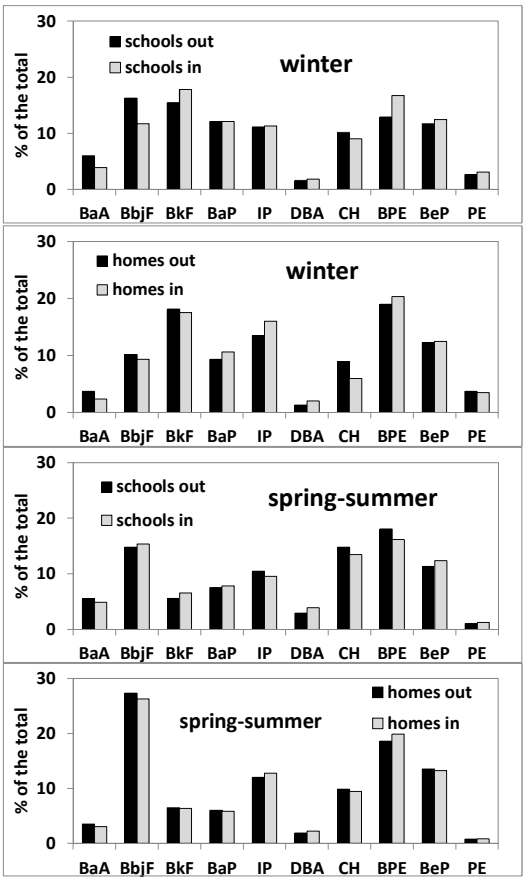

Figure 1. Indoor and outdoor PAH percentages.

Conclusions

The PAH indoor/outdoor concentration ratios and percent distributions in Rome change with site and year time, which modified the congener contribution to ambient toxicity.

http://www.ispesl.it/expah/

Seasonal and weekly modulations of Psychotropic Substances (PSs) in Rome, Italy

Romagnoli P [1], Sacco F [2] , Balducci C [1], Perilli M [1], Cecinato A[1]

[1] Institute of Atmospheric Pollution Research, CNR, Monterotondo Stazione RM, I-00015, Italy
[2] Regional Agency for Environmental Protection of Lazio, Rieti, I- 02100, Italy
Key words: Psychotropic substances; airborne particulates; indoor air contaminants; atmospheric pollution;
Presenting author e.mail: romagnoli@iia.cnr.it

In the frame of the LIFE+(Environment and Health) Programme, CNR participates to EXPAH project (co-ordinator: INAIL, Rome, Italy), aimed at assessing the true exposition of population to airborne toxicants.

Although the principal objective of the project were polynuclear aromatic hydrocarbons (PAHs), a set of ancillary toxicants were investigated, comprising licit and illicit drugs, to elucidate the true role played by compound classes (Cecinato et al 2011) As for psychotropic substances, the study was focussed on nicotine (NIC), caffeine (CAF), cocaine (COC) and cannabinoids (CBs), i.e. the sum of cannabinol, cannabidiol and Δ^9-tetrahydrocannabinol. Measurements were made in Rome, Italy, at schools, private houses and offices (non-industrial workplaces) both indoors and outdoors (Table 1). The ambient data were compared to those detected at the monitoring stations belonging to Regional Pollution Network of ARPA Lazio. This kind of measurements was accompanied by those of regulated toxicants ($PM_{2.5}$, O_3, NO_2), to account for possible interferences.

Table 1. Timetable of sites investigated (2011-12)

year time	schools	offices	houses
Nov-Dec	3	0	0
Jan-Feb	0	1	4
May-Jun	3	1	0
Jun-Jul	0	0	4

Measurements were made in winter and spring-summer seasons, in order to confirm the different concentration levels usually detected.

All procedures adopted in this study, previously validated by CNR-IIA (Cecinato et al 2009), were modified to be applied to indoor environments. They included the PM collection over 24h (starting at 08:00h), sample pooling, solvent extraction, alumina column chromatography, and GC-MSD (EI-SIM) analysis. Two time schedules were chosen for this investigation, i.e. five-day (Monday to Friday) and two-day (Saturday and Sunday), to discriminate weekdays from weekends.

Results

Nicotine, caffeine and cocaine were detected at all sites investigated, and indoor concentrations were comparable to those detected outdoors. None site was known as subjected to inner sources of cocaine and CBs, as a consequence external illicit psychotropic substances efficiently penetrated indoor environment. Generally, seasonal trends were observed with winter levels higher than the spring-summer ones. The decrease was particularly relevant for CBs. Remarkable is the finding that CBs inside appear higher than outside, suggesting an effect of accumulation (see Fig.1) (Cecinato et al 2012) . Different ratios indoor/oudoor concentration can be found according to the site and the substances taken in account. Differences can be observed also according to the days of the week.

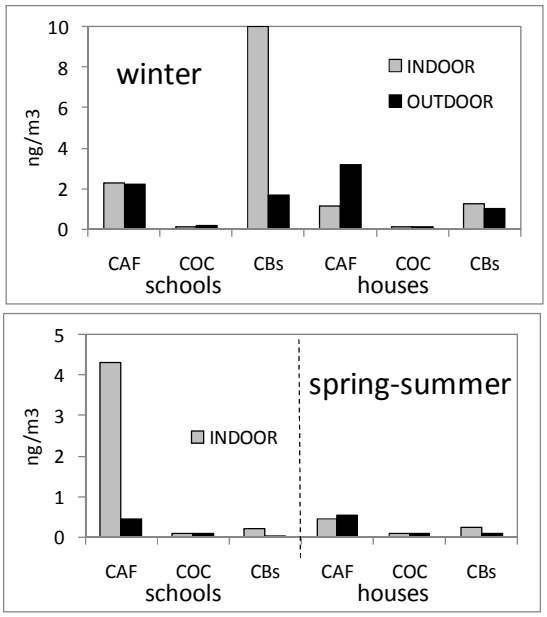

Figure 1. Winter and spring/summer levels of airborne psychotropic substances valued indoors and outdoors

Conclusions

PSs (comprising the illicit ones) affect indoor environments degrees often higher than outdoor air.

This investigation was supported by EC through the *LIFE+ Environment and Health* Programme

Cecinato A., Balducci C., Nervegna G. (2009) *Sci. Total Environ.* **407**, 1683-1690.

Cecinato, A. Balducci C., Guerriero E., Sprovieri F., Cofone F. (2011) *Sci. Total Environ.* **412-413,** 87–92.

Cecinato A.,Catia Balducci C., Romagnoli P., Mattia Perilli (2012) Environ. Pollut. 171, 140-147

Spatial and seasonal variation of nitrogen dioxide and ozone in modern office buildings

T. Szigeti[1], V.G. Mihucz[1], P.M. Bluyssen[2], P. Carrer[3], A. Cattaneo[4], D. Cavallo[5], H.J.M. Cornelissen[6], S. Dimitroulopoulou[7], S. Fossati[3], C. Mandin[8], E. Oliveira de Fernandes[9], K.K. Kalimeri[7], Y. de Kluizenaar[6], R. Pereira[9], Y. Sakellaris[7], D.E. Saraga[7] and J.G. Bartzis[7]

[1]Department of Analytical Chemistry, Institute of Chemistry, Eötvös Loránd University, Budapest, 1117, Hungary
[2]Department of Architectural Engineering and Technology, Delft University of Technology, Delft, 2628 BL, The Netherlands
[3]"L. Sacco" Department of Biomedical and Clinical Sciences, Università degli Studi di Milano, Milan, 20122, Italy
[4]Department of Clinical Sciences and Community Health, Università degli Studi di Milano, Milan, 20122, Italy
[5]Department of Science and High Technology, Università degli Studi dell'Insubria, Como, 22100, Italy
[6]TNO, Delft, PO Box 49, 2600 AA,The Netherlands
[7]Department of Mechanical Engineering, University of Western Macedonia, Kozani, 50100, Greece
[8]CSTB - Centre Scientifique et Technique du Bâtiment, Marne-la-Vallée Cedex 2, 77447, France
[9]Institute of Mechanical Engineering, Faculty of Engineering, University of Porto, Porto, 4200-465, Portugal
Keywords: indoor air quality, passive sampling, mechanical ventilation, air pollution
Presenting author email: tamas.szigeti@yahoo.com

Lately, there is an increasing concern on indoor air quality (IAQ), as in our modern world, people are spending about 80% of their time in a built environment.

OFFICAIR is a European collaborative project focusing on IAQ and its effects in modern office buildings in the following countries: Finland, France, Greece, Hungary, Italy, Portugal, Spain and The Netherlands. In each partner country, around 20 office buildings were selected according to strictly established selection criteria and a general survey was carried out focusing on the assessment of the IAQ and health and comfort perception at work. Finally, 36 buildings were selected for further monitoring and health outcome evaluation.

One of the tasks was the determination of nitrogen dioxide and ozone by passive sampling using Gradko and Radiello samplers for 5 consecutive working days in 4 offices/building and 1 outdoor location, preferably close to the air intake of the HVAC systems. Sampling was done in summer 2012 and it was repeated in winter 2012/2013. Both nitrogen dioxide and ozone were determined spectrophotometrically. Nitrogen dioxide and ozone samples were measured at Gradko (UK) and at the Department of Analytical Chemistry of Eötvös Loránd University, respectively. Two duplicate samples per compound and per country were made. Field and travel blanks were also prepared for each building and shipped to the centralised laboratories.

In the lack of certified reference material, as a validation aspect, the results of O_3 samples collected on the roof (30-65 m high) of the office buildings in Hungary were compared with simultaneously performed on-line measurements of ozone at a station of the Hungarian Air Quality Network Service considered as urban background for Budapest. Mean of relative standard deviations for O_3 measurements was 21%. In the case of duplicate samples, deviation was between 7 and 34%.

In the case of Greece, Hungary and the Netherlands, higher outdoor ozone values were determined during the summer campaign due to the heat wave of mid June – July of 2012. Generally, in France and Spain, indoor ozone levels fell under the detection limit.

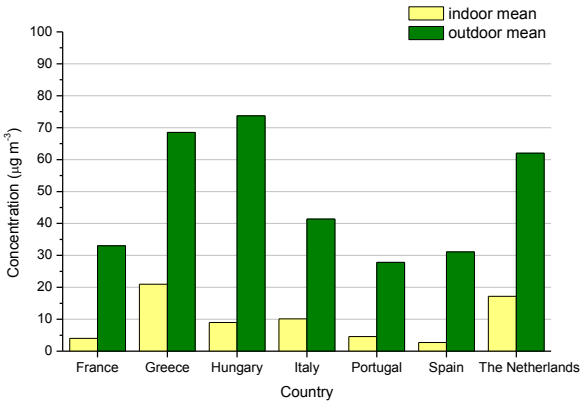

Figure 1. Indoor and outdoor ozone levels in office buildings monitored in the OFFICAIR project during summer 2012.

In most cases, the indoor / outdoor ratios were higher for NO_2 than for O_3 which indicates the higher reactivity of ozone in the indoor environment. The outdoor O_3 and NO_2 levels were mainly building location dependent.

This work was supported from the project "OFFICAIR" (On the reduction of health effects from combined exposure to indoor air pollutants in modern offices) funded by the European Union 7th Framework (Agreement 265267) under Theme: ENV.2010.1.2.2-1.

Indoor air quality in Lahore, Pakistan

Ian Colbeck[1], Zaheer A.Nasir[2], Zulfiqar Ali[3] and Sidra Safdar[3]
[1]School of Biological Sciences, University of Essex, Colchester, Essex, CO4 3SQ, UK
[2]Department of Civil, Environmental and Geomatic Engineering, University College London, WC1E 6BT, UK
[3]Department of Zoology, University of the Punjab, Lahore, Pakistan
Keywords: Pakistan, particulate matter, indoor air
Presenting author email: colbi@essex.ac.uk

Lim et al. (2012) have estimated that globally 3.2 million people died from air pollution in 2010. They suggest that over 2.1 million premature deaths and 52 million years of healthy life lost in 2010 were due to fine particle air pollution in Asia. In addition indoor air pollution from solid fuel usage kills 3.5 million people annually.

Very few studies have been conducted in Pakistan regarding indoor air quality (Colbeck et al. 2010). It is not recognized as an environmental hazard at government level. Lahore (31.55°N and 74.34°E) is the second biggest city of Pakistan and the provincial capital of Punjab. It is one of the most densely populated cities of the world with an estimated population of 10,000,000.

The current study was undertaken to monitor the concentration of fine particulate matter ($PM_{2.5}$) in different residential settings within Lahore and to identify the major sources of pollution.

Twenty four houses were selected as study sites. Two real time aerosol monitors (TSI DustTrak 8520) were run in parallel; one in the kitchen and another in the living room. Fine particulate concentration in all study sites was monitored for 72 hours each in the kitchens and living rooms beginning from January 2012 to January 2013. There were nine small houses ($\leq$ 2510.6 m^2), nine medium sized houses (> 2510.6 m^2 to 5021.2 m^2) and six large sized houses (> 5021.2 m^2). The number of occupants varied from 3 to 13individuals in the different households.

The results are summarised in Table 1. The average concentrations of $PM_{2.5}$ were higher in the kitchens as compared to the living rooms. The highest mean concentration (1003 µg/m³) occurred in a kitchen in which a window faced a furniture factory; this was probably a source of fine PM throughout the day. The lowest average concentration (63 µg/m³) was in a kitchen that was not in use. In the living rooms the highest value of $PM_{2.5}$ (984 µg/m³) was observed in a house in a semi-urban industrial area, the head of the family was a smoker and there were 13 occupants. The lowest value (68 µg/m³) was found in a house with only 6 occupants and they spent most of their time outdoors resulting in low concentrations of PM. No significant difference was observed between the day and night averages.

Cooking, cleaning, smoking, and space heating were observed to be the major sources from the indoors environment while outdoor sources also played an important role especially in houses located in industrial and semi-urban areas and near high traffic roads.

Table 1. Average $PM_{2.5}$ concentrations (µg/m³) in kitchens and living rooms in Lahore.

Number of occupants	KITCHEN			LIVING ROOM		
	24 hr avg	Day	Night	24 hr avg	Day	Night
12	1003	1091	885	463	372	489
4	249	254	264	206	217	207
6	227	207	248	141	118	161
8	347	387	283	198	204	185
7	189	186	192	148	142	153
6	363	336	485	237	207	314
3	185	150	226	166	133	205
7	187	219	145	172	186	140
8	63	68	53	120	118	117
6	74	58	93	68	58	70
7	237	276	131	117	119	112
12	136	136	136	177	194	154
6	211	145	377	123	131	108
8	201	217	172	216	235	170
5	135	138	129	135	134	133
7	336	361	297	333	341	340
6	194	228	151	193	287	154
13	433	377	525	517	370	653
5	314	238	388	344	282	767
4	439	306	551	474	343	585
8	858	717	977	984	848	1096
6	753	658	849	921	895	985
3	516	408	647	701	558	388
13	383	395	323	439	500	388

Colbeck, I., Nasir, Z.A. and Ali, Z. (2010) *Environmental Science and Pollution Research* **17**, 49-63.

Lim, S.S. et al. (2013) *The Lancet* **380**, 2224-2260.

INDOOR AIR QUALITY IN UNIVERSITY

Chen. SW[1], Mena, KD[2] and Chen.PS [1*]

[1] Department of Public Health, Kaohsiung Medical University
[2] Epidemiology, Human Genetics, and Environmental Sciences, School of Public Health, The University of Texas Health Science Center at Houston
Keywords: Ultrafine, PM, Classroom.
Presenting author email:ann78929@hotmail.com

In the previous studies, indoor air quality in classroom was found to affect learning efficiency and health status of students by questionnaire investigation. Air pollutants and environmental factors such as carbon dioxide (CO), temperature, relative humidity (RH), ozone (O_3), particulate matter (PM), fungal bioaerosol, bacterial bioaerosols and ventilation rate were the factors of concern. It was indicated that poor air quality in office building decreased workers' working efficiency in the range of 6%-9%. The ventilation type of classroom in university is similar to office buildings. However, little studies concerned this issue. Therefore, the purpose of this study is to investigate the indoor air quality in the classrooms in a university.

We selected 9 classrooms in 2 academic buildings (Building A, building B) in a university from September to December in 2008. CO_2, CO, Relative Humidity, temperature (Indoor Air Quality Meters, TSI INCORPORATED, USA), wind speed, ventilation rate (TSI INCORPORATED, USA), O3 (Ozone Monitor, BUD INDUSTRIES, USA), PM_{10}、PM_4、$PM_{2.5}$、PM_1 (Dust Trak, TSI INCORPORATED, USA), and ultrafine particles (P-Trak, TSI INCORPORATED, USA) were measured indoor and outdoor simultaneously before and after mechanical ventilation turning on in the morning and noon. Airborne bacteria and fungi were also sampled by impaction method and cultured in Malt Extract Agar and Tryptic Soy Agar, respectively.

Our results showed that the concentration of PM_{10}, PM_4, $PM_{2.5}$, PM_1, fungal bioaerosols and bacterial bioaerosols before mechanical ventilation turning on were higher than it turned on. For CO_2 concentration, 9.52% and 33.33% samples in building A and building B, respectively, were exceeded the recommendation of indoor air quality from Taiwan Environmental Protection Agency. In addition, O_3 concentration of building B was significant higher than building A (p=0.0169). A lot of plants nearby building B might be the reason.

Table1. Failure rate of building A, and B when comparing with Taiwan EPA's guideline of indoor air.

	Building A(n=21)	Building B(n=6)
CO	0%	0%
CO_2	10%	33%
$PM_{2.5}$	33%	0%
PM_{10}	14%	0%
O_3	0%	0%
Fungi	0%	0%
Bacteria	0%	0%

Table2. Before and after turning on mechanical ventilation in classrooms.

	Before	After	
	Median	Median	p-value
Temp.(℃)	22	22	0.0379*
RH(%)	64	64	1.0000
CO(ppm)	4	4	0.5071
CO_2(ppm)	535	511	0.7239
Wind Speed(m/s)	0.03	0.10	0.0004*
Ultrafine(PT/cm^3)	11360	13300	0.3314
PM_1(μg/m^3)	530	440	0.5962
$PM_{2.5}$(μg/m^3)	550	500	0.6270
PM_4(μg/m^3)	600	500	0.5961
PM_{10} (μg/m^3)	660	600	0.5961
O_3(ppb)	2	1	0.3745
Fungi (CFU/m^3)	90	60	0.0422*
Bacteria (CFU/m^3)	206	146	0.1331

* p<0.05 (Wilcoxon Sign Rank Test)

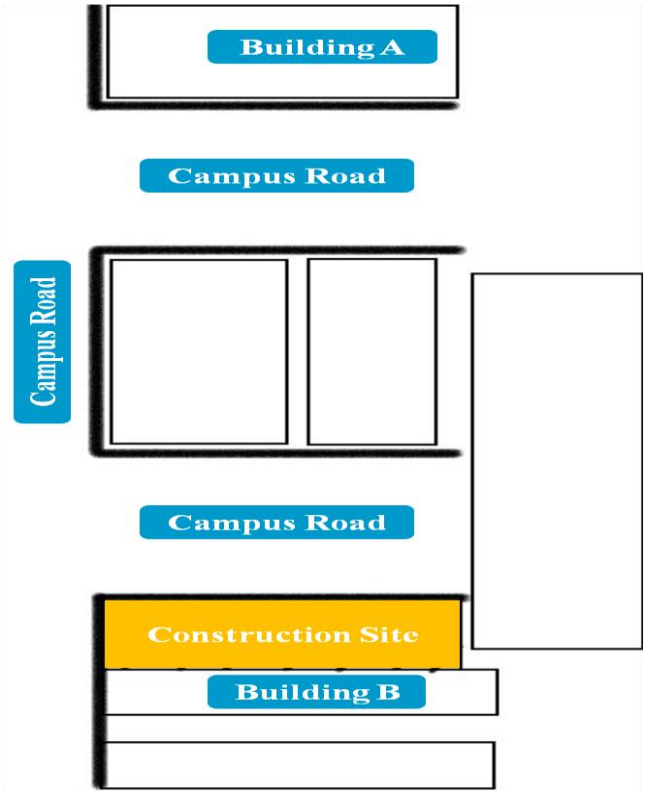

Figure 1. floor layout

Concentrations of Indoor Submicrometer and Supermicrometer Particulate Matter in a Primary School in Prague.

J. Stolcpartova, M. Branis, J. Hromadka

Institute for Environmental Studies, Charles University, Prague 2, 128 01, Czech Republic
Keywords: school, submicrometer particles, indoor air quality
Email: stolcpar@natur.cuni.cz

Children are susceptible to environment pollution and school is the second environment when they spent most of their time (Silvers *et al.*, 1994). Therefore, pollution in the school environment can affect their health, wellbeing and even their school results (Mendell and Heath, 2005). Particle matter (PM) in schools could have both indoor and outdoor origin. Indoor generated particles are mostly coarse and are produced by resuspension. In urban areas the majority of outdoor PM have its source in traffic. These particles contain a number of hazardous substances and generally and their aerodynamic diameter is usually below 1 micron. It has been repeatedly shown that they easily penetrate into classrooms (Avigo *et al.*, 2008; Branis *et al.*, 2009). However, it was also documented, that submicrometer particles can be produces by children and by the activity they perform (Morawska *et al.*, 2009). The present work investigated concentrations of aerosol particles, in specialized classrooms in an elementary school situated in the centre of Prague.

Mass concentration of PM was measured by DustTrak DRX 8533$^{(TSI)}$ nephelometers while the number concentrations of particles below 1μm were monitored by a P-Trak$^{(TSI)}$ condensation particle counter. The instruments measured in two pairs, one set was situated in the studied classroom and the second one outdoors. The measurement integration time was set to 5 minutes. In total, eight four-day measuring campaigns were performed in 2011/2012 from November to July. The school was situated in a park near the centre of Prague. The traffic was rather low in the school vicinity. Student occupancy data were collected in cooperation with teachers. Measurements took place in three classrooms – Computer classroom 50.7m^2 (ground floor); Art/Music classroom 57.5m^2 (2nd floor), Biology/Chemistry classroom 55.7m^2 (2nd floor).

It was found that mass concentrations of submicrometer particles were dependent on outdoor concentrations (regression, p-value<0.002 or less for all classrooms), in contrast to supermicrometer particles which were affected mainly by students. The outdoor concentration had a very limited influence. Because of smooth transition between submicrometer and supermicrometer particles, a multivariate statistical approach was selected. Students had a significant effect on particles concentrations (RDA, p-value<0.01; outdoor concentrations were set as covariates). The strongest effect was documented for number concentrations of submicrometer particles and supermicrometer mass concentrations (Figure 1). It has to be noticed, that all relationships were week. It is assumed that the level of submicron aerosol pollution in the classrooms depended mainly on outdoor concentrations. Students or/and their activity during lessons had only a weak effect. In contrast, the supermicron mass concentrations of aerosol were more affected by classroom occupancy.

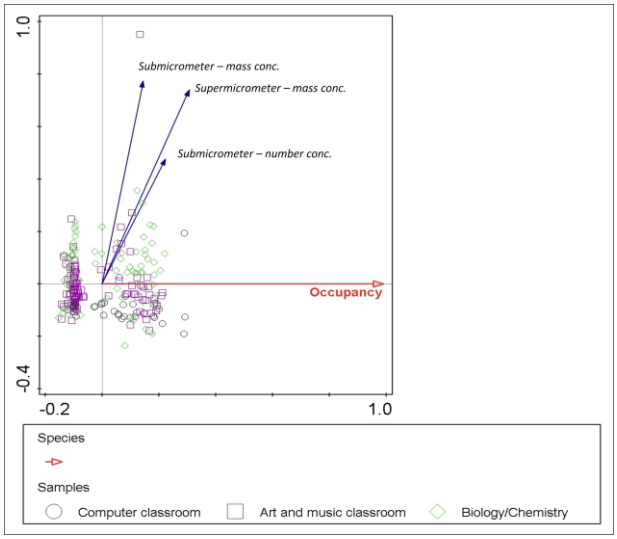

Figure 1. Graph of multivariate analysis RDA (statistical software Canoco)

Avigo, D. Jr, Godoi, A.F., Janissek, P.R., Makarovska, Y., Krata, A., Potgieter-Vermaak, S., Alfoldy, B., Van Grieken, R. and Godoi R.H. (2008) Anal. Bioanal. Chem. **391**, 1459-1468.

Branis, M., Safranek, J. and Hytychová, A. (2009) *Build. Environ.* **44**, 1246–1252.

Mendell, M.J. and Heath, G.A (2005) *Indoor Air* **15**, 27–52.

Morawska, L., He, C., Johnson, G., Guo, H., Uhde, E. and Ayoko, G. (2009) Environ. Sci. Technol. **43,** 9103–9109.

Silvers, A., Florence, B.T., Rourke, D.L. and Lorimor, R.J. (1994) *Risk Anal.* **14**, 931–944.

$PM_{2.5}$ in modern office buildings: elemental characterization and oxidative potential

T. Szigeti[1], C. Dunster[2], F.J. Kelly[2], Zs. Kertész[3], A. Cattaneo[4], Gy. Záray[1] and V.G. Mihucz[1]

[1]Department of Analytical Chemistry, Institute of Chemistry, Eötvös Loránd University, Budapest, 1117, Hungary
[2]MRC-HPA Centre for Environment and Health, King's College London, London, SE1 9NH, UK
[3]Laboratory of Ion Beam Applications, Institute of Nuclear Research, Debrecen, 4100, Hungary
[4]Department of Clinical and Community Sciences, Università degli Studi di Milano, Milan, 20122, Italy
Keywords: indoor/outdoor particles, PIXE, air pollution, occupational health
Presenting author email: tamas.szigeti@yahoo.com

OFFICAIR is a European collaborative project focusing on indoor air quality in modern office buildings throughout Europe. It started on 1st November 2010 and it will end on 31st October 2013.

One of the main tasks of the project was the collection of indoor and outdoor $PM_{2.5}$ aerosol samples for detailed analysis. In Hungary, $PM_{2.5}$ sampling was performed in 5 selected offices (one/building) with a Skypost high-volume aerosol sampler (TCR Tecora Srl, Milan, Italy). Corresponding outdoor sampling was also undertaken close to the air intake of the of HVAC system situated on the roof of each building. Sampling time was 8 hours / day coinciding more or less with the daily shift of the workers (from 9 AM to 5 PM). Sampling was conducted with two filter types (both 47 mm) quartz fibre filters (Whatman QM-A) and Teflon (Whatman). Filters were conditioned at 20 ± 1 °C and 50 ± 5% relative humidity. Each day, 18.34 m^3 of air was pumped through the filters. Field blanks inserted into the sampling head were also employed.

The first analysis was the determination of the mass concentration. Indoor $PM_{2.5}$ mass concentration values ranged between 3.0 μg m^{-3} and 22.7 μg m^{-3} whereas outdoor concentrations (with one exception) were always higher and ranging from 4.7 to 28.2 μg m^{-3}. Outdoor $PM_{2.5}$ mass concentration values were comparable with our previous study (Szigeti *et al.* 2013) conducted in Budapest. Independently of the filter material, indoor / outdoor (I/O) mass concentration ratios varied between 0.26 and 0.96 (one exception: 1.47). This outcome is also in good agreement with literature data: 0.37-0.88 (Horemans *et al.* 2008). In 4 out of 5 buildings, relatively uniform I/O ratios were observed. Further, one building characterized with equilibrated I/O values (Figure 1) indicating proper ventilation a finding supported by perfluorocarbon tracer (PFT) measurements performed at BRE (UK).

After the $PM_{2.5}$ gravimetric analysis, samples were shipped on ice to Kings' College London where they were subjected to oxidative potential analysis (Godri et al, 2011). This consisted of a 4-h incubation at 37 °C of 5-mm discs cut from the loaded filters in 0.5 mL of a model solution simulating the respiratory tract lining fluid containing as antioxidants 200 μmol dm^{-3} of urate (UA), ascorbate (AA) and glutathione each. After centrifugation, the remaining amounts of UA and AA were determined by reversed-phase high performance liquid chromatography with electrochemical detection. Glutathione (GSX, GSSG, GSH) was determined by enzyme-linked 5,5'-Dithio-bis(2-nitrobenzoic acid) (DTNB) assay by using a microplate reader.

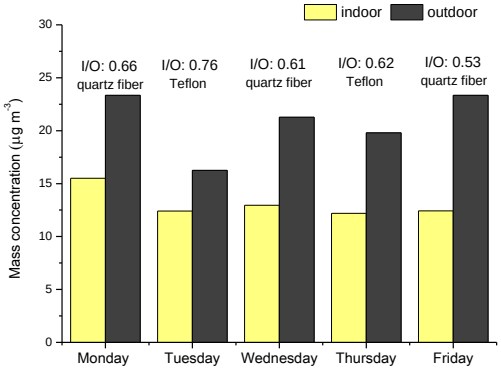

Figure 1. Daily indoor/outdoor $PM_{2.5}$ mass concentration ratios (I/O) calculated for samples collected onto quartz fibre filter and Teflon filters in one building in Hungary.

Particle induced X-ray emission was applied for the quantification of some major and minor elements in the collected aerosol samples. In the case of samples collected onto Teflon filters, elements ranging from Al to Zn could be determined. In spite of the high blank values for Fe, Ca, Cl, K and S in the aerosol samples collected onto quartz fibre filters, a wider range of elements could be determined (from Al to Pb).

This work was supported from the project "OFFICAIR" (On the reduction of health effects from combined exposure to indoor air pollutants in modern offices) funded by the European Union 7th Framework (Agreement 265267) under Theme: ENV.2010.1.2.2-1. The authors are grateful to Sani Dimitroulopoulu and Stuart Upton (BRE, UK).

Horemans, B., Worobiec, A., Buczynska, A., Van Meel, K. and Van Grieken, R. (2008) *J. Environ. Monitor.* **10**, 867-876.
Szigeti, T., Mihucz, V.G., Óvári, M., Baysal, A., Atılgan, S., Akman, S. and Záray, G. (2013) *Microchem. J.* **107**, 86-94.
Godri, K.J., Harrison, R.M., Evans, T., Baker, T., Dunster, C., Mudway, I.S., Kelly F.J. (2011) *PLoS ONE* **6**, e21961. doi:10.1371

Characterization of the bacterial and fungal bioaerosols in three elementary schools in Kaohsiung

Wang. MC[1], Mena. KD[2] and Chen. PS[1*]

[1]Department of Public Health, Kaohsiung Medical University, Kaohsiung, Taiwan
[2] Epidemiology, Human Genetics, and Environmental Sciences, School of Public Health, The University of Texas Health Science Center at Houston

Keywords: fungi, bacteria, elementary school.
Presenting author email: asdf800525@hotmail.com

Introduction

Recently, indoor air quality (IAQ) including bioaeorosls at school had drawn much attention by people. In South Taiwan, the average temperature and total cumulative rainfall in 2009 is 23.7℃ and 1756.3 mm. It's a great environment for fungi and bacteria. Therefore, we tried to characterize the distribution of the fungal and bacterial bioaeorosols in classrooms in three elementary schools in Kaohsiung and their determine factors.

Materials and Methods

Three primary schools, industrial, traffic, and reference school, were selected to assess PM_{10}, $PM_{2.5}$, and PM_1 concentration. The distance between EPA's Monitoring Station and industrial, traffic, and reference school, is about 300 m, 0 m, and 537 m, respectively.

Nine classrooms of each school to a total number of 62 classrooms was evaluated both indoor and outdoor during April 13th to Jun 13th and September 18th to October 16th , 2009. Bacterial and fungal bioaerosols were sampled at 8 am and 3 pm（MAS-100 ; MERCK, USA）and cultivated in Tryptic soy agar（TSA）and Malt extract agar（MEA）, respectively. Colony-Forming Unit (CFU) after 24hr and 48hr were counted for bacteria and fungi, respectively.

Results and Discussion

The average concentration of bacterial bioaerosols

Inside classroomsin traffic, industry, and reference school was 960±492 CFU/m^3 (means±S.D), 879±1042 CFU/m^3, 1769±1545 CFU/m^3,respectively, whereas the average concentration of bacterial bioaerosols outside classrooms was 640±394 CFU/m^3, 296.5±111 CFU/m^3, 940.6±1026 CFU/m^3 , respectively (table1). It was shown that indoor concentration was higher than the outdoor concentration in most cases. The percentage of higher indoor bacterial concentration was 80%, 66.67%, and 77.78% in traffic, industry, and reference school, respectively. Table2 showed the I/O ratio of bacterial bioaerosols. The average I/O ratio of three schools was all higher than 1. It may be affected by whether the classrooms near the restrooms and stairs. For fungal bioaerosols, the average indoor concentration at traffic, industry, and reference school was 505±248 CFU/m^3 (means±S.D), 323±156 CFU/m^3 and 1658±1258 CFU/m^3, respectively, whereas the average concentration of bacterial bioaerosols outside classrooms was 473±309, 283±159, 1510±799 (teble1), respectively.

Similar trend was observed for both fungi and bacteria. The percentage of the higher indoor fungal bioaerosols at traffic, industry, and reference school, was 75%, 30%, and 66.67% respectively. Table2 Showed the I/O ratio of fungal bioaerosols.In comparison with the guideline value of IAQ in Taiwan, the the rate of classroom above the standard of bacterial bioaerosols at traffic, industry, and reference school was 19.05%, 0%, and 28.57%, respectively, and the failure rate of fungal bioaerosols was 9.52%, 5%, and 85.17%, respectively.

Table1. The Descriptive statistics and the rate of classroom exceed the guideline of Taiwan EPA

		Mean	Median	Std.	Min.	Max.	Above the standard
Indoor bacteria (CFU/m^3)	Traffic	960	713	492	286	1993	90%
	Industry	879	493	1042	241	4293	45%
	Reference	1769	1123	1545	218	5650	85.7%
Outdoor bacteria (CFU/m^3)	Traffic	640	582	394	149	1608	
	Industry	296	270	111	160	533	
	Reference	940	640	1026	170	4949	
Indoor fungi (CFU/m^3)	Traffic	505	435	248	171	945	0%
	Industry	323	319	156	81	636	0%
	Reference	1658	1353	1258	475	5725	66.7%
Outdoor fungi (CFU/m^3)	Traffic	473	416	309	128	1396	
	Industry	283	230	159	67	674	
	Reference	1510	1230	799	377	3860	

Table2. I/O ratio of traffic, industry, and reference school in the morning and afternoon

		Morning					Afternoon				
	School(N)	Mean	Median	Std.	Min.	Max.	Mean	Median	Std.	Min.	Max.
Bacteria	Traffic (21)	2.2	1.9	1.5	0.1	5.8	3.0	1.8	4.6	0.3	21.2
	Industrty (20)	3.5	1.7	5.5	0.4	25.8	2.5	1.2	3.5	0.5	3.7
	Reference (21)	3.9	2.59	4.9	0.3	22.4	1.7	1.4	1.3	0.2	4.9
Fungi	Traffic (21)	1.2	1.1	0.6	0.2	2.4	1.5	1.4	0.9	0.2	3.1
	Industrty (20)	1.4	1.0	0.9	0.5	16.0	2.0	1.2	3.1	0.3	14.7
	Reference (21)	1.4	1.1	1.14	0.1	5.3	1.2	1.0	0.7	0.3	2.7

Exposure Assessment of Ozone in Elementary Schools in Kaohsiung, Taiwan

Lin, YC[1], Mena. KD[2] and Chen, PS [1*]

[1]Department of Public Health, Kaohsiung Medical University, Kaohsiung, Taiwan
[2] Epidemiology, Human Genetics, and Environmental Sciences, School of Public Health, The University of Texas Health Science Center at Houston
Keywords: ozone I/O ratios
Presenting author email:yanchelin@gmail.com

In the previous studies, children's health effect was related to ozone. Kaohsiung daily average ozone concentration is much higher than the average of Taiwan. The objective of this study is to evaluate the ozone concentration in classrooms in elementary schools in Kaohsiung, Taiwan.

From April to June (spring) and September to November (autumn) in 2009, 62 classrooms were selected from three elementary schools in Kaohsiung to monitor indoor and outdoor ozone by Ozone Monitor Model 202 (2B Technologies, lnc) in real-time for continuous eight hours.

Poor correlation between the concentration inside classroom and air monitoring station was shown in both Spring and Autum (Table 1 and Table 2). In spring, the indoor and outdoor ozone concentration were from 6.06 to 93.52 ppb and 11.78 to 53.33 ppb, respectively, with failure rate of 58% and 0%, respectively, when comparing to the recommendation of Taiwan Environment Protection Administration (30ppb). In fall, the indoor and outdoor ozone concentration was from 7.6 to 86.1 ppb and 7.14 to 94.57 ppb, respectively, with failure rate was 77% and 46%, respectively.

The concentration of ozone rose in the morning and the maximum value appeared between 11:00 to 12:00. In autumn, the outdoor ozone concentrations were slightly higher than indoor in three schools. Indoor/Outdoor ratios (I/O ratios) of ozone varied in a range from 0.9 to 1.1. I/O ratios observed in our studies were higher than that in other previous studies. From our studies, high failure rate and high I/O ratio observed in spring and autumn in Kaohsiung implied that indoor ozone exposure of children in classroom should be an important issue and need further studies of its health effect.

The concentration of ozone rose in the morning and the maximum value appeared between 11:00 to 12:00. We need to pay more attention on indoor ozone concentration in elementary schools in Kaohsiung. It may be a problem by using the data from air monitor station to estimate the exposure of children.

Table 1. Correlation between indoor ozone concentration and air quality station in spring.

	Background		Traffic		Industry	
	R	*p*-value	R	*p*-value	R	*p*-value
08:00	-.033	0.39	0.87	0.002	0.88	0.003
09:00	0.85	0.004	1.00	<0.0001	0.50	0.253
10:00	0.82	0.007	0.83	0.005	0.74	0.04
11:00	0.80	0.010	0.88	0.002	0.89	0.01
12:00	0.91	0.002	0.95	<0.0001	0.83	0.01
13:00	1.00	<0.0001	1.00	<0.0001	0.81	0.64
14:00	0.96	<0.0001	0.88	0.002	0.64	0.09
15:00	0.80	0.010	0.88	0.002	0.76	0.03

Table 2. Correlation between indoor ozone concentration and air quality station in autumn.

	Background		Traffic		Industry	
	R	*p*-value	R	*p*-value	R	*p*-value
08:00	0.40	0.20	0.35	0.29	0.28	0.38
09:00	0.81	0.001	0.76	0.01	0.54	0.07
10:00	0.90	<0.001	0.86	<0.001	0.62	0.03
11:00	0.95	<0.001	0.92	<0.001	0.61	0.04
12:00	0.66	0.01	0.97	<0.001	0.18	0.58
13:00	0.76	0.001	0.89	<0.001	-0.06	0.85
14:00	0.98	<0.001	0.93	<0.001	0.28	0.40
15:00	0.96	<0.001	0.88	<0.001	-0.17	0.60

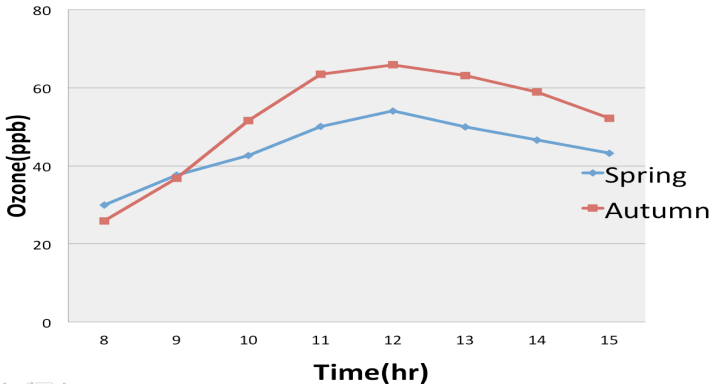

Fig1. The trend of the 8hr average indoor concentration of ozone

Real-time Monitoring Of $PM_{2.5}$ In Primary School

Lin, YC[1], Mena, KD[2] and Chen, PS [1*]

[1]Department of Public Health, Kaohsiung Medical University
[2] Epidemiology, Human Genetics, and Environmental Sciences, School of Public Health, The University of Texas Health Science Center at Houston

Keywords: $PM_{2.5}$, primary school, indoor and outdoor
Presenting author email:yanchelin@gmail.co

PM2.5 may increase the risk of heart disease, stroke and some cardiovascular diseases. In this study, we monitored PM2.5 in the classrooms of the primary schools in Kaohsiung, Taiwan.

Three primary schools, industry, traffic, and reference school, were selected to assess PM_{10}, $PM_{2.5}$, and PM_1 concentration. The distance between EPA's Monitoring Station and industry, traffic, and reference school, is about 300 m, 0 m, and 537 m, respectively. Real-time monitoring of $PM_{2.5}$ from 08:00 to 16:00 was held simultaneously indoor and outdoor of the classroom to a total of 26 and 35 classrooms during April 13th to Jun 13th, 2009 and September 7th to November 6th, 2009, respectively (DUSTTRAK™ Aerosol Monitor ; Model 8520, TSI USA).

We found that the trends of indoor and outdoor $PM_{2.5}$ were the same, and the concentration of indoor $PM_{2.5}$ is higher than outdoor $PM_{2.5}$ in the classrooms of the schools. The concentrations of indoor and outdoor $PM_{2.5}$ in fall were significantly higher than in spring. For I/O ratio, the indoor concentrations of $PM_{2.5}$ were significantly higher than outdoor $PM_{2.5}$ concentrations in both spring and fall in traffic, and reference school. The relationship between the indoor concentrations of $PM_{2.5}$ in classrooms and the data from monitoring stations was not significant. The typical trend of hour average $PM_{2.5}$ in the classrooms was shown in Figure 1.The hour-average trend of indoor and outdoor concentration was similar and the indoor concentration was higher than outdoor. But the data from the monitoring station was lower than the indoor and outdoor hour-average concentrations in classrooms. It was indicated that the data from the monitoring stations could not represent of the actually exposure of school children.

Table 1. The correlation of data of AQ monitoring stations and indoor $PM_{2.5}$ in primary schools in spring.

	Reference		Traffic		Industry	
	R	*p*-value	R	*p*-value	R	*p*-value
08:00	0.857	0.006	0.687	0.060	0.700	0.036*
09:00	0.976	<.0001	0.577	0.104	0.283	0.460
10:00	0.646	0.083	0.617	0.077	0.167	0.668
11:00	0.706	0.050	0.720	0.029	0.418	0.262
12:00	0.809	0.014	0.786	0.021	0.567	0.112
13:00	0.738	0.036	0.929	0.003	0.733	0.025*
14:00	0.952	0.0003	0.410	0.273	0.762	0.028*
15:00	1	<.0001	0.671	0.048	0.617	0.077

Table 2. The correlation of data of AQ monitoring stations and indoor $PM_{2.5}$ in primary schools in autumn.

	Reference		Traffic		Industry	
	R	*p*-value	R	*p*-value	R	*p*-value
08:00	0.857	0.028	0.811	0.001	0.906	<0.001
09:00	0.472	0.120	0.767	0.003*	0.890	<0.001
10:00	0.437	0.154	0.790	0.002*	0.872	<0.001
11:00	0.296	0.376	0.802	0.001*	0.888	<0.001
12:00	0.801	0.001	0.341	0.303	0.760	<0.001
13:00	0.751	0.004	0.563	0.071*	0.829	<0.001
14:00	0.803	0.009	0.640	0.046*	0.466	0.173
15:00	0.321	0.307	0.842	0.002*	0.482	0.132

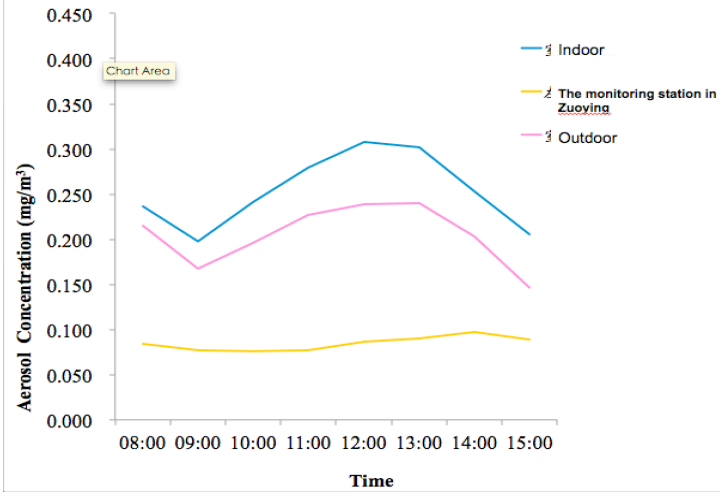

Figure 1. The trend of the average concentration of $PM_{2.5}$ from indoor, outdoor and the monitoring station.

Ultrafine particles counts in elementary school in Taiwan

Wang, MC[1], Mena, KD[2] and Chen, PS[1*]

[1]Department of Public Health, Kaohsiung Medical University, Kaohsiung, Taiwan
[2] Epidemiology, Human Genetics, and Environmental Sciences, School of Public Health, The University of Texas Health Science Center at Houston

Keywords: ultrafine particles, elementary school, I/O ratio.
Presenting author email: asdf800525@hotmail.com

Introduction

Previous studies showed that exposure to ultrafine particles have adverse health effects in children. Ultrafine particles also play an important role in asthma symptoms of children. Kaohsiung is a heavy industrial city with high particulate matter concentration. Therefore, it is important to assess children's exposure to ultrafine particles in Kaohsiung, Taiwan. In this study, we aimed to measure ultrafine particles concentration in the classrooms of elementary schools in Kaohsiung. Real-time monitoring of ultrafine particles for eight hours was performed. In addition, indoor and outdoor concentration was simultaneously measured in the morning and afternoon.

Materials and Methods

Three elementary schools, reference, industry and traffic schools, was selected in Kaohsiung, Taiwan. Nine classrooms were randomly selected in each elementary school with a total sample size of twenty- seven classrooms. Ultrafine particles concentration was monitoring in real-time from 8 am to 4 pm between April 2009 and June 2009 (TSI P-trak model 8525, TSI, USA). We also measured ultrafine particles concentration indoor and outdoor of classroom at 8 am and 4 pm. For comparison of indoor and outdoor concentration, Indoor/Outdoor ratio (I/Oratio) of ultrafine particles was calculated.

Results and Discussion

The average concentration for ultrafine particles in reference, industry and traffic school was 7.8×10^3 (pt/cc), ranging from 2.9×10^3 (pt/cc) to 1.2×10^4 (pt/cc), 1.7×10^4(pt/cc), ranging from 4.3×10^3 (pt/cc) to 3.5×10^4 (pt/cc), and 1.7×10^4 (pt/cc), ranging from 2.7×10^3 (pt/cc) to 4.0×10^4(pt/cc), respectively (Table 1.) . Our results showed that the average concentration in industry and traffic school was significantly higher than that of reference school ($p<0.0001$). More sources of pollutants around traffic and industry school may be the reason. For the concentration profile (Figure 1) from 8 am to 4 pm, similar trend was observed among all the 27 classrooms that ultrafine particles concentration was the highest in the morning and decreased with time. Hourly average concentration of ultrafine particles in reference school was all lower than that of industry and traffic school.

The study showed that eight hours average concentration of ultrafine particles in industry and traffic school was significantly higher than that of reference school. For the trend of an hour average concentration, ultrafine particles concentration was the highest in the morning. In addition, the I/O ratio of ultrafine particles was all below 1.

Table 1. The eight hours average concentration for ultrafine particles in reference, industry and traffic school (N=9)

	Mean (pt/cc)	Median (pt/cc)	SD	C.V.%	Minimum (pt/cc)	Maximum (pt/cc)
Industry school	7.8×10^3	7.8×10^3	3.1×10^3	3.9×10^1	2.9×10^3	1.2×10^4
Reference school	1.7×10^4	1.6×10^4	7.5×10^3	4.3×10^1	4.3×10^3	3.5×10^4
Traffic school	1.7×10^4	1.6×10^4	8.3×10^3	4.6×10^1	2.7×10^3	4.0×10^4

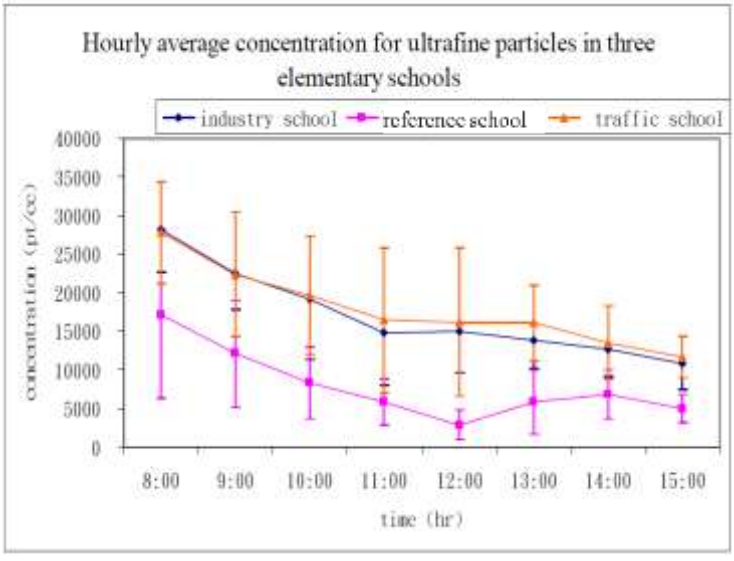

Figure 1. Hourly average concentration for ultrafine particles in three elementary schools

The distribution of PM_{10}, $PM_{2.5}$, and PM_1 concentrations in primary schools in Kaohsiung, Taiwan

Chen, SW[1], Mena, KD[2] and Chen, PS [1*]

[1] Department of Public Health, Kaohsiung Medical University
2 Epidemiology, Human Genetics, and Environmental Sciences, School of Public Health, The University of Texas Health Science Center at Houston

Keywords: Ultrafine, PM, Classroom.
Presenting author email:ann78929@hotmail.com

PM_{10}, $PM_{2.5}$ and PM_1 may increase the risk of heart attack, stroke and some cardiovascular diseases. Lung function of school children, the susceptible groups, could be decreased by particulate matter. So far, there's little study aiming the particular matter exposure of the elementary school children in classroom. Therefore, the purpose of this study is to evaluating PM_{10}, $PM_{2.5}$, and PM_1 concentration profiles in school children's classrooms in Kaohsiung, an industrial city in Taiwan.

Three primary schools, industry, traffic, and reference school, were selected to assess PM_{10}, $PM_{2.5}$, and PM_1 concentration profiles. Real-time monitoring of PM_{10}, $PM_{2.5}$, PM_1 from 08:00 to 16:00 was held in the classroom to a total of 26 and 35 classrooms during April 13th to Jun 13th, 2009 and September 7th to November 6th, 2009, respectively (DUSTTRAK™ Aerosol Monitor ; Model 8520, TSI USA). In addition, PM_{10}, $PM_{2.5}$, and PM_1 concentration were simultaneously monitoring indoor and outdoor in the morning and afternoon.

The concentrations of PM_{10}, $PM_{2.5}$, and PM_1 in fall were significantly higher than that in spring. The differences of seasons in industry and traffic school were more obvious than that of reference school. In Spring, the mean value of PM_1/PM_{10} was 0.84, 0.81, and 0.86 in industry, traffic, and reference school, respectively; whereas the mean values of $PM_{2.5}/PM_{10}$ was 0.87, 0.84, and 0.88 in industry, traffic, and reference school, respectively. In fall, the mean values of PM_1/PM_{10} was 0.91, 0.90, and 0.88, in industry, traffic, and reference school, respectively; whereas the mean values of $PM_{2.5}/PM_{10}$ was 0.93, 0.91, and 0.88 in industry, traffic, and reference school, respectively. The mean of the ratio in fall was significantly higher than that in spring. There was no significant correlation of the PM_{10} concentration between monitoring stations and classroom in spring. But in fall, there was significantly medium positive correlation of the PM_{10} concentration between monitoring stations and classroom in traffic and industry school.

The concentrations of PM_{10}, $PM_{2.5}$, and PM_1 and the ratios of the PM_1/PM_{10}, and $PM_{2.5}/PM_{10}$ were higher in fall than in spring. The correlation between the concentration of PM_{10} in the classrooms and data from air monitoring station indicated that the data from the air monitoring station may not exactly represent the exposure of school children in the classroom.

Table 1. Concentration of PM in three primary schools in Spring and Autumn

	Spring				Autumn				Difference
	N	Mean	S.D	Range	N	Mean	S.D	Range	
Industry school									
PM_{10}(mg/m^3)	862	0.09	4.70	0.02－0.24	1055	0.15	5.55	0.06－0.22	Autumn>Spring*
$PM_{2.5}$(mg/m^3)	862	0.08	4.60	0.01－0.22	1055	0.14	5.18	0.05－0.21	Autumn>Spring*
PM_1 (mg/m^3)	862	0.08	4.50	0.01－0.22	1055	0.14	5.21	0.05－0.20	Autumn>Spring*
Traffic school									
PM_{10}(mg/m^3)	857	0.08	3.80	0.02－0.20	1160	0.18	6.80	0.05－0.41	Autumn>Spring*
$PM_{2.5}$(mg/m^3)	857	0.07	3.30	0.01－0.18	1160	0.16	6.72	0.04－0.39	Autumn>Spring*
PM_1 (mg/m^3)	857	0.07	3.30	0.01－0.18	1160	0.16	6.72	0.04－0.39	Autumn>Spring*
Reference school									
PM_{10}(mg/m^3)	782	0.08	5.24	0.01－0.15	1163	0.10	5.61	0.02－0.30	Autumn>Spring*
$PM_{2.5}$(mg/m^3)	782	0.07	5.06	0.01－0.14	1163	0.09	5.27	0.02－0.29	Autumn>Spring*
PM_1 (mg/m^3)	782	0.07	5.05	0.01－0.14	1163	0.09	4.92	0.02－0.29	Autumn>Spring*

Clean air delivery rate (CADR) analysis based on energy consumption for different air flow rates of air cleaners

B. Han[1,2], J.S. Kang[1,2] , H.J. Kim[1] and Y.J. Kim[1]

[1]Environmental & Energy Systems Research Division, Korea Institute of Machinery & Materials, Daejeon, 305-343, Republic of Korea
[2]Department of Environmental & Energy Mechanical Engineering, University of Science & Technology, Daejeon, 305-343, Republic of Korea
Keywords: cleaners, energy, saving, performance
Presenting author email: bhan@kimm.re.kr

Recently, it has been further important to save energy for electrical devices owing to global warming and lack of hydrocarbon resources. Thus, the energy efficiency has started to be classified as its rated classes such as US EPA's Energy Star for the different household electrical devices such as air conditioners and refrigerator. The main performance of air clenaers has been expressed as their clean air delivery rate (CADR), which indicates the fraction of particles (of a particular size distribution) that have been removed times the air flow rate through the device. The CADR of air cleaners has a linear relationship with air flow rate (Q) and particle collection effiency (η) and thus CADR ~ ηQ. Therefore, a large-scale air cleaner with a high air flow rate can obtain a high CADR value. However, the high CADR would not be appropriate from an energy efficiency point of view because a high flow rate probably leads to a high power consumption. In the present study, the CADR of air cleaners has been investigated based on power or energy consumption to understand which air cleaner is better or which air flow rate of operation is better at a fixed air cleaner.

Figure 1 shows the CADR (m^3/min) divided by power consumption (W) at the maximum flow rates (m^3/min) for ten different filter-type air cleaners. The data of CADR/Watt was scattered between 0.08 and 0.18 (m^3/min)/W and thus it showed little relationship between the CADR/Watt and the maximum air flow rates of the air cleaners. This result probably suggests that the energy efficiency of air cleaners may be rarely related to their air flow rates and it is just dependent on the different models of air cleaners. Figure 2 shows the CADR/Watt with different flow rates for the identical air cleaners which have maximum air flow rates of 2.9, 5.9 and 16.3 m^3/min, respectively. For the identical air cleaner, the highest CADR/Watt was found at the smallest air flow rate regardless of three models of air cleaners. It decreased with exponential forms as air flow rate increased. Furthermore, the air cleaner with a higher maximum air flow rate had a higher CADR/Watt for the fixed air flow rate. Therefore, it could be concluded that the CADR/Watt of air cleaners is highly dependent on their air flow rates as well as the models (types of filters and fans) of the air cleaners. This result suggests that the air cleaner having a higher maximum air flow rate is profitable to a higher energy saving as operated with the smallest air flow rate.

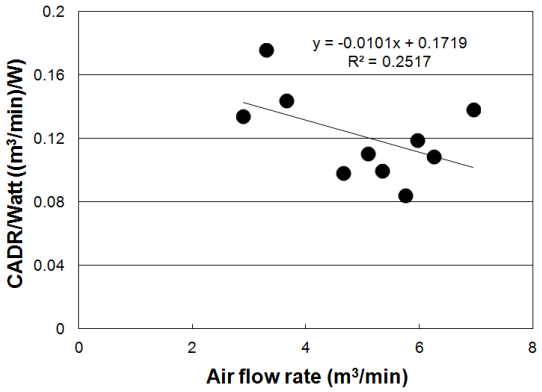

Figure 1. CADR/Watt at the maximum air flow rates for ten different air cleaners.

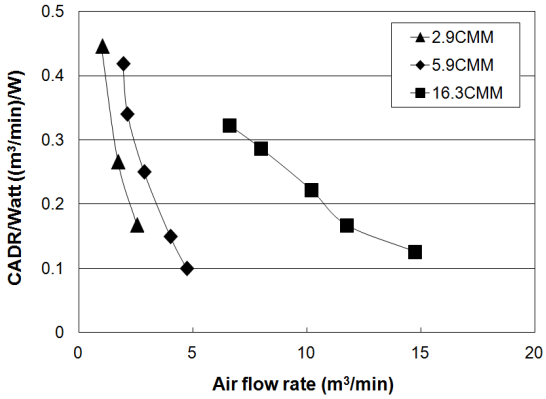

Figure 2. CADR/Watt at different air flow rates for three air cleaners.

This work was supported by the Basic Project (SC0960) of Korea Institute of Machinery and Materials (KIMM).

Shaughnessy, R. J., Levetin, E., Blocker, J., Sublette and K. L. (2004) *Indoor Air* **4**, 179-188

Shanghnessy, R. J. and Sextro, R. G. (2007) *Journal of Occupational and Environmental Hygiene* 3, 169-181.

Sanchez, M. C., Brown, R. E., Webber, C. and Homan, G. K. (2008) *Energy Policy* **36**, 2098-2108.

Characterization of particular matters in subway HAVC system

S. Huang and Y.M. Jo

Department of Environmental engineering, Hyunghee University, Yonggin-si, Geyonggi-do, 446701, South Korea
Keywords: inhalable particles, subway, magnetic property, characterization.
Presenting author email: coral-119@163.com

Underground subway microenvironments have been a great concern as metro is an important public transportation in metropolis. Subway aerosol particles, which are generated mainly by the movement of trains and passengers, and accumulated in a closed environment (Jung *et al*, 2012), resulted in high concentrations of indoor particular matter (PM). Particles of less than 25μm are known to be dominant size distribution of inhalable particles. They are responsible for atmospheric environment and human health effects. Usually, HVAC systems are applied to refresh the underground subway system with filtration.

To achieve better underground subway air quality, this article is devoted to analyzing the air quality in subway HVAC system, characterizing the properties of PM. Since there is no any investigation on magnetic performance of particle aggregation, the magnetic agglomeration of inhalable particles in the external magnetic field prior to filtration by CFD and experiment will be suggested and carried out in further study, serves as a tool for the design of environmental control systems indoor.

Particle samples used in this study were collected from the eletret filter in subway HVAC system (Taechong station, Jeki station). The magnetic fraction was separated by a magnet of 5000 Oe which wrapped with a weighing paper. Herein, the magnetic particles were defined as those attracted to the magnet.

X-ray diffraction (XRD) patterns of magnetic particles were obtained by D8 Advance (Bruker) using Cu Kα radiation. The 2θ scanning range was 10-100° with an increment of 0.02^o (2θ), scanning speed was 3 ^{o}/min. Mineral identification was based on reference JCPDS card.

The morphology was observed by a scanning electron microscope (SEM, Stereoscan 440) with an energy dispersive X-ray detector (EDX, Oxford 7060) for chemical analyses. Measurement of particle size distributions was carried out by Malvern with MSS0010 model working in a light scattering regime.

Results turned out that all of particles collected in subway HVAC system were magnetic, indicating that the sources of them were present near the rails. It alarms public the close relationship between the atmospheric and indoor air quality. Figure 2 showed that the size of sampling particles were in the range of 0.01-200μm, and the average size was 22 μm while the 90% size were below 65μm. XRD patterns and SEM/EDX spectrums demonstrated that Fe_2O_3 (its strongest peak is at 33.9^o 2θ) and Fe_3O_4 (its strongest peak is at 35.5^o 2θ) (see Figure 1) existence. Most of the particles were Fe-containing particles mixed with Ti, Si, Ca, S and C, as shown in Figure 3. These results were agreed with Kukier's (2003) which stated that magnetic fractions contained magnetite, hematite and also quartz. Due to the magnetic properties of particles, external magnetic field will be applied to study the agglomeration of particles in subway HAVC system prior to filtration in following paper.

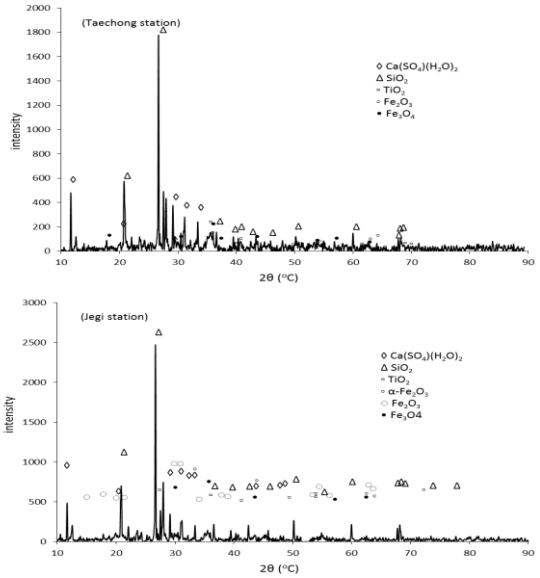

Figure 1. XRD patterns of Taechong and Jegi samples.

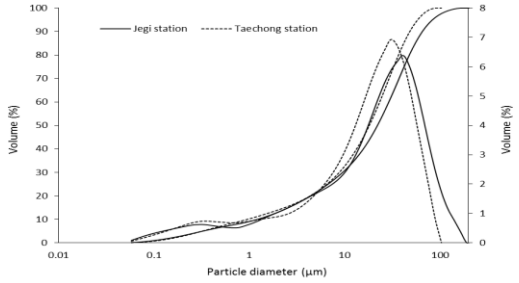

Figure 2. Size distribution of subway samples

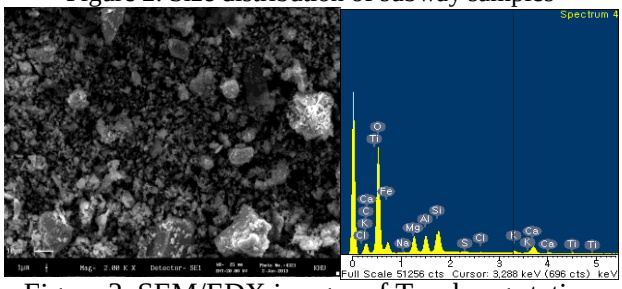

Figure 3. SEM/EDX images of Taechong station

Hae-Jin Jung, et al (2012) *Journal of hazardous materials* **213-214**, 331-340.

Urszula Kukier, et al (2003) *Environmental pollution* **123**, 255-266.

The effect of controlled indoor activities on the particulate matter mass and number concentrations

S.E. Chatoutsidou[1,2], N. Serfozo[1], I. Kopanakis[1], T. Glytsos[1], and M. Lazaridis[1]

[1]Department of Environmental Engineering, Technical University of Crete, Polytechneioupolis, 73100 Chania, Greece
[2]Norwegian Institute for Air Research (NILU), PO Box 100, Kjeller, Norway
Keywords: indoor aerosols, indoor aerosol emissions
Presenting author email: lazaridi@mred.tuc.gr

Characterization of indoor particulate matter is complex and requires knowledge of particle origin, sink, temporal and spatial variation, and dynamics. Source characterization and emission rates from different indoor activities are factors which affect the indoor concentration of particulate matter.

The objective of the current study was to determine the influence of different controlled indoor activities on the number and mass particle concentrations. Burning candle and incense, smoking, printing and boiling water were chosen as typical indoor activities.

Number concentration was measured using a P-Track (TSI) instrument, while, $PM_{2.5}$ mass concentration was measured using a Dust-Track II (TSI) instrument. All measurements took place in a laboratory room.

Table 1 shows the average number concentration of particles before (background level) the emissions and during the emission period. Indoor activities produce aerosol particle, which are emitted to ambient air and therefore influence the background concentration. The results are in agreement with previous experimental studies (Hussein, 2006, Glytsos, 2010).

Table 1. Average number concentration of particles before the emissions (Background) and during emission periods for each activity source.

Source	Background, #/cm^3	Emission period, #/cm^3
Candle burning	1411	2019
Incense burning	5276	30563
Smoking	2818	41435
Printing	5186	10468
Water boiling	2498	4908

An increase of the aerosol concentration was observed in all experiments. The increase fluctuated from 30% to 93%. The highest increase on the concentration was observed during burning of an incense stick and smoking cigarette with measured number concentrations equal to 61,828 particles/cm^3 and 65,830 particles/cm^3 respectively.

Increase of the particle mass concentration was also observed during the simulated activities. Figure 1 presents the particle number and mass concentration in parallel versus time for incense burning and cigarette smoking.

The average mass concentration during incense burning was 174 ± 92 μg/m^3. Before the start of the experiment the average ambient concentration was 26 μg/m^3. This indicates an increase of 85% in mass concentration of particles. Moreover, the aerosol mass concentration remained high for several minutes after the end of the incense burning.

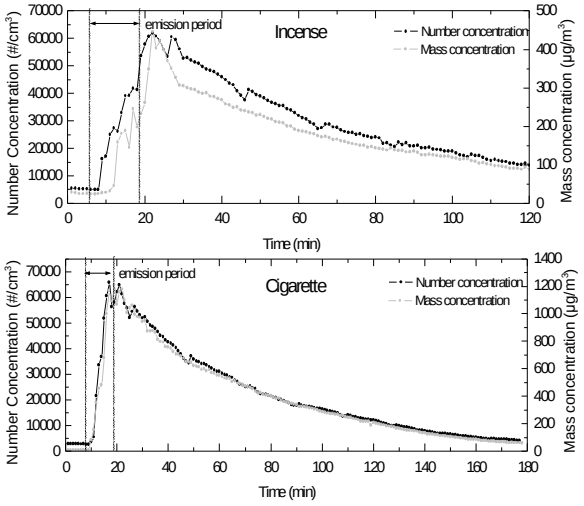

Figure 1. Number and mass concentration versus time for incense burning and cigarette smoking.

The highest indoor aerosol mass concentration was observed during cigarette smoking with total average mass concentration 376 ± 309 μg/m^3. The aerosol mass concentration before the activity was 16 μg/m^3 and on average 802 μg/m^3 during the emission activity.

From this study, major particulate sources identified to be incense burning and smoking cigarette. Future studies will focus on the effect of indoor sources on the aerosol particle number size distribution under specific scenarios.

The research leading to these results has received funding from the European Union Seventh Framework Programme HEXACOMM *FP7/2007-2013* under *grant agreement* n° *315760.*

Hussein, T., Glytsos, T., Ondrá_cek, J., Dohányosová, P., _Zdímal, V., Hämeri, K., Lazaridis, M., Smolík, J., Kulmala, M. (2006) *Atmospheric Environment* **40**, 4285-4307.

Glytsos T, Ondráček J, Džumbova L, Kopanakis I, Lazaridis M. (2010) *Atmospheric Environment* **44**, 159–49.

Survivability of yeast in an electrodynamic balance

Y.M. Kuo[1], S.H. Huang[2] W.Y. Lin[3], S.C. Teng [4] and C.C. Chen[2]

[1]Department of Occupational Safety and Health, Chung-Hwa University of Medical Technology, Tainan, Taiwan
[2]Institute of Occupational Medicine and Industrial Hygiene, National Taiwan University, Taipei, Taiwan
[3]Institute of Environmental Planning and Management, National Taipei University of Technology, Taipei, Taiwan
[4]Graduate Institute of Microbiology, College of Medicine, National Taiwan University, Taipei, Taiwan
Keywords: electrodynamic balance, bioaerosol, yeast, survivability.
Presenting author email: ccchen@ntu.edu.tw

Previous studies on survivability of microorganisms were mainly carried out by placing microbial-laden liquid, such as serum, on the surface. However, these viability test data could not reflect the survivability of microorganisms suspended in the air because the environmental stress levels would be different. Electrodynamic balance (EDB) has long been used to characterize the physical and chemical properties of single particle fixed and airborne in the chamber by electrostatic forces ((Sageev *et al.*, 1986). With the assistance of video capture and automatic feedback control system, the EDB became more advanced and versatile. In the present study, an EDB system was used, probably for the first time, to evaluate the survivability of yeast cell.

The experimental system, as shown in Figure 1, consisted of (1) a double-ring EDB chamber which was designed to levitate one particle with DC and AC field, (2) a laser beam (I= 0~100 mW, λ= 532nm) to illuminate particle, and a digital camera (400X) to capture image of the target particle, and (3) an automatic control system written in Labview 8.2. Before introducing bioaerosol to EDB, the system was tested and optimized by using monodisperse (5, 10, 15 μm) acrylic powders. The operating DC and AC voltages were 200~1000 V and 1.3 kV/frequency= 350~1000 Hz, respectively. Yeast cell (Saccharomyces cerevisiae YPH499) was chosen for its size, falling right into the working range of EDB (3 to tens μm). The yeast aerosols were generated by using a Wright nozzle modified for maximum aerosol output. A retrieving probe was made to capture the yeast cell levitated in the EDB. The retrieved cell was then cultivated to examine the viability. Laser light intensity, chamber temperature, humidity, and retention time in the chamber are among the principal operating parameters.

The results showed that the EDB system could retain super-micrometer-sized (5, 10, 15 μm) acrylic powders and yeast aerosols in the chamber for hours or even days. The survival rate of yeast cells was around 5%, after retrieved from the EDB chamber with RH= 20% and then cultivated on YEPD agar. The survival rate increased (from 5 to 26%) with increasing relative humidity (from 20 to 75%) in the EDB chamber. The survival rate decreased with increasing retention in the chamber, for example, from 28% of 5 min down to 22% of 30 min. These survival rates are much lower than yeast cells in distilled water before aerosolization (90%) and yeast cells after aerosolization (80%). However, it should be noticed that both high survival rates were based on viability test following methylene blue staining procedure, which might not be exactly the same with YEPD agar cultivation method.

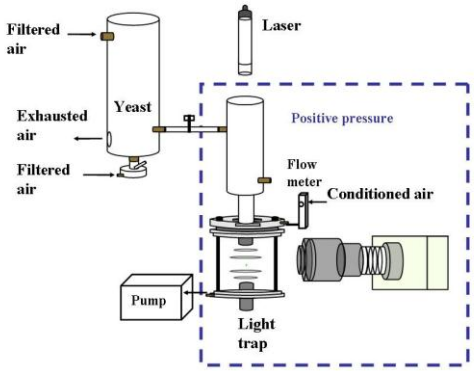

Figure 1. Schematic diagram of the electrodynamic balance system

This work was supported by the National Science Council of Taiwan.

Sageev, G., J. H. Seinfeld and R. C. Flagan (1986). "Particle sizing in the electrodynamic balance." Review of Scientific Instruments 57(5): 933-936.

Evaluation on removal performance of air cleaning devices against airborne allergen particles using an optical particle counter and ELISA method

H.J. Kim, B. Han, and Y.J. Kim*

Department of Eco-Machinery System, Korea Institute of Machinery and Materials (KIMM), Daejeon, 171 Jangdong, Yuseong-gu, 305-343, Korea
Keywords: allergen, airborne, removal, air cleaning
*Presenting and corresponding author's email: yjkim@kimm.re.kr

In this study, we evaluated the aerodynamic characteristics of airborne allergen particles both with and without air-cleaning devices, i.e., a dehumidifier and an air conditioner, using artificially created allergen powders that contained the proteins Del p 1 and Fel d 1 which are believed to play important roles in the etiology of asthma by dogs and cats. Figure 1 shows the experimental set-up for this sutudy. Measurements were taken using a real-time optical particle counter and a closed chamber (4 x 3 x 2.5 m^3). The CADR (Clean Air Delivery Rate) was measured both with and without operating air-cleaning devices for a variety of particle sizes. Time- and size-dependent particle-removal performance was evaluated using an optical particle counter, and the results were compared with measurements taken using the ELISA (two-site enzyme-linked immunosorbent assay) method, which is commonly used for allergen measurements but can not analyze the real-time size-dependent aerodynamic properties of the removal devices.

Figure 2 shows the CADRs with and without an operating dehumidifier and air conditioner. The CADRs, which are a universal air-cleaning performance metric, were linearly proportional to particle size, and the removal of airborne allergen particles was significantly enhanced, by 4 and 7 times on average, by the operation of a dehumidifier and an air-conditioner, respectively.

Shown in Figure 3, the removal efficiency of the air conditioner obtained by ELISA and the optical particle counter based on particle number in the peak size and on total volume were 1.06, 1.14, and 1.05 times higher than comparable values for the dehumidifier. Also, the difference between the removal efficiencies of the air-cleaning devices for allergen particles calculated from total mass measured by ELISA and from total volume measured by an optical particle counter were 0.32% for the dehumidifier and 5.97% for the air conditioner.

These results indicate that our simple measurement method, which used an in-situ optical particle counter, could easily predict values of air-cleaning performance against airborne allergens that were obtained by the time-consuming ELISA method. Also, the performance of the test for air-cleaning devices using these in-situ measurements is more realistic because airborne allergen particles cause allergic diseases via respiratory organs, such as the nose. This method is a promising tool for measuring air-cleaning performance for airborne allergen particles in indoor environments.

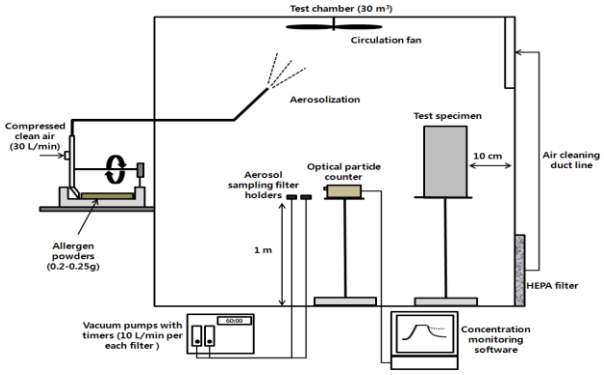

Figure 1. Experimental set-up for this study.

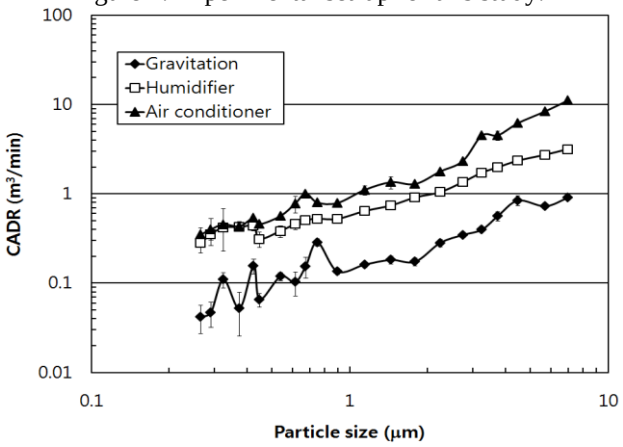

Figure 2. CADRs with and without an operating dehumidifier and air conditioner

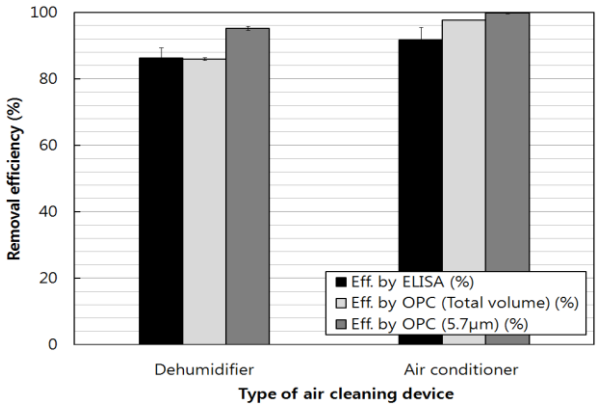

Figure 3. Comparison of the removal efficiencies of the dehumidifier and air conditioner calculated using mass by the ELISA, numeric concentration of 5.7-μm particles, and the total volumetric concentration by an optical particle counter.

This work was supported by a General Research Fund (SC0960) of the KIMM.

Aerosol Particles in the Indoor Environment of the Týn Church in Prague

L. Mašková[1,2] and J. Smolík[1]

[1]Department of Aerosol and Laser Studies, Institute of Chemical Process Fundamentals AS CR, v.v.i., Rozvojová 135, 165 02, Prague 6, Czech Republic
[2]Charles University in Prague, Faculty of Science, Institute for Environmental Studies, Benátská 2, 12 801, Prague 2, Czech Republic
Keywords: Indoor particles, number size distribution.
Presenting author email: maskova@icpf.cas.cz

Particulate matter inside cultural heritage buildings possesses different degrees of risk to materials. Particles not only cause soiling but are abrasive, provide sites for surface reactions and have a potential to damage artifacts due to their hygroscopic nature (Hachtfield, 2005, Nazaroff *et al.*, 1990). The aim of this study was to investigate concentrations and sources of airborne PM in the indoor environment of the Týn Cathedral in Prague.

Measurement was performed during the exhumation of remains of the astronomer Tycho Brahe (5 days intensive campaign in November 2010). The measurements included particle number concentrations and size distributions determined by a Scanning Mobility Particle Sizer (TSI, USA) and an Aerodynamic Particle Sizer (TSI, USA), covering the size range 10 – 20,000 nm. During the campaign the traditional Christmas markets took place in front of the cathedral. The markets started every day at 9 AM a finished around 8 PM. On 15 November the tomb was opened and the remains were exhumed. During the next 3 days the church was closed for public. On 19 November the remains was deposited back into the tomb during a celebration.

Time behaviour of coarse particles (> 2.5 μm) showed work at opening of the tomb and visitors as a source. The time behaviour of submicron particles concentration (< 200 nm) showed periodical increase starting at about 9 AM, with maxima at about 8 PM, followed by subsequent decrease to initial values. It indicates outdoor origin with close markets as the most probable source. During the celebration significant contribution of submicron particles from burning candles and incense was observed (Fig. 1).

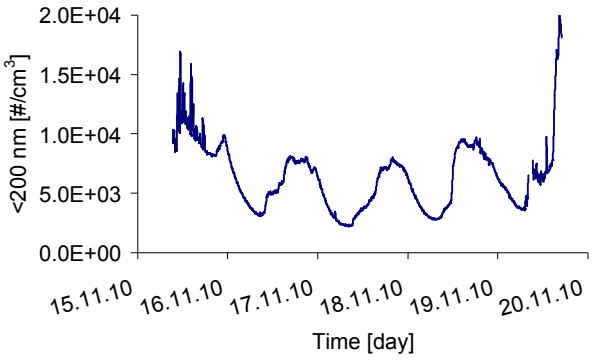

Figure 1. Time series of indoor number concentration of particles < 200 nm.

To describe in detail sources of fine particles in the indoor environment measurements of spatial and temporal variation of those particles were performed during the Easter markets (April 2011). The measurements were done by a P-TRAK (TSI, USA) during three periods in a day: (a) early morning (8 AM) – before markets and visiting hours started; (b) in the beginning of visiting hours and markets (10 AM); (c) during the full operation of markets and visiting hours (12 AM). Scheme of the church with average values recalculated to spatial distributions of concentrations during these periods is shown in Fig. 2a,b,c. The results revealed that in early morning the indoor concentration is homogeneous (2a) and started to grow close doors (points A, C, E, G) after the beginning of the markets (2b). Another source of fine particles is lighting of candles by visitors (point J in Fig. 2c).

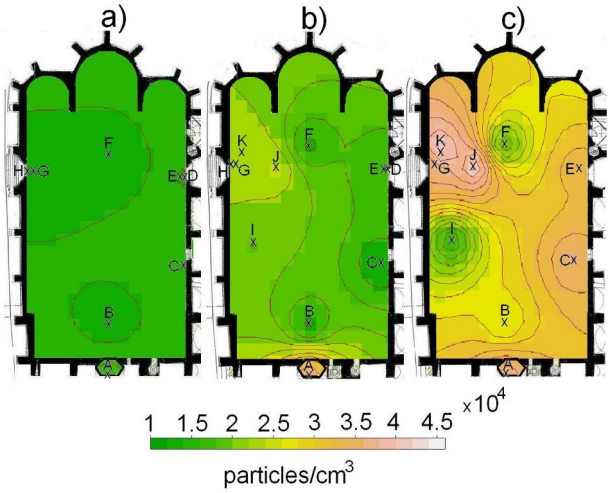

Figure 2. Scheme of the cathedral with measuring points and average values recalculated to spatial distributions of concentrations during the three periods of the measurement.

Hatchfield, P. B. (2005) *Pollutants in the Museum Environment.* Archetype Publications, London.
Nazaroff, W. W., Salmon, L. G. and Cass, G. R. (1990) *Environ. Sci. Technol.*, 24, 66-77.

Air Quality in Different Types of Archives

L. Mašková[1,2] and J. Smolík[1]

[1]Department of Aerosol and Laser Studies, Institute of Chemical Process Fundamentals AS CR, v.v.i., Rozvojová 135, 165 02, Prague 6, Czech Republic
[2]Charles University in Prague, Faculty of Science, Institute for Environmental Studies, Benátská 2, 12 801, Prague 2, Czech Republic
Keywords: Indoor/outdoor particles, number size distribution, ventilation rate.
Presenting author email: maskova@icpf.cas.cz

Aerosol particles are one of the major pollutants in outdoor and indoor air. They may negatively influence health, but also have negative effects on ecosystems and cultural heritage. Particulate matter (PM) can be harmful for works of art by causing soiling and chemical damage, depending on particle size and chemical composition (Hatchfield, 2005).

The study includes indoor/outdoor monitoring of the air quality in four archives in the Czech Republic, which representing different outdoor environments: Zlatá Koruna (rural), Třeboň (small city with seasonal tourism), Teplice (industrial area), and Prague (large city with traffic). The aim of this study is to investigate concentrations and sources of airborne PM and gaseous pollutants in the indoor environment of the archives, and to establish the relationship between the indoor and outdoor environment. In 2012 the measurements were performed at Třeboň and Zlatá Koruna during 4 intensive campaigns in different seasons of the year.

The results indicated outdoor air as the most probable source of particles in the indoor environment of both archives. Average values for the indoor/outdoor ratios of the particle number concentration had a maximum between particle diameters of 0.1– 1 μm (Fig. 1), which indicates a maximum penetration factor and low indoor deposition velocity of these particles. The penetration at Třeboň was higher probably due to simple windows with gaps, compared to double glassed windows at Zlatá Koruna.

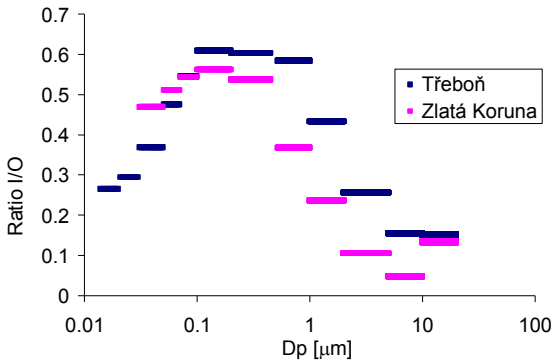

Figure 1. Indoor/outdoor ratios of particle number concentrations versus particle size at Třeboň and Zlatá Koruna during the winter campaign.

These results were confirmed by measurements of the ventilation rate, which was at Třeboň in average three times higher than at Zlatá Koruna (Fig. 2). The ventilation rate was lower in summer than in winter at both archives, probably due to lower temperature difference between indoor and outdoor environment.

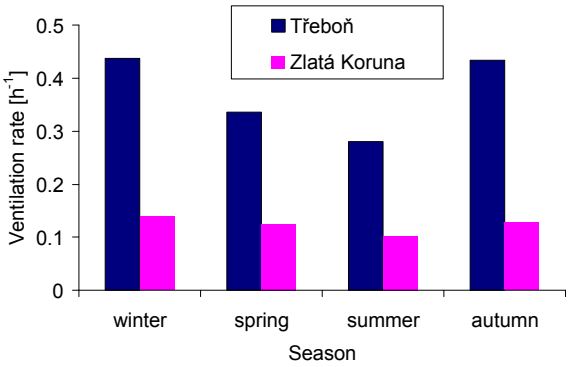

Figure 2. Ventilation rates measured at Třeboň and Zlatá Koruna in different seasons of the year.

This work was supported by the Ministry of Culture under grant DF11P01OVV020.

Hatchfield, P. B. (2005) *Pollutants in the Museum Environment.* Archetype Publications, London.

Alveolar dose of ultrafine particles for children in urban environments

M. Mazaheri[1], S. Clifford[1,2], M. A. Megat Mokhtar[1], F. Fuoco[3], G. Buonanno[3], L. Morawska[1]

[1]International Laboratory for Air Quality and Health, Institute of Health and Biomedical Innovation, Queensland University of Technology, Brisbane, Queensland 4001, Australia
[2]Centre for Air Quality & Health Research and Evaluation, 431 Glebe Point Rd, Glebe 2037, Australia
[3]Department of Civil and Mechanical Engineering, University of Cassino, Cassino, Italy
Keywords: ultrafine particles, alveolar dose, children, urban environment.
Presenting author email: m.mazaheri@qut.edu.au

The aim of this study was to quantify school children's exposure to ultrafine particles (UFP) in urban environments. The study was conducted as part of a larger epidemiological project aiming to determine the association between exposures to UFPs and children's health, titled "Ultrafine Particles from Traffic Emissions and Children's Health"[1] (UPTECH). School children aged 8-11 years old at 24 state schools within the Brisbane Metropolitan Area participated in the present study. This paper presents the methodology and results for calculating deposited UFP surface area in the alveolar region (dose), where UFP deposition is more efficient for particles larger than 6 nm (ICRP 1994, Buonanno et al. 2012).

The alveolar surface area doses were derived using measured time-series of UFP number concentrations, $N(t)$, and average particle diameters, $d_{p,av}$, using Philips Aerasense Nano Tracers at 16 s sampling intervals. The doses were determined for the following activity microenvironments in a typical school day (recorded with an activity diary): school (in and outdoors), home (eating/cooking times, sleeping and other), other non-schooling activities (in and outdoors) and commuting.

The total dose for each activity within the 24 hour period of measurement for a child aged A, $\delta_{A,k}$, is calculated as

$$\delta_{A,k} = \sum_{j=1}^{J} \mathrm{IR}_{A,k} \int_{t_{1j}}^{t_{1j}} \int_{0}^{\infty} g\left(d_p,t\right) \mathrm{d}d_p \, \mathrm{d}t$$

where IR is the inhalation rate of activity k and $g(d_p,t)$ is the product of the estimated particle size distribution, the particle number concentration, per-particle surface area, πd_p^2, and the deposition ratio (Hinds 1999). The estimated particle size distribution is log-normal with mean $d_{p,av}(t)$ and standard deviation, σ_k, dependent on the activity (Buonanno et al. 2012).

Figure 1 shows the results of total dose and dose relative intensity (fraction of daily dose divided by fraction of daily time for that activity) calculations for the 39 children at the first 12 schools whose activity diaries comprise at least 23 hours of non-missing information. While most activities provide a similar contribution to the daily total dose, they do so with varying intensities and durations. The lowest median dose intensity is during sleeping, a time with very few sources of particles. The highest median dose intensity occurs during outdoor times at school, when particle number concentration (PNC) is moderately high and children are more active (higher breathing rate). The second highest dose intensity is commuting due to high PNC during commutes. Even though commuting dose intensity does not contribute highly to the total dose because of its short duration (3% of the day), it confirms the significance of exposure to traffic emissions .

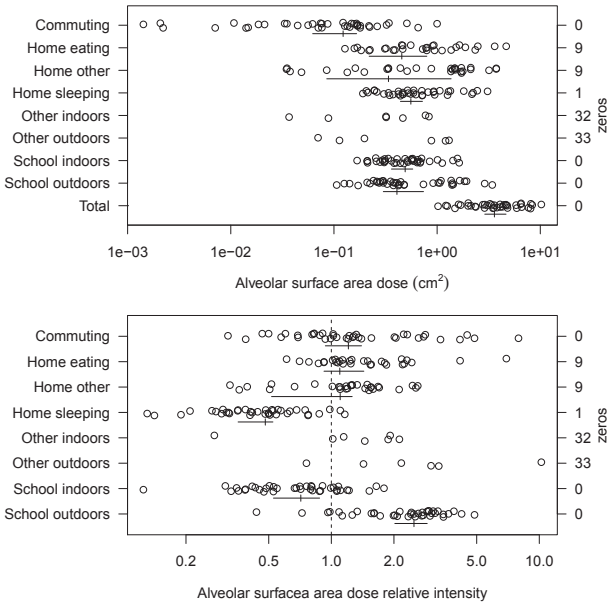

Figure 1: Calculated alveolar surface area dose and dose relative intensity with bootstrapped medians and their 95% CIs. Zeros account for the number of children whose activity diaries do not record any instances of that activity.

This work was supported by the Australian Research Council (ARC), QLD Department of Transport and Main Roads (DTMR) and QLD Department of Education and Training (DET) through a Linkage Grant LP0990134.

G. Buonanno, L. Morawska, L. Stabile, L. Wang, and G. Giovinco. A comparison of submicrometer particle dose between Australian and Italian people. *Environmental Pollution*, 169:183 – 189, 2012. ISSN 0269-7491

ICRP. *Human Respiratory Tract Model for Radiological Protection: A Report of a Task Group of the International Commission on Radiological Protection*. Elsevier Science Ltd., Oxford, U.K., 1994

W.C. Hinds. *Aerosol technology: properties, behavior, and measurement of airborne particles*, chapter 11, Respiratory Deposition, pages 233–259. Wiley-Interscience. Wiley, 1999

[1]http://www.ilaqh.qut.edu.au/Misc/UPTECH%20Home.htm

Subway platform air quality: assessing the influences of tunnel ventilation, train "piston effect" and station design

T. Moreno[1], N. Pérez[1], C. Reche[1], E. de Miguel[2], M. Capdevila[2], S. Centelles[2], J. Jaume[2], A. Alastuey[1] and X. Querol[1]

[1]Inst. of Environmental Assessment and Water Research, IDAEA, CSIC, C/Jordi Girona 18-24, 08034 Barcelona, Spain
[2]Transports Metropolitans de Barcelona, TMB Santa Eulalia, Av. del Metro s/n L'Hospitalet de Llobregat, 08902, Spain
Keywords: subway, air quality, piston effect, Barcelona.
Presenting author email: teresa.moreno@idaea.csic.es

It is known that air quality in underground rail transport systems, especially with regard to inhalable particulate matter (PM) concentrations, is highly variable but commonly extremely poor. There are, however, few specific data investigating potentially controlling influences on PM levels in subways, such as the effects of underground ventilation, train movement, and different station designs. With this in mind, an intensive, high resolution air quality measurement campaign was conducted in 10 stations along Line 2 of the Barcelona metro system under (a) normal ventilation conditions, and (b) with daytime tunnel ventilation systems shut down. Fifteen different PM size ranges (0.3-20 µm) were measured at 6-second intervals for one hour in four different sampling sites along each of the 10 platforms, together with concentrations of CO and CO_2. The data confirm that subway air quality is extremely variable, with average PM_{10} platform concentrations ranging from 11 to 95 µg/m^3 and transient peaks in several stations regularly rising into the 100-200 µg/m^3 range. The stations with poorest air quality were those with only a single platform and narrow tunnel containing a single line, and with lateral (rather than end) exit points, and there was always a notable spatial increase in PM_{10} levels at the end of the station furthest from the entrance (in those stations with only one exit). In these stations with the poorest air quality, average levels of PM_{10} rose when tunnel ventilation was turned off, in some cases doubling in concentration. This increase was despite the fact that outside air background concentrations in Barcelona were 30% lower during this phase of the experiment: clearly outside conditions were not significantly affecting air quality underground. The ratio of fine to coarse PM recorded by PM_3/PM_{10} (ranging between 0.6-0.7) was unaffected by the presence or absence of tunnel ventilation. Levels of CO and CO_2 under normal ventilation conditions were unexceptional (typically c.0.4ppm and 400-550ppm respectively), in most cases staying similar or falling when the ventilation was turned off. The main conclusion of the study is that the various combinations of station design and tunnel ventilation are the dominant factors controlling underground air quality in the Barcelona metro, with the "piston effect" induced by trains producing a perceptible through-draught but having less influence on actual air quality in terms of PM concentrations.

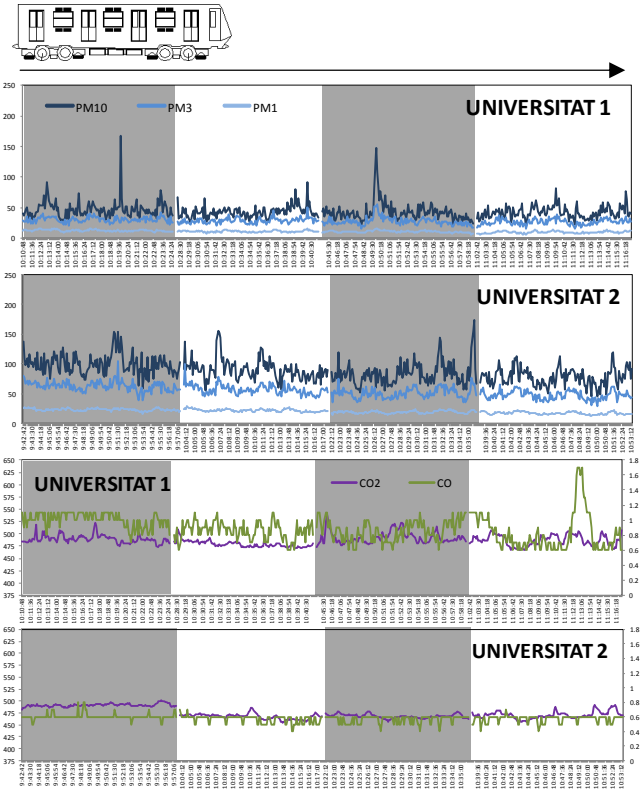

Figure 1. Example of PM concentrations in µg/m^3, and CO2 (left axes) and CO (right axes) in ppm, measured every 6 seconds in 4 different points along the subway platform. Data are shown for the Universitat station (with single train line and single platform) in the week 1 with tunnel ventilation (Universitat 1), and week 2 without tunnel ventilation (Universitat 2).

This work was supported by the Spanish Ministry of Economy and Competitiveness within the I+D Project CGL2012-33066, and the Metropolitan Transport Services of Barcelona (TMB).

The effect of biomass burning on PM exposure during wintertime

D.A. Sarigiannis[1,2], S. Karakitsios[1] and M. Kermenidou[1]

[1]Department of Chemical Engineering, Aristotle University of Thessaloniki, Thessaloniki, 54124, Greece
[2]Centre for Research and Technology Hellas (CE.R.T.H.), Thessaloniki, 57001, Greece
Keywords: PM exposure, biomass burning
Presenting author email: denis@eng.auth.gr

Over the last couple of years, the use of biomass as heating source was allowed in Greece as a CO_2-neutral means of space heating in the large metropolitan areas of Athens and Thessaloniki affecting more than half of the country's population. At the same time the use of light heating diesel was heavily taxed. In the same period Greece faces a financial crisis with significant repercussions on the average household income. This combination resulted in reduced traffic loads but excessive biomass use for domestic heating. In this context, the current study deals with the assessment of the seasonal variability of PM exposure in the city of Thessaloniki.

A combination of measured and modeled data of outdoor and indoor PM10 and PM2.5 were generated, feeding a composite integrative exposure assessment framework that takes into account indoor air quality modeling, time activity patterns and activity based inhalation rates. The measurements campaign included the assessment of outdoor and indoor air quality and the evaluation of biomass use (in open fireplaces) for domestic heating. Outdoor measurements highlighted a significant increase of PM10 (from 30.1 to 73.1 μg/m^3) and PM2.5 (from 19.4 to 62.7 μg/m^3) concentrations during the transition from the warm to the cold period of the year 2012, in contrast to the previous year (2011) where this transition was accompanied by a smaller increase of 12 μg/m^3 for both PM10 and PM2.5. Between the two years, there is a significant difference in the PM emission patterns; in 2012 the traffic component is reduced, while during the colder period the component associated with the biomass heating dramatically increases. The latter is verified by the positively correlated levoglucosan concentrations to ambient air PM concentrations. Indoor concentrations followed a similar pattern, while in the case of fireplace use, average daily concentrations rise up to 10 μg/m^3 and 14 μg/m^3 for PM2.5 and PM10 respectively. Concentrations tend to rise significantly during the fireplace operation, accompanied by an average increase of 65 and 85 μg/m^3 for PM2.5 and PM10 respectively; however this increase is more prominent in PM of lower aerodynamic diameter as identified by particle size measurements (Figure 1). Average indoor air concentrations seemed to be significantly affected by the outdoor air quality rather than moderate indoor air biomass burning emissions, as estimated by IAQ modeling and verified by the respective measurements.

Personal exposure (Figure 2) is determined by the overall indoor air quality, since people spend about 85% of their time indoors. Tracking intra-day variability (Figure 3), shows that peaks of ambient PM concentrations do not necessarily reflect peaks of actual exposure and intake (red line), since the timing and the location where people perform their activities is also important.

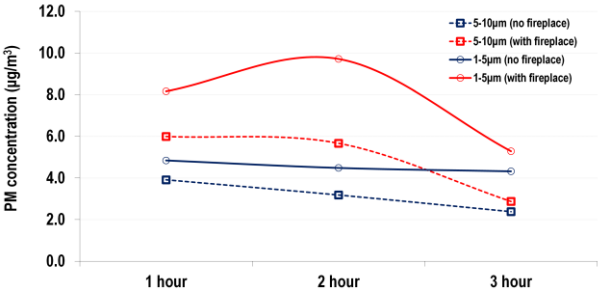

Figure 1. Comparative concentration profiles of open fireplace operation for different PM size fractions (PM1-5 and PM5-10).

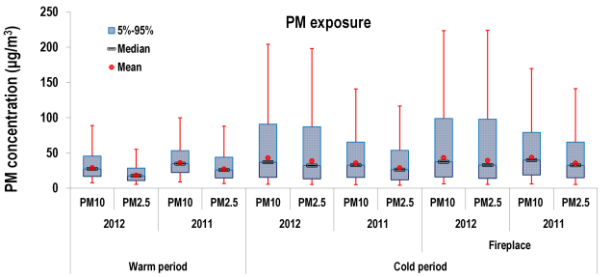

Figure 2. Seasonal variability of exposure to PM for the years 2011 and 2012.

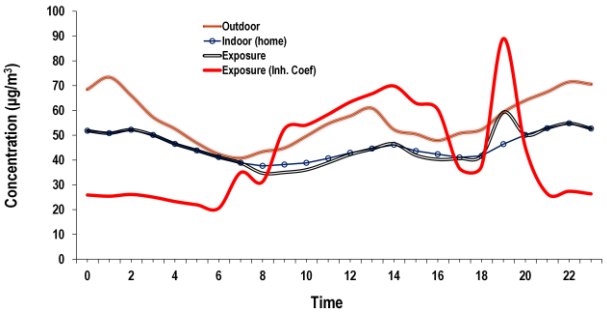

Figure 1. Typical wintertime intra-day variability profile of PM10 concentration and personal exposure.

Late night peaks of ambient PM concentrations (related to domestic heating emissions) do not correspond to peaks of actual intake, since people spend a large part of the time sleeping thus inhalation rate is very low. On the contrary, peaks of exposure (and potential intake) are related to specific activities performed outdoor (e.g. commuting by any transportation means) or indoors (use of open fireplace).

Particle release from open ethanol fireplaces into the indoor environment

T. Schripp[1], E. Uhde[1], S. Wientzek[1], M. Wensing[1] and T. Salthammer[1]

[1]Dept. Material Analysis and Indoor Chemistry, Fraunhofer WKI, Braunschweig, Lower Saxony, 38108, Germany
Keywords: ethanol, combustion, lung deposition, FMPS.
Presenting author email: erik.uhde@wki.fraunhofer.de

The indoor use of open ethanol burning fireplaces is a common decorative trend. In contrast to wood burning fireplaces that feature enclosure and/or chimneys, all combustion products that ethanol fireplaces generate are released into the indoor environment. Due to the fact that the fuel is burned in liquid or gel form, complete combustion can be expected. Even though the fireplaces show no significant visible smoke they can be assumed to be strong sources for (ultra)fine particles (UFP). The present study reports emission test chamber experiments of ethanol fireplaces with a series of liquid and gel fuels.

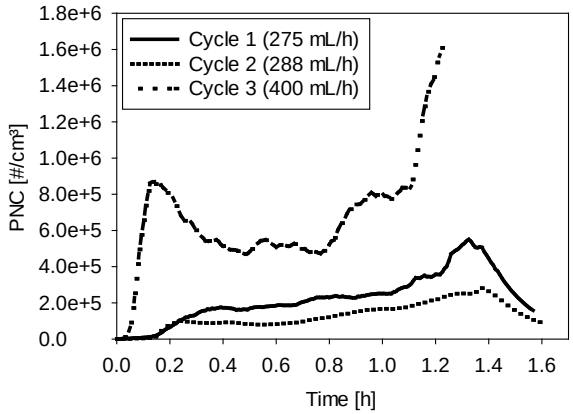

Figure 1. Development of the particle number concentration (PNC, FMPS) during the burning phase of 3 measurement cycles of sample "1/fluid" (500 mL). The observed ethanol consumption is given in brackets.

The open fire places were tested in a ventilated 48 m³ stainless-steel emission test chamber according to the recommendations of the manufacturer and DIN 4734-1. Three liquid and five gel samples were tested. Before each experiment, the heating value of each fuel was measured. The burning phases lasted between 70 - 240 min. The emission was monitored during and until 12 h after the burning phase. The following parameters were continuously measured: particles, NO_x, CO, CO_2 and formaldehyde. In addition volatile organic compounds were measured via a thermal desorption GC/MS method. The particles were continuously measured via Fast Mobility Particle Sizer (FMPS, 5.6 nm – 560 nm) and Grimm Aerosol Spectrometer (0.3 µm – 20 µm). The particle exposure assessment was performed on the basis of the lung deposition model of the International Council on Radiological Protection (ICRP, 1994). The longest burning time observed was 240 min and, thus, the assumed exposure scenario comprised a duration of 4 h for all tested devices without further consideration of the burning time.

Operation of the ethanol fireplaces significantly affected the air quality in the test chamber. During the operation of some devices the German guideline values for CO_2 (2000 ppm) and NO_2 (350 µg/m³) were exceeded. Some systems showed considerable release of formaldehyde. Peak particle concentrations ranged between $6.2 \cdot 10^3$ #/cm³ and $2.3 \cdot 10^6$ #/cm³ for the sum of particles in the size range of the FMPS. The devices were not constant emitters of particles and - in some cases - showed significant differences between different measurement cycles (Fig. 1). The count median diameter (CMD) of the particles during the burning phase ranged between 10 nm and 65 nm. This low particle size allows deep lung penetration down to the alveolar region. For the present aerosols, approx. 60% of the total lung particle deposition is expected to occur in the lower alveoles (AI). The calculated particle surface deposition ranges from 0.1 cm²/4h (AI) to 6.2 cm²/4h (AI) within an estimated exposure time of 4 h for a sitting male. Buonanno et al. (2011) estimated the daily alveolar particle intake for Italian in the range between 22.8 cm²/d (AI) and 25.1 cm²/d (AI) (3.8 cm²/4h – 4.2 cm²/4h) for several indoor activities, such as cooking and cleaning. The operation of an ethanol fireplace induces a particle exposure that adds between 1% and 155% to this common "background" exposure. (Fig. 2) This further illustrates that open ethanol fireplaces are a strong source for ultra-fine particles indoors in some cases.

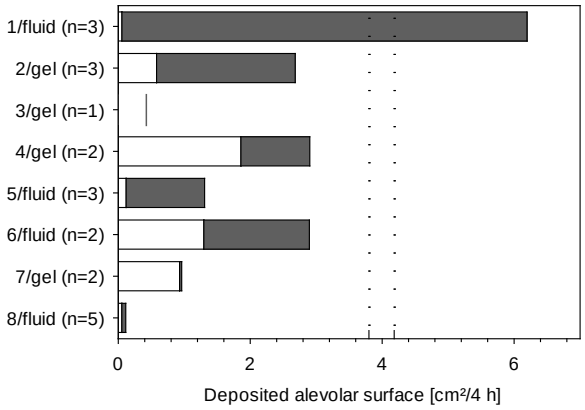

Figure 2. Estimated particle surface deposited in the alveoles of the human lung. The dashed lines mark the range of estimated particle deposition (4 h) by Buonanno et al.

Buonanno, G., Giovinco, G., Morawska, L., et al. (2011) *Atmospheric Environment*, **45**, 6216-6224.
ICRP (1994) *Annals of the ICRP*, **24**, 36-54.

Nanoparticle Enhanced PCR Detection of Bacterial Aerosols

Siyu Xu and Maosheng Yao*
State Key Joint Laboratory for Environmental Simulation and Pollution Control,
College of Environmental Sciences and Engineering
Peking University, Beijing 100871, China

Keywords: NanoPCR, Bacteria, Bioaerosol.

Presenting author email: yao@PKU.edu.cn

Bioaerosol detection is of great importance in many fields, yet their low quantity in complex samples makes such an effort difficult. Here, we have investigated the use of nanoparticles (AgNPs, TiO2NPs and their combination) assisted PCR (nanoPCR) in enhancing the efficiency. Pure bacterial species E. coli and B. subtilis with serial dilutions were tested for obtaining optimal parameters such as nanoparticle concentration and the volume of the nanoparticle mixture. These optimal parameters were then applied to detecting indoor and outdoor bacterial aerosols collected using a liquid impinger. The PCR products were subsequently subjected to agarose gel electrophoresis and DNA stain.

The results showed that the enhancements varied with nanoparticle type, concentration level, and DNA template concentration. Data with E. coli and B. subtilis revealed that the optimal parameters were: 0.6 nM for TiO2NPs, 0.9 nM for AgNPs, 2 uL for the mixture, and diluted DNA templates. Our data also suggest that the mixture of AgNPs and TiO2NPs performed better compared to their individual ones especially for lower DNA levels when coupled with qPCR. BacLight DNA stain results showed that use of nanoparticles could form nanoparticle-DNA clusters, which led to concentrating local DNA and thus enhancing PCR detection. Our environmental bioaerosol monitoring data suggest that NanoPCR technique can be immediately applied to detecting 45 low quantity of airborne biological materials with up to 500 times enhancement. The developments in this work can further broaden qPCR applications in bioaerosol research fields.

Acknowledgements: The authors acknowledge the supports from National Science Foundation of China Grant 21077005.

Direct Viral Aerosol Inactivation by Microwave Irradiation and its Mechanisms

Yan Wu and Maosheng Yao*
State Key Joint Laboratory for Environmental Simulation and Pollution Control,
College of Environmental Sciences and Engineering
Peking University, Beijing 100871, China

Keywords: Microwave Irradiation, Viral Aerosol

Presenting author email: yao@PKU.edu.cn

Previously, we have studied the bacterial and fungal aerosol inactivation by direct microwave irradiation at 2450 MHz. Here, we further investigated its inactivation of airborne virus in laboratory controlled conditions. MS2 coliphage used as a human model virus were aerosolozied using a Collison Nebulizer and exposed to the direct microwave irradiation for ~ 2 min at three different power levels (700 , 385, 119 W) in this work. The microwave irradiation unit investigated in our previous studies was used here. In addition to the survival rate, the viral envelope surface proteins with and without the microwave irradiation were also examined using PCR and gel electrophoresis.

Experimental data showed that direct exposure of MS2 virus in airborne state to the microwave irradiation at 700 W for less than 2 min resulted in more than 90% inactivation efficiency, and about 50% at the lowest power level (199 W). Water-borne MS2 virus exposure to the microwave irradiation revealed that the inactivation rate depended on the power level and irradiation time. Scanning electron images showed visible damages to the viral envelope. Results from PCR and gel electrophoresis showed that severe damages occurred to the viral envelope surface proteins such as the A protein, the capsid protein and the replicase protein, among which the A protein was completely damaged. Damages to these functional proteins would result in the loss of viral ability to mount an infection. This study demonstrated that even without the filtration the direct microwave irradiation could also achieve high inactivation efficiency for viral aerosols. Among many efforts including the development of viral vaccines, engineering control solutions could provide unlimited potential in the battle against the emerging viral threats.

Acknowledgements: The authors acknowledge the supports from National Science Foundation of China Grant 21077005.

Improving the Efficiencies of Andersen Impactors Using Mineral-Oil-Spread Agar Plate

Maosheng Yao*, Zhenqiang Xu, Kai Wei, Yan Wu, Fangxia Shen, Qi Chen, Mingzhen Li
State Key Joint Laboratory for Environmental Simulation and Pollution Control, College of Environmental Sciences and Engineering
Peking University, Beijing 100871, China
Keywords: Microwave Irradiation, Viral Aerosol
Presenting author email: yao@PKU.edu.cn

As a bioaerosol sampling standard, Andersen type impactor is widely used since its invention in 1950s, including the investigation of the anthrax attacks in the United States in 2001. However, its related problems such as impaction and desiccation stress as well as particle bounce have not been solved. Here, we improved its biological collection efficiencies by plating a mineral oil layer (100 μL) onto the agar plate. An Andersen six-stage sampler and a BioStage impactor were tested with mineral-oil-spread agar plates in collecting indoor and outdoor bacterial and fungal aerosols. The effects of sampling times (5, 10 and 20 min) were also studied using the BioStage impactor when sampling environmental bioaerosols as well as aerosolized Bacillus subtilis (G+) and Escherichia coli (G-). In addition, particle bounce reduction by mineral-oil-plate was also investigated using an optical particle counter (OPC). Experimental results revealed that use of mineral-oil-spread agar plate can substantially enhance culturable bioaerosol recoveries by Andersen type impactors (p-values<0.05). The recovery enhancement was shown to depend on bioaerosol size, type, sampling time and environment. In general, more enhancements (extra 20%) were observed for last stage of the Andersen six-stage samplers compared to the BioStage impactor for 10 min sampling. When sampling aerosolized B. subtilis, E. coli and environmental aerosols, the enhancement was shown to increase with increasing sampling time, ranging from 50% increase at 5 min to ~100% at 20 min. OPC results indicated that use of mineral oil can effectively reduce the particle bounce with an average of 66% for 10 min sampling. Our work suggests that enhancements for fungal aerosols were primarily attributed to the reduced impaction stress, while for bacterial aerosols reduced impaction, desiccation and particle bounce played major roles. The developed technology can readily enhance the agar-based techniques including those high volume portable samplers for bioaerosol monitoring.

Acknowledgements: This study was supported by the National Science Foundation of China (Grants 21277007, 21077005 and 20877004), and special fund of State Key Joint Laboratory of Environment Simulation and Pollution Control.

Cancer risk assessment for the inhalation exposure to particulate matters and polycyclic aromatic hydrocarbons from household cooking in northern Taiwan

K.-P. Yu[1], K.R. Yang[1], S. C. Lung[2] and C.-H, Liu[2]

[1]Institute of Environmental and Occupational Health Sciences, National Yang-Ming University, Taipei, 11221, Taiwan
[2]Research Center for Environmental Changes, Acadimia Sinica, Taipei, 11529, Taiwan
Keywords: exposure, MOUDI, cooking, risk.
Presenting author email: kpyu@ym.edu.tw

Food cooking generates lots of harmful fine and ultrafine particles (Torkmahalleh *et al*., 2012). Many occupational studies have shown that the incremental lifetime cancer risk (ILCR) caused by exposure to polycyclic aromatic hydrocarbons (PAHs) in cooking fume was much higher than the suggested acceptable limit of 10^{-6} (See *et al*., 2006; Zhao *et al.*, 2011). However, the result of occupational studies is based on higher exposure level, including concentration, frequency and duration, and cannot represent the exposure of the general population. The exposure to cooking fume generated from daily household cooking may be more representative and such data were relatively limited in Taiwan.

In this study, we selected five families without smoker in northern Taiwan as the sampling sites. We took the particle samples during cooking periods by using a Micro-Orifice Uniform-Deposit Impactors and monitored the 24-hour particle concentrations profile by using a Scanning Mobility Particle Sizer and a 6-channel optical particle counter. The gaseous PAHs were collected by a glass cartridge packed with polyurethane foam and Amberlite XAD-16 polymeric adsorbent. After being Soxhlet-extracted with a mixed solvent (*n*-hexane and dicloromethane; vol/vol, 1:1), both the particulate and gaseous PAHs samples were analyzed by the gas chromatography mass spectrometry.

Table 1 shows the PAHs concentration (mean and range) emitting from household cooking. Although gaseous PAHs contributed more than 85% of the total PAHs, particulate PAHs percentage increased with number of ring and contributed most of the $B[a]P_{eq}$. The $B[a]P_{eq}$ is significantly positive correlated with the PM of larger particles (>3.2 μm) but negative correlated with that of particles smaller than 0.056μm, indicating that most toxic PAHs deposited on larger particles (Fig. 1).

The ILCR was evaluated as the following:

$$\mathrm{ILCR} = \frac{(\mathrm{C} \times \mathrm{IR} \times \mathrm{EF} \times \mathrm{ED})}{\mathrm{BW} \times \mathrm{AT}} \times \text{Slope factor} \quad (1)$$

where, C is the PAHs concentration; IR is the inhalation rate; EF is the exposure frequency; ED is exposure duration; BW is the body weight; AT is the averaging time for carcinogen (25550 day=70 yrs); SF is the slope factor.

Table 1. PAHs from household cooking.

	PAH conc.(μg/m³)	*Particulate PAHs*
Total PAHs	11.481 (1.456—57.012)	13.27%
[a]LM-PAHs	9.857 (1.145—50.212)	3.50%
[b]MM-PAHs	1.074 (0.091—5.280)	75.58%
[c]HM-PAHs	0.549 (0.181—1.520)	95.09%
[d]B[a]P$_{eq}$	0.098 (0.055—0.230)	**94.76%**

a: 2 & 3 rings; b: 4 rings; c: >4 rings; d: banzo[a]pyrene equivalent concentration

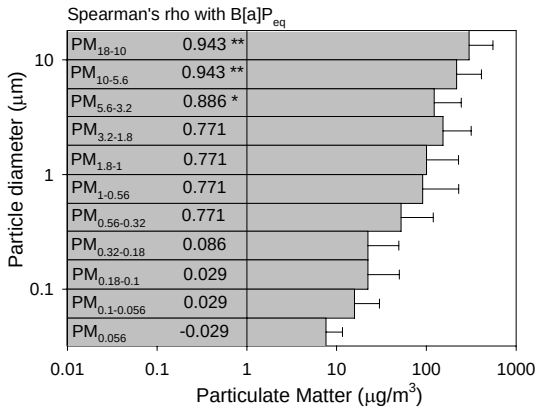

Fig. 1. Particulate matters (PM) emit from household cooking and their Spearman's rho with $B[a]P_{eq}$

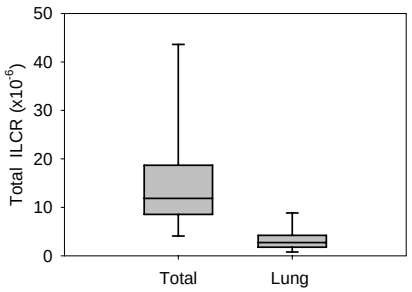

Fig. 2. ILCR caused by exposure to total PAHs (Total) and alveolar deposited PAHs (Lung) from cooking. (PAHs conc. Lognormal (LN) distr., IR: 1.75 m^3/h×2 h/day = 3.5 m^3/day, EF: (LN) 252 day/yr, Geo. Std.=1.01, ED=50 yr, BW: (LN) 59.78 kg, Geo. Std.=1.07)

Fig. 2 demonstrates that distribution of ILCR based on Monte Carlo simulation result. The ILCR is much lower than those reported by occupational studies. However, the ILCR is higher than the recommended acceptable limit of 10^{-6}, implying that even the exposure to PAHs to daily household cooking could result in a significant cancer risk.

This work was supported by the National Science Council of Taiwan under grant NSC 100-2221-E-010-003-MY3.

See, S., Karthikeyan, S. and Balasubramanian, R. (2006) *J. Environ. Monit.* **8**, 369-376.

Torkmahalleh, M., Goldasteh, I., Zhao, Y., Udochu, N., Rossner, A. and Hopke, P. (2012) *Indoor Air* **22**, 483-91.

Zhao, P., Yu, K.-P. and Lin C.-C. (2011) *International Archives of Occupational and Environmental Health* **84**, 231-237.

Enhancement effect of O_3 on the antifungal efficacy of nano-metals supported TiO_2 on resistant mold spores

K.-P. Yu, Y.-T. Huang, S.-C. Yang

Institute of Environmental and Occupational Health Sciences, National Yang-Ming University, Taipei, 11221, Taiwan
Keywords: Antifungal, ozone, *Aspergillus niger*.
Presenting author email: kpyu@ym.edu.tw

Increasingly tremendous rainfall events due to climatic changes have caused serious water damages and extensive dampness in indoor environments, which lead to molds growth. For example, the indoor fungal concentration in remediated houses can reach as high as 2×10^5 spores/m^3 several weeks after the flood (Hsu *et al.*, 2011). Exposure to home dampness and molds is a risk factor for irritation, allergy, infection and respiratory diseases. To remediate microbial pollution, antimicrobial efficacy of nano-metals has been extensively studied (Sondi and Salopek-Sondi, 2004; Morones *et al.*, 2005; Egger *et al.*, 2009). However, most of the relative studies focused on the bactericidal efficacy. Molds, especially their spores, are more resistant than bacteria. Therefore, an expansively evaluation of the antifungal efficacy of this technique is necessary.

In this study, the nano-metals (Ag, Cu and Ni) supported catalysts were successfully prepared by the simple and low-cost incipient wetness impregnation method, while the titanium dioxide (Degussa (Evonik) P25) nanoparticle was served as the support (Fig 1). The prepared catalysts were denominated as 0.5wt%Ag/P25, 5wt%Ag/P25, 2wt%Cu/P25 and 5wt%Ni/P25, respectively, according to the species and the amount of loaded metals.

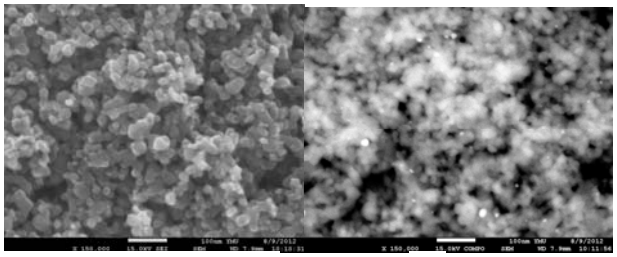

Fig.1. SEM images of 0.5wt%Ag/P25 (a), SEI (secondary Electron Image) (b) COMBO mode (SEI and Back Scatted Electron Image) Bright spots in the COMBO mode are Ag particles

The antifungal experiments of *Aspergillus niger* spores were conducted on two surfaces (quartz and putty) in the darkness with and without ozone exposure. The critical Ag concentration to inhibit the germination and growth of *Aspergillus niger* spores of 5wt% nano Ag catalyst was 65 mg/mL, which was lower than several cases reported in previous studies (Egger *et al.*, 2009).

The antifungal kinetics fitted the Chick-Watson model:

$$SR = \exp(-kt) \quad (1)$$

in which SR is the survival ratio of *Aspergillus niger* spores; k is the inactivation rate constant; t is the elapsed time. The inactivation rate constants of *Aspergillus niger* spores on nano-metals (Ag, Cu and Ni) supported catalysts in the presence of ozone (Fig.2(b) k=0.475~0.966 h^{-1}) were much higher than those in the absence of ozone (Fig.2(a) k= 0.001~0.268 h^{-1}). However, on the surface of TiO_2 particles, no antifungal effect was observed until 6-hour exposure to ozone. Consequently, ozone has a synergetic effect on nano-metal antifungal effectiveness.

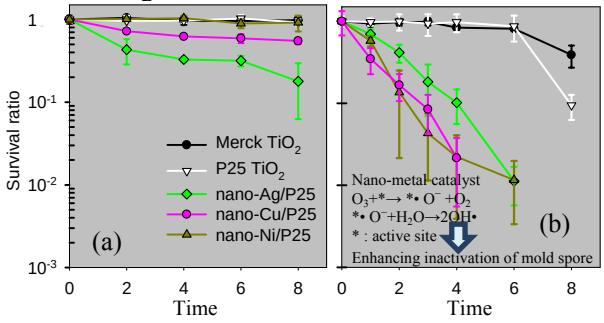

Fig. 1 Time profiles of the survival ratio of *Aspergillus niger* spore on the surface of catalysts and quartz chip (a) in the darkness (Dark); (b) exposed to 5-ppm ozone

Antifungal experimental result of the catalysts on putty was shown in Fig. 3. Nano-Ag and -Cu catalysts did inactivate the *Aspergillus niger* spores when being applied on putty, but the inactivation rate constants were lower than those applied on the quartz chips. This may result from the fact that the Ag and Cu ions could form complexes with the alkalinity of the putty which reduced the diffusivity of the nano-Ag and Cu.

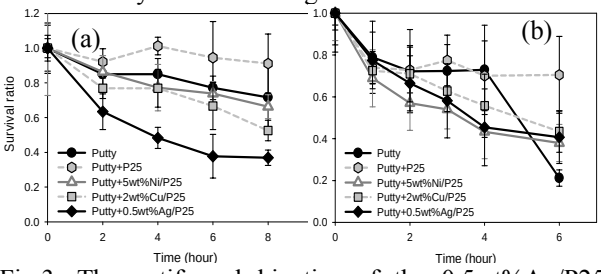

Fig.3. The antifungal kinetics of the 0.5wt%Ag/P25, 2wt%Cu/P25 and 5wt%Ni/P25 catalysts against *Aspergillus niger* spore when being applied on the putty (a) in the darkness (Dark); (b) exposed to 5-ppm ozone

This work was supported by the National Science Council of Taiwan under grant NSC 99-2221-E-010-005-

Hsu, N.Y., Chen, P.Y., Chang, H.W., Su, H.J. (2011) *Science of The Total Environment* **409**, 1677-1682.

Egger, S., Lehmann, R.P., Height, M.J., Loessner, M.J., Schuppler, M. (2009) *Applied and Environmental Microbiology* **75**, 2973-2976.

Sondi, I., Salopek-Sondi, B., (2004) *Journal of Colloid and Interface Science*, **275,** 177-182.

Morones, J.R., Elechiguerra, J.L., Camacho, A., Holt, K., Kouri, J.B., Ramírez, J.T., Yacaman, M.J., (2005) *Nanotechnology*, **16,** 2346-2353.

Organic composition of indoor/outdoor particles in an elementary school

C.A. Alves[1], R.C. Urban[2], P.N. Pegas[1] and T. Nunes[1]

[1]Centre for Environment and Marine Studies, Department of Environment, University of Aveiro, 3810-193 Aveiro, Portugal

[2]Faculty of Philosophy, Sciences and Languages of Ribeirão Preto, University of São Paulo, 14040-901 Ribeirão Preto, SP, Brasil

Keywords: PM_{10}, classroom, organic tracers.

Presenting author email: celia.alves@ua.pt

The impact of air pollution on school children's health is currently one of the key focus of international organisations. Children spend up to ten hours per day at school and the health impact of air pollutants is much higher for pupils than for adults in similar environments (Guo *et al*., 2010). Particulate matter is one of the most important pollutants in indoor air. In spite of the various studies performed worldwide to assess the pupils' exposure to indoor particles, only a few aimed at characterising their chemical composition and most of them were mainly focused on the elemental content (e.g. Almeida *et al*., 2011). Comparatively almost nothing is known about the organic matter in particulate matter, which can encompass irritant, carcinogenic and/or mutagenic compounds.

In this study, an intensive sampling campaign of indoor and outdoor airborne particulate matter (PM_{10}) was carried out in a primary school of Aveiro, Portugal, from February 28 to March 27, 2011, to investigate mass concentrations and organic composition and to evaluate the influence of outdoor air pollution on the indoor air. The organic speciation was performed by gas chromatography-mass spectrometry after multi-solvent extraction, fractionation of the organic extracts in a silica gel column and application of derivatisation techniques to the more polar compounds.

The weekly indoor PM_{10} concentrations during occupancy periods ranged from 75 to 145 μg m^{-3}, whereas much lower levels, from 20 to 62 μg m^{-3}, were registered outdoors. The dominant organic compound classes were acids, sugars, polyols and *n*-alkanes (Fig. 1). Polycyclic aromatic compounds were detected at indoor and outdoor concentrations of 893±650 and 830±421 pg m^{-3}, respectively, never exceeding the benzo[a]pyrene equivalent carcinogenic threshold of 1 ng m^{-3} set by the World Health Organisation.

It can be clearly seen that concentrations of most organic compounds were many times higher than their homologous outdoor levels. The ratio between indoor and outdoor (I/O) concentrations gives an indication whether the generation is from indoors or derived from the outdoor environment. Air exchange rates below 1 h^{-1}, such as those registered in this study, have been reported to give higher I/O ratios for particles (Rojas-Bracho *et al*., 2000).

Carbon preference indices of *n*-alkanes around 1, both indoors and outdoors, and the presence of biomass combustion tracers (e.g. levoglucosan, L, mannosan, M, and galactosan, G) in indoor particles suggest that infiltration of outdoor particulates leads to contamination of classrooms with vehicle emissions and biomass burning smoke likely coming from biofuel use in nearby restaurants and bakeries.

The L/M and L/(M+G) ratios are within the ranges reported for softwood burning (Fine *et al*., 2004). The input of this source is also confirmed by fluoranthene/(fluoranthene+pyrene) ratios > 0.5.

The indoor and outdoor concentrations of organic compounds were closely correlated (r^2=0.5-0.8). The slopes of the linear regressions indicate that 12-22% of the indoor levels are of outdoor origin.

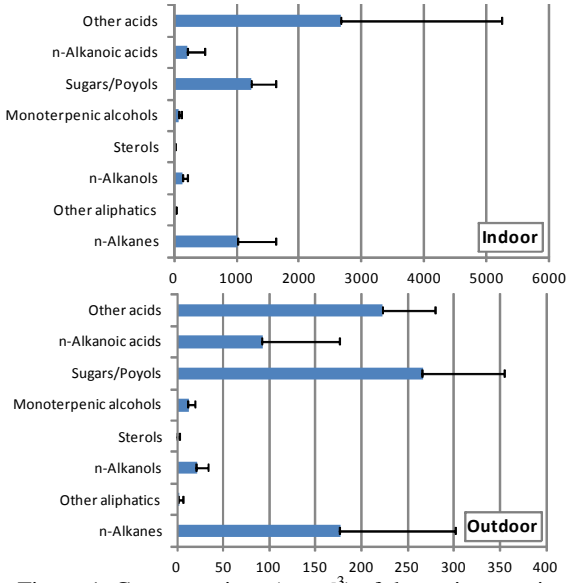

Figure 1. Concentrations (ng m^{-3}) of the main organic compound classes in PM_{10}.

R.C. Urban and P.N. Pegas acknowledge the PhD grants, respectively, from FAPESP and the Portuguese Science Foundation (FCT).

Almeida, S.M., Canha, N., Silva, A., Freitas, M.C., Pegas, P., Alves, C., Evtyugina, M. and Pio, C. (2011) *Atmos. Environ*. **45**, 7594-7599.

Fine, P.M., Cass, G.R. and Simoneit, B.R.T. (2004) *Environ. Eng. Sci*. **21**, 387-409.

Guo, H., Morawska, L., He, C., Zhang, Y.L., Ayoko, G. and Cao, M. (2010) *Environ. Sci. Poll. Res.* **17**, 1268-1278.

Rojas-Bracho, L., Suh, H.H. and Koutrakis, P. (2000) *J. Expo. Anal. Env. Epid.* **10**, 294-306.

Indoor air quality in school buildings in the city of Sosnowiec, Poland

P.Z. Brewczyński[1], E. Krakowiak[1], J. Kurek[2], A. Wlazło[1], M. Zaciera[2]

[1]Department of Biohazards and Immunoallergology & [2]Department of Chemical Hazards and Genetic Toxicology, Institute of Occupational Medicine and Environmental Health, Sosnowiec, 41-200, Poland
Keywords: school, indoor air pollutants.
Presenting author email: p.brewczynski@imp.sosnowiec

Children spend about 6-8 h daily in school more than in any other indoor environment except home. For that reason indoor air quality in classrooms influences quality of life and health of pupils. Major sources of indoor air pollution are building construction, decoration materials, furnishings, and the occupants themselves and their activities. Other major outdoor contributing factors include traffic-related and industrial pollution, as well as the type of ground on which the school sits.

The aim of this study was to assess the level of the indoor air quality parameters (PM2.5, formaldehyde, benzene, toluene, xylene, NO_2, O_3, CO, CO_2, benzo(a)pyrene, radon) in a naturally ventilated school buildings in the city of Sosnowiec.

Studies were carried out in three schools (in 9 classrooms). The main criterion of the schools selection was their location, type of construction and operating conditions. Monitoring was performed during the winter months, since heating plays a crucial role on indoor air pollution level. The concentrations of formaldehyde, NO_2, O_3, and volatile organic compounds were measured with the use of passive diffusion samplers. The concentrations of formaldehyde were measured using AT 1200 High Performance Liquid Chromatograph with diode array detector. The concentrations of benzo(a)pyrene were detected using AT 1200 High Performance Liquid Chromatograph with fluorescence detector. Volatile organic compounds like benzene were measured using Varian Star 3600 Cx Gas Chromatograph with Flame Ionization Detector. Radon was determined by passive – track counts on film exposed method. The concentrations of nitrogen dioxide and ozone were measured using spectrophotometer analysis. Concentrations of PM2.5 were measured from Monday to Friday (during teaching hours) using filter-based samples charged with a pump and by gravimetric analysis of PTFE filter samples.

PM2.5 concentrations were usually lower indoors than outdoors (I/O ratio less than 1), because no indoor sources were detected. However, higher indoor concentrations (I/O ratio value was 1.1) were found in one school where the air exchange was not efficient, as confirmed by indoor CO_2 data significantly higher than in other schools.

Benzene and formaldehyde concentrations inside of schools were much higher in comparison to outdoor concentrations which shows that the emission source of these harmful chemicals are furnishings, building materials or finishing materials.
Trichloroetylene, tetrachloroetylene and naphthalene did not exceed limit threshold values of methods used for their determination.

Table 1. Selected IAQ parameters.

IAQ parameters	Range	
	Indoor	Outdoor
PM2.5 ($\mu g/m^3$)	34.31-113.55	38.00-127.17
Formaldehyde ($\mu g/m^3$) *	13.87-53.30	1.58-4.82
Benzene ($\mu g/m^3$)	9.58-38.03	5.53-10.42
Toluene ($\mu g/m^3$) *	2.61-100.71	2.19-5.90
Xylene ($\mu g/m^3$) *	0.00-9.94	0.00-2.84
NO_2 ($\mu g/m^3$) *	8.81-26.97	17.10-58.50
O_3 ($\mu g/m^3$) *	2.7-6.7	21.9-166.4
Radon (Bq/m^3)	40-107	40-90
B(a)P ($\mu g/m^3$) *	0.006-0.045	0.015-0.026
CO (ppm)	0.0-1.1	0.2-1.0
CO_2 (ppm) *	1158-2590	383-532
RH (%) *	31.9-49.2	76.9-85.1
Temperature (ºC) *	19.0-23.3	-1.6-3.5

*$p < 0.05$ for a statistical analysis the non-parametric Mann-Whitney U test was used.

Faulty working ventilation may distribute pollutants from any sources to other parts of the building, too.

Nitrogen dioxide, ozone, and benzo(a)pirene concentrations are higher outdoors than indoors (in classrooms) therefore so the source of their formation can be attributed to atmospheric air.

The worst outdoor air quality was found in one school located in the city centre with high traffic flow and naturally high car fumes generation.

The majority of presented pollutants, are potentially capable to induce toxic processes leading ultimately after a long exposure to long term clinical effects triggered by even small doses. And because of this it is extremely important to identify the possible threat and undertake the relevant preventive measures.

This study was supported by the SINPHONIE project, Schools Indoor Pollution and Health: Observatory Network in Europe & IOMEH statutory activity.

References available by the authors

Assessing the contribution of indoor particulate matter sources in residential homes in a northern province of Italy

P. Fermo[1], A. Piazzalunga[1,2], J. Tarlassi[1] , A. Cattaneo[3], P. Urso[4], M.G. Perrone[2]

[1]Department of Chemistry, University of Milan , 20133, Milan, Italy
[2]Department of Environmental Science, University of Milano Bicocca, 20126 Milano, Italy
[3]Department of Clinical Sciences and Community Health, University of Milan, 22100 Milano, Italy
[4]Biomedical and Clinical Science Department "L.Sacco" University of Milano 20157 Milano, Italy

Keywords: particulate matter, indoor pollution, PAH, ions
Presenting author email: paola.fermo@unimi.it

Many hazardous chemicals produced by different anthropogenic sources and emitted in the environment may cause adverse effects on human health (Kampa et al., 2008). Particulate matter (PM) effects on human health are well known. Because people spend most of their time indoors, indoor PM exposure is a relevant health concern. Indoor residences greatly contribute to total daily exposures because people spend 80 to 90% of their time in confined environments (Schweizer et al. 2007). The health effects are strictly correlated to the chemical composition since PM contains classes of compounds, such as PAHs, recognized as carcinogen by IARC.

Aim of this study was to assess the chemical composition of $PM_{2.5}$ and PM_{10} samples collected in residential homes in a Northern province of Italy (Lodi) in order to identify the main sources of indoor exposure and the contribution of outdoor particles. 24-h samples were collected in 29 homes by means of GK2.05 and GK2.69 samplers (Cattaneo et al. 2011) during both winter and summer. Characteristics of the buildings, including location (e.g. proximity to roads with high traffic) were recorded. Furthermore a time-activity diary containing each activity that could influence indoor PM levels (occupants number, heating system, ventilation, number of cigarettes smoked, time spent for cooking food, time spent on housework, etc.) was available.

The concentrations of 8 ions (Ca^{2+}, Mg^{2+}, K^{+}, NH_4^{+}, Na^{+}, SO_4^{2-}, NO_3^{-} and Cl^{-}) and 15 PAHs considered as "priority" for the U.S. EPA (naphthalene, acenaphthene, fluorene, phenanthrene, anthracene, fluoranthene, pyrene, benzo (a) anthracene, chrysene, benzo (b) fluoranthene, benzo (k) fluoranthene, benzo (a) pyrene, dibenzo (a, h) anthracene, benzo (g, h, i) perylene and indeno (1,2,3, cd) pyrene) were quantified.

The impacts of outdoor sources is attested by the high contribution of sulphate and nitrate during both seasons. This is confirmed by what reported for the regional emissions (INEMAR 2007) according to which traffic in Lodi province corresponds to approximately 47% of the total emissions of both $PM_{2.5}$ and PM_{10}. Therefore the traffic volume on neighboring roads heavily affects indoor PM levels.

It is worth noting that in Lodi province there is also a big impact of agricultural responsible for high ammonia emissions.

The concentrations of PAHs as sum of the 15 examined species were found, with few exceptions, to be below 5 ng m^{-3} and 2 ng m^{-3} in winter and summer respectively.

In order to identify possible PAHs sources, three different methodologies were applied:

1. diagnostic ratios of PAH isomers (Alves et al. 2012, Venkataraman, et al. 1994),
2. linear mixed models for repeated measurements (summer and winter) aimed at identifying main determinants (Urso et al., in press)
3. Chemical Mass Balance (Belis et al., 2011)

The characteristic of buildings and the activities was used to select the variables to be included in the tested models.

Preliminary results have shown that meat cooking represents an important source of indoor PAHs, in addition to gasoline and diesel combustion due to outdoor sources.

Kampa, M. et al. (2008) Environ. Poll., **151**, 362-367.
Schweizer, C. et al. (2007) J. Expo. Anal. Environ. Epidemiol., **17**, 170-181
Cattaneo et al. (2011) Indoor Air, **21**, 489–500
INEMAR (INventarioEMissioniARia-Regione Lombardia). Available: http://www.ambiente.regione.lombardia.it/inemar/webdata/elab_standard_prov.seam?cid=34934
Alves et al.(2012) Atmos. Environ., **59**, 243-255.
Venkataraman, et al. (1994) J. Air & Waste Manage. Assoc,. **44**, 1103-1108.
Urso et al. (2013), Atmos. Environ., in press
Belis et al. (2011) Atmos. Environ., **45**, 7266-7275.

Thursday, September 5, 2013

Poster session C: PMx, Posters C155 – C201

Assessment of population exposure to $PM_{2.5}$ and PM_{10} in the Athens metropolitan area

V. Aleksandropoulou and M. Lazaridis

Department of Environmental Engineering, Technical University of Crete, Chania, Polytechneioupolis, 73100, Greece
Keywords: exposure, urban aerosols.
Presenting author email: vic.aleksandropoulou@enveng.tuc.gr

PM_{10} levels have dropped significantly during the last decade in the Athens metropolitan area, however still are areas where the EU Air Quality Standards (AQS) for the protection of human health are frequently exceeded (Aleksandropoulou *et al.* 2012). Moreover, the average exposure indicator for $PM_{2.5}$ concentrations exceeded the target value of 25 μg/m^3 in 2010. The objective of this work is to evaluate the population exposure to PM_{10} and $PM_{2.5}$ at local outdoor and indoor residential environments in Athens, during the period 2000 – 2010. A preliminary assessment of the exposure to local outdoor PM_{10} during 2010 is presented.

The methodology used for the spatiotemporal allocation of PM_{10} concentrations is based on a data interpolation approach thus probably cannot capture the spatial variation within the urban area. However, it is based on common procedures and is appropriate in calculating population exposure estimates (Horalek *et al* 2007). The variables were selected based on evaluation of model performance. In particular, the exposure concentration was estimated using monitor and modelling data. Monitor data were available from the Hellenic Ministry for the Environment, Energy and Climate Change, whereas the PM_{10} background levels were retrieved from the EMEP Unified model results database (EMEP/MSC-W). The metropolitan area was divided to rural and urban/suburban land based on the Corine Land Cover (CLC) 2000 database and the geographical distribution of population of the EEA dataset was used. Multivariate statistical analysis was used for the spatiotemporal allocation of PM_{10} concentrations at rural areas, using as variables the anthropogenic primary emissions of PM_{10} (compiled based on Aleksandropoulou *et al* 2011), the variation in rural monthly averaged PM_{10} concentrations and the day-to-day variation in background suburban concentrations. At artificial surfaces, the local outdoor PM_{10} levels were estimated using the inverse-squared-distance weighted average of the background suburban monitor values scaled with anthropogenic primary PM_{10} emissions. Monitor values at traffic stations affect the PM_{10} concentration gradient only in their vicinity.

The results, as regards the model performance were 0.88 and 0.79 index of agreement (IA) for the annual averaged concentrations and the number of exceedences, respectively. Likewise, the root mean squared error (RMSE) is equal to 4.15, 0.81, 0.01 and 2.2 for the annual averaged concentrations at all monitoring stations, at background and traffic stations and for the number of exceedences, respectively.

It was found that the annual averaged concentrations over rural and urban areas were 19 μg/m^3 and 45.4 μg/m^3, respectively. More than 69% of the population living in the area is exposed to PM_{10} concentrations above the annual AQS of 40 μg/m^3, whereas 83% of the population lives in areas where the daily AQS of 50 μg/m^3 was exceeded more than 35 times during 2010. The estimated probability of exceedence of the daily AQS in the area during 2010 is shown in Figure 1. The hot spots correspond to urban areas and areas with significant primary PM_{10} emissions. In addition, the distribution of the normalised population load (Walker *et al* 1999) is depicted in Figure 2 which reflects populated areas with concentrations above the daily AQS.

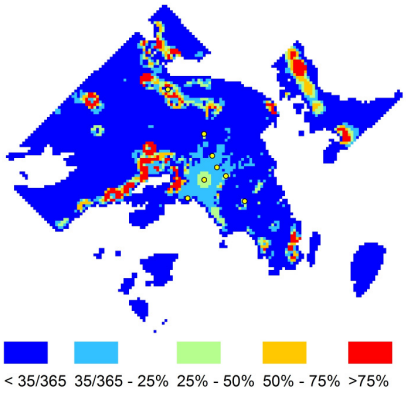

Figure 1. Probability of exceedence of daily AQS.

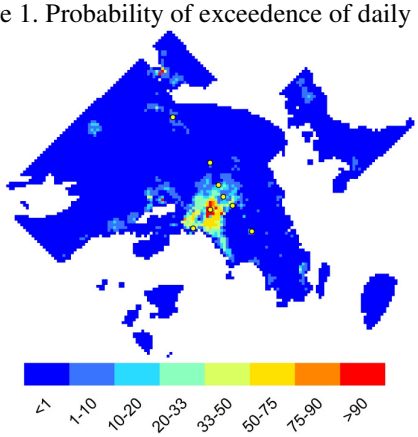

Figure 2. Normalised population load distribution (%).

This work was supported by the European Union's LIFE Programme under grant LIFE 09 ENV/GR/000289.

Aleksandropoulou, V., Torseth, K. and Lazaridis, M. (2011*) Water Air Soil Pollut.* **153**, 15-34.

Aleksandropoulou, V., Eleftheriadis, K., Diapouloi, L., Torseth, K. and Lazaridis, M. (2012*) J. Environ. Monit.*, DOI: 10.1039/C1EM10673B.

Walker, S.E.., Slordal, L.H., Guerreiro, C., Gram F. and Gronskei, K.E (1999) *J. Environ. Monit.* **1**, 321-326.

Horalek, J., Denby, B., Smet, P., de Leeuw, F., Kurfurst,, P., Swart, R. and van Noije, T. (2007) *Spatial mapping of air quality for European scale assessment,* ETC/ACC Technical Paper.

Measurement of Non-Volatile Particulate Matter Mass Emission Indices of Aircraft Gas Turbine Sources

B.T. Brem[1,2], L. Durdina[1,2] and J. Wang[1,2]

[1]Air Quality and Particle Research Group, Empa, Dübendorf, CH-8600, Switzerland
[2]Institute of Environmental Engineering at ETH Zürich, Zürich, CH-8093, Switzerland
Keywords: aircraft emissions, particulate matter
Presenting author email: benjamin.brem@empa.ch

Particulate matter (PM) emissions from aircraft gas turbines are a concern for human health, environmental pollution and climate change. Expected future regulations on emissions require a reliable determination and understanding of particulate matter emission factors under variable thrust and environmental conditions.

This work presents the measurements and preliminary results of non-volatile PM mass emission indices (mass PM/ mass fuel) for aircraft gas turbine sources. Such measurements are challenging due to the high temperature (up to 750ºC) and pressure conditions in the turbine exhaust. A state-of-the-art sampling system shown in Figure 1 was installed at the engine test cell at SR Technics, Zurich Kloten.

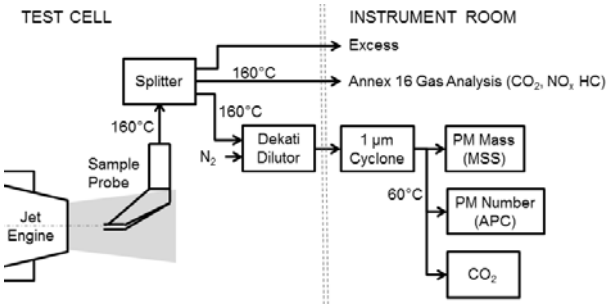

Figure 1. Simplified schematic of the aircraft gas turbine PM mass sampling system installed at SR Technics

PM laden exhaust was continuously sampled by an Inconel sampling probe at the engine exit plane. The aerosol sampled was then diluted with dry nitrogen by a factor of eight to ten and transported via temperature controlled lines to minimize condensation, particle agglomeration, and gas-to-particle conversion. Non-volatile PM mass was determined with a micro soot sensor (MSS, Model 483, AVL Inc.) based on the photo acoustic detection principle. In parallel to the MSS, an AVL particle counter (APC) and a CO_2 analyzer (Model 410i, Thermo Inc.) provided PM number and CO_2 concentrations emitted. The emitted CO_2 concentration was used in the PM mass emission index calculation according to Lobo *et al.* (2007).

The aircraft gas turbines tested to date include a CFM International 56-5B4/2P engine for the dedicated tests and a CFM International 56-7B24/3 and a Pratt and Whitney 4168A engine for piggy-back tests. Dedicated tests consisted of a series of engine thrust conditions defined by the turbine inlet temperature and rotational speed.

Preliminary results of the sampled PM mass concentration and engine thrust of a dedicated CFM 56-5B4/2P engine test are provided in Figure 2.

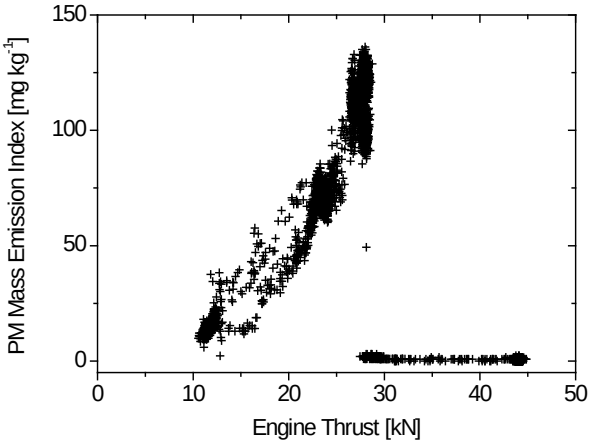

Figure 2. Measured PM mass emission index vs. engine thrust of a CFM 56-5B4/2P engine

Figure 2 indicates that the PM mass emission index increases for thrust levels up to 28 kN. Above 28 kN thrust, a sudden drop in emissions to an index near the detection limit of the instrumentation (< 5 mg kg^{-1}) is observable. This phenomenon is explained by the staged double annular combustor of the CFM 56-5B4/2P. This type of combustor is unique with respect to PM emissions: at low powers, only a pilot combustor zone is fuelled with a rich fuel mix to ensure combustion stability, resulting in high PM emissions; at high powers both the pilot and main combustor zones are fuelled with a lean combustor mix which results in low PM emissions.

Besides the determination of emission indices for various models of engines, current work investigates the effects of variable environmental conditions such as humidity and temperature, so a robust dataset can be provided to policy makers and climate modelling communities.

This work is supported by the Swiss Federal Office of Civil Aviation (FOCA)

Lobo, P.; Hagen, D. E.; Whitefield, P. D.; Alofs, D. J. (2007), Physical characterization of aerosol emissions from a commercial gas turbine engine, *J. Propul. Power*, **23**, 919– 929

Dynamic Changes of the Aerosol Composition and Concentration During Different Burning Phases of Wood Combustion

M. Elsasser[1], C. Busch[1], J. Orasche[1], C. Schön[2], H. Hartmann[2], J. Schnelle-Kreis[1] and R. Zimmermann[1]

[1]Joint Mass Spectrometry Centre / Chair of Analytical Chemistry, University of Rostock, 18051 Rostock, Germany, Helmholtz Zentrum München, 85764 Neuherberg, Germany
[2]Technology and Support Centre in the Centre of Excellence for Renewable Resources (TFZ), 94315 Straubing, Germany

Keywords: wood combustion, emission, AMS, burning phases.
Presenting author email: michael.elsasser@helmholtz-muenchen.de

Wood combustion is an important contributor to the ambient aerosol, especially during the wintertime. (Elsasser *et al*., 2012). However, its contribution to the ambient pollution might be underestimated since emissions often have been approximated as a constant emission disregarding any compositional changes in the burning process.

Different on-line mass spectrometry-based methods with a high-time resolution were applied to investigate changes in the composition of the aerosol gas-phase and particle-phase during wood combustion. The experiments were carried out with a logwood boiler and a logwood stove at the Technology and Support Centre (TFZ) in Straubing, Germany. Different fuel types (spruce and beech) and burning conditions (normal, overloaded feed, oxygen-deficiency) were investigated. A Photo Ionisation (PI) Time-of-Flight Mass Spectrometer (ToF-MS) was applied for selective detection of aromatic organic compounds in the gas phase by Resonance Enhanced Multi Photon Ionisation (REMPI, Heger *et al.*, 1999). The aerosol particle phase of the non-refractory compounds was analysed by a High Resolution Time-of-Flight Aerosol Mass Spectrometer (HR-ToF-AMS, Aerodyne Research Inc., DeCarlo *et al*., 2006). Together with FTIR measurement of the gas phase a comprehensive characterisation of the dynamic of wood combustion was achieved.

This dynamic could be described in four different burning phases, during which the aerosol compounds and concentration changed significantly. The novel approach of this study is to separate and categorize the phases of a whole batch based on observed chemical changes in the gas phase. For the first time positive matrix factorisation (PMF) was applied to separate different emission pattern from wood combustion.

The observation of the four different burning phases showed for example for the first phase (ignition phase), which was linked to the guaiacol signal, the highest concentrations of organic mass (figure 1). The following "harsh combustion phase", which was linked to the naphthalene signal, showed a maximum of the relative amount of the "wood combustion marker" signal at mass-to charge-ratio (m/z) 60. Additionally, the inorganic compounds like sulphate and chloride had their maxima during this second phase and the following "stable combustion phase". The start of the char burnout was indicated by an increase of the carbon monoxide concentration in the gas phase. The organic mass was the main contributor to the total non-refractory mass in all the phases; however it decreased from 99% to 80% in the subsequent phases. This study demonstrates an overview of the impact of the dynamic phases of wood combustion on the composition and concentration of emitted aerosols. Additionally, it showed that burning conditions can significantly change the characteristics of emission. For example, an overloaded stove experiment showed a four-fold higher particle mass emission of non-refractory compounds (figure 1, below).

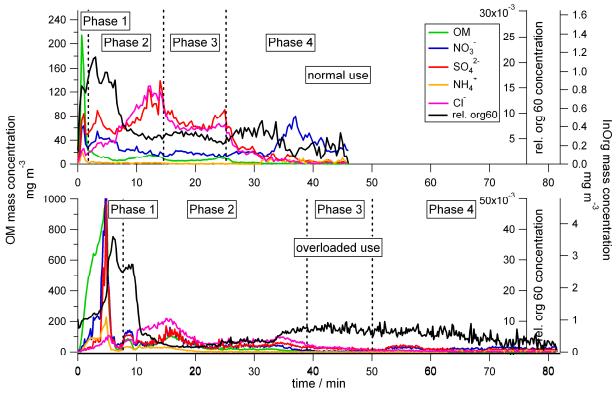

Figure 1. Variation with time of non-refractory aerosol components concentrations measured by AMS from a logwood stove experiment with beech: (top) wood under normal combustion conditions and (below) an overloaded stove experiment.

This work was supported by the Helmholtz Virtual Institute of Complex Molecular Systems in Environmental Health (HICE) and the Technology and Support Centre, Straubing, Germany.

Elsasser, M., Crippa, M., Orasche, J., DeCarlo, P.F., Oster, M., Pitz, M., Cyrys, J., Gustafson, T., Pettersson, J.B.C., Schnelle-Kreis, J., Prévôt, A.S.H. and Zimmermann, R. (2012) *Atmos. Chem. Phys.* **12**, 6113-6128.

Heger H. J., Zimmermann, R., Dorfner, R., Beckmann, M., Griebel, H., Kettrup, A., and Boesl, U. (1999) *Anal. Chem.* **71**, 46-57.

DeCarlo, P. F., Kimmel, J. R., Trimborn, A., Northway, M. J., Jayne, J. T., Aiken, A. C., Gonin, M., Fuhrer, K., Horvath, T., Docherty, K., Worsnop, D. R., and Jimenez, J. L. (2006) *Anal. Chem.* **78**, 8281–8289, 2006.

PM_{10} chemical composition in at street canyon and urban locations in London, UK

David C Green and Anja H Tremper
MRC HPA Centre for Environment and Health, King's College London, London, SE1 9NH, UK
Keywords: metals, PM_{10}, non-exhaust emissions
Presenting author email: david.c.green@kcl.ac.uk

Introduction

Concentrations of a number of elements have been used as tracers for non-combustion sources of PM in London[1]. By 2020 non-combustion sources are predicted to rise to 80-90% of vehicle emissions[2], are highly uncertain and despite being predominantly found in the coarse fraction, have been associated with health end points[3]. Previous studies have been campaign based, however this study quantifies the concentrations of these elements at a background and a street canyon location over a 12 month period.

Methods

PM_{10} samples were collected every 24 hours onto mixed cellulose esters filters using Partisol samplers. This was undertaken at urban background (North Kensington) and street canyon (Marylebone Road) locations between Jan 11 and Jan 12. The samples were digested using hydrofluoric acid and analysed using ICP-MS for a range of elements (Al, Ba, Ca, Cr, Cu, Fe, Mg, Mn, Mo, Na, Ni, Pb, Sb, Sr, Ti, V and Zn). A traffic increment was calculated as the difference between the contemporaneous daily measurement from North Kensington and Marylebone Road.

Results and discussion

Mean concentrations ranged over three orders of mangnitude; Fe was the most abundant element measured, 430 ngm^{-3} at the background site and a traffic increment of 1720 ngm^{-3} while Ni was the least abundant 1.3 ngm^{-3} at the background site and a traffic increment of 1.7 ngm^{-3}. The relative abundance of each element is shown in Figure 1. Elements can be grouped into broad source categories based on the concentrations measured at the two sites and what is known about their origins.

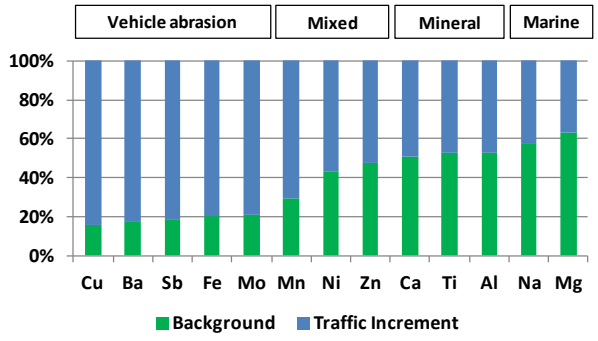

Figure 1: Relative abundance of selected elements in background and traffic increment

The correlations between NO_X and the elements associated with vehicle abrasion emissions (Ba, Cu, Fe, Sb, Mo) is shown in Table 1 for both the background site and in the traffic increment; this demonstrates the traffic related source of these elements.

Table 1: Correlation of vehicle abrasion elements with NO_X ; background in green, traffic increment in blue

	NO_X	Ba	Cu	Fe	Sb	Mo
NO_X		0.81	0.81	0.80	0.81	0.80
Ba	0.75		0.96	0.92	0.97	0.94
Cu	0.82	0.88		0.92	0.96	0.93
Fe	0.87	0.81	0.84		0.91	0.89
Sb	0.78	0.88	0.83	0.80		0.94
Mo	0.91	0.81	0.85	0.95	0.82	

Many of the elements, such as those which are predominantly mineral in origin (Al, Ca, Ti) have regional, as well as local sources. The local sources are highly dependent on wind speed and direction. The bivariate polar plot in Figure 2 demonstrates the wind direction and wind speed dependence of the Al and Ca traffic increment concentrations

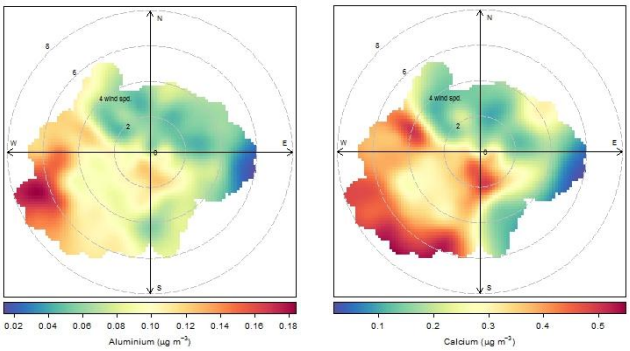

Figure 2: Bivariate polar plot of Al traffic increment concentration.

Together with the additional chemical characterization measurements made at these sites, this dataset will allow a detailed examination of the sources and processes governing the non-exhaust PM concentrations measured at these sites.

References

1. Harrison, R.M. et al (2012) Estimation of the Contributions of Brake Dust, Tire Wear, and Resuspension to Non-exhaust Traffic Particles Derived from Atmospheric Measurements. ES&T. DOI: 10.1021/es300894r

2. Rexeis M. et al. Trend of vehicle emission levels until 2020 – Prognosis based on current vehicle measurements and future emission legislation. Atmos. Env. 2009, 43, 4689-4698.

3. Malig, B.J.et al. Coarse particles and mortality: evidence from a multi-city study in California. OEM 2009;66:832-839.

Particles in road and railroad tunnel air - properties, sources and abatement possibilities

M. Gustafsson[1], S. Abbasi[2], G. Blomqvist[1], A. Gudmundsson[3], S. Janhäll[1], C. Johansson[4,5], M. Norman[5], U. Olofsson[2], B. Sjövall[5], H. Wilhelmsson[1]

[1]VTI - Swedish National Road and Transport Research Institute, Linköping, SE 581 95, Sweden
[2]KTH Machine Design, SE 100 44, Stockholm, Sweden
[3]Division of Ergonomics and Aerosol Technology, Lund University, SE 221 00, Lund, Sweden
[4]Department of Applied Environmental Science, Stockholm University, SE 106 91, Stockholm, Sweden
[5]Stockholm Environment and Health Administration, SLB-analys, SE 104 20, Stockholm, Sweden

Keywords: particle, tunnel, road, railroad
Presenting author email: mats.gustafsson@vti.se

Particulate air pollution in road tunnels is often very high due to high emissions and restricted air exchange (e.g. Gëller *et al.*, 2005). Also subway and railroad subterranean environments have been shown to suffer from high particle concentrations (e.g. Gustafsson *et al.*, 2012). The particle sources differ substantially, though. Road traffic particles have both exhaust and non-exhaust sources such as tires, pavement and brakes, while non-exhaust sources totally dominate the rail road particle emissions (e.g. Abbasi *et al.*, 2011).

In an on-going research project, airborne particles in a railroad and a road tunnel are characterized regarding concentrations, size distributions and elemental composition in relation to traffic. The aim is to characterise and identify the main particle sources to be able to suggest abatement measures regarding material and system use as well as measures regarding traffic.

Particle properties were studied during campaigns on the platform of Arlanda Central station (railroad tunnel below Arlanda airport, Stockholm) and in the Söderledstunneln (road tunnel in central Stockholm). At Arlanda C, a new photo cell based system for detecting train arrivals, their deceleration and length was used (Figure 1).

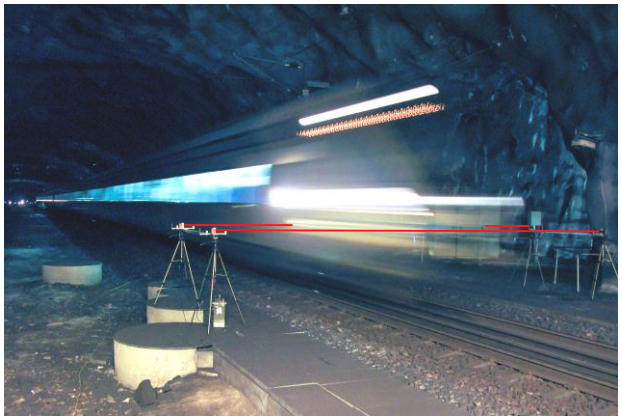

Figure 1. Train detection system at Arlanda Central (red beams illustrating infrared light).

From the measurements at Arlanda C it is clear that certain train types and/or train individuals affect mass and number concentration of particles very differently. While some trains do not seem to contribute to increased concentrations, others result in mass concentration increases and some also to obvious particle number concentration increases, without NO_x concentrations rising (no exhaust contribution) (Figure 2). Previous studies show that the main sources for railroad particles are wear of brakes, wheels and rail and are as such rather coarse (> 0.5 µm). The source(s) of the ultrafine mode (approx. 20 nm) contributing to high particle number are therefore of special interest.

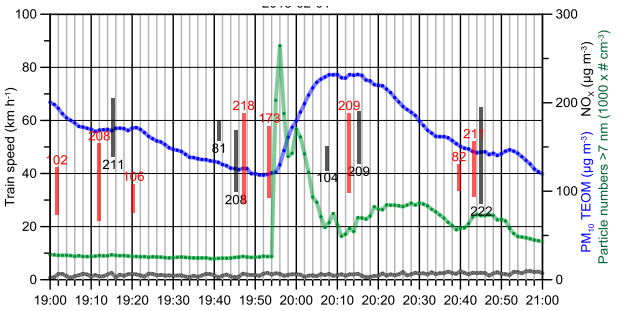

Figure 2. PM_{10} (blue), particle number (green), NO_x (grey), and trains (red = southbound, black = northbound) during two hours on 1st of February, 2013. Note the particle concentration response of the 173 m long train at 19:54.

In Janhäll *et al.* (these proceedings) data from the road tunnel study is presented. Further work will describe differences between road and railroad tunnel particle emissions, size resolved particle composition, source apportionment and abatement strategies.

This work was supported by the BVFF; a research program financed by the Swedish Transport Administration, The Royal Institute of Technology, KTH, and the Swedish National Road and Transport Research Institute, VTI.

Abbasi, S., Wahlström, J., Olander, L., Larsson, C., Olofsson, U. and Sellgren, U. (2011). *Wear*; **273**: 93-99.

Gëller, M.D., Sardar, S.B., Phuleria, H., Fine, P.M. and Sioutas, C. (2005) *Environmental Science and Technology*; **39**: 8653-8663.

Gustafsson, M., Blomqvist, G., Swietlicki, E., Dahl, A. and Gudmundsson, A. (2012). *Transportation Research Part D: Transport and Environment*; **17**: 277-285.

Study on design optimization of HI-FILTER SYSTEM by using CFD

Youn Suk Kang[1, 2], Hye Mi Lim[1], Cheol-Gyu Lee[1], Du-Hun Jang[1]

[1]Research Centre, J -E Tech. Co., Ltd., Ansan-si, Gyeonggi-do, 426-901, Republic of Korea
[2]Department of Environmental Energy Systems Engineering, Kyonggi University, Seoul, 120-702, Republic of Korea
Keywords: Filter Bag, Electrostatic Precipitator, HI-FILTER, CFD, fine dust, Guide Vane
Presenting author email: hansoltanpi@nate.com

Among existing dust removal technologies, dust collector of filter bag is the most efficient one. But, it needs to be replaced filter bag periodically so, the maintenance cost is excessive, also problem such as the increase of operational costs occurs as air pulsing cycle becomes short.

In order to solve this problem, by reducing the dust load that inflows to dust collector of filter bag, so the pressure loss stays low, and the number of cleaning and intensity should be reduced. So, by combining an electrostatic precipitator with filter bag into one-equipment, study on the development of HI-FILTER system which minimizes the problems such as the emission of fine dust and reattachment of dust secession from filter bag, short replacement cycle of filter bag etc. and its characteristics are conducted.

In order to review the problem of pressure loss which can happen in dust collector of HI-FILTER, by using computing fluid analysis, this study examined the structure of gas inflow distributor.

Gas distributor which deals the gas flowing in the dust collector generally uses a fixed size plate. However, according to this study, if the perforated plates are used to deal the gas that flows in through the duct with 90° in the sub, there is a tendency of the air leaning to one side, so we could confirm that high pressure down happened. In order to disperse this biased flow as evenly as possible, we assumed 2 forms: one is a perforated plate structure with many holes of reduced upper size and enlarged lower opening port, the other is the duct with guide vane and then we performed CFD. We confirmed that remodelled perforated plate could improve biased gas a little but the pressure loss was still strong. Yet, in guide vane (case4), we could solve the problems of biased gas flow and pressure down. (See the Table 1. and Figure 1.)

Table 1. Pressure drop according to gas distribution plate structure.

NO.	Models.	Inlet (m^3/min)	Pressure Loss (mmH_2O)
1	Case1	1,100	41.6
2	Case1	1,000	41.4
3	Case2	1,100	41.0
4	Case3	1,100	39.8
5	Case3	1,000	32.9
6	Case4	1,000	31.8

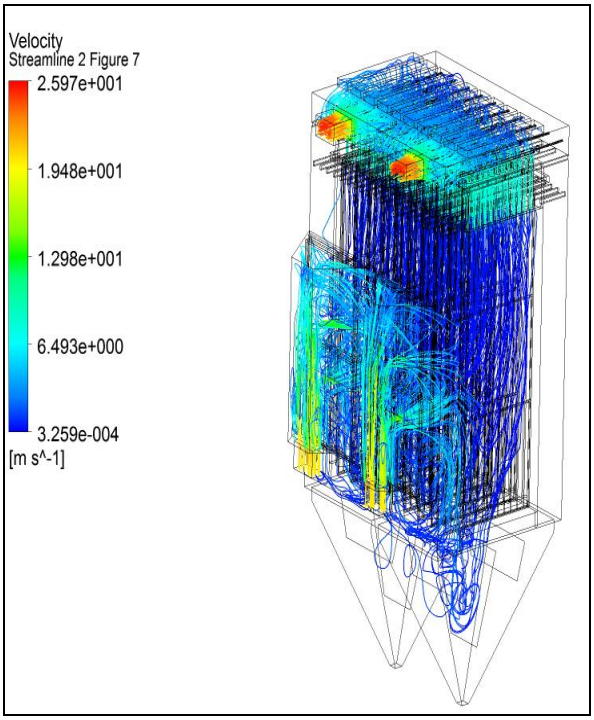

Figure 1. Velocity streamline of Case 4.
(Inlet air: 1000 Sm^3/min, without filter)

This subject is supported by Korea Ministry of Environmental as “The Eco-Innovation Project”.

Fluent Inc., FLUENT v6.1 User`s Guide.
Brian J. Dumont, et al. (2001) *8th Int. Conf. on Electrostatic Precipitation.*
Jin Uk Lee, et al. (2003) *1st CAE Conf.*, Electrostatic Precipitation Simulation Test.

PM trends, chemical composition and source apportionment of particulate matter in Mediterranean countries: Results from the Med-Particles project

A. Karanasiou [1,2] X. Querol [2] A. Alastuey [2] C. Perrino[3] J. de la Rosa [4], G. Berti[5], B. Artiñano[6], J. Sunyer[1] F. Forastiere[7] M. Stafoggia[7], the Med-Particles Study Group

[1] Centre for Research in Environmental Epidemiology (CREAL), Barcelona, Spain
[2] Institute of Environmental Assessment and Water Research (IDAEA-CSIC), Barcelona, Spain
[3] C.N.R. Institute of Atmospheric Pollution Research, Rome, Italy
[4] University of Huelva, Spain
[5] Regional Protection Environmental Agency, Piedmont Region, Turin, Italy
[6] Environment Department, CIEMAT, Madrid, Spain
[7] Department of Epidemiology, Lazio Region Health Service, Rome, Italy

Keywords: PM, chemical composition, source apportionment, emission sources
Presenting author email: angeliki.karanasiou@idaea.csic.es

The Mediterranean Basin, (MB) is characterised an air pollution hotspot, located at a crossroad of air masses coming from Europe, Asia and Africa (Lelieveld et al., 2002). Pollution in the area results from traffic and industrial sources and domestic heating. Dust storms coming mainly from the Sahara desert and to a lesser extent from the Middle East, transport high quantities of mineral aerosols increasing significantly the levels of particulate matter (Pey et al., 2013). Forest fires and agricultural burning emissions are also affecting the area. Moreover, marine aerosols and ship emissions are considered to be an important contributor to the MB aerosol burden. The large variety of aerosol sources coupled with the complex orography and atmospheric dynamics gives rise to a complex mixture of gaseous and particulate matter (PM) pollutants that merits further investigation.

In the framework of the Med-Particles project http://www.epidemiologia.lazio.it/medparticles/index.php/en/). Ambient concentrations of $PM_{2.5}$, PM_{10}, gaseous pollutants and also chemical components were collected from traffic and urban background sites in MB countries: Spain (Barcelona, Madrid, Huelva), France (Marseille), Italy (Rome, Turin, Bologna, Milan) and Greece (Athens, Thessaloniki) for the period 2001-2010. The objective of Med-Particles is to investigate the health effects of long-term exposure to ambient air pollution in the Mediterranean Basin. Specific emission sources will be investigated in order to assess the health effects in the MB and point out any differences between North and South Europe.

Firstly the air quality of the MB and the pollution sources were investigated. The long-term trends of PM_{10} and $PM_{2.5}$ show a decreasing trend for all the traffic sites in the MB despite the important variability of the concentration values, Figure 1 (Carslaw and Ropkins 2011). This decreasing trend could be attributed to the effectiveness of the vehicular emission control strategies that have been implemented in Europe and the improvement in motor engine characteristics. Again the role of economic crisis in the region should be taken into account as traffic intensity has been reduced due to the increase of fuel price.

Source apportionment by PMF provided 6 common sources for $PM_{2.5}$ and PM_{10}, namely, local dust, secondary aerosol, mobile source, biomass burning, coal combustion, and minor industrial emission. Among these sources, the mineral source (road dust and soil) is the major contributor to PM_{10}, up to 40% of its mass concentration, while for fine particles traffic and secondary aerosol are the main sources contributing 25% and 30% correspondingly to the $PM_{2.5}$ mass concentrations. Regarding the background sites, crustal particles are the dominant constituent.

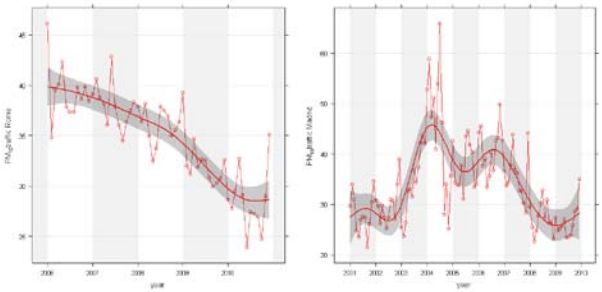

Figure 1. PM_{10} trend analysis in representative traffic sites in Rome and Madrid

This work was supported by the European Community (LIFE + Environment Policy and Governance, LIFE10 ENV/IT/327)

Carslaw, D., Ropkins, K., 2011. Openair: Open-source tools for the analysis of air pollution data. Available at: http://www.openair-project.org.

Lelieveld J., Berresheim H., Borrmann S., Crutzen P.J. et al., 2002, *Science* Vol 298, pp 794–799

Pey, J., Querol, X., Alastuey, A., Forastiere, F., Stafoggia, M., 2013, *Atmos. Chem. Phys.* Vol 13(3), pp. 1395-1410

Overview of the AIRUSE project: Testing and Development of air quality mitigation measures in Southern Europe

A. Karanasiou[1], F. Amato[1], T. Moreno[1], A. Alastuey[1], M. Viana[1], F. Lucarelli[2], S. Nava[2], G. Calzolai[2], C. Pio[3], C. Alves[3], T. Nunes[3], K. Eleftheriadis[4], E. Diapouli[4], V. Vasilatou[4], E. Monfort[5], I. Celades Lopez[5], R.M. Harrison[6], D. Beddows[6] and X. Querol[1]

[1]Institute of Environmental Assessment and Water Research (IDAEA-CSIC), Barcelona, Spain
[2]Department of Physics and Astronomy and INFN, University of Florence, Sesto Fiorentino, 50019, Florence, Italy
[3]Centre for Environmental and Marine Studies (CESAM), Department of Environment, University of Aveiro, 3810-193 Aveiro, Portugal
[4]ERL, Institute of Nuclear and Radiological Science & Technology, Energy & Safety, NCSR Demokritos 15310, Attiki, Greece
[5]Asociacion de Investigacion de las industrias Ceramicas, Instituto de Tecnologia Ceramica, Campus Riu Sec, Castellon, Spain
[6]Division of Environmental Health & Risk Management, University of Birmingham, Edgbaston, Birmingham B15 2TT, United Kingdom

Keywords: mitigation measures, particulatte matter, emission sources, air quality
Presenting author email: angeliki.karanasiou@idaea.csic.es

Air pollution due to particulate matter (PM) is a multi-effect problem with detrimental consequences for human health and the environment. The current policy efforts, at EU and national level, have not fully delivered the expected results. Many urban areas especially in Southern Europe do not meet the air quality standards (2008/50/EC Directive). The AIRUSE project aims to test existing and future mitigation measures and develop new strategies for the improvement of air quality in Southern European countries (www.airuse.eu). The project involves public and private institutions of Spain, UK, Portugal, Italy and Greece.

Typical anthropogenic source contributions in PM, widely affecting European urban air quality are: road transport, biomass burning and industrial emissions. In Mediterranean cities there is an important contribution of urban dust from deposited dust arising from brake, tyre and road abrasion, construction/demolition, diffuse industrial emissions, and soil dust resuspension (Karanasiou et al., 2011and 2009; Amato et al., 2009). Other specific features of Southern European cities are: high population and car density, low vegetation cover, high levels of urban ammonia (giving rise to high fine PM levels), high photochemical activity, and elevated shipping emissions. Based on the above, measures to reduce ambient PM concentrations and protect human health in Southern European cities require a different approach from those measures applied in central Europe.

AIRUSE will firstly harmonize PM monitoring and modelling methods to determine the contribution of air pollution sources in Spain, Portugal, Italy and Greece. Four urban areas have been selected for this purpose: Barcelona (Spain), Athens (Greece), Porto (Portugal), Florence (Italy).

The measures to be tested and developed during the lifetime of the project AIRUSE are:

1. Use of Calcium Magnesium Acetate (CMA) solution, $MgCl_2$ and $CaCl_2$ as dust suppressants given their binding properties for particles deposited on roads.
2. Road wetting/moistening to reduce road dust resuspension from urban paved roads. Road wetting will be tested at different rates and frequencies in order to estimate the best cost-benefit approach.
3. The optimization of solid fuel combustion for domestic heating by introduction of continuously controlled conditions (automatic fuel feeding, distribution of combustion air) and modification of the fuels granulation. The use of catalytic converters or filter technologies.
4. Best available techniques for industries that exceed the threshold limit values in the AIRUSE implementation area

AIRUSE aims to:

• Support Southern Europe member states in implementing the Directive 2008/50/EC
• Improve existing air mitigation measures
• Recommend new measures for the improvement of air quality, based on innovative approaches
• Supply the decision makers in Southern Europe member states with a valuable tool for environmental planning
• Stimulate the allocation of European funds for the implementation of new mitigation strategies

Aknowledgements

This work was supported by the European Community (LIFE + Environment Policy and Governance, LIFE11 ENV/ES/584)

Amato, F., Pandolfi, M., Escrig, A., Querol, X., Alastuey, A., Pey, J., Perez, N., Hopke, P.K. 2009, *Atmos. Environ.*, Vol 43(17), pp. 2770-2780

Karanasiou A., Moreno T., Amato F., Tobías A., Boldo E., Linares C., Lumbreras J., Borge R., Alastuey A., Querol X., 2012, *Atmos. Environ.* Vol 54, pp 465-469

Karanasiou A.A., Siskos P.A, Eleftheriadis K., 2009, *Atmos. Environ*, Vol 43, pp 3385-3395

Particle size distributions of combustion aerosol of various local fuel mixtures

E. Krugly[1], E. Puida[2], K. Buinevičius[2], L. Kliučininkas[1], I. Stasiulaitienė[1], A. Minikauskas[1] and D. Martuzevičius[1]

[1] Department of Environmental Engineering, Kaunas University of Technology, Kaunas, LT-50254, Lithuania
[2] Department of Thermal and Nuclear Energy, Kaunas University of Technology, Kaunas, LT-44312, Lithuania
Keywords: Fuel combustion, aerosol, PSD.
Presenting author email: edvinas.krugly@ktu.lt

Introduction

Biomass is increasingly popular fuel for individual and district heating boilers in Lithuania. Consumption of this type of fuel grows constantly due to rising prices of fossil fuels. Use of biomass as a local and "clean fuel" in individual heating boiler and in municipal central heating system boilers is supported by the state.

Despite of its near-zero carbon balance, the combustion of biomass can be significant source of fine aerosol particles, VOC, PAH and other products of incomplete combustion that has negative effect on human health.

Aim of this study was to investigate emissions of aerosol particles and gaseous pollutants generated during combustion of local biomass fuels and their mixtures, including wood pellets, sunflower shell pellets, straw pellets, municipal waste water treatment sludge and others in small scale heating boilers.

Methods

The laboratory fuel combustion experiments were conducted in a small scale (13 kW) grate-type heating boiler. During experiment the following types of fuel were used: wood pallets (humidity content - 7.1 %, ash content - 0.42 %, calorific value – 16907 kJ/kg), straw pellets (12.3 %, 6.1 %, 14133 kJ/kg), rapeseed and other grain waste, sunflower shell pellets, dried wastewater sludge, as well as mixtures of these fuels. The laboratory heating boiler was equipped with controlled fuel supply, removal of ash, air supply, and water circulation. The supply of fuels was kept in a range of 2.5-3.5 kg/h. Flue gas temperature and velocity was measured using temperature and velocity probes. Samples of aerosol and gaseous pollutants were taken through sampling ports in the exhaust tube.

Aerosol PSDs were measured using ELPI+ with double injector dilution system (Dekati Ltd., Finland) with dilution ratio of ~50. Gaseous pollutants were measured using flue-gas analyzer IMR2000 (Environmental Equipment Inc., USA). Measurements of pollutant emissions were conducted during stable and optimal regime of combustion process.

Results

As expected, various fuels exhibited different emission patterns based on their chemical composition. Figures 1 and 2 present PSDs of aerosols obtained the combustion of wood pallets (Fig. 1) and a mixture of wood pellets and wastewater sludge (humidity content - 5 %, ash content - 38 %, calorific value – 11107 kJ/kg, Fig. 2). According to number concentration, PSD obtained from wood pallets a clear mode was observed at 0.154 μm, ($1.59 \cdot 10^8$ #/cm^3). In case of the calculated volume concentration, the PSD was bimodal (0.26 μm, $1.05 \cdot 10^4$ μm^3/cm^3; 9.88 μm, $6.8 \cdot 10^4$μm^3/cm^3). Number concentration PSD obtained from mixture fuel burning was clearly bimodal (0.0272 μm, $428 \cdot 10^5$ #/cm^3; 0.154 μm, $960 \cdot 10^5$ #/cm^3), as well as volume PSD (0.0545 μm, $6.38 \cdot 10^2$ μm^3/cm^3; 9.88 μm, $5.0 \cdot 10^6$ μm^3/cm^3).

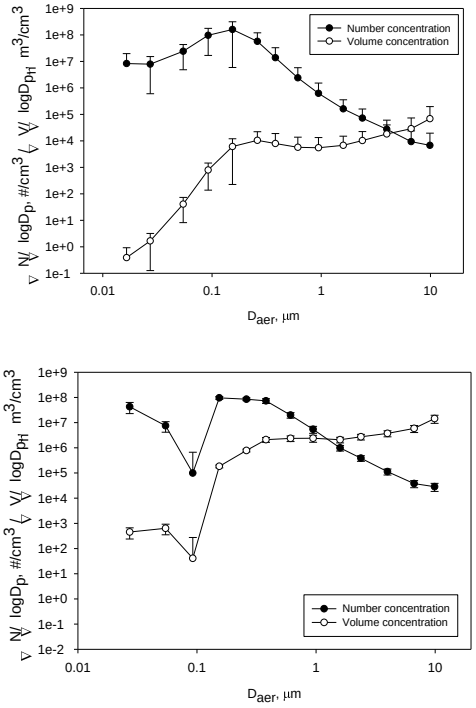

Figure 1. Number and volume concentration PSDs of aerosol particles emitted during combustion of a) wood pellet, b) mixture of 50% wood pellets and 50% wastewater sludge

The following concentrations of gaseous compounds were registered for the above cases: wood pellets: O_2 – 11.4±1.1%, CO – 121±22 mg/m^3, CO_2 – 9.3±2.5 %, NO - 171±24.3 mg/m^3, NO_x - 38±4.6mg/m^3, SO_2 - 270±26.4 mg/m^3; wood pallets and wastewater sludge mixture: O_2 – 12.5±1.3%, CO – 994±92 mg/m^3, CO_2 – 8.2±2.7 %, NO - 521±44.7 mg/m^3, NO_x - 832±37.9 mg/m^3, SO_2 - 1477±166.1 mg/m^3.

The results provide valuable information on the evaluation of environmental impact of the combustion of the researched fuels as well as data on optimization of combustion processes.

This work was supported by Research Council of Lithuania under grant "Pollution Control in Biomass Combustion: from Pollutant Formation to Human Exposure" (BioMassPoll), project No. ATE05/2012.

Analysis of intrapersonal variance of hourly PM exposures

P. Lipponen[1],O. Hänninen[1], J. Kolomazníková[2] and M. Braniš[2]

[1]National Institute for Health and Welfare (THL), Department of Environmental Health, Kuopio, P.O. Box 95, Finland
[2] Charles University in Prague, Faculty of Science, Institute for Environmental Studies, Albertov 6, 128 43 Prague 2, Czech Republic

Keywords: PM, personal exposure, intra and inter personal variance components.

Presenting author email: pasi.lipponen@thl.fi

Table 1. Statistics for predicting personal exposures using fixed station data from Riogrovy sady school.

Data statistics	$PM_{2.5}$ Exposure		Fixed	Model - all		Model - filtered		Model statistics		
	E1h	E1hf	site PM_{10}	PredE	ResidE	PredE	ResidE	Statistic	All	Filtered
mean (µg m^{-3})	54.9	37.3	26.9	53.3	1.6	37.0	17.8	**R**	0.139	0.557
sd (µg m^{-3})	175.4	29.1	18.5	21.3	174.1	15.5	174.2	**R2**	0.019	0.311
min (µg m^{-3})	1.3	1.3	0.0	20.8	-150.6	13.5	-104.3	**ß0**	19.6	12.6
max (µg m^{-3})	5453.3	174.6	142.0	195.6	5422.5	140.5	5432.6	**ß1**	1.2	0.9
count	5270	5150	4632	5270	5270	5270	5270	**n**	5270	5169

E1h: hourly personal exposure, E1hf: E1h filtered for high-end outliers, FSM : fixed site monitoring (PM_{10})

Long-term exposures to air pollution, especially particulate matter (PM), have been shown to be significant determinants of cardiovascular events and potentially associated with the onset of the development of corresponding diseases. Personal exposure studies have clearly shown that especially for short-term exposures the ambient measurements are poor predictors. For long-term exposures this relationship is not known, as direct measurements of long-term exposures is not possible for practical reasons.

The current work uses a 1-year time series of personal $PM_{2.5}$ exposures of a one individual to estimate the relationship of the personal and ambient air variance components according to equation 1:

Eq 1. $$\sigma_{Tot}^2 = \sigma_P^2 + \sigma_A^2$$

Personal $PM_{2.5.}$ mass concentrations were collected by non-smoking female adult by using a portable, real-time photometric aerosol monitor (TSI DustTrak 8520) from February 2006 to January 2007 (Branis *et al*. 2010). The monitor with rechargeable battery was carried by the person daily and in nighttime or during special activities, it was placed in her close vicinity. The sampling interval was set to 5 minutes. The equipment was switched off only during periods where measurements could not be made. The original 5-minute time series was transformed into 1-hour averages and combined with the corresponding fixed site PM_{10} measurements from the Riogrovy sady school, located South-East from the Prague Central Railway Station and approximately 1.5 km from the city center. Fixed site data extended from February to December in 2006.

Personal exposure levels peaked at 8.5 mg m^{-3} with maximum 1-hour average being over 5400 µg m^{-3}. When all data is included in the regression analysis, the fixed site data explains only 1.9% of the variance (Table 1), suggesting that the personal activities dominate exposure variability. However, when the extreme high exposures above 175 µg m^{-3} are filtered from the data as being related with high exposure events, the coefficient of determination of the regression model reaches 31%, suggesting that almost one third of intrapersonal exposure variance can be attributed to ambient air quality when excluding highest events. The remaining 69% of intrapersonal variance in this case is attributable to the personal behavior, including time-activity.

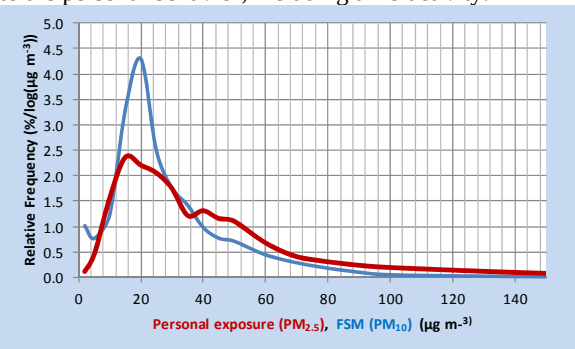

Figure 1. Probability distributions of $PM_{2.5}$ personal exposure levels and PM_{10} fixed site monitoring data.

The probability distribution of personal exposures exhibits a clearly multimodal shape (Figure 1), suggesting that microenvironments visited during the year can be divided into several domains and that division of time-use between these domains would be a significant predictor of the exposure variance and levels.

Acknowledgements. This work has been supported by Ministry of Education, Youth and Sports of the Czech Republic under Research Scheme No. NPVII 2B08077, Life+ -project EXPAH (Contract ENV/IT/000082; 2009), EU Contract FP7-ENV-2009-1-243406 (TRANSPHORM), and Academy of Finland Contract 133792 (PM Sizex).

Braniš, M. and Kolomazníková, J. (2010) *Atm. Env.* **44**, 2865 – 2872.

Real-time relationship between digital visibility and PM2.5 at the middle of Taiwan

C.-H. Luo[1*] and S. Yang[2]

[1]Department of Safety, Health and Environmental Engineering, Hungkuang University, Taichung, 43302, Taiwan (ROC)
[2]Center of General Education, Toko University, Chiayi, 61363, Taiwan (ROC)
Keywords: atmospheric visibility, air quality, PM2.5, digital image processing.
Presenting author email: andyluo@hk.edu.tw

Atmospheric clarity presents the visual quality of the atmospheric environment and has been quantitatively detected by several digital visibility indexes investigated by several image processors (Luo *et al* 2005, Luo *et al* 2011). Visibility impairment due to airborne submicro-sized aerosols has been studied over the past years. Real-time digital visibility and PM2.5 monitoring were investigated, and their relationship was analyzed at the middle of Taiwan in this study.

Atmospheric visibility was detected the Long Path Visibility Transmissometer (LPV-4, OPTEC, Inc., US) and the images of related landscape were recorded at the same time. The digital visibility was calculated by the image processor and presented by the image index (Figure 1).

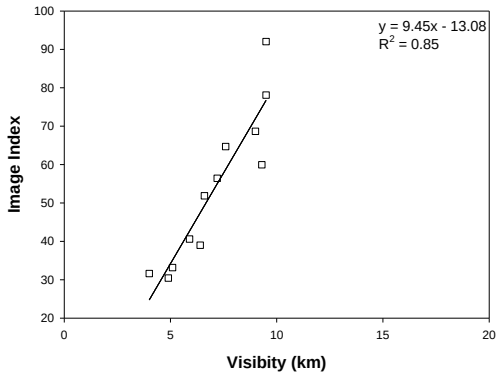

Figure 1. The linear relationship between the atmospheric and digital visibility values.

Figure 2 shows the images and the related digital index values. PM2.5 data was collected from the nearby monitoring station.

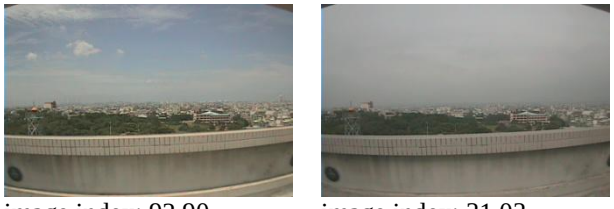

image index: 92.90 image index: 31.03

Figure 2. The atmospheric images and related digital image index values.

The coefficient of variation (CV) of the hourly level changes of digital visibility and PM2.5 concentration for two week measurements was normalized in the following equation.

$$CV = \frac{hourly\ \ value - mean\ \ value}{mean\ \ value}$$

Finally, sixth-order curve fitting function was used to analyze and build the relationship between digital visibility index and PM2.5 concentration in Figure 3. According to the results, the change of PM2.5 show a downward trend, but digital visibility value presents the change in the rising trend around 8:00. From 11:00 to 14:00, PM2.5 changed downwards, and digital visibility value showed the upward change. A time delay of change trends appeared and should be discussed more in depth.

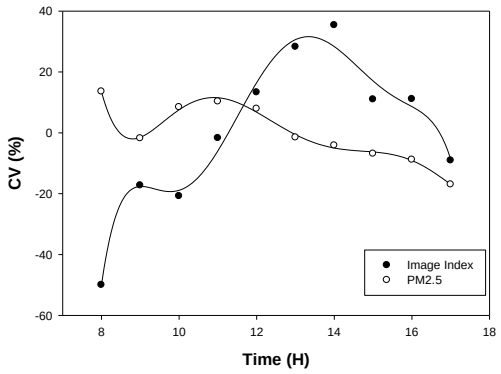

Figure 3. This is a comparison between digital image index and PM2.5 concentration.

This work was supported by the National Science Council of Taiwan under contract no. NSC 100-2628-E-241-001.

Luo, C.-H., Liaw, J.-J., Wen, C.-Y., Yuan, C.-S. and Lo, C.-C. (2005) *Atmos. Environ.* **39**, 2545-2552.

Luo, C.-H., Lin, K.-H., Wen C.-Y., Chiu S.-H., Yuan C.-S. and Yang S. (2011) *INT. J. REMOTE. SENS.* **32**, 9801-9810.

On the fine and the coarse fractions of atmospheric aerosol

M. Manigrasso[1], A. Febo[2] and P. Avino[1]

[1]INAIL Settore Ricerca, Certificazione e Verifica, via Urbana 167, 00184 Rome, Italy
[2]Istituto Inquinamento Atmosferico, Area della Ricerca del C.N.R. di Roma, 00016 Monterotondo Scalo, Italy
Keywords: fine particles, coarse particles, PM2.5, PM1.
Presenting author email: m.manigrasso@inail.it

The fine mode of PM is dominated by both primary anthropogenic pollution from combustion processes and gas-to-particle conversion, whereas the coarse mode is mainly related to wind erosion, mineral dust emission and long-range transport from desert areas (natural events). Pope et al (2002) observed that 10 µg m^{-3} increments of fine PM (PM2.5) were associated to increased risk of all-cause, cardiopulmonary and lung cancer mortality, respectively of about 4%, 6% and 8% in metropolitan areas in the United States. The same authors found that coarse particles were not consistently associated with mortality. Toxicological and epidemiological studies have established a link between the components associated to fine PM (PAHs, carbonaceous PM, metals) and adverse health effects. Then, it is crucial to know when fine PM measurements are affected by coarse natural sources.

To this purpose we analyzed a PM pollution event occurred on February 2009, characterized by a strong advection of Saharan dust. PM10, PM2.5 and PM1 measurements were performed in the northern periphery of Rome on January-February 2009, both as mass concentrations by β attenuation technique (SWAM 5a Dual Channel Monitor, FAI) and size resolved number concentrations (APS 3321, TSI). β-radioactivity of short-lived decay products of Radon was measured (PBL Mixing Monitor. FAI) to obtain information about the pollutant vertical mass transport in the Planetary Boundary Layer (PBL). PM10 and PM2.5 concentrations higher respectively than 250 and 100 µg m^{-3} were measured on February 3rd.

Figure 1 shows the temporal trends of 0.58, 1.03, 2.45, 4.06 µm size channels of an Aerodynamic Particle Sizer (APS) along with the trends of natural radioactivity. On February 02nd at 06 am the natural radioactivity suddenly dropped, coherently with the increased degree of atmospheric dilution, fine mode aerosol (represented by 0.58 µm size channel) dropped as well. In the next hours, radioactivity kept at low levels (high PBL mixing height), aerosol size fractions remained at low levels too for some hours and then started increasing, until February 03rd, when they reached maximum values. This occurrence can be explained only admitting that a higher atmospheric layer rich of coarse dust got mixed with surface aerosol, due to the increase of PBL mixing height. Although the one described is clearly a coarse event, it influenced to some extent also fine mode aerosol: to minor extent 0.58 µm and more significantly 1.03 µm size fraction. So, in the period considered we have observed a "coarse" source extending its contribution in what we generally call the "fine" region, below 1 µm, as clearly shown in Figure 2, where the aerosol mass size distribution is reported before and during the Saharan dust event.

PM2.5 can be completely misleading as indicator of fine mode aerosol. PM1 rather than PM2.5 should be preferred to represent anthropogenic pollution. It should be kept in mind that the separation between fine and coarse aerosol can be below 1 µm, so that also PM1 can be influenced by natural sources of coarse aerosol.

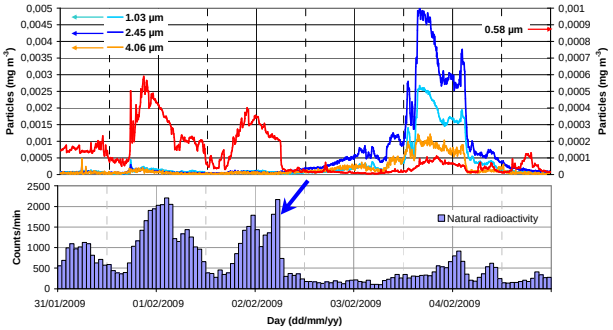

Figure 1. Daily trends of 0.58, 1.03, 2.45, 4.06 µm APS size fractions and of natural radioactivity in the period January 31st-February 04th, 2009.

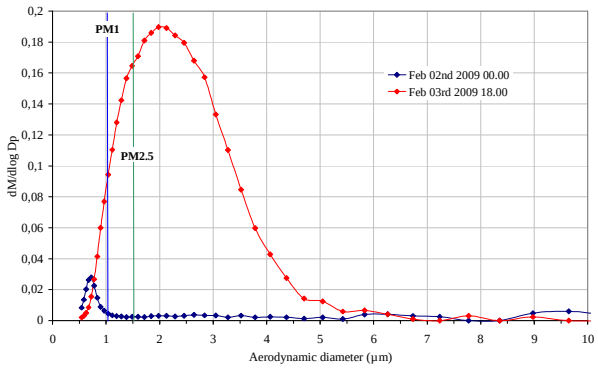

Figure 2. aerosol mass size distributions before (blue curve) and during (red curve) the Saharan dust episode.

This work was supported by INAIL under grants P20L09 and P20L01.

Avino, P., Brocco, D., Lepore, L. and Pareti, S. (2003) *Ann. Chim. (Rome)* **93**, 589-594.

Manigrasso, M., Febo, A., Guglielmi, F., Ciambottini, V. and Avino, P. (2012) *Env. Poll.* **170**, 43-51.

Pope, C.A., Burnett, R.T., Thun, M.J., Calle, E.E., Krewski, D., Ito, K. and Thurston, G.D. (2002) *JAMA* **287**, 1132-1141.

Nanoparticle contribution to elemental concentration in atmospheric particulate matter

S. Canepari[1,2], M.L. Astolfi[1], M. Marcoccia[1], D. Frasca[1] and C. Perrino[2]

[1]Department of Chemistry, Sapienza University of Rome, 00185, Italy
[2] CNR Institute of Atmospheric Pollution Research, Monterotondo St. (Rome), 00015, Italy

Keywords: nanoparticles, elemental concentration, aggregates, size distribution.
Presenting author email: melissa.marcoccia@libero.it

Several epidemiological studies suggest that health diseases due to the exposure to atmospheric particulate matter (PM) are mainly associated with the inhalation of particles able to penetrate deeply into the respiratory tree. Among these, particular attention has been recently paid to particles smaller than 100 nm in diameter (nanoparticles, NPs). Because of their peculiar morphology, chemical composition, minute size and high surface area NPs are very reactive towards their environment and able to penetrate living cells. Moreover, they are able to adsorb and carry heavy metals and other carcinogenic compounds.

Due to their high surface area, atmospheric NPs easily aggregate to form large clusters; when in contact with biological systems, however, clusters may disaggregate again releasing free NPs able to translocate across the respiratory epithelium and enter the lymphatic and the circulatory system. For this reason, the quantitative relevance of aggregated NP contribution to PM is of great importance in air quality and health studies.

Instruments measuring atmospheric NP concentration select incoming particles on the basis of their physical characteristics (optical diameter, electric mobility or aerodynamic diameter). When using these techniques, aggregated NPs are fatally neglected, as clusters physically behave as a single, wider particle (generally between 0.1 and 1 μm). Environmental studies would thus benefit from the availability of a chemical method able to evaluate the contribution of insoluble NP contained in aggregates to atmospheric PM.

We have developed a method able to fractionate the total elemental concentration in atmospheric PM into three contributes: the water-soluble fraction, the insoluble non-nanometric fraction and the fraction due to insoluble NPs, both individual and contained into larger clusters. The application of the method to size-segregated real atmospheric PM samples is described.

The method consists in the following procedure. PM samples are disperded in deionized water, exposed to ultrasounds and then filtered to separate the insoluble coarser particles from the suspended fraction, which contains elements both as suspended solid NPs and in water-soluble form. The insoluble fraction is subjected to microwave-assisted acid digestion and analysed by ICP-MS. The suspended fraction is divided into two aliquots: one is directly analysed by ICP-MS, the other one is injected into a chromatograph equipped with an anion exchange cartridge and then analysed by ICP-MS. NP contribution to the total elemental concentration is evaluated as the difference between the results obtained before and after the elution from the cartridge.

The application of the method to size-segragated atmospheric samples collected in the urban atmosphere of Rome, Italy, has highlighted three possible behavior of the analyzed elements.

For some elements, which show a dimensional distribution almost completely in the coarse range (e.g.: Na, Li, Mg, Ba, Mn, Sr), the ICP results obtained before and after passing the chromatographic pre-column agreed well, indicating that the suspended fraction contained only soluble species of these elements. A second group (e.g.: Rb, Tl, K) was mainly confined in the fine fraction; again, the ICP results obtained before and after the elution were in quite good agreement. These elements were thus contained in fine particles as soluble species, not retained by the chromatographic pre-column. A third group of elements (e.g.: Sb, Cd, V, As, Sn, Pb) also exhibited a relevant fine contribution, but the values obtained after the elution were markedly lower than those obtained from the direct analysis. All these elements are likely contained in a NP fraction that is analyzed by ICP-MS, as well as the soluble fraction, but is retained by the chromatographic pre-column. The latter behaviour is shown by most of the elements typically emitted from combustion sources, which are considered as the main responsible for NP emission in the atmosphere.

Although the proposed method needs a wider field application, these results are of environmental and toxicological relevance because the health and environmental effects of the elements identified in the NP fraction (As, Cd, Sb, V, Pb) could be considerably different from the effects caused by the same elements in soluble forms or contained in coarser particles (Cho et al., 2012; Mukhtar and Limbeck, 2013) Furthermore, this fractionation scheme may allow an increase of elemental selectivity as tracers of PM sources responsible for emission of inorganic NPs, as waste incineration.

Cho, W.S., Duffin, R., Thielbeer, F., Bradley, M., Megson, I.L., MacNee, W., Poland, C.A., Tran, C.L., Donaldson, K. (2012) *Toxicol. Sci*. **126**, 469–477.

Mukhtar, A., Limbeck, A. (2013) *Anal. Chim. Acta*, in press, doi:10.1016/j.aca.2013.02.008.

Primary aerosols from ship diesel engine exhaust within the framework of HICE measurement campaign

L. Mueller[1,2,3], G. Jakobi[1,3], M. Elsasser[1,2,3], B. Stengel[3,4], R. Rabe[3,4], O. Sippula[3,5], E. Karg[1,3], M. Sklorz[2,3], T. Streibel[2,3], J. G. Slowik[6], A.S.H Prevot[6], J. Schnelle-Kreis[1,3] and R. Zimmermann[1,2,3]

[1]Joint Mass Spectrometry Centre, Cooperation Group Comprehensive Molecular Analytics, Helmholtz Zentrum München, Ingolstädter Landstr. 1, 85764 Neuherberg, Germany
[2]Joint Mass Spectrometry Centre / Chair of Analytical Chemistry, University of Rostock, 18051 Rostock, Germany
[3]HICE –Helmholtz Virtual Institute of Complex Molecular Systems in Environmental Health – Aerosols and Health, www.hice-vi.eu
[4]Fakultät für Maschinenbau und Schiffstechnik Lehrstuhl für Kolbenmaschinen und Verbrennungsmotoren, Albert-Einstein-Str. 2, Universität Rostock, 18059 Rostock, Germany
[5]Department of Environmental Science, University of Eastern Finland, Kuopio, Finland
[6]Laboratory of Atmospheric Chemistry, Paul Scherrer Institute, 5232 Villigen, Switzerland
Keywords: ship, emission, non-refractory
Presenting author email: laarnie.mueller@helmholtz-muenchen.de

Particulate matter attributed to ship emissions has been correlated to adverse health effects worldwide (Corbett, 2007). Due to the complexity and limited knowledge on the composition of the emitted aerosols from ship emissions, it has been difficult to correlate their chemical components to toxic effects in humans. Thus, there is a need for a high-time resolution and high throughput of chemical information on the emissions from ships in order to identify the processes related to ship operation on the evolution of chemicals that may affect biological systems. In this study, the time-resolved chemical characteristics of primary emitted aerosols from a ship diesel engine were investigated using the High-Resolution Time-of-Flight Aerosol Mass Spectrometer (HR-TOF-AMS, Aerodyne Research Inc., DeCarlo *et al*., 2006).

A set of state-of-the art online instrumentation measuring gases, size distribution and chemical composition were used in conjunction with the cell exposure system (Air-Liquid-Interface) during the Helmholtz Virtual Institute of Complex Molecular Systems in Environmental Health (HICE) measurement campaign that took place in Rostock on November 19-30, 2012 to investigate the characteristics of the emitted primary aerosols and their effects on lung epithelial cells. In particular, the HR-TOF-AMS has been used to investigate the non-refractory components of the ship engine exhaust particles. Heavy Fuel Oil (HFO 180) and Destillate fuel (EN 590) were used as fuels in a one-cylinder ship diesel engine operated at different loads according to ISO 8187-4 E2 for emission testing.

Corresponding weighting factors were used to define the duration of each operation point resulting in a test cycle that is representative to sea operation. Higher loads (>50% of nominal output) represent a normal operation for ships sailing across the sea. Lower loads used in this study are typical for operation close to the coast or within harbours. This allows the investigation of the effects of engine loads at constant speed and fuel types to the emitted non-refractory aerosols. Fig. 1 shows the response of the AMS to the two types of fuels and engine loads. The 75% load represents “sailing” condition whereas the 25% denotes the “idling” operation. Organics and sulphate compounds were detected by the AMS in the HFO experiment whereas only organic compounds were detectable in the DF experiment. The evolution of non-refractory compounds differs between the HFO and DF with the engine operation. Elevated concentrations of organics were observed at 25% load in the HFO whereas the highest concentration was observed at 75% for DF.

High resolution data analysis and comparison with other online techniques will be shown in details.

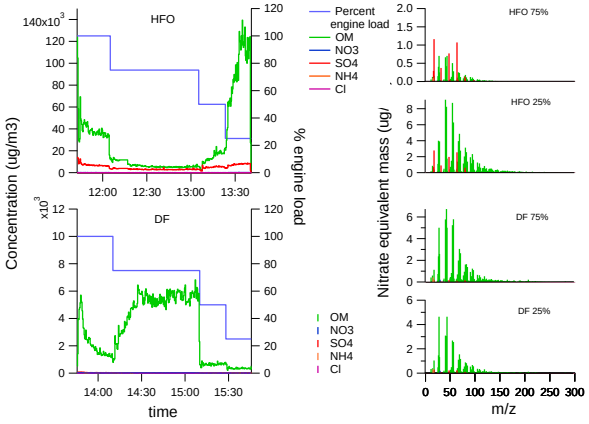

Fig.1. Progression of the measured non-refractory components with the ISO load operation in HFO (*top left)* and DF (*bottom left)*. The average mass spectra for load 75% and 25% for HFO *(top right)* and DF *(bottom right,)* respectively.

This work is part of the Helmholtz Virtual Institute of Complex Molecular Systems in Environmental Health, HICE. Health effects of organic compounds in aerosols are currently being investigated in the framework of HICE.

Corbett, J., Winebrake, J.J., Green, E. H., Kasibhatla, P., Eyring, V., Lauer, A. (2007). *Environ. Sci. and Technol.* **41**, 8512–8518.

DeCarlo, P. F., Kimmel, J. R., Trimborn, A., Northway, M. J., Jayne, J. T., Aiken, A. C., Gonin, M., Fuhrer, K., Horvath, T., Docherty, K., Worsnop, D. R., and Jimenez, J. L. (2006) *Anal. Chem.* **78**, 8281–8289, 2006.

Study of the aerosol elemental composition with high time resolution: preliminary results from the AIRUSE LIFE+ Project

S.Nava[1], G. Calzolai[1], M. Chiari[1], F. Lucarelli[1], F. Amato[2], A. Karanasiou[2], X. Querol[2], C. Alves[3], M. Duarte[3], T. Nunes[3], C. Pio[3], K. Eleftheriadis[4], D. Beddows[5] and R.M. Harrison[5]

[1]Department of Physics and Astronomy, University of Florence and INFN, Sesto Fiorentino, 50019, Italy
[2]Institute of Environmental Assessment and Water Research (IDAEA-CSIC), Barcelona, 08034, Spain
[3]Centre for Environmental and Marine Studies (CESAM), Department of Environment, University of Aveiro, Aveiro, 3810-193, Portugal
[4]ERL, Demokritos National Center of Scientific Research, Institute Attiki, Athens, 15310, Greece
[6]Division of Environmental Health & Risk Management, University of Birmingham, Edgbaston, Birmingham, B15 2TT, United Kingdom
Keywords: PIXE, hourly composition, source apportionment
Presenting author email: nava@fi.infn.it

Atmospheric aerosols are of great concern because they can have negative effects both on environment and on human health. In Europe, the current policy efforts have not fully delivered the expected results and many urban areas still do not meet the air quality standards (2008/50/EC Directive). This is especially true for Southern Europe, where both anthropogenic and natural (Saharan dust, marine aerosols, etc.) sources give important contributions to particulate matter (PM).

The AIRUSE project, which involves public and private institutions of Spain, UK, Portugal, Italy and Greece, aims at testing existing and future mitigation measures and to develop new strategies for the improvement of air quality in Southern European countries (www.airuse.eu). The project includes PM sampling in four urban sites in Barcelona (Spain), Athens (Greece), Porto (Portugal), and Florence (Italy), for long periods (~1 year), on a daily basis. It will allow us to obtain a time-extensive data set, which is mandatory in order to get an overall representative picture of the PM composition in these urban sites.

However, it should be noted that most particulate emissions as well as atmospheric transport and dilution processes change within a few hours and daily samples are not capable of tracking these rapid changes. High-time resolved detailed characterisation allows a better insight on processes such as formation, transport, removal, deposition and chemical reactions in the atmosphere. Moreover, high-time resolution allows a direct comparison with meteorological parameters and gaseous pollutants, which are generally monitored on hourly basis. High-time resolved samplings can also give further information about source emissions: these can heavily impact on air quality with very high emission loadings of elements or compounds during a few hours in a day, and the knowledge about the timing and intensity of specific episodes may be important to assess human exposure. Furthermore, source apportionment receptor models need a series of samples containing material from the same set of sources in differing proportions and increasing the time resolution of the measurements typically provides samples that have greater between-sample variability in the source contributions than samples integrated over longer time periods.

For these reasons, intensive high time resolution PM samplings are also included in the AIRUSE project. The fine (< 2.5 μm) and coarse (2.5-10 μm) fractions of particulate matter are collected with hourly time resolution by means of ''streaker'' samplers (PIXE International Corporation). PIXE analyses, performed with a 3 MeV proton beam from the 3 MV Tandetron accelerator of the INFN-LABEC laboratory, allow the assessment of the concentrations of several elements (Na, Mg, Al, Si, P, S, Cl, K, Ca, Ti, V, Cr, Mn, Fe, Ni, Cu, Zn, Br, Sr and Pb), including important source tracers, with hourly time resolution (Fig. 1).

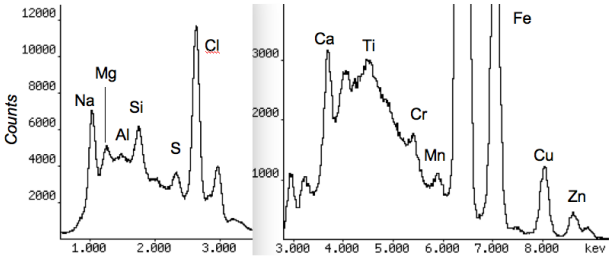

Figure 1. Example of X-ray spectra obtained by PIXE analysis of the aerosol (coarse fraction) collected during one hour sampling in Porto.

Two wintertime intensive sampling campaigns, of about 3 weeks each, have been carried out in Florence and Porto. Summertime campaigns are scheduled in all the AIRUSE sampling sites, while wintertime campaigns in Barcelona and Athens will be carried out next winter.

In this work preliminary results will be shown. In particular, hourly data will be used to investigate:

- the impact of industrial emissions, which produce short intense pollution peaks;
- the effects of road transport: exhaust and not-exhaust emissions and dust resuspension (which is particularly important in South European urban environments due to the lower precipitation and higher solar irradiation);
- the impact of biomass burning (hourly resolution daily patterns of fine K, fine Cl, and other elements may help in disentangling this source).

This work was supported by the European Community (LIFE + Environment Policy and Governance, LIFE11 ENV/ES/584).

Characterisation of winter aerosols in the Helsinki region by TEM/EDX individual particle analysis

J.V. Niemi[1], S. Saarikoski[2], K. Saarnio[2], A. Frey[2], A. Kousa[1], H. Kuuluvainen[4], L. Pirjola[3], T. Rönkkö[4] and R. Hillamo[2]

[1]Helsinki Region Environmental Services Authority, P.O. Box 100, FI-00066 HSY, Helsinki, Finland
[2]Air Quality Research, Finnish Meteorological Institute, P.O. Box 503, FI-00101 Helsinki, Finland
[3]Department of Technology, Metropolia University of Applied Sciences, P.O. Box 4021, FI-00180 Helsinki, Finland
[4]Department of Physics, Tampere University of Technology, P.O. Box 692, FI-33101 Tampere, Finland

Keywords: particle composition and sources, electron microscopy, SP-AMS, mobile measurements
Presenting author email: jarkko.niemi@hsy.fi

The detailed monitoring of aerosol particle properties in urban and suburban areas is a challenging task, since particle concentration, size, composition and sources vary strongly in time and space. As a part of MMEA Programme (Measurement, Monitoring and Environmental Assessment, 2010-2014), we have conducted field campaigns in the poor air quality hot spot areas of the Helsinki region, i.e. city centre street canyons (Dec 2010 campaign; Pirjola et al. 2012), major roads (Oct-Nov 2012) and densely populated small house areas with local wood burning (Feb 2012). During the campaigns, stationary and mobile online measurements (laboratory van 'Sniffer') have been performed, focusing on particle composition, size distribution and volatility. Furthermore, particle samples have been collected for transmission electron microscopy coupled with energy-dispersive X-ray microanalysis (TEM/EDX). The combined application of several methods enables us to obtain a comprehensive view on aerosol properties and sources as well as to test new measurement methods.

We will present detailed TEM/EDX individual particle view, complemented with other methods, on typical winter aerosols in the Helsinki region. Four periods for TEM/EDX analysis were selected during the campaign in February 2012;

1. very clean period (CLEAN) at urban background site on seashore due to air flows from the Atlantic Ocean (Feb 21 morning),

2. strong long-range transported pollution episode (LRT-EPI) at urban background site on seashore due to air flows from eastern Europe (Feb 18 evening),

3. fresh smoke plumes from biomass burning (SMOKE) in suburban small house area mixed with LRT pollution (Feb 18 evening), and

4. fresh emissions from traffic (TRAFFIC) at kerbside of busy street in Helsinki city centre during morning rush hour (Feb 24 morning).

Description of aerosol properties

Aerosol properties were measured by Sniffer along the selected research routes. Online PM_1 chemical composition was monitored with a soot particle aerosol mass spectrometer (SP-AMS) and an aethalometer. Particle size distributions were measured with an electrical low pressure impactor (ELPI). During the 15 min samplings for TEM/EDX, the mobile laboratory was parked. The size-segregated particle samples (6 size fraction between 56 and 1 800 nm) for TEM/EDX were collected with a rotating MOUDI impactor.

The volume size distributions (Fig. 1) and PM_1 bulk chemical compositions (Fig. 2) of particles show the general view on aerosol properties for the four periods.

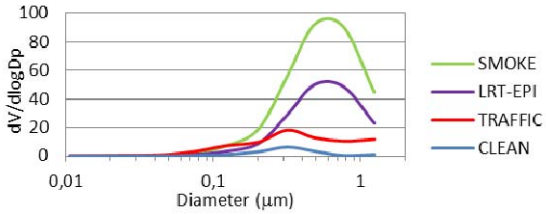

Figure 1. Particle volume size distributions (ELPI).

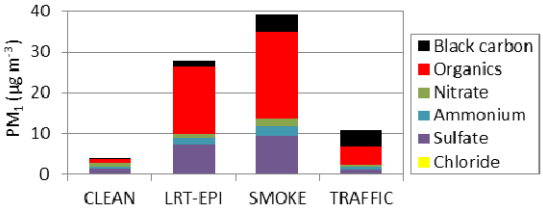

Figure 2. PM_1 bulk chemical compositions (SP-AMS).

The individual particles (# ~ 1100) analyzed with TEM/EDX were classified into several groups (particle types) based on their elemental composition, morphology, internal structure and susceptiblity to damage by an electron beam. The major particle groups were 1) tar balls, 2) K/C-rich, 3) soot, 4) soot mixed with secondary material, 5) S/C-rich secondary, 6) Ni-V-Fe with secondary, 7) Fe-rich, 8) Si-Al-rich, 9) sea salt, and 10) NaCl street-deicer rock salt. Figure 3 shows two TEM images, as an example for LRT-EPI and TRAFFIC periods. The detailed size-segrated particle classification and TEM-images will be shown in the EAC.

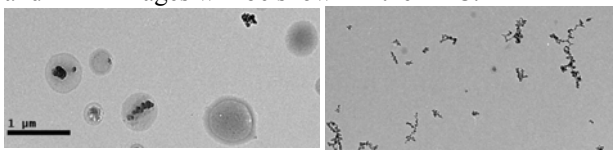

Figure 3. TEM images; LRT-EPI (left), STREET (right).

This study was partly funded by MMEA Programme. MMEA is supported by Tekes (the Finnish Funding Agency for Technology and Innovation) and coordinated by the Finnish Energy and Environment Cluster.

Pirjola, L., Lähde, T., Niemi, J.V., Kousa, A., Rönkkö, T., Karjalainen, P., Keskinen, J., Frey, A., Hillamo, R. (2012) *Atmos. Env.* **63**, 156−167.

Development of a non-destructive method based on infrared analysis for quantification of ionic components in atmospheric particulate matter

A.Piazzalunga[1,2], D.Ballabio[2], V. Bernardoni[1,3], P. Fermo[1], U. Molteni[1], P. Prati [4], R. Vecchi[3], G.Valli[3],

[1]Department of Chemistry, Università degli Studi di Milano , 20133, Milan, Italy
[2]Department of Environmental Science, University of Milano Bicocca, , 20126 Milano, Italy
[3]Department of Physics, Università degli Studi di Milano , 20133, Milan, Italy
[3]Department of Physics, Università di Genova, 16146, Genova, Italy

Keywords: particulate matter, FTIR, ions quantification
Presenting author email: andrea.piazzalunga@unimib.it

Among the analytical technique developed so far for atmospheric aerosol characterization, Fourier Transform Infrared spectroscopy (FTIR) allows to determine both organic fraction (functional groups) and some inorganic components (ammonium, nitrate, sulfate, silicates, carbonates). The FTIR analysis on particulate matter collected on filters has encountered great success since the method is basically not destructive so that the sample can be analyzed further using other techniques. It is worthy to note that the approaches used in the literature to determine the above mentioned aerosol components generally involve rinsing the sample with appropriate solvents (Maria et al., 2002; Russel et al., 2009).

In this work we focus on the quantification of the inorganic components of PM (NO_3^-, SO_4^{2-}, NH_4^+) by FTIR and therefore avoiding any sample pre-treatment.
Of each sample was recorded in the absorption spectrum transmittance. To obtain quantitative information from the FTIR spectra, a multivariate approach based on Partial Least Squares (PLS) has been applied.
The samples themselves were used as standards for the training of the multivariate model; input data were obtained analyzing the samples with ion chromatography (Piazzalunga et al., 2013).

The development of PLS models was performed on a database of 300 filters collected in several measurement campaigns carried out in Milan and Genoa between 2010 and 2012.

A preliminary analysis of IC data with Principal Component Analysis (PCA) shows how the first two principal components explain 98% of the total variance.
Five different PLS models were tested. The number of latent variables for each model was chosen minimizing RMSECV (error in cross validation).

The models for the examined species show a good agreement with IC data, in figure 2 is reported the comparison between FTIR and IC sulphate quantification.

In conclusion, coupling FTIR with PLS methods allows to quantify major ions in PM samples without pre-treatment reducing costs and time of analysis.

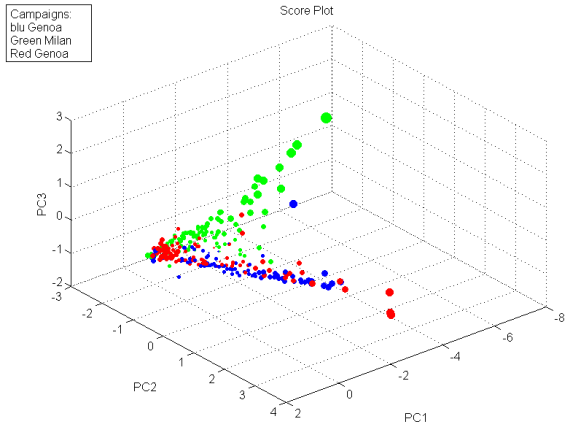

.
Figure 1: score plot obtained from PM compositional data (sulphate, nitrate and ammonium); variance explained by PC1 and PC2: 98%

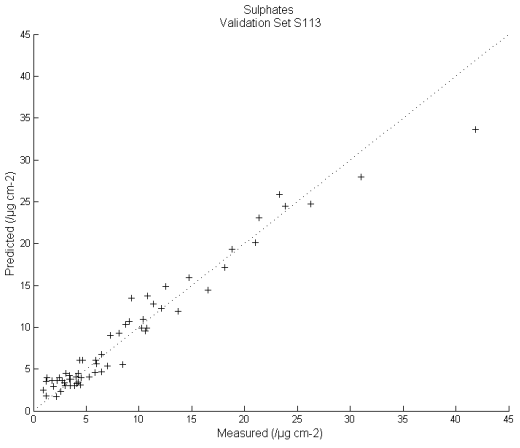

Figure 2: Comparison between FT-IR (y axis) and ion chromatography (x axis) sulphate quantification

References

Piazzalunga et al., 2013, Anal. Bio. Chem. 405, 1123 - 1132
Russell et al., 2009, Atmospheric Environment, 43(38), 6100–6105
Maria et al., 2002, Atmospheric Environment, 36(33), 5185–5196

Micromarkers of source-specific combustion aerosols

O.B. Popovicheva[1], E.D. Kireeva[1], N.M.Persiantseva[1]

[1]Institute of Nuclear Physics, Moscow State University, Moscow, 119991, Russia
Keywords. combustion aerosols, characterization, source of emission
Presenting author email: polga@mics.msu.su

Aerosols generated by incomplete combustion of fossil fuels (FF) and biomass burning (BB) are major air pollutants. Open BB relating to wildfires contributes to almost a half of the combustion aerosol global inventory. Aerosol emissions of transport systems are currently acknowledged to be a largest source of uncertainties in understanding the impacts on the regional air quality. Ship emission is among the world's highest polluting sources per quality of fuel consumed. Combustion aerosols may serve tracers allowing a link to distinct combustion sources in apportionment studies if their key physico-chemical characteristics representative the emission sources are defined. The estimations of the source contribution to ambient particulates assume specific markers different from other combustion sources.

A complexity of multicomponent and source-specific PM emissions requires the characterization of individual particles. The classification of combustion aerosols may be done by representative particle types according to their chemical specification. This approach allows quantifying the various diesel and biomass burning sources and identifying the specific characteristic features that can serve as micromarkers emission source.

Presently, the hierarchical cluster analysis (HCA) is a data analysis technique which is used for the interpretation of electron microprobe analysis data and the determination of particle types in ambient air with a large number of pollution sources. Here, we present the development of HCA for characterization the FF and BB emissions by classification of individual particle data on characteristic groups with similar morphological and chemical composition according to the source and type of fuel used. Scanning electron microscopy (SEM) coupled with energy-dispersive X-ray spectroscopy (EDX) is used for characterization of morphology and composition of a large number of individual particles. FTIR spectroscopy and ion content measurements provide the bulk composition data for clustering expert analysis that assures that the mean composition of a cluster is close to physico-chemical identifiable type of particles. Impact of Fe content in laboratory-produced soot aerosol on its composition and structure was analysed in Bladt *et al.* (2012) to demonstrate the elaborated approach for separation individual particles into characteristic groups representing the particle types in dependence of iron content in soot.

This review presents micromarkers of source-specific combustion aerosols emitted by transport systems (road and marine diesel engines) and in open fire experiments. Microscopic and chemical characterization of Opel Astra diesel engine exhaust operated at 35 km/h speed and used diesel B0 fuel with various lube oil (low and high SAPS) and biodiesel fuel B20 with high SAPS are performed. The most abundant group (around 50%) in each exhaust is polluted soot. In diesel B0 exhaust particles, low SAPS groups of silicates, iron and aluminum oxides are found. Using high SAPS with larger ash content leads to abundance of groups of Al oxide and Al fused with Fe. The most prominent impact of high SAPS using relates with presence of well-separated groups of Nb oxides and W particles. Biodiesel exhaust particles, high SAPS contain groups of Fe and Zn oxides, and W particles. The source specific micromarker of biodiesel particles is a separate group enriched by Cl, K, and Na, the elements which are commonly recognized as biomarkers of biofuel combustion.

Exhausts from the main and auxiliary engines operated onboard of a RoRo/casetter carrier ship during TRANSFORM campaign, burning heavy and distillated fuels, respectively, are analyzed (Popovicheva *et al*., 2012). SEM/EDX observations of emitted aerosols indicate carbonaceous particles internally and externally mixed with inorganic species in the combination of spherical and irregular shapes. The composition of individual particles is varying in a wide concentration range of major elements (C, O) and impurities (S, Fe, Si, Ca, Zn, V, Ni, K, Mn) representative the origin of fuels. In distillated fuel (DF)-derived aerosols we identify groups of soot, Ca- and Fe/Si-rich particles. Calcium sulfate/oxide/carbonates and iron oxides are found to compose the group of Ca- and Fe-rich particles, respectively, while silicon oxide and silicate determine the group of Si-rich particles in heavy fuel (HF)-derived emission. Transition metals (V, Ni) containing particles specify the separate group which may serve as a specific micromarker of heavy fuel combustion.

Characterization of freshly-generated smoke particles produced in small-scale spruce open fire experiments shows the groups of soot, Ca- and Fe-rich particles while K- and Mn- rich groups identify the specific micromarkers of BB.

Thus, state-of-the-art characterization of complex multicomponent aerosols improves the quantification of contribution of various fossil fuel and biomass burning emissions to ambient particulates and the identification of a source type in the apportionment studies.

This work was supported by RFBR projects 12-05-00395_a and 12-05-92002.

Bladt, H., Schmid, J., Kireeva, E., Popovicheva, O.B. et al. (2012). *Aerosol Science and Technology*, 46, 1337-1348.

Popovicheva O., Kireeva E. et al. (2012). *J. Environ. Monit.*, **14**, 3101 – 3110.

Meteorological and chemical factors triggering an exceptional PM pollution episode in wintertime in the Po Valley, Italy

V. Poluzzi[1], D. Bacco[2], G. Bonafé[1], C. Maccone[1], S. Ferrari[1], R. Vecchi[3], S. Decesari[4] and I. Ricciardelli[1]

[1]Emilia-Romagna Region Agency for Prevention and Environment (ARPA), Bologna, I-40138, Italy
[2]Department of Chemical and Pharmaceutical Sciences, University of Ferrara, Ferrara, I-44121, Italy
[3]Department of Physics, Università degli Studi di Milano, Milan, I-20133, Italy
[4]Institute of Atmospheric Sciences and Climate, National Research Council (CNR), Bologna, I-40129, Italy
Keywords: PM, atmospheric aerosol, pollution episode.
Presenting author email: iricciardelli@arpa.emr.it

An exceptional pollution episode interested the Po Valley (Northern Italy) from 15th to 19th February 2012, and was responsible for very high PM concentrations (Figure 1), principally in its western and southern parts. In particular in Parma and Milan, PM_{10} concentrations reached about 250 µg/m^3. From the meteorological point of view the Po Valley was interested by heavy snowfalls from 1st to 12th February in particular in its southern area. A period characterized by atmospheric stagnation followed until 19th, but interrupted from an outbreak of northerly dry winds on the lee side of the Alps (foehn) on 15th and 16th. Observed PM concentrations started to increase from 15th February, reaching a maximum on 19th February. Starting from 20th February, PM concentrations significantly decreased in the entire Po Valley due to the rainfall.

The present work deals with the results of chemical analyses performed on PM_1 and $PM_{2.5}$ samples collected at urban and rural background sites in southern Po Valley. Moreover, the aerosol mass closure on the chemical species was calculated for the analyzed period. The results for Bologna urban background station are shown in Fig 2.

Furthermore it has been analyzed the Particles Number Concentrations (PNC) observed in the urban and rural background sites in Bologna measured by Optical Particle Counters (FAI-Instruments OPC Multichannel Monitor) in a range between 280 nm and 10 µm.

The analysis of meteorological factors and of the chemical dataset indicates that a gradual accumulation of aerosols progressed from 15th to 19th February mainly due to lowering of mixing height, while the factors responsible for the second maximum observed after 16th February are more complex. The chemical composition in this second period was characterized by a large fraction of ammonium nitrate particles (up to 70%) suggesting that chemical processes beside the meteorological factors came into play. In this study it was examined the following possible explanation for the peak concentrations of PM: a) contribution of transboundary transport of pollutants, b) manure spreading on agricultural land and consequent increase of ammonia concentration in atmosphere, c) snow melting and releasing of aerosol precursors in the atmosphere.

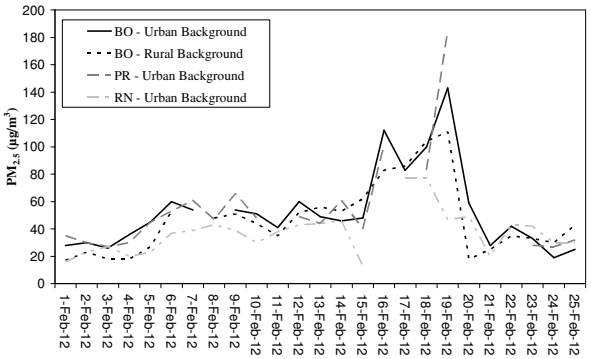

Figure 1. $PM_{2.5}$ mass concentrations in four cities of Po Valley in February 2012.

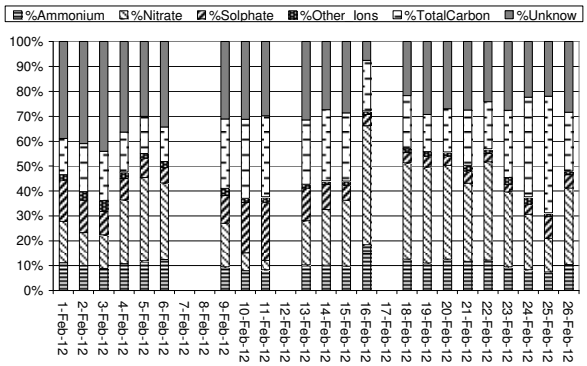

Figure 2. Aerosol mass closure on the chemical species, $PM_{2.5}$ samples collected in Bologna urban background site in February 2012.

This research was conducted as part of the "Supersito" Project, which was supported and financed by Emilia-Romagna Region and Regional Agency for Prevention and Environment under Deliberation Regional Government n. 428/10.

Comparison of particle number concentration and $PM_{2.5}$ chemical species in urban and rural sites in Po Valley (I) during measurement program in the Supersito project

I. Ricciardelli[1], D. Bacco[2], F. Scotto[1], A. Trentini[1], A. Vagheggini[3] and V. Poluzzi[1]

[1]Emilia-Romagna Region Agency for Prevention and Environment (ARPA), Bologna, I-40138, Italy
[2]Department of Chemical and Pharmaceutical Sciences, University of Ferrara, Ferrara, I-44121, Italy
[3]Department of Statistical Sciences "Paolo Fortunati", University of Bologna, I-40126, Italy
Keywords: correlation, number size distribution, $PM_{2.5}$, chemical composition
Presenting author email: iricciardelli@arpa.emr.it

Under the framework of the Supersito project, continuous monitoring of physical and chemical parameters takes place in two sites located in the Po Valley (Northern Italy): an urban background site (BMS) situated in Bologna, a big town in the Valley near Apennines mountains, and a rural background site (SPC) located in the countryside 40 km North East of Bologna.

This work has the purpose of assessing differences between two environmental conditions from a statistical point of view. This approach allows the achievement of size segregated information on the aerosol main chemical components, useful for source attribution, without performing additional analysis on size fractionated aerosol samples.

Aerosol number concentration and size distribution data of three months in fall-winter 2011/2012 are analyzed. Data are collected by an Optical Particle Counter (FAI OPC Multichannel Monitor) that classifies particles in 8 size bins in the 0.28 – 10 µm size range.

PM_1 and $PM_{2.5}$ daily concentrations are monitored in both sites and a complete characterization of $PM_{2.5}$ composition is achieved by the determination of ions (NH_4^+, NO_3^-, SO_4^{2-}, K^+, Na^+, Ca^{2+} and Cl^-), total carbon and metals (As, Fe, Ni and Zn).

Daily patterns of total particle concentration in the two sites in the whole period reveal a good correlation coefficient (r=0.91). The total particle concentration mean values in the two sites are clearly similar (BMS=773 cm^{-3}, SPC=763 cm^{-3}).

Mean $PM_{2.5}$ levels in BMS and SPC are, respectively, 47 and 40 µg m^{-3} while PM_1 are 26 and 24 µg m^{-3}.

Concerning the chemical composition of $PM_{2.5}$, the aerosol mass closure on the chemical species for the analyzed period is presented in Figure 1.

Particle number size ranges and chemical species are examined using correlation matrices to study the partitioning of species in the different size classes and to analyze time trends of aerosol constituents, in order to identify similarities or differences between the two sites.

PM_1 and, mostly, $PM_{2.5}$ in BMS show high correlations with size channels up to optical diameter d_o<2 µm while in SPC these good correlations are observed only up to d_o<0.7 µm.

High correlations (r>0.80) are observed between NH_4^+ and NO_3^- with fine particles channels (d_o<1.1 µm) both in BMS and SPC. Conversely, SO_4^{2-} presents only in BMS a good correlation (r>0.70) with particle number d_o<0.7.

Ca^{2+} shows a good correlation with the largest fraction of particles (d_o>5 µm) both in BMS (r=0.83) and in SPC (r=0.81). Other ions (K^+, Na^+ and Cl^-) have a fairly good correlation, only in SPC, with greater particle size.

Total carbon concentration (sum of organic and elemental carbon) doesn't show a clear association with a single particle size range but, anyhow, its correlations with each size bins are higher in BMS than in rural site.

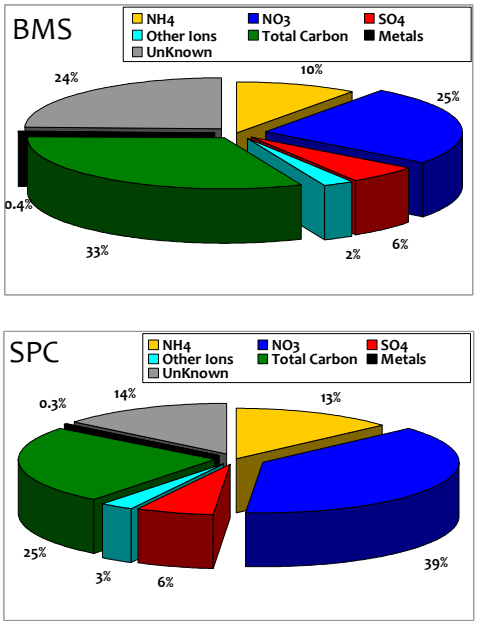

Figure 1. $PM_{2.5}$ mass closure on chemical species

Among metals, As and Fe show better correlations with coarse particles (d_o>1.1 µm), in SPC than in BMS. Conversely the correlations of the same metals with fine particles (d_o<1.1µm) are higher in BMS than in SPC.

This research was conducted as part of the Supersito Project, which was supported and financed by Emilia-Romagna Region and Regional Agency for Prevention and Environment under Deliberation Regional Government n. 428/10.

Pey, J., Alastuey, A., Querol, X. and Rodriguez, S. (2010) *Atmospheric Environment.* **44,** 4879-4890

Fang, G-C., Wu, Y-S., Rau, J-H, Huang, S-H. (2006) *Atmospheric Research.* **80**, 294-308

Organic aerosols from residential wood burning emissions analysed by Ultra-high resolution mass spectrometry

A. G. Rincón[1], C. Alves[2], M. Dietzel[3] and M. Kalberer[1]

[1]Department of Chemistry, University of Cambridge, Cambridge, Cambridgeshire, CB2 1EW, United Kingdom
[2]Centre for Environmental and Marine Studies, Department of Environment, University of Aveiro, Aveiro, 3810-193, Portugal
[3]Institute of Nano- and Microfluidics, Center of Smart Interfaces, Technical University Darmstadt, D-64287 Darmstadt, Germany

Keywords: organic aerosols, biomass burning, chemical analysis, mass spectrometry.
Presenting author email: agr36@cam.ac.uk

Biomass burning (BB) is considered as one of the largest primary sources of organic aerosols in the atmosphere. The chemical composition of BB aerosol is diverse and depends e.g., on the chemical composition of the burning material. Emissions from residential fireplace combustion of wood have been shown to be major contributors to air pollution during winter months. The fraction of BB particle mass is not easily identified with conventional analytical techniques due to the highly complex compound mixtures in organic aerosols.

Here we present results of ultra-high resolution mass spectrometry (UHR-MS), which has unique capabilities to characterize complex samples (Nizkorodov, 2011), (Rincón, 2012). UHR-MS allows identifying unambiguously the elemental composition of thousands of compounds in a single analysis and gaining information about the structure and formation mechanisms of organic compounds in aerosols.

The BB sample was collected from a typical open fire stove used in Portugal for residential heating. The burning test was made using a predominant tree species in Portugal *Pinus pinaster* (Maritime pine) and it was carried out at the combustion facility of the University of Aveiro. The complete description of the facility and other parameters continuously monitored during the experiment are published elsewhere (Goncalves, 2011). Particulate matter with aerodynamic diameters below 2.5µm was collected onto quartz fibre filters.

The water-soluble organic fraction of the filter extracts was separated from inorganic ions by a solid phase extraction step and re-dissolved in acetonitrile-water prior to analysis. UHR-MS analyses were performed using an LTQ Orbitrap Velos, with an accuracy below 2ppm, using an electrospray ionisation source. Mass spectra were measured by direct infusion, in negative and positive polarities and recorded within the range of 50-500m/z. Molecular formulas were assigned to the exact masses of more than 3000 compounds in a single sample using the XcaliburTM software and additional software written in-house.

Figure 1 shows a van Krevelen plot of H/C versus O/C of the compounds containing carbon, hydrogen and oxygen, detected in negative and positive polarity. Compounds with high H/C ratio (H/C>2) and a double bond equivalent (DBE) of zero are measured mostly in positive mode. They correspond to saturated oxygenated species, which contain at least 6 carbon and 3 oxygen atoms in each formula. Possible compounds could be long chain polyalcohols. The lower left corner of the diagram contains the most unsaturated compounds (DBE>8) with low O/C and H/C ratios likely oxidized polyaromatic hydrocarbons. Compounds with O/C≥1 were detected mainly in negative polarity and include dicarboxylic, hydroxy and ketocarboxylic acids with less than 7 carbon atoms. Other signatures of the samples consist of a variety of carboxylic acids, phenolic compounds and carbonyl compounds.

Mass spectral pattern of these samples are also compared to ambient samples to identify the BB signatures in the ambient samples. More highly oxidized compounds, including organo sulfates and organo nitrates are more abundant in ambient samples compared to BB samples. In contrast a higher number of components from BB samples exhibit an olefinic and aromatic nature than in ambient samples. These findings are consistent with the lack of aging in the BB samples.

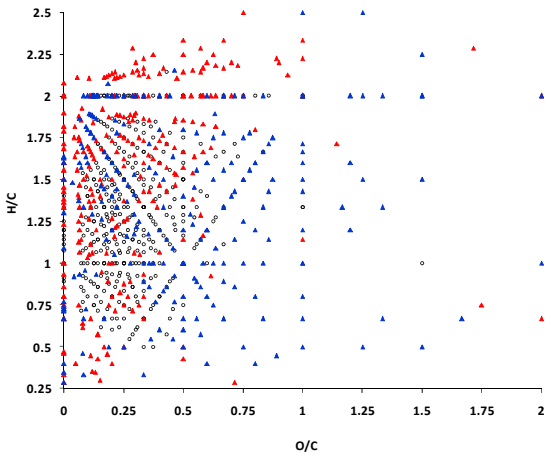

Figure 1. Van Krevelen diagram of $C_cH_hO_o$ containing organics measured in negative (▲), positive (▲) MS mode and compounds measured in both polarities (○).

Nizkorodov, S.A., Laskin, J., and Laskin, A. (2011). *Phys. Chem. Chem. Phys.,* **13**, 3612-3629.

Rincón, A. G., Calvo, A. Dietzel, M. and Kalberer, M. (2012) *Environ. Chem.* **9**, 298-319.

Goncalves, C., Alves, C., Fernandes, A. P., Monteiro, *et al.* (2011) *Atmos. Environ.,* **45**, 4533-.4545.

A highway study of PM and black carbon (BC) in Flanders (Belgium)

D. Roet, J. Vercauteren, C. Matheeussen and E. Roekens

Flemish Environment Agency (VMM), Kronenburgstraat 45, 2000 Antwerpen, Belgium

Keywords: PM, black carbon (BC), highway

Presenting author email: d.roet@vmm.be

From April 2012 until February 2013 the Flemish Environment Agency (VMM) carried out measurements near a **busy highway** as part of the European Life+ ATMOSYS project. Four mobile instrument vans were placed along a perpendicular transect oriented along the dominant south-west wind direction near the busy E40 highway in Affligem (Flanders, Belgium). Each mobile instrument van was equipped with automated monitors to measure **PM_{10}** and **$PM_{2.5}$** as well as **black carbon** (BC). Additionally passive samplers were used to determine the concentrations of **NO_2**, **NH_3** and volatile organic compounds (**VOC**). This highway campaign focused on determining the pollutant contributions coming from the highway as well as their **concentration gradients**.

Experimental setup:

In total 4 mobile instrument vans were used of which one was placed upwind (at 14m from the highway) and the other three downwind (at 6m, 55m and 96m from the highway respectively). Measurements of PM were done with TEOM-FDMS monitors and black carbon with MAAP monitors. Passive sampler measurements were also done at the locations of the mobile instrument vans and two additional downwind locations for the determination of NO_2, NH_3 and VOC. The local meteorological parameters wind speed and wind direction were also measured at a height of 9m at the upwind location.

Figure 1 One of the mobile instrument vans placed downwind with a Leckel alongside (left).

Additionally sampling with Leckel SEQ 47/50 low volume samplers was done for 24h at 2.3 m^3/h on 47mm Pallflex® Tissuquartz™ 2500 QAT-UP filters. Alongside each mobile instrument van such a Leckel was placed (see *Figure 1*) in order to compare the daily PM_{10} mass concentrations to those reported by the TEOM-FDMS monitors.

Results:

The importance of black carbon (BC) on health and climate effects is known from scientific literature (see for example[1]). It is a very good tracer for combustion due to vehicle exhaust. Our **first results** show that there is a **very strong gradient of BC** as a function of distance to the highway (see *Figure 2*).

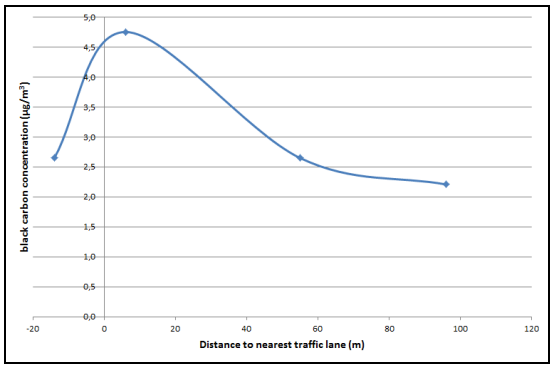

Figure 2: Gradient of black carbon (BC) measured near a busy highway.

Results for the other measured pollutants (PM, NO_2, NH_3 and VOC) will be presented along with a detailed analysis including traffic numbers and meteorological conditions.

[1] Health effects of black carbon, WHO (2012), http://www.euro.who.int/en/what-we-publish/abstracts/health-effects-of-black-carbon

Urban organic aerosols ultrafine particles compositions: a high-resolution mass spectrometry characterization

G. Salque-Moreton[1], R. Jacob[1], D. Voisin[1], F. Donnaz[1], J.-L. Jaffrezo[1], J.-L. Besombes[2] and R. Thissen[3]

[1] UJF / CNRS, Laboratoire de Glaciologie et Géophysique de l'Environnement, Grenoble, France

[2] Université Savoie, Laboratoire de Chimie Moléculaire et Environnement, Chambéry, France

[3] UJF / CNRS-INSU, Institut de Planétologie et d'Astrophysique de Grenoble, Grenoble, France

Keywords: SOA, PMx, urban aerosols, ESI-HRMS.

Presenting author email: guillaume.salque@ujf-grenoble.fr

Organics compounds represent the major fraction of atmospheric aerosol particles; a large part is still not well characterized. A detailed understanding of the sources, transformations processes and fates of organics aerosols is needed.

Investigating the chemical composition of fine and ultrafine particle matter can be expect by using electrospray ionization coupled with high-resolution linear ion trap Orbitrap™ (Thermo Corp.) mass spectrometer (ESI-HRMS). ESI-HRMS is an innovative, recent and powerful tool for describing the organic matter. Chemical and physical properties of organic aerosols are determined with ESI-HRMS by molecular composition. We present here the chemical composition of ultrafine aerosols particles collected on filters at an urban site in Grenoble, France, during winter and summer 2012.

Prior to the MS analysis, aerosols are sampled and segregated upon three sizes (<0.1 µm; 0.1 to 1 µm; 1 to 2.5 µm) using a DA-80 DIGITEL™ collector and a BGI High Volume Cascade Impactor. Firstly, chemical speciation is run on each sample to measure EC, OC, ions and metals. The water-soluble fraction is isolated using Accelerated Solvent Extractor (ASE 200 – Dionex) and diluted in acetonitrile before the ESI injection.

Orbitrap-HRMS provides a resolution of 100,000 at m/z 400, with a mass range 50 – 2000 amu. The ESI-HRMS is known as a "soft" ionization method, leading to very little fragmentation. Thus this technique is more used for the chemical characterization of individual molecules in complex mixtures of SOA. Acquisition is made for both positive and negative ionization mode.

For our moderately complex mixture (~ 2000 peaks), containing O, C, H, N, S and Na, unambiguous elemental formula assignments were established below 350 Da within 1 mDa using a custom computer software (Attributor v1.05) developed by F.R. Orthous-Daunay (2011) and described in Danger et al. (submitted). It is based on a suite of scripts that allow to evaluate the most probable attribution of a high resolution peak, based on its mass, the presence and relative intensity of isotopic peaks, as well as chemical rules (nitrogen rule, even electron ions, etc.) Using a Kendrick analysis (Hughey et al., 2001) based on the CH2 and C2H4O pattern on the unambiguous attribution of most peaks below 350 Da as shown in figure 1, series of regularly spaced peaks were identified in the spectrum, and used to extend the formula attribution toward higher masses. This extension into Kendrick series was also checked against isotopic patterns. Typical standard deviation of the Kendrick mass defect in any such identified series was lower than 0.5 mDa which ensures the proper attribution of all the members of a series, to within less than 1 mDa in the full mass range explored (i.e. 50-800 Da).

The identified elemental formulas are classified into elemental sub-groups referring to the CHONS composition. The obtained results show seasonal variation of chemical moieties and allow a comparison upon particle size. Finally, a comparison will be realized on ambient OA collected at an urban kerbside site (Grenoble, France) in the course of the MOCOPO .

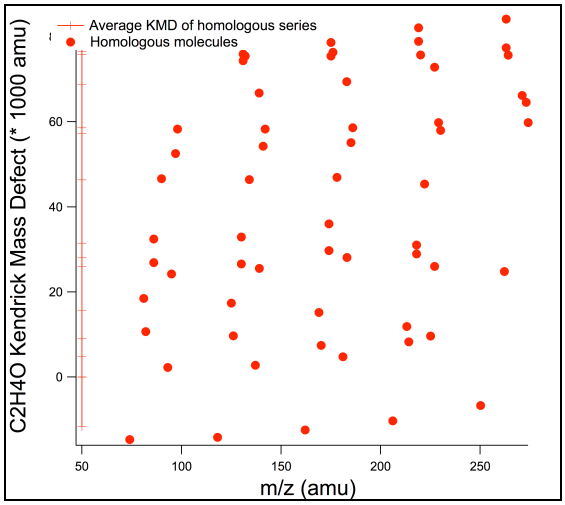

Figure 1. C2H4O Homologous series by ESI(+)-HRMS

G. Salque-Moreton thanks the French Région Rhône-Alpes for his PhD grant.

Gelencsér, A., May, B., Simpson, D., Sánchez-Ochoa, A., Kasper-Giebl, A., Piot, C., Legrand, M., (2007). *J. Geophys. Res.* **112**, D23S04.

Goldstein, A.H., Galbally, I.E., (2007). *Environmental Science & Technology* **41**, 1514–1521.

Rincón, A.G. et al., 2012. *Environmental Chemistry*, 9(3), p.298-319.

Organic and elemental carbon associated to PM_{10} and $PM_{2.5}$ in the urban atmosphere - Estimation of secondary organic carbon

C. Samara[1], D. Voutsa[1], A. Kouras[1], K. Eleftheriadis[2], Th. Maggos[2], D. Saraga[2], M. Petrakakis[3]

[1]Aristotle University of Thessaloniki, Department of Chemistry, Environmental Pollution Control Laboratory, University Campus, 54124 Thessaloniki, Greece
[2]National Centre of Scientific Research "Demokritos", Institute of Nuclear Technology and Radiation Protection, Environmental Research Laboratory, 15310 Ag. Paraskevi, Attiki, Greece
[3]Environmental Department, Municipality of Thessaloniki, Paparigopoulou 7, Thessaloniki 54630, Greece

Keywords: Carbonaceous particles; elemental carbon; organic carbon, PM10/PM2.5
Presenting author email: csamara@chem.auth.gr

Organic carbon (OC) and elemental carbon (EC) constitute major components of atmospheric particles with sum contribution in European urban areas reaching up to 25-40% and 30-50% of total PM_{10} and $PM_{2.5}$ masses, respectively (Putaud et al., 2004). Thessaloniki, Greece (40°62´E, 22°95´N) is a densely populated city suffering from high concentrations of airborne particulate matter. Previous studies indicated that organic matter constituted a significant fraction of the PM_{10} mass (23% and 18% at an urban-traffic and an urban-industrial site, respectively), while EC had a lower contribution at both sites (6.3% and 3.6 %, respectively) (Terzi et al., 2010).

The aim of the present study was to further investigate OC and EC in the urban atmosphere. For this purpose, PM_{10} and $PM_{2.5}$ fractions were collected from an urban-traffic (UT) and an urban-background (UB) site of Thessaloniki, usually exhibiting the max and min levels of air pollutants. At both sites, PM_{10} and $PM_{2.5}$ samples were concurrently collected during the warm and the cold months of the year (July-Sept 2011 and Febr-April 2012). Sampling was carried out according to EN12341 and EN14907 using Low Volume Samplers operating at constant flow rate 2.3 m^3/h. PM_{10} and $PM_{2.5}$ fractions were collected on Φ 47 mm high purity quartz filters prefired at 500 ^oC for 4 hours. Each sampling had a 24-h duration starting at 00:00. OC and EC were determined by the Thermal Optical Transmission method in a Sunset Laboratory OCEC Analyzer.

Summary statistics for OC and EC associated with $PM_{2.5}$ and PM_{10} are shown in Table 1. UB exhibited significantly lower concentrations than UT for both carbonaceous species with EC_{10} levels being towards the lowest among reported values for traffic impacted urban European sites (Grivas et al., 2012) and $OC_{2.5}$ levels within the range of reported values for urban background sites in Europe (Viana et al., 2006; Reche et al., 2012).

Table 1. Mean±SD for concentrations of PM_{10}, $PM_{2.5}$ and associated OC and EC ($\mu g/m^3$)

	OC_{10}	EC_{10}	$OC_{2.5}$	$EC_{2.5}$
UT (N=57)	11±4.6	6.4±2.1	9.0±4.8	5.4±1.7
UB (N=54)	6.6±4.6	0.9±0.6	5.7±4.4	0.7±0.4

Average contributions of OC and EC to total PM_{10} mass were 21% and 14% at UT *vs.* 19% and 2.7% at UB, respectively. The corresponding contributions of OC and EC to total $PM_{2.5}$ mass were 27% and 19% at UT *vs.* 23% and 3% at UB. It was found that 89% and 81% of EC associated to PM_{10} is distributed in the fine particle fraction at UT and UB, respectively, while the corresponding percentages for OC were and 88% and 86%, respectively. The mean OC/EC ratio at UT was 1.9±1.1 in PM_{10} and 1.9±1.4 in $PM_{2.5}$, whereas a clear prevalence of OC over EC was found at UB with mean OC/EC ratios 7.5±2.8 in PM_{10} and 8.1±2.6 in $PM_{2.5}$

EC_{10} and $EC_{2.5}$ levels at UT permanently exceeded the corresponding values at UB revealing that locally generated road traffic emissions are superimposed upon the urban EC background. UT also exceeded UB concerning OC_{10} and PM_{10}, however, a negative increment appeared for $PM_{2.5}$ and $OC_{2.5}$ during February possibly indicative of local emissions from residential wood burning.

Secondary organic carbon (OC_{sec}) was estimated by the EC tracer method (Turpin and Huntzicker, 1995; Pio et al., 2011). As seen in Table 2, the OC_{sec} contributions to OC at UB were higher than at UT averaging 59% and 43% in PM_{10}, and 61% and 46% in $PM_{2.5}$ in the cold and the warm period, respectively. The higher concentrations of OC_{sec} in winter than in summer might be suggestive of long-range transport and temperature influence, as well as to miscellaneous OC in winter, including secondary aerosols from traffic plus primary and secondary aerosols from stationary combustion.

Table 2. Secondary organic carbon (OC_{sec}) concentrations at the urban-traffic (UT) and urban background (UB) sites

		Warm season		Cold season	
		OC_{sec} ($\mu g\ m^{-3}$)	OC_{sec}/OC (%)	OC_{sec} ($\mu g\ m^{-3}$)	OC_{sec}/OC (%)
UT	PM_{10}	3.4±2.6	35±19	7.3±4.5	50±23
	$PM_{2.5}$	2.7±2.4	39±22	7.1±5.1	54±25
UB	PM_{10}	1.9±1.1	43±19	5.0±3.7	55±17
	$PM_{2.5}$	1.6±1.2	46±17	3.5±3.2	40±16

References

Grivas, G. et al. (2012). *Sci. Total Environ.*, **414**, 535-45.
Pio, C.A. et al. (2011). *Atmos. Environ.*,**45**, 6121-32.
Putaud, J.-P. et al. (2004). *Atmos. Environ.*, **38**, 2579-2595.
Reche, C. et al. (2012). *Sci. Total Environ.*, **427-428**:175-190.
Terzi, E. et al. (2010). *Atmos. Environ.*, **44**, 2231-2239.
Turpin, B.J., Huntzicker, J.J. (1995). *Atmos. Environ.* **29**, 3527-3544.
Viana, M. et al. (2006). *Atmos. Environ.*, **40**, 2180-2193.

Aknowledgements

This work was supported by the European Community (LIFE + Environment Policy and Governance).

The influence of children jumping on the bed on PM10/PM2.5/PM1 concentration profile

Yeh, CL[1], Mena, KD[2], and Chen, PS[1*]

[1]Department of Public Health, Kaohsiung Medical University, Kaohsiung, 80708,Taiwan
[2]Department of Public Health, University of Texas Health Science Center, Houston, El Paso, 79902,USA
Keywords: schoolchildren, suspended particulate matter, PM
Presenting author email: protamine1199@yahoo.com.tw

Introduction

Recently, the harmful effects of suspended particulate matter (PM) on human's respiratory system were observed. When children jump on the bed at home, it may resuspend PM. Therefore, the purpose of the present study was to evaluate the influence of children jumping on the bed on $PM_{10}/PM_{2.5}/PM_1$ concentration profile at schoolchildren's house.

Materials and Methods

20 schoolchildren's houses in Kaohsiung city in Taiwan were evaluated. Firstly, $PM_{10}/PM_{2.5}/PM_1$ concentration was simultaneously monitored over the first five minutes to obtain background concentration profiles. Then, a common cane was used to tap the bed for about one minute, followed by keeping motionless in 7 to 10 minutes to let PM settle down. Then, we made children's bed by raising bed sheets for about one minute, followed by keeping motionless in 7 to 10 minutes. This evaluation was conducted by the same person for consistency of the beating strength, beating frequency, and beating location.

Results and Discussion

Our results showed that the concentration of PM_{10}, $PM_{2.5}$ and PM_1 were immediately arising when tapping bed was started, and the peak was kept at least one minute. The mean background concentration of PM_{10}, $PM_{2.5}$ and PM_1 was 89, 80, 80 ug/m^3, respectively. When tapping bed, the mean concentration of PM_{10}, $PM_{2.5}$ and PM_1 was 1561, 1457, 1456 ug/m^3, respectively. When making bed, the mean concentration of PM_{10}, $PM_{2.5}$ and PM_1 was 179, 156, 156 ug/m^3, respectively. When tapping-bed, PM concentration was 27, 28, and 28 times higher than that of background concentration for PM_{10}, $PM_{2.5}$ and PM_1, respectively. When making bed, PM concentration was 2.6, 2.5, and 2.5 times higher than that of background concentration for PM_{10}, $PM_{2.5}$ and PM_1, respectively. Mite may be one of the majority components of these resuspended PM.

Conclusion

In conclusion, jumping on the bed and making bed significantly increased PM concentration. These actions may increase the risk of respiratory symptoms, especially for asthma children.

Table 1. PM concentration of background, tapping and making bed

	PM_1	$PM_{2.5}$	PM_{10}	PM_{10}-$PM_{2.5}$	$PM_{2.5}$-PM_1
	PM_1	$PM_{2.5}$	PM_{10}	PM_{10}-$PM_{2.5}$	$PM_{2.5}$-PM_1
Background (μg/m^3)	80	80	89	9	0
Tapping bed (μg/ m^3)	1456	1457	1561	104	1
Making bed (μg/ m^3)	156	156	179	22	1
Tapping bed - Background (μg/ m^3)	1376	1376	1472	95	1
Making bed - Background (μg/ m^3)	75	76	90	14	0
Tapping bed/Background	18.2	18.1	17.5	12.2	3.3
Making bed/Background	1.9	1.9	2.0	2.6	2.5
Background (μg/ m^3)	80	80	89	9	0
Tapping bed (μg/ m^3)	1456	1457	1561	104	1
Making bed (μg/ m^3)	156	156	179	22	1
Tapping bed - Background (μg/ m^3)	1376	1376	1472	95	1
Making bed - Background (μg/ m^3)	75	76	90	14	0
Tapping bed/Background	18.2	18.1	17.5	12.2	3.3
Making bed/Background	1.9	1.9	2.0	2.6	2.5

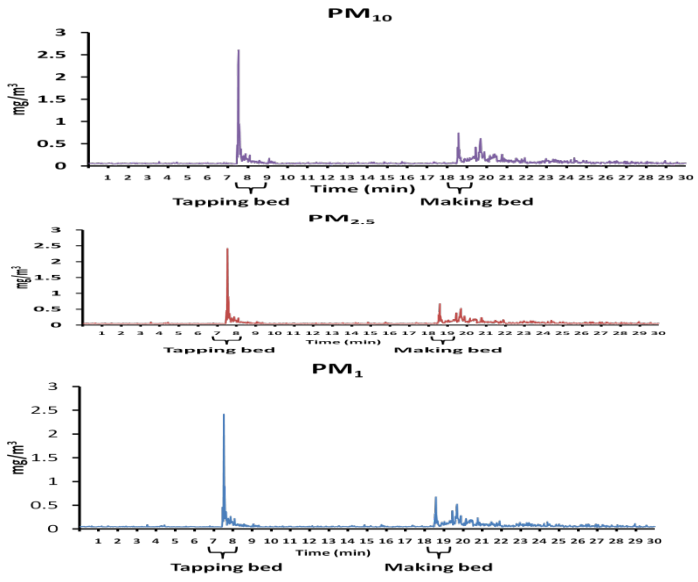

Figure 1. Time serial distribution of PM10, PM2.5, PM1

Summer and winter time aerosol levels at an urban Mediterranean environment: Impacts of biomass burning.

[1,2]M. Psichoudaki, [1,2]E. Kostenidou, [3]A. Bougiatioti, [4]S. Bezantakos, [4]G. Biskos, [3]A. Nenes, [1,2,5]S.N. Pandis

[1]Department of Chemical Engineering, University of Patras, Patras, 26500, Greece
[2]Institute of Chemical Engineering and High Temperature Chemical Proccesses (ICE-HT), Foundation of Research and Technology Hellas, Patras, 26504, Greece.
[3]Schools of Earth & Atmospheric Sciences and Chemical & Biomolecular Engineering, Georgia Institute of Technology, Atlanta, Georgia, USA.
[4]Department of Environment, University of the Aegean, Mytilene, 81100, Greece
[5]Department of Chemical Engineering, Carnegie Mellon University, Pittsburgh, PA 15213, USA.

Keywords: organic aerosol, biomass burning.
Presenting author email: mpsichoudaki@chemeng.upatras.gr

The mass concentration, composition, physical and chemical properties (e.g., extent of oxidation of organic particulate matter) can vary significantly during the year. Patras is coastal urban area with around 200,000 inhabitants, located in western Greece, with light industry. Local traffic has been long assumed to be the major local aerosol source. Due to the high photochemical intensity throughout year but especially during the summer, significant production of secondary aerosol mass is expected.

Winter and summertime intensive measurements have been carried out to investigate the differences on the levels, sources, and chemical processing of ambient particles in this urban area of the Eastern Mediterranean. Aerosol mass, chemical composition and hygroscopicity were monitored during the summer by combining a High Resolution Aerosol Mass Spectrometer (HR-AMS), a Scanning Mobility Particle Sizer (SMPS), a Scanning Flow CCN Counter (SFCA, Moore and Nenes, 2009), a Hygroscopic Tandem Differential Mobility Analyzer (HTDMA). 24-hour filter samples were analyzed for the determination of Organic Carbon (OC), Elemental Carbon (EC) and Water Soluble Organic Carbon (WSOC). The summer measurements took place from 8 to 27 June 2012. Winter-time sampling included day (8:00-18:00) and night (18:00-8:00) filter collection. The winter measurements were carried out from 10 of January until 10 of February of 2013.

Significant differences in the submicron aerosol levels were observed between summer and winter. The $PM_{0.5}$ concentrations are shown at Figure 1. Higher concentrations and variability were observed during the winter period. The mean concentration of $PM_{0.5}$ during the winter intensive campaign was 17.8±16.2 μg m^{-3} and 5.2±2.3 μg m^{-3} for the corresponding period during the summer. The low summertime concentrations are partially due to lower pollutant emissions in Greece due to the financial crisis. The very high levels during the winter are due to high biomass burning emissions from both fireplaces and also agricultural burning of olive tree branches (Kostenidou et al., 2013). These do cause high concentrations of PM and the corresponding gas-phase pollutants during specific periods and days. For example, the PM usually started increasing at around 18:00, reaching a peak at 23:00 and returning to lower levels by 3:00. This variation is consistent with the increased use of fireplaces for home heating. The low mixing heights during the winter also help enhance the pollutant concentrations.

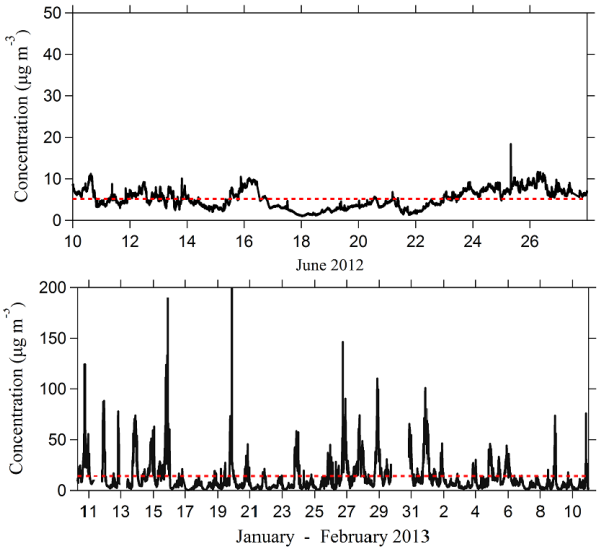

Figure 1. Summer (upper curve) and winter (lower curve) levels of $PM_{0.5}$ aerosol. Dashed lines show the average concentration for the corresponding sampling period.

Differences in the diurnal profiles and variation for the different periods will be discussed and the hygroscopicity of the aerosols will be inspected for the two sampling periods.

This work was supported by the Pan-European Gas Aerosols Climate Interaction Study, PEGASOS.

References

Kostenidou, E., Kaltsonoudis, C., Tsiflikiotou M., Louvaris, E., Russell, L.M. and Pandis, S.N. (2013) *ACPD*, submitted.

Moore R.H. and Nenes, A. (2009) *Aerosol Sci. Technol.* 43, 12, 1192-1207.

An integrated source apportionment study: Positive Matrix Factorization vs. the Chemical Transport Model CAMx

M.C. Bove, P. Brotto, F. Cassola, E. Cuccia, D. Massabò, A. Mazzino and P. Prati

Department of Physics & INFN, University of Genoa, via Dodecaneso 33, 16146, Italy

Keywords: source apportionment, receptor models, chemical transport models
Presenting author email: mcbove@ge.infn.it

The contribution of particular emission sources to PM levels can be highlighted by two different tools: Receptor Models and Chemical Transport Models, both widely adopted even if rarely with a synergic approach. Actually, a satisfying methodology to compare the results and even the categorizations of the two approaches is still missing and highly desirable. In the framework of the MED APICE project (http://www.apice-project.eu/), the Department of Physics (DIFI) of the University of Genoa was involved in the evaluation of the impact of harbor activities on the urban air quality and the definition of strategies to reduce air pollution in port cities. This gave the opportunity to use both Source Apportionment approaches to integrate their potentialities. Receptor Models allow to obtain the evaluation of atmospheric pollutants apportionment from different sources, based on ambient data at monitoring sites whereas Chemical Transports Models (CTMs) extend the assessment on the formation of secondary aerosols on the whole studied territory with a certain resolution too.

For this purpose, a PM2.5 sampling campaign was carried out collecting daily PM2.5 samples for a six month period (May- October 2011) in the urban area of Genoa in three sites (two immediately outside the harbour area and one inland in the northern area of the city) selected considering the direction of prevailing winds. Subsequent compositional analyses produced a large database for a Receptor Model analysis. Positive Matrix Factorization, PMF (Paatero et al, 1994), was used to identify and characterize the major PM2.5 sources. Particular attention was given to the evidence of emissions from heavy fuel oil combustion by ships, known to be an important source of secondary sulphate aerosol.

Also, a meteorological and air quality modelling system has been implemented at DIFI, based on the mesoscale NWP model WRF (Skamarock, 2008) and the Eulerian CTM CAMx (ENVIRON, 2010). Through subsequent nesting, meteorological and pollutant concentration fields are obtained up to resolutions of order of 1 km. During the campaign, a large amount of data has been collected and analysed while simulations have been ran over the whole monitoring period.

Source apportionment for PM2.5 was evaluated by CAMx in the same period of the monitoring campaign through the specific Particulate Source Apportionment Technology (PSAT) tool. PSAT uses reactive tracers to apportion primary and secondary PM and gaseous precursors to secondary PM among different source categories and source regions.

Source apportionment outcomes allowed a comparison with the results obtained by Receptor Models. Table 1 shows the average contribution of the resolved sources to PM2.5 levels in the monitoring sites.

Table 1. Comparison between average sources apportionment obtained by PMF and CAMx.

PM2.5 Sources	PMF	CAMx - PSAT
Maritime/harbour	(13 ± 5) % coastal (9 ± 3) % inland	9% coastal 5% inland
Energy production and Industry	(30 ± 10) %	20%
Road transport	(40 ± 15) %	45%
Residential/tertiary	Not identified	5 %
Others (sea salt, dust, etc.)	(15 ± 5) %	20%

The PM2.5 source apportionment analysis by PMF and CTMs produced a quite comparable picture. In particular, focusing on the mail goal of the APICE project, i.e. the impact of maritime activities on air quality, the two approaches were in fair agreement both near the harbour sites and inland. The evaluation of the uncertainties of the CAMx apportionment is presently in progress and it will be discussed during the Conference.

This work has been founded by the Programme MED under the APICE grant.

ENVIRON 2010 *User's Guide, Comprehensive Air Quality Model with Extensions (CAMx). Version 5.30*, ENVIRON International Corporation, Novato, CA.

Paatero, P., Tapper, U. (1994) *Positive matrix factorization: a non-negative factor model with optimal utilization of error estimates of data values*. Environmetrics **5**, 111-126.

Skamarock, W. C., Klemp, J. B., Dudhia, J., Gill, D. O., Barker, D. M., Huang, X. Z., Wang, W., Powers ,J. G. 2008. *A Description of the Advanced Research WRF Version 3. Technical report, Mesoscale and Microscale* Meteorology Division, NCAR, Boulder, Colorado

Characterization of PM_{10} sources in the central Mediterranean Basin

G. Calzolai[1], S. Nava[1], M. Chiari[1], F. Lucarelli[1], S. Becagli[2], R. Traversi[2], M. Marconi[2], F. Rugi[2], R. Udisti[2], A. di Sarra[3], G. Pace[3], D. Meloni[3], C. Bommarito[4] and D. M. Sferlazzo[5]

[1] Department of Physics and Astronomy, University of Florence & INFN-Florence, Sesto F.no, Florence, I-50019, Italy

[2] Department of Chemistry, University of Florence, Sesto Fiorentino, Florence, I-50019, Italy

[3] ENEA Lab. for Earth Observations and Analyses, S. Maria di Galeria, Roma, I-00123, Italy

[4] ENEA, Laboratory for Earth Observations and Analyses, Palermo, I-90141, Italy

[5]ENEA, Laboratory for Earth Observations and Analyses, Lampedusa, I-92010, Italy

Keywords: Mediterranean Basin, aerosol sources, PM_{10}, PMF.

Presenting author email: calzolai@fi.infn.it

The Mediterranean Basin is characterized by heavy atmospheric pollution, due to the insistence on the area of relevant environmental stress factors of both natural and anthropogenic emission. This work aims at assessing the contributions of the different aerosol sources affecting the Central Mediterranean Basin by a PMF (Positive Matrix Factorization) analysis on a 2-years PM_{10} data set collected at the Global Atmosphere Watch Station of Lampedusa.

Lampedusa Island is centrally located in the Mediterranean Basin, being more than 100 km far from the nearest coast. Such a geographical position makes Lampedusa an ideal site for the study of the aerosol affecting the Central Mediterranean Basin, as it is far from every continental pollution source. Moreover, in Lampedusa, at the Station for Climate Observations maintained by ENEA (Italian Agency for New Technologies, Energy and Sustainable Economic Development), continuous observations of greenhouse gases concentration, total ozone, ultraviolet irradiance, aerosol properties and other climatic parameters are performed (Becagli *et al.*, 2012).

PM_{10} samples are collected on a daily basis since 2007; data from years 2007 and 2008 (accounting for totally 562 samples) were used in this study. After mass gravimetric measurements, samples were fully characterized by analysing different portions with different analytical techniques: in detail, the ionic content was determined by Ion Cromatography (IC), soluble metals were detected by Inductively Coupled Plasma Atomic Emission Spectrometer (ICP-AES), and the total (soluble + insoluble) elemental composition was assessed by Particle Induced X-ray Emission (PIXE).

PMF was run with the algorithm PMF2 (Paatero1997) in the robust mode. Solutions from 5 to 10 factors were systematically explored and a seven-factors solution was selected. The resolved sources are the following ones: sea-salt, mineral dust, biogenic emissions, primary ship emissions, secondary sulphate, secondary nitrate, and biomass burning emissions (see Figure 1). The observed relative ratios and enrichment factors are consistent with literature data for such sources hence strengthening the results of the analysis.

Average source contributions to total PM_{10} mass are estimated to be about 5% for primary ship emissions, biogenic emissions and biomass burning; 10% for secondary nitrate and secondary sulphate; 25% for mineral dust and 40% for sea salt.

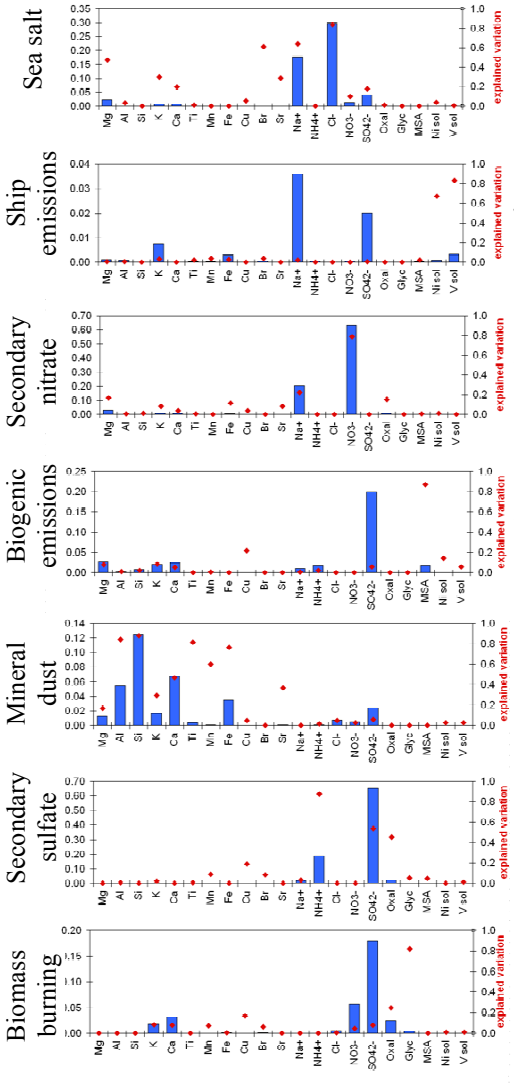

Figure 1. Source profiles and explained variations.

Becagli S., Sferlazzo D. M., Pace G., di Sarra A., C. Bommarito C., Calzolai G., Ghedini C., Lucarelli F., Meloni D., Monteleone F., Severi M., Traversi R., Udisti R. (2012) *Atmos. Chem. Phys.* 12, 3479–3492

Paatero, P. (1997) *Chemometrics and Intelligent Laboratory Systems* 37, 23-35

Size-segregated source apportionment of aerosol using water soluble components

D. Cesari[1], D. Contini[1], A. Genga[2], M. Siciliano[2], P. Ielpo[1,3], M. R. Guascito[2] and M. Conte[1]

[1]Istituto di Scienze dell'Atmosfera e del Clima, ISAC-CNR, Lecce, Apulia, 73100, Italy
[2]Dipartimento di Scienze e Tecnologie Biologiche e Ambientali, Università del Salento, Lecce, Apulia, 73100, Italy
[3]Istituto di Ricerca Sulle Acque, IRSA-CNR, Bari, Apulia, 70132, Italy
Keywords: size-segregated aerosol, MOUDI, EPA PMF3.0, Source Apportionment.
Presenting author email: d.cesari@isac.cnr.it

The aerosol size distributions and the contents of chemical species in the different size-ranges play an important role in determining visibility, air quality and human health effects. The aim of this work is to perform a Source Apportionment (SA) study to evaluate the source contributions to each size range using only water soluble major components and discussing the potentiality and the limits of the approach used. Aerosol samples were collected in an urban background site (Lecce, SE of Italy), using a 10-stages Micro-Orifice Uniform Deposit Impactor (MOUDI II, MSP, Model 120R) operating at 30 l/m. The impactor was equipped with aluminium substrates (47 mm, MSP Corporation) and the 10 stages had nominal cut-off sizes (in μm): 10, 5.6, 3.2, 1.8, 1.0, 0.56, 0.32, 0.18, 0.10 and 0.056. Teflon filters (47 mm, Pall Corporation) were used as back-up filters as well as sampling substrates for simultaneous measurement with a standard low-volume PM10 sampler (Tecora) used for evaluation of losses in the impactor. The average loss resulted in 19% (± 2%) with the major losses associated to nitrate (35% ± 10%). Between February and October 2011, 21 samples were collected: 18 samples were sampled for 48 h and 3 sample for 72 h. Collected samples were stored in Petri dishes at 4 °C until analysed. Gravimetric analysis was performed using a microbalance (Sartorius CP2/F, sensitivity 1μg). Soluble ionic species were determined via High Performance Ion Chromatography (HPIC, Dionex DX-500 System), for SO_4^{2-}, NO_3^-, NH_4^+, Cl^-, Na^+, K^+, Mg^{2+} and Ca^{2+}, and with a Shimadzu TOC analyzer (model 5050), for Water Soluble Organic Carbon (WSOC) and Water Soluble Inorganic Carbon (WSIC) fractions. Chemical analysis show that measured ions accounted, on average, for 39.6% of PM10, WSOC accounts for 13.1% while WSIC for 1.8% of PM10.

The average size distributions of collected aerosol and of water soluble species were fitted to lognormal distributions. Aerosol presented a bimodal distribution that include an accumulation mode (Mass Median Diameter = 0.35 ± 0.02 μm), accounting in average terms for 51 ± 4 % of PM10, and a coarse mode (MMD = 4.5 ± 0.4 μm), accounting in average terms for 49 ± 4 % of PM10. A bimodal distribution was observed for SO_4^{2-}, $NH4^+$, WSOC and K^+ (more abundant in the accumulation mode) and for Cl^-, Ca^{2+}, WSIC and NO_3^- (more abundant in the coarse mode). Na^+ and Mg^{2+} presented a mono-modal distribution in the coarse range. Size-segregated composition of collected aerosol was used for SA using the EPA PMF3.0 software. A different procedure was used with respect to similar works reported in literature (Chan et al., 2000; Fang et al., 2006), using two input datasets, representing the accumulation mode and the coarse mode. The concentrations of a specific species in the different size ranges were considered as independent samples of the same species in the PMF analysis rather than independent species of the same sample. Five sources were individuated in the accumulation mode (marine, crustal, sulphate, nitrate and combustion/traffic emission) and four sources in the coarse mode (marine, crustal, sulphate and nitrate). The size-segregated contributions were reported in Figure 1. There are some differences in the sources observed in the two modes: the accumulation mode nitrate, of secondary origin, is different from the nitrate observed in the coarse mode, that is mainly sodium nitrate and nitrate salts associated to crustal dust. Results showed that it has been possible to evaluate the source contributions in the different size-ranges as well as the contribution to the accumulation and coarse mode separately. In general, SA results were in agreement with indirect estimates of marine and ammonium sulphate contributions. However, there are limits to the application of the PMF model limited to the water soluble species. Specifically, in the accumulation mode it was not possible to distinguish between traffic source and the contribution of other combustion sources (i.e., biomass burning). In the coarse mode it was not possible to separate the sodium nitrate factor from a contribution of nitrate of crustal/resuspension origin.

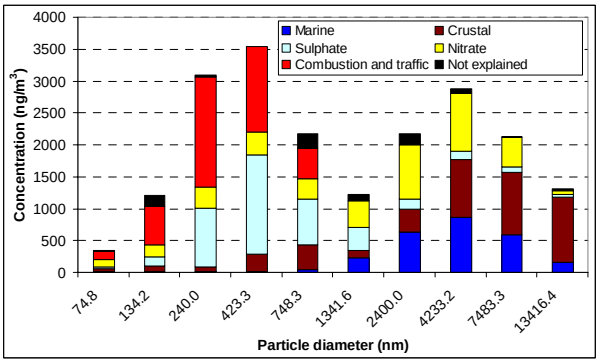

Figure 1. Size-segregated source apportionment (the indicated diameters are the geometric mean diameters).

Chan, Y.C., Vowles, P.D., McTainsh, G.H., Simohen, D.D., Bailey, G.M., and McOrist, G.D. (2000) *Sci. Total Environ.*, **262**, 5-19.

Fang, G.C., Wu, Y.S., Rau, J.Y., and Huang, S.H. (2006) *Atmos. Res.*, **80**, 294-308.

The Impact of Select Pollutant Sources on Air Quality for Ostrava and the Moravian-Silesian Metropolitan Region by the Positive Matrix Factorization model

L. Černikovský[1], J. Novák[1], H. Plachá[1], B. Krejčí[1], I. Nikolova[1], E. Chalupníčková[1], T. Conner[2], G. Norris[2], K. Kovalcik[2], D. Olson[2], J. Turlington[2], C. Croghan[2], R. Willis[2], R. Williams[2]

[1]Czech Hydrometeorological Institute, Prague, Czech Republic
[2] U.S. Environmental Protection Agency, Research Triangle Park, North Carolina, USA
Keywords: Moravian-Silesian Region, source apportionment, positive matrix factorization, PMF
Presenting author email: cernikov@chmi.cz

The Ostrava region of the Moravian-Silesia metropolitan area of the Czech Republic represents one of the most highly industrialized areas in Eastern Europe with a large number of coke oven plants, blast furnaces, steel plants, and rolling mills being present. Ostrava is the third largest city in the Czech Republic containing 214 km^2 and with the country's third largest population (app. 300K). This equates to a population density about 1400 inhabitants/km^2. Its documented history dates back to the period of the 13th century. The discovery of high quality black coal in the mid 1700's and its access to four major river systems established the future direction of the area with respect to its industrial development. The primary metropolitan area is bordered by the Beskydy and Jeseniky mountain ranges. The presence of the large number of coal-related industries in addition to geographical conditions often results in weather-related pollution inversions which have a serious impact on local air quality. The region is connected with the Silesian voivodship in Poland which belongs to highly polluted areas by particulate matter and benzo*[a]*pyrene in Europe as well.

The Czech Hydrometeorological Institute (CHMI) working collaboratively with the U.S. Environmental Protection Agency (EPA) have designed a source apportionment study to determine the impact of regional as well as local sources on overall air quality for the region. Intensive (daily 12-hr day-night) fine particulate matter ($PM_{2.5}$), semi-volatile organic compounds (SVOCs), polycyclic aromatic hydrocarbons (PAHs), organic and elemental carbon (OC/EC), pollutant gases and meteorology were monitored for approximately a seven week period during the summer of 2012 and the late fall/early winter of 2012 at three primary monitoring locations (Poruba - background suburban in residential area; Radvanice - industrial suburban, downwind of prevailing winds from large industrial source; Vratimov – residential area upwind of prevailing winds from the same large industrial source). All the locations are highly polluted by PM and PAHs as well in the long term.

A variety of multivariate source apportionment models, such as positive matrix factorization (PMF), were be used to develop preliminary source impact categories. Findings associated with a preliminary source apportionment effort will be presented and will include summaries of the spatial (upwind versus downwind) and temporal (seasonal) variability of key source markers observed to influence local air quality.

In summer, large difference between $PM_{2.5}$ and PAHs was found between day and night in terms of concentrations and content as well. Average 12-hr PAHs concentration was 1,97 ng.m^{-3} in Radvanice and 0,87 ng.m^{-3} in Vratimov; maximum 12-hr concentrations were 13,18 and 11,05 ng.m^{-3} respectively. Relevant concentrations were much lower in Poruba, an average of 0,37 ng.m^{-3} and a maximum of 2,71 ng.m^{-3}, An example of one day PAHs content is below. The content of light PAHs was much higher in the night sample of 27 May.

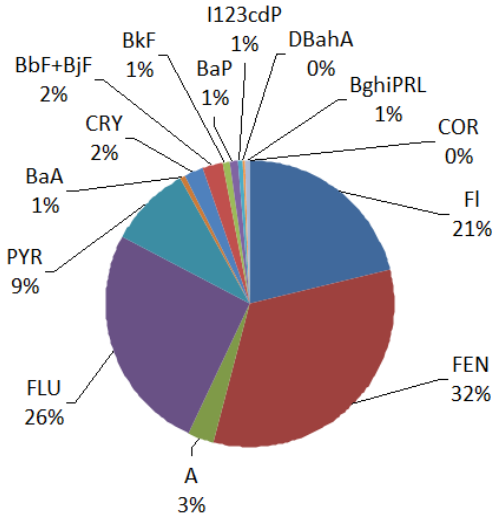

Figure 1. Radvanice, 27. 5. 2012, day: $PM_{2.5}$ = 15,26 µg.m^{-3}, PAHs = 44,4 ng.m^{-3}

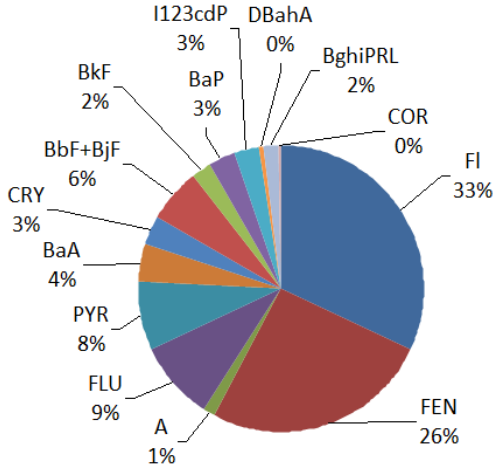

Figure 2. Radvanice, 27. 5. 2012, night: $PM_{2.5}$ = 19,58 µg.m^{-3}, PAHs = 191,2 ng.m^{-3}

The Impact of Select Pollutant Sources on Air Quality for Ostrava and the Moravian-Silesian Metropolitan Region by the Positive Matrix Factorization model

L. Černikovský[1], J. Novák[1], H. Plachá[1], B. Krejčí[1], I. Nikolova[1], E. Chalupníčková[1], T. Conner[2], G. Norris[2], K. Kovalcik[2], D. Olson[2], J. Turlington[2], C. Croghan[2], R. Willis[2], R. Williams[2]

[1]Czech Hydrometeorological Institute, Prague, Czech Republic
[2] U.S. Environmental Protection Agency, Research Triangle Park, North Carolina, USA
Keywords: Moravian-Silesian Region, source apportionment, positive matrix factorization, PMF
Presenting author email: cernikov@chmi.cz

The Ostrava region of the Moravian-Silesia metropolitan area of the Czech Republic represents one of the most highly industrialized areas in Eastern Europe with a large number of coke oven plants, blast furnaces, steel plants, and rolling mills being present. Ostrava is the third largest city in the Czech Republic containing 214 km^2 and with the country's third largest population (app. 300K). This equates to a population density about 1400 inhabitants/km^2. Its documented history dates back to the period of the 13th century. The discovery of high quality black coal in the mid 1700's and its access to four major river systems established the future direction of the area with respect to its industrial development. The primary metropolitan area is bordered by the Beskydy and Jeseniky mountain ranges. The presence of the large number of coal-related industries in addition to geographical conditions often results in weather-related pollution inversions which have a serious impact on local air quality. The region is connected with the Silesian voivodship in Poland which belongs to highly polluted areas by particulate matter and benzo*[a]*pyrene in Europe as well.

The Czech Hydrometeorological Institute (CHMI) working collaboratively with the U.S. Environmental Protection Agency (EPA) have designed a source apportionment study to determine the impact of regional as well as local sources on overall air quality for the region. Intensive (daily 12-hr day-night) fine particulate matter ($PM_{2.5}$), semi-volatile organic compounds (SVOCs), polycyclic aromatic hydrocarbons (PAHs), organic and elemental carbon (OC/EC), pollutant gases and meteorology were monitored for approximately a seven week period during the summer of 2012 and the late fall/early winter of 2012 at three primary monitoring locations (Poruba - background suburban in residential area; Radvanice - industrial suburban, downwind of prevailing winds from large industrial source; Vratimov – residential area upwind of prevailing winds from the same large industrial source). All the locations are highly polluted by PM and PAHs as well in the long term.

A variety of multivariate source apportionment models, such as positive matrix factorization (PMF), were be used to develop preliminary source impact categories. Findings associated with a preliminary source apportionment effort will be presented and will include summaries of the spatial (upwind versus downwind) and temporal (seasonal) variability of key source markers observed to influence local air quality.

In summer, large difference between $PM_{2.5}$ and PAHs was found between day and night in terms of concentrations and content as well. Average 12-hr PAHs concentration was 1,97 ng.m^{-3} in Radvanice and 0,87 ng.m^{-3} in Vratimov; maximum 12-hr concentrations were 13,18 and 11,05 ng.m^{-3} respectively. Relevant concentrations were much lower in Poruba, an average of 0,37 ng.m^{-3} and a maximum of 2,71 ng.m^{-3}, An example of one day PAHs content is below. The content of light PAHs was much higher in the night sample of 27 May.

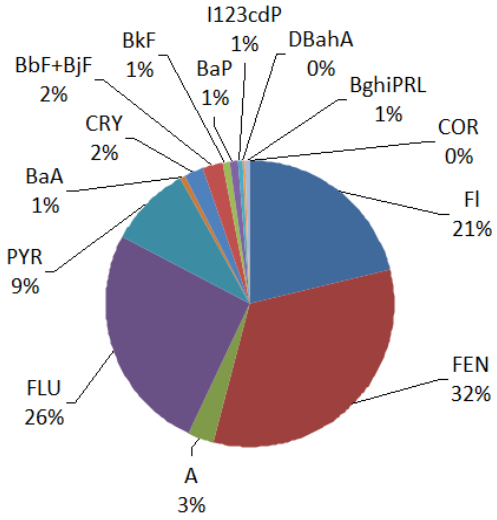

Figure 1. Radvanice, 27. 5. 2012, day: $PM_{2.5}$ = 15,26 µg.m^{-3}, PAHs = 44,4 ng.m^{-3}

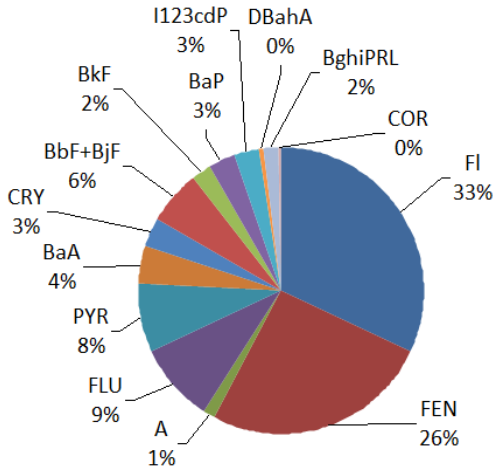

Figure 2. Radvanice, 27. 5. 2012, night: $PM_{2.5}$ = 19,58 µg.m^{-3}, PAHs = 191,2 ng.m^{-3}

Source apportionment of PM2.5 at Abu Dhabi sites

C. Hak and S. López-Aparicio

NILU – Norwegian Institute for Air Research, Kjeller, 2007, Norway
Keywords: PM2.5, source apportionment, PMF, Abu Dhabi.
Presenting author email: ch@nilu.no

Particulate matter (PM) is one of the most concerning pollutants in the United Arab Emirates. Air quality monitoring showed that concentrations of particulate matter are high in Abu Dhabi and frequently exceed international air quality limit and guideline values for the protection of human health. A considerable fraction expectedly originates from the natural background. Nearly 80% of Abu Dhabi consists of sandy desert and the north and west is composed of an extensive area of evaporite deposits (AGEDI, 2012; Glennie, 2001). Local industrial sources and traffic as well as long-range transported aerosol are also expected to contribute to the particle mass observed.

To our knowledge, no source apportionment study has been carried out in the area so far. For an efficient abatement strategy, a clear identification of the sources and their contributions to PM mass is needed.

The objective of this study is to identify and quantify the major sources to fine particle mass at two sites in the Emirate of Abu Dhabi. Positive Matrix Factorisation (PMF), a widely recognised receptor modelling method, was applied on chemically speciated data to find multiple sources of particles in the area and possible differences between the sites.

To achieve this, particle sampling was carried out at two sites in Abu Dhabi. One of the selected sites was a residential urban background site (Khalifa) in the city of Abu Dhabi. The other site was an urban background site (Bida Zayed) in the Western Region of the Emirate of Abu Dhabi. The measurements took place between March and November 2012.

Method

PM2.5 was sampled during 24 hours periods on a daily basis with sequential filter samplers using Teflon filters and Quartz fibre filters. 70 sampling days from each of the sites were analysed chemically. In order to determine the concentrations of elements and inorganic ions, Teflon filters were analysed by Inductively Coupled Plasma Mass Spectrometry (ICP-MS) and ion chromatography (IC; Table 1), respectively. Quartz fibre filters were analysed applying Thermal Optical Analysis (TOA; Table 1).

Table 1. Analytical methods and analysed species.

Elements (ICP-MS) Li, Be, Mg, Al, Si, K, Ti, V, Cr, Mn, Fe, Co, Ni, Cu, Zn, As, Se, Br, Rb, Sr, Y, Mo, Cd, Sn, Sb, Cs, Ba, Tl, Pb, Bi, Th, U
Inorganic ions (IC) SO_4^{2-}, NH_4^+, NO_3^-, Na^+, Cl^-, Mg^{2+}, Ca^{2+}, K^+
Carbonaceous fractions (TOA) OC1, OC2, OC3, OC4, PyrOC, EC1, EC2, EC3, Carbonate

The speciated PM2.5 data from both sites were analysed through EPA PMF3 to identify the PM sources.

Results and Conclusions

The median concentrations of individual compounds were very similar at both sites. Only for carbonate, a clear difference could be observed, showing higher concentration at Bida Zayed compared to Khalifa, pointing to different geological contributions.

An additional step was introduced into TOA in order to take into account carbonates, which are a non-negligible fraction of mineral dust in the area.

The study shows that secondary aerosol is a major contribution at both sites. The common source factors that were found at both sites were

- mineral dust, characterised by high loading of Ti, Fe, Al, Li, Mg, Y, Th etc
- traffic, characterised by non-exhaust markers (Zn, Cu, Sb, Mo) and carbonaceous fractions
- secondary aerosol, characterised by sulphate and ammonium and combustion signatures.

An industrial source factor was identified at both sites, although with different signatures, which can be interpreted as influence of different industries.

A sea salt factor was only identified at Khalifa. This site is located on the island housing the city of Abu Dhabi, whereas Bida Zayed is located about 50 km from the coast, explaining why a sea salt factor was not resolved.

The geology of the surface of Abu Dhabi is quite heterogeneous. An additional source factor, characterising natural contribution was only found at Bida Zayed and pointing to evaporite deposits. This is likely explained by the higher occurrence of sabkhas in the Western Region.

This work was financed by the Environment Agency Abu Dhabi (EAD), United Arab Emirates.

Glennie, K.W. (2001) *Evolution of the Emirates Land Surface: an Introduction in United Arab Emirates: A new perspective,* Trident Press.

AGEDI Abu Dhabi Global Environmental Data Initiative (2012) http://www.agedi.ae/Pages/index.aspx.

Comparison of PMx collected at sites with different level of air pollution using iron oxides as magnetic tracers

E. Petrovsky[1], B. Kotlik[2], A. Kapicka[1], M. Mikesova[2], R. Zboril[3] and H. Grison[1]

[1]Institute of Geophysics ASCR, Bocni II/1401, Prague 4, 14131, Czech Republic
[2]National Institute of Public Health, Srobarova 48, Prague 10, 10042, Czech Republic
[3]Regional Centre of Advanced Technologies and Materials, Palacky University, Slechtitelu 11, 783 71 Olomouc, Czech Republic
Keywords: PMx, magnetite, concentration, pollution
Presenting author email: b.kotlik@szu.cz

Iron oxides of both natural and anthropogenic origin form significant part of atmospheric dust and, depending on the source, transport pathways and deposition, may coexist with harmful substances, such as heavy metals. In case of specific situation, e.g. close neighbourhood of steel works, they may serve as magnetic tracer of the particular major source of air pollution. Therefore, knowledge on their form, concentration and grain size and shape may provide useful information in assessing the character and source of pollution. Methods developed in rock and environmental magnetism are very sensitive to minute amount of ferrimagnetic iron oxides (magnetite and maghemite) and have potential to provide this information (e.g., Sagnotti et al., 2006, 2009; Górka-Kostrubiec et al., 2012).

In our contribution we show typical differences in PMx properties collected at Czech sites with different level of air pollution during different periods. Sampling sites include industrial site (Bartovice – close to major steel works and Branany – close to open mine pit), traffic site (next to outer highway circle around Prague), urban site (Prague downtown) and rural site (town of Nove Hrady). Sampling periods include typically summer and winter period, one sampling campaign at Bartovice was during smoggy period when concentrations of PM10 significantly exceeded the daily limits. We typically sampled total suspended particles (TSP), PM10, PM2.5 and PM1. In addition to standard data on PMx concentration a range of laboratory magnetic measurements was carried out in order to reveal the type of iron oxides, their concentration and grain size. These measurements were complemented by scanning electron microscopy and Mossbauer spectroscopy. In all the cases, particles of typical spherical shape, rich in iron oxides, were observed (Fig. 1). Concentration of iron oxides reflects well general trends in air pollution, reflected by the concentration of PM10. Magnetic parameters sensitive to grain-size distribution of Fe-oxides are different for summer and winter PM10 samples in articular in the rural site, with clear shift towards finer particles in summer. This may reflect different source of PM, with dominant natural particles from agriculture and land-use activities in summer, compared to those produced by domestic heating in winter. No clear differences in grain size distribution of iron oxides were observed in the case of industrial site of Bartovice.

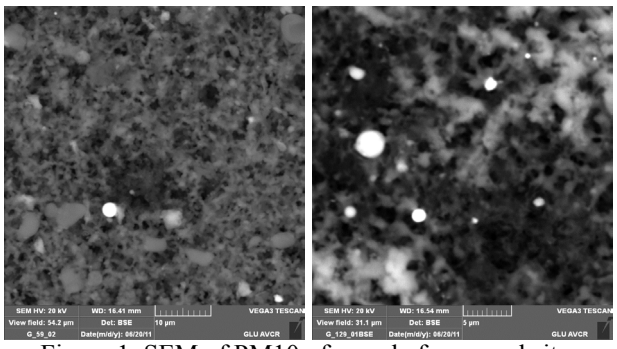

Figure 1. SEM of PM10 of sample from rural site, collected in non-heating (left) and heating (right) period.

Our results suggest that magnetic minerals (ferrimagnetic iron oxides – magnetite and maghemite) reflect well specific site and seasonal characteristics of air pollution and provide additional information related to relative contribution of major pollution sources.

This work was supported by the Czech Science Foundation under grant P210/10/0554.

Górka-Kostrubiec, B., Król, E. and Jeleńska, M., (2012) *Stud. Geophys. Geod.* **56**, 861-877, DOI: 10.1007 /s11200-010-9094-x

Sagnotti, L., Macri, P., Egli, R. and Mondino, M., (2006) *J. Geophys. Res.* **111**, B12S22, DOI: 10.1029 /2006JB004508

Sagnotti, L., Taddeucci, J., Winkler, A. and Cavallo, A., (2009) *Geochem. Geophys. Geosyst.* **10**, Q08Z06, DOI: 10.1029/2009GC002563 (2009)

Seasonal variability of the PMx chemical composition and ammonia concentration in loose-housing cowshed

M. Maasikmets[1, 2], A. Kaasik[3], A. Ruus[4], E. Teinemaa[1]

[1]Estonian Environmental Research Centre (EERC), Marja 4d, 10617 Tallinn, Estonia; [2]Estonian University of Life Science, Institute of Agricultural and Environmental Sciences, Kreutzwaldi 5, 51014 Tartu, Estonia; [3]Estonian University of Life Science, Institute of Veterinary Medicine and Animal Science, Kreutzwaldi 62, 51014 Tartu, Estonia; [4]Tallinn University of Technology (TUT), Tartu College of TUT, Department of Technology, Puiestee 78, 51008 Tartu, Estonia

Keywords: PMx, ammonia, livestock

Presenting author email: marek.maasikmets@klab.ee

Livestock housing is an important source of primary particulate matter (PM) emissions and contributing to secondary PM levels through emission of precursor gases such as ammonia (NH_3). Elevated levels of PM and NH_3 are harmful to environment, as well as to the human and livestock health. NH_3 can also participate in atmospheric reactions (e.g., gas-to-particle conversion) once airborne, forming ammonium aerosols such as ammonium sulphate, -nitrate, -chloride, which tend to have longer atmospheric residence lifetimes (1–15 days) due to a decrease in dry deposition velocity (Aneja et al. 1998) and therefore may be transported and deposited further downwind from the source (Blunden et al., 2008). PM emissions from livestock housings vary with type of housing and livestock. To assess impact to PM levels and contribution to secondary PM suitable emission factors (EF) is necessary to identify NH_3 levels in cowshed. The aim of the current study was to create emission factors and emission database for loose housing cowsheds as this is dominant type of housing used in Estonia. As indoor air of loose housing cowsheds are strongly influenced by ambient air patterns of PM10 and PM2.5, also ambient levels of PM were measured. Results enabled to identify actual emissions of the loose housing system during the whole year.

Microclimate parameters (temperature, °C; relative humidity, %); CO_2 and NH_3 concentration, (ppm) as well as fractional distribution of particulate matter (PM) mass ($\mu g/m^3$) and number (1/cm3) concentrations (size classes with aerodynamic diameter less than 10, 8.17, 5.18, 3.12, 1.97, 1.24, 0.77, 0.49, 0.32, 0.20, 0.12, 0.07 and 0.04 µm) were measured continuously at 2.5 meter height from the floor in semi-insulated loose housing cowshed in Märja, Estonia.

An electrical low pressure impactor (ELPI^{TM}, Dekati) with the sampling rate of 29.25 l/min was used for the measurements of mass and number concentration of the PM fractions. The minimum detection level at 1 stage for the mass concentration is 0.01 $\mu g/m^3$ and for the number concentration 142 $1/cm^3$. The upper concentration limit at 13 stage for the mass concentration is 8269 mg/m^3 and for the number concentration 2.7E+04 $1/cm^3$. At the particle inlet the Dekati® Dryer DD-600 was used. Ionic composition of the particles fractions were analyzed by ion chromatography (Dionex DX2000 and DX2100).

For the NH_3 the Picarro G2103 (Picarro) analyzer was used, which uses for the NH_3 detection the Wavelength-Scanned Cavity Ringdown Spectroscopy (WS-CRDS), with the range from 1 ppb to 50 ppm.

Wind direction and speed inside the cowshed was measured with 2D ultra-sonic anemometers (WMT-52, Vaisala), for the humidity measurement Vaisala HUMICAP® 180R sensors (HMT 130, Vaisala) were used, for the temperature measurements Pt1000 RTD Class F0.1 IEC 60751 sensors were used and for CO_2 measurements NDIR sensors were used (GMT 220, Vaisala).

For the PM10 and PM2.5 ambient measurement BAM 1020 (Met One Instruments Inc.) was used, which measures ambient particulate concentration using beta ray attenuation with 1 h resolution from 1 $\mu g/m^3$ to 1000 $\mu g/m^3$.

Results

Within measurement campaign was a significant correlation between measured NH_3, PMx and CO_2 concentrations and within NH_3, PM10 and RH significant correlation was found. This indicates that indoor concentrations are directly influenced by the ventilation rate. NH_3 in the air inside the cattle shed was more strongly correlated with the concentration of the fine fractions up to 1 µm of PM. Background concentrations of PM and NH_3 should be taken into account, which is not always the case if EF are calculated.

This work was supported by the Estonian Environmental Investment Fund and Estonian Science Foundation project BioAtmos.

Aneja, V. P., Murray, G. C. & Southerland, J. (1998). Atmospheric nitrogen compounds: emissions, transport, deposition, and assessment. Environmental Manager.

Blunden, J., Aneja, V. P. & Westerman, P. W. (2008). Measurement and analysis of ammonia and hydrogen sulfide emissions from a mechanically ventilated swine confinement building in North Carolina. Atmospheric Environment, 42(14), 3315-3331.

Contribution from wood burning to the PM10 aerosol at four urban background sites in Flanders, Belgium

W. Maenhaut[1,2], R. Vermeylen[2], M. Claeys[2], J. Vercauteren[3], C. Matheeussen[3] and E. Roekens[3]

[1]Department of Analytical Chemistry, Ghent University, Gent, BE-9000, Belgium
[2]Department of Pharmaceutical Sciences, University of Antwerp, Antwerpen, BE-2610, Belgium
[3]Flemish Environment Agency (VMM), Antwerpen, BE-2000, Belgium
Keywords: PM10, OC, EC, levoglucosan, wood burning.
Presenting author email: willy.maenhaut@ugent.be

In an earlier one-year study (2010-2011) the contribution from wood burning to the PM10 aerosol was assessed for 7 sites in Flanders, Belgium (Maenhaut *et al.*, 2012). As a follow-up of that work, a new one-year study was performed, whereby PM10 samplings were made every fourth day from 30 June 2011 until 2 July 2012 at a background site in each of the following cities: Antwerpen, Gent, Brugge, and Oostende. The site in Gent was also used in the earlier study, but the other sites were new ones. The samplings were done for 24 h and 47-mm diameter Pallflex® Tissuquartz™ 2500 QAT-UP filters were used. After sampling the PM10 mass concentration was determined by weighing; organic and elemental carbon (OC and EC) were measured by thermal-optical transmission analysis using the NIOSH protocol (Birch and Cary, 1996) and the wood burning tracers levoglucosan, mannosan, and galactosan were determined with gas chromatography / mass spectrometry.

As in the earlier study, the three wood burning tracers were very highly correlated with each other at each of the sites (all r> 0.95). There was little difference in the levoglucosan to mannosan (L/M) ratios of the 4 sites. The annual mean L/M ratios ranged from 8.9 to 9.9. These ratios are larger than in the 2010-2011 study, where they ranged from 6.2 to 7.1 for the 7 sites. From our L/M ratios we derived the relative contributions of softwood and hardwood burning, thereby using the same approach as used by Schmidl *et al.* (2008). It was found that softwood burning accounted, on average, for about 50%, and there was little variation in this percentage with site or with season. In the 2010-2011 study, the annual mean percentages were higher, i.e., around 70%. It is estimated that the uncertainty in those percentages is of the order of 10% points and that it is largely of a systematic nature (i.e., resulting from the calibration curves for levoglucosan and mannosan in the current and earlier studies). The difference between the 50% and 70% of the two studies may therefore not be significant.

Similarly as in the 2010-2011 study, the concentrations of the three anhydrosugars showed a pronounced seasonal variation with highest levels in winter and lowest ones in summer. The anhydrosugar data of the 4 sites were highly correlated with each other. For example, the between site correlation coefficients for levoglucosan were in the range 0.92-0.97 for 3 of our 4 sites (Antwerpen, Gent, and Oostende), while the correlation coefficients between the levoglucosan data from Brugge and those of the other 3 sites were in the range 0.79-0.83. High site-by-site correlation coefficients were also observed in the 2010-2011 study, where they were in the range 0.80-0.96 for 6 of the 7 sites (Maenhaut *et al.*, 2012). Like in the earlier study it can again be concluded that wood burning in Flanders is a regional scale phenolmenon and that it is probably taking place in many individual houses on similar occasions (e.g., on cold days, weekends or holidays). The slopes of the regression lines (forced through the origin) of the levoglucosan data of Gent, Brugge, and Oostende on the data from Antwerpen were 1.11, 1.06, and 0.77, respectively, and thus close to 1, which is again consistent with a regional phenomenon with many wood burning sources throughout Flanders. The lower slope for Oostende is attributed to the proximity to the North Sea, so that the air there is often diluted by maritime air.

The levoglucosan data were used to assess the contribution from wood burning to the OC and the PM10 mass (Schmidl *et al.*, 2008). More specifically, levoglucosan was multiplied by factors of 5.59 of 10.9 to obtain respectively the OC and PM10 mass concentrations from wood smoke. These contributions varied substantially with season (with for the contribution to the OC the largest percentage in winter, followed by autumn, spring, and summer), but there was little difference between the contributions of the 4 sites. The seasonal means of the contribution from wood burning to the OC were 15-19%, 3.6-5.8%, 20-25%, and 34-41% for spring, summer, autumn, and winter, respectively, whereby the ranges are the ranges of the means for the 4 sites. As to the PM10 mass, the seasonal means of the contribution from wood smoke were 2.3-3.3%, 0.55-1.3%, 5.9-9.0%, and 6.5-9.8% for spring, summer, autumn, and winter, respectively, whereby the lowest mean percentage in each season was observed for Oostende. Both for OC and the PM10 mass, the results of the current study show good resemblance to the results from the 2010-2011 study.

Birch, M.E. and Cary, R.A. (1996) *Aerosol Sci. Technol.* **25**, 221-241.

Maenhaut, W., Vermeylen, R., Claeys, M., Vercauteren, J., Matheeussen C. and Roekens, E. (2012) *Sci. Total Environ.* **437**, 226-236.

Schmidl, C., Marr, I.L., Caseiro, A., Kotianová, P., Berner, A., Bauer, H., Kasper-Giebl, A. and Puxbaum, H. (2008) *Atmos. Environ.* **42**, 126-141.

Characterization of submicron organic aerosol in Prague by ME 2 factor analysis of summer AMS data

O. Makeš[1], P. Vodička[1], J. Schwarz[1] and F. Canonaco[2], A.S.H. Prévôt[2], V. Ždímal[1]

[1]The Institute of Chemical Process Fundamentals of ASCR, v.v.i, Prague 6 - Suchdol, 165 02, Czech Republic
[2]Laboratory of Atmospheric Chemistry, Paul Scherrer Institut, 5232 Villigen PSI, Switzerland
Keywords: AMS, organic aerosol, PMF, ME-2
Presenting author email: makes@icpf.cas.cz

Real-time measurement of submicron aerosol was performed at Prague – Suchdol site (Czech Republic) during six weeks in June and July 2012. Highly time-and-size resolved data were obtained from measurements carried out by a Compact Time-of-Flight Aerosol Mass Spectrometer (C-ToF-AMS, Aerodyne). The retrieved organic data were deconvoluted using the Multilinear Engine (ME-2) algorithm (Paatero, 1999), and analyzed with the newly developed GUI provided by Paul Scherrer Institute (Canonaco *et al.* in prep.). The preliminary results are presented in this abstract.

The first step consisted of an unconstrained positive matrix factorization (PMF) on the organic aerosol (OA) data, of which main sources could be identified as a hydrocarbon-like organic aerosol (HOA), an oxygenated organic aerosol (OOA) and a biomass burning organic aerosol (BBOA). The identified PMF factors were compared with the aerosol and gaseous tracers (e.g. NO, O_3, CO, NO_3, SO_4) from collocated instruments.

In the second step, the PMF factor solutions were compared with reference spectra and an analysis of the data by the chemical mass balance (CMB) model followed. It was found that the four-factor solution obtained from PMF explained more than 95% of all the variance in the data.

In the next step, the four-factor solution attained by the previous analyses (PMF, CMB) was used to be further treated by constraining techniques. In this case we exploited the *a*-value approach (Lanz *et al.* 2007), which can be viewed as a combination of PMF and CMB. An external factor profile (a reference spectrum) and *a*-value were defined for each factor. The *a*-value determines the extent to which the output factor profile is allowed to vary from the input factor profile. These four factors, related to four aerosol sources, were fixed by the ME-2 model: HOA factor (*a*-val = 0,3) related to the road traffic, BBOA factor (*a*-val = 0,5), and two kinds of oxygenated organic aerosol factors (OOA I and OOA II). OOA I factor (*a*-val = 0,9) is most frequently interpreted as an aged aerosol with low volatility. On the contrary, diurnal patterns of OOA II factor (*a*-val = 0,9) exhibit maxima at night and high anti-correlation with temperature. Therefore it can be assumed that OOA II factor represents a volatile fraction of OOA.

Acknowledgement:
Financial support by the Czech Science Foundation (CSF P209/11/1342) is gratefully appreciated.

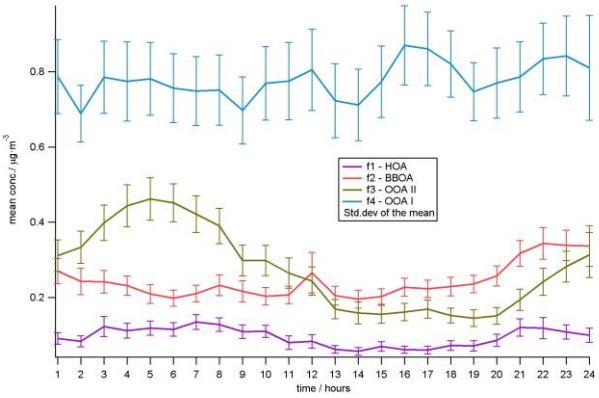

Fig. 1. Diurnal means and standard deviations of the contributions of all identified factors

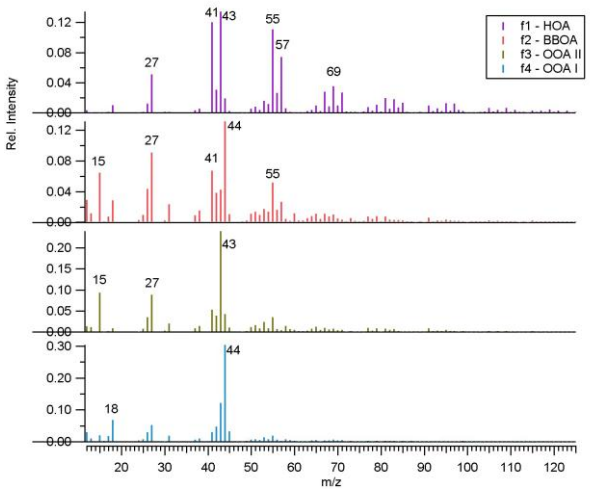

Fig. 2. Spectra of the four identified factors

References:
Canonaco F., et al. A newly developed interface for analyzing generalized Multilinear engine (ME-2) results: An example on aerosol mass spectrometer data over several months, in prep.

Lanz VA, et al. Source apportionment of submicron organic aerosols at an urban site by factor analytical modeling of aerosol mass spectra. Atmos Chem Phys. 2007; 7:1503–1522.

Paatero, P. The multilinear engine – a table-driven least squares program for solving multilinear problems, including the n-way parallel factor analysis model. J Comput Graph Stat. 1999;8:854–888.

Source apportionment in suburban environment during summer

L. Marmureanu[1], J. Vasilescu[1], D. Nicolae[1], F. Canonaco[2], J.G. Slowik[2], A.S.H. Prévôt[2]

[1] National Institute of Research and Development for Optoelectronics, Magurele, 077125, Romania
[2]Laboratory of Atmospheric Chemistry, Paul Scherrer Institut, 5232 Villigen PSI, Switzerland
Keywords: organic aerosols, mass spectrometry, levoglucosan fraction
Presenting author email: mluminita@inoe.ro

The atmospheric load of anthropogenic aerosol species is determined by factors such as emission, aging, convective transport and deposition processes, the level of scientific understanding being recognized to be medium to low (IPPC, 2007).

This study aims to identify the sources of aerosols in a suburban area near Bucharest, Romania, during the EMEP summer campaign, 7th June to 18th July 2012. Continuous measurements of submicron non-refractory aerosol composition with 10 minute time resolution from a C-Tof–AMS (Drewnik et al., 2005) and meteorological data (temperature) were used to characterize the local suburban aerosol.

The Hysplit trajectory model (Draxler R.R., et al, 2012) suggested that the site area was influenced by air masses coming mostly from west and south of Europe, therefore Saharan dust, aerosols from vegetation fires but also urban polluted aerosols could be present over the measurements' location during this campaign. Locally the agriculture activities are the most important sources of organic aerosols, mainly biomass burning.

In order to identify the main sources of aerosols at our site location we used the ME-2 algorithm to deconvolve the measured AMS organic mass spectra as described by Canocaco et al. (2013) and Lanz et al. (2008). Measurements influenced by high humidity and m/z 29 and 30 peaks due to air fragmentation were excluded from the entire dataset. Two factors were constrained during ME-2 analysis: biomass burning organic aerosol (BBOA) and hydrocarbon-like organic aerosol (HOA), and two unconstrained factors were also found: low-volatility oxygenated organic aerosol (LV-OOA) and semi-volatile oxygenated organic aerosol (SV-OOA).

BBOA was present during the entire measurement period. The ratio of organic m/z 60 (a characteristic fragment of sugars such as levoglucosan) to the total organics (denoted *f60*) often exceeded 0.003, the background level found by Cubison et al. (2011). The *f60* values exceeded this threshold for almost 70% of the measurements. In Figure 1, we show *f44* versus *f60*, which suggests the presence of BBOA and low volatility oxygenated organic aerosols (LV-OOA) organic aerosols (Cubison et al., 2011). BBOA likely derives from a combination of local agricultural activities and long-range transport.

The second constrained factor, HOA, is related to traffic activity and may be influenced by the ring road around Bucharest situated approximately 1 km from the sample location.

The time series of SV-OOA, correlation with NO_3 and diurnal pattern (not shown) indicate more local origin. LV-OOA has a more regional character, without a diurnal pattern, being correlated with long range transport (DeCarlo et al., 2010).

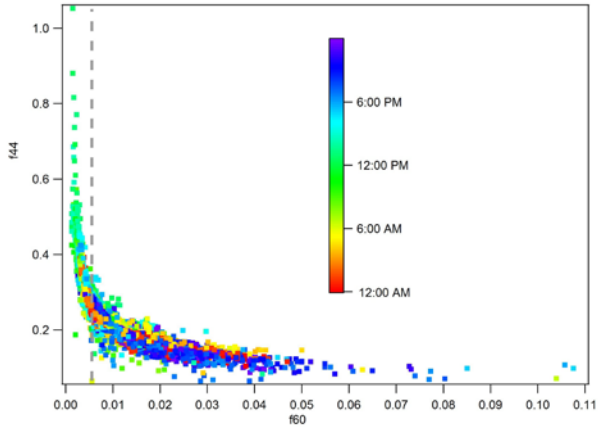

Figure 1 *f44* versus *f60* ratios for the entire campaign, 7th of June-18th of July

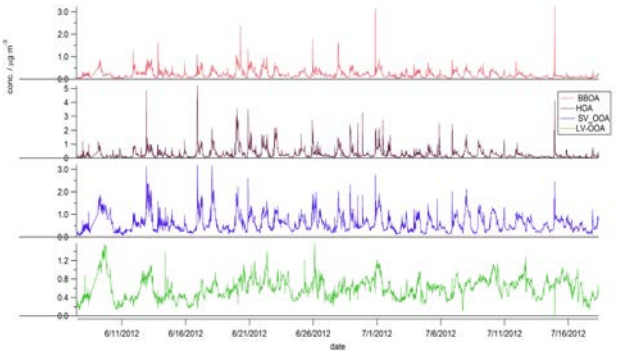

Figure 2 Time series of source apportioned organic components

This work was partially supported by the Romanian National Authority for Scientific Research, CNCS – UEFISCDI, project number PN-II-RU-PD-2011-3-0082, and the Romanian-Swiss project AEROS (AErosols in ROmania and Switzerland).

Canonaco et al.,(2013) Atmos. Chem. Phys, in prep.
Cubison, M. J., et al (2011) Atmos. Chem. Phys., 11, **12049–12064**
DeCarlo et al., (2010) Atmos. Chem. Phys.,10, 5**257-5280**
Draxler R.R., et al, (2012), HYSPLIT (HYbrid Single-Particle Lagrangian Integrated Trajectory) Model access via NOAA ARL READY Website
Drewnick, F., S.S. et al., (2005) Aerosol Science and Technology, **39:637–658**,
Lanz, V.A., M.R. et al., (2008) Environmental Science & Technology, 42(1), **214-220**.

The contribution of winter sanding to PM_{10} concentrations at traffic stations in the Czech Republic in 2011

Leona Matoušková[1]

[1]Air Quality Protection Division, Czech Hydrometeorological Institute, Prague 4, 143 06, Czech Republic
Keywords: PM_{10}, winter sanding
Presenting author email: leona.matouskova@chmi.cz

Air pollution caused by PM_{10} remains one of the main problems of air quality assurance in the Czech Republic. The exceedance of the daily limit value for PM_{10} in 2011 at least in one locality was recorded in all zones and agglomerations. Of the total number of 157 localities in which PM_{10} measurements were carried out in 2011, 89 localities reported exceedances of 24-hour PM_{10} limit value.

The concentrations of PM_{10} show a clear course with the highest concentrations in the cold months of the year. Higher concentrations of PM_{10} in the ambient air during the cold part of the year may be influenced both by higher emissions of particles from seasonal sources (e.g. the share of local heating as concerns PM_{10} emissions is more than 30 %), and by deteriorated dispersion conditions. The maximum concentrations in February and November correspond with bad dispersion conditions in these months (Matoušková and Ostanická eds., 2012).

According to EC (2011), higher concentrations of during the cold part of the year may be also influenced by the re-suspension of particulates following winter sanding or salting of roads. This guidance recommends methods for the determination of the contributions of these processes to the ambient concentrations of PM. Member States may designate zones or agglomerations within which limit values for PM_{10} are exceeded in ambient air due to the re-suspension of particulates following winter-sanding (EC, 2008). The proposed method (based on results from Northern Europe) assumes the contribution from winter sanding to be 50 % of the coarse fraction (PM_{10}-$PM_{2.5}$) for each exceedance day with an identified impact from winter sanding. This contribution can be subtracted from the observed PM_{10} concentration if the following criteria apply (EC, 2008): there was road sand or the remains of it actually on the road or adjacent footpaths; $PM_{2.5}$ measurements at the same site at which the PM_{10} exceedance has been observed if it is possible; the road surface was dry; the $PM_{2.5}/PM_{10}$ ratio is equal or less than 0.5. This criterion selects days with high local contributions of coarse particles and excludes high contributions from long-range transport.

On the assumption that these conditions were met, the analysis for five traffic stations in the Czech Republic has been possible to carry out. The averages of $PM_{2.5}/PM_{10}$ ratio at these five sites are higher than 0.5. They range from 0.52 to 0.84. Furthermore, lower ratio approaching the value 0.5 occurs mostly from April to September. Further, we take into the account the period January-March and November-December according to Austrian study (EC, 2011) for the subtraction of the contribution of winter sanding to PM_{10} concentrations. Consequently, it was possible to identify only a few days, where both the conditions of the $PM_{2.5}/PM_{10}$ ratio less than 0.5 and the concentrations of PM_{10} higher than daily limit value (50 $\mu g.m^{-3}$) were met (Table 1).

Table 1. The contribution of winter sanding to PM_{10} concentrations at five traffic sites in the Czech Republic

Monitoring site	Days > 50 $\mu g.m^{-3}$	Days with the ratio < 0,5 and PM_{10} > 50 $\mu g.m^{-3}$	Days > 50 $\mu g.m^{-3}$ after reduction
Brno-Svatoplukova	85	1	85
Brno-Zvonařka	59	0	59
Hradec Králové	49	0	49
Prague 9-Vysočany	**46**	**14**	**36**
Beroun	**53**	**21**	**40**

Based on these results, the contribution of winter sanding to PM_{10} concentrations in the Czech Republic is neglected. The achievement of maximal 35 exceedances of the daily limit value has not been met at sites suitable for this analysis. Our results are consistent with the conclusion that more sophisticated methods might be needed in Central European countries for attributing an exceedance to winter sanding (EC, 2011).

EC (2008) *Directive 2008/50/EC of the European Parliament and the Council relating to Air Quality and Clean Air for Europe*

EC (2011) *Working paper establishing guidelines for determination of contributions from the resuspension of particulates following winter sanding or salting of roads under the Directive 2008/50/EC on ambient air quality and cleaner air for Europe*

Ostatnická, J., Matoušková, L. eds. (2012) *Znečištění ovzduší na území České republiky v roce 2011 (Air Pollution in the Czech Republic in 2011)*, Czech Hydrometeorological Institute

Size distributed metallic elements in submicron and ultrafine atmospheric particles from urban and industrial areas: a source assessment

S. Mbengue [1,2], L. Alleman [1,2] and P. Flament [1,3]

[1] Univ Lille Nord de France, F-59000 Lille, France
[2] Mines Douai, CE, F-59508 Douai, France
[3] ULCO, LPCA, F-59240 Dunkerque, France
Keywords : particles, size distribution, metallic elements, enrichment factor
saliou.mbengue@mines-douai.fr

In recent decades, studies have evidenced the relationship between high concentrations of airborne particles (PM) and increased mortality and morbidity related to respiratory and cardiovascular diseases (Künzli *et al.,* 2000; Pope et Dockey, 2006). PM_{10} and $PM_{2,5}$ are usually selected as the monitoring parameters for air quality evaluations. However metallic elements associated with inhalable particles, particularly in the finest fraction, have been shown to increase human lung and cardiopulmonary injuries (Schaumann *et al.,* 2004; Osornio-Vargaset *et al.*, 2003). In toxicology and source assessment, particle size is a key parameter. The objective of the present study is to give new insights about the size distribution and source emissions of potentially toxic heavy metals in an urbano-industrial area representative of other major industrial regions in Europe.

The $PM_{10,}$ PM_1 and $PM_{ultrafine}$ fractions were collected under "industrial" and "urban-traffic" wind sectors, in one of the largest industrial cities of France (Dunkirk) during winter 2012. The PM were sampled using low pressure cascade impactors and elemental analyses were performed by ICP-AES (Al, Ca, Fe K, Mg and Na) and ICP-MS (As, Ba, Cd, Co, Cr, Cu, La, Mn, Mo, Ni, Pb, Rb, Sb, Sr, Ti, V and Zn).

Both, meteorological conditions and emission sources variability were found to be important parameters that control the size distribution and the chemical composition of particles. The PM_{10}, PM_1 and $PM_{0.29}$ mass concentrations were respectively 23.6 ± 6.0, 10.1 ± 4.1 and 2.4 ± 1.1 µg/m^3, under industrial influence and 29.8 ± 4.1, 16.6 ± 3.9 and 5.8 ± 2.1 µg/m^3 under urban-traffic influence. Regarding the relative concentration of the twenty three elements investigated, the submicron fractions (PM_1 and $PM_{0.29}$) accounted respectively for about 41.8 ± 10.8% and 9.8 ± 2.4% of the PM_{10} mass for the industrial sector and 56.8 ± 16.2% and 20.2 ± 9.3% for the urban-traffic one. This comparison suggests that urban sources produce, in average, finer particles and in a larger amount than industrial sources. Regarding the relative concentration of metallic elements, the submicron fractions (PM_1) represented 46 ± 24 % for industrial and 52 ± 23 % for urban-traffic sectors, with generally higher proportions for the ultrafine fraction ($PM_{0.29}$) under an urban-traffic sector influence (14 ± 8% and 24 ± 9%, respectively), associated to sources located within the city and suburban traffic.

This result imply that, even for an urban environment potentially influenced by the proximity of metallurgical activities, traffic within the urban district and nearby house heating may overwhelmingly influence the metallic content of atmospheric nanoparticles. However, industrial processes may significantly affect the neighboring urban atmosphere with metal-rich particles, especially in the accumulation mode ($PM_{0.29-1}$). They have been attributed, in this size range, to primary particles emitted by steelworks and metal refinery processes. These aerosols can easily reach our sampling site located in the nearby urban area (2000 m). We also evidenced that vehicular emissions remain the main sources of Cu and Sb in the submicron fraction.

This work was part of a program from the "Institut de Recherche en ENvironnement Industriel" (IRENI) and was financially supported by the Nord-Pas-de-Calais Regional Council, the French Ministry of Higher Education and Research, the European Regional Development Fund (ERDF) and Ecole des Mines de Douai.

Künzli, N., Kaiser, R., Medina, S., Studnicka, M., Chanel, O., Filliger, P., Herry, M., Horak Jr, F., Puybonnieux-Texier, V., Quénel, P., Schneider, J., Seethaler, R., Vergnaud, J-C. Sommer, H. (2000) *The Lancet* **356**, 795-801.

Osornio-Vargas, A., Bonner, J. C., Alfaro-Moreno, E., Martinez, L., Garcia-Cuellar, C., Poncede-Leon Rosales, S., et al., (2003) *Environ. Health Perspect.* 111, 1289–1293.

Pope, A.C., Dockery, D.W., (2006) *Air & Waste Manage. Assoc.* **56**,709–742.

Schaumann, F., Borm, P.J.A., Herbrich, A., Knoch, J., Pitz, M., Schins, R.P.F., Luettig, B., Hohlfeld, J.M., Heinrich, J., Krug, N. (2004) *Am. J. Respir. Crit. Care Med.* **170**, 898–903.

Estimation of Non-Exhaust Emissions in PM_{10} Road Dust in Birmingham, UK

Pallavi Pant[1] and Roy M. Harrison[1,2]

[1]School of Geography, Earth and Environmental Studies, University of Birmingham, Edgbaston, Birmingham, B15 2TT, UK
[2]Department of Environmental Sciences/Centre of Excellence in Environmental Studies, King Abdulaziz University, PO Box 80203, Jeddah(21589), Saudi Arabia
Keywords: road dust, traffic, PM_{10}, non-exhaust emissions
Presenting author email: pxp024@bham.ac.uk

Non-exhaust emissions constitute an important fraction of total road traffic emissions and becoming increasingly important to achieve air quality targets (Denier van der Gon *et al.*, 2013). Road dust consists of primarily coarse-sized particles derived from different sources such as wear and tear of vehicle components (brakes, tyres and clutches) and road surface, engine corrosion, tailpipe emissions, crustal dust and other emissions sources. The aim of this study was to characterize the metal concentrations in road dust in a busy traffic tunnel in UK.

Sampling of PM_{10} road dust was conducted in the Queensway Tunnel in Birmingham, UK in September 2012 using the dust resuspension chamber (Amato *et al.*, 2009). The samples were collected using 47mm PTFE filters and extracted using reverse aqua regia. A total of 14 elements were analysed including Si, Al, S and Fe with energy-dispersive x-ray fluorescence (EDXRF) and Zn, Cu, Ba, Sb, Mn, Cd, Ni, using inductively coupled plasma mass spectrometry (ICP-MS). Details of the chemical analysis methodology are presented in Gietl et al. (2010).

Based on Pearson correlation analysis, two major groups of elements were identified, each with statistically significant correlations among the elements in the group: crustal elements including Al, Si and Fe (r^2>0.99) and traffic-related elements such as Cu, Zn, Sb, Ba and Mn. Interestingly, while Ti was found to be correlated to traffic-related elements, Ni was not found to be correlated to either group. S showed higher correlation to the crustal elements (r^2>0.91) compared to traffic-related elements (r^2>0.60-0.64). The traffic-related elements could not be subdivided into tyre/brake wear categories based on correlation analysis.

Table 1: Elemental Ratios for PM_{10}

	Si/Al	Fe/(Al+Si)	Cu/Sb
Average	3.91	0.21	7.44

A diagnostic ratio of 7.0 ±1.9 has been proposed for brake wear particles (Amato *et al.*, 2009) and in the current study, a Cu/Sb value of 7.5 was observed indicating the contribution of brake wear particles. The Si/Al ratio was also observed to be corresponding to previously reported values in the literature.

Using Ba and Zn as markers for brake wear and tyre wear and the conversion ratios reported in Harrison et al. (2012), contributions of brake dust and tyre dust to PM_{10} were calculated to be 6.6% and 15.6% respectively. However, the percentage of tyre dust might be an over-estimate owing to the several different sources of Zn.

Similar measurements are currently being made in roads with different traffic loads to estimate the contribution of traffic emissions to PM_{10} under different traffic conditions.

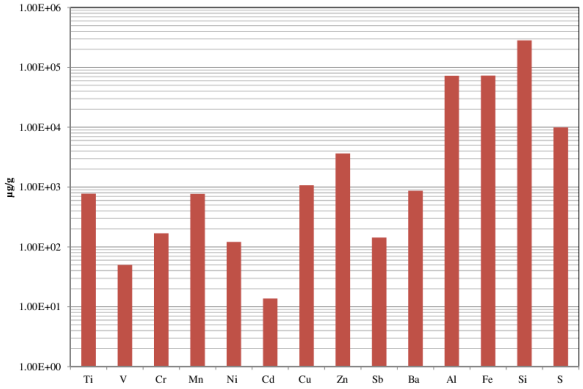

Figure 1: Average concentrations of trace metals in PM_{10} road dust

The authors would like to thank Amey and Massimiliano Mascelloni (University of Birmingham) for assistance during sampling and Dr. Stephen Baker for help with chemical analysis. Pallavi Pant gratefully acknowledges financial support from the University of Birmingham.

Amato, F., Pandolfi, M., Viana, M., Querol, X., Alastuey, A. and Moreno, T. (2009) Atmos. Env. 43, 1650-1659.

Denier van der Gon, H., Gerlofs-Nijland, M.E., Gehrig, R., Gustafsson, M., Janssen, N., Harrison, R.M., Hulskotte, J., Johansson, C., Jozwicka, M., Keuken, M., Krijgsheld, K., Ntziachristos, L., Riediker, M. and Cassee, F.R. (2013) *J. Air Waste Manage. Assoc.* **63(2)**, 141-146.

Gietl, J., Lawrence, R., Thorpe, A.J. and Harrison, R.M. (2010) *Atmos. Env.* **44**, 141-146.

Harrison, R.M., Jones, A.M., Gietl, J., Yin, J. and Green, D.C. (2012) *Env. Sci. Tech.* **46(12)**, 6523-6529.

Elemental composition and source identification of $PM_{0.09-0.26}$ in European air pollution hot-spot

P. Pokorná[1], J. Hovorka[1] and P.K. Hopke[2]

[1] Institute for Environmental Studies, Faculty of Science, Charles University in Prague, Benátská 2, 128 01, Prague 2, Czech Republic

[2]Center for Air Resources Engineering and Science, Clarkson University, Box 5708, Potsdam, NY 13699-5708, USA

Keywords: Highly time resolved aerosol elemental composition, DRUM, PMF, Source identification.

Presenting author email: petra.karkulin@post.cz

The ambient aerosol source composition is particle size dependent (Dodd, 1991). Therefore, to improve the accuracy of aerosol source apportionment, size segregated aerosol measurement with high time resolution is required (Han, 2005; Peré-Trepat, 2007). Usually, mode of aerosol particle number distribution is within 80-130 nm the objective of presented study was to identify sources of $PM_{0.09-0.26}$ in industrial city Ostrava in Czech Republic, Central Europe.

Measurements were conducted from 26th Jan to 21st Feb 2012 in Ostrava city in the north-east part of the Czech Republic. Mainly due to accumulation of steel industry and coke plants, the city counts among the worst air quality region in EU.

$PM_{0.09-0.26}$ was sampled by the 8 stage Davis Rotating-drum Uniform-size-cut Monitoring (8DRUM) with 2-h time resolution (last stage of 8DRUM). The 120 minute integrates of aerosol mass within the desired size range was calculated from five minute data by Scanning mobility Particle Sizer, (SMPSL-3936, L-25, TSI) Also $PM_{2.5}$ by 7 laser photometers DustTrak, DT (8520, TSI) were measured to evaluate PM2.5 middle-scale variability. Complete meteorology wind speed (WS) wind direction (WD), temperature (T), relative humidity (RH), global radiation (GR), precipitation (P) were also concurrently recorded.

A bilinear receptor model, EPA PMF 4.2.0.0, was used to resolve the possible sources for 120 minutes integrations of mass concentrations with size interval 91.4 – 259.5 nm and elemental composition for 28 elements analyzed by S-XRF at the Advanced Light Source, Lawrence Berkeley National Laboratory, CA.

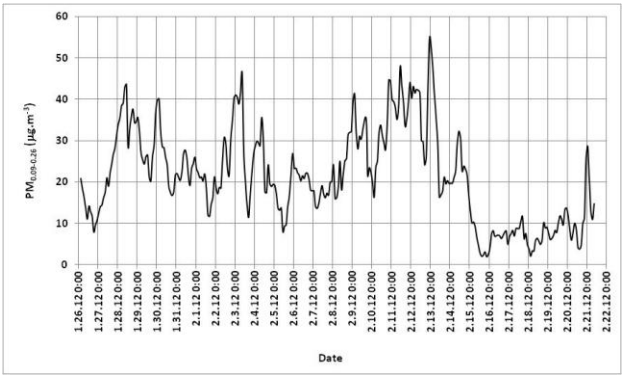

Figure 1. Dynamics of two hours averages of $PM_{0.09-0.26}$ in Ostrava 26.1-22.2. 2012.

According to the different meteorological condition and $PM_{0.09-0.26}$ concentration is it possible to separate the measuring campaign to two periods. The smog period characterised by low T (median=-14.8 °C), WS (median=0.7 $m.s^{-1}$), WD prevailing from NE and high $PM_{0.09-0.26}$ (median=23.4 $\mu g.m^{-3}$) lasted from 26th Jan to 14th Feb. The after smog period (15th – 21st Feb) was characterised by grow of T (median=-1.7 °C), WS (median=1.1 $m.s^{-1}$), WD prevailing from NW to SW and precipitation, which resulted in $PM_{0.09-0.26}$ decrease (median=7.4 $\mu g.m^{-3}$) (Figure 1.). The $PM_{0.09-0.26}$ median values of elements with highest total mass concentration measured during the sampling campaign are quoted in the Table 1.

Table 1. The $PM_{0.09-0.26}$ median values of main elements.

Element	Median ($ng.m^{-3}$)	Element	Median ($ng.m^{-3}$)
Na	65.2	K	63.5
Si	13.3	Fe	5.3
S	285.1	Zn	17.5
Cl	19.9	Pb	6.9

The $PM_{2.5}$ inter-DT differences in the course of measurement were not statistically significant. As result the monitoring station position was eligible and air monitoring data representative for the urban environment.

The PMF resolved six possible factors of them two were identified to account for about 70 % and 20 % of $PM_{0.09-0.26}$ mass respectively. The first was related to Pb, Cu, Co and S and the second to As, Zn, K and S. Both the sources were attributed to high temperature processes.

This work was supported by the Grant Agency of the Czech Republic under the project GAP503/12/G147.

Dodd, J.A., Ondov, J.M., Tuncel, G., Dzubay, T.G., Stevens, R.K. (1991) *Environ. Sci. & Techol.* **25**, 890-903.

Han, J.S., Moon, K.J., Ryu, S.Y., Kim, Y.J., Perry, K.D. (2005) *Atmos. Environ.* **39**, 3113–3125.

Peré-Trepart, E., Kim, E., Paatero, P., Hopke, P.K. (2007) *Atmos. Environ.* **41**, 5921-5933.

$PM_{2.5}$ chemical composition and source apportionment in the Po Valley: the Med Particles and Supersito projects preliminary results

F. Scotto[1], S. Ferrari[1], I. Ricciardelli[1], R. Vecchi[2], G. Valli[2], A. Piazzalunga[3] and V. Poluzzi[1]

[1]Regional Agency for Environmental Protection in the Emilia-Romagna region, Bologna, I-40138 Italy
[2]Department of Physics, Università degli Studi di Milano, Milan, I-20133 Italy
[3]Department of Earth and Environmental Sciences, University of Milano-Bicocca, Milan, I-20126 Italy

Keywords: source apportionment, atmospheric aerosol, $PM_{2.5}$, PMF
Presenting author email: iricciardelli@arpa.emr.it

Recent studies claim that PM10 is responsible for the most significant short-term effects on human health, while PM2.5 is likely responsible for the most severe health effects overall. Therefore, well-characterized PM2.5 data are requested by epidemiological studies to better understand the relationship between air pollution and adverse health effects.

Med Particles and Supersito projects aim at a better understanding of the PM air pollution characteristics in some European cities of the Mediterranean region and their interconnections with human health. A common goal of the two projects is to perform the PM2.5 mass closure and source apportionment in an area where scarse information on this size fraction is still available.

In this paper we discuss preliminary results about the PM2.5 chemical composition and its source apportionment obtained for Bologna urban area. The city of Bologna is located in the south-eastern part of the Po valley (Italy), a region which is considered a pollution hot spot as many exceedances of the 50/2008 EU Directive daily limit value for PM10 are registered.

The sampling period has been from October 2012 to March 2013. This is typically a period when the Po valley weather is characterized by several days of thermal inversion, fog, absence of wind and low temperature.

Parallel 24-h samplings have been carried out on quartz fibre and PTFE filters at the urban station in Bologna.

Ions (nitrate, sulphate, ammonium, sodium, potassium, magnesium, calcium, chloride, bromide and phosphate) have been analysed by ion chromatography on quartz fibre filters.

Elemental and Organic Carbon (EC/OC) have been analysed on quartz fibre filters with a transmittance thermal-optical instrument (Sunset Laboratory inc.) using the EUSAAR-2 thermal protocol.

Levoglucosan, mannosan and galactosan have been determined on PTFE filters using high performance anion-exchange chromatography coupled with pulsed amperometric detection following the procedure described in Piazzalunga et al. (2010).

Elemental analysis (Na, Mg, Al, Si, S, Cl, K, Ca, Ti, V, Cr, Mn, Fe, Ni, Cu, Zn, Ga, Ge, As, Se, Br, Rb, Sr, Y, Zr, Mo, Ba, Pb) has been performed by ED-XRF spectrometry on PTFE filters.

The chemical characterization performed on about 200 samples allows to detect specific components or sources of particulate matter such as marine aerosol (Na, Cl, Mg), mineral dust (Al, Si, Ca, Ti, Sr), secondary inorganic components (e.g. sulphates and nitrates), biomass burning products (levoglucosan, K^+, Zn, Rb), heavy oil combustion (V, Ni), incinerator emissions (K, Zn, Pb), traffic (EC, OC, Cu, Fe, Mn), and industrial emissions (EC, OC, Mn, Ni, Zn, Pb).

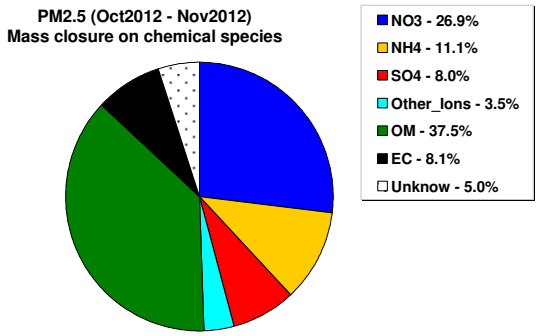

The whole dataset is analysed by Positive Matrix Factorization to identify major PM2.5 sources impacting the area and to obtain source apportionment.

This study was funded by the EC LIFE Environment Program under the project "Med-Particles - Particles size and composition in Mediterranean countries: geographical variability and short-term health".

Funding has been also obtained from the project "Supersito" approved and financed by Regione Emilia-Romagna and Regional Agency of Environmental Protection (Arpa) of Emilia-Romagna (DGR 428/2010).

Piazzalunga A., Fermo P., Bernardoni V., Vecchi R., Valli G., De Gregorio M.A. (2010). *Intern. J. Environ. Anal. Chem.,* **90** (12): 934–947

Traffic-generated changes in the chemical composition of 13 fractions of PM in an urban area of Upper Silesia, Poland.

W. Rogula-Kozłowska

Institute of Environmental Engineering, Polish Academy of Sciences, 34 M. Skłodowska Curie St., 41-819 Zabrze, Poland

Keywords: chemical mass closure, traffic, size-resolved chemical composition.

email: wioletta@ipis.zabrze.pl

Within urbanized areas, the growth of road traffic intensity is correlated with the growth of the ambient concentrations of particulate matter (PM) and its components. The aim of the study was to determine the influence of road traffic on chemical composition of 13 fractions of PM in a typical urban area of Upper Silesia.

PM was sampled simultaneously at two sites in Katowice (Upper Silesia, Poland). One of the measuring points, located in the city centre, represented so-called urban background (UB). The second point (HW), located near the A4 motorway, was directly exposed to the traffic emission. PM was sampled in summer 2012 using two thirteen-stage DEKATI cascade impactors. The samples were analyzed for carbon (organic and elemental), water soluble ions (Na^+, NH_4^+, K^+, Mg^{2+}, Ca^{2+}, Cl^-, NO_3^-, SO_4^{2-}) and concentrations of 24 elements by using, respectively, a Sunset Laboratory carbon analyzer, a Herisau Metrohm AG ion chromatograph, and a PANalitycal EPSILON 5 X-ray fluorescence spectrometer.

To perform the mass closure calculations for each dust fraction in the measuring period the PM chemical components were categorized into seven classes (Tab. 1) according to Rogula-Kozłowska et al. (2012; 2013).

Table 1. Chemical mass closure for 13 dust fractions at HW and UB in Katowice.

	EC	OM	SIA	NaCl	CM	TE	UM
HW	**%**						
>10	5.5	28.6	7.2	5.6	18.3	3.7	31.2
6.8-10	6.7	31	8.6	9.7	18	3.8	22.2
4.4-6.8	12.1	48.8	9.3	5.5	23.6	4.1	-3.4
2.5-4.4	9.8	36.1	8.5	3.3	20.2	2.8	19.4
1.6-2.5	6.9	37.5	13.9	3.3	7.2	9.7	21.5
1-1.6	3.3	53.4	21	2.8	2.4	4	13
0.65-1	2.4	51.9	22.5	2.5	0.8	1.8	18
0.4-0.65	2.6	43.4	21.3	2.4	1	1.4	27.9
0.26-0.4	3.4	37.8	17.6	2.5	1.4	1.3	36
0.17-0.26	8.3	33.5	15	2.9	1.3	1.6	37.5
0.108-0.17	13.7	32	10.9	3.3	2	2.5	35.6
0.06-0.108	10.2	24.2	8.9	3	2.1	3.2	48.5
0.03-0.06	10.6	38.3	13.4	4.8	4.1	7	21.9
UB	**%**						
>10	5.1	32.2	12.3	7	19.9	4.9	18.5
6.8-10	8.1	43.1	13.5	5.6	16.7	6.1	6.9
4.4-6.8	8.5	41.5	12.2	5	21.5	4.5	6.8
2.5-4.4	5.7	33.9	11.2	4.3	17.6	3	24.3
1.6-2.5	3.4	37	16.9	3.6	6.6	6	26.5
1-1.6	2	52.9	19.1	2.7	2	3.7	17.6
0.65-1	1.6	52.4	23.6	2.5	0.8	1.8	17.2
0.4-0.65	1.7	42.9	21	2.4	1	1.3	29.7
0.26-0.4	1.3	38.8	17.6	2.4	1.7	1.2	37
0.17-0.26	2.1	30.8	15.6	2.6	2	1.7	45.2
0.108-0.17	2.6	34.2	14.6	4.7	3.7	3.9	36.3
0.06-0.108	3.2	34.9	18.1	6.9	8.4	7.3	21.2
0.03-0.06	3.1	39.6	19.8	9.7	12.1	11.6	4.1

EC-elemental carbon, OM – organic matter, SIA – secondary inorganic aerosol, CM – crustal matter, TE – trace elements, UM – unidentified matter

The concentrations of PM_1, $PM_{2.5}$, PM_{10} and of total PM did not differ significantly between the measuring points. The concentrations of the particles with the aerodynamic diameters smaller than 1 µm differed more explicitly.

The effect of traffic at HW showed as the high concentrations of elemental carbon (EC, significantly higher than at UB, Fig. 1). $PM_{0.108\text{-}0.17}$- and $PM_{0.06\text{-}0.108}$-bound EC had the ambient concentrations 8 times greater at HW than at UB and the mass contributions to PM--6 times. In Katowice, because of municipal emission and poor quality of the vehicle fleet, also the coarse fraction of dust was enriched in EC. Such a phenomenon is unusual if compared with other European regions.

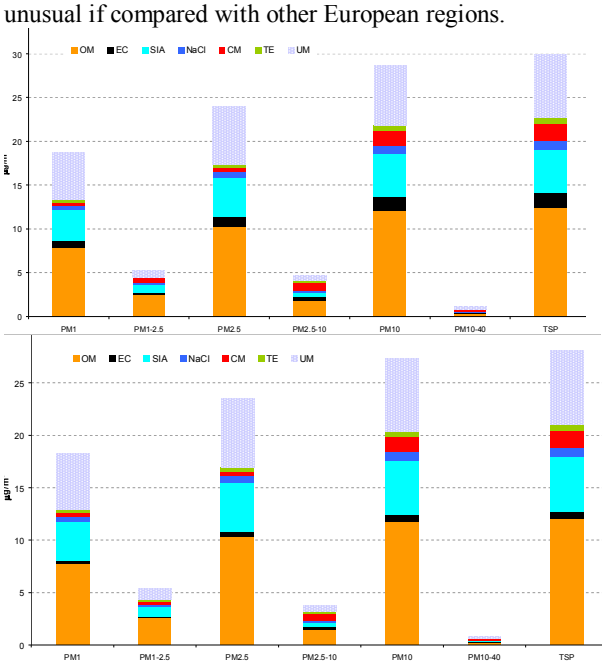

Figure 1. Concentrations of PM components in selected dust fractions at HW (top diagram) and UB (bottom diagram).

The work was supported by the grant No. N N523 564038 from the Polish Ministry of Science and Higher Education.

Rogula-Kozłowska W., Klejnowski K., Rogula-Kopiec P., Mathews B., Szopa S. (2012) *Bull. Environ. Contam. Toxicol.*, 88, 722–729.

Rogula-Kozłowska W., Klejnowski K. (2013) *Bull. Environ. Contam. Toxicol.*, 90, 103-109.

PM_1 chemical and mineralogical characterization near a crude oil pre-treatment plant (Agri Valley) during an emergency procedure

S. Trippetta[1], R. Caggiano[1], S. Margiotta[1], S. Sabia[1], A. Speranza[1], V. Summa[1]

[1]IMAA, Istituto di Metodologie per l'Analisi Ambientale, CNR, C.da S. Loja, Z.I., 85050, Tito Scalo (PZ), Italy
Keywords: PM_1, trace elements, mineralogy.
Presenting author email: serena.trippetta@imaa.cnr.it

Systematic PM_1 (i.e., aerosol particles with aerodynamic diameter less than 1 μm) measurements have been performed in Agri Valley (Basilicata Region - Southern Italy) since December 2011.

This area is of great concern in environmental and health-related studies since it houses the largest European on-shore reservoir and one of the largest crude oil pre-treatment plant within an anthropized area. In this plant, identified as Centro Olio Val d'Agri (COVA), oil stabilization and gas conditioning are performed implying continuous gaseous and particulate emissions. Moreover, emergency procedures aimed at plant depressurization occasionally occur involving great concern in population living near the COVA plant due to the rise of the height of the control flames that continuously burn in the system of torches. These events, besides having an high visual impact, could also represent risks for environment and human health (Mourad *et al.*, 2009).

In this context, PM_1 daily concentrations and its content in 14 chemical elements (Al, Be, Ca, Cr, Fe, K, Li, Mg, Mn, Na, P, Ti, S and Zn) recorded in Viggiano (the nearest town to the COVA plant at about 2 km away from it) immediately before, during and immediately after the activation of an emergency procedure occurred on 28 September 2012 were analysed. Chemical analysis was performed by Inductively Coupled Plasma-Optical Emission Spectrometry (ICP-OES).

Geochemical and mineralogical characterization of the PM_1 by means of Scanning Electron Microscope Field Emission Gun (FEG) are being carried out as well.

During the period under consideration, the PM_1 daily concentrations ranged between 1.6 μg m^{-3} and 8.0 μg m^{-3}, with a mean value of 4.5 μg m^{-3}.

The role of the potential sources of crustal and anthropogenic components can be identified by applying the Enrichment Factor (EF) technique using Al as reference crustal element (Caggiano *et al.*, 2011). Enrichment Factor (EF) mean values show that Fe, K, Mg, Mn, Na and Ti were of prevailing natural origin (EF≤10) while Be, Ca, Cr, Li, P, S and Zn mainly originated by anthropogenic sources (Figure 1).

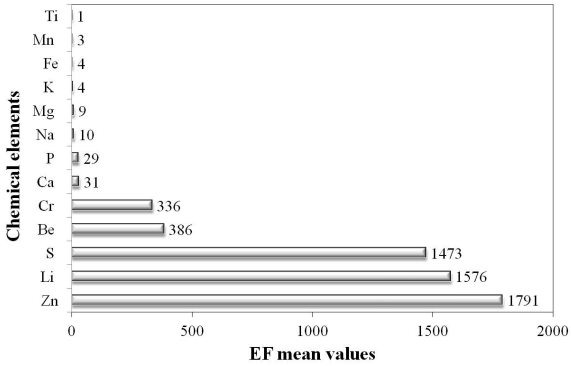

Figure 1. EF mean values.

Focusing on 28 September, S concentrations increased reaching the highest value of the entire study period. This could suggest also a contribution of the safety procedure activation occurred on this day to the PM_1 measured.

This work was carried out in the framework of the research agreement between "Regione Basilicata - Osservatorio Ambientale della Val d'Agri" and "Istituto di Metodologie per l'Analisi Ambientale" of the National Research Council (CNR).

Caggiano, R., Macchiato, M. and Trippetta, S. (2010) *Sci. Total Environ.* **408**, 884-895.

Mourad, D., Ghazi, O. and Noureddine, B. (2009) *Korean J. Chem. Eng.* **26(6)**, 1706-1716.

Sources and trends of atmospheric pollutants at Pallas, Finland, during 1996-2009

M. Vestenius[1], P. Anttila[1], S. Leppänen[1], K. Hansson[2], E. Brorström-Lunden[2] and H. Hakola[1].

[1]Finnish Meteorological Institute, P.O. BOX 503, FI-00101 HELSINKI, FINLAND
[2] IVL Swedish Environmental Research Institute Ltd., Box 5302, SE-400 14 GÖTEBORG, SWEDEN

Keywords: POP, PAH, PMF, AIR QUALITY

Presenting author email: mika.vestenius@fmi.fi

Introduction

Source apportionment of atmospheric pollutants was studied at the Finnish Meteorological Institute's (FMI) Global Atmosphere Watch (GAW) station, Pallas (67°58´N, 24°06´E). The station is located at the northernmost limit of the northern boreal forest zone and represents well the continental background air of the subarctic region (Hatakka et al., 2003).

The atmospheric pollutants data set contains aerosol samples for persistent organic pollutants (POP) and polycyclic aromatic hydrocarbons (PAH) data with the major inorganic ions and metal data from EMEP filter samples as well as ozone, nitrogen dioxide and sulphur dioxide.

Positive Matrix Factorization (PMF) was applied in source apportionment and the source sector frequency distribution using EMEP air mass trajectories was calculated for each PMF factor in order to identify source directions.

Results and discussion

PMF-analysis of weekly samples yielded five potential source factors, which were identified as Kola factor (F1), insecticide factor (F2), sea spray factor (F3), soil factor (F4) and traffic and LRT factor (F5).

Factor 1 contains large amount of trace elements (As, Ni, Cu, Pb, V, Zn) with most of gaseous SO_2 and 30-40% of the heavier PAH pollution. These pollutants are characteristic to the industries in Kola peninsula and air masses for this factor came from east.

Factor 2 contains most of the insecticides a-HCH and g-HCH (lindane) with high summer contribution, but without any specific source direction. This factor had a decreasing trend due to the reduction of the production and use of these compounds (Li et al., 2002).

Factor 3 is the sea spray factor without clear seasonal variation. Over 60% of PM_{10} was associated to this factor, i.e. maritime air masses and sea salt particles. The source direction was the Arctic Ocean and the northern Atlantic Ocean. Intrestingly, majority of organochlorine compounds and 30% of the lighter PAH compounds were associated with this factor. This might be an evidence of that these compounds are evaporating from the waters of melting glaciers.

Factor 4 is a soil source; high loadings of aluminium, manganese, ammonium, potassium and PCBs with a systematic summer maximum. PCBs are found in particles and/or evaporation from the soil (Yi et al., 2008). The air masses related to this factor originated mainly from south and west.

Factor 5 includes approximately half of PAHs and NO_2. The factor contribution was highest in winter and the dominating source directions were south and southwest. The high loadings of NO_2 and long-range transfer (LRT) nitrate and ammonium particles suggest reasonably remote traffic sources. The high contribution of DDT and DDE also refers to LRT air masses from the southern areas, where DDT is still in use (ATSDR, 2002).

References

Hatakka, J., Aalto, T., Aaltonen, V., Aurela, M., Hakola, H., Komppula, M., Laurila, T., Lihavainen, H., Paatero, J., Salminen, K. & Viisanen, Y. (2003) *Boreal Env. Res.* **8**, 365–383.

Li Y-F, Macdonald RW, Jantunen LMM, Harner T, Bidleman TF, Strachan WMJ (2002) *Sci Total Environ* **291**:229–4

Yi, S.-M., Reddy Pagilla, S., Seo, Y.-C., Mills, W.J., Holsen, T.M. (2008) *Chemosphere* **71**, p.1028.

ATSDR, (2002) *Toxicological Profile for DDT, DDE, and DDD.* Agency for Toxic, Substances and Disease Registry, Atlanta, US.

High-time resolved characterization of $PM_{1.0}$ in a peri-urban site near Rome, Italy

R. Salzano[1], M. Giusto[1], M. Montagnoli[1], M. Catrambone[1], E. Rantica[1], T. Sargolini[1] and C. Perrino[1]

[1]Institute of Atmospheric Pollution Research, C.N.R., Montelibretti (Rome), 00015, Italy
Keywords: HR-ToF-MS, $PM_{1.0}$, real-time, chemistry
Presenting author email: salzano@iia.cnr.it

The chemistry of sub-micron particles with high time-resolution was investigated in a peri-urban site close to the city of Rome (Italy). The "A. Liberti" Observatory is an experimental facility included in the EMEP network that is located in Central Italy 25 km far from the metropolitan area. The study site is positioned in the eastern edge of the Tiber valley in front of the Sabini mountains (50 m a.s.l.). The area is characterized by a low density of industrial emissions and by particular meteorological conditions that favour the occurrence of anthropogenic aerosols emitted in the metropolitan area (Perrino et al, 2009).

The submicron particulate mass at the considered measuring station is constituted by a large fraction (20 – 90 %) of organic aerosol (OA) whereas the rest of the mass consist of soot, inorganic salts and elements. As well known PM constituents can be divided in primary, directly emitted in the atmosphere by anthropogenic sources (e.g., traffic, industries and domestic combustion), and secondary, that are formed in the air through physical-chemical processes (e.g., oxidation, nucleation or condensation). While submicron secondary inorganic aerosols are mainly composed of ammonium nitrate and sulfate (Seinfeld and Pandis, 2006), secondary organic aerosol (SOA) may be composed of thousands of compounds, many of which are unknown (Goldstein et al, 2008), and further uncertainties exist in SOA formation pathways (Hallquist et al, 2009).

The integration between different techniques, in-line and off-line, highly time resolved and accumulated over long periods, represents a promising approach for filling the cognitive gap about direct emission sources and secondary formation mechanisms.

The experimental campaign (30 days) started in January and terminated in early February of the current year. The scheduling was defined in order to join this activity to the EMEP – ACTRIS intensive measuring winter period. The in-line data were obtained sampling from a Nafion-dried line and analysing the resulting aerosol with an Aerodyne HR-ToF-MS, configured to acquire information in V and W modes, and with a Scanning Mobility Particle Sizer (SMPS). Additional real-time information were obtained using an optical particle counter and gas analyzers (O_3, NO_x, CO_2). Meteoclimatic information were recorded using a standard meteorological station and monitoring atmospheric stability conditions with a Rn-daughters detector (PBL). Off-line determinations were carried out on PM_{10} and $PM_{2.5}$, collecting samples on both teflon and quartz membranes, accumulated on a 24h basis and on 3h intervals for only three days. Filters were successively analyzed by X-ray Fluorescence (XRF), Inductively Coupled Plasma Mass Spectrometry (ICP-MS), Ion Chromatography (IC) and thermo-optical analysis in order to determine major elements, micro and trace metals, soluble ions and elemental/organic carbon content respectively.

This campaign is the first attempt to characterize the submicron aerosol near Roma on real-time. The availability of such large amount of information represents a good opportunity to integrate data derived from AMS measurements and obtained by traditional off-line techniques. In details traditional techniques have been used for obtaining the mass closure and consequently estimating the PM macro-sources (i.e. crustal, organic, anthropogenic, sea-salt and secondary inorganic). At the same time, real-time data have also provided an estimation of different aerosol components. OA can be separated into oxygenated OA (OOA), hydrocarbon-like OA (HOA), and sometimes other components such as biomass burning OA (BBOA). Furthermore, an additional important comparison can be done on the secondary inorgaic aerosol (i.e. ammonium, sulphates and nitrates), which are clearly detected by AMS.

This preliminary results evidenced the possibility to complete the description of aerosol dynamics at different time scales. The traditional investigations made on PM10 and PM2.5 at daily and at 3 hours basis were integrated with real-time measurements that supported the detection of high-time resolved aerosol variations close to the city of Rome.

Goldstein, A.H., Worton, D.R., Williams, B.J., Hering, S.V., Kreisberg, N.M., Panic, O. and Gorecki, T. (2008) *J. Chromatogr. A*, **1186**, 340–347.

Hallquist, M., Wenger, J.C., Baltensperger, U., Rudich, Y., Simpson, D., Claeys, M., Dommen, J., Donahue, N.M., George, C., Goldstein, A.H., Hamilton, J. F., Herrmann, H., Hoffmann, T., Iinuma, Y., Jang, M., Jenkin, M.E., Jimenez, J.L., Kiendler-Scharr, A., Maenhaut, W., McFiggans, G., Mentel, Th.F., Monod, A., Prevot, A.S.H., Seinfeld, J.H., Surratt, J.D., Szmigielski, R. and Wildt, J. (2009) *Atmos. Chem. Phys.*, **9**, 5155–5236.

Perrino, C., Canepari, S., Catrambone, M., Dalla Torre, S., Rantica, E. and Sargolini, T. (2009) *Atmos. Env.* **43(31)**, 4766–4779.

Seinfeld, J.H. and Pandis, S.N. (2006) *From Air Pollution to Climate Change*, John Wiley & Sons.

Thursday, September 5, 2013

Poster session C:
Reserve Posters, C202 – C216

Urban particulate matter monitoring on a mobile platform: a real time experiment on a long term scale

B. Moroni[1,2], E. Scocchera[1], A. Piazzalunga[3], M. G. Ranalli[4] , S. Castellini[5], and D. Cappelletti[2,5]

[1]DICA, Università di Perugia, Perugia, Italy
[2]Centro di Eccellenza SMAArt, Università di Perugia, Perugia, Italy
[3]DISAT, Università di Milano Bicocca, Milano, Italy
[4]Dipartimento di Economia, Finanza e Statistica, Università di Perugia, Perugia, Italy
[5]Dipartimento di Chimica, Biologia e Biotecnologie, Università di Perugia

Keywords: mobile platform, urban pollution, real time monitoring, traffic rates
Presenting author email: david.cappelletti@unipg.it

In this paper we propose an innovative approach to the study of urban pollution dynamics, with a particular emphasis to vehicular traffic and generated aerosols. In synthesis, a mobile monitoring platform has been developed exploiting the urban transport system in Perugia (Italy), called Minimetrò. It is based on a monorail train, exploiting a relatively high number of cabins (in average 20) driven by a wire rope continuously running at medium low speed (4-5 m/s) along a radial transect (~3 km, in approx. 20 minutes) over the city. The cabins travel on a monorail built 5 meters above the road level. The cabin path starts from a large suburban parking area, it crosses various heavy traffic roads and road crossings, passes through a park, climbs Perugia hill, and finally reaches the city center inside a terminal tunnel. All these features make the Minimetrò system a good mobile platform for real time investigation of the dynamics of formation and dispersion of pollutants in the urban area.

The basic idea has been to customize and integrate an Optical Particle Counter (OPC, 6 sec. resolution, 22 size classes) inside the cabin. To complement the information coming from the mobile station, two other fixed OPCs (FAI Instruments) have been installed at both ends of the Minimetrò line. Moreover the Minimetrò line passes at short distance (50 m) from the urban background and traffic monitoring stations of air quality. These provide hourly averaged O_3, NO_x, Benzene and CO concentrations, as well as 24h PM_{10} and $PM_{2.5}$ data records. In addition, the main weather parameters are recorded as well as a PBL stability monitor (FAI Instruments) has also been installed in this station. Finally, traffic rates are recorded continuously in two points along the Minimetrò line with a 5 minutes time resolution.

An example of aerosol data is shown in Figure 1, where the number concentration of coarse fraction particles (D_P>1 μm) is shown, for a particular day, as a function of the position along the path (*y* axis, in meters) and time of the day (*x* axis). The color code are number concentration of particles per volume of air. In this particular example the variable impact of a Saharan dust intrusion occurring in the late afternoon is evidenced in different areas of the city. In addition, higher particles concentrations (red areas in the graph) are observed near heavy traffic roads, which point to a role of particle resuspension.

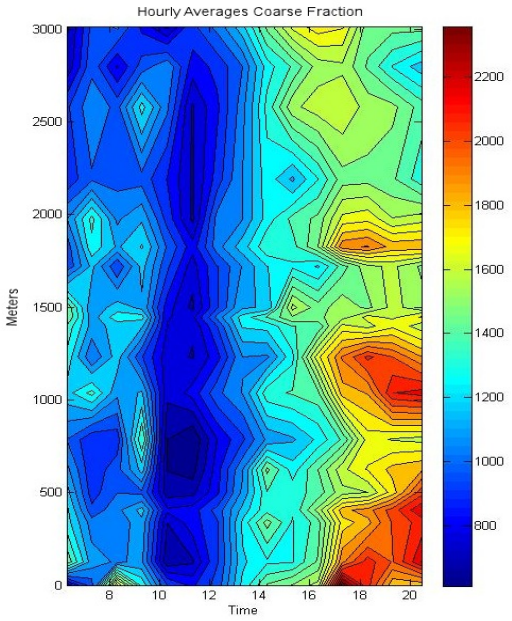

Figure 1 - Spatial – temporal distribution of coarse fraction particles recorded in date 20/10/2012.

The data acquisition started in September 2012 and will last one year. Ad-hoc statistical techniques are employed to fully exploit this large amount of information: functional data analysis can handle high frequency time series, while additive models can produce maps as those in Figure 1 and explain the contribution of covariates.

Special interest has been paid to the characterization of the aerosols in the underground paths of the Metro line in order to analyze the impact of degrading metal and rubber parts of the system. In this case the specific emission of the Metro system has been characterized, exploiting two HVS multistage impactors which allowed simultaneous samplings inside and outside the tunnel for metals and IPA size distributions. Moreover EC/OC ratios, black carbon as well as morphological a mineralogical assessments via electron microscopy on samples taken inside the tunnel have been used to integrate the mobile cabin data. Detailed results will be presented at the Conference.

Characterisation of the aerosol sources in Brindisi (Italy) harbour area within the CESAPO project: an overview of the experimental results

D. Contini[1], D. Cesari[1], A. Donateo[1], A. Gambaro[2], A. Genga[3], G. Giovanelli[4], R. Giua[5], F.M. Grasso[1], E. Gregoris[6], P. Ielpo[1,7], S. Masieri[4], E. Merico[1], E. Morabito[2], A. Nocioni[5], T. Pastore[5], and M. Siciliano[3]

[1] Istituto di Scienze dell'Atmosfera e del Clima, ISAC-CNR, Lecce, 73100, Italy
[2] Dipartimento di Scienze Ambientali, Informatica e Statistica, Università ca' Foscari Venezia, Venezia, 30123, Italy
[3] Dipartimento di Scienze e Tecnologie Biologiche e Ambientali, Università del Salento, Lecce, 73100, Italy
[4] Istituto di Scienze dell'Atmosfera e del Clima, ISAC-CNR, Bologna, 40129, Italy
[5] Agenzia Regionale per la Prevenzione e la Protezione dell'Ambiente, ARPA Puglia, Bari, 70126, Italy
[6] Istituto per la Dinamica dei Processi Ambientali, IDPA-CNR, Venezia, 30123, Italy
[7] Istituto di Ricerca sulle Acque, IRSA-CNR, Bari, 70132, Italy
Keywords: ship emissions, source apportionment, PM2.5, number particle concentration.
Presenting author email: d.contini@isac.cnr.it

The harbour areas are economic centres and transport hubs, that bring together different transport modes (sea, road, railway transport) and, often, include relevant industrial activities. Emissions of ships and of harbour-related activities could have potential negative impact on air quality especially for fine and ultrafine atmospheric particles (Contini at al., 2011; Healy et al., 2010).

At the beginning of 2012 it was started the research project CESAPO (Contribution of Emission Sources on the Air quality of the POrt-cities in Greece and Italy), within the framework of Interreg Greece-Italy 2007/2013, having among its objectives the quantification of the contribution to atmospheric particles of emission sources in two important Mediterranean port-cities: Patra (Greece) and Brindisi (Italy) using state-of-the-art modelling and experimental approaches. Here, an overview of the experimental results obtained in Brindisi will be presented. The area studied is influenced by several emissions: an industrial area, three power plants, an airport and an harbour with a freight traffic and total goods movement that accounted for more than 9.5 million tons and over 520,000 passengers in 2011. Experimental activities in CESAPO were based on an intensive observation period (IOP) of 5 months (June-October 2012). During the IOP the data of 10 fixed monitoring stations (the regional network managed by ARPA Puglia) and those from two additional stations specifically installed during the project inside the harbour area were collected. A station was used to characterize the chemical composition of PM2.5 (metals, major water soluble ions and carbon content) and PAHs (in the gaseous and aerosol phases) and the other was devoted to high temporal resolution (1 second) measurements of PM2.5 mass, number concentrations of submicron particles and diurnal spatially integrated gaseous concentrations using a remote sensing DOAS system (Premuda et al., 2011).

Results of source apportionment based on PM2.5 composition, using the Positive Matrix Factorization (EPA PMF3.0), and on high temporal resolution measurements will be presented and compared with other harbour areas in Italy and Europe. Preliminary results indicate that average PM10 and PM2.5 concentrations in the harbour area are smaller than those observed in the urban area but SO_2 concentrations associated to oil combustion and shipping emissions were larger. The secondary non-sea-salt-sulphate was essentially ammonium sulphate and accounted for about 32% of PM2.5. The detailed contributions of ship traffic and of harbour activities (loading/unloading of ships) were analysed using high temporal resolution measurements. The two contributions appear to be of the same order of magnitude and sporadic in nature being due to numerous short concentrations peaks (durations variable between 10 and 100 minutes) in PM2.5 and in the number of sub-micron particles. An example of peaks to due ships is reported in Figure 1. These peaks were analysed using a statistical methodology that takes into account the wind direction and the actual ships traffic to quantitatively characterize the contribution of vessels traffic and of harbour activities.

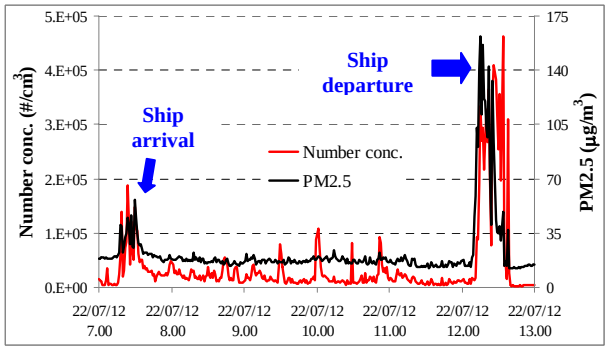

Figure 1. Example of ship emissions contribution to PM2.5 and number particle concentrations.

This work was supported by the Interreg Greece-Italy 2007-2013 program under grant I1.32.06.

Contini, D., Gambaro, A., Belosi, F., De Pieri, S., Cairns, W.R.L., Donateo, A., Zanotto, E., Citron, M. (2011) *J. Environ. Manage.* **92**, 2119-2129.

Healy, R.M., Helleburst, S., Kourtchev, I., Allanic, A., O'Connor, I.P., Bell, J.M., Healy, D.A., Sodeau, J.R., Wenger, J.C. (2010) *Atmos. Chem. Phys.* **10**, 9593-9613.

Premuda, M, Masieri, S., Kostadinov I., Bortoli, D., Petritoli A., Giovanelli, G. (2011) *Atmos. Environ.* **45**, 5212-5219.

An experimental approach to measure particle deposition in large circular ventilation ducts

G. Da[1], E. Géhin[1], M. Ben-Othmane[2], M. Havet[3], C. Solliec[4], C.Motzkus[1]

[1]CERTES, Université Paris-Est, Créteil, 94010, France
[2]Clauger, Brignais, 69530, France
[3]Umr GEPEA, Oniris, 44322, Nantes, France
[4]Umr GEPEA, Ecole des Mines de Nantes, 44300, Nantes, France
Keywords: Bio-aerosol, Particle deposition, Ventilation ducts, Food-industries.
Presenting author email: guillaume.da@u-pec.fr

This study was a part of the French project CleanAirNet, which aimed at producing new knowledge, models and techniques to help controlling the safety of the food products, through a better control of aerosol particle (bioaerosols) transport and deposition in the ventilation networks of the food industry. A small body of experimental literature has been reported on large ventilation ducts (Sippola, 2004). The purpose of this paper was to investigate particle deposition experiments in large circular ducts for fully developed turbulent flow.

An experimental setup (called MIDAS) was designed in a laboratory to validate a theoretically based model predicting particle deposition velocities for fully developed turbulent flow in an horizontal with circular cross-section (Ben Othmane, 2010).

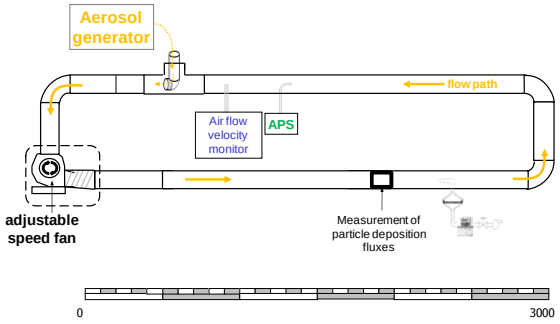

Figure 1. The experimental bench to investigate particle deposition velocity.

The experimental bench proposed in this study included a ventilation system, a monodisperse fluorescent aerosol generation system (VOAG, TSI), and direct-reading instruments to monitor the following parameters in real time: air-velocity, temperature, relative humidity, particle aerodynamic diameter (APS, TSI). The deposition of particles mass onto different surface orientations (with respect to gravity) was calculated by wiping the fluorescent particles and subsequently by measuring their concentrations by spectrofluorometry (FluoroMax, HORIBA). The particle mass deposited on filter was also determined by fluorescent techniques.

Experiments conducted at (5.0 ± 0.3) m/s in the circular duct system (160 mm in diameter, Reynolds number of 5.3×10^5) showed great stability for the generation of particles with nominal size of (0.92 ± 0.01) (2.12 ± 0.03), (3.47 ± 0.03) and (6.02 ± 0.11) µm; with trials lasted for 72, 4, 3 and 1 hour respectively.

The fluorescent technique allowed measuring deposited mass particle down to ($4.8\text{x}10^{-11}$ ± $1.1\text{x}10^{-11}$) kg. The deposition velocities obtained with 6 µm particles showed maximum uncertainty and variability of 35% and 26% respectively.

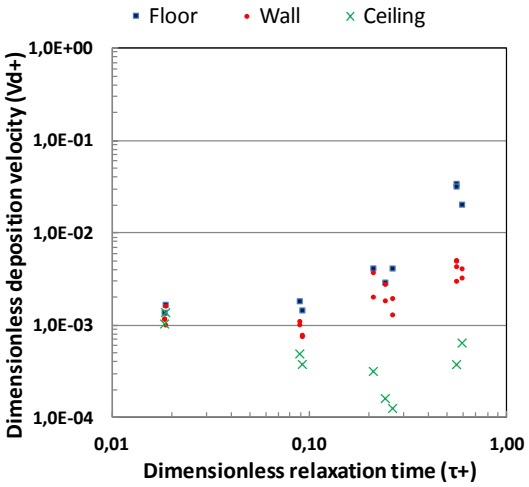

Figure 2. The influence of surface orientation in the circular duct, on dimensionless velocity.

The measured dimensionless deposition velocity showed the influence of the surface orientation (floor, wall and ceiling), in which a clear effect of the particle diameter is demonstrated. The experimental approach proposed in this study can be used to validate models on particle deposition in ventilation ducts from food factories, by considering large circular sections, turbulent flows, and thermal gradients for thermophoresis.

This work was supported by the French National Research Agency under the project CleanAirNet: “Hygienic design of ventilation duct networks in food factories”.

Ben Othmane, M., Havet, M., Géhin, E. and Solliec, C. (2010) *Aerosol Sci. Technol.* **44**, 775-784.
Sippola, M.R. and Nazaroff, W.W. (2004) *Aerosol Sci. Technol.* **38**, 12.

PMF source apportionment for fine and coarse PM in Athens, Greece: Evolution of source contributions over the last decade

K. Eleftheriadis[1], E. Diapouli[1], A. Karanasiou[2], S. Vratolis[1], V. Vasilatou[1], M. Gini[1], D. Saraga[1], S. Pateraki[1], Th. Maggos[1]

[1] Institute of Nuclear & Radiological Sciences & Technology, Energy & Safety,
National Centre of Scientific Research "Demokritos", 15310 Ag. Paraskevi, Attiki, Greece
[2] Institute of Environmental Assessment and Water Research, Spanish Research Council, 08034 Barcelona, Spain
Keywords: $PM_{10}/PM_{2.5}$, source apportionment, PMF, source evolution.
Presenting author email: eleftheriadis@ipta.demokritos.gr

Particulate air pollution remains a significant environmental problem in big urban centres in Europe and around the world. The development of effective control policies calls for the identification of the main particulate matter (PM) sources, as well as the quantification of their contribution to elevated concentration levels. The city of Athens has been known to face severe air pollution problems due both to the presence of multiple particle sources and to the meteorological conditions and topography that promote pollutants build-up. The presence of significant natural sources further complicates the efforts to apply effective mitigation measures and to ensure compliance with air quality guidelines. The objective of the present work was to identify the major PM sources in the Athens area, quantify their relative contribution to coarse and fine particle concentrations and examine their evolution over the last decade.

Source apportionment by positive matrix factorization (PMF) analysis was performed on two $PM_{10}/PM_{2.5}$ datasets from 2002 and 2012. Both datasets covered warm and cold period. The 2002 measurement campaign included 24-hr gravimetric measurements from three urban residential sites. The collected teflon filters were analysed for a number of elements by electrothermal atomic absorption spectrometry (Cd, Pb, V, Ni, Mn, Cr, Cu, Fe and Al) and flame atomic absorption spectrometry (Ca, Mg, K and Na), as well as for major anions (Cl^-, NO_3^- and $SO4^{2-}$) by ion chromatography. In addition, black carbon (BC) data were obtained by means of an aethalometer (AE-9, Maggee Sci). The 2012 campaign was conducted at two urban background sites. 24-hr gravimetric measurements were performed with two different filter substrates (teflon and quartz) in order to allow for a more extensive chemical characterization of the aerosol fractions. Elemental composition was again quantified by electrothermal and flame atomic absorption spectrometry. Ionic species (Na^+, Mg^{2+}, Ca^{2+}, K^+, NH_4^+, SO_4^{2-}, NO_3^-, Cl^-) were quantified by ion chromatography, while elemental (EC) and organic (OC) carbon were also measured by thermal-optical methodology.

Two-dimensional Positive Matrix Factorisation (PMF) has been applied to each dataset. Details on input data preparation are provided in Karanasiou et al. (2009). Two PMF models were used, PMF2 (Version 4.2) and EPA PMF 3.0, and the obtained results were compared. Analysis was performed for different numbers of factors and the best solution was chosen based on goodness of fit parameters (Q value and the explained variation of the matrix F) as well as by examining the obtained factors profiles with respect to the possibility of associating them with specific source. In addition, multiple values of Fpeak (in the range -2.0 to 2.0) were examined in order to explore different rotations of the solutions.

In general the two models applied showed good agreement of results. Vehicular traffic was found the main contributor to fine particle concentrations, with marine aerosol also playing a major role. Fossil fuel combustion and traffic contributions were similar. Coarse particles concentrations seemed unaffected by all combustion-related sources and were attributed to a large extent to natural sources (sea salt, soil). (Figure 1)

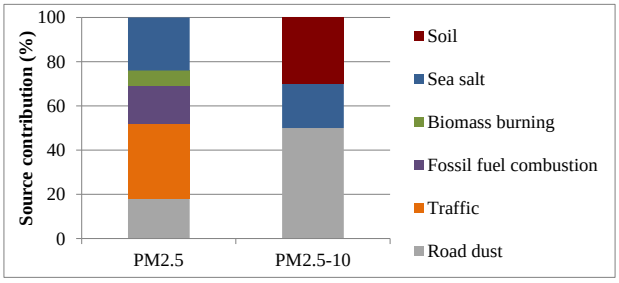

Figure 1. Relative contribution (%) of each source to PM concentration levels (Year 2002).

PMF analysis on the 2012 dataset is still in progress but initial results indicated a differentiation in PM source contributions over the last decade. This is also evident by the reduced concentration levels, attributed to a decrease in anthropogenic emissions either because of efficient mitigation measures (new-technology "cleaner" vehicles, traffic regulations etc.) and/or lower anthropogenic activity due to the financial crisis of the last two years. The final results are expected to provide an interesting insight into the present air pollution situation in the city and the potential "new" major contributors to the observed daily exceedances of air quality guidelines.

This work was supported by the European Commission LIFE+ Environment Policy and Governance programme.

Karanasiou, A.A., Siskos, P.A. and Eleftheriadis, K. (2009) *Atmos. Environ.* **43**, 3385–3395..

Toxicological effects of the particulate emissions from diesel engines and wood combustion are affected by used technology

P.I. Jalava[1], M.S. Happo[1], T. Brunner[2], I. Obernberger[2], T. Murtonen[3], P. Aakko-Saksa[3], J. Mäki-Paakkanen[4], J. Jokiniemi[1,3] and M-R. Hirvonen[1,4]

[1]University of Eastern Finland, Department of Environmental Science, FI-70211, Kuopio, Finland
[2]Graz University of Technology, Bioenergy 2020+, Graz, Austria.
[3] VTT Technical Research Centre of Finland, Fine Particles, FI-02044 VTT, Espoo, Finland
[4]National Institute for Health and Welfare, Department of Environmental Health, FI-70701, Kuopio, Finland
Keywords: Health effects of aerosols, Biofuels, Particulate matter, Toxicology

Particulate air pollution is one of the major public health concerns worldwide. Emissions from traffic and energy production are among the most important sources of these harmful particles. Especially residential wood combustion has increased in the same time as other emissions e.g. from traffic have been decreasing. The combustion emissions are associated with a large variety of adverse health effects, including both cardiac and respiratory symptoms. Recently IARC declared diesel engine emission to be carcinogenic to human but the biomass combustion emissions do not have the same status yet. This decision concerning diesel engine emissions is based mostly on the data from very old technologies. However, the engines have gone through significant improvements during recent years but the development of small scale combustion has been much slower.

We have investigated several modern and old technology heating appliances as well as different diesel engine types for the physicochemical and toxicological properties of the emitted particulate matter (PM). The studies included three types of diesel engines, Euro 2 small industrial engine, a large Euro IV truck engine and CNG powered bus. The conventional diesel fuel (EN590), rapeseed methyl ester (RME) and hydrotreated vegetable oil (HVO) was used as fuels in the two former and the catalyst aftertreatment was applied. Biomass furnaces were old and modern technology logwood boilers, old and new technology stoves and wood chip and pellet burning boilers. Particulate samples (Dp<1μm) for both toxicological and chemical characterization were collected from the diluted emissions. RAW 264.7 macrophage cell line was exposed to the particulate samples for 24h. Inflammatory parameters, TNFα and chemokine MIP-2 were analyzed. Cytotoxicity was analyzed with MTT assay and flow cytometric methods (PI exclusion and cell cycle analysis). Genotoxicity was determined with comet assay and intracellular oxidative species were detected in flow cytometric analyses of DCF oxidation. There were large differences in the magnitude of the toxicological responses. Old technology biomass combustion samples were up to 30 times more potent inducers of genotoxic responses than the modern technologies. The results from the engines were not as drastic but they revealed up to 8-fold differences in genotoxicity, respectively. The magnitude of the toxicological responses was generally slightly higher by the biomass combustion samples than the engine emission samples.

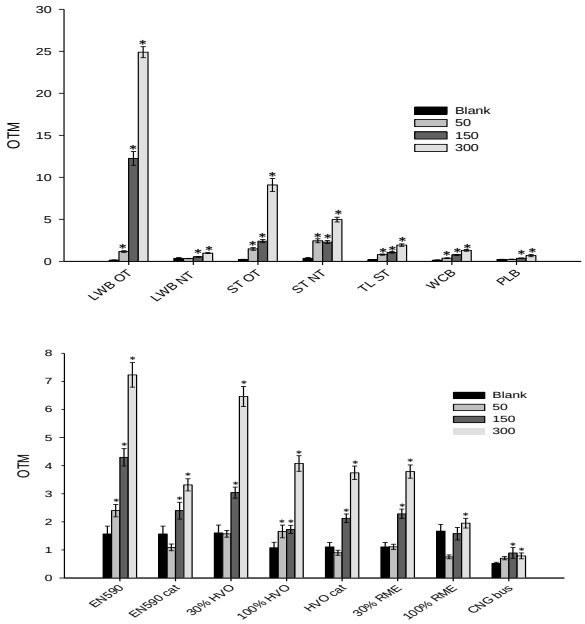

Genotoxicity assessed with comet assay after 24h exposure to PM_1 emission samples from different situations. Bars show blank and three doses (50, 150 and 300μg/ml) ± SEM. Upper figure presents the results from biomass combustion whereas the lower figure is for the engine emissions.

The old technologies had in most cases larger emissions than the technologically developed alternatives. This emphasizes the differences between the samples. The modern technologies can be considered less harmful than the old, but also the emissions from modern technologies can cause harmful effects. From the toxicological perspective the emissions from at least the old technology biomass combustion should not be considered as less harmful than the emissions from the engines.

Jalava PI, Tapanainen M., Kuuspalo K, et al. (2010) *Inhal. Toxicol.* **22** (S2) 48-58.
Jalava PI., Happo M, Kelz J, et al. (2012a). *Atmos. Environ.* **50**: 24-35.
Jalava P.I., Aakko-Saksa P., Murtonen T., et al. (2012b). *Part. Fibre Toxicol.* 9: 37.
Uski O., Happo M.S., Jalava P.I et al. (2012). *Inhal. Toxicol.* **24 14**: 952-965.
Happo MS, Uski O, Jalava PI, et al. (2013). *Sci. Total Environ.* **443:** 256-266.

Diurnal variation of small and large ion concentrations in an urban location

E.R. Jayaratne, X. Ling and L. Morawska

International Laboratory for Air Quality and Health. Institute of Health and Biomedical Innovation.
Queensland University of Technology. Brisbane 4000. Australia.
Keywords: ions, particles, attachment, charged aerosols
Presenting author email: r.jayaratne@qut.edu.au

A Neutral cluster and Air Ion Spectrometer (NAIS) was used to monitor the concentration of airborne ions on 258 full days between Nov 2011 and Dec 2012 in Brisbane, Australia. The air was sampled from outside a window on the sixth floor of a building close to the city centre, approximately 100 m away from a busy freeway. The NAIS detects all ions and charged particles smaller than 42 nm. It was operated in a 4 min measurement cycle, with ion data recorded at 10 s intervals over 2 min during each cycle. The data were analysed to derive the diurnal variation of small, large and total ion concentrations in the environment. We adapt the definition of Horrak et al (2000) and classify small ions as molecular clusters smaller than 1.6 nm and large ions as charged particles larger than this size.

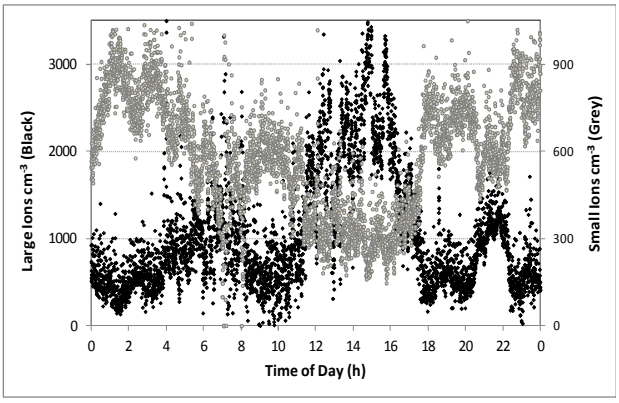

Figure 1: Diurnal variation of large and small ion concentrations on 3 February 2012 in Brisbane.

Fig 1 shows the large and small ion concentrations on a typical day. The large ion concentration generally peaked during the middle of the day, especially when there was secondary particle formation due to nucleation of organic precursors from motor vehicle emissions. On this day, a condensation particle counter showed a particle number concentration (PNC) of about 2 x 10^4 cm^{-3} between 12h and 14h. It is well known that small ions rapidly attach to particles in the air. There is an apparent negative correlation between the large and small ion concentrations in Fig 1. The maximum small ion and minimum large ion concentrations generally occurred between midnight and 4 am when the air was relatively clean (PNC of about $3x10^3$ cm^{-3}), while the maximum large ion and minimum small ion concentrations were observed soon after mid day when the PNC was a maximum ($1\text{-}3x10^4$ cm^{-3}).

Fig 2 shows the mean hourly total ion concentrations over the entire measurement period. The error bars show the corresponding standard deviations. The total ion concentration was fairly constant between $1x10^3$ and $2x10^3$ cm^{-3} right through the night and showed maximum concentrations of between $3x10^3$ and $4x10^3$ cm^{-3} shortly after mid day.

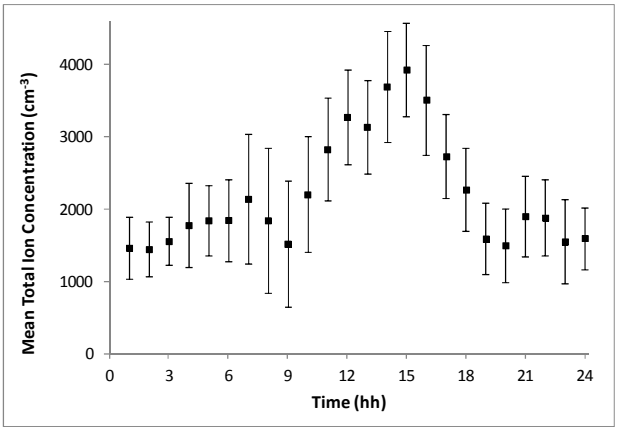

Figure 2: Mean hourly values of the total ion concentration with standard deviations.

The health effects of ions and charged particles are still largely unknown. Some studies have shown that, during inhalation, charged particles are more likely to be deposited in the human lungs than similarly sized uncharged particles (Cohen et al, 1998). While there have been several reports of small ion concentrations in urban environments (Retalis et al, 2009, Ling et al, 2010), there have not been many similar studies dealing with large ions and charged particles (Hirssiko et al, 2007, 2011). We believe that this is the first study of charged particles in an urban environment in the Southern Hemisphere.

Cohen, B.S., Xiong, J.Q., Fang, C., Li, W. (1998) *Health Physics*. 74, 554-560.
Hirsikko, A., Juuti, T.Y, et al (2007) *Boreal Environ Res.* 12, 295-310.
Hirsikko, A., Nieminen, T., et al. (2011) *Atmos Chem Phys.*, 11, 267-798.
Horrak, U., Salm, J., Tammet, H. (2000) *J Geophys Res.* 105(D7), 9291-9302.
Ling, X., Jayaratne, E.R., Morawska, L. (2010) *Atmos Environ*. 44, 2186-2193.
Retalis, A., Nastos, P., Retalis, D. (2009) *Atmos Res*. 91, 219-228.

Particulate Matter in Indoor Air in two Schools in Vienna, Austria

A. Kasper-Giebl[1], N. Jankowski[1,2], K. Kassin[1,3], E. Can Cetintas[1], H. Bauer [1,†] and H. Grothe[4]

[1]Institute of Chemical Technologies and Analytics, Vienna University of Technology, Vienna, A-1060, Austria
[2]now at: Amag, Austria Metal AG, Braunau am Inn - Ranshofen, A-5282, Austria
[3]now at: Umweltbundesamt, Vienna, A-1090, Austria
[4]Institute of Materials Chemistry, Vienna University of Technology, Vienna, A-1060, Austria

Keywords: indoor air, source apportionment, chemical composition, carbonaceous aerosols
Presenting author email: akasper@mail.tuwien.ac.at

Sampling of particulate matter was performed in two schools in Vienna in 2011. The first campaign started in January and lasted until April, the second from October till December, respectively. Particulate matter (PM10) was collected in parallel with a high-volume sampler (Digitel DHA80) using quartz fibre filters, a low-volume sampler (Leckel, SEQ47/50) using cellulose acetate filters and a beta particulate monitor (ESM, Eberline). In addition to the characterization of indoor air the sampling equipment was also installed outside the buildings for at least one week during both campaigns. This allowed to determine the ambient PM10concentrations in the vicinity of the two schools and to compare them with the air quality network in Vienna. This comparison showed very good agreement and allowed to take data from the air quality network as ambient concentration data for the time of the indoor sampling. Filter samples were analysed for aerosol mass, water soluble ions, carbon parameters (total carbon, elemental carbon, organic carbon, carbonates) selected anhydrosugars and other saccharides, cellulose, humic like substances and metals using protocols described in Bauer et al. (2007).

Both sampling sites were located in the western part of Vienna. The vicinity of HBLVA Rosensteingasse (RG) can be characterized as a densely populated residential area with some influence of local traffic. The other site, BG Fichtnergasse (FG), is also a residential area with a large number of single family houses and private gardens around. Average concentrations of particulate matter in the ambient were ranging from 20 µg/m³ (April at FG) to 81 µg/m³ (November at RG). Sampling times comprised most of the exceedances of the 24h-limit value of PM10 observed in Vienna during 2011.

As expected indoor particulate matter concentrations showed distinct daily and weekly cycles reflecting the activity of students and teachers moving around the building and vaccations or weekends. Superimposed to these short time fluctuations the concentrations are driven by the ambient air concentrations monitored within the air quality network in Vienna.

Chemical analyses accounted for approx. 90 % of aerosol mass using a macro-tracer model (Bauer et al. 2007) which allows to quantify the contributions of inorganic secondary aerosols, mineral dust, wood smoke, other organic material and traffic to aerosol mass. For indoor samples organic material gave the highest contribution to aerosol mass, with cellulose being the most dominant single compound measured. Furthermore pronounced differences of saccaride concentration patterns were observed by comparing indoor and ambient air samples. Thus sugar alcohols being tracers for fungal spores (Bauer et al. 2008) were only determined outside, while e.g. glucose, fructose and succrose were only determined in indoor air samples. In FG mineral dust and in RG inorganic ions were the second important contributors to aerosol mass, respectively. Traffic showed a similar and rather small contribution at both sampling sites.

For ambient air samples inorganic secondary aerosol is the most important contributor to aerosol mass, followed by mineral dust, wood smoke and other organic material.

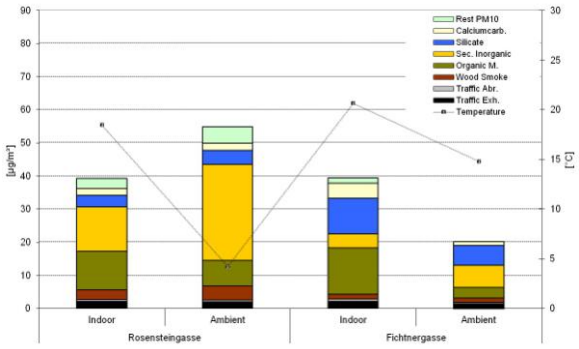

Figure 1. Source apportionment in the first campaign.

This work was supported by the Austrian Federal Ministry for Science and Research, within the Sparkling Science programme (SPA03-33). We thank the Environment Agency Austria and the municipal authority (MA22) for providing part of the sampling equipment. Support in the lab by H. Zbiral, C. Ramirez Santa Cruz, J. Firmkranz, L. Sampaio Cordeiro Wagner, J. Kirchbacher, B. Meixner, L. Striok and N. Wolf is gratefully acknowledged.

Bauer H. et al. (13 authors) (2007) AQUELLA Steiermark, Report LU08/07 (available at: http:// umwelt.steiermark.at/)
Bauer H. et al. (2008) *Atmos. Environ.* **42**, 588-593

Organic aerosol speciation with in-situ thermal desorption gas chromatography: a brief history of the TAG instrument

N.M. Kreisberg[1], S.V. Hering[1], A.P. Teng[1], G. Isaacman[2], Y. Zhao[2], D.R. Worton[2], A.W.H. Chan[2], B.J. Williams[3], J.T. Jayne[4], A.T. Lambe[4], T. Hohaus[4], J.R. Kimmel[4], D.T. Sueper[4], W. Brooks[4], L.R. Williams[4], A.M. Trimborn[4], D.R. Worsnop[4] and A.H. Goldstein[2]

[1]Aerosol Dynamics Inc., Berkeley, CA, 94806, USA
[2]Depart. of Environmental Science, Policy & Management, University of California, Berkeley, CA, 94720, USA
[3]Depart. of Energy, Environmental & Chemical Engineering, Washington University in St. Louis, MO, 63130, USA
[4]Aerodyne Research Inc., Billerica, MA, 01821, USA
Keywords: organic aerosol, thermal desorption, gas chromatography, mass spectrometry
Presenting author email: nathan@aerosol.us

Speciation at the molecular level is necessary to more fully understand the sources, sinks, transport and transformation of organic matter in the atmosphere. The thermal desorption aerosol gas chromatograph (TAG) is a mature instrument successfully deployed in five distinct field campaigns and offers a proven method for in-situ, hourly speciation of organic aerosols.

Multiple versions of this evolving instrument will be reviewed but all have in common the use of chemical separation using gas chromatography following thermal desorption. The first TAG to be deployed relied on inertial impaction to collect particulates and filter blanks to estimate vapour adsorption. Figure 1 illustrates the ability to acquire hourly time series of useful aerosol markers (primary norhopane and secondary phthalic acid) in the LA basin as part of the SOAR campaign (Williams et al., 2010). A subsequent deployment in the California Sierra Foothills (Worton et al., 2011) provided important information about the interaction of biogenic primary gases with anthropogenic pollutants that dominates secondary organic aerosol production.

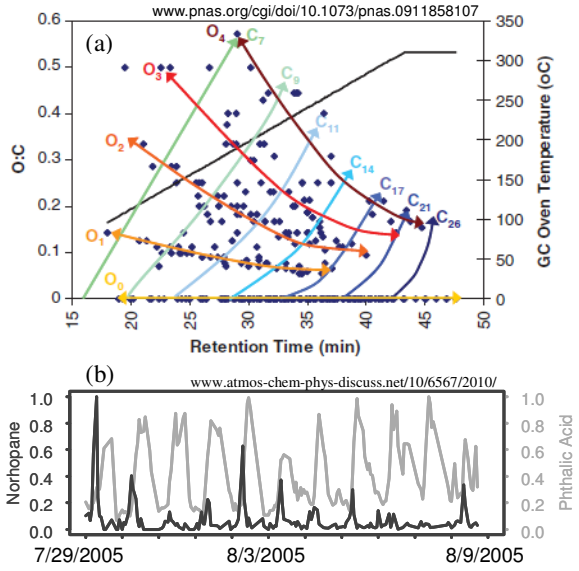

Figure 1. (a) O:C ratio, carbon and oxygen numbers vs. volatility as indicated by column retention time for ~300 compounds and (b) time series of representative source markers as measured in Riverside, CA in 2005.

To measure semi-volatile organics, which are important to secondary aerosol formation, a new version of the instrument has been developed to collect both particle and semi-volatile vapor phases (Zhao et al., 2013). Using a high efficiency carbon-based gas phase denuder and a new collection system with a reusable metal-fiber filter, alternate samples with and without the denuder provide direct partitioning measurements of organic compounds.

A parallel development has focussed on adapting the TAG instrument to function as a parallel collection system to be added to the Aerodyne Aerosol Mass Spectrometer (AMS; Canagaratna et al., 2007). This hybrid instrument (Williams et al., 2013) shares a detector to provide simultaneous size-dependent bulk and speciated organic aerosol information in one instrument. Comparing measurements from these separate instruments has proven the utility of being able to identify individual marker species corresponding to traditional AMS organic classes based on oxygen to carbon ratios such as HOA, OOA etc. (Williams et al., 2010; Worton et al., 2011).

Current efforts are directed towards expanding the range of compounds that can be analysed using in-situ derivatization of highly polar species. A dual cell version of the semi-volatile oriented instrument for initial deployment as part of a southeast US summer of 2013 field campaign seeks to ascertain the origin and fate of the large secondary organic aerosol levels present throughout the region. The paired filter cells provide simultaneous collection of denuded and undenuded aerosol streams for unique hourly measurements of derivatized SOA markers stemming from the oxidation of isoprene and other (bio-)anthropo-genic precursors.

Work supported under U.S. DOE SBIR/STTR grants DE-FG02-02ER83825, DE-FG02-05ER 86235, DE-FG02-08ER86335 and DE-FG02-08ER85160 and California Air Resources Board award number 03-324.

Canagaratna et al (2007) *Mass Spec Revs, 26*, 185-222.
Williams et al (2010) *Atmos Chem Phys, 10*, 11577-603.
Worton et al (2011) *Atmos Chem Phys, 11*, 17071-125.
Zhao (2013). *Aerosol Sci Technol, 47*(3), 258-266.
Williams et al (2013) submitted *Aerosol Sci and Technol*

Particle characterization during abrasive treatment of composite material containing fibres by Cryo HRTEM

K.I. Lieke[1], M. Levin[1,2], K.A. Jensen[1] and I.K. Koponen[1]

[1]National Research Center for the Working Environment, 2100 Copenhagen, Denmark
[2]Department of Nanotechnology, Technical University of Denmark, 2800 Kgs. Lyngby, Denmark
Keywords: nano fibre composite, production emission, HRTEM, cryo.
Presenting author email: KirstenLieke@gmx.de

Composite material including nano particles and fibres is today used in production and sealing of surfaces. Highly stressed surfaces such as of cars, boats and light aircrafts need to provide properties that demand the use of new materials including nano fibres, that enhance stability. Manufacturing of these surfaces involves abrasive treatment, during which material is emitted. We characterized particles from treatment of composite material including nano fibres. Nano particles can have an adverse health effect (Donaldson et al., 2002) when inhaled by humans exposed to emissions during manufacturing and surface treatment.

Particles were collected using a micro intertial impactor set similar to the one described by Kandler (2009). Sampling was performed on 2 stages (upper cut off 0.89 µm and lower cut off 0.047 µm diameter) on Ni-TEM grids with Formvar carbon foil (Plano, Wetzlar, Germany).

Transmission electron microscopy (TEM) was used for analysis of particles on 12 samples from 6 tests in total. Overview and high-resolution (HR) microscopic images were recorded using a Tecnai T20 G2 (FEI, Eindhoven, the Netherlands) at the Center for Electron Nanoscopy, Technical University of Denmark, operating at 200kV. Due to beam sensitive material a nitrogen cooled cryo transfer holder (Gatan Inc. Ca. USA) was used to keep the sample below -80 degrees Celsius during analysis. It was accounted for possible beam damage and hydro carbon deposition by using low beam current densities and short acquisition time. Energy dispersive X-ray detection (EDS) was carried out on single particles using an Oxford 80mm silicon drift detector.

Scanning electron microscopy (SEM) was performed on samples collected from deposited material (powder) with a ESEM Quanta 200 FEG (FEI, Eindhoven, the Netherlands).

Online measurements with FMPS, ELPI, CPC and GRIMM dust monitor were conducted in parallel.

Particles in the size range from 40 nm up to 500 nm (average geometric diameter) were analysed and classified based on their structure, morphology, beam stability and chemical composition.

Particles originating from the composite proofed to be partly crystalline material (Figure 1). Few nanometer thin fibres were found in agglomerates of few hundred nanometers, parts of them sticking out of the bulk. Single fibers of 100 nm in width and several 100 nanometers in length were less abundant.

Ammonium sulfate, sodium chloride and soot particles that were found in high abundances on the substrates were classified as background particles. However, composite particles, as well as fibres were sometimes found internally mixed with background particles.

Particles revealed inhomogeneous composition and irregular shape and morphology. Size, surface area and density determination will be discussed for the different materials.

SEM investigations on deposited material revealed extreme charging of particles, especially of the fibrous material. Potential issues regarding the detection by instruments using electric mobility sizing will be critically discussed.

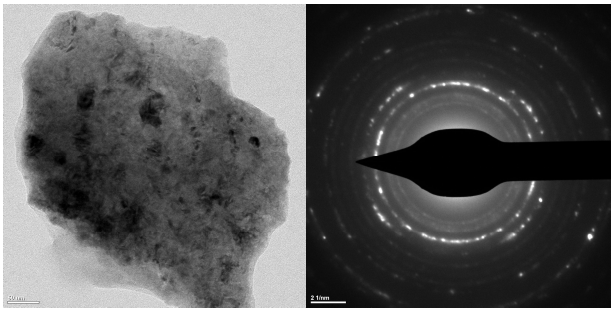

Figure 1. TEM bright field image (left) and diffraction pattern (right) of a nano particle originating from abrasive treatment of composite material.

The authors like to thank Signe Hjortkjær Hansen for technical support. We gratefully acknowledge excellent microscopy conditions at Center for Electron Nanosccopy (CEN), Technical University of Denmark and technical support by Wilhelmus Huyzer. This work was supported by the NanoSafetyCenter and Nanovalid.

Donaldson et al.,2002, Inflammation caused by particles and fibers, Inhalation tox. **9**, 5-27

Kandler, K., 2009. An aerosol sampler for single particle analysis. Presentation at the European Aerosol Conference 2009, Karlsruhe, Germany. Abstract T092A04.

Trace elements bioaccessibility in fine and ultrafine particles from the industrial area of Dunkirk (France) during the NANO-INDUS project

S. Mbengue [1,2], L. Alleman [1,2] and P. Flament [1,3]

[1] Univ Lille Nord de France, F-59000 Lille, France
[2] Mines Douai, CE, F-59508 Douai, France
[3] ULCO, LPCA, F-59240 Dunkerque, France
Keywords: Fine particles, Trace elements, bioaccessibility, lung fluid.
saliou.mbengue@mines-douai.fr

Inhalable atmospheric particles (< 10 µm) may contain high concentrations of trace elements (TE) that could induce adverse cardiovascular and respiratory effects (Donaldson *et al.*, 2002). Fine and ultrafine particles (smaller than 2.5 and 0.1 µm, respectively) are suspected to be more harmful, because of their small size and high specific surface, allowing them to penetrate deeply in our respiratory tract and even pass through the cellular membrane. After penetrating in our body, particulate TE can be partially or completely dissolved upon contact with the lung fluids (Costa and Dreher, 1997). Particle size, shape, chemical composition and potentially toxic bioaccessible content are the main characteristics to consider in the PM-induced biological impacts (Oberdörster *et al.*, 2005). Trace metal pulmonary bioaccessibility assessment requires the use of extraction solutions mimicking the physiological fluids (Caboche *et al.*, 2011). The purpose of this study was to assess TE bioaccessibility in different size fractions of PM, collected according to emission sources using a synthetic lung fluid (Gamble solution, pH = 7,4 et ≈ 37 °C). Coarse, fine and ultrafine PM were collected in the vicinity of metallurgical plants (at 500 and 2000 m from the chimneys) and in traffic influenced urban area nearby, using cascade impactors (DEKATI - 3 and 13 stages). Bioaccessible fractions and total concentrations of a large set of elements, selected according to their potential toxicity and their property of source markers (Al, As, Ba, Cd, Co, Cr, Cu, Fe, K, La, Mg, Mn, Mo, Ni, Pb, Rb, Sb, Sr, Ti , V and Zn), were analyzed by ICP-AES and ICP-MS.

Overall, total concentrations in PM_{10} increased with the industries proximity, implying the large contribution of industrial sources in PM_{10} TE concentrations. Pulmonary bioaccessibility results show that metal solubility would depend on the source types. Indeed, the solubility in the Gamble solution for Mn, Pb, Rb and Zn (associated to the metallurgical emissions) in PM_{10} were higher in the vicinity of industrial plants than in urban area where, inversely, traffic related elements (Cu and Sb) showed higher dissolution percentages. For elements associated to industrial emissions, bioaccessibility in PM_{10} decreased with the distance from the sources that could be linked (1) to the change of elemental speciation during PM transport or (2) the increasing contribution of others/more refractory sources. In the industrial and "urban-traffic" areas, the bioaccessibility increased toward smaller PM, particularly for anthropogenic elements like Cd, Co, Mn, Ni, Pb, Rb, Sb and Zn.

These results indicate that the bioaccessibility may vary according to the type and distance from the sources, in addition to the size of PM and the chemical form of TE. Our current works move at the moment to a better estimate of these two parameters within industrial plumes.

This work was part of a program from the "Institut de Recherche en ENvironnement Industriel" (IRENI) and was financially supported by the French Environment and Energy Management Agency (ADEME), the Nord-Pas-de-Calais Regional Council, the French Ministry of Higher Education and Research, the European Regional Development Fund (ERDF) and Ecole des Mines de Douai.

Costa, D.L., Dreher, K.L. (1997) Environ. Health Persp. **105**, 1053-1060.
Caboche, J., Perdrix, E., Malet, B., Alleman, L. Y. (2011) *J. Environ. Monit.* **13**, 621-30.
Donaldson, K., Tran, C.L., MacNee, W. (2002) *Eur. Respir. Mon.* **21**, 77–92.
Oberdörster, G., Oberdörster, E., Oberdörster, J. (2005) *Environ Health Perspect.* **113**, 823-39.

Free energy barrier in the growth of sulfuric acid clusters

T. Olenius[1], O. Kupiainen[1], I.K. Ortega[1] and H. Vehkamäki[1]

[1]Department of Physics, University of Helsinki, Helsinki, FI-00014, Finland
Keywords: sulfuric acid, molecular clusters, modeling, new particle formation
Presenting author email: tinja.olenius@helsinki.fi

Formation of secondary atmospheric particles begins with the clustering of gas phase molecules into small molecular clusters, which can grow by colliding with gas molecules and each other. As experimental observation of the smallest clusters is extremely difficult, theoretical methods provide necessary tools to study the properties of these clusters.

We have used first principles quantum chemistry combined with a dynamic model to study the kinetics of sets of small clusters containing either sulfuric acid (H_2SO_4) and ammonia (NH_3) or sulfuric acid and dimethylamine (DMA, $(CH_3)_2NH$) molecules. The model (Atmospheric Cluster Dynamics Code; McGrath *et al*, 2012) solves the steady-state of the system considering all possible collision and evaporation processes. Collision rates are calculated as in the kinetic gas theory, and evaporation rates are derived from quantum chemical Gibbs free energy of formation of the clusters (Ortega *et al*, 2012). We included in the simulations clusters containing in principle up to four acid and four base molecules for DMA; for ammonia, the behavior of the system was not as straightforward as for DMA and therefore the set was extended to include clusters with up to five acids and five bases in order to better understand the system. Both sets were studied with and without electrically charged clusters.

We performed the simulations in atmospherically relevant conditions. The base concentration was fixed by setting a constant base monomer concentration, whereas the acid concentration was set by fixing the sum of all neutral clusters containing one acid and any number of base molecules, as the instrument for measuring the acid concentration (CIMS; Chemical Ionization Mass Spectrometer) is likely to detect also these clusters as acid monomers. We tracked the main clustering pathways in each system and converted the quantum chemical Gibbs free energies of formation of the growing clusters to the acid and base concentrations used in the simulations.

Figure 1 shows the Gibbs free energy of formation of the growing clusters as a function of growth step in the studied systems. In the system with sulfuric acid and ammonia, there are energy barriers in the main growth pathways both in the electrically neutral and ionic systems. Charged clusters dominate the clustering routes in the ionic system by growing out as negative or positive cluster ions and forming neutral clusters by recombination. In the acid-DMA system the growth along the most significant pathways is barrierless and occurs via electrically neutral clusters also when ions are present.

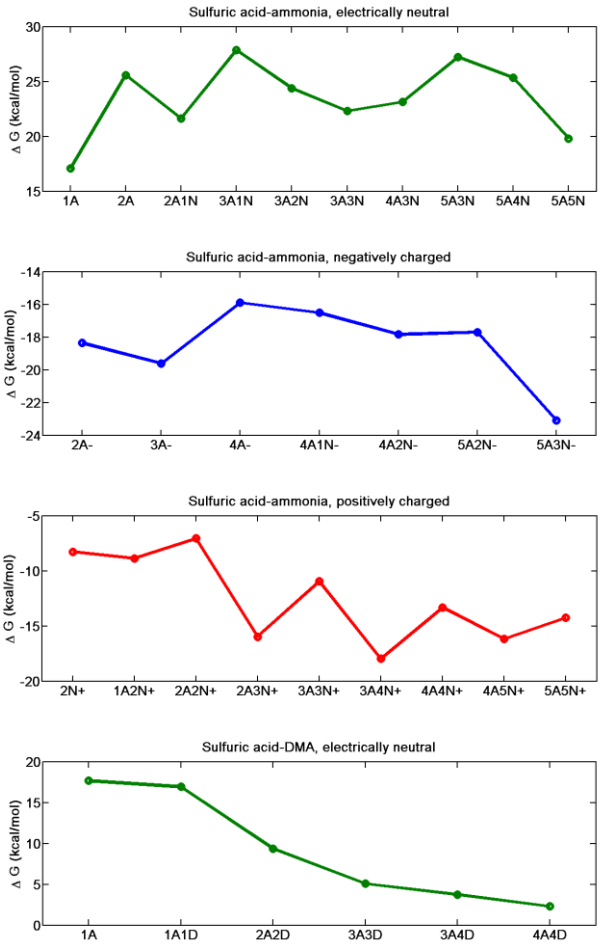

Figure 1. Gibbs free energy of formation as a function of growth step along the most significant growth routes in the sulfuric acid-ammonia and sulfuric acid-DMA systems at T=5 °C, $[H_2SO_4]=10^6$ cm^{-3} and $[NH_3]$=100 ppt or [DMA]=1 ppt. For ammonia, both electrically neutral and charged growth routes are shown; for DMA, only the neutral route is shown as the contribution of ions is insignificant. Acid, ammonia and DMA molecules are denoted with A, N, and D, respectively.

This work was supported by FP7-MOCAPAF project No 257360, FP7-ATMNUCLE project No 227463, Väisälä Foundation and Academy of Finland. The authors thank CSC- IT Center for Science in Espoo, Finland for the computing time.

McGrath, M.J. *et al* (2012) *Atmos. Chem. Phys.* **12**, 2345-2355.

Ortega, I.K. *et al* (2012) *Atmos. Chem. Phys.* **12**, 225-235.

Evaporation and growth dynamics of layered droplets: Theory and experiments

H. H. Tu and A. K. Ray

Department of Chemical and Materials Engineering, University of Kentucky
Lexington, KY 40506 U.S.A. Country
Keywords: two phase droplets, interfacial mass transfer, light scattering
email: akray@engr.uky.edu

Many physical and commercial processes involve evaporation and growth of two phase layered droplets of partially miscible components. In many cases, a volatile droplet is coated with an immiscible layer to create a diffusional barrier in order to retard evaporation of the core droplet. The presence of a layer, however, brings about a number of rate-controlling mechanisms for the transfer of species from the core droplet to the surrounding gas phase and induces markedly different effects on the evaporation rate of the core droplet, including enhancement of the rate (Ray et al., 1991). To understand evaporation and growth dynamics of layered droplets we have experimentally studied droplets of a number of immiscible systems to determine the determine evaporation characteristics of volatile core droplets coated with layers of nonvolatile components and developed a pseudo steady state model for evaporation and growth kinetics of a two phase droplet of two partially miscible components, exposed to a stagnant gas phase.

The theoretical analysis show the rate of evaporation or growth of a core droplet may increase, decrease or show a maximum with increasing layer thickness, depending the physical properties (e.g., vapour pressure, diffusion coefficients and miscibility limits) of the binary system. Criteria for various scenarios that arise during the evaporation or growth of a layered droplet have been developed in terms of analytical expressions. We have also examined evaporation of single layered droplets suspended in an electrodynamic balance (EDB) under vapour-free atmospheres. Droplets were generated from a homogeneous solution that was prepared by dissolving two immiscible components in a highly volatile common solvent. With the evaporation of the volatile solvent two phases in a suspended droplet separated to form a layered droplet. Droplets of di-ethylene glycol (DEG), tri-ethylene glycol (TEG), diethyl phthalate (DEP), and dimethyl phthalate (DMP) coated, respectively, with dioctyl phthalate (DOP), dibutyl phthalate (DBP), and squalane were studied. A suspended droplet was illuminated by a polarized laser beam, and scattered light from the droplet was by monitored by two photomultiplier tubes (PMTs). Resonances (i.e., peaks) observed in the elastic scattering intensity versus time spectra from a suspended droplet were interpreted using elastic light scattering theory to obtain outer and core radii of the droplet as functions of time (Ray and Nandakumar, 1995; Tu and Ray, 2006). The results obtained from core droplets of DEG and TEG coated with DOP as well as DBP layers show that the core evaporation rate monotonically increases as the layer thickness increases, and the evaporation rate of a core droplet can exceed the rate of an uncoated droplet of the same size. The results from DEP droplets coated with squalane layers show the core evaporation rate increases to a maximum, and then decreases as the layer thickness increases. The experimental results are highly reproducible and agree well with the model predictions. Because of the relatively low volatility of the core compounds involved in the study, a monotonic decrease in the core evaporation rate with increasing layer thickness, one of the scenarios indicated by the model, was not observed. In this study, we show that miscibility limits of nearly of immiscible binary systems, and the unknown parameters of a binary activity coefficient model can be evaluated from the evaporation data on layered droplets such binary systems.

This work was supported by the National Science Foundation and the National Institute for Occupational Safety and Health.

Ray A. K., Devakottai B., Souyri A. and Huckaby J. L. (1991) Evaporation Characteristics of Droplets Coated with Immiscible Layers of Non-volatile Liquids, *Langmuir*, **7**, 525-531.

Ray, A. K. and Nandakumar, R. (1995) Simultaneous Determination of Size and Wavelength-dependent Refractive Indices of Thin Layered Droplets,, *Applied Optics*, **34**, 7759-7771.

Tu, H. H. and Ray, A. K. (2006) Investigation of concentrically and eccentrically layered droplets by light scattering, *Appl. Opt.* **45**, 7652-7656.

Atmospheric tar balls: primary droplets from biomass burning?

Á. Tóth[1], A. Hoffer[2], I. Nyírő-Kósa[2], M. Pósfai[1], and A. Gelencsér[1, 2]

[1] Department of Earth and Environmental Sciences, University of Pannonia, Veszprém, P.O. Box 158, H-8201, Hungary
[2] MTA-PE Air Chemistry Group of the Hungarian Academy of Sciences, University of Pannonia, Veszprém, P.O. Box 158, H-8201, Hungary
Keywords: tar ball, formation mechanism, primary emission, biomass burning.
Presenting author email: ubul.toth@gmail.com

Biomass burning is a globally important source of anthropogenic carbonaceous aerosol. Atmospheric tar balls occur in large numbers in relatively fresh biomass burning plumes (Pósfai *et al* 2003). These particles can be easily recognized by transmission electron microscopy (TEM) by their shape and composition. In contrast to other spherical aerosol types such as sulphates the amorphous, spherical tar ball particles are stable and do not volatilize under the electron beam. These particles differ from soot particles as well, since they do not contain a microstructure of concentric graphene-like layers. Due to their absorption properties tar ball particles have an important role in the Earth's radiation budget (Alexander *et al* 2008). These particles typically occur externally mixed with other particles in the atmosphere. According to elemental analyses of individual particles, tar balls consist mostly of carbon, with a minor amount of oxygen and may contain only traces of sulphur, potassium, chlorine and silicon. The average C/O molar ratio is about 10 (Pósfai, *et al* 2004).

It has been hypothesized that tar ball particles form in secondary processes from pyrolysis products in the atmosphere (Pósfai, *et al* 2004). However, these particles are homogenous, they do not contain an internal core and form a distinct group of particles with diameters up to 500 nm. On the basis of these features we now hypothesize that tar ball particles are ejected as droplets of tar, produced during the pyrolysis and are emitted from inside the vascular tissues and other pores of the burnt plants.

In this study we carried out a laboratory experiment to produce tar ball particles under conditions simulating the hypothesized formation mechanism but with the total exclusion of flame or fire. A closed all-glass apparatus was constructed in which droplets were generated from tar-water emulsion by bubbling purified air or nitrogen through it. The droplets were passed through a heated zone at 450 ^{o}C to simulate thermal processes occurring in the fire zone. Then the airflow was cooled and dried with excess dry air and the particles were collected on grids for TEM analysis.

The tar-water emulsions used in the experiments were prepared previously by dry distillation of various plants (e.g. needles of *Pinus ponderosa* and logs of Turkey oak).

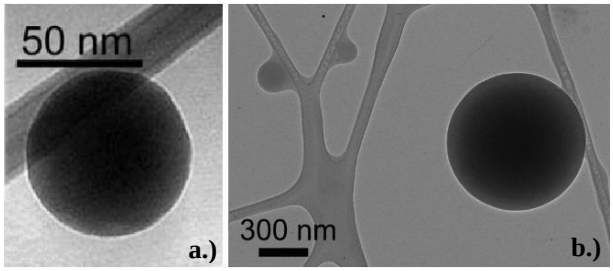

Figure 1. Bright-field TEM images of (**a.**) atmospheric tar ball (Pósfai *et al.*, 2004); (**b.**) laboratory-generated tar ball.

The morphology and elemental compositions of the particles were studied using TEM with energy-dispersive X-ray spectrometry (EDS). The generated particles were perfectly spherical and similarly to atmospheric tar ball particles, they were homogeneous (did not contain a condensation core) as it can be seen in *Figure 1b*. The C/O molar ratio of the laboratory-generated tar ball particles were also in the range reported for atmospheric tar balls. Our results imply that the suggested primary mechanism may be a feasible pathway of tar ball formation in biomass burning, but further studies are clearly warranted.

Present work was published in the frame of the project ***TÁMOP-4.2.2.A-11/1/KONV-2012-0064***. The project is realized with the support of the European Union, with the co-funding of European Social Fund.

Alexander, D. T. L., P. A. Crozier, J. R. Anderson, (2008), Brown Carbon Spheres In East Asian Outflow and Their Optical Properties, *Science*, **321**, 833.

Pósfai, M., R. Simonics, J. Li, P. V. Hobbs, and P. R. Buseck (2003), Individual aerosol particles from biomass burning in southern Africa, 1, Compositions and size distributions of carbonaceous particles, *J. Geophys. Res.*, **108** (D13), 8483.

Pósfai, M., A. Gelencsér, R. Simonics, K. Arató, J. Li, P. V. Hobbs, and P. R. Buseck (2004), Atmospheric tar balls: Particles from biomass and biofuel burning, *J. Geophys. Res.*, **109**, (D06213).

Application of broadband optical cavity methods to studying the optical properties of aerosols at short wavelengths

E. M. Wilson[1,2], J.C.Wenger[1,2], D. S. Venables[1,2]

[1] Department of Chemistry, University College Cork, Cork, Ireland
[2] Environmental Research Institute, University College Cork, Cork, Ireland

Keywords: optical properties, near-ultraviolet, optical cavity, IBBCEAS, nitroaromatic, nitrophenol, SOA, simulation chamber
Presenting author email: eoin.wilson@umail.ucc.ie

There is currently much interest in light absorption by atmospheric aerosols. Recent research has shown that some types of atmospheric particles start to absorb strongly at blue and ultraviolet wavelengths, but there are few techniques to probe the aerosol optical properties at these wavelengths. Varma et al. (2009) first showed that *incoherent broadband cavity-enhanced absorption spectroscopy* (IBBCEAS) is a promising approach to measure aerosol extinction with high sensitivity. Several groups are now using IBBCEAS for studying aerosol optical properties across a continuous spectral region and at short wavelengths (Washenfelder et al., 2012; Zhao et al., 2013). Our aim in this presentation is to describe our recent work to extend IBBCEAS aerosol measurements to very short wavelengths (Chen et al., 2011; Wilson et al., 2012).

A schematic of the experimental system is shown in Fig. 1. The IBBCEAS system was coupled directly across a 4 m^3 atmospheric simulation chamber in the Centre for Research into Atmospheric Chemistry at University College Cork. The system is unusual in that it is a single channel optical cavity spectrometer with continuous spectral coverage from 320 to 405 nm. The 4 m long optical cavity partially compensated for the reduced mirror reflectivity across this broad range. A xenon short arc lamp was used as a light source across the spectral region.

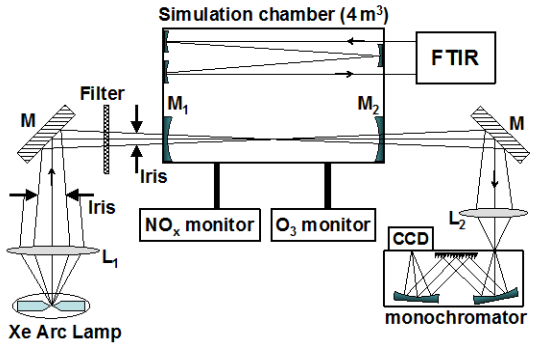

Figure 1. Layout of the atmospheric simulation chamber, IBBCEAS spectrometer, and ancillary equipment.

The stability and sensitivity of the system's extinction measurements were evaluated in a series of SOA experiments. The SOA was formed by photolysing strongly absorbing nitroaromatic compounds, which have been implicated in reducing levels of actinic radiation in large urban centres. The analysis of the total extinction spectrum is discussed, particularly how the contributions of gas phase absorption and particle extinction can be separated. We consider key elements of the experimental system and compare our approach to those of other groups. Finally, the future prospects for using IBBCEAS in field and chamber studies are assessed.

We gratefully acknowledge financial support from Science Foundation Ireland through grant 11/RFP/GEO3200.

Chen, J., Wenger, J.C., and Venables, D.S. (2011) *J. Phys. Chem. A*, **115**, 12235–12242.
Varma, R.M., Venables, D.S., Ruth, A.A., Heitmann, U., Schlosser, E., Dixneuf, S. (2009) *Appl. Opt.* **48**, B159.
Washenfelder, R.A., Flores, J.M., Brock, C.A., Brown, S.S., and Rudich, Y. (2012) *Atmos. Meas. Tech. Discuss.*, **6**, 113-157.
Wilson, E.M., Chen, J., Varma, R.M., Wenger, J.C. and Venables, D.S. (2012); *Proc. Int. Rad. Symp.*, AIP (in press).
Zhao, W., Dong. M., Chen, W., Gu, X., Hu, C., Gao, X., Huang, W., and Zhang, W. (2013) *Anal. Chem.*, **85**, 2260.

Release of fine particles from birch pollen grains following impaction

N. Visez[1], M. Choël[2], G. Loubert[1], G. Chassard[1], D. Petitprez[1]

[1]PhysicoChimie des Processus de Combustion et de l'Atmosphère, UMR 8522 CNRS Université Lille 1, Villeneuve d'Ascq, 59655, France
[2]Laboratoire de Spectrochimie Infrarouge et Raman, UMR 8516 CNRS Université Lille 1, Villeneuve d'Ascq, 59655, France
Keywords: Birch pollen, Ozone, Asthma, Granule.
Presenting author email: nicolas.visez@univ-lille1.fr

Dispersion of pollen allergens in the fine (ie. respirable) particle fraction is a major concern for allergenic asthma. Release of cytoplasmic particles may occur through hydration or germination of the pollen (Schäppi *et al*, 1997). Moreover, air pollution has been shown to facilitate pollen rupture (Motta *et al*, 2006). In this work, we have investigated rupture of the pollen and subsequent release of cytoplasmic particles following a mechanical stress generated with a PM_{10} impactor.

Experimental conditions. Birch pollen grains (ca. 20 µm) were aerosolized in the laboratory into a synthetic air flow of 10 $L.min^{-1}$ and sent into an impactor (Dekati) equipped solely with a PM_{10} stage. Particle size distributions were measured at the outlet of the impactor with an Aerosol Particle Sizer (TSI 3321). Impaction tests were also done with pollen grains artificially polluted with 3 ppm of ozone for 4 hours. Particle size distributions were normalised to show an equal number of pollen grains at 17 µm. All experiments were done in triplicate. For the purpose of FEG-SEM imaging, experiments were done with PM_{10} and PM_1 stages. Particles impacted were collected onto adhesive conductive carbon tapes for investigation of structural damage of the grains.

Results. Comparison of size distributions for native pollen and impacted pollen shows formation of an aerosol composed of fine particles with two size modes centred at 0.7 and 2.0 µm (figure 1). Formation of those particles was surprisingly smaller with ozone-polluted pollen. Pollen has been probably dried by the flow of synthetic air during the ozone exposure suggesting a role of the water content of the grain.

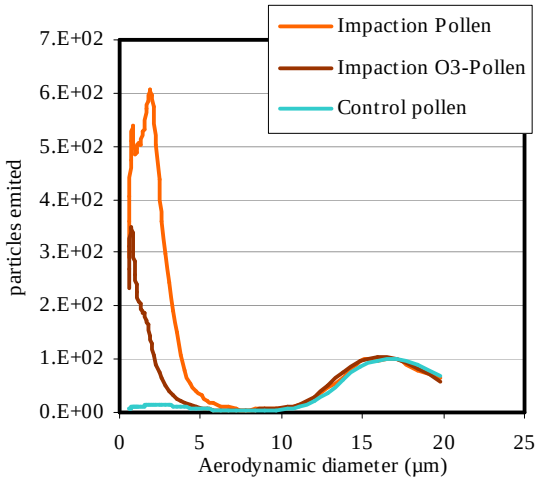

Figure 1. Normalised particle size distributions measured for aerosolized pollen (control run) and for pollen impaction (O_3-polluted or not).

Morphological examination of the sampling on PM_{10} stage by SEM revealed that a number of birch pollens were broken (figure 2). Small particles of micrometric size and ovoid shape were observed in PM_1 fraction (not shown).

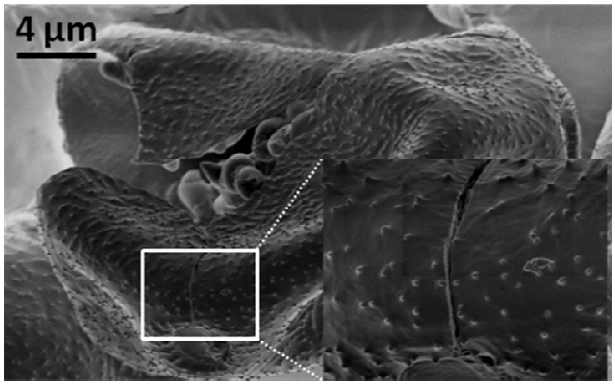

Figure 2. SEM image of a damaged pollen grain exhibiting a large fracture enabling the release of cytoplasmic granules. Insert: enlarged view of a crack in the exine.

Conclusion. Our results show that impaction on a solid surface at wind speed of about 3 $m.s^{-1}$ can induce birch pollen grain rupture. To the best of our knowledge, we gave evidence for the first time of a new mechanism for the release of respirable particles from birch pollen directly in an aerosol phase. Mechanical rupture may occur for pollen through wind transportation but also during pollen sampling by impaction. This latter is of particular importance for an artefact-free detection of allergens on fine particles by use of a multi-stage cascade impactor.

This work was supported by Région Nord Pas-de-Calais, Ministère de l'Enseignement Supérieur et de la Recherche, CNRS, Université Lille 1, European Regional Development Fund (ERDF) and IRENI (Institut de Recherche en ENvironnement Industriel).

Motta, A., Marliere, M., Peltre, G., Sterenberg, P., Lacroix, G. (2006). *Int. Arch. Allergy Immunol.*, 139, 294-298.

Schäppi, G.F., Taylor, P.E., Staff, I.A., Suphioglu, C., Knox, R.B. (1997). *Sex. Plant Reprod.*, 10, 315-323.

Friday, September 6, 2013

Plenary lecture: Urban aerosol: tendencies and challenges
By Imre Salma

Urban aerosol: tendencies and challenges

Imre Salma

Institute of Chemistry, Eötvös University, H-1518 Budapest, P.O. Box 32, Hungary
Keywords: environmental Kuznets curve, ultra-fine aerosol, nucleation strength factor, WSOC, SOA
Presenting author email: salma@chem.elte.hu

Approximately 47% of word population lives in urban areas, and this ratio is expected to grow further in time. In more developed countries, it is already 73%. Hence, the air quality in large urban zones affects the health and life of many people as well as the built environment and cultural heritage. Population growth, urbanisation, economic and industrial developments, road traffic and environmental management policies definitely influence the urban atmospheric environment. Temporal evolution of air pollution, however, shows tendencies or patterns which can be generalized to many large cities.

One of the most important criteria air pollutants in urban environments is atmospheric aerosol. Urban-type aerosol contains a mixture of particles which originate from a large variety of local (i.e. urban), regional (e.g. biogenic, geogenic or marine) emission sources and formation processes, and of particles that are advanced to cities by long-range transport. Combustion processes in homes and residential places, vehicular exhaust emissions of particulate matter and gaseous compounds and their interactions in the air usually contribute substantial to particulate matter. The complexity of particles makes it challenging to understand the role the urban aerosol and its production types play in many environmental and climate issues on different temporal and spatial scales, as well as to assess their relevance and consequences for human health. Are there dedicated or typical properties, behaviour and transformation processes for urban-type aerosol? What makes it different from the other aerosol types, and what are its peculiar environmental and health effects? Primary particles such as coarse particles with specific chemical composition, soot particles or some particulate organic compounds can be characteristic for urban activities. Some secondary organic components and the abundance of water-soluble organic carbon seem also to be linked to urban features. As far as the ultra-fine size fraction is concerned, its contribution to the total particle number is relatively large (above 75%) in cities. These particles likely also have different chemical composition with respect to the other aerosol types. There are feasible methods to distinguish between the two major production types of ultra-fine aerosol, i.e., between direct emissions and atmospheric nucleation as indicated in Figure 1.

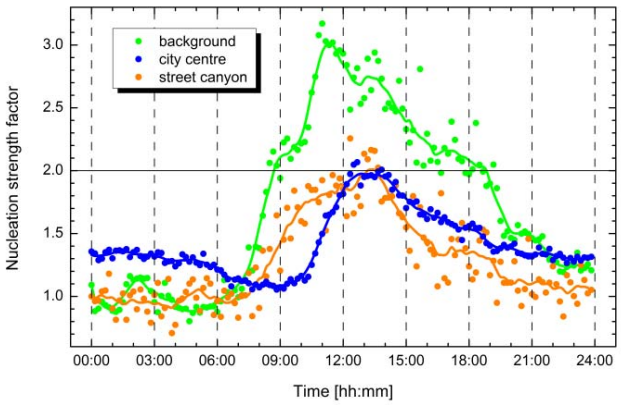

Figure 1. Diurnal variations of nucleation strength factor for the near-city background, city centre and street canyon environments in Budapest. The curves were obtained by one-hour smoothing. The horizontal line indicates the value at which atmospheric nucleation becomes the major production type for ultra-fine particles.

Micro-meteorology, geography and topology of urban agglomerations advance or restrict the transport and dispersion of particles. As a result, substantial differences in concentrations and other properties can occur among various urban environments within a city as far as both the particle number and mass are concerned.

In the lecture, the issues mentioned above will be discussed in more detail with selected examples for large European urban zones.

Financial support of the Hungarian Scientific Research Fund (contract K84091) is appreciated.

Friday, September 6, 2013

Session: Atmospheric Aerosols,
Aerosol-cloud interaction and climate effects of aerosols

Simplifying the water-affinity and CCN activation of complex organic aerosols: A model study

I. Riipinen[1, 2], N. Rastak[1] and S. N. Pandis[2, 3]

[1]Department of Applied Environmental Science, Stockholm University, Stockholm, Sweden
[2]Center of Atmospheric Particle Studies, Carnegie Mellon University, Pittsburgh, PA, United States
[3]Department of Chemical Engineering, University of Patras, Patras, Greece
Keywords: Water-solubility, organic aerosol, CCN activation
Presenting author email: ilona.riipinen@itm.su.se

Introduction

The solubility in water is one of the key properties governing the water-absorption and CCN activation behaviour of aerosol particles.

Organics contribute a large fraction (20-90%, depending on the environment) of atmospheric submicron particulate mass, which is the part of the aerosol size distribution that typically dominates the CCN numbers. Atmospheric organic compounds have a wide range of solubilities, spanning from practically insoluble material to highly water soluble compounds (e.g. Raymond and Pandis 2003). To accurately predict the water content and CCN activation of atmospheric OA information on the dissolution behaviour and aqueous phase interactions of these complex mixtures is needed.

We introduce a theoretical framework (Solubility Basis Set, SBS) representing the mixture components with a continuous distribution of solubilities, similar to the VBS (Donahue et al., 2006). Using this framework, we investigate the dissolution behaviour of complex organic mixtures and furthermore their CCN activity. Particularly, we investigate the response of the CCN-activation to varying solubility ranges, distributions, and numbers of components in the mixture. We also present a simple relationship between the dissolved fraction and the apparent κ value. Furthermore, we provide recommendations for reasonable simplifications of the dissolution behaviour or organic mixtures, specifically in relation to interpretation of experimental CCN studies and activation predictions of SOA.

Methods

We consider a monodisperse population of spherical aerosol particles consisting of an internal mixture of organic compounds. When exposed to water vapour, these particles grow reaching a thermodynamic equilibrium between the water vapour and the particle phase according to the Köhler theory. The wet particle is allowed to consist of maximum two phases: the insoluble organic phase and the aqueous phase. The compositions of the organic and aqueous phases are determined by the equilibrium between the aqueous phase and the water vapour, and the equilibrium of the aqueous phase with the organic insoluble phase assuming an ideal mixture of the organics. Critical supersaturations and the dissolution behaviour at the point of CCN activation were calculated from the Köhler theory predictions.

We investigated the dissolution behaviour and CCN of 68 different organic mixtures with varying solubility distributions. We varied the range of pure component water solubilities present in the mixture, the shape of the solubility distribution, and the number of components *n* in the distribution.

Results

Figure 1 displays an example of the model results, namely the relationship between the apparent hygroscopicity parameter κ (as derived from fits to the model output) and the dissolved organic fraction ε at the point of activation. The dependence of κ on ε follows a simple linear relationship, and in fact could explain some of the apparent discrepancy between the κ values derived from hygroscopicity vs. CCN activation measurements. Futhermore, we present a criterion for complete solubility at the point of activation, considerably simplifying the theoretical predictions of the CCN activation of complex organic mixtures.

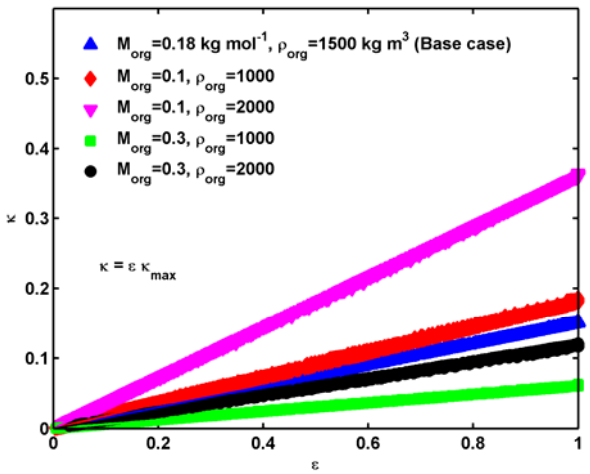

Figure 1. The hygroscopicity parameter κ vs. the dissolved fraction at the point of CCN activation.

Donahue, N. M., Robinson, A. L., Stanier, C. O., and Pandis, S. N., (2006), Environ. Sci. Technol., 40, 2635–2643, 2006

Goldstein, A., and Galbally, I., (2007) *Environ. Sci. Technol.*,40 (5), 1514–1521.

Raymond, T. M., and S. N. Pandis (2003) *J. Geophys. Res.*, 108 (D15), 4469.

Marine Cloud Brightening – do implementation assumptions change its effectiveness?

A.K.L. Jenkins[1], P.M. Forster[1]

[1]School of Earth and Environment, University of Leeds, Leeds, United Kingdom

Keywords: marine cloud brightening, large-eddy simulation, WRF/Chem, geoengineering

Presenting author email: eeaklj@leeds.ac.uk

We present the impacts of two implementation assumptions on the potential albedo enhancements achievable through the proposed Marine Cloud Brightening (MCB) scheme (Latham, 2002; Salter et al., 2008).

In the MCB proposal, sea water droplets would be emitted from close to the sea surface into the marine stratocumulus-topped boundary layer. These droplets would evaporate to form sea salt aerosols, which are intended to increase cloud albedo via the first and second indirect aerosol effects.

By using the WRF/Chem model in the large-eddy simulation configuration at small domain sizes, we interrogate two assumptions:

1) Emitting DRY aerosols vs. WET droplets

Previously, the emitted aerosols have been simulated as DRY aerosols. By instead simulating the emission as WET droplets, we find rapid evaporation and associated latent heat fluxes. These result in local temperature decreases and short-lived cold pools which suppress the height of the aerosol plumes by up to a third.

Omitting this plume height suppression by assuming that the emitted aerosols are DRY creates an overestimation in cloud albedo increase, producing a 94.1% increase in cloud albedo for our weakly precipitating case compared to an 88.5% increase when the emission is simulated as WET droplets.

Whilst this DRY versus WET sensitivity reduces the number of aerosols reaching the cloud base by half during the early morning, it is of less importance during the more uncoupled daytime. At this time, cloud-top-originating turbulence decreases, and poor transport of both the emitted aerosols, and moisture from the surface leads to low cloud albedo enhancement regardless of aerosol emission assumption.

2) Aerosol processes in the emitted plume

Previous studies, at a global scale, have shown that the albedo enhancement is sensitive to a combination of assumed emitted aerosol size distribution and number concentration, and the background aerosol conditions (Rasch et al., 2009; Korhonen et al., 2010; Alterskjær et al., 2012; Jones and Haywood, 2012; Partanen et al., 2012).

Here, we focus first on producing more realistic size distributions and number concentrations by using higher-resolution simulations (0.5m horizontal resolution) to capture the behaviour of the plume on emission into the boundary layer wind (figure 1).

By simulating the dynamics and aerosol processes within these plumes, we find a growth of larger aerosols, with an associated reduction in aerosol number concentration.

We then utilise these new aerosol size distributions and number concentrations in cloud simulations, in order to assess how the inclusion of this implementation detail affects the albedo perturbation under several background aerosol conditions.

These outcomes are intended to inform both future modelling work, and potential engineering design considerations.

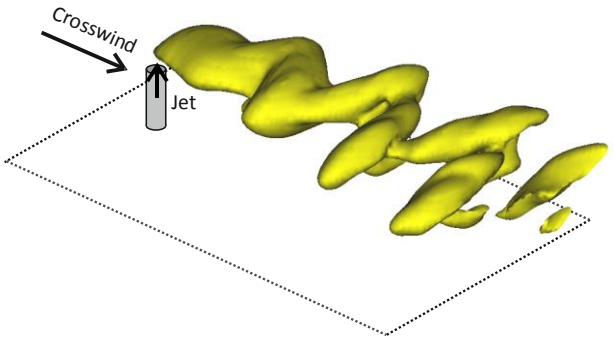

Figure 1. Annotated isosurface schematic of aerosol plume (yellow) in a crosswind

This work is supported by the EPSRC and NERC through the 'Integrated Assessment of Geoengineering Proposals' (IAGP, http://www.iagp.ac.uk). A.K.L.J. is supported through a Met Office CASE Studentship.

Alterskjær, K., Kristjánsson, J. E., and Seland, Ø.: Atmos. Chem. Phys., 12, 2795-2807, 2012.
Jones, A., and Haywood, J. M.: Atmos. Chem. Phys., 12, 10887-10898, 2012.
Korhonen, H., Carslaw, K. S., and Romakkaniemi, S.: Atmos. Chem. Phys., 10, 4133-4143, 2010.
Latham, J.: Atmospheric Science Letters, 3, 52-58, 2002.
Partanen, A.-I., Kokkola, H., Romakkaniemi, S., Kerminen, V.-M., Lehtinen, K. E. J., Bergman, T., Arola, A., and Korhonen, H.: J. Geophys. Res., 117, D02203, 2012.
Rasch, P. J., Latham, J., and Chen, C. C.: Environ. Res. Lett., 4, 2009.
Salter, S., Sortino, G., and Latham, J.: Philosophical Transactions of the Royal Society A: Mathematical, Physical and Engineering Sciences, 366, 3989-4006, 2008.

The importance of organic compounds for the first aerosol indirect effect: sensitivity to cloud formation parameterizations and meteorological fields.

R.E.P. Sotiropoulou and E. Tagaris

Environmental Research Lab, INT-RP, N.C.S.R. Demokritos, Aghia Paraskevi, Greece
Keywords: Aerosol-cloud interaction, CCN, organics, radiative forcing, clouds, modeling.
Presenting author email: rsot@ipta.demokritos.gr

Atmospheric aerosols are a focus of attention because of their important impacts on clouds and climate change. Organic aerosols represent an important fraction of tropospheric aerosol; in polluted regions organic aerosols are the second most abundant component by mass of the aerosol burden (Ramanathan et al., 2001). A number of studies have shown that organics play an important role in the aerosol indirect effect (AIE) which is one of the greatest sources of uncertainty in the assessment of anthropogenic climate change. Given that ambient organic aerosols may consist of hundreds of species, their representation in global climate models is typically limited to a few classes; this leads to further challenges in simulating AIE. In addition, much uncertainty also arises from the relationship used to link aerosol with cloud droplet number concentration (CDNC) and the variability in the predicted meteorology that contribute significantly to the differences in predicted AIE between GCM studies. Here it is assessed the importance of organic aerosols for the first AIE under different cloud droplet formation parameterizations and meteorological fields.

For this, the 3D NASA Global Modeling Initiative (GMI) chemical-transport model is used. GMI allows easy interchange of different model components while maintaining all others identical allowing a direct intercomparison of results obtained between alternate representations of aerosol, chemistry and transport processes. CDNC is computed using both empirical correlations (i.e., Menon et al., - LB (2002)), and physically-based parameterizations (i.e., Abdul-Razzak and Ghan - AG (2000), and Fountoukis and Nenes - FN (2005)). Emissions from the IPCC CMIP5 (CMIP) are used. Sensitivities are examined under two meteorological fields (i.e., NASA GEOS4 finite volume GCM (FVGCM) and NASA GEOS1-STRAT (GEOS)) for the same time period. Computed CDNC is used to calculate the effective radius (Re). The CLIRAD-SW solar radiative transfer model is used online to calculate the cloud optical depth (COD) and the shortwave fluxes from the surface to the top of the atmosphere (TOA). COD is calculated as a function of the effective radius. Evaluation of modeling results (i.e., Re, COD) is performed against satellite products from Moderate Resolution Imaging Spectroradiometer (MODIS) platform.

Depending on the combination of meteorological field and cloud scheme used the annual mean CDNC ranges between 63 and 189 cm^{-3} (Figure 1) with larger differences seen over heavily polluted regions (e.g., Europe, China, NE USA), regions affected by long range transport of pollution (e.g., Atlantic Ocean) or by biomass burning (e.g., S. Africa, S. America). Simulations without taking into account organics lead to a reduction in CDNC over S. America and S. Africa that are affected by biomass burning; lower CDNC values are also seen in eastern Asia because of the use of fossil fuels. The impact of organics on the first AIE is mixed: in pristine regions organics increase CCN increasing AIE, while in polluted areas particles grow larger, decreasing CCN and therefore counteracting AIE.

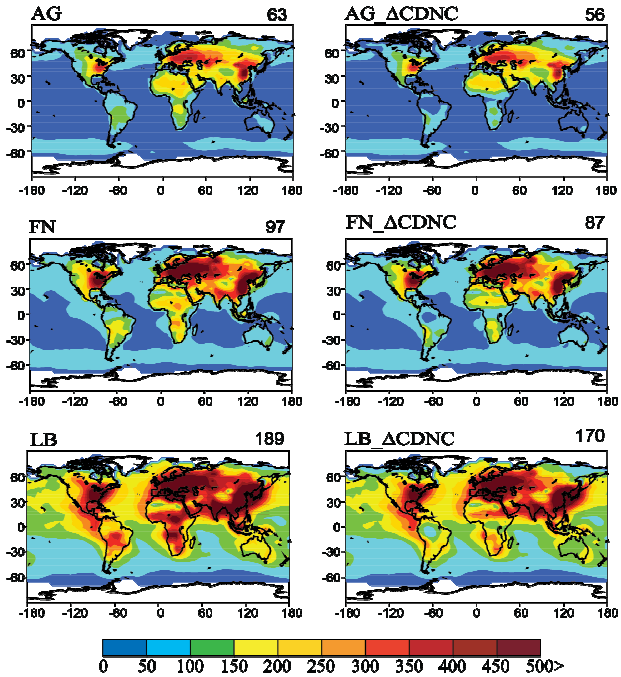

Figure 1. Simulated annual mean CDNC (cm^{-3}) for all droplet formation schemes used under the GEOS meteorological field (right panel) and relative change in CDNC when neglecting organic aerosol, (i.e., $CDNC_{tot}$ – $CDNC_{OC}$) (left panel). Global averages are shown in the upper right hand corner of each panel

This work was supported by the National Strategic Reference Framework (NSRF) 2007-2013 grand No 09SYN-31-667.

Abdul-Razzak, H. and Ghan, S. (2002), *J. Geophys. Res.*, **107**.

Fountoukis, C. and Nenes, A. (2005), *J. Geophys. Res.*, **110**(D11212), doi:10.1029/2004JD005 591.

Menon et al. (2002), *J. Atmos. Sci.*, **59**, 692-713

Ramanathan V., P.J. Crutzen, J.T. Kiehl and D. Rosenfeld (2001), *Science*, 294, 2119

Local geological topsoil dust in the area of Rome: linking mineral composition, aerodynamic size and optical properties

A. Pietrodangelo[1], R. Salzano[1], C. Bassani[1], S. Pareti[1] and C. Perrino[1]

[1]Institute of Atmospheric Pollution Research, C.N.R., Montelibretti (Rome), 00015, Italy
Keywords: mineral dust, size distribution, optical properties, radiative transfer model.
Presenting author email: pietrodangelo@iia.cnr.it

Airborne mineral dust plays a key role in energy exchange processes of the Earth's system. Understanding these phenomena requires deep knowledge of physical, chemical, morphological and size properties of mineral aerosols. However, large knowledge gap is currently recognized about these issues, e.g. the scatter and absorption of solar and terrestrial radiation by mineral dust, affecting also the reliability of modelling estimates (Hansell *et al*., 2011). In this view, an effort has been made in this study to link the aerodynamic behaviour and the optical properties of a suspended PM_{10} purely crustal dust. Topsoil mineral dust samples representative of major geological domains (Volcanics, Siliciclastic, Travertine) in the area of Rome (Italy) were collected from selected outcropping rocks. Chemical profiles of dust were previously obtained (Pietrodangelo *et al*., 2013). A micro-analytical approach based on Scanning Electron Microscopy and Energy Dispersive X-ray microanalysis (SEM-EDX) has been then applied, leading to define at once mineralogical composition and morphological features of more than 500 individual dust particles per sample. These were quantified by EDX microanalysis and X-ray spectra were matched with mineral EDX spectra of geochemical archives. Quantified particles were thus assigned to different mineral groups. Aerodynamic size distributions of each mineral groups and of major geological domains were finally built up by means of mineral densities (site-related) and of individual particle morphological data. Consistency of this approach was assessed by comparison with results of X-ray Diffraction (XRD) analysis of the same samples. In figure 1 the number size distribution of Volcanics and Travertine is reported.

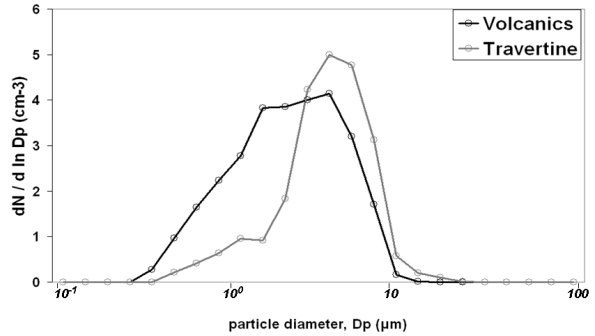

Figure 1. Number size distribution of Volcanics and Travertine PM_{10} with respect to aerodynamic diameter.

Awareness of mineralogical features of dust aerosols is also crucial in evaluating their optical and radiative behaviour. In this study, the optical properties of crustal dust were simulated by the 6SV atmospheric radiative transfer code (Kotchenova *et al*., 2008; Vermote *et al*., 1997), which computes aerosol optical properties (single-scattering albedo, asymmetry parameter, extinction coefficient, scattering coefficient and phase function) by the Mie Theory. Volume size distributions and refractive indexes related to dust samples of this study were used as model input data, respectively representing dust micro-physical and chemical properties. Conditions of dryness and of spherical particle shape were applied to all parts of this work, as this choice meets requirements both of SEM-EDX microanalysis and of the 6SV code to estimate particle scattering and absorption of the electromagnetic waves.
In figure 2 the single-scattering albedo and the extinction coefficient of the Volcanics and Travertine PM_{10} is reported.

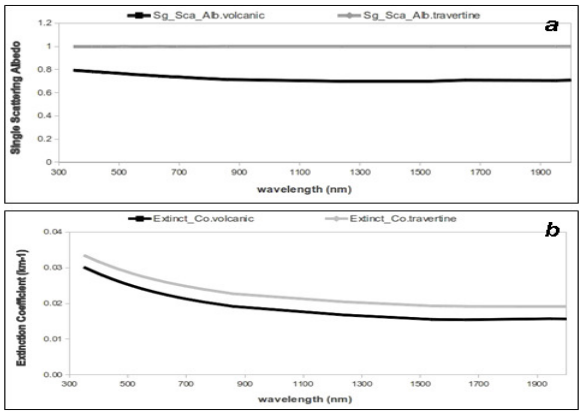

Figure 2. Single-scattering albedo (a) and extinction coefficient (b) of Volcanics and Travertine.

The single-scattering albedo highlights the weak absorption of Travertine along the visible and near-infrared spectral domain. The extinction coefficient shows a similar spectral dependence of Volcanics and Travertine on the extinction of electromagnetic waves with respect to the direction of propagation.

Hansell, R.A., Reid, J.S., Tsay, S.C., Rousch, T.L. and Kalashnikova, O.V. (2011) *Atmos. Chem. Phys*. **11**, 1527-1547.

Pietrodangelo, A., Salzano, R., Rantica, E. and Perrino, C. (2013) *Atmos. Env*. **69**, 1-14.

Kotchenova, S.Y., Vermote, E.F., Levy, R., Lyapustin, A. (2008) *Appl. Optics* **47**, 2215-2226.

Vermote, E.F., Tanrè, D., Deuzè, J.L., erman, M., Morcrette, J.J. (1997) *IEEE Trans. Geosci. Remote Sens*. **35**, 675-686.

Modeling aerosol water uptake in the Arctic and its direct effect on climate

N. RASTAK[1], A. EKMAN[2], S. SILVERGREN[4], P. ZIEGER[3], U. WIDEQVIST[1], J. STRÖM[1], B. SVENNINGSSON[4], P. TUNVED[1] and I. RIIPINEN[1]

[1]Department of Applied Environmental Science and Bert Bolin Centre for Climate research, Stockholm University, Sweden
[2]Department of Meteorology (MISU), Stockholm University, Sweden
[3] Paul Scherrer Institute (PSI), Laboratory for Atmospheric Chemistry, 5232 Villigen, Switzerland
[4]Division of Nuclear Physics, Lund University
Keywords: hygroscopicity, scattering coefficient, HTDMA, nephelometer
Presenting author email: narges.rastak@itm.su.se

Introduction

Water uptake or hygroscopicity is one of the most fundamental properties of atmospheric aerosols. Aerosol particles containing soluble materials can grow in size by absorbing water in ambient atmosphere. Hygroscopic growth depends on the dry size of the particle, its chemical composition and the relative humidity in the ambient air (Fitzgerald, 1975; Pilinis et al., 1995). One of the typical problems in aerosol studies is the lack of measurements of aerosol size distributions and optical properties in ambient conditions. In this study we try to bridge the gap between measurements performed under dry conditions and aerosol properties in the humid atmosphere. To do this we utilize a hygroscopic model which calculates the hygroscopic growth of aerosol particles at Mt Zeppelin station, Ny Ålesund, Svalbard during 2008.

Methods

A hygroscopic growth model was built on the κ-Köhler theory (Petters and Kreidenweis, 2007). The monthly chemical composition of the aerosol particles is represented by observations of inorganic ions obtained from the Norwegian Institute for Air Research (NILU) and filter sample analysis for the organic and elemental carbon (OC/EC) concentration (Silvergren et al., unpublished manuscript). The assumed components are: soluble and insoluble organics, sulfate, sea salt and soot. Internally mixed aerosol particles with homogenous chemical composition are assumed. After using the hygroscopic model, the radiative properties and radiative influence of the aerosols on the Arctic environment are studied using a Mie scattering model (Wiscombe, 1979) and a radiative transfer model (Richiazzi et al., 1998). A scheme of the models and inputs is shown in Fig 1.

Conclusions

The evaluation of the hygroscopic model calculations with HTDMA measurements from September 2007- August 2008 (Silvergren et al., unpublished manuscript) and the Mie scattering model calculations with humid nephelometer measurements during a 90 days campaign at Zeppelin station (Zieger et al., 2010) show a good agreement.

Sensitivity tests show that the model calculations are more sensitive to relative humidity and particle's size than its chemical composition. The hygroscopic growth of aerosol particles in ambient atmosphere increases the annual mean scattering coefficient by about a factor of 5 compared with calculations on completely dry aerosols. Hygroscopic growth should therefore be considered in all comparisons between in situ measurements, satellite products and model predictions of aerosol optical thickness. Our results also indicate that the RH profiles and variation are key parameters needed for correct predictions of aerosol optical properties.

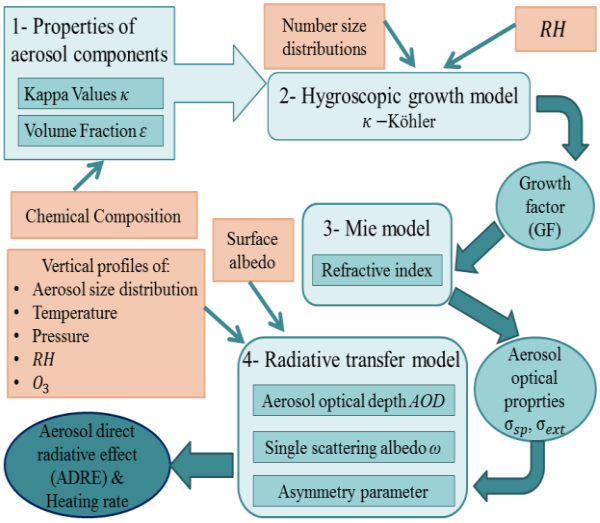

Figure 1. Scheme of the models and inputs, starting from defining the individual components of the aerosol particles and ending to calculate the aerosol direct radiative effect (ADRE) and heating rate profiles.

Petters, M. D., Kreidenweis, S. M.(2007), *Atmos. Chem. Phys.*, 7, 1961–1971.
Wiscombe, W., (1979), Available from National Technical Information Service as NTIS PB 301388.
Richiazzi, P., et al. (1998) *B. Am. Meteorol. Soc.*, 79, 2101–2114.
Zieger, P., et al. (2010), *Atmos. Chem. Phys.*, 10, 3875–3890.

Pre-Industrial atmospheric background black carbon concentrations in North America.

Liaquat Husain[1,2] and Tanveer Ahmed[1,2]

[1]Wadsworth Center, New York State Department of Health, Albany, NY 12201-0509, USA, and
[2]Department of Environmental Health Sciences, School of Public Health, State University of New York, Albany, NY, 12222, USA

Black carbon (BC) aerosols in the atmosphere absorb solar radiation, and cause heating of the atmosphere, may alter Earth's cloud cover, and impact precipitation cycle. The best estimate for radiative forcing from BC with 90% certainty is + 1.1 Wm^{-2} (+ 0.17 to 2.1 Wm^{-2}), second only to that of CO_2. A major uncertainty in the estimation is a serious lack of atmospheric BC measurements. Currently, models are used to estimate BC emissions into the atmosphere based on energy consumption and emission factors for variety of fuels and combustion methods used. Here we report long term measurements of BC in the atmosphere, over a period of several centuries using lake sediments, which contain records of atmospheric aerosols over thousands of years, if not longer. Retrieval of such records provides an invaluable source for understanding changes in the atmosphere with time. Several studies have been conducted with such an objective. Owing to a lack of knowledge of deposition rates of atmospheric aerosols into the lake sediments, a major shortcoming of these studies have been an inability to convert the measurements of chemical species in lake sediments into the atmosphere. We have developed a technique to overcome this shortcoming by measuring black carbon in atmospheric aerosols, and in lake sediment cores. The concentrations of BC were determined in daily filters collected at Whiteface Mountain, NY, from 1978 to 2005. Cores from two lakes around Whiteface Mountain, NY, were collected. Cores were (1) sectioned in thin slices, (2) freeze dried, (3) dated using the ^{210}Pb technique, (4) BC chemically separated, and (5) concentrations measured using the thermal-optical method. The deposition rate of BC from the atmosphere to the lakes was determined by comparing the BC concentration in air and the sediments for the 1978 -2005 period. The deposition rate so determined was used to concert the BC in the sediment into the atmosphere for the ~1978 to ~1100 period. The BC concentrations for the industrial period, ~1850 was low but rapidly increased from ~1900, peaked ~1925, decreased very slowly up to ~ 1980, followed by a sharp decrease, Fig 1. Concentration has remained fairly steady since, ~70 ngm^{-3}. A comparison of BC so determined is made with BC emissions estimated by NASA's global circulation model GISS GCM Model E (Koch et al, J. of Climate, 24, 2693-2714, 2011), and the European Atmospheric Chemistry Transport Model Oslo CTM2 (Skeie et al, ACP, 11, 6809-6836, 2011), using energy consumptions. Both model predictions agree reasonably well from ~1900 to about 1925, but under-predict by factors of 2 ~1950 and by a factor of 3 to 4 ~1980. These estimates are crucial for evaluating climate models against the *true* long-term measurements and will help seriously improve their predictive capability to simulate future warming trends. The 'natural' background of BC in the atmosphere for the ~1100 to ~1800 period was also fairly steady, with a notable spike ~1400, at 50ngm^{-3}, only slightly lower than the current measurements at Whiteface Mountain, 70 ngm^{-3}. The control measures in North America clearly have reduced atmospheric BC concentrations from ~700ngm^{-3} ~ 1950s.

Figure 1. Comparison of atmospheric BC concentrations determined using lake sediments with model estimates.

Historical $[EC]_{atm}$ measurements reconstructed from lake sediments of WP. These were compared with the modeled derived atmospheric BC concentration BC_{atm} data from *Skeie et al.* [2011].

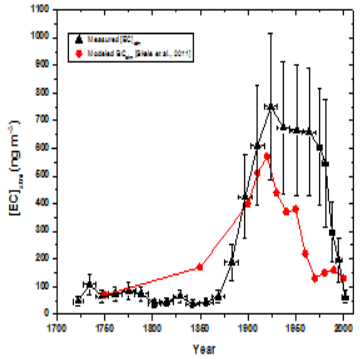

Global model simulations of the impact of transport sectors emissions on atmospheric aerosol and climate

M. Righi[1], J. Hendricks[1] and R. Sausen[1]

[1]Deutsches Zentrum für Luft- und Raumfahrt (DLR), Institut für Physik der Atmosphäre, Oberpfaffenhofen, Germany
Keywords: global aerosol modelling, transport sector emissions, climate impacts.
Presenting author email: mattia.righi@dlr.de

Emissions from the transport sectors (land transport, shipping and aviation) are among the major sources of tropospheric aerosol. Aerosol particles can have a significant impact on climate and can affect air quality, in particular in urban, densely populated areas, resulting in adverse health effects. The emissions from the transport sectors are expected to grow in the near future, especially in the developing countries. At the same time, various mitigation strategies are being applied in order to reduce air pollution and climate impacts.

In this work we use the EMAC-MADE global aerosol model to quantify the impact of transport emissions on global aerosol (Figure 1). We consider a present-day (2000) scenario and four future (2030) RCP scenarios from the CMIP5 emission dataset developed in support of IPCC AR5. Number emissions are also included in the model and derived from mass emissions under different assumptions on the size distribution of particles emitted by the three transport sectors. Additional sensitivity experiments are performed to quantify the effects of the uncertainties related to such assumptions.

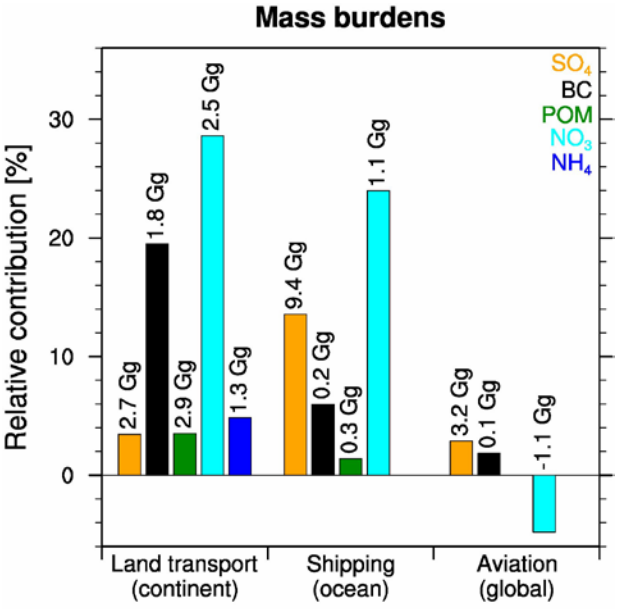

Figure 1. Relative contributions of the transport sectors to the multi-year average mass burdens of different aerosol components for the three transport sectors. The value on top of each bar shows the corresponding absolute contributions. The analysis is based on global simulations considering year 2000 emissions.

The model simulations show that the impact of the transport sectors closely matches the emission patterns. Land transport is the most important source of black carbon pollution in the USA, Europe and the Arabian Peninsula (Figure 2). Shipping strongly contributes to aerosol sulphate concentrations along the most-travelled routes of the northern Atlantic and northern Pacific oceans, with a significant effect also along the coastlines. The impact of aviation is mostly confined to the upper-troposphere (7 – 12 km), in the northern mid-latitudes, although significant effects are also simulated at the ground, due to the emissions from landing and take-off cycles.

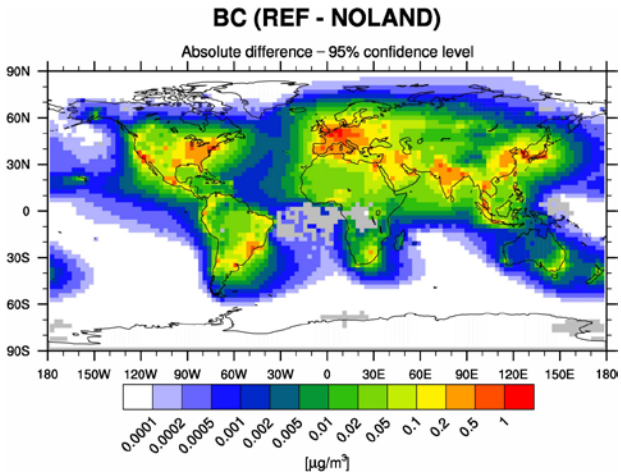

Figure 2. Absolute impact of land transport on BC surface-level concentration for year 2000 emissions. Non-significant grid-points are masked out in gray.

The simulations further reveal that transport-induced perturbations of particle number concentrations are very sensitive to the assumptions on the size distribution of emitted particles, with the largest uncertainties simulated for the land transport sector.

The climate impacts, due to aerosol direct and indirect radiative effects, are strongest for the shipping sector, as a consequence of large effects of sulphate aerosol on low marine clouds.

This study has been conducted in the framework of the DLR project VEU and of the EU project TRANSPHORM.

Variations of levels of atmospheric electrical and meteorological parameters and natural radioactivity in response to heavy smog due to forest fires

M.S. Cherepnev[1], A.V. Vukolov[1], I.I. Ippolitov[2], M.V. Kabanov[2], P.M. Nagorsky[2], Yu.A. Phalagov[3], S.V. Smirnov[2] and V.S. Yakovleva[1]

[1]Department of Applied Physics, Tomsk Polytechnic University, Tomsk, 634050, Russian Federation
[2]Institute of Monitoring of Climatic and Ecological System SB RAS, Tomsk, 634050, Russian Federation
[3]Institute of Atmospheric Optics, SB RAS, Tomsk, 634050, Russian Federation
Keywords: forest fires, aerosol, light ions, radioactivity.
Presenting author email: maxcherepnev@gmail.com

Extreme weather conditions created in summer in the European part of Russia in 2002 and 2010 and in Siberia in 2004 and 2012 due to forest fires led to the large number of forest and peat fires accompanied by extreme smoke of atmosphere.

Tropospheric aerosol together with greenhouse gases is an important climate-making factor influencing the radiation balance of the Earth. An important mechanism of variations of atmosphere electrical parameters (electric intensity E and polar conductivities $\lambda_{\pm}$) is the change in the number of light ions that are the main charge carriers due to their outflow onto the atmospheric aerosol. Decrease in the number of light ions in their outflow onto aerosol particles should lead to a decrease of $\lambda_{\pm}$ and to an increase of electric field intensity E. Ionization of air molecules in the atmosphere surface layer takes place mainly due to the natural radioactivity.

Based on a joint analysis of the variations of ionizing radiation levels (α-, β-, γ-background) in the atmosphere at heights of 5, 10 m and 25 m and depths of 0.1, 0.2, 0.5 and 1 m in the soil, meteorological and atmospheric electrical parameters in the summer smog due to summer forest fires in Siberia (2012) it was found that an increase of intensively smokiness and related with it decrease of visual range (S_m, Fig. 1, panel 1) and fall of solar radiation flux (I, panel 2) in the visible and UV ranges is followed by a decrease of λ_+ (panel 3) and the level of α-background radiation (panel 4). The clear dependence of β-, γ-background radiation level (panel 5) on S_m was not found.

Analysis of observation data of atmospheric electrical parameters during periods with maximal smog aerosol concentrations in the urban atmosphere surface layer due to long-term forest fires allowed for the first time to find out the effect of daily inversions of the electric field intensity with a changing range of 300 V/m and more in the daytime, of -300 V/m at night (panel 6). The observed effect of daily variations of the electric field in the atmosphere surface layer differs from the known effects by that it was detected in the smog conditions when forest fires covering large areas often for a long time in many regions. The proposed interpretation of this effect does not contradict the well-known diffusion-kinetic model of the ion charge aerosol.

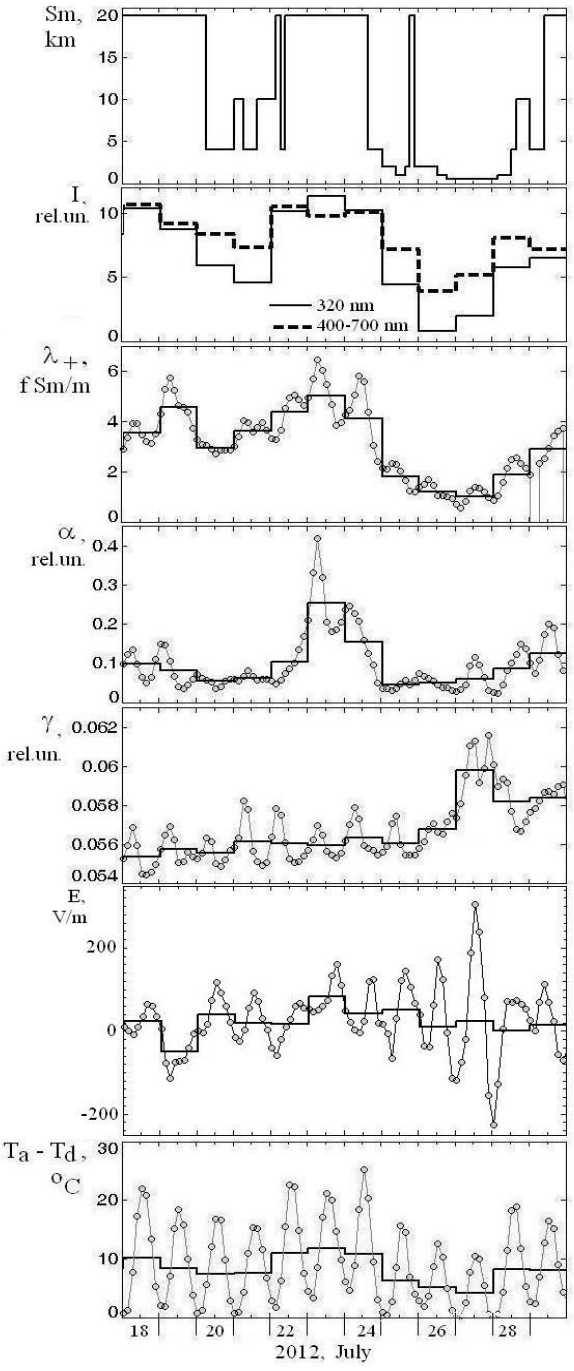

Figure 1. Variations of α-, γ-radiation components and meteorological quantities (S_m, I, λ_+, E, T_a -T_d) during the smog due to summer forest fires

Friday, September 6, 2013

Session: Atmospheric Aerosols,
Mineral dust, marine aerosols and others

Below-cloud scavenging by snow and mixed precipitation events calculated from high temporal resolution *in situ* measurements

G. Depuydt[1], O. Masson[1], J.L. Brenguier[2], C. Piot[3], J.L. Jaffrezo[3]

[1]IRSN/PRP-ENV/SESURE/LERCM, Cadarache, BP3, 13115 St Paul lez Durance, France
[2]CNRM/GMEI, Météo-France, 42 Av Coriolis, 31057 Toulouse cedex 1, France
[3]LGGE, 54, rue Molière, BP 96, 38402 Saint-Martin d'Hères cedex, France
Keywords: snow scavenging, aerosol size distribution, in-situ measurements
Presenting author email : guillaume.depuydt@irsn.fr

Below-cloud scavenging by snow (snowout) is well identified as an efficient wet deposition process. In case of snow events, accidental releases of pollutants or radionuclides can have serious impacts on biosphere. The recent nuclear accident at the Fukushima-Daiichi Nuclear Power Plant in March 2011 has highlighted the need for snowout coefficient determination when releases of radioactive materials or pollutants occurred in mountainous regions.

Many snowout studies realised till now are laboratories experiments (Knutson et al., 1976, Sauter et al., 1989) whereas few *in situ* studies are available (Kyrö et al., 2009 ; Paramonov et al., 2011). Determination of below-cloud scavenging of atmospheric aerosol particles by snow using *in situ* measurements is needed for a better understanding of this process.

During three winter seasons, optical particle counters were installed on two French sites to record aerosol concentrations from 0.25 to 32 µm with high temporal resolution (a spectra of 31 size classes each minute). Simultaneous use of a PARSIVEL disdrometer at these sites have allowed to identify snow events or events characterized by solid hydrometeors (snowflakes) and liquids (raindrops) coexistence ("mixed events").

For the recorded events (19 snowy and 27 mixed), scavenging coefficient Λ was calculated with the formulation used in previous *in situ* studies (Laakso et al., 2003, Paramonov et al., 2011) :

$$\Lambda(d_p) = \frac{1}{\Delta t} \ln\left[\frac{c_0(d_p)}{c_1(d_p)}\right] \qquad (1)$$

where Δt is the duration of the event, d_p the particle diameter, and c_0 and c_1 the concentration of particle before and after snow or mixed events, respectively. Such method is named "global approach".

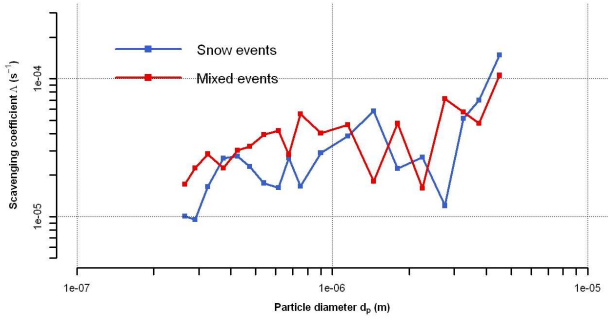

Figure 1. Scavenging coefficient Λ of aerosol according to their size, for snow and mixed events

In the 0.25 to 32 µm size range, mean and median scavenging coefficients Λ were $2.9\ 10^{-5}$ and $1\ 10^{-5}\ s^{-1}$ for snow events, and $1.8\ 10^{-4}$ and $1.7\ 10^{-5}\ s^{-1}$ for mixed events. These values are similar to those reported by Kyrö (2009) and Paramonov (2011). For the same sizes range, previous work on below-cloud scavenging by rain have shown mean values of Λ which range between $6.2\ 10^{-5}\ s^{-1}$ and $3\ 10^{-4}\ s^{-1}$, but data were recorded during events with higher intensities. Higher mean scavenging efficiency for mixed events observed here was also shown by Paramonov et al. (2011). As shown in figure 1, no great difference is observed in the distribution of Λ according to the particle diameter between 0.25 and 4.5 µm (no enough data usable below this size).

To improve these results which do not take into account the meteorological conditions variability during snow or mixed events, another similar approach was used. High temporal resolution measurements allowed us to fit decreasing aerosol concentrations to an exponential function for a large number of shorts periods (typical duration of some few minutes). Those for which this fitting is good (relative difference less than few %) were selected, and other processes that scavenging (advection in particular) were considered as negligible. Results were compared with those computed of the "global approach" and with below-cloud scavenging by rain coefficients.

This work was cofunded by Meteo-France and with the financial support of the Water Agency "Rhône Mediterrannée et Corse".

The air quality monitoring Association ATMO-PACA and The staff of the Laboratory of Glaciology and Geophysics of the Environment of Grenoble (LGGE) are also greatly thanked.

Knutson, E.O., Sood, S.K., Stockham, J.D., 1976. *Atmos. Environ.* (1967) 10, 395–402.

Kyrö, E.-M., Grönholm, T., Vuollekoski, H., Virkkula, A., Kulmala, M., Laakso, L. (2009) *Boreal Environ. Res.* **14**, 527–538.

Laakso, L., Grönholm, T., Rannik, U., Kosmale, M., Fiedler, V., Vehkamäki, H., Kulmala, M., (2003) *Atmos. Environ.* **37**, 3605–3613.

Paramonov, M., Grönholm, T., Virkkula, A. (2011) *Boreal Environ. Res.* **16**, 304–320.

Sauter, D.P., Wang, P.K. (1989) *J. Atmos. Sci.* **46**, 1650–1655.

Diurnal and seasonal variations of (nano)aerosols in the Škocjan Caves, Slovenia, a natural treasure of planet Earth

Irena Grgić[1], Ivan Iskra[2], Boštjan Podkrajšek[3], Vanja Debevec Gerjevič[4]

[1]Laboratory for Analytical Chemistry, National Institute of Chemistry, SI-1000 Ljubljana, Slovenia
[2]A.P.E Research, BioNanoLab, Area Science Park, 34149 Trieste, Italy
[3] Institute of Occupational Safety, Chengdujska cesta 25, 1260 Ljubljana – Polje, Slovenia
[4]Škocjan Caves Regional Park, Department for Research and Development, Škocjan, Divača, Slovenia

Keywords: cave aerosols; nano-particles; PM_{10}; size distribution; particle number concentration
Presenting author email: irena.grgic@ki.si

The Škocjan Caves are one of the most important cave systems in the world; they represent the most significant underground phenomena in the Karst region and Slovenia as well. Since 1986 Škocjan Caves were on the UNESCO's list of natural and cultural world heritage sites. Since the caves are opened to the public for a longer time, the possible pollution coming from the outside ambient air and additionally the influence of visitors can represent a real danger for this natural treasure. The important activity of the Škocjan Caves Regional Park, Slovenia is to monitor the parameters over the long period of time as it will be possible to detect the negative effects on the environment, and further timely react and prevent the potential damage.

In addition to the climatic conditions and radon activity concentration usually measured in the caves (e.g. Sainz et al. 2007), aerosol particles should also be measured as important factor. However, due to the extreme conditions in the caves (e.g. high relative humidity), especially if the sampling instrument is not adapted for such conditions, difficulties in aerosol measurements can be expected. This is likely the reason for low number of papers on aerosols in the caves (Kertész et al. 2002).

In this study, the continuous aerosol measurements during three different sampling periods were performed in the Škocjan Caves. To get information about the background aerosol concentration, the first measurement campaign on PM_{10} and size distribution of aerosols was carried out in December 2011. During June and August 2012, when a higher number of visitors is usually expected, the aerosol size distribution and number concentration of nano particles were additionally followed. Furthermore, PM_{10} measurements were performed also outside the cave to observe the possible influence of atmospheric particles.

Background concentration of PM_{10} was found to be about 4 µg m^{-3}; higher concentration was measured in June, and particularly in August 2012. It can be suggested that the increase in the aerosol concentration inside the cave was connected to both, the polluted atmospheric air which enters the cave with opening the door and to the higher number of visitors. Measurements of nano particles with SMPS additionally confirmed these findings. During summer period a severe raise in total aerosol concentration was determined (up to 18,000 particles cm^{-3}). Our results demonstrated that we were really able to detect very small changes and variations in aerosol concentration inside the cave. To our knowledge these are the first results on nano aerosols in the cave at all, and we believe should be considered seriously to protect the cave environment against their potential negative effects.

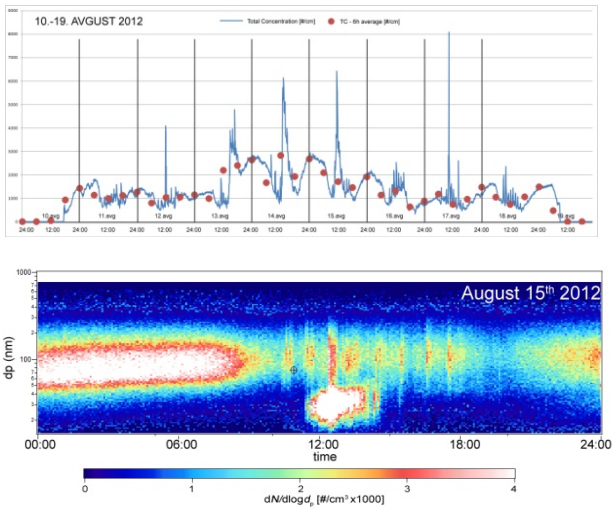

Figure 1. Total number conc. of particles between 14 nm and 710 nm for period 10 - 19 August 2012; and number conc. (particles cm^{-3}) and size distribution of the particles measured in the Škocjan Caves, Slovenia on 15 August 2012, using SMPS (TSI).

This work was supported by the Slovenian Research Agency (Contract no. P1-0034-0104). We thank the Škocjan Caves Park Public Service Agency, Slovenia for the permission and possibility to install the instruments in the Škocjan Caves.

Sainz, C., Quindós, LS., Fuente, I., Nicolás, J., Quindós, L. (2007) *J. Hazard. Mater*. **145**, 368-371.

Kertész, Zs., Balásházy, I., Borbély-Kiss, I., Hofmann, W., Hunyadi, I., Salma, I., Winkler-Heil, R. (2002) *Nucl. Instr. and Meth. B* **189**, 221-226.

Aerosol Processes in PAH Infiltration and Population Exposure in Rome

P. Lipponen[1], O. Hänninen[1], R. Sorjamaa[1], M. Gherardi[2], M.P. Gatto[2], A. Gordiani[2], A. Cecinato[3], P. Romagnoli[3] and C. Gariazzo[2]

[1]National Institute for Health and Welfare (THL), Department of Environmental Health, Kuopio, P.O. Box 95, Finland
[2] Italian Workers' Compensation Authority (INAIL), Monte Porzio Catone (RM), 00040, Italy
[3] National Research Council of Italy, Institute of Atmospheric Pollution Research (CNR-IIA), P.O. Box 10, Monterotondo Stazione 00015, Rome, Italy
Keywords: PAH, infiltration, exposure, seasonal variation.
Presenting author email: pasi.lipponen@thl.fi

Polycyclic aromatic hydrocarbons (PAHs) are known to be harmful to human health e.g. by causing lung cancer (Vineis *et al*, 2004). Spatial variability of the emissions, atmospheric dispersion, infiltration of the particles from outdoor to indoors, and population time-activity defines the exposures. Since the time spent indoors is typically 80-90%, exceeding times spent in traffic and outdoors, indoor exposures and thus particle infiltration from outdoors is a key issue (e.g. Hänninen *et al*, 2004).

Infiltration from outdoors to indoors, as well as lung deposition, is largely affected by particle size (Hänninen *et al*, 2012). Recently, accumulation mode particle deposition to alveolar region has been noticed to be the largest contributor to the PAH uptake (Zhang *et al*, 2012).

The aim of the work is to quantify the main aerosol processes that modify infiltration and respiratory tract deposition.

$PM_{2.5}$-bound PAH concentration measurements carried out in Rome, Italy, were used to evaluate the indoor-to-outdoor relationships of PAHs. A mass-balance model is used to estimate infiltration and indoor sources. Additional results regarding the indoor-outdoor behavior of PAH are presented in a parallel paper by Gatto *et al*.

High, up-to 30-40 fold differences in outdoor and indoor PAH concentrations were observed between non-heating and heating seasons. Indoor-to-outdoor ratios of PAH concentration between different microenvironments were noticed to vary much less, but between different seasons the variation of indoor-to-outdoor ratios for examined homes was significant. Indoor sources played only a minor role in PAH exposures.

As can be seen from Figure 2, accumulation mode particles, i.e. the particles of which demonstrate high infiltration rate indoors and the particles of which are able to penetrate alveolar parts of human lungs are also the particles consisting high mass concentrations.

Seasonal heating emissions contribute almost 90% of the PAH exposure yearly in Rome metropolitan area followed by traffic and waste incineration. The variation in the PAH indoor-outdoor relationship is significant between different seasons, but there is only little variations between different microenvironments. Majority of the PAH mass is in accumulation mode and ultrafine particle size ranges. The latter is affected more by infiltration.

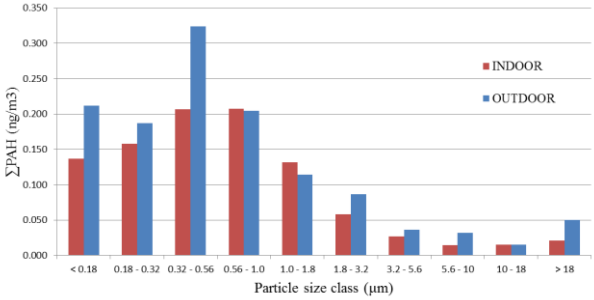

Figure 1. Measured Σ_{11}PAH concentration as a function of particle size distribution.

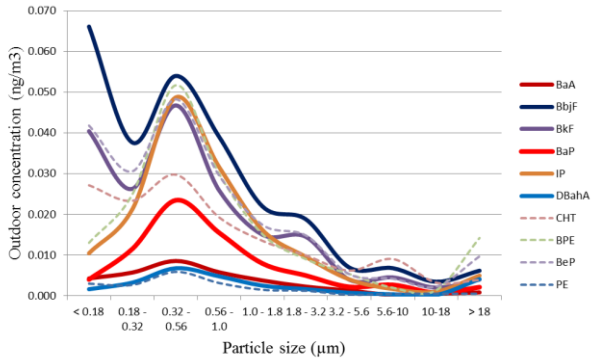

Figure 2. Outdoor concentration as a function of particle size distribution for all PAH compounds.

This work has been supported by Life+ -project EXPAH (Contract ENV/IT/000082; 2009), EU Contracts FP7-ENV-2009-1-243406 (TRANSPHORM), ENV4-CT95-0205 (ULTRA) and Academy of Finland Contract 133792 (PM Sizex).

Gatto M *et al*. (2013), Seasonal behavior of indoor and outdoor PAHs in different microenvironments of Rome, Italy. Parallel presentation at EAC.

Hänninen, O., Lebret, E., Ilacqua, V., Katsouyanni, K., Künzli, N., Srám, R.J. and Jantunen, M. (2004) *Atm.Env.* **38**, 6411 - 6423

Hänninen, O., Sorjamaa, R., Pekkanen, J., Lanki, T. and Cyrys, J. (2012) *Proc. Of Congress on Air Quality*, Athens, Greece.

Vineis, P., Forastiere, F., Hoek, G. and Lipsett, M. (2004) *Int. J. Cancer* **111**, 647-652.

Zhang, K., Zhang, B.-Z., Li, S.-M., Wong, C. and Zeng, E.Y. (2012) *Sci. Tot. Env.* **431,** 245-251.

Two years of measured vertical profiles in the Arctic (Svalbard): results from 2011-2012 spring-summer campaigns

L. Ferrero[a], D. Cappelletti[b], B. Moroni[b], V. Vitale[c], R. Udisti[d], G. Sangiorgi[a], M.G. Perrone[a], M. Busetto[c], C. Lanconelli[c], M. Mazzola[c], A. Lupi[c], S. Becagli[d], R. Traversi[d], D. Frosini[d], M. Maturilli[e], R. Neuber[e], C. Ritter[e], J. Graeser[e], M. Fierz[f], G. Mocnik[g] and E. Bolzacchini[a]

[a]POLARIS research centre, DISAT, University of Milano-Bicocca, Piazza della Scienza 1, 20126, Milano, Italy.
[b]DICA, University of Perugia, Via G. Duranti 93, 06125 Perugia, Italy.
[c]ISAC CNR Viale Gobetti 101, 40129, Bologna, Italy.
[d]University of Florence, Via della Lastruccia 3, 50019, Sesto Fiorentino, Florence Italy.
[e]Alfred-Wegener Institut für Polar- und Meeresforschung (AWI), Forschungsstelle Potsdam, Telegraphenberg 43A, 14473 Potsdam, Germany.
[f]University of Applied Sciences Northwestern, Switzerland, Windisch, Switzerland.
[g]Aerosol d.o.o., Kamniska 41, SI-1000 Ljubljana, Slovenia

Keywords: Vertical profiles, Arctic, Planetary Boundary layer, Black Carbon.
Presenting author email: luca.ferrero@unimib.it

Aerosols properties (i.e. size distribution, chemical composition, Black Carbon fraction) and their load along the air column influence the climate forcing (IPCC, 2007; Corrigan et al., 2008). In order to study the effect of the Planetary Boundary Layer (PBL) dynamics on the particulate concentration, aerosol vertical profiles were conducted over Svalbard (Ny-Ålesund, Gruvebadet Station) along 2 summer (March-September) campaigns (2011 and 2012) in the framework of the CICCI program (Cooperative Investigation of Climate-Cryosphere Interaction; http://ny-niflheim.nilu.no/cicci//).
A helium-filled tethered balloon was fitted with: a miniaturized electrical nanoparticle detector (miniDiSC); a novel micro-Aethalometer (AE51, Magee Scientific) for Black Carbon (BC) absorption measurements; an Optical Particle Counter (GRIMM *1.107*; 31 size classes between 0.25 to 32 μm); a miniaturized cascade impactor (Sioutas SKC with 2 impaction stages: <1 μm, >1 μm) to collect samples of particulate matter; a meteorological station (Vaisala Tethersonde TTS 111).
In spring, 84 profiles (up to ~1 km height) were analyzed evidencing multilayered aerosol structures. Aerosol stratification heights were detected for three broadsize ranges (d_p<250 nm, 250 nm<d_p<1000 nm, d_p>1000 nm) by a gradient method; their frequency distribution is resumed in Figure 1.

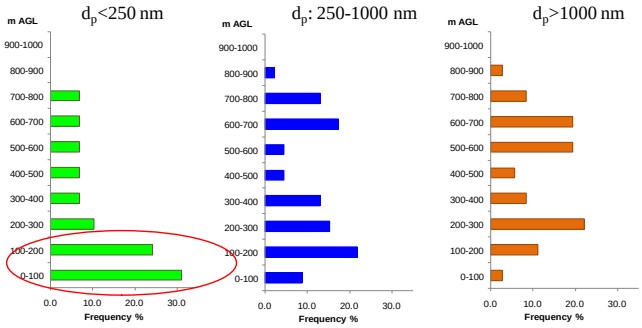

Figure 1. Frequency of aerosol stratifications along height as a function of size.

Finest particles (d_p<250 nm) were layered manily closer to the ground, where they showed higher concentration compared to accumulation mode particles (250-1000 nm; Figure 2). Often this behaviour was accompanied by a decrease of BC concentration. This behaviour was driven by the thermal structure of the lower troposphere characterized by both ground-level and high altitude thermal inversions. A case study is reported in Figure 2, as an example of the aforementioned behaviours. As a results aerosols of different sizes were layered in a different way in the lower troposphere.

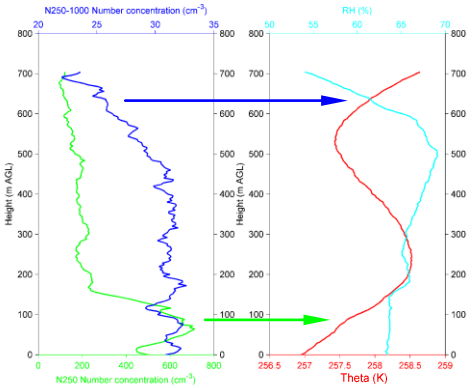

Figure 2. Vertical distribution of nanoparticles (greeen, left) accumulation mode particles (blue, left) on 6th April 2011 together with the thermal structure of the atmosphere (red, right).

In summer, 112 vertical profiles were carried out. BC and aerosol data pointed out that a total of 60 days were characterized by values 100-1000 times higher than background, due to the ship emissions in the port and in the harbour. This result demontrates that this anthropic source heavily affects the environment of the Ny Alesund area and suggesting its possible relevant role in the pollution of so critical Arctic regions.

This work was supported by the Italian National Research Council (CNR). We are also grateful for the help and logistical support to the German Alfred-Wegener-Institut (AWI).

Corrigan et al. (2008). Atmos. Chem. Phys., 8, 737–747.
IPCC: Climate Change 2007.

EMEP intensive measurements on mineral dust in PM_{10}, summer 2012 and winter 2013

W. Aas[1], X. Querol[2], F. Lucarelli[3], A. Alastuey[2], N. Pérez[2], H. Areskoug[4], V. Balan[5], J. N. Cape[6], M. Catrambone[7], D. Ceburnis[8], S.Conil[9], L. Gevorgyan[10], J.L. Jaffrezo[11] , C. Hueglin[12], N. Mihalopoulos[13], M. Mitosinkova[14], T. Moreno[2], J.-P. Putaud[15], V. Riffault[16], K. Sellegri[17], G. Spindler[18]

[1]NILU-Norwegian Institute for Air Research, 2027 Kjeller, Norway
[2]Institute of Environmental Assessment and Water Research (IDAEA-CSIC), Barcelona, Spain
[3]Dipartimento di Fisica e Astronomia and INFN, 50019 Sesto Fiorentino (Firenze), Italy
[4]Stockholm University, ITM, 106 91 Stockholm, Sweden
[5]Hydrometeorologic State Service, Ministry of Ecology and Natural Resources, Chisinau, Moldova
[6]Centre for Ecology and Hydrology (CEH), Bush Estate EH26 0QB, UK
[7]CNR, The Institute for Atmospheric Pollution, 00015 Monterotondo Stazione (Rome), Italy
[8]School of Physics, National University of Ireland Galway, Galway, Ireland
[9]ANDRA - DRD - Observation Surveillance, Observatoire Pérenne de l'Environnement, 55290 Bure, France
[10]Environmental Impact Monitoring Center, Yerevan, Armenia
[11]Laboratoire de Glaciologie et Géophysique de l'Environnement, 38 402 St Martin d'Hères Cedex, France
[12]Air Pollution, Environmental Technology EMPA, 86000 Dübendorf, Switzerland
[13]Environmental Chemical Processes Laboratory Dept of Chemistry, University of Crete, 71003 Heraklion, Greece
[14]Slovak Hydrometeorological Institute, 83315 Bratislava, Slovak Republic
[15]European Commission – DG Joint Research Centre, Ispra, Italy
[16]Département Chimie et Environnement, Ecole des Mines de Douai, 59508 Douai Cedex, France
[17]Laboratoire de Météorologie Physique LaMP-CNRS/OPGC, 63170 Aubiere, France
[18]Leibniz Institute for Tropospheric Research (TROPOS) 04318 Leipzig, Germany

Keyword: EMEP, mineral dust, chemical speciation, aerosols
Presenting author email: waa@nilu.no

The European Monitoring and Evaluation Programme (EMEP) under the UN-ECE CLTRAP, periodically arrange intensive monitoring periods (Aas *et al*, 2012), and in 2012-2013 one of the major focus was to measure chemical speciation in PM_{10} with special emphasis on mineral dust, with daily sampling for two one-month periods: 8. June - 12 July 2012, and 11 Jan - 8. Febr. 2013. The campaign was arranged in cooperation with the EU projects ACTRIS, ChArMEx and PEGASOS.

Fourteen regional sites across Europe (Figure 1) participated, and this unique dataset enables an extensive evaluation of transport, sources and regional distribution of mineral dust across the continent.

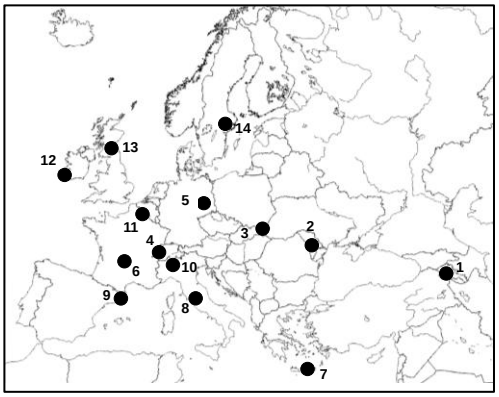

Figure 1. Sites participating in the EMEP intensive periods

PM_{10} samples were collected using low volume samplers, and were subsequently analysed for major and trace elements using PIXE at the INFN laboratory in Florence.

The chemical composition of PM_{10} mineral dust across Europe during the spring-summer period is described, and correlated with possible dust origin changes.

Important variations on the Si/Al, Mg/Al, K/Al are detected and correlated with possible source origin features. Fe-Al and Ti-Al showed a very good correlation independently of the site indicating that both Fe and Ti have a major aluminium-silicate mineral affinity.

Results allowed evidencing the impact of two African dust outbreaks occurring during the study period on the levels and composition of PM_{10} across south-western and central Europe (Figure 2). During these episodes, mineral dust composition was very similar in the affected sites. Composition is compared with the original mineral dust sampled at different African locations in prior studies

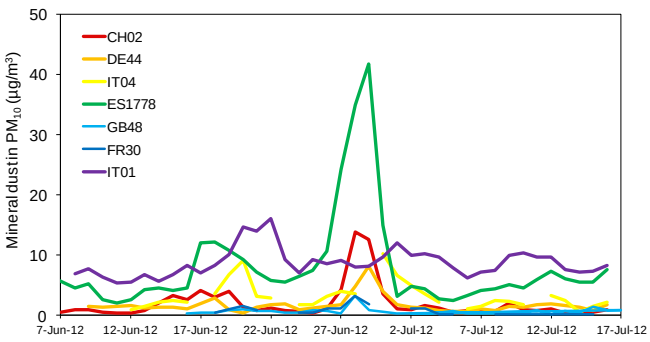

Figure 2. Time trends showing Sahara dust episode across Western Europe.

Aas W, et al. (2012) *Atmos. Chem. Phys.*, **12**, 8073-8094.

The effect of hexanoic acid on the hygroscopic properties of sodium halide aerosols

Lorena Miñambres*, Estíbaliz Méndez, María N. Sánchez, Fernando Castaño and Francisco J. Basterretxea

Department of Physical Chemistry, University of the Basque Country UPV/EHU, Leioa, Biscay, 48940, Spain

Keywords: marine aerosol, heterogeneous nucleation, hygroscopicity.
Presenting author email: lorena.minambres@ehu.es

Atmospheric aerosols generally consist of inorganic species with a wide variety of organic compounds and elemental carbon. One of the types of aerosol in which we have focused our attention is sea salt aerosol. Those aerosols are mainly caused by ocean wave action and constitute the second most abundant type of naturally suspended particulate matter in the troposphere after dust aerosol (Seinfeld & Pandis, 1998). In addition, an appreciable fraction of organic material is present in marine sea salt particles. Much of the organic fraction correspond to water insoluble fatty acids (Donaldson & Vaida, 2006), such as hexanoic acid (HA) that is an intermediate between soluble and highly insoluble organic acids, and has higher vapor pressure than the atmospherically more abundant acids. Fatty acids are presented as surface films on marine aerosols and that can affect properties such as hygroscopicity, phase transition or chemical reactivity. Despite the importance of this subject there is a lack of knowledge in the physical changes.

In the present work we study the hygroscopic properties of some submicrometric sea salt aerosols (NaCl, NaBr and NaI) coated with HA by Fourier-transform infrared spectroscopy in a flow cell. Infrared spectroscopy is a sensitive technique to characterize aerosol composition, water content and particle phase. With this study we provide physicochemical information of the influence of halogen atoms in the NaX/HA system, spectroscopic results about the dynamic of heterogeneous nucleation and a complete study of hygroscopic processes in NaX/HA/H_2O system.

HA phase in the particles has been spectroscopically monitored at given values of both relative humidity (RH) and HA/NaX solute mass ratio. The obtained results indicate that the gaseous HA easily nucleates onto dry and aqueous NaX particles. Furthermore, our results show that the amount of dissolved HA in the aqueous particles is negligible compared to the total amount of deposited HA. For this reason, we assume that practically all HA will be found on the surface of the particles. On the other hand, the evolution of the amounts of liquid HA on aerosols with RH shows that gaseous water molecules tend to displace HA molecules away from the particle surface, to energetically stabilize the system as the RH is increased.

Another important point is that the results on water uptake and release in HA covered particles reveal that the organic compound does not appreciably alter the hygroscopic processes for NaCl/HA with respect to the pure NaCl particles, whereas NaBr and NaI particles covered by HA deliquesce at higher RH and uptake water more abruptly than the pure inorganic particles. In contrast, efflorescence process in NaX aqueous particles is not substantially affected by the presence of HA.

Our results suggest that the surface properties of sea-salt particles may be more complex than model predictions, because, as bromide and iodine ions tend to segregate to the surface of particles, the effect of fatty acids can different for each $Cl^-/Br^-/I^-$ ions. Moreover, at given conditions of atmospheric RH, the amount of liquid water and the phase of sea-salt particle outer core may vary with respect to the expected behavior of pure NaCl particles. We are extending our investigation to more organic compounds to study the influence of the chain length of the fatty acid.

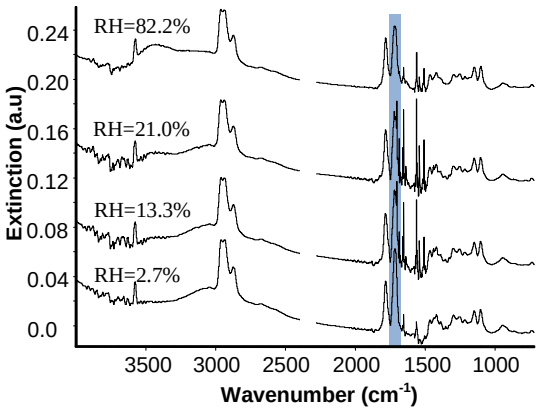

Figure 1. Infrared extinction spectra of NaI particles after passing through a heated cell containing HA exposed to different RHs. The presence of liquid water can be detected by the broad band centered at near 3400 cm^{-1}. It can be seen that the band intensities of liquid HA (≈1710 cm^{-1}, coloured) decrease as RH increase.

This work was supported by Ministerio de Ciencia e Innovación (Madrid, CGL2011-22441 and Consolider CSD-2007-00013), by Gobierno Vasco/Eusko Jaurlaritza (Vitoria-Gasteiz, IT520-10), and UPV/EHU for UFI11/23 and general support. L.M. thanks UPV/EHU for a postdoctoral research grant.

References

Seinfeld, J. H., Pandis, S. N. (1998) *Atmospheric Chemistry and Physics*; John Wiley; New York.

Donaldson, D. J., Vaida, V., 2006, *Chem. Rev.*, 106(4) doi: 10.1021/cr040367c.

Marine Aerosol Hygroscopicity and Volatility, Measured on the Chatham Rise (New Zealand)

L. Cravigan[1], M. Mallet[1], Z.D. Ristovski[1], P. Vaattovaara[2], N. Talbot[4], G. Olivares[4], M. Harvey[3], C. Law[3]

[1]ILAQH, Queensland University of Technology, Brisbane, 4000, Australia
[2]Department of Applied Physics, University of Eastern Finland, Kuopio, FI-70211, Finland
[3]National Institute of Water and Atmospheric Research, Auckland,1010, New Zealand
[4]National Institute of Water and Atmospheric Research, Wellington, 6021, New Zealand
Keywords: Marine Aerosols, Volatility, Hygroscopic Growth
Presenting author e-mail: z.ristovski@ qut.edu.au

Composition of the abundant Aitken and accumulation mode remote marine aerosol has important direct and indirect climate influences (Andrea and Rosenfeld 2008). Modeling indicates that the marine organic aerosol parameterization has a significant impact on the aerosol indirect forcing (Gantt *et al* 2012). Despite the importance of this aerosol source there are significant uncertainties surrounding the production mechanisms, processing and resulting ultrafine marine aerosol composition.

This study considers the composition of Aitken and accumulation mode remote marine particles observed at the Chatham Rise (East of New Zealand; latitude 42°S- 44°S, longitude 174°E-177°E). These observations were undertaken during the IGBP- SOLAS Surface Ocean Aerosol Production (SOAP) voyage in February/March 2012 on board the research vessel RV-Tangaroa (NIWA, Wellington, New Zealand). The Chatham Rise is located in the southern Pacific Ocean and is characterized by intensive summer phytoplankton blooms. These blooms lead to high organic concentration in the water and high dimethyl sulfide concentrations in the water and gas phase.

Atmospheric ultrafine particles (30-150nm) were studied using a Volatility Hygroscopicity Tandem Differential Mobility Analyser (VH-TDMA) (Johnson *et al* 2008). The VH-TDMA uses parallel SMPS's to examine particles of a pre-selected size that have been conditioned to high humidity and/or high temperature. Compositional information was obtained by exposing particles to a controlled relative humidity (20-90%) and observing the resultant hygroscopic growth. Further information is obtained from changes in the size and hygroscopic growth as particles are exposed to high temperature (25-550°C). The VH-TDMA was also capable of conducting deliquescence measurements were the relative humidity was ramped from 50-90%.

In addition the remote marine aerosol distribution and concentration was characterized using an SMPS and 2 condensation particle counters (CPC3007, CPC3010 and WCPC3781). Black carbon measurements were taken with an Aetholometer as a marker for ship pollution. Complementing the VH-TDMA measurements are observations from an ultra-fine organic TDMA (UFO-TDMA). This instrument examines the change in preselected particle size (<50nm) after being exposed to alcohol vapor, providing information on the organic content.

In addition to the atmospheric observation a number of experiments were conducted using a bubble bursting chamber. The aim of these experiments were to analyse the influence of the sea water composition on the production of primary marine aerosols. Same detailed analysis of the particle properties as for the atmospheric particles was conducted for the particles from the bubble bursting chamber.

The RV-Tangaroa route was designed to maximize the time spent in waters with high biological productivity (see Figure 1.) and efforts were made to minimize the influence of ship pollution on atmospheric measurements. This resulted in the examination of areas with a broad range of water biology and chemistry under a variety of meteorological conditions.

Results will be presented on both the remote marine aerosols as well as the primary aerosols generated from the bubble bursting chamber.

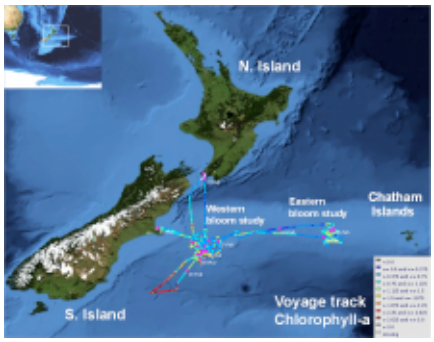

Figure1. :SOAP voyage track showing the concentration of Chlorophyll-a.

The SOLAS-SOAP experiment was funded by the NIWA program on Oceanic Control of Atmospheric Composition and supported by funding from NZ Ministry of Primary Industries. Logistic support to enable these measurements was provided by the Royal Society of New Zealand International Mobility Fund Contract IMF11A-70. QUT participation was partly funded by the NZ RS&T 2011-12 International Mobility Fund. PV was also supported by the Center of Excellence of Finnish Academy.

Andreae, M. O. and Rosenfeld, D. (2008) *Earth-Science Reviews,* **89**, 13–41.
Gantt, B., et al. (2012) *Atmos. Chem. Phys.* **12**, 6555–6563.
Johnson, G. R., et al. (2008) *J. Aero. Sci.* **39**, 850–861.

Assessment of emission sources in an industrial area using instrumental and biomonitoring techniques

J.Lage[1], S.M.Almeida[1], M.A. Reis[1], P.C. Chaves[1], M.C. Freitas[1], T. Ribeiro[1], S. Garcia[2], J.P. Faria[3], B.G. Fernández[3], H.Th. Wolterbeek[4]

[1]URSN, IST-CTN, Instituto Superior Técnico, Universidade Técnica de Lisboa, Sacavém, 2686-953, Portugal
[2]Instituto de Soldadura e Qualidade, Portugal; [3] Global R&D – ArcelorMittal, Spain;
[4] Delft University of Technology, The Netherlands
Keywords: PM_{10}, biomonitors, source apportionment, industry.
Presenting author email: joanalage@ctn.ist.utl.pt

The objective of this study was to assess the air quality and the contribution of emission sources in the vicinity of an industrial area placed in the North of Spain, which is affected by a steelwork, a cement factory and a power plant. For that complementary tools were used:

1) Metal concentrations were mapped in the surroundings of the industrial area using passive biomonitors;

2) Geographic Information System was used to evaluate the relations between the spatial distribution of the elements, contamination factors, land use and topography and to identify the sources and processes associated with the pollutants' formation;

3) PM_{10} was sampled in the industrial area and a temporal database of aerosol species was built to evaluate the seasonal variations of metal concentrations;

4) Receptor models were used to identify and quantify the contributions of the industrial operations to metal concentration in the local ambient air.

The spatial distribution of the chemical elements assessed by the biomonitors showed an increase of Al, Ca, Cl, Cu, Fe, I, Mn, Na, Sb and V in the industrial area. Elements associated with the soil also presented increased concentrations in this area probably due to re-suspension caused by the heavy traffic of trucks (Fig.1).

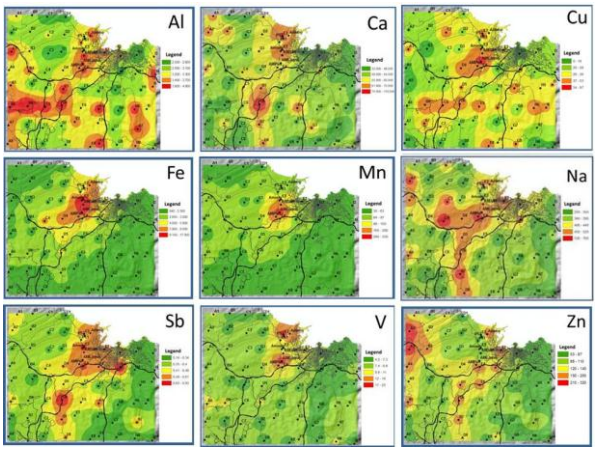

Figure 1. Spatial distribution of the Al, Ca, Cu, Fe, Mn, Na, Sb, V and Zn concentrations measured in the exposed biomonitores.

PMF applied to the PM_{10} compounds identified 7 emission sources. The first source clearly reflected the sea-spray composition, having high shares of Cl and Na, and contributed on average to 22% of the PM_{10} mass. The second source, which contributed on average to 11% of the total PM_{10} mass, was mainly composed of As, Cr, Cu, Ni, Pb, Sb and Zn and was attributed to mixed combustion processes and traffic. The third source contained high percentages of NH_4^+ that derives from gas to particle conversion processes. The contribution of this factor to PM_{10} mass was on average 12%. The fourth factor is made of Br and contributed for 1.8% of the total PM_{10} mass. The fifth source is dominated by NO_3^- and SO_4^{2-} and contributed on average for 19% of the PM_{10} mass concentration. The sixth source carries high percentages of Al, Ca, La, Si, Ti and V and account for 14% of the PM_{10}. These are the major constituents of soil and point out the fingerprint of mineral dust. The seventh factor was associated with steel production as it is defined by Fe and Mn. This source accounted for 21% of PM_{10} mass concentration (Fig.2).

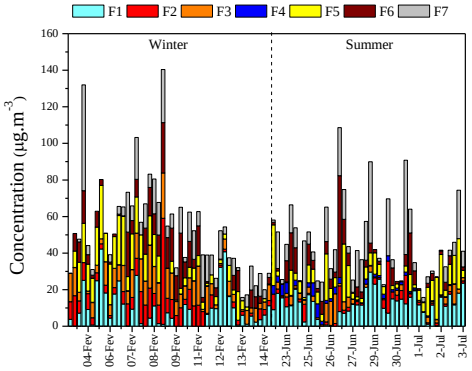

Figure 2. Source contribution for PM_{10} total mass concentration time series (µg.m^3).

This work showed that the use of complementary tools is essential in the assessment of the air quality. Atmospheric particles are usually measured instrumentally. However, particles sampling and characterization is necessarily performed by a limited number of sampling stations due to the associated high costs. As a result, vast areas are not covered by any monitoring system. Therefore, in one hand biomonitoring offers unique advantages - the ability to perform high-density sampling at any spatial scale at low cost and the measurement of a wide range of pollutants. In the other hand, instrumental measurements inform about the absolute air concentrations and the temporal trend of the pollutants.

This work was supported by the Portuguese "Fundação para a Ciência e Tecnologia" under the J. Lage PhD fellowship SFRH/BD/79084/2011. The research leading to these results has received funding from the European Community's Research Fund for Coal and Steel (RFCS) under grant agreement no RFSR-CT-2009-00029.

Friday, September 6, 2013

Session: Fundamentals,
Aerosol properties and dynamics

Evolution of the charge state z and the cross section W of mobility-selected protein ions held for tens of ms at temperatures from 25 to 100 °C.

J. Fernandez de la Mora[1] and M. Attoui[2]

[1]Yale University Mechanical Engineering Department New Haven CT USA

[2]University Paris Est Creteil, University Paris-Diderot, LISA, UMR CNRS 7583, France
attoui@univ-paris12.fr
keywords : protein mobility charge state

A first differential mobility analyzer (DMA_1) is used to select dimer and tetramers ions of the protein concanavalin A, electrosprayed into CO_2 from water solutions containg 100 mM triethylammonium formate. These selected ions are then subject for tens of ms to heating in an atmospheric pressure flow tube, and finally analyzed in a second DMA (DMA_2)where the drift gas is air at room temperature. The first DMA (DMA_1) flat DMA type (high resolution and high transmission DMA) works in closed loop. The second DMA (DMA_2) half mini type runs in open loop with air of the lab at room temperature.

Approximately 10% reduction in protein cross section (in ambient air) is found for all ions after exposing them to air at 100°C in the transfer tube. This substantial compaction is approximately linear with the change in temperature, and is far from being saturated at 100 °C. This notion that an even greater compaction would be achieved by further heating is confirmed by estimates of the effective density of the gas phase proteins, which evolves from about 0.85 g/cm^3 at room temperature to about 1 g/cm^3 at 100 °C. While unusually high for protein ions, this 1 g/cm^3 is still far from the theoretical density of 1.3 g/cm^3 determined based on the volume displaced by proteins dissolved in water.

The thermally induced compaction observed suggests that gas phase proteins are relatively malleable under the action of capillary forces. On the other hand, full compaction, if at all possible, requires substantial heating during substantial periods. This fact confirms the widely held notion that there are substantial barriers resisting conformational changes of proteins following their transfer from solution to the gas phase.

A surprisingly high level of charge reduction takes place in the transfer tube, even at room temperature, which is only moderately accelerated at 100 °C. For instance, selected dimer ions originally in charge states z =10 (2^{+10}) reach DMA_2 in charge states 10, 9 and 8 (2^{+10}-2^{+8}), with comparable charge loss observed for other dimer (2^{+9} and 2^{+8}) and tetramer ions (4^{+13}). We argue that the observed charge reduction cannot be due just to deprotonation of the protein by triethylamine vapors present. Rather, removal of the protonated amine from the protein must overcome a substantial activation barrier.

Evaluation of the role played by multiple scattering on the radiative properties of soot fractal aggregates

J. Yon[1], F. Liu[2], A. Bescond[1], C. Caumont-Prim[1], C. Rozé[1], F.-X. Ouf[3], A. Coppalle[1]

[1]UMR 6614 CORIA, CNRS, Université et INSA de Rouen, Saint Etienne du Rouvray, BP12, 76801, France
[2]Black Carbon Metrology, Measurement Science and Standards, National Research Council Ottawa, Ontario, Canada
[3]Institut de Radioprotection et de Sûreté Nucléaire (IRSN), PSN-RES, SCA, LPMA, Gif-Sur-Yvette, 91192, France.
Keywords: light scattering, soot, fractal aggregates, multiple scattering.
yon@coria.fr

Soot particles are well known for their toxicological impact due to their ultrafine size and content in carcinogenic molecules (PAH) and more recently for their strong influence on the global warming (Bond, et al., 2013). These particles appear like aggregates composed of primary spheres with optical properties similar to the graphitic carbon. Their specific spatial layout permits to establish a fractal like behaviour, *i.e.* a power law relationship between the aggregate mass and its size.

There is a rise in the use of optical diagnostics for *in-situ* characterization of soot particles. Indeed, measurement of light extinction by soot particles is often considered as a reliable way to determine the soot volume fraction. Laser induced incandescence is widely used to measure soot volume fraction in many applications or to evaluate the wavelength dependence of soot radiative properties. Angular light scattering is also used to determine the particle size or fractal dimension d_f (morphological parameter). Because of the complex morphology of these particles, the evaluation of their exact radiative properties is difficult and time consuming. For this reason, it is highly desirable to employ a simple yet adequately accurate theory, namely the Rayleigh Debye Gans theory for fractal aggregates (RDG-FA) in the interpretation of the detected angle resolved scattering signals or extinction measurements to infer morphological parameters.

The RDG-FA theory predicts that light absorption is related to the number of primary spheres N_p in the aggregates (proportional to the particle volume) and the light scattering to N_p^2. The angular dependence of the scattered light is described by a structure factor f (red curve in figure 1) which depends on the particle size and fractal dimension (Dobbins and Megaridis, 1991). This theory appears to be reliable relatively to the experimental uncertainties (Chakrabarty, et al., 2007); however, several important hypotheses are made including that radius of the primary sphere has to be smaller than the wavelength (Rayleigh regime), each primary spheres is supposed to be exposed to the incident light source and multiple scattering inside the aggregate is neglected. Although the role played by multiple scattering has been observed (Liu and Smallwood, 2010; Yon, et al., 2008), to our knowledge, how these assumptions affect the evaluation of the soot radiative properties has not been investigated. The present study was motivated by this observation.

In this study, the absorption and scattering properties of 150 aggregates generated by diffusion limited cluster-cluster aggregation (DLCA) are calculated by the discrete dipoles approximation (DDSCAT) (Draine and Flatau, 2010). The results are compared to those determined by RDG-FA in order to demonstrate the influence of multiple scattering and the shielding effect on the soot radiative properties for 7 wavelengths (from 266 to 1064 nm). For example, figure 1 presents the comparison between the structure factor numerically determined for each aggregates for the wavelength 266 nm (with multiple scattering) and the corresponding RDG-FA one (without).

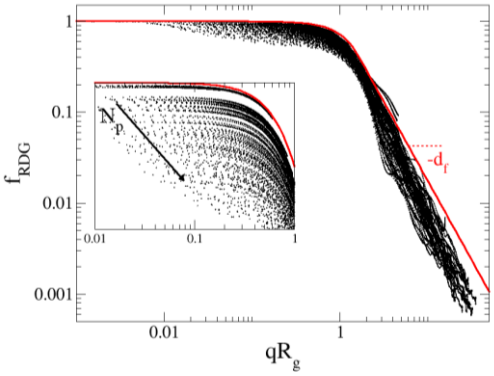

Figure 1. Comparison between structure factors evaluated by DDA approach and RDG-FA (red curve).

This figure shows that multiple scattering can affect the slop of the structure factor in the power-law regime and consequently the determination of the fractal dimension. This deviation from the RDG-FA theory is explained by a phenomenological approach involving the scaling approach introduced by Sorensen (q-region, 2013) by adding the role played by multiple scattering. We finally show that multiple scattering also has a strong impact on the evaluation of absorption and total scattering cross sections.

Bond, T.C., *et al.* (2013) *Journal of Geophysical Research: Atmospheres*.
Chakrabarty, R.K., *et al.* (2007) *Applied optics*, **46**, 6990-7006.
Dobbins, R.A. and Megaridis, C.M. (1991) *Applied optics*, **30**, 4747-4754.
Draine, B.T. and Flatau, P.J. (2010).
Liu, F. and Smallwood, G.J. (2010) *Journal of Quantitative Spectroscopy and Radiative Transfer*, **111**, 302-308.
Sorensen, C.M. (2013) *Journal of Quantitative Spectroscopy and Radiative Transfer*.
Yon, J., Roze, C., Girasole, T., Coppalle, A. and Mees, L. (2008) *Particle & Particle Systems Characterization*, **25**, 54-67.

The role of the scaling-law prefactor in the morphology of fractal aggregates

A.D. Melas[1 2], A.G. Konstandopoulos[1 3], L. Isella[4] and Y. Drossinos[2]
[1]Department of Chemical Engineering, Aristotle University, 50006 Thessaloniki, Greece
[2]European Commission, Joint Research Centre, 21027 Ispra (VA), Italy
[3]Aerosol & Particle Technology Laboratory, CERTH/CPERI, P.O. Box 60361, 57001 Thessaloniki, Greece
[4]European Commission, DG Energy, 2530, Luxemburg
Keywords: fractal prefactor, shape anisotropy, fractal dimension.
Presenting author email: Anastasios.Melas@jrc.ec.europa.eu

Fractal-like aggregates created via agglomeration (aerosols) or flocculation (colloids), obey a scaling law, $N = k(R/R_1)^{d_f}$ where N is the number of primary particles, R_1 the primary particle radius, and d_f the fractal dimension. The factor R is a characteristic length scale which can be either the radius of gyration (R_g), or the geometric radius (R_{geo}) which is the radius of the largest sphere encompassing the cluster centered at its center of mass, or the maximum distance in a fractal aggregate (L). A generalized prefactor corresponds to each characteristic length scale: these prefactors are the fractal prefactor (k_f), the inverse of the filling factor ($1/f$) and the packing fraction (ϕ) respectively. The physical meaning of these prefactors and more specifically the importance of k_f has been stressed recently (Wu and Friedlander, 1993). In this study, we relate large and small-scale structure properties to N, d_f and k_f changes.

For the needs of our study we created fractal aggregates with a mimic cluster-cluster algorithm (Filippov et al., 2000). The use of this algorithm gives us the advantage to create very fast fractal aggregates that have precisely prescribed number of primary particles, fractal dimension and fractal prefactor. We study the effect of N, d_f and k_f on shape anisotropy (A_{13}), mean angles (θ_{ijk}) and average number of near neighbors (c_N). Anisotropy is a large-scale indicator, a measure of the cluster stringiness. It is calculated from the principal radii of gyration R_i ($i = 1,2,3$) by diagonalizing the aggregate's inertial tensor. An indicator of a cluster's small-scale structure is the probability distribution of the angles formed by three monomers. The angles are specified by two intersecting lines passing through a central monomer i and two (j,k) monomers pairwise touching it. For every monomer i we calculated the number of its neighbors k, to which we associated $k(k-1)/2$ angles (possible pairwise combinations). In Fig. 1 we present distributions of angles for different N, d_f and k_f.

An alternative indicator of local compactness is the mean number of nearest neighbors, or coordination number, defined as the average number of contacts of a particle in a fractal aggregate. The synthetic fractals analyzed herein have coordination number close to 2, a consequence of our algorithm that requires that two clusters have only one sticking point. Since the coordination number is approximately constant we calculated the average number of

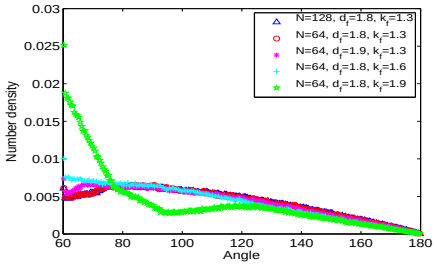

Figure 1: Ensemble-averaged probability distributions of three-monomer cluster angles.

near neighbors (c_N) at a fixed distance $5R_1/2$. The parameter choices are summarized in Table 1. The results are averaged over 5000 fractal aggregates.

Table 1: Mean characteristic structural parameters: shape anisotropy $< A_{13} >$, three-monomer angle $< \theta_{ijk} >$, and number of neighbors c_N.

	N	(d_f, k_f)	R_g/R_1	$\langle A_{13} \rangle$	$\langle \theta_{ijk} \rangle$	c_N
1	128	(1.8, 1.3)	12.8	3.78	105.8	2.63
2	64	(1.8, 1.3)	8.7	3.76	105.6	2.60
3	64	(1.9, 1.3)	7.8	3.30	104.0	2.73
4	64	(1.8, 1.6)	7.8	3.61	101.1	2.96

The effect of d_f is shown by comparison of rows 2 and 3, whereas k_f from the rows 2 and 4. These effects may be considered comparable as clusters (1.9, 1.3), row 3, and (1.8, 1.6), row 4, have the same radius of gyration. These comparisons indicate that changes of d_f produce larger changes of A_{13}, and a change of k_f large changes in the mean three-monomer angles and c_N. Hence, in general, the fractal dimension is an indicator of the overall aggregate's shape (large-scale aggregate morphology), while the prefactor becomes an indicator of local structure (small-scale morphology).

This work was supported by a European Commission Doctoral Fellowship (ADM).

M. Wu, S.K. Friedlander, J. Colloid Int. Sci. 159 (1993) 246.

A.V. Filippov, M. Zurita, D.E. Rosner, J. Colloid Interface Sci. 229 (2000) 261.

The Collision Frequency of Fractal-like Aerosols in the Free Molecular Regime

M.L. Eggersdorfer and S.E. Pratsinis

Department of Mechanical and Process Engineering, ETH Zurich, CH-8092 Zürich, Switzerland

Keywords: Coagulation, Discrete Element Method Simulation, Self-preserving Size Distribution, Sintering.
Presenting author email: sotiris.pratsinis@ptl.mavt.ethz.ch

Aerosol technology is used routinely in large scale production of commodities like pigmentary titania, carbon black and fumed silica. Recent advances in combustion and aerosol sciences have led to aerosol synthesis of sophisticated materials from catalysts to gas sensors, biomaterials and even nutritional products (Strobel and Pratsinis, 2007).

The manufacturing of some of these simple oxide commodities have taught us that the dynamics of aerosol reactors and the product nanoparticle characteristics span 10-15 orders of magnitude in length and time. So systematic process design requires interconnected models for different length and time scales that can be distinguished into continuum, mesoscale, molecular dynamics and quantum mechanics, comprising the so-called multiscale process design (Buesser and Pratsinis, 2012). One important, if not the most important, design criterion is the *high temperature particle residence time*. It determines the nanoparticle growth by gas and surface reaction, coagulation and sintering. Typically gas phase chemistry is so rapid that coagulation and sintering control particle growth. So knowing particle dynamics is necessary to design processes for particle manufacture.

The coagulation rate of spherical particles is reasonably well understood. However nanoparticles form fractal-like aggregates (chemically- or sinter-bonded) and agglomerates (physically bonded) of primary particles (Eggersdorfer and Pratsinis, 2013). Typically the collision radius of such structures is approximated with the radius of gyration, r_g, of equivalent spheres in the classic coagulation rate. Langevin Dynamics simulations corroborated the notion that r_g scales the collision radius in the free molecular regime (Pierce et al., 2006) but Mulholland et al. (1988) found that the actual collision radius is ~21% larger than r_g.

Here, the formation of nanoparticles by coagulation and sintering is simulated in the free molecular regime by a discrete element method (DEM, mesoscale). The particles follow random ballistic trajectories with the mean thermal velocity according to kinetic theory at volume fraction, $\phi = 10^{-7}$. The formation of agglomerates is traced in time to extract the detailed collision frequency, also for non-spherical particles. The system is doubled in size once the number of agglomerates halved (Figure 1). Simulations were carried out continuously to determine the collision frequency and agglomerate mass and size distributions for coagulation-agglomeration. Modified collision kernels for the detailed and overall collision frequency are extracted.

Aggregate sintering is modeled by a multiparticle viscous flow sintering mechanism accounting for the PP

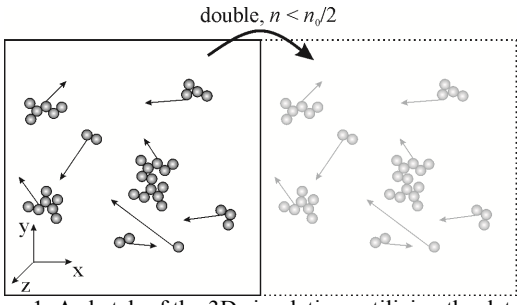

Figure 1. A sketch of the 3D simulations utilizing the detailed coordinates of each particle: The domain is doubled once the agglomerate number is halved from its initial value.

polydispersity and aggregate structure (Eggersdorfer et al., 2011). The ratio of characteristic sintering time, τ_s, to collision time, τ_c, solely defines the aggregate structure independent of T. Furthermore, the detailed aggregate size distributions can be determined quantitatively to get the detailed fractions of spherical particles, aggregates and agglomerates (Fig. 2).

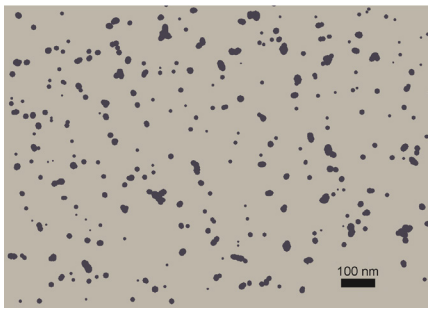

Figure 2: TEM-like image of SiO_2 nanoparticles grown by coagulation and sintering at 1900 K for *0.02* s simulated with up to $16 \cdot 10^6$ PPs. Mostly spherical particles are present at these conditions, though some of the larger have been aggregated already.

Buesser, B. and Pratsinis, S.E. (2012) *Annu. Rev. Chem. Biomol. Eng.* **3**, 103-127.

Eggersdorfer, M.L., Kadau, D., Herrmann, H.J. and Pratsinis, S.E. (2011) *Langmuir* **27**, 6358-6367.

Eggersdorfer, M.L. and Pratsinis, S.E. (2013) *AIChE J.* in press.

Mulholland, G.W., Samson, R.J., Mountain, R.D. and Ernst, M.H. (1988) *Energy Fuels* **2**, 481-486.

Pierce, F., Sorensen, C.M. and Chakrabarti, A. (2006) Phys. Rev. E 74, 021411.

Strobel, R. and Pratsinis, S.E. (2007) *J. Mater. Chem.* **17**, 4743-4756.

Collision Cross Section Calculation and Differential Mobility Analysis-Mass Spectrometry (DMA-MS) of Po-210 and Electrospray Generated Ions

Carlos Larriba-Andaluz[1], Hui Ouyang[1], Mark J. Meredith[1], Derek R. Oberreit[1], and Christopher J. Hogan Jr.[1]

[1]Department of Mechanical Engineering, University of Minnesota, Minneapolis, Minnesota, 55455, USA
Keywords: Ion Mobility Spectrometry, Ion Generation, Density Functional Theory, Gas Molecule Scattering
Presenting author email: hogan@me.umn.edu

In the free molecular regime, the collision cross section of charged particles and ions, Ω, can be related to electrical mobility, Z_p, via the relationship:

$$Z_p = \frac{3ze}{4\rho_{gas}\bar{c}\Omega} \quad (1)$$

where z is the integer charge on the particle/ion, e is the unit electron charge, ρ_{gas} is the background gas mass density, and c is the mean thermal speed of the particle/gas molecule reduced mass. The collision cross section in turn, can be calculated from polyatomic (all-atom) model structures for particles via gas molecule scattering simulations, and with proper calculation techniques, mobility measurements can be used to distinguish possible particle candidate structures from one another.

However, such gas molecule scattering simulations require an input model for the manner in which gas molecules scatter from a particle surface (both in terms of the scattering angle and reemission speed), when particles are modeled as fixed polyatomic structures. Here, we present new, efficient computational approaches for collision cross section calculation from polyatomic models, which can invoke any set of predefined gas molecule scattering rules. In the results presented, two specific scattering models are examined: (1) elastic hard sphere scattering (EHSS) which has been frequently invoked for comparison to collision cross section measurements made on ~1.0 nm ions in Helium background gas, and (2) diffuse hard sphere scattering (DHSS), which, when applied to a spherical particles, leads to results in excellent agreement with the free molecular limit of the semi-empirical Stokes-Millikan equation. With both scattering models, the influence of gas molecule polarization (the ion-induced dipole potential) is accounted for in calculations.

The described calculation procedures are applied to determine the collision cross sections of singly and doubly charged Sodium, Potassium, Rubidium, and Cesium Iodide cluster ions (positively charged). These ions are selected for examination because they have reasonably well-defined local-minima structures which can be determined via ab initio and density functional theory calculations. EHSS and DHSS predicted collision cross sections for these ions are compared to the measured collision cross sections in dry air for these ions, measured with a high resolution parallel-plate differential mobility analyzer coupled to a time of flight mass spectrometer (DMA-MS). Salt cluster ions are produced via electrospray ionization of salt solutions in methanol, and mass measurement subsequent to mobility analysis enables clear identification of the atomic composition and charge state of each examined cluster. Figure 1 plots the ratio of the DMA-MS measured collision cross sections to the calculated collision cross sections for these salt ions, as a function of the number of neutral ion pairs per cluster ion. In general, DHSS predictions are found in better agreement with measurements than are EHSS predictions, though the measurement agreement with DHSS predictions and disagreement with EHSS predictions both decrease with increasing cation mass in cluster ions.

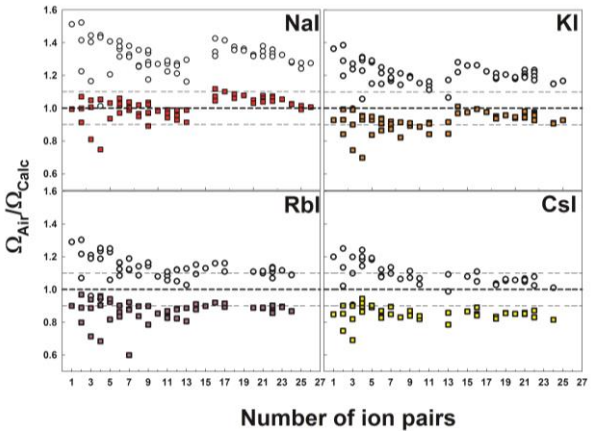

Figure 1. Comparison of measured (Ω_{air}) to calculated (Ω_{calc}) collision cross sections for positively charged salt cluster ions. Open symbols: EHSS calculations. Closed symbols: DHSS calculations.

DMA-MS measurements, density functional theory structure calculations, and collision cross section calculations are also performed on Po-210 generated positive and negative ions. Ions are generated in water-free "zero" air with clean metal tubing connecting the ion source to the DMA-MS (though the Po-210 is housed with plastic). Generally, Po-210 ions are found to be 50-300 Da organic ions, formed via protonation/deprototation or electron loss/gain. Similar to salt cluster ions. The predicted collision cross sections with DHSS calculations are found to be in better agreement with measurements for Po-210 ions. Overall, the presented work suggests that mobility-mass measurement in combination with structural modeling and collision cross section calculation from gas molecule scattering is a promising route to the examination of particles in the nanometer size range.

A new approach to the theory of Brownian coagulation

M.S. Veshchunov, I.B. Azarov

Nuclear Safety Institute (IBRAE) of Russian Academy of Sciences,
Moscow, 115191, Russia
Keywords: Brownian coagulation; kinetic equation.
Presenting author email: vms@ibrae.ac.ru

The new approach to the Brownian coagulation theory developed in the authors papers (Veshchunov, 2010) and (Veshchunov and Azarov, 2011), is overviewed. The traditional diffusion approach to calculation of the collision frequency function for coagulation of Brownian particles is critically analyzed. In particular, it is shown that the diffusion theory (Smoluchowski, 1917), (Chandrasekhar, 1943) is applicable only to the special case of coalescence between large and small particles, $R_1 >> \bar{r} >> R_2$ (where $\bar{r} \approx n^{-1/3}$ is the mean inter-particle distance), and becomes inappropriate to calculation of the coalescence rate for particles of comparable sizes, $R_1, R_2 << \bar{r}$.

In the latter, more general case of comparable size particles, coalescences occur mainly in the kinetic regime (rather than in the diffusion one) characterized by random (homogeneous) spatial distribution of particles (rather than by their concentration profiles), owing to their rapid diffusion mixing in-between collisions. This kinetic regime is realized in a wide range of the particles concentrations, obeying the basic assumption of the theory $n^{1/3}R << 1$, this allows calculation of the collision rate in various modes of the kinetic regime (continuum, free molecular and transition) within the same approach.

In the kinetic regime the original multi-particle problem is rigorously reduced to consideration of two-particle collisions. This justifies the phenomenological form of the pair-wise kernel $\beta(R_1, R_2)$ in the Smoluchowski kinetic equation, derived for spatially homogeneous systems.

In the continuum mode of the kinetic regime, corresponding to $a << R$, where a is the particle persistent length, the calculated coalescence rate formally (and, in fact, fortuitously) coincides with the expression $\beta_{dif}(R_1, R_2) = 4\pi(D_1 + D_2)(R_1 + R_2) \equiv 4\pi D_{12} R_{12}$ derived by Smoluchowski (1917) for the diffusion regime that is relevant only in the particular case of large and small particles coalescences. This formal coincidence apparently explains a reasonable agreement of predictions of the kinetic equation derived in the traditional approach with experimental measurements of the Brownian particles coalescence rate.

In the opposite range $a >> R$, the standard free molecular expression for the collision frequency function β_{fm} is valid. Since the transition interval $a \approx R$ also belongs to the kinetic regime characterized by homogeneous spatial distribution of particles, it can be described by the interpolation formulas derived within the new analytical approach with fitting parameters that can be specified numerically, avoiding semi-empirical assumptions of the existing models.

Numerical calculations of the coalescence rate β/β_{fm} as a function of a_{12}/R_{12} are performed using the Monte Carlo method (by evaluation of the sweeping rate $\beta/\beta_{fm} = (\delta V/\delta t)/(\delta V_0/\tau_{12})$ of randomly distributed immobile point markers by migrating Brownian particle), generalizing the analytical approach applied to the limiting cases $a << R$ and $a >> R$, in two subsequent approximations of the random walk theory. The calculated points can be approximated by analytical expressions with 2 and 4 fitting parameters, Figure 1.

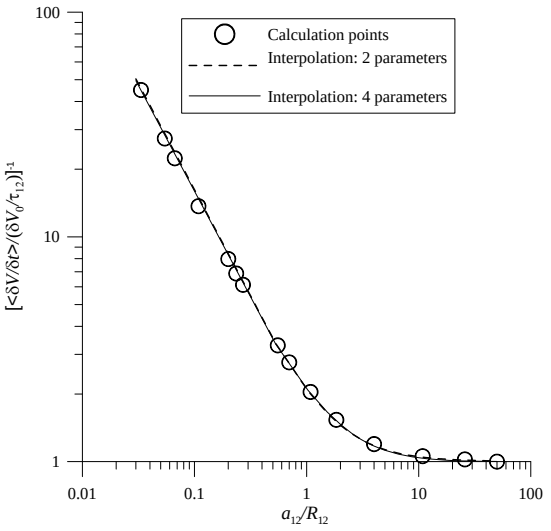

Figure 1. Dependence of the steady-state values of the inverse coalescence rate on the parameter a/R using interpolation curves, in comparison with the calculated points (centers of circles).

References

Chandrasekhar, S. (1943) *Reviews of Modern Physics*, **15**, 1-89.

Smoluchowski, M. (1917) *Zeitschrift für Physikalische Chemie*, **92**, 129-154.

Veshchunov, M.S. (2010) *Journal of Aerosol Science*, **41**, 895-910.

Veshchunov, M.S., Azarov, I.B. (2012) *Journal of Aerosol Science*, **47**, 70–77.

Oblique Impact Fragmentation of Nanoparticle Agglomerates

M. Gensch and A.P. Weber

Department of Particle Technology, Clausthal University of Technology, 38678 Clausthal-Zellerfled
Keywords: nanoparticle agglomerate, oblique impaction, single stage low pressure impactor, fragmentation
Presenting author email: manuel.gensch@tu-clausthal.de

In order to avoid particle agglomeration or condensation of gaseous components on the particle surface during online sampling from high temperature processes the aerosol has to be heavily diluted. Therefore, the particles usually exhibit high gas velocities in the sampling inlet. Beside high shearing strain particles may impact at different angles on the walls of the sample inlet. Up to now it is unknown, if this mechanical loading is sufficient to change the particle size and morphology, thus, if the sample is still representative for the aerosol.

If agglomerates impact angular, there are two velocity components (schematically shown in figure 1 left). The tangential component impress an additionally shear motion on the agglomerate.

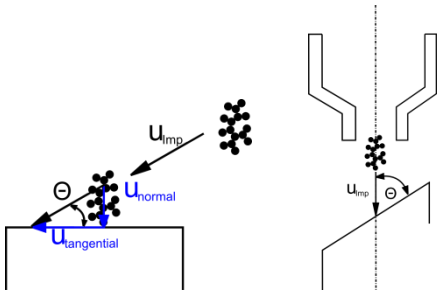

Figure 1. left: oblique Wall impaction of a fractal like agglomerate; right: schematically drawing of a low pressure impactor with an oblique impaction plate

The effect of impact angle on the fragmentation behaviour of nanoparticle agglomerates is poorly investigated. For agglomerates produced in granulation processes with grain sizes in the micron range and agglomerate sizes in millimetre range, it is known, that granules which are sensitive to shear stress, show an increased fragmentation with decreasing impact angle (Samini et. al.).

In order to investigate the role of impact loading and impact angle on the morphology of aerosol particles, their rebound and fragmentation behaviour is investigated in a modified Single Stage Low Pressure Impactor (SS-LPI). The feasibility of agglomerate fragmentation in SS-LPI has already been shown in a number of publications. Particles are impacted on the impaction target with a defined velocity and occurring fragmentation is investigated by determination of the fragment size distribution using Transmission Electron Microscopy. Compared to other studies, the current study also focusses on the rebound of particles after particle wall collisions. Therefore, also the rebound probability of the fragments and their respective size distribution are investigated using a low pressure sampling unit. The fragments are collected until the sampling unit is saturated. Afterwards, the pressure is relaxed to ambient conditions allowing the use of ambient pressure measurement devices such as SMPS. In order to quantify the effect of shear, agglomerates are impacted with different collision angles.

Fractal like platinum agglomerates with a fractal dimension of D_f=1,8 and mobility diameters of x_{ME}=50nm and x_{ME}=70nm were impacted in a single stage low pressure impactor under different impact angles (schematically shown in figure 1 right). The impact velocity is estimated by transferring a three parameter model developed for perpendicular impaction (Rennecke et. al.). First results indicate that the impact angle influence the fragmentation behaviour of nanoparticle agglomerates.
Particles with low fractal dimension tend rather to adhere to surfaces upon collision, while more dense particles are less affected by adhesion force and may easier be re-entrained in the aerosol flow. Further research will focus on the determination of fragmentation threshold and bouncing probabilities of agglomerates of different structures and inter-particle bond strength.

Samini, A., Moreno, R., Ghadiri, M., (2004) Powder Technology “Analysis of impact damage of agglomerates: effect of impact angle”

Rennecke, S., Weber, A.P., (2013) Journal of Aerosol Science, vol. 55, pp: 89-103

Evaporation and growth dynamics of layered droplets: Theory and experiments

H. H. Tu and A. K. Ray

Department of Chemical and Materials Engineering, University of Kentucky
Lexington, KY 40506 U.S.A. Country
Keywords: two phase droplets, interfacial mass transfer, light scattering
email: akray@engr.uky.edu

Many physical and commercial processes involve evaporation and growth of two phase layered droplets of partially miscible components. In many cases, a volatile droplet is coated with an immiscible layer to create a diffusional barrier in order to retard evaporation of the core droplet. The presence of a layer, however, brings about a number of rate-controlling mechanisms for the transfer of species from the core droplet to the surrounding gas phase and induces markedly different effects on the evaporation rate of the core droplet, including enhancement of the rate (Ray et al., 1991). To understand evaporation and growth dynamics of layered droplets we have experimentally studied droplets of a number of immiscible systems to determine the determine evaporation characteristics of volatile core droplets coated with layers of nonvolatile components and developed a pseudo steady state model for evaporation and growth kinetics of a two phase droplet of two partially miscible components, exposed to a stagnant gas phase.

The theoretical analysis show the rate of evaporation or growth of a core droplet may increase, decrease or show a maximum with increasing layer thickness, depending the physical properties (e.g., vapour pressure, diffusion coefficients and miscibility limits) of the binary system. Criteria for various scenarios that arise during the evaporation or growth of a layered droplet have been developed in terms of analytical expressions. We have also examined evaporation of single layered droplets suspended in an electrodynamic balance (EDB) under vapour-free atmospheres. Droplets were generated from a homogeneous solution that was prepared by dissolving two immiscible components in a highly volatile common solvent. With the evaporation of the volatile solvent two phases in a suspended droplet separated to form a layered droplet. Droplets of di-ethylene glycol (DEG), tri-ethylene glycol (TEG), diethyl phthalate (DEP), and dimethyl phthalate (DMP) coated, respectively, with dioctyl phthalate (DOP), dibutyl phthalate (DBP), and squalane were studied. A suspended droplet was illuminated by a polarized laser beam, and scattered light from the droplet was by monitored by two photomultiplier tubes (PMTs). Resonances (i.e., peaks) observed in the elastic scattering intensity versus time spectra from a suspended droplet were interpreted using elastic light scattering theory to obtain outer and core radii of the droplet as functions of time (Ray and Nandakumar, 1995; Tu and Ray, 2006). The results obtained from core droplets of DEG and TEG coated with DOP as well as DBP layers show that the core evaporation rate monotonically increases as the layer thickness increases, and the evaporation rate of a core droplet can exceed the rate of an uncoated droplet of the same size. The results from DEP droplets coated with squalane layers show the core evaporation rate increases to a maximum, and then decreases as the layer thickness increases. The experimental results are highly reproducible and agree well with the model predictions. Because of the relatively low volatility of the core compounds involved in the study, a monotonic decrease in the core evaporation rate with increasing layer thickness, one of the scenarios indicated by the model, was not observed. In this study, we show that miscibility limits of nearly of immiscible binary systems, and the unknown parameters of a binary activity coefficient model can be evaluated from the evaporation data on layered droplets such binary systems.

This work was supported by the National Science Foundation and the National Institute for Occupational Safety and Health.

Ray A. K., Devakottai B., Souyri A. and Huckaby J. L. (1991) Evaporation Characteristics of Droplets Coated with Immiscible Layers of Non-volatile Liquids, *Langmuir*, **7**, 525-531.

Ray, A. K. and Nandakumar, R. (1995) Simultaneous Determination of Size and Wavelength-dependent Refractive Indices of Thin Layered Droplets,, *Applied Optics*, **34**, 7759-7771.

Tu, H. H. and Ray, A. K. (2006) Investigation of concentrically and eccentrically layered droplets by light scattering, *Appl. Opt.* **45**, 7652-7656.

Friday, September 6, 2013

Session: Aerosol Chemistry,
Chemical characterisation techniques for aerosols

Novel Viscosity Measurement Technique for Atmospheric Aerosols using Fluorescence Lifetime Imaging Microscopy (FLIM)

C. Fitzgerald[1], N. Hosny[2], M. Kalberer[1], M. Kuimova[2], F. Pope[3]

[1]Department of Chemistry, University of Cambridge, Cambridge, CB2 1EW, England
[2]Department of Chemistry, Imperial College, London, SW7 2AZ, England
[3]School of Geography, Earth and Environmental Science, University of Birmingham, Birmingham, B15 2TT, England
Keywords: organic aerosol, viscosity, fluorescence molecular rotors, fluorescence lifetime
Presenting author email: cf355@cam.ac.uk

Analysis of the phase of atmospheric organic aerosol (OA) has become important in recent years due to the suggestion that secondary organic aerosols (SOAs) can adopt a non-crystalline, amorphous solid or highly viscous liquid state, as opposed to assuming they are a well-mixed liquid (Virtanen, 2012). The presence of such a highly viscous phase will have significant implications for diffusion rates for gases in/out of OA, rates of reaction in the condensed phase, formation rates of OA and other properties such as their ability to act as cloud condensation nuclei.

A quantitative method that can measure viscosity changes of organic aerosol particles is therefore important for a comprehensive understanding of aerosol processes in the atmosphere and currently no method exists to measure directly the viscosity of micrometer size droplets.

Here we present a new technique to quantitatively measure the viscosity of organic aerosol particles in the micron size range using fluorescence dyes called 'molecular rotors' combined with fluorescent lifetime imaging microscopy (FLIM). This technique has already been applied successfully to the measurement of viscosity in biological systems (Kuimova, 2012).

This new technique was first tested with sucrose particles with 10 to 100 μm diameters exposed to varying relative humidity. The viscosity increase of sucrose droplets that is expected during a decreasing RH from 90 to 75 % was compared with literature data.

The viscosity change of oleic acid droplets during ozonolysis was also measured online with FLIM (Fig. 1). An increase in viscosity was observed between 100-1000 mPa.s, which can be explained by the formation of oligomers and increased hydrogen-bonding of oxidation products. A size dependence was observed with larger droplets reacting more slowly to the exposure of ozone. This effect was more pronounced when exposed to lower ozone concentrations.

This study was extended to the measurement of the viscosity of the SOA formed from the ozonolysis of α-pinene, when exposed to different ozone concentrations and relative humidity.

Results will also be presented of the first attempts to couple FLIM with optical laser trapping, which allows for a measurement of viscosity changes in a contact-free environment using a suspended aerosol droplet.

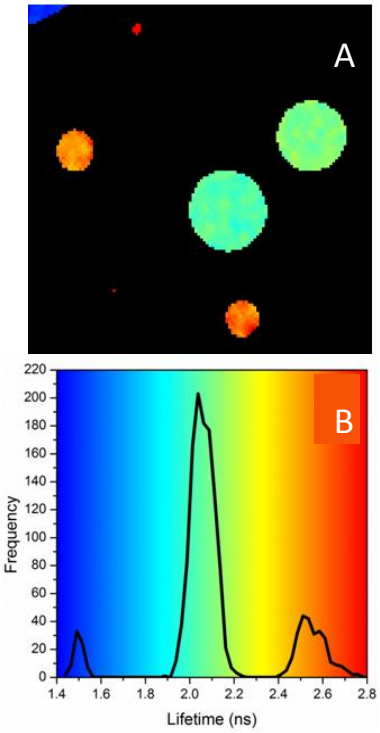

Figure 1. Oleic acid particles (containing the fluorescence molecular rotor BODIPY-C10), exposed to ozone (~1.5 ppm) for 15 mins. (A) Fluorescence Lifetime image. Smaller droplets show a longer lifetime corresponding to a higher viscosity compared to the larger droplets in the same field of view. (B) Lifetime histogram (Hosny, 2013).

This work was supported by the National Environmental Research Council.

Honsy, N., Fitzgerald, C., Kalberer, M., Kuimova, M., Pope, F. (2013) *Faraday Discussions*, submitted.
Kuimova, M. (2012) *PCCP* **14**, 12671–12686.
Virtanen, A. *et al.* (2102) *Nature* **467**, 824-827.

Extractive electrospray ionisation: A novel mass spectrometry technique for the online characterisation of organic aerosol composition and reactivity

P.J. Gallimore and M. Kalberer

Centre for Atmospheric Science, Department of Chemistry, University of Cambridge, CB2 1EW, UK
Keywords: Aerosol chemistry, mass spectrometry, online measurement, SOA
Presenting author email: pjg48@cam.ac.uk

Organic compounds are often the dominant fraction of tropospheric aerosol. Despite this, our understanding of the composition of organic aerosol is limited. A lack of detailed knowledge of the chemical composition of aerosols limits our understanding of their effect on climate and air quality.

We present a new technique for online measurement of the compounds present in organic aerosol: Extractive Electrospray Ionization (EESI) coupled to Mass Spectrometry (MS). In this method, a plume of charged solvent droplets is generated using an Electrospray Ionisation source. Aerosol particles are directed into this spray and particle-into-droplet extraction occurs, dissolving the soluble aerosol components. The volatile solvent evaporates and gas-phase aerosol analyte ions are formed and sampled at the MS inlet (Figure 1). We present here a custom-designed EESI source which has been designed and optimized to interface with a commercial Ultra-High Resolution Mass Spectrometer.

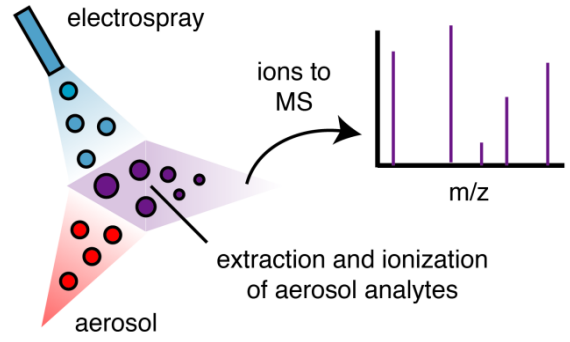

Figure 1: Illustration of the EESI-MS principle applied to organic aerosols.

EESI-MS offers a number of advantages: The online ionization mechanism provides composition information on aerosols in flow-tube and chamber studies with a time resolution of seconds, without the potentially large sampling artefacts introduced by collecting aerosols onto substrates for offline analysis. The ionization process produces molecular ions with minimal fragmentation, which greatly aids the interpretation of spectra for complex mixtures.

We have demonstrated that the MS ion signal scales linearly with particle mass concentration in the range tested and is independent of particle diameter and liquid water content, suggesting that the entire particle bulk is extracted for analysis. High sensitivity for aerosols composed of oxygenated organic compounds is achieved. For example, tartaric acid aerosol can be detected in the sub-µg/m^3 range, with a dynamic range of about 3.5 orders of magnitude, using tandem MS experiments[1].

EESI was also used to understand the chemical mechanisms of reactions occurring in the particle phase. These are increasingly being recognized as making an important contribution to observed organic aerosol composition. Measurements of oleic acid aerosol (20µg/m^3) after ozonolysis reveal the formation of a variety of oxidation products in good agreement with previous offline studies. Time-resolved measurements of the same system reveal the growth of oligomers as the reaction time between aerosol and ozone is increased. The average molecular weight and oxygen:carbon ratio of these oligomers increase over time (Figure 2), which has implications for particle viscosity, hygroscopicity and phase.

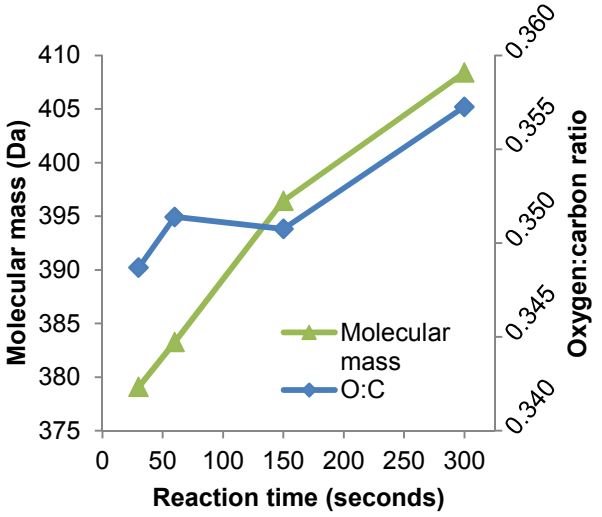

Figure 2: Time-resolved EESI-MS measurements of oligomers formed during oleic acid ozonolysis reveal that on average they become heavier and more oxygenated at longer reaction times.

Future work will study the product-resolved kinetics of aerosol-phase chemistry at a molecular level and implement a simple model to obtain rate constants for oligomer formation and other reactions in particles. This will allow us to assess their importance in influencing the chemical composition of aerosols.

This work was supported by the Natural Environment Research Council, UK.

[1] Gallimore, P.J. and Kalberer, M. (submitted).

A Unique On-line Method to Infer Water-Insoluble Particulate Mass-Fractions

Daniel Short[1,3], Michael Giordano[1,3],Yifang Zhu [4], Phillip Fine[2], Andrea Polidori[2] and Akua Asa-Awuku[1,3]

[1]Department of Chemical and Environmental Engineering, University of California, Riverside, California, 92521, USA
[2]South Coast Air Quality Management District, California, USA
[3]Center for Environmental Research and Technology (CE-CERT), University of California, Riverside, California, 92507, USA
[4]University of California-Los Angeles, Los Angeles, California

Keywords: hygroscopicity, butanol CPC, water-based CPC, size distributions
Presenting author email: akua@engr.ucr.edu

The mass, size, and water-insoluble chemical composition of particulate matter below 2.5μm (PM2.5) significantly effects air quality, climate, and human health. Carbonaceous material, such as Black Carbon (BC) can contribute to water-insoluble PM2.5 and their subsequent effects. BC is formed from the incomplete combustion of fossil fuels and biomass (Novakov et al. 2000) and tends to be emitted below 30 nm (Akhter et al. 1985). BC is defined by optical properties and in this study, it is quantified by an ability to absorb energy at 670 nm wavelengths. BC aerosol is water-insoluble when freshly emitted (~ 1 day) but can add water-soluble materials in surface oxidation and condensation reactions during its atmospheric lifetime (Koehler et al. 2009). Hence as a BC particle ages, it can modify the overall insoluble fraction, hygroscopic properties, and reduce the critical water-vapor required to initiate heterogeneous nucleation

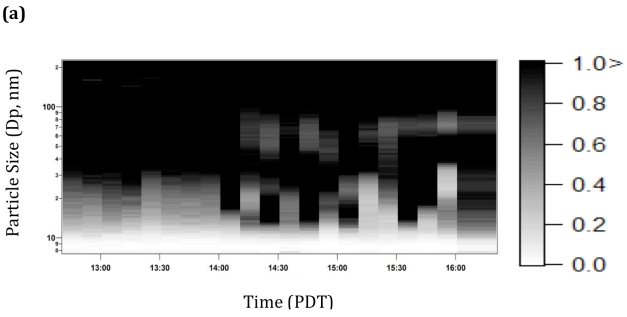

Figure 1. The comparison of water to butanol particle counts for weekday measurement.

Particle number, size, and composition information is important for constraining aerosol effects on air quality, climate, and health. The composition of particles, especially from vehicular sources, may contain insoluble black carbon (BC) material that modify particle nucleating properties. For this study, ambient aerosol was sampled from the South Coast Air Quality Management District (SCAQMD) instrument station located 15 m from the I-710 freeway in Long Beach, California. A water-based condensation particle counter (CPC) and a butanol-based CPC provided particle number concentration data. Both instruments were coupled with a Scanning Mobility Particle Sizer (SMPS) and particle number and size were recorded. Real time particle insoluble mass fractions are estimated with the SMPS data sets; theoretical mass fractions are calculated from ideal hygroscopicty single parameter , κ - values. This is the first time that this experimental method has been employed and used to infer online insoluble mass fractions.

Akhter, M.S., Chughtai, A.R. and Smith, D.M. (1985),. *Spectroscopic studies. Applied Spectroscopy.* 39(1):143-153

Novakov, T., Andreae, M. O., Gabriel, R., Kirchstetter, T. W., Mayol-Bracero, O. L., & Ramanathan, V. (2000). *Geophys. Res. Lett* **27.** 24: 4061-4064.2000)

Koehler, K. A., DeMott, P. J., Kreidenweis, S. M., Popovicheva, O., Petters, M. D., Carrico, C. M., Kireeva, E., Khokhlova, T., and Shonija, N (2009, *Atmospheric Chem. Phys.,* **11**, 7906–7920, doi:10.1039/b905334b, 2009

Surface site density versus nucleation rate approaches of formulating ice formation in clouds – a comprehensive analysis based on AIDA cloud simulation experiments

O. Möhler, N. Hiranuma, K. Höhler, C. Hoose, M. Hummel, M. Niemand, C. Oehm, T.Schmitt, I. Steinke and R. Wagner

Institute for Meteorology and Climate Research, Karlsruhe Institute of Technology, Karlsruhe, Germany
Keywords: Ice, nucleation, cloud, parameterisation
Presenting author email: Ottmar.moehler@kit.edu

A more detailed understanding and formulation of cloud microphysical processes is still one of the major challenges for improving atmospheric cloud, weather, and climate models. These include homogeneous freezing of water and solution droplets, though this part is considered to be well understood and formulated for models (Pruppacher et al., 1997; Koop et al., 2000) as well as the various modes of heterogeneous ice nucleation (Vali, 1985) like deposition nucleation, condensation freezing, immersion freezing and contact freezing, which involve solid atmospheric aerosol particles as heterogeneous ice nuclei (IN).

The fact that only a very minor fraction of the solid atmospheric aerosol particles is active as ice nuclei, in particular at high temperatures (Pruppacher and Klett, 1997) makes it difficult to quantify and formulate the temporal and spatial distribution of ice nuclei for models. Another complication is related to the complex mixture and high variability of the atmospheric aerosol particles concerning size, chemical composition, morphology, and surface coating, which makes it difficult to formulate and calculate the IN concentration not only as a function of temperature and humidity, but also as a function of aerosol parameters.

During the previous years, an increasing number of laboratory experiments investigated ice nucleation processes for a broad variety of aerosol types (Hoose and Möhler, 2012; Murray et al., 2012). Different concepts and approaches have been developed and applied to fit the experimental data, in order to use such fit results as parameterizations of ice formation in atmospheric models. Some of them are relying on classical nucleation rate theory (Pruppacher and Klett, 1997), others describe the ice nucleation activity as function of ice-active sites on the aerosol particle surface (Connolly et al., 2009).

The nucleation rate approaches calculate the formation rate of ice directly as a function of time and particle surface area, but in most cases have to consider an empirical variation of the activation energy or freezing probability over the particle surface area at a given temperature. This is due to weaker temperature dependence of the ice formation rate in most experiments than predicted by classical nucleation rate theory with just one activation energy or contact angle (e.g. Marcolli et al., 2007).

The active site approaches consider a temperature dependent variation of the freezing probability per particles surface area and calculate the formation rate of ice particles mainly as function of the rate of temperature change (Connolly et al., 2009; Niemand et al., 2012). Up to now it appears to be unclear which approach is more appropriate to formulate and predict the abundance of ice nuclei and ice particles in the atmosphere.

Since 2003, the AIDA cloud chamber was used for comprehensive series of ice nucleation experiments with a variety of different aerosols like soot, organics, minerals or biological particles, and in wide ranges of temperature, relative humidity and cooling rate. The AIDA team has started consistent and comprehensive re-analysis of the 10 year data set to provide a uniform compilation of parameters for formulating the ice formation in atmospheric models as function of aerosol properties, temperature and humidity. The conference contribution will include an overview and discussion of the experimental data set, selected results and some basic concepts.

The work has been funded by the Helmholtz Association ATMO research program and through the Virtual Institute on Aerosol-Cloud Interactions (VI-ACI, VH-VI-233). Part of this work was also funded by the Deutsche Forschungsgemeinschaft (DFG, grants MO668/1-1, MO668/1-2, MO668/2-1, and MO668/4-1).

Pruppacher, H. R. and Klett, J. D. (1997) *Microphysics of clouds and precipitation*, Kluwer Academic Publishers, Dordrecht, The Netherlands.

Koop, T, Luo, B., Tsias, A. and Peter, T. (2000) *Nature* **406**, 611-614.

Vali, G. (1985) *Bull. Am. Met. Soc.* **66**, 1426-1427.

Hoose, C. and Möhler, O. (2012) *Atmos. Chem. Phys.* **12**, 9817-9854.

Murray, B. J., O'Sullivan, D., Atkinson, J. D., and Webb, M. E. (2012) *Chem. Soc. Rev.* **41** (19), 6519-6554.

Connolly, P. J., Möhler, O., Field, P. R., Saathoff, H., Burgess, R., Choularton, T., and Gallagher, M. (2009) *Atmos. Chem. Phys.* **9**, 2805-2824.

Marcolli, C., Gedamke, S., Peter, T., and Zobrist, B. (2007) *Atmos. Chem. Phys.* **7** 5081-5091.

Niemand, M., Möhler, O., Vogel, B., Vogel, H., Hoose, C., Connolly, P, Klein, H., Bingemer, H., DeMott, P. J., Skrotzki, J., and Leisner, T. (2012) *J. Atmos. Sci.* **69**, 3077-3092.

X-ray study of freshly emitted carbonaceous nano-aerosols by synchrotron radiation.

F.-X. Ouf[1], F.-A. Barreda [2, 3], A. Coppalle[4], D. Ferry[5], X.-J. Liu[3], B. Marcillaud[1], C. Miron[3], J.-B. A. Mitchell[6], T. Mostefaoui[7], C. Nicolas[3], M. Patanen[3], P. Parent[8], E. Robert[3], O. Sublemontier[2], J. Yon[4]

[1]Institut de Radioprotection et de Sûreté Nucléaire (IRSN), PSN-RES, SCA, LPMA, Gif-Sur-Yvette, 91192, France.
[2]CEA/IRAMIS/SPAM/Laboratoire Francis Perrin, CEA Saclay, Gif-sur-Yvette Cedex, 91191, France.
[3]Synchrotron SOLEIL, Saint Aubin, BP 48, Gif-sur-Yvette Cedex, 91192, France.
[4]UMR 6614 CORIA, INSA de Rouen, Avenue de l'université, B.P. 8, Saint-Etienne du Rouvray, 76801, France.
[5]CINaM-CNRS UMR 7325, Campus de Luminy, Marseille, 13009, France.
[6]Institut de Physique de Rennes, UMR 6251, Université Rennes 1, Rennes Cedex, 35042, France.
[7]Université de A. Mira, Route de Targa ou Zemmour, Bejaia 6000, Algérie.
[8]LCPMR, Université Paris VI/CNRS, 11 rue Pierre et Marie Curie, Paris, 75005, France.
Keywords: surface chemistry, soot particles, XPS, XANES
Presenting author email: francois-xavier.ouf@irsn.fr

Over the last few decades, much research has been conducted on the toxicological and global warming influences of combustion generated aerosols. Due to their complex composition and morphology, their reactivity and more especially their hygroscopicity are not well understood. Beyond the question of soot reactivity, pioneering work has been devoted in the last decades to the surface analysis of soot particles by XPS (Toosi et al., 1992; Kirchner et al., 2003) and to the identification of chemical entities attached to the soot surface, which could improve our understanding on soot hydrophilicity (Vander Wal et al., 2011). Nevertheless, in all these studies, measurements have been performed on particles deposited on substrates and, even if high-resolution soft X-ray photoelectron spectroscopy is a powerful characterization tool, hydrophilicity can only be examined using isolated nanoparticles, with no interaction with a substrate. The major aim of this study is to demonstrate the potential of XANES/XPS analysis of airborne carbonaceous aggregates above the C (1s) and O (1s) thresholds, and to compare these results with those obtained from conventional bulk analysis.

These experiments have been carried out with soft X-rays at the PLEIADES beamline of the SOLEIL synchrotron in France. The aerosol source is an industrial propane diffusion flame apparatus (combustion aerosol standard mini-CAST Jing Ltd). Particles were injected through a diffusion dryer prior to entering an aerodynamic lens. Alignment of the aerodynamic lens with the X-ray synchrotron beam was carried out by using SiO_2 nanoparticles generated by atomization, and the particle concentration in the interaction chamber was monitored with a Faraday Cup/electrometer.

Due to the demonstrative aspect of this first attempt of XPS/XANES of airborne soot particles, several technical issues have been considered during the experiment but we were successful in acquiring some photoemission and absorption spectra. Four different fuel-to-oxygen ratios were investigated for XANES and two for XPS, corresponding to a contribution of organic carbon (OC) components to the total mass of carbon ranging from 8 % to 35 %. Only XANES spectrum will be discussed in this abstract and examples of spectra are presented in Figure 1.

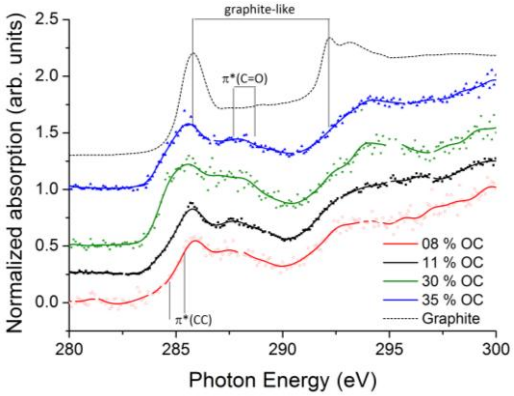

Figure 1. XANES spectrum as a function of OC

Beyond the proof of feasibility, XANES spectra obtained here for different operating conditions of the CAST burner are promising. One interesting point is the drift to lower energy of the C=C region as the OC content increases, together with a slight decrease in intensity around 292 eV. If one compares this to spectra for graphite, this shows that the graphite-like contribution of the nanoparticle decreases to the benefit of aliphatic-like carbon of the OC phase, including double and triple CC moieties. For each sample, we also observe a significant contribution of π* (C=O) resonances at 287.5-288.5 eV; further assignment is still in progress.

A discussion, concerning the technical difficulties encountered during the alignment of the carbonaceous nanoparticles beam and the less effective focusing power of the aerodynamic lens for this type of nanoparticles, will be done. Beyond these experimental difficulties, leading to a limited resolution of the obtained spectra, the feasibility of XPS and XANES analysis of freshly emitted airborne carbonaceous aggregates is demonstrated and opens the way to further investigation on the surface chemistry and reactivity of soot particles.

Toosi R. et al. *Combust. Flame*. **90** (1992) 1-10.
Kirchner U. et al. *J. Aerosol Sci.* **34** (2003) 1323-1346.
Vander Wal R.L. et al. *Analyt. Chemist.* **83** (2011) 1924-1930.

Micro-Raman monitoring of photoevolution and hygroscopicity of single particles by using an environmental acoustic levitation cell

Y.A. Tobon, M. Moreau, S. Sobanska and J. Barbillat

Laboratoire de Spectrochimie Infrarouge et Raman, UMR CNRS 8516, Université de Lille 1 Sciences et Technologies, Bât. C5, 59655 Villeneuve d'Ascq Cedex, France
Keywords: levitation, single-particles, photoreactivity, Raman
Presenting author email: yeny.tobon-correa@univ-lille1.fr

In atmospheric chemistry, aerosols play an essential role mainly concerning the heterogeneous chemistry in the atmosphere (Andreae and Crutzen 1997). However, studying the aerosol properties remains a challenge and it's indispensable to try to understand the chemical processes which occur at the particle or at the surface scale. Laboratory experiments are the most common way to go towards to real processes under controlled conditions, and it's necessary to look for techniques or combination of techniques which permit to simulate the conditions occurring in the atmosphere.

Raman spectroscopy is a non-destructive technique that provides detailed molecular and structural information with a spatial resolution of about $1 \mu m^3$, and it is a valuable tool to follow real-time evolutions of volume or surface structures under controlled conditions. Micro-Raman spectroscopy, coupled to an environmental levitation cell, is especially useful for studying, at micrometric scale, the *in-situ* modifications of aerosol when exposed to reactive environments or humidity without the influence of a contacting surface (Krieger, et al. 2012). Moreover, photochemical transformation can be followed by irradiation of the particles.

In this presentation, we used an environmental acoustic levitation cell coupled to the micro-Raman spectroscopy to monitor the physical and chemical processes occurring in particles of atmospheric interest when exposed both, to humidity and UV-Vis light. Physical and chemical changes can be followed at the interface or deeper depending on the optical properties of the particle. Particles, as small as 20 µm, can be levitated and studied by micro-Raman spectroscopy. Hygroscopic property evolution of nitrate containing aerosols (NH_4NO_3) when irradiated with UV-Vis light was investigated by using this experimental set up.

Environmental levitation cell coupled to micro-Raman spectroscopy

An ultrasonic levitator (APOS BA 10, Tec5, Germany) was modified to be installed within a small dimension environmental levitation cell and was horizontally coupled to the Raman microscope as shown in figure 1. The cell consists of 4 optics accesses, and transparent quartz windows allowing the exposure to UV radiation. Two inlet/outlet valves are used for gas supplies to modify the environment inside the cell. The relative humidity and the temperature are measured within the cell by using an adapted sensor.

The spectrometer used for the coupling is a Horiba Scientific LabRam HR visible, equipped with a CW 633 nm laser and a Liquid Nitrogen-cooled CCD camera. We used the micro arrangement in backscattering mode.

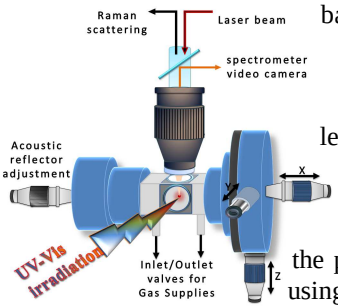

Figure 1. Schematic diagram of environmental levitation cell coupled to the Raman microscope

The size evolution of the particles was measured by using the spectrometer video camera and the growth factor was calculated by comparing geometric diameter evolution for various RH. The chemical evolution, i.e liquid versus solid and NO_3 to NO_2, was followed through Raman spectra acquired with time steps ranging between 2 and 10 s.

Hygroscopicity and photochemical transformation

Deliquescence and efflorescence processes of NH_4NO_3 were evidenced by the transformation of the Raman spectra. The shift on the NO_3 symmetric stretching vibration near to 1040 cm^{-1} is the most common change reported on the literature as an evidence of the transitions. However, our experiments showed that other structural changes occur before shifting of the 1040 cm^{-1}-band is produced. By using spectral data treatments the transformation rate was drawn.

The levitated aerosol particles were exposed to broad-band UV-visible radiation ($250 \leq \lambda \leq 800$ nm). The Raman spectrum was recorded for different times of irradiation to closely scrutinize any decay of the nitrate bands due to the photo-degradation of the aerosol and the growth of bands due to the nitrite photoproduct. The experiment was reproduced for various RH and compared. The influence of humidity on the nitrate photo-degradation was demonstrated for individual particles.

These experiments have permitted to validate the ensemble and the smooth running of the device, giving us access to study the reactivity and the physical chemistry processes occurring on the interfaces of single aerosol particles.

This work was supported by funds from the "Laboratoire d'Excellence (LABEX) -CaPPA- and IRENI program.

Andreae, M. O., and Crutzen, P. J. (1997). *Science* **276,** 1052-1058.

Krieger, U. K., Marcolli, C., and Reid, J. P. (2012). *Chem. Soc. Rev.* **41,** 6631-6662.

Measurements of Oxidized Organic Compounds using Nitrate Chemical Ionization Time-of-Flight Mass Spectrometry coupled to an Atmospheric Pressure interface (NO_3-CI-APi-ToF)

P.Massoli[1], A. Lambe[1,2], T. Hohaus[1], M. Canagaratna[1], P. Chaabra[1], H. Stark[1,3], J. Kimmel[1,4], J. Jayne[1], and D. Worsnop[1]

[1]Aerodyne Research Inc., 45 Manning Road, Billerica, MA 01821, USA
[2]Department of Chemistry, Boston College, Chestnut Hill, MA 02467, USA
[3]Cooperative Institute for Research in Environmental Sciences, University of Colorado, Boulder, CO 80303, USA
[4] Tofwerk, AG, Uttigenstrasse 22 CH-3600 Thun, Switzerland
Keywords: organic molecules, mass spectrometry, secondary organic aerosols

Presenting author email: pmassoli@aerodyne.com

We present laboratory and ambient measurements of gaseous organic compounds by means of nitrate ion (NO_3^-) based chemical ionization (CI) coupled with a atmospheric pressure interface time-of-flight mass spectrometer, APi-ToF (Junninen *et al.*, 2010). This technique, namely NO_3-CI-APi-ToF allows to selectively detect gas-phase species with greater acidity than nitric acid (HNO_3), e.g., highly oxidized organic molecules and sulfuric acid (H_2SO_4), via clustering with the NO_3^- ion and its high order clusters ($NO_3^-(HNO_3)_n$) (Kurten *et al.*, 2011; Jokinen *et al.*, 2012).

The capability of making such highly selective measurements is important because both H_2SO_4 and organic vapors have a recognized key role in new particle formation (NPF) processes (Riipinen *et al.*, 2012), and likely have an important role in particulate phase chemistry and formation of secondary organic aerosols (SOA).

The NO_3-CI-API-ToF was deployed during the Southern Oxidant and Aerosol Study (SOAS) at the forest supersite in Centreville, AL. The main goal of the SOAS campaign is to investigate the composition, sources, and pollution dependence of SOA formation in the Southeast US. This site is affected both by substantial biogenic volatile organic compounds (BVOC) emissions (dominated by isoprene) and anthropogenic emissions. Isoprene and other BVOCs are known to contribute to the organic aerosol (OA) budget in this region (Goldstein and Galbally, 2007).

During SOAS, the NO_3-CI-API-ToF will be deployed along with many other state of the art instruments to address these scientific questions. The instrument will operate in dual mode, i.e., switching between the NO_3-CI-API-ToF configuration and a simple APi-ToF (without CI). The latter configuration provides additional information on the concentration and composition of negative and positive ambient ions (e.g. Ehn *et al.*, 2010, 2012).

We also compare ambient NO_3-CI-API-ToF results with laboratory measurements, where oxidized organic vapors are produced using a Potential Aerosol Mass flow reactor (Lambe *et al.*, 2011) by the OH oxidation of biogenic and anthropogenic gas-phase precursors over multiple days of equivalent atmospheric exposure. The effect of NO_x levels on the gaseous oxidation products is also investigated.

Acknowledgements: this work is supported by the National Science Foundation (NSF).

References

Ehn, M., Junninen, H., Petaja, T., Kurten T., Kerminen, V.M., Schobesberger, S., Manninen, H.E., Ortega, I., Vehkamaki, H., Kulmala, M., and Worsnop, D. (2010) *Atmos. Chem. Phys.*, **10**, 8513-8530

Ehn, M., Kleist, E., Junninen, H., Petaja, T., Lonn, G., Schobesberger, S., DalMaso, M., Trimborn, A., Kulmala, M., Worsnop, D. Wahner, A., Wildt, J., and Menthel, T. (2012) *Atmos. Chem. Phys.*, **12**, 5113-5127

Jokinen, T., Sipila, M., Junninen, H., Ehn, M., Lonn, G., Hakala, J., Petaja, T., Mauldin, R.L., Kulmala, M., and Worsnop, D. (2012), *Atmos. Chem. Phys.*, **12**, 4117-4125

Junninen, H., Ehn, M., Petaja, T., Luosujarvi, T., Kotiaho, T., Kostiainen, R., Roghner, U., Gonin, M., Fuhrer, K., Kulmala, M., and Worsnop, D. (2010), *Atmos. Meas. Tech.*, **3**, 1039-1053

Kurten, T., Petaja, T., Smith, J., Ortega, I., Sipila, M., Junninen, H., Ehn, M., Vehkamaki, H., Mauldin, R.L., Worsnop, D., and Kulmala, M. (2011), *Atmos. Chem. Phys.*, **11**, 3007-3019

Goldstein, A.H., and Galbally, I.E. (2007), *Env. Sci. Technol.*, **41**, 5, 1514 - 1521

Lambe, A. T., Ahern, A. T., Williams, L. R., Slowik, J. G. , Wong, J. P. S., Abbatt, J. P. D., Brune, W. H., Ng, N. L., Wright, J. P., Croasdale, D. R., Worsnop, D. R., Davidovits, P., and Onasch, T. B. (2011), *Atmos. Meas. Tech.*, **4**, 445-461

Riipinen, I., Yli-Juuti, T., Pierce, J. R., Petäjä, T., Worsnop, D. R., Kulmala M., and Donahue N. M. (2012), *Nat. Geo.*, 2012, **5**, 453-458.

Quantitative single particle mass spectrometry with the Aerodyne aerosol mass spectrometer: development of a new classification algorithm and application to field data

F. Freutel[1], F. Drewnick[1], J. Schneider[1], T. Klimach[1], and S. Borrmann[1,2]

[1]Particle Chemistry Department, Max Planck Institute for Chemistry, 55128 Mainz, Germany
[2]Institute of Atmospheric Physics, Johannes Gutenberg University Mainz, 55128 Mainz, Germany
Keywords: single particle aerosol mass spectrometry, classification algorithm, MEGAPOLI.
Presenting author email: fr.freutel@mpic.de

Single particle mass spectrometry using laser desorption / ionization instruments is well established; however, this method is typically not capable of providing quantitative information about the chemical composition of the individual particles. Efficient single particle mass spectrometry using the Aerodyne aerosol mass spectrometer (AMS) has become possible with the introduction of the light scattering probe by Cross *et al* (2009). Here, the particles are flash vaporized on a hot surface and ionized by electron impact ionization. This method provides reproducible fragmentation patterns of individual chemical species, and therefore enables quantification of different, non-refractory chemical compounds within the single particles (diameters ~300 - 1000 nm).

So far, published cluster algorithms like principal component analysis (Cross *et al*, 2009) or k-means clustering (Liu *et al*, 2012) have been used for the analysis of AMS single particle data. In these studies quantitative information on the content of different aerosol species has been acquired separately by using the same procedures as applied to AMS ensemble mass spectra. No unambiguous method was used yet to both quantify the contents of organic and inorganic species and to identify and separate different organic species within single particles.

Here, we present the development, laboratory validation, and field application of a new method for AMS single particle analysis, which provides both quantitative information about the contents of different organic and inorganic species within single particles and classification of particles into different particle types.

In a first step the single particle mass spectra are compared to reference mass spectra for typical particle components (i.e., NH_4NO_3, $(NH_4)_2SO_4$, glucose as biomass (burning) proxy, oleic acid as cooking proxy, oxygenated organic aerosol OOA from ambient measurements, and gasoline engine exhaust). To obtain quantitative information on the content of these components in the particles, the corresponding mass spectra are subtracted proportionately from the single particle mass spectra. Depending on the components found in every single particle it is assigned to a certain particle type. This approach allows an unambiguous detection of different species within the single particle mass spectra, and, unlike clustering algorithms, does not depend on the specific dataset analyzed.

In laboratory measurements this method was tested and validated. Species in laboratory-generated single particle mass spectra are reasonably well identified and separated, as long as sufficient signal is available.

The new single particle analysis method was applied successfully to AMS data acquired during field measurements which took place in July 2009 in Paris within the MEGAPOLI project. About 90% out of ~26,000 single particle mass spectra have successfully been classified according to their composition (Fig. 1). Particles originating from primary emissions (i.e. cooking and traffic) are found to be externally mixed with internally mixed particles of OOA, nitrate and sulphate. Only for a small fraction of particles, mixtures of different organic species or organics other than OOA with inorganics were found ("mixed organics" in Fig. 1).

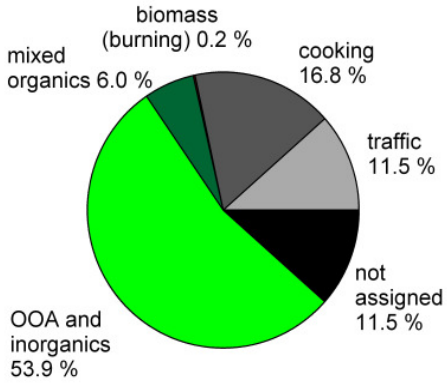

Figure 1. Classification of the AMS single particle mass spectra acquired during the MEGAPOLI campaign.

Comparison of averaged single particle composition with results from ensemble measurements showed good agreement. In addition to direct information about aerosol mixing state and consequently potential particle sources, this method provides valuable data on absolute concentrations of certain species within individual particles and their temporal variations.

We thank E.S. Cross, D. Sueper, T.B. Onasch, and J. Kimmel for providing the basic data analysis and the data acquisition software, respectively.

Cross, E.S., Onasch, T.B., Canagaratna, M., Jayne, J.T., Kimmel, J., Yu, X.-Y., Alexander, M.L., Worsnop, D.R., and Davidovits, P. (2009) *Atmos. Chem. Phys.* **9**, 7769-7793.

Liu, S., Russell, L.M., Sueper, D.T., and Onasch, T.B. (2012) *Atmos. Meas. Tech. Discuss.* **5**, 3047-3077.

Friday, September 6, 2013

Session: Particle-Lung Interactions,
PM toxicity

Translocation of fluorescently labelled SiO_2 nanoparticles across human bronchial epithelial monolayers

I. George[1], S. Vranic[1], S. Boland[1], and A. Baeza-Squiban[1]

[1] Laboratoire des Réponses Moléculaires et Cellulaires aux Xénobiotiques (RMCX), Unité Biologie Fonctionnelle et Adaptative (BFA), EAC CNRS 4413, Université Paris Diderot, Sorbonne Paris Cité, 5 rue Thomas Mann 75205 Paris cedex 13.

Keywords: Nanoparticles, Calu-3, NHBE, Barriers

Presenting author email: isabelle.george.rmcx@gmail.com

Potential effects of nanomaterials on human health and especially their ability to cross physiological barriers have to be determined because of applications of nanotechnologies in many fields. Inhalation is a frequent mode of exposure to nanoparticles (NPs) and there is evidence of their ability to cross epithelial barriers to reach secondary organs via the bloodstream. Our aim is the study of NP translocation across human bronchial epithelial cells using SiO_2 NPs of three different sizes (16, 50, and 100 nm).

We used the Calu-3 cell line which is able to form an efficient bronchial barrier when seeded onto a porous membrane. By evaluation of the transepithelial electrical resistance (TEER), as well as by monitoring the paracellular transport of a fluorescent marker (Lucifer Yellow), we have shown that Calu-3 cells have the ability to form a tight epithelial monolayer after 2 weeks in culture when they were seeded on 3 µm-polycarbonate Transwell membranes.

Fluorescently labelled SiO_2 NPs (SiO_2-FITC NPs) were used to quantify translocation, and we first investigated their ability to cross the porous membrane in the absence of cells. Whatever the NP size, 24 hours after applying NPs to the apical chamber, the NPs were recovered in the basal chamber with an increasing NP concentration (up to 10%) when the applied apical concentrations were decreasing. By confocal microscopy we observed that the majority of the NPs remained trapped in the membrane. Upon addition of foetal calf serum or dipalmitoyl lecithin, the transport of NPs increased by 5 or 30 times, respectively.

For concentrations up to 10 µg/cm² SiO_2-FITC NPs were non cytotoxic for the Calu-3 cell line and had no pro-inflammatory effect after 24 hours of treatment as shown by studying Interleukine-8 release. However they dose-dependently induced the expression of a specific bronchial mucin, MUC5AC. The translocation of NPs was size-dependent: 6% of the NPs applied to the apical chamber were recovered in the basal chamber when cells were exposed to the 16 nm-sized NPs whereas this percentage fell to 2% for 100 nm SiO_2 NPs. Confocal microscopy experiments were used to confirm NP internalization.

Experiments were also performed on primary Normal Human Bronchial Epithelial cells (NHBE). Quantitative translocation assays cannot be done as these cells must be grown on low porosity membranes (0.4 µm pores). Only morphological studies by confocal microscopy were performed on NHBE cells which exhibit normal (mucociliary) or pathological (squamous and mucosal) differentiation. Preliminary results have shown that NP retention inside the monolayer was differentiation-dependent with a very important retention inside the mucosal epithelium.

In conclusion, SiO_2-FITC NPs can cross in a low amount the bronchial epithelial barrier at non cytotoxic concentrations, without inducing cellular inflammation and affecting epithelial integrity. The mechanisms involved in this translocation are now under investigation. The Calu-3 cell line revealed to be a suitable model to characterize the ability of NPs to cross epithelial barriers according to their physico-chemical characteristics.

This work was supported by grants from Anses project N° PNR-EST-2010/2/79 (TiSiTrans) and National Grant “Nanotrans” (N°EST-2010/2/079) and by Région Ile de France / DIM SEnT for I. George PhD funding and FP7 project ENPRA (n°228789) for S. Vranic PhD funding.

Air-liquid interface exposure system for in vitro toxicological studies of wood combustion aerosols

S. Mülhopt[1], M. Dilger[2,3], C. Schlager[1], R. Zimmermann[3], S. Diabaté[2], C. Weiss[2], H.-R. Paur[1]

[1]Institute for Technical Chemistry, Karlsruhe Institute of Technology, 76021 Karlsruhe, Germany
[2]Institute of Toxicology and Genetics, Karlsruhe Institute of Technology, 76021 Karlsruhe, Germany
[3]HICE – Helmholtz Virtual Institute of Complex Molecular Systems in Environmental Health – Aerosols and Health, www.hice-vi.eu

Keywords: Exposure, Health effects of aerosols, Human lung cells, Combustion aerosols
Presenting author email: muelhopt@kit.edu

Background:
Exposure to ambient aerosols can epidemiologically be linked to increased morbidity and mortality rates, while aerosols formed during combustion processes seem to be the most potent hazards [1]. Current attempts to replace fossil fuels by regenerative sources create new additional sources for emissions of combustion derived aerosols. Despite of their high impact on human health, combustion aerosols, especially from regenerative sources, are insufficiently characterized. The aerosol components responsible for the adverse effects as well as the underlying mechanisms are yet to be identified. Addressing this knowledge gap, the "Helmholtz Virtual Institute of Complex Molecular Systems in Environmental Health" (HICE) conducts joint measurement campaigns wherein controlled aerosol generation by combustion of different fossil fuels (e.g. wood, diesel) is combined with comprehensive on-line characterization of the aerosols and in vitro investigations of their effects on human cells.

Material and Methods:
Most in vitro studies on aerosol health effects rely on submerged exposure of collected particulate matter, suspended in the medium. This method alters many characteristics of the aerosol. In contrast, the use of an air-liquid interface (ALI) exposure system allows on-line exposure experiments during aerosol generation while maintaining most of the physical and chemical characteristics of the aerosol components. Additionally, the possibility to separate the particulate phase from the whole aerosol is an important tool to study the relevance of gaseous components. For the reproducible assessment of lung toxicity of airborne particle emissions from combustion processes the Karlsruhe Exposure System was developed as described in detail before [2]. To cope with the high number of samples including controls needed for the biological characterization during the HICE measurement campaigns, a new ALI exposure system with up to 18 sampling positions has been built. As an option, electrostatic deposition can be used to increase the particle dose on the cells per time unit.

Figure 1. HICE exposure system for air-liquid interface exposure of human lung cells towards combustion derived particle emissions

Preliminary results of wood smoke exposed A549 human lung epithelial cells show no cytotoxicity but an induction of xenobiotic-metabolizing enzymes, attributable to the particulate matter.

Acknowledgement:
This work was supported by the Helmholtz Association within the virtual institute HICE. Further Informations: www.hice-vi.eu

References:
[1] Paur, H.-R., Cassee, F. R., Teeguarden, J., Fissan, H., Diabate, S., Aufderheide, M., Kreyling, W. G., et al. (2011). *Journal of Aerosol Science*, 42(10), 668–692. doi:10.1016/j.jaerosci.2011.06.005
[2] Paur, H.R., Mülhopt, S., Diabaté, S., Weiss, C. (2008) *Journal für Verbraucherschutz und Lebensmittelsicherheit*, 3, 319-329

Nanotoxicological studies in the Air-Liquid Interface using engineered metal NPs – Protein corona, gene analysis and dose response

C.R. Svensson[1],S. Ameer[2], J.H. Pagels[1], T. Cedervall[3], M. Kåredal[2], L. Ludvigsson[4], K. Broberg[2], B.O. Meuller[4], M.E. Messing[4], J. Rissler[1]

[1]Ergonomics and Aerosol Technology, Lund University, Lund, SE 221 00, Sweden
[2]Occupational and Environmental Medicine, Lund University, Lund, SE 221 00, Sweden
[3]Biochemistry and Structural Biology, Lund University, Lund, SE 221 00, Sweden
[4]Divison of Solid State Physics, Lund University, Lund, SE 221 00, Sweden
Keywords: Nanoparticles, Air Liquid Interface, Characterization, Toxicology
Presenting author email: Christian.Svensson@design.lth.se

There is an ongoing discussion whether traditional toxicological methods are sufficient to evaluate the risk of inhalable nanoparticles. Since the use of manufactured nanoparticles is increasing, the need for toxicological data is great. There is also an increased interest in metal nanoparticles for targeted drug delivery. This has led to the emergence of Air-Liquid Interface toxicology. Here aerosol NPs are administered directly from air and deposited upon cellular cultures, or relevant media, providing a more realistic in vitro environment for toxicological studies, especially for lung deposition – one route of exposure that has been pinpointed as important in risk assessments.

This work takes on a holistic approach towards the toxicology of metal NPs. The NPs are characterized in aerosol phase with regards to both mass, size and morphology. The NPs are then deposited unto cellular cultures or into physiological media using a commercialised deposition chamber, *Nano Aerosol Chamber In Vitro Toxicity* (NACIVT), a chamber based on the work by Savi (2008). When deposited into cellular media, blood serum or into lung fluid the NPs characteristics in solution can be studied using several methods. By using UV-Vis spectroscopy the relative degree of agglomeration is determined and by using dynamic light scattering and particle tracking analysis the hydrodynamic size is determined. Upon deposition onto cellular cultures, both primary and standardized cell lines, endpoints of varying sensitivity is investigated to determine the NP effects. Cellular viability and cytotoxicity is determined using standard assays. Protein expression from the cells will be investigated in the surrounding media, cytokines, interleukins etc. In addition state of the art gene analysis techniques will be employed, both towards a whole genome perspective and single genes. The rationale is that as particles may not be directly terminal towards the cells, they still react in characteristic ways expressing various genes.

One type of NP that will be used is agglomerate and sintered silver (AgNP) generated by a spark discharge system, described by Meuller (2012). The system is capable of generating aerosols of a variety of different metal particles with different shapes properties. The aerosol is generated polydisperse as agglomerates, by using a sintering furnace the agglomerates can be compacted to varying degrees. This results in metal NP aerosols with the varying total surface areas, while retaining the same total mass.

In order to characterize a sintered AgNP aerosol it was connected to a laminar flow diluter (model 3302, TSI Inc.) and the NACIVT was coupled in parallel with a TEOM and an SMPS system. The dilution system allowed for a stable dilution up to 15 times. Also AgNP was deposited in the NACIVT on silicon surfaces for electron microscopy and determination of deposition efficiency, Figure 1A.

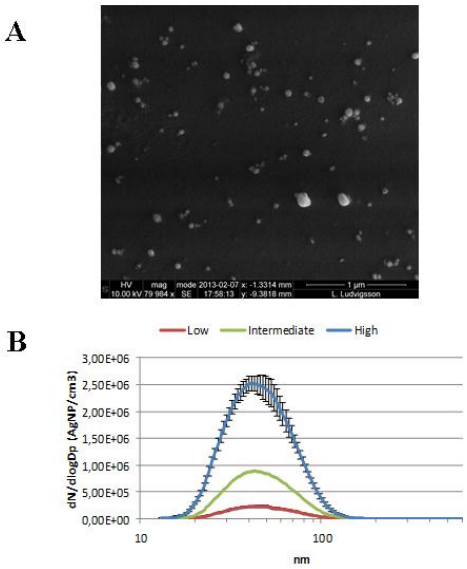

Figure 1. A) Sintered AgNPs deposited onto a SEM grid in the nacivt chamber. B) Average SMPS scan of sintered AgNP at three concentrations tested.

The cell exposures were performed at three concentration levels, exposing the cells placed in the NACIVT chamber during one hour. The SMPS system scanned the size distributions continuously, shown in Figure 1B, The AgNP aerosol was stable during the events and deposition efficiency approximately 15-20%. By TEOM the mass concentrations with std was 1520(180), 467(97) and 99(20) µg/m3.

In conclusion a stable aerosol of AgNP agglomerates was generated for exposure of cells during 1h duration, with endpoints including state of the art gene analysis and standard assays.

This work was supported by the Nanometer Structure Consortium at Lund University (nmC@LU) and the Swedish research council FAS through project 2009-1291 and the FAS-centre METALUND

Savi, M. (2008).Environ. Sci. Technol. ***42****, 5667-5674*
Meuller, B.O. (2012). Aerosol Sci. Technol. ***46****, 1256-1270*

Aerosol characterisation of e-cigarettes

R. Cabot[1], A. Koc[1], C.U. Yurteri[1] and J.J. McAughey[1]

British American Tobacco, Group R&D Centre, Regents Park Road, Southampton, SO15 8TL, UK
Keywords: e-cigarette, smoke, particle size, particle concentration
Presenting author email: john_mcaughey@bat.com

E-cigarettes are a new category of inhaled consumer product rapidly gaining popularity with adult cigarette smokers. Electronic cigarettes (also known as e-cigarettes or electronic nicotine delivery systems (ENDS)) are typically cigarette shaped battery-powered electronic devices which produce an aerosol containing nicotine generated by an electrically powered heating element which vaporizes a liquid formulation. The condensable material used to generate the bulk aerosol is normally a formulation of water, nicotine with glycerol, propylene glycol (PG) or a mixture of each. A coloured LED at the end is lit when the device is puffed. The system heaters are normally activated on puffing via an internal pressure detector.

Particle size measurements were conducted on a glycerol, water and nicotine based commercial e-cigarette bought from retail sources in the UK. One complication for testing is that there are no accepted standard puffing regimes for analytical testing of this new product category and hence puffing regimes similar to those used for cigarette testing were used but with some differences. In practice, there is a delay from the onset of puffing for the pressure sensor to actuate and effective heating to commence. Ingebrethsen *et al.* (2012) report this to be of the order of 1s which matches our experience. Therefore puff regimes were of 3s duration and 30s intervals rather than the 2s durations normally used for cigarette smoking. Puff volumes were 50 mL, equivalent to mouth volume in the ICRP66 inhalation model. A minimum of 144 consecutive puffs were taken on 3 examples of a commercial e-cigarette, in line with reported capacities, and tested by electrical mobility. Light scattering measurements were confined to 12 puff replicates.

Measurements were conducted by electrical mobility using the Model DMS-500 with Smoking Cycle Simulator (Cambustion, UK) and by light scattering using the Spraytec (Malvern, UK).

Table 1: Electrical mobility (EM: n=432) and light scattering (LS: n=12) measurements for e-cig aerosol.

	Count Median Diameter (nm)	Volume Median Diameter (nm)	Particle Number per puff
EM	63 ± 9	252 ± 11	4.99e10 ±2.26e9
LS		435 ± 39	

Measured geometric standard deviations (σ_g) are 1.55–1.65 and good precision is observed for both measures.

The volumetric mean particle diameter data are similar for the two methods given their different physical operating principles. The electrical mobility analyser operates at reduced pressure and there is scope for evaporation from the glycerol / nicotine / water droplets. This was observed by Ingebrethsen *et al.* (2012) who reported typical geometric mean diameters of 17-28 nm by electrical mobility. The Ingebrethsen, 2012 work used a high level of secondary dilution (200:1) and hence total dilution (3 400-5 500:1), in contrast to our own work where secondary dilution was absent. The observed data are consistent with increased evaporation at higher dilution levels as might be expected. The presence of particles for measurement was consistently observed for 2.0-2.1s of the 3s puff supporting the hypothesis of a delayed onset of approximately 1s from puff initiation to aerosol delivery. Particle number per puff are of the same order between these and the Ingebrethsen data (2.7-7.4e9.cm^{-3}), when corrected for puff volume.

For light scattering, it is known that scatter intensity from aerosol droplets decreases markedly below the wavelength of visible light and therefore there is some scope for smaller particles in the distribution to be under-represented, potentially elevating the average diameter. Reported data from this study are again similar to those of the Ingebrethsen study where measurements of diameter of average mass by a multi-wavelength light extinction apparatus were in the region of 272–351 nm.

In conclusion, the measurement data suggest that the aerosol plume from e-cigarettes can be characterised with good precision, by real-time analytical methods using commercially available equipment. Further work is clearly necessary to agree standard testing regimes between industry and regulators and further scientific investigation is required to understand and develop the most appropriate measurement technique.

This work was conducted in-house by British American Tobacco.

Ingebrethsen, BJ., Cole, SK and Alderman, SL (2012) *Inhal Toxicol.* **24**(14):976-84.

International Commission for Radiological Protection ICRP Publication 66 : (1994) *Ann. ICRP* **24** (1-3).

Ecotoxicity of various types of urban particulate matter

B. Jancsek-Turóczi[1], A. Hoffer[2], Á. Tóth[1], N. Kováts[1], A. Ács[1], and A. Gelencsér[1]

[1]Institute of Environmental Sciences, University of Pannonia, Veszprém, H-8201, Hungary
[2]Air Chemistry Group of the Hungarian Academy of Sciences, Veszprém, H-8201, Hungary
Keywords: PM_{10}, ecotoxicity, health effects
Presenting author email: turoczi.beatrix@indamail.hu

The health effects of urban air pollution are evaluated on the basis of time-weighted average concentrations of criteria pollutants (e. g. NO_x, CO, SO_2, O_3, $PM_{2.5}/PM_{10}$). The PM_{10} is identified as one of the most dangerous pollutants on human health by the EU new directive on air quality (2008/50/CE). The hazard posed by urban PM is generally linked to the presence of toxic metals, carcinogenic and mutagenic compounds, thus it depends on the sources of PM that vary by season.

Bioluminescence inhibition bioassays were successfully deployed for the assessment of potential health effects of organic extracts of particulate matter collected from vehicular exhaust (Vouitsis *et al*, 2009). However, these studies only assess the ecotoxicity of a subfraction of $PM_{2.5}/PM_{10}$, and the deployment of organic solvents such as dimethyl-sulphoxide or dichloromethane, combined with Soxhlet extraction does not represent a realistic environmental exposure route.

Therefore a simple method was developed for the direct assessment of the bulk ecotoxicity of $PM_{2.5}/PM_{10}$ (Kováts *et al*, 2012). This method is based on the kinetic version of the *Vibrio fischeri* bioluminescence inhibition bioassay (Lappalainen *et al*, 1999). Contrary to previous other measurements, the bulk samples are assayed without prior extraction, and no organic solvents are applied.

During different aerosol sampling methods aerosols of various types were collected: winter and summer urban PM_{10}, diesel engine emission aerosol of passenger cars and buses, biomass and cigarette smoke samples and resuspended road dust.

During ecotoxicity bioassays aqueous suspensions of aerosol samples were measured with Thermo Luminoscan Ascent unit. Ecotoxicity (EC_{50} values) of samples were calculated using Ascent Software provided by Aboatox Co. EC_{50} of a sample was determined as the absolute mass of aerosol particles that causes 50 % reduction in the bioluminescence output of the test organisms relative to the control under the given experimental conditions. EC_{50} is expressed in units of mg. The lower EC_{50} value indicates higher ecotoxicity of the sample.

Fresh biomass and cigarette smoke samples proved to be the most ecotoxic among all aerosol types. Surprisingly, the most diesel engine emission samples were less ecotoxic than biomass smoke samples. EC_{50} values of diesel emission samples of passenger cars showed more scatter due to different engine types, conditions and fuel qualities. Ecotoxicity of diesel engine emission samples of buses showed very high correlation with engine standards: ecotoxicity of EURO 0 and 1 engines were found to be the highest and that of EURO 4 engine was not measurable. Resuspended road dust was the least ecotoxic due to the high fraction of inert mineral phases (Jancsek-Turóczi *et al*, 2013).

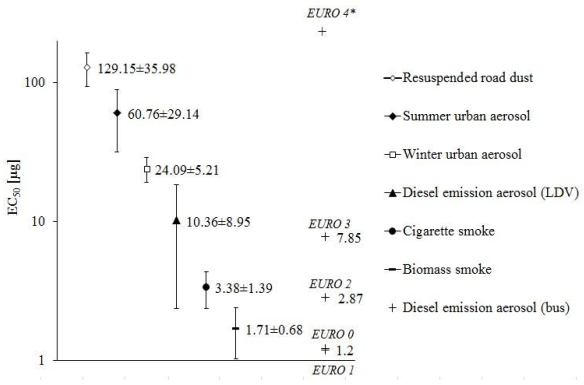

Figure 1. Comparison of EC_{50} values of aerosols of various types.

Winter urban PM_{10} samples showed significantly higher EC_{50} values than summer PM_{10} due to high contribution of vehicular and wood burning emissions which were also ecotoxic. In summer the biomass burning emission is substituted with secondary organic aerosol which reduces the ecotoxicity. Furthermore, the higher degree of atmospheric mixing in summer reduces the share of primary emission particulates and increases the contribution of atmospheric transport. Bioaerosol particles of probably negligible ecotoxicity are also more abundant in summer than in winter (Turóczi *et al*, 2012).

The authors are grateful for the financial support of the grants of the Hungarian Research Fund OTKA K 101484.

Jancsek-Turóczi, B., Hoffer, A., Nyírő-Kósa, I. and Gelencsér, A. (2013*) J. Aerosol Sci.* (in review)

Kováts, N., Ács, A., Kovács, A., Ferincz, Á., Turóczi, B. and Gelencsér, A. (2012) *Environ. Toxicol. Pharmacol*. **33**, 223–228.

Lappalainen, J., Juvonen, R., Vaajasaari, K, and Karp, M. (1999) *Chemosphere*, **38** (5), 1069–1083.

Turóczi, B., Hoffer, A., Tóth, Á., Kováts, N., Ács, A., Ferincz, Á., Kovács, A. and Gelencsér, A. (2012) *Atmos. Chem. Phys.* **12**, 7365–7370.

Vouitsis, E., Ntziachristos, L., Pistikopoulos, P., Samaras, Z., Chrysikou, L., Samara, C., Papadimitriou, C., Samaras, P. and Sakellaropoulos, G. (2009) *Environ. Pollut.* **157**, 2320–2327.

The respiratory toxicity of coal fly ash

T.P. Jones[1], P. Brown[2] and K.A. BeruBe[2]

[1]School of Earth and Ocean Sciences, Cardiff University, Cardiff, Wales, CF10 3YE, UK
[2]School of Biosciences, Cardiff University, Cardiff, Wales, CF10 3AX, UK
Keywords: combustion, DNA damage, fly ash, mullite, physicochemistry, reactive oxygen species.
Presenting author email: berube@cardiff.ac.uk

The combustion of coal for the generation of electricity has many environmental implications. Coal fly ash (CFA; Figure 1) is a product of coal combustion, formed from the incombustible mineral matter contained within the coal. CFA is respirable (i.e. <2.5µm diameter) and known to be detrimental to human respiratory health upon exposure (Brown, 2011).

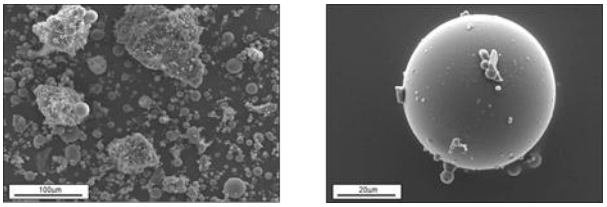

Figure 1. Scanning electron micrograph of CFA: Bulk (left|) and PM10 (right) fractions, respectively.

The aim of this study was to compare the relative respiratory toxicity of CFA samples obtained from three Chinese coal-burning power stations to CFA obtained from a UK coal-burning power station; both bulk and respirable PM_{10} samples were tested. In order to elucidate CFA toxicity, a multi-disciplinary approach was taken, thereby considering geochemical aspects of the fly ash as well as biochemical properties.

Geochemical analysis was used to determine the composition, morphology and solubility of metallic components. Total analysis, carried out using FLUXY ICP-MS, identified the bulk elements present, X-ray diffraction (XRD) identified crystalline phases present in the particles, and the overall morphology was evaluated by scanning electron microscopy (SEM).

Three *in vitro* biochemical techniques were used to elucidate the samples relative bioreactivity. The samples were tested on their capability to a) generate reactive oxygen species (ROS), using a DCFH assay, b) cause haemolysis of red blood cells (RBCs) via a haemolysis assay, and c) cause damage to plasmid DNA, by use of a plasmid scission assay (PSA).

The geochemical analysis showed the samples differ very little in composition between bulk and PM_{10} fractions and the overall solubility of metals was low (Figure 2). XRD identified the presence of mullite (Figure 3) in all samples with increased levels seen in one particular Chinese sample. SEM showed the particles to be spherical in shape and respirable in size, with 18% of the UK PM_{10} samples in the fine particle size range, able to reach the most distal regions of the respiratory system.

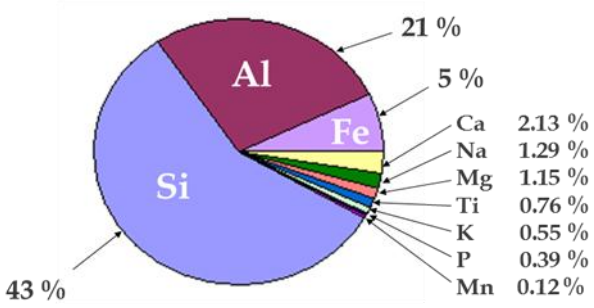

Figure 2. Elemental composition of a UK PM_{10} fly ash sample. The level of leachable metals is very low.

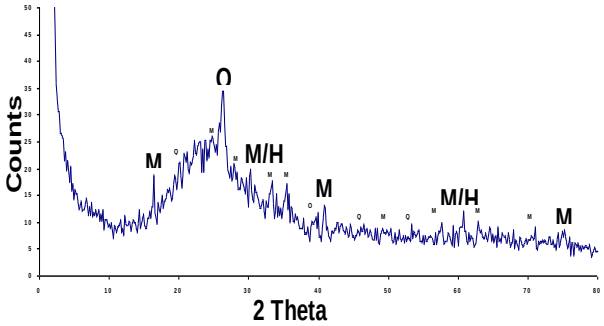

Figure 3. XRD showing mullite (M) and hematite (H).

The biochemical assays showed the Chinese samples to be more reactive, especially one PM_{10} sample, which gave 66% haemolysis for a 15mg dose and 49% damage to plasmid DNA. The relative toxicity of technogenic particles is often dependent on the bioavailability of metals, which generate ROS via Fenton-redox mechanisms. CFA metals appear tightly bound within the spheres, suggesting forms of crystalline silica may provide the platform for toxicity.

PM_{10} can remain airborne, travel long-distance and penetrate into the thoracic region of the lungs. CFA is known to contain toxic heavy metals, e.g. As, Hg, Pb, Cd, Se, which are associated with cancer and neurological problems. Fly ash is put into landfills and lagoons which can leach heavy metals, risking contamination of ground water and water supplies. Effective particulate removal technology and waste management is critical to removing any potential threat to human health.

This work was supported by the Medical Research Council (MRC), UK.

Brown, P. (2011), *Respiratory Toxicity of Coal Fly Ash*. PhD Thesis, Cardiff University, Wales, UK.

Trace elements bioaccessibility in fine and ultrafine particles from the industrial area of Dunkirk (France) during the NANO-INDUS project

S. Mbengue [1,2], L. Alleman [1,2] and P. Flament [1,3]

[1] Univ Lille Nord de France, F-59000 Lille, France
[2] Mines Douai, CE, F-59508 Douai, France
[3] ULCO, LPCA, F-59240 Dunkerque, France
Keywords: Fine particles, Trace elements, bioaccessibility, lung fluid.
saliou.mbengue@mines-douai.fr

Inhalable atmospheric particles (< 10 µm) may contain high concentrations of trace elements (TE) that could induce adverse cardiovascular and respiratory effects (Donaldson *et al.*, 2002). Fine and ultrafine particles (smaller than 2.5 and 0.1 µm, respectively) are suspected to be more harmful, because of their small size and high specific surface, allowing them to penetrate deeply in our respiratory tract and even pass through the cellular membrane. After penetrating in our body, particulate TE can be partially or completely dissolved upon contact with the lung fluids (Costa and Dreher, 1997). Particle size, shape, chemical composition and potentially toxic bioaccessible content are the main characteristics to consider in the PM-induced biological impacts (Oberdörster *et al.*, 2005). Trace metal pulmonary bioaccessibility assessment requires the use of extraction solutions mimicking the physiological fluids (Caboche *et al.*, 2011). The purpose of this study was to assess TE bioaccessibility in different size fractions of PM, collected according to emission sources using a synthetic lung fluid (Gamble solution, pH = 7,4 et ≈ 37 °C). Coarse, fine and ultrafine PM were collected in the vicinity of metallurgical plants (at 500 and 2000 m from the chimneys) and in traffic influenced urban area nearby, using cascade impactors (DEKATI - 3 and 13 stages). Bioaccessible fractions and total concentrations of a large set of elements, selected according to their potential toxicity and their property of source markers (Al, As, Ba, Cd, Co, Cr, Cu, Fe, K, La, Mg, Mn, Mo, Ni, Pb, Rb, Sb, Sr, Ti , V and Zn), were analyzed by ICP-AES and ICP-MS.

Overall, total concentrations in PM_{10} increased with the industries proximity, implying the large contribution of industrial sources in PM_{10} TE concentrations. Pulmonary bioaccessibility results show that metal solubility would depend on the source types. Indeed, the solubility in the Gamble solution for Mn, Pb, Rb and Zn (associated to the metallurgical emissions) in PM_{10} were higher in the vicinity of industrial plants than in urban area where, inversely, traffic related elements (Cu and Sb) showed higher dissolution percentages. For elements associated to industrial emissions, bioaccessibility in PM_{10} decreased with the distance from the sources that could be linked (1) to the change of elemental speciation during PM transport or (2) the increasing contribution of others/more refractory sources. In the industrial and "urban-traffic" areas, the bioaccessibility increased toward smaller PM, particularly for anthropogenic elements like Cd, Co, Mn, Ni, Pb, Rb, Sb and Zn.

These results indicate that the bioaccessibility may vary according to the type and distance from the sources, in addition to the size of PM and the chemical form of TE. Our current works move at the moment to a better estimate of these two parameters within industrial plumes.

This work was part of a program from the "Institut de Recherche en ENvironnement Industriel" (IRENI) and was financially supported by the French Environment and Energy Management Agency (ADEME), the Nord-Pas-de-Calais Regional Council, the French Ministry of Higher Education and Research, the European Regional Development Fund (ERDF) and Ecole des Mines de Douai.

Costa, D.L., Dreher, K.L. (1997) Environ. Health Persp. **105**, 1053-1060.
Caboche, J., Perdrix, E., Malet, B., Alleman, L. Y. (2011) *J. Environ. Monit.* **13**, 621-30.
Donaldson, K., Tran, C.L., MacNee, W. (2002) *Eur. Respir. Mon.* **21**, 77–92.
Oberdörster, G., Oberdörster, E., Oberdörster, J. (2005) *Environ Health Perspect.* **113**, 823-39.